Final Report

Project Title: Mississippi State University Sustainable Energy Research Center, Phases I - IV
Award Number: DE-FG36-06GO86025

Recipient: Mississippi State University
Project Location: Mississippi State University, Starkville, Mississippi

Reporting Period: June 1, 2006 – June 30, 2014
Date of Report: September 26, 2014
Written by: W. Glenn Steele

Principal Investigator: W. Glenn Steele

Mississippi State University
DOE Project DE-FG36-06GO86025
Sustainable Energy Research Center

Lessons Learned

Most significant successes and advances in this project:

The Sustainable Energy Research Center (SERC) project at Mississippi State University included all phases of biofuel production from feedstock development, to conversion to liquid transportation fuels, to engine testing of the fuels. The significant successes and advances for each are discussed below.

The feedstocks work focused on non-food based crops and yielded an increased understanding of many significant Southeastern feedstocks. An emphasis was placed on energy grasses that could supplement the primary feedstock, wood. Two energy grasses, giant miscanthus and switchgrass, were developed that had increased yields per acre. Each of these grasses was patented and licensed to companies for commercialization.

The fuels work focused on three different technologies that each led to a gasoline, diesel, or jet fuel product. The three technologies were microbial oil, pyrolysis oil, and syngas-to liquid-hydrocarbons.

The microbial oil technology resulted in a process to increase the oil accumulation by the microbes. This process was demonstrated at a pilot-scale of one gallon per day of finished fuel and a patent was obtained for the technology. The patent has been licensed to a company for commercialization.

The pyrolysis oil work resulted in both an economical boiler fuel and in a gasoline, diesel, jet fuel mixture with a low oxygen content. An auger-fed fast pyrolysis system was developed and was demonstrated in a one ton per day pilot-scale facility. This facility includes all phases of the fuel production process: feedstock preparation and transport, bio-oil production, and conversion process to produce liquid transportation fuels.

The syngas-to-liquid hydrocarbons work resulted in several multifunctional catalysts for gasoline range, diesel range, or jet fuel range hydrocarbons production. The technology was demonstrated in a pilot-scale facility that included a gasifier, a gas clean-up system, and a one gallon per day reactor. Patents were obtained for the catalysts, and a license has been issued to a company for commercialization of the diesel fuel technology.

The engine testing work resulted in significant advances in the understanding of the combustion process for mixed biofuel/conventional fuel engine firing. The results

showed performance and emissions benefits from the mixed fuels. These tests were run at the micro-level in a rapid compression machine, in a single cylinder research engine, and at scale in spark-ignition and diesel engines.

Areas where project came up short and why:

The SERC project met all the contract goals and objectives. A local goal that was above and beyond the contract goals was to have each fuel technology patented and licensed to a company for commercialization. The pyrolysis oil technology has seen significant interest but has no active licenses at this time. A major barrier in the commercialization of these new technologies is the financial risk in taking a new product to market. In addition, the declining price of fossil fuel has made it challenging for biofuels to be competitive.

Future work:

As noted under project short comings, the financial risks in commercializing a new technology are great. Usually the science is understood, but the engineering hurdles to full scale operation can be insurmountable. Related to the SERC fuel technologies, future work could include small steps toward eliminating these engineering hurdles. The SERC pilot-scale facilities answered much about the initial scale-up issues. A few intermediate scales between the pilot and full-scale operation could increase the probability of success in the final commercialization of the technologies.

Final Report

Project Title: Mississippi State University Sustainable Energy Research Center
Award Number: DE-FG36-06GO86025

Recipient: Mississippi State University
Project Location: Mississippi State University, Starkville, Mississippi

Reporting Period: June 1, 2006 – December 1, 2008
Date of Report: March 31, 2009
Written by: William D. Batchelor and W. Glenn Steele

The goal of the Sustainable Energy Research Center (SERC) at Mississippi State University (MSU) is to build multi-disciplinary teams to conduct research needed to exploit the ability of the state and region to generate biomass for energy production and to develop economic and environmentally sustainable energy conversion systems to support the emerging sustainable energy industry in the Southeast. The work under this contract, DE-FG36-06GO86025, is divided into twelve different tasks ranging from feedstock development, to fuel production, to product utilization. The complete listing of projects and tasks is provided in the table below. Following the table a complete final report is provided for each of the A through L task areas.

Number of Task, subtask(s), or	Title of task, subtask or milestone.	Task or Milestone Completion Criteria (to include cost and performance metrics)	Actual accomplishments
A	Biodiesel		
A.DL.1	Final Report		Complete
A.1	Conversion of waste sludge to biodiesel	Producing ASTM Biodiesel	Crude biodiesel was generated from sewage sludge. This biodiesel is being refined to comply with the ASTM standard.
A.1.ML.1	Produce ASTM Biodiesel from sewage sludge	Producing ASTM Biodiesel	Crude biodiesel was generated from sewage sludge. This biodiesel is being refined to comply with the ASTM standard.
A.2	Identification and grow of oleagenous microorganisms	Production of lipids >20% dry weight of microbes	Numerous oleagineous microorganisms were identified and grown using lignocellulose sugars and glycerine.
A.2.ML.1	Microbial production of oils using glycerine	Production of lipids >20% dry weight of microbes	Several oleaginous microorganisms were examined to produce oil from glycerine. Some of the evaluated microorganisms produced more than 20% of their dry weight in oil.
A.3	Evaluation of lipid capture strategies	Provide list of adsorbents	Numerous adsorbents were identified with the potential to remove oils from water.
A.3.ML.1	Identify adsorbents to remove lipids from wastewaters	Provide list of adsorbents	Based on chemical and physical properties three adsorbents were selected for further examination of lipids removal from water. These adsorbents were kenaf, cellulose acetate, and polyethylene.
A.3.ML.2	Enhance adsorption capacity and selectivity via surface modification	Enhance lipid removal over baseline (non-modified adsorbents)	The surface of selected adsorbents was modified using strong oxidizers. The adsorption capacity of the selected adsorbents toward lipids increased after surface modification.
A.4	Biodiesel from Chinese tallow, castor, rape, and tall oil	Producing ASTM Biodiesel	ASTM biodiesel was produced from tall oil. Chinese tallow and Castor oil are still being evaluated. Biodiesel produced from castor oil does not meet ASTM quality because of high viscosity. One option to be evaluated is the blending of castor oil biodiesel with soy biodiesel to meet the viscosity test.
A.4.ML.1	Optimize process parameters	Producing ASTM Biodiesel	Process parameters were optimized for producing biodiesel from tall oil. Optimum parameters to produce biodiesel from Chinese tallow and castor oils are being determined and will be included in the final report.
A.4.ML.2	Determine process economics	Report process economic for producing ASTM biodiesel	Process economics will be calculated using the optimum process parameters and will be included in the final report.
A.5	Developing culturing techniques for lipid bearing plants	Cultivate crops	Culturing techniques were developed for castor, sunflower, okra, and crambe.
A.5.ML.1	Identify and culture south east high oil content crops	Cultivate crops	Castor was identified as a summer crop.
A.5.ML.2	Genetically modified plants to produce more oils	Enhance oil production compared to baseline (non-genetically modified)	Genes that increase branching in plants were indentified and tested. The increase of branching would increase seed numbers per plant, and consequently, oil production.
A.5.ML.3	Develop ricin-free castor	Reduce ricin concentration	Genetic, chemical, and physical methods were examined to deactivate and/or reduce ricin concentration in castor seeds.
A.6	Development of lipid extraction models using supercritical fluids	Report model predictions	Vapor pressure predictions for three phospholipids were completed: 1,2-Distearoyl-sn-glycero-3-phosphotidylethanolamine (CAS # 1069-79-0); 1,2-Dioleoyl-sn-glycero-3-phosphotidylcholine (CAS # 56648-95-4); 1,2-Dipalmitoyl-sn-glycero-3-phosphotidylethanolamine (CAS # 923-61-5).
A.6.ML.1	Determine experimental and theoretical solubility of model lipids	Comparison between predictive models and experiments	Predictions and experimental solubility of phospholipids in conventional solvents, and in supercritical carbon dioxide/methanol mixtures were completed.
A.7	Determine stability of non-traditional lipid feedstocks	Report stability of oils and biodiesel	Catfish oil was evaluated for stability. The best oil source is a non-heated source as a byproduct of an organic feed manufacturer.
A.7.ML.1	Correlate oil oxidation measurements with shelf life	Report correlation of stability and shelf life	Conducting tests at 80C results in good predictability of stability of oils and biodiesel.
A.8	Develop heterogeneous catalyst for transesterification	Producing ASTM Biodiesel	Numerous heterogenous catalysts were examined to produce biodiesel. ASTM quality was not achieved.
A.8.ML.1	Produce biodiesel using heterogeneous catalysts	Producing ASTM Biodiesel	FAMES were generated using several heterogenous catalyst and soybean oil. ASTM quality was not achieved. The catalysts were deactivated in a relatively short time.
A.9	Techniques to reduce NOx emissions	Model NOx emissions	Modeling results indicated some of the biodiesel properties that could enhance NOx formation.
A.9.ML.1	Perform emission studies using ethano/biodiesel blends	Model NOx emissions	NOx emmisions from several ethanol/biodiesel blends were measured.
A.9.ML.2	Validate a proposed mechanism for NOx generation	Report modeling results	Experiments were conducted to validate NOx generation mechanisms.

A.10	Conversion of glycerin into value-added chemicals	Higher yield and selectivity compared to sugars	Although the by-products identified were not propanediol or lactic acid, their by-products were valuable non-the less. All cultures tested showed the ability to produce acetic acid with the highest concentration of 1.2 g/l medium. Two cultures showed the ability to produce butanoic acid in addition to the acetic acid. One of the four cultures tested was able to produce a third metabolic by-product, propanoic acid.
A.10.ML.1	Optimize production of 1,3-propanediol and lactic acid using neat and crude glycerine	Higher yield and selectivity compared to sugars	Lactic acid and 1,3-propanediol were not produced efficiently from the using the evaluated cultures.
A.10.ML.2	Develop a kinetic model for converting glycerine into 1,3-propanediol or lactic acid	Report modeling results	Since the cultures evaluated did not produce 1,3-propanediol or lactic acid, the task was foused on acetic acid rate of production. The rate of acetic acid production was determined to be 0.174 mg acetic acid/g of cells/ h.
A.11	Separation of nutraceutical fatty acids	High selectivity for unsaturated fatty acids	Different metal ions were evaluated for the extraction of omega-3 fatty acid methyl esters. Metal complexes with very high selectivity toward the unsaturated omega-3-fatty acids were identified.
A.11.ML.1	Evaluate different transition metal ions on silica gel for the separation of FAMEs	High selectivity for unsaturated fatty acids	Sorbents were successfully applied to extract and enrich polyunsaturated fatty acid methyl esters (PUFAMEs) including EPA and DHA with both high selectivity and high capacity.
A.11.ML.2	Evaluate biphasic solvent as extraction media	High selectivity for unsaturated fatty acids	Ionic liquids were used to extract polyunsaturated fatty acids from solution with high selectivity.
A.12	Removal of biodiesel impurities (metals) using silane compounds	Producing ASTM Biodiesel	The results from synthesis experiments utilizing sodium dodecyl benzene sulphonate (SDBS) as a linking agent between the Cu surface and tetraethoxysilane (TEOS) indicated that the silane concentration greatly impacts the silica shell thickness and porosity.
A.12.ML.1	Sinthesize silane compounds capable of removing impurities from biodiesel	Producing ASTM Biodiesel	Transmission electron microscopy images of the metal-silicate core-shell nanostructures were utilized to compile average particle diameter, silica shell thickness, and overall morphology of the core-shell nanostructures.
Number of Task, subtask(s), or	Title of task, subtask or milestone.	Task or Milestone Completion Criteria (to include cost and performance metrics)	Actual accomplishments
B	Bio-oil		
B.DL.1	Final Report		
B.1	Characterization of bio-oils produced from southern forestry and agricultural feed stocks	Bio-oils from the specified southern forestry and agricultural feed stocks characterized	For 4 southern biomass types feed stocks, bio-oils and pyrolysis chars were physically and chemically analyzed.
B.1.DL.1	Harvest and dry feed stocks and perform ash and inorganic tests	Feed stocks obtained, dried and ground for pyrolysis	Pine, sweetgum, white oak and switchgrass feed stocks were harvested, dried to 10% moisture content and pyrolyzed.
B.1.DL.2	Perform py-GC/MS on 4 feed stocks	Py-GC/MS analyses performed	Py-GC/MS analyses were performed as initial data prior to performance of laboratory-scale auger pyrolysis reactor runs.
B.1.DL.3	Pyrolize 4 feed stocks and perform chemical and physical tests on bio-oils and char	Bio-oils produced and bottled for analysis	Auger pyrolysis reactor runs were performed to produce bio-oil and char for each of the 4 species studied. Some chemical and physical analyses were performed at MSU and some by independent laboratories.
B.2	Bio-oil hydrogenation and co-pyrolysis for fuels and co-products	Bio-oils upgraded by HDO, methylation or esterification and one or more value-added chemical products developed	Catalytic HDO was successfully performed; esterification was performed by homogeneous and heterogenous catalysis.
B.2.DL.1	Test bio-oil fractionation methods to produce lignin and aqueous fractions; analyze fractions	Chemical analyses of fractions complete	Fractionation of bio-oils was found to be unnecessary in order to apply HDO successfully; these experiments were, therefore, terminated.
B.2.DL.2	Perform HDO on raw bio-oils and lignin fractions with standard and new catalysts	HDO performed with 2 standard and 4 new catalysts; products identified	HDO was performed with 2 standard and numerous new catalysts. A commercial catalyst not previously applied for bio-oil HDO was selected as the most economic catalyst.
B.2.DL.3	Establish transesterification reaction conditions for various homogeneous and heterogeneous catalysts; screen catalysts and select system with highest	Subset of catalysts identified and chemical analyses completed	Several heterogeneous and homogeneous esterification catalysts were tested and the catalyst with highest yield was identified. Chemical analyses are complete.
B.2.DL.4	React raw bio-oils with methanol/catalyst and distill; chemically and physically characterize methylation products	Chemical and physical analysed of methylated products completed	Chemical and physical analyses of methylated products were completed. Methylation required large percentages of alcohol and long reaction times. The methylation approach was abandoned in favor of the more economic esterification process developed in another task.
B.2.DL.5	Perform py-GC/MS co-pyrolysis of polypropylene with oak and pine feed stocks; analyze results	Chemical analyses of copyrolysis products complete	Copyrolyis of 3 plastic types was completed and chemical and physical tests completed. Results indicated significantly increased hydrogen content, and therefore upgrading, for bio-oils produced from copyrolysis of a 1 to 1 blend of wood and plastic.

B.3	Upgrading pyrolysis vapor via catalysis and filtration	Pyrolysis vapor catalysis and filtration to the stage that petroleum refining can be applied to produce fuels and chemicals	Vapor catalysis has been tested with 4 catalysts; catalytic coking was minor at approximately 10%. Vapor catalyzed bio-oils with relatively high water contents were produced indicating potential hydrodeoxydation from catalysis reaction. Vapor filtration with a new media appears promising. There was some delay in starting this project due to unavailability of the Gen I pyrolysis reactor. However, upon completion of the Gen II reactor the Gen I reactor is completely dedicated to vapor catalysis and the research is progressing well.
B.3.DL.1	Design, fabricate and test vapor phase reactor and filter	Vapor phase reactor tested with a single catalyst	A single vapor phase catalyst was tested early in the research.
B.3.DL.2	Test vapor-phase reactor with a limited number of catalysts	Five catalysts tested with vapor phase reactor	Five catalysts were tested and coking and bio-oil physical and chemical tests were performed.
B.4	Bio-oil pretreatment with supercritical fluids	Separation of wood feed stocks into cellulose, hemicellulose and lignin components; bio-oil upgrading completed	Hemicellulose was completely separated from the cellulose and lignin components; bio-oil upgrading by supercritical water was unsuccessful as the method was not selective for undesirable compounds.
B.4.DL.1	Design and test supercritical reactor	Reactor operational with one solvent	Water was tested as the initial supercitical solvent.
B.4.DL.2	Down select 2 supercritical solvents	Best solvents selected, named and characterized	Methanol was tested with water to attempt to improve the supercritical fluid selectivity for bio-oil compounds but this was unsuccessful.
B.4.DL.3	Perform supecritical treatments of biomass and bio-oil	A minimum of 4 treatments completed and chemical and physical analyses of products perfromed	Twenty-five treatments were completed at various temperature, residence time, and water contents.
B.5	Fuel and chemical production from CCA-treated lumber	Separation for reuse and/or disposal of CCA metals; production of fuels and chemicals from produced pyrolysis oils	Electrokinetic separation of CCA metals from CCA treated wood was successful. The microreactor for production of pyrolysis oils produced oils that will be analyzed in future research with non-SERC funding.
B.5.DL.1	Assemble equipment and collect, prep and charactierize feed stock	Initial test of equipment setups complete	Equipment was assembled for fabrication; CCA-treated wood was chemically characterized.
B.5.DL.2	Fabricate and test electrokinetic cells and microreactors	Initial test of equipment setups complete	The electrokinetic system was fabricated and successfully tested early in the project; the pyrolysis microreactor was problematic to fabricate and was tested in the 3rd quarter of the last year of the research program.
B.5.DL.3	Conduct initial electrokinetic and thermal studies	Data from 3 replicated experiments completed and analyzed	Electrokinetic studies completed; CCA metals are successfully separated by this method. Pyrolysis of CCA woods successful in the microreactor.
B.5.DL.4	Conduct mass balance studies to determine terminal distribution of metals	Data from 3 replicated experiments completed and analyzed	Mass balance study of electrokinetic experiments completed; mass balance studies of pyrolysis oils produced in microreactor are ongoing.
Number of Task, subtask(s), or	Title of task, subtask or milestone.	Task or Milestone Completion Criteria (to include cost and performance metrics)	Actual accomplishments
C	Ethanol		
C.DL1	Final Report		Complete
C.1	Optimization of the Acid Hydrolysis Process for Ethanol and Biodiesel Production	Development of Acid -Hydrolysis Method	A method was developed and a hydrolyzate was produced for the production triglycerides via the oleaginous microorganism *Rhodotorula glutinis.*
C.1.DL.1	Selection of a suitable biomass source and depolymerization using traditional acid hydrolysis	Development of acid-hydrolysis process and the accompaning analytical analysis for the sugars	Based on the suggestion of the plant and soil scientist switchgrass was selected as the biomass source.
C.2	Optimization of Ethanol Production from Acid Hydrolysates	Development of Acid -Hydrolysis Conversion Method	Ethanol was produced in a low pH medium with glucose as the source of carbon.
C.2.ML.1	Acclimation and evaluation of acid tolerant ethanol producing microorganisms	Development of a procedure for identifying low pH fermenting microbes	At least one low pH acclimated fermenting microorganism was isolated.
C.2.ML.2	Evaluate biological pretreament of acid hydrolysate to increase the concentration of fermentable sugars and in vessel removal of ethanol for increased production	Development of a procedure to evaluate the efficacy of biologically treating non-fermentables	No biological pretreatment tested sucessfully increased the fermentable sugars percentages by removing the non-fermentable because the oleaginous microorgnaisms tested would selectively remove hexoses first followed by the removal of pentoses.
C.3	Isolation and Optimization of Microorganisms Capable of Fermenting Syngas to Ethanol	Development of some Tools to Evaluate syngas utilizing microorganisms	Several organisms were isolated with the ability to utilize components of syngas and produce trace amounts of ethanol
C.3.ML.1	Isolation, cultivation, and evaluation of known and MSU isolated syngas fermenting microorganisms.	Development of procedures for isolating, cultivating, and evaluatingknown and MSU isolated syngas fermenting microorganisms	Numerous microorganisms including ones in MSU's possesion, isolated by MSU, or purchased were evaluated and some found to produce ethanol.
C.3.ML.2	Begin the development of molecular tools to identify the genetic limitations of syngas fermentations by evaluating	Identification of key enzymes	Several key enzymes were evaluated and the molecular tools to evaluate them were developed and utilized.
C.4	Optimization of Reactor design and Operation for Syngas Fermentation	Development of Techniques for Evaluating Reactor Design and Operation for Syngas Conversion	Some of the techniques explored were successful e.g. surfactant to increase the solubility while selectively removing some gas components while others were not successful e.g. the in situ removal of ethanol via propane extraction.

C.4.ML.1	Evaluation of different operational parameters for modeling the system using a 5 L fermentor.	Development of preliminary models	Development of these models meet with limited success due in large part to the in ability of the cultures to produce significant quantities of ethanol from syngas constitiuents.
C.4.ML.2	Evaluate several surfactants and hydrates for increasing the solubility of syngas in the aqueous phase and separation of the syngas constituents.	Development of procedures for evaluating surfactants and hydrates	Gas Hydrates showed some promise of separating syngas components aided by surfactants. In situ separation of ethanol from water was in hibited by the immediate freezing of water in the exhaust line and was abandoned because of this.
Number of Task, subtask(s), or	Title of task, subtask or milestone.	Task or Milestone Completion Criteria (to include cost and performance metrics)	Actual accomplishments
D	Syngas to Gasoline		
D.DL.I	Final Report		Complete
D.1	Screening Catalysts	Identified Catalysts	Secured commercial catalysts for making methanol (Cu/Al_2O_3) and for making gasoline from methanol, H-ZSM-5. These catalysts will be baseline catalysts.
D.1.ML.1	Catalyst Characterization	Show that extraframe work Al content is low	The framework silica/alumina ratio was 35/1 whereas the atomic ratio was 23/1. This means that 1/3 of Al is extra-framework. The actual acid site density is directly related to the framework alumina density.
D.2	Catalyst Preparation	Prepared novel catalysts	Completed as proposed: Cu/ZSM-5. This work showed that only over-exchanged Cu catalysts would make methanol which is the intermediate to gasoline.
D.2.ML.1	Characterize M-ZSM-5 Catalyst	Calculate the proton density before and after Cu exchange	Was able to accomplish before Cu exchange. Could not achieve afterwards because target amine also adsorbed to Cu ions.
D.3	Evaluate Catalyst Activity	Compared activity with literature data	We observed compareable acitivty and selectivity with literature for the zeolite; however, the methanol synthesis catalyst showed a little too much CO_2.
D.3.ML.1	Reproduce optimum reaction conditions	Total conversion of MeOH with minimum light gas yields	Did not obtain as the light gas yields were to much..
D.3.ML.2	Examine effects of impurities	Less than 10% decrease in yields	Was not realized, as both Cu/Zn and Cu/Co/Cr catalysts were totally poisoned by H_2S.
D.4	Examine Impurity Effects	Show yield effects for impurity in feed	Sulfur caused permanent poisoning, but ammonia was reversible poison.
D.4.ML.1	Examine effect of H2S and NH3	Less than 10% decrease in yields	Was not realized for exposure to sulfur. Need to develop a sulfur tolerant catalyst or remove S from feedstock.
D.5	Evaluate Novel Catalyst Activity	Gasoline produced	Yes. (R+M)/2 octane number was 96; API gravity was 50°; Reid Vapor Pressure was 13.5 psig; ASTM initial distilllation temperature was 78 ^{o}F; final temperature was too high, >410°F.
Number of Task, subtask(s), or	Title of task, subtask or milestone.	Task or Milestone Completion Criteria (to include cost and performance metrics)	Actual accomplishments
E	Syngas	An Improved Gasification System	System Improved
E.DL.1	Final Report		Completed
E.1	Modify Existing Down Draft Unit	Modified Down Draft Unit	System modified
E.1.ML.1	Design and Procure equipment for Online Tar Analysis	Ability to collect Tar and Particulates using the updated protocol	Tar and prarticulate system developed and protocal updated
E.1.DL.1	Fabricate Interface between the genset and gasification	Collection of data from the genset	Data collect from the genset
E.2	Improve Current Gas Sampling Protocol and Capability	An Improved Gasification System	Gasification system Improved
E.2.ML.1	Identify optimal gas sampling protocol	Generation of Detailed Tar and Particulate Data	Tar and particulate system used collect samles and data generated
E.2.ML.2	Procure and fabricate sampling train	Gas sampling Equipment to Support Gasification Studies	Gas samplinge equipment adquired and tested
E.2.DL.1	Proof testing of new sampling train	Testing of the New Gas Sampling Protocol	New gas sampling protocal tested
E.3	Procure and instrument a lab scale fluidized bed gasifier	Acquisition of a Lab Scale FBG for use to support Gasification Research	Funding redirected and system not developed
E.3.ML.1	Assemble FBG Team	Scientific Team to address the needs of a FBG	Team assembled and detains of FBG developed
E.3.ML.2	Specify design	A detailed design for the laboratory scale fluidized bed gasifier	System designed and cold model tested
E.3.DL.1	Acquire parts for the FBG	Parts Acquisition for the FBG	Parts for the cold model obtined
E.4	Syngas Conditioning	Development of a Treatment train for Syngas Cleaning	System design and installed on the down draft unit
E.4.ML.1	Identify existing tolerances for end-use devices	Assessment of effective syngas treatment methodology	Technology accessed
E.4.DL.1	Test cool gas adsroption for gas polishing	Cool gas Polishing Mythology	System designed
E.5	Surfactant assisted syngas separation	Surfactant assisted syngas separation methodology	Surfactants designed and tested
E.5.ML.1	Procurement of the Parr system	Acquisition of the Parr Reactor	Reacor aquired
E.5.DL.1	Testing of lab syngas for hydrate separation	Determination of the effectiveness of hydrate separation	Hydrate tested and determine to be effective
E.6	Ash Utilization	Protocol for Ash Utilization	Ash utiliztion protocal evaluated
E.6.ML.1	Characterization of ash	Data for Ash Characterization	Ash Characterized
E.6.DL.1	Testing of ash blends	Data for testing of Ash Blends	Ash blending initiated
E.7	Oxygen looping catalyst system	Development and evaluation of an Oxygen Looping Catalyst System	Oxygen looping catalyst developed
E.7.ML.1	Selection and Characterization of metal oxides	Data for Metal Oxide Characterization	Metal Oxides Characterized
E.7.DL.1	Testing of Catalytic oxides	Assessment of effective Catalytic Oxides for Oxygen looping	Oxygen looping assessed
E.8	Pyrolysis/Syngas conversion	Micro Scale Physical Modeling system for Pyrolysis/Syngas Conversion	Micor Scale Physical Model construced and tested
E.8.DL.1	Fabrication of micro reactors for two-stage pyrolysis-	Generation of a micro reactor for use in pyrolysis/gasification studies	System fabricated
E..9	Peletization/densificaiton of feed-stocks	Generation of Pelletized Feed-stock for gasification Studies	Pelletized feedstock developed

E.9.DL.1	Generation of pellets form switch-grass, Mischantus and	Generation of Pelletized switch-grass, Mischantus and elephant grass Feeds	Pelletized switchgrass, Miscanthus and elephant grass evaluated
E.9.DL.2	Generation of pellets form cotton-gin waste and wood	Generation of Pelletized Feedstock form cotton-gin waste and wood feeds	Pelletized cotton-gin waste and wood feeds evaluated
Number of Task, subtask(s), or	Title of task, subtask or milestone.	Task or Milestone Completion Criteria (to include cost and performance metrics)	Actual accomplishments
F	Biomass Utilization		
F.DL.1	Final Report		Complete
F.1	detailed Mathematical Model of biomass thermal	Develop first order biodiesel combustion model	
F.1.ML.1	Conduct an extensive literature review	A review of existing combustion models related to biofuels	An extensive literature review of existing thermodynamic diesel combustion models has been performed and a detailed table of literature has been compiled.
F.1.ML.2	Create a database of physical and chemical properties	a detailed database of physical and chemical properties to be used in modeling combustion processes	A database of physical and chemical properties of biodiesel fuel has been developed. For instance, variation of physical properties such as viscosity etc.with temperature and pressure are available to be used in developing a detailed phenomenological model
F.1.ML.3	Develop a first order combustion model	A basic first order combustion model for biodiesel engine	A basic first order diesel and biodiesel combustion model has been developed. In particular, various conventional Arrhenius type diesel ignition delay sub models were evaluated and it was found that they either under-or over-predicted biodiesel ignition delay times. Therefore, the reduced chemistry Shell Autoignition model was adopted for predicting biodiesel ignition delays.
F.1.ML.4	Validate the combustion model for engine performance	A validated combustion model	The first order combustion model was validated using experimental data from straight diesel and biodiesel experiments from open literature..
F.1.ML.5	Develop and validate a Nox model	A validated model to predict NOx emission	NOx emission prediction sub model based on Zeldovich kinetics has been developed.
F.2	Experimental study and analysis of biomass combustion	Experimental data of biomass fuel	
F.2.ML.1	Procure and install a single-cylinder engine	Installation of a single-cylinder engine	A single cylinder variable compression ratio diesel engine has been procured and installed.
F.2.ML.2	Instrument the engine	instrument the engine with the required transducers	Various transducers have been procured, and an AC dynamometer has been identified (yet to be ordered) to perform engine experiments.
F.2.DL.3	develop a data acquisition system to obtain mearuments	A data acquisition system for data collection	A lab view based data acquisition system has been developed
F.2.ML.4	Develop a detailed experimental matrix	A detailed experimental matrix to guide engine testing	A detailed experimental matrix for baseline diesel/biodiesel and syngas testing has been developed.
F.2.ML.5	Debug various engine subsystems	Calibrate and debug the engine subsystems	We are still awaiting the procurement of an AC dynamometer and control system. The single cylinder engine will be coupled to the dynamometer to perform extensive engine testing described in the experimental matrix.
F.2.ML.6	Obtain baseline performance and emissions data for diesel combustion	Base line performance data obtained	Baseline performance data has not yet been obtained since we are awaiting the purchase of the AC dynamometer.
F.3	Uncertainty analysis of the developed models and experimental data	uncertainty analysis to determine the controling variables	A general uncertainty analysis has been performed and important variables have been identified.
F.3.ML.1	determine the unvcertaing of the cdombustion model	determine the uncertainty associated with the combustion model	A detailed uncertainty analysis of the combustion model is complete, and the most sensitive parameters of the combustion model have been identified.
F.3.ML.2	determine the uncertainty of the model based on the input uncertainties	determine the uncertainty of the model based on the input uncertainties	a dynamic uncertainty analysis has been performed and the time-varying uncertainties of various variables were identified. It was found that the most sensitive parameter of the combustion model was the temperature dependent specific heat ratio of combustion gases.
F.3.ML.3	Determine combustion model validity	validate the combustion model	The combustion model was validated using data from experiments available in the open literature.
F.3.ML.4	perform general uncertainty analysis of the engine	Engine test system uncertainty analysis	
F.3.ML.5	Perform a detailed uncertainty analysis of the engine system	Perform a detailed uncertainty analysis of the engine system	A detailed uncertainty analysis of a standard engine test system has been performed, and important guidelines to choose transducers and sensors has been outlined.
F.3.ML.6	determine the uncertainty of the baseline performance data	determine the uncertainty of the baseline performance data	Since performance data was not acquired, this task could not be completed.
F.4	Evaluate DME and glycerin derivatives as alternative spark ignition fuels	Evaluate DME and other fuels as alternative spark ignition engine fuels	Phase-diagrams depicting stable combinations of glycerol derivatives as spark ignition fuels were developed.
F.4.ML.1	Recruit a PhD student	Recruit a PhD student	Completed
F.4.ML.2	Acquire raw materials	Obtain the raw material to conduct the evaluation of alternative fuels	Completed
F.4.ML.3	Develop experimental design and preliminary testing	Develop experimental design and validate the apparatus	Completed
F.4.ML.4	Testing various DME blends with gasoline in a spark ignition engine	perform experimental testing of DME blends	This task will be completed upon instrumenting the single cylinder research engine
Number of Task, subtask(s), or	Title of task, subtask or milestone.	Task or Milestone Completion Criteria (to include cost and performance metrics)	Actual accomplishments

G	Distributed Generation (DG)		
G.DL.1	Final Report		Complete
G.1	Develop Simulations to quantify technical and economic benefits and costs of biomass DG	Simulation developed and verified	Simulations for technical assessments were developed in several packages including LINGO, HOMER, MATLAB, CymDist, and MSU software. There was a lack of a comprehensive biomass generator model so it was not possible to do system level economic assessments. Some initial economics related to storage are documented in G.2.
G.1.ML.1	Testing and Analysis of Technical Impact of DG	Report on Testing and Analysis Results, Procedure for Evaluating Technical Impact	As mentioned above analysis was done with several packages. Research activities have created a single optimization stability index, integration of storage and power electronics analysis and initial activities for particle swam optimization for a multi-objective optimization. Theses in G2 and G3 provide details.
G.1.ML.2	Testing and Analysis of Economic and Economic/Technical Impact of DG	Report on Testing and Analysis Results for Economics and Tool for Phase 1 Technical and Economic Analysis for DG	Due to the lack of a biomass generator model for electrical interconnection and economic costs, we were not able to do the system level economic analysis. Some initial work related to storage is provided under G2.
G.2	Investigate technical and economic solutions related to energy storage and power conditioning devices of biomass-generated energy	Develop a list of solutions	Students have developed the models for the power electronics related to two-way converters so power can go back and forth between the biomass source and its support system and the utility grid. One student worked an internship at NREL based on his work for seven months.
G.2.ML.1	Testing and Analysis of Impacts of DG on Transients	Report on Testing and Analysis of Impact of DGs on Transients	Transient stability was studied for three different systems. Power system, power electronic and storage models were combined to evalute the impact of these systems. Full results are available in the MS thesis by Aarthi Asok Kumar (http://sun.library.msstate.edu/ETD-db/theses/available/etd-11142008-151157/)
G.2.ML.2	Hardware-in-the-loop testing and Costs/Benefit options for storage	Report on Modeling and Cost/Benefit Options, Models for integrated storatge/biomass DG options	Developed models for several storage techniques including battery and ultracapacitor. Developed initial biomass DG model. Hardware-in-the-loop testing was not accomplished as hardware purchase was beyond the scope of the project.
G.3	Run simulations to quantify siting DG impact on the power grid and provide optimization methods for siting related to stability, voltage support, decrease losses and other key criteria	Simulations completed	Optimization was done using the stability index. Initial studies and the foundational work for the multi-objective optimization relating to other issues has been done and will be finished in a student's PhD work (beyond this project).
G.3.DL.1	Report on Literature Review and Initial Analysis of DG Impact on Stability	Report on Literature Survey and Testing/Analysis on DG impact of stability	Literature review was developed and sent as a previous report. Initial stability index has been developed and was implemented in LINGO for the IEEE 13 node test case considering one DG. Report for G.3.DL.2 has initial and comprehensive results.
G.3.DL.2	Report on results of power flow/stability and optimization of DG placement	Report on Stability/Power Flow and Optimization Results, Phase I Stability Index	Optimal placement was evaluated related to size and location using LINGO on the IEEE 13 node and 37 node feeders. Results will be reported in papers. Full results available in MS Thesis by Abhilash R. Masanna gari (http://sun.library.msstate.edu/ETD-db/theses/available/etd-11142008-135719/)
Number of Task, subtask(s), or	Title of task, subtask or milestone.	Task or Milestone Completion Criteria (to include cost and performance metrics)	Actual accomplishments
H	Chemicals		
H.DL.1	Final Report		Complete
H.1	Development of Catalytic Reformer and Modeling	A functional fuel reformer with at least 80% hydrogen selectivity and >80%	
H.1.DL.1	Active catalysts for glycerol reforming	80% hydrogen selectivity and 80% glycerin conversion	Ni/Al_2O_3 catalyst gave a hydrogen selectivity of 80% and a maximum glycerol conversion of 94%
H.1.DL.2	Glycerin droplet modeling	A functional model than can predict glycerin droplet size distribution	Molecular Dynamics simulations showed that the lifetime is related to the theory fit to the experimental data. A paper decribing this advanced simulation technique has been submitted to Physical Review E (http://arxiv.org/abs/0807.4759).
H.2	Poduction of biohydrogen	A biological hydrogen reforming system with acceptable hydrogen yield	
H.2.DL.1	Substrate development for Asotobactor vivendi	Micromoles of H_2 per hour per gram of protein	A biowaste-based medium with no added nitrogen or carbon source was developed for growing hydrogen producing *A. vinelandii*. Expected rate of H_2 production under these conditions is 66microM/gram cell protein/min. A hydrogenase biobrick that generates H_2 at the rate of 6 mol H_2/mole of sucrose was introduced into this bacterium to increase hydrogen production. Experiments are ongoing to determine the exact H_2 generation by this genetically engineered bacterium when grown on biowaste containing medium.

H.2.DL.2	Gene Cloning	His-tagged Fe-Hydrogenase gene will be verified	His-tagged Fe-hydrogenase gene was constructed. It was introduced in A. vinelandii. Expression of the hydrogenase was verified by Western blotting and probing with anti-His-antibody.
H.2.DL.3	Bacterial and algal co-culture development	A successful lead algae would produce H_2 at >20% efficiency	This project was formally terminated after the 2nd quarter of funding due to difficulty securing graduate students.
H.2.DL.4	Real Time monitoring of genetically engineered bacteria	Observable LIF signal from Azotobactor	Successfully recorded auto-fluorescence spectra from *Azotobacter vinelandii* grown under conditions that activate (nitrogen minus) or inactivate (nitrogen plus) *nif* gene expression. The spectra changes clearly show the difference of growth conditions by a factor of 10 at 402-nm with 325-nm excitation wavelength.
H.3	Hydrogen Storage Materials Development	Successful storage of hydrogen in solid state materials (criteria not yet	
H.3.DL.1	Hydrogen adsorption characterization of nano-	Hydrogen adsorption data	This project was terminated following the death of the PI.
H.4	Production of Speciality Chemicals	Successful selective cleavage of phosphate ester bonds and development of	
H.4.DL.1	Selective Phosphate-ester Cleavage in Phospholipids	>50% phospho-ester cleavage without secondary cleavage or reaction.	Cleavage reactions examined on phosphatidyl choline (PC), serine (PS), and ethanolamine (PE) using 6 different metal halide catalysts. Phosphate ester cleavage≥ 50% for PC and PE using lithium chloride under mild reaction conditions.
H.4.DL.2	Determine dielectrophoretic parameters to separate phosphate ester from fatty acid / glycerol backbone	Most viable fluorescent phosphate sensors will have rapid binding (<2 min) with free phosphate and be easily detectable on a fluorescent microscope.	Molecular Probe's PiPer Phosphate Assay was used as a fluorescent indicator of O-phospho-L-serine in glycerol in dielectrophoretic fields. Fluorescence was able to track presence and position in the field, but could not be used to quantify phosphate molecules per unit area due to time dependent light / field interactions. However, qualitative results indicate concentration of O-phospho-L-serine in high electric field density regions.
H.4.DL.3	Crystallization of fatty acids from bulk solutions	Provide solubility data over a range of at least 20 oC with composition repeatable with ±10% accuracy	Solubility data for linoleic acid (LA) had a standard deviation of 10.8% at low solubilties of 1.45 g LA/100 g solvent.
H.5	Polymers for bioplastics	Development of feasible methods to produce polymers from recalcitrant	
H.5.DL.1	Design and evaluate polymerization techniques for the development of bioplastics	Suitable polymerization method(s) would provide MWs > 5K	Copolymers produced from a series of biomass-derived monomers with MWs > 5kDa and yields as high as 98% using melt polycondensation reactions.
Number of Task, subtask(s), or	Title of task, subtask or milestone.	Task or Milestone Completion Criteria (to include cost and performance metrics)	Actual accomplishments
I	Feedstocks		
I.DL.1	Final report	Final Report and all data sets completed for the Feedstocks Thrust	Complete
I.1	Characterize lignocellulosic crops for use as bioenergy crops in MS	Yield trials conducted and analyzed	One to 2 year yield trials at multiple locations completed and analyzed. Yields of biomass grasses assessed at multiple locations
I.1.DL.1	Dataset on characteristics and yield of lignocellulosic crops in MS	Data assembled on characteristics and yield of lignocellulosic crops	Final reports describe crop production hurdles and potential biomass dry matter production
I.2	Characterize oilseed crops for use as bioenergy crops in	Yield trials conducted and analyzed	One to 2 year yield trials at multiple locations completed and analyzed
I.2.DL.1	Dataset on characteristics and yield of oilseed crops in MS	Data assembled on characteristics and yield of oilseed crops	Final reports describe crop production hurdles and potential oil yield from various crops
I.3	Characterize physiological limits of select bioenergy	Yield trials conducted and analyzed	Physiological responses by bioenergy crops measured and reported
I.3.DL.1	Dataset on the physiological limitations specific bioenergy crops	Data assembled on the physiological limitations of specific bioenergy crops	Algorithms developed which mathematically describe bioenergy crop response to environmental stresses
I.4	Modify cell walls for cost efficient bio-fuel production	Experiments completed	Transgenic rice has been generated. Further verification is required.
I.4.DL.1	Dataset on the biological means to degrade cell walls of	Data assembled on the biological means to degrade cell walls of bioenergy	Database search completed
I.4.DL.2	A scientific system to study rice cell walls	A scientific system to study rice cell walls	Systems for proteome analysis of cell synthesis regulatory proteins has been established, including total protein and nuclear protein analysis.
I.5	Study the pelletization process as a means to densify biomass	Successful development of pellets	An Sprout-Waldron 125 hp pellet mill was purchased, installed, and tested as the test platform for biomass pelleting studies. Material handling equipment were assembled to complete the biomass pelleting system. Pelleting studies on this installed system were focused on switchgrass as the feed material. Studies on pelleting such other biomass as wheat straw, giant Miscanthus, elephant grass, cotton gin trash, and softwood forest trimmings were undertaken in collaboration with ADM Alliance Nutrition in Illinois. Results of that effort identified biomass moisture content, grind size, and pellet mill die speification as critical parameters in pelletization. Informal collaboration on the pelleting of biomass was established with Andritz Sprout (formally Sprout-Waldron).

I.5.DL.1	Dataset on the properties of biomass and biomass pellets	Data assembled on the properties of biomass and biomass pellets	Studies on pelleting such other biomass as wheat straw, giant Miscanthus, elephantgrass, cotton gin trash, and softwood forest trimmings were undertaken in collaboration with ADM Alliance Nutrition in Illinois. Results of that effort identified biomass moisture content, grind size, and pellet mill die specification as critical parameters in pelletization. Particle size upon grinding was affected by the biomass but particle size distribution analysis through standard mechanical sieving was incapable of characterizing the fibrous grinds that would provide data for size reduction and densification operations. A sieveless particle size distribution analysis method using computer vision was therefore developed.
I.6	Evaluate forestry products as a possible biomass source	Evaluation completed	Final report submitted
I.6.DL.1	Dataset on the availability and production costs of	Data assembled on the availability and production costs of woody biomass	Dataset compiled
Number of Task, subtask(s), or	Title of task, subtask or milestone.	Task or Milestone Completion Criteria (to include cost and performance metrics)	Actual accomplishments
J	Economic and Policy Analysis		
J.DL1	Publish combined report of Economics and Policy	Combined report completed	Complete
J.1	Estimate quantities, harvest & transport costs of woody		
J1.1.DL1	Estimate quantities of woody residues	Woody residue inventory completed	Completed woody residue inventory.
J.1.DL2	Create a budget estimating woody residue harvest and transport costs	Budget completed for estimating woody residues harvest and transport cost	Completed budget for estimating woody residue harvest and transport cost.
J1.DL3	Estimate maximum transport distances of woody resiues	Mileage charts for transporting woody residues completed	Completed mileage charts for transporting wood residues.
J.2	Evaluate poulty litter, cotton gin trash and soybean as		
J.2.DL1	Develop a GIS map of poultry litter concentrations in Mississippi	GIS map depicting quantities and locations of poultry litter completed for Mississippi	County level GIS map completed displaying the amount/tons of poultry litter produced/available in Mississippi.
J.2.DL2	Develop a GIS map of cotton gin trash concentrations in Mississippi	GIS map depicting quantities and locations of cotton gin trash completed for Mississippi	County level GIS map completed displaying the amount/tons of cotton gin trash produced/available in Mississippi.
J.2.DL3	Develop a GIS map of soybeans concentrations in Mississippi	GIS map depicting quantities and locations of soybeans completed for Mississippi	County level GIS map completed displaying the amount/bushels of soybeans produced/available in Mississippi.
J.3	Develop biomass crop enterprise budgets for biomass		
J.3.DL1	Identify the cost of cultural practices used to produce biomass crops	Collected of costs and cultural practices for biomass production completed	Completed a comprehensive review of agronomic cultural practices and related costs used to produce biomass/feedstock grasses.
J.3.DL2	Estimate costs and returns for biomass crops	Biomass crop enterprise budgets with costs & returns completed	Complete detailed crop enterprise budget for switchgrass and giant miscanthus to determine costs of delivery to biofuels plant
J.4	Estimate environmental costs and impacts of biomass		
J.4.DL1	Assemble table of emission factors per ton from	Table of biomass production emission factors completed	Completed table of biomass production emission factors
J.4.DL2	Assemble table of emission factors per ton from biomass harvest, etc.	Table of biomass harvest, transport and storage emission factors completed	Completred table of biomass harvest, transport, and storage emission factors
J.4.DL3	Assemble table of emission factors per ton from	Table of biomass conversion to biofuels emission factors completed	Completed table of biomass conversion to biofules emission factors
J.4.DL4	Combine table of emission factors per ton from all biomass activities	Combined Table of emission factors related to biomass to biofuel completed	Completed combined table of emission factors related to biomass to biofuel processes.
J.5	Conduct analyses of domestic and international energy		
J.5.DL1	Design interactive web interface for producing energy trade flow maps	Interactive web interface for creating energy trade flows maps complete	Completed interactive web interface for creating energy trade flows maps
J.5.DL2	Identify policies influencing energy and ag product production and trade	Identifiaction of trade policies influencing energy trade and ag production completed	Completed identification of trade prolicies influencing energy trade and ag production
J.5.DL3	Use model to predict impacts of price and policies on energy markets	Conceptual model developed to predict price and policies impacts completed	Conceptual model developed to predict price and policies impacts nearing completion.
J.6	Identify economic & environmental policies promoting		
J.6.DL1	Conduct economic literature review analyzing biomass and bioenergy	Literature review of economic research related to biomass/biofuels completed	Completed literature review and published a report describing/citing sources of published economic research related to biomass/biofuels
J.6.DL2	Identify policies in all 50 states used to promote biomass/bioenergy	Identification of state/public policies used to promote biomass/biofuels completed	Posted on website a listing of local/state/federal policies influencing the increased use of biofuels and development of biofuel industries
J.6.DL3	Estimate price elasticities for various bioenergy products	Consumer acceptance/attitudes and price elasticities for biofuels completed	Completed a national survey of 3,000 consumers designed to ascertain the willingness-to-pay for E10 and E85 ethanol products
Number of Task, subtask(s), or	Title of task, subtask or milestone.	Task or Milestone Completion Criteria (to include cost and performance metrics)	Actual accomplishments
K	Social Policy	Technical Report	Completed technical paper as this report, presented at conference.
K.DL.1	Final Project Report	Final Technical Report	Completed as attached.
K.1	Construction of Biomass Crop Databases	Completion of Biomass Crop Databases	Completed as proposed.
K.1.DL.1	Update 1992 ORNL data to 1997 & 2002	Completion of ORNL estimates for 1997 & 2002 Ag Census Data	Completed as proposed.
K.2	Identify Optimal Agronomic Biomass Zones, Value-	Identification of optimal biomass zones using spatial criteria	Completed as proposed and described in a conference paper.
K.2.DL.1	Use LISA approach to ID biomass zones	Completion of statistically significant LISA analyses	Completed as proposed and described in a conference paper.
K.3	Determine Reduced Optimal Biomass Zones & Impact on Disadvantaged Populations	Determination of overlap between disadvantaged farm populations and optimal biomass zones using spatial criteria	Work is on-going on this problem due to data issues with disadvantaged farm populations; optimal biomas zones completed as proposed.

K.4	Assess Contours of Political Support for Emergent Biomass Industry	Completion of spatial contours estimation using wombling method	Work is on-going on this problem due to data issues with completing the political support indicators. Data are currently being validated for completion at a future date.
K.4.DL.1	Construct Political Databases	Completion of political power, voter ratings databases	Work is on-going on the political power metrics although voter ratings database was completed as proposed.
Number of Task, subtask(s), or	Title of task, subtask or milestone.	Task or Milestone Completion Criteria (to include cost and performance metrics)	Actual accomplishments
L	Environmental Sustainability		developed and validated methods for determining environmental sustainability for production of feedstock, specifially switchgrass
L.DL.1	Final Report	Final Report Completed	Final report summarizing results was produced. The project also resulted in one published paper and two theses.
L.1	Meteorological Data Collection	Complete Data Set	Raw daily climate data were acquired and quality checked.
L.1.DL.1	Develop Meteorological Data Set	Complete Data Set	Derived weather data was generated by the ALMANAC model as needed.
L.2	Identify Suitable Basin for SWAT Model	Basin Selected	Spatial analysis was expanded to the entire state of Mississippi, and research showed that the ALMANAC yield model was more appropriate for this project than the SWAT model.
L.3	Determine Hydrologic Response Gradient	Additional Basins Analyzed	Analysis determined that climate was not a limiting factor for the growth of switchgrass in Mississippi.
L.3.DL.1	Response Gradient Analysis	Slope/Gradient Analysis of Basins	Spatial analysis of GIS layers showed the best locations throughout the state for switchgrass production.
L.4	Production of Statewide GIS Layers	Layers Complete	Statewide GIS layers that were needed for the spatial analaysis of feedstock production were produced.
L.4.DL.1	Data Layers for SWAT Inputs and Outputs	Complete Set of GIS Layers	All GIS data layers were processed and formatted for use with the ALMANAC model, which replaced the use of the SWAT model in this project.

Sustainable Energy Research Center
Biodiesel Thrust Area Final Report for 2006-2008

1. Project Title, name of principal investigator, and all team members: A. Novel Processes and Feedstocks for Producing Biodiesel

Rafael Hernandez, Todd French, Sandun Fernando, Hossein Toghiani, Rebecca Toghiani, Keisha Walters, Dr. Adrienne Minerick, Tingyu Li, Dwane Braasch, Juan Silva, and Brian Baldwin

2. List authorized distribution notices: The information contained in the section of the Sustainable Energy Research Center report is available to be distributed as the Department of Energy deems necessary.

3. Executive Summary:

Municipal wastewater treatment plants in the United States produce over 6.2 million metric tons of dried sewage sludge every year. This microorganism rich sludge is often landfilled or used as fertilizer. Recent restrictions on the use of sewage sludge, however, have resulted in increased disposal problems. Extraction of lipids from sludge yields an untapped source of cheap feedstock for biodiesel production. Solvents used for extraction in this study include *n*-hexane, methanol, acetone, and supercritical CO_2. Gravimetric yield of oil was low for non-polar solvents but addition of polar solvents gave a considerably increased yield. However, the percent of saponifiable material was less. Extraction of lipids with a mixture of *n*-hexane, methanol, and acetone gave the largest conversion to biodiesel for a solvent system, 4.41% based on total dry weight of sludge. *In Situ* transesterification of dried sludge resulted in a yield of 6.23%. Assuming a 10% dry weight yield of FAMEs the amount of biodiesel available for production in the United States is 1.4 million cubic meters per year. Outfitting 50% of municipal wastewater plants for lipid extraction and transesterification could result in enough biodiesel production to replace 0.5% of the national petroleum diesel demand (0.7 million cubic meters).

Other sources of lipids investigated were Black mustard, birdseed rape, canola, Camelina, Crambe, flax, and *Hesperis.* These plants were selected based on their oil content and their capability to grow in the US Southeast. Genetic procedures were developed to increase the oil content of these plants. Of the species investigated, canola, sunflower, and okra have the greatest potential. However, it should be noted that even record yields of all the crops mentioned above will not come close to fully replacing the U.S. need for oil/petroleum.

Extraction procedures were developed to recover nutritional components, such as omega-3 fatty acid eicosapentaenoic acid (EPA) and docosahexaenoic acid (DHA), from oil and biodiesel. Additionally, a method was developed to isolate another value added product, Vitamin E, from oils. The methods developed were based on differences in binding between polyunsaturated fatty acid methyl esters and the transition metal ions. More than 90% EPA was recovered using using AgBF4/SiO2●Im+●$PF6^{-}$. After a consecutive two-step stripping by ethyl ether and then 1-hexene, the concentration of EPA increased from 7% in the feed stock solution to about 90% in the 1-hexene stripping solvent. After five recycles, the sorbent is still usable.

Ordered mesoporous adsorbents were prepared by physically coating functionalized ionic liquids onto mesoporous silica gel. These adsorbents were successfully applied to the selective extraction and separation of vitamin E from a model mixture of soybean oil deodorizer distillate. Five adsorbent recycle tests showed good reusability of this ionic liquid-modified mesoporous adsorbent.

Another approach to improve the overall economic feasibility of biodiesel production is the conversion of glycerine into value added chemicals. Microorganisms capable of converting glycerine to 1,3-propanediol and lactic acid were isolated from various environments ranging from manure to sewage treatment plants. There was one notable isolate that co-produce both products and one in particularly high concentrations. This culture with more understanding of its metabolic pathways could prove a useful biological agent for the conversion of glycerol.

Homogeneous acid or base catalysts dissolve fully in the glycerol layer and partially in the fatty acid methyl esters (biodiesel) layer in the triglyceride transesterification process. Heterogeneous (solid) catalysts, on the other hand, can prevent catalyst contamination making product separation much simpler. In the present work, the transesterification kinetics of five different solid catalysts with soybean oil is presented. It was determined that heterogeneous catalysts require much higher temperatures and pressure to achieve acceptable conversion levels when compared to using homogeneous catalysts. Subsequent to preliminary investigations, transesterification was conducted for selected high performance solid catalysts, i.e., MgO, CaO, BaO, PbO, and MnO_2 in a high pressure reactor up to a temperature of 215°C. The yield of the fatty acid methyl esters and the kinetics (rate constant and order) of the reaction were estimated and compared for each catalyst.

Meeting sustainable energy demand with minimum environmental impact is a major area of concern in the energy sector. Alternative fuels such as biodiesel, ethanol etc. have been quite promising for fulfilling both these aspects. While biodiesel reduces emissions of CO, life cycle CO_2, SO_x, volatile organic compounds (VOC) and particulate matter (PM) significantly, the propensity for the production of NO_x is an important problem that requires extensive research. NO_x emission from a direct-injection diesel engine is mainly due to formation of thermal NO that is described by Zeldovich mechanism. Thus, studying temperature profile during biodiesel combustion can provide useful insights to the formation and destruction of NO_x. The main objective of this work is to investigate the effect of component methyl esters of biodiesel on open air flame temperature distribution and the effect of blending biodiesel with diesel and oxygenates (ethanol and methyl acetate) on open air flames. This objective was achieved by obtaining thermocouple measurements and thermal infrared imaging of local flame temperatures of wick-generated open air flames. A relationship between blend proportions and relative flame temperatures were obtained. In general, it was found that blending oxygenates such as ethanol and methyl acetate into petroleum diesel tended to increase the flame temperature in comparison with straight diesel fuel. The analyses of relative flame temperatures of different components of biodiesel were performed to evaluate the effect of unsaturation level and the hydrocarbon chain length on the flame temperature. It was found that the saturated methyl esters resulted in greater flame temperatures in comparison to unsaturated methyl esters. It was also revealed that shorter chained fatty acid methyl esters lead to higher flame temperatures as compared to its longer chained counterparts.

The monoalkylesters of fatty acids derived from vegetable oils or animal fats, are considered as an attractive alternative fuel for diesel engines. This interest is based on a number of properties of biodiesel including the fact that it is produced from a renewable resource and its potential to reduce exhaust emissions. Although several studies have been performed on biodiesel emissions, the results have been contradictory with some studies reporting a reduction of NO_x emissions while others reporting an increase. Also, thus far, there has been no promising method on record which has been successful in reducing biodiesel related NO_x emissions. The objective of this study was to evaluate the effect of blending biodiesel and ethanol into conventional diesel fuel on exhaust gas emissions. Ethanol could be added to diesel in limited quantities along with biodiesel since biodiesel stabilizes the ternary system by acting as an amphiphile. This paper illustrates the emission characteristics of diesel-biodiesel-ethanol (DBE) fuel blends on one used and two brand new engines. DBE is a new form of oxygenated diesel fuel blend and has a potential to reduce NO_x emissions and to be an alternative to diesel fuel. The blend ratio (diesel: Biodiesel: ethanol) by volume used in this study was 70:25:5, 70:20:10 and 70:15:15. The results from the operation of diesel engine with DBE showed a significant reduction in NO_x emissions in new engines with increased ethanol concentration where as with the old engine under similar conditions, an increased NO_x emissions profile was observed. CO emission increased with increasing ethanol proportion in the blends in both new and old engines.

Project Background:

Biodiesel is defined as “mono-alkyl esters of long chain fatty acids derived from vegetable oils or animal fats which conform to ASTM D6751 specifications” for use in diesel engines. Biodiesel utilization has increased significantly over the last 10 years mainly due to environmental benefits and a national energy policy directed towards reducing dependence of foreign oil via development of renewable and alternative fuels. The use of biodiesel reduces emissions of CO_2, CO, SO_2, and particulates from operating diesel engines. Under a sustainable energy policy by the US Department of Interior, over 20 national parks operate boats, trucks, heating systems, electricity generators, and other fuel related systems on 100% biodiesel and/or biodiesel/petroleum diesel blends. Numerous school districts, transit authorities, public utility companies, and recycling companies also have successfully used biodiesel. The US military has begun to procure biodiesel for use in on-base vehicles. These numerous experiences with the use of biodiesel have clearly shown the environmental and high performance characteristics of biodiesel.

The future of biodiesel based on its current status appears to provide limited impacts to truly reduce foreign oil dependency because of high production costs (approximately $2.50 per gallon for soy oil) and relatively low US production capacity (if all of the existing oleochemical capacity within the US is utilized, only 500 million gallons of biodiesel could be produced per year; yet, the US burned over 40 billion gallons of petroleum-based biodiesel last year). Lipid feedstocks represent over 70% of biodiesel production costs. This project will focus on developing microbial-, animal-, and plant-derived lipid feedstocks and their applicability to produce high quality biodiesel (defined based on performance using ASTM testing and economic assessments). These new lipid feedstocks will be characterized by high oil yield and the potential to generate billions of gallons of oil for biodiesel production. Environmentally friendly extraction/separation techniques will be developed to cost effectively extract the lipids and separate high value

compounds contained in the oil prior to transesterification. Another focus area of the project is the synthesis of heterogeneous catalysts for the transesterification reaction and glycerine conversion into value added chemicals. The latter also will be conducted via the development of robust fermentation techniques. The integration of new feedstocks, extraction/separation techniques, and generation of value added chemicals from glycerine will transform the current biodiesel industry into a true biorefinery. To accomplish the above stated efforts, developmental tasks will be performed by a research team consisting of chemical engineers, mechanical engineers, plant scientists, biochemists, economists, chemists, biologists, and microbiologists.

Project Goals and Objectives

The main objective of the proposed research is to reduce the cost per gallon of biodiesel to levels competitive with wholesale prices of petroleum diesel via development of a research base within Mississippi that can address key technology barriers associated with feedstock availability and process limitations. To accomplish the above stated overall goal, a multi-disciplined research team consisting of chemical engineers, mechanical engineers, plant scientists, biochemists, economists, chemists, biologists, and microbiologists has been organized. Academic units from Mississippi State University (MSU) participating with this project include those from the MSU Bagley College of Engineering (Dave C. Swalm School of Chemical Engineering and the Agricultural and Biological Engineering Departments); Mississippi Agricultural and Forestry Experiment Station (Departments of Plant and Soil Science, Biochemistry, Agricultural Economics, and Food Science, Nutrition, and Health Promotion); and The MSU College of Arts and Science (Chemistry Department). Specific objectives include:

(1) Evaluation of sewage sludges from wastewater treatment facilities as a source of lipids for producing ASTM D6751 biodiesel. These facilities generate billions of pounds of sewage sludge annually. Previous research conducted at MSU indicates that these sludges contained approximately 30% by weight lipids. Successful utilization of this lipid source for producing biodiesel could result in generation of billions of gallons of the fuel and an innovative solution to the sludge disposal problem faced by numerous states.

(2) Identification and isolation of oleaginous microorganisms with the capability to use glycerol and sugars (i.e., pentose and xylose) for lipids production. Utilization of glycerine for oil production would eliminate the excess market supply of this chemical, which has caused a significant reduction in price and an excess inventory crisis for biodiesel producers. The use of all sugars contained in lignocellulose could potentially add billions of gallons of lipids for biodiesel production.

(3) Design and evaluation of nano-encapsulation techniques for removing heavy metal impurities from biodiesel production processes. These impurities are present at varying concentrations in biodiesel generated using a wide variety of feedstock sources, including sewage sludge and oleaginous yeast.

(4) Evaluation of commercial adsorbents and absorbents to collect lipids contained in food processing industry wastewaters. The food processing industry generates

million of gallons of wastewater containing lipids which could be used for biodiesel production. The adsorption capacity of the adsorbents/absorbents toward lipids will be measured via preparation of adsorption isotherms. Surface modification techniques will be applied to enhance the adsorption/absorption properties of selected adsorbents/absorbents.

(5) Optimization of biodiesel production using Chinese tallow tree, rapeseed, castor, and tall oil. The Chinese tallow tree and castor generate seeds with naturally high lipid yields. These non-traditional crops grow well in the south and could contribute significant amounts of lipids in a relatively small area. The methodology to genetically modified these plants to enhance lipid production and biomass yield will be developed using canola as a model plant. Additionally, the plasmid construct for castor will be developed to shut down ricin production.

(6) Study the cultivation techniques and harvesting economics for flax, camelina, mustard, and Canola as additional lipid sources for the Southeast United States.

(7) Development of environmentally friendly lipids extraction techniques. Previous research in MSU indicates that conventional extraction techniques, such as hexane extraction and Bly Dyer extraction, are not effective for the extraction of lipids (phospholipids) contained in microbial feedstocks. Techniques involving supercritical fluids, compressed gases, and integration of extraction/reaction will be evaluated as extraction alternatives for the proposed non-traditional lipid feedstocks.

(8) Examine the effect of extraction techniques on oil stability. Shelf life is an important factor to consider by biodiesel producers using non-traditional feedstocks for biodiesel production. Rancid oil could consume catalyst, generate soaps during base catalyzed transesterification, and increase biodiesel production cost. Data will be generated on the effect of extraction techniques on quality and shelf life of catfish, Chinese tallow tree, soybeans, and sewage sludge oil. A method to discern oil and biodiesel stability will be standardized.

(9) Synthesis of heterogeneous catalysts for the transesterification reaction. Additionally, activation techniques will be applied for previously discovered catalysts. The application of heterogeneous catalysis for producing biodiesel could reduce biodiesel production cost, generate better quality glycerine, and facilitate the application of continuous production processes.

(10) Examine the NOx forming reaction dynamics when using biodiesel as the fuel in compression ignition engines. Most studies indicate an increase in NOx emissions during biodiesel combustion. Elucidation of the physico/chemical cause(s) of the increase could be correlated to biodiesel composition, and thus, the potential production of a low NOx biodiesel blend.

(11) Isolate/grow microorganisms with the capability to efficiently convert glycerine into propanediol or lactic acid. Non-biological routes alternatives also will be evaluated to convert glycerine to propanediol, ethanol, and methanol.

Task A.1. MSU Research on Biodiesel from Wastewater Sludge

1. Introduction

The production of biodiesel in the United States has increased substantially in the last three years; from 75 million gallons in 2005, to 250 million gallons in 2006, and 450 million gallons in 2007 (National Biodiesel Board, 2007a). Biodiesel production plants are continuously being built all over the United States, and the total capacity is expected to reach well over 1 billion gallons in the next few years. This unprecedented increase in interest and demand for biodiesel and other fuels derived from renewable biomass is driven by rising petroleum fuel costs, increasing concern for the environmental impact of emissions from the combustion of conventional fossil fuels, increasing reliance on foreign oil sources, and decline in domestic oil production (Nelson and Schrock, 2006).

Biodiesel is a petroleum diesel substitute produced by the base- or acid-catalyzed transesterification of vegetable oils and animal fats that yields the methyl esters of the fatty acids of the lipid feedstock (Knothe, 2005). It is known to be biodegradable and has an energy content comparable to No.2 biodiesel when used as a B20 blend (National Biodiesel Board, 2007b). Furthermore, the flash point of regular No. 2 petroleum diesel is 125°F, while the flash point of pure biodiesel is above 200°F; making biodiesel safer and easier to use, handle, and store (National Biodiesel Board, 2007c). Engine emissions such as unburned hydrocarbons, carbon monoxide, and particulate matter could be reduced by 67, 48, and 47 % respectively if biodiesel is used in a conventional engine (National Biodiesel Board, 2007d).

As an effect of the increasing demand for biodiesel, the demand for lipid feedsctocks such as soybean, canola, rapeseed, sunflower, palm, and coconut oils have also increased. Among these feedstocks, soybean oil is the most widely-used in the United States. In 2007, around 19.4 billion pounds out of a total soybean oil production of 20.2 billion pounds (or roughly 96%) were consumed by the food industry (American Soybean Association, 2007). This has led to concerns about providing enough feedstock to cater to the increasing demands for biodiesel in the next few years at the expense of the food manufacturing industry. Moreover, a major challenge for the commercialization of biodiesel production using these feedstocks is the high cost of pure vegetable or seed oils, which constitutes between 70 and 85 % of the overall biodiesel production cost (Haas and Foglia, 2005). Thus, in order to reduce the cost per gallon of biodiesel, alternative feedstocks that are readily available in large quantities and at low cost must be used.

Among the alternate lipid feedstocks that have been investigated were non-edible crops such as *Jatropha curcas* (Foidl *et al.,* 1996); animal fats such as lard (Lee *et al.,* 2002), and beef tallow (Nelson and Shrock, 2006); and waste cooking oil (Kulkarni and Dalai, 2006). This study investigated the possibility of using municipal sewage sludge as a lipid feedstock for biodiesel production. Wastewater treatment facilities produce approximately 6.2 million metric tons (dry mass) of sludge in the United States annually (WEF, 2002). As shown in Figure 1, there are two main sludge streams in a typical wastewater treatment facility employing an activated sludge process. The primary sludge is a combination of floating grease and solids collected at the bottom of the primary clarifier of a wastewater treatment plant after screening and grit removal, while the secondary, or activated, sludge is mainly microbial cells and suspended solids produced during the aerobic biological treatment of wastewater and is collected from the secondary clarifier. A portion of the collected activated sludge stream, typically 50 to 75 % of the

average wastewater flowrate, is recycled back to the aeration basins to maintain a sufficient concentration of microorganisms required for a certain degree of treatment (Tchobanoglous *et al.,* 2003). The remainder of the sludge stream is then wasted and further treated and stabilized by aerobic or anaerobic digestion before being disposed by incineration or land application.

The amount of sewage sludge is expected to increase in the future due to increasing urbanization and industrialization. Hence, sludge handling, treatment, and disposal are formidable environmental challenges that have to be faced. Sludge incineration results in emissions that contain dioxins and heavy metals, while land application and landfill disposal raise similar concerns with the accumulation of heavy metals and toxic organic pollutants in soils and plants. One viable alternative to these disposal methods is to utilize the sludge as a source of lipid feedstock for biodiesel production. Municipal sewage sludge contains a significant amount of organic matter which is predominantly proteins and carbohydrates. These account for approximately 90 % of the volatile suspended solids after the sludge is concentrated by settling at 4°C for 24 hr (Yuan *et al.*, 2006). The lipid fraction of the municipal wastewater sludge is a composite organic matrix originating from the direct adsorption of lipids from domestic and industrial wastes to the sludge, and/or from the phospholipids in the cell membranes of microorganisms, their metabolites and by-products of cell lysis. Jardé *et al.* (2005) studied 48 samples of sewage sludge from different wastewater treatment plants and extracted and fractionated them into aliphatic, aromatic, and polar fractions. The polar fractions, which comprised up to 36.8 % wt. of the dry sludge, showed the presence of fatty acids and steroids. The fatty acids were predominantly in the range of C_{10} to C_{18}, which are excellent for the production of methyl esters. Boocock *et al.* (1992) obtained 17 to 18 % wt. lipids from raw sewage sludge by boiling solvent extraction. Approximately 65 % wt. of the extracts were found to be free fatty acids and 7 % wt. were glyceride fatty acids. On the other hand, Shen *et al.* (2003) investigated the pyrolysis of secondary sewage sludge under inert conditions. They obtained a maximum of 30 % wt. oil from dry sludge at a temperature of 525ºC and a gas residence time of 1.5 s. In the study by Dufreche *et al.* (2007), it has been demonstrated that lipids can be extracted from secondary sludge through use of organic solvents with different polarities or with supercritical carbon dioxide. They further concluded that the integration of lipid extraction processes in 50 % of all existing municipal wastewater treatment plants in the United States, and transesterification of the extracted lipids could produce approximately 1.8 billion gallons of biodiesel, which is roughly 0.5 % of the yearly national petroleum diesel demand. Since municipal wastewater sludges are readily available at practically no cost, the cost of biodiesel production may be reduced as well, along with helping solve some environmental issues associated with sludge treatment and disposal.

In this study, an *in-situ* transesterification procedure was applied on dried primary and secondary sludge samples. The *in-situ* process eliminated the need to extract and separate the lipids and fatty acids contained in the sludge since the fatty-acid containing lipids are simultaneously extracted and transesterified. Thus the reaction time and the amount of solvent and samples required are reduced compared to a separate lipid extraction and transesterification process. In a previous study, Haas *et al.* (2004) performed a base-catalyzed *in-situ* transesterification on soy flakes for biodiesel production. More recently, the same authors achieved 97 % of the theoretical maximum yield of FAMEs by using soybean flakes with 2.6 % moisture as the raw material (Hass *et al.*, 2007).

The purpose of this research was to investigate the feasibility of using an acid-catalyzed *in-situ* transesterification process on primary and secondary sewage sludge to produce biodiesel. The effect of operating conditions such as reaction temperature, H_2SO_4 catalyst concentration, and the mass ratio of methanol to sludge used on the fatty acid methyl ester (FAME) yield in percent mass per mass of sludge were examined. Kinetic analysis on the FAME yields with respect to time was also conducted to determine the effects of the three factors mentioned on the reaction rate. Finally, an economic analysis was conducted to estimate the cost per gallon of the biodiesel obtained using municipal sewage sludge as the lipid feedstock.

2. Methods

2.1. Chemicals

For the *in-situ* transesterification experiments, HPLC-grade methanol, sulfuric acid (H_2SO_4), sodium chloride, and *n*-hexane were purchased from Fisher Scientific (Pittsburgh, PA, USA) and used as received. A mixture of 37 reference fatty acid methyl esters (FAMEs) in the range of C_4 to C_{24}, including saturated, mono-unsaturated and polyunsaturated FAMEs was purchased from Supelco (Bellefonte, PA, USA) and used for the preparation of GC calibration standards.

2.2. Sample preparation

The primary and secondary sewage sludge samples were collected from a municipal wastewater treatment plant employing an activated sludge process for BOD_5 (Biochemical Oxygen Demand) removal located in Tuscaloosa, AL, USA. After collection, both the primary and secondary sludge samples were concentrated by settling at 0ºC for 24 hr. The supernatant liquid was discarded and the wet sludges were centrifuged using a Marathon 3000 centrifuge (Fisher Scientific, Pittsburgh, PA, USA) at 3000 RPM for 20 minutes. The dewatered sludges were spread into trays and allowed to freeze for three days at -18°C in a ColdTech freezer (Jimex Corp., Hayward, CA, USA). The frozen sludges were then freeze-dried in a bulk tray freeze dry system (LABCONCO, Kansas City, MO, USA). Afterwards, the freeze-dried sludge samples were crushed, homogenized and stored in the freezer prior to use. The solids content of the freeze-dried sludge was measured to be approximately 95 % on average using an Ohaus Model MB45 infrared heater (Ohaus, Pine Brook, NJ, USA).

2.3. In-situ transesterification

Although an alkali-catalyzed transesterification employing soluble metal hydroxides or methoxides is much faster than an acid-catalyzed transesterification and is most often used commercially (You *et al.,* 2008), problems such as soap formation and difficulty in product separation can arise due to the possibility of having a high concentration of free fatty acids (FFA) in the sewage sludge samples. Freedman *et al.* (1986) recommended using an acid catalyst for lipid feedstocks with >1% FFA, hence an acid-catalyzed transesterification (Figure 2) was used for producing biodiesel from the sewage sludge samples. The primary sludge and secondary sludge were treated separately using the exact same procedure. Five grams of freeze-dried sludge were weighed into each of eight 500-mL flasks. The sludge samples were then randomly treated with the eight treatment combinations of reaction temperature (50 and 75°C), H_2SO_4 concentration (1 and 5 % v/v), and mass ratio of methanol to dried sludge (8:1 and 12:1). A 25-mL volume of hexane was added to improve the lipid solubility in the reaction mixture. The sludge was then suspended in solution using a magnetic stirring bar and the mixture was heated to the set temperature using a hot water bath. The loss of methanol

and hexane due to evaporation was minimized by using a condenser with water at 20°C. Four replicates of each treatment combination of temperature, acid concentration, and mass ratio of methanol to sludge were performed each at different reaction times (0, 4, 8, and 24 hours).

After the reaction was stopped, the mixture was allowed to cool and the flask contents were transferred into a 125-mL bottle. Then, 5 mL of saturated NaCl solution and 50 mL of hexane were added and the bottle was shaken vigorously for three minutes. The mixture was then centrifuged at 3000 RPM for three minutes and the supernatant hexane phase was withdrawn and transferred into a 250-mL separatory flask. The extraction procedure was repeated three times. Afterwards, the total volume of the collected supernatant was washed with 10 mL of a 2 % (w/v) potassium bicarbonate solution and the aqueous phase was allowed to settle. The bottom layer was then discarded and the upper layer (hexane layer) was passed through a filter paper containing anhydrous sodium sulfate and collected into a 500-mL round-bottom flask. A 10-mL aliquot of the hexane phase was pipetted into a test tube for FAME analysis and the remainder was subjected to solvent removal under a vacuum using a Büchi R205 Rotary Evaporator (Büchi Labotechnik, Switzerland) at 320 mbar and 40°C. After all the hexane was removed, the flask was flushed with nitrogen to remove any remaining hexane in the gas phase and then weighed to determine the weight of the residue by difference.

2.4. FAME Analysis

The FAMEs in the hexane phase were analyzed using an Agilent 6890 gas chromatograph equipped with a flame ionization detector (Agilent, Santa Clara, CA, USA). The column used was a 100 m $\times$ 0.25 mm $\times$ 0.2 μm Supelco SP 2380 capillary column (Supelco, Bellefonte, PA, USA) with stabilized poly (90% biscyanopropyl/10%cyanopropylphenyl) siloxane as the stationary phase. The column temperature was programmed to increase from 110°C to 140°C at 10°C/min; maintained at 140°C for 4 minutes; then ramped from 140°C to 240°C at 2°C/min; and finally maintained at 240°C for 40 minutes. The detector temperature was set at 260°C. The carrier gas used was helium (14 psi) at a flow rate of 45.0 mL/min, while the sample injection volume was 1.0 μl with a split ratio of 100:1. The internal standard used was 1,3-dichlorobenzene (Fisher Scientific, Pittsburgh, PA, U.S.A.). Calibration curves between peak area and concentration were established by injecting reference FAME samples of known concentrations into the GC-FID.

3. Results and Discussion

3.1. Effect of operating conditions on FAME yield from primary sludge

The FAME yield (mass of FAME/mass of sludge) as a function of reaction time for the transesterification of primary sludge at the different combinations of reaction temperature, H_2SO_4 concentration, and mass ratio of methanol to sludge are plotted in Figure 3. As shown in the figure, the methyl ester yield increased as the length of reaction time was increased. However, the decreasing slope of the yield curves at $t > 8$ hours may be attributed to the decrease in the reaction rate with time as the concentration of the fatty acids in the sludge decreased due to its conversion to methyl esters. A three-way analysis of variance (ANOVA) with respect to temperature, H_2SO_4 concentration, and mass ratio of methanol to sludge revealed a significant interactive effect ($p < 0.0001$) of the three factors investigated. Therefore, the data were analyzed by pooling the FAME yield data at each of the eight combinations of the three factors. A t-test on the means revealed that the combination of 75°C reaction temperature, 5 % (v/v) H_2SO_4, and a 12:1 methanol to

sludge ratio produced the significantly highest yield for the transesterification of the primary sludge while the combination of 50°C, 1 % (v/v) H_2SO_4, and 8:1 methanol to sludge ratio produced the lowest. It may be speculated that the increase in the yield of the methyl esters was due to the combined effects of increasing the temperature, the presence of a greater amount of catalyst, and a greater excess of methanol that led to the initial jump in the reaction rate at the reaction time less than 8 hours. Moreover, the higher concentration of methanol may have also contributed to the higher FAME yield by driving the equilibrium of the transesterification reaction forward towards the formation of the methyl ester.

3.2. Effect of operating conditions on FAME yield from secondary sludge

The FAME yield as a function of the reaction temperature, H_2SO_4 concentration, and methanol to sludge mass ratio were plotted in Figure 4 in the same manner as with the primary sludge data. However, the three-way ANOVA revealed no significant ($p >>> 0.05$) two- or three-factor interaction effects among the three variables investigated. Instead, the FAME yield was found to be significantly affected by the independent effects of temperature ($p = 0.0025$), H_2SO_4 concentration ($p < 0.0001$), and methanol to sludge mass ratio ($p < 0.0001$). A t-test on the means found that the yield could be maximized by applying any of the high levels of the factors (75°C, 5 % v/v H_2SO_4, or 12:1 methanol to sludge mass ratio).

On the average, the FAME yields obtained from the transesterification of primary sludge were significantly higher than those obtained from secondary sludge, possibly due to the higher concentration of free fatty acids and triglycerides in the form of bound fats and grease in the primary sludge. On the other hand, the secondary sludge is mostly composed of microbial cells, and the methyl esters produced from the transesterification of secondary sludge may have originated from the phospholipids in the cell membranes of these microorganisms.

The amount of the microbial phospholipids that can be converted to biodiesel depends on the sludge residence time in the activated sludge reactor of the wastewater treatment facility. A long residence time leads to the conversion of organic matter in the wastewater into CO_2, water, and some cell mass. Reducing the sludge residence time would lead to the production of more microbial cells, and therefore, more phospholipids due to more carbon being diverted from cell mass production as opposed to CO_2.

3.3. Reaction kinetics for the transesterification of primary sludge

The lipids in primary sludge are composed mostly of triglycerides, with some diglycerides and monoglycerides. For simplicity of the kinetic analysis of the data, it is assumed that all the FAMEs produced were derived from triglycerides. Transesterification of a triglyceride requires three moles of methanol for every mole of triglyceride and results in the production of three moles of fatty acid methyl esters and one mole of glycerol. Hence, the rate of disappearance of triglycerides is given by:

$$-\frac{dC_{TG}}{dt} = k' C_{TG}^{\alpha} C_{methanol}^{\beta} \qquad (1)$$

where α and β are the reaction orders with respect to triglyceride and methanol, respectively, and k' is an empirical reaction rate constant. Assuming that there is no change in the volume of the reaction mixture in the liquid phase, the concentrations of each reactant, triglyceride and methanol were expressed in terms of conversion (x_{TG}), and initial concentration (C_{TG0}) as the following:

$$C_{TG} = C_{TG0}(1 - x_{TG}) \tag{2}$$

$$C_{FAME} = 3C_{TG0}x_{TG} \tag{3}$$

The rate of production of the FAMEs is given by:

$$\frac{dC_{FAME}}{dt} = 3k' C_{TG}^{\alpha} C_{methanol}^{\beta} \tag{4}$$

where C_{FAME} is the concentration of FAMEs in the reaction mixture at time *t*. Substitution of equations (2) to (4) into equation (1) results into:

$$\frac{dx_{TG}}{dt} = \frac{k'}{C_{TG0}} C_{TG0}^{\alpha}(1 - x_{TG})^{\alpha} C_{methanol}^{\beta} \tag{5}$$

In this present work, it was assumed that the methanol is present in great excess with respect to the triglycerides in the sludge, and its concentration remained constant over the course of the experiment. The concentration of methanol is combined with *k'*, and the $C_{TG0}^{\alpha-1}$ term, yielding a pseudo-reaction rate constant, *k*. Thus, equation (5) can be simplified as

$$\frac{dx_{TG}}{dt} = k(1 - x_{TG})^{\alpha} \tag{6}$$

Using the assumption that all the lipids in the primary sludge are triglycerides, and that the maximum conversion of these triglycerides into FAMEs ($x_{TG} = 1$) is achieved at *t* = 24 h, the initial concentration of the triglycerides is estimated by:

$$\lim_{t \to \infty} \left(\frac{C_{FAME}(t \to \infty)}{3C_{TG0}} \right) = 1 \tag{7}$$

The conversion at any time *t*, is thus evaluated from:

$$x_{TG}(t) = \left(\frac{C_{FAME}(t)}{3C_{TG0}} \right) \tag{8}$$

Integral analysis of the conversion data versus reaction time was performed by assuming 0, 1, and 2 as the reaction order α. The most linear trend ($R^2 = 0.99$) was obtained with a second-order assumption ($\alpha = 2$), thus, the data were fit into the equation

$$\frac{x_{TG}}{1 - x_{TG}} = kt \tag{9}$$

The values of the pseudo-rate constants and their corresponding coefficients of determination (R^2) were obtained by linear regression for the different experimental conditions and summarized in Table 1. A *t*-test at the 0.05 significance level was performed on the calculated rate constants pooled between the two levels of each of the factors investigated. The results of the test indicated no significant differences on the rate constants between the two levels of temperature ($p = 0.5092$) and between the two levels of the methanol to sludge mass ratio ($p = 0.8148$). However, the rate constants at 5 % (v/v) of H_2SO_4 were found to be significantly higher ($p \leq 0.0001$) than at 1 % (v/v); therefore, it can be inferred that only the amount of the acid catalyst had a significant effect on the rate at which the triglycerides in the primary sludge were converted to methyl esters. This observation may be attributed to the increase in the rate of formation of the reaction intermediates (as shown in Figure 5) caused by the presence of a greater amount of catalyst. It was expected that increasing the amount of methanol added to the reaction mixture would increase the reaction rate by shifting the equilibrium of the transesterification reaction towards the formation of the products. However, the amount of methanol supplied with the two levels of the methanol to sludge mass ratio were already in excess, hence its effect on the reaction rate was negligible.

3.4. FAME analysis of biodiesel from primary and secondary sludge

The fatty acid composition of the lipids from the primary and secondary sludge was inferred from the results of the FAME analysis of the biodiesel produced from the *in-situ* transesterification of the sludge samples. As shown in Figure 6, there appears to be no substantial difference in the fatty acid composition of primary and secondary sludges that were transesterified. Analysis of biodiesel samples from both types of sludge indicated the occurrence of significant amounts of the methyl esters of palmitic acid (C16:0), stearic acid (C18:0), and oleic acid (C18:1). The observed differences were the occurrence of around 25 % (mol/mol sample) C16:1 (palmitoleic acid) methyl ester in the secondary sludge biodiesel as compared to 3 % in the primary sludge biodiesel; and around 7 % C18:2 (linoleic acid) methyl ester in primary sludge biodiesel as compared to 1 % in secondary sludge biodiesel. These results were in agreement with the findings of Dufreche *et al.* (2007) on the fatty acid composition of secondary (or activated) sludge taken from the same municipal wastewater treatment plant as in this study.

3.5 Biodiesel from Sludge

In-situ transesterification of lipid from dry sludge was conducted using methanol with sulfuric acid as catalyst. The experiments were conducted using 1:12 mass ratio of dried sludge to methanol at 60°C, 400 rpm for 24 hours with 1.3% catalyst. A biodiesel yield of 9.25±0.54% was obtained with 4.58% bound glycerin. Reesterification of the obtained biodiesel using sulfuric acid using 1:6 mole ratio of triglyceride (as triolein) was done at 60°C for 24 hours with same catalyst loading. The partial results of ASTM tests for the biodiesel obtained from *in-situ* and reesterification are summarized in Table 3. It is important to notice that even though the biodiesel prepared from the sludge extract did not pass ASTM, the re-esterification results suggest that refining of the crude biodiesel could be conducted to meet ASTM standards. Biodiesel was not generated in large enough quantities to conduct all the battery of analysis necessary for ASTM certification.

3.6. Economic analysis

A complete breakdown of the estimated costs associated with the *in-situ* transesterification of municipal wastewater sludge is shown in Table 2. Due to the close similarity of the fatty acid composition of primary and secondary sludge as presented in the previous section, it may be feasible to combine the two sludge types into a single

feedstock for biodiesel production. The annual capacity of 3.07×10^5 gallons of biodiesel per year (1.16×10^6 L/yr) for a proposed biodiesel plant utilizing municipal wastewater sludge as the lipid feedstock was based on the rated annual treatment capacity of the wastewater treatment plant in Tuscaloosa, AL (from which the sludge samples were obtained) which is approximately 30 million gallons of wastewater/day. The total sludge production was estimated using the ratio of 0.65 kg of sludge produced/kg BOD_5 removed (Rittman and McCarty, 2001), assuming that the total BOD_5 removal from the wastewater treatment steps (primary sedimentation, aerobic oxidation, secondary clarification) was 95 %. The yield of FAMEs was assumed to be 10 % wt. of the total sludge produced, and the amount of sludge wasted was assumed to be 20 % of the total annual sludge production. Based on the results of the statistical analysis (Sections 3.1 and 3.2), the amounts of methanol and sulfuric acid to be used were calculated using the 5 % (v/v) H_2SO_4 and 12:1 methanol to sludge mass ratio. It was also assumed that the methanol used for the *in-situ* transesterification were recovered and reused for approximately 40 batch cycles. An important factor for estimating the total capital investment (TCC) and total annual production costs (TAPC) is the fixed capital cost (FCC). The FCC, which represents the cost of constructing a new facility, was estimated as the sum of the total equipment cost, contingencies and fees, and costs of auxiliary facilities (You *et al.,* 2008). Equipment costing was done using the same method and assumptions used by You *et al.* (2008), with the exception of the 15 % transportation, insurance, and tax fees required to deliver all pieces of equipment from the United States to Taiwan. The auxiliary facilities costs, which includes purchase of land, installation of electrical and water systems, and construction of all internal roads, may be significantly lowered if the biodiesel facility can be built on the site of or adjacent to the wastewater treatment facility. This set-up can also minimize or eliminate entirely the cost of transporting the feedstock (sludge) into the biodiesel production facility. Based on the estimated TAPC corresponding to the proposed annual biodiesel production capacity of 3.07×10^5 gallons/yr, a break-even price of $3.23/gallon of processed biodiesel was calculated. Profits, income taxes, and product transportation cost effects on the final selling price per gallon of the sludge biodiesel were not considered in this study. Although the raw municipal wastewater sludges are available at practically no cost, the cost of sludge pretreatment by dewatering prior to an *in-situ* transesterification process still constitutes a significant portion of the total production costs at 53 %. However, this is lower than when the biodiesel feedstock used is soybean oil, which constitutes around 65 to 75 % of the total production cost (You *et al.,* 2008). Moreover, the estimated price per gallon of the sludge biodiesel is significantly lower that the current average price of petroleum diesel fuels (around $4.80/gallon) and refined soy biodiesel, which averages between $4.00 to $4.50/gallon. A complete optimization study of the *in-situ* transesterification of municipal wastewater sludge to increase the yield on FAMEs is necessary to further improve the cost-competitiveness of the process and the biodiesel product.

4. Conclusions

It has been demonstrated that biodiesel can be produced through the *in-situ* transesterification of municipal primary and secondary sludges. The yield of FAMEs from primary sludge was found to be significantly affected by the interactive effects of temperature, acid catalyst concentration, and methanol to sludge mass ratio, while the yield of FAMEs from secondary sludge was significantly affected by the independent effects of the three factors investigated. The maximum yields of FAMEs for primary (14.5

% wt.) and secondary sludge (2.5 % wt.) were both obtained at 75°C, 5 % (v/v) H_2SO_4, and 12:1 methanol to sludge mass ratio. Kinetic analysis of the FAME yield data from the *in-situ* transesterification of primary sludge revealed that the reaction was second-order with respect to reaction time, and that an increase in the concentration of the acid catalyst significantly increased the reaction rate. Analysis of the methyl esters by gas chromatography indicated a similarity between the fatty acid composition of the primary and secondary sludge. The results were also in agreement with the findings of a previous study by Dufreche *et al.* (2007) on the fatty acid composition of the sludge samples taken from the same wastewater treatment plant. The price of biodiesel obtained from these feedstocks was estimated to be $ 3.23/gallon, which is comparatively lower than the costs of petroleum diesel and soybean biodiesel. Thus, it can be concluded that municipal wastewater sludges have a high potential as a cost-competitive and abundant feedstock for the production of biodiesel.

References:

American Soybean Association, 2007. Soy Stats 2007. http://www.soystats.com/2007/Default-frames.htm.

Boocock, D.G.B., Konar, S.K., Leung, A., Ly, L.D., 1992. Fuels and chemicals from sewage sludge: 1. The solvent extraction and composition of a lipid from raw sewage sludge. Fuel 71(11), 1283-1289.

Dufreche, S., Hernandez, R., French, T., Sparks, D., Zappi, M., and Alley, E., 2007. Extraction of lipids from municipal wastewater plant microorganisms for production of biodiesel. J. Am. Oil Chem. Soc. 84, 181-187.

Foidl, N., Foidl, G., Sanchez, M., Mittelbach, M., Hackel, S., 1996. *Jatropha curcal* L. as a source for the production of biofuel in Nicaragua. Bioresour. Technol. 58, 77

Freedman, B., Butterfield, R.O., Pryde, E.H., 1986. Transesterification kinetics of soybean oil. J. Am. Oil Chem. Soc. 63, 1375-1380.

Haas, M.J., Scott, K.M., Marmer, W.N., Foglia, T.A., 2004. *In-situ* alkaline transesterification: an effective method for the production of fatty acid esters from vegetable oils. J. Am. Oil Chem. Soc. 81, 83-89.

Haas, M.J., Foglia, T.A., 2005. Alternate feedstocks and technologies for biodiesel production, in: Knothe, G., Krahl, J., Gerpen, J.V. (Eds.), The Biodiesel Handbook. AOCS Press, Illinois, pp. 42-61.

Haas, M.J., Scott, K.M., 2007. Moisture removal substantially improves the efficiency of *in-situ* biodiesel production from soybeans. J. Am. Oil Chem. Soc. 84, 197-204.

Jardé, E., Mansuy, L., Faure, P., 2005. Organic markers in the lipidic fraction of sewage sludges. Water Res. 39, 1215-1232.

Knothe, G., 2005. Introduction: What is biodiesel?, in: Knothe, G., Krahl, J., Gerpen, J.V. (Eds.), The Biodiesel Handbook. AOCS Press, Illinois, pp. 1-3.

Kulkarni, M.G. Dalai, A.K., 2006. Waste cooking oil – an economic source for biodiesel: A review. Ind. Eng. Chem. Res. 45, 2901-2913.

Lee, K.-T., Foglia, T.A., Chang, K.-S., 2002. Production of alkyl esters as biodiesel fuel from fractionated lard and restaurant grease. J. Am. Oil Chem. Soc. 79, 191-195.

National Biodiesel Board, 2007a. Fuel facts sheets. http://www.biodiesel.org/pdf_files/fuelfactsheets/backgrounder.PDF

National Biodiesel Board, 2007b. Energy content. http://www.biodiesel.org/pdf_files/fuelfactsheets/BTU_Content_Final_Oct2005.pdf.

National Biodiesel Board, 2007c. Sample material safety sheet. http://www.biodiesel.org/

pdf_files/fuelfactsheets/MSDS.pdf.
National Biodiesel Board, 2007d. Biodiesel emissions. http://www.biodiesel.org/pdf_files/fuelfactsheets/emissions.pdf.
Nelson, R.G., Schrock, M.D., 2006. Energetic and economic feasibility associated with the production, processing, and conversion of beef tallow to a substitute diesel fuel. Biomass Bioenergy 30, 584-591.
Rittman, B.E., McCarty, P.L., 2001. Environmental Biotechnology: Principles and Applications. McGraw-Hill, New York.
Schuchardt, U., Sercheli, R., Vargas, R.M., 1998. Transesterification of vegetables: a review. J. Braz. Chem. Soc. 9, 199-210.
Shen, L., Zhang, D.K., 2003. An experimental study of oil recovery from sewage sludge by low-temperature pyrolysis in a fluidised-bed. Fuel 82, 465-472.
Tchobanoglous, G., Burton, F.L., Stensel, H.D., 2003. Wastewater Engineering: Treatment and Reuse. McGraw-Hill, New York.
Water Environment Federation, 2002. Activated sludge MOP OM-9, second ed. Water Environment Federation, Virginia.
Yuan, H., Chen, Y., Zhang, H., Su, J., Zhou, Q., Gu, G., 2006. Improved bioproduction of short-chain fatty acids (SCFAs) from excess sludge under alkaline conditions. Environ. Sci. Technol. 40, 2025-2029.
You, Y., Shie, J., Chang, C., Huang, S., Pai, C., Yu, Y., Chang, C.H., 2008. Economic cost analysis of biodiesel production: Case in soybean oil. Energy Fuels 22, 182-189.

Tables

Table 1
Pseudo second-order rate constants for the *in-situ* transesterification of primary sludge.

Temperature (°C)	H_2SO_4 concentration (% v/v)	Methanol to sludge mass ratio	k (L/mol·h)	R^2
50	1	8:1	3.0111	0.9907
50	5	8:1	4.2471	0.9978
50	1	12:1	3.1044	0.9814
50	5	12:1	4.3487	0.9931
75	1	8:1	3.4023	0.9919
75	5	8:1	4.5206	0.9889
75	1	12:1	3.5156	0.9923
75	5	12:1	4.6312	0.9613

Table 2
Annual cost estimates for the *in-situ* transesterification of municipal wastewater sludge. Basis: 3.07×10^5 gallons/yr (1.16×10^6 L/yr).

A. Total capital investment cost, TCC (FCC + WCC)[a]		**$488,177.48**
1. Equipment cost, EC		$276,728,91
a. Transesterification reactor		$74,652.67
b. Neutralization reactor		$8,008.65
c. Washing column		$46,641.16
d. FAME distillation column		$85,574.42
e. Heat exchangers		$2,089.35
f. Pumps		$29,536.78
g. Others		$30,225.89
2. Contingencies and fees, CFC (18 % of EC)		$49,811.20
3. Total basic module cost, TBMC (EC + CFC)		$326,540.12
4. Auxiliary facility cost, AFC (30% of TBMC)		$97,962.04
5. Fixed capital cost, FCC (TBMC + AFC)		$424,502.16
6. Working capital, WCC (15 % of FCC)		$63,675.32
B. Total annual production cost, TAPC (DOC+IOC+DEPC+GE)[b]		**$992,327.00**
1. Direct operating costs, DOC		$768,386.52
a. Feedstock (sludge) preparation, centrifugation, and drying[c]	$1.72/gal	$528,040.00
b. Methanol	$0.08/gal	$102,578.33
c. Acid catalyst and solvent	$0.15/gal	$58,880.00
d. Labor[c]	$0.10/gal	$30,700.00
e. Heating oil[d]	$0.008/L	$9,295.96
f. Electricity[d]	$0.002/L	$2,323.99
g. Cooling water[d]	$0.0013/L	$1,510.59
h. Steam[d]	$0.0009/L	$1,045.80
i. Wash water[d]	$0.0001/L	$116.20
j. Maintenance and repairs (6 % of FCC)		$25,470.13
k. Operating supplies (15 % of maintenance and repairs)		$3,820.52
l. Lab charges (15 % of labor)		$4,605.00
2. Indirect operating costs, IOC		$26,910.04
a. Overhead, packing, storage (60% of labor)		$18,420.00
b. Local taxes (1.5 % of FCC)		$6,367.53
c. Insurance (0.5 % of FCC)		$2,122.51
3. Depreciation, DEPC (10 % of FCC)		$42,450.22
4. General expenses, GE		$154,580.22
a. Administrative expenses (25 % of overhead)		$4,605.00
b. Distribution and selling (≈10 % of TPC)		$99,983.48
c. Research and development (≈5 % of TPC)		$49,991.74
Price of biodiesel per gallon to break even		**$3.23**

[a]Costs were estimated based on the values reported by You *et al.* (2008) using the conversion equation of capacity: $Cost_B = Cost_A(Capacity_B/Capacity_A)^{0.65}$.
[b]Itemized production costs were based on the costs reported by You *et al.* (2008) unless specified otherwise.
[c]Dufreche *et al.* ,2007.
[d]Nelson and Schrock, 2006.

Table 3. ASTM testing results.

Property	Method	Limits	*In-situ*	Reesterified	Units
Flash Point, Closed Cup	D93	93 min	33.33 (92°F)	-	°C
Methanol Content	EN14110	0.2 max	0.011	0.001	% vol
Kinematic Viscosity, 40°C	D445	1.9 – 6.0	3.87	-	mm^2/s
Total Sulfur	D5453	0.05 max	0.5933	0.4712	%wt
Copper Strip Corrosion	D130	No. 3 max	No. 4c	No. 4b	
Cloud Point	D2500	Report	cannot be determined	cannot be determined	°C
Carbon Residue	D4530	0.05 max	1.65	-	%wt
Acid Number	D664	0.50 max	3.63	-	mg KOH/g
Free Glycerin	D6584	0.020 max	0.181	0.112	%wt
Total Glycerin	D6584	0.024 max	4.759	0.114	%wt
Vacuum Distillation End Point	D1160	360 max	400	-	°C

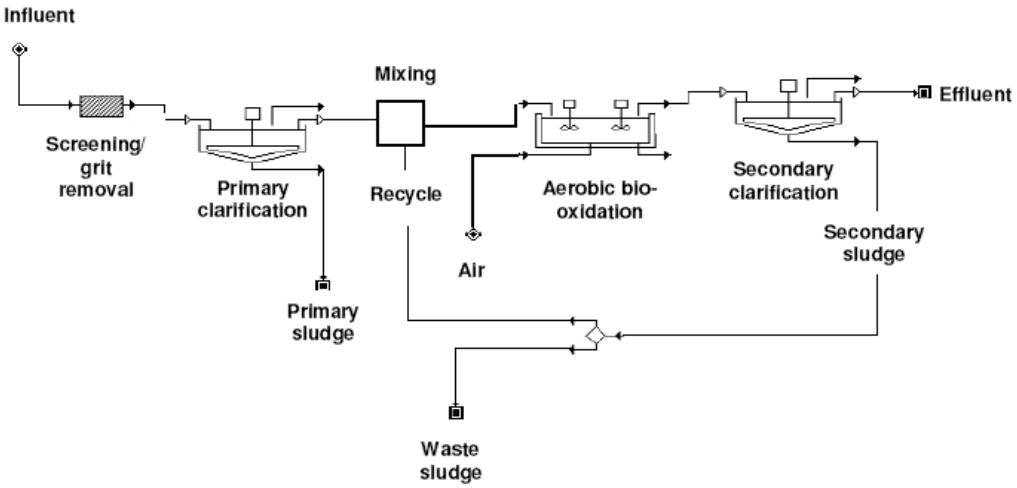


Fig. 1. Schematic diagram of a conventional municipal wastewater treatment plant.

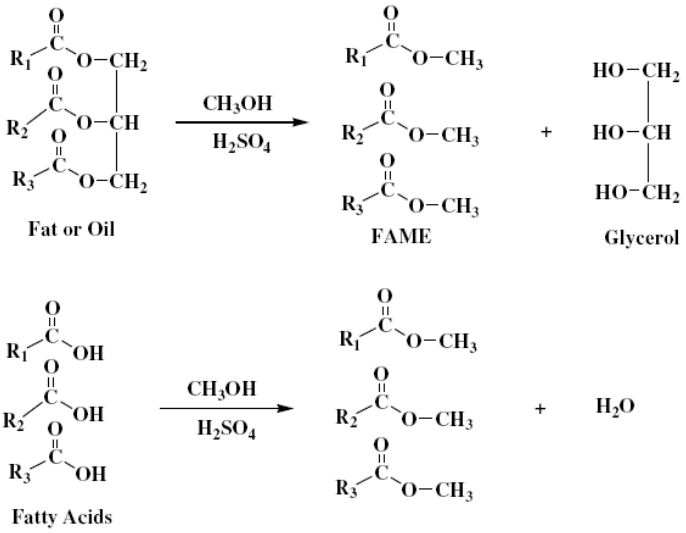


Fig. 2. Acid-catalyzed transesterification of triglycerides and free fatty acids.

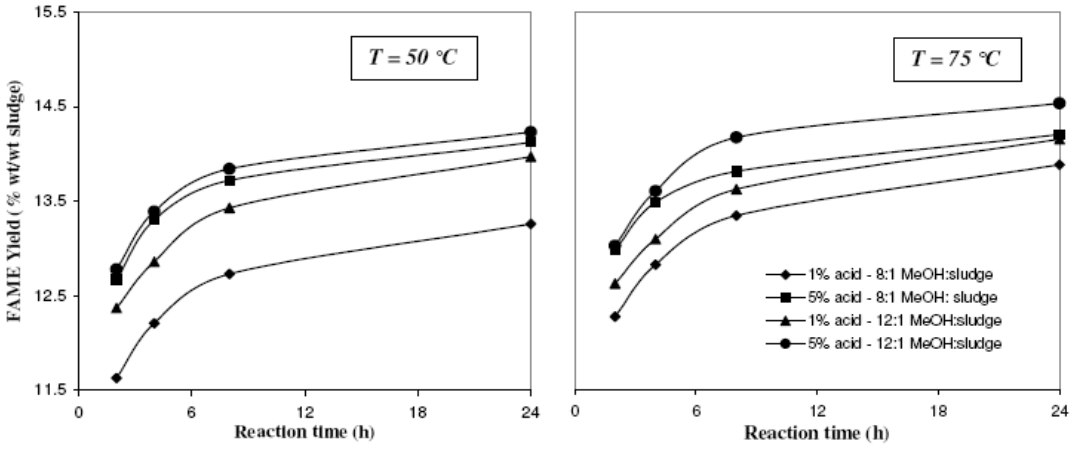


Fig. 3. FAME yield versus reaction time for the *in-situ* transesterification of municipal primary sludge.

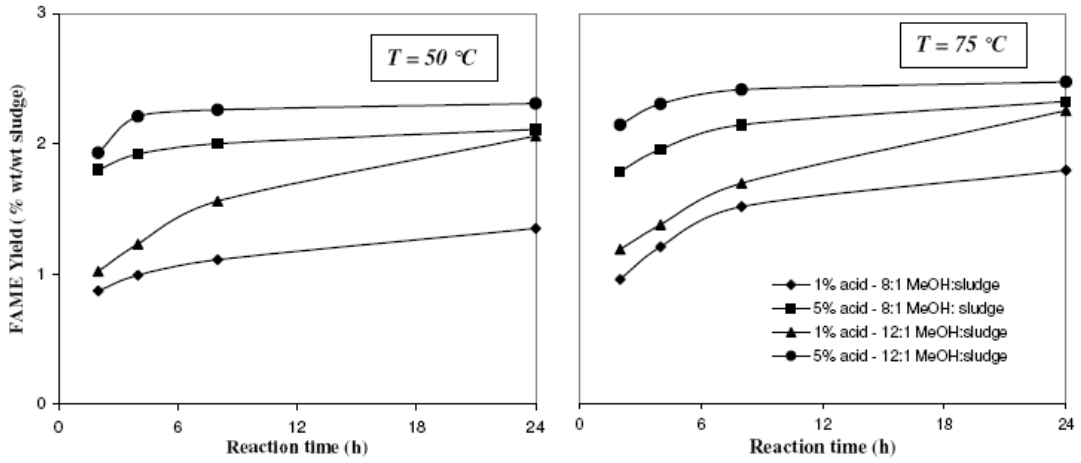


Fig. 4. FAME yield versus reaction time for the *in-situ* transesterification of municipal secondary sludge.

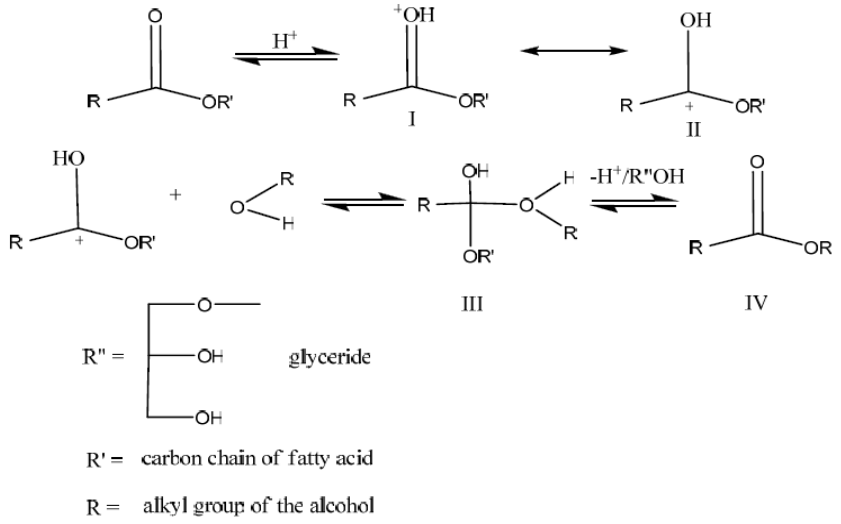


Fig. 5. Mechanism of the acid-catalyzed transesterification of vegetable oils (Schuchardt *et al.*, 1998).

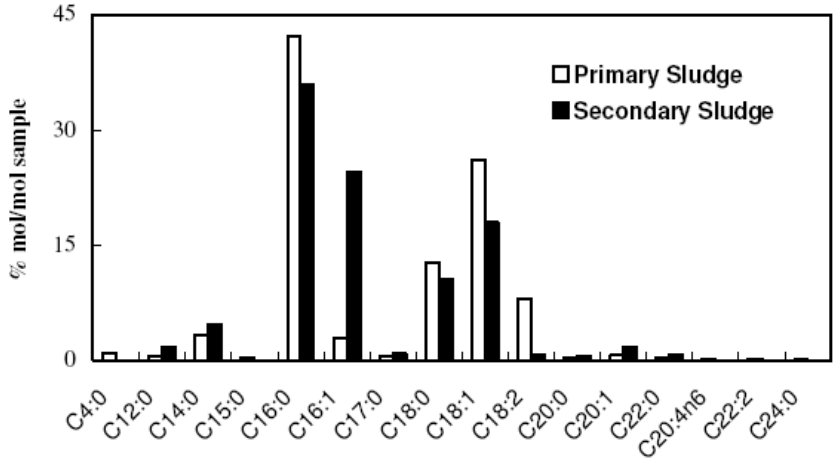


Fig. 6. FAME analysis of biodiesel obtained from the *in-situ* transesterification of municipal primary and secondary sludge at 4 h reaction time, 50 °C, 5 % (v/v) H_2SO_4, and 8:1 methanol to sludge mass ratio.

Task A.2. MSU Research on Oleaginous Microorganisms

A.2. Project 1

1. Introduction

The inevitable depletion of the world's conventional fossil energy sources and concerns over global climate change due to greenhouse gas emissions have refocused scientific research worldwide on the development of sustainable biofuels from biomass (Perlack et al. 2005; Wyman, 2003; Campbell and Laherrere, 1998; Kerr, 1998). In particular, bioethanol derived from biomass and biodiesel derived from plant oils and animal fats have attracted a large amount of attention (Hamelinck et al. 2005; Reaney et al., 2005; Sun and Cheng, 2002; Turkenburg, 2000; Wheals, et al., 1999). Widely available lignocellulosic materials, such as crop residues, grasses, sawdust, wood chips, and solid animal waste, are promising candidates for ethanol production (Sun and Cheng, 2002; Mosier et al. 2005; Hamelinck, et al., 2005). There are four main stages in the process of converting lignocellulosic biomass to ethanol: pretreatment, hydrolysis, fermentation, and product separation/purification. Lignocellulosic biomass is composed of 40~60% cellulose, 20~40% hemicellulose, and 1~25% non-hydrolysable lignin (Hamelinck, et al., 2005). Hydrolysis of cellulose produces primarily glucose. In contrast, the hydrolysis of hemicellulose from angiosperm plants produces mainly xylose and arabinose, which are not readily fermented to ethanol by many naturally occurring organisms (Mosier, et al., 2005; Gong, 1983). Further more, the hydrolysis product mixture (hydrolysate) contains a wide spectrum of compounds having inhibitory effects on ethanol fermentation microorganisms (Bakker, et al., 2004; Luo, et al., 2002; Larsson, et al., 1999). This inhibition also reduces the ethanol productivity, thus increasing the cost of the product. Naturally occurring biochemical pathways need to be identified that can convert all of the sugars in lignocellulosic biomass to a fuel or fuel feedstock with limited inhibition of the other constituents of acid hydrolysates.

Oleaginous microorganisms are considered as an alternative source of oils and fats (Ratledge and Wynn, 2002; Leman, 1997). Some of them are reported to be able to accumulate substantial amount of oils, up to 87% of the cellular dry weight, which could be further transesterified to make biodiesel (Alvarez, et al., 1996). The focus of this study was to determine if *R. glutinis* could produce lipids from sugars contained in acid hydrolysate from switchgrass, particularly, utilizing pentose sugar in the acid hydrolysate. The combination of xylose conversion to microbial lipids or valuable cellular materials with fermentation of hexose sugar to ethanol would increase the yield from lignocellulosic biomass, thereby effecting a cost reduction.

2. Experiments

2.1 Preparation of acid hydrolysate from switchgrass

Switchgrass was obtained from the Department of Plant and Soil Sciences, Mississippi State University. The as-received switchgrass was subjected to size reduction and then sieved to collect material in the size range of 40 mesh to 60 mesh. A 72% (w/w) sulfuric acid solution was prepared from concentrated sulfuric acid (98.5% w/w, Fisher Scientific) by dilution with deionized water. A 10 g sample of switchgrass was mixed with 50 g of the 72% (w/w) sulfuric acid solution in a 1000 mL round-bottomed flask. After the switchgrass and 72% sulfuric acid solution were thoroughly mixed, the resulting mixture was stored in a refrigerator for 24 hours. Deionized water in the amount of 300 mL was then added to the flask in order to produce a mixture, containing approximately 10 % by weight sulfuric acid. This diluted mixture was then heated in a water bath at 95 °C for 3 hours. The liquid hydrolysate was filtered into a glass receiver. Calcium carbonate powder was used to adjust the pH of the hydrolysate to approximately 7.

2.2 Lipid production from acid hydrolysate by oleaginous yeast

The oleaginous yeast *Rhodotorula glutinis* (ATCC 15125) was used in all experiments. The yeast was grown initially in artificial acid hydrolysate medium at a pH of 5.5 and 30 °C, which contained (per liter): yeast extract,1.0 g; $Na_2HPO_4 \cdot 12H_2O$, 1.0 g; KH_2PO_4, 1.0 g; $MgSO_4 \cdot 7H_2O$, 0.4 g; $(NH_4)_2SO_4$, 4.0 g; trace mineral solution, 10 ml; $FeSO_4$ solution, 6.0 ml; sugar, 20 g; acetic acid, 5.2 g; furfural, 0.60 g. The trace mineral solution consisted of (per liter): $CaCl_2 \cdot 2H_2O$, 3.6 g; $ZnSO_4 \cdot 7H_2O$, 0.75 g; $CuSO_4 \cdot 5H_2O$, 0.13 g; $MnSO_4 \cdot H_2O$, 0.50 g; $CoCl_2 \cdot 6H_2O$, 0.13 g; $Na_2MoO_4 \cdot 2H_2O$, 0.17 g. The $FeSO_4$ solution contained 4.0 g/L $FeSO_4 \cdot 7H_2O$. The 20 g of sugar is composed of: glucose, 10.7g; xylose, 8.2 g; galactose, 0.3 g; arabinose, 1.0 g; mannose, 0.1 g (Bakker, et al., 2004). Once the culture reached the stationary phase, the cells were harvested by centrifugation at 2500 RPM for 15 minutes. The yeast cells were then transferred to a fresh medium made of 90% (v) of acid hydrolysate product and 10% (v) of the concentrated nitrogen-free mineral salt solution for the lipid accumulation at pH 5.5 and 30 °C. The concentrated mineral salt solution was composed of (per 100 ml): $Na_2HPO_4 \cdot 12H_2O$, 1.0 g; KH_2PO_4, 1.0 g; $MgSO_4 \cdot 7H_2O$, 0.4 g; trace mineral solution, 10 ml; $FeSO_4$ solution, 6.0 ml.

2.3 Analytical methods

Cell dry weight determination was performed by centrifuging the cells at 6000 RPM for 15 min, washing twice with DI water and drying in a freeze-dry system to constant weight. The lipid content of the cell was obtained by the gravimetrical method described by Bligh & Dyer (1959). The lipid transesterification and fatty acid methyl ester (FAME) extractions were carried out following the procedures described by Christie (2003).

The FAMEs were analyzed using an Agilent 6890 series Gas Chromatograph equipped with a Supelco SP 2380 capillary column(100 m x 0.25 mm x 0.2 micron, model number

Supelco 24317) and a flame ionization detector (FID). Details are described by (Need another reference)Easterling et al. (in print).

Glucose and xylose were analyzed by high pressure liquid chromatography (Agilent 1100 Series) equipped with an evaporative light scattering detector (model 200, SofTA Corporation). The column used was a Grace-Prevail Carbohydrate ES 5u (produced by Alltech) with a length of 250 mm, I.D.of 4.6 mm, particle size 5 micrometer and pH range 2-13. The guard column was 7.5 mm long and I.D. was 4.6 mm. Both were operated at room temperature. The mobile phase was water/ acetonitrile (35:65, v/v) with a flow rate of 1ml/min. The isocratic, spray chamber was controlled at 25 °C, drift tube at 55 °C. The injection volume was 2 µL.

3. Results and Discussion

3.1 Acid hydrolysate from switchgrass.

The sugars produced by the concentrated acid hydrolysis of switchgrass are primarily composed of glucose and xylose (Bakker et al., 2004). In this work, only glucose and xylose were analyzed. Figure 1 provides a HPLC-ELSD chromatogram for the hydrolyzate from this study, indicating the presence of both xylose and glucose. Quantification of these provided concentrations of 10.6 g/L and 9.6 g/L for glucose and xylose, respectively. Consideration of the amount of hydrolyzate produced (750 mL) from 30 g of switchgrass allows determination of glucose yield and xylose yield of 26.5% and 24 %, respectively (concentration * hydrolyzate volume/raw biomass).

3.2 Lipid production by Rhodotorula glutinis growing on acid hydrolysate from switchgrass

Lipid accumulation in oleaginous microorganisms begins when it has exhausted the nutrients, particularly nitrogen, in the medium, but with a surfeit of carbon still remaining. At first, the cells grow rapidly until the nitrogen is consumed followed by the conversion of excess of carbon in the medium into lipids. In this study, the process included two stages. The first stage was characterized by the cell growth. Once the culture reached the stationary phase, the cells were transferred to a fresh nitrogen-free medium. In the second stage, the cells were expected to accumulate lipids as no exogenous nitrogen was added to the medium.

As shown in Figure 2, in the first stage, *Rhodotorula glutinis* grew very rapidly in the artificial acid hydrolysate medium in the presence of 5.2 g/L acetic acid and 0.6 g/L furfural, which could inhibit the growth of ethanol yeast. The culture reached the stationary phase within 40 hours with a lag phase of 14 hours. At point A (Figure 2), the cells were collected and transferred to a fresh medium for lipid accumulation.

In the second stage for lipid accumulation, cell mass and the lipid content of the cellular materials are shown in Figure 3. As presented in Figure 3, the cell mass in the culture increased from 2.05 g/L to 5.74 g/L. Figure 4 displays sugar consumption by *R. glutinis* over time. The growth of the yeasts indicated that nitrogen was presented in the medium, although no exogenous source of nitrogen was added to the medium. The analysis on nitrogen performed by 4500-N_{org} B. Macrokjeldahl method (Greenberg, 2005) indicated that 73 mg/L of nitrogen was present in the actual acid hydrolysate solution. This low concentration of nitrogen in the acid hydrolysate suggests that the main nitrogen presented in the culture was most likely transferred by yeast from the first stage of growth phase.

The lipid content of cells remained almost constant at approximately 5.4% of the cellular dry weight (Figure 3). Zalashko et al. (1988) reported that the presence of compounds inhibiting oxidative phosphorylation and glycolysis decreased biomass and lipid production. In this study, the low lipid content was mainly due to the low sugar concentration. As shown in Figure 4, glucose was consumed within the first 50 hours and then xylose was metabolized during the succeeding 27 hours. A higher lipid accumulation by *R. glutinis* is expected by utilizing a new acid hydrolysate with higher concentration of sugars. *R. glutinis* is reported to be able to

accumulate lipids up to 60.69% growing on glucose of 100 g/l as carbon source (Dai et al. 2007).

3.3. Fatty acid composition

In Table 1 is the fatty acid composition of *R. glutinis* grown on acid hydrolysate. These data indicated that the fatty acid composition remained almost constant except for a slightly higher proportion of unsaturated fatty acids when grown on acid hydrolysate. The fatty acid mixture consists of 25% (wt%) saturated palmitic acid (C16:0), stearic acid (C18:0) and lignoceric acid (C24:0), 49%(wt%) monounsaturated oleic acid and cis-11-eicosenoic acid and 26% (wt%) polyunsaturated linoleic acid and cis-11,14-eicosadienoic acid. The accumulated lipids are storage forms of fuel in many organisms. As observed by Ganger et al. (1992, 1993) as long as nitrogen was present in the culture medium, the lipid content in the cell of *R. glutinis* was constant low due to the cell growth and fatty acid composition of the lipid remained almost same with a high proportion of unsaturated fatty acids. This is consistent with our experimental results. It was also reported that when nitrogen was exhausted completely, the growth slowed down, and the lipid content of the yeast *R. glutinis* started to increase with a decreasing proportion of unsaturated fatty acids (Granger, et al., 1992, 1993). Therefore, provided with an enough higher sugar concentration in the actual acid hydrolysate, the lipid content in the tested *R. glutinis* would increase with an increasing proportion of saturated fatty acids after a complete exhaustion of nitrogen.

In summary, the growth of *Rhodotorula glutinis* in the artificial and actual acid hydrolysate mediums suggests that it is possible to produce lipids by the tested oleaginous yeast growing on the acid hydrolysate of switchgrasss.

References:

Alvarez, H.M., Mayer, F., Fabritius, D., Steinbüchel, A., 1996. Formation of intracytoplasmic lipid inclusion by *Rhodooccus opacus* strain PD630. Arch. Microbiolo. 165, 377-386.

Bakker, R.R., Gosselink, R.J.A., Maas, R.H.W., de Vrije, T., De Jong, E., van Groenestijn, J. W., Hazewinkel, J.H.O., 2004. Biofuel production from acid-impregnated willow and switchgrass. The 2nd World Conference on Biomass for Energy, Industry and Climate Protection, 10-14 May, Rome, Italy, 1467-1470.

Bligh, E.G., Dyer, W. J., 1959. A rapid method of total lipid extraction and purification. Canadian Journal of Biochemistry and Physiology. 37(8), 911-917.

Campbell, C.J., Laherrere, J. H., 1998. The end of cheap oil. Scientific American. 3, 78–83.

Christie, W., 2003. Lipid Analysis, Third ed., The Oily Press, Bridgewater, England

Dai, C. C., Tao, J., Xie, F., Dai, Y.J., Zhao, Mo., 2007. Biodiesel generation from oleaginous yeast *Rhodotorula glutinis* with xylose assimilating capacity. African Journal of Biotechnology. 6(18), 2130-2134.

Easterlin, e.R., French, W.T., Hernandez, R., Licha, M., 2008, The effect of glycerol as a secondary substarte on the growth and fatty acid composition of *Rhodotorula glutinis*. Biosource Technology. (in print).

Gong, C.S., 1983. Recent advances in D-xylose conversion by yeasts. In: Tsao, G.T. Ed., Annual Reports of Fermentation Processes, vol. 6. Academic Press, 253-291.

Granger, L.M., Perlot, P., Goma, G., Pareilleux, A., 1992. Kinects of growth and fatty acid production. Appi Mircrobol. Biotechnol. 37, 13-17.

Granger, L.M., Perlot, P., Goma, G., Pareilleux, A., 1993. Effect of various nutrient limitations on fatty acid production by *Rhodotorula glutinis*. Appl. Microbiol Biotechnol. 38, 784-789.

Greenberg, A., Ed. 2005. 4500-Norg B. Macro-Kjeldahl method in Standard Methods for the Examination of Water and Wastewater, 21st Edition. American Water Works Association, 4-131-4-132

Hamelinck, C. N., Van Hooijdonk, G., Faaij, A. P.C., 2005. Ethanol from lignocellulosic biomass: techno-economic performance in short-, middle- and long-term. Biomass and Bioenergy. 28(4), 384-410.

Leman, J. 1997. Oleaginous microorganisms: An assessment of the potential. Advances in Applied Microbiology, 43,195-243.

Kerr RA, 1998. Geology: The next oil crisis looms large-and perhaps close. Science. 281:1128-1131.

Larsson, S., Palmqvist, E., Hahn-Hagerdal, B., Tengborg, C., Stenberg, K., Zacchi, G., Nilvebrant, N.O., 1999. The generation of fermentation inhibitors during dilute acid hydrolysis of softwood. Enzyme and Microbial Technology. 24(3/4), 151-159.

Luo, C., Brink, D. L., Blanch, H. W., 2002. Identification of potential fermentation inhibitors in conversion of hybrid poplar hydrolyzate to ethanol. Biomass and Bioenergy, 22(2), 125-138.

Mosier, N., Wyman, C., Dale, B., Elander, R., Lee, Y. Y., Holtzapple, M., Ladisch, M., 2005. Features of promising technologies for pretreatment of lignocellulosic biomass. Bioresource Technology. 96, 673-686.

Perlack, R.D., Wright, L.L., Turhollow, R.F., Graham, R.L., Stokes, B.J., Erbach, D.C., 2005. Biomass as feedstock for a bioenergy and bioproducts industry [electronic resource] : the technical feasibility of a billion-ton annual supply, Oak Ridge, Tenn. : Oak Ridge National Laboratory (http://www.ornl.gov/~webworks/cppr/y2001/rpt/123021.pdf).

Ratledge C., Wynn, J. P., 2002. Biochemistry and molecular biology of lipid accumulation in oleaginous microorganisms. Advances in Applied Microbiology, 51,1-51.

Reaney, M. J. T., Hertz, P. B., McCalley, W. W., 2005. Vegetable oils as biodiesel. Bailey's Industrial Oil and Fat Products (6th Edition). 6, 223-257.

Sheehan, J., 2001, The Road to Bioethanol: A Strategic Perspective of the U.S. Department of Energy's National Ethanol Program. In: Himmel, M.E., Baker, J.O. and saddler, J. N. (Eds), Glycosy hyhrolases for biomass conversion. American Chemical Society, pp. 2-25.

Sun, Y., Cheng, J.Y., 2002. Hydrolysis of lignocellulosic materials for ethanol production: a review. Bioresource Technology. 83, 1-11.

Wyman, C.E., 2003. Potential synergies and challenges in refining cellulosic biomass to fuels, chemicals, and power. Biotechnology Progress. 19, 254-262.

Turkenburg, W.C., 2000. Renewable energy technologies. In: Goldemberg J, Baker JW, Khatib H, Ba-N'Daw S, Popescu A, Viray FL, editors. World Energy Assessment; energy and the challenge of sustainability. New York NY, USA: United Nations Development Programme UNDP. p. 219–72 (Chapter 7).

Wheals, A. E., Basso, L. C., Alves, D. M. G., Amorim, H. V., 1999. Fuel ethanol after 25 years. Trends in Biotechnology. 17(12), 482-487.

Zalashko, M. V., Koroleva, I. F., Andreevskaya, V. D., 1988. Lipid and carotenoid synthesis by *Rhodotorula glutinis* in the presence of compounds inhibiting oxidative phosphorylation and glycolysis. Mikrobiologiya. 57(4), 693-5

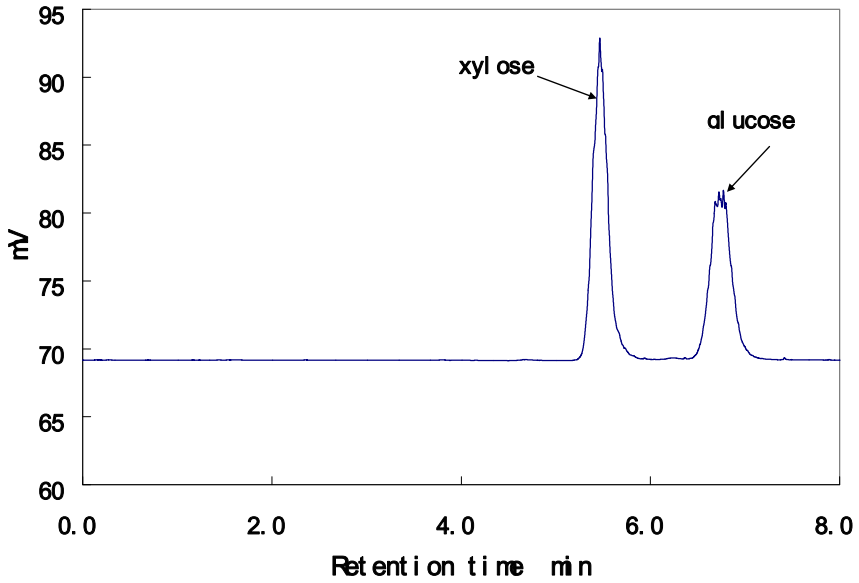


Figure 1. HPLC-ELSD spectra of the acid hydrolysate from switchgrass

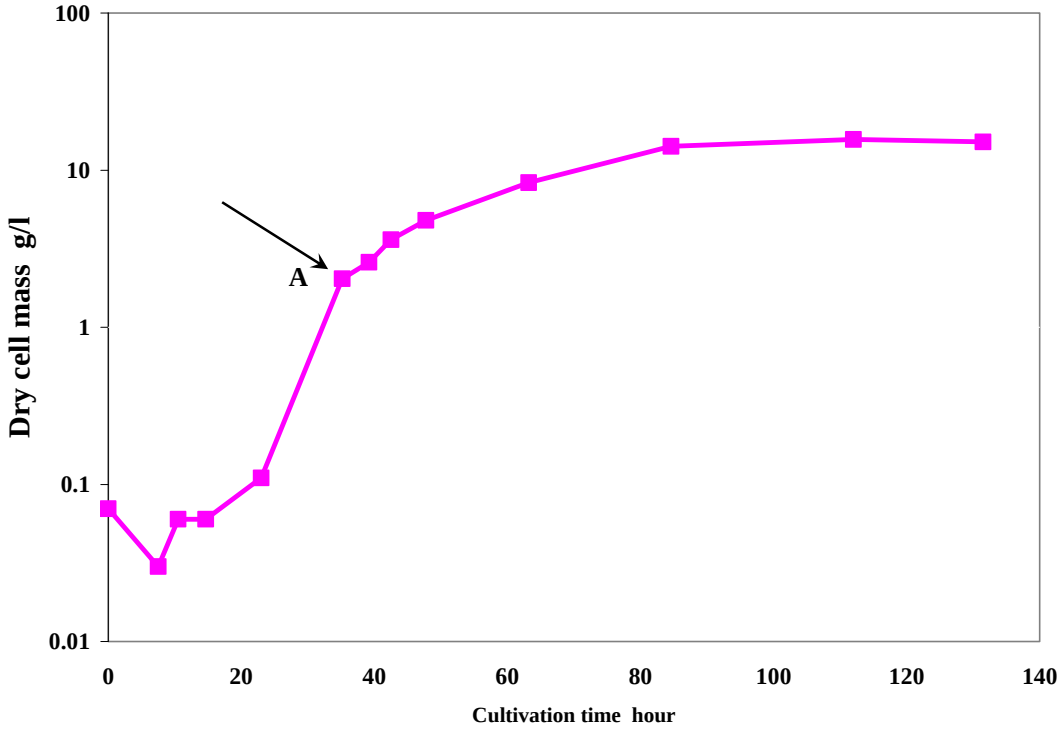


Figure 2 Cell growth in the nitrogen-rich artificial acid hydrolysate medium. Point A signifies the beginning of the oil accumulation period.

A.2. Project 2

1. Introduction

Biodiesel is one of the alternative fuels currently being produced in the United States and elsewhere around the World (Sheehan, et a.l., 1998, Van Gerpen, 2004). A chemical process called transesterification, is used to make biodiesel, this is a process in which the glycerol is separated from the triacylglycerides in fats or vegetable oils (National Biodiesel Board, 2006). Glycerol is 10% of the product output (Fortenberry, 2005), or 1 lb of glycerol for each gallon of biodiesel fuel. The future supplies and usage of glycerol are expected to increase as biodiesel plants increase production, and the output will greatly outpace demand. Biodiesel production has already had a significant impact on the price of refined glycerol (Virent, 2006). A major concern of glycerol producers is the reduced price of glycerol resulting from the increased production of biodiesel. Some alternative uses for this glycerol that have been investigated are substrates for fermentation process or the production of biosurfactants (Ashby, 2006, Solaimanet al., 2006). Another alternative use for glycerol is as a growth substrate for the cultivation of oleaginous yeasts. Oleaginous yeasts are single-celled fungi defined as having at least 20% of their dry weight made up of lipids (Ratledge, 1977). Not only do these yeasts contain membrane lipids, but they accumulate lipid in the form of triacylglycerol (TAG) (Gill et al., 1977). *Rhodotorula glutinis* is an oleaginous yeast which is able to activate non-esterified fatty acids for the synthesis of triacylglycerol (Gangar et al., 2001). In *R. glutinis,* fatty acids are activated in an ATP dependent manner prior to being used. Gangar et al. (2002) have demonstrated that an enzyme, acyl-acyl carrier protein (ACP) plays a role in activating fatty acids for triacylglycerol biosynthesis. There is plenty evidence to suggest that this organism has the potential to be a source of fatty acids for the production of biodiesel. Oleaginous yeasts have the ability to grow and accumulate lipids when grown on glycerol (Meesters et al., 1996), have short generation times, and very minimal nutrient requirements. While purified glycerol has many possible uses, the crude glycerol produced during biodiesel manufacturing contains macro elements such as calcium, potassium, magnesium, sulfur and sodium (Thompson et al., 2005). In order to minimize unknown variables introduced through the use of crude glycerol, initial studies to determine whether or not glycerol could be used as substrate or co-substrate for growth were conducted using purified glycerol. Using the glycerol to produce fatty acids to be used as biodiesel feedstock would provide an added bonus of offsetting costs of production.

The objectives of this work were: 1. determine the effect of pure glycerol on the growth of the yeast *R. glutinis*, 2. assess the effects of pure glycerol on the lipid accumulation of the yeast, and 3. determine the effect of using pure glycerol as a sole or secondary carbon source on the fatty acid methyl ester (FAMEs) content for *R. glutinis*.

2. Experimental Procedures

Organism

The yeast *Rhodotorula glutinis* (ATCC 204091) was used in all experiments (ATTC, 2006a).

Media

All media was sterilized in a Steris® (Mentor, Ohio) autoclave for 15 minutes at 121°C and 15 psi. *Stock culture medium*. *R. glutinis* was cultured overnight on yeast peptone dextrose media (Fisher Scientific, hereinafter referred to as YPD) pH 6.5, 35°C to maintain a stock culture.

Cell mass accumulation medium. Basal Medium (BM) (containing per 1 liter distilled water: 0.2 g KH_2PO_4, 0.15 g yeast extract, and 8.0g NH_4Cl) based on ATCC Minimal Medium protocols (ATCC 2006 b ATTC 2006b) and contained experimental carbon source(s),

dextrose, xylose, glycerol, or mixtures of two sugars, at C/N molar ratios of 10/1. This BM was used to culture *R. glutinis* to accumulate cell mass in preparation for inoculating the test media. *Test medium.* The test media used in the experiments was based on the BM but was amended (per 1 liter distilled water: 0.4 g KH_2PO_4, 0.3 g yeast extract, and 2.0g NH_4Cl) and contained the experimental carbon sources so that the C/N molar ratios were 10/1. The pH of the media was adjusted to 6.0 with 10% HCl (vol/vol).

Inoculum Preparation

R. glutinis subcultures were used to inoculate 3-500 mL batches of each culture medium. After 6 days of growth, the cultures were centrifuged (20 min at 6000 rpm and 22°C). The pellet was washed three times with physiological saline (0.85% NaCl). The concentrated cells were used to inoculate a test media containing the appropriate carbon source(s). The media was inoculated to a cell density of 0.5 mg/mL which correlated to an absorbance of 0.5 at 600 nm.

Experiment Design

The carbon sources tested were: dextrose, xylose, and glycerol, the carbon sources in mixtures tested were: dextrose plus xylose, xylose plus glycerol, and glycerol plus dextrose. Three replicate cultures of *R. glutinis* with each of the six carbon sources were incubated at 35°C on a New Brunswick Rotary Shaker/Incubator (Edison, New Jersey) set at 112 rpm for 48 h.

Measurement of Growth

Every 24 h , for 48 h a 1 mL sample was removed from each experimental replicate and the absorbance of light at 600 nm wavelengths was measured for each sample via Spectronic* Genesys* 20 Spectrophotometer (Thermo*Electron). Cell mass of the *R. glutinis* cultures was correlated to A_{600} prior to experimenting with test medium.

Lipid Extraction

To monitor lipid content of the cells, yeast grown on the test media (Table 1) were extracted every 24 h as described by Bligh and Dyer, 1959.

Gravimetric Analysis of Lipids

The lipid transesterification and fatty acid extractions were carried out following the procedures described by Christie , 2003.

Gas Chromatography/ Flame Ionization Detection of FAMEs.

The FAMEs were analyzed using an Agilent 6890 series Gas Chromatograph equipped with a Supelco SP 2380 (100m x 0.25mm x 0.2 micron, model number Supelco 24317) capillary column and a flame ionization detector (FID). The inlet temperature was set at 260°C with a pressure of 40 psi in split mode (100:1). Helium served as the carrier gas with a flow of 126 mL/min (total flow, 130.3 mL/min). The oven temperature program ramped from 110°C (held the initial temperature for 4 min) to 140°C at 10°C per min, from 140°C to 220°C at 2°C per min, and finally from 220°C to 240°C at 2°C per min. The temperature was held at 240°C for 40 min. The detector temperature was maintained at 260°C with a hydrogen flow of 40 mL/min and air flow of 450 mL/min with constant makeup flow at 45 mL/min. A 10 μL Hamilton glass syringe was used to inject a 1 μL sample of hexane containing the unknown FAMEs and 1 mg/mL 1, 3-dichlorobenzene as the internal standard.

3. Results and Discussion

The effect of glycerol as a secondary substrate on the growth of R. glutinis. When glycerol was provided as a carbon source along with dextrose, *R. glutinis* accumulated more cell mass after 48 h. (38% cell mass increase) than when either carbon source was provided singly (Table 1). Compared to dextrose, glycerol is less favorable as an energy source, which is

verified by our findings that dextrose grown *R. glutinis* increased cell density 24% when given dextrose and 18% when given glycerol as the sole carbon source. Using xylose and glycerol simultaneously as carbon sources resulted in 14% cell density increase which was a lower percent increase than when the carbon sources were used alone (18% increase for both xylose grown and glycerol grown).

The greatest cell mass increase of 49% was observed with dextrose plus xylose grown culture and was followed by a 38% increase in cultures given glycerol plus dextrose. The results indicate that growth on dextrose can be enhanced through the simultaneous addition of glycerol. With the output of glycerol increasing as new biodiesel plants come online and additional studies using crude glycerol, processes of this type could make beneficial use of the surplus glycerol. Biodiesel production has already had a significant impact on the price of refined glycerol (Virent, 2006).

The effect of glycerol on the lipid accumulation of R. glutinis. Although iron, zinc, phosphorus, nitrogen, and concomitant limitations of nitrogen and phosphorus or magnesium have resulted in lipid accumulation (Fortenberry, 2005, Granger et al., 1993, Ykema et al., 19889), nitrogen limitation has been used more extensively to create an environment conducive to lipid hoarding. Carbon has been determined to be limiting at C/N molar ratios of 4/1 and surfeit for oleaginous yeast C*ryptococcus curvatus* at C/N molar ratios of 25/1 (Meesters, et al., 1996). A C/N ratio of 10/1 was provided in the test media used in these *R. glutinis* batch culture experiments, therefore, rather than optimizing lipid production, the goal was to observe the basic lipid producing capability of the yeast when given different carbon sources.

The lipid contents (as % dry cell weight) of the *R. glutinis* cultures are shown Figure 1. The data demonstrates differences in oil accumulation by R. glutinis between those cultures provided single carbon sources and those provided mixtures of carbons sources. When comparing the 24 and 48 h data for all experiments, lipid content of the glycerol grown *R. glutinis* increased on average 12.97% while dextrose grown and xylose grown *R. glutinis* decreased 8.56% and 9.08% respectively. The dextrose plus xylose grown culture increased 1.11% from 24 to 48h. While the data suggests that using glycerol as a sole carbon source may result in greater lipid production by the oleaginous yeast *R. glutinis* the standard error shows there is not sufficient evidence to determine whether using glycerol in conjunction with a six or five carbon sugar will cause the oleaginous yeast *R. glutinis* to produce more lipid than when the carbon sources are used individually. It can be submitted, however, that glycerol grown *R. glutinis* accumulates more lipid under these experimental conditions than dextrose grown and xylose grown cultures.

The lipid accumulating properties of *R. glutinis* has been explored extensively (Gangar et al., 2002Granger e al., 1992,Solaiman et al., 20064, Yoon and Rhee, 1983) especially when considered a source of fatty acids in the nutritional supplement arena. The use of glycerol as a carbon substrate, due to its prospective surplus and decreased value, has been appraised (Gill et al., 1977, Nouredini et al., 1988, Papanikolau et al., 2002).The implications of recycling glycerol for use as a substrate on which to grow oleaginous yeasts for the production of lipids should be investigated more thoroughly, for its potential is outstanding. While over 70% of biodiesel production costs are due to the expense of feedstocks such as soybean and rapeseed oil (Haas et al., 2006), using a renewable lipid source such as that from oleaginous yeast could also help to cut the costs of production.

The research presented here compares the lipid accumulating capabilities of *Rhodotorula glutinis* when grown on substrates such as dextrose, xylose, glycerol and their combinations has not been previously considered. Our findings validate that glycerol is a viable carbon source for the production of lipid by the oleaginous yeast *R. glutinis*.

The effect of different growth substrates used on the FAME saturation of R. glutinis. Figure 2a shows the results of the fatty acid saturation content of *R. glutinis* grown on each of the six carbon source(s) tested. After 24 hrs of incubation, at least 50% of the total FAMES present in each culture were saturated in nature except in the case of the glycerol and dextrose grown *R. glutinis* which had a content of 48% (SD=0.82) saturated FAMEs. The xylose grown and the glycerol grown *R. glutinis* contained the greatest fraction of saturated FAMEs at 69% (SD=1.88) and 68% (SD=9.00), respectively.

At 24 h when glycerol was present as a secondary carbon source, there was an increase in polyunsaturated fats for the xylose plus glycerol grown *R. glutinis* compared to the fatty acid composition of only xylose grown *R. glutinis*. An increase in monounsaturated fatty acids in the fatty acid composition for *R. glutinis* was observed when the cells grown on dextrose plus glycerol when compared to cells grown on dextrose or glycerol solely . The addition of glycerol as a carbon source along with dextrose or xylose resulted in a decrease in the amount of saturated fatty acids.

At 48 h (Figure 2b) the xylose grown and the dextrose plus xylose grown cultures contained the greatest percent saturated FAMEs at 76% (SD=7.97) and 71% (SD=5.96), respectively, with the dextrose grown *R. glutinis* follwing at 70% (SD=5.58) (Fig 2b). The glycerol grown *R. glutinis* and the glycerol and dextrose grown *R. glutnis* contained 46% (SD=4.26) and 46% (SD=3.15) saturated fatty acids, respectively. The degree of fatty acid saturation still decreased when comparing single carbon sources to mixed sugar sources, except in the case of the dextrose plus xylose grown *R. glutinis*.

The effect of time on fatty acid saturation. When comparing the 24 h profiles to the 48 h (Table 2, Table 3) compositions, the saturated fatty acids derived from glycerol grown *R. glutinis* decreased from 68% (SD=9.0) to 46% (SD=4.26). The saturation of the FAMEs from the xylose plus dextrose grown yeast increased 62% (SD=7.9) to 71% (SD=5.96) and xylose grown cultures increased in saturation 69% (SD=1.88) to 76% (SD=7.97). The FAME saturation of the dextrose grown, glycerol plus dextrose grown, and xylose and glycerol grown *R. glutinis* cultures did not change significantly over time.

When glycerol was used along with dextrose as carbon substrates, the saturation of the FAMEs derived from *R. glutinis* was less than when dextrose was used alone, but was comparable to the saturation levels of glycerol grown *R. glutinis.* The xylose grown yeast produced the most saturated FAMEs and the effect of adding glycerol as a secondary carbon substrate in the media was that the unsaturated FAME's increased.

Our results indicate that mixing glycerol with either of the other two carbon sources serves to decrease the saturation of FAMEs produced by *R. glutinis* and that with time the saturation of the glycerol grown cultures decrease. One possible explanation is that glycerol metabolism activates the expression of different enzymes used in fatty acid synthesis. Microarray analysis would be able to confirm or disprove this theory.

The effect of glycerol on the FAME profile of R. glutinis grown. Five fatty acids commonly reported in the literature for different oils are the saturated fatty acids, palmitic acid (C16:0) and stearic acid (C18:0); the monounsaturated fatty acid, oleic acid (C18:1); and the polyunsaturated fatty acids linoleic acid (C18:2) and linolenic acid (C18:3) (26,28,29,30). The fatty acids produced by *R. glutinis* in the above experiments were predominantly palmitic acid and stearic acid. Compared to soybean oil and rapeseed oil, which are used in the U.S. and the E.U. respectively as feedstocks for biodiesel production, the FAMEs derived from *R. glutinis* were more saturated. Soybean oil contains mostly C18:2 (53.7%) and C18:1 (23.3%) while rapeseed oil consists of mainly the same fatty acids at 23.3% and 64.4%, respectively (O'Brien, 1988).

When considering whether biodiesel derived from yeast lipids is suitable for use as a fuel, several factors should be analyzed. The fatty acid structures of the alky esters that make up biodiesel lend specific properties to the fuel that must conform to standards set by American Society of Testing and Materials (ASTM, 2006). The cetane number (CN), cloud point, pour point, heat of combustion, and lubricity are some of the properties influenced by fatty acid structure and the standards for 100% biodiesel are outlined in the method ASTM D 6751 (ASTM, 2006). Saturated fatty acids tend to give favorable properties to the biodiesel such as increseased cetane value, decreased NOX emissions, shorter ignition delay time, and oxidative stability; while unsaturated fatty acids lend better cold flow and pour point values (ASTM, 2006, Knothe, 2005).

This study has demonstrated that pure glycerol can be combined with other carbon sources such as dextrose and xylose to serve as a carbon and energy source for the oleaginous yeast *R. glutinis*. The results of this study also indicate the fatty acid composition can be affected from the type of carbon source provided. The ability of *R. glutinis* to convert pure glycerol into fatty acids and TAG is the first step needed to using the crude form of glycerol produced during biodiesel production.

References:

American Type Culture Collection http://www.atcc.org/common/catalog/numSearch/numResults.cfm?atccNum=204091 (accessed July 2006).

American Type Culture Collection http://www.atcc.org/common/documents/mediapdfs/1199.pdf (accessed August 2006).

American Type Culture Collection http://www.atcc.org/common/documents/mediapdfs/846.pdf (accessed September 2006).

Ashby, R.D., Solaiman, D., Foglia, T. A., 2006. New uses for glycerol: fermentation substrates for value-added product synthesis [abstract]. Annual Meeting and Expo of the American Oil Chemists' Society. p. 72.

ASTM D6751 Specification for biodiesel blend stock (B 100) for distillate fuels. http://wetestit.com/ASTM%20D6751.htm. (Accessed July 2006).

Bligh, E.G., Dyer, W. J., 1959. A rapid method of total lipid extraction and purification. Canadian Journal of Biochemistry and Physiology. 37(8), 911-917.

Christie, W., 2003. Lipid Analysis, Third ed., The Oily Press, Bridgewater, England.

Davoli, P., Mierau, V., Weber, R. S. W. 2004. Carotenoids and fatty acids in ard yeasts *Sporoblomyces rosus* and *Rhodotorula glutinis*. Applied Biochemistry and Microbiology. 40, 392-397.

Fortenbery, T.R., 2005. Biodiesel Feasibility Study: An evaluation of biodiesel feasibility in Wisconsin, Department of Agribusiness, University of Wisconsin – Madison.http://64.233.187.104/search?q=cache:dlPIj5Su9.

Gangar, A., Karande, A. A., Rajasenkharan, R., 2001. Purification and characterization of acyl-acyl carrier protein synthetase from oleaginous yeast and its role in tryacylglycerol biosynthesis. Biochemical Journal. 360, 471-479.

Gangar, A., Raychaudhuri, S., Rajasekhran, R., 2002. Alteration in the cytosolic triacylglycerol biosynthetic machinery leads to decreased cell growth and triacylglycerol synthesis in oleaginous yeast. Biochemistry Journal. 365, 577-589.

Gill, C. O., Hall, M. J., Ratledge, C., 1977. Lipid accumulation in oleaginous yeast (*Candida* 107) growing on glucose in a single stage continuous culture. Applied and Environmental Microbiology. 33(2), 235-239.

Granger, L.-M., Perlot, P., Goma, G., Pareilleux, A. 1992. Kinetics of growth and fatty acid production of *Rhodotorula glutinis*. Applied Microbiology and Biotechnology. 37, 13-17.

Granger, L.-M., Perlot, P., Goma, G., Pareilleux, A., 1993. Efficiency of fatty acid synthesis by oleaginous yeast: prediction of yield and fatty acid cell content from consumed C/N ratio by simple method. Biotechnology and Bioengineering. 42,1151-1156.

Haas, M.J., McAloon, A. J., Yee, W. C., Foglia, T. A., 2006. A process model to estimate biodiesel production costs. Bioresource Technology. 97, 671-678.

Hassan M., Blanc, P.J., Granger, M., Pareilleux, A., Goma, G., 1993. Lipid production by an unsaturated fatty acid auxotroph of the oleaginous yeast *Apiotrichum curvatum* grown in a single stage continous culture. Appl Microbiol Biotechnol 40, 483-488.

Knothe, G., 2005. Dependence of biodiesel fuel properties on the structure of fatty acid alkyl esters, fuel processing technology 86,1059-1070.

Noureddini, H., Dailey, W. R., Hunt, B.A., 1998. Production of ethers of glycerol from crude glycerol- the byproduct of biodiesel production. Papers in Biomaterials University of Nebraska, Lincoln.

Meesters, P. A., Huijberts, G.N.M., Egglink, G. 1996. High-cell-density cultivation of the lipid accumulating yeast *Cryptococcus curvatus* using glycerol as a carbon source. Applied Microbiology and Biotechnology 45, 575-579.

O'Brien, R.D., 1988. Fats and oils, first ed., Lancaster Technomic Publishing Co., United Kingdom, pp. 206–207 .

Papanikolaou, S., Munilglia, L., Chevalot, I., Aggelils, G., Marc, I., 2002. *Yarrowia lipolytica* as a Potential Producer of Citric Acid from Raw Glycerol. *Journal of Applied Microbiology.* 92, 737.

Ratledge, C., 1977. Microbial Lipids in Biotechnology, second ed. by H.J Rehm and G. Reed, vol 7, VCH Germany., pp. 133-197.

Sheehan, J., Dunahay, T., Beneman, J., Roessler, P., 1998. A Look Back at the U.S. Department of Energy Aquatic Species Program: Biodiesel from Algae, National Renewable Energy Laboratory.

Solaiman, D., Ashby, R. D., Zerkowski, J. A., Hotchkiss, T. A., Foglia, T.A., Marmer, W. N., 2006. Bioconversion of Soy-Based Feedstocks into Biopolymers and Biosurfactants [abstract]. Annual Meeting and Expo of the American Oil Chemists' Society. p. 14 .

The official Site of the National Biodiesel Board. Biodiesel. http://www.biodiesel.org/resources/biodiesel_basics/default.shtm (accessed July 2006).

Thompson, J. C., B. B. He, B. B., 2005. Characterization of Crude Glycerol from Biodiesel Production from Multiple Feedstocks. Food and Process Engineering Institute Division of ASABE.

Van Gerpen, J., 2004. Business Management for Biodiesel Producers, Iowa State University Under Contract with the National Renewable Energy Laboratory.

Virent. (accessed July 2006). Conversion of Glycerol Stream in a Biodiesel Plant Background. www.virent.com/whitepapers/Biodiesel%20Whitepaper.pd.

Ykema, A., Verbree, E. C., Kater, M. M., Smit, H., 1988. Optimization of Lipid production in the Oleaginous Yeast *Apiotrichum curvatum* in Whey permeate. Applied Microbiology and Biotechnology 29, 211-218.

Yoon, S.H., Rhee, J.S. 1983. Lipid from Yeast Fermentation: Effects of Culture Conditions on Lipid Production and its Characteristics of *Rhodotorula glutinis*. Journal of the American Oil Chemists' Society 60 (7), 1281-1286.

1. TABLE 1

The effect of carbon source and mixtures of carbon sources on the cell mass accumulation of *Rhodotorula glutinis* when grown at 35°C with agitation (112 rpm)

Carbon Source	0 hr (mg)	24 hr (mg)	48 hr (mg)	Overall Cell Mass Increase (%)
Dextrose	17.47 ± 1.42	17.86 ± 2.03	22.81 ± 0.26	24
Xylose	13.25 ± 2.03	13.05 ± 0.95	16.05 ± 0.17	18
Glycerol	20.21 ± 0.26	22.15 ± 0.72	24.41 ± 1.08	18
Dextrose/Xylose	18.28 ± 0.25	25.63 ± 1.57	35.52 ±1.46	49
Xylose/Glycerol	18.87 ± 0.05	21.40 ± 0.48	21.84 ± 0.49	14
Glycerol/ Dextrose	14.01 ± 0.34	17.96 ± 0.91	22.56 ± 0.95	38

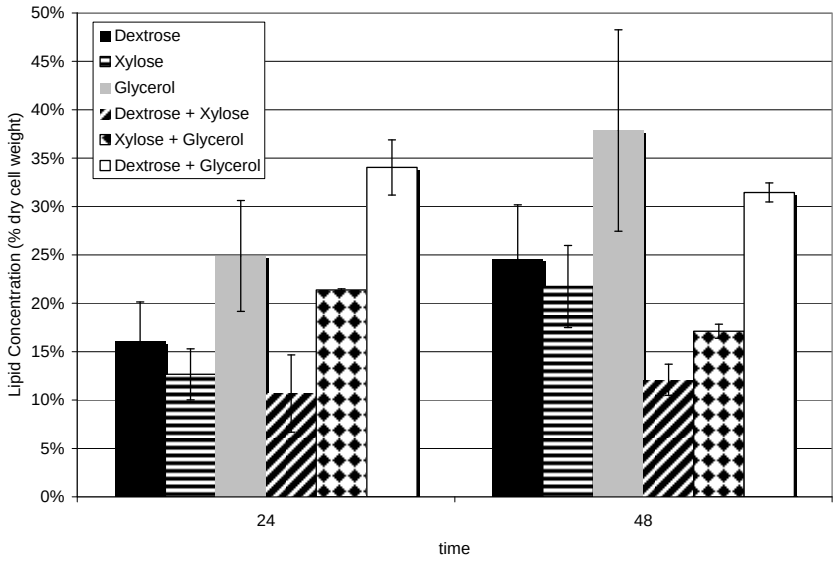


Figure 1. The effect of glycerol and culture duration on the total lipid production of *Rhodotorula glutinis* when grown at 35°C with agitation (112 rpm)

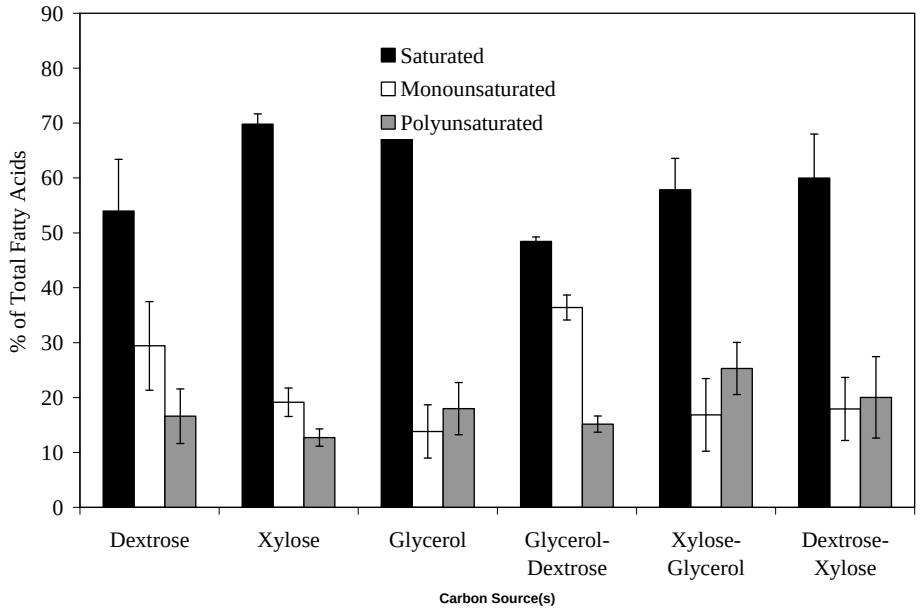


Figure 2a. The effect of carbon source on the saturation of fatty acids produced by *Rhodotorula glutinis* after 24 h of agitated (112 rpm) incubation at 35°C

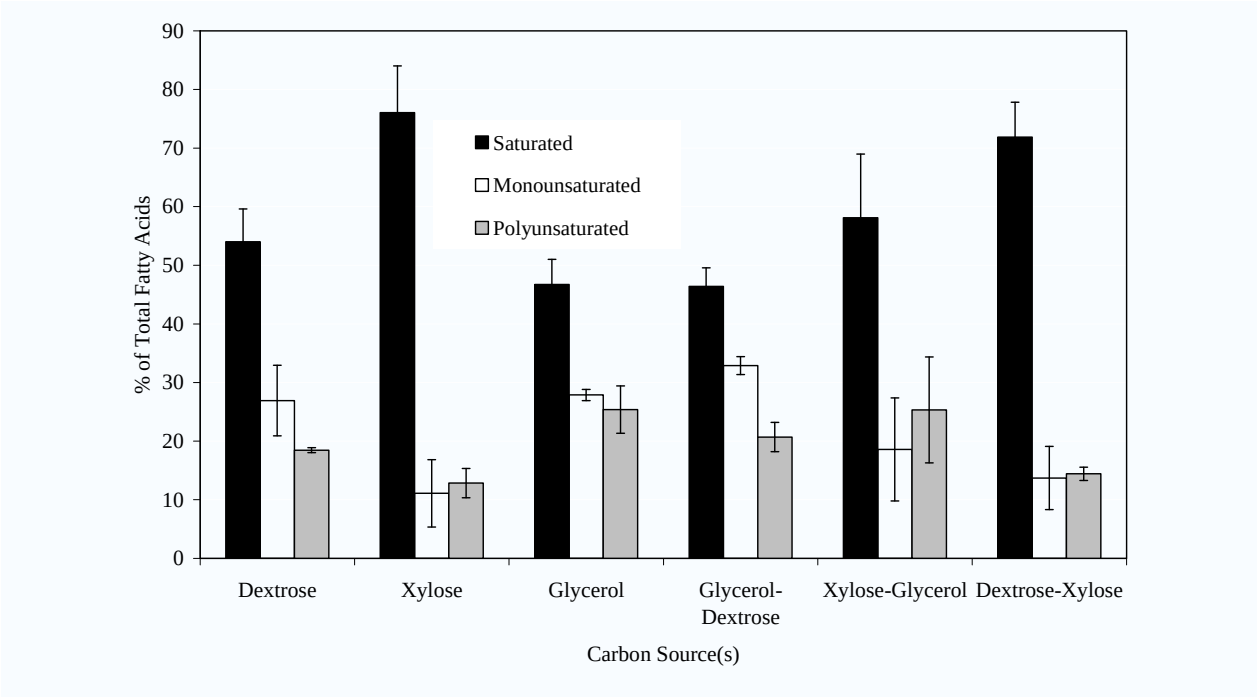


Figure 2b. The effect of carbon source on the saturation of fatty acids produced by *Rhodotorula glutinis* after 48 h of agitated (112 rpm) incubation at 35°C

Table 2. A comparison of the total percent of selected fatty acid methyl esters produced by *Rhodotorula glutinis* when grown on different carbon sources at 24 h

Carbon Source	Dextrose*	Xylose*	Glycerol**	Gly+Dex*	Xyl+Gly*	Dex+Xyl**
C16:0 Palmitic	26.30 ± 4.65	30.06 ± 1.80	12.35 ± 6.87	18.81 ± 0.74	11.09 ±1.66	12.17 ± 7.84
C18:0 Stearic	35.37 ± 7.64	24.88 ± 1.02	38.63 ± 7.02	19.80 ± 1.18	39.65 ± 7.76	45.42 ± 8.62
C18:1 Oleic	18.76 ± 4.25	14.5 ± 4.25	6.58 ± 2.91	28.46 ± 4.58	3.07 ± 2.62	7.42 ± 1.34
C18:2 Linoleic	3.04 ± 1.93	8.01 ± 0.87	4.04 ± 1.64	3.80 ± 0.71	4.35 ± 0.8	4.32 ± 1.52
C18:3 Linoleic	0	0	1.74 ± 0.66	0.72 ± 0.08	3.80 ± 0.71	3.05 ± 1.62

Table 3. A comparison of the total Percent of selected fatty acid methyl esters produced by *Rhodotorula glutinis* when grown on different carbon sources at 48 h

Carbon Source	Dextrose*	Xylose*	Glycerol**	Gly+Dex*	Xyl+Gly*	Dex+Xyl**
C16:0 Palmitic	24.88 ± 3.27	38.24 ± 1.05	16.01 ± 0.92	17.48 ± 1.28	12.22 ± 6.56	18.02 ± 2.22
C18:0 Stearic	32.30 ± 1.19	28.04 ± 3.29	21.86 ± 3.56	20.96 ± 3.51	39.05 ± 8.40	49.54 ± 6.31
C18:1 Oleic	24.76 ± 4.88	7.37 ± 3.77	18.05 ± 3.02	27.62 ± 4.36	8.97±12.92	8.17 ± 5.53
C18:2 Linoleic	0.26 ± 0.02	5.02 ± 1.97	15.91 ± 4.25	2.71 ± 1.99	5.91± 4.41	2.64 ± 1.05
C18:3 Linoleic	0.42 ± 0.21	0	1.76 ± 0.50	0.86 ± 0.26	2.71± 1.99	1.61 ± 0.33

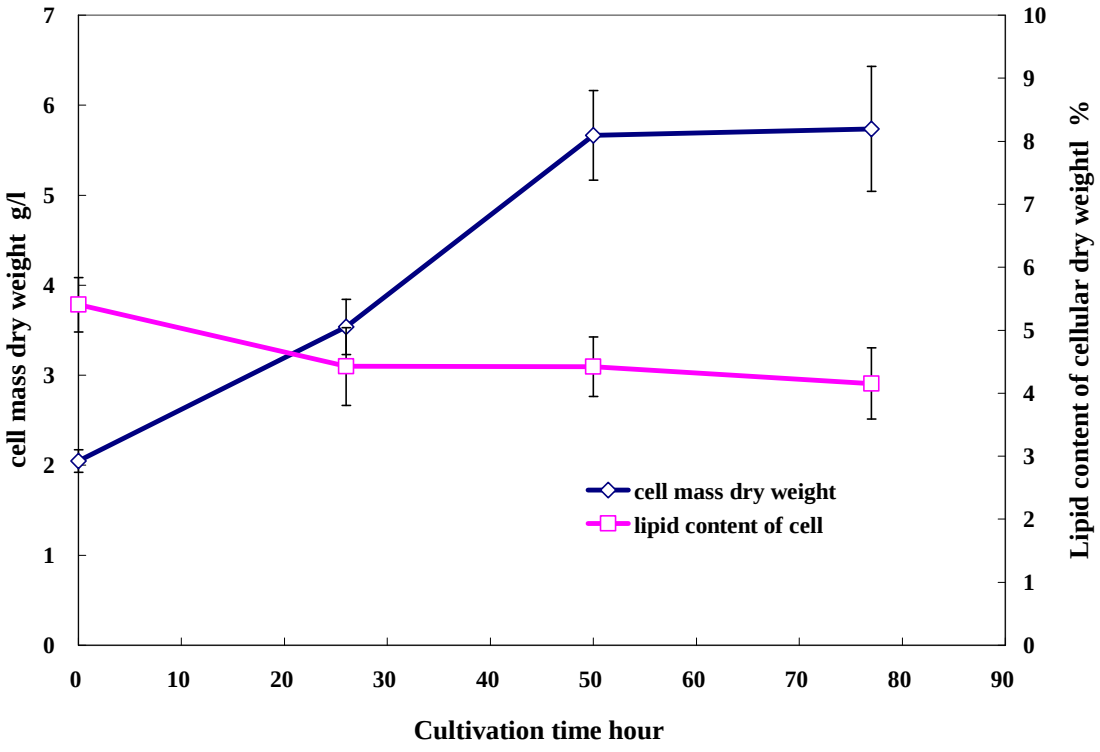


Figure 3 Cell mass in the culture for lipid accumulation and the lipid content of the cellular dry weight

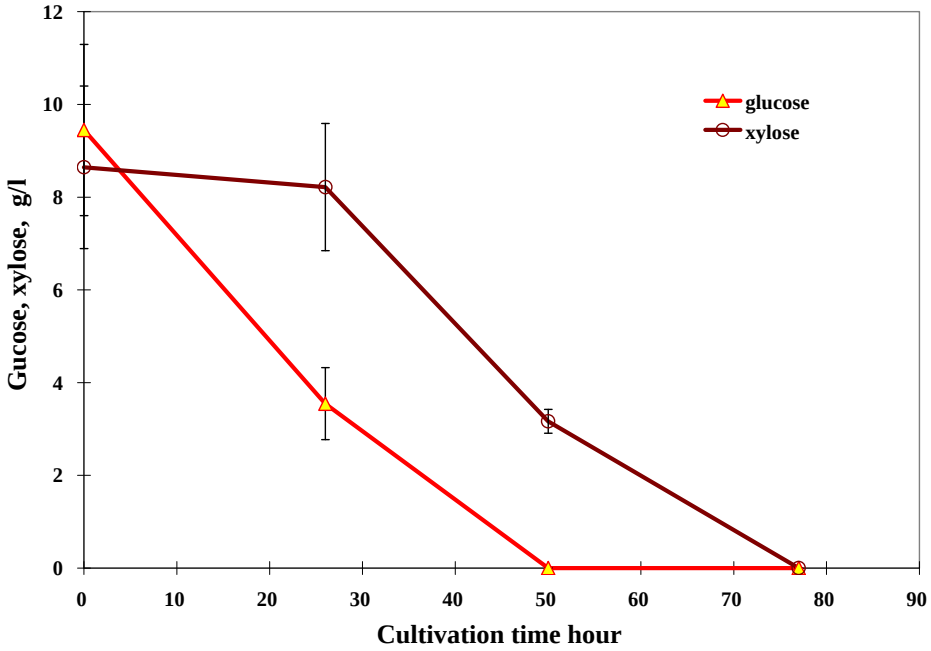


Figure 4 Concentration of glucose and xylose in the culture for lipid accumulation.

Table 1 Fatty acid composition of microbial lipids in *Rhodotorula glutinis* growing on acid hydrate from switchgrass

Fatty acid composition	Cultivation time hour				average
	0	26	50	77	
C14:0		0.3±0.3	0.7±0.0	0.6±0.0	
C16:0	12.8±5.9	10.2±0.4	15.9±0.2	16.3±1.6	
C18:0	9.8±7.9	11.4±4.5	8.6±0.9	5.6±1.3	
C18:1	41.1±4.5	42.9±0.2	47.6±1.8	35.2±3.0	
C18:2	27.1±0.8	23.2±3.4	19.0±1.7	32.6±8.5	
C20:1	8.2±8.0	8.6±3.2	4.4±0.5	6.2±2.2	
C20:2			0.5±0.1	0.4±0.4	
C24:0	0.4±0.4	1.6±0.7	10.5±0.3	1.0±0.3	
Saturated %	23.7±13.0	25.0±6.2	27.6±1.0	24.5±3.3	25.2±2.4
Monounsaturated %	49.3±12.6	51.7±2.9	52.7±1.3	42.2±0.8	49.0±6.8
Polyunsaturated %	27.0±0.8	23.3±3.3	19.6±1.5	33.3±4.1	25.8±7.5

Task A.3. MSU Research on Commercial Adsorbents to Collect Lipids from Wastewaters

1. Introduction

The main goal of this phase of the project was to evaluate commercial adsorbents to collect lipids contained in industry wastewaters, specially the food processing industry. This industry generates million of gallons of wastewater containing lipids which could be used for biodiesel production. The adsorption capacity of the adsorbents/absorbents toward lipids was measured via preparation of adsorption isotherms.

The Kenaf (core) used in this experiment was provided by the Kengro® corporation out of Charleston, Mississippi. The following treatments were evaluated during the past year (2007):

Kenaf

1. Mechanically Separated (MS) 3 hours – Agitated using an over head electric mixer (500 rpm). Water changed every hour for a maximum of 3 hours.
2. Control no Modification (Bag) – Kenaf material pulled straight out of the bag directly from the Kengro Corporation.
3. Kenaf ozonation (O^3) – A 40% (w/w) aqueous slurry with appropriate amounts of distilled water added. The slurries were placed into a sparging tank and ozonated using a corona discharge ozone generator (with a voltage that produced a 4% (w/w) ozone in an oxygen carrier stream).
4. Kenaf ozonation w/ Hydrogen Peroxide (H_2O_2) – ozonation as described above along with the initial, batch-added dosing of 500 mg/L hydrogen peroxide.

Cellulose Acetate

5. Control no Modification – Cellulose material pulled straight out of the bottle.
6. Cellulose Acetate ozonation (O^3) – A 40% (w/w) aqueous slurry with appropriate amounts of distilled water added. The slurries were placed into a sparging tank and ozonated using a corona discharge ozone generator (with a voltage that produced a 4% (w/w) ozone in an oxygen carrier stream).

Polyethylene

7. Control no Modification – Polyethylene material pulled straight out of the bottle.
8. Polyethylene ozonation (O^3) – A 40% (w/w) aqueous slurry with appropriate amounts of distilled water added. The slurries were placed into a sparging tank and ozonated using a corona discharge ozone generator (with a voltage that produced a 4% (w/w) ozone in an oxygen carrier stream).

Kenaf, Cellulose acetate, and Polyethylene were modified using the above techniques and were then dried for 24 hours at 80° C. The modified adsorbent (for each technique) was then placed in 60ml glass vials in duplicate samples of 0.1, 0.07, 0.05, 0.03, 0.01 grams. An emulsion of soybean oil and distilled water (40ml) was then placed into the vials which contained the adsorbent. The experimental protocol is listed bellow.

2. Experimental Protocol

1. Place adsorbent into 60ml vial.
2. Add 40ml of emulsified soybean oil and distilled water (200, 400, 800, 1600 mg/L)
3. Place on wrist shaker for 3 hours
4. Remove the vial from the wrist shaker and then remove a 10ml sample and place into another 60ml vial.
5. 15ml of chloroform coupled with an internal standard (C_{20}) was placed into the 60ml vial with 10ml of the sample.

6. An aliquot (1ml) was then taken form the vials and used for the analysis.

3. Analysis

Soybean oil standards were created using a serial dilution from 2000 ppm to 200 ppm and analyzed using an HP 5890 Series II Gas Chromatograph (GC). The column used in the GC was Restek® triglyceride column (Rtx® 65TG 15 meter). Figure 1 illustrates the standards used throughout the experiment.

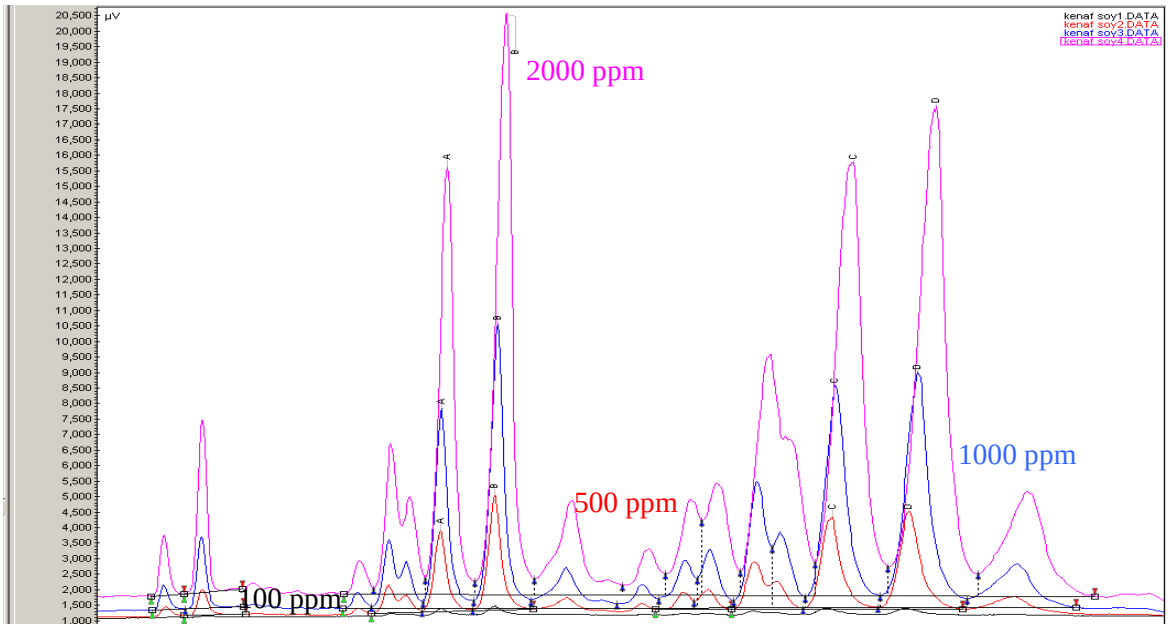


Figure 1. Soybean oil standards from the HP 5890 Series II GC.

The information from the chart indicates the four peaks that were used to identify the presence of the Soybean oil (Peak A, B, C, and D). The standards were run every time prior to any of the samples. Varian® Galaxie chromatography data system computer software calculated a ppm for each sample using these standards. Control samples (solution of soybean oil and water only no adsorbent) were run for every set. Figure 2 illustrates the data analysis of a control sample at 2000 ppm.

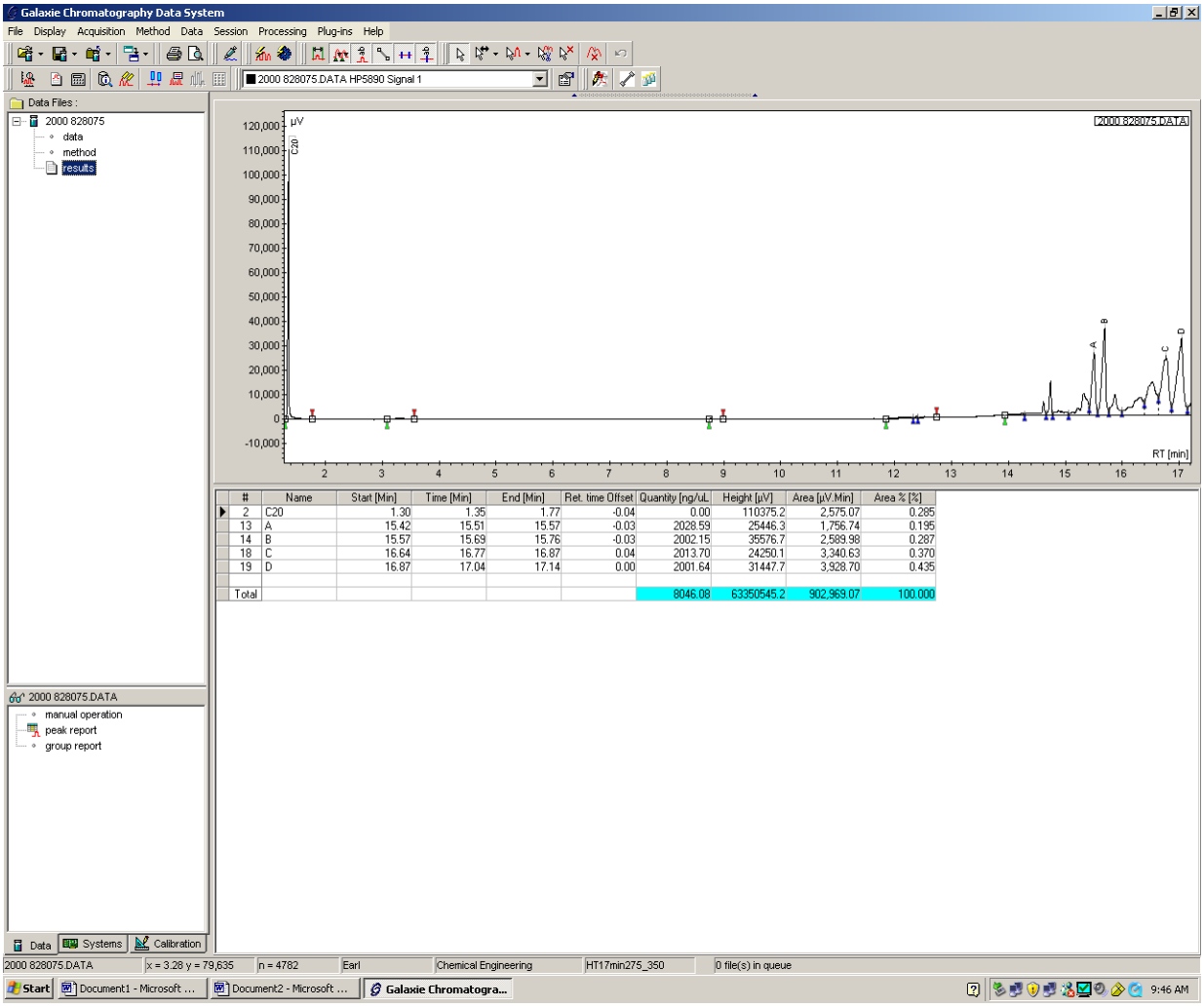


Figure 2. Chromatograph data analysis

The first retention time of 1.30 minutes indicates the internal standards presence within the sample and following peaks have retention times ranging from 15 – 17 minutes represents the soybean oil. After data collection of all the samples from the GC the duplicates were averaged together and are shown in table 1.

Table 1. shows the averaged numbers for each washing technique.

	Kenaf	Recovered		y	x
Kenaf Core @ 200 ppm soybean oil	mass (g)	Soy (mg/L)	K Loading	Ln K	Ln C
MS 3 hours	0.1	52.01	88.794	4.486319	3.951436
MS 3 hours	0.07	61	109	4.691348	4.110874
MS 3 hours	0.05	63	164	5.099866	4.143135
MS 3 hours	0.03	74	252	5.529429	4.304065
MS 3 hours	0.01	76	798	6.682109	4.330733
O3	0.1	86	74	4.304065	4.454347
O3	0.07	100	86	4.454347	4.60517
O3	0.05	106	112	4.718499	4.663439
O3	0.03	114	172	5.147494	4.736198
O3	0.01	119	486	6.186209	4.779123
O3 H_2O_2	0.1	56.75	85.95	4.453766	4.038656
O3 H_2O_2	0.07	58.95	121	4.795791	4.07669
O3 H_2O_2	0.05	62	166	5.111988	4.127134
O3 H_2O_2	0.03	63	274	5.613128	4.143135
O3 H_2O_2	0.01	96	624	6.43615	4.564348
No Modification	0.1	93	64.2	4.162003	4.532599
No Modification	0.07	98	87	4.465908	4.584967
No Modification	0.05	100	120	4.787492	4.60517
No Modification	0.03	187	26	3.258097	5.231109
No Modification	0.01	197	18	2.890372	5.283204
Kenaf Core @ 400 ppm soybean oil	mass (g)	Soy (mg/L)	K Loading	Ln K	Ln C
MS 3 hours	0.1	208	835.2	6.727671	5.337538
MS 3 hours	0.07	232.5	1172.143	7.066589	5.44889
MS 3 hours	0.05	278	1586.4	7.369223	5.627621
MS 3 hours	0.03	309	2582	7.85632	5.733341
MS 3 hours	0.01	311	7734	8.953381	5.739793
O3	0.1	67.54	440	6.086775	4.21272
O3	0.07	70.98	625	6.437752	4.262398
O3	0.05	80.65	863	6.760415	4.390119
O3	0.03	105	1390	7.237059	4.65396
O3	0.01	117.64	4094	8.317278	4.767629
O3 H_2O_2	0.1	85.8	429	6.061457	4.452019
O3 H_2O_2	0.07	92.69	606	6.40688	4.529261
O3 H_2O_2	0.05	123.06	812	6.6995	4.812672
O3 H_2O_2	0.03	154.93	1290.14	7.162506	5.042973
O3 H_2O_2	0.01	184	3696	8.215006	5.214936
No Modification	0.1	133	160	5.075174	4.890349
No Modification	0.07	148	216	5.375278	4.997212
No Modification	0.05	189	253	5.533389	5.241747
No Modification	0.03	245	310	5.736572	5.501258
No Modification	0.01	262	828	6.719013	5.568345
Kenaf Core @ 800 ppm	mass (g)	Soy (mg/L)	K Loading	Ln K	Ln C

soybean oil					
MS 3 hours	0.1	312.214	292.67	5.679046	5.743689
MS 3 hours	0.07	321.976	409.74	6.015523	5.774477
MS 3 hours	0.05	368.941	517.271	6.248567	5.910637
MS 3 hours	0.03	395.618	808.764	6.695507	5.980449
MS 3 hours	0.01	452	2088	7.643962	6.113682
O3	0.1	221.908	346.85	5.848892	5.402263
O3	0.07	217.698	499.12	6.212847	5.383109
O3	0.05	235.493	677.41	6.518277	5.461681
O3	0.03	312	976	6.883463	5.743003
O3	0.01	526.47	1641.18	7.403171	6.266194
O3 H_2O_2	0.1	182.06	370.764	5.915566	5.204336
O3 H_2O_2	0.07	196.76	517.063	6.248165	5.281985
O3 H_2O_2	0.05	302.76	596.688	6.391394	5.71294
O3 H_2O_2	0.03	425.075	749.85	6.619873	6.052266
O3 H_2O_2	0.01	588.42	1269.48	7.146363	6.377441
No Modification	0.1	510	294	5.68358	6.234411
No Modification	0.07	536	398	5.986452	6.284134
No Modification	0.05	629	445	6.098074	6.444131
No Modification	0.03	707	586	6.37332	6.561031
No Modification					
Kenaf Core @ 1600 ppm					
soybean oil	0.01	768	1392	7.238497	6.64379
MS 3 hours	0.1	482	671	6.508769	6.177944
MS 3 hours	0.07	531	917	6.821107	6.274762
MS 3 hours	0.05	NA	NA	NA	NA
MS 3 hours	0.03	711	1778	7.483244	6.566672
MS 3 hours	0.01	900	4200	8.34284	6.802395
O3	0.1	241	815.4	6.703679	5.484797
O3	0.07	219	1183.74	7.076434	5.389072
O3	0.05	294	1567.2	7.357046	5.68358
O3	0.03	453	2294	7.738052	6.115892
O3	0.01	510	6540	8.785692	6.234411
O3 H_2O_2	0.1	177	853.8	6.749697	5.17615
O3 H_2O_2	0.07	219	1183.74	7.076434	5.389072
O3 H_2O_2	0.05	223	1652.4	7.409984	5.407172
O3 H_2O_2	0.03	365	2470	7.811973	5.899897
O3 H_2O_2	0.01	490	6660	8.803875	6.194405
No Modification	0.1	550	630	6.44572	6.309918
No Modification	0.07	712	761	6.634633	6.568078
No Modification	0.05	736	1036.8	6.943894	6.60123
No Modification	0.03	741	1718	7.448916	6.608001
No Modification	0.01	1124	2856	7.957177	7.024649
Cellulose Acetate @ 200 ppm	mass (g)	Soy (mg/L)	K Loading	Ln K	Ln C
O3	0.1	148	31	3.433987	4.997212
O3	0.07	162	33	3.496508	5.087596
O3	0.05	168	38	3.637586	5.123964

O3	0.03	176	48	3.871201	5.170484
O3	0.01	187	78	4.356709	5.231109
No Modification	0.1	164	21.6	3.072693	5.099866
No Modification	0.07	173	23	3.135494	5.153292
No Modification	0.05	174	31.2	3.440418	5.159055
No Modification	0.03	181	38	3.637586	5.198497
No Modification	0.01	192	48	3.871201	5.257495
Cellulose Acetate @ 400 ppm	mass (g)	Soy (mg/L)	K Loading	Ln K	Ln C
O3	0.1	143	154	5.036953	4.962845
O3	0.07	173	195	5.273	5.153292
O3	0.05	220	216	5.375278	5.393628
O3	0.03	269	262	5.568345	5.594711
O3	0.01	318	492	6.198479	5.762051
No Modification	0.1	197	122	4.804021	5.283204
No Modification	0.07	199	173	5.153292	5.293305
No Modification	0.05	210	228	5.429346	5.347108
No Modification	0.03	265	270	5.598422	5.57973
No Modification	0.01	318	492	6.198479	5.762051
Cellulose Acetate @ 800 ppm	mass (g)	Soy (mg/L)	K Loading	Ln K	Ln C
O3	0.1	643	94	4.543295	6.466145
O3	0.07	657	122	4.804021	6.487684
O3	0.05	696	125	4.828314	6.54535
O3	0.03	721	158	5.062595	6.580639
O3	0.01	769	186	5.225747	6.645091
No Modification	0.1	196	362	5.891644	5.278115
No Modification	0.07	195	519	6.251904	5.273
No Modification	0.05	233	680	6.522093	5.451038
No Modification	0.03	244	1112	7.013915	5.497168
No Modification	0.01	519	1686	7.430114	6.251904
Cellulose Acetate @ 1600 ppm	mass (g)	Soy (mg/L)	K Loading	Ln K	Ln C
O3	0.1	1157	386	5.955837	7.053586
O3	0.07	1247	474	6.161207	7.128496
O3	0.05	1257	652	6.480045	7.136483
O3	0.03	1393	814	6.70196	7.239215
O3	0.01	1624	1056	6.962243	7.392648
No Modification	0.1	198	841.2	6.734829	5.288267
No Modification	0.07	194	1205	7.094235	5.267858
No Modification	0.05	277	1588	7.370231	5.624018
No Modification	0.03	213	2774	7.928046	5.361292
No Modification	0.01	465	6810	8.826147	6.142037
Polyethylene @ 200 ppm	mass (g)	Soy (mg/L)	K Loading	Ln K	Ln C
O3	0.1	352	28	3.332205	5.863631
O3	0.07	361	32	3.465736	5.888878
O3	0.05	364	43	3.7612	5.897154
O3	0.03	378	44	3.78419	5.934894

O3	0.01	391	54	3.988984	5.968708
No Modification	0.1	153	34	3.526361	5.030438
No Modification	0.07	162	41	3.713572	5.087596
No Modification	0.05	172	45	3.806662	5.147494
No Modification	0.03	187	46	3.828641	5.231109
No Modification	0.01	202	48	3.871201	5.308268
Polyethylene @ 400 ppm	mass (g)	Soy (mg/L)	K Loading	Ln K	Ln C
O3	0.1	169	18	2.890372	5.129899
O3	0.07	179	18	2.890372	5.187386
O3	0.05	182	22	3.091042	5.204007
O3	0.03	187	26	3.258097	5.231109
O3	0.01	195	30	3.401197	5.273
No Modification	0.1	301	67	4.204693	5.70711
No Modification	0.07	326	75	4.317488	5.786897
No Modification	0.05	351	75.6	4.325456	5.860786
No Modification	0.03	376	76	4.330733	5.929589
No Modification	0.01	399	90	4.49981	5.988961
Polyethylene @ 800 ppm	mass (g)	Soy (mg/L)	K Loading	Ln K	Ln C
O3	0.1	810	302	5.710427	6.697034
O3	0.07	919	338	5.823046	6.823286
O3	0.05	965	419	6.037871	6.872128
O3	0.03	1055	518	6.249975	6.961296
O3	0.01	1224	540	6.291569	7.109879
No Modification	0.1	598	113	4.727388	6.393591
No Modification	0.07	632	132	4.882802	6.448889
No Modification	0.05	676	133	4.890349	6.516193
No Modification	0.03	719	136	4.912655	6.577861
No Modification	0.01	763	144	4.969813	6.637258
Polyethylene @ 1600 ppm	mass (g)	Soy (mg/L)	K Loading	Ln K	Ln C
O3	0.1	1425	354	5.869297	7.261927
O3	0.07	1587	367	5.905362	7.369601
O3	0.05	1701	378	5.934894	7.438972
O3	0.03	1817	398	5.986452	7.504942
O3	0.01	1939	462	6.135565	7.569928
No Modification	0.1	928	223	5.407172	6.833032
No Modification	0.07	940	309	5.733341	6.84588
No Modification	0.05	1015	342	5.834811	6.922644
No Modification	0.03	1119	362	5.891644	7.020191
No Modification	0.01	1221	474	6.161207	7.107425

Isotherms were developed to provide a measure of impact of the candidate washing techniques. The isotherms were prepared using the Freundlich's equation:

$X/M = K*C^{1/n}$

where,
X = milligrams of glycerine

M = Mass of adsorbent
C = Concentration of glycerine, mg/L
K and n = Freundlich Coefficients

These coefficients can be determined from the laboratory data (Table 1) by plotting Ln (X/M) Ln (C). The equation below illustrates a linear version of the above equation that when plotted can be used to calculate the coefficients using simple linear regression:

Ln (X/M) = Ln K + 1/n Ln C

Figures 3–11 show the isotherms for the chosen candidate washing techniques. The adsorption capacity for kenafs affinity to adsorb Lipids is apparently better than the other adsorbent candidates. Adsorption capacity does increase after surface oxidation techniques. Table 2 gives the Ln (X/m) values.

Table 2. Ln (X/m)

	Ln (X/M) = Ln K + 1/n Ln C
Kenaf Core @ 200 ppm soybean oil	
MS	Ln(X/m) = 4.929(1/n)-15.247
O3	Ln(X/m) = 4.993(1/n)-18.244
O3 H_2O_2	Ln(X/m) = 3.338(1/n)-8.7052
No Modification	Ln(X/m) = 8.055(1/n)-32.376
Kenaf Core @ 400 ppm soybean oil	
MS	Ln(X/m) = 4.1329(1/n)-15.456
O3	Ln(X/m) = 3.3804(1/n)-8.1015
O3 H_2O_2	Ln(X/m) = 2.4263(1/n)-4.7624
No Modification	Ln(X/m) = 1.7946(1/n)-3.7153
Kenaf Core @ 800 ppm soybean oil	
MS	Ln(X/m) = 4.8482(1/n)-22.17
O3	Ln(X/m) = 1.4849(1/n)-1.8185
O3 H_2O_2	Ln(X/m) = 0.878(1/n)-1.437
No Modification	Ln(X/m) = 3.0529(1/n)-13.365
Kenaf Core @ 1600 ppm soybean oil	
MS	Ln(X/m) = 2.8395(1/n)-11.041
O3	Ln(X/m) = 1.8967(1/n)-3.4335
O3 H_2O_2	Ln(X/m) = 1.8312(1/n)-2.7089
No Modification	Ln(X/m) = 2.1775(1/n)-7.3347
Cellulose Acetate @ 200 ppm	
O3	Ln(X/m) = 3.8693(1/n)-16.06
No Modification	Ln(X/m) = 5.4201(1/n)-24.61
Cellulose Acetate @ 400 ppm	
O3	Ln(X/m) = 1.2556(1/n)-1.2562
No Modification	Ln(X/m) = 2.3114(1/n)-7.1673
Cellulose Acetate @ 800 ppm	
O3	Ln(X/m) = 3.463(1/n)-17.773
No Modification	Ln(X/m) = 1.3073(1/n)-0.6341

Cellulose Acetate @ 1600 ppm	
O3	Ln(X/m) = 2.906(1/n)-14.442
No Modification	Ln(X/m) = 1.8847(1/n)-2.8445
Polyethylene @ 200 ppm	
O3	Ln(X/m) = 3.9132(1/n)-17.262
No Modification	Ln(X/m) = 1.1067(1/n)-1.9622
Polyethylene @ 400 ppm	
O3	Ln(X/m) = 5.9172(1/n)-31.308
No Modification	Ln(X/m) = 0.8425(1/n)-0.597
Polyethylene @ 800 ppm	
O3	Ln(X/m) = 1.558(1/n)-4.7162
No Modification	Ln(X/m) = 0.8257(1/n)-0.5025
Polyethylene @ 1600 ppm	
O3	Ln(X/m) = 0.7854(1/n)-0.1319
No Modification	Ln(X/m) = 2.1013(1/n)-8.7899

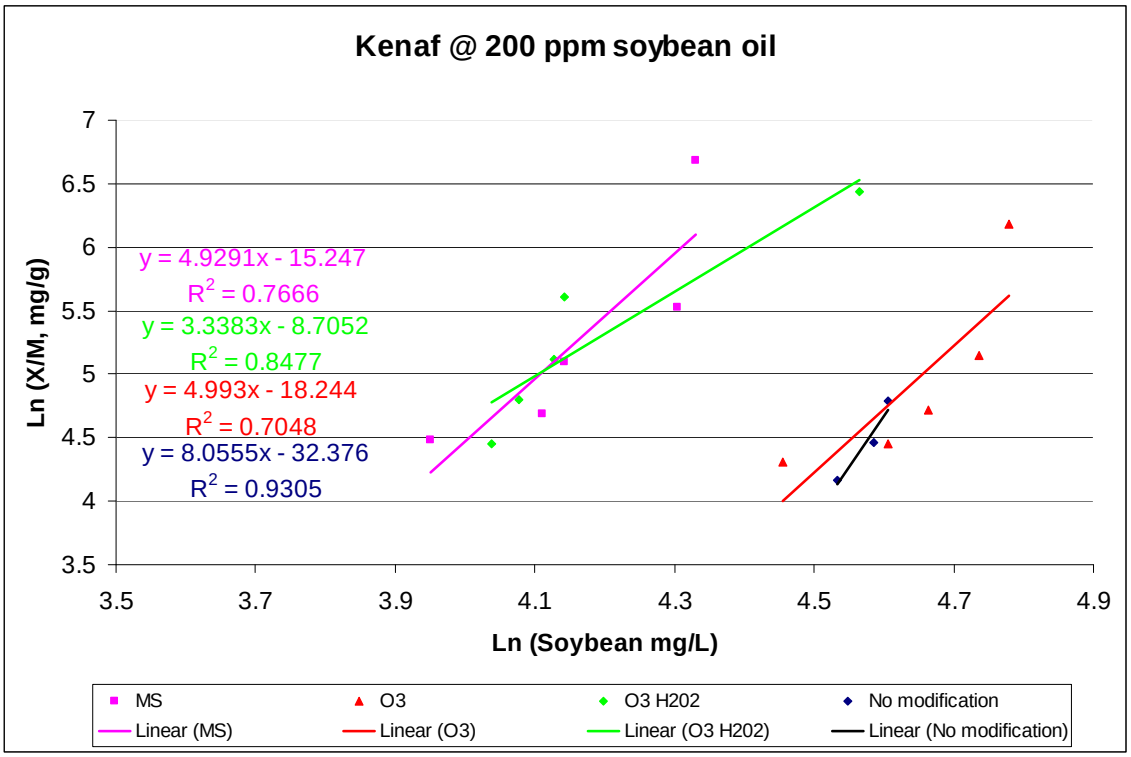


Figure 3. surface modification techniques on adsorption capacity

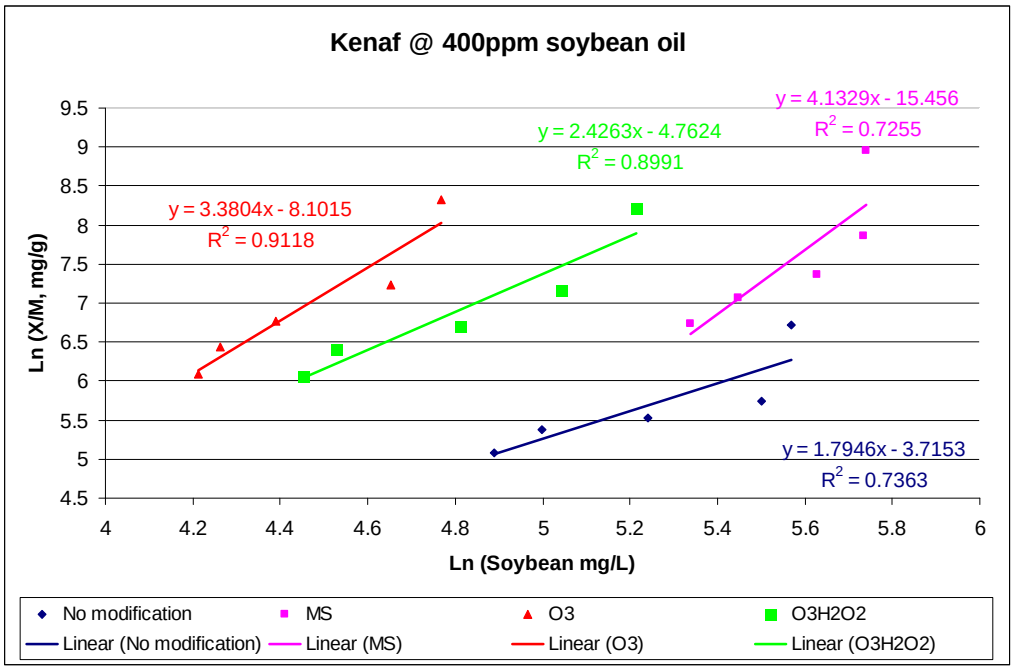


Figure 4. surface modification techniques on adsorption capacity

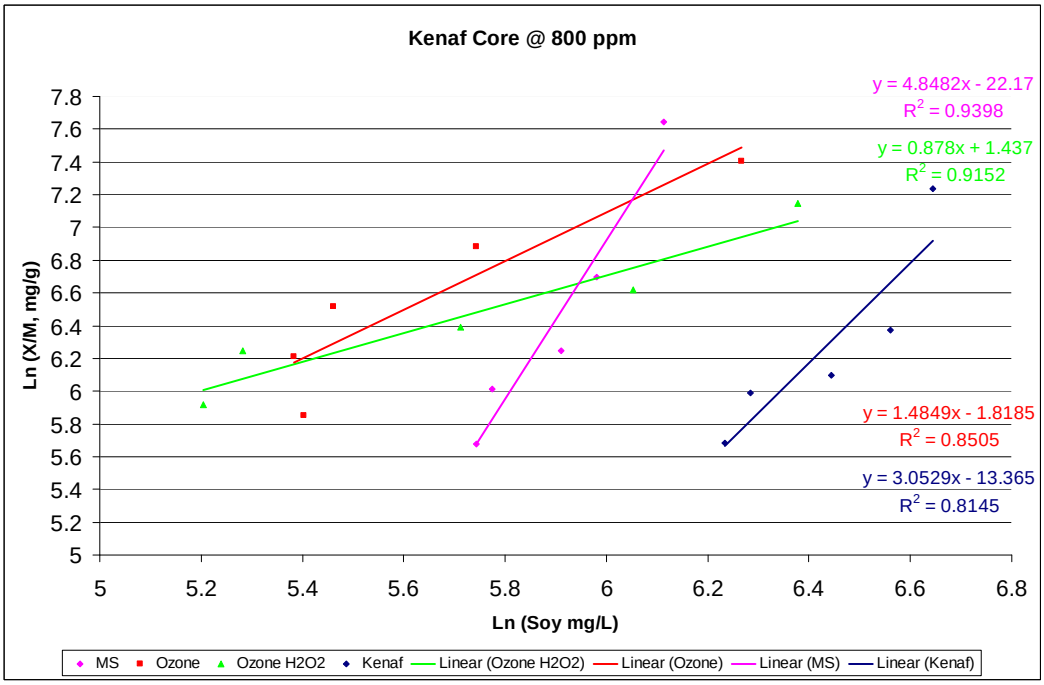


Figure 6. surface modification techniques on adsorption capacity

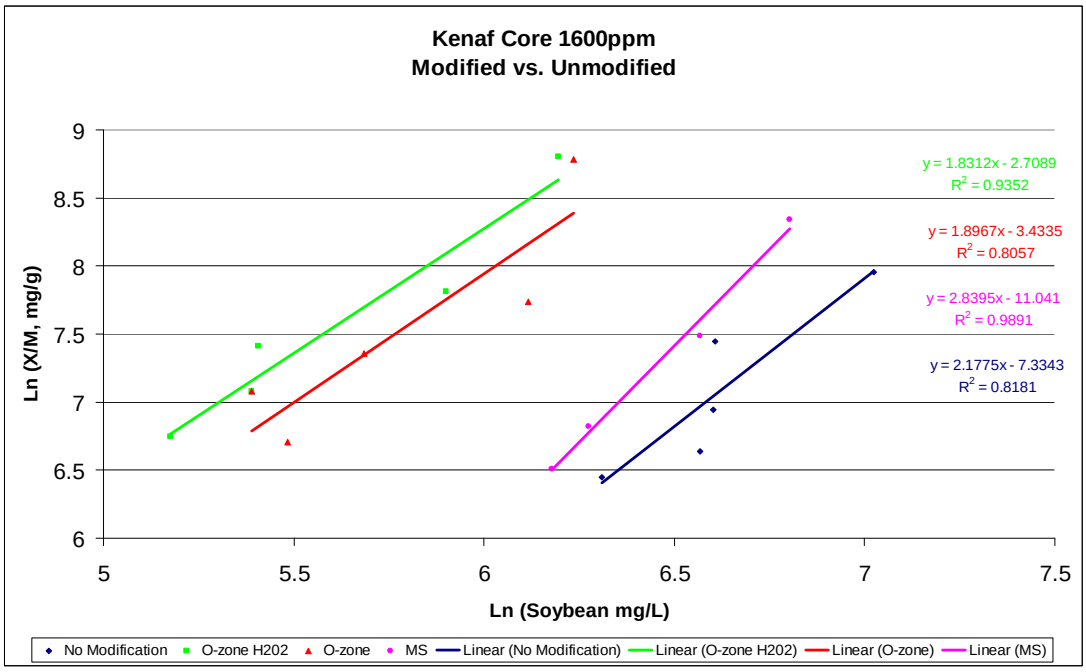


Figure 7. surface modification techniques on adsorption capacity

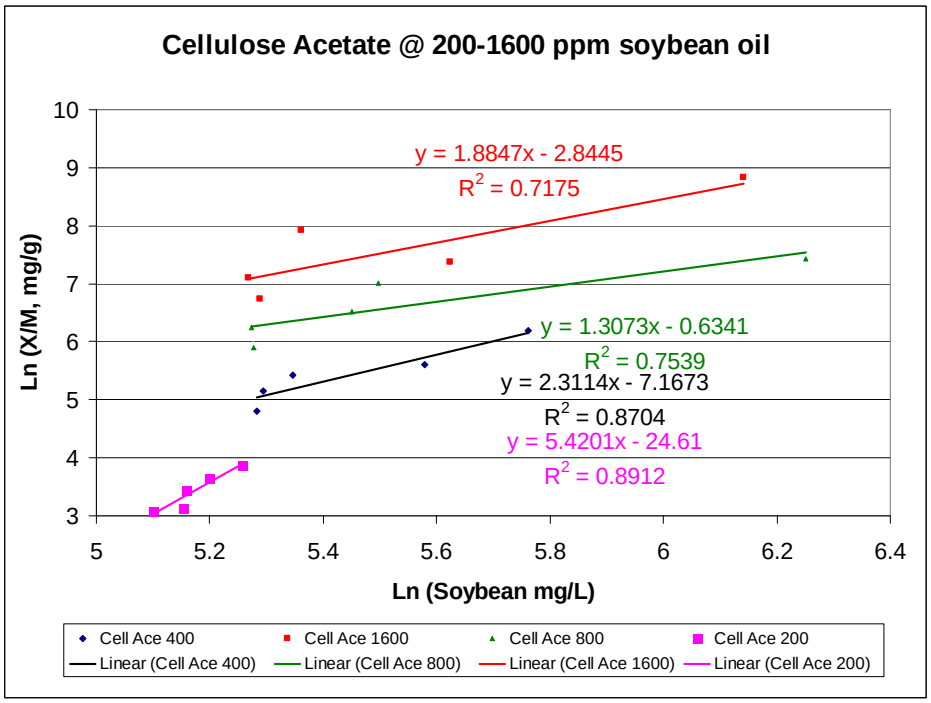


Figure 8. surface modification techniques on adsorption capacity

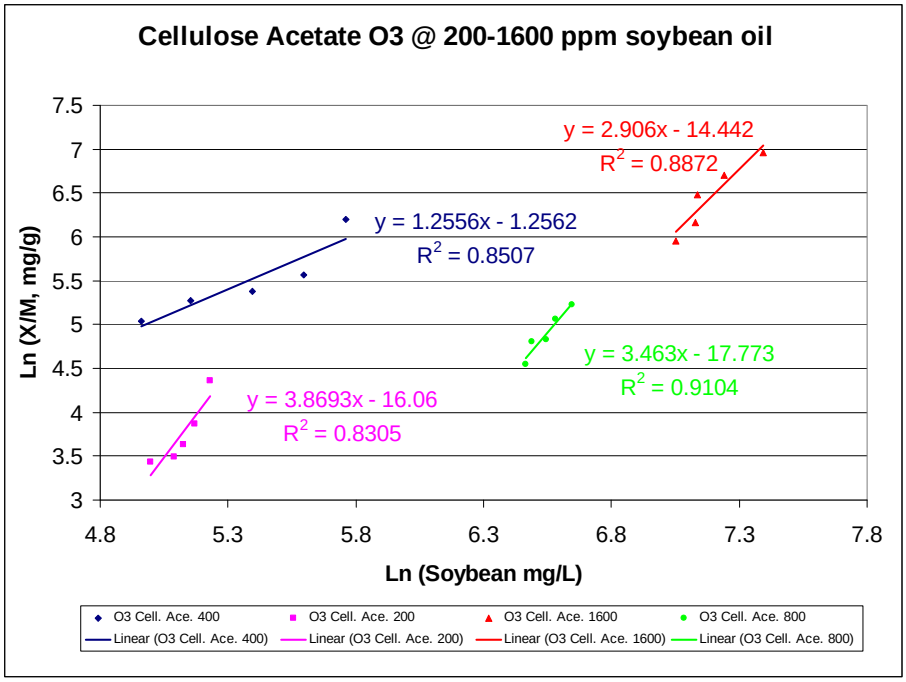


Figure 9. surface modification techniques on adsorption capacity

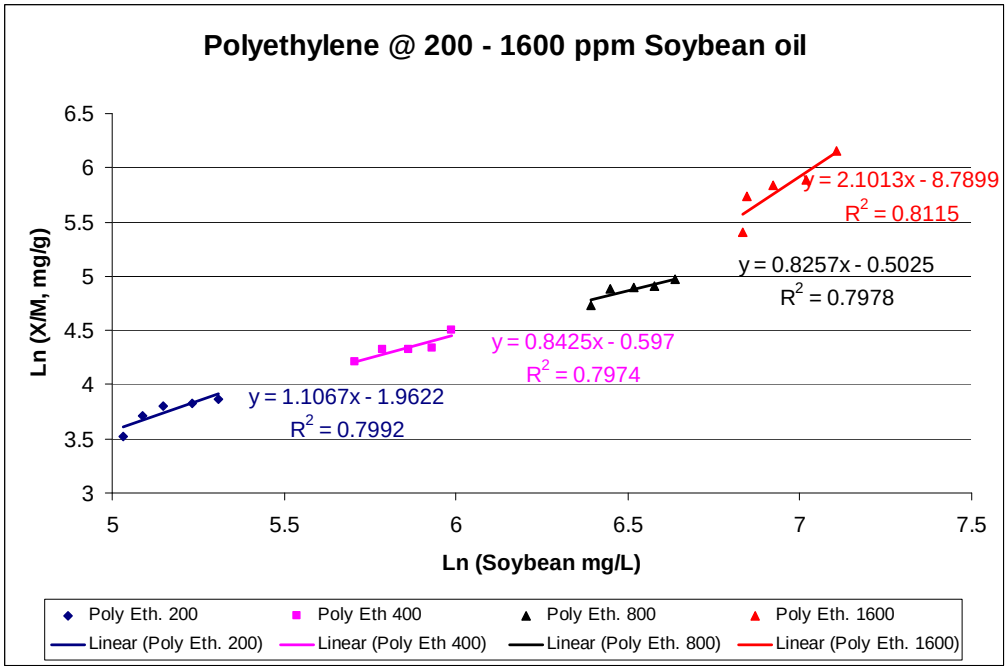


Figure 10. surface modification techniques on adsorption capacity

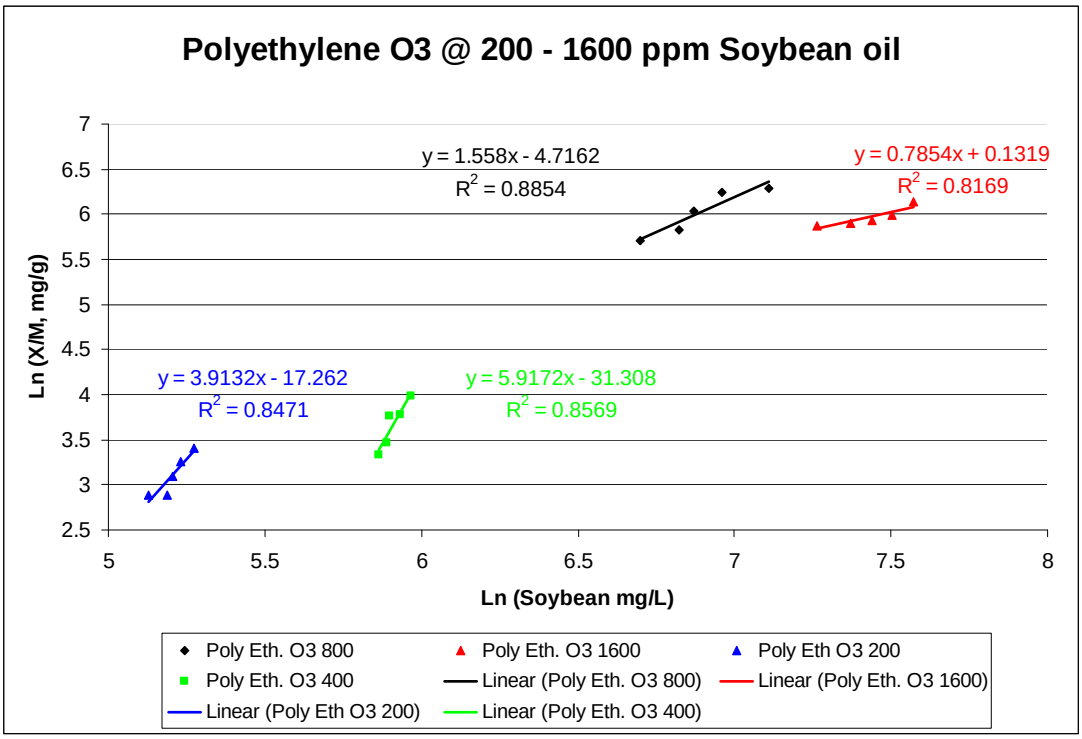


Figure 11. Surface modification techniques on adsorption capacity

4. Conclusion

The adsorbent evaluated were not efficient to remove lipids from water. Surface modification via oxidation improved the adsorption capacity of the kenaf but not to a level that would transform positively the technical feasibility of the technology.

Task A.4. Optimization of biodiesel production using Chinese tallow tree, rapeseed, castor, and tall oil.

1. Introduction

The need for alternative energy becomes greater as petroleum reserves become depleted [Pahl, 2005]. According to the Energy Information Administration, the United States currently uses 20% of the world's petroleum. More than 60% of this domestic use comes from imports [EIA, 2006]. The government has begun to see the importance of renewable energy in the U.S. economy. Alternative energy has three main drivers for future development: (1) depletion of nonrenewable fossil fuels, (2) environmental benefits, and (3) enhance of homeland security. Price stability and security issues related to foreign crude oil supply has led to the implementation of energy policies supporting the development of a domestic, renewable energy. The Energy Policy Act (EPAct) of 1992 was the first policy act by the government to strongly support renewable energy with its requirement for government fleets to use a certain percentage of alternative fueled vehicles. This act was amended in 1998 to again apply credits for the use of biodiesel in conventional vehicles [NBB, 2006]. In late 2004, the U.S. Congress passed a biodiesel tax incentive allowing distributors of biodiesel to compete with petroleum markets. The tax incentive was due for expiration at the end of 2006 but Congress passed an

extension during the EPAct of 2005 along with several other incentives for alternative energy growth [U.S. DOE, 2006].

Application of renewable energy can be seen in the transportation industry. As the biodiesel industry expands more research is needed in developing alternative feedstocks to ensure continuous growth. Vegetable oils are currently the lead suppliers for the biodiesel industry. The current market is controlled by a small sector of suppliers and could inhibit the growth of renewable energy.

Biodiesel

Biodiesel has come to the forefront of the energy community as a clean-burning, renewable energy that can displace the use of diesel fuels. Biodiesel is "a fuel composed of mono alkyl esters that are derived from vegetable oils or animal fats, designated B100, and meeting the requirements of the American Standard Testing and Materials (ASTM) D 6751-06" (ASTM D 6751, 2006). Biodiesel is usually produced by the reaction of oil with an alcohol in the presence of a catalyst. This source of energy is listed by the Environmental Protection Agency (EPA) as an alternative fuel and fuel additive. It can be produced from a wide range of renewable oils and fats with many desirable traits over petroleum diesel. The positives aspects of biodiesel use include:

- Renewable
- Biodegradable
- Carbon neutral
- Improved lubricity
- Higher cetane number
- Blending capability with No. 2 Diesel

The carbon cycle is a model of the amount of carbon above the crust of the earth, and its movement to and from the atmosphere. The extraction of crude oil from subsurface reserves increases the amount of existing carbon in the cycle. It is believed to contribute to the increase in carbon dioxide in the atmosphere and global warming. Biodiesel emissions are produced from carbon in the atmosphere and considered neutral in the carbon cycle.

Biodiesel has the capability of being blended with petroleum diesel. This ability is a positive for the introduction of biodiesel on a small scale thus progressively building the industry. Blends of biodiesel and petroleum diesel are recognized with the symbol B-XX. The XX is replaced by the volume percentage of biodiesel in a blend. The example of a common blend is 20 percent biodiesel with 80 percent petroleum would be labeled B-20. Pure or neat biodiesel is often referred to as B-100. Biodiesel is also an excellent lubricant which may help as low-sulfur petrodiesel fuels have poor lubricity. The cetane number, which is a characteristic of how well a fuel will ignite, is higher with biodiesel allowing for a more complete combustion over petroleum diesel. A B-20 blend has also shown to reduce net CO_2 emissions by 16 percent [Sheehan, 1998]. Along with lower sulfur, emissions, and aromatics, biodiesel is an ideal fuel to help lower the U.S.'s dependence on foreign oil. Biodiesel is typically produced from virgin vegetable oils that carry a high cost. By utilizing lower cost lipid feedstocks, biodiesel could build a larger, more diverse production base.

Tall Oil

Tall oil is a by-product of the manufacturing of pulp and paper products and is categorized as a part of the Naval Stores Industry. Tall oil is one possible feedstock not commonly studied for biodiesel production. The Naval Stores Industry encompasses the utilization of wood products including: tall oil, gum rosin, and terpenes. This collective group of products was originally used for sealing boats in the naval industry. Tall oil was identified in the late 1800's as a natural product of pine wood. Tall oil comes from the ether extractable portion

of trees that are a mixture of free fatty and rosin acids with some neutrals. Tall oil comes from the Swedish word “talloja” meaning “pine oil” which helps to differentiate it in the United States from terpene alcohols [Watkins, 2000]. The tall oil content in most pine species is about 3% weight of the dry wood. During the pulping process the lipid and rosin portion of the extractives are saponified and removed from the pulping process. The soap is composed of roughly 55% fatty acid salts and the remainder being the resin acids. This crude oil is acidulated using sulfuric acid to produce a free acid form. The crude tall oil (CTO) can be separated into the major fatty acid and rosin acid fractions. Resin acids are used to produce emulsifiers, inks, and paper sizing agents while the fatty acids fraction competes with the current vegetable oil markets for specialty chemical manufacturing [Sjostom, 1993].

Production of CTO in the United States is roughly 213 million gallons per year. Georgia Pacific, Arizona Chemical Company, and Eastman Chemical Company are the main producers of crude tall oil in the United States. The current market value of crude tall oil $0.08 per lb., while tall oil fatty acids are in the range of $0.23 per lb [Chemical Market Reporter, 2005]. This is roughly $0.04 per lb below the current price of vegetable oil. The tall oil fatty acids that could be utilized for biodiesel represent close to 50% of total crude tall oil production [Zinkel and Russell, 1989]. In terms of total production, tall oil could supply around 100 million gallons of biodiesel per year. A downside of using tall oil is that the processing techniques used in pulping add sulfur to the oil. This will affect its performance on emissions quality when converted to biodiesel. Another downside is that the production of tall oil is dependent upon the industry and results in fluctuations. These two downsides could turn around, first due to improved environmental regulations leading to less sulfur input during pulp processing. Another aspect is increased recovery of crude tall oil which is not always performed in the industry. These two possible benefits could help tall oil become a more competitive alternative fuel feedstock.

As the demand for biodiesel increases, more sources of oil will need to be available to meet the market demand. Characterizing different oils and their process variables introduces flexibility into large scale biodiesel production. Evaluating alternative oils ensures that the expanding biodiesel market will continue to have feedstock that will meet the quality demands set by ASTM D 6751. Publications relating to biodiesel have mainly involved the study of operating conditions, fuel performance, emissions, and physical properties more so than kinetics. The free fatty acid kinetic studies that have been performed involved triglycerides. A detailed study monitoring and modeling acid-catalyzed esterification will help determine the optimal conditions for free fatty acid conversion to biodiesel.

This research project was undertaken to evaluate the production of tall oil as a feedstock for biodiesel. In order to evaluate tall oil as a candidate for biodiesel, the objectives of this research were to optimize the parameters for tall oil fatty acid conversion, evaluate and model the kinetics of the conversion, and perform ASTM quality testing on the produced biodiesel. Optimizing the conversion parameters ensures that the most effective combination of feedstocks, catalyst, and operating conditions are found for the reaction. Modeling the kinetics of conversion provides the data to scale up and fine tune the reaction for peak production. Performing quality test on the tall oil biodiesel produced identifies any potential problems with the fuel.

Process Chemistry

Plant and animal oils have to be modified in order to be used in a modern diesel engine. The triglycerides in oils have a molecular weight between 660 and 980. These molecules bind together to create a liquid roughly ten times more viscous than diesel fuel [Peterson, 1983]. To reduce the viscosity, the glycerol bonds need to be hydrolyzed and replaced. Lower alcohols are used to take the place of the glycerol.

Transesterification is a process used to convert acylglycerols into the fatty acid alkyl esters (FAAE) that make up biodiesel. The fatty acid may be named depending on the type of alcohol employed. If methanol is used, then the product is called a “fatty acid methyl ester”. Ethanol and methanol are the most popular low molecular weight alcohols used for this process. The alcohol utilized is mainly a function of cost and availability. Methanol is the primary alcohol in the U.S. because of its cost. In processing, the alcohol quickly reacts with the fatty acids as they are released from the glycerol. The reaction is catalyzed by either an alkaline or acid catalyst. Base catalysts are mainly used to aid in the removal of the glycerol. These include sodium hydroxide (NaOH), potassium hydroxide (KOH), and sodium methoxide ($NaCH_2OH$). The base catalyst for triglycerides works by removing a proton from the alcohol group which becomes very reactive and takes the place of the glycerol attached to the carbonyl group of the fatty acid. Acid catalysts are extremely slow to react with TG in comparison to base catalyst, but they are resistant to some impurities. Acid catalyzed reactions do not remove a proton but donate a proton to the carbonyl group of the fatty acid by which the alcohol will attach. The overall transesterification reaction of a triglyceride with alcohol is represented by the general equation in Figure 1. The reaction is reversible and to shift the equilibrium to the right, processing conditions need to be utilized. First, a large excess of alcohol may be used to drive the reaction to the right. Another method for increased conversion is to remove the glycerol product as it is produced. By applying one or two of these methods, the reaction may be driven to completion and all the oil converted into biodiesel.

Along with transesterification there are three other possible reactions in biodiesel processing. These include saponification, esterification, and hydrolysis. Saponification is the conversion of a carboxylic acid into its salt form. Free fatty acids that are present in unrefined vegetable oils will undergo this reaction during alkaline-catalyzed transesterification of triglycerides. A proton is removed from the free fatty acid by the base and the alkaline salt attaches to the fatty acid instead of the alcohol. This reaction is shown in Figure 2 as a fatty acid is converted to its sodium salt.

Esterification is the reaction of a carboxylic acid with an alcohol to form water and an alkyl ester. The reaction is usually catalyzed by a strong acid. This reaction can be used to convert the free fatty acids into biodiesel. The acid catalyst protonates the carbonyl group which allows the alcohol to be received. The reaction is faster for the free fatty acids since there is no obstruction from a glycerol alcohol as in triglycerides. Esterification is represented by the general equation in Figure 3. The reaction is reversible and by using an excess of alcohol or by removing water as it is formed will drive the reaction to completion.

Hydrolysis is the production of free fatty acids from acylglyerols or fatty acid alkyl esters. It will reduce a triglyceride to a free fatty acid and a diglyceride as in Figure 4 or remove the alcohol of biodiesel to produce a free fatty acid which is the reverse of esterification. This is considered an operation problem if oil is used that contains water.

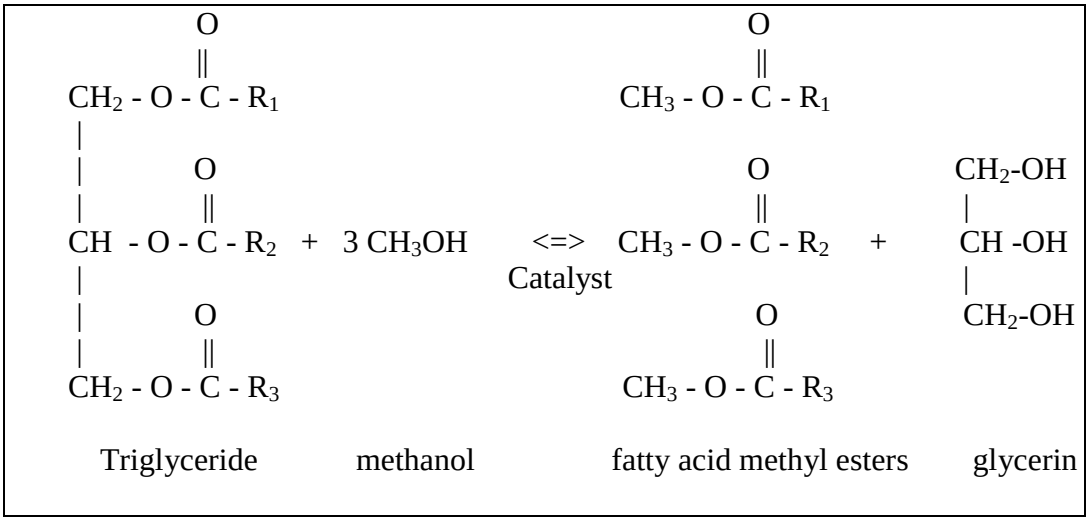


Figure 1. Conversion reaction of triglyceride to fatty acid methyl esters.

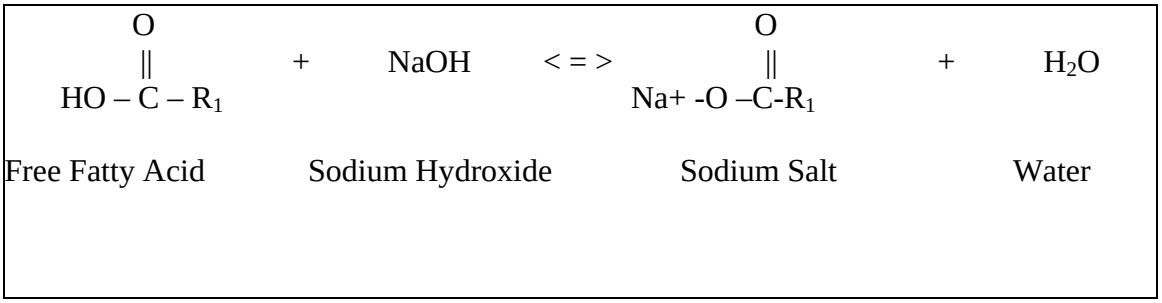


Figure 2. Saponification of a fatty acid with sodium hydroxide

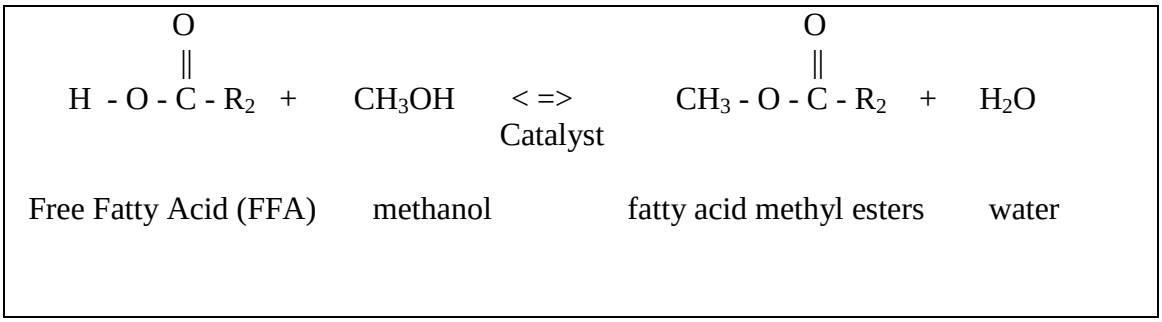


Figure 3. Conversion of free fatty acids to fatty acid methyl esters

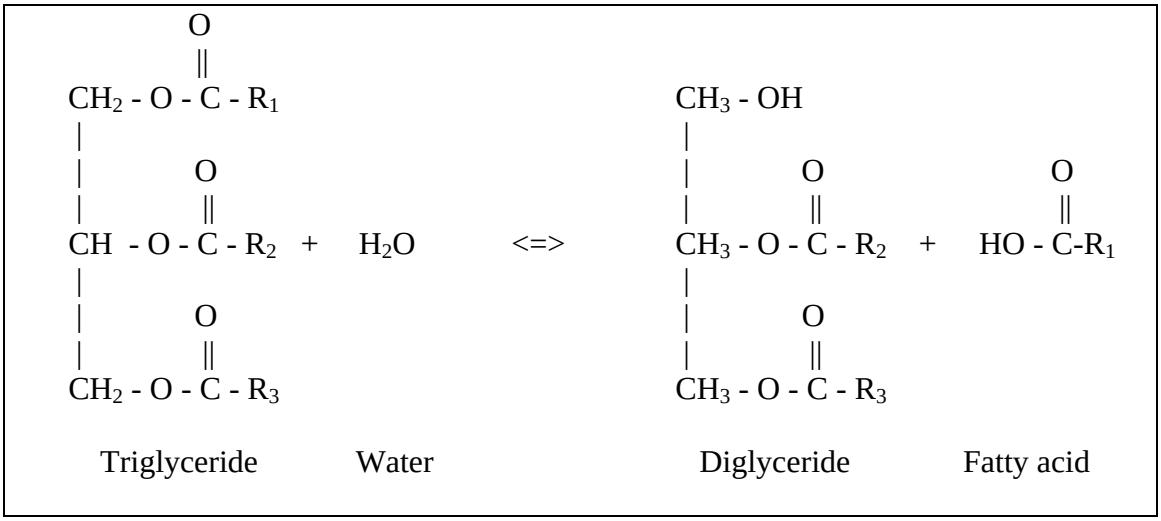


Figure 4 Hydrolysis reaction for a triglyceride

2. Methods and Materials

Parametric effects and reaction kinetics of biodiesel production were evaluated using fatty acids isolated from tall oil and methanol as reactants. All experiments were conducted using a batch reactor. The parametric effects were compared using statistical analysis to determine optimum operating conditions. Kinetics studies were conducted using the optimal conditions to gather information on reaction rates and modeling characteristics. Finally, ASTM quality tests were performed on the tall oil biodiesel that was produced at the optimum conditions. The tall oil tested in this study had a low resin acid content. Sulfuric acid was used as the acid catalyst because of its wide industrial use and availability. The experimental design was laid out and performed in a completely random order to ensure non-bias testing.

Factorial Design of Experiments

Initial experiments to study the optimal conditions of biodiesel production were designed using factorial analysis. A 2^4 factorial experimental design was used to determine the optimum values of temperature, catalyst amount, rate of agitation, and alcohol amount. Each parameter was evaluated at a low and high value, and the four variables studied by performing (2^4= 16) sixteen experiments with replicates. The design matrix (Table 1) outlines the two levels of the variables and the response. The (-1) represents the low level and the (+1) represents the high level of operation. The levels were chosen based on previous experiments and literature reviews. The temperatures cover the usual range of operation found in biodiesel production. The low temperature level was chosen as 30°C while 60°C was the high level. The 1% and 5% sulfuric acid concentrations evaluated the activity needed for effective conversion. The methanol to oil molar ratio has been commonly studied to provide the minimum value needed for optimal conversion. The molar ratios of alcohol to oil were 6:1 and 60:1. Mixing effects were studied to ensure that mass transfer limitations would not be involved during kinetic

experiments. The data from the factorial experiments were processed using statistical analysis software.

Kinetic Experiments

Kinetics experiments were performed on the tall oil with optimal parameters based off the results of the factorial design of experiments. The methanol to oil ratio was 6:1, and the sulfuric acid was 5 % weight of the tall oil. The temperatures studied for the kinetics ranged from 30°C to 60°C. 60°C was chosen as the highest temperature because it was a few degrees below the boiling point of methanol (64.7^{o}C). The experiments were studied at atmospheric pressure so the boiling point of methanol was not exceeded during this study.

Chemicals

Tall oil was purchased from Arizona Chemical (Sylfat 2; Savannah, GA) as one of their distributed products. Typical analysis gives an acid value of 194 with less than 3.3% rosin acid and 2.4% unsaponifiables. The major fatty acid components of the tall oil are: 44% oleic acid (C18:1), 34% linoleic (C18:2), 9% linolenic (C18:3), 5% saturated fatty acids, 8% other fatty acids. From these components, an average molecular weight of 281.47 was determined for later calculations. These and other characteristics of tall oil are listed in Table 2. The tall oil was stored under a nitrogen blanket at a pressure of 4 psi to prevent any oxidation. Methanol optima grade was purchased from Fisher Scientific. It was kept in the original amber glass bottle. Methanol was poured into graduated cylinders for measurement and excess was stored in another bottle to prevent any contamination. Sulfuric acid A.C.S. plus was purchased from Fisher Scientific. It was stored and careful attention was provided to ensure safety and that moisture did not contaminate the acid. The hexane used in the experiments was optima grade (Fisher Scientific. It was stored in the original amber bottle. During sample preparation the hexane was dispensed from a wash bottle. Distilled water was used during sample preparation to stop the reaction, remove the methanol, and neutralize the sulfuric acid. It was also used in batch preparation for the water washing step to remove the acid and methanol.

Experimental Apparatus

The esterification reactions took place in two identical Chemglass jacketed reactors (Figure 5) purchased from Fischer Scientific, Inc. The reactors had a working volume of 1 liter and were equipped with four ports on the top. The center port supported a glass rod which was controlled by a digital stirrer. The three side ports were used to connect a thermocouple, a condenser, and a sampling port. The thermocouple was routed through a temperature controller and controlled the heating mantle. Cold tap water was supplied to the condenser and a rubber septum in the sampling port allowed for the removal of samples.

Experimental Procedures

The tall oil was first weighed out in a glass beaker. This amount was predetermined based on the methanol ratio to ensure an optimum reaction volume in the reactor roughly 80% of the total volume or 800 mL. The oil sample was placed in the reactor with the thermocouple and heated to the desired reaction temperature. Meanwhile the proper amount of methanol and sulfuric acid were measured and combined, this mixture was also heated to the reaction temperature on a hot plate. The digitally controlled stirrer was adjusted to the correct speed while the glass reactor with the oil was being heated to the reaction temperature. Once the reactants reached the reaction temperature, the methanol with the sulfuric acid was added to the reactor through the sample port. The mixer and timers were started after all the reactants were in the reactor and the septum was back over the sample port.

Sample Preparation

Variable samples were taken from the reactor at 1, 5, 10, 15, 20, 30, 60, 120, 180, 240, 300, and 360 minutes. The 2 mL samples were withdrawn from the reactor with a 16 gauge, 12” stainless steel lock tip needle attached to a 20cc micro-mate hypodermic glass syringe

(Fischer Scientific, Inc.). The samples were placed into 125 mL separatory funnels where 2 mL of distilled water was added to stop the reaction. 5 mL of hexane was immediately added and the funnel gently shaken for around 30 seconds. The mixture was allowed to settle and the lower layer of methanol, water, and sulfuric acid was drained. A 5 mL methanol/water (90/10 % v/v) mixture was added to the funnel and again agitated to further remove any acidity of the mixture. Once the lower layer was removed the hexane layer containing the tall oil fatty acids, and methyl esters was placed in a Pyrex 16 x 125 mm vial and put on a Turbovap (Model LV; Zymark, MA) to remove the hexane. The Turbovap used helical gas flow of nitrogen in a 40°C constant temperature bath to evaporate the hexane. Once the hexane was removed, the neat biodiesel was ready for storage (0°C), analysis, or preparation.

Analysis of TOFA and Methyl Esters

Gas Chromatograph (GC)

An Agilent gas chromatograph (Model 6890N; Palo Alto, CA) with an FID detector was used to determine the quantity of individual fatty acid methyl esters produced from tall oil. Separation of the individual fatty esters was performed over a Supelco fused-silica capillary column (SP-2380; Bellefonte, PA) composed of stabilized poly (90% biscyanopropyl / 10% cyanopropylphenyl siloxane) and dimensions of 100 m x 0.25 mm xx 0.2 mm. The calibration curve was prepared using a Supelco 37 FAME mixture. The known concentrations were prepared and injected along with 1,3-Dichlorobenzene as the internal standard.

The method for the gas chromatograph began with a 1 mL injection and a split ratio of 100:1. A nonlinear column temperature gradient starting at 110°C and ending at 240°C was run for 60 min. Helium was the carrier gas for the GC while hydrogen and air were supplied to the FID. Tall oil methyl ester samples were prepared in hexane with a concentration around 3 mg oil/ml and a concentration of 1mg/ml of 1,3 Dichlorobenzene. The total concentration of 3 mg/ml was in the range of calibration for the GC. Table 5.2 lists the individual fatty acids and their respective concentrations in the sample.

Attenuated Total Reflectance-Fourier Transform Infrared

The neat oil samples were analyzed for fatty acid methyl esters and free fatty acids by a PerkinElmer ATR-FTIR (Model 100; Wellesley, MA). The Spectrum 100 was a self-contained unit that used a Helium Neon laser to emit a continuous, visible wave radiation. The optical system allows the collection of data over the range of 7,800-370 cm^{-1}. The detector was a mid infrared detector of deuterated triglycine sulphate. The ATR was a combination of Diamond and Zinc Selenide (ZnSe) crystals.

A spectrum over the range of 4,000 cm^{-1} to 650 cm^{-1} was performed on each sample. The background was taken before each set of samples over the same sample range. The computer program automatically adjusted the background as the base for the final spectrum. Before and after each set of samples, a quality test was performed on the diamond to ensure that it was clean.

The FTIR allows for the quantification of material based on the vibration of the functional group. Different functional groups absorb infrared light at different wavelengths. The tall oil methyl ester's alcohol functional group exhibits vibrations at around the 1741 cm^{-1} wavelength, while the tall oil fatty acids themselves exhibit vibrations at 1706 cm^{-1} as a result of the carboxylic acid functional group.

The use of Beer's Law which correlates concentration to absorbance was used to quantify the conversion of tall oil fatty acids. A set of standards were prepared for the calibration of the 1,741 cm^{-1} wavelength which corresponds to the methyl ester functional group. Tall oil was initially characterized by its acid value. These values were also analyzed using the American Oil Chemists' Society (AOCS) Official Method Ca 5a-40 for free fatty acid content.

The tall oil fatty acids were then completely esterified with methanol in the presence of sulfuric acid. The fatty acid methyl ester product was purified and the acid value was again analyzed. Table 3 lists the acid value for several samples of the tall oil before and after conversion. The average acid value of the tall oil correlates to 97.6% free fatty acids initially. After the esterification reaction, the acid value fell to 0.143 which corresponds to less than 0.07% free fatty acids. Weight fraction of TOFA and TOME were weighed out in 10 percent increments from 0% to 100%. The ATR-FTIR values for peak height at wavelength 1,741 cm^{-1} were correlated to conversion based off comparison to the acid value tests. Concentration vs. absorbance was plotted and a trend-line produced. The equation to calculate conversion from the peak height of absorbance at 1741 cm^{-1} is:

$$\%\ Conversion = X_{FAME} = \frac{N_{moles\ FAME\ produced}}{N_{moles\ oil\ (time=0)}} = 473.3 \times Peak\ Height - 14.07$$

The R^2 value is 0.9995 and suggests that Beer's Law is followed in this calibration.

Quality Standards

Several tests were available for testing biodiesel under ASTM D 6751-06 standards. Tests were performed to determine the quality of the biodiesel produced from tall oil. This includes sulfur analysis, cold flow, carbon residue, vacuum distillation, copper corrosion, flash point, and viscosity. All equipment was purchased through PAC (Houston, TX).

Cloud Point

The CPP 5Gs was the automated instrument used for measuring the cloud determined by ASTM D 2500. 45 mL of biodiesel were required to run a test for cloud point. The sample was placed in the container and the preprogrammed setup ran the test. The cloud point program increased the temperature of the sample to 45°C and then incrementally decreased the temperature until crystals formed in the sample. A set of probes emitted light through the sample to detect the crystal formation.

Carbon Residue

A micro carbon residue tester (MCRT) model 160 was used to measure the carbonaceous matter in the fuel. Free and total glycerol left in the biodiesel will produce the ash and build up in a diesel engine. Roughly 1.5 g of biodiesel was burned and measured in accordance with ASTM D 4530. The differences in weight of the vials and weight of the sample are used to calculate the residual ash after the test.

Vacuum Distillation

The Herzog automated vacuum distillation (Model HDV 632) analyzes a 200 mL sample for the boiling curve of the distillation products following ASTM D 1160. Methyl esters of fats boil in the small range from 330 to 357°C at atmospheric pressure. This ASTM test provides another precaution against high boiling contaminants with a maximum specification of 360°C.

Viscosity

Viscosity was measured in an ISL temperature bath. The temperature was kept constant at 40°C while four different capillaries were used to measure the viscosity. The Cannon-Fenske Routine viscometer capillaries were 50, 75, 100, and 150 for measurements. 7 mL of tall oil biodiesel were placed in each tube and allowed to heat to 40°C in the temperature bath. The sample was then drawn up into the capillary tube and the time recorded for the fluid

to pass from the upper line to the lower line of calibration. The time in seconds is then multiplied by the calibration factor to calculate the viscosity in mm^2/second. The calibration factor if for the individual tube measured at the factory.

Sulfur Analysis

Sulfur analysis was performed using an ANTEK sulfur analyzer (Model 9000) which was also supplied by PAC. The system is composed of a sampler, a furnace, and detector. The furnace was operated at 1050^oC using oxygen and argon. An 8 uL sample was injected and analyzed. The high temperature completely gasified the sample which was combined with O_2 to form: CO_2, H_2O, NO, SO_2, and other oxides. For sulfur analysis the SO_2 was exposed to ultraviolet radiation at a specific wavelength. The electrons that were impacted by the radiation shifted to a higher energy level. After the sample passed through the radiation the electrons dropped back down to their ground state and emitted light that was measured in a photomultiplier tube. The wavelength of the light emitted was specific for sulfur and was also proportional to the amount of sulfur in the sample. Sulfur in iso-octane at 5, 10, 25, and 50 ppm were purchased from ANTEK Instruments (Houston, TX) and used as calibration standards.

Flash Point

The Flash point was performed in a Pensky Martens analyzer built by Herzog (Model HFP 360). The test cup was filled with 75 mL of biodiesel. The cup was placed in the heating block and the electric igniter, thermocouple, and stir rod were attached to the cup. Once the program was started the sample was heated at a constant rate while continuously being stirred. The stirrer was stopped while the small electric flint was introduced into the cup at regular intervals. The flash point was measured as the lowest temperature of the liquid at which the vapor above the sample will ignite from the introduction of the electric flint.

Copper Corrosion

Copper corrosion was analyzed using 45 mL of biodiesel sample. Copper strips are representative of fuel system components and may be an indication of possible metal corrosion problems. The strips were finely polished and added to the biodiesel sample in a glass vial. The vial was placed into a 50^oC constant temperature bath and left for 3 hours. At the end of the test the copper strip was visually compared to standards. The degree of tarnish is reported as it compares to the standards. The maximum allowable degree of tarnish is labeled as number 3 and is designated dark tarnish.

Table 1. Design matrix for 2^4 experimental design

Parameters	Levels	
	Low(-1)	High(+1)
1-Agitation	100 RPM	400 RPM
2-Temperature	30 ^{o}C	60°C
3-Sulfuric Acid Catalyst	1%	5%
4-Methanol	6:1	60:1

Experiment No.	Parameters			
	1	2	3	4
1	-1	-1	-1	-1
2	+1	-1	-1	-1
3	+1	+1	-1	-1
4	+1	+1	+1	-1
5	-1	-1	-1	+1
6	-1	-1	+1	+1
7	-1	+1	+1	+1
8	-1	+1	-1	+1
9	+1	-1	+1	-1
10	-1	+1	+1	-1
11	+1	-1	-1	+1
12	+1	-1	+1	+1
13	+1	+1	-1	+1
14	-1	-1	+1	-1
15	-1	+1	-1	-1
16	+1	+1	+1	+1

Table 2. Tall oil fatty acid characterization

Acid Value	196
Saponification Value	197
Iodine value	131
Composition:	
Moisture, %	<0.1
Ash, %	<0.01
Rosin Acids, %	3.3
Unsaponifiables, %	2.4
Fatty Acids Total, %	95
Fatty Acid Composition	
Oleic, %	44
Linoleic, %	34
Linolenic, %	9
Saturated, %	5
Other, Fatty Acids, %	8
Specific Gravity	0.906

Table 3. Acid values for tall oil titration calibrations

(mg KOH/g)

sample #	Tall Oil Fatty Acids	Tall Oil Methyl Esters
1	195.7	0.13
2	194.9	0.16
3	195.2	0.14
Average	195.3	0.143

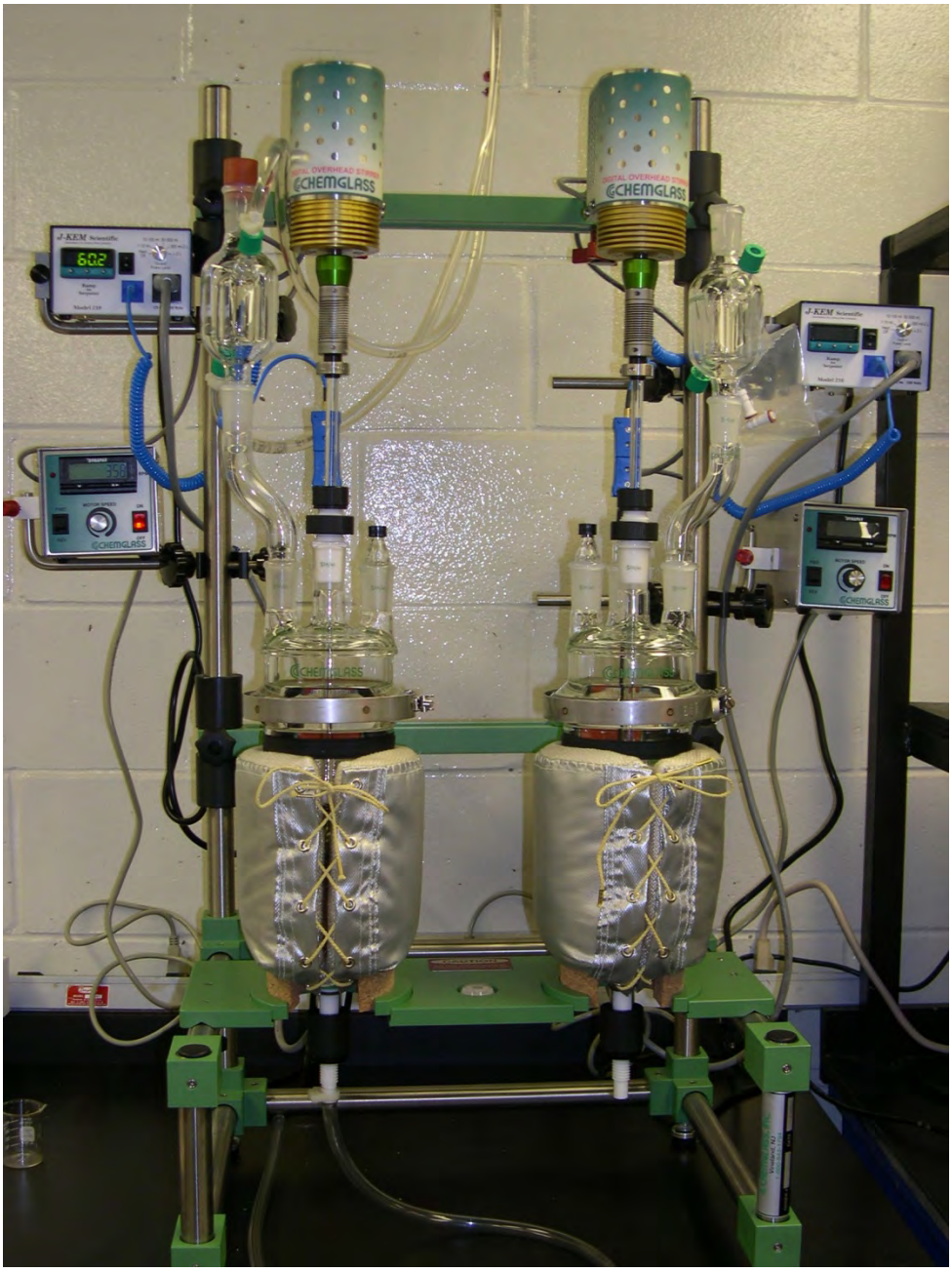


Figure 5. Experimental glass reactor apparatus

3. Results and Discussion

Results and Discussion of Factorial Design Analysis

The evaluation of tall oil as a feedstock for biodiesel production was split into three main areas. The first was the statistical analysis of the combined effects of alcohol, temperature, mixing, and catalyst. The optimal conditions of the statistical analysis lead to the kinetic study in order to obtain the reaction rates and activation energy. Finally, ASTM D 6751 based tests evaluated the quality of the biodiesel produced from tall oil.

Factorial Design Evaluation

The factorial design of experiments at two levels was a simple yet powerful tool in evaluating the operating parameters of tall oil conversion. It answers the question, "How does temperature, alcohol, catalyst, and degree of agitation affect the conversion of tall oil into biodiesel?". All the factors and their responses were evaluated based on the analysis of variance (ANOVA). ANOVA is a statistical method that combines the sum of squares with the variance of the data to relate the impact an independent variable(s) has on the dependent variable [Montgomery, 2003].

Figure 6 illustrates the individual effects of the four variables. The positive effect of the variables can be seen. The plot of temperature on conversion has the greatest slope followed by alcohol concentration, then catalyst amount. The effects of these variables were all positive as the values of the parameters went from the low level to the high level of analysis. The agitation is a straight line with no significant effect on conversion as the agitation was adjusted from 100 to 400 RPMs. This led to the conclusion that no significant mass transfer limitations were observed in this reaction setup. An agitation speed of 400 RPM was therefore used for subsequent testing.

ANOVA was performed on the above significant variables to evaluate their effects of interaction. Alcohol, temperature, catalyst, and their respective interactions significantly affect the conversion of tall oil into biodiesel. Figure 7 is a cube plot of the significant main effects holding agitation at the high level (400 RPM). The edges mark the changing independent variables while the corners identify the average conversion under the given conditions. For example, the lower left corner achieved 66.26% conversion of tall oil at 1% weight sulfuric acid, a 6:1 molar ratio of methanol to oil, and a temperature of 30°C. This is one type of visual recognition of the statistical data.

Figure 8 is a plot of the two way interactions between the independent variables alcohol and catalyst. The interaction between alcohol and catalyst is fairly proportional. The increase in conversion from a 1% catalyst to 5% at a 6:1 molar ratio is 4.38% (dX1) while the increase at a 60:1 molar ratio is a change of 6.58% (dX2). That is only a difference of 2.2% conversion from changing the catalyst from 1% to 5%. The same was true for the interaction between temperature and catalyst with a difference of only 2.12% conversion. The interaction between alcohol and temperature was not proportional (see Figure 9). As temperature increased from 30°C to 60°C at a 6:1 molar ratio conversion increased by 25.11%. This was a larger increase than observed at the 60:1 molar ratio. It was only an increase of 9.67%. The difference between these two interactions was 15.44% conversion.

Evaluating this data lead to the parameters used in studying the kinetics of the reaction. A catalyst concentration of 5% weight of the oil was used because the catalyst concentration increased proportionally with both the increases in alcohol and temperature. This is similar to past research in acid catalyzed esterification. If too much acid is used the structure of the oil may be affected. Because the 6:1 molar ratio of alcohol to oil showed a larger increase in conversion over the temperature range evaluated it was used in the kinetic study. If the 60:1 molar ratio of alcohol to oil was used the kinetic model might have been overshadowed by using the large excess of alcohol.

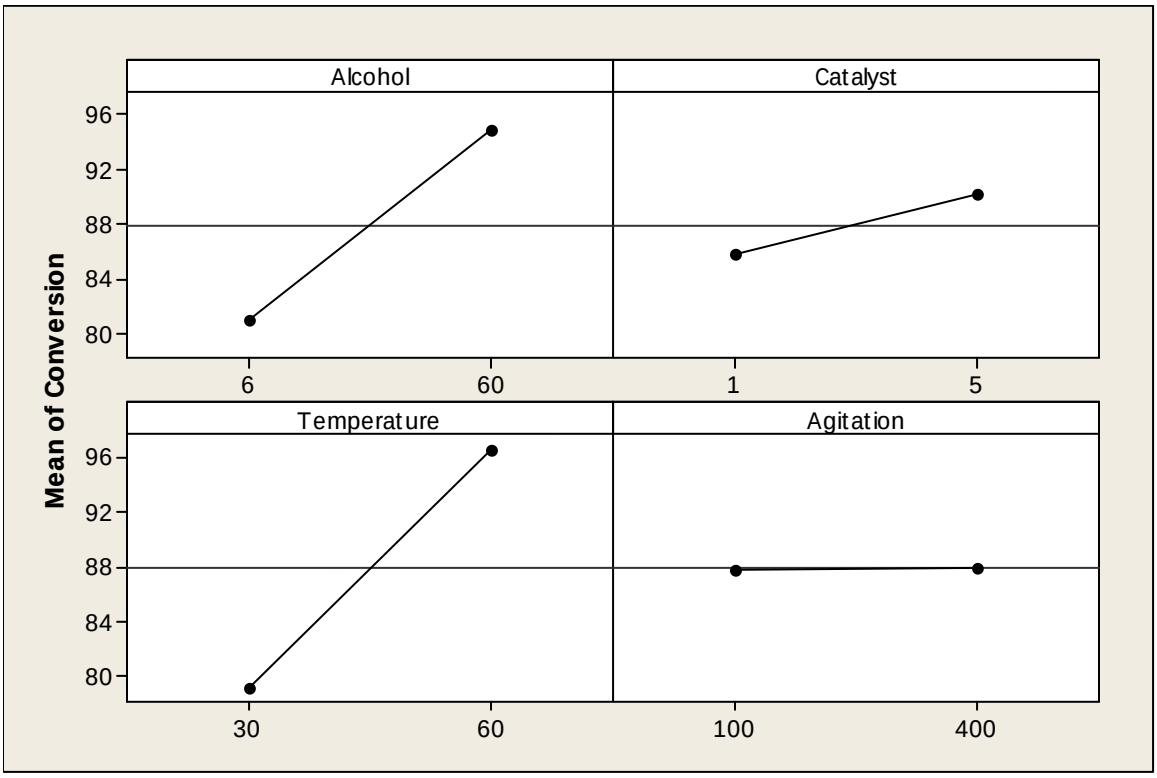


Figure 6 Individual main effects plot versus conversion

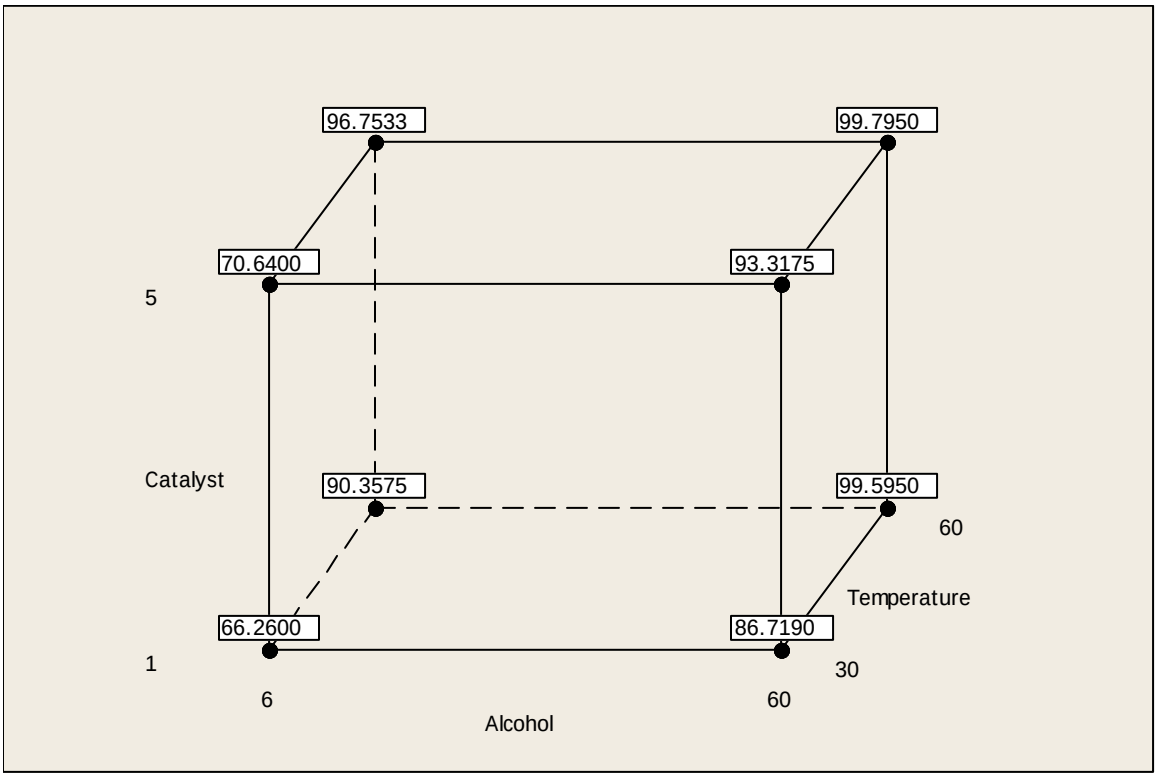


Figure 7 Cube plot of significant effects and conversion

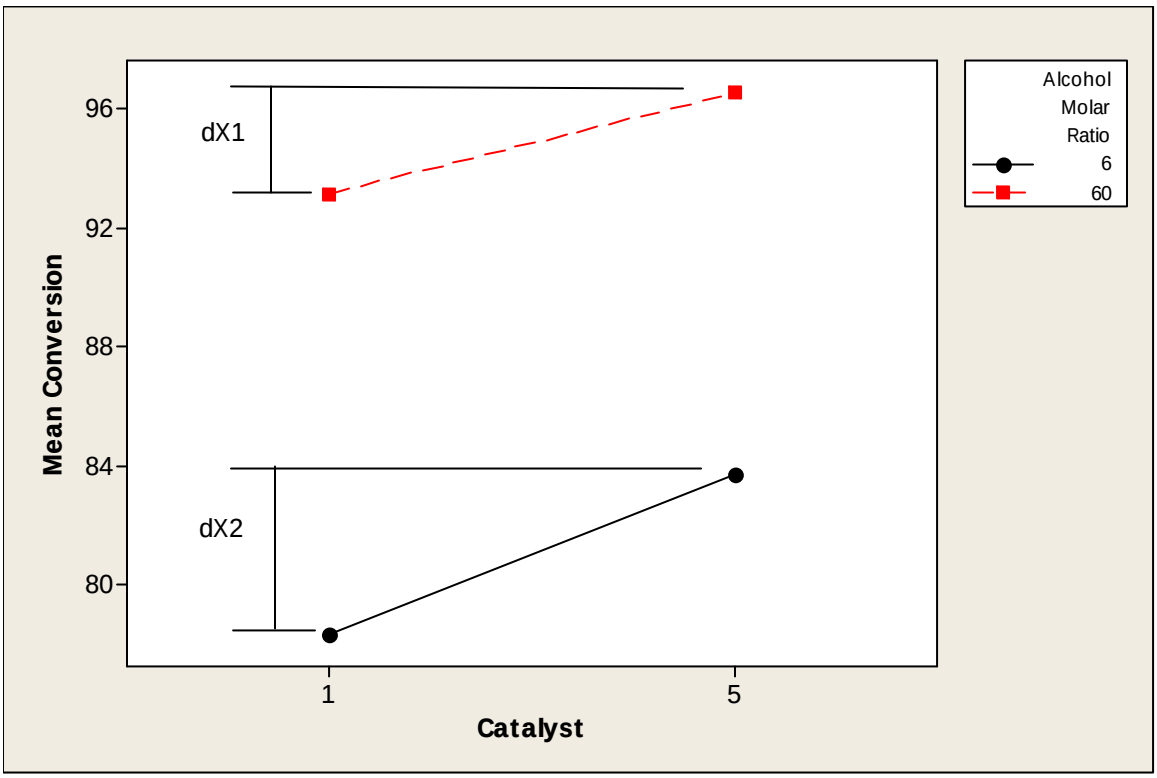


Figure 8 Interaction plot of catalyst and alcohol versus conversion

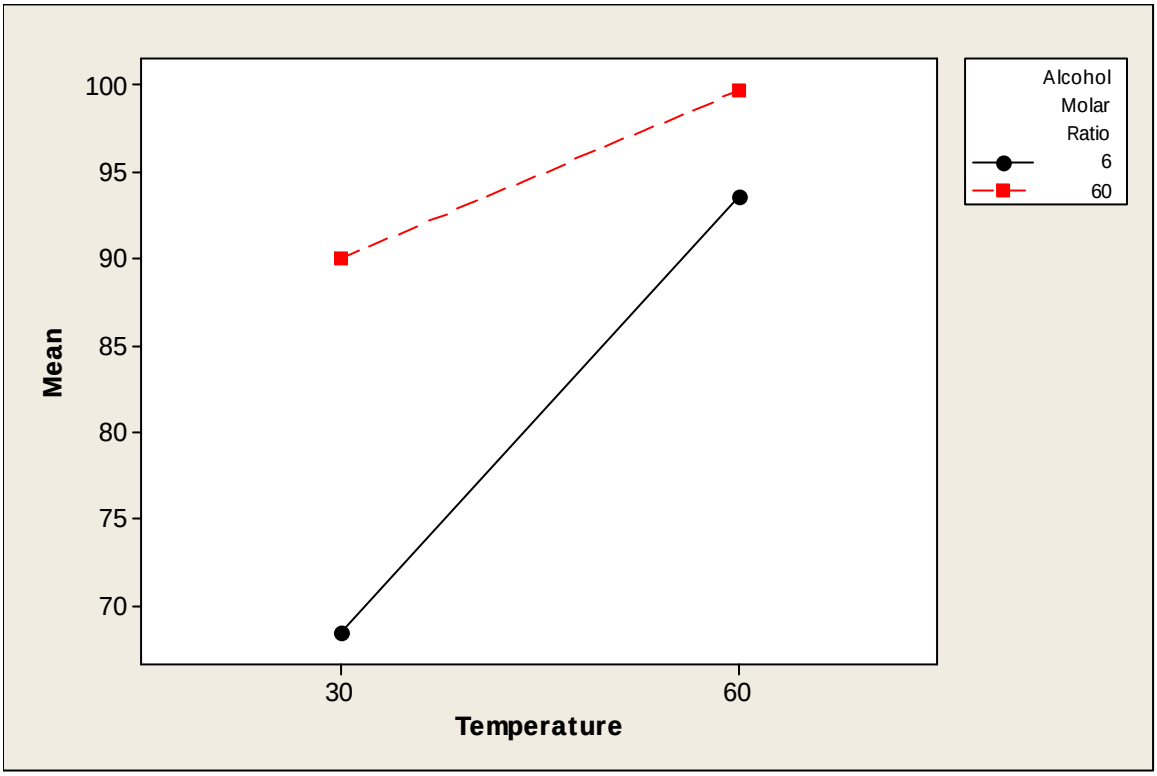


Figure 9. Interaction plot of alcohol and temperature versus conversion

Results and Discussion of Kinetic Analysis

Kinetic Model

Kinetic analysis involves determining the temperature effect of the reaction. To evaluate this, the same process conditions were repeated at different temperatures. Reaction conditions were based on the results of the factorial design of experiments. Mixing was held constant at 400 RPM's throughout the reaction. A 5% by weight sulfuric acid was utilized as the catalyst with a 6:1 molar ratio of methanol to oil. The reaction of tall oil fatty acids with methanol in the presence of sulfuric acid is represented is given by:

$$Tall\ Oil\ Fatty\ Acids + Methanol \overset{sulfuric\ acid}{\Leftrightarrow} Tall\ Oil\ Methyl\ Esters + Water$$

The conversion versus time data at the temperatures 30, 40, 50, and 60°C were collected. Figure 10 is the graph of these conversions versus time. Utilizing the elementary reaction of esterification, a pseudo-homogeneous second-order equilibrium model was used for modeling the
experimental runs [Fogler, 1999]. The rate of the reaction can be characterized by the second order reversible reaction.

$$-r_a = -\frac{dC_a}{dt} = k_1 \cdot C_a \cdot C_b - k_2 \cdot C_c \cdot C_d$$

where,

$-r_a$ = the rate of disappearance of tall oil fatty acids as a function of time

k_1 = the forward rate constant (Liters * mol^{-1} * $minute^{-1}$)

C_a = the concentration of tall oil fatty acids (mol * $Liter^{-1}$)

C_b = the concentration of methanol (mol * $Liter^{-1}$)

k_2 = the reverse rate constant (Liters * mol^{-1} * $minute^{-1}$)

C_c = the concentration of tall oil methyl esters (mol * $Liter^{-1}$)

C_d = the concentration of water (mol * $Liter^{-1}$)

This model has shown to be able to describe esterification reaction kinetics for liquid catalysts [Tesser et al., 2005]. It appears that the reaction rate is the highest during the first 30 minutes then approaches an asymptote value as equilibrium is approached. This type of behavior is exhibited due to the reversible nature of the esterification reaction.

Reaction Rates

The rates of the reaction for the degradation of the tall oil fatty acids were calculated by differential analysis on the conversion data. The concentration data is a function of time and the rate of the reaction is the change in concentration with respect to time (-dCa/dt). Since the sample times were not equally spaced the graphical differentiation technique described by Folger (1999) was employed to differentiate the conversion versus time data. First, the average slope DCa/Dt was calculated for each sample interval. This value was plotted as a histogram versus time. A best fit curve was applied to the histogram and the rate data $(dCa/dt)_t$ as a function of time was obtained from the plot.

The rates of the reaction at the four temperatures are summarized in Table 4. The rate of the reaction decreases significantly during the first 30 minutes of conversion. For example, the rate of reaction falls from 1.2 to 0.0041 mol * min^{-1} *L^{-1} at a temperature of 60°C. This reaffirms the idea of the reversible nature of the reaction. As the reaction proceeds to completion, the rate drops because of the competing reverse reaction.

Polymath is a mathematical program that was used to model nonlinear regression of the rate of the reaction. It uses the Levenberg-Marquardt Algorithm to minimize the sum of squares for the nonlinear functions. The second order reversible model was fitted to the data to calculate the two unknown rate constants in rate equation. Rate constants, k_i, for the forward and reverse reactions were determined at each temperature. The R^2 values range from 0.9107 to 0.9585 which suggest the pseudo-homogeneous second-order equilibrium model physically describes the rate of reaction at these temperatures.

The forward reaction rate constants for 30°C, 40°C, 50°C, and 60°C are: 0.89706, 1.2541, 1.55172, and 1.76925 (L*mol^{-1} * min^{-1})*10^{-2}. The reverse reaction rate constants for these temperatures were also calculated. The reverse reaction rate constants for 30°C, 40°C, 50°C, and 60°C are: 4.426, 2.36263, 1.4706, and 1.03861 (L*mol^{-1} * min^{-1})*10^{-2}. Appendix C also contains the Polymath reports for the statistical parameters at each of the four temperatures evaluated.

Activation Energy

The Arrhenius equation was applied to the rate constants in order to determine their temperature dependence. The Arrhenius Equation relates the reaction coefficients to the operating temperature:

$$k = A \cdot \exp\left(-\frac{E_a}{RT} \right)$$

where,

A = the pre-factor

E_a = the activation energy

T = the temperature in Kelvin

R = the constant.

Plotting the Ln(k) vs. 1/T gives a linear correlation between the two parameters and is known as the Arrhenius plot. The slope of the line is therefore equal to $-E_a/R$ and the pre-factor (A) is equal to the natural log of the intercept. Figure 11 represents the effect of temperature on the reaction rate constants. The activation energy for the forward rate constant was calculated to

be 19.73 kJ/mol, and the pre-exponential factor was 23.6. Sendzikiene et al. (2004) obtained an activation energy of 13.3 kJ/mol and a pre exponential factor of 1.27. While the activation energies are close, the difference in the value of A might be related to the environmental differences between the two studies. Sendzikiene et al. esterified free fatty acids in the presence of triglycerides with a 1% weight sulfuric acid. This study only involved the free fatty acid environment and utilized a 5% weight sulfuric acid catalyst. This could contribute to the larger frequency factor represented by the pre exponential factor A.

Table 4. Changing rates of reaction at the various

Temperatures units (mol * min^{-1} * L^{-1})

Time	**30°C**	**40°C**	**50°C**	**60°C**
0	0.4200	0.7500	0.9100	1.2000
1	0.2585	0.4990	0.6313	0.7530
5	0.0556	0.0375	0.0510	0.0358
10	0.0315	0.0263	0.0265	0.0255
15	0.0180	0.0141	0.0149	0.0160
20	0.0109	0.0109	0.0105	0.0088
30	0.0072	0.0067	0.0058	0.0041

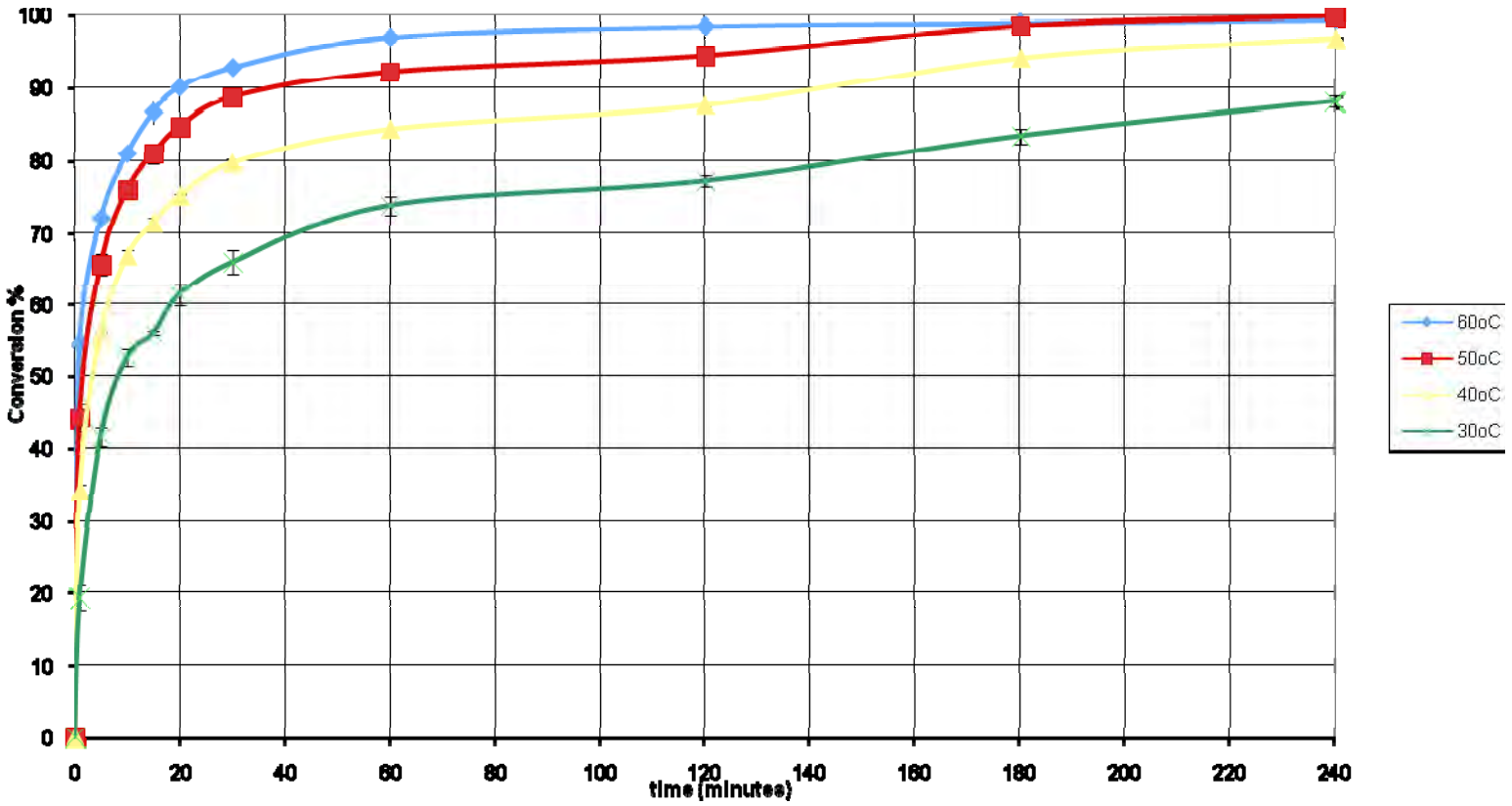


Figure 10. Conversion versus time graph for kinetic experiments

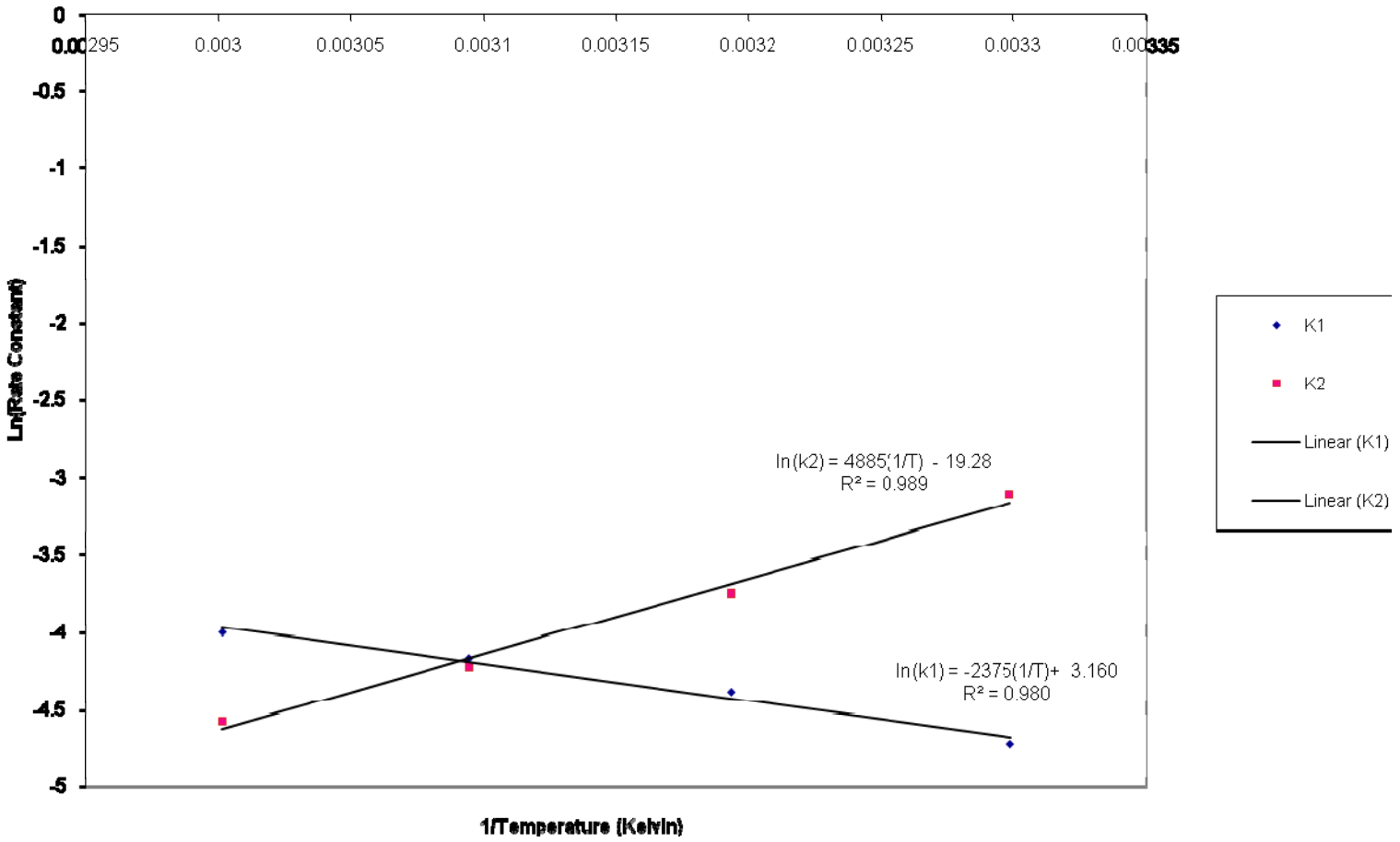


Figure 11. Arrhenius plot for reaction rate constants

ASTM D 6751 Results

Several quality standards were performed on the final tall oil methyl ester product. Random batch processes were evaluated throughout the course of the experimental analysis of the tall oil conversion. The results for cloud point, carbon residue, vacuum distillation, cetane number, viscosity, sulfur analysis, flash point, and copper corrosion were performed on the final tall oil product.

Cloud Point

The cloud point is the temperature at which clouds of wax crystals first appear in a liquid sample when it is subjected to decreasing temperatures. The average cloud point for tall oil methyl ester was found to be -10.7^{o}C (see Table). Number 2 diesel fuel's cloud point is around -12°C, while soybean methyl esters have cloud points around 0°C [Lee et al., 1995; Fukuda et al., 2001]. The reason for tall oil methyl esters lower cloud point is due to relatively low concentrations of saturated fatty acid esters. The total concentration of saturated fatty acids in soybean oil is 17% which is 10% higher than the tall oil saturated fatty acids. The relationship between lower crystallization temperatures and higher concentrations of branched chain esters explains the lower cloud point for tall oil methyl esters. Rosin acids are usually a crystalline structure at room temperature and may inhibit the low cloud point if higher percentages are used in the final product. The lower cloud point is a positive aspect for the biodiesel produced from tall oil because it will perform better in colder weather.

Carbon Residue

The carbon residue is formed from fuel exposure to high temperatures in the absence of oxygen. It is a measure of the tendency of a fuel to deposit a carbon rich residue in the engine injection components. The maximum limit is 0.05% weight. Tall oil methyl ester samples ranged from 0.01-0.03% mass. This indicates that a quality produced tall oil biodiesel will meet the specification of the carbon residue test.

Vacuum Distillation

The fatty acids in biodiesel all have relatively close boiling points and do not represent a curve as petroleum diesel components. The ASTM D 1160 distillation temperature is used to determine if there are any high boiling contaminants in the fuel. The maximum allowable value is 360°C. All tall oil methyl esters samples were below this value with an average of 352.6^{o}C.

Cetane Number

The cetane number is a dimensionless number used to describe how well a diesel fuel will ignite. The higher the number the more complete combustion in the engine. Petroleum diesel must meet a minimum cetane number of 40 while biodiesel must meet a minimum of 47 according to ASTM D 613. Tall oil biodiesel produced a cetane number of 48.74 which is within the quality limits of ASTM testing. Tall oil could be blended with no. 2 petroleum diesel as a cetane improver to increase ignition quality.

Viscosity

The viscosity of a diesel engine fuel must be within a certain range because it will affect the atomization of the fuel. If the viscosity is too high, there will not be enough fuel in the ignition chamber. The viscosities of most biodiesel overlaps with those of petroleum diesel. ASTM test method D 445 for the kinematic viscosity of biodiesel limits range from 1.9-6.0 mm^{2}/s. Petroleum diesel number 2 ranges from 1.9-4.1 mm^{2}/s. The average viscosity for tall oil methyl esters was 5.15 mm^{2}/s. This is within the acceptable limits for quality biodiesel.

Sulfur Analysis

Sulfur in biodiesel can affect emissions systems performance and is limited to a very small quantity. Vegetable oil biodiesel are essentially free of sulfur and easily meet ASTM requirements. The average concentration of sulfur in the tall oil biodiesel was 49.02 parts per million (ppm). This is above the low grade ASTM limit and may pose problems with this fuels

production and utilization. The low grade S15 has a sulfur limit of 15 ppm while the S500 grade has a limit of 500 ppm. The tall oil evaluated in this study meets the fuel requirements under the grade S500 and may be utilized off-road fuel vehicles. Additional processing was performed on the tall oil methyl esters to evaluate sulfur removal. These results will be presented in a future publication.

Flash Point

The flash point analysis is used to determine if the substance is flammable. Biodiesel must have a flash point above 130°C according to ASTM D 93. This method may be used to test for the presence of residual alcohol contamination. If the alcohol used in esterification is not removed during processing of the final product and the flash point falls below 130°C, then safety and transportation regulations are violated. The flash points of various tall oil methyl esters ranged from 168.9-178.3^{o}C. All flash points exceed the minimum requirement of 130°C and indicate that it represents a low fire hazard.

Copper Corrosion

Several components in a diesel injection system are susceptible to corrosion. Copper is used as an indicator for corrosion. ASTM D130 outlines the use of copper strips to characterize the tendency of the fuel to corrode engine components. The maximum allowable indication is No. 3 which represents dark tarnish. All the tall oil methyl ester samples represented 1A which is slight tarnish. This gives the estimation that tall oil biodiesel will not be a corrosive fuel in diesel engines.

Summary

Tall oil methyl esters meet the specifications of all the ASTM standards tested. Table 5 compares the ASTM standards of tall oil methyl esters with the methyl esters from soybean oil. Tall oil methyl esters show a dramatic advantage over soybean oil methyl esters in the cloud point analysis. This could allow tall oil biodiesel to be used in colder climates where soy methyl esters would cause problems.

Table 5 ASTM D 6751-06 for tall oil and soy oil methyl esters

Property	Method	Limits	Tall Oil BD	Soy Oil BD	Units
Flash point, closed cup	D 93	130 min	173.24	n/a	° C
Kinematic viscosity, 40 ° C	D 445	1.9 - 6.0	5.15	4.59	mm2/s
Total Sulfur	D 5453	15 (S15 Grade) 500 (S500 Grade)	49.02	5	ppm
Copper strip corrosion	D 130	No. 3 max	1A	1A	
Cetane number	D 613	47 min	48.74	50.4	
Cloud point	D 2500	Report to customer	-10.7	0	° C
Carbon residue	D 4530	0.050 max	0.02	0.01	wt. %
Acid number	D 664	0.80 max	0.08	0.15	mg KOH/g
Vacuum distillation end point T-90	D 1160	360 °C max, at	352.6	n/a	oC

4. Conclusions

The results of this research provide the basis for the production of biodiesel from tall oil fatty acid feedstocks. Three studies were performed on the tall oil fatty acid feedstock. Factorial design analysis was initially performed to evaluate the effects of significant parameters on conversion. Alcohol, acid, temperature, and agitation were evaluated using this statistical analysis. The optimal parameters from the analysis were then used to determine the kinetic

model for tall oil esterification. The final tall oil methyl ester product was analyzed for quality under the standards set by ASTM D 6751-06.

The conclusions made from this research are:

- The factorial design analysis showed that alcohol, acid, and temperature all have a significant effect on conversion.
- The range of agitation did not show a significant effect on conversion. It was concluded that mass transfer limitations were not involved in this kinetic study.
- Based on statistical analysis, the optimal conditions for esterification were a catalyst weight of 5%, alcohol to oil ratio of 6:1, and the agitation kept at 400 RPM's. Ninety-nine percent conversions could be achieved under these conditions with the temperature at 60°C and a residence time of 2 hours.
- The kinetics of esterification of tall oil fatty acids at the optimal parameters followed second order kinetics.
- The rate of reaction increased with increasing temperature. The forward reaction rate constants for 30, 40, 50, and 60°C are: 0.89706, 1.2541, 1.55172, and 1.76925 (L*mol^{-1} * min^{-1})*10^{-2}.
- All the ASTM D 6751-02 standards tested except sulfur analysis passed with traditional water wash processing.

Similar experiments were conducted with Chinese tallow tree and castor oils. The ASTM standard was not met with these oils. Blending of biodiesel from these oils with soy bean oil biodiesel was considered as an option to meet the ASTM standard.

References:

Boocock, D.G.B., S. K. Konar, V. Mao, C. Lee, and S. Buligan. (1998) Fast Formation of High-Purity Methyl Esters from Vegetable Oils. JAOCS, 75 (9), 1167-1171.

Brown, W. H., and C. S. Foote. (2002). Organic Chemistry (3rd edition). New York: Harcourt College Publishers.

Bryan, T. (2005, March). Adsorbing It All. Biodiesel Magazine, 40-43.

Campbell, C. J. (2004). The Coming Oil Crisis. Essex, England: Petroconsultants S. A.

Canakci, M., and J. V. Gerpen. (1999). Biodiesel Production via Acid Catalysis. Trans of the ASAE, 42 (5), 1203-1210.

Canakci, M. and J. V. Gerpen. (2001). Biodiesel Production from Oils and Fats with High Free Fatty Acids. Transactions of the ASAE, 44 (6), 1429-1436.

Cetinkaya, M., and F. Karaosmanoglu. (2004). Optimization of Base-Catalyzed Transesterification of Used Cooking Oil. Energy and Fuels, 18 (6), 1888-1895.

Chemical Market Reporter, (2005, December). 266 (18).

Conley, R. (1970). Infrared Spectroscopy (2nd Edition). Boston, MA: Allyn and Bacon, Inc.

Cvengros, J., Z. Cvengrosova. (2004). Used Frying Oils and Fats and Their Utilization in the Production of Methyl Esters of Higher Fatty Acids. Biomass and Bioenergy, 27, 173-181.

Darnoko, D., and M. Cheryan. (2000). Kinetics of Palm Oil Transesterification in a Batch Reactor. JAOCS, 77 (12), 1263-1267.

Diesel, R. (1912). The Diesel Oil-Engine, Engineering, 93: 395-406, Chem. Abstr. 6: 1984.

Dube, M. A., S. Zheng, D. McLean, and M. Kates. (2004). A Comparison of Attenuated Total Reflectance-FTIR Spectroscopy and GPC for Monitoring Biodiesel Production. JAOCS, 81 (6), 599-603.

EIA Annual Energy Outlook 2006
Accessed Online: 9/3/2006
http://www.doe.eig.gov/aeo2006/

Firestone, D. (1999). Physical and chemical characteristics of oils, fats, and waxes, AOCS Press.

Fogler, H. S. (1999). Elements of chemical reaction engineering (3rd edition). Upper Saddle River, NJ: Prentice Hall.

Foglia, T. C., and K. C. Jones. (1997). Quantitation of Neutral Lipid Mixtures Using High Performance Liquid Chromatography with Light Scattering Detection. J. Liq. Chromatogr. Relat. Technol., 20 (12), 1829-1838.

Formo, M. W. (1954). Ester Reactions of Fatty Materials. JAOCS, 31, 548-559.

Freedman, B., R. O. Butterfield, and E. H. Pryde. (1986). Transesterification Kinetics of Soybean Oil. JAOCS, 63 (10), 1375-1380.

Freedman, B., E. H. Pryde, and T. L. Mounts. (1984). Variables Affecting the Yields of Fatty Esters from Transesterified Vegetable Oils. JAOCS, 61 (10), 1638-1643.

Fukuda, H., A. Kondo, and H. Noda. (2001). Biodiesel Fuel Production by Transesterification of Oil. J. Biosci. Bioeng., 92, 405-416.

Haas, M. J., A. J. McAloon, W. C. Yee, and T. A. Foglia. (2006). A Process Model to Estimate Biodiesel Production Costs. Bioresource Technology, 671-678.

Haas, M. J. (2005). Improving the Economics of Biodiesel Production Through the Use of Low Value Lipids as Feedstock: Vegetable Oil Soapstock. Fuel Processing Technology, 86, 1087-1096.

Hass, M. J., P. J. Michalski, S. Runyon, A. Nunez, and K. M. Scott. (2003). Production of FAME from Acid Oil, A By-Product of Vegetable Oil Refining. JAOCS, 80 (1), 97-102.

Haas, M. J., S. Bloomer, and K. Scott, Simple. (2000). High-Efficiency Synthesis of Fatty Acid Methyl Esters from Soapstock, JAOCS, 77 (4), 373-379.

ICIS Chemical Business. (2006, October). 1 (38).

Knothe, G. (1999). Rapid Monitoring of Transesterification and Assessing Biodiesel Fuel Quality by Near-Infrared Spectroscopy Using a Fibre-Optic Probe. JAOCS, 76 (7), 795-800.

Knothe, G. (2000). Monitoring a Progressing Transesterification Reaction by Fiber-Optic Near Infrared Spectroscopy with Correlation to H^1 Nuclear Magnetic Resonance Spectroscopy. JAOCS, 77 (5), 489-493.

Leclercq, E., A. Finielsand, and C. Moreau. (2001). Transesterification of Rapeseed Oil in the Presence of Basic Zeolites and Related Catalysts. JAOCS, 78, 1161-1165.

Lee, I., L. A. Johnson, and E. G. Hammon. (1995). Use of Branched-Chain Esters to Reduce the Crystallization Temperature of Biodiesel. JAOCS, 72, 1155-1160.

Ma, F., L. D. Clements, and M. A. Hanna. (1998). The Effects of Catalyst, Free Fatty Acids, and Water on Transesterification of Beef Tallow. Trans of the ASAE, 41 (5), 1261-1264.

Mittelbach, M. (1996). Diesel Fuel Derived from Vegetable Oils, VI: Specifications and Quality Control of Biodiesel, Bioresource Technology, 56, 7-11.

Montgomery, D. C., and G. C. Runger. (2003). Applied Statistics and Probability for Engineers (3rd edition). New York: John Wiley & Sons.

National Biodiesel Board, Fuel Fact Sheets, Benefits of Biodiesel.
Accessed online 8/12/2006:
http://www.biodiesel.org/pdf_files/fuelfactsheets/Benefits%20of%20Biodiesel.Pdf

Noureddini, H. and D. Zhu. (1997). Kinetics of Transesterification of Soybean Oil. JAOCS, 74 (11), 1457-1463.

Nye, M. J., T. W. Williamson, S. Deshpande, J. H. Schrader, W. H. Snively, T. P. Yurkewich, and C. L. French. (1983). Conversion of Used Frying Oil to Diesel Fuel by Transesterification: Preliminary Tests. JAOCS, 60 (8), 1598-1601.

Nye, M. J. and P. H. Southwell. (1983). Esters from Rapeseed Oil as Diesel Fuel. Proceedings from the Vegetable Oil as Diesel Fuel Seminar III, Northern Agricultural Energy Center, Peoria, IL, 1983.

Obibuzor, Jude U., Abigor, Roland D., and Okiy, Dere A. (2003). Recovery of Oil via Acid-Catalyzed Transesterification. JAOCS, 80, 77-80.

Ozgul-Yucel, S., and S. Turkay. (2003). FA Monoalkylesters from Rice Bran Oil by in situ Esterification. JAOCS, 80, 81-84.

Pahl, Greg. (2005). Biodiesel: growing a new energy economy. (1st Edition). Chelsea Green Publishing.

Peterson, C. L., D. L. Auld, and R. A. Korus. (1983). Winter Rape Oil Fuel for Diesel Engines: Recovery and Utilization. JAOCS, 60 (8), 1579-1587.

Ryan, T. W., L. G. Dodge, and T. J. Callahan. (1984). The Effect of Vegetable Oil Properties on Injection and Combustion in Two Different Diesel Engines. JAOCS, 61, 161.

Sheehan, J., V. Camobreco, J. Duffield, M. Graboski, and H. Shapouri. (1998). Life Cycle Inventory of Biodiesel and Petroleum Diesel for Use in an Urban Bus. NREL/SR-580-24089, Golden, CO: National Renewable Energy Laboratory.

Sendzikiene, E., V. Makareviciene, P. Janulis, S. Kitrys. (2004). Kinetics of Free Fatty Acids Esterification with Methanol in the Production of Biodiesel Fuel. Eur. J. Lipi Sci. Technol., 106, 831-836.

Sjostrom, Eero. (1993). Wood Chemistry: Fundamentals and Applications (2ND Edition). San Diego, CA: Academic Press.

http://www.me.iastate.edu/biodiesel/Technical Papers/Tech_papers.html

Srivastava, A., and R. Prasad. (2000). Triglyceride-based Diesel Fuels. Renewable and Sustainable Energy Reviews, 4, 111-133.

Standard specifications for Biodiesel Fuel (B100) Blend Stock for Distillate Fuels. (2006). Designation: D6751-06. Annual Book of ASTM standard: Philadelphia, PA.

Tapasvi, D., D. Wiesenborn, and C. Gustafson. (2005). Process Model for Biodiesel Production from Various Feedstocks. Transactions of the ASAE, 48 (6), 2215-2221.

Tesser, R., M. D. Serio, M. Guida, M. Nastasi, and E. Santacesaria. (2005). Kinetics of Oleic Acid Esterification with Methanol in the Presence of Triglycerides. Ind. Eng. Chem. Res., 44 (21), 7978-7982.

USDA Oil Crops Situation and Outlook Yearbook: OCS-2006/May 2006 Economic Research Service, USDA
Accessed on-line: October 18, 2006 [http://usda.mannlib.cornell.edu/usda/current/OCS-yearbook/OCS-yearbook-05-31-2006.pdf]

U. S. DOE, EPAct 2005 laws.
Accessed online: August 22, 2006
[www.eere.energy.gov/afdc/laws/epact_2005.html]

Watanabe, Y., Y. Shimada, A. Sugihara, H. Noda, H. Fukuda, and Y. Tominaga. (2000). Continuous Production of Biodiesel Fuel from Vegetable Oil Using Immobilized *candida antarctica* Lipase. JAOCS, 77, 355-359.

Watkins, Catherine. (2000). Tall oil fatty acids, Inform, 11, 580-588.

Yang, H., and J. Irudayaraj. (2001). Comparison of Near-Infrared, Fourier Transform-Infrared, and Fourier Transform-Raman Methods for Determining Olive Pomace Oil Adulteration in Extra Virgin Olive Oil. JAOCS, 78 (9), 889-895.

Zinkel, D. F., and J. Russell., eds. (1989). Naval stores: production, chemistry, utilization.. New York, NY: PCA.

Zullaikah, Siti, Lai, Chao-Chin, Ramjan Vali, and Ju, Yi-Hsu. (2005). A Two-step Acid-catalyzed Process for the Production of Biodiesel from Rice Bran Oil. Bioresource Technology, 96, 1889-1896.

Zheng, S., Kates, M., Dube, M.A., and Mclean, D.D. (2006). Acid-catalyzed Production of Biodiesel From Waste Frying Oil. Biomass and Bioenergy, 30 (3), 267-272.

Task A. 5. Study the cultivation techniques and harvesting economics for Southeast Feedstocks

1.Introduction

Oilseed crops are most commonly grown for edible oil production, but also have the potential to serve as feedstock for biodiesel. Oilseed crops; especially winter annual oilseeds, such as canola, or "catch-up" crops (planted after early harvest of one crop, while there is still season to grow another) like okra and sunflower; could provide expanded rotation options on prime farmland. Production orientated research across the state on oilseed crops has provided a greater understanding of feedstock growing potential as well as challenges faced in the cultivation of bioenergy crops.

A.5.1 Identify and culture Southeast high oil content crops

Sunflower yield and oil content were affected by date of planting, nitrogen fertilization and location of production. Oil yields ranged from 483 to 1388 L ha $^{-1}$. Productivity of winter canola, winter mustard, and coriander were equal to or exceeded average yields reported in the literature. Flax was slightly less. Crambe, and camelina did not perform well in Mississippi although manipulations in cultural practices offer the possibility for greater success.

A.5.2 Genetically modified plants to produce more oils

Duration of funding was not sufficient to explore both enhancing oilseed yield in brassicas and enhancing over expression of lipid biosynthesis. Research was focused on generation of transgenic rice that over expresses a regulatory gene in lipid metabolic pathway.

A.5.3 Develop ricin free castor

First steps of this research were realized. Methods of examining and deactivating ricin from expressed meal cake were achieved. Chronological developmental accumulation and localization of ricin, and native degradation of ricin have been characterized.

2.Methods and Results

Additional information can be found in Section I (Feedstocks) and I.2 (Characterization of oilseed crops). Recently, canola, sunflower, and a number of other oilseed crops have received consideration for biodiesel production in North America. For use in diesel engines, biodiesel is typically blended with fossil diesel fuel (2-30%), but it may also be used in pure form. Biodiesel is also used for heating.

Our goal was to develop agronomically, economically, and environmentally sustainable cropping systems for production of oilseed energy (biodiesel) crops in Mississippi. The long-term (5-year) objectives of this study were: (1) To screen varieties from several species of oilseed crops for the ecological conditions of Mississippi; (2) To compare extraction efficiency from various oilseed crops; (3) Economic evaluation of various cropping systems and recommendations to Mississippi growers.

A.5.1 Identify and culture southeast high oil content crops

A study was designed to evaluate several oilseed cultivars including: canola, oriental mustard (*Brassica juncea*), sunflower (*Helianthus annuus*), coriander (*Coriandrum sativum* L.), crambe (*Crambe abyssinica* Hochst), and camelina (*Camelina sativa* (L.) Crantz.) over two-year period as dual-use crops for Mississippi growers. Overall, our results indicated that sunflower,

winter canola, winter mustard and coriander can be successfully grown under Mississippi climatic and soil type conditions. Productivity of these crops was equal to or exceeded average yields reported in the literature. Canola and mustard can provide yields of 1100 L ha $^{-1}$ (about 120 gal ac $^{-1}$) or more of oil per year. Flax, crambe, and camelina did not perform very well in Mississippi. However, more research on seeding dates may prove feasibility of these crops.

Sunflower was investigated for the effects of fertilizer N rates of 0, 67, 134, and 202 kg ha^{-1}, and cultivar (DKF3875, DKF2990, DKF3510 and DKF3901) and their interaction on seed yield, oil content, and oil composition of sunflower grown at five sites in Mississippi (Newton, Starkville, Stoneville, and two sites in Verona: Verona site 1(silty clay loam soil) and Verona site 2 (sandy loam soil). Tested cultivars had dissimilar fatty acid composition. Oleic acid concentration in the original seed oil of the four cultivars DKF3875, DKF2990, DKF3510 and DKF3901 was 29, 26, 85 and 41%, respectively. Cultivar and fertilizer N rate differences were significant with respect to seed yields at Stoneville, Newton and Verona site 2, N rate was significant at Stoneville, and cultivar x N interaction was significant at Starkville and Verona site 1. At Stoneville, Newton, and Verona site 2, DKF3510 had the highest yields. DKF2990 provided lower yields in Stoneville and in Verona site 2. Seed oil concentration was higher in DKF3875 and DKF2990 (43-47%) and lower in DKF3510 and DKF3901 (40-44%) at Stoneville and Verona site 2. However, at Newton, oil concentration was highest in DKF2990, lower in DKF3510 and DKF3901 and lowest in DKF3875. Overall, increasing fertilizer N rates reduced seed oil content, but increased seed yields and subsequently oil yield per area. Relative to the concentration of oleic acid in the original seed used for planting, oleic acid increased in all locations and cultivars, with only one exception in one cultivar at one location. As expected, there was a corresponding decrease in the concentration of linoleic acid. Also, concentration of stearic acid decreased relative to the original seed. These results suggest that sunflower under the hot humid climate of Mississippi may accumulate a higher concentration of oleic acid (which may improve health benefits) and lower concentrations of linoleic and stearic acids. In most cases, fertilizer N rate, cultivar, or N x cultivar interaction resulted in altered concentration of other fatty acids (palmitic, arachidic, gondoic, behenic, and lignoceric) in sunflower oil. Oil yields varied between 483 and 1388 L ha^{-1} and calculated biodiesel oil per area was 386 to 1,110 L ha^{-1} (41 to 119 gal ac^{-1}) with the different treatments and locations. Sunflower can be a viable crop in most parts of Mississippi for production of cooking oil or biodiesel. Further research is needed on sunflower management practices and on the possibility of double cropping of oilseeds in southeastern US.

A.5.2 Genetically modified plants to produce more oils

Project 1

We proposed genetically modification of rice straw (*Oryza sativa*) cell wall so that we can cost effectively process the cellulose biomass into bio-fuel while maintaining high grain yield production in agriculture. It has been shown that high moisture in straw and thus slow burning rate is the primary obstacle in direct syngas production from rice straw. To resolve the problem, we have generated transgenic rice that over expresses a regulatory gene in lipid metabolic pathway. The expression of this gene is expected to reduce the moisture of straw and facilitate burning of straws. Although the moisture of straw remains to be tested in the transgenic rice, we find that the per-thousand grain weight increased about 15% in the transgenic rice and the plants appeared to be healthier. Our research probably opens a new approach to increase both seed yield and biofuel production.

A.5.2 Genetically modified plants to produce more oils

Project 2

The goal of our project is to use *Arabidopsis thaliana* as a model organism to screen for genes with the potential of improving the seed yield and quality of canola (rape seed). *Arabidopsis thaliana* and canola are within the same mustard/crucifer family. The close relationship makes it possible to apply the research results obtained in *Arabidopsis* to canola.

We have identified two multiple branch mutants (*mub1* and *mub2*). These mutants have over two folds of more branches and produce 1 to 2.5 folds more seeds per plants. In addition, these plants are slightly shorter and occupy less space to grow. Therefore, genes whose mutation caused the phenotype should have great potential in improving seed yield and plant structure of mustard plants. Because these two mutants are recessive mutants, our plan was to clone these two genes in *Arabidopsis* and canola and knockout the homologous genes in canola.

We have cloned these two genes in *Arabidopsis*. One of the genes is a transcription factor and the other gene is a peptidase. While, we were cloning the homologous genes in Canola, the funding got terminated. We were unable to continue this project. Therefore, we have not got the results published.

Our studies in *Arabidopsis* have proven that a single gene can result in substantial improvement in seed yield and plant architecture. There is a great potential of using *Arabidopsis* as a model organism to identify genes critical to seed yield improvement.

Development of environmentally friendly lipids extraction techniques.

This effort represents the first application of COSMO-RS for the prediction of the solubility of complex biological molecules in a supercritical fluid. This work provides a basis for predictive screening of supercritical solvent mixtures and identification of operating conditions suitable for economical recovery of phospholipids from a complex matrix. The extremely high cost of phospholipids of high purity motivates the use of computational methods to perform preliminary optimization of experimental conditions best suited for phospholipids recovery. Experiments to determine the solubility of phospholipids can then be focused on those conditions that are most likely to result in greater recovery of these biological molecules from a complex matrix.

Introduction

The use of supercritical fluids for extraction of phospholipids from biomass, in particular from waste sewage sludge, has the potential to provide an additional feedstock for biodiesel production. One of the challenges in developing a competitive, economical recovery process using supercritical fluids is the identification of optimal temperature and pressure for the recovery operation. Use of a predictive model can provide a means to narrow the scope of conditions (temperature and pressure) as well as supercritical solvent composition that are examined experimentally. One essential physical property for the prediction of a component's solubility in a supercritical fluid is the vapor pressure of the pure component. For most common chemicals, the vapor pressure data are available in the literature. However, for phospholipids, these data are not readily available and would be prohibitively expensive due to the cost and limited availability of purified compounds. What are available for these phospholipids of interest are their chemical structures.

The use of chemical structure as a means to predict physical and transport properties as well as physicochemical properties has been the subject of intense research in recent years. Physical and transport properties examined include vapor pressure,[i] melting point and density[ii], as well as viscosity, surface tension and thermal conductivity.[iii] Physicochemical properties examined include the octanol-water partition coefficient,[iv,v] aqueous solubility,[vi,vii,viii] soil-sorption coefficient,[ix] and Henry's law constant.[x] A recently developed approach by Klamt[xi] provides for *a priori* predictions of thermophysical data for chemical systems. Based on the "Conductor-like Screening for Real Solvents", COSMO-RS has a strong quantum chemical and statistical thermodynamics basis, that allows a physically meaningful description of the interactions between molecules in a solution. It has been employed for prediction of pure component physical properties, physicochemical properties including aqueous solubility,[xii] soil sorption coefficients,[xiii], gas solubilities and partition coefficients,[xiv] as well as phase equilibrium for binary mixtures.[xv,xvi,xvii]

In this project, prediction of the solubility of select phospholipids in supercritical solvents of differing compositions was undertaken. This effort combined the use of chemical structure for estimation of essential physical properties of the phospholipids with the use of COSMO-RS for the prediction of pure component vapor pressure of phospholipids and solubilities of phospholipids in solvents. A computational tool for estimation of solubility in supercritical fluids was developed. A key component of this project was validation of the computational approach. To this end, literature solubility data for fatty acids, fatty acid methyl esters and fatty acid ethyl esters in conventional solvents, and where available, in supercritical solvents, were used to validate the computational approach.

A comprehensive search of the literature provided solubility data for fatty acids, fatty acid methyl esters and fatty acid ethyl esters in a variety of conventional solvents, including water, ethanol, methanol, hexane, toluene, DMSO, chloroform). Limited data were identified for fatty acid solubility in supercritical fluids. TURBOMOLE computations were undertaken for each of the compounds listed in Table 1.

Table 1. Compounds Used for Validation of Approach

Fatty Acids	Fatty Acid Methyl Esters	Fatty Acid Ethyl Esters
Azelaic Acid		
Lauric Acid	Methyl Laurate	Ethyl Laurate
Linoleic Acid	Methyl Linoleate	Ethyl Linoleate
Myristic Acid	Methyl Myristate	Ethyl Myristate
Oleic Acid	Methyl Oleate	Ethyl Oleate
Palmitic Acid	Methyl Palmitate	Ethyl Palmitate
Pelargonic Acid	Methyl Pelargonate	
Stearic Acid	Methyl Stearate	Ethyl Stearate

For the majority of these compounds, necessary physical property data were available. Necessary physical property data included: melting temperature, latent heat of fusion, boiling temperature, critical temperature and pressure, and vapor pressure. To validate group contribution approaches for estimation of any or all of these physical properties, suitable methods were identified in the literature and used for prediction. A comparison of experimental data and predictions was used to identify those predictive methods that would be employed for the phospholipids.

Solubility of each compound in a variety of conventional solvents was computed using COSMOTHERM. These predictions were performed as a function of temperature, and compared with available literature data. When literature solubility data were available for a compound in a supercritical fluid, predictions of solubility were undertaken and compared with the experimental measurements. This approach of comparison with experimental data, whenever possible, provided validation of the computational scheme employed for solubilities in conventional solvents, as well as in supercritical fluids.

Initially, three model phospholipids compounds were identified in consultation with Dr. Earl Alley. These were distearoyl phosphatidylcholine (CAS# 816-94-4) dipalmitoyl phosphatidylcholine (CAS #63-89-8) and dipalmitoyl phosphatidylethanolamine (CAS # 5681-36-7). These were chosen so that subtleties associated with differences in the attached acyl groups (palmitoyl versus stearoyl) and in the group attached to the phosphate head group (choline versus ethanolamine) could be elucidated. Later three additional phospholipids were identified: 1,2-Dipalmitoyl-sn-glycero-3-phosphoethanolamine (DPPE; CAS # 923-61-5); 1,2-

Distearoyl-sn-glycero-3-phosphoethanolamine (DSPE; CAS # 1069-79-0) and 1,2-Dioleoyl-sn-Glycero-3-phosphocholine (DOPC; CAS # 56648-95-4). Structures were obtained for each of these compounds, and prepared for input to TURBOMOLE (V5.9). TURBOMOLE computations for the electron density distribution for these compounds were completed.

Results from the TURBOMOLE computations were used as input to COSMOTHERM V01.06. Additional predictions of the latent heat of fusion, critical properties, and the vapor pressure of each compound were completed. Solubilities of each of the phospholipids in conventional solvents (water, chloroform, DMSO, ethanol, methanol and toluene) were completed. Solubilities in supercritical carbon dioxide and supercritical carbon dioxide/methanol mixtures were also completed.

A.5.3 Develop ricin-free castor

Castor is a full-season summer crop which would compete for cotton, corn, and soybean acres. The percentage oil in its seed (55-60%) makes it hard to ignore as a potential oil feedstock crop. Mean yields of 2200 kg ha^{-1} (1100+ kg oil ha^{-1}) of castor seed were achieved at locations north of Starkville. Presence of ricin in the extracted meal raises substantial safety concerns. Side studies have been conducted to evaluate ricin accumulation and catabolism. Evaluation by Western blot indicated that, contrary to published accounts, ricin is not in all parts of the castor plant. We were never able to detect ricin in any plant part (except seed). Also, ricin cannot be detected in the developing seed until 28 days post pollination. Peak accumulation was reached at 40 days post-pollination. Upon planting the seed (or otherwise simulating germination) ricin degrades. Ricin is not detectable 10 days after the onset of germination (when the plant emerges from the ground). This information coupled with chemical and heat denaturation work on castor meal will make safer handling of castor seed possible.

For projects involving computer modeling, provide the following information:

a. Model description, key assumptions, version, source and intended use
   - TURBOMOLE, V5.9 – available from COSMOLOGIC – performs quantum mechanical DFT computations
   - COSMOTHERM V 01.06 – available from COSMOLOGIC – based on 'Conductor-like Screening Model for Real Solvents'.

b. Performance criteria for the model related to the intended use
   Detailed in summary of work

c. Test results do demonstrate the model performance criteria were met (e.g., code verification/validation, sensitivity analyses, history matching with lab or field date, as appropriate
   Detailed in summary of work

d. Theory behind the model, expressed in non-mathematical terms

e. Mathematics to be used, including formulas and calculation methods

f. Whether or not the theory and mathematical algorithms were peer reviewed, and, if so, include a summary of theoretical strengths and weaknesses
   TURBOMOLE and COSMOTHERM are extensively peer reviewed

g. Hardware requirements
   - Nextcom Computing, LLC., Next Dimension Next Demand-II Computer System – high end graphics work station, featuring dual processing capabilities

h. Documentation (e.g., users guide, model code).

References

[1] Basak, S.C., Mills, D., *J. Chem. Inf. Comput. Sci.*, 41, 692-701, (2001).
[1] Trohalaki, S., Pachter, R., Drake, G.W., Hawkins, T., *Energy & Fuels*, 19, 279-284, (2005).
[1] Kauffman, G.W., Jurs, P.C., *J. Chem. Inf. Comput. Sci.*, 41, 408-418, (2001).

[1] Marrero, J., Gani, R., *Ind. Eng. Chem. Res.*, 41, 6623-6633, (2002).
[1] Derawi, S.O., Kontogeorgis, G.M., Stenby, E.H., *Ind. Eng. Chem. Res.*, 40, 434-443, (2001).
[1] McElroy, N.R., Jurs, P.C., *J. Chem. Inf. Comput. Sci.*, 41, 1237-1247, (2001).
[1] Ran, Y., Jain, N., Yalkowsky, S.H., *J. Chem. Inf. Comput. Sci.*, 41, 1208-1217, (2001).
[1] Liu, R., So, S.S., *J. Chem. Inf. Comput. Sci.*, 41, 1622-1639, (2001).
[1] Delgado, E.J., Alderete, J.B., Jana, G.A., *J. Chem. Inf. Comput. Sci.*, 43, 1928-1932, (2003).
[1] English, N.J., Carroll, D.G., *J. Chem. Inf. Comput. Sci.*, 41, 1150-1161, (2001).
[1] Klamt, A., Eckert, F., *Fluid Phase Equilibria*, 172, 43-72, (2000).
[1] Klamt, A., Eckert, F., Hornig, M., Beck, M.E., Burger, T., *J. Computational Chemistry*, 23(2), 275-281, (2002).
[1] Klamt, A., Eckert, F., Diedenhofen, M., *Environmental Toxicology and Chemistry*, 21, 2562-2566, (2004).
[1] Maassen, S., Arlt, W., Klamt, A., *Chemie-Ingenieur-Technik*, 67(4), 476-479, (1995).
[1] Eckert, F., Klamt, A., *Ind. Eng. Chem. Res.*, 40, 2371-2378, (2001).
[1] Putnam, R., Taylor, R., Klamt, A., Eckert, F., Schiller, M., *Ind. Eng. Chem. Res.*, 42, 3635-3641, (2003).
[1] Constantinescu, D., Klamt, A., Geana, D., *Fluid Phase Equilibria*, 231, 231-238, (2005).

Task A.6 - Solubility of Phospholipids in Supercritical CO_2

1. Summary

Supercritical carbon dioxide extraction of lipids and phospholipids from sewage sludge was investigated and accomplished in this project. The solubility of lipids and phospholipids in supercritical carbon dioxide is dependent on temperature, pressure and the co-solvent concentration. Methanol was employed as co-solvent in this work. Fractionation of lipids and phospholipids from sewage sludge was accomplished using a two-step supercritical extraction process. This process first employed neat supercritical carbon dioxide to extract lipids from the sewage sludge, and then employed using supercritical carbon dioxide with co-solvent methanol to extract phospholipids from sewage sludge. This two-step approach provides a technically viable mechanism to fractionate these entities during recovery from sewage sludge for further processing and treatment. Significant cost reductions in biodiesel production cost are anticipated if this widely available resource (sewage sludge) can used as feedstock for biodiesel production. Such a two-step recovery method also provides the means by which valuable byproducts such as the omega-3 fatty acids, eicosapentaenoic acid (EPA) and docosahexaenoic acid (DHA), can be recovered simultaneously.

Sewage sludge and model compounds (soybean lecithin, 2-Distearoyl-sn-Glycero-3-Phosphatidylcholine ($C_{44}H_{88}NO_8P$; abbreviated as DSPC) and 1,2-Dioleoyl-*sn*-Glycero-3-Phosphocholine ($C_{44}H_{84}NO_8P$, abbreviated as DOPC)) were extracted with neat supercritical carbon dioxide and with supercritical carbon dioxide/methanol co-solvent. The solubility of two phospholipid model compounds in the supercritical fluid(s) was determined experimentally.

2. Introduction

Phospholipids are complex molecules consisting phosphorous in the polar head group and one or two aliphatic chains. They are ubiquitous to living organisms and serve as the main component of cell membranes in these organisms. A cell membrane is comprised of two layers of phospholipid molecules, which together are known as the phospholipid bilayer. This bilayer forms because the phospholipid molecules have unique character at either end of the molecule. One end of the molecule is hydrophilic due to phosphorous polar head group and the other end is hydrophobic due to the non-polar hydrocarbon tail. The function of the phospholipid bilayer is to separate the cell interior from its environment.

Carbon dioxide is the supercritical fluid of choice in many applications due to the relatively mild conditions required to induce the supercritical fluid state (temperature of 304.2 K, slightly above room temperature; and pressure of 73.8 atm). Another advantage of supercritical carbon dioxide extraction is the ease of separation between supercritical solvent and solute upon expansion back to atmospheric pressure; the solute either condenses or precipitates in neat form, with essentially no contamination of the carbon dioxide solvent. However, it is well known that supercritical carbon dioxide is a poor solvent for polar constituents. Addition of a polar compound as a modifier to the carbon dioxide serves to improve the ability of the supercritical fluid mixture to solvate polar species, such as phospholipids. Suitable polar compounds to serve in this modifier, or co-solvent, role are methanol (critical temperature of 512.6 K, critical pressure of 79.9 atm) and ethanol (critical temperature of 513.9 K, critical pressure of 60.7 atm).

Sludge generated in wastewater treatment facilities consists of a variety of microorganisms. The main components of microorganism membranes are phospholipids such as phosphatidylcholine and phosphosphatidylethanolamine. Research on lipid and phospholipids solubility in supercritical carbon dioxide allows evaluation of the use of supercritical fluid extraction as a means to recover lipids and phospholipids from primary sludge and secondary sludge.

3. Experimental

Materials. Freeze-dried waste secondary sewage sludge collected from a municipal wastewater treatment plant located in Tuscaloosa, AL was used in two step supercritical carbon dioxide extraction process to recover lipids and phospholipids. Commercially available soybean lecithin (A mixture consisting phosphatidylcholine (PC), phosphosphatidylethanolamine (PE), phosphatidylinositol (PI), phosphatidic acid (PA), phosphatidylserine (PS), triglycerides, carbohydrates, sphingolipids) from Fisher Scientific, 1,2-Distearoyl-sn-Glycero-3-Phosphatidylcholine ($C_{44}H_{88}NO_8P$) (DSPC) (Figure 1) and 1,2-Dioleoyl-*sn*-Glycero-3-Phosphocholine ($C_{44}H_{84}NO_8P$) (DOPC) (Figure 2) from Avanti Polar Lipids, Inc. were used as model compounds to study the solubility of these species in supercritical CO_2. Methanol (HPLC grade) was obtained from Fisher Scientific. Carbon dioxide (99.5% purity) and nitrogen (ultrahigh purity) were supplied by NexAir (Memphis, TN).

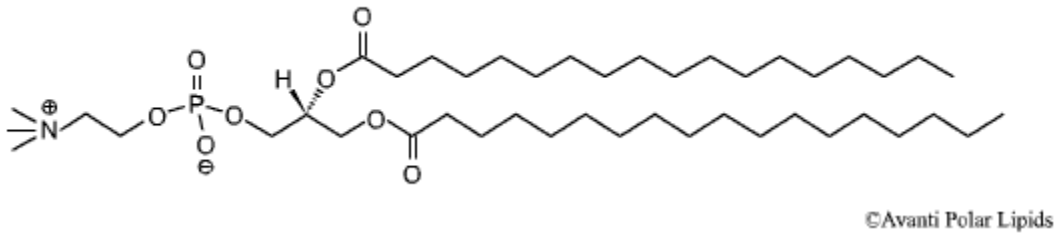


Figure 1. Structure of 1,2-Distearoyl-*sn*-Glycero-3-Phosphocholine (DSPC)

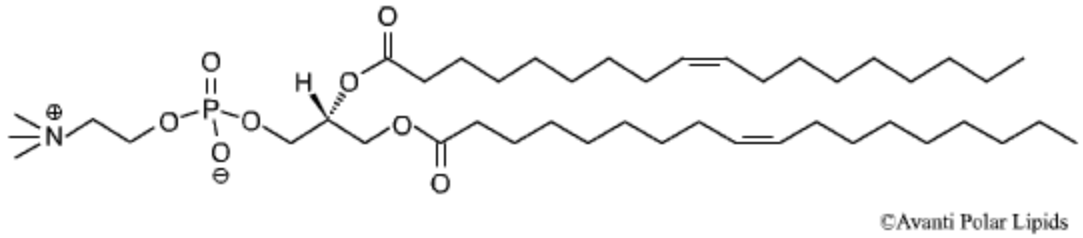
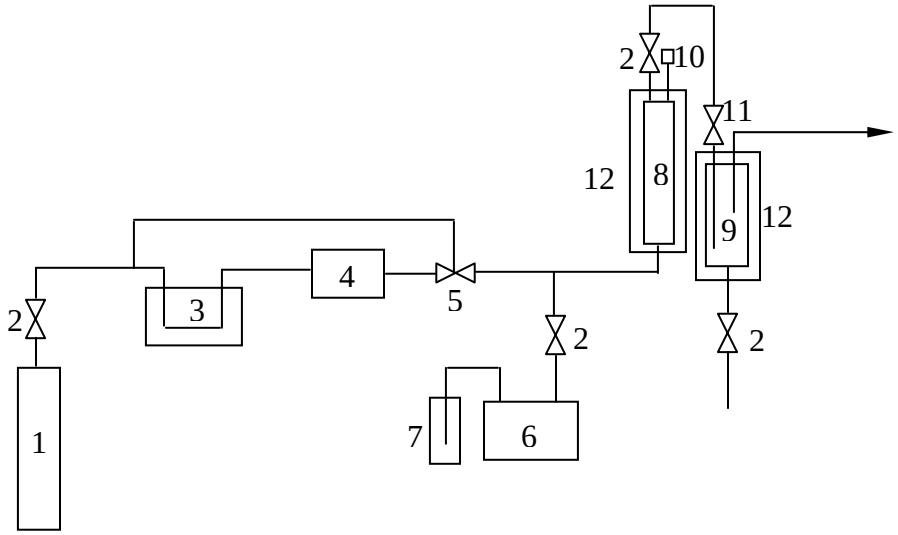


Figure 2. Structure of 1,2-Dioleoyl-*sn*-Glycero-3-Phosphocholine (DOPC)

Procedure. The extraction and solubility experiments were carried out in a SFE-100 unit from Thar Technologies (Figure 3). A dynamic technique was used to determine the solubility of model compounds in supercritical carbon dioxide (SC-CO_2).



1- CO_2 tank	5- pressure regulator	9- cyclone
2- valve	6- methanol pump	10- rupture disc
3- cooler	7- methanol reservoir	11- depressurization valve
4- CO_2 pump	8- extractor	12- temperature controller

Figure 3. Flow diagram of the supercritical fluid extraction unit.

Analytical methods. The lipids contained in the product extract were converted to fatty acid methyl esters (FAMEs) by acid catalysis using a modified version of Christie's method. A 20 mg lipid sample was dissolved in 1 ml hexane containing 1,3-dichlorobenzene as the internal standard in a test tube. 2ml of 1% sulfuric acid in methanol solution was added the test tube. The tube was closed and incubated at 50 °C overnight. 5 ml of 5% sodium chloride in water solution was then added to the mixture. The FAMEs were extracted with 5 ml hexane twice. The obtained hexane extracts were combined, washed with 4 ml 2% potassium bicarbonate in water solution and oven dried over anhydrous sodium sulfate. The FAME samples were analyzed on a Supelco capillary column (SP 2380, 100m $\times$ 0.25 mm $\times$ 0.2 μm) with stabilized poly(90%

biscyanopropyl/10%cyanopropylphenyl siloxane as the stationary phase. The column was installed in a 6890N gas chromatograph (Agilent) equipped with a flame ionization detector. The column was temperature programmed from 110 °C to 140 °C at 10 °C/min and was maintained at 140 °C for 4 min, then ramped from 140 °C to 240 °C at 2 °C/min and was maintained at 240 °C for 40 min. The detector temperature was 260 °C. The carrier gas was helium (40.24 psi) at a flow rate of 45.0 ml/min; the sample size was 1 μl with a split ratio of 100:1. Peaks were identified by comparing the relative retention time of each peak with those of standard fatty acid methyl esters.

Fourier Transform Infrared Spectroscopy (FTIR)-attenuated total reflectance (ATR) measurements were conducted on a Perkin Elmer instrument at room temperature over the wavenumber range of 4000-600 cm^{-1} with 4 cm^{-1} spectral resolution by averaging 32 scans. The reference background was collect in the absence of any sample.

Solution H^1 NMR spectra were obtained on a Bruker AMX-300 spectrometer using $CDCl_3$ as solvent with tetramethylsilane (TMS) as internal reference.

Phosphorus analysis using a wavelength of 470 nm on UV-VIS Perkin-Elmer machine was used to qualitatively analysis lipids and phospholipids in the extract.

4. Discussion of Results

Freeze-dried secondary sludge

Figure 4 shows the total amount of oil extracted from sequential supercritical CO_2 extraction of freeze-dried secondary sludge as a function of the mass of CO_2 used. The extraction rate was fastest at the beginning of the supercritical extraction process. As more CO_2 passed through the extractor, more oil was extracted from the freeze-dried secondary sludge. The extraction rate decreased as the amount of oil left in the freeze-dried secondary sludge decreased. After the passage of ~ 3000 g of CO_2, the majority of the oil had been removed from the freeze-dried secondary sludge. This de-oiled freeze-dried secondary sludge was left in the extractor. Subsequently, five additional supercritical CO_2 extractions were performed which employed 5, 10 and 15 wt% methanol co-solvent.

Figure 5 shows the amount of extract from supercritical CO_2 extraction from de-oiled freeze-dried secondary sludge with 5, 10 and 15 wt% methanol as co-solvent, respectively. The mass of extract is for total individual extraction. The mass of extract increased monotonically as more CO_2 passed through the extractor. Due to the polarity of methanol, both phospholipids and polar lipids were extracted when methanol was present as co-solvent. Thus, the yield of supercritical CO_2 extraction can be enhanced by increasing the polarity of the supercritical fluid. Also, the mass of extract increased as the weight percentage of methanol increased in the supercritical carbon dioxide/methanol mixture. The observed increase was greater for the runs with 5 wt% and 10 wt% than the observed increase for the runs with 10 wt% and 15 wt%.

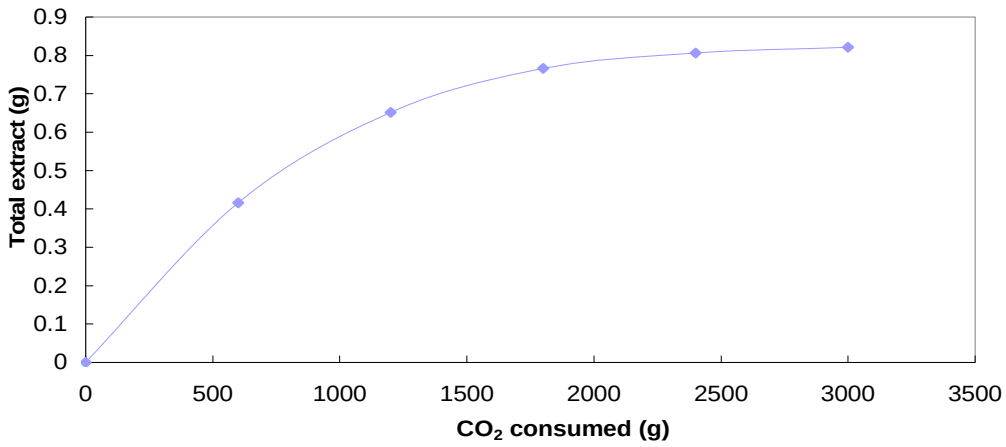


Figure 4. Total oil extracted as a function of CO_2 consumed for freeze-dried secondary sludge at P=200 bar, T=40 ºC, CO_2 flow rate=20 g/min

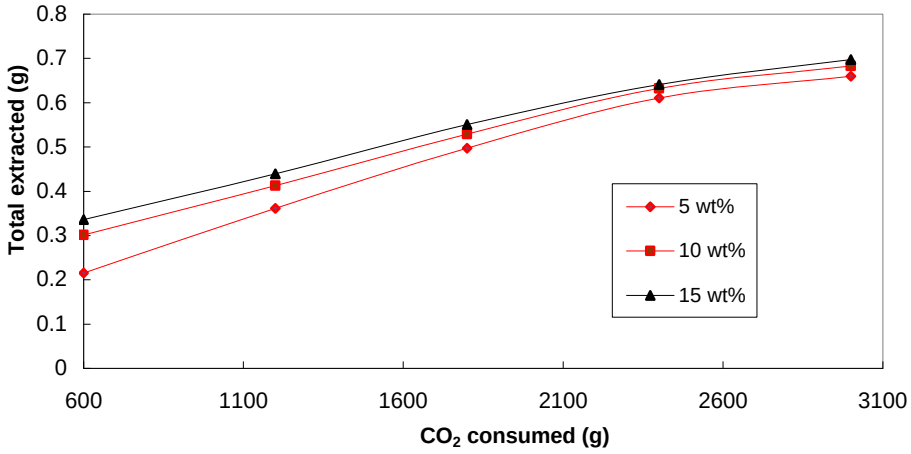


Figure 5. Amount of oil and phospholipids extracted from supercritical CO_2 extraction of de-oiled freeze-dried secondary sludge as a function of CO_2 consumed with 5 wt% methanol as co-solvent (P=200 bar, T=40 ºC, CO_2 flow rate=20g/min).

Phosphorus analysis using a wavelength of 470 nm on UV-VIS Perkin-Elmer machine was used to qualitatively analysis phosphorus and phospholipids in the extract. Tables 1 - 3 show the weight and percentage of phosphorus and phospholipids in each extract. The weight and percentage of phospholipids are calculated by assuming phosphatidylcholine (C18:1n,

$C_{42}H_{82}NO_8P$, MW=760) accounted for the majority of the phospholipids. As shown in Tables 1 - 3, phospholipids were not extracted by neat supercritical CO_2. Thus, phospholipids are not soluble in neat CO_2 due to their polar nature. Different amounts of phosphorus were extracted in extracts from experiments M1-5 to M5-5, M1-10 to M5-10, and M1-15 to M5-15. The weight percentage of phosphorus in the extract increased as the extraction was taking place and then decreased. The higher percentage of methanol in the solvent/co-solvent mixture was more effective in extraction of phospholipids from sludge, especially when the concentration of methanol increased from 5 wt% to 10 wt%.

Table 1. Weight of phosphorus and phospholipids in each extraction (5 wt% of methanol as co-solvent after pure CO_2 extraction).

	1-5	2-5	3-5	4-5	5-5	M1-5	M2-5	M3-5	M4-5	M5-5
phosphorus mg	0	0	0	0		2.2	1.8	1.6	0.6	0.3
phosphorus wt%	0	0	0	0		1.02	1.23	1.18	0.53	0.60
phospholipids g	0	0	0	0		0.048	0.039	0.035	0.013	0.007
phospholipids wt%	0	0	0	0		22.19	26.77	25.55	11.53	13.11

1-5, 2-5, 3-5, 4-5 and 5-5 are the five sequential extractions with pure CO_2
M1-5, M2-5, M3-5, M4-5 and M5-5 are the five sequential extractions with 5 wt% methanol as co-solvent

Table 2. Weight of phosphorus and phospholipids in each extraction (10 wt% of methanol as co-solvent after pure CO_2 extraction).

	1-10	2-10	3-10	4-10	5-10	M1-10	M2-10	M3-10	M4-10	M5-10
phosphorus mg	0	0	0	0		3.1	2.1	1.7	0.7	0.3
phosphorus wt%	0	0	0	0		1.03	1.89	1.45	0.68	0.59
phospholipids g	0	0	0	0		0.0673	0.0456	0.0369	0.0152	0.007
phospholipids wt%	0	0	0	0		22.34	41.08	31.55	14.76	12.80

1-10, 2-10, 3-10, 4-10 and 5-10 are the five sequential extractions with pure CO_2
M1-10, M2-10, M3-10, M4-10 and M5-10 are the five sequential extractions with 10 wt% methanol as co-solvent

Table 3. Weight of phosphorus and phospholipids in each extraction (15 wt% of methanol as co-solvent after pure CO_2 extraction).

	1-15	2-15	3-15	4-15	5-15	M1-15	M2-15	M3-15	M4-15	M5-15
phosphorus mg	0	0	0	0		3.5	2.3	1.7	0.8	0.4
phosphorus wt%	0	0	0	0		1.04	2.23	1.52	0.88	0.71
phospholipids g	0	0	0	0		0.0673	0.0499	0.0369	0.0174	0.009
phospholipids wt%	0	0	0	0		22.61	48.49	33.11	19.15	15.51

1-15, 2-15, 3-15, 4-15 and 5-15 are the five sequential extractions with pure CO_2
M1-15, M2-15, M3-15, M4-15 and M5-15 are the five sequential extractions with 15 wt% methanol as co-solvent

Soybean lecithin

Figure 6 shows the total amount of oil extracted from sequential supercritical CO_2 extraction of soybean lecithin as a function of the mass of CO_2 used. The extraction rate was fastest at the beginning of supercritical extraction. As more CO_2 passed through the extractor, more oil was extracted from soybean lecithin. The extraction rate decreased as the amount of oil left in soybean lecithin decreased. After the passage of ~ 4500 g of CO_2, the majority of the oil had been removed from the soybean lecithin. De-oiled soybean lecithin was left in the extractor for subsequent treatment with supercritical CO_2 containing methanol as co-solvent.

Figure 7 shows the amount of extract from supercritical CO_2 extraction from de-oiled lecithin with methanol as co-solvent. The mass of extract contained in the figure is for each individual extraction. The mass of extract increased as the weight percentage of methanol used as co-solvent increased. The mass of the last extract from sequential supercritical CO_2 extraction of soybean lecithin was 0.01344 g (Figure 6). However, the mass of extract from the de-oiled soybean lecithin with 5 wt% of methanol as co-solvent was 0.193 g. This increase in the extract mass must due to extraction of phospholipids in addition to a small amount of oil from the de-oiled soybean lecithin. The amount of phospholipids extracted increased as the mass fraction of methanol in supercritical CO_2 extraction increased. This is due to the polarity of phospholipids and the presence of the polar co-solvent, methanol. Thus, the yield of supercritical CO_2 extraction can be increased by increasing the polarity of the supercritical fluid.

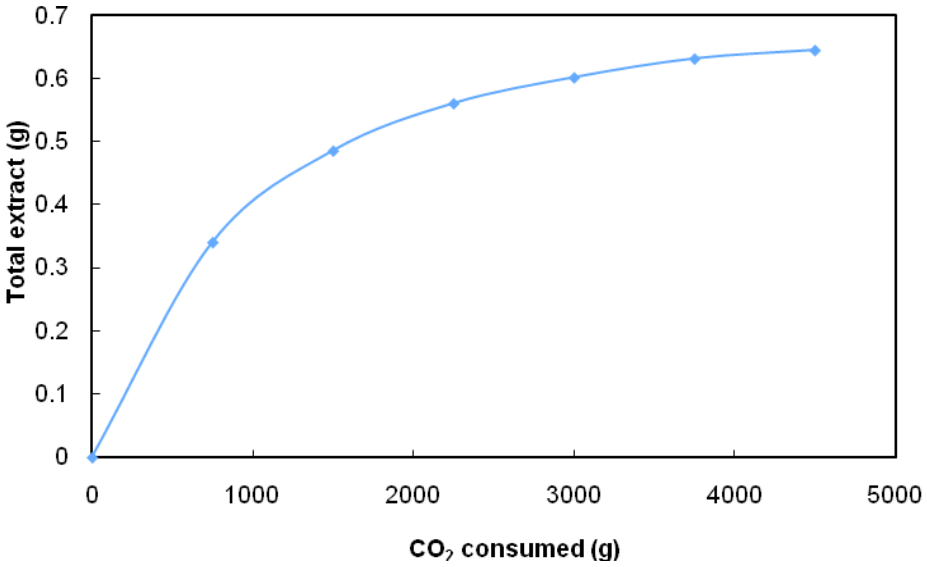


Figure 6. Total oil extracted as a function of CO_2 consumed for soybean lecithin at P=200 bar, T=30 ºC, CO_2 flow rate=25 g/min

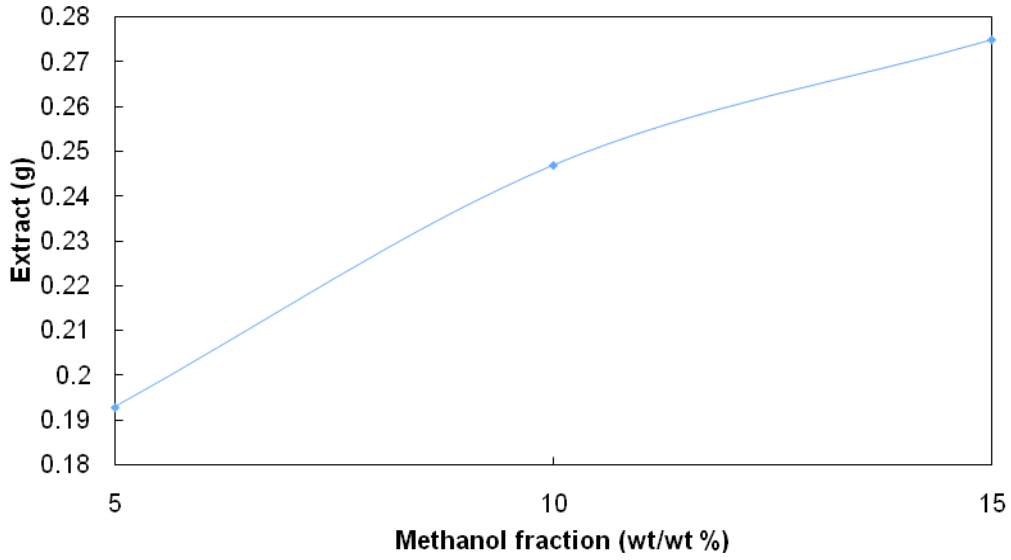


Figure 7. Amount of oil and phospholipids extracted from supercritical CO_2 extraction of de-oiled soybean lecithin as a function of methanol mass fraction in the supercritical fluid phase (P=200 bar, T=30 ºC, CO_2 flow rate=25g/min).

The fatty acid composition from GC-FID for the raw soybean lecithin, first extracted neat carbon dioxide, then extracted with 5, 10 and 15 wt% methanol as co-solvent is shown in Figure 8. Saturated vs. unsaturated fatty acid composition from GC-FID for the raw soybean lecithin, first extracted with neat carbon dioxide, then extracted with 5, 10 and 15 wt% methanol as co-

solvent is shown in Figure 9. The various triglycerides and phospholipids that make up soybean lecithin contain both saturated and unsaturated fatty acids ranging in carbon number from 16 to 18. One of the objectives of this study was to find out how the fatty acid composition changed as a function of mass fraction of methanol used as co-solvent for the supercritical CO_2 extraction. The fatty acids from the first extractions from soybean lecithin using neat CO_2 were mainly composites of C18:1, while those extracts obtained by supercritical CO_2 extraction with methanol as co-solvent contained a higher percentage of C18:2. The mole percentage of C18:2 increased as the mass fraction of methanol in supercritical CO_2 extraction increased. Oil enriched in C18:1 fatty acid was more readily extracted with neat supercritical CO_2. Normally, the solubility decreased with increasing carbon number or molecular weight. The presence of a double bond in C18:1 decreases the melting point of the compound considerably. This results in greater solubility in supercritical carbon dioxide of compounds with C18:1 compared to the solubility of compounds with C16:0. Since the extracts of supercritical CO_2 extraction with methanol as co-solvent are mainly phospholipids, the fatty acids in phospholipids in mainly C18:2. Also, the unsaturated and monounsaturated fatty acids decreased as the mass fraction of methanol in supercritical CO_2 increased.

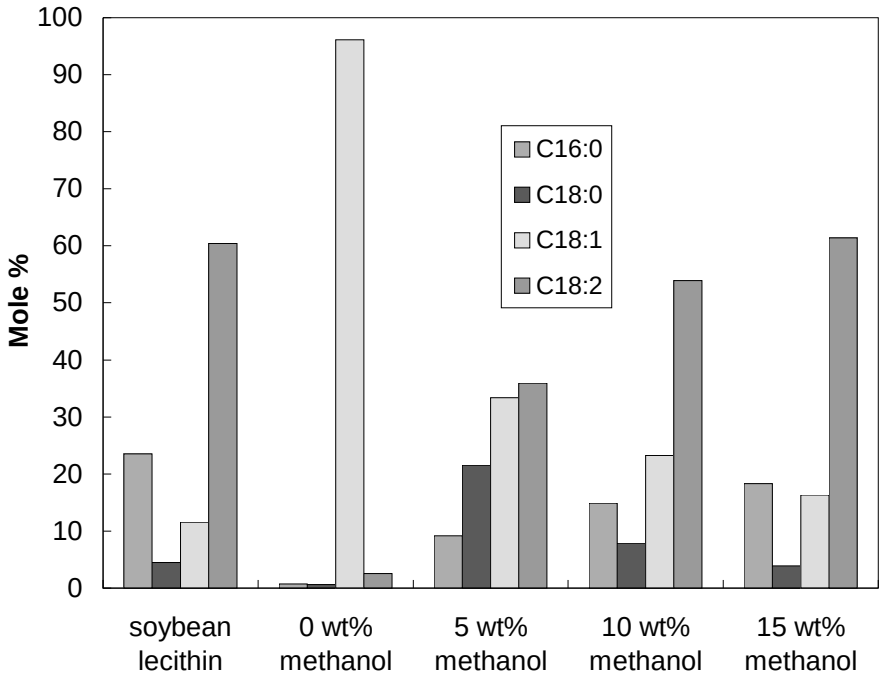


Figure 8. Fatty acid composition from GC-FID for the raw soybean lecithin, first extract without methanol as co-solvent and the extract with 5, 10 and 15 wt% methanol as co-solvent.

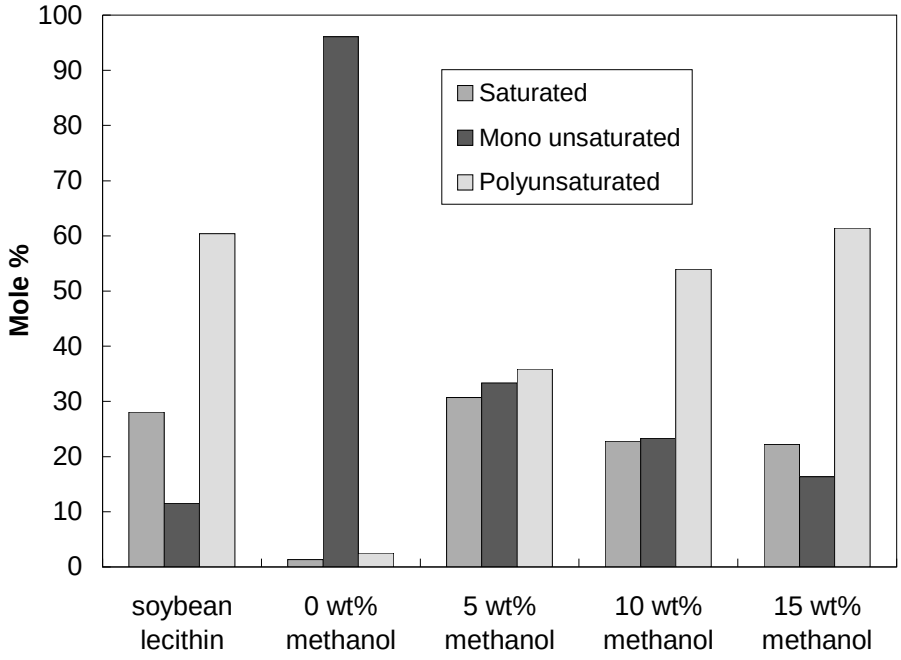


Figure 9. Saturated vs. unsaturated fatty acid composition from GC-FID for the raw soybean lecithin, first extract without methanol as co-solvent and the extract with 5, 10 and 15 wt% methanol as co-solvent.

FTIR spectra of the first extract, obtained without methanol as co-solvent, and the extracts from runs with 5, 10 and 15 wt% methanol as co-solvent, respectively, are shown in Figure 10. Long chain fatty acids have bands between 2960 and 2850 cm^{-1} due to the asymmetric C-H stretching of methyl (2960 cm^{-1}, shoulder) and methylene (2925 cm^{-1}) groups, and symmetric C-H stretching of methylene (2850 cm^{-1}) groups of the hydrocarbon chain. The unsaturated carbon-hydrogen bond exhibits a weak band at 3000 cm^{-1} (=C-H). The medium intensity bands at 1459 and 722 cm^{-1} are due to the CH_2 scissoring deformation and rocking vibration, respectively. Phospholipids in extract with 5, 10 and 15 wt% of methanol as co-solvent exhibit a strong band at 1025 cm^{-1} due to the aliphatic P-O-C vibration of phosphate group. They also exhibit medium PO_2 vibration at 971 cm^{-1}. These bands are absent in the FTIR spectrum of the first extract without methanol as co-solvent. Thus, no phospholipids are extracted by pure supercritical CO_2 without methanol as co-solvent.

H^1 NMR spectra of the raw soybean lecithin first extract were obtained without methanol as co-solvent, and the extract obtained with 5, 10 and 15 wt% methanol as co-solvent. The chemical shift of the terminal methyl group fatty acid hydrocarbon chain was found at 0.85-0.89 ppm. The methylene groups of the hydrocarbon chain was found at 1.25-1.29 ppm for all the extract H^1 NMR spectra. The NMR spectra of extracts with methanol as co-solvent exhibit signals of the $-N(CH_3)_3$ from phosphatidylcholine (PC) at 3.3-3.4 ppm and $–NH_3$ from phosphatidylethanolamine (PE) at 3.1 ppm. These chemical shifts were absent in the NRM spectrum of the first extract, obtained without methanol as co-solvent. Thus, H^1 NMR spectrum further confirms that no phospholipids were extracted by pure supercritical CO_2 without methanol as co-solvent. The area ratios of the peaks of $-N(CH_3)_3$ from PC at 3.3-3.4 ppm and $–NH_3$ from PE at 3.1 ppm over that of the methylene peak from extracts with methanol as co-

solvent are all higher than those observed for raw soybean lecithin. Therefore, the extracts with methanol as co-solvent were enriched in phospholipids. Moreover, the area ratios of the peaks of -N(CH_3)$_3$ from PC at 3.3-3.4 ppm over that of –NH_3 from PE at 3.1 ppm from extracts with methanol as co-solvent were different. The extract with 5 wt% of methanol as co-solvent was enriched in PC, the extract with 10 wt% of methanol as co-solvent was enriched in both PC and PE, and that with 15 wt% of methanol as co-solvent was enriched in PE. PC was more readily extracted by supercritical CO_2 with methanol as co-solvent than PE. The solubility difference of PC and PE may be due to lower estimated cohesive energy density of PC than that of PE.

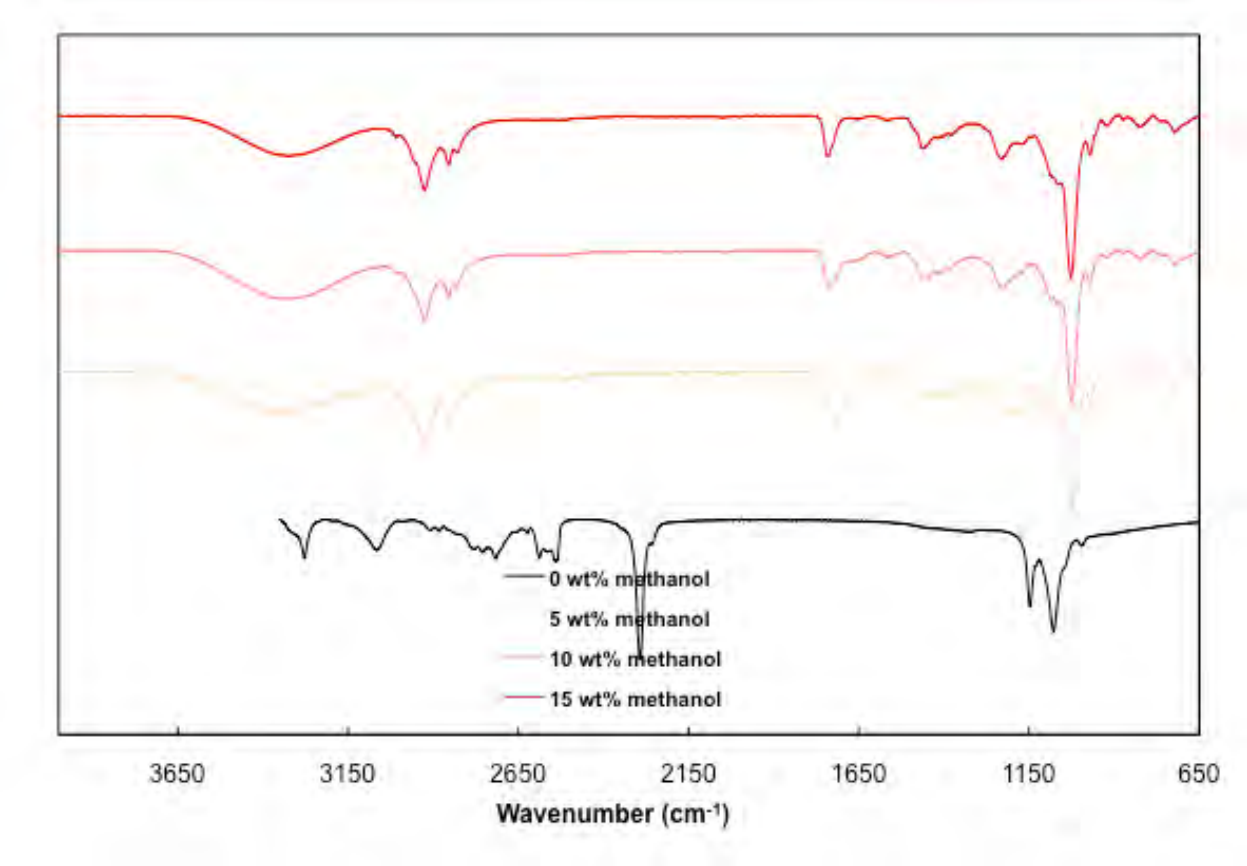


Figure 10. FTIR spectra of first extract without methanol as co-solvent and the extract with 5, 10 and 15 wt% methanol as co-solvent.

Model compounds DSPC and DOPC

Experimental conditions were established using literature data for the critical point of methanol/carbon dioxide mixtures (Liu et al., 2003). These data are shown in Figure 12 for completeness. For a 5 mole % methanol/95 mole % carbon dioxide mixture, the critical temperature for the mixture was estimated to be ~ 320 K and the critical pressure to be ~ 9 MPa. Two temperatures were selected (323.15 K and 333.15 K) and a series of four pressures, ranging from 12 MPa to 30 MPa, were employed. Measurements were conducted for each combination of temperature and pressure, using neat supercritical carbon dioxide, and using a carbon dioxide/5 mole % methanol mixture.

Two series of experiments were conducted: one series employing neat supercritical carbon dioxide; one series employing a 5 mole % methanol/95 mole % carbon dioxide mixture. When neat supercritical carbon dioxide was employed as the supercritical fluid, no measurable

amount of either model compound (DSPC and DOPC) was present in the mixture removed from the cyclone separator and then subjected to solvent evaporation in the TurboVap.

When supercritical CO_2 with 5 mol% methanol as cosolvent was employed as the supercritical fluid, the results shown in Table 4 were obtained. For each 30 minute interval, the mass of model phospholipid was measured, and the appropriate molecular weight, the mole fraction of the phospholipid in the supercritical fluid phase was calculated. For DSPC, the molecular weight is 790.16 g/gmol; for DOPC, the molecular weight is 786.15 g/gmol.

The addition of methanol as a co-solvent resulted in the supercritical fluid mixture being better able to solubilize the polar phospholipid compounds. The solubility of DSPC and of DOPC in the carbon dioxide/methanol supercritical fluid mixture is shown in Figures 13 and 14, respectively. The solubility was found to increase with increasing pressure for each experimental temperature examined for either compound. The solubility of DOPC at any temperature/pressure combination was greater than the solubility of DSPC at the same conditions. This was due to the presence of two double bonds in the structure of DOPC. The presence of the double bonds usually will lower the melting point of the compound comparing to that of compound with similar structure.

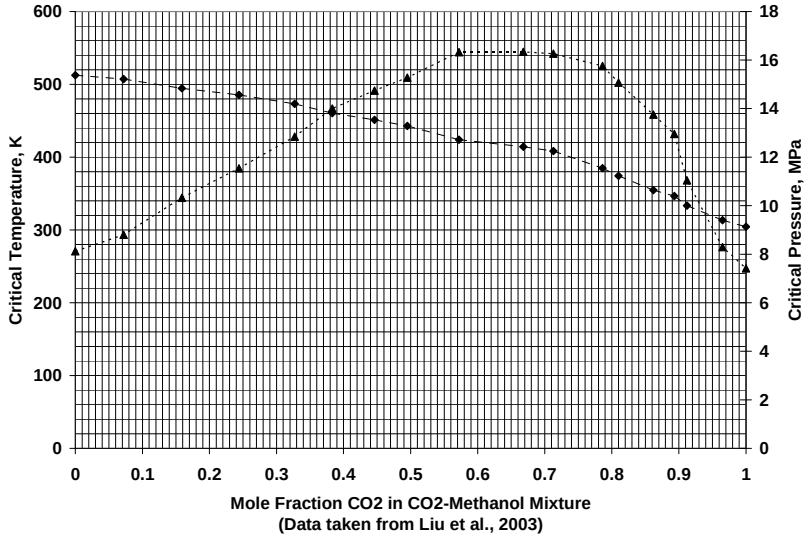


Figure 12. Critical Temperature and Critical Pressure for Methanol/Carbon Dioxide Mixtures (Liu et al., 2003).

Table 4. DSPC and DOPC solubility in supercritical CO_2 with 5 mol% methanol as cosolvent (mole fraction)

Temperature T/K	Pressure P/MPa	Phospholipid Solubility, $y_{phospholipid}$	
		DSPC	DOPC
323.15	12	0.2258×10^{-6}	0.3794×10^{-6}
323.15	15	1.418×10^{-6}	2.332×10^{-6}
323.15	20	2.477×10^{-6}	2.782×10^{-6}
323.15	30	3.053×10^{-6}	3.355×10^{-6}
333.15	12	0.1111×10^{-6}	0.1933×10^{-6}
333.15	15	0.5054×10^{-6}	1.402×10^{-6}
333.15	20	1.596×10^{-6}	2.789×10^{-6}
333.15	30	3.820×10^{-6}	4.290×10^{-6}

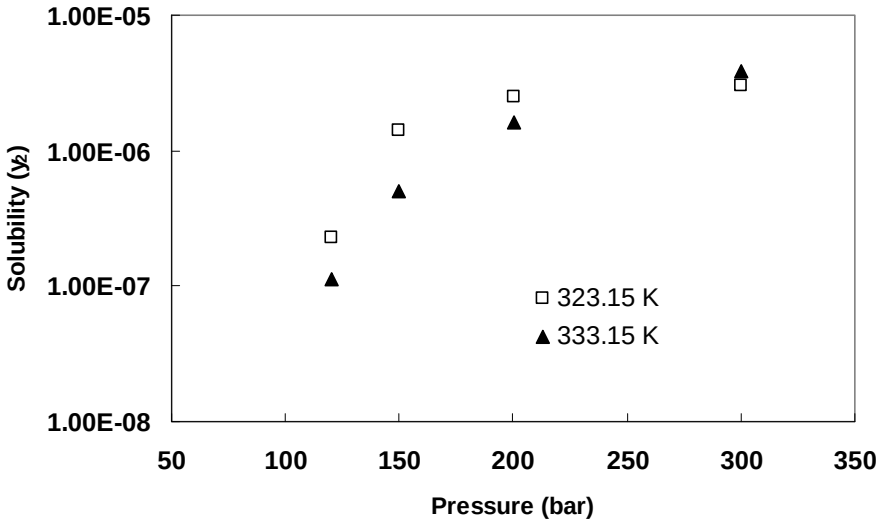


Figure 13. Model compound DSPC solubility in in supercritical CO_2 with 5 mol% methanol as cosolvent.

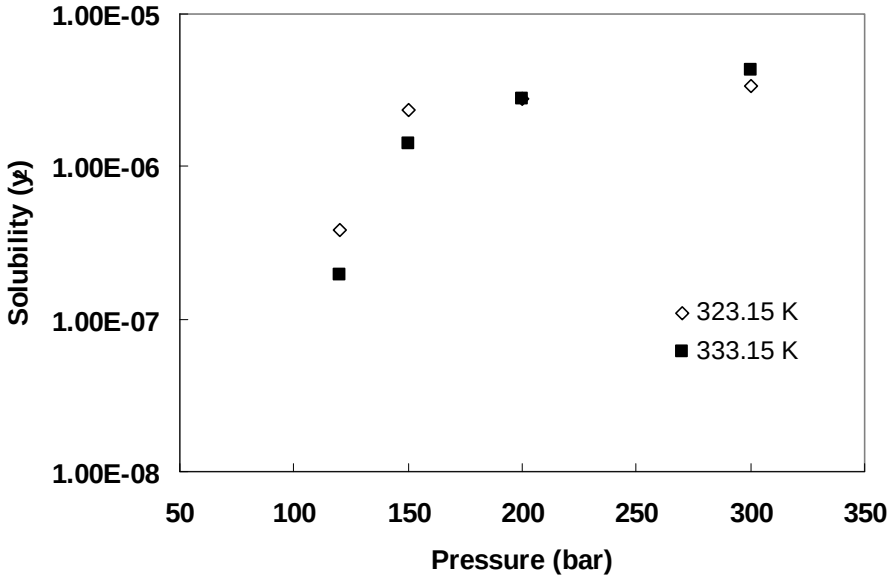


Figure 14. Model compound DOPC solubility in supercritical CO_2 with 5 mol% methanol as cosolvent.

Conclusion

No phospholipids were extracted from freeze-dried secondary sludge when neat supercritical carbon dioxide was employed and the oil exteaction rate from freeze-dried secondary sludge decreased due to decreased oil in the sludge as the extraction continued. The fatty acid composition in each extract was different. C16 and C18 fatty acids comprised the majority of fatty acids identified. Also, different amounts of phosphorus were extracted in each extract when methanol was used as co-solvent.

Similar to the behavior of freeze-dried secondary sludge, there were no phospholipids extracted from soybean lecithin when only neat supercritical carbon dioxide was employed. C16 and C18 were the majority fatty acids in soybean lecithin. The extracts enriched in different amounts of PE and PC were obtained when different concentrations of methanol was used as co-solvent.

The solubility of model compounds, DSPC and DOPC, in supercritical carbon dioxide with 5 mole % methanol as co-solvent, was studied experimentally. Experiments with neat supercritical carbon dioxide indicate that DSPC and DOPC are not soluble (at detectable levels) at either temperature examined (323.15 K and 333.15 K) over the pressure range examined (12 MPa to 30 MPa). The solubility of both DSPC and DOPC were greatly enhanced by adding 5 mol% methanol as cosolvent.

Task A.7. Examine the effect of extraction techniques on oil stability.

2. Methods

Various antioxidants and levels on various biodiesels were evaluated to devise the best ones to prevent oxidation. These were the nonnatural antioxidants, since the natural antioxidants like tocopherol and ascorbic/erythorbic acid did not have much effect on delaying oxidation as per the indution point test.

2. Results and Conclusions

Comparison of extraction process on yield and characteristics of plant and animal lipid:
Hexane was the best extraction process for biodiesel stability
Stability test for feedstocks and biodiesel:
The Rancimat test proved to be effective, when conducted with precautions.
Development of a process for catfish derived biodiesel comparing various catfish oil feeds:
The best oil source is a non-heated source as a byproduct of an organic feed manufacturer
Compare stability tests for lipids and biodiesel:
Accelerated stability test for biodiesel
Conducting tests at 80 ^{o}C results in good predictability of stability of oils and biodiesel
Screen antioxidants for oil and biodiesel stability:
TBHQ at 800 ppm was the best antioxidant/concentration for biodiesel stability, with over 6 months at normal conditions in MS.
Compare accelerated vs. normal stability tests:
The accelerated stability test proved more reliable than normal conditions test (normal aging).

Task A.8. Research on Reaction Kinetics of Soybean Oil Transesterification Using Heterogeneous Metal Oxide Catalysts.

1. Introduction

Biodiesel is generally produced by the transesterification of a triglyceride (vegetable oil, animal fat etc.) with alcohol in the presence of a catalyst (basic, acidic, enzymatic etc). The products are fatty acid alkyl esters (biodiesel) and glycerol. The stoichiometric reaction requires 1 mol of a triglyceride and 3 moles of alcohol. However, excess alcohol is used in order to drive the reaction forward (since the transesterification is a reversible reaction) to increase the yields of the alkyl esters and to allow phase separation from the glycerol formed. Figure 11 depicts a generalized reaction for the transesterification reaction.

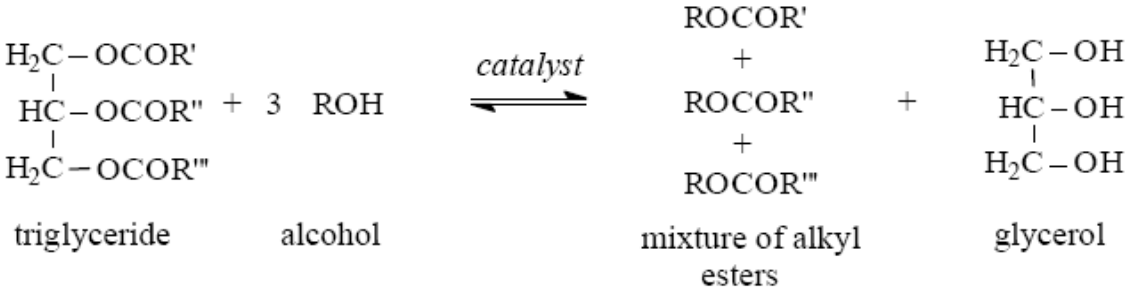


Figure 11. Transesterification of soybean oil into biodiesel.

In transesterification, the selection of catalyst depends on the amount of free fatty acid present in the source oil. When the free fatty acid content is less than approximately 1% , an alkali catalyzed reaction is preferred due to better conversion rates. For higher amounts of free fatty acid content, acid catalyzed esterification followed by transesterification is better suited. Conventionally homogeneous catalysts (like NaOH, KOH etc.) are used for the transesterification. However, there are drawbacks associated with homogeneously catalyzed processes. The catalyst dissolves fully in the glycerin layer and partially in the FAME layer. As a

result, biodiesel should be cleaned through a slow, tedious and environmentally unfriendly water washing process. Catalyst contaminated glycerin has little value in today's market and is increasingly becoming a disposal issue. Another negative aspect of the homogeneously catalyzed process is that the catalysts are not re-usable. Heterogeneous catalysts, on the other hand, makes product separation easier and makes catalysts re-usable. Also, heterogeneous catalysts have the potential to simplify the production process by enabling usage of continuous packed bed reactors.

In most of the solid catalyzed experiments, the reaction proceeded at a relatively slow rate [43]. The presence of heterogeneous catalysts makes the reaction mixture a three-phase system, oil-methanol-catalyst, which for mass transfer reasons, protracts the reaction. At the same time, heterogeneous catalysis requires relatively harsher reaction conditions, i.e., high pressures and high temperatures. For example, some experiments have been carried out at temperatures as low as 78 K and as high as 1000 K and high pressures, with high pressure and temperature favoring better conversion [44]. The overall goal of this study was to identify a heterogeneous oxide catalyst that gives satisfactory FAME yields at intermediate conditions compared to above.

Biodiesel Production Using Solid Catalysts

There have been several studies on the transesterification of vegetable oils using heterogeneous catalysts. In one study, rapeseed oil was transesterified by methanol using basic alkaline-earth metal compounds: calcium oxide, calcium methoxide and barium hydroxide [43]. It was found that these were effective in the transesterification reaction and the reaction rate could be enhanced by ultrasound as well as by introducing an appropriate reagent into a reactor to promote methanol solubility in the triglyceride [43].

Biodiesel from jatropha curcas oil was produced with a heterogeneous solid super base catalyst, calcium oxide [45]. The results showed that the base strength, $pK_{B,}$ of calcium oxide was more than 26.5 after calcination, following immersion in an ammonium carbonate solution. Optimization of reaction conditions were studied for the transesterification of jatropha curcas oil. It was found that under the optimum conditions for catalyst calcinations, i.e. a temperature of 900°C, reaction temperature of 70°C, reaction time of 2.5 h, catalyst loading of 1.5%, and a methanol/oil molar ratio of 9, the oil conversion was 93%. However, a different study [46] concluded that using calcium oxide calcined in air only resulted in a 10% methyl esters yield after 4h. The catalyst samples were prepared by calcination of the precipitated calcium carbonate at 900°C in the prescribed atmosphere, an ambient air or helium gas flow. Calcination in a helium gas flow markedly intensified the activity of calcium oxide yielding acceptable ester yields in 2 h.

In a different study, biodiesel was produced by transesterification of soybean oil with methanol using ZnO loaded with KF as a solid base catalyst [47]. The catalyst with 15% KF loading and calcined at 873°K showed the best activity. The results also showed that the activity of the catalysts correlated with their basicity. The transesterification of soybean oil using alumina loaded with potassium iodide (35% w/w) as a solid base catalyst [48] showed that after calcination at 773 K for 3 h, the catalyst gave the highest basicity and the best catalytic selectivity for this reaction. The conversion was found to be 96% under the optimum reaction conditions. In other work, a heterogeneous base catalyst, $Na/NaOH/\gamma\text{-}Al_2O_3$, showed comparable results to a homogenously catalyzed NaOH process [49]. Although screening studies have been carried out on potential heterogeneous catalysts, the kinetics of the heterogeneously catalyzed process has not yet been analyzed in depth. This study is an attempt to fill this gap in knowledge to a selected group of solid oxide catalysts.

Reaction Kinetics of Transesterification Reaction

Although the importance of biodiesel as an alternative fuel has grown during the last twenty years, the chemical kinetics of transesterification, very important for process design, remain controversial. Kinetics describes the rate of chemical reactions. Rate equations are typically written in terms of the concentration of the reactants. In the past, it has been observed that the base catalyzed transesterification is a second order reaction [50]. This has been confirmed in a different work for the transesterification of soybean oil with methanol using sodium hydroxide a homogeneous catalyst [51]. In this work, it was assumed that transesterification is a three-step, reversible process, and the reaction rate constants and activation energies were determined for all the forward and reverse reactions.

In a different work, the rate constants and the reaction order were determined for each of the steps in the presence of a catalyst with a computerized kinetics program [52]. It was found that the forward reactions appear to be pseudo-1st order or 2nd order depending upon conditions used. Reverse reactions appeared to be 2nd order. At a MeOH/oil molar ratio of 6:1, a shunt reaction was observed. Activation energies were determined for all forward and reverse reactions under a variety of experimental conditions for plots of log k vs. $1/T$ (where k = rate constant and T =temperature)**.**

In the present work, the fatty acid methyl esters yields from the transesterification of soybean oil with methanol in the presence of different solid catalysts were determined. The reaction kinetics (rate constant and reaction order) of the transesterification reactions was proposed.

2. Materials and Methods

Reagents

Solvent-extracted degummed soybean oil donated by Bungi Corporation Marks, MS, USA, was used as the triglyceride. The basic catalysts (PbO, MgO, MnO_2, BaO & CaO) and methanol (99.9 %) used in the study was purchased from Fisher Scientific, USA.

Equipment

The transesterification was carried in a fully automated high-pressure high-temperature batch reactor (PARR Instrument, 4843). The equipment consists of a high pressure cylindrical chamber, a heater, a water line (in order to control the temperature) and a stirrer.

Soybean oil and Methanol solution

A mixture of 30 mL methanol and 100 mL of soybean oil and 2 g of solid catalyst was used in each experimental unit.

Transesterification

Two different methods of transesterification were followed. For the first three catalysts, (PbO, MgO & MnO_2), the mixture (oil, methanol and catalyst) was first heated to 215°C (it was found that there was a very little conversion of 3 to 4% in the ramping period). Then the reaction was carried out for 2 hours in the high-pressure reactor. Samples were taken out in 15-minute intervals and the fatty acid methyl esters yield was measured with gas chromatography. For the last two catalysts, (CaO, BaO), it was observed that significant conversions took place during the first few minutes of the reaction (46% and 20% respectively) while ramping up the temperature to 215°C. Accordingly, the method was changed for these two, in this case the oil was first heated with the catalyst to 215°C, then 30 mL of methanol was injected using a HPLC pump at a flow rate of 10 mL/min for 3 minutes. Then the experiments were carried out for the next 14 minutes at a sampling interval of 2 minutes. The product (a mixture of fatty acid methyl esters and glycerol) was separated and then was transferred to a freezer before being sent for gas chromatography (GC) analysis.

Gas Chromatography Analysis

The top layer of each sample, after stabilization, was analyzed for FAME composition at the Mississippi State Chemical Laboratory, Mississippi State University, with gas chromatography.

Determination of Reaction Kinetics

The transesterification reaction is a reversible reaction and therefore, excess methanol is used to drive the reaction forward. Equation 1 shows the generalized transesterification reaction, where A is the triglyceride, B is methanol, C is FAME and D is glycerol. The equation also shows the stoichiometric relationship between the reactants and the products.

$$A + 3\,B \Leftrightarrow C + D \tag{1}$$

The general rate equation for the Equation 1 will be,

$$-\frac{\mathrm{d}C_A}{\mathrm{d}t} = kC_A{}^{\alpha}C_B{}^{\beta} \tag{2}$$

Where,

$-\frac{\mathrm{d}C_A}{\mathrm{d}t}$ = the consumption of reactant A per unit time

k = rate constant

C_A = concentration of A after time t

C_B = concentration of B after time t

α = reaction order of reactant A

β = reaction order of reactant B

Also,

$$C_A = C_{A0}(1 - X) \tag{3}$$

$$C_B = C_{A0}(\theta_B - 3X) \tag{4}$$

$$\theta_B = C_{B0} / C_{A0} \tag{5}$$

Where,

C_{A0} = initial concentration of A

C_{B0} = initial concentration of B

X = conversion

θ_B = the ratio of C_{B0} to C_{A0}

Equation 2 can be written as

$$\frac{\mathrm{d}\,X}{\mathrm{d}\,t} = kC_{A0}^{(\alpha+\beta-1)}(1-X)^{\alpha}(\theta_B - 3X)^{\beta} \qquad (6)$$

In the present work, 8 different cases were analyzed in order to get the reaction order. These case were,

$(\alpha=0,\ \beta=0)$; $(\alpha=1,\ \beta=0)$; $(\alpha=0,\ \beta=1)$; $(\alpha=1,\ \beta=1)$; $(\alpha=2,\ \beta=0)$; $(\alpha=0,\ \beta=2)$; $(\alpha=2,\ \beta=1)$; $(\alpha=1,\ \beta=2)$.

For each case, definite integrals of Equation 6 were calculated from a conversion of X=0 to a conversion of X=X in the time span of t = 0 to t = t. Then the calculated equation for each case was transferred into a linier equation passing through origin (*y=mx*). The transferred equations for all the 8 cases are as follows:

Case 1: $(\alpha=0,\ \beta=0)$

$$C_{A0}X = kt \qquad (7)$$

Case 2: $(\alpha=1,\ \beta=0)$

$$\ln\left(\frac{1}{1-X}\right) = kt \qquad (8)$$

Case 3: $(\alpha=0,\ \beta=1)$

$$-\frac{1}{3}\left[\ln\frac{(\theta_B - 3X)}{\theta_B}\right] = kt \qquad (9)$$

Case 4: $(\alpha=1,\ \beta=1)$

$$\frac{1}{(\theta_B - 3)}\ln\left[\frac{(\theta_B - 3X)}{(1-X)\theta_B}\right] = kC_{A0}t \qquad (10)$$

Case 5: $(\alpha=2,\ \beta=0)$

$$\frac{X}{(1-X)} = kC_{A0}t \qquad (11)$$

Case 6: (α =0, β =2)

$$\frac{X}{(\theta_B - 3X)\theta_B} = kC_{A0}t \qquad (12)$$

Case 7: (α =2, β =1)

$$\frac{1}{(\theta_B - 3)}\{\frac{X}{(1-X)} - \frac{3}{(\theta_B - 3)}\ln[\frac{(\theta_B - 3X)}{(1-X)\theta_B}]\} = kC_{A0}{}^2t \qquad (13)$$

Case 8: (α =1, β =2)

$$\frac{1}{(3-\theta_B)}\{\frac{3X}{(\theta_B - 3X)\theta_B} - \frac{1}{(3-\theta_B)}\ln[\frac{(1-X)\theta_B}{(\theta_B - 3X)}]\} = kC_{A0}{}^2t \qquad (14)$$

For Equations 7 through 14, if it is assumed that the left side component is an ordinate (y variable) and *t* (for Eq. 7 to 9), $C_{A0}t$ (for Eq. 10 to 12) and $C_{A0}{}^2t$ (for Eq. 13 to 14) are abscissas (x variable) respectively, the equations are in the form of *y=mx* (a straight line passing through origin). For all 8 cases, the y variable was plotted against the corresponding x variable and the coefficient of determination was determined. In all the cases (Eq. 7 to 14), the slope of the straight line is the rate constant (k) for the reaction. The highest correlation coefficient (R^2) for each case was observed and the case that gave the highest correlation coefficient was used to determine the reaction order.

Determination of Surface Area of the Catalysts

Surface area is an attribute that is used by catalyst manufacturers and users to monitor the activity and stability of catalysts. There are different methods used to measure surface area, most methods are based on the isothermal adsorption of nitrogen. Either a single point or multipoint method can be used to calculate the surface area. In our case the multipoint Brunauer, Emmett and Teller (BET) method was used to measure total surface area of these metal oxides by the use of nitrogen adsorption/desorption isotherms at liquid nitrogen temperature and relative pressures (P/Po) ranging from 0.04-0.4.

3. Results

Biodiesel Yield

The biodiesel yield (FAME %) from gas chromatography analysis showed a large variation among different solid catalysts. Figure 12 shows the biodiesel yield (FAME) for all the catalysts, PbO, MgO, MnO_2, BaO and CaO, over 2 hours of transesterification. For PbO the yield was found to be more than 84% after 1 hour, for MgO the maximum yield was found to be approximately 66% after 2 hours and for MnO_2 the yield surpassed 80% after 2 hours.

For BaO and CaO, the biodiesel yield was found to be more than 95% and 75% within 15 and 30 minutes respectively. Cracking of the methyl esters was observed subsequent to these time periods. The initiation of reduction of methyl esters yield could be attributed to the pretense that the rate of cracking exceeded the rate of transesterification for BaO and CaO after

15 and 30 minutes respectively under the provided reaction conditions. As a result, only 2 data points for BaO and 3 data points for CaO were at hand to calculate the reaction order and rate constant - which was not sufficient (Figure 12). Consequently, in order to capture the trend, the method was modified for these two catalysts. The data was collected in 2 min intervals for 14 minutes after attaining a temperature of 215°C. It could be noted that according to Figure 13, the FAME yield for the BaO catalyst surpassed 85% after 14 minutes and for catalyst CaO, the yield was found to be approximately 78% after 2 minutes.

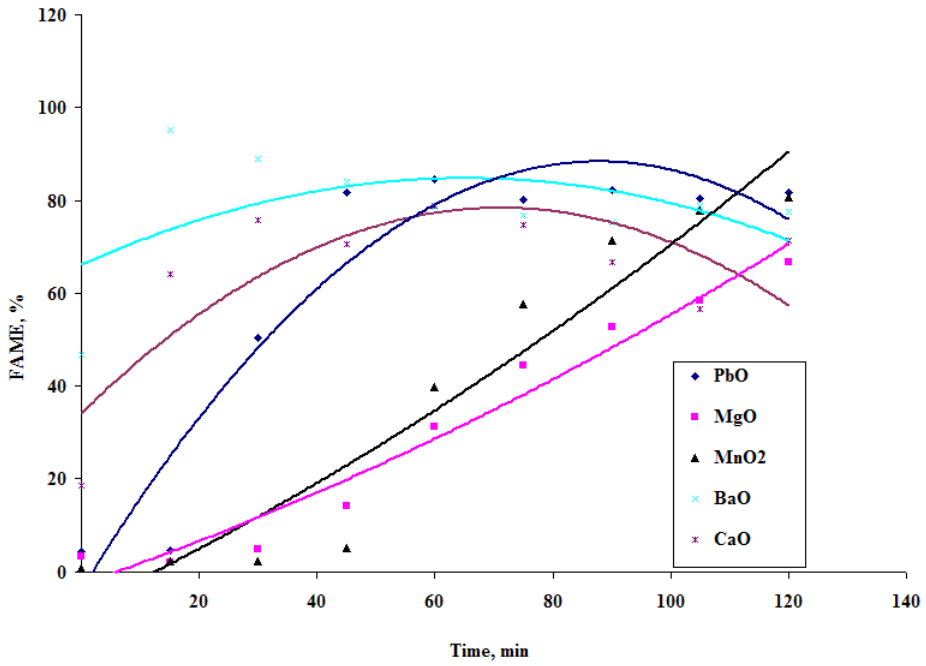


Figure 12. FAME Yield for PbO, MgO, MnO_2, BaO and CaO (reaction times denoted

represent time after reactants reached 215°C).

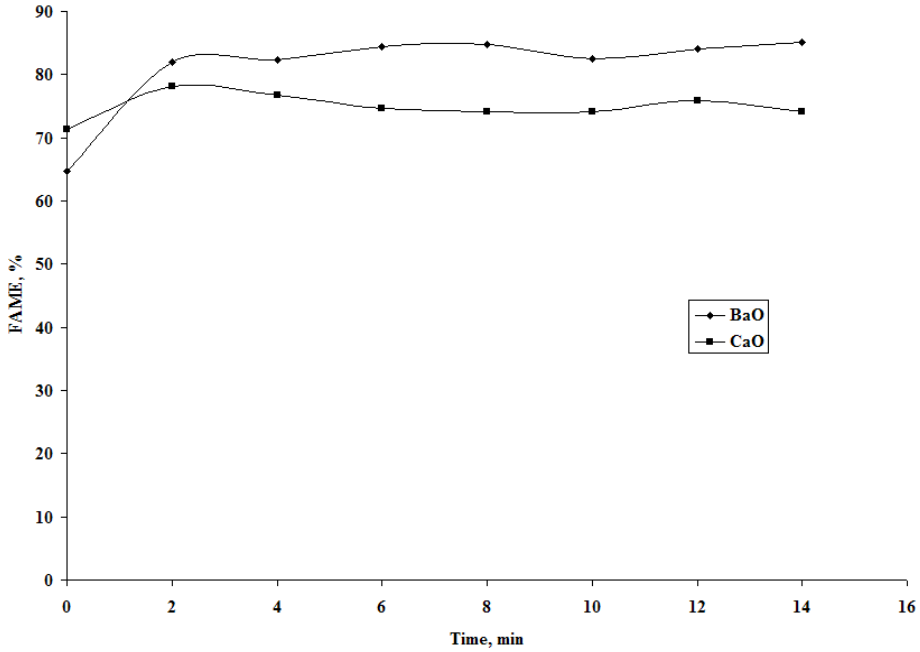


Figure 13. FAME Yield for BaO and CaO (reaction times denoted represent time after reactants reached 215°C).

Reaction Kinetics

Based on the principle discussed above, all eight cases for each catalyst were plotted and the coefficient of correlation (R^2) was determined for each case. Finally the case with the highest coefficient of correlation (R^2) was selected for the determination of rate constant and reaction order. Table 8 gives the R^2 values of all eight cases for each of the 5 catalysts.

For some experimental units, Table 8 renders an array of R^2 values because the data has been transferred in the form of $y=mx$ in order to model the reaction order based on Equation 7 to 14. For each catalyst, the highest R^2 value is selected out of the 8 cases and the corresponding values of slope were determined. Table 9 gives the reaction order of the transesterification w.r.t. each of the reactants, as well as the overall reaction order and the value of rate constant for each of the 5 catalysts.

Surface Area of the Catalysts

Table 10 shows the surface area of the catalysts based on the nitrogen adsorption /desorption method (multipoint BET), and it was found that MgO had the largest area of 157.4 m^2/g whereas the PbO had the minimum of 0.55 m^2/g.

4. Conclusions

The base catalyzed transesterification of soybean oil using solid catalysts produces biodiesel under high pressure and high temperature conditions. A maximum biodiesel yield of 85% was obtained by BaO in 14 minutes, whereas, PbO, MnO_2, CaO and MgO gave a maximum yields of 84%, 80%, 78% and 66% respectively at 215°C. The overall reaction order of PbO, MnO_2, BaO, CaO and MgO was found to be 1, 1, 3, 1 and 1 respectively. The highest rate constant was observed for BaO which was 0.0085 $g^2.mole^{-2}.min^{-1}$.

Table 8. The Value of Coefficient of Correlation (R^2) of All Eight Cases for Each Catalyst.

Catalysts → Cases ↓	PbO	MgO	MnO2	BaO	CaO
1	0.90	0.91	0.87	0.39	0.48
2	0.89	0.90	0.85	0.49	0.45
3	0.91	0.93	0.88	0.41	0.49
4	0.88	0.88	0.83	0.51	0.44
5	0.83	0.83	0.77	0.61	0.41
6	0.90	0.91	0.86	0.42	0.46
7	0.81	0.80	0.74	0.63	0.41
8	0.86	0.85	0.80	0.53	0.44

Table 9. Reaction Order of the Transesterification w.r.t. Each of the Reactant as well as Overall and the Rate Constant.

Catalyst	Order w.r.t. Triglyceride	Order w.r.t. Methanol	Overall Order	Rate Constant
PbO	0	1	1	0.0032, min^{-1}
MgO	0	1	1	0.0011, min^{-1}
MnO_2	0	1	1	0.0014, min^{-1}
BaO	2	1	3	0.0085, $g^2.mole^{-2}.min^{-}$
CaO	0	1	1	0.0046, min^{-1}

Table 10. Surface Area of the Metal Oxides

Catalyst	Surface area, m^2/g
PbO	0.55
MgO	157.4
MnO_2	50.55
BaO	0.76
CaO	61.39

Task A.9. Research on Exhaust Emissions Using Diesel-Biodiesel-Ethanol Blends in New and Used Compression Ignition Engines

1. Introduction

The current scenario of rapidly increasing energy demand across the world has led many countries to search for renewable fuel sources other than fossil fuels. Also, the heightened awareness of harmful effects associated with ambient air pollution compels introduction of more stringent environmental regulations worldwide. Beginning in 2007, the United States, heavy-duty diesel engine emission regulations will be phased in with a NO_x standard of 0.27 g/kW-hr (0.2 g/bhp-hr) and a particulate standard of 0.01 g/kW-hr (0.01 g/bhp-hr). In Europe, the 2005 European Union (EU) 4 standard is 3.5 g/kW-hr (2.6 g/bhp-hr) for NO_x and 0.2 g/kW-hr (0.15 g/bhp-hr) for particulate with a change (EU 5 standard) to 2 g/kW-hr (1.5 g/bhp-hr) for NO_x in 2008 [79,80].

Although discrepancies exist, there is a general agreement in the research community that biodiesel reduces particulates, emissions of CO, SO_2 and HC. However, it has been reported that biodiesel increases oxides of nitrogen (NO_x) emissions by as much as 10.3% for 100% biodiesel [81]. McCormick stated that newer engines increase NO_x emission in comparison to older engines, where the increase in the emissions level could be as high as 31% vs 10% [82]. NO_x emissions in a Detroit Diesel 2-stroke engine increased with the addition of methyl soyester while particulate emissions decreased [83]. Using a 1991 6V-92TA DDEC II engine, NO_x emissions were found to increase by 3.5%, 5.5%, 13.4% and 15% respectively for 10%, 20%, 30% and 40% blends. Graboski and coworkers tested methyl soyate and diesel blends in a 1991 Detroit Diesel Series 60 (4-stroke) engine. For 35% biodiesel, the composite NO_x emissions increased by nearly 1%, while the composite particulate emissions decreased by 26% relative to the reference diesel. For 100% biodiesel, the composite NO_x increased by 11% while PM was decreased by 66% [84]. Signer and coworkers reported a 3 to 4% increase in NO_x for a 3.5% increase in fuel density using the EEC 13-mode test cycle [85]. Cetane number and fuel aromatic content are well known to influence NO_x and PM emissions from diesel engines [86].

There are various effective engine direct-emission control methods used in the past, but they are still inadequate to guarantee meeting the proposed emissions reduction regulations. Some catalytic devices have been devised to purify the exhaust from engines. Due to additional cost, they are not practical nor do they prove satisfactory for engine manufacturers to meet the 2007 emission standards. Changing the fuel properties of biodiesel using different blends of oxygenates is another approach which is found to be economic and efficient in reduction of emissions [87-89]. This study, attempted to understand the effect of adding ethanol as an oxygenate into biodiesel on the tailpipe emissions profile. Ethanol has a much lower cetane number and energy value (26.98 MJ/kg) than biodiesel, yet, it has beneficial fuel properties. One of the disadvantages of biodiesel is its high cloud point, which makes it unsuitable for cold weather conditions. Ethanol tends to reduce the cloud point when blended with biodiesel [90,91].

Due to the low calorific value of ethanol, E-diesel blend is believed to reduce engine power. Interestingly, some studies have shown that not much variation is observed in brake horsepower, depending on blend concentrations. There was no significant power reduction in an engine operated on E-diesel blends up to 20% [92]. Abu-Qudais and group found an increase of 3.6% in brake thermal efficiency and 43.3%, 34%, and 32% reductions in CO, HC, and soot emissions, respectively at an optimum percentage of 15% E-diesel blends [93]. E-diesel yielded significant reductions in particulate matter (PM) [94,95]. Recent studies conducted on E-diesel confirmed substantial reductions in PM, at times up to 40%, depending on the test methods, operating conditions, and ethanol concentrations [96-100]. Marek and Evanoff also found reductions in NO_x emissions ranged from 0-5% and 0-4% for 15% and 10% ethanol blends respectively [98]. However, another engine test showed considerable variations in both PM and NO_x over the load-speed range of the engine with reductions varying 22-75% and 60-84% respectively. Ajiv and coworkers observed a reduction in the carbon monoxide (CO) and nitrogen oxides (NO_x) emissions when a 20% blend of E-diesel was used in a constant-speed stationary diesel engine as opposed to diesel fuel [101].

The major drawback of adding ethanol into diesel is its immiscibility in diesel over a wide range of temperatures. Additionally, the miscibility of ethanol in diesel depends on factors such as pressure, relative humidity, and ethanol concentration. Buchholz et al. reported that the limited solubility of ethanol in diesel fuel required either an emulsifier (Span 85) or co-solvent (*n*-butanol) to prepare ethanol-in-diesel blends [102]. Commercially, various surfactants are used as emulsifiers to form an ethanol-diesel emulsion. Ali and Hanna determined the ratio of beef tallow (methyl tallowate) to ethanol that gave the same viscosity as No. 2 diesel fuel [103]. They found that tallow ester:ethanol:diesel should be 16.25:8.75:75 to get a stable emulsion that had a viscosity similar to that of diesel fuel. Looking into the phase behavior of the biodiesel-ethanol-diesel ternary system, Fernando and Hanna suggested that biodiesel could be effectively used as an amphiphile in an ethanol-diesel blend [104]. Aforementioned work laid the foundation for investigating the concept of using ethanol to reduce NO_x emissions.
The objective of this study is to evaluate the effect of neat biodiesel and blends of diesel-biodiesel-ethanol (DBE) emulsions on exhaust gas emissions

2.Materials and Methods

Engine and Instrumentation

The study was performed using the following three engines: Ford 4000, John Deere 5103 and John Deere 4039DF008 multi-fuel engine. The Ford was a 45 year old engine with less than 200 hours run time and the two John Deere engines were brand new. Each of the engines was a direct injection type. Specifications of the engines are presented in Table 12. The engines were coupled to a hydraulic dynamometer. Engine torque was adjusted and set using the dynamometer. Engine speed was controlled using the throttle. A NOVA Logger II analytical gas analyzer was used to investigate the emissions from the engines.

Table 12. Engine Specifications.

Specification	Ford 4000	John Deere 5103	John Deere 4039DF008
No. of Cylinder	3	3	4
Bore, mm	111.75	106.5	106.5
Stroke, mm	111.76	110	110
Displacement, litre	3.294	2.9	3.9
Compression ratio	16.5:1	17.8:1	17.8:1
Rated HP	42.7	38	41
Rated speed	2200	2400	1800
Fuel Injection Pump	Distributor-type	Stanadyne K5	Stanadyne K5

Fuel Blends

The experiments were carried out using pure diesel, neat biodiesel, diesel-biodiesel (70:30) blend and three different DBE (Diesel-Biodiesel-Ethanol) blends in proportions of 70:25:5 (D70BD25E5), 70:20:10 (D70BD20E10) and 70:15:15 (D70BD15E15) respectively. The fuel properties tests such as flash point, kinematic viscosity, cloud point, carbon residue, copper corrosion, calorific value, density, cetane number, acid number and Reid vapor pressure of each fuel combination were performed. Specific blend compositions and their properties are given in Table 13.

The methyl soy ester employed was a commercially available biodiesel known as “Soygold” that conformed to the ASTM D 6751-03 biodiesel standard. The following tests were conducted at the Biodiesel Testing Facility in Swalm School of Chemical Engineering at Mississippi State University: Carbon Residue Test (ASTM D 4530), Cloud Point (ASTM D 2500), Copper Corrosion (ASTM D 130), Flash Point (ASTM D 93A) and Viscosity (ASTM D 445). Tests of other parameters like Cetane Number (ASTM D613), Acid Number (ASTM D664) and Reid Vapor pressure were conducted at Southwest Research Institute, San Antonio, TX.

Table 13. Fuel Properties of Diesel, Biodiesel, and Blends.

Property	Diesel	Biodiesel	D70BD30	D70BD25E5	D70BD20E10	D70BD15E15
Calorific Value, kJ/kg	42026	33622	39364	39098	38827	38554
Cetane Number	43.3	51.7	46.7	42.6	40.8	36.2
Flash point	71	145	95	39	30	23
Acid Number	<0.05	0.21	0.08	0.11	0.07	0.06
Reid Vapor Pressure, kPa	1.68	0.33	0.41	1.67	2.96	3.44
Density, g/litre	846.2	915.0	866.84	861.24	854.74	848.69
Kinematic Viscosity, cSt	2.677	4.127	3.04	2.767	2.42	2.29
Carbon residue, %	0.0759	0.185	0.076	0.0623	0.0487	0.0778
Cloud Point, °C	-29	1	-9	-11	-12	-14
Copper Corrosion	1A	1A	1A	1A	1A	1A

Several concerns have been raised regarding potential adverse effects of the use of ethanol on engine performance and durability. Ethanol has fuel properties that are different than both biodiesel and diesel fuel, and does not meet either ASTM D 6751-03 for biodiesel fuel or ASTM D975 specification for diesel fuel. Thus, addition of ethanol in diesel-biodiesel blends may fail to meet standard fuel specifications. The data in Table 13 show that flash point decreased significantly with the rise in ethanol proportions. Adding ethanol increased the Ried vapor pressure of the blend extensively, making the fuel blends more volatile and vapor lock can be a problem. This means that DBE has more stringent storage requirements than conventional diesel. In fact, DBE must be stored and handled more like gasoline.

Biodiesel and ethanol, with low calorific values resulted in a reduction of blend calorific value. D70BD15E15 has lower cetane number than the diesel fuel specifications i.e. less than 40. The kinematic viscosity of D70BD20E10 and D70BD15E15, while being slightly lower than that for a typical diesel, met both the diesel and biodiesel specifications. The corrosivity as measured by copper strip corrosion method for each blends were the same as typical diesel, and also within specifications. The cloud points for the biodiesel and all the other blends were significantly higher than for typical diesel. However, it can be seen that addition of ethanol into diesel-biodiesel blends resulted in a decrease of the cloud point.

Testing Procedures

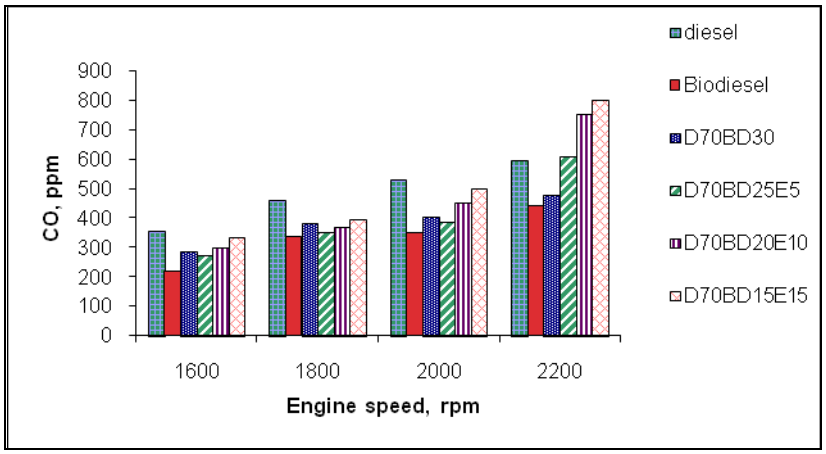
The NOVA gas analyzer was turned on 10 minutes prior to collection of data to allow the instruments to stabilize. The engine was started and warmed-up, at low idle, long enough to establish correct oil pressure and was checked for any fuel, oil, water and air leaks.

The speed was then increased to chosen engine rpm and load was set using the dynamometer. Data were taken while the engine was at constant load for different speeds. For the John Deere 5103, the selected engine speeds were 1400, 1700, 2000 and 2400 rev/min. Engine rpm of 1600, 1800, 2000 and 2200 were selected for Ford 4000. For John Deere multi-fuel engine, there was an automatic engine rpm set at 1800. The engine was run at the specified speeds and loads for a minimum of 15 min before data were collected during the last one hour of operation. The procedure was repeated for all the selected fuel types. The experiment was replicated three times and the average values were reported. The testing was done at the Mississippi State University Department of Agricultural and Biological Engineering.

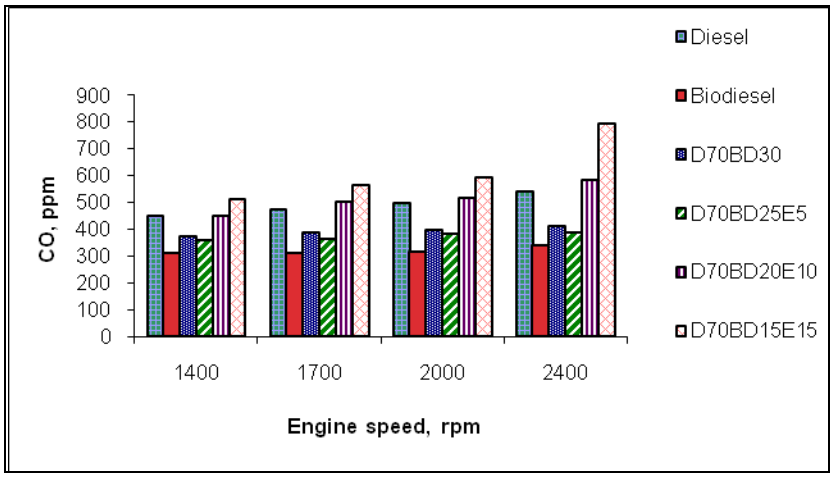
3. Results

CO Emissions

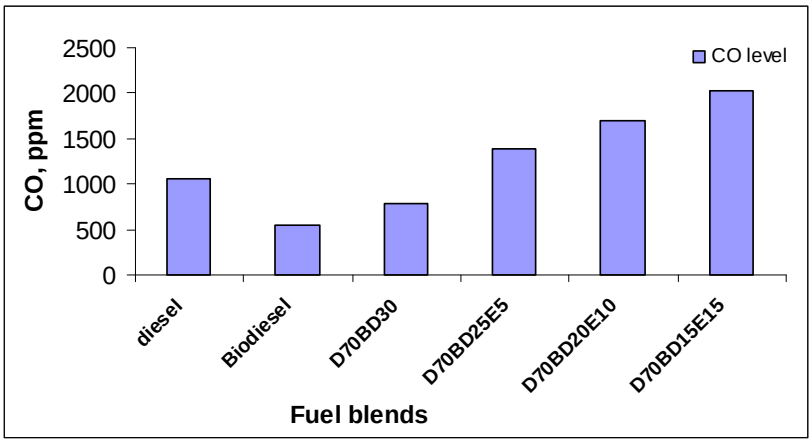
Ethanol has the potential to significantly lower CO emissions from diesel engines due to the high oxygen content. This has not been systematically observed since ethanol simultaneously both increases oxygen content and decreases the cetane number of a fuel. In some cases, the adverse impacts of a lower cetane number outweigh the benefits of an increased oxygenate content. A comparison of emissions using different fuel combinations in the three engines is shown in Figure 23. Compared to diesel fuel, the CO emissions of the biodiesel-diesel-ethanol blends increased with the increase in blend ethanol proportions. The increase of CO emissions with the increase of ethanol percentage in the blend could be attributed to respective reduction of the cetane numbers. It can be seen that biodiesel causes significantly less CO emissions. These lower emission levels were likely due to the fact that biodiesel contains about ten percent oxygen by weight, and this ample availability of oxygen helps to completely oxidize hydrocarbons in the cylinder. Also as engine rpm increased at the same load level, the CO emission level increased significantly.



a. Ford 4000 Tractor Engine



b. John Deere 5103 Tractor Engine

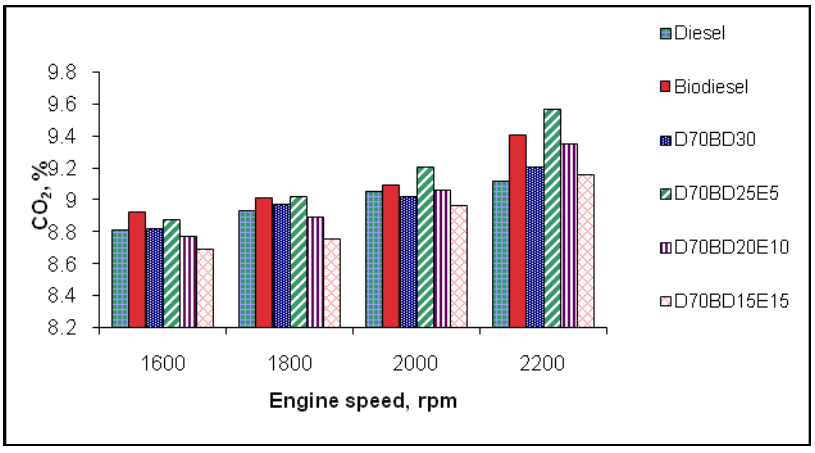


c. John Deere multi-fuel gen-set engine

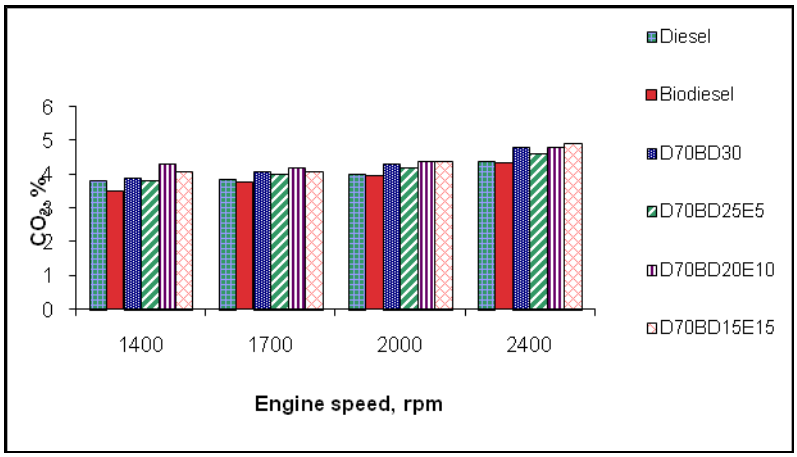
Figure 23. Comparison of the Carbon Monoxide Level.

CO_2 Emissions

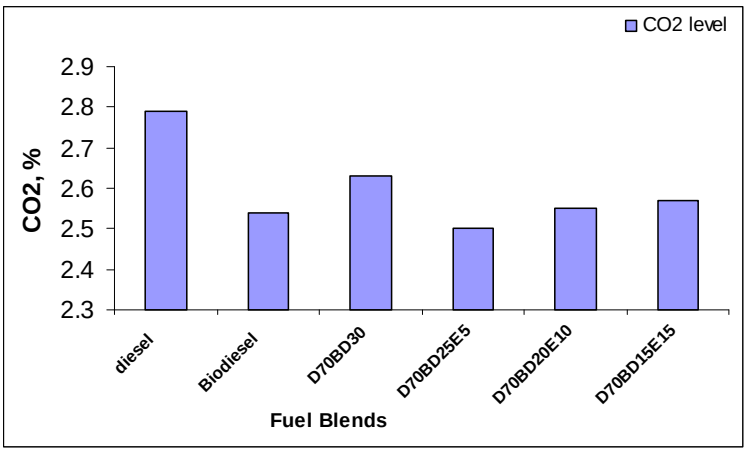
Figure 24 shows the variation of engine-out CO_2 emissions caused by the differences in fuel compositions in the presence of ethanol and biodiesel. CO_2 emissions increased with the increase in engine speed. It was found that the CO_2 emissions among different fuel combinations were not significantly different.



a. Ford 4000 Tractor Engine



b.John Deere 5103 Tractor Engine



c. John Deere multi-fuel gen-set engine

Figure 24. Comparison of the Carbon Dioxide Level.

Oxides of Nitrogen

Nitrogen oxides (NO_x) collectively refer to both NO and NO_2. Nitrogen oxides formation generally increases with the increase in flame temperature and slower flame speed. Nitrogen oxide emissions also increase with reduced engine speed. While high temperatures and pressures are desirable for high efficiency operation of a diesel engine, they are also the prime cause for the formation of NO_x gasses. According to literature, the NO_x emissions behavior of biodiesel in unmodified diesel engines varies widely. Several reports show NO_x is increased with biodiesel. However, in chassis dynamometer tests with the Cummins B 5.9 L, a reduction in NO_x with a corresponding increase in PM was found [105,106]. The variability in NO_x response for biodiesel may be due to individual variables in the engines themselves. Sharp and co-

workers stated that there is “a strong link between increasing cetane numbers and reducing NO_x emissions, but the response varies from engine to engine [107,108].”

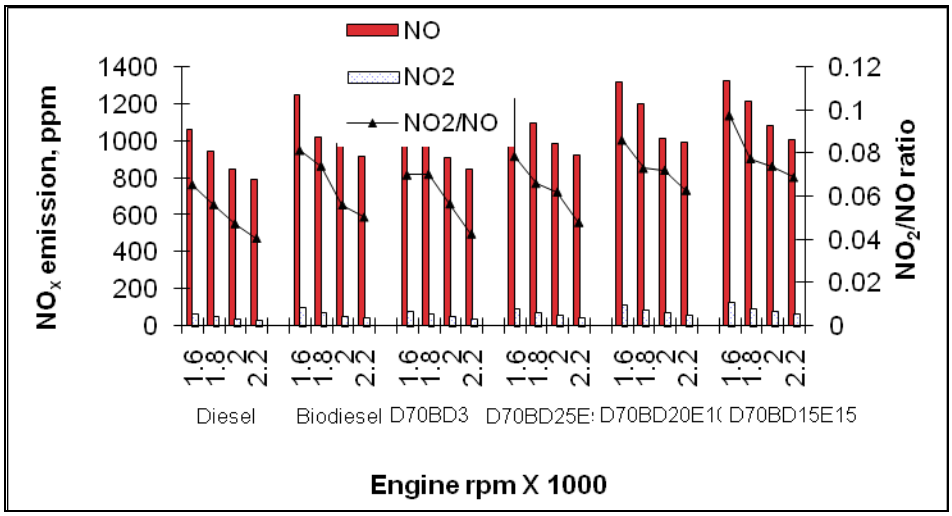
The NO_x exhaust emissions are shown in Figure 25. The NO_x emissions were higher for biodiesel and DBE blends in respect to diesel fuel in old ford 4000 engine. The increased NO_x emissions could be associated with the oxygen content of the methyl esters, since the fuel oxygen may provide additional oxygen for NO_x formation. Mittelbach and Tritthart tested used frying oil methyl ester and they found increased NO_x emissions compared to No. 2 diesel fuel [109]. Rickeard and Thompson [110] and Monyem [111] stated that the NO_x emissions increased for the biodiesel fuels.

Increasing ethanol fraction increased both NO and NO_2 emission and simultaneously raised NO_2/NO in the old Ford 4000 engine. NO_x emission and NO_2/NO reduced with increase in rpm. When compared with D70BD30, the D70BD25E5 blend showed an average increase in NO_x emission of 16%. On similar comparison, D70BD20E10 indicated an average increase of 21% and a 24% rise using D70BD15E15.

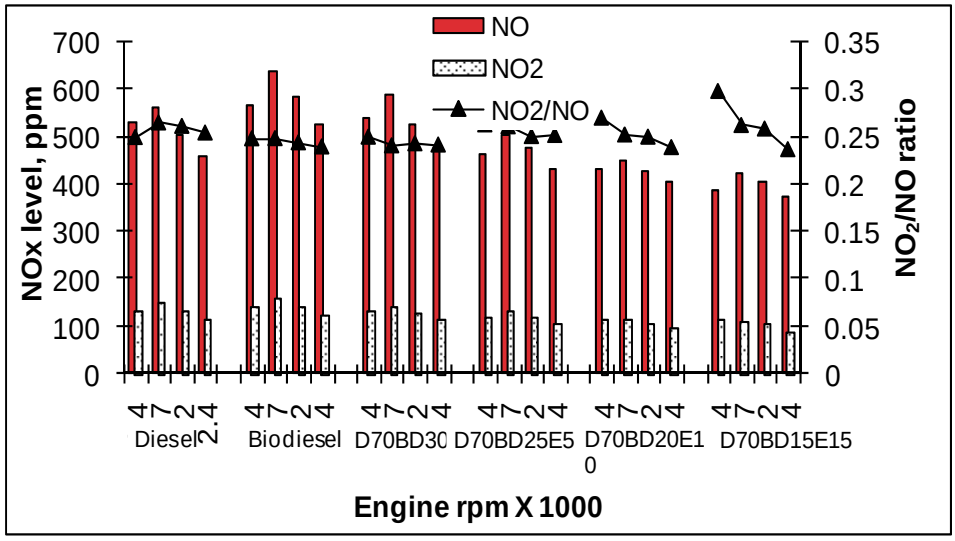
In contrast to the old Ford 4000 engine, the new John Deere 5103 tractor engine showed a reduction in NO and NO_2 emissions with increasing ethanol proportions in the fuel blend. An increment in NO_2/NO was observed in this case. NO_x level and NO_2/NO ratio declined with increase in engine speed. There was an average reduction of 12% of NO_x emission using D70BD25E5 in comparison to D70BD30. Similarly, a drop of 16% NO_x emission was observed using D70BD20E10 while a decrease of 22% was found using D70BD15E15. This clearly indicates that within the ranges tested, increased ethanol concentrations favor a reduction in NO_x emissions.

The John Deere multi-fuel engine also showed a similar trend - increased ethanol concentrations resulted in a reduction of levels of NO_x and NO_2/NO. When compared with D70BD30, 12%, 21% and 29% reduction in NO_x was observed using D70BD25E5, D70BD20E10 and D70BD15E15 respectively.

The three engines were obtained at different times and therefore it is not statistically accurate to compare results between the engines. However, the difference can be attributed to different engine specifications in three different engines. Dissimilar Compression ratios and fuel injection systems can be the vital explanations for the dissimilar trend in different engines. The increase in NO_2/NO level with addition of ethanol can be accredited to the fact that on addition of ethanol, a greater amount of NO was oxidized to NO_2. This may be due to the better oxidizing ability of ethanol. Moreover, it was noted that an increase in engine rpm at the same load level reduced the NO_x emission level significantly. This may be due to reduced air:fuel mixture at a higher speed. A super-lean mixture at low rpm burns very hot and produces a lot of NO_x. The richer the mix, the cooler the combustion zone and hence, lower NO_x at higher rpm. Also, this could be the reason behind the reduced NO_2/NO level with increase in engine rpm.



a. Ford 4000 Tractor Engine



b. John Deere 5103 Tractor Engine

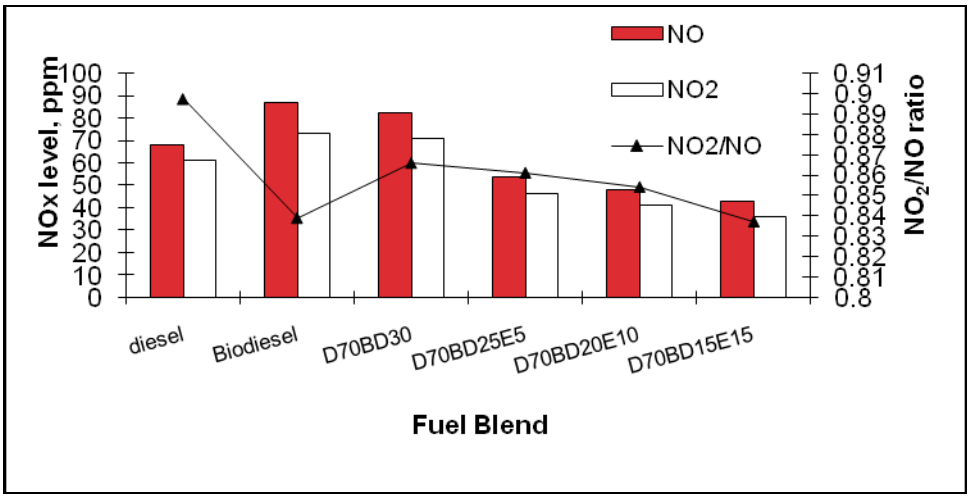


Figure 25. Comparison of the NO_x Level

4. Conclusions

Based on the data collected, several general conclusions may be reached regarding the effect of ethanol-biodiesel-diesel emulsions on exhaust emissions. Increase in the ethanol percentage in the biodiesel-diesel blends caused significant changes in fuel properties like cetane number, flash point and Reid vapor pressure demanding more stringent storage requirements than conventional diesel. Biodiesel was associated with lower CO emissions levels compared to levels associated with diesel fuel. Adding ethanol however increased CO emissions. Using biodiesel generally tended to increase NO_x emissions. Substituting neat biodiesel for diesel fuel, resulted in an increase of NO_x emissions by roughly 10-20 percent. Adding ethanol showed two different trends in NO_x emissions. With new engines, increase in ethanol proportion in the fuel blend resulted in a decline of NO_x emissions, although the old Ford 4000 engine demonstrated an almost reverse trend in NO_x emissions. It is possible that other properties of ethanol and biodiesel or interaction with characteristics of the combustion process and combustion chamber dynamics may have caused this variation in the expected trend toward NO_x emissions. More research is needed to fully understand the dependence of NO_x emissions on the diesel-biodiesel-ethanol and other parameters.

Task A.10. Research on Extraction of Nutritional Components from Biodiesel

1. Introduction

Our goal is the extraction and separation of novel secondary products, such as polyunsaturated fatty acid methyl esters (including DHA and EPA) from bio-diesel (and bio oils).

We have achieved our stated goal, as we have developed efficient methods to isolate polyunsaturated fatty acid methyl esters from bio-diesel and bio-oils. In addition, we have developed a method to isolate another value added product, Vitamin E, from bio-oils, which is not in our original plan.

Part 1: Extractive separation of polyunsaturated fatty acid methyl esters including omega-3 fatty acid eicosapentaenoic acid (EPA) and docosahexaenoic acid (DHA)

Our hypothesis to isolate this class of fatty acids, which are used as popular dietary supplements and prescription medicine (OMACOR), is that they bind transition metal ions much stronger than their harmful saturated analogs. To solve the solubility problem associated with these metal ions, we devised a biphasic extraction system involving novel ionic liquids. In our procedure, fatty acid methyl esters dissolved in hexanes are extracted with transition metal ions dissolved in ionic liquids. Because of the binding between polyunsaturated fatty acid methyl esters and the transition metal ions, the polyunsaturated fatty acids methyl esters are extracted selectively into ionic liquids, thus separated from the saturated fatty acid methyl esters which stayed in hexanes. After layer separation, polyunsaturated fatty acid methyl esters could be back extracted with 1-hexene. The procedure worked very well.

The first experiment was done using silver salt (Ag+) as the transition metal ion. Ionic liquid proved essential in this extraction, as other solvents worked poorly (Figure 1).

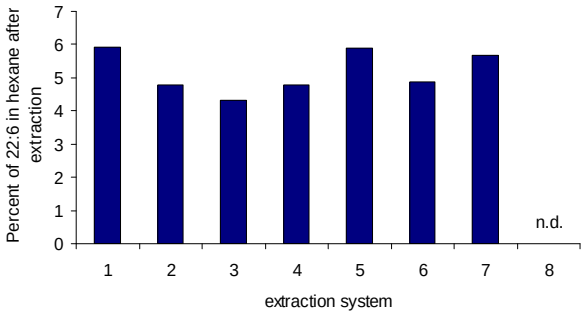


Figure 1. Comparison of various extraction systems. Column 1, percent of DHA in hexane before extraction; 2, pure [hmim][PF_6](no silver salt); 3, $AgBF_4$/water; 4, $AgBF_4$/ethylene glycol; 5, $AgNO_3$/water; 6, $AgNO_3$/(water: methanol=1:4); 7, $AgBF_4$/(water: methanol=1:4); 8, $AgBF_4$/[hmim][PF_6]. Initial fatty acid methyl ester compositions in hexane: 16:0=21.70%, 18:0=22.66%, 18:1=25.50%, 18:2=24.25%, DHA (22:6) = 5.95%. 10 mg of silver salt (0.05 mmol) was used

We have also evaluated different metal ions for the extraction of omega-3 fatty acid methyl esters (Figure 2), since it is known that other transition metals could also exhibit some coordination ability with the double bond. Seven metal complexes in ionic liquids were selected to extract unsaturated fatty acid methyl esters in hexane solvent. The extraction ability of the metal complex was assayed by the EPA (20:5) concentration in hexane. The stronger the extraction ability, the lower the concentration of EPA in hexane becomes. $PdCl_2$, $NiCl_2$ and CuCl showed low extraction ability for EPA in ionic liquids [hmim][PF_6]. The latter transition metal complex, H_2PtCl_6, $PdCl_2(TPP)_3$ and $RhCl(TPP)_3$ exhibited moderate extraction for EPA in [hmim][PF6]. $AgBF_4$ in [hmim][PF6] showed very high extraction for EPA. It is apparent that $AgBF_4$ has the highest extraction ability among all the metal ions tested.

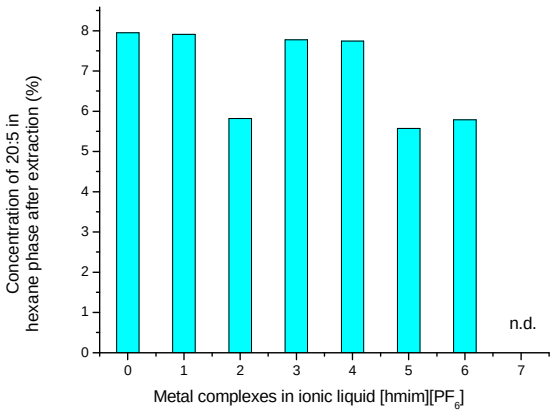


Figure 2. Comparison of extraction of EPA (20:5) in hexane with metal ions in ionic liquids. 0, no metal, control experiment; 1, $PdCl_2$; 2, H_2PtCl_6; 3, $NiCl_2$; 4,CuCl; 5, $PdCl_2(TPP)_3$; 6, $RhCl(TPP)_3$; 7, $AgBF_4$. n.d, not determinable.

We then studied the isolation of EPA and DHA by covalently immobilizing ionic liquids (ILs) onto silica gel and then coating this silica-supported ILs with silver salts. These sorbents were successfully applied to extract and enrich polyunsaturated fatty acid methyl esters (PUFAMEs) including EPA and DHA with both high selectivity and high capacity. The enrichment of PUFAMEs was investigated using a simple three-step procedure consisting of (1) sorbent pretreatment, (2) sample extraction onto the sorbent and (3) stripping the sorbent by 1-hexene. Only 5 mg of the sorbent (AgBF4/SiO2●Im+●PF6¯) completely adsorbed 0.33 mg of EPA (20:5) in 5 min from the feed mixture solution. The saturated extraction capacity for EPA by using this AgBF4/SiO2●Im+●PF6¯sorbent was 120.0 mg/g as determined by its adsorption isotherm. After a consecutive two-step stripping by ethyl ether and then 1-hexene, the concentration of EPA increased from 7% in the feed stock solution to about 90% in the 1-hexene stripping solvent. After five recycles, the sorbent is still usable.

To further increase the extraction capacity, we have also studied mesoporous silica gel complexing sorbents. For this purpose, we prepared and characterized mesoporous silica gel. Compared with similar experiment described in the last paragraph, much higher extraction capacities were obtained.

Part 2. Separation of vitamin E from soybean oil

Ordered mesoporous adsorbents were prepared by physically coating functionalized ionic liquids onto mesoporous silica gel. These adsorbents were successfully applied to the selective extraction and separation of vitamin E from a model mixture of soybean oil deoderizer distillate. Various parameters affecting the adsorption process, such as adsorption time, ionic liquid structures and loadings, the adsorption isotherm, and adsorbent reusability were investigated using liquid-solid extraction. α-Tocopherol capacities as high as 211 mg/g adsorbent were obtained through the adsorption isotherm tests using [emim][Gly]/SBA-15 as the adsorbent. The anion of glycine was employed as the counteranion to 1-ethyl-3methyl-imidazolium ([emim]). When this functionalized ionic liquid was coated on traditional microporous silica gel, the extraction capacity of the [emim][Gly]/SiO2 dropped to 105 mg/g adsorbent. The substantial extraction capacity enhancement of [emim][Gly]/SBA-15 adsorbent was ascribed to its larger pore size and surface area versus traditional silica gel.

[emim][Gly]/SBA-15 also exhibited a very high adsorption selectivity for α-tocopherol. The ratio of distribution coefficients between α-tocopherol and the major interfering component glyceryl triundecanate (Kd(α-tocopherol) /Kd(triglyceride)) was 10.5. The concentration of α-tocopherol was significantly increased from 15.6 (wt%) in original feedstock solution to 73.0% after stripping the adsorbed product with diethyl ether. The original feedstock solution also contained fatty acid methyl esters, triglyceride and α-tocopherol. Five adsorbent recycle tests showed good reusability of this ionic liquid-modified mesoporous adsorbent. The distribution coefficient for α-tocopherol, Kd(α-tocopherol), went down from 199 ml/g in the first cycle to 148 ml/g in the fifth cycle.

Task A.11. Research on Glycerol Fermentation

1. Introduction

Due to the world's decreasing supply of fossil fuels, alternative fuel sources must be found. Biodiesel fuel is steadily becoming a viable alternative to petroleum diesel. Glycerol is a key product from the production of biodiesel. It is produced during the transesterification process by cleaving the fatty acids from the glycerol backbone (the fatty acids are used as part of the biodiesel, which is a fatty acid methyl ester). Glycerol is a non-toxic compound with many uses; however, if a surplus exists in the future, more uses for the produced glycerol needs to be found. Also, for biodiesel production processes that incorporate animal wastes, the glycerol byproduct could negatively impact the quality of the glycerol and require expensive cleaning steps. As a consequence the crude glycerol form these feedstocks would not be desirable for use in many of its current applications in foods, cosmetics, pharmaceuticals, etc. These limitations again illustrate the need for new, more profitable uses of glycerol to be discovered.

The goal of this phase of the project was to find an add-on process to the biodiesel production process that will convert the glycerol by-product into more valuable substances for end uses other than food or cosmetics, focusing at present on 1,3-propanediol and lactic acid. Experiments using bacteria that are known to ferment glycerol into these compounds has been performed in order to establish a benchmark for comparison against other types of bacteria. For this work the three benchmark cultures (*Clostridium acetobutylicum, Clostridium beijerinckii, and Clostridium pasteurianium*) were utilize as benchmark organisms to compare to MSU isolates producing these compounds. Some of the isolates tested from MSU's Chemical Engineering culture collection were isolated during a US DOE EPSCoR project whose focus was to find a microorganism capable of economically converting syngas to ethanol. During the EPSCoR project >20 cultures were isolated from various environments ranging from manure to sewage treatment plants. In addition to these microorganisms as potential glycerol-fermenting microorganisms, attempts were made to isolate glycerol-fermenting microorganisms from Winogradsky columns. Winogradsky columns are an old technique of developing microbial biofilms that allows microorganisms to develop in their native state thereby encouraging the growth of larger variety of microorganisms. Reported here are the findings of those experiments.

2. Materials and Methods

Glycerol-Fermenting Cultures: *Clostridium acetobutylicum* ATCC 824*, Clostridium beijerinckii* ATCC 14823*, and Clostridium pasteurianium* ATCC 6013 were purchased from the American Type Culture Collection and cultivated on ATCC 1500 culture medium. Isolates from the previous EPSCoR work were removed from storage at 0ºC

on slants and placed into fresh ATCC 1500 medium and incubated at 35ºC and 100 rpm. In order to increase the genetic pool of glycerol-fermenting microorganisms other microorganisms with this ability were also screened. The sources of these microorganisms were the biofilms that had formed in the Winogradsky columns that MSU had been developing for several years (Figure 6). These cultures were isolated by first selecting a Winogradsky column that distinctly developed biofilms (this is an indication of fully developed column). Based on the known the development of colors in the columns samples were selected from a zone in the columns known to be anaerobic. Since this was the early phase little efforts were placed on identification of the isolates. Emphasis was placed on the ability of each organism to convert glycerol into industrial products and the efficiencies of these conversions.



Figure 6. Fully Developed Winogradsky Column with Distinct Biofilm Layers and Glycerol-Fermenting Microorganisms Label Clostridium.

Isolation of Glycerol-Fermenting Cultures: Traditional enrichment techniques were utilized to isolate candidate cultures. Using a modified ATCC 1500 medium (glycerol as the carbon source instead of corn starch) either 1 mL of inoculum or 1 g of soil was initially added to 30 mL of the sterile medium contained in 40mL volatile organic acid (VOA) vials under anaerobic conditions. Vials were initially allowed to incubate for 5 days before the first enrichment transfer was made. Enrichments of this culture were made by transferring 1 mL of the fluid to sterile ATCC 1500 glycerol medium under anaerobic conditions followed by a 3 day incubation period. Anaerobic conditions were maintain via the use of a Coy Flexible Anaerobic Chamber that was equipped with an automatic airlock system and 4 sets of arm ports (Figure 7). The chamber contains an atmosphere of 95% N_2 and 5% H_2. Workers were able to transfer cultures into fresh medium via pipette inside the anaerobic chamber and avoid the cultures from being exposed to oxygen for which they are very sensitive to it.



Figure 7. Worker Transferring Cultures in the Coy Flexible Anaerobic Chamber.

Following three enrichments, an aliquot of the cell suspension was transferred to 100 mm diameter Petri plates containing ~25 mL of ATCC 1500 medium solidified with 18 g/L bacto agar. Using traditional streak plate techniques the individual cultures were isolated from members of their consortium. These cultures were incubated in the glove bag to ensure anaerobic conditions for a minimum of five days. Using an inoculation loop individual colonies from the surface of the solidified medium were transferred to liquid 40 mL VOA vials containing 30 mL of fresh sterile ATCC 1500 glycerol medium. These cultures were incubated for 3 days before being transferred to fresh ATCC 1500 glycerol medium. After the third transfer cultures were tested for the presences of lactic acid and/or 1,3-propanediol.

Glycerol GC-FID Analytical Method: These samples were shot in triplicates for GC-FID analysis. An Agilent 6890 gas chromatography (GC) system with a Flame Ionization Detector (FID) and autosampler (Agilent Inc., Palo Alto, CA) was used. The system was controlled by the Agilent GC Chemstation software; version B.01.03. The system was operated with Ultra High Purity hydrogen gas (NexAir LLC, Columbus, MS) and compressed air (NexAir) at flow rate of 40 mL/min and 400 mL/min respectively. Ultra High Purity hydrogen gas was used as makeup gas on the system. The final combined flow was regulated to 35.0 mL/min. A Restek Stabilwax-DA capillary column (30 m length, 250 um inner diameter, 0.25 um film thickness, and maximum temperature of 260ºC) was used for separation of the compounds. During the injection cycle, the syringe was washed twice with a 50% Acetonitrile solvent, and injections of 1 µl were made with a 10 µl syringe. Post injection, the syringe was washed again twice with the solvent. The inlet was run in split mode in a 40:1 ratio with an initial temperature of

255ºC. The oven was programmed to hold the initial temperature of 50ºC for 2 minutes and then ramp with 22ºC/min to the final temperature of 250ºC and hold for 7 minutes. The total runtime was 18.09 minutes.

Lactic Acid and 1,3-Propanediol Analysis with HPLC: Lactic acid and 1,3-propanediol in the liquid phase was quantified using a Waters HPLC System (Milford, Massachusetts). The Waters System consisted of a 515 Pump, a 717-Plus Autosampler, and a 2487 Dual λ Absorbance Detector. The HPLC used a Waters YMC ODS-AQ S-5 120 Å column (150 x 4.6 I.D., S-5 µm, 12nm), and the corresponding Waters YMC ODS-AQ S-5 120 Å guard column (4.0 x 23 mm threaded guard). The mobile phase for the HPLC was 20 mM NaH_2PO_4 with a pH of 3.5.

Correlating Cell Mass to Optical Density: Cultures were inoculated for growth into 200 mL of ATCC 1500 glycerol medium under anaerobic conditions. These cultures were grown for three weeks to achieve a large amount of cell mass. After this period the cultures were placed in a centrifuge at 2000 rpm for 20 minutes. This sample was resuspended in 50 mL of medium without glycerol. At this point a serial dilution was made by placing volumes of the cell suspension into blank medium to achieve dilutions of 1:1, 1:2, 1:5, and 1:10. Ten mL of the resuspend cell pellet was placed on aluminum weigh dishes and dried overnight at 60ºC. Dilutions were examined for optical density using a Genesys 20 spectrophotometer at 546 nm wavelength. A curve was generated by plotting optical density measurements vs cell mass concentrations for all three of the ATCC purchased cultures. These curves are presented in Figures 8-10.

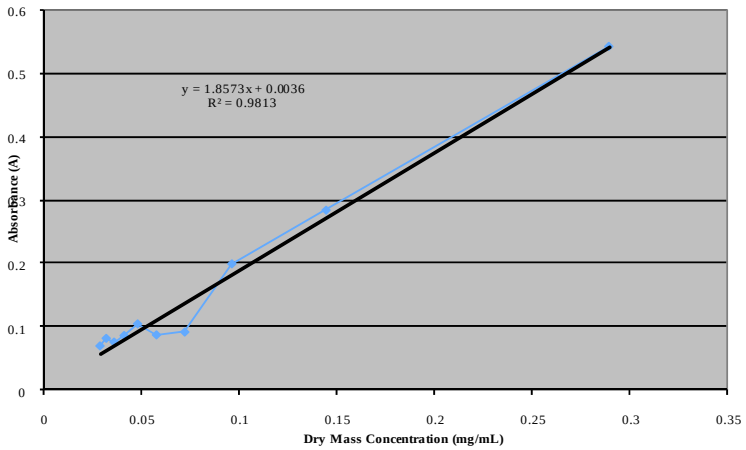


Figure 8. Correlation of Absorbance to Dry Mass Concentrations for *Clostridium acetobutylicum.*

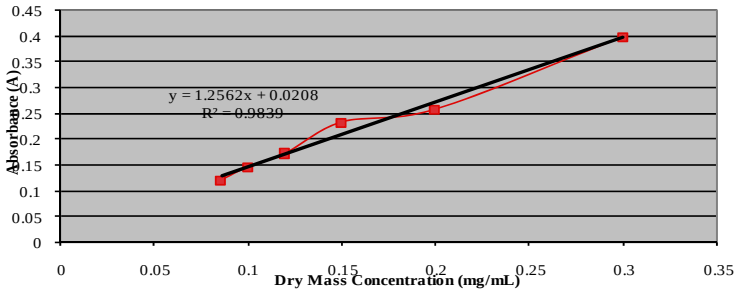


Figure 9. Correlation of Absorbance to Dry Mass Concentrations for *Clostridium beijerinckii.*

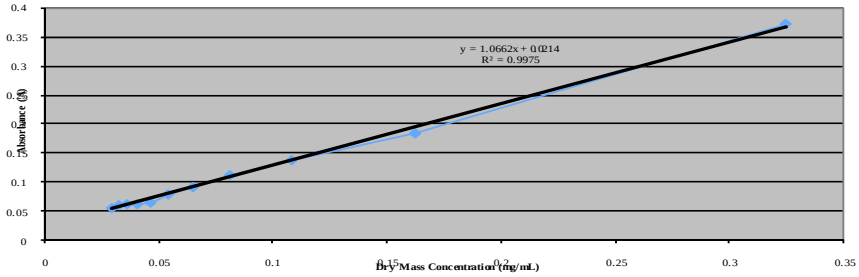


Figure 10. Correlation of Absorbance to Dry Mass Concentrations for *Clostridium pasteurianium.*

3. Results

Glycerol Conversion by C. acetobutylicum, C. beijerinckii, and C. pasteurianium:

The results of these experiments are given in Table 6 below. These assays were conducted in 40 mL VOA vials containing 30 mL of ATCC glycerol medium. The concentration of glycerol used in this study was 2.5 g/L. The results of these experiments demonstrate the ability of *C. acetobutylicum* and *C. beijerinckii* to convert glycerol into lactic acid at concentration greater than 100 mg/L. However *C. beijerinckii* was capable of simultaneously producing 1,3-propanediol from the fermentation of

glycerol. With a more fundamental understanding of the genetic regulations this microorganism offers the potential to produce either product depending on the market price. *C. pasteurianum* by far produced the largest concentration of 1,3-propanediol of all the microbes purchased from ATCC or isolated by MSU. *C. pasteurianum* failed to produce any detectable amounts of lactic acid during the time tested.

BACTERIA	**1,3-PROPANEDIOL PRODUCED (ppm)**	**LACTIC ACID PRODUCED (ppm)**
Clostridium acetobutylicum	none	145.35
Clostridium beijerinckii	43.32	179.31
Clostridium pasteurianum	545.58	none

Table 6. Final Concentration of 1,3-Propanediol and Lactic Acid in the Fermentation Medium When the ATCC Cultures Were Offered ATCC 1500 Glycerol Medium (2.5 g/L glycerol).

The yield of product per mole of glycerol also demonstrated that *C. pasteurianum* was much more efficient at converting glycerol to 1,3-propanediol than was *C. acetobutylicum* or *C. beijerinckii* at converting glycerol to either product. *C. pasteurianum* yielded 0.27 mol of 1,3-propanediol per mol of glycerol. Where *C. acetobutylicum* only yielded 0.06 mol of lactic acid per mol of glycerol and *C. beijerinckii* yielded 0.08 mol and 0.02 of lactic acid and 1,3-propanediol respectively per mol of glycerol. Of these three tested *C. pasteurianum* produced the highest yield and final concentration of product when offered 2.5 g/L glycerol.

Glycerol Conversion by MSU Isolates: Of the >20 cultures tested only 8 showed any measurable amounts of either lactic acid or 1,3-propanediol in the fermentation broth. These cultures were designated J1, J2, J6, J7, J8, J9, J10, and J13 and the concentration of either lactic acid or 1,3-propanediol is given in Table 7. It is very apparent that the cultures isolated were very well suited for the conversion of glycerol to lactic acid as all but 2 of the MSU isolates produced the compound. Three cultures (J6, J1, and J13) produced more lactic acid than the benchmark organisms. With yields greater than 20 mol lactic acid per mol of glycerol for all three microorganisms. Three cultures (J6, J7, and J9) demonstrated the ability to produce 1,3-propanediol during glycerol fermentation. However all three MSU cultures produced products at concentrations below that of the benchmark microorganisms. There was one notable isolate the caught the eye of the investigators and that was culture J6 due to the ability of this microorganism to co-produce both products and one in particularly high concentrations. This culture with more understanding of its metabolic pathways could prove a useful biological agent for the conversion of glycerol.

These results demonstrate the potential for undiscovered microorganisms to

carryout significant biochemical pathways. It also demonstrates the importance of being able to culture the microorganisms from its environment as was demonstrated using the Winogradsky columns. The metabolic ability of the microbial community is vast and could have tremendous potential.
All of the cultures isolated during this study were placed in the freezer in glycerol medium for use in subsequent experiments.

Table 7. Final Concentration of 1,3-Propanediol and Lactic Acid in the Fermentation Medium When Offered ATCC 1500 Glycerol Medium (2.5 g/L glycerol) to the MSU Isolates.

BACTERIA	1,3-PROPANEDIOL PRODUCED (ppm)	LACTIC ACID PRODUCED (ppm)
J6	78.89	509.56
J7	214.22	none
J9	50.89	none
J1	none	476.43
J2	none	131.12
J8	none	148.41
J10	none	119.78
J13	none	794.44

Task A.12 - Removal of biodiesel impurities (metals) using silane compounds

1. Introduction

The goal for this project was to develop and evaluate nano-encapsulation techniques for removal of heavy metal impurities from biodiesel production processes. While a number of impurities are present at low concentrations in biodiesel as a direct consequence of the feedstock source including Cu, Pb, Mn, Fe, B and Co, this effort focused on copper because the chemistry was unknown and copper is present in higher concentrations in primary sludge for biodiesel. If a reaction scheme could be developed for this metal, it would be easier to port to other metals. An extensive literature search was conducted on (1) silanizing agents and silica self-assembly in core shell nanotechnology and (2) alternative strategies to remove trace levels of heavy metals contaminants from other processes.

Based upon silica / metal chemistry described, two compounds were selected to bind to the copper colloid surface and then simultaneously bind to free silicate in solution. The compounds chosen to have an affinity for both copper and silicate were sodium dodecyl benzene sulphonate (SDBS-technical grade, CAS#25155-30-0) and poly vinylpyrrolidone of average molar masses of 8kg/mol (PVP-8, CAS#9003-39-8) were selected. Free silicate was obtained in the form of tetraethoxysilane (TEOS, 99.999%, CAS#78-10-4), which readily binds on top of itself to form a thick silicate layer.

Synthesis experiments were conducted with a Cu colloid suspension having average particle sizes of 125 nm. A panel of experiments was conducted where particles were functionalized with polyvinylpyrrolidone (PVP) at various concentrations. A second panel was conducted with particles functionalized with sodium dodecyl

benzene sulphonate (SDBS). The PVP or SDBS chemically linked the Cu surface to tetraethoxysilane (TEOS) which then grew upon itself to form a silica shell around the particle. The resulting core-shell nanostructures were characterized by transmission and scanning electron microscopy to assess average particle diameter, silica shell thickness, and overall morphology of the core-shell nanostructures. Reactant concentrations and synthesis conditions were optimized to maximize silica shell thickness, morphology, and nanoparticle dispersion. Further, characterization of the chemical bonding between the copper, linker molecule (PVP and SDBS) and silane and the formation of a silicate shell was conducted with Fourier Transform Infrared spectroscopy.

Synthesis experiments determined that sodium dodecyl benzene sulphonate (SDBS) yielded more consistently reliable results than polyvinylpyrrolidone (PVP). Further, results from synthesis experiments utilizing sodium dodecyl benzene sulphonate (SDBS) as a linking agent between the Cu surface and tetraethoxysilane (TEOS) indicated that the silane concentration greatly impacts the silica shell thickness and porosity.

The synthesis procedure is as follows:

(a) Functionalization:

PVP dissolved in water

PVP + Colloidal solution + Stirring

Functionalized colloidal particles

(b) Stabilization:

Functionalized particles are transferred into ethanol

Solution of PVP-stabilized particles centrifuged/sedimented

(c) Synthesis of Silica Shell:

Sediments redispersed in a solution of NH_3 in C_2H_5OH

TES solution added during slow stirring

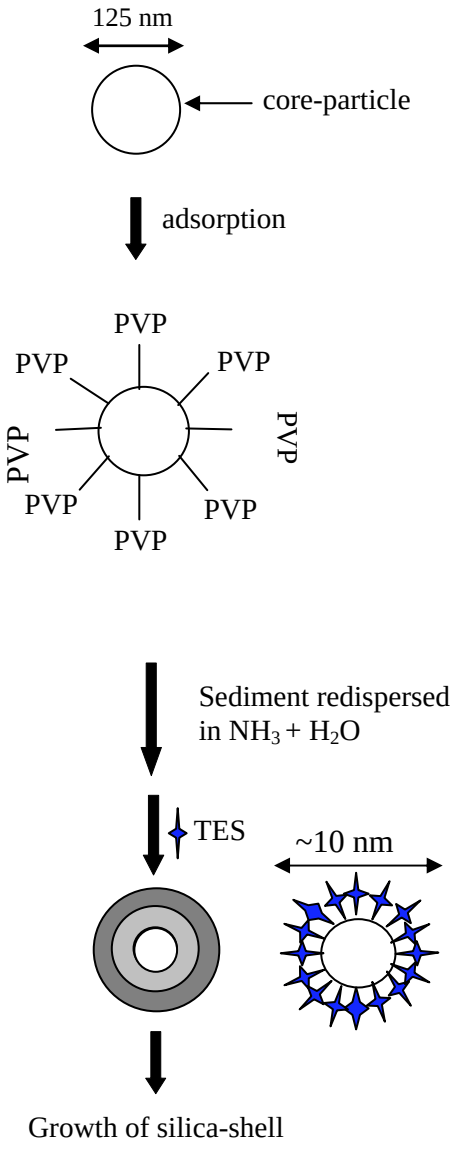


Figure 1. Schematic of colloid coating process showing the (a) functionalization, (b) stabilization, and (c) synthesis steps.

Technical Presentations:

Aich, S., K.B. Walters, and A.R. Minerick. "Rendering Trace Metal Particulates Inert Via Nanoencapsulation In Biological Processes" Biology-Inspired Nanotechnology Session at the Institute of Biological Engineers, St. Louis, MO: 6 Mar. 2007.

Aich, S., K.B. Walters, and A.R. Minerick. "Effect of Stabilizers on Encapsulation of Metallic Colloidal Nanoparticles," Regional Poster Session: Society of Plastics Engineers: 6 Mar. 2007.

Aich, S.,K.B. Walters, and A.R. Minerick. "An Electron Microscopy Study of Cu/SiO2 Core-Shell Nanoparticles." Annual Meeting of the Southeastern Microscopy Society, Decatur, GA: 12 Apr. 2007.

Aich, S., F. Schulz, K.B. Walters, and A.R. Minerick. "Synthesis and Characterization of Cu-SiO2 Core-Shell Nanoparticles." Functional Nanoparticles and Nanocoatings on Particles-II (03D03) – Particle Technology Forum: American Institute of Chemical Engineers Annual Conference (AIChE); Nov. 2007.

Aich, S. K.B. Walters, and A.R. Minerick. "Nano-Encapsulation of Trace Metal Impurities in Biodiesel." Chemistry and Chemical Engineering: Mississippi Academy of Science, 23 Feb. 2007.

Baldwin, B.S. 2007. Oil feedstocks for the Southeast (What is feasible?). First Ann Miss. State Univ. Biofuels Conf. Starkville, MS. 27 Aug.

Barnes, D. S. Ganji, D.S. Horton, B.S. Baldwin, D.A. Braasch. 2007. Modification of castor for use in biodiesel: Knocking out the toxin. First Ann Miss. State Univ. Biofuels Conf. Starkville, MS. 27 Aug.

Benson, T., Hernandez, R., French, T., and Zappi, M., "Production of Biodiesel from Wastes Associated with Meat Butchering Processes," Presented at the 2005 AIChE Annual Meeting, Cincinnati OH.

Brown, A. B. Rogers, B.Baldwin, D. Braasch, W. Holmes. 2007. Characterization of hesperis and black mustard oil as possible biodiesel feedstock. Amer. Oil Chem. Soc. Conf. Quebec City Quebec. May 1-3.

Brown, A.E., W.E. Holmes, E.C. Rogers, T Verlotl, and B.S. Baldwin. 2007. FAME analysis of *Hesperis matronalis*: GCXGC-TOFMS better resolution. Amer. Soc. Mass Spec. Conf., Indianapolis, IN. 3-7 Jun.

Brown, A. B. Rogers, B.Baldwin, D. Braasch, W. Holmes. 2007. Characterization of hesperis and black mustard oil as possible biodiesel feedstock. Amer. Oil Chem. Soc. Conf. Quebec City Quebec. 1-3 May.

Crymble, S.D., R. Hernandez, W. T. French, M.E. Zappi, B.S. Baldwin, and D. Thomas. 2006. Kinetic Study of biodiesel production from Chinese tallow tree oil. Amer. Inst. Chem. Eng. Ann. Conf. San Francisco, CA. Nov 12-17.

Dufreche, S., Hernandez, R., Zappi, M., French, T., Sparks, D., Alley, E., “Production of Low-Cost Biodiesel Using a Novel Bacterial-Based Feedstocks,” 97th AOCS Annual Meeting & Expo, April 30-May 3, 2006, St.Louis, Missouri.

Dufreche, S., Hernandez, R., French, T., Zappi, M., Sparks, D., and Alley, E., “Production of Low-Cost Biodiesel Using a Novel Bacterial-Based Feedstock,” Presented at the 2005 AIChE Annual Meeting, Cincinnati OH.

French, W.T., Hernandez, R., Zappi, M., Dufreche, S.T., Sparks, D.L., “Production of Biodiesel from Wastwater Treatment Sludge,” World Renewable Energy Congress IX, 19-25 August 26 Florence, Italy.

French, T., Hernandez, R., Easterling, E., and Zappi, M., “Extraction and Production of Value-Added Products from Waste Feedstocks,” Presented at the 2005 AIChE Annual Meeting, Cincinnati OH.

Hernandez, R., Zappi, M., French, T., Whitlock, J., and Alley, E., “Production of Biodiesel Using an Integrated Extraction Reaction Method,” Presented at the 2005 AIChE Annual Meeting, Cincinnati OH.

Hernandez, R., “Novel Processes and Feedstocks for Producing Biodiesel,” Energy Summit Sponsored by Congressman Chip Pickering, Pearl, Mississippi.

Hernandez, R., Sparks, D., French, T., Toghiani, H., Toghiani, R., Zappi, M., “Production of Value-Added Chemicals via Oxidation of Lipids in Supercritical Carbon Dioxide,” 97th AOCS Annual Meeting & Expo, April 30-May 3, 2006, St.Louis, Missouri.

Hernandez, R., “Biodiesel from Non-Traditional Feedstocks,” Southeast Diesel Collaborative Meeting Sponsored by the Environmental Protection Agency, April 26, Atlanta, GA.

Hernandez, R., French, T., Dufreche, S., Sparks, D., Zappi, M., “MSU Biodiesel Production Process,” 2006 Bioproducts Conference Sponsored by the Mississippi Biomass Council, April 23, 2006, Philadelphia, Mississippi.

Hernandez, R., and French, W.T., “Overview of the Biodiesel Industry,” Mississippi Young Farmers Association, 21st January, 2006, Jackson MS.

Hernandez, R., French, T., Sparks, D., Dufreche, S., “Biodiesel Production Using Alternative Feedstocks,” 87th Annual Convention of the Southern Seed Association,” January 15, 2006, San Antonio, TX.

Liang, K.; Toghiani, H.; Hernandez, R. “Supercritical CO_2 Extraction Lipids and Phospholipids from Sewage Sludge”, 2007 AICHE Annual Meeting. (November 4-9, 2007, Salt Lake City, Utah, USA)

Liang, K., Toghiani, H.; Hernandez, R.; Sparks, D. “Supercritical CO_2 Extraction for Lipid and Phospholipid Recovery from Sewage Sludge”, 98th AOCS Annual Meeting. (May 12-17, 2007, Quèbec City, QC, Canada)

Schulz, F., S. Aich, K.B. Walters, and A.R. Minerick. "Synthesis and Characterization of Cu-SiO2 Core-Shell Nanoparticles." Final Symposia of the NSF REU Site Chemistry - Chemical Engineering: The Bonds Between Us; 27 July 2007.

Sebastian, T., B.S. Baldwin, D.S. Horton, and C.L. Webber. 2007. Estimation of pollen dispersal and gene flow in the potential biofuel crop castor (*Ricinus communis* L.). First Ann Miss. State Univ. Biofuels Conf. Starkville, MS. 27 Aug.

R. K. Toghiani, **Prediction of Phospholipid Solubilities in Conventional Solvents**, 7th Southern School on Computational Chemistry and Materials Science, Jackson, MS, April 6-7, 2007.

R.K. Toghiani, **Prediction of Phospholipid Solubility in Supercritical Fluids**, 11th International Conference on Properties and Phase Equilibria for Product and Process Design PPPEPPD 2007, Hersonissos, Crete, Greece, May 20-25, 2007.

R.K. Toghiani, **Estimation of Phospholipid Solubility in Conventional Solvents and in Supercritical Fluids**, 2007 AIChE Annual Conference, Salt Lake City, UT, November 4-9, 2007.

Zhang, G., W.T. French, R. Hernandez, H.Toghiani, J. Carmical, W. Homes, A. Brown, and B. Baldwin. 2007. Lipid production from acid hydrolysate of lingocellulosic biomass using *Rhodotorula glutinis*. AIChe Annual Meeting. Salt Lake City, UT. 4-7 Nov.

Zheljazkov, V.D, B. Baldwin, W. Ebelhar, N. Buehring, and C. Coker. 2007. Sunflowers as an oil seed crop for biodiesel production in Mississippi. Southern Amer. Agron. Society Association Annual Meeting. Mobile, AL, 3-6 Feb.

Refereed Proceedings

1. Holmberg, K.B., K.D. Jones, B.S. Baldwin, J.L. Douglas, J.M. Grabowski. 2006. Progress and Problems in Selecting Six Native Grass Species. Pp. (Proc.) Fifth Eastern Native Grass Symposium. Harrisburg, PA. Oct 10-13.

Edited Proceedings

1. Oldham, L.O., B.S. Baldwin, D.J. Lang, and M. Collins. Biofuel research efforts in Mississippi. *In* Carl Crozier ed. Southern Plant Nutrient Management Conference Proceedings. October 2-3, 2007. Olive Branch, MS. Publisher: The Noble Foundation.

Journal articles:

Baldwin, B.S. and R.D. Cossar. 2008. Castor (*Ricinus communis* L.) yield in response to planting date at four locations in the South-central U.S. Industrial Crops and Prod. (Accepted).

Danviriyakul, S., S Jongrattananon, J McGillivray,' JL Silva. Quality and oxidative stability of biodiesel produced from catfish oil by-product from meal feed industry. Submitted, JAOCS

Brown, Ashli E, Supanee Danviriyakul, Elizabeth C. Rogers, Juan L. Silva, and William E. Holmes. Oxidation byproducts from catfish biodiesel (In review).

Danviriyakul, S., S Jongrattananon, JL Silva. Accelerated storage for prediction of biodiesel stability. (In review).

Dufreche, S., Hernandez, R., French, T., Sparks, D., Zappi, M., and Alley, E., "Extraction of Lipids from Municipal Wastewater Plant Microorganisms for Production of Biodiesel," *J. Amer Oil Chem Soc*, 2007, 84, 181-187.

Jeliazkov, V.D., B. Baldwin, W. Ebelhar, J. Miller, N. Buehring, 2008. Assessment and yield of sunflower (*Helianthus annuus* L.) grown at multiple locations in Mississippi. Agon. J. 100(3):635-642.

Li, M., Wang, T., Pham, P.J., Pittman, Jr., C.U., Li, T., "Liquid Phase Extraction and Separation of Noble Organometallic Catalysts by Functionalized Ionic Liquids," *Separation Science and Technology*, 2008, 43, 1-14.

Li, M., Pham, P.J., Li, T., "Extraction and Concentration of Omega-3 Fatty Acid Methyl Esters by Ionic Liquids Containing Silver Salt," *Separation Science and Technology*. Conditionally accepted. Revision required.

Liang, K., Toghiani, H., Hernandez, R., French, W.T., Dufreche, S., Mondala, A., "Biodiesel Production by *In-Situ* Transesterification of Primary and Secondary Sludge," *Bioresource Technology*, Submitted June 2007. Conditionally accepted. Revision required.

Min Li, Tao Wang, Patrisha J. Pham, Charles U. Pittman, Jr., Tingyu Li, "Liquid phase extraction and separation of noble organometallic catalysts by functionalized ionic liquids", Separation Science and Technology, **2008**, 43, 828-841.

Min Li, Tingyu Li "Enrichment of Omega-3 polyunsaturated fatty acids methyl esters by ionic liquids containing silver salt", Separation Science & Technology, **2008**, 43, 2072-2089.

Min Li, Patrisha J. Pham, Charles U. Pittman, Jr., Tingyu Li "Selective Solid-Phase Extraction of α-Tocopherol by Functionalized Ionic Liquid-Modified Mesoporous SBA-15 Adsorbent", Anal. Sci., in press.

Min Li, Patrisha J. Pham, Charles U. Pittman, Jr., Tingyu Li; "SBA-15-supported ionic liquids containing silver salts: Novel mesoporous pi-complexing sorbents for separating polyunsaturated fatty acid methyl esters",Microporous and Mesoporous Materials, in press.

Oldham, L.O., B.S. Baldwin, D.J. Lang, and M. Collins. Biofuel research efforts in Mississippi. *In* Carl Crozier ed. Southern Plant Nutrient Management Conference

Proceedings. October 2-3, 2007. Olive Branch, MS. Publisher: The Noble Foundation.

Paraschivescu, M.C., Alley, E.G., French, W.T., Hernandez, R, Armbrust, K., "Determination of Methanol in Biodiesel by Headspace Solid-Phase Microextraction," *Bioresource Technology*, Accepted for Publication, September 2007.

Singh, A.K., Fernando, S., and Hernandez, R., "Base-Catalyzed Fast Transesterification of Soy Bean Oil Using Ultrasonication," *Energy & Fuels*, 2007, 21, 1161-1164.

Singh, S.K., V.G. Kakani, D. Brand, B. Baldwin, K.R. Reddy. 2008. Assessment of cold and heat-tolerance of winter-grown canola cultivars by pollen based parameters. J. Agron. Crop Sci. 194:225-236.

Other Publications:

National Winter Canola Variety Trail. 2007. Report of Progress 973. Kansas State Uni. Agric. Expt. Stat. And Coop. Ext. Ser. Contribution No. 07-187-S.

National Winter Canola Variety Trail. 2006. Report of Progress 973. Kansas State Uni. Agric. Expt. Stat. And Coop. Ext. Ser. Contribution No. 07-187-S.

Horton D. S., B. S. Baldwin and K. B. Holmberg. 2006. Determination of optimum planting date of seven species of winter oilseeds in Mississippi (A preliminary study). ASA-CSSA-SSSA International Meetings, Indianapolis, IN. 12-16 Nov.

McGillivray, J, Jl Silva, R Hernandez. 2006. The Study of Oxidative Stability of Biodiesel and Their Feedstocks. Miss. Academy Sci. mtg, Vicksburg, MS Feb. 23-24. J Miss. Academy Sci. 51(1):24-25.

Silva, JL, T French, R Hernandez, S Dean. 2006. Catfish by-products as a source of Biodiesel- Availability, sources, quality. 5th Annual Southern BioProducts Conf., Choctaw, MS April 3-4.

McGillivray, J, R Hernandez, JL Silva. 2006. Oil Stability Index as a Measure of Lipid and Biodiesel Quality. 5th Annual Southern BioProducts Conf., Choctaw, MS April 3-4.

Danviriyakul, Supanee, S. Jongrattananon and J.L. Silva. 2006. Oxidative stability of catfish and soybean biodiesel. 2006 MSU Bioddiesel Workshop, MSU, August 24.

McGillivray, John, JL Silva and R Hernandez. 2006. Extraction method affects oxidation of catfish and soybean oils. 2006 MSU Biodiesel Workshop, MSU, August 24.

Danviriyakul, S., S, Jongrattanon, S., Silva, JL. 2007. COMPARISON OF STORAGE STABILITY OF CATFISH BIODIESEL WITH AND WITHOUT ANTIOXIDANT. Miss. Academy Sci. mtg, MSU, MS Feb. 22-23. J Miss. Academy Sci. 52(1): 81.

Danviriyakul, S, Jongrattanon, S., Silva, JL. 2007. OXIDATIVE STABILITY OF CATFISH AND SOYBEAN BIODIESEL. Miss. Academy Sci. mtg, MSU, MS Feb. 22-23. J Miss. Academy Sci. 52(1): 70.

Danviriyakul, S.; Jongrattanon, S.; Patel, M, Kim, T., Silva, J.L. 2007**.** Oxidative Stability of Catfish and Soybean Biodiesel. 2007 MSU Biofuels Conf., Aug. 24, MSU (poster).

Danviriyakul, S.; Jongrattanon, S.; Silva, J.L. 2007. Comparison of Storage Stability of Catfish Biodiesel with and without Antioxidant. 2007 MSU Biofuels Conf., Aug. 24, MSU (poster).

Danviriyakul, Supanee, Saowalee Jongrattananon and JuanL. Silva. 2008. Stability of catfish antioxidant-containing biodiesel under accelerated storage conditions. Miss. Academy Sci. mtg, Olive Branch, MS Feb. 21-22. J Miss. Academy Sci. 53(1): 51-52 (Abst. P3.05, student competition).

Theses and Dissertations:
Holmberg, Kyle B. Selection for reduced seed dormancy in seven native grass species. M.Sc. Mississippi State Univ. Plant and Soil Sci. Dec. 2007.

McGillivray, John. 2006. The Oxidative Stability of Soybean and Catfish Methyl Esters and their Feedstocks. MS Thesis, FNH, MSU.

Website:

a. Web site or other Internet sites that reflect the results of this project
   Research projects are reflected under:
   http://www.che.msstate.edu/research/MDERL/
   A Research Experiences for Undergraduates (REU) student also worked on this project and the information is featured on: http://www.msstate.edu/org/reubonds/
b. Networks or collaborations fostered
   Networks and contacts were made through the MSU Electron Microscope Center for completion of TEM and other electron microscope characterizations.

Networks Fostered:
National
There are six Land Grant scientists in the US that work with castor (2 in TX, 1 in MS, 2 in NY, 1 in IL). We have formed a working group to make solicitation of funding more likely.
Regional

Southeastern Regional Bioenergy Group based in Tifton GA

Main Research Product: New way to isolate omega-3 fatty acid, new way to isolate Vitamin E

Inventions/Patent Applications, licensing agreements: provisional patent application filed on Method for Isolating and Enriching Polyunsaturated Fatty Acid Methyl Esters from a Mixture of Fatty Acids.

Sustainable Energy Research Center
Bio-oil Thrust Area Final Report for 2006-2008

1. **Project title, principal and co-investigators:** B. Development of Fuels and Chemical Co-Products from Bio-Oils

Principal investigator: Philip H. Steele
Co-investigators: Mark Bricka, Sandun Fernando, Leonard Ingram,
Moon Kim, Charles Pittman, Hossein Toghiani, Rebecca Toghiani

2. **List of authorized distribution:** The information contained in this report is available for distribution as DOE deems necessary.

3. **Executive Summary**

Task B.1: Characterization of bio-oils produced from southern forestry and agricultural feed stocks
Several southern forestry and agricultural biomass types were tested as pyrolysis feed stocks. Feed stocks, bio-oils and chars were pyrolyzed and chemically and physically analyzed. Yields of bio-oil ranged from 35.2 percent to 60.1 percent for the various feed stocks. Char yields varied widely by feed stock type and ranged from 12.1 to 34.6 percent. Water content, acid value, viscosity, and percent solids varied among bio-oils by feed stock type; specific values are reported in the full summary and in publications resulting from this research.

Task B.2: Bio-oil hydrogenation and co-pyrolysis for fuels and co-products
Hydrodeoxygenation (HDO) catalysts developed and tested in a batch reactor at various temperature, residence time and pressure regimes. A catalyst and processing system was developed that produced HDO bio-oil in 30 minutes or less. Yield of HDO bio-oil was 35% by weight and the HDO bio-oil contained 72% of the original energy of the raw bio-oil. This HDO treatment reduced water from 20 to 5%, while viscosity remained approximately the same. HHV was more than doubled and acid value was reduced by 67%. The chemical properties of the HDO bio-oil were shown by FTIR to be similar to the aromatics and alkanes spectral regions to petroleum diesel.

A bio-oil esterification method developed that reduces bio-oil water content and acidity while significantly increasing HHV. The increase in HHV moves bio-oil to an energy level of 80% of No. 2 fuel oil, making the upgraded bio-oil much more competitive as a liquid fuel than is raw bio-oil.

Copyrolysis of waste plastics with wood showed that a 50:50 mixture produced a mildly upgraded bio-oil. Carbon content was increased while oxygen content was significantly decreased; water content remained about the same but acid value was reduced to nearly one half of that of raw bio-oil.

Task B.3: Upgrading pyrolysis vapor via catalysis and filtration
Prior to continuous catalytic upgrading of pyrolysis vapor directly from the auger reactor batch phase catalytic vapor phase experiments were conducted using bio-oil model compounds, simulated bio-oil mixtures, and crude bio-oil co-fed with solvents. Subsequent continuous-flow catalytic treatment studies employed a packed bed reactor. Following the packed-bed reactor experiments, a fixed-bed up-flow reactor was designed for pyrolysis vapor phase treatment. This reactor was installed at the outlet of the auger reactor; thus, the pyrolysis vapor entering the fixed bed flow reactor were typical of bio-oil pyrolysis vapors. Six catalysts were tested with some indicating relatively low coking. Water content is high with some presumably from successful HDO reactions. Over pyrolysis may also be occurring and will need to be addressed in future research. A proprietary ceramic filter was used to successfully filter char.

Task B.4: Bio-oil treatment with supercritical fluids
Supercritical water treatment of bio-oil was tested to attempt to selectively decompose compounds known to rapidly coke catalysts during HDO catalysis. Our experimental results indicate that such selective degradation is not possible utilizing the supercritical conditions that we tested. The supercritical water environment results in significant degradation of all compounds present in the bio-oil. However, furfural, vanillin and levoglucosan, which are known to contribute significantly towards coke formation, were effectively eliminated as a result of the treatment. Thus, it may be possible to significantly shorten treatment time and effect a less complete degradation of the bio-oil.

Task B.5: Fuel and chemical production from pyrolysis of CCA-treated lumberA micro pyrolysis system was designed and fabricated to produce the bio-oil for the electrokinetic tests. EK test results indicate that 99% of the copper, 95% of the arsenic, and 88% of the chrome could be removed.

4. Comparison of goals and actual activities

See attached spreadsheet.

5. Summary of activities

Task B.1: Characterization of bio-oils produced from southern forestry and agricultural feed stocks

The hypothesis under which the research on characterization of bio-oils produced from southern feed stocks was performed was that forms of southern forestry and agricultural feed stocks should be tested to determine their potential. Utilization of ground whole-tree and harvest residue were hypothesized to have potential problems for the production of bio-oil that should be identified.

Feed stocks, pyrolysis char and bio-oil characterization by GC/MS and pyrolysis gas chromatography (Py-GC/MS) were performed. Py-GC/MS experiments were performed on kenaf, switchgrass, sweet gum, white oak, pine and corn stover. Py-GC/MS analyses were also performed on feed stock mixtures of switchgrass/white oak, switchgrass/sweet gum, kenaf/sweet gum and kenaf/sweet gum.

Analyses of bio-oils and chars produced by the MSU auger bio-oil reactor were also performed. Feed stocks pyrolyzed and chemically and physically analyzed were white oak, sweet gum, switchgrass, and kenaf, bundled pine harvested from mature stand, 1st thinning harvest, 2nd thinning harvest, corn stalks, pine needles, cottonwood cottonwood whole tree, cottonwood bark, and cottonwood leaves. Table 1 gives a summary of selected results from the chemical and physical analyses performed on the bio-oils.

Table 1. Selected chemical and physical analysis results for southern forestry and agricultural feed stocks.

Sample ID	%Water	Acid Value	pH	Density	Viscosity	Solids
				kg/l	cSt	%
White Oak	12.7	119	2.72	1.21	72.1	1.23
Sweet Gum	23.8	130	2.81	1.18	28.3	0.72
Switchgrass	11.2	105	3.10	1.15	42.5	1.92
Pine wood	13.0	82	3.10	1.19	80.7	0.12
Mature Stand	18.9	116	2.94	1.19	36.7	0.96
1st Thinning	22.4	111	2.95	1.19	38.8	1.08
2nd Thinning	19.6	116	2.91	1.20	30.0	0.75
Pine bark	19.8	84	3.20	1.17	very high	2.10

Bio-oil yields of bio-oil ranged from 35.2 to 60.1 %. Bark feedstocks typically gave a lower yield than feedstocks from wood or wood mixed with bark or leaves or needles components. Pine wood gave the highest bio-oil yield. Char yields varied widely by feed stocks type and ranged from 12.1 to 34.6 %.

Bio-oil water content, acid value, viscosity, and percent solids were variable by feed stock type. Water content was highest for sweetgum and 1st thinning pine and lowest for pine clear wood and switchgrass. The pH for all bio-oils was fairly consistent in the range of 2.7 to 4.2. Acid values are probably a better indicator of sample acidity because dissociation of weak acids can be influenced by solution characteristics. Bio-oil made from sweetgum had the highest acid value. Pine bark produced a bio-oil that was extremely viscous. Bio-oil from pine bark and switchgrass also contained the highest non-filterable solids. Weight average molecular weights were determined by gel permeation chromatography and ranged from 330 to 470. GC/MS analysis results showed that the bio-oils were a complex mixture of organic acids, aldehydes, ketones, alcohols, furans, and substituted phenols. Bio-oils HHVs ranged from 7125 to 9410 Btu/lb ; for char the HHVs ranged from 11,352 to 15,392 BTU/lb.

Task B.2: Bio-oil hydrogenation and co-pyrolysis for fuels and co-products

We hypothesized that screening of additional HDO catalysts, combined with application of new temperature and pressure regimes, would allow identification of a successful HDO catalyst.

Hydrodeoxygenation (HDO) catalysts previously reported as performing bio-oil HDO were tested to prove repeatability of previous studies. Additional commercial catalysts as well as catalysts synthesized in our laboratory were tested.

Our research to date has resulted in our development of a catalyst and catalysis system that produces HDO bio-oil in 2 h or less in a batch reactor. The yield of HDO bio-oil is 35% by weight with this product containing 72% of the original energy of the raw bio-oil. The physical and chemical properties of our raw bio-oil are compared to HDO bio-oil are given in Table 2. Water content was significantly reduced from 20 to 5% and acid value was reduced to about one-third of the original value of 97. Viscosity was somewhat reduced. The HHV of HDO bio-oil was roughly twice that of the raw bio-oil, increasing from 17 to 35 MJ/kg.

Table 2. Physical and chemical properties of HDO compared to raw bio-oil from southern pine feed stocks.

Parameters	Raw bio-oil	HDO bio-oil
Water (wt %)	20	5
Acid value (mg KOH/g)	97	32
pH	3.2	4.0
Oxygen content (wt%)	45	5
Viscosity at 400C (cSt)	12.0	10.4
HHV (Mj/kg)	17	35
Ash (wt %)	0.04	0.04

The chemical properties of the HDO bio-oil are compared to both petroleum diesel and raw bio-oil in the FTIR spectra shown in Figure 1. Comparison of these spectra indicates that, in the aromatics area of the spectrum (< 1400 wavenumber), the raw bio-oil is similar to diesel in chemical character. This is also true in the alkanes region (> 2900 wavenumber).

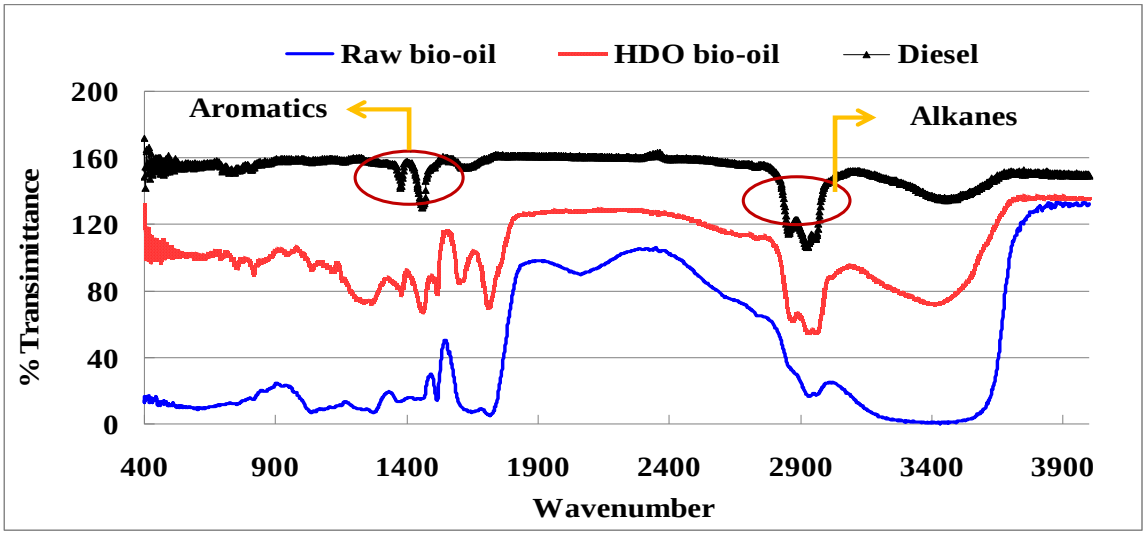


Figure 1. FTIR spectrum of petroleum diesel vs raw and HDO bio-oils.

A bio-oil esterification method was developed that reduces water content and acidity while significantly increasing HHV. Table 3 gives the properties of the upgraded bio-oil versus the properties of raw bio-oil. Upgraded bio-oil acid value and water content were reduced by more than half, from 19.6 to 9.0% for water content and from 89 to 4.4 for acid value; HHV was increased by 36% from 17.5 to 23.8; flash point was reduced from 106 to 90^{0}C. Viscosity increased slightly from 30 to 38 but remains well within the acceptable range for fueling a liquid-fueled boiler. A decrease in acid value will eliminate the corrosion issue involved with utilization of bio-oil as a liquid fuel. Reduced water content and flash point will significantly improve the upgraded bio-oil combustibility. The increase in HHV moves bio-oil to an energy level of 80% of No. 2 fuel oil, making the upgraded bio-oil much more competitive as a liquid fuel than is raw bio-oil. The ash content of raw bio-oil is a very low 0.04% and upgraded bio-oil maintains this level. Low ash content eliminates a source of deposition on boiler parts.

Table 3. Physical and chemical properties for the bio-oil produced from pine wood.

	Raw bio-oil	Esterified bio-oil
Water (%)	19.6	9.04
Acid value (mg KOH/g)	89	4.37
Higher heating value (MJ/kg)	17.51	23.83
Flash point (°C)	106	90
Viscosity at 40^{0}C (cSt)	29.95	38
Ash (wt %)	0.04	0.04
Specific gravity at 20^{0}C (g/ml)	1.25	1.22

Waste plastics (polystyrene, high density polyethylene and polypropylene) were copyrolyzed with pine wood to determine the bio-oil upgrading potential. Py-GC/MS analyses were initially performed on wood

and plastic combined in five ratios: 100:0, 25:75, 50:50, 75:25 and 0:100 (w/w). Results indicated that chemical product distribution was strongly influenced based the specific wood-to-plastic ratio. Inspection of the chemical species produced for all wood/plastic ratios showed no new chemical compounds beyond those formed during the pyrolysis of the wood and plastics alone. Thus, there was no evidence of the occurrence of chemical cross-reactions between wood and plastic vapors at the conditions tested. Py-GC/MS results indicated that a 50:50 plastic to wood ratio was the optimum mix of those tested; temperature of 450 °C was the best temperature for both wood and plastic pyrolysis.

Elemental analysis of each wood/plastic bio-oil was compared with the pine bio-oil. The amounts of carbon present in the pine wood/polystyrene (PS), pine wood/high density polyethylene (HDPE) and pine wood/polypropylene (PP) bio-oils were 66.27, 68.59 and 79.7%, respectively. Thus, the carbon contents were increased by 15.8 to 38.5% compared to pine bio-oil (carbon content 57.2%). The amounts of oxygen present in the pine wood/plastic bio-oils were significantly lower compared to the pine bio-oil alone. The oxygen content of the pine wood/PP bio-oil was only 9.55 % which is a 70.34% reduction versus that in pine bio-oil (oxygen content 32.2%). The oxygen content of the pine wood/PS and pine wood/HDPE bio-oils were 27.02 and 22.9%, respectively, which were 16.08% and 28.8% lower compared to the oxygen content of the pine bio-oil alone. The polyolefinic plastics, used for the copyrolysis, were long chain hydrocarbons that do not contain oxygen. When pine wood was copyrolyzed with each plastic in 50:50 (w/w) ratio, the only source of the oxygenated compounds were the 50 wt% of pine wood. Therefore, the amount of oxygen was lowered and carbon and hydrogen content increased in the pine wood/plastic bio-oil compared to the pine bio-oil alone.

The water content, pH, acid value, density and viscosity of the pine wood bio-oil, pine wood/PS, pine wood/HDPE and pine wood/PP bio-oils were determined. The pine wood/PP copyrolysis bio-oil had water content of 5.44 %. This amount was significantly lower than the water present in the pine wood/HDPE and pine wood/PS bio-oils. The amounts of water present in the pine wood/HDPE and pine wood/PS bio-oils were 15.7 and 9.47%, respectively. The pine wood bio-oil had a 13 % water content. The pine wood/PS bio-oil's pH was slightly lower (pH=2.82) than that of the pine wood/HDPE bio-oil (pH=3.03) and pine wood/PP bio-oil (pH=3.02). The acid value of pine wood/HDPE bio-oil was 72.53, much higher than the pine wood/PS bio-oil (30.62) and pine wood/PP bio-oil (38.12). The pine bio-oil had a pH of 3.1 and acid value of 82. The higher acid value indicates the presence of the higher amounts of carboxylic acids in the bio-oil.

Task B.3: Upgrading pyrolysis vapor via catalysis and filtration

The hypothesis under which upgrading of bio-oils via vapor catalysis was performed was that new catalysts, beyond those tested in previous research, should be screened and new processes developed in an attempt to circumvent the rapid catalyst deactivation from coking experienced by previous researchers. Investigators believed that methodical studies employing bio-oil simulants would allow elucidation of the mechanisms underlying rapid catalyst coking and provide insight as to the means to circumvent this coking. The hypothesis underlying vapor filtration was that the proper media must be developed to allow filtration of char particles from the hot pyrolysis vapor stream. This filtration was expected to assist in reduction of catalyst deactivation.

Vapor phase batch reactor studies were undertaken to provide rapid catalyst screening under controlled operating conditions. A Parr batch reactor was employed. Catalytic hydrotreating (HDT) reactions of four model bio-oil components versus catalyst composition, temperature, pressure, and time elucidated the conversion and product distribution for each model compound. 2-Furaldehyde (aldehyde), anisole (phenol), cyclopentanone (ketone), and acetic acid (carboxylic acid) were employed as model compounds.

A bio-oil simulant was employed to allow determination of the bio-oil components that result in rapid deactivation of the catalysts in previous research. The bio-oil simulant was a mixture of methanol (5%), acetaldehyde (12%), acetic acid (14%), glyoxal (4%), acetol (8%), glucose (8%), guaiacol (17%), furfural (4%), vanillin (8%), and water (20%), all by weight. The pH of the simulated bio-oil was approximately 2.3.

Seven commercial catalysts and our synthesized HDT catalysts were screened for upgrading of the bio-oil simulant. Anisole was very reactive on all the HDT catalysts. No coking occurred from HDT of anisole for the catalysts tested. Furfural was found to be stable at 300 °C over cracking catalysts. Furfural showed extensive coking over both cracking and HDT catalysts compared to anisole, cyclopentanone, and acetic acid. Acetic acid was very stable below 300 °C on all the HDT catalysts tested. C_2 and C_3 gaseous hydrocarbons from acetic acid were formed only at 350 °C or above.

Extensive coking of the catalysts and formation of char were observed in all the catalytic upgrading experiments using bio-oil simulant-a. Furfural gave maximum catalyst coking and also the formation of char at the bottom of the reactor. A second bio-oil simulant-b was prepared without furfural. Furfural was replaced by excess addition of methanol. All the experiments were carried out for 60 min.

Batch phase catalytic HDT reactions with raw bio-oil as the substrate were conducted using select HDT catalysts as a function of initial hydrogen partial pressure and hydrogen donor solvent. Three hydrogen donor solvents (tetralin, cyclohexane, ethyl acetate) were tested without hydrogen and with hydrogen at a raw bio-oil/solvent ratio of 1 to 3. Catalyst coking occurred fairly rapidly at temperatures above 270 °C. This coke development occurred with raw bio-oil, bio-oil simulant, or oxygenated model compounds. Partial deoxygenation occurred, resulting in the formation of CO, CO_2, and H_2O. Cyclohexane as a hydrogen donor gave a yellow liquid product compared to a black liquid observed when either tetralin or ethyl acetate was the hydrogen donor. Cyclohexane and tetralin proved to be effective hydrogen donor solvents while ethyl acetate did not.. Several oxygenates were reduced using cyclohexane and tetralin.

Flow reactor studies were conducted to achieve significantly shorter residence times. Initial work employing 100 % bio-oil were not encouraging with either HDT catalysts or cracking catalysts. Catalytic studies co-feeding ethanol or methanol were conducted. One catalyst produced gasoline weight compounds with alcohols as a hydrogen donor. When bio-oil (2 wt %) was cofed with either ethanol or methanol, rapid catalyst coking was due to the polymerization of bio-oil compounds. The majority of phenolic compounds also disappeared.

Construction of a heated upflow catalytic vapor phase reactor, attached to the outlet of the auger-fed bio-oil reactor, was completed and catalytic reactions were performed. Bio-oil from wood pyrolysis exited the auger reactor at ~ 450 °C and entered the catalytic heated upflow reactor, where the temperature was raised to a predetermined temperature (nominally 450 to 650 °C). A proprietary ceramic filter was utilized and was very effective for filtration of char. Following filtration the vapor passed upward through a packed catalyst bed and then to a condenser. The condensed products were analyzed by GC/MS.

Several commercial catalysts and our synthesized catalysts were tested in the upflow catalytic. For select catalysts, only a small portion of the bio-oil vapors entering the catalytic reactor were lost to coke formation on the catalyst. A large amount of gas was produced during the combined auger reactor pyrolysis plus vapor phase catalytic treatment, presumably because the catalytic reactor subjected the vapors to temperatures higher than optimum for fast pyrolysis, thereby further gasifying some of the products. The product distribution in one typical gas sample run with one catalyst was hydrogen (8.37%), carbon monoxide (40.8%), carbon dioxide (15.4%), and % methane (9.8%).

The water content in the liquid phase product from our vapor phase catalysis experiments varied from 42.8 to 66.4 %. Apparently, as upgrading proceeded and more gasification and deoxygenation occurred, additional water was produced as might be expected. The raw bio-oil produced when no catalyst was present was 48 %. Our select catalysts appeared to lowerthe acid value of the liquid product via promotion of decarboxylation of carboxylic acids.

Cracking of biomass-derived compounds was observed during in-situ catalytic upgrading of bio-oil vapor resulting in dehydration, decarboxylation, and decarbonylation reactions, which indicates the deoxygenation of bio-oil. One catalyst demonstrated significant cracking of biomass compounds resulting in the formation of hydrocarbons including toluene, xylene, indene, as well as higher molecular weight compounds including 2-methyl naphthalene, and naphthalene. One catalyst also resulted in significant decrease in the amount of carbonyl and acidic functional groups in the treated bio-oil. One support type showed a maximum decrease in carbonyls in the treated bio-oil, but did not result in formation of any non-oxygenated hydrocarbons. Qualitative GC/MS results indicated the formation of non-oxygenated aromatics such as toluene, xylenes, phenolics, and catechols. Two catalysts resulted in low coke formation and surface area reduction ~ 10 % upon regeneration.

Task B.4: Bio-oil treatment with supercritical fluids

The hypothesis underlying bio-oil treatment with supercritical fluids was that bio-oil could be processed under supercritical water conditions to transform the bio-oil chemical composition. This transformation was directed at upgrading to a form that would allow easier HDO of the product. A second hypothesis was that biomass feed stocks could be fractionated into products that would subsequently allow more successful upgrading by HDO or other means. Initial supercritical bio-oil treating experiments were performed on a bio-oil simulant while subsequent studies employed crude bio-oil obtained from the Forest Products Department.

All experiments were performed with a Parr high pressure/high temperature batch reactor, suitable for studies at pressures up to 5000 psi and temperatures up to 500 °C. Analytical support was provided by the Forest Products Department's analytical laboratory.

Supercritical Water Treatment Experiments

Computations with Chemcad (process simulation software, Chemstations, Inc., Houston, TX) were performed to determine the appropriate charge of solvent (water) and bio-oil to the reactor to achieve supercritical conditions. The bio-oil stimulant was a mixture of methanol (5%), acetaldehyde (12%), acetic acid (14%), glyoxal (4%), acetol (8%), glucose (8%), guaiacols (17%), furfural (4%), vanillin (8%) and water (20%), all by weight.. This formulation incorporated compounds containing the important functional groups comprising bio-oil.

Experiments were designed to examine the effect of operation temperature, bio-oil/water mass ratio and reaction time on the bio-oil composition. A series of experiments were performed examining the temperature range of 300 to 420 °C, bio-oil/water mass ratios of 0.01/1 to 1/1, and reaction times ranged from 30 minutes to 5 hours. Care was taken during charging of the reactor to ensure an inert atmosphere prior to introduction of the reactants. Early experiments employed the bio-oil stimulant, while later experiments employed raw bio-oil.

Experimental results indicated that, with supercritical water treatment, furfural was effectively converted to products along with formation of coke. Approximately 80% of furfural was converted, independent of

operating temperature. Vanillin conversion was essentially complete at all operating conditions examined, with an average conversion of 99.88%. Guaiacol, 4-ethyl 2-methoxy phenol and 4-methyl 2-methoxy phenol are likely products from vanillin conversion and were identified in the treated product. Levoglucosan has been reported in the literature to be a major precursor leading to coke formation. Levoglucosan conversion was only 15.7% at 300 °C, and for a one-hour reaction time. However, almost complete conversion of levoglucosan was achieved at near/supercritical conditions (380 and 420 °C).

Catechol was one of the prominent compounds produced from the supercritical conditions tested.The formation of catechol was significantly higher at 420 °C, reasonably high at 380 °C and notably lower at 300 °C. One explanation is that the formation of this compound and of other substituted phenols is from phenol. The low yield of catechol at 300 °C can be explained by the low phenol yield at the same operating temperature. Acetol, one of the compounds present in the bio-oil stimulant, was only partially converted at sub-critical treatment conditions (300 °C). In contrast, during the treatments at near-supercritial and supercritical conditions, complete conversion was achieved.

In general, the intensity and diversity of reactions occurring increased with an increase in bio-oil/water mass ratio, as expected. Unreacted acetic acid, guaiacol and acetol along with 3-methyl phenol were the most prominent products in the liquid phase with 1 wt.% bio-oil. In contrast, with 5 and 10 wt%, a broad spectrum of products including phenol, methyl and ethyl phenols, catechol and propenoic acid were present in the liquid phase and acetaldehyde, lower alkanes, alkenes, cycloalkanes and carbon oxides were present in the gas phase. The range of products was even greater with 25 wt% bio-oil. This was expected as there are a number of reactions that occur simultaneously or can occur sequentially as formed intermediate products undergo reaction with unreacted components to produce other chemical species. Also of interest is the increased rate of gas products formation with higher bio-oil composition in the feed. The increased gas production rate was assumed to be due to cracking reactions that were aided by the availability of bio-oil components at the higher bio-oil/water mass ratio.

Raw bio-oil produced from pyrolysis of clear pine wood was treated subsequent to the experiments utlilizing simulated bio-oil. Experiments were designed to examine the effect of operating temperature, bio-oil/water mass ratio and reaction time on the product distribution. Mass ratios of 1/1 to 1/3 were examined with operating temperatures between 300 and 420 °C.

Furfural was converted with a conversion of 93.8% with treatment at subcritical temperature (300 °C). The conversion at near-supercritical conditions (380 °C) was slightly less at 90.3% while treatment at 420 °C gave an average conversion of 92.4%. Conversions achieved using raw bio-oil were greater than achieved with the simulant. Guaiacol conversion was almost complete at 420 °C with an average conversion of 99.3% while that at near-supercritical conditions (380 °C) the rate was less at 89.6%. Subcritical treatment was not very effective in converting guaiacols with an average conversion of only 69.9%. An increase in bio-oil/water mass ratio resulted in greater conversion, possibly due the fact that higher bio-oil loading facilitates more numerous and effective collisions that promote the desirable reactions.

Phenol conversions were greater at subcritical conditions (300 °C) compared to those achieved at higher temperatures. This distinction, however, disappeared during the longer reaction time. The conversion of catechol was not significantly impacted by the reaction temperature. Catechol and other substituted phenols are most likely formed from phenol. This may explain the lower catechol conversions achieved during the longer reaction time due to the lower phenol conversions that could occur in a short reaction period. Conversion of vanillin was complete regardless of operating conditions. Guaiacol is most likely the major product formed by disproportionation of vanillin; 4-ethyl 2-methoxy phenol and 4-methyl 2-methoxy phenol were also likely formed from vanillin. Levoglucosan was completely converted, regardless of operating conditions.

Experiments aimed at studying the temporal behavior of the reaction system concluded that majority of reactions occur rapidly and have essentially gone to completion within the first hour of reaction time. These findings were similar to those obtained with the bio-oil simulant.. The conversions achieved at a 5-hour reaction time are essentially equivalent to those achieved at 1-hour reaction time. These results may also indicate that the reaction mixture has achieved a quasi-equilibrium state as most of the components present do not undergo further reactions or conversion during the extended reaction time.

From the experimental results, it was evident that treatment with near-supercritical and supercritical water significantly altered the bio-oil composition. Some compounds were effectively removed by the treatment, and as they disappeared, other compounds were formed. Examination of the product distribution provideed a means to evaluate the treatment process. As no effort was undertaken to separate the treated bio-oil from the water employed in the treatment process, the samples submitted for analysis were diluted and thus, concentrations reported by the Forest Products Laboratory in these samples were much lower than for raw bio-oil. These lower concentrations were due in part to the water present in the sample; as the amount of water added for supercritical treatment was determined by the bio-oil/water mass ratio, direct comparison of concentrations between runs was not possible, nor was comparison of concentrations in the raw bio-oil and treated sample.

Qualitative analysis of both the liquid products and captured gas samples from the reactor were performed. Among products in the liquid phase, while guaiacol formation was more pronounced at the lower treatment temperature, substituted phenols were more prominent with treatment at higher temperatures. This could also be due to the fact that conversion of guaiacol to phenols is more favored at the higher temperatures. Acetic acid and propanoic acid were formed at all treatment conditions. However, during the longer treatment time (5 hours), acetic acid was partially converted with treatment at 380 and 420 ^{o}C. Aliphatic compounds were generally formed only at higher operating temperatures (420 ^{o}C). For products in the gas phase, a wider spectrum of products was formed during the longer treatment time as a result of cracking reactions.

Biomass Fractionation Experiments

Examination of pretreatment strategies to fractionate biomass into its three primary constituents was proposed. A two step process was envisioned, with hemicellulose extracted first, followed by extraction of lignin from cellulose. Hydrothermal treatment of biomass was used to effectively solubilize the hemicellulose from raw biomass.

Pine wood chips were obtained from the Forest Products Department and used as the biomass feedstock. The wood chips were sieved with a mechanical shaker. Three particle sizes were collected for use in experiments - < 0.425 mm, 0.425-1 mm, > 1 mm. Lignin, hemicellulose and cellulose contents of the wood chips were determined for each collected fraction. Hemicellulose content varied between 12.6 to 14.0 %, cellulose content varied between 49.1 to 50.9 % and the lignin content varied between 24.7 to 32.7 %. Moisture content before and after drying was measured to determine the bound and unbound moisture content. Moisture contents ranged from 7.3 to 8.0 % before drying and between 2.8 to 3.6 %, with an average unbound moisture content of 4.5 % and average bound moisture content of 3.2%.

Surface area measurements of each particle range were also performed. An automated Quantachrome Autosorb Gas Sorption system was employed for these measurements. Surface area was dependent on the nominal particle size, as expected. Surface areas of 0.642 m^2/g, 0.567 m^2/g and 0.317 m^2/g were measured for < 0.425 mm, 0.425 – 1 mm, and > 1 mm, respectively.

Biomass/water mass ratios (1/20 to 1/1) and reaction temperatures (170-230 °C) were chosen as control variables and reaction time was fixed at 30 minutes for all experiments. The effect of mixing in the hydrothermal treatment was also examined through use of controlled stirrer speed (150-500 RPM). The experiment was performed by charging weighed quantities biomass into the reactor. After the reactor was sealed, it was then flushed with nitrogen gas a few times to displace any air present inside the reactor. A vacuum pump was then evacuated the residual air and nitrogen present inside the reactor. Water was then metered into the reactor via the liquid sampling valve the heating cycle initiated. The reactor contents were heated to the desired operating temperature and maintained for the thirty-minute reaction time. The reaction was then quenched by circulating cool water through the reactor cooling loop.

The treated biomass, recovered from the reactor, was weighed and dried. The products were submitted for analysis of hemicellulose, cellulose and lignin. As the treatment temperature was increased, the recovery of hemicellulose decreased. At the lowest temperature examined, 170 °C, essentially complete isolation of hemicellulose from the biomass was accomplished, with little or no removal of cellulose or lignin. As the temperature was increased, cellulose was also partially solubilized from the biomass. A higher biomass/water ratio also was desirable; greater recovery of hemicellulose was achieved at the highest biomass/water mass ratio. These studies indicated that it is possible to partition the complex biomass into a hemicellulose fraction by hydrothermal treatment, leaving cellulose and lignin exclusively in the biomass residue.

Task B.5: Fuel and chemical production from pyrolysis of CCA-treated lumber

The hypothesis underpinning the pyrolysis of CCA treated wood for fuels and chemicals was that the large volumes of this wood arriving at landfills can be pyrolyzed by small on-site reactors. This would reduce the presence of this debris in the landfills and prepare for the day when disposal in this manner is not allowed.

The micro pyrolysis system to produce the bio-oil for the electrokinetic tests was fabricated and tested. The system produced bio-oil within the experimental temperature range of 400-550 °C. Experiments with CCA-treated wood were conducted after the optimization studies were completed. A complete mass balance was developed for the CCA-metals across the system. Initial testing indicated that Cr and As are removed in the gas stream while Cu is removed with the char.

Microwave assisted acid digestions (modified EPA Method 3051) were performed to determine the metal content of CCA-treated wood, and the generated samples were analyzed by ICP. Moisture contents of the untreated and treated wood were determined by drying the wood samples in a forced air oven at 105 °C until the weight of the samples became constant. Table 4 gives a summary of the test results. EK test results indicate that 99% of the copper, 95% of the arsenic, and 88% of the chrome could be removed.

Table 4. Results of metal analysis and moisture content testing

	Untreated Wood	**CCA-treated Wood**
Moisture Content	16%	12%
Chromium	N/A	5200 ppm
Copper	N/A	3000 ppm
Arsenic	N/A	5500 ppm

6. Products developed and technology transfer activities:

Patents: None.

Publications:

L. Ingram, D. Mohan, P. Steele, D. Strobel, B. Mitchell, J. Mohammad, K. Cantrell, and C.U. Pittman, Jr. 2008. Pyrolysis of wood and bark in an auger reactor: Physical properties and chemical analysis of the produced bio-oils. *Energy and Fuels* 22(1): 614-625.

Ingram, L.I., D. Mohan, P. Steele, D. Strobel, B. Mitchell, J. Mohammad, K. Cantrell, and C.U. Pittman, Jr. 2008. Pyrolysis of wood and bark in an auger reactor: Physical properties and chemical analysis of the produced bio-oils. *Energy and Fuels* 22(1): 614-625

Leightley, L. and P. H. Steele. 2005. Energy and chemicals from wood biomass – an industry of the future for Mississippi. Tree Talk 27(4):15-16. The Mississippi Forestry Assoc., Jackson, MS.

Mitchell, B.K., L.L. Ingram, J.A. Soria, P.H. Steele and D. Strobel. 2008. Chemical and physical characteristics of bio-oils from pine and oak feed stocks. In Proc: Woody Biomass Utilization: Challenges and Opportunities. 60th Int'l Meeting of the Forest Products Research Society. June 25-27, Newport Beach, CA. Forest Products Society, Madison, WI. 103 p.

Mohan, D., C. U. Pittman and P. H. Steele. 2006. Single, binary and multi-component adsorption of copper and cadmium from aqueous solutions on Kraft lignin – a biosorbent. J. of Coloid and Interface Science, Issue 297, p 489-504.

Mohan, D., C.U. Pittman, M. Bricka, F. Smith, B. Yancey, J. Mohammad, P. H. Steele, M.F. Alexandre-Franco, B. Gomez-Serrano, H. Gong. 2007. Sorption of arsenic, cadmium, and lead by chars produced from fast pyrolysis of wood and bark during bio-oil production. J. of Colloid and Interface Science. 310 (2—7) 57-73.

Mohan, D., C. U. Pittman and P. H. Steele. 2006. Pyrolysis of wood/biomass for bio-oil: a critical review. Energy and Fuels 20(3):848-889

Steele, P. H., B. K. Mitchell and J. E. Cooper. 2007. Bundled slash: a potential new biomass resource for fuels and chemicals. In Proc. of the 29th Symposium on Biotechnolgy for Fuels and Chemicals. April 29-May2, Denver, CO. Society of Industrial Microbiology.

Steele, P.H., B.K. Mitchell, J.E. Cooper, S. Arora. 2008. Bundled slash: A potential new biomass resource for fuels and chemicals. Applied Biochemistry and Biotechnology 148 (1):1-13.

Yu, F., R. Ruan, P.H. Steele. 2008. Consecutive reaction model for the pyrolysis of corn cob. Transactions of the American Society of Agricultural and Biological Engineers. Vol. 51(3): 1023-1028.

Presentations:

Bhatttacharya, Priyanka, Moon Kim, Philip H. Steele, Leonard Ingram, and Charles Pittman, Jr. 2007. Fast pyrolysis of waste plastics with woody biomass. D5 IUFRO, Taipei Taiwan, November 2007.

Bhattacharya, P., P.H. Steele, L.L. Ingram and C.U. Pittman. Development and fuels and value-added chemicals form pyrolysis of wood and waste plastic mixtures. 235th American Chemical Society National Meeting & Exposition. April 6-10. New Orleans, LA.

Bhattacharya, P., P. H. Steele, L. L. Ingram and C.U. Pittman, Jr. 2008. The influence of plastic addition to wood biomass for production of pyrolysis liquid fuels. Mississippi State University. The Southeastern Natural Resources Graduate Student Symposium. March 26-28. Starkville, MS.

Bhatttacharya, Priyanka, Philip H. Steele, Leonard Ingram, and Charles Pittman, Jr. 2007. Co-pyrolysis of pine wood with three waste plastics. 61st Int'l Meeting of the Forest Products Society. June, 2007. Knoxville, TN.

Gajjela, S.K., F. Yu, E.M. Hassan and P.H. Steele. The application of NiMo and CoMo catalysts to the hydrodeoxygenation of bio-oils. Mississippi State University. The Southeastern Natural Resources Graduate Student Symposium. March 26-28. Starkville, MS.

Gajjela, S.K. 2008. The influence of water content on hydrodeoxygenation of bio-oil by NiMo and CoMo catalysts. 62nd Int'l Convention of the Forest Products Society. June 22-24. St. Louis, MO.

Gajjela, S.K., E.M. Hassan, F. Yu, P.H. Steele 2008. Hydrodeoxygenation of wood-based bio-oils on reduced NiMo / Al_2O_3 and CoMo / Al_2O_3 catalyst. Mississippi State University. Graduate Student Association, 6th Annual research symposium. April 4. Starkville, MS.

Guda, V.K, R. Challa, H. Toghiani, C.U. Pittman, Jr., A.C. Gujar, P.H. Steele. 2007. Catalytic upgrading of bio-oil AIChE National Meeting. Salt Lake City, UT, November 4-9.

Ingram, L., P. H. Steele, D. Strobel, and B. Mitchell. 2006. Characterization and analysis of bio-oils produced with wood and bark feed stocks using an auger fed reactor. Mississippi Biomass Council 5th Annual Southern Bio-Products Conference. April 3-4. Pearl River Resort, Choctaw, MS.

Ingram, L. and P. H. Steele. 2006. Wood-based bio-oil for fuel. SmallWood 2006. May 16-18, Richmond, VA. Forest Products Society, Madison, WI.
Li, Q., F. Yu, E.M. Hassan, L. L. Ingram, and P.H. Steele. 2008. Solid acid catalytic upgrading of bio-oils. Mississippi State University. The Southeastern Natural Resources Graduate Student Symposium. March 26-28. Starkville, MS.

Li, Q., F. Yu, E.M. Hassan, L.L. Ingram, Jr. and P.H. Steele. Bio-oil upgrading to remove acid by solid acid catalysis. Forest Products Society International Convention. June 22-24. St. Louis, MO.

Mitchell, B.K., P.H. Steele, J.E. Cooper, S. Arora. 2007. Components and aging characteristics of bundled southern pine slash. Arkansas Forum on the Productivity of the John Deere slash bundler. School of Forest Resources, University of Arkansas at Monticello. May 15. Monticello, AR.

Steele, P. H. 2004. The potential for developing a bio-oil industry in Mississippi. Southern Bio-Products Conference. March 4-6. Biloxi, MS.

Steele, P. H. 2005. Forest biomass feed stock availability. 2005 Southern Bio-Products Conference. March 22-23. Jackson, MS.

Steele, P. H. 2006. Current and future products from pyrolysis oils. 2006 Bioenergy and Wood Products Conference. March 14-16. Denver, CO. Society of Industrial Mycology.

Steele, P. H., B. K. Mitchell and J. E. Cooper. Bundled slash: a potential new biomass resource for fuels and chemicals. 29th Symposium on Biotechnolgy for Fuels and Chemicals. April 29-May 2, Denver, CO. Society of Industrial Microbiology.

Steele, P.H., B.K. Mitchell and S. Arora. 2007. Yield, composition, curing and pyrolysis of bundled southern pine harvesting slash. Wood Biomass Technical Interest Group: Utilization Challenges and Opportunities. June 10-13, Knoxville, TN. 61st International Forest Products Society Convention.

Steele, P.H., E.M. Hassan, F. Yu, B.K. Mitchell, L.L. Ingram, Jr. 2008. The potential for whole-tree utilization for bio-oil production. 62nd Int'l Forest Products Society International Convention. June 22-24. St. Louis, MO.

Steele, P.H. and B. Mitchell. 2008. Bundled slash: a potential new biomass resource for energy, fuels and chemicals. 2008 Mid-South Forestry Equipment Show: Woody Biomass Seminar. June 5. Starkville, MS.

Steele, P.H. and B.K. Mitchell. 2008. Bundled slash: a potential new biomass resource for energy, fuels and chemicals. Woody Biomass Conference: Fueling the Future. June 5. Mississippi State University, Starkville, MS.

Steele, P.H., S. Gajella and F. Yu. 2008. A pyrolytic path to hydrocarbons. Mississippi State Universsity. 3rd Biofuels Conference. Aug. 14-15. Starkville, MS.

Steele, P.H., E.M. Hassan, F.Yu, B.K. Mitchell and L.I. Ingram. 2008. The potential for whole-tree utilization for bio-oil production. The 62nd Int'l Convention of the Forest Products Society. St. Louis, MO. June 22-24.

Steele, P.H. 2008. Biofuels from Mississippi forest resources. Mississippi State University, Forest and Wildlife Research Center Technology Transfer Conference. August 5-6. Starkville, MS.

Toghiani, R.,K , A.K. Sekar, P. Steele. 2007. Improvement of bio-oil stability. Forest Products Biorefineries II session at the 2007 AIChE Annual Conference, Salt Lake City, UT, November 4-9, 2007.

Poster Forums

Bhattacharya, P. Utilization of waste plastic to upgrade wood-derived bio-oil products. Seventh Annual Southern Bio Products and Renewable Energy Conference. April 14-15. Choctaw, MS. Mississippi Biomass Council, Jackson, MS.

Bhattacharya, P., P.H. Steele, Ingram, L.I., and C.U. Pittman, Jr. 2007. Upgrading bio-oil by co-pyrolysis of woody biomass with selected polymers. Mississippi State University. 2nd Biofuels Conference. August 27, 2007. Starkville, MS.

Bhattacharya, P. P. Steele, K Cantrell, and L. Ingram. 2007. Improvement of bio-oil quality by removal of acids and water. Mississippi State Univ. 2nd Biofuels Conference. August 27, 2007. Starkville, MS.

Bhattacharya, P., P. Steele, L. Ingram and C.U. Pittman, Jr. 2007. Upgrading of bio-oil by co-pyrolysis wood biomass with.selected polymers. Mississippi State Univ. 2nd Biofuels Conference. August 27, 2007. Starkville, MS.

Bricka, M. 2008. Design of a laboratory-scale pyrolysis system for evaluating the recycle potential of CCA-treated wood waste. Mississippi State University. 1st Energy Synergy Workshop. June 17. Starkville, MS.

Guda, V.K., H. Toghiani, C.U. Pittman, Jr., .U., A. Gujar, C. R. Challa, P. Steele. 2007. Catalytic upgrading of bio-oil vapor. Mississippi State Univerisity. 3rd Biofuels Conference. Aug. 14-15. Starkville, MS.

Gajjela, S.K., E.M. Hassan, F. Yu, P.H. Steele 2008. Upgrading pyrolysis derived wood-based bio-oils on different commercial hydrotreating catalysts. Mississippi State University. 1st Energy Synergy Workshop. June 17. Starkville, MS.

Gajjela, S. Upgrading pyrolysis derived wood-based bio-oils on commercial hydrotreating catgalysts. Seventh Annual Southern Bio Products and Renewable Energy Conference. April 14-15. Choctaw, MS. Mississippi Biomass Council, Jackson, MS.

Gajjela, S.K., E.M. Hassan, F. Yu and P.H. Steele. 2008. Second generation bio-fuels: study of hyddrodeoxygenation of bio-oils from the fast pyrolysis of pine wood. Mississippi State Univerisity. 3rd Biofuels Conference. Aug. 14-15. Starkville, MS.

Guda, V.K., H. Toghiani, C.U. Pittman and P. H. Steele. 2008. Catalytic upgrading of pyrolysis vapor. 3rd Biofuels Conference. Aug. 14-15., Starkville, MS.

Hall, J.W., B.K. Mitchell, P.H. Steele, E.M. Hassan. 2007. Production of bio-oil from bundled pine harvested slash. Mississippi State University. 2nd Biofuels Conference. August 27, 2007. Starkville, MS.

Hassan, E.M., L.L. Ingram, Jr., P.H. Steele. 2008. Chemical pretreatment applications of pine feed stocks to modify bio-oil chemical speciation. Mississippi State University. 1st Energy-Synergy Workshop. April 17. Starkville, MS.

Hassan, E.M., L.L. Ingram, Jr., P.H. Steele. 2008. Chemical characterization of fast pyrolysis bio-oils produced from pretreatments of pine wood feed stocks. 30th Symposium on Biotechnology for Fuels and Chemicals. May 4-7. New Orleans, LA.

L. Ingram, D. Mohan, P. Steele, D. Strobel, B. Mitchell, J. Mohammad, K. Cantrell, and C.U. Pittman, Jr. 2008. Pyrolysis of wood and bark in an auger reactor: Physical properties and chemical analysis of the produced bio-oils. Energy and Fuels 22(1): 614-625.

Li, Q. Upgrading of bio-oils with sulfate-promoted iron oxide. Seventh Annual Southern Bio Products and Renewable Energy Conference. April 14-15. Choctaw, MS. Mississippi Biomass Council, Jackson, MS.

Li, Q. , F. Yu, E.M. Hassan, L.L. Ingram, Jr. and P.H. Steele. 2008. Sulfur-promoted iron oxide catalysis for upgrading of bio-oils. Mississippi State University. 1st Energy-Synergy Workshop. April 17. Starkville, MS.

Li, Q., F. Yu, E.M. Hassan, L. L. Ingram, and P.H. Steele. 2008. Soil acid catalytic upgrading of bio-oils. The Southeastern Natural Resources Graduate Student Symposium. March 26-28. Starikville, MS.

Li, Q., F. Yu, E.M. Hassan, L. L. Ingram, and P.H. Steele. 2008. Differential sugar allocation by a py-GC/MS study of pretreated pine wood. Mississippi State University. 3rd Biofuels Conference. Aug. 14-15., Starkville, MS.

Mitchell, B.K., P.H. Steele, E.M. Hassan. 2008. Collecting and utilizing southern pine post-harvest residue. Mississippi State University. 1st Energy-Synergy Workshop. April 17. Starkville, MS.

Sekar, A.K., Toghiani, R.K., Steele, P. 2007. Improvement of bio-oil stability using bcritical/supercritical water treatment. Mississippi State Univ. Bioenergy Conference, Mississippi State University, August 27, 2007.

Sekar, A., R.K. Toghiani and P.H. Steele. 2008. Effect of supercritical water on the composition of bio-oil. 3rd Biofuels Conference. Aug. 14-15. Mississippi State Univerisity, Starkville, MS.

Steele P. H. 2004 BioOil: The natural energy source for our forests. Conference for Biomass Utilization as the South's Industry of the Future. Oct. 25-26/ Paul W. Bryant Conf. Center. Tuscaloosa, AL.

Tripathi, M.M., E.M..Hassan, L. Ingram and P. Steele. 2007. Application of NIR spectroscopy for monitoring bio-oil polymerization. Mississippi State University. 2nd Biofuels Conference. August 27, 2007. Starkville, MS.

Sustainable Energy Research Center
Ethanol Thrust Area Final Report for 2006-2008

1. Project title, principal and co-investigators: C. Conversion of Lignocellulosic Biomass to Ethanol Using Novel Processes

Principal investigator: Todd French
Co-investigators: Rafael Hernandez, Hossein Toghiani, Cliff George, Mark Bricka, Bill Elmore, Susan Bridges, Yoginder Dandass, James Warnock, Dwaine Braasch, Yean-Sung Jung, Shane Burgess, **Error! Reference source not found.**, and Lewis R. Brown

2. List of authorized distribution

The information contained in the section of the Sustainable Energy Research Center report is available to be distributed as the Department of Energy deems necessary.

3. Executive Summary

Task C.1: Optimization of the Acid Hydrolysis Process for Ethanol and Biodiesel Production

Based on the work conducted by the feedstock group, switchgrass was selected as the source of lignocellulosic biomass. A method was developed and a hydrolyzate was produced for the co-production of ethanol and triglycerides via ethanolagens and oleaginous microorganism *Rhodotorula glutinis*.

Task C.2: Optimization of Ethanol Production from Acid Hydrolysates

The objective of this task was to determine the scientific feasibility of coupling ethanol production with triglyceride production using an acid hydrolysate from lignocellulosic biomass. Ethanol was produced in a low pH medium with glucose as the source of carbon. This was a good first step if the oleaginous microorganisms had the ability to selectively remove only non-fermentable components. What was discovered was the oleaginous microorganisms would selectively remove the glucose prior to the removal of the non-ferementable portion. What this meant was if the two process were to be coupled it would require the fermentation of the fermentable sugars to occur first followed by a conversion of the non-fermentables by the oleaginous microorganisms.

Task C.3: Isolation and Optimization of Microorganisms Capable of Fermenting Syngas to Ethanol

A second process also under development is thermally depolymerize biomass to produce syngas (CO, CO_2, H_2, etc.). This is a very promising technology given the wide range of feedstocks that can be gasified and subsequently converted to ethanol. There exist microorganisms with the ability to metabolically convert CO and H_2 to ethanol or acetic acid depending on the conditions of their environment. Estimated yields of ethanol are 75-80 gallons per dry ton of biomass. Several organisms were isolated with the ability to utilize components of syngas and produce trace amounts of ethanol. Using one of these microorganisms genetic markers were developed to aid in indentifying other candidate microorganisms and genetic limitations to converting syngas components to ethanol.

Task C.4: Optimization of Reactor design and Operation for Syngas Fermentation

Since syngas is a gas and it is the substrate for the microorganisms several reactor designs and operational conditions were tested to determine if it would have a positive effect on ethanol production. Some of the techniques explored were successful *e.g*. surfactant to increase the solubility while selectively removing some gas components while others were not successful e.g. the in situ removal of ethanol via propane extraction.

4. Comparison of goals and actual activities

See attached spreadsheet.

Task C.1: Optimization of the Acid Hydrolysis Process for Ethanol and Biodiesel Production

(1) Optimization of the acid hydrolysis process by looking at the degrees of depolymerization. Recent discoveries at MSU suggest that there may not be a need to be as aggressive on the acid pretreament.

Sub-Task: Depolymerization of Lignocellulose

The conversion of biomass (including municipal solid wastes) by concentrated acid hydrolysis to biofuel for transportation has been a major research focus in the past at MSU[i;ii]. Over the past decade, examination of fast growing crops for their potential as a source of renewable fuels have been of interest in the state of Mississippi and in other regions.[iii] This research focuses on concentrated acid hydrolysis of these biomass resources.

Optimized conditions under which to conduct acid hydrolysis of biomass samples were identified through this experimental effort. An acid:biomass ratio of 3:1, combined with a pretreatment time of 6 hrs with 72% H_2SO_4, followed by hydrolysis for 6 hours under reflux at 95 °C in ~ 10 % H_2SO_4 solutions provided acceptable sugar yields (glucose and xylose).

Feed Stock Selection

President Bush, in his state of the union address, affirmed the need for our nation to develop technology "for producing ethanol, not just from corn, but from wood chips, and stalks or switchgrass". In the state of Mississippi, wood waste (chips and sawdust) is a resource of significant quantity due to the presence of the furniture manufacturing and pulpwood manufacturing industries. Switchgrass and giant miscanthus are also potentially viable feedstocks, as they possess yields of 8-12 tons/acre and could be planted on over a million acres/year in Mississippi, as feedstocks.[iv] The hollocellulose (cellulose and hemicellulose) content of miscanthus is greater than that of switch grass, and the ash content is lower as well. Thus, giant miscanthus offers an opportunity for a feedstock with potentially greater glucose yields. Experimental efforts were focused on two feedstocks: switchgrass and giant miscanthus.

Size Reduction

The as-received biomass samples possessed broad size ranges. Four different mesh size screens were used to classified biomass into 4 size ranges: 20 mesh, 40 mesh, 60 mesh and 80 mesh. The as-received switch grass sample and the switch grass sample with the size range -40/+60 mesh (420-250 μm) are shown in Figure 1.



As-received switch grass from the supplier with random size

As-received switch grass with the size range -40/+60 mesh (420-250 μM)

Figure 1. Comparison of switch grass sample before and after size reduction

Biomass samples with uniform and narrow size range provide a means to control the feedstock in order to optimize the further chemical/physical treatment and characterization analysis. NREL had developed a series of standard laboratory analytical procedures (LAP) for biomass projects.[v] In this series of LAPs, the acceptable size range for biomass samples is 20-80 mesh.

Effect of Order of Solvent Addition on Extractive Content

The impact of solvent addition order on extractive content for two feedstocks was also examined. It was found that use of water as the first stage solvent, followed by ethanol as the second stage solvent, resulted in the largest degree of extractives removal from the feedstocks examined (switch grass and giant miscanthus). A two stage extraction process was employed with ethanol and with water as the solvent in each stage. A series of experiments were conducted on two feedstocks, switch grass and giant miscanthus, to examine the impact of the order of solvent addition on the total amount of material extracted from the biomass sample. Experimental results are shown in Table 1 for switch grass feedstock and in Table 2 for giant miscanthus feedstock. For either feedstock, when water was employed as the solvent in the first extraction stage, the total amount of material extracted from the biomass sample was greater than when ethanol was used as the solvent in the first extraction stage.

Table 1. Switch Grass: Effect of Order of Solvent Addition on Extractive Content.

Extraction order	Extractives content in water (%)	Extractives content in ethanol (%)	Total extractives content (%)
1st water and 2nd ethanol	8.04	2.49	10.53
1st ethanol and 2nd water	6.86	2.78	9.64

Table 2. Giant Miscanthus: Effect of Order of Solvent Addition on Extractive Content.

Extraction order	Extractives content in water (%)	Extractives content in ethanol (%)	Total extractives content (%)
1st water and 2nd ethanol	4.60	1.93	6.53
1st ethanol and 2nd water	2.38	2.98	5.36

Determination of Moisture Content [9]

A MB45 Moisture analyzer was used to analyze the % dry matter of the biomass samples. Duplicate measurements were performed. The experimental data are listed in Table 3.

Table 3. Dry Matter Content of Biomass.

Biomass sample	Dry Matter Content (%)
Switch grass in 20-40 mesh (as-received)	91.01
Switch grass in 40-60 mesh (as-received)	91.10
Switch grass in 60-80 mesh (as-received)	91.51
Switch grass in 20-80 mesh (as-received)	91.18
Switch grass in 40-60 mesh (extractives free)	99.34
Elephant grass in 20-40 mesh (as-received)	93.30
Elephant grass in 40-60 mesh (as-received)	93.75
Elephant grass in 60-80 mesh (as-received)	93.40
Giant miscanthus in 20-40 mesh (as-received)	93.64
Giant miscanthus in 40-60 mesh (as-received)	93.64
Giant miscanthus in 60-80 mesh (as-received)	93.48

Based on the analysis results of the dry matter content of the biomass samples, the moisture content was independent of the mesh size.

BET Surface Area

The surface area of each sample was measured using an AUTOSORB-1 system (Quantachrome Instruments. Krypton and nitrogen were used as adsorbates. Results are shown in Table 4 for the four biomass samples (as-received switch grass, extractives-free switch grass, as-received giant miscanthus and extractives-free giant miscanthus). Measurements were performed in duplicate for each adsorbate.

Table 4. BET Surface Area of Biomass Samples.

Biomass Sample	Adsorbate Gas	Surface Area (m^2/g)	Correlation Coefficient
As-received Switch grass (40-60 mesh)	Krypton	0.96	0.999389
	Nitrogen	1.36	0.999219
Extractives-free Switch grass (40-60 mesh)	Krypton	0.96	0.999442
	Nitrogen	1.64	0.999414
As-received Giant Miscanthus (40-60 mesh)	Krypton	0.67	0.999420
	Nitrogen	0.65	0.999525
Extractives-free Giant Miscanthus (40-60 mesh)	Krypton	0.41	0.999189
	Nitrogen	0.39	0.999821

The surface areas determined are fairly low and are typical of biomass materials, based on previous experience with measurement of saw dust, chicken litter, kenaf, etc.

Morphology Study

Scanning electron microscopy (SEM) and energy dispersive X-ray (EDAX) were employed to examine the surface morphology of the pre- and post-treated samples.

Scanning electron microscope (SEM)

The SEM images of as-received and extractives-free switch grass sample are shown in Figure 2 and of giant miscanthus are shown in Figure 3. The degree of crystallinity is not impacted by the removal of extractives. From the appearance of the surfaces in the two figures, the removal of extractives results in a smoother surface. The pore volume appears to have changed with treatment for the giant miscanthus, but this finding is not supported by the surface area measurements.

Energy Dispersive X-Ray (EDAX)

Extractives are relatively low molecular weight organic and inorganic species. Pretreatment to remove these compounds is desirable as they will consume a portion of the acid employed to hydrolyze cellulose and hemicellulose during acid hydrolysis. Table 5 provides EDAX results of surface elemental composition for switch grass and giant miscanthus, for both as-received and extractives-free samples. On the surface of the as-received switch grass sample, Mg, Si, Cl, K and Ca are present in small amounts. Extraction results in removal of Mg, Cl and K. In giant miscanthus, the elements present on the surface of as-received sample include Al, Mg, Si, K and Ca. Extraction removes Mg and K.

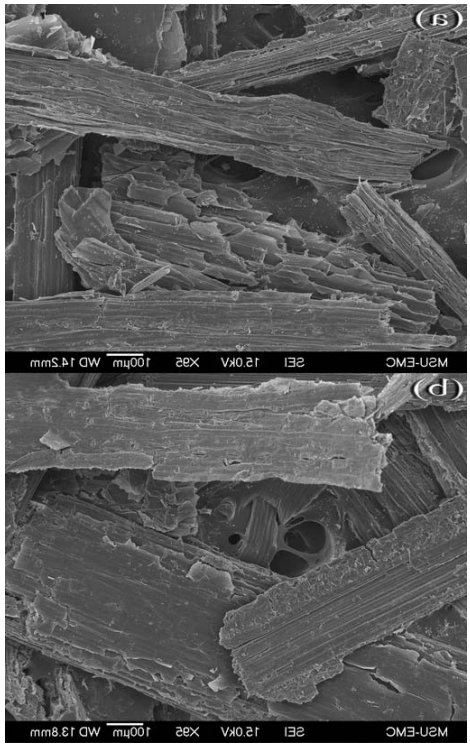


Figure 2. SEM images of as-received (a) and extractives-free (b) switch grass samples.

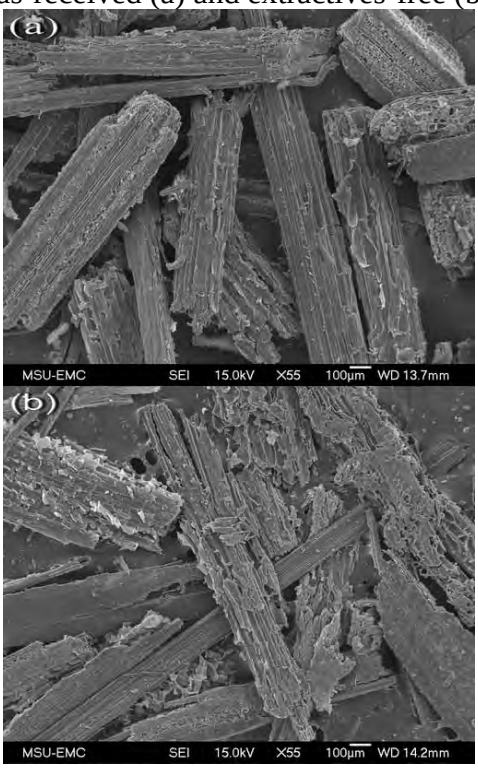


Figure 3. SEM images of as-received (a) and extractives-free (b) giant miscanthus samples.

Table 5. Elemental composition and weight percent in the biomass samples.

Element	As-received Switch grass	Extrative-free Switch grass	As-received giant miscanthus	Extrative-free giant miscanthus
C	49.33	49.55	53.03	49.96
O	45.33	44.89	42.85	43.68
Al	/	/	1.53	2.69
Mg	0.26	/	0.19	/
Si	0.63	4.19	1.17	2.30
Cl	0.95	/	/	/
K	1.50	/	0.42	/
Ca	1.99	1.37	0.80	1.37

Characterization of Biomass

A study of the use of FTIR to qualitatively determine cellulose, hemicellulose and lignin content of biomass samples was undertaken. Switch grass samples with -20/+80 mesh size range were analyzed using a Perkin-Elmer Spectrum 100 FTIR. The scan range was from 4000 cm^{-1} to 600 cm^{-1}. The FTIR spectrum of the switch grass sample in the size ranges of 20-80 mesh is shown in Figure 4.

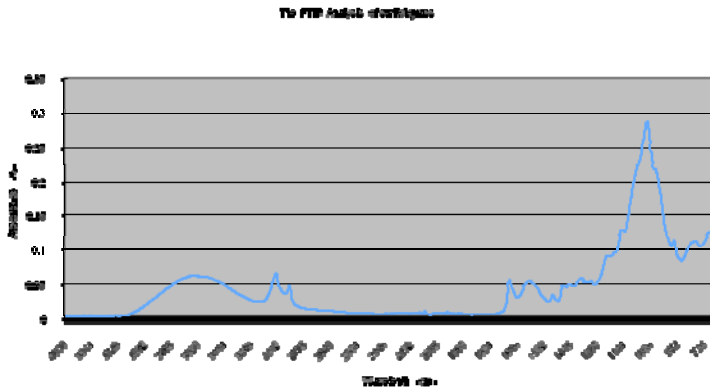


Figure 4. FTIR spectrum of switch grass sample in the size range of -20/+80 mesh.

Conventional determination of lignocellulosic content such as glucose, xylose and lignin is a lengthy, multi-step process. Schultz and co-workers at MSU were first to explore FTIR as a method for determination of glucose, xylose and lignin contents in sweetgum and white oak with their diffuse Reflectance Fourier Transform Infrared Spectrometry (DRIFT).[vi] Following their method, the DRIFT spectra of lignocellulosic samples were collected and analysis initiated.

Determination of protein, ash, NDF, ADF contents and gross energy

The measurements of protein, ash, NDF, ADF contents and gross energy of the biomass samples were completed by an external laboratory. The data are shown in Table 6.

Table 6. Characterization of Biomass Samples.

Biomass sample	Protein (%)	Ash (%)	NDF (%)	ADF (%)	Gross energy (cal/g)
Switch grass in 20-40 mesh (as-received)	3.27	4.53	83.76	48.25	4050.49
Switch grass in 40-60 mesh (as-received)	4.39	4.74	82.53	45.18	/
Switch grass in 60-80 mesh (as-received)	4.84	4.85	81.69	44.91	/
Switch grass in 20-80 mesh (as-received)	3.68	4.48	83.70	47.86	/
Switch grass in 40-60 mesh (extractives-free)	2.99	3.02	91.73	52.97	/
Elephant grass in 20-40 mesh (as-received)	0.98	4.02	85.83	53.72	4181.89
Elephant grass in 40-60 mesh (as-received)	1.16	4.53	84.87	52.63	/
Elephant grass in 60-80 mesh (as-received)	1.75	5.02	83.72	52.47	/
Giant miscanthus in 20-40 mesh (as-received)	1.13	4.35	86.06	53.26	4105.77
Giant miscanthus in 40-60 mesh (as-received)	1.62	4.47	86.46	54.57	/
Giant miscanthus in 60-80 mesh (as-received)	1.47	4.37	85.87	54.46	/

Protein and ash are minor components of the grass feedstocks, and cannot be hydrolyzed to the monosaccharides. The determination of protein and ash contents helps to construct the complete composition of a grass feedstock and allows effective hydrolysis yield of fermentable sugars to be estimated. NDF is the sum of cellulose, hemicellulose, lignin and ash.[vii] ADF is the sum of cellulose, lignin and ash.[7] The difference between NDF and ADF represents the hemicellulose content in biomass. ADL (Acid Digestible Lignin) is the sum of the lignin and ash content.[7] Gross energy is also reported.

Acid Hydrolysis Activities

The use of concentrated acid on biomass samples causes a disruption in the hydrogen bonding network that exists between chains of cellulose.[viii] As a result, the crystallinity of the sample is significantly reduced, and the end result is an amorphous state for the cellulose.[8] Hydrolysis of the cellulose to glucose, through introduction of water to the sample at low to moderate temperatures, is rapid and complete.[8] Alternately, the reaction kinetics of acid hydrolysis have been verified to follow a series depolymerization sequence where the cellulose polymer is partially fragmented to form oligosaccharide chains, which undergo further reaction to form monosaccharides and other decomposition productions. The formation of oligosaccharides from cellulose during primary hydrolysis in concentrated acid

has been hypothesized by numerous investigators to occur through a reversible reaction where depolymerization and repolymerization of glucose occurs. The reaction scheme for primary hydrolysis is:

$$\text{Cellulose} \xrightarrow{70-85\%\,H_2SO_4} \text{Cellulose-Acid Complex} \underset{\text{Re polymerization}}{\overset{\text{Depolymerization}}{\Leftrightarrow}} \text{Oligosaccharides}$$

For secondary hydrolysis, the pertinent scheme is:

$$\text{Oligosaccharides} \xrightarrow[\approx 100^{\circ}C]{\text{Heat}} \text{Glucose} \xrightarrow[\approx 100^{\circ}C]{\text{Heat}} \text{Decomposition Products}$$

Acid Hydrolysis of Biomass

A biomass sample (either switch grass or giant miscanthus) of ~1.00 g was mixed with ~3.00 g of 72% sulfuric acid solution in a 100 mL round flask. The acid:biomass ratio was 3:1 for this experiment. The ratio was varied from 2:1 to 10:1. The mixture in the flask was placed in the refrigerator and maintained at temperature for the prescribed pretreatment time of 24 hours. Then the appropriate amount of distilled water was added to the flask to produce an approximately 10% H_2SO_4 solution. The mixture was heated in a water bath at 95°C under total reflux conditions for the desired hydrolysis time (3, 6, or 12 hours).

After the hydrolysis period was completed, the mixture was filtered using a crucible filter with the aid of water suction. Deionized water was used to rinse the solid residue in the crucible filter three times. The combined filtrate was transferred into a 100 mL volumetric flask. Addition deionized water was then added to the volumetric flask so that the final amount of diluted hydrolyzate was 100 mL. This diluted hydrolyzate contains all sugars produced from the initial biomass sample. A few milliliters of hydrolyzate was transferred to a 50 Erlenmeyer flask, where barium carbonate powder was added to the solution to neutralize it to a pH of 7. The neutralized hydrolyzate was then filtered through a 0.2μm filter into a sample vial for HPLC analysis.

The solid residue produced from the acid hydrolysis of the biomass sample was collected in a weighed crucible. The solid residue was then dried in an oven at 105 °C for 24 hours, and then moved to a dessicator. The solid residue/crucible was weighted on an analytical balance once it had cooled to room temperature.

An HP Agilent 1100 HPLC system equipped with an ELSD detector was used to analyze the glucose and xylose concentrations in the produced hydrolyzate. The column used was a Grace Preveil Carbonhydrate ES 5u column. The mobile phase in this column is a solution of 35% H_2O/65% CH_3CN. The flowrate of the mobile phase was 1 mL/min. Analysis was performed at room temperature.

Impact of Acid:Biomass Ratio on Biomass Conversion

Two types of grass biomass samples, as-received switch grass and giant miscanthus, were employed in the concentrated acid hydrolysis process. The weight ratio of the 72% H_2SO_4 to biomass sample (Acid:Biomass Ratio) was adjusted from 2:1 to 10:1 for each biomass examined. The pretreatment time and hydrolysis time were 24 hours and 3 hours, respectively. For this set of experiments, the only manipulated variable was the acid:biomass ratio, the weight ratio of the biomass sample to the amount of 72% H_2SO_4 solution employed.

Upon completion of the hydrolysis and subsequent filtering and drying, the solid residue mass was measured for each sample.

Two different approaches can be employed to estimate the sugar yield in the hydrolyzate. One approach is to directly measure the sugar concentrations in the hydrolyzate using HPLC. The other approach is to evaluate the extent of depolymerization of cellulose and hemicellulose in the original biomass sample. If the minor depolymerization/dissolution of lignin is neglected, then the reduction in mass between the original biomass sample and the solid residue may be equated with the amount of cellulose/hemicellulose transferred by hydrolysis to the hydrolyzate. Table 7 provides a summary of experimental results from the examination of acid:biomass ratio.

Table 7. Impact of Biomass:acid Ratio on Degree of Conversion of Cellulose and Hemicellulose.

Sample	Mass of Biomass Sample (g)	Mass of 72% H_2SO_4 (g)	Acid to Biomass Ratio	Mass of solid residue (g)	Mass loss (g)	Degree of Conversion (%) (% mass hydrolyzed)
Switch grass	0.73	7.33	10:1	0.352	0.378	51.8
	0.92	7.40	8:1	0.449	0.471	51.2
	2.00	10.00	5:1	0.937	1.063	53.2
	2.18	6.60	3:1	0.982	1.198	55.0
	2.00	4.03	2:1	0.967	1.033	51.6
Giant miscanthus	0.50	5.10	10:1	0.264	0.236	46.9
	1.12	5.64	5:1	0.624	0.496	44.3
	1.21	3.67	3:1	0.628	0.582	48.1
	1.38	2.80	2:1	0.740	0.640	46.4

Note: All trials were carried out with a pretreatment time of 24 hours in 72% H_2SO_4 in the refrigerator, followed by hydrolysis at 95 °C for 3 hours.

The degree of conversion as a function of acid:biomass ratio showed similar trends for both switch grass and giant miscanthus. The largest degree of conversion (defined as initial mass of sample minus mass of solid residue divided by the initial sample mass) was obtained for a acid:biomass ratio of 3:1. The trends obtained are shown in Figures 5 (switch grass) and 6 (giant miscanthus).

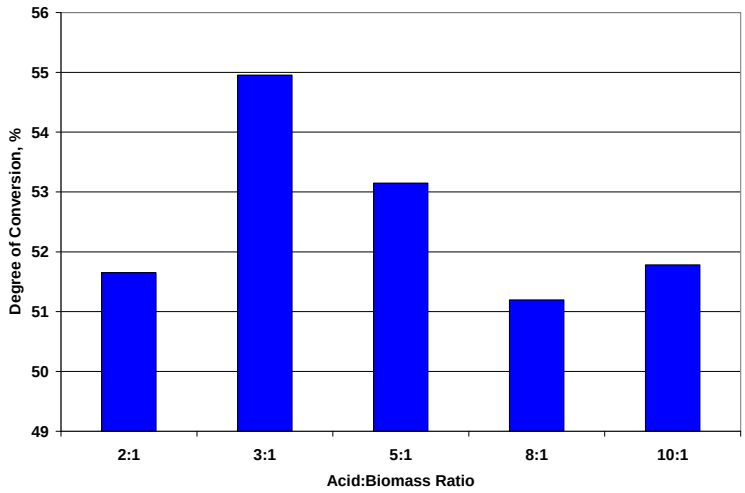


Figure 5. Effect of Acid:Biomass Ratio on % Mass Hydrolyzed for Switch Grass

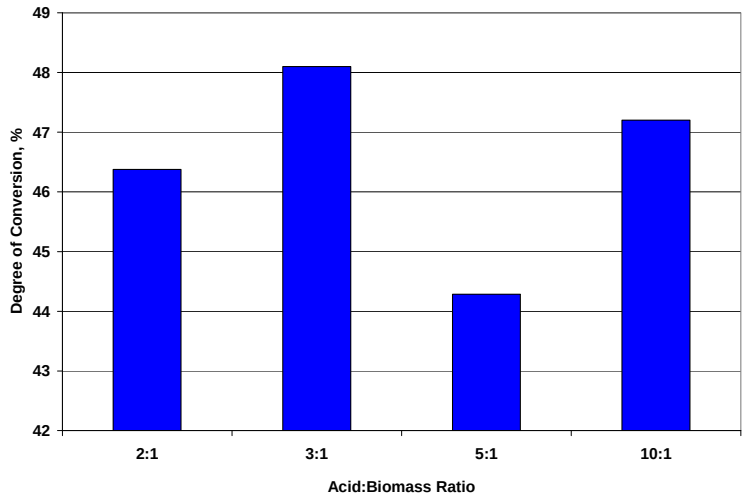


Figure 6. Effect of Acid:Biomass Ratio on % Mass Hydrolyzed for Giant Miscanthus

Impact of Concentrated Acid-Petreatment Time

In these experiments, the acid:biomass ratio was controlled at 3:1 for all samples, and the subsequent hydrolysis was conducted at 95 °C for 3 hrs. The manipulated variable for this set of experiments was the length of time allotted for pretreatment using concentrated sulfuric acid. For these experiments, the glucose and xylose concentrations in the resulting hydrolyzate were measured using HPLC, and these values were used to calculate the degree of conversion obtained for a given biomass sample.

The pretreatment of biomass with concentrated sulfuric acid was conducted using differing treatment times to determine the impact of pretreatment time on the degree of conversion. After combining the biomass sample and 72% sulfuric acid, the mixture is maintained for the pretreatment time at room temperature. The pretreatment time was varied from 1 hour to 24 hours. During the pretreatment period, the concentrated sulfuric acid converts the crystalline regions in cellulose fibers to amorphous structure. The amorphous cellulose along with the

hemicellulose in the biomass sample is more readily hydrolyzed by 10% H_2SO_4 solution to monosaccharides. After filtration and drying, the solid residue was weighed. The sugars' (glucose and xylose) concentrations in the hydrolyzate were determined by HPLC. These data are then used to calculate the yield of sugars, which is comparable to the degree of conversion. The experimental data are shown in Table 8.

Table 8. Impact of pretreatment time of 72% H_2SO_4 on sugars yield from switch grass

Trial Number	1	2	3	4	5
Mass of switch grass (as-received) (g)	1.226	0.998	1.146	1.314	1.336
Mass of 72% H_2SO_4 (g)	3.749	3.021	3.497	4.39	4.19
Acid:biomass ratio	3:1	3:1	3:1	3:1	3:1
Pretreatment time (hour)	1	3	6	10	24
Added DI water (g)	22.1	17.8	20.8	25.5	24.7
Acid wt% after water addition	10.44	10.44	10.36	10.56	10.45
Hydrolysis time (hrs)	3	3	3	3	3
Volume of Hydrolyzate (ml)	100	100	100	100	100
Glucose Concentration in hydrolyzate (mg/ml)	2.46	3.00	3.87	4.07	4.22
Xylose concentration in hydrolyzate (mg/ml)	2.74	2.85	3.14	3.13	3.27
Concentration of total sugars in hydrolyzate (g/100 ml)	0.520	0.585	0.701	0.720	0.749
Yield of fermentable sugars (glucose+xylose) =(sugar mass/sample mass)*100	42.4	58.6	61.2	54.8	56.0
Mass of solid residue (gram)	0.511	0.291	0.260	0.295	0.315
Degree of Conversion =[(sample mass -solid residue mass)/sample mass]*100	58.3	70.8	77.3	77.5	76.5

Pretreatment conducted with 72 % H_2SO_4 at room temperature; Hydrolysis conducted at 95 °C.

The highest yields of glucose and xylose were obtained with a pretreatment time of 6 hours. The trend is shown more clearly in Figure 7. A similar trend is observed in the degree of conversion, but the degree of conversion based on solid residue mass overestimated the sugars yield.

During the pretreatment period, the high concentrated sulfuric acid converts the crystalline regions in cellulose fibers to an amorphous structure. Thus, longer pretreatment times should imply a greater conversion of the more crystalline cellulose to the amorphous structure, with greater amounts of glucose released during the following hydrolysis period. The experimental data obtained in this work do not support this supposition. One possible explanation is that a longer pretreatment time may lead to decomposition of the sugar, resulting in a drop in sugars yield.

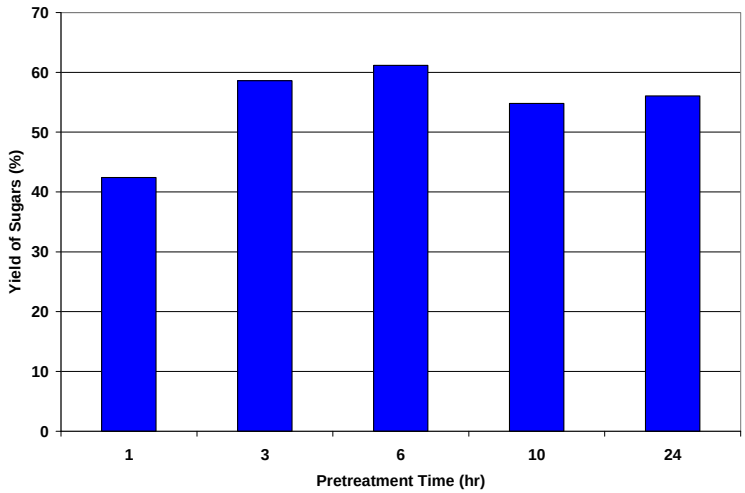


Figure 7. Effect of Pretreatment Time on Yield of Sugars

Impact of Acid Hydrolysis Time on Sugar Yield

The impact of acid hydrolysis time was examined in the final series of experiments. During these experiments, the acid:biomass ratio was held constant at 3:1 and the pretreatment time was held constant at 6 hours. Acid hydrolysis times of 3, 6, and 12 hours were examined to determine its impact on sugars yield. Experimental data are shown in Table 3.3.

The sugars yield was greatest (66.1%) for a hydrolysis time of 6 hours. However, the sugars' yields for all runs were similar. The concentrations of glucose and of xylose in the hydrolyzate depend on the initial amount of biomass sample employed. After hydrolysis, the volume of hydrolyzate was increased to 100 ml by addition of deionized water. Thus, larger biomass samples would give rise to greater concentrations of sugars in the hydrolyzate. The determination of yield normalizes the obtained amount of sugars using the initial biomass sample; thus, the sugars yield values can be directly compared.

Optimized Acid Hydrolysis Conditions

Experiments have been performed to identify favorable conditions under which to conduct hydrolysis of biomass samples. An acid:biomass ratio of 3:1, combined with a pretreatment time of 6 hrs with 72% H_2SO_4, followed by hydrolysis for 6 hours under reflux at 95 °C in ~ 10 % H_2SO_4 solutions provided sugar yields of > 65 %.

Table 9. Impact of hydrolysis time of 10% H_2SO_4 on the yield of sugars from switch grass

Trial Number	1	2	3
Mass of switch grass (as-received) (g)	1.146	0.989	1.262
Mass of 72% H_2SO_4 (g)	3.497	3.012	3.806
Acid:biomass ratio	3:1	3:1	3:1
Pretreatment time (hr)	6	6	6
Added DI water (g)	20.8	17.8	22.6
Acid wt% after water addition	10.36	10.41	10.39

Hydrolysis time (hr)	3	6	12
Volume of Hydrolyzate (ml)	100	100	100
Concentration of glucose in hydrolyzate (mg/ml)	3.87	3.63	4.21
Concentration of xylose in hydrolyzate (mg/ml)	3.14	2.91	3.17
Concentration of total sugars in hydrolyzate (g/100 ml)	0.701	0.654	0.738
Yield of fermentable sugars (glucose+xylose)) =(sugar mass/sample mass)*100	61.2	66.1	58.5
Mass of solid residue (g)	0.260	0.221	0.276
Degree of Conversion =[(sample mass -solid residue mass)/sample mass]*100	77.3	77.7	78.1

Pretreatment conducted with 72 % H_2SO_4 at room temperature; Hydrolysis conducted at 95 °C.

Task C.2 – Optimization of Ethanol Production from Acid Hydrolysates

(1) Development of acid- and alcohol-tolerant ethanol producers through aggressive molecular and culturing techniques. Ethanol-producers with these abilities would have the potential to decrease the cost of the acid hydrolysis pretreatment by decreasing the need for neutralizing the acids.
(2) Evaluation of the oleaginous microorganisms developed in the biodiesel efforts as a secondary pretreatment step to remove the pentoses, furan, phenolic compounds, and acetic acid may increase ethanol production while simultaneously providing a feedstock from which biodiesel could be produced.

In these experiments, the sugar to lipid processes is a two-stage culture system. In the first stage, the yeast was grown initially in a nitrogen-rich medium with 20 g/l of total sugars. Once the culture reached the stationery phase, the cells were harvested by centrifugation at 2500 RPM for 15 minutes. In the second stage, yeasts harvested were transferred to a fresh nitrogen-free media for the lipid accumulation. In the second stage, the cells were expected to accumulate lipids as no exogenous nitrogen was added to the medium. Pure glucose or xylose or artificial acid hydrolysate of switchgrass were tested as sole carbon and energy sources.

The oleaginous yeast *Rhodotorula glutinis* (ATCC 15125) was used in all experiments. The yeast was grown initially in nitrogen-rich medium at a pH of 5.5 and 30 , which contained (per liter): yeast extract,1.0 g; $Na_2HPO_4 \cdot 12H_2O$, 1.0 g; KH_2PO_4, 1.0 g; $MgSO_4 \cdot 7H_2O$, 0.4 g; $(NH_4)_2SO_4$, 4.0 g; trace mineral solution, 10 ml; $FeSO_4$ solution, 6.0 ml; 20 g of glucose or xylose, or artifical acid hydrolysate with 0.3 ml furfural and 20 g of total sugar. The trace mineral solution consisted of (per liter): $CaCl_2 \cdot 2H_2O$, 3.6 g; $ZnSO_4 \cdot 7H_2O$, 0.75 g; $CuSO_4 \cdot 5H_2O$, 0.13 g; $MnSO_4 \cdot H_2O$, 0.50 g; $CoCl_2 \cdot 6H_2O$, 0.13 g; $Na_2MoO_4 \cdot 2H_2O$, 0.17 g. The $FeSO_4$ solution contained 4.0 g/L $FeSO_4 \cdot 7H_2O$. Per 20 g of sugar in acid hydrolysate is composed of: glucose, 10.7g; xylose, 8.2 g; galactose, 0.3 g; arabinose, 1.0 g; mannose, 0.1 g; acetic acid, 5.2 g.

The fresh nitrogen-free medium for the lipid accumulation consists of (per liter) $Na_2HPO_4 \cdot 12H_2O$, 1.0 g; KH_2PO_4, 1.0 g; $MgSO_4 \cdot 7H_2O$, 0.4 g; trace mineral solution, 10 ml; $FeSO_4$ solution, 6 ml; and pure glucose or xylose of various concentration (30 to 60) or acid hydrolysate with various amount of total sugar (30g to 60 g) and 0.3 ml furfural.

Analytical methods

Cell dry weight determination was performed by centrifuging the cells at 6000 RPM for 15 min, washing with DI water and drying in a freeze-dry system to constant weight. The lipid content of the cell was obtained by the gravimetrical method described by Bligh & Dyer.

The fatty acid methyl ester (FAME) transesterified from the microbial lipid were analyzed using an Agilent 6890 series Gas Chromatograph equipped with a Supelco SP 2380 capillary column(100 m x 0.25 mm x 0.2 micron, model number Supelco 24317) and a flame ionization detector (FID).

Glucose and xylose were analyzed by high pressure liquid chromatography equipped with an evaporative light scattering detector. The column used was a Grace-Prevail Carbohydrate ES 5u with a length of 250 mm, I.D.of 4.6 mm, particle size 5 micrometer and pH range 2-13. The guard column was 7.5 mm long and I.D. was 4.6 mm. Both were operated at room temperature. The mobile phase was water/ acetonitrile (35:65, v/v) with a flow rate of 1ml/min. The isocratic, spray chamber was controlled at 25 °C, drift tube at 55 °C. The injection volume was 2 µL.

The growth of *Rhodotorula glutinis*

As shown in Figure 1, the oleaginous microorganism *Rhodotorula glutinis* grew very well in the media made of acid hydrolysate with ethanol yeast inhibitor of acetic acid and furfural. It reached stationery phase within 16.5 hours (point A in figure 1). The yeast were then harvested at the time of point A and transferred to nitrogen-free medium for lipid accumulation.

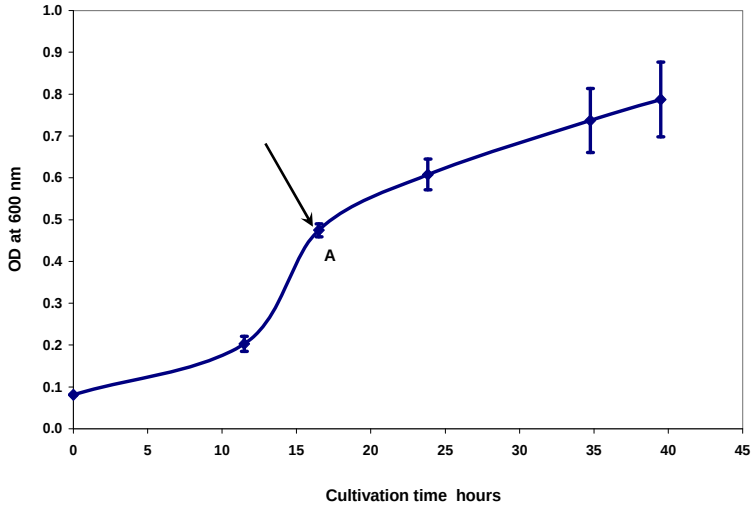


Figure 1, Growth of *Rhodotorula glutinis* in the nitrogen-rich medium with acid hydrolysate as carbon and energy source at pH 5.5 and 30 .

Lipid production by *Rhodotorula glutinis* grown on pure glucose.

The lipid accumulation in *Rhodotorula glutinis* grown on glucose of 24.4 g/l or 31.80 g/l or 60 g/l as sole carbon and energy source was shown in Figures 2, 3, and 4, respectively.

When 24.4 g/l glucose was added to the medium, the yeast cell mass increased within 96.2 hours from initial 3.89 g/l with 4.54 % of lipid (wt%, based on dry cell mass) to 10.94 g/l with 15.57% of lipid when glucose was exhausted.

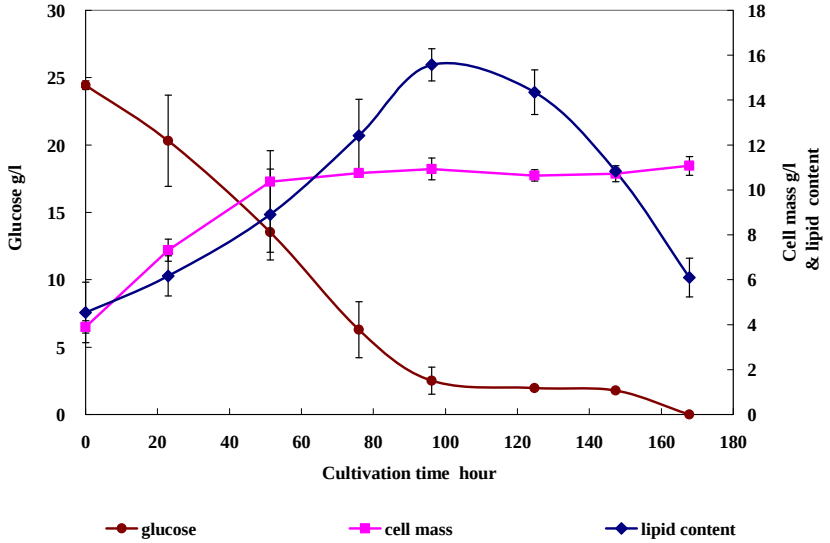


Figure 2 Lipid production by *Rhodotorula glutinis* grown on 30 g/l of glucose at 30

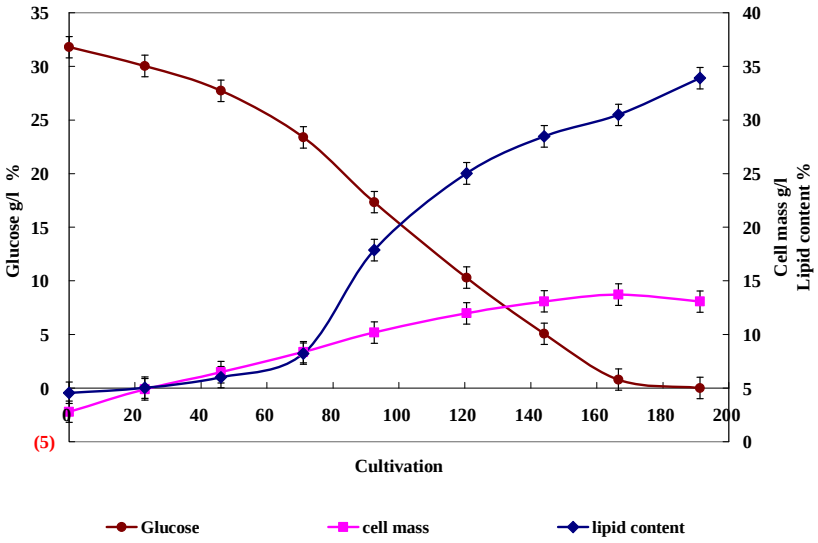


Figure 3 Lipid production by *Rhodotorula glutinis* grown on 30 g/l of glucose at 30

When the initial glucose concentration rose to 31.80 g/l, the cell mass increased from initial 2.78 g/l to 13.72 g/l, lipid in cell was accumulated from 2.78 % to 33.90% while glucose was exhausted. The cells started to accumulate lipid quickly as the cell mass increase rate leveled off after 92.5 hours. When the initial glucose was added up to 60 g/l, cell mass concentration increased to 14.93 g/l, and lipid in dry cell mass was accumulated up to 44.96% (shown in Figure 4). These results indicated that with higher sugar concentration more lipids can be accumulated in the cell.

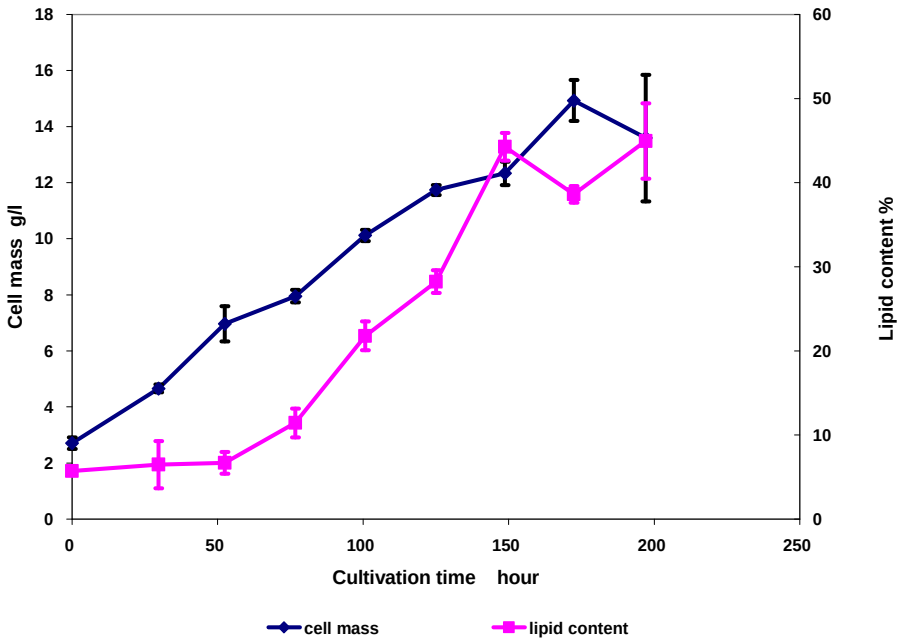


Figure 4 Lipid production by *Rhodotorula glutinis* grown on 60 g/l of glucose at 30

Lipid production by *Rhodotorula glutinis* grown on pure xylose at 30 .

Xylose fermentation to ethanol has not been demonstrated with naturally occurring microorganisms. However there exist a pathway that nature has selected and that pathway is the conversion of xylose into triglycerides. The lipid accumulation by *Rhodotorula glutinis* grown on initial xylose concentrations of 23.76 g/l and 30.63 g/l was tested and the results are presented in Figures 5 and 6, respectively.

When grown on a xylose concentration of 23.76 g/l, the cell mass of *Rhodotorula glutinis* increased from 2.84 g/l to 8.76 g/l with lipid content of dry cell mass rising from 1.37% to 25.44% until xylose was exhausted within 96.5 hours. When the initial xylose was increased to 30.63 g/l, cell mass concentration rose to 9.20 g/l with lipid content increasing to 44.02%.

These results demonstrate that the oleaginous microorganism *Rhodotorula glutinis* has higher lipid production while grown on xylose than on glucose. This can be pontential be explained by the fact that pentose metabolism generates more NADPH, which is required in fatty acid synthesis, than glucose metabolism.

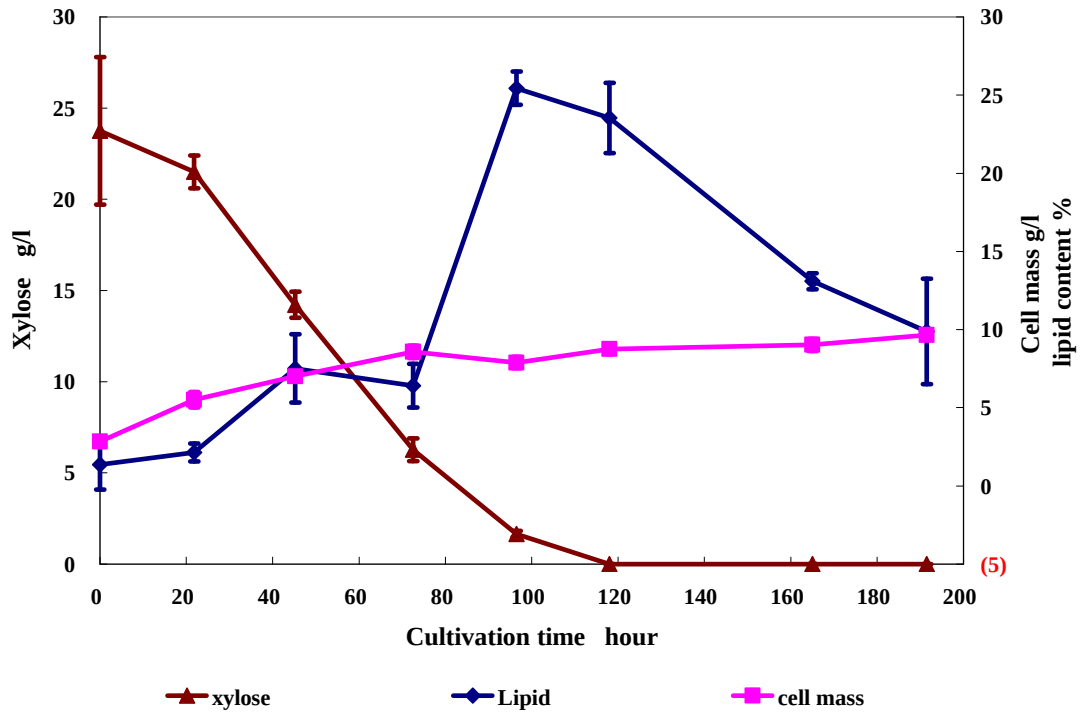


Figure 5 Lipid production by *Rhodotorula glutinis* grown on 30 g/l of xylose at 30 .

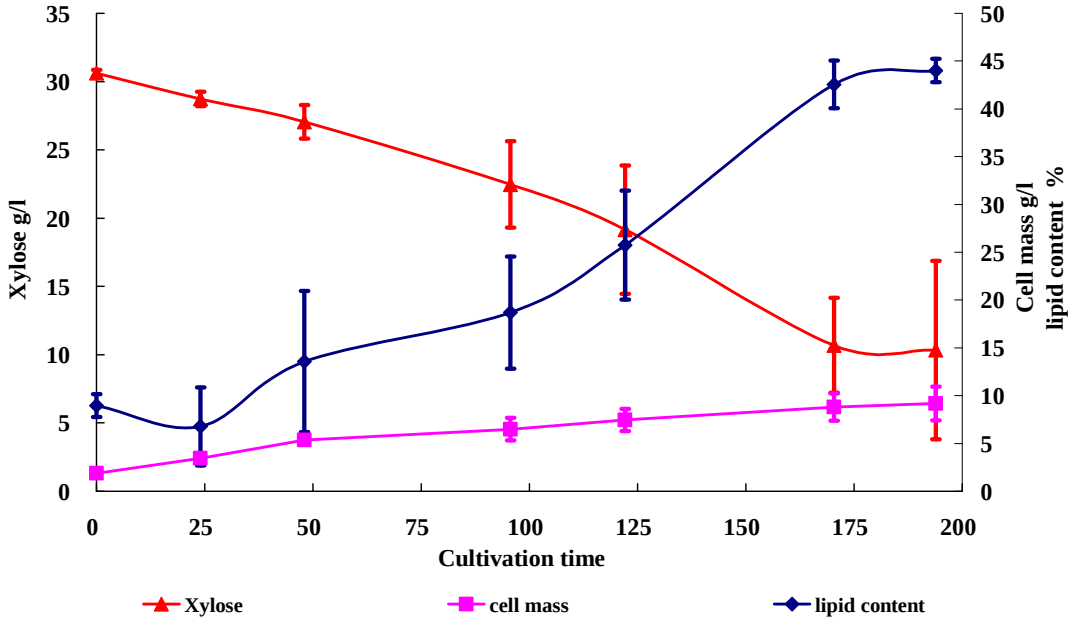


Figure 6 Lipid production by *Rhodotorula glutinis* grown on 45 g/l of xylose at 30

<u>Lipid production by *Rhodotorula glutinis* growing on artificial acid hydrolysate.</u>

As presented above, *Rhodotorula glutinis* was grown very well in the media using acid hydrolysate as sole carbon and energy source with acetic acid and furfural, which are inhibitors for ethanol yeast, but also accumulated lipid from glucose and xylose, and has a higher lipid accumulation in cells from xylose than from glucose.

In the experiments, acid hydrolysate with total sugar of 30 g/l, 45 g/l and 60 g/l in the media was added for the lipid accumulation. The cell mass, lipid content in dry cell mass and the sugar consumption in the medium were measured during the fermentation. The results were presented in Figures 7, 8, and 9.

When the total sugar concentration added was 30 g/l, cell mass increased from initial 1.49 g/l to 6.25 g/l with lipid content increasing from 2.12% to 16.67%. If the initial total sugar concentration was 45 g/l, cell mass increased from 2.58 g/l to 10.31 g/l, the lipid content in dry cell mass also increased from 3.62% to 29.78%. When initial total sugar concentration increased further to 60 g/l, the lipid accumulated in the cell reached 38.97% of the dry cell mass

It also showed that the oleaginous microorganism *R. glutinis* metabolized the glucose first, then the xylose when glucose was exhausted. The lipid accumulated in the cells had a maximum value followed by a slight decrease while the glucose was exhausted, and then the cells started to accumulate lipid again by metabolizing xylose.

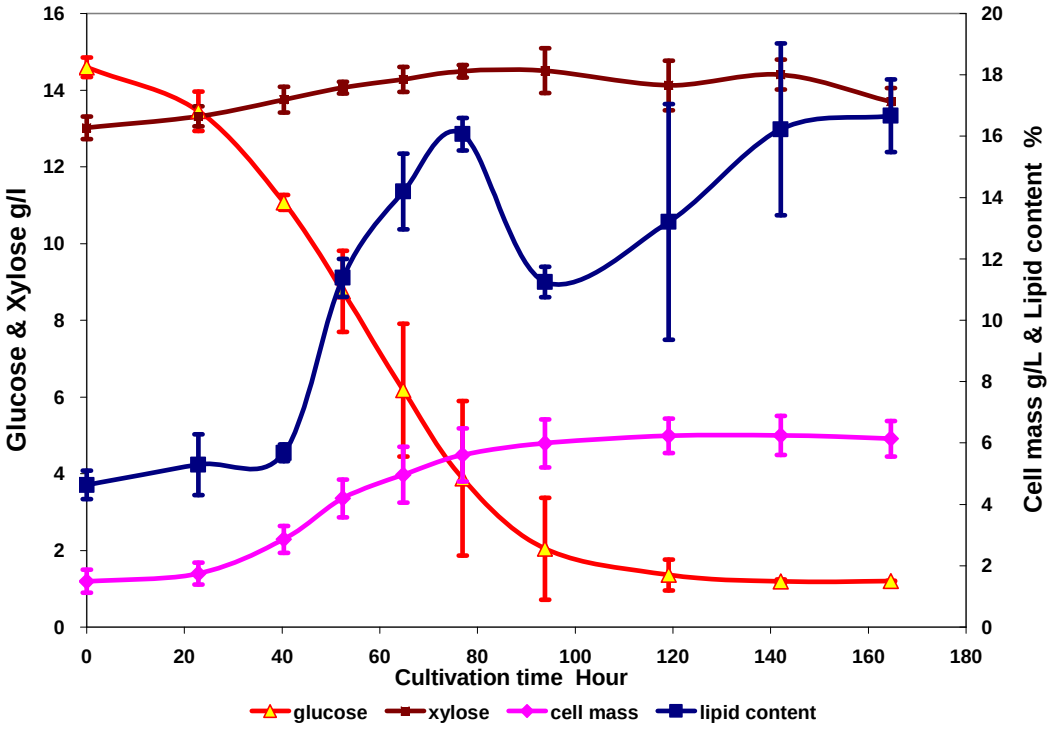


Figure 7 Lipid production by *Rhodotorula glutinis* grown on acid hydrolysate with 30 g/l of total sugar at 30

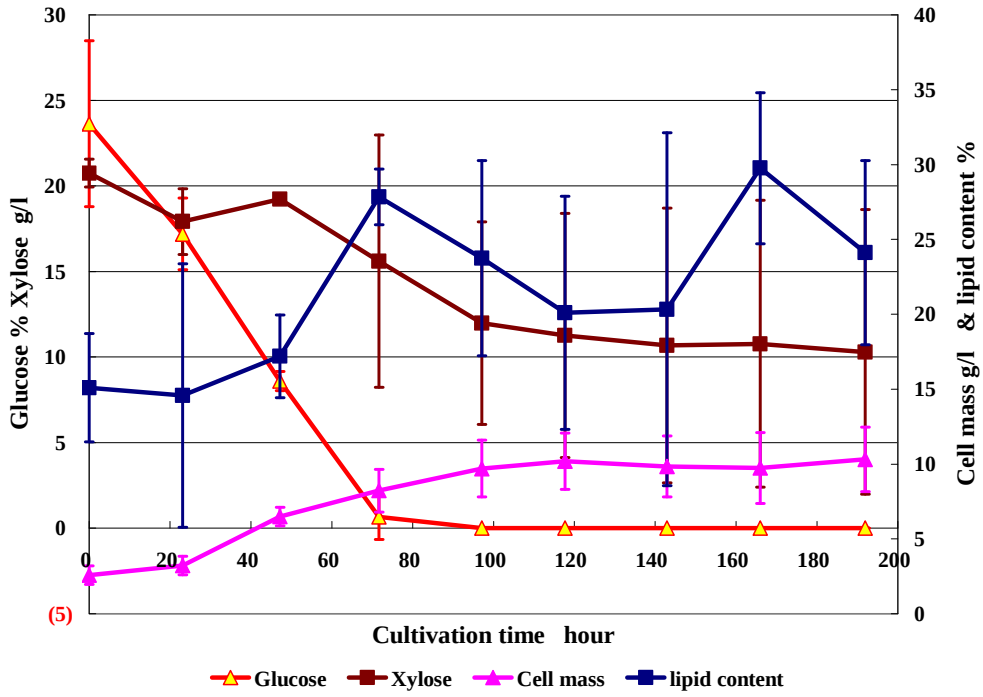


Figure 8 Lipid production by *Rhodotorula glutinis* grown on acid hydrolysate with 45 g/l of total sugar at 30

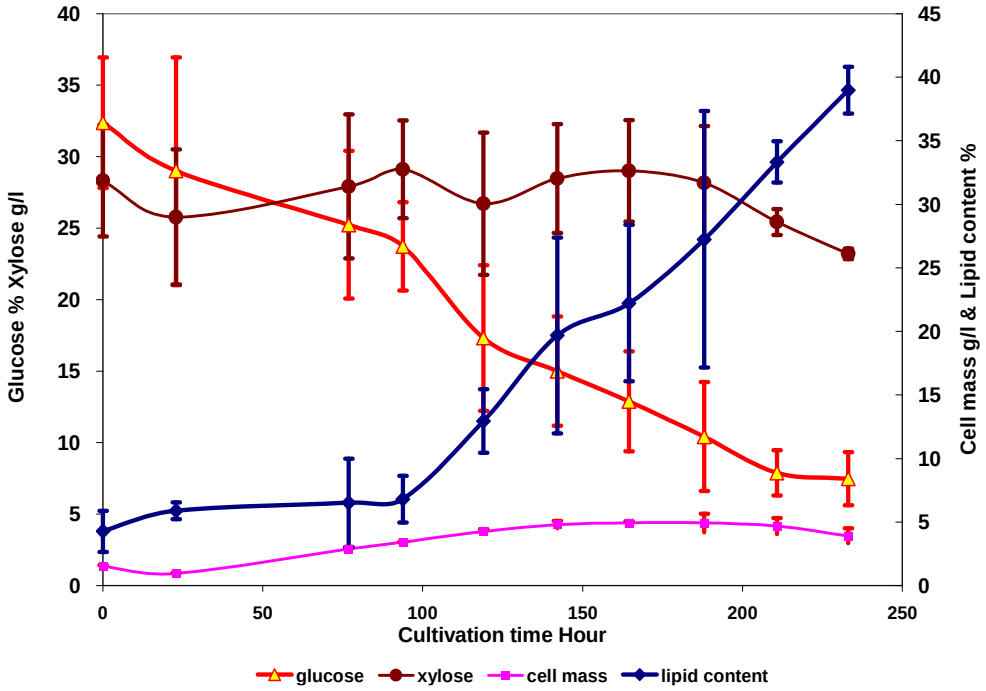


Figure 9 Lipid production by *Rhodotorula glutinis* grown on acid hydrolysate with 60 g/l of total sugar at 30

Task C.3 – Isolation and Optimization of Microorganisms Capable of Fermenting Syngas to Ethanol

(1) Isolation and optimization of microorganisms capable of producing ethanol from syngas. Efforts will focus on the isolation of microorganisms capable of producing ethanol and will be compared to benchmark microorganisms that are known syngas fermenters such as *Clostridium ljungdahlii* strain P7. To enhance these efforts genetic tools will be utilized to focus the search for microorganisms with these abilities.

(2) Development of technologies to overcome the mass transfer limitations due to low solubilities of syngas in fermentation broth. Two approaches will be investigated to address this issue. The first approach will look to optimize gas sparging and mixing for maximum distribution of syngas into the aqueous phase. The second approach will utilize biological and synthetic surfactants to increase gas solubility.

(3) Genetic tools will be developed to optimize syngas fermentation by first looking at the genes involved in the pathways. An additional benefit is the genetic tools developed will also aid in the search for more efficient syngas producers.

Isolation of novel syngas fermenting microorganisms

Work on this project began with previously isolated enrichment cultures. The 30ºC enrichment cultures were obtained from soil from a hog waste lagoon in Crawford, MS. while the 90ºC enrichment cultures were obtained from cutting from a well drilled in Washington Co., AL, at a depth of 11,000 feet. The medium employed is shown in Table 1. All of these cultures produced ethanol from carbon monoxide under anaerobic conditions.

Table 1. Medium Formulation

NH_4Cl	0.50 g
KCl	0.05 g
$MgSO_4 \cdot 7H_2O$	0.10 g
NaCl	0.40 g
KH_2PO_4	0.05 g
$CaCl \cdot 2H_2O$	10.00 mg
Distilled Water	495.00 ml
Trace Mineral Solution (ATCC)	2.50 ml
Vitamin Solution (ATCC)	2.50 ml

Chemicals are added to the distilled water and then the pH is adjusted to a final pH of 6.8. Medium is distributed in 10 ml aliquots into Wheaton Bottles containing crushed pyrite and then autoclaved. Trace and vitamin solutions are then added (0.1 ml of each per bottle) in the anaerobic chamber.

Initially, all of the 30ºC enrichment cultures failed to grow upon subculture, even though they had been carried in the same medium for several years. The only difference in the medium was a lack of alabandite in the medium upon which the organisms liked to grow as shown in Figure 1. The company from which the alabandite was purchased went out of business and no new supplier has been found. Previous experience in growing the cultures with pyrite rather than

alabandite was successful, but growth appeared to be slightly less that with the alabandite. Nevertheless, from this point forward, pyrite was substituted for alabandite.



Figure 1. Growth on pieces of alabandite from an enrichment culture producing ethanol from carbon monoxide at 30ºC anaerobically.

Using the newly acquired anaerobic chamber, colonies on plates of solid medium (See Figure 2) streaked from enrichment cultures grown on carbon monoxide were picked into vials of mineral salts medium and grew well as shown in Figure 3. Gram stains made of these enrichment cultures revealed the presence of gram positive, rod-shaped bacteria as shown in Figure 4. In addition to visual evidence of growth, analysis of the atmosphere of the vials proved carbon monoxide utilization and tests of the liquid medium demonstrated the presence of ethanol.



Figure 2. Colonies on the surface of mineral salts agar plates streaked from an enrichment culture that produced ethanol from CO at 30ºC in mineral salts medium.



Figure 3. Sealed Vials containing enrichment cultures in mineral salts medium grown on CO at 30ºC. (Second vial from the left contains uninoculated mineral salts medium.)

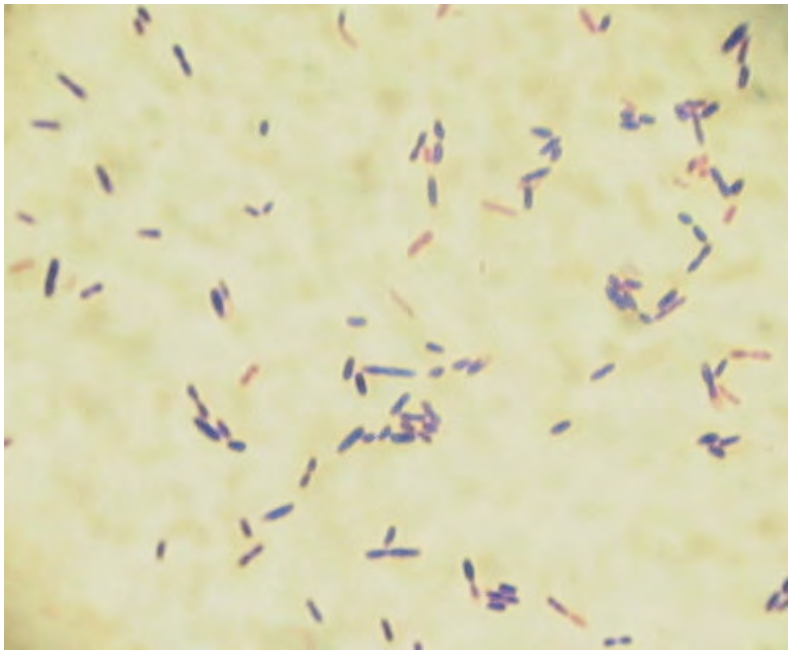


Figure 4. Gram stain of an enrichment culture grown in mineral salts medium at 30ºC anaerbically. The culture used carbon monoxide for growth.

Because of the difficulty in maintaining growth of cultures producing ethanol from carbon monoxide, some transfers of enrichment cultures were made into mineral salts medium containing sterile soil as a source of potentially necessary nutrients. These studies did not

indicate a lack of nutrients in the medium and the practice was abandoned. Additionally, Smith Tubes containing pyrite were employed as culture vessels (See Figure 5) since quick observation can determine if gas is being consumed without having to rely on more time-consuming gas chromatographic analyses.

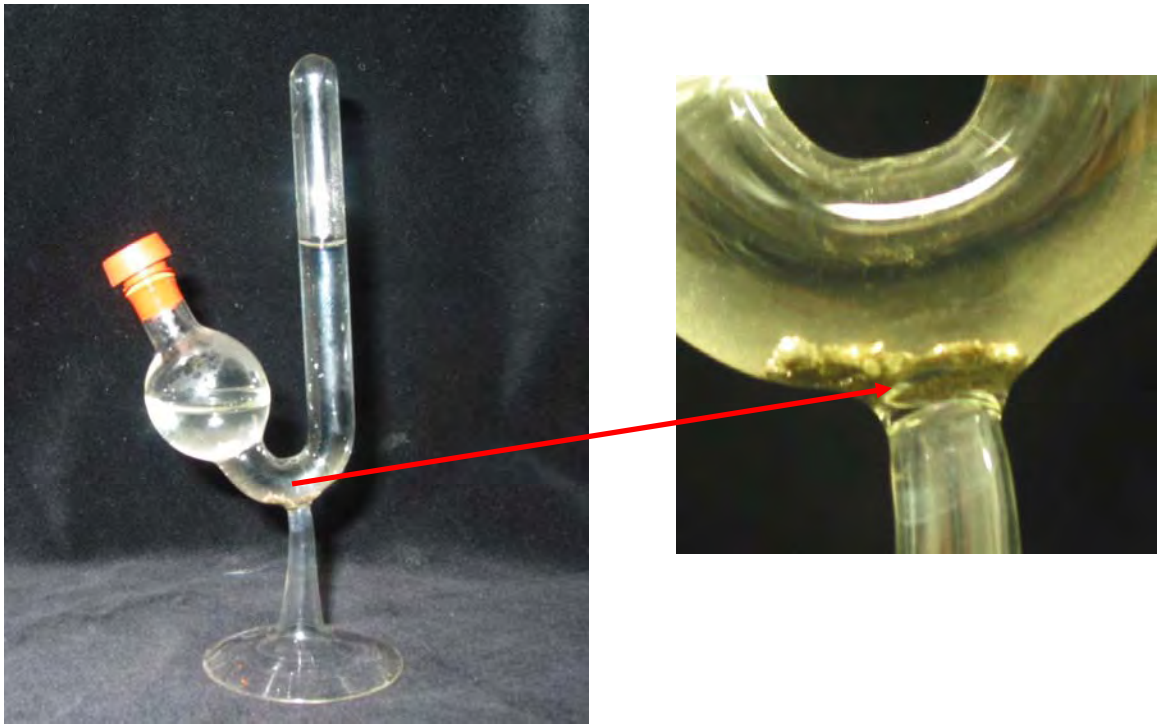


Figure 5. Picture of Smith Tube on left and a close up of the alabandite in the Smith Tube on the left.

Other work in the laboratory has shown that by replacing the main energy source (CO), removing CO_2, and not replacing other nutrients has resulted in the continual utilization of the energy source at a constant rate. Also, there has been evidence that the water employed to prepare the medium might have an impact on the production of ethanol. Therefore, the following experiment was conducted. The conventional medium was prepared with distilled water from either the Biological Sciences Laboratory or the Chemical Engineering Laboratory. Ten ml of each medium was placed into each of two 70-ml vials and inoculated with one ml of a new enrichment culture. The vial was flushed with syngas, which contains carbon monoxide.

All work was carried out in an anaerobic chamber. Incubation was carried out at 30ºC. Periodically, samples of the liquid were analyzed for ethanol using the Analox Alcohol Analyzer AM1. Samples of the atmosphere were analyzed for carbon monoxide and carbon dioxide using a Fisher Model 1200 Gas Partitioner. The vials were opened in the anaerobic hood and the atmosphere removed and replaced with new syngas.

Carbon monoxide was consumed and carbon dioxide produced by the cultures in all of the vials and the results of the alcohol analyses are shown in Figure 6. As may be seen, the samples using medium prepared with water from the Biological Sciences Laboratory had a slightly greater ethanol content that did the samples using medium prepared with water from the Chemical Engineering Laboratory.

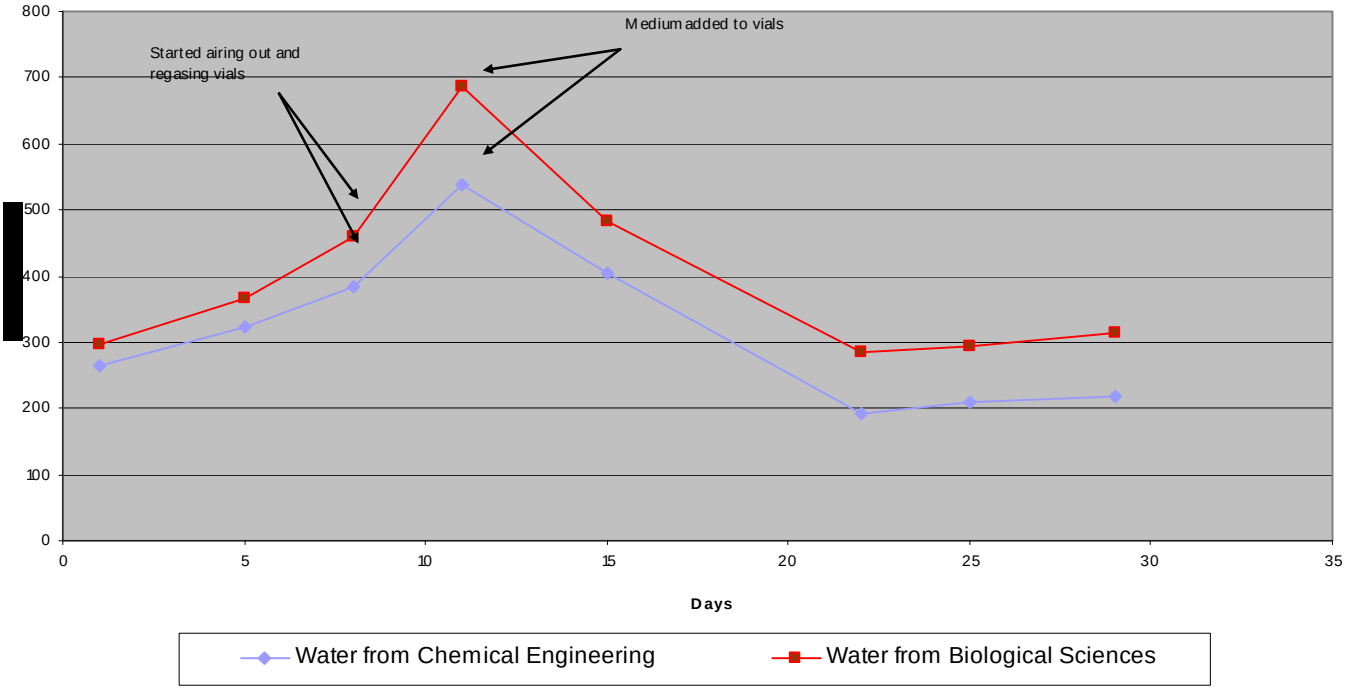


Figure 6. Ethanol production at 30ºC in 70-ml vials using medium prepared with distilled water from two different sources.

Of special interest is the fact that the ethanol in both systems increased with each exchange of atmosphere after the first three samplings. At the fourth sampling, liquid medium was added to each vial to replace the liquid lost by sampling. As may be observed, the concentration of ethanol decreased for the next two samplings. Whether this finding is due to addition of more nutrients or simply a change in the metabolism of the microorganisms to begin using the ethanol is not known at this time. This experiment was repeated and, as may be seen in Figure 7, the results confirmed that medium prepared using water from the Biological Sciences Laboratory resulted in more ethanol production by the carbon monoxide-utilizing culture than did the medium prepared using water from the Chemical Engineering Laboratory, although the amount of ethanol produced was reduced in both cases. Therefore, the experiment was repeated a third time and once again the Biological Sciences Laboratory water resulted in a greater

amount of ethanol production. These data suggest that there is a difference in the chemical content of the two waters. Whether this is because the Biological Sciences water has one or more compounds in it that enhance ethanol production or whether the Chemical Engineering water has one or more compounds that slightly inhibit ethanol production is not known at this time. Since the water is distilled water, the compound(s) involved is probably inorganic in nature. A similar situation has been experienced in other cases in this laboratory in dealing with cultures growing in mineral salts media and using single simple substrates, e.g.. methane, ethane, hydrogen, etc.

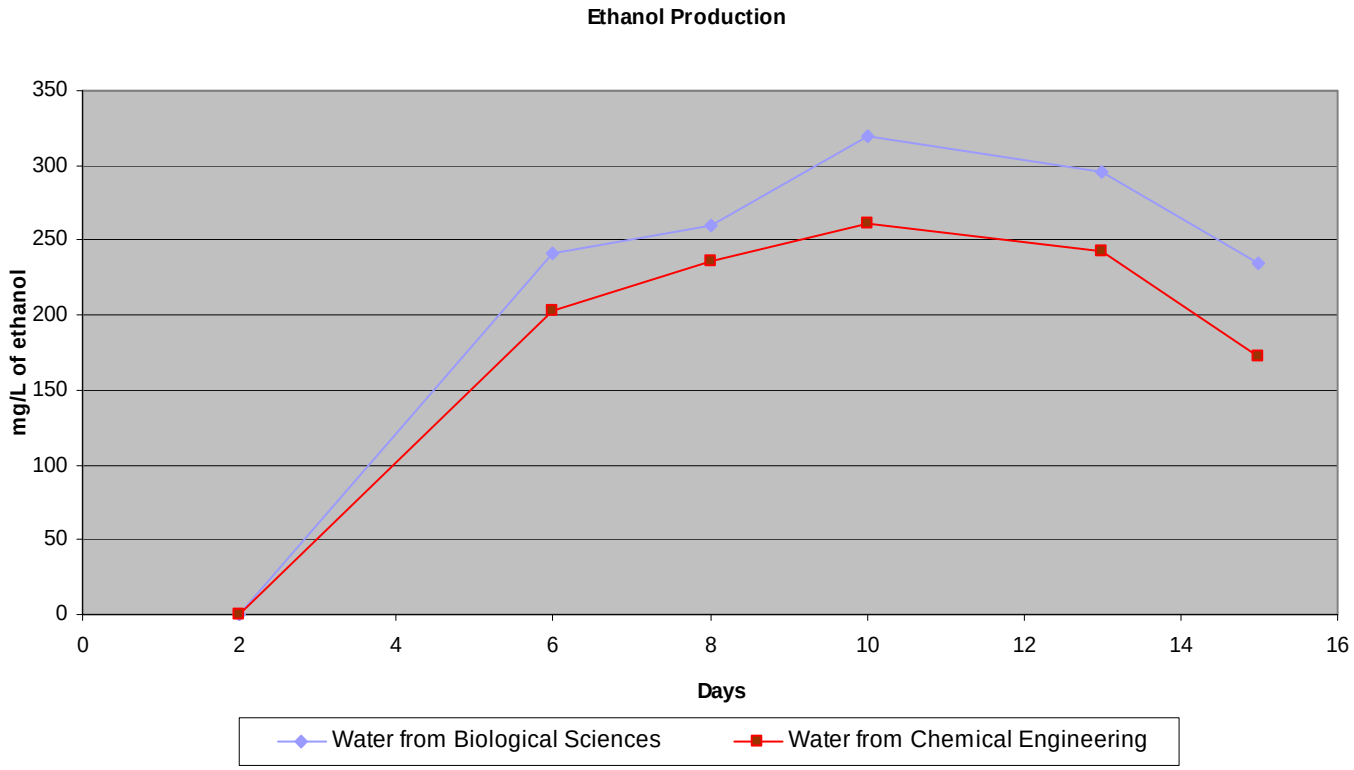


Figure 7. Ethanol production at 30ºC in 70-ml vials using medium prepared with distilled water from two different sources.

There also has been some evidence that ethanol production is influenced by the concentration of carbon monoxide in the atmosphere. Presently, there are three cultures that grow well with no problems like in the past. Two cultures are being maintained in ethanol medium made with water from the Chemical Engineering Laboratory and one culture is being maintained in medium made from water from the Biological Sciences Laboratory. It was reported above that cultures grown in medium made with water from Biological Sciences produced more ethanol in the growth medium than they did when grown in medium made with water from Chemical Engineering. This trend is still holding true. The two waters were mixed in different concentrations to determine the effect on growth and ethanol production but no significant difference was observed and therefore, water from the Biological Sciences Laboratory is now used for the medium. So far, the greatest amount of ethanol detected in any of the 30ºC

cultures is 690 mg/L. It should be pointed out however, that while ethanol production is low, no attempt has been made to increase ethanol production and the figures for ethanol production are for ethanol production in the growth medium, not in ethanol production medium nor under conditions optimal for ethanol production.

The 90ºC enrichment cultures that produce ethanol from carbon monoxide fail to yield microscopic evidence of cellular material even when gas chromatographic analyses demonstrate that carbon monoxide is being consumed. It appears that the cells are below the size detectable with the light microscope (0.2µ). Therefore, attempts were made to demonstrate the presence of microbial cells in the culture using a flagella stain wherein the stain may increase the size of the cell such that it is more visible. The culture suspension to be stained was vigorously vortexed to help separate some of the cells from their attachment to solid material (pyrite) in the culture medium and then passed through a 0.45 µ membrane filter. The filtrate was then filtered through a 0.22 µ membrane filter and the material on the filter suspended in distilled water. The distilled water suspension was allowed to air dry on a slide and the slide flooded with Leifson's Flagella Stain until a precipitate formed (usually within 10 min). The stain was gently washed from the slide and the slide viewed under oil immersion on the light microscope. As may be observed in Figure 8, using the flagella stain did not improve the situation significantly. Therefore, samples of the 90ºC enrichment cultures were examined using the electron microscope.

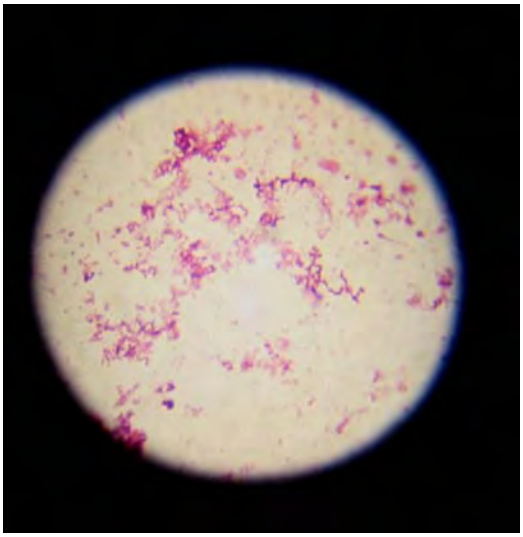


Figure 8. Leifson Flagella Stain of a 90°C enrichment culture as seen under oil-immersion.

Figures 9 and 10 are electron micrographs of samples from the 90ºC enrichment culture. It can be seen that the cells are extremely small (approximately 150 nm in diameter) and almost completely spherical.

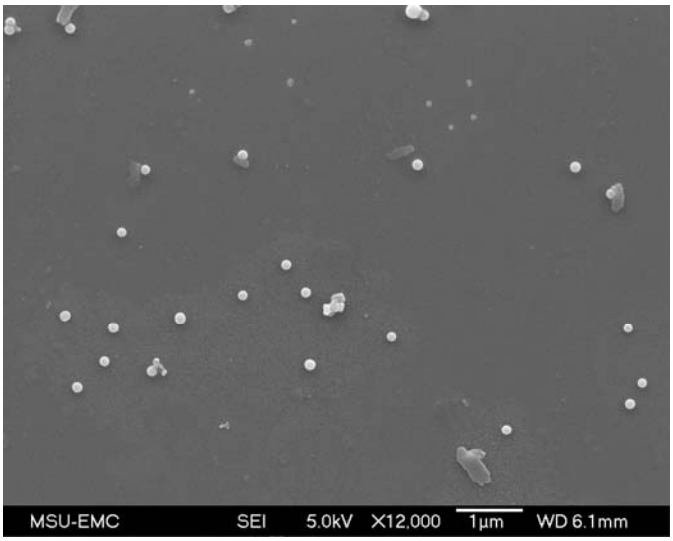


Figure 9. Photomicrograph (x12,000) of 90°C culture grown on syngas.

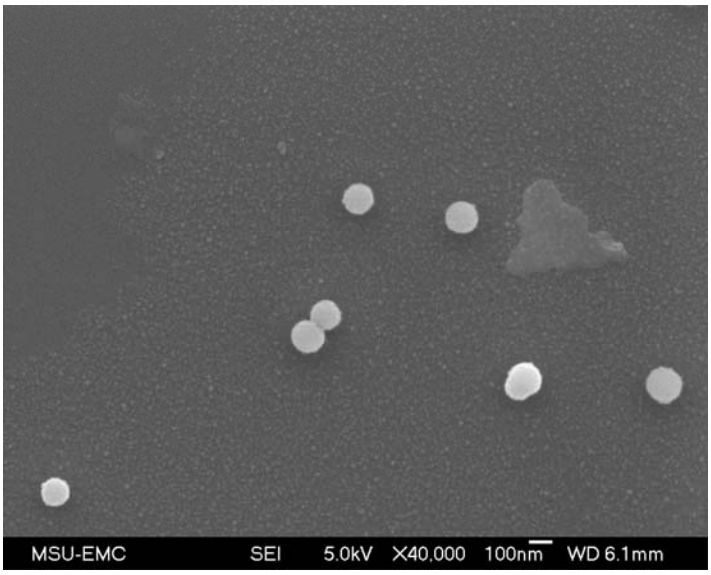


Figure 10. Photomicrograph (x40,000) of 90°C culture grown on syngas.

It was then decided to prove that these particles were indeed cellular material by staining the particles with a DNA stain that only stains DNA, a constituent of biological matter, not inanimate matter. Figure 11 is a photograph of material stained with DAPI (4'-6-diamidino-2phenylindole) taken using the scanning electron microscope with regular white light. Figure 12 shows the exact same picture using ultraviolet light rather than white light. As seen, some of the

particles are fluorescing blue which indicates that they contain DNA, thereby verifying that some of the particles are microbial cells.

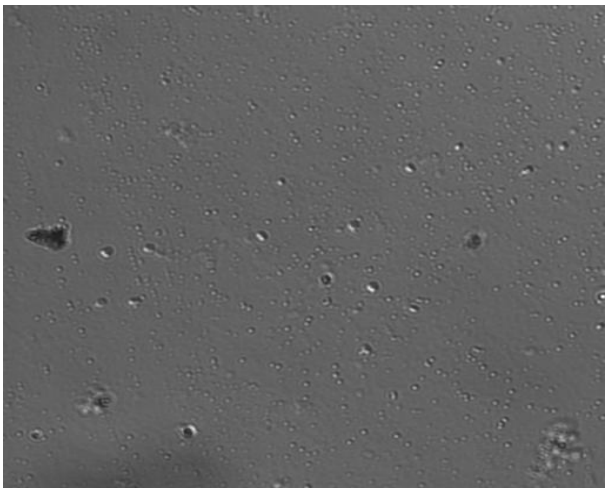


Figure 11. Electron micrograph of 90°C culture showing particles in a sample stained with DAPI (4'-6-diamidino-2-phenylindole) and viewed using white light.



Figure. 12 The exact same electron micrograph of 90°C culture shown in Figure 11 stained with DAPI (4'-6-diamidino-2-phenylindole) and viewed using ultraviolet light.

Development of molecular tools to identify the genetic limitations of syngas fermentations by evaluating the expression of key enzymes

Aerobic Models

Microorganisms which are capable of sequestering carbon monoxide and or carbon dioxide may be able to reduce pollutants, while yielding alternative energy sources such as ethanol. A gene cluster responsible for the assimilation of carbon has been identified. The Cox gene cluster encodes for a multifunctional enzyme known as carbon monoxide dehydrogenase (CODH) which is responsible for the aerobic assimilation of carbon monoxide (CO) into organic cellular carbon. This gene cluster has been found on chromosomal and extra-chromosomal elements. The Cox gene cluster is divided into three domains Cox M, Cox S and Cox L, which code for a Flavoprotein, FeS protein and a copper/molybdenum protein respectively, Figure 1. Collectively this enzymes complex facilitates the reversible oxidative conversion of carbon monoxide to carbon dioxide. Carbon dioxide in solution is subsequently converted back to carbon monoxide while bound to a molybdenum cationic center and presumably passed on to a neighboring acetyl-CoA synthase (ACS) enzyme resulting in the metabolically valuable form of carbon, acetyl-CoA. Acetyl-CoA is a key intermediate in the catabolism of carbon which can result in the formation of ethanol.

Using *Oligotropha carboxidiovorans*, as a starting point, we have used bioinformatics to elucidate additional information related to the fixation of CO (Figures 1 & 2). In general, aerobic and anaerobic organisms exist which have pathways that can sequester CO. The aerobic strains utilize a Cu/Mo center, while the anaerobic strains favor the use of a Ni center. In the later, the CODH activity has been associated with the ACS activity and is likely in physical contact which enhances substrate channeling leading to more efficient conversion of CO to Acetyl-CoA. Nucleic acid sequence alignments did not exhibit substantial sequence homology within or between the aerobic or anaerobic species. Therefore traditional PCR primer design was not a feasible route. Reverse engineering from the protein sequence was pursued as a means to develop primers with sufficient homology within the two different classes of CODH. Using the protein alignments, we deduced four domains of conserved sequence for the aerobic species containing CODH (Figure 3).

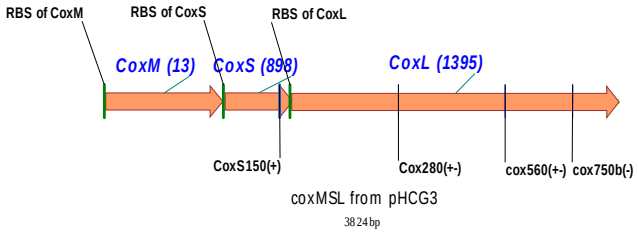


Figure 1. Arrangement of genetic subunits M, S, and L within the gene cluster for CODH.

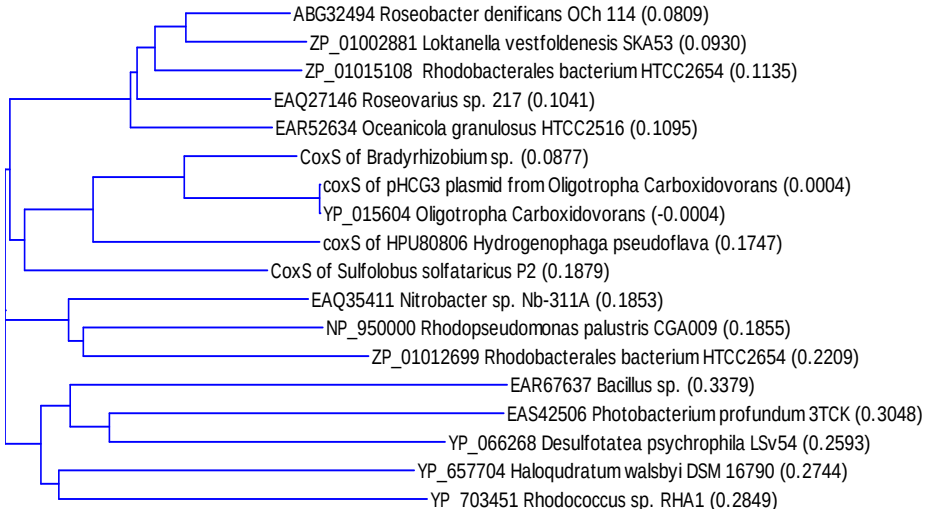


Figure 2. Phylogenetic linkage of species containing the aerobic form of the CODH gene cluster.

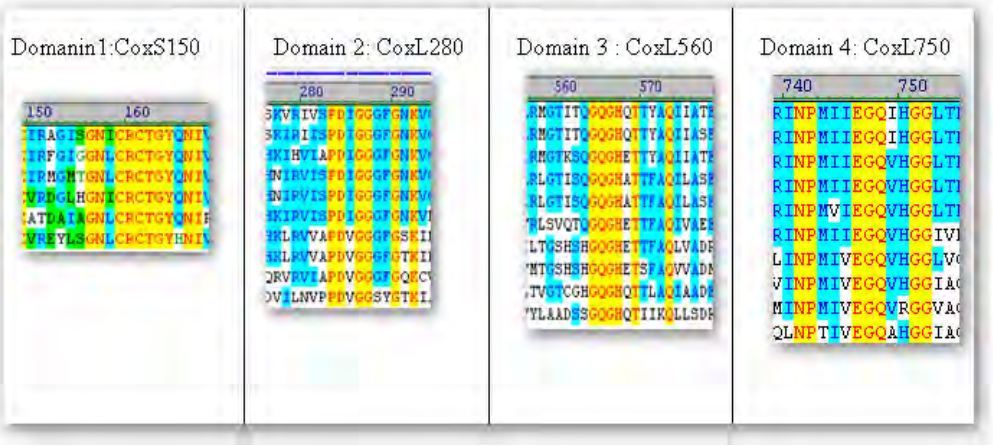


Figure 3. Identified domains of conserved protein sequence of the CODH gene cluster.

We focused our efforts on the aerobic class of CODH and expanded our species list from *Oligotropha carboxidiovorans* to include *Aspergillus oryzae, Stappia aggregate, Rhodococcus opacus and Bradyrhizobium sp.*, in addition to challenging numerous negative controls (Table 1). Seven second generation PCR primers for the determination of the Cox M, S, and L subunits of CODH have been tested. Primers were designed using reverse translation and a codon bias for bacterial genomes. The protein sequences were aligned and four domains identified which contained conserved amino acids (Figure 3). Primers were designed around those conserved residues and we used wobble design for the remaining bases (Table 2).

Table 1. Microbial list of genomes used for Cox gene cluster primer validation.

Microorganism	**Identity**
Aspergillus flavus (oryzae)	ATCC 42149
Bradyrhizobium sp.	ATCC 42149
Stappia aggregata	ATCC 25650
Staphylococcus aureus	ATCC 49476
Streptococcus pneumoniae	ATCC 49619
S. bovis	ATCC 9809
Serratia marcescens	ATCC 13880
Proteus vulgaris	ATCC 13315
Shigella sonnei	ATCC 9290
S. flexneri	ATCC 12022
Salmonella choleraesuis	ATCC 14028
S. typhimurium	ATCC 14028
Enterococcus faecalis	ATCC 29212
E. faecium	ATCC 35667
E. hirae	ATCC 8043
E. casseliflavus	ATCC 700327
E. durans	ATCC 6056
E. gallinarum	ATCC 49573
E. saccharolyticus	ATCC 43076
E. avium	ATCC 14025
Lactococcus lactis	ATCC 11454
Oligotropha carboxidovorans	ATCC 49405

Screening of the organisms (Table 1) has confirmed that the primers for the CoxL domain are specific and unique. Amplification of a single 520bp amplicon was observed for *Bradyrhizobium sp., Stappia aggregate* and *Oligotropha carboxidovorans* (Figure 5). Each organism was cultivated in the ATCC preferred medium and the genomic DNA isolated using the Gram positive DNA purification system from Epicentre Biotechnologies Madison, WI. Amplification was performed with all combinations of primer pairs (Table 2) using genomic DNA or single enzyme digested DNA which was re-precipitated and quantified as template. PCR conditions were optimized based upon the determined Tms of the primers and the amplification results. Standard PCR and touchdown PCR protocols were utilized. Rare base cutters were utilized to limit the number of fragments, providing a more accessible template for amplification while retaining fragment sizes which more readily precipitated.

Table 2. Wobble designed PCR primers for the amplification and detection of CODH.

Several sets of primers were tested including: CoxS150+/CoxL280-, CoxL280+/CoxL560-, CoxL560+/CoxL750a-, and CoxL560+/CoxL750- (Table 2). The most

Name	Sequence	Tm $_{min}$ °C	Tm $_{max}$ °C	Tm $_{ave}$ °C
CoxS150(+)	5'- TB TGY CGN TGY ACC GGN TAY -3'	50.9	65.7	58.6
CoxL280(+)	5' - CCN GAY RTN GGN GGS RGC TW - 3'			
CoxL280(-)	5' – WA GCY SCC NCC NAY RTC NGG -3'	52.00	70.60	61.90
CoxL560(+)	5'- GGN CAG GGV CAY SMN AC - 3'			
CoxL560(-)	5' – GT NKS RTG BCC CTG NCC -3'	48.90	66.00	58.00
CoxL750a(-)	5' –NCC YTC NAY NAY NRT NGG RTT -3'			
CoxL750b(-)	5' – CC NCC NYG NRY CTG NCC YTC -3'	40.10	63.40	52.30

successful primer pair was CoxL560+/CoxL750b- which produced an amplicon of 520 base pairs. The amplicon represents one of the most likely successful amplification products since both primers reside within the same genetic subunit. Optimization of template preparation and template to primer ratios revealed that 200ng of EcoRV digested template resulted in more specific amplification compared to non-digested template from *Bradyrhizobium sp.* Figure 4, compare lanes 4 and 5 undigested and digested. Changing the restriction enzyme to XbaI required a slight modification of the PCR protocol for complete optimization while HindIII digested potential templates in regions that interfered with amplification (data not shown). Template DNA that was precipitated after digestion resulted in cleaner more specific amplification compared to non-precipitated template (Figure 5 compare lanes 4 and 6) and that as little as 20ng of non-precipitated template was adequate for amplification of a specific product according to the touchdown PCR protocol depicted in table 3.

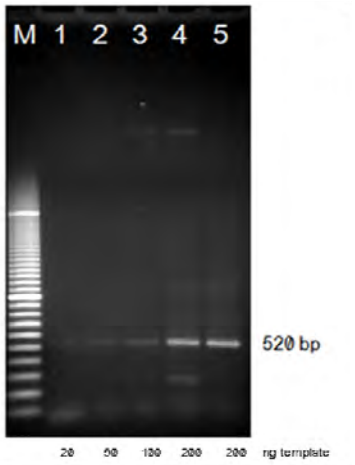


Figure 4 .Dose responses of undigested (1-4) and digested genomic *Bradyrhizobium sp* DNA.

Table 3 Touchdown PCR protocol for amplification of CODH Cox L subunit with CoxL560+/CoxL750b- primers.

Temperature	Time	Cycles
97◦	3 min.	1
95◦ C	20 sec	
60◦ C (-0.5◦ C/cycle	25 sec	10
72◦ C	35 sec	
95◦ C	20 sec	
55◦ C (-0.5◦ C/cycle	25 sec	35
72◦ C	35 sec	
72◦ C	2 min	
4◦ C	Hold	

Extending the above touchdown PCR protocol to test 18 negative controls and three CODH positive strains resulted in the amplification of only CODH positive strains (Figure 5, lanes 20-23) the primer pair of CoxL560+/CoxL770- thus represents a unique primer pair that is capable of detecting the presence of the CoxL subunit of the CODH complex. Further work is needed to extend the detection to the other two subunits or a mega amplicon which spans all three subunits.

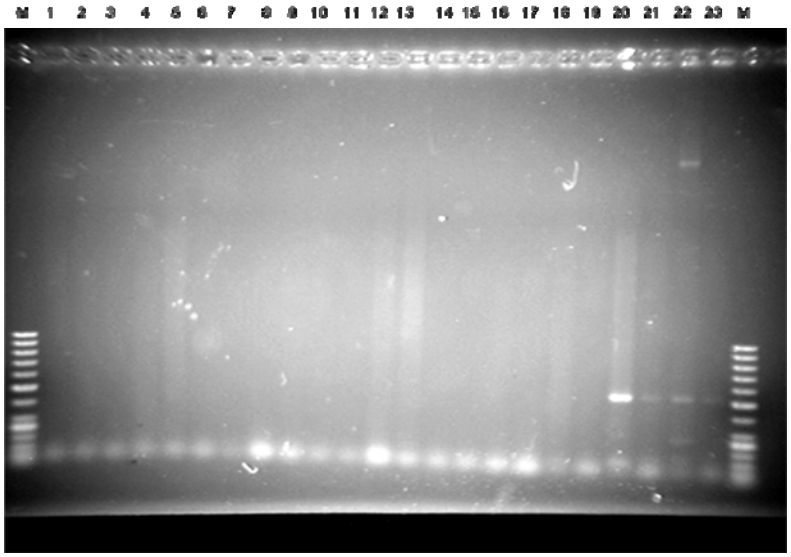


Figure 5 PCR Amplification of 18 negative control strains (1-18) and three positive CODH strains (20 EcoRV digested *Stappia aggregata* , 21 EcoRV Digested *Bradtrhyzobium sp.*, 22 undigested *Bradyrhyzobium sp.*, and 23 Undigested *Oligotropha carboxidovorans*

To validate the PCR, we next examined the inclusion of a 16S ribosomal DNA amplification product as an internal control and reference for Q-PCR applications. We utilized two sets of 16S rRNA primers (Table 4) during these investigations[1]. Examination of four negative control strains (*Shigella sonnei*, *Serratia marcescens, E. saccharolyticus, and E. faecium*) all resulted in the appropriate amplicon of 700 and 300 bp respectively for the respective primer sets (Table 4). Likewise, the strains positive for CODH resulted in the appropriate amplicons. Amplicons of the *O. carboxidovorans* was approximately $1/4^{th}$ that of all other strains tested with the ribosomal DNA primers (data not shown).

The goal of using the internal control was to perform multiplexing PCR capable of amplifying both the ribosomal DNA target and the CoxL subunit of CODH simultaneously. We again relied on the touchdown PCR protocol described in Table 3 using 4-5 times the concentration of CoxL primers (400nM) relative to the 16S rDNA primers (100nM). Figure 6 clearly deppicts that there was no interference in amplification during the multiplex PCR. The specificity of both primer pairs remained intact with the temperature profile used and thus we have successfully developed a primer set for the amplification and detection of carbonmonoxide hehydrogenase (CODH) which is now ready for screeening of environmental samples. Screening of additional samples will be necessary for identifying isolates which have the potential for sequestering CO and or CO_2 into cellular carbon sources. We had anticipated moving this research into the screening phase however, the funding for this project was not renewed.

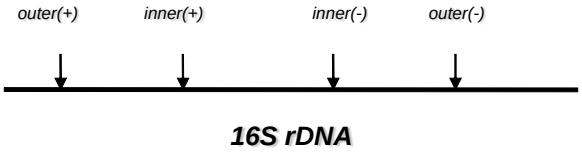


Figure 6. Diagram of 16S Ribosomal primer relationships

Table 4. 16S Ribosomal DNA primers and expected amplicon

Name	Sequence	Expected Amplicon
16S-rDNA-outer +	GTGTAGCGGTGAAATGCG	700bp
16S-rDNA-outer -	ACGGGCGGTGTGTACAA	
16S-rDNA-inner +	GGTGGAGCATGTGGTTTA	300
16S-rDNA-inner -	CCATTGTAGCACGTGTGT	

CODH is an important enzyme in cell function. The ability to obtain carbon and energy is the most important function in cell growth and maintenance. In addition, the ability to produce ethanol for use in bio-fuel production is important to the energy crisis facing the world. CODH allows organisms to solve both of these problems. Through specific pathways, cells are able to use carbon monoxide to create ethanol or use carbon dioxide to make ATP and a cellular carbon

source. Research into the utilization of CODH and the identification of more organisms with CODH capacity should be reevaluated as an important focus of research related to biofuel Figure 6. Multiplex PCR with CoxL560+/CoxL750b- in conjunction with 16S rDNA inner and outer primers. Lane 1, 16S outer primers concomitant with CoxL primers with *S. aggregate* template DNA. Lane 2 16S outer primers concomitant with CoxL primers with *E. saccharolytica* template DNA. Lane 3, 16S inner primers concomitant with CoxL primers with *S. aggregate* template DNA. Lane 4, 16S inner primers concomitant with CoxL primers with *E. saccharolytica* template DNA. M is a DNA molecular weight marker.

production.

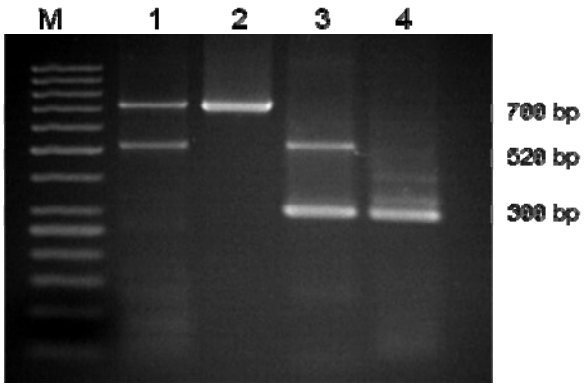


Figure 6. Multiplex PCR with CoxL560+/CoxL750b- in conjunction with 16S rDNA inner and outer primers. Lane 1, 16S outer primers concomitant with CoxL primers with *S. aggregate* template DNA. Lane 2 16S outer primers concomitant with CoxL primers with *E. saccharolytica* template DNA. Lane 3, 16S inner primers concomitant with CoxL primers with *S. aggregate* template DNA. Lane 4, 16S inner primers concomitant with CoxL primers with *E. saccharolytica* template DNA. M is a DNA molecular weight marker

Comparison of *Oligotrpha carboxidovorans* to *Clostridium cardoxidivorans*

Microorganisms with the best genetic tools for ethanol production are central to economic bio-fuel production. In particular, it is critical for successful industrial scale ethanol production from syngas that the bio-fermentation ecology balance in syngas fermentors be maintained. In this sub-task, we used genomic technologies to identify enzymes that are potentially important for fermentation of syngas.

Clostridium carboxidivorans and *Oligotropha carboxidovorans* are bacterial species that are capable of fermenting syngas (CO, H_2, and CO_2) and converting it into biofuels. In this project, our long-range goal was to identify the genetic networks and/or specific genes used during syngas fermentation by *C. carboxidivorans* and *O. carboxidovorans* so that the fermentation process can be enhanced either by genetic manipulation or by specific small molecule chemical metabolic inhibitors. The **three biological aims** for this project were to **1)** Sequence the *O. carboxidovorans* genome; **2)** Sequence the *C. carboxidivorans* genome; **3)** Define the functional proteome during syngas fermentation under different environmental

conditions. Furthermore, because the datasets that the proteomics datasets we produced in aim 3 are so large, and our computational methods sub-optimal, our **fourth aim** was to develop a novel computational methods for proteomics analysis and a method for to accelerate analysis.

Completion and annotation of *Oligotropha carboxidovorans* genome sequence.

Syngas is a mixture of CO, CO_2, and H_2 that results from gasification of organic wastes, and microbial fermentation of this gas mixture could serve as a source for biofuels (3). *O. carboxidovorans* is capable of utilizing these gases for chemolithoautotrophic growth. Therefore, the *O. carboxidovorans* genome sequence is allowing investigations into how it is able to assimilate carbon that is fixed by chemolithoautotrophy into its metabolism, which will benefit the future use of syngas for biofuel production. These studies would not be possible from the sequence of the megaplasmid alone. In addition, this genome sequence is enabling studies to determine how the metabolism of *O. carboxidovorans* functions under heterotrophic conditions versus chemolithoautotrophic conditions and how it is able to switch between these two contrasting lifestyles.

The complete genome sequence of *Oligotropha carboxidovorans* strain OM5 was determined using a combination of standard 454 pyrosequencing and paired end 454 sequencing at 454 Life Sciences (Roche) to generate a scaffolded assembly. 1,242,155 reads from standard sequencing and 536,302 reads from paired end sequencing were assembled using Newbler assembler (Roche). Five scaffolds containing 62 contigs were obtained after paired end sequencing, two of which were comprised of sequences belonging to the megaplasmid pHCG3, and the remaining three formed the chromosome. The gaps between contigs were closed by PCR amplification followed by Sanger sequencing with primer walking (Eurofins MWG Operon). Sanger reads were incorporated into the assembly using Sequencher (Gene Codes) and SeqManPro (Lasergene). Bases in the assembled contigs carried a Phred-equivalent quality score of 40 or above, which means that the level of accuracy was 99.99%. After gap closure, the circular chromosome was comprised of 2 contigs.

The *O. carboxidovorans* OM5 chromosome sequence contains 3,745,772 bp, had average sequencing depth of ~27x, and contained 3754 putative open reading frames (ORFs). The sequence was annotated using TIGR Annotation Engine, which used a Interleaved Markov model (Glimmer) (1) for gene prediction, and it was manually curated using Manatee (TIGR) for accuracy. The genome has been deposited in DDBJ/EMBL/GenBank under the project accession ABKN00000000.

The genome contains 49 tRNA genes and a single rRNA operon. The 3.7 Mb circular chromosome has a G+C content of 62.4%. No plasmids were found except the megaplasmid pHCG3 (2). Genes encoding metabolic enzymes involved in energy metabolism, biosynthesis of amino acids/ fatty acids, nucleotide metabolism, transcription and DNA metabolism, protein synthesis and degradation, and signal transduction were identified on the chromosome. The chromosome also contains genes encoding enzymes that allow heterotrophic growth on organic acids such as acetate, pyruvate, lactate, crotonate, malate, succinate , formate, and glyoxylate as substrates. The megaplasmid pHCG3 contains genes for chemolithoautotrophic utilization of CO and CO_2 (carboxidotrophy), H_2 and CO_2 (hydrogenotrophy), and CO_2 fixation under aerobic conditions (2).

Completion of *Clostridium carboxidivorans* draft genome.

C. carboxidivorans growth was very slow under anaerobic conditions and was very sensitive to very slight amounts of oxygen. Thus, cultivation was very difficult and prone to either death of the bacteria or contamination. Another difficulty encountered is that the genomic DNA is prone to degradation after isolation. Thus, this organism presented considerable challenges for genome sequencing.

To overcome these hurdles, genomic DNA was amplified following isolation to supply enough for sequencing. The actual sequencing strategy used was similar to that used for *O. carboxidovorans* using 454 Life Sciences. A total of 429,680 high quality shotgun reads were generated along with 111,154 high quality paired reads for scaffolding, resulting in 216 large contigs that were organized in 73 scaffolds. A large number of these gaps have been closed by PCR amplification and Sanger sequencing. Total genome size is approximately 5,646,053 bp. Genome annotation is in progress. *C. carboxidivorans* is an example of an organism that genomic analysis has the potential to greatly accelerate identification of enzymes and pathways involved in syngas fermentation because characterization by traditional phenotypic analyses would be very technically challenging.

Identification of *Oligotropha carboxidovorans* enzymes for syngas fermentation by comparing protein expression under syngas, acetate, and syntrophic conditions.

Oligotropha carboxidovorans OM5 grows under chemolithoautotrophic conditions by utilizing CO + H_2 in syngas and also it grows heterotrophically on acetate medium. During growth on these substrates, the organism expresses different amounts of enzymes that specifically utilize these substrates and assimilate them into their metabolism. We performed fatty acid methyl ester (FAME) analysis to determine whether useful fatty acids are produced by *O. carboxidovorans* under syngas conditions. We also analyzed protein expression by *O. carboxidovorans* under syngas conditions using two dimensional liquid chromatography electrospray ionization tandem mass spectrometry to identify enzymes produced during sygas fermentation.

FAME analysis showed that *O. carboxidovorans* produces three fatty acid methyl esters, hexadecanoic acid (Palmitic acid C_{16}), octadecanoic acid (Stearic acid C_{18}) and octadecenoic acid (positional isomer of Oleic acid C_{18}), when grown in the presence of syngas and acetate. The amount of these fatty acids was higher when grown on syngas. Under heterotrophic growth, the fatty acid profile was quite different. Palmitic acid and oleic acid were absent, and the relative amount of stearic acid present was comparatively less. Instead, octanoic acid methyl ester (caprylic acid) and octadecatrienoic acid were produced. Both of these were not present when grown in acetate or syngas. Thus, in the presence of syngas, *O. carboxidovorans* produced more of the fatty acids that are components of biodiesel.

Table 1. Results of FAME analysis of *O. carboxidovorans* under heterotrophic, syngas, and acetate growth conditions.

FATTY ACID METHYL ESTER		Amount (ng/ml)		
		TSB	SYNGAS	ACETATE
Octanoic acid methyl ester	Caprylic acid	6.337	0	0
Hexadecanoic acid methyl ester	Palmitic acid	30.05	105.3	19.91
Hexadecenoic acid methyl ester	Palmitoleic acid	0	55.16	18.99
Octadecanoic acid methyl ester	Stearic acid	10.5	14.37	33.89
Octadecenoic acid methyl ester	Oleic acid	12.58	40.77	58.20
Octadecatrienoic acid methyl ester	α-Linolenic acid	1.373	0	0

It appears that, in the presence of syngas, CO_2 is available in abundance to *O. carboxidovorans*, and CODH fixes CO_2 to acetyl CoA, which becomes the starting point of fatty acid synthesis (Figure 1). Fatty acid biosynthesis necessitates a 3-C precursor, malonyl-coenzyme A (CoA), which is derived from acetyl-CoA by the action of acetyl CoA carboxylase. Malonyl-CoA is transacylated to malonyl-acyl carrier protein (ACP) by malonyl-CoA acyl carrier protein transacylase. Significant expression of these two proteins in the presence of syngas marks the initiation of fatty acid biosynthesis in the bacterium. ACP plays a major role in phospholipid and rhamnolipid synthesis apart from playing central roles in other biosynthetic processes. Thereafter, fatty acid elongation begins involving cycles of a condensation reaction followed by reduction, dehydration and a second reduction, leading to the formation of palmitic acid (C16) that was found during FAME analysis.

Significant changes in expression of proteins involved in both biosynthesis and oxidation of amino acids were detected. Because *O. carboxidovorans* is not oleaginous, the genes responsible for oxidation of fatty acids were also produced significantly along with biosynthesis genes.

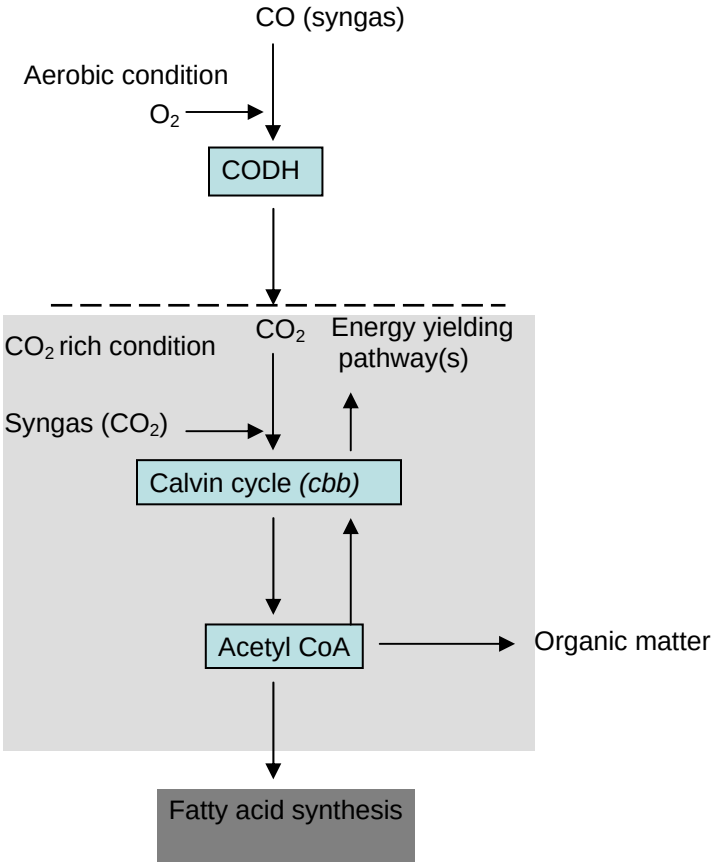


Fig. 1. Graphical representation of the roles of *O. carboxidovorans* enzymes in CO and CO_2 utilization to synthesize fatty acids.

Accelerating String Set Matching in FPGA Hardware for proteomics

At the core of proteomics is a string set matching problem: mass spectra are matched with strings of amino acids in a database. A correlation is calculated for all potential matches and this is used as the basis of a probability calculation. Here we designed and implemented a novel technique to accelerate the performance of the string set matching problem with particular emphasis on applications in computational proteomics. The process of matching peptide sequences against a genome translated in six reading frames is part of a proteogenomic mapping pipeline and was is used as a case-study. The Aho-Corasick algorithm was adapted for execution in field programmable gate array (FPGA) devices in a manner that optimizes space and performance. In this approach, the traditional Aho-Corasick finite state machine (FSM) is split into smaller FSMs, operating in parallel, each of which matches up to 20 peptides in the input translated genome. Each of the smaller FSMs is further divided into five simpler FSMs such that each simple FSM operates on a single bit position in the input (five bits are sufficient for representing all amino acids and special symbols in protein sequences).This bit-split organization of the Aho-Corasick implementation enabled efficient utilization of the limited random access memory (RAM) resources available in typical FPGAs. The use of onchip RAM (as opposed to FPGA logic resources) for FSM implementation also enabled rapid reconfiguration of the FPGA without the place and routing delays associated with complex digital designs. Experimental

results showed storage efficiencies of over 80% for several data sets. Furthermore, the FPGA implementation executing at 100 MHz was nearly 20 times faster than an implementation of the traditional Aho-Corasick algorithm executing on a 2.67 GHz workstation.

Developing new algorithms for proteogenomic mapping, protein quantification, and computation of protein coverage

The proteogenomic mapping pipeline is complete, has been tested and the Oligotropha annotation using proteogenomic mapping is underway. We have also developed new computational tools to improve the quality of protein identifications and to enable eventual protein quantification of the organisms grown under different conditions (e.g. different aerobic chemolithoautotrophic conditions). Development of a protein quantification tool (ProtQuant) has been completed and the tool has been installed and tested at CVM. An article describing this tool has been published in *BCM Bioinformatics* (see publications). Another tool, PepFly, has been developed to determine which peptides in a complex mixture are likely to be detected by mass spectrometry in a MudPIT experiment. We have used this tool for systems biology experiments in other organisms to determine if a protein we expected to see but did not was likely to be detectable. An article describing this tool has also been published in *BCM Bioinformatics*.

Task C.4 – Optimization of Reactor Design and Operation for Syngas fermentation

(1) Evaluation of reactor design/operation for the rapid removal of ethanol *in situ* to optimize ethanol production from acid hydrolysate or syngas. The utilization of a pressurized vessel containing a layer of liquid propane on the surface would effectively remove ethanol from the aqueous phase as it was produced could reduce the inhibitory effects exhibited by some ethanol-producing microorganisms. A secondary benefit that may be realized is the removal of phenols or tars from the fermentation broth.

<u>Optimization of Reactor design and operation of syngas fermentation.</u>
Evaluation of different operational parameters for modeling the system.

Effect of Carbon Source and Agitation on Ethanol Production: This study hypothesized that the conversion of syn-gas to ethanol by the P7 bacteria would be less efficient than the conversion of CO the ethanol but that agitation would improve conversion rates by increasing mass transfer. To test this hypothesis P7 was cultured in liquid medium under strict anaerobic conditions and sparged with CO every two days. Cultures were agitated at 200rpm on a shaker platform housed in a 37°C incubator. Control samples were cultured under identical conditions but remained static. A parallel set of experiments was performed but CO was substituted with syn-gas. Experiments were run for a total of 11 days and samples were collected at regular intervals for measurement of ethanol. Ethanol content was quantified by gas chromatography.
In all experiments the ethanol content showed a statistically significant increase. When P7 was cultured with CO the ethanol content peaked after 3 days and remained constant thereafter. When syn-gas was used to culture P7, ethanol content reached its maximum content after 9 days. These trends were the same regardless of whether the cultures were static or agitated. The

highest mean concentration of ethanol was found in cultures incubated with syn-gas plus agitation. However, due to the variance in the data no significant difference was detected between the highest mean values in the other samples. The lowest mean maximum concentration was found in agitated cultures sparged with CO. This was significantly lower than the maximum concentrations in static cultures sparged with CO or syn-gas. The results are shown in the following figure.

In conclusion, the highest ethanol concentrations were found when P7 was gassed with syn-gas. However, agitation did not significantly improve ethanol concentration in these cultures. Ethanol production was more rapid when P7 was gassed with CO. In these cultures, agitation lowered the maximum mean concentration of ethanol.

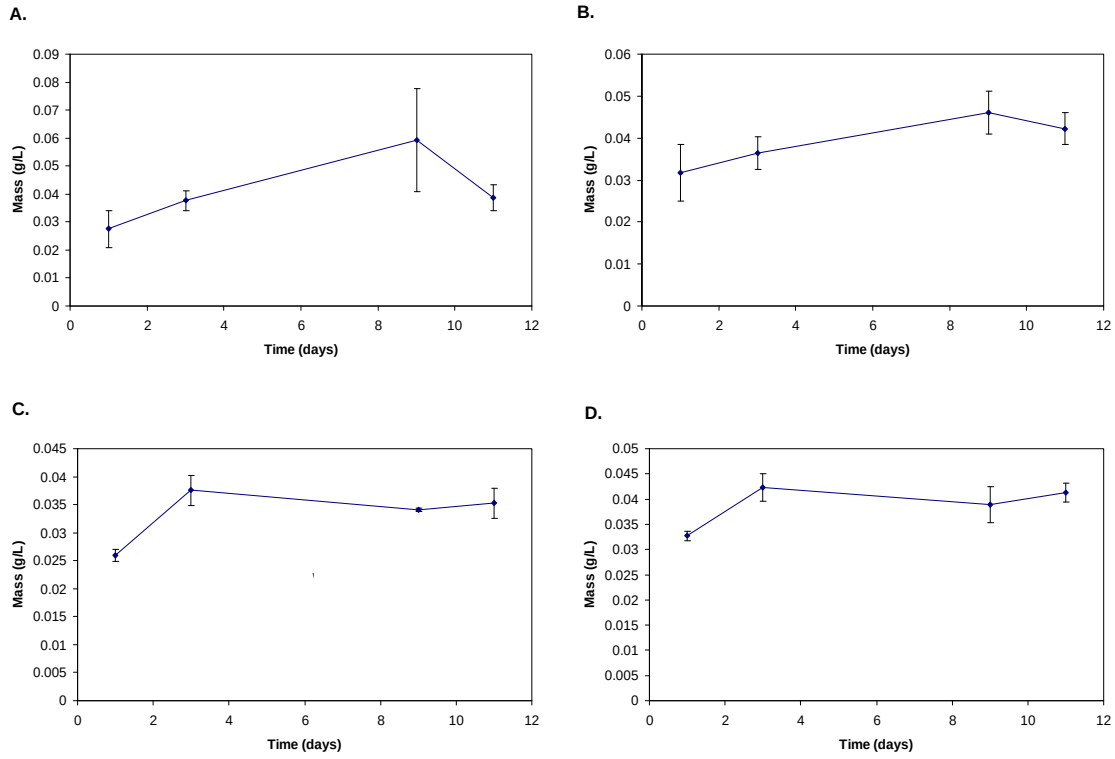


Figure 1: Ethanol production from P7 bacteria vs. time. A) P7 grown with syn-gas and agitation; B) P7 grown with syn-gas under static conditions; C) P7 grown with CO and agitation; D) P7 grown with CO under static conditions. Data points represent mean values ± standard deviation, n = 3.

Evaluate several surfactants for increasing the solubility of syngas in the aqueous phase and separation of the syngas constituents.

For the first time, CO_2 gas separations from a syngas were demonstrated by a surfactant-assisted gas hydrate process. Trisiloxanes, biosurfactant and sodium dodecyl sulfate (SDS) were screened for effectiveness in the process. The most effective surfactant was found to be SDS used in multiple stages of gas hydrate formation; a 75% reduction of the original CO_2 content of a gas mixture was achieved with a 3-stage hydrate process.

The separation of gases in a surfactant-assisted gas hydrate process was shown to be technically effective. The goal to achieve at least a 33% separation of CO_2 from a syngas was exceeded by a large margin. The study introduced economic enhancements to the hydrate

process that included a non-stirring process to form the hydrates; tetrahydrofuran in conjunction with a siloxane surfactant showed promise in lowering required pressures to form hydrates.

Gas separations are an important unit operation in the chemical process industries. This study introduces a new means to achieve some of these separations in a surfactant-assisted gas-hydrate process. The study for the first time demonstrated use of siloxane surfactants in a gas hydrate process. The results present a new novel means for industrial gas separations.

Screening Surfactants for Creating CO_2 Hydrates

The following surfactants were screened for their efficacy in promoting CO_2 gas hydrates—the goal being to preferentially remove CO_2 from a gas mixture: (1) sodium dodecyl sulfate, (2) two members of the trisiloxane family, i.e., Silwet L-77 and Silwet 408, and (3) the biosurfactant rhamnolipid. There are two properties of surfactants that are important in the hydrate separations—adsorption on solid surfaces at the gas/water interface and absorption of CO_2. Unless the surfactant adsorbs on the solid surface at the water/gas interface, stirring is necessary as hydrates form.

Trisiloxane surfactants that solubilize CO_2 were evaluated for promoting CO_2 hydrate formation. Trisiloxane forms micelles and accumulates CO_2 at nucleation sites. This family of surfactants was found to be very effective for rapidly generating carbon-dioxide-gas-hydrates in a stirred vessel. Trisiloxane Silwet L-77 increased hydrate formation three-fold over the control. The improvement continued as the trisiloxane concentration was increased to a concentration of 1000 ppm in water.

An unusual characteristic of Silwet L-77 to adsorb and initiate hydrates on Teflon hydrophobic surfaces was found.

Rhamnolipid biosurfactant was evaluated for forming CO_2 gas hydrates in a quiescent system, but rhamnolipid was found not to adsorb on metal surfaces at the gas/water interface, necessitating a chemical modification to establish this property.

Sodium dodecyl sulfate (SDS) adsorbs readily on metal surfaces to promote hydrates.

It is feasible to improve surfactant adsorption properties through chemically modifying their structures by attaching a phosphate group. This chemical modification was attempted on the anionic surfactants that had shown minimal adsorption properties during screening.

Chemical Modification of Surfactants

Two CO_2-philic trisiloxanes, Silwet 408 and Silwet L-77, were evaluated. One trisoloxane was modified by chemically substituting a phosphate group to increase adsorption. A phosphate group was reacted with Silwet 408 trisiloxane. Pressure drop data during hydrate formation showed that hydrate formation increased by a factor of 5.2 because of the added adsorption properties from the implanted phosphate group.

The biosurfactant Rhamnolipid was reacted with phosphoric acid. Its adsorption properties were improved from addition of the phosphate group.

Achieve at least a 33% Separation of CO_2 from Gas Mixtures with Hydrates

Initial separation tests were made with SDS. These first tests gave a 28% removal of the CO_2 present in a 60/40 CH_4/CO_2 initial gas mixture. Sodium dodecyl sulfate was then used in hydrate formation to separate CO_2 from a hydrogen/nitrogen/carbon monoxide/methane/carbon dioxide gas mixture of 9.36/12.75/2.93/53.28/22.18 molar percent, respectively. In 3

experimental runs, 40.6%, 49.8% and 39.3% of the CO_2 content of this free gas was removed by a first stage of hydrate formation assisted by SDS surfactant.

Next, Silwet L-77, a carbon dioxide solubilizing surfactant, was used in a concentration of 1000 ppm in distilled water to achieve the desired separation of carbon dioxide from a gas mixture with methane. A 33 1/3% separation of CO_2 from a CO_2/CH_4 40.26/59.74 gas mixture was accomplished in the hydrate process to reach the goal of Task #3. The initial free gas contained 40.26% CO_2 and the final free gas after hydrate formation contained 26.85 % CO_2 (Run # CMGH201).

Finally, a series of hydrate stages were used to affect the CO_2 separation from a gas mixture. Multiple stages of hydrate formation were used to separate a 50% CO_2 – 50% CH_4 initial gas composition. At the end of a 3rd stage of hydrate formation, the CO_2 concentration in the gas mixture had been reduced from 50% to 12.45% in the gaseous phase. This represents a 75% reduction in the original carbon dioxide content in the original gas. The results indicate a trend whereby additional stages would reduce the CO_2 contaminant to a negligible value.

Evaluate Tetrahydrofuran Effect on Hydrate Separation Process

Tetrahydrofuran (THF) is known to decrease the pressure required for stable hydrate formation, which would help economics of a hydrate separation process. We cursorily evaluated THF with the trisiloxane surfactant and found a surprising positive effect of the combination on CO_2 hydrate formation. THF retarded CO_2-hydrate formation without surfactant, but with Silwet–77 present, hydrate formation was improved substantially.

Although the trisiloxane-THF combination looks promising, the goal to completely evaluate Task 4 was not reached. Getting the new test cell online proved to be a time-limiting factor in further evaluating THF in Task 4.

A new hydrate test cell was designed and put in operation to study gas hydrate separations of syngas. The hydrates forming in the test cell could be viewed. Effectiveness of the hydrate separation was measured by gas chromatographic analysis of the headspace gas remaining in the test cell. The test cell performed as desired.

Hydrates formed in the absence of surfactants will make some separations of gas mixtures. However, surfactants selectively enhance gas separations as well as increase reaction rate and reduce process costs. Representative surfactants from different families of surfactants were screened to improve efficiency of CO_2 removal from the gas phase. Those families were selected that could selectively absorb CO_2 from the free gas phase above the water-surfactant solution. Trisiloxanes, biosurfactant, and sodium dodecyl sulfate were representative surfactants evaluated.

Only SDS demonstrated the desired property of adsorption and hydrate formation on metal surfaces that effectively increases hydrate formation rates and reduces process costs (eliminates stirring). The trisiloxanes, as well as the biosurfactant, were chemically modified with phosphate groups to improve the adsorption property.

Separation of gas mixtures were demonstrated in stirred as well as non-stirred systems in a single hydrate formation stage. Finally, multiple stages of hydrate formation demonstrated a high degree of CO_2 separation from gas mixtures.

6. Products developed and technology transfer activities:

Patents: None

Publications:

1. Easterling, E. R., French, W. T.*, Hernandez, R., and Licha, M. 2009. "The effect of glycerol as a secondary substrate on the growth and fatty acid composition of *Rhodotorula glutinis*". Bioresource Technology. 100, 356-361.

Presentations:

1. Todd French, Rafael Hernandez, Jaclyn Hall, and Andro Mondela 2007. "Wastewater Treatment Facilities: a Novel Biorefinery for the Production of BioCrude" American Oil Chemist Society, May 2007
2. Jaclyn Hall, Todd French, and Rafael Hernandez 2007 "Cultivating Oleageneous Yeast Using Municipal Wastewater" American Oil Chemist Society, May 2007
3. Stephen Dufreche, Rafael Hernandez, Bill Holmes, Earl Alley, and Todd French 2007 "Influence of Phosphorous on the Heterogeneous Catalytic Cracking of Phospholipids for Green Diesel Production" American Oil Chemist Society, May 2007
4. Darrell Sparks, Rafael Hernandez, Antonio Estevez, and Todd French 2007 "Kinetics of Oleic Acid Oxidation in a Supercritical Fluid" American Oil Chemist Society, May 2007
5. Bill Holmes, Tracey Benson, Rafael Hernandez, Mark White, and Todd French 2007 "Online Mass Spectrometry Analysis of a Catalytic Cracking Reactor" American Oil Chemist Society, May 2007
6. Todd French and Rafael Hernandez. 2007 "Wastewater Treatement Facilties: Next Generation Biorefineries" CleanTech 2007, June 2007
7. Robert McComas, Mark Bricka, and Todd French 2007 "Preliminary Investigation Of Cellular Lipid Extraction Using Electroporation As An Enhancement Technique" American Institute for chemical Engineering Annual Conference, November 2007
8. Andro Mondala, Rafael Hernandez, and Todd French "Ozone Disinfection And Biodegradability Enhancement Of Primary Wastewater Effluent" American Institute for chemical Engineering Annual Conference, November 2007
9. Earl Alley, Rafael Hernandez, Todd French, Bill Holmes, and Mari Parachevavue "Kinetics Of Transesterification Reactions Of Lipids" American Institute for chemical Engineering Annual Conference, November 2007
10. Stephen Dufreche, Rafael Hernandez, Todd French, Mark G. White, Earl G. Alley, William E. Holmes Effect of Phosphorus on Acid Cracking of Lipids for the Production of Green Diesel American Institute for chemical Engineering Annual Conference, November 2007
11. Darrell Sparks, Antonio Estevez, Rafael Hernandez, Todd French, and Earl Alley, Synthesis Of Renewable Chemicals From Oleic Acid American Institute for chemical Engineering Annual Conference, November 2007

12. Guochang Zhang, Todd French, Rafael Hernandez, Lynn Prewitt, Lew Brown, and Magan Green, Combining Microbially Enhanced Oil Recovery With CO2 Sequestration American Institute for chemical Engineering Annual Conference, November 2007
13. Guochang Zhang, Todd French, Rafael Hernandez, Earl Alley, and Bill Holmes Lipid Production From Acid Hydrolysate Of Lignocellulosic Biomass Using Rhodotorula Glutinis American Institute for chemical Engineering Annual Conference, November 2007
14. Jaclyn Hall, Todd French, Rafael Hernandez, Earl Alley, and Bill Holmes, Conversion of Wastewater Treatment Facilities into Biorefineries American Institute for chemical Engineering Annual Conference, November 2007
15. Kaiwen Liang, Rafael Hernandez, Hossein Toghiani, and Todd French Biodiesel From Sewage Sludge American Institute for chemical Engineering Annual Conference, November 2007
16. Tracey Benson, Rafael Hernandez, Mark White, Todd French, Bill Holmes Development Of A Laboratory Scale Catalytic Cracking Reactor American Institute for chemical Engineering Annual Conference, November 2007
17. Tracey Benson, Rafael Hernandez, Mark White, Todd French, Bill Holmes Identification Of The Cracking Mechanism Of Mono-, Di-, And Triglycerides Over H-Zsm-5 Catalyst American Institute for chemical Engineering Annual Conference, November 2007

APPENDIX

References:

Taherzadeh, M. J., Liden, G., Gustafsson, L., and Niklasson, C. 1997. The effects of panthenate deficiency and acetate addition on anaerobic batch fermentation of glucose by S*accharomyces cerevisiae. Appl. Microbiol. Biotechnol.* 46:176-182

Rallu, F., Gruss, A., Ehrlich, S. D., and Magulin, E. 2000. Acid-and multistress-resistant mutants of *Lactococcus lactis*: identification of intracellular stress signals. *Mol. Microbiol*. 35:517-528

De Angelis, M., Bini, L., Pallini, V., Cocconcelli, P.S., and Gobbetti, M. 2001. The acid-stress response in *Lactobacillus sanfrancisscensis* CB1. *Microbiology* 14:1863-1873

Arnold, C. N., McElhanon, J.j Lee, A., Leonhart, R and Siegele, D. A. 2001. Global analysis of *Escherichia coli* gene expression during the acetate-induced acid tolerance response. *J. Bacteriol*. 183:2178-2186.

Audia, J. P., Webb, C. C., and Foster, J. W. 2001. Breaking through the acid barrier: an orchestrated response to proton stress by enteric bacteria. *Int. J. Med. Microbiol*. 291:97-106

Alfantanzi, A. M. and Pickles, C. A. 1992., Materials at High Temperature, 10 (1):51-59.

Aranda, P., Chen, Wen-Janq, Martin, C. R., 1995, *Memb. Sci., 99,* 185-95.

Arora, D. et al., 1997, *Production of Ethanol from Refinery Waste Gases*, DOE Final Report (DOE-AL-98770-3)

1. Sauer, P., Gallo, J., Kesselova, M., Kolar, M., and D. Koukalova. 2005. Universal Primers for Detection of Common Bacterial Pathogens Causing Joint Infection. *Biomed Pap Med Fac Univ Palacky Olomouc Czech Repub* 149(2):285–8.

Arora, D., Basu, R., Breshears, F. S., Gaines, L. D., Hays, K. S., Phillips, J. R., Wilkstrom, C. V., Clausen, E. C., and Gaddy, J. L. 1996. AProduction of Ethanol from Refinery Waste Gases. Final Report, April 1994 B July 1997@. DOE/AL/98770-3 (DE98003194).
Arora, D., Basu, R., Phillips, J. R., Wilkstrom, C. V., Clausen, E. C., and Gaddy, J. L. 1995. AProduction of Ethanol from Refinery Waste Gases. Phase II. Technology Development@. DOE/AL/98770-1 (DE97006845).
Ayea, E., He, D., and Wang, J., 1993, App. Catal. A: General, V104, pp. 77-85.
Bashir, S. and Lee, S., 1994, *Fuel Sci. and Tech. Inter*., 12, 11/12.
Bauer, M.W., L. E. Driskill, W. Callen, Snead, M.A., E. J. Mathur, and R.M. Kelly, *1999, J. Bacteriol. 181*, 284-90.
Bioengineering Resources, Inc. 1995. ABench-Scale Demonstration of Biological Production of Ethanol from Coal Synthesis Gas. Topical Report 5: Process Analysis@. DOE/PC/92118-T14 (DE96007018).
Blanch, H. and Clark, D., 1997, *Biochemical Engineering*, Marcel Dekker Inc.
Borja, R., Banks, C., and Sanchez, E., 1996, *J. Biotech*., 45, 2.
Bredwell, M. and Worden, M., 1998, Biotech. Prog., V14, pp. 31-38.
Bredwell, M., Srivastava, P., and Worden, M., 1999, Biotech. Prog., V15, pp. 834-844.
Broder, J.D., J. W. Barrier, G. E. Farina, and G. Lightsey, 1985 , *Acid Hydrolysis Experimental Facility Results with Corn Stover,* ASAE Paper No. 85-30083.
Brooks, T. and Ingram, L., 1995, Biotech. Prog. V11, pp. 619-625.
Bryjak, M., Pozniak, G., Trochimczuk, W., *1992, Agnew. Makromol. Chem. 200* , 93-108.
Bryjak, M. Trochimczuk, W., 1992, *Agnew. Makromol. Chem. 200,* 111-21.
Business Trends, Nov. 1998, 20, 6.

Business Trends, July 1999, 40, 7.
Cabasso, I.; Liu, Z.Z.; Makenzie, T., 1986, *J. Membrane Sci., 28*, 109.
Carder, J. H., 1986, *Anal. Biochem., 153*, 75-9.
Choi, H.S. ; Hino, T. ; Shibata, M. ; Negishi, M. ; Ohya, H., 1992, *J. Membrane Sci., 72*, 259.
Claassen, P, van Lier, J., Lopez, A., van Niel, E., Sijtsma, L., Stams, A., de Vries, S., and Weusthuis, R, 1999, Appl. Microbiol. Biotech., V52, pp. 741-755.
Coffin, J. M. 1984. AIndustrial Coal Gasification: Applications and Economy@. Energy Prog., 4:131-137.
Dai, Y-R., D.Reed, J.Millstein, P.Hartzell, D. Grahame, and D. DeMoll, 1988, *Arch. Microbiol*. 169: 525-529.
Datta, R. and Zeikus, J. G. 1982. Dev. Ind. Microbiol., 23:131-140.
Davidson, B. and Wyman, C., 1994, *Sixteenth Symposium on Biotechnology for Fuels and Chemicals*, Humana Press
Dobbek, H., L. Gremer, O. Meyer, and R. Huber, 1999, *Proc. Natl. Acad. Sci. USA 96*: 8884-8889.
DOE, 1999, Website - biofuels.nrel.gov/bioethanol
DOE, 1999, Website - ott.doe.gov/ofd/ethanol
DOE, 1999, Website - nrel.biotech_symposium
DOE, 1999, Website - nrel.gov/research/indutrial_tech/biomass.html
DOE, 1999, Website - rredc.gov/biomass/doe/rbep/wis.ethanol
Dunning, J. W., and Elbert C. Lathrop, 1984, *Process for Saccharifying Plant Materials,* Pat. No. 2,450,586.
Dunning, J. W., and Elbert C. Lathrop, 1945, *The Saccharification of Agricultural Residues*, *Ind. Eng. Chem.*, 24-9.
Elmaleh, S. and Abdelmoumni, L., 1998, *Water Sci. Tech*., 38, 8/9.
Engler, C., Walawender, W., and Fan, L., 1975, Environmental Science and Technology, V9, N13.

Erena, J., Arandes, J., Bilbao, J., Olazar, M., and de Lasa, H., 1998, J. Chem. Tech., V72, pp. 190-196.
Exxon Co., USA. 1979. AEnergy Outlook 2000@. Houston, TX, USA. In Bioprocessing of Coal-derived Synthesis Gases by Anaerobic Bacteria= by A. J. Grethlein and M. K. Jain, TIBTECH, vol 10, p. 418-423, December 1992.
Fraga, M. and Jordao, E., 1998, React. Kinet. Catal. Letters, V64, N2.
Gaddy, et al., AProduction of Ethanol from refinery waste gases,@ DOE/AL/98770-3 DE 98003/94 Final Report to DOE under cooperative agreement DE-FC 04-94AL98770, August 1997
Gaddy, J. L. and Clausen, E. C. 1992. A*Clostridium ljungdahlii*, An Anaerobic Ethanol and Acetate Producing Microorganism@. US Patent # 5,173,429, issued on Dec 22, 1992.
Goodwin, S. and Zeikus, 1987, *J. Bacteriol. 169*, 2150-7.
Grethlein, A. J. and Jain, M. K. 1992. ABioprocessing of Coal-Derived Synthesis Gases by Anaerobic Bacteria@, TIBTECH, 10:418-423.
Harris, E., Hajny, G., Hannan, M., and Rogers, S., 1946, Industrial and Engineering Chemistry, V38, N9.
Hester, R. and Farina, G, 1995, Patent No. 5,407,580, US Patent Office, Washington DC.
Hirano, A., Ueda, R., Hirayama, S. and Ogushi, Y., 1997, Energy, V22, N2/3.
Hikmet, R. M., Callister, S., Keller, A., 1988, *Polymer 29*, 1378- 88.
Horikoshi, K and W.D. Grant, 1998, *Extremophiles; Microbial Life in Extreme Environments* Wiley - Liss, NY ISBN 0-471-02618-2.
Hsu, Y. and Shieh, W., 1993, *Biotechnology and Bioengineering*, 41, 347-353.

Ingram et al., 1999, *J. Biotech*., 15, 855-868.
Jiang, M.; Gronowski, A.A.; Yeager, H.L.; Wu, G.; Kim, J.S.; Eisenberg, A, 1994,. *Macromolecules*, *27*, 6541.
Jo, W.H.; Kang, Y.S.; Kim, H.J., 1993, *J. Membrane Sci.*, *85*, 81.
Jørgensen, S., C. E. Vorgias and G. Antranikian, 1997, *J. Biol. Chem. 272*, 16335-42.
Kadam, K. and Newman, M., 1997, *Appl. Microbiol. Biotech*., 47, 625-629.
Kang, B.S. and Y.M.Kim, 1999, *J. Bacteriol*. 181: 5581-5590.
Kawabata, N.; Oda, H., 1989, *Biotechnol. Bioeng*., *34*, 1045.
Kawabata, N., 1992, *Prog. Polym. Sci*., *17*, 1.
Kawagoe, M., Kawakami, K., Nakamura, Y., Naoe, K., Miki, K., and Noda, H., 1999, Journal of Bioscience and Bioengineering, V87, N1, pp. 116-118.
Kesava, S. and Panda, T., 1996, J. Industrial Micro., V17, pp. 11-14.
Kesting, R. E., 1971, *Synthetic Polymer Membranes*, McGraw-Hill Inc.
Kim, J. T., Anderson, J. L., 1989, *J. Memb. Sci. 47*, 163-82.
Kim, H., Bellows, P., Datta, R., and Zeikus, J., 1984, Applied and Env. Micro., V48, N4.
Kita-Borsa, T., Pacas, D., Selim, S., and Cowley, S., 1998, *Ind. Engr. Chem. Res*., 37, 3366-3374.
Kitani, O., and Hall, *C., 1989, Biomass Handbook*, Gordon and Breach Pub. Co., p. 434-51.
Klasson, K., Ackerson, M., Clausen, E., and Gaddy, J., 1991, *Fuel*, 70, 5.
Klasson, K., Ackerson, M., Clausen, E., and Gaddy, J., 1993, *Fuel*, 72, 12.
Klasson, K. T., Gupta, A., Clausen, E. C., and Gaddy, J. L. 1993. AEvaluation of Mass-Transfer and Kinetic Parameters for *Rhodospirillum rubrum* in a Continuous Stirred Tank Reactor@, Appl. Biochem. Biotechnol., 39/40:549-557.
Koch, R., P. Zabowski, A. Spreinat, and G. Antranikian, 1990, *FEMS Microbiol. Lett. 71*, 21-6.
Koros, W.J.; Fleming, G.K.; Jordon, S.M.; Kim, T.H.; Hoehn, H.H., 1988, *Prog. Polym. Sci.*, *13*, 339.
Kunduru, M. and Pometto, A., J. Ind. Micro., V16, pp. 249-256.
Lightsey, G. R., C.E. George and A.G. Wehr, *Evaluation of Cotton Seed Processing Wastes as Feedstocks for the TVA Concentrated Acid Hydrolysis Process*, 1991, Final Report to Ms. Dept.of Economic and Comm. Dev.
Lepkowski, W. 1991. Chem. Eng. News.,V69:20-31.
Lewis, R., 1997, Hawley=s Condensed Chemical Dictionary, Van Nostrand Reinhold Pub.
Lin, C. and Chang, R., 1999, J. Chem. Tech. Biotech., V74, pp. 948-500.
Linden, J. C. 1988. In >Handbook on Anaerobic Fermentations=, L. E. Erickson and Y.-C. D. Fung (Eds.), pp. 59-80, Marcel Dekker.
Lorowitz, W. H. and Bryant, M. P. 1984. Appl. Environ. Microbiol., 47:961.
Lundberg, R. D., Phillips, R. R., 1982, *J. Polym. Sci, Polym. Phys. Ed., 20*, 1143-54.
Lynd, L., Cushman, J., Nichols, R., and Wyman, C., 1991, *Science*, 251, 4999 1318.
Machio, G., Koufopanos, C., and Lucchesi, A. 1992., Bioresources Technol., 42:219-231.
Madhukar, G. R., Elmore, B. B., and Huckabay, H. K. 1996. AMicrobial Conversion of Synthesis Gas Components to Useful Fuels and Chemicals@, Appl. Biochem. Biotechnol., 57/58:243-251.
Markov, S., Weaver, P., and Seibert, M., 1997, Applied Biochemistry and Biotechnology, V63 - 65.
Marlatt, J. and Datta, R., 1986, *Biotech. Progress*, 2, 1.
Matsudaira, P.T, ed., 1988, *A Practical Guide to Protein and Peptide Purification for Microsequencing*, Academic Press NY. ISBN 0-12-480280-X.
Maupin-Furlow, J and J. G. Ferry, 1996, *J. Bacteriol*. 178: 6849-6856.

McCullough, G. R., Roberts, S. C., and van der Burgt, M. J. 1982. Energy Progr., 2:69-72. In >Bioprocessing of Coal-derived Synthesis Gases by Anaerobic Bacteria= by A. J. Grethlein and M. K. Jain, TIBTECH, vol 10, p. 418-423, December 1992.
Meyer, C., Ross, J., and Papoutsaki, E., 1986, *App. Micro. Biotech*., 24, 159-167.
Mississippi State University, 1996, *Production and Utilization of Industrial Wood and Bark Residues in Mississippi*, MDEQ and MSU Extension Service.
Nishio, N., Solveria, R., Hamato, K., and Nagai, S., 1993, *J. Fermentation and Bioengineering*, 75, 4.
Ono, H., Fujiwara, K., Sugiyama, E., and Yoshida, K., 1990, *Inter. Chem. Engr*., 30, 3.
Pasternak, M.; Dorawala, T.G., 1991, *J. Polym. Sci., Part A, 29*, 915.
- Peters, M. and Timmerhaus, K., 1991, Plant Design and Economics for Chemical Engineers, McGraw-Hill Inc., New York, NY.
Pereira, E. and Martin, G., 1993, App. Catal. A.: General, V108, pp. 291-309.
Philipidis, G., Smith, K., and Wyman, C., 1993, Biotech. And Bioengr., V41, pp. 846-853.
Phillips, J. R., Klasson, K. T., Clausen, E. C>, and Gaddy, J. L. 1993. ABiological Production of Ethanol from Coal Synthesis Gas B Medium Development Studies@, Appl. Biochem. Biotechnol., 39/40:559-571.
Redkar, S., Kuberkar, V., Davis, R., *1996, J. Membrane Sci., 121*, 229-42.
Reinmert, R., 1985, Synthetic Fuels, pp. 135-163.
Rogers, P. 1986. AGenetics and Biochemistry of *Clostridium* Relevant to Development of Fermentation Processes@, Adv. Appl. Microbiol., 31:1-60.
Rondleman, C. and Hohman, N., 1993, *Agribusiness*, 9, 3.
Salin, M.L. and N.J. Brown-Peterson, 1995, *The Archaea: A Laboratory Manual*, (F.T. Robb, A.R. Place, K.R. Sowers, H.J. Schreier, S. DasSarma and E.M. Fleischmann eds.), Cold Spring Harbor Press, NY. ISBN 0-87969-397-5.
Sata, T., 1991, *J. Appl. Electrochem*, *21*, 283.

---

[i] Lightsey, G.R., Toghiani, H. “Conversion of Hazardous Biomass Wastes to Ethanol”, Final Report, USDA, Contract # 94-34142-0428, September 1995.

[ii] Lightsey, G.R., Toghiani, H., Hill, D.O. “Feasibility of Ethanol Production from Grains, Agricultural By-Products, Wood Wastes and Energy Crops, proposal submitted to Mr. Dave Swalm, Texas Petrochemical Corporation, August 1994.

[iii] Yat, S.C., Berger, A., Shonnard, D.R. *Bioresource Technology*, 99, 3855-3863, 2008.

[iv] Columbus, E. P., Baldwin, B. S. Mississippi Bioenergy Roundtable, 2004.

[v] National Renewable Energy Laboratory, LAP: Preparation of Samples for Compositional Analysis; LAP-001: Determination of Total Solids in Biomass; LAP-010: Determination of Extractives in Biomass.

[vi] Schultz, T. P., Templeton, M. C., McGinnis, G. D. *Anal. Chem.*, 1985, 57, 2867-2869.

[vii] Richards, D. J., Ivanova, L. K., Smallman, D. J. Zheng, B. Assessment of waste degradation using acid digestible fibre analysis, International Workshop “Hydro-Physico-Mechanics of Landfills", March 2005, Grenoble, France.

[viii] Sheehan, J. “Glycosyl Hydrolases for Biomass Conversion (edited by M. E. Himmel, J. O. Baker, and J. N. Saddler), American Chemical Society. 2001, 2-25.

Sustainable Energy Research Center
Syngas to Gasoline Thrust Area Final Report for 2006-2008

1. **Project title, principal and co-investigators:** Task D. Syngas to Gasoline

Principal Investigator:	Mark G. White, Ph. D.; Director of Dave C. Swalm School of Chemical Engineering and Earnest W. Deavenport, Jr. Endowed Professor
Additional Investigator:	Hossein Toghiani, Ph. D.; Associate Professor of Dave C. Swalm School of Chemical Engineering
Team Members:	Amit C. Gujar, Ph. D.; Shetian Liu, Ph. D.; Prashant Daggolu; Peter Thomas

2. **List of authorized distribution**
Unlimited distribution.

3. **Executive Summary**

Task D.1 Screening Catalysts: This project fits into the larger research effort to convert the vast supplies of lignocelluloses present in the Southeastern United States into liquid hydrocarbons. The lignocelluloses may be gasified into a mixture that is rich in carbon monoxide and hydrogen, which is known commonly as synthesis gas. The technology developed here reveals that enhanced yields of liquid hydrocarbons can be developed from the catalytic conversion of synthesis gas, providing that alcohols containing two to four carbons were the intermediates in a one-bed, catalytic converter operated at > 50 bar and at temperatures between 300 and 375°C. These results led us to seek a catalytic function that selectively converts synthesis gas to C_2 – C_4 alcohols. Preliminary results with a Cu/zeolite, Cu/Co/CrO_x and Cu/Co/CrO_x catalysts were promising in that these higher molecular weight alcohols were formed, but these catalysts were deemed unsatisfactory in that too much methane was also formed. Work completed previously at another university suggested that another supported transition metal oxide might be a good higher-alcohols catalyst function that could be incorporated into a support that affects alcohol dehydration as well.

Task D.2 Catalyst Preparation: The catalysts listed were prepared by standard techniques described in the publications arising from this work. The prepared catalysts were characterized for metal content, surface area, and for proton density.

Task D.3 Evaluation of Catalyst Activity. The catalysts listed above were evaluated for activity to convert a feedgas of carbon monoxide and hydrogen to hydrocarbon products. All catalyst produced liquid hydrocarbons in the gasoline boiling range but with different yields of carbon dioxide, methane, and light hydrocarbon gases.

Task D.4 Examine Feed Gas Impurity Effects. The Cu-based catalysts were all poisoned irreversibly by a feed containing 50 ppm hydrogen sulfide. The same catalysts were reversibly poisoned by ammonia in the feed stream (50 ppm).

Task D.5 Evaluation of Novel Catalyst Activity. When two catalytic agents (alcohol-forming and alcohol-dehydration) were employed as separate heterogeneous catalysts in a single

converter, our data revealed the unexpected result that the quality of the liquid hydrocarbons could be much improved if the alcohol-forming catalyst was placed upstream of the alcohol-dehydration catalyst. This separation of catalyst functions could be an alternative to placing both catalyst functions on a single support and more work will be necessary to define better the optimum placement of catalytic functions.

Preliminary characterizations of the hydrocarbon liquids produced by this technology shows that it is an excellent blending stock for high octane gasoline in that its octane number is very high (101) and its Reid vapor pressure is also high (13.5 psig) while it shows a heavier component that could be blended into jet fuel and diesel. The characteristics of the formed hydrocarbon liquids can be adjusted by the choice of zeolite to be the metal support. For example, a liquid rich in aromatics result from a catalyst supported on H-ZSM-5 and some of these aromatics demonstrate a high degree of *para*-regioselectivity such as *para*-xylene. A liquid composed mainly of *iso*-paraffins and cycloparaffins develops when the zeolite support is Y-zeolite.

4. Comparison of goals and actual activities

See attached spreadsheet.

5. Summary of activities

Task D.1 Screening Catalysts and Task

The original hypothesis was to combine the established technology of methanol synthesis catalysis with the known chemistry of acid-catalyzed dehydration[1] so as to achieve the conversion of synthesis gas to hydrocarbon liquids in one catalyst contained in a single catalytic converter. Challenges to this hypothesis included the normal operating temperatures and pressures of the two catalytic reactions. The optimum temperature for each catalyst differed by 150°C (250°C for MeOH synthesis and 400°C for alcohol dehydration), and the alcohol dehydration reaction had only been confirmed at low pressures (*ca.*, 1-2 atm); whereas, the alcohol synthesis catalysts were successful only at higher pressures (50-70 bar). While the original hypothesis was partially successful, a discovery early in the program convinced us to seek a supported metal catalyst that would convert synthesis gas into C_2-C_4 alcohols. It was found that these higher alcohols could be converted, *via* acid-catalyzed dehydration, into liquid hydrocarbons at much higher rates (8-10 times) than what could be achieved using methanol as the intermediate and the octane numbers of the liquid products were the same (RON = 92), regardless of the alcohol used. With this finding in mind, we altered the original research plan to include the evaluation of supported metal catalysts which were active over the same temperature range that the alcohol dehydration catalysts were active (300-400°C). Doan showed that synthesis gas could be converted to higher alcohols over an alumina-supported $Cu/Co/CrO_x$ at temperatures higher than 325°C.[2] With these results in hand, we examined the performance of single bed, pipe flow reactor packed with an intimate mixture of particles from the $Cu/Co/CrO_x$ and H^+-ZSM-5 (silica/alumina ratio = 23).

Task D.2 Preparation and Characterization of Catalysts: Catalyst Characterization of CuO-CoO-Cr_2O_3/H^+-ZSM-5 Bifunctional Catalysts.

[1] Chang, C. D. Lang, W. H. Silvestri, A. U.S. Patent 4 096 163, 1978.

[2] Doan, P. T.,Characterization of Cu-Co-Cr-K catalysts, Master thesis, Mississippi State: Mississippi State University, Starkville, MS, 2001.

Physical Properties of the Catalysts. Table 1 lists the surface areas, pore volume, and average pore diameter of H^+/ZSM-5, CuO-CoO-Cr_2O_3, and CuO-CoO-Cr_2O_3/H^+-ZSM-5. From Table 1 it can be seen that H^+/ZSM-5 has the largest BET area of 303 m^2/g. BET surface areas of CuO-CoO-Cr_2O_3, fresh C3Z, used CuO-CoO-Cr_2O_3 and used C3Z are 38.75, 169.38, 26.62, and 147.25 m^2/g, respectively. The surface area of used CuO-CoO-Cr_2O_3 is less than that of fresh CuO-CoO-Cr_2O_3, which confirms earlier 400°C activity and lifetime performance indicating that sintering may occur during reaction, thus resulting in modification of the catalyst structure.

TABLE 1: Physical Properties of the Catalysts

Catalyst	BET surface area (m^2/g)	pore volume (cm^3/g)	pore diameter (μm)
H^+-ZSM-5	303.2	0.15	2.8
Fresh C3	38.8	0.202	0.123
Used C3	26.6	0.249	0.174
Fresh C3Z	169.4	0.179	1.82
Used C3Z	147.3	0.21	2.1

XRD Analysis. X-ray diffraction spectroscopy, XRD, was used to identify the crystalline phases present on the ZSM-5, Cu-Co-Cr oxides, and CuOCoOCr_2O_3/ZSM-5 catalysts before and after reaction. Figure 7 shows the XRD patterns of the samples. The XRD peaks corresponding to CuO at 2θ of 35.5° and 38.7° are observed in the fresh catalyst sample. Cobalt and chromium are found as Co_3O_4 and Cr_2O_3 crystallites in the fresh sample. Cu0 (at 2θ = 43.3°, 50.4°, and 74°, JCPDS-4-836) is clearly detected by XRD in the used catalyst samples. XRD of used samples indicates that Co_3O_4 was converted to CoO after reaction, whereas the reflection lines of Cr_2O_3 are unchanged after reaction, meaning Cr_2O_3 is not reduced under reaction conditions.

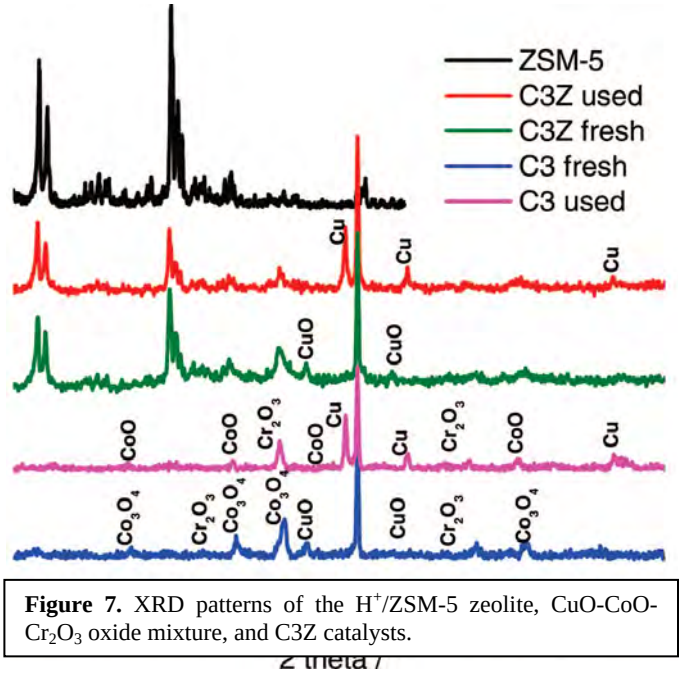


Figure 7. XRD patterns of the H^+/ZSM-5 zeolite, CuO-CoO-Cr_2O_3 oxide mixture, and C3Z catalysts.

XPS Analysis. *Copper High-Resolution Spectra.* The binding energies of the detected elements obtained from XPS high-resolution spectra are calibrated based on 284.8 eV, the adventitious carbon 1s. The Cu $2p^{3/2}$ XPS spectra taken from the fresh, reduced, and used catalysts were deconvoluted based on the assumption that the peaks are Gaussian. The Cu $2p^{3/2}$ peak has a BE value of 932.5 eV, which corresponds to either Cu^0/Cu^+ species. Only through examination of Auger transition parameters can the differentiation of Cu^+ and Cu^0 species be obtained.[3] A shoulder in the Cu peak is evident at 933.7 eV which is due to the presence of Cu^{2+}.[4] The high-resolution spectra of the fresh catalyst showed that copper mainly exists as Cu^{2+}. However, these Cu^{2+} species disappeared with exposure to H_2 at 275°C, and Cu^0 species

[3] Sheffer, G. R.; King, T. S. *J. Catal.* **1989**, *115*, 376.
[4] Moulder, J. F.; Stickle, W. F.; Sobol, P. E.; Bomben, K. D. *Handbook of X-ray Photoelectron Spectroscopy*; Chastain, J., Ed.; Perkin-Elmer Corporation, MN, 1992.

in the near-surface increased. A summary of atomic concentrations of Cu $2p^{3/2}$ peaks based on model area is shown in Table 2. The Cu^{2+} species totally disappeared, and only Cu^0, with a much more intensified and narrower peak, was detected in the catalyst after reaction. These effects may be due to the reduction of Cu^{2+} species to copper metal. Also, reduction in the Cu^{2+} shoulder indicates that the catalysts are reduced under higher temperature. The results agree with Monnier et al.,[5] who observed that reduction of CuO in the Cu-Cr oxide catalyst to Cu^0 occurs upon exposure to H_2 at 270 °C. Likewise, Apai et al.[6] and Capece et al.[7] have also stated that the CuO in Cu/Cr_2O_3 catalysts is reduced to Cu^0 upon pretreatment. According to the literature, the amount of stable surface Cu^+ sites was directly related to methanol production rate.[8,9] Both Cu^0 and Cu^+ sites are required for methanol synthesis since the Cu^0 and Cu^+ sites are essential for H_2 and CO adsorption, respectively. Courty et al.[10] speculated that Cu+ species were stabilized in the spinel or as copper chromate phases, which were responsible for CO adsorption, while Cu^0 was responsible for CO desorption and C-C bond formation. The Cu peak observations also agree with Calafat et al.,[11] who stated that Cu^{2+} species in CuZnCr catalyst were completely reduced after the reaction. Also, surface Cu species increased in the catalyst after reaction indicating that no loss in activity was observed because, according to Chinchen et al.,[12] the activity of the catalyst is a function of copper metal concentration.

TABLE 2: Copper Species Concentration of Cu $2p^{3/2}$ Peaks

	Cu^0-Cu^{1+}	Cu^{2+}	Cu^0-Cu^{1+}/Cu^{2+}
fresh	61.62	38.38	1.61
reduced at 275°C	88.55	11.45	7.74
used	100.00	0.00	

Cobalt High-Resolution Spectra. XPS high-resolution spectra of Co are shown in Figure 8. The primary peaks are assigned to Co^{2+}/Co^{3+} with the shoulder of Co^0 species. Co^{2+}/Co^{3+} species differentiation could not be obtained due to the closeness of their binding energies. The spectra investigation do not agree with Sheffer et al.[5] that satellite peaks of $2p^{3/2}$ are more intensified in the reduced catalyst compared to fresh catalyst, and much more intensified in used catalyst. Frost et al.[13] stated that the high-intensity, satellite peaks indicated the presence of Co^{2+} species, and less intense satellite structures of Co^{3+} species. Thus, Co in fresh catalysts was present as Co^{3+}, indicated by a low-intensity satellite structure at about 9.4 eV from the $2p^{3/2}$ main peak. Likewise, observation of used catalysts is in agreement with Calafat et al.[13] that Co was present as Co^{2+} species, mainly proven by the high-intensity satellite peak at about 6 eV from the $2p^{3/2}$ peak. After reduction in situ by H^2, no significant changes in satellite peaks were observed, which indicated no significant reduction from Co^{3+} to Co^{2+} at the reduction temperature of 275 °C. At 400°C, Fornasari et al.[14] observed the reduction of Co^{3+} to Co^{2+} in

[5] Monnier, J. R.; Hanrahan, M. J.; Apai, G. *J. Catal.* **1985**, *92*, 119.
[6] Apai, G.; Monnier, J. R.; Hanrahan, M. J. *J. Chem. Soc., Chem. Commun.* **1984**, 212.
[7] Capece, F. M.; Di Castro, V.; Furlani, C.; Mattogno, C.; Fragale, C.; Gargano, M.; Rossi, J. *J. Electron Spectrosc. Relat. Phenom.* **1982**, *27*, 119.
[8] Klier, K.; Chatikavanij, R. G.; Herman, R. G.; Simmons, G. W. *J. Catal.* **1982**, *74*, 343.
[9] Monnier, J. R.; Hanrahan, M. J.; Apai, G. *J. Catal.* **1984**, *88*, 523.
[10] Courty, P.; Durnad, D.; Freund, E.; Sugier, A. *J. Mol. Catal.* **1982**, *17*, 241.
[11] Calafat, A.; Laine, J. *J. Catal.* **1994**, *147*, 88.
[12] Chinchen, G. C.; Mansfield, K.; Spencer, M. S. *CHEMTECH* **1990**, 692.
[13] Frost, D. C.; McDowell, C. A.; Woolsey, I. S. *Mol. Phys.* **1974**, *27*, 1473.
[14] Fornasari, G.; Huysser, A. D.; Mintchev, L.; Trifiro, F.; Vaccari, A. *J. Catal.* **1992**, *135*, 386.

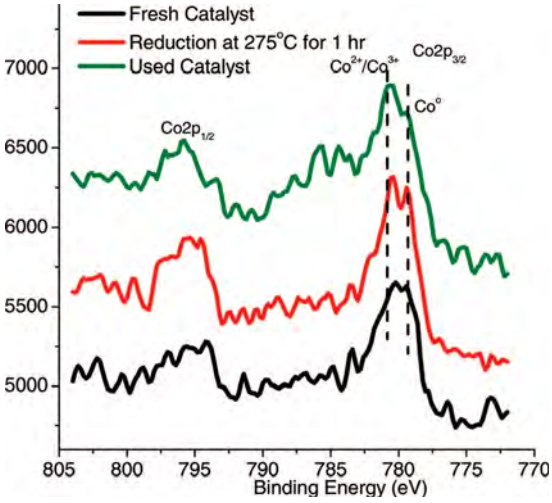


Figure 8. Co XPS high-resolution spectra of C3Z catalysts

that had the capability of producing ethanol, as well as propanol.

Chromium High-Resolution Spectra. The high resolution XPS Cr $2p^{3/2}$ spectra are shown in Figure 9. The broad peak width indicates that a mixture of chemical states is present near the surface. They appear to be Cr^0, Cr^{3+}, $Cr(OH)_x$, and Cr^{6+} at binding energies of 574.8, 576.5, 577.5, and 578.3 eV, respectively. Reduction of Cr^{6+} species was observed with exposure to H_2. Cr^{6+} to Cr^{3+} reduction is expected since a strong oxidizer metal salt was used to form the catalyst recursor.[12] $Cr(OH)_x$ species are also observed at increasing pretreatment temperature. The change in Cr^{3+} shoulder shape indicates a reduction in Cr^{3+} since Cr^{3+} species are reducible.[19] The increase in the shoulder at the Cr^0 species region and shift in the binding energy indicate that other Cr species may be partially reduced to Cr^0 species. After the reaction, more Cr^0 species are exhibited in the near-surface region.

Cu-Zn-Cr catalyst, and Sugi et al.[15] also observed that some Co^{2+} species are reduced to the metallic state at 300°C in modified cobalt catalysts with the presence of Ru. On the basis of the observation and overlapping of O auger features/Co $2p^{3/2}$, no conclusive results about Co reduction could be made. In general, Co species on the near-surface region are less than those deeper in the bulk. Castner et al.[16],[17] also emphasized that Co species at near-surface regions can be substantially different from those in the bulk, and the direct comparison by using a fraction of surface Co reduction is not advisable. Otherwise, the Co spectra investigation showed that the surface Co peaks varied significantly in size and shape with the temperature of reduction. Stiles et al.[18] stated that a tolerable quantity of cobalt may produce a catalyst

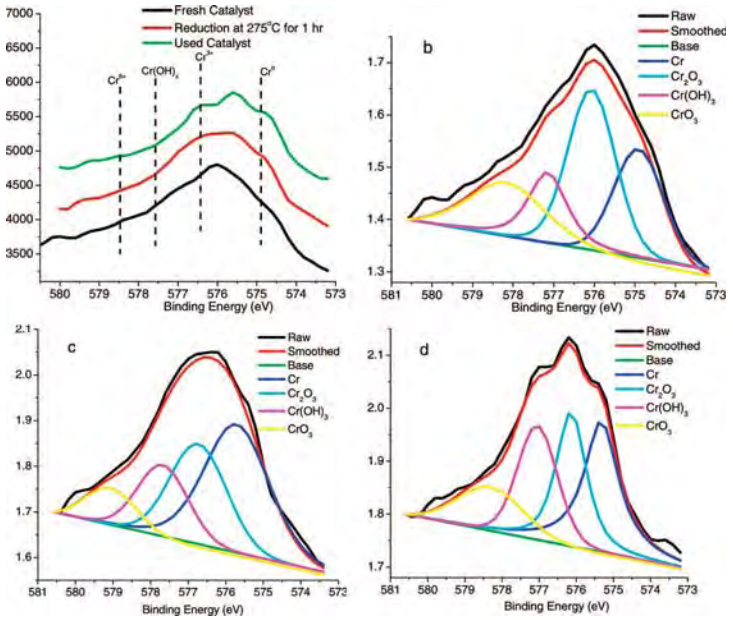


Figure 9. XPS of C3Z catalysts: (a) high-resolution spectra of Cr $2p^{3/2}$, Cr $2p^{3/2}$ peak deconvolutions of (b) fresh catalyst and (c) after 1 h reduction at 275 °C, and (d) used catalyst.

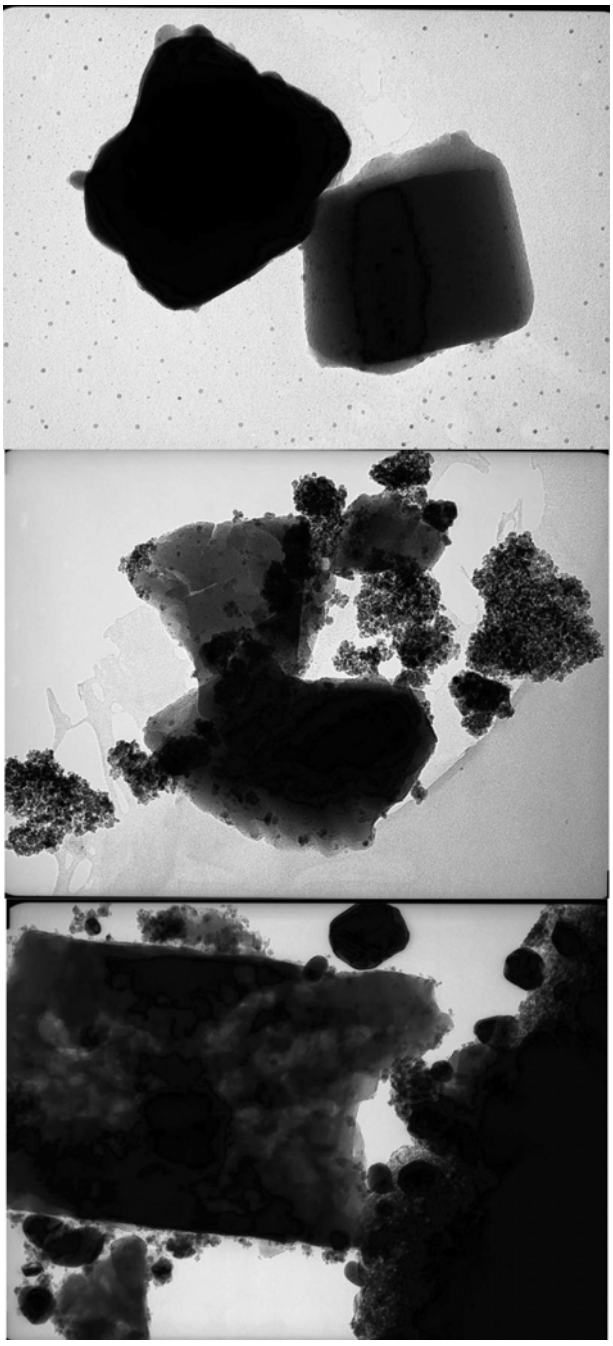
15 Sugi, Y.; Takeuchi, K.; Matsuzaki, T.; Arakawa, H. *Chem. Lett.* **1985**, 1315.

16 Castner, D. G.; Santilli, D. S. *Catalytic Materials*; Whyte, T., Dalla Betta, R., Derovane, E., Baker, R., Eds.; ACS Symp. Ser. No. 248; American Chemical Society: Washington, D.C., 1984; Vol. 42.

17 Castner, D. G.; Watson, P. R.; Chan, I. Y. *J. Phys. Chem.* **1989**, *93*, 3188.

18 Stiles, A. B.; Chen, F.; Harrison, J. B.; Hu, X.; Storm, D.; Yang, H. X. *Ind. Eng. Chem. Res.* **1991**, *30*, 811.

19 Tauster, S. J.; Fung, S. C.; Baker, R. T. K.; Horsley, J. A. *Science* **1981**, *221*, 1121.



Transmission Electron Microscope (TEM). The particle size of C3 species and their level of dispersion on the zeolite particle in C3Z catalysts before and after reaction were compared. A Jeol JEM-100CXII TEM was used for the analysis the Cu-Co-Cr-ZSM-5 catalysts. Micrographs of fresh and used catalysts are shown in Figure 10. Zeolite particles are between 0.1 and 1 μm in the fresh H+/ZSM-5. Cu-Co-Cr and ZSM-5 were well-mixed in the fresh sample; Cu-Co-Cr mixture oxides were both porous and nanosized. Copper particles grow to an average size of 30-50 nm after reaction at 350 °C for 170 h. At this temperature, aggregation of copper particles becomes larger due to sintering and is accompanied by partial separation from CoO-Cr_2O_3 and zeolite. Therefore, at higher reaction temperatures, copper particles sinter, and so the number of copper crystallites is decreased. This implies that sintering of the catalyst takes place at higher temperature; consequently, the number of active sites is decreased. Figure 10 shows the TEM images of the used C3Z catalyst (after 300 h of reaction under 375 °C). In these micrographs, evidence of sphere-shape particles is present. These particles are between 30 and 50 nm in size. TPR results showed that only CuO was reduced at temperatures under 450 °C; thus, it is hypothesized that these distinctive particles are reduced metal copper that has partially separated from the Cu-Co-Cr oxides after 170 h of reaction. Copper is sintering and segregated from both CoO-Cr_2O_3 and H^+-ZSM-5.

Figure 10. TEM images of H^+/ZSM-5 (top, 100K mag), fresh C3Z catalyst (middle, 100K mag), and used C3Z catalyst (bottom, 67K mag).

Task D.3 Evaluation of Catalyst Activity.

Effect of Temperature on the Catalyst Performances. The temperatures studied are 275, 300, 325, 350, 375, and 400°C, with the remaining conditions maintained at the values previously indicated. Figure 1a shows the variation of CO conversion, C_1-C_6^+ selectivity with temperature, the other variables remaining constant. Figure 1a shows that the influence of

temperature on CO conversion is very important. CO conversion increases from 28% at 300 °C to 66% at 375°C; however, it decreases to 63% at 400°C. Although temperature favors the kinetics of hydrocarbon formation reactions, according to the thermodynamics only the light hydrocarbons, like methane, show higher stability in these conditions. Figure 1 shows high temperature up to 375°C is more favorable for the CO conversion. Therefore, higher temperature enhances productivity of hydrocarbons, but it may lead to catalyst deactivation due to copper sintering.[20] The decrease in conversion as temperature is increased above 375°C is most likely due to the thermodynamic restrictions of the exothermal reaction and Cu sintering, which leads to partial loss of catalyst activity. The hydrocarbon concentration in the effluent increases with temperature, as expected. Selectivity toward gasoline (C_5^+) first increases when the temperature increases from 275 to 375°C, and then decreases after 375°C. This may result from the fact that either the activation energies for the condensation steps are smaller than those for hydrogenation of light hydrocarbons, or that there are hydrocracking reactions, which are favored by temperature. No temperature gradients were observed along the catalyst bed during pretreatment, but during the introduction of the syngas process, excessive exotherms were observed. The catalyst zone temperature of the C3Z reaction rapidly rose to 325°C in 5 min after the reaction start with a temperature of 275°C. This was most likely due to the methanation or low hydrocarbon formation. Figure 1b clearly shows the hydrocarbon distribution changes with temperature, the light hydrocarbons (mainly methane) being favored at higher temperatures. Higher hydrocarbons are more sensitive to temperature, undergoing cracking and dealkylation

[20] Jin, Y.; Datyen, A. K. *J. Catal.* **2000**, *196*, 8.

reactions that become increasingly important with increasing temperature. Selectivity toward gasoline (C_5^+ fraction) increases first when the temperature increases from 275 to 375°C (Figure 1a). With respect to the higher hydrocarbons and aromatic products (toluene, xylenes, 1,2,3-trimethylbenzene, and 1,2,4,5-tetramethylbenzene, *etc.*) (Figure 1b), as the temperature increases the C_5^+ fractions increase, and the C_8 fraction reaches a maximum value at 375°C and then decreases with increasing temperature. The aromatic fractions increase with temperature, especially above 350°C. This result is in agreement with data already published on syngas conversion over a cobalt-based catalyst mixed with H^+-ZSM-5 zeolite.[21]

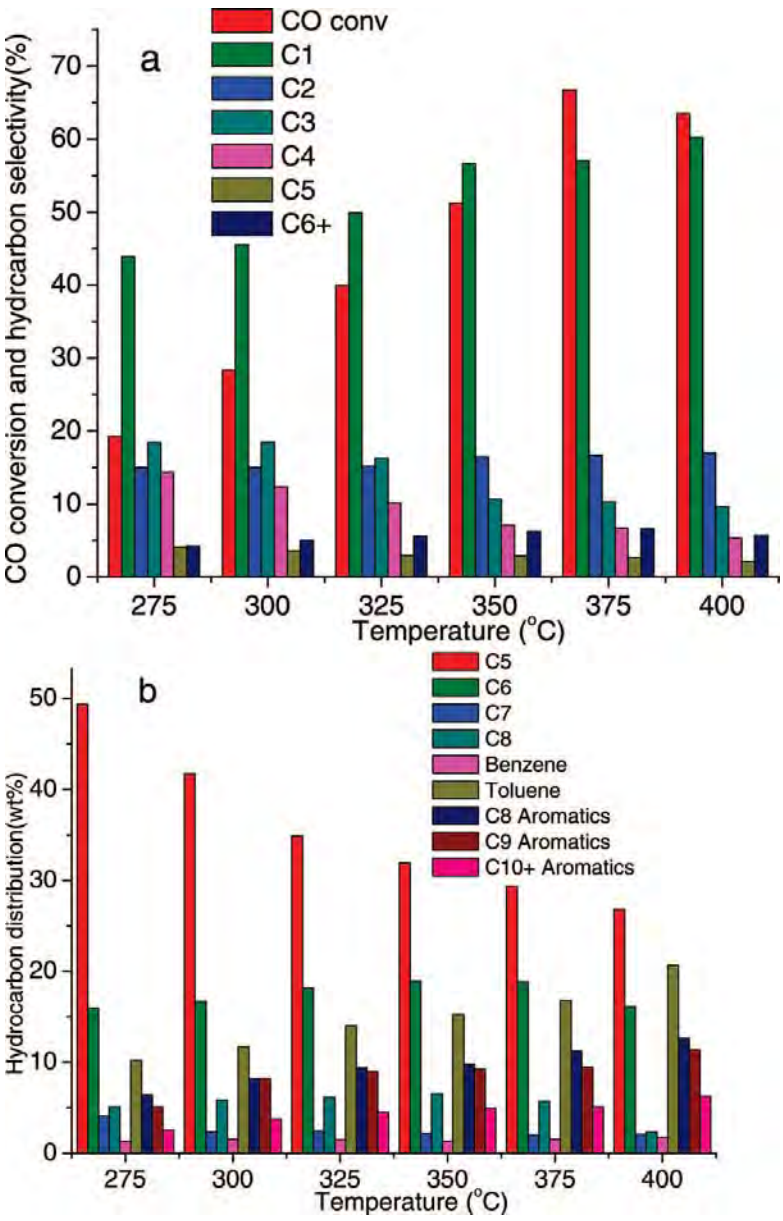


Figure 1. Effect of temperature on (a) CO conversion, selectivity and (b) higher hydrocarbon distribution at 1000 psig, H_2/CO) 1, and 600 h^{-1}; 5 g 50 wt % CuO-CoO-Cr_2O_3-50 wt % H^+-ZSM-5 was used in the reaction.

Role of CO/H_2 Molar Ratio on the Catalyst Performances. The synthesis gas ratio is an important parameter in higher hydrocarbon synthesis. It can affect both reaction rates and activity. A lower H_2/CO ratio tends to decrease CO conversion while increasing higher hydrocarbon selectivity. A change in the ratio will also affect the partial pressure of H_2 and CO under constant total pressure, thus the stoichiometry will be different for each reaction. Higher hydrogen partial pressure will eliminate coke formation, thus better activity will be obtained. Higher carbon monoxide partial pressure favors the formation of high molecular weight compounds. By decreasing the H_2/CO ratio, CO insertion and C-C chain growth are more favorable, which then enhance the production of higher hydrocarbons. The feed H_2/CO molar ratio of 2 to 1 has been used, and its effect on CO conversion and hydrocarbon distribution has been investigated. In Figure 2, the CO conversion and hydrocarbon have been compared with a H2/CO molar ratio of 1 to 2 in the feed. CO conversion was 66% at 375°C for H_2/CO of 1, while 70% for 2. Therefore, when the H_2/CO ratio increases, CO conversion clearly increases. Figure 2b compared C_5^+ product distributions of

[21] Varma, R. L.; Bakhshi, N. N.; Mathews, J. F.; Ng, S. H. *Ind. Eng. Chem. Res.* **1987**, *26*, 183.

different H_2/CO molar ratio. It was concluded that a higher H_2/CO ratio favored the formation of products of lower C/H ratio (straight chain of paraffin), while a lower H_2/CO ratio favored higher C/H ratio products (aromatics). For a higher H_2/CO ratio the gasoline fraction clearly increases at the expense of the lighter fractions in the product stream. For a lower H_2/CO molar ratio, a higher selectivity toward aromatics is observed when the H_2/CO molar ratio is 1. These results are due to the fact that a decrease in the H_2/CO molar ratio favors the condensation steps over the hydrogenation steps. Consequently, products of greater C/H ratio are formed and an increase in selectivity toward hydrocarbon components of the gasoline takes place.

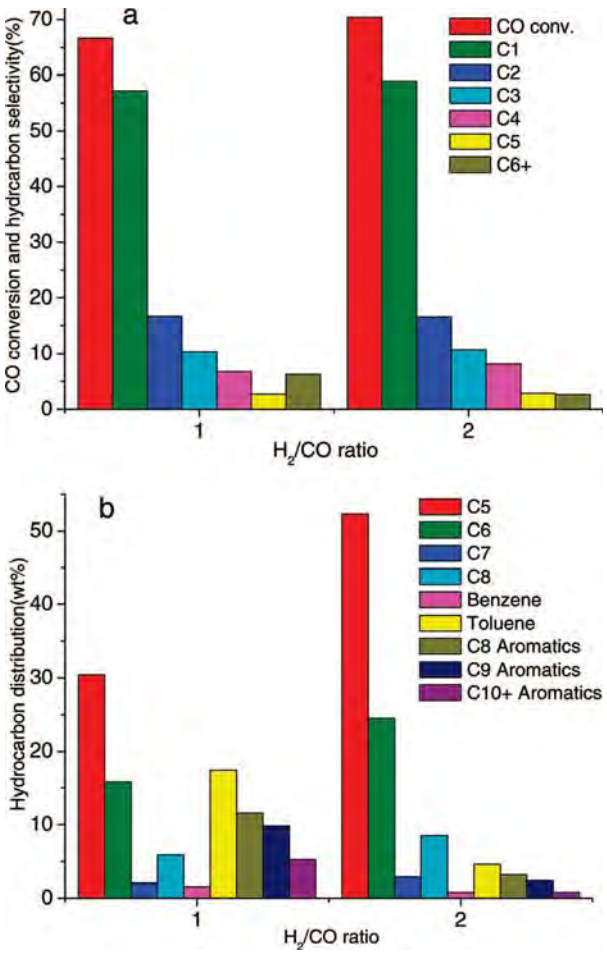


Figure 2. Effect of H_2/CO molar ratio on (a) CO conversion, selectivity and (b) higher hydrocarbon distribution at 1000 psig, 600 h^{-1} and 375°C; 5 g 50 wt % CuO-CoO-Cr_2O_3-50 wt % H+-ZSM-5 was used in the reaction.

Influence of Pressure on the Catalyst Performance. An increase in total pressure will increase the equilibrium toward the product side, and increase the conversion. The change in
Gibbs free energy will always be negative when pressure increases. Furthermore, a change in total pressure will not affect the water gas shift reaction but will change the equilibrium product distribution. Experiments under pressures of 700, 850, 1000, and 1200 psig have been carried out. The other operating conditions are the following: temperature 375°C; CO/H_2 molar ratio 1; and gas space velocity 600 h^{-1}. The effect of pressure on both CO conversion and process selectivity shows that when pressure increases, CO conversion increases (figure is not shown here). Within the C_5^+ fraction, an important effect of pressure on selectivity is observed. The increase in pressure clearly favors the formation of C_5^+ and aromatics, while C_1-C_3 gaseous hydrocarbons clearly decrease with an increase of pressure.

Comparison of Catalytic Performance for the Catalyst Bed of Bifunctional Cu-Co-Cr/H^+-ZSM-5 and the Two-Layer Bed of Cu-Co-Cr Oxides and H+-ZSM-5. The performance of the C3Z sample and that of C3 + ZSM-5 (C3 on the top of the catalyst bed, H+/ZSM-5 on the bottom of the catalyst bed) were compared in Figure 3. The CO conversion of the C3Z bifunctional catalyst was higher than that of the two-layer-bed system of Cu-Co-Cr and H+/ZSM-5. C3Z was found to favor the formation of tetramethylbenzene and trimethylbenzene, while C3 + ZSM-5 would produce more toluene and *p*-xylene under the same conditions. The synergism between CuO-CoO-Cr_2O_3 and H^+/ZSM-5 of the bifunctional catalyst could enhance the CO conversion or enable the effect.

Lifetime Performance and Impact of Contaminant H_2S on the Catalyst Performance. ***Time-on-Stream Performance.*** The effect of time on stream on the performance of the catalyst was studied at 350°C over a period of 170 h. The evolution of CO conversion and hydrocarbon distribution with time on stream are shown in Figure 4 for a C3Z catalyst. The activity of the catalyst reached a steady state after a period of approximately 2 h under operating conditions. The reaction temperature was set to 300 °C in the beginning of the reaction since the temperature went up 30-50°C when feeding syngas to the fresh reduced catalyst. The temperature then was slowly adjusted to 350°C. The catalyst was continuously run for 1 week. Figure 4 also shows the corresponding hydrocarbon distribution at different times. After 170 h, the CO conversion drops by ~5%, but the selectivity toward C_5^+ hydrocarbons is more affected by the time on stream. The increase in the proportion of methane during the aging process is observed. The proportion of aromatics in the C_5^+ fraction remains constant. These results indicate a slow deactivation of the catalyst, probably due to copper sintering on the surface of the CoO + Cr_2O_3 oxides and the ZSM-5 zeolite.

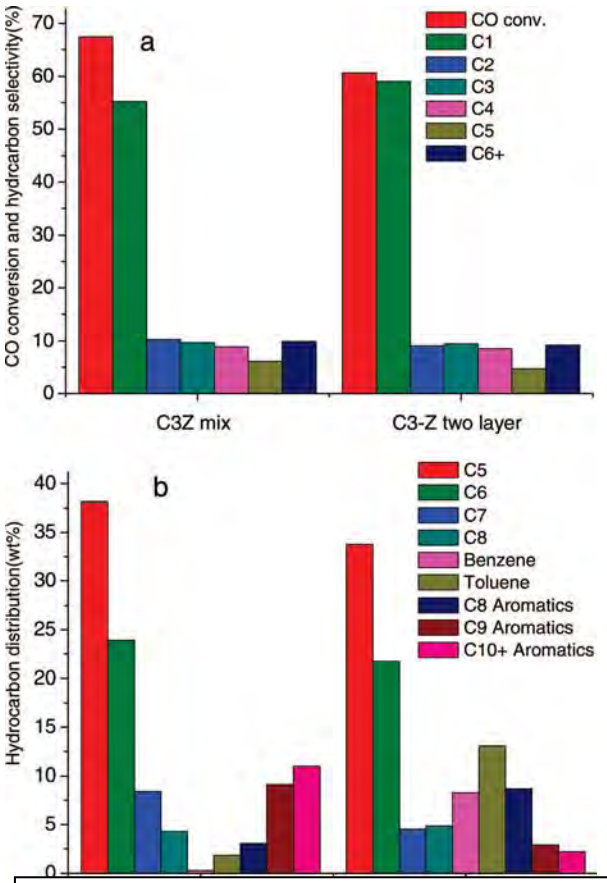


Figure 3. Comparison of (a) CO conversion, selectivity and (b) higher hydrocarbon distribution at 375°C and 600 h^{-1} over C3Z (physical mixture) catalyst bed and C3 + ZSM-5 (C3 on the top of catalyst bed, ZSM-5 on the bottom of the catalyst bed) two-layer catalyst bed under 375°C and 1350 psig, 600 h^{-1} GHSV.

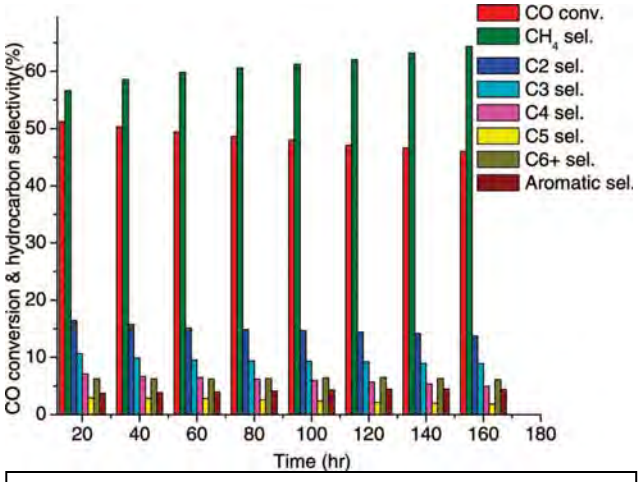


Figure 4. Time on stream of CO conversion and hydrocarbon selectivity on a C3Z catalyst at 350°C, 1000 psig, 600 h^{-1}, and H_2/CO) 1/1.

Task D.4 Examine Feed Gas Impurity Effects. ***Impact of H_2S on the Catalyst Performance.***

To investigate the impact of H_2S on Cu-Co-CrO_x/H^+-ZSM-5 catalyst performance, 3.6 g of C3Z catalyst (Cu-Co-Cr /ZSM = 1 weight ratio) was charged to the reactor. This catalyst contained 0.72 g of CuO (0.009 mol of Cu). The catalyst was first prereduced at 300°C with hydrogen for 1 h. Then sulfur-free syngas was passed over the catalyst at 300°C for 3 h. The reaction temperature was then adjusted to 375°C and the system pressure was raised to 1110 psig. After achieving steady-state conditions with the sulfur-free synthesis gas, the feed to the reactor was changed to a premixed synthesis gas, containing H_2S at ppm levels (56.5 ppm; CO/H_2 ratio ca. 1/1). The H_2S-contaminated synthesis gas was fed to the reactor at a flow rate of 300 mL/min for 2 h. At this time, the cumulative moles of hydrogen sulfide fed to the reactor are equivalent to a molar ratio of H_2S/Cu of 1/100. The feed was switched back to sulfur-free synthesis gas for 12 h at a flow rate of 100 mL/min. A gas sample of reactor effluent was then analyzed. These steps were repeated, to examine H_2S/Cu molar ratios of 1/20 (10 h), 1/10 (20 h), 1/5 (40 h), 1/2 (100 h), 3/4 (150 h), and 1/1 (200 h). A gas sample was taken after each molar ratio, after sulfur-free synthesis gas had passed through the reactor for 12 h at a flow rate of 100 mL/min. The CO conversion and CO_2 yield after each exposure are shown in Figure 5a. CO conversion decreased with increased exposure to H_2S. This may be due to sulfur reacting with the active copper sites to form copper sulfide ($Cu + H_2S \rightarrow CuS + H_2$; $Cu^{2+} + S^{2-} \rightarrow CuS$; $CuO + H_2S \rightarrow CuS + H_2O$). The catalyst was found to completely lose its activity (CO conversion around 2%) after running 300 h (H_2S/Cu= 1.5/1). CO_2 yield was almost constant if the H_2S/Cu ratio was less than 1/2. The CO_2 yield increased a little after H_2S/Cu exceeded 1/2. Selectivity to hydrocarbons was illustrated in Figure 5b. It was found that with the increase of fed H_2S (1/100 to 1/2), CH_4 selectivity decreased slowly, and CH_4 selectivity decreased significantly after H_2S/Cu = 1/2. C_2H_6 and C_3H_8 selectivity were found to be almost constant with a increase of fed H_2S (1/100 to 1/2). However, the selectivity increased after a H_2S/Cu ratio higher than 1/2. C_4^+ selectivity increased with the increase of fed H_2S. Hydrocarbon distribution from on line GC-FID signals (not shown here) as a function of the total amount of H_2S fed during the reactions proved that with the increase of fed H_2S (1/100 to 1/20), higher aromatics, i.e., tetramethylbenzene, decreased first, while toluene and *p*-xylene and part of the straight chain of paraffin increased a little. However, if the fed H_2S increased further (1/10 to 1/2), all the hydrocarbons decreased due to total CO conversion decrease.

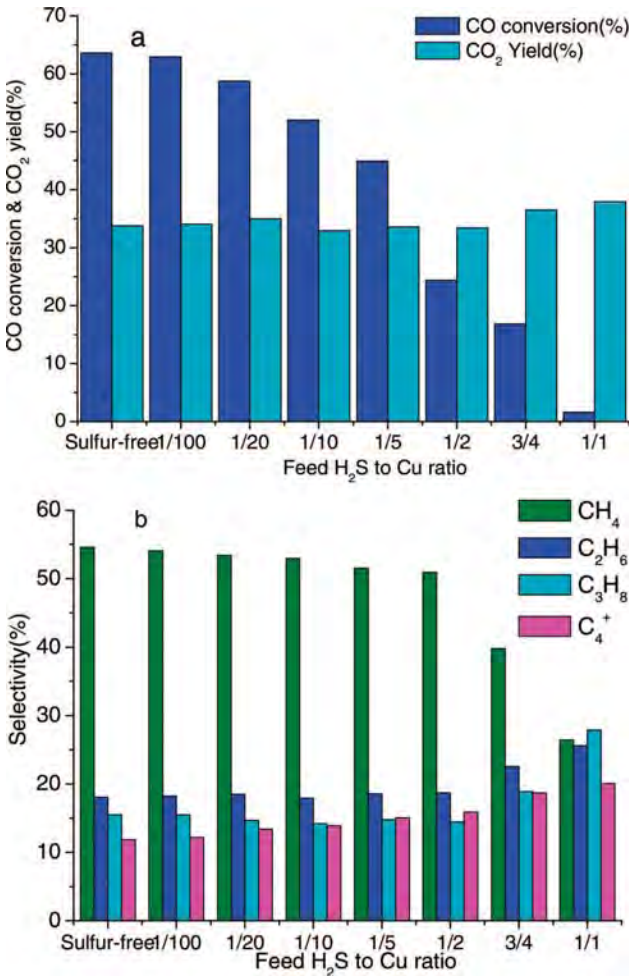


Figure 5. Effect of H_2S (56.5 ppm; H_2/CO) 1/1) on (a) CO conversion, CO_2 yield and (b) hydrocarbon selectivity of a C3Z catalyst for syngas to hydrocarbons at 1100 psig, and 375°C; 3.6 g 50 wt % CuO-CoO-Cr_2O_3-50 wt % ZSM-5 was used in the reaction.

Task D.5 Evaluate Novel Catalyst: Bifunctional C3Z Catalysts.

Bifunctional transition metal oxide-ZSM-5 catalysts are capable of converting syngas to gasoline in a single reaction step for they contain both the CO hydrogenatuion function (Cu-Co-Cr oxides) and the hydrocarbon synthesis function (ZSM-5). There are two steps involved in the conversion of syngas to hydrocarbons over the bifunctional catalyst. First, alcohols are synthesized from the syngas over a Cu-Co-Cr oxide catalyst. Cu-Co-Cr-based catalysts are utilized for the production of higher alcohols. In the following step, alcohols are converted to higher hydrocarbons over zeolite ZSM-5. The ZSM-5 catalyst dehydrates the alcohols including methanol and rearranges the remaining hydrogen and carbon atoms into a concentrated high energy fuel. Although alcohols themselves have been used in motor fuels both as an octane booster to conventional gasoline and in their pure form, each gallon of gasoline has twice the energy content of a gallon of methanol. A lot of work has been done with the conversion of methanol to gasoline. However, little work has been done with the conversion of higher alcohols to gasoline so far. Some primary results have been reported in our laboratory on conversion of higher alcohols to higher hydrocarbons;[22] it was found that the methanol reaction over H^+/ZSM-5 gave aromatics including *p*-xylene, 1,2,3-trimethylbenzene, and 1,2,4,5-tetramethylbenzene and oxygenates including dimethyl ether, 3-methyl-2-butanone, and acetone among others. The reaction of ethanol under similar conditions gave ethyl-ubstituted aromatic compounds including 1,3-diethylbenzene and 1,2-diethylbenzene and alkanes such as 3-methylheptane and 4-methyloctane among others. When ethanol was used, the production of oxygenates was less than that obtained for methanol. Propanols when reacted over H^+-ZSM-5 resulted in different product distributions for 1-propanol and 2-propanol. Employing 1-propanol as the reactant resulted in product distribution almost exclusively composed of alkenes and branched alkanes like 2-methyl-1-propene, 4-methylhexane, and 4-methylheptene among others. No traces of aromatic compounds were observed. In contrast, employing 2-propanol as a reactant resulted in a product distribution containing both aromatics including p-xylene and 1-ethyl-2-methylbenzene and olefins including 3-methyl-2-hexene and 3-methyl-2-pentene, *etc.* Another interesting observation was the presence of 2-propanol in the product when 1-propanol was used as a feed. Of all the butanols reacted over H^+-ZSM-5, only 2-methyl-2-propanol (*tert*-butanol) gave significant aromatic yield. The remaining butanol isomers mainly gave branched alkanes and alkenes. Thus, it is concluded that the tendency for aromatics formation over ZSM-5 increases as follows: tertiary alcohol >secondary alcohol > primary alcohol.[22]

The conversion of syngas into higher alcohols as well as hydrocarbons is strongly dependent on the process variables. Selectivity toward gasoline (C_5^+ fraction) increases first when the temperature increases from 275 to 375°C (Figure 1a). With respect to the higher hydrocarbons and aromatic products (toluene, xylene, 1,2,3-trimethylbenzene, and 1,2,4,5-tetramethylbenzene) (Figure 1b), as the temperature increases the C_5^+ fractions increase, and the C_8 fraction reaches a maximum value at 375°C and then decreases with increasing of temperature. The aromatic fractions increase with temperature, especially above 350°C. From these results it can be said that there is a balance between two trends: the CO hydrogenation reactions yielding alcohols, mainly due to the Cu-Co-Cr metal oxides, with an optimum temperature of 250-300°C and the acid function-based reactions, *i.e.,* conversion of oxygenates to hydrocarbons or aromatization, mainly due to the ZSM-5 zeolite, with an optimum temperature of 350-400°C. A compromise between these two trends leads to an optimum reaction temperature to give the maximum C_5^+ yield. On the other hand, although the C_5^+

[22] White, M. G.; Gujar, A. C.; Nolan, M.; Guda, V. K.; Yan, Q.; Toghiani, H. The AIChE 2007 Annual Meeting, Salt Lake City, UT, November 7, 2007.

fraction decreases in absolute terms, the aromatic fraction increases relative to the total C_5^+ fraction when the temperature increases above 375°C, that is, the liquid fraction becomes richer in aromatics. This result is in agreement with data already published on syngas conversion over a cobalt-based catalyst mixed with H^+-ZSM-5 zeolite.[23] It has been proven that for all FT catalysts having an increase in operating temperature results in a shift in selectivity toward lower carbon number products and to more hydrogenated products.[24] The degree of branching increases and the amount of secondary products formed such as ketones and aromatics also increases as the temperature is raised.[25] These shifts are in line with thermodynamic expectations and the relative stability of the products. As Co is a more active hydrogenating catalyst the products in general are more hydrogenated and also the CH_4 selectivity rises more rapidly with increasing temperature.[26] The synthesis rates of both alcohols and hydrocarbon are dependent on the syngas pressure over C3 catalyst. Therefore, increasing syngas partial pressure results in an increased productivity of all products with the exception of CO_2, which is not very sensitive to the change in syngas pressure. In the present study, a stoichiometric H_2/CO ratio of 1 seems to be an appropriate syngas composition for the synthesis of hydrocarbons.

Reactive Sites of C3Z Catalysts for Syngas to Hydrocarbons. Cu-Co-Cr based catalysts are utilized for the production of higher alcohols. The chain growth of higher alcohol formation is favored at high cobalt concentration or low copper content, and/or alkali metal content.[27] Many reported that the selectivity of higher alcohols is directly related to the Cu-Co interaction.[28,29,30,31,32,33,34] In another words, the cobalt ions in combination with metallic Cu or the interaction phase are important to oxygenate synthesis. The Cu-Co interaction formed after reduction is the active site for the reaction[35] as mentioned earlier. Also, some researchers mentioned that the unreduced cobalt ions are responsible for higher alcohol synthesis.[32-34] XRD results show metallic copper and CoO probably are active components for CO hydrogenation. It has been proven that Cu^0/Cu^+ is the active species in the synthesis of methanol over conventional Cu-based catalysts. XPS results show copper species are mainly present as Cu^{2+} in fresh catalyst. When exposed to H_2, Cu^0 species in the near-surface region increased while the Cu^{2+} shoulder was reduced. Likewise, higher near surface Cu^0 peaks are noticed while the Cu^{2+} peak totally disappeared in the catalyst after reaction. The cobalt species in fresh catalyst is Co^{3+}, and in used catalyst it is Co^{2+}. Moreover, no significant reduction from Co^{3+} to Co^{2+} is observed during the reduction procedure. In general, fewer cobalt species are on the surface compared to in the bulk. Chromium features in the near-surface region appeared to be Cr^0, Cr^{3+}, $Cr(OH)_x$, and Cr^{6+}. Cr^{3+} could not be differentiated. Nevertheless, the presence of Cr^{3+} species has been proven by others, and reduction in Cr^{3+} species is observed. Increasing treatment temperature results in Cr^{6+} to Cr^{3+} reduction. Other Cr species are also partially reduced to Cr^0

[23] Varma, R. L.; Bakhshi, N. N.; Mathews, J. F.; Ng, S. H. *Ind. Eng. Chem. Res.* **1987**, *26*, 183
[24] Liu, Z.-W.; Li, X.; Asami, F.; Fujimoto, K. *Fuel Proc. Technol.* **2007**, *88*, 165.
[25] Dry, M. E. In *Catalic Science and Technology*; Anderson, J. R., Boudart, M., Eds.; Springer: Berlin, Germany,1981; Vol. 1, p 159
[26] Calleja, G.; de Lucas, A.; van Grieken, R. *Fuel* **1995**, *74*, 445.
[27] Courty, P.; Forestiere, N.; Kawata, N.; Ohno, T.; Raimbault, C.; Yoshimoto, M. *Industrial Chemicals* V*ia C1 Processes*; Fahey, D., Ed.;
ACS Monograph 328; American Chemical Society: Washington, D.C., 1987; Chapter 4.
[28] Courty, P.; Durand, D.; Freund, E.; Sugier, A. *J. Mol. Catal.* **1982**, *17*, 241.
[29] Xu, X.; Scholten, F. *Appl. Catal.* **1992**, *82*, 91.
[30] Di Cosimo, J. I.; Apestegufa, C. R. *J. Catal.* **1989**, *116*, 71.
[31] Baker, E.; Burch, R.; Niu, Y. *Appl. Catal.* **1991**, *73*, 135.
[32] Di Cosimo, J. I.; Marchi, A. J.; Apestegufa, C. R. *J. Catal.* **1992**, *134*, 594.
[33] Baker, E.; Burch, R.; Hibble, J.; Loader, K. *Appl. Catal.* **1990**, *65*, 281.
[34] Baker, E. Burch, R., Golunski, E. *Appl. Catal*. **1989,** *53*, 279.
[35] Dalmon, J. A.; Chaumette, P.; Mirodatos, C. *Catal. Today* **1992**, *15*, 101.

species. Finally, more Cr^0 species in aged catalyst existed in the near-surface region. In higher alcohol synthesis, copper sites are responsible for hydrogen dissociative chemisorption and CO associative adsorption since these are the main elements in methanol synthesis. Metallic cobalt sites are responsible for CO dissociation, carbon-carbon chain growth, and hydrogenation since cobalt is the FT synthesis metal. By surface migration, the adsorbed CO molecule moves to an adsorbed alkyl group and inserts between metal sites and the alkyl group. Hence, cobalt and copper sites must be close to each other for the possibility of this surface migration. Separation of the two metals or the heterogeneous distribution during catalyst preparation will cause selectivity deterioration for alcohol synthesis, hence, higher hydrocarbon production.[36]

Stability of the C3Z Catalysts. The effect of temperature on syngas to higher alcohol reactions over Cu-Co-Cr oxides has been reported both in the thermodynamics and experimental. High temperature is more favorable for the average alcohol production rate. Therefore, higher temperature enhances productivity of alcohols, but can also lead to catalyst deactivation due to sintering, or simply the alcohol synthesis reaction will change to the methanation synthesis or another hydrocarbon synthesis. The catalysts have a limited range of operating temperature from 275 to 300°C since the catalyst deactivation due to sintering is normally a concern above 300°C for copper catalysts.[36] The sintering of copper metal was the main contribution to the decreasing of CO conversion of the C3Z catalyst at temperatures above 375°C. Figure 1 shows high temperature is more favorable for the CO conversion. Therefore, higher temperature enhances the productivity of hydrocarbons, but it may lead to catalyst deactivation due to sintering. The decrease in conversion as temperature is increased above 375°C is due, first, to the thermodynamic restrictions of the exothermal reaction and, second, to Cu sintering, which leads to partial loss of catalyst activity. The presence of larger metallic copper crystallites may be a contributing factor in enhancing selectivity to gaseous hydrocarbons in the lifetime performance case, in contrast to the synthesis of higher alcohols that decreases as the copper dispersion is decreased. Moreover, both alcohol and hydrocarbon yields decreased monotonically with reaction time, demonstrating the lower catalytic stability of the catalyst at higher temperature. This can be explained by the possibility that the metal surface is sintered gradually during the reaction process. It is also noted that the catalyst lifetime is dependent on the sulfur level in synthesis gas. It has been generally assumed that catalysts for CO hydrogenation such as the FT process and methanol synthesis are poisoned by a small amount of sulfur compounds in the feed.[37,38] It was reported a $Cu/ZnO/Al_2O_3$ catalyst loses its methanol synthesis activity even in the presence of a 1.6 ppm concentration of H_2S.[38] Sulfur content in the syngas is seriously high especially when the syngas is produced from a coal and heavy oil. The syngas produced from biomass and waste materials that are thought to be promising carbon resources for the future contains H_2S to some extent also. Berg et al.[39] reported that the H_2S content is in a range from 20 to 200 ppm when the syngas is produced from a noncatalytic gasification of biomass while the syngas from waste plastics contains H_2S and COS in 300 ppm concentration.[40] To avoid the sulfur poisoning, conventional plants are equipped with a huge desulfurizer unit that removes the sulfur compounds almost completely from the feed. Considering these situations, the development of sulfur-tolerant catalysts is expected to contribute to increasing the versatility of the syn-fuel process.

---

[36] Xiaoding, X.; Doesburg, E.; Scholten, *J. Catal. Today* **1987**, *2*, 125.

[37] Fischer, F. *Brennst.-Chem.* **1935**, *16*, 1.

[38] Wood, B. J.; Isakson, W. E.; Wise, H. *Ind. Eng. Chem. Prod. Res. De*V. **1980**, *19*, 197.

[39] Berg, M.; Koningen, J.; Sjostrom, K.; Waldheim, L. In *DeVelopment in Thermochemical Biomass ConVersion*; Blackie Academic & Professional: London, UK, 1997; p 1117.

[40] Jahnek, F. C. *PETROTECH* **1999**, *22*, 943.

Conclusions

CO hydrogenation to hydrocarbons was examined over a bifunctional C3Z catalyst in a fixed bed flow reactor, operating at 275 to 400 °C temperature, 300 to 1200 h-1 gas hourly space velocity (GHSV), and 700 to 1500 psig pressure. It was found that CO conversion increases from 28% at 300°C to 66% at 375°C; however, it decreases to 63% at 400°C. Selectivity toward gasoline (C_5^+ fraction) increases first when the temperature increases from 275 to 375°C. With respect to the higher hydrocarbons and aromatic products (toluene, xylenes, 1,2,3-trimethylbenzene, and 1,2,4,5-tetramethylbenzene, etc), as the temperature increases the C_5^+ fractions increase, and the C_8 fraction reaches a maximum value at 375°C and then decreases with increasing temperature. CO conversion decreases with increasing of GHSV, while C_5^+ selectivity also decreases. It can be concluded that CO conversion decreases with the increasing of space velocity. The gasoline fraction (C_5^+) continuously decreases with increasing space velocity. CO conversion and hydrocarbon have been compared with H_2/CO molar ratio of 1 and 2 in the feed. CO conversion was 60% at 350°C for H_2/CO of 1, while it was 70% for 2. It was found higher the H_2/CO ratio favored the formation of products of lower C/H ratio (straight chain of paraffin), while lower H_2/
CO ratio favored higher C/H ratio products (aromatics). For a lower H2/CO molar ratio, a higher selectivity toward aromatics is observed when the H_2/CO molar ratio is 1. CO conversion increases as pressure increases. The increase in pressure clearly favors the formation of C_5^+ and aromatics, while C_1-C_3 gaseous hydrocarbons clearly decrease with increasing pressure. The C3Z bed favored the formation of tetramethylbenzene and trimethylbenzene, while the C3 + ZSM-5 two-layer catalyst bed would produce more toluene and *p*-xylene under the same

conditions. The CO conversion drops by ~5% over the C3Z catalyst after running for 170 h, but

the selectivity toward the C_5^+ hydrocarbons is more affected by the time on stream. The increase in the proportion of methane during the aging process is observed. The proportion of aromatics in the C_5^+ fraction remains constant. These results indicate a slow deactivation of the catalyst, probably due to copper sintering on the surface of the CoO + Cr_2O_3 oxides and the ZSM-5 zeolite. The catalyst was investigated under a syngas containing 56.5 ppm of H_2S and it was found that the catalyst lost its activity with increasing S/Cu ratio. The surface area of used CuO-CoO-Cr_2O_3 is less than that of the fresh CuO-CoO-Cr_2O_3, which confirms that catalyst sintering may occur during reaction, thus resulting in modification of the catalyst structure. XRD results demonstrated that Cu, Co, and Cr are mainly present as CuO, Co_3O_4, and Cr_2O_3 in the as-prepared catalysts, copper oxide was reduced to copper metal, Co_3O_4 was reduced to CoO, while Cr_2O_3 remained unchanged after reaction. XPS results showed Cu, Co, and Cr mainly present as Cu^{2+}, Co^{2+}/Co^{3+}, and Cr^{3+} in the fresh catalyst samples, almost 100% copper is Cu^0 in the used catalyst surface and cobalt mainly exists as Co^{2+} after reaction, and chromium is almost unchanged after reaction. SEM and TEM images proved copper sintering and segregation from $CoOCr_2O_3$ and H-ZSM-5 zeolite, which leads to the deactivation of the catalyst.

6. END OF SUMMARY SECTION.

Patents: None.

Publications:

A. Qiangu Yan, Phuong Thanh Doan, Hossein Toghiani, Amit C. Gujar, and Mark G. White, "Synthesis Gas to Hydrocarbons over CuO-CoO-Cr_2O_3/H^+-ZSM-5 Bifunctional Catalysts", *J. Phys. Chem. C,* **112,** 3, Pages: 11847-11858, (2008).

Presentations:

A. Gujar, Amit C. and M. G. White, "Reaction of Alcohols over H^+ZSM-5", North American Catalysis Society Meeting, Houston, TX (June 17-20, 2007).
B. Gujar, Amit C. and M. G. White, "Syngas to Gasoline", Second Biofuels Conference at Mississippi State University, Mississippi State, MS. August 14, 2007.
C. Gujar, Amit C. and M. G. White, "Batch Reactor Studies of Methanol to Gasoline over H^+ZSM-5", paper 6z, Annual Meeting of the AIChE, Salt Lake City, UT, November, 2007.
D. Gujar, Amit C, and Mark G. White, "Batch Reactor Studies of Methanol to Gasoline over Metal Oxides Supported on H^+ZSM-5", paper 420f, Annual Meeting of the AIChE, Salt Lake City, UT, November, 2007.
E. Mark G. White, Amit C. Gujar, Vamshi K. Guda, Qiangu Yan, Hossein Toghiani, "Reaction of Alcohols over H^+ZSM-5", paper 420 e, Annual Meeting of the AIChE, Salt Lake City, UT, November, 2007.
F. Shetian Liu and Mark G. White, "Novel Catalyst for Synthesis Gas to Gasoline", Third Biofuels Conference at Mississippi State University, Mississippi State, MS. August 13, 2008.
G. Shetian Liu and Mark G. White, "Fischer-Tropsch Synthesis over Mo/HZSM-5 Catalysts", 236 ACS Meeting, August 17, 2008.

II. Websites: http://www.che.msstate.edu/academics/faculty_staff/index.php?facultyID=25

III. Networks or collaborations: We are in the process of forming a collaboration with Dr. Jim White at Pacific Northwest National Laboratories. The immediate goal is to arrange a visit by my graduate student, Mr. Prashant Daggolu, to PNNL so as to use some of the facilities there to help with his Ph D research which is related to the DoE sponsored work here.

IV. Technologies developed: The current work seeks to extend the present knowledge base on converted synthesis gas to liquids by going through a higher alcohols intermediates. It is conjectured that this pathway may lead to flexibility in the types of hydrocarbons that can be formed from chemicals to fuels.

V. Inventions, patent applications, etc.

A. Provisional patent: Novel Fischer-Tropsch Catalysts and Process for Liquid Hydrocarbon Fuel Production, filed August 14, 2008.

VI. Other products: none.

Sustainability Energy Research Center
Syngas Thrust Area E. - Final Report for 2006-2008

1. Project title, Principal and co-investigators: E. Investigation of Technical Barriers Effecting Bio-based Syngas Production, Utilization, and Conversion

Principal Investigator
Dr. R. Mark Bricka – Dave C. Swalm School of Chemical Engineering

Co-Principal Investigators
Dr. Sandoon Fernando –Department of Agricultural and Biological Engineering
Dr. Rudy Rogers - Dave C. Swalm School of Chemical Engineering
Dr. Filip To - Department of Agricultural and Biological Engineering
Dr. Clifford George - Dave C. Swalm School of Chemical Engineering
Dr. Tom White – Department of Civil Engineering
Mr. Eugene Columbus - Department of Agricultural and Biological Engineering

2. List of authorized distribution: The information contained in the section of the Sustainable Energy Research Center report is available to be distributed as the Department of Energy deems necessary.

3. Executive Summary

Task E.1 Many modifications were made to the existing down draft gasification unit to improve the operation and enable better data collection and increase the flexibility of the unit. These modifications proved to be effective and assisted in the generation of materials and data for Tasks E.2, E.4, E.6, E.8 and E.9 Results of this task were successful.

Task E.2 Improved gas sampling protocol was developed and the equipment to conduct this sampling was obtained. Tar and particulate results obtained using the new tar sampling procedure were compared with the results obtained from the previous procedure being used. Results indicated that better recoveries of the new tar sampling protocol are much higher. In additional laboratory methods for computational analysis of the tars were validated. The improved sampling protocol has been implemented and is now currently being used for all subsequent gas analysis.

Task E.3 A cold flow model circulating fluidized bed gasifier was built out of clear PVC piping. The solid circulation rates were determined using a bed material diversion method. The average riser voidage was calculated at steady state conditions as well as the average particle velocities inside the riser solids circulation rates and suspension densities of the fluidized media. Results of the cold flow model indicate that no fluidization occurred until the superficial velocity exceeded 2 m/s. Based on the data collected from the cold flow model

operation and design, data were generated for the construction or procurement of the FBG system.

Task E. 4 Syngas conditioning was one of the most effective tasks undertaken by this syngas thrust area. Results of this research developed zeolite metal catalysts which (in the laboratory) have proven to be very effective for tar destruction. In addition, this work lead to the investigation of other naturally occurring catalysts that are also very effective for tar destruction and are very low cost. Research must continue, but scale up of these catalysts is very feasible and must be pursued. Patents will be sought as part of this research effort.

Task E. Surfactant-assisted hydrate separations add another dimension of making group removals of specific families of gases. The results of the project achieved a significant removal of CO_2 (41 %) from the original amount in the syngas due to SDS-surfactant-assisted hydrate formation. At the same time, that syngas had its original hydrogen content increased by 56.7% during the 1-step hydrate process. The process is safe. The process separates the syngas mixture, but also individually sequesters the separated gases. The process holds promise for capturing and sequestering nuisance gases such as carbon dioxide, hydrogen sulfide, sulfur dioxide, carbon monoxide, and NO_x compounds that are encountered in numerous industrial processes.

Task E.6 Ash generation is an unavoidable part of gasification. Currently, the mixing of biomass generated ash with coal ash limits its use due to ASTM definitions of ash and its use. Results of this investigation indicate that the properties of coal ash are not diminished by blending biomass produced ash with coal produced ash. Steps are currently being initiated to introduce modified standards to incorporate the mixing of coal and biomass ash.

Task E.7 Oxygen looping using metal oxides was evaluated and proved to have limited application to gasification. Further research in this area is discouraged.

Task E.8 As a result of this task a micro-reactor for the production of pyrolysis liquid was fabricated and operated. Pyrolysis liquid was generated and gasified. Results indicate that this is a cost effective approach for producing energy from biomass.

Task E.9 – Densified feedstocks for gasification studies were produced via pelleting or briquetting and subsequently gasified. Investigations indicated that pelleting is effective for densifying feedstocks but is an energy intensive process. Many difficulties were uncovered regarding densification and many technical obstacles must still be resolved. Additional work is needed before densification can be utilized on a wide scale.

4. Comparison of goals and actual activities

See attached spreadsheet

5. Summary of activities

Task E.1 – Modify Existing Down Draft Unit

Many modifications were made to the existing down draft gasification unit to improve the operation and enable better data collection and increase the flexibility of the unit. First the feed system was changed to provide the ability to feed a verity of materials. In addition the particulate removal system was improved as well as a knock out container was constructed to remove excess condensation in the syngas prior to flaring or transport to the genset. A gas compression system was also fabricated and installed. Ports were also installed to allow real time sampling of the syngas stream. The genset was completely re-instrumented as part of this task and testing of the genset was conducted. This task did not generate data directly but was necessary to enable tasks 2 -9 to be conducted effectively. Numerous runs of the gasifier were conducted to improve the system operation, develop a thorough understanding of the system operational parameters, and to generate syngas under a variety of conditions for subsequent use in other tasks under this thrust area.

Task E.2 – Improve Current Gas Sampling Protocol and Capability

A tar sampling method was identified after thorough literature review of the various tar sampling techniques currently being used worldwide. A tar sampling method was chosen "Guideline for sampling and analysis of tars and particulates in biomass producer gases, Version 3.3, Energy project ERK6-CT1999-20002 (Tar protocol)", which is being standardized in Europe. Efforts are underway to standardize this guideline in the United States as well. During this year equipment, chemicals, and supplies necessary for the tar sampling protocol have been finalized and have been procured. We established contact with Steve Deutch (NREL) and John Neeft (Biofuels program coordinator, The Netherlands), who have been involved with the development of this method. They helped us with their advice and suggestions with equipment procurement and fabrication. Design and fabrication was done to meet the specific requirements of the method, which included fabrication of heated sampling lines, thimble filter assembly, glassware etc. Tar analysis system was put together and tested. We encountered some problems with the setup during the shakedown testing. There was a very high-pressure drop across the glass impingers used. This pressure drop was attributed to the frits, which were provided at the bottom of the impinger tubes. These problems have been addressed and the system has been tested successfully. Tar sampling guideline is now being used at our facility to determine both qualitative, and quantitative analysis of tars and particulates. A picture of the new sampling system while in operation is provided in Figure 1. Methods have been developed to detect phenols (phenol, creosol, xylenols, etc.), aromatics (benzene, toluene, ethyl benzene, etc.), and polynuclear aromatic hydrocarbons (naphthalene, phenanthrene, coronene, etc.) on Gas Chromatograph (Flame Ionization Detector). These are the common organic compounds detected in tars [1].

Tar and particulate results obtained using the new tar sampling procedure were compared with the results obtained from the previous procedure being used. Comparison of tars and particulates determined from the two procedures for hard wood are provided in Table 1. Also,

the most common compounds present in these tars were benzene, toluene, camphene, naphthalene, 2.methylnapthalene, 1-methylnapthalene, 2-chloronapthalene, acenapthylene, acenapthene, florene, and phenanthrene. Comparison of the results shows that there was a significant difference in the amount of tars and particulates measured. There was an approximate two-fold increase in the amount of particulates measured in comparison to the previous method. The old procedure did not employ isokinetic sampling technique, which, might have contributed to this variation. The new tar sampling guideline will be followed for all future tar and particulates analysis.

Table 1: ***Comparison of tars and particulates between the tar sampling procedures***

	Old Procedure	Tar Sampling Guideline
Average Tars, mg/m^3	**51.14**	**119**
Average Particulates, mg/m^3	**93.89**	**9750**

Also, analysis of the tars provided a detailed list of different individual compounds present. Table 2, provides a list of the contaminants detected in the tars quantitatively for an experiment performed with softwood. The new sampling method is being employed to sample tars and particulates presently and will be used in the future for all tar and particulate analysis.

Table 2: ***Qualitative Analysis for Tars Generated from Softwood Experiment***

Compound	**% Tars**
Benzene	21.2
Napthalene	38.9
2-Methylnapthalene	5.4
1-Methylnapthalene	2.9
2-Chloronapthalene	3.5
Acenapthylene	10.1
Florene	2.3
Phenanthrene	7.1
Anthracene	1.7
Pyrene	2.5

Figure 1: ***Tar Sampling System***





Task E.3 – Procure and instrument a lab scale fluidized bed gasifier (FBG)

The goal of Task E.3 was to design, construct, and instrument a laboratory scale fluidized bed gasifier for the gasification of biomass. A circulating fluidized bed gasifier (CFBG) was chosen as the gasifier configuration. CFBG's have several advantages (Figure 2) when compared to other gasifier types that make them suitable for biomass gasification, including high heat transfer rates, high gas solid interactions, little restriction on particle size and moisture content, etc.

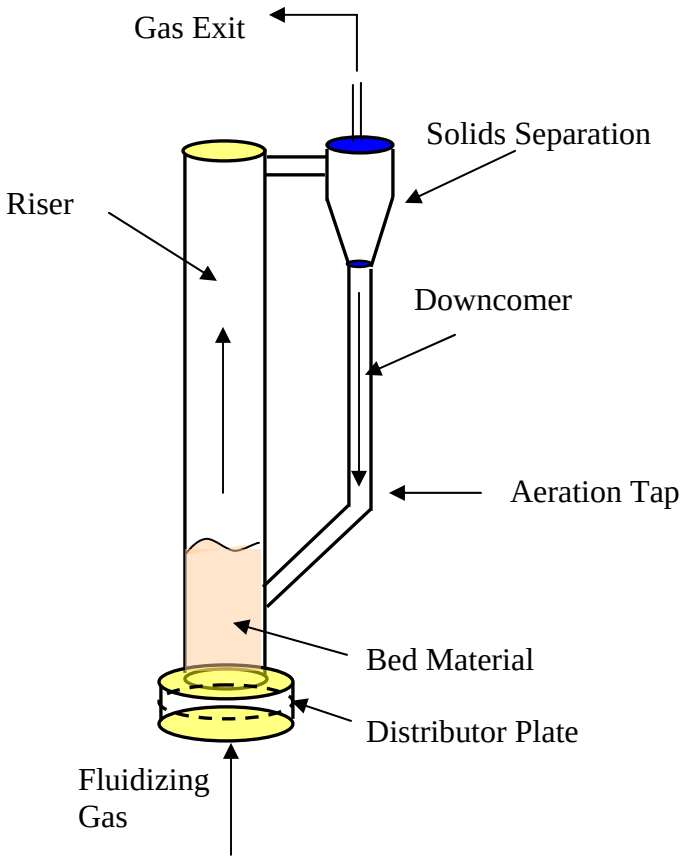


Figure 2. Circulating Fluidized Bed Gasifier

Task E.3 was further broken down into two subtasks. The first subtask was to design and construct a laboratory scale circulating fluidized bed cold flow model to aid in the design of the laboratory scale CFBG. Several operating parameters were to be studied using the cold flow model, and a set of optimal operating conditions was to be determined. These parameters were as follows: solids circulation rates (SCR), riser flow regimes, suspension densities, and bed material diameters. The second subtask was to design, construct, and instrument a laboratory scale CFBG. Upon completion of this, biomass was to be fed to the gasifier under a variety of operating conditions to determine their effect on the composition of syngas produced.

Subtask 1: Cold Flow Model Gasifier

A cold flow model circulating fluidized bed gasifier was built out of clear PVC piping so that the hydrodynamics of the system were visible. The specifications of the cold flow model can be found in Table 3. Experiments were then used to determine the

Table 3. Cold Flow Model Specifications

Riser Inner Diameter	2 (in)
Riser Height	144 (in)
Downcomer Diameter	2 (in)
Recycle Geometry	Y-Valve
Particle Separations Device	Cyclonic Filter
Bed Material	Silica Sand
Bed Material Diameter (average)	200 microns, 500 microns
Solids Recycle Control	Gate Valve

optimal operational conditions for the laboratory scale CFBG. The solid circulation rates were determined using a bed material diversion method, in which the bed material (once having passed through the riser and into the downcomer) was diverted into a separate holding container over a set amount of time. This process was triplicated at a variety of riser superficial gas velocities, and for both the 200-micron and 500-micron bed material diameters. The average riser voidage was calculated using a similar method, in which once the model was operating at steady state at a known superficial velocity, the air flow to the bottom of the cold flow model, as well as the valve controlling the solids recycle, were shut off simultaneously. The volume of bed material left behind in the riser was then determined and averaged over the entire volume of the riser. This, along with the SCR at given riser superficial velocities, allowed for the calculation of the average particle velocities inside the riser.

Upon completion of subtask 1, a laboratory scale circulating fluidized bed gasifier was to be constructed and instrumented. However, the second allotment of funding was redirected before subtask 1 was finalized. Therefore, further development of the laboratory scale gasifier was terminated.

Results of the cold flow model indicate that the SCR as a function of the riser superficial velocity can be found in Figure 3. For both 500 and 200 micron silica sand diameters, no solids recycle was found until a riser superficial velocity of approximately 3 m/s. The SCR for the 200 micron sand was higher at a given riser velocity than for the 500 micron sand. However, the 500 micron sand showed a steadier operation, with a smaller variation at each measured superficial velocity. The average riser voidage as a function of superficial riser velocity can be found in Figure 4. For both the 200 and 500-micron sand, the riser voidage increases almost linearly with an increase in superficial velocity. It is also important to note that there is little difference between the voidages at a given riser velocity for either diameter sand.

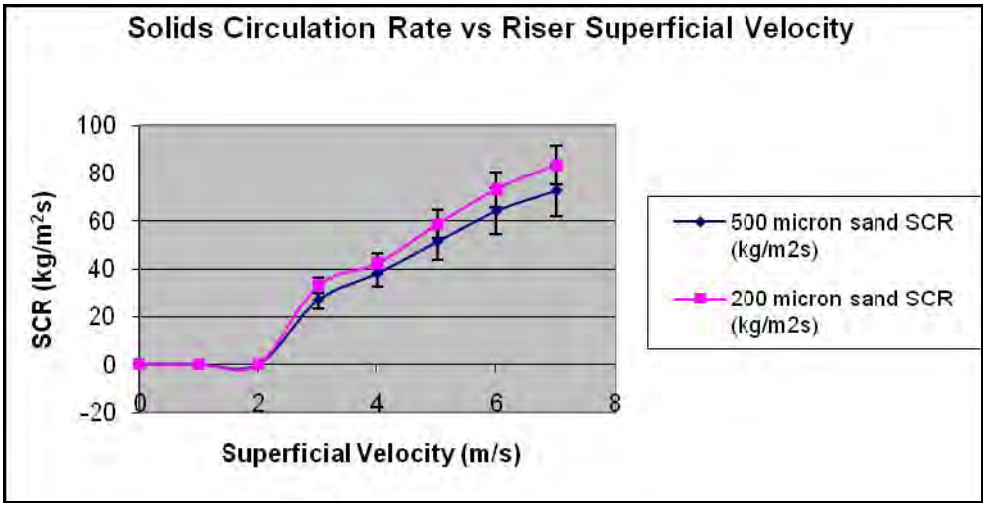


Figure 3. SCR vs Riser Superficial Velocity

Average riser particle velocity as a function of riser superficial velocity can be found in Figure 5. As expected, the 200-micron particles have higher riser velocities than the 500-micron particles. The difference in particle velocities becomes more significant as the riser superficial velocity increases. This leads to smaller particles having lower residence times inside the reactor than larger particles, possibly causing conversion to be higher with larger particles.

Based upon the collected data, the following Table 4 gives a summary of the suggested operational parameters and gasifier design information. Depending on the equivalence ratio used during gasification, the use of these operational parameters would lead to the various amounts of syngas produced (estimated), as shown in Figure 6. Also shown is the approximate amount of biomass needed at each equivalence ratio for a given riser superficial velocity.

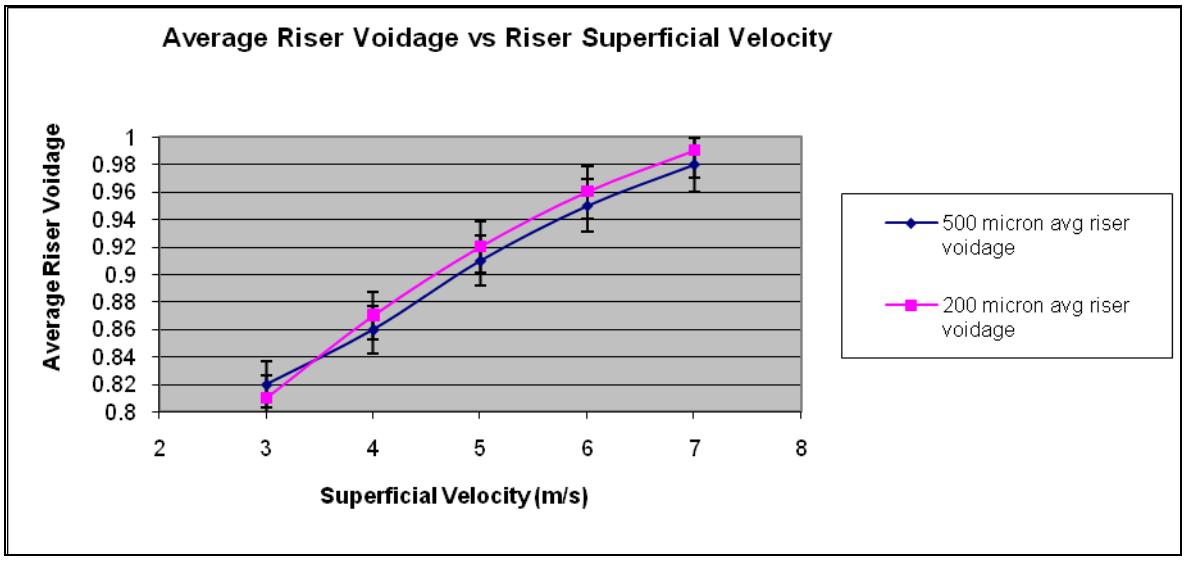


Figure 4. Average Riser Voidage vs Riser Superficial Velocity

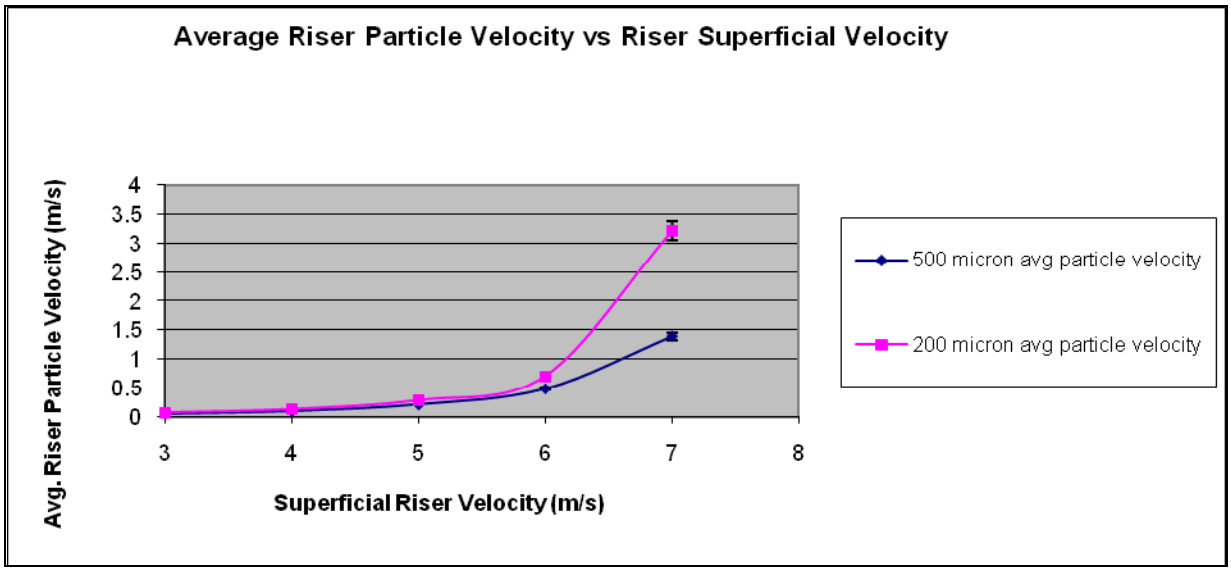


Figure 5. Avg. Riser Particle Velocity vs. Superficial Riser Velocity

Table 4. Laboratory Scale CFBG Parameters and Design Information

Riser Height	144 (in)
Riser ID	2 (in)
Solids Separation	Dual Cyclone System
Downcomer Geometry	2 in ID with a 24 x 5 in solids reservoir
Return Geometry	Y-valve
Solids Recycle Control	Globe Valve
Riser Superficial Velocity	4-6 (m/s)
Bed Material	Silica Sand (2600 kg/m^3)
Bed Material Avg. Diameter	500 microns
Solids Circulation Rate	40-60 (kg/m2s)
Riser Particle Velocity	<1 (m/s)
Average Riser Voidage	.85-.95

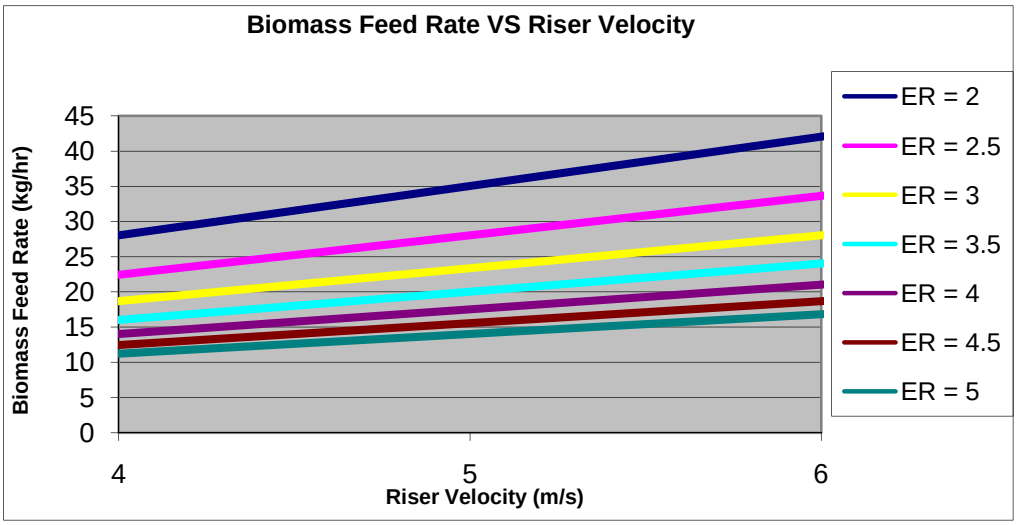


Figure 6. Biomass Feed Rate vs Riser Superficial Velocity

Task E.4 – Syngas Conditioning

A laboratory scale catalytic reactor was designed and fabricated to evaluate a suitable catalyst for tar destruction both in terms of activity and cost. Figure 7 shows a picture of the lab scale

catalytic reactor. Several catalysts have been tested to evaluate the catalytic activity for the removal of tars. Table 5, provides a list of zeolite-based catalysts that have been tested. Also, several nickel supported clay catalysts were evaluated due to the low cost associated with clay supports (Ni supported Montmorillonite and Bentonite). The experimental conditions for the experiments performed are provided below.

Temperature: 550, 650, 750 ^{o}C
Pressure: Atmospheric
Model Compound: Naphthalene
Syngas Flowrate: 150 cc/min.
Naphthalene Input: 12 mg/min. (10.54 g/m^3)
Water Input: 0.015 ml/min.
Steam/Carbon: 5.9
Gas Hourly Space Velocity: 9450 h^{-1} (3.34 kg/m^3)
Catalysts Tested: 7.5% Ni on ZY-80, ZY-5.2, SiO_2/Al_2O_3
Catalyst Size: 20-40 mesh
Catalyst Weight: 500 mg
Experiment Duration: 2.5, 97 hours

Catalysts were prepared in the laboratory and tested for tar removal activity. The prepared catalysts were characterized by X-ray diffraction (XRD), surface area analysis (BET), temperature programmed reduction (TPR), transmission electron microscopy (TEM), Inductively coupled plasma atomic emission spectroscopy (ICP) techniques and the post run (spent) catalysts were characterized by BET, XRD, TEM, fourier transform infrared spectroscopy (FTIR), and thermo gravimetric analysis (TGA), to further investigate reasons behind the catalytic activity. Also, naphthalene analysis was accomplished using a gas chromatograph flame ionization detector (GC-FID) and the gas compositions by a gas chromatograph thermal conductivity detector (GC-TCD).

Figure 7: ***Lab Scale Catalytic Reactor***



Table 5: ***Pore size and Surface area of zeolite based catalysts evaluated***

Catalyst	**SiO_2/Al_2O_3**	**Pore Size, A^o**	**Surface Area, m^2/g**
Zeolite Y 5.2	5.2	7.4 X 7.6	750
Zeolite Y 30	30	7.4 X 7.6	750
Zeolite Y 80	80	7.4 X 7.6	780
Zeolite β	25	6.6 X 6.7	680
ZSM 5	24	5.3 X 5.6	425
Chabazite	4	3.7 X 4.1	520
SiO_2/Al_2O_3	28	-	381
7.5% Ni on ZY 5.2	5.2	7.4 X 7.6	481
7.5% Ni on ZY 30	30	7.4 X 7.6	646
5, 7.5, 10 % Ni on ZY 80	80	7.4 X 7.6	673
7.5% Ni on Chabazite	4	3.7 X 4.1	283
7.5% Ni on SiO_2/Al_2O_3	28	-	401
10 % Ni on Zβ	25	6.6 X 6.7	-
7.5 % Ni on ZSM5	24	5.3 X 5.6	-

Some of the results from the experiments performed are presented in Tables 6 and 7. Results from Table 6 show that there was an increase in the activity of the catalyst with increasing temperature. Also, there was an increase in the naphthalene removal efficiencies with a decrease in the acidity of the zeolites. The activity of Ni supported montmorillonite was comparable with ZY 80 as shown in Table 6, which is relatively cheaper catalyst support. Thermogravimetric analysis (TGA) was performed on the used catalysts from experiments performed at 650 and 750 ^oC to determine the effect of coke deposition on the catalyst. Coke analysis in provided in Table 7, the results of which suggest that there was a decrease in the amount of coke formation with increasing temperature. This could be due to the steam reforming and dry reforming reactions taking place at higher temperatures. Table 7 also shows an increase in the amount of coke deposited on the catalyst with an increase in the acidity of zeolites. Although, the results from the table directly do not correspond to an increase in the coke formation with decreasing acidity, a comparison of the amount of naphthalene removed with coke formation would be more indicative of the higher coke formation with a decrease in the acidity. X ray diffraction (XRD) analysis was done on fresh and used catalysts to determine the effect of temperature on the zeolite stability. The results from XRD analysis suggested that the zeolite structure was stable at the operating conditions at which the tests were performed. Also, the presence of nickelaluminate was not observed from XRD analysis. The formation of nickelaluminate would have reduced catalyst activity irreversibly, which was not the case. XRD and TGA analysis further substantiate the possible explanation for the decreased catalytic

activity with an increase in the acidity of the zeolites, the main reason being coke formation, under the conditions tested.

The suggested mechanisms that might be involved in the removal of naphthalene from syngas are shown below.

Steam Reforming

$C_{10}H_8 + 10H_2O \leftrightarrow 10CO + 14H_2$…….(1)

Dry Reforming

$C_{10}H_8 + 10CO_2 \leftrightarrow 20CO + 4H_2$……(2)

Thermal Cracking

$C_{10}H_8 \rightarrow C^* + Gas + Lower\ Hydrocarbons$…….(3)

Hydrocracking

$C_{10}H_8 + H_2 \leftrightarrow CO + H_2 + CH_4 + Coke$……..(4)

Water-Gas Shift Reaction

$CO + H_2O \leftrightarrow CO_2 + H_2$……(5)

Methane Reforming [High Temp., 700 C]

$CH_4 + H_2O \rightarrow CO + 3H_2$……..(6)

Methanation [Low temp, 500 C]

$CO + 3H_2 \rightarrow CH_4 + H_2O$……..(7)

Dry Reforming of Methane

$CO_2 + CH_4 \rightarrow 2CO + 2H_2$…….(8)

Long-term tests were carried out to evaluate the stability of the catalysts for the removal of tars. Figure 8, presents the naphthalene removal efficiencies of different catalysts over 97 hours. The results show that all the catalysts tested had a stable activity with different removal efficiencies, except chabazite. The activity of Ni chabazite steadily decreased from 99 % to 33 % over 97 hours, which could be due to the structural collapse of chabazite at higher temperatures and smaller pore size. The results also show that ZY-80 and ZY-30 had the best naphthalene removal efficiencies. Also, removal efficiencies of montmorillonite were comparable with ZY-30 and ZY-80. However, lower cost and availability makes 7.5% Ni on montmorillonite a better candidate for tar removal. Hence, further experiments are being carried out with montmorillonite to further improve the catalyst performance.

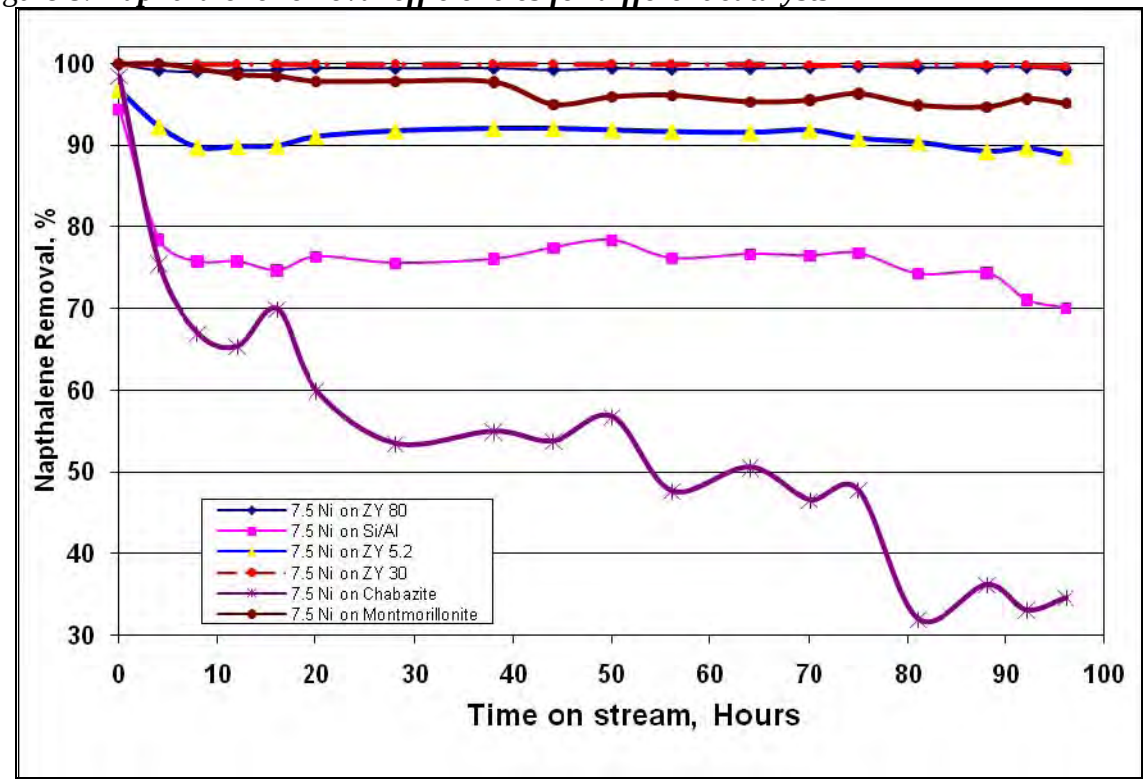
Table 6: ***Napthalene removal efficiencies for tests performed for 150 minutes***

	Temperature, ^oC		
Catalyst	***550***	***650***	***750***
7.5 % Ni on Montmorillonite	94.3%	91.2%	96.2%
7.5 % Ni on ZY 5.2	61.0%	68.2%	82.9%
7.5 % Ni on ZY 30	89.6%	73.9%	80.3%
7.5 % Ni on ZY 80	85.0%	89.5%	96.9%
7.5 % Ni on SiO_2/Al_2O_3	67.5%	76.2%	74.8%

Table 7: ***Coke Analysis***

Catalyst	Coke Deposited, %	
	650° C	**750° C**
7.5 % Ni on ZY 5.2	*8.93 %*	2.62 %
7.5 % Ni on ZY 30	*7.74 %*	1.21 %
7.5 % Ni on ZY 80	*9.00 %*	0.70 %
7.5 % Ni on SiO_2/Al_2O_3	*2.30 %*	0.72 %
7.5 % Ni on Bentonite	1.35 %	--
7.5 % Ni on Montmorillonite	3.01 %	--

Figure 8: ***Naphthalene removal efficiencies for different catalysts***



Task E.5- Surfactant assisted syngas separation

The Parr high-pressure, hydrate test cell was designed, constructed, and set up for operations in the laboratory. Procurement of the Parr high pressure system allowed the viewing and filming of hydrate formation in the test cell as planned in the proposal and this proved to be a valuable analysis tool for such operations. It allows the formulation and verification of a mechanism for hydrate formation that can be correlated with data on successful syngas separation.

A second task, "Screening and selection of surfactant for hydrated-assisted separations" was completed on schedule. The trisiloxane *Silwet L-77* to solubilize carbon dioxide and the sodium dodecyl sulfate *SDS* to solubilize hydrocarbon gases were chosen from the screenings of

surfactants. Both surfactants promote hydrate formation. Besides these two surfactants, Silwet 408 (another siloxane), rhamnolipid (a biosurfactant), Silwet Q2-5211(a third siloxane), and modifications of all these by adding phosphate groups to their structures were tested. The screenings allowed the project to proceed to the next step of testing laboratory pure syngas with the surfactant for hydrate formation and separation.

Another phase of testing involved the use of laboratory pure syngas with surfactants for hydrate formation and separation. This work involved an initial syngas molar composition of about 9.36% hydrogen, 12.75% nitrogen, 2.93% carbon monoxide, 53.28% methane, and 22.18% carbon dioxide. A surfactant sodium dodecyl sulfate (SDS) was used with 1000 ppm in water solution and gas hydrates were formed from syngas pressurizing the solution. Nine experimental runs were made using SDS as the only surfactant in the hydrate separation process. After a first stage separation with this gas-water composition, carbon dioxide content was reduced by 40.9% in the syngas free gas phase and hydrogen content was increased by 56.7% in the syngas free gas phase. See Fig. 9.

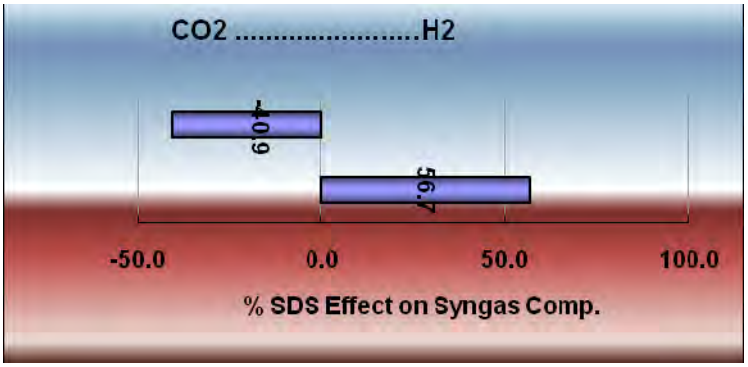


Fig. 9. SDS surfactant assists in the separation of syngas during gas-hydrate formation.

A surfactant L-77 siloxane was used with 1000 ppm in water solution and gas hydrates were formed from syngas pressurizing the solution. After a first stage separation with this gas-water composition, carbon dioxide content was reduced in the syngas free gas phase and hydrogen content was increased in the syngas free gas phase to a much lesser extent than with the SDS surfactant. See Fig. 10.

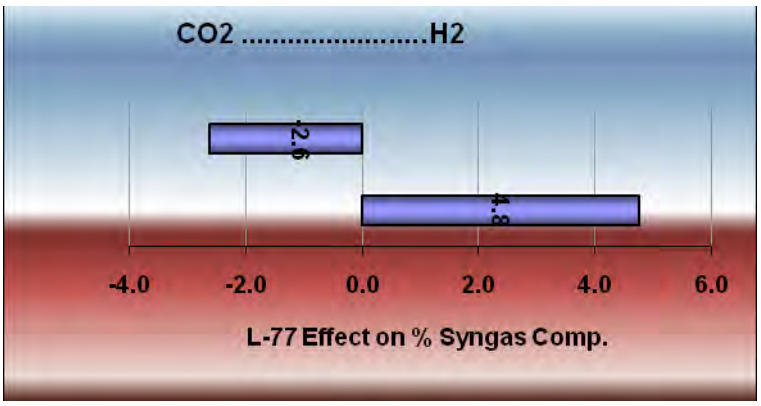


Fig. 10. L-77 siloxane surfactant assists in the separation of syngas during gas-hydrate formation.

Note that hydrogen is one of the few gases that will not form stable gas hydrates because of its diminutive molecular size. The 56.7% increase in the syngas's H_2 composition from hydrate formation in only one stage using SDS is an excellent result. The increase is mostly due to the scavenging of CO_2 by the surfactant-assisted hydrate formation. Both the increase of hydrogen and the decrease of carbon dioxide in the syngas are highly positive results.
Overall, the results were good, but it is anticipated that a hydrogen concentration could be substantially increased in the syngas and a carbon dioxide concentration correspondingly decreased in the syngas with a multi-stage process.

The last phase of testing involved the establishment of the potential of THF to improve gas separation. The appeal of using THF in water solution as hydrates form is that formation pressures may be decreased. A 4% THF-water solution was evaluated for forming gas hydrates to separate syngas. Without surfactant, THF appeared to retard hydrate formation with carbon dioxide as the pressurizing gas. With the siloxane Silwet-77 in the THF, carbon dioxide hydrate formation was improved. Only minor success in attaining project goals was realized in the THF experiments.

The project demonstrated the potential of a novel means of separating syngas via surfactant-assisted gas hydrate formation. The process holds promise of other uses.

Task E.6 – Ash Utilization

Fly ash used in concrete construction material applications has a very large market. When used as partial replacement of more expensive cement, the upper replacement limit is about twenty-five percent. Fly ash also imparts other properties that improve PCC properties.

Because of its wide spread use there are American Society for Testing and Materials (ASTM) specifications and test procedures for fly ash and pozzolanic materials. These standards are used to insure such materials have desired properties. These standards are ASTM C 618-03. Standard Specifications for Coal Fly Ash and Raw or Calcined Natural Pozzolan for use in Concrete and ASTM C 311-02, Standard Test Methods for Sampling and Testing Fly Ash or

Natural Pozzolans for Use in Portland-Cement Concrete. These standards arc limited to two types of fly ash produced from coal fired generating plants, Class F and Class C. Class F is produced from burning anthracite coal and Class C is produced from burning lignite or subbituminous coal. ASTM standards prohibit use of fly ash not produced from firing coal alone.

This task was conducted to evaluate the ash product of co-firing biomass and coal for use in the concrete materials industry. Currently, a proposed bill, H.R. 1945, would require all coal-fired electric power plants start co-firing in 2009. The percent of biomass would start at 1% in 2009 and increase incrementally to 20% by 2020. As of 2007, the European Standard EN 450 allows co-fired fly ash in concrete, but with additional requirements to those for fly ash produced from coal alone.

Advantages of co-firing

- Many biomass sources are waste products and co-firing them avoids landfill use.
- These waste products are often cheaper than coal.
- Co-firing lowers sulfur and mercury levels in both emissions and fly ash.

Disadvantages of co-firing

- The BTU value per unit weight of biomass/coal blend is less than from coal alone.
- Steady and homogenous sources of biomass can be difficult to find.
- Logistics can sometimes make the total cost of using biomass more expensive than using coal.

Fly ash as a partial replacement for cement in concrete increases strength, mitigates expansion, reduces heat of hydration, and improves workability of the concrete. Fly ash mitigates expansion by reducing the heat of hydration and controlling the alkali silica reaction (ASR). The sum of $SiO_2 + Al_2O_3 + Fe_2O_3$ is the main factor in how well the fly ash is able to mitigate concrete expansion.

To document the properties of co-fired fly ash samples were obtained from two power plants. The first plant (Colbert Fossil Plant) is owned by the Tennessee Valley Authority (TVA) and is located in Tuscumbia, AL. The second plant (Gadsden Steam Plant) is owned by Southern Company and is located in Gadsden, AL. Samples of fly ash from the Colbert Fossil Plant were produced by co-firing 4% (by weight) wood chips as the biomass source. Samples of fly ash from the Gadsden Steam Plant were produced by co-firing 8%, 10%, and 15% (by weight) wood chips as the biomass source. A sample of fly ash from 0% biomass (coal only) was also provided from both power plants in order to have a reference point to measure the effects of co-firing.

An oxide analysis was performed using x-ray fluorescence (XRF). The Loss on Ignition test (LOI) indicates how much carbon is in the ash. In terms of LOI, the effects of co-firing at the Colbert Fossil Plant appear to be greater than the Gadsden Steam Plant even though the Colbert Fossil Plant only co-fired with 4% biomass. High carbon contents can have adverse affects on concrete strength development. Analysis results are shown in Table 8.

Tests were conducted to examine the effects of co-fired fly ash on shrinkage and expansion. Compressive and flexural strength tests were performed on concrete specimens produced using co-fired fly ash as partial replacement of cement. Specimens in this project are both moist cured and air dried. The length changes caused by air drying (shrinkage) will be compared to the length changes caused by ASR (expansion). Length changes due to air drying (shrinkage) are usually larger in magnitude than the length changes due to ASR (expansion). To further examine how well the fly ashes control the ASR effect, the fly ashes were combined with hi-alkali cement in addition to the standard type I cement. Room humidity and temperature during air drying was approximately 50% and 72 ºF, respectively. Water-cement ratio used in all specimens was 0.40. To date only the Gadsden Steam Plant fly ash has been tested. Four replicate specimens were prepared and tested for compressive strength while six replicate specimens were tested for flexural strength. A higher replication of tests was used for flexural strength because there is slightly more variation in the test results.

Table 8 Chemical Composition of Fly Ash

Oxide	Colbert Coal Fly Ash - Class F	Colbert Co-Fired Fly Ash - 4% Biomass	Gadsden Coal Fly Ash - Class C	Gadsden Co-Fired Fly Ash- 8% Biomass	Gadsden Co-Fired Fly Ash- 10% Biomass	Gadsden Co-Fired Fly Ash- 15% Biomass
SiO_2	47.68	55.66	48.98	50.14	47.74	49.22
Al_2O_3	17.59	18.83	26.50	25.61	26.29	25.30
Fe_2O_3	18.33	4.40	11.47	11.40	10.81	10.77
Sum	83.60	78.89	86.95	87.16	84.83	85.29
TiO_2	0.99	0.80	1.29	1.21	1.19	1.20
P_2O_5	0.10	0.35	0.44	0.36	0.32	0.37
CaO	7.43	5.82	1.24	1.07	1.21	1.11
MgO	0.85	1.98	1.06	1.09	1.08	1.04
Na_2O	0.60	1.50	0.23	0.24	0.22	0.23
K_2O	2.25	1.19	2.51	2.74	2.59	2.65
SO_3	1.68	0.51	0.11	0.12	0.13	0.10
BaO	0.03	0.16	0.31	0.30	0.28	0.28
SrO	0.02	0.14	0.13	0.09	0.09	0.09
Total	97.55	91.34	94.27	94.36	91.95	92.37
LOI	2.47	8.71	5.72	5.62	8.06	7.58

In specimens containing fly ash, 20% of the cement was replaced. The 20% replacement is common in practice and is the standard replacement called for in ASTM C 618 – 05 to measure the strength activity index of the fly ash. The strength activity index is measured by comparing the compressive strength of concrete specimens without fly ash to specimens with fly ash. Results are shown in Tables 9 and 10.

Two replicate beams were produced for each material combination and curing condition to monitor the length changes. Length changes of the two beams were averaged for a result. The length comparator device used measures to 1/10,000th of an inch and the variation of length change between two beams of the same type was low. The magnitude of the length changes due to air drying (shrinkage) was higher than for ASR (expansion).

The data collected indicates that a significant amount of biomass (wood) can be co-fired with coal and still produce an acceptable fly ash. In most cases the co-fired fly ash performed as well or better than the standard coal fly ash. ASTM C 618 should be modified or changed to allow co-fired fly ash in concrete as long as it meets all the same physical property criteria set forth for coal fly ash.

Many coal-fired power plants now inject lime into the coal burning process to reduce sulfur emissions. As the CaO content of the fly ash increases, the fly ash becomes more cementious which makes it useful for some applications, but ASTM C 618 specifically prohibits the use of fly ash that has been produced from a plant with lime injection. So, for these plants and others whose fly ash already fails to meet ASTM criteria; the effect of co-firing might be a non-issue.

Table 9 Compressive Strength for Gadsden Steam Plant Fly Ash (psi)

		Four Samples Each	Cement Only	0% Biomass Fly Ash	8% Biomass Fly Ash	10% Biomass Fly Ash	15% Biomass Fly Ash
Standard Cement	Moist Cured	7 day	5,741±310	5,442±449			
		28 day	7,800±889	5,856±485	5,842±985	6,082±640	5,530±682
		90 day		7,343±1,576			
	Air Dried	7 day	6,336±1,282	6,550±714			
		28 day	8,593±380	7,953±602	6,654±654	6,320±523	5,933±255
		90 day					
Hi-Alkali Cement	Moist Cured	7 day	5,392±576	5,106±219	4,661±614	5,449±561	4,767±324
		28 day	6,588±881	5,331±805	5,894±444		
		90 day					
	Air Dried	7 day	7,152±494	5,504±123	4,883±752	5,834±620	4,417±1,002
		28 day	8,100±1,250	6,023±413	5,735±241		
		90 day					

Table 10 Modulus of Rupture (M_R) for Gadsden Steam Plant Fly Ash (psi)

		Six Samples Each	Cement Only	0% Biomass Fly Ash	8% Biomass Fly Ash	10% Biomass Fly Ash	15% Biomass Fly Ash
Standard Cement	Moist Cured	7 day	1,476±254				
		28 day	1,572±245	1,647±?	1,288±226	1,535±193	1,403±177
		90 day					
	Air Dried	7 day	600±352	622±138			
		28 day	1302±478	1661±401	1021±353	1342±197	1112±159
		90 day					
Hi-Alkali Cement	Moist Cured	7 day	1,283±138	1,134±82	1,020±50	1,305±151	1,160±214
		28 day	1,300±238	1,538±60	1,388±90		
		90 day					
	Air Dried	7 day	1,191±409	1,014±126	905±207	1,035±98	990±104
		28 day	1,629±576	1,408±287	953±89		
		90 day					

Task E.7- Oxygen looping catalyst system

In current gasification systems, air is used to partially oxidize the biomass feed. This air contains nitrogen which in turn dilutes the producer gas significantly lowering its total energy value. In this study a chemical oxygen carrier was used to strip oxygen from air by adsorption, transport the stripped air into the gasifier, and release the oxygen by desorption to facilitate combustion. This study targeted the ability of selected metal oxides to adsorb oxygen from air and desorb oxygen at working temperatures of biomass gasification systems. As part of this investigation four specific objects were targeted:

1. To evaluate the optimum oxygen uptake conditions (oxidation mode) of selected metal oxides
2. To evaluate the optimum oxygen release conditions (reduction mode) of selected metal oxides
3. To investigate the stability of the catalytic oxides subjected to repeated oxidation-reduction cycles
4. To Characterization of promising catalytic oxides.

While not all objects of this task were achieved, studies did revealed that the metal oxides can degrade to release oxygen. In this study over 8 metal oxidants were evaluated. These included V_2O_5, IrO_2, CuO, LaO, CeO_2, ZrO2, CeO2 and TiO_2. Decomposition studies using thermogravimetric analysis (TGA) were used to identify the temperature at which decomposition of the metal oxides occurred. An example graph of such studies is provided in Figure 11. Many of the metal oxidants decomposed at high temperatures (greater than 800°C).

Conclusion

Out of the transition metal oxides tested, TiO_2 showed the best Redox potential although it was not adequately repeatable. Most of the other metal oxides we analyzed did not show good results. The practicality of this work is questionable and future research in this area is discouraged.

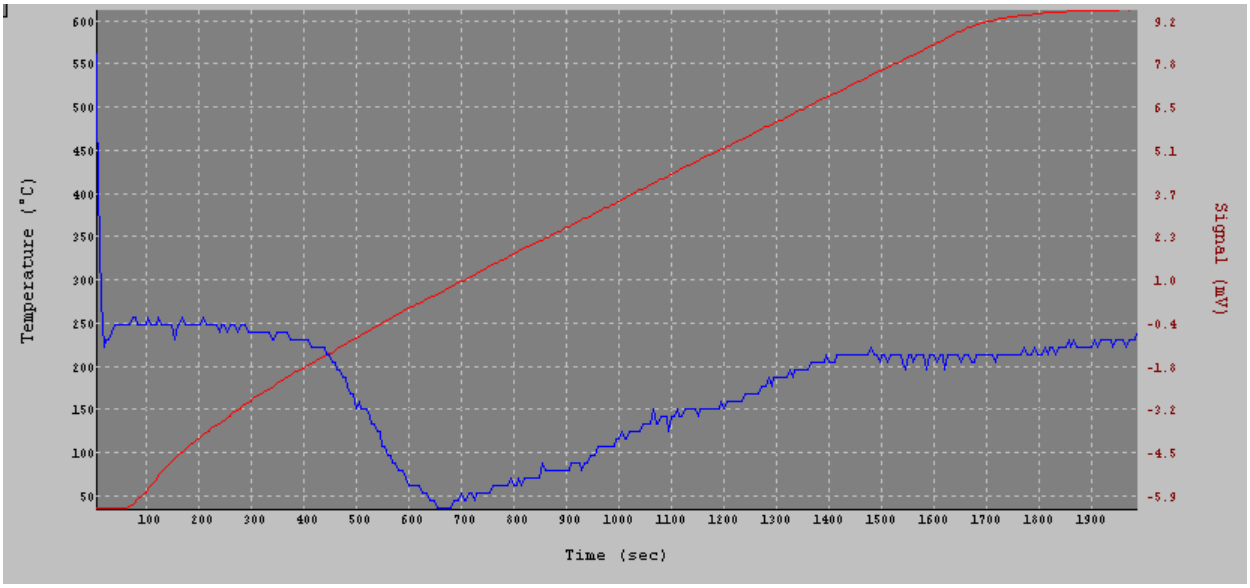


Figure 11. Temperature Programmed Decomposition, Run 1 at 600oC for the CeO_2 catalyst

Task E.8 – Pyrolysis/Syngas conversion

This task focused on the two stage gasification of biomass. It was desired to produce a pyrolysis liquid and to investigate the gasification of the liquid. The first step of this process was to develop a micro scale reactor for use to produce the pyrolysis liquid. As part of this task CCA-treated wood was target as the feed for this system. Results of this investigation are detailed as follows. Specific tasks associated with Pyrolysis/Syngas research effort are provided in Table 11.

Table 11. Research Tasks

Assemble equipment and collect, prepare, and characterize feedstock
Fabricate and test microreactors
Conduct initial thermal studies
Conduct mass balance studies to determine terminal distribution of metals

<u>Feedstock Collection, Preparation, Characterization and Micro R actor Design and Fabrication</u>

An out-of-service cylindrical utility pole (treated with CCA) was donated for research to Mississippi State University by Starkville Electric Company. The pole was chipped and the smaller diameter fraction was then ground into sawdust for use in microwave assisted acid

digestions, moisture content studies, and pyrolysis experiments. Microwave assisted acid digestions (modified EPA Method 3051) were performed to determine the metal content of the CCA-treated wood, and the generated samples were analyzed using a Perkin Elmer Instruments Optima 4300 DV Inductively Coupled Plasma Optical Emissions System (ICP-OES). Moisture content of the CCA-treated wood waste was determined using the method provided in Table 12.

Table 12. Method for Determining Moisture Content

1	Weigh sample tin (a)
2	Add wet wood sample to tin and weigh the tin (b)
3	Place sample tin + wood sample in a forced air oven at 103°C for at least 3 hours
4	Remove sample tin + wood sample from the oven and place in dessicator for 15 minutes
5	Weigh sample tin + dry wood sample (c)
6	Repeat steps 3-5 until sample weight becomes constant
7	Calculate moisture content using equation 1

$$\%\ \text{Moisture} = \frac{(b-a)-(c-a)}{(c-a)} \times 100 \qquad \text{Equation 1}$$

After completing an extensive literature review of existing laboratory-scale pyrolysis systems, the current system was designed to consist of three primary units: the reactor, condensers, and sampling train. The reactor is made of 316 stainless steel pipe and has dimensions of 2 inches (diameter) by 8 inches (length). In the current set-up, the reactor is heated using a Fisher Isotemp Muffle Furnace, and operates under nitrogen purge. Two condensers are used in series to cool the pyrolysis vapors and collect the pyrolysis oil. The sampling train consists of a mixed cellulose ester filter (employed to collect any possible particulates that have passed through the system) and impingers containing sodium sulfide (to assist in capturing arsenic). Figure 12 is a photograph of the lab-scale pyrolysis system, and Figure 13 shows the reactor inlet.

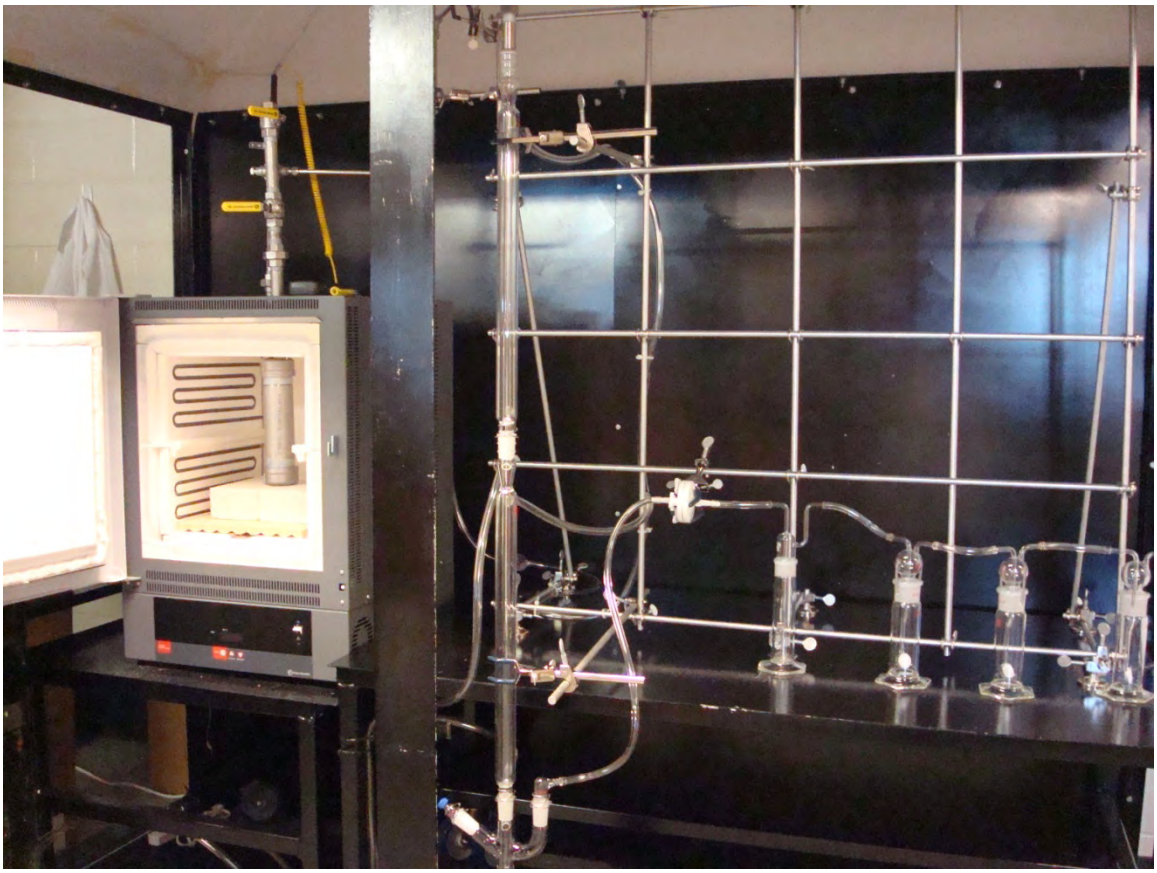


Figure 12. Lab-scale Pyrolysis System Without Insulation



Figure 13. Reactor Inlet With Insulation

The system was initially operated with untreated wood to determine the optimal operating conditions for bio-oil production, and these are provided in Table 13. These operating parameters were used to carry out all of CCA-treated wood experiments.

Table 13. System Operating Parameters

Warm-up Time	2.25 hours for 350°C set point; 3.5 hours for 550°C set point (on average)
Cool-down Time	5 hours (on average)
Loading Capabilities	≤ 5 grams of sawdust at a time
Gas Flow	No higher than 5 L/min

Each of the products generated during the pyrolysis experiments were subjected to analysis. All materials were subject to microwave assisted acid digestions. Modified EPA Method 3051 was used for all of the solid materials (char, filter, etc.), while EPA Method 3052 and Method 3015A were used for the liquid materials (bio-oil and impinger solutions). The samples generated from these experiments were analyzed on the ICP-OES.

Conclusions

Overall research has been successful. A micro scale reactor capable of generating pyrolysis liquid and the gasification of this liquid has been initiated. Wood chips generate a good material which has great potential to generate a pyrolysis liquid for gasification. This investigation indicates that the gasification of pyrolysis liquid is a very cost effective method to generate energy from a wood source.

Task E.9- Polarization/densification of feed-stocks

Densified feedstocks for gasification studies were produced through pelleting or briquetting at MSU, in collaboration with USDA-ARS, or in collaboration with industry. The goal was to obtain a diversity of feedstocks in terms of type and form and investigate if these factors affect the resultant syngas produced from a typical air blown, fixed-bed, downdraft gasifier or the gasifier operation. Switchgrass pellets were produced in the MSU pilot plant as well through a contract production. Prioritizing gasification work on switchgrass and wood chips and wood pellets deferred the need for giant Miscanthus and elephant grass pellets that was indicated in the study plan. Densified cotton gin trash in the form of briquettes were available from the USDA-ARS Cotton Production and Processing Research Unit in Lubbock, Texas while wood pellets were available from commercial collaborators and so these were utilized advantageously to meet project timelines.

6. Products developed and technology transfer activities:

Patents: None

Publications:

Igathinathane, C., A. R. Womac, L. O. Pordesimo, and S. Sokhansanj. Mold appearance on selected corn stover components during moisture adsorption. Bioresource Technology. (in press)

Igathinathane, C., L. O. Pordesimo, W. D. Batchelor, E. P. Columbus, and S. Methuku. 2008. Shape identification and size distribution of particles from basic shape parameters using ImageJ. Computers and Electronics in Agriculture 63:168-182.

Buchireddy, Prashanth, and Bricka, R. Mark "Overview of different methods for the removal of tars from biomass gasification" in preparation.

Presentations:

Blakely, John Alex (2008) "Cold Flow Model Circulating Fluidized Bed Reactors" Paper presented at the American Institute of Chemical Engineers Southern Regional Conference in Auburn, Alabama, April 5, 2008.

Blakely, John Alex (2008) "Operation and Characterization of a Cold Flow Model Circulating Fluidized Bed Gasifier" Poster presented at the American Institute of Chemical Engineers Annual Meeting in Philadelphia, Pennsylvania on November 17, 2008.

Bricka, R. Mark, 2008. "Environmental Impacts of Alternative Energy Sources,, AWMA Southern Section Annual Meeting and Technical Conference, 05Aug – 08 Aug, 2008, Biloxi, MS

Bricka, R. Mark 2007. "State of the Art Review for Distributed Biomass Gasification," Six Annual Southern BioProducts Conference, April 16-18, 2007, Pearl River Resort, Choctaw, MS.

Bricka, R. Mark, 2007. "Design of a Partial Oxidation Methanol Production Plant," American Institute of Chemical Engineers, 2007 Annual Meeting, November 4-9, 2007, Salt Lake City, Utah.

Bricka, R. Mark, Singletary, Monty. 2007. "Increasing the Economic Efficiency of Feedstock Used for Greenhouse Heating," American Institute of Chemical Engineers, 2007 Annual Meeting, November 4-9, 2007, Salt Lake City, Utah.

Bricka, R. Mark. 2007. "State of the Art Review for Distributed Biomass Gasification," Proceedings of the Sixth Annual Southern BioProducts Conference, April 16-18, 2007, Pearl River Resort, Choctaw, MS.

Brooks, Bryant (2008) "Evaluation of the Potential of Surfactant Aided Conversion of Synthesis Gas to Ethanol" Poster presented at the First Annual Energy-Synergy Workshop at Mississippi State University on April 17, 2008.

Buchireddy, Prashanth R., and Bricka, R. Mark, 2008. "Biomass Gasification: Catalytic Tar Removal Using Ni-Zeolite Catalysts," Proceedings of the 2008 AICHE Annual Meeting and Centennial Celebration, November 16-21, 2008, Philadelphia, PA

Buchireddy, Prashanth (2008) "Biomass Gasification: Removal of tars from producer gas" Poster presented at the First Annual Energy-Synergy Workshop at Mississippi State University on April 17, 2008.

Buchireddy, Prashanth (2008) "Biomass Gasification: Removal of tars using FCC catalysts" Poster was presented at the 2008 Biofuels Conference at Mississippi State University

Buchireddy, Prashant, R. Mark Bricka, Columbus, Eugene, and Wooten, James. 2007. "Production of Clean Synthetic Gas From Biomass Using a Downdraft Gasifier," Six Annual Southern BioProducts Conference, April 16-18, 2007, Pearl River Resort, Choctaw, MS.
Buchireddy, Prashant R., Bricka, R. Mark, Wooten, James, and Columbus, Eugene, P. 2006. " Production of Clean Synthetic Gas from Biomass Using a Downdraft Gasifier," Presented at the 2006 Annual American Institute of Chemical Engineers Fall Meeting, Nov 12 -17, 2006, San Francisco CA.

Cook, Melissa (2008) "Design of a Laboratory Scale Pyrolysis System for Evaluating the Recycle Potential of CCA-Treated Wood Waste" Paper presented at the American Institute of Chemical Engineers Southern Regional Conference in Auburn, Alabama April 5, 2008.

Cook, Melissa (2008) "Design of a Laboratory Scale Pyrolysis System for Evaluating the Recycle Potential of CCA-Treated Wood Waste" Poster presented at the American Institute of Chemical Engineers Annual Meeting in Philadelphia, Pennsylvania on November 17, 2008.

Igathinathane, C., L. O. Pordesimo, M. W. Schilling, and E. P. Columbus. 2008. Fast and simple measurement of cutting energy requirements for plant stalk cutting. Paper No. 084111. Paper No. 083975. Presented at the ASABE Annual International Meeting, Providence, Rhode Island, June 29-July 2. St. Joseph, Michigan: ASABE.

Igathinathane, C., L. O. Pordesimo, and W. D. Batchelor. Ground biomass sieve analysis simulation by image processing and experimental verification of particle size distribution. For presentation at the 2008 ASAE Annual International Meeting, Providence, Rhode Island, June 29-July 2, 2008

Jones, Jared (2008) “Biomass Gasification: Catalytic tar removal using Fe and Ni supported Zeolites” Paper presented at the American Institute of Chemical Engineers Southern Regional Conference in Auburn, Alabama, April 5, 2008.

Lusk, Richard (2008) “Cold Flow Model Circulating Fluidized Bed Gasification” Poster presented at the Annual SPE Meeting at Mississippi State University on March 13, 2008.

Lusk, Richard (2008) “Design and Construction of a Cold Flow Model Circulating Fluidized Bed Gasifier: A Technical Overview” Poster presented at the First Annual Energy-Synergy Workshop at Mississippi State University on April 17, 2008.

Lusk, Richard, and Bricka, R. Mark, 2007. “Biomass Gasification in a Circulating Fluidized Bed,” Six Annual Southern BioProducts Conference, April 16-18, 2007, Pearl River Resort, Choctaw, MS.

Lusk, Richard D., and Bricak, R. Mark, 2007. “Design and Construction of a Cold Flow Circulating Fluidized Bed Gasifier: A Technical Overview,” American Institute of Chemical Engineers, 2007 Annual Meeting, November 4-9, 2007, Salt Lake City, Utah.

Lusk, Richard, Bricka, R. Mark, and Columbus, Eugene. 2007. “Gasification Technology Overview.” Presentation at the Sixth Annual Southern BioProducts Conference, April 16-18, 2007, Pearl River Resort, Choctaw, MS.

Rice, Derek J. 2008. “Techniques to improve the Use of Biomass Fuels Used to provide heating to the Facilities at the Natchez Trace Greenhouses,” Proceedings of the 2008 AICHE Annual Meeting and Centennial Celebration, November 16-21, 2008, Philadelphia, PA

Parker, Amy. 2008. “Design of a Laboratory Scale Pyrolysis System for Evaluating the Recycle Potential of CCA-Treated Wood Waste” Poster presented at the First Annual Energy-Synergy Workshop at Mississippi State University on April 17, 2008.

Parker, Amy. 2008. “Evaluation of the Recycle Potential for CCA-treated Wood Waste Using Pyrolysis Techniques” Paper presented at the Southern Section Air & Waste Management Association Annual Conference in Biloxi, Mississippi on August 7, 2008

Parker, Amy M., and Bricka, R. Mark, 2008. “Laboratory-Scale Fast Pyrolysis of CCA –Treated Wood Waste,” Proceedings of the 2008 AICHE Annual Meeting and Centennial Celebration, November 16-21, 2008, Philadelphia, PA

Parker, Amy M., and Bricka, R. Mark, 2007. “Evaluation of the Recycle Potential for CCA Treated Wood Waste Using Pyrolysis Techniques,” American Institute of Chemical Engineers, 2007 Annual Meeting, November 4-9, 2007, Salt Lake City, Utah.

Pordesimo, L. O., J. R. Wooten, P. R. Buchireddy, C. Igathinathane, L. Wei, and R. M. Bricka. 2008. Feedstock effects on syngas quality and production in a downdraft gasifier. Paper No. 084474. Presented at the ASABE Annual International Meeting, Providence, Rhode Island, June 29-July 2. St. Joseph, Michigan: ASABE.

Pordesimo, L. O., L. Wei, J. R. Wooten, C. Igathinathane, R. M. Bricka, E. P. Columbus. 2008. Process performance of a downdraft gasifier burning hardwood chips. Paper No. 084474. Presented at the ASABE Annual International Meeting, Providence, Rhode Island, June 29-July 2. St. Joseph, Michigan: ASABE.

Pordesimo, L. O., L. Wei, J. R. Wooten, C. Igathinathane, R. M. Bricka, E. P. Columbus. 2008. Process performance of a downdraft gasifier burning hardwood chips. Paper No. 084474. Presented at the ASABE Annual International Meeting, Providence, Rhode Island, June 29-July 2. St. Joseph, Michigan: ASABE.

Pordesimo, L. O., J. R. Wooten, P. R. Buchireddy, C. Igathinathane, L. Wei, and R. M. Bricka. 2008. Feedstock effects on syngas quality and production in a downdraft gasifier. Paper No. 084474. Presented at the ASABE Annual International Meeting, Providence, Rhode Island, June 29-July 2. St. Joseph, Michigan: ASABE.

Singletary, Monty, and Bricka, R. Mark. 2007. "Phosphate Stabilization of Lead from Small Arms Ranges to Reduce Groundwater and Surface-Impacts," Mississippi Water Environment Association's 50th Annual Meeting and Technical Conference, May 29- June 1, 2007, BancorpSouth Conference Center, Tupelo, MS.

Singletary, James, and Bricka, R. Mark. 2007. "Tar and Particulate Removal From a Novel Gasification Unit Using Saw Dust as the Feed Stock," Presentation at the Sixth Annual Southern BioProducts Conference, April 16-18, 2007, Pearl River Resort, Choctaw, MS.

Singletary, James, and Bricka, R. Mark. 2006. " Tar and Particulate Removal from a Novel Gasification Unit Using Sawdust as a Feedstock," Presented at the 2006 Annual American Institute of Chemical Engineers Fall Meeting, Nov 12 -17, 2006, San Francisco CA.

Thomas, Heather (2008) "Evaluation of Life Cycle Analysis as Applied to Bio-Oil Synthesis" Poster presented at the First Annual Energy-Synergy Workshop at Mississippi State University on April 17, 2008.

Thomas, Heather S., and Bricka, R. Mark, 2008. "Life Cycle Assessment of Bio-Oil production by Pyrolysis of Wood," Proceedings of the 2008 AICHE Annual Meeting and Centennial Celebration, November 16-21, 2008, Philadelphia, PA

Thomas, Heather, Bricka, R. Mark, Singletary, Monty, and Steele, Phil, 2007. "Life Cycle Analysis of a Renewable Lumber Preservative," American Institute of Chemical Engineers, 2007 Annual Meeting, November 4-9, 2007, Salt Lake City, Utah.

Wei, L., C. Igathinathane, L. O. Pordesimo, J. Lee, and W. D. Batchelor. 2008. Developing a novel method for determining surface area of ground biomass particles. Paper No. 084571. Presented at the ASABE Annual International Meeting, Providence, Rhode Island, June 29-July 2. St. Joseph, Michigan: ASABE.

Wooten, James, R., Prashanth R. Burchireddy, and Eugene P. Columbus. The Effects of Ash Content on the Burning of Biomass in a Downdraft Gasifier. Annual International Meeting of ASABE, Minneapolis, MN, June 17-20, 2007, Paper no. 076198

Wooten, J. R., L. O. Pordesimo, C. Igathinathane, and E. P. Columbus. 2008. Classification of wood chips using image processing texture analysis. Paper No. 084467. Presented at the ASABE Annual International Meeting, Providence, Rhode Island, June 29-July 2. St. Joseph, Michigan: ASABE.

Yang, Peilin, Eugene P. Columbus, James Wooten, William D. Batchelor, Prashanth R. Buchireddy, Lin Wei. Evaluation of Syngas Storage under Different Pressures and Temperatures. Annual International Meeting of ASABE, Minneapolis, MN, June 17-20, 2007, Paper no. 076199.

Sustainable Energy Research Center
Biomass Utilization Final Report for 2006-2008

1. **Project title, principal and co-investigators:** F. Biomass Utilization

Principal investigator: Louay M. Chamra
Co PI: Kalyan K. Srinivasan, Sandun Fernando

2. **List of authorized distribution**

The information contained in this report is deemed non-confidential and non-sensitive and can be disclosed to individuals as deemed appropriate by DOE.

3. **Executive Summary**

The major objective of this research is to identify pathways to utilize biomass fuels manufactured in the state of Mississippi to develop environmentally friendly, high efficiency combustion engines, using both experimental methods and phenomenological combustion simulations. Combustion in engines occurs by complex thermo-chemical reactions that are primarily governed by the physical and chemical properties of fuel molecules taking part in those reactions. It is therefore important to know probable variations in the chemical fuel composition. A database of physical and chemical properties of various biofuels has been developed to aid in the development of thermodynamic phenomenological combustion models. These combustion models employ phenomenological equations to characterize the nature of ignition, combustion and pollutant formation phenomena in biofuel combustion processes. In particular, since the behavior of ignition processes of biofuels is not very well understood, it is of paramount interest to understand if standard ignition delay correlations developed for petroleum-based diesel fuels can be applied to predict the ignition behavior of biofuels or if other chemistry-based ignition delay models need to be investigated to develop a new framework for predicting the ignition behavior of biofuels. In this regard, both conventional Arrhenius type ignition delay correlations and more specific reduced chemistry based ignition delay correlations were investigated in this study. A phenomenological first order biodiesel combustion model was developed with the aforementioned ignition delay models to predict the behavior of biodiesel combustion. This model was validated using experimental data obtained from the open literature. Additionally, detailed verification and validation of the combustion model was performed to identify the most sensitive model parameters that affect model predictions. Finally, a nitrogen oxide chemistry model was developed independently and validated using a phenomenological model for natural gas combustion. The results from the first order combustion simulation indicate that standard Arrhenius type ignition delay correlations are not suitable to predict the ignition delay times of biodiesel combustion and therefore reduced chemistry ignition delay models are required to adequately quantify the ignition behavior of biodiesel type fuels. The verification and validation efforts clearly indicate that model parameters such as initial pressure, in-cylinder mass and ratio of specific heats play a significant role in determining the nature of combustion heat release and cylinder pressure. It was also found that the first order combustion model, owing to its simplicity, will have to be further developed into a multizone combustion model in order to accurately predict the nitrogen oxide trends from biodiesel and syngas combustion. The ultimate goal of developing the combustion model is to provide a guideline for optimizing biofuel combustion for performance improvement and emissions reduction. A robust combustion model can identify parameters that need to be optimized without resorting to costly experimental techniques. Upon identification of these parameters, selective experimentation can be performed to arrive at optimal biofuel combustion solutions. To accomplish this objective a variable compression ratio, single cylinder research engine has been purchased to perform advanced combustion diagnostics to realize clean and efficient combustion using biofuels. It is anticipated that the benefits from the modeling and experimental efforts will enable the development of hitherto unexplored advanced combustion strategies that exhibit considerable potential for *extremely low NO_x and PM emissions, diesel-like fuel conversion efficiencies (~45%),* and *substantial usage (~ 99 percent) of renewable biodiesel and*

ethanol fuels instead of petro-diesel, which are important goals of the recently launched *Advanced Energy Initiative* of the US DOE. Upon successful completion of the proposed research, it is expected that its efficiency and emissions benefits will be of significant interest to the *light-duty automobile engine industry* (e.g., GM and Ford, which currently have renewed ethanol car programs) and the *heavy-duty truck and bus engine industry* (e.g., Caterpillar, Cummins, International Truck, PACCAR, etc.) as well as large-scale *ethanol manufacturers* such as ADM.

4. Comparison of goals and actual accomplishments

Please see attached XLS spreadsheet for details

5. Summary of Activities for Entire Period of Funding

Task 1: A detailed mathematical model of biomass/biofuel thermal processes and validation of the modeling results using proper experimental means will be performed. The validation of the model predictions is an essential part of the work. The proposed model will also consider the environmental regulations currently faced by industry.

Subtask 1.1: Conduct extensive literature review of existing thermodynamic diesel engine combustion models with specific relevance to biofuels

Over fifty research papers were reviewed to develop the comprehensive literature review, which addresses combustion modeling using thermodynamics based models in diesel engines. A database of this literature review is available and can be presented upon request. The entire database of the literature review is omitted from this summary to preserve the brevity of this document.

Subtask 1.2: Create a database of physical and chemical properties of various biodiesels and biodiesel-diesel mixtures. These physical and chemical properties will be used in modeling combustion of pure biodiesel and biodiesel-diesel mixtures.

A physical properties database has been developed. The database lists physical properties of various biodiesel blends available in literature today and is omitted from this document to maintain brevity of presentation. This database of physical properties can be made available upon request.

Subtask 1.3: Develop first order biodiesel engine combustion model.

A first order engine combustion model incorporates simple phenomenological approximations to the actual combustion processes occurring inside the cylinder of an internal combustion engine.

Figure 1 shows the system of thermodynamic analysis. A closed system with constant mass is considered. The following equations describe the compression, compression and expansion processes.

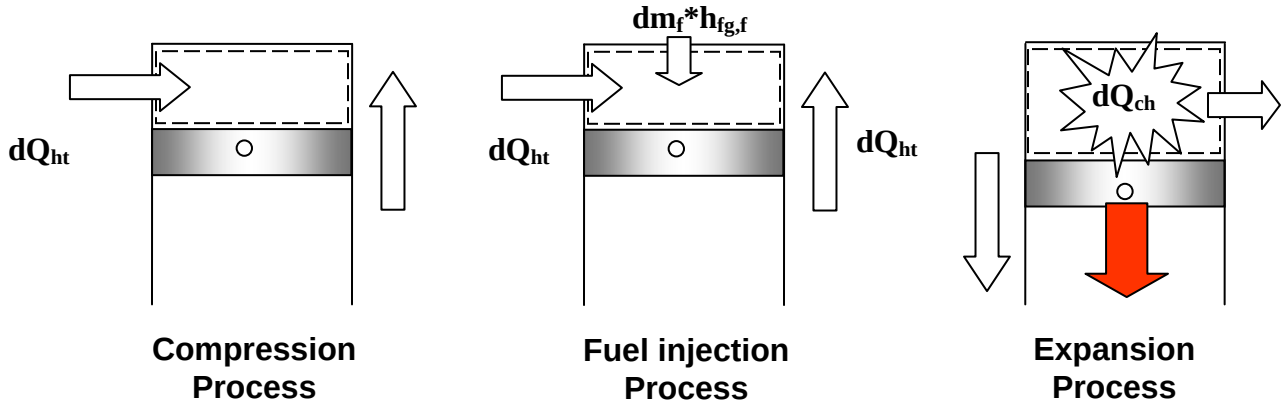


Figure 1

Table 1: Assumptions and Equations used in the First Order Phenomenological Combustion Simulation

Process	Crank angle	Equations	Assumptions	Comments
Compression and Fuel Injection	$IVC \leq \Theta \leq FIS$ $FIS \leq \Theta \leq SOC$ – Estimation of ignition delay time	1. $PV = mRT$ 2. $dU = dQht - dW$ (for details see Appendix I) 3. When fuel injection starts, the latent heat of vaporization of the fuel needs to be considered since this will cool the cylinder contents, therefore another term needs to add to eqn (2) upon fuel injection, $dm_{f,inj}*h_{fg,\,f}$ 4. Ignition delay time estimate (see Appendix I)	⇒ The in-cylinder contents are assumed to be at uniform state. As a first step we assume that the contents at the start of compression are only air. ⇒ Pressure (P) at IVC is assumed to be the same as intake manifold pressure. ⇒ Temperature (T) at IVC is assumed to be intake manifold temperature ⇒ Using P and T we estimate the initial mass (m) at IVC ⇒ As the mass is compressed, there is heat transfer between the cylinder walls and the gases ⇒ The heat transfer rate is estimated using a heat transfer (**dQht**) correlation, typically Woschni's ⇒ The compression work is estimated from first law for a closed system ⇒ Fuel injection is treated as a lumped parameter, i.e. all the fuel is injected between FIS and FIE (a profile can be assumed) ⇒ Ignition Delay time (τid), which is defined as the time elapsed, typically in milliseconds (ms) between FIS and SOC is calculated using an ignition delay correlation	⇒ IVC-Crank angle corresponding to intake valve closure (User Specified) ⇒ TDC – Top Dead Center (=360° for 4-stroke engine) ⇒ FIS – Fuel Injection Start Crank angle, typically this starts before TDC ⇒ FIE – Fuel Injection End Crank angle, typically this ends after TDC ⇒ SOC – Start of Combustion Crank angle, this is estimated as the time at which, $\sum_{FIS}^{FIS+\Delta t} \tau_{id}\,\Delta t = 1$
Combustion	$SOC \leq \Theta \leq EVO$	5. $dU = dQch - dQht - dW + dm_f*h_{fg,f}$, technically the fuel	⇒ Use a Wiebe Function to model heat release rate in the combustion	⇒ EVO – Crank angle corresponding

		6. **dQch** is estimated using the equation in Appendix I		

Subtask 1.4: Validate the combustion model for engine performance using appropriate experimental results

From the literature reviewed in activity 1.1, it was decided to develop a simple thermodynamic model based on assumed burn rates given by Wiebe functions. The various subroutines needed in this model such as ignition delay, temperature dependent physical properties, and combustion stoichiometry were identified and a graduate student developed these subroutines in FORTRAN/Mathcad as part of his dissertation. This model is complete and has been validated against experimental results obtained from literature.

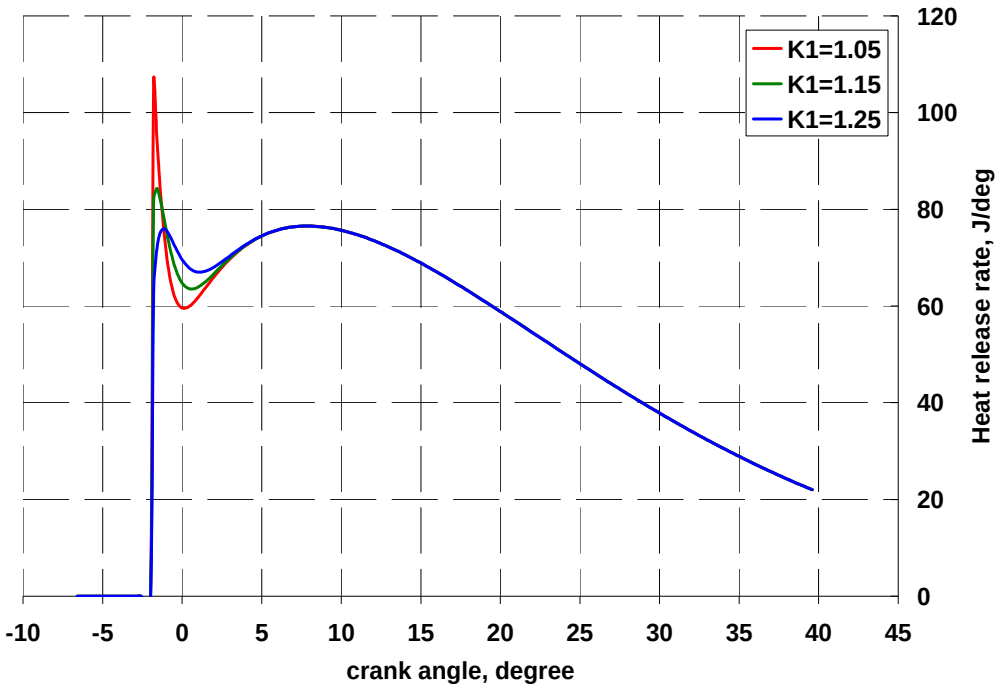


Fig.2. Effect of different premixed reaction rate

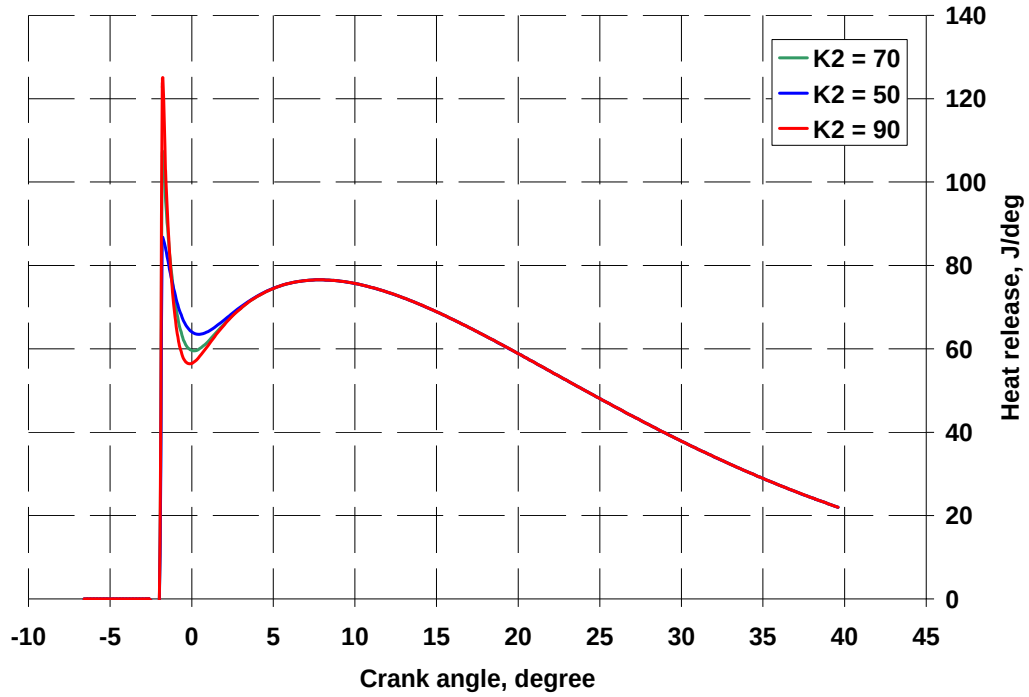


Fig.3. Effect of different peak time for premixed reaction

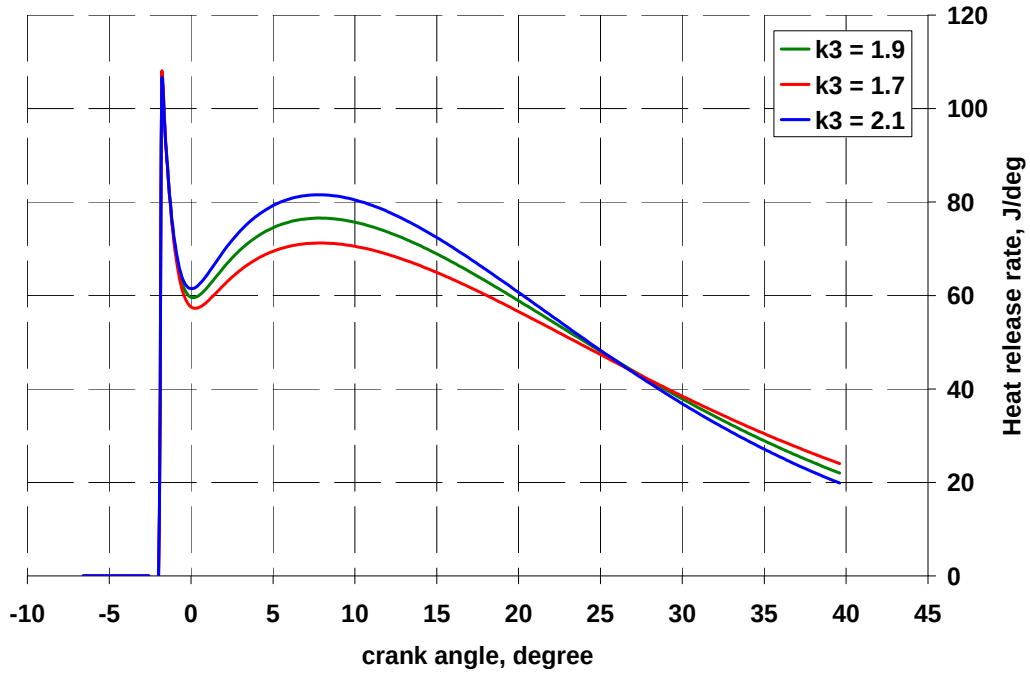


Fig.4. Effect of different diffusive reaction rate

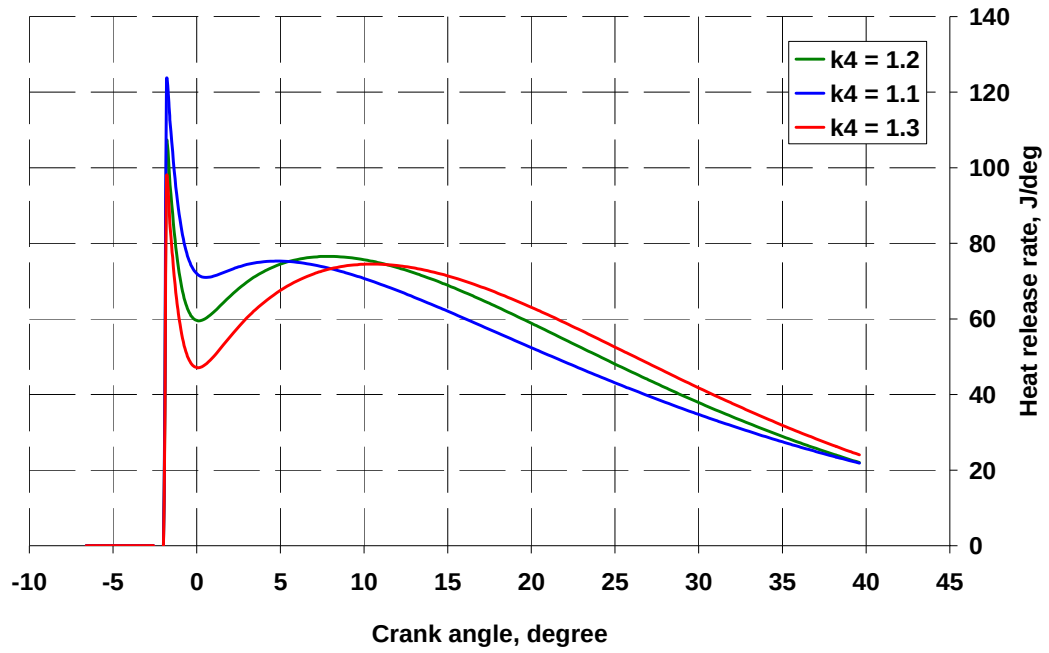


Fig. 5. Effect of different peak time for diffusive reaction

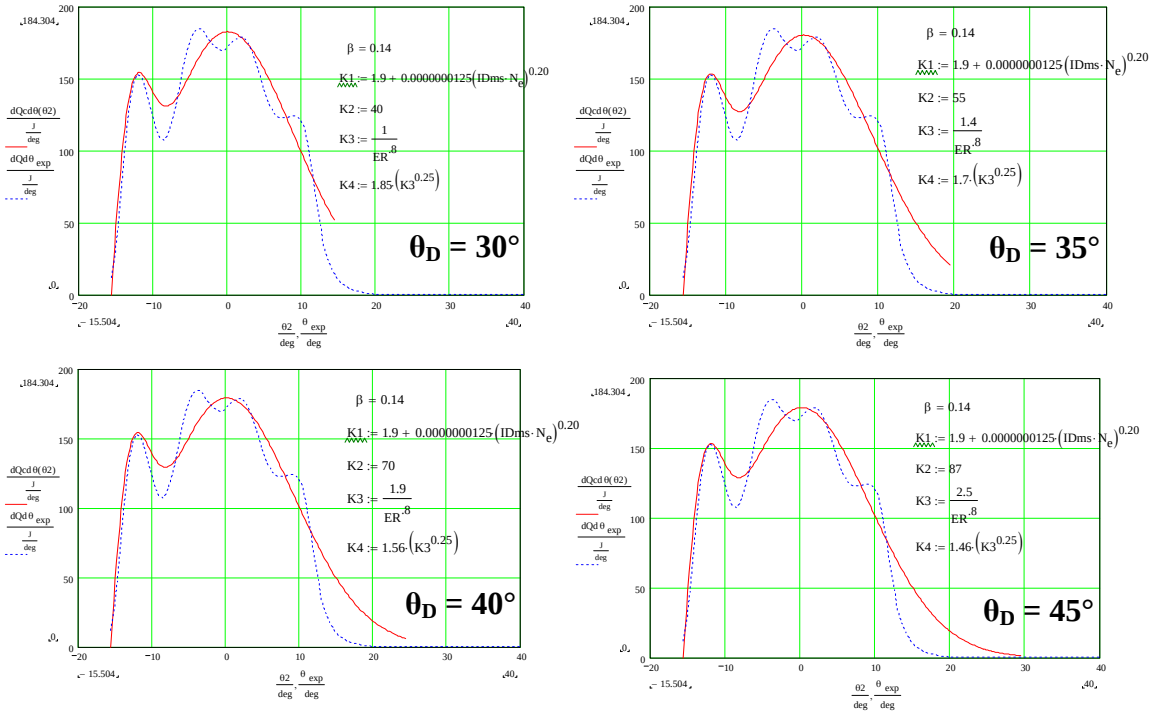


Fig.6. Effect of combustion duration, θ_D at $\beta = 0.14$

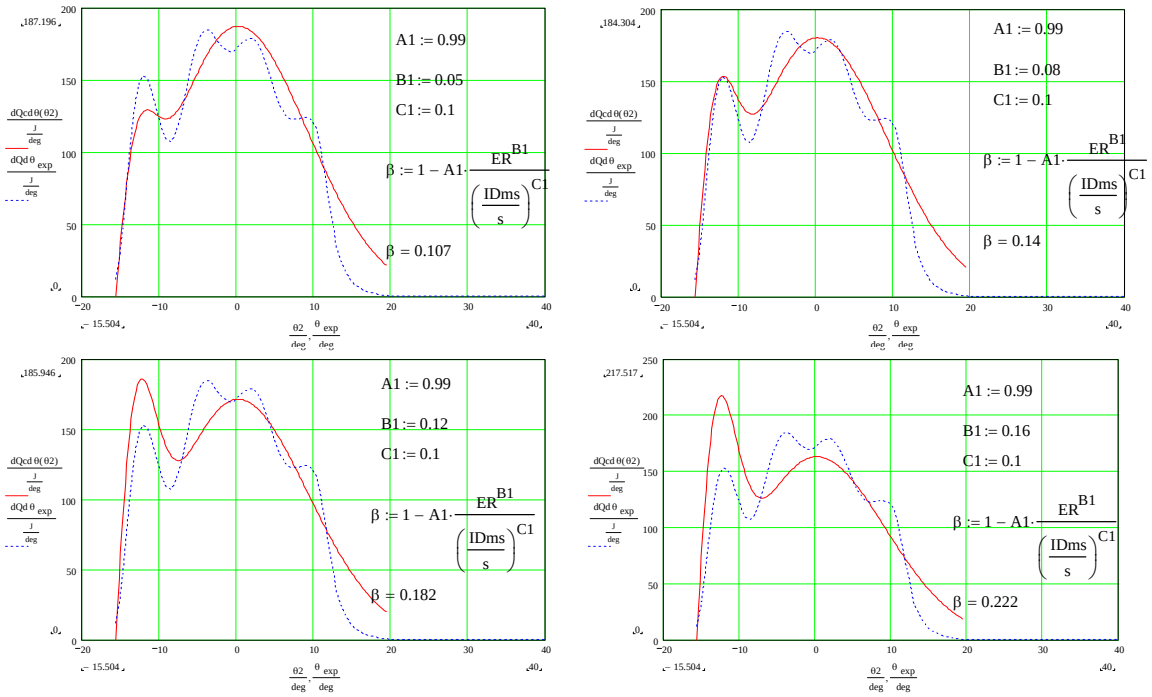


Fig.7 Effect of ratio of premixed and diffusive mass burned rate fraction (β) at θ_d= 35°CA

Ignition Delay Models: A comparison between standard Arrhenius Ignition Delay Correlations and Experimental Ignition Delay

The autoignition phase affects engine efficiency as well as exhaust pollutant emissions by influencing the overall combustion process and timing,. Autoignition of diesel sprays is usually described in terms of autoignition delay and autoignition location. Although the autoignition may be considered as a continuous process it is a widely accepted that autoignition is the beginning of the thermal explosion that follows a physical delay (mixing of fuel with ambient gas) and a chemical delay (chemical reactions leading to the onset of a flame).

Two main parameters that describe the autoignition process are the initial temperature at which the autoignition can develop and the time delay before the start of autoignition t_{del}. Both strongly depend on pressure, fuel composition, the condition of internal surface of the engine, and other factors.

Majority of the expressions for the definition of the ignition delay are based on selection of the appropriate values of pressure and temperature in related to the different state of engine, for example, pressure and temperature at start of the injection process. Additionally, it has been found that an influence of the engine load defined by the equivalence air/fuel ratio during compression stroke is determined using state of air (Ti and Pi) at the intake valve closing (sometimes using coefficient of residual gases), while speed loads has an influence directly on Ti and Pi. Selection of P and T on this way could introduce a certain error in the correlation expressions.

Taking into consideration the fact that all correlation expressions presented in the literature are semi-empirical and achieved by the measurements on certain engines, on a certain speed and load regimes, using a certain fuel type, a question regarding its universality for application in other cases could be raised.

This work analyzes frequently used semi- empirical expressions from the literature. The intention is to check application of these expressions on the diesel engine in the case of the diesel and biodiesel fuel use.

Preliminary studies with the simulation showed that prediction of the onset of ignition with the appropriate ignition model was a very critical requirement to guarantee satisfactory heat release and cylinder pressure predictions [8]. So the first step in model calibration was to obtain a good prediction of the timing of the onset of ignition over the entire range of different set of input conditions. Both Arrhenius-type empirical ignition delay correlations and the Shell model were used to predict the onset of ignition and the results are discussed below. In spite of the discrepancies between the findings, due to the different methods used, similar correlations relating the autoignition delay to the ambient gas condition have been found. One of these correlations is given by the relation [9]:

$$\tau_{ign} = AP^{n}\phi^{m}\exp\left(\frac{E}{RT}\right) \qquad \ldots 1$$

where, τ_{ign} is instantaneous the ignition delay time (calculated at each crank angle), A is a pre-exponential factor, P is the in-cylinder pressure, φ is the total equivalence ratio, m and n are empirical exponents, E is the activation energy of the fuel (diesel in the present case) in kJ/mol, R is the universal gas constant, and T is the temperature. Six different ignition delay correlations [10] were investigated using the following metric:

$$\text{Variation}(\%) = \frac{\text{Prediction} - \textit{Experimental}}{\textit{Experimental}} \times 100$$

From the table below it is clear that while the ignition delay correlations match up pretty well with diesel, they cannot be directly extended to biodiesel combustion since the chemical composition of the fuel is different and fundamental experiments need to be performed to obtain ignition delay correlations for biodiesel.

Table. 1 Comparison of ignition delay predictions using various Arrhenius-type ignition delay correlations with experimental ignition delay values.

	Arrhenius expression	Variation (%)	
		Diesel	Biodiesel
Spadaccini and Tvelde (1982)	$\frac{2.43\times10^{-9}}{P^{2}}\exp\left(\frac{20926}{T}\right)$	-52.84	-83.93
Spadaccini and Tvelde (1982)	$\frac{4\times10^{-10}}{P}\exp\left(\frac{20080}{T}\right)$	-53.4	-83.93
Stringer et al.(1970)	$\frac{0.0405}{P^{0.757}}\exp\left(\frac{5473}{T}\right)$	5.65	65.711
Wolfer et al. (1938)	$\frac{0.44}{P^{1.19}}\exp\left(\frac{4650}{T}\right)$	-3.36	33.17
Hirayasu et al. (1980)	$\frac{0.0276}{P^{1.23}}\exp\left(\frac{7280}{T}\right)$	2.98	28.19
Watson et al. (1980)	$\frac{3.45}{P^{1.02}}\exp\left(\frac{2100}{T}\right)$	-21.51	26.38
Hardenberg and Hase	$(0.36+0.22.U)\exp\left(E_{a}.\left(\frac{1}{R.T}-\frac{1}{17190}\right).\left(\frac{21.2}{P-12.4}\right)^{0.63}\right)$	-45.33	-30.19

Subtask 1.5: Develop and validate a predictive NOx emissions model using Zel'dovich kinetics.

This model was developed and validated using a multizone phenomenological combustion model for natural gas combustion. At this stage, the first order combustion model developed for biofuel combustion is inadequate to accommodate the Zeldovich kinetics NOx sub model because the NOx model requires spatially resolved temperatures in the combustion chamber to predict with any accuracy. Since the first order combustion model is a single zone model, the cylinder temperature is only an average temperature and hence is not representative of the hot NOx formation zones. Therefore, the model will under predict NOx emissions. On the other hand, a multizone model, which will be developed during the next phase, will allow for more detailed NOx predictions. However, to validate the fidelity of the NOx model, it was coupled to another independent multizone phenomenological natural gas combustion simulation and the results are presented below. Combustion in the natural gas engine was initiated using a small diesel pilot, and the simulation accounted for ignition and combustion behavior of diesel fuel in predicting the NO emissions trends

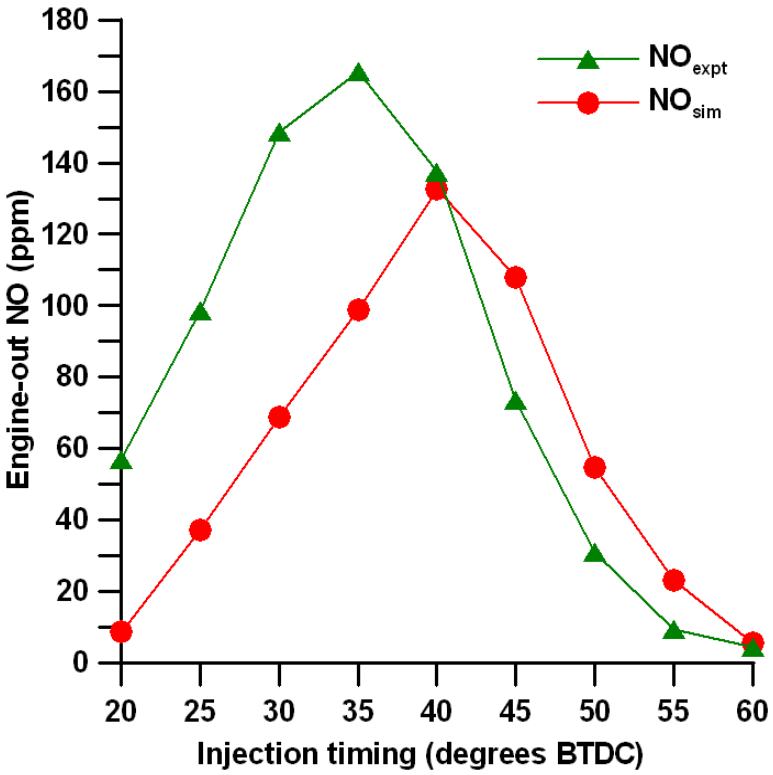


Fig 1. Comparison between Zeldovich mechanism nitrogen oxide predictions versus actual Engine Experiments conducted on a natural gas fired engine. The experiments were done at constant power of 21 kW and 1700 rev/min. The injection timing of diesel pilot was varied between 15° to 60° BTDC.

Task 2. Experimentally study and analyze the different combustion processes of biomass fuel, i.e. syngas, direct burning of wood or garbage, biodiesel, bio-oil. These experiments will allow us to

determine the energy efficiency of each process as well as the emissions generated during the combustion process. Also, valuable information about the use of biomass such as net efficiency of the energy conversion process will be evaluated in this section. A detailed uncertainty analysis of the experimental results will be performed in this part of the investigation.

Subtasks 2.1: Procure and install a single-cylinder diesel engine, a.c dynamometer and engine control system.

- A Single Cylinder (compression ignited) Research Engine \has arrived on MSU campus. The following are the key specifications of the SCRE:
- Mode of combustion – compression ignition
- Displacement 1.875 L and baseline compression ratio 17:1
- Optical module to visualize combustion in real-time has been procured in addition to the base engine described above
- An A.C. dynamometer with motoring capabilities has been ordered and the expected date of delivery is 18 weeks. The AC dynamometer will be installed and commissioned at the MSU combustion engines laboratory. The fidelity of coupling between the AC dynamometer and the SCRE will be tested.
- A completely flexible cooling and lubrication system for the SCRE has procured and coupled to the single cylinder research engine.
- An AVL smoke meter has been procured to ascertain smoke emissions from future biofuels when used in a diesel engine
- A five gas emissions bench has been procured and is awaiting commissioning to enable the measurement of pollutant emissions such as oxides of nitrogen, unburned hydrocarbons, carbon monoxide, carbon dioxide, and oxygen from internal combustion engines.

Subtask 2.2: Instrument engine with the required temperature and pressure sensors, flow meters, and emission monitor.

- A "virtual engine" on paper has been instrumented and all the required measurements and devices have been identified.
- All supporting instrumentation has been ordered to complete the instrumentation of the single cylinder research engine. However, without the arrival of the dynamometer complete instrumentation will not be possible. This task will be carried over to the next period of funding for completion.

Subtask 2.3: Develop a digital data acquisition system with LabView interface to obtain real-time measurements from the engine.

- A comprehensive digital data acquisition has been designed using Lab View to acquire in-cylinder pressure. However, they have not been tested since the single cylinder research engine has to be coupled with the dynamometer before this can be done. This will be carried on to the next period of funding for completion.

Subtask 2.4: Develop detailed experimental matrix to guide engine testing.

Subtask 2.5: Debug the various engine subsystems and ensure seamless integration of all mechanical and electrical components

Subtask 2.6: Obtain baseline performance and emissions data for straight diesel combustion

- These subtasks were not completed owing to the fact that the both the engine dynamometer and emissions bench are still on order. They will be completed upon coupling the engine and the dynamometer and installing the emissions bench.

Task 3. Uncertainty analysis of the developed models will be performed to determine the uncertainty associated with the comparison error between the model and experimental results. This uncertainty analysis will determine if further improvements or modifications need to be

performed in the proposed model. In addition, uncertainty analysis will be used to determine which variable or variables have to be properly controlled to improve the performance of the combustion of biomass.

Subtask 3.1: Obtain data for task 1.4 and determine data uncertainty.

Subtask 3.2: Determine uncertainty of engine combustion model based on model input uncertainties

Detailed uncertainty estimates of cylinder pressure estimates from the simple combustion model were obtained by perturbing twenty model parameters. This was done to identify critical model parameters. It was found that the ratio of specific heats and initial pressure and temperature estimates were the most important parameters and the accuracy of the model predictions were dependent on the accuracy of the initial estimates of these parameters. This task is complete insofar as diesel combustion is concerned. A basic framework has been established, and this can be changed easily to accommodate other fuels. The purpose of the verification and validation (V&V) process is twofold.

1) verification - the process of assessing the numerical error and code implementation of a model
2) validation - process of assessing how accurately the model represents the real world quantity(s) of interest

Considerations also should be made for the definitions of prediction and uncertainty. *Prediction* refers to inferences made about a simulation of a quantity of interest that differs from cases that have been validated, and *uncertainty* is defined as the interval about a measured quantity that bounds the true value of that quantity 95 out of 100 times.

The techniques that will be used in the V&V process for the combustion model were initially proposed for use in the computational fluid dynamics field, but can be generalized for use in many disciplines (Coleman and Stern). Using these techniques, we can attempt to validate the model at multiple realizations using benchmark experimental data along with simulation results at similar conditions. Any inferences we make outside these realizations are not validated by the V&V process. We can simply state that the model is valid or invalid at the particular realizations being investigated.

Since this combustion model is relatively complex physically and mathematically, we will need to estimate uncertainty intervals associated with model inputs, initial conditions, numeric solutions, use of previous data, physical approximations, etc... The uncertainty associated with the model inputs and initial conditions will be estimated using the parameters measured during the validation experiments. There are widely accepted methods for estimated uncertainties associated with numerical error (probably negligible in this case anyhow).

In addition to modeling uncertainties, there are also uncertainties associated with the benchmark experiments/analysis which must be considered in the validation process. The main concern in this case is the pressure measurement associated with the combustion chamber. Due to the nature of the pressure measurement, estimating the uncertainty interval that bounds the true pressure in the combustion chamber may be difficult. A good grasp of the physics involved in this measurement is crucial.

The following figure shows some basic framework for the verification and validation processes.

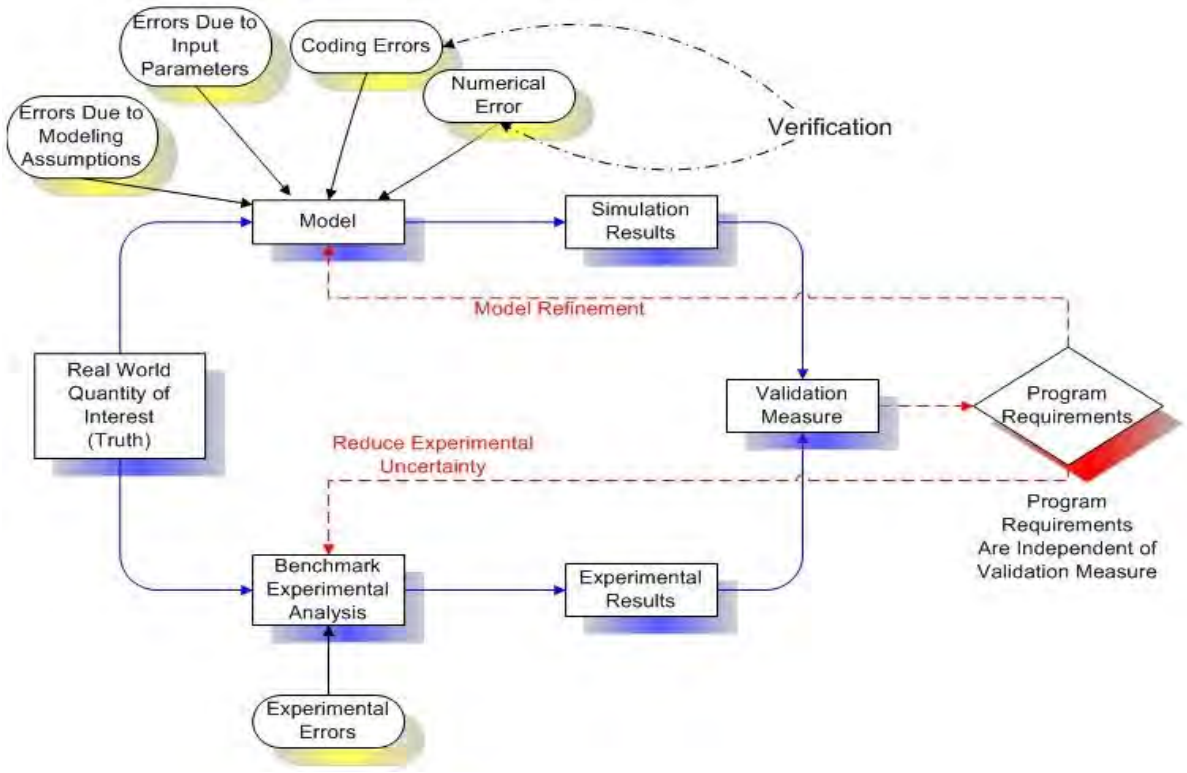


Figure 8: Schematic of Verification and Validation of models.

In our case, initial experimental data has been recorded; therefore, the reduction of experimental uncertainty is not applicable. However, if the V&V effort does not meet the program requirements, the model can be refined to decrease the uncertainty associated with modeling assumptions. This process may be repeated until all realizations have been validated.

<u>The following uncertainties are associated with the model inputs</u>
Geometric parameters:

1) CR-compression ratio ($V_{displaced}$, $V_{clearance}$)
2) R (connecting rod length, L, stroke, S)
3) θ – crank angle (θ_d, θ_s, etc…)
4) N – engine speed
5) $A_{cylinder\ head}$
6) A_{piston}

Initial Conditions:

1) Initial pressure, P_1
2) Initial temperature, T_1

Properties:

1) CN – cetane number
2) γ – specific gravity
3) φ – fuel-air equivalence ratio (m_f, m_a)

Other Considerations:

1) τ_{id} – ignition delay time (T@ TDC, P@ TDC, CN, U_p)
2) T_∞ - temperature of the cylinder wall
3) ω – average angular velocity ($P_m(\theta)$, V_r, R_r, T_r)
4) Q_{in} – heat addition (Qlhv, m_f, m_a)

<u>Summary of the verification and validation processes</u>

The verification process involves assessing the errors stemming from code implementation and numeric solutions.
In the validation effort, we first define a comparison error, E = D-S, as the difference between the simulation and experimental results. Furthermore, we need to define an uncertainty interval that bounds E.

$$U_E^2 = \left(\frac{\partial E}{\partial D}\right)^2 U_D^2 + \left(\frac{\partial E}{\partial S}\right)^2 U_S^2 = U_D^2 + U_S^2$$

or

$$U_E^2 = U_D^2 + U_{SN}^2 + U_{SPD}^2 + U_{SMA}^2$$

U_D is the experimental uncertainty, U_{SN} is the uncertainty associated with the numeric solution, U_{SPD} is the uncertainty associated with input of previous experimental data, and U_{SMA} is the uncertainty associated with modeling assumptions.

The purpose of the validation process is to assess the uncertainty associated with the modeling assumptions. A validation uncertainty, U_{VAL}, is defined which is the metric used in the Coleman and Stern validation approach.

$$U_{VAL}^2 = U_E^2 - U_{SMA}^2 = U_D^2 + U_{SN}^2 + U_{SPD}^2$$

If $E<U_{VAL}$, we are below the noise level of the validation experiment and do not have evidence to reject the model as valid. If $E>U_{VAL}$, we may need to refine the model or reevaluate our uncertainty calculations to make sure that uncertainties were not neglected.

We can calculate U_D using our knowledge of the combustion chamber pressure measurement. U_{SN} for this first order model is very small if not totally negligible. In order to calculate USPD we must calculate the partial derivative of the result (combustion chamber pressure, $P(\theta)$) with respect to each variable. We can do this in Mathcad using the finite-difference approximation.

$$\left.\frac{\partial r}{\partial X_1}\right|_{X_2, X_3 \ldots X_J const} \cong \frac{r_{X_1+\Delta X, X_2 \ldots X_J} - r_{X_1, X_2 \ldots X_J}}{\Delta X_1}$$

Once we obtain converged derivative estimates, the equation for the uncertainty in the result becomes.

$$U_r{}^2 \cong \left(\frac{\Delta r}{\Delta X_1} U_{X_1}\right)^2 + \left(\frac{\Delta r}{\Delta X_2} U_{X_2}\right)^2 + \ldots + \left(\frac{\Delta r}{\Delta X_J} U_{X_J}\right)^2$$

In the case of the first order combustion model, this will be the uncertainty associated with the model inputs. The uncertainty associated with each variable will depend on the measurements recorded during the validation experiments.

Preliminary First-Order Combustion Model

A preliminary first-order combustion model with heat transfer has been developed. Moreover, a sensitivity analysis was conducted to evaluate the uncertainty magnification factor (UMF) and uncertainty percent contribution (UPC) of each variable in the model.

The UMF and UPC values for each variable as a function of crank angle are presented on the following page. The uncertainty analysis was conducted assuming a 1% total uncertainty for each variable in the model. The UPC values were averaged over an entire cycle as well as calculated at each crank angle increment. The UMF values were also calculated at each crank angle increment.
Due to the large number of variables considered, variables which did not contribute significantly to the total uncertainty in the result were left out of the UPC bar graph.

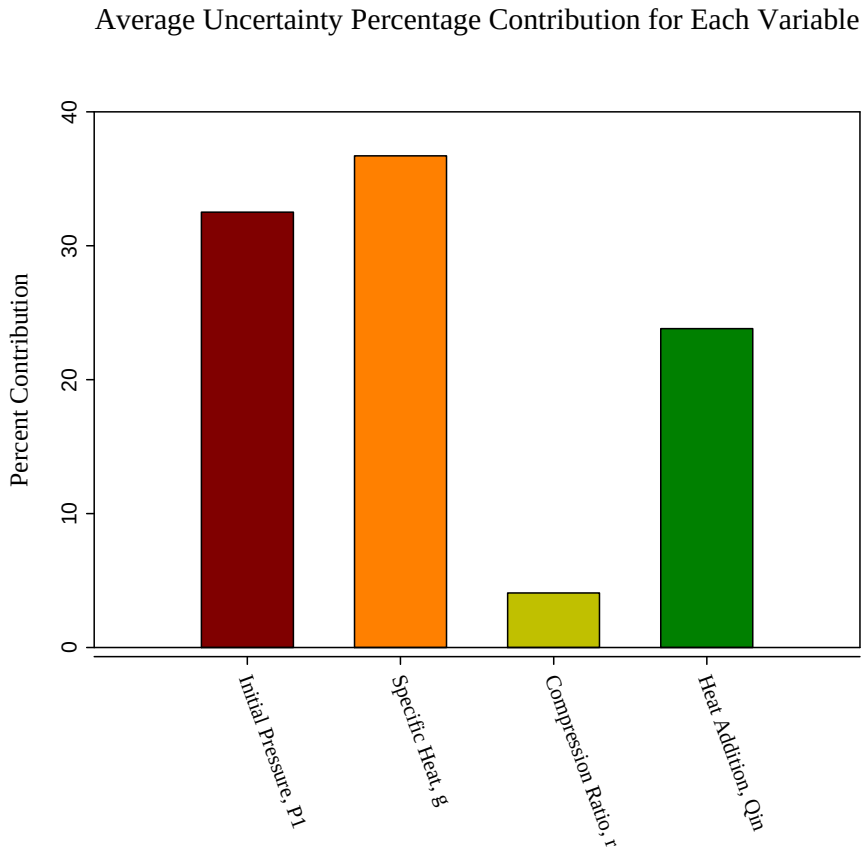


Figure 9: Comparison of uncertainty contribution to the heat release computed from experimental analysis of cylinder pressure data

Subtask 3.3: Determine combustion model validity.

A detailed uncertainty analysis of experimental cylinder pressure data has been performed. It was found that the accuracy of the heat release rate estimates from the pressure data depends on accuracy of the estimation of trapped cylinder mass, which in turn depends on accurate determination of valve timing, intake manifold temperature and pressure. Moreover, the phasing of the crank angle encoder, which is a device that counts the degrees of rotation in a crankshaft, and in-cylinder pressure referencing, were identified as critical parameters that affect the estimates of heat release rates from combustion. In Fig.10, the uncertainty intervals are plotted with the simulated and measured in-cylinder pressures to check the validity of the simulated results. The results in Figure show that most values of the measured in-cylinder pressure are within the uncertainty region, especially where the combustion process occurs, i.e., in between 165 and 188 degrees of crank angle. However, some measured values in between 150 and 165

degrees are slightly missed by the uncertainty intervals. Interestingly, the uncertainty curve shown in Fig. 3 forms a very similar shape of the simulated in-cylinder pressure curve shown in Fig. 4 but a little bit of phase change. It makes sense that the transient uncertainty values follow the pattern of the outcome from the equations instead of having the constant uncertainty value because the uncertainty errors propagate throughout the equations.

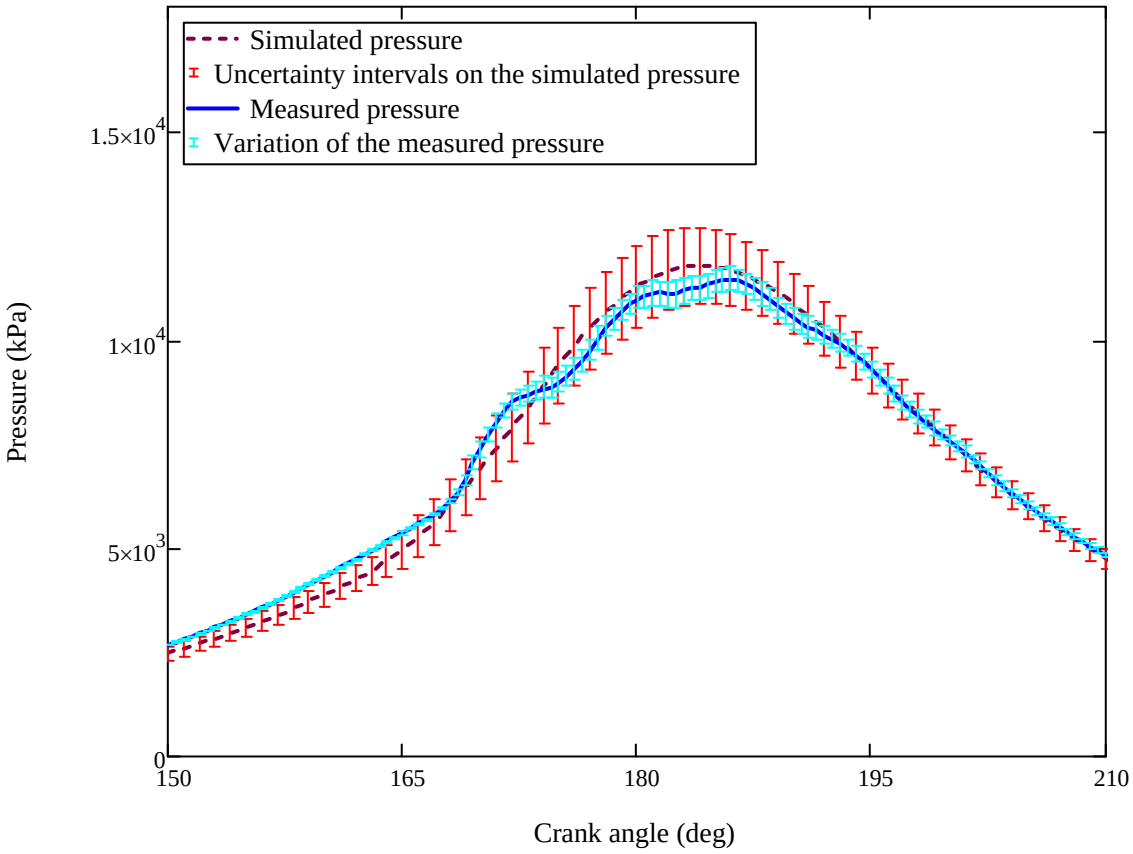


Figure 10. Simulated and measured in-cylinder pressure with uncertainty interval vs. crank angle

Subtask 3.4: Perform general uncertainty analysis of engine test system.

A single cylinder diesel engine being purchased that has the following specifications:

Engine Power	54 horsepower
Engine Speed	2,200 revolutions per minute (RPM)
Engine Torque	129 foot pounds (calculated at 2,200 RPM)

Contributing hardware to the uncertainty in the engine's thermal efficiency has been estimated below:

Hardware	**Uncertainty in Measurement**
Dynamometer	Engine torque and speed
Drive shaft with coupling	Engine torque and speed
Air flow meter	Air flow rate
Mass flow meter(s)	Diesel and natural gas fuel flow rates
Pressure sensor(s)	Differential and gauge pressures
Type-K thermocouple(s)	Temperature of coolant, oil, and gases (intake and exhaust)
Crank encoder	Crank angle

In determining the engine's thermal efficiency two methods can be applied, (1) volumetric flow rate and/or (2) mass flow rate method(s).

The equation of thermal efficiency via volumetric flow rate through implementing a volumetric flow meter is as follows:

$$\eta = \frac{P}{\rho V_d \ f \ Q_{lh}} \tag{B.1}$$

where η = thermal efficiency
P = Power
ρ = density
V_d = flow meter displacement
f = flow meter frequency
Q_{lh} = lower heating value

The equation of the thermal efficiency via mass flow rate through implementing a mass flow meter is given below:

$$\eta = \frac{P}{\dot{m} Q_{lh}} \tag{B.2}$$

where η = thermal efficiency
P = Power
$\dot{m}$ = mass flow rate
Q_{lh} = lower heating value

Both Equations B.1 and B.2 are first order data reduction equations and can be simplified as follows for uncertainty analysis:

$$\left(\frac{U_\eta}{\eta}\right)^2 = \left(\frac{P}{\eta}\frac{\partial \eta}{\partial P}\right)^2\left(\frac{U_P}{P}\right)^2 + \left(\frac{\rho}{\eta}\frac{\partial \eta}{\partial \rho}\right)^2\left(\frac{U_\rho}{\rho}\right)^2 + \left(\frac{V_d}{\eta}\frac{\partial \eta}{\partial V_d}\right)^2\left(\frac{U_{V_d}}{V_d}\right)^2 + \left(\frac{f}{\eta}\frac{\partial \eta}{\partial f}\right)^2\left(\frac{U_f}{f}\right)^2 + \left(\frac{Q_{lh}}{\eta}\frac{\partial \eta}{\partial Q_{lh}}\right)^2\left(\frac{U_{Q_{lh}}}{Q_{lh}}\right)^2 \tag{B.3}$$

$$\left(\frac{U_\eta}{\eta}\right)^2 = \left(\frac{P}{\eta}\frac{\partial \eta}{\partial P}\right)^2\left(\frac{U_P}{P}\right)^2 + \left(\frac{\dot{m}}{\eta}\frac{\partial \eta}{\partial \dot{m}}\right)^2\left(\frac{U_{\dot{m}}}{\dot{m}}\right)^2 + \left(\frac{Q_{lh}}{\eta}\frac{\partial \eta}{\partial Q_{lh}}\right)^2\left(\frac{U_{Q_{lh}}}{Q_{lh}}\right)^2 \tag{B.4}$$

From the data reduction equations, it is known that all variables contributing to the thermal efficiency are of the same order and thereby the determining factor in the overall thermal efficiency uncertainty will be the variable with the most uncertainty.

In the above equations, power (P) and density (ρ) can be determined by evaluating secondary equations which are as follows:

$$P = N \tau \tag{B.5}$$

where N = Engine Speed
τ = Engine Torque

$$\rho = \frac{P_r}{Z(R/M)T} \tag{B.6}$$

where P_r = Pressure
Z = Compressibility Factor
R = Gas Constant
M = Molecular Weight
T = Temperature

The data reduction equation of Equations B.5 and B.6 are as shown, respectively:

$$\left(\frac{U_P}{P}\right)^2 = \left(\frac{N}{P}\frac{\partial P}{\partial N}\right)^2\left(\frac{U_N}{N}\right)^2 + \left(\frac{\tau}{P}\frac{\partial P}{\partial \tau}\right)^2\left(\frac{U_\tau}{\tau}\right)^2 \quad \text{(B.7)}$$

$$\left(\frac{U_\rho}{\rho}\right)^2 = \left(\frac{P_r}{\rho}\frac{\partial \rho}{\partial P_r}\right)^2\left(\frac{U_{P_r}}{P_r}\right)^2 + \left(\frac{T}{\rho}\frac{\partial \rho}{\partial T}\right)^2\left(\frac{U_T}{T}\right)^2 + \left(\frac{Z}{\rho}\frac{\partial \rho}{\partial Z}\right)^2\left(\frac{U_Z}{Z}\right)^2 + \left(\frac{M}{\rho}\frac{\partial \rho}{\partial M}\right)^2\left(\frac{U_M}{M}\right)^2 \quad \text{(B.8)}$$

It should be noted that in Equation B.8 the gas constant (R) is assumed to be a given constant and thereby has no uncertainty associated with its value thereby it can be removed from the data reduction equation.

Without the actual hardware in hand, only general estimates of uncertainty can be made at this point in time. Using an average from multiple inquiries to manufactures a table has been constructed showing estimated uncertainties of the proposed hardware (See Table B.1).

From Table B.1 it can be seen that the engine torque and the fuel pressure contribute the most uncertainty to the thermal efficiency equation. As a result, when purchasing hardware for the engine the dynamometer and crank shaft precision and biased uncertainties will contribute the most to the uncertainty in the torque measurement while the uncertainty associated with the pressure sensor(s) (both differential and gauge) will determine the overall uncertainty in the fuel pressure measurement. With that in mind, purchasing the most precise and accurate devices for these measurements will greatly improve the overall uncertainty in the thermal efficiency of the engine. Manufactures of these hardware devices have been called and specifications of their device including uncertainty analysis should arrive via email within the next couple of days.

Table B.1. Estimated uncertainties of the proposed hardware

Variable		***Estimated Uncertainty***
Engine Speed	(N)	0.1 % of full scale
Engine Torque	(τ)	1.0 % of full scale
Fuel Mass Flow Rate	($\dot{m}$)	±1.0 % of reading 0.5 % of full scale
Flow Meter Frequency	(f)	0.5 % of full scale
Flow Meter Displacement	(V_d)	±1.0 % of reading
Fuel Temperature	(T)	± 1.1 °C
Fuel Pressure	(P_r)	1.5 % of full scale
Fuel Molecular Weight	(M)	0.5 % of value
Fuel Gas Compressibility Factor	(Z)	0.1 % of value
Fuel Lower Heating Value	(Q_{lh})	0.5 % of value

Subtask 3.5: Perform detailed uncertainty analysis of engine test system.
Subtask 3.6: Determine uncertainty of baseline performance data in Subtask 2.6

The subtasks 3.5 and 3.6 are in progress and will be completed upon acquiring experimental data from the single cylinder research engine.

Task 4: Evaluate DME and glycerin derivatives as alternative spark ignition fuels

Subtask 4. 1. Recruit a Ph. D. student

This subtask is completed and the student has been graduated with a Dissertation titled, "Steam Reforming of Oxygenated Hydrocarbons for Hydrogen Production over Metal Catalysts,"

Subtask 4. 2: Acquire raw materials

This subtask has been partially completed. Hardware for bench testing of alternative fuels testing has been completed. Instrumentation such as FTIR, gas analyzers and GC has been procured. However, the single cylinder research engine that procured still needs to be coupled to a dynamometer to complete testing. The remainder of this task will be completed during the next phase of activities.

Subtask 4.3: Develop experimental design and preliminary testing

A test matrix to evaluate blends of DME and glycerol based additives on the bench has been developed and preliminary testing has been performed to evaluate the octane rating and calorific values of blends of glycerol based additives and gasoline. This study attempted to identify the possibility of blending glycerol and glycerol based co-products, such as propanediol and propanol with gasoline as oxygenates. The study revealed that there is a possibility to use glycerol and its derivatives with gasoline as an automotive fuel. Octane number and the heating value of different mixtures of gasoline, ethanol, and glycerol and its derivatives are presented. Major conclusions from this preliminary are,

- The phase study revealed that the amount of glycerol that could be successfully blended with gasoline varied widely depending on the amount of n-propanol amphiphile present.
- Analyses for primary fuel properties of glycerol, propanediol, propanol, ethanol, and gasoline blends suggest that certain blends could be used as spark ignition fuels.
- The octane numbers of most of the sample blends were greater than 100.

Detailed results from this study have been published in a paper titled, "Glycerol based automotive fuels from future biorefineries," (please see the publications section 6 for complete citation)

Subtask 4.4: Testing various DME blends with gasoline in a spark ignition engine

This task is a work in progress at this stage since the single cylinder research engine intended to test these new fuel blends is being instrumented with appropriate sensors. Once the engine is coupled to the A. C. dynamometer this task will be completed.

6. Publications from this effort

1. H. Yang, S. R. Krishnan, K. K. Srinivasan, K. C. Midkiff, 2006, "Sensitivity Analysis of NOx Formation from Micro-pilot Ignited Natural Gas Engines," *ASME Journal of Engineering for Gas Turbines and Power*, 129 (1), pp. 261-270
2. Srinivasan, K. K., Mago, P. J., Zdaniuk, G. J., Chamra, L. M., and Midkiff, K. C. (2008). "Improving the Efficiency of the Advanced Injection Low Pilot Ignited Natural Gas Engine Using Organic Rankine Cycles," Journal of Energy Resources Technology, Trans. ASME, vol.130, doi 10.1115/1.2906123.
3. J.B., Weathers, B.T. Marvel, K. K. Srinivasan, P.J. Mago, L. M. Chamra, W. G. S Steele, "Error Propagation in Heat Release Analysis of Pilot Ignited Natural Gas Combustion," Proc. of the ASME IMECE, Nov 11-14, 2007, Seattle, Wa.,
4. K. K. Srinivasan, P. J. Mago, G. J. Zdaniuk, L. M. Chamra, K. C. Midkiff, "Improving the Efficiency of the Advanced Injection Low Pilot Ignited Natural Gas Engine using Organic Rankine Cycles," ASME Energy Sustainability Conference, Long beach CA, Jun 24-29, 2007[1]
5. S. R. Krishnan, K.K. Srinivasan, Y. Qi., H. Yang, K. C. Midkiff, "Phenomenological modeling of low-temperature advanced low pilot ignited natural gas combustion," SAE 2007-01-0942

[1] This paper won the Best Paper Award in the track Energy Systems Miniaturization, Micro and Nano Scale Transport in the Energy Sustainability 2007 conference, long beach, Ca. Jun 24-30, 2007.

6. H. Cho, R. Luck, S. R. Krishnan, K. K. Srinivasan, “Dynamic uncertainty analysis of a first order diesel engine combustion model”, *under review* Journal of Automobile Engineering
7. K. K. Srinivasan, G. A. Adebiyi, C. M. Gibson, Thermodynamic performance optimization of reciprocating internal combustion engines, Accepted for publication in the Proc. of the ASME IMECE, Nov 1-6, 2008, Boston, Ma.
8. Uncertainty Analysis of Net Heat Release Rate Predictions in a Single Cylinder Pilot Compression Ignited Natural Gas Engine, M. S. Thesis, B. T. Marvel, Mississippi State University, 2008.
9. Sandun Fernando *, Sushil Adhikari, Kiran Kota, Ranjitha Bandi, “Glycerol based automotive fuels from future biorefineries,” Fuel, vol. 86, pp. 2806-09, 2007

Sustainable Energy Research Center

Distributed Generation Area Final Report for 2006-2008

1. **Project title, name of principal investigator, and all team members:** G: Distributed Generation
Dr. Noel Schulz, Dr. Anurag Srivastava

2. **List of authorized distribution limitation notices, such as patentable material or protected data.**
Material provided does not have any distribution limitations.

3. **Executive summary**

Task G.1: Develop simulations to quantify technical and economic benefits and costs of biomass DG
Traditionally simulations for the inclusion of distributed generation (DG), such as biomass, have only looked at the avoided generation costs and not quantified the comprehensive technical and economic benefits related to the penetration of biomass DG within the electric grid. The research team within the Mississippi State Electrical and Computer Engineering Department has developed several resources and tools that can be used to evaluate the biomass DG impact on the grids. Several documents provided in earlier reports outlined technical, economic and political opportunities and challenges related to the inclusion of biomass related energy sources with the power grid, particularly in Mississippi.

Simulations related to the technical impacts of the biomass DG have been developed in multiple software tools including LINGO, HOMER, MATLAB, CymDist, and MSU developed software. Standard test cases have been used to evaluate how the size and location of distributed generation impacts various electrical characteristics and may lead to more reliable and higher quality electric power systems. Initial development of a stability index and multi-objective optimization techniques will help provide the owners of DG and electric utilities with additional technical information to help facilitate the connection of DG into the power grid. Inclusion of the DG sources including biomass can help provide a more flexible grid that can eventually reduce the cost of electricity, increase the penetration on alternative energy sources and provide back-up power during catastrophic events such as terrorist attacks or extreme weather.

Task G.2: Investigate technical and economic solutions related to energy storage and power conditioning devices of biomass-generated energy

One of the challenges related to many distributed generation sources including renewable energy sources is providing consistent electrical energy to the power grid. Depending on the technology, the electricity may not be produced at an optimal time. Related to this it is important to understand how to integrate energy storage devices with biomass related DG to make the most of the energy produced. Additionally biomass DG sources can be connected two ways – utility connected or islanding.

Simulation models have been developed for energy storage devices (batteries and ultracapacitors) as well as the power electronic interfaces between the energy storage devices and biomass DG to allow for simulations of the system to see how the presence of biomass DG within an interconnected system may impact the way that the system reacts to faults and maintaining stability. These models and the comprehensive simulations help provide a full picture of the impacts of DG and related to the goals of Task G.1.

Task G.3: Run simulations to quantify siting DG impact on the power grid and provide optimization methods for siting related to stability, voltage support, decrease losses and other key criteria.

While some biomass DG may need to be sited near a fuel source, others have the flexibility to be sized and sited where needed. Most studies before this research only focused on the decrease in power losses provided by additional penetration of distributed resources. In our research work we have developed two different approaches to quantifying the impact on stability as well as a multi-objective optimization related to stability, voltage support and decreased losses. The single objective optimization has been tested on two different IEEE test systems to identify the best sites and sizes for DG penetration.

4. **Comparison of goals and actual accomplishments.**

See attached spreadsheet. Funding for this task was provided for only first time interval of project. Extension of work has been accomplished with other Department of Energy funds.

5. **Summarization of activities for entire period of funding**

Project Objective: Develop simulations to investigate the impact of biomass-distributed generation on the electric power grid. Impacts include technical, policy and economic. Technical impacts include steady state, stability and transient analysis and energy storage requirements. Policy and economics issues include investigating how tariffs within Mississippi and the southeast will impact the economic feasibility of biomass distributed generation penetration into the power grid.

Task G.1 Develop Simulations to quantify technical and economic benefits and costs of biomass DG

In evaluating DG on a distribution system, DG placement and sizing are critical factors in improving the overall performance of the power system (i.e. minimizing losses, increasing voltage stability, minimizing impact on fault current, etc…). Simulations of the IEEE 13 Node Test Feeder were implemented in the power analysis software package, CYME. Again, the purpose of modeling the IEEE Test Feeders in CYME is to obtain the power flow solution for a distribution system with the presence of DG (i.e. voltages, losses, fault current, etc.). The results obtained from CYME will be used to help formulate a multi-objective optimization problem to determine the optimal placement and sizing of DG. Result tables of the CYME simulations are below. These results will help provide a basis for the technical impact of DG to allow our research team to place economic benefits related to penetration of the DG.

One of the main objectives of the project is to improve the performance and accuracy of an existing optimization algorithm (i.e. particle swarm) when solving a multi-objective DG sizing and placement problem.

[1] Previously, the research team reviewed the following optimization techniques with applications in power systems: Tabu Search, Genetic Algorithm, Simulated Annealing, Evolutionary, Particle Swarm, and Ant Colony.

[2] Of these popular optimization techniques, particle swarm and genetic algorithm were chosen for further evaluation in our research efforts. MATLAB codes for particle swarm and genetic algorithm were downloaded and will be used to better understand the mathematical and computational methods associated with each technique.

[3] The software LINGO will be used in future activities to prove to be helpful in these research efforts in solving a multi-objective optimization problem without have to utilize a particular optimization technique.

[4] Finally, the research team discussed DG related issues with engineers from Alabama Power, a subsidiary of Southern Company. The discussion focused mainly on the technical and economic issues related to their experience of evaluating the possible installation of 2 x 1 MW Synchronous Generators (bio-gas: Landfill) on their distribution system. The following are some of the issues discussed: protection schemes, synchronization, equipment ratings, fault current, power flow, equipment connection, cost of building tie-lines, and peak/valley loads. The dialog also highlighted some issues related to the utilization of CYME to evaluate DG on a distribution system.

IEEE 13 Node Test Feeder:

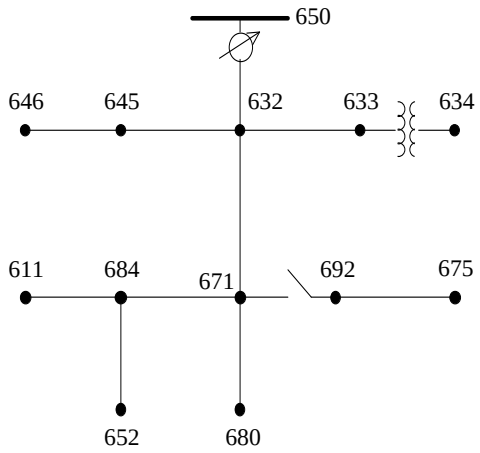


Figure 1: IEEE 13 Node Test Feeder One Line Diagram

Section Id	Equipment Id	Equip Code	Total Load (kW)	Total Load (kVAR)	Total distance (miles)
IEEE13	IEEE_13_XFM	Substation			0
650-632	BY_PHASE,556_ACSR_26/7,556_ACSR_	Conductor			0.4
632-633	BY_PHASE,4/0_ACSR_6/1,4/0_ACSR_6	Conductor			0.5
633-634	BY_PHASE,DEFAULT,DEFAULT,DEFAULT	Conductor	400	290	0.5
632-645	BY_PHASE,NONE,1/0,1/0,1/0,505	Conductor	170	125	0.5
645-646	BY_PHASE,NONE,1/0_ACSR_6/1,1/0_A	Conductor	230	132	0.5
632-671	BY_PHASE,556_ACSR_26/7,556_ACSR_	Conductor	1355	776	0.8
671-680	BY_PHASE,556_ACSR_26/7,556_ACSR_	Conductor			0.9
671-684	BY_PHASE,1/0,NONE,1/0,1/0,505	Conductor			0.8
684-611	BY_PHASE,NONE,NONE,1/0,1/0,510	Conductor	170	80	0.9
684-652	1/0(19X)	Cable	128	86	1
671-692	BY_PHASE,DEFAULT,DEFAULT,DEFAULT	Conductor	170	151	0.8
692-675	250(37X)AA_CN	Cable	843	462	0.9
		Total Load	**3466**	**2102**	

Table 1: IEEE 13 Node Test Feeder Load & Conductor Information

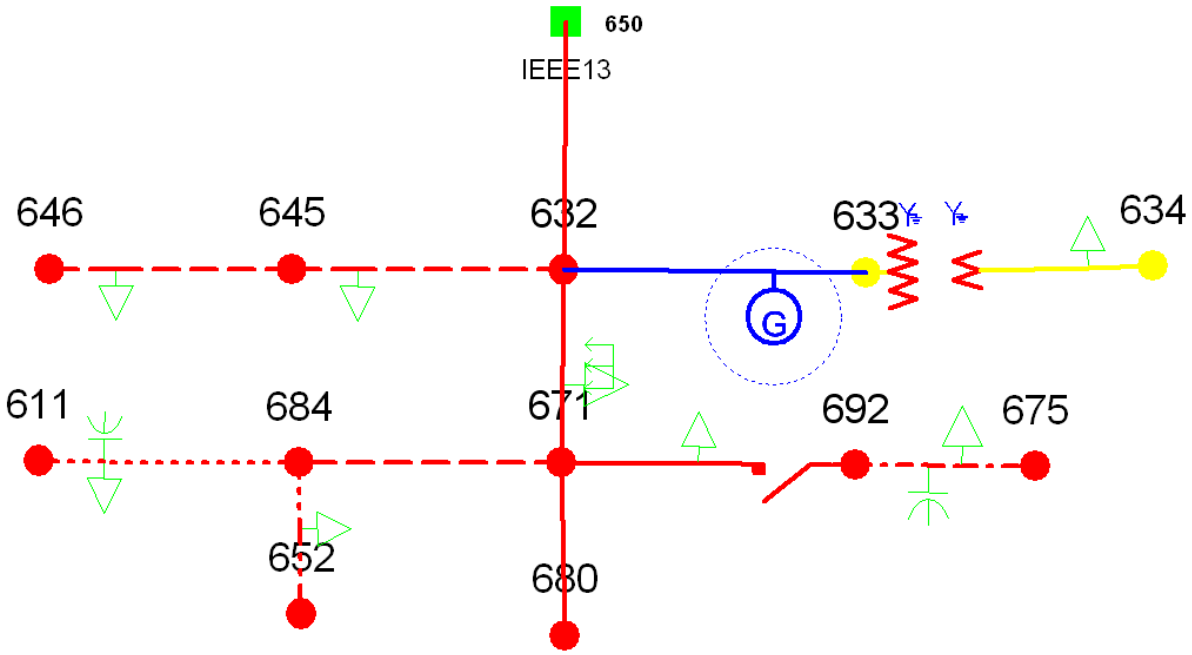
CYME Simulation Notes:

- No Voltage Regulators @ Node 650 to observe the impact of the DG only on the node voltages
- Synchronous Generators can only be installed at 3-phase node locations (Nodes: 632, 633, 671, 680, 692)
- Synchronous Generator Power Factor @ 85% (Typically 85% – 95%)
- The power flow solutions were solved with one DG on the system at a time.
- DG penetration level of 0%, 25%, 50%, & 75% of Total Load (~3466 kW)

DG Penetration Level (%)	Real Power (kW)	Reactive Power (kVar) @ pf = 85%
0 %	0	0
25 %	866.5	557.9
50 %	1733	1115.98
75 %	2599.5	1673.8

- Simulation Results at different DG sizes & locations:
  1) Node Voltages
  2) System Losses
  3) Node Fault Currents
- Acceptable Voltage Level: $.95 < V < 1.05$

CYME SIMULATION
RESULTS:



IEEE 13 Node Test Feeder:
Phase C
Voltage Profile
Synchronous Generator @ 25% DG Penetration

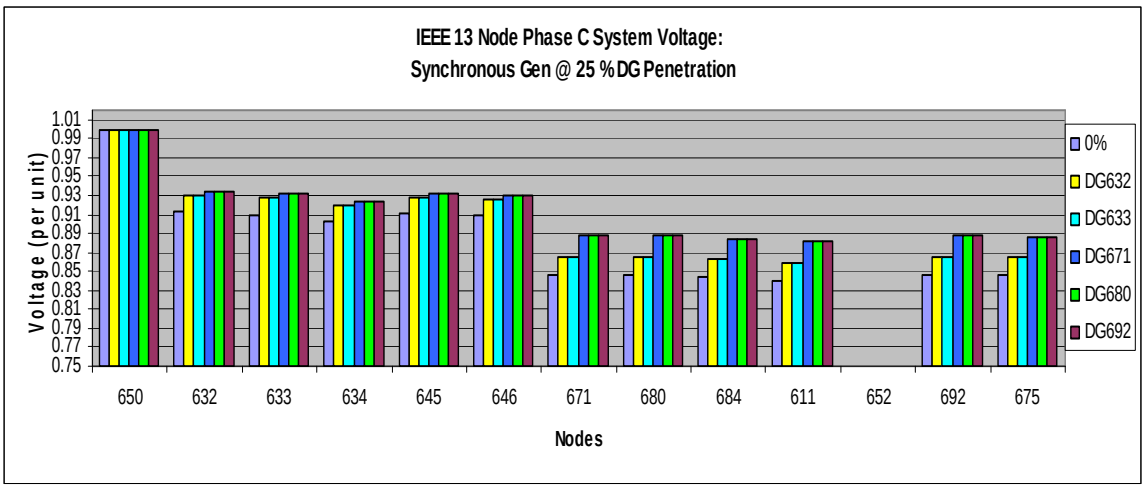


Figure 2: Voltage Profile of Phase C @ 25% penetration level @ different DG Locations

Table 2: Voltage Profile of Phase C @ 25% penetration level @ different DG Locations

Section Id	Code	NO DG	DG632 Phase C Volt (pu)	DG633 Phase C Volt (pu)	DG671 Phase C Volt (pu)	DG680 Phase C Volt (pu)	DG692 Phase C Volt (pu)	Total distance (miles)
650	Substation	1	1	1	1	1	1	0
632	NODE	0.913	0.931	0.931	0.935	0.935	0.935	0.4
633	NODE	0.91	0.928	0.928	0.932	0.932	0.932	0.5
634	NODE	0.902	0.92	0.92	0.924	0.924	0.924	0.5
645	NODE	0.911	0.928	0.928	0.932	0.932	0.932	0.5
646	NODE	0.909	0.926	0.926	0.93	0.93	0.93	0.5
671	NODE	0.847	0.866	0.866	0.888	0.888	0.888	0.8
680	NODE	0.847	0.866	0.866	0.888	0.888	0.888	0.9
684	NODE	0.844	0.862	0.862	0.885	0.885	0.885	0.8
611	NODE	0.84	0.859	0.859	0.881	0.881	0.881	0.9
652	NODE							1
692	NODE	0.847	0.866	0.866	0.888	0.888	0.888	0.8
675	NODE	0.846	0.865	0.865	0.887	0.887	0.887	0.9

- All voltages slightly improved with the presence of DG, but the red indicates that the voltages are below an acceptable level (V < .95)
- The size of DG is not large enough to provide adequate voltage support for system
- Voltage levels at DG locations 671, 680, 692 are identical (close proximity to each other). This means that the placement of a DG at any one of these locations would provide the same amount of voltage support; therefore, other deciding factors such as fault current levels and losses would be used to determine optimal location of DG.

Synchronous Generator @ 50% DG Penetration

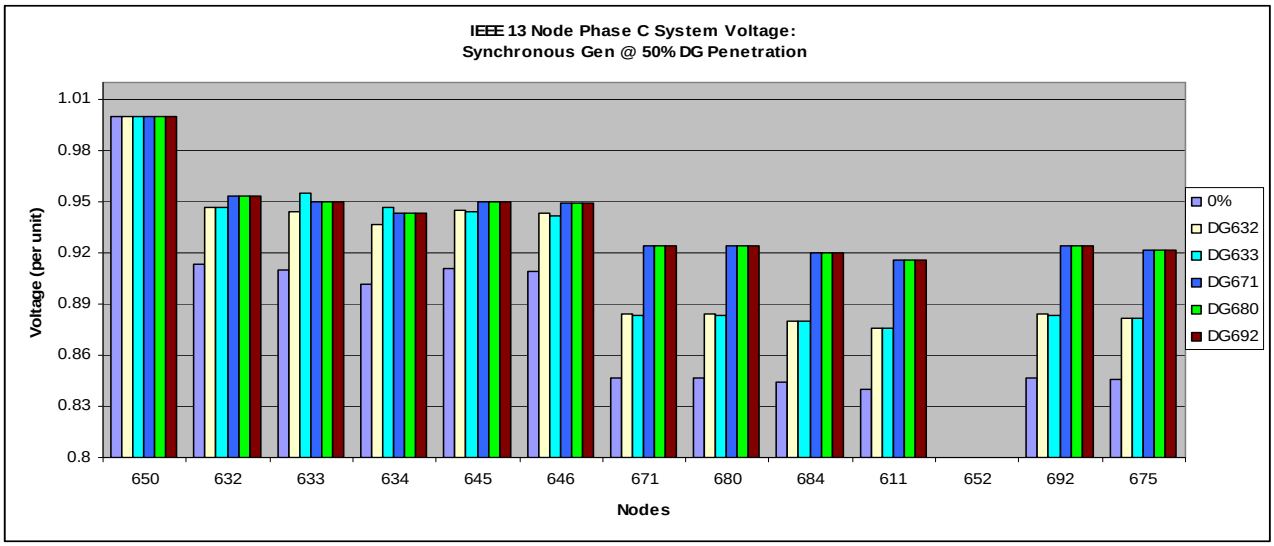


Figure 3: Voltage Profile of Phase C @ 50% penetration level @ different DG Locations

Table 3: Voltage Profile of Phase C @ 50 % penetration level @ different DG Locations

Feeder Id	Section Id	Code	NO DG	DG632 Phase C Volt (pu)	DG633 Phase C Volt (pu)	DG671 Phase C Volt (pu)	DG680 Phase C Volt (pu)	DG692 Phase C Volt (pu)	Total distance (Miles)
IEEE13	650	Substation	1	1	1	1	1	1	0
IEEE13	632	NODE	0.913	0.947	0.947	0.953	0.953	0.953	0.4
IEEE13	633	NODE	0.91	0.944	0.955	0.95	0.95	0.95	0.5
IEEE13	634	NODE	0.902	0.937	0.947	0.943	0.943	0.943	0.5
IEEE13	645	NODE	0.911	0.945	0.944	0.95	0.95	0.95	0.5
IEEE13	646	NODE	0.909	0.943	0.942	0.949	0.949	0.949	0.5
IEEE13	671	NODE	0.847	0.884	0.883	0.924	0.924	0.924	0.8
IEEE13	680	NODE	0.847	0.884	0.883	0.924	0.924	0.924	0.9
IEEE13	684	NODE	0.844	0.88	0.88	0.92	0.92	0.92	0.8
IEEE13	611	NODE	0.84	0.876	0.876	0.916	0.916	0.916	0.9
IEEE13	652	NODE							1
IEEE13	692	NODE	0.847	0.884	0.883	0.924	0.924	0.924	0.8
IEEE13	675	NODE	0.846	0.882	0.882	0.922	0.922	0.922	0.9

- The voltages in red are below acceptable level (V < .95)
- The DG is not providing enough reactive power to provide proper voltage support.
- Voltage decreases with respect to distant from the substation (source). The lowest system voltages are farthest from the source.

Synchronous Generator @ 75% DG Penetration

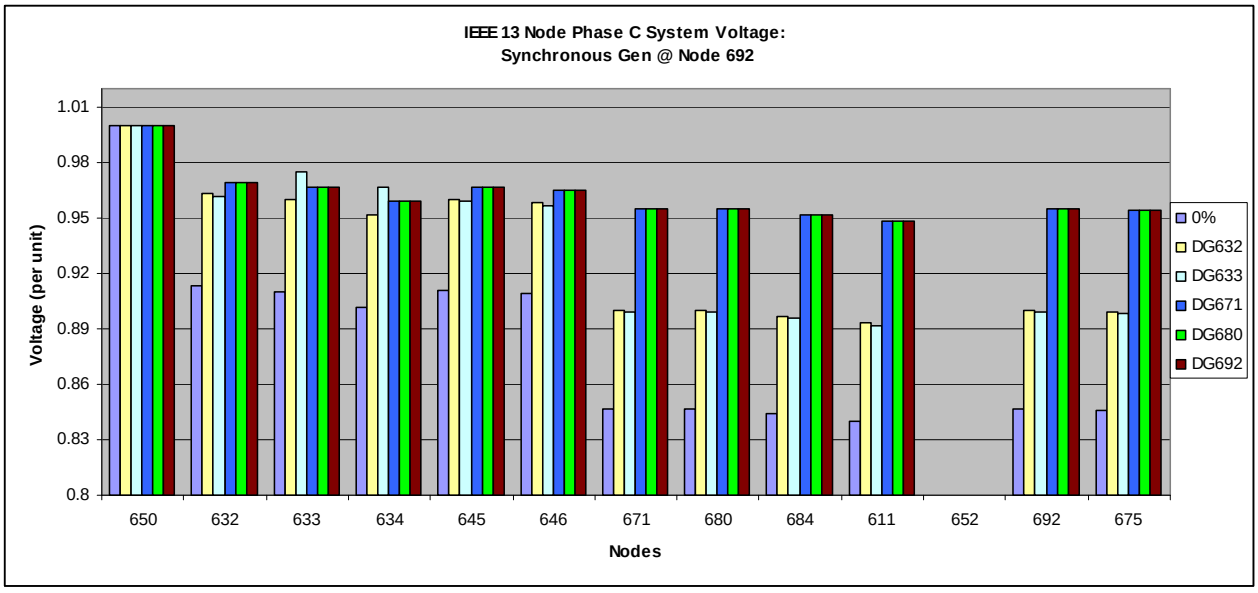


Figure 4: Voltage Profile of Phase C @ 75% penetration level @ different DG Locations

Table 4: Voltage Profile of Phase C @ 75 % penetration level @ different DG Locations

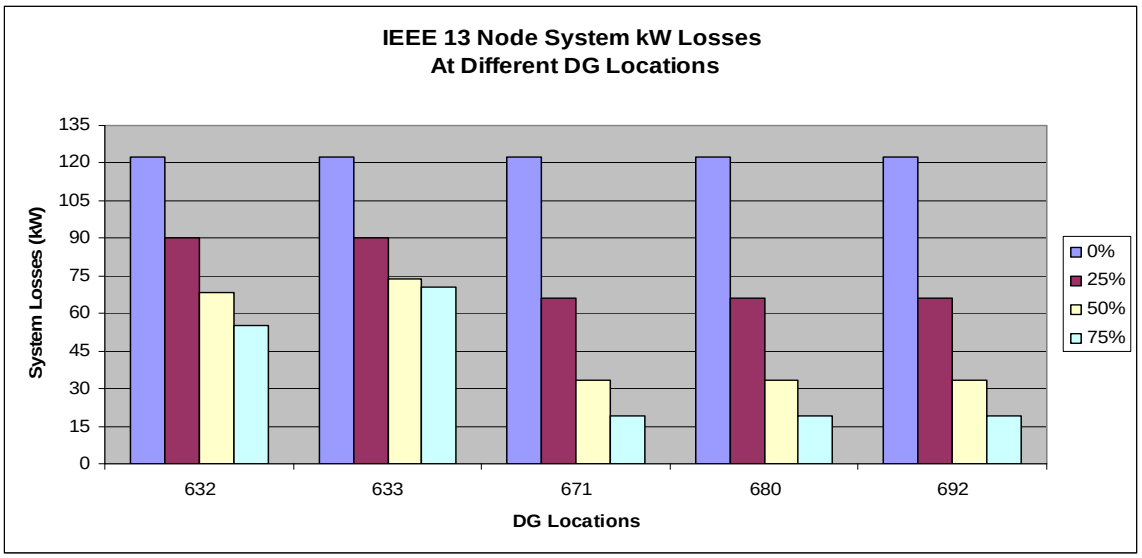
Feeder Id	Section Id	Code	NO DG	DG632 Phase C Volt (pu)	DG633 Phase C Volt (pu)	DG671 Phase C Volt (pu)	DG680 Phase C Volt (pu)	DG692 Phase C Volt (pu)	Total distance (Miles)
IEEE13	650	Substatio	1	1	1	1	1	1	0

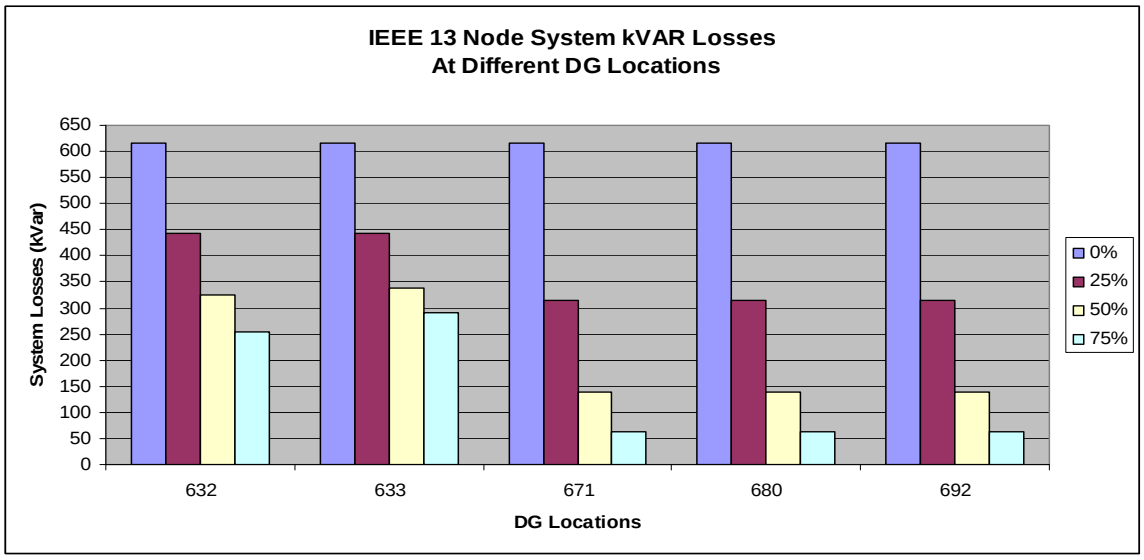
		n							
IEEE13	632	NODE	0.913	0.963	0.962	0.969	0.969	0.969	0.4
IEEE13	633	NODE	0.91	0.96	0.975	0.967	0.967	0.967	0.5
IEEE13	634	NODE	0.902	0.952	0.967	0.959	0.959	0.959	0.5
IEEE13	645	NODE	0.911	0.96	0.959	0.967	0.967	0.967	0.5
IEEE13	646	NODE	0.909	0.958	0.957	0.965	0.965	0.965	0.5
IEEE13	671	NODE	0.847	0.9	0.899	0.955	0.955	0.955	0.8
IEEE13	680	NODE	0.847	0.9	0.899	0.955	0.955	0.955	0.9
IEEE13	684	NODE	0.844	0.897	0.896	0.952	0.952	0.952	0.8
IEEE13	611	NODE	0.84	0.893	0.892	0.948	0.948	0.948	0.9
IEEE13	652	NODE							1
IEEE13	692	NODE	0.847	0.9	0.899	0.955	0.955	0.955	0.8
IEEE13	675	NODE	0.846	0.899	0.898	0.954	0.954	0.954	0.9

- A slight improvement in system voltages, but still less than desirable.
- Since voltage decreases with respect to distance, a generator placed farther from the substation (source) will be able to provide better voltage support.

IEEE 13 Node Test Feeder:
System Losses

IEEE 13 Node System Losses:
At Different DG Location @ Various DG Penetration Levels

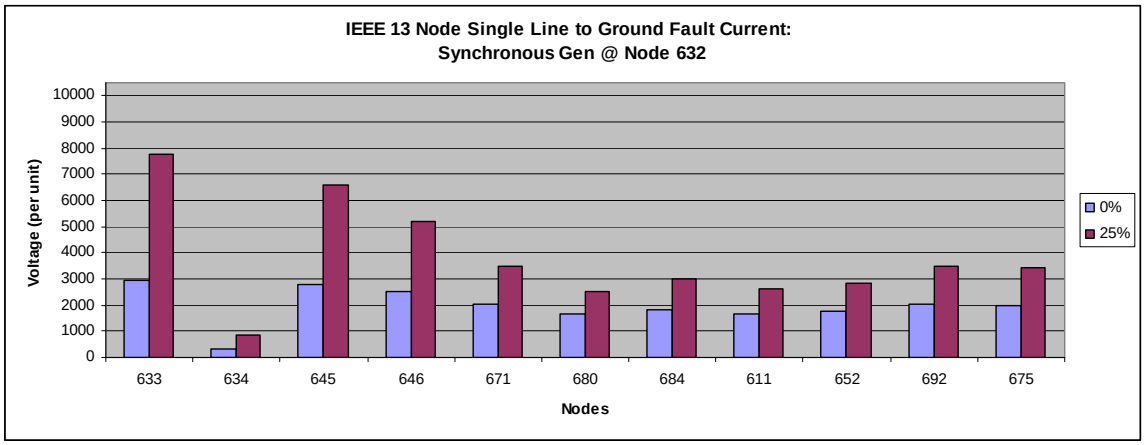




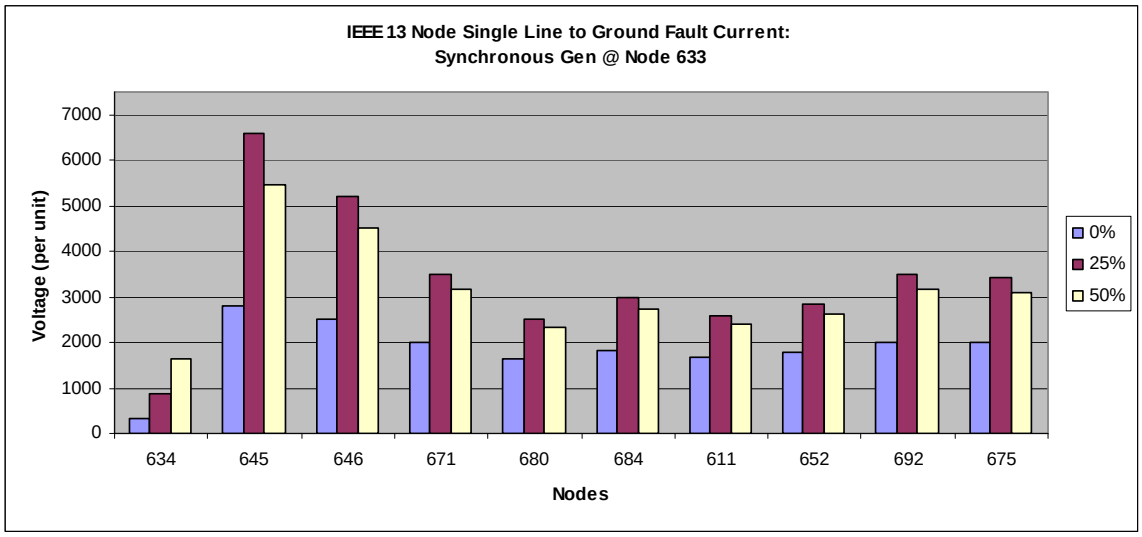
- As DG size increases, the overall system losses decreases
- DG placed at locations farthest from substation provides a larger reduction in system losses.

IEEE 13 Node Test Feeder: Single Line to Ground Fault Currents

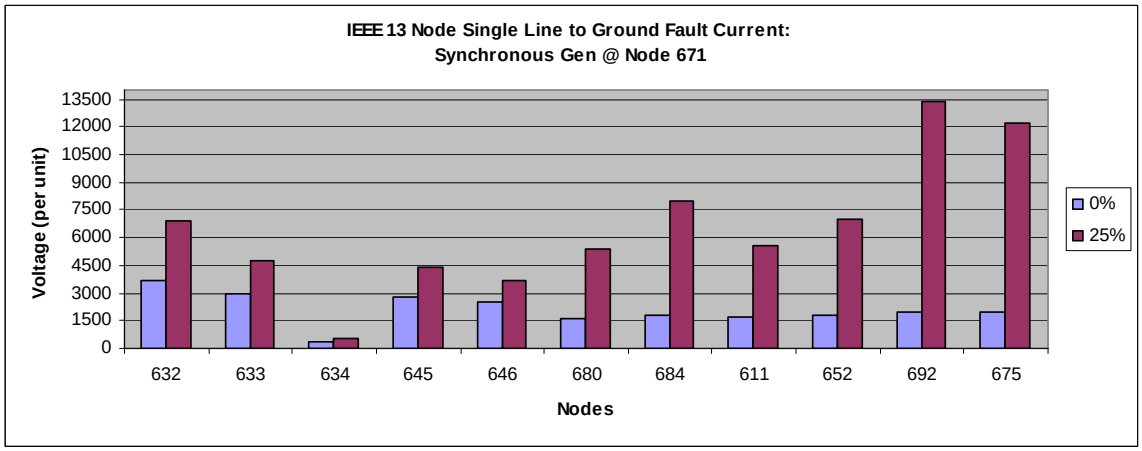
Synchronous Generator @ Node 632



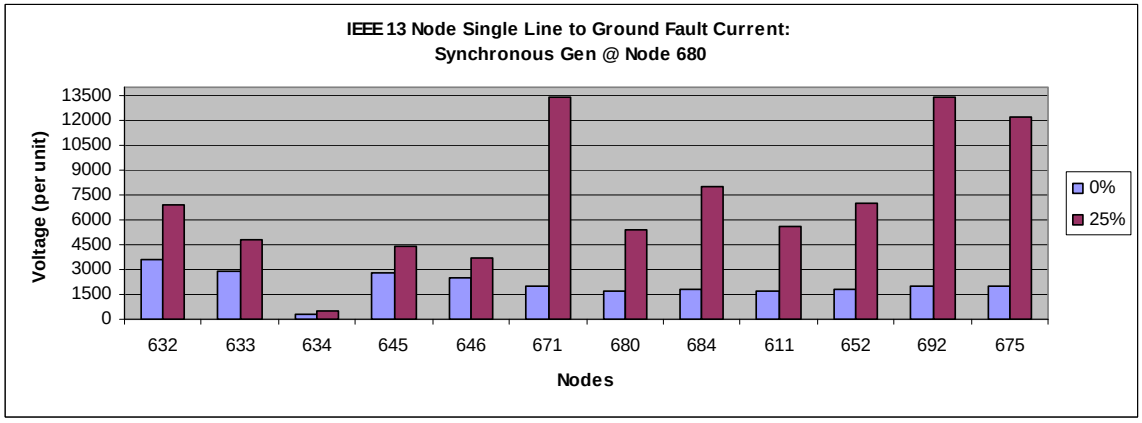
Synchronous Generator @ Node 633



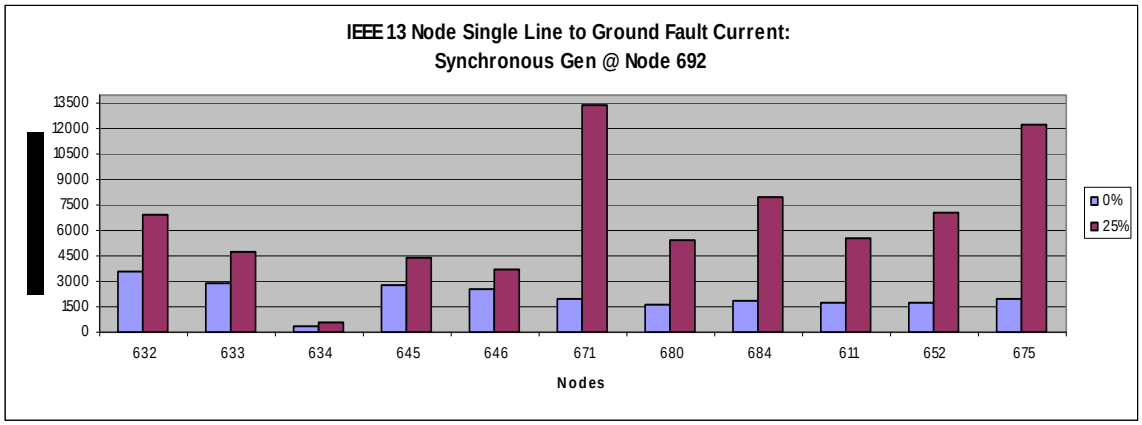
Synchronous Generator @ Node 671



Synchronous Generator @ Node 680



Synchronous Generator @ Node 692



- Protection schemes & Equipment Ratings are affected by the fault current levels throughout the power system

- A drastic change in fault currents will result in changes in equipment (i.e. fuses, reclosers, sectionalizers) & re-engineering of protection scheme.

- Since the fault current for higher penetration levels were similar, only 25% was selected for comparisons

- Single Line to Ground Faults were selected at random for comparisons

- Other types of Faults:

    a. 3 Phase (LLL)
    b. Double Phase (line-to-line)
    c. Double Phase to Ground (LLG)

Task G.2 Investigate technical and economic solutions related to energy storage and power conditioning devices of biomass-generated energy

The overall goals towards the end of this funding cycle were to accomplish the following

1) Analyze the rotor angle and voltage stability due to different types of faults and for different penetrations of DG.
2) Work to develop a mathematical model of the battery including electrical and thermal features
3) Work on developing a system in RSCAD to allow hardware-in-the-loop testing using ultracapacitors.

Rotor angle stability:

Three different types of faults (Three phase fault, Line-Ground fault, Double Line- Ground fault) were applied to the system for a period of 100 ms and the resulting change in the rotor angle of the machines were analyzed. This procedure was repeated for different penetration levels of the DG (5% to 50%). The rotor angle due to three phase fault and with 10% and 40% penetration of DG are given in Figures 1 and 2, respectively. Similar results have been obtained for different types of faults and different penetration levels. From the results that were obtained, it could be seen that an increase in the penetration level of DG decreases the deviation in the rotor angle.

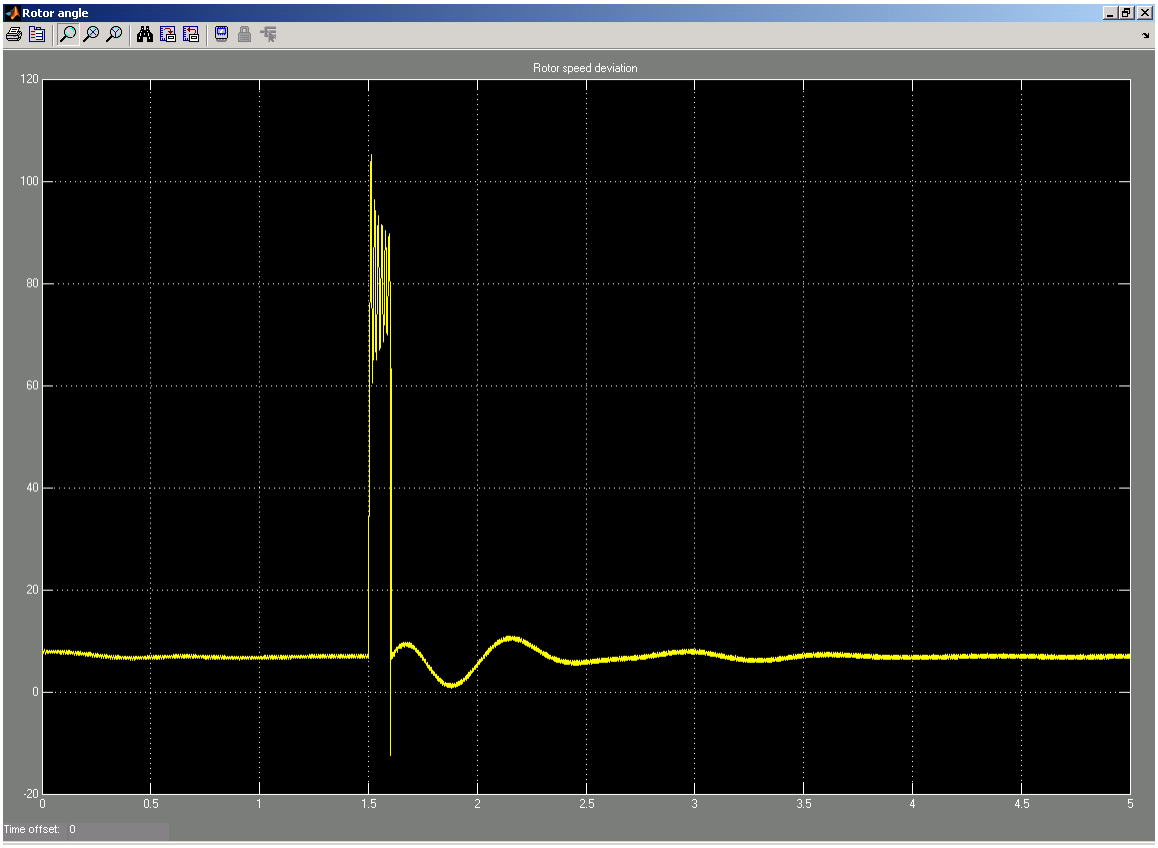


Fig 1. Deviation in Rotor angle due to 3ph fault with 10% penetration of DG

From the figures it can be seen that, when a fault is applied at time t = 1.5 s. The change in the rotor angle is less with 40% penetration of DG compared to 10% penetration. After the clearance of fault, the time taken to settle to normal is less with 40% penetration of DG.

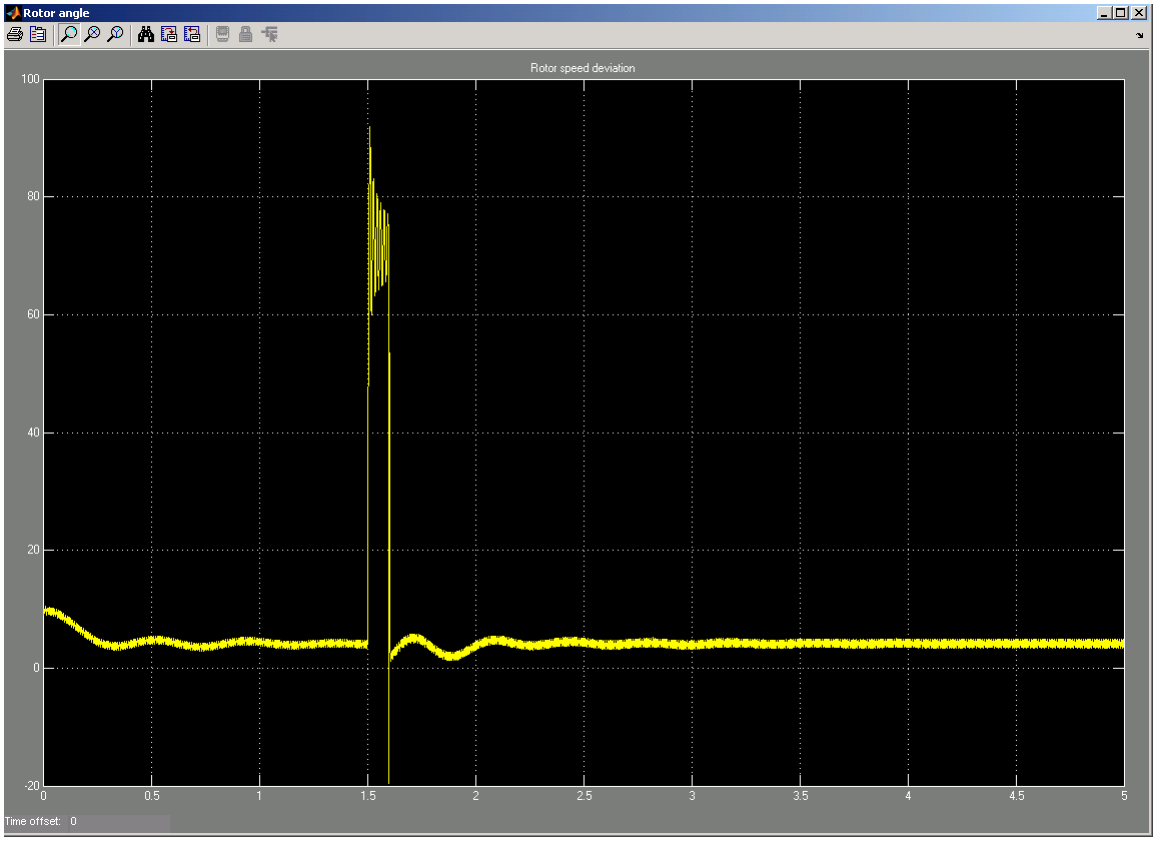


Fig 2. Deviation in Rotor angle due to 3ph fault with 40% penetration of DG

Voltage stability

Fig 3 shows the system that has been used in the voltage stability analysis. This system has the induction motor loads included in it. Similar to rotor angle analysis, different types of faults were applied to the system for a period of 100 ms and the terminal voltage of DG's were obtained. A similar procedure was repeated for different penetration levels of the DG. Analysis of the stability of the voltage was done in terms of the amount of drop in voltage during fault period and the time taken to return to normal operating voltage after the clearance of fault.

The terminal voltage of the DG due to three phase fault with 10% and 40% penetration of DG is given in Figures 4 and 5, respectively. It can be seen that as the penetration level of DG increases the amount of drop in voltage during a fault and the time taken to return to normal operating voltage after clearance of fault decreases. Therefore the voltage stability is seen to increase with the increase in penetration level of DG. Figures 6 to 11 show the amount in voltage drop and time taken to return to normal, for different types of faults and different penetration levels of DG.

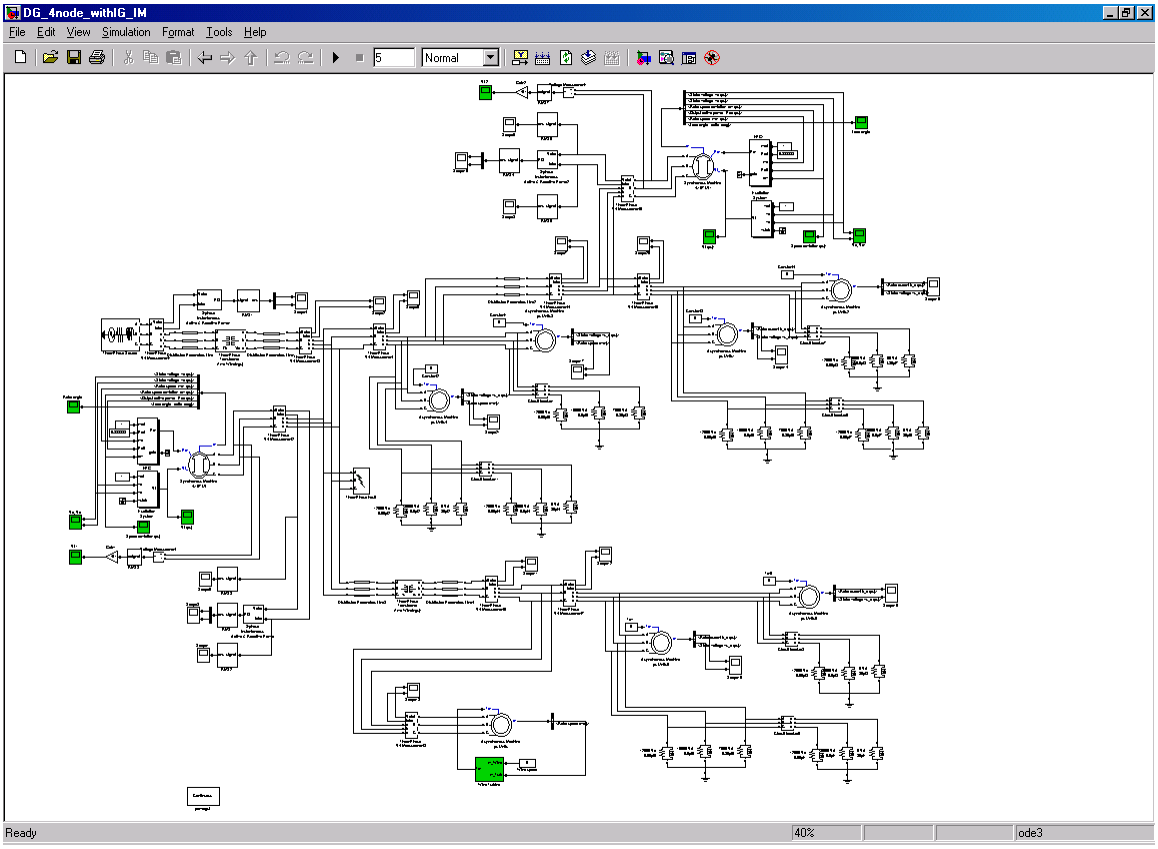


Fig 3 System used for voltage stability analysis (includes induction motor loads)

Amount of drop in voltage during different types of fault

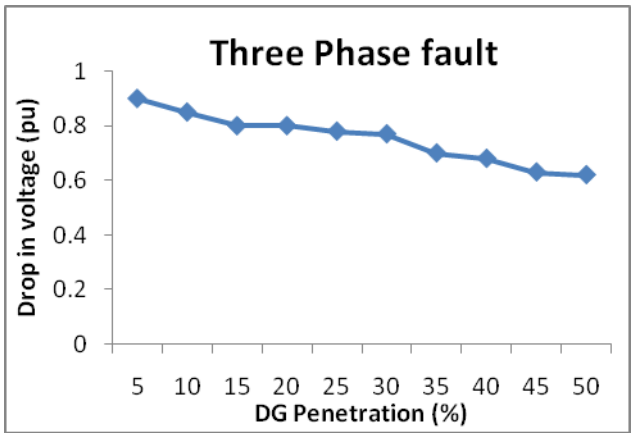


Fig 6. Drop in voltage due to 3 phase fault

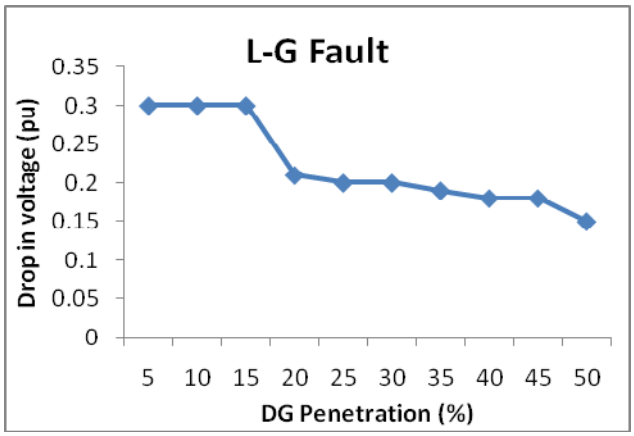


Fig 7. Drop in voltage due to L-G fault

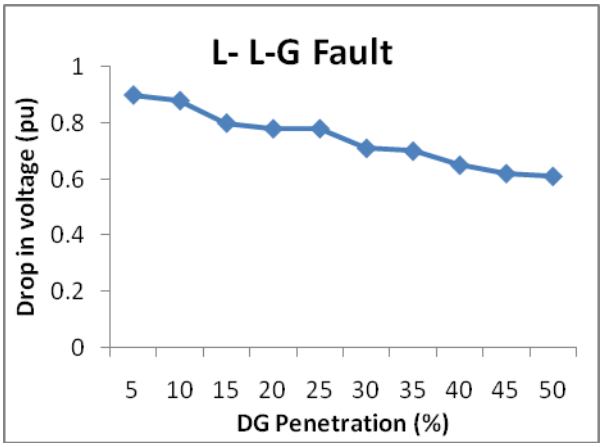


Fig 8. Drop in voltage due to L-L-G fault

Time taken to return to normal operating voltage after the clearance of fault

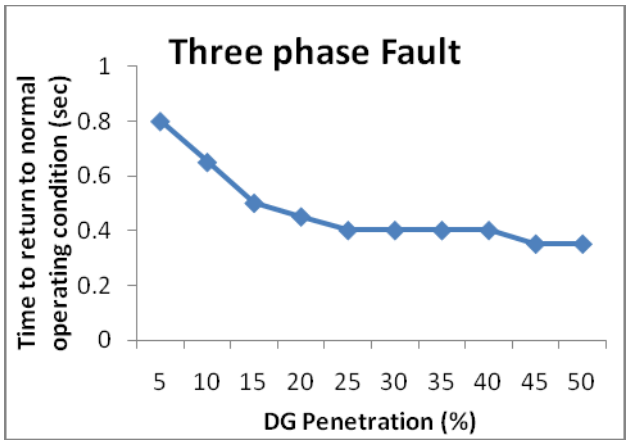


Fig 9. Time taken to return to normal voltage due to Three phase fault

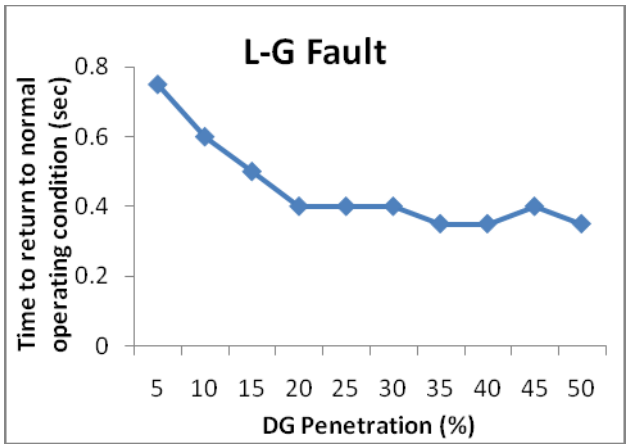


Fig 10. Time taken to return to normal voltage due to L-G fault

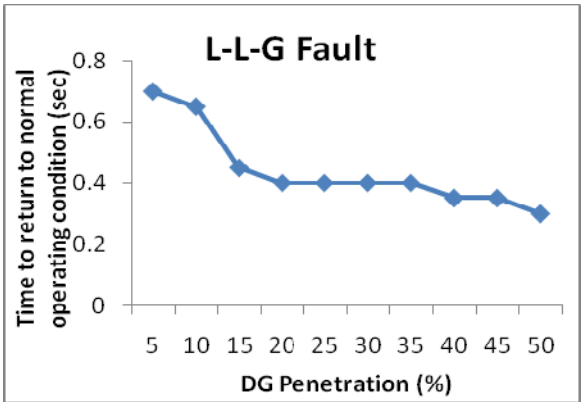


Fig 11. Time taken to return to normal voltage due to L-L-G fault

Development of Battery model in Simulink

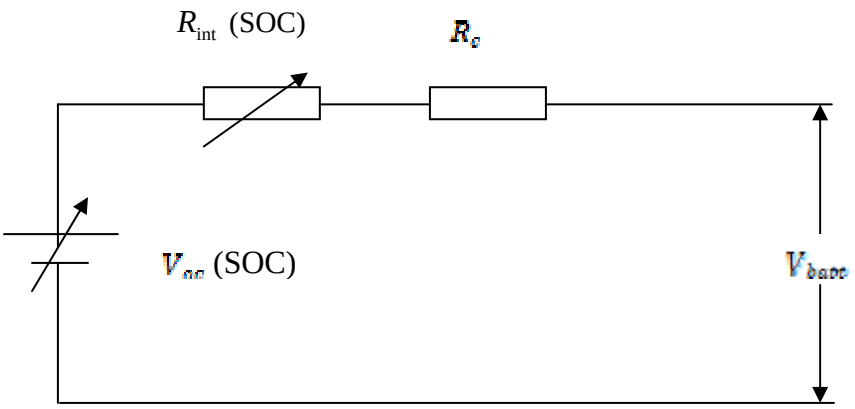


Fig 12. Equivalent circuit of battery

For the equivalent circuit given above, the equations that are necessary to develop a mathematical model are given below.

State Of Charge, $SOC = -\frac{1}{Q_{max}} \int i(t)dt$ (1)

Battery voltage, $V_{batt} = V_{oc}$ (SOC) – { R_{int} (SOC) + R_c } i (t) (2)

Thermal energy balance equation, given below, governs the temperature change of the battery,

$m \cdot c_p \cdot \frac{dT(t)}{dt} = i(t)^2 \cdot R_{int} - h_c \cdot A\,[T(t) - T_a]$ (3)

where

m	Battery mass (kg)
c_p	Specific heat (J/kgK)
T	Temperature of the battery (K)
R_{int}	Battery internal resistance (Ω)
hc	Heat transfer coefficient (W/m²K)
A	Battery surface area (m²)
Ta	Ambient temperature (K)

Using these equations, model of the battery was developed in Simulink (fig 13)

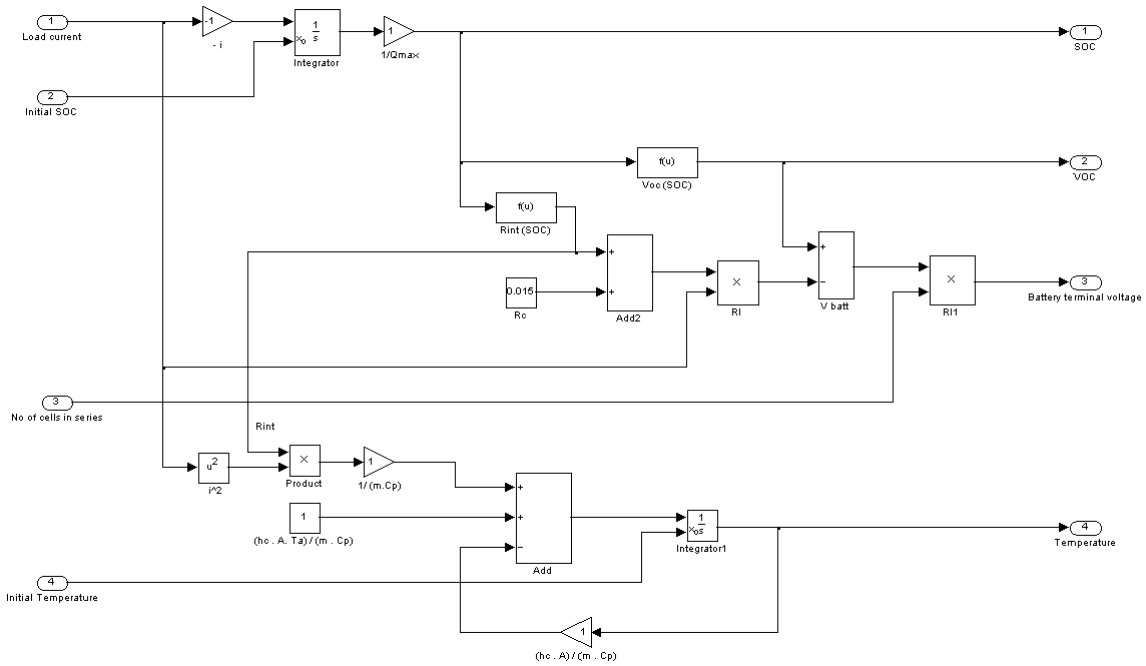


Fig 13. Battery model in Simulink

This project was continued via other funding sources and the final results are presented in the student's MS thesis (provide in section 6, publications #3). This is available on-line at http://sun.library.msstate.edu/ETD-db/theses/available/etd-11142008-151157/

Task G.3 Run simulations to quantify siting DG impact on the power grid and provide optimization methods for siting related to stability, voltage support, decrease losses and other key criteria

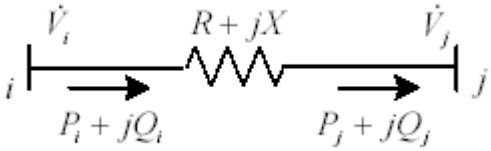
The overall goals for the final funding cycle were:

- Finish the optimization of both sizing and location of DG for 13-node system.
- Implement the above for larger systems.
- Start formulation on the multi objective function addressing various issues like voltage support, reduced losses and stability.

The size of the Distributed Generation is defined as the ratio of the total power supplied by all the DG's connected to the grid to the total load. Oversizing of the DG or multiple DG's and improper location leads to the injection of the overcurrents and overvoltages that causes instability in the system. Hence the sizing and siting of the DG has to be dealt seriously and in this part of the work the size of the DG is optimized first and then the location of the DG is optimized using the optimized size obtained from the first part. Optimization here is to find the best size and location of the DG such the stability of the system is maximum giving the best voltage profile.

Many approaches are being used by the researchers to find the best location and size, which include optimizing the size such that cost of generation is reduced or losses are reduced. In this part of the work the best size and location are found by minimizing the stability index, which was selected from the literature review. The selected index is derived from the two-line diagram as shown below

The stability index derived from the above is



$$L = 4[ViVj\cos(\theta i-\theta j) - Vj^2\cos(\theta i-\theta j)^2]/Vi^2$$

where $Vi\angle\theta i$ and $Vj\angle\theta j$ are the voltages at node 'i' and node 'j'. The above index can be extended to any larger system and the stability index can found for all the nodes and if

$L > 1$; the system is stable.

$L < 1$; the system is unstable.

This stability index can be used to maximize the stability and is being implemented using the optimization software, LINGO. LINGO is a simple tool for utilizing the power of linear and nonlinear optimization to formulate large problems concisely, solve them and analyze the solution. The IEEE 13 node feeder is being used as the test case and the test case as well as the unbalanced power flow equations are modeled in LINGO, which gives the voltages and voltage angles at all the nodes. LINGO does accept complex numbers hence power flow equations were modeled for both real and imaginary parts separately. The voltages that are found from the power flow will be in real and imaginary parts. But the stability index is in polar form, so the index was reduced to

$$L(i) = \frac{4[(V_{1aR}V_{2aR}+V_{1aI}V_{2aI})(V_{1aR}^2+V_{1aI}^2)-(V_{1aR}V_{2aR}+V_{1aI}V_{2aI})^2)]}{(V_{1aR}^2+V_{1aI}^2)^2}$$

Where V_{1aR}, V_{1aI} are real and imaginary parts of voltages of node 1 for phase A and V_{2aR},V_{1aI} are real and imaginary parts of voltages of node 2 for phase A.

Two DG's modeled as negative loads were connected to the test case and the total penetration of the DG is increased from 10% to 60% of the total load in steps of 5% and at each stage the power flow was run and the objective function is minimized using the voltages obtained from the power flow. The modeling of the objective function and the constraints are shown below:

Objective function:

Min (i) = @Min ((Volt1R (i), Volt2R (i)/qualifier/: (L (i)) for phase A

Contraints:

1) $V(i)_{min} <= V(i) <= V(i)_{max}$, Voltage limits

2) $P(DG)_{min} <= P(DG) <= P(DG)_{max}$, DG limits
and here it is from 10% to 60% of total load.

3) L (i) < 1.0, stability should be less than 1.0.

The objective function loops to get the achieve the minimum stability index value for all the cases of DG penetration and the objective function is modeled as

Initial implementation of this objective function found limits in LINGO's capabilities. A new upgrade of LINGO is being purchased to allow looping and fix the problem allowing advanced simulations.

This project was continued via other funding sources and the final results are presented in the student's MS thesis (provide in section 6, publications #4). This is available on-line at http://sun.library.msstate.edu/ETD-db/theses/available/etd-11142008-135719/

6. **Identify products developed under the award and technology transfer activities**, such as:
   a. Publications (list journal name, volume, issue), conference papers, or other public releases of results.

Publications

1. Aarthi Asok Kumar, Anurag Srivastava and Noel N. Schulz, "Impact of Biomass Based Distributed Generation with Energy Storage on Transient Stability of Grid", *Proceedings of Power Systems Conference 2008*, Clemson University, March 2008.
2. Abhilash Masannagari, Anurag Srivastava and Noel N. Schulz, "Optimizing Siting and Sizing of Distributed Generation to Maximize Grid Stability," *Proceedings of Power Systems Conference 2008*, Clemson University, March 2008.
3. Aarthi Asok Kumar, "Technical and Economic Impacts of Distributed Generators and Energy Storage Devices on the Electric Grid," M.S. Thesis, Department of Electrical and Computer Engineering, Mississippi State University, December 2008.
4. Abhilash R. Masannagari, "Optimizing the Size and Location of Distributed Generators to Maximize the Grid Stability," M.S. Thesis, Department of Electrical and Computer Engineering, Mississippi State University, December 2008.

Presentations

1. Aarthi Asok Kumar, Anurag K. Srivastava and Noel N. Schulz, "Transient Impact of the Distributed Generation with Energy Storage on the Electric grid," *IEEE Transmission and Distribution Conference and Exposition*, Chicago, Illinois, April 21 – 23, 2008 (Poster).
2. Abhilash R. Masannagari, Anurag K. Srivastava and Noel N. Schulz, "Optimizing the DG Size to Maximize the Grid Stability using LINGO," *IEEE Transmission and Distribution Conference and Exposition*, Chicago, Illinois, April 21 – 23, 2008 (Poster).
3. Shravana K. Musunuri, Herbert Ginn and Noel N. Schulz, "Power Electronic Interface of Energy Sources to Utility Grid," *IEEE Transmission and Distribution Conference and Exposition*, Chicago, Illinois, April 21 – 23, 2008 (Poster).
4. Shravana K.. Musunuri, Herbet Ginn and Noel N. Schulz, "Power Electronics interface of multiple energy sources to utility grid," Seventh Annual Southern Bio Products and Renewable Energy Conference. April 14-15, 2007, Choctaw, MS. Mississippi Biomass Council, Jackson, MS, (Poster).
5. Derrick Cherry and Noel N. Schulz, "Technical, Economic and Policy Evaluation of Distributed Generation on the Mississippi Power Grid," Seventh Annual Southern Bio Products and Renewable Energy Conference, April 14-15, 2007, Choctaw, MS. Mississippi Biomass Council, Jackson, MS, (Poster).
6. Abhilash R. Masannagari, Anurag K. Srivastava and Noel N. Schulz, "Simulations to quantify siting DG impact on the power grid," Seventh Annual Southern Bio Products and Renewable Energy Conference,April 14-15, 2007, Choctaw, MS, Mississippi Biomass Council, Jackson, MS, (Poster).
7. Aarthi Asok Kumar, Anurag K. Srivastava and Noel N. Schulz, "Investigation of technical and economic solutions related to energy storage and power conditioning devices of biomass – generated energy," Seventh Annual Southern Bio Products and Renewable Energy Conference. April 14-15, 2007, Choctaw, MS. Mississippi Biomass Council, Jackson, MS, (Poster).

8. Derrick Cherry and Noel N. Schulz, “Evaluation of Renewable Distributed Generation on the Mississippi Power Grid,” Workshop on Renewable Energy for Minnesota, McNamara Alumni Center, University of Minnesota, Minneapolis, Thursday October 12, 2006 (Poster).

b. Web site or other Internet sites that reflect the results of this project
None

c. Networks or collaborations fostered
Collaborative research activities with the MSU micro-CHP team were started as an extension of the SERC activities. One graduate student spent seven months at NREL doing a summer internship. Developed relationships with local electric co-op (4 County Electric Cooperative).

d. Technologies/Techniques
None

e. Inventions/Patent applications, licensing agreement
None

f. Other products, such as data or databases, physical collections, audio or video, software or netware, models, educational aid or curricula, instruments or equipment.
None

Sustainable Energy Research Center
Value-Added Chemicals Thrust Area Final Report for 2006-2008

1. Project title, principal and co-investigators: H. Value Added Chemicals from Biomass

Principal Investigator: Keisha B. Walters
Co-investigators: Dwaine Braasch, Bruce Cain, Sandun Fernando, Nara Gavini, Priscilla Hill, Adrienne Minerick, Mark Novotny, Lakshmi Pulakat, Jadish P. Singh, F.Y. Yueh

2. List of authorized distribution:

The information contained in the section of this Sustainable Energy Research Center report is available to the distributed as the Department of Energy deems necessary.

3. Executive summary:

Task H.1: *Development of Catalytic Reformer and Modeling*
Efforts to develop a chemical reforming system with fast output rates were successful, with the development of a model to predict glycerol conversion and the identification and testing of a Ni-Al_2O_3 catalyst which provided a hydrogen selectivity of 80% and maximum glycerol conversion of 94%. In addition, molecular dynamics simulations were used determine lifetime models for glycerin/water nanodroplets.

Task H.2: *Production of Biohydrogen*
Biological reforming uses only a fraction of energy from what is required for a chemical reformer and by using a mixed culture can be tailored to accept a variety of feedstocks with varying compositions. Studies into biological reformation showed that both wild type and mutant *A. Vinelandii* were able to grow well under conditions targeted to increase the expression of Fe-nitrogenase, a primary factor in efficient biohydrogen production. These conditions included the use of lignin and biowaste as carbon sources. On the other hand,. Genetic manipulation of *A. Vinelandii* was performed to increase expression of Fe-nitrogenase and the growth of these genetically engineered bacterium were monitored using a specially designed laser induced fluorescence (LIF probe).

Task H.3: *Hydrogen Storage Materials Development*
This project was terminated following the death of the PI.

Task H.4: *Production of Specialty Chemicals*
Efforts involved cleavage chemistries, specialty separations, crystallization, and polymer synthesis to achieve this objective. In order to remove phosphorous from biofuels streams and provide additional feedstock materials (fatty acid chains and phosphate head groups) for subsequent processes, cleavage and separation studies were performed on phospholipids (PL) and fatty acid analogs. Efforts to cleave PL ester groups varied based on the specific PL and reaction conditions, but cleavage yields as high as 82% were achieved. The cleavage phosphate headgroups were then used to synthesize novel phosphate polymers. An innovative technique was applied to the separation of the cleaved fatty acid and phosphate head group components, namely dielectrophoretic (DEP) trapping. In additional, crystallization techniques were also studied to effective produce high purity fatty acids, which have significant value in the pharmaceutical and nutraceutical industries. Both DEP trapping and crystallization separation techniques were not found to be amenable to the fairly large molecular weight fatty acid molecules.

Task H.5: *Polymers for Bioplastics*

Methods were investigated to utilize by- and waste-products of biofuels processing as monomeric materials for renewable polymers (bioplastics). The methods developed allowed for several linear and branched copolymers to be developed. By varying reaction conditions, the chemical composition, processing parameters, and degradation rates can be modified which allows for tailoring these bioplastics to a given application.

4. Comparison of goals and actual accomplishments:

See the attached report spreadsheet for details.

5. Summary of activities:

Task H.1: *Development of Catalytic Reformer and Modeling*

Use of biodiesel and its production are expected to grow steadily in the future. With the increase in production of biodiesel, there would be a glut of glycerol in the world market. Glycerol is a potential feedstock for hydrogen production because one mole of glycerol can produce up to four moles of hydrogen. However, less attention has been given for the production of hydrogen from glycerol via steam reforming process. Steam reforming of glycerol for hydrogen production involves complex reactions (Figure 1). As a result, several intermediate byproducts are formed and end up in the product stream affecting final purity of the hydrogen produced. Furthermore, the yield of the hydrogen depends on several process variables, such as system pressure, temperature, and ratio of reactants. Thermodynamic analysis would predict favorable reaction conditions for hydrogen production. As a result of this study several robust catalysts that are highly selective towards hydrogen production from glycerol were developed.

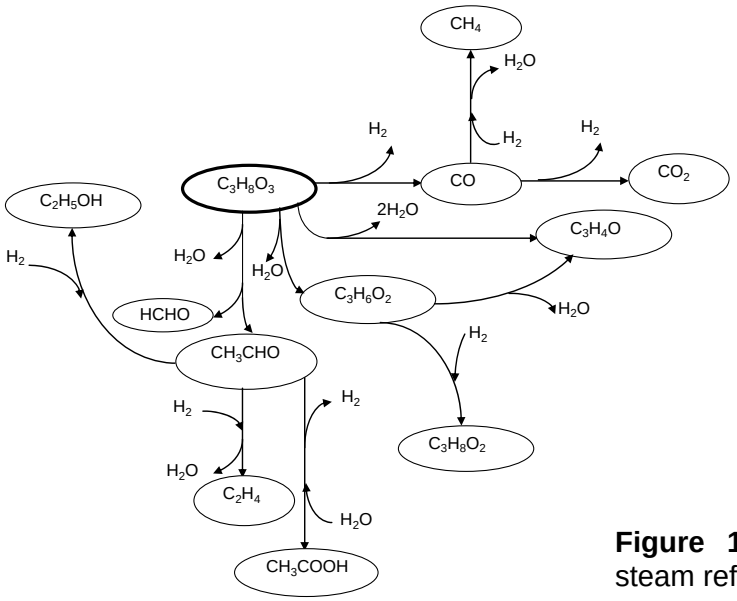


Figure 1: Reaction pathways in glycerol steam reforming.

A thermodynamic equilibrium analysis was performed for the steam reforming process of glycerol over the following variable ranges: pressure 1-5 atm, temperature 327-727 ^{o}C (600 – 1000 K), and water to glycerol feed ratio 1:1-9:1. The equilibrium concentrations of different compounds were calculated by the method of direct minimization of the Gibb's free energy. The study revealed that the best conditions for producing hydrogen is at a temperature > 627 ^{o}C (900 K), atmospheric pressure, and a molar ratio of water to glycerol of 9:1. Under these conditions methane production is minimized, and the carbon formation is thermodynamically inhibited.

As a part of catalysts screening, 14 catalysts were on a ceramic foam monoliths (92% Al_2O_3, and 8% SiO_2) using incipient wetness technique. Effects of these catalysts on hydrogen selectivity and glycerol conversion in temperatures ranging from 600-900 ^oC were discussed. Furthermore, the effects of glycerol/water ratio, metal loading, and feed flow rate (space velocity) were analyzed for the two best performing catalysts. Under the reaction conditions investigated, Ni/Al_2O_3 and $Rh/CeO_2/Al_2O_3$ were found as the best performing catalysts in terms of hydrogen selectivity and glycerol conversion. About 80% of hydrogen selectivity was obtained with Ni/Al_2O_3, whereas the selectivity was 71% with $Rh/CeO_2/Al_2O_3$ at 9:1 water/glycerin molar ratio, 900 ^oC temperature, and 0.15 ml/min feed flow rate (15300 GHSV). Although higher metal loading increased glycerin conversion for both catalysts, hydrogen selectivity remained relatively unaffected. At 3.5 wt% of metal loading, the glycerin conversion was about 94% in both the catalysts.

Effects of hydrogen production from glycerol via steam reforming process over different supports were studied on Ni/CeO_2, Ni/MgO, and Ni/TiO_2 catalysts. Catalysts were characterized using various techniques. Ni/CeO_2 catalyst had the highest surface area (67.0 m^2/gm) followed by Ni/TiO_2 (64.9 m^2/gm), and Ni/MgO (50.2 m^2/gm). Also, Ni/CeO_2 showed the highest metal dispersion (6.14 %) compared to Ni/MgO (0.38 %), and Ni/TiO_2 (0.29 %). Effects of reaction temperatures, feed flow rates, and water/glycerol molar ratios on hydrogen selectivity and glycerol conversion were analyzed. Ni/CeO_2 was found to be the best performing catalyst compared to Ni/MgO and Ni/TiO_2 under the experimental conditions investigated. Ni/CeO_2 gave the maximum hydrogen selectivity of 74.7 % (5.22 moles of H_2 out of 7) at water/glycerol molar ratio of 12:1, temperature of 600 ^oC, and feed flow rate of 0.5 ml/min compared to Ni/MgO (38.6%) and Ni/TiO_2 (28.3%) under the similar conditions.

The activation energy of glycerol reforming reaction was found to be 103 kJ/mol and the reaction order with respect to glycerol was 0.23 over Ni/CeO_2 catalysts based on the power law. The power law model was used to predict glycerol conversions and the model-predicted results are plotted along with experimental data in Figure 2.

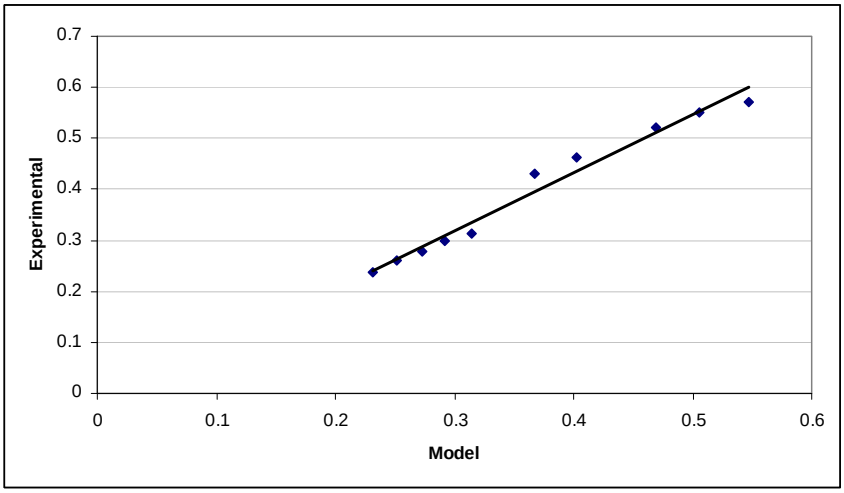


Figure 2: Experimental and model-predicted glycerol conversions showing an average deviation of 6.7% between the experimental and model-predicted conversion values.

The proposed glycerin droplet modeling work has been completed including investigations of molecular dynamics simulations for the lifetime nanoscale glycerin/water droplets, both at zero pressure and under ambient pressure supplied by nitrogen molecules. The findings are in agreement with the expected results; however, the atomistic simulation results also show that for the small nanodroplets a statistical interpretation of the lifetime data is required. A short paper on these simulations is currently in the draft form. On the other front, we have been able to develop and understand and confirm a theory for how rejection-free dynamic Monte Carlo algorithms perform as a function of inter-atomic potential and density. We have also devised a long-time dynamic Monte Carlo algorithm based on the Projective Dynamics method. Articles on each of these algorithmic advances are in draft form, and should become part of the theses of the two graduate students involved in these projects. We have evaluated the results we have and are deciding currently whether or not they will fit into an article, given the non-continuation of the project.

The activities were two-fold

- Molecular dynamics simulations of glycerin water nanodroplets
  - Constructed force fields for glycerin, water, and nitrogen using AMBER gaff
  - Devised methodology to equilibrate nanodroplets
  - Performed trial simulations of nanodroplet lifetimes, to compare with published results for nanodroplet lifetimes
    - Most droplets started with 1 nm or 2 nm radius
    - Mixtures of glycerin:water of 1:2 and 1:1 by number of molecules
  - Observed that the nanodroplets evaporated almost exclusively by only the water molecules leaving the nanodroplets in the time frame of the simulations
- Advanced algorithms for long-time simulations for nanodroplets
  - Obtained methodology for dynamic Monte Carlo simulations of interacting particles, building on those devised for hard particles
  - Advanced the methodology of Projective Dynamics, significantly enhancing its applicability in molecular dynamics, stochastic Brownian, and dynamic Monte Carlo simulations

Task H.2: *Production of Biohydrogen*

The aim of this task was to develop a biowaste-based medium for cheap, large-scale growth of the soil bacterium *Azotobacter vinelandii* with the bacterium serving as a source of biohydrogen. Nitrogenase of *A. vinelandii* produces hydrogen as a byproduct. *A. vinelandii* DJ54 is an *A. vinelandii* mutant that has the capability to generate biohydrogen at a better rate because a) the Mo-Nitrogenase is non-functional in this mutant, b) the V-nitrogenase could be inactivated by the absence of Vanadium in the medium, and c) the Fe-nitorgenase that produces hydrogen at a higher rate could be activated by the addition of excess Fe^{++} in the medium (in the absence of Molybdenum). Based on the growth rate information for wild-type *A. vinelandii*, further analysis was carried out to test the growth of both wild type and mutant *A. vinelandii* (*A. vinelandii* DJ54) using bio-waste based media. The bio-waste based media were devoid of added sugar or nitrogen. Thus, the sugar content essential for the growth of this *A. vinelandii* was obtained from the bio-waste material (Figure 3). Since the cells were grown in the absence of added ammonium (an essential component of Burke's $nitrogen^{+}$ medium in which the mutant *A. vinealndii* strain normally grows), it is expected that the biological nitrogen fixation was carried out by the activated Fe-nitrogenase.

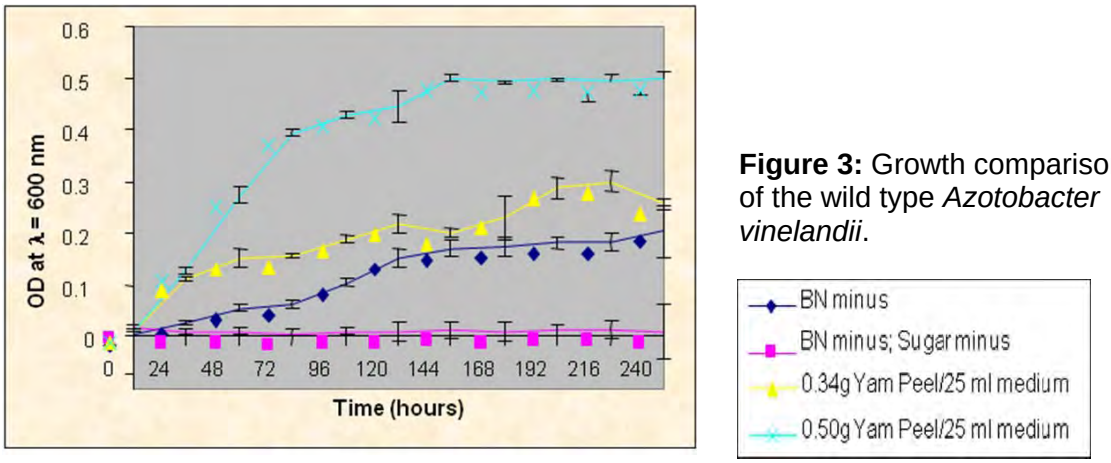


Figure 3: Growth comparison of the wild type *Azotobacter vinelandii*.

It was observed that the best growth medium for *A. vinelandii* DJ54 was corn-husk based medium with no added sugar, nitrogen, Molybdenum, or Vanadium (Figure 4). Moreover, *A. vinelandii* DJ54 could be maintained for several sub-culturing experiments on bio-waste based media in the absence of Molybdenum and in the presence of excess iron, a condition that activates the Fe-nitrogenase. We also developed medium that contains up to 2% lignin that could support diazotrophic growth of *A. vinelandii*. The significance of these observations is that we can use a bio-waste based media reliably for the growth of *A. vinelandii* that will serve as the hydrogen producing bacterium. To monitor expression of *nif* genes under these conditions (because the biomass-based medium could carry some nitrogen source), we developed a biomarker using *lacZ* gene cloned under the transcriptional regulation of *nif* promoter. Extent of expression of this biomarker correlates with the expression of the *nif* genes responsible for the production Fe-nitrogenase. According to literature, the average active rate of hydrogen evolution by Nitrogenase is 66mM/g cell protein/min and our future goal is to determine whether this level of hydrogen evolution is achieved when the cells are grown on biowaste-based medium.

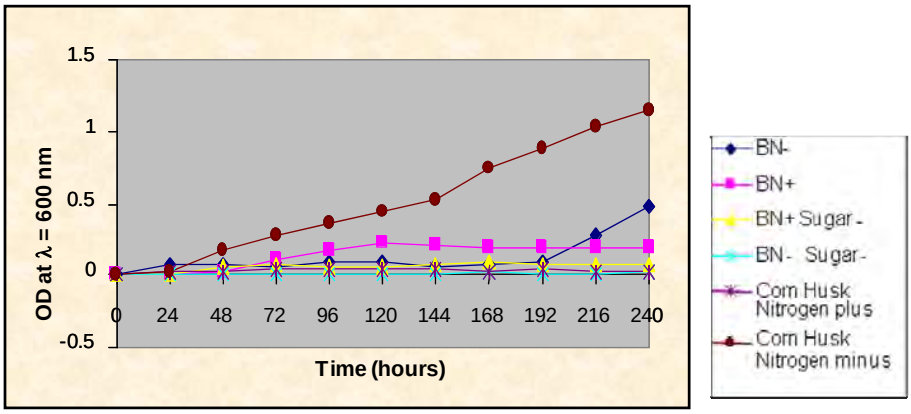


Figure 4: The Fe-nitrogenase over-expressing *A. vinelandii* mutant strain DJ54 grows most efficiently in corn husk-based media in the absence of added sugar, N, and Mo.

Gene cloning and the expression of the Fe-hydrogenase gene was also attempted. Specifically, our aim was to construct a hydrogenase biobrick to express the HydA a highly efficient, single unit hydrogenase from *E. cloacae,* an anaerobic bacterium, in the aerobic *A. vinelandii.* This task was completed. The *hydA* gene from *E. cloacae* was cloned under the transcriptional regulation of the *nifH* promoter and as a His-Tag fusion. The construct was made by cloning the

complete sequence as a blunt-end fragment in the Sma1 site of pUC57. The fragment contained built-in restriction sites for the restriction enzymes *EcoR*1 and *Hind*III at 5' and 3' respectively for further sub-cloning into other plasmids. The built-in *Bam*H1 site was used to insert a kanamycin resistance marker to use as a marker during the integration of this gene into *A. vinelandii* chromosome via homologous recombination between the construct and the *nifH* on the chromosome. The gene was flanked by the *nifH* promoter sequence at 5' side and the sequence starting from the stop codon of *nifH* and part of *nifD* sequence at the 3' region. The construct was released from the pUC57 by restriction digesting with appropriate enzymes and were subcloned either into pUC57 or pBHR1. A. vinelandii strains carrying the hydA biobrick were generated by transforming A. vinelandii strains OP (wild type) or DJ54. Expression of the HydA in nitrogen limiting conditions was monitored by Western blotting of the lysates from these strains and probing with anti-His antibody. Results of these experiments showed that HydA was efficiently expressed in aerobic *A. vinelandii.*

Production of hydrogen from biological systems dates back to the early nineteen sixties. Since that time a wealth of basic science has been conducted using a variety of organisms to produce bio-hydrogen. Much of the work on biological hydrogen production for commercial sales focuses on the green alga *Chlamydomonas reinhardtii* and some photosynthetic bacteria such as *Rhodospirillum rebrum*. However, there are some natural selective conditions which prohibit the production of hydrogen; most significantly is the sensitivity to oxygen and or ammonia and the slow release of hydrogen. This project focused on the co-culture of bacterial strains and algal cultures for the development of a sustainable photosynthetic system capable of producing high yields of bio-hydrogen. The use of both aerobic and anaerobic mesophilic and thermophilic algal and bacterial strains in developing the co-culture consortia and so exploiting both nitrogenase and hydrogenase enzyme systems was proposed; of specific interest were the marine algae and photosynthetic bacteria. The research will focus on identifying specific strains containing nitrogenase and or hydrogenase activities as they relate to hydrogen production and release. The specific aims were to: 1) determine if co-culturing of algae and bacterial strains can complement each other for the purpose of hydrogen production. 2) determine the specific elements that are involved and 3) develop and engineer alternative pathways for the production of biohydrogen. A combination of genetic transformation and knock out techniques and gene expression profiling were proposed as methods to identify key changes. This project was formally terminated after the second quarter of funding due to difficulty in securing graduate students.

A highly sensitive and specific optical fiber sensor based on laser induced fluorescence (LIF) was developed as an analytic tool to study changes in the physiological conditions of *Azotobacter vinelandii* in response in different growing media. This optical fiber sensor has the capability to quickly, non-invasively, and quantitatively probe biochemical transformations in accordance with growth conditions of *Azotobacter vinelandii.* A Y-shaped probe was used to deliver the excitation radiation to illuminate the sample cell at normal incidence to induce auto-fluorescence and then sent the collected fluorescence to detector. It has one launching fiber and six surrounding collecting fibers. The absorption spectra difference had close relationships with fluorescence spectral difference. From the absorption spectra of *Azotobacter vinelandii*, we found the excitation wavelength for distinguishing different growth condition should be in the range of 300-425 nm. To optimum the sensor performance we have evaluate different fluorescence excitation sources which included a 325 nm continuous wave (CW) He-Cd laser, a 355 nm frequency tripled pulsed Nd:YAG laser, a 405 nm CW diode laser, and a 442 nm CW He-Cd laser and a 532 nm CW-DPSS Nd:YAG laser. The performance of the laser systems were compared by recording the absorption and auto-fluorescence spectra from *Azotobacter vinelandii* grown under conditions that activate (nitrogen minus) or inactivate (nitrogen plus) *nif* gene expression under similar design configuration but with different excitation excitation light

source. The fluorescence emission spectra for *Azotobacter vinelandii* suspended in sterile saline suspension which had subtracted with background (fluorescence spectra with growth media) with different excitation wavelengths were recorded. To study shape difference, fluorescence spectra were normalized with respect to the fluorescence primary peak intensity in order to compare spectral features under different growth conditions. By comparing LIF spectra of *Azotobacter vinelandii* with the excitation wavelength of 325, 355, 405 and 425 nm, we found the most noticeable fluorescence spectra difference by a factor of ~10 at 402nm with 325-nm excitation wavelength. These results show that LIF can be used as a tool to differentiate between same bacteria that exhibit different physiological and biochemical parameters. Effects of various influential experimental parameters and configurations were investigated in order to optimize sensor performance.

In conclusion, we have demonstrated LIF based optical fiber sensor for distinguishing and identifying *Azotobacter vinelandii* corresponding to different growth environments that alter the expression of nitrogenase in *Azotobacter vinelandii*. This study has demonstrated that LIF spectra can offer preliminary information about the physiological and biochemical status of bacteria. Based upon the problem, LIF sensor can be modified and improved for better analysis. We expect these optical fiber sensor developments will have important implications on the development of better biosensors for the areas of bio-chemistry, chemistry, genetics research and agricultural industry.

Task H.3: *Hydrogen Storage Materials Development*

The reliable and efficient storage of hydrogen is a significant technological challenge for the successful integration of biomass feedstock in a renewable energy system. Despite significant research efforts over the past decade to obtain materials and design combinations for cost effective hydrogen storage capacity, significant gaps remain in terms of storage system weight, size, and reliable long-term integrity. This project proposed to bridge this gap using new combinations of nano-material technologies verified through experimental evaluation. A new class of micro- and nano-laminated nano-composites was to be designed and tested that incorporated zeolytes, catalyst, and fullerene-based carbon nanotube composites. This new material was to be tested in a high temperature and high-pressure reactor test-bed using accelerated cyclic loading/unloading to evaluate its performance in comparison with other solid-state storage materials under consideration. This project was terminated following the death of the PI.

Task H.4: *Production of Specialty Chemicals*

Selective cleavage of phosphate ester in phosphatidyl choline (PC), phosphatidyl ethanolamine (PE) and phosphatidyl serine (PS) (Figure 5) were investigated using the combined effect of lithium and zinc halide with potassium hydroxide in chloroform at moderate reaction temperatures (21-60 ^{o}C) and times (2-4 h). The catalytic effect of the resultant lithium and zinc hydroxide on carbonyl and phosphonyl ester cleavage was evaluated using FTIR, XPS and NMR. To qualitatively and quantitatively determine ester bond cleavage, FTIR peaks were identified and correlated to the functional groups present in the neat (un-reacted) and reacted phospholipid samples. Peak height

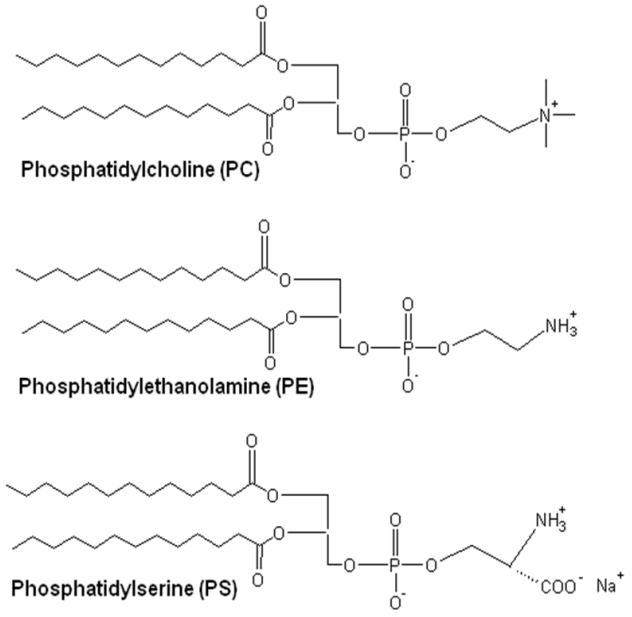


Figure 5: Phospholipid structures of phosphatidly choline (PC), phosphatidyl ethanolamine (PE), and phosphatidylserine (PS).

ratios (PHR) were then calculated and compared between reactions involving the phospholipids, catalysts, and reaction conditions tested. Carbonyl (C=O) and phosphonyl (P=O) stretching was observed for the ester functionalities present in these phospholipids at 1740 cm^{-1} and in the region of 1230-1000 cm^{-1}, respectively. Ratios of the C=O and P=O peak heights to the height of the aliphatic hydrocarbon (C-H scissoring bend) peak at 1465 cm^{-1} allowed the carboxylate ester and phosphate ester cleavage to be monitored and quantified. A decrease in the PHR of a particular functional group indicates that scission or chemical modification of that functional group or a related bond has occurred. Qualitative and quantitative analysis of reacted sample spectra revealed the formation of asymmetric carboxylate anion stretch (1577 cm^{-1}) and symmetric phosphonyl dianion stretch (1006 cm^{-1}) due to cleavage of the carbonyl and phosphonyl ester bonds.

Qualitative analysis revealed that ester bond cleavage was achieved in PC using lithium chloride and lithium bromide as the catalyst. In PE, only lithium chloride was found to bring about a significant cleavage of the ester bonds. In PS, no significant cleavage was observed with either lithium chloride or lithium bromide. Quantitative FTIR spectral analysis using PHRs confirmed significant cleavage of both carboxylate and phosphate ester bonds in (1) PC reacted with lithium chloride, (2) PC reacted with lithium bromide, and (3) PE reacted with lithium chloride. The success of these reactions is likely due to higher reactivity of lithium chloride versus lithium bromide and lithium iodide and polar interactions between the PS head group and the catalytic species which prevent ester attack. Reaction with lithium chloride at 60 ^{o}C for 4 h gave 82, 33, and 2% reductions in carboxylate ester groups in PE, PC, and PS, respectively. Under these same conditions, 65, 50, and 9% reductions in phosphonyl ester content were seen for PE, PC, and PS, respectively. None of the zinc halides studied produced significant ester bond cleavage; this is likely due to the lower reactivity of zinc halides in comparison to corresponding lithium halides. It was also found that reaction time and temperature did not have any significant effect on the cleavage of ester bonds as the cleavage reaction proceeds quickly at room temperatures.

A secondary goal of this project was to investigate use of the cleaved polar phosphate molecule in the synthesis of phosphate functionalized polymers. Substrates were formed by first depositing a thiol self assembled monolayer (SAM) on gold coated silicon wafers (Si-Au) and then grafting end-functionalized polymer to which phospholipid head groups will be substituted. The surface modified gold wafers were analyzed using external reflectance (ER) FTIR spectroscopy and static contact angle measurements (SCA).

Using a direct deposition method, amine end-functionalized polypropylacrylic acid (PPAA-NH_2) was grafted to gold substrates via thiol self assembled monolayers (SAMs) at 50 ^{o}C for 6, 12, 24 or 48 hours. The acrylic acid pendant groups in PPAA-NH_2 were substituted with phospholipid headgroups, namely phosphocholine, phosphorylethanolmine and phosphor-DL-serine. The substitution reaction was performed at 50 ^{o}C for 6, 12, 24 or 48 hours using methanol as the solvent. ER-FTIR spectra indicated successful thiol SAM deposition, PPAA-NH_2 grafting, and phosphate head group substitution. As only preliminary studies were conducted, the grafting density and robustness of the tethered polymer layers are not clear at this stage.

Additional, efforts were made to determine optimal operating parameters for the spatial separation of o-phospho-l-serine from 1,2-dioleoyl-sn-glycerol (two components comprising the phospholipid phosphatidyl serine, Figure 6(a)). The original tasks were to conduct literature searches to obtain information on other phosphate separation techniques, complete background on dielectrophoretic manipulation of molecules, and applicable fluorescent phosphate sensors. Simultaneously, the design and implementation of equipment for dielectrophoretic experiments was completed. Microdevice fabrication was also necessary to be able to then experimentally

test frequencies from 50 to 80 GHz and monitor phosphate ester response in the dielectrophoretic microdevices. Each of these tasks is discussed in turn.

Phosphatidyl-serine compounds are present in high concentrations in biofuels produced from sewage waste and similar sources. However, phosphates are undesirable in the finished fuels due to fouling and reduced octane ratings. A tandem project explored the chemistry of cleaving the phosphate headgroup from the lipid backbone. 1,2-O-phospho-l-serine (Figure 6b; CAS # 407-41-0) was chosen because it is similar in structure to phosphatidyl serine and allowed coordination with the cleavage project. 1,2-Dioleoyl-*sn*-glycerol (Figure 6c; Avanti Lipids) was chosen for its similar molecular weight & structure (mass weight of 620.538) to the lipid from phosphatidyl serine.

Exploration of dielectrophoresis (DEP) was chosen as a novel separation tool that selectively traps molecules of specific sizes and conductivities based on the frequency used in the non-uniform, AC electric field that is applied. The dielectric force is powerful because any electric field is squared for DEP force movement.

$$F_{DEP} = \tfrac{1}{2}\alpha\upsilon\nabla\left|E_e\right|^2$$

Theory predicts four dispersion regions and our o-phopsho-l-serine molecule was expected to be manipulated in the gamma dispersion region in the microwave frequencies (GHz) because these dispersions rely heavily on the internal characteristics (orientation relaxation of molecules).

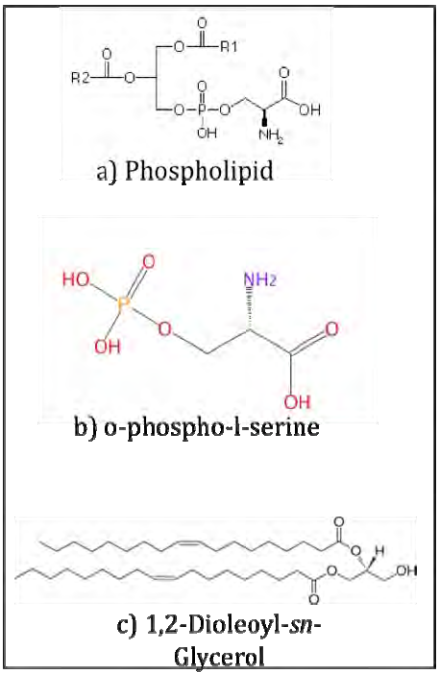


Figure 6: Chemical compounds investigated with dielectrophoresis (DEP).

Equipment to complete the dielectrophoretic experiments were purchased and properly installed. Electronic equipment included an Agilent CSA spectrum analyzer (N1996A-503), two Agilent analog signal generators with a frequency range of 250 kHz to 3 GHz (N581A-503), Agilent high resistance meter (4339B), and MiniCircuits combiners and amplifiers. Concurrently, fabrication of microdevices necessary to conduct the experiments was pursued and existing facilities (MCASP) at MSU were consulted to fabricate the devices. AUTOCAD drawings for fabrication masks were completed, but it was found that each generation of mask micromachined from this facility would be prohibitively expensive. Therefore, the lab invested in soft photolithography equipment (single wafer spin processor, Lindberg vacuum oven, vacuum pump, polydimethylsiloxane, and silicon wafers) which was installed and used to construct prototype microdevices for mounting on the fluorescent microscope stage. Microdevice masks were redesigned to minimize sample sizes and fluorescent light contamination.

Fluorescent controls were conducted for dielectrophoretic (DEP) trapping of a phosphate ester (o-phospho-l-serine) from 1,2-dioleoyl-sn-glycerol. Molecular Probes' PiPer Phosphate Assay Kit, a fluorescent detection kit, which excited and emitted light only in the presence of phosphate was found to increase its fluorescent intensity with time in the presence of o-phospho-l-serine in aqueous solution (Figure 7). This time dependent fluorescence added another dimension to the control experiments and ultimately made it impossible to quantify o-phospho-l-serine concentrations spatially in the dielectrophoretic field; qualitative data was collected instead. Calibration curves for fluorescent emission (at a fixed time of 15 minutes) of free phosphates both with and without the presence of 1,2-dDioleoyl-sn-glycerol (50/50 mixture) were completed. Phosphate molecules were fluorescently tagged and their behavior imaged in the

dielectrophoretic field from 50 to 80 GHz under our fluorescent video optical microscope. Fluorescent spatial images on the red channel (~600 nm) indicated positive identification of o-phospho-l-serine near the high field density electric field region. Fluorescence was able to track presence and position in the field, but could not be used to quantify phosphate molecules per unit area due to time dependent fluorescent emission changes. In conclusion, higher frequencies (near 80 GHz) produced the greatest separation as judged by spatial color changes. Voltage requirements are high (> 100 V/mm) to due to the small molecule diameter. Lipid manipulation would require less energy, lower frequencies.

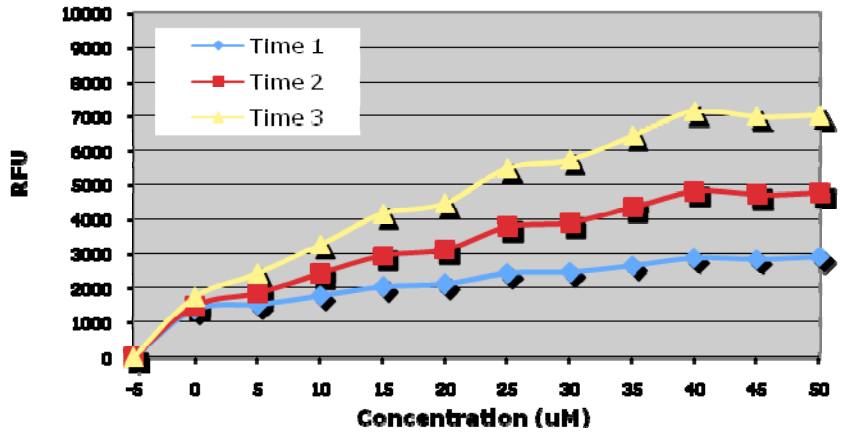


Figure 7: Fluorometer and video optical microscopy for o-phospho-l-serine at λ = 600 nm.

It was hypothesized that fatty acids could be crystallized from solution of suitable quality to be used in nutraceutical applications. For analysis purposes, GC calibration curves were developed for measuring the quantities of oleic, stearic, linoleic, and linolenic acids in hexane and in acetonitrile. Linoleic acid is highly soluble in hexane and requires very low temperatures to obtain separation. Specifically, the solubility is 53 g linoleic acid per 100 g hexane at -30 ^{o}C. To achieve good separation, a crystallizer would have to be operated at lower temperatures which would require significant refrigeration. In contrast, linoleic is much less soluble in acetonitrile with a solubility of 11.2 g linoleic acid per 100 g acetonitrile at 10 ^{o}C. Since it is much more practical to operate at higher temperatures, subsequent work focused on crystallization from acetonitrile. For linolenic acid, the literature solubility value was 3.33 g linolenic acid per 100 g acetonitrile at -22.5 ^{o}C. Due to the very low temperatures required to crystallize linolenic acid, it was not feasible to study linolenic acid. Therefore, the research focused on linoleic acid.

Work continued with both oleic acid (OA) and linoleic acid (LA) being crystallized from acetonitrile (ACTL). The solubility values for linoleic acid had a standard deviation of 0.155, which is about 10.8 % of the average solubility value. All of the data is at -10 ^{o}C. For oleic acid, GC results of 0.88 g OA/100 g ACTL are close to the literature data of Hoerr and Harwood (1952) of 1.1 g OA/100 g ACTL. It should be noted that the literature data was published in 1952 and that differences could well be due to advances in measurement techniques. For linoleic acid, current measurement values of 1.45 g LA/100 g ACTL are lower than the Hoerr and Harwood (1952) value of 4.9 g LA/100 g ACTL. This difference is also likely due to measurement techniques.

One key part of this work is determining the purity of the crystals formed. Experiments were performed with cooling rates ranging from 0.2 to 0.6 K/min. For all cases, the quantities of the materials added to the crystallizer were weighed. The crystals were recovered by using vacuum filtration. The concentrations of the solution and the crystals were measured by a GC at the end of the experiment. A mass balance on the system was performed to verify that concentration

measurements were consistent and reasonable. For both solutes, the purity was highest at the slowest cooling rate. The oleic acid crystals contained significant quantities of acetonitrile. The crystals were only about 20% oleic acid. Linoleic acid exhibited much higher purity with crystals that were 80 % linoleic acid when a cooling rate of 0.2 K/min was used (Figure 8). However, it is clear that a high purity cannot be obtained by crystallization for either one of these crystals. Since it was clear that the desired purities could not be obtained, detailed crystallization kinetics studies were not performed.

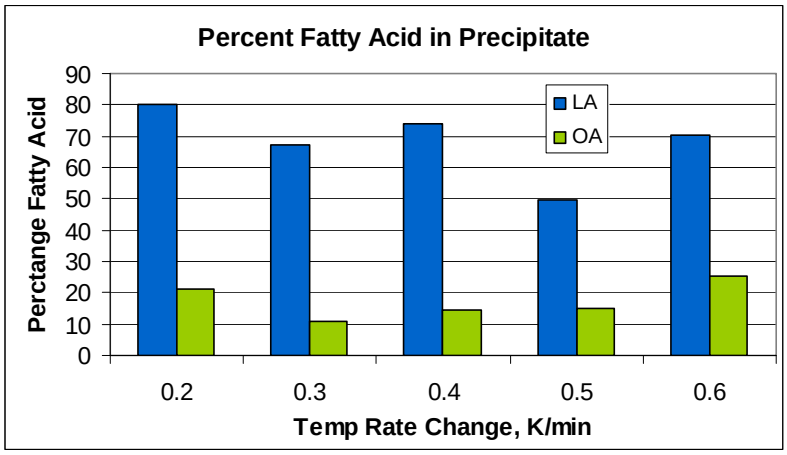


Figure 8: Percentages of linoleic (LA) and oleic (OA) acids present in the crystals precipitate.

Monomers from renewable (biomass and biofuel byproducts; Figure 9) can be polymerized into bioplastics through various synthesis chemistries, including melt polycondensation. The initial work on this project focused on the selection of catalysts to determine the most viable catalyst for the remainder of the research. Lewis acids that had little or no environmental impact and were readily available at low cost were screened as possible candidates for catalysts. The catalyst selection was done by co-polymerizing a diol and diacid at varying temperatures from 25 °C to 175°C with a 5 g reaction weight. The yields for each catalyst, determined by weight of polymer produced divided by theoretical yield, over a range of temperatures was used as the determining factor for further study. It was found that there was no statistical difference between the catalysts with a maximum yield of ~ 37%; however, these results were for small scale reactions conducted under mass transfer limited conditions. Based on the usage conditions and polycondensation results in the literature, aluminum chloride was chosen as the catalyst for the remainder of the studies. Mass transfer limitations were removed through use of a larger reaction vessel, higher monomer charge (50 g), stirring, and vacuum which resulted in increased reaction yields and molecular weights, as determined by gel-permeation chromatography.

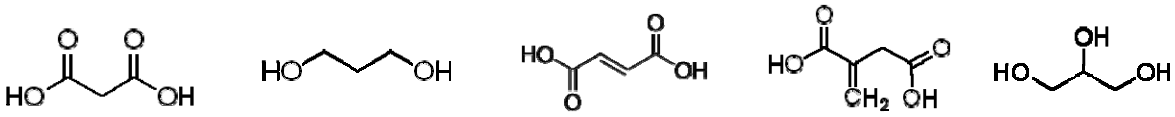


Figure 9: Poly-alcohol and acid monomers tested which are available as biomass platform chemicals.

Poly-alcohols and poly-acids were then copolymerized under the modified conditions (larger reaction vessel, higher monomer charge (50 g), stirring, and vacuum). Additional reaction parameters included the use of aluminum chloride as the catalyst, temperatures between 125

and 175 °C at 10 °C intervals, and a 1:100 monomer to catalyst ratio. Results from this set of reactions indicated that reaction yield and molecular weight were functions of temperature with yields reaching a maximum of 80% and molecular weights greater than 5 kDa. Time was also examined as a variable; copolymerizations were performed from 2 to 32 hours at a specified temperature and catalyst to monomer ratio. These results showed reaction time was a significant factor for these copolymerizations when trying achieve molecular weights greater than 5 kDa and yields greater than 80%. The alcohol to acid molar ratio was varied to determine the influence of the concentration of functional groups on yield and molecular weight. The ratio was varied from 90% to 10% alcohol molar concentration at a fixed temperature and reaction time. The data showed that higher alcohol concentrations produced the highest yields, which is supported by the literature.

The final set of polymerizations were run using variations in the monomer to catalyst molar ratio. The ratio was varied from 1:100 to 1:10,000 at a fixed temperature and reaction time. Upon increasing the ratio, the reaction yields fell off dramatically indicating a need for lower monomer to catalyst molar ratios.

An preliminary degradation study was performed where uniform polymer coupons were placed in water at varying pH values, times, and temperatures. It was demonstrated from these degradation experiments that hydrolytically degradable bioplastics have been developed with degradation rates that are dependent on time, temperature and pH.

The products of the polymerization reactions were analyzed with Fourier transform infrared (FTIR) spectroscopy to determine chemical composition and gel-permeation chromatography (GPC) to detemrine molecular weight and polydispersity index. Select samples were analyzed with proton nuclear magnetic resonance (NMR) and X-ray photoelectron spectroscopy (XPS) to further verify the chemical structure and differential scanning calorimetry (DSC) to determine glass transition and melting point temperatures. The condensate from select reactions was analyzed with liquid chromatography-mass spectroscopy (LC-MS) for insight into the side products of these reactions. Chemical characterization of the polymers with FTIR, NMR and XPS has allowed for the deduction of the kinetic mechanisms behind these polymerization reactions.

Using FTIR spectroscopy, it has been demonstrated that not only is the (expected) ester linkage present in the backbone of these polymers, but there is also evidence of a substantial amount of anhydride and ether linkages. The ability to control the linkage type will influence the crystallinity and the rate of degradation for these polymers. The polymer composition also provided insight into the reactivity of the (poly)acid and (poly)alcohol monomers studied. It was initially assumed that the acids would only react with the alcohols, but this was disproven. Furthermore, the determination of the concentration of each linkage type gives insight into the validity of the equal reactivity assumption, which is common in polycondensation reactions. The chemical analysis also showed that the resultant chemical composition of the polymers was dependent on time, temperature, alcohol to acid molar ratios, and monomer to catalyst molar ratios. FTIR spectroscopy was also used to demonstrate that the anhydride bonds degrade first and so the degradation rate can be controlled by controlling the anhydride concentration. NMR spectroscopy was performed in deuterated chloroform with TMS as a reference. NMR verified the chemical structures determined by FTIR. Investigation of whether the surface composition of these polymers was different from the bulk chemical composition was done by XPS. Analysis of the XPS spectra showed no significant difference in the surface chemical composition from the bulk (as determined by FTIR). By analyzing the polymerization condensate with LC-MS further verified that all three linkages (ester, ether, and anhydride) are present and that the aluminum chloride was chlorinating both the alcohols and acids.

Characterizations using GPC allowed for determination of molecular weights and showed that the reactions had multimodal distributions. For some of the copolymers, the multimodal

distribution can be explained by branching of the polymers produced from poly-ols and unsaturated monomers. For the linear polymers, the multimodal distribution, with at least one of the components being greater than 20 kDa, is explained by a combined reaction scheme involving both step-growth and chain-growth polycondensation routes. Normally when performing melt polycondensation, yields greater than 99% are needed to achieve molecular weights greater than 5 kDa. If both routes exist simultaneously, higher molecular weights can be achieved at lower yields. It was also demonstrated that the dominant synthesis route was dependent on reaction time, reaction temperature, alcohol to acid molar ratios, and monomer to catalyst molar ratios and could be controlled to achieve molecular weights greater than 5 kDa. DSC was used to determine a glass transition temperature below -20 °C and a melting point above 30 °C for the linear polymers. The branched polymers glass transition and melting point temperatures could not be determined using DSC.

A series of novel degradable, renewable copolymers (bioplastics) were synthesized from biomass-based monomers (Table 1) with controllable chemical structures, yields and molecular weights dependent on time, temperature, alcohol to acid molar ratios, and monomer to catalyst molar ratios.

Table 1: Summary of bioplastics synthesized including yields, molecular weight distributions, and polymer structure.

Copolymer	Yield	Mw (Bimodal)	Structure
PDO-MA	2% – 90%	1 – 10 kDa, 20 – 50 kDa	Linear, saturated polymer
PDO-IA	9% – 90%	1 – 3 kDa, 20 – 65 kDa (branched polymers)	Branched, unsaturated polymer
GLY-FA	18% – >99%	N/A (insoluble polymer)	Highly branched, unsaturated polymer

6. Products Developed and Technology Transfer Activities:

Patents: None

Publications:

Adhikari, S., Fernando, S., and Haryanto, A., "Production of hydrogen by steam reforming of glycerin over alumina supported metal catalysts," *Catalysis Today*, **2007**, 129 (3-4), 355-364.

Adhikari, S., Fernando, S., Gwaltney, S., Filip To, S.D., Bricka, R.M., Steele, P.H., and Haryanto, A., "A thermodynamic analysis of hydrogen production by steam reforming of glycerol," *Int. Journal of Hydrogen Energy*, **2007**, 32(14), 2875-2880.

Adhikari, S., Fernando, S., and Haryanto, A., "Glycerin steam reforming for hydrogen production," *Transactions of ASABE*, **2007**, 50(2), 591-595.

Adhikari, S., Fernando, S., and Haryanto, A., "A comparative thermodynamic and experimental analysis on hydrogen production by steam reforming of glycerin," *Energy & Fuels*, **2007**, 21(4), 2306-2310.

Adhikari, S., Fernando, S., and Haryanto, A., "Hydrogen production from glycerin by steam reforming over nickel catalysts," *Renewable Energy*, **2008**, 33(5), 1097-1100.

Adhikari, S., Fernando, S., Filip To, S.D., Bricka, R.M., Steele, P.H., and Haryanto, A., "Conversion of glycerol to hydrogen via steam reforming process over nickel catalysts," *Energy & Fuels,* **2008**, 22(2), 1220-1226.

Adhikari, S. and Fernando, S., "Nanoparticles Production from Glycerin via Electrospray and Size Measurement Techniques," *Transactions of ASAE*, **2006**, 49(4):1269-1272.

Adhikari, S., Fernando, S., and A. Haryanto, "Thermodynamic and Experimental Analysis on Hydrogen Production by Steam Reforming of Glycerin," *Energy and Fuels*, **2007**, 21(4), 2306-2310.

Fernando, S. Adhikari, S., and S. Chandrapal, "Biorefineries: Current Status, Challenges and Future Directions," *Energy and Fuels*, 2006, 20*,* 1727-1737.

Haryanto. A, Fernando, S. and S. Adhikari. 2007. "Ultrahigh Temperature Water Gas Shift Catalysts to Increase Hydrogen Yield from Biomass Gasification," *Catalysis Today*, **2007**, 129(3-4) 269-274.

Kim, C.K., Yueh, F.Y., Singh, J.P., Dong, H., Gavini, N., and Pulakat, L., “Optical Sensor for studying the differences between auto fluorescence spectra of nitro-fixing and non-nitrogen fixing *Azotobacter Vanelandii*,” submitted to *Applied Spectroscopy*.

Lahiri, S., Pulakat, L., and Gavini, N., “Functional Participation of a nifH-arsA2 Chimeric Fusion Gene in Arsenic Reduction by *Escherichia coli*,” submitted to *J. Bacteriology*.

Minerick, A.R. “DC Dielectrophoresis in Lab-on-a-Chip Devices,” in the Encyclopedia of Micro- and Nanofluidics, Li, Dongqing (ed), Springer, Berlin Heidelberg New York, in press.

Minerick, A.R., Ugaz, V.M., Murthy, S., Posner, J.P., "Review of Electrophoresis and BioMEMS in 2007: American Electrophoresis Society 24th Annual Meeting," *Journal of Capillary Electrophoresis and Microchip Technology*, **2008**, accepted and in press.

Mohan, V., Gandy, J.M.; Crosby, S.E.; Hubbard, L.E.; Walters, K.B. “Selective Ester Cleavage in Phospholipids,” manuscript in preparation.

Reeves, S.M. and Hill, P.J., “Cooling Rate Effect on the Crystallization of C18 Fatty Acids,” manuscript in preparation.

Rowe, M. D., Walters, K. B., “Synthesis and Characterization of Copolymers based on 1,3-Propane Diol, Malonic Acid, and Itaconic Acid,” manuscript in preparation.

Adhikari, S., Fernando, S., and Haryanto, A., “Hydrogen Production from Renewable Alcohols over Pt and Ni Catalysts,” ASABE Annual International Meeting, Minneapolis, MN. June 17-20, 2007, paper # 076001.

Adhikari, S., Fernando, S.D., and Haryanto, A., “Steam reforming of glycerin for hydrogen production over Ni catalyst,” Preprints of Symposia, American Chemical Society, Division of Fuel Chemistry, 2007, 52(1), 180-181.

Adhikari, S. and Fernando, S.D., “Nanoparticle production from glycerin via electrospray and size measurement,” Annual International Meeting ASABE, Portland OR, July 9-12, 2006, paper # 066073.

Adhikari, S. and Fernando, S.D., “Glycerin Steam Reforming for Hydrogen Production,” Annual International Meeting ASABE, Portland OR, July 9-12, 2006, paper # 066222.

Adhikari, S., Fernando, S., Haryanto, A., “Sugar steam reforming for hydrogen production,” Abstracts of Papers, 232nd ACS National Meeting, San Francisco, CA, United States, Sept. 10-14, 2006.

Adhikari, S., Fernando, S., Gwaltney, S.R., Haryanto, A., “A thermodynamic analysis of hydrogen production by steam reforming of glycerol,” Abstracts of Papers, 232nd ACS National Meeting, San Francisco, CA, United States, Sept. 10-14, 2006.

Haryanto, A. and Fernando, S., “Producing Sustainable Hydrogen from Biomass Gasification Coupled with Wager Gas Shift Catalysts,” Annual International Meeting ASABE, Portland OR, July 9-12, 2006, paper # 066226.

Jha, S.K. and Fernando, S., “Analysis of Diesel Engine Exhaust Fueled with Blends of Biodiesel and Ethanol,” Annual International Meeting ASABE, Portland OR, July 9-12, 2006, paper # 066138.

Rowe, M.D., Smith, E.M., Walters, K.B., “Development of Renewable Polymers From 1,3-Propane Diol and Malonic Acid,” Proceedings of ANTEC – Society of Plastics Engineers, Cincinnati, OH, (2007), 65, 1562-1568.

Singh, A. and Fernando, S., “Base Catalyzed Transesterification of Soybean Oil Using Ultrasonication,”A nnual International Meeting ASABE, Portland OR, July 9-12, 2006, paper # 066220.

Kim, Chan Kyu "Development of biophotonics sensor based on laser induced fluorescence," Ph.D. Dissertation, Department of Physics, Mississippi State University, December 2007.

Mohan, V., "Selective Ester Cleavage in Phospholipids," M.S. Thesis, Swalm School of Chemical Engineering, Mississippi State University, August 2008.

Presentations:

Adhikari, S., Fernando, S., and Haryanto, A., "Hydrogen Production from Renewable Alcohols over Pt and Ni Catalysts," ASABE Annual International Meeting, Minneapolis, MN, June 17-20, 2007 (paper # 076001).

Adhikari, S. and Fernando, S.D., "Nanoparticle production from glycerin via electrospray and size measurement," Annual International Meeting ASABE, Portland OR, July 9-12, 2006 (paper # 066073).

Adhikari, S. and Fernando, S.D., "Glycerin Steam Reforming for Hydrogen Production," Annual International Meeting ASABE, Portland OR, July 9-12, 2006 (paper # 066222).

Adhikari, S., Fernando, S., and Haryanto, A., "Steam reforming of glycerin for hydrogen production over Ni catalyst," American Chemical Society Meeting, Division of Fuel Chemistry, Chicago, IL March 25-29, 2007.

Adhikari, S., Fernando, S., and Haryanto, A., "Production of hydrogen by steam reforming of glycerin over alumina supported metal catalysts," Institute of Biological Engineering Meeting, St. Louis, MO, March 30-April 1, 2007.

Adhikari, S., Fernando, S., Haryanto, A., "Sugar steam reforming for hydrogen production," 232nd ACS National Meeting, San Francisco, CA, United States, Sept. 10-14, 2006.

Adhikari, S., Fernando, S., Gwaltney, S.R., Haryanto, A., "A thermodynamic analysis of hydrogen production by steam reforming of glycerol," 232nd ACS National Meeting, San Francisco, CA, United States, Sept. 10-14, 2006.

Adler, K.L.; Mathew Rowe, M.D.; Walters, K.B. "Surface Characterization of Tethered Responsive Polyamine Films for Biomedical Applications," 2007 MSU Chemistry:Chemical Engineering – The Bonds Between Us REU Poster Symposium, July 27, 2007.

Álvarez Lugo, E.L.; Rowe, M.D.; Walters, K.B. "Physio-Chemical Properties of Lung Tissue," 2007 MSU Chemistry:Chemical Engineering – The Bonds Between Us REU Poster Symposium, July 27, 2007.

Dong, H., Matthews, A., Cunningham, M., Gavini, N., and Pulakat, L., "Optimization of Organic Waste Based Media Sustainable to Biohydrogen Production," Mississippi Academy of Sciences Annual Meeting, February 21-23, 2007.

Dong, H., Matthews, A., Pulakat, L., and Gavini, N., " Role of NIFH GLU112 in Binding to NIFK of Nitrogenase Complex," Mississippi Academy of Sciences Annual Meeting, February 21-23, 2007.

Haryanto, A. and Fernando, S., "Producing Sustainable Hydrogen from Biomass Gasification Coupled with Wager Gas Shift Catalysts," Annual International Meeting of ASABE, Portland OR, July 9-12 (paper # 066226).

Jamnekar, G.V., Pulakat, L., and Gavini, N. "Folding Pathway of the Fe-Protein: Effect of Amino Acid Replacements on NIFM Independent Fe-Protein Conformation," Mississippi Academy of Sciences Annual Meeting, February 21-23, 2007.

Jha, S.K. and Fernando, S., “Analysis of Diesel Engine Exhaust Fueled with Blends of Biodiesel and Ethanol,” Annual International Meeting of ASABE, Portland OR, July 9-12 (paper # 066138).

Mohan, V., Hubbard, L; Gandy, J; Crosby, S.; Walters, K.B. “Selective Ester Cleavage in Phospholipids –Towards the Development of Phosphate Polymers,” American Institute of Chemical Engineering (AIChE), Salt Lake City, Utah, November 4-9, 2007.

Mohan, V.; Hubbard, L.; Walters, K.B. “Selective Phosphate Ester Cleavage in Phospholipids,” MSU ESCAPE Conference, March 2-4, 2007.

Mohan, V., Hubbard, L.; Crosby, S.; Walters, K.B. “Selective Ester Cleavage in Phospholipids -- Towards the Development of Phosphate Polymers,” National Polymer Graduate Research Conference sponsored by the American Chemical Society (ACS) Division of Polymer Chemistry, Oak Ridge National Lab, Oak Ridge TN, June 2007.

Mohan, V., Hubbard, L., Walters, K. B., “Reaction Conditions for the Selective Cleavage of Phosphate Esters in Phospholipids,” MSU GSA Research Symposium, March 30, 2007.

Mohan, V., Hubbard, L., Walters, K. B., “Phosphate Ester Cleavage in Phospholipids,” MS Academy of Sciences 71st Annual Meeting, February 21-23, 2007.

Novotny, M.A., “Physics Research at MSU and Grassroots Advocacy and the American Competitive Initiative (ACI),” invited presentation, Mississippi Association of Physicists, Mississippi State University, Mississippi State, MS, Oct. 21, 2006.

Novotny, M.A., “Non-equilibrium Statistical Physics Applied to Parallel Computing,” invited presentation, 3rd International Workshop on Simulational Physics, Zhejiang University, Hangzhou, China, Nov. 16-18, 2006.

Proctor, G., P.T. Jouben, and Minerick, A.R., "Fluorescence in Cellular Microfluidic Devices," Final Symposia of the NSF REU Site Chemistry - Chemical Engineering: The Bonds Between Us, July 27, 2007.

Pulakat, L. and Gavini, N., “Expression of Functional *hydA* from Anerobic *Enterobacter cloacae* into Aerobic *Azotobacter vinelandii*,” 108th General Meeting, American Society for Microbiology, June 2008, Boston, MA.

Reeves, S.M. and Hill, P.J., “Effect of Cooling Rate on Oleic and Linoleic Acid Crystal Compositions,” accepted for presentation, AIChE Annual Meeting, November 2008.

Rowe, M.D.; Walters, K.B. “Synthesis and Characterization of Renewable Copolymers: Poly(glycerol-fumarate) and Poly(trimethylene-malonate),” presented National Polymer Graduate Research Conference sponsored by the American Chemical Society (ACS) Division of Polymer Chemistry, Oak Ridge National Lab, Oak Ridge TN, June 2007.

Rowe, M. D., Smith, E. M., Walters, K. B., “Development of Renewable Polymers From 1,3-Propane Diol and Malonic Acid,” ANTEC - Society of Plastics Engineers - Cincinnati, OH, May 6-11, 2007.

Rowe, M. D., Walters, K. B., “Synthesis and Characterization of Bioplastics,” ANTEC - Society of Plastics Engineers - Cincinnati, OH, May 6-11, 2007.

Rowe, M.D., Terrell, L.B., Smith, E.M., Walters, K.B., “Synthesis, Characterization, and Degradation of Renewable Copolymers,” poster presented at the 2007 American Institute of Chemical Engineers Annual Meeting, Salt Lake City, UT, November 2007.

Rowe, M.D., Smith, E.M., Terrell, L.B., Walters, K.B., “Synthesis and Characterization of Renewable Copolymers: Poly(Glycerol-Fumarate) and Poly(Trimethylene-Malonate),” poster

presented at the 2007 American Institute of Chemical Engineers Annual Meeting, Salt Lake City, UT, November 2007.

Rowe, M.D.; Smith, E.M.; McMaster, A.; Walters, K.B. "Development of Renewable Polymers from 1,3-Propane Diol and Malonic Acid," poster presented at the 2007 AIChE Southern Regional Conference, March 30-April 1, 2007.

Rowe, M.D.; Smith, E.M.; Walters, K.B. "Renewable Polymer Development Using 1,3-Propane Diol, Glycolic Acid, and Malonic Acid," MSU ESCAPE Conference, March 2-4, 2007.

Rowe, M.D.; Smith, E.M.; Terrell, L.B.; Walters, K.B. "Development of Renewable Polymers from 1,3-Propane Diol and Malonic Acid," poster presented at the 2007 SPE Mississippi Chapter Meeting, March 6, 2007.

Rowe, M. D., Smith, E. M., Walters, K. B., "Development of Renewable Polymers From 1,3-Propane Diol and Malonic Acid," MS Academy of Sciences 71st Annual Meeting; Journal of the Mississippi Academy of Sciences, February 21-23, 2007.

Rowe, M. D., Smith, E. M., Walters, K. B., "Synthesis and Characterization of Renewable Polymers Produced From 1,3-Propane Diol, Glycolic Acid, and Malonic Acid," Presented at the MSU GSA Research Symposium, March 30, 2007.

Rowe, M. D., Smith, E. M., Terrell, L., McMaster, A., Walters, K. B., "Development of Renewable Polymers Produced From 1,3-Propane Diol, Glycolic Acid, and Malonic Acid," Poster presentation at the American Institute of Chemical Engineers (AIChE) Southern Regional Conference, March 30-April 1, 2007.

Rowe, M.D., Crosby, S., Walters, K.B., "Dependence of Hydrolytically degradable Poly(ester-anhydride) Copolymers on Temperature and Time," accepted for presentation at the Annual Meeting of AIChE, Philadelphia, PA, November 16-21, 2008.

Rowe, M.D., Walters, K.B., "Development and Characterization of Copolymers from Renewable Resource Monomers," accepted for presentation at the Annual Meeting of AIChE, Philadelphia, PA, November 16-21, 2008.

Rowe, M.D., Walters, K.B., "Hydrolytic Degradation of Renewable Copolymers," accepted for presentation at the Annual Meeting of AIChE, Philadelphia, PA, November 16-21, 2008.

Rowe, M.D., Walters, K.B., "Development and Characterization of Renewable Copolymers Poly(glycerol-fumarate) and Poly(trimethylene-malonate) from By-products of Biorefineries," Joint AIChE-ACS Meeting, AIChE 2008 Spring National Meeting and 235th ACS National Meeting, New Orleans, LA, April 6-10, 2008.

Rowe, M.D., Walters, K.B., "Synthesis, Characterization, and Degradability of Renewable Copolymers," 2007 American Institute of Chemical Engineers Annual Meeting, Salt Lake City, UT, November 2007.

Singh, A. and Fernando, S., Base Catalyzed Transesterification of Soybean Oil Using Ultrasonication," Annual International Meeting ASABE, Portland OR, July 9-12, 2006 (paper # 066220).

Tiwari, V.S., Yueh, F.Y., Singh, J.P., Cunningham, M., Pulakat, L., and Gavini, N., "Study of Bacteria using Raman Spectroscopy," SPIE-Optics East 2006, October 1-4, 2006, Boston, MA.

Tiwari, V.S., Yueh, F.Y., Singh, J.P., Cunningham, M., and Pulakat, L., "Spectroscopic Methods for Identifying Bacteria Cells," MS Academy of Sciences 71st Annual Meeting, February 21-23, 2007.

Web sites:

Electrophoresis project (Subtask H.4.2) was described at http://www.che.msstate.edu/research/MDERL/ from March 07 to July 08.

Development of renewable polymers (Task H.5) project is described at http://www.che.msstate.edu/research/PolySEL/research.html.

Networks or collaborations fostered:

Collaboration between simulation and experimental groups for glycerol reforming and modeling (Subtask H.1.2).

In order to complete the controls for the fluorescence work, it was necessary to cooperate with the people at the Life Sciences Biotechnology Institute. The spatial recording of fluorescence in a dielectrophoretic field has formed the basis for collaboration with David Wipf, MSU chemistry (Subtask H.4.2).

Other products:

A highly sensitive and specific optical fiber sensor based on laser induced fluorescence (LIF) has been developed as an analytic tool to study changes in the physiological conditions of *Azotobacter vinelandii* in response in different growing media (Subtask H.2.4).

7. Computer modeling:

For glycerin/water modeling efforts (Subtask H.1.2):

Nanodroplet Molecular Dynamics Simulations

a) Model used AMBER gaff force fields, the program NAMD for the simulations, and the program VMD for visualization; assumed that molecular dynamics simulations would be adequate to test certain predictions of nanodroplet production and nanodroplet lifetimes
b) The actual simulations of a 2 nm radius nanodroplet took on the order of five months on 48 processors to achieve physical simulation times of tens of nanoseconds
c) Tested against estimates from statistical mechanical calculations
d) The theory is to use the computer to integrate Newton's equations of motion for a system composed of many atoms with realistic force fields between the atoms
e) Well established, see documentation for program NAMD
f) Well established procedure
g) Many months of simulation time on many tens of processing elements were required, even for the test runs that were performed
h) N/A

Rejection-free Dynamic Monte Carlo for Continuous Systems

a) Realistic two-body forces between atoms, with a Brownian dynamic caused by lighter particles
b) Showed that the algorithm would perform much better than normal algorithms in the low-temperature, high-density regime
c) Yes, the theoretical predictions and the simulations agreed for the algorithmic speedup
d) The theory used absorbing Markov Chains, Brownian dynamics, and event-driven simulation methodologies
e) Formulas in the paper on http://arxiv.org/abs/0807.4759
f) Submitted for peer review to Physical Review E
g) Required months of simulation time on a single powerful workstation
h) In the preprint on arxiv

Enhancements to the Projective Dynamics Algorithm

a) Assumes a time-dependent development from a starting state to a set of absorbing states, and that the average lifetime is required between these two, for any physical system
b) Currently have just showed that the algorithmic method produces the correct results, so no speed-up yet
c) Test results in one-dimension, where we could compare with exact solutions, and in two dimensions validate the results
d) The theory uses ideas of a particular type of absorbing Markov chain, which has the property of being almost weakly lumpable
e) Theory requires about two pages of mathematics to give outline of method
f) Paper is currently being written
g) Proof-of-concept required only months on a fast workstation
h) Will be in the paper submitted for publication in the technical literature

Sustainable Energy Research Center
Feedstocks Thrust Area Final Report for 2006 - 2008

1. Project title, principle and co-investigators: Section I. Feedstocks (Oilseeds and Lignocellulosic)

Thrust Leader: Mike Collins, Jac J. Varco
Co-investigators: Brian S. Baldwin, D.L. Grebner, Dwight Kanter, David Lang, Bisoondat Macoon, Zhaohua Peng, K. Raja Reddy, Mark W. Shankle, Tim Walker

2. List of authorized distribution: Unlimited distribution

3. Executive Summary

Feedstocks research was conducted with an emphasis on sustainable agronomic production potential of bioenergy-specific crops which offer the possibility of being grown on land less desirable for traditional food crop production.

Task I. 1: Characterized lignocellulosic crops for use as bioenergy crops in MS
Dry matter yield trials of of lignocellulosic crops (switchgrass and giant miscanthus) at Raymond, Newton, Pontotoc and Starkville, MS locations. Additionally, energycane, naipergrass and sweet sorghum were tested at Starkville. Switchgrass and giant miscanthus have an advantage in that they dry down in fall, making harvest and storage easier.

Task I.1 DL.1: Dataset on characteristics and yield of lignocellulosic crops in MS
Post-establishment year dry weight yields ranged from 2900-9430 kg ha^{-1}. Switchgrass was the lowest yielding, followed by sweet sorghum, giant miscanthus. Dry weight yield of energycane cultivars ranged from 8300 - 26,100 kg ha^{-1} at Starkville. A late spring frost seemed to severely compromise naipergrass yield. Ash was substantially lower in switchgrass and giant miscanthus vs. sorghum, naipergrass, and energycane. This will have implications in fertility requirements of the crop.

Task I.2: Characterize oilseed crops for use as bioenergy crops in MS
See Section A5. Castor (*Ricinus communis*), okra (*Ablemosheus esculentus*), and sunflower (*Helianthus annuus*) were investigated as summer crops. Canola (*Brassica napus*) , oriental mustard (*B. juncea*), coriander (*Coriandrum sativum* L.), crambe (*Crambe abyssinica* Hochst), and camelina (*Camelina sativa* (L.) Crantz.) Were evaluated as potential winter crops. Castor is a full season high oil seed. Availability of determinant types of sunflower and okra allow for their use (June planting dates) following winter annual species (May harvest dates).

Task I.2.DL. 1: Dataset on characteristics and yield of oilseed crops in MS

See Section A5. Sunflower yield and oil content were affected by date of planting, nitrogen fertilization and location of production. Oil yields ranged from 483 to 1388 L ha^{-1}. Blackbird predation was severe on late planted fields. Productivity of winter canola, winter mustard, and coriander were equal to or exceeded average yields reported in the literature. Flax was slightly less, but has the advantage of linen as a bioproduct. Crambe, and camelina did not perform well in Mississippi although manipulations in cultural practices and genetics offer the possibility for greater success. Okra yields were limited by weather. Oil content of the 22 cultivars tested ranged from 9 to 14.5% oil. Fatty acid profile was similar to cottonseed, but individual fatty acids varied by cultivar.

Task I.3: Characterize physiological limits of select bioenergy crops in MS
Crambe was not cold hardy enough to survive winter. Canola, crambe, and mustards could not tolerate waterlogged soils; thought modification of cultural practices would ameliorate these issues. Warm spring temperatures followed by a spring frost severely damaged canola yields. Screening of 12 field-grown canola cultivars identified cold- and heat-tolerant cultivars. Yields of castor seed peaked at Starkville and Memphis sites, similar latitudes to that in which the cultivar was developed.

Task I.3. DL.1: Dataset on the physiological limitations of specific bioenergy crops in MS
Crambe, which is typically grown as a summer annual in the North, has a low temperature threshold of 4.5°C. Critical leaf N values which are needed to optimize N fertilization rates were determined for switchgrass and castor and a system for detection using remote sensing technology is in the early phases of development. Various weed control options in switchgrass establishment. Through selective breeding, switchgrass precoious germination has been increased from 0.8 to 70%. Interseeding of switchgrass with legumes has shown some benefit.

Task I.4: Modify cell walls for cost efficient bio-fuel production
It has been shown that high moisture in straw and thus slow burning rate is the primary obstacle in direct syngas production from rice (*Oryza sativa*) straw. To resolve the problem, we have generated transgenic rice that overexpresses a regulatory gene in lipid metabolic pathway.

Task I.4.DL.1: Dataset on the biological means to degrade cell walls of crops
A study to better understand the colonization process of soil bacteria on rice residues was conducted through ~150d period. Rice seems to be colonized during the first several weeks by specific microbial groups. Investigations in using naturally occurring degraders found in the soil have shown promise for pre-treatment of rice and switchgrass residues.

Task I.4.DL.2: A scientific system to study rice cell walls
Using our new culturing technique we detected that 25% (12 out of 48 clones) had less than 95% sequence similarity to those bacteria previously cultured in the Ribosomal Database Project. Four of the clones had sequence similarities of less than >89% compared to those previously cultured by the RDP. We have also developed a unique

method that has allowed us to probe for novel bacterial types that may represent new metabolic capabilities useful for breaking down celluloses.

Task I.5 Study the pelletization process as a means to densify biomass
I.5.DL.1 Dataset on the properties of biomass and biomass pellets
Completion of this project will provide economical data on the harvesting, processing, densifing, and transportation of biomass from the production area to the biorefinery or gasification site. Parameters for producing pellets and/or cubes from biomass will be determined that will enable producers to provide quality products to the biorefinery.

Task I.6 Evaluate forestry products as a possible biomass source
I.6.DL.1 Dataset on the availability and production costs of woody biomass
This study evaluated woody biomass from logging residues, small-diameter trees, mill residues, and urban waste as a feedstock for cellulosic ethanol production in Mississippi. The focus on Mississippi is to assess in-state regional variations and provide accurate information of biomass estimates for those industries interested in locating in Mississippi. Supply and cost of four woody biomass sources were derived from Forest Inventory Analysis (FIA) information, a recent forest inventory conducted by the Mississippi Institute for Forest Inventory, and primary production costs. According to our analysis, about 4.0 million dry tons of woody biomass is available for production of up to 1.2 billion liters of ethanol each year in Mississippi. The feedstock consists of 69% logging residues, 21% small-diameter trees, 7% urban waste, and 3% mill residues. Of the total, 3.1 million dry tons (930 million liters of ethanol) can be produced for \$30 dry ton^{-1} or less. Woody biomass from small-diameter trees are more expensive than other sources of biomass. Transportation costs accounted for the majority of total production costs. A sensitivity analysis indicates that the largest impacts in production costs of ethanol are stumpage price of woody biomass and technological efficiency. These results provide a valuable decision support tool for resource managers and industries in identifying parameters that affect resource magnitude, type, and location of woody biomass feedstocks in Mississippi. Impacts on local economies may result in additional jobs, tax revenues, and infrastructural improvements.

4. Comparison of goals and actual accomplishments

Duration of the research reported in Section I.1 - I.4.2 is derived from research conducted from June 2006 through November 2007. Crop production and field analysis are tied to season and weather without exception. Most crop production reports are limited to a single year's data. Funding arrived in June 2006. That funding allowed field researchers to plant late season crops, winter crops and establish perennial grasses. During the 2007 funding year (through November) those perennial grasses matured and data was obtained. All project leaders were instructed to release all personnel funded from this earmark, as subsequent funding was not awarded. Crop projects that could continue were funded from other sources. Harvested plant materials (seed or biomass) were provided to other researchers to allow them to continue their research. Transgenic material development was either severely truncated or reduced to a single objective.

5. Summary of activities

Task I. 1: Characterized lignocellulosic crops for use as bioenergy crops in MS

The overall objective of a series of studies involving lignocellulosic crops was to develop economically viable management practices that could easily be implemented throughout Mississippi to deliver a high quality and consistent feedstock for the bioenergy industry. Most pertinent was the compilation of a yield database of candidate species for bioenergy production grown across environments in Mississippi. Post-establishment year dry weight yields ranged from 2900-9430 kg ha^{-1}. Switchgrass was the lowest yielding, followed by sweet sorghum, giant miscanthus. Dry weight yield of energycane cultivars ranged from 8300 - 26,100 kg ha^{-1} at Starkville. A late spring frost seemed to severely compromise naipergrass yield. Ash was substantially lower in switchgrass and giant miscanthus vs. sorghum, naipergrass, and energycane. This will have implications in fertility requirements of the crop. Additionally, the truly deciduous nature of switchgrass and giant miscanthus seem to allow scavenging of nutrients from the above ground plant materials which will also affect sustainability.

Task I.1 DL.1: Dataset on characteristics and yield of lignocellulosic crops in MS

Plots were established on 2 May 2006 at Raymond and 23 May 2006 at Newton. Entries consisted of five elite breeding lines and five released cultivars of switchgrass, and a Miscanthus hybrid in four replications. Switchgrass entries were seeded at a rate of 5.6 kg pure live seed per hectare. Plots were 5 × 3 m with a 2-m alleyway between blocks. Morphological observations included occurrence of flowering, pests and diseases. Switchgrass stands were weak during the establishment year, but were much stronger in the second year. This has implications for how soon producers can start seeing economic returns from the crop. Giant miscanthus and two commercial cultivars, 'Kanlow' and 'Trailblazer' did not establish well and continued to perform poorly, and data from these entries were eliminated from statistical analysis. Overall, at both locations switchgrass breeding lines yielded greater biomass (5540 - 8010 kg ha-1) than commercial cultivars 'Cave-in-Rock' (3210 kg ha-1) and 'Shawnee' (2900 kg ha-1), but yield of 'Alamo' (5030 kg ha-1), the cultivar currently recommended for our region, was intermediate between the breeding lines and the low yielding commercial cultivars. The two top yielding entries at Newton (average=9540 kg ha-1) had about 50% greater biomass yield than the same entries at Raymond (6400 kg ha-1), but all the other entries had similar yields across locations, suggesting that the genetic potential of those two entries may be affected by environment. Chemical characteristics of the plants are to be analyzed.

A trial was conducted in 2006 and 2007 at the Pontotoc Ridge-Flatwoods Experiment Station in Pontotoc County, Mississippi to evaluate commercially available switchgrass varieties, Noble Foundation breeding lines of switchgrass, johnsongrass, and giant miscanthus. The trial was established on an Atwood silt loam (fine-silty, mixed, thermic Typic Paleududalfs). On May 15, 2006 switchgrass was planted at 5.6 kg pure live seed (PLS)/ha and johnsongrass was planted at 16.8 kg/ha. Atrazine, a preemerge herbicide was applied at 2 qt/A following planting. No fertilizer was applied in 2006 to minimize weed pressure. Pendimethalin herbicide was applied at 2.5 pt/A on Feb. 23, 2007.

Fertilizer was applied at 67-34-34 kg/ha actual N-P-K on May 4, 2007. Harvests were January 11, 2007 for the 2006 growing season and December 11, 2007 for the 2007 growing season. Variety and breeding lines treatments included NF/GA991, NF/GA992, NF/GA993, NF/GA001, NF/G05-1, Alamo, Cave-in-rock, Kanlow, Shawnee, Trailblazer, johnsongrass, giant miscanthus with shoots, and giant miscanthus without shoots.

In 2006, yield ranged from 0 to 5346 kg/ha for giant miscanthus with/without shoots and NF/GA001, respectively. All breeding line varieties being developed by the Noble Foundation and Alamo yielded greater than 3930 kg/ha, which was higher than all other treatments. In 2007, yield ranged from 1382 to 12,155 kg/ha for giant miscanthus without shoots and NF/G05-1, respectively. All breeding line varieties and Alamo yielded greater than 9430 kg/ha. This research indicates that the Alamo variety is the best switchgrass variety commercially available for use as a feedstock in North Mississippi and that yield is comparable for several new varieties that may be available in the future. In addition, the profit margin may be narrow during the establishment year due to low biomass production, but yield of biomass will at least double during the second year.

A trial was conducted in 2007 at the Pontotoc Ridge-Flatwoods Experiment Station in Pontotoc County, Mississippi to evaluate fertilizer N rate effects on switchgrass yield. The trial was established on an Atwood silt loam (fine-silty, mixed, thermic Typic Paleududalfs). 'Alamo' switchgrass seed at 6.7 kg/ha/A was planted on May 15, 2006. No fertilizer was applied in 2006 due to the potential increase in weed pressure by fertilization in the establishment year. In 2007, pendimethalin (prowl) was applied at 2.5 pt/A on February 23. Nitrogen treatments in the form of Ammonium Nitrate (34%) were applied on May 4, 2007. Treatments included 60, 120, 180, and 240 kg N/ha. In addition, 168 kg/ha 0-20-20 was applied to the entire trial area. A 0.91-m X 1.82-m section was harvested out of each plot on December 11, 2007. Yield ranged from 8982 to 13,090 kg/ha for the untreated check and 240 kg-N/ha, respectively. A simple economic assessment was conducted based on $40/ton switchgrass and $435/ton for fertilizer N. When subtracting the cost of fertilizer N from the gross returns, the untreated check was the most profitable with returns of $160/A. This return was greater than all treatments receiving N. This suggests that it may not be economically feasible to apply fertilizer N when switchgrass is grown on this soil type in a dry-land situation.

In 2006 and 2007, several herbicides with different classes of chemistry were evaluated for use during the establishment year in switchgrass production. In 2006, Alamo switchgrass was planted with a drill on June 1st. Herbicides applied PRE included photosynthesis inhibitors (triazines) atrazine, simazine, and ametryn; protox inhibitors flumioxazin and sulfentrazone; and mesotrione, which inhibits 4-HPPD that affects carotenoid biosynthesis. Herbicides applied POST either alone, as a tank mix, or followed by a PRE treatment included the synthetic auxins 2,4-D and dicamba; and ALS inhibitors chlorimuron-ethyl and imazethapyr. The PRE treatments were applied immediately following planting and POST treatments were applied on August 18.

Ratings of percent stand and yield were used to determine herbicide tolerance. Percent stand was at least 40% in August for the untreated check. Therefore, switchgrass was considered to have tolerance to herbicides applied PRE if 40% stand was recorded. Based on these guidelines, switchgrass was not tolerant to any herbicide applied PRE in this study. Switchgrass yield was highest with dicamba, Clarity (POST) and sulfentrazone, Spartan (PRE) fb chlorimuron-ethyl, Classic (POST). Yield with several other treatments was no different than the untreated, which indicates that some injury early may be acceptable to achieve weed control and promote late season growth. However, environmental conditions were extremely dry during the 2006 season. In 2007, several PRE treatments that were terminated from the study due to unacceptable crop injury involved simazine and ametryn (triazines); and the 4-HPPO inhibitor mesotrione. Also, the herbicide rimsulfuron was added as a PRE treatment. All POST treatments remained in the study with several additions, which included ALS inhibitors metsulfuron, rimsulfuron, nicosulfuron, and halosulfuron. Alamo switchgrass was planted on April 19th with PRE treatments being applied within 24hrs and POST treatments being applied on June 21st to switchgrass with at least 4 leaves and an average plant height of 12 inches. At 63 and 93 DAP, percent stand of switchgrass was lower with all PRE treatments compared to the untreated check. However, yield was similar for all treatments and ranged from 7163 to 8273 kg/ha. In regard to the POST applications, only imazethapyr (Pursuit), nicosulfuron (Accent), and rimsulfuron (Resolve) injured switchgrass 27, 40, and 40%, respectfully at 2 WAT. The metsulfuron (Ally) treatment applied POST yielded the highest biomass at 9137 kg/ha. All treatment combinations that included nicosulfuron injured switchgrass 40% at 2 weeks after POST application. Biomass yield with all combination treatments was lower compared to the untreated check.

Seed and biomass yield were determined on nine switchgrass cultivars planted in August 2006 at Starkville. First seed yield ranged from 50 to 125 kg/ha. Biomass yield after seed harvest ranged from 7000 to 15,000 kg/ha and varied with cultivar. Nutrient uptake of switchgrass fertilized with 67 kg N, 4.5 kg P and 37 kg K/ha harvested in December averaged across cultivars was 156 kg N, 16 kg P and 33 kg K/ha grown in a Marietta soil. An existing stand of 'Alamo' switchgrass was harvested as hay in June, as seed in October and as biomass in early winter of 2006 and 2007. Forage quality of switchgrass harvested in June was acceptable as livestock feed for beef animals. Seed yield of pure live seed (PLS) was 31 to 39 kg/ha in 2006 and 6 to 68 kg/ha in 2007. Full season switchgrass in December 2006 had a dry matter yield of 17,800 kg/ha and of 15,600 kg ha in November 2007 following seed harvest. Total nutrient uptake of switchgrass for two harvest in 2006 was 122 kg N, 14 kg P and 82 kg K/ha. Full season switchgrass fertilized with 67 kg N, 4.5 kg P and 37 kg K/ha harvested once in December 2006 removed 82 kg N, 6 kg P and 35 kg K/ha grown on a Savannah soil.

Multiple uses of switchgrass as livestock hay and for seed production provides producers with economic returns during feedstock development for biomass utilization. Switchgrass contained 7500 BTU, 0.03 to 0.05 % S, and 3 to 5% ash.

Two tasks detailed in the statement of work were worked on in 2006 and 2007 and are being repeated in 2008. These were 'Study on seed production potential of new and existing lines of switchgrass in Mississippi' and 'Maintain existing Alamo switchgrass plots.' Seed yield data was collected from 9 cultivars of switchgrass planted in 2006 on a Marietta soil from 1 m2 quadrats as physiological maturity occurred in September and October, 2007. Seed were cleaned and analyzed for % germination and purity. Biomass was harvested for yield in December and February. First seed yield ranged from 50 to 125 kg/ha. Gross energy, digestibility, ash and minerals were analyzed. Biomass yield after seed harvest ranged from 7000 to 15,000 kg/ha and varied with variety. Nutrient uptake of switchgrass harvested in December averaged across cultivars was 156 kg N, 16 kg P and 33 kg K/ha.

'Alamo' switchgrass established in 1999 on a Savannah soil was utilized in 2006 to determine biomass and seed yield and was repeated in 2007. Plots were split to harvest biomass in June and December and for seed in October. Plots harvested for biomass in June (half season) had a yield of 6200 kg/ha in 2006 and 8600 kg/ha in 2007 or the equivalent of 3 to 4 tons acre-1 of hay during a time of drought when other summer grasses had yield of less than 2000 kg ha-1.

Double utilization of switchgrass as both a bio-energy crop and as emergency livestock feed enhances the likelihood that farmers will develop acreage during feedstock startup. Seed harvested in October had a disappointing yield in both 2006 and 2007. After cleaning, seed yield of pure live seed (PLS) was 31 to 39 kg/ha in 2006 and 6 to 68 kg/ha in 2007. Biomass harvested in December 2006 had a yield of 7000 kg/ha and yield of 2200 kg/ha in November 2007 if harvested in June. Full season switchgrass in December 2006 had a yield of 17,800 kg/ha and of 15,600 kg/ha in November 2007. Biomass in 2006 and 2007 was analyzed for energy value (BTU), sulfur, ash, minerals and digestibility. Nutrient uptake of switchgrass harvested twice in 2006 was 122 kg N, 14 kg P and 82 kg K/ha. Full season switchgrass harvested once in December 2006 removed 82 kg N, 6 kg P and 35 kg K/ha. Samples from 2007 are pending analysis.

Progress in increasing germination rate has been substantial for switchgrass, but slower for big bluestem and indiangrass (Table 1). Increasing the germination could improve stand establishment of these native grasses. We have made significant progress with switchgrass currently at 6 cycles of selection = 70% precocious germination. Indiangrass and big bluestem are just starting their 4th cycle.

Table 1. Changes in germination rate via selection for precocious germination.

	Percentage 2007 Germination						
Species	Cycle of Selection						
	0	1	2	3	4	5	6
Lowland switchgrass	1.0	5.8	39.0	43.8	43.8	30.1	70.1
Big bluestem	1.6	2.8	2.0	16.0	16.3	-	-

Indiangrass	0.3	11.8	7.2	11.0	18.7	-	-

In 2006, a small emergence trial was established to determine if our selection procedure does indeed increase precocious emergence compared to a number of commercially available lines. We have maintained that test and now use it for yield trials (Table 2). Cycles 2 and 3 tested in the top group. It is unknown why Cycle 4 had such low yield. Please note that Cycle 3 yielded better than four of the five commercial varieties and Cycle 4.

Table 2. Relative yield of switchgrass varieties selected for improved germination.

Population	Cycle3	Cave IR	Cycle2	Trail-blazer	Cycle4	Shawnee	Alamo	Kanlow
2007 Relative Yield	3.63	2.47	2.43	2.3	2.1	1.8	1.7	1.2
LSD grouping	a	ab	abc	bc	bc	bc	bc	c

Legume interseeding with switchgrass is being evaluated to evaluate benefits such as increased N availability and lower reliance on commercial fertilizers. Results indicate that both white clover and crimson clover provide the equivalent N of between 56 to 112 kg N/ha (Table 3). Relative yield with ball clover and arrowleaf clover treatment were equivalent to less than 56 kg N/ha. Additional testing should decrease variance and allow greater precision in assessment.

Table 3. Relative yield of switchgrass interseeded with various legume species and selected fertilizer N rates.

Treatment	112 kg N ha^{-1}	White clover	Crimson clover	56 kg N ha^{-1}	0 kg N ha^{-1}	Ball clover*	Arrowleaf clover*
2007 Relative Yield	13.95	11.10	10.40	10.13	8.10	7.95	7.25
LSD grouping	a	ab	ab	b	b	b	b

* Ball and arrowleaf clover failed to establish in the test.

Sweet sorghum has the potential to serve as a direct feedstock source to produce ethanol. The extracted juices can be fermented and the stalks can serve as either for fuel for distillation, or as a raw material for cellulosic ethanol production. Twelve cultivars of sweet sorghum were chosen for the experiment: Bale All, Bundle King, Dale, Della, Keller, M81-E, Pace Setter, Simon, Sugar Drip, Sugar Top, Theis, and Topper. These

cultivars have been developed in Mississippi and Kentucky. Cultivars were planted at a density of thirteen seed per meter (4 seed per linear foot) on thirty six inch rows twenty feet long and arranged in four row plots. Each row in the plot was randomly designated for ripener and deheading treatments, while the remaining two rows were designated for Brix sampling and a control. Severe winds in August caused extensive lodging. We did collect Brix data and some yield data. Brix increased over the course of the summer until mid-Oct. then started to decline. The high range for Brix in sweet sorghum is 16 to 22%. At our location, Dale yielded the greatest ethanol per aliquot fermented. We also submitted samples of sap from each of the cultivars for lab analysis. Being related to maize, sorghum does contain fructose, and like maltose, is not fermented by first generation yeast (limits ethanol production). There are distinct differences among cultivars for fructose, with Della and Dale being highest in fructose at roughly 30%.

In another study involving energycane, we have been working with USDA-ARS-SRC, Houma, LA and other locations in the Southeast determining yield and cold hardiness. We are currently the most northerly location testing energycane. Sugarcane and energycane are established in the early fall (late Aug. to Sept.) by burying canes in furrows allowing sprouting and maintaining that field into the next year when yield is possible. We have been monitoring sugar accumulation, growth, yield, and hardiness for two years, all nine genotypes (seven energycane and two sugarcane) have survived at Starkville. While all have survived, four of the nine have consistently poor emergence and subsequent yield. Yields ranged from 5390 to 9475 kg ha^{-1} dry matter (normally sugarcane is harvested wet). Moisture content of these cane varieties exceeds 80%, so wet tonnage would range from 26,945 to 47,155 kg ha^{-1}. Brix is substantially lower for energycane (6.4- 10.9%) than sweet sorghum (14.3-22.4%). The five genotypes designated for continued testing based on ability to reestablish from winter are US 02-144, US 02-147, US 06-9001, US 06-9002 and US 72-114.

Task I.2: Characterize oilseed crops for use as bioenergy crops in MS
See Section A5. Castor (*Ricinus communis*), okra (*Ablemosheus esculentus*), and sunflower (*Helianthus annuus*) were investigated as summer crops. Canola (*Brassica napus*) , oriental mustard (*B. juncea*), coriander (*Coriandrum sativum* L.), crambe (*Crambe abyssinica* Hochst), and camelina (*Camelina sativa* (L.) Crantz.) were evaluated as potential winter crops. Castor is a full season high oil seed. Availability of determinant types of sunflower and okra allow for their use (June planting dates) following winter annual species (May harvest dates).

Task I.2.DL. 1: Dataset on characteristics and yield of oilseed crops in MS
See Section A5. Sunflower yield and oil content were affected by date of planting, nitrogen fertilization and location of production. Oil yields ranged from 483 to 1388 L ha^{-1}. Blackbird predation was severe on late planted fields. Productivity of winter canola, winter mustard, and coriander were equal to or exceeded average yields reported in the literature. Flax was slightly less, but has the advantage of linen as a bioproduct. Crambe, and camelina did not perform well in Mississippi although manipulations in cultural practices and genetics offer the possibility for greater success.

Task I.3: Characterize physiological limits of select bioenergy crops in MS

A study on sunflower investigated the effects of fertilizer N rates of 0, 67, 134, and 202 kg ha^{-1}, and cultivar (DKF3875, DKF2990, DKF3510 and DKF3901) and their interaction on seed yield, oil content, and oil composition of sunflower grown at five sites in Mississippi (Newton, Starkville, Stoneville, and two sites in Verona: Verona site 1(silty clay loam soil) and Verona site 2 (sandy loam soil). Tested cultivars had dissimilar fatty acid composition. Oleic acid concentration in the original seed oil of the four cultivars DKF3875, DKF2990, DKF3510 and DKF3901 was 29, 26, 85 and 41%, respectively. Cultivar and fertilizer N rate differences were significant with respect to seed yields at Stoneville, Newton and Verona site 2, N rate was significant at Stoneville, and cultivar x N interaction was significant at Starkville and Verona site 1. In Stoneville, Newton, and Verona site 2, DKF3510 had the highest yields. DKF2990 provided lower yields in Stoneville and in Verona site 2. Seed oil concentration was higher in DKF3875 and DKF2990 (43-47%) and lower in DKF3510 and DKF3901 (40-44%) at Stoneville and Verona site 2. However, at Newton, oil concentration was highest in DKF2990, lower in DKF3510 and DKF3901 and lowest in DKF3875. Overall, increasing fertilizer N rates reduced seed oil content, but increased seed yields and subsequently oil yield per area. Relative to the concentration of oleic acid in the original seed used for planting, oleic acid increased in all locations and cultivars, with only one exception in one cultivar at one location. As expected, there was a corresponding decrease in the concentration of linoleic acid. Also, concentration of stearic acid decreased relative to the original seed. These results suggest that sunflower under the hot humid climate of Mississippi may accumulate a higher concentration of oleic acid (which may improve health benefits) and lower concentrations of linoleic and stearic acids. In most cases, fertilizer N rate, cultivar, or N x cultivar interaction resulted in altered concentration of other fatty acids (palmitic, arachidic, gondoic, behenic, and lignoceric) in sunflower oil. Oil yields varied between 483 and 1388 L ha^{-1} and calculated biodiesel oil per area was 386 to 1,110 L ha-1 (41 to 119 gal ac^{-1}) with the different treatments and locations. Sunflower can be a viable crop in most parts of Mississippi for production of cooking oil or biodiesel. Further research is needed on sunflower management practices and on the possibility of double cropping of oilseeds in southeastern US.

Castor is a full-season summer crop which would compete for cotton, corn, and soybean acres. The percentage oil in its seed (55-60%) makes it hard to ignore as a potential oil feedstock crop. Mean yields of 2200 kg ha^{-1} of castor seed were achieved at locations north of Starkville.

Crambe is generally a spring planted crop in the northern US. However, it has substantial potential as an oilseed crop because of a high concentration of eurusic acid in its oil profile. Winter planting and published reports indicated that crambe can not tolerate winter temperatures less than - 4.5 C (24 F). Greater than 99% of all crambe plants succumbed to the cold weather. Seed of remaining plants were collected as a base population for a winter crambe line.

Winter-grown canola (*Brassica napus* L.) production is limited mostly by frost and winter kill in the southern canola growing regions of the United States. Therefore, tolerance to cold and heat were assessed by studying percentage of pollen viability (PV), in-vitro pollen germination (PG) and pollen tube length (PTL) for twelve field-grown cultivars. Freshly collected pollen from all cultivars were incubated in artificial solid growth media at a constant temperature ranging from 10 to 35°C at 5°C interval for 24 h to determine PG and PTL. A modified bilinear model best described the temperature response functions of PG and PTL. Canola cultivars showed significant variability ($P < 0.001$) for PV (61.3 to 89.7 %), PG (29.0 to 48.2 %) and PTL (463 to 931 µm). The average cardinal temperatures, T_{min}, T_{opt}, and T_{max}, for PG and PTL were 6.4, 24.3, and 33.7°C, respectively. The principal component analysis revealed that maximum PG, PTL, T_{min}, and T_{opt} of both PG and PTL were the most important factors in determining cold-tolerance, whereas T_{max} of PG and PTL, and maximum PG and PTL were more responsible in separating the cultivars for heat-tolerance. The canola cultivar, KS3077 was the most cold-tolerant with the lowest T_{min} and the widest temperature adaptability range, and the cultivar, Kadore was the most heat-tolerant with the highest T_{max} for the PG (Fig. 2 and 3). The identified cold- and heat-tolerant cultivars may be useful in canola breeding programs to develop cultivars suitable for a niche environment.

Task I.4: Modify cell walls for cost efficient bio-fuel production

Cereal crop straws and stalks are highly abundant agricultural byproducts that are composed of mainly plant cell walls. The cell wall biopolymers include cellulose, hemicellulose, lignin, pectin, and proteins, which are usually cross-linked with each other and tightly packaged. The rigid structure of cell wall makes it very difficult to extract the polysaccharides and break them into monosaccharides that can be easily converted into bio-fuel. We propose to genetically modify the cell wall so that we can cost effectively process the cellulose biomass into bio-fuel while maintaining high grain yield production in agriculture.

It has been shown that high moisture in straw and thus slow burning rate is the primary obstacle in direct syngas production from rice (*Oryza sativa*) straw. To resolve the problem, we have generated transgenic rice that overexpresses a regulatory gene in lipid metabolic pathway. The expression of this gene is expected to reduce the moisture of straw and facilitate burning of straws. Although the moisture of straw remains to be tested in the transgenic rice, we find that the per-thousand grain weight increased about 15% in the transgenic rice and the plants appeared to be healthier. Our research probably opens a new approach to increase both seed yield and biofuel production.

Task I.4.DL.1: Dataset on the biological means to degrade cell walls of crops

A study to better understand the colonization process of soil bacteria on rice residues was conducted through ~150d period. The incubation experiment was completed in July 2008 and the process of evaluating the composition of the bacterial and microbial communities will take place over the next year. By extracting and sequencing 16S rRNA genes, preliminary investigations on the colonization process during the first several weeks suggest that the rice residues select for specific microbial groups and that the bacterial

community is dynamic during the decomposition process.

We have also had some success culturing and describing (16S rRNA gene) novel bacteria through the use of a cellulosic media in direct contact with the soil. Cultures using standard cellulose culture media resulted in the detection of commonly found phylotypes and typically had >99% sequence similarity among the 48 separate clones that we evaluated. In contrast, using our new culturing technique we detected that 25% (12 out of 48 clones) had less than 95% sequence similarity to those bacteria previously cultured in the Ribosomal Database Project. Four of the clones had sequence similarities of less than >89% compared to those previously cultured by the RDP. Other methods that will more specifically probe the nature of the cellulose degraders, such as the use functional gene probes and microarrays may be helpful but could also be biased because of our current limited knowledge about the diversity of cellulose degraders. We thus feel that our current investigations are worthwhile and economical given our objectives and goals.

Our central premise is that having co-evolved with terrestrial plants over the past 500 million years, microorganisms in soil serve as a reservoir of metabolic and genetic capacities that can help solve the problems inherent in the transformation of feedstocks for production of biofuels. Numerous cellulose degrading microorganisms have been isolated from environmental habitats, however we also know that we have only scrapped the surface (<1%) of the natural diversity of these organisms. Many of these uncultured microorganisms may have evolved specific capabilities that help them overcome the inhibitory influence of lignin and more efficiently degrade celluloses in the presence of lignin. We thus proposed to study the diversity of bacteria capable of colonizing cellulosic residues and attempt to culture novel cellulose degraders. We have partial described the dynamics of bacterial communities on decomposing rice straw residues and seek to further this understanding through longer periods of residue aging. We have also developed and would like to further refine a unique method that has allowed us to probe for novel bacterial types that may represent new metabolic capabilities useful for breaking down celluloses.

Woody Biomass as Biofuels: A study was conducted to evaluate woody biomass from logging residues, small-diameter trees, mill residues, and urban waste as a feedstock for cellulosic ethanol production in Mississippi. The focus on Mississippi is to assess in-state regional variations and provide accurate information of biomass estimates for those industries interested in locating in Mississippi. Supply and cost of four woody biomass sources were derived from Forest Inventory Analysis (FIA) information, a recent forest inventory conducted by the Mississippi Institute for Forest Inventory, and primary production costs. According to our analysis, about 4.0 million dry tons of woody biomass is available for production of up to 1.2 billion liters of ethanol each year in Mississippi. The feedstock consists of 69% logging residues, 21% small-diameter trees, 7% urban waste, and 3% mill residues. Of the total, 3.1 million dry tons (930 million liters of ethanol) can be produced for $30 dry ton-1 or less. Woody biomasses from small-diameter trees are more expensive than other sources of biomass. Transportation costs accounted for the majority of total production costs. A sensitivity analysis indicates

that the largest impacts in production costs of ethanol are stumpage price of woody biomass and technological efficiency. These results provide a valuable decision support tool for resource managers and industries in identifying parameters that affect resource magnitude, type, and location of woody biomass feedstocks in Mississippi. Impacts on local economies may result in additional jobs, tax revenues, and infrastructural improvements.

Task I.4.DL.2: A scientific system to study rice cell walls

See also I.4. A major problem in lignocellulosic bioethanol production is that the tight cell wall structure prevents cell wall degradation enzymes to penetrate into the interior of the cell wall to degrade polymers. A cell wall structure change, loosen the cell wall, will allow cellulases and other digestion enzymes gain better access to the interior of the cell wall to release saccharides for ethanol fermentation. Consequently, the efficiency of ethanol production from rice straw will be improved. To achieve the goal of modifying the cell wall structure, we have examined the proteome and expression profile in rice suspension cells and protoplasts to search for regulatory proteins involved in cell wall synthesis. The results obtained in this project have helped us obtain a DOE competitive grant.

The long term goal of this project is to modify plant cell walls for cost efficient bio-fuel production from the by-products cereal crops, such as rice straw and maize stover. While trying to create transgenic rice with better quality for syngas production, we also proposed to systematically investigate the regulatory mechanisms of cell wall synthesis using genomic approaches in rice. We believe that the understanding of cell wall synthesis regulatory mechanism will lead to improvement of cell wall characteristics and yield.

We have successfully generated transgenic rice lines. We have found that the transgenic rice produces larger seeds than the wild type. While the per-thousand seed weight of the wild type is 20.2g, the per-thousand seed weight of the transgenic rice is 23.2g. The molecular characterization of the transgenic lines is in progress. Chromatin proteome analysis has been completed. A paper has been published (Tan, F, Li, G., Chitteti, R. B., and Peng, Z. (2007) Proteome and Phosphoproteome Analysis of Chromatin Associated Proteins in Rice (Oryza sativa). Proteomics. 7(24):4511-27.We have also completed proteome quantitative comparison between suspension cells and protoplasts. Data analysis and paper preparation is in progress. This part of work has helped us obtain a DOE competitive grant.

Task I.5 Study the pelletization process as a means to densify biomass

A Sprout-Waldron 125 hp pellet mill was purchased, installed, and tested as the test platform for biomass pelleting/densification studies. Material handling equipment was assembled to complete the biomass pelleting system. Bulk amounts of switchgrass, wheat straw, giant Miscanthus, elephant grass, cotton gin trash, and softwood forest trimmings were collected, processed (grinding), and stored for densification studies. For comparative purposes, hardwood and softwood chips/pellets were also collected. All

these biomass feedstocks were physico-chemically characterized. Effect of exposure to weathering on physico-chemical properties were also investigated using hardwood chips and switchgrass as test materials. The data collected was tabulated and analyzed. Particle size upon grinding was affected by the biomass but particle size distribution analysis through standard mechanical sieving was incapable of characterizing the fibrous grinds that in turn provides data for size reduction and densification operations. A sieveless particle size distribution analysis method using computer vision was therefore developed.

Pelleting studies on the installed pelleting system were focused on switchgrass as the feed material. Studies on pelleting such other biomass as wheat straw, giant Miscanthus, elephant grass, cotton gin trash, and softwood forest trimmings were undertaken in collaboration with ADM Alliance Nutrition in Illinois. Results of that effort identified biomass moisture content, grind size, and pellet mill die specification as critical parameters in pelletization. Informal collaboration on the pelleting of biomass was established with Andritz Sprout (formally Sprout-Waldron).

Task I.6 Evaluate forestry products as a possible biomass source
The initial efforts of this study leveraged efforts by scientists in the MSU Department of Forestry and the Mississippi Forestry Commission's Mississippi Institute for Forest Inventory (MIFI). MIFI conducted a state wide forest resource assessment of standing timber. A stratified random sampling schemes was employed across 5 pre-defined geographic regions of the state. These regions are Northeast, Central, Southwest, Southeast, and Delta. Drs. Thomas Matney and Emily Schultz, members of the research team along with MIFI staff, worked on data processing and the website's updating.

Results of the study were presented at the 13th International Symposium on Society and Resource Management in Park City. A manuscript on woody biomass estimates and production costs for the state of Mississippi was submitted to *Biomass and Bioenergy* for review and potential publication. We presented the results of this study at the 2007 Southeast Bioenergy Conference in Tifton, GA and at the 2007 Biofuels Conference in Mississippi State University. We also submitted a manuscript for the 2007 SAF National Convention proceedings in October 2007 in Portland, OR.

In addition, a manuscript was prepared for an edited book on renewable energy from forest resources in the United States. This manuscript retook concepts analyzed in previous manuscripts, with special emphasis on production costs variability and sensitivity analysis, and impacts of developing cellulosic ethanol industry in Mississippi.

A Master thesis was completed by Zhimei Guo during this period. The title of the thesis is "Economic and policy perspectives of biofuel as an emerging use of forest biomass in Mississippi. Part of Zhimei's thesis was published in the *International Forestry Review* with the title: "Utilization of forest derived biomass for energy production in the U.S.A.: status, challenges, and public policies." Digital copies are available at: http://sun.library.msstate.edu/ETD-db/theses/available/etd-09072007-125135/.

Potential Project Impacts

Given world instability and the United States heavy dependence on importing foreign oil, this research may have an important impact for a forest resource rich state such as Mississippi. Although much research exists about the development of the technologies for converting woody biomass into bio-fuels such as ethanol and bio-oil, this study will provide information useful to policy makers at the state level to aid their efforts in building potential bio-energy conversion facilities. The potential use of bio-fuels such as bio-oil as a heating fuel or ethanol as a gasoline substitute or additive could provide non-industrial and industrial private landowners with an alternative market for their small diameter trees. The information provided by this study will aid state policy makers in developing policy instruments to advance the development of this emerging fuel market. In addition, this work on bio-fuels will serve as a basis for evaluating its potential as a zero net emitter of carbon dioxide into the atmosphere. This information would be useful in strategically position Mississippi's economy in the emerging carbon trading market.

6. Products developed and technology transfer activities:

a. Publications:

Baldwin, B.S. and R.D. Cossar. 2008. Castor (*Ricinus communis* L.) yield in response to planting date at four locations in the South-central U.S. Industrial Crops and Prod. (Accepted).

Guo, Z., **Grebner, D.L.**, Sun, C., and S.C. Grado. (In Review). Evaluation of alternative forest management regimes for supply woody biomass for biofuel production in Mississippi. Submitted to *Southern Journal of Applied Forestry* on December 4, 2008.

Singh, S.K., V.G. Kakani, D. Brand, B. Baldwin, K.R. Reddy. 2008. Assessment of cold and heat-tolerance of winter-grown canola cultivars by pollen based parameters. J. Agron. Crop Sci. 194:225-236.

Igathinathane, C., L. O. Pordesimo, W. D. Batchelor, E. P. Columbus, and S. Methuku. 2008. Shape identification and size distribution of particles from basic shape parameters 2009. using ImageJ. Computers and Electronics in Agriculture 63:168-182.

Jeliazkov, V.D., B. Baldwin, W. Ebelhar, J. Miller, N. Buehring, 2008. Assessment and yield of sunflower (*Helianthus annuus* L.) grown at multiple locations in Mississippi. Agon. J. 100(3):635-642.

Jones, T.L., Schultz, E.B., Matney, T.G., **Grebner, D.L.**, and D.L. Evans. (Accepted). A forest product/bioenergy mill location and decision support system based on a county-

level forest inventory and geo-spatial information. Chapter 7, In: Gan, J., S. Grado, and I. Munn (Editors). Global Change and Forestry: Economic and Policy Impacts and Responses. Nova Science, NY.

Grebner, D.L., Perez-Verdin, G., Henderson, J.E., and A.J. Londo. (In Review). Bioenergy from woody biomass, potential for economic development, and the need for extension. Submitted to the Journal of Extension on May 16, 2008. Received preliminary comments on 8/4/08.

Perez-Verdin, G., Grebner, D.L., Munn, I.A., Sun, C., and S.C. Grado. (In Review). Economic impacts of woody biomass utilization for bioenergy in Mississippi. Submitted to Forest Products Journal on May 7, 2008. Received comments on 7/23/08.

Perez-Verdin, G., Grebner, D.L., Sun, C., Munn, I.A., Schultz, E.B., and T.G. Matney. (In Review). Woody biomass availability for bioethanol conversion in Mississippi. Submitted to Biomass and Bioenergy, August 21, 2007. Revision submitted 7-29-08.

Guo, Z., Sun, C., and D.L. Grebner. 2007. Forest-derived woody biomass utilization for bioenergy production in the United States: status, challenges, and government policies. International Forestry Review. 9(3): 748-758.

Tan, F, Li, G., Chitteti, R. B., and Peng, Z. (2007) Proteome and Phosphoproteome Analysis of Chromatin Associated Proteins in Rice (*Oryza sativa*). Proteomics. 7(24):4511-27.

Kakani, V. G. and K. R. Reddy. 2007. Temperature response of C4 species big bluestem (*Andropogon gerardii*) is modified by growing carbon dioxide concentration. Environmental and Experimental Botany 61: 281-290.

Kakani, V.G., K.R Reddy and D Zhao. 2006. Deriving a simple spectral ratio R1689/R1657 for spatial and temporal determination of cotton leaf water potential. Journal of New Seeds 8: 11-27.

Grebner, D.L., Perez-Verdin, G., Sun, C., Munn, I.A., Schultz, E.B., and T.G. Matney. (In Press.) Woody biomass feedstock availability, production costs and implications for bioenergy conversion in Mississippi. Book Chapter 12, In: Renewable Energy From Forest Resources in the United States. Edited by Barry Solomon and Valerie Luzadis. Submitted on October 15, 2007. Revision submitted on March 15, 2008. Expected publication date fall 2008.

Guo, Z., **Grebner, D.L.**, Sun, C., and S.C. Grado. (Accepted). Biofuel production impacts on the management of southern pine plantations in Mississippi. Chapter 8, In: Gan, J., S. Grado, and I. Munn (Editors). Global Change and Forestry: Economic and Policy Impacts and Responses. Nova Science, NY.

Perez-Verdin, G., *Grebner, D.L.,* ***Munn, I.A., Sun, C., and S.C. Grado. (Accepted). Economic impacts of woody biomass utilization for bioenergy in Mississippi. Chapter 6, In: Gan, J., S. Grado, and I. Munn (Editors). Global Change and Forestry: Economic and Policy Impacts and Responses. Nova Science, NY.***

Grebner, D.L., Perez-Verdin, G., Henderson, J.E., and A.J. Londo. (In Press). Bioenergy from woody biomass, potential for economic development, and the need for extension. Submitted to the *Journal of Extension* on May 16, 2008. Accepted January 29, 2009.

Perez-Verdin, G., **Grebner,** D.L., Sun, C., Munn, I.A., Schultz, E.B., and T.G. Matney. 2009. Woody biomass availability for bioethanol conversion in Mississippi. *Biomass and Bioenergy*, 33(3): 492-503.

Grebner, D.L., Perez-Verdin, G., Sun, C., Munn, I.A., Schultz, E.B., and T.G. Matney. 2009. Woody biomass feedstock availability, production costs and implications for bioenergy conversion in Mississippi. Chapter 12, In: Solomon and Luzadis, eds. Renewable Energy from Forest Resources in the United States. Routledge, London. 330 p.

Perez-Verdin, G., **Grebner, D.L.,** Munn, I.A., Sun, C., and S.C. Grado. 2008. Economic impacts of woody biomass utilization for bioenergy in Mississippi. *Forest Products Journal*, 58(11): 75-83.

Guo, Z., Sun, C., and **D.L. Grebner**. 2007. Forest-derived woody biomass utilization for bioenergy production in the United States: status, challenges, and government policies. *International Forestry Review*. 9(3): 748-758.

Other Publications:

Oldham, L.O., B.S. Baldwin, D.J. Lang, and M. Collins. Biofuel research efforts in Mississippi. In Carl Crozier ed. Southern Plant Nutrient Management Conference Proceedings. October 2-3, 2007. Olive Branch, MS. Publisher: The Noble Foundation.

National Winter Canola Variety Trail. 2007. Report of Progress 973. Kansas State Uni. Agric. Expt. Stat. And Coop. Ext. Ser. Contribution No. 07-187-S.

National Winter Canola Variety Trail. 2006. Report of Progress 973. Kansas State Uni. Agric. Expt. Stat. And Coop. Ext. Ser. Contribution No. 07-187-S.

Grebner, D.L., Perez-Verdin, G., Sun, C., Munn, I.A., Schultz, E.B., and T. G. Matney.

2008. An approach for estimating the availability, production costs, and implications of bioenergy development in the United States Mid-South. In: Proceedings, International Symposium on Emerging needs of society from forest ecosystems: towards the opportunities and dilemmas in forest managerial economics and accounting. Sponsored by the IUFRO Unit 4.05.00 Managerial Economics and Accounting at the University of Ljubljana, Ljubljana, Slovenia in May 22-24, 2008.

Jones, T.L., Schultz, E.B., Matney, T.G., Grebner, D.L., and D.L. Evans. 2008. A forest product/bioenergy mill location and decision support system based on a county-level forest inventory and geo-spatial information. In: Proceedings, Southern Forest Economics Workshop, San Antonio, TX on March 5-6, 2007.

Perez-Verdin, G., Grebner, D.L., Sun, C., Munn, I.A., Schultz, E.B., and T.G. Matney. 2008. Woody biomass feedstock supplies and management for bioenergy in Mississippi. In: Proceedings, Southern Forest Economics Workshop, San Antonio, TX on March 5-6, 2007.

Guo, Z., Grebner, D.L., Sun, C., and S.C. Grado. 2008. Biofuel production impacts on the management of southern pine plantations in Mississippi. In: Proceedings, Southern Forest Economics Workshop, San Antonio, TX on March 5-6, 2007.

Perez-Verdin, G., Grebner, D.L., Sun, C., Munn, I.A., Schultz, E.B., and T.G. Matney. 2007. The potential woody biomass supply for biofuel generation in Mississippi. In: Proceedings, Society of American Foresters National Convention, Portland, OR, October 23-27, 2007.

Macoon, B., and T. Steed. 2008. Cultivar, location, and harvest timing effects on switchgrass production. In Annual Meeting Abstracts [CD-ROM]. ASA, CSSA, SSSA. Madison, WI. (In press).

Henderson, J.E., I.A. Munn, G. Perez-Verdin, and D.L. Grebner. (In Press). Forestry in Mississippi: The impact of the forest products industry on the post-Katrina Mississippi Economy: An input-output analysis. Forest and Wildlife Research Center, Research Bulletin FO-XXX, Mississippi State University.

Perez-Verdin, G., Grebner, D.L., Sun, C., Munn, I.A., Schultz, E.B., and T.G. Matney. 2007. Woody biomass inventories for biofuels use in Mississippi. In: Book of Abstracts, 13th International Symposium on Society and Resource Management, Park City, UT, June 17-21, 2007.

Lang, D.J. and V. Temu. 2007. Effect of Mid-Season Harvest on Seed Quality of Switchgrass. IN: Proceedings American Forage Grassland Council. Alison, W. (ed). 16:99. State College, PA 24-26 June, 2007

Reddy, K.R., S.K. Matcha, S.K. Singh, D. Brand and R. Seepaul. 2008. Quantifying the

effects of temperature and nitrogen on swticgrass growth and development. The 38th Biological Systems Simulation Modeling Meeting Conference, 8-10 April 2008, Temple TX, USA, pp. 24-25.

Grala, R.K., Nepal, P., and D.L. Grebner. 2008. Utilization of logging residues for producing Bioenergy and reducing carbon dioxide emissions. In: Proceedings, Society of American Foresters National Convention, Reno, NV, November 4-9, 2008.

Theses:

Guo, Z. 2007. Analysis of bio-fuel as an emerging wood use. Masters of Science Thesis. Mississippi State University. 80p.

Satyasai Kumar Matcha. 2007. Effects of Nitrogen Defficiency on Plant Growth, Leaf Photosynthesis, and Hyperspectral Reflectance Properties in Castor (Ricinus communis L.). December 2007, Mississippi State University, Mississippi State, Mississippi, MS

Professional Presentations:

Igathinathane, C., L. O. Pordesimo, M. W. Schilling, and E. P. Columbus. A novel method of rapid measurement of cutting energy of corn stalks using torque wrench. Poster presentation at the 1st MSU Energy-Synergy Workshop, Mississippi State, Mississippi, April 17, 2008.

Pordesimo, L. O., G. Holt, C. Igathinathane, and E. P. Columbus. Densification of herbaceous bioenergy feedstocks for transportation and handling. Poster presentation at the 1st MSU Energy-Synergy Workshop, Mississippi State, Mississippi, April 17, 2008.

Igathinathane, C., L. O. Pordesimo, E. P. Columbus, and W. D. Batchelor. Machine vision methods of determining size and size distribution of biomass and agricultural materials. Poster presentation at the 7th Annual Southern BioProducts and Renewable Energy Conference, Choctaw, Mississippi, April 14-15, 2008

Wei, L., C. Igathinathane, L. O. Pordesimo, W. D. Batchelor, and J. Lee. A novel method for determination of surface area of biomass particles. Poster presentation at the 7th Annual Southern Bioproducts and Renewable Energy Conference, Choctaw, Mississippi, April 14-15, 2008. (3rd PLACE POSTER COMPETITION WINNER).

Pordesimo, L. O., C. Igathinathane, E. P. Columbus, J. D. Davis, W. D. Batchelor, J. R. Wooten, and L. Wei. Feedstock engineering: critical component of the energy from biomass industry. Poster presentation at the 1st MSU Energy-Synergy Workshop, Mississippi State, Mississippi, April 17, 2008.

Pordesimo, L. O., G. Holt, C. Igathinathane, and E. P. Columbus. Densification of herbaceous bioenergy feedstocks for transportation and handling. Poster presentation at the 1st MSU Energy-Synergy Workshop, Mississippi State, Mississippi, April 17, 2008.

Pordesimo, L. O., S. Capareda, S. Sokhansanj, and S. Fernando. 2008. Enhancement and stabilization of biomass feedstock quality through utilization/recycling biological waste streams. Paper No. 159. Presented at the 236th ACS National Meeting & Exposition, August 17-21, Philadelphia, Penn. (Invited)

J. R. Wooten, L. O. Pordesimo , C. Igathinathane, E. P. Columbus. Classification of Wood Chips Using Image Processing Texture Analysis. Annual International Meeting ASABE, Providence, Rhode Island, June 29 – July 2, 2008. Paper No. 084467.

Igathinathane Cannayen, Lester O Pordesimo, M W Schilling, Eugene P Columbus. Fast and Simple Measurement of Energy Requirements for Plant Stalk Cutting. Annual International Meeting ASABE, Providence, Rhode Island, June 29 – July 2, 2008. Paper No. 084111.

Lester O. Pordesimo, Lin Wei, James R. Wooten, C. Igathinathane, R. Mark Bricka, Eugene P. Columbus. Process Performance of a Downdraft Gasifier Burning Hardwood Chips. Annual International Meeting ASABE, Providence, Rhode Island, June 29 – July 2, 2008. Paper No. 084474.

Shah, A., Srinivasan, R., To, F., Fernando, S.D., Columbus, E., Wooten, J., and Yang, P. 2008. Performance Parameters of Syngas Operated Personal Power System. Annual International Meeting ASABE, Providence, Rhode Island, June 29 – July 2, 2008. Paper No. 084444.

Horton D. S., B. S. Baldwin and K. B. Holmberg. 2006. Determination of optimum planting date of seven species of winter oilseeds in Mississippi (A preliminary study). ASA-CSSA-SSSA International Meetings, Indianapolis, IN. 12-16 Nov.

Zhang, G., W.T. French, R. Hernandez, H.Toghiani, J. Carmical, W. Homes, A. Brown, and B. Baldwin. 2007. Lipid production from acid hydrolysate of lingocellulosic biomass using Rhodotorula glutinis. AIChe Annual Meeting. Salt Lake City, UT. 4-7 Nov.

Brown, A. B. Rogers, B.Baldwin, D. Braasch, W. Holmes. 2007. Characterization of hesperis and black mustard oil as possible biodiesel feedstock. Amer. Oil Chem. Soc. Conf. Quebec City Quebec. May 1-3.

Zheljazkov, V.D, B. Baldwin, W. Ebelhar, N. Buehring, and C. Coker. 2007. Sunflowers as an oil seed crop for biodiesel production in Mississippi. Southern Amer. Agron. Society Association Annual Meeting. Mobile, AL, 3-6 Feb.

Sebastian, T., B.S. Baldwin, D.S. Horton, and C.L. Webber. 2007. Estimation of pollen dispersal and gene flow in the potential biofuel crop castor (*Ricinus communis* L.). First Ann Miss. State Univ. Biofuels Conf. Starkville, MS. 27 Aug.

Barnes, D. S. Ganji, D.S. Horton, B.S. Baldwin, D.A. Braasch. 2007. Modification of castor for use in biodiesel: Knocking out the toxin. First Ann Miss. State Univ. Biofuels Conf. Starkville, MS. 27 Aug.

Brown, A.E., W.E. Holmes, E.C. Rogers, T Verlotl, and B.S. Baldwin. 2007. FAME analysis of *Hesperis matronalis*: GCXGC-TOFMS better resolution. Amer. Soc. Mass Spec. Conf., Indianapolis, IN. 3-7 Jun.

Crymble, S.D., R. Hernandez, W. T. French, M.E. Zappi, B.S. Baldwin, and D. Thomas. 2006. Kinetic Study of biodiesel production from Chinese tallow tree oil. Amer. Inst. Chem. Eng. Ann. Conf. San Francisco, CA. Nov 12-17.

Perez-Verdin, G., Grebner, D.L., Sun, C., Munn, I.A., Schultz, E.B., and T.G. Matney. 2008. Woody biomass feedstock supplies and management for bioenergy in Mississippi. Presented at the Southern Forest Economics Workshop for presentation in Savannah, GA on March 9-11, 2008.

Perez-Verdin, G., Grebner, D.L., Sun, C., Munn, I.A., Schultz, E.B., and T.G. Matney. 2007. The potential woody biomass supply for biofuel generation in Mississippi. Paper presented at the SAF National Convention in Portland, OR on October 23-27, 2007.

Perez-Verdin, G., Grebner, D.L., Sun, C., Munn, I.A., Schultz, E.B., and T.G. Matney. 2007. Woody biomass inventories for biofuels use in Mississippi. Presented at the 13th International Symposium on Society of Resource Management, Park City, Utah, June 17-21, 2007.

Temu, V. and D.J. Lang. 2008. Potential of Switchgrass for Seed Production During the First Growing Season in Mississippi. IN: Proceedings American Forage Grassland Council. Alison, W. (ed). Louisville, KY 25-29 January, 2008.

Lang, D.J. and V. Temu. 2007. Seed Production Potential of Switchgrass in the Southeast USA. Southern Section American Society Abstracts Meeting, Mobile, AL. 3-7 February 2007.

Shankle, M.W., T.F. Garrett, and J.L. Main. 2008. Switchgrass feedstock production systems for Mississippi. The 1st Energy-Synergy Workshop, organized by the MSU Energy Working Group.

Shankle, M.W., 2008. Switchgrass production and weed management in Mississippi. Mississippi Agricultural Pest Management Associations, Joint Conference, Weed Science Session.

Maia Mula and Mark A. Williams. 2007. Bacterial community composition during early decomposition of lignocellulosic residue. Sixth Annual Southern Bioproducts and Renewable Energy Conference, Philadelphia, MS.

Maia Mula, Mark A. Williams, Kamlesh Jangid, Barny Whitman. Bacterial composition and diversity during decomposition of rice straw. 2008. Joint meeting of American Society of Agronomy and Geological Society of America, Houston, TX.

Reddy, K.R., S.K. Matcha, and V.R. Reddy. 2008. Remote sensing algorithms for nitrogen deficiency in bioenergy crops, caster and switchgrass. 5th International Crop Science Congress, 13-18 April, 2008, Jelu, Korea.

Matcha, S.K. and K.R. Reddy. 2007. Derivation of reflectance algorithms and best wavebands to study N deficiency in bioenergy crops, castor and switchgrass. The ASA-CSSA-SSSA International Annual Meetings, 4-8 November 2007, New Orleans, Louisiana, USA.

Matcha, S.K. and K.R. Reddy. 2007. Changes in pigments, photosynthesis, and reflectance properties of castor (*Ricinus communis* L.) leaf senescence. The ASA-CSSA-SSSA International Annual Meetings, 4-8 November 2007, New Orleans, Louisiana, USA.

Singh, S.K., V.G. Kakani, D. Brand, B. Baldwin and K.R. Reddy. 2007. Assessment of cold and heat tolerance of field-grown canola cultivars by pollen-based parameters. The ASA-CSSA-SSSA International Annual Meetings, 4-8 November 2007, New Orleans, Louisiana, USA.

Matcha, S.S.K. and K.R. Reddy. 2007. Effects of nitrogen deficiency on leaf reflectance and selection of optimum wavebands for N detection in castor and switchgrass. The 6TH Annual Southern BioProducts and Renewable Energy Conference, April 16 - 18, 2007, Pearl River Resort - Golden Moon Casino & Hotel, Choctaw, Mississippi, USA.

Matcha, S. S. K., V. G. Kakani and K. R. Reddy. 2007. Nitrogen deficiency alters growth, development, physiology, and leaf reflectance properties in switchgrass. The 5th Annual Graduate Student Association Research Symposium, March 30, 2007, Mississippi State University, Mississippi State, MS, USA.

Matcha, S.S.K., V.G. Kakani and K.R. Reddy. 2007. Effects of nitrogen deficiency on plant growth and photosynthesis, and selection of reflectance properties for physiology in switchgrass. 37th Biological Systems Simulation Conference, April 17-19, 2007, Beltsville, Maryland, USA.

Matcha, S.K. and K.R. Reddy. 2007. Effects of nitrogen deficiency on plant growth, leaf photosynthesis, and hyper spectral reflectance properties in castor (Ricinus communis).

Southern Branch of the American Society of Agronomy Annual Meetings, Feb 3-7, 2007, Mobile, AL, USA.

Baldwin, B.S. 2007. Oil feedstocks for the Southeast (What is feasible?). First Ann Miss. State Univ. Biofuels Conf. Starkville, MS. 27 Aug.

Grebner, D.L., Schultz, E.B., and T.G. Matney. 2008. State forest inventory and potential for enabling economic impact. Presented at the Forest and Wildlife Research Center Technology Transfer Conference & Mississippi Forestry Association Board of Directors Meeting, Franklin Center, Mississippi State, MS August 5-6, 2008.

Grebner, D.L., Perez-Verdin, G., Sun, C., Munn, I.A., Schultz, E.B., and T.G. Matney. 2008. Economic considerations and current status of woody biomass feedstock availability in Mississippi. Presented at the MSU Department of Agricultural Economics Seminar Series, MS on April 18, 2008.

Grebner, D.L., Perez-Verdin, G., Sun, C., Munn, I.A., Schultz, E.B., and T.G. Matney. 2008. Economic considerations and current status of woody biomass feedstock availability in Mississippi. Presented at the Seventh Annual Southern Bioproducts and Renewable Energy Conference in Choctaw, MS on April 14-15, 2008.)

Grebner, D.L., Perez-Verdin, G., Sun, C., Munn, I.A., Schultz, E.B., and T.G. Matney. 2008. Woody biomass and the potential for bio-fuel production for Mississippi. Presentation will be given at the annual meeting of the Southern Hardwood Research Group, Stoneville, MS, on February 12, 2008.

Grebner, D.L., Perez-Verdin, G., Sun, C., Munn, I.A., Schultz, E.B., and T.G. Matney. 2007. Woody biomass inventories for biofuels use in Mississippi. Presented at the Southeast Bioenergy Conference 2007, Tifton, GA, July 31-August 2, 2007.

Perez-Verdin, G., Grebner, D.L., Sun, C., Munn, I.A., Schultz, E.B., and T.G. Matney. 2007. Woody biomass feedstock supplies and management for bioenergy in Mississippi. Presented at the Department of Plant and Soil Sciences, Mississippi State on February 22, 2007.

Zheljazkov, V.D., B. Vick, W. Ebelhar, N. Buehring, B. Baldwin, T. Astatkie, and J. Miller. 2007. Effect of N, Cultivar and their Interaction on Sunflower Yield, Oil Content, and Composition. ASA-CSSA-SSSA Annual International Meeting, November 4-8, 2007, New Orleans, LA.

Zheljazkov, V.D., B. Baldwin, W. Ebelhar, N. Buehring, and C. Coker. 2007. Sunflowers as an Oil Seed Crop for Biodiesel Production in Mississippi. SAAS and Annual Meeting Amer. Soc. Agron. Southern Branch. Feb 3-7, Mobile, AL. Available: http://a-c-s.confex.com/crops/2007srb/techprogram/S3241.HTM

Shanmugam S.G., and V.D. Zheljazkov. 2007. Oilseed Crops as Potential Biodiesel Crops for Mississippi. SAAS and Annual Meeting Amer. Soc. Agron. Southern Branch. Feb 3-7, Mobile, AL.

Reddy, K.R. Crop responses to abiotic responses: Tools and methods. Crop Genetics and Production Research Unit, USDA-ARS, 30 May 2008, Stoneville, Mississippi, USA.

Reddy, K.R. 2007. Climate change and crop productivity: Challenges and opportunities. The Digital Biology Learning Community (DBLC), John Gresham Room, Mississippi State University Library, 11 September 2007, Mississippi State, MS, USA.

Reddy, K.R. and V.R. Reddy. 2007. Controlled environment facilities for plant process quantification and modeling: Advantages and limitations. The ASA-CSSA-SSSA International Annual Meetings, 4-8 November 2007, New Orleans, Louisiana, USA.

Reddy, K.R. 2007. Searching for genotypic variability among crops to global environmental change. 104th Annual Meeting of The Southern Association of Agricultural Scientists, Biochemistry and Biotechnology Division, Mobile Convention Center, February 5, 2007, Mobile, AL, USA.

Reddy. K.R. 2006. Climate change and crop productivity: Challenges and opportunities. Students and faculty, Natural Resources and Ecology Laboratory and the USDA-UV-B Monitoring Program, Colorado State University, 11 April, 2006, Fort Collins, Colorado, USA.

Reddy, K.R. Crop responses to abiotic responses: Tools and methods. Crop Genetics and Production Research Unit, USDA-ARS, 30 May 2008, Stoneville, Mississippi, USA.

Reddy, K.R. 2007. Climate change and crop productivity: Challenges and opportunities. The Digital Biology Learning Community (DBLC), John Gresham Room, Mississippi State University Library, 11 September 2007, Mississippi State, MS, USA.

Reddy, K.R. and V.R. Reddy. 2007. Controlled environment facilities for plant process quantification and modeling: Advantages and limitations. The ASA-CSSA-SSSA International Annual Meetings, 4-8 November 2007, New Orleans, Louisiana, USA.

Reddy, K.R. 2007. Searching for genotypic variability among crops to global environmental change. 104th Annual Meeting of The Southern Association of Agricultural Scientists, Biochemistry and Biotechnology Division, Mobile Convention Center, February 5, 2007, Mobile, AL, USA.

Jones, T.L., E.B. Schultz, T.G. Matney, D.L. Grebner, D.L. Evans, C.A. Collins. 2008. A forest product/bio-energy mill location and decision support system based on a county-level forest inventory and geo-spatial information. Poster presented at the Forest and Wildlife Research Center Technology Transfer Conference & Mississippi Forestry

Association Board of Directors Meeting, MS on August 5-6, 2008.

Perez-Verdin, G., Grebner, D.L., Sun, C., Munn, I.A., Schultz, E.B., and T.G. Matney. 2008. Economic impacts of woody biomass utilization for bio-energy development in Mississippi. Poster presented at the Forest and Wildlife Research Center Technology Transfer Conference & Mississippi Forestry Association Board of Directors Meeting, MS on August 5-6, 2008.

Jones, T.L., E.B. Schultz, T.G. Matney, D.L. Grebner, D.L. Evans, C.A. Collins. 2008. A forest product/bio-energy mill location and decision support system based on a county-level forest inventory and geo-spatial information. Poster presented at the First Annual Energy-Synergy Workshop at Mississippi State, Mississippi on April 17, 2008.

Perez-Verdin, G., Grebner, D.L., Sun, C., Munn, I.A., Schultz, E.B., and T.G. Matney. 2008. Economic impacts of woody biomass utilization for bio-energy development in Mississippi. Poster presented at the First Energy-Synergy Workshop in Starkville, MS on April 17, 2008.

Jones, T.L., E.B. Schultz, T.G. Matney, D.L. Grebner, D.L. Evans, C.A. Collins. 2008. A forest product/bio-energy mill location and decision support system based on a county-level forest inventory and geo-spatial information. Poster presented at the Seventh Annual Bioproducts and Renewable Energy Conference in Choctaw, Mississippi on April 14-15, 2008.

Perez-Verdin, G., Grebner, D.L., Sun, C., Munn, I.A., Schultz, E.B., and T.G. Matney. 2008. Economic impacts of woody biomass utilization for bio-energy development in Mississippi. Poster presented at the Seventh Annual Southern Bioproducts and Renewable Energy Conference in Choctaw, MS on April 14-15, 2008.

Perez-Verdin, G., Grebner, D.L., Sun, C., Munn, I.A., Schultz, E.B., and T.G. Matney. 2008. Economic impacts of woody biomass utilization for bio-energy development in Mississippi. Poster presented at the Mississippi SAF Annual Meeting in Tunica, MS on April 1-3, 2008.

Jones, T.L., E.B. Schultz, T.G. Matney, D.L. Grebner, D.L. Evans, C.A. Collins. 2008. A forest product/bio-energy mill location and decision support system based on a county-level forest inventory and geo-spatial information. Poster presented at the North Mississippi Research and Extension Center Producer Advisory Council Meeting in Tupelo, Mississippi on February 21, 2008.

Perez-Verdin, G., Grebner, D.L., Sun, C., Munn, I.A., Schultz, E.B., and T.G. Matney. 2007. Woody biomass feedstock supplies and management for bioenergy in Mississippi. Poster presented at the Sixth Annual Southern Bioproducts and Renewable Energy Conference in Choctaw, MS on April 16-18, 2007.

Perez-Verdin, G., Grebner, D.L., Sun, C., Munn, I.A., Schultz, E.B., and T.G. Matney. 2007. Availability and feasibility of woody biomass for bioethanol conversion in Mississippi. Poster presented at the First Annual MSU Biofuels Conference in Starkville, MS on August 27, 2007.

Jones, T.L., Schultz, E.B., Matney, T.G., Grebner, D.L., Evans, D.L., and C.A. Collins. 2007. A forest product/bioenergy mill location and decision support system based on a county-level forest inventory and geo-spatial information. Poster presented at the Joint MS & LA SAF meeting in Natchez, MS on April 17-19, 2007.

Perez-Verdin, G., Grebner, D.L., Sun, C., Munn, I.A., Schultz, E.B., and T.G. Matney. 2007. Woody biomass feedstock supplies and management for bioenergy in Mississippi. Poster presented at the Joint MS & LA SAF meeting in Natchez, MS on April 17-19, 2007.

b. Websites or other Internet sites that reflect the results of this project

Mississippi State University Plant and Soil Sciences Department
http://www.msstate.edu/dept/pssfeedstocks/
http://www.pss.msstate.edu/soilmicro

Modified MIFI Data Reporter: http://www.mifi.ms.gov/

Information developed from our study is available on this website:
http://www.sebioenergy.org/2007/speakers.htm

c. Networks or collaborations fostered

Six Land Grant scientists in the US that work with castor (2 in TX, 1 in MS, 2 in NY, 1 in IL). We have formed a working group to make solicitation of funding more likely.

Southeastern Regional Bioenergy Group based in Tifton GA

The key technology developed in the research was the modification of the Mississippi Institute for Forest Inventory Dynamic Reporter. See link: http://www.mifi.ms.gov/ . The reporter allows users to estimate woody biomass by county or user defined region or polygons within Mississippi.

Sustainable Energy Research Center
Economic and Policy Analysis Final Report for 2006 -2008

1. Project Title: J: Sustainable Energy Center – Economic and Policy Analysis for Renewable and Sustainable Energy

Principal Investigators: Herndon, Cary W. and Coble, Keith H.

Team Members: Drs. Sanjoy Bhattacharjee, Benjamin Blair, Keith Coble, Laura Grace, Robert Grala, C.W. "Bill" Herndon, Kenneth Hood, Darren Hudson, Gregory Ibendahl, Randall Little, Andrew Muhammad, Daniel Petrolia, Jon Rezek, and William Stuart.

2. None/Not Applicable

3. Executive Summary

The production and collection of biomass feedstocks that are used to produce renewable bio-energy fuels and/or value-added products holds potential to generate income for resource owners, provide economic growth and rural development, and provide energy sources to help reduce dependence on non-renewable petroleum based fuels. Development of alternative fuel sources, while reducing dependence on foreign oil and increasing availability of domestically produced renewable bio-energy, would increase national economic and environmental security. Creating biomass and bio-energy industries in the U.S. would generate employment and promote economic development in rural communities. It is critical that these renewable feedstocks and bio-energy fuels are produced so that the environment is protected and land, air, and water quality is not harmed. Sustainability and success of these renewable energy systems depends on their economic profitability, competitiveness with alternative fuel sources and uses for the inputs, environmental benefits, and U.S. policies that influence investment, development, and operations of the industries that emerge.

The proposed research is designed to evaluate the costs of producing and/or collecting various biomass feedstocks that could be used to manufacture biorenewable fuels. Additionally, research will focus on evaluating and designing an assortment of local, state and national public and private policies employed to facilitate the development of sustainable bioenergy industries in Mississippi, the Southeast and in the US.

Several investigators analyzed the economic viability of utilizing various feedstocks in a lignocellulousic plant producing ethanol. The costs of producing, harvesting, and transporting of various grasses were estimated to determine the value of selected feedstocks at the conversion plant. Sensitivity analyses were conducted using various ethanol yields from feedstocks and selected conversion plant construction costs to estimate the value of the feedstock at various prices for ethanol. Other research investigated the amounts and locations of various types of cellulousic feedstocks (poultry litter and forest residues) and used this information to determine probable least-cost transportation biofuel conversion plant sites in Mississippi. Finally, initial results were published analyzing a survey of U.S. consumers' willingness to pay for E10 and E85 ethanol products. Survey findings report that consumers in states located in the Northeast and MidWest are willing to pay more for these "green" biofuel products.

The research conducted by the Economic and Policy Analysis investigators provides estimates of the locations of various feedstocks and the costs of producing, harvesting, transporting these feedstocks to proposed least-cost transport cost plant

sites. Comprehensive economic analyses were conducted to determine the various types of costs related to these activities using crop budgeting, harvest and storage cost analyses, transportation modeling, and amortization of capital equipment to estimate to break-even price for ethanol need to pay for all these costs in a proposed lignocellulousic facility. Sensitivity analyses were also conducted to allow for parameterization of various factors, including: (1) a variety of ethanol yield rates per ton of feedstock, and; (2) a range of ethanol plant construction costs per gallon of annual plant capacity. Econometric techniques were utilized to estimate consumers' willingness-to-pay for E10 and E85 collected from a national survey of 3,000 Americans.

The Economic and Policy Analyses research conducted is vitally important to consumers, business and industries, and local, state and federal policymakers who are investing time and capital into the biofuel sector. Rigorous economic analyses is paramount in evaluating the long-term viability and sustainability of renewable energy alternatives and determining the types of government policies needed to promote these biofuel industries. Renewable fuels hold the promise for decreasing our dependence of foreign oil/energy and also would create employment, investment and enhanced economics activity in rural areas searching for economic development opportunities.

4. Comparison of goals and actual accomplishments. All goals achieved

5. Summarization of activities for entire period of funding.

Task J.1: Economic Availability of Woody Residues for Utilization by Mills in Mississippi Robert K. Grala, Laura A. Grace, and William B. Stuart
Department of Forestry, Mississippi State University

The goal of this task was to examine distribution of woody residues in Mississippi and determine quantities that can be potentially utilized by mills located in the state for heat and electricity generation. This task was accomplished by generating maps illustrating distribution of woody residues within the state and mill procurement zones, determining transportation and extraction costs, and quantifying availability of woody residues at selected mill prices (gate prices).

Task J.1.DL1: Generating a map illustrating availability of woody residues.
This task required utilization of information available from several sources. The volumes of logging residues available in Mississippi at county level were determined using a Timber Products Output – an online reporting tool maintained by the USDA Forest Service. The volume information was converted to weight (green tons) and linked with spatial information on Mississippi counties in ArcGIS environment to generate map illustrating distribution of logging residues (Figure 1). In the next step, a spatial data on location of wood using mills in Southern U.S. was obtained from Southern Research Station of the USDA Forest Service. This information was overlaid on previously developed map to illustrate location of Mississippi mills in relation to available logging residues (Figure 2). In total, 107 facilities were located in Mississippi. These mills were used to determine statewide procurement zones for logging residues utilizing ArcGIS Network Analyst. We utilized an existing road network available within ArcGIS to establish procurement zones for 10, 20, 30, 40, 50, and 60-mile maximum hauling distances. An example of 30-mile procurement area for all mills located in Mississippi is presented in Figure 3. The obtained spatial information was used to determine quantities of logging residues available in each procurement zone. Because volumes of logging residues were available at county level, it was assumed that they were uniformly

distributed within each county. A proportion of county area allocated to specific procurement zone was used to determine quantity of logging residues available within that zone (Table 1). Results show that a 10-mile procurement zone accounts for 30% of logging residues available within the state, whereas 20-mile and 30-mile zones account for 80% and 92%, respectively. Increasing hauling distance beyond 30 miles resulted in a relatively small increase of available logging residues (an additional 4.6% at 60-mile hauling distance). This was because this model accounted only for logging residues available in Mississippi, whereas longer hauling distances would require recovery of logging residues from neighboring states.

Task J1.DL2: Determining the costs of transporting woody residues.
An existing road network was used to determine costs for transporting woody residues from the harvest site to the closest mill. However, an extremely large number of potential harvest sites resulted in even greater number of potential transportation routes. Even routes with the same hauling distance might represent different transportation costs due different combination of road types. To simplify the process, 25 randomly selected harvest sites were generated for each procurement zone totaling to 150 harvest sites. An ArcGIS Network Analyst was used to determine the shortest hauling distance from each harvest site to closest mill. Each routed was examined to determine road types on the hauling route. Transportation costs for each route were determined using Route Chaser – a spreadsheet program developed by the Wood Supply System Group of MSU College of Forest Resources. This program takes into account various components such equipment, labor and fuel costs, repair, maintenance, taxes, financing, insurance, and a road type. Because transportation costs depend on many factors such distance, road type, slope, and weather, they can vary significantly for each harvest site. Consequently, four statistics (minimum, maximum, mean, and median transportation costs) were used to determine feasibility scenarios for transporting logging residues. Transportation costs varied significantly ranging from $4.10/green ton (at fuel cost of $2.85/gallon) to $38.63/green ton (at fuel cost of $5.00/gallon). Increasing hauling distance from 10 to 30 miles doubled transportation cost, whereas further increase to 60 miles increased the transportation cost threefold. This important because majority of mills operate at longer hauling distances. A logging residue gate price at the mill for each procurement zone was determined as a sum of following costs: stumpage price, recovery of woody residues from the harvest site, chipping, and hauling. These costs can vary significantly, depending whether softwood or hardwood species are harvested. A range of likely costs was used to determine lower and upper limit for gate prices for woody residues recovered from each procurement zone (Table 2).

J.1.DL3: **Mileages for transportation of woody residues.**
Predetermined gates prices of $15, $30, and $45 per green ton of delivered logging residues were used to determine economic availability of woody residues in Mississippi. A maximum hauling distance was determined for each gate price by subtracting stumpage price, recovery and chipping costs and determining transportation costs. This step allowed calculating a maximum hauling distance at predetermined gate price. A cost map illustrating procurement zones at examined gate prices is presented in Figure 4, whereas availability of logging residues is presented in Table 3.

Table 1. Availability of logging residues in Mississippi at predetermined hauling distances

Hauling Distance (miles)	**Logging Residues Available within the Hauling Distance**			**Percentage of Total State's Logging Residues** (%)
	Softwood (green tons)	**Hardwood** (green tons)	**Total** (green tons)	
10	365,206	365,029	730,235	29.8
20	949,755	963,108	1,912,863	78.0
30	1,113,824	1,147,653	2,261,477	92.3
40	1,140,532	1,209,039	2,349,572	95.9
50	1,133,697	1,202,245	2,335,942	95.3
60	1,134,235	1,230,667	2,364,902	96.5

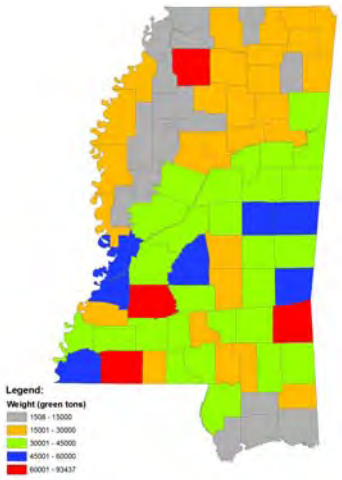


Figure 1.

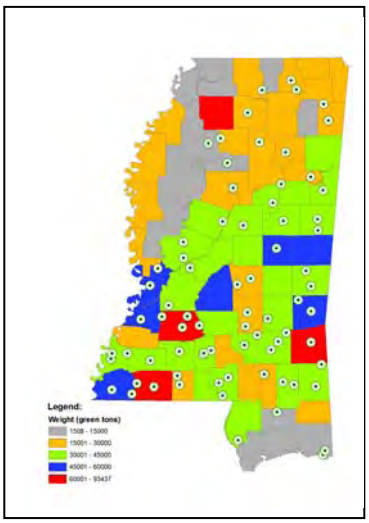


Figure 2.

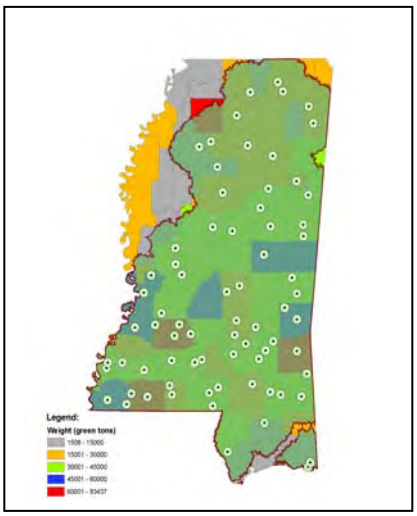


Figure 3.

Table 2. Mill gate prices for woody residues at varied recovery and fuel costs calculated for randomly selected mill in Mississippi.

Hauling Distance (miles)	Stumpage Price ($/green ton)	Recovery from Forest ($/green ton)	Chipping ($/green ton)	Transport ($/green ton)			Gate Price ($/green ton)		
				$2.85/gallon	$4.00/gallon	$5.00/gallon	$2.85/gallon	$4.00/gallon	$5.00/gallon
10									
low cost	3.00	6.00	5.00	4.10	4.20	4.29	18.10	18.20	18.29
average cost	3.50	9.00	6.00	4.86	5.05	5.22	23.36	23.55	23.72
high cost	4.00	12.00	7.00	5.76	6.06	6.32	28.76	29.06	29.32
20									
low cost	3.00	6.00	5.00	4.17	4.27	4.36	18.17	18.27	18.36
average cost	3.50	9.00	6.00	6.23	6.60	6.91	24.73	25.10	25.41
high cost	4.00	12.00	7.00	7.99	8.56	9.05	30.99	31.56	32.05
30									
low cost	3.00	6.00	5.00	4.68	4.86	5.01	18.68	18.86	19.01
average cost	3.50	9.00	6.00	7.51	8.02	8.47	26.01	26.52	26.97
high cost	4.00	12.00	7.00	10.56	11.49	12.29	33.56	34.49	35.29
40									
low cost	3.00	6.00	5.00	4.66	4.84	4.99	18.66	18.84	18.99
average cost	3.50	9.00	6.00	7.97	8.54	9.04	26.47	27.04	27.54
high cost	4.00	12.00	7.00	10.54	11.43	12.21	33.54	34.43	35.21
50									
low cost	3.00	6.00	5.00	5.59	6.04	6.28	19.59	20.04	20.28
average cost	3.50	9.00	6.00	9.43	10.22	10.87	27.93	28.72	29.37
high cost	4.00	12.00	7.00	15.30	16.78	18.07	38.30	39.78	41.07
60									
low cost	3.00	6.00	5.00	6.14	6.47	6.76	20.14	20.47	20.76
average cost	3.50	9.00	6.00	10.64	11.57	12.37	29.14	30.07	30.87
high cost	4.00	12.00	7.00	15.63	17.25	18.67	38.63	40.25	41.67

Table 3. Availability of logging residues in Mississippi at predetermined gate prices and fuel cost of $2.85 per gallon.

Gate Price ($/green ton)	**Transportation and Recovery Cost Scenario**	**Availability of Logging Residues** (green tons)
20		
	Low cost	2,027,705
	Average cost	50,947
	High cost	0[a]
30		
	Low cost	2,353,265
	Average cost	1,394,269
	High cost	26,102

[a] Price was too low to recover and transport any quantity of logging residues.

Task J.2: Evaluate poultry litter, cotton gin trash and soybean as feedstocks for biofuel production.

To accomplish task J.2, Mississippi State University researchers and extension specialists conducted an inventory of existing poultry, cotton, and soybean production, by county, in the state of Mississippi, 2006. Production data was then used to calculate the total annual tons of poultry litter, cotton gin waste, and soybeans produced per county. Extension poultry specialist with the Poultry Science Department at Mississippi State University provided conversion numbers used to determine the amount of poultry litter available based on the production numbers for Mississippi. Conversion numbers used to calculate gin waste was provided by research and extension agricultural engineers with the department of Agricultural and Biological Engineering at Mississippi State University. Total soybean production numbers were taken from production data reported by the National Agricultural Statistical Service (NASS). The data collected was used by GeoResources Institute at Mississippi State University to develop maps illustrating tons per county of each feedstock. The maps can be used to determine total annual feedstock available in Mississippi and designate major concentration points within the state for collection and distribution to bio-energy processing facilities.

The following data is summary of totals for each feedstock:
Broilers
Production/tons of litter

year	chicks placed 1000's	Mortality rate 7.50%	No. Broilers 1,000's	ton/litter conversion (1.6/1000 birds)	tons of litter
2001	793,480	0.075	59,511	1.6	95,217
2002	804,475	0.075	60,335	1.6	96,537
2003	826,451	0.075	61,983	1.6	99,174
2004	873,979	0.075	65,548	1.6	104,877

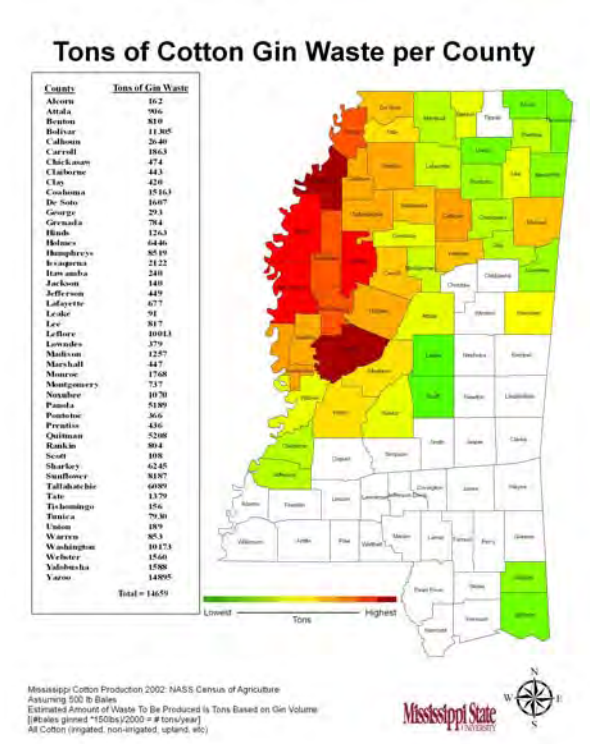
2005	878,268	0.075	65,870	1.6	105,392

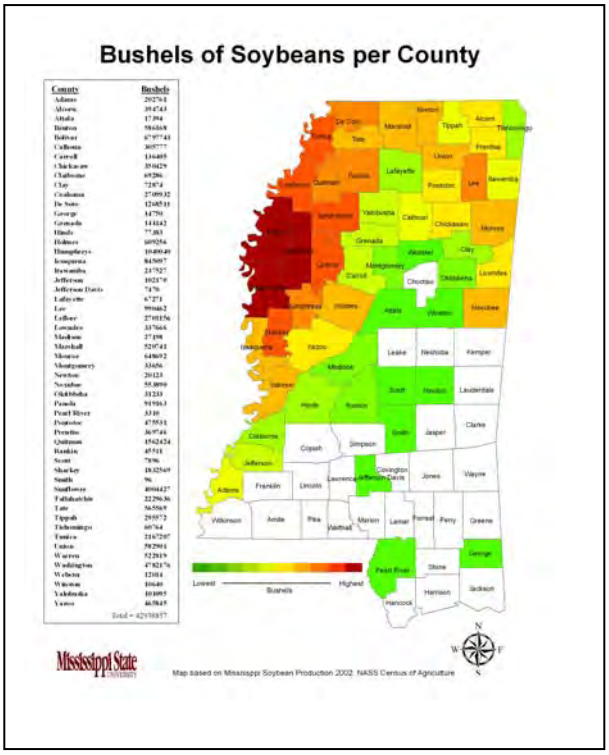
Cotton
Assuming 500 lbs per bale
Estimated gin waste produced in tons:
{[(#bales ginned*150lbs)/2000]= #tons gin waste per year}

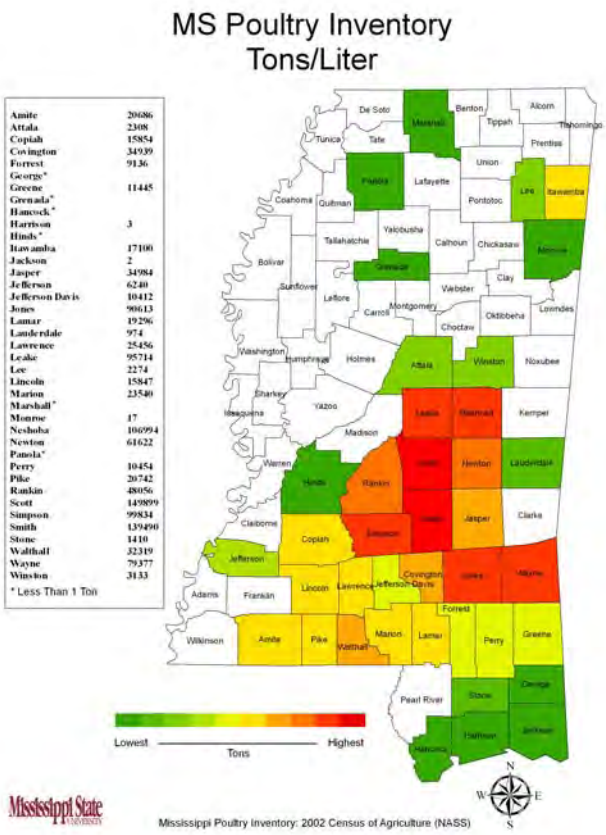
Mississippi total	Cotton	tons
5-year avg.	Bales	gin trash
2001-2005	2,188,800	164,160

Soybeans

Mississippi Total	bushels
5–year avg.	51,221,000
2001-2005	







<u>Task J.3:</u> Develop cost of production estimates, e.g., enterprise budgets, for selected alternative biomass feedstocks that could be produced in the state and region.

The United States has become dependent on nonrenewable resources such as nuclear, coal, and crude oil as major sources of energy and fuel. Ethanol has been identified as a renewable fuel source that may help alleviate this dependence. Recent technological advances have developed a method to produce ethanol from lignocellulosic biomass. The purpose of this study is to determine production and transportation costs of switchgrass, eastern gammagrass, and giant miscanthus using Mississippi and Oklahoma data. This study also estimated the returns above the cost of feedstock for a biorefinery and the incentive package needed to pay for feedstock and construction cost. Results indicate cost difference across species, method of harvest, and location. The biorefinery returns and the incentive package explain the amount of capital needed for a biorefinery to compensate for the cost of feedstock and construction.

To estimate yield and production cost per acre for switchgrass, giant miscanthus, and eastern gammagrass, experimental plot level yield data are collected from Experiment Station research plots in Stillwater, Oklahoma and Starkville, Mississippi. The agronomic data from Mississippi are provided by Dr. Brian Baldwin, while the agronomic data from Oklahoma are provided by Dr. Francis Epplin. The agronomic data from both locations include the field operations associated with production and the yields

measured in dry tons per acre for each species of LCB. The yield data represent harvests in 2003, 2004, and 2005, providing three seasons of harvest data.

Each of the three species of LCB was planted with four replications for both the single and dual harvest methods in 2002, providing four data points for each year, LCB specie, and harvest method. Tables 4.1 and 4.2 display the summary statistics for the yields observed in both locations: Starkville, Mississippi; and, Stillwater, Oklahoma.

Yield data summary statistics for LCB grown in Mississippi.

Species	Harvest	Mean	Std Dev	Minimum	Maximum
		(Tons per Acre)			
Switchgrass	SH	12.49	3.03	4.57	21.01
	DH	14.97	6.32	7.12	30.14
Giant Miscanthus	SH	14.47	5.52	7.84	29.13
	DH	16.45	6.32	7.20	27.41
Eastern Gammagrass	SH	4.76	4.57	0.80	16.64
	DH	8.74	0.36	8.35	9.19

Yield data summary statistics for LCB grown in Oklahoma.

Species	Harvest	Mean	Std Dev	Minimum	Maximum
		(Tons per Acre)			
Switchgrass	SH	7.08	1.31	5.23	9.22
	DH	6.88	1.28	4.75	9.21
Giant Miscanthus	SH	5.53	0.84	4.14	6.50
	DH	5.82	0.73	5.03	7.13
Eastern Gammagrass	SH	4.24	1.37	1.61	5.69
	DH	4.42	1.43	2.01	6.41

These summary statistics describe the data that are used to estimate the tons per acre produced. The means from Table 4.1 show that, across all species grown in Mississippi, a dual harvest system produces more tons per acre than single harvest systems. Giant miscanthus grown under a dual harvest system produces the most per acre of the LCB species grown in Mississippi. Eastern gammagrass yields are nearly twice as much with a dual harvest system as compared to a single harvest system. To explain the difference, when eastern gammagrass is left in the field too long before harvesting it begins to wilt and decay in the field. Thus, in a single harvest system, there are substantial in-field losses prior to harvest. Therefore, earlier first cut in the dual harvest system minimizes losses because the grass is harvested before starting to wilt.

As for the LCB produced in Oklahoma, the means from Table 4.2 show that switchgrass grown under a single harvest system produces the highest yield, measured in tons per acre, of the systems studied. Giant miscanthus and eastern gammagrass both produced higher yields under a dual harvest system.

Cost data summary statistics for LCB grown in Mississippi with the establishment year cost amortized over a 15-year stand life.

		Mean	Std Dev	Minimum	Maximum
		(Cost per ton in dollars)			
Switchgrass	SH	28.50	14.37	14.22	65.40
	DH	25.66	10.58	10.93	46.33
Giant Miscanthus	SH	27.35	11.06	11.34	42.13
	DH	25.74	11.49	13.17	50.16
Eastern Gammagrass	SH	122.14	108.71	17.93	372.10
	DH	37.62	1.53	35.75	39.33

Cost data summary statistics for LCB grown in Oklahoma with the establishment year cost amortized over a 15-year stand life.

		Mean	Std Dev	Minimum	Maximum
		(Cost per ton in dollars)			
Switchgrass	SH	35.16	6.56	26.17	46.14
	DH	40.87	8.06	29.54	57.27
Giant Miscanthus	SH	57.13	9.43	47.52	74.61
	DH	59.14	1.41	47.63	67.52
Eastern Gammagrass	SH	66.85	33.11	42.97	151.87
	DH	70.30	28.40	42.94	136.94

Since the construction cost per annual gallon of ethanol produced for a lignocellulosic biorefinery has not been published, this study displays how sensitive this cost is to a lignocellulosic biorefinery. The biorefinery biomass feedstock, operating, and construction costs are used to estimate the price per gallon of ethanol needed for the biorefinery to breakeven. While these cost are not all of the components to a biorefinery's total cost of production, other costs such as feedstock storage or any post production cost associated with ethanol production are assumed to be zero in this study. Two different cost scenarios were used to provide a range from a lower to a higher cost scenario. The lower cost scenario took advantage of less expensive biomass feedstock and operating costs, while the higher cost scenario utilized the more expensive feedstock and operating costs.

Using the following equation: $$P_E = \frac{\mathrm{B}}{\delta} + \mathrm{X} + \Phi$$

P_E is the breakeven price per gallon of ethanol. B represents the price of the delivered stock. The production costs were estimated using the establishment cost, maintenance cost, harvesting cost, and moving the LCB to an in-field location for the transport vehicle. The transportation costs estimates assume the feedstock is loaded on a semi-truck in the field and hauled to the biorefinery. The loading and transporting cost is divided by the assumed weight of the truck load, to calculate transportation cost per ton. Production data used, was agronomic data collected at Mississippi State University and Oklahoma State University through the Biomass-Based Energy research project. Transportation cost data, from the field to the plant, was collected from survey data conducted on trucking companies in Mississippi. δ represents the gallons produced per ton of feedstock. X is the construction cost per annual gallon. Φ is the operating cost per gallon. Some biorefineries are eligible for tax incentives to produce ethanol.

	Construction Cost per Annual Gallon								
	$1.00	$1.50	$2.00	$2.50	$3.00	$3.50	$4.00	$4.50	$5.00
Gallon/ton	Price per gallon of Ethanol Needed (In Dollars)								
150	2.80	3.30	3.80	4.30	4.80	5.30	5.80	6.30	6.80
140	2.85	3.35	3.85	4.35	4.85	5.35	5.85	6.35	6.85
130	2.91	3.41	3.91	4.41	4.91	5.41	5.91	6.41	6.91
120	2.98	3.48	3.98	4.48	4.98	5.48	5.98	6.48	6.98
110	3.06	3.56	4.06	4.56	5.06	5.56	6.06	6.56	7.06
100	3.16	3.66	4.16	4.66	5.16	5.66	6.16	6.66	7.16
90	3.28	3.78	4.28	4.78	5.28	5.78	6.28	6.78	7.28
80	3.43	3.93	4.43	4.93	5.43	5.93	6.43	6.93	7.43
70	3.62	4.12	4.62	5.12	5.62	6.12	6.62	7.12	7.62
60	3.87	4.37	4.87	5.37	5.87	6.37	6.87	7.37	7.87
50	4.23	4.73	5.23	5.73	6.23	6.73	7.23	7.73	8.23
40	4.76	5.26	5.76	6.26	6.76	7.26	7.76	8.26	8.76
30	5.66	6.16	6.66	7.16	7.66	8.16	8.66	9.16	9.66
20	7.44	7.94	8.44	8.94	9.44	9.94	10.44	10.94	11.44

This chart explains the upper bound incentives needed to breakeven. The prices were calculated by using a price of delivered feedstock of $107.15, and a per gallon operating cost of $1.75. These results include the tax incentive package of $.66. Currently, the average facility produces about 30 gallons of ethanol per ton of feedstock. If construction costs are at $3.00 per annual gallon, then the price per gallon of ethanol needed to breakeven is $7.66.

	Construction Cost per Annual Gallon								
	1.00	1.50	2.00	2.50	3.00	3.50	4.00	4.50	5.00
Gallon/ton	Price per gallon of Ethanol Needed (In Dollars)								
150	1.07	1.57	2.07	2.57	3.07	3.57	4.07	4.57	5.07
140	1.08	1.58	2.08	2.58	3.08	3.58	4.08	4.58	5.08
130	1.10	1.60	2.10	2.60	3.10	3.60	4.10	4.60	5.10
120	1.12	1.62	2.12	2.62	3.12	3.62	4.12	4.62	5.12
110	1.15	1.65	2.15	2.65	3.15	3.65	4.15	4.65	5.15
100	1.18	1.68	2.18	2.68	3.18	3.68	4.18	4.68	5.18
90	1.22	1.72	2.22	2.72	3.22	3.72	4.22	4.72	5.22
80	1.27	1.77	2.27	2.77	3.27	3.77	4.27	4.77	5.27
70	1.33	1.83	2.33	2.83	3.33	3.83	4.33	4.83	5.33
60	1.41	1.91	2.41	2.91	3.41	3.91	4.41	4.91	5.41
50	1.53	2.03	2.53	3.03	3.53	4.03	4.53	5.03	5.53
40	1.70	2.20	2.70	3.20	3.70	4.20	4.70	5.20	5.70
30	1.99	2.49	2.99	3.49	3.99	4.49	4.99	5.49	5.99
20	2.57	3.07	3.57	4.07	4.57	5.07	5.57	6.07	6.57

This chart shows the lower bound incentives needed to breakeven. The prices were calculated by using a price of delivered feedstock of $34.61 and a per gallon operating cost of $.50 It also includes the tax incentives package of $.66. If the plant produces 30 gallons of ethanol per ton of feedstock, and assumes a $3.00 construction cost per annual gallon, the plant needs a price of $3.99 to breakeven

Task J.4: Estimate environmental costs and benefits for proposed feedstocks and bioenergy processes to evaluate environmental sustainability.

This analysis presents estimated emissions produced during production, harvest, and transport of switchgrass, giant miscanthus, Eastern Gammagrass, poultry litter, and cotton gin trash, candidate feedstocks for ethanol production. Crop production included all field practices including harvest. Because the first year of production is for establishment of the grass, no harvest occurs. Therefore transportation began in year 2 after harvest when the crop was transported off the farm. Emissions from hauling were converted to a per-acre basis by multiplying emissions from hauling per ton by the average yield per acre. Major parameters assumed for this analysis are shown in Table 1.

Emissions due to crop production were estimated based on fuel-use requirements of production equipment. Production included all practices from crop establishment to harvest and "on-farm" transportation (moving bales to edge of field). Totals for five-year production for Switchgrass and Giant Miscanthus, and three-year for Eastern Gammagrass, were estimated for two harvest regimes: single harvest and double harvest. Average yields from the three grasses (used to calculate values in Table 2) All variables are considered "as is" for this table, meaning that moisture content of feedstock will be the same as it is at harvest.

All transportation after "on-farm" transportation was included in the Transportation section (Table 3). Fuel requirements (gallons per acre) were multiplied by emissions factors, taken from GREET (2006) to yield quantity (pounds/gallon/acre) of each pollutant produced.

Emissions estimates due to feedstock transport were based on the quantity of fuel consumed by the vehicles used to transport the feedstocks. Fuel economy assumptions were based on several estimates taken from personal interviews of local truck drivers. Specifically, transport emissions were estimated as follows:

$$X = \frac{\dfrac{\text{miles traveled}}{\text{miles per gallon}}}{\dfrac{\text{tons feedstock per truck}}{\text{emissions per unit}}}$$

X = lbs. of emissions per ton of feedstock.

We assumed three transport distances in order to present a range of emissions: 10 miles, 25 miles, and 50 miles. For each distance, we included both the trip to the destination with the truck loaded and the return trip with the truck empty. Cargo weight per truck was taken from Busby et al. (2007) Poultry litter and cotton gin trash are by-products of poultry and cotton production, and thus, no production and harvest operations are assumed for these feedstocks. Emissions estimates commences at transport. Cargo weight was assumed to be 12 tons per truck for poultry litter and 14 tons per truck for gin trash. The density of gin trash was assumed to be equal to that of garden mulch. This figure was multiplied by maximum volume capacity of a truck trailer to find out whether a full load would exceed the legal weight limit. Trucks hauling poultry litter could carry 12 tons per load, and trucks hauling cotton gin trash could haul 14 tons per truck, both below the legal limit.

Total emissions over production, harvest, and transport were estimated by adding the average emission per year from feedstock production and harvest (over year 1 and years 2-5, etc) to the emissions per acre yielded from off-farm transportation of the crop (Table 4).

Table 1. Feedstock Production and Harvest Parameters Parameters

Truck Fuel Economy	6 mpg
Cargo weight of the truck	14.6 tons
Density of garden mulch	25.93 lbs/ft^3

Table 2

Crop Production	Fuel Use	VOC	CO	NOx	PM10	SOx	CH4	N2O	CO2	GHG
	(gal/A)	0.02	0.10	0.19	0.02	0.00	0.00	0.00	21.90	21.98
Switchgrass		Calculated by: Amount of fuel used in year x emissions factors								
Year 1 Establishment	3.47	0.07	0.36	0.67	0.06	0.01	0.00	0.00	76.00	76.28
Years 2-5 Single Harvest	7.57	0.15	0.78	1.47	0.13	0.02	0.00	0.00	165.72	166.34
Years 2-5 Double Harvest	14.89	0.29	1.53	2.88	0.26	0.03	0.00	0.00	326.04	327.25
Single Harvest 5 Year Total	33.74	0.66	3.47	6.54	0.59	0.08	0.01	0.01	738.89	741.63
Double Harvest 5 Year Total	63.02	1.23	6.48	12.21	1.11	0.14	0.01	0.02	1380.16	1385.27
Giant Miscanthus		Calculated by: Amount of fuel used in year x emissions factors								
Year 1 Establishment	16.94	0.33	1.74	3.28	0.30	0.04	0.00	0.00	371.06	372.43
Years 2-5 Single Harvest	7.32	0.14	0.75	1.42	0.13	0.02	0.00	0.00	160.32	160.91
Years 2-5 Double Harvest	14.64	0.29	1.50	2.84	0.26	0.03	0.00	0.00	320.63	321.82
Single Harvest 5 Year Total	46.22	0.91	4.75	8.96	0.81	0.11	0.01	0.01	1012.32	1016.08
Double Harvest 5 Year Total	75.50	1.48	7.76	14.63	1.33	0.17	0.01	0.02	1653.59	1659.72
Eastern Gammagrass		Calculated by: Amount of fuel used in year x emissions factors								
Year 1 Establishment	1.94	0.04	0.20	0.38	0.03	0.00	0.00	0.00	42.45	42.60
Year 2-3 Single Harvest	7.57	0.15	0.78	1.47	0.13	0.02	0.00	0.00	165.72	166.34
Year 2-3 Double Harvest	14.89	0.29	1.53	2.88	0.26	0.03	0.00	0.00	326.04	327.25
Single Harvest 3 Year Total	32.20	0.33	1.75	3.31	0.30	0.04	0.00	0.00	373.89	375.28
Double Harvest 3 Year Total	61.48	0.62	3.26	6.15	0.56	0.07	0.01	0.01	694.52	697.10

*GHG: CO2 equivalents (CO2, CH4,N2O)

Table 3

Transport	Fuel Use	VOC	CO	NOx	PM10	SOx	CH4	N2O	CO2	GHG
**accounts for to and from trips		0.02	0.09	0.26	0.00	0.01	0.00	0.00	44.06	44.41
Transport (per ton)	(gal/ton/mile)	Calculated by: ((Miles travled/fuel economy of truck)/tons per truck) x emissions factors								
10 Miles	0.11	0.00	0.01	0.03	0.00	0.00	0.00	0.00	5.03	5.07
25 Miles	0.29	0.00	0.02	0.07	0.00	0.00	0.00	0.00	12.57	12.67
50 miles	0.57	0.01	0.05	0.15	0.00	0.00	0.00	0.00	25.15	25.35
Poultry Litter (12 tons/truck)	(gal/ton/mile)	Calculated by: ((Miles travled/fuel economy of truck)/tons per truck) x emissions factors								
10 Miles	0.14	0.00	0.01	0.04	0.00	0.00	0.00	0.00	6.12	6.17
25 Miles	0.35	0.01	0.03	0.09	0.00	0.00	0.00	0.00	15.30	15.42
50 miles	0.69	0.01	0.06	0.18	0.00	0.00	0.00	0.00	30.60	30.84
Gin Trash (14 tons/truck)	(gal/ton/mile)									
10 Miles	0.07	0.00	0.01	0.02	0.00	0.00	0.00	0.00	3.19	3.22
25 Miles	0.18	0.00	0.02	0.05	0.00	0.00	0.00	0.00	7.98	8.05
50 miles	0.36	0.01	0.03	0.09	0.00	0.00	0.00	0.00	15.96	16.09

*GHG: CO2 equivalents (CO2, CH4,N2O)

Table 4

Production + Transport Emissions for Grasses (per year average)										
Switchgrass (Single Harvest)	Average Yield:	12.49	Tons/Acre	(Average yearly emissions per acre)				+ (Emissions per Acre from transport)		
10 Miles	10.67	0.21	1.07	2.16	0.17	0.03	0.00	0.00	265.28	266.54
25 Miles	12.81	0.24	1.26	2.70	0.18	0.04	0.00	0.01	359.51	361.52
50 miles	16.37	0.30	1.57	3.61	0.20	0.06	0.01	0.01	516.56	519.83
Switchgrass (Double Harvest)	Average Yield:		14.97	Tons/Acre						
10 Miles	16.53	0.32	1.70	3.36	0.27	0.04	0.00	0.01	406.01	407.84
25 Miles	18.66	0.37	1.92	4.02	0.29	0.06	0.01	0.01	518.95	521.68
50 miles	22.23	0.44	2.29	5.11	0.31	0.08	0.01	0.01	707.18	711.42
Giant Miscanthus (Single Harvest)	Average Yield:		14.47	Tons/Acre						
10 Miles	10.90	0.21	1.09	2.21	0.17	0.03	0.00	0.00	275.24	276.58
25 Miles	13.37	0.25	1.31	2.84	0.18	0.04	0.00	0.01	384.41	386.62
50 miles	17.50	0.32	1.67	3.90	0.20	0.07	0.01	0.01	566.35	570.02
Giant Miscanthus (Double Harvest)	Average Yield:		16.45	Tons/Acre						
10 Miles	16.98	0.33	1.71	3.41	0.28	0.04	0.00	0.01	413.45	415.34
25 Miles	19.79	0.38	1.96	4.12	0.29	0.06	0.01	0.01	537.56	540.44
50 miles	24.49	0.46	2.36	5.32	0.31	0.09	0.01	0.01	744.39	748.94
Eastern Gammagrass (Single Harvest)	Average Yield:		4.67	Tons/Acre						
10 Miles	6.97	0.08	0.40	0.80	0.06	0.01	0.00	0.00	98.27	98.73
25 Miles	7.77	0.09	0.47	1.00	0.07	0.02	0.00	0.00	133.50	134.25
50 miles	9.11	0.11	0.58	1.34	0.07	0.02	0.00	0.00	192.22	193.44
Eastern Gammagrass (Double Harvest)	Average Yield:		8.74	Tons/Acre						
10 Miles	13.29	0.22	1.17	2.30	0.19	0.03	0.00	0.00	275.47	276.68
25 Miles	14.79	0.25	1.30	2.68	0.20	0.04	0.00	0.01	341.40	343.14
50 miles	17.29	0.29	1.52	3.32	0.21	0.05	0.01	0.01	451.30	453.92

Task J.5: Perform a competitive analysis of selected biofuels by investigating the market structure and participants, trade flows, and pricing mechanisms for various fuels and energy products.

The general purpose of Task J5 is to create a platform for examining recent developments in the production, consumption, and trade flows of energy and agricultural products related to biorenewables. This project is comprised of three main components. The first component compiles recent data on various aspects of energy and agricultural markets. The second component is a collection of international economic policies and goals aimed at the development and functioning of renewable energy markets. The final component focuses on ethanol - the most widely available biorenewable fuel in the U.S. A conceptual model is created that graphically details the linkages and interactions between the ethanol market and various other markets and policies. Each of these components is packaged on an interactive CD for dissemination to researchers, educators, and policy makers.

Information pertinent to international renewable energy production and trade flows was collected from various sources by the project investigators and a graduate student funded by the grant. These sources included databases established by the International Energy Agency, the U.S. Department of Energy, Energy Information Administration, and the Food and Agriculture Organization of the United Nations. The data include country-specific information on conventional energy production, consumption, and trade, as well as, similar information for renewable energy sources including: municipal waste, industrial waste primary solid biomass, biogas, liquid biofuels, geothermal, solar thermal, hydro, solar photovoltaics, tide-wave-ocean, and wind power. In addition, country-level data on agricultural production, consumption, prices and trade flow data was also incorporated onto the CD.

Economic policies regarding the development of biorenewable energy markets and the rules governing those markets are quite various worldwide. In developed economies these policies include capital grants, tax incentives, and tradable certificates. Policies in developing countries are sparse and generally consist of rural electrification programs. The most comprehensive source for these policies was the biorenewable policy database maintained by the International Energy Agency. Available data through 2006 for 39 countries was collected from this database by the project investigators and a graduate student funded by this grant. The data cataloged on the CD can serve as an important resource for researchers interested in analyzing the effectiveness of various policies in promoting the development of biorenewable energy production and markets.

The final component of this project consists of a conceptual model of a specific biorenewable market. In particular, this model investigates the linkages and feedbacks in the market for ethanol. It includes various endogenous and exogenous variables such as the markets for co-products, feedstock and other production costs, trade policy, foreign production, crude oil prices, domestic crop and livestock markets and domestic and foreign energy and environmental policy. An emphasis was placed on the impact of ethanol from Brazil - the largest producer of fuel ethanol in the world. The purpose of this model is to provide a visual representation of the factors that affect and are affected by changes in domestic production, consumption and imports of fuel ethanol. This model can be used by researchers to more thoroughly investigate particular linkages and relationships. It can also be used by policy makers to discern the effects of proposed policy changes on various markets and to formulate more efficient policy alternatives.

Each of the three main components are collected on a single CD which provides access to the country-specific information, and the conceptual model through an intuitive user interface. This interface includes six main sections described below.

- WELCOME
  - Provides information regarding the purpose of the research, the title of the project and the source of funding.

- COUNTRY INFO
  - Provides access to country specific biorenewable energy and crop data, including production, consumption, and export/import data, and a catalog of price information and economic policies. Users access data via drop-down menus.

- CONCEPTUAL MODEL
  - Provides a conceptual model of the U.S. ethanol market that visually represents the linkages and interconnections important in driving U.S. ethanol prices, consumption, production, and imports. Clickable links direct users to more detailed analysis of various components of the model.

- REFERENCES
  - Provides a list of the research and data sources used to compile this compendium.

- ABOUT US
  - Provides the professional background of the researchers involved in the project.

- CONTACT
  - Provides contact information for the two principal investigators responsible for this component of the overall project.

Two minor changes were made from the original proposed tasks. First, instead of placing our final product on the web, a CD containing the project information was produced. This was done due to concerns about web hosting and upkeep of the website. Second, we focused solely on the ethanol market in our conceptual model, excluding biodiesel. This was done for two main reasons. First, the biodiesel market is relatively underdeveloped in the U.S. relative to the ethanol market. Many of the same linkages apply for biodiesel, although the volume produced is lower. Second, biodiesel is not traded in large quantities outside Europe. Since this Task focused mainly on international biorenewable policies and trade flows and how they affect the U.S., we concentrated on ethanol, which is more relevant in this country.

Task J.6: Describe sensitivity of the production of biorenewable feedstocks to changes in petroleum prices, substitute crop prices, and market structure variables, including analyses of policy alternatives at the local, state, regional, national and international levels.

Studies concerning the impact of U.S. Ethanol Production on Feed Cost and Livestock and Animal Industries

Justification: Feed costs, which are a core part of animal production, play a key role in determining livestock prices. Feed costs represent 50% to 70% of livestock production expenses and are a critical component of livestock profitability (Wright et al., 2007). Renewable energy has created a new agricultural environment that is rapidly changing. Given the concerns of higher feed costs, the primary objective of the following studies were to determine the

sensitivity of U.S. broiler production and U.S. catfish production to changes in corn prices induced by an expansion in U.S. ethanol production.

Overview and Outputs: The following is a summary of two studies conducted under the SERC Economic and Policy Analysis Project. The primary objective of the first study was to assess the impact of rising corn prices on U.S. broiler production. The second paper is still ongoing where the objective is to assess the how rising feed cost due to increased ethanol production has impacted the U.S. catfish industry.

Summary of Broiler Study: Given the concerns of higher feed costs due to increase ethanol production, the objective of this study was to determine the sensitivity of U.S. broiler production to changes in corn prices. Elasticity estimates indicated that percentage increases in feed cost decreased U.S. broiler production by 0.06 percent and percentage increases in corn cost decreased U.S. broiler production by 0.042 percent. Simulation results project that if corn prices increased from $2.50 to $4.50, U.S. broiler production would decrease from 11.67 billion lbs to 11.38 billion lbs, an overall decrease of 3 percent, which represents a loss of $133.2 million for the industry.

Given results, assumptions can be made as to the relative small decrease in broiler supply. Among these are poultry relationships with other meats and contractual agreements. Given that corn is a major component of feeds for all meats, corn prices will affect the supply of beef and pork as well as poultry. Meat prices will likely increase, which should increase the consumption of poultry relative to beef and pork. Vertical integration may also have an effect on poultry supply. Poultry processors often contract with many grower operators. The integrator supplies the chicks and feed, among other aspects of production, to the grower. These companies have invested much time and money into research that has created a very efficient production process. Since 1920, mortality rates have decreased from 18 percent to 4 percent in 2005 (NCC, 2006). The increase in productivity may likely have keep production strong in the face of significant increases in corn prices. This suggest that the results of this study should be taken with some caution given that producers may be more responsive to present changes corn prices resulting from ethanol production than price changes in the past. Therefore the impact of rising corn prices on broiler production may be greater than results suggest.

Summary of Catfish Study: Corn is a key ingredient in making the least-cost and most nutritious catfish feed. For instance, feed for food size catfish, which is 32% protein, typically contains 32.1% corn grain and 41.4% soybean meal (Robinson et al., 2006). Given the importance of corn in catfish feed production, corn prices should significantly influence feed costs, and production and prices at the farm and wholesale level.

In recent years, the demand for corn has increased due to growing ethanol production. Form 2000 to 2006, ethanol production increased from 1.6 billion gallons to approximately 5 billions, an increase of 212.5%. Ethanol production is projected to increase even further (Collins, 2007). Because corn is the primary ingredient for U.S. ethanol production, corn production has expanded and corn prices have significantly increased. According to National Agricultural Statistics Service (NASS), the average farm level corn price in 2005 was $1.96 per bushel. Corn prices increased from $2.00 per bushel in January 2006 to $3.01 in December 2006. As of June 27, 2007 corn futures (Dec 08 contract) settled at $7.87 per bushel.

Due to rising corn prices, the catfish industry is facing rising feed costs. This study assesses the impact of corn prices on catfish feed cost, and the impact of rising feed cost on catfish production and prices at the wholesale and farm level. From results we infer the impact of the Ethanol boom on the catfish industry. Preliminary results show that for every percentage increase in corn prices, feed cost for the catfish industry rises by 0.13%.

Study analyzing the demand for Ethanol blended fuel by US consumers

U.S. ethanol production has increased from less than 2 billion gallons in 2000 to 6 billion gallons in 2007 (RFA 2007), due in part to high oil prices and increased government subsidies. In spite of the surge in its production, very little work has examined ethanol demand. Although an opinion poll was conducted by Harris Interactive on behalf of the Biotechnology Industry Organization (2006) and a report on consumer opinion was published on the Renewable Fuels Association website (2007), there was no research study focused on identifying the key characteristics that drives demand for ethanol blended fuel. Our study bridges this gap. The primary focus of this study was to identify peoples' preferences for alternative fuels, particularly ethanol blended fuel, identify the factors that shape peoples' preferences and influence to pay premium and calculate peoples' willingness to pay (WTP) a premium for ethanol blended fuel.

In order to collect the necessary data for this study, we developed and administered a nationwide contingent-valuation survey of consumer preferences for E-10 (a blend of 10% ethanol and 90% gasoline) and E-85 (a blend of 85% ethanol and 15% gasoline) to estimate willingness-to-pay for both fuels and to identify key characteristics driving demand. Between April & June of 2007 a Contingent Valuation (CV) mail survey was conducted on a 3000-person stratified (weighted by state population) random sample selected across all 50 US states.

Survey Results

The survey generated 748 returns (a 25% response rate). In comparison to the national statistics, our survey sample was skewed slightly in favor of middle-aged, educated, upper-middle-class males. Median U.S. household income (in 2004) was $44,334, whereas the mean household income level of our sample was about $60,000. The average U.S. household size (in 2000) was 2.59, whereas the mean household size for our sample was 2.5. Forty-nine percent of the U.S. population (in 2006) was male, whereas 69% of our sample was male. Median U.S. age (in 2000) was 35.3. However, we were interested in persons 18 years of age or older, which comprise 74.3% of the population. Accounting for this share, the adjusted median age is 48. The mean age of our sample was 58. , Fifteen and one-half percent of the U.S. population (in 2000) held a bachelor's degree and 8.9% held a master's degree. Fifty-four percent of our sample had a high-school degree or less, 24% had completed a bachelor's degree, and 22% had a graduate degree. Thirty-six percent of respondents in the sample lived in a city with a population above 50,000, 31% live in a city with population between 10,000 and 50,000, 14% live in towns under 10,000 residents, and 18% live in a rural/farm area. The mean number of vehicles owned per household was just above 2. Thirty-eight percent of respondents described themselves as politically conservative, 17% as liberal, 28% as neither conservative nor liberal, and 17% chose "I would rather not say". We adjusted the sample representation bias while estimating the mean willingness to pay (WTP) a premium for ethanol blended fuel.

Forty-seven percent of respondents said they would derive more satisfaction from using E-10 relative to conventional gasoline, 31% said they were not sure if they would, and 22% said they would not. Forty percent of respondents indicated that they would also derive more satisfaction from using a blend with greater than 10% ethanol relative to E-10, but 43% said they were unsure, and 18% said they would not. Almost 23 % respondent said that they are not sure whether they prefer E-10 over regular gasoline or a fuel using a blend with greater than 10% ethanol relative to E-10. This result implies that demand for E-10 may be a reasonable proxy for demand for a blend with greater than 10% ethanol. However, 12% of respondents indicated that although they derived additional satisfaction when switching from gasoline to E-10, they were unsure of whether they would derive additional satisfaction when switching to a higher-ethanol blend.

Individuals were asked why the federal government should pursue alternative-fuels program. We also asked them what they think as the best approach to reducing gasoline consumption. Table 1 shows a two-way relationship between the two responses.

Table 1: Individual and Joint Percentage Breakdown of Primary Reason for Pursuing an Alternative-Fuels Program by Preferred Alternative Policy (N = 567)

		Why should the federal government pursue alternative-fuels program?				
		Economic	Environmental	National Security	No reason	Total
Best approach to reducing gasoline consumption	Increased Public Transport	3%	10%	9%	2%	24%
	More ethanol	6%	7%	11%	0%	25%
	Hybrids, fuel-cell cars, etc.	10%	22%	17%	2%	51%
	Total	18%	40%	38%	4%	100%

From table 1 40% of respondents indicated that the federal government should pursue an alternative-fuels program for environmental reasons, 38% said for national-security reasons, and 18% said for economic reasons. Finally, although the percentage differences are small, those who support increased ethanol use tend to support alternative fuels for national-security reasons, whereas those that support hybrid cars, etc., tend to support alternative fuels for environmental reasons. The results to the alternative-fuels program question are more interesting, however, if broken down according to political orientation. Table 2 shows such relationship.

Table 2: Individual and Joint Percentage Breakdown of Primary Reason for Pursuing an Alternative-Fuels Program by Political Orientation (N = 598)

		Why should the federal government pursue alternative-fuels program?				
		Economic	Environmental	National Security	No reason	Total
Political Orientation	Conservative	9%	10%	17%	2%	38%
	Neither conservative nor liberal	4%	13%	11%	1%	29%
	Liberal	2%	12%	3%	0%	17%
	Did not reveal	3%	5%	7%	1%	16%
	Total	18%	40%	38%	4%	100%

Self-described political “liberals” overwhelmingly choose the environment as the main reason to pursue alternative fuels, whereas conservatives choose national security. Moderates choose the environment slightly over national security, whereas those that chose to conceal their political identity did the opposite.

Individuals were asked whether they perceived any positive impact of more usage of E-10 relative to conventional gasoline. Most respondents, do, however, perceive increased ethanol use to have some positive impact on the country. Sixty-eight percent, 60%, and 54% of the respondents indicated that increased ethanol use would have a positive impact on the

nation's environment, economy, and national security, respectively; whereas only 8%, 12%, and 1% said the impact would be negative.

Willingness to pay questions and other related issues:

In order to estimate the mean willingness to pay, each respondent was asked whether he would be willing to pay $PE10 for E-10, or choose conventional gasoline at price $PGAS. The E-10 price was constructed according to energy equivalence, based on the U.S. Department of Energy's conversion yield of 1.52 times more mileage per gallon of conventional gasoline than 100% ethanol (2005). The price of conventional gasoline was held constant at $2.55 per gallon across all surveys (this was the prevailing national average price of regular gasoline when the survey was sent out in the spring of 2007); thus the energy-equivalent price for E-10 was calculated as $2.55 [0.9 + (0.1/1.52)] = $2.46. Subsequently added to this amount was a randomly-assigned premium of 5, 10, 15, 20, or 25 ¢ per gallon to arrive at the stated E-10 price, PE10. The WTP question for E-85 was worded and prices calculated in a similar manner. The energy equivalent price for E85 was $1.81. Although the premium varied across surveys, the premium each individual was asked to pay was the same for the two fuels (i.e., if the premium was 25¢ for E-10, it was also 25¢ for E-85). Respondent understanding of energy equivalence and its relationship to price was critical; thus each respondent was given detailed information about energy equivalence and was asked questions to confirm understanding.

In order to get an unbiased estimate of WTP, it was necessary to know whether an individual does not want to pay a particular premium because of the premium itself or simply because the individual does not want to buy the good at any price. Our survey, therefore, contained a follow-up question to individuals who refused to pay the premium.

Although most vehicles require no modification to use E-10, most require some engine modification to use E-85 (unless the owner happens to own a flex-fuel vehicle, which was not the case for most respondents). The survey was designed such that changes in respondents WTP from E-10 to E-85 should be influenced by the change in ethanol concentration, not by engine compatibility issues. However, to account for the possible influence of the compatibility issue on WTP, we asked them the WTP question for E-85 first, then provided information about car engine compatibility and gave them estimated costs for engine modification. Those that responded positively to the WTP question were then asked to update their response, i.e., whether they would also incur the necessary expenditure (either to modify their existing engine or buy a flexible-fuel vehicle) within a year in order to be able to consume E-85.

Out of the 748 respondents, 594 individuals (79%) responded to both WTP questions. Of those that responded, 134 respondents (23%) stated that they were willing to pay some premium for both E-10 and E-85, 151 individuals (25%) were ready to pay a premium for E85 but not E10, 15 individuals (3%) were willing to pay a premium for E10 but not E85, and 294 (49%) said they would not pay any premium for either of the fuels.

As mentioned earlier, although the premia vary across individuals, the amount of the premium each individual has been asked to pay for each of the two fuels is the same, and WTP questions were based upon a choice between E-10 versus regular gasoline and E-85 versus regular gasoline. The results in Table 3 indicate that respondents are more willing to pay a premium for E85 than for E10, regardless of stated preferences.

Table 3. WTP response by bid and follow-up response (willingness to pay for E-10/E-85 at any price < bid)

	E-10			E-85		
Premium	N	Yes	Pr(Yes)	N	Yes	Pr(Yes)

5¢	117	51	0.44	109	66	0.61
10¢	123	39	0.32	117	64	0.55
15¢	146	36	0.25	138	62	0.45
20¢	116	15	0.13	104	37	0.36
25¢	148	17	0.11	136	61	0.45
Total	650	158	0.24	604	290	0.48
			Adjusted for E-85 compatibility issue:		46	0.08
Any price < Bid	433	262	0.60508	283	137	0.48
			Adjusted for E-85 compatibility issue:		3	0.01

Estimation:

Regression analyses were conducted to estimate parameters and mean WTP for E-10 and E-85. The WTP equation was a function of the bid, age, gender, preference dummy, and political preference variable of the respondents. The selection equation was a function of the middle class income, policy standpoint, age, education, and gender of the respondents. We also employed a non-parametric method to calculate the mean WPT premium value. Table 4 shows these results.

Table 4. Estimated WTP premium ($/gallon) for E-10 and E-85

	E-10	E-85
Log-linear Model		
Mean	$0.124	$0.152
Median	$0.119	$0.135
Turnbull (Non-parametric)		
Mean	$0.062	$0.131
Lower bound	$0.054	$0.120
Upper bound	$0.070	$0.142

Conclusions:

First, we wish to repeat that our survey had a response rate of 25%; thus 3 out of 4 would-be respondents did not contribute their opinions, and thus our results may not necessarily be representative of the general public. However, in as much as our sample represents the general population, the following can be said.

The results of this survey indicate that the overall perception of ethanol is positive. The majority of respondents perceived ethanol to have a positive influence on the environment, the economy, and on national security. Additionally, results indicate that there exists a positive WTP a premium for both E-10 and E-85, with apparently stronger preferences (i.e., greater WTP) for E-85. Additionally, results indicate that demand for E-85 is more price inelastic relative to E-10, with this result being driven by some consumers with no preference at all for E-10 but strong preferences for E-85 that appear to be non-responsive to price increases. Results also indicate that those consumers who are unsure about the micro-level benefits of E-85 are nonetheless more inclined to pay a premium, i.e., to err on the side of more ethanol.

These results, however, must be kept in perspective. In spite of these positive results, it is also apparent that ethanol is not the globally-preferred transportation-energy alternative: most consumers indicated a preference for increased public transit or non-ethanol-based energy sources over ethanol, even among those with a positive WTP for ethanol blends. These results, then, indicate that the push by industry and government to promote ethanol use may run counter to public demand: although consumers have some preferences for ethanol blends, they would nonetheless prefer something else even more.

Finally, the results of the econometric modeling indicate that acceptance and WTP for E-10 can be explained by demographic and other preference variables, but acceptance and WTP for E-85 can not (at least with the variables used here). Thus, although preferences for E-85 appear to be universally stronger than those of E-10, the reason why is not yet apparent. It is left to future research to identify the key drivers of demand for E-85.

6. Identify products developed under the award and technology transfer activities, such as:

a. Publications/Theses/Presentations

Busby, David P., Randall D. Little, Saleem Shaik, Francis Epplin, Brian S. Baldwin, and Cary W. Herndon. “Costs of Producing Ethanol from a Lignocellulosic Biomass.” Research Paper accepted for presentation at the 2007 Annual Meeting of the Southwestern Economics Association. March 14-17, 2007, Albuquerque, New Mexico

David Busby, Saleem Shaik, Angelina Martins, Francis Epplin, Randall D. Little, Charles M. Taliaferro, Brian S. Baldwin, and Seonghuyk Hwang. “Yield and Production Costs for Three Potential Dedicated Energy Crops in Mississippi and Oklahoma Environments.” Selected Paper accepted for presentation at the 2007 Annual Meeting of the Southern Agricultural Economics Association. February 4-7, 2007, Mobile, Alabama.

Busby, David P., Randall D. Little, Saleem Shaik, Francis Epplin, Brian S. Baldwin, and Cary W. Herndon. “Cost of Producing Biomass for Lignocellulosic Ethanol Production.” Research Poster presentation at the American Farm Bureau Federation Annual Convention. January 7-8, 2007, Salt Lake City, Utah.

Whittington, Andrew and C.W. Herndon. "Biomass and Biofuels Literature Bibliography for Economic and Policy Analysis." Department of Agricultural Economic Research Report, Mississippi State University, December, 2006.

Whittington, Andrew, Kenneth Hood and C.W. Herndon. "Availability of Poultry Litter as an Alternative Energy Feedstock: The Case for Mississippi." Selected Paper accepted for presentation at the 2007 Annual Meeting of the Southern Agricultural Economics Association. February 4-7, 2007, Mobile, Alabama.

Whittington, Andrew and C.W. Herndon. "Poultry Litter as an Alternative Energy Feedstock.” Research Poster Presentation, American Farm Bureau Meetings. Salt Lake City, Utah January 7-9, 2007.

Blair, Benjamin and Jon Rezek. “The Effects of Hurricane Katrina on Pass-Through for Gulf Coast Gasoline.” Research Paper presentation at the 2007 American Economic Association Annual Meetings. January 3, 2007. Chicago, IL.

Muhammad, Andrew, Andrew Whittington, John Anderson and C.W. Herndon. “The Impact of Feed Cost on U.S. Poultry Production: Implications for the Impact of Increased Ethanol Production.” Research Paper presentation at the 2007 Bio-Fuels, Food and Feed Tradeoffs Conference. April 13, 2007, St Louis, MO.

Grala, R.K., Grace L.A. and W.B. Stuart. 2007. Logging Residues as Bioenergy Feedstock: A broad perspective. 2007 Southern Forest Economics Workshop. San Antonio, TX, March 4-6, 2007.

Busby, David P., Cost of Producing Lignocellulosic Biomass for the Production of Ethanol . **Master of Science Thesis**, Department of Agricultural Economics, Mississippi State University, July 2007.

Busby, David P., and C.W. Herndon. “Cost of Producing Biomass for Lignocellulosic Ethanol Production”, Poster Paper presented at Mississippi State University Biofuels Conference, Starkville, Mississippi, August 29, 2007

Busby, David P., and C.W. Herndon. “Biorefinery Production Feasibility using Lignocellulosic Biomass”, Poster Paper presented at Mississippi State University Biofuels Conference, Starkville, Mississippi, August 29, 2007

Petrolia, Dan. “Impact of the Ethanol Industry on U.S. Agriculture”, Invited Paper presented at Mississippi State University Biofuels Conference, Starkville, Mississippi, August 29, 2007

Muhammad, Andrew, Andrew Whittington, John Anderson and C.W. Herndon. “The Impact of Feed Cost on U.S. Poultry Production: Implications for the Impact of Increased Ethanol Production.” Submitted for journal publication to the ***Review of Agricultural Economics***, Review in progress and publication pending.

Herndon, C.W. “The Booming Ethanol and Bioenergy Industry: Fad or Revolution for Agriculture” Presented at the Agriculture Wealth Management, Accounting and Taxation Conference, Stoneville, Mississippi, January 11, 2008.

Bhattacharjee, Sanjoy, Dan Petrolia and C.W. Herndon “Analysis of U.S. Consumers’ Willingness to Pay for E10 fuel: Contingent Valuation Approach.” Selected Paper presented at the Southern Agricultural Economics Association Annual Meeting, Dallas, Texas, February 2-5, 2008

Blair, Benjamin and Jon Rezek. “The Effects of Hurricane Katrina on Pass-Through for Gulf Coast Gasoline.” ***Economics Letters***, forthcoming.

Bhattacharjee, Sanjoy, Dan Petrolia and C.W. Herndon. “Do Americans Want Ethanol? A Comparative Contingent Valuation Study of Wiingness-to-Pay for E-10 and E-85.“ Submitted for publication to the ***Review of Agricultural Economics***, (under review).

Denly, Jonathan and C.W. Herndon “Financial Analysis of Implementing an Anaerobic Digester and Free Stall Barn System on a Mississippi Dairy Farm” ” Selected Paper presented at the Southern Agricultural Economics Association Annual Meeting, Dallas, Texas, February 2-5, 2008

Busby, David P., Andrew Phillips and C.W. Herndon. “Construction Cost Sensitivity of a Lignocellulosic Ethanol Biorefinery” Selected Paper presented at the Southern Agricultural Economics Association Annual Meeting, Dallas, Texas, February 2-5, 2008

Herndon, C.W. “The Booming Ethanol and Bioenergy Industry: Fad or Revolution for Agriculture” Presented at the Agriculture Wealth Management, Accounting and Taxation Conference, Stoneville, Mississippi, January 11, 2008.

Herndon, C.W. “The Ethanolization of Agriculture and the Roles for Agricultural Economists” Presidential Address presented at the Southern Agricultural Economics Association Annual Meeting, Dallas, Texas, February 2-5, 2008

Petrolia, Daniel R. “The Economics of Harvesting and Transporting Corn Stover for Conversion to Fuel Ethanol: A Case Study for Minnesota.” ***Biomass and Bioenergy*** 32(2008): 603-12.

Petrolia, Daniel R. “An Analysis of the Relationship between Demand for Corn Stover as an Ethanol Feedstock and Soil Erosion.” ***Review of Agricultural Economics*** (forthcoming).

Petrolia, DR, Bhattacharjee, S, D Hudson, and CW Herndon. Do Americans Want Ethanol? A Comparative Contingent Valuation Study of Willingness-to-Pay for E-10 and E-85. submitted for review to the ***Review of Agricultural Economics***.

Bhattacharjee, S and D.R. Petrolia. "The Environment, the Economy, or National Security: What’s Driving Americans to Drive on Ethanol?", Working Paper, Department of Agricultural Economics, Mississippi State University.

“Do Americans Want Ethanol? A Contingent-Valuation Study of Demand for E-10 and E-85”, by Daniel Petrolia, Sanjoy Bhattacharjee, Darren Hudson, and Bill Herndon. Departmental Seminar Series, Department of Agricultural Economics & Agribusiness, Louisiana State University, March 7, 2008

Herndon, C.W. “The Ethanolization of Agriculture and the Roles for Agricultural Economists” Southern Agricultural Economics Association Presidential Address, Journal of Applied and Agricultural Economics, (Forthcoming August 2008 issue).

Anderson, J.D. and K.H. Coble, "Impact of Renewable Fuels Standard Ethanol Mandates on the Corn Market." Working Paper, Department of Agricultural Economics, Mississippi State University, July 2, 2008

Liang, Y, K.H. Coble, A. Harri. "Is the Southeastern Region the Residual Supplier of U.S. Crops?: The Policy Implications of Crop Supply Responses under Risk." Working Paper, Department of Agricultural Economics, Mississippi State University.

Herndon, C.W., David Busby, and Randy Little. “Biomass Cost of Production and Construction Cost Sensitivity of a Lignocellusic Ethanol Biorefinery.” 2008 Biofuels Conference, Mississippi State University, August 14, 2008.

Bhattacharjee, Sanjoy, Dan Petrolia, and C.W. Herndon. “ Do Americans Want Ethanol.” Selected Poster, American Agricultural Economics Assosciation Meetings, Orlando, Florida, July 28, 2008.

Sustainable Energy Research Center
Social Policy Thrust Area Final Report for 2006-2008

1. Project title, name of principal investigator, and all team members:

Task K. Social Policy Elements of Biomass Energy Crop Potentials in the Southeastern United States

Frank M. Howell, PI. Jerry Emison, Co-PI, Jeremy R. Porter, Ph.D. Student, Philip B Mason, Ph.D. Student, Erin Holmes, Ph.D. student.

2. List of authorized distribution limitation notices, such as patentable material or protected data.

Unlimited distribution.

3. Executive summary

The recent and projected status of energy production and consumption in the U.S., resulting in substantial dependencies upon foreign oil, has continued to provide pressure on domestic energy security. All told, bio-energy systems, and biomass crop production in particular, will be important elements of national security, economic vitality, and public policy. Using biomass crop estimates based upon models developed at the Oak Ridge National Laboratory and the DOE National Renewable Energy Laboratory, we identify potential biomass crop production zones using spatial analysis methods. The Midwest and the South are, by far, the largest regions of potential production. Once potential biomass crop yield is made proportional to estimated land and production costs, the South's optimal crop zones fall along the Gulf Coast and Atlantic Seaboard whereas in the Midwest, they are largely in non-metropolitan localities. In this study, we explore where traditional farming practices and metropolitan influence will compete for land use against farmland located in these optimal biomass crop production zones. We use overlapping LISA statistics to identify significant clusters of counties facing conflict for land use is. To measure competition for land use in counties located within biomass zones circa 2000, we use population growth and housing data from Census Bureau estimated, farmland data from the Census of Agriculture, and remotely sensed land use/cover data from the USGS. The implications of these factors and how they will potentially affect biomass crop production are discussed.

4. Comparison of goals and actual accomplishments.

See attached Spreadsheet.

5. Summary of activities.

K.1 Construction of Biomass Crop Databases

Focus and Objectives. The spatial identification of agronomically-optimal biomass crop zones is the main focus of this study. Within this framework we have three objectives: (a) the

identification of significantly high-likelihood spatial clusters of counties or "zones" for biomass crop production; (b) determining the proximity of these biomass zones to metropolitan areas, and (c) the estimation of the economically optimal crop production zones when crop yield potential is weighed against land-value and production costs so as to assess patterns of potential land-use conflict in the future. By combining two sets of data estimating overlapping definitions of biomass crop sources, the results provide the best information available with a nationwide scope on where the bio-economy is best likely to develop.

Sources of Data. Data were obtained from several sources, all pertaining to the county-level for the 48 contiguous states. Counties are used as the primary unit of analysis based on the fact that this was the geographic level at which data was available. The main sources of biomass crop data come from Graham et al. from the Oak Ridge National Laboratory [ORNL] (1996) and Milbrandt of the National Renewable Energy Laboratory [NREL] (2005). The estimates for biomass crops, switchgrass (SG) and short-rotation, wood crops (SWRC), produced by Robin Graham and her associates pertained to 1992. We obtained those data from Dr. Graham and produced similar estimates for 1997 and 2002 using the same procedures but updating the key variables (e.g., CRP acres, harvest acres, etc.) from the successive Censuses of Agriculture. We also obtained the biomass crop estimates produced by Milbrandt (2005) circa 2005.

Both Graham and Milbrandt's data are important in this analysis as they paint somewhat different pictures of potential biomass production based on their sources. The ORNL data provided by Graham is an estimate of potential biomass production acres from the growth of switchgrass and short rotation woody crops, while the NREL data obtained from Milbrandt takes into account the potential effects of harvesting urban residues. The majority of the current analysis will examine the ORNL data provided by Graham due to the availability of accompanying variables used in categorizing counties based on their production potential. However, it is important to introduce both data sources to fully understand the different contexts in which biomass is opertationalized and where they are located in space across the U.S.

Information on region, metropolitan proximity, county landmass, and total cropland in acres were respectively taken from the Census Bureau, the USDA Economic Research Service, and the Census of Agriculture for 1997 and 2002.

Measurement. Potential biomass crop estimates pertain only to switchgrass and short-rotation, woody crops (SRWC) such as hybrid poplars and willows, based upon the ORNL model published by Graham et al. (1996) whereas the "total technical biomass resources" available in the county is based upon Milbrandt's work (2005) at NREL. The NREL source contains a broader set of potential biomass sources than simply two major crops, including: agricultural residues from crops and methane from manure management; wood residues from forestry, primary and secondary mills, and urban wood residues; and municipal discards including methane emissions from landfills and domestic wastewater treatment. We briefly summarize the measurement of these variables but more details are available in the source citations for interested readers.

ORNL Data. The total switchgrass (SG) potential based on the ORNL model is expressed in acres as is the total potential for short-rotation, woody crops (SRWC). Switchgrass and SRWC acreage overlapped in many areas where soil type and climate are conducive to both crops. However, in some areas one is dominantly more likely to grow than the other. In order to

identify, for each county, the total amount of land which could be dedicated to biomass production regardless of the crop type, we created a variable which represents the total potential biomass acreage in a county. The resulting variable was equal to the total number of potential acres, where the two crops were equally likely to grow, and the crop specific acreage of the dominant crop, where one crop was more likely to grow than another.

In order to identify optimal zones for the production of biomass crops in the form of switchgrass and SRWC, three variables in particular are of interest. First, in order to be an optimal area of crop production it is assumed that obtaining the land will be economically feasible, or low land rent value. Land rent is simply measured as the local price of land per acre. Next, it is important to understand where yield profits are high enough to persuade farmers to convert farming operations to switchgrass and SRWC. Yield prices are measured as the crop-specific pay a farmer can expect in exchange for a dry ton of crop. Lastly, it is important to know where production costs are lowest. This final variable in the rubric is an estimate of the local price per year (minus land rent) of a given crop per acre. The combination of these three variables will lead to an ordinal categorization of 'most' to 'least' optimal counties identified for the potential production of biomass crops.

NREL Data. Milbrandt (2005: 59) describes the "technical" biomass potential as being "based on the accessible biomass with respect to constraints of land use, and the majority of the quantity depends on assumptions and factors that relate population to the amount of residue generation. These factors are often local and subject to the level of technology (harvest, collection etc.) available, and vary between different studies." Using a complex modeling scheme based upon a wide variety of sources and modeled estimation procedures on each potential source, she produced two data elements of interest to this study: the amount of switchgrass and the total potential biomass from all sources, both expressed in dry tons. (See Milbrandt 2005 for more details.)

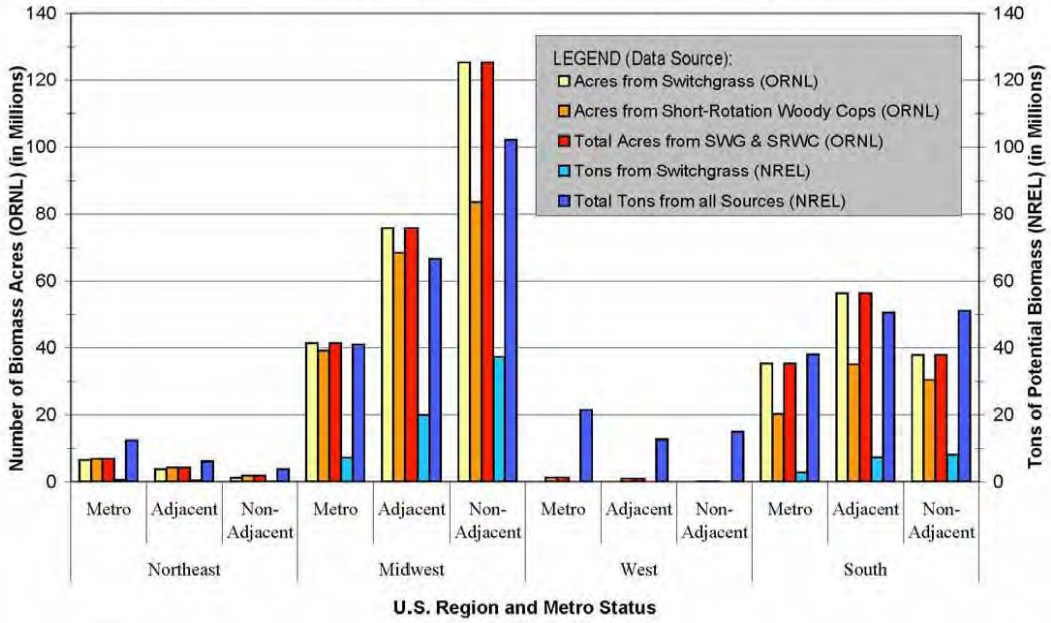
Demographic Controls. County designations for metropolitan proximity used the USDA ERS urban influence taxonomy (Ghelfi and Parker 1997). Counties were collapsed into three groups: metropolitan, non-metropolitan but adjacent to a metro area, and non-metropolitan and non-adjacent. The 1993 metropolitan status taxonomy was deemed appropriate due to the fact that the ORNL data originated in 1992 and the newer 2003 definition is not comparable to previous definitions based incompatibility stemming from new criteria for defining metropolitan status. "This latest reclassification reflects not only a decade of urban growth and restructuring, but also extensive modification of the rules governing metro and nonmetro status" (ERS 2003). Region corresponds to the four U.S. Census regions (Northeast, Midwest, South, and West). While it is understood that large variation exists within these geographic units, here they will allow for a better understanding of the spatial demography and distribution of potential biomass production zones.

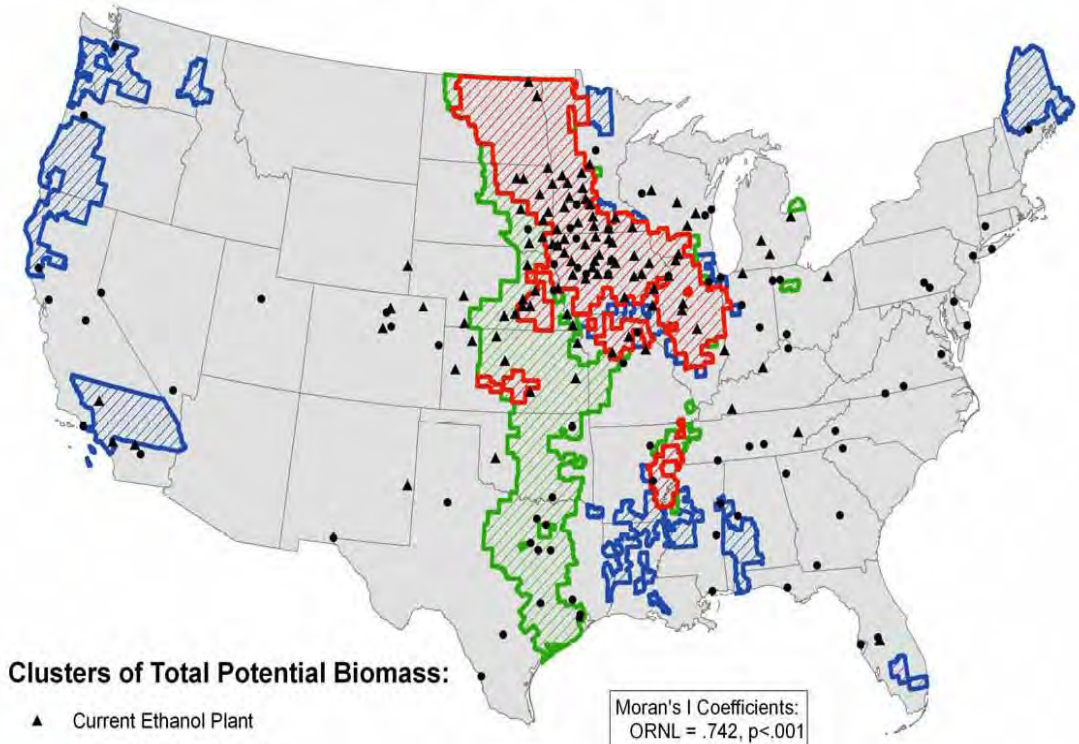
Results. Shown in Figure 1 in the upper panel is the potential for U.S. regions to participate in the crop production component of the bio-economy and it is largely restricted to the Midwest and the South. The Northeast could utilize some 5 to 10 million acres for these two biomass crops, mostly concentrated in metropolitan areas, while the West has some 2 to 3 million such acres, however the Midwest and South, by far, dominate the potential for growing these two biomass crops. The crop-only results are much the same in relation to the tons of potential biomass using the NREL data. However, the metropolitan areas in both the West and Northeast show a greater biomass potential. This is especially true in the West where the tons of

potential biomass from NREL sources dwarf the potential from the biomass crops using the ORNL data. This difference can primarily be attributed to the diversity of biomass sources, especially those related to high population centers (urban wood residues, landfill residues, etc.).

Consistent with the report by Thomas and Howell (2003) who found substantial agricultural production within the confines of metropolitan areas, the results in Figure 1 show that between 35 and 40 million acres in either the Midwest or the South could be devoted to bio-energy crop production. The main difference between the South and Midwest is the latter's relative concentration of biomass crop acreage being situated in rural counties that are not adjacent to large urban population centers. The South's largest potential crop acreage lies in clear proximity to metropolitan areas, a recipe for significant land-use conflict and competition. The NREL estimates are consistent with the spatial patterns in the ORNL estimates in the metropolitan proximity and regional totals. This sensitivity analysis using disparate approaches suggests that the general patterns of acres and tons of volume yield complementary estimates.

Figure 1. Spatial demography of potential biomass production





In order to identify where these areas are situated in geographic space the LISA results are also presented in the figure as shaded outlines around groups of counties where specific significant clusters were identified. For ORNL estimates, containing only switchgrass and short-rotation, woody crops the significant spatial clusters are presented in green, and for the NREL estimates, containing a broader array of potential biomass sources they are presented in blue. Also, an area in red, which identifies the overlap in clusters of counties with high potential for biomass production, regardless of the data source (both ORNL and NREL) is presented. Lastly, the locations of bio-refinery plants processing either ethanol or bio-diesel are overlaid on the map to illustrate this sector's spatial proximity to input sources.

For the ORNL data on switchgrass and short-rotation wood crops, the global Moran's I coefficient is .74, a very large coefficient (see Anselin 1995), quantifying the extreme positive clustering pattern in the map. This can be more clearly interpreted as those counties with high potential biomass acreage are surrounded by counties with high potential biomass acreage. These significant spatial clusters of biomass potential are located in the upper and lower Midwest, in the Heartland, in eastern Texas, and along the Mississippi River Delta. Two pockets of high acreage of potential biomass crops are observed in South Carolina and in Pennsylvania.

Regarding the broader NREL biomass measure, the distribution has a significant Moran's I coefficient equal to 0.399. It is not as large as the one for the ORNL data but, nevertheless, is a strong level of spatial clustering (Anselin 1995). While there are indeed significant non-random clusters of potential biomass materials in the upper Midwest and in the South, there are also smaller significant clusters in the Northeast and in the Northwest. Finally, as can also be observed in Figure 1, the emergent bio-economy as revealed by private-sector investments in bio-refineries is largely locating in these significant clusters of potential biomass crop zones, further evidence of the spatial impact likely to emerge from this industry.

These results do not take into account production costs, competitive land uses, land rents, and so forth (see Downing and Grahm 1996; Jolley 2006) in the production of bio-fuels. We now present an optimization assessment of the ORNL data for switchgrass and short-rotation, woody crop production, taking into account estimated land rent value and production costs. (The more broadly defined NREL data do not have such data associated with them).

K.2 Identification of optimal biomass crop production zones.

In Figure 2, the optimization rules are displayed along with a bar chart of the distribution of acres (in millions) and the number of counties in each region associated with each optimal classification zone. The four zones with *high projected yield* are ranked in the top half of this scheme, each varying in terms of the land rent value and costs of producing the crop. The bottom half contains varying classifications of costs with *low projected yields*. These categorizations of high and low are based on the global mean for each category and for each crop type respectively, and are presented in Figure 2.

The most optimal zone is one with low input costs (low land rent and production costs) and high yield, labeled as production classification zone # 1 "Most Optimal". This zone characterizes almost 75 million acres of potential switchgrass and 20 million acres of short-rotation, woody crops. The modal production zone is # 4, defined as high yield but also "Expensive Biomass" in terms of high land rental values and production costs and applies to

both biomass crops. Finally, areas categorized as having low yield and high associated costs are labeled #8 “Least Optimal”. The most optimal, expensive biomass, and least optimal zones are listed in order with the intermittent zones being more arbitrarily placed in between based on some desired and some undesired characteristics.

Figure 2. Optimization breakdown and descriptives of production classification zones*

Economic and Production Optimization Classification Scheme

Optimization Variables				Number of Counties in Classification Zone by U.S. Region										
					SWG Optimal Zone					SRWC Optimal Zone				
Variable	Rent	Yield	Production Costs	Northeast	Midwest	West	South	Total	Northeast	Midwest	West	South	Total
Median SWG	$50.73/acre	$35.84/dry ton	$1216.44/acre/yr.										
Median SRWC	$50.73/acre	$65.62/dry ton	$1443.40/acre/yr.										
Classification Zone #													
1 (Most Optimal)	**Low**	**High**	**Low**	**0**	**615**	**0**	**62**	**677**	**11**	**615**	**35**	**5**	**666**
2	Low	High	High	39	96	0	123	258	5	4	0	209	218
3	High	High	Low	0	55	0	0	55	13	50	0	0	63
4 (Expensive Biomass)	**High**	**High**	**High**	**0**	**84**	**0**	**94**	**178**	**0**	**21**	**0**	**125**	**146**
5	Low	Low	Low	0	19	0	101	120	47	75	0	23	145
6	Low	Low	High	39	4	196	244	483	15	40	161	293	509
7	High	Low	Low	0	22	0	290	312	82	84	0	24	190
8 (Least Optimal)	**High**	**Low**	**High**	**139**	**160**	**218**	**0**	**517**	**44**	**166**	**414**	**710**	**1,334**

* Low and high cutpoints based in relation to the U.S. median of the specific variable.

From the figure it is easy to see that the Midwest has a huge advantage in term of the number of counties in the "Most Optimal" zone. Within the region, the vast majority of its counties are located in the "Most Optimal" zone, while the only other 'player' in the biomass

production game, in terms of switchgrass on SRWC production, is the South. The South shows promise in that much of its potential lies in highly optimal zone number two with low production costs but high land rents. This could be indicative of a spatial clustering around metropolitan areas.

This is examined in greater detail in Table 1. The results from the table show that, again, the greatest number and percent of the specified regions counties in the "Most Optimal" zone are in the Midwest. Furthermore, they tend to be distributed pretty evenly across all three metropolitan status types. On the other hand the counties in the high production zones in the South region tend towards being metropolitan counties. Thus the initial perceived association between higher land rents for the more optimal southern zones of biomass crop production.

Table 1. Comparison of Count and Percent of Counties by Optimal Production Zones Between the Midwest and South Regions & Metro Status

Switchgrass

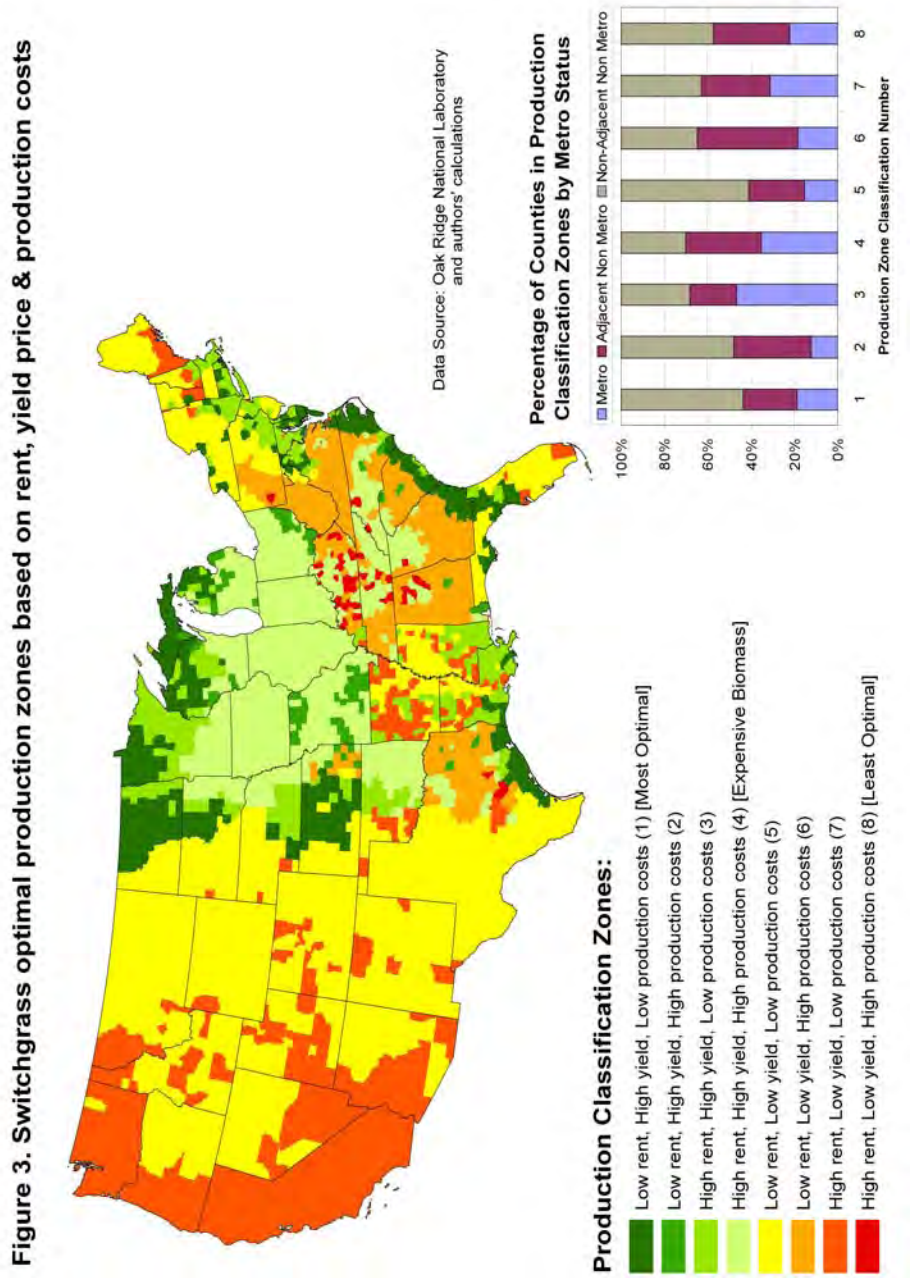
Optimization Categories	Region and Metropolitan Proximity											
	South (*n = 1,374*)						Midwest (*n = 1,055*)					
	Metro		Adjacent		Non-Adjacent		Metro		Adjacent		Non-Adjacent	
	Num.	%	Num.	%	Num.	%	Num.	%	Num.	%	Num.	%
1 (Most Optimal)	**36**	**2.6**	**0**	**0.0**	**11**	**0.8**	**190**	**18.0**	**224**	**21.2**	**201**	**19.1**
2	76	5.5	36	2.6	11	0.8	17	1.6	23	2.2	56	5.3
3	0	0.0	0	0.0	0	0.0	4	0.4	18	1.7	33	3.1
4 (Expensive)	**29**	**2.1**	**29**	**2.1**	**36**	**2.6**	**4**	**0.4**	**14**	**1.3**	**66**	**6.3**
5	36	2.6	33	2.4	32	2.3	3	0.3	5	0.5	11	1.0
6	67	4.9	79	5.7	98	7.1	0	0.0	1	0.1	3	0.3
7	54	3.9	136	9.9	100	7.3	0	0.0	9	0.9	13	1.2
8 (Least Optimal)	**83**	**6.0**	**192**	**14.0**	**200**	**14.6**	**3**	**0.3**	**15**	**1.4**	**142**	**13.5**
Total	381	27.7	505	36.8	488	35.5	221	20.9	309	29.3	525	49.8

Short-Rotation Woody Crops

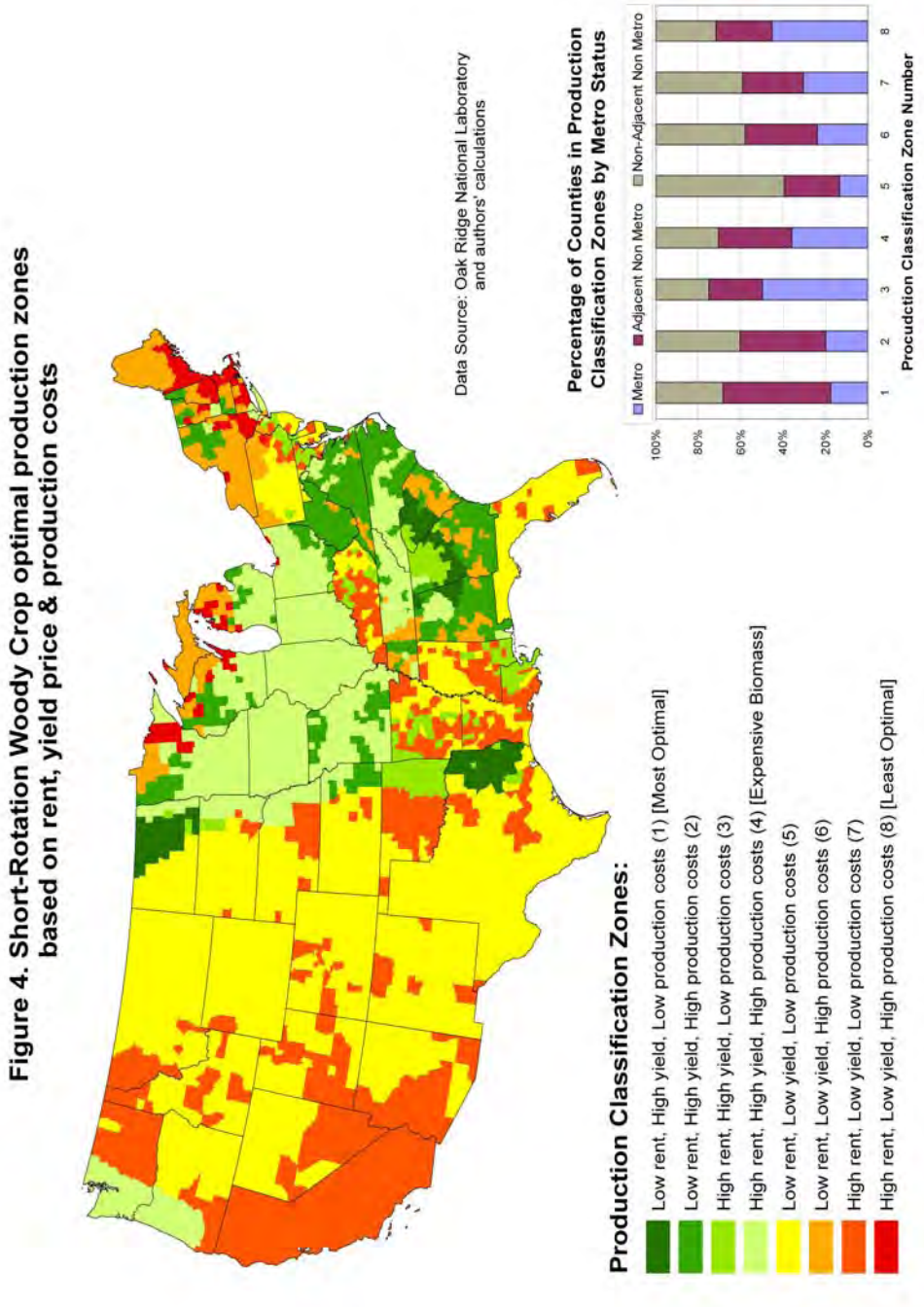
Optimization Categories	Region and Metropolitan Proximity											
	South (*n = 1,374*)						Midwest (*n = 1,055*)					
	Metro		Adjacent		Non-Adjacent		Metro		Adjacent		Non-Adjacent	
	Num.	%	Num.	%	Num.	%	Num.	%	Num.	%	Num.	%
1 (Most Optimal)	**5**	**0.4**	**0**	**0.0**	**0**	**0.0**	**192**	**18.2**	**221**	**20.9**	**202**	**19.1**
2	109	7.9	58	4.2	42	3.1	0	0.0	1	0.1	3	0.3
3	0	0.0	0	0.0	0	0.0	5	0.5	20	1.9	25	2.4
4 (Expensive)	**33**	**2.4**	**65**	**4.7**	**27**	**2.0**	**0**	**0.0**	**3**	**0.3**	**18**	**1.7**
5	7	0.5	9	0.7	7	0.5	16	1.5	27	2.6	32	3.0
6	94	6.8	96	7.0	103	7.5	2	0.2	4	0.4	34	3.2
7	3	0.2	12	0.9	9	0.7	2	0.2	18	1.7	64	6.1
8 (Least Optimal)	**130**	**9.5**	**280**	**20.4**	**300**	**21.8**	**4**	**0.4**	**15**	**1.4**	**0**	**0.0**
Total	381	27.7	505	36.8	488	35.5	221	20.9	309	29.3	525	49.8

K.3 Spatial illustration for optimal biomass crop production zones.

The overall picture for growing switchgrass, amortized against principal input costs, shifts from what was obtained from simply considering potential yields. In Figure 3, the production zone classifications show that the most optimal zone (# 1) is spatially concentrated in the upper Midwest, in Kansas, along the Gulf Coast, and the Eastern Seaboard. There are also pockets of counties throughout the eastern half of the U.S. also meeting the criteria in this classification zone. The more expensive high yield classification (# 4) tends to be located in the Midwest where it is the higher land rent values and crop production costs that reduce the high acreage with potential for biomass crop to a slightly less optimal status for switchgrass.



The optimized outlook for short-rotation, wood crops are shown in Figure 4. Whereas the Midwest tended to dominate the most optimal classification (# 1) for switchgrass, it is the Southeast, long a dominant forest region, which has the highest concentrations of this class of counties. Most of the zone 1 counties are located adjacent to metropolitan areas (see clustered bar chart in Figure 4). The most "expensive" but high yield class (# 4) tends to be located in the Midwest. Thus, in both switchgrass (Figure 3) and short-rotation, woody crops (Figure 4), the Midwest is likely to face higher input cost factors than is the Southeast.



K. 4 Metropolitan Influence and Land Use Conflict in Potential Biomass Crop Production.

In this study, we explore where traditional farming practices and metropolitan influence will compete for land use against farmland located in these optimal biomass crop production zones. We use overlapping LISA statistics to identify significant clusters of counties facing conflict for land use is. To measure competition for land use in counties located within biomass zones circa 2000, we use population growth and housing data from Census Bureau estimated, farmland data from the Census of Agriculture, and remotely sensed land use/cover data from the USGS.

Conceptual Background. In the United States, researchers have already identified areas that are likely to produce the highest yields. Like any crop, a successful harvest of biomass is in part determined by several key environmental factors, namely the soil quality, temperature, length of growing season, and availability of adequate water quantity (van Ittersum and Rabbinge 1997; Clifton-Brown, Stampfl, and Jones 2004). Accounting for environmental differences, scientists have predicted that initially, successful switchgrass production could occur in the Lake States, North Plains, South Plains, and Southeast (Walsh et al. 1998, 5). But, as the market matures, and the value of switchgrass increases, the Midwest is expected to have a key role in the industry due to its agronomic potential, in spite of its expensive production costs (Walsh et al. 1998, 5). However, in areas where switchgrass will not grow well, some have hypothesized that optimal biomass crop production can be performed through short-rotation woody crop (SRWC) harvests (Weih 2004). Tennessee, Louisiana, Minnesota, Oregon, and the Northeast and Lake States are particularly anticipated as having the potential to become important contributors to the SRWC industry (Walsh et al. 1998, 5).

Most recently, researchers have identified optimization zones for biomass production as a way to move toward a more spatialized understanding of the emerging bioenergy industry (Howell et al. 2007). Their general findings include the following. First, key biomass production zones are located in the Midwest and the South. Second, a spatial relationship exists between some characteristics of counties and their projected agronomic potential. Third, after accounting for land rent, expected yield size, and estimated production costs, Howell et al. (2007) found that a majority of the “most optimal” (low rent, high yield, low production costs) counties are adjacent to metropolitan areas. In general, counties in the Midwest and Southeast are expected to produce large yields, but at a generally high cost. For comparative purposes, however, input costs are less in the South than they are in the Midwest and may provide opportunities for greater profits and economic development. This suggests that the impact that urbanization has on land use competition and potential biomass crop production will likely vary by region. Therefore, we need to more thoroughly investigate what effects urbanization will contribute to the likelihood of these “optimal” biomass growing zones.

Purpose. The literature clearly suggests that spatial propinquity to urban centers will likely be a critical factor in understanding land-use competition and the use of agricultural land in biomass production. This study examines these questions through three specific objectives. First, we explore where traditional farming practices and metropolitan influence will compete for land use in farmland located within previously defined optimal biomass crop production zones. Second, we identify significant clusters of counties where land use conflict is likely to exist.

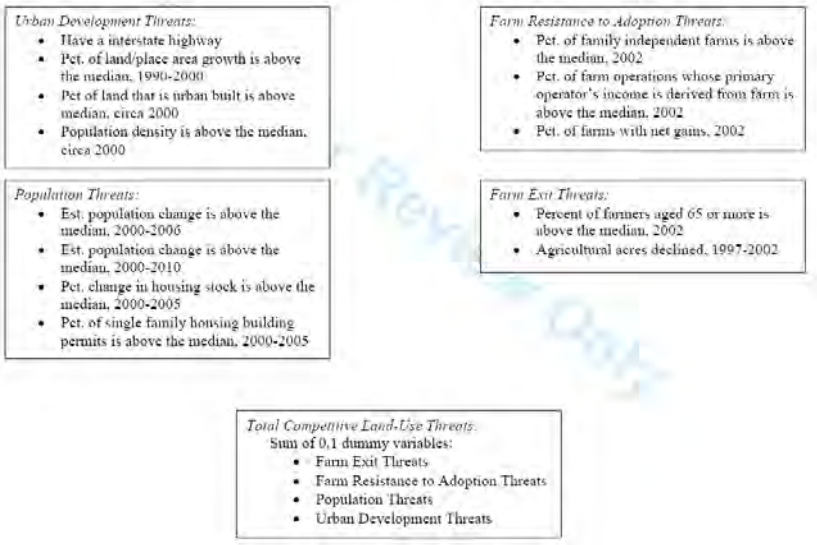
Thirdly, we examine the implications of these factors and how they will potentially affect biomass crop production as this industry emerges.

Procedures. Data at the county-level were obtained from several sources for the 48 conterminous states. Biomass crop data comes from two sources: Graham et al. (1996), and Howell et al. (2007). Graham et al. initially provided estimates for biomass crops, switchgrass (SWG) and short-rotation, woody crops (SRWC) for 1992. Howell et al. (2007) provided similar potential crop estimates for 1997 and 2002 using similar procedures using successive years of the Census of Agriculture. Information regarding population growth, building permit data, number of acres in farmland, land use/cover, and metropolitan proximity were obtained from the Census of Agriculture, Census Bureau, U.S. Geological Survey and the USDA Economic Research Service. Lastly, data was obtained from the U.S. Census Bureau (2006) to compute highway information.

Variable Measurement. Potential biomass crop estimates and total technical biomass resources are consistent with previous research designs (Graham, Allison, and Becker 1996; Howell et al. 2007; Milbrandt 2005). These data estimates only SWG and SRWC production as biofuel sources (Graham, Allison, and Becker 1996). Using procedures adopted from the Howell et al. (2007) study, we calculate the agronomic yield potential of a county and cross-classified this with land rent and production costs. From this table, we computed four categories that describe the potential optimization level that a county has for biomass crop production. They are: "high yield, cheap cost" (low rent, high yield, low production cost (=1)); "high yield, moderate cost" (low rent, high yield, high production cost, or high rent, high yield, low production cost (=2)); "high yield, expensive cost" (high rent, high yield, high production cost (=3)); and "not high yield" (=0).

In this study, we conceptualize biomass crop production as facing four different types of threats; urban development threats, population threats, farm resistance to adoption threats, and farm exit threats (see Figure 1). Within each of these dimensions of land use competition, there are several indications constructed as discrete variables (0,1). These dummy variables are summed to estimate the level of threat from each dimension. Population threats is composed of four dummy variables created from Census Bureau data: whether the estimated population change in the county is above the median between 2000-2006 (=1); or 2000-2010 (=1); the percent change in housing stock is above the median from 2000-2005 (=1); and whether the percent of single family housing building permits is above the median for 2000-2005 (=1).

Figure 1: Competitive Land-Use Threats Defined



The urban development threat is composed of four dichotomous variables: Whether the county has an interstate highway (=1); percent of land/place area growth is above the median between 1990-2000 (=1); the percent of land that is urban built is above the median, circa 2000 (=1); and if the population density is above the national median, circa 2000 (=1). The farm resistance to adoption threat is constructed from three variables. They are whether the percent of family independent farms in 2002 is above the median (=1); the percent of farm operations in 2002 whose primary operator's income is derived from the farm is above the median (=1); and the percent of farms with net gains in the county is above the median (=1) in 2002. The farm exit threat consists of two parts: whether the percent of farmers aged 65 or more in 2002 is above the median (=1); and whether the number of agricultural acres declined in the county between 1997 to 2002i (=1).

Metro status (circa 2002) was measured via a categorical variable: metro (metropolitan), adjacent (non-metropolitan but adjacent to a metro area), and not adjacent (non-metropolitan and non-adjacent). Additional variables used in this study were production costs, non-rent production costs, potential biomass acres, and metro status.

Lastly, to measure the Total Competitive Land Use Threats due to metropolitan influences, all Urban Development Threats, Population Threats, Farm Exit Threats, and Farm Resistance to Adoption Threats were summed. Higher values indicate counties that, pose a higher risk of land use competition with biomass production.

Analytic Procedures. In this study, we use Geographic Information Systems (GIS) analyses to visualize the spatial distribution of population and metropolitan-status variables in relation to the optimal biomass zones. Most of the analytic procedures used are descriptive but we do include statistical significance tests in the spatial clustering analyses. In addition we identified significant clusters of counties where conflict for land use exists within statistically significant clusters of contiguous optimal biomass production zones. This was done by overlapping Anselin's LISA statistic (1995) which deconstructs the global Moran's I coefficients into the county level. We also cross-classify biomass related variables by U.S. region and the county's proximity to metropolitan statistical areas.

Results. Shown in Figure 2, counties in the Midwest have many more potential high yield acres to dedicate to SWG and SRWC than the South. However, most of these acres are in counties that will make biomass production expensive. This is particularly the case for SRWC. Figure 1 also shows the expected pattern that the number of threats facing competitive land-use is highest in metro areas and lowest in not adjacent areas. Of particular interest is the result that the Midwest has more than 30 million potential high yield switchgrass acres with five or fewer metropolitan threats. For the short-rotation woody crop production, the South contains about the same number of potential acres at a cheap or moderate cost relative to the Midwest. These findings suggest while the Midwest could become a key player in switchgrass production, the South could also have an important role in short-rotation woody crops. Yet, these findings are for the regions as a whole. At this point, we turn the focus of our study towards investigating specific types of threats and where high threat clusters exist, paying particular attention to counties that have many agricultural acres that are surrounded by counties with many acres. We term this area as the potential agronomic biozone (see Figure 2).

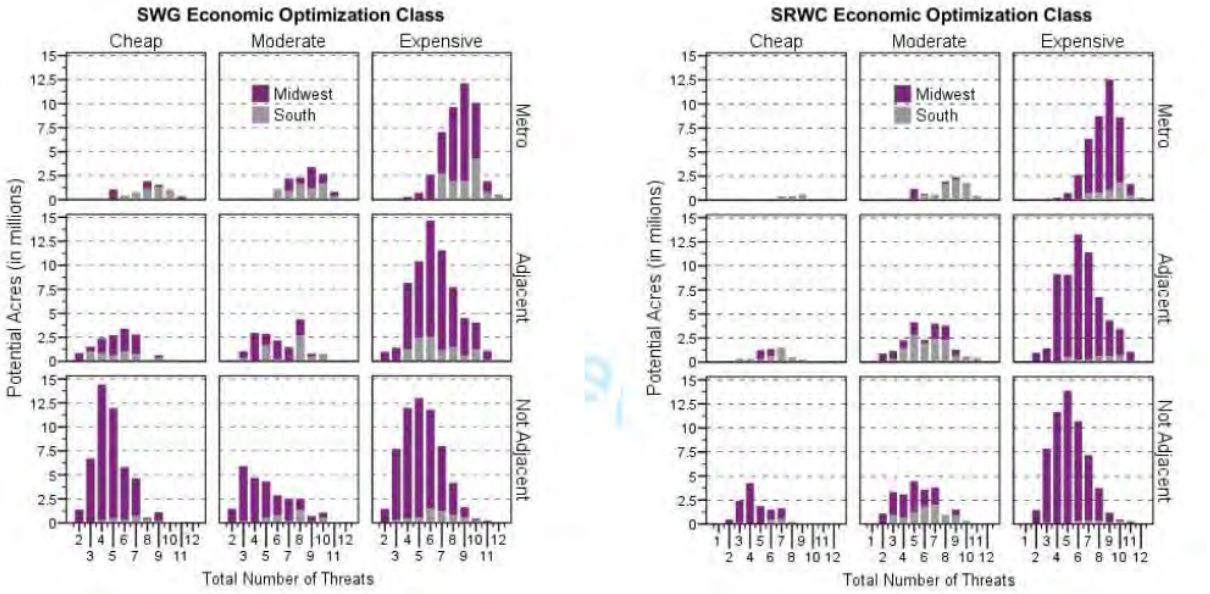


FIGURE 2 Total Competitive Land-use Threats for switchgrass (SWG) and short-rotation woody crops (SRWC) high yield economic optimization, potential acres and metro status: Midwest and South, circa 2002

The first dimension of threats examined is urban development threats (see Figure 3). Our analyses inform us that the occurrence of this threat is relatively low throughout most of the identified agronomic biozone. The Moran's I coefficient is 0.434 ($p<0.001$), thereby indicating that the positive clustering observed in the map is not random. Given the relatively low frequency within the agronomic biozone, these results show that there are, however scattered urban development threat clusters reaching significance in this biozone. These are located adjacent to most of metropolitan Illinois, Dallas, Memphis, Minneapolis and the Southern coastal region.

Other analyses not shown reveal that as the acreage of farmland increases, the number of urban development threats increase. However, this pattern occurs only in the South and only marginally in the Midwest. In all, the Midwest has about 34 million potential SWG acres and nine million SRWC potential acres located in cheap production zones that have no urban development threats. By contrast, the South has only 2 million potential WG acres and less than 1 million SRWC potential acres in cheap production zones without urban threats. The results for population threats are not surprisingly similar to those of broader urban development patterns. But they are not spatially identified further show Population Threats to be similar to the Urban Development Threats (see Figure 3). For example, within the agronomic biozone, we see that that the Midwest has significantly (Moran's I-0.434; $p<0.001$) far fewer population threat clusters than the South (Moran's I=0.458; $p<0.001$). Interestingly, where Illinois was largely covered with urban development threats clusters, it only has a few small Population Threat clusters. In contrast, the Dallas and Saint Paul area had high threat areas under both types of threat.

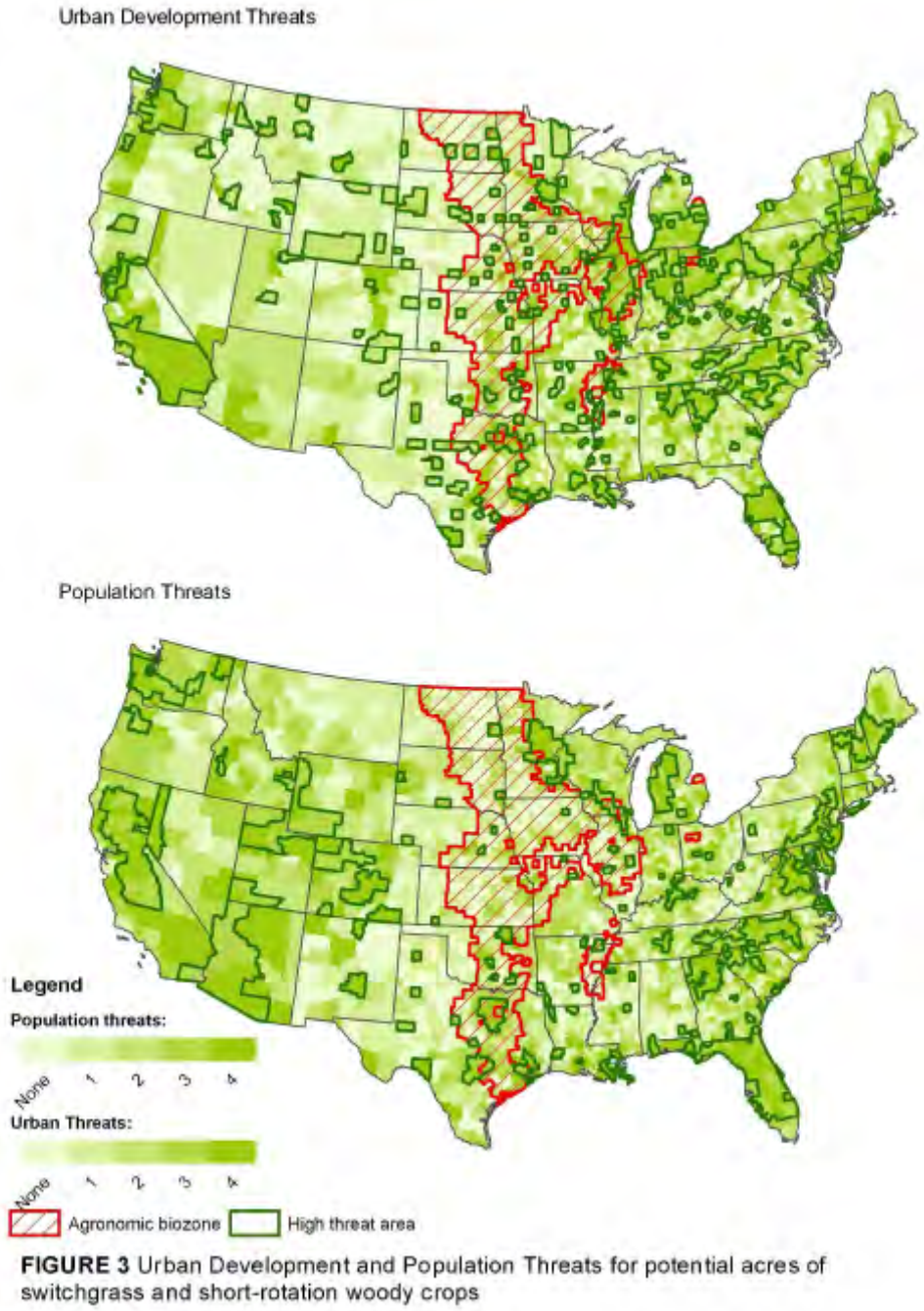


FIGURE 3 Urban Development and Population Threats for potential acres of switchgrass and short-rotation woody crops

The next phase of analysis examined the spatial distribution of farm exit threats. These results show that despite the nation as a whole experiencing farm exit threats, counties within the agronomic biozone are relatively stable in terms of these threats (see Figure 4). However, as the Moran's I (0.269; $p<0.001$) suggests, farm exit threat clusters are not randomly distributed. Interestingly, where the Dallas area in the past analyses has been shown to be significantly threatened, no such clusters appear under this indicator.

The last dimension of threats that we examined in this study is farm resistance to adoption threats. Our results illustrate that while most of the country has few such threats, most

of the Midwest is confronted with all three components of this variable type (see Figure 4). Examining the Moran's I (=0.424; p<0.001) clearly shows that these distributions are not random. In fact, nearly all of the Midwest that lies within the optimal agronomic zone is also circumscribed by a farm resistance to adoption threats cluster. In stark contrast, not only are there few clusters in the Southern part of the agronomic biozone. In general there are also few farm resistance to adoption threats clusters in the South. Lastly, there are very few acres that are available to either the Midwest or the South that have one or less farm resistance threats.

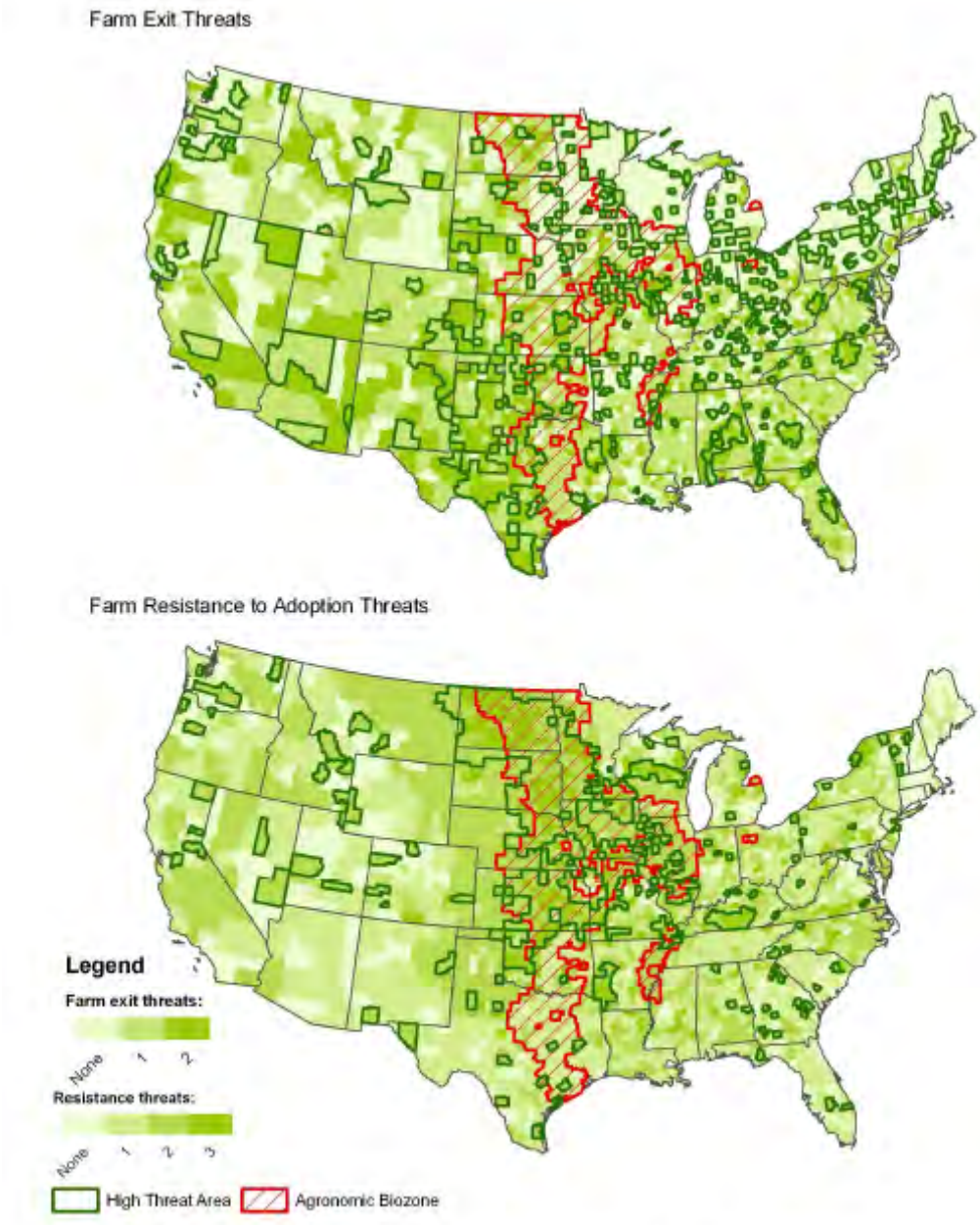


FIGURE 4 Farm Exit and Farm Resistance to Adoption Threats for potential acres of switchgrass and short-rotation woody crops

In the final phase of analysis, we turn to the total competitive land-use threats (i.e. the sum of urban development threats, population threats, farm resistance to adoption threats, and

farm exit threats). As is illustrated on Figure 5, there is substantial variation in the distribution of threats, but as the Moran's I coefficient of 0.392 indicates, there is significant ($p<0.001$) positive clustering. The majority of these threat clusters are located outside of the optimal agronomic biozone with the exceptions of Chicago and Dallas being faced with a large threat cluster. Several other smaller threat clusters present themselves in the Minneapolis area and throughout North and South Dakota. Lastly, the bar charts in Figure 5 indicate that the relatively higher volume of biomass potential in the Midwest is contained within expensive production areas. On the other hand, the Midwest has more than 20 million potentially high yield acres in cheap production areas available for switchgrass that are minimally threatened (4 or fewer threats). Regarding the comparison of how total competitive land-use threat clusters and high yield economic optimization are related to SWG and SRWC production specifically, we now turn to our results shown on Figure 6. This figure illustrates that although the Midwest has many more potential high yield SWG acres in the agronomic biozone, they tend to be located in the expensive production zones. However, we also see that most of North Dakota and Kansas offer high yield SWG acreage in cheap production areas while remaining relatively unthreatened by urbanization. These results also reveal that cheap production areas running from Georgia through the Carolinas remain relatively unthreatened, while those on the neighboring counties of the Eastern seaboard are highly threatened.

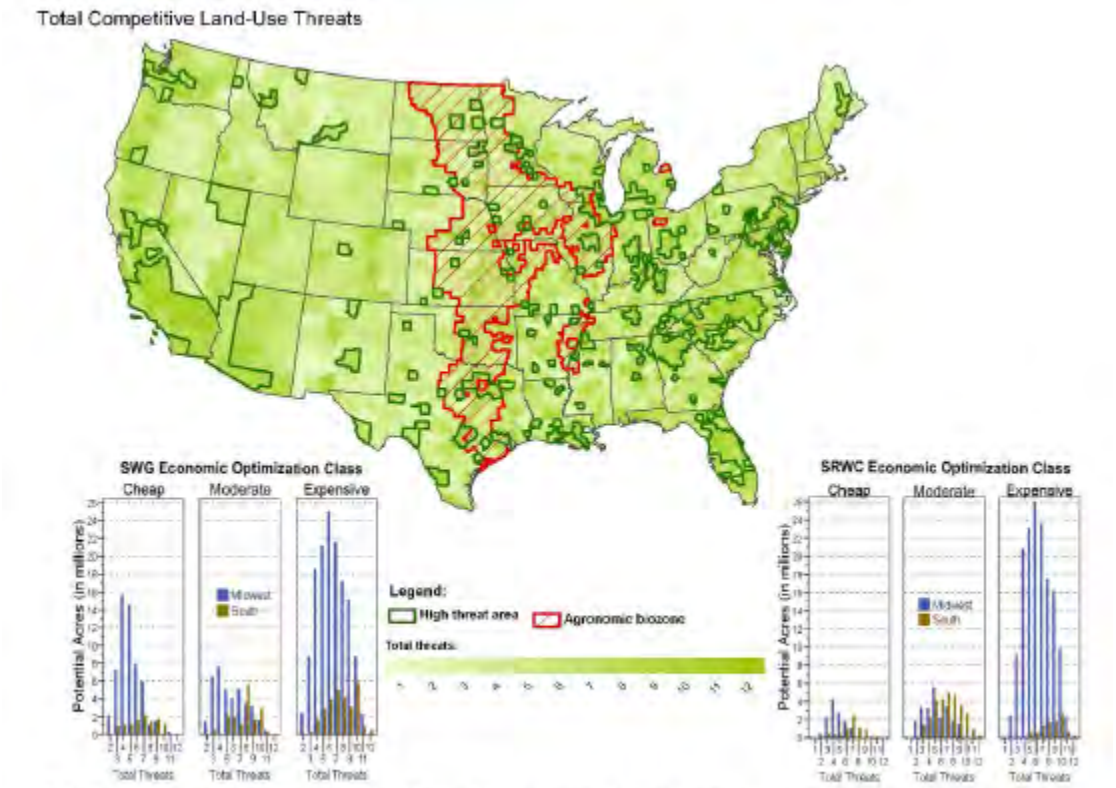


FIGURE 5: Total Competitive Land-Use Threats for potential acres of switchgrass and short-rotation woody crops production, and high yield economic optimization

Turning our focus to the SRWC model, there are some important contrasts to the results for SWG. We see that the majority of Kansas is no longer classified as a high yield cheap producer (see Figure 6). In contrast, much of North Dakota remains so suggesting that this state could affectively produce both biomass crops. Additionally, high yield SRWC production is projected to be feasible in the Northwest and throughout much of the South. While substantial portions of these moderate producers are circumscribed in high threat cluster areas, much of it is

not in terms of SRWC.

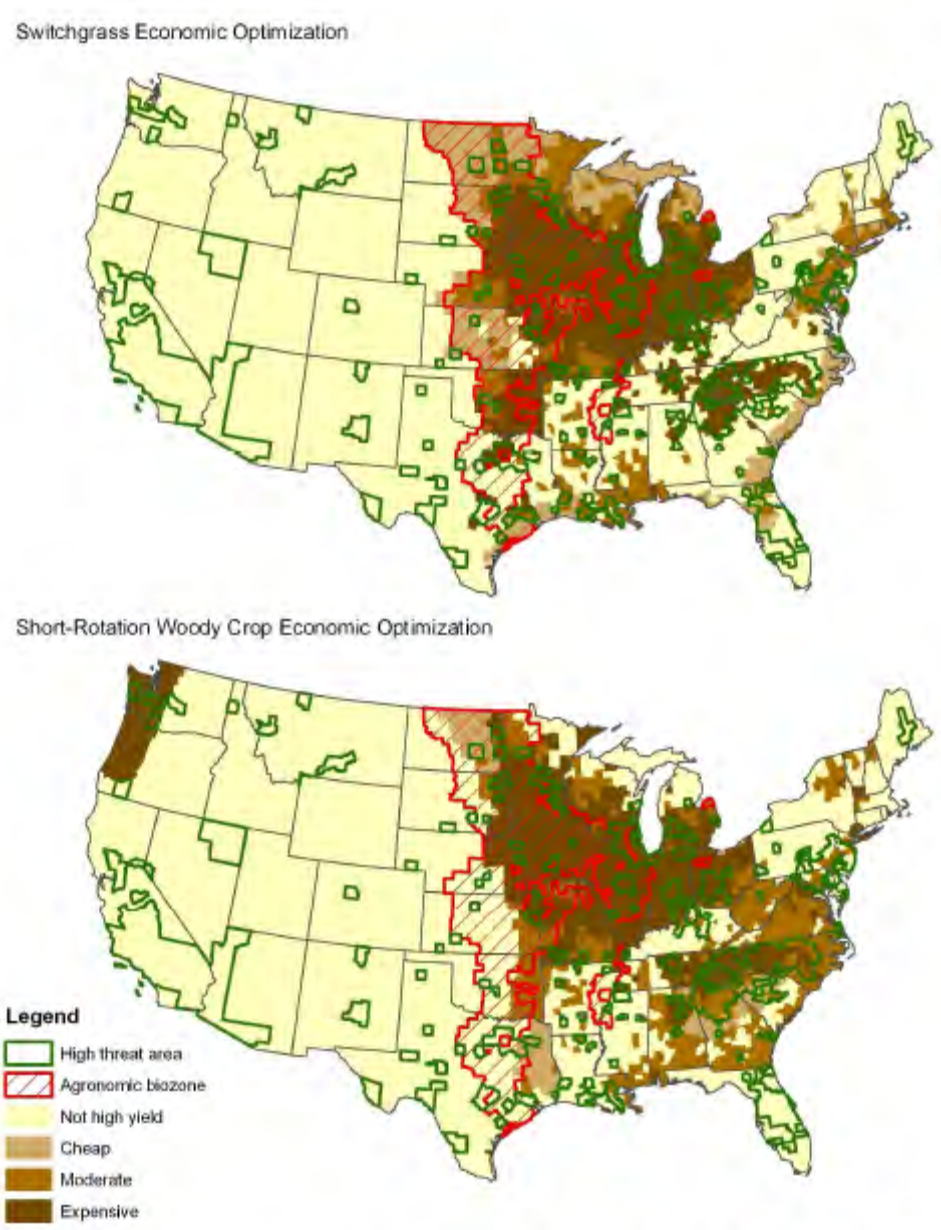


FIGURE 6 Total competitive land-use threats for potential acres of switchgrass and short-rotation woody crops by high yield economic optimization

6. Publications

Howell, F. M., J. R. Porter, P. B Mason, and T. C. Blanchard. 2007. Spatial contours of potential biomass crop production in the U.S. Paper read at *Southern Rural Sociological Association*, Mobile, Alabama, 3-7 February 2007.

Frank M. Howell, Jeremy R. Porter, Philip B Mason, and Troy C. Blanchard. 2008. Spatial Contours of Potential Biomass Crop Production: An Examination of Variations by U.S. Region. Under review at Southern Rural Sociology (SRSA Official Journal, Auburn University).

Phil B. Mason, Frank M. Howell, and Jeremy R. Porter. 2008. Metropolitan Influence and Land Use Conflict in Potential Biomass Crop Production: A Spatial Demographic Analysis.. Under review at Society & Natural Resources (Taylor & Francis).

Other products of this grant were the construction of the Spatial Analysis Laboratory in the Department of Sociology, Rm. 375 Bowen Hall, Mississippi State University. This laboratory consists of four workstations, two file servers, two network-addressable-servers (NAS), and color and monochrome laser printing. The total disk space available for file storage and backup to online disk is 10 terabytes (TB).

All project data, raw and enhanced, is stored on the NAS devices in the Spatial Analysis Laboratory.
The documentation of the data and analytic results are stored along with the data file system in the SAL.

Sustainable Energy Research Center
Environmental Sustainability Thrust Area Final Report for 2006-2008

1. Project title, name of principal investigator, and all team members

Project Title: L. Environmental Sustainability in Bioenergy

Principal Investigators: Drs. Jonathan Pote (lead), Charles Wax, Thomas Cathcart, Bill Cooke, and Brian Baldwin.

2. List of authorized distribution limitation notices, such as patentable material or protected data.

None.

3. Executive summary

This research presents a spatial analysis useful for identifying the best locations for growing bio-energy feedstocks in Mississippi and the environmental impact of the extensive planting of those feedstocks. Sets of climate, soil, elevation, slope, land use, drainage and other environmental databases were developed to use in GIS layers to spatially evaluate levels of productivity potential. Spatial depictions of statewide environmental suitability were produced using both fuzzy logic and linear weighted additive methods in GIS analyses of each individual variable. Comprehensive results from both methods pinpoint locations in the state most suitable for growth of feedstocks.

The technical effectiveness of the methods used for the spatial analyses was validated by use of the Agricultural Land Management Alternatives with Numerical Assessment Criteria – ALMANAC – model developed by the United States Department of Agriculture to estimate potential yields. This computer simulation model is used to estimate plant productivity for plant species such as switchgrass. Seven years of field data associated with soil and weather were used as inputs in the ALMANAC model. The model simulated switchgrass mean yields at 575 locations that were distributed proportionally as a function of the area of each soil series present in Mississippi.

Yield and suitability were correlated under different modeling conditions. Sensitivity analysis was used to obtain the best correlation between potential switchgrass yield and the suitability model to identify the best coefficients for each parameter. Analysis of variance (ANOVA) implemented through SAS 9.2 statistical software resulted in R-square = 0.7075 and Adj R –Square = 0.7072. The correlation procedure in SAS resulted in a Pearson correlation coefficient for suitability of 0.84 with ($P<0.0001$). Finally, Arc MAP 9.2 (GIS software) was used to process the input soil data as grids. The resulting output product was a final map (5 rank levels) of soil suitability across Mississippi for switchgrass.

This research benefits the public by showing that the State of Mississippi has few environmental limitations on the production of feedstock like switchgrass, and has many locations that are highly suitable to production of such crops. Further, the analyses allow precise location of areas within the state where sufficient acreage is available in highly suitable production categories to make switchgrass economically viable. Prevalence of environmental suitability for production of bio-energy feedstocks in Mississippi may lead to alternative crops for Mississippi producers, and put Mississippi in a position to aid in U.S. energy independence.

4. Comparison of goals and actual accomplishments

See spreadsheet attached.

5. Summary of activities

L. The original hypothesis of this project was that certain geographic regions of Mississippi would be better for growing biofuel feedstocks.

L.1 In order to confirm the hypothesis, environmental databases such as soils, land use, and climate were produced.

L.1.DL.1 Where applicable, these datasets were obtained in or converted to a GIS format.

L. 2 As the datasets were being obtained and processed, the spatial analyses were expanded to the entire state of Mississippi, rather than limiting the analyses to one basin. Two investigators completed a trip to Texas A&M University for training by the developers of the SWAT and ALMANAC models. During the training, it was determined that the ALMANAC model was better suited than the SWAT model for predicting estimated switchgrass yields, so the ALMANAC model was substituted for the SWAT model in the methodology of this project.

L.3 and L.3.DL.1 The remaining two objectives of the project were to use the environmental databases and GIS layers to model the environmental productivity potential for switchgrass and then spatially evaluate and display the potential for switchgrass growth throughout Mississippi using two models – a weighted linear model and a fuzzy logic model. Raw daily weather data was acquired and quality checked. Derived weather data was generated by the Almanac model as needed. A model to predict evaporation from other measured parameters was created for use in locations where no evaporation data were available. A manuscript documenting this activity has been accepted for publication.

L.4 Final GIS layers for soil, land use, slope, roughness, and competitive use were completed.

L.4.DL.1 Two different multi-criteria analyses have been developed for statewide site suitability analyses – a weighted linear model and a fuzzy logic model. Each of these analyses resulted in a M.S. thesis. A GIS analysis and associated data layers of statewide site suitability for switchgrass production based on the fuzzy logic model were completed (Figure 1). A GIS analysis and associated data layers of statewide soil suitability for switchgrass production based on the weighted linear model were also produced (Figure 2).

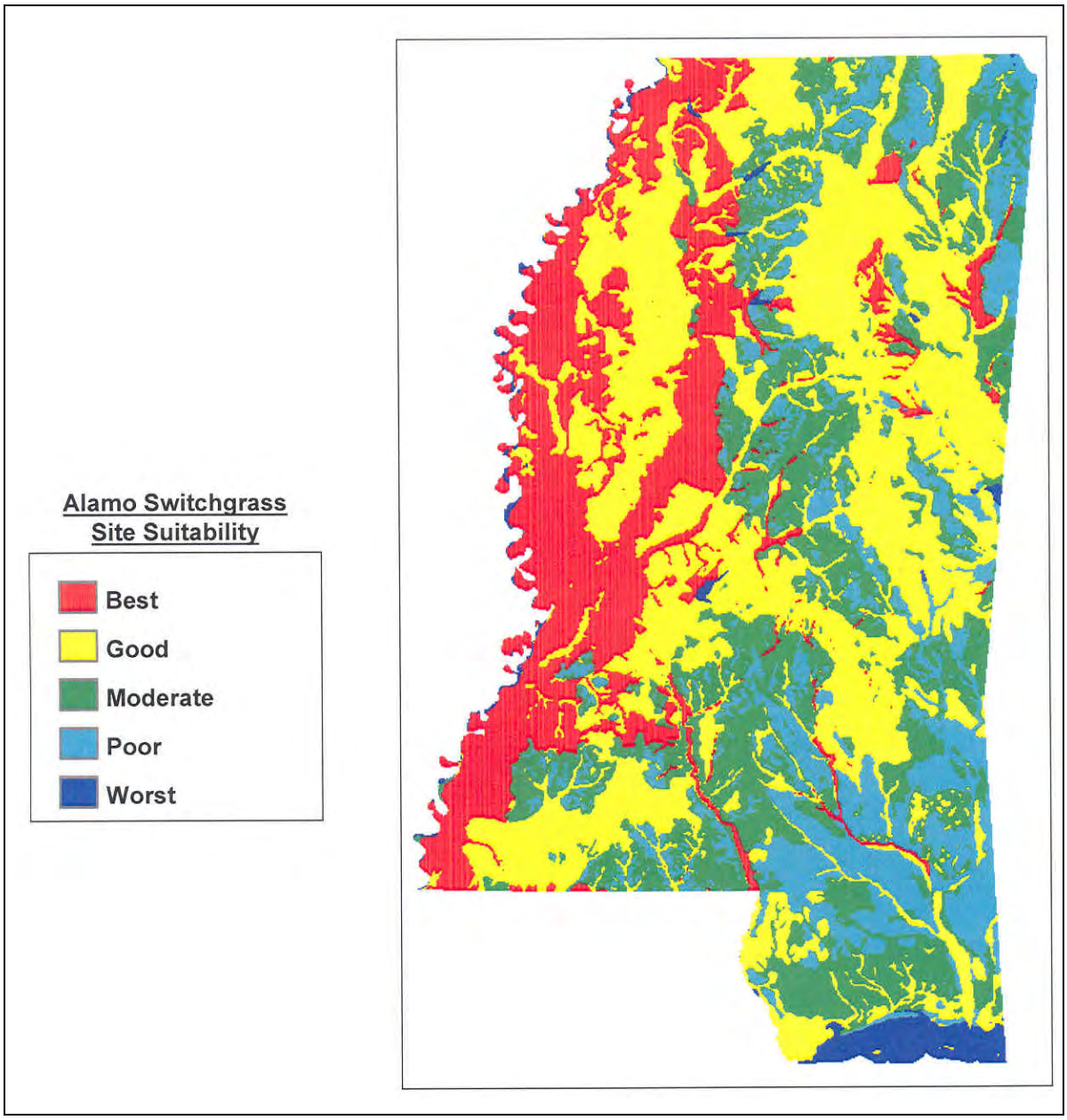


Figure 1. Environmental suitability for switchgrass production in Mississippi.

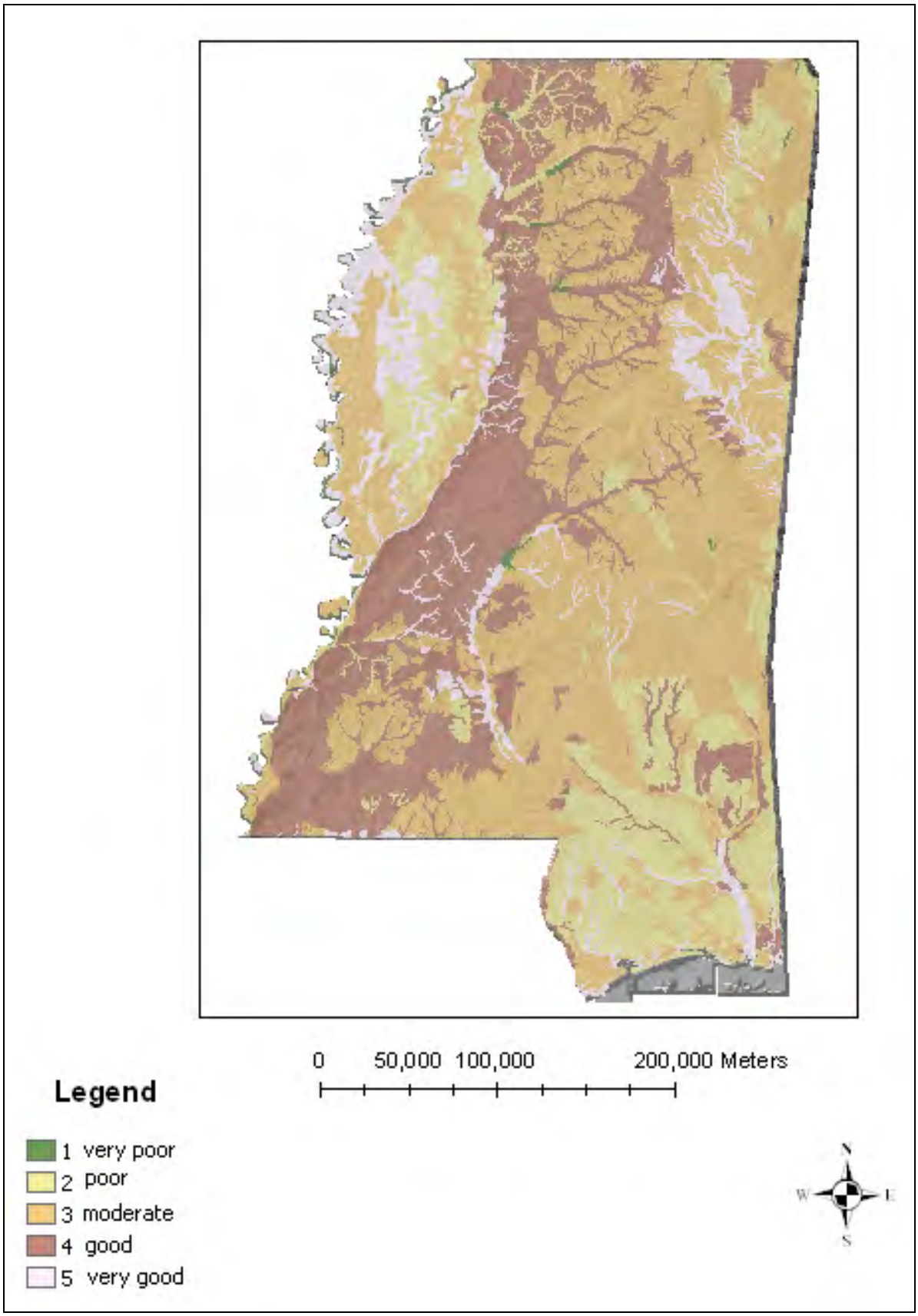


Figure 2. Soil suitability for switchgrass production in Mississippi.

6. Identify products developed under the award and technology transfer activities, such as:

a. **Publications**

In press. Cooke, W.H., K. Grala and C.L. Wax. "A Method for Regional Estimates of Evaporation for Use in GIS-Based Dynamic Forest Fire Risk Models." Southeastern Geographer.

Theses in fulfillment of requirements of M.S. degree, Department of Geosciences:

"Fuzzy Logic Techniques Applied to a Switchgrass Ecological Site Suitability Model for the State of Mississippi." Michele Maxson. Defense held in October, 2007.

"Determination of Soil Suitability in the State of Mississippi to Grow Switchgrass Using GIS - Modeling, Multicriteria Analysis and Sensitivity Analysis." Eduardo Arias. Defense held in March 2008.

b. Web site or other Internet sites
c. Networks or collaborations fostered
d. Technologies/Techniques

Some of the techniques for generating information layers may be unique. The method for estimating evaporation and the GIS layers using statewide soil associations to model specific elements such as soil moisture and pH are cases in point.

e. Inventions/Patent applications, licensing agreement
f. Other products, such as data or databases, physical collections, audio or video, software or netware, models, educational aid or curricula, instruments or equipment.

The weather database is now one of the most complete of its kind for the prototype location.

Final Report

Project Title: Mississippi State University Sustainable Energy Research Center, Phase II
Award Number: DE-FG36-06GO86025

Recipient: Mississippi State University
Project Location: Mississippi State University, Starkville, Mississippi

Reporting Period: January 1, 2008 – June 30, 2011
Date of Report: July 31, 2011
Written by: W. Glenn Steele

Program Manager: W. Glenn Steele
Principal Investigators: W. Glenn Steele

DOE Project Team
DOE-HQ contact:
DOE Field Project Officer: Gene Petersen 303-275-4937 gene.petersen@go.doe.gov
DOE Contract Specialist: Brenda Dias 303-275-6043 brenda.dias@go.doe.gov
DOE Project Engineer: Nicholas Frasier 303-275-4772 nicholas.frasier@go.doe.gov

Acknowledgment: This material is based upon work supported by the Department of Energy under Award Number DE-FG36-06GO86025.

Disclaimer: This report was prepared as an account of work sponsored by an agency of the United States Government. Neither the United States Government nor any agency thereof, nor any of their employees, makes any warranty, express or implied, or assumes any legal liability or responsibility for the accuracy, completeness, or usefulness of any information, apparatus, product, or process disclosed, or represents that its use would not infringe privately owned rights. Reference herein to any specific commercial product, process, or service by trade name, trademark, manufacturer, or otherwise does not necessarily constitute or imply its endorsement, recommendation, or favoring by the United States Government or any agency thereof. The views and opinions of authors expressed herein do not necessarily state or reflect those of the United States Government or any agency thereof.

DOE Award Number: DE-FG36-06GO86025
Name of Recipient: Mississippi State University
Project Title: Mississippi State University Sustainable Energy Research Center
Principal Investigator: W. Glenn Steele

The data and information contained in Pages 1-231 of this report have been submitted in confidence and contain trade secrets and/or patentable intellectual property.

Executive Summaries

The goal of the Sustainable Energy Research Center (SERC) at Mississippi State University (MSU) is to build multi-disciplinary teams to conduct research needed to exploit the ability of the state and region to generate biomass for energy production and to develop economic and environmentally sustainable energy-conversion systems to support the emerging sustainable-energy industry in the Southeast. The work under this contract, DE-FG36-06GO86025, is divided into seven tasks ranging from feedstock development to fuel testing. The complete listing of projects and tasks is provided in the table below. Following the table a complete final report is provided for each of the A through G tasks.

Bio-oil

Subtask A.1 Design, build, and operate a mobile pyrolysis reactor
The proposed mobile reactor was designed, built and installed in a 38-foot-long enclosed trailer. Testing confirms production of bio-oil at 65% yield with capability to process 10 kg/h of biomass. A char furnace to provide 50% of pyrolysis heat was designed and tested. The required temperature of 700 ^{o}C was attained satisfying the goal of providing more than 50% of pyrolysis energy. All milestones were achieved.

Subtask A.2 Raw bio-oil upgrading
Hydroprocessing catalysts were developed, allowing application of two-stage hydrotreating/hydrocracking raw bio-oil upgrading to a hydrocarbon mixture. The mixture has a color similar to refined petroleum fuels with zero oxygen and water and with a neutral pH. Higher heating value is equivalent to petroleum fuels at approximately 44.5. Detailed hydrocarbon analyses, simulated distillation, and spinning band distillation show that the fuel is composed of approximately equal proportions of hydrocarbons' molecular weights in gasoline, jet, and diesel petroleum fuels. All milestones were achieved.

Subtask A.3 Space heating application
Two lignocellulosic boiler fuels were developed with improved properties. One fuel is an esterified product while the second is olefinated. The esterified fuel contains slightly higher water content due to the esterification reaction. However, acid value is reduced by 50% and higher heating value is increased by 30% due to esterification of acids to esters. The olefinated product contains dramatically lower water content at 6% with a higher heating value of approximately 70% of that of petroleum heating oil. The acid value of the olefinated product is also 50% lower than that of raw bio-oil. The yield of both boiler fuels is 100% with no loss to gases or char. Boiler tests with slightly modified boilers showed good performance with immediate ignition and clean burning. All milestones were achieved.

Subtask A.4 Feedstock and bio-oil characterization with pretreatment
Yellow poplar and black willow woods and giant miscanthus and elephant grass feedstocks were characterized by analyzing both feedstocks and their resulting pyrolysis products. Pine wood was utilized as a benchmark by which to compare the yields and chemical properties of the tested feedstock bio-oils. Results indicated that giant miscanthus and yellow poplar gave relatively high yields of bio-oil at 57 and 56%, respectively, compared to 60.1% for pine wood. Elephant grass and black willow provided relatively low yields at 43 and 44%, respectively. Yellow poplar produced a bio-oil with low water content while the giant miscanthus bio-oil had somewhat higher water content; the black willow and elephant grass bio-oils had very high water contents. The low yields combined with high water content values for the elephant grass eliminates it as a biomass type suitable for pyrolysis. The feedstock type that compared most favorably with pine wood as a feedstock, with the exception of the relatively high water content, was giant miscanthus. Black willow will probably be marginal as a feedstock for production of bio-oil. However, refinements of pyrolysis temperature levels and residence time may increase yield and reduce water content to a level that black willow could be considered as an acceptable pyrolysis feedstock. Pretreatment of four feedstocks in two particle sizes resulted in eight feedstock types treated with seven acid and base chemical pretreatments (0.5, 1, and 2% concentrations of phosphoric acid; 1% hydrochloric acid; and 0.5 and 1% sulfuric and 0.5% sodium hydroxide). Phosphoric acid treatment at 1% concentration provided the highest sugar-yield pine wood. Sulfuric acid pretreatment at 1% provided a bio-oil with the best properties. All milestones were achieved.

Subtask A.5 Determine petroleum refinery bio-oil characteristics
Interaction with petroleum refineries allowed us to determine the characteristics of upgraded bio-oil acceptable for refining. Proposals for applying these upgrading steps in the refineries were made to funding agencies with two refineries. The projects were not funded, but future application of our upgrading technology is promising with considerable interest from refiners. All milestones were achieved.

Biocrude

Subtask B.1 Develop wastewater treatment operational strategies to maximize production of biocrude
The prospect of utilizing municipal sewage activated sludge microorganisms for the production of biodiesel feedstock lipids via aerobic fermentation was investigated. Biomass yields decreased and lipid contents increased with increasing C:N ratio (10:1-70:1) while both variables were highest at 40 and 60 g L^{-1} glucose loadings. Kinetic analysis indicated a greater influence of growth-associated lipid production on lipid concentration and yield coefficient. Overall, activated sludge grown in C:N ratio 40 and 60 g L^{-1} glucose loading produced a maximum of 2.2 g L^{-1} lipids. Fatty acid methyl ester (FAME) analysis showed improved biodiesel quality and higher lipid and biodiesel yields of 18 and 10% CDW, respectively, compared to raw activated sludge. Fermentation experiments were conducted at C:N ratio 70 and 60 g L^{-1} glucose loading. Several engineering aspects of the proposed fermentation process for the enhancement of lipid and biodiesel yields from municipal sewage activated sludge are discussed in order to determine its feasibility in industrial applications. Continuous process simulations were performed using computer software to obtain projected biomass and lipid productivities, biodiesel yields, and substrate consumption rates. Preliminary design calculations were then made to estimate the required bioreactor size for specific calculation bases, specifically the assumed substrate conversion or yield coefficients for lipids and biodiesel production. An economic analysis was conducted to determine capital investment, production costs, and optimal product selling price. Sensitivity analysis on the effect of sugar cost on

biodiesel break-even price showed that a lignocellulose sugar cost between $0.12 and $0.14/lb (DOE Target) would be needed to reduce the biodiesel cost below the $3.00/gal mark ($2.80/gal), which was lower than the average diesel price of $3.07 in the United States during the period of conducting the study. Therefore, further studies must be conducted to determine suitable low-cost fermentation substrates for the production of biocrude in order to enhance the cost-competitiveness of the proposed biocrude production process from activated sludge systems.

The production of biodiesel from dried (95% solids) activated sludge obtained from Tuscaloosa, AL was optimized based on the yield of FAMEs. *In situ* transesterification process was used with sulfuric acid as a catalyst. A general factorial of 4 x 6 x 5 for temperature, methanol to sludge ratio, and catalyst concentration, respectively, was considered for optimization. Results showed that biodiesel yield can be adequately described by the *quadratic response surface model* with R^2 of 0.8432 and statistically insignificant lack of fit (*p=0.1523*). Furthermore, results indicated significant acid-catalyzed polymerization of unsaturated fatty acids or their esters at temperatures above 60 ^{o}C thereby decreasing biodiesel yield. Numerical optimization was conducted, and the results showed that an optimum biodiesel yield of 4.88% can be obtained at 55 ^{o}C, 25 methanol to sludge ratio and 4% volume sulfuric acid. The optimum experimental biodiesel yield was indeed obtained at that condition but with a value of 4.79 ± 0.02%.

The production of biodiesel from wet activated sludge obtained from Tuscaloosa, AL was optimized based on the yield of FAMEs. *In situ* transesterification process was used with sulfuric acid as catalyst. An orthogonal central composite response design was considered to investigate the effects of temperature, moisture content, methanol to sludge ratio, and catalyst concentration and their interaction effects on the yield of biodiesel. Results showed that the biodiesel yield can be satisfactorily described by the *quadratic response surface model* with a R^2 of 0.836 and a statistically not significant lack of fit (*p=0.254*). Coded regression coefficients, main effect plots, and surface plots indicated that a maximum biodiesel yield may be obtained at 75 °C, 30 mL/g (methanol/sludge) and 10% volume (catalyst concentration). Numerical optimization was conducted, and the results showed that at this reaction condition, a biodiesel yield of 3.78% (weight) can be obtained. Experimental verification gave a biodiesel yield of 3.93 ± 0.15% (weight) giving a model error of 7.35%. This indicates high reliability of the model. Economic analysis showed that the *in situ* transesterification of activated sludge without water removal (84.5% moisture) is less economical than the *in situ* transesterification of dried sludge (5% moisture). However, sensitivity analysis indicated that the process presented in this study can be made more economical by reduction of water to 50% (weight). At this level of moisture, a biodiesel break-even price of around $7.00/gal is attainable, which is still more expensive than petroleum-based diesel (~$2.95/gal). For the biodiesel from activated sludge to be economically competitive, a biodiesel yield of greater than 10% (weight) is necessary, which could be achieved using the enhanced sludge technique.

Subtask B.2 Development of an oleaginous microbial consortium for use as a return activated sludge in biocrude production

A combination of an oleaginous consortium and raw activated sludge improved overall cell mass concentration. This combination could be used to increase oil yield. The use of just the oleaginous consortium did not meet the target of $3.00/gal biodiesel.

Subtask B.3 Produce quality transportation fuels defined by the American Society for Testing and Materials Standard

Catalytic cracking experiments were conducted using the three fractions obtained from Soxhlet extraction. The same conditions and catalysts were employed for all experiments. Results

showed that only the methanol fraction with ZSM-5 as catalyst gave an appreciable yield of hydrocarbons. The separation of the extract based on polarity alone is not enough for its conversion to fuel. This is probably due to inherent complexity of the extract, and it might be necessary to separate the extract based on compound class (i.e., hydrocarbons, wax esters, steryl esters, fatty acids, acylglycerides, phospholipids, etc.). After separation, determination of cracking conditions and catalyst might be necessary for each class.

Subtask B.4 Design cost efficient biomass and biofuels supply chains
One objective of this study was to design and evaluate the performance of the supply chain for biocrude production from activated sewage sludge in wastewater-treatment facilities. Experimental results indicate that feeding wastewater activated sludge with high sugar load and establishing a high carbon-to-nitrogen ratio in the wastewater could enhance biocrude yield and quality from the sludge. The biocrude will be further refined and converted to biodiesel. The optimization part of the optimization-simulation framework that we propose uses a mixed integer program to identify locations for sugar plants as well as the assignment of wastewater-treatment plants to sugar plants and refineries. The objective is to minimize total supply-chain-related costs. We use the solution from the optimization model (the structure of the supply chain) to build a discrete-event simulation model. The simulation captures the seasonal and random nature of biomass supply. We use a case study that designs the supply chain for biocrude in Mississippi given the availability of lignocellulosic biomass and the locations of harvesting sites, wastewater-treatment plants, and refineries.

Lignocellulosic Conversion

Subtask C.1 Determination of sugar conversion kinetics into triglycerides
The results presented herein demonstrate the ability of oleaginous microorganisms (e.g., *Rhodotorula glutinis*) to utilize lignocellulosic sugars for the intracellular production of lipids (a biofuel feedstock). In Subtask C.1, this work demonstrates that this particular yeast can consume all of the glucose and xylose to below detectable limits when offered singularly. However, when offered simultaneously, this particular yeast will preferentially choose glucose over xylose. Once the glucose has been consumed, the xylose can be consumed to below detectable limits. This work has demonstrated that it is possible to consume the major sugar components of lignocellulosic material using wild-type microorganisms for the production of biofuel feedstock. Because sugars are not the only compounds resulting from hydrolysis of biomass, studies were conducted to determine the effect of acetic acid and furfural on *R. glutinis'* ability to metabolize these sugars into lipids. The data demonstrates that inhibition by these compounds does occur; however, it seems to be more pronounced with glucose metabolism. When xylose is the sole substrate, the effects of the acetic acid and furfural are not as noticeable as indicated by the cell mass and lipid production compared to the controls without inhibitors present. This information could be very useful in developing a strategy for inputting sugars into the fermentors for maximum yield of oil with minimal inhibition effects. Much work has been done by others to identify metabolic pathways for the production of ethanol (a gasoline displacement technology) from lignocellulosic feedstocks. The work presented here provides additional information for the production of a diesel displacement technology using oleaginous microorganisms that consume lignocellulosic derived sugars for the production of microbial lipids.

Subtask C.2 Isolation and characterization of novel oleaginous microorganisms
In addition to the known oleaginous microorganisms, we believed it could be beneficial to identify additional oleaginous microorganisms with the potential for expanded metabolic capabilities (e.g., utilization of different substrates or faster lipid production rates). Towards this

end, a novel source of microorganisms was investigated. Using subsurface core materials, some of which were obtained on past Department of Energy-funded projects, were used as a novel source of microorganisms for lipid production. These efforts unfortunately have not identified any additional oleaginous microorganisms but have provided a method and some molecular probes to continue the search for additional oleaginous microorganisms.

Subtask C.3 Evaluation of non-lethal oil extraction technologies

Because oleaginous microorganisms store their lipid intracellularly, the cells must be ruptured to release the oils for separation. Efforts were placed on developing a mutant oleaginous microorganism that could secrete lipids without having to go through the energy intensive steps of water removal and cell lysis. Although some of these energy requirements might be circumvented, there would be some energy required to separate and purify the oil from the aqueous phase. In order for this to be considered an oleaginous microorganism with the ability to secrete, the oil was necessary. Using *Rhodococcus opacus*, a mutant was developed that appeared to release oil compared to the wild-type while leaving the cell alive as determined by staining. Additional tests would be required to confirm this ability.

Subtask C.4 Evaluation of the cellulose and hemicellulase production ability of these oleaginous microorganisms

One of the major costs associated with producing oils from lignocellulosic sugars is the cost of the sugar inputs. Depolymerizing lignocellulosic sugars is costly and energy intensive. If the oleaginous microorganisms could utilize natural fibers for oil accumulation, they might positively affect the economics of producing oil from this feedstock. The first step in the process was to understand the genetic makeup of *R. glutinis* to determine if this organism possessed the ability to produce cellulase or hemicellulase. The genome of *R. glutinis* has been sequenced and can now be used to determine if the genes are present for this process.

This work has proven the ability of *R. glutinis* to utilize the sugars that make up lignocellulosic material even in the presence of inhibitors. This work has also demonstrated the potential to produce a mutant with the ability to secrete the oils it produces intracellularly. Having the genome of *R. glutinis* sequenced will allow us to determine what the metabolic capabilities are and what makes it oleaginous.

<u>Synthesis Gas</u>

Subtask D.1 Catalyst development

Novel heterogeneous catalytic systems were evaluated and tested for production gasoline range fuels from syngas. Because the nitrogen level of the biomass-derived syngas can be up to 60%, in the catalytic converting syngas to gasoline process, work has concentrated on the development of catalysts for the production of liquid fuels from nitrogen-rich syngas. Previous work demonstrated that the Mo/HZSM-5 catalyst (the second-generation catalyst) was active in Fischer–Tropsch synthesis (FTS) when using syngas without a nitrogen component. Mo/HZSM-5 catalyst was continually evaluated for FTS, but using a high-level nitrogen-containing syngas. Liquid hydrocarbons formed on the Mo/HZSM-5 were composed mainly of alkyl-substituted aromatics and lower branched and cyclized alkanes. Lower hydrocarbons produced included mainly methane, ethane, propane, and *iso*-butane. However, the CO conversion and selectivity of liquid hydrocarbons from biomass-derived syngas were not satisfied when comparing to pure syngas (without nitrogen).

A third-generation catalyst has been prepared and evaluated for catalytic converting nitrogen-rich syngas and biomass-derived syngas to gasoline range hydrocarbons. The catalytic process occurs at a temperature of 250-400 °C, a gas volume hourly space velocity (GHSV) of 500 to 5,000 h^{-1} and a pressure of 500-1500 psi. The CO conversion, selectivity of CO_2 and hydrocarbon, and hydrocarbon distribution were measured in a fixed-bed flow reactor. It was found that the catalyst has relatively high activity and selectivity in producing liquid hydrocarbons when running with nitrogen-rich syngas and biomass-derived syngas. The CO conversion, hydrocarbon selectivity, and hydrocarbon distribution as a function of temperature, pressure, GHSV, composition of the feed, and reaction time were examined. The increase of temperature and pressure favors CO conversion and formation of more hydrocarbons. The conversion of CO in the syngas was 73% under a reaction temperature of 310 °C and a pressure of 1000 psi and 58% under a reaction pressure of 500 psi when using a model syngas (19% H_2, 20% CO, 12% CO_2, 2% CH_4, balanced N_2.). This catalyst gave higher conversion efficiency under a lower CO-H_2 pressure. The conversion into hydrocarbons reached about 70 mol% while the conversion into CO_2 was about 30 mol%. The resultant hydrocarbons were hydrocarbons of the gasoline boiling point range, containing 40 to 50 wt% of light hydrocarbons (C_1-C_4), which is significantly lower than in the case of using the Mo/HZSM-5 catalyst, producing more than 70% light hydrocarbons. According to detailed hydrocarbon analysis, the composition of gasoline fraction contained up to 40 wt% aromatics, 15 wt% of olefins, and 40 wt% of paraffins while more than 90% of the liquid hydrocarbons were aromatics in the case of the Mo/HZSM-5 catalyst. The compositions of liquid hydrocarbon mixture products can be adjusted through the operating conditions. Time-on-stream results showed the catalyst was stable. CO conversion reached 74% after a 20-hr run at 310 ^{o}C, and kept constant after a 120-hr run. Biomass-derived syngas was also tested for hydrocarbon production. The CO activity and selectivity was similar to that of the model syngas. The composition of the gasoline phase was also similar to the model syngas except there were more aromatics and less olefins in the biomass-derived syngas product.

Subtask D.2 ASTM characterization of the gasoline product

A sufficient quantity of liquid hydrocarbon was collected to permit a battery of ASTM tests to be completed. These tests showed an octane number (R+M)/2 equaling 96, an API gravity of 50°, and a Reid vapor pressure of 13.5 psi. The ASTM distillation curve was consistent with that of a 410 F endpoint gasoline mixed with a heavy catalytic cracked gasoline fraction.

Biomass Utilization

Economic, environmental, and strategic interests have refocused IC engines research on increasing efficiencies, reducing pollutant emissions, and identifying renewable alternative fuels. In the proposed project, the feasibility of using biomass-derived renewable fuels (biodiesel and syngas) as sustainable energy alternatives to conventional petroleum-derived fuels in IC engines was investigated. Novel combustion strategies were attempted to achieve high fuel efficiencies and engine power densities while simultaneously realizing extremely low engine-out emissions.

This research, which had both simulation and experimental components, sought to achieve several objectives: (i) Experiments with different injection strategies to investigate, diesel, B20, biodiesel, and syngas combustion over a range of engine loads, (ii) Development and validation of phenomenological combustion simulations of diesel, biodiesel, and syngas combustion. These objectives were accomplished in three subtasks over the project duration of three years.

The major anticipated benefits of the technologies in this research are fuel efficiency improvements (up to 40%), good power densities (BMEP ~ 10 bar), strategies to achieve low NOx and PM emissions, and development of high fidelity models to investigate advanced combustion strategies for future IC engines. In general, the project efforts demonstrated that dual fuel combustion is a promising strategy for alternative fuel utilization and can provide good fuel conversion efficiencies and low NOx and PM emissions without major modifications to the engine architecture. However, the project results also established the need to continue these investigations to understand and optimize advanced dual fuel combustion strategies to achieve further performance and emissions improvements.

Subtask E.1 Advanced low-temperature combustion experiments with biodiesel and diesel-biodiesel blends
Phase I of Subtask E.1 involved experiments with B20 and B100 fuelling and measurement of nitrogen oxides, carbon monoxide, smoke emissions, and other performance parameters, such as fuel conversion efficiencies and rate of heat release profiles, to establish a baseline. Phase II of Subtask E.1 involved detailed experimentation to identify optimal combinations of fuel injection strategies and appropriate intake manifold conditions with B100 and B20 blends to achieve low emissions (as mandated by EPA Tier 4 (non-road)) and high fuel conversion efficiencies.

Subtask E.2 Phenomenological low temperature engine combustion simulation development
Phase I of Subtask E.2 involved the development of fundamental, predictive phenomenological biodiesel (B100) combustion simulation while Phase II of Subtask E.2 involved the development of computer simulations to predict B100-ignited syngas combustion.

Subtask E.3 Evaluation of biodiesel-ignited syngas low temperature combustion
Phase I of Subtask E.3 involved experiments with B100-syngas fuelling and measurement of nitrogen oxides, carbon monoxide, smoke emissions, and other performance parameters, such as fuel conversion efficiencies and rate of heat release profiles, to establish a baseline. Phase II of Subtask E.1 involved detailed experimentation to identify optimal combinations of fuel injection strategies and appropriate intake manifold conditions with B100-ignited syngas to achieve low emissions (as mandated by EPA Tier 4 (non-road)) and high fuel conversion efficiencies.

Feedstocks

Subtask F.1 Field trials
Feedstocks research was conducted with an emphasis on sustainable agronomic production potential of bioenergy-specific crops that offer the possibility of being grown on land less desirable for traditional food-crop production. Production-orientated research across the state on high biomass and sugar crops has provided a greater understanding of feedstock growing potential as well as challenges faced in the cultivation of bioenergy crops. Dry matter yield trials of lignocellulosic crops at the Raymond and Mississippi State, MS locations indicated switchgrass breeding lines yielded greater biomass than the commercially available cultivars ‘Shawnee’ and ‘Cave-in-Rock.’ ‘Alamo,’ which is the currently recommended cultivar for our region, yielded slightly less than the breeding lines. Miscanthus at the Raymond location did not establish well, and yields were not reported. Ratios of N:P usage were 10:1, while N:K ratios were from 4.7 to 16.4 when harvested in December. Harvesting in January reduced K uptake values the greatest. Fertilizer N application generally increased yield, but response was

inconsistent across years. Fertilizer N application increased switchgrass biomass yield 20 and 30% with rates of 56 and 112 kg/ha, respectively, compared to the control. Switchgrass biomass yield was not compromised by mid-season harvesting for forage purposes, which suggests that dual purpose usage could be feasible during feedstock development. Monitoring of above-ground and below-ground growth of switchgrass is providing important information on C sequestration and N dynamics within the plant system from shoots to crowns to roots. A direct comparison of switchgrass versus giant miscanthus demonstrated the importance of the need for multiple years of data collection as giant miscanthus yielded less than a third ('Illinois clone') to slightly more than a third ('Freedom') than switchgrass. Additionally, switchgrass cultivars have shown a yield increase from Year 1 to Year 3 of growth. Progress has also been made in selective breeding for greater germination rates of switchgrass, indiangrass, and big bluestem. Interseeding of switchgrass with legumes has shown some benefit. Physiological studies on switchgrass indicated genotypes, which differ in germination response to temperature with some being tolerant of high temperatures and some being tolerant of low temperatures. Genotypes also varied significantly in their response to drought stress and could aid in optimizing selection for regions differing in relative moisture status. Research on big bluestem demonstrated the effects of N availability on physiological parameters. A deficiency of N reduces biomass production through a reduction in photosynthesis, tiller number, and leaf dry weight. Remote sensing results demonstrated the ability to evaluate big bluestem stands for overall plant health, which could prove useful in managing vast areas for feedstock production. Crop residues, which remain following harvest, offer an alternative source of biomass although the woody nature of the materials makes it difficult to extract cellulosic compounds and convert them to fermentable sugars. Investigations in using naturally occurring degraders found in the soil have shown promise for pre-treatment of rice residues. Genomic analysis and genetic modification of cell walls has resulted in a transgenic rice, which has a greater grain weight, and progress has been made in understanding regulatory proteins important in cell wall synthesis. A Timber Disaster Recovery and Wood Utilization Response Tool was developed: the Wind Wood Web site (**windwoodutilization.org**) was designed to provide information relating to the preparation for, response to, and recovery of downed and damaged timber and woody debris from major wind events.

Subtask F.2 Feedstock Engineering

Work conducted within the Feedstock Engineering Group consisted of grass densification efforts, environmental impact modeling, and spatial distribution and economic modeling of potential bioenergy crops. Densification is a key step in reducing the transportation costs of biomass feedstocks. In-field hay cubing was examined as a way to reduce the number of steps in achieving a densified feedstock. To date, we have not been able to effectively cube switchgrass. Efforts have focused on cubing Bermuda grass as a model for energy crops. In-field cubing achieved a production efficiency of 73.6% using Bermuda grass. Cubing efficiency was increased by 5.3% (78.9%) using a lignin sulfonate binder applied at 50lb/ton. Secondly, the environmental impacts and the ultimate sustainability of biomass production for conversion to biofuels is being modeled. A key approach that we have examined is the use of net energy value (NEV) to measure the sustainability of bioenergy produced from a particular source. A larger NEV value indicates more nonrenewable energy replaced, and a positive value is an indication of sustainability. We have investigated different factors that affect variability in corn stover productivity in the Mississippi Delta region and found that NEV was positive indicating that the corn stover-based ethanol production system in the Delta region is sustainable. Finally, spatial distributions of the potential bio-energy crops and their environmental impact in Mississippi watersheds are being studied for their potential in syngas production. The sustainability and modeling efforts also consider developing and using economic models, such as a "Cost Calculator," to evaluate pilot-scale bio-gasification systems.

Number of Task, subtask, or milestone	Title of Task, subtask, or milestone	Task or Milestone Completion Criteria	Actual Accomplishments
A.	Bio-oil		
A.1	Design, build and operate a mobile pyrolysis reactor		The mobile reactor was designed, fabricated and tested and exceeded the milestone by 5%. Similarly, 10 kg/hr capacity exceeded target by 100%. A novel char furnace was designed and produced 60% of reactor heat.
A.1.ML.1	Design and fabricate a mobile reactor that processes 5kg/hr of biomass with a raw bio-oil yield of approximately 60%.	Bio-oil yield tested for production of 1 gal of bio-oil	The mobile reactor was designed, fabricated and tested. Yield was 65% exceeding milestone by 5 percentage points. The pyrolysis capacity is 10 kg/h exceeding target by 100%.
A.1.ML.2	Attempt to utilize char and pyrolysis gas to produce up to 50% of required reactor pyrolysis energy.	Required temperature of 500C attained on test bed	A novel char furnace was designed, fabricated and tested. A temperature of 700C produced approximately 80% of required pyrolysis heat exceeding milestone by 60%.
A.2	Raw bio-oil upgrading		Novel hydroprocessing catalysts produced and tested in a batch reactor. It produced zero oxygen hydrocarbons and heating value equal to petroleum fuels; olefination produced upgraded bio-oil and the milestone was achieved.

A.2.ML.1	Reduce oxygen content of catalyzed bio-oils; the addition of olefins will reduce bio-oil water content; the addition of reactive alcohols will produce a moderately upgraded bio-oil with reduced water content and increased stability compared to standard alcohols addition results. Pyrolysis vapor will be filtered to remove char particles from raw bio-oil; some mechanisms responsible for the high instability of bio-oils produced from leaves and barks will be identified.	Oxygen content reduced to <1% by HDO;weigh organics after centrifugation to determine % increased solubility;compare pH of alcohol-reacted bio-oils to those with simple addition; determine % char removal by microscopic examination;phenomenon causing bark	Novel hydroprocessing catalysts produced zero oxygen hydrocarbons; olefination produced upgraded bio-oil with HHV at 70% of petroleum fuels; alcoholation research allowed production of a stable boiler fuel with pH 50% of that of raw bio-oil; research into properties of bark bio-oil instability identified several potential mechanisms and a path to solution. Milestones met or exceeded.
A.2.ML.2	Reduce oxygen content of catalyzed bio-oils; the addition of olefins will increase solubility of bio-oil organics in a hydrocarbon blend; the addition of reactive alcohols will produce a moderately upgraded bio-oil with reduced acidity and increased stability compared to standard alcohols addition results. Pyrolysis vapor will be filtered to remove char particles from raw bio-oil; the mechanisms responsible for high instability of bio-oils produced from leaves and barks will be identified and solutions will be proposed or tested.	Oxygen content reduced to <1% by HDO;weigh organics after centrifugation to determine % increased solubility;compare pH of alcohol-reacted bio-oils to those with simple addition; determine % char removal by microscopic examination;phenomenon causing bark	Novel hydroprocessing catalysts produced zero oxygen hydrocarbons; olefination produced upgraded bio-oil with HHV at 70% of petroleum fuels; alcoholation research allowed production of a stable boiler fuel with pH 50% of that of bio-oil; research into properties of bark bio-oil instability identified several potential mechanisms. Milestones met or exceeded.
A.3	Space heating application		A 10 gal/h semi-batch esterification system was designed and tested; 40 total hours of heating time were performed on a modified boiler. Milestones were met or exceeded.

A.3.ML.1	Design and fabrication of a 10-gal/hr semi-batch transesterification system.	Production rate of 10-gal per hour reached.	A 10 gal/h semi-batch esterification system was designed and tested. Milestone met or exceeded.
A.3.ML.2	Increase esterified bio-oil production system to 20/gal per hour and to achieve a 40-hour continuous test of upgraded bio-oil firing of a commercial furnace in conjunction with a current industry partner.	Large quantity of esterified bio-oil produced and 40 hour heating test completed.	Large quantities of esterified boiler fuel were produced during the research period. 40 total hours of heating time were performed on a modified boiler. Milestone met or exceeded.
A.4	Feedstock and bio-oil characterization with pretreatment		Four agricultural feedstocks were characterized; four forestry and agricultural feedstocks were pretreated by five chemical pretreatments; particle sizes were manipulated to provide tests of 3 feedstock particle sizes ranging from steam exploded to 1-2 mm. All bio-oils produced were chemically and physically characterized.
A.4.DL.1	Characterize two new forestry or agricultural feedstocks; four model forestry and agricultural feedstocks will be pretreated by five chemical pretreatments with chemical and physical tests of the resulting bio-oils; particle size methods will be developed to produce three categories of particle size ranging from steam exploded to 1-2mm.	All feedstocks characterized fully and resulting bio-oils chemically and physically characterized	Four agricultural feed stocks were characterized; four forestry and agricultural feedstocks were pretreated by five chemical pretreatments; particle sizes were manipulated to provide tests of 3 feedstock particle sizes ranging from steam exploded to 1-2 mm. All bio-oils produced were chemically and physically characterized.

A.4.DL.2	Characterize two new forestry or agricultural feedstocks; four model forestry and agricultural feedstocks will be pretreated by the particle reduction techniques developed in year one and the three chemical pretreatments tested will be increased to 10 and particle reduction and chemical pretreatments will be tested to determine influence on bio-oil characteristics. Characteristics measured will be water content, viscosity, viscosity stability over time and temperature, pH and total acid number. Chemical analyses by GPC, GC/MS, HPLC and FTIR will be performed.	All feedstocks characterized fully and resulting bio-oils chemically and physically characterized	Eight agricultural feed stocks were characterized and pretreated with seven chemical pretreatments. All bio-oils produced were chemically and physically characterized. Experimental results allowed identification of two pretreatments that produced superior bio-oil properties. Milestones were met or exceeded.
A.5	Determine petroleum refinery bio-oil characteristics		The upgraded bio-oil characteristics were determined. During the research period MSU met with the management of two refineries; we developed proposals with each of these two refineries to fund the refining of MSU biocrude. Milestones were met or exceeded.
A.5.DL.1	Determine bio-oil characteristics required for refining in current petroleum refineries. Based on the characteristics determined as necessary for refining MSU will develop refined catalysis and feedstock pretreatment plans to attempt to produce these characteristics as closely as possible.	Meet with one or more petroleum refineries.	The biooil characteristics required for refining in current petroleum refineries were determined. During the research period MSU met with the management of two refineries; we developed proposals with each of these two refineries to fund the refining of MSU biocrude. Milestones were met or exceeded.

A.5.DL.2	To provide a supply of bio-oil as closely as possible to refinery specifications. This bio-oil will refined by a test-scale FCC system capable of refining small amounts of crude fuels.	Third party report returned to allow comparison with refinery desired characteristics.	The refineries with whom we cooperated desired an oxygen value as close to zero as possible. MSU produced this biocrude and a detailed hydrocarbon analysis was produced fully describing the 360 hydrocarbons that it contained. This cooperation allowed us to develop two proposals for further development of this technology at refinery pilot scale. Milestones were met or exceeded.
B.	Biocrude		
B.1	Develop wastewater treatment operational strategies to maximize production of biocrude.	Increase lipid production of traditional activated sludge by 50%	Lipid production was increased by 400%
B.1.ML.1	To achieve 60% of the theoretical conversion of the sugars into biocrude. Currently, theoretical conversion of sugars into oils is 35%.		A maximum yield of 6% was obtained using batch mode operation. Simulations using a continuous stirred tank reactor yielded a 25% lipid production.
B.1.ML.2	The production of refined biocrude from lignocellulosic sugars at approximately $3.00/gal. An estimate of the cost of refining biocrude will be determined and included as part of this task.		Assuming a sugar cost of $0.10 per pound (DoE Target) the cost of biocrude was estimated at $2.80 per gallon.
B.2.	Development of an oleaginous microbial consortium for use as a return activated sludge in biocrude production	Accumulate over 40% by weight lipids using the oleginous consortium grown on wastewater	An oleaginous consortium was developed that increased the production of lipids when combined with raw sludge.
B.2.ML.1	To attempt the achievement of 60% conversion of the BOD component of wastewater into cells.		Over 60% of the BOD introduced in the system was consumed by the oleaginous consortium.

B.2.ML.2	The production of biocrude from lignocellulosic sugars at approximately $3.00/gal. An estimate of the cost of refining biocrude will be determined and included as part of this task.		A combination of the oleaginous consortium and raw sludge could meet the target. The oleaginous consortium by it self did not meet the target.
B.3	Produce quality transportation fuels defined by the American Society for Testing Materials Standard.	Meet ASTM standard for fuel production	Biodiesel was produced from wet and dry sludge mixtures.
B.3.DL.1	Evaluate hydro-deoxygenation to remove some heteroatoms.		Cracking of the oil extracts produced hydrocarbons.
B.3.DL.2	Evaluate denitrification to remove some heteroatoms.		Cracking of the oil extracts produced hydrocarbons.
B.4	Design cost efficient biomass and biofuels supply chains		A model was developed for biocrude chain supply economics.
B.4.DL.1	Identify the appropriate model for conducting these analyses.	Model of biocrude costs considering chain supply economics	A model was developed for biocrude chain supply economics. The model is included as part of the report.
B.4.DL.2	Estimate the cost of supply biomass, cost of distributing the fuel and sensitivity of the logistic cost to biomass yield, biomass price, biocrude price and biorefinery size.		See model results.
C.	Lignocellulosic Conversion		
C.1	Determination of sugar conversion kinetics into triglycerides.		The oleaginous microorganisms evaluated achieved the conversion goals set for this task.
C.1.ML.1	To attempt the achievement of 60% conversion of the theoretical lignocellulosic sugars into triglycerides.	To attempt the achievement of 60% conversion of the theoretical lignocellulosic sugars into triglycerides	The process was able to convert greater than 90% of the individual sugars
C.1.ML.2	To attempt the achievement of 75% conversion of the theoretical lignocellulosic sugars into triglycerides.	To attempt the achievement of 75% conversion of the theoretical lignocellulosic sugars into triglycerides	The process was able to convert greater than 75% of the sugars when offered in a mixture

C.2	Isolation and characterization of novel oleaginous microorganisms.		Several isolates were obtained and evaluated from various environments however only one was capable of producing 10% of its dry weight in triglycerides.
C.2.DL.1	To screen ten environmental samples for novel triglyceride accumulating microorganisms.	To screen ten environmental samples for novel triglyceride accumulating microorganisms	Ten isolates from subsurface oil wells were screened for their ability to accumulate triglycerides
C.2.DL.2	To screen ten additional environmental samples for oleaginous microorganisms.	To screen ten additional environmental samples for novel triglyceride accumulating microorganisms	Ten isolates from manure, pond water, and sludge were screened for their ability to accumulate triglycerides
C.3	Evaluation of non-lethal oil extraction technologies		A mutant of Rodococcus opacus was obtained and demonstrated the ability to produce triglycerides and place them in the medium.
C.3.ML.1	To attempt to achieve 15% oil release with 40% survivability of the cells.	To attempt to achieve 15% oil release with 40% survivability of the cells.	With the techniques employed the mutant Rhodococcus opacus released greater than 15% of their oil with greater than 40% surviving cells
C.3.ML.2	To attempt to achieve 30% oil release with 60% survivability of the cells.	To attempt to achieve 30% oil release with 60% survivability of the cells	The Rhodococcus opacus mutant released all other triglyceride into the medium with greater than 60% survivability compared to the wild type
C.4	Evaluation of the cellulase and hemicellulase production ability of these oleaginous microorganisms.		The sequence of Rhodotorula glutinis's has been obtained and will provide information about its ability to produce cellulases and hemicellulases.
C.4.ML.1	Screen six of the oleaginous microorganisms for the ability to accumulate oil and degrade 20wt% of the lignocellulose.	To screen six of the oleaginous microorganisms for the ability to accumulate oil and degrade 20wt% of the lignocellulose	Six oleaginous microorganisms were screened for their ability to consume lignocellulose but were unsuccessful in achieving the 20wt%

C.4.ML.2	To attempt to achieve 30wt% degradation of the lignocellulose while achieving triglycerides production.	To attempt to achieve 30wt% degradation of the lignocellulose while achieving triglycerides production.	Rhodotorula glutinis's genome was sequenced and will be used to determine the presence of important lignocellulosic degrading enzymes. Since the 20wt% was not obtained neither was the 30.
D.	Gasoline derived from synthesis gas		
D.1	Catalyst development		Two syngas to gasoline catalysts were developed. A provisional patent (for 2nd generation catalyst) was filed (61,189,084), a patent disclosure (for 3rd generation catalyst) was prepared.
D.1.ML.1	To attempt to achieve 50% conversion of CO with at least 20% yield of gasoline product.	Achieved milestone to improve liquid yields to 20%	Five metal catalysts were screened for syngas conversion to liquid hydrocarbons. At least three catalysts were successful in achieving the 50% CO conversion rate with 20% selectivity to liquid hydrocarbon.
D.1.ML.2	To attempt to achieve 70% conversion of CO with at least 40% yield of gasoline product.	Did not achieve milestone to improve liquid yields to 40%	The effects of reaction temperature, pressure and syngas flow rate were performed to determine the CO conversion rate and selectivity to liquid hydrocarbon. However, no catalyst was successfully obtained in achieving the 70% CO conversion rate with 40% selectivity.
D.2	ASTM characterization of the gasoline product		GC and GC-MS methods based on ASTM standards were established to characterize the gasoline product.
D.2.ML.1	To attempt to achieve a research octane number of 90.	Achieved milestone to hit octane target of 90	ASTM method was established for hydrocarbon determination. Octane number of 90 hydrocarbon was obtained by the ASTM method.
D.2.ML.2	To attempt to achieve a research octane number of 93.	Achieved milestone to hit octane target of 93	Octane number of 93 hydrocarbon was obtained by selected metal catalyst on syngas conversion.
E.	Biomass Utilization		

E.1	Advanced low temperature combustion experiments with biodiesel and diesel-biodiesel blends	Investigate diesel and biodiesel blends to establish baseline	Baseline with diesel, B20 and B100 established
E.1.ML.1	Measure baseline fuel efficiencies and engine-out Nox, CO and HC emissions with conventional B100 and B20 engine operation.	measure baseline fuel efficiencies and engine-out NOx, CO and HC emissions	Measured fuel conversion efficiencies, Nox, HC, CO and PM emissions
E.1.ML.2	Identify optimal combinations of fuel injection strategies and appropriate intake manifold conditions (temperature and pressure) to achieve low temperature combustion of B100 and B20 blends and measure performance as indicated by mean effective pressures, rate of heat release schedules, fuel conversion efficiences, and emissions (both PM and NOx) approaching US EPA Tier 4 (non-road) standard of 0.4 g/k Wh.	measure performance as indicated by mean effective pressures and rate of heat release schedules and fuel conversion efficiencies, and emissions	Detailed performance parameters were obtained over a range of engine loads and fuel injection timings
E.2	Phenomenological low temperature engine combustion simulation development.		Phenomenological simulation validated for neat diesel and biodiesel combustion
E.2.ML.1	To predict B100 combustion heat release rates and pressure histories accurately and validate the predictions against baseline experimental data obtained in Subtask 1.5 to within 10 percent error.	predict B100 combustion heat release rates and pressure histories accurately and validate the predictions against baseline experimental data	Developed a detailed phenomenological combustion simulation to predict B100 performance
E.2.ML.2	To complete simulation of biodiesel-ignited syngas low temperature combustion, validate predictions with baseline experimental results from Subtask 5.3 to within 10 percent error and determine best operating	validate predictions with baseline experimental results to within 10 percent error	Validated phenomenological combustion simulation against experimental data and quantified uncertainties

	parameters to optimize biodiesel-ignited syngas		
E.3	Evaluation of biodiesel-ignited syngas low temperature combustion	Investigate biodiesel-syngas combustion performance and emissions	Investigated diesel-ignited syngas combustion for performance and emissions
E.3.ML.1	To baseline the performance (fuel efficiency and power density) and engine-out Nox, CO and HC emissions from biodiesel-ignited syngas combustion.	baseline the performance (fuel efficiency and power density) and engine-out NOx, CO and HC emissions	Measured fuel conversion efficiencies, Nox, HC, CO and PM emissions
E.3.ML.2	Achieve optimized combinations of biodiesel-syngas fueling coupled with innovative biodiesel injection strategies to realize low temperature combustion with best tradeoffs between fuel conversion efficiency (up to 40%), power density and Nox emissions (up to 40%), power density and NOx emissions (up to 0.4 g/k Wh).	achieve optimized combinations of biodiesel - syngas fuelling to achieve best tradeoffs between fuel conversion efficiency (up to 40%), power density and NOx emissions (up to 0.4 g/kWh).	Achieved maximum syngas substitution of 32% at low engine loads. Higher substitutions not possible due to poor syngas heating values and excessive engine instabilities
F.	Biomass Feedstock Development	Final Report and all data sets completed for biomass utilization	
F.1	Yield Trials	Data assembled on characteristics and yield of lignocellulosic crops	Limited success of these. Extreme drought compromised establishment of some tests.
F.1.DL.1	Measuring yield response to annual performance of yield as a function of environment and management practices and compiling those measurements into a representative yield estimate of biomass available for conversion to transportation fuel.	Yield trials conducted and analyzed	Perennial deciduous grasses are candidates for low inputs. 50 to 60 lbs of N, 20 lbs of P and 60 lbs of K

F.2	Feedstock engineering	Investigated densification, net energy value for sustainability and spatial distribution of potential energy crops
F.2.DL.1	Quantification of the expected cost of providing three Southeastern-based feedstocks to refinery/biorefinery company gate.	Developed a densified bermudagrass cube through in-field cubing, increased cubing efficiency from 74% to 79% using a binder. Was unable to cube switchgrass and giant miscanthus successfully in the field.
F.2.DL.2	Quantification of the expected cost of providing three additional Southeastern-based feedstocks to refinery/biorefinery company gate.	Net energy value was used to examine sustainability of biomass production. Spatial distribution of energy crops were studied.
G.	Project Management and Reporting	
G.1	Quarterly reports for this project for two years	Quarterly reports were submitted.
G.1.DL.1	Quarterly reports	Quarterly reports were submitted.
G.2.	Final reports for each task	Final report is complete.
G.2.DL.1	Final reports	Final report is complete.
G.3	Develop partnerships with national laboratories, industries and other research groups	A number of partnerships and collaborative relationships were developed that promote SERC technologies.
G.3.DL.1	Provide leadership to each task to develop partnerships with national laboratories, industries and other research groups and report these in quarterly reports.	SERC representatives met with over fifty agencies and organizations to promote collaboration and established over ten Memorandums of Understanding/Non-disclosure Agreements with collaborating agencies.

Sustainable Energy Research Center
Bio-oil Thrust Area Final Report for 2008-2010

A. Principle investigator and co-investigators: Philip H. Steele, Richard Patton, Priscilla Hill, Radha Srinivasan, Leonard Ingram, Charles Pittman, Jr., Keisha Walters, El-Barbary Hassan, Rebecca Toghiani, Hossein Toghiani

B. Summarization of Activities

Subtask A.1 Design, build, and operate a mobile pyrolysis reactor

1. Planned Activities

A.1.ML.1 Year 1 milestone is to design and fabricate a mobile reactor that processes 5kg/hr of biomass with a raw bio-oil yield of approximately 60%.

A.1.ML.2 Year 2 milestone will be to attempt to utilize char and pyrolysis gas to produce up to 50% of required reactor pyrolysis energy.

2. Summarization of Activities

The mobile reactor was designed, built, and installed in a 38-foot-long enclosed trailer. The reactor has been fully tested by numerous pyrolysis tests producing bio-oil from pine wood particles. The reactor provides yields equivalent to our laboratory static reactor (65% from pine wood). However, the production rate is increased to 10 kg/h compared to 7 kg/h for the laboratory static reactor. The reactor is now completed. A prototype char furnace was tested. A temperature of 700 ^{o}C was attained, indicating that sufficient heat can be produced to supply sufficient heat to reduce pyrolysis heat supplied by other sources by more than 50%.

Subtask A.2 Raw bio-oil upgrading

1. Planned Activities

A.2.ML.1 Year 1 milestones are to reduce oxygen content of catalyzed bio-oils; the addition of olefins will reduce bio-oil water content; the addition of reactive alcohols will produce a moderately upgraded bio-oil with reduced water content and increased stability compared to standard alcohols-addition results. Pyrolysis vapor will be filtered to remove char particles from raw bio-oil; some mechanisms responsible for the high instability of bio-oils produced from leaves and barks will be identified.

A.2.ML.2 Year 2 milestones are to reduce oxygen content of catalyzed bio-oils; the addition of olefins will increase solubility of bio-oil organics in a hydrocarbon blend; the addition of reactive alcohols will produce a moderately upgraded bio-oil with reduced acidity and increased stability compared to standard alcohols addition results. Pyrolysis vapor will be filtered to remove char particles from raw bio-oil; the mechanisms responsible for high instability of bio-oils produced from leaves and barks will be identified, and solutions will be proposed or tested.

***2.* Summarization of Activities**

Alcoholation

The use of methanol or other alcohols to prevent the increase in viscosity of bio-oil during aging is well documented in literature published prior to this research. Two of the major objectives of this study were to further investigate the chemical reactions of methanol with selected components of bio-oil and to determine if the fuel quality of bio-oil can be improved

by injecting methanol directly into the pyrolyzer during production. Because aldehydes and alcohols react to form acetals, which leads to the formation of viscous polymers, the reaction of methanol with aldehydes was of primary interest.

One of the problems in using bio-oil for fuel is that the viscosity increases during storage over a period of a few weeks or months. Fluids with high viscosity are difficult to pump through transfer lines and may eventually clog pumps and pipes. Combustion of bio-oil with fuel injectors or spray nozzles is also difficult or impossible with viscous fluids. The addition of methanol is of interest because of the initial decrease in viscosity and contribution to the long-term stability of bio-oil. For this project, hydroxyacetaldehyde (HA) was an aldehyde of intense interest because previously reported concentrations in bio-oil were as high as 10 to 15%. This aldehyde is capable of reacting with itself or other alcohols and aldehydes to form dimers, trimers, and higher molecular compounds. Relative to the capability of methanol to prevent an increase in viscosity during storage, one hypothesis is that methanol reacts with the aldehyde functional group of HA and inhibits polymer formation. The concentration of HA in bio-oil is difficult to measure, so the reaction product of methanol and bio-oil, 2, 2-dimethoxyethanol (DME), was used to determine the extent of the reaction.

The reaction of methanol with organic acids present in bio-oil was also of interest because these reactions can compete with the formation of acetals. In laboratory experiments at 60 ^{o}C, small amounts of strong mineral acids, such as sulfuric and hydrochloric (7×10^{-4} M), catalyzed the reaction of methanol with HA and organic acids. Similar concentrations of p-toluene sulphonic acid and methyl sulphonic acid also exhibited catalytic properties. Weaker acids, such as phosphoric and the organic acids already present in bio-oil, had little or no effect on the reaction rates. When bio-oil was filtered prior to these experiments, the formation of DME was not observed unless a strong mineral or organic acid was used as the catalyst. The chemical and physical properties of bio-oil treated with 0, 5, 10, and 20%methanol were studied in great detail. With the 90 ^{o}C accelerated aging test, bio-oil viscosity was not improved with the 0 and 5%methanol treatments. With the addition of 10 and 20%treatments of methanol, the viscosity was unchanged after three days but increased slightly over the entire five-day test period. These results suggest that a threshold quantity of about 5%methanol may be required to produce stabilization effects during long-term storage of bio-oil.

One possible explanation for this observation is that some of the mono-functional organic acids in bio-oil may react more readily with methanol than the poly-functional compounds. This reaction would result in chain termination or the prevention of dimer and trimer formation that could lead to the formation of high-molecular-weight viscous compounds.

In the second part of this project, methanol was injected directly into the pyrolysis reactor in five different concentrations relative to the amount of bio-oil produced from southern pine. Approximately 100 ml of bio-oil was produced in these experiments. A high-pressure liquid chromatograph (HPLC) pump coupled to an automotive type fuel injector was calibrated to deliver the required weight of methanol based on the production rate of bio-oil. The chemical and physical properties of bio-oil produced during the injection methanol without a catalyst and methanol with sulfuric acid catalyst were determined. Viscosity measurements from accelerated aging tests at 90 ^{o}C for five days indicated that injection rates of 3-4%concentrations of methanol prevented a significant increase in bio-oil viscosity. The use of a sulfuric-acid catalyst may have had little effect on the aging characteristics.

In the third phase of this project, three different treatments of bio-oil were produced for test burning in a small waste-oil burner. Southern pine was pyrolyzed to produce approximately 3 l of bio-oil with the following treatments applied during pyrolysis: (1) Injection of 5.6%methanol with no catalyst, (2) Injection of 5.6%methanol with sulfuric acid catalyst, and (3) no methanol treatment. Observation of the flame from the bio-oil burner indicated that the bio-oil that had been treated with methanol was more completely combusted than the untreated material. The detailed chemical and physical analysis of these samples also indicated that the methanol-treated bio-oil was more suitable for use as fuel than the un-treated samples.

Bio-oil Hydroprocessing to Hydrocarbons

MSU has developed a proprietary two-stage catalyst with 100% hydrocarbon characteristics that will be reported here. Current results are for mostly batch-reactor experiments with some data available from continuous packed-bed reactor experiments. Hydrodeoxygenation was performed on raw bio-oil produced from both pine wood and giant miscanthus feedstocks. Raw bio-oil was produced in an auger reactor utilizing feedstock particles of 1-3 mm diameter. These were fast pyrolyzed at approximately 500 ^{o}C. Yield for pine and giant miscanthus feedstocks were 65 and 60% dry-weight basis, respectively. The raw bio-oil was stored at 4 ^{o}C immediately after production and maintained at this temperature until hydroprocessing experiments were performed. Physical properties of pH, water content, acid value, density, viscosity, and higher heating value (HHV) were measured. Percent water was determined by ASTM Method D-1744. Viscosity was determined with a Stony Brook Model PDVa-100 viscometer at 50 ^{o}C. Acid value was obtained by dissolving 1 g of bio-oil in an isopropanol/water mixture and titrating to a pH of 8.5 with 0.1 N KOH. The pH was determined indirectly by adding one gram of bio-oil to 50 ml of water, stirring, and measuring the pH with an Orion Model EA920 pH meter. The density of bio-oil was determined at 20 ^{o}C. The calorific value was measured as higher heating value (HHV) by an Ika-5000 bomb calorimeter. Elemental analyses of raw bio-oil were determined by using a CE-440 elemental analyzer. FTIR spectra of raw bio-oil and hydrocarbons were determined with a Varian 3100 FTIR analyzer with standard KBR disc technique. Upgraded HDO bio-oil was characterized by gas chromatography coupled with mass spectrometry (GC/MS) to identify individual chemical compounds. Two-stage catalytic hydroprocessing was performed with MSU proprietary catalysts with a first-stage hydrotreating step followed by a more severe second-stage hydrocracking step. All hydrogenation tests were performed in a high-pressure autoclave in batch mode or in a packed-bed reactor developed at MSU. Our preliminary research with these catalysts investigated temperatures between 200 and 500 ^{o}C at 5-25 MPa of hydrogen pressure. Tables A.2.1 and A.2.2 summarize the characteristics of the GM raw bio-oil prior to the hydrogenation application. The raw giant miscanthus bio-oil contained 55.8% oxygen; viscosity was 7.15 cSt. Bio-oil acid value was 113 mg KOH/g with pH of 2.75 Bio-oil HHV was approximately 12 MJ/kg. The raw pine bio-oil contained 43.5%; viscosity was 53 cSt with density of 1.15 g/ml. Bio-oil pH was 2.3, and acid value was 94. Bio-oil HHV measured was 17.0.

For both pine and giant miscanthus bio-oils, the hydrocracked product produced from the application of the two-stage catalytic processing of the raw bio-oil was a light yellowish hydrocarbon mix. A minor amount of char residue, considered to be uncatalyzed carbon, was contained in this product but was easily removed by brief centrifugation. No water was detected in this final hydrocracked product. The properties of the final hydrocracked giant miscanthus product had an oxygen content of 0.3%; viscosity decreased to 2.65, very close to that of petroleum diesel (2.60). The pH of the hydrocarbon was a nearly-neutral 6.5, which is confirmed by the very low total acid number of less than 0.1. The properties of the

final hydrocracked product from the pine bio-oil had an oxygen content less than 0.1%; viscosity decreased to 2.6, very close to that of petroleum diesel. Density was 0.77, about midway between the values for petroleum gasoline and diesel. The pH of the hydrocarbon was a nearly-neutral 6.5, which is confirmed by the very low total acid number of less than 0.1. A detailed hydrocarbon analysis showed that, as expected, the raw bio-oil chemical composition differs a great deal from that of the hydrocarbon mix produced by our final hydrocracking treatment. In raw bio-oil, phenols and phenolic derivatives are major oxygenated compounds. In the hydrocracked bio-oil, olefinic compounds, oxygenated compounds, phenolic compounds, carbohydrates, and their derivatives that were present in raw bio-oil converted to hydrocarbons.

Table A.2.1. Physical and chemical properties of raw giant miscanthus and upgraded bio-oil.

Property	GM raw bio-oil	Upgraded bio-oil
Oxygen (wt%)	55.8	<0.3
Viscosity (cSt) at 40 ^{o}C	7.15	2.65
pH	2.75	6.5
Acid value (mg KOH/g)	113	~0.1
Water content (wt%)	35.7	0.0
HHV (MJ/kg)	~12	44.6

Table A.2.2. Physical and chemical properties of raw pine wood and upgraded bio-oil.

Property	Raw	Upgraded
Oxygen	43.5	<0.1
Viscosity	53.0	2.6
Density	1.15	0.7
pH	2.3	6.5
Acid	94	~0.1
Water	23.5	0.0
HHV	17.0	45.4

A simulated distillation GC analysis was performed on the same pine hydrocarbon mixture analyzed for the detailed hydrocarbon analysis. This analysis showed that the distilled fuel weights corresponding to petroleum fuels were gasoline 37%, jet fuel 27%, diesel 25%, and heavy fuel oil 11%. Therefore, the results of our two-stage hydroprocessing experiments with MSU catalysts indicate that both pine and giant miscanthus raw bio-oils can be hydroprocessed to produce a hydrocarbon mixture containing numerous hydrocarbon types. The hydrocarbon products described should be able to be refined in current petroleum refineries with minimal infrastructure modifications. In addition, that sharp cuts of this hydrocarbon mix will allow production of fuels nearly identical to petroleum diesel, gasoline, and jet fuel such that these biomass-based fuels can be easily blended with petroleum fuels appears very feasible.

Bio-oil Aging Study

Cottonwood and pine biomass, bio-oil, and char were characterized and compared for similarities and differences between bio-oil properties. Biomass and char samples were analyzed by elemental analysis and DRIFTS. Bio-oil pH, density, water content, viscosity, and ATR-FTIR spectra were all collected and compared. Differences in pH, density, and viscosity were observed when comparing the neat pine and cottonwood bio-oils produced from various parts of the tree (clear wood, bark needles, and leaves). In addition, when

comparing total bio-oil, fractionated bio-oil, and water condensate of pine and cottonwood, the results suggested the incorporation of forestry residue (bark and/or leaves/needles) moderately affects the composition and properties of the bio-oil, as discussed in the following sections.

The elemental analysis of the cottonwood biomass showed that there was nitrogen present in all of the samples, with higher carbon and lower oxygen contents seen for clear wood and whole tree biomass when compared to bark and leaves if remainder of percentage (R) is assumed to be oxygen. Neat pine bark fractioned [PBF] and cottonwood clear wood fractionated [CCWF] bio-oil underwent a serial filtration by vacuum filtration [20-25 μm] followed by centrifugal filtration [0.2 μm]. Neat pine clear wood total [PCWT] and fractionated [PCWF] bio-oils also underwent a serial filtration by vacuum filtration [20-25 μm] followed by a second vacuum filtration [2.5 μm] and concluded with a centrifugal filtration [0.2 μm]. Unfiltered and filtered bio-oils were then aged at 80 °C for 6, 12, 24, 168, 336, and 504 hours. Unfiltered and filtered sample characterizations included pH, water content, and viscosity measurements, and attenuated total reflectance Fourier transform infrared (ATR-FTIR) spectroscopy, gel permeation chromatography (GPC), and coupled gas chromatography-mass spectroscopy (GC/MS) were utilized to identify and monitor chemical composition. Neat PWTF bio-oil samples flowed with visually low viscosity and little to no bottom phase present. The unfiltered samples separated into two phases at 50 vol% split bottoms at 168 h and 90 vol% bottoms after 336 h. At 504 h, there was a combined phase. The filtered samples remained one phase even after 504 h of aging, indicating the bio-oil bottoms phase was filtered from the samples or filtration prevented any reactions that originally increased viscosity for the bottoms phase. Water-content data showed an initial decrease in unfiltered samples and then a steady increase after 168 h of aging. Filtered samples possessed larger water contents at 168 and 336 h, but the 504 h data was not obtained due to the samples' insolubility in the titration solvent. Filtration may have removed material that resulted in an increase in water weight percent. The pH values for the filtered and unfiltered bio-oils showed very little difference until 504 h of aging, when the unfiltered samples had a slightly higher pH (2.47 versus 2.3). Average pH of the PWTF bio-oil decreased slightly from 2.75 to 2.3 over the 504 h of aging. All the filtered samples showed similar increases in water content to those of unfiltered samples. This suggests that the filtration did not slow/stop water formation and may have encouraged it.

PBF, PCWT, PCWF and CCWF all exhibited unexpected increases in viscosity likely due to decreased water content as the result of water retention by the filter. PBF viscosity decreased after filtration by 23% (corresponding to the 12% decrease in water content) post filtration. Between 336 and 504 h, phase separation occurred in both unfiltered and filtered samples resulting in 30-50 vol% bottom phase, subsequently decreasing the viscosities by 64 and 75%, respectively. After 504 h, both unfiltered and filtered PCWT decreased in viscosity significantly, a result of phase separation where the top and bottom phases were approximately 50/50 v/v. When comparing neat PCWF to PCWT, the fractionated oil has a 370% larger viscosity and 67% lower water content. Both unfiltered and filtered PCWF viscosities increased during aging, resulting in increases of 800 and 481%, respectively, after 504 h. After 504 h, CCWF viscosities for unfiltered and filtered oil increased by 153 and 423%, respectively. All molecular weights increased, during aging in both unfiltered and filtered samples for all four bio-oils with filtration not having a significant effect. Samples that phase separated experienced an increase in molecular weights in the bottom phase while the top phase molecular weight returned to the original molecular weight. The PBF samples had the largest molecular weights and the largest increase after 504 h of aging. FTR spectra comparison showed no significant changes during aging. Filtered and unfiltered samples

resembled one another, indicating that filtration did not change anything in the bio-oil. Peak height ratios (PHRs) showed that the samples follow the same trends as exhibited in the phase separation study. Decreases in primary alcohol peaks and increases in C=O bonds or aromatic ring peaks. As for previous results, filtration seemed to change the aging reactions. Cottonwood whole tree total [CWTT] and cottonwood bark total [CBT] bio-oil samples were used to investigate the rheological effects of solids added to bio-oil. Particles added included ground char produced along with the bio-oils, white quartz sand, fumed silica, and silica packing. All particles were added to 10 ml of bio-oil to obtain 3.5, 1.75, and 0.875 vol% samples. Rheological data was then collected for forward and reverse stepped shear experiments over the range 0.1 to 1000 1/s. Both neat and altered bio-oil samples displayed positive and negative viscosity hysteresis effects, which were most noticeable in the CWTT bio-oil samples. Particle size distribution analysis revealed all samples were similar with particle shapes pointing towards a spherical configuration. There was not a large change in particle diameters, for even the char was crushed with a pestle and mortar before being added. There was little to no difference in the ATR spectral comparison between the neat and solids-added bio-oil samples except for the CBT-silica packing samples where the primary alcohol peak showed a small difference. Therefore, it was determined that no chemical changes occurred in the samples due to the particle addition and so should not impact the aging process in terms of chemical compositional changes.

Neat pine and cottonwood bio-oils produced from clear wood, whole tree, bark, and needles/leaves were examined before and after accelerated aging at 80 °C for 24 h and 504 h. Minitab software was used with a 2^k factorial statistical method to examine the effects of tree type, forestry residue (bark needles and/or leaves), oil type, and aging time on bio-oil properties such as pH, water content, viscosity and molecular weight. P values were used to evaluate the importance of each factor using an alpha = 0.05 (95% confidence). For phase-separated samples, the extremes of property values were used, water content from the top and molecular weight from the bottom samples. The control samples indicated that tree type has a significant impact on pH and forestry residue influenced the water content the most, but the interaction of the two are not that important. Whether the oil is fractionated or total, sample impacts water content and molecular weight significantly and the oil containing the water condensate affects all four properties with the largest impact on viscosity and initial molecular weight. Aged samples showed slightly different results, with tree type having significant effect on pH, water content, and molecular weight. Forestry residue no longer had any effect on water content, but did affect pH results. Aging for 24 h affected all four properties, with the largest effect on molecular weight. After 504 h of aging, the viscosity was the most affected factor and the water content is no longer affected. This suggests that water condensation reactions occur in the shorter aging times, while the polycondensation reactions occur in the longer aging times, making viscosity not as important until around 504 h of aging. It was determined that forestry residue present in biomass prior to pyrolysis affects the water content of un-aged bio-oil. In addition, the tree type (cottonwood or pine) had no impact on the pyrolysis properties, and the bio-oil collection method (total vs. fractionated oil) played a larger role. Total oil, fractionated oil plus water condensate, affects all of the properties examined and had the largest impact on viscosity and initial molecular weight. After 24 h of accelerated aging, a correlation was only found with increased molecular weight while 504 h of aging correlated to changes in pH, water content, viscosity, and molecular weight. FTIR analysis indicated that leaf and bark biomass contains more aromatic compounds than clear wood and whole tree biomass while char contains more aromatic, alcohol, ether, and/or ester-containing compounds.

When comparing neat bio-oils produced from pine and cottonwood, there were differences in the pH, density, and viscosity depending on the part(s) of the tree used. Preliminary comparisons of (i) pine and cottonwood feed stocks and (ii) total bio-oil, fractionated bio-oil, and water condensate suggest that the incorporation of bark and/or leaves/needles alters the chemical composition and properties of the bio-oil and could lead to large differences between these materials during aging. Tests indicated that the presence of forestry residue (bark needles and/or leaves) in the biomass affects the water content of unaged bio-oil while the tree species, at least for cottonwood and pine, had no impact. Bio-oil collection (total, fractionated, water condensate) was shown to play a large role where the total oil containing the water condensate affects all of the properties with the largest impact on viscosity and initial molecular weight. During aging, both unfiltered and filtered samples increased in viscosity with the filtered samples having larger viscosities than the unfiltered samples throughout aging. In addition, once PCWT and PBF phase separated, the viscosity decreased drastically due to the introduction of two separate layers with very different properties. Molecular weight also increased during aging in all samples and in phase separated samples: the bottom phase had larger molecular weights—that continued to increase during aging—and the top phase molecular weight decreased to reach the initial molecular weight of the sample. Etherification during aging was determined by GC-MS and FTIR in the PWTF bio-oil. Both aromatic ethers and phenolic compounds were formed in both the filtered and unfiltered bio-oil samples.

In the second filtration study, ATR-FTIR peak-height ratios showed a general trend in the reactions occurring in PCWT, PCWF, PBF, and CCWF oils during aging where all exhibited decreases in primary or secondary alcohols and/or ethers in addition to an increase in aromatics and ketones or carboxylic acids. GC/MS analysis showed that filtration does alter the aging reactions by moderating in composition within PBF, PCWF, and PCWT, but not CCWF. This suggests that the removal of the solids (along with the material coating the solids) may prevent one reaction but also could allow for other reactions to proceed. Addition of particles to cottonwood whole tree total (CWTT) and cottonwood bark total (CBT) bio-oils along with rheological studies demonstrated that char addition will elevate viscosities prior to aging, but not to the extent that is observed in aging. In addition, bio-oil displayed positive and negative viscosity hysteresis effects that were most noticeable in the CWTT bio-oil samples. Given the collected data hysteresis did not appear to be dependent on particle size in the bio-oils investigated, and the viscosity increases observed in aging studies cannot be due merely to the presence or formation of solids particles.

Supercritical Fluids Upgrading

Conversion of both pine wood particles (1-3 mm) and raw bio-oil to liquid products by supercritical alcohol treatment was performed. Eight types of alcohols were utilized: methanol, ethanol,1-propanol, 2-propanol, 1-butanol, 2-butanol, 2-methyl-2-propanol, and 1-methyl-2-propanol. 10 wt% Co-Mo/H^+ZMS-5 and 10 wt% Co-Mo/MgO catalysts were tested to catalyze the supercritical alcohol reaction with pine chips and bio-oil. All supercritical reactions were performed in a high temperature and pressure autoclave. In each experiment, pine particles or raw bio-oil were charged to the reactor, accompanied either 5 wt% of catalyst or without catalyst. Following oxygen purging, alcohols were then introduced into the reactor and heated to an operating temperature, which was established as $1.1T_c$ of the alcohol under study. Heating was accomplished with 80% heater power at a ramp rate of about 4-5 °C/min. Once the operating temperature was achieved, the power was adjusted to hold the reactor at the operating temperature for a specific period (30 min in most experimental trials). The self-generated pressure in the reactor was controlled at the desired operating pressure by adjusting the amounts of bio-oil and alcohol charged to the reactor. After the specified reaction time, the autoclave was cooled to ambient temperature and gases produced during the reaction were vented into a Tedlar bag through the gas sample valve. The liquid and solid products were collected after the sealed reactor was opened. The liquid product was separated from the solid residue by filtration and analyzed by elemental and GC/MS. In general, increased chain length in the alcohol for C_2+ alcohols was associated with increases in both carbon and hydrogen content of the produced liquid as compared to pinewood chips. The increased hydrogen and carbon content, and reduced oxygen content indicated that co-processing of wood chips with C_2+ alcohols has the potential to produce a liquid fuel. Acid values were determined for these liquid products. The acid value of crude bio-oil was reported as 94.9 mg KOH/g. For the liquid products produced by the coprocessing of alcohols and wood chips, acid values ranged from 3.97 to 10.3. These values are much lower than that for crude bio-oil. The water content for the liquid products produced by the supercritical alcohol reactions were much lower than for crude bio-oil (38.5%) and ranged from 14.5 to 26.5%.

Four alcohols with branched chain structures (2-propanol, 2-butanol, isobutanol, and *tert*-butanol) were examined in their supercritical states for processing wood chips. Processing pine wood chips with supercritical *tert*-butanol did not yield a liquid product. Two Co-Mo catalysts, acidic Cata8 and basic Cata9, were examined for processing wood chips with supercritical alcohols. The use of the acidic catalyst resulted in the formation of only solid and gaseous products for all alcohols employed except methanol. The use of the basic catalyst gave rise to the formation of a liquid product for all of the straight chain alcohols, as well as three of the four branched alcohols examined (exception being *tert*-butanol). No definitive trends relating alcohol structure with liquid product characteristics were identified. The application of supercritical alcohols to upgrade raw bio-oil produced liquids that were tested by elemental analysis as a first screening test. The elemental analysis results indicated that the supercritical alcohol treatments did not improve the bio-oil properties. This was the result regardless of the utilization of catalyst to accelerate the reaction. The use of catalyst had no significant impact on the elemental composition distribution for any of the alcohols examined for either the pine particle or bio-oil supercritical treatments. Supercritical treatment of biomass with C_2+ alcohols appears promising. In general, increased chain length in the alcohol for C_2+ alcohols was associated with increases in both carbon and hydrogen content of the produced liquid as compared to pine wood chips. The increased hydrogen and carbon content and reduced oxygen content indicate that co-processing of wood chips with C_2+ alcohols has the potential to product a liquid fuel. However, use of supercritical alcohols to upgrade crude bio-oil was not successful.

Vapor Catalysis

The objective of the proposed research was to upgrade pyrolysis vapors to hydrocarbon-rich products by catalytic cracking. The project was organized as a series of tasks beginning with the installation of a three-zone fixed-bed catalytic reactor on the top of the auger reactor so that the pyrolysis vapors from the auger reactor exit pass through the catalyst bed. An initial set of experiments was performed to screen catalysts to check their efficacy in upgrading pyrolysis vapors. Then, selecting catalyst with best performance from the catalyst screening step, the effect of process variables (catalyst bed temperature and catalyst to feed ratio) on product distribution of upgraded bio-oil was studied. Finally, physical and chemical analysis of the upgraded bio-oil was conducted. Physical analysis experiments included determination of stability (viscosity), water content, and pH of the bio-oils produced. Analysis by GC/MS was conducted . Fresh, spent, and regenerated catalysts were characterized using BET and XRD.

Vapor-phase batch-reactor studies were undertaken to provide rapid catalyst screening under controlled operating conditions. A Parr batch reactor was employed. Catalytic HDO reactions of four model bio-oil components were conducted as a function of catalyst composition, temperature, pressure, and time elucidated the conversion and product distribution for each model compound. 2-Furaldehyde (aldehyde), anisole (phenol), cyclopentanone (ketone), and acetic acid (carboxylic acid) were selected as the model compounds. Catalysts employed were MCM-41 800 m^2/g, Co/Mo 117 m^2/g, H-ZSM-5 354 m^2/g, Mg-Al Layered Double Hydroxides (LDH) 135.53 m^2/g, Ni-ZSM-5, Ni-Mo 171.47 m^2/g,Pd/Al_2O_3. A bio-oil stimulant was employed in early experiments; it consisted of a mixture of methanol (5%), acetaldehyde (12%), acetic acid (14%), glyoxal (4%), acetol (8%), glucose (8%), guaiacol (17%), furfural (4%), vanillin (8%), and water (20%), all by weight. The pH of the oil was approximately 2.3. Extensive coking of the catalyst and formation of char was observed in all the catalytic upgrading experiments using bio-oil simulant A [BS^a]. Furfural gave rise to maximum catalyst coking and also to the formation of char at the bottom of the reactor. A second bio-oil simulant B [BS^b] was prepared without furfural. Furfural was replaced by methanol. All experiments were carried out for 60 min. Batch phase catalytic HDO reactions using raw bio-oil as the substrate were conducted using hydrotreating catalysts (Pd/Al_2O_3, $Co\text{-}Mo/Al_2O_3$, $Ni\text{-}Mo/Al_2O_3$) as a function of initial hydrogen partial pressure and hydrogen donor solvent. Three hydrogen donor solvents (tetralin, cyclohexane, ethyl acetate) were examined with and without hydrogen at a raw bio-oil/solvent ratio of 1 to 3.

Flow reactor studies were conducted to achieve significantly shorter residence times. Initial work employing 100% bio-oil were not encouraging with either HDO catalysts or cracking catalysts. Catalytic studies co-feeding ethanol or methanol were also conducted. An auger reactor of 7.6 cm in diameter and 102 cm in length was employed for the purpose of producing bio-oil vapor. The distance between the screws (i.e., between the augers) is about 3 in. The auger speed was 11-12 RPM at the desired auger pyrolysis temperature. The particle size of the pine sawdust used in the pyrolysis was 1-2 mm. The gases produced from biomass pyrolysis pass through a 1-in. diameter, 24-in.-long packed bed mounted on the top of the auger reactor. This packed-bed reactor was enclosed in a three-zone furnace to keep the catalyst at the desired temperature. Bio-oil vapor flow was also facilitated by the N_2 gas flow controlled by a mass flow controller. Usually, the N_2 gas flow was restricted to 1-2 L/min. The effluent pyrolytic vapors from the PBR were condensed by passing them through a 5-ft-long stainless-steel tube (.5 in. I.D) enclosed by a jacket of coolant (50% ethylene glycol solution maintained at -8 °C) before reaching a set of five

impingers kept in the constant-temperature bath having coolant maintained at -8 °C. To maximize bio-oil vapor condensation, a two-mouthed round-bottom flask was used as the fifth impinger, where one mouth (exit) was attached to two long condensers connected in series (to provide more surface area for heat transfer). This condensation set-up aided in effective trapping of bio-oil vapors produced in the experiments carried out at low biomass feed rates. Moreover, ethyl acetate, methanol, and acetone were used as solvents in second, third, and fourth impingers for improved trapping of pyrolysis vapors as well as fractionation of bio-oil vapor. Char is formed as a solid by-product. The bio-oil vapors passed through a layer of ceramic filter (25 g) to remove the very fine char before passing through the catalyst. Then, each layer of catalyst (10 g) was followed by a layer of ceramic filter (10 g) until the desired amount of the total catalyst was loaded in the packed bed reactor. This dilution of the catalyst with the ceramic filter material helped to mitigate issues with reactor plugging. The ceramic filter also acted as a support screen to prevent the catalyst bed from falling into the auger reactor pipe.

As the first task of this project, we performed experiments to determine the optimum temperature to perform fast pyrolysis of pine sawdust to produce maximum bio-oil yield. Experiments were performed at temperatures of 400, 450, and 500 °C. Maximum yield was obtained for a temperature of 450 °C. Cracking of pyrolysis vapors and the removal of oxygen in the form of carbon oxides, especially CO_2, is required to produce a pyrolysis oil rich in hydrocarbons. Rejection of oxygen in the form of CO or H_2O uses more carbon or hydrogen to eliminate oxygen. Zeolite catalysts, especially HZSM-5 catalysts, were shown to be an active cracking catalyst in deoxygenation of pyrolysis vapors, but coking was reported to be a major setback. The Si/Al support used in the present study was expected to increase catalyst life by filtering the char from the pyrolysis vapors. The preliminary experimental set using a range of catalysts including Si/Al, γ-alumina, HZSM-5, Zeolite-Y (HY) was concluded, and HZSM-5 was found be the best catalyst in obtaining hydrocarbons. Later experiments tested the efficacy of iron-supported catalysts, Fe-ZSM5 and Fe-HY. The effect of catalyst-bed temperature and catalyst to feed ratios on the chemical composition of pyrolysis product oil is the subject of extensive literature. High catalyst bed temperatures favor gaseous to liquid products, but marginally hinder catalyst coking. With HZSM catalyst, a moderate to high catalyst-to-feed (C/F) ratio is required to obtain liquid hydrocarbons by cracking pyrolysis vapors. Although high C/F ratios favor the formation of more water and gaseous yields, a liquid product with less oxygenates and rich in hydrocarbons can be obtained. The C/F ratio is dependent on the catalyst composition; therefore, the optimum may vary from one catalyst to the other. The catalysts that performed best from catalytic screening tests were investigated further at various catalyst bed temperatures (400-600 °C) and C/F ratios. For each catalyst, the optimum process variables to be used in obtaining a high-quality liquid product from cracking pyrolysis vapors were determined. The catalytically treated pyrolysis oils were chemically characterized using GC/MS techniques and gel permeation chromatography (GPC). GC/MS was used to identify the chemical composition of upgraded oils whereas GPC was used to obtain general molecular weight information of chemical species present in upgraded pyrolysis oil.

Other tests conducted included physical characterization of deoxygenated pyrolysis oils, including elemental analysis, acid value, water content analysis and viscosity tests. These results were compared to the physical and chemical characteristics of untreated pyrolysis oil. HZSM-5 resulted in a significant decrease in the amount of carbonyl and acidic functional groups in the treated bio-oil but also showed significant cracking of biomass compounds, resulting in the formation of hydrocarbons including toluene, xylene, and indene as well as higher MW compounds including 2-methyl naphthalene and naphthalene. More

phenols were present in the HZSM-5 upgraded liquid product. Cracking of guaiacols, vanillins, and acetovanillones was the predominant reaction set that occurred during *in situ* catalytic upgrading of pyrolytic vapor over the HZSM-5 catalyst. Qualitative data indicated the formation of non-oxygenated aromatics, such as toluene, with much lower amounts of xylenes, phenolics, and catechols. The following conclusions can be drawn from the catalyst screening experiments: 1) Partial deoxygenation of bio-oil was achieved by *in situ* catalytic upgrading of bio-oil vapor over different catalysts through dehydration (main route), decarboxylation, and decarbonylation reactions. 2) Catalytic upgrading of bio-oil vapor over HZSM-5 resulted in a very small conversion of lighter organics to non-oxygenated aromatics, such as toluene and xylene, and substituted benzenes, such as 1-propynyl benzene,1-ethynyl-4-methyl benzene, and indene. The formation of such aromatics is believed to be through a carbenium ion mechanism, i.e. by oligomerization of cracked fragments, alkylation, ismomerization, cyclization, followed by aromatization. 3) γ-Alumina showed a decrease in the carbonyls through decarbonylation (main route) and decarboxylation. γ-alumina upgrading of pyrolytic oil did not show any formation of hydrocarbons. On γ-alumina, catechols were not significantly cracked to phenolics, but some catechol to phenol conversion occurred over HZSM-5. These resultsindicate that HZSM-5 is a better cracking catalyst than γ-alumina. 4) Carbonyl groups (aldehydes, ketones) are one of the very reactive functional groups present in the bio-oil. A decrease in the carbonyl functional group in the product bio-oil occurred over γ-Alumina. The broad conclusion from these studies is that HZSM-5 was the best performing catalyst. In catalytic upgrading experiments, as shown in Figure A.2.1, a decrease in liquid product and an increase in gas products were observed with increasing catalyst bed temperature. At higher temperatures, cracking of larger molecules, condensation reactions, and cleavage of side chains are expected to occur on acid catalysts. This is also evident from the water-content analysis. With respect to acid catalysts, the presence of Bronsted acid sites results in the formation of more water due to hydrolysis and condensation processes. Thermal cracking may also contribute to the formation of water and gaseous products. As upgrading proceeds and more gasification and deoxygenation occurs, we expect more water to form. Formation of more water is an indication of bio-oil deoxygenation.

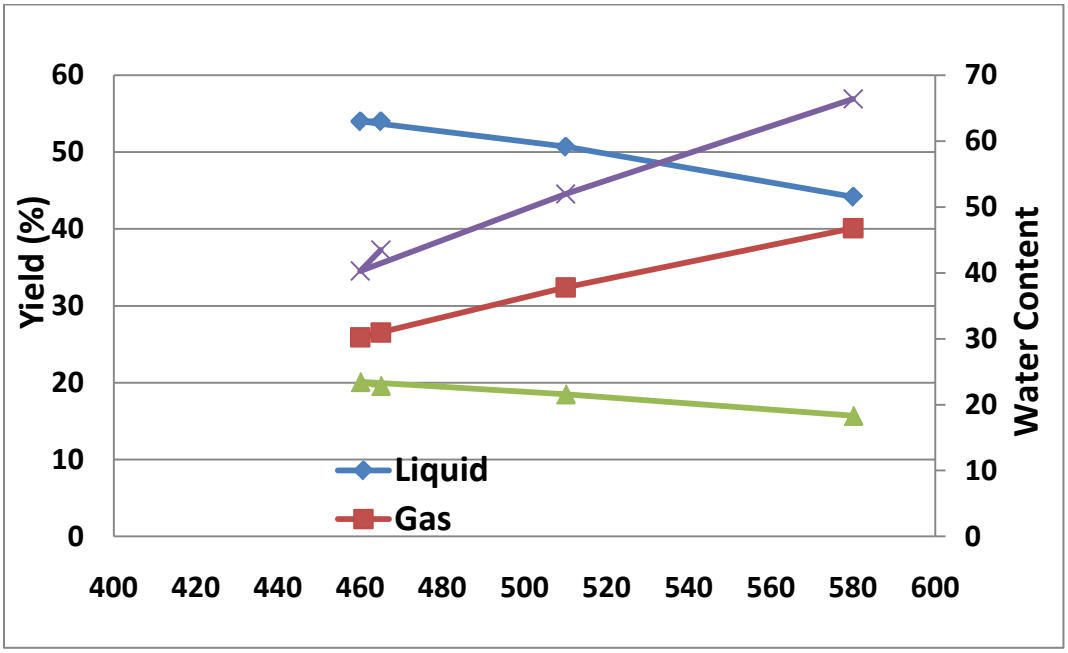


Figure A.2.1. Product distribution vs. catalyst bed temperature in HZSM-5 upgrading experiments.

The formation of carbonyls increased at higher catalyst bed temperatures due to the greater conversion of anhydrosugars to carbonyl family compounds (furfural, furfuryl alcohol, substituted furfural compounds, and substituted cyclopentenones). Higher catalyst temperatures also favored the conversion of guaiacols and eugenols to catechols and phenols. Phenols were reported earlier to be the primary reaction product in cracking of pyrolytic oil over acidic HZSM-5 catalyst, but the present results were found to differ, where diols (catechols and resorcinol) were found to be predominant compared to phenols. This may be due to the rapid coking of catalyst reaction sites from anhydrosugars and carbonyl family, predominantly at higher temperatures (especially 580 °C), thereby inhibiting further cracking of catechols to phenols and benzene. Cracking of guaiacols, vanillins, and acetovanillones is the predominant reaction set that resulted in the formation of catechols that occurred during *in situ* upgrading of pyrolytic vapor using HZSM-5. Moderate cracking of biomass-derived compounds was observed during in-situ catalytic upgrading of bio-oil vapor, resulting in dehydration (formation of more water), decarboxylation, and decarbonylation reactions (increase in noncondensable gas yields), which indicates the deoxygenation of bio-oil. The chemical composition of the liquid product in the experiment using regenerated HZSM-5 at 450 °C showed close resemblance to the fresh HZSM-5-treated liquid product; the product distribution as well remained almost the same. The fresh catalyst showed a slightly better activity than regenerated catalyst. This indicates sufficient regeneration of the catalyst. GC/MS analysis was performed on the liquid product obtained from thermal treatment of pyrolysis vapor (blank runs) as well as *in situ* catalytic upgrading experiments, yielding both quantitative and qualitative information. Phenols were earlier reported to be the primary reaction product in the cracking of pyrolytic oil over acidic HZSM-5 catalyst, but the present results were found to contrast, with diols (catechols and resorcinol) found to be predominant over phenols. This may be due to rapid coking of catalyst reaction sites from anhydrosugars and carbonyl family, predominantly at higher temperatures, thereby inhibiting further cracking of catechols to phenols and benzene.

Previous experiments showed that the cracking of guaiacols, vanillins, and acetovanillones was the predominant reaction set that resulted in the formation of catechols. Moderate cracking of biomass derived compounds was observed during thermal treatment (blank runs) of bio-oil vapor, resulting in dehydration (formation of more water) and non-oxygenated aromatic hydrocarbons, such astoluenes and xylenes. Thermal and catalytic deoxygenation occurred primarily due to decarboxylation and decarbonylation reactions (increase in noncondensable gas yields), which indicated the deoxygenation of bio-oil. GC-MS peak area percentages of the non-oxygenated compounds present in the oils show that the chemical composition of the bio-oils significantly changed when the pyrolysis vapors were upgraded over different zeolites. The concentration of undesirable bio-oil compounds (furans, levoglucosan type sugars, etc.) decreased for both zeolites compared to the non-catalytic pyrolysis experiments. Also, zeolites facilitated the formation of a significant amount of gasoline-range non-oxygenated hydrocarbons. The gasoline compounds consisted entirely of alkylated benzenes. The composition of gasoline-range aromatic hydrocarbons formed in the present catalytic experimental set matches closely with the results reported by previous researchers. In the catalytic pyrolysis experiments, HZSM-5 showed better performance than the ZY catalyst, but at the expense of liquid product yield. The strong Bronsted acidity of HZSM-5 is responsible for its higher cracking efficiency. Coking of the catalysts occurred, and the rate of coking was observed to be similar in both zeolites cases.

Bio-oil Olefination

A novel means of olefinating bio-oil to improve fuel properties was tested. A GC/MS analysis of the olefinated/esterified product of the current example identifies 17 esters. These 17 esters comprised more than 22% of the total area % described in the GC/MS results. Phenolic compounds present in the original raw bio-oil, such as phenol, 2-methylphenol, 2-methoxyphenol, 2-methoxy-4-methyl phenol, etc. are also present. A comparison of the properties of the olefinated bio-oil product is compared to raw bio-oil in Table A.2.3. The water content of raw bio-oil was 28.6 compared to only 6.0 for olefinated bio-oil. This low water content results largely from the conversion of water to esters by the reaction. HHV is increased as a result of water reduction and the energy added by the esters produced from the reaction. Other contributions also assist in the increase in HHV but proprietary issues prevent their disclosure here. Deoxygenation of the raw bio-oil is indicated by the increase in carbon from 52.1 to 65.0% and hydrogen from 6.4 to 10.3%. Oxygen value decreased from 43.5 to 24.5%. This deoxygenation resulting from the reaction is likely the cause of increased energy content as well as increased stabilization, explained below in the discussion of Table A.4.1 results.

Table A.2.3. Fuel properties of olefinated bio-oil compared to raw bio-oil.

Properties	Raw bio-oil	Olefinated bio-oil
Water %-wt	28.6	6.0
HHV(MJ/kg)	17.2	32.8
pH value	2.30	3.3
C (%)	52.1	65.0
H (%)	6.4	10.3
O (%)	43.5	24.5

Accelerated aging tests to monitor viscosity changes for both raw bio-oil and olefinated bio-oil were performed to determine the impact of olefination on bio-oil stability over time. The accelerated aging test subjected control and olefinated product to 90 ^{o}C for 24 h. Properties were measured initially and every 6 h up to 24 h. These results showed that both initial viscosity and viscosity over time were dramatically reduced by olefination. Initial viscosity of the olefinated product was only 5.6 compared to 7.15 cST at the initial condition. Over the 24 h of accelerated aging, the viscosity of the olefinated product increased by only 0.4 cSt to 6.00. The raw bio-oil by contrast hardened so much that after the first 6 h of aging it was impossible to perform the viscosity test. These results indicate that olefination of bio-oil produces a high-energy fuel with very favorable aging properties and should make an excellent boiler fuel.

Subtask A.3 Space heating application

1. Planned Activities

A.3.ML.1 Year 1 milestone is the design and fabrication of a 10-gal/hr semi-batch transesterification system.

A.3.ML.2 Year 2 milestone is to increase the esterified bio-oil production system to 20/gal per hour and to achieve a 40-hour continuous test of upgraded commercial furnace bio-oil firing in conjunction with a current industry partner.

2. Summarization of Activities

Two lignocellulosic boiler fuels (LBF) were successfully developed, one based on esterification and one on olefination reactions. Esterified and olefinated boiler fuels properties are provided in Table A.3.1. These results show that the water content of raw bio-oil, at 24.2%, increases to about 1.5% due to the esterification reaction that is known to create water. By contrast, the olefinated bio-oil had water content reduced from 24.2 to 6.0% due mainly to the conversion of water to alcohols during the olefination reaction. Both the esterification and olefination reactions reduced acid value by nearly 50%, from 89 to about 46 mg KOH/g. Viscosity of both esterified and olefinated fuels were reduced. The esterified product had viscosity reduced by half, from 14.5 for raw bio-oil to 7.4 cSt for esterified bio-oil; olefinated bio-oil viscosity was reduced to approximately 1/3 of that of raw bio-oil at 5.6 cSt. HHV of raw bio-oil (17.5 MJ/kg) was increased by 36% to 23.8 MJ/kg while that for the olefinated fuel was increased by nearly 100% to 32.8 MJ/kg. These results indicate that the fuel properties of esterified bio-oil are improved moderately while those of olefinated bio-oil are improved dramatically.

Table A.3.1. Properties of esterified bio-oil compared to olefinated bio-oil.

Property	Raw bio-oil	Esterified bio-oil	Olefinated bio-oil
Water Content (%)	24.2	25.6	6.0
Acid value (mg KOH/g)	89	46	46.8
Viscosity (cSt @ 40 ^{o}C)	14.53	7.37	5.6
HHV (MJ/kg)	17.5	23.8	32.8

Both LBFs were test burned in boilers converted with retrofit high aeration injection of compressed air. Both fuels burned well, leaving with immediate ignition and no residual in the boiler. The esterified LBF was licensed to an industrial firm that will produce and market it for industrial and agricultural heating applications.

Subtask A.4 Feedstock and bio-oil characterization with pretreatment

1. Planned Activities

A.4.DL.1 Year 1 deliverables are to characterize two new forestry or agricultural feedstocks; four model forestry and agricultural feedstocks will be pretreated by five chemical pretreatments with chemical and physical tests of the resulting bio-oils; particle size methods will be developed to produce three categories of particle size ranging from steam exploded to 1-2 mm.

A.4.DL.2 Year 2 deliverables are to characterize two additional forestry or agricultural feedstocks; the four model forestry and agricultural feedstocks will be pretreated by the particle reduction techniques developed in year one; the three chemical pretreatments tested will be increased to 10; and particle reduction and chemical pretreatments will be tested to determine influence on bio-oil characteristics. Characteristics measured will be water content, viscosity, viscosity stability over time and temperature, pH and total acid number. Chemical analyses by GPC, GC/MS, HPLC, and FTIR will be performed.

2. Summarization of Activities

Characterization

Four feedstocks were analyzed to characterize both biomass and bio-oil yields and properties. The biomass types characterized were black willow, giant miscanthus, elephant grass, and yellow poplar. These feedstocks were dried followed by grinding to a 1-3 mm particle size. A 200g subsample was randomly collected from the total produced for each sample and was further ground to 40-80 mesh to allow performance of elemental and chemical composition analysis. The elemental composition of each of the feedstocks is given in Table A.4.1.

Table A.4.1. Elemental composition of the four study feedstock and pine wood.

Sample	Carbon	Hydrogen	Nitrogen	Remainder
Pine wood (control)	40.3	7.53	0.06	52.1
Black Willow	34.25	4.66	1.94	59.14
Yellow Poplar	44.26	5.3	1.36	49.07
Elephant Grass	40.06	5.06	1.48	53.4
Giant Miscanthus	37.59	4.94	1.66	55.81

Bio-oil, char, and gas yields resulting from pyrolysis of the four study feedstocks and pine wood are given in Table A.4.2. Giant miscanthus and yellow poplar gave relatively high yield of bio-oil at 57 and 56%, respectively, compared to 60.1% for pine wood. Elephant grass and black willow gave relatively low yield compared with pine wood, 43 and 44% for elephant grass and black willow, respectively, as compared to 60.1% for pine wood.

Table A.4.2. Bio-oil, char, and gas yields resulting from pyrolysis of the four study feedstocks and pine wood.

Sample	Bio-oil yield (%)	Char yield (%)	Gas yield (%)
Pine wood (control)	60.1	19.1	20.8
Black Willow	44.0	21.0	35
Yellow Poplar	56.0	16	28
Elephant Grass	43.0	29	28
Giant Miscanthus	57.0	24	21

Physical properties of water content, acid value, viscosity, pH, and density were determined for each bio-oil as provided in Table A.4.3. The water content of the elephant grass bio-oil was very high at 55.6%.

Table A.4.3. Physical properties of the bio-oils produced from the four study feedstocks and pine wood.

	Physical properties				
Sample	water %	Acid Value	Viscosity	Density	pH
Pine wood (control)	25.0	92.0	14.35	1.15	3.2
Giant Miscanthus	37.8	109.6	4.21	1.13	3.48
Elephant Grass	55.6	97.5	1.89	1.09	3.32
Yellow Poplar	27.4	121.9	8.66	1.16	3.22
Black Willow	44.8	104.7	3.22	1.1	3.2

The water content for the four feedstocks was somewhat high relative to that of pine wood. For the grasses, this can be attributed to a higher cellulose and lower lignin content compared to pine wood. It may also be due to the fact that the MSU reactor utilizes temperature and residence times optimized for pine wood. Further research to optimize these to increase yield and to minimize water production may be possible for those who select these as pyrolysis feedstocks. The water content of the elephant grass and black willow bio-oils was very high. Water content at this level will normally cause self fractionation of the bio-oil either shortly after production or over time during storage. A solution to this high water content will be necessary for these two feedstocks to be utilized commercially. The viscosities of all of the four study feedstock bio-oils were considerably lower than for pine wood bio-oil. The viscosity values appear to be a direct function of the magnitude of water content of each bio-oil.

Table A.4.4. Chemical property characteristics of the four study feedstocks and pine wood.

Peak No.	Compound	Concentration (ug/ul)				
		Pine Wood (Control)	Giant Miscanthus	Elephant Grass	Yellow Poplar	Black Willow
1	Phenol	125.23	60.21	21.33	46.81	55.11
2	3-methylphenol	96.72	61.03	6.29	47.57	58.68
3	2,4-dimethylphenol	55.49	27.89	1.15	23.50	27.47
4	2,6-dimethoxyphenol	190.15	112.53	25.47	94.43	113.99
5	Acetovanillone	785.83	2.93	1.25	3.22	26.49

The chemical properties (Table A.4.4) or the produced bio-oil was also determined by GC/MS spectral analysis. By comparison to pine bio-oil the concentration of phenolic chemical compounds in the four study bio-oils were much lower, between 50 to 100% lower. Again, the relative concentrations of phenolic compounds are directly linked to the lignin

content of the respective feedstocks with pine biomass containing the largest percentage of lignin and the grasses containing considerably less. Giant miscanthus contains significantly more lignin than does elephant grass as illustrated in its stiff stems. For this reason, Giant miscanthus had phenol concentrations at about the same level as black willow and yellow poplar. Elephant grass contains much less lignin and much higher cellulose than the other feedstocks, which explains the lower concentration of phenols and the higher water content of the bio-oil. These results indicate that, of the four feedstocks compared to pine wood, giant miscanthus has the most closely comparable properties in terms of yield, physical properties (Table A.4.5), and chemical speciation. Yellow poplar also produced a bio-oil with only slightly lower yield than for pine wood. Water content was low. With the exception of a high acid value, 40% higher than pine, the physical properties of yellow poplar bio-oil are similar to those of pine. The content of phenolic chemical species is about half of the values for pine and about two thirds of that for giant miscanthus. Black willow feedstock produced a bio-oil with relatively high water content but with acid value equivalent to pine bio-oil. Phenolics concentration of black willow bio-oil is about the same as for yellow poplar and is approximately half that of pine wood bio-oil. Elephant grass produces low yield and very low water content due to a preponderance of cellulose content above lignin. Elephant grass will not make a good feedstock for bio-oil production due to its low yield and high water content.

Table A.4.5. Physical property characteristics of the four study feedstock types.

	Physical properties				
Sample	water %	Acid Value	Viscosity	Density	pH
Giant Miscanthus	37.8	109.6	4.21	1.13	3.48
Elephant Grass	55.6	97.5	1.89	1.09	3.32
Yellow Poplar	27.4	121.9	8.66	1.16	3.22
Black Willow	44.8	104.7	3.22	1.1	3.2

The four study bio-oils were chemically characterized using GC/MS and the chemical concentrations of most abundant chemical components were determined.

Biomass Pretreatments

Chemical and physical pretreatments were performed in a consistent manner on four feedstocks comminuted to three particle sizes to determine their influence on bio-oil characteristics. Feedstocks tested were pine wood, sweetgum wood, switchgrass, and corn stover. Pine wood samples were pretreated in a heated phosphoric acid aqueous solution at three acid concentrations (0.5, 1, and 2 wt. %) at 100 ^{o}C for 1 h. After the pretreatment, samples were washed with distilled water until pH=7 and then dried in the open air at room temperature for 72 h to 10% moisture content. A control sample was prepared by washing pine wood with the same amount of distilled water as used for pretreated samples followed by drying as previously discussed. The optimal pretreatment condition determined for the phosphoric acid pretreatment was then applied for the sulfuric acid and hydrochloric acid pretreatments for comparison to determine the best inorganic acid type for pretreatment to produce increased anhydrosugars yield during fast pyrolysis. Pretreated biomass and control samples were tested by Py-GC/MS to obtain chemical products yield after pyrolysis. Pine wood flour samples were pretreated with three different phosphoric acid concentrations (0.5, 1, and 2 wt. %) at 100 ^{o}C for 1 h. Py-GC/MS yields were determined in terms of area % from the GC/MS spectra. The pine flour was pyrolyzed at 450 ^{o}C, a residence time of 10 s, and a heating rate of 10 ^{o}C/ms. The main focus in these tables was on sugars increase as a result of treatment. The yield of levoglucosan increased from 11.6 to 20.5% when the

phosphoric acid concentration increased from 0.5 to 1% and only slightly increased from 20.5 to 20.92% when the phosphoric acid concentration increased from 1 to 2%. The yield of levoglucosenone was slightly decreased as the phosphoric acid concentration increased from 0.5 to 2%. The yield of furfural decreased slightly with a higher acid concentration, and slight increases were observed for the yields of acetic acid, hexadecanoic acid, and 2-methoxy-4-propyl-phenol. Thus, phosphoric acid pretreatment concentration of 1 wt % was selected as the most efficient of the three tested. Product types and distributions were determined as % of GC/MS spectral area for the pyrolysis of pine wood flour pretreated with three different acids (phosphoric acid, sulfuric acid, and hydrochloric acid). Pine wood flour samples were pretreated by 1% of three different acid solutions (phosphoric acid, sulfuric acid, and hydrochloric acid) at 100 ^{o}C for 1 h. Phosphoric acid pretreatment gave the highest yield of levoglucosan (20.5%) and lowest yields of acetic acid and 2-methoxy-4-propyl-phenol. In contrast to phosphoric acid pretreatment, hydrochloric acid pretreatment gave the lowest yield of levoglucosan (15.8%) and highest yields of acetic acid and 2-methoxy-4-propyl-phenol among the three different acid pretreatments. Sulfuric acid pretreatment gave levoglucosan yield of 16.23%. Pine wood flour samples were pretreated with three different phosphoric acid concentrations (0.5, 1, and 2 wt %) at 100 ^{o}C for 1 h. Phosphoric acid pretreatment removed most of the mineral content from the raw pine wood. The mineral content, especially for calcium, potassium, and magnesium, was significantly decreased after phosphoric acid pretreatment. The optimal pretreatment condition of pine wood for high yield of anhydrosugars was determined for 1% phosphoric acid at 100 ^{o}C for 1 h, which produced 20.5% of levoglucosan. Inductively coupled argon plasma spectrometry (ICAPS) was used to test the dominant metal ion contents of control and pretreated pine wood flour samples, including Ca, Mg, P, K, Na. It was found that demineralization of pine wood by mild acid pretreatment increased levoglucosan yield from 1.8% for the untreated sample and 20.5% for the pretreated sample. Pretreated pine wood flour with lower mineral content gave higher levoglucosan yield after fast pyrolysis.

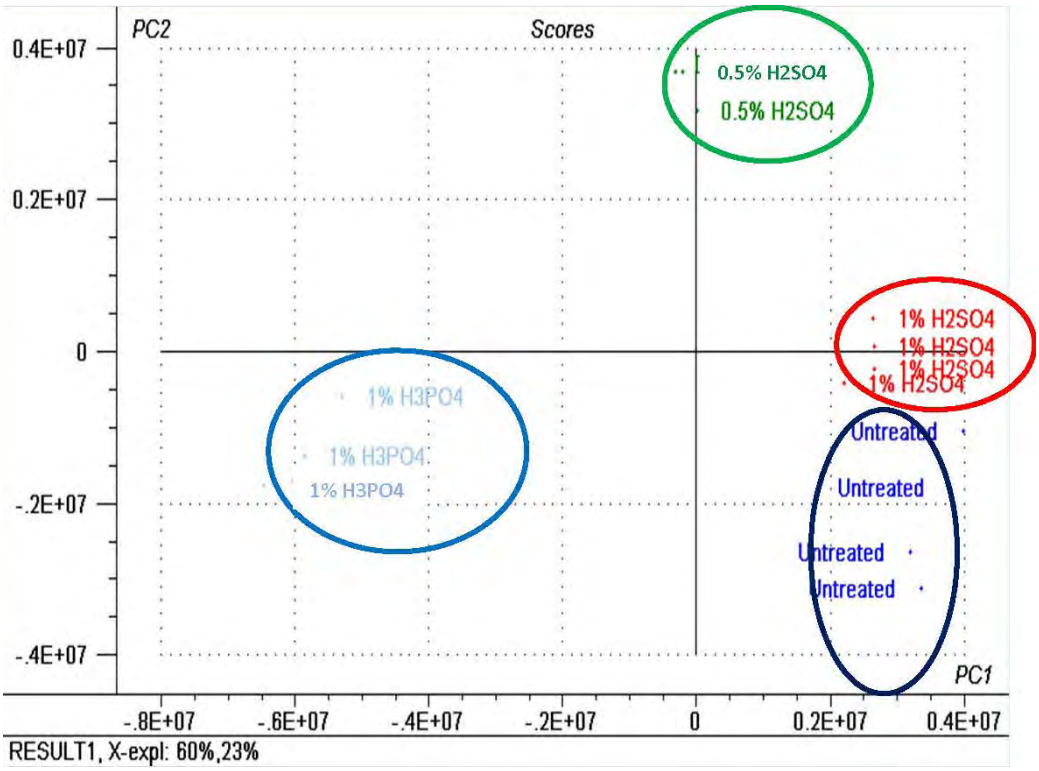


Figure A.4.1. Principal Component Analysis results.

Among the three pretreatments carried out in this study, phosphoric acid pretreatment resulted in bio-oil with the lowest acid value and highest viscosity. Phosphoric acid pretreatment also gave the highest anhydrosugars yield, at 28.41% in the bio-oil sample. Principal component analysis (PCA) of GC/MS spectra showed that the products from pretreatment of pine wood with 0.5% H_2SO_4, 1% H_2SO_4, and 1% phosphoric acid differed significantly in chemical properties in terms of GC/MS spectra (Figure A.4.1). In additional experiments, three more feedstocks, corn stover, switchgrass, and sweetgum, were pretreated in a heated 1% phosphoric acid aqueous solution at 100 ^{o}C for 1 h. After the pretreatment, samples were washed with distilled water until pH=7 and then dried in the open air at room temperature for 72 h to 10% moisture content. The pretreated feedstocks were dried and pyrolyzed as previously described. Among the three feedstocks, sweetgum gave the highest bio-oil yield of 53 wt % during fast pyrolysis, compared with corn stover and switchgrass with respective bio-oil yields of 38 wt % and 47 wt %. The physical and chemical properties of the bio-oils showed that sweetgum bio-oil had the highest water content of 55.07 wt % and lowest acid values of 85.25 mg KOH/ g oil, compared to corn stover bio-oil with water content of 36.42 wt % and acid value of 89.55 mg KOH/ g oil, and switchgrass bio-oil with water content of 33.88 wt % and acid value of 91.95 mg KOH/ g oil.

Bio-oil produced from pinewood by fast pyrolysis has the potential to be a valuable substitute for fossil fuels. Pretreatment prior to the fast pyrolysis process has been shown to alter the structure and chemical composition of biomass. To determine the influence of biomass pretreatment on bio-oil produced during fast pyrolysis, we tested three pretreatments, dilute acid, dilute alkali and steam explosion. The chemical pretreatments applied in this phase of the research were 0.5% and 1% H2SO4 and 0.5% NaOH. Particle-size treatments were also applied in terms of steam explosion and 1-2 mm particle size. Bio-

oils were produced from untreated and pretreated pine wood feedstocks in an auger reactor at 450 ^{o}C. The bio-oil's physical properties of pH, water content, acid value, density, viscosity, and heating value were measured. Chemical characteristics of the bio-oils were determined by gas chromatography-mass spectrometry. Results showed that bio-oil yield and composition were significantly influenced by biomass pretreatment. Of the three chemical pretreatment methods, 1% H_2S04 pretreatment resulted in the highest bio-oil yield and best bio-oil quality. The physical characteristics of pH, density, acid value, water percent, viscosity, and calorific values for the bio-oils are summarized in Table A.4.6. Untreated, large-size pine wood produced bio-oil with a pH value of 2.7 and an acid value of 90.1. Acid, alkaline, and steam-explosion pretreatments had little effect on the density of the bio-oils, which ranged from 1.14 to 1.18 ml/g. Pretreatment increased the water content of bio-oils compared to the control. This increase was of a magnitude of 31.8 to 40.8% with the exception of NaOH pretreatment, which resulted in an increase of 166.8%. The bio-oils produced by the 1 and 0.5% sulfuric acid increased viscosity above that of the control (6.5 cSt) with values of 7.1 and 7.3, respectively. The high viscosity for the acid-treated bio-oils indicated that the acid treatments resulted in additional polymerized bio-oil components with resulting higher bio-oil viscosity. In contrast to the increased bio-oil viscosity resulting from the acid pretreatments, the viscosity of the alkaline and steam-explosion pretreated bio-oils decreased. The viscosities of the alkaline and steam-explosion pretreated bio-oils were 1.5 and 3.9, with respective reductions of 77 and 39.4%. The calorific higher heating values (HHV) of the acid pretreated study bio-oils were 15.0 and 16.5 MJ/kg, similar to control bio-oil HHV of 16.0. Bio-oil HHV values were approximately one-half of the 42 MJ/kg value for petroleum fuels.

Table A.4.6. Physical properties of bio-oils from different pretreatments of large-size pine wood.

Samples	Bio-oil of untreated pine wood	Bio-oil of 1% H_2SO_4 treatment	Bio-oil of 0.5% H_2SO_4 treatment	Bio-oil of 0.5% NaOH treatment	Bio-oil of Steam-explosion treatment
pH	2.7	2.8	2.5	3.2	2.8
Acid Value	90.1	65.1	65.2	41.2	64.2
Density (g/ml)	1.17	1.18	1.20	1.09	1.14
Viscosity (cSt at 50 °C)	6.5	7.3	7.1	1.5	3.9
Water (%)	20.8	27.5	29.5	55.6	29.3
HHV (MJ/kg)	16.1	16.5	15.0	0*	0 *

The HHVs of bio-oils produced from biomass pretreated with NaOH and steam explosion could not be determined because of the high water content. As shown in Table A.4.6, bio-oil from 1% H_2SO_4 had higher HHV, higher viscosity, and lower acid value compared to other pretreatments. It can be concluded that 1% H_2SO_4 pretreatment resulted in bio-oil with the most desirable physical characteristics.

Subtask A.5 Determine petroleum refinery bio-oil characteristics

1. Planned Activities

A.5.DL.1 Year 1 deliverable is to determine bio-oil characteristics required for refining in current petroleum refineries. Based on the characteristics determined as necessary for refining, MSU will develop refined catalysis and feedstock pretreatment plans to attempt to produce these characteristics as closely as possible.

A.5.DL.2 Year 2 deliverable is to provide a supply of bio-oil as closely as possible to refinery specifications. This bio-oil will be refined by a test-scale FCC system capable of refining small amounts of crude to fuels.

2. Summarization of Activities

Interaction with petroleum refineries allowed us to determine the characteristics of upgraded bio-oil acceptable for refining. The result was development of a hydrocarbon mixture capable of direct input to the refining process just prior to the distillation process. Proposals for applying these upgrading steps in the refineries were made to funding agencies with two refineries. The projects were not funded, but future application of our upgrading technology is promising with considerable interest from refiners.

C. Products developed under the award and technology transfer activities.

Publications

Bhattacharya, P., E.B. Hassan, P.H. Steele, J. Cooper, and L.L. Ingram, Jr. 2010. Effect of acid catalysts and accelerated aging on the reaction of methanol with hydroxy-acetaldehyde in bio-oil. BioResources 5(2):908-919.

Bhattacharya, P., P.H. Steele, E.M. Hassan, B. Mitchell, L. Ingram, and C.U. Pittman, Jr. 2009. Wood/plastic copyrolysis in an auger reactor: Chemical and physical analysis of the products. Fuel 88:1251-1260.

Gajjela, S., E.M. Hassan, F. Yu, and P.H. Steele. 2010. Production of zero-oxygen hydrocarbons from bio-oil produced from biomass. Environmental Progress & Sustainable Energy. (In Press).

Hassan, E.M., P.H. Steele, and L.L. Ingram, Jr. 2009. Characterization of fast pyrolysis bio-oils produced from pretreated pine wood. Applied Biochemistry and Biotechnology 154:182-192.

Hassan, El Barbary M., Fei Yu, Leonard Ingram and Philip H. Steele. 2009. The potential use of whole-tree biomass for bio-oil fuels. Energy Sources, Part A, 31:1829-1839.

Mohan, D., J. Shi, D.D. Nicholas, C.U. Pittman, Jr., P.H. Steele and J.E. Cooper. 2008. Fungicidal values of bio-oils and their lignin-rich fractions obtained from wood/bark fast pyrolysis. Chemosphere 71:456-465.

Patterson, D.W., M.H. Pelkki, and P.H. Steele. 2008. Productivity of the John Deere slash bundler in removing in-forest residues from pine harvest sites in the mid-South: Four case studies. Forest Products Journal 58(7/8):31-36.

Patterson, D.W., J.I. Hartley, M.H. Pelkki and P.H. Steele. 2010. Effects of 9 months of weather exposure on slash bundles in the mid-South. Forest Products Journal 60(3):221-225.

Patton, Richard, Philip Steele and Fei Yu. 2010. Coal vs. charcoal-fueled diesel engines: A review. Energy Sources, Part A, 32:315-322.

Steele, P. H. 2010. Past, present and future of pyrolytic production of bio-oil. International Conference on Woody Biomass Utilization. Mississippi State University. Forest Products Society. Madison, WI. (In press)

Steele, P., S. Gajjela, F. Yu, G. Gresham. 2009. Hydrocarbon production via biomass pyrolysis and hydrodeoxygenation. In Proc. of Clean Technology Conference & Expo 2009. May 3-7. Houston, TX. pp. 82-85.

Sukhbaatar, B., P.H. Steele, L.L. Ingram and M.G. Kim. 2009. An exploratory study on the removal of acetic and formic acids from bio-oil. BioResources 4(4):1319-1329.

Sukhbaatar, B., P.H. Steele and M.G. Kim. 2009. Use of lignin separated from bio-oil in oriented strand board binder phenol-formaldehyde resins. BioResources 4(2):789-804.

Tripathi, M.M., E.M. Hassan, F. Yueh, J.P. Singh, P.H. Steele. 2010. Study of the effect of ultraviolet exposure on bio-oil by laser-induced fluorescence spectroscopy. Energy Fuels 24:6187-6192.

Tripathi, M.M., E.M. Hassan, F.Y. Yueh, J.P. Singh, P.H. Steele, and L.L. Ingram, Jr. 2009. Reflection-absorption based near infrared spectroscopy for predicting water content in bio-oil. Sensors and Actuators B: Chemical 136(1):20-25.

X-L. Yang, C.U. Pittman, Jr., X-F. Zhu. 2009. Model reactions with olefins for bio-oil upgrading over solid acid catalysts. Accepted in Chemical Journal of Chinese Universities.

X-L. Yang, S. Chatterjee, Z-J. Zhang, X-F. Zhu and C.U. Pittman, Jr. 2010. Reactions of phenol, water, acetic acid, methanol and 2-hydroxymethyl-furan with olefins as models for bio-oil upgrading. Industrial and Engineering Chemistry Research 49:2003-2013.

Yu, F., R. Ruan and P. Steele. 2009. Microwave pyrolysis of corn stover. American Society of Agricultural and Biological Engineers Vol. 52(5):1595-1601.

Zhang, J., H. Toghiani, D. Mohan, C.U. Pittman, Jr. and R.K. Toghiani. 2007. Product analysis and thermodynamic simulations from the pyrolysis of several biomass feedstocks. Energy Fuels 21:2372-2385.

Z. Zhang, X. Yang, Q. Wang and C. U. Pittman, Jr. 2010. Upgrading bio-oil by additions across olefins over solid acid catalysts. In Proc. of the Conference on China's Technological Development of Renewable Energy Sources. *Vol 1: 381-386.* Scientific Research Publishing, USA, ISBN: 978-1935068-51-8.

Zhang, Z., Q-W. Wang, X-L. Yang, S. Chatterjee, and C.U. Pittman, Jr. 2010. Sulfonic acid resin-catalyzed addition of phenols, carboxylic acids and water to olefins: Model reactions for catalytic upgrading of bio-oil. Bioresource Technology 101:3685-3695.

Presentations

Bhattacharya, P., L. Ingram, E.B. Hassan, and P.H. Steele. 2009. Effect of acid catalysts on the reaction of methanol and other alcohols with hydroxyacetaldehyde in bio-oil. 238th American Chemical Society National Meeting and Exposition. August 16-20. Washington, DC.

Bhattacharya, P., L.L. Ingram, Jr., E.M. Hassan, P.H. Steele. 2009. Study of the reactions of methanol and other alcohols with hydroxy-acetaldehyde in bio-oil. 8th Annual Southern BioProducts and Renewable Energy Conference. May 20-21. Jackson, MS.

Bhattacharya, P., L.L. Ingram, Jr., E.M. Hassan, P.H. Steele. 2010. Improvement of bio-oil stability for use as fuel by injection of methanol during pyrolysis of southern yellow pine. Poster presented at 2010 MSU Biofuels Conference. August 12-13. Jackson, MS.

Bricka, M. 2008. Design of a laboratory-scale pyrolysis system for evaluating the recycle potential of cca-treated wood waste. 1st Energy Synergy Workshop, Mississippi State University, Starkville, MS, June 17.

Chatterjee, S., E. M. Hassan, X. Yang and C.U. Pittman, Jr. 2009. Bio-oil upgrading by the addition of olefins. National Meeting of the American Chemical Society, Division of Fuel Chemistry. August. Washington, DC.

Chatterjee, S., Z. Zhang, E.M. Hassan, and C.U. Pittman, Jr. 2010. Olefination of bio-oil: upgrading bio-oil using olefins from refineries. 9th Annual Southern Bioproducts and Renewable Energy Conference, Tunica, MS, April 13-14.

Columbus, E., and P.H. Steele. 2010. Wood to bio-oil. 12th Annual National Value-added Agriculture Conference, Biloxi, MS, June 27-29.

Cooper, J.E., E.M. Hassan, P.H. Steele and B.K. Mitchell. 2009. Wood preservatives from wood-based pyrolysis oil. International Conference on Wood Biomass Utilization, Mississippi State University. August 4-5. Starkville, MS.

Gajjela, S., E.M. Hassan, F. Yu, and P.H. Steele. 2010. Catalytic production and analysis of aviation fuels from biomass-derived bio-oil. 239th American Chemical Society National Meeting, San Francisco, CA, March 21-25.

Gajjela, S., E.M. Hassan, F. Yu, and P.H. Steele. 2010. Production of zero-oxygen hydrocarbons from biomass-based bio-oil. 239th American Chemical Society National Meeting, San Francisco, CA, March 21-25.

Gajjela, S.K., E.M. Hassan, F. Yu, P.H. Steele. 2009. Biomass to fuels: Upgrading of pyroligneous fraction of bio-oil to second-generation bio-fuels. Eighth Annual Southern Bio Products and Renewable Energy Conference, Mississippi Biomass Council. May 20-21. Jackson, MS.

Gajjela, S.K., P.H. Steele, E.M. Hassan, F. Yu. 2009. Poster. Wood to fuels: Catalytic upgrading of fast pyrolysis bio-oil to second-generation bio-fuels. Graduate Research Symposium, Mississippi State University. November 6. Mississippi State, MS.

Gajjela, S.K., Q. Li, E.M. Hassan, P.H. Steele. 2010. Production of biomass fuels for co-processing in standard refineries. Poster presented at 2010 MSU Biofuels Conference, Jackson, MS, August 12-13.

Guda, V.K., H. Toghiani, C.U. Pittman, and P.H. Steele. 2008. Catalytic upgrading of pyrolysis vapor. 3rd Biofuels Conference, Mississippi State University, Starkville, MS, Aug. 14-15.

Hall, J.W., B.K. Mitchell, D.R. Parish, P.H. Steele. 2010. Production of pyrolysis energy by combustion of char. Poster presented at 2010 MSU Biofuels Conference, Jackson, MS, August 12-13.

Hall, J.W., B.K. Mitchell, D. Parish, and P.H. Steele. 2010. Production of pyrolysis energy by combustion of char. 9th Annual Southern Bioproducts and Renewable Energy Conference, Tunica, MS, April 13-14.

Hassan, E.M., S.K. Gajjela, F. Yu, P.H. Steele. 2009. Chemical characterization of catalytic hydrogenated bio-oil and their distilled fractions. 2009 AICHE Annual Meeting. November 8-13. Nashville, TN.

Hassan, El Barbary, Philip Steele, Brian Mitchell, and Qi Li. 2010. Production and characterization of fast pyrolysis bio-oil from giant miscanthus feedstock. Forest Products Society 64th International Convention, Madison, WI, June 20-22.

Li, Q., F. Yu, E.M. Hassan, L.L. Ingram, Jr., P.H. Steele. 2009. Dilute acid pretreatment of pine wood to increase levoglucosan production by fast pyrolysis. 2nd Energy Workshop. April 15. Mississippi State, MS.

Li, Q., F. Yu, E.M. Hassan, L.L. Ingram, Jr., P.H. Steele. 2009. Dilute acid pretreatment of biomass for enhancement of anhydrosugar production by fast pyrolysis. Eighth Annual Southern Bio Products and Renewable Energy Conference, Mississippi Biomass Council. May 20-21. Jackson, MS.

Li, Q., F. Yu, P.H. Steele, E.M. Hassan, B.K. Mitchell. 2009. Production and application of anhydrosugars from fast pyrolysis of pre-treated biomass. Forest Products Society 63rd International Convention. June 21-23. Boise, ID.

Li, Q., P.H. Steele, F. Yu, B.K. Mitchell, E.M. Hassan. 2009. Carbon implications of production of ethanol from pyrolysis of lignocellulosic biomass. Forest Products Society 63rd International Convention. June 21-23. Boise, ID.

Li, Q., P.H. Steele, F. Yu, E.M. Hassan. 2010. Enhancing anhydrosugars yield for ethanol production from lignocellulosic biomass via a pyrolytic route. Poster presented at 2010 MSU Biofuels Conference, Jackson, MS, August 12-13.

Li, Q., P.H. Steele, E.M. Hassan, F. Yu, and B. Mitchell. 2010. The effect of dilute acid pretreatment on bio-oil properties produced by fast pyrolysis of lignocellulosic biomass. Forest Products Society 64th International Convention, Madison, WI, June 20-22.

Li, Q., F. Yu, E.M. Hassan, B. Mitchell, and P.H. Steele. 2010. Production of bio-ethanol from lignocellulosic biomass via a pyrolytic route. Forest Products Society 64th International Convention, Madison, WI, June 20-22.

Li, Q., F. Yu, B. Mitchell, and P.H. Steele. 2010. PY-GCMS study of the chemical products from fast pyrolysis of dilute acid pretreated lignocellulosic biomass. 9th Annual Southern Bioproducts and Renewable Energy Conference, Tunica, MS, April 13-14.

Livingston, R., F. Yu, Q. Li, P.H. Steele. 2010. Production of lignocellulosic ethanol from pyrolytic anhydrosugars. Poster presented at 2010 MSU Biofuels Conference, Jackson, MS, August 12-13.

Naske, C.D., S.E. Crosby, and K.B. Walters. 2009. Initial aging studies of pyrolysis bio-oil produced from pine and cottonwood. Undergraduate Research Symposium, Mississippi State University, April 21.

Naske, C.D., S.E. Crosby, and K.B. Walters. 2009. Initial aging studies of pyrolysis bio-oil produced from pine and cottonwood. AIChE Southern Regional Conference, University of Alabama, Tuscaloosa, AL, April 3-4.

Naske, C.D., S.E. Crosby, A. McMaster, and K.B. Walters. 2009. Preliminary chemical and physical characterizations of bio-oil aging. Poster submitted for presentation at the Mississippi State University 2nd Energy Workshop, April 15.

Naske, C.D., J. Speed, Z. Wynne, S.E. Crosby and K.B. Walters. 2009. Effects of char particles on the aging of bio-oil produced from timber biomass pyrolysis. Poster presentation given at the AIChE 2009 Annual Student Conference, Nashville, TN, November 9.

Naske, C.D., S.E. Crosby, A. McMaster and K.B. Walters. 2009. Preliminary studies of ph and char particle content on bio-oil aging. Podium presentation given at the AIChE 2009 Annual Meeting, Nashville, TN, November 11.

Naske, C.D., S.E. Crosby, J. Speed, Z. Wynne, and K.B. Walters. 2009. Examination of char particle effects on bio-oil aging reactions. Podium presentation given at the Mississippi State University 8th Annual Graduate Research Symposium, November 6.

Naske, C.D., A. Onwubiko, and K.B. Walters. 2010. Monitoring molecular weight and polydispersity changes during the aging of pine and cottonwood pyrolysis oil. Poster presentation at the Summer 2010 Undergraduate Research Symposium, Mississippi State University, July 29.

Naske, C.D., P. Polk, J. Speed, W.E. Holmes, and K.B. Walters. 2010. Evolution of phase separation during aging in pine pyrolysis oil. Poster presentation at the Summer 2010 Undergraduate Research Symposium, Mississippi State University, July 29.

Naske, C.D., J. Speed, Z. Wynne, and K.B. Walters. 2010. Effects of methanol addition on the aging of bio-oil produced from pine needles. Mississippi State University Annual Undergraduate Research Symposium, Mississippi State, MS, April 22.

Platt, J.A., P.H. Steele, B.K. Mitchell and D.L. Grebner. 2009. Pyrolysis oil produced from southern pine plantation understory vegetation. Forest Products Society 63rd International Convention. June 21-23. Boise, ID.

Puettmann, M. and P.H. Steele. 2009. Carbon sequestration in wood products treated with bio-oil wood preservatives systems. Forest Products Society 63rd International Convention. June 21-23. Boise, ID.

Sekar, A., R.K. Toghiani, and P.H. Steele. 2008. Effect of supercritical water on the composition of bio-oil. 3rd Biofuels Conference, Mississippi State Univerisity, Starkville, MS, Aug. 14-15.

Steele, P. H and S.K. Gajjela. 2010. Refinery options for hydrocarbons from hydroprocessed bio-oil. Southeastern Biomass Conference. November 3. Atlanta, GA.

Steele, P.H. 2009. Development of fuels from bio-oils. Department of Energy Thermochemical Portfolio Review. April 14-16. Denver, CO.

Steele, P.H. 2009. West Alabama - East Mississippi: Northern region county level forest products industrial production and economic impact. Workshop for West Alabama - East Mississippi Economic Development. April 1. Thomasville, AL.

Steele, P.H. 2009. West Alabama - East Mississippi: Southern region county level forest products industrial production and economic impact. Workshop for West Alabama - East Mississippi Economic Development. April 2. Starkville, MS.

Steele, P.H. 2009. Bio-oil upgrading and pretreatment. TCBiomass 2009. September 16-18. Chicago, IL.

Steele, P.H. 2009. Production of bio-oil and derivative bio-fuels from biomass. Southern Virginia Bioenergy: Making Innovation Work. Institute for Advanced Learning and Research. October 6. Danville, VA.

Steele, P.H. 2009. Production of multiple biofuel types from upgraded pyrolysis oil. Mississippi State University Biofuels Conference. August 6-7. Jackson, MS.

Steele, P.H. 2010. Development, progress and scale up of pyrolytic processes. 2010 MSU Biofuels Conference. August 12-13. Jackson, MS.

Steele, P.H. 2010. From trees to biofuels: The future bio-oil bonanza. Society of American Foresters. September 30. Starkville, MS.

Steele, P.H. and S.K. Gajjela. 2010. Production of jet fuel from wood-based pyrolysis oil. Forest Products Society 64th International Convention, Madison, WI, June 20-22.

Steele, P.H. 2009. Development of fuels from bio-oils. DOE Thermochemical Portfolio Review. Denver, CO, April 14-16.

Steele, P.H. 2009. West Alabama-East Mississippi: Northern region county level forest products industrial production and economic impact. Workshop for WAEM Economic Development Sponsored by The Montgomery Institute, Thomasville, AL, April 1.

Steele, P.H. 2009. West Alabama-East Mississippi: Southern region county level forest products industrial production and economic impact. Workshop for WAEM Economic Development Sponsored by The Montgomery Institute, Starkville, MS, April 2.

Steele, P.H., F. Yu, Q. Li, and E.M. Hassan. 2009. Increasing aqueous fraction anhydrosugars yields during fast pyrolysis. 238th American Chemical Society National Meeting and Exposition. August 16-20. Washington, DC.

Steele, P.H., S. Gajjela, F. Yu, and E.M. Hassan. 2009. Hydrocarbon fuel production via biomass pyrolysis. 237th American Chemical Society National Meeting, Salt Lake City, Utah, March 22-26.

Steele, P.H., S.K. Gajjela, E.M. Hassan. 2010. Comparison of hydroprocessed bio-oil gasoline, diesel and jet fuel fractions characteristics to ASTM standards for drop-in fuels. 240th American Chemical Society National Meeting, Boston, MA, August 22-26.

Steele, P.H., S.K. Gajjela, F. Yu, E.M. Hassan, and G. Gresham. 2009. Hydrocarbon production via biomass pyrolysis and hydrodeoxygenation. Clean Technology Conference & Expo 2009. May 3-7. Houston, TX.

Steele, P.H., S.K. Gajjela, F. Yu, E.M. Hassan. 2009. Hydrocarbons production via Biomass fast Pyrolysis and Hydrodeoxygenation. 2009 AICHE Annual Meeting. November 8-13. Nashville, TN.

Tao, J., D.R. Parish, F. Yu, P.H. Steele. 2010. Upgrading bio-oil by esterification over acid catalyst for greenhouse heating. Poster presented at 2010 MSU Biofuels Conference, Jackson, MS, August 12-13.

Tao, Jingming, Qi Li, Fei Yu and Philip Steele. 2010. Upgrading pyrolytic oils from lignocellulosic biomass by esterification. Forest Products Society 64th International Convention, Madison, WI, June 20-22.

Tao, Jingming, Don Parish, and Philip Steele. 2010. Greenhouse heating with esterified bio-oil. Forest Products Society 64th International Convention, Madison, WI, June 20-22.

Tao, Jingming, Fei Yu and Philip Steele. 2010. Upgrading bio-oil derived from southern yellow pine wood by esterification. 9th Annual Southern Bioproducts and Renewable Energy Conference, Tunica, MS, April 13-14.

Waggoner, Charles and Philip Steele. 2009. Pyrolysis of cellulosic materials for production of alternative transportation fuels. Joint Conference: International Thermal Treatment Technologies/Hazardous Waste Combustors (IT3). May 18-21. Cincinnati, OH.

Wang, H., R. Srinivasan, A. Aryanto, P.H. Steele, F. Yu, E.M. Hassan and B.K. Mitchell. 2010. Steam explosion pretreatment of biomass for bio-oil production. Poster presented at 2010 MSU Biofuels Conference, Jackson, MS, August 12-13.

Yang, C.J. and A. R. Minerick. 2009. Deoxygenation of bio-oil via electrocatalysis. 2009 MSU Biofuels Conference. August 6-7. Jackson, MS.

Yang, C.J. and A.R. Minerick. 2009. Reduction of bio-oil via electrocatalysis. AES Poster Session - American Institute of Chemical Engineers Annual Conference (AIChE). November.

Yang, Chungja and A.R. Minerick. 2009. Bio-oil deoxygenation via electrocatalytic reduction. Society of Plastics Engineers Mississippi Chapter Meeting, March.

Yang, Chungja and A.R. Minerick. 2009. Bio-oil deoxygenation via electrocatalytic reduction. Physical Science Division, 7th Annual GSA Symposium, April.

Yu, F., P.H. Steele, Q. Li and E.M. Hassan. 2009. Cellulosic ethanol production from anhydrosugars by fast pyrolysis. 25th Annual International Fuel Ethanol Workshop & Expo. June 14-18. Denver, CO.

Yu, F., P.H. Steele, S.K. Gajjela, E.M. Hassan. 2009. Production of hydrocarbons from fast pyrolysis of pine wood. 2009 ASABE Annual International Meeting. June 21-24. Reno, NV.

Networks or other collaborations fostered

The SERC Bio-oil thrust interacted with numerous individuals and organizations during the research period:

- Ergon, Inc. refining at Vicksburg, MS. Collaborated on a biorefinery proposal to upgrade bio-oil at their site.
- Hunt Refinery at Tuscaloosa, AL. Collaborated on a bio-oil stabilization proposal.
- Kior, Inc. collaborating on improvements to the Kior pyrolysis and upgrading process for plants to be located in Mississippi.
- Collaborated on a $45 million grant proposal submitted to AFRI; pyrolysis oil production and upgrading was MSU responsibility.
- Collaborated with faculty at Washington State and North Dakota Universities on an AFRI grant proposal to produce a co-product from bio-oil.
- Collaborating with Piedmont Bioproducts to provide license to MSU auger pyrolysis reactor technology and license to Lignocellulosic Boiler Fuel production technology.
- Collaborating with Chemical Products Company to license auger reactor design to produce char for production of industrial chemicals.
- Collaborating with Parker Towing Company to develop a solid boiler fuel produced with pyrolysis oil components.

- Collaborating with Membrane Specialties Company to provide bio-oil for a competitively funded project.
- Collaborating with Eclipse Renewables to advise on upgrading pyrolysis products; possibly will license technology.

Inventions/Patent applications, licensing agreements

Steele, P.H., F. Yu, B. Mitchell and Q. Li. Patent Pending. Method of increasing anhydrosugars, pyroligneous fractions and esterified bio-oil. U.S. Pat. Off., Washington, D.C.

Steele, P.H., C. Pittman, L. Ingram, S. Gajjela, Z. Zhang and P. Bhattacharya. Patent Pending. Method to upgrade bio-oils to fuel and biocrude. U.S. Pat. Off., Washington, D.C.

- MSU has licensed its novel auger pyrolysis reactor technology and its Lignocellulosic Boiler Fuel technology to Piedmont Bioproducts.

- MSU has licensed its novel auger pyrolysis reactor technology to Chemical Products Company.

Sustainable Energy Research Center
Biocrude Thrust Area Final Report for 2008-2010

A. Principle investigator and team members: Rafael Hernandez, Todd French, Sandra Eksioglu

B. Summarization of Activities

Subtask B.1 Develop wastewater treatment operational strategies to maximize production of biocrude

1. Planned Activities

B.1.ML.1 Year 1 milestone is to achieve 60% of the theoretical conversion of the sugars into biocrude. Currently, the theoretical conversion of sugars into oils is 35%.

B.1.ML.2 Year 2 milestone is the production of refined biocrude from lignocellulosic sugars at approximately $3.00/gal. A preliminary cost estimate has been published in the Journal of the American Oil Chemist Society (2007) 84:181-187. It was reported that unrefined oil could be produced at approximately $2.10/gallon. It is expected that refining biocrude to the quality necessary before biofuels production may cost over $1.00/gallon. An estimate of the cost of refining biocrude will be determined and included as part of this task.

2. Summarization of Activities

B.1. ML. 1: The potential for enhanced biocrude production by the indigenous microbial consortium in municipal wastewater activated sludge was initially evaluated via batch cultivations using synthetic wastewater media supplemented with glucose as the sole carbon source. Theoretically, oil production by microorganisms occurs in media in which the carbon source is present in excess relative to a nutrient, which is usually nitrogen. At the time when the limiting nutrient is exhausted with a surfeit of the carbon source still present in the culture, the excess carbon is diverted to the production of intracellular lipids as a form of energy storage. Hence, the initial hypothesis of this sub-project was that one or more member/s of the activated sludge microbial community would be able to exhibit the lipid accumulation phenomenon when subjected to similar conditions of nutrient limitations and excess carbon. Furthermore, the use of mixed cultures from wastewater sludges could potentially reduce biocrude production costs as opposed to using pure oleaginous yeast strains because the need for media sterilization could be eliminated. The use of wastewater as fermentation media could also minimize the costs associated with nutrient supplementation due to the naturally-occurring nitrogen and phosphorus levels in the wastewater. The normal operating conditions at which raw activated sludges are grown are usually low carbon-to-nitrogen ratio (C:N) and low substrate loading (in terms of BOD or COD). Therefore, high, medium, and low levels of the carbon-to-nitrogen ratio (C:N) and glucose loading were tested for their effects on biomass growth and lipid accumulation by the activated sludge microorganisms, and our findings have been accepted for publication in the AIChE Journal after an initial review and resubmission with revisions. The results showed enhanced biocrude production from activated sludge cultivated in high C:N ratio (70:1) and high glucose loading (60 g/L) media. As shown in Figure B.1.1, the total biocrude production at these levels amounted to an 80% increase from 10% CDW in raw activated sludge (RAS) to 18% CDW in cultivated activated sludge at C:N 70:1 and 60 g/L initial glucose loading. The saponifiable fraction of the total lipids (biocrude) or the fraction that can be converted to biodiesel or green diesel also increased by as much as 400% from

around 2% CDW in RAS to 10% CDW in enhanced sludge grown under the same conditions. Figure B.1 also shows the resulting fatty acid profiles of the saponfiable fractions of biocrude obtained at the different C:N ratios investigated. The biocrude produced from activated sludge showed high palmitic (C16:0) and oleic acid (C18:1) contents similar to plant oils and similarly making it suitable for use as a biofuel feedstock.

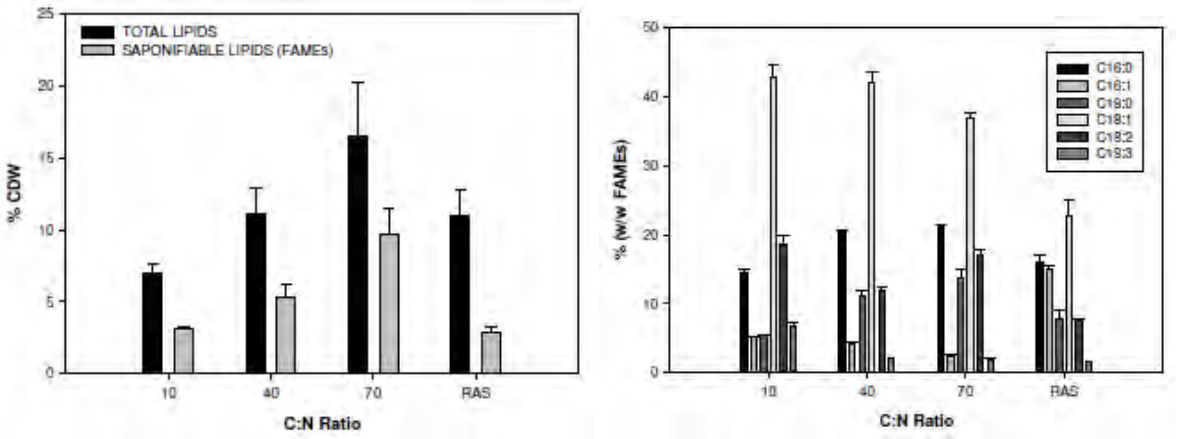


Figure B.1.1. Effect of C:N ratio on biocrude production by activated sludge and fatty acid profile of the saponifiable fraction. (RAS = raw activated sludge).

Following analysis of the fermentation kinetic data, the overall maximum conversion of glucose to biocrude or the lipid yield coefficient ($Y_{P/S}$) was 0.038 g/g glucose consumed obtained from C:N 70:1 - 60 g/L glucose loading run, which is significantly less than the theoretical conversion of 0.21 g/g. However, it was found that in the batch fermentation runs using this treatment, the majority of the conversion of glucose to biocrude occurred during the stationary phases (0.063 g/g), which is higher than during the lag and exponential phases (0.019 g/g). Although biomass lipid contents were improved, the cell biomass concentration needs to be sufficiently high as well to increase biocrude yield coefficient. Therefore, a fermentation strategy that was considered involved an initial cultivation of the activated sludge in low initial glucose loading and C:N ratio up to the exponential phase to accumulate maximum cell biomass concentration followed by semi-batch or continuous feeding of substrate media with high C:N ratios. The following approach will have the advantage of a gradual feeding of substrate to minimize potential substrate inhibition due to shock loading and enhance the conversion of efficiency of glucose to biocrude by the activated sludge. However, our initial attempts to perform these experiments were unsuccessful for the most part as the semi-continuous processing mode produced only a slight increase in $Y_{P/S}$ (around 0.5 g/g), while the continuous fermentation experiments resulted in washout, despite operating at a low dilution rate to match the estimated maximum specific growth rate of the activated sludge microorganisms. These failures have been attributed to the lack of nutrients in the feeding media, which limited biomass growth and hence the maintenance of a viable microbial cell concentration that could continuously produce biocrude. Current experiments are underway to evaluate this proposed solution in order to attain the goal of 0.21g/g conversion to biocrude using this approach and to establish the necessary design foundations for incorporating the proposed biocrude accumulation process in a continuously operating biological wastewater treatment process.

B.1. M.L. 2: The use of pure glucose as the sole carbon source for biocrude accumulation in activated sludge has been considered to be impractical due to its relatively high cost

contribution to the final product. To address this issue, low-cost alternative sources of sugars, such as lignocellulose hydrolyzates, have been considered as potential substrates. The findings are to be found in a paper that has been accepted for submission by the AIChE Journal, which contains the results of our investigation on the effects of artificial mixtures of lignocellulose biomass hydrolysis products on biocrude production by activated sludge. However, previous studies have shown that the degradation of lignocellulose produces chemical by-products that are known to be toxic to microbial growth; hence, their effects on activated sludge microorganisms were evaluated as well.

Pentose sugars are also liberated in the process, and although most microbial lipid accumulations such as that with activated sludge microorganisms utilize glucose (a hexose sugar) as the primary substrate, experiments need to be conducted to assess the capabilities and efficiency of pentose sugar utilization by activated sludge for biocrude production. Representative inhibitor compounds (furfural and acetic acid) and pentose sugar (xylose) were tested for their individual and combined effects. Figure B.1.2 shows that furfural (a), acetic acid (b), and their combinations (c) reduced the total biocrude and biodiesel yield from activated sludge grown in synthetic wastewater with glucose as the primary carbon source. On the other hand, xylose was successfully utilized as a sole carbon source and co-utilized with glucose for enhanced biocrude production by activated sludge with statistically similar total and saponifiable lipids yields (d). The fatty acid profile of the biocrude were very similar with that obtained using glucose as the sole carbon source and with conventional plant oil sources, such as soybean; hence, it could be likewise applicable for biodiesel or green diesel application. The subsequent challenge, therefore, was to reduce the toxic effects of the inhibitors on the microbial process. The conventional process for preventing this problem involves the use of physical or chemical detoxification methods, such as evaporation or over-liming. The use of such methods, however, would add to the substrate cost. Therefore, the use of a gradual substrate feeding scheme to reduce the instantaneous levels of inhibitors in the culture throughout the duration of the fermentation runs was implemented. This was specifically the use of semi-continuous and continuous fermentation modes for the cultivation of the activated sludge. However, similar to what was seen previously with glucose, the implementation of these fermentation schemes should have required the addition of nutrient supplements in the feed solutions and not just the substrate itself because no viable microbial cell concentration was maintained and washout was observed. Further experiments will still be conducted to verify these observations.

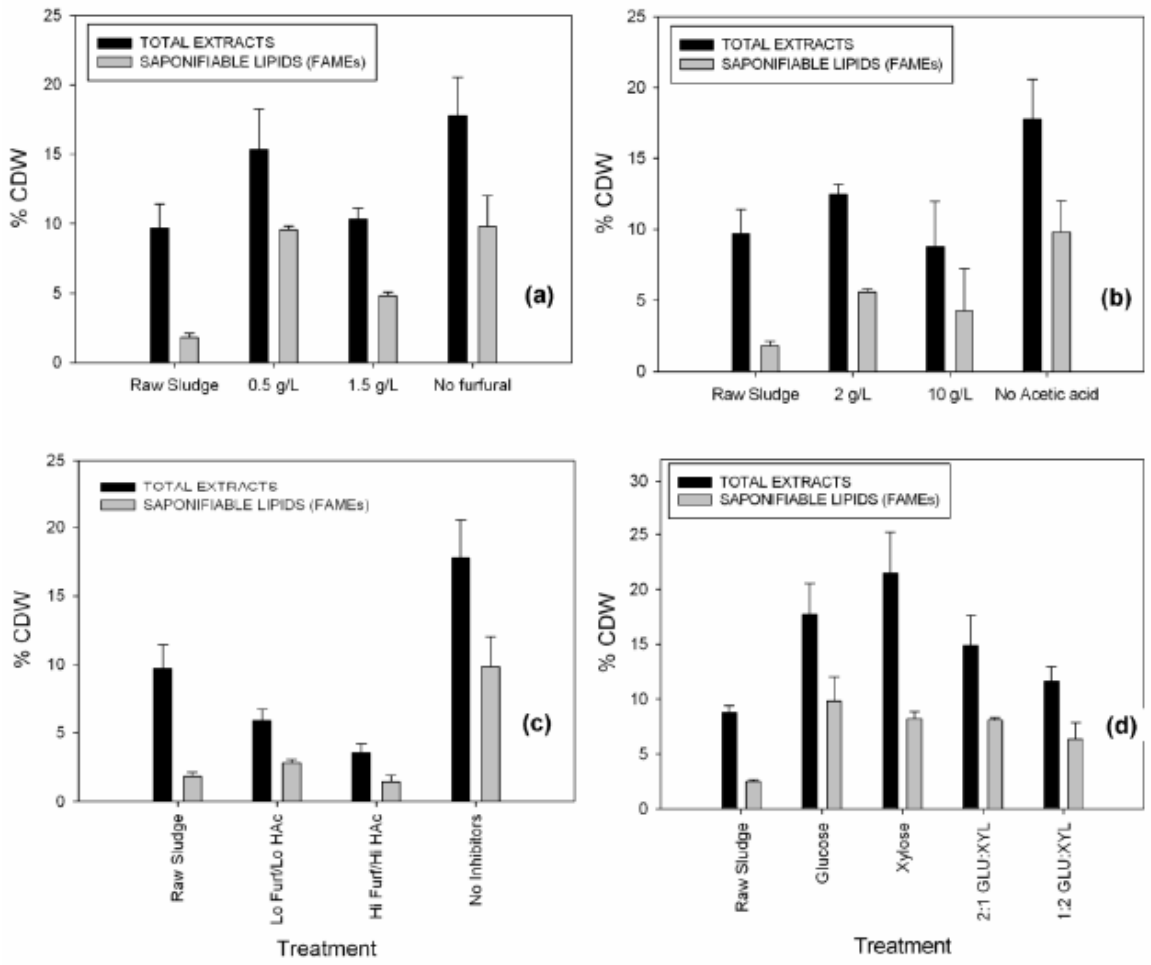


Figure B.1.2. Effect of lignocellulose hydrolysis products on total biocrude production and saponifiable lipid fraction in activated sludge.

Table B.1.2: Cost estimate for *in-situ* transesterification of activated sludge with enhanced biocrude yields. Basis: 1.25 x 10^6 gallons/yr biodiesel production capacity.

Item	Unit Cost	Total Cost
A. Total capital investment cost, TCC (FCC + WCC)[a]		$788,376.10
1. Equipment cost, EC (In $1000/8000 ton annual cap.)		$186,126.08
a. Transesterification reactor	$284.75	$14,502.89
b. Neutralization reactor	$21.25	$68,612.18
c. Washing column	$97.75	$109,977.71
d. FAME distillation column	$153.85	$2,459.44
e. Heat exchangers	$3.40	$32,839.70
f. Pumps	$45.05	$32,381.90
g. Others	$44.20	$186,126.08
2. Contingencies and fees, CFC (18 % of EC)		$80,441.98
3. Total basic module cost, TBMC (EC + CFC)		$527,341.87
4. Auxiliary facility cost, AFC (30% of TBMC)		$158,202.56
5. Fixed capital cost, FCC (TBMC + AFC)		$685,544.43
6. Working capital, WCC (15 % of FCC)		$102,831.66
B. Total annual production cost, TAPC (DOC+IOC+DEPC+GE)[b]		$6,034,992.06
1. Direct operating costs, DOC		$5,709,099.79
a. Sugars for fermentation[c]	$2.52/gal	$3,150,860.10
b. Feedstock (sludge) preparation, centrifugation, and drying[d]	$1.72/gal	$2,147,746.12
c. Methanol	$0.08/gal	$102,578.33
d. Acid catalyst and solvent	$0.15/gal	$58,880.00
e. Labor[d]	$0.10/gal	$124,868.96
f. Heating oil[e]	$0.008/L	$37,810.32
g. Electricity[e]	$0.002/L	$9,452.58
h. Cooling water[e]	$0.0013/L	$6,144.18
i. Steam[e]	$0.0009/L	$4,253.66
j. Wash water[e]	$0.0001/L	$472.63
k. Maintenance and repairs (6 % of FCC)		$2,147,746.12
l. Operating supplies (15 % of maintenance and repairs)		$102,578.33
m. Lab charges (15 % of labor)		$58,880.00
2. Indirect operating costs, IOC		$88,632.26
a. Overhead, packing, storage (60% of labor)		$74,921.38
b. Local taxes (1.5 % of FCC)		$10,283.17
c. Insurance (0.5 % of FCC)		$3,427.72
3. Depreciation, DEPC (10 % of FCC)		$68,554.44
4. General expenses, GE		$168,705.56
a. Administrative expenses (25 % of overhead)		$18,730.34
b. Distribution and selling (≈10 % of TPC)		$99,983.48
c. Research and development (≈5 % of TPC)		$49,991.74
C. Total revenues from biosolids fertilizer sale	$35.80/ton[f]	$961,475.09
D. Net annual production costs (B-C)		$5,073,516.98
Price of biodiesel per gallon to break even		**$4.06**

[a]Costs were estimated based on the values reported in $1000 per 8000 tons of biodiesel per yr using the conversion equation of capacity: $Cost_b = Cost_a(Capacity_b/Capacity_a)^{0.65}$ [You, et al., 2008].
[b]Itemized production costs were based on the costs reported by You *et al.* (2008) unless specified otherwise.
[c]Sugar cost of $0.22/lb converted to per gallon of biodiesel produced [IMF, 2010]
[d][Dufreche, et al., 2007].
[e][Nelson and Schrock, 2006].
[f][Sullivan, et al., 2007].

Economic and cost analyses were conducted to determine the cost of biodiesel production from enhanced biocrude via fermentation of lignocellulose sugars by activated sludge and compare it with those previously found by Dufreche et al. (2007) and Mondala et al. (2009) for biodiesel production from raw activated sludge. Table B.2 shows the details of the cost analysis, and it was determined that the cost of the sugar substrate along with the total biocrude yield or conversion ($Y_{P/S}$) are the most important factors that affect the break-even biodiesel cost. With the current cost of sugars set by DOE ($0.20/lb), the calculated biodiesel cost per gallon with enhanced sludge biocrude was higher ($4.06) than the

$3.00/gal projected in the previous studies. Further sensitivity analysis on the effect of the sugar cost on the biodiesel break-even price showed that a lignocellulose sugar cost between $0.12 and $0.14 per lb (DOE Target) would be needed to reduce the biodiesel cost below the $3.00/gal mark ($2.80/gal), which was lower than the average diesel price of $3.07 in the United States during the study period. Therefore, further studies must be conducted to determine suitable low-cost fermentation substrates for the production of biocrude in order to enhance the cost-competitiveness of the proposed biocrude production process from activated sludge systems.

Subtask B.2 Development of an oleaginous microbial consortium for use as a return activated sludge in biocrude production

1. Planned Activities

B.2.ML.1 Year 1 milestone is to attempt the achievement of 60% conversion of the BOD component of wastewater into cells.

B.2.ML.2 Year 2 milestone is the production of biocrude from lignocellulosic sugars at approximately $3.00/gal. An estimate of the cost of refining biocrude will be determined and included as part of this task.

2. Summarization of Activities

Because the members of the oleaginous consortium require a eutrophic environment and traditional municipal wastewaters are historically deficient in terms of carbon, municipal wastewater was amended with glucose to determine the ability of a consortium of known oleaginous microorganisms to grow and produce lipids. A study conducted by Mondala et al. showed that oleaginous microorganisms contained in the return activated sludge began to proliferate when the sugar concentrations were raised to 60 gL^{-1}. Therefore, this experiment focuses on the growth of the consortium on raw wastewater amended with 60 gL^{-1} of glucose to increase the survivability of the members of the oleaginous consortium. The results of this research showed that the consortium with indigenous microorganisms improved overall cell mass concentration compared to the positive and negative controls. Figure B.2.1 shows the cell mass production throughout the 120 hr cultivation period. The first 24 hr for both the treatments and the controls shows the lag phase or acclimation period where the microorganisms typically develop the enzymes to utilize the nutrients in the wastewater while competing with the indigenous microorganisms. The exponential growth phase for the treatment is from the 24-hr point to the 72-hr point. At 72 hr, stationary phase is apparent until the end of the experiment. The positive control shows a steady increase in cell mass concentration from 24 hours until the completion of the experiment. The negative control also shows a similar result to the positive control. The maximum cell mass concentration of the treatment is 5.3 g/L, whereas the maximum for the positive control is 1.7 g/L and for the negative control is 0.96 g/L. The cell mass produced by the consortium and indigenous microorganisms is approximately five times the amount that is produced by either of the controls. Thus, the combination of the consortium microorganisms with the indigenous microorganisms results in a significant amount of cell mass concentration produced.

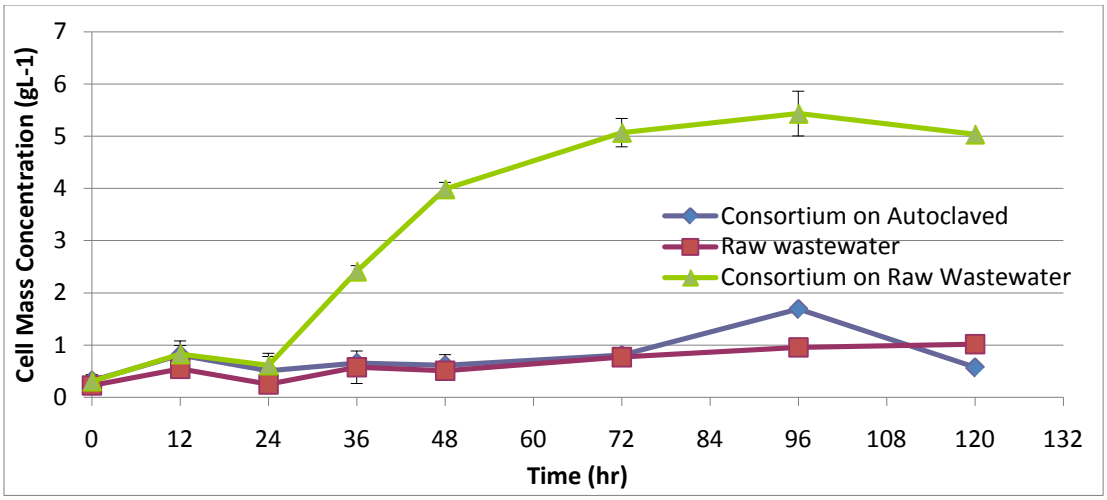


Figure B.2.1: Cell mass production of the consortium on raw wastewater (triangles), consortium on autoclaved wastewater (diamonds), and raw wastewater (squares).

In addition to cell mass concentration, glucose concentration was also measured throughout the experiment to determine if the indigenous microorganisms have an effect on the consortium's ability to consume glucose. Because COD would be significantly impacted by this amount of sugar added to these experiments, the analysis of sugar was examined instead of COD. Figure B.2.2 shows the consumption of the supplemented glucose in the varying treatments. The sugar consumption shows that the consortium with indigenous microorganisms consumes the additional 60g/L of glucose within 72 hours of cultivation. This consumption of glucose supports the significant amount of cell mass produced (Figure B.2.1). The positive control shows a steady decrease until the 36-hr point where it shows a slowing of glucose being consumed. From 36 to 120 hr, the positive control shows an increased consumption rate. The positive control also showed 33g/L of glucose remaining in the wastewater at the end of the experiment. The negative control shows a similar trend to the positive control for the first 36 hr. After 36 hr, the negative control shows a slower decrease in glucose concentrations until the 96 hr, where it remains constant at 20 gL-1 at 120 hr. This steady decrease supports the slight increase in cell mass concentration (Figure B.2.1).

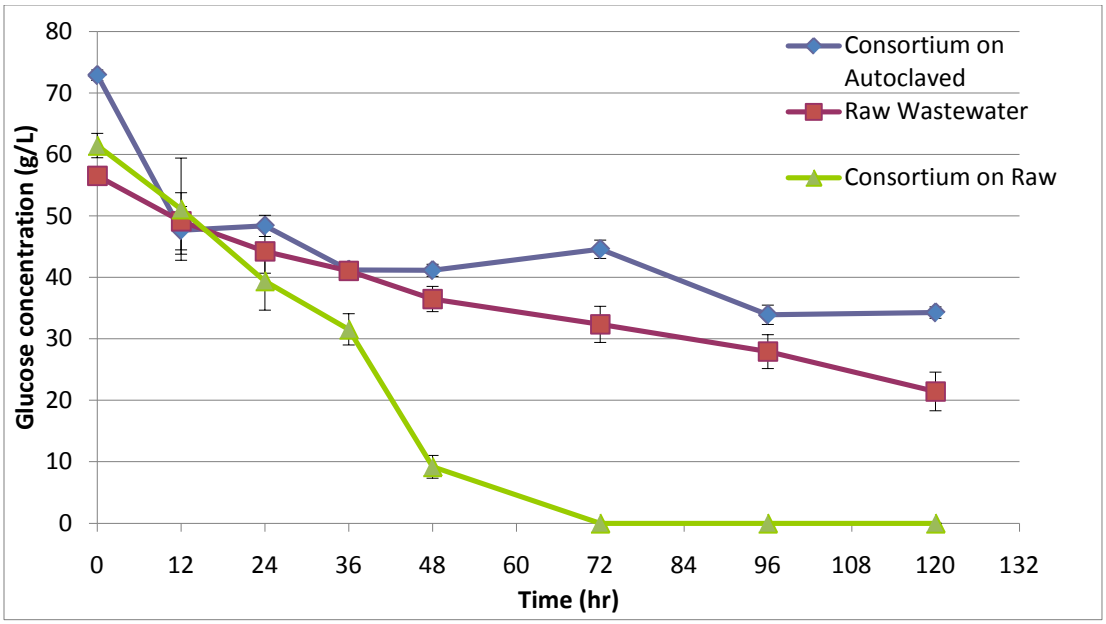


Figure B.2.2: Glucose concentration of the consortium on raw wastewater (triangles), consortium on autoclaved wastewater (diamonds), and raw wastewater (squares).

In order to determine the effect indigenous microorganisms have on the consortium's ability to accumulate oil, lipid mass concentrations were measured. Figure B.2.3 shows the production of lipids over time for each treatment. The consortium with indigenous microorganisms shows the largest amount of lipid production of 0.25g/L after only 36 hr of cultivation. The amount of lipid remained steady from 12 hr to 120 hr. This result shows that the microorganisms are not using the metabolic pathway for lipid production but instead are using the pathway for replication/cell mass production, supporting the cell mass concentration (Figure B.2.1). Because these experiments were conducted in flasks, aeration occurred only as a result of surface transfer. This deficiency in aeration is believed to contribute to the glucose remaining in the autoclaved and raw controls. Because the consortium on raw completely consumed the sugar whereas the consortium on autoclave did not, it is possible that the autoclaving procedure reacted or volatilized some needed component from the wastewater. The positive control shows lipid production within the first 12 hr, then showing a steady decrease until 96 hr. The maximum lipid produced by the positive is 0.15 gL^{-1}. The negative control shows a sharp increase from 0 hr to 12 hr. At 12 hr, it shows a constant decrease until 72 hr. The negative control reaches a maximum of 0.14 gL^{-1} at the 12-hr point. The negative control then shows a stationary lipid production from the 72-hr to 96-hr point. The varying trends show that the combination of the microorganisms in the consortium and in the raw wastewater produces the largest amount of lipids within the first 12 hr.

When comparing the treatment to the negative control, the trends are similar in the fact that they produce a large amount of lipid within the first 12 hr of cultivation. This result could potentially show that the indigenous microorganisms outcompete some of the microorganisms within the consortium. However, because the consortium on raw wastewater shows a larger increase in cell mass production and lipid production than the negative control, the microorganisms are obviously forming a symbiosis relationship within the first 12 hr to promote growth, glucose consumption, and lipid production.

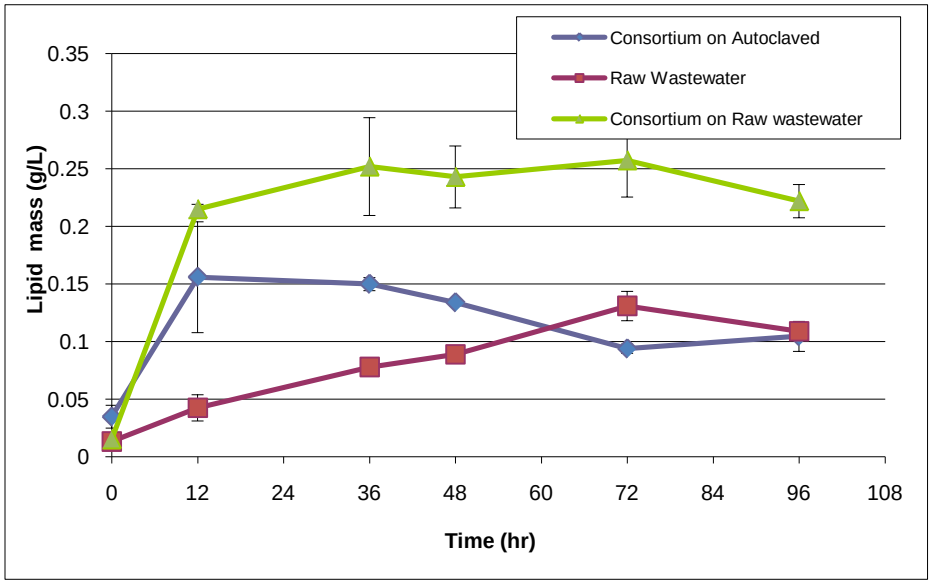


Figure B.2.3: Lipid concentration of the consortium on raw wastewater (triangles), consortium on autoclaved wastewater (diamonds), and raw wastewater (squares).

After the lipids were extracted from the cell mass, they were transesterified into FAMEs. Figure B.2.4 shows the total FAMEs produced by each treatment over the duration of the experiment. The total FAMEs for the consortium grown on raw wastewater shows a steady increase from 0.17 gL^{-1} at 0 hr to 1.8 gL^{-1} at 120 hr. The amount produced for the treatment is seven times larger than the total FAMEs produced compared to both controls. The combination of consortium microorganisms and indigenous microorganisms produced the largest amount of total FAMEs when compared to the controls, which supports the lipid mass concentration data (Figure B.2.3). The positive control shows a steady increase until 48 hr but decreased at 120 hr. The negative control showed a steady increase until 120 hr where it produced $1gL^{-1}$.

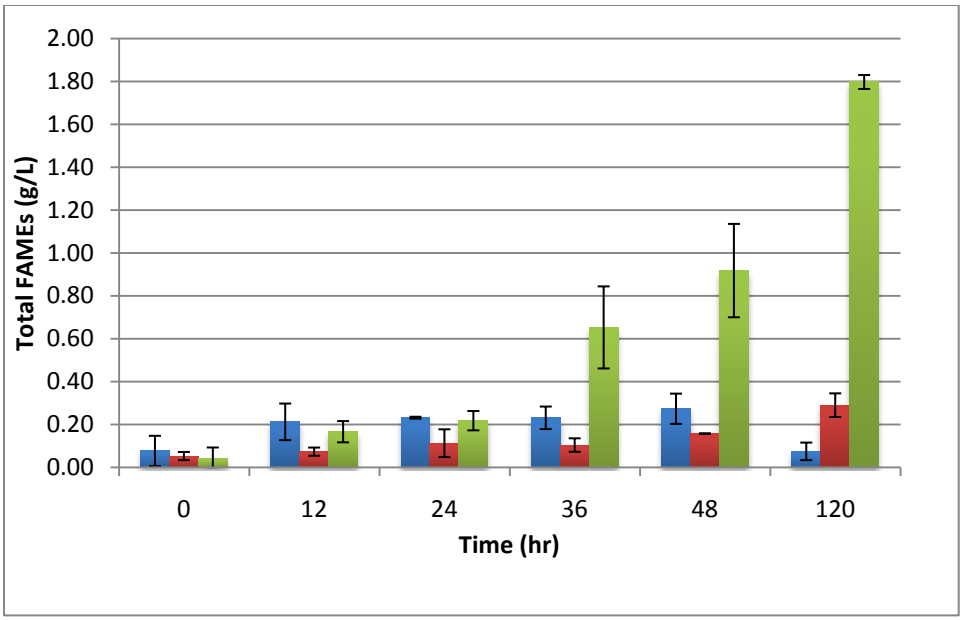


Figure B.2.4: Total FAMEs from the consortium on raw wastewater (green), consortium on autoclaved wastewater (blue), and raw wastewater (red).

Along with the total FAMEs, the fatty acid profiles for the controls and the treatment were measured. Table B.2.1 shows the fatty acid profile results for the consortium grown on autoclaved and raw wastewater compared to raw wastewater. The profile from the consortium grown on raw wastewater shows the majority consisting of palmitic, oleic, and linoleic acid. The positive control profile includes high percentages of palmitic, heptadecanoic, and oleic acid. The negative control shows a majority of palmitic, stearic, oleic, and linoleic acid. Each sample showed a large percentage of palmitic and oleic acid, which is a fatty acid commonly found in oleaginous microorganisms. In addition, each sample also showed heptadecanoic acid, which can be related to a common oleaginous bacterium, *R. opacus*. Overall, these profiles show that the raw wastewater potentially contains oleaginous microorganisms because the fatty acids found in the raw wastewater are similar to oleaginous microorganisms.

These results demonstrate that the consortium has the potential to use wastewaters amended with significant amounts of sugar for growth and the production of lipids that can be transesterified for the production of biodiesel. The addition of this amount of sugar also introduces an additional cost to the utilization of the wastewater infrastructure, nutrients, and water for the production of biofuels.

Subtask B.3 Produce quality transportation fuels defined by the American Society for Testing and Materials Standard

1. **Planned Activities**

   B.3.DL.1 Year 1 deliverable is to evaluate hydro-deoxygenation to remove some heteroatoms.

   B.3.DL.2 Year 2 deliverable is to evaluate denitrification to remove some heteroatoms.

2. **Summarization of Activities**

   Raw activated sludges were collected from a Tuscaloosa, AL wastewater treatment facility. The solid content of the activated sludges was concentrated by gravity settling followed by either vacuum filtration or centrifugation. A portion of the centrifuged sludge was freeze-dried prior to extraction. Extractions were conducted using either centrifuged or freeze-dried sludges as will be discussed below.

   Initial focus was given to the *in situ* transesterification of freeze-dried activated sludge with a solid content of ~95% weight. The process was optimized by varying reaction temperature (45, 55, 65, and 75°C), methanol loading (5, 10, 15, 20, 25, and 30 mL/g solid), and catalyst (sulfuric acid) loading (0.5, 1, 2, 4, and 6% volume/volume). A full factorial experimental design was considered for optimization. Reactions were carried out using Instatherm block system for 24 h. One gram of freeze-dried activated sludge was weighed into screw-capped reaction vials with a capacity of at least two times the reaction volume. Treatments were then randomly assigned to each of the vials. Then, the assigned volume of methanolic sulfuric acid was added, and the mixture was heated to the desired temperature at ambient pressure. The solids were kept suspended in solution using a magnetic stirring bar.

   After 24 h, the mixture was allowed to cool to room temperature. The mixture was then centrifuged at 3000 rpm for 5 min, and the supernatant was transferred into a 60-mL vial. To recover any FAMEs adhered to the solid residue, it was washed two times with 5 mL of methanol, vortex-mixed for 2 min, and centrifuged at 3000 rpm for 5 min. The supernatants were pooled with the first one, after which the methanol was removed at 45°C under 15 psi stream of N_2. The residue was re-dissolved in 15 mL of *n*-hexane and washed three times with 5 mL of distilled water. Vigorous mixing was done during water washing and any emulsions formed were broken by centrifugation at 1500 rpm for 5 min. The hexane layer was then transferred to a 20 mL screw-capped test tube passing through ~2 g of anhydrous sodium sulfate to remove traces of water. The hexane was removed under N_2, and the residue was re-dissolved in 10 mL of toluene with 200 ppm 1,3-dichlorobenzene, and 100 ppm BHT. The 1,3 dichlorobenzene was used as the internal standard for FAME analysis while BHT was added primarily because of its antioxidant property. The FAMEs analyses were carried out using an Agilent 6890 gas chromatograph equipped with flame ionization detector (GC-FID) and using a Restek Stabilwax-DA capillary column.

   Numerical optimization results showed that an optimum biodiesel yield of 4.88% weight may be obtained at 55 °C, 25 mL methanol/g sludge, and 4% (volume) sulfuric acid. Experimental verification showed a yield of 4.79 ± 0.02% (weight) at the optimum condition.

   The *in situ* transesterification process was then applied on a partially dewatered (by centrifugation) sludge. It is well documented in the literature that water has a negative effect on transesterification. However, the extent of that effect is still unknown especially on the *in*

situ transesterification process. Initial results of economic analyses indicated that the drying of the sludge constitute more than 50% of the break-even price of biodiesel. If the drying process can be eliminated, the cost of the biodiesel from activated sludge may significantly decrease. On the other hand, it is anticipated that higher methanol and catalyst loadings might be necessary due to the dilution effect of the water present. The hypothesis is that the cost associated with the drying step is more than enough to compensate for the costs of additional methanol and sulfuric acid.

The optimization of the *in situ* transesterification of wet activated sludge (~15.50% weight solids) was conducted using an orthogonal central composite response design following the same procedure for freeze-dried activated sludge. Temperature (45-75 °C), methanol loading (5-30 mL/g solids), and sulfuric acid concentration (1-10% volume based on methanol) were considered for the optimization. A maximum biodiesel yield of 3.93 ± 0.15% (weight) at 75 °C, 30 mL methanol/g solids and 10% (volume) sulfuric acid.

The break-even price of biodiesel from the *in situ* transesterification of dry and wet sludges were compared. Analyses showed that the biodiesel from the dry process ($7.42 per gal) is still more economical than the biodiesel from the wet process ($14.48 per gal). This is primarily due to higher methanol and catalyst and larger equipments required for the wet process. Based on the results obtained on the dry and wet processes, sensitivity analyses were conducted. First, the effect of moisture content on the break-even price of biodiesel was determined. Results indicated that a lowest break-even (~$7.00/gal) price may be obtained at 50% (weight) moisture content (Figure B.3.1). Still, this price cannot compete with petroleum-based diesel. And so, the effect of biodiesel yield on the break-even price was determined. It was found out that for this feedstock to be economically competitive, a yield of at least 10% (weight) is needed. At 10% yield, a break-even price of ~$2.90/gal is attainable (Figure B.3.2).

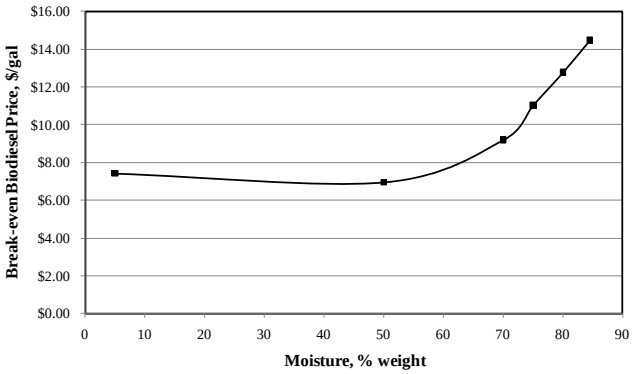


Figure B.3.1. The impact of moisture content of activated sludge on the break-even price of biodiesel.

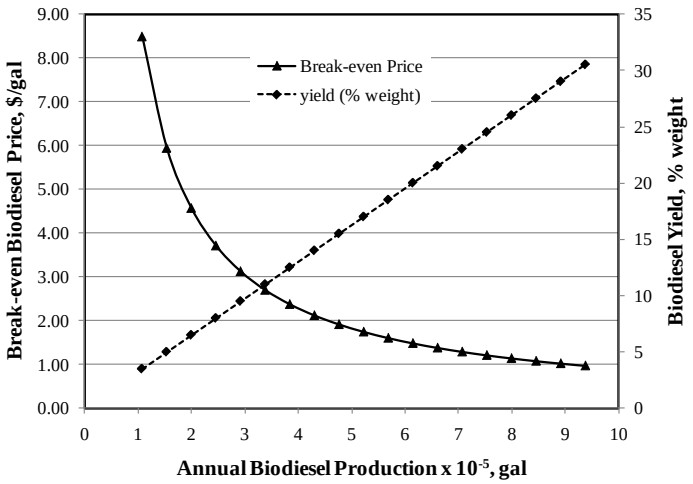


Figure B.3.2. The influence of yield on the break-even price of biodiesel form activated.

The results of the *in situ* transesterification experiments showed that other compounds might be present in the activated sludge as indicated by high gravimetric yield (as high as 15% weight). The activated sludge is a mix of different microorganisms, the majority of which are heterotrophic bacteria. Aside from fatty acids and acylglycerides, most bacteria are known to produce other compounds, such as sterols, polyhydroxyalkanoates, waxes, alkyl benzene, polycyclic aromatic hydrocarbons, etc. These compounds might be accountable for high gravimetric yield of extracts from *in situ* transesterification. If these compounds can be converted to biofuel, the 10% yield could be attained. However, only free fatty acids and free fatty acid-containing compounds (i.e. acylglycerides, wax esters, steryl esters and polyhydroxyalkanoates) can be converted to biodiesel. Other compounds present in the sludge might need a different route (e.g., catalytic cracking) for fuel conversion.

Prior to application of catalytic cracking on the extract from activated sludge, different extraction procedures were explored. This was to maximize the gravimetric extract yield of activated sludge. Particularly, extraction procedures that would not modify/change the identity of compounds present in the activated sludge were tested. Accelerated solvent extractions using either pure *n*-hexane or a solvent system consisting of 60/20/20 (by volume) *n*-hexane/acetone/methanol were tested on freeze-dried sludge. Bligh & Dyer extractions on both wet and dried sludges were also conducted. The Bligh & Dyer extraction of wet sludge gave the highest extraction yields (~13% weight gravimetric and ~4% weight biodiesel yields) (Figure B.3.3).

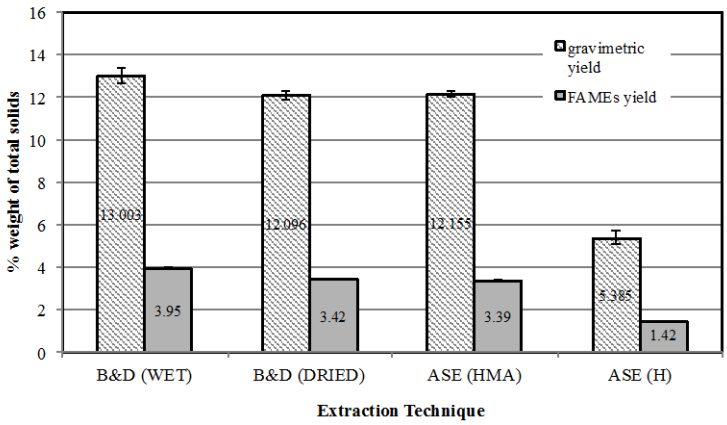


Figure B.3.3. Comparison of different activated sludge extraction techniques.

Catalytic cracking experiments utilizing Quatra-C® (Figure B.3.4) were conducted using three catalysts (ZSM-5, Zeolite-Y, and Silica-Alumina). The extract obtained from the Bligh & Dyer procedure was used for all the experiments. For all the experiments, a 1:20 (by weight) extract:catalyst ratio was used. Results showed the complexity of the extract from activated sludge as indicated by a very small (almost negligible) yield of hydrocarbons. Even when the injector (feed) temperature was increased to 500 °C, no appreciable production of hydrocarbons was observed.

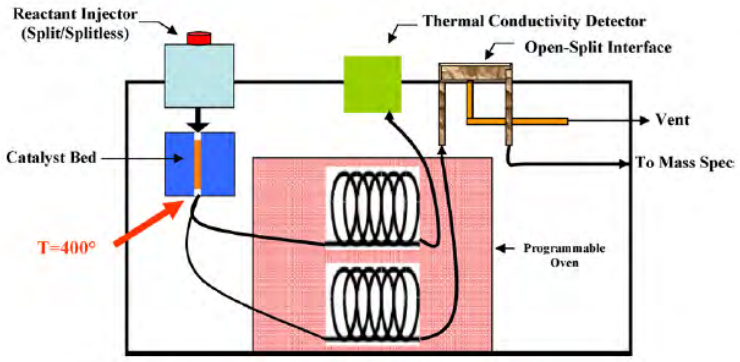


Figure B.3.4. Diagram of the Quatra C illustrating the use of dual chromatographic columns along with TCD and MS detectors.

As shown in Figure B.3.4, the extract that was used in catalytic cracking has ~ 30% (weight) yield of FAMEs. Because of this, it was expected that considerable production of hydrocarbons would be observed during catalytic cracking of this extract. However, the presence of other high-boiling components might have added to the complexity of the extract and prevented the volatilization of the fatty acids and fatty acid-containing compounds. Thus, a different approach was explored.

The extract was subjected to a modified Soxhlet extraction prior to catalytic cracking. The extract (2 g dissolved in 25 mL of chloroform) was mixed with 8 g of silica gel in a round-bottom flask. The mixture was stirred for an hour, after which the solvent was removed by evaporation at reduced pressure. The silica gel-extract mixture was then loaded to a glass

thimble and was introduced to a 150 mL Soxhlet extractor and extraction was carried out at 75 °C, using several solvents. Nonpolar compounds were extracted with 250 mL hexane. This fraction (35.83% weight of extract) contains hydrocarbons, wax esters, steryl esters, triglycerides, and sterols. Polar compounds were extracted with 250 mL ethyl acetate followed by 250 mL of methanol. The ethyl acetate fraction (27.93% weight of extract) contains di-, monoglycerides, and fatty acids while the methanol fraction (36.99% weight of extract) mainly contains free fatty acids and phospholipids.

Catalytic cracking experiments were then conducted using the three fractions obtained from Soxhlet extraction. The same conditions and catalysts were employed for all experiments. Results showed that only the methanol fraction with ZSM-5 as catalyst gave an appreciable yield of hydrocarbons (Figure B.3.5). The separation of the extract based on polarity alone is not enough for its conversion to fuel. It is probably due to the inherent complexity of the extract, and it might be necessary to separate the extract based on compound class (i.e., hydrocarbons, wax esters, steryl esters, fatty acids, acylglycerides, phospholipids, etc.). After separation, determination of cracking conditions and catalyst might be necessary for each class.

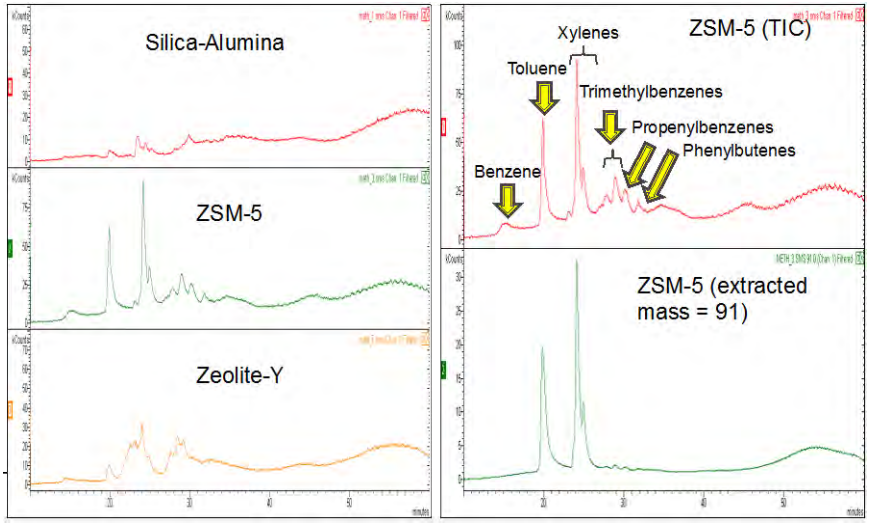


Figure B.3.5. Catalytic cracking of methanol fraction of activated sludge extract.

Subtask B.4 Design cost efficient biomass and biofuels supply chains

1. **Planned Activities**

   B.4.DL.1 Year 1 deliverable is to identify the appropriate model for conducting these analyses.

   B.4.DL.2 Year 2 deliverables are to estimate the cost of supply biomass, cost of distributing the fuel and sensitivity of the logistic cost to biomass yield, biomass price, biocrude price, and biorefinery size.

2. **Summarization of Activities**

   Managing the supply chain for production of biocrude is challenging due to a number of

uncertainties we observe in this chain. Biomass is an agricultural product, and as such, its production yields are subject to weather conditions, insect populations, plant diseases, etc. Demand for biocrude and costs are also uncertain. These characteristics cannot be captured by optimization models, such as mixed integer programs (MIP) as they are deterministic in nature. For this reason, we propose an optimization-simulation model for designing and managing the supply chain of biodiesel. Simulation-optimization tools in supply chains use simulation models to evaluate and improve the results of an optimization model. Typically, these models feed each-other iteratively until a predefined termination criterion (such as, optimality gap, or running time) is reached (Ding, 2004). In these studies, the simulation model evaluates static solutions obtained by the optimization model in dynamic/stochastic environments. We adopted a similar approach in evaluating the results of our optimization models. A number of articles in the literature (Keskin et al., 2010; Karabakal et al., 2000; and Ding et al., 2004) indicate that optimization-simulation models are capable of capturing the dynamics and representing the stochastic nature of supply chains. Simulation-optimization models are scarce in the literature of biomass-to-biofuel supply chain design and management. De Mol et al. (1997) developed an optimization-simulation model for the biomass-to-biofuel logistics management. While in principle the model proposed by De Mol et al. is similar to ours, there are a number of differences. The type of biofuel considered, the structure of the corresponding supply chain, and the methodology used to solve the optimization model are different. In this study, we use the optimization model to identify locations for the sugar plants and identify facility assignments. The simulation model allows us to include uncertain (stochastic) variables in our model and to represent the dynamic behavior of the system.

Figure B.4.1 presents the supply chain for production of biodiesel. This chain has three lignocellulosic biomass supply sides, two sugar plants, one WWT facility, and two refineries. The optimization model that we propose identifies a supply chain structure that minimizes expected investment and logistics costs (such as transportation and inventory costs). Particularly, this model identifies: (a) the location of sugar plants given the supply and distribution of biomass, and location of WWT facilities; (b) the capacity and number of sugar plants required to make use of the available biomass; (c) the assignment of biomass supply sites to each sugar plant; (d) the assignment of sugar plants to supply a particular WWT facility; and (e) the assignment of WWT facilities to refineries where the biocrude will be shipped for further processing.

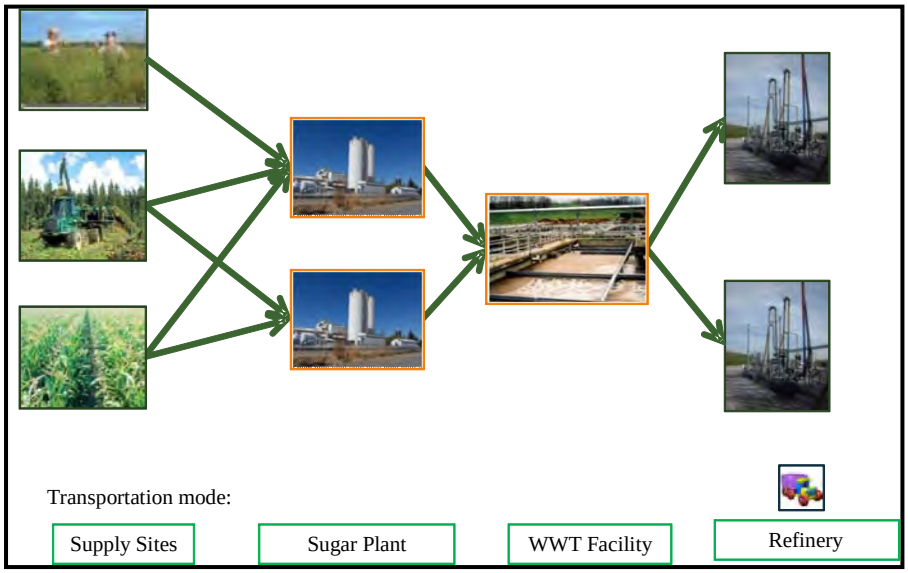


Figure B.4.1. Supply Chain Structure.

The discrete-event simulation model simulates the movement of biomass and biocrude in the supply chain. The simulation model captures the seasonality and randomness of biomass supply and incorporates fluctuations on transportation and production capacities to give a more realistic estimate of supply chain-related costs. The simulation model identifies a biomass-harvesting schedule based on information about weather conditions and forest inventory. Figure B.4.2 provides a schematic representation of the optimization-simulation model we have developed.

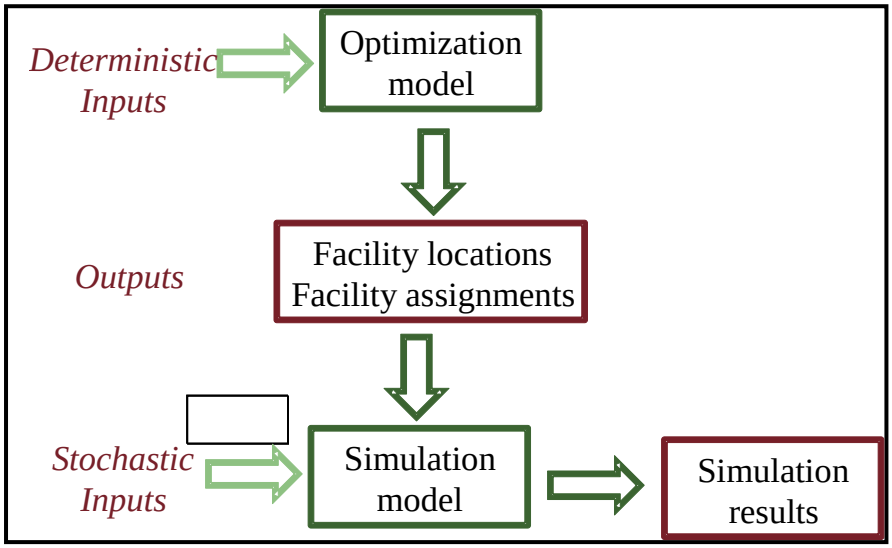


Figure B.4.2. Optimization-Simulation Approach.

In order to estimate supply chain-related costs, we collected data and then ran the optimization and simulation models we build using this data. In this report, we summarize the data collected below. In Section G, we give details about the model developed. We have estimated the cost of producing biodiesel. We also have completed a sensitivity analysis. The results are presented below.

Input Data

Locations

Harvesting Sites: We consider forest residues to be the lignocellulosic biomass feedstock used to produce sugar due to the abundant amount of forest residues available in Mississippi. Mississippi Institute for Forest Inventories (2010) provides information about forest inventories in each county of Mississippi. Therefore, each county is considered to be a supply point in our problem. A total of 44 counties from the Central, Southwest, and Southeast regions of Mississippi are considered as harvesting sites. These counties are also potential locations for the sugar plants that will be opened.

Waste Water Treatment Plants: Mississippi Department of Environmental Quality (2010) provides information about the maximum amount of water that each municipal WWT facility can treat in a particular day. We have identified 65 different municipal WWT facilities located in Mississippi with maximum capacity of treating anywhere from 2 million gallons of water a day (MGD) to 46 MGD.

Refineries: We assume that the existing petroleum and diesel refineries (a total of 20) located in Mississippi and the neighboring states will be used.

Costs

Sugar: The Department of Energy and private industries have invested over the last 10 years in research on enzymatic hydrolysis of lignocellulosic biomass for production of sugars. The data related to sugar production (such as plant investment costs and capacities, biomass to sugar conversion rates, and processing costs) that we use here come from the article of Knutsen and Davis (2004).

Biocrude: The data related to biocrude production costs and conversion rates comes from Ding et al. (2004). The work by Mondala et al. (2009) updates the technology proposed by Dufreche et al. (2007) by treating waste waters with lignocellulosic sugars. Mondala et al. (2009) show that this update in technology results in higher biocrude yields. This improvement came at a higher price due to the additional cost of producing lignocellulosic sugar. However, the expectations are that the amount of sugar needed to produce 1 gal of biocrude will decrease. In our notation, the technologies being tested (1, 2, 3, and 4) refer to a usage of 9, 8, 5, and 4 lb of sugar respectively per gallon of biocrude.

Transportation: Agricultural Marketing Service (AMS) (2010) provides information about transportation costs of agricultural products using trucks for the South Central region of the U.S. Based on this data, for distances less than 25 miles, the average truck rate is $3.6/mile/ton; for distances between 25 and 100 miles, $2.35/mile/ton; and for distances between 100 and 200 miles, $1.90/mile/ton.

Considering the amount of water being treated daily at municipal WWT facilities in Mississippi, we estimate that the potential biocrude production is 50 MGY. We have estimated the amount of sugar required (and as a consequence the amount of biomass harvested) to produce 50 MGY biocrude. Table B.4.1 summarizes these results. These results indicate that as the technology improves the amount of biomass harvested is smaller. For example, using Technology 4 requires about 3.8 million dry tons of forest residues to produce 50 MGY biocrude. Note that Perez at al. (2009) have estimated that the

total annual amount of residues available for biofuel production in Mississippi is 3.9 million dry tons.

Table B.4.1. Biomass and Sugar Requirements for 50 MGY of Biocrude Production in Mississippi.

Technology 1		Technology 2		Technology 3		Technology 4	
Sugar (tons)	Biomass (tons)	Sugar (tons)	Biomass (tons)	Sugar (tons)	Biomass (tons)	Sugar (tons)	Biomass (tons)
1,632,328	8,958,988	1,414,684	7,764,456	848,810	4,658,674	679,048	3,726,939

Results from Optimization Model

One of the major goals of this research is to understand the relationship between logistics-related costs (such as transportation and inventory costs) and technology improvements. Other goals are to design a cost-efficient supply chain for biodiesel, understand what drives transportation costs in this chain, and analyze the impact of logistics costs on biodiesel total delivery costs.

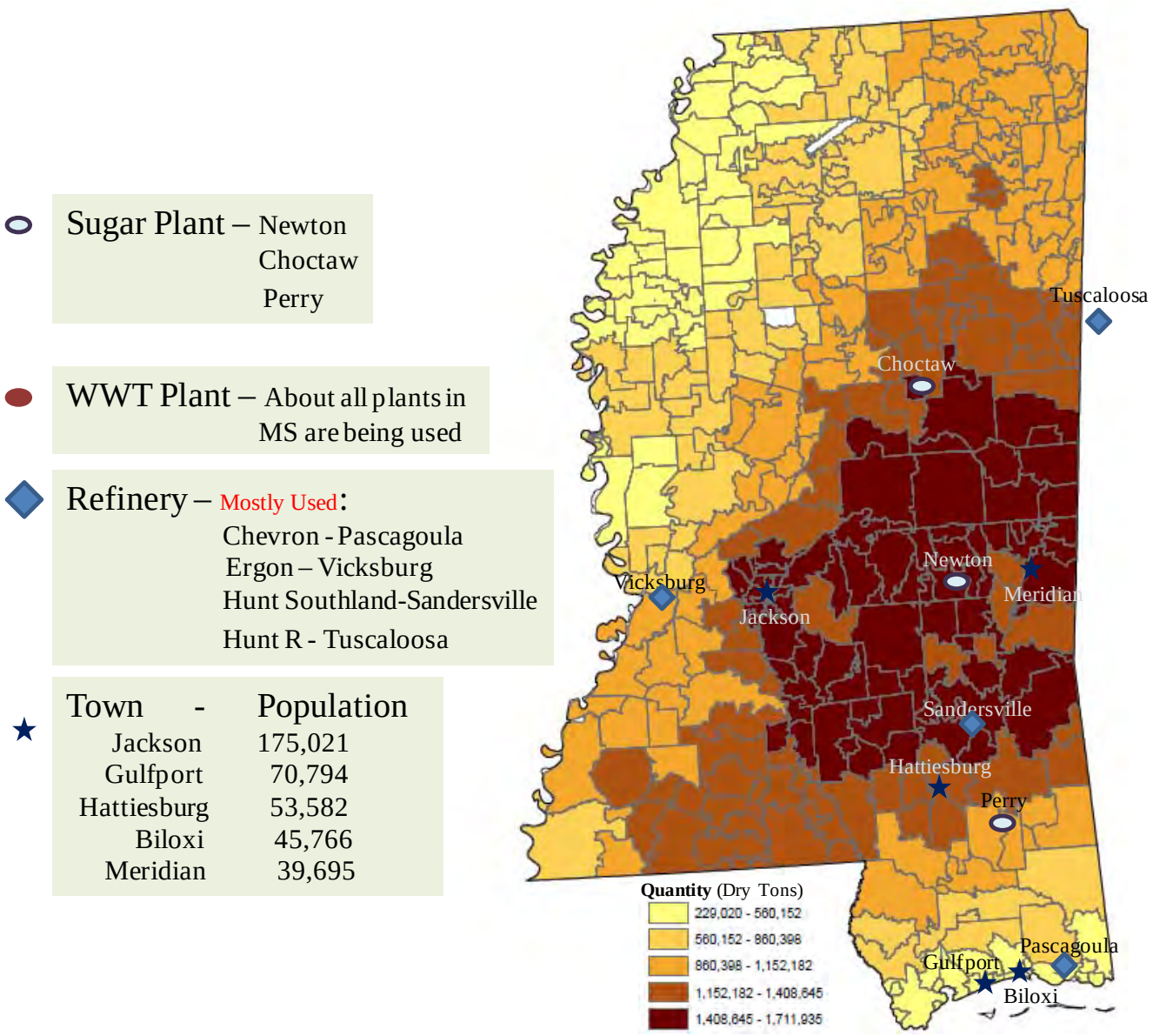


Figure B.4.3. Biodiesel Supply Chain for Mississippi.

The results of the optimization model identify where the sugar plant(s) should be located and which WWT facilities and the refineries should be assigned to that sugar plant (Figure B.4.3). In the scenario when Technology 1 is utilized and biodiesel production is 15 MGY, the sugar plants should be opened in the counties Newton, Choctaw, and Perry. All of the WWT refineries are assigned to these sugar plants. The refineries mostly used are in Pascagoula, Vicksburg, Sandersville, and Tuscaloosa. The results of this figure are an indicator of the validity of our model. South and Central Mississippi are rich with forest residues. The counties that make the top of the list with respect to biomass supply are located in the Central part of Mississippi (for example, Attala, Kemper, Smith, and Lauderdale). The largest towns in Mississippi are mainly located in the South (by the coastline) and Central Mississippi.

Our solution assigns one sugar plant in the South (Perry County), one in the Center (Choctaw County), and one between South and Central Mississippi (Newton County). These locations guarantee minimal system-wide costs by being located centrally to biomass supply and sugar demand points (WWT facilities).

Table B.4.2. Transportation costs for biodiesel.

Technology	Biodiesel Production (MGY)		
	2	4	6
	Transportation costs ($/gal)		
1	1.26	1.30	1.50
2	1.05	1.11	1.25
3	0.57	0.72	0.69
4	0.44	0.56	0.63

Table B.4.3. Transportation distance from harvesting to sugar plant.

Technology	Biodiesel Production (MGY)		
	2	4	6
	Transportation distances (mil)		
1	20.52	22.86	26.74
2	19.25	21.82	25.14
3	13.26	20.46	20.93
4	10.42	19.11	22.17

Tables B.4.2-5 present the results from the optimization model. The unit transportation cost for biodiesel increases as the amount of biodiesel produced increases from 2 and 6 MGY (Table B.4.2). This is mainly due to the increased transportation distances to provide the biomass required to produce lignocellulosic sugars (Table B.4.3). It is interesting to note that as the technology for production of biocrude improves (going from Technology 1 to 4), the transportation costs in the supply chain decrease. Improvements in technology imply that the amount of sugar (and as a consequence the amount of biomass) required per unit of biocrude reduces. As a result, the transportation distances (Tables B.4.3 and 4) and transportation costs will reduce.

Table B.4.4 presents the total distance traveled and the number of sugar plants opened as the technology improves and as the amount of biodiesel produced increases. These results indicate the trade-offs that exist between transportation and investment costs. When biodiesel is produced in smaller quantities, and as the technology of producing biocrude improves, the amount of biomass used (transported) is relatively small. Therefore, the overall supply-chain costs are minimized by opening one single sugar plant. This obviously is not the case as the amount of biodiesel produced increases, as opening one additional sugar plant (which increases investment costs) decreases overall transportation costs. Table B.4.5 presents transportation distances from the sugar plant to the WWT facilities. These distances depend on the number of sugar plants opened.

Table B.4.4. Total Transportation Distances and Number of Sugar Plants Opened.

Technology	Biodiesel Production (MGY)					
	2		4		6	
	Dist.	Nr. Plants	Dist.	Nr. Plants	Dist.	Nr. Plants
1	90.09	1	74.45	2	81.91	2
2	88.45	1	73.84	2	78.45	2
3	78.98	1	89.47	1	72.40	2
4	72.95	1	86.97	1	89.99	1

Table B.4.5. Transportation Distance from Sugar Plant to WWT Facility

Technology	Biodiesel Production (MGY)		
	2	4	6
	Transportation distances (mil)		
1	20.02	15.14	15.23
2	19.61	13.63	15.21
3	25.19	32.71	17.13
4	35.34	36.41	30.63

Results from Simulation Model

The optimization model proposes opening three sugar plants. Based on this model, the supply chain of each sugar plant is independent. That means, a sugar plant does not share biomass supply points with other plants, or does not ship to the same WWT facility. The main reason for such a structure is the capacity of a sugar plant with respect to the capacity of farms, and WWT facilities. The farms in Mississippi are of small and medium size; therefore, each farm supplies a single sugar plant. Similarly, WWT facilities are of small capacity; therefore, each facility is solely supplied by a sugar plant. This is the reason why the simulation model we created in FlexSim mimics the supply chain consisting of one sugar plant supplied by 12 farms. For each plant, one can build a similar model. Tables B.4.6 and 7 present the results from the simulation models. In this model, we consider that the amount of biomass available to harvest changes from one period to the other. In Table B.4.6, these fluctuations are 85-100% of the expected biomass available whereas in Table B.4.7, the range is 100-125%. The simulation model uses the data about the precipitation and bulb temperature of a TMY to identify days one cannot harvest due to weather.

Table B.4.6. Simulation Results: Biodiesel Production
For Biomass Supply between 85% to 100% of Expected

	Nr. of Transportation Vehicles Available		
	1	2	3
Tech 1	1,333,290	2,069,197	2,069,197
Tech 2	1,539,525	2,386,552	2,386,552
Tech 3	2,571,640	3,978,547	3,978,547
Tech 4	3,211,668	4,974,337	4,974,337

Table B.4.7. Simulation Results: Biodiesel Production
For Biomass Supply between 100% to 125% of Expected

	Nr. of Transportation Vehicles Available		
	1	2	3
Tech 1	1,333,290	2,499,775	2,499,775
Tech 2	1,539,525	2,884,158	2,884,158
Tech 3	2,571,640	4,807,123	4,807,123
Tech 4	3,211,668	6,009,336	6,009,336

Based on the results of the simulation, the amount of biodiesel produced initially increases as we go from using one to two transportation vehicles. The main reason is the limitation imposed by having one truck at a farm to deliver residues to the sugar plant. As a result, the sugar plant does not receive the amount of residues required to work at its full capacity. This limitation impacts the total amount of biocrude produced and, as a consequence, the total amount of biodiesel. Statistical analyses indicate that when the number of vehicles increases from one to two, the difference in the amount of biodiesel produced is statistically significant at 95% confidence level. When we increase the number of vehicles from two to three, the difference in the amount of biodiesel produced is not statistically significant. This is an indication that increasing the number of vehicles used to three is not necessary. Two vehicles can handle the flow of biomass to the sugar plant. Therefore, the optimal number of vehicles to utilize at a facility is two.

Comparing the results from Tables B.4.6 and 7, we see that increasing the amount of biomass available for production of biofuel in Mississippi and improving the conversion technology used have the potential to positively impact production of biodiesel. Statistical analysis indicates that the difference between the amounts of biodiesel produced under the low (Table B.4.6) and high (Table B.4.7) biomass availability scenarios is statistically significant only when two and three vehicles are available to ship biomass (95% confidence level). When one vehicle is being used, due to limitations on transportation capacity, the increase in the amount of biomass available does not impact the production of biodiesel.

Results from Sensitivity Analysis

We performed a sensitivity analysis with respect to a number of parameters and estimated the corresponding cost of producing 1 gal of biodiesel. We changed drying, extraction,

product refining at the refinery, and centrifuge costs to see their impact to the cost of producing biodiesel (see Tables B.4.8-11). We have built 16 different scenarios to consider what happens to supply chain-related costs as the conversion technology improves (going from Technology 1 to 4), as production level increases, and other costs change. Tables B.4.8-11 present the different scenarios we have created. Table B.4.12 summarizes the results of the sensitivity analysis. Based on these best case-scenario results (when Centriguge/separation is $0.20/gal; Drying is $0.0/gal; Extraction is $0.10/gal; and Biocrude Processing Refinery is $0.25/gal), the total cost of biodiesel varies anywhere between $2.55 and $5.84, depending on the production capacity and the conversion technology used. In the worst case scenario (when Centriguge/separation is $0.43/gal; Drying is $1.0/gal; Extraction is $0.34/gal; and Biocrude Processing Refinery is $0.60/gal), the total cost of biodiesel is anywhere between $4.34 and $7.25, depending on the production capacity and the conversion technology used.

Table B.4.8. Scenarios Developed for Centrifuge

Scenarios	Drying	Extraction	Refinery	Tech	Prod
1	1.00	0.34	0.60	1	Low
2	0.00	0.10	0.60	1	Low
3	1.00	0.34	0.25	1	Low
4	0.00	0.10	0.25	1	Low
5	1.00	0.34	0.60	4	Low
6	0.00	0.10	0.60	4	Low
7	1.00	0.34	0.25	4	Low
8	0.00	0.10	0.25	4	Low
9	1.00	0.34	0.60	1	High
10	0.00	0.10	0.60	1	High
11	1.00	0.34	0.25	1	High
12	0.00	0.10	0.25	1	High
13	1.00	0.34	0.60	4	High
14	0.00	0.10	0.60	4	High
15	1.00	0.34	0.25	4	High
16	0.00	0.10	0.25	4	High

Table B.4.9. Scenarios Developed for Drying

Scenarios	Centrifuge	Extraction	Refinery	Tech	Prod
1	0.43	0.34	0.60	1	Low
2	0.20	0.10	0.60	1	Low
3	0.43	0.34	0.25	1	Low
4	0.20	0.10	0.25	1	Low
5	0.43	0.34	0.60	4	Low
6	0.20	0.10	0.60	4	Low
7	0.43	0.34	0.25	4	Low
8	0.20	0.10	0.25	4	Low
9	0.43	0.34	0.60	1	High
10	0.20	0.10	0.60	1	High
11	0.43	0.34	0.25	1	High
12	0.20	0.10	0.25	1	High
13	0.43	0.34	0.60	4	High
14	0.20	0.10	0.60	4	High
15	0.43	0.34	0.25	4	High
16	0.20	0.10	0.25	4	High

Table B.4.10. Scenarios Developed for Extraction

Scenarios	Centrifuge	Drying	Refinery	Tech	Prod
1	0.43	1.00	0.60	1	Low
2	0.20	0.00	0.60	1	Low
3	0.43	1.00	0.25	1	Low
4	0.20	0.00	0.25	1	Low
5	0.43	1.00	0.60	4	Low
6	0.20	0.00	0.60	4	Low
7	0.43	1.00	0.25	4	Low
8	0.20	0.00	0.25	4	Low
9	0.43	1.00	0.60	1	High
10	0.20	0.00	0.60	1	High
11	0.43	1.00	0.25	1	High
12	0.20	0.00	0.25	1	High
13	0.43	1.00	0.60	4	High
14	0.20	0.00	0.60	4	High
15	0.43	1.00	0.25	4	High
16	0.20	0.00	0.25	4	High

Table B.4.11. Scenarios Developed for Refining

Scenarios	Centrifuge	Drying	Extraction	Tech	Prod
1	0.43	1.00	0.34	1	Low
2	0.43	0.00	0.34	1	Low
3	0.43	1.00	0.10	1	Low
4	0.20	0.00	0.10	1	Low
5	0.43	1.00	0.34	4	Low
6	0.43	0.00	0.34	4	Low
7	0.43	1.00	0.10	4	Low
8	0.20	0.00	0.10	4	Low
9	0.43	1.00	0.34	1	High
10	0.43	0.00	0.34	1	High
11	0.43	1.00	0.10	1	High
12	0.20	0.00	0.10	1	High
13	0.43	1.00	0.34	4	High
14	0.43	0.00	0.34	4	High
15	0.43	1.00	0.10	4	High
16	0.20	0.00	0.10	4	High

Table B.4.12. Summary Results from Sensitivity Analysis

Drying Costs	Biodiesel costs															
Costs	**Sc 1**	**Sc 2**	**Sc 3**	**Sc 4**	**Sc 5**	**Sc 6**	**Sc 7**	**Sc 8**	**Sc 9**	**Sc 10**	**Sc 11**	**Sc 12**	**Sc 13**	**Sc 14**	**Sc 15**	**Sc 16**
1.00	7.25	6.79	6.86	6.40	5.60	5.15	5.22	4.77	6.96	6.50	6.57	6.12	4.34	3.89	3.96	3.51
0.80	7.06	6.61	6.67	6.22	5.41	4.96	5.03	4.58	6.76	6.31	6.38	5.93	4.15	3.70	3.77	3.32
0.60	6.87	6.40	6.47	6.02	5.22	4.77	4.84	4.38	6.57	6.12	6.19	5.73	3.96	3.51	3.58	3.12
0.40	6.66	6.22	6.28	5.84	5.03	4.58	4.65	4.20	6.38	5.93	5.99	5.55	3.77	3.31	3.38	2.93
0.20	6.48	6.03	6.10	5.64	4.84	4.39	4.45	4.00	6.19	5.74	5.80	5.35	3.58	3.13	3.19	2.74
0.00	6.30	5.84	5.90	5.45	4.65	4.19	4.26	3.81	6.00	5.55	5.61	5.16	3.38	2.93	3.00	2.55

Extraction Cos	Biodiesel costs															
Costs	**Sc 1**	**Sc 2**	**Sc 3**	**Sc 4**	**Sc 5**	**Sc 6**	**Sc 7**	**Sc 8**	**Sc 9**	**Sc 10**	**Sc 11**	**Sc 12**	**Sc 13**	**Sc 14**	**Sc 15**	**Sc 16**
0.30	7.49	6.03	7.11	5.64	5.84	4.38	5.46	4.00	7.19	5.74	6.81	5.35	4.58	3.12	4.20	2.74
0.26	7.46	5.99	7.07	5.61	5.81	4.35	5.42	3.96	7.16	5.70	6.77	5.31	4.54	3.09	4.16	2.70
0.22	7.40	5.96	7.03	5.57	5.77	4.31	5.38	3.92	7.12	5.66	6.74	5.28	4.51	3.05	4.12	2.66
0.18	7.38	5.91	6.99	5.54	5.73	4.27	5.35	3.89	7.08	5.62	6.69	5.24	4.47	3.01	4.09	2.62
0.14	7.34	5.88	6.95	5.49	5.69	4.23	5.31	3.85	7.06	5.59	6.66	5.20	4.43	2.97	4.04	2.59
0.10	7.29	5.84	6.91	5.45	5.65	4.19	5.27	3.81	7.04	5.55	6.62	5.16	4.39	2.93	4.01	2.55

Refinery Cos	Biodiesel costs															
Costs	**Sc 1**	**Sc 2**	**Sc 3**	**Sc 4**	**Sc 5**	**Sc 6**	**Sc 7**	**Sc 8**	**Sc 9**	**Sc 10**	**Sc 11**	**Sc 12**	**Sc 13**	**Sc 14**	**Sc 15**	**Sc 16**
1.05	7.52	7.24	6.06	5.84	5.88	5.60	4.42	4.19	7.23	6.95	5.77	5.55	4.62	4.34	3.15	2.93
0.65	7.15	6.87	5.68	5.45	5.50	5.22	4.03	3.81	6.85	6.57	5.38	5.16	4.24	3.96	2.77	2.55

Centrifuge Costs	Biodiesel costs															
Costs	**Sc 1**	**Sc 2**	**Sc 3**	**Sc 4**	**Sc 5**	**Sc 6**	**Sc 7**	**Sc 8**	**Sc 9**	**Sc 10**	**Sc 11**	**Sc 12**	**Sc 13**	**Sc 14**	**Sc 15**	**Sc 16**
0.43	7.52	6.06	7.15	5.68	5.88	4.42	5.50	4.03	7.23	5.77	6.85	5.38	4.62	3.15	4.24	2.77
0.40	7.49	6.02	7.12	5.64	5.85	4.38	5.47	4.00	7.21	5.73	6.82	5.35	4.59	3.12	4.21	2.74
0.37	7.46	6.00	7.08	5.61	5.83	4.36	5.44	3.97	7.18	5.70	6.79	5.32	4.56	3.09	4.18	2.71
0.34	7.44	5.96	7.06	5.59	5.80	4.33	5.41	3.95	7.15	5.68	6.77	5.29	4.53	3.06	4.15	2.68
0.31	7.41	5.94	7.03	5.56	5.77	4.30	5.38	3.91	7.12	5.65	6.73	5.26	4.50	3.04	4.12	2.65
0.28	7.38	5.91	7.00	5.54	5.74	4.27	5.35	3.89	7.09	5.62	6.71	5.24	4.48	3.01	4.09	2.62
0.25	7.36	5.89	6.97	5.50	5.71	4.24	5.32	3.86	7.06	5.59	6.68	5.21	4.45	2.98	4.06	2.59
0.22	7.32	5.86	6.94	5.47	5.68	4.21	5.30	3.83	7.03	5.56	6.64	5.18	4.42	2.95	4.03	2.56
0.19	7.30	5.82	6.91	5.44	5.65	4.18	5.27	3.80	7.00	5.53	6.62	5.15	4.39	2.92	4.00	2.54

References

Ahuja, R, A., Magnanti, T. Orlin, J. (1993). *Network Flows*. New Jersey: Prentice Hall.

Benson, T.J., Holmes, W.E., White, M.G., French, W.T., Alley, E.G. and Hernandez, R. Development of a heterogeneous catalytic cracking reactor utilizing online mass spectrometry analysis. *J Chromatogr A* **1172**: 204-208 (2007).

De Mol, R. M., Jogems, M.A., Van Beek, P., Gigler, J.K. (1997). Simulation and Optimization of the Logistics of Biomass Fuel Collection. Netherlands Journal of Agricultural Science*.* 45, 219–228.

Ding, H., Benyoucef, L., Xie, X. (2004). A Simulation - Based Optimization Method for Production - Distribution Network Design. 2004 IEEE International Conference on Systems, Man and Cybernetics. 4521–4526.

Dufreche, S., Hernandez, R., French, T., Sparks, D., Zappi, M., Alley, E. Extraction of lipids from municipal wastewater plant microorganisms for production of biodiesel. *J Amer Oil Chem Soc*. 2007; 84: 181-187.

Ekşioğlu, S.D., Acharya, A., Leightley, L.E., Arora, S. (2009). Analyzing the Design and Management of Biomass-to-Biorefinery Supply Chain. Computers and Industrial Engineering. 57, 1342-1352.

Hu, C., Zhao, X., Zhao, J., Wu, S., Zhao, Z.K. Effects of biomass hydolysis by-products on oleaginous yeast Rhodosporidium toruloides. Bioresour Technol. 2009; 100: 4843-4847.

Huang, C., Zong, M-h., Wu, H., Liu, Q-p. Microbial oil production from rice straw hydrolysate by Trichosporon fermentans. Bioresour Technol. 2009; 100: 4535-4538.

Karabakal, N., Gunal, A., Ritchie, W. (2000). Supply Chain Analysis at Volkswagen of America. Interfaces, 30, 46-55.

Keskin, B. B., Melouk, S. H., Meyer, I. L. (2010). A Simulation Optimization Approach for Integrated Sourcing and Inventory Decisions. Computers & Operations Research , 37 (9), 1648-1661.

Knutsen, J. S., Davis, R.H. (2004). Cellulase Retention and Sugar Removal by Membrane Ultrafiltration During Lignocellulosic Biomass Hydrolysis. Applied Biochemistry and Biotechnology*.* 113 – 116, 585–599.

Mississippi Department of Environmental Quality. Active Permit and Coverage Search. http://opc.deq.state.ms.us/search_ai_alt.aspx. Accessed Feb 1, 2010.

Mississippi Institute for Forest Inventories. District Reports. http://www.mifi.ms.gov. Accessed Feb 1, 2010.

Mondala, A., Liang, K., Toghiani, H., Hernandez, R., French, T. Biodiesel production by *in situ* transesterification of municipal primary and secondary sludges. *Bioresour Technol*. 2009; 100: 1203-1210.

Mondala, A.H., Hernandez, R., French, T., McFarland, L., Santo Domingo, J.W., Meckes, M., Ryu, H., Iker, B. Enhanced lipid and biodiesel production from glucose-fed activated sludge: kinetics and microbial community analysis. Published online 6 May 2011. *AIChE J* 2011; 57: n/a/ doi: 10.1002/aic.12655

Mondala, A. Enhanced lipid production and biodiesel yields from activated sludge via fermentation of lignocellulose hydrolyzate. Ph.D. dissertation, Mississippi State University, United States -- Mississippi. Retrieved May 11, 2011, from Dissertations & Theses: Full Text.(Publication No. AAT 3432248).

NREL, Renewable Resource Data Center. National Solar Radiation Database. http://rredc.nrel.gov/solar/old_data/nsrdb/. Accessed Feb 1, 2010.

Perez-Verdin, G., D.L. Grebner, C. Sun, I.A. Munn, E.B. Schultz, T.G. Matney, 2009. Woody Biomass Availability for Bioethanol Conversion in Mississippi. Biomass and Bioenergy, Vol. 33, pg. 492-503.

Revellame, E., Hernandez, R., French, W., Holmes, W., Alley, E. Biodiesel from activated sludge through *in situ* transesterification. *J Chem Technol Biotechnol* **85**: 614-620 (2010).

Revellame, E.D., Hernandez, R., French, W.T., Alley, E.G., Holmes, W.E. The conversion of lipids derived from activated sludge into biofuels, in 2010 AIChE Annual Meeting, Salt Lake City, UT (2010).

Revellame, E., Hernandez, R., French, W., Holmes, W., Alley, E., Callahan, Ii R. Production of biodiesel from wet activated sludge. *J Chem Technol Biotechnol* **86**: 61-68 (2011).

Sokhansanj, S., Kumar, A., Turhollow, A.F. (2006). Development and implementation of integrated biomass supply analysis and logistics model (IBSAL). Biomass and Bioenergy. 30(10), 838–847.

USDA, Agricultural Marketing Service. Truck Transportation. http://www.ams.usda.gov/AMSv1.0/getfile?dDocName=STELPRDC5069739&acct=graintransrpt. Accessed Feb 1, 2010.

C. Products developed under the award and technology transfer activities:

Publication

Ekşioğlu, S.D., G. Palak, A. Mondala, A. Greenwood "Supply Chain Designs and Management for Biocrude Production Via Wastewater Treatment." Environmental Progress & Sustainable *Energy* (submitted Oct. 2010, 1st revision submitted May 25).

Presentations

Ekşioğlu, S.D., "Tools for Supply Chain Design and Logistics Management of Biofuels." 2010 Mississippi State University Biofuels Conference, August 12 -13, 2010, Jackson, Mississippi.

Ekşioğlu, S.D., G. Palak "Supply Chain Designs for Biocrude Production via Wastewater Treatment." IIE Annual Meeting, May 2010, Cancun, Mexico.

Palak, G., S.D. Ekşioğlu, “An Optimization-Simulation Tool for Supply Chain Design and Management of Biocrude Production.” INFORMS Annual Meeting, Nov. 2010, Austin, TX.

Poster Presentations

Palak, G., S.D. Ekşioğlu “An Optimization – Simulation Tool for Biocrude Supply Chain Design and Management.” 2010 Mississippi State University Biofuels Conference, August 12 -13, 2010, Jackson, Mississippi.

Palak, G., S.D. Ekşioğlu “An Optimization – Simulation Tool for Biocrude Supply Chain Design and Management.” 2nd Annual Transportation Workshop, March 2010, Mississippi State University.

Palak, G., S.D. Ekşioğlu “An Optimization – Simulation Tool for Biocrude Supply Chain Design and Management.” 2010 MAS/INFORMS Southern Regional Conference, April 2010, Huntsville, Alabama.

D.a.1 Optimization Model Description, key assumptions and intended use

The network in Figure D.d.1 represents the network flow model we developed. This is a three-dimensional network that allows us to capture not only movement of flow within supply chains, but also system dynamics from one time period to the next. We consider time to be the third dimension in addition to x and y coordinates we use to identify the location of a facility. This third dimension is discrete (rather than continuous). Within each time period (time t, and $t + 1$), the network structure is the same and represents the structure of the supply chain. Different time periods are connected together through inventory arcs that represent the inventories available at a facility from the previous time period. The length of a time period could be as long as one day, one week, or one month. The selection depends on the system dynamics (certain problem parameters should change from one period to the next) and availability of data. The length of the time horizon for our study is one year. The reason for selecting such a time horizon is that planting and harvesting of biomass and agricultural products in general is done on a year-to-year basis. The main objective of this model is to identify a supply chain design that minimizes the costs of flowing products from the supply to the demand nodes.

Note that there are no inventory arcs for harvesting sites. In this model, we consider that lignocellulosic biomass is being used to produce lignocellulosic sugar. Forest residues can be collected year round, other than during two months of the winter. Therefore, there is no need for storage facilities. The sugar plant itself has some storage capacity to handle fluctuations in biomass supply. Similarly, municipal waste is available year round. Our supply chain ends at refineries, and the output from a refinery is biodiesel.
The mathematical model we propose assumes deterministic demand, supply, and costs. Demand, supply, and costs can, however, change dynamically from one period to the next. We assume that the transportation and inventory costs are linear. Investment costs are assumed to be of a fixed-charge nature.

We envision that Economic Development Offices (such as Mississippi Technology Alliances) will use these models to add business professionals (who plan to invest in the area of biofuels in Mississippi) and make better decisions about facility location and capacity. We

expect that the user of these models will input his/her specific data with respect to supply, demand, technology, and costs and identify supply-chain designs that optimize system-wide performance.

D.b Performance criteria for the model related to intended use
The optimization model we discuss is a deterministic model. We use CPLEX (a commercial solver) to solve the problem. The solutions we present here are the optimal solutions presented by CPLEX. CPLEX guarantees solutions with 0% optimality gap.

D.c Test the results to demonstrate the model performance criteria were met.
The results of the optimization model are validated mathematically and visually. We have run our model for very small supply chains and obtained the same results as certain manual calculations. For the large supply chains, the validation is also made visually. We believe that the results in Figure B.4.3 can be used to visually validate our model. Mississippi is known for having an abundant (3.8 million dry ton annually) amount of residues (mainly forest residues) available for biofuel production (Perez et al., 2009). These residues are mainly located in south and central Mississippi. Considering this information, it seems intuitive that all sugar plants would be located mainly in south and central Mississippi to minimize the transportation of biomass. However, sugar needs to be shipped to WWT facilities, which are located in nearly every county of Mississippi. The biggest cities in Mississippi are Jackson, Gulfport, Hattiesburg, Biloxi, and Meridian, which are mainly in central and south Mississippi. Therefore, the sugar plants are not located centrally with respect to biomass only (one – Choctaw - is shifted toward the north and the other – Perry – toward the south). The location of the sugar plants guarantees the minimization of the distance traveled. This model is all about balancing transportation, location, and inventory costs. The locations of sugar plants (and facility assignment) seem to have achieved the goal.

The simulation models intend to estimate the effects of adding transporters and randomness in supply costs. For the validation of the simulation model, we ran the model with deterministic inputs. The optimization model and the deterministic simulation model gave the same biodiesel output and the unit cost per gallon of biodiesel for the same supply-chain scenarios. This ensured us of the correctness of the simulation model.

D.d. Theory behind the model, expressed in non-mathematical terms
Due to the structure of the supply chain, we use a network flow-based model for this problem (Ahuja et al., 1993). Consider the supply chain presented in Figure B.4.1. In this supply chain, the supply points are forests and farmlands, which provide biomass (such as forest residues, agricultural residues, and energy crops) for production of lignocellulosic sugars. Sugars are transported to WWT facilities where they are used to treat activated sludge to produce biocrude. The amount and content of water treated in a WWT facility determines the biocrude production capacity of the facility. For example, WWT facilities located near largely populated areas or industrial food-processing complexes treat wastewater that is rich in food waste and glycerin. Thus, the amount of lipids extracted from activated sludge in these facilities is higher. Finally, biocrude is transported to refineries for further processing to biodiesel.

Figure D.d.1 Network representation of the model.

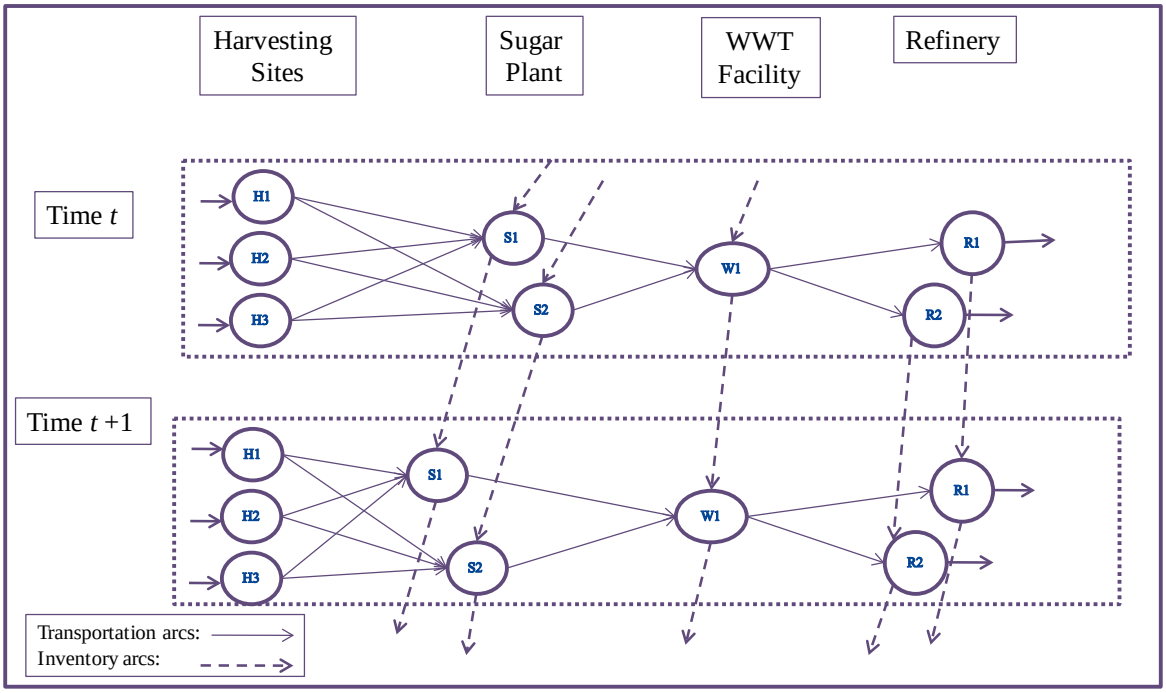


Figure B.4.1 illustrates a small supply chain that consists of three harvesting sites, two potential locations for sugar plants, one WWT facilities, and two refineries. This supply chain can be represented by a network, where a facility is a node, and the transportation links between facilities are the arcs of this network. For example, biomass harvesting sites are the supply nodes; potential locations for sugar plants and WWT facilities are transshipment nodes; refineries are the demand nodes. The links that connect harvesting sites to sugar plants, sugar plants to WWT facilities, WWT facilities to refineries are the transportation arcs. These arcs represent the movement of biomass, sugar, and biocrude in the network. When products flow on these arcs, transportation and inventory costs occur. Our objective is to flow products (for example, lignocellulosic biomass, sugar, and biocrude) in this supply chain and incur the minimum costs. The mathematical models we develop identify where facilities should be located, production capacity of a facility, how much biomass should be harvested in a period, and how much biomass should be transported in order to minimize the overall supply chain-related costs of the final product.

C.e. Mathematics to be used, including formulas and calculations methods

We now describe the MIP formulation that we propose. The *decision variables* are: x_{jl} a binary variable that takes the value 1 if a sugar plant of size *l* is located at site *j*, and takes the value 0 otherwise; z_{jbt} the amount of biomass type *b* stored at the sugar plant at location *j* in period *t*; z_{jt}^{1} the amount of sugar stored at the sugar plant *j* in period *t*; z_{it}^{2} the amount of sugar stored at WWT plant *i* in period *t*; z_{it}^{3} the amount of biocrude stored at WWT plant *i* in period *t*; y_{kjbt} the amount of biomass type *b* shipped from harvesting site *k* to sugar plant *j* in period *t*; y_{jit}^{1} the amount of sugar shipped from sugar plant *j* to WWT facility *i* in period *t*; y_{igt}^{2} the amount of biocrude shipped from WWT facility *i* to diesel refinery *g* in period *t*; w_{jbt} the amount of biomass *b* processed at sugar plant *j* in period *t*; e_{jt} the amount of sugar

produced at plant *j* in period *t*; ζ_{it} the amount of sugar processed at WWT facility *i* in period *t*; η_{it} the amount of biocrude produced at WWT facility *i* in period *t*.

The *parameters* are: ψ_{jl} the amortized annual cost of constructing and operating a sugar plant of size *l* at *j* (in $); h_b^1 the unit inventory holding cost for biomass feedstock *b* (in $/ton); h^2 the unit inventory holding cost for sugar (in $/ton); h^3 the unit inventory holding cost for biocrude (in $/ton) ; p_b the unit cost of planting, growing and harvesting biomass feedstock type *b* (in $/ton); c_{kjb} the unit transportation cost of biomass type *b* from harvesting site *k* to sugar plant *j* (in $/ton); c_{ji}^1 the unit transportation cost of sugar from plant *j* to WWT facility *i* (in $/ton); c_{ig}^2 the unit transportation cost of biocrude from WWT facility *i* to refinery *g* (in $/ton); ω_b^1 the unit processing cost of biomass feedstock *b* at a sugar plant (in $/ton) ; ω^2 the unit processing cost at a WWT facility; ω^3 the unit processing cost at a refinery; λ_{kbt} the amount of biomass *b* available at the harvesting site *k* in period *t* (in ton); α biomass deterioration rate (in %); β_b the conversion rate from biomass feedstock *b* to sugar (in ton/ton); γ_i the conversion rate from sugar to biocrude at WWT plant *i* (in gal/ton); σ the conversion rate from biocrude to biodiesel (in gal/gal); d_t demand for biocrude in period *t*; PC_l the production capacity of sugar plant of size *l* (in ton); SC_l the storage capacity at a sugar plant of size *l* (in ton); WC_i the production capacity at a WWT facility located at *i* (in gal).

$$\text{minimize}\left[\sum_{j=1}^{J}\sum_{l=1}^{L}\psi_{jl}x_{jl}+\sum_{b=1}^{B}h_b^1\left(\sum_{t=1}^{T}\sum_{j=1}^{J}z_{jbt}\right)+h^2\left\{\sum_{t=1}^{T}\left\{\sum_{j=1}^{J}z_{jt}^1+\sum_{i=1}^{I}z_{it}^2\right\}\right\}+h^3\left\{\sum_{t=1}^{T}\sum_{i=1}^{I}z_{it}^3\right\}+\right.$$

$$\left.\sum_{t=1}^{T}\left(\sum_{b=1}^{B}\sum_{k=1}^{K}\sum_{j=1}^{J}\left(p_b+c_{kjb}\right)y_{kjbt}+\sum_{j=1}^{J}\sum_{i=1}^{I}c_{ji}^1y_{jit}^1+\sum_{i=1}^{I}\sum_{g=1}^{G}(c_{ig}^2+\omega^3)y_{igt}^2\right)+\sum_{j=1}^{J}\sum_{b=1}^{B}\sum_{t=1}^{T}\omega_b^1w_{jbt}+\omega^2\sum_{i=1}^{I}\sum_{t=1}^{T}\eta_{it}\right]$$

Subject to:

$$\sum_{j=1}^{J} y_{kjbt} \le \lambda_{kbt} \qquad k=1,...K; b=1,...,B; t=1,...,T \qquad (1)$$

$$\sum_{k=1}^{K} y_{kjbt} + (1-\alpha) z_{jb,t-1} = w_{jbt} + z_{jbt} \qquad j=1,...J; b=1,...,B; t=1,...,T \qquad (2)$$

$$e_{jt} \le \sum_{b=1}^{B} \beta_b w_{jbt} \qquad j=1,...J; t=1,...,T \qquad (3)$$

$$e_{jt} + z^1_{j,t-1} = \sum_{i=1}^{I} y^1_{jit} + z^1_{jt} \qquad j=1,...J; t=1,...,T \qquad (4)$$

$$\sum_{j=1}^{J} y^1_{jit} + z^2_{i,t-1} = \zeta_{it} + z^2_{it} \qquad i=1,...I; t=1,...,T \qquad (5)$$

$$\eta_{it} \le \gamma_i \zeta_{it} \qquad t=1,...,T \qquad (6)$$

$$\eta_{it} + z^3_{i,t-1} = \sum_{g=1}^{G} y^2_{igt} + z^3_{it} \qquad i=1,...I; t=1,...,T \qquad (7)$$

$$\sum_{i=1}^{I} \sum_{g=1}^{G} \sigma y^2_{igt} = d_t \qquad t=1,...,T \qquad (8)$$

$$\sum_{b=1}^{B} z_{jbt} \le \sum_{l=1}^{L} S_l x_{jl} \qquad j=1,...J; t=1,...,T \qquad (9)$$

$$e_{jt} \le \sum_{l=1}^{L} C_l x_{jl} \qquad j=1,...J; t=1,...,T \qquad (10)$$

$$\eta_{it} \le WC_i \qquad i=1,...I; t=1,...,T \qquad (11)$$

$$\sum_{l=1}^{L} x_{jl} \le 1 \qquad j=1,...J \qquad (12)$$

$$\phi, z, y, w, e, \eta, \xi \ge 0 \qquad (13)$$

$$x \in \{0,1\} \qquad (14)$$

The objective of this MIP model is to minimize the total annual costs, which consist of: (a) biomass harvesting, storing, transporting, and processing; (b) sugar processing, storing, and transporting; (c) biocrude processing, storing, and transporting; and (d) investment and operating costs of sugar plants. Constraints (1) indicate that the amount of biomass shipped to all sugar plants cannot exceed what is available. Constraints (2) are the flow conservation constraints for biomass at a sugar plant. Constraints (3) indicate that the amount of sugar produced in a period depends on the amount of biomass processed and the corresponding conversion rate. Constraints (4) and (5) are the flow conservation constraints for sugar at a sugar plant and WWT facility. Constraints (6) indicate that the amount of biocrude produced in a period depends on the amount of sugar processed and the amount of sugar needed to produce 1 t of biocrude. Constraints (7) and (8) are the flow conservation constraints for biocrude at a WWT facility and refinery. Constraints (9), (10), and (11) are storage and production capacity constraints at sugar plants and WWT facilities, respectively. Constraints (12) indicate that a single sugar facility will be open in a particular location. Constraints (13) are the non-negativity constraints, and (14) are the binary constraints.

D.a.2 Simulation Model Description

The discrete event simulation model is built in FlexSim. This model replicates the supply-chain structure identified by the optimization model. FlexSim has the capability to use geographical coordinates to set the exact locations of facilities and farms in the model. These coordinates are then used to calculate transportation times and distances. In the simulation model, we also set transportation and production capacities to mimic the reality. For example, we experiment with the total number of transportation vehicles available to ship lignocellulosic biomass and present the impact that transportation capacity has on total costs and lead time. The simulation runs on a day-to-day basis. This approach helps monitoring biomass and biocrude inventory levels closely.

The amount of biomass available in a particular day is subject to the amount of biomass inventory and weather conditions. The data we use in this model to estimate biomass supply comes from Mississippi Institute of Forest Inventory (2010). These reports provide data about the available forest inventory in Mississippi at the county level. We use this information to estimate a sustainable amount of residues to collect in each county (see Ekşioğlu et al., 2009). The simulation model allows us to consider fluctuations of the amount of biomass harvested. We consider this amount to fluctuate between an upper and a lower bound. These bounds are set 10% under and above the expected biomass available for production of biofuels. The National Solar Radiation Data Base provided by National Renewable Energy Laboratory (2007) provides data about the weather of a typical meteorological year (TMY). We use this data to determine rain precipitation and the dry-bulb temperature on a particular day and then determine if we harvest that day. The simulation model follows the practice that biomass is not harvested on very cold days [for example, days when temperatures are below -10 ^{o}C (Sokhansanj et al., 2006)] or on rainy days.

We run the simulation model for the whole time horizon, which is one year. We observe the fluctuations of the inventory level for sugar and biocrude during this time period. We also keep track of the inventory and transportation costs in the supply chain.

D.f. Whether or not the theory and mathematical algorithms were peer reviewed and, if so, include a summary of theoretical strengths and weaknesses.

The work presented in this report has been submitted for publication to *Environmental Progress and Sustainable Energy*. We received positive reviews and have resubmitted the revised paper.

Similar models to the ones proposed here exist in the literature of supply-chain design and management for industrial products. From a theoretical point of view, this work is unique because it captures the specific nature of sludge/biocrude and its supply chain. The value of the models we propose stands not only in estimating biocrude supply-chain costs and understanding trade-offs. These models can be used by decision makers to design and manage biomass-to-biofuels supply chains. For example, we envision that Economic Development Offices (such as Mississippi Technology Alliances) will use these models to add business professionals (who plan to invest in the area of biofuels in Mississippi) to making better decisions about facility location and capacity. We expect that the user of these models will input his/her specific data with respect to supply, demand, technology and costs, and identify supply chain designs that optimize system wide performance.

The simulation and optimization models we propose can be enhanced. The following are a number of problem extensions that can be explored to increase the value of these models. In the simulation model, we assume that the amount of biomass available for production of

lignocellulosic sugar fluctuates within a lower and upper bound. Distribution functions can be developed to better represent these fluctuations. Similarly, incorporating distribution functions that better represent fluctuations of transportation, inventory, and production costs will increase the value of the simulation model. The optimization model we propose is capable of capturing certain supply chain dynamics as we move from one period to the next. However, it does not capture the stochastic nature of biomass supply and costs. Two-stage location-allocation stochastic programming models can be used to improve the quality of the results from the optimization model.

D.g. Hardware requirements.

The algorithms were executed on a desktop computer, Intel(R) Core(TM)2 CPU processor -- 2.66GHz CPU each -- 4.00GB of RAM.

D.h. Documentations

We have attached the code we developed for our optimization and simulation model at the end of the document. In the optimization model, we have included comments to help the reader understand. The simulation model is in FlexSim, which has a user friendly interface. The reader familiar with Flexim will find it easy to use the model.

Sustainable Energy Research Center
Lignocellulosic Conversion Thrust Area Final Report for 2008-2010

A. Principle investigator and co-investigators: Todd French, Guochang Zhang, Rafael Hernandez, Lewis R. Brown, Susan Diehl, Janet Donaldson, Mark Lawrence, Debarti Paul, Susan Bridges, Shane Burgess, Yoginder Dandarass

B. Summarization of Activities

Subtask C.1 Determination of sugar conversion kinetics into triglycerides

1. Planned Activities

C.1.ML.1 Year 1 milestone is to attempt the achievement of 60% conversion of the theoretical lignocellulosic sugars into triglycerides.

C.1.ML.2 Year 2 milestone is to attempt the achievement of 75% conversion of the theoretical lignocellulosic sugars into triglycerides.

2. Summarization of Activities

Microorganism and the media

The oleaginous yeast *Rhodotorula glutinis* (ATCC 15125) was used in all experiments. Therefore, *R. glutinis* was grown initially in nitrogen-rich medium at a pH of 5.5. The nitrogen rich medium contained (per liter): yeast extract,1.0 g; $Na_2HPO_4 \cdot 12H_2O$, 1.0 g; KH_2PO_4, 1.0 g; $MgSO_4 \cdot 7H_2O$, 0.4 g; $(NH_4)_2SO_4$, 4.0 g; $FeSO_4$ solution (4.0 $g.l^{-1}$ $FeSO_4 \cdot 7H_2O$), 6.0 ml; and trace mineral solution, 10 ml. The trace mineral solution consisted of (per liter): $CaCl_2 \cdot 2H_2O$, 3.6 g; $ZnSO_4 \cdot 7H_2O$, 0.75 g; $CuSO_4 \cdot 5H_2O$, 0.13 g; $MnSO_4 \cdot H_2O$, 0.50 g; $CoCl_2 \cdot 6H_2O$, 0.13 g; $Na_2MoO_4 \cdot 2H_2O$, 0.17 g. For the carbon and energy source, sugars were mixed to produce an artificial acid hydrolysate that was composed of: glucose, 10.7g; xylose, 8.2 g; galactose, 0.3 g; arabinose, 1.0 g; mannose, 0.1 g. A total of 20 g l^{-1} of this sugar mixture was added to the medium along with furfural 0.3 ml. l^{-1} and 0.26 g of acetic acid per gram of sugars.

Analytical

Cell Dry Weight: Cell dry weight determination was performed by centrifuging the cells at 6037 $\times$ g for 15 min, washing with DI water, and drying in a freeze-dry system to constant weight.

Lipid Extraction: The lipid content of the cellular materials was obtained by extracting the lipids from the cell mass using a method modified from the one described by Bligh and Dyer.

Lipid Identification: The microbial lipids were transesterified to fatty acid methyl esters (FAME) by reacting with methanol having 20 $cm^3.dm^{-3}$ H_2SO_4 as catalyst at 60 $^{\circ}C$ for 2 h. After being neutralized with $KHCO_3$ solution, the FAMEs were extracted by toluene and analyzed using an Agilent 6890 series Gas Chromatograph. The FAME peaks were identified and quantitated by comparing the unknown responses to those generated from known standards.

Sugar Analysis: Glucose and xylose are the major components (> 95%) of the sugars in acid hydrolysate of switchgrass. These two sugars' concentrations were analyzed by high pressure liquid chromatography (Agilent 1100 series).

Ammonium Analysis: The concentration of nitrogen (ammonium) was determined by ion chromatograph (IC, ICS 3000 ion chromatograph DIONEX).

Experimental results

Yeast Growth

In this study, the process included two stages. The first stage was characterized by the cell growth. During this stage, the nitrogen was in excess compared to sugar. The C:N ratio is 9.6:1 (wt). The lipid production in the cells during this stage was constant and below 5% (wt%). Once the culture reached the stationary phase as determined by no significant change in the optical density, the cells were transferred to a nitrogen-free medium for lipid accumulation. During the second stage, the cells were expected to accumulate lipids as no exogenous nitrogen was added to the medium and a surfeit of carbon was available.

As shown in Figure C.1.1, the lag phase was about approximately 5 h and cell mass concentration reached 2.16 g. l^{-1} within 20 h. As indicated by the cell mass concentration and the OD value, the culture reached stationary phase within 20 h. As demonstrated in Figure C.1, *R. glutinis* metabolized glucose even with the presence of both glucose and xylose. These results in Figure C.1.1 indicate that the oleaginous microorganism *R. glutinis* was able to grow in the media containing sugars from artificial acid hydrolysate with the known inhibitors acetic acid and furfural present. Based on these results, the yeast could be harvested at 20 h from a nitrogen-rich medium and transferred to the nitrogen-free medium for lipid accumulation.

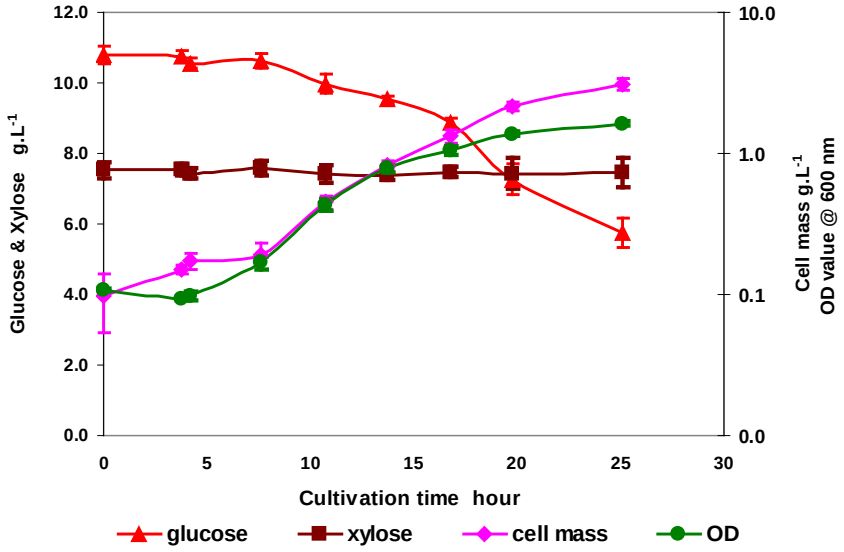


Figure C.1.1 - Growth as determined by gravimetric and optical density measurements of *Rhodoturula glutinis* in the nitrogen-rich medium with sugars from an artificial acid hydrolysate as carbon and energy source including acetic acid and furfural at 30˚C. [At 20 h, the cells reach the stationary growth phase].

In this study, the acetic acid and furfural as a product of acid hydrolysis of switchgrass were studied for its effect on the growth of *R. glutinis*. Toward this end, the growth of *R. glutinis* on pure glucose and xylose of 20 g. l^{-1} were compared to the growth using glucose or xylose with 0.3 ml. l^{-1} fufural and 0.26 g acetic acid/g of sugar present. The results of dry cell mass concentration with time are presented in Figure C.1.2. These results clearly show that there is some effect on *R. glutinis*' ability to metabolize glucose during the growth phase as indicated by a decrease in the cell mass in the presence of these inhibitors. The effect was not observed with cultures growing on xylose with or without the inhibitors present.

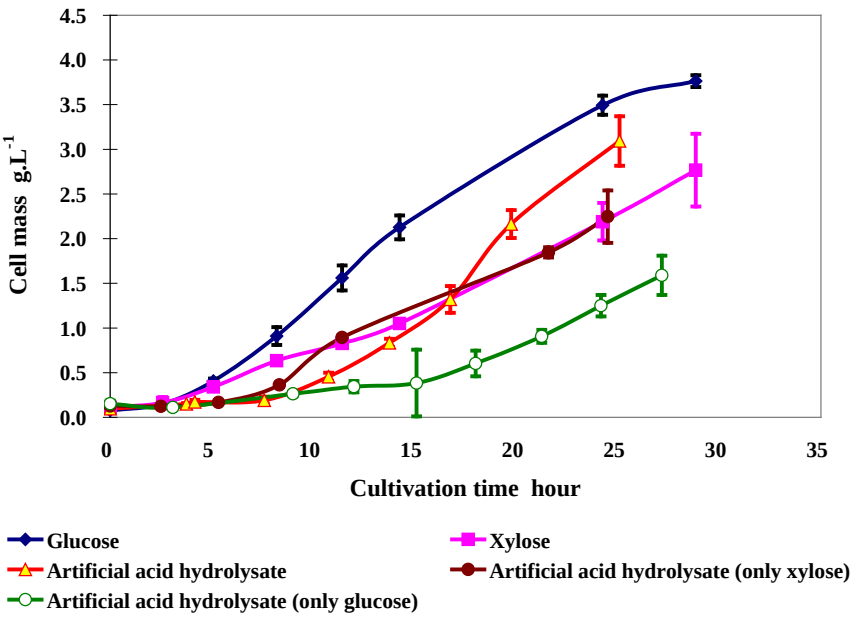


Figure C.1.2 - The effect of acetic acid and furfural on growth of *R. glutinis* when grown with various carbon sources at 30 ˚C.

Lipid accumulation

During the first stage, *R. glutinis* reached stationary phase after 20 h of growth using the sugars in the artificial acid hydrolysate as sole carbon and energy source. In the experiments, pure glucose, or pure xylose, or artificial acid hydrolysate with total sugar of 30.0 g. l^{-1} or 45.0 g. l-1, or 60.0 g. $l^{-1}$was added to the *R. glutinis* from the first stage for the lipid accumulation during the second stage. The cell mass, lipid content of the dry cell mass, and the sugar concentrations remaining in the medium were measured during this experiment. The results are presented in Figures C.1.3, C.1.4 and C.1.5.

Lipid production by Rhodotorula glutinis growing on pure glucose

The lipid accumulation in *Rhodotorula glutinis* grown on glucose of 24.4 g/l or 31.80 g/l or 60 g/l as sole carbon and energy source was shown in Figures C.1.3, 1.4, and 1.5, respectively. While adding 24.4 g/l glucose to the medium, the yeast cell mass increased within 96.2 h from initial 3.89 g/l with 4.54 % of lipid (wt%, based on dry cell mass) to 10.94 g/l with 15.57% of lipid when glucose was exhausted.

When the initial glucose concentration rose to 31.80 g/l, the cell mass increased from initial 2.78 g/l to 13.72 g/l, lipid in cell was accumulated from 2.78 % to 33.90% until glucose was exhausted. The cells started to accumulate lipid quickly as the cell mass increased, rate leveled off after 92.5 h. When the initial glucose was 60 g/l, cell mass concentration increased to 14.93 g/l and lipid in dry cell mass was accumulated up to 44.96% (Figure C.1.4). It indicated that with higher sugar concentration more lipids will be accumulated in the cell.

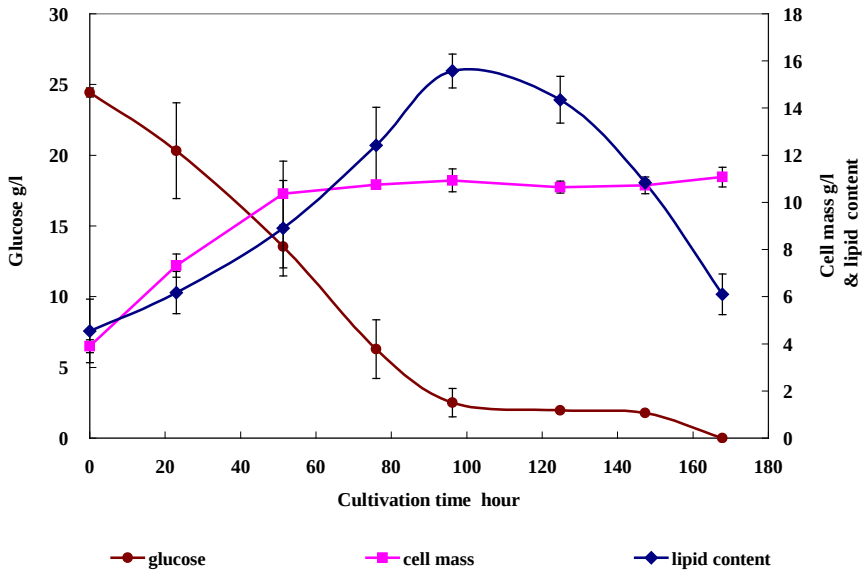


Figure C.1.3. Lipid production by *Rhodotorula glutinis* grown on 24.4 g/l of glucose at 30 ℃

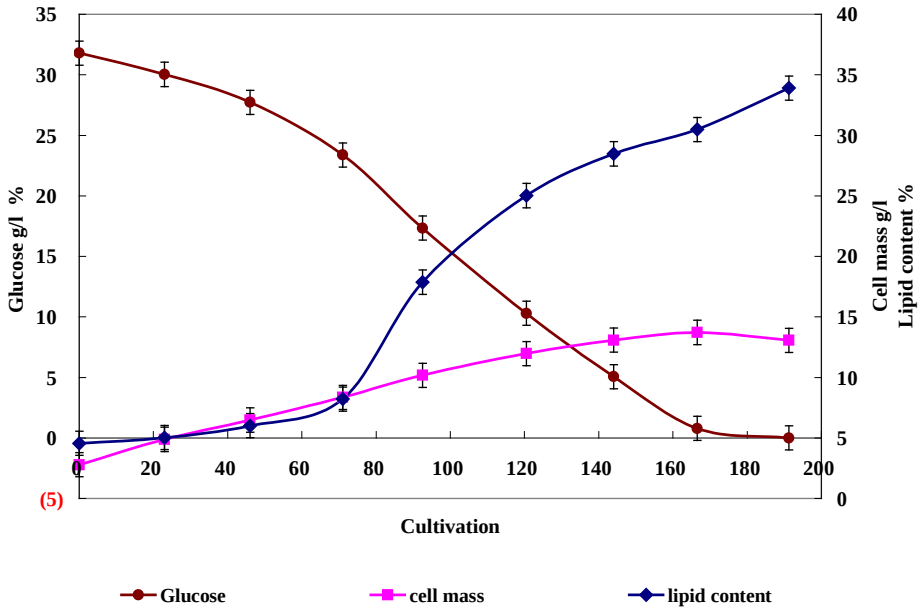


Figure C.1.4 Lipid production by *Rhodotorula glutinis* growing on 31.8 g/l of glucose at 30 ℃

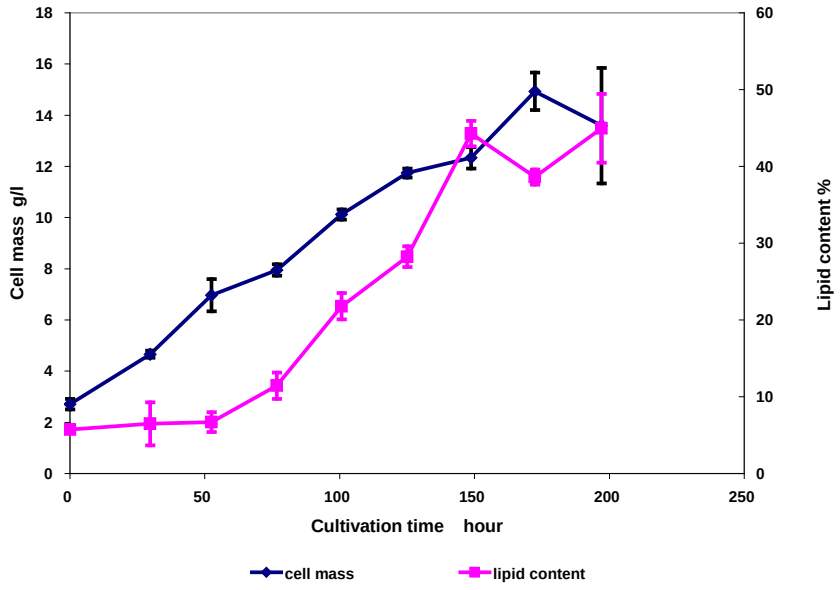


Figure C.1.5 Lipid production by *Rhodotorula glutinis* growing on 60 g/l of glucose at 30 ℃

Lipid production by Rhodotorula glutinis grown on pure xylose at 30 ℃

Pentose cannot be converted to ethanol by naturally occurring microorganisms but can be easily converted to microbial lipid. The lipid accumulation by *Rhodotorula glutinis* grown on xylose of initial 23.76 g/l and 30.63 g/l was tested, and the results are presented in Figures C.1.6 and C.1.7, respectively.

While grown on xylose of 23.76 g/l, the cell mass of *Rhodotorula glutinis* increased from 2.84 g/l to 8.76 g/l with lipid content of dry cell mass rising from 1.37% to 25.44% until xylose was exhausted within 96.5 h. When initial xylose was added up to 30.63 g/l, cell mass concentration rose to 9.20 g/l with lipid content increasing to 44.02%. These results showed that the oleaginous microorganism *Rhodotorula glutinis* has higher lipid production while grown on pentose of xylose than on glucose.

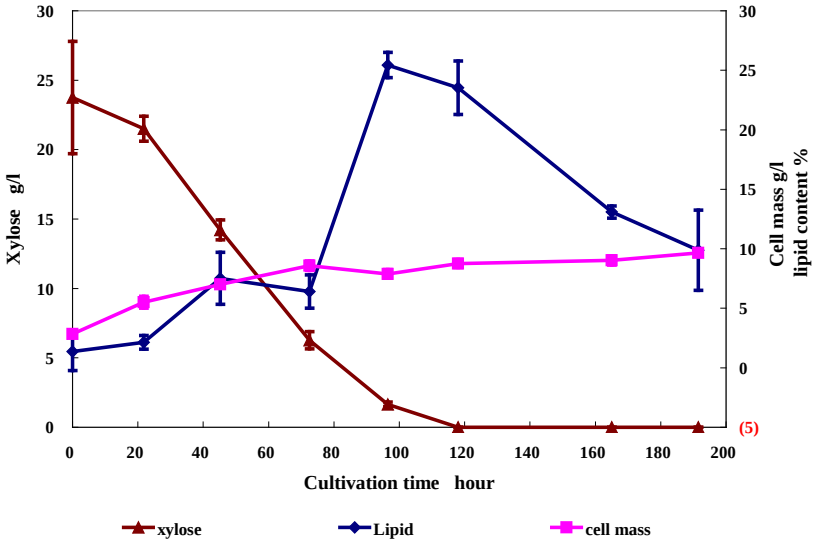


Figure C.1.6 Lipid production by *Rhodotorula glutinis* grown on 30 g/l of xylose at 30 ℃.

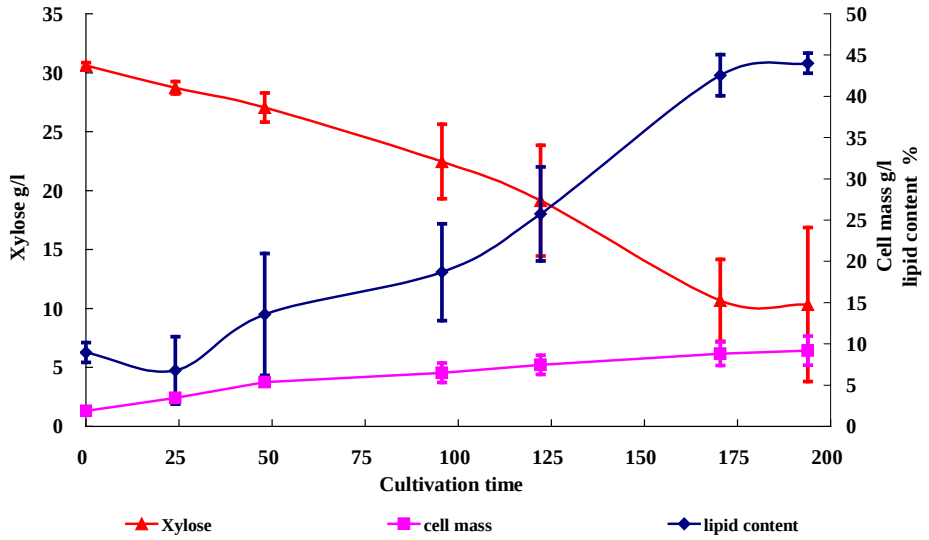


Figure C.1.7 Lipid production by *Rhodotorula glutinis* grown on 45 g/l of xylose at 30 ℃

Lipid production by Rhodotorula glutinis growing on artificial acid hydrolysate

As presented above, *Rhodotorula glutinis* was grown very well in the media using acid hydrolysate as sole carbon and energy source with acetic acid and furfural, which are inhibitors for ethanol yeast. Under these conditions, *R. glutinis* also accumulated lipid from glucose and xylose and had a higher lipid accumulation in cells from xylose than from glucose.

In the experiments, acid hydrolysate with total sugar of 30 g/l, 45 g/l, and 60 g/l in the media was added for the lipid accumulation. The cell mass lipid content in dry cell mass and the sugar consumption in the medium were measured during the fermentation. The results are presented in Figures C.1.8, C.1.9, and C.1.10.

When the total sugar concentration added was 30 g/l, cell mass increased from initial 1.49 g/l to 6.25 g/l with lipid content increasing from 2.12% to 16.67%. If the initial total sugar concentration was 45 g/l, cell mass increased from 2.58 g/l to 10.31 g/l, the lipid content in dry cell mass also increased from 3.62% to 29.78%. When initial total sugar concentration increased further to 60 g/l, the lipid accumulated in the cell reached 38.97% of the dry cell mass

The results of the sugar analysis also showed that the oleaginous microorganism *R. glutinis* metabolized the glucose first, then the xylose when glucose was exhausted. The lipid accumulated in the cells had a maximum value followed by a slight decrease while the glucose was exhausted. Then the cells started to accumulate lipid again by metabolizing xylose.

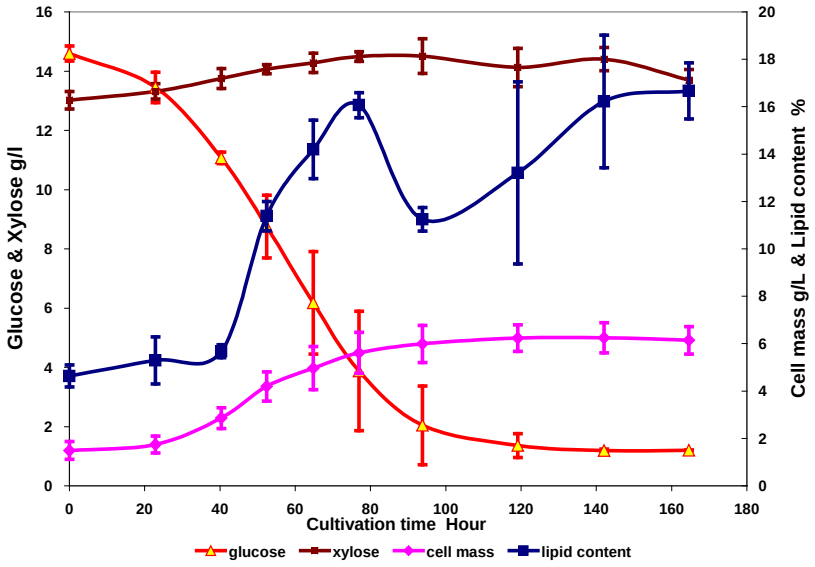


Figure C.1.8 Lipid production by *Rhodotorula glutinis* grown on acid hydrolysate with 30 g/l of total sugar at 30 ℃

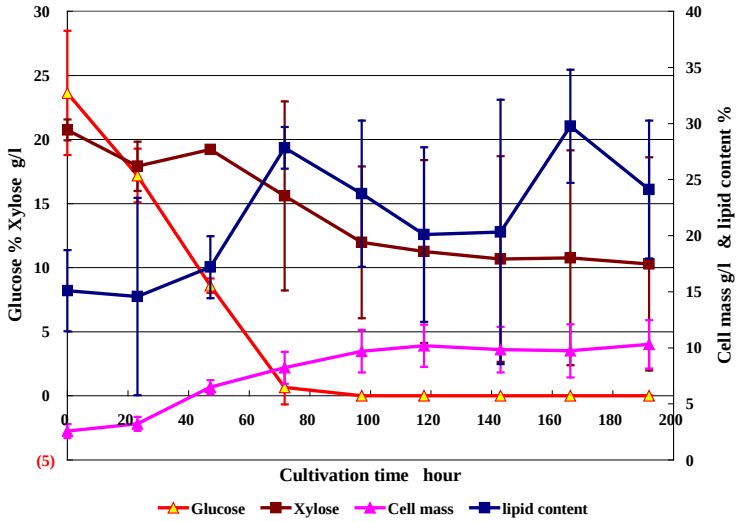


Figure C.1.9 Lipid production by *Rhodotorula glutinis* grown on acid hydrolysate with 45 g/l of total sugar at 30 ℃

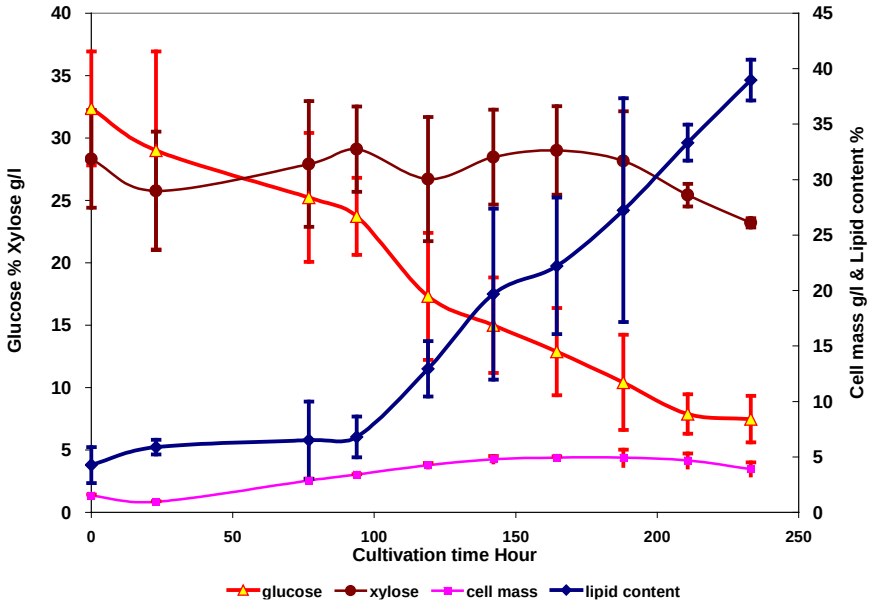


Figure C.1.10 Lipid production by *Rhodotorula glutinis* grown on acid hydrolysate with 60 g/l of total sugar at 30 ℃

Lipid production by Rhodotorula glutinis growing on artificial acid hydrolysate with 20 g/L of total sugar

In the growth and lipid production by R. glutinis with artifical acid hydrolysate with 30 to 60 g/L of total sugar, a great amount of sugar still remains in the cultures. In this study, acid hydrolysate with a lower concentration of 20 g/L total sugar were evaluated for growth and lipid accumulation. The sugar added in media is listed in Table C.1.1. In all the tests, both acetic acid and furfural were added to investigate the influences on the cell growth and lipid accumulation from glucose and xylose. The results were compared with tests having 45 g/l of total sugars and shown in Figures C.1.11-C.1.14. The summary of the results is as follows.

The 20 g/L pure glucose was depleted within four days; the cell mass concentration reached 9.35 g/L ; the xylose of 20 g/L was metabolized in about five days; and, finally, the cell mass concentration increased to 8.45 g/L.

While having 10.8 g/l glucose and 8.2 g/L xylose in a mixture of total 20 g/l sugars from artificial hydrolysate of switchgrass, glucose was consumed with 96 h, and xylose was depleted 48 h later. The maximum cell mass concentration was 7.43 g/L.

Table C.1.1 Components of sugars added to the media.

Test	Initial concentration of lignocellulosic sugars							
	Glucose g	Xylose g	Galactose g	Arabinose g	Mannose	Total g	Acetic acid g	Furfural
SGGX-20	10.6998	8.155	0.3324	0.9937	0.1048	20		
SGXG-20	8.155	10.6998	0.3324	0.9937	0.1048	20	5.2	0.3 ml/L
SGG-20	20					20		
SGX-20		20				20		
SGGX-45	24.0746	18.3488	0.748	2.2358	0.2358	45	11.7	

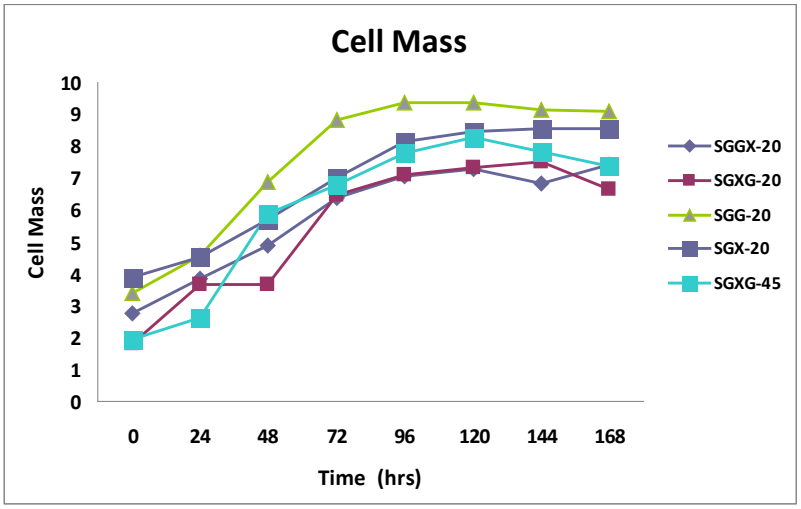


Figure C.1.11 Growth of *R. glutinis* at 30 ˚C with 20 g/L of total sugars

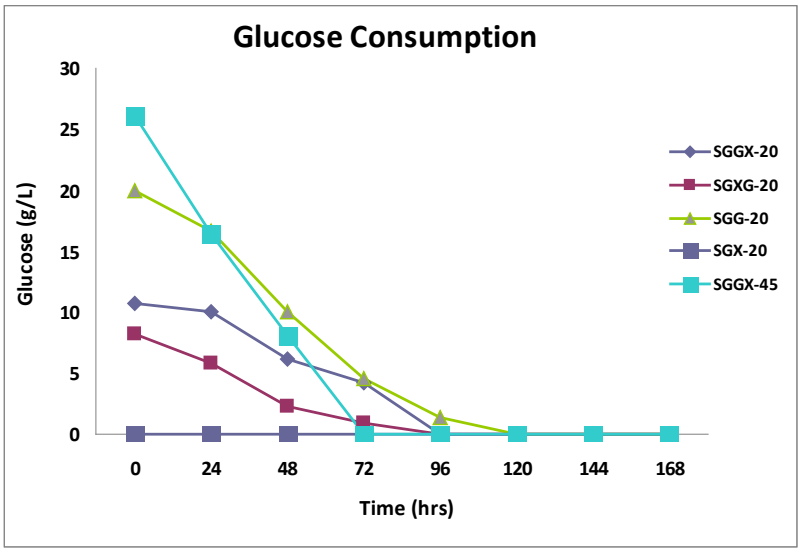


Figure C.1.12 Glucose consumption by *R. glutinis* at 30 ˚C with 20 g/L of total sugars

In the media added 10.8 g/l xylose and 8.2 g/L glucose with 20 g/l of total sugar, the glucose was eaten up in about 72 h and xylose was almost used up in the following 48 h. The maximum cell mass concentration rose to 7.51 g/L.

For all the tests with 20 g/l total sugars, the lipid content in the cells was constant low because the sugar was depleted before the microorganism entering the lipid accumulation phase.

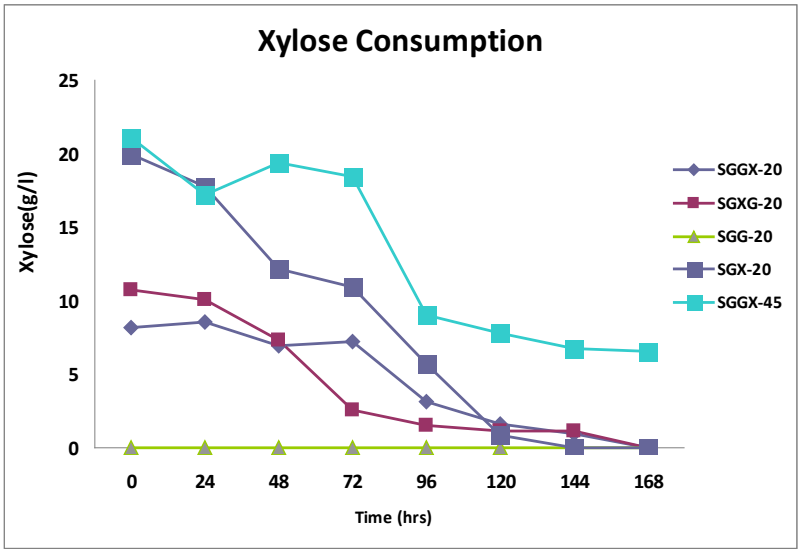


Figure C.1.13 Xylose consumption by *R. glutinis* at 30 ˚C with 20 g/L of total sugars

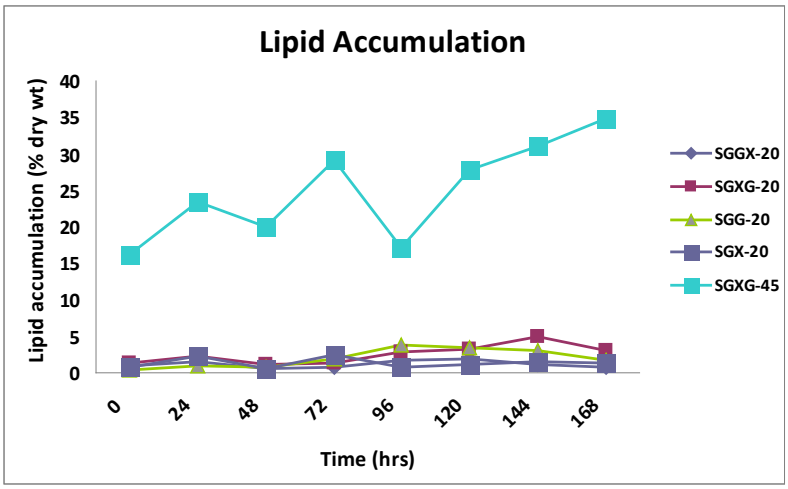


Figure C.1.14 Lipid accumulation by *R. glutinis* at 30 ˚C with 20 g/L of total sugars

1.2.4 Fatty acid composition of microbial lipids

While using microbial lipid to produce biodiesel, the properties of the fuel are determined by the structure of its component fatty esters, particularly the fatty acid composition. In Table C.1.2, the fatty acid composition of the methyl esters generated from the microbial lipids of *R. glutinis* grown on the artificial acid hydrolysate of switchgrass with 60 g. l^{-1} of total sugar are presented. The major fatty acids are Hexadecanoic acid (C16:0), Octadecanoic acid (C18:0), (9Z) Octadec-9-enoic acid (C18:1), cis, cis-9,12-octadecadienoic acid (C18:2), and

all-cis-6,9,12-octadecatrienoic acid (C18:3). These data show that the fatty acids that make up the triacyglycerols in microbial oil are also present in soy bean oil and only different in the total percentages.

Table C.1.2 - Fatty acid composition of microbial lipids in *Rhodotorula glutinis* growing on acid hydrate from switchgrass with total sugar of 60 g/l

Cultivation time, hour	0.0	22.8	76.9	93.8	119.1	142.1	164.6	188.1	210.8	233.1
Lipid content, %	4.3	5.9	6.5	6.8	13.0	19.7	22.2	27.3	33.3	39.0
Octanoic acid (C8:0)	0.4	0.0	0.1	0.1	0.1	0.1	0.0	0.0	0.0	0.1
Decanoic acid (C10:0)	1.4	1.6	0.7	0.3	0.2	0.1	0.1	0.1	0.1	0.2
Dodecanoic acid (C12:0)	1.9	0.4	0.3	0.1	0.2	0.3	0.2	0.2	0.2	0.3
Tetradecanoic acid (C14:0)	2.3	1.9	1.4	1.1	1.2	1.3	1.2	1.3	1.3	1.4
Hexadecanoic acid (C16:0)	8.2	12.5	15.0	16.9	18.2	19.0	19.3	19.4	19.6	18.7
Hexadec-9-enoic acid (C16:1)	1.7	1.6	1.0	0.7	0.5	0.6	0.5	0.4	0.5	0.6
Octadecanoic acid (C18:0)	22.3	9.7	16.2	16.6	15.7	15.0	15.2	15.6	14.2	13.2
(9Z) Octadec-9-enoic acid (C18:1n9c)	26.9	41.1	44.1	44.2	44.7	44.5	44.6	44.0	43.9	43.8
cis, cis-9,12-octadecadienoic acid (C18:2n6c)	8.5	12.2	9.0	9.6	9.9	10.4	10.7	11.1	12.1	12.7
all-cis-6,9,12-octadecatrienoic acid (C18:3n6)	5.3	4.2	3.2	3.8	4.3	4.6	4.8	5.0	5.2	5.5
Icosanoic acid (C20:0)	3.9	3.4	2.0	1.6	1.3	1.0	0.9	0.9	0.8	1.0
Docosanoic acid (C22:0)	5.5	3.9	2.3	1.4	1.2	1.0	0.9	0.7	0.8	0.8
(Z)-Docos-13-enoic acid (C22:1n9)	3.5	1.2	0.9	0.9	0.7	0.6	0.4	0.3	0.3	0.5
Tetracosanoic acid (C24:0)	8.1	6.4	3.8	2.7	1.8	1.5	1.2	1.1	1.1	1.3
Total:	100.0	100.0	100.0	100.0	100.0	100.0	100.0	100.0	100.0	100.0
saturated lipid	54.0	30.1	25.7	24.2	24.2	24.4	23.9	23.7	23.8	23.7
mono unsaturated lipid	32.2	43.8	46.0	45.8	46.0	45.6	45.5	44.7	44.7	44.9
polyunsaturated lipid	13.8	16.4	12.2	13.4	14.2	15.0	15.4	16.0	17.2	18.2

Subtask C.2 Isolation and characterization of novel oleaginous microorganisms

1. Planned Activities

C.2.DL.1 Year 1 deliverable is to screen 10 environmental samples for novel triglyceride accumulating microorganisms.

C.2.DL.2 Year 2 deliverable is to screen 10 additional environmental samples for oleaginous microorganisms.

2. Summarization of Activities

The initial approach to isolate novel oleaginous microorganisms was to screen cores from petroleum-bearing formations for the desired microbes. This decision is based on the assumption that some of the microbes responsible for the production of crude oil millions of years ago may still be present, probably in the form of ultramicrobacteria (UMB). A total of 11 cores were employed resulting in 62 cultures isolated. The locations from which cores were obtained range from the United States to Ecuador and Kuwait and from depths of 4,000-11,000 ft.

Another approach to finding microorganisms producing large quantities of triclycerides was to evaluate organisms in our stock culture collection of microbes that grew on the gaseous hydrocarbons propane, n-butane, and isobutane. A total of 4 propane, 16 n-butane, and 6 isobtane cultures were screened for triglycerides.

The challenge was to find a suitable method to examine the cultures for the presence of triglycerides. Efforts to quantitate the triglyceride content of cultures using a Triglyceride Quantification Kit from BioVision Products did not produce satisfactory results. Some

cultures were analyzed using the Bligh Dyer method, but a large amount of cellular material is needed for this test to receive satisfactory results. In order to increase the quantity of biomass, tests (using the four propane cultures) were undertaken to compare biomass production using growth in liquid medium, growth on the surface of agar, and biphasic growth. The media employed in this experiment was Bacto Tryptic Soy Broth (TSB) and Bacto Tryptic Soy Agar (TSA). The inoculum was 0.2 ml of MSM culture of each microorganism grown under an atmosphere of propane, oxygen, and carbon dioxide for five days at 30 ºC. The cultures were incubated on the shaker while the petri plates were incubated in conventional fashion. After spreading the inoculum on the biphasic plates, 14 ml of TSB were placed on the plates, and the plates incubated on a VWR Scientific Products Rocking Platform model 200. All cultures were incubated at 30 ºC for five days. After incubation, cells were harvested and the dry weight of cells determined. The results are given in Table C.2.I.

Table C.2.1. Dry Weight of Cells Produced After Five Days of Growth at 30 ºC.

Propane Culture No.	TSB (g of cells)	TSA (g of cells)	Biphasic Growth (TSA covered with TSB) (g of cells)
3	0.05	0.05	0.31
32	0.04	0.11	0.59
33	0.03	0.11	0.27
34	0.05	0.05	0.40

In order to expedite the testing of cultures for the presence of lipids, we decided to test hydrophobicity as a preliminary screening technique. The test for hydrophobicity involves increasing the percent light transmission of an aqueous culture by exposing it to hexadecane. We found this method to be only partially successful because while it will differentiate between cells of the same organisms in terms of fat content, it will not do so for cells of different species.

Another hydrophobicity test (Serebryakova, E.V. et al., Microbiology 2002, 71:202-204) was used and found to be more accurate. The test uses the Hydrophobicity Index (HI) of the microbial cells showing relative amounts of lipid in cultures. The HI is calculated by the formula:

$$HI = \frac{100 - E \times 100}{Eo}$$

Eo = the initial optical density of the cell suspension
E = the optical density of the aqueous phase after its separation from the chloroform phase

All cultures on hand were screened using this method. We found that n-butane cultures 2, 6, and 33 had a Hydrophobicity Index (HI) of 77%, 93%, and 82%, respectively, and that isobutane cultures 13 and 12 had a Hydrophobicity Index of 87% and 83%, respectively. All other cultures had an HI below 80%.

Using known oleaginous microorganisms such as *Rhodotorula glutinis, Cryptococcus curvatus,* etc., molecular probes development was begun under this funding. These probes

were to be used to screen environmental samples for the presence of these and closely related oleaginous microorganisms. The first objective was to quantify the specific species within the microbial consortium and determine how they change with the differing conditions. One of the only ways to quantify changes in individual species in a mixed population is through quantitative real time PCR. Initially a list of 10 yeasts and 9 actinobacteria was provided, and subsequently 6 more yeast were added to the list. Sequence information was obtained from the NCBI Web site for 22 of the 25 species in the consortium. There was no sequence information for two of the isolates (*Acinetobacter* sp strain HO1-N and *A.* sp. Strain 211). Up to 20 sequences were obtained for each species (if possible) and aligned with MegAlign (Lasergene software). Consensus sequences were brought into BEACON DESIGNER software and primers designed for quantitative real time PCR. There was one departure from the original plan. Originally, the plan was to multiplex the assays. However, after extensive discussion with LSBI, the advice was not to multiplex. Optimizing multiplex assays can take longer and is much more difficult than running a series of singleplex assays. Therefore, primers were designed, so the PCR assay conditions were the same for more than one species, if possible, allowing for the running of multiple species in a given PCR run. In order to validate the primers for specificity, pure cultures (or DNA) were needed. Unfortunately, pure cultures could not be obtained for all species, so primers were optimized for 12 of the available species. It is not simply the presence, absence, or change of a species that determines increased production of triglycerides, but what species are actively expressing enzymes involved in triglyceride synthesis. The next series of studies were designed to determine what media conditions turns on or off select key genes that code for triglyceride synthesis. Due to limited sequence information on GenBank, the two species evaluated were *Rhodococcus opacus* and *Yarrowia lipolytica*, with a possibility for *Cryptococcus albidus* or *Cryptococcus curvatus* based on sequence information for *C. neoformis*. Quantitative real time PCR primers were developed for one or all of the above species for the following enzymes: acetyl CoA carboxylase, beta-ketoacyl ACP synthase, enoyl ACP reductase, wax ester synthase, 1-acylglycerol-3-phosphate acyltransferase, and glycerol-3-phosphate acyltransferase. The primers have been optimized using cDNA from RNA extracted from the species of interest. After validation, the cultures will be exposed to changes in the media composition to determine how that impacts the expression levels of select genes.

Subtask C.3 Evaluation of non-lethal oil extraction technologies

1. Planned Activities

C.3.ML.1 Year 1 milestone is to attempt to achieve 15% oil release with 40% survivability of the cells.

C.3.ML.2 Year 2 milestone is to attempt to achieve 30% oil release with 60% survivability of the cells.

2. **Summarization of Activities**

Background and rationale

The goal of this subtask was to develop a method to extract lipids from oleaginous microorganisms that would retain cell viability. Instead of trying to use mechanical means to accomplish this task, we employed the use of molecular techniques. Advancements in molecular biology are now allowing researchers to focus on alternative methods to optimize biofuel sources and production (Fischer, Klein-Marcuschamer et al. 2008; Clomburg and Gonzalez 2010; Dellomonaco, Fava et al. 2010). However, most other laboratories using

this method have focused on using modified common laboratory microorganisms, which has proven to have several limitations, including potential toxicity of the end product in large concentrations and extraction of the product. The best means to extract the usable product from these modified microbes is to lyse the cells, which requires high-energy processes. Therefore, we took an alternative approach to accomplish this goal, which entailed modifying an oleaginous microorganism to be able to accumulate extracellular lipids.

Approaches used to accomplish goal

Rhodococcus opacus is an oleaginous microorganism capable of producing up to 76% of its cell weight in triacylglycerides (TAGs) (Waltermann, Luftmann et al. 2000; Alvarez and Steinbuchel 2002). This microbe accumulates these specialized lipids in inclusion bodies within its cytoplasm. In this project, *R. opacus* was genetically modified through treatment with ethyl methanesulfonate (EMS) and was subsequently found to accumulate extracellular lipids. This was initially determined through the growth of the auxotrophic mutant KD115, which was only able to grow if an external source of triglycerides were provided. In a mixed culture with both the modified *R. opacus* (JD103) and KD115, this auxotrophic mutant was able to grow. This suggested that the cells were either lysing or secreting lipids extracellularly for the use by this microorganism. To determine which of these possibilities was responsible for the growth of the auxotroph, JD103 was further analyzed by flow cytometry, microscopy and mass spectrometry to determine if JD103 produces extracellular lipids while retaining viability.

Using fluorescent microscopy to identify the location of bacteria and lipids, we were able to determine that JD103 had large lipid bodies extracellular, which was not observed in the wild-type strain (Figure C.3.1). Growth of this mutant was also very similar to the wild-type *R. opacus* (Figure C.3.2). Glucose consumption was also compared between R. opacus wildtype and JD103. Our results in Table C.3.1 indicate that JD103 consumed less glucose than the wild-type strain.

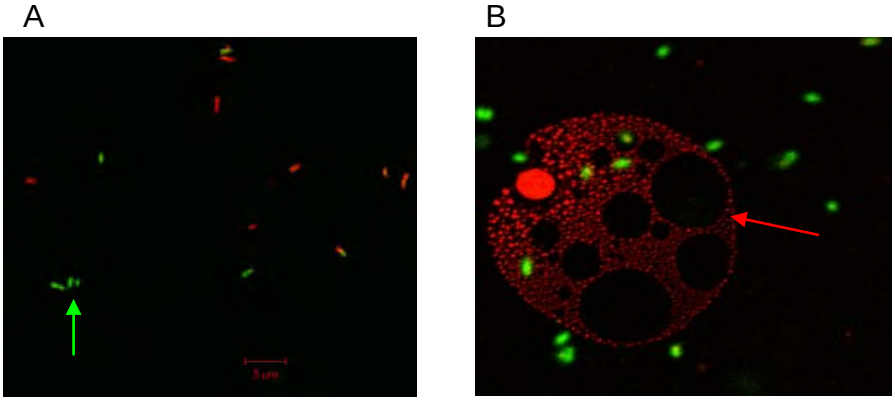


Figure C.3.1. Lipid formation by *R. opacus* WT (A) and JD103 (B) after a 24 hr incubation as observed by confocal microscopy. Cells were stained with nile red (lipid stain, red) and SYTO 9 (nucleic acid stain, green). Green arrows indicate location of bacterial cells; red arrow indicates extracellular lipids.

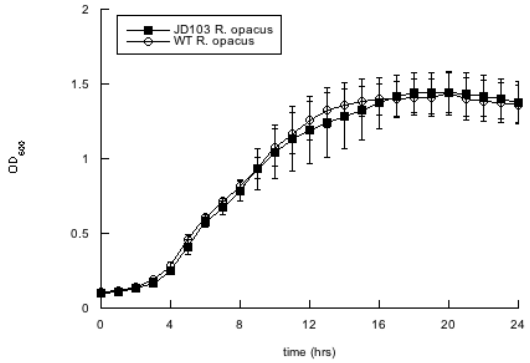


Figure C.3.2. Growth analysis of *R. opacus* WT (■) and JD103 (○). Growth curves represent the average of three independent replicates.

Our results in Table C.3.1 suggest that the cells are not as metabolically active as wild type, even though our growth analysis in Fig. C.3.2 suggests otherwise. Because of our conflicting results between cell viability and glucose consumption, we further analyzed JD103 to verify that these cells were viable. Viability of JD103 was further confirmed to be similar to the wild-type strain using the *Live/Dead* stain (Invitrogen). Briefly, ~1x10^7 cells were stained with the LIVE/DEAD *BacLight*^{TM} bacterial viability kit consisting of SYTO 9 and propidium iodide. Cells were then analyzed by a BD FASCaliber flow cytometer using Cell Quest software (BD Biosciences, San Jose, CA). Analyses were performed on 4500 to 5000 cells (gated events) using instrument parameters previously described by others (Gunasekera, Veal et al. 2003). Percent viability was determined by a two-parameter comparison of green (live cells) and red (dead cells) fluorescent emissions for individual bacteria using the formula described by the manufacturer: [% live green-emitting cells/ (% dead red-emitting cells + % live green-emitting cells)] x 100. Three independent replicates were performed for each strain. Our results showed that at 24 h, both WT and JD103 had similar viability (~78% cells viable).

Table C.3.1. Amount of glucose consumed after 24 h of growth

Strain	%Glucose consumed	±StdDev
WT *R. opacus*	99.51%	0.02113
JD103	85.86%	0.30762

The data presented above all indicate that JD103 is viable and may be accumulating extracellular lipids. To quantify the amount of triglycerides that were produced extracellularly did exceed these observed by the wild-type strain, cells were grown for 24 h and were pelleted by centrifugation. The supernatants were removed from the cell pellets, and lipids from both the supernatants and cell pellets were isolated using the Bligh & Dyer lipid extraction method as described previously. Our initial attempt at this method did not result in a significant difference in extracellular lipids, but did indicate that the mutant had fewer lipids intracellularly. We hypothesized that this might be due to the lipophilic behaviour of the lipids being retained near the cell pellet, causing loss during the extraction process. We, therefore, repeated the assay with an additional wash of the cell pellet with chloroform. This was added to the collected supernatant and lipid extractions were performed. Weights of the resulting lipid extractions were determined (in lieu of “media only” controls) to obtain the yield of lipid production as compared to sugar consumption (Table C.3.1). The results indicated that even though the cell mass per gram of sugar consumed was higher for WT

following a 24-h incubation, JD103 consumed less sugar (also correlates with Table C.3.1) and also accumulated a significantly higher amount of lipids in the surrounding media (Table C.3.2).

Table C.3.2. Yield of lipids produced

Strain	Yield extracellular lipid:sugar	Yield cell mass:sugar	Cells: sugar consumed
WT *R. opacus*	0.098glipid/g sugar	0.0803g cells/g sugar	$4.62x10^{11}$ CFU/g sugar
JD103	0.353g lipid/g sugar	0.0588g cells/g sugar	$1.56x10^{11}$ CFU/g sugar

Gas chromatographic (GC) analysis of the lipids extracted indicated that a predominant portion of the supernatant was monoglycerides for both JD103 and WT (Table C.3.3). There was a significant increase in the amount of monoglycerides in the supernatant of JD103 compared to WT. However, comparing the cell pellet (intracellular) lipid composition from JD103 to WT indicated that JD103 had a significant decrease in the intracellular amount of both monoglycerides and triacylglycerides. No significant difference was observed in the concentration of diglycerides present in the JD103 cells as compared to the WT intracellular lipid composition. The overall quantities of extracellular and intracellular fatty acid methyl esters for JD103 were also not significantly different from WT (Table C.3.4). A significant increase was observed in the extracellular concentration of lignoceric acid methyl ester in JD103 as compared to WT. However, this concentration increase was relatively minor in relation to the total concentration of FAMEs (1.8%).

Table C.3.3. Extracellular and intracellular lipid profiles

	WT intracell[a]		WT extracell[b]		JD103 intracell[a]		JD103 extracell[b]	
Lipid	Conc µg/mL	StDev	Conc µg/mL	StDev	Conc µg/mL	StDev	Conc µg/mL	StDev
Monoglycerides	17.32	2.85	56.15	0.19	12.27*	0.81	98.23*	3.40
Diglycerides	8.27	0.95	16.03	2.32	10.65	1.40	18.52	1.44
Triglycerides	43.28	0.01	3.83	0.21	28.74*	0.22	5.21*	1.41

[a]Intracellular concentrations of lipids are based on 20 mL cell pellets collected from 24 h cultures of WT or JD103. StDev represents ± standard deviations.
[b]Extracellular concentrations of lipids are based on 10 mL of supernatant collected from 24 h cultures of WT or JD103. StDev represents ± standard deviations.
*Indicates significant change ($p < 0.05$) in concentration in JD103 compared to WT.

Table C.3.4. FAMEs present in WT and JD103 *R. opacus*.

	WT intracell[b]		WT extracell[c]		JD103 intracell[b]		JD103 extracell[c]	
FAME	%	StDev	%	StDev	%	StDev	%	StDev
Myristic AME (C14:0)	3.59	0.07	2.43	0.15	3.36	0.14	2.66	0.38
Palmitic AME (C16:0)	36.35	0.57	28.68	0.89	35.16	0.72	29.99	2.53
Palmitoleic AME (C16:1)	1.88	0.06	ND		1.96	0.22	0.39	0.59
Stearic AME (C18:0)	19.28	0.72	46.05	1.56	20.75	3.31	38.90	4.51
Oleic AME (C18:1)	13.85	0.63	3.54	1.03	13.26	1.32	5.70	2.44
Linolenic AME (C18:3)	2.52	0.14	ND		2.27	0.44	0.41	0.61
Erucic AME (C22:1)	ND[a]		ND		ND		0.15	0.46
Lignoceric AME (C24:0)	0.14	0.41	0.25	0.74	0.38	0.57	1.80*	0.48
Total Unknowns (based on C16:0)	22.40	0.81	19.05	1.29	22.87	1.15	20.00	2.66
Total FAMEs (μg/mL)	76.63	4.35	72.24	2.72	73.83	9.32	86.51	14.96

[a]ND: Not detected
[b]Intracellular concentrations of lipids are based on 20 mL cell pellets collected from 24 h cultures of WT or JD103. StDev represents ± standard deviations.
[c]Extracellular concentrations of lipids are based on 10 mL of supernatant collected from 24 h cultures of WT or JD103. StDev represents ± standard deviations.
*Indicates significant change ($p < 0.05$) in concentration in JD103 compared to WT.

Subtask C.4 Evaluation of the cellulose and hemicellulase production ability of these oleaginous microorganisms

1. Planned Activities

C.4.ML.1 Year 1 milestone is to screen six of the oleaginous microorganisms for the ability to accumulate oil and degrade 20wt% of the lignocellulose.

C.4.ML.2 Year 2 milestone is to attempt to achieve 30wt% degradation of the lignocellulose while achieving triglycerides production.

2. Summarization of Activities

The oleaginous and oxidative red yeast *Rhodotorula glutinis* was selected for genome sequencing due to its potential to improve efficiency of lignocelluloses degradation and triglyceride production. High throughput genome sequencing of *R. glutinis* was conducted using 454 GS-FLX Titanium. One standard run and one paired end run were completed, resulting in a genome that was organized in 384 large contigs (500 bp or larger) and 29 scaffolds. Subsequent PCR and Sanger sequencing closed 176 gaps, resulting in an assembly with 208 contigs. To improve the assembly, an Illumina sequencing run was conducted. Raw Illumina data was assembled with the 454 paired end sequencing data using Sequencher, which resulted in our final assembly containing 169 contigs organized in 28 scaffolds. The genome size of ~20 MB was covered with average depth of~ 40X.

For annotation, the genome was the parsed through RepeatMasker to mask known repetitive elements. GeneMark gene prediction program was used to predict putative genes from *Rhodotorula glutinis*. GeneMark is self-training and was able to provide more than 200 annotated genes that we used to train Augustus and Glimmer. We also used BLAST (homology-based search) in addition to the three ab-initio gene finders to search for gene models from the whole genome. Apollo browser was used to manually annotate the best

model based on evidence presented by the gene finders and BLAST. The final *R. glutinis* genome has the following characteristics:

Genome size: 20,657,952 bp
GC content: 61.88 %
Percentage of putative genic regions: 17,229,291 bp (83%)
Percentage of repeats: 244,690 bp (1.18 %)
Total number of putative genes: 6110
Average distance between putative genes: 3951 bp

As typical for eukaryotic genomes, the *R. glutinis* genome contained a number of repetitive elements (Table C.4.1).

Table C.4.1. Repetitive elements in the *Rhodotorula glutinis* genome

Element Type	**Number in genome**	**Total length**	**Percent of genome**
Retroelements	17	6064 bp	0.03 %
DNA transposons	1	56 bp	0.00 %
Unclassified	1	101 bp	0.00 %
Total interspersed repeats	**19**	**6221 bp**	**0.03 %**
Small RNA	2	5217 bp	0.03 %
Simple repeats	845	45760 bp	0.22 %
Low complexity*	2198	188122 bp	0.91 %

*mostly regions that are poly-purine, AT, GC and other repeats not included in simple repeats

The final *R. glutinis* assembly has been submitted to GenBank and is awaiting assignment of an accession number. Pathway analysis and metabolic reconstruction is currently in progress. High-priority pathways for analysis are lipid biosynthesis and storage pathways as well as lignocellulose degradation pathways. Functional genomics are also being used to identify regulatory pathways controlling lipid accumulation by investigating gene expression in modified Czapek Dox broth with C/N ratios of 10:1, 30:1, 40:1, and 50:1 using glucose as the carbon source and sodium nitrate as nitrogen source.

Impact

Pathway analysis and functional genomics investigations of *Rhodotorula glutinis*, which are enabled by the genome sequence, will allow identification of regulatory mechanisms controlling lipid accumulation. Our goals are to improve the lignocellulose degradation/lipid accumulation efficiency of *R. glutinis*, develop a mechanism to control lipid accumulation using environmental signal(s), and possibly develop a method to trigger triglyceride secretion. Alternatively, pathways for lipid accumulation and/or secretion will be transferred to other microorganisms that are more efficient at lignocellulose degradation.

C. Products developed under the award and technology transfer activities, such as:

Publications

G. Zhang, *French, WT., Hernandez, R., Alley, E., and Paraschivescu, M., "Lipid Production from Acid Hydrolysate of Lignocellulosic Biomass by Rhodotorula glutinis," Biomass and Bioenergy 2011, Vol. 35, p.734-740.

Hall, J. I., Hetrick, M.; French*, W. Todd; Hernandez*, Rafael A.; Donaldson, Janet; Mondala, Andro; Holmes, William. Oil Production by a consortium of oleaginous microorganisms grown on primary effluent wastewater. Journal of Chemical Technology and Biotechnology 2011, Vol. 86, p.54-60.

Sustainable Energy Research Center
Syngas to Gasoline Thrust Area Final Report for 2008-2010

A. Principle investigator and co-investigators: Fei Yu and Todd Mlsna

B. Summarization of Activities

Subtask D.1 Catalyst development

1. Planned Activities

D.1.ML.1 Year 1 milestone is to attempt to achieve 50% conversion of CO with at least 20% yield of gasoline product.

D.1.ML.2 Year 2 milestone is to attempt to achieve 70% conversion of CO with at least 40% yield of gasoline product.

2. Summarization of Activities

There are two strategies to convert syngas to a wide range of fuels and chemicals. Fischer−Tropsch (FT) synthesis is a major part of gas-to-liquids (GTL) technology, which converts syngas into liquid fuels with a wide range of liquid hydrocarbon fuels and high-value added chemicals. However, the FT products are controlled by the Anderson−Schulz−Flory (ASF) polymerization kinetics, resulting in a nonselective formation of any hydrocarbons. Another approach is first to convert syngas to methanol over a methanol synthesis catalyst and subsequently polymerize methanol to hydrocarbons over ZSM-5. Syngas is first converted to methanol over a copper-based hydrogenation catalyst. In the second stage, methanol is converted to gasoline over a ZSM-5 catalyst. During the recent years, many investigations have demonstrated the advantages of the one-stage processes by using bifunctional catalysts compared with the two-stage and three-stage processes of synthesis gas conversion to gasoline. The use of a bifunctional catalyst allows for simultaneously carrying out the synthesis of methanol from syngas over the metallic function and the transformation of methanol into hydrocarbons over the acidic function. The fulfillment of both steps in the same reaction medium promotes the displacement of the thermodynamic equilibrium of methanol synthesis. Also, the shape selectivity of the acidic function provides a high selectivity that cannot be reached in the FT synthesis. Moreover, previous syngas to gasoline technologies are based mostly on using pure syngas or low-nitrogen syngas, which mainly derive from natural gas or coal. There are limited publications using nitrogen-rich syngas and/or biomass-derived syngas to produce hydrocarbons. The existing MSU downdraft gasifier is producing syngas from biomass, such as hardwood chips, switchgrass, miscanthus, municipal solid waste, etc. Currently, the syngas from the gasifier contains about 20% H_2, 19% CO, 12% CO_2, 2% CH_4, and 47% N_2. The nitrogen content is too high for the hydrocarbon synthesis if we use existing technologies, including catalysts. Developing high activity and high stability catalysts is the key for a better overall performance when using the biomass-derived syngas.

The second- and third-generation catalysts were both developed for a single-stage hydrocarbon mixture production process from biomass-derived syngas and are illustrated below.

Catalysts preparation

Preparation of transition metal deposited zeolite

A typical zeolite used in the present invention is ZSM-5. First, at least one of the transition metals is deposited or ion-exchanged onto the zeolite by one of the methods as the

conventional impregnation, traditional ion exchange, hydrothermal ion exchange, solid state ion exchange, or chemical vapor deposition. These transition metals are generally in the forms of salts. Usually, these transitional metal salts are water-soluble halides or nitrates or ammine complex salts that are commercial available. After the transitional metal is deposited on the zeolite, the mixture is calcined at 400 °C for 3 h, after which the transition metal deposited zeolite is ready for use.

Promoted with potassium

The prepared above catalyst is promoted with 1-4 wt% potassium by impregnation method. The final obtained bifunctional catalyst is first calcined at 400°C for 5 h, then crushed and pelletized to tablets.

Syngas Preparation

Three types of model syngas obtained from Airgas (Columbus, MS) were used for catalytic conversion of syngas to liquid hydrocarbons:

- 50% H_2, 50% CO
- 50% H_2, 50% CO, 60% N_2
- 19% H_2, 20% CO, 12% CO_2, 2% CH_4, 47% N_2

To prepare the biomass-derived syngas, woodchips were converted to syngas with a down-draft gasifier (Community Power Corporation Bio-Max, Littleton, CO). Unlike the model syngas, the biomass-derived gas contained certain impurities. This biomass-derived syngas was made up of a near 1:1 mole ratio of H_2 to CO (19% H_2, 20% CO, 12% CO_2, 2% CH_4, 47% N_2).

Catalytic conversion of syngas to liquid hydrocarbons

The synthesis gas conversion reaction was carried out in a fixed-bed reactor. Three grams of the catalyst were loaded to the reactor. The system was first purged by a helium flow for 30 min, followed by prereducing with a syngas mixture at 400 °C for 8 h; then syngas was fed in until reaching the desired pressure with slow adjustment of the system to the desired temperature. The reaction was operated under the following conditions: 250- 400 °C, a gas volume hourly space velocity (GHSV) of 500 to 5,000 h^{-1}, and a pressure of 500-1500psi.

Liquid hydrocarbons production from model syngas 1 (50% H_2, 50% CO)

The second-generation catalyst (Mo/HZSM-5) has been found active in FT synthesis. The catalyst was evaluated under various reaction conditions with low H_2/CO molar ratio (~1.0) model syngas 1 (50% H_2, 50% CO) because typically biomass-derived syngas contains H_2 and CO with molar ratio of 1. Liquid hydrocarbons formed on the Mo/HZSM-5 were composed mainly of alkyl-substituted aromatics and lower-branched and cyclized alkanes. Aliphatic hydrocarbons were detected only in trace amounts. Lower hydrocarbons produced included mainly methane, ethane, propane, and iso-butane. Higher alcohols and carboxylic acids (C1-C6) were detected in the water phase liquids from FT synthesis. It is supposed that the formation of hydrocarbons on Mo/zeolite is through bifunctional-zeolite acidity and molybdenum metal catalysis via mixed alcohols as the intermediates. Investigation of the zeolite structure's effects indicated that zeolite Y is also an excellent support for Mo in the FT synthesis.

Table D.1.1. Mo/zeolite catalysts for FT synthesis at 623K, 500 psi and 573K, 1000 psi (H2/CO = 1.0).

Catalyst	$SiO2/Al_2O_3$	T (K)	P (psi)	CO Conversion (%)	Products Distribution*	
					C1-3	Liq. Products
5%Mo/HZSM-5	23	573	1000	10.5	0.26	0.05
		623	500	47.5	0.87	---
	50	573	1000	15.2	0.49	0.52
		623	500	31.8	0.68	0.25
	80	573	1000	32.4	0.43	0.18
		623	500	51.2	0.73	0.01
	280	573	1000	20.6	0.38	0.16
		623	500	44.6	0.59	0.03
10%Mo/HZSM-5	23	573	500	15.8	0.53	0.27
5%Mo/zeolite-Y	80	573	1000	13.9	0.79	0.80
5%Mo/zeolite-β	25	573	1000	13.5	0.64	---
		623	500	39.1	0.63	---

* Product distribution was based on carbon basis and one mole CO_2 formation

Liquid hydrocarbons production from model syngas 2 (20%H_2, 20%CO and 60% N_2)

Mo/HZSM-5 has also been evaluated for catalytic converting model syngas 2 (20%H_2, 20%CO and 60% N_2) to gasoline-range hydrocarbons. The CO conversion, hydrocarbon selectivity, and hydrocarbon distribution as a function of temperature, pressure, GHSV, composition of the feed, and reaction time were examined.

Effects of temperature on catalytic performance

The tests were carried out at different temperatures, they were 300, 320, 340, 350, 360, and 380 ^oC, with other parameters maintained the same at 600 h^{-1} and 1000 psi. Figure D.1.1 shows CO conversion rate changed with temperature variation. Generally, CO conversion rate was significantly influenced by temperature. It increased from 12% at 300 ^oC to 65% at 350 ^oC. The rate fluctuated from 350 to 380 ^oC. It decreased to 63% at 360 ^oC and then increased to 67% at 380 ^oC, which was the highest CO conversion rate among the tested temperature range. The rate increased at a high pace from 300 ^oC to 350 ^oC. However, it slowed down at higher temperatures. This result suggested that although the catalyst will be more active at higher temperatures, the difference generated by temperature will be limited,

mostly because of catalyst deactivation caused by sintering the Mo catalyst at higher temperatures.

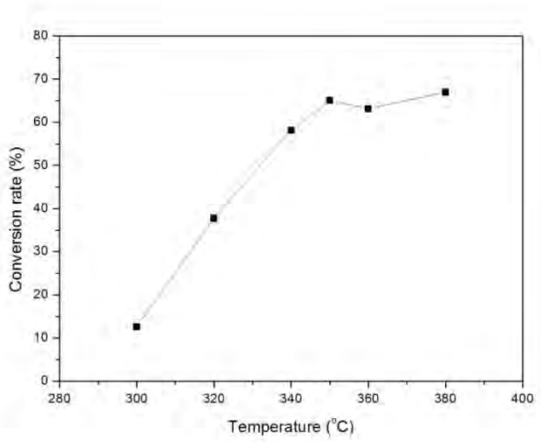


Figure D.1.1. The effect of temperature on CO conversion rate at 600 h^{-1} and 1000 psi.

Figures D.1.2 and 3 showed the selectivity and yield to CO_2, light hydrocarbons (C1-C3), and higher hydrocarbons (C4+). Although selectivity to CO_2 decreased when temperature went up, the CO_2 yield showed an increase from 300 ^oC to 380 ^oC. Therefore, higher temperatures will produce more CO_2, which will aggravate the carbon lost and reduce carbon utilizing efficiency. The thermodynamics suggest that only light hydrocarbons can keep stable in higher temperatures. Figures D.1.2 and 3 well illustrate this point. The selectivity and yield of light keep increasing among the temperature range and achieve 27% and 11% respectively at 380 ^oC, mostly due to their stability in such conditions. However, the selectivity and yield of higher hydrocarbons have an increase from 300 to 350 ^oC, then a drop from 350 to 380 ^oC; 31% and 20%, respectively, were observed at 350 ^oC as a maximum.

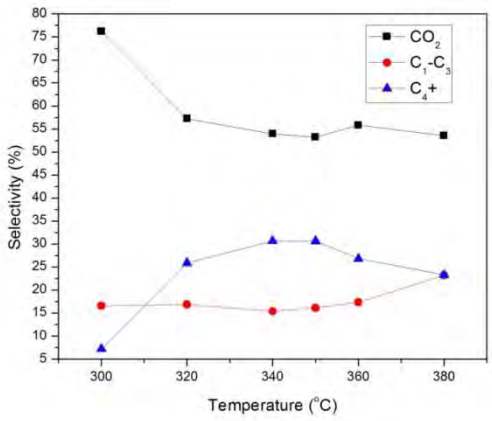


Figure D.1.2. The effect of temperature on product selectivity at 600 h^{-1} and 1000 psi.

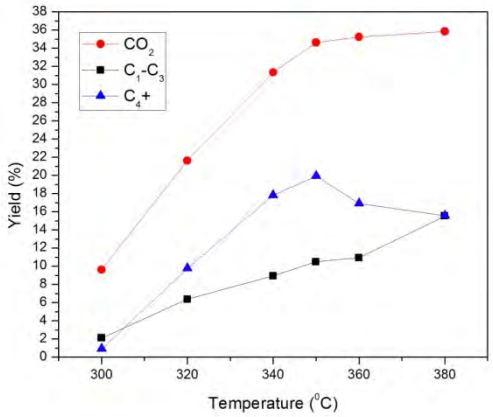


Figure D.1.3. The effect of temperature on yield at 600 h^{-1} and 1000 psi.

Effects of pressure on catalytic performance

The tests were also carried out at different pressures from 500 psi to 1000 psi with other parameters maintained the same at 600 h^{-1} and 350 ^{o}C. Figure D.1.4 shows CO conversion rate changed with pressure variation. CO conversion rate increased from 27% at 500 psi to 65% at 1000 psi, which suggests that Mo/ZSM-5 favored higher CO conversion rate at higher pressure.

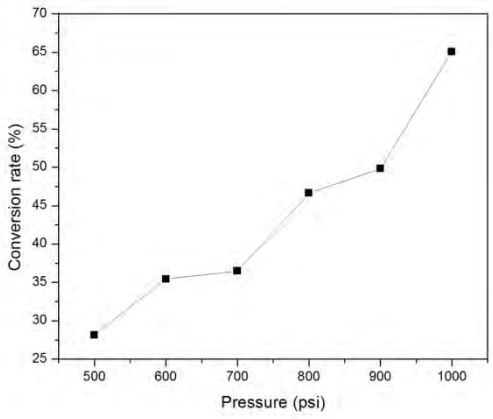


Figure D.1.4. The effect of pressure on CO conversion rate at 600 h^{-1} and 350 ^{o}C.

Figure D.1.5 and 6 showed the CO selectivity and yield to CO_2, light hydrocarbons (C1-C3) and higher hydrocarbons (C4+). CO selectivity to CO_2 increased when pressure increased from 500 psi to 600 psi, then decreased when pressure went up to 1000 psi. However, the CO_2 yield showed an increase from 500 psi to 1000 psi. Therefore, higher pressure will produce more CO_2, which will aggravate the carbon lost and reduce carbon utilizing efficiency. The CO selectivity to light hydrocarbons kept decreasing among the pressure range and achieved 15.5% at 1000 psi. However, the CO selectivity and yield of higher hydrocarbons had an increase from 500 psi to 1000 psi; 31% and 18%, respectively, were observed at 1000 psi as a maximum.

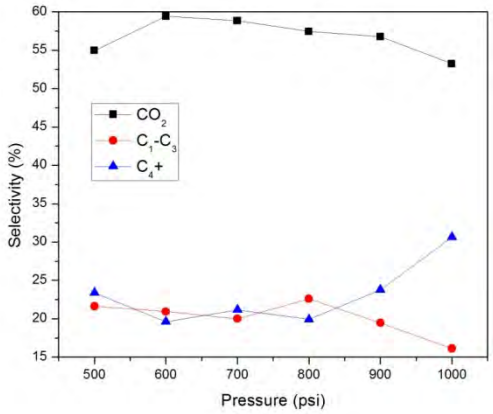


Figure D.1.5. The effect of pressure on product selectivity at 600 h^{-1} and 350 ^{o}C.

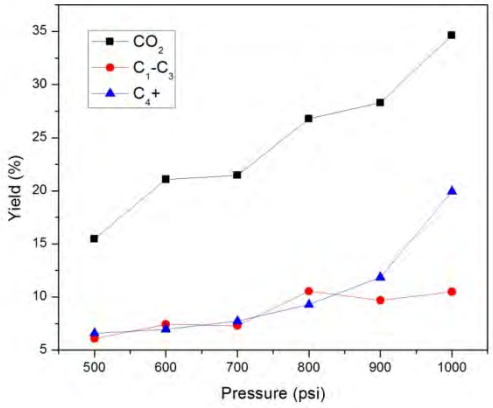


Figure D.1.6. The effect of pressure on yield at 600 h^{-1} and 350 ^{o}C.

Effects of flow rate on catalytic performance

The tests were also carried out at different syngas flow rate from 600 h^{-1} to 2400 h^{-1} with other parameters maintained the same at 1000 psi and 350 ^{o}C. Figure D.1.7 shows CO conversion rate changed with pressure variation. Figures D.1.8 and 9 show the CO selectivity and yield to CO_2, light hydrocarbons (C1-C3), and higher hydrocarbons (C4+). CO conversion rate decreased from 65% at 600 h^{-1} to 23% at 2400 h^{-1}. Both CO selectivity and yield of higher hydrocarbons decreased from 600 h^{-1} to 2400 h^{-1}; 30% and 20%, respectively, were observed at 600 h^{-1} as a maximum.

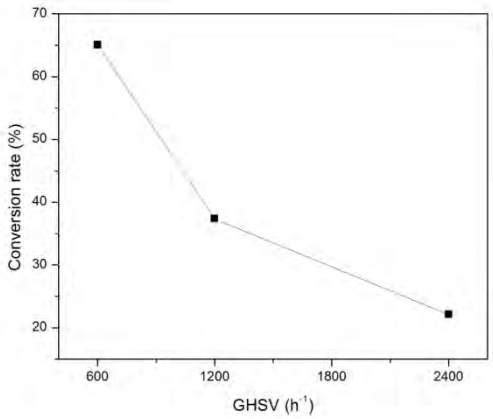


Figure D.1.7. The effect of GHSV on CO conversion rate at 1000 psi and 350 ^{o}C.

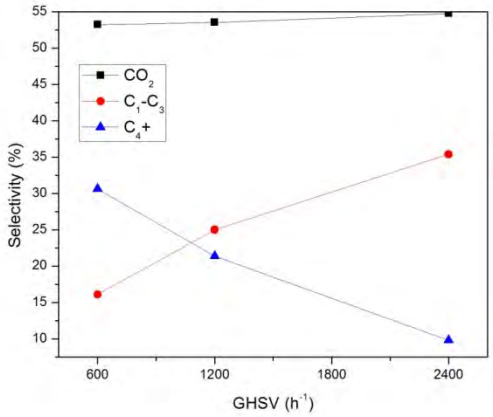


Figure D.1.8. The effect of GHSV on product selectivity at 1000 psi and 350 ^{o}C.

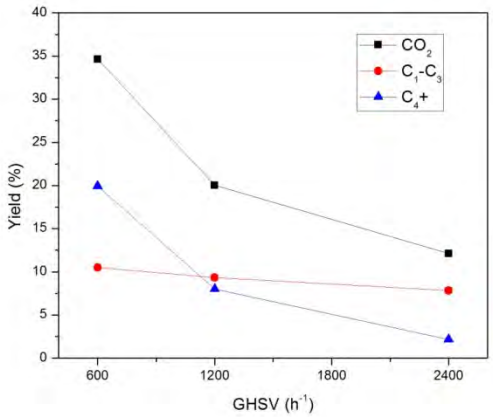


Figure D.1.9. The effect of GHSV on yield at 1000 psi and 350 ^{o}C.

Liquid sample analysis

GC-MS analysis of oil-phase results showed that more than 70 hydrocarbons were detected (Figure D.1.10). Those hydrocarbons can be classified into four groups: (1) Paraffin, such as Pentane, Hexane, and Heptane; (2) Iso-Paraffin, such as iso-butane, 2-Methylbutane, and

2,4-Dimethylpentane; (3) Aromatics, such as Benzene, Toluene, Ethylbenzene, and Naphthalene; (4)Naphthenes, such as 1, 3-dimethyl-cyclopentane, and 1, 4-dimethyl-cyclohexane. Interestingly, there was no olefin detected in our liquid sample, which appeared in traditional syngas to hydrocarbon synthesis. Some oxygenates were also detected in the water phase by GC-MS, such as ethanol and acetone. It suggested a possible alcohol to hydrocarbon mechanism of conversion over the Mo/HZSM-5 catalyst.

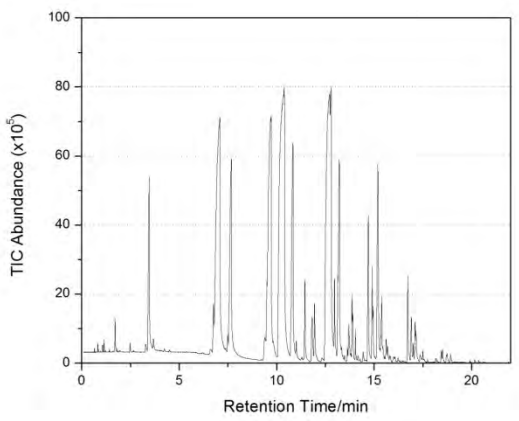


Figure D.1.10. GC-MS result of oil phase from reaction on Mo/HZSM-5 catalyst at 350 ^{o}C, 1000 psi, 600 h^{-1} for 120 h.

Liquid hydrocarbons production from model syngas 3 (19% H_2, 20% CO, 12% CO_2, 2% CH_4, 47% N_2)

Mo/HZSM-5 has also been evaluated for catalytic converting both model syngas 3 (19% H_2, 20% CO, 12% CO_2, 2% CH_4, 47% N_2) and biomass-derived syngas to liquid hydrocarbons. However, CO conversion rate and CO selectivity to liquid hydrocarbons were at a low level. Then the third-generation catalyst was developed and evaluated for catalytic converting model syngas (19% H_2, 20% CO, 12% CO_2, 2% CH_4, 47% N_2) to gasoline range hydrocarbons. The CO conversion, hydrocarbon selectivity, and hydrocarbon distribution as a function of temperature, pressure, GHSV, composition of the feed, and reaction time were examined. The catalytic process occurs at a temperature of 250- 400°C, a gas volume hourly space velocity (GHSV) of 500 to 5,000 h^{-1}, and a pressure of 500-1500 psi. The CO conversion, selectivity of CO_2 and hydrocarbon, and hydrocarbon distribution were measured in a fixed-bed flow reactor. It was found that the catalyst has relatively high activity and selectivity in producing liquid hydrocarbons when running with this type of model syngas (Figures D.1.11-14). The increase of temperature and pressure favors CO conversion and formation of more hydrocarbons. The conversion of CO in the syngas was 73% under a reaction temperature of 310 °C, and a pressure of 1000 psi and 58% under a reaction pressure of 500 psi. This catalyst gave higher conversion efficiency under a lower CO-H_2 pressure. The conversion into hydrocarbons reached about 70 mol% while the conversion into CO was about 30 mol%. The resultant hydrocarbons were hydrocarbons of the gasoline boiling point range, which contained 40 to 50 wt% of light hydrocarbons (C_1-C_4), significantly lower than in the case of using the Mo/HZSM-5 catalyst (second-generation catalyst), which produced more than 70% light hydrocarbons. According to detailed hydrocarbon analysis, the composition of gasoline fraction contained up to 40 wt% aromatics, 15wt % of olefins, and 40wt % of paraffins while more than 90% of the liquid hydrocarbons were aromatics in the case of the Mo/HZSM-5 catalyst. The compositions of

liquid hydrocarbon mixture products can be adjusted through the operating conditions. Time-on-stream results showed the catalyst was stable. CO conversion reached 74% after 20 h at 310 ^{o}C, and kept constant after 120 h (Figure D.1.15).

Effect of temperature

The temperatures studied were: 290, 300, 310, 320, 330, and 350 ^{o}C with the remaining conditions maintained at the values previously indicated. Figure D.1.16a shows the variation of CO conversion, C_1 - C_5^+ selectivity with temperature, the other variables remaining constant. Figure D.1.16a shows how influential temperature was on CO conversion. CO conversion increased from 55% at 290 ^{o}C to 83% at 350 ^{o}C. Figure D.1.16b clearly shows the hydrocarbon distribution changed with temperature, the light hydrocarbons being favored at higher temperatures. Higher hydrocarbons were more sensitive to temperature, undergoing cracking and dealkylation reactions that became increasingly important with increasing temperature.

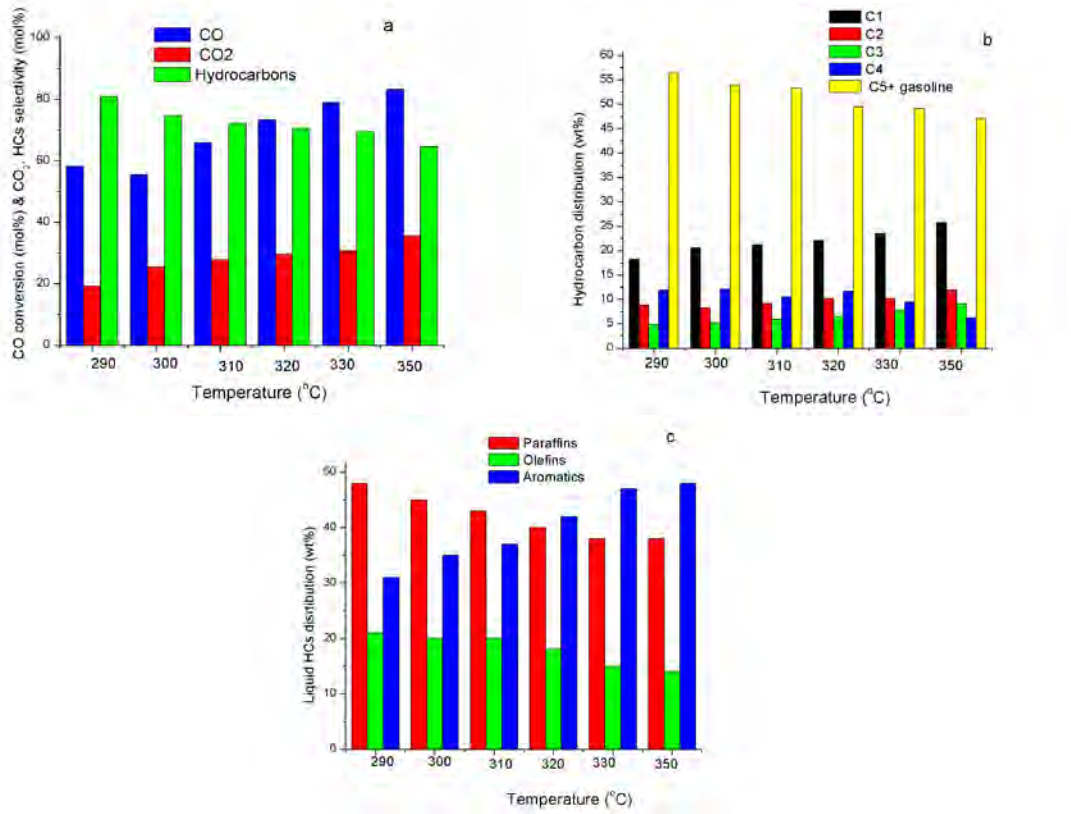


Figure D.1.16. Effect of temperature on (a) CO conversion, CO_2 and hydrocarbon selectivity, (b) hydrocarbon distribution, and (c) liquid hydrocarbon distribution at 1000psi, with model syngas of 19% H_2, 20% CO, 12% CO_2, 2% CH_4, 47% N_2, GHSV of 2000 h^{-1}; 3 g of 3rd generation catalyst was used in the reaction. Time on stream of 48-100 h.

Influence of pressure on the catalyst performances

An increase in total pressure will increase the equilibrium towards the product side and increase the conversion. The change in Gibbs free energy will always be negative for a system where the change in number of moles upon reaction is negative and when pressure increases. Furthermore, a change in total pressure will not affect the water gas shift reaction

but will change the equilibrium product distribution. Experiments under pressures of 500, 750, 1000, and 1250 psi have been carried out. The other operating conditions were: temperature, 310 ^{o}C; gas space velocity 2000 h^{-1}, with model syngas of 19% H_2, 20% CO, 12% CO_2, 2% CH_4, 47% N_2.The effect of pressure on both CO conversion and process selectivity showed that when pressure increased, CO conversion increased (Figure D.1.17). Within the C_5^+ fraction, an important effect of pressure on selectivity was observed. The increase in pressure clearly favored the formation of C_5^+, while C_1~C_3 gaseous hydrocarbons clearly decreased with increasing of pressure.

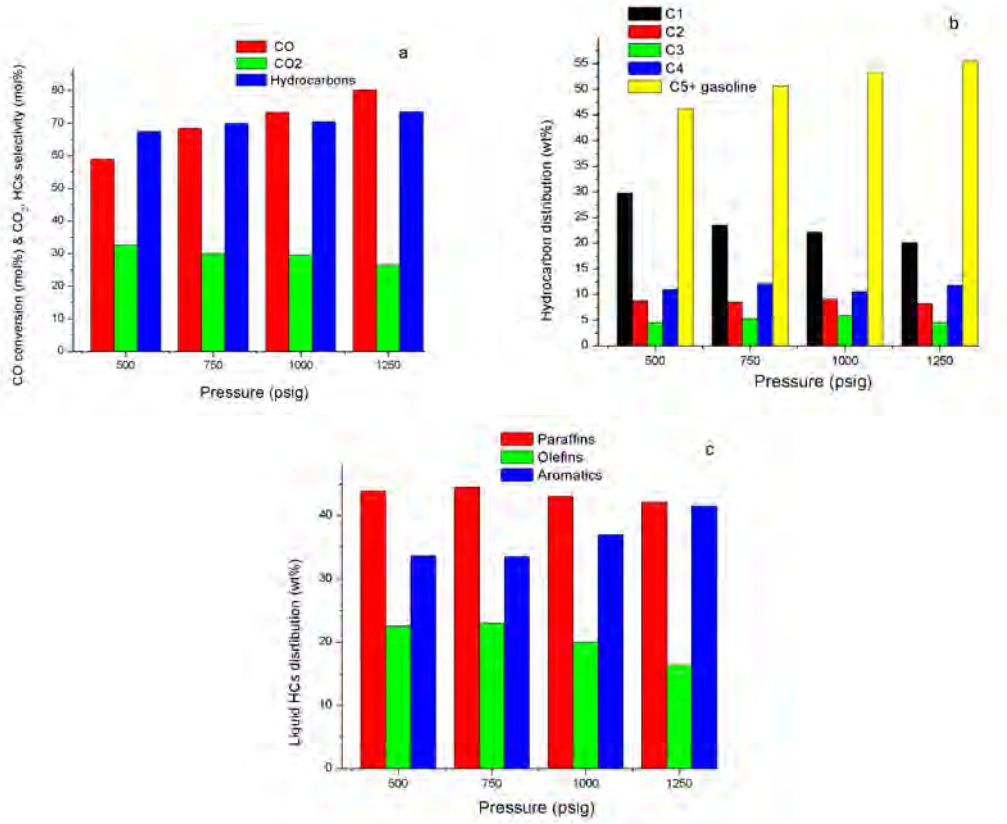


Figure D.1.17. Effect of pressure on (a) CO conversion, CO_2 and hydrocarbon selectivity, (b) hydrocarbon distribution, and (c) liquid hydrocarbon distribution at 310 ^{o}C, with model syngas of 19% H_2, 20% CO, 12% CO_2, 2% CH_4, 47% N_2, GHSV of 2000 h^{-1}; 3 g of 3rd generation catalyst was used in the reaction. Time on stream 48-100 h.

<u>Impact of space velocity on the catalyst performances</u>

Experiments were completed with different GHSV, 500, 1000, 2000, 2500, and 3000 h^{-1}, and the remaining operating conditions have been maintained at 310 ^{o}C, 1000 psi, CO/H_2 = 1. The effect of the space velocity on CO conversion and hydrocarbon distribution showed that when the space velocity increased, CO conversion decreased as expected (Figure D.1.18). At the same time, C_5^+ selectivity also decreased. It can be concluded that CO conversion decreased with the increasing of space velocity. The effect of space time on product distribution was significant. It was observed that the yields of hydrocarbons decreased with increasing of space velocity. The gasoline fraction (C_5^+) continuously decreased with increasing space velocity.

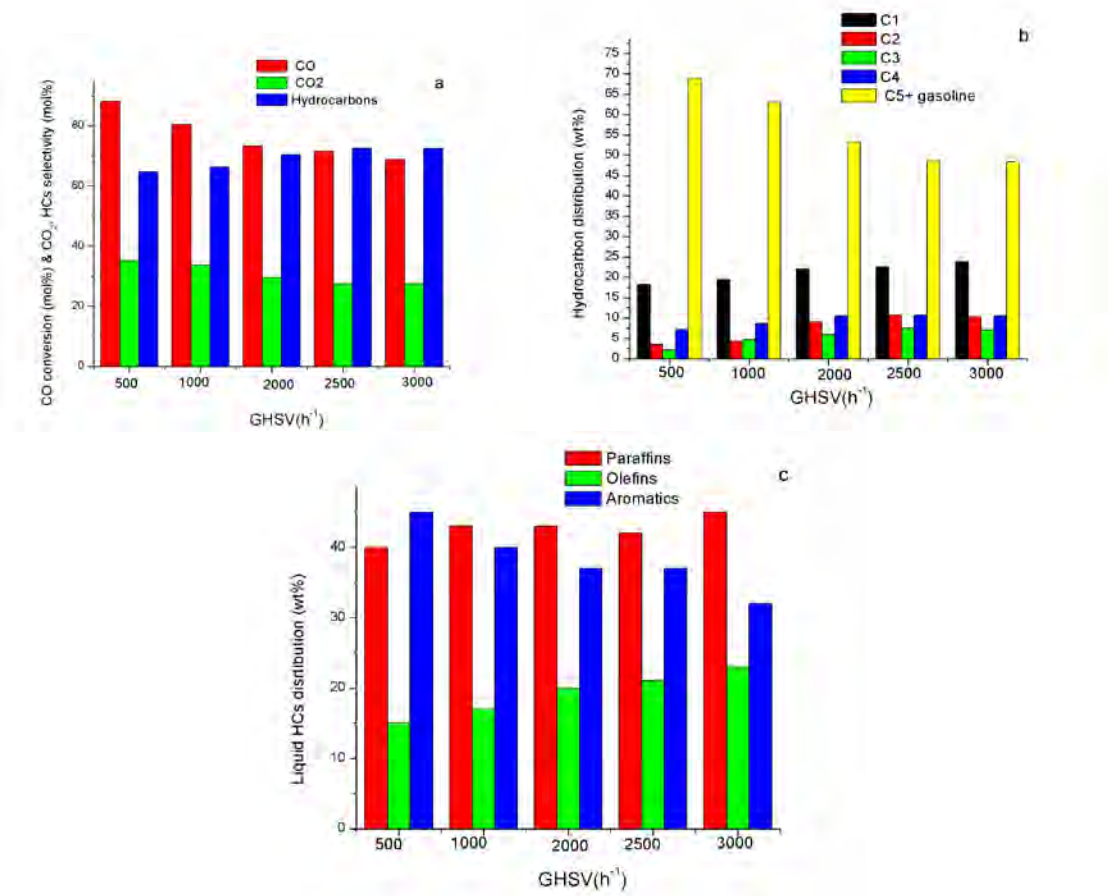


Figure D.1.18. Effect of gas hourly space velocity (GHSV) on (a) CO conversion, CO2 and hydrocarbon selectivity, (b) hydrocarbon distribution, and (c) liquid hydrocarbon distribution at 310 ^{o}C, 1000 psi, with model syngas of 19% H_2, 20% CO, 12% CO_2, 2% CH_4, 47% N_2; 3 g of 3rd generation catalyst was used in the reaction.

Role of syngas composition on the catalyst performances

Syngas composition is an important parameter in higher hydrocarbon synthesis. It can affect both reaction rates and activity. It was found that the catalyst had relatively high activity and selectivity in producing liquid hydrocarbons when running with nitrogen-rich syngas (Figure D.1.19).

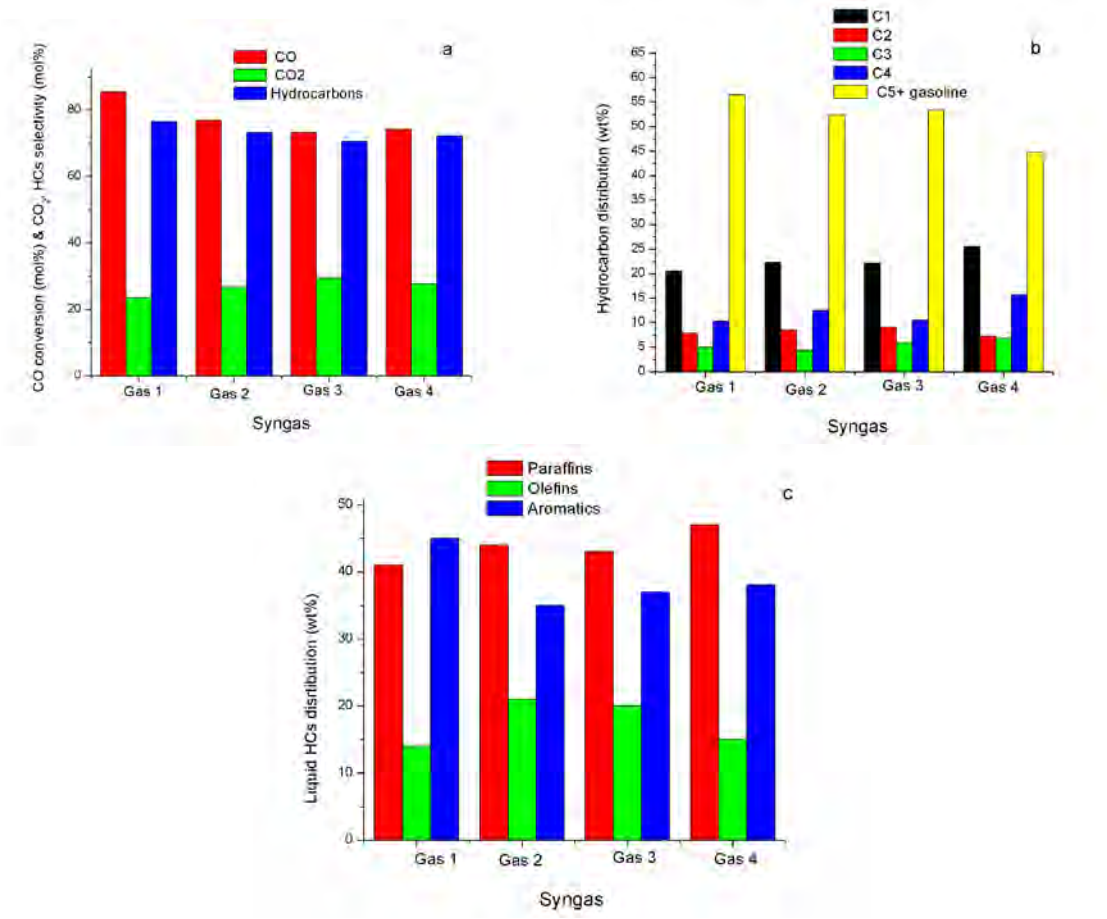


Figure D.1.19. Effect of syngas composition on (a) CO conversion, CO2 and hydrocarbon selectivity, (b) hydrocarbon distribution, and (c) liquid hydrocarbon distribution at 310 ^{o}C, 1000 psi, GHSV of 2000 h^{-1}; 3 g of 3rd generation catalyst was used in the reaction. (Model syngas 1: 50% H_2, 50%CO; Model syngas 2: 20.1%H_2, 20%CO, 60% N_2; Model syngas 3: 19% H_2, 20% CO, 12% CO_2, 2% CH_4, 47% N_2; Model syngas 4: 40%H_2, 20%CO, 12% CO_2, 2%CH_4, balance N_2.)

Time-on-Stream Performance

The effect of time on stream on the performance of the catalyst was studied at 310 °C over a period of 120 h. The evolution of CO conversion and hydrocarbon distribution with time on stream are shown in Figure D.1.20 for the third-generation catalyst. The activity of the catalyst reached a steady state after a period of approximately 20 h under operating conditions. Time-on-stream results showed the catalyst was stable. CO conversion reached 74% after 20 h at 310 ^{o}C, and kept constant after 120 h.

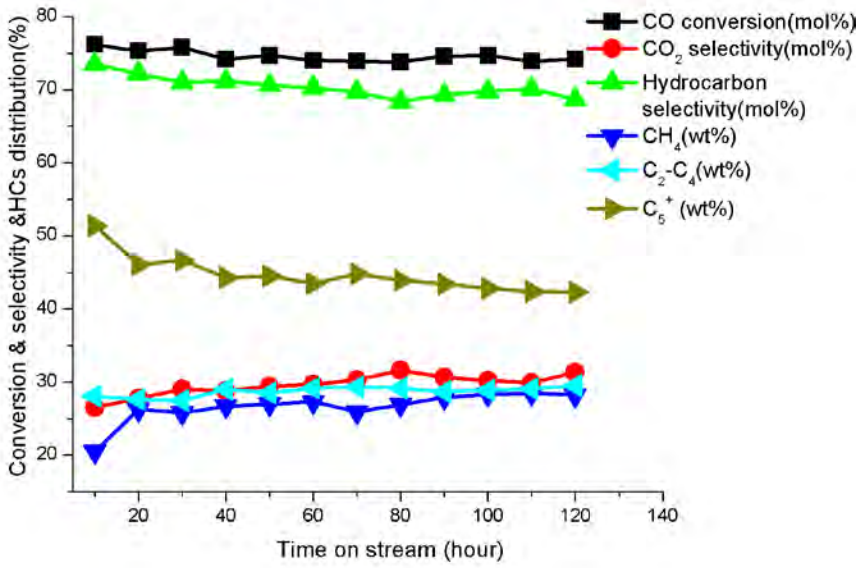


Figure D.1.20. Time on stream of CO conversion, hydrocarbon selectivity and distribution on the 3rd generation catalyst at 310°C, 1000 psi, 2000 h^{-1} with model syngas of 19% H_2, 20% CO, 12% CO_2, 2% CH_4, 47% N_2.

Liquid hydrocarbons production from biomass derived syngas (19% H_2, 20% CO, 12% CO_2, 2% CH_4, 47% N_2)

A downdraft gasifier is producing biomass-derived syngas from wood chips and other biomass. The biomass-derived syngas contains about 19% H_2, 20% CO, 12% CO_2, 2% CH_4, 47% N_2 if using wood chips as biomass feedstock. In addition to the gases listed above, the biomass derived syngas also contains trace amounts of tars, NH_4, H_2S, O_2, and particulates as impurities. Biomass-derived syngas was cleaned by bubbling through water-containing tanks before compressed up to 1800 psi. The compressed biomass-derived syngas was fed to a fixed-bed reactor for liquid hydrocarbon production. The biomass-derived syngas activity and selectivity was similar to that of the model syngas (19% H_2, 20% CO, 12% CO_2, 2% CH_4, 47% N_2), as shown in Figures D.1.21-23. Liquid product samples were collected and analyzed. The composition of the gasoline phase was also similar to the model syngas except there were more aromatics and less olefins in the biomass-derived syngas product.

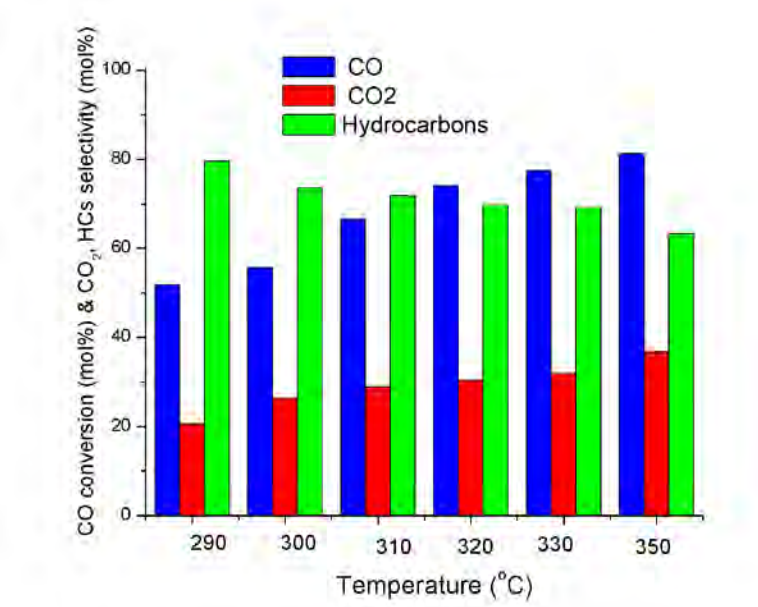


Figure D.1.21. Effect of temperature on CO conversion, CO_2 and hydrocarbon selectivity at 1000 psi, with biomass derived syngas (19% H_2, 20% CO, 12% CO_2, 2% CH_4, 47% N_2), GHSV of 2000 h^{-1}; 3 g of 3rd generation catalyst was used in the reaction. Time on stream of 24-48 h.

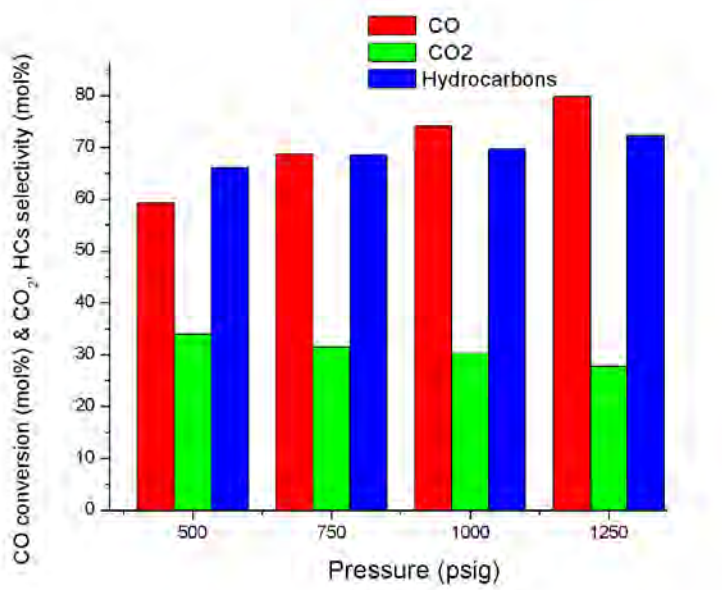


Figure D.1.22. Effect of pressure on CO conversion, CO_2 and hydrocarbon selectivity, at 310 ^{o}C, with biomass derived syngas (19% H_2, 20% CO, 12% CO_2, 2% CH_4, 47% N_2), GHSV of 2000 h^{-1}; 3 g of 3rd generation catalyst was used in the reaction. Time on stream 24-48 h.

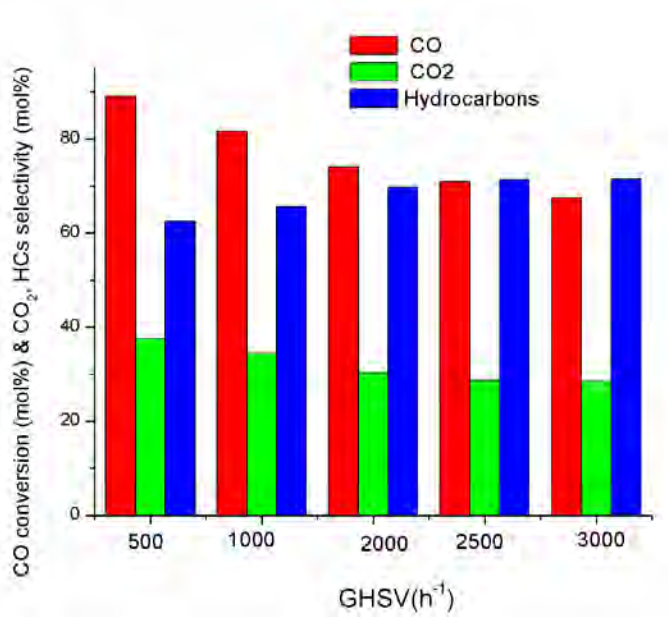


Figure D.1.23. Effect of gas hourly space velocity (GHSV) on CO conversion, CO2 and hydrocarbon selectivity, at 310 ^{o}C, 1000 psi, with biomass derived syngas (19% H_2, 20% CO, 12% CO_2, 2% CH_4, 47% N_2); 3 g of 3rd generation catalyst was used in the reaction.

Subtask D.2 ASTM characterization of the gasoline product

1. Planned Activities

D.2.ML.1 Year 1 milestone is to attempt to achieve a research octane number of 90.

D.2.ML.2 Year 2 milestone is to attempt to achieve a research octane number of 93.

2. Summarization of Activities

We produced a liter of gasoline-range hydrocarbons for ASTM analysis. The gravity was 50 oAPI, and the octane numbers reported from knock engine analysis were as follows: MON = 88 and RON = 103 for a value of (R+M)/2 = 95.5. The Reid vapor pressure was 13.5 psi, which is greater than the normal vapor pressure for a 410 F end-point gasoline of 7-10 psi.

The ASTM distillation of this liquid is shown in Figure D.2.1. On the same plot, we show the ASTM distillation of a 410 °F end-point gasoline. It is clear that the liquid produced from this technology is a mixture of a gasoline with another hydrocarbon mixture having a higher boiling-point curve. The preliminary data suggest that this liquid would be an excellent blending component for refinery products.

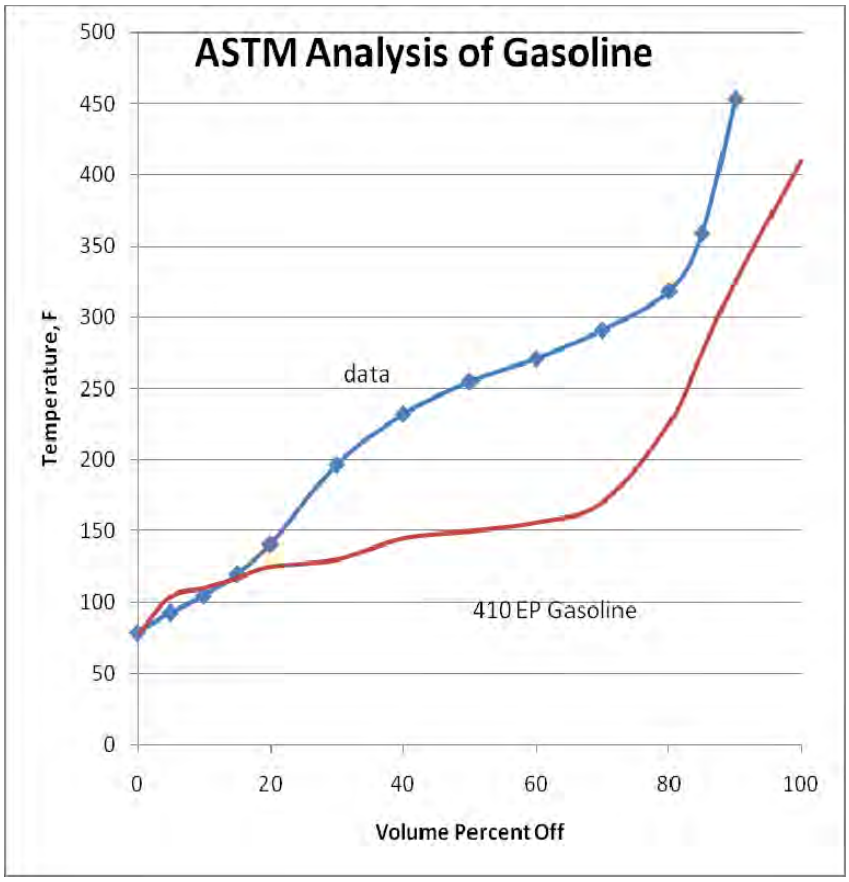


Figure D.2.1. ASTM Distillation of liquid hydrocarbon compared with a 410 °F End-Point Gasoline.

A sufficient quantity of liquid hydrocarbon was collected to permit a battery of ASTM tests to be completed. These tests showed an octane number (R+M)/2 equaling 96, an API gravity of 50°, and a Reid vapor pressure of 13.5 psi. The ASTM distillation curve was consistent with that of a 410 °F endpoint gasoline mixed with a heavy catalytic cracked gasoline fraction.

C. Products developed under the award and technology transfer activities.

Publications

Hu, J., F Yu, et al. Catalytic Conversion of Simulated Biomass-derived Syngas to Gasoline-range Hydrocarbons over Mo/HZSM-5 Catalysts. (Submitted to *Bioresource Technology*)

Liu, S., A Gujar, P Thomas, H Toghiani, M White. *2009.* Synthesis of Gasoline-Range Hydrocarbons over Mo/H+-ZSM-5 Catalysts. *Applied Catalysis, A*:*General. 357:*18-25.

Street J. F Yu, et al. Gasoline-Range Hydrocarbon Production using Gasified Biomass over Mo/HZSM-5. (Submitted to *Fuel*)

Yan, Q., P Doan, H Toghiani, A Gujar, M White. *2008.* Synthesis Gas to Hydrocarbons over CuO-CoO-Cr2O3/H+-ZSM-5 Bifunctional Catalysts. *J. Phys. Chem. C.* 112:11847-11858.

Presentations

Benson, T., Hernandez. R., French, T., White, M., Holmes, W. Elucidation of Mechanism for the Cracking of Unsaturated Lipids Using a Benchmark Catalyst and Commercial Catalysts. 99th American Oil Chemist Society Meeting, May 16-20, 2008, Seattle, Washington.

Gujar, A. C. and M. G. White, Reaction of Alcohols over H+ZSM-5. North American Catalysis Society Meeting, Houston, TX. June 17-20, 2007.

Gujar, A. C. and M. G. White. Syngas to Gasoline. Second Biofuels Conference at Mississippi State University, Mississippi State, MS. August 14,2007.

Gujar, A. C. and M. G. White. Batch Reactor Studies of Methanol to Gasoline over H+ZSM-5. paper 6z, Annual Meeting of the AIChE, Salt Lake City, UT, November, 2007.

Gujar, A. C, and M. G. White. Batch Reactor Studies of Methanol to Gasoline over Metal Oxides Supported on H+ZSM-5. paper 420f, Annual Meeting of the AIChE, Salt Lake City, UT, November, 2007.

Hu, J., Yu, F., Wei, L., Columbus, E., and Batchelor, W. Preliminary Study of the Conversion of Biomass Gasification Syngas to Gasoline-range Hydrocarbons over Mo/HZSM-5. Paper 1008573, ASABE 2010 Annual International Meeting, Pittsburgh, Pennsylvania, June 20-23, 2010.

Liu, S. and M. G. White. Novel Catalyst for Synthesis Gas to Gasoline. Third Biofuels Conference at Mississippi State University, Mississippi State, MS. August 13, 2008.

Liu, S. and M. G. White. Fischer-Tropsch Synthesis over Mo/HZSM-5 Catalysts. 236 ACS Meeting, August 17, 2008.

Sparks, D., Hernandez, R., Estevez, A., Alley, E., French, T. Utilization of a Supercritical Fluid Medium for the Generation of Renewable Chemicals from Oleic Acid. 99th American Oil Chemist Society Meeting, May 16-20, 2008, Seattle, Washington.

Street, J., Columbus, E., Warnock, J., Wooten, J., White, M. Scale-Up of Gasoline-range Hydrocarbons over Mo/H-Y and Mo/HZSM-5 Catalysts. An IBE Poster Presentation presented for IBE 2010 Conference. Cambridge, MA, March 4-6, 2010.

Street, J., Columbus, E., Warnock, J., Wooten, J., White, M., Yu, F. Scale-Up of Gasoline-Range Hydrocarbon Production over Mo/HZSM-5 using Synthesis Gas. A Poster Presentation presented for the Mississippi State 2010 Biofuels Conference. Jackson, MS, August 12-13, 2010.

Street, J., Columbus, E., Warnock, J., Wooten, J., White, M. Preliminary Parameters to Produce Gasoline-range Hydrocarbons from Synthesis Gas. Paper: BIO-097999, An ASABE Meeting Presentation written for the 2009 Bioenergy Engineering Conference, Seattle, Washington, October 11-14, 2009.

White, M. Conversion of Syngas to Gasoline. An Oral Presentation presented for the Mississippi State 2010 Biofuels Conference. Jackson, MS, August 12-13, 2010.

White, M. G. A. C. Gujar, V. K. Guda, Q. Yan, H. Toghiani. Reaction of Alcohols over H+ZSM-5. paper 420 e, Annual Meeting of the AIChE, Salt Lake City, UT, November, 2007.

Yu, F., Q. Yan, J. Hu, Y. Lu, L. Wei, J. Wooten, E. Columbus and W. Batchelor. 2010. Mixed Hydrocarbons from Biomass Gasification Syngas over Mo/HZSM-5 Catalyst. 9th International Conference on Sustainable Energy Technologies (SET). Shanghai, China. August 24-27.

Yu, F., Q. Yan, J. Hu, L. Wei, E. Columbus and J. Wooten. 2010. Mixed Hydrocarbon Production from Biomass-derived Syngas over A Bi-functional Catalyst. International Symposium on Renewable Feedstock for Biofuel and Bio-based Products. Austin, TX, August 11-13.

Sustainable Energy Research Center
Biomass Utilization Thrust Area Final Report for 2008-2010

A. Principle investigator and team members: Kalyan K. Srinivasan and Sundar R. Krishnan

B. Summarization of Activities

Subtask E.1 Advanced low-temperature combustion experiments with biodiesel and diesel-biodiesel blends

1. Planned Activities

E.1.DL.1 Year 1 deliverables are to measure baseline fuel efficiencies and engine-out NO_x, CO, and HC emissions with conventional B100 and B20 engine operation.

E.1.DL.2 Year 2 milestone is to identify optimal combinations of fuel injection strategies and appropriate intake manifold conditions (temperature and pressure) to achieve low temperature combustion of B100 and B20 blends and measure performance as indicated by mean effective pressures, rate of heat release schedules, fuel conversion efficiencies, and emissions (both PM and NO_x) approaching US EPA Tier 4 (non-road) standard of 0.4 g/kWh).

2. Summarization of Activies

All experiments were performed on a four-cylinder turbocharged diesel engine fitted with an EDC rotary fuel-injection pump. The fuel injection was controlled by an ECU. The ECU did not allow for full control over injection timing, pressure, quantity and duration of injection; therefore, the range of operation of the fuel-injection pump was limited, which seriously influenced the optimization of engine performance and emissions. All experiments were performed at a constant engine speed of 1800 rev/min. The complete experimental matrix is provided in Table E.1.1 below. Table E.1.2 shows the properties of diesel fuel #2 and biodiesel used to obtain B20 and/or straight biodiesel (B100), which served as fuels for the experiments reported in this research.

Table E.1.1. Engine experimental test matrix for B20 and B100 operation at constant engine speed of 1800 rev/min

BMEP (bar)	2.5			5.0			7.5			10.0		
Inj. Tim. (°btdc)	0°	4°	10°	0°	4°	10°	0°	4°	10°	0°	4°	10°
B20	X			X			X			X		
B100	X			X			X			X		

Table E.1.2. B100 and Diesel #2 fuel properties (measured at the Mississippi State Chemical Lab)

	Diesel#2	B100
API Grav	32.710	27.830
Kinematic Viscosity (cs)	2.708	4.685
Flash Point (F)	155.000	290.000
Cetane Index	44.300	49.900
Cetane Number	47.700	57.980

Figure E.1.1 discusses the smoke-NOx trade-off with B20 and B100 operation at four different engine loads (2.5, 5., 7.5, and 10 bar b.m.e.p) and three different injection timings (10°, 4°, and 0°btdc). It is clear that with B100 fuelling the smoke emissions are lower than the corresponding B20 values at all engine loads while NOx emissions are comparable if not higher than corresponding B20 levels. These are attributable to the fact that B100 fuelling, due to the presence of fuel-bound oxygen, tends to produce significantly lower smoke emissions.

The lower smoke emissions are also responsible for the corresponding increase in NOx emissions. In fact, the reason for increased NOx emissions is a highly debated topic and many reasons have been offered for its increase with B100 fuelling relative to straight diesel levels. Of these, a probable explanation is attributed to the suppression of soot radiation due to soot oxidation, as a result of which the in-cylinder temperatures are higher than they would be for straight diesel operation, and, hence, have higher NOx emissions. In this study, there is some evidence of that fact; although not conclusive, it can provide some insight (as discussed in Figures E.1.7a and E.1.7b later in this document).

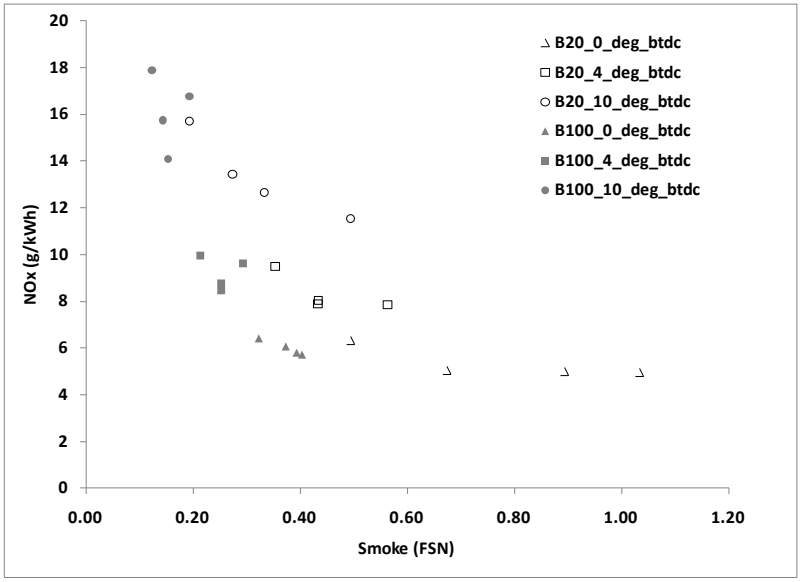


Figure E.1.1. Smoke-NOx trade-off for B20 and B100 operation over a range of injection timings and loads

Figure E.1.2 below shows the brake specific carbon monoxide emissions (BSCO) for B100 and B20 operation over a range of loads and injection timings at a constant engine speed of 1800 rev/min (see Table 1 above for more details). There is little difference between BSCO values between B20 and B100 fuelling; however, at higher loads, B100 BSCO is considerably lower than B20. This again could be attributed to higher bulk gas temperatures with B100 fuelling, which could possibly help oxidize CO emissions to CO_2.

Figure E.1.3 shows the fuel conversion efficiencies from B100 and B20 combustion at 1800 rev/min over a range of injection timings at different engine loads. As expected, the B20 efficiency values are consistently higher than B100. From Table E.1.3 below, it can be seen that in all operating conditions, the ignition delay time of B100 is much shorter than that of B20 and it also has a relatively earlier Ca50% phasing; this indicates that the ignition phasing of B100 is almost always at TDC. This is due to the higher cetane rating of B100 (see Table E.1.2). Moreover, the calorific value of diesel is about 10% higher than that of B100; therefore, the fueling requirement to produce the same power is higher for B100 than for diesel, which could be the reason for consistently lower fuel conversion efficiencies of B100 compared to B20.

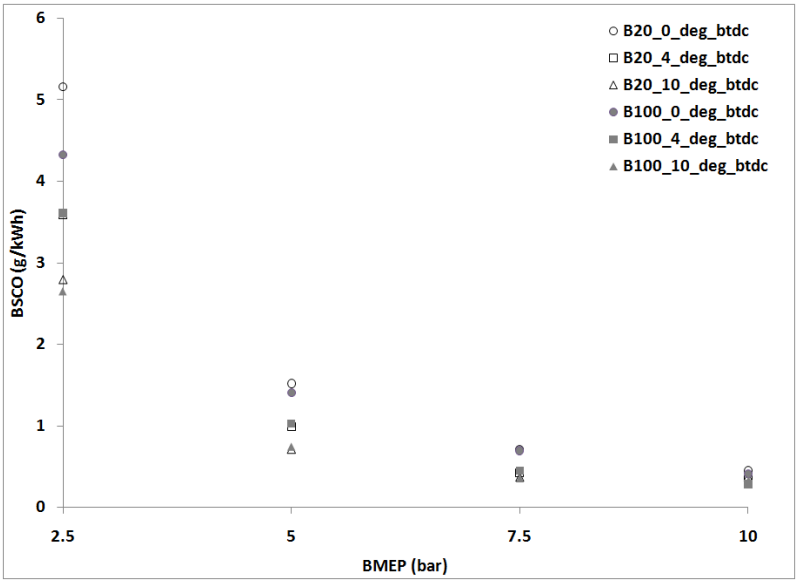


Figure E.1.2. Brake Specific Carbon Monoxide emissions for B20 and B100 operation over a range of injection timings and load

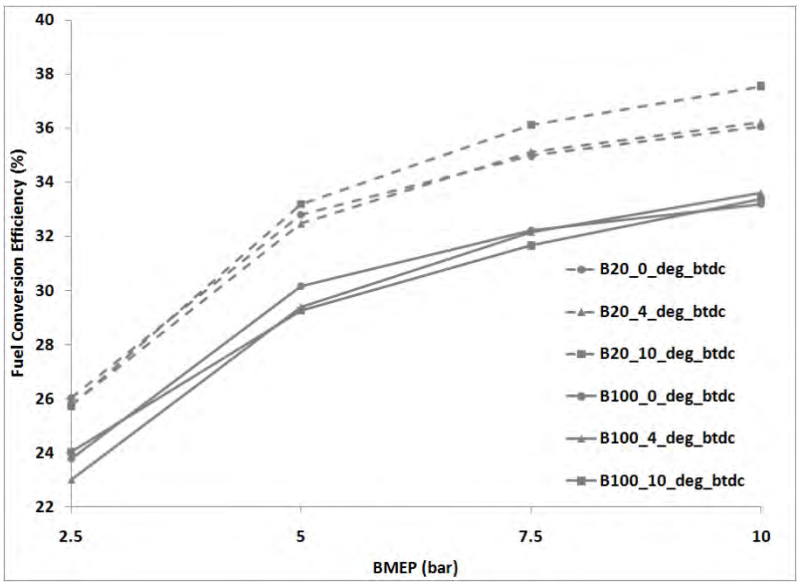


Figure E.1.3. Fuel conversion efficiency vs. Brake mean effective pressure (load) for B20 and B100 operation over a range of injection timings

Figures E.1.4-7 show the in-cylinder pressure, heat release rate, and average cylinder temperature profiles for B20 and B100 combustion at 10°btdc injection timing as indicated in Table E.1.1. Table E.1.3 summarizes the ignition delay times and Ca50% location for all experimental conditions. At all operating conditions, the following observations are true: 1) the ignition delay times are shorter for B100 combustion, and 2) the crank angle corresponding to 50% heat release is also advanced compared to B20 combustion. In particular, for all conditions, the averaged cylinder temperature, which is representative of the bulk gas temperature, is much higher for B100 combustion. In particular, it is instructive to compare Figures E.1.7a and E.1.7b, respectively. These figures show the incylinder heat release, cylinder pressure and average cylinder temperature profiles from straight B100 and B20 combustion at 10 bar bmep and 10°btdc injection timing. At this condition, the B100 NOx values are atleast 10–15% higher than corresponding B20 values. While the smoke emissions are lower than corresponding B20 values by about 40%. From Figures E.1.7a and E.1.7b, it can be seen that the bulk gas temperature (or the average cylinder temperature) for B100 combustion is much higher than B20; therefore, it can be argued that although this is an average temperature, its higher magnitude points to local cylinder temperatures being high also. This might offer a plausible explanation for increased NOx emissions with straight B100 fuelling compared to B20 or even straight diesel fuel.

From these observations, it can be said that NOx emissions will likely be higher for B100 combustion, owing to a likely reduced soot radiation due to the lower observed soot emissions compared to B20 combustion.

Table E.1.3. Ignition delay times and crank angle corresponding to 50 percent heat release for B20 and B100 operation at different engine loads and injection timings.

Injection timing (deg btdc)	BMEP (bar)	Ignition Delay (CAD)		Ca50% (CAD)	
		B20	B100	B20	B100
10°	2.5	1.5	1	4.5	3
	5	1.5	0.5	5.5	4
	7.5	1.5	0	6.5	4.5
	10	1	0	7.5	5.5
4°	2.5	1.5	0.5	9	8.5
	5	1.5	0.5	10.5	10
	7.5	1	0.5	11.5	11
	10	1	0.5	12.5	11
0°	2.5	2	0.5	13	12.5
	5	1	0	14.5	14
	7.5	1	0	15.5	15
	10	0.5	0	16.5	15.5

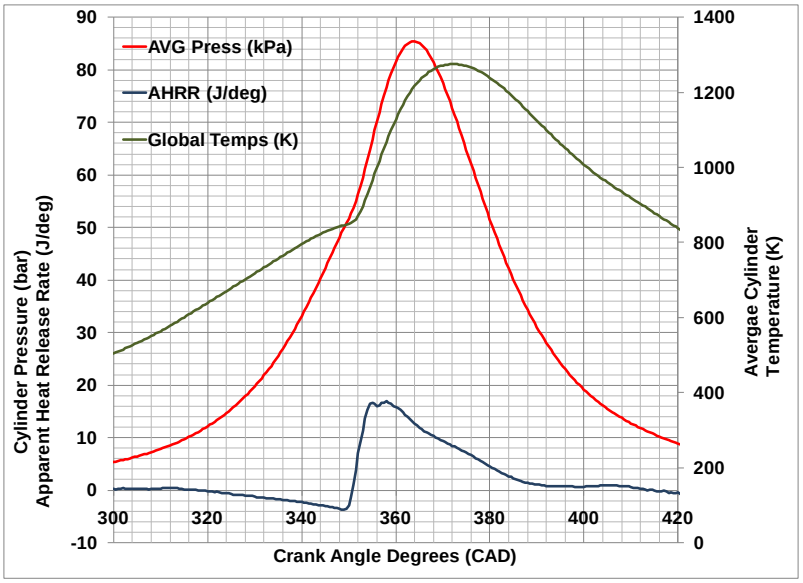


Figure E.1.4a. Crank resolved apparent heat release rate, cylinder pressure and average cylinder temperature schedules for B100 combustion with FIS = 10°btdc and at 2.5 bar b.m.e.p.

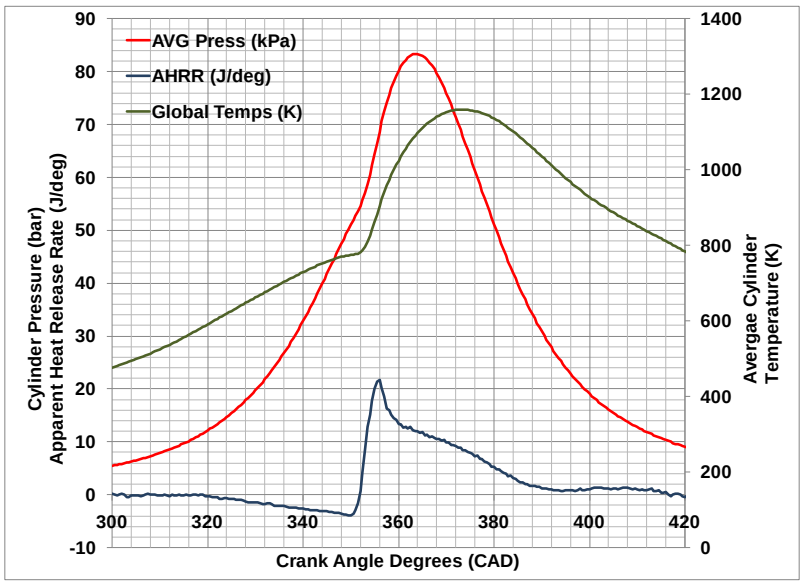


Figure E.1.4b. Crank resolved apparent heat release rate, cylinder pressure and average cylinder temperature schedules for B20 combustion with FIS = 10°btdc and at 2.5 bar b.m.e.p.

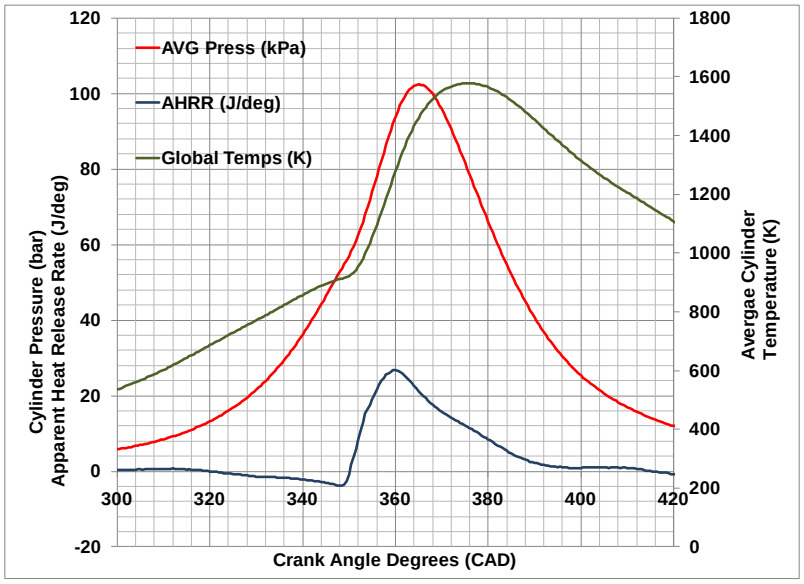


Figure E.1.5a. Crank resolved apparent heat release rate, cylinder pressure and average cylinder temperature schedules for B100 combustion with FIS = 10°btdc and at 5 bar b.m.e.p.

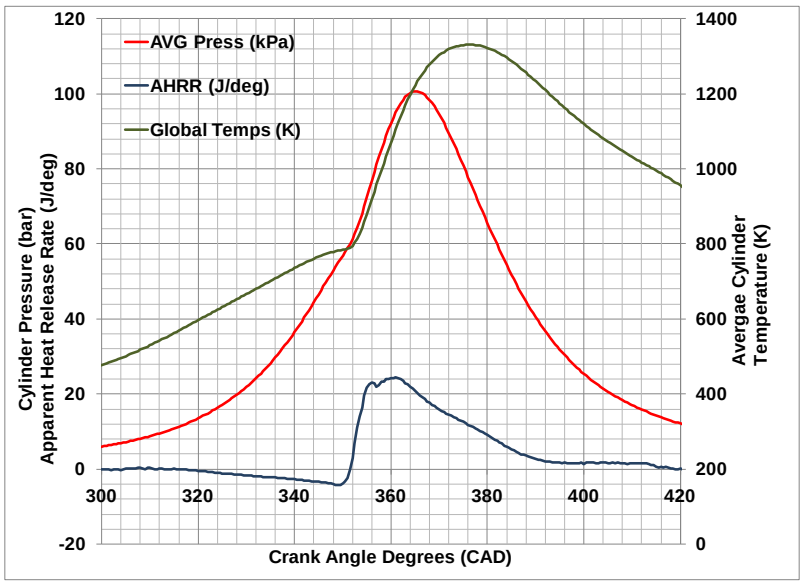


Figure E.1.5b. Crank resolved apparent heat release rate, cylinder pressure and average cylinder temperature schedules for B20 combustion with FIS = 10°btdc and at 5 bar b.m.e.p.

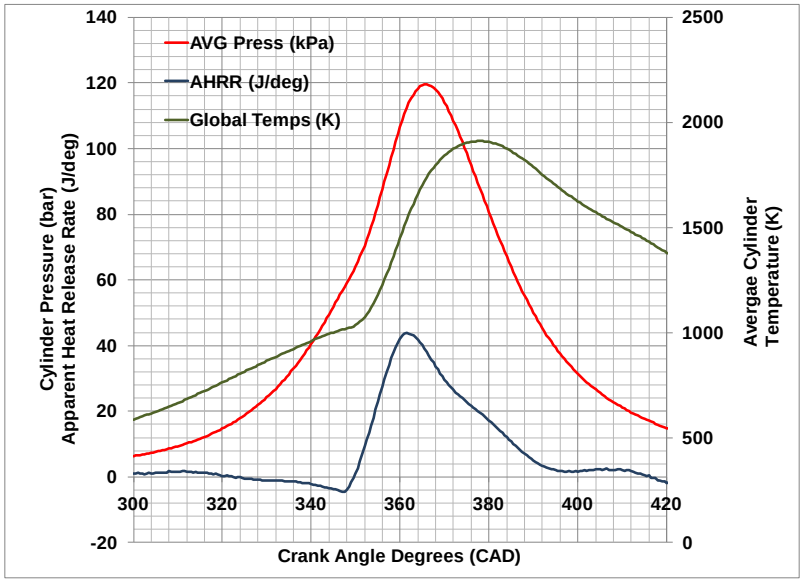


Figure E.1.6a. Crank resolved apparent heat release rate, cylinder pressure and average cylinder temperature schedules for B100 combustion with FIS = 10°btdc and at 7.5 bar b.m.e.p.

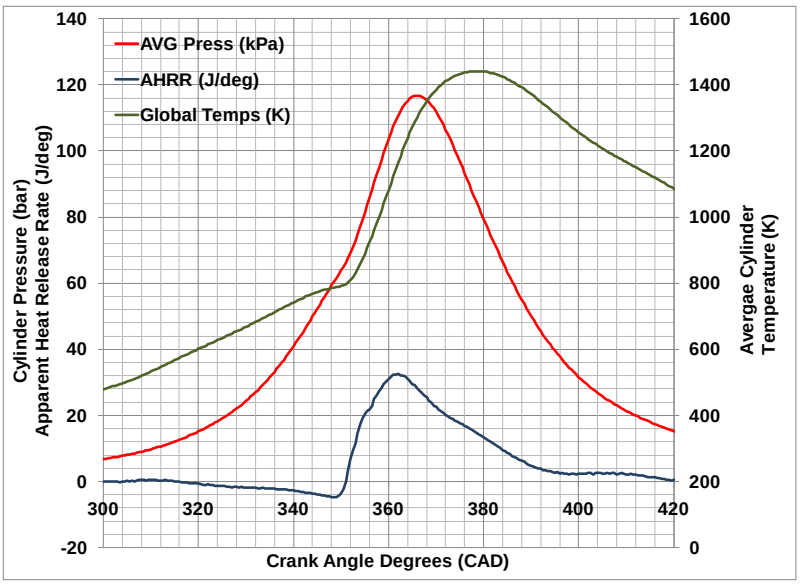


Figure E.1.6b. Crank resolved apparent heat release rate, cylinder pressure and average cylinder temperature schedules for B20 combustion with FIS = 10°btdc and at 7.5 bar b.m.e.p.

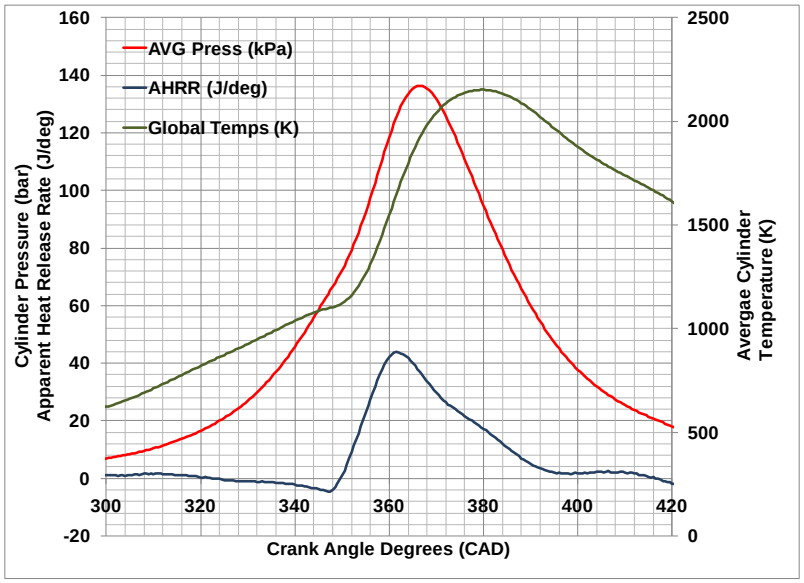


Figure E.1.7a. Crank resolved apparent heat release rate, cylinder pressure and average cylinder temperature schedules for B100 combustion with FIS = 10°btdc and at 10 bar b.m.e.p.

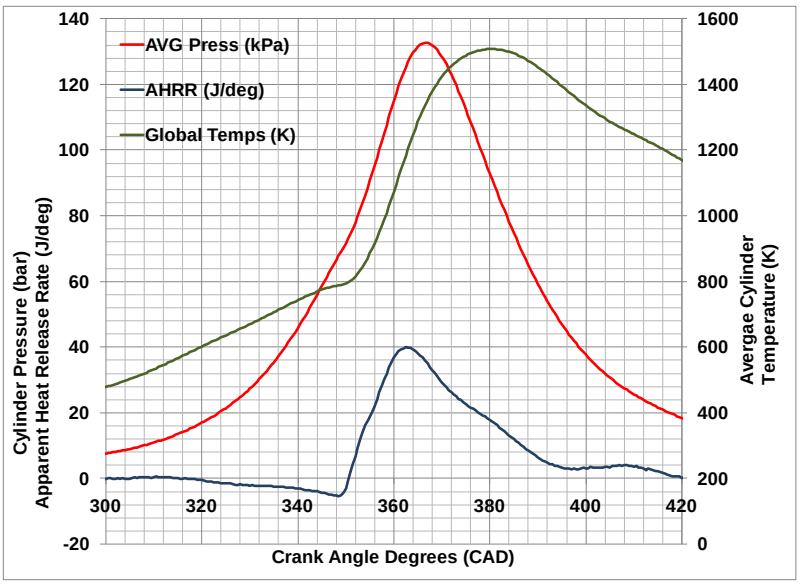


Figure E.1.7b. Crank resolved apparent heat release rate, cylinder pressure and average cylinder temperature schedules for B20 combustion with FIS = 10°btdc and at 10 bar b.m.e.p.

Figures E.1.8-11 show the in-cylinder pressure, heat release rate, and average cylinder temperature profiles for B20 and B100 combustion at 4°btdc injection timing as indicated in Table E.1.1. Table E.1.3 summarizes the ignition delay times and ca 50% location for all experimental conditions. At all operating conditions, the following observations are true: 1) the ignition delay times are shorter for B100 combustion, and 2) the crank angle corresponding to 50% heat release is also advanced compared to B20 combustion. Also, relative to the 10°btdc injection timing, the ca 50% locations are much more advanced. This means that combustion occurs at a much slower rate compared to the 10° btdc timing and perhaps that the bulk of the combustion energy release occurs much later in the expansion stroke, thereby also at lower cylinder temperatures, which might explain the relatively lower NOx emissions for both B20 and B100 combustion. However, the B100 NOx still remains higher than B20 NOx emissions.

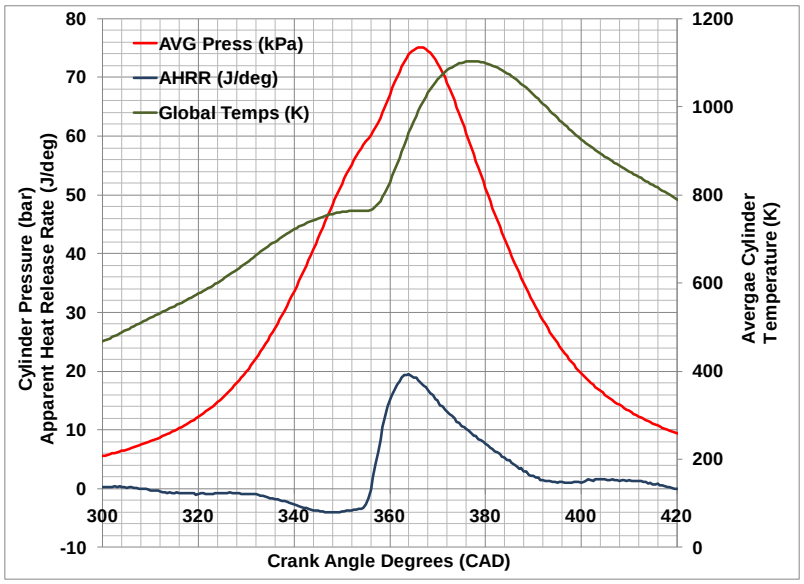


Figure E.1.8a. Crank resolved apparent heat release rate, cylinder pressure and average cylinder temperature schedules for B100 combustion with FIS = 4°btdc and at 2.5 bar b.m.e.p.

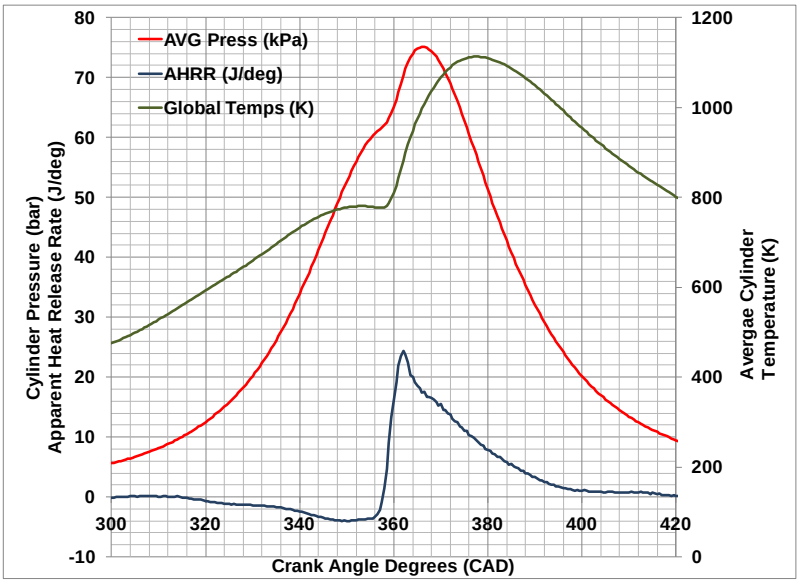


Figure E.1.8b. Crank resolved apparent heat release rate, cylinder pressure and average cylinder temperature schedules for B20 combustion with FIS = 4°btdc and at 2.5 bar b.m.e.p.

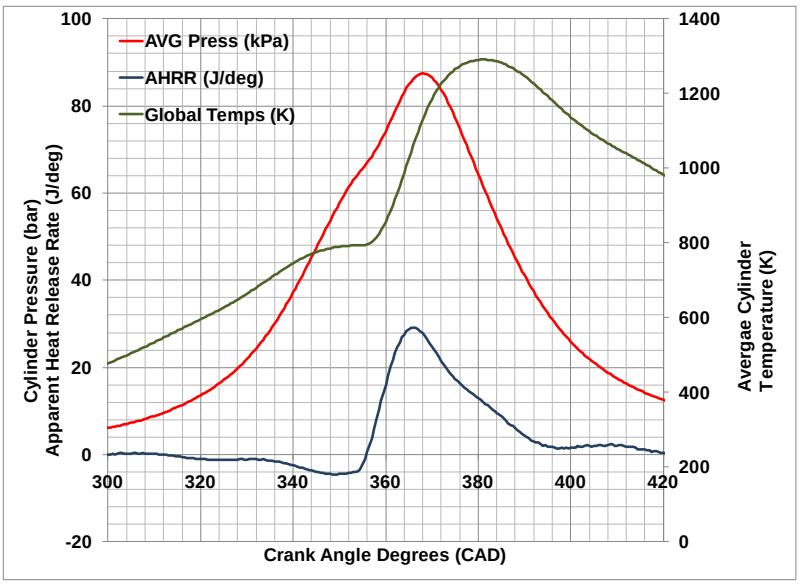


Figure E.1.9a. Crank resolved apparent heat release rate, cylinder pressure and average cylinder temperature schedules for B100 combustion with FIS = 4°btdc and at 5 bar b.m.e.p.

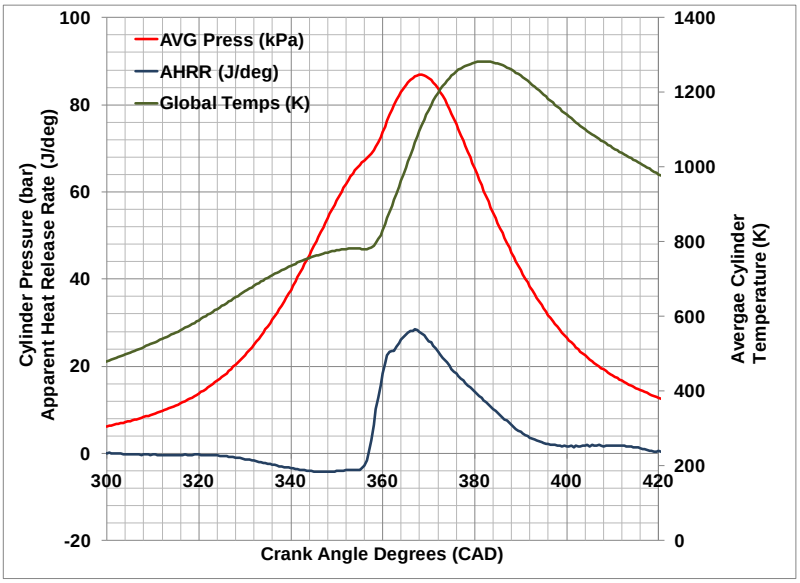


Figure E.1.9b. Crank resolved apparent heat release rate, cylinder pressure and average cylinder temperature schedules for B20 combustion with FIS = 4°btdc and at 5 bar b.m.e.p.

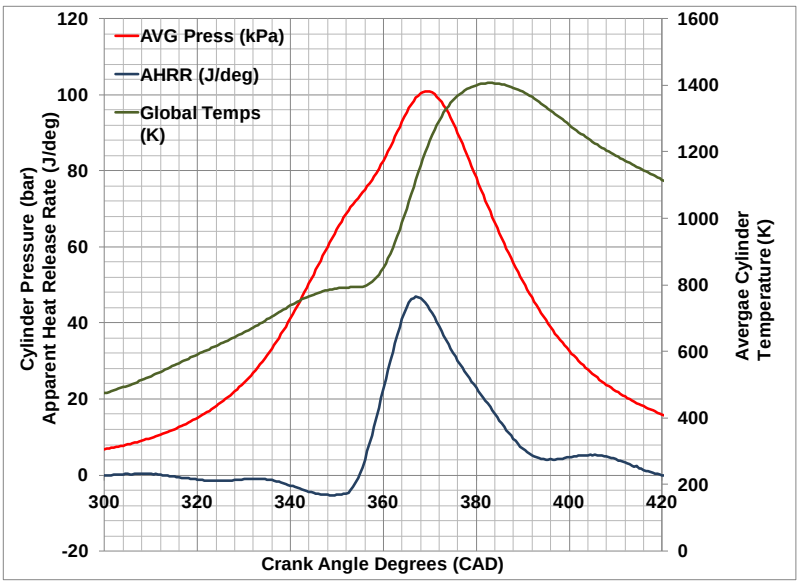


Figure E.1.10a. Crank resolved apparent heat release rate, cylinder pressure and average cylinder temperature schedules for B100 combustion with FIS = 4°btdc and at 7.5 bar b.m.e.p.

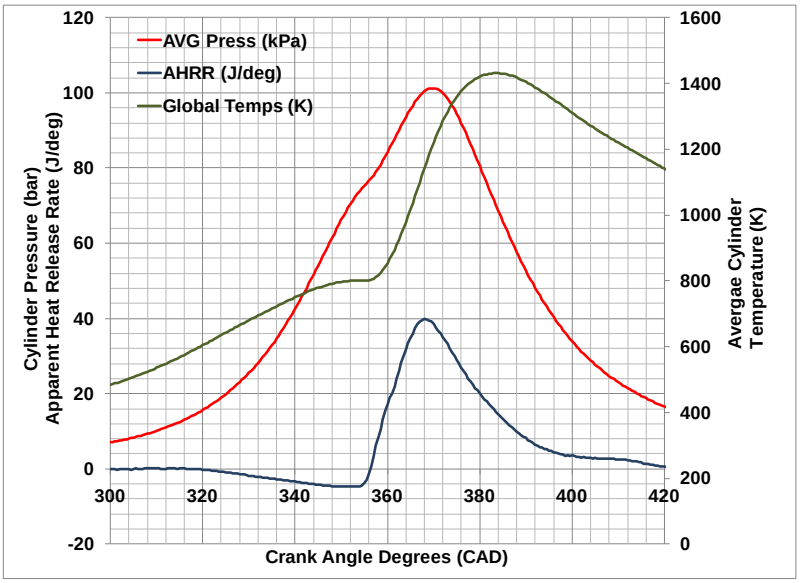


Figure E.1.10b. Crank resolved apparent heat release rate, cylinder pressure and average cylinder temperature schedules for B20 combustion with FIS = 4°btdc and at 7.5 bar b.m.e.p.

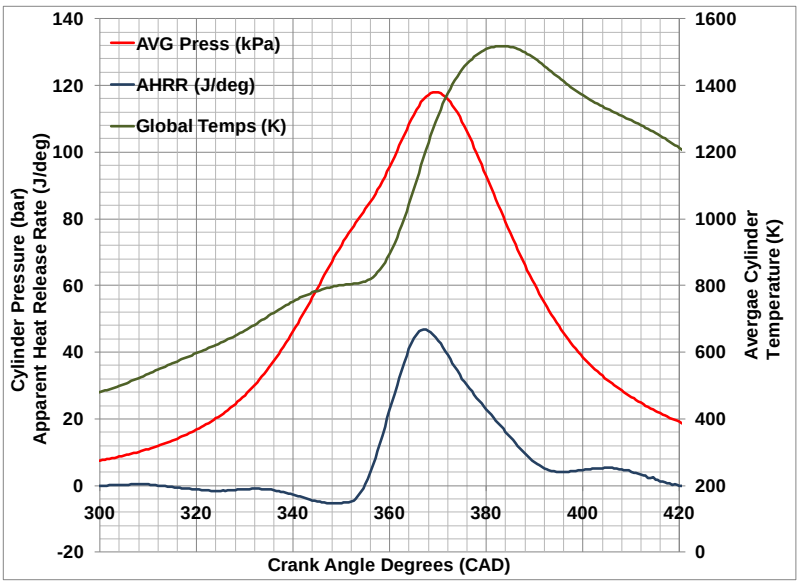


Figure E.1.11a. Crank resolved apparent heat release rate, cylinder pressure and average cylinder temperature schedules for B100 combustion with FIS = 4°btdc and at 10 bar b.m.e.p.

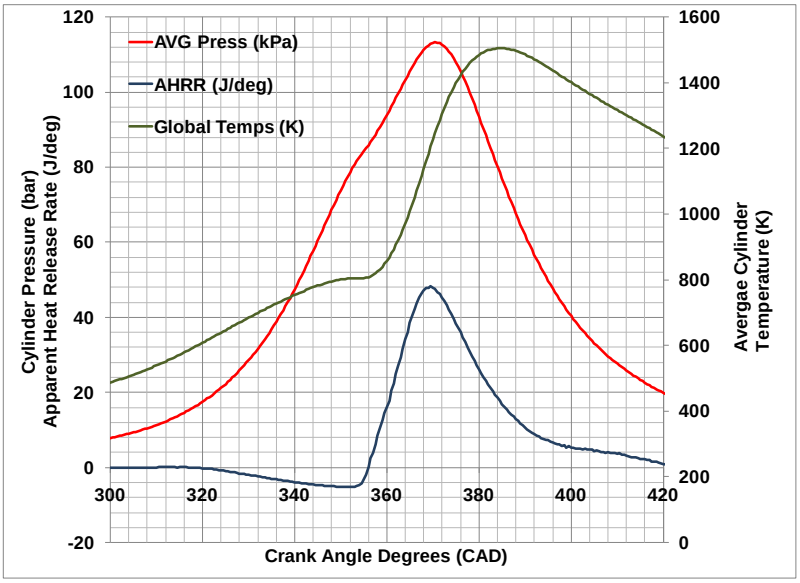


Figure E.1.11b. Crank resolved apparent heat release rate, cylinder pressure and average cylinder temperature schedules for B20 combustion with FIS = 4°btdc and at 10 bar b.m.e.p.

Figures E.1.11-15 show the in-cylinder pressure, heat release rate and average cylinder temperature profiles for B20 and B100 combustion at 0°btdc injection timing as indicated in Table E.1.1. Table E.1.3 summarizes the ignition delay times and ca 50% location for all experimental conditions. At all operating conditions, the following observations are true: 1) the ignition delay times are shorter for B100 combustion, and 2) the crank angle corresponding to 50% heat release is also advanced compared to B20 combustion. Also, relative to the 10°btdc and 4°btdc injection timings, the ca 50% occurs much later in the

expansion stroke, thereby also at lower cylinder temperatures, which might explain the relatively lower NOx emissions for both B20 and B100 combustion. However, the B100 NOx still remains higher than B20 NOx emissions.

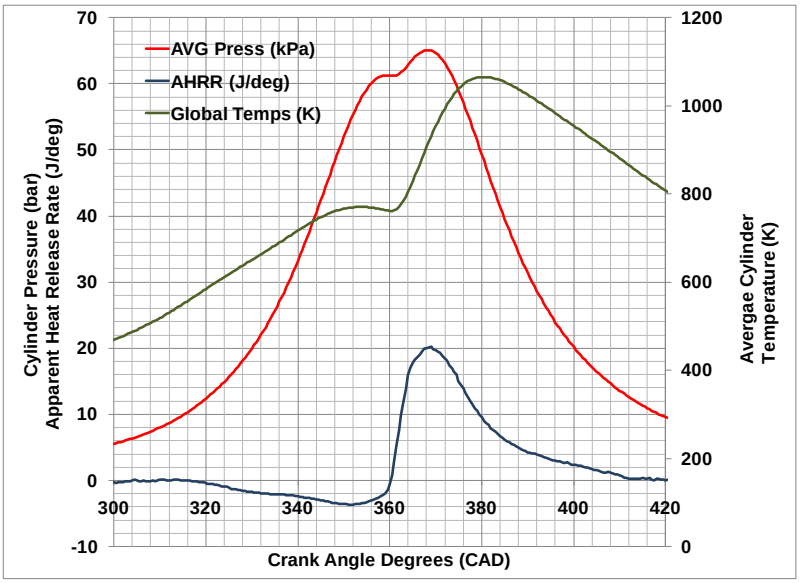


Figure E.1.12a. Crank resolved apparent heat release rate, cylinder pressure and average cylinder temperature schedules for B100 combustion with FIS = 0°btdc and at 2.5 bar b.m.e.p.

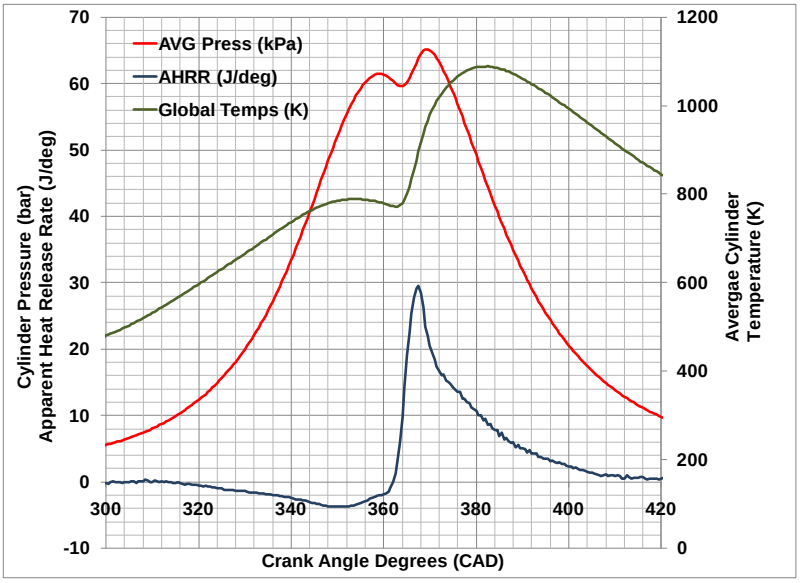


Figure E.1.12b. Crank resolved apparent heat release rate, cylinder pressure and average cylinder temperature schedules for B20 combustion with FIS = 0°btdc and at 2.5 bar b.m.e.p.

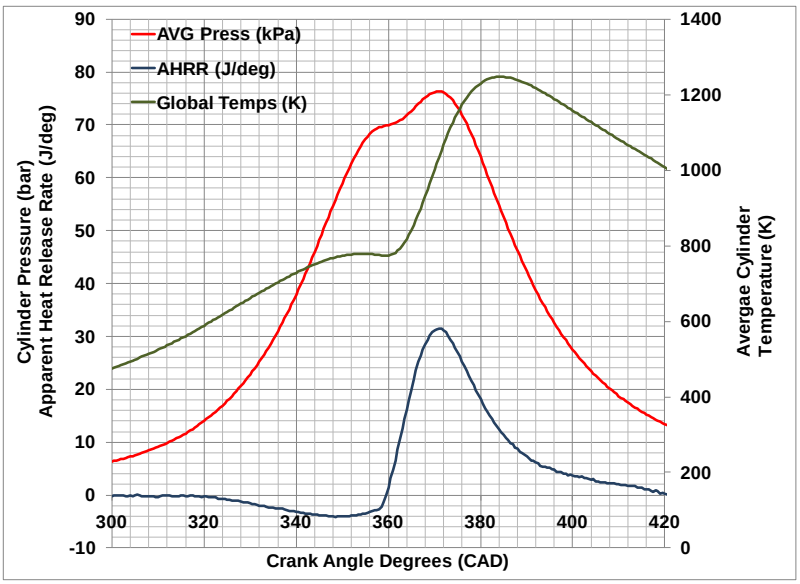


Figure E.1.13a. Crank resolved apparent heat release rate, cylinder pressure and average cylinder temperature schedules for B100 combustion with FIS = 0°btdc and at 5 bar b.m.e.p.

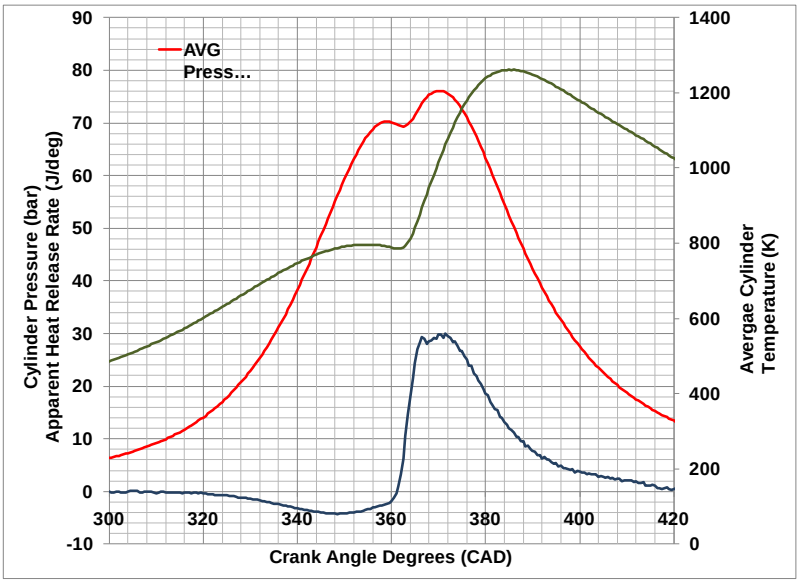


Figure E.1.13b. Crank resolved apparent heat release rate, cylinder pressure and average cylinder temperature schedules for B20 combustion with FIS = 0°btdc and at 5 bar b.m.e.p.

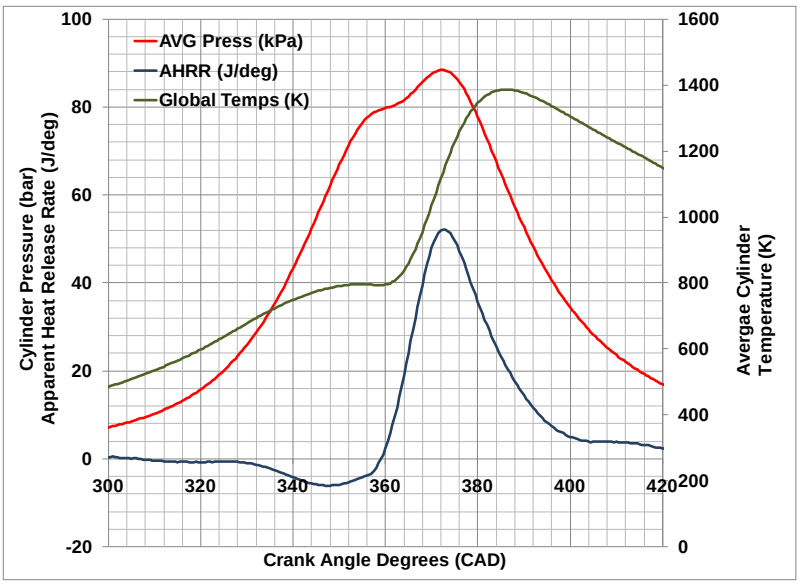


Figure E.1.14a. Crank resolved apparent heat release rate, cylinder pressure and average cylinder temperature schedules for B100 combustion with FIS = 0°btdc and at 7.5 bar b.m.e.p.

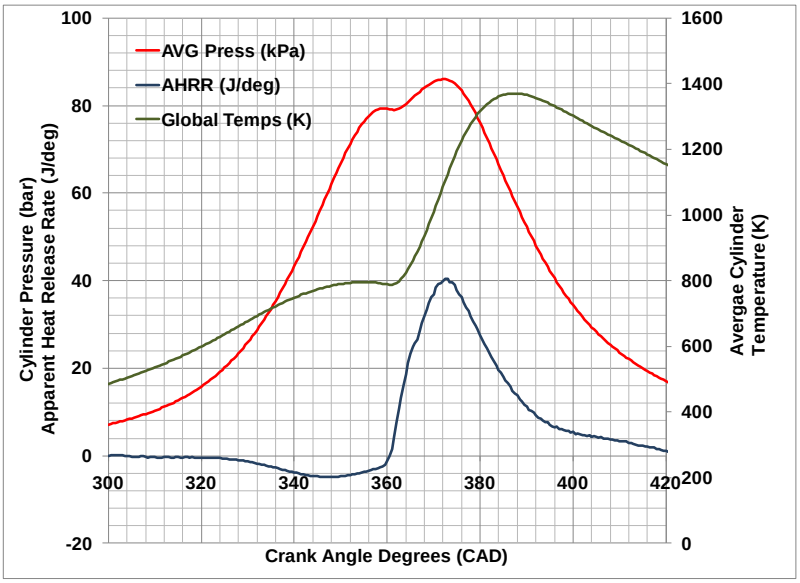


Figure E.1.14b. Crank resolved apparent heat release rate, cylinder pressure and average cylinder temperature schedules for B20 combustion with FIS = 0°btdc and at 7.5 bar b.m.e.p.

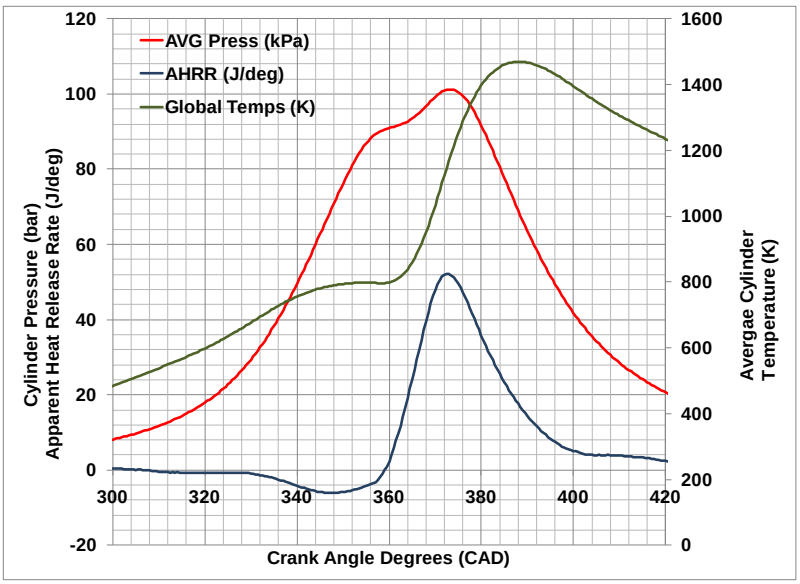


Figure E.1.15a. Crank resolved apparent heat release rate, cylinder pressure and average cylinder temperature schedules for B100 combustion with FIS = 0°btdc and at 10 bar b.m.e.p.

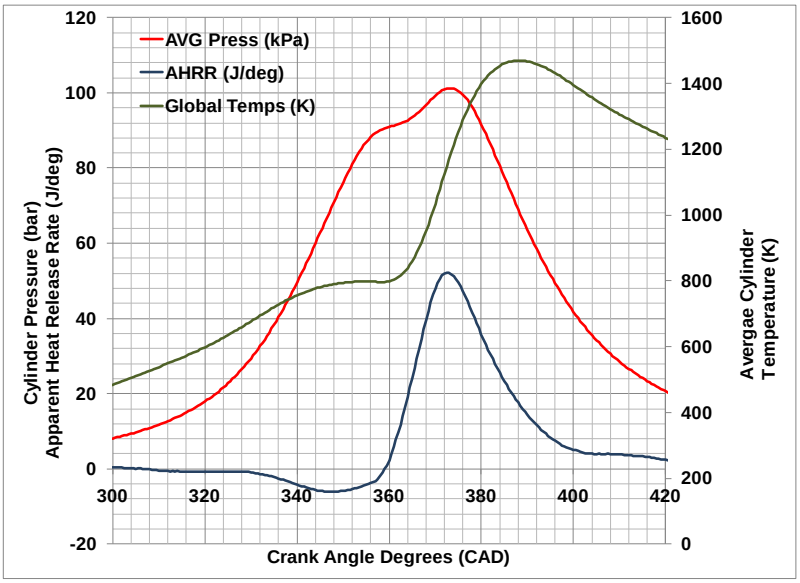


Figure E.1.15b. Crank resolved apparent heat release rate, cylinder pressure and average cylinder temperature schedules for B20 combustion with FIS = 0°btdc and at 10 bar b.m.e.p.

In summary, it is clear that with B100 fuelling the NOx emissions were generally higher than for B20 fuelling; however, with increasing injection timing retard, it is possible to obtain lower NOx emissions albeit with significant fuel efficiency penalties. Also, since B100 has a lower heating value compared to both B20 and straight diesel fuel, the fuel conversion efficiencies were generally lower. At this point, it is noteworthy to mention that the test engine had to be

rebuilt on several occasions due to severe engine knock while performing some dual fuel investigations (see Figures E.1.16-18). Therefore, the compression ratios were modified from baseline values, which explain the low fuel conversion efficiencies. Also, the fact that the diesel engine uses a fuel-injection pump that did not allow for any control of injection parameters, such as fuel injection timing, fuel injection pressure, fuel injected quantity, and number of fuel injection pulses, a full optimization of B100 and B20 combustion could not be performed. As a result, the reported emissions were the best possible values obtained under the constraints of the fuel injection pump. However, one interesting trend that is clearly demonstrated is the significant lowering of NOx emissions with injection retard (in line with observations in the open literature). Therefore, a clear relationship between fuel injection and NOx emissions has been established, and there is further room to achieve significantly lower NOx emissions with a fully electronic injection system controller. In addition, the cylinder pressure and average cylinder temperature traces for B100 help corroborate earlier findings in research about increasing NOx emissions with B100 fuelling. In particular, at 10 bar bmep operation because the average cylinder temperatures are much higher than corresponding B20 operation, it is clearly plausible that the overall cylinder temperatures are generally higher, possibly due to reduced soot radiation because the fuel-bound oxygen in B100 tends to oxidize soot without allowing for larger soot particles to be produced, which would radiate away more energy from the flame front. As a consequence, the flame temperatures are higher, and this might result in higher NOx emissions with B100 combustion.

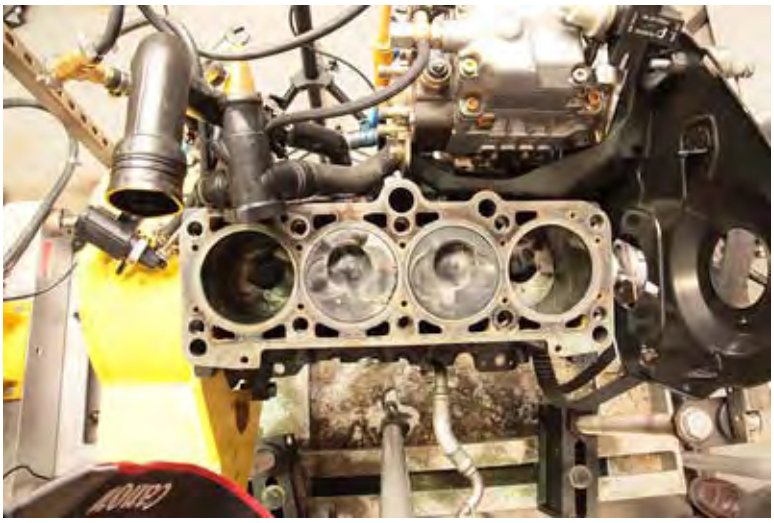


Figure E.1.16. Engine disassembled after severe damage to pistons due to end gas knock



Figure E.1.17. Close-up examination of the extent of piston damage due to engine knock



Figure E.1.18. Hi-resolution image of chipping of metal due to severe engine knock

Subtask E.2 Phenomenological low temperature engine combustion simulation development

1. Planned Activities

E.2.ML.1 Year 1 milestone is to predict B100 combustion heat release rates and pressure histories accurately and validate the predictions against baseline experimental data obtained in Subtask 5.1 to within a 10% error.

E.2.ML.2 Year 2 milestone is to complete simulation of biodiesel-ignited syngas low temperature combustion, validate predictions with baseline experimental results from Subtask 5.3 to within a 10% error and determine the best operating parameters to optimize biodiesel-ignited syngas combustion.

2. Summarization of Activities

Phenomenological simulations were developed to predict B100 heat release rates and cylinder pressure schedules. The simulations were developed using MATHCAD and FORTRAN programming languages. In spray-guided combustion, such as in conventional diesel and biodiesel engines, it is very important to model the ignition delay time that characterizes the autoignition event, which initiates the combustion process. Therefore, a separate ignition delay model based on the Shell autoignition model (an eight-step, generic, hydrocarbon autoignition mechanism that captures chain propagation and chain branching in the pre-ignition chemical reactions) was developed in MATHCAD along with a zero-dimensional, single-zone combustion model to address B100 combustion. This model was then further improved to include two zones to capture dual fuel low temperature combustion, as in diesel or biodiesel pilot ignited natural gas and syngas combustions. The models were validated using experimental data (both acquired in-house on our B100 fuelled multi-cylinder engine and our own previously published data on a dual fuel diesel-pilot ignited natural gas engine (Krishnan et al.). Following these validation efforts, a more updated multi-zone phenomenological model that captures the spray behavior and flame propagation in the subsequent gas-air mixture was developed and validated using published data[1]. The details of the two-zone phenomenological model were published in a peer-reviewed conference paper (Jha et al.). The details of the multi-zone phenomenological simulation are described later in the document and were also published in an award-winning peer-reviewed journal article (Krishnan and Srinivasan). The model is robust enough to tackle a variety of liquid fuel and gaseous fuel combustion scenarios; however, because there are no reliable flame speed correlations available for syngas and because its composition is highly variable and dependent on the biomass gasification process, it was difficult to validate any syngas combustion data accurately. However, the current framework is capable of predicting syngas combustion performance once reliable flame propagation parameters are obtained in the open literature.

Figures E.2.1-4 show the in-cylinder pressure histories and heat release rate schedules from B100 combustion at different loads (depicted in terms of brake mean effective pressures, BMEP) and at different fuel injection timings (10°, 4° and 0°BTDC). In each set of figures, the measured and predicted cylinder pressure histories are shown first (Figure E.2.1a), followed by the experimentally derived and predicted heat release schedules (Figure E.2.1b). The convention followed in the legends is as follows: e.g., BD_10_356_Experiment refers to experimental results for biodiesel (B100) operation at 10 bar BMEP and 356 absolute crank angle degrees (or 4°BTDC) while BD_10_356_Simulation refers to the corresponding simulation results. In general, it is clearly evident from these figures that the single-zone simulation with a Wiebe function-based combustion model was able to predict cylinder pressure histories for B100 operation very well (a near-perfect match is evident) for all injection timings and engine loads (BMEPs). The heat release predictions (especially the combustion duration and peak heat release rates) are also very good for high loads (BMEP = 7.5 bar and BMEP = 10 bar). However, for lower BMEPs (5 bar and 2.5 bar), the single-zone combustion model overpredicts the peak heat release rates, despite predicting combustion durations quite well. This may be attributed to the fact that the single-zone combustion model does not capture all of the complicated physics of the combustion process as other two-zone and multi-zone combustion models. This formed the basis for developing two-zone and the more sophisticated multi-zone phenomenological combustion models described below.

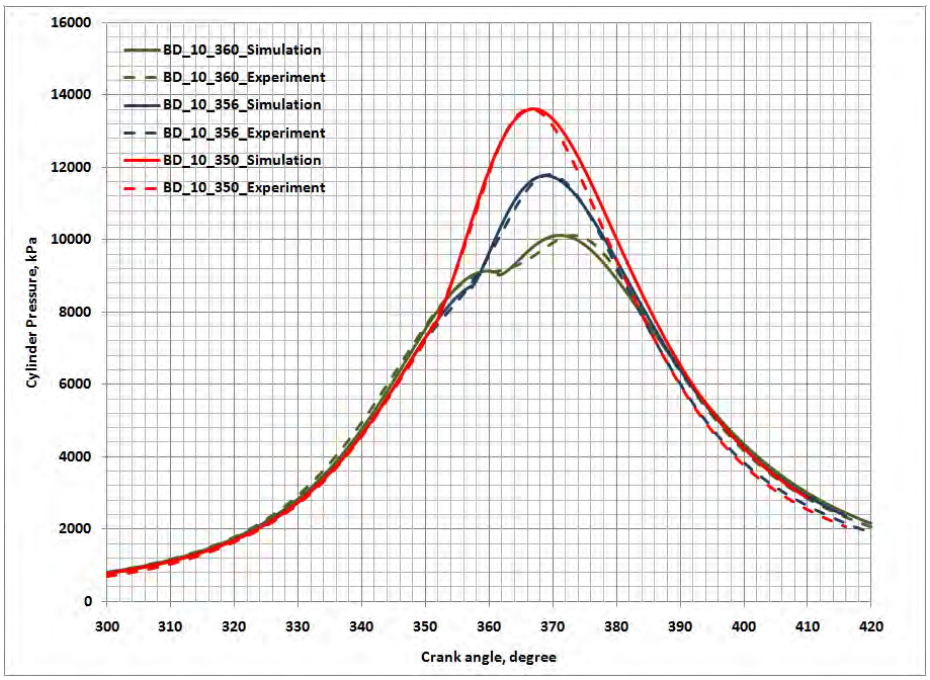


Figure E.2.1a. Comparative B100 experimental and simulated crank resolved cylinder pressure schedules at 2.5 bar bmep

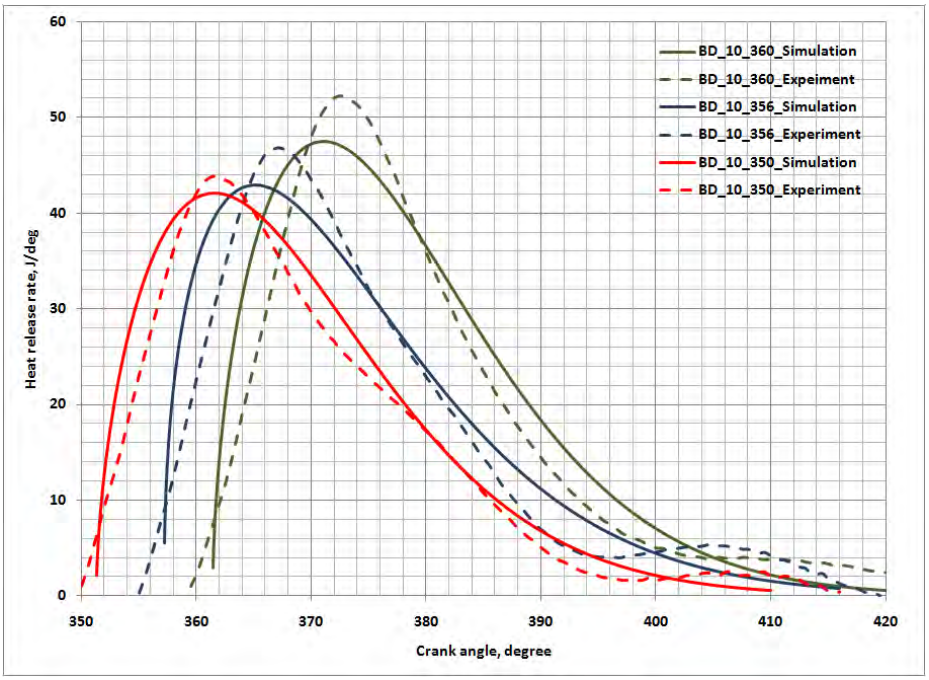


Figure E.2.1b. Comparative B100 experimental and simulated crank resolved apparent heat release rate schedules at 2.5 bar bmep

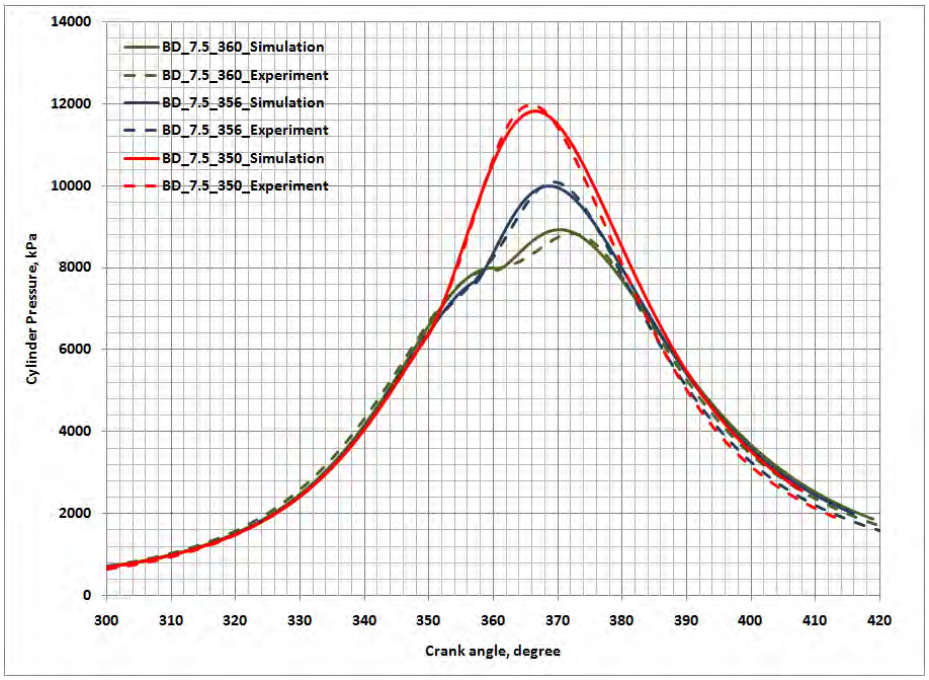


Figure E.2.2a. Comparative B100 experimental and simulated crank resolved cylinder pressure schedules at 5 bar bmep

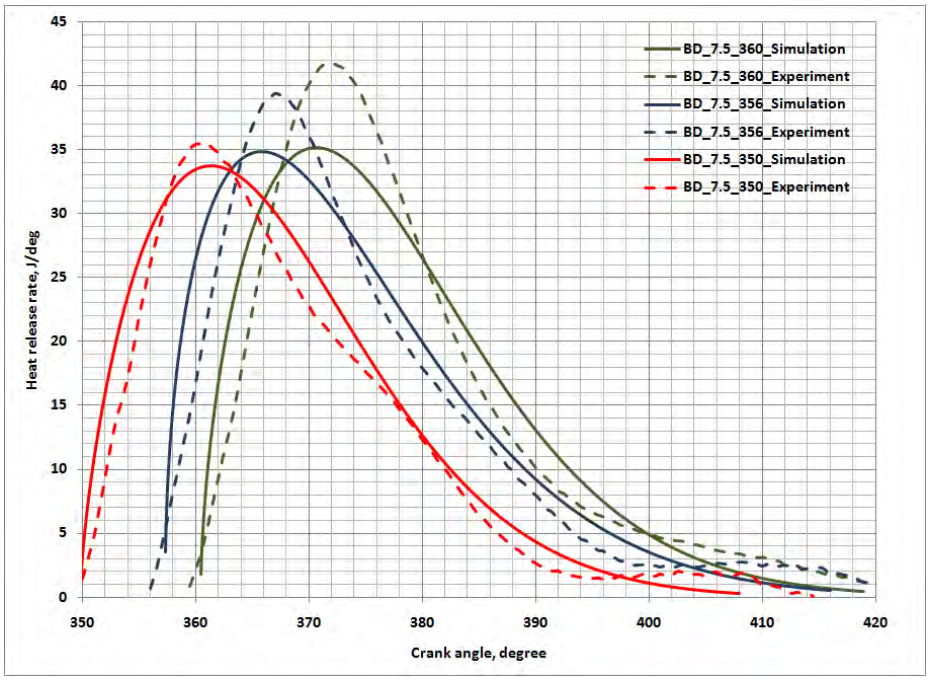


Figure E.2.2b. Comparative B100 experimental and simulated crank resolved apparent heat release rate schedules at 5 bar bmep

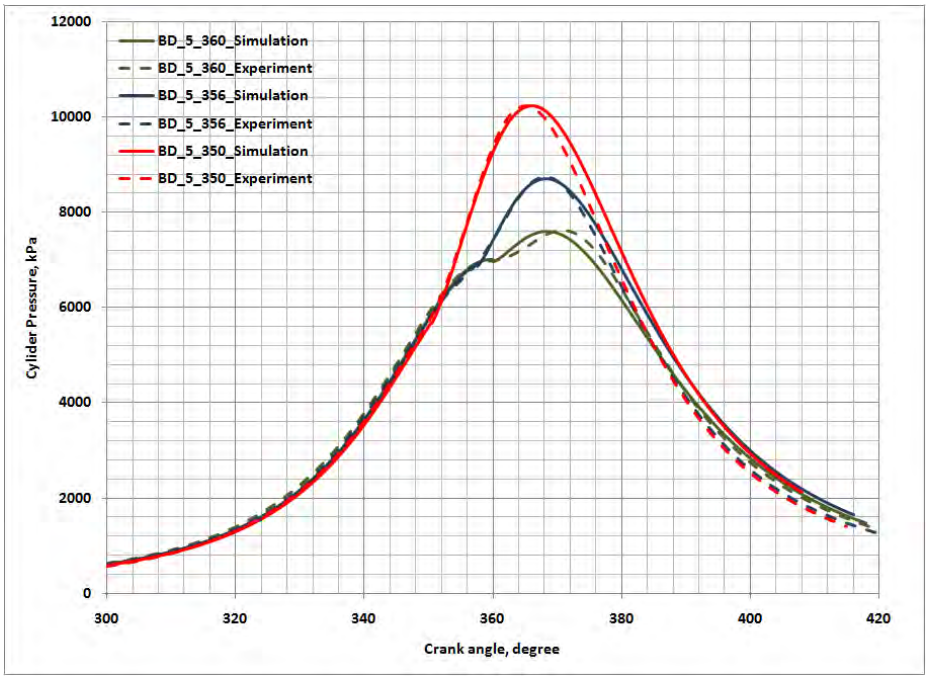


Figure E.2.3a. Comparative B100 experimental and simulated crank resolved cylinder pressure schedules at 7.5 bar bmep

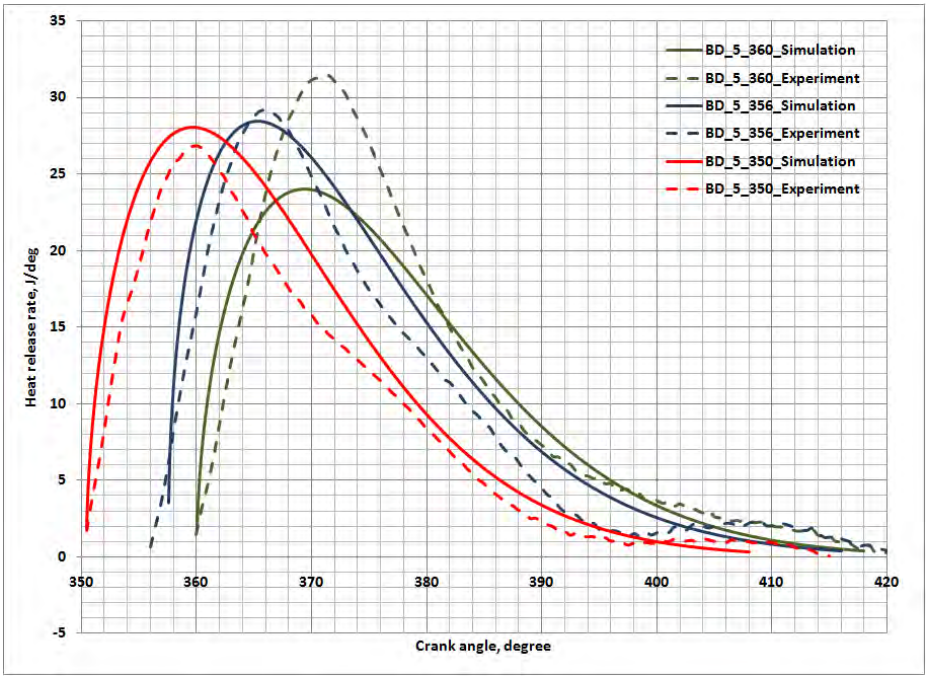


Figure E.2.3b. Comparative B100 experimental and simulated crank resolved apparent heat release rate schedules at 7.5 bar bmep

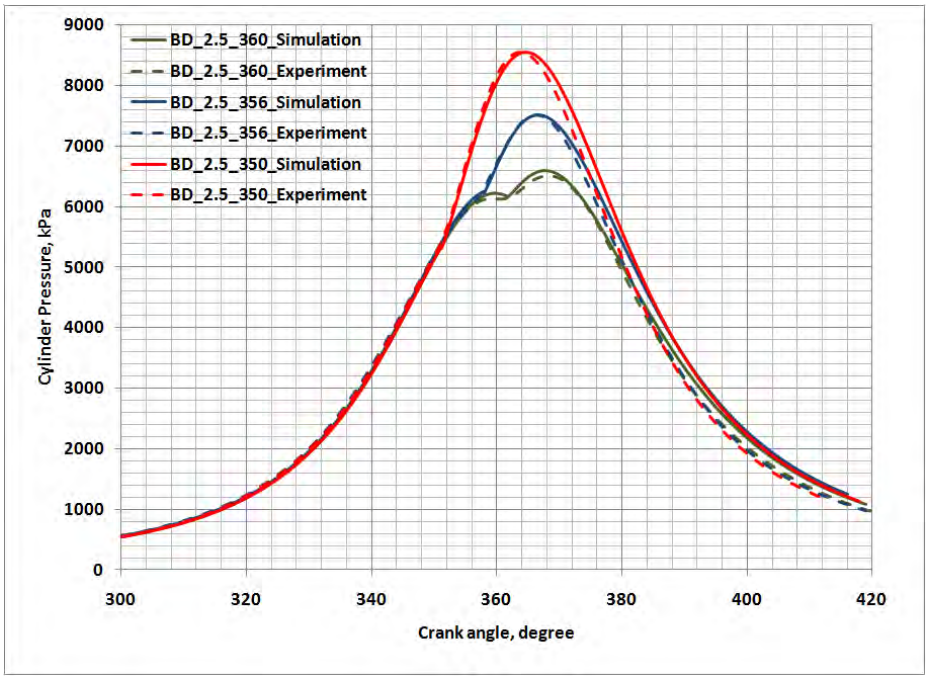


Figure E.2.4a. Comparative B100 experimental and simulated crank resolved cylinder pressure schedules at 10 bar bmep

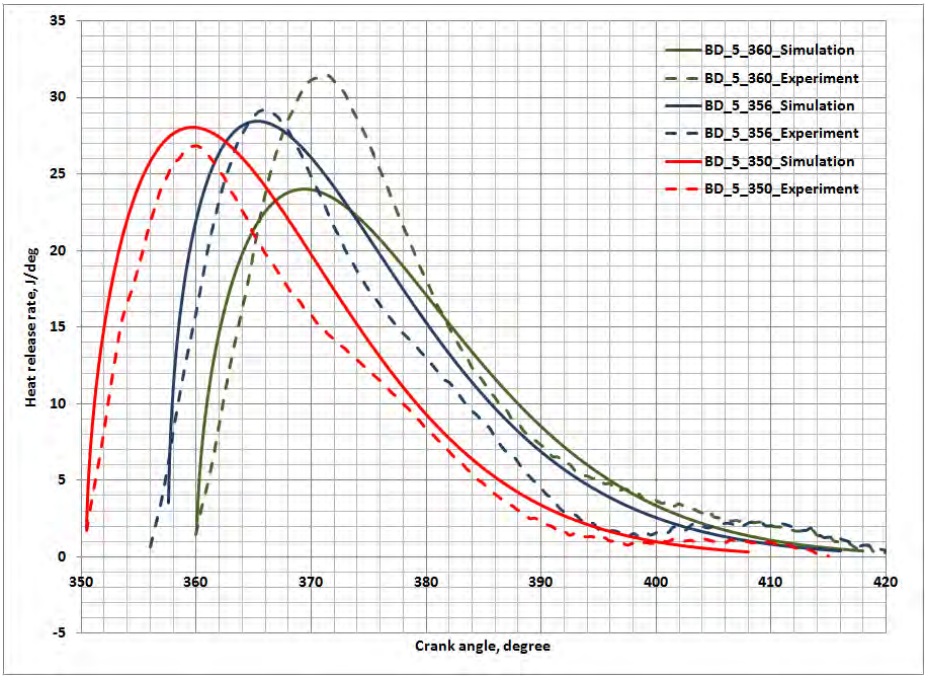


Figure E.2.4b. Comparative B100 experimental and simulated crank resolved apparent heat release rate schedules at 10 bar bmep

Quasi-two-zone combustion model

To complement the single-zone combustion model, a quasi-two-zone combustion model was developed and validated with experimental data available for dual fuel pilot-ignited natural gas low temperature combustion (LTC). The essential feature of dual fuel pilot-ignited natural gas LTC is the presence of distributed ignition centers that enable faster combustion rates in lean, premixed natural-gas air mixtures. Distributed ignition centers present a unique challenge in modeling dual fuel LTC with a phenomenological approach. Several simplifying assumptions have been made to model ignition phenomena in dual fuel LTC:

1. The quasi-two-zone model considers the closed thermodynamic system between IVC and SOC. No attempt has been made to model the intake process.
2. The closed system is a mixture of ideal gases.
3. After beginning of pilot injection (BOI), the combustion chamber is divided into two zones: the autoignition zone and the main reaction zone.
    a. In the autoignition zone, pilot diesel sprays undergo evaporation and ignition in the presence of natural gas and air. The autoignition zone is an ensemble of all the autoignition sites (distributed ignition centers) present in the combustion chamber. Evaporation of diesel sprays is modeled using an isolated droplet evaporation model. Further, the diesel sprays are assumed mono-disperse with droplets of uniform Sauter Mean Diameter (SMD). Finally, to capture the effect of distributed ignition centers without resorting to a detailed entrainment model, it is assumed that upon evaporation, diesel mixes adiabatically with the surrounding natural gas-air mixture at a user specified autoignition zone equivalence ratio (φ_{auto}). The autoignition zone equivalence ratio is a model parameter, whose effect on the predicted ignition delay (ID) was investigated, and an optimal φ_{auto} was determined.
    b. The bulk of the combustion occurs in the “main reaction” zone, which includes unburned reactants, diluents (from EGR), and post-combustion products. Upon diesel ignition, the overall combustion phenomenon is modeled using a simple Wiebe function.
4. The quasi-two-zone model is assumed to investigate the behavior of “knock-free” combustion conditions only. Therefore, the pressures of the autoignition zone and the main reaction zone are equal at any given crank angle.
5. The autoignition zone ceases to exist as soon as pilot diesel ignites and combustion of the premixed natural gas-air mixture begins in the main reaction zone.

For a more detailed account of the various sub-models, please see our conference publication (Jha et al. (2010), Paper No. ICEF2010-35127, Proc. of ASME IC Eng. Div. 2010 Fall Tech. Conf. Sep 12-15, San Antonio, TX). In the following paragraphs, the effects of one important model parameter and one experimental parameter are discussed to provide a general idea of the model behavior.

As mentioned above, φ_{auto} is an important model parameter in the quasi-two-zone combustion model. The effect of φ_{auto} on ID predictions is shown as percent relative error trends in Figure E.2.5. The relative error in ID was calculated as the difference between predicted ID and experimental ID for a given BOI and φ_{auto}, normalized with the experimental ID, and expressed as a percent relative error in the predicted ID. For this parametric study, φ_{auto} was varied from lean to rich values while other engine variables were held constant: engine speed, N_e = 1700

rpm, cylinder pressure at IVC, P_{IVC} = 212 kPa, intake temperature, T_{in} = 75° C, SMD = 30 µm, diesel injected mass, m_d = 3.94 mg/cycle, and EGR = 0%. The purpose of this study was to determine the optimal φ_{auto}, which provided the least percent relative error over the range of BOIs encountered in ALPING LTC. Figure E.2.5 shows that the stoichiometric autoignition zone equivalence ratio (φ_{auto} = 1.0) resulted in the least error (±10%) in predicted IDs between 20° and 60° BTDC injection timings. Consequently, the optimal φ_{auto} for the present model was assumed to be 1.0 over the range of BOIs in dual fuel LTC. The percent relative error trends also show that the impact of φ_{auto} variation on predicted IDs was more pronounced at retarded BOIs, possibly due to the increased importance of the physical component of ID at retarded BOIs.

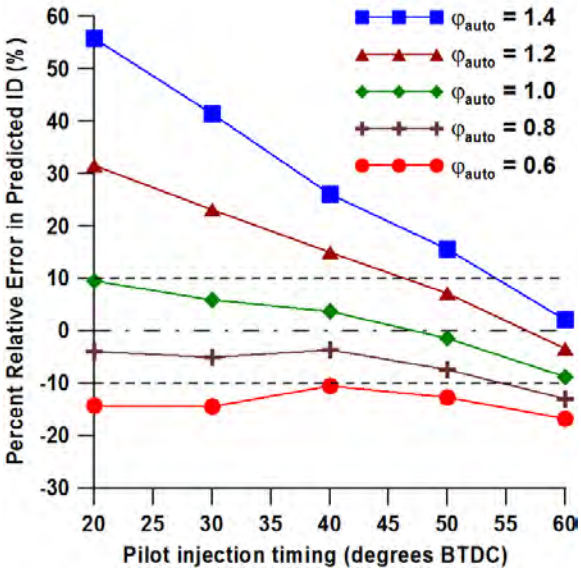


Figure E.2.5. Relative error in predicted ignition delays vs BOI for different autoignition zone equivalence ratios (φ_{auto}) at half load (BMEP = 6 bar); 1700 rpm, P_{IVC} = 212 kPa, SMD = 30 µm, T_{in} = 75° C, EGR(%) = 0

Modeling EGR Effects

Exhaust gas recirculation (EGR) involves slip-streaming some of the exhaust back into the intake manifold to mix with fresh intake charge to reduce NOx emissions. The amount of EGR in the total intake charge is usually expressed as EGR %, which is defined as: EGR (%) = (m_{EGR} / m_i) * 100, where $m_i = m_a + m_{NG} + m_{EGR}$ and m_{EGR} is the mass of EGR. Because diesel engines do not employ any intake throttling, they operate at 95-100% volumetric efficiencies at most engine operating conditions. The use of EGR results in displacement of a portion of air, causing a reduction in the air available for combustion. This decreased combustion air lowers the air-fuel ratio at which the engine operates and can affect exhaust emissions significantly. Also, when uncooled, EGR is mixed with the air delivered to a diesel engine, the temperature of the charge increases and can considerably affect the compressed charge temperature and the combustion process. The displacement of intake charge with CO_2 and H_2O can impact the combustion process in many ways. For instance, addition of EGR can lead to a net reduction in intake oxygen concentration, which influences the flame temperature and, thus, NOx emissions. On the other hand, the higher specific heats of both CO_2 and H_2O in comparison to that of O_2 and N_2 being displaced results in a net diluent effect. In dual fuel LTC, when the intake natural gas-air mixture mixes at T_{in} with recycled, uncooled, exhaust gas at a higher temperature (T_{EGR}), the resulting natural gas-air-EGR mixture temperature (T_{mix}) will be higher. Also, both CO_2 and

H_2O can potentially dissociate into radicals at the high temperatures encountered during combustion. In particular, these dissociation reactions could be one cause for the increase in ID with increasing EGR, and, consequently, a larger portion of the fuel could burn in the premixed phase. Another important effect while using EGR can be a net stratification in temperature and/or composition of the final intake mixture. However, the extent of homogenization of the in-cylinder mixture is dependent on available mixing times.

Figure E.2.6 shows both experimental and simulated IDs as a function of BOI at different EGR substitutions. A reduction in ID was observed with increasing percent EGR for the entire range of BOIs except the most retarded BOI of 20° BTDC. There may be several competing factors that led to this behavior. For example, increasing hot EGR substitutions led to higher intake charge temperatures, thereby causing shorter ignition delays for most BOIs. On the other hand, oxygen concentrations also decreased as percent EGR was increased; therefore, the charge was hotter and depleted of oxygen when it entered the combustion chamber. Also, the higher specific heats (C_p) of CO_2 and H_2O introduced by EGR increased the effective C_p of the intake mixture. This increase in effective C_p resulted in lower temperatures at the time of pilot diesel injection. Lower temperatures at BOI coupled with oxygen depletion resulted in lower preignition energy release in the autoignition zone. This decrease in preignition energy release competed with the effects of higher intake charge temperatures at different BOIs, affecting the actual ignition delay times. However, from Figure E.2.6, it is clear that ID decreases with increasing EGR substitutions for most BOIs. This demonstrates that for most BOIs the most significant effect of uncooled EGR is a net increase in intake charge temperature, and, therefore, a net reduction in IDs. For the most retarded BOI of 20° BTDC, the experimental ID increased with increasing EGR, indicating the potentially more significant impact of higher C_p, lower temperatures at BOI, and oxygen depletion on ID compared to intake charge temperatures. However, the simulated IDs do not follow the experimental trends for 20° BTDC BOI but continue to show a decreasing trend with increasing EGR. These differences indicate a potential shortcoming of the present quasi-two-zone model.

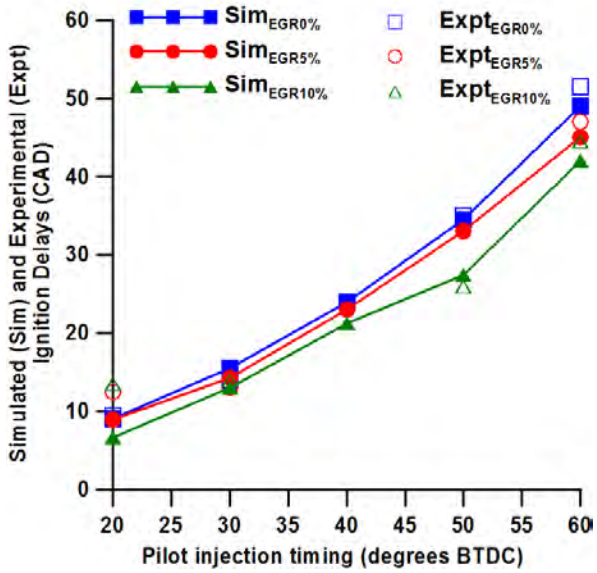


Figure E.2.6. Ignition delay and $\Delta\theta_{evap}$ vs BOI for different EGR (%) at half load (BMEP = 6 bar); 1700 rpm; P_{IVC} = 212 kPa, T_{in} = 75° C, SMD = 30 μm, φ_{auto} = 1.0

Uncertainty Analysis of Quasi-Two-Zone Model

Figures E.2.7-9 show uncertainty percentage contributions (UPC) of important model parameters and experimental variables. Of the pre-exponential factors, A_{p3} and A_q accounted for about 90% of the overall uncertainty in IDs for all BOIs (see Figure E.2.7). Among activation energies, E_q alone contributed to about 85% of the overall uncertainty for all BOIs while, E_b, E_{p2}, and E_{p3} each contributed less than 10% to the overall uncertainty. Among experimental variables, the UPC contributions of T_{in} were 40-50% while the UPCs for φ_{auto} were 20-30% over the range of BOIs. By comparison, the UPCs for compression ratio (CR) and the carbon chain length in diesel surrogate (n_{RH}) were less than 10%. The droplet diameter (d_D) showed significant UPC (~ 30%) only for 20° BTDC BOI, for which the physical component of ID was more important.

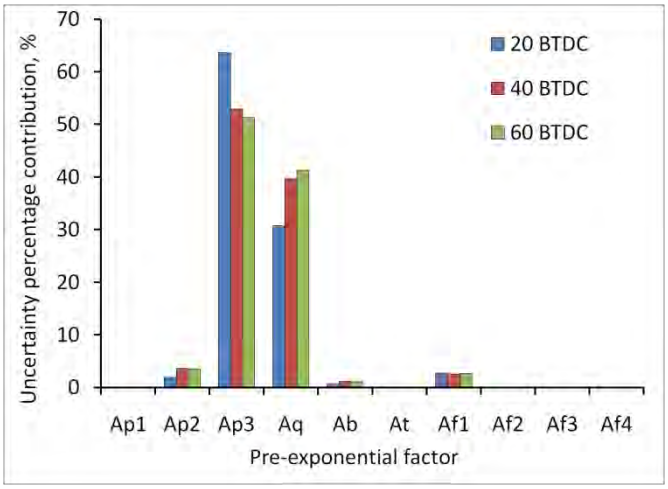


Figure E.2.7. UPC (%) of pre-exponential factors used in modified H&R model at different BOIs.

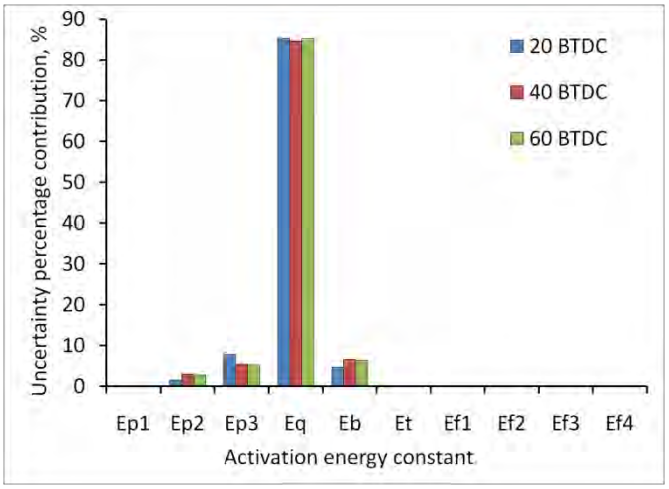


Figure E.2.8. UPC (%) of activation energies used in modified H&R model at different BOIs.

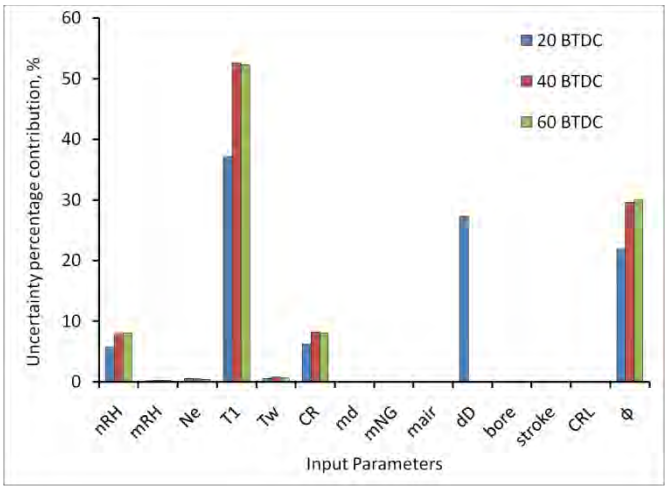


Figure E.2.9. UPC (%) of experimental input variables used in modified H&R model at different BOIs.

Summary

A modified version of a generic hydrocarbon autoignition model was used in a quasi-two-zone combustion model to simulate diesel ignition delays (ID) for partially premixed dual fuel LTC. The effects of hot EGR on predicted and measured IDs in dual fuel LTC were evaluated. Finally, a detailed uncertainty analysis of the ID model was performed to identify critical model parameters and experimental input variables. The following conclusions can be drawn from the predicted and measured ID results at a medium load (BMEP = 6 bar), engine speed of 1700 rpm, and intake manifold temperature (T_{in}) of 75°C:

1. With the present ID model, predicted IDs matched measured IDs (within ± 10 percent error) over a range of BOIs from 20° to 60° BTDC, with only the activation energy for chain initiation (E_q) modified to 2.7×10^4 from the baseline value of 4.159×10^4.
2. Diesel evaporation times ($\Delta\theta_{evap}$) increased with increasing droplet SMD. Initial droplet SMDs of the monodisperse diesel spray influenced IDs at retarded BOIs but had very little or no impact at advanced BOI.
3. Increasing T_{in}, which was the most sensitive among all experimental input variables, led to a reduction in both the physical ($\Delta\theta_{evap}$) and chemical components of ID.
4. Hot EGR led to shorter predicted and measured IDs over the range of BOIs, except 20° BTDC. In general, thermal effects of hot EGR were found to be more pronounced than either dilution or chemical effects for most BOIs.
5. Uncertainty analysis results indicated that ID predictions were most sensitive to model parameters A_{P3}, A_q, and A_{f1}, and E_q and the experimental input variable T_{in}, which also contributed the most to overall uncertainties in IDs.

Multi-Zone Phenomenological Combustion Model

A multi-zone phenomenological combustion model that simulates closed-cycle engine processes has been developed. The primary objective of the model is to simulate dual fuel low temperature combustion (LTC). In dual fuel LTC, the initial pilot combustion phase is somewhat similar to diesel spray combustion while the subsequent natural gas combustion phase involves premixed turbulent combustion by flame propagation (similar to a spark-ignited engine). Therefore, the present model incorporates phenomenological aspects of both diesel spray combustion and premixed turbulent flame propagation.

The simulation starts from intake valve closure (IVC) and proceeds until exhaust valve opening (EVO). Depending on the stage of the simulation, the cylinder contents are divided into one or

more of the following zones: an unburned zone, pilot fuel zones (packets), a flame zone, and a burned zone. Because the simulation is only quasi-dimensional and is not capable of providing spatial resolution of the cylinder contents, it does not require any of these zones to be continuous or contiguous. To solve for various properties in each zone, the conservation of mass, conservation of energy, overall volume conservation, and the ideal gas equation of state are employed. For example, the generic form of the energy equation for a given zone *i* (an open thermodynamic system) is

$$\frac{d\left(m_i c_{vi} T_i\right)}{d\theta} = \sum_{net\ in} \frac{dQ_i}{d\theta} - \frac{PdV_i}{d\theta} + \sum_{net\ in} h_i \frac{dm_i}{d\theta}$$

where, m_i is the mass, c_{vi} is the specific heat at constant volume, T_i is the temperature, and all derivatives are with respect to crank angle (θ). The first term on the right hand side of the above equation is the net heat input into the zone, which includes heat transfer from/to the cylinder walls and, if applicable, energy lost due to diesel evaporation and added due to combustion in packets or the flame zone. The second and third terms represent boundary work output and the net enthalpy input due to any mass transfer, respectively. Of these energy interactions, heat transfer and boundary work are experienced by all zones. Specific details of energy and mass interactions, and the sub-models used in different zones are discussed in the following journal article: Krishnan, S.R. and Srinivasan K.K. (2010) Proc. Inst. Mech. Engrs: Part D J. Automobile Engr. 224, pp. 1597-1622.

Model Assumptions

Important assumptions of the phenomenological dual fuel LTC combustion simulation used for modeling diesel-ignited natural gas combustion are listed below.

1. Each zone is treated as an open thermodynamic system consisting of a mixture of ideal gases.
2. Heat transfer occurs only between each zone and the cylinder walls. Although, mass transfer is allowed between zones, inter-zonal heat transfer is neglected.
3. Because the natural gas used in dual fuel LTC experiments was largely composed of methane (98% by volume), methane is assumed to represent natural gas in the simulation and n-dodecane is assumed to represent diesel fuel. *However, it is important to note that the simulation can be easily modified to work with a combination of several different pilot and main fuels.*
4. When diesel and natural gas burn in any zone, they are converted into products of complete combustion (CO_2 and H_2O).
5. End of combustion (EOC) is attained when the unburned zone mass becomes very small (less than 0.001% of its initial value) or more than 99.9% of the total entrained mass in the flame zone has been burned.

Example Model Results

In this section, example results are presented from the multi-zone combustion simulation. For a more detailed account, please see our exhaustive journal article on this topic: Krishnan, S.R. and Srinivasan K.K. (2010) Proc. Inst. Mech. Engrs: Part D J. Automobile Engr. 224, pp. 1597-1622. *In this regard, it is perhaps pertinent to point out that this journal article was awarded the 2010 SAGE Best Paper Award by the Editor and Editorial Board of the Proceedings of the Institute of Mechanical Engineers: Part D, Journal of Automobile Engineering.*

Figure E.2.10 shows the predicted (subscript sim) and experimental (subscript expt) pressures and heat release rates for different BOIs for dual fuel LTC. The only parameter that was

changed with BOI was that responsible for radial stratification of the spray J_{tot}, whose specific value at each BOI is shown in the corresponding figure. In Figure E.2.10, slight discrepancies may be noted between some of the experimental and simulated pressure curves even before ignition. The primary experimental causes for these discrepancies were: (a) the long valve overlap period (~ 45 CAD) in the single-cylinder engine used for the experiments and the relatively late IVC (37° ABDC) that led to inaccuracies in the calculation of total mass trapped inside the cylinder at IVC from measured intake manifold conditions or flow rates, and (b) the location of the cylinder pressure transducer, which was mounted via connecting passages to the combustion chamber (not flush-mounted), due to lack of direct access ports in the cylinder head of the single-cylinder engine. Although the model was calibrated with motoring pressure traces, the best match still showed some discrepancies between measurements and predictions. These same discrepancies were also observed when the measured and predicted combustion pressure traces were compared.

For the late BOI of 20° BTDC, Figure E.2.10a shows that predicted pressures match measured pressures quite well but the peak heat release rate is underpredicted. While start of combustion (SOC) is predicted well, peak heat release rates are underpredicted and combustion rates are slower. The reason for slower combustion at 20° BTDC BOI is evident when packet equivalence ratios are examined closely. For 20° BTDC BOI, all packets are richer-than-stoichiometric at SOC, with nearly 50% of the packets richer than the equivalence ratio of 2.0. Therefore, they exhibit slower heat release rates and, consequently, attain lower peak temperatures compared to intermediate BOIs. Cooler packets reduce the effective flame area, lead to slower flame combustion, thus resulting in lower peak heat release rates. However, the overall heat release duration is predicted fairly well despite the overprediction of heat release rates toward EOC for 20° BTDC.

As shown in Figures E.2.10b and E.2.10c, the overall heat release rates are predicted better for 30° BTDC and 40° BTDC BOIs compared to 20° BTDC but the peak pressures are slightly overpredicted. The predicted heat release durations matched well with the experimental durations for both 30° BTDC and 40° BTDC. For 30° BTDC, the peak pressures are overpredicted because the initial heat release rates are overpredicted. Compared to 20° BTDC, the packet equivalence ratios for 30° BTDC are much closer to stoichiometric, so the packet temperatures are much higher, leading to faster combustion rates. However, the peak heat release rates are still slightly underpredicted. On the other hand, for 40° BTDC both cylinder pressure and heat release rate predictions are better. The peak heat release rates are predicted satisfactorily and the initial heat release rates are only slightly overpredicted. Almost 70% of the packets lie within the equivalence ratio range of 0.8-1.1 for 40° BTDC. Therefore, combustion rates are faster, and packet temperatures are also the highest for 40° BTDC. It must be noted that the J_{tot} value used for 40° BTDC is increased from 3 to 4 for the same I_{tot} value (of 41) as 30° BTDC to account for the higher number of potential ignition centers for the earlier BOI.

Figures E.2.10d and E.2.10e show model predictions for the early BOIs of 50° BTDC and 60° BTDC, which were obtained with J_{tot} values of 7 and 12, respectively. As mentioned before, one important objective of the simulation is to predict combustion at early BOIs, which yielded the best NO_x – efficiency tradeoffs in the dual fuel LTC experiments. For 50° BTDC, both heat release rates and cylinder pressures are predicted very well. A slight delay in the occurrence of peak heat release rate may be observed along with a slight underprediction of the heat release duration. The heat release prediction for 60° BTDC is even better. The model predicts SOC, heat release duration, initial heat release rates, and peak heat release rates very well, with the only downside being a slight overprediction of the peak pressure for 60° BTDC. Overall, the

predictions at early BOIs are much better compared to late and intermediate BOIs, thus satisfying the main objective of the model development effort. It is also interesting to note that the experimental heat release profiles for 50° BTDC and 60° BTDC BOIs do not exhibit the initial heat release peak that was visible for late and intermediate BOIs. Similarly, the heat release spikes that were noted in the predicted heat release curves for late and intermediate BOIs are virtually absent at 50° BTDC and 60° BTDC. For early BOIs, diesel has sufficient time to mix with the surrounding lean natural gas-air mixture during the long ignition delay periods; therefore, it is possible that upon ignition, pilot diesel combustion occurs simultaneously with natural gas combustion by localized flame propagation. Consequently, there is no distinct initial heat release peak in the experimental heat release curves. In the simulation, the long ignition delay periods for 50° BTDC and 60° BTDC resulted in packet combustion at substantially leaner equivalence ratios, thus smoothing out the initial heat release spikes that were observed at late and intermediate BOIs. A majority of packets for 50° BTDC BOI and virtually all packets for 60° BTDC were leaner-than-stoichiometric at SOC, with almost 60% of packets lying in the 0.6-0.7 equivalence ratio range at SOC for 60° BTDC. These lean packets led to lower peak packet temperatures at early BOIs.

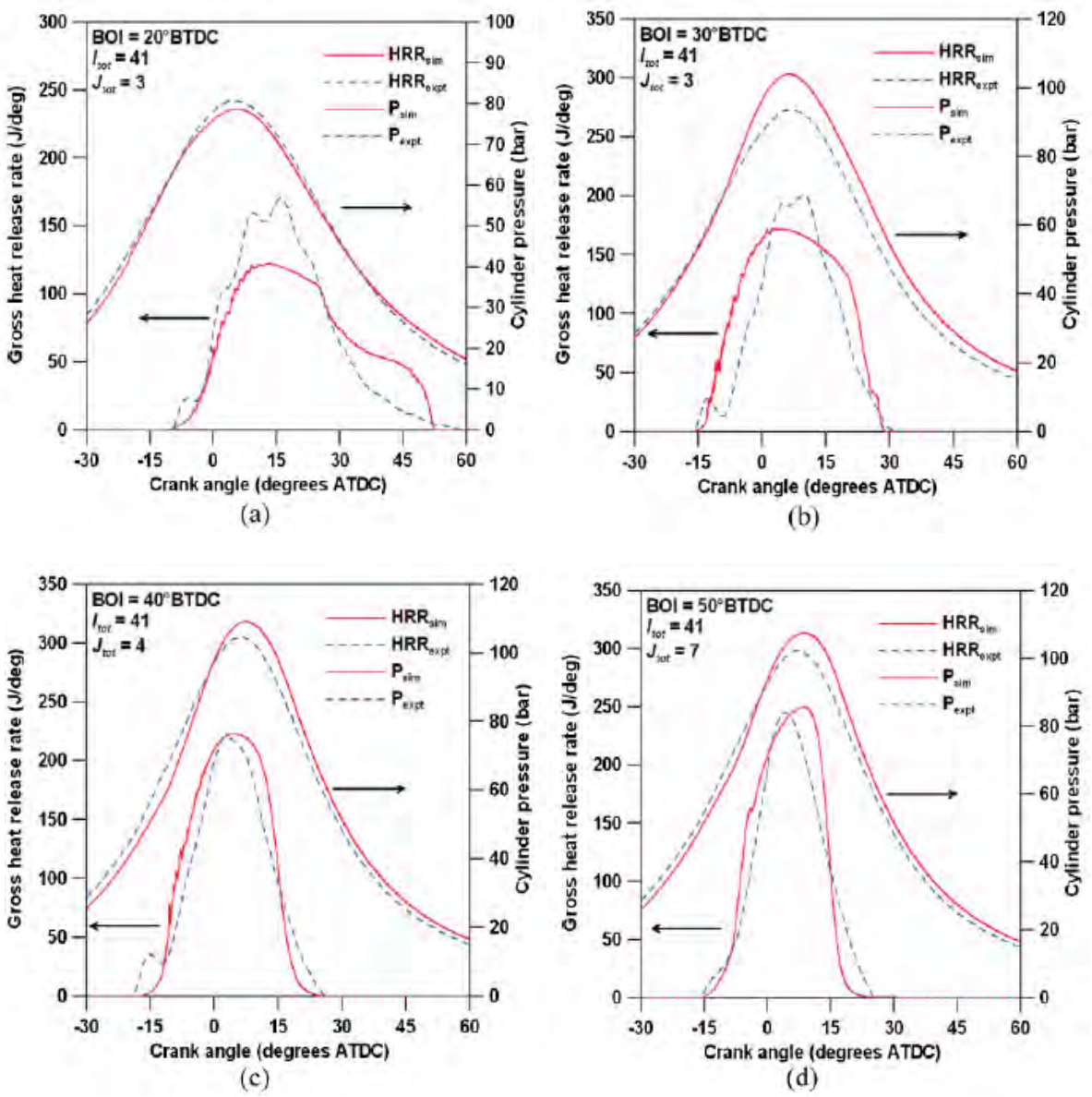


Figure E.2.10a-e. Experimental and predicted cylinder pressure histories and heat release schedules for pilot-ignited natural gas combustion at different BOIs.

Summary

A multi-zone phenomenological simulation has been developed to simulate partially premixed advanced injection dual fuel low temperature combustion (LTC). This simulation combined, in a novel way, several modeling aspects of diesel spray combustion and premixed turbulent flame propagation. The cylinder contents were divided into an unburned zone, pilot fuel zones (or "packets") that account for diesel combustion, a flame zone for natural gas combustion, and a burned zone. Predictions from the simulation were validated against experimental results and parametric studies were performed, leading to the following significant conclusions:

1. The simulation predicted dual fuel LTC satisfactorily over a wide range of pilot injection timings (BOI) from 20° BTDC to 60° BTDC.

2. The onset of ignition (predicted with the Shell autoignition model) and heat release profiles (especially combustion durations) were predicted accurately for the entire BOI range but peak pressures were slightly overpredicted for 30°, 40°, and 50° BTDC BOIs. Both combustion pressure and heat release profiles were predicted better at early BOIs, which yielded very low NO_x emissions in ALPING combustion experiments.
3. A strong coupling was observed between pilot spray combustion in packets and premixed turbulent combustion in the flame zone because pilot diesel combustion in packets directly affected flame area and, consequently, flame zone combustion. Further, it was shown that the number of ignition centers (packets) had a profound influence on overall heat release rates and flame zone combustion.
4. The highest in-cylinder temperatures were obtained in packets, indicating that *pilot diesel spray combustion is likely the dominant source of NO_x emissions in dual fuel LTC*. Measured engine-out NO_x emissions were extremely low at 60° BTDC BOI, likely due to relatively low temperature packets that persisted longer in the combustion process; further, the average peak packet temperature (TP_{PEAK_AVG}) was only 1720 K, much lower than the critical NO_x formation temperature ($T_{critical_NOx}$) of 2000 K. By comparison, at 20° BTDC and 40° BTDC, peak temperatures of long residence time packets were much higher (TP_{PEAK_AVG} values for 20° BTDC and 40° BTDC were 2480 K and 2700 K, respectively), resulting in substantially higher NO_x emissions.
5. Although approximately 90% of combustion energy release occurred in the flame zone, the predicted peak flame temperature was only about 1650 K (due to the very lean flame zone equivalence ratio of ~ 0.38), indicating the *near-zero potential for NO_x formation in the flame zone*.
6. Increasing intake charge temperature (T_{in}) and pilot fuel quantity (Q_{inj}) led to faster combustion, higher peak heat release rates, and higher TP_{PEAK_AVG} values at 60° BTDC BOI, confirming their relative importance vis-à-vis NO_x emissions. However, increasing natural gas equivalence ratios (ϕ_{NG}) at fixed T_{in} and Q_{inj}, only led to higher peak heat release rates without affecting TP_{PEAK_AVG} values significantly. These results are in agreement with experimentally measured trends for NO_x emissions, which were relatively unaffected as ϕ_{NG} was increased (at fixed Q_{inj}) to attain engine loads as high as 12 bar BMEP.

Subtask E.3 Evaluation of biodiesel-ignited syngas low temperature combustion

1. Planned Activities

E.3.DL.1 Year one deliverable is to baseline the performance (fuel efficiency and power density) and engine-out NO_x, CO and HC emissions from biodiesel-ignited syngas combustion.

E.3.DL.2 Year two milestone is to achieve optimized combinations of biodiesel - syngas fueling coupled with innovative biodiesel injection strategies to realize low temperature combustion with best tradeoffs between fuel conversion efficiency (up to 40%), power density and NO_x emissions (up to 0.4 g/kWh).

2. Summarization of Activities

This subtask was designed to evaluate syngas as a potential fuel for low temperature combustion. First, we evaluated the feasibility of using syngas for conventional dual fuel combustion with diesel as the pilot ignition source before attempting any low temperature combustion experiments. Consequently, a series of dual fuel experiments were designed and performed on the multi-cylinder 1.9L Volkswagen TDI engine used for Subtask E.1. As mentioned before in task E1, Figures E.1.16-18, this multi-cylinder engine had experienced

extensive damage due to knock and had to be re-built several times. These contingencies restricted the range of experiments performed with syngas as the main fuel.

The syngas used in this study was generated using a fixed bed, down draft atmospheric pressure gasifier – "Renewable Fuel Gas Generator (RFGG)," purchased from Community Power Corporation in Littleton, Colorado. The capacity of the RFGG was 18 kW (electrical equivalent) with a gas flow rate output ranging from 30 to 60 normal cubic meters per hour (Nm_3/h). The syngas purification unit was also embedded in the RFGG gasifier unit. The composition (v/v) of the generated syngas was 22.16% CO, 17.55% H_2, 3.07% CH_4, 11.89% CO_2, and 45.33% N_2. While this manufacturing process possessed the advantages of flexibility and relative ease, because air (containing 79% nitrogen by volume) was used as the oxidizer, the syngas that was produced contained substantial concentrations of nitrogen (an inert gas species that does not contribute to the fuel's heating value). The properties of syngas obtained from the RFGG are tabulated in Table E.3.1 below.

Table E.3.1. Average Properties of Syngas generated by RFGG

Parameters	Units	Average
LHV	MJ/Nm^3	5.79
Tars	mg/Nm^3	14.06
Particulates	mg/Nm^3	3.05

On account of the fairly low heating value of syngas and the significantly high nitrogen concentrations, a standard full bottle of syngas (compressed to 400 psig) lasted only for about 20 to 30 minutes of actual engine testing at a given time. Therefore, it was quite difficult and laborious to perform these experiments. In addition, as mentioned above, the engine knock/rebuilding problems restricted the range of experiments possible with syngas fueling. *Most importantly, the onset of excessive engine instabilities with syngas fuelling severely curtailed the maximum possible syngas substitutions.* Therefore, we decided to focus on conventional dual fuel experiments instead of LTC experiments.

The major results from diesel-ignited syngas dual fuel combustion for various engine loads (BMEPs of 2.5 bar, 5 bar, and 7.5 bar) are presented below in Figures E.3.1-4. In these figures, PES refers to the percent energy substitution (i.e., replacement of diesel) by syngas. For all BMEPs, the maximum substitution of syngas was uniformly limited by the onset of engine instabilities. For example, while a maximum PES of about 32% was possible at 2.5 bar BMEP, the maximum PES at 7 bar BMEP was only 10%. As shown in Figure E.3.1, with increasing PES of syngas, the fuel conversion efficiency was reduced, ostensibly due to the deterioration of the combustion process. Clearly, syngas burned slower than diesel, thus prolonging combustion durations and reducing fuel conversion efficiencies.

Figure E.3.2 shows a tradeoff between NOx and smoke emissions (measured in Filter Smoke Number or FSN) for various syngas PES and engine loads. As evident from this figure, increasing syngas PES led to a monotonic decrease in both NOx and smoke emissions for all loads. While this is clearly desirable, these potential emissions benefits must be viewed in the proper context. Figures E.3.3 and E.3.4 illustrate that both carbon monoxide (CO) and unburned hydrocarbon (HC) emissions increased significantly with increasing PES of syngas. For example, at 2.5 bar BMEP, diesel-ignited syngas combustion at 32% PES led to a six-fold increase in CO emissions and five-fold increase in HC emissions. Therefore, the potential for reduced NOx and smoke emissions with diesel-

ignited syngas dual fuel combustion is tempered by significant increases in CO and HC emissions.

In summary, the quality of syngas (especially its lower heating value and inert gas [nitrogen] content) has a substantial impact on its performance as an engine fuel. Because the syngas used in these experiments had over 40% by volume of nitrogen, its lower heating value was quite low. Therefore, only conventional dual fuel experiments were attempted, and the performance and emissions characteristics of diesel-syngas dual fuel combustion were quantified.

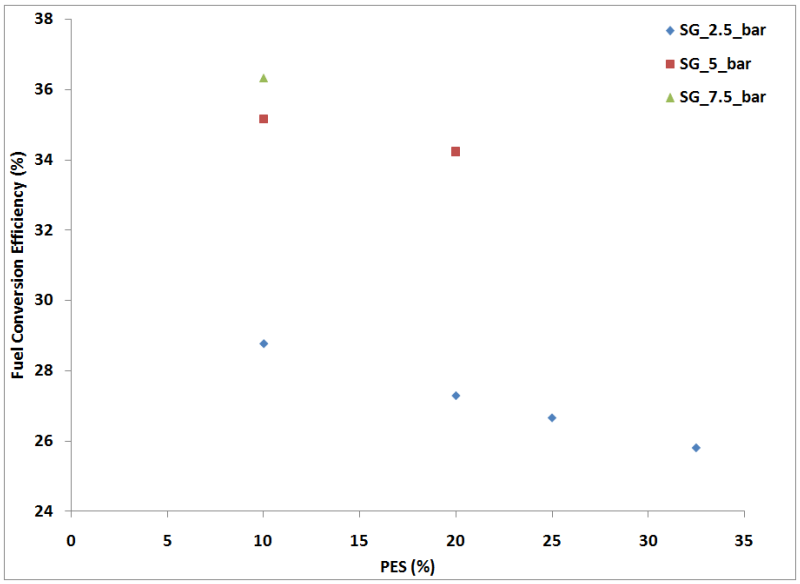


Figure E.3.1. Fuel conversion efficiency versus percent energy substitution (PES) for diesel-ignited syngas operation for different engine loads (BMEPs of 2.5 bar, 5 bar, and 7.5 bar).

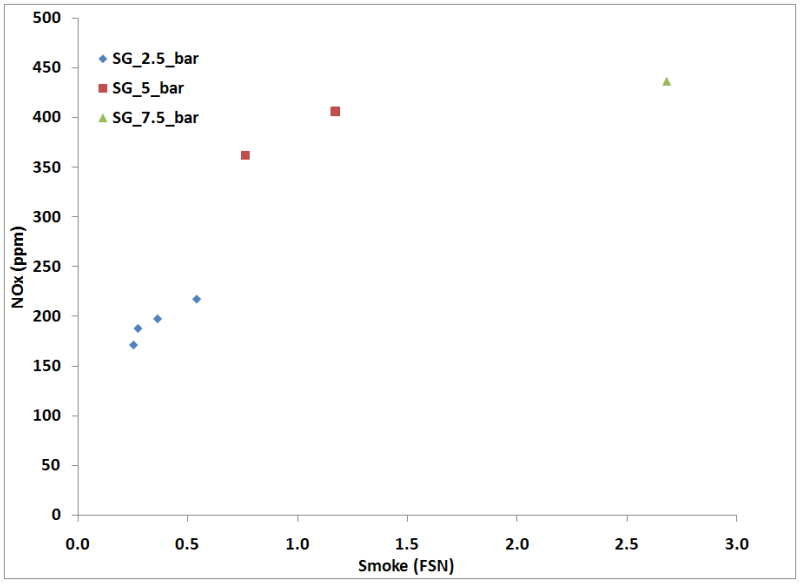


Figure E.3.2. NOx emissions versus smoke emissions (FSN) for diesel-ignited syngas operation for different PES and engine loads (BMEPs of 2.5 bar, 5 bar, and 7.5 bar).

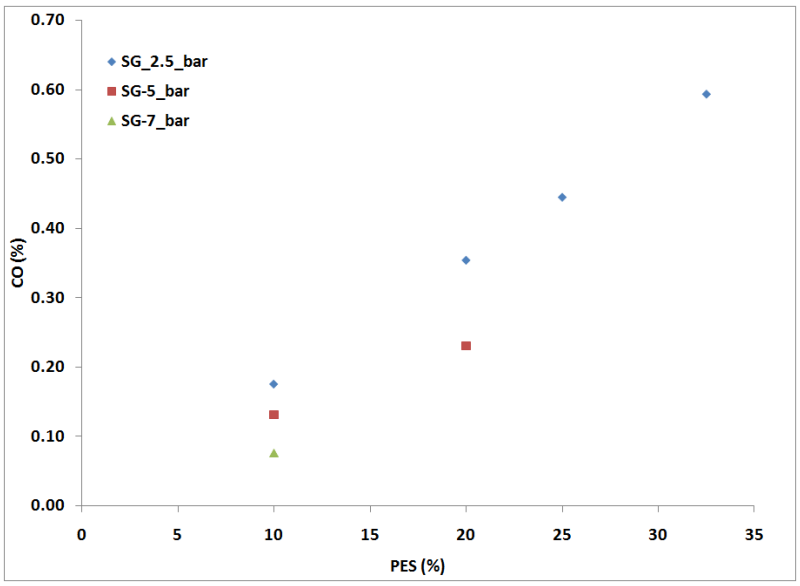


Figure E.3.3. Carbon monoxide (CO) emissions versus percent energy substitution (PES) for diesel-ignited syngas operation for different engine loads (BMEPs of 2.5 bar, 5 bar, and 7.5 bar).

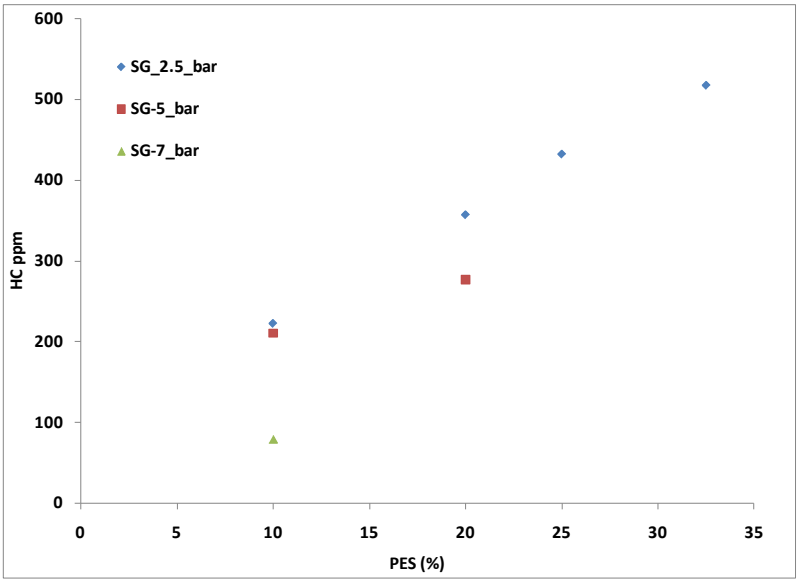


Figure E.3.4. Unburned hydrocarbon (HC) emissions versus percent energy substitution (PES) for diesel-ignited syngas operation for different engine loads (BMEPs of 2.5 bar, 5 bar, and 7.5 bar).

References

Krishnan et al. (2004), ASME J Gas Turb. & Pow., 126(3), pp.213-218

Krishnan S.R. and Srinivasan K.K. (2010) Proc. Inst. Mech. Engrs: Part D J. Automobile Engr. 224, pp. 1597-1622

Jha et al. (2010), Paper No. ICEF2010-35127, Proc. of ASME IC Eng. Div. 2010 Fall Tech. Conf. Sep 12-15, San Antonio, TX

C. Products developed under the award and technology transfer activities.

Publications

Cho, H, Krishnan, S. R., Luck, R., and Srinivasan, K. K., 2009 "Comprehensive uncertainty analysis of a Wiebe function-based combustion model for pilot-ignited natural gas engines," *Proceedings of the Institution of Mechanical Engineers, Part D: Journal of Automobile Engineering*, Volume 223, Number 11 / 2009, pp. 1481-1498, DOI: 10.1243/09544070JAUTO1103

Gibson, C.M., Polk, A., Shoemaker, N., Srinivasan, K.K., and Krishnan, S.R. 2011, "Comparison of Propane and Natural Gas Performance and Emissions in a Turbocharged Direct Injection Dual Fuel Engine," ASME Journal of Engineering for Gas Turbines and Power, 133, 092806

Harrod, J., Mago, P.J., Srinivasan, K.K., and Chamra, L.M., 2009 "First and Second Law Analysis of a Stirling Engine with Imperfect Regeneration and Dead Volume," *Proceedings of the Institution of Mechanical Engineers, Part C: Journal of Mechanical Engineering Science*, 2009, Vol 223, No. 11, pp. 2595-2607

Krishnan, S. R. and Srinivasan, K. K. (2010). Multi-Zone Modeling of Partially Premixed Low Temperature Combustion in Pilot-Ignited Natural Gas Engines. *Proc. Instn. Mech. Engrs.: Part D: Journal of Automobile Engineering, 224, pp. 1597-1622 (This paper won the 2010 SAGE Best Paper Award by the Editor and Editorial Board of Proceedings of the Institution of Mechanical Engineers, Part D: Journal of Automobile Engineering)*

Srinivasan, K. K., Mago, P. J., Krishnan, S. R., 2010 "Analysis of Exhaust Waste Heat Recovery from a Dual Fuel Low Temperature Combustion Engine using an Organic Rankine Cycle," *Energy, Vol. 35, pp. 2387-2399, doi:10.1016/j.energy.2010.02.018*

Presentations

Gibson, C.M., Polk, A., Shoemaker, N., Srinivasan, K.K., and Krishnan, S.R. 2010, "Comparison of Propane and Natural Gas Performance and Emissions in a Turbocharged Direct Injection Dual Fuel Engine," Paper No. ICEF2010-35128, Proceedings of the ASME IC Engines Division 2010 Fall Technical Conference (ICEF2010), September 12-15, San Antonio, TX; *Presenter – C. M. Gibson*

Jha, S.K., Krishnan, S.R., Srinivasan, K.K. 2010, "Quasi-Two-Zone Modeling of Diesel Ignition Delay in Pilot-Ignited Partially Premixed Low Temperature Natural Gas Combustion," Paper No. ICEF2010-35127, Proceedings of the ASME IC Engines Division 2010 Fall Technical Conference (ICEF2010), September 12-15, San Antonio, TX; *Presenter – S. K. Jha*

Krishnan, S.R., Srinivasan, K.K., and Midkiff, K.C. “Ignition In Pilot-Ignited Natural Gas Low Temperature Combustion: Multi-Zone Modeling and Experimental Results,” 2009, Proceedings of the ASME Internal Combustion Engines Division, Spring 2009 meeting, Milwaukee, WI, May 2009; *Presenter – S. R. Krishnan*

Knizley, A.A., Srinivasan, K.K., and Krishnan, S.R. “Fuel and Diluent Effects on Entropy Generation in a Constant Internal Energy-Volume (UV) Combustion Process,” presented at the 7th US National Technical Meeting of the Combustion Institute, Hosted by the Georgia Institute of Technology, Atlanta, GA, March 20-23, 2011.

Tripathi, M.M., Krishnan, S.R., Srinivasan, K.K., Yueh, F.-Y., and Singh, J.P. “Development of a Robust Sensor for Monitoring Equivalence Ratio in Premixed Flames Using Chemiluminescence and Multivariate Data Analysis,” presented at the 7th US National Technical Meeting of the Combustion Institute, Hosted by the Georgia Institute of Technology, Atlanta, GA, March 20-23, 2011.

Networks or collaborations fostered

KiOR Fuels, Inc.

Current research with SERC has fostered a symbiotic collaboration with KiOR fuels, who have invested in a long-term collaboration with MSU to investigate the combustion behavior of their patented ReCrude™ fuel.

PACCAR Engines and Propane Education Research Council

Current research performed at SERC has enabled the leveraging of a three-way partnership between PACCAR, PERC, and MSU (CAVS (Center for Advanced Vehicular Systems) and SERC) to perform advanced low temperature dual fuel combustion research in a 12.9 liter PACCAR engine at MSU.

DENSO corporation, NA

SERC research has been leveraged to obtain research and teaching equipment funding to the tune of $100,000 from DENSO Foundation, NA.

Argonne National Lab

Engine combustion research as SERC has resulted in several collaborative proposals and research articles with the Center for Transportation Research at Argonne National Laboratory.

D. A multi-zone phenomenological combustion model (see Figure D.1) that simulates closed-cycle engine processes has been developed. The simulation starts from intake valve closure (IVC) and proceeds until exhaust valve opening (EVO). Depending on the stage of the simulation, the cylinder contents are divided into one or more of the following zones: an unburned zone, pilot fuel zones (packets), a flame zone, and a burned zone, as shown schematically in Figure D.1. While the different zones are illustrated as continuous and contiguous for ease of visualization, it should not be construed that they are necessarily so; in fact, at advanced injection timings, packets can be dispersed throughout the cylinder

forming distributed ignition centers. Because the simulation is only quasi-dimensional and is not capable of providing spatial resolution of the cylinder contents, it does not require any of these zones to be continuous or contiguous.

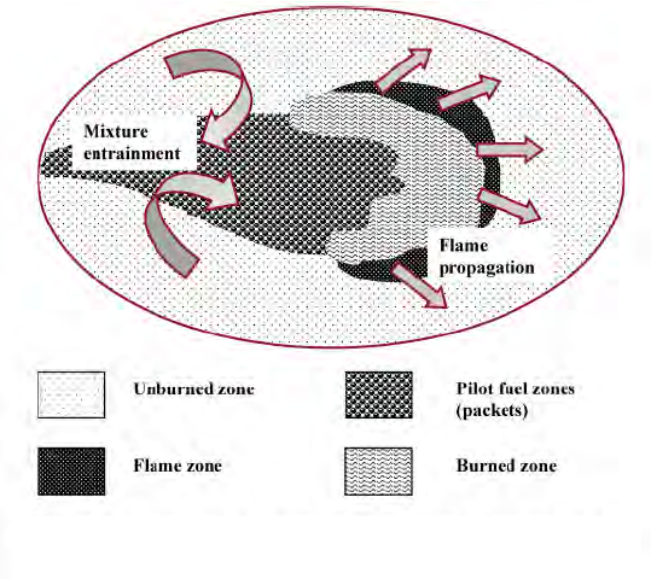


Figure D.1. Schematic representation of various zones in the combustion simulation

The generic form of the energy equation for a given zone *i* (an open thermodynamic system) is

$$\frac{d\left(m_i c_{vi} T_i\right)}{d\theta} = \sum_{net\ in} \frac{dQ_i}{d\theta} - \frac{PdV_i}{d\theta} + \sum_{net\ in} h_i \frac{dm_i}{d\theta} \qquad (1)$$

where, m_i is the mass, c_{vi} is the specific heat at constant volume, T_i is the temperature, and all derivatives are with respect to crank angle (θ). The first term on the right side of Equation 1 is the net heat input into the zone, which includes heat transfer from/to the cylinder walls and, if applicable, energy lost due to diesel evaporation and added due to combustion in packets or the flame zone. The second and third terms represent boundary work output and the net enthalpy input due to any mass transfer, respectively. Of these energy interactions, heat transfer and boundary work are experienced by all zones.

Model Assumptions

Important assumptions of the phenomenological combustion simulation are listed below.

1. Each zone is treated as an open thermodynamic system consisting of a mixture of ideal gases.
2. Heat transfer occurs only between each zone and the cylinder walls. Although mass transfer is allowed between zones, inter-zonal heat transfer is neglected.
3. Combustion in any zone is assumed complete, i.e., fuel is converted to products of complete combustion (CO_2 and H_2O).
4. End of combustion (EOC) is attained when the unburned zone mass becomes very small (less than 0.001% of its initial value) or more than 99.9% of the total entrained mass in the flame zone has been burned.

The simulation model was developed using both Mathcad and FORTRAN programming languages. The objectives of this simulation were to be able to use it as a predictive tool to obtain *apriori* information on new combustion strategies before subjecting them to experimentation. For instance, the simulation could be used to evaluate the potential of a particular fuel injection strategy to obtain low NOx emissions even before performing detailed and costly experiments. The framework of this simulation package also includes detailed uncertainty analysis to allow for the quantification of model parameter uncertainties. Finally, this simulation is designed to evaluate both conventional spray combustion processes, such as diesel and biodiesel combustion, and more advanced low temperature combustion concepts.

The model should be able to predict combustion heat release rates and pressure histories accurately and validate the predictions against baseline experimental data within a 10% error.

Figures D.2-4 show the verification and validation and sensitivity analyses done with various sub-models of the phenomenological simulations that were developed in this research effort. As shown in the figures below, the phenomenological simulation was validated using a variety of published and actual experimental data. Figure D.2 shows the fidelity of the predicted ignition delay time validated against experimental data acquired on a dual fuel low temperature combustion strategy that uses a small diesel pilot spray to ignite a lean natural gas-air mixture.

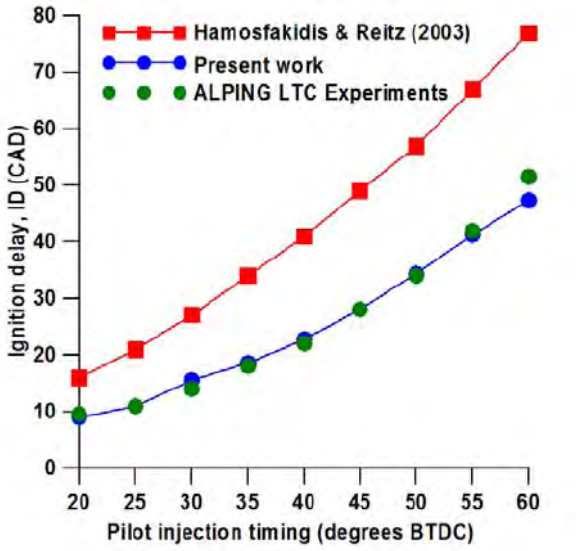


Figure D.2. Comparison of experimental and model-predicted ignition delay times for low temperature dual fuel combustion at half load operation

Figure D.3 compares predicted and measured cylinder pressure histories for ALPING combustion at -60° ATDC SOI. Also shown in this figure are crank angle-resolved uncertainty intervals of predicted cylinder pressures and the variation of measured cylinder pressures. As evident from Figure D.3, the simulated pressure curve for the present case matches quite well with the average measured pressure curve. Further, results from the uncertainty analysis show that the measured cylinder pressure values mostly lie within the predicted uncertainty intervals for the simulated pressure curve.

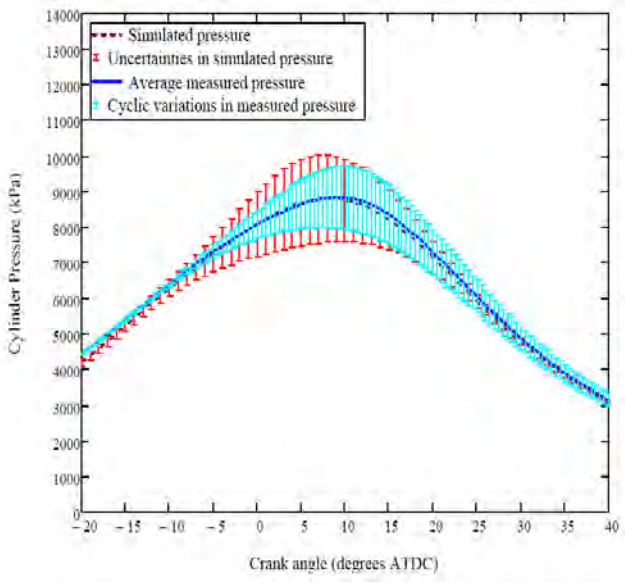


Figure D.3. Crank resolved uncertainties of predicted cylinder pressures and measured cylinder pressure data for dual fuel low temperature combustion

Figure D.4 shows the predicted heat release rate against experimental heat release rate for biodiesel (B100) combustion at 5 bar bmep and 1800 rev/min. The fuel injection timing was 4°BTDC. Clearly, the model captures the phasing and peak heat release rate locations fairly accurately; however, the HRR is over predicted during the expansion phase of the combustion process. This is attributed to the difficulty in accurately modeling the wall heat transfer process during the combustion process.

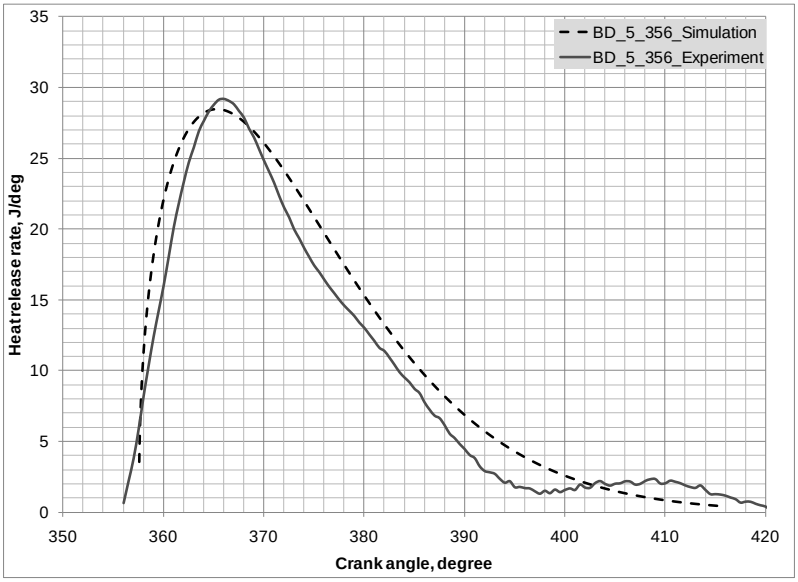


Figure D.4. Comparison of predicted heat release rate against experimental heat release rate for biodiesel (B100) combustion at 5 bar bmep and 1800 rev/min

The phenomenological combustion simulation developed in this research is a collection of many sub-routines written in the FORTRAN language. The simulation is performed between intake valve closure and exhaust valve opening, which makes it closed cycle. The in-cylinder mass is a constant throughout the simulation process. No attempt has been made to model the intake and exhaust processes. The simulation sub-models and the general flow of the computer simulation are represented in the flow chart below in Figure D.5. As seen from the flow chart below, the simulation is a sequential call to many sub-routines such as gas entrainment, spray evaporation, ignition delay, flame propagation, and NOx formation. The simulation starts by calling a subroutine to initialize all variables used in the program. This is followed by preliminary calculations, where constants, etc. are declared, which is followed by the simulation of compression process. This is followed by a call to inject packets, which represents the fuel injection process in spray combustion processes. As the spray is injected, the fuel droplets begin to evaporate due to the difference in temperature between the fuel droplets and the surrounding air. This is followed by a call to ignition delay, which is defined as the time between fuel injection start and the first instance of combustion in the cylinder. This is then followed by calls to manage both premixed and mixing controlled phases of combustion and finally an estimation of NOx emissions using extended Zeldovich kinetics.

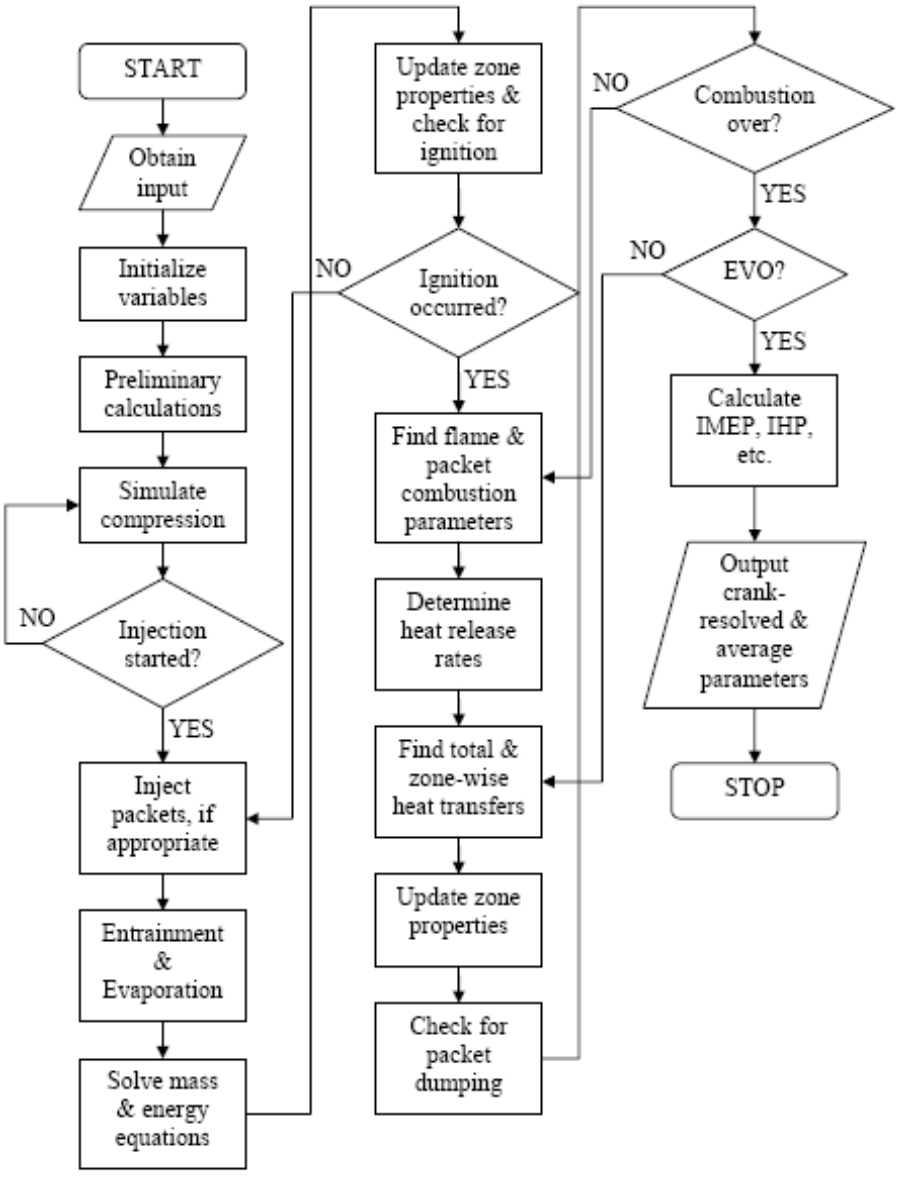


Figure C.5. Flow chart of the combustion simulation

The mathematical formulation of the combustion simulation is presented with a brief explanation of various subroutines.

Unburned zone

At Intake Valve Closure (IVC), the premixed natural gas-air mixture trapped in the cylinder constitutes the unburned zone. Mass is transferred from the unburned zone to packets after Beginning of Injection (BOI) and to the flame zone after Start of Combustion (SOC). The state of the unburned zone is tracked as long as there is some unburned mass in the cylinder.

Pilot fuel zones (Packets)

At BOI, the packets, which account for combustion of diesel and some natural gas entrained in the diesel spray, come into existence. The lifetime of a packet depends on the fulfillment of certain "dumping criteria" that are discussed later (see description of burned zone). A user-specified number of packets is sequentially injected throughout the injection duration and an axisymmetric diesel spray is assumed. As shown in Figure D.6, packets are classified based on their time of entry into the cylinder (*I*) and the anticipated radial stratification in unburned mixture entrainment across the spray (*J*). In other words, *J* packets of equal diesel mass are injected every time step over the duration of injection, leading to a constant rate of fuel injection. A higher value of *I* indicates that the packet is injected relatively later in the injection process, while a higher value of *J* indicates that the packet's location is closer to the spray axis and less capable of entraining the unburned mixture. Although spatial packet locations are not determined in this model, this method of packet identification allows for appropriate stratification of mixture entrainment across the spray, and in this sense, the entrainment model is quasi-dimensional. In the following paragraphs, various sub-models relevant to the packets including mixture entrainment, diesel evaporation, ignition, and diesel and natural gas combustion are discussed.

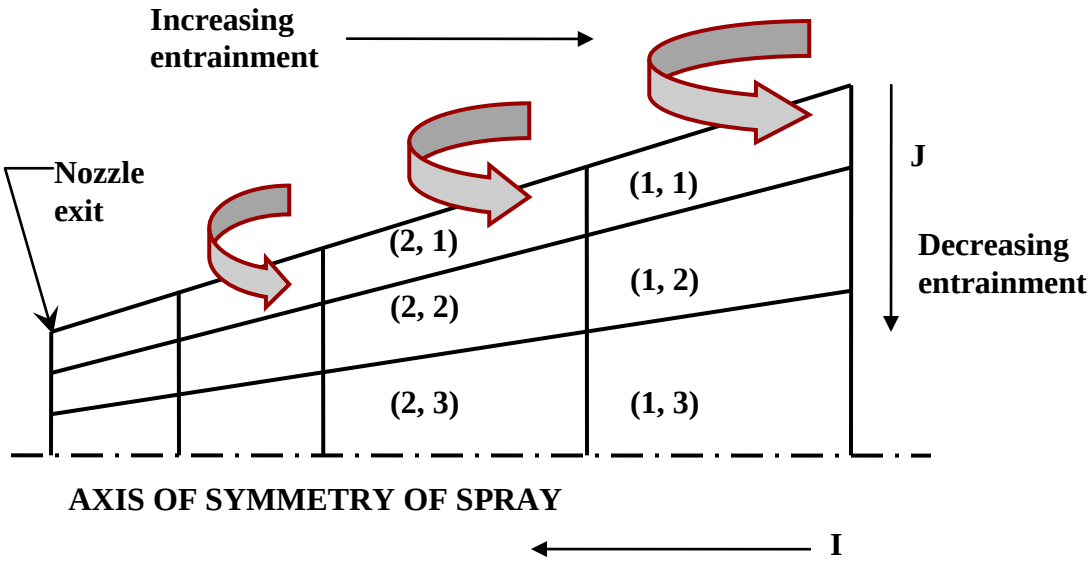


Figure D.6. Schematic of packets showing spray entrainment and radial stratification.

Mixture entrainment model

The phenomenological basis of the entrainment model is the recognition that the mixture entrainment into the spray is simultaneously governed by several factors. Because the spray can entrain the unburned mixture only if it is available, the entrainment rate is proportional to the unburned zone mass, m_u. Further, all of the available unburned mixture can be entrained into the spray in a characteristic entrainment time, θ_{ch}, which is assumed to be the time taken (in crank angle degrees) for the spray to penetrate a characteristic entrainment distance equal to the cylinder bore radius. From a physical perspective, θ_{ch} can be interpreted as the time taken to completely entrain the surrounding fluid into the diesel spray or the time taken for the diesel spray to engulf the entire combustion chamber volume. From the aforementioned scaling arguments, the total rate of unburned mass entrained into the spray ($dm_{tot\text{-}ent}/d\theta$) must be directly proportional to the unburned zone mass and

inversely proportional to the characteristic entrainment time and can be written as follows:

$$\frac{dm_{tot-ent}}{d\theta} \propto \frac{m_u}{\theta_{ch}} \tag{2}$$

Becuase the total unburned entrained mass is distributed among a total number of $I_{tot} \times J_{tot}$ packets, $dm_{tot\text{-}ent}/d\theta$ is divided by $I_{tot} \times J_{tot}$. Also, proper stratification in mixture entrainment must be ensured in the direction normal to the spray axis and for packets injected later in the injection process. Finally, the decay of spray entrainment as the spray disintegrates and loses its initial momentum must be captured. Based on these considerations, the mass of mixture entrained (m_{ent}) into any packet (I, J) in one calculation step ($\Delta\theta$) is expressed as follows:

$$m_{ent}(I,J) = K \frac{m_u}{I_{tot} J_{tot} (1+Y)} \frac{\Delta\theta}{\theta_{ch}} \exp\left(-\frac{I}{I_{tot}} \frac{J}{J_{tot}} \right) \tag{3}$$

where, K is the entrainment constant, which is an important model parameter that influences the net spray momentum, Y is the ratio of time elapsed since BOI to the total injection duration, and I_{tot} and J_{tot} are the maximum values of I and J, respectively. The exponential term in Equation 3 accounts for stratification of entrainment across the spray and progressively lower entrainment in packets that are injected later in the injection process (higher I values). The term $(1+Y)$ ensures that the overall rate of mixture entrainment in the spray decreases with increasing elapsed time since BOI. This mimics reality because as the spray penetrates into the surroundings its velocity decreases and eventually mixture entrainment into the spray decreases.

Diesel evaporation model

The total amount of pilot diesel fuel is initially divided equally among all packets, which are tracked separately thereafter. However, only evaporated diesel is allowed to enter the packets. All fuel droplets are initialized with the same initial, user-specified Sauter mean diameter (*SMD*). Droplet evaporation rates are calculated using a quasi-steady, isolated droplet evaporation model in which evaporation rates adjust instantly to temperature and species concentration changes. At the end of each time-step, droplet diameters in each packet are updated based on the remaining liquid volumes.

The steady-state energy and mass conservation equations (in spherical coordinates) for evaporation of a single diesel droplet are

$$\frac{d}{dr}\left(\rho_g \alpha_g 4\pi r^2 \frac{dT}{dr} \right) - \frac{d}{dr}\left([\dot{W}'' 4\pi r^2] C_g T \right) = 0 \tag{4}$$

$$\frac{d}{dr}\left(\rho_g D_F 4\pi r^2 \frac{dY_F}{dr} \right) - \frac{d}{dr}\left([\dot{W}'' 4\pi r^2] Y_F \right) = 0 \tag{5}$$

where, T is the temperature, r is the droplet radius, Y_F is the mass fraction of vapor diesel; α_g, C_g, and ρ_g are the thermal diffusivity, specific heat at constant-pressure, and density of gas mixture in the ambient, respectively; and D_F is the diffusion coefficient of diesel vapor in the diesel-natural gas-air mixture. Assuming a Lewis number of one, the dimensionless mass transfer number can be expressed as

$$B = \frac{C_g\left(T - T_\infty\right)}{[L + C_l\left(T_w - T_R\right)]} = \frac{\left(Y_F - Y_{F\infty}\right)}{\left(Y_{Fw} - Y_{FR}\right)} \tag{6}$$

where, subscripts ∞, *w* and *R* correspond to far away from droplet surface, at the droplet wall, and in the interior of the droplet respectively, *B* is the transfer number, C_l is the specific heat of liquid diesel, and *L* is the latent heat of vaporization of diesel. Thus, diesel mass evaporation rate per unit area is

$$\dot{W}'' = \frac{h^0}{C_g}\ln(1+B) \tag{7}$$

where, h^0 is the average heat transfer coefficient for heat transfer between each droplet and its surroundings, which is calculated based on an assumed constant Nusselt number of 2.0.

Ignition model

The Shell autoignition model developed by Shell to predict knocking tendency in fuels was used to model ignition in each packet. The Shell model employs generic species in a global, eight-step, chain-branching reaction mechanism of hydrocarbon ignition and includes reactions for chain initiation, propagation, branching, and termination. The original model coefficients for 90 research octane number (RON) fuel (assuming n-dodecane stoichiometry) were used with the exception of the pre-exponential factor (A_{p3}) controlling fuel consumption in the propagation cycle, which was modified from the original value of 1×10^{13} to 8×10^{11} to provide better ignition delay predictions.The eight-step chain-branching reaction schemes involved in this model are shown here:

$$RH + O_2 \xrightarrow{k_q} 2R^* \tag{8}$$

$$R^* \xrightarrow{k_P} R^* + P + q \tag{9}$$

$$R^* \xrightarrow{f_1.k_p} R^* + B \tag{10}$$

$$R^* \xrightarrow{f_4.k_p} R^* + Q \tag{11}$$

$$R^* + Q \xrightarrow{f_2.k_p} R^* + B \tag{12}$$

$$B \xrightarrow{k_b} 2R^* \tag{13}$$

$$R^* \xrightarrow{f_3.k_p} out \tag{14}$$

$$2R^* \xrightarrow{k_t} out \tag{15}$$

Here RH represents hydrocarbon fuel (C_nH_{2m}), R* the radical, B the branching species, Q the intermediate species, and P the products. A very notable assumption in the SAI model is that although the radicals R* refer to different radicals encountered before ignition; they are treated as a single group.

The five conservation equations that describe the above mechanisms are as follows:

$$\frac{d[R^*]}{dt} = 2\left(k_q[RH][O_2] + k_B[B] - k_t[R^*]\right) - f_3 k_p[R^*] \tag{16}$$

$$\frac{d[B]}{dt} = f_1 k_p[R^*] - k_B[B] + f_2 k_p[Q][R^*] \tag{17}$$

$$\frac{d[Q]}{dt} = f_4 k_p [R^*] - f_2 k_p [Q][R^*] \quad (18)$$

$$\frac{d[O_2]}{dt} = -p k_p [R^*] \quad (19)$$

$$RH = \frac{[O_2] - [O_2]_{t=0}}{pm} + [RH]_{t=0} \quad (20)$$

The specific reaction rate constants obtained using Arrhenius expressions with pre-exponential factors (*A*) and activation energies (*E*) are expressed as $k_i = A_i \exp(-E_i/RT)$. On the other hand, the rate constant, k_P in the rate expressions is obtained as $k_p = (1/(k_{P1}[O_2]) + 1/k_{P2} + 1/(k_{P3}[RH]))^{-1}$. The factor f_i can be expressed as $f_i = A_{fi}.exp(-E_i/RT).[O_2]^{xi}.[RH]^{yi}$. Exothermicity, *q*, of the reaction is calculated as the heat release during the propagation cycle for oxidation of a single -CH2- fuel molecule from the fuel assuming a fixed proportion (λ) of CO and CO_2 in the products. Effect of species R*, B and Q were neglected in the energy and mass balances in the original SAI model. The oxygen consumption rate which is one of the important rate determining steps is defined as

$$p = \frac{[n(2-\lambda)+m]}{m} \quad (21)$$

Twenty six kinetic parameters were used and optimized for the simulation of autoignition in the original SAI model.

Packet combustion model

After a packet ignites, diesel is allowed to burn according to the following single-step global reaction mechanism:

$$\dot{m}_{d-ij} = A_{pd} \exp\left(\frac{-E_A}{RT_{ij}}\right)\left[C_{12}H_{26}\right]_{ij}^{0.25}\left[O_2\right]_{ij}^{1.5}\frac{V_{ij}MW_d}{\omega} \quad (22)$$

where, $\dot{m}_{d-ij}$ is the diesel reaction rate in packet (*I*, *J*) in g/rad, the pre-exponential factor A_{pd} is assumed to be 2.5×10^{10} $(\text{moles/cm}^3)^{-0.75}$/s (this is lower than the value of 3.8×10^{10} recommended for decane), the activation energy E_A is 30 kcal/mole, $[C_{12}H_{26}]_{ij}$ is packet diesel (n-dodecane) vapor concentration (in moles/cm^3), $[O_2]_{ij}$ is packet oxygen concentration (in moles/cm^3), T_{ij} is packet temperature in K, V_{ij} is instantaneous packet volume in cm^3, *R* is the universal gas constant (kcal/mol-K), MW_d is the molecular weight of n-dodecane, and ω is the crankshaft angular velocity in rad/s.

Burned zone

The burned zone is formed one time step after SOC and contains burned products transferred every time step from the flame zone. The burned products in a packet are not transferred to the burned zone until the following conditions are satisfied: (a) the packet temperature is lower than a critical temperature (1900 K), below which NO_x formation rates will become negligible, and (b) more than 90% of diesel in a packet has burned *or* its reaction rate becomes less than 1 percent of their maximum values. When both conditions (a) and (b) are satisfied, all packet contents are allowed to mix instantaneously and adiabatically with the burned zone. This mixing process (termed “dumping”) is expected to capture hot regions of burned products in packets, which lead to most of the NO_x formed

during combustion. When all packets are dumped, flame area becomes zero, flame zone ceases to exist, and combustion is terminated.

Heat transfer model

The overall heat transfer rate ($dQ_{tot}/d\theta$) from cylinder gases to cylinder walls is determined using Woschni's heat transfer correlation [53] and the average cylinder temperature (T_{avg}). Heat transfer rate ($dQ_i/d\theta$) from each zone i is obtained by weighting $dQ_{tot}/d\theta$ with the area (computed as volume raised to the two-thirds power) and temperature (T_i) of that zone:

$$\frac{dQ_i}{d\theta} = \frac{dQ_{tot}}{d\theta} \frac{V_i^{2/3}\left(T_i - T_{wall}\right)}{\sum_i V_i^{2/3}\left(T_i - T_{wall}\right)} \tag{23}$$

where, V_i is the zone volume, and T_{wall} is the cylinder wall temperature (~ 480 K).

The phenomenological simulation has been developed to analyze both spray guided combustion, such as in diesel engines, and dual fuel combustion, as in diesel pilot-ignited natural gas, propane, syngas, or any other liquid fuel with high octane rating. The submodels have been evaluated rigorously against experimental data in a peer-reviewed journal publication (Krishnan, S. R. and Srinivasan, K. K. (2010). Multi-Zone Modeling of Partially Premixed Low Temperature Combustion in Pilot-Ignited Natural Gas Engines. Proc. Instn. Mech. Engrs.: Part D: Journal of Automobile Engineering, 224, pp. 1597-1622).

The computer simulation can be run on a Windows XP machine in a matter of a few minutes. The simulation requires a FORTRAN compiler, which may be obtained from Intel Corp.

Sustainable Energy Research Center
Feedstocks Thrust Area Final Report for 2008-2010

A. Principle investigator and team members: Jac J. Varco, Brian S. Baldwin, Eugene Columbus, Jeremiah Davis, D.L. Grebner, David Lang, Rocky Lemus, Bisoondat Macoon, Prem Parajuli, Joel Paz, Zhaohua Peng, K. Raja Reddy, Mark Shankle, Jim Shepard, and Mark Williams

B. Summarization of Activities

Subtask F.1 Field Trials

1. Planned Activities

F.1.DL.1 Years 1 and 2 deliverables consist of measuring yield response to annual performance of yield as a function of environment and management practices and compiling those measurements into a representative yield estimate of biomass available for conversion to transportation fuel.

2. Summarization of Activities

Physiological limitations of specific bioenergy crops in MS using controlled environments

Switchgrass (Panicum Virgatum L.) intraspecific variation and thermotolerance classification using in vitro seed germination assay

The objectives of this study were to (a) quantify the effects of temperature on seed germination capacity and rate, (b) determine the cardinal temperatures for seed germination capacity and rate, and (c) classify genotypes for temperature tolerance using cumulative temperature response index concept. The seed germination and temperature dependent functional algorithms developed are a prerequisite for modeling the germination of switchgrass genotypes adapted to different climatic zones. Methodology included germination of stratified seed of 14 switchgrass genotypes at seven constant temperatures from 15 to 45 °C and under a constant light intensity of 35 µmol m^{-2} s^{-1} for 12 h d^{-1}. Germination was recorded at 6-h intervals in all treatments. Results included maximum seed germination (MSG) and germination rate (GR), estimates by fitting sigmoidal function to germination-time series data (Figure F.1.1), varied among genotypes. Quadratic and bilinear models best described the MSG and GR responses to temperature, respectively (Figures F.1.2 and F.1.3). The mean cardinal temperatures, T_{min}, T_{opt}, and T_{max}, were 8.1, 26.6, and 45.1°C for MSG and 11.1, 33.1, and 46.0 °C for GR, respectively. Cardinal temperatures for MSG and GR, however, varied significantly among genotypes. Genotypes were classified as sensitive ('Cave-in-rock', 'Dacotah', 'Expresso', 'Forestburg', 'Kanlow', 'Sunburst', 'Trailblazer,' and 'Warrior'), intermediate ('Alamo', 'Blackwell', 'Carthage', 'Shawnee', and 'Shelter') and tolerant ('Summer') to high temperature based on cumulative temperature response index (CTRI) estimated by summing individual response indices estimated from the MSG and GR cardinal temperatures (Table F.1.1). Similarly, genotypes were also classified as sensitive (Alamo, Blackwell, Carthage, Dacotah, Shawnee, Shelter, and Summer), moderately sensitive (Cave-in-rock, Forestburg, Kanlow, Sunburst, and Warrior), moderately tolerant (Trailblazer), and tolerant (Expresso) to low temperatures.

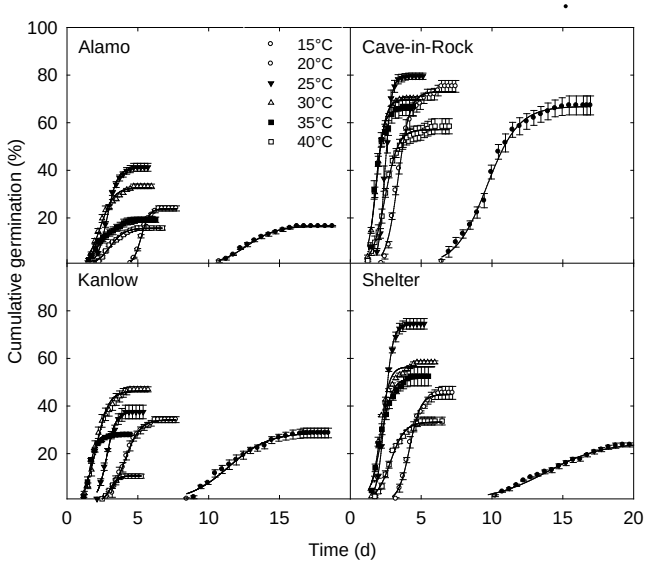


Figure F.1.1. Germination time courses for seeds of Alamo, Cave-in-Rock, Kanlow, and Shelter switchgrass germinated at a range of temperature (15-40°C). The symbols indicate the observed cumulative germination data and the lines indicate the germination time courses fitted using a three-parameter sigmoidal function. Data are means and ± SE of four replications.

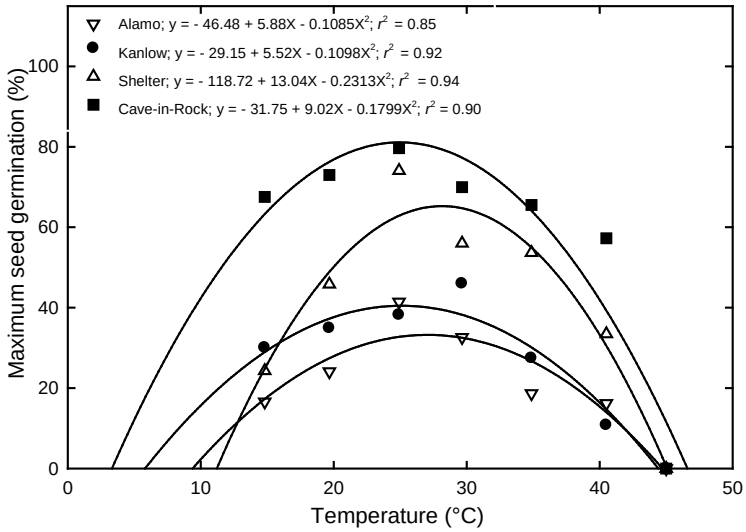


Figure F.1.2. Influence of temperature on maximum seed germination and along with the fitted quadratic equations of four switchgrass genotypes (Alamo, Kanlow, Shelter, and Cave-in-Rock). The symbols are recorded maximum germination percentages and the curves are fitted lines using quadratic functions.

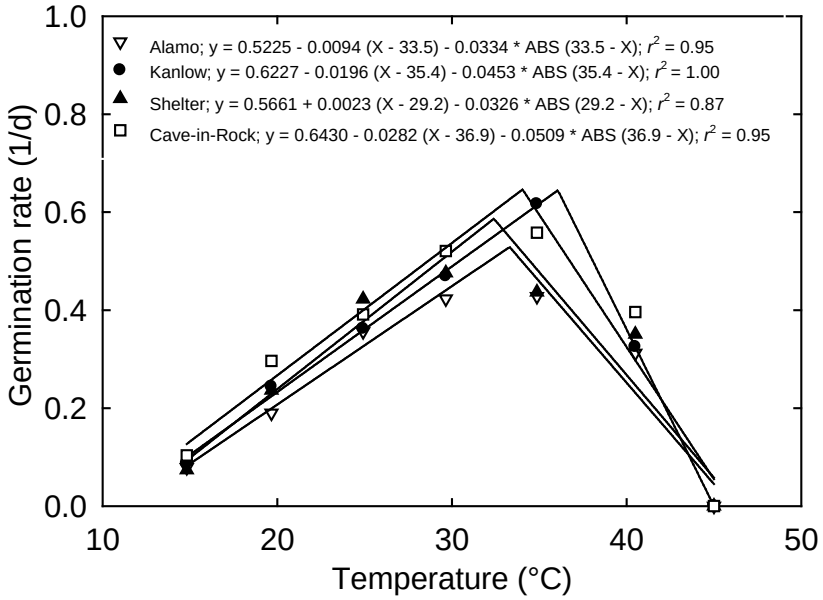


Figure F.1.3. Effect of temperature on germination rate along with the fitted modified bilinear fitted lines and equations of four switchgrass genotypes (Alamo, Kanlow, Shelter and Cave-in-Rock). The symbols are the derived germination rate, and the lines are predicted values by the fitted modified bilinear equations.

Table F.1.1. Classification of switchgrass genotypes into (A) heat-tolerance and (B) cold-tolerance groups based on cumulative temperature response index (CTRI; unitless) along with individual scores in parenthesis.

(A) Heat-tolerance classification based on CTRI

Heat-sensitive (CTRI = 4.83 - 5.43)	**Intermediate (CTRI = 5.44 -5.74)**	**Heat-tolerant (CTRI = 5.75 - 6.05)**
Expresso (4.83)	Alamo (5.45)	Summer (5.78)
Trailblazer (4.85)	Blackwell (5.47)	
Sunburst (5.0)	Shawnee (5.51)	
Cave-in-Rock (5.01)	Carthage (5.56)	
Kanlow (5.03)	Shelter (5.59)	
Tusca (5.06)		
Forestburg (5.16)		
Dacotah (5.36)		

(B) Cold-tolerance classification based on CTRI

Cold-sensitive (CTRI = 4.74 - 5.03)	**Moderately cold-sensitive (CTRI = 5.04 - 5.32)**	**Moderately cold-tolerant (CTRI = 5.33 -5.62)**	**Cold-tolerant (CTRI = 5.63 - 6.21)**
Shelter (4.74)	Forestburg, (5.08)	Trailblazer (5.52)	Expresso (5.64)
Summer (4.74)	Tusca (5.19)		
Carthage (4.78)	Kanlow (5.21)		
Shawnee (4.8)	Cave-in-Rock (5.24)		
Blackwell (4.82)	Sunburst (5.26)		
Alamo (4.84)			
Dacotah (5.0)			

In conclusion, the cardinal temperature estimates would be useful to improve switchgrass models for field applications. Additionally, the identified cold- and heat-tolerant genotypes can be selected for niche environments and in switchgrass breeding programs to develop new genotypes for low- and high-temperature environments.

Influence of drought stress on seed germination of diverse switchgrass genotypes

The objectives of this study were to investigate the influence of drought stress on switchgrass seed germination and to develop a model for switchgrass to be used in field management decisions. An experiment was conducted to quantify the moisture stress tolerance of four switchgrass genotypes (Alamo, Kanlow, Shelter, and Cave-in-Rock) during germination by subjecting seeds to simulated well watered, but drought conditions. Four replicates of 100 stratified seed were germinated in varying concentrations (0-1.2 MPa) of polyethylene glycol (PEG 1600), and seed germination was monitored at 6-h intervals from

initial incubation. Results included estimations of maximum seed germination (MSG) and germination rate (GR) by fitting a three-parameter sigmoid function to germination time, which defined the germination percentage, shape of the response, and germination speed (Figure F.1.4). The cultivar Shelter did not germinate at -0.8 MPa while the other genotypes did not germinate beyond -0.8 MPa. Genotypes and water potential treatments interacted significantly and affected both MSG ($P < 0.001$) and GR ($P < 0.001$) (Figure F.1.4). Generally, incremental increases in water potential significantly decreased both MSG ($P < 0.001$) and GR ($P < 0.001$) across genotypes (Figures F.1.5 and F.1.6). Relative to the control (0 MPa), Alamo MSG decreased by 12, 26, 23, and 189% at -0.2, -0.4, -0.6, and -0.8 MPa, respectively. Similar trends were observed for the other genotypes. MSG ($r^2 = 0.95$) and GR ($r^2 = 0.98$) responses to water potential were best described by quadratic models with genotype-specific response algorithms determined (Figures F.1.5 and F.1.6).

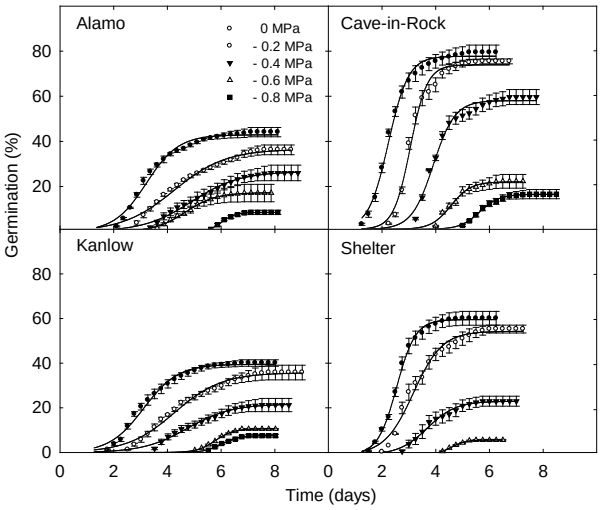


Figure F.1.4. Switchgrass seed germination time courses for (A) Alamo, (B) Kanlow, (C) Shelter, and (D) Cave-in-Rock genotypes at a range of water potentials.

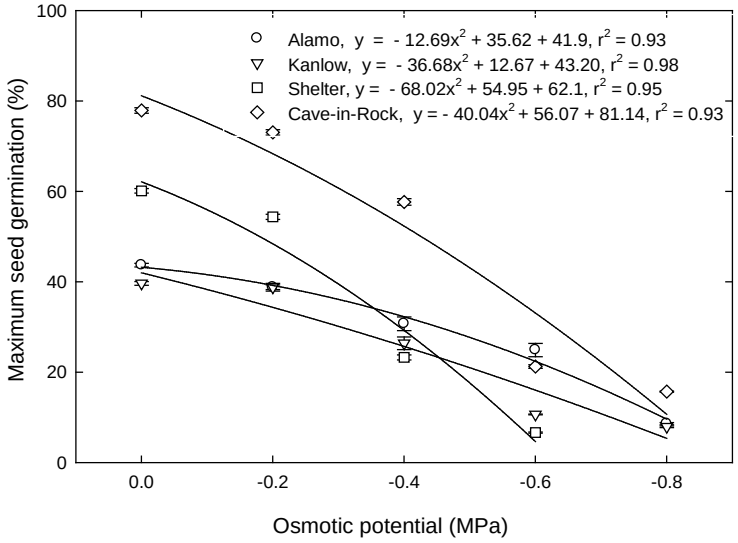


Figure F.1.5. Effect of water potential on maximum seed germination along with the fitted quadratic lines and equations of four switchgrass genotypes (Alamo, Kanlow, Cave-in-Rock, and Shelter). The symbols are the derived maximum seed germination from the seed germination-time course analysis, and the lines are predicted values by the fitted quadratic equations.

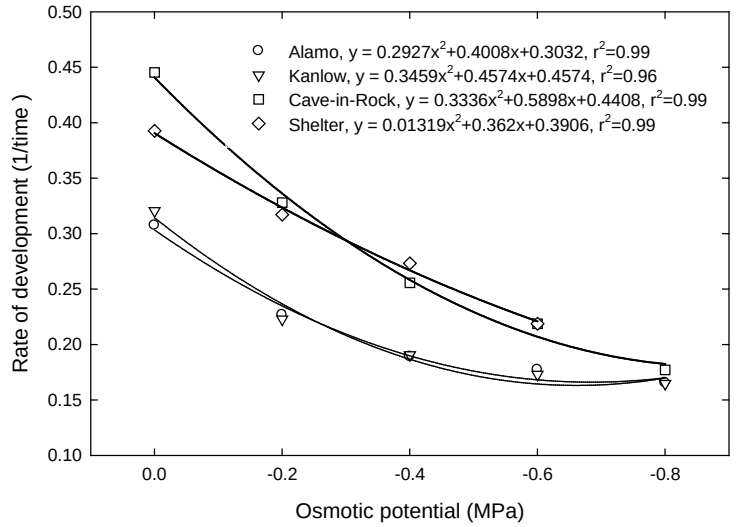


Figure F.1.6. Effect of water potential on rate of development of seed germination along with the fitted quadratic lines and equations of four switchgrass genotypes (Alamo, Kanlow, Cave-in-Rock, and Shelter).

In conclusion, water deficits significantly affected the germination capacity of switchgrass genotypes. Genotypes varied significantly in their response to drought stress. The genotype-specific algorithms developed can be used in modeling seed germination under variable moisture conditions. Also, the data can be used to plant switchgrass genotypes, depending

on the soil moisture level at a given location, to maximize seedling establishment.

Temperature effects on switchgrass growth, development, and reproductive potential

The objectives of this study were to investigate the influence of temperature on switchgrass growth, physiology, and development in order to understand the limitations of abiotic stress effects on biomass production. This study was conducted in sunlit, controlled-environment chambers known collectively as the Soil-Plant-Atmosphere-Research (SPAR) facility to quantify the effects of temperature on switchgrass (Figure F.1.7). Four SPAR chambers were maintained at 20/14, 28/20/ 34/26, and 40/32 °C day/night cycles and at 400 µmol mol^{-1} of CO_2. Plant heights and number of leaves were measured weekly throughout the experiment. Leaf areas and dry weights were obtained at 21, 42, and 69 days after treatment and 103 days after sowing.



Figure F.1.7. Soil-Plant-Atmosphere-Research (SPAR) facility, North Farm Mississippi State University.

The results indicated that mainstem elongation, leaf addition and growth, and biomass accumulation rates were very responsive to temperatures. Major growth rates (stem elongation, leaf area growth, biomass, and photosynthesis) increased linearly with increases in temperature up to 29 °C. The rates remained unaltered/or declined slightly at the highest temperature tested (40/32 °C) (Figures F.1.8 and F.1.9). Developmental rates such as leaf addition and tiller numbers increased linearly between 18 and 35 °C (Figure F.1.9). Switchgrass reached panicle maturity in 80 days at 34/26 °C but required 96 and 87 days at 28/20 and 40/32 °C, respectively. Panicles did not initiate at 22/14 °C during this experimental period (103 days of sowing). The highest panicle dry weight was observed at 34/26 °C. Panicle dry weights declined by 72 and 35% at 28/20 and 40/32 °C, respectively, compared to plants grown at 34/26 °C (Table F.1.2). Decreased panicle weights at the lower (28/20 °C) and higher (40/32 °C) temperatures were due to fewer and smaller panicles per plant.

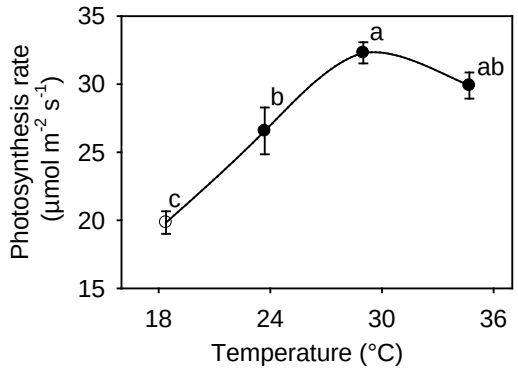


Figure F.1.8. Temperature effects on photosynthetic rate of switchgrass measured 64 days after treatment. The letters indicate significance level at P = 0.05 level.

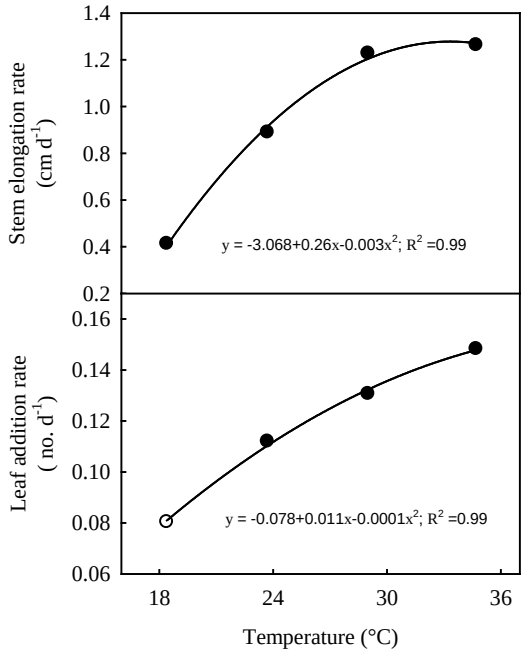


Figure F.1.9. Temperature effects on stem and leaf elongation rates of switchgrass measured during the experimental period.

Table F.1.2. Influence of temperature on various growth processes of switchgrass (CV. Alamo), 103 days after treatment temperature treatment.

Parameter	Temperature treatments (day/night °C)				LSD
	22/14	28/20	34/26	40/32	
Leaf dry weight(g plant^{-1})	3.27 ± 0.37^{b}	6.92 ± 0.84^{b}	13.55 ± 1.12^{a}	15.34 ± 1.42^{a}	30***
Stem dry weight (g plant^{-1})	4.46 ± 0.57^{c}	14.2 ± 2^{b}	28.57 ± 2.42^{a}	30.62 ± 3.34^{a}	27.51***
Panicle dry weight (g plant^{-1})	0 ± 0^{c}	0.80 ± 0.29^{bc}	2.94 ± 0.63^{a}	1.9 ± 0.4a^{b}	9.2***
Total dry weight (g plant^{-1})	7.73 ± 0.93^{c}	20.8 ± 2.94^{b}	45.06 ± 3.62^{a}	47.66 ± 4.85^{a}	31***
Panicles (no. plant^{-1})	0 ± 0^{b}	3.0 ± 0.6^{b}	7.7 ± 1.0^{a}	6.0 ± 0.6^{a}	25***
Panicle partitioning (%)	0 ± 0^{c}	2.14 ± 0.46^{bc}	5.93 ± 0.81^{a}	3.86 ± 0.6^{ab}	17***
50% panicle initiation (Days)	0 ± 0^{c}	96 ± 3.2^{a}	80 ± 2.6^{b}	87 ± 2.0^{b}	450***

Significantly different means within a parameter at P<0.001 (***) are separated by different letters.

In conclusion, temperature affected several growth and developmental processes in switchgrass. Seed and feedstock production was drastically reduced at the highest temperature tested. The temperature-specific functional relationships developed in this study for various growth and developmental processes would be useful for modeling switchgrass growth and development in a changing real world environment.

Hyperspectral reflectance properties, growth, leaf photosynthesis and electron transport of nitrogen deficient big bluestem (Andropogon gerardii)

The objectives of this current study are to (a) understand responses of big bluestem growth and leaf photosynthesis under N deficiency and (b) identify spectral signatures that best describe N and chlorophyll concentrations, which can be used to detect big bluestem health. This experiment is being conducted under outdoor pot-culture conditions to determine effects of N deficiency on big bluestem growth, photosynthesis, and leaf hyperspectral reflectance properties. Big bluestem, cv. 'Bonelli', was seeded in 120 12-l pots filled with fine sand and irrigated with Hoagland's nutrient solution. Treatments initiated at 60 days after sowing (DAS) included: (1) continued applying Hoagland's nutriend solution to the control (100N); (2) reduced N to 20% of the control (20N); and (3) withheld N from the solution (0N). Chlorophyll (Chl), N, and hyperspectral reflectance of the uppermost fully expanded leaves were determined at 10-d intervals from 60 to 115 DAS during the N treatments. Plant growth and developmental parameters were measured at the end of the experiment, 115 DAS (Table F.1.3).

Table F.1.3. Effects of N deficiency on big bluestem photosynthetic parameters derived from light response curves, measured between 80 and 85 days of sowing and 20 and 25 days after N (100N = control, 20N = 20% and 0N = 0% N of control, respectively) treatments.

Parameter	Nitrogen treatment		LSD	
	0N	20N	100 N	
*A*max (µmol CO_2 m^{-2} s^{-1})	19.5	33.6	40.1	11.0
*R*d (µmol CO_2 m^{-2} s^{-1})	1.14	3.31	2.65	0.85
Φ (µmol CO_2 µmol^{-1} photons)	0.0323	0.0568	0.06	0.01
θ (curvature; unit less)	0.997	0.583	0.42	0.18
LCP (µmol photons m^{-2} s^{-1})	35.4	58.3	41.9	8.6**
LSE (µmol photons m^{-2} s^{-1})	638	651	674	115^{N}
*ETR*max (µmol electrons m^{-2} s^{-}	65.9	94.9	123.	20.5

* and ** indicate significance at *P* = 0.01, and 0.05% level, and ^{NS} = not significant.

Results indicate that N deficiency caused a reduction in leaf Chl content, photosynthesis (*A*), electron transport rate (*ETR*), and dry weight of biomass components (Table F.1.3). Leaf and panicle dry weight contained the greatest decrease while root dry weight had the smallest decrease under N deficiency (Table F.1.4). Deficit N increased leaf reflectance at 555 (R555) and 715 (R715) nm and caused a red-edge shift to shorter wavelengths (Figure F.1.10). Leaf N and Chl concentrations were linearly correlated with not only the reflectance ratios of R545/R1605 (r^2 = 0.82) and R555/R405 (r^2 = 0.81), respectively, but also the first derivatives of the reflectance (dR/dλ) in red-edge centered 690 or 700 nm (r^2 = 0.74 - 0.83) (Figure F.1.11). These specific reflectance ratios (dR/dλ) may be used for rapid and non-destructive estimation of leaf Chl and plant N status of big bluestem to detect changes in N for appropriate nitrogen management strategies during the growing season.

Table F.1.4. Effects of N deficiency on big bluestem plant growth and dry matter accumulation, harvested 115 days of sowing and 55 days after N treatment.

Parameter	Nitrogen treatment			LSD
	0N	20N	100N	
Plant height (cm)	175.5	191.8	178.8	13.8**
Tillers (no. plant^{-1})	23.7	38.3	50.8	7.38***
Panicle bearing tillers (no. plant^{-1})	5.5	10.7	22.0	3.36***
Total panicles (no. plant^{-1})	15.8	29.4	64.0	10.32***
Leaf dry weight (g plant^{-1})	13.2	29.1	35.6	5.25***
Stem dry weight (g plant^{-1})	25.7	48.6	73.9	9.67***
Panicle dry weight (g plant^{-1})	2.03	4.73	9.52	2.00***
Root dry weight (g plant^{-1})	47.2	57.0	92.8	^{NA}
Biomass (g plant^{-1})	88.7	142.5	207.7	44.4***

** and *** indicate significance at *P* = 0.01, and 0.001% level, and ^{NA} = not analyzed.

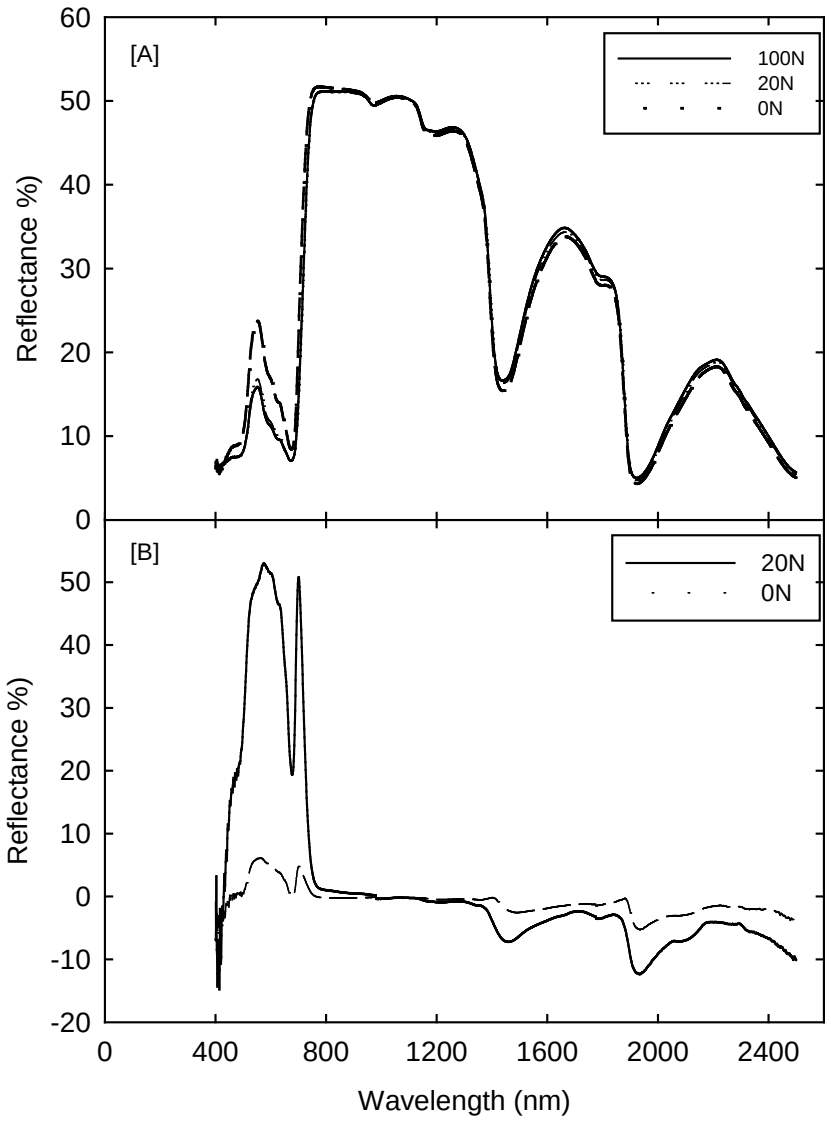


Figure F.1.10. Nitrogen deficiency effects on big bluestem leaf reflectance properties: (A) leaf spectral reflectance and (B) reflectance sensitivity to N deficiency. Data are means of five sampling dates and 20 leaves at each date from 60-115 days after sowing. The reflectance sensitivity = [(Rλ of N-deficient treatment − Rλ of the control)/Rλ of the control × 100%] (λ = 405, 415, 425 . . . 2495).

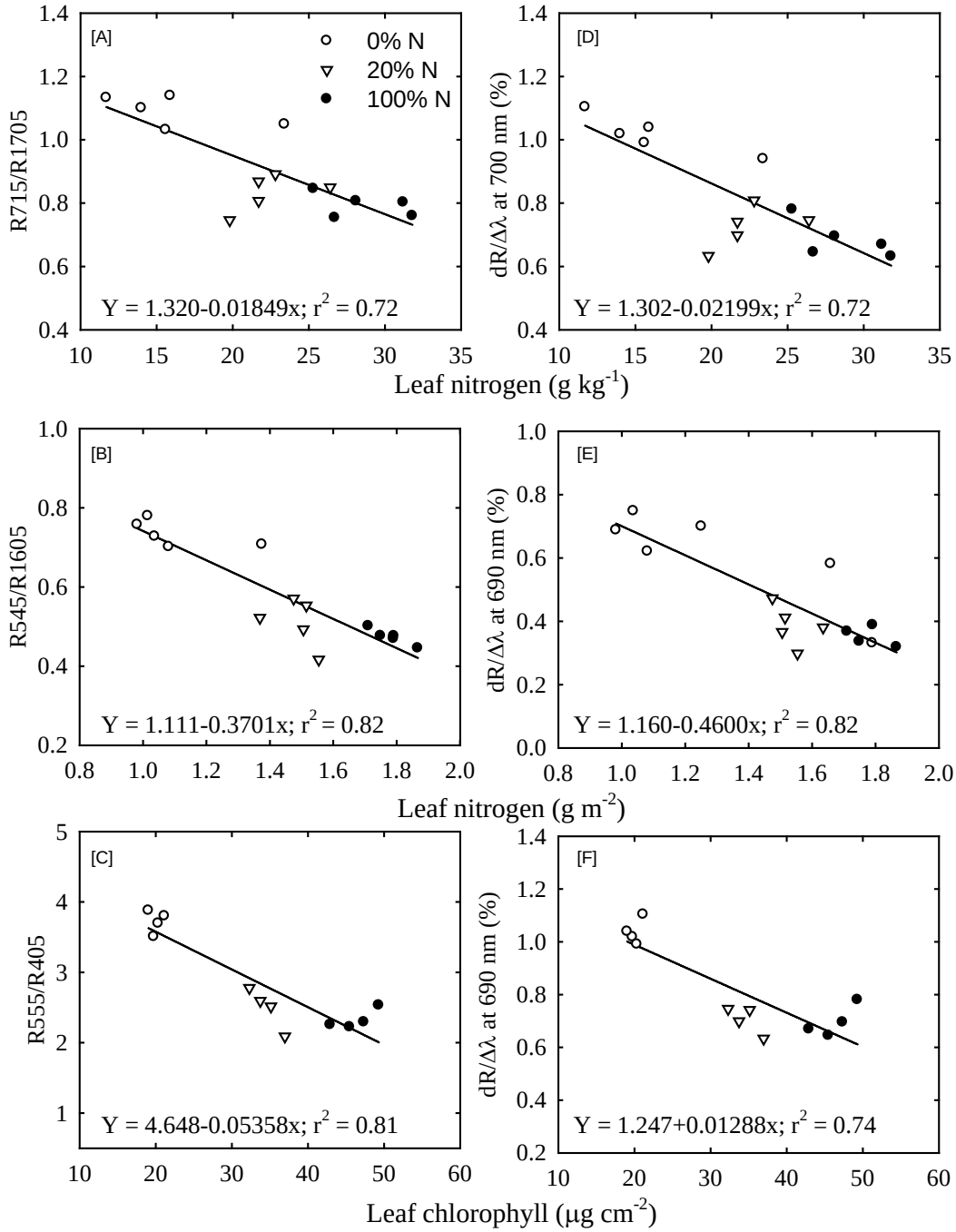


Figure F.1.11. Linear regression of big bluestem (A and D) leaf dry weight-based N, or (B and E) leaf area-based nitrogen concentrations, or (C and F) leaf chlorophyll, with (A - C) a given reflectance ratio or with (D - F) the first derivative of reflectance (dR/dλ) at 680 or 700 nm, which has the greatest r^2 value with leaf chlorophyll or nitrogen concentrations. Data are pooled over the three treatments and five sampling dates from 60 to 115 days after sowing (n = 15 for leaf nitrogen and n = 12 for chlorophyll).

In summary, N deficiency significantly lowered biomass production in big bluestem through a reduction in leaf photosynthesis, tiller number, and leaf dry weight. The study also reveals that N deficiency of big bluestem would reduce sequestration of atmospheric CO_2 and availability of forage as big bluestem is a dominant species in the natural ecosystems of North America and in managed systems if removed N through feedstocks is not replaced. The identified spectral ratios for leaf N and chlorophyll can be used to detect the health of the species in a given ecosystem and appropriate management measures can be adopted. Therefore, remote sensing can be used to monitor and maintain the health of big bluestem naturally as well as in managed feedstock production systems.

Seed Yield of Switchgrass

Seed yield data was collected from nine varieties of switchgrass planted in 2006 on a Marietta soil from 1 m^2 quadrats as physiological maturity occurred in September and October. Seed were cleaned and analyzed for % germination and purity. Biomass was harvested for yield in December and February 2007. Seed yield (pure live seed-PLS) ranged from 5 kg ha-^{1} for 'Kanlow' to 158 kg ha^{-1} for 'Alamo' in 2007 (Table F.1.5) and from 19 kg ha^{-1} for Kanlow to 52 kg ha^{-1} for Alamo in 2008 (Table F.1.6). Seed was lost in 2009 due to heavy fall rainfall, but seed in 2010 looks promising and is awaiting processing. Gross energy was similar at 8000 BYU lb^{-1} (Table F.1.10), Ash was 4.1% in December and 3.3% in February and Sulfur dropped from 0.05% in December to 0.03% in February (Table F.1.8). Biomass yield after seed harvest ranged from 7.0 to 18.0 Mg ha^{-1} and varied with variety (Tables F.1.7, F.1.9, F.1.11 and F.1.12). Nutrient uptake of switchgrass harvested in December averaged across varieties was 112 kg N (Table F.1.7), 11 kg P and 24 kg K ha^{-1} in 2007 and 82 kg N, 8 kg P and 5 K ha^{-1} in 2008 (Table F.1.9).

Table F.1.5. Seed Yield and Quality of Nine Switchgrass in September and October, 2007

	Gross	PLS	Purity	Germination	Dormant	Viable
Variety	-------- kg ha^{-1} ----------		---------- % ----------			
Alamo	400	158	67.4	55.0	7.0	62.0
Cave-in-Rock	164	51	66.7	40.8	7.0	47.8
Kanlow	16	5	68.7	48.5	10.0	58.5
NA Shawnee	70	22	78.5	41.8	8.5	50.2
NF/GA-991	91	22	56.0	42.0	5.2	47.2
NF/GA-992	159	86	79.4	56.8	6.2	63.0
NF/GA-993	141	31	46.8	38.5	4.0	42.5
NF/GA-001B)	246	85	65.9	51.8	4.0	55.8
NFSG05-1	473	158	54.7	53.8	6.2	60.0
LSD (0.05)	207	85	21.5	17.8	5.0	17.8
Mean	195	69	64.9	47.6	6.5	54.1

Table F.1.6. Seed Yield and Quality of Nine Switchgrass in September and October, 2008

	Gross	PLS	Purity	Germination	Dormant	Viable
Variety	-------- kg ha^{-1} ----------		---------- % ----------			
Alamo	292	52	77.8	4.5	29.8	34.2
Cave-in-Rock	51	20	68.8	5.5	46.0	51.5
Kanlow	92	19	79.3	13.0	25.5	38.5
NA Shawnee	45	19	96.3	5.0	49.5	54.5
NF/GA-991	181	29	84.3	4.0	29.5	33.5
NF/GA-992	292	28	59.3	5.0	20.5	25.5
NF/GA-993	180	38	60.6	17.0	21.0	38
NF/GA-001B)	328	70	75.6	2.5	26.8	29.3
NFSG05-1	290	35	41.7	4.5	34.5	39.0
LSD (0.05)	86	39	45.6	10.1	19.9	23.4
Mean	197	38	72.2	6.1	32.1	38.4

Seed was lost in 2009 due to heavy rains in September and October, 2009
Seed yield in 2010 pending processing

Table F.1.7. Biomass Yield and Nutrient Uptake/Removal of Switchgrass harvested in December 2007 and February 2008

	December 2007				February 2008			
	Biomass	N Uptake	P Uptake	K Uptake	Biomass	N Uptake	P Uptake	K Uptake
Variety	---------- kg ha^{-1} ----------							
Alamo	12482	108	11	23	13178	106	8	2
Cave-in-Rock	9164	81	8	17	7115	56	4	1
Kanlow	9072	81	8	16	6655	54	4	1
NA Shawnee	7910	69	7	15	6836	55	4	1
NF/GA-991	15569	136	14	29	12850	103	8	2
NF/GA-992	14224	125	13	26	10939	87	7	1
NF/GA-993	15489	134	14	29	12191	96	8	2
NF/GA-001B	18156	159	16	34	12566	101	8	2
NFSG05-1	13345	116	12	25	10330	82	6	1
LSD (0.05)	3881	32	3	10	2841	25	2	1
Mean	12834	112	11	24	10296	82	6	1
CV %	20.7	19.7	20.1	27.6	18.9	21.6	19.1	48.9

Fertilized with 448 kg 15-5-10 ha^{-1} in March 2007; Marietta Soil
February biomass was left to weather since December.

Table F.1.8. Nutritive Value, Energy and Minerals of Switchgrass harvested in December 2007 and February 2008

	BTU	ADF	Lignin	IVDMD	ASH	N	P	K	S	Ca	Mg
Harvest	Cal lb^{-1}	---------- % ----------									
December	7550	51.4	10.0	25.8	4.1	0.88	0.09	0.18	0.05	0.33	0.15
February	7613	55.0	11.1	18.5	3.3	0.80	0.06	0.01	0.03	0.33	0.08
P < 0.05	NS	*	*	*	*	NS	*	*	*	NS	*
Mean	7575	52.8	10.4	22.9	3.8	0.84	0.08	0.12	0.04	0.33	0.12

Table F.1.9. Biomass Yield and Nutrient Uptake/Removal of Switchgrass harvested in December 2008 and January 2009

	December 03, 2008				January 26, 2009			
	Biomass	N Uptake	P Uptake	K Uptake	Biomass	N Uptake	P Uptake	K Uptake
Variety	---------- kg ha^{-1} ----------							
Alamo	14279	91	9	7	20591	143	15	10
Cave-in-Rock	7304	50	6	3	10081	68	9	5
Kanlow	10972	57	6	2	11014	62	7	4
NA Shawnee	9436	71	6	3	7598	44	4	2
NF/GA-991	15087	100	8	8	15329	88	7	6
NF/GA-992	13743	88	8	10	14630	87	9	10
NF/GA-993	15382	105	10	2	15859	115	11	3
NF/GA-001B)	14189	86	7	6	19576	142	12	7
NFSG05-1	16823	96	11	8	17455	116	12	8
LSD (0.05)	4485	66	6	14	4620	66	7	16
Mean	13024	82	8	5	14681	96	9	6
CV %	23.6	35.0	35.4	119.8	21.6	30.4	33.2	116.6

Fertilized with 448 kg 15-5-10 ha^{-1} in March 2008;
Soil: Marietta
January biomass was left to weather since December.

Table F.1.10. Nutritive Value, Energy and Minerals of Switchgrass harvested in December 2008 and January 2009

	BTU	ADF	Lignin	IVDMD	ASH	N	P	K	S	Ca	Mg
Harvest	Cal lb^{-1}	---------- % ----------									
December	7982	47.5	6.5	31.7	4.0	0.59	0.10	0.13	0.030	043	0.11
February	8060	50.3	7.3	27.2	3.2	0.65	0.06	0.04	0.017	0.32	0.07
P < 0.05	*	*	*	*	*	*	*	*	*	NS	*
Mean	8021	48.9	6.9	24.4	3.6	0.62	0.08	0.08	0.024	0.38	0.09

Table F.1.11. Biomass Yield of Nine Switchgrass Varieties, 2009 at Starkville, MS

	November 18, 2009	Standing	February 3, 2010	Standing
Variety	kg ha^{-1}	DM %	kg ha^{-1}	DM %
Alamo	14678	53.6	10854	84.6
Cave-in-Rock	6842	60.9	6988	78.2
Kanlow	11813	57.9	11117	85.5
NA Shawnee	8950	59.3	6683	79.9
NF/GA-991	12238	52.8	11193	85.2
NF/GA-992	15334	54.9	11851	83.6
NF/GA-993	12172	55.9	9646	85.2
NF/GA-001B)	13878	53.8	12264	83.6
NFSG05-1	14515	54.0	14248	84.1
LSD (0.05)	2662	2.1	4177	7.7
Mean	12269	55.9	10538	83.3

Planted: 25 August, 2006 Soil: Marietta
Fertilizer: 448 kg ha^{-1} 15-5-10 in March, 2009 (1x)

Table F.1.12. Biomass Yield of Nine Switchgrass Varieties, 2010 at Starkville, MS

	December 3, 2010	Standing	February 2011	Standing
Variety	kg ha^{-1}	DM %	kg ha^{-1}	DM %
Alamo	14829	71.9		
Cave-in-Rock	8348	74.8		
Kanlow	14118	75.7		
NA Shawnee	7809	76.4		
NF/GA-991	13928	71.8		
NF/GA-992	16988	77.9		
NF/GA-993	14764	80.4		
NF/GA-001B)	15572	73.2		
NFSG05-1	15041	75.7		
LSD (0.05)	4276	7.4		
Mean	13488	75.3		

Biomass and Seed Yield of Switchgrass Harvested Half and Full Season

'Alamo' switchgrass established in 1999 on a Savannah soil was utilized in 2006 to determine biomass and seed yield from 2006 to 2010. Plots were split to harvest biomass in

June and December and for seed in October across all years. Plots harvested for biomass in June (half season) had an average yield of 6.2 to 9.4 Mg ha^{-1}. Total full season yield ranged from 9.0 to 20.8 Mg ha^{-1}. Average seed yield of pure live seed (PLS) was 31 to 39 kg ha^{-1} in 2006 (Table F.1.15), 6 to 68 kg ha^{-1} in 2007 (Table F.1.16), and 26 to 29 kg ha^{-1} in 2008 (Table F.1.17) for half and full season, respectively. Seed was lost in 2009 due to excessive fall rainfall. Gross energy ranged from 7500 to 8000 BTU lb^{-1}; average Sulfur content was 0.028% for full-season switchgrass harvested in November and 0.05 to 0.07% for half season switchgrass harvested in June or November (Tables F.1.13 and F.1.14). Half season switchgrass harvested in June was suitable as forage for beef animals. Nutrient uptake of switchgrass harvested in June and November ranged from 122 to 158 kg N, 14 to 20 kg P, and 82 to 133 kg K ha^{-1}. Full-season switchgrass harvested once in December removed averages of 74 to 82 kg N, 6 to 13 kg P, and 35 to 58 kg K ha^{-1}.

Table F.1.13. Biomass Yield of Alamo Switchgrass in 2008 Harvested Half (2x) or Full Season (1x) as Affected by Harvest Frequency in 2006-2007.

	June	November	Total Season	Harvest Frequency	
	---------- kg ha^{-1} ----------			2006-07	2008
Full to Full	0 c[†]	14620 a	14620 bc	1x	1x
Full to Half	13683 a	7072 c	20755 a	1x	2x
Half to Full	0 c	10973 b	10973 c	2x	1x
Half to Half	10627 b	4827 c	15454 b	2x	2x
LSD (P<0.05)	2299	2600	3724		

[†] Full season plots not harvested in June Soil: Savannah
Fertilizer: 336 kg ha^{-1} 15-5-10: March and June

Table F.1.14. Biomass Yield of Switchgrass in 2009 Harvested Half (2x) or Full Season (1x) as Affected by Harvest Frequency in 2006-2007.

	June	November	Total Season	Harvest Frequency	
	---------- kg ha^{-1} ----------			2006-07	2008-09
Full to Full	0 b[†]	9831 a	9831 b	1x	1x
Full to Half	9409 a	3372 b	12781 a	1x	2x
Half to Full	0 b	9089 a	9089 b	2x	1x
Half to Half	9179 b	3201 a	12380 a	2x	2x
LSD (P<0.05)	788	1315	1689		

[†] Full season plots not harvested in June Soil: Savannah
Fertilizer: 300 lbs $acre^{-1}$ 15-5-10: Full Season 1x in March; Half Season 2x in March and June

Table F.1.15. Biomass Yield of Alamo Switchgrass in 2010 Harvested Half (2x) or Full Season (1x) as Affected by Harvest Frequency.

	June	November	Total Season	Harvest Frequency	
	---------- kg ha^{-1} ----------			2006-07	2008-10
Full to Full	0 b[†]	11269 a	11269 a	1x	1x
Full to Half	8540	2302 b	10842 a	1x	2x
Half to Full	0 b	10621 a	10621 a	2x	1x
Half to Half	7981	2057 b	10038 a	2x	2x
LSD (P<0.05)	906	1569	1990		

[†] Full season plots not harvested in June Soil: Savannah
Fertilizer: 336 kg ha^{-1} 15-5-10: March and June

Table F.1.16. Energy and Nutritive Levels of 'Alamo' Switchgrass as Affected by mid-season harvest, 2008

	Protein	NDF	ADF	Lignin	IVDMD	Sulfur	ASH	BTU
Harvest	---------- % ----------							Cal lb^{-1}
June-Half	7.22	74.4	38.9	3.8	56.9	0.058	4.6	8046
Nov -Half	4.42	78.8	44.8	5.2	38.9	0.050	4.0	7993
Nov- Full	2.84	81.3	44.8	4.9	37.0	0.022	3.4	8025

Table F.1.17. Energy and Nutritive Levels of Alamo Switchgrass as Affected by mid-season harvest, 2009

	Protein	NDF	ADF	Lignin	IVDMD	Sulfur	ASH	BTU
Harvest	---------- % ----------							Cal lb^{-1}
June - Half	6.8	75.1	40.6	3.0	43.5	0.070	4.5	7576
Nov - Half	5.6	74.4	40.3	3.5	33.0	0.067	4.0	7689
Nov - Full	4.0	80.3	43.8	4.3	26.1	0.035	3.1	7695

Table F.1.18. Seed Yield of 'Alamo' Switchgrass as affected by mid-season harvest, 2006.

Season	Yield	Pure live seed	Purity	Germination	Dormant	Total viable
	---------- kg ha^{-1} ----------		---------- % ----------			
Half	46	31	94.7	63.6	6.6	70.2
Full	64	39	86.1	59.5	6.1	65.6
LSD $_{(0.05)}$	29	22	9.8	15.1	3.7	16.1

Table F.1.19. Seed Yield of 'Alamo' Switchgrass as affected by mid-season harvest, 2007

Season	Yield	Pure live seed	Purity	Germination	Dormant	Total viable
	--------- kg ha^{-1} ----------		---------- % ----------			
Half	24	6	44.3	55.6	4.2	59.9
Full	315	68	53.5	46.8	2.6	49.4
LSD $_{(0.05)}$	80.2	12.6	9.9	11.2	1.3	11.8

Table F.1.20. Seed Yield of 'Alamo' Switchgrass as affected by mid-season harvest, 2008

Season	Yield	Pure live seed	Purity	Germination	Dormant	Total viable
	--------- kg/ha ----------		---------- % ----------			
Half	56	29	68.9	9.1	31.2	40.4
Full	97	26	75.5	8.1	26.0	34.1
$LSD_{(0.05)}$	22	8	12.5	3.9	5.8	8.2

Results indicate that seed yield was low and subject to losses due to excessive fall rainfall in two of the four years, indicating that there would be a 50% chance of obtaining harvestable seed. Biomass yield was not compromised by mid-season harvest for forage, indicating that dual-purpose usage of switchgrass would be feasible during feedstock development.

Selection for precocious germination (reduced seed dormancy)

In reduced seed dormancy research, progress was substantial for switchgrass but slower for big bluestem and indiangrass. The overall goal was to allow for ease of establishment of native grasses, resulting in increased feedstock production. Significant progress was accomplished with lowland switchgrass, and after seven cycles of selection, pre-stratification germination levels equalled 94% in four days. Indiangrass and big bluestem completed their sixth cycle (data pending). Precocious germination for Cycle 5 indiangrass and big bluestem equalled 14% and 55%, respectively. Cycle 7 upland switchgrass (Expresso) has been licensed to Ernst Conservation Seeds, Meadville, PA (main office)/ Live Oak, FL (SE office). Foundation seed fields will be established in New Bern, AL in spring 2011.

Germplasm/seed increase and testing

Regarding germplasm research, half the Cycle 6 nucleus (breeders) seed was sent to NRCS – PMC in Coffeeville for increase at DCDC, and clones of parents of Cycle 7 were sent to Calvin Ernst (license pending).

Nitrogen replacement/low input switchgrass using cool season legumes

Previous data seemed to indicate that both white clover and crimson clover provide average nitrogen equivalents of 50 to 100 lb N. Ball clover and arrowleaf clover provide less than adequate N levels at 100 lb N. Additional testing should decrease variance and allow greater precision in assessment of N contents. Additional tests have been undertaken in fall 2010 (SERC III funds) to further assess nitrogen replacement using cool-season legumes, including a variety of clovers and vetches.

Direct yield comparisons of switchgrass and giant miscanthus (M*x*g)

Recent studies have suggested that biomass yields of switchgrass are half that of giant miscanthus (M*x*g). A study was introduced in 2009 in Starkville to directly compare yields of switchgrass and M*x*g. 'Freedom' giant miscanthus (MSU variety), "Illinois clone" giant miscanthus (University of Illinois Champaign), and 'EG1101'(Ceres, Inc.) switchgrass were included in the study. Plants were grown over winter in greenhouses and transplanted in May 2009 to provide a competitive advantage against summer weeds. 'EG1101' plots included 1600 plants, while 'Freedom' and "Illinois clone" plots consisted of 400 plants. Plants varying in maturity were harvested at the end of 2009. 'EG1101' switchgrass yielded highest with an average of 33.8 Mg/ha; 'Freedom' yielded an average of 12.05 Mg/ha; and "Illinois clone" yielded lowest at 8.98 Mg/ha. Greater yields for switchgrass are not uncommon for the establishment year. Complete maturation of giant miscanthus requires

two or three years, resulting in substantially greater yields than the initial establishment year.

Proprietary – Screening switchgrass (cv. Alamo) for resistance to imazapic herbicide (Plateau)

Potential for licensing (and perhaps patent) is high. New patenting system will allow for patents to be applied to the parents the cultivar released from this work.

The overall objective was to screen for individuals that show resistance to the herbicide, thus generating a population of plants that could establish under a broad-spectrum herbicide that normally kills or alters switchgrass growth/establishment. This process is different than transgenics because it contains extensive screening of naturally occurring variation in a cross-pollinated crop. 364,650 Alamo seedlings have been screened by applying 8.0 fl oz/acre of imazapic herbicide. Of the 364,650 seedlings screened, 78 survived. A second application of imazapic was made at a rate of 14.0 oz/acre (the highest labeled rate for tolerant species) to eliminate any variability of tolerance. Eleven of the selected population did not survive from the second application. Sixty-seven highly tolerant parents will generate a population of resistant offspring (a selection intensity of 0.0187%). Resistance to this herbicide is a qualitative trait that must be "stacked;" therefore, additional screening of elite individuals is necessary to boost resistance for subsequent generations. This additional screening is being accomplished through agar screening (germinating second-generation seed in agar that contains imazapic). Selection of individuals through this method is pending. The project was started with SERC monies but has been transferred to other funds due to lack of funding.

Seed Safener Research

Seed safeners protect against certain herbicides that will control troublesome weeds during planting and establishment periods. Preliminary field trials demonstrated the effectiveness of the seed safener Concep III® (Syngenta). It protects against the herbicide metolachlor (Dual Magnum®). Field trials were conducted in spring of 2009 that evaluated seedling survival, weed control, and yield of several switchgrass varieties. Results include no significant differences in safener protection between varieties; however, there were yield differences discovered in the method of safener application to the seed (Figure F.1.12). The project was implemented with SERC funds, but is now funded by leveraged funds (DOE NC Region SunGrant), which resulted in a thesis (J. Brett Rushing) and a competitive grant (DOE NC Region SunGrant).

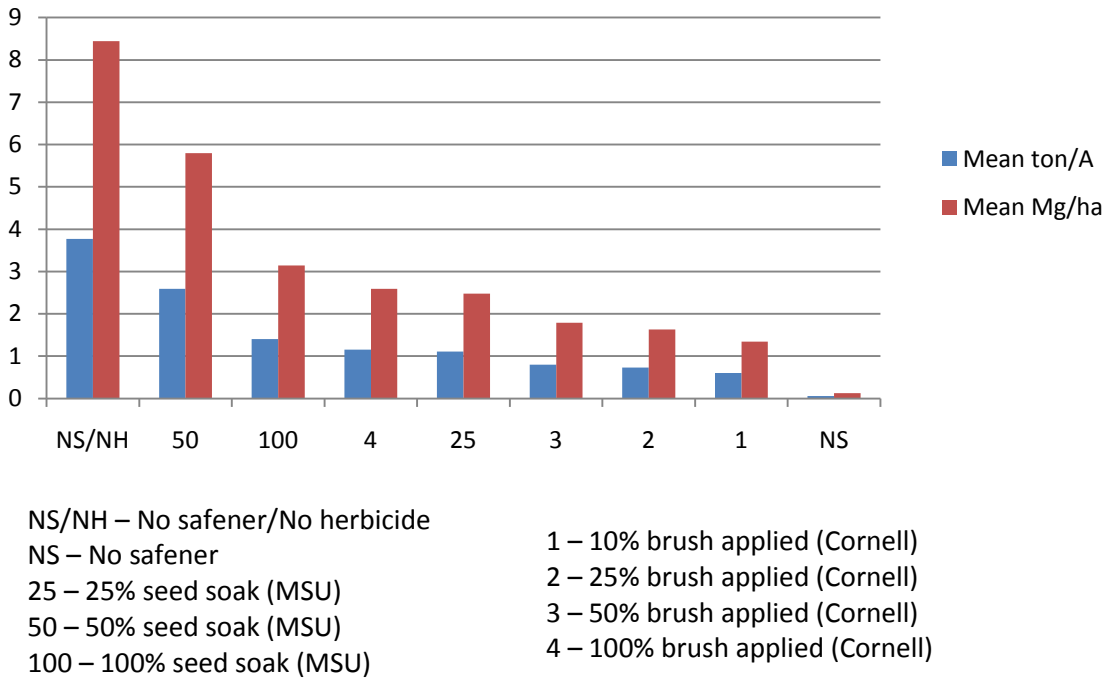


Figure F.1.12. Mean Yield of 'Alamo' Switchgrass Seed Safener Trial at Starkville, MS in 2009

Sweet sorghum as a direct source of ethanol

The objectives of this study were to (a) grow and use sweet sorghum as a direct source of ethanol by fermenting the epressed sap and (b) use the stalks either for fuel to distill or as a raw material for cellulosic ethanol. Twelve cultivars of sweet sorghum were chosen for the experiment: Bale All, Bundle King, Dale, Della, Keller, M81-E, Pace Setter, Simon, Sugar Drip, Sugar Top, Theis, and Topper. These cultivars have been developed in MS and KY. They were planted at a density of 13 seed/m on 0.91 m rows, 6.4m long by four rows wide. Each row was randomly designated for ripener and deheading treatments while the remaining two rows were designated for ºBrix sampling and a control. Strong winds caused moderate to severe lodging of the field similar to previous years. ºBrix increased over the course of the summer, peaked in mid-October, then declined. High range for ºBrix in sweet sorghum is 16-22%. At the MS location in 2009, Dale yielded the greatest ethanol per aliquot and fermented an average of 8.3mL of ethanol per 400mL of wort (Table F.1.22). Sap samples were submitted from each of the cultivars for lab analyses. Apart from maize, a close counterpart, sorghum does contain fructose. There are distinct differences among cultivars for percentage fructose, with Della and Dale being highest in fructose at 30%, respectively.

Table F.1.22. Two-year fresh weight (kg/ha), mean extractable sap (lt/ha), mean EOS (end of season), °Brix, and mean ethanol (lt/ha) of 11 sweet sorghum (*Sorghum bicolor*) cultivars during the 2008 - 2009 growing seasons.

Cultivar	Fresh Weight (kg/ha)	Mean extractable sap (lt/ha)	Mean EOS °Brix	Mean ethanol (lt/ha)
Bale All	1804.02 CD†	1717.10 D	7.68 E†	137.70 C†
Bundle King	2985.23 BC	2487.80 CD	12.09 D	409.03 ABC
Dale	3724.43 AB	3817.40 BC	15.87 AB	807.14 A
Della	3586.76 AB	3893.40 BC	14.78 ABC	706.02 A
Keller	3623.47 AB	3918.30 BC	17.06 A	561.85 AB
M81-E	4141.48 AB	5174.90 AB	15.31 AB	800.60 A
Simon	1054.91 D	1634.50 D	11.08 D	123.30 C
Sugar Drip	1399.09 CD	2388.00 CD	12.75 CD	273.06 BC
Sugar Top	4945.69 A	5997.90 A	14.81 ABC	788.35 A
Theis	3600.89 AB	4024.80 BC	14.53 BC	602.75 AB
Topper	3657.80 AB	4557.80 AB	15.53 AB	735.05 A

Energycane Research

New germplasm of energycane is being screened for USDA-ARS-SRRC, Houma, LA to determine yield and cold hardiness of new energycane (*Saccharum spontenaum* x *S.domesticum*) hybrids. This study is separate from the DOE Herbaceous Feedstocks Partnership (five original genotypes). The MS site is the farthest north testing location for energycane. In 2009, 13 new genotypes were planted in Starkville. The severity of the winter killed all but four genotypes (HoCP 72-114, Ho 02-113, Ho 00-06, and Ho 99-48). Sugar and energycane were established in early fall 2010 by burying canes in furrows, monitoring new growth from the planted biomass, and maintaining the field into the next year when yield will occur. Sugar accumulation, growth, yield, and hardiness have all been monitored.

Weed management in switchgrass as a bio-feedstock in Pontotoc, MS

Switchgrass was harvested from plots that had some measurable weed control. Biomass yield was determined (Table F.1.23). A tank-mix of Accent + Ally at 0.66 and 0.1 oz ai/A, respectively, was applied postemergence and controlled broadleaf signalgrass 86% at three weeks after treatment. In addition, yield and percent stand the following spring was higher for this treatment when compared to all others.

Table F.1.23. Switchgrass yield, percent stand, and weed control at the Pontotoc Ridge-Flatwoods Experiment Station in 2009-2010.

Treatment	Rate	App. Time	broadleaf signalgrass 1 WAT	broadleaf signalgrass 3 WAT	prickly sida 1 WAT	prickly sida 3 WAT	smallflower m-glory 1 WAT	smallflower m-glory 3 WAT	Injury 1 WAT	Injury 3 WAT	Yield	Stand 2nd Year April 2010
			----------% Control----------						%	%	Lbs/A	%
Untreated			0	0	0	0	0	0	0	0	0	18
Atrazine	1.0 qt/A	PRE	15	0	100	100	100	100	0	0	0	14
Atrazine	1.5 qt/A	PRE	43	20	100	100	99	100	0	0	0	20
Atrazine	2.0 qt/A	PRE	58	33	100	93	100	89	0	0	156	53
Atrazine COC	1.0 qt/A 1 % v/v	POST	10	5	33	66	89	100	0	0	0	9
Atrazine COC	1.5 qt/A 1 % v/v	POST	3	8	48	71	78	100	0	0	265	35
Atrazine COC	2.0 qt/A 1 % v/v	POST	0	15	48	85	98	100	0	0	886	50
Atrazine Atrazine COC	0.5 qt/A 1.0 qt/A 1 % v/v	PREPOSTPOST	28	16	100	100	100	100	0	0	632	41
Atrazine Atrazine	0.5 qt/A 1.5 qt/A	PR	15	11	100	95	100	100	0	0	76	23

COC	1 % v/v	EPOSTPOST									2	
Atrazine Atrazine COC	0.5 qt/A 2.0 qt/A 1 % v/v	PREPOSTPOST	28	23	100	100	100	100	1	0	686	35
Atrazine Atrazine COC	1.0 qt/A 1.0 qt/A 1 % v/v	PREPOSTPOST	40	33	100	100	100	100	0	0	1245	44
Ally NIS	0.1 oz wt/A 0.25 % v/v	POST	0	10	38	70	33	75	0	0	421	30
Ally Accent NIS	0.1 oz wt/A 0.66 oz wt/A 0.25 % v/v	POST	48	86	33	66	23	70	24	19	2080	86
Ally Accent NIS	0.1 oz wt/A 0.33 oz wt/A 0.25 % v/v	POST	28	45	26	40	18	38	25	10	1521	47
Accent NIS	0.33 oz wt/A 0.25 % v/v	POST	43	65	33	0	10	5	28	13	211	39
Accent NIS	0.66 oz wt/A 0.25 % v/v	POS	50	81	34	3	16	0	25	36	247	66

		T										
Beacon NIS	0.38 oz wt/A 0.25 % v/v	POST	8	3	25	8	23	50	21	23	0	16
Beacon NIS	0.76 oz wt/A 0.25 % v/v	POST	5	3	30	20	30	57	21	42	0	10
Ally Beacon NIS	0.1 oz wt/A 0.38 oz wt/A 0.25 % v/v	POST	15	10	38	69	29	79	25	26	356	22
Ally Beacon NIS	0.1 oz wt/A 0.76 oz wt/A 0.25 % v/v	POST	8	8	40	70	35	100	20	40	0	6
Axial XL NIS	8.2 fl oz/A 0.25 % v/v	POST	40	10	0	0	0	0	38	80	0	8
Accent Atrazine NIS	0.66 oz wt/A 0.5 qt/A 0.25 % v/v	POST	20	73	33	3	43	29	24	29	290	26
KIH-485 NIS	2.0 oz wt/A 0.25 % v/v	POST	0	0	0	0	0	0	0	0	0	11
LSD (0.05)			21.3	25.2	18.2	12.7	15.4	25.8	6.8	13.5	104 0.2	33.6

Evaluation of fertilizer N rate in switchgrass for use as a bio-feedstock source in Pontotoc, MS

This study will be ongoing into SERC III. The switchgrass planted in August of 2009 for establishment for this study in 2010 did not survive the extreme temperatures due to a non-extensive root system. Re-establishment occurred in spring 2011.

Varietal evaluation of switchgrass and *Miscanthus* species at Brown Loam and Newton locations

Plots were established on 2 May 2006 at Raymond. Entries consisted of five elite breeding lines and five released cultivars of switchgrass, and a Miscanthus hybrid in four replications. Switchgrass entries were seeded at a rate of 5.6 kg pure live seed per hectare. Plots were 5 × 3 m with a 2-m alleyway between blocks. Morphological observations included occurrence of flowering, pests and diseases. Switchgrass stands were very poor during the establishment year, but were better in the second year, which holds implications on how soon producers can start seeing economic returns from the crop. Miscanthus and two commercial switchgrass cultivars, 'Kanlow' and 'Trailblazer' did not establish well and continued to perform poorly, so data from these entries was eliminated from statistical analyses. For biomass yield data in 2007-2009, yields increased with age of stands. By 2009, yields ranged from 9.4 to 31.2 Mg ha^{-1} (Table F.1.24). Alamo and the improved experimental lines yielded greater than the counterpart varieties of Cave-in-Rock and Shawnee. Chemical characteristics of the plants are to be analyzed in the near future.

Table F.1.24. Biomass yield from a single end-of-season harvest of eight switchgrass entries during the 2007, 2008, and 2009 growing seasons at Raymond, MS.

	Year		
Entry†	**2007**	**2008**	**2009**
	- Mg ha^{-1} -		
Alamo	5.83	17.93	28.04
Cave-in-Rock	4.11	9.56	9.36
NF/GA-001	5.80	24.08	29.50
NF/GA-991	6.67	15.62	23.40
NF/GA-992	7.35	22.10	31.23
NF/GA-993	6.63	14.14	21.38
NFSG05-1	6.42	13.18	21.77
Shawnee	4.45	7.81	9.46
LSD (0.05)	1.82	3.52	5.11
Mean	5.95	15.05	21.77

Nitrogen fertilizer management effects on switchgrass production at Brown Loam

Four fertilizer N rates were imposed on four switchgrass entries in a 4 x 4 factorial arrangement of a randomized complete block design experiment with four replications. The N rates included 0, 80, 160, and 240 kg N ha^{-1} applied all at once annually in May and the four entries consisted of two experimental lines, NFGA011 and NFGA992, and two commercial cultivars, Alamo and Cave-in-Rock. Plots were seeded on 2 May 2006 at Brown Loam at a rate of 5.6 kg pure live seed per hectare. Fertilizer N treatments were imposed in 2008, and the study was conducted for two growing seasons, 2008 and 2009. Alamo and the two experimental entries consistently had greater yields (23.5 to 25.5 Mg ha^{-1} in 2008 and 18.5 to 21.6 Mg ha^{-1}in 2008) than Cave-in-Rock (10.5 and 10.0 Mg ha^{-1} in 2007 and 2009, respectively). In 2008, yield increased by 66% (from 14.7 to 24.5 Mg ha^{-1}) from zero N application to 80 kg N ha^{-1}, but there were no further yield increases with additional

increments of N fertilizer. In 2009, however, there was a linear increase in biomass yield from 13.9 to 19.9 Mg ha^{-1} with increasing N rate.

Nitrogen fertilizer management and harvest frequency effect on switchgrass production at Brown Loam

Alamo switchgrass was planted in 5 × 3-m plots in a 4 x 2 factorial arrangement of a randomized complete block design experiment with three replications. Treatments were four harvest frequencies (1, 2, 3, or 6 harvests per year) and two N fertilizer application rates (80 and 240 kg N ha^{-1}). Plots were seeded on 2 May 2006 at Brown Loam at a rate of 5.6 kg pure live seed per hectare. The seeds were drilled in rows at 15 cm spacing. Drought conditions throughout the summer after seeding of the plots resulted in extremely poor germination and seedling establishment, and plant density in plots were undesirable even in the second year. Stands were much improved in spring of 2008, so treatment imposition and data collection began. Results indicate that harvests done twice per year or once at the end of the season had similar yield, but total annual yield decreased with more frequent harvest. Another year of data collection is ongoing and the study has been expanded to include quantification of soil carbon sequestration.

Explanation of Variance: Imposition of treatments did not start until 2008 season (third year after planting) instead of during the second year because the switchgrass stands were not sufficiently established by the second year after planting. As a result, the study is still ongoing.

Nitrogen Uptake, Residual Effects, and N Translocation in Alamo Switchgrass Measured by ^{15}N-labelled Fertilizer

The objectives of the study were: (a) to determine N translocation in switchgrass throughout the growing season and (b) to determine best nutrient management practices by estimating N residual effects on biomass production, quality, and timing of fertilizer N applications. A small-scale field study was developed to address issues related to nutrient management in switchgrass as a bioenergy crop. A 12-year plot of Alamo switchgrass was used to conduct the experiment at the Henry A. Leveck Animal Research Center in Starkville, MS. A N^{15} tracer technique for measuring N translocation and storage in switchgrass was used. The experimental design was a randomized complete block design replicated four times. Three N treatments (0, 56, and 112 kg N ha^{-1}) were applied to plots (0.91 m x 3 m) as ammonium nitrate to measure seasonal yields and residual effects in November of 2009 and 2010. These N treatments were applied to 0.91 m^2 plots using double-labeled ammonium nitrate (^{15}N @ 2.5% enrichment) in May 2009. Plots containing N^{15} were harvested at quarterly sampling dates throughout 2009 and 2010. Samples [shoot, root (crown + root) and soil] were collected in August and November of 2009 and in February, May, August, and November of 2010. Shoot samples were collected in close proximity to ground level. Root samples were collected using a 0.30 m^2 area to a 15 cm depth along with 10 soil core samples within each plot to a 15 cm depth. Soil samples were weighed and air-dried after sampling to obtain soil bulk density and soil water content. Soil samples were then ground to pass a 2-mm mesh and prepared for analyses. Root samples were washed and separated into crown and root and dried at 65 °C. Total C and N in the soil and tissue samples were determined using a dry combustion Carlo Erba Analyzer. Soil, root, and biomass samples will also be analyzed for N^{15} enrichment using a dry combustion mass spectrometer analyzer coupled to an isoprime in the near future.

Results include a linear increase in seasonal yields but no available significant mean separations in 2009 or 2010 (Figure F.1.13). No significant differences were observed in

total biomass production in 2009 and 2010. Average yields indicated a 20% and 30% increase for the 56 and 112 kg N ha^{-1} application rates when compared to the control. All collected samples are being analyzed for N^{15}, C, P, and K. The amount of N removed from the system was directly related to biomass yield and was significantly affected by harvest time and species. Importantly, overall there were no significant changes in N content between an early winter harvest (November) and a late winter harvest (February). This study indicates the benefits of N translocation soon after senescence; therefore, there is no reason to risk yield losses by delaying harvest over the winter.

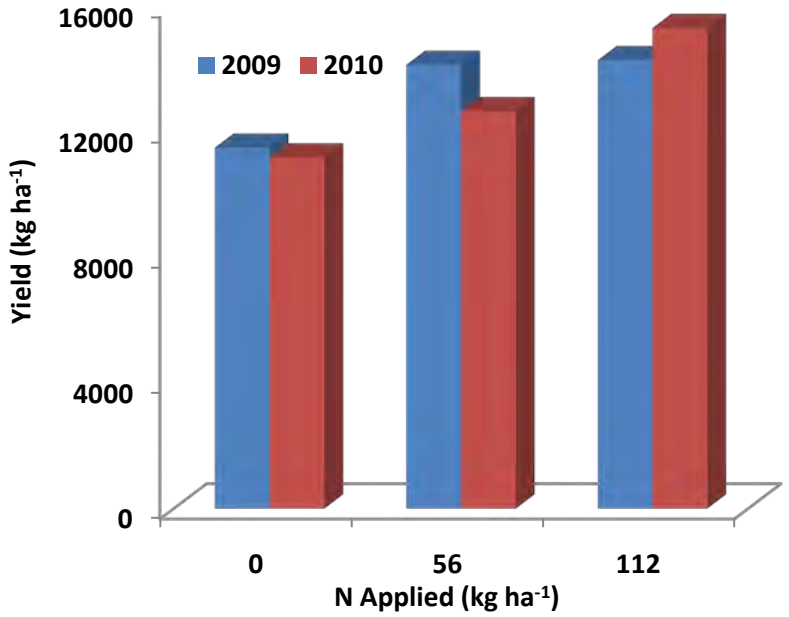


Figure F.1.13. Total switchgrass biomass yields at different fertility levels

There were significant differences in yield, nitrogen content, and carbon content across sampling dates (Table F.1.25). No significant differences were observed in N rates. N and C content increased late in the season. The below-ground canopy at 15 cm depth indicated that 63% of the biomass was allocated to crowns while 37% was allocated to roots. A significant below-ground biomass type x date interaction was observed in the percent of biomass distribution (Table F.1.26). Crowns had a higher nitrogen (64 g m^{-3}) content than roots (37 g m^{-3}). Nitrogen content was also affected by sampling date and N rate (Table F.1.27). Nitrogen applications did not affect N content of the crowns or roots. Carbon pool was 34% higher in the roots than in the crown. Significant interactions of biomass type (crown and roots) was observed across sampling dates for C pools. A sampling date x N rate interaction was also observed for C pool.

Table F.1.25. Yield, nitrogen and carbon content of above-ground biomass from August 2009 to November 2010.

Sampling Date	Yield	N Content	C Content
	---------- g cm^{-2} ----------		
Aug-09	904	9.9	454
Nov-09	954	5.4	481
Feb-10	872	5.3	443
May-10	434	2.8	216
Aug-10	2197	13.4	1123
Nov-10	2153	--	--
$LSD_{0.05}$	332.7	2.2	135

Table F.1.26. Biomass distribution of crowns and roots across different sampling dates in 2009 and 2010. Samples were taken at a 15-cm depth.

Sampling Date	Crown	Root	$LSD_{0.05}$
	---------- % Biomass ----------		
Aug-09	62.78	37.22	4.28
Nov-09	64.30	35.70	6.04
Feb-10	57.63	42.37	7.90
May-10	65.22	34.78	8.88
Aug-10	65.54	34.36	5.00
Nov-10	63.86	36.14	4.88
$LSD_{0.05}$	5.61	5.61	--

Table F.1.27. Changes in N pool of below-ground biomass at different sampling dates and N rates in 2009 and 2010. Samples were taken at a 15-cm depth.

	N applications rate (kg ha^{-1})			
Sampling Date	0	56	112	$LSD_{0.05}$
		N (g m^{-3})		
Aug-09	51.00	37.36	48.71	NS
Nov-09	49.93	42.60	42.20	NS
Feb-10	52.38	62.04	39.12	NS
May-10	62.15	43.92	40.42	21.34
Aug-10	62.85	47.48	66.25	NS
$LSD_{0.05}$	NS	18.29	23.14	--

Significant changes in N concentrations were observed between above-ground biomass and below-ground constituents across sampling dates (Table F.1.28), but no significant differences were observed between crown and root. N concentration was affected by rates in both above- and below-ground biomass (Table F.1.29). N concentration fluctuated over the sampling dates with higher concentrations towards the beginning of the growing season and declining at the end of the season. There was a fluctuation in soil water content throughout the season due to wet weather conditions in August and September 2009 and

dry in August 2010 (Table F.1.30). Soil N content was observed to be higher in November 2009 and February 2010 when compared to other sampling dates. Carbon content increased at the end of season due to accumulation of more lignocellulosic material. This data indicates that there is a large pool of total N with potential mineralization to maintain low N inputs for well-established switchgrass.

Table F.1.28. Nitrogen concentration of above- and below-ground constituents across different sampling dates. Roots samples were collected at a 15-cm depth.

	Biomass Type			
		Belowground		
Sampling Date	**Aboveground**	**Crown**	**Root**	**$LSD_{0.05}$**
	---------- % N ----------			
Aug-09	1.08	0.63	0.69	0.08
Nov-09	0.56	0.57	0.54	NS
Feb-10	0.63	0.79	0.66	0.09
May-10	1.52	0.59	0.63	0.08
Aug-10	0.61	0.66	0.74	0.08
$LSD_{0.05}$	0.09	0.08	0.07	--

Table F.1.29. Seasonal changes in N concentration among above- and below-ground (crown and root) biomass due to N applications.

	N Applications rate (kg ha^{-1})			
Sampling Date	**0**	**56**	**112**	**$LSD_{0.05}$**
	---------- % N ----------			
Aug-09	0.77	0.83	0.79	NS
Nov-09	0.60	0.54	0.52	0.04
Feb-10	0.71	0.69	0.67	NS
May-10	0.93	0.91	0.89	NS
Aug-10	0.69	0.66	0.66	NS
$LSD_{0.05}$	0.20	0.80	0.10	--

Table F.1.30. Soil water content (SWC), bulk density (BD), N content and C content during sampling periods in 2009 and 2010. Samples were taken at a 15-cm depth.

Sampling Date	SWC	BD	N Content	C Content
	%	g cm^{-3}	Mg ha^{-1}	
Aug-09	18.10	1.11	1.17	15.24
Nov-09	17.84	1.20	1.32	17.91
Feb-10	19.46	1.31	1.50	19.91
May-10	14.19	1.18	1.42	18.82
Aug-10	9.19	1.00	1.13	14.30
Nov-10	10.19	1.70	--	--
$LSD_{0.05}$	2.58	0.09	0.16	2.00

The ability of switchgrass to remain viable at low levels of applied N is attributed to its internal nutrient cycling. Because of the accelerated mineralization of soil organic matter due to the extensive switchgrass root system and symbiotic relationships with soil and plant microbes and atmospheric deposition, the available nitrogen pool could be larger than what has been estimated. However, due to the deep rooting ability of switchgrass, soil and root samples should be taken to a depth of 1 to 2 m in order to more accurately assess available soil N and in result increase precision of fertilizer inputs.

In conclusion, the data suggests that N cycling in switchgrass may be more influential for affecting global climatic change than carbon cycling. Even with this internal cycling, harvest inevitably would remove some nutrients from the system. There is no biofuel crop that can withstand such losses without soil fertilizer inputs. The acquisition and retention of C and N are key determinants of GHG fluxes that need to be associated with bioenergy crops. Although switchgrass appears to be sustainable in the short-term with limited N, the long-term ecological consequence of harvesting switchgrass without fertilizer inputs remains unknown.

Degredation of lignocellulosic residues using cultured bacteria

Widespread utilization of lignocellulosic biomass for ethanol production is impeded by the absence of low-cost technology for overcoming its natural recalcitrance. The central premise of the research is that having co-evolved with terrestrial plants over the past 500 million years, microorganisms in soil serve as a reservoir of metabolic and genetic capacities that can help solve the problems inherent in the transformation of feedstocks for production of biofuels. The overall objective was to identify novel bacterias that may be useful for the preparatory degradation of feedstocks common to the southeastern United States, and which could offer these products a competitive advantage in a burgeoning cellulosic ethanol market.

The objective of this study was to determine whether growth of bacteria in association with their native soil habitat would increase the cultivability of novel and diverse types of taxa. It was hypothesized that the soil provides a diverse suite of microbial-derived metabolites, signaling molecules and nutrients for microbial growth, so that bacteria grown in close association with a soil habitat would show greater levels of diversity and richness than bacterial communities grown on a common Cellulose Congo Red medium. It was also hypothesized that the most important effect of the soil habitat would be related to the biotic

component of the soil. Sterile soil would thus have different community composition and lower levels of diversity and richness, and fewer previously uncultivated members than a community grown next to a living and microbial-rich soil.

Inoculated regenerated cellulose filters (RCF) were used as a carbon source and physical support for microorganisms and then tightly coupled to the soil habitat. The soil habitat and the RCF growth medium were separated by a polycarbonate membrane (0.02 µm) to prevent the movement of bacteria and larger organisms. Three treatments of RCF filters were coupled to: 1) unsterilized soil habitat ($Biotic_{RCF}$), 2) sterilized soil habitat ($Abiotic\text{-}HN_{RCF}$), and 3) soluble soil C without a soil habitat ($Abiotic\text{-}LN_{RCF}$). A more conventional cellulose Congo red agar (CA) plate was also used for comparison. Following 20 days of incubation, the developing communities from all the treatments were characterized using 16S rDNA clone libraries. A total of 112 OTU's (D=0.03) were derived from approximately 341 clones. Different treatments supported the growth of significantly different communities (Libshuff, $p<0.0019$). However, compared to the other cultivation techniques, diversity indices were much greater in the RCF incubated in association with unsterilized soil. For example, the Simpson's inverse diversity was 3 to 6 X greater in the unsterilized treatment ($1/D = 33.6$) compared to the other RCF and traditional plating methods ($1/D \sim 5$ to 10). Hence, the presence of a living and metabolizing microbial community appears to have an important impact on the cultivation of bacteria. Previously uncultured members included those in the phyla *Proteobacteria, Bacteroidetes, and Planctomycetes*. This method shows considerable promise for cultivation and eventually the isolation of previously uncultured microorganisms and also hints at the importance of microbial interactions to support bacterial growth.

Genomic analysis and genetic modification of cell wall for cost efficient bio-fuel production in rice (Oryza sativa)

The long term goal of this project was to modify plant cell walls for cost-efficient bio-fuel production from the by-products cereal crops, such as rice straw. Objectives included: 1) Making transgenic plants with putative regulatory genes involved in cell-wall synthesis, 2) Establishment of a nuclear and chromatin proteome map of rice suspension cells, and 3) Identification of differentially expressed nuclear proteins via comparison of the protoplast (without cell wall) and suspension cell (with cell wall) nuclear sub-proteomes.

Multiple rice and Arabidopsis transgenic lines with genes involved in cell wall degradation and synthesis have been generated and several transgenic lines with substantial changes in cell wall content in both Arabidopsis and rice have been identified. However, due to the termination of funding, the research was stopped and literature was delayed. Most of the nuclear and chromatin proteome mass analyses have been completed. Part of the research has been published.

Subtask F.2 Feedstock Engineering

1. Planned Activities

F.2.DL.1 Year 1 deliverable is the quantification of the expected cost of providing three Southeastern-based feedstocks to refinery/biorefinery company gate.

F.2.DL.2 Year 2 deliverable is the quantification of the expected cost of providing thess additional Southeastern-based feedstocks to refinery/biorefinery company gate.

2. Summarization of Activities

Evaluation of the Supply and Cost of Woody Biomass for Bio-Energy Production in Mississippi

The study focused on the post-harvest recovery and utilization of logging residuals. Some influential attributes landowners associate with this process include bioenergy production, cleanliness of the harvest site, reduction of fire and pest risks, environmental effects on the harvest site, and the dollar value of the actual logging residues. The removal and utilization of logging residuals to create bioenergy can have an indirect utility to landowners through a 'warm-glow' effect by helping to reduce fossil fuel use and protecting the environment. By removing the logging residues, a cleaner post-harvest site would be produced, which could be important to landowners concerned with aesthetics. It can also reduce the need for some site-preparation activities that might not have been necessary otherwise and significantly reduce re-planting costs. With the removal of slash and downed woody-debris comes a reduction of the fuel load that can make wild fires more dangerous. It also removes an attractive habitat and food source for wood-boring insects that can damage or kill other trees in the area. There is also an issue of increased sediment runoff, which can be detrimental to water quality and soil compaction from using more heavy equipment than usual. Another important attribute is the dollar value of these logging residuals. Bioenergy production facilities' willingness to pay landowners a considerable amount for the residues could significantly influence their harvesting decision. Conversely, the transportation and processing costs for these products is not well defined and, hypothetically, could reduce the landowner's income. By using conjoint analysis, estimation of the influence the individual attributes have on the landowner's harvesting decision can be determined.

To reach the desired study population, a random selection of private forest landowners, owning at least 100 acres of forestland, was acquired from a MS timber tax database. A mail-based questionnaire was established as the survey instrument. The survey was designed to use contingent valuation (CV) methods to determine NIPF landowners' preferences concerning the utilization of logging residuals and divided into six sections concerning the landowners' forest characteristics, environmental preferences, management objectives, and socio-demographic information. Two different CV methods were also included as separate sections. Due to the complicated nature of the contingent valuation sections, the questionnaire was field tested, throughout Mississippi, at local county forestry association (CFA) meetings in Yalobusha, Clay, and Greene County to get feedback from the target audience. The initial survey used three versions of contingent valuation including a choice model, a contingent ranking, and a contingent rating. The contingent ranking section was found to be the least useful due to confusion with the other variations. Therefore, it was deemed unnecessary and discarded from the questionnaire. The contingent rating was found to be the best method to reach the objectives of this study. After finalizing the questionnaire, the first mailing went out 9 November 2009 with a reminder postcard following one week later. A second mailing was sent to non-respondents on 2 December 2009

The contingent rating section of the survey used the hypothetical timber harvesting situations to elicit landowners' likeliness to harvest under each of the four scenarios. The subjects were asked to rate each scenario from 1(Not likely to harvest) to 5(Likely to harvest). Scenario 1 is a standard clearcut, where the landowner receives the estimated fair market value ($3000/ac) and residue was left in the field. Scenarios 2, 3, and 4 involve a clearcut on the same hypothetical timber stand. In this situation, however, logging residuals and non-merchantable timber are removed to produce biofuel. The only difference between

2 and 3 is the price received by the landowner. In Scenario 2, the landowner would receive fair market value identical to Scenario 1 ($3000/ac). In Scenario 3, he or she would receive additional income from selling the logging residuals for profit ($3200/ac). The $200/ac increase was used because it is a rate high enough to have a significant influence on landowners' decisions and it assumes a delivered price for the woody biomass at a rate between full pulpwood price and half pulpwood prices at the time of the survey. Scenario 4 involves a situation where the landowner would receive less than fair market value from the harvest ($2800/ac). This was designed under a hypothetical idea that transport and harvesting costs for utilizing woody biomass could reduce the landowners' total income. Intuitively, the only reason a landowner would be more likely to harvest in this situation, rather than a standard clearcut, is if he or she preferred the associated benefits of biomass utilization over monetary benefits (Table F.2.1).

Table F.2.1. A comparison of attributes within the contingent rating scenarios of a survey of NIPF landowners in Mississippi. Subjects were asked to rate (from 1 to 5) their likeliness of harvesting timber in each scenario.

	Scenario 1 (Standard Clearcut)	**Scenario 2**	**Scenario 3**	**Scenario 4**
Biofuel produced	no	yes	yes	yes
Clean harvest site	no	yes	yes	yes
Decrease fire & pest risk	no	yes	yes	yes
Site prep required	intensive	minimal	minimal	minimal
Price received at harvest	$3000/ac	$3000/ac	$3200/ac	$2800/ac

Given world instability and the U.S. having heavy dependence on importing foreign oil, this research may have an important impact for a forest resource-rich state, such as MS. Although much research exists about the development of the technologies for converting woody biomass into biofuels, such as ethanol and bio-oil, this study will provide information useful to policy makers at the state level to aid their efforts in building potential bio-energy conversion facilities. The potential use of biofuels, such as bio-oil as a heating fuel or ethanol as a gasoline substitute or additive, could provide non-industrial and industrial private landowners with an alternative market for their small diameter trees. The information provided in this study will aid state policy makers in developing policy instruments to advance the development of this emerging fuel market. In addition, this work will serve as a basis for evaluating its potential as a zero net emitter of carbon dioxide into the atmosphere. This information would be useful in strategically positioning Mississippi's economy in the emerging carbon-trading market.

Subtask F.3 Biomass Feedstock Development

1. Planned Activities

F.2.DL.1 Year 1 deliverable is to quantify the expected cost of providing three Southeastern-based feedstocks to a refinery/biorefinery company gate.

F.2.DL.2 Year 2 deliverable is to quantify the expected cost of providing three additional Southeastern-based feedstocks to a refinery/biorefinery company gate.

2. Summarization of Activities

Densification through In-Field Hay Cubing

Work was completed to determine the efficiency of in-field hay cubing as a method to densify grasses for further biofuels processing. The objectives were to develop an in-field cubing test platform and determine if the use of binding agents increased cubing efficiency. A John Deere 425 Hay Cuber was refurbished and modified to provide the cubing platform (Figures F.3.1 and F.3.2). Major systems (mechanical, hydraulic, electrical, and water application) were modified or upgraded with newer technology to improve reliability. The cubing dies were replaced with a tapered die to improve cubing of grass materials as compared to alfalfa for which the machine was created. A preliminary investigation showed correlations between the moisture content of the biomass and its ability to be densified into cubes (Figure F.3.3). The best cube production was demonstrated from 9-15% moisture content (Figure F.3.4). Maintaining die temperature was a function of continuous operation (Figure F.3.5).

A study was developed to evaluate the effectiveness of applying a binder to improve in-field cubing of Bermuda grass as a model for other energy grasses (Table F.3.1 and Figure F.3.6). Lignin sulfonate binder was applied at a rate of 25 kg/t (50 lb/t). The treatments of no binder and with binder resulted in cube production of 73.6 ± 1.0% and 78.9 ± 1.0%, respectively. The treatment with binder improved cube production by 5.3% as compared to no binder. Cubing without a binder resulted in no correlation between measured parameters of initial moisture content, cube moisture content, ambient temperature, die temperature, and feed rate on percent cubes. However, cubing with a binder accounted for 84% of the variation in our regression model. The regression model for percent cubes (binder) resulted in significant terms of cube moisture content and feed rate. To improve the effectiveness of cubing, a binder must be used.

Table F.3.1. Day-by-day treatment comparison of means

	Means					
Treatment	**Day**	**$MC_{initial}$**	**MC_{cube}**	**T_{amb}**	**T_{die}**	**FR (kg/min)**
No Binder	**1**	9.40	20.48	90.67	186.95	8.62
	2	8.05	15.40	91.67	181.42	11.18
	3	11.65	15.59	91.18	178.42	15.71
	4	10.04	15.57	91.12	183.73	9.45
Binder	**1**	8.63	20.58	89.60	192.44	9.97
	2	9.08	14.92	93.10	173.04	11.86
	3	11.20	15.43	90.52	182.98	16.04
	4	10.58	15.74	88.99	180.34	9.54



Figure F.3.1. Illustration of the 1974 John Deere Hay Cuber in its initial condition.



Figure F.3.2. The 1974 machine with new paint and modifications completed.



Figure F.3.3. Student collecting output from chute of cuber into plastic containers.

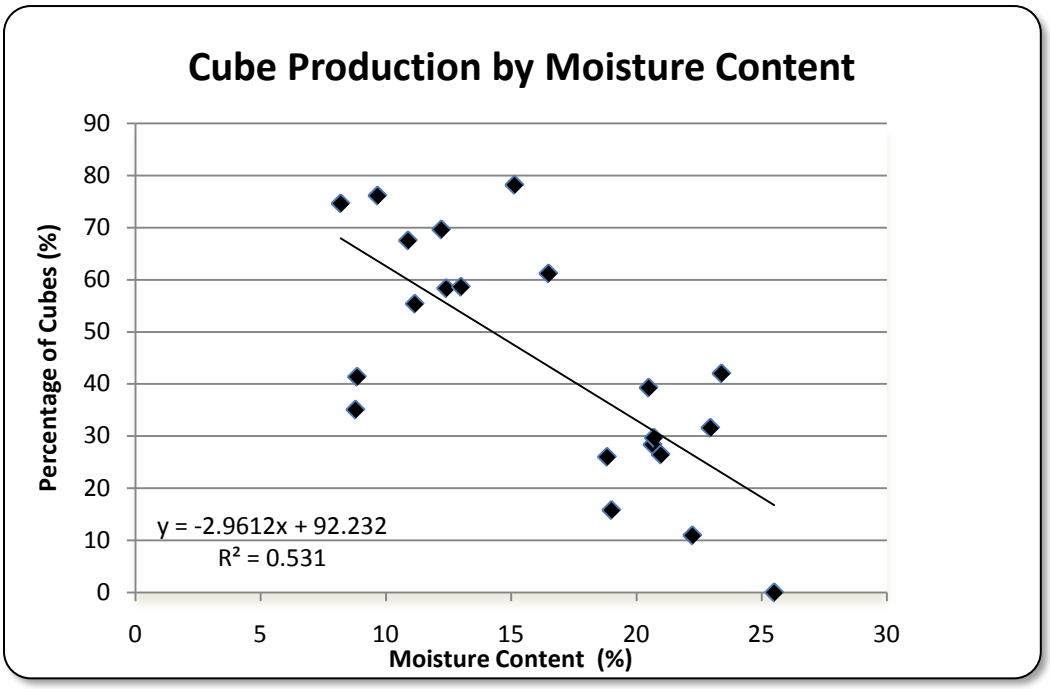


Figure F.3.4. Regression of cube production with moisture content

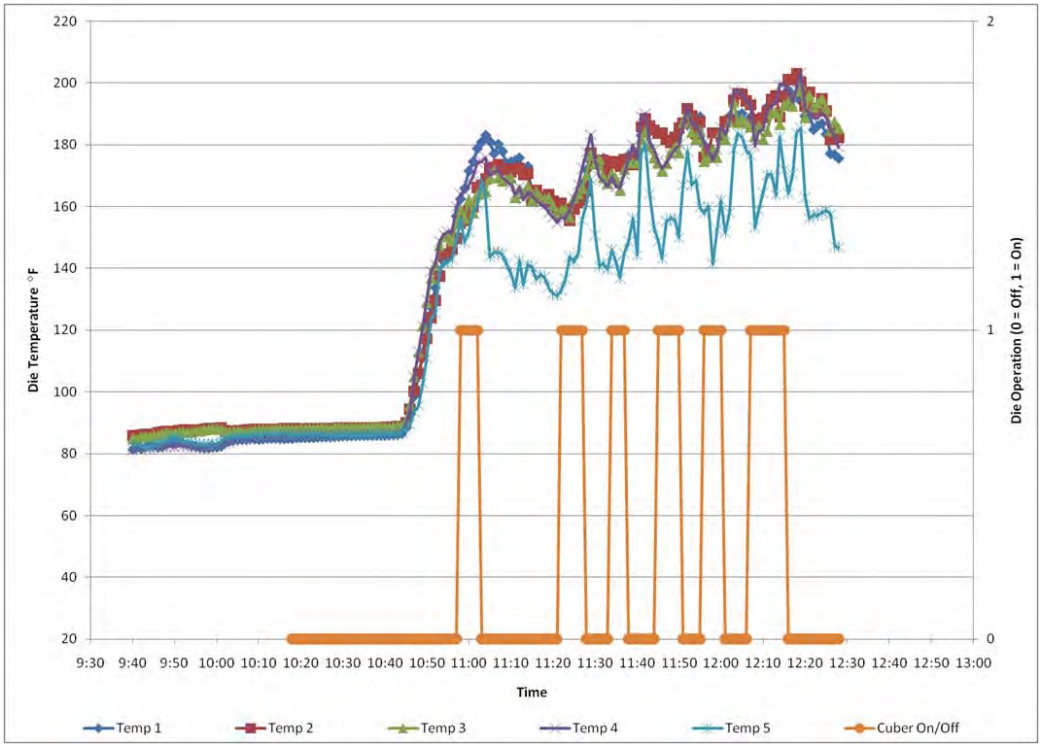


Figure F.3.5. Illustration of die temperatures as a function of cuber operation.

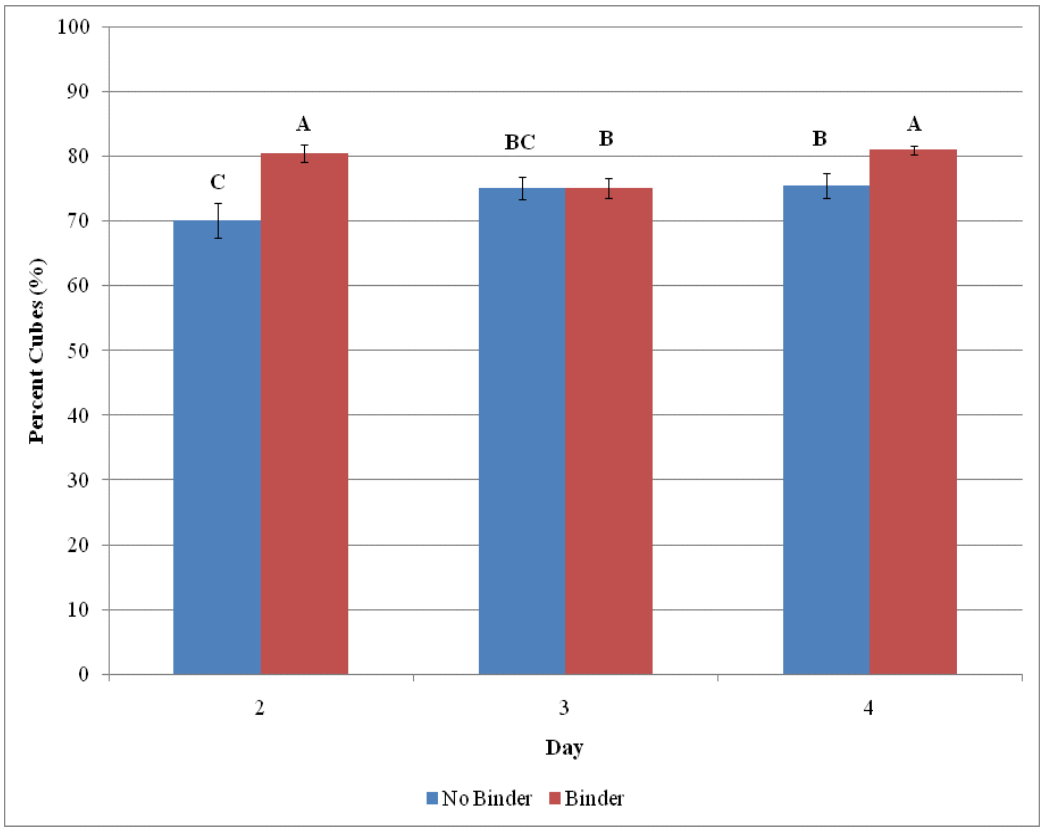


Figure F.3.6: Illustration of cube production (% Cube) for each day and treatemtn. A, B, C denote significant difference ($p<0.05$).

Sustainability Analysis of Biomass Production Using Net Energy Value

The inherent variability in maize stover productivity due to variations in soils and crop management options might contribute to variations in the sustainability and environment friendliness of maize stover-based bioethanol production systems, which are not known especially for the Delta region of Mississippi, a major maize production area in the state. The goal of this study was to examine how variations in soils and crop management options would affect maize-stover yield (MSY) and, accordingly, the sustainability and environment friendliness of the stover-based bioethanol production systems in the Delta region. Based on geographical representation, potential acreage, and data availability, three locations in the region were selected. Using CERES-Maize, a widely used and tested crop model, and historical weather data of 30 years, MSYs for these locations were simulated for several scenarios of soils, cultivars, planting dates, and irrigation amounts.

Two indicators were established for determining the sustainability and environment friendliness of the stover-based ethanol production systems. Net energy value (NEV), computed as “renewable energy produced” minus “nonrenewable energy used,” was used as an indicator for sustainability whereas carbon credit balance (CCB), computed as “carbon credits earned” minus “carbon credits used,” was used as an indicator for environment friendliness. The parameters used for estimating NEV and CCB for the Delta region are shown in Tables F.3.2 and F.3.3, respectively. For each scenario, values of NEV and CCB were computed from MSYs. The effects of soils, cultivars, irrigation amounts, and planting

dates on MSY, NEV, and CCB were determined using Analysis of Variance (ANOVA) and LSD tests and regression analyses. The values of MSY, NEV, and CCB each associated with the three soils – sandy loam, silt loam, and silty clay loam – were significantly different from each other in all locations, as were the values of each of these variables associated with high-, mid-, and low-yielding cultivars. With an increase in irrigation amount, values of MSY, NEV, and CCB initially increased, reached a peak, and then decreased. Similarly, these variables increased for each shift in planting date from the first week of March through a date at which they peaked and declined thereafter. A third-degree polynomial relationship was found between planting date and MSY, NEV, and CCB (Figures F.3.7 and F.3.8). By moving from the lowest production scenario to the highest, values of MSY, NEV, and CCB could be increased by as high as 86-553%, depending on location and weather conditions.

In general, stover yields could be increased gradually by shifting from the lowest production scenario to the one with silt-loam soil, DynaGro-High cultivar, 50% moisture content threshold for irrigation, and the optimum planting date. The effect of variation in soils and crop management options on NEV and CCB were the same as on MSY because of a linear relationship between MSY and NEV or CCB. Although values of both NEV and CCB decreased with an increase in traveling distance, these indicators did not vary significantly across locations because of little contribution of transportation relative to those of the other activities combined. The NEV and CCB were positive for all scenarios, indicating that a stover-based ethanol production system in the Delta region is both sustainable and environmentally friendly.

Table F.3.2. Values of various parameters used for estimating net energy value for the Delta region.

Parameter	Value	Unit	Source
Stover to ethanol conversion ratio (r)	0.30	m^3/t (l/kg)	Kim & Dale (2004); Luo *et al*. (2009); Luo *et al*. (2010)
Energy from ethanol (e_e)	21.20	GJ/m^3	Hammerschlag (2006); Luo *et al*. (2009); Luo *et al*. (2010)
Energy from co-product (e_c)	2.60	GJ/m^3	Lavigne & Powers (2007)
Energy for harvesting (e_h)	1.20	GJ/m^3	Sokhansanj *et al*. (2006)
Energy for densification (e_d)	0.86	GJ/m^3	Morey *et al*. (2010)
Energy for transportation (e_t)	2.75	MJ/m^3/km	Morey *et al*. (2010)
Energy for processing (e_p)	0.30	GJ/m^3	Lavigne & Powers (2007)

Table F.3.3. Values of various parameters used for estimating CCB for the Delta region.

Parameter	Value	Unit	Source
Fraction of carbon in stover (f)	0.41	w/w	Sakala *et al*. (2000); Bunemann *et al*. (2004); Johnson *et al*. (2006); Makumba & Akinnifesi (2008)
CO_2 emission from harvesting (c_h)	26.77	kg/t	Sokhansanj *et al*. (2006)
CO_2 emission from densification (c_d)	19.69	kg/t	Morey *et al*. (2010)
CO_2 emission from transportation (c_t)	202.66	g/t/km	Morey *et al*. (2010)
CO_2 emission from processing (c_p)	49.06	kg/t	Morey *et al*. (2010)

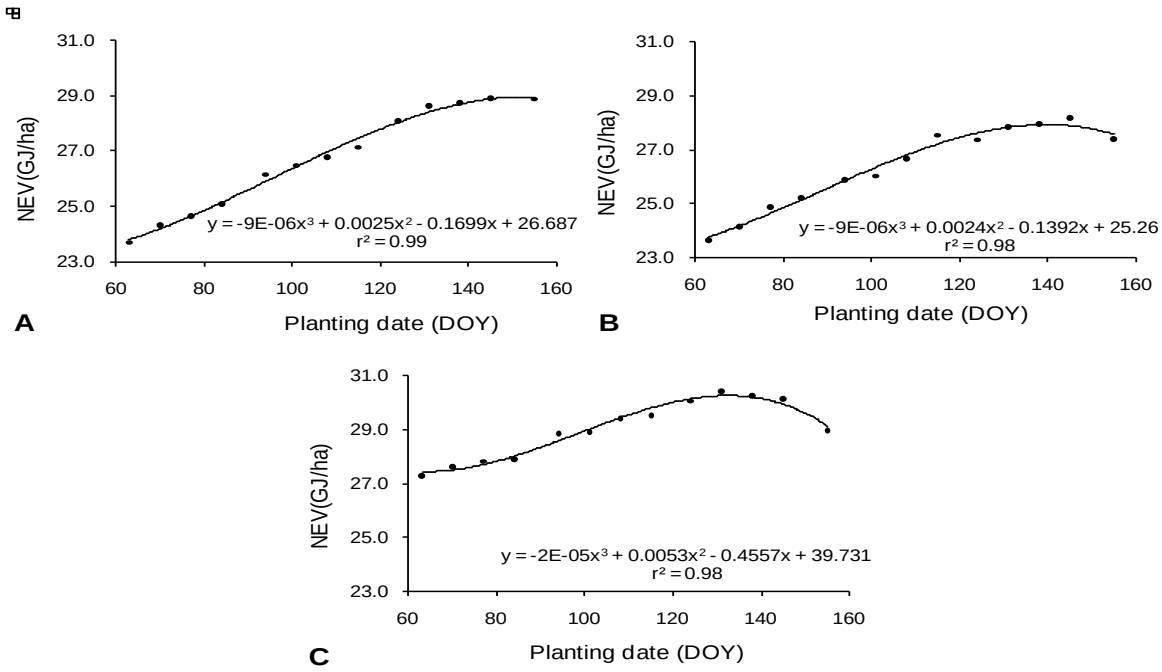


Figure F.37. Net energy value (NEV), y, as a function of planting date, x, for three locations in the Delta region of Mississippi: A) Tunica, B) Moorhead, and C) Vicksburg. DOY = day of year.

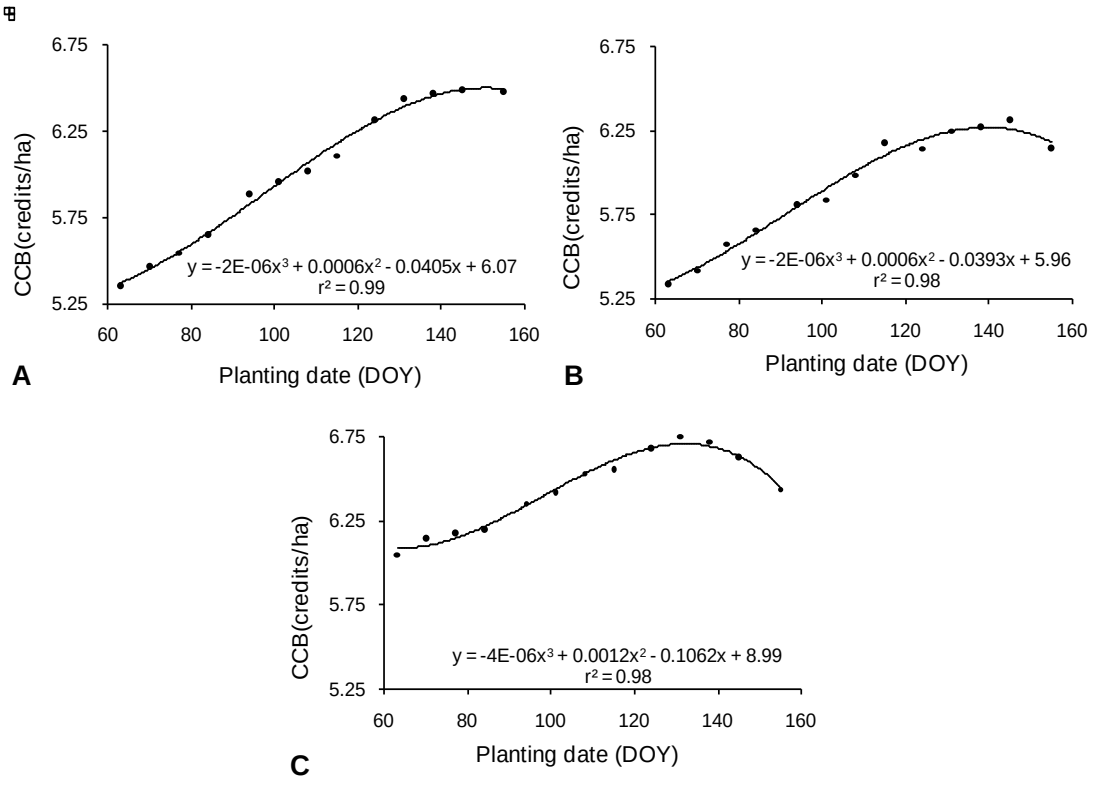


Figure F.3.8. Carbon credit balance (CCB), y, as a function of planting date, x, for three locations in the Delta region: A) Tunica, B) Moorhead, and C) Vicksburg. DOY = day of year.

Spatial Distribution of Energy Crops

The long-term goal of this study was to determine the spatial distribution of the potential bio-energy crops and their environmental benefits, such as soil organic carbon (SOC) and water quality in Mississippi for renewable fuels through economic modeling and analysis. Our work towards meeting those objectives will be continued in the SERC III project. The current objective of this research is to monitor SOC due to the change of agricultural management practices in the agricultural fields and use a model to identify the relationships between SOC and other hydrologic and water-quality parameters. The model's purpose is to predict bio-energy crop feedstock yield at the large-scale watersheds in Mississippi.

Preliminary carbon analysis of the soil samples determined that the majority of carbon was found in the 6-in.depth (compared to 12 and 24 in.); more carbon was found in the forestland and pastureland than in the cropland. Model simulations from the two watersheds (Town Creek and Upper Pearl River) determined the negative correlation between available moisture content and carbon content in the soil, which may be sample-size dependent. The economic model, including a cost calculator (Figure F.3.9), was developed for the economic analysis of bio-gasification systems. Preliminary results of the economic analysis using this model and model sensitivity were presented at the Institute of Biological Engineering annual conference in Atlanta, GA.



Figure F.3.9. Illustration of computer-based cost calculator with input fields

C. Products developed and technology transfer activities

Publications

Anderson, W.F., Michael D. Casler, and Brian S. Baldwin. 2008. Improvement of perennial forage species as feedstock for bioenergy. *In* Genetic Improvement of Bioenergy Crops, Vermerris, Wilfred (Ed.) Spring Publishing. pp. 420.

Baldwin, B.S. and R.D. Cossar. 2009. Castor (*Ricinus communis* L.) yield in response to planting date at four locations in the South-central U.S. Industrial Crops and Prod. 29:316-319.

Barnes, Daniel J., Brian S. Baldwin, and Dwaine A. Braasch. 2009. Degradation of ricin in castor seed meal by temperature and chemical treatment. J. Ind. Crop Prod. 29:509-515.

Barnes, Daniel J., Brian S. Baldwin, and Dwaine A. Braasch. 2009. Ricin accumulation and degradation during castor seed development and late germination. J. Ind. Crop Prod. 30:254-258

Chouvarine, P. A.M. Cooksey, F.M. McCarthy, D.A. Ray, B.S. Baldwin, SM. Burgess, D.G. Peterson. 2010. Phylogenetic and fuctions analysis of *Miscanthus*. BioMed Central; Plant Biology. (Accepted).

Grala, R.K., Nepal, P., and D.L. Grebner. 2008. Utilization of logging residues for producing Bioenergy and reducing carbon dioxide emissions. In: Proceedings, Society of American Foresters National Convention, Reno, NV, November 4-9, 2008.Grebner, D.L., Perez-Verdin, G., Sun, C., Munn,

I.A., Schultz, E.B., and T.G. Matney. 2009. Woody biomass feedstock availability, production costs and implications for bioenergy conversion in Mississippi. Chapter 12, In: Solomon and Luzadis, eds. Renewable Energy from Forest Resources in the United States. Routledge, London. 330 p.

Grebner, D.L., Perez-Verdin, G., Henderson, J.E., and A.J. Londo. 2009. Bioenergy from

woody biomass, potential for economic development, and the need for extension. *Journal of Extension*. Available online at: http://www.joe.org/joe/2009december/a7.php.

Gruchy, S.R., Grebner, D.L., Munn, I.A., and I.A. Hussain. (In preparation). Landowner willingness to harvest woody biomass for an incipient cellulosic biofuels industry in Mississippi. Intend to submit to the *Southern Journal of Applied Forestry*.

Guo, Z., Grebner, D.L., Sun, C., and S.C. Grado. 2010. Biofuel production impacts on the management of southern pine plantations in Mississippi. Chapter 11, In: Gan, J., S. Grado, and I. Munn (Editors). Global Change and Forestry: Economic and Policy Impacts and Responses. Nova Science, NY. 332 p. Guo, Z., Grebner, D.L., Sun, C., and S.C. Grado. 2010. Evaluation of loblolly pine management regimes in Mississippi for biomass supplies: a simulation approach. *Southern Journal of Applied Forestry,* 34(2): 65-71.

Jones, T.L., Schultz, E.B., Matney, T.G., Grebner, D.L., and D.L. Evans. 2010. A forest product/bioenergy mill location and decision support system based on a county-level forest inventory and geo-spatial information. Chapter 9, In: Gan, J., S. Grado, and I. Munn (Editors). Global Change and Forestry: Economic and Policy Impacts and Responses. Nova Science, NY. 332 p.

Joshi, O, Grebner, D.L., Munn, I.A., Hussain, A., and S.R. Gruchy. (In Preparation). Determinants of landowners' choice for preferred harvesting methods of supplying woody biomass in Mississippi. Intend to submit to *Forest Science*.

Kakani, V. G. and K.R. Reddy. 2010. Hyperspectral reflectance properties, growth, leaf photosynthesis and electron transport of nitrogen deficient big bluestem (*Andropogon gerardii*). Journal of Agronomy and Crop Science196:379-390.

Kakani, V. G., G.K. Surabhi and K.R. Reddy. 2008. Photosynthesis and fluorescence responses of C_4 plant *Andropogon gerardii* acclimated to temperature and carbon dioxide. Photosynthetica 46: 420-430. Lemus, R. 200x. Establishing and Managing Switchgrass as a Forage. Mississippi State Univ. Coop. Ext. Serv. Ext. Pub. (in review).

Perez-Verdin, G., Grebner, D.L., Munn, I.A., Sun, C., and S.C. Grado. 2010. Economic impacts of woody biomass utilization for bioenergy in Mississippi. Chapter 10, In: Gan, J., S. Grado, and I. Munn (Editors). Global Change and Forestry: Economic and Policy Impacts and Responses. Nova Science, NY. 332 p.

Perez-Verdin, G., Grebner, D.L., Sun, C., Munn, I.A., Schultz, E.B., and T.G. Matney. 2009. Woody biomass availability for bioethanol conversion in Mississippi. *Biomass and Bioenergy.* 33(3): 492-503. Perez-Verdin, G., Grebner, D.L., Munn, I.A., Sun, C., and S.C. Grado. 2008. Economic impacts of woody biomass utilization for bioenergy in Mississippi. *Forest Products Journal*. 58(11): 75-83.

Ramdeo, S., Macoon, B., K.R. Reddy, and B. Baldwin. 2010. Switchgrass (*Panicum virgatum* L.) intraspecific variation and thermotolerance classification using *in vitro* seed germination assay. AOB Plants (Submitted).

Reddy, K.R. and S.K. Matcha. 2010. Remote sensing algorithms for castor bean nitrogen and pigment assessment for fertility management. Industrial Crops and Products 32: 411-419.

Reddy, K.R. and S.K. Matcha. 2010. Quantifying nitrogen effects on castor (*Ricinus communis* L.) development, growth, and photosynthesis. Industrial Crops and Products. 31: 185-191.

Schultz, E.B., T.G. Matney, and D.L. Grebner. 2009. User Manual for A Tree Biomass and Carbon Estimation System: Carbon Calculator and Associated Growth and Yield Systems. Carbon Short Course, Mississippi State University, Extension Service. 7/15/2009. Mississippi State, MS. http://fwrc.msstate.edu/software.asp

Schultz, E.B., Matney, T.G., and D.L. Grebner. (In Press). A tree biomass and carbon estimation system. In: Proceedings, 15th Biennial Southern Silvicultural Research Conference, Hot Springs, AR, November 17-20, 2008.

Singh, S.K., V.G. Kakani, D. Brand, B. Baldwin, K.R. Reddy. 2008. Assessment of cold and heat-tolerance of winter-grown canola cultivars by pollen based parameters. J. Agron. Crop Sci. 194:225-236.

Tan F, Zhang K, Mujahid H, Verma DP, Peng Z. (2010) Differential Histone Modification and Protein Expression Associated with Cell Wall Removal and Regeneration in Rice (Oryza sativa). J Proteome Res. 2010 Nov 19. [Epub ahead of print]

Williams, Mark. Soil Biology and Biochemistry article, Submitted Dec 2010.

Woli, P. and J.O. Paz. 2011. Assessing the effects of soils and crop management options on maize stover yield, net energy value, and carbon credit balance associated with bioethanol production in the Mississippi Delta. Journal of Agricultural Science (*In Review*)Zheljazkiov, V.D., B.A. Vick, B.S. Baldwin, N. Buehring, T. Astatkie, and B. Johnson. 2010. Oil Productivity and Composition of Sunflower as a Function of Hybrid and Planting Date. J. Indus. Crops Prod. (Accepted)

Zheljazkiov, V.D., B.A. Vick, B.S. Baldwin, N. Buehring, T. Astatkie, and B. Johnson. 2010. Effect of planting date, N rate, and hybrid sunflower (*Helianthus annuus* L.) J. Plant Nutr. (Accepted)

Zheljazkov V.D., B. Vick, B.S. Baldwin, N. Buehring, T. Astatkie, and B. Johnson. 2009. Yield, oil and oleic acid content of sunflower (*Helianthus annuus* L.) as a function of planting date, N rate, and hybrid. Agron J. 101(4):1003-1010.

Zheljazkov, V.D., B. Baldwin, W. Ebelhar, J. Miller, N. Buehring, 2008. Assessment and yield of sunflower (*Helianthus annuus* L.) grown at multiple locations in Mississippi. Agon. J. 100(3):635-642.

Bulletins and Brochures

Henderson, J.E., I.A. Munn, G. Perez-Verdin, and D.L. Grebner. 2008. Forestry in Mississippi: The impact of the forest products industry on the post-Katrina Mississippi Economy: An input-output analysis. Forest and Wildlife Research Center, Research Bulletin FO 374, Mississippi State University. 31pp.

(http://www.fwrc.msstate.edu/pubs/forestryinmississippi06.pdf)

Perez-Verdin, G., Grebner, D.L., Munn, I.A., Sun, C., and S.C. Grado. 2008. Economic impacts of woody biomass utilization for bioenergy in Mississippi. *Forest Products Journal*. 58(11): 75-83. http://www.fwrc.msstate.edu/pubs/10487.pdf)

Theses Compiled by Graduate Students

Gruchy, S.R. (In Progress). Landowner willingness to harvest woody biomass for an incipient cellulosic biofuels industry in Mississippi. Masters of Science Thesis. Mississippi State University. Defense date schedule for 12/14/10.

Joshi, O. (In Progress). Woody biomass and bioenergy opportunities in Mississippi. Doctor of Philosophy Dissertation. Mississippi State University.

Presentations

Auld, D. et al. 2009. Genetic improvement of castor in the western hemisphere. International Castor Oil Assoc. Barcelona, Spain. 3-5 May.

Baldwin, B. 2010. Biomass for bioenergy: Where the industry appears to be going. Seventh Eastern Native Grass Symp. Knoxville, TN. Oct 5-8.

Baldwin, B. 2010. Biomass energy crops for the Southeast. MSU Biofuels Conference. Jackson, MS. 11-13 Aug.

Baldwin, Brian S., J. Brett Rushing, Edward Richard, Thomas Tew, Anna Hale, 2010. Energycane: Sugarcane gone North. Seventh Annual Bioenergy Feedstock Symposium. Champaign, IL. 11-12 Jan.

Baldwin, B., and P. Steele. 2009. Bamboo as a bio-energy feedstock. Delta Bamboo Supply Chain Summit. 9-10 Jun.

Baldwin, Brian S. and Phil Steele. 2009. Bamboo Cultivation and Bio-oil from Lignocellulosic Materials. Delta Bamboo Supply Chain Summit. Stoneville, MS. 9-10 Jun.

Baldwin, Brian S. 2008. Fuel from biomass: Alternatives and current state of development. Plenary speaker. Sixth Eastern Native Grass Symposium, Columbia SC. 7-10 Oct.

Baldwin, Brian. S., D. Scott Horton, J. Brett Rushing. 2008. Rivercane propagation workshop. Presentation to: Revitalization of Traditional Cherokee Artisan Resources and Resources and Center for Cherokee Plants. Kituwah, Cherokee Reservation, NC 14-15 Apr.

Baldwin, B., D.K. Lee, V. Owens, W. Rooney, T. Voigt. 2009. U.S. Dept. of Energy Regional Biomass Feedstocks Partnership. 21st Annual Meeting Assoc. Adv. Indus. Crops. Termas de Chillán, Chillán, Chile 14-19 Nov.

Baldwin, Brian S. 2008. Biomass crops for Mississippi. MAFES/MSU-ES Annual Meeting 5-7 Nov.

Baldwin, Brian S., Daniel J. Barnes, and Dwaine A. Braasch. 2008 Accumulation of ricin in developing castor seed, and subsequent degradation during germination. AAIC 20th Ann. Meeting, College Station, TX. 7-11 Sep.

Fleisher, D., D. Timlin, K.R. Reddy, V.R. Reddy, Y. Yang, and S.H. Kim. 2009. Effects of CO_2 and temperature on Crops: Lessons from growth chambers. ASA-CSSA-SSSA Annual International Meetings, 1-5 November, 2009, Pittsburgh, PA, USA.

Grado, S.C. and D.L. Grebner. 2008. Status of Research by the MSU Department of Forestry Forest Economics and Management working group. Presented at the MSU Department of Forestry Annual Advisory Committee Meeting, November 18, 2008.

Grebner, D.L. 2009. Woody biomass feedstock availability, production costs and implications for bioenergy conversion in Mississippi. Presented at the 52th Annual Southern Forest Insect Work Conference, Gulfport, MS July 28-31, 2009. (Invited)

Gruchy, S.R., Grebner, D.L., Munn, I.A., and Hussain, A. 2010. Preliminary assessment of non-industrial private forest landowner willingness to harvest in support of biofuel processing in Mississippi. Poster presented at: 9th Annual Southern BioProducts & Renewable Energy Conference; Tunica, MS, Apr 13-14, 2010.

Gruchy, S.R., D.L. Grebner, Munn, I.A., and A. Hussain. 2010. Assessing non-industrial private landowner's willingness to harvest woody biomass in support of biofuel processing in Mississippi: Preliminary results. Presented at Southern Forest Economics Workshop, Pinehurst, NC, March 15-17, 2010.

HakKwan Kim, Parajuli P. B., Fei Yu, Joel O. Paz, and Eugene Columbus. 2011. Economic Model for Evaluating Syngas Production Cost of Bio-gasification Facility. IBE Annual Conference, Loews Atlanta, March 3-5, 2011, Atlanta, GA.Huddleston J. W. 2010. Management Options for Wind Generated Biomass. Smallwood 2010 Conference, Hot Springs, Arkansas, Arlington Resort Hotel & Spa, pp.19-20.

Huddleston J. W. 2009. Hurricane Katrina: Impacts on Forests and Lessons Learned. Mississippi State University Department of Forestry & Mississippi RC&D Council, Hattiesburg, Mississippi, Lake Terrace Convention Center.

Joshi, O. and D.L. Grebner. 2010. An assessment of potential economic impacts associated with wood-based bioenergy industries in Mississippi. Poster presented at 9th Annual Southern BioProducts & Renewable Energy Conference, Tunica, MS, April 13-14, 2010.

Joshi, O. and D.L. Grebner. 2010. An assessment of potential economic impacts associated with wood-based bioenergy industries in Mississippi. Poster presented Southern Forest Economics Workshop, Pinehurst, NC, March 15-17, 2010.

Kakani, V.G., K.R. Reddy, K.J. Boote and D.J. Lang. 2008. Leaf and canopy photosynthesis and biomass of big bluestem and bahiagrass in response to temperature. The Pan American Congress on Plants and Bioenergy, June 22-25, 2008, Merida, Mexico.

Kakani, V.G., K.J. Boote, K.R. Reddy and D. Lang. 2008. Effect of below-optimum temperature on canopy photosynthesis, growth, and forage quality of bahiagrass (*Paspalum notatum* Flueggé). The GSA and ASA Joint Annual Meetings, 5-9 October, 2008, Houston, Texas, USA.

Knoll, J.E. W. F. Anderson, B. Baldwin, E. Richard. 2010. Harvest date effects on biomass yield and quality of new energycane (*Saccharum* hybrid) genotypes in the southeastern USA. ASA/CSSA/SSA Meetings. Long Beach, CA. 31 Oct - 4 Nov.

Lang, D.J. and V. Temu. 2007. Seed Production Potential of Switchgrass in the Southeast USA. Southern Section American Society Abstracts Meeting, Mobile, AL. 3-7 February 2007.

Lang, D.J. and V. Temu. 2007. Effect of Mid-Season Harvest on Seed Quality of Switchgrass. *IN*: Proceedings American Forage Grassland Council. Alison, W. (ed). 16:99. State College, PA 24-26 June, 2007.

Lang, D.J., Shankle, B, Oswalt, E., Duckworth, J. Sanborn, Buell, R. and B. Robertson. 2010. Establishment and Evaluation of Switchgrass on Reclaimed Minesoil. *IN:* R.I. Barnhisel (Ed.) Proc. 2010 National Meeting of the American Society of Mining and Reclamation. Pittsburgh, PA. 27:536-550. peer reviewed

Lemus, R. Utilizing Switchgrass in a Grazing System. 2010 Native Warm-season Grass Forage Tour. USDA/NRCS. Plant Material Center. Coffeeville, MS. September 14, 2010.

Lemus, R. Nutrient Management for Bioenergy Crops. Mississippi Crop College. Mississippi State University. February 19, 2009.

Lemus, R. and R. Rosseau. Carbon Sequestration and Carbon Credits for Forage and Forestry Production in MS. Clay Co. Forestry Association. West Point, MS. December 18, 2008.

Lemus, R., L. Oldham, K. Crouse. 2008. Soil Nutrient Recommendations for Switchgrass Production in Mississippi. *In* Annual Meeting Abstracts [CD-ROM]. Southern Plant Nutrient Management Conference State Report. Olive Branch, Mississippi, November 4-5, 2008

Lemus, R. and R. Rosseau. Potential Carbon Sequestration and Carbon Credits for MS. Clay Co. Forestry Association. West Point, MS. November 11, 2008.

Lowe, J.W., J.D. Davis, D. Chesser, and E. Columbus. 2009. Investigation of In-field cubing for Biomass Densification. Presentation for the 2009 ASABE International Meeting, June 21- 24. Reno, NV.

Lowe, J.W., J.D. Davis, G.D. Chesser, E.P. Columbus. 2009. Effect of moisture content on in-field cubing of grass for biomass densification. Abstract for the MSU Biofuels Conference. August 6-7. Jackson, MS. (poster)

Lowe, J.W., J.D. Davis, G.D. Chesser, J.K. Ward, E.P. Columbus. 2009. Effects of moisture content on in-field cubing quality. Abstact for the MSU 8th Annual Graduate Research Symposium. Nov. 6th. Starkville, MS.Macoon, B., and T. Steed. 2008. Cultivar, location, and harvest timing effects on switchgrass production. *In* Annual Meeting Abstracts [CD-ROM]. ASA, CSSA, SSSA. Madison, WI.

Parish, D.J. and R. Lemus. 2008. Nutrient Cycling in Switchgrass Grown for Bionass. *In* Annual Meeting Abstracts [CD-ROM]. ASA, CSSA, and SSSA, Madison, WI. Houston, TX. October 5 – 9, 2008.

Reddy, K. R. 2010. Environmental plant physiology research at Mississippi State University, Mississippi, USA. 21st September, 2010, Faculty and Students, Department of Botany, Sri Venkateswara University, Tirupati, A.P., India.

Reddy, V.R., D. Fleisher, D. Timlin, and K.R. Reddy. 2010. Climate information, crop modeling and sectoral perceptions on food security. GTZ & Colombo meeting, Colombo, 6-11 June 2010, Sri Lanka. Reddy, V.R., D. Fleisher, D. Timlin, V. Ambumozhi, K.R. Reddy, and Y.Yang. 2009. Monitoring the vulnerability and the need for adaptation planning for food security, Regional Workshop on Mainstreaming Climate Change Adaptation into Developmental Planning, 14-17 April 2009, Asian Development Bank Institute, Tokyo, Japan.

Reddy, K. R. 2009. Climate change and crop productivity: what is at stake? Students and faculty, Department of Agriculture, Alcorn State University, 23 February**,** 2009, Alcorn State, MS, USA**.**

Reddy, K.R. 2009. Controlled environment facilities for plant process quantification and modeling, Southern Association of Agricultural Scientists – Biochemistry and Biotechnology Division, 31st January to 3rd February, 2009, The Westin Peachtree Plaza, Atlanta, GA, USA.

Reddy, K.R. and V.G. Kakani. 2008. Searching for genotypic variability among crops to global environmental change: Challenges and opportunities. Golden Jubilee Conference on Challenges and Emerging Strategies for Improving Plant Productivity, Indian Society for Plant Physiology, 12-15 November, 2008, New Delhi, India.

Reddy, K. R. Climate change and crop productivity: What is at stake? Students and faculty**,** Birsa Agricultural University, 14 November, 2008, Ranchi, Jharkhand, India.

Reddy, K.R. 2008. Climate change and crop productivity: Challenges and opportunities. Students and faculty, Sri Venkateswara Agricultural College, 19 November, 2008**,** Tirupati, India.

Reddy, K.R. 2008. Crop responses global climate change: Challenges and opportunities. Students and faculty, Tamil Nadu Agricultural University, 23rd November, 2008, Coimbatore, TN, India.

Reddy, K.R. 2008. Controlled environment facilities for plant process quantification, global change, and crop modeling. Students and faculty, Tamil Nadu Agricultural University, 23rd November, 2008, Coimbatore, TN, India.

Reddy, K.R. 2008. Crop productivity in changing world: Challenges and opportunities. Students and faculty, Acharya N.G. Ranga Agricultural University, 4th December, Rajendra Nagar, Hyderabad, India. Reddy, K.R. Crop responses to abiotic responses: Tools and methods. Crop Genetics and Production Research Unit, USDA-ARS, 30 May 2008, Stoneville, Mississippi, USA.

Reddy, K.R., R. Seepaul, B. Gajanayake, and D. Brand. 2009. Growth and *in vitro* temperature-dependent functional algorithms for corn, cotton, soybean, and big bluestem seed germination. 39th Biological Systems Simulation Conference, Biological Systems Simulation Group and The University of Georgia, 11 – 13 May, 2009, Griffin, GA, USA, pp. 16-17.

Reddy, K.R., S.K. Singh, D. Brand, R. Seepaul and B. Macoon. 2008. Developing temperature-dependent functional algorithms for switchgrass growth and development for modeling. The GSA and ASA Joint Annual Meetings, 5-9 October, 2008, Houston, Texas, USA.

Reddy, K.R. 2008. Quantifying the Effects of environmental factors on crop growth using environmental productivity concept. The GSA and ASA Joint Annual Meetings, 5-9 October, 2008, Houston, Texas, USA.

Reddy, K. R., S. K. Matcha, and V. R. Reddy. 2008. Remote sensing algorithms for nitrogen deficiency in bioenergy crops, caster and switchgrass. 5th International Crop Science Congress, 13-18 April, 2008, Jelu, Korea.

Reddy, K.R., S.K. Matcha, S.K. Singh, D. Brand and R. Seepaul. 2008. Quantifying the effects of temperature and nitrogen on switchgrass growth and development. The 38th Biological Systems Simulation Modeling Meeting Conference, 8-10 April 2008, Temple TX, USA, pp. 24-25.

Seepaul, R., B. Macoon, K.R. Reddy, and B. Baldwin. 2010. A simple *in vitro* seed germination assay to classify switchgrass genotypes for thermotolerance. American Society of Agronomy Southern Branch Annual Meetings, Wyndham Orlando Resort, 7-10 February, 2010, Orlando, Florida, USA.

Seepaul, R., B. Macoon, K.R. Reddy, and B. Baldwin. 2010. Switchgrass selection for temperature tolerance. Producer Advisory Annual Meeting, North Mississippi Research and Extension Center, Lee County Agri-Center, 18 February, 2010, Verona, Mississippi, USA.

Seepaul, R., B. Macoon, K.R. Reddy, and B. Baldwin. 2009. Assessing genotypic variability of switchgrass seed germination in response to temperature. ASA-CSSA-SSSA Annual International Meetings, 1-5 November, 2009, Pittsburgh, PA, USA

Schultz, E.B., Matney, T.G., and D.L. Grebner. 2008. A tree biomass and carbon estimation system. Presented at 15th Biennial Southern Silvicultural Research Conference, Hot Springs, AR, November 17-20, 2008.

Temu, V. and D.J.Lang. 2008. Potential of nine *Panicum virgatum* (Switchgrass) varieties for seed production based on first year performance at Mississippi State University.

Presented at the joint meeting of the Society of Range Management and American Forage and Grassland Council, 25-29 January, 2008. Louisville, KY.

Yangyang Deng, and Parajuli P. B. 2011. Economic Evaluation of Electricity Generation from a Small-Scale Bio-Gasification Facility using an Optimization Model. IBE Annual Conference, Loews Atlanta, March 3-5, 2011, Atlanta, GA.

Zheljazkov, V.D., B.A. Vick, B. Baldwin, N. Burhring, W. Ebelhar, T. Astatkie, T. Horgan, and B. Johnson. 2009. Effect of seeding date and N rate on sunflower yields, oil content and composition. SAAS 31 Jan - 3 Feb.

Web sites or other Internet sites that reflect the results of this project
http://www.pss.msstate.edu
http://www.msstate.edu/dept/pssfeedstocks/
http://www.pss.msstate.edu/soilmicro
http://www2.msstate.edu/~dlang/Switchgrass%20for%20Biomass.htm

Networks or collaborations fostered
MSU has been the only university partner of the federal interagency Woody Biomass Utilization Group.
National
DOE SunGrant Initiative, Herbaceous Feedstocks Partnership, Energycane Group. Eastern Native Grass Alliance.
Regional
Southeastern Regional Bioenergy Group based at UGA, Tifton GA. Germplasm exchanges with ARS, Tifton GA; Houma LA; Univ. Ill. Campaign Urbana

Techniques/Technologies
New method of growing bacteria to cultivate previously uncultivated taxa.

D. For projects involving computer modeling, provide the following information

1. Model Description, key assumptions, version, source and intended use
<u>The Empirical Model</u>
To make the contingent rating scenarios comparable, the woody biomass utilization models (Scenarios 2, 3, and 4) were individually compared to the standard clearcut model (Scenario 1). The dependent variable was created by forming an index from the difference between the biomass utilization scenarios and the standard clearcut scenario. The results were summarized into indices of 0, 1, or 2, indicating whether the subject is less likely, equally likely, or more likely to harvest than in a standard clearcut (Scenario 1). If a respondent rated the standard clearcut scenario higher than another scenario, then it was assigned a 0, which indicates a preference to the standard clearcut scenario. If a respondent rated the standard clearcut equal to another scenario, then it was assigned a 1. If the other scenario was rated higher than the standard clearcut, then it was assigned a 2, which indicates it is preferred over the base model. The dependent variables for each of the 3 models include the index difference between Scenario 2 and Scenario 1 (V2V1), the index difference between Scenario 3 and Scenario 1 (V3V1), and the index difference between Scenario 4 and Scenario 1 (V4V1).

The independent variables include a range of descriptive information to determine what influences these NIPF landowners' preferences. The ACRES and PREVHARV variables are based on the landowners' forest characteristics. ACRES is a continuous variable indicating how many total acres of forested land the respondent owns. PREVHARV is a dummy variable indicating whether the landowner had harvested timber on his or her land in the past. CLIMATE is also a dummy variable indicating whether the respondent thought global climate change was a serious issue that needed to be addressed. This variable was used to address the landowners' environmental preferences. HABITAT, AESTH, FINANC, and INVEST were used to understand the landowners management objectives. These variables were transformed from a discrete choice, rating variable, into dummy variables indicating whether the objectives are thought to be important (1) or unimportant (0). AGE, EDU, and INCOME are demographic variables used to help understand NIPF landowners' decisions, and to determine whether the sampled population was an accurate representative of the total population. AGE and INCOME are continuous variables, while EDU is categorical. The age data was collected from an open-ended question. The income and education questions required the respondents to select their answers from a prepared range of choices. The income question provided fourteen choices ranging from less than $30,000 annually to more than $150,000 annually. The selection categories were broken into $10,000 ranges to increase response rate by making the answer less revealing to the respondents specific income while still providing enough detail for our research purposes. The responses were converted into a continuous variable by using the median of the range selected as a real number. The education question presented eight choices ranging from "less than high school," to "professional degree." This data was assigned a continuous variable format by assigning a number scale (1 – 8) as the education level increased.

Due to the ordinal nature of the dependent variables, the ordered logit model is used to analyze the data. The probabilities of the indices (V2V1, V3V1, and V4V1) are estimated from the model. The ten independent variables previously described are used to explain these probabilities. Three ordered logit models were used to determine the influence of utilizing logging residuals on NIPF landowner decisions:

$$V2V1 = \beta_0 + \beta_1 ACRES + \beta_2 PREVHARV + \beta_3 CLIMATE + \beta_4 HABITAT + \beta_5 AESTH + \beta_6 FINANC + \beta_7 INVEST + \beta_8 AGE + \beta_9 EDU + \beta_{10} INCOME + \varepsilon \quad (1)$$

$$V3V1 = \beta_0 + \beta_1 ACRES + \beta_2 PREVHARV + \beta_3 CLIMATE + \beta_4 HABITAT + \beta_5 AESTH + \beta_6 FINANC + \beta_7 INVEST + \beta_8 AGE + \beta_9 EDU + \beta_{10} INCOME + \varepsilon \quad (2)$$

$$V4V1 = \beta_0 + \beta_1 ACRES + \beta_2 PREVHARV + \beta_3 CLIMATE + \beta_4 HABITAT + \beta_5 AESTH + \beta_6 FINANC + \beta_7 INVEST + \beta_8 AGE + \beta_9 EDU + \beta_{10} INCOME + \varepsilon \quad (3)$$

Once these models are estimated, the effects from individual variables will be analyzed to determine their effects on the dependent variables. This will indicate the landowners' preferences for the woody biomass utilization harvesting attributes as they compare to standard clear-cutting. The Brant Test of parallel regression assumption will be used to indicate whether this model is suitable. The ordered logit model runs multiple equations at the same time. For the assumption of parallel regression to be true, the different coefficients derived from the multiple equations must not vary considerably.

The total response rate was 703 returns from 2,438 successful mailings (28.8%). The usable response rate was 511 usable returns from 2,438 successful mailings (20.1%). To check for non-response bias, demographic variables from the first and second mailings were compared to check for significant differences. The bias was found to be inconsequential after performing t-tests on the total acreage, age, and income variables from the first and second mailings (Table D.1.1).

Table D.1.1. T-test statistics of demographic variables between the first and second survey mailings to NIPF landowners in Mississippi. They are insignificant at 5%, therefore, non-response bias is inconsequential.

	Mean	**Variance**	**t-stat**	**P(T<=t)**
ACRES 1	554.39	1995306.48	1.31	0.09
ACRES 2	422.17	494225.63		
AGE 1	65.90	155.71	0.88	0.19
AGE 2	65.01	158.27		
INCOME 1	85.47	1898.23	1.05	0.15
INCOME 2	81.46	1858.47		

Descriptive statistics and variable definitions for the independent variables used to explain the model are described (Table D.1.2). This information provides a general idea of the study population's demographics, as well as common responses, and the degree of variability. The average total acreage of the study population was 461.8 acres, with a high degree of variation. The average age was 65, and the average household income was around $86,000 per year. The average education fell between the associate's degree and achelor's degree categories. About 87% of the study population had previously had timber harvested on their land. Less than 40% of the study population thought that global climate change was an issue that should be seriously addressed. Over 80% thought that providing wildlife habitat, receiving financial gain, and maintaining forestland as an investment of assets were important objectives as a forest landowner. Less than 75% thought that improving aesthetic value was an important objective.

For the study of landuse and agricultural management change effects on soil carbon, we have been using the Soil and Water Assessment Tool (SWAT) model supported by USDA (Arnold et al., 1998). For the preliminary economic analysis and modeling, we have developed a model using parametric equations and C^{++} computer programming language (Kim et al., 2011; Deng et al., 2011). Some equations are presented below in Table D.1.2.

Table D.1.2. Equations used in the model for calculating syngas production, and economic analysis.

	Cost factor	Equation
•	Total capital cost (C_{TC})	$C_{FC}+C_{FC}$
o	Fixed capital cost (C_{FC})	
1.	Direct project costs (C_{DC})	
(a)	Equipment (f.o.b) (C_{EQ})	C_{EQ}
(b)	Materials for installation (C_{MI})	$0.2C_{EQ}$
(c)	Building and construction (C_{BC})	$0.35C_{EQ}$
2.	Indirect project costs (C_{IC})	

(a) Freight, insurance, and taxes (C_{FIT})	$0.08C_{EQ}$
(b) Construction overhead (C_{CO})	$0.05C_{EQ}$
(c) Contractor engineering costs (C_{CE})	$0.15(C_{EQ}+C_{MI})$
3. Other costs (C_{OT})	
(a) Contingency and fee cost (C_{CF})	$0.18(C_{DC}+C_{IC})$
(b) Auxiliary facilities cost (C_{AF})	$0.3(C_{DC}+C_{IC}+C_{CF})$
o Working capital cost (C_{WC})	$0.13C_{FC}$
• Annual capital charge (C_{AC})	C_{TC} ×Capital recovery factor
• Total Operating cost (C_{AO})	$C_{DO}+C_{FO}+C_{GC}$
1. Direct operating costs (C_{DO})	
(a) Raw materials (C_{RM})	C_{RM}
(b) Waste treatment (C_{WT})	C_{WT}
(c) Utilities (C_{UT})	C_{UT}
(d) Operating labor (C_{OL})	C_{OL}
(e) Supervisory and clerical labor (C_{SC})	$0.15C_{OL}$
(f) Maintenance and repairs (C_{MR})	$0.06C_{FC}$
(g) Operating supplies (C_{OS})	$0.15C_{MR}$
(h) Laboratory charges (C_{LC})	$0.15C_{OL}$
(i) Patents and royalties (C_{PR})	$0.03C_{AO}$
2. Fixed operating costs (C_{FO})	
(a) Local taxes (C_{LT})	$0.15C_{FC}$
(b) Insurance (C_{IS})	$0.005C_{FC}$
(c) Overhead cost (C_{OH})	$0.6(C_{OL}+C_{SC}+C_{MR})$
3. General costs (C_{GC})	
(a) Administration costs (C_{AD})	$0.15(C_{OL}+C_{SC}+C_{MR})$
(b) Distribution and selling costs (C_{DS})	$0.10C_{AO}$
(c) Research and development (C_{RD})	$0.05C_{AO}$
• By-product credit (C_{PC})	C_{PC}
• Annual production cost	$C_{AC}+C_{AO}-C_{PC}$

Table D.1.3. Descriptive statistics for explanatory variables used to determine NIPF landowners' likeliness to harvest when utilizing logging residuals to produce bioenergy in Mississippi.

Variables	Variable Description	Mean	Std. Dev.
ACRES	Continuous variable indicating total acres of forested land owned by the respondent	461.81	1097.28
PREVHARVEST	Dummy variable indicating if respondent has previously harvested timber on his/her land	0.87	0.34
CLIMATE	Dummy variable indicating if respondents think global climate change is a serious issue	0.39	0.49
HABITAT	Dummy variable indicating if habitat management is an important objective for the landowner	0.80	0.40
AESTH	Dummy variable indicating if aesthetic value of the forest is important to the landowner	0.74	0.44
FINANC	Dummy variable indicating if financial benefit is an important objective for the landowner	0.83	0.38
INVEST	Dummy variable indicating if maintaining the forestland as an investment of assets is important to the landowner	0.83	0.37
AGE	Continuous variable indicating the age of the respondent in years.	64.80	12.41
EDU	Categorical variable indicating the education level of the respondent	4.34	1.86
INCOME	Continuous variable indicating the annual household income of the respondent in thousands of U.S. dollars.	86.17	43.30
*511 observations *20.96% response rate	usable		

The Brant Test was used to prove that the ordinal logit was an appropriate model that does not violate the parallel regression assumption. In model, V2V1, the p-value for chi^2 was 0.7, for Model V3V1, the p-value of chi^2 was 0.4 and in Model V4V1, the p-value for chi^2 was 0.3. All chi-square values were insignificant. This indicates that the parallel regression assumption has not been violated, and that the ordered logit model is suitable for the data (Table D.1.3).

Table D.1.3. Chi-square statistics from the Brant Test of parallel regression assumptions for survey data of NIPF landowners in Mississippi. Insignificant p-values indicate that the assumption is not violated.

	V2V1 MODEL		V3V1 MODEL		V4V1 MODEL	
	chi^2	**$p>chi^2$**	**chi^2**	**$p>chi^2$**	**chi^2**	**$p>chi^2$**
All	7.32	0.695	10.42	0.404	11.28	0.336
ACRES	0.21	0.65	0.12	0.73	0.13	0.721
PREVHARVEST	0.65	0.42	0	0.95	2.77	0.096
CLIMATE	1.45	0.23	5.78	0.02	1.65	0.199
HABITAT	0	0.98	0.22	0.64	0.55	0.46
AESTH	1.28	0.26	1.93	0.17	0.21	0.648
FINANC	0.52	0.47	0.1	0.76	0.4	0.529
INVEST	0.04	0.85	0.04	0.84	0.14	0.707
AGE	0.01	0.93	0.17	0.68	0.49	0.485
EDU	0.42	0.51	1.06	0.3	0.11	0.74
INCOME	1.18	0.28	0.38	0.54	0.66	0.415

The log-likelihood ratios of all three models used in the study were significant at 1% alpha level. This indicates a good fit for the models, and therefore a rejection of the hypothesis that all the predictors' regression coefficients would be equal to zero. The predicted outcomes of the 3 models were all within two percent of the observed outcomes, which indicates that the model was successful in predicting NIPF landowners' decisions (Table D.1.4).

Table D.1.4. A comparison of predicted and observed frequencies of landowner decisions from three ordered multinomial logit models based on survey data of NIPF landowners in Mississippi.

	Model 1 (V2V1)		Model 2 (V3V1)		Model 3 (V4V1)	
	% Pred	**% Obs**	**% Pred**	**% Obs**	**% Pred**	**% Obs**
0 (less likely)	2.32	2.74	2.41	2.94	24.55	25.44
1 (equally likely)	35.97	36.40	25.46	26.61	44.37	42.47
2 (more likely)	61.71	60.86	72.13	70.45	31.09	32.09

Table D.1.5 gives a comparison of significant variables, within at least the 90% confidence level, and their signs across all three models. This allows for evaluation of trends between the models, and is a good indicator of landowner preferences. The highly significant likelihood ratio probabilities, and the insignificant Brant test probabilities indicate that all models are well fitted, and do not violate parallel regression assumptions. The table shows that all significant variable signs were consistent across the three models. This shows that landowners' preferences were consistent across the models, which is an intuitive sign that the data works well with the model.

Table D.1.5. Comparison of the coefficient signs of variables found to be significant in at least 90% confidence from ordered logit models based on survey data of Mississippi NIPF landowners.

	Model 1 (V2V1)	**Model 2 (V3V1)**	**Model 3 (V4V1)**
ACRES	**-**	**-**	**-**
PREVHARVEST			**-**
CLIMATE	**+**	**+**	
HABITAT	**+**	**+**	**+**
AESTH	**-**	**-**	
FINANC	**+**	**+**	
INVEST			**-**
AGE	**-**	**-**	
EDU	**+**	**+**	
INCOME	**+**		
LR Prob > chi2	0.0000	0.0000	0.0002
Brant Prob > chi2	0.6950	0.4040	0.3360

2. Whether or not the mathematical algorithms were peer reviewed:
Analytical approaches were used. Currently all of the work in is in the peer-reviewed process.

3. Hardware requirements:

4. Software used:
Limdep (statistical software package)
SAS
Microsoft Excel

Sustainable Energy Research Center
Project Management Final Report for 2008-2010

A. Principle Investigator: W. Glenn Steele

B. Summarization of Activities

Subtask G.1 Quarterly reports for this project for two years

1. Planned Activities

O.1.DL.1 Year 1 and Year 2 deliverables are quarterly reports for the project.

2. Summarization of Activities

Quarterly reports were submitted.

Subtask G.2 Final reports for each task

1. Planned Activities

O.2.DL.1 Year 2 deliverables are final reports for each task.

2. Summarization of Activities

Final report is complete.

Subtask G.3 Develop partnerships with national laboratories, industries and other research groups

1. Planned Activities

O.3.DL.1 Year 1 and Year 2 deliverables are to provide leadership to each task to develop partnerships with national laboratories, industries, and other research groups and report these in quarterly reports.

2. Summarization of Activities

SERC representatives met frequently with companies and agencies to promote collaboration and commercial development of SERC-developed technologies. Below is a list of collaborating/partnering agencies:

DOE Laboratories: ORNL, PNNL, NREL, INL
Government Agencies: EPA, USDA, DOE(FE, EERE), HS(SERRI), Air Force, Navy, Army
Petroleum: Ergon, PERC
Biofuels: Bunge-Ergon, KiOR, EnerSysNet, General Atomics, Bio Energy LLC, Harrelson & Associates, Hunt Refinery
Agriculture: Wayne Farms, Reprieve Renewables, Conservation Seeds
Brewery: Lazy Magnolia
Timber: International Paper
Chemicals: Enerkem, Renewable Opportunities
Utilities: Entergy, Mississippi Power, Southern Company, TVA, Atmos
Instrumentation & Equipment: Bruker, Savery LLC, Piedmont Biofuels, Chemical Products
Universities: Florida, NC State, Ohio State, Missouri, Puerto Rico, Hohenheim (Germany), Washington State, North Dakota

SERC established MOU/NDAs with Hy-Tekbio, EnerSysNet, Mississippi Power, KiOR, ROI, Inc., Chemical Products Co., JBS United, AST, Inc., Piedmont BioProducts, Inc., Eclipse Renewables, and United Technologies Corporation.

Final Report

Project Title: Mississippi State University Sustainable Energy Research Center, Phase III
Award Number: DE-FG36-06GO86025

Recipient: Mississippi State University
Project Location: Mississippi State University, Starkville, Mississippi

Reporting Period: January 1, 2010 – June 30, 2012
Date of Report: July 31, 2012
Written by: W. Glenn Steele

Principal Investigator: W. Glenn Steele

The data and information contained in Pages 8-49 of this report have been submitted in confidence and contain trade secrets and/or patentable intellectual property.

Acknowledgment: This material is based upon work supported by the Department of Energy under Award Number DE-FG36-06GO86025.

Disclaimer: This report was prepared as an account of work sponsored by an agency of the United States Government. Neither the United States Government nor any agency thereof, nor any of their employees, makes any warranty, express or implied, or assumes any legal liability or responsibility for the accuracy, completeness, or usefulness of any information, apparatus, product, or process disclosed, or represents that its use would not infringe privately owned rights. Reference herein to any specific commercial product, process, or service by trade name, trademark, manufacturer, or otherwise does not necessarily constitute or imply its endorsement, recommendation, or favoring by the United States Government or any agency thereof. The views and opinions of authors expressed herein do not necessarily state or reflect those of the United States Government or any agency thereof.

Number of Task, Subtask or Milestone	Title of Task, Subtask or Milestone	Task or Milestone Completion Criteria	Actual Accomplishments
H.	Bio-oil		
H.1	Develop one ton per day pilot scale pyrolysis reactor and bio-oil upgrading system		
H.1.1.	Design, build and test a one ton/day fast pyrolysis unit with esterification and HDO upgrading unit operations. The pyrolyis reactor will attain 65% yield based on clear pine feedstock. Bio-oil water content will be less than 28%. Solids content will be less than 0.5%. HDO bio-oil will have an acid value less than 1, oxygen content less than 1% and an HHV of greater than 44 Mj/kg. The esterified bio-oil will meet ASTM bio-oil heating oil standards at the No. 4 level. Tests will be performed to determine these characteristics of the bio-oils produced from two other feedstocks and compared to the results for clear pine feed.	Design, build and test a one-ton per day pyrolysis reactor. Attain 65% bio-oil yield from the new reactor with water content below 28%, solids content less than 0.5%. HDO bio-oil will have an HHV above 44 MJ/kg. Esterified bio-oil will meet ASTM No. 4 boiler fuel grade. Two feedstocks will be tested in the new reactor to be compared to clear pine wood feedstock.	The pyrolysis reactor is designed, built and is being tested. Bio-oil has been produced at a test rate. Bio-oil yield and characteristics will be determined during SERC IV activities. Fuel production and quality tests must also be performed during SERC IV when the reactor produces the required bio-oil.
H.2	Develop laboratory scale catalytic pyrolysis reactor		
H.2.1.	The bio-oils produced by this method will be partially hydrogenated with resultant characteristics of 30% less oxygen and acid value and than for raw bio-oils, and 30% of emulsified water will be partially fractionated from the product.	Bio-oils partially hydrogenated will contain 30% oxygen and acid value than raw bio-oils; 30% of water will be fractionated from the final partially upgraded product.	Bio-oils were partially hydrogenated with 10% reduction of oxygen value and 33% reduction of acid value; 10% of water was fractionated from the product. Further conversion improvements will be pursued during SERC IV.
H.3	Maximize bio-oil anhydrosugars for production of ethanol		
H.3.1.	Replicated experiments will optimize the initial results that provided the 50% increase in anhydrosugars to attempt to attain a yield of 55%. The specific anhydrosugars produced by the procedure will be identified. The process to produce monmeric sugars will be refined and yields determined precisely. Inhibitors will be identified and removed to allow ethanol to be produced at one-half the level obtained by grain ethanol practices.	55% yield of anhydrosugars will be achieved. Inhibitors will be identified. Inhibitors will be removed by filtration with activated carbon; target level of ethanol produced microbially was one-half of that obtained currently by grain ethanol practices.	55.6% yield of anhydrosugars were produced. 90% of inhibitors were identified by HPLC. 90% of inhibitors were removed and ethanol was produced at about one-half the level of that obtained by grain ethanol practices.
H.4	Produce hydrogen from process and pyrolysis process heat		
H.4.1.	Produce hydrogen at a cost equivalent to that for production from current methane systems at 2006 prices. Hydrogen purity will be equivalent to methane system industrial hydrogen.	Produce hydrogen at the cost of current methane systems. Hydrogen purity will be equivalent to industrial hydrogen.	Bio-oil was utilized for hydrogen production by catalytic reforming. Production cost was close to that for hydrogen from current methane systems.
I.	Biocrude		
I.1	Biocrude production using a pilot facility		The design and construction of the Biocrude pilot facility was completed successfully. It has been running since November 2011 producing Biocrude from domestic wastewaters.
I.1.1	Design, development and testing of a 1 gal/week pilot scale facility.		The 1 gallon/week Biocrude production was validated using single cultures and wastewater treatment microbial consortiums.

I.1.2.	Economic analysis of the cost of producing oil in the pilot facility.		The economic analysis indicated Biocrude production at less than $3.00/gallon.
I.2	Evaluation of growth conditions on various biowaste feedstocks		Biocrude was produced successfully using switch grass and baggasse hydrolyzates with resulting yields (lb oil/lb of dry cells) over the 15% target..
I.2.1.	Development of a report ranking the characteristics and potential of various sources of wastewaters, agricultural crops, and residue for use as a feedstock supplement, characterization of microbial consortia, and performance metrics of various feedstocks.		Several sources of carbon to produce Biocrude has been identified and will be evaluated in 2012-2013.
I.2.2.	Oil accumulation above 15% by weight evaluated for microbial biomasses grown on pulp and paper and food processing industrial wastes. Economic analyses indicate that microbial content above 15% by weight generate Biocrude under $3.0/gallon.		Pulp and paper wastewaters has been shown as a viable growth media for Biocrude production.
I.3	Examine non-conventional oil separation techniques		Promising biocrude extraction results were obtained using two novel and non-conventional extraction techniques; electrostatic coalescense and in-situ transesterification. Performance of these extraction technologies will continue to be evaluated during 2012-2013.
I.3.1.	Achieve 80% oil extraction with the target of extracting oil at $0.30/lb.		
I.4	Produce quality transportation fuels defined by the American Society for Testing and Materials Standard		Transportation fuels were produced from Biocrude and microbial cells.
I.4.1	Complete a 70% mass balance of Biocrude components and cracking products using petroleum refining catalysts.		Over 70% mass balance of compounds resulting from catalytic cracking of microbial oils and microbial media were identified.
I.5	Design cost efficient biomass and biofuels supply chains		Supply chain models were developed to assess the impact of logistics on biocrude production cost using domestic wastewaters. The models were also used to determine the impact of logistics on biodiesel produced from biocrude.
I.5.1.	Identify the appropriate model for conducting these analyses.		
I.5.2.	Estimate the cost of supply biomass, cost of distributing the fuel and sensitivity of the logistic cost to biomass yield, biomass price, biocrude price and biorefinery size.		
J.	Microbial Oil		
J.1	Confirmation of microbial growth and carbon conversion kinetics at the pilot scale	To determine the growth rate at the pilot	Task completed.
J.1.1.	Achieve a mass of 10 g/L of the R. glutinis in the pilot reactor.	Achieve 10 g/L of cell mass in the pilot scale fermentors	10 g/L cell mass.

J.1.2	Achieve 20% dry wt. oil content R. glutinis in the pilot reactor.	Of the 10 g/L cell mass the goal was to achieve a lipid content of 20%	20 % was achieved
J.2	Determination of optimal temperature for lipid accumulation using lignocellulosic sugars.	Several temperature were evaluated to determine the optimum for R. glutinis	30 C was determined to yield the highest cell mass.
J.2.1.	To determine the optimum temperature for producing lipids using R. glutinis on lignocellulosic sugars.	Several temperature were evaluated to determine the optimum for R. glutinis	30 C was determined to yield the highest cell lipid percentage.
J.3	Commercialization plan	Using the data determine a commercialization path	From the data it was determined that industrial wastewaters offer the best path
J.3.1.	Development of a complete economic analysis of a commercial scale facility	Perform an economic analysis	The economic analysis determined current sugar cost were too high to produce microbial oils from this feedstocks.
K.	Hydrocarbons derived from synthesis gas		
K.1	Larger scale catalyst testing using actual synthesis gas		
K.1.1.	Achieve 50% conversion of CO with 30% selectivity to liquid hydrocarbons using 2nd generation catalyst to determine its performance with real synthesis gas from a downdraft gasifier.	Achieve milestone to 50% conversion of CO with 30% selectivity to liquid hydrocarbons	The 3rd generation catalyst was developed for bio-syngas conversion to liquid hydrocarbons. 50% CO conversion rate with 30% selectivity to liquid hydrocarbon was achieved.
K.1.2.	Determine the catalyst life-time in extended, time-on-stream testing with real synthesis gas obtained from a downdraft gasifier.	Determine the catalyst life-time by time-on-stream testing	The time-on-stream effect on the performance of the 3rd generation catalyst was studied for a period of 160 h. No further change such as catalyst deactivation was observed.
K.1.3.	Determine the effect of trace amounts of H2S in the actual synthesis gas upon yields.	Determine the effect of H2S on the hydrocarbon yield	After bio-syngas cleaning, there is no H2S that affect the hydrocarbon yield.
K.2	Process design and economic analysis		
K.2.1.	Complete process design for a commercial plant to make liquid hydrocarbons from synthesis gas derived from biomass-synthesis gas.	Complete process design of pilot reactor	The pilot FCC reactor was designed and installed.
K.2.2.	Complete economic analysis for the plant described in milestone one assuming a “brown-field” installation.	Complete economic analysis for the plant	The economic analysis was completed. Based on the syngas production capacity of 10,000 Nm3/h, the product unit cost of gas (Light Hydrocarbons), oil (Liquid Hydrocarbons) and aqueous (Oxygenates) were $2.01 /MMBTU, $1.59 /Gallon and $1.33 /Gallon, respectively.
L.	Biomass Combustion		
L.1	5.1 Investigate ignition and combustion signatures of non-food biomass-derived fuels and/or relevant surrogates in a rapid compression machine		Three peer-reviewed journal articles, two peer-reviewed conference papers, and one non-peer-reviewed conference paper were published.
L.1.1.	To measure ignition and combustion pressure histories of carefully chosen biomass fuel surrogates.	measure ignition and combustion pressure histories	Two optical diagnostic techniques (natural chemiluminescence and LIBS) were investigated in atmospheric, premixed methane-air flames in a rectangular slot burner.
L.1.2	To characterize ignition delays and combustion behavior of non-food biomass fuels at various engine-like operating conditions.	characterize ignition delays and combustion behavior	Ignition characteristics in diesel-ignited methane and diesel-ignited propane dual fuel combustion were quantified.

L.2	Demonstrate fuel injection and engine combustion strategies for non-food biomass-derived fuels		Four peer-reviewed journal articles, two peer-reviewed conference papers, and four non-peer-reviewed conference papers and posters.
L.2.1.	To investigate fuel injection and engine combustion strategies for surrogate blends of non-food biomass-derived fuels.	Study fuel injection and engine combustion strategies for surrogate blends of non-food biomass-derived fuels	Four different alternative fuels were tested in a VW 1.9L TDI engine: biodiesel, methane, propane, and a renewable non-food biomass-derived distillate fuel. A multi-zone model of dual fuel low temperature combustion (LTC) was developed and published in an award-winning article in the Journal of Automobile Engineering. Cyclic variations in dual fuel LTC and entropy generation in a constant internal-energy-volume combustion vessel were also studied.
L.2.2.	To measure baseline engine performance, combustion heat release, and exhaust emissions from non-food biomass-derived fuels and/or suitable surrogate blends.	Measure baseline engine performance, combustion heat release, and exhaust emissions	Ignition, combustion, fuel conversion efficiencies, and engine-out exhaust emissions were measured for straight biodiesel fueling and for biodiesel-ignited methane and propane dual fuel combustion. Additional experiments are underway for understanding the combustion of other non-food biomass-derived fuels.
M.	Biomass Feedstocks Development		
M.1	Testing, establishment of candidate species, and conversion of pasture/CRP land to candidate species		Testing underway and continuing on conversion of range land to biomass crops at Red Hills Coal Mine (Ackerman, MS). Safener work with seeded switchgrass is successful.
M.1.1.	Successful establishment of Uniform Variety Trials at six to eight locations around Mississippi, with continued testing of herbicides to enhance successful establishment under both tillage and no-tillage conditions.		Field tests have been established at eight locations in Mississippi. Several herbicides have been identified for use in controlling weeds in switchgrass and giant miscanthus.
M.2	Management, nutrient cycling, and char usage		Greenhouse studies completed indicate char must be nutrient charged before application.
M2.1.	Provide a second year assessment of the movement of N within feedstock species, assessing feedstock species' potential of associative nitrogen fixation, determine N value of legume mediated nitrogen fixation, and obtain baseline data on appropriate char application rates.		Nutrient (N) movement hypothesis confirmed. Associative nitrogen fixation experiments inconclusive, but appear to show that switchgrass is an associative nitrogen fixer. Cool season legumes are a viable option as a low input nutrient management scheme. Hairy vetch is the best option.
M.3	Wood residue assessments		Potential sources of "waste" wood have been identified.
M.3.1.	Development of a survey and data regarding recoverable wood residue for bioenergy conversion.		Developed survey.
M.4	Feedstock engineering		

M.4.1.	Define several potential harvesting and delivery systems that could be implemented in the SE-US.		A maize stover yield model was used to determine its potential as a feedstock. Net energy value and carbon credit balance were positive for corn in the western region of the Mississippi Delta. Spatial distribution of potential bio-energy crops and their environmental benefits, such as soil organic carbon (SOC) and water quality in Mississippi for renewable fuels were studied through economic modeling and analysis.
M.4.2.	Develop economic and performance data for at least one feedstock system that could be reasonably implemented for grass crops in the SE-US taking into account farm size, equipment availability, and farmer acceptance		Energy grasses (switchgrass and giant miscanthus)can be successfully used as a poultry bedding. Farmer interest increased due to direct market potential in addition to energy production.
N.	Pilot Plant Construction and Support		
N.1	Completion of construction and commissioning of a building housing two pilot plants.		The SERC building has been completed and commissioned. Utility systems have been constructed and tested. Process areas for the Bio-oil and Biocrude Projects have been established, Equipment for each project has been installed, connected to utilities, and commissioned. Support for each project is ongoing.
O.	Project Management and Reporting		
O.1	Quarterly reports for this project for two years		
O.2	Final reports for each task		
O.3	Develop partnerships with national laboratories, industries and other research groups		The SERC team met frequently with companies and agencies to promote economic development of the institute's technologies. Representatives from SERC met with a number of companies, laboratories, government agencies, and universities to discuss collaboration.

Begin Confidential Information.

Task H. Bio-oil

Principle Investigators and team members:

Philip H. Steele, Dept of Forest Products
C. U. Pittman, Jr., Dept of Chemistry
Fei Yu, Dept of Agricultural & Biological Engineering
E. M. Hassan, Dept of Forest Products
Keisha B. Walters, Dept of Chemical Engineering
Radhakrishnan Srinivasan, Dept of Agricultural & Biological Engineering
Sanjeev Gajjela, Dept of Forest Products
Brian Mitchell, Dept of Forest Products

The goal of this task is to produce and characterize high-quality bio-oils from southern forestry and agricultural feedstocks. The focus of this project is to scale up to a one ton per day pilot scale pyrolysis reactor and to scale up the two successful bio-oil upgrading technologies developed by Mississippi State University. These technologies are Lignocellulosic Bio-Oil to produce a boiler fuel and HDO Bio-Oil to produce transportation fuel.

The entire bio-oil task section contains patentable and protected data. The use of this confidential information is limited to utilization by the program manager to evaluate the task results. Disclosure of any of the confidential material discussed here is a violation of the confidentiality guaranteed by this distribution limitation notice.

Executive Summary:

The research results produced by the Mississippi State University (MSU) DOE-funded Sustainable Energy Research Center (SERC) add significantly to the general and specific understanding of both bio-oil production and bio-oil conversion to fuels. To date, MSU has patents filed and pending on a novel auger pyrolysis reactor design (scalable to 50 tons per day production). This design is licensed and in operation at the facility of one of our industrial cooperators. A pilot plant at 5-8 tons per day production is currently being installed on the MSU campus. This facility will have biomass processing, a pyrolysis reactor, centrifugal bio-oil filtration, and conversion capabilities to produce both esterified and hydroprocessed fuels. This pilot bio-oil facility will demonstrate bio-oil technology to the public including industry professionals and researchers. The capital cost for building an auger reactor is estimated to be 65% of that required for fluidized bed reactors. Therefore, this auger reactor technology will strengthen the economic feasibility of bio-oil production. A patent for a novel bio-oil esterification technology, olefination, has been filed and is pending. We have excellent results from production of a high-energy boiler fuel from this technology. This fuel requires no hydrogen to produce and no hydrotreater. For this reason the cost of this fuel will be much lower than for hydroprocessed bio-oil, making this technology potentially viable at today's petroleum fuel costs. With regard to MSU's anhydrosugars research, we have filed a patent that is pending on a method to increase anhydrosugars by a standard mild-acid pretreatment followed by pyrolysis with a modified pyrolysis reactor that rapidly cools the vapor stream. This rapid cooling prevents the breakdown of the anhydrosugars contained in the vapor. Our research indicates that levoglucosan yields from the bio-oil water fraction are increased from 36 to 51%, an increase of 42% by this technology. Anhydrosugars can be hydrolyzed to nearly 100% yield of glucose. Glucose can be utilized to produce ethanol and hydrogen as well as biochemical products. We produced ethanol and hydrogen from the glucose obtained from bio-oil. While our formal

economic research will be performed in the near future, we estimate that our breakthrough in preserving anhydrosugars during pyrolysis will make the bio-oil liquid fraction an economically viable source of sugars due to the dramatically increased sugar yield that it allows. An alternative to production of sugars from bio-o3333il was investigated by separating hemicellulose from wood by hydrothermolysis. This sugar from this hemicellulosic product was then separated via membrane filtration followed by purification. We will optimize this technology during SERC IV. Research by MSU on the mechanisms involved in polymerization of bio-oil will assist industries and researchers with a more complete description of the progression of the process over time. MSU appears to be the first organization to pyrolyze torrefied wood as a feedstock able to provide a high hydrocarbon yield in raw bio-oil. Two catalysts produced hydrogen contents of 75 and 69% respectively in bio-oil produced from torrefied wood. Success in utilizing torrefied feedstocks to increase initial hydrogen content of raw bio-oil offers the potential for substantially reducing the cost of hydrogen applied in subsequent hydroprocessing steps. This research will be scaled up from micro-reactor to laboratory scale in SERC IV. In summary, MSU has developed several novel technologies to produce fuels, or the precursors to fuels, during the SERC III phase of its bio-oil research. We look forward to refining these technologies during SERC IV. While our hydroprocessing research was somewhat derivative, we did improve on the technology to obtain 0% oxygen hydrocarbons. In addition, during the work to develop our hydroprocessing techniques, we developed novel and exciting fuels that will have the potential to revolutionize bio-oil upgrading technology to produce drop-in fuels.

Subtask H.1 Develop a one ton per day pilot scale pyrolysis reactor and bio-oil upgrading system

Both MSU hydrodeoxygenated (HDO) bio-oil hydrocarbons and lignocellulosic biodiesel require relatively large-scale testing to determine commercial viability. This will require hundreds of gallons to be produced per month. Scale up of the MSU pyrolysis reactor to one ton per day to produce 130 gallons per day of pyrolysis oil will be performed to provide this raw bio-oil. Both the MSU HDO and lignocellulosic bio-oil systems will also be scaled up to process 130 gallons of bio-oil per day to provide the fuels required for both engine and boiler testing. Hydrogen for the pilot-scale HDO bio-oil upgrading will be produced by hot water electrolysis at temperatures from simulated and actual industrial processes. Multiple biomass types produced by the SERC Feedstocks Thrust will be pyrolyzed in the pilot plant to produce bio-oil and upgraded bio-oils. Engine and boiler testing for the two fuel systems will be undertaken to characterize both engine and boiler performance and emissions. A post-filtration system successfully tested by MSU at the bench scale will be scaled up to remove micro-particles of char from hot bio-oil produced by the pyrolysis reactor. Chemical and physical analyses of raw bio-oil and the upgraded biofuels will be performed in the MSU Bio-oil Chemical Analytical Laboratory or by an independent laboratory. Cooperation of MSU faculty and staff will be provided for development of a one ton per day pyrolysis reactor at an industrial site with process heat providing pyrolysis heat.

Planned Activities:

H.1.ML.1 Design, build, and test a one ton per day fast pyrolysis unit with esterification and HDO upgrading unit operations. The esterification and HDO upgrading methods will be improved during SERC III to allow the development of scaled-up pilot plant production of these fuels during the final construction of the pilot plant. The pyrolysis reactor will attain 65% yield based on clear pine feedstock. Bio-oil water content will be less than 28%. Solids content will be less than 0.5%. HDO bio-oil will have an acid value less than 1, oxygen content less than 1% and an HHV of greater than 44 Mj/kg. The esterified bio-oil will meet ASTM bio-oil heating oil standards at the No. 4 level. Tests will be performed to determine these characteristics of the

bio-oils produced from two other feedstocks and compared to the results for clear pine feed. The bio-oil produced in the pilot plant will be post-filtrated to remove most of the entrained particulate matter.

Summarization of Activities:

Accomplishment of analysis of the bio-oils preceeding and following post filtration required analysis. For an easy reference, Table H1 lists the methods used for bio-oil characterization. All measurements were performed a minimum of three times to get an average value and standard deviation when possible. Not all methods were used, but all are available for future testing if desired. Analytical methods used in investigating filtration methods were MIM analysis, ash wt% analysis, FTIR (ATR and DRIFTS), GPC, calorimetry analysis, and elemental analysis. Calorimetry and elemental analysis were used sparingly due to time constraints. Previous testing included bio-oil produced from pine (P) and cottonwood (C) trees and included different tree parts as the biomass feedstock: whole tree (WT), bark (B), clear wood (CW), and leaves/needles (L or N). Bio-oil was also collected from the condensers either as whole (W) that included all three condensers or was split into fractionated (F) and water condensate (WF) samples. The WF sample was collected separately from the condenser with the highest water content and the remainder (from the other two condensers) makes up the F sample. While some of the work shown involves those samples, the testing of the scaled-up filtration system primarily involves pine clear wood. In terms of woody biomass, pine is one of the easiest and most inexpensive biomass feedstocks. Other biomass types will be processed (cottonwood trees, miscanthus grass, etc.), and different feedstocks will need to be tested in the future. Clear wood was chosen as a feedstock due to the relative ease in processing/obtaining the biomass and the properties of the resultant bio-oil. Clear wood biomass consists of the trunk of the tree only, without bark or leaves/needles. Bark and leaves/needles were shown from previous testing to produce bio-oil with undesirable and inconsistent properties, such as lower pH values, higher water content, lower heating values, and higher viscosity. Bark and leaves/needles inherently have higher variability in properties and also tend to have higher ash, particulate, and water contents. Since the goal of SERC III is to test a one ton per day facility in efficiently producing useable, upgraded bio-oil, it was determined that clear wood would be the only type of tree part tested at this time.

Table H1: Summary of testing methods utilized in evaluating pyrolysis oil properties.

Measurement type or device	**Parameters**
Pyrolysis	MSU Forest Products Lab; auger pyrolysis reactor under vacuum at 400 °C; average flow rate of 15-20 L/min; 25 °C water condensers
Density	Weighing known volumes of bio-oil
FTIR Spectroscopy using Thermo Electron Nicolet 6700; attenuated total reflectance Fourier transform infrared (ATR-FTIR) spectroscopy using MIRacle accessory	Sample placed on Diamond/Zn 45 deg ATR crystal; liquid N_2 cooled MCT-A* detector, 4 cm^{-1} resolution, 256 scans, 1.8988 optical velocity, 7000-800 cm^{-1} wavenumber range
Molecular weight determination by gel permeation chromatography (GPC) using custom built instrument [Varian Star 9040 refractive index detector, Waters 610 Fluid pump and 600 Controller, Varian Mesopore guard columns (50x4.6mm ID and 250 x 4.6mm ID)]	Sample prepared at 1-2 mg/mL concentration in Optima grade tetrahydrofuran (THF), sonicated, and filtered with 0.45 µm syringe filter before injection; 50 µL injection volume; flow rate at 0.3 mL/min; nine-point polystyrene calibration; internal standard used to account for pressure changes and retention time shifts

GC/MS analysis using Varian 3600 gas chromatogram with Varian Saturn 2000 mass spectrometer and fused silica column Rtx-1 MS (30 m x 0.25mm)	50 – 300 °C temperature range; helium carrier gas with 1.2 mL/min volumetric flow rate; 250°C detector temperature; NIST 2005 organic compound database used for compound identifications
Centrifugal filtration using an Eppendorf 5810R centrifuge	Grace 50 mL filter centrifuge tubes; 2500 rpm for up to 30 min; tubes used with and without filter insert to mimic pilot plant-scale centrifuge
Ash content	DIN EN 7 method: 10-20 g sample placed in porcelain crucible, dried in vacuum oven (Fisher Sci Isotemp Model 285A) at 105 °C for 4 hours to remove water and higher volatiles, held at 775 °C for 1 hour (ThermoLyne 1400 furnace) to ensure complete combustion, and then cooled. Remaining sample weighed to determine ash weight content.
MIM content	Bio-oil to MeOH ratio of 1:10 to ensure bio-oil mostly dissolved; 1 micron pore size filters heated in oven for 15 min and cooled in dessicator before use; solution filtered with excess of methanol; after filtration, filters dried in air for 15 min and then in oven at 107 °C for 30 minutes; placed at RT in dessicator for 10 min; weighed to determine MIM.
Calorimetry	Adiabatic PARR 1535EA oxygen bomb calorimeter operated at 115V and 60 Hz following ASTM D 240-92 in which sample burned and temperature change recorded and used for HHV values.

Data from previous characterization showed that large variations in properties were observed for whole tree pyrolysis oil. The bark content of the pyrolysis oil was determined to be the main source of the variation. The bark of the tree contains more metal and ash content, and so the emphasis focus of this pyrolysis filtration work was pine clear wood. Wood samples were debarked before chipping, drying, and further processing. To further show the extent of polymerization that occurs when bio-oil is stored for long periods of time, samples were aged for 3 months at 80 °C and characterized by GPC and rheology to determine the impacts that aging has on the bio-oil. The results are shown in Table H2 for pine whole tree and clear wood samples both filtered and unfiltered prior to aging. Due to the long aging times, there is a large variation in the data and there was visible phase separation that occurred for one of the samples (pine whole tree). Phase separation is due to polymerization reactions that occur during aging. These reactions increase the water content and lead to the formation of a top aqueous layer and a bottom organic layer. These results clearly demonstrate the need for a filtration system to hinder the aging reactions that occur in the storage of bio-oil.

Table H2: Summary of MW and viscosity of unfiltered/unfiltered and unaged/aged (3 mos. at 80 °C) pine bio-oil samples. Shaded cells in the table correspond to unfiltered samples.

Sample Name	MW (Da)	Viscosity (cP)
Pine, whole tree, whole oil, NOT filtered, aged for 3 mos. at 80 °C, top phase	531.67 ± 34.32	2.56 ± 0.075
Pine, whole tree, whole oil, NOT filtered, aged for 3 mos. at 80 °C, top phase	1480.57 ± 167.97	12,706 ± 6,030
Pine, whole tree, fractionated oil, NOT filtered, NOT aged	1200 ± 56	12.6
Pine, whole tree, fractionated oil, FILTERED, NOT aged	1120 ± 47	11.4
Pine, clear wood, whole oil, NOT filtered, NOT aged	551 ± 21	17.59 ± 2.9
Pine, clear wood, whole oil, FILTERED, NOT aged	514 ± 7	27.8 ± 0.62

Methanol insoluble material (MIM) and ash content analyses were performed on bio-oil filtered and control samples to determine if post-condensation filtration significantly affected the bio-oil characteristics. Samples included pine clear wood whole (PCWW), pine clear wood fractionated (PCWF), pine bark fractionated (PBF), and cottonwood clear wood fractionated (CCWF). The fractionated samples indicate that one high-water content cell in the condenser system condenser stream was not added to the sample. This condenser stream was included for the whole samples. Post-condensation filtration was performed on the samples and the impact of filtration on MIM and ash content was assessed both prior to and after accelerated aging at 80°C for 3 weeks. The MIM content data is summarized in Figure H1. Samples with 95% confidence interval (CI) error bars have been tested in triplicate and average MIM values are shown. One limitation in testing of MIM content is the sample volume needed. Samples with single data points were not available in sufficient quantity to allow for testing replicates. The new reactor is expected to provide for higher bio-oil production and generate enough material for extended testing.The MIM data shows that the filtration did reduce the methanol insoluble material content for the unaged samples. The MIM content is lower than the filtered neat unaged samples. Due to the absence of replicated data for some samples and the large measured deviations in other samples, it is difficult to determine if the filtration affected the MIM content after those samples had been aged. For PCWF and PCWW, no difference existed in the MIM levels of any of the tested samples regardless of filtration or aging condition. For CCWF, a trend could not be determined in the aging of the unfiltered samples since both of the unfiltered samples have only single data points. For the filtered CCWF samples, there was a statistically significant increase in the MIM content upon aging. This increase points to chemical conversions occurring within the sample as the result of aging that result in increased MIM content. Data for the pine bark fractionated (PBF) samples were distinct from the other three sample sets without an identifiable trend related to the use of hard vs. soft wood biomass or the collection of fractionated vs. whole bio-oil. PBF showed highly elevated initial unfiltered, unaged levels of MIM content (~1 wt. %) as compared to the other sample types (≤0.25 wt. %). Filtration of the PBF sample reduced the MIM content to the sample levels found in the other samples. After aging, however, the PBF MIM content measured was at least as high as the initially measured levels. These results for the pine bark-based bio-oil may be due to the inherent

variations in pine bark composition between locations on the same tree, tree-to-tree variations, and between different stands of trees. This large variation in MIM content for bio-oil samples produced from pine bark samples matches our prior results showing both large material property variations within the batch and marked deviations from values measured for bio-oil that did not contain bark.

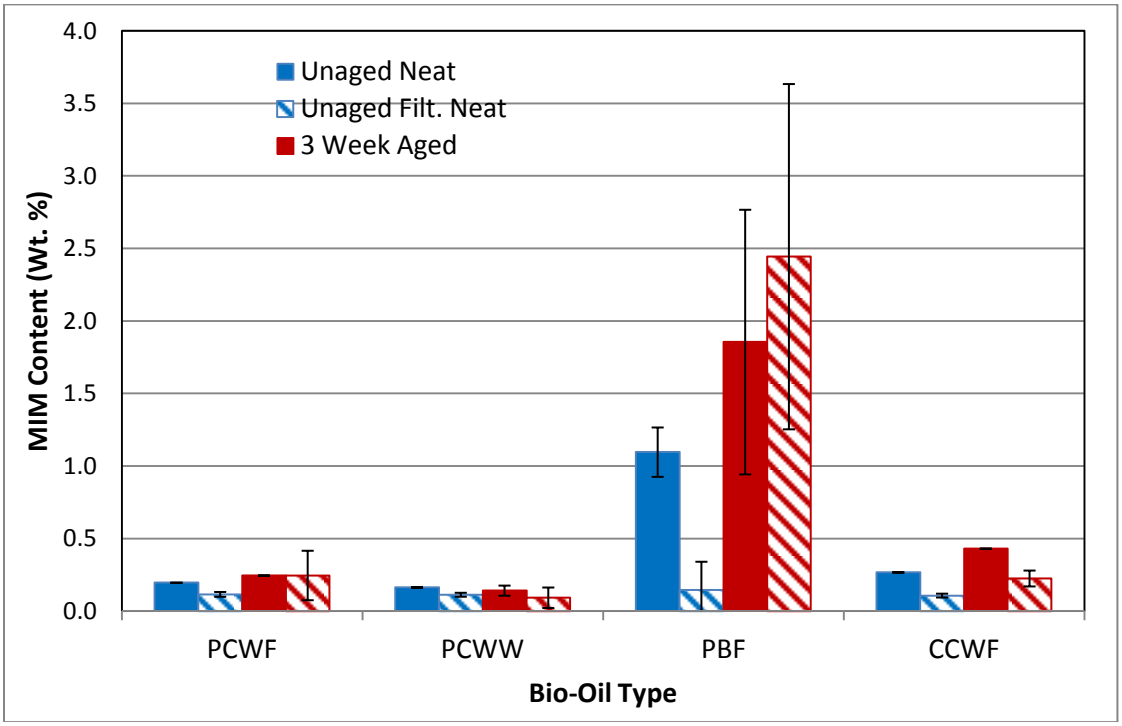


Figure H1: MIM data for unaged/aged and unfiltered/filtered bio-oil samples: pine clear wood whole (PCWW), pine clear wood fractionated (PCWF), pine bark fractionated (PBF), and cottonwood clear wood fractionated (CCWF).

As a corollary to the MIM study, ash content data was measured to determine if filtration reduced the resultant ash content for these bio-oil samples. Ash content data is given in Table H3 and Figure H2 for unfiltered (C) and filtered (FC) samples of pine bark fractionated (PBF), cottonwood clear wood fractioned (CCWF), and pine clear wood whole (PCWW) bio-oil. Standard deviations and 95% confidence intervals were calculated when multiple data points (replicates) could be collected. However, due to the large sample mass needed for a single ash content measurement, some samples could only be tested once.

Table H3: Ash content (wt. %) measurements for unfiltered / control and filtered PBF, CCWF, and PCWW bio-oil samples.

Sample	Avg Ash Content (wt %)	Std Dev	95%CI
PBF-Control	0.0273	N/A	N/A
PBF-Filtered	0.0086	N/A	N/A
CCWF-Control	0.0153	0.0025	0.0035
CCWF-Filtered	0.0179	0.0018	0.0025

PCWW-Control	0.0153	0.0050	0.0069
PCWW-Filtered	0.0310	0.0222	0.0252

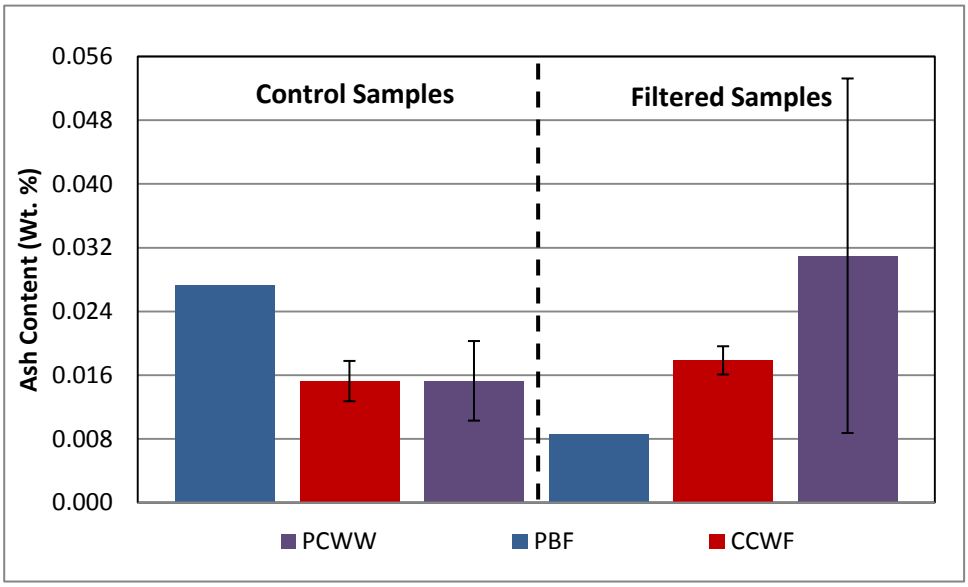


Figure H2: Ash content (wt%) for unfiltered/control samples and filtered samples of PBF, CCWF, and PCWW bio-oil samples.

The data indicate that filtration will remove materials that contributed to the ash content, but further study is needed. For PBF, the control (unfiltered) sample had significantly more ash content than the filtered sample. Neither CCWF nor PCWW showed statistically significant differences in ash content between the filtered and unfiltered/control samples. However, the lack of replication (small sample volume available) as well as the large variance measured for some samples means a definitive conclusion cannot be reached regarding the relationships between filtration and ash content using this data. To help determine the chemical composition of the solid materials that were removed during the filtration of bio-oil, DRIFTS FTIR characterization was performed on the removed solids. Representative spectra for the washed solids from PWTF, PCWW, PBF, and CCWW are shown in Figure H3. The spectra of solids from different feedstocks were generally similar to one another and also showed little difference from the spectra for bio-oil, for which the data is not given in this report. The two peaks at 1715 cm^{-1} and 1600 cm^{-1} indicate less carboxylic acid content (C=O) and higher aromatic ring content in the solids versus the corresponding oils. There is correspondingly a peak at 3058 cm^{-1} that indicates aromatic C-H stretching. The peaks seen in the range of 1452-1165 cm^{-1} are stronger for the solids and correspond to conjugated bonds of C-O and C-C bending and C-C and C-H deformation of aromatic rings. These groups can contribute to aging-related reactions, so filtration is expected to aid in retarding aging reactions during bio-oil storage by removing the char particulate matter that can catalyze these reactions.

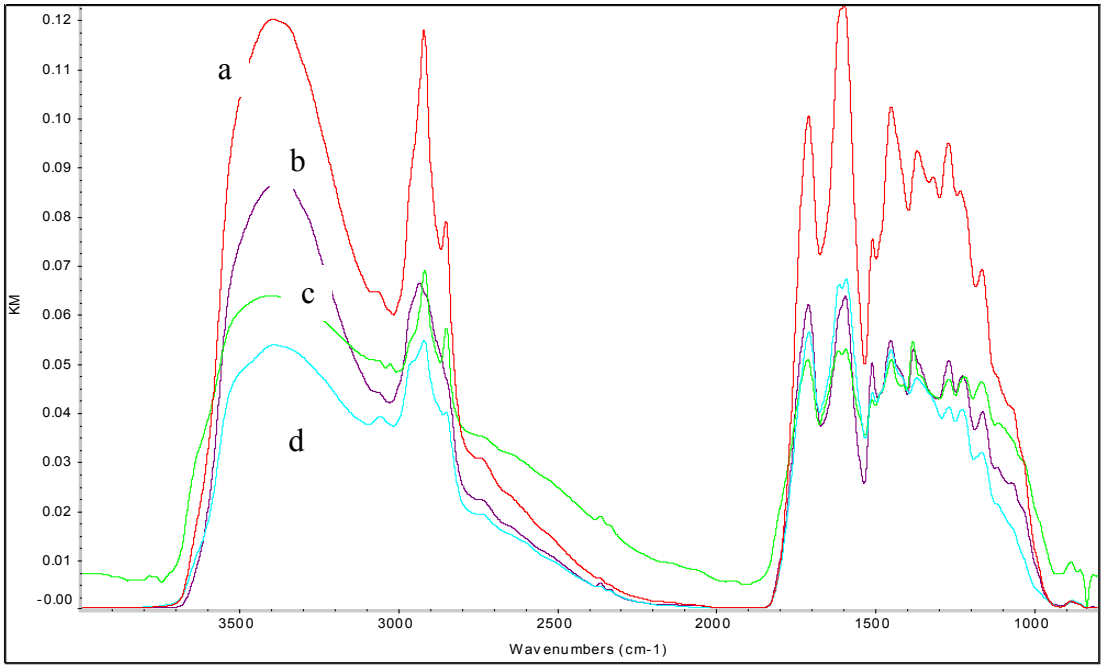


Figure H3: Spectra of filtered solids from (a) PWTF, (b) PCWW, (c) PBF, and (d) CCWW.

To help with standardization of bio-oil produced from the MSU SERC facility, tables were constructed listing characteristics of bio-oil received from the auger reactor system and the biomass used to produce them. Table H4 lists the approximate composition of the pine and cottonwood samples used as feedstock and Table H5 lists the approximate conversion of the biomass to pyrolysis oil and char by weight. Table H6 shows the elemental data for biomass, char, and selected bio-oil samples and Table H7 lists the properties of the neat samples and filtered samples using the previously discussed characterization methods. Data in Table H7 is averaged over 3 characterizations per sample, except for elemental analysis and MIM content. The MIM content required large amounts of sample such that testing could only be performed one to two times per sample to conserve sample volume for other characterization methods.

Table H4: Estimated wt% of tree parts used as feedstock for cottonwood (CW) and pine samples.

	Component	**Wt%**
CW	Clear Wood	56.5
	Bark	18.9
	Stems	8.5
	Leaves	3.4
Pine	Clear Wood	65.6
	Bark	8.8
	Stems	17.6
	Needles	8

Table H5: Estimated biomass conversion/yield (wt.%) using the FP standard-size pyrolysis reactor.

Biomass	Bio-Oil (Wt.%)	Char (Wt.%)	Bio-oil + Char (Wt.%)	Losses (Wt.%)
Cottonwood Whole Tree	49.9	23.4	73.3	26.7
Cottonwood Clear Wood	53.3	24.7	78.0	22.0
Cottonwood Bark	37.6	33.9	71.5	28.5
Cottonwood Leaves	26.7	51.8	78.5	21.5
Pine Whole Tree	56.0	26.0	82.0	18.0
Pine Clear Wood	59.0	23.0	82.0	18.0
Pine Bark	40.0	40.0	80.0	20.0
Pine Needles	51.0	48.0	99.0	1.0

Table H6: Elemental analysis summary for biomass, char, and pyrolysis oil samples.

	Elemental Composition (ppm)					
Material	**Ca**	**K**	**Mg**	**Na**	**P**	**S**
Pine Clear Wood Biomass	838	630	225	105	95	91
Pine Whole Tree Biomass	2116	1552	479	63	308	207
Pine Bark Biomass	2532	1832	607	115	294	265
Cottonwood Clear Wood Biomass	3494	2409	467	98	163	342
Pine Clear Wood Char	3444	2308	878	124	348	167
Pine Whole Tree Char	4352	3944	1074	155	701	140
Pine Bark Char	1830	1359	1491	145	685	231
Cottonwood Clear Wood Char	4573	3252	1994	174	896	583
Pine Clear Wood pyrolysis Oil	407	67	92	119	0	86
Pine Whole Tree pyrolysis Oil	237	102	63	156	17	147
Pine Bark pyrolysis Oil	261	115	71	119	0	172

Table H7: Summarized physicochemical data for unfiltered (neat) and filtered samples.

Unfiltered Properties	PCWF	PCWT	PWTF	PBF	CCWF
Density (g/mL)	1.48 ± 0.01	1.43 ± 0.01	1.33 ± 1.1	1.2 ± 0.01	1.4 ± 0.11
pH	2.12 ± 0.02	2.97 ± 0.03	2.74 ± 0.06	2.47 ± 0.02	3.07
Water Content (wt%)	17.6 ± 1.2	29.5 ± 1.8	34.2 6± 3.2	35.8 ± 5.3	19.8 ± 3.8
Dynamic Viscosity (cP)	96 ± 9.7	17.59 ± 2.9	12.6	22.23 ± 5.6	42.63 ± 3.8
Methanol Insoluble Solids, MIM (wt%)	0.152 ± 0.094	0.16	0.58 ± .41	1.1 ± 0.236	0.27
Weight Average Molecular Weight (Da)	538 ± 26	551 ± 21	1200 ± 56	575 ± 65	610 ± 26

Elemental Analysis (%)					
C	49.9	40.7	33.6	36.7	46.9
H	7.0	7.7	8.3	7.8	7.4
N	0.1	0.1	0.2	0.3	0.1
O (R)	43.0	51.6	58.0	55.2	45.6
Elemental Analysis by ICP (%)					
C	48.2	44.0	31.5	43.1	46.8
N	0.3	0.3	0.5	0.4	0.3
S	0.1	0.1	0.2	0.1	0.2
Filtered Properties	**PCWF**	**PCWT**	**PWTF**	**PBF**	**CCWF**
pH	2.29 ± 0.02	2.2 ± 0.11	2.83 ± 0.12	2.33 ± 0.5	2.43 ± 0.06
Water Content (wt%)	9.11 ± 1.4	22.95 ± 0.83	34.26 ± 3.2	31.3 ± 2.3	14.3 ± 0.9
Dynamic Viscosity (cP)	345.4 ± 19	27.8 ± 0.62	11.4	17.14 ± 0.46	91.9 ± 5.4
Methanol Insoluble Solids, MIM (wt%)	0.162 ± 0.067	0.11 ± 0.015	-	0.041 ± 0.011	0.062 ± 0.054
Weight Average Molecular Weight (Da)	514 ± 14	514 ± 7	1120 ± 47	514 ± 23	603 ± 43

Analytical results showed that room temperature liquid (post-condensation) filtration of bio-oil through filter membranes will remove materials that contributed to the ash content, but further study should be performed comparing post-filtered bio-oil to improvements in bio-oil properties following hot gas filtration and/or liquid filtration just after condensation at elevated temperatures. The solid material found in the bio-oil indicates polymerization has occurred in the samples, which agrees with literature results. Due to the studies of liquid filtration problems at room temperature and the promising studies of filtration at higher temperatures cited in the literature of a centrifuge filtration system, provided by Westfalia Separators, Inc., filtering char particles from hot bio-oil immediately following condensation was considered an effective alternative to room temperature filtration. The condensed bio-oil will be at approximately 40-50 °C immediately following condensation. This temperature will lower viscosity and ensure the pyrolysis liquid does not plug up the system. To determine if the system could work in removing micron and submicron particles, a spin test was performed at Westfalia Separators, Inc. in Northvale, NJ, to determine the short-term effects of commercial centrifuge filtration. A spin test is an experiment that uses a test tube to hold a sample of bio-oil which is spun at high g-forces to determine the percent solids removed, the particle size distributions, and differences in solids types that exists between the material that is filtered and the material that is retained in the samples. Initial spin test results showed there were some settable solids present in the bio-oil that could be removed with centrifugation. This result indicates that a commercial centrifuge system should be able to remove solids from the 40-50 °C bio-oil. A major concern about the spin testing and centrifuge filtration is the bio-oil's low pH (2-3) that could damage wetted parts. Some studies, per literature review, indicate that stainless steel and Teflon are not affected by pyrolysis oil, but other materials such as brass, copper, cobalt, aluminum, and some polymers such as polyethylene can be greatly affected, especially at higher temperatures. Because of this concern, pyrolysis oil was produced from the auger reactor system and sent to Germany for

further testing to confirm that the pyrolysis oil does not affect the wetted parts or that the wetted parts do not alter the bio-oil's intrinsic chemistry. Further testing is also being done on spin tested samples (Figures H4 and H5). Results are pending. Attempts were made to determine the temperature versus centrifuge filtration relationship for MSU bio-oil. However, difficulties were found in maintaining the pyrolysis oil temperature. Various methods used in laboratory scale testing were found to be highly inaccurate and unable to replicate the conditions in the large-scale filtration unit.



Figure H4: Bio-oil samples before spin testing.



Figure H5: Bio-oil samples after spin testing showing significant removal of solids by centrifugation.

The large-scale filtration unit was approved as a sole source order by the state of Mississippi. The PO has been issued to GEA Westfalia by MSU. The unit is in production with an estimated shipping date provided by Westfalia of 10/25/12. Corrosion testing has not yielded any concerns, as low chloride contents (36 mg/L) were measured. During large-scale heated spin testing by the GEA Westfalia Separator Group in Oelde, Germany, the following spin conditions were used: 80 °C centrifugal cups; 6000 rpm; mean centrifugal acceleration of 4,500 × g (m/s²); spin times of 0.5, 1 and 2 min. The pyrolysis oil separated into three phases (top: water-rich, light brown/translucent, ~ 20 vol.% with ρ = 1.177 g/cm³ at 20°C; middle: oil-rich, dark brown/opaque, ~ 79.5 vol.%, pH = 2.7, ρ = 1.185 g/cm³ at 20°C; bottom: solids, black, ~ 0.5 vol.%). Similar separation results were observed with the addition of 0.1% citric acid/2 vol.% water prior to spin testing with 1.2 vol.% solids achieved (Figure H6). This information has led to modification in the equipment being ordered such that the equipment will now have variable configuration. The equipment can be configured to act as a simple centrifugal filter (clarifier) or

as a three-phase separator. The ability to separate the solids and also the water-rich and oil-rich phases of the pyrolysis oils will provide a higher quality oil and additional opportunities for downstream upgrading.

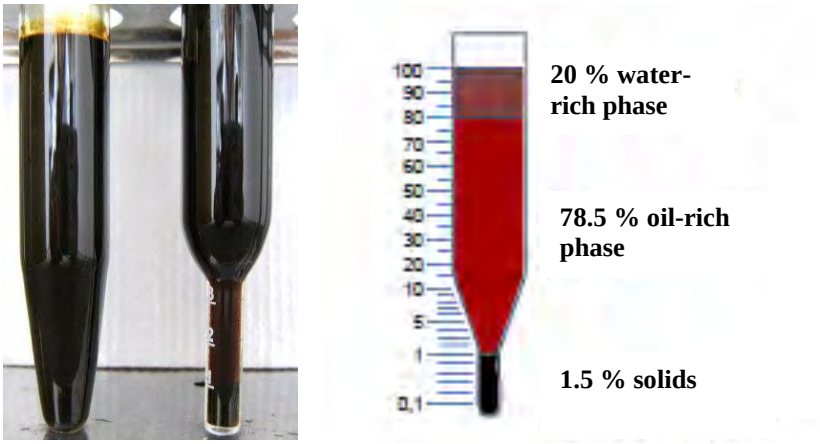
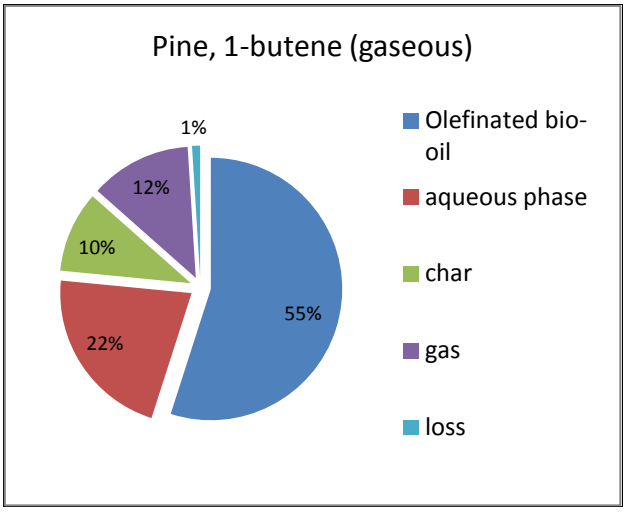


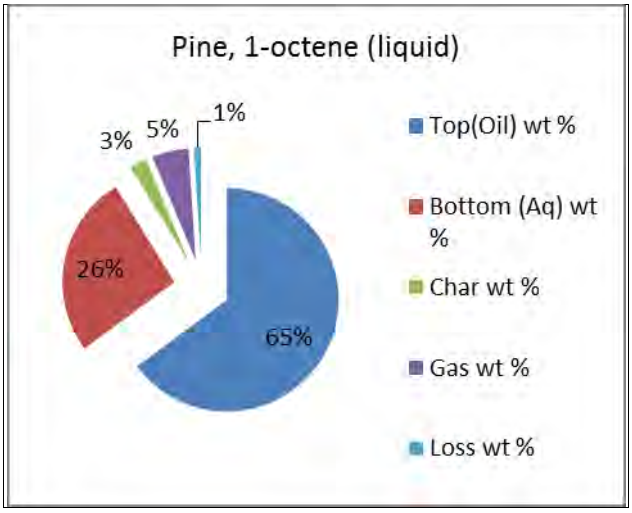
Figure H6: Bio-oil samples after large-scale heated (80 °C) spin testing showing significant removal of solids by centrifugation and separation of two liquid phases.

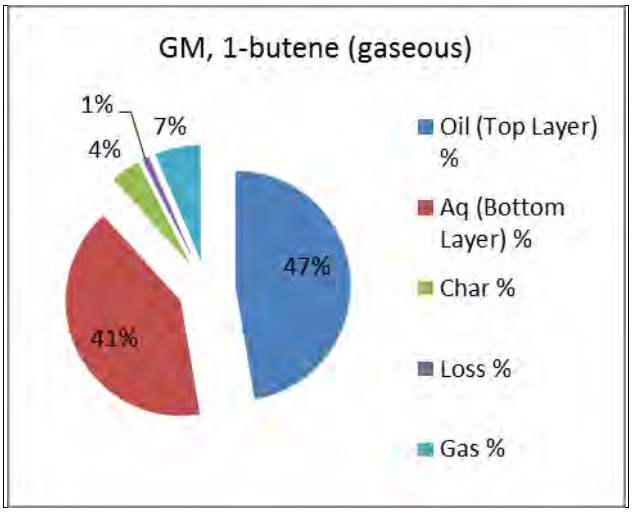
Once the unit is installed, it will be tested to determine separation efficiency, compatibility with auger produced bio-oil by MSU FP, and equipment integration and operation, both in batch and continuous operation modes. Locations of filtration equipment, associated tanks, piping and valves, electrical and air connections, and disposal mechanism for the filtered solids are being determined in conjunction with Energy Institute personnel.

Olefinated esterified bio-oil was produced from both pine wood and Giant Miscanthus (GM) bio-oil. Both liquid and gaseous olefins were combined with the bio-oil that was then catalytically treated in a heated stirred autoclave. Successful production of a viable esterified product requires addition of 20 to 30% alcohol(s) to prevent phase separation of the final esterified product. The liquid olefin tested was octane at 10% wt basis and the gaseous olefin was butane at 20 psi. The combined bio-oil, olefins, and alcohol were placed in a high pressure autoclave and stirred and maintained for 2 hours at the desired temperature. Water is fractionated during the olefination reaction, which is one of the strengths of the technology. Therefore, a two-phase liquid is produced. One phase is an esterified bio-oil fraction and the second phase is a water fraction. Char is also produced during this reaction. The water and esterified bio-oil fractions and char are easily separated by centrifuging the mixture followed by pouring off the two phases. This leaves the char which settles to the bottom of the centrifuge tubes. The water and esterified bio-oil are cleanly fractionated by the centrifuge process and the water is removed with a separation funnel. Physical and chemical properties (acid value, water content, and higher heating value) for each esterified/olefinated product were determined by ASTM D7544 standard specification for pyrolysis liquid boiler fuel and compared to the properties of a raw bio-oil as control. The mass balance of the esterification/olefination reactions is shown in Figure H7. For pine wood, gaseous olefin produced a 55 wt% yield of the esterified bio-oil while liquid olefin produced 65 wt%. Therefore, gaseous olefin yielded 15 wt% less than liquid olefin. For GM, gaseous olefin produced a 47 wt% yield of the esterified bio-oil while liquid olefin produced 53 wt%. Therefore, gaseous olefin yielded 11 wt% less than liquid olefin. Physical and chemical properties of raw bio-oil and upgraded bio-oil are listed in Table H8. The acid value of the pine bio-oil with liquid octene and gaseous butene was reduced by 36.4 and 52.6 wt%, respectively. For GM, the initial acid value was much higher than for pine wood at about 120 mg/g KOH. Following olefination, the GM acid value was reduced from 117.3 to about 56 mg/g KOH.

GC/MS analyses of raw bio-oil and pine and GM esterified product were compared.This comparison showed that the bio-oil carboxylic acid and aldehydes and ketones reacted with the olefins and alcohols to produce an esterification reaction. The products of this reaction were esters and acetals. The olefination reaction also dramatically reduced the initial bio-oil water content that ranged from 26% for pine bio-oil to 44% for GM bio-oil. Following the olefination reaction, water content in the esterified product was reduced to approximately 7% to 10%. The esters and acetals produced from the esterification reaction combined with the water content reduction resulted in a large increase in higher heating value (HHV) from their initial range of 5 to 14 MJ/Kg to a range of approximately 28 to 32 MJ/kg. These results are preliminary and we will continue to refine the olefination process in SERC IV.







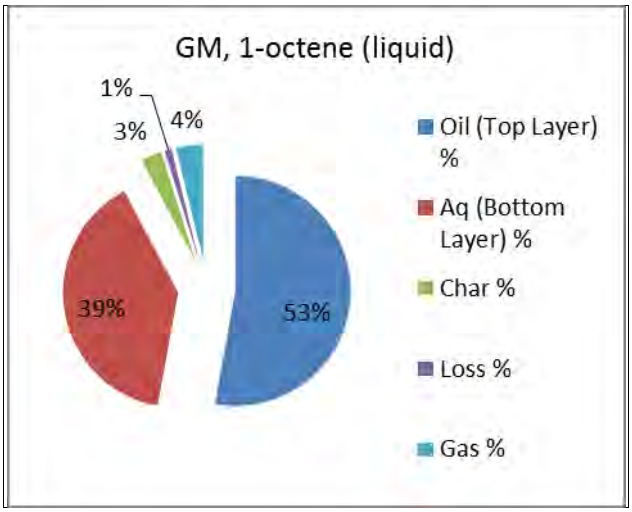


Figure H7: Mass balance of the esterification/ olefination reactions.

Table H8: Physical and chemical properties of raw bio-oil and upgraded bio-oil using 1-butene and 1-octene.

Physical and chemical properties	Raw	1-butene	1-octene
	Pine		
Acid Value (mg KOH/ g)	90.92	43.08	57.86
Water Content (wt %)	27.86	6.9442	6.03
HHV (MJ/kg)	14.35	30.4	32.72
	Giant Miscanthus		
Acid Value (mg KOH/ g)	117.28	59.09	56.63
Water Content (wt %)	44.06	7.16	13.42
HHV (MJ/kg)	7.76	31.44	27.8

Raw bio-oil is highly acidic and has high oxygen content. Upgraded bio-oil suitable as a transportation fuel has been produced from hydrodeoxygenated oil (HDO) to produce mixed hydrocarbons with zero oxygen and zero acid value. This process can be performed by two

methods:application of HDO in a batch reactor and application of HDO with a continuous packed bed reactor. Batch reactors can be used at the lab scale and are easy to operate. Batch reactors are used primarily to perform the initial experiments of catalysts to determine their feasibility for HDO upgrading. All industrial processes utilize continuous reactors to render the HDO process economical. Our current HDO research was performed in a high-pressure continuous packed bed reactor fabricated at MSU. Various catalysts were prepared by the impregnation method to test the HDO process in the packed bed reactor. The bio-oil was passed through the packed bed reactor at 350 ^{o}C temperature utilizing hydrogen gas at 1000 psi to react in the catalyst bed in the reactor column. The oil from the packed bed was cooled in a condenser and collected for analysis. We analyzed the bio-oils produced in the packed bed reactor for acid value, oxygen content, hydrogen content, carbon content, nitrogen content, and HHV. The results obtained from the HDO process are shown in Figure H8 and Table H9. In Figure H8 the results are compared with the bio-oil as control and 1st HDO obtained from batch process (in batch process the bio-oil is treated in a stirred reactor at 350 ^{o}C for 3 hours at 1500 psi of hydrogen to produce the 1st stage HDO).

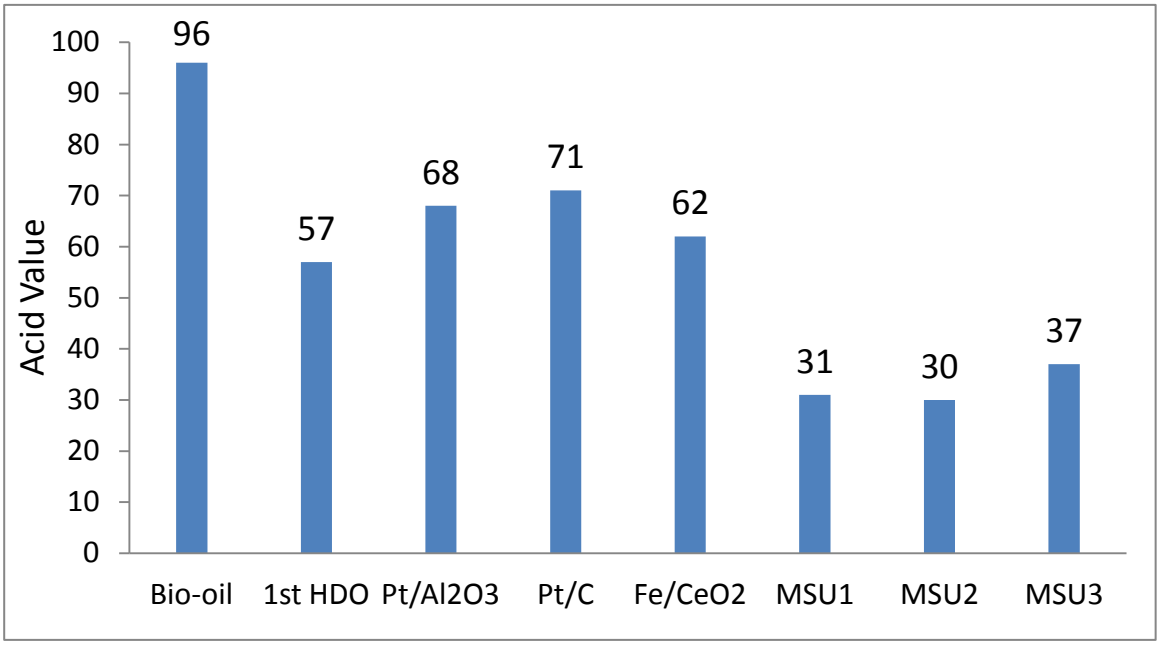


Figure H8: Acid value by catalyst type for the catalysts tested in the packed bed reactor

Figure H8 gives the acid value for the catalysts tested. These acid values indicated that there was a relatively substantial reduction in acid value that ranged from 26 to 69% as compared to the value of 96 mg/g KOH for raw bio-oil. The process showed promising results based on lower acid value, using MSU1 and MSU2 based on lower acid value, higher HHV, higher carbon content and higher hydrogen content. In addition, water content for these two catalysts was below 2%.

Table H9: Chemical analysis of HDO oil from packed bed reactor.

	Acid value	HHV MJ/kg	% C	% H	% N	% Remaining	% water content
Raw bio-oil	90.84	12	37.5	7.7	0.03	54.63	29.41
1st HDO	57.53	33.26	72.3	9.75	0.2	17.71	3.38

MSU1 catalyst	31	41.31	79	10.62	0	10.37	1.86
MSU2 catalyst	30.67	38.06	76.26	10.23	0.36	13.15	1.88
MSU3 catalyst	37.69	37.19	70.77	10.22	0	19.33	2.49

The MSU1 and MSU2 catalysts indicate very promising results toward the goal of producing a transportation fuel by means of HDO applied by a continuous packed bed reactor. Future experiments will be performed in SERC IV to otimize the catalysts with various other combinations to achieve production of mixed hydrocarbons of drop-in fuel quality.

The patented MSU pyrolysis reactor design was fabricated to a 5-ton per day scale (see Figure H9). The reactor is fully computer controlled to allow most of the operation to be performed from the operator's booth (Figure H10). The reactor was thoroughly tested to determine that computer instructions to motors, heaters, etc. function properly. Biomass has been pyrolyzed and bio-oil made. A continuous stirred reactor of 5-gallon capacity was custom built by a vendor to allow both first-stage HDO and esterification to be performed at large scale.



Figure H9: Photograph of scaled-up MSU pyrolysis reactor.



Figure H10: Computer control modules automating the scaled-up MSU pyrolysis reactor.

Subtask H.2 Develop laboratory scale catalytic pyrolysis reactor

Partial upgrading of bio-oil by deoxygenation during the pyrolysis step has the potential to produce a product useable directly as heating fuel and one that is stabilized for transport. In addition, the partially deoxygenated product will be more easily upgraded by full deoxygenation at a later stage. A proprietary MSU technology to increase the reaction speed of low-cost catalysts in the pyrolysis reactor for partial deoxygenation of bio-oil will be developed in an existing 10 kg/h pyrolysis reactor.

1. Planned Activities:

H.2.ML.1 The bio-oils produced by this method will be partially hydrogenated with resultant characteristics of 30% less oxygen and acid value compared to raw bio-oils, and 30% of water content will be partially fractionated from the product.

2. Actual Accomplishments:

We hypothesized that catalytic pyrolysis of torrefied wood may produce a relatively highly upgraded bio-oil compared to bio-oil that is normally produced. Our initial research to test our hypothesis was performed at micro-scale by py-GC/MS methods. Pine wood was torrefied in the MSU auger reactor. We tested seven catalysts produced by impregnation method to perform the py-GC/MS catalytic pyrolysis. These catalysts are listed in Table H10. Loblolly pine wood was utilized to perform the catalytic pyrolysis at both the micro and laboratory scale with the pine wood ground to powder. The catalytic pyrolysis py-GC/MS studies were performed with catalysts in a 1:1 (w:w) ratio with the pine wood. The pine flour was mixed with the catalysts and placed in a quartz tube and pyrolyzed with the vapor entrained into the CDS pyroprobe and on into the GC/MS. The pyrolysis temperature was maintained at 550^{0}C with a heating rate of 10°C/ms and residence time of 10 sec. Table H11 summarizes the area percentages by functional group. The most important functional group in our results is the hydrocarbon functional group. The hydrocarbon yields for these catalysts is very low or zero. Therefore, we concluded that these catalysts were relatively ineffective at the catalyst proportion tested for catalytic pyrolysis as we applied it in this experiment. Due to the relatively high cost of these catalysts, we did not test higher catalyst ratios for these catalysts. For these reasons, no further

analysis or additional testing were performed for these catalysts for pine wood, and we decided to focus on a new approach.

Table H10: Catalyst types tested to determine catalytic activity and products.

Cat. No.	Catalyst name
1	Palladium
2	Ruthenium
3	Ni-HZSM-5
4	5% platinum on AC
5	Ni-Si-Al
6	MSU catalyst
7	1% platinum on Al

Table H11: Catalytic pyrolysis yields in area percentage by functional group.

Treatments	Ketones	Acid	Hydrocarbon	Phenol	Ester	Furan	Aldehyde
Control	8.809	1.415	0	15.772	0	0	2.297
Palladium	6.117	0.548	4.194	44.069	0	0	0
Ruthenium	12.177	0.797	1.842	39.175	0	1.716	0
Ni-HZSM-5	2.023	1.82	1.487	33.53	0	0	7.049
Platinum on AC	6.807	2.075	1.528	49.943	0	2.177	0
MSU 1	14.027	0	4.413	35.627	0	2.823	0
MSU	14.034	5.065	0	12.645	1.148	6.058	12.307
Platinum on Al	12.799	1.928	0	23.701	0	3.126	6.047

Based on Table H11, results at a biomass to catalyst ratio of 1:1, the hydrocarbon yield for all the catalysts was low. We next increased the biomass to catalyst ratio to 1:5. For this higher ratio of catalyst, we showed the best results for a zeolite catalyst. The hydrocarbon yield was 67.2%, as shown in Figure H11. The py-GC/MS results for the zeolite catalyst with torrefied wood are very promising. In SERC IV we will continue these SERC III catalytic pyrolysis tests to apply our method at larger scale.

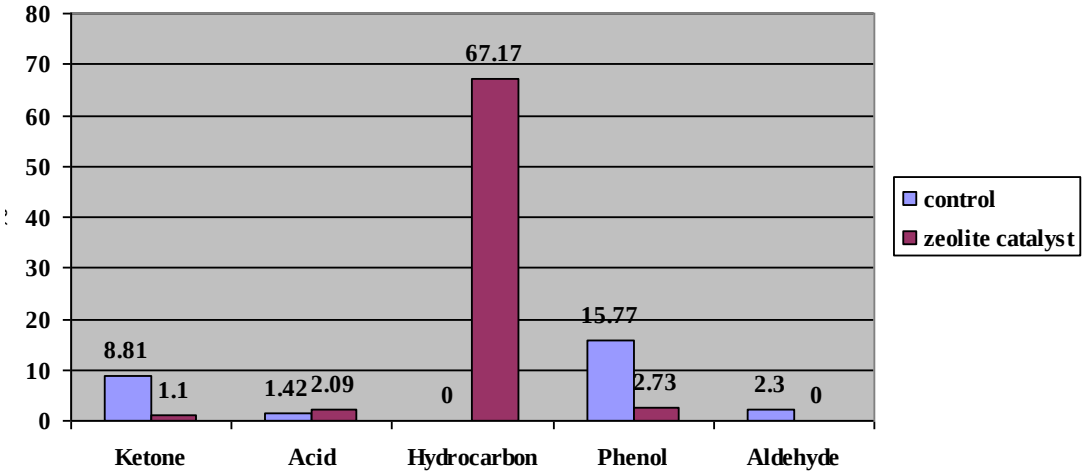


Figure H11: Results of pyrolysis on zeolite catalyst for biomass to catalyst at 1:5 ratio.

Our new approach was to test catalytic pyrolysis with torrefied wood. This was followed by performing catalytic pyrolysis on the torrefied wood. Torrefied wood produces bio-oil with reduced oxygen content and removes most of the hemicellulose and biomass moisture. Therefore, producing torrefied wood prior to pyrolysis allowed us to start with a less recalcitrant feedstock for the bio-oil produced. We could locate no previous studies that applied catalytic pyrolysis to torrefied wood, so we had no previous data as to how this less recalcitrant feedstock may respond to the catalytic pyrolysis treatments. We tested the catalytic pyrolysis of torrefied wood utilizing the same 7 catalysts plus 2 combinations of these same catalysts to perform catalytic pyrolysis. The proportion of catalyst to biomass was maintained at a 1:1 ratio and the same py-GC/MS conditions of 550^0C with a heating rate of 10^oC/ms and residence time of 10 seconds were applied. Code names for the catalysts (Table H12) were utilized to prevent loss of any intellectual property related to the catalysts mixed together.

Table H12: Code names of catalysts utilized in the experiments.

Cat. No.	Catalyst name
1	Cat 1
2	Cat 2
3	Cat 3
4	Cat 4
5	Cat 5
6	Cat 6
7	Cat 7
8	Cat 8
9	Cat 9

Table H13 gives the results in terms of area percent by functional group for each of the 9 catalysts tested. Examination of the hydrocarbons produced shows that two of the catalysts were far superior to the remaining seven. The yields for these catalysts were approximately 69 wt% and 74 wt% for Catalysts 3 and 2, respectively.

Table H13: Catalytic pyrolysis py-GC/MS area percentage yields by functional group.

	Acid	Alcohol	Aldehyde	Ester	Furan	Hydrocarbon	Ketone	Phenol
Control	9.565	0.469	8.421	2.518	7.202	4.293	28.532	19.088
Cat 1	8.444	11.108	4.908	3.376	8.871	21.842	8.277	3.262
Cat 2	4.72	0.47	0.329	0.974	0.332	74.299	0.847	0
Cat 3	0	1.523	2.111	1.133	0.703	68.709	0	0
Cat 4	0.306	2.064	8.768	3.546	0	0	0	58.505
Cat 5	0.684	0.738	1.965	0	5.986	41.231	16.792	5.362
Cat 6	0	0.383	5.85	4.409	2.086	4.351	13.558	52.344
Cat 7	1.148	0.735	1.313	1.006	0	48.519	17.77	4.184
Cat 8	2.519	0.829	5.698	0	25.658	28.191	6.534	1.435
Cat 9	2.323	0	0.666	1.443	20.534	20.9	20.939	8.583

These py-GC/MS results show highly promising results compared to catalytic pyrolysis of non-torrefied pine wood.

Subtask H.3 Maximize bio-oil anhydrosugars for production of ethanol

1. Planned Activities:

H.3.ML.1 Replicated experiments will optimize the initial results that provided the 50% increase in anhydrosugars to attempt to attain a yield of 55%. The specific anhydrosugars produced by the procedure will be identified. The process to produce monomeric sugars will be refined and yields determined precisely. Inhibitors will be identified and removed to allow ethanol to be produced at one-half the level obtained by grain ethanol practices.

2. Summarization of Activities:

Levoglucosan is the major anhydrosugar component of bio-oil produced by fast pyrolysis. Previous research has shown that levoglucosan yield can be greatly increased if a mild acid pretreatment is applied to demineralize the feedstock prior to pyrolysis. The interest in levoglucosan production provides a route to production of monomeric sugars, primarily glucose, which can be utilized to produce biochemically derived fuels (ethanol, butanol, etc). This study developed a new method based on pyrolysis of clear pine wood particles with acid pretreatment and modification of the pyrolysis process. This new method resulted in a 15.1% increase in levoglucosan yield in a single condenser (Condenser 2.) when water spray was applied with a novel condenser temperature manipulation method. The results indicated that this method successfully condensed large fractions of the sugar-rich bio-oil aqueous fraction into a single condenser (Condenser 2.). Most importantly, a significantly greater than 10% yield increase in anhydrosugars in the total bio-oil was produced by the water spray method. This increase may change the process economics of production of anhydrosugars via pyrolysis. The experimental treatments applied in this study are given in Table H14: pine biomass untreated with acid and

without spray applied, pine treated with acid and without spray applied, pine treated with acid and with spray applied, and pine untreated with acid and with spray applied. The biomass weights pyrolyzed and the weights of water spray applied for the control and spray treatments are also given in Table H14. The yield of char, bio-oil, and gases is shown in Table H15 for the four treatments.

Table H14: Treatments and biomass and spray volumes applied.

Treatment no.	Control and spray treatments	Biomass weight (g)	Water spray weight (g)
1	Biomass untreated; no spray	2070	0
2	Biomass pretreated; no spray	1359	0
3	Biomass untreated; spray	1562.5	183
4	Biomass pretreated; spray	1567.5	170

As see from Table H15, acid pretreatment increased char yield slightly, resulting in a small decrease in the yield of bio-oil. Table H16 results indicate that acid pretreatment significantly reduced the formation of carbon monoxide, carbon dioxide, and methane during fast pyrolysis. Reduced pyrolysis gas formation may have resulted because acid pretreatment removes minerals from biomass which may serve as catalysts for more complete carbohydrate thermal degradation into non-condensable gases, particularly carbon monoxide, carbon dioxide, and methane. Relatively high nitrogen content in the non-condensable gases was expected due to the fact that nitrogen was utilized to purge the reactor of oxygen. For oxygen and ethane, the concentration levels were almost the same among the four treatments.

Table H15: Percentage yields of bio-oil, char, and non-condensable gases based on feedstock weight.

Treatments	Percentage yield based on feedstock weight (wt. %)		
	Whole bio-oil	Char	Non-condensable Gases[a]
Biomass untreated; no spray	64	21	15
Biomass pretreated; no spray	60	22	18
Biomass untreated; spray	61	21	18
Biomass pretreated; spray	59	26	15

[a]The yield of non-condensable gases was not measured but calculated by subtraction.

Table H16: Non-condensable gas composition for the four treatments.

Treatments	Gas components in mole percentage (%)							
	H2	O2	N2[a]	CH4	CO	CO2	C2H6	Unknown[b]
Biomass untreated; no spray	0	0.31	42.59	5.75	28.08	18.18	0.49	4.6
Biomass pretreated; no spray	0	0.11	72.69	2.07	11.97	10.01	0.16	2.99
Biomass untreated; spray	0	0.42	43.65	5.65	27.38	18.05	0.51	4.34
Biomass pretreated; spray	0	0.47	75.08	1.53	10.49	9.91	0.1	2.42

[a] High percentage of nitrogen was due to the initial purging of nitrogen into the pyrolysis reactor system prior to each run.
[b] The percentage of unknown gases was calculated by subtraction.

The levoglucosan concentration increased from 8.66% for Treatment No. 1 (Biomass untreated without spray) to 14.04% for Treatment No. 2 (Biomass pretreated without spray), and further increased to 15.52% for Treatment No. 4 (Biomass pretreated with spray). From the GC

analysis results of non-condensable gases in the previous section, acid pretreatment significantly reduced the formation of carbon monoxide, carbon dioxide, and methane that appeared to result from acid pretreatment removal of minerals from biomass which serve as catalysts for carbohydrate complete degradation into non-condensable gases. Therefore, liquid production of levoglucosan replaced decomposition of levoglucosan into gases. Our results also indicate that the novel application of appropriate condenser temperatures by this method successfully condensed large fractions of the sugar-rich bio-oil aqueous fraction into a single condenser. Levoglucosan weight percentage yield by treatment for each of Condensers 1 to 4 is given in Table H17. Table H17 shows that the levoglucosan yields provided were much higher for condensers 1 and 2 as compared to those for Condensers 3 and 4. The levoglucosan content of Condenser 2, however, is accompanied by high water content. It was found that this high water content bio-oil in Condenser 2 self-fractionated, allowing the capture of the aqueous fraction. The pyroligneous fraction can be utilized for various purposes, but by our preferred embodiment, this fraction is to be combined with the bio-oil contents of Condensers 1, 3, and 4.

Table H17: Levoglucosan distribution by weight percentage by treatment for each of condensers 1 to 4.

Treatment applied	levoglucosan content (percent)			
	Cond. 1	Cond. 2	Cond. 3	Cond. 4
Biomass untreated; no spray	41.72	42.03	11.77	4.49
Biomass pretreated; no spray	39.2	46.62	9.84	4.34
Biomass untreated; spray	43.46	41.59	7.91	7.04
Biomass pretreated; spray	34.02	53.68	8.82	3.47

Table H18 shows the results of the application of our preferred method in terms of total water content contained in the bio-oil contents of Condensers 1, 3, and 4 combined with the self-fractionated pyroligneous fraction from Condenser 2.These values show that total water content by each treatment range between 12 and 16%. These low water content values will give a starting bio-oil a water content 10 or more percentage points lower than the approximate 25% water content assumed for well-manufactured bio-oil of high quality. Finally, a high-quality bio-oil with low water content that is more easily converted to fuels results from the combination of all products but the self-fractionated aqueous fraction from Condenser 2.

Table H18: Water content (weight percentage) contained in the bio-oil contents of condensers 1, 3, and 4 combined with the self-fractionated pyroligneous fraction from condenser 2.

Water content (percent)	Treatment applied
12.27	Biomass untreated; no spray
14.88	Biomass pretreated; no spray
13.79	Biomass untreated; spray
15.55	Biomass pretreated; spray

Table H19 compares the yield increase of levoglucosan for the water spray method to that without water spray for biomass that has been pretreated as described above. The increase for Condenser 2 condensate from the water spray treatment was 53.68 wt% compared to 46.62 wt% for the treatment without water spray. Therefore, the water spray treatment resulted in a levoglucosan yield increase of 15.1%. The increased yield from the total bio-oil production was obtained by combining the contents of Condensers 1 to 4 for both treatments. The levoglucosan yield for the no-spray treatment was 14.04 wt%, while that for the spray treatment was 15.52 wt%. Therefore, the yield increase for the total bio-oil was 10.5%.

Table H19: Levoglucosan content (weigh percentage) of combined bio-oils from condensers 1-4 and from condenser 2.

Condenser 2 only (percent)	Condensers 1-4 (percent)	Treatment applied
46.62	14.04	Biomass pretreated; no spray
53.68	15.52	Biomass pretreated; spray

The device and method developed in this study provides a means to greatly increase anhydrosugars yield produced from pyrolysis of biomass feedstock. This increase is achieved by injection of a liquid spray into the vapor stream of any pyrolysis reactor type just prior to the reactor condensers. A fractional condensation system employed by our pyrolysis reactor is also a novel element of this study. This system condenses bio-oil pyrolysis vapors to various desired fractions by manipulation of condenser temperature applied by differential heating or cooling of the condensers. An embodiment of our fractional condensation system makes it possible to condense most of the water contained in a pyrolysis vapor stream into a single condenser. The high amount of water contained in this condenser causes self-fractionation, which allows separation of the aqueous and pyroligneous fractions of bio-oil. The aqueous fraction contains a high percentage of anhydrosugars that may be utilized to produce fuels or chemicals. The pyroligneous fraction, with the removal of compounds that foul catalysts, is more easily utilized for catalysis to hydrocarbon fuels. The primary problem with the fermentation of lignocellulosic hydrolysate is the presence of inhibitors that slow or stop microbial growth. These inhibitors must be removed or inactivated in order to detoxify the sugar containing aqueous fraction enough to be fermented. Complicating this issue is the fact that there are over one hundred different compounds present in the lignocellulosic hydrolysate, and many of them have the capability to slow microbial growth to prevent ethanol production. Also, when these compounds are present together, they have more of an inhibitory effect than when present alone. Therefore, this research also seeks to remove as many inhibitory compounds as possible while maintaining a high glucose concentration in the hydrolyzed water fraction of high-sugar bio-oil. Microorganisms can also be developed to resist the effects of inhibitory compounds such as phenols, carboxylic acids, and furans. Genetically engineered yeasts or bacteria can be used for this purpose. Also, adaptive evolution is a technique utilized to increase resistance to the presence of inhibitors. Activated carbon is a form of carbon that is usually derived from charcoal. It is a very porous material, thus it has a large surface area in which a vast array of chemicals can adhere to it. It is commonly used to remove toxic materials from gasses and liquids. Although it is capable of removing phenolic compounds, it can also remove the sugars present in the hydrolysate. Researchers are trying to find a method to utilize activated carbon to remove inhibitory compounds while removing as little sugar as possible. There are several factors that can affect the efficiency of the adsorption to the activated carbon. Temperature, residence time, and amount of activated carbon all can affect how well the inhibitors can be removed. Lian et al. claim to have used activated carbon to detoxify the hydrolysate while maintaining a glucose concentration of 70 g/L (w/v) of glucose. Air stripping is a technique used to convert volatile liquids into gases. It is often used in the cleanup of wastewater containing volatile compounds. Volatile compounds are characterized by a low aqueous solubility and a high vapor pressure. Volatile compounds have a high Henry's constant. Compounds with high Henry's constants are more capable of being removed by air stripping methods. An increase in temperature results in an increase in the Henry's law coefficient. Thus, utilizing air stripping for volatile compound removal becomes more efficient at higher temperatures. Residence time and pH can also affect inhibitor removal using air stripping. At a lower pH, volatile acids can be removed, while at a higher pH, ammonium can be removed. However, when longer residence

times and higher temperatures are utilized, evaporation of water becomes a problem with this method. Overliming is a process that can reduce the presence of phenol and furan derivatives by utilizing pH. The hydrolysate pH is adjusted from an approximate pH of 3 to 10-11. This results in a solid precipitate that can be filtered out. This precipitate contains a mixture of furan and phenol containing compounds. The pH can then be adjusted back down to approximately 5. This can result in more phenol and furan precipitation that can be removed. However, this technique can also result in a loss of fermentable sugars as well. As with the above methods, residence time and temperature can affect the efficiency of overliming techniques. An increase in temperature can increase the removal of phenols and furans; however, it also increases the amount of acetic and formic acid produced during the reaction. This technique is used to target specific chemicals to be removed from a solution based on the solubility of the chemicals. Two phases result due to the immiscibility of the different solutions. Usually the two phases consist of water and an organic solvent. Non-polar and polar solvents can be utilized to remove different chemicals present in the lignocellulosic hydrolysate. In some cases, multiple solvents are used to increase efficiency or to extract multiple compounds. One problem associated with using this technique is that it can introduce more inhibitory compounds to the mixture. Also, the solvent must be removed prior to extraction. Another potential removal technique is to use microbes that can digest inhibitory compounds without consuming the glucose. This method is desirable as it would not introduce more compounds to the system that would inhibit fermentation. The problem with this method is that there are very few known microbes that can digest phenols without consuming glucose. However, a bacterium known as Cupriavidus basilensis has recently been found to consume dichlorophenol, benzene, phenol, toluene, furfural, and hydroxymethylfurfural (HMF) without consuming glucose. This has the potential to remove some of the more potent inhibitors while maintaining glucose. Furthermore, this bacteria has proven to convert furan derivatives, namely HMF, into 2,5-furandicarboxylic acid. This compound is now considered one of the priority chemicals for green energy of the future by the U.S. Department of Energy. It is a renewable chemical that can take the place of terephthalic acid for the production of aromatic polymers and polyesters. Thus, advances in this research could yield a dual purpose result in producing a renewable polymer building block and detoxifying the lignocellulosic hydrolysate for ethanol fermentation. Adaptive evolution results from mutations that can occur in an organism as a result of exposure to environmental challenges. In this case, the ethanol producing microorganisms could adapt to develop a resistance to the inhibitors present in the aqueous fraction of bio-oil. This could eliminate the need for a detoxification step if the microbes could adapt to grow and produce ethanol in the presence of inhibitory compounds. Temperature, pH, low substrate concentrations, and inhibitors can all cause microbial evolution. There are several mutation models that can be used to portray the adaptation process. The first is the cryptic growth model. Here, the environmental conditions do not cause the mutations. However, the mutations occur randomly, and most of the mutated organisms are the ones that survive. Next is the directed mutation model. In this model, genetic mutations are targeted to directly alleviate the environmental stress. Finally, the hypermutation model hypothesizes that there are many mutations along the genome. Although many of the mutations do not relieve environmental stresses, some of them are helpful, and those that have helpful genes survive. These theories can be used to model microbial growth as several generations of colonies can be grown in stressful conditions to create a mutant that is resistant to the presence of phenol and furan derivatives. Below is the result of detoxification of bio-oil hydrolysate by using activated carbon, air stripping, overliming, and solvent extraction. Tests were conducted to determine the exact concentration of bio-oil hydrolysate that was necessary to inhibit the yeast from growing in the medium. The YPD medium was autoclaved separately to ensure the chemical composition would not change for the most accurate results. Pure glucose YPD medium, 1% (v/v) aqueous fraction in YPD medium, 5% (v/v) aqueous fraction in YPD medium, 10% (v/v) aqueous fraction in YPD medium, and 20% (v/v) aqueous fraction in YPD

medium, and 30% (v/v) aqueous fraction were all tested for glucose consumption after 24 hours. The results are shown in Table H20. The inhibitory compounds present in the aqueous fraction of bio-oil are able to completely inhibit the yeast growth in concentrations greater than 10% hydrolysate.

Table H20: Effect of bio-oil hydrolysate on glucose consumption.

Medium	Glucose consumed (g)
0% hydrolysate	19.82
1% hydrolysate	17.76
5% hydrolysate	4.97
10% hydrolysate	0.8
20% hydrolysate	0.00
30% hydrolysate	0.00

Even at levels as low as 5% of hydrolysate, only about 25% of the glucose is consumed by the yeast. This analysis demonstrates the necessity of detoxification of the bio-oil hydrolysate in order to efficiently be capable of fermenting all of the glucose into ethanol. Activated carbon, air stripping, overliming, and solvent extraction methods are common ways of attempting to remove the inhibitors from the bio-oil hydrolysate. As mentioned earlier, the success of these methods is based on the amount of the compound quantified by a GC/MS and the retention of fermentable glucose measured by HPLC. The targets of these results are the phenolics, furan derivatives, and volatile organic acids. Activated carbon shows promising results in removing inhibitory compounds. The prior test resulted in successful fermentation of aqueous fraction treated with activated carbon. When removing the phenolics and furan derivatives, however, glucose was also removed. When 1% (w/v) of activated carbon was mixed with the aqueous fraction, the glucose was maintained while inhibitory compounds were significantly removed. Glucose concentration remained at 35 g/L, while the acetic acid concentration decreased from a GC/MS percent area of 10.67 to 0.88 and the furfural concentration decreased from a GC/MS percent area of 2.45 to 0.55. This is a 92% reduction in acetic acid and a 78% reduction in furfural on the GC/MS area percentage basis. Air stripping methods did not result in sufficient volatile acid removal. At temperatures of both 25°C and 60°C, the glucose concentration increased as a result of evaporation of water from the hydrolysate. Glucose rose from 35 g/L to 39 g/L at 25°C and from 35 g/L to 60 g/L at 60°C. This method was only analyzed for glucose concentration. After the glucose concentration increased, it can be assumed that the concentration of other heavy molecules in the solution increased as well. Therefore, even if the acetic acid present in the aqueous fraction was removed, the phenol and furan concentration increased as well. As these are both significant inhibitory factors, air stripping cannot sufficiently remove enough compounds to allow for successful fermentation. Overliming methods were utilized to attempt to remove inhibitory compounds. After the pH was elevated and allowed to settle over night, the phenols present in the aqueous fraction were removed. However, the glucose concentration was also cut in half. This method can also introduce other compounds that can inhibit the fermentation of the bio-oil hydrolysate. Thus, this method is inconclusive until the resulting treated hydrolysate can be tested for fermentation. Solvent extraction methods included equal portions of linoleic acid and hydrolysate and equal portions of hexane and hydrolysate. The linoleic acid extraction resulted in maintenance of 35 g/L of glucose while acetic acid is reduced by 73% and furfural is reduced by 61% on the basis of GC/MS area. Hexane extraction of the bio-oil hydrolysate also maintained the glucose concentration of 35 g/L, an acetic acid reduction of 78%, and a furfural reduction of 38% by GC/MS area. These methods both significantly removed microbial inhibitors. However, they could have also added new compounds that could potentially hurt cell growth. The GC/MS and HPLC results are displayed in Tables H21 and H22.

Table H21: Glucose concentration after treatment.

Treatment	Glucose (g/L)
None	37.87
Hexane	35.39
Linoleic Acid	36.17
Air Strip at 25°C	38.71
Air Strip at 60°C	70.82
Activated carbon	36.4

Table H22: Acetic acid and furfural gc/ms area percentage after treatment.

Treatment	Acetic acid (area %)	Furfural (area %)
None	10.67	2.45
Hexane	2.33	1.51
Linoleic Acid	2.88	0.95
Activated carbon	0.88	0.55

Cupriavidus basilensis was aseptically placed into a broth containing 50% (v/v) of the aqueous hydrolysate and allowed to grow for three days. The GC/MS results show that little, if any, phenolic or furan compounds were consumed by the bacteria. Also, no furan dicarboxylic acid was found. This could largely be in part to the high concentration of acetic acid that was present even after the media was neutralized by NaOH. Even though about 2 g/L of cell mass was produced in the medium after three days, no phenolics, furans, or glucose was consumed. This method of inhibitor removal was not effective in this study. However, it could be more efficient if combined with other removal methods. Adaptive evolution techniques were conducted by inoculating plates ranging from 10% (v/v) to 20% (v/v) hydrolysate and exposing some plates that grow colonies to UV light to produce mutations that could help the yeast become resistant to the aqueous fraction. After ten inoculations to attempt to attain inhibitor resistance, the 10% (v/v) hydrolysate plates were the most in which the yeast could grow. 20% (v/v) hydrolysate plates show no colony growth. And even on the 10% (v/v) hydrolysate plates, the colonies were significantly smaller than the pure YPD agar colonies. This method needs significantly more transfers to show any results of improved cell growth at higher hydrolysate concentrations. This is shown below in Figure H12.

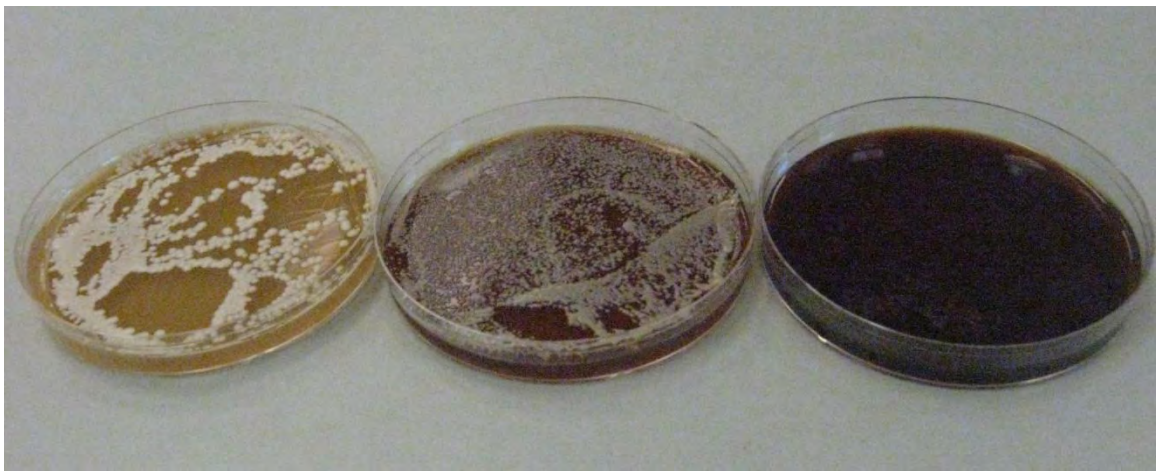


Figure H12: Image of yeast colony growth after 10 transfers. Notes: from left to right: pure glucose YPD agar, 10% (v/v) hydrolysate, 20% (v/v) hydrolysate.

The compositional analysis of the green pine wood was performed according to National Renewable Energy Laboratory Technical Report NREL/TP-510-42618 (Table H23).

Table H23**:** Compositional analysis for green pine wood.

Sample	Moisture Content	Elemental analysis				Sugars, %				
		% C	% H	% N	% O	Glucan	Xylan	Galactan	Arabinan	Mannan
Green Pine wood	69.0	40.3	7.53	0.06	52.1	43.81	5.42	1.39	1.38	13.68

In order to optimize the pretreatment conditions, green pine wood was pyrolyzed without any pretreatment (control) and also treated with 1% phosphoric acid at different biomass/treatment solution ratio (1:3, 1:4.5 and 1:6). The yields of oil, char, and gas were determined and recorded in Table H24.

Table H24: Oil, char, and gas yields of different pyrolyzed green pine wood.

Pretreatment ratio	Oil Yield, %	Char Yield, %	Gas yield*, %
Control	52	18	30
1:3	65	20	15
1:4.5	63	20	17
1:6	63	20	17

Catalyst Concentration= 1%
Mixing time: 1 hr at room temperature, temp.: 95°C for 2 hrs.
* By Difference

The aqueous fraction bio-oil was isolated and the sugar contents were determined using HPLC chromatography. Sugars in aqueous fraction bio-oils were hydrolyzed using sulfuric acid according to the reported method by National Renewable Energy Laboratory (NREL). The results of sugar analysis are shown in Table H25. From these results, we conclude that the biomass to pretreatment solution (1:4.5) was the optimum ratio. In order to determine the optimum catalyst concentrations, green pine wood was treated with 3 different concentrations of phosphoric acid catalyst (0, 0.5, 1 and 2%). The results are given in Table H26.

Table H25: Sugar content for the aqueous fraction bio-oil prepared at different biomass to treatment solution ratios.

Condition	Glu-cose	Xy-lose	Galac-tose	Arabin-ose	Man-nose	Levo-glu-cosan	Total conc. (g/100 g bio-oil)	MW
(Control)	6.15	1.09	1.24	1.59	2.87	2.52	15.46	160
(1:3)	9.80	1.01	1.57	0.68	4.31	0.30	17.67	160
(1:4.5)	14.92	4.09	0.43	0.83	2.28	0.69	23.23	160
(1:6)	10.35	1.09	1.70	0.68	5.17	1.46	20.45	160

Table H26: Oil, char, and gas yields of different pyrolyzed green pine wood.

Catalyst concentration	Oil Yield, %	Char Yield, %	Gas yield*, %
0 (control)	52	18	30

0.5%	68	17	15
1%	65	20	15
2%	47	23	30

Biomass/treated solution ratio=1:3
Mixing time; 1 hr at room temperature, temp.; 95°C for 2 hrs.

The aqueous fraction bio-oil was also isolated and the sugar contents were determined using HPLC chromatography. The results of sugar analysis are shown in Table H27.

Table H27: Sugar content for the aqueous fraction bio-oil prepared at different catalyst concentrations.

Condition	Glu-cose	Xy-lose	Galact-ose	Arabin-ose	Man-nose	Levo-glu-cosan	Total conc. (g/100 g bio-oil)	MW
(Control)	6.15	1.09	1.24	1.59	2.87	2.52	15.46	160
0.5%	12.91	4.00	0.95	0.91	2.49	2.77	24.03	160
1%	9.80	1.01	1.57	0.68	4.31	0.30	17.67	160
2%	13.13	2.91	1.04	0.77	2.12	2.80	22.77	160

From the above results we concluded that:

- 0.5% is the optimum catalyst concentration
- 1:4.5 is the optimum biomass to pretreated solution ratio.

Aqueous fraction hydrolysis was aimed at identifying the hydrolysis conditions to improve overall free monomeric sugars in the aqueous fraction samples. The aqueous fraction bio-oil was isolated by mixing the bio-oil and water in a ratio of 1:1. Bio-oil water mixture was left overnight to allow separation of bio-oil into bio-oil and aqueous fractions. The aqueous fraction of eight different bio-oils (control and seven pretreated bio-oils) were isolated and used for the next hydrolysis steps. The amount of sulfuric acid used for hydrolysis was determined based on the pH for each aqueous fraction sample according to the standard method of National Renewable Energy Laboratory for determination of sugars byproduct in liquid fraction (NREL/TP-42623).
The difference between aqueous fraction sugar composition before and after hydrolysis steps are shown in Figures H13 and H14. Figure H13 shows that most of the sugars in the aqueous bio-oil fraction exist as anhydrosugars, especially levoglucosan. Separation of anhydrosugars from the aqueous fraction is very difficult. Therefore, a sulfuric acid hydrolysis step was performed to convert most of the anhydrosugars into monomeric sugars as shown in Figure H3. Separation of all low molecular weight sugars from the aqueous fraction bio-oil can then be achieved by reverse osmosis (RO) membrane. RO membrane technology was utilized to separate the monosugars produced from the hydrolyzed aqueous fraction.

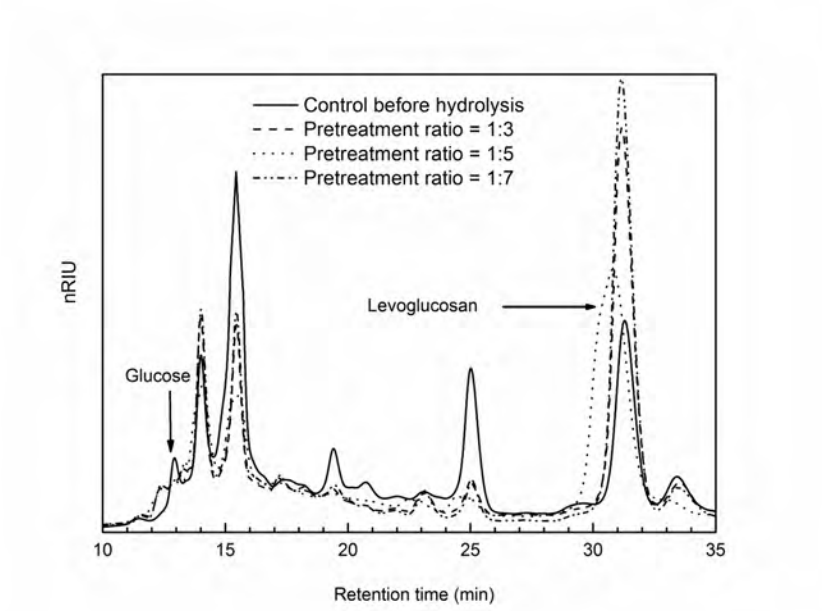


Figure H13: Effect of treatment conditions on the sugar concentrations of aqueous fraction bio-oil before hydrolysis.

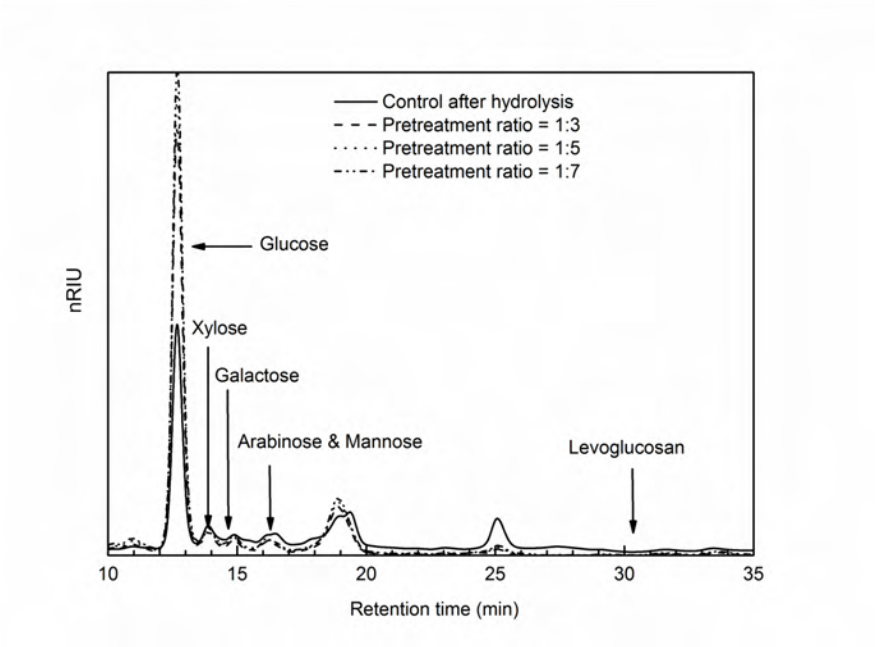


Figure H14: Effect of treatment conditions on the sugar concentrations of aqueous fraction bio-oil after hydrolysis.

Monosugars recovery from the aqueous fraction solutions was achieved in single stage RO filtration process. The specific objectives of this part of study were to investigate the ability of the RO membrane to concentrate hydrolyzed monomeric sugars in aqueous fraction solutions enough to be easily separated in powder form by using freeze drying. To evaluate the process parameters and the efficiency of membrane, the filtration experiments were performed for aqueous fraction solutions by using a flat sheet RO membrane filtration unit (Alfa Laval Test

Unit M20) with an active surface area of 0.018 m^2 (Alfa Laval-RO90). The flow mode in this filtration unit was cross flow. In this cross flow filtration system the feed solution was pumped from the feed tank (volume 3.0 L) to the membrane module by using a Hydra-cell pump. The pressure over the membrane can be varied by using a control valve. During filtration, the retentate flows back to the feed tank. The filtration runs were performed with RO membrane to investigate the membrane ability to concentrate monosugars in the retentate at constant temperature. The pure water flux (PWF) tests were performed at the beginning and at the end of the run to detect any membrane fouling. The fouling was determined based on the difference between the pure water flux before (PWFb) and after (PWFa) the process solution filtration.

$$\text{Fouling (\%)} = \frac{PWFb - PWFa}{PWFb} \cdot 100\%$$

The mass flux (Jm) for the membrane can be determined by the following equation.

$$J_m = \frac{m_p}{A_m}$$

m_p: mass flow rate of permeate (Kg/h)
A_m: membrane surface area (m^2)

The selectivity of the membrane for a solute is described by rejection. The rejection which can be observed (Ro) is defined by equation:

$$R_o = 1 - \frac{C_p}{C_b}$$

Where:
C_p: concentration of solute in permeates.
C_b: concentration of solute in the solution on high pressure side of membrane (feed side).

Table H28: Sugar analysis of aqueous fraction bio-oil, permeate, and retentate after the RO membrane filtration process and determination of the selectivity of the membrane toward sugars.

	Glucose	Levoglucosan	Other Sugars*	Total Sugars	Fouling (%)
Feed	15.09	0.51	9.47	24.97	
Permeate	4.30	0.44	2.53	8.34	25.0
Retentate	7.92	0.67	4.28	12.89	
Rejects(R_0)	0.73	0.13	0.73	0.66	

* Xylose, mannose, galactose and arabinose

RO membrane experiments were performed to concentrate the monosugars in the aqueous fraction, i.e. reducing the volume of the water solvent. The results of the first experiment represented in Table H28 showed that the hydrolysate fouled strongly (25 %). According to Table H28, the rejection factor for the total sugars was 0.66, and the rejection factor for glucose, other sugars, and levoglucosan were 0.73, 0.62, and 0.13, respectively. Thus, the RO membrane has higher selectivity toward glucose and other sugars than towards levoglucosan. The presence of low molecular weight lignin fragments (phenolic compounds) with monosugars in the concentrated aqueous solution prevented extraction of the monosugars in pure form, in addition to the strong sticky property of the sugars after the freeze drying stage. Also, the

phenolic compounds represent a protective barrier that prevents enzymes or bacteria for conversion of monosugars to fuel. For the conversion of sugars portion in the aqueous fraction to fuel, the monosugars must be extracted without contamination by phenolic compounds and other fermentation inhibitors so that microorganisms can utilize the pure extracted monosugars. The prevalence of dimeric to tetrameric phenolic lignin, produced from pyrolytic decomposition, in hydrolyzed aqueous fraction with water and a plethora of compounds of many classes caused hindrance to separate the monosugars in pure form and also caused inefficient performance via RO membrane separation. Due to the presence of such phenolic compounds in the hydrolyzed aqueous fraction, monosugars acquired a hygroscopic property. This task was aimed to determine whether it was technically feasible to apply a solvent-solvent separation technique which was dependent on using immiscible organic solvents with the hydrolyzed aqueous solution containing a mixture of chemical species having various solubility capabilities in the aqueous phase and immiscible organic solvent phase. Two layers (organic layer and aqueous layer) were formed due to the addition of immiscible organic solvent to the hydrolyzed aqueous solution. The immiscible organic solvent was able to extract phenolic compounds from the aqueous phase to form an organic layer and consequently the concentration of phenolic compounds in the aqueous phase was reduced. As a result, the aqueous solution, containing monosugars, after solvent-solvent separation can be concentrated by using the RO membrane, and subsequently the monosugars can be purified from a big portion of related phenolic compounds by freeze drying. In our study, two organic solvents were used (n-butanol and ethyl acetate) with the hydrolyzed aqueous solution in solvent-solvent separation processes. The quantity of each solvent was added to a known volume of the aqueous solution based on the volume of organic solvent to the volume of aqueous solution (1:1). The addition of required amount of solvent was added in a 2L separating funnel. The upper layer was the organic solvent layer which was rich with phenolic compounds and the lower layer was the aqueous layer which was rich with monosugars. After the solvent-solvent separation process, the remaining phenolic compounds in the aqueous layer were checked by using UV/visible spectrophotometry. The monosugars in the produced aqueous layer were concentrated by performing the RO membrane filtration process and then the concentrated solution was freeze dried to obtain a yellowish white powder. Effect of utilization of ethyl acetate in the solvent separation stage is shown in Table H29. Use of ethyl acetate reduced the rejection factor of the total sugars (0.62) experienced earlier. The permeate flux (108 $Kg/h.m^2$) and fouling of membrane (16.44%) in case of ethyl acetate separation were still higher than for not performing the solvent separation stage. The produced monosugars after ethyl acetate treatment possessed a sticky property which strongly hindered the effectiveness of the purification step. The effect of butanol separation stage on the membrane performance and sugars concentration is shown in Table H30. With *n*-butanol treatment, the phenolic content was reduced in the solution. After the *n*-butanol separation step, the amount of phenolic compounds was negligible and there was an improvement in membrane performance which exhibited itself as a higher rejection factor than that in the absence of butanol. Also, the permeate flux was 165 $Kg/h.m^2$ and the fouling factor was13.7%. Therefore, the use of butanol in the separation stage enhanced the selectivity of the membrane towards the monosugars concentration and enabled us to obtain monosugars mixed with traces of polyphenolic compounds in addition to disappearance of the sticky property related to the presence of phenolic compounds (Figure H15). Comparing the membrane performance for both *n*-butanol and ethyl acetate, we found that *n*-butanol separation stage had higher phenolic extraction efficiency than did ethyl acetate treatment. Also, the amount of phenolic compounds associated with the monosugars produced after the ethyl acetate separation stage was higher than for the *n*-butanol separation stage. Therefore, separation by n-butanol is the superior method for obtaining monosugars with maximum purification.

Table H29: Effect of solvent separation stage on the concentration of sugars after membrane filtration.

Solvent		Glucose	Levoglucosan	Other Sugars*	Total Sugars
	Feed	15.09	0.51	9.47	24.97
Ethyl Acetate	Permeate	2.26	0.24	5.08	9.38
	Retentate	7.68	0.11	5.16	12.84
	Rejects(R_0)	0.85	0.52	0.46	0.62
n-butanol	Permeate	4.08	0.14	3.91	8.13
	Retentate	10.43	0.38	6.9	17.71
	Rejects(R_0)	0.73	0.71	0.58	0.67

* Xylose, mannose, galactose and arabinose

Table H30: Effect of solvent stage on membrane fouling.

	Mass flow rate of permeate (kg/h)	Mass flux (kg/hm^2)	PWFb (kg/hm^2)	PWFa (kg/hm^2)	Fouling (%)
Ethyl Acetate	1.08	108	335	280	16.4
n-butanol	1.65	156	315	272.7	13.7



Figure H15: Sugar isolated after ethyl acetate purification step (left) and sugar separated after n-butanol purification step (right).

UV spectrophotometer analysis of the aqueous layer was performed following solvent separation. Figure H16 shows UV analysis to determine the effect of using ethyl acetate and *n*-butanol for minimizing the phenolic compound concentration in hydrolyzed aqueous solution. UV analysis was applied on four aqueous fraction solutions: aqueous fraction solution without solvent separation stage, aqueous fraction solution after ethyl acetate separation (1:1), aqueous fraction after butanol separation, and aqueous fraction solution after *n*-butanol separation (1:1 and 3:1). The results demonstrated the success of the solvent-solvent separation technique to reduce the concentration of phenolic compounds in the aqueous phase of the hydrolyzed solution. As shown in Figure H16, soluble lignin fragments and phenolic compounds have a very characteristic peak at 272 cm-1 wave number. The intensity of this peak, and accordingly the concentration of lignin and phenolic compounds, was remarkably decreased applying solvent-solvent separation. The concentration of phenolic compounds in the aqueous layer for *n*-butanol

separation was lower than that in case of ethyl acetate separation at the same solvent to aqueous fraction ratio (1:1). In case of n-butanol separation with solvent to aqueous (3:1), the remaining phenolic concentration in aqueous layer was negligible, which was demonstrated by the flat peak in UV analysis representing phenolic compounds. Therefore, the use of *n*-butanol enabled us to obtain an aqueous fraction solution containing monosugars without phenolic compounds. This is considered an important stage in order to separate monosugars in pure form.

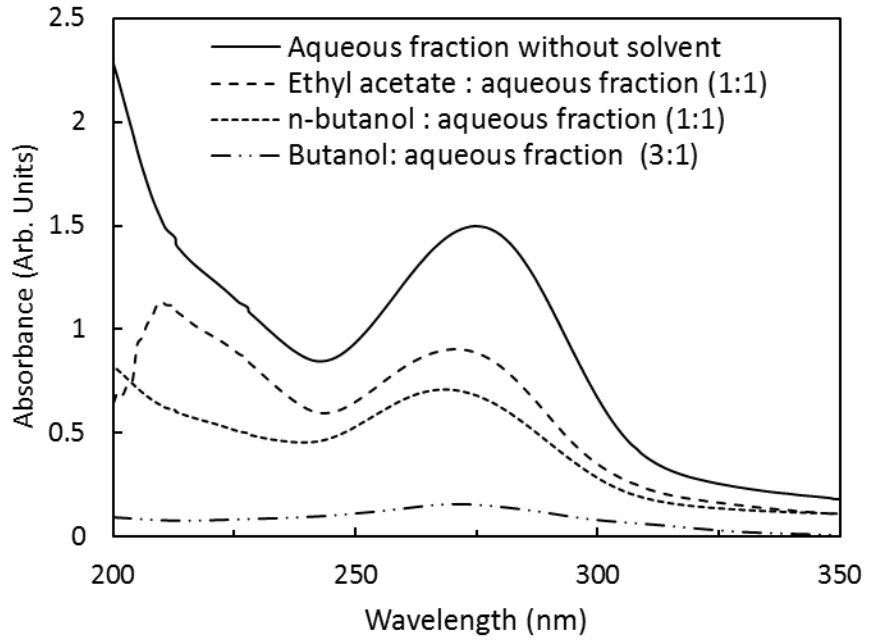


Figure H16: UV absorbance for aqueous fraction bio-oil before and after solvent separation step.

GC-MS analysis was performed to determine the nature of organic compounds existing in the organic layer after the solvent-solvent separation step and in the bio-oil before the water fractionation step (raw bio-oil). The results of GC-MS analysis for raw bio-oil, the organic layer of ethyl acetate and *n*-butanol fractions are shown in Figure H16 and Table H30. As expected, raw bio-oil and both organic layers were composed of many lignin and carbohydrate degradation products such as ketones, aldehydes, phenols, organic acids, esters, and aromatic compounds. GC-MS data shows that raw bio-oil contains a considerable amount of anhydrosugars (Area % = 25.59) compared with very small amounts of anhydrosugars (Area % $\approx$ 1%) after fractionation and the solvent separation step. These results coincide with the HPLC data showing that more than 25% of anhydrosugars were produced at the optimum pretreatment step. The results also show that high molecular weight fatty acids (tetradecanoic acid, oleic acid) and terpenoid (stigmastan-3,5-diene) compounds appear only in the raw bio-oil. This result means that the water fractionation step was very effective in eliminating high molecular weight compounds from the aqueous fraction bio-oil. Low molecular weight compounds such as furfural and non-aromatic ketones which were mainly produced from carbohydrate fraction or lignin degradation phenolic compounds exist in both unfractionated (raw bio-oil) and the organic layer of fractionated bio-oil. We note that non-aromatic ketones consisted principally of saturated and unsaturated cyclic ketones such as 2-cyclopetene-1,4-dione, 1,2 cyclopentanedione-3-methyl, 2-furylhydroxymethyl ketone, and levoglucosenone predominated in the aqueous fraction solution because they possessed higher percentage of *n*-

butanol or ethyl acetate layer than that in raw bio-oil. Lignin degradation phenolic compounds such as phenol and phenol derivatives existed mainly in the hydrolyzed aqueous fraction bio-oil rather than the oil fraction because of their high percentage in both *n*-butanol and ethyl acetate layers. One chemical compound (2-furanethanol, beta-methoxy) showed a very high tendency at retention time 11.55 min in case of ethyl acetate layer compared with *n*-butanol and raw bio-oil. From the above results one can conclude that the aqueous phase from fast pyrolysis contained mostly low molecular weight phenolic degradation products. Nonaromatic ketones and phenols are the main organic compounds that were identified in the hydrolyzed aqueous phase.

Subtask H.4 Produce hydrogen from process and pyrolysis process heat

Production of hydrotreated bio-oil requires an economical source of hydrogen to render this an economic technology. MSU will utilize process heat from pyrolysis and other industrial sources to produce hot water at near 1000°C. Water at this temperature can utilize electrolysis to split the water molecules to produce hydrogen with about half the electrical energy normally required. This source of energy can, therefore, produce hydrogen from the water produced during bio-oil hydrotreating. The project will begin with experiments with hot water heated by other means than from combustion of pyrolysis byproducts.

1. Planned Activities:

H.4.ML.1 Produce hydrogen at a cost equivalent to that for production from current methane systems at 2006 prices. Hydrogen purity will be equivalent to methane system industrial hydrogen.

2. Summarization of Activities:

Catalytic reforming of bio-oil model compound (acetic acid) was performed using nanonickel/γ-Al_2O_3 catalyst. Effects of various process variables, including reaction temperature, pressure, and feed flow rate (FFR) were studied by taking 20 wt% acetic acid aqueous solutions. While high temperatures favored the production of hydrogen and CO, lower temperatures increased the yield of methane and carbon oxides such as CO_2. Production of CO in the product gas was evident only at temperatures above 500 °C, and yield increased with reaction temperature. Increasing reaction pressure decreased hydrogen yields and increased the production of CH_4 and CO_2.While complete conversion of acetic acid to gas products was achieved at temperatures higher than 550 °C, ketonization reactions leading to the formation of acetone took place at lower temperatures. Thermogravimetric analysis performed on the used catalysts showed that increasing acetic acid concentrations in the feed increases catalyst coking. Catalysts can be completely regenerated at 650-675 °C. A nickel nanocatalyst (NNG) was prepared by mechanical mixing of required loading (10 wt%) of nickel nanoparticles (<100 nm particle size) (Sigma-Aldrich) with the catalyst support (γ-Al_2O_3). The nickel nanocatalyst (NNG) was directly used without any pre-treatments. Catalytic reforming experiments were carried out in a fixed bed continuous up-flow reactor (316 SS – 0.5" O.D) system, consisting of a HPLC pump (Shimazdzu LC-20) to pump the aqueous acetic acid solution, a flow controller unit (three mass flow controllers), the reactor unit, and the analysis unit (Shimadzu GC equipped with FID and TCD detectors). The experiments were performed under N_2 flow controlled using an MFC. The liquid feed is aqueous acetic acid solution of known composition which is mixed with the N_2 gas stream and passes through a pre-heating zone maintained at ~320 ^{o}C at the bottom of the reactor before entering the catalytic reactor. Catalyst of 1g with particle size of 500-1000 μm is placed at the center of the reactor with Quartz wool at both the ends. Remainder of the reactor

is filled with glass beads to maintain uniform temperature through the reactor. Heating of the reactor was provided using an electrical furnace. Catalyst bed temperature was monitored by a K-type thermocouple placed inside the reactor. Catalyst performance experiments were conducted as a function of reaction temperature (°C), feed flow rates "FFR" (mLpm), and reaction pressure "P" (Psig), keeping the acetic acid concentration constant (20 wt%). At each process variable the reaction was carried out for at least five hours, such that steady state conditions were achieved. The composition of gas product was analyzed by Shimadzu GC equipped with thermal conductivity detector (TCD) and flame ionization detector (FID). GC-MS analysis was performed on the liquid product samples. TGA was performed on the used catalysts to determine the amount of residual carbon deposited on the catalyst surface. A Shimadzu TGA-50 instrument was used to perform the TG analysis. A required amount of catalyst was placed on an alumina pan and a temperature program from room temperature to 1000 ^{o}C at a ramping rate of 5 ^{o}C/min was used. The runs were performed under a N_2 flow of 30 mL/min. Percentage weight loss of the used catalysts was determined from TGA analysis.

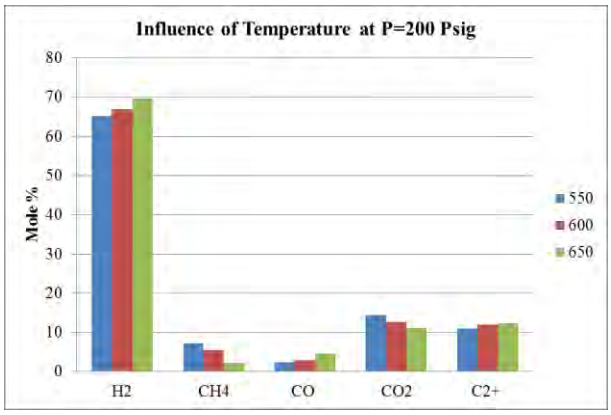


Figure H17: Influence of reaction temperature on the product distribution at P=200 Psig.

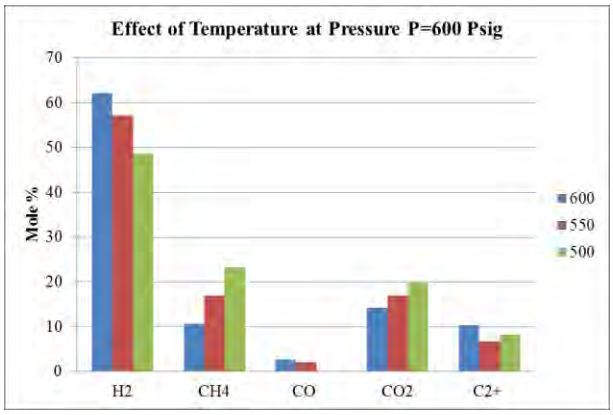


Figure H18: Influence of reaction temperature on the product distribution at P=600 Psig.

The influence of reaction temperature on the catalytic behavior of NNG catalyst in the conversion of acetic acid to hydrogen rich product gas was studied at two different reaction pressures (200 and 600 Psig). From Figures H17 and H18, significant differences in terms of activity and product distributions could be noticed as a function of temperature. High reaction temperatures clearly favored the production of hydrogen and CO, while lower temperatures increased the production of CH_4 and CO_2. Not only did the temperature affect acetic acid conversion, but it also significantly influenced the product distribution. At temperatures of 550 ^{o}C and lower, formation of acetone was evident from the liquid sample analysis, indicating that the

ketonization reactions occurred at low reaction temperatures. Increase in the yield of methane at low temperatures indicates that methanation of CO occurs and therefore decreases the hydrogen yield in the product gas. Catalytic reforming involved the cleavage of both C-C and C-H bonds in acetic acid molecule on the metal surface of the catalyst thereby resulting in the formation of H_2, CO, CO_2, CH_4 and C_{2+} gases as products. From Figure H18, it is evident that CO production is not favored at low reaction temperatures (500 ^oC). This indicates that the water gas shift reaction is sensitive to temperature, and is more favorable at lower temperatures.

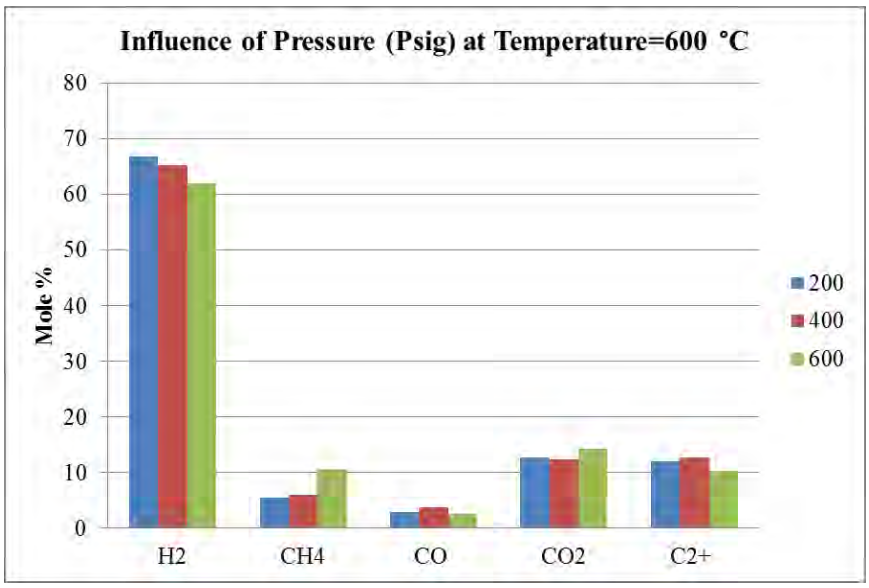


Figure H19. Influence of reaction pressure on the product distribution at T=600 ^oC.

Influence of three different pressures on the catalytic performance was investigated at 600 ^oC, keeping the FFR constant at 0.2 mLpm. Results shown in Figure H19 indicate that low pressures are favorable for attaining maximum conversion of acetic acid to hydrogen rich product. While low to moderate pressures (200-400 Psig) favored the production of hydrogen, the experiments conducted at 600 Psig produced high yields of methane (methanation) and CO_2 in the product gas. Increase in the yields of CH_4 and CO_2 at high reaction pressures might be due to CO methanation and the decomposition of acetic acid, thereby indicating that high reaction pressures favor methanation and decomposition reactions. Conversion of acetic acid to H_2 rich product gas was found to be a function of FFR. Figure H20 shows that H_2 production increased with flow rate and the methanation reactions and the production of CO_2 increased with decrease in FFR. At low space velocities (higher residence time), CO and H2 molecules produced by the cleavage of C-C and C-H bonds in the acetic acid molecule tends to undergo methanation reactions on the catalyst surface with increasing residence time, and therefore form more CH_4. Increasing yields of CO_2 with decreasing FFR might be due to two reasons: 1.) higher residence time might facilitate the decomposition reactions; 2.) since the effect of FFR was studied at 500 ^oC where water-gas shift reactions are quite favorable, more CO_2 is formed from CO and H_2O in the feed.

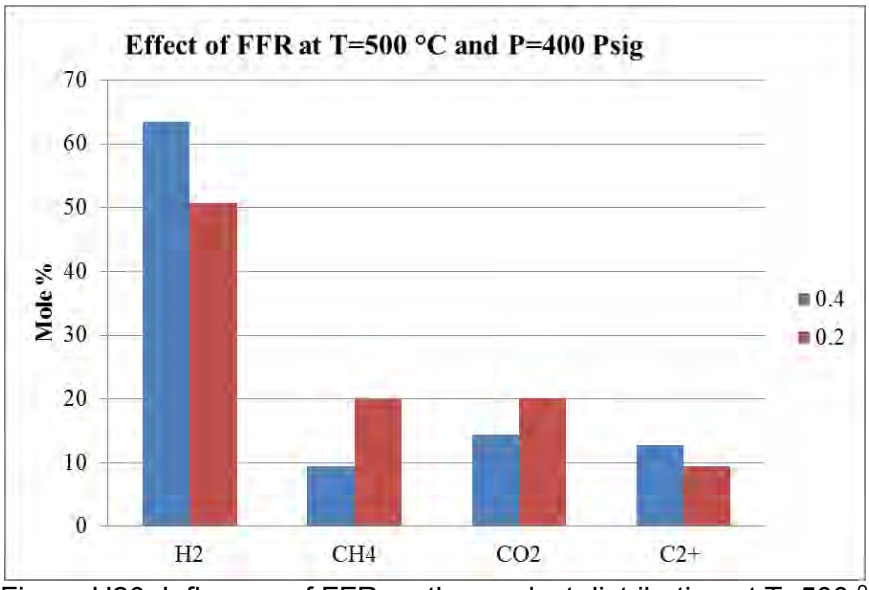


Figure H20: Influence of FFR on the product distribution at T=500 °C and P=400Psig.

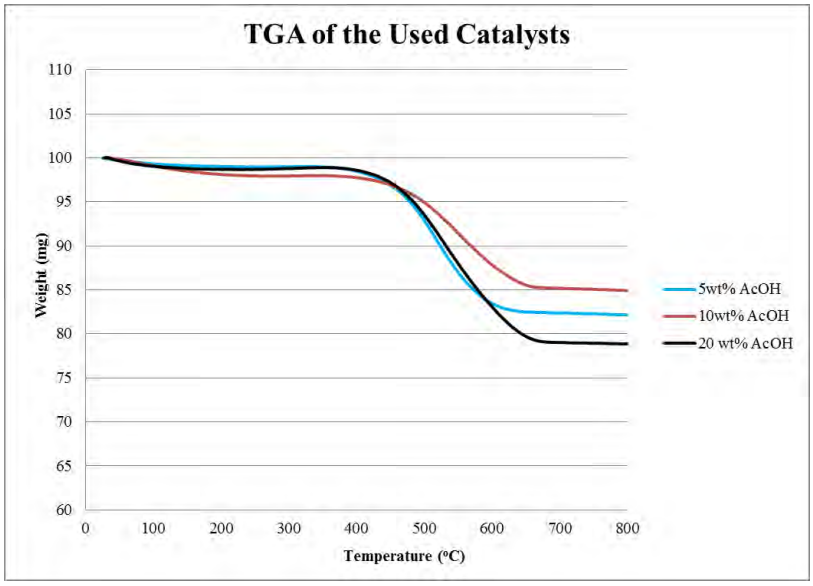


Figure H21: TGA curves of the used catalysts.

Thermogravimetric analysis was performed on the nickel nanocatalysts used for reforming acetic acid aqueous solutions of three different concentrations (5, 10 and 20 wt%). Figure H21 shows that carbon deposition on the catalyst surface (coking reactions) increased with increasing concentration of acetic acid in the feed. The initial weight loss of the catalyst samples at 100-120 °C is due to the evaporation of adsorbed water from the catalyst. Increase in acetic acid concentration results in the greater amount of reactions to occur on the active sites of the catalyst. Some of the C_{2+} hydrocarbons or CH_4 produced during reforming reactions tends to undergo aromatization within the catalyst pores and therefore form polyaromatics. These polyaromatics cannot escape the catalyst pores due to their larger size, and hence get deposited inside the pores. Coking may also occur on the catalyst surface. The TG curves indicate that catalysts can be completely regenerated at 650-675 °C.

Patents:

Three patent applications.

Publications:

Badger, P., S. Badger, M. Puettmann, P. Steele and J. Cooper. 2011. Techno-economic analysis: Preliminary assessment of pyrolysis oil production costs and material energy balance associated with a transportable fast pyrolysis system. BioResources 6(1):34-47.

Gajjela, Sanjeev K., E.B.M. Hassan, B. Mitchell, and P.H. Steele. 2011. Hydrocarbons from woody biomass. In Woody Biomass Utilization: Proceedings of the International Conference on Woody Biomass Utilization, Starkville, MS, August 4-5. 2009. Edited by John R. Shelly (Madison, WI. Forest Products Society), pp.23 – 30. ISBN-13:978-1-892529-60-2.

Lippke, Bruce, R. Gustafson, R. Venditti, T. Volk, E. Oneil, L. Johnson, M. Puettmann, P.H. Steele. 2011. Sustainable biofuel contributions to carbon mitigation and energy independence. Forests (2):861-874.

Mao, A., S.Q. Shi, P.H. Steele. 2011. Flakeboard bonded with PMDI/bio-oil adhesive systems. Forest Products Journal 61(3):240-245.

Mohan, D., S. Rajput, V.K. Singh, P.H. Steele and C.U. Pittman, Jr. 2011. Modeling and evaluation of chromium remediation from water using low cost bio-char, a green adsorbent. Journal of Hazardous Materials 188:319-333.

Mohan, D., A. Saraswat, V.K. Singh, M. Alexandre-Franco, C.U. Pittman, Jr. 2011. Development of magnetic activated carbon from almond shells for trinitrophenol removal from water. Chemical Engineering Journal. Published on-line: doi:10.1016/j.cej.2011.06.054.

Steele, Philip H., F. Yu, and S. K. Gajjela. 2011. Past, present, and future production of bio-oil. In Woody Biomass Utilization: Proceedings of the International Conference on Woody Biomass Utilization, Starkville, MS, August 4-5. 2009. Edited by John R. Shelly (Madison, WI. Forest Products Society), pp.17 – 22. ISBN-13:978-1-892529-60-2.

Wang, H., Srinivasan, R., Yu, F., Steele, P., Li, Q., and Mitchell, B. 2011. Effect of acid, alkali and steam explosion pretreatments on characteristics of bio-oil produced from pinewood. Energy and Fuels. 25:3758-3764.

Wang, H., R. Srinivasan, F. Yu, P. Steele, Q. Li, B. Mitchell, A. Samala. 2012. Effect of acid, steam explosion and size reduction pretreatments on bio-oil production from sweetgum, switchgrass and corn stover. Applied Biochemistry and Biotechnology (accepted).

Zhang, Z., Q. Wang, P. Tripathi, C.U. Pittman, Jr. 2011. Catalytic upgrading of bio-oil using 1-octene and 1-butanol over sulfonic acid resin catalysts. Green Chemistry. 13:940-949.

Hassan, E., Abouyousef, H., and Steele, P. H. (2011) Increasing the Efficiency of Fast Pyrolysis Process through Sugar Yield Maximization and Separation from Aqueous Fraction Bio-oil *Fuel Processing Technology*, **(In Review)** The FWRC manuscript number FP 625.

Mohan, D., R. Sharma, V.K. Singh, P.H. Steele, C. Pittman. 2012. Fluoride removal from water using bio-char, a green waste, low-cost adsorbent: Equilibrium uptake and sorption dynamics modeling. Industrial & Engineering Chemistry Research. 51(2):900-914.

Naske, C.D., P. Polk, P.Z. Wynne, J. Speed, W.E. Holmes, K.B. Walters. 2012. Postcondensation filtration of pine and cottonwood pyrolysis oil and impacts on accelerated aging reactions. Energy & Fuels 26(2):1284-1297, DOI: 10.1021/ef200541d.

Penmetsa, K., P.H. Steele. 2012. Preliminary findings for the production of water repellent torrefied wood pellets with pyrolysis oil. Environmental Progress & Sustainable Energy. 31(2):235-239.

Pittman, C.U., Jr., D. Mohan, A. Eseyin, Q. Li, L. Ingram, E. M. Hassan, B. Mitchell, H. Guo and P. H. Steele. 2012. Characterization of Bio-oils Produced from Fast Pyrolysis of Corn Stalks in an Auger Reactor. *Energy & Fuels, dx.doi.org/1021/ef30039221.*

Conference Proceedings:

Gajjela, S.K., P.H. Steele, E.M. Hassan, B.K. Mitchell. 2011. Production of hydrocarbons via catalytic hydroprocessing of giant miscanthus bio-oil. American Chemical Society, Division of Fuel Chemistry 56(1):24-26.

Yu, F., E.M. Hassan, L.L. Ingram, Jr., P.H. Steele. 2008. Esterification of bio-oils in the presence of sulfated iron oxide catalyst. American Chemical Society, Division of Fuel Chemistry 53(2):859-860.

Scientific/Professional Papers/Presentations:

Gajjela, S.K., P.H. Steele. 2011. Production of heating and transportation fuels via fast pyrolysis of biomass. Southeastern Society of American Foresters Annual Meeting. 2/20/2011 - 2/22/2011. Tallahassee, FL.

Hassan, E.M., P.H. Steele, Q. Li, B.K. Mitchell. 2011. Optimization of fast pyrolysis process towards more sugars as an alternative route for chemicals and fuels. 31st Southern Forest Tree Improvement conference. 6/13/2011 - 6/16/2011. Biloxi, MS.

Li, Q., P.H. Steele, E.M. Hassan, B.K. Mitchell. 2011. Characterization of bio-oils produced from fast pyrolysis of lignocellulosic biomass. Southeastern Natural Resources Graduate Student Symposium. 3/2/2011 - 3/4/2011. Starkville, MS. Plenary.

Li, Q., P.H. Steele, F. Yu. 2011. Converting biomass to sugars via pyrolysis. BIT's 1st Annual World Congress of Bioenergy - 2011. 4/25-30/2011. Dalian, CHINA.

Livingston, D., F. Yu, Q. Li, and P. Steele, 2011. Ethanolic Fermentation of Bio-oil Hydrolysate. S1041 (The Science and Engineering for a Biobased Industry and Economy) Symposium. August 2, 2011. Stillwater, OK.

Parapati, D., S.K. Gajjela, P.H. Steele. 2011. Electrocatalytic upgrading of biomass derived bio-oil produced from fast pyrolysis of woody biomass. Southeastern Natural Resources Graduate Student Symposium. 3/2/2011 - 3/4/2011. Starkville, MS.

Penmetsa, K., S.K. Gajjela, B.K. Mitchell, E.M. Hassan, Q. Li, P.H. Steele. 2011. Production of bio-fuels from giant miscanthus feedstock. 2011 American Chemical Society Conference. 3/27/2011 - 3/31/2011. Anaheim, CA.

Steele, P.H. 2011. Pyrolysis oil and drop-in fuels with Freedom. REPREVE Renewables: Freedom Giant Miscanthus Field Day. 1/13/2011 - 1/13/2011. Soperton, GA.

Steele, P.H. 2011. From trees to biofuels: The future of bio-oil in Mississippi. Macon Rotary Club. 1/18/2011 - 1/18/2011. Macon, MS.

Steele, P.H. 2011. From trees to biofuels: The future of bio-oil in Mississippi. Winston County Forestry Association. 2/1/2011 - 2/1/2011. Louisville, MS.

Steele, P.H. 2011. Development of fuels from bio-oils. DOE Thermochemical Conversion Platform. 2/16/2011 - 2/18/2011. Denver, CO.

Steele, P.H. 2011. Future timberland owner benefits from commercialization of bio-oil technology. Annual meeting of the Oktibbeha County Forestry Association. 3/10/2011 - 3/10/2011. Starkville, MS.

Steele, P.H. 2011. Production of boiler and transportation fuels via pyrolysis of southern pine biomass. 58th Annual Southern Hardwood Forest Research Group Meeting. 3/15/2011 - 3/15/2011. Stoneville, MS.

Steele, P.H., Q. Li, S.K. Gajjela. 2011. Producing transportation and heating fuels from catalysis of wood and grass pyrolysis oils. Beijing Forestry University. 4/19-20/2011. Beijing, CHINA.

Steele, P.H., S.K. Gajjela. 2011. Production of gasoline, diesel and aviation fuels from catalyzed wood and grass bio-oils. BIT's 1st Annual World Congress of Bioenergy - 2011. 4/25-30/2011. Dalian, CHINA.

Steele, P.H. 2011. Bio-oil's future as a consumer of Mississippi timber. Southern Forest Tree Improvement Conference 2011. 6/13/2011 - 6/16/2011. Biloxi, MS. Plenary.

Steele, P.H., J.E. Cooper, M. Puettmann. 2011. An Aspen process model: Producing liquid fuels from pyrolysis of woody biomass. Forest Products Society 65th International Convention. 6/19/2011 - 6/21/2011. Portland, OR. Plenary.

Steele, P.H. 2011. Fuels and bioproduct development using pyrolysis oil. Biomass and Bioenergy Short Course. 8/4/2011 - 8/4/2011. Mississippi State, MS. Invited.

Steele, P.H. 2011. Scale-up of pyrolytic processes. 2011 Biofuels Conference. 10/5/2011 - 10/7/2011. Mississippi State, MS.

Tao, J., S.K. Gajjela, P.H. Steele. 2011. Production of boiler fuels from bio-oil via esterification and olefination reaction pathways. Southeastern Natural Resource Graduate Student Symposium. 3/2/2011 - 3/4/2011. Starkville, MS. Plenary.

Tao, J., B.K. Mitchell, F. Yu, P.H. Steele. 2011. Alcohol injection into the pyrolytic vapor stream as a method to rapidly produce esterified bio-oil. Forest Products Society 65th International Convention. 6/19/2011 - 6/21/2011. Portland, OR. Plenary.

Wynne, Z., K. Walters, C. Naske, P. Polk. 2011. Preliminary Investigations of Pyrolysis Oil Filtration Methods. 2011 Biofuels Conference. 10/5/2011 - 10/7/2011. Mississippi State, MS.

Poster Presentations:

Hafez, I.H., E.M. Hassan, M.G. Kim, P.H. Steele. 2011. Poster. Hydrothermal Liquefaction of Perennial Biomass Feedstocks for Production of Transportation Fuels. 31st Southern Forest Tree Improvement conference. 6/13/2011 - 6/16/2011. Biloxi, MS.

Hassan, E.M., B. Sukhbaatar, S.P. Mun, M.G. Kim, P.H. Steele. 2011. Poster. Optimization of hot-compressed water (HCW) pretreatment and membrane filtration processes to isolate and characterize southern pinewood hemicelluloses. Forest Products Society 65th International Convention. 6/19-21/2011. Portland, OR.

Hassan, E.M., E. El-Giar, B.K. Mitchell, P.H. Steele. 2011. Poster. Characterization of fast pyrolysis bio-oils from white oak and sweetgum woods. Forest Products Society 65th International Convention. 6/19-21/2011. Portland, OR.

Hassan, E.M., K.F. El-Tahlawy, Q. Li, P.H. Steele. 2011. Poster. New route for fuels and chemicals from aqueous fraction bio-oil. Forest Products Society 65th International Convention. 6/19-21/2011. Portland, OR.

Hassan, E.M., H. Abouyousef, Q. Li, P.H. Steele. 2011. Poster. Increasing the Efficiency of Fast Pyrolysis Process through Sugars Isolation from Aqueous Fraction Bio-oil. MSU Biofuel conference. 10/5/2011 - 10/7/2011. Mississippi State, MS.

Li, Q., P.H. Steele, F. Yu, E.M. Hassan. 2011. Poster. High-performance liquid chromatography method for determination of anhydrosugars and other degradation products derived from fast pyrolysis of lignocellulosic biomass. Pittcon Conference and Expo 2011.
3/14/2011 - 3/17/2011. Atlanta, GA.

Li, Q., P.H. Steele. 2011. Poster. Conversion of lignocellulosic biomass to sugars via a thermal chemical route. Tenth Annual Southern BioProducts and Renewable Energy Conference. 5/10-11/2011. Biloxi, MS.

Li, Q., P.H. Steele, F. Yu, E.M. Hassan. 2011. Poster. Determination of levoglucosan and other degradation products derived from fast pyrolysis of lignocellulosic biomass. Forest Products Society 65th International Convention. 6/19-21/2011. Portland, OR.

Li, Q., P.H. Steele, S.K. Gajjela, F. Yu, B.K. Mitchell. 2011. Poster. Prevention of anhydrosugars decomposition to increase levoglucosan production during fast pyrolysis of lignocellulosic biomass. 2011 Biofuels Conference. 10/5/2011 - 10/7/2011. Mississippi State, MS.
Parapati, D., P.H. Steele. 2011. Poster. Production of torrefied wood pellets with biomass compounds. Tenth Annual Southern BioProducts and Renewable Energy Conference. 5/10-11/2011. Biloxi, MS.

Parapati, D., S.K. Gajjela, P.H. Steele. 2011. Poster. Electrocatalytic upgrading of biomass derived bio-oil. 2011 Biofuels Conference. 10/5/2011 - 10/7/2011. Mississippi State, MS.

Steele, P.H., P. Bhattacharya, B.K. Mitchell, Q. Li. 2011. Poster. Production of fuels from pine plantation understory biomass. Forest Products Society 65th International Convention. 6/19-21/2011. Portland, OR.

Tanneru, S., S.K. Gajjela, P.H. Steele. 2011. Poster. Exploratory studies on boiler fuel production from bio-oil using liquid olefins. 2011 Biofuels Conference. 10/5/2011 - 10/7/2011. Mississippi State, MS.

Tao, J., P.H. Steele. 2011. Poster. Developing boiler fuel by injecting alcohol into pyrolytic vapor stream. Tenth Annual Southern BioProducts and Renewable Energy Conference. 5/10-11/2011. Biloxi, MS.

Tao, J., P.H. Steele, B.K. Mitchell, F. Yu. 2011. Poster. Production and characterization of esterified bio-oil by injecting alcohol into the pyrolytic vapor stream. Forest Products Society 65th International Convention. 6/19-21/2011. Portland, OR.

Tao, J., S.K. Gajjela, P.H. Steele. 2011. Poster. Developing boiler fuels from bio-oil by gaseous olefination. 2011 Biofuels Conference. 10/5/2011 - 10/7/2011. Mississippi State, MS.

End Confidential Information.

Task I. Biocrude

Principle Investigators and team members:
Rafael Hernandez, Dave C. Swalm School of Chemical Engineering, PI
Sandra Eksioglu, Dept. of Industrial and Systems Engineering, Co-PI
Todd French, Dave C. Swalm School of Chemical Engineering, Co-PI

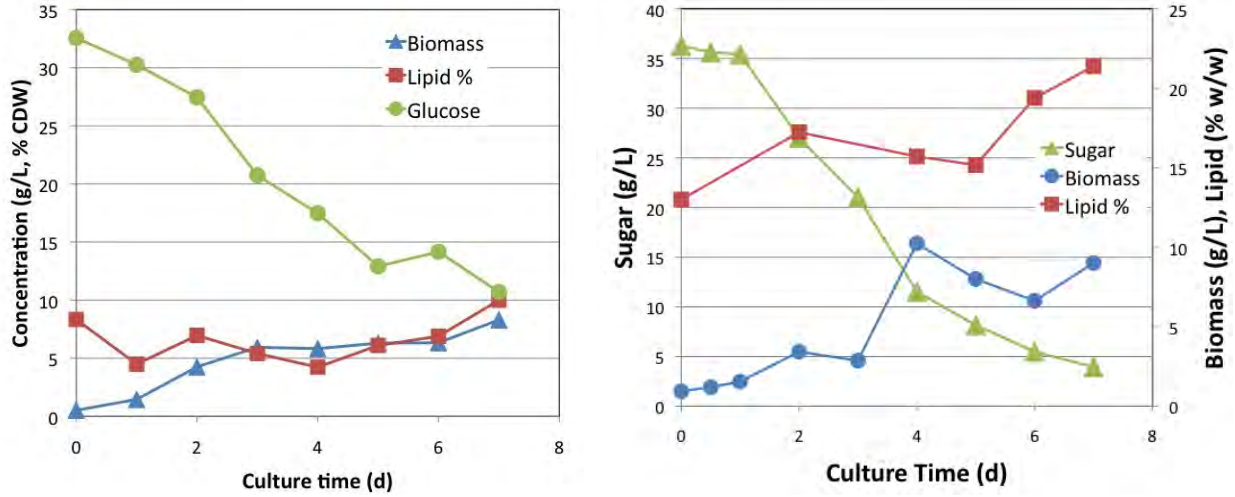
Executive Summary:
The overall objective of this task is to explore the utilization of existing waste streams in conventional wastewater treatment for producing bio-crude oil, and to refine this oil into biofuel. Traditionally, these waters have been considered an energy consuming waste. They are treated by wastewater treatment facilities before they are returned to surface water bodies. Due to the composition of domestic and most industrial wastewaters, biological treatment is the most applied treatment option. During biological treatment, microorganisms use the carbon and nutrients in the wastewater for growth and energy. Consequently, in the process of treating the water, one of the by-products is microbial cells. Previous studies conducted by the PIs indicated that some of the microorganisms present in that sludge have a high potential to turn waste (*e.g.* lignocelluloses, industrial effluents and sewage) into fuel feedstock. This group of microorganisms has been termed oleaginous due to their ability to accumulate more than 20% of their dry mass as acylglycerols. These lipids can be used to produce renewable diesel using processes similar to petroleum refining. The residual biomass can be further utilized in the production of liquid fuels, heat and electricity by combustion, fermentation or thermochemical gasification. The resulting biofuels will be tested for their applicability to be used as fuel for transportation. Further, the range of wastewaters and carbon sources usable as a feedstock for these microorganisms needs to be explored, identified and characterized for their possible carbon loads to get a clear estimate of the contribution of the proposed technology to the overall goal of displacing significant quantities of fossil fuels.

Subtask I.1 Biocrude Production Using a Pilot Facility
Experiments and test runs were conducted using the pilot scale biocrude production facility in order to evaluate the performance of its component process equipment and the overall plant process. The main components of the SERC pilot scale biocrude production facility that were tested were three 400-L mixing tanks, two 500-L volume (400-L maximum capacity) fermenter/bioreactors, the membrane separator with a maximum capacity of 500 L/h, the spray dryer, and the solvent recovery/product concentration unit.

1.1. Fermentation Experiments and Bioreactor Performance Tests
For the fermentation test runs, return activated sludge (RAS) and a pure oleaginous yeast culture of *Rhodotorula glutinis (R. glutinis)* were used as inocula, and the experiments were conducted as follows. The *R. glutinis* inoculum used to seed the fermenter was prepared by first preparing three 1-L shake flask cultures of *R. glutinis* obtained from stock cultures in YM broth media. These flask cultures were incubated for two days at 27°C and 100 RPM shaking. Each of these 1-L seed cultures was used to inoculate three 9-L YM broth media in each of three BIOFLO 410 fermenters. These fermenter cultures were then cultivated for two days at 27°C, 100 RPM agitation rate, 5 SPLM aeration rate, and uncontrolled pH. Within these four days of inoculum preparation, the 500-L fermenter was initialized and prepared prior to inoculation with the *R. glutinis* cultures. The sugar media was prepared by dissolving 18 kg of glucose (60 g/L initial concentration in 300 L culture volume) in 260 L of warm water in the sugar mixing tank and then pumping the solution in the fermenter. The fermenter containing the sugar solution was then sterilized in place (SIP) following the recommended protocols in the equipment instruction manual and the programmed SIP procedure in the fermenter control panel. A

concentrated solution of the modified synthetic wastewater (SWW) medium (components were weighed on a 300-L volume) was prepared in 10-L solution contained in a glass carboy and sterilized in an autoclave. The amount of glucose and the nutrients added correspond to an initial carbon-to-nitrogen (C:N) ratio of 70:1, which in laboratory batch tests was found to be optimum for lipid accumulation. The sterile SWW medium was then pumped into the sterile and cooled fermenter medium and mixed. The mixed medium was aerated and the fermenter pH and DO probes were calibrated. The *R. glutinis* seed cultures in the BIOFLO 410 fermenters were then harvested and transferred aseptically into the 500-L fermenter using the built-in peristaltic pumps to create a total culture volume of 300-L.
For the fermentation experiments using RAS, approximately 60 L of activated sludge were obtained from the sludge recycle line at the Hilliard Fletcher Wastewater Treatment Plant in Tuscaloosa, AL, and pumped directly into the fermenter containing the cooled sterile SWW medium. The 300-L fermentation culture was then run for 7 days, and samples were taken daily for laboratory analysis. Temperature was maintained at 25°C, agitation at 100 RPM, aeration at 3 SLPM, and the headspace pressure at approximately 10 psig.

Figure I1 shows representative fermentation profiles from five pilot-scale fermentation runs of the oleaginous yeast *Rhodotorula glutinis* and RAS. For the *R. glutinis* run, the maximum achieved biomass concentration after the seven-day fermentation run was around 8 g/L from an initial biomass level of 0.5 g/L, which was lower than the intended initial level.



(A) (B)

Figure I1: Fermentation profiles of representative *Rhodotorula glutinis* (A) and return activated sludge (B) pilot-scale fermentation cultures for lipid accumulation.

The exponential growth phase occurred between 1-3 days of cultivation after which the stationary phase commenced. The lipid content profile showed an initial level of around 8.34% w/w that decreased to 4.23% w/w after 4 days, which then increased to 10% after 7 days. The residual sugar profile showed a diluted initial level of around half the initial intended amount of 60 g/L. The sugar was consumed at a fast rate until 5 days, in which the sugar consumption was reduced gradually. The final residual sugar level after 7 days was approximately 10 g/L. The lower than expected lipid yields could be attributed to the diluted initial sugar concentration. The cause of this dilution was most likely the inaccurate liquid level readings in the fermentation vessel that measures the head pressure to determine the liquid level inside the fermenter. Another probable cause could be the amount of water added to the fermenter to compensate for the evaporated water following SIP. The amount of water lost post-sterilization was found to be unintentionally high due to the premature aeration of the sterile media immediately following

SIP. In spite of this, extending the fermentation run beyond 7 days could have most likely improved lipid yields due to the increasing trend and a residual sugar level one-third the initial amount.

However, the resulting fermentation profiles from the pilot-scale fermentation run of RAS (B) showed a maximum achieved biomass concentration of around 15 g/L from an initial biomass level of 1 g/L achieved at 4 days corresponding to the exponential phase. After this, an appreciable decline and recovery of the biomass concentration to 10 g/L describing the stationary phase was observed. The lipid content profile showed an initial level of around 13% CDW that reached a maximum level of around 22% CDW. Similar to the *R. glutinis* runs, a recurring problem based on several trials is the overestimation of the initial sugar substrate (glucose) concentration, which led to around 36 g/L instead of the intended 60 g/L initial level. In spite of this, glucose was consumed at a fast rate until 7 days, leading to a final residual sugar level of around 4 g/L. Overall biomass and lipid yields based on glucose consumption using RAS were 25 and 6% (g/g glucose consumed), respectively, which shows that RAS cultures performed better on pilot-scale fermentation runs in terms of lipid accumulation compared with *R. glutinis* cultures. Further improvements in fermentation experiment set-up and media and inocula preparation, optimization of fermentation conditions for both types of inocula such as temperature, agitation rate, pH control, etc., and evaluation of fed-batch and continuous fermentation modes are currently being investigated with the aim of further improving the biocrude yield for activated sludge and *R. glutinis.*

Initial SIP trials were successful for both Fermenters 1 and 2. Heating to sterilization temperature took around 10-15 minutes, and sterilization temperature maintenance was within ±1°C. The main problems encountered were leaks in the cooling water and steam lines, premature aeration of sterile culture resulting to loss of liquid volume, and difficulty in achieving set cooled temperature (25°C) due to inadequate cooling capacity of installed in-line chiller. Savery and ICET personnel have repaired the leaks as of March 2012. Furthermore, modifying the SIP protocol to introduce aeration only when the hot sterile media has been cooled down to normal operating temperature has minimized the loss of sterile media volume. The cooling capacity issue has been resolved by installing a three-way connection that supplied process water for initial cooling of the hot sterile media to the fermenter jacket and discarding the hot water from the jacket to the drain. After the sterile media in the fermenter was cooled to around 40-50°C, the three-way valve was set to circulate chilled (10°C) water through the jacket. This approach greatly reduced the cooling time needed to achieve the 25°C operating temperature to around 30 minutes. Furthermore, the SIP procedure proved to be effective, as no evidence of contamination on the *R. glutinis* culture was observed visually. Cleaning-in-place (CIP) operation was conducted successfully as well as using a 1% caustic solution. The difficulty in accessing the CIP connections in the air exhaust line on the fermenter vessel lids were resolved through the installation of a catwalk/accessway that provides easier and safer access when switching the air exhaust and CIP lines prior to the CIP operation. The difficulties of pumping antifoam and base were resolved by reducing the vessel backpressure to < 10 psi during pumping operations. Higher RPM inoculum pumps were also installed to assist in overcoming vessel backpressure and increase the rate of delivering the culture inocula into the fermentation medium.

1.2. Downstream Processing Tests

After the 7-day fermentation run, the culture was automatically pumped in batches to the membrane separator to concentrate the *R. glutinis* cells. The retentate stream from the membrane separator consisting of concentrated *R. glutinis* cells were pumped in batches into the spray dryer for a total of two days, and the dried biomass was collected and subjected to

laboratory analysis for moisture content, lipid extraction, and FAME analysis. The permeate stream was discarded in the sump. Lipids (biocrude) from the dried biomass were extracted using various solvent and solvent mixtures such as pure hexane or 60:20:20 (by volume) hexane:methanol:acetone (HMA) mixtures using a stirred tank vessel. The solvent extracts were processed using the solvent recovery unit in order to separate the solvents and concentrate the lipid product.

Membrane separator performance was tested using both RAS and *R. glutinis* biomass generated from the fermentation tests. Images from the initial tests using *R. glutinis* are shown in Figure I2, which shows the membrane separator in operational mode with the clear permeate stream and the retentate stream rich in the *R. glutinis* biomass. The membrane separator increased the cell biomass concentration of the feed culture from 10 g/L to approximately 20 g/L in 35-L batches. The retentate batches were stored in sterile glass carboys prior to feeding in the spray dryer. However, this harvesting scheme proved to be unfeasible and inefficient since it led to stoppages in membrane separator operation and exposed the cell-rich retentate to the environment. Therefore, the membrane separator was retrofitted with a 10-gallon steel holding tank to hold the retentate stream while feeding it slowly to the spray dryer. This allowed for a continuous feeding of broth from the fermenter and feeding of retentate to the spray dryer. This scheme has since been implemented in processing the succeeding RAS and R. glutinis fermentation cultures.



Figure I2: Left – The membrane separator in operation mode. Right – Collection bottles showing permeate (clear) and retentate (pink) streams.

Performance tests conducted on the membrane separator have shown that using a 25 psi pressure differential, the membrane separator was able to process approximately 240 L/h (~4 L/min), and when the system rate slowed down to 1 L/min, the process was stopped. Table I2 shows further that increasing the pressure differential led to a faster rate of processing. As the retentate was unloaded, the flow of permeate was restored to initial value. The retentate was then transferred by gravity to the said holding tank, but soon it became apparent that a pump needed to be installed along the retentate-to-holding tank line to overcome the head pressure formed by the retentate liquid accumulating in the holding tank. After one hour of processing time, the temperature of the culture had increased to 50°C, possibly due to fluid friction. It is not known yet whether this phenomenon, as well as the high pressure differential, has a detrimental effect on the lipid content of the microbial biomass, i.e. if high operating pressures could cause cell rupture and leakage of intracellular lipids into the permeate. GCFID analysis of the retentate and permeate streams was conducted to verify this issue. Figure I3 is a comparison of the retentate and permeates after FAME analysis showing no lipids in thepermeate. In addition to this, Figure I4 shows no difference in lipid profiles in comparison of change in pressure differential across the membrane. The recommendation is to run at highest delta P of 25 to 28 to

shorten process time. Overall, fermentation broth solids concentration was increased from 1.5-2% w/v to approximately 3.0% w/v. Further experiments are being conducted to increase the solids concentration to 5-10% w/v.

Table I1: Effect of set pressure differential on membrane separator performance.

Differential Pressure (Psi)	Initial Permeate Flow Rate (L/min)	Final Permeate Flow Rate (L/min)	Temperature	Operating Time (min)	Retentate ((g/L)/min)
10	3.34	2.1	47	41	2.622
22	6.25	2.5	49	28	4.702
28	6.12	2.94	47	22	5.571

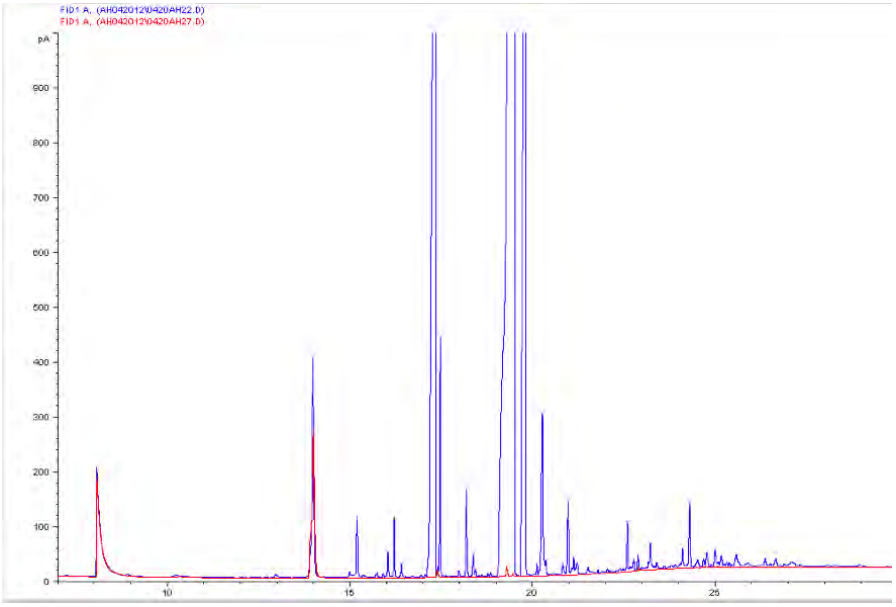


Figure I3: Comparison of retentate (blue) and permeate (red) FAME composition showing no detectable fatty acids in the permeate stream.

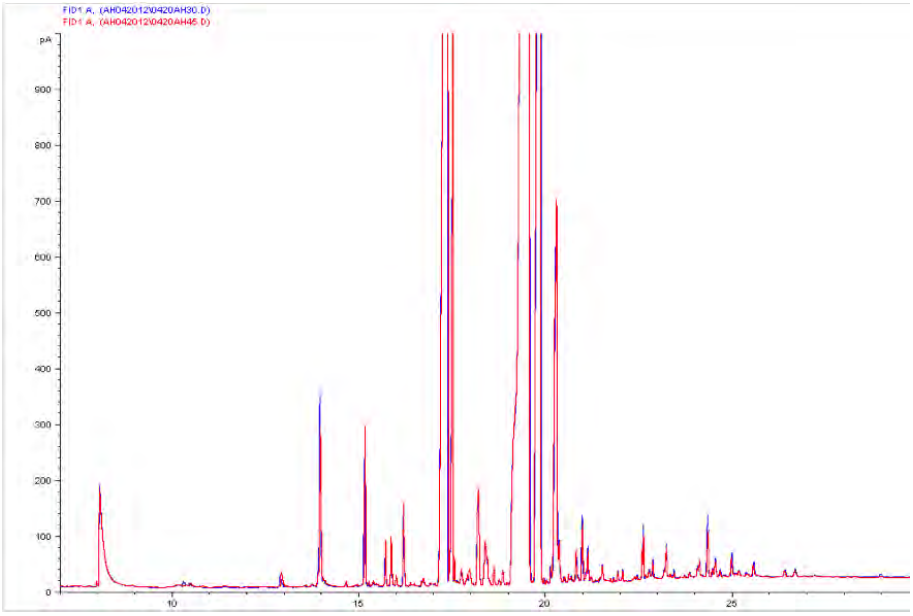


Figure I4: Comparison of retentate FAME composition a 10 psi (blue) and 28 psi (red) set pressure differential across membrane.

Initial spray drying tests were conducted using the retentate containing *R. glutinis* biomass-rich broth. The spray dryer proved to be the bottleneck process for the pilot production process as the available peristaltic pump and tubing could only pump a maximum of 10 L/h of the concentrated *R. glutinis* culture into the spray dryer nozzle. This could be remedied by the selection of a higher RPM pump and bigger diameter tube. The first test run in the spray dryer resulted in a pasty and sticky biomass that adhered to the interior wall of the spray dryer due to the absence of high pressure nebulizing air. This initial run necessitated the dismantling and manual clean up of the cyclone separator and the inner walls of the dryer. The next runs conducted utilized a 20-psig air for spray nebulization. The inlet air was initially set at 250°F. The resulting “dry” cells on this initial run had a cakey texture and an average moisture content of 15% by wt. In the next runs, the inlet air temperature was increased to around 300°F. The resulting moisture contents of the different batches of dried *R. glutinis* cells are summarized in Figure I5, and images of the collected dried cells are shown in Figure I6. The dried cell batches were also analyzed for lipid content using the Bligh and Dyer extraction method, and the results are summarized in Figure I5. Based on the results, the higher the temperature of the inlet air is the lower the moisture content will be, but at the expense of a lower gravimetric yield from Bligh and Dyer Extraction. This could most likely be due to decomposition of the lipids due to high drying temperatures. Therefore, further optimization of the drying operations will be conducted to balance drying efficiency with lipid content. Among the operational variables that will be optimized are nebulizing air pressure, spray nozzle rotational speed, and feed pump speed, in addition to the inlet air temperature.

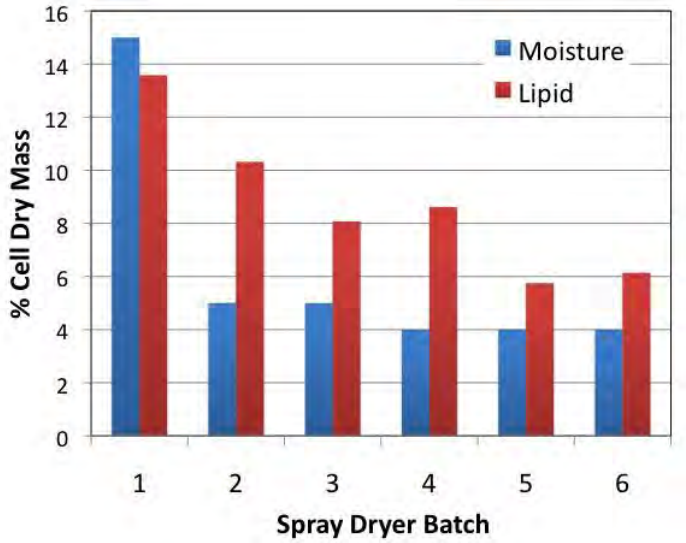


Figure I5: Spray dryer performance and effect on gravimetric lipid yield from Bligh & Dyer extraction per drying batch conditions. Batch 1 – inlet air temperature 250°F, batches 2 to 6 - inlet air temperature 300°F. Pump speed constant at 50 RPM. Nebulizing air at 20 psi.



Figure I6: Top left – Dried *R. glutinis* cells in cyclone separator collection container. Top right and bottom – Details of collected dry *R. glutinis* cells from spray dryer.

Optimization experiments for spray drying performance were conducted using retentate obtained from a representative RAS-inoculated lipid accumulation culture. Response surface methodology was used to design an experiment testing the individual and interactive effects of the following variables: inlet air temperature, nebulizer rotation speed, and feed pump speed on the moisture removal efficiency and lipid content of the dried biomass. The goal was to determine the optimum spray dryer conditions that would maximize moisture removal but result in minimal reduction in lipid content of the biomass. The results are summarized in Table I2.

Table I2: Experimental data for spray dryer operation optimization.

Run No.	Inlet Air Temp (°C)	Nebulizer Rotational Speed	Feed Pump Speed	Moisture Removal Efficiency (%)	Lipid Content of Dried Biomass

		Rating (%)	Rating (%)		(% CDW)*
1	150	40	65	85.2%	5.37
2	150	60	65	75.0%	5.35
3	250	40	65	88.3%	5.31
4	250	60	65	92.9%	5.23
5	200	40	50	93.1%	3.84
6	200	40	80	88.3%	4.31
7	200	60	50	91.1%	4.46
8	200	60	80	89.5%	5.14
9	150	50	50	89.8%	4.98
10	250	50	50	94.7%	4.99
11	150	50	80	78.2%	4.93
12	250	50	80	90.0%	5.22
13	200	50	65	91.5%	3.61
14	200	50	65	91.1%	4.12
15	200	50	65	91.1%	4.13

*Compared against biomass lipid content of 6% w/w obtained via freeze drying and Bligh and Dyer extraction.

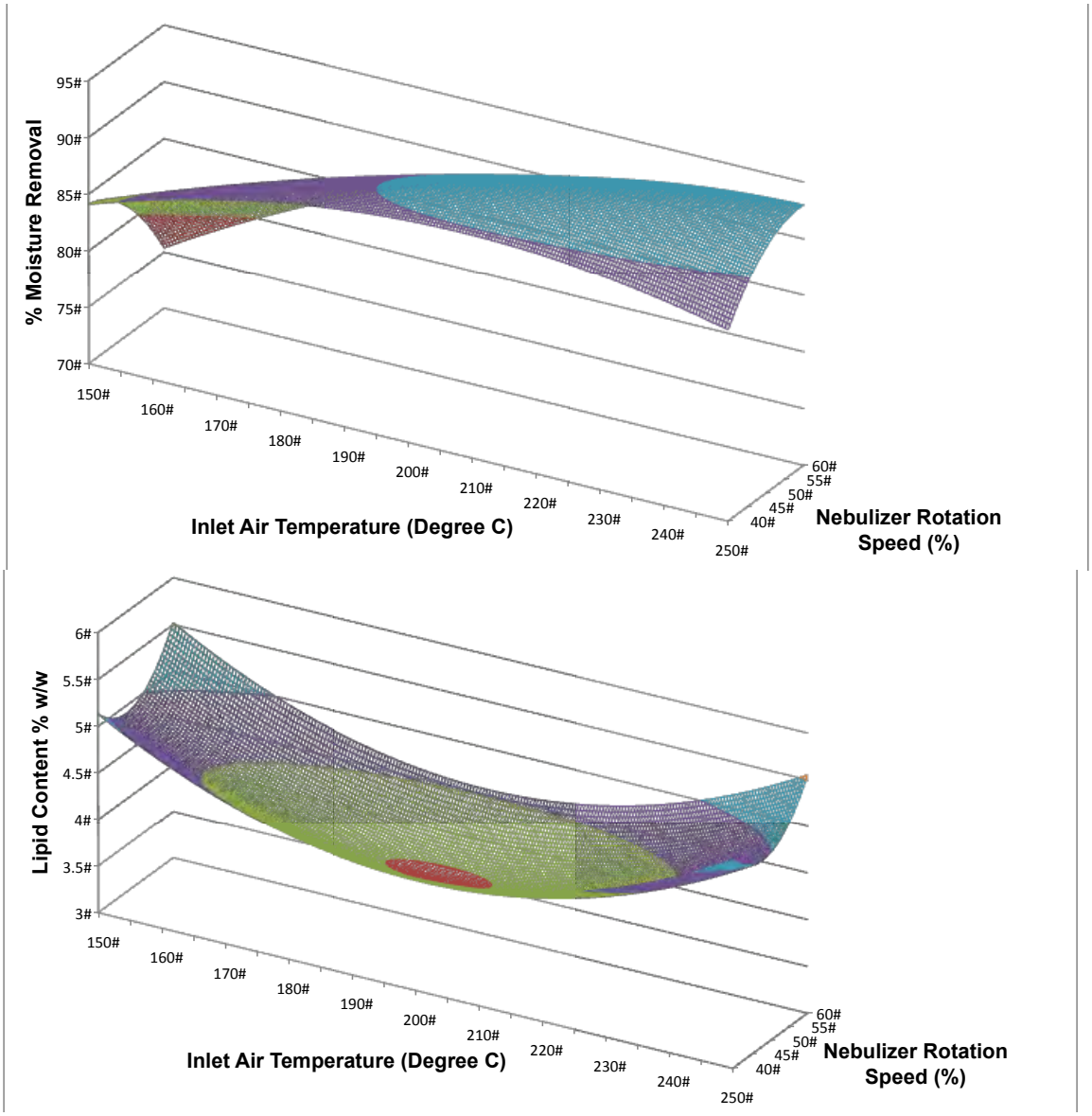


Figure I7: Response surface plot of the interactive effect of inlet air temperature and nebulizer rotation speed on moisture removal efficiency (top) and biomass lipid content (bottom). Pump speed = 68%.

As shown in Table I2, the spray dryer run operated at 250°C inlet air temperature, 50% nebulizer rotational speed, and 50% pump speed showed maximum moisture removal efficiency of 94.7%. However, the highest lipid content of the biomass (i.e. minimal reduction in lipid content compared with laboratory scale freeze-drying and Bligh and Dyer extraction procedure) was obtained at 150°C inlet air, 40% nebulizer rotational speed, and 65% feed pump speed. Analysis of Variance (ANOVA) of the response surface model and data showed that the interaction between the inlet air temperature and nebulizer speed and the individual effect of pump speed were the only factors that significantly affected the moisture removal efficiency at the 95% confidence level. The optimum conditions for maximum moisture removal calculated via canonical analysis were inlet air temperature of 250.6°C, nebulizer speed of 58.8%, and pump speed of 68%. The analysis also showed that increasing the pump speed has an inverse

(negative) effect on the moisture removal efficiency while the interactive effect of inlet air temperature and nebulizer speed has a positive effect on the moisture removal efficiency. However, the lowest lipid content of the biomass was predicted at 201°C inlet air temperature, 48.4% nebulizer speed, and 53% feed pump speed. This means that this set of spray dryer operating conditions is detrimental to the lipid content of the biomass, and the quadratic temperature factor has the only significant effect on the lipid content of the biomass at the 95% confidence level. Factor levels higher and lower than those conditions at the predicted minimum could be beneficial for reducing the negative effect of the spray drying on the lipid content. Based on these results and the surface plots shown in Figure I7, the spray dryer could be operated in the region of 250°C inlet air temperature and 40-50% nebulizer speed at 68% pump speed to maximize moisture removal while minimizing lipid loss during spray drying.

Preliminary tests on the lipid extraction and solvent recovery process equipment have been conducted initially using cooking oil in hexane. The test solution was mixed in the extraction and vessel and pumped into the vacuum-assisted solvent recovery system. Based on the initial tests, ≈90% recovery of the cooking oil and ≈80% recovery of hexane were obtained. Extraction tests using the spray-dried biomass of *R. glutinis* produced the results summarized in Table I3. The data shows excellent solvent recovery for neat samples containing vegetable oil and satisfactory recovery of the initial oil supplied. With the *R. glutinis* extract, however, the solvent recovery was between 50–65%. The percent recovery values of lipids from the biomass extracts were 20 and 5% for hexane-methanol-acetone (HMA) and hexane, respectively, showing that the majority of the extractables from the HMA solvent mixture were polar in nature. Figure I8 shows the high temperature GC chromatogram of the HMA-extracted lipids from *R. glutinis*. The chromatogram shows significant amounts of triacylglycerols and some free fatty acids and FAMEs.

Table I3: Solvent recovery data using extracts from dried *Rhodotorula glutinis* biomass.

Run #	Run 4	Run 5
Solvent (L)	10	10
Mass of *R. glutinis* cells (g)	500	500
Bag Weight (g)	155.6	155
Temp Range (°C)	60-65	60-65
Time (h)	24	24
Vacuum (mmHg)	325	325
Composition	HMA	H
Results:		
Solvent Recovered (L)	5.14	6.56
Mass oil recovered (g)	100	25
Solvent recovery (%)	51.4	65.6
Oil Recovery %	20	5

A= Acetone, M= Methanol,
C= Chloroform, H= Hexane

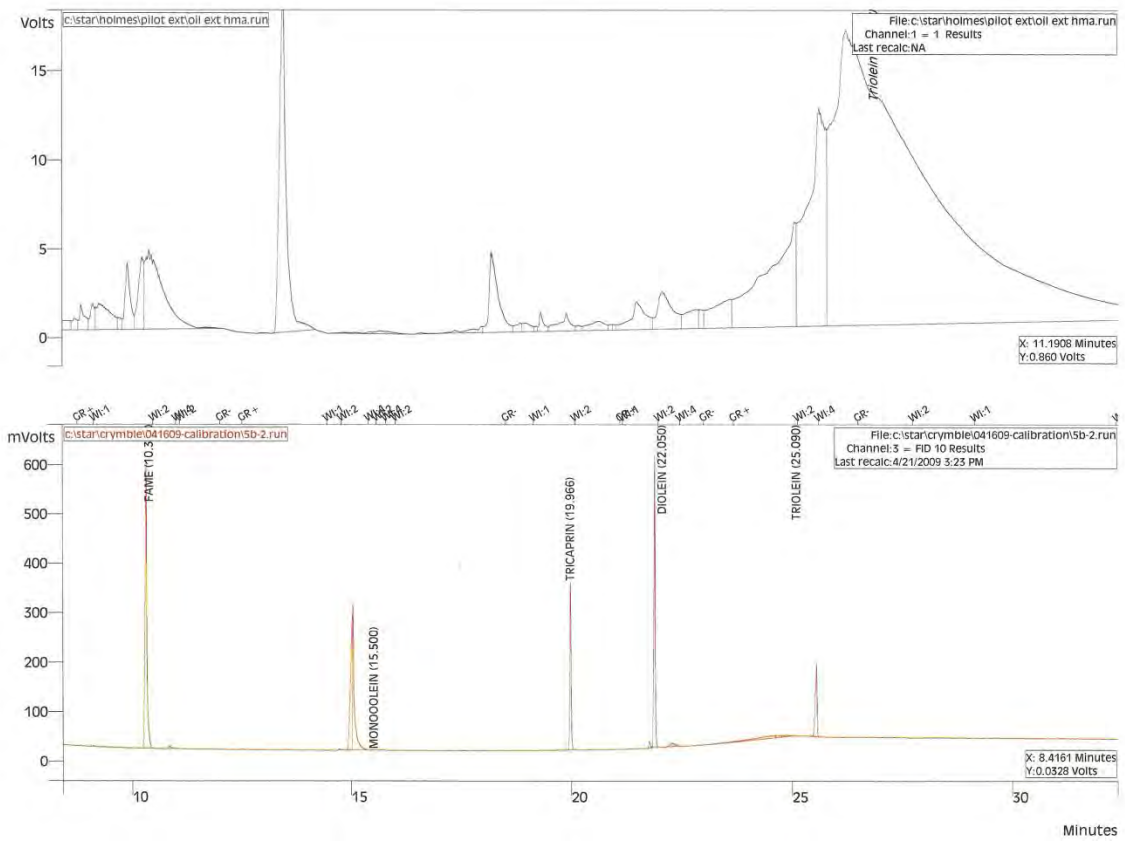


Figure I8: High temperature GC chromatogram of *R. glutinis* lipid concentrated using the solvent recovery unit (top) compared with a standard (bottom).

Addressing Milestone 1: Design, development, and testing of a 1 gallon/week pilot scale facility
So far, the biocrude production yield of the pilot facility has yet to reach the 1 gallon per week rate. With the current experiments performed in batch mode, the average lipid production rate obtained was between 0.2 – 0.3 gallons per week. Further batch tests will still be conducted to determine biomass production, lipid accumulation, and sugar consumption kinetic parameters that will be optimized and used for the implementation of fed-batch, semi-continuous, continuous fermentation modes, as well as full and/or partial cell recycling. These fermentation strategies could be applied to maximize biomass and lipid production and optimized sugar conversion to the desired product. In addition to optimizing the fermentation process, downstream process equipment parameters are still continuously being evaluated and optimized in order to minimize product biocrude loss and degradation.

Addressing Milestone 2: Economic analysis of the cost of producing oil in the pilot facility
Initial attempts of analyzing the economics of the pilot-scale production of biocrude resulted in relatively higher production costs due to the utilities costs attributed to aeration and mixing in the bioreactors. These items were eliminated in the economic analysis of a full-scale biocrude production process in an existing and operational wastewater treatment facility as the aeration and mixing energy expenditures for lipid production could be incorporated into the requirements of the existing aerobic bio-oxidation basins for the reduction of wastewater BOD. The main goal of testing the pilot facility is to demonstrate that the laboratory-scale biocrude production could be scaled-up from the bench (5 L) to the pilot scale (500 L) and to industrial scale levels while attaining similar biomass and lipid production rates and yields. The results obtained in the pilot

facility validated the batch data. The detailed economic analysis of the process is presented in the next section.

Subtask I.2 Evaluation of Growth Conditions on Various Biowaste Feedstocks

In order to reduce the cost of producing biocrude-based biofuels via sugar fermentation, alternative feedstocks and carbon sources were evaluated for lipid production by oleaginous microorganisms and enhanced activated sludge cultures. A sensitivity analysis of the effect of the carbon substrate on proposed biocrude production process (Table I4) has shown that the carbon substrate comprises a major fraction of the total biofuel production cost and further reduction of the carbon source would result in reduction of feedstock fraction cost and biofuel breakeven price. Therefore, the alternative feedstocks should be relatively low cost and widely available. Some potential candidates are sugars derived from waste lignocellulose biomass and high strength industrial wastewaters such as from pulp and paper, livestock and meat processing, and biofuel facilities.

Table I4: Effect of carbon source on cost of biodiesel from biocrude.

Sugar Cost ($/lb)	Feedstock Cost Fraction (%)	Break Even Price ($/gallon)
0.20	87.8	4.06
0.18	87.1	3.81
0.16	86.4	3.56
0.14	85.5	3.31
0.12	84.6	3.05
0.10	83.5	2.80
0.08	82.2	2.55
0.06	80.8	2.30
0.04	79.1	2.04

2.1. Waste Lignocellulose Biomass as Substrate

The objective was to determine the suitability of using hydrolyzate from sugarcane bagasse and switchgrass, both agricultural waste biomass materials, as substrates for microbial production of biocrude. Three batch fermentation set-ups were prepared using the following treatments: two set-ups for (1) activated sludge inoculum, and 1 set-up for (2) concentrated activated sludge. Treatments (1) and (2) were set up as follows. A synthetic wastewater medium (240 mL) was prepared and sterilized in two 5-L BIOFLO 310 fermenter vessels using xylose (60 g/L) as the carbon source and ammonium sulfate (1.62 g/L) as the nitrogen source. The initial C:N ratio was 70:1. The sterile media was inoculated with 60 mL of return activated sludge (RAS) obtained from Tuscaloosa, AL. The fermentation was run for 7 days with periodic sampling. Xylose was used as the carbon source in order to acclimate the microorganisms in the sludge and the yeast to the sugar, which is dominant in both the switch grass and sugarcane bagasse hydrolyzate. After 7 days, the culture volumes were reduced to 2 L and approximately 1 L of the switchgrass hydrolyzate was added to each of the two vessels. Treatment (1) was then allowed to incubate for 7 more days with periodic sampling. Treatment (2) was set up parallel to treatment (1) by inoculating a synthetic wastewater medium with concentrated RAS obtained via vacuum filtration to match the biomass concentration of (1) after the first 7 day acclimation period. Subsequently, approximately 1 L of the switch grass hydrolyzate/sugarcane bagasse was added into vessel (3) and the culture was allowed to incubate for 7 days.

Figures I9 and I10 show the two-stage batch fermentation experiments wherein the activated sludge cultures were acclimated to xylose during the first 7 days and fed with the lignocellulose hydrolyzate at day 7 with additional nutrients. In both cases, biomass lipid contents increased significantly to reach maximum levels of around 30-45% CDW. However, due to the low initial sugar concentration of the switchgrass hydrolyzate, which was fully utilized after 8 days (Figure I9), the lipid content of the enhanced activated sludge biomass utilizing switchgrass hydrolyzate decreased significantly. We saw similar results when sugarcane bagasse hydrolyzate was used regardless of whether additional nutrients were added (Figure I10) or not (Figure I11). This could be attributed to the relatively higher sugar concentration of the bagasse hydrolyzate than the switch grass hydrolyzate. The calculated kinetic parameters summarized in Table I5 show improved sugar conversion to lipids when using xylose and renewable sugars obtained from the waste material sugarcane bagasse. The results indicate that lignocellulose biomass hydrolyzates are suitable carbon sources for lipid accumulation by activated sludge mixed cultures provided that there is a prior xylose adaptation step. Control runs in which activated sludge was not acclimated to xylose prior to hydrolyzate feeding showed no appreciable lipid production.

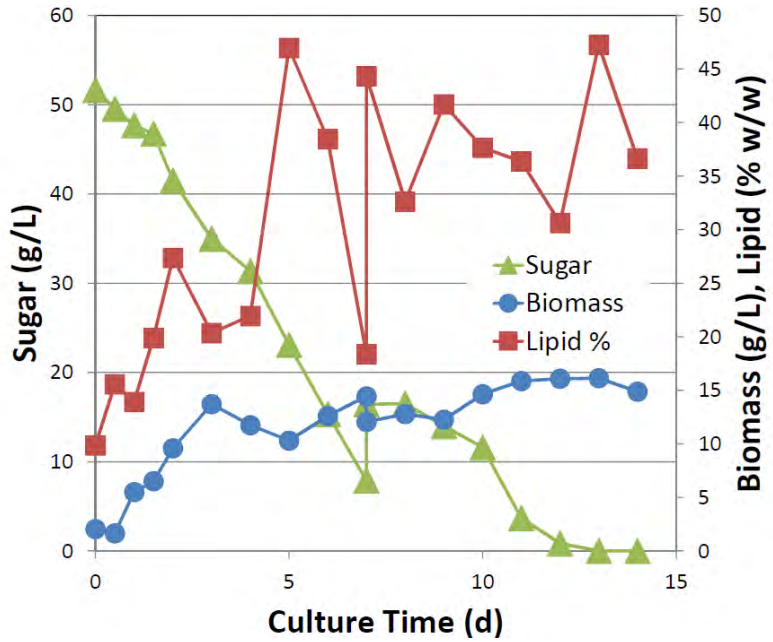


Figure I9: Fermentation profiles of RAS culture fed with switch grass hydrolyzate from GA. Xylose acclimation day 0-7. Switch grass hydrolyzate feeding with additional nutrients at day 7-14.

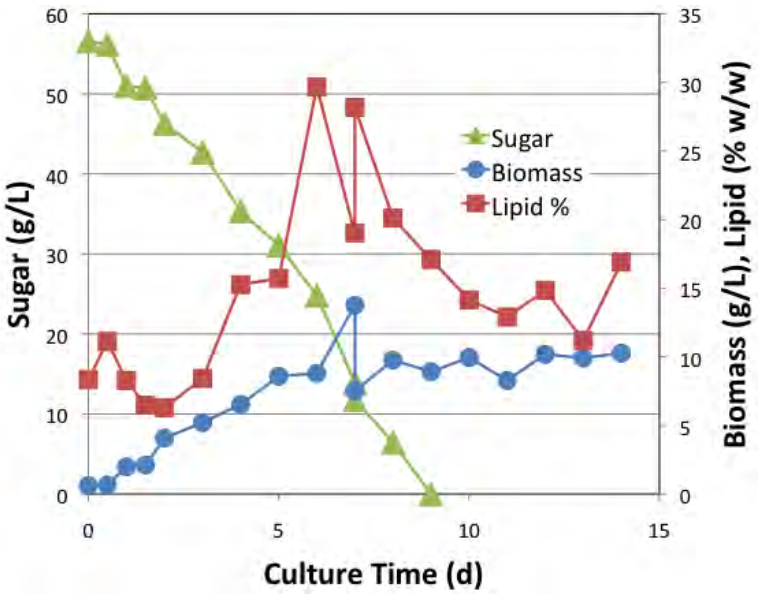


Figure I10: Fermentation profiles of RAS culture fed sugarcane bagasse hydrolyzate. Xylose acclimation from day 0-7. Bagasse hydrolyzate feeding with additional nutrients from day 7-14.

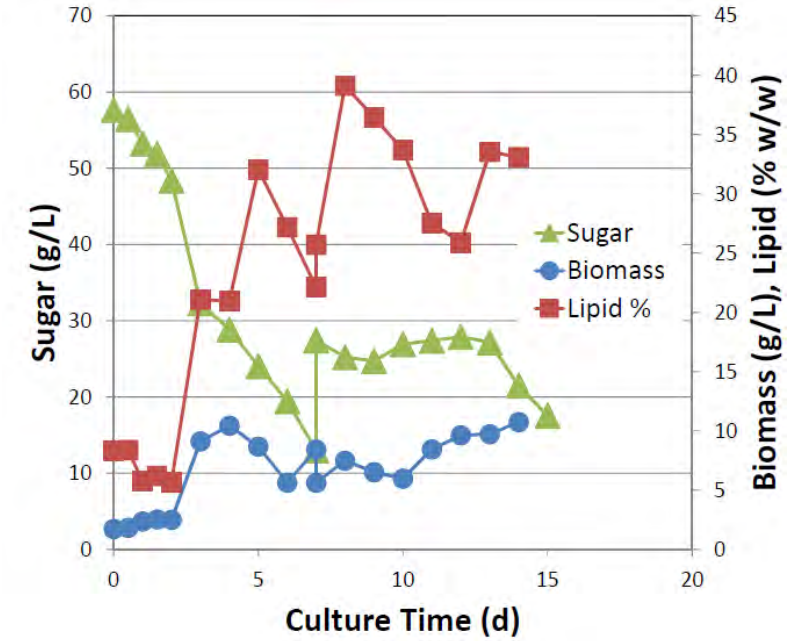


Figure I11: Fermentation profiles of RAS culture fed sugarcane bagasse hydrolyzate. Xylose acclimation from day 0-7. Switch grass hydrolyzate feeding without additional nutrients from day 7-14.

Table I5: Kinetic and yield parameters of biocrude production via fermentation of various carbon substrates.

Parameters	Treatment Glucose	Xylose Acclimation(7 d)	Bagasse Feeding (7 d)
μ_{max} (h^{-1})*	0.042	0.074	0.023

X_0 (g/L)*	0.885	1.05	6.78
X_{max} (g/L)*	7.12	8.97	9.85
m	0.466	0.136	0.110
n	5.79×10^{-4}	1.62×10^{-3}	1.04×10^{-4}
P_{max} (g/L)	5.12	4.85	7.63
Maximum lipid content (% CDW)	44.2	47.0	47.3
Lipid productivity (g/L·h)	0.030	0.034	0.032
Maximum Sugar Uptake Rate g/(L·h)	0.198	0.260	0.098
% Sugar Utilized	56	85	100
$Y_{X/S}$ Overall (g/g)*	0.195	0.227	0.285
$Y_{P/S}$ Overall (g/g)	0.150	0.128	0.139
α	4.29	0.546	0.867
β	8.71×10^{-3}	0.030	0.010
k_e (g/g·h)	4.85×10^{-3}	1.77×10^{-2}	9.42×10^{-3}
Overall biomass productivity (g/L·h)	0.061	0.073	0.028
Maximum biomass concentration (g/L)	11.6	14.4	16.1

*Based on non-lipid biomass (non lipid biomass = total biomass – lipid mass).

2.2. High Strength Industrial Wastewaters as Substrates for Biocrude Production

High BOD and COD wastewaters from various industries could prove to be excellent sources of water, nutrients, and carbon for production of renewable biocrude via fermentation by oleaginous microorganisms and enhanced activated sludge cultures. Pulp and paper wastewater has been evaluated in this project as it ranks as a top producer of huge amounts of wastewater effluents amounting to approximately 20000 – 60000 gallons per ton of product. The three different types of pulp and paper wastewaters were tested: pulp wash sewer water, mixed wastewater containing all effluent streams in the plant, and the anaerobic digestion pond effluent. The wastewaters were characterized for BOD_5 and COD using standard AWWA/APHA methods. Residual sugar concentration (glucose and xylose) was analyzed using the YSI 2900 Biochemistry Analyzer, and nutrient (ammonium, nitrite, nitrate, phosphate) levels were analyzed by ICS 3000 ion chromatograph. The information on the total carbon (as residual sugar or COD) and nutrient levels was used to formulate the amount of sugar and nutrient amendments on the wastewaters to establish a high C:N ratio conducive to lipid accumulation by the microorganisms under consideration. Results have shown that the three types of wastewaters contain non-detectable amounts of N and P nutrient ions and sugars but contain appreciable amounts of sodium and sulfate ions, presumably originating from the pulping and cooking processes. The COD levels were (in mg/L) 1478 for pulp wash, 1361 for the mixed wastewater, and 410 for the anaerobic lagoon effluent. These valuesindicate the necessity for supplementation with sugars and nutrients. Waste activated sludge obtained from the Tuscaloosa WWTF stored and aerated in a glass jar up to 24 hours was used as inoculum. Sixty grams per liter of glucose, 1.62 g/L of ammonium sulfate, 1.5 g/L of sodium phosphate monobasic, and 1.0 g/L of potassium phosphate dibasic were added into each of the wastewaters. The amended WW were then transferred into the fermenter vessel, and the initial pH adjusted to 6.5. RAS was added to give 20% v/v inoculum concentration. The fermentation run was commenced during the point of inoculation and allowed to proceed for 7 days. The temperature was controlled at 25°C, the aeration rate at 3 vvm, and the agitation rate at 300

rpm, and was adjusted to maintain a DO level no lower than 60% saturation. Duplicate samples were collected and analyzed for biomass concentration (centrifugation and freeze-drying), lipid content (Bligh and Dyer extraction method and solvent evaporation by Turbovap), residual sugar (YSI 2900), residual ammonium, nitrite, nitrate, phosphates (IC), and residual COD (Standard digestion method). DO and pH were monitored using the built-in probes in the fermenters. The lipid extracts (biocrude) are currently being processed for GCFID analysis of biodiesel yield (saponifiable fraction) and fatty acid profile.

The results shown in Figures I12 to I14 indicate that the activated sludge microbial cultures were able to grow and increase their lipid content and produce biocrude using the pulp and paper wastewaters supplemented with sugar and nutrients as media. Biomass production was comparable for all wastewaters, but a maximum lipid yield of 40% w/w was obtained using the anaerobic digestion pond effluent as the media (Figure I12). This could indicate the presence of some recalcitrant inhibitory compounds in the pulp wash and mixed wastewater that limit lipid accumulation that are not present in the pond effluent. Presumably, the anaerobic digestion process could have eliminated these recalcitrant compounds as evident in its lower initial COD. Experiments and analyses are still ongoing to verify these claims and to present the lipid accumulation performance of pure oleaginous yeast strains (*R. glutinis*) when using amended pulp and paper wastewater as substrate for lipid accumulation. The collected biocrude samples will be analyzed for biodiesel fraction and lipid profile and the BOD and COD reduction efficiency will be determined.

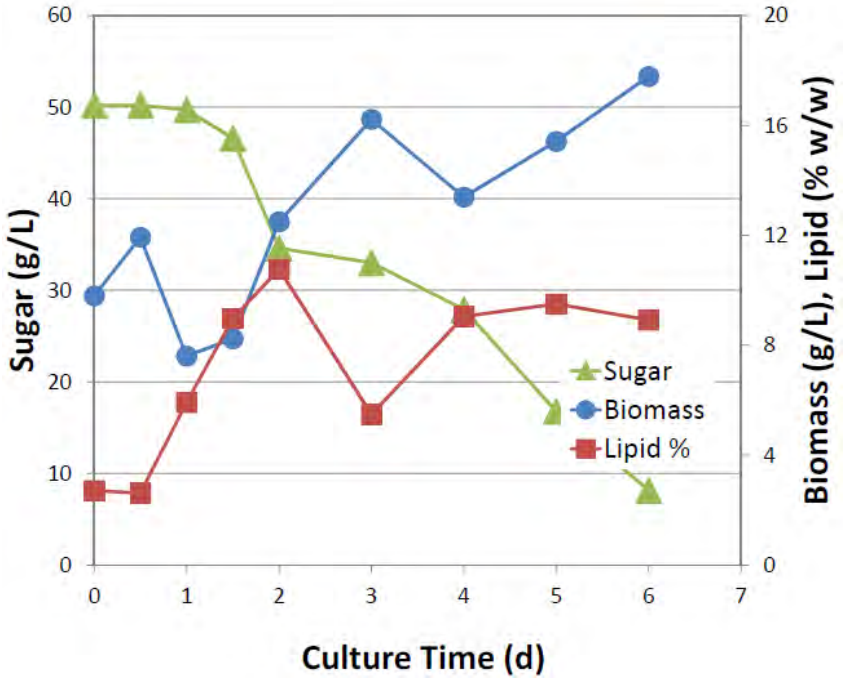


Figure I12: Fermentation profiles of RAS culture in pulp wash amended with glucose and nutrients.

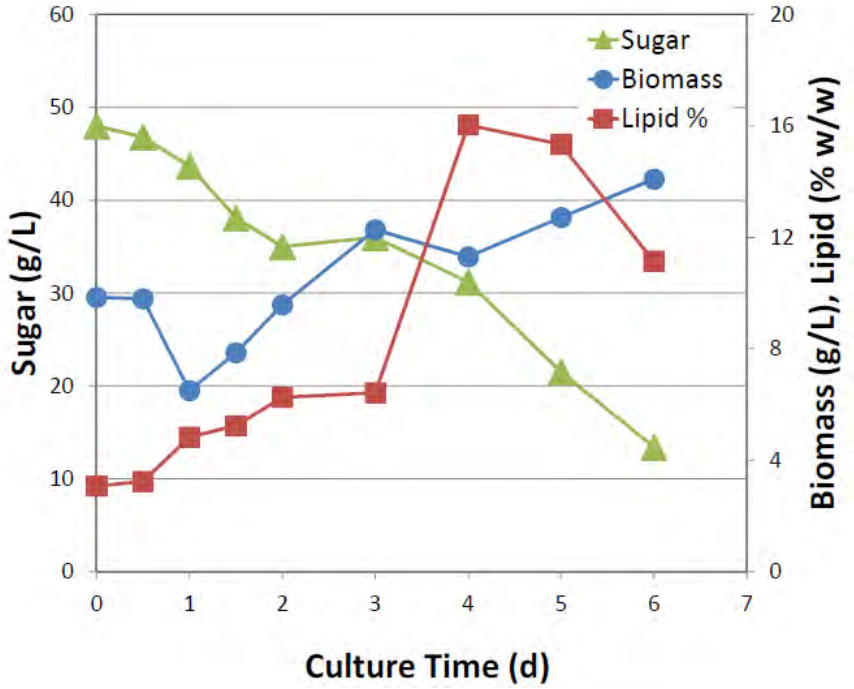


Figure I13: Fermentation profiles of RAS culture in mixed pulp and paper wastewater amended with glucose and nutrients.

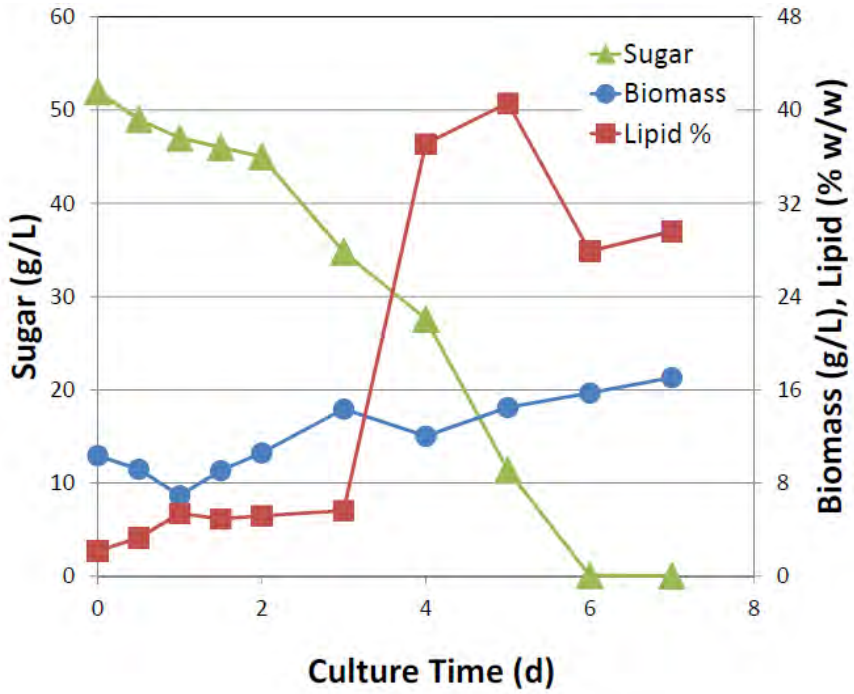


Figure I14: Fermentation profiles of RAS culture in anaerobic digestion pond effluent amended with glucose and nutrients.

Addressing Milestone 1: Development of a report ranking the characteristics and potential of various sources of wastewaters, agricultural crops, and residue for use as a feedstock supplement, characterization of microbial consortia, and performance metrics of various feedstocks.

Different types of industries producing high strength wastewaters in Mississippi were surveyed to determine the industrial source that could produce a high BOD loading rate that could potentially be used for the cultivation of enhanced activated sludge cultures for biocrude production. The top two sources in terms of pounds of BOD per day of influent are pulp and paper mills and poultry processing wastewaters. Values of BOD loadings of representative companies from these industries are presented in Tables I6 and I7. Therefore, pulp and paper wastewaters were tested as fermentation substrates, and performance metrics were determined as shown in Figures I12, I13, and I14. Poultry wastewaters have similarly been tested, but initial tests indicated a high presence of chloride ions possibly originating from bleaching and disinfection of slaughtered poultry and processing areas, thus potentially inhibiting microbial growth. Further studies are being conducted to possibly include pretreatment processes to remove inhibitory compounds in the wastewater to enhance microbial growth of the lipid-accumulating microorganisms.

Data on the comparison of agricultural crops and residue as potential sources of fermentable sugars for the enhanced biocrude production process were obtained via supply chain and logistics analysis and modeling studies conducted by Dr. Sandra Eksioglu and her team at the Department of Industrial and Systems Engineering and were the basis for selection of the biomass hydrolyzates tested in this study. Fermentation parameters and performance metrics are presented in Section 2.1.

Table I6: BOD_5 loading (lbs/day) of representative pulp and paper mill wastewaters in Mississippi.

Company Name	Location	2008	2009	2010
AbittibiBowater Newsprint South Inc.	Grenada	2,030.75	1,185.75	2,010.00
Burrows Paper Corp.	Pickens	32.67	37.58	43.50
Coastal Paper	Wiggins	100.00	100.00	100.00
Georgia Pacific Corp.	Monticello	11,663.92	6,644.33	6,976.00
Leaf River Cellulose	New Augusta	504.42	488.33	571.50
Mississippi River Corp.	Natchez	3,521.27	3,725.93	3,917.35
Weyerhaeuser Co., Columbus Modified Fiber Div.	Columbus	443.58	289.75	201.90
Weyerhaeuser Co., Pulp and Paper Complex	Columbus	2,360.75	2.953.50	2,260.08

Table I7: BOD_5 loading (lbs/day) of representative poultry processing wastewaters in Mississippi.

Company Name	Location	2008	2009	2010
DG Foods, LLC	Hazlehurst	173.08	278.25	743.17
Koch Foods of Mississippi, LLC	Morton	3,465.00	2,625.50	3,156.75
Marshall Durbin Food Corp.	Hattiesburg	539.50	1,302.83	1,926.67
Peco Foods	Canton	9,325.75	7,359.50	8,753.67
Sanderson Farms, Inc.	Laurel	16,118.58	12,444.33	14,481.42
Wayne Farms, LLC	Laurel	12,085.65	13,311.54	13,455.40

Addressing Milestone 2: Oil accumulation above 15% by weight evaluated for microbial biomasses grown on pulp and paper and food processing industrial wastes. Economic analyses indicate that microbial content above 15% by weight generate Biocrude under $3.0/gallon.

Several engineering aspects of the proposed fermentation process for the enhancement of lipid and biodiesel yields from municipal sewage activated sludge are discussed in order to determine its feasibility in industrial applications. Continuous process simulations were performed using computer software to obtain projected biomass and lipid productivities, biodiesel yields, and substrate consumption rates. Preliminary design calculations were them made to estimate the required bioreactor size required for specific calculation bases, specifically the assumed substrate conversion or yield coefficients for lipids and biodiesel production. An economic analysis was conducted to determine capital investment, production costs, and optimal product selling price. Based on the results of the laboratory-scale cultivation experiments conducted in this study, the proposed fermentation process for the conversion of lignocellulose sugars into storage lipids could be applied to aerobic activated sludge bioreactors for the enhancement of its lipid content and subsequently its saponifiable lipid fraction or biodiesel yield. Single stage batch kinetic parameters obtained at an initial C:N ratio of 70:1 and substrate (hydrolyzate) concentration of 60 g/L were used to design a large scale continuous lipid accumulation process and estimate the fermentation profiles under the same initial conditions. These kinetic parameters and their corresponding values shown in Table I8 were used to generate the continuous fermentation profiles in Figure I15 and the steady state values and performance parameters shown in Table I9. Calculations were carried out using the Runge-Kutta-Fehlberg algorithm of the ordinary differential equations program of Polymath® Professional 6.1 (CACHE Corpn., USA). These numerical values can then be applied to the design of a large scale lipid accumulation process in a wastewater treatment plant employing the activated sludge process.

Table I8: Single-stage batch fermentation kinetic parameters at 60 g hydrolyzate per L initia l loading and C:N ratio 70:1 used for estimation of continuous culture profiles.

Parameter	**Symbol**	**Units**	**Value**
Maximum specific growth rate	μ_{max}	h^{-1}	0.018
Saturation constant	K_S	g/L	14.0
Empirical constant for growth-associated lipid production	m	g/g	0.223
Empirical constant for non growth-associated lipid production	n	g/g·h	3.5×10^{-4}
Non lipid biomass yield coefficient	$Y_{X/S}$	g.g	0.39
Optimum dilution rate	D_{opt}	h^{-1}	0.01

Table I9: Performance parameters of model simulated continuous fermentation of lignocellulose hydrolyzate for enhanced lipid accumulation of activated sludge.

Dilution rate, D	h^{-1}	0.01
Feed Substrate Concentration S_0	g/L	60
Initial Non Lipid Biomass Concentration, X_0	g/L	1.0
Initial Lipid Content,	% CDW	9.1
Initial Lipid Concentration P_0	g/L	0.1
Steady State		
Time to Reach Steady State	h (d)	3243 (135)
Non Lipid Biomass Concentration X	g/L	32.4
Lipid Content	% CDW	20.5

Lipid Concentration *P*	g/L	8.4
Substrate Concentration *S*	g/L	18.2
Non Lipid Biomass Productivity	g/L·h	0.32
Lipid Productivity	g/L·h	0.08
Substrate Loading Rate	g/L·h	0.61
Substrate Effluent Rate	g/L·h	0.18
Substrate Consumption Rate	g/L·h	0.43
Non Lipid Biomass Yield Based in Substrate Consumed $Y_{X/S}$	g/g	0.39
Lipid Yield Based on Substrate Consumed $Y_{P/S}$	g/g	0.20

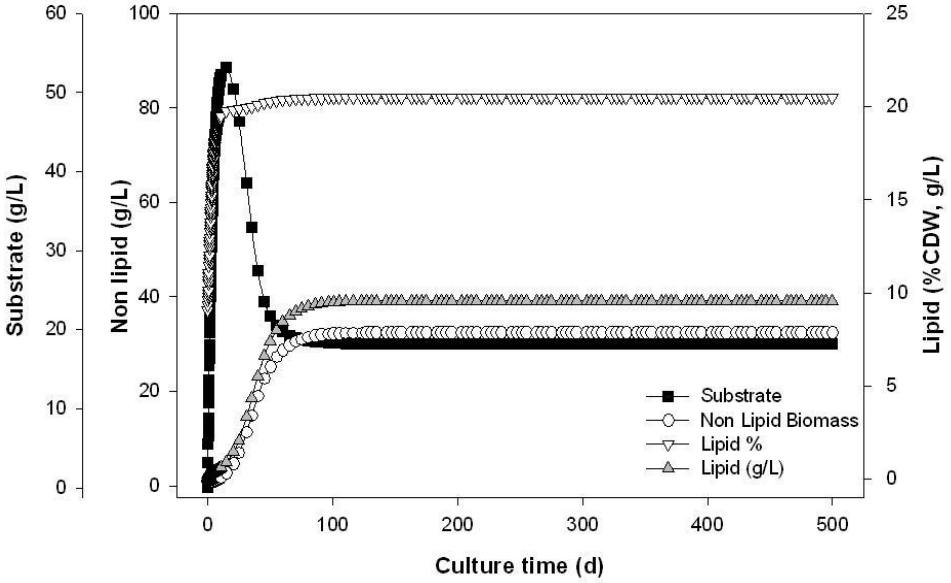


Figure I15: Model simulation for the continuous fermentation of model lignocellulose hydrolyzate at 60 g/L hydrolyzate feed concentration, C:N ratio 70:1, D = 0.01 h^{-1}.

For the process scale-up calculations, the municipal wastewater treatment plant from which the activated sludges used in this study were obtained was considered. This wastewater treatment plant is located in Tuscaloosa, AL, USA, and is rated with an average daily capacity of 30 MGD (million gallons per day). For the proposed lipid enhancement process for activated sludge, 2% of the total average daily capacity was assumed to be used as the influent media stream, hence the basis of the design was:

$$\begin{aligned}\text{Design influent flow rate } &= 0.02(30) = 0.6\,\text{MGD} \\ &= 80{,}200\ \text{ft}^3/\text{d} \\ &= 2.3\times10^6\ \text{L/d}\end{aligned} \tag{2}$$

The total substrate loading rate shown in Table I2 (0.61 g/L·h) was obtained by multiplying the influent substrate concentration (S_0 = 60 g/L) with the design dilution rate (0.01 h^{-1}). Thus, the substrate loading for the proposed large scale process was calculated as

$$\text{Total substrate loading} = FS_0$$
$$= \left(2.3\times10^{6}\ \text{L/d}\right)\left(60\times10^{-3}\ \text{kg/L}\right)$$
$$= 1.4\times10^{5}\ \text{kg/d}$$
$$= 5.0\times10^{7}\ \text{kg/yr} \qquad (3)$$

To express these parameters in terms of BOD_5, the conversion factor of 224 mg/L BOD_5 for a standard 300 mg/L of glucose solution for the standard BOD_5 analysis method was used [APHA, et al., 1998] and the calculated BOD_5 equivalent of the initial substrate concentration of 60 g/L was 44800 mg BOD_5/L . Hence, the BOD_5 loading was calculated as 681 lb BOD_5/1000 ft^3·d. The required total working volume of the bioreactor or aeration basin for the proposed process was then calculated from the dilution rate and design flow rate as

$$V_R = \frac{F}{D} = \frac{9.5\times10^{4}\ \text{L/h}}{0.01\ \text{h}^{-1}} = 9.3\times10^{6}\ \text{L}$$
$$= 9.3\times10^{3}\ \text{m}^3$$
$$= 3.3\times10^{5}\ \text{ft}^3$$
$$= 2.5\times10^{6}\ \text{gal} \qquad (4)$$

or, based on the equivalent BOD_5 loading,

$$V_R = 2.2\times10^{5}\ \frac{\text{lb BOD}_5}{\text{d}}\left(\frac{1000\ \text{ft}^3\ \text{d}}{681\ \text{lb BOD}_5}\right)$$
$$= 2.5\times10^{6}\ \text{gal}$$
$$= 3.3\times10^{5}\ \text{ft}^3 \qquad (5)$$

The bioreactor/aeration basin dimensions were then sized based on the design guideline for completely-mixed systems, wherein the typical length-to-width ratios are between 1.5:1 and 2:1 at depths less than 5 m (15 ft) [Celenza, 2000]. Although most activated sludge aeration basins are designed in plug flow configurations having length-to-width ratios of at least 5:1 or, in many cases, even greater than 10:1, the use of the plug flow for this particular application was considered inappropriate due to the existence of concentration gradients along the length of the basin [Celenza, 2000]. Assuming a liquid depth of 5.5 m (15 ft) and length-to-diameter ratio of 2:1, the bioreactor length and width are calculated to be 58.2 m (191 ft) and 29.1 m (95.4 ft), respectively. The effluent substrate flow rate was calculated as

$$\text{Effluent substrate flow rate} = FS$$
$$= \left(2.3\times10^{6}\ \text{L/d}\right)\left(18.2\times10^{-3}\ \text{kg/L}\right)$$
$$= 4.1\times10^{4}\ \text{kg/d}$$
$$= 1.5\times10^{7}\ \text{kg/yr} \qquad (6)$$

Hence, the overall substrate consumption can be estimated by taking the difference of the total substrate loading and the effluent substrate loading to obtain 9.9×10^4 kg/d or 3.5×10^7 kg/yr. Similarly, the BOD_5 concentration and loading of the effluent was calculated as 13580 mg BOD_5/L and 206.5 lb BOD_5/1000 ft^3·d. These levels are still too high for discharge in stabilization ponds; hence, the effluent should be routed back to the head of the wastewater treatment plant for further BOD_5 degradation. Moreover, due to its significant residual substrate content, the

effluent could likewise be recycled into the fermentation process for further utilization by the activated sludge microorganisms for lipid production, therefore lowering the sugar requirement and costs. The non lipid biomass and lipid production rates were also calculated from steady state data as

$$\begin{aligned}\text{Non lipid biomass production} &= FX \\ &= \left(2.3\times10^{6}\ \text{L/d}\right)\left(32.4\times10^{-3}\ \text{kg/L}\right) \\ &= 7.5\times10^{4}\ \text{kg/d} \\ &= 2.7\times10^{7}\ \text{kg/yr}\end{aligned} \tag{11.5}$$

and

$$\begin{aligned}\text{Lipid production} &= FP \\ &= \left(2.3\times10^{6}\ \text{L/d}\right)\left(8.4\times10^{-3}\ \text{kg/L}\right) \\ &= 1.5\times10^{4}\ \text{kg/d} \\ &= 5.4\times10^{6}\ \text{kg/yr}\end{aligned} \tag{11.6}$$

In this instance, lipid production can also be calculated by multiplying the lipid yield coefficient $Y_{P/S}$ with the sugar consumption rate using the assumed value of 0.20 g lipids/g substrate consumed and by multiplying the non lipid biomass production rate with the lipid content by mass of the enhanced sludge biomass. The milestone objective aims to test lipid contents above 15% by mass, but the calculations presented in this economic analysis use the predicted value of 20.5% w/w as shown in Table I9. In order to determine the economic feasibility of the proposed process, a cost analysis approach employed previously [Mondala, et al., 2009] was used in the current study to estimate the production cost and price per gallon of biocrude obtained from the enhanced sludge; the results are shown in Table I10. The basis for the cost analysis is one year of continuous operation of the sequential lipid accumulation cultures of activated sludge. The sugar cost is also assumed to be the only contribution to the total direct operating cost (DOC). No additional construction of bioreactors was necessary since the fermentation process could be conducted in available activated sludge aeration basins in the wastewater treatment plant; hence, no equipment and capital costs were incurred in this manner. The sugar cost was estimated at $0.20/lb, the average of the monthly sugar price from Jan. – Sep. 2010 as found in the International Monetary Fund webpage listing of fuel and non-fuel commodity prices [IMF, 2010]. Additionally, the process effluent stream still contains significant quantities of the substrate (18.2 g/L); the effluent streams were assumed to have recycled following separation of the oil-rich sludge biomass to fully incorporate the sugar supply into the process. All the sludges being produced were harvested and processed for biocrude extraction, and there was no sludge recycle stream.

Table I10: Annual cost estimates for biocrude production of enhanced activated sludge. Bases: 1.58×10^6 gallons/yr (5.97×10^6 L/yr) capacity, 20 % w/w lipid content.

Item	Unit Cost	Total Cost
A. Total capital investment cost, TCC (FCC + WCC)[a]		$723,384.01
1. Equipment cost, EC (ln $1000/8000 ton annual cap.)		$410,058.39
a. Extraction vessel	$284.75	$219,791.30
b. Solvent recovery/Product concentrator	$153.85	$118,752.91
c. Heat exchangers	$3.40	$2,624.37
d. Pumps	$45.05	$34,772.95
e. Others	$44.20	$34,116.86

2. Contingencies and fees, CFC (18 % of EC)		$73,810.51
3. Total basic module cost, TBMC (EC + CFC)		$483,868.90
4. Auxiliary facility cost, AFC (30% of TBMC)		$145,160.67
5. Fixed capital cost, FCC (TBMC + AFC)		$629,029.57
6. Working capital, WCC (15 % of FCC)		$94,354.44
B. Total annual production cost, TAPC (DOC+IOC+DEPC+GE)[b]		$6,068,566.69
1. Direct operating costs, DOC		$5,378,131.14
a. Sugars for fermentation[c]	$2.00/gal	$3,150,860.10
b. Biomass preparation, i.e., drying[d]	$1.06/gal	$1,671,408.00
c. Extraction	$0.21/gal	$331,128.00
d. Labor[d]	$0.10/gal	$157,680.00
e. Maintenance and repairs (6 % of FCC)		$37,741.77
f. Operating supplies (15 % of maintenance and repairs)		$5,661.27
g. Lab charges (15 % of labor)		$23,652.00
2. Indirect operating costs, IOC		$107,188.59
a. Overhead, packing, storage (60% of labor)		$94,608.00
b. Local taxes (1.5 % of FCC)		$9,435.44
c. Insurance (0.5 % of FCC)		$3,145.15
3. Depreciation, DEPC (10 % of FCC)		$62,902.96
4. General expenses, GE		$520,344.00
a. Administrative expenses (25 % of overhead)		$23,652.00
b. Distribution and selling (≈10 % of TPC)		$473,040.00
c. Research and development (≈5 % of TPC)		$23,652.00
C. Total revenues from biosolids fertilizer sale	$35.80/ton[f]	$961,475.09
D. Net annual production costs (B-C)		$5,107,091.60
Price of biodiesel per gallon to break even		**$3.24**

[a]Costs were estimated based on the values reported in $1000 per 8000 tons per yr using the conversion equation of capacity: $Cost_B = Cost_A(Capacity_B/Capacity_A)^{0.65}$ [You, et al., 2008].
[b]Itemized production costs were based on the costs reported by You *et al.* (2008) unless specified otherwise.
[c]Sugar cost of $0.22/lb converted to per gallon of biocrude produced [IMF, 2010]
[d][Dufreche, et al., 2007].
[e][Nelson and Schrock, 2006].
[f][Sullivan, et al., 2007].

For estimation of the operating costs, it was assumed that there were minimal to zero capital costs related to the fermentation process since existing aeration basins and settlers in the WWTP could be used. Therefore, the fixed capital investment cost (FCC) only accounted for the fabrication of biocrude extraction equipment based on the calculated production capacity and their respective contingencies, fees, and auxiliary facilities according to the methods employed in another paper [You, et al., 2008]. The FCC was then used to estimate the total capital investment cost (TCC) and total annual production cost (TAPC) as seen in Table I10 Items A and B, respectively, using the approach used by You and colleagues [2008]. As mentioned previously, the auxiliary facilities cost, which includes the purchase of land, installation of electrical and water systems, and construction of internal roads (AFC, Table I10 Item A.4.) as well as the feedstock transportation costs [Mondala, et al., 2009], may be significantly lowered if the biocrude extraction facility was built in the same site or within close proximity of the wastewater treatment plant. In order to recover some of the TAPC and reduce the fraction of feedstock cost attributed to the sugars, the use and sale of the spent biomass (biosolids) after

lipid extraction as fertilizer replacement has been considered. These solids theoretically still contain nitrogen and phosphorus from the microbial cell materials that may be utilized nutrient sources for agricultural applications at an estimated cost of $35.80 per dry ton [Sullivan, et al., 2007]. Based on the overall non lipid biomass output of the fermentation and transesterification, assuming complete separation of lipidic materials (2.7×10^4 tons/yr), the estimated yearly revenues from the sale of the spent biosolids was projected to be $961,475.09, and subtracting this value from the TAPC gives the net annual production cost (Table I3 Item D). Therefore, the break-even price of the biocrude exclusive of profits, income taxes, and product transportation cost was calculated as $3.24/gallon of processed biocrude at 20% w/w lipid content of the enhanced sludge biomass with a sugar cost of $0.20/lb. Sensitivity analysis was conducted to determine the effect of target biomass lipid content and sugar cost on the biocrude break-even price per gallon and the conditions needed to attain a price below $3.00/gallon. The results are summarized in Figure I16. Based on the results shown in Table I10, a lignocellulose sugar cost between $0.15 and $0.18/lb is needed to reduce the biocrude price below the $3.00/gallon mark.

Subtask I.3 Examine non-conventional oil separation techniques

Lipid feedstocks coming from microorganisms (i.e. bacteria, yeast, and microalgae) contain membrane lipids (e.g. phospholipids) in addition to the target lipidic compound (mainly triacylglycerides) [1]. Phospholipids are amphiphilic compounds which could act as surfactant/emulsifier in the presence of water, complicating lipid extraction processes (see Figure I16). To eliminate this complication, microbial feedstocks are subjected to drying to a certain moisture level to minimize formation of emulsions. However, drying of feedstocks containing high levels of water is not economically feasible. For example, a study on the biodiesel production from activated sludge, which contains ~98% weight water, indicated that the cost of water removal accounts to more than 50% of the fuel cost [2]. Thus, alternative processes that do not require complete water drying to limit emulsion formations (demulsification) must be explored.

Electrostatic coalescence is a widely used process in the petroleum industry for accelerating the separation of water from water-in-oil emulsions by the application of an electric field. This separation technique, is not, however, very common in separating water from water-in-(lipid-rich oil) or (lipid-rich oil)-in-water emulsions. With the growing interest in producing biofuels and other specialty chemicals from lipidic material, electrostatic coalescence might be a useful tool for efficient lipid extraction from different feedstocks prior to product conversion(s).

A laboratory scale electrostatic coalescer was built to evaluate the electrocoalecense of a model ternary system that contains emulsion.

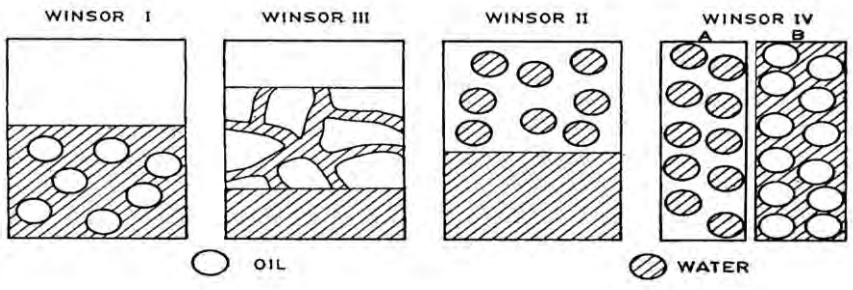


Figure I16: Representation of different emulsions [3].

A ternary mixture containing (by weight) 90% decane, 2.5% lecithin, and 7.5% water was prepared. Based on the study conducted by Angelico et al. (2004), this mixture forms a Winsor III–type emulsion [4]. However, after sonication overnight at ~23°C, the prepared mixture resulted in a homogenous, single-phase system (see Figure I17). This homogeny could be due to possible differences in the composition of the lecithin used, particularly the fatty acid moiety. Furthermore, this could be due to differences in homogenization temperature used, 23°C for this study versus 25°C for the study conducted by Angelico et al.

The mixture (~45mL) was loaded into a rectangular cuvette and was then subjected to electro-coalescence at different DC field strength (1, 5, 10 and 20kV) for a period of 5 minutes. The set-up shown in Figure I18 was used for this experiment. To observe the progress of the process, <0.5% (weight) Sudan III dye was added to the mixture. Sudan III is a red-colored dye that is soluble in hydrocarbons (i.e. decane), even in the presence of high concentration of phospholipids, but is not soluble in water. Due to density differences, the water that will be separated out during the process was expected to settle at the bottom of the reaction vessel. Without the dye, however, this would not be observed visually, and the process evaluation would require complicated analytical procedure. GC-MS and/or LC-MS could be needed for a speciation-type performance of the system. However, for initial evaluation, visual observation would suffice.

The effect of the applied voltages on the separation of the emulsion was evaluated based on the observed time of the on-set of separation and the time of the cessation of the separation.



Figure I17: Decane-water-lecithin mixture containing <0.5% (weight) Sudan III prior to high voltage electrocoalescer.

The electrostatic coalesce set-up is shown in Figure I18. It includes two power supplies, each of which can supply voltages ranging from -20 to +20 kV. This allows the system to give a maximum of 40kV field strength. The reaction vessel was caged in a 1-ft^3 acrylic box for safe operation. The reaction vessel, which is a glass vessel, has a maximum capacity of 56 mL (40 × 20 × 104 mm). Two electrode geometries were considered in this study: (bare) ⅛-in diameter stainless steel rod and (bare) 55mm ×10 mm × 1.6mm stainless steel plate. The distance between the electrodes was kept constant at 5 cm. Different parts of the set-up are labeled in Figure I18.

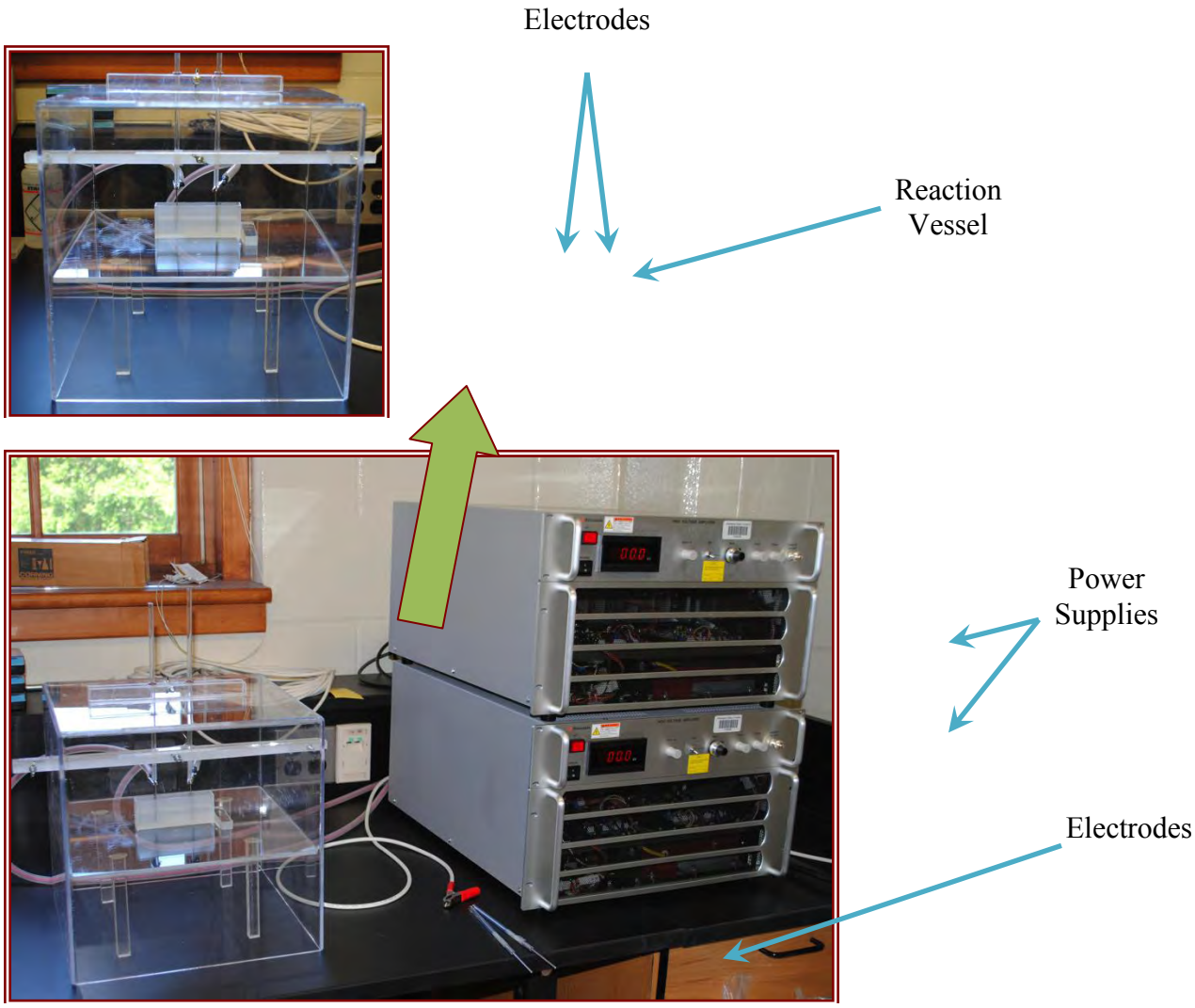


Figure I18. The high-voltage electrostatic coalescer set-up.

The progress of the process was monitored for a period of 5 minutes. During the process, vertical and horizontal movements were observed for both electrode geometries, which are possibly due to re-orientation of lecithin emulsion (micelles). The vertical movements induced water separation, which settled as droplets at the bottom of the vessel (Figure I19), and increased as the voltage applied was increased. Similarly, the horizontal movements were greater for higher voltages applied (almost negligible for 1 and 5kV). These horizontal movements resulted to tightening of a gel-like mass (possibly compacted lecithin emulsion) in the inter-electrode distance. More compacted lecithin emulsions were observed as voltage applied was increased, regardless of the electrode geometry. These observations indicated that electrostatic coalescence could be used not only for removal of water but also for lecithin purification from decane + water + lecithin emulsion.

The separation on-set was faster for plate electrode (Table I11). This is possibly due to a more uniform field for the plate electrode, which, with the dimensions used, covered almost the entire width of the vessel. However, separation cessation was faster for rod electrode. It is suspected that the longer cessation time for plate electrode was due to the higher separation efficiency as compared to the rod electrode at the same field strength. This is also due to a more uniform field for plate electrode.

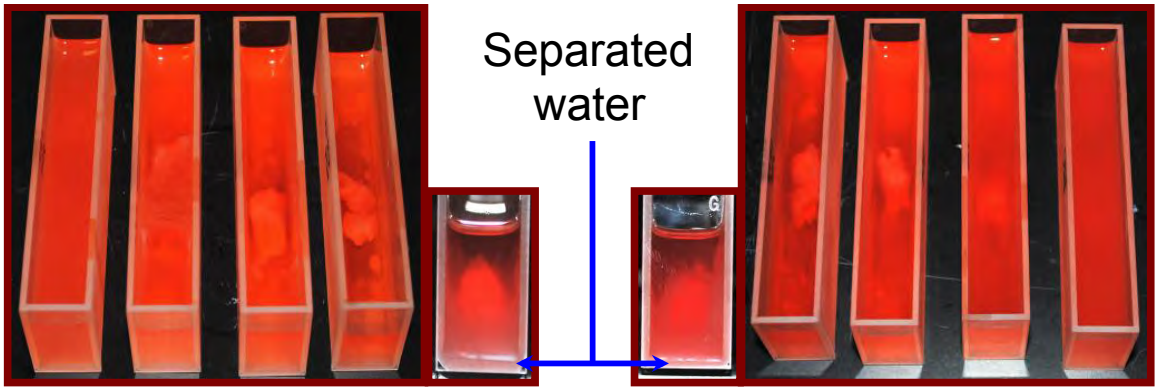


Figure I19. Effect of field strength on the demulsification of decane + water + lecithin emulsion. (a) Plate electrode (b) Rod electrode.

Table I11. Effect of field strength on the demulsification on-set and demulsification cessation of decane + water + lecithin emulsion

Electrode Geometry	Applied Voltage (kV)	Separation On-set (s)	Separation Cessation (s)
Plate	1	20	130
	5	17	115
	10	15	107
	20	7	75
Rod	1	25	102
	5	19	95
	10	12	90
	20	8	80

In studying the electrostatic coalescence of lipid emulsions, it is important to have an established phase diagram(s) for the lipid systems being considered in this study. Phase diagrams will provide concentration region(s) where and what type of emulsions are present. This, in turn, will serve as a basis of how much water should be removed from the feedstock and how much solvent should be added prior to electrostatic coalescence. Due to limited available literature about these phase diagrams, they have to be established before further experimentations.

For these reasons, the electrostatic coalescence was not applied to an actual sample and thus, the milestone (Achieve 80% oil extraction with the target of extracting oil at $0.30/lb) was not met. Six ternary systems are currently under investigation to establish phase diagrams. These

are Phospholipid + Decane + Water, Phospholipid + Hexadecane + Water, Triacetin + Decane + Water, Triacetin + Hexadecane + Water, Soybean oil + Decane + Water, and Soybean oil + Hexadecane + Water. The data will be included in the SERC IV final report.

Application of Liquid Propane as an Extraction Fluid

Introduction:
The separation of lipids from an aqueous environment often incurs a large percentage of the total operating and production costs associated with reclamation and enhancement of lipids in microbial and other wastewater. Among other non-conventional oil separation techniques that were considered to reduce this cost, liquid propane was evaluated to determine its technical and economic feasibility to extract lipids from mixtures containing water.

In order to more effectively plan and model experiments that involve using liquid propane to extract lipids directly from complex slurries or mixtures, the solubility of various pure lipid components in liquid propane was necessary. These pure lipid components would be model compounds to represent those typically found in microbial or other lipid sources, such as triglycerides, free fatty acids, and phospholipids.

Materials and Methods:
Extractions were performed with a lab-scale extractor manufactured by Thar Technologies, (Model SFE-500F-1-FMC50; Pittsurgh, PA). This equipment was designed for extractions with supercritical carbon dioxide and also included an additional pump to be used for co-solvents. Initial experiments were planned to measure the solubility of lipids in a mixture of supercritical carbon dioxide and near-critical liquid propane. Further extraction experiments were planned to only use the co-solvent pump to deliver near-critical liquid propane.

The equipment operates using a dynamic, flow-through method to determine solubility. This technique assumes the solvent is fully saturated with the solute within the sample vessel at the specified temperature, pressure, and flow rate. The stainless-steel 500-mL sample vessel was charged with an excess of the desired lipid sample between two layers of glass wool (Fisher Scientific), with the remaining void volume filled with 2-mm diameter borosilicate glass beads (Chemglass, Vineland, NJ). The charged vessel was then heated to the specified temperature. The solvent then passed through the sample vessel at the set temperature, pressure, and flow rate for a known amount of time. The solvent and the dissolved lipid solute then flowed into a cyclone collector, where the solute remained as the solvent vaporized. The solute was collected in one or more tared glass vials by rinsing the cyclone collector with hexane and/or chloroform. After evaporating the rinse solvent under a stream of nitrogen, the mass of extracted lipid solute was determined gravimetrically. This solute mass was divided by the total mass of the solvent that passed through the sample vessel to determine the solubility at the specified temperature and pressure.

The first lipid component to be tested was a phospholipid mixture obtained from a commercial vendor (Avanti Polar Lipids, Alabaster, AL) and used without further purification. This product is a soy phospholipid extract that is composed of phosphatidylcholine (PC, 97.2%) and lysophosphatidylcholine (LPC, 2.8%). The fatty acid distribution is given in Figure I20.

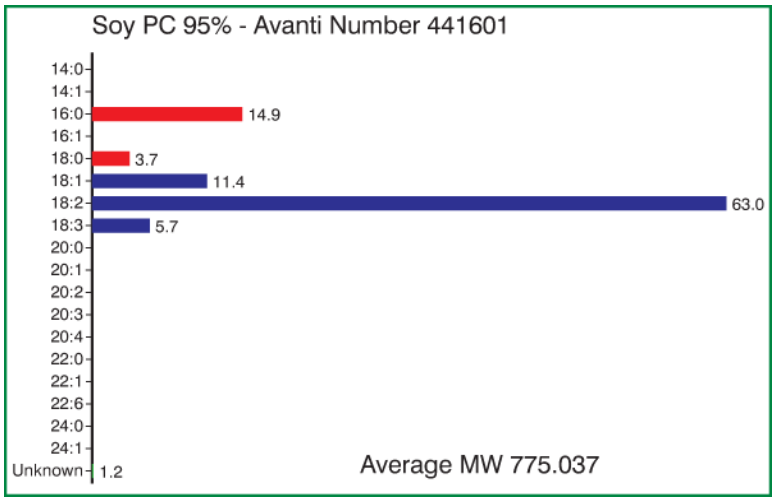


Figure I20: Fatty Acid Distribution of Soy PC 95% - Avanti Number 441601.

This phase of the study examined the effect of three variables—temperature, pressure, and ratio of propane to supercritical carbon dioxide—on the solubility using a 3^3 design of experiments, where 27 experiments each of three replicates were conducted. These 27 experiments include all combinations of the three levels of each of the three variables: (35 °C, 50 °C, 65 °C; 8 MPa, 21.5 MPa, 35 MPa; 0%, 25%, 50% propane). No further statistical analysis was performed on the data set, but rather it was used to model the solubility of lecithin with the Chrastil Equation and similar density-based models. Figure I21 shows a plot of solubility vs. density for these 27 data points. Each point represents the mean of the three replicates, and the error bars represent one standard deviation. Although both axes of Figure I21 are nondimensionalized, it should be noted that the absolute solubility is very small. Of the 5 g of sample that is loaded into the apparatus, the collected sample amount is typically less than 20 mg.

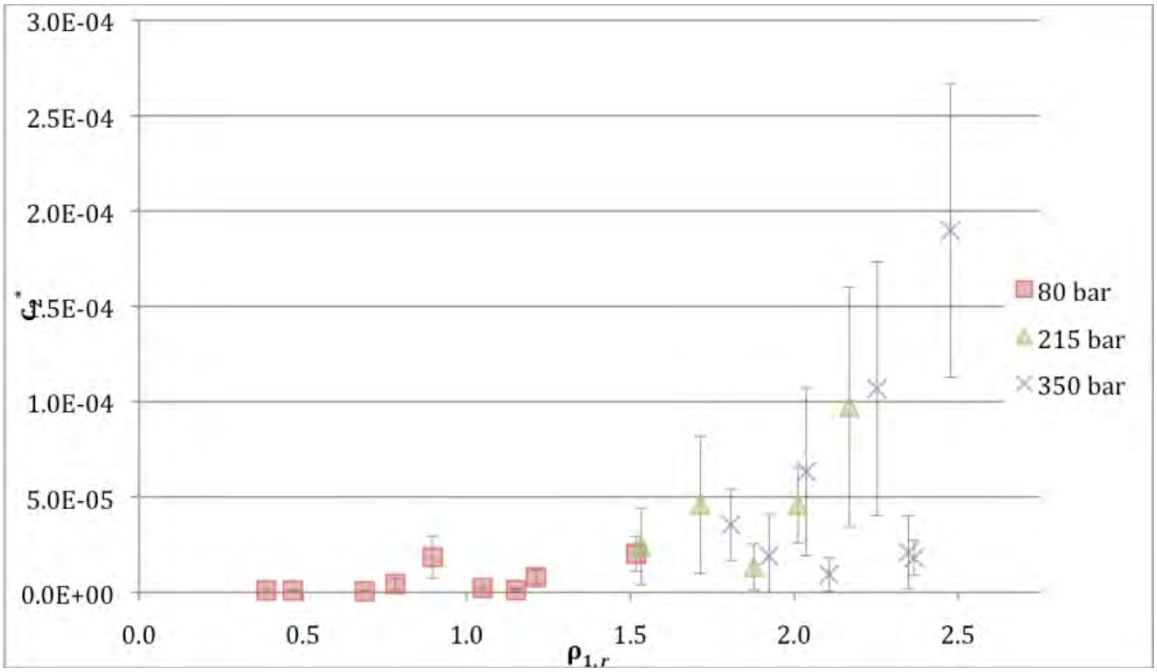


Figure I21: Solubility of Lecithin vs. Density of CO2/Propane Solvent (nondimensionalized).

Research Challenges:
Upon further inspection of the data and methods of the experiment, two major flaws became apparent. First, there was a pattern in each data point where the measured solubility was highest for the first replicate, with the value of each successive replicate being dramatically lower. Also, upgrades to the apparatus revealed that the actual amount of propane being used in the experiment was significantly lower than the amount assumed to have been used in each run.

Replicate issue:
As mentioned above, the measured solubility of each set of conditions decreased from one replicate to the next. This effect can be seen in Figure I22, which contains a subset of the previous mean solubility data from Figure I21 plus data points representing each of the three replicates. In each case, the first replicate was near or above one standard deviation above the mean, the second replicate was at or below the mean, and the third replicate was near one standard deviation below the mean.

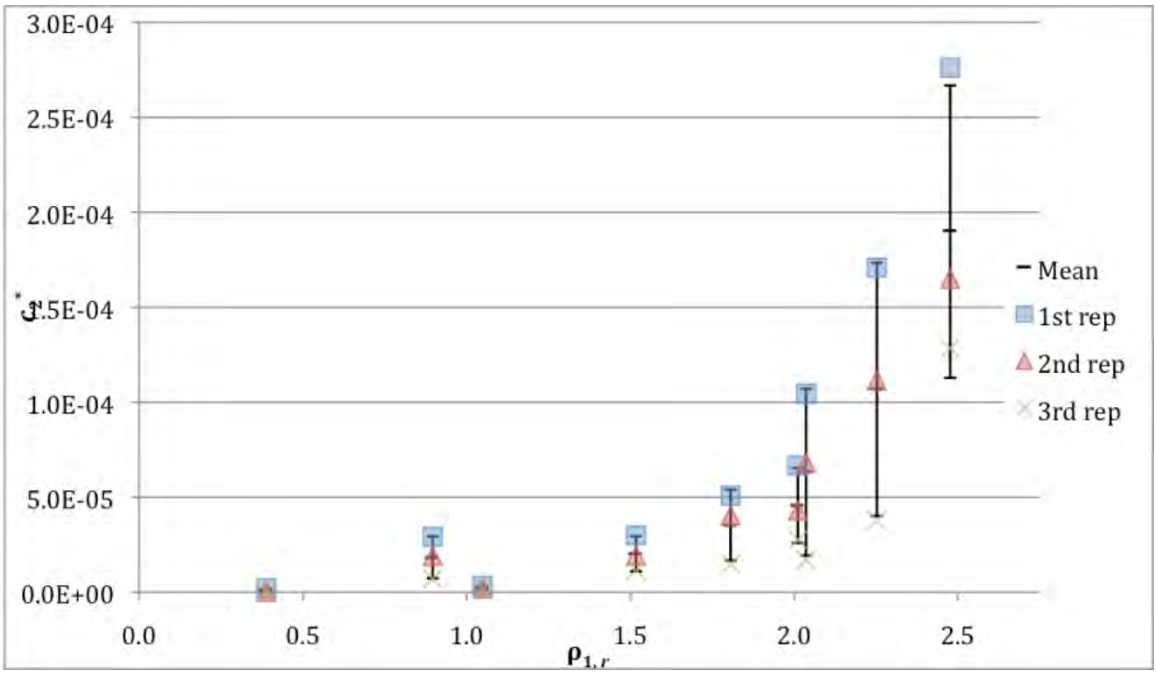


Figure I22: Replicate Repeatability of Solubility vs. Solvent Density Data.

A series of experiments was designed to isolate the cause of the data anomalies, all conducted at 8 MPa, 35°C, and with no propane, with 20 g/min CO_2 for 25 min.

- Consecutive Replicates: the normal method where the system remains pressurized between replicates (five replicates instead of the usual three)
- Successive Replicates: system is depressurized between replicates but the same sample loading is used (four replicates)
- Isolated Replicates: system is depressurized, cleaned, and repacked with a fresh sample loading between replicates (four replicates)

Consecutive Replicates:
This test was conducted using more replicates than usual to see if the diminishing-solubility effect would level off over enough replicates, although after five replicates, the effect was still

ongoing. Figure I23 shows the results of this test, where the error bars represent the standard deviation of all five replicates.

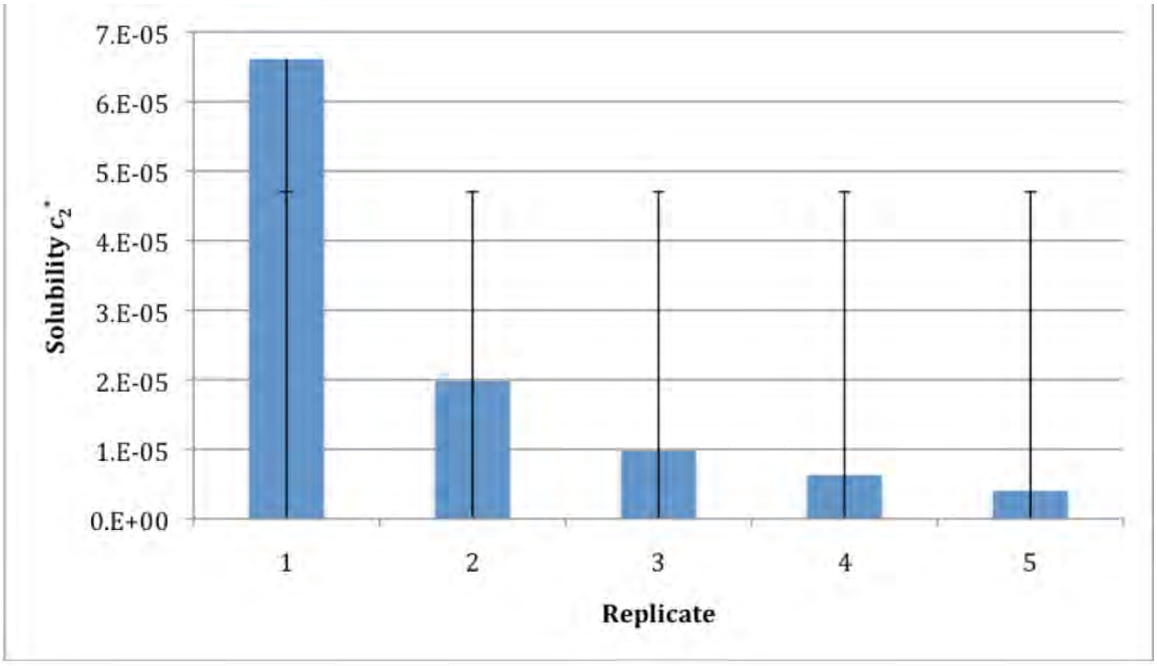


Figure I23: Solubility vs. Consecutive Replicates.

Successive Replicates:
Since the usual method of running the experiment involves leaving the system pressurized, this test was conducted to determine if depressurizing the system between runs would prevent the diminishing-solubility effect. The results shown in Figure I24 indicate that it does not.

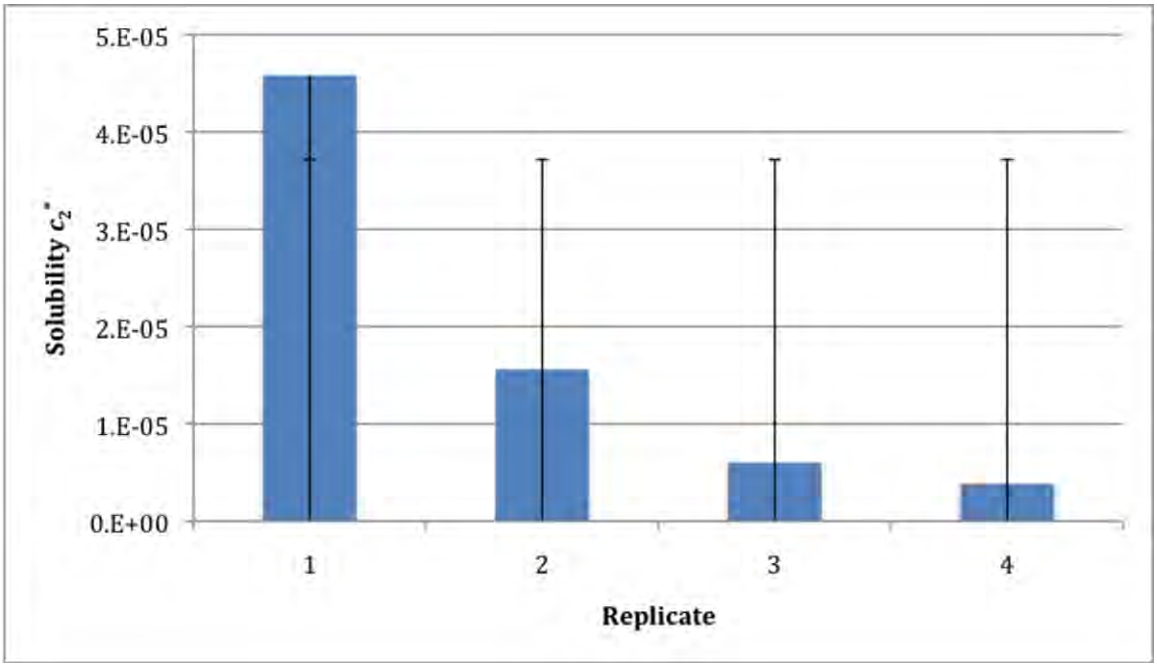


Figure I24: Solubility vs. Successive Replicates.

Isolated Replicates:
This test acted as a control, since it is essentially a series of first replicates only. Although there was some experimental variability across the replicates, the results all fell within one standard deviation of the mean. There was no diminishing-solubility effect present, as shown in Figure I25.

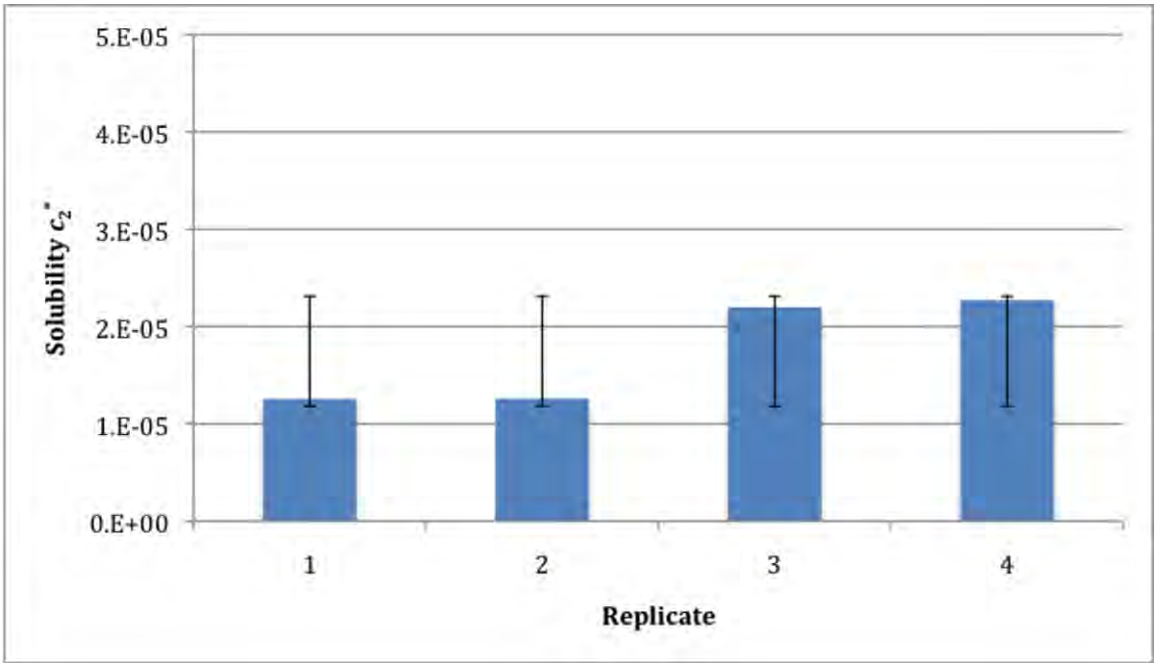


Figure I25: Solubility vs. Isolated Replicates.

Discussion:
Several hypotheses were developed as to why the solubility of a given sample loading was decreasing over time:

1. Oxidation of unsaturated fatty acids in the phosphatidylcholine sample
2. Selective solubility of phospholipids with specific fatty acid configurations
3. Exposure to nonpolar solvent that produce reverse micelles that inhibit solubility

Hypotheses 1 and 2 were in consideration because the lecithin sample used in the experiments is not a pure compound. Although the sample is 97% phosphatidylcholine, these phosphatidylcholine molecules contain a distribution of fatty acids in the two remaining positions on the phospholipid molecule's glycerol backbone. The fatty acid profile provided by the manufacturer is given in Figure I20.

According to hypothesis 1, any of these unsaturated fatty acids are vulnerable to oxidation, which may affect the solubility of the mixture over time. According to hypothesis 2, particular fatty acid combinations may be solubilized more readily, leaving behind the less-soluble components.

Both of these hypotheses have been addressed by running a consecutive replicate experiment with a new sample that contains a pure phosphatidylcholine configuration, namely with a palmitic acid at each of the two fatty acid positions of the glycerol backbone (dipalmitoylphosphatidylcholine, DPPC; Avanti Polar Lipids, Alabaster, AL). Since palmitic acid is completely saturated, it is not vulnerable to oxidation in the same way an unsaturated fatty acid would be. Furthermore, since the sample consists of only one fatty acid configuration, there

is no possibility for selective solubility. As shown in Figure I26, the results of this experiment exhibit the same diminishing-solubility effect. Hypotheses 1 and 2 can both be rejected. It is unlikely that either the oxidation of unsaturated bonds or the selective extraction of phospholipids with preferred fatty acid configurations contribute to the diminishing-solubility effect.

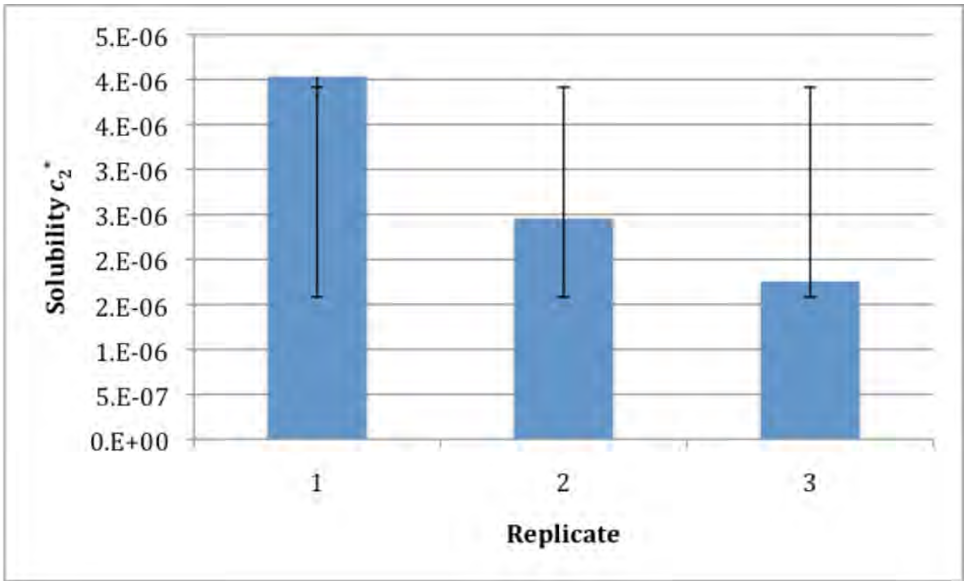


Figure I26: Effect of number of replicates on the solubility of dipalmitoylphosphatidylcholine in supercritical carbon dioxide.

According to hypothesis 3, the nonpolar CO_2 solvent is inducing the production of reverse micelles that inhibit the solubility of the phospholipid. This hypothesis was proposed because of the known behavior of this type of phospholipid when present in an aqueous (polar) environment where it forms micelles and/or bilayer membranes. The polar phosphate head groups align outward toward the polar water, while the nonpolar fatty acid chains align inward with themselves. In the reverse micelle hypothesis, the reverse occurs in the presence of the nonpolar CO_2 solvent. The hydrophobic fatty acids would project outward toward the hydrophobic solvent, shielding the hydrophilic phosphate head groups, which are repelled to the interior of the reverse micelle.

Computer simulations of molecular dynamics of CO_2 and phospholipids were studied to determine if this hypothesis is feasible. A monolayer of ten phospholipid molecules (palmitoyl-oleoyl-phosphatidylcholine, POPC) was surrounded by a bath of 4979 carbon dioxide molecules. The temperature and pressure of the system were maintained at 35°C and 80 bar, respectively, matching the conditions of many of the supercritical CO_2 laboratory experiments. The molecular dynamics software package NAMD was used to simulate the movement of these particles for one million time steps, where each time step spans two femtoseconds. Figure I27 shows the before and after visualizations of this simulation. In the before image, the monolayer is oriented such that the nonpolar fatty acid chains are aligned on the right (carbon: aqua, hydrogen: white), while the polar head groups are aligned on the left (nitrogen: blue, oxygen: red, phosphorus: brown). Over time, the hydrophobic fatty acid chains begin to move around the monolayer to shield the hydrophilic head groups from the nonpolar solvent. The after image shows the reverse micelle, in which the polar head groups comprise a core that is surrounded by the fatty acid chains, which project outward into the supercritical carbon dioxide solvent. The solvent is not shown.

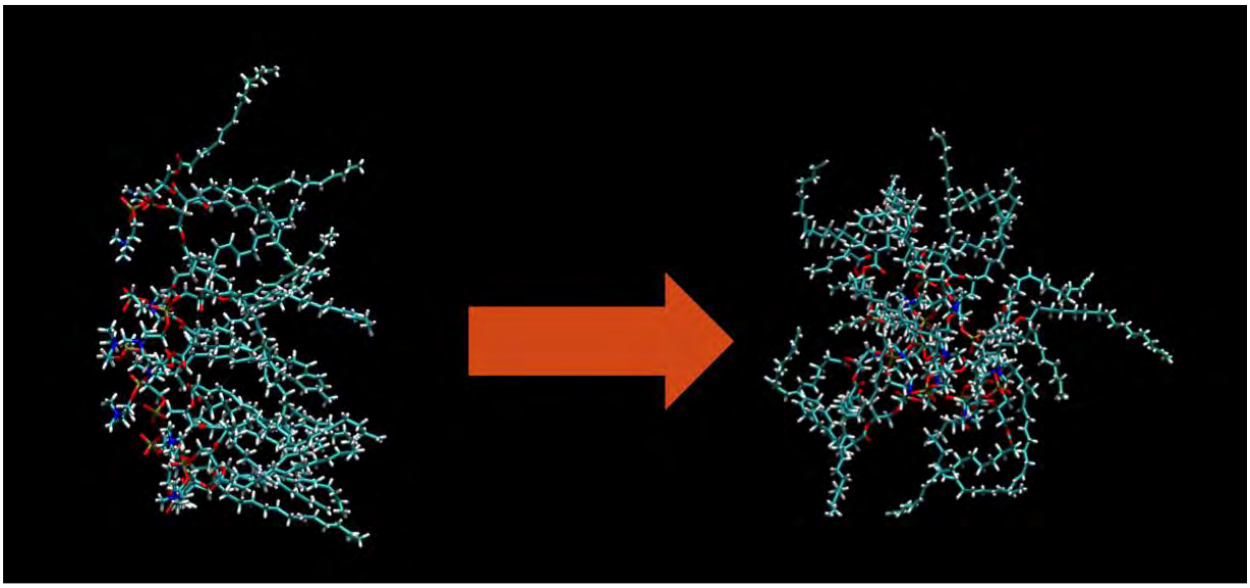


Figure I27: Reverse Micelle Formation of 10 POPC Molecules in Supercritical CO_2.

In the simulation, the reverse micelle equilibrates very quickly (less than two nanoseconds), while the experimentally observed diminishing-solubility effect persists on a time scale of minutes to hours. This discrepancy is possibly due to the large bulk of sample in the actual experiments compared to the single layer of ten molecules in the simulation. The effects of the supercritical CO_2 on the 5 g of phospholipid in the laboratory experiments take longer to propagate through the entire sample, whereas in the simulation all of the phospholipid molecules are exposed to the solvent during the entire process.

Although the results of this simulation are qualitative, they indicate that the reverse micelle hypothesis is feasible. The link between reverse micelle formation and the diminishing-solubility effect is not fully elucidated, but a plausible explanation can be proposed. Initially, the phospholipid sample is in equilibrium with the surrounding air in the atmosphere at room temperature. When the supercritical carbon dioxide is first introduced to the sample, the higher temperature and pressure induce the sample to undergo changes in the configuration of its constituent molecules. During this period, the system is in a high-energy state compared to its equilibrium state. Some of the phospholipid molecules on the periphery of the sample are vulnerable to being solubilized by the CO_2 before the bulk of the sample can shield itself from the solvent by configuring its molecules into orientations analogous to the reverse micelle observed in the simulation. This hypothesis would explain not only the diminishing-solubility effect, but also the low solubility measurements relative to the amount of sample used.

Propane Equipment and Safety Issue:
The original equipment does not have a flow meter on the propane line to directly control the co-solvent flow rate. The co-solvent pump speed is set proportional to the pump speed of the CO_2 pump, which is controlled by a flow meter on the CO_2 line. The propane experiments were operated on the assumption that this approximation was adequate. In order to check the accuracy of this assumption and to have better control over the propane flow rate, a work-around was devised. A scale was installed to weigh the propane tank that feeds the apparatus. The difference in scale readings between the start and end of an experiment can be used to give an average flow rate over the course of the experiment. For the amounts of propane

planned for the experiments, the scale readability limitations would introduce an error of less than 1%.

However, the scale did not show the propane usage that had been anticipated. The amount used over three replicates, projected to be approximately 375 g, only gave a reading of 16 g. To rule out whether the scale was malfunctioning, it was tested by weighing the CO_2 cylinder during an experiment. The mass readings of the scale were consistent with the amounts measured by the flow meter. The conclusion is that the scale is functioning properly, and the amount of propane being pumped into the system is dramatically lower than anticipated.

Safety Concerns:
Upon inspection of the pump, it was discovered that the piston rods were damaged, likely rendering the pump inoperable. After having the pump repaired, the scale began to indicate that the pump was indeed pumping liquid propane into the system. An explosive gas detector was directed at the gas outlet downstream of the cyclone collector where it indicated the presence of propane. The equipment was then ready to perform extractions with propane; however, the amount of propane being discharged into the hood exceeded the hood's capacity to adequately vent the propane. Since the discharged propane gas is heavier than air, the propane began to surround the electrical equipment in the hood used to power the extractor. At this point the experiments were halted to avoid any risk of accident.

Conclusion:
Despite having performed extensive experiments to determine the solubility of lecithin in supercritical carbon dioxide and propane, flaws in the equipment and methodology have been revealed that cast doubt onto the validity of the data. Once these issues were isolated and resolved, the presence of the venting propane became too great of a risk to continue any further experimentation.

References
[1] J Liu, J Huang, Z Sun, Y Zhong, Y Jiang, F Chen, Differential lipid and fatty acid profiles of photoautotrophic and heterotrophic Chlorella zofingiensis: assessment of algal oils for biodiesel production, *Bioresour Technol*, 102:1 (2011) 106-110.
[2] S Dufreche, R Hernandez, T French, D Sparks, M Zappi, E Alley, Extraction of lipids from municipal wastewater plant microorganisms for production of biodiesel, *J Am Oil Chem Soc*, 84:2 (2007) 181-187.
[3] JR Baran, Winsor I⇔III⇔II Microemulsion Phase Behavior of Hydrofluoroethers and Fluorocarbon/Hydrocarbon Catanionic Surfactants, *J Colloid Interface Sci*, 234:1 (2001) 117-121.
[4] R Angelico, A Ceglie, G Colafemmina, F Delfine, U Olsson, G Palazzo, Phase Behavior of the Lecithin/Water/Isooctane and Lecithin/Water/Decane Systems, *Langmuir*, 20:3 (2004) 619-631.

Subtask I.4 Produce quality transportation fuels defined by the American Society for Testing and Materials Standard

Catalytic cracking plays a vital role in petroleum refinery processes. It is the most extensively used process for conversion of heavy oils into valuable products like gasoline and other lighter products. Typically, catalytic cracking reactions are carried out at 290-400°C and 1200-2000 psig [1]. For this process, zeolite catalysts are known to have high selectivity and activity, which translate to profitable liquid product yields and high cracking capacity. However, modifications of the catalyst's surface (i.e. removal of some aluminum atoms from the framework) are sometimes necessary to meet industrial demands and specifications (i.e. higher octane rating) [2].

Not until recently has the investigation on catalytic cracking of oxygenated compoundsgained much attention. Most research had focused on compounds present in vegetable oils and bio-oil, a product of wood pyrolysis. Reports indicated that vegetable oil cracking is a promising alternative route for the preparation of 1st generation biofuels that are within the boiling range of gasoline compounds [3-6].

Lipids are oxygenated organic compounds that may also contain nitrogen and phosphorus. In addition to these, lipidic material considered for production of 2nd generation biofuels might also contain considerable amount of metals (i.e. calcium, potassium, magnesium) that may poison cracking catalysts. Aside from the removal of oxygen, another major challenge would be the purification of these feedstocks with variable compositions prior to catalytic cracking [7].

In catalytic cracking of lipidic compounds, ZSM5, particularly H^+ZSM5 (Figure I28), is one of the most commonly used zeolites [3, 8-12]. ZSM5 is a shape-selective catalyst developed by Mobil Research and Development Corp. in the mid-1970s. Due to its shape selective characteristics, ZSM5 is being used for materials that require minor cracking which would result in higher proportion of liquid relative to gaseous products [13]. The role of H^+ZSM5 in a catalytic cracking unit is normally as an octane-boosting additive due to its higher selectivity towards aromatic hydrocarbons [14].

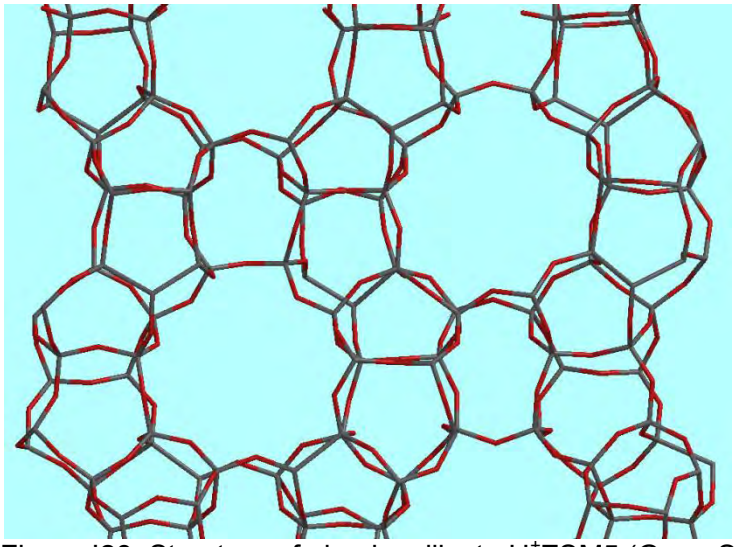


Figure I28: Structure of alominusilicate H^+ZSM5 (Gray, Silicon/Aluminum; Red, Oxygen).

Most studies on the conversion of lipidic materials into renewable fuel by catalysis were focused on vegetable oils (which are mostly triacyglycerides), fatty acids (including their esters), and bio-oil (a by-product of wood pyrolysis). However, for an effective utilization of 2nd generation biofuel feedstocks (i.e. waste oils and microbial oils), the cracking of other compounds present in the feedstock must also be understood. The study conducted by Revellame et al. (2012) showed that fatty alcohols (associated with wax esters) were consistently present in raw activated sludges obtained from a municipal wastewater treatment facility [15]. These compounds are not converted to fuel and thus considered as waste during transesterification reaction.

Fatty alcohols are important oleochemicals for manufacture of a variety of products, and thus their occurrence in activated sludge makes it a very attractive petroleum alternative. However, their utilization as raw material for production of everyday commodities might be subjected to public scrutiny. The production of 1st generation biofuels, particularly biodiesel, had caused disturbances in the oleochemical industry. The utilization of all compounds present in 2nd generation feedstock (i.e. activated sludge) for fuel production could avoid disturbances of the oleochemical industry supply and demand structure. Thus, it is important to study possible routes for their conversion to fuel.

This study dealt with catalytic cracking of a model compound that is present in activated sludge, particularly 1-octadecanol. This fatty alcohol is a saturated 18-carbon compound, which is solid at ambient condition. Activated sludge contains C14 – C18 fatty alcohols with octadecenol as the dominant one [15]. Nevertheless, octadecanol was chosen as the model compounds due to its possible unreactivity. For example, the study conducted by Benson (2008) on the super acid trifluoromethanesulfonic acid (triflic acid) cracking of fatty acids showed a highly unreactive behavior of palmitic acid, a 16-carbon saturated fatty acid. Furthermore, it is long established that alkane cracking, although similar to alkene cracking, proceeds with slow reaction rates [13]. It was anticipated that catalytic cracking of octadecanol would be difficult as compared to octadecenol, and thus the former was chosen as model compound.

The cracking mechanism for the conversion of 1-octadecanol to fuel using H^+ZSM5 was developed to support its utilization as fuel. Although H^+ZSM5 is not an industrially used catalyst due to its instability at high temperature, its intrinsically high acidity (mostly Brønsted) made it suitable for development of catalytic cracking mechanisms [13]. Zeolitic Brønsted acid sites are the active species in different hydrocarbon transformations including cracking, isomerization, and alkylation [16].

Reactions and analyses were performed using Quatra C (Cryogenic Capillary Catalytic Cracker), which is an in-house built reactor/analyzer (see Figure I29). This system is a modified Varian 3600 (Walnut Creek, CA, U.S.A.) gas chromatograph with front and rear injectors being used for reactant injector and reactor (catalyst bed), respectively. This system can take samples in solid, liquid, or gas form. Liquid and gas reactants are injected using syringes, while solid reactants are loaded in a glass crucible and are directly injected using a Varian ChromatoProbe (see Figure I30).

The catalyst bed (reactor) is normally operated up to 400°C. This is a dual-column system equipped with a Saturn 3 mass spectrometer (Varian, Walnut Creek, CA, U.S.A.) and a thermal conductivity detector (TCD). This feature of the system allows automatic analyses of reaction products including fixed gases. To maintain constant flow to the mass spectrometer, an open-split interface, manufactured by SGE Analytical Science (Victoria, Australia) was utilized. The

open-split interface allows only 1 mL/min of flow to the mass spectrometer and thus offers flexibility of the system to higher gas flowrates across the catalyst bed.

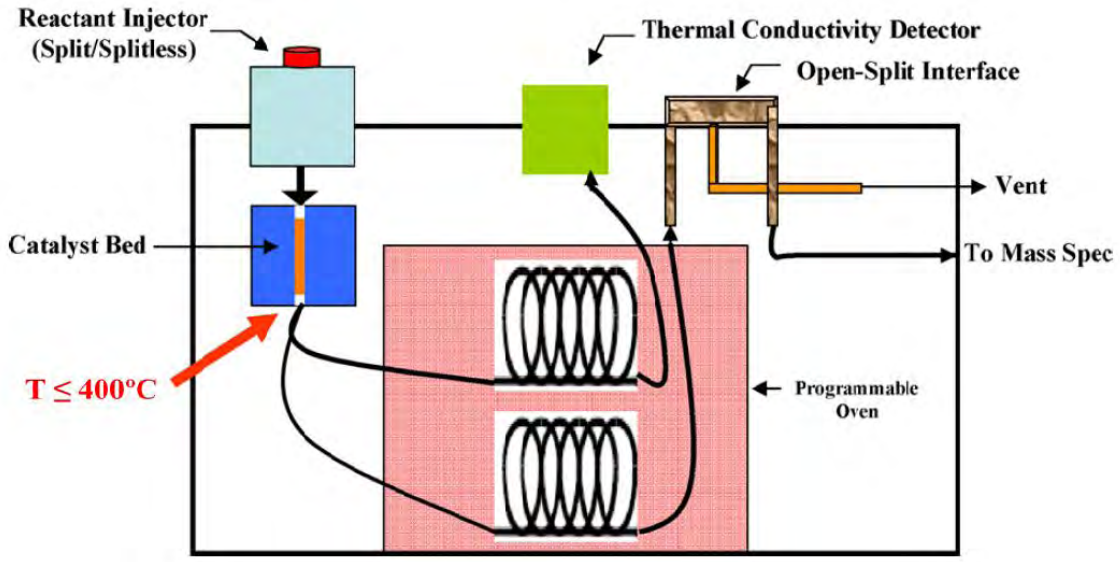


Figure I29: Diagram of the Quatra C illustrating the use of dual chromatographic columns [17].

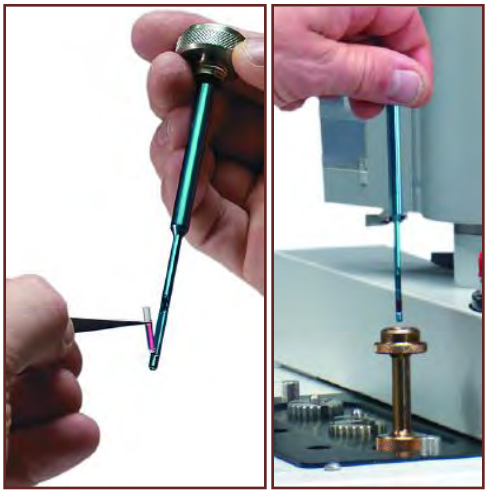


Figure I30. Sample introduction using ChromatoProbe [18].

Cracking reactions were performed by first adding the catalyst to the reaction tube. The reaction tube was a ¼ in. O.D. glass tubing (7.2 cm length x 3.9 mm I.D.) that was subjected to sonication with acetone and chloroform for one hour each and then heated in a furnace at 500°C. Catalyst amounts were varied from 0 – 20 mg. Silanized glass wool was used to hold the catalyst in place and to reduce channeling through the catalyst. For catalyst loading less than 20 mg, silica gel (200/400 mesh) was added in an appropriate amount to keep the amount of solids inside the tube constant. This was done to maintain constant hydrodynamics inside the reactor.

The catalyst-loaded reaction tube was then placed inside the reaction zone of the Quatra C. The desired temperature was set, and the catalyst was given time for off gassing of air and adsorbed water vapor. The air/H_2O indicator of the mass spectrometer was monitored, and once within

acceptable levels (≤ 0.5 amu for air and ≤ 5% H_2O^+/H_2O for water), the reaction/analysis was initiated. High levels of air and water can burnout the filament in the mass spectrometer.

Due to the limitation of the Quatra C and the nature of the reactant, the injection procedure was modified to inject the reactant directly to the catalyst bed. It was necessary to keep the reactant in liquid form. This was accomplished by mildly heating the reactant in a hot plate until it melted. Direct reactant injections were accomplished by using a syringe heated isothermally by a heating tape that was controlled by a rheostat (see Figure I31). Air bubbles inside the syringe were eliminated, after which the syringe was cooled down and weighed. Prior to injection, the syringe was mildly heated again to melt the reactant. The amount of reactant injected was determined by getting the difference of the weights before and after injection. This modification allowed GC oven programming down to -40°C.

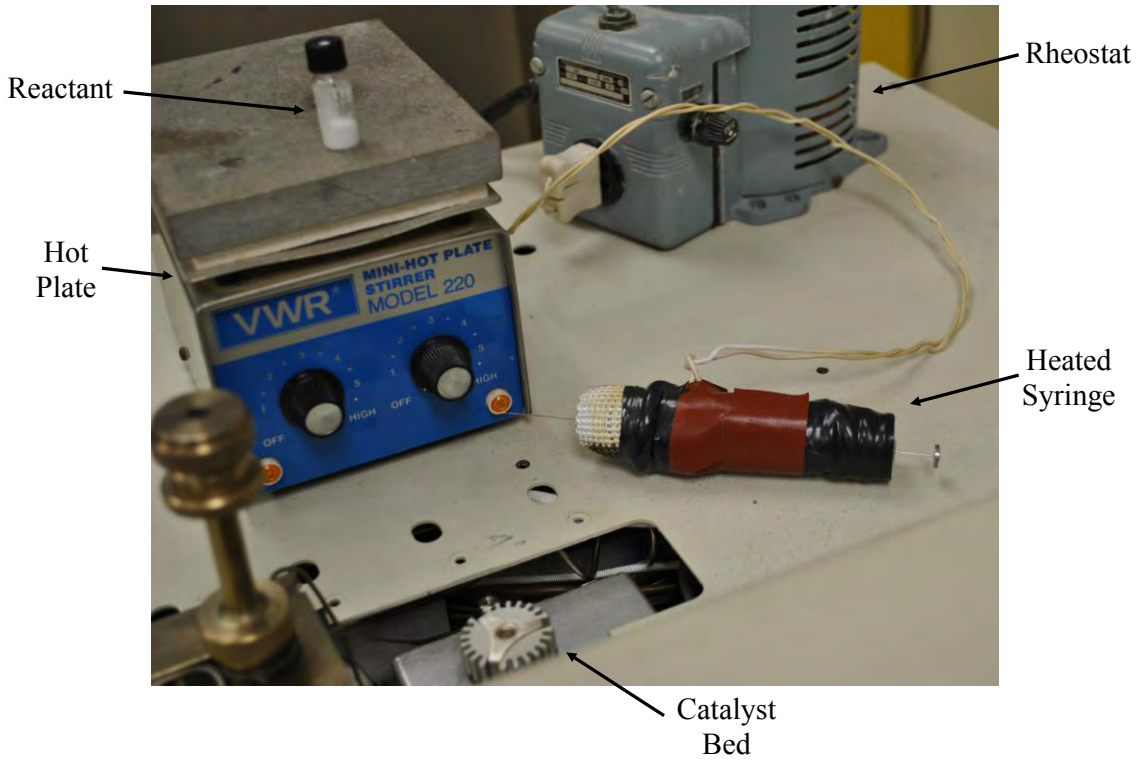


Figure I31: Direct injection of 1-octadecanol to the catalyst bed using a heated syringe.

Chromatographic analysis was conducted using helium as carrier gas. The flow of helium through the catalyst bed and through the chromatographic columns was adjusted to ~15 mL/min using an Intelligent Digital Flowmeter (Varian, Walnut Creek, CA, U.S.A.). The GC oven was programmed with an initial temperature of 0°C for 10 minutes and was then ramped to 50°C at 5°C/min, then to 100°C at 3°C/min, and finally to 300°C at 10°C/min and was held at 300°C for 3.34 minutes.

Quantitation was performed using calibration curves from standard compounds. For all the experiments, the mass spectrometer was configured to operate only in electron impact (EI) mode. Reaction runs were segmented to analyze for different mass-charge (m/z) ranges. Low molecular weight compounds eluting during the first 10 minutes were scanned from 10 – 80 m/z and for the rest of the chromatographic run, the mass range was 40 – 350 m/z to analyze high molecular weight compounds.

Thermal Cracking:
Experiments were conducted to determine the range of temperatures suitable for the study of catalytic cracking mechanism of 1-octadecanol. For these experiments, ~ 1 mg of 1-octadecanol was injected to the catalyst bed containing 20 mg silica gel (no H^+ZSM5). The temperature of the catalyst bed was varied from 325 to 400°C.

It has long been known that in thermal decomposition of alcohols, two reactions predominate: dehydration and dehydrogenation (Figure I32). Studies indicated that these two reactions can be greatly enhanced by catalysts. These catalysts were subdivided into three categories: dehydrating, dehydrogenating, and mixed. Some of the dehydrating catalysts include thorium, tungsten, and aluminum. Ethanol pyrolysis over reduced copper leads to the formation of acetaldehyde as dominant product. Silica, on the other hand, is considered to be a mixed catalyst that enhances both dehydration and dehydrogenation of alcohols [19, 20].

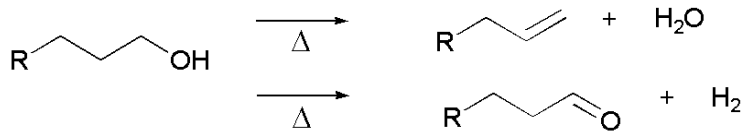


Figure I32: Thermal decomposition (pyrolysis or thermal cracking) of alcohols [20].

The results of the thermal cracking experiments are shown in Figure I33 (see also Figure I34). It can be seen that at 400°C around 90% of the initial reactant was converted to two other compounds (labeled Unknown 1 and Unknown 2 in Figures I33 and I34). Since silica gel was used for these experiments, it was suspected that Unknown 1 and Unknown 2 were octadecene and octadecanal, respectively. Octadecene will be the product of octadecanol dehydration, while octadecanal will be produced by octadecanol dehydrogenation. Nevertheless, further analysis of these two unknown peaks was not conducted at this part of the study. As also shown in Figure I6, the extent of octadecanol conversion decreases with temperature and is almost negligible at 325ºC. Thus, for the catalytic cracking experiments, temperatures from 325 to 375°C were initially considered.

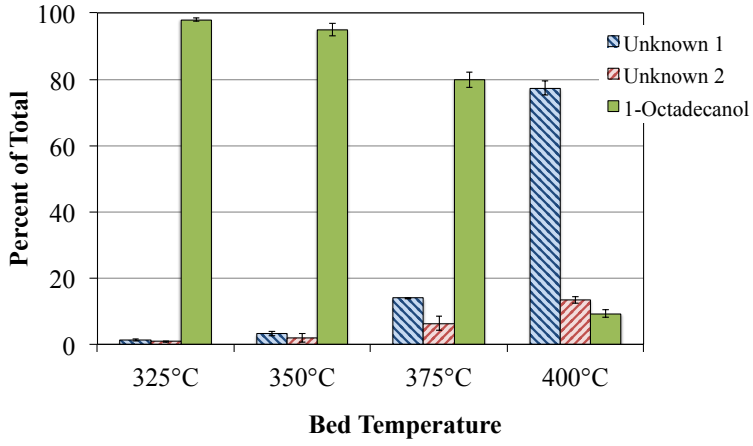


Figure I33: Thermal cracking of 1-octadecanol.

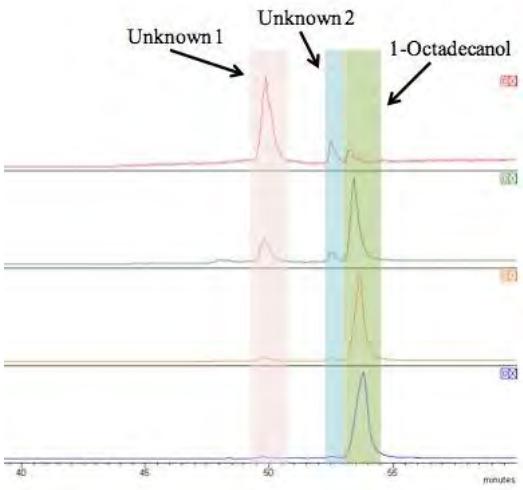


Figure I34: Effect of temperature on the thermal cracking of 1-octadecanol.

Catalytic Cracking:
Catalytic cracking of any compound using a shape selective catalyst, like H^+ZSM5, is greatly affected by the compounds geometry. For example, dehydration of 1-butanol using zeolite-A catalyst is easier compared to 2-butanol. The linear geometry of 1-butanol allows it to enter the catalyst pores, access the active sites, and undergo dehydration more easily [21].

The catalyst used in this study had a pore diameter of 5.5 Å. As evident by the AM-1 molecular geometry calculations, which were conducted using Spartan software (Wavefunction, Irvine, CA, USA), the 1-octadecanol is small enough to enter the pores of the H^+ZSM5 catalyst (Figure I35). However, there might still be some site restrictions due to the length of the molecule, which is about 25 Å. Thus, initial cracking of this molecule could be the sum of contributions from cracking inside and outside the pores of the H^+ZSM5 catalyst.

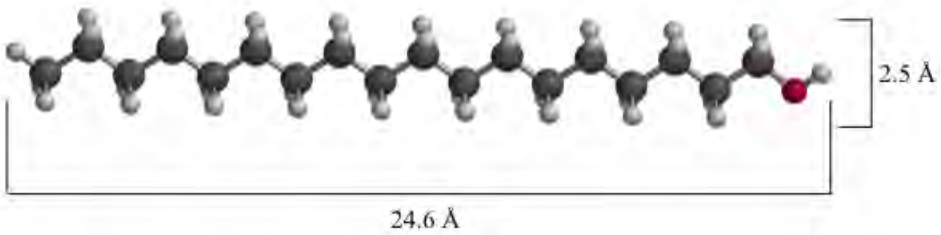


Figure I35: Equilibrium geometry of 1-octadecanol (calculated from semi-empirical AM-1 calculations using Spartan '06.

Effect of Temperature:
As mentioned earlier, temperatures from 325 to 375ºC were considered for catalytic cracking of 1-octadecanol over H^+ZSM5. However, no significant conversion was observed at 325ºC. Thus experiments were conducted between 350 and 375°C using 2.5 mg H^+ZSM5. The main aim of this set of experiments was to determine the temperature at which cracking intermediates would be observed. It was anticipated that catalytic cracking of 1-octadecanol would be faster than that of vegetable oils (i.e. triacylglycerides) due to high molecular weight and molecular geometry of the latter. Thus, a low catalyst loading (2.5 mg) was used for this set of experiments.

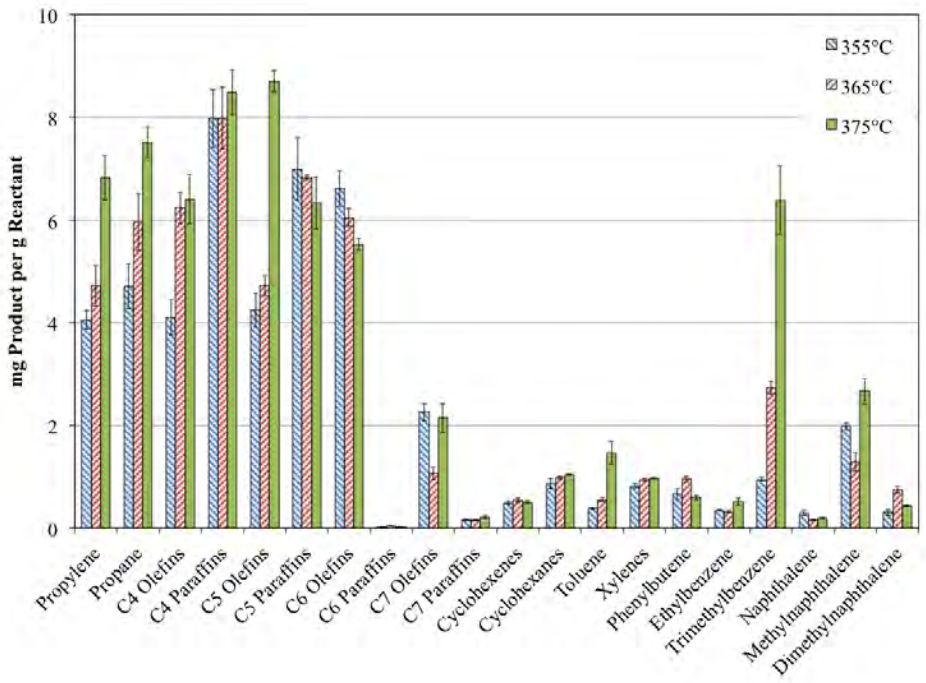


Figure I36: Effect of temperature on the catalytic cracking of 1-octadecanol using 2.5 mg H^+ZSM5.

The effect of temperature on the catalytic cracking of 1-octadecanol is shown in Figure I36. It can be seen that, except for C5 paraffins and C6 olefins, all the cracking products increased with temperature. This increase in product formation could be due to increase in kinetic energy of the 1-octadecanol at higher temperatures. Increase in kinetic energy means increase collision between the reactant (and/or initial cracking products) and the active sites of the catalyst, resulting in a higher reactant conversion. The decrease in the formation of C5 paraffins and C6 olefins at a higher temperature suggests that they serve as intermediates for the production of other products (i.e. cyclic hydrocarbons and eventually to aromatic hydrocarbons). However, this could not be confirmed since this set of experiments was conducted with a constant amount of catalyst. This translates to constant retention time of the reactant in the catalyst bed.

Effect of Catalyst Loading:
To better understand the cracking mechanism of 1-octadecanol, the catalyst loading was varied from 2.5 to 20 mg. As was shown in the previous section, the qualitative profile of cracking products were the same for the three temperatures investigated. However, as shown in Figure I33, thermal cracking is still significant at 375°C. Thus, 365ºC was chosen for this set of experiments to minimize the effect of thermal cracking while ensuring high reactant conversion. Varying the amount of catalyst does not provide kinetic data. Nonetheless, at constant bed diameter, increasing the catalyst loading means increase in reactant retention time.

The results of this set of experiments are shown in Figure I37. Generally, all the cracking products increased with catalyst loading, except for C6 olefins. Unlike what was observed in the previous section, the C5 paraffins increased with catalyst loading which indicates that this group of compounds is not the major intermediate(s) for the catalytic cracking of 1-octadecanol over H^+ZSM5. This suggests that C6 olefins serve as main intermediates for catalytic cracking of 1-octadecanol.

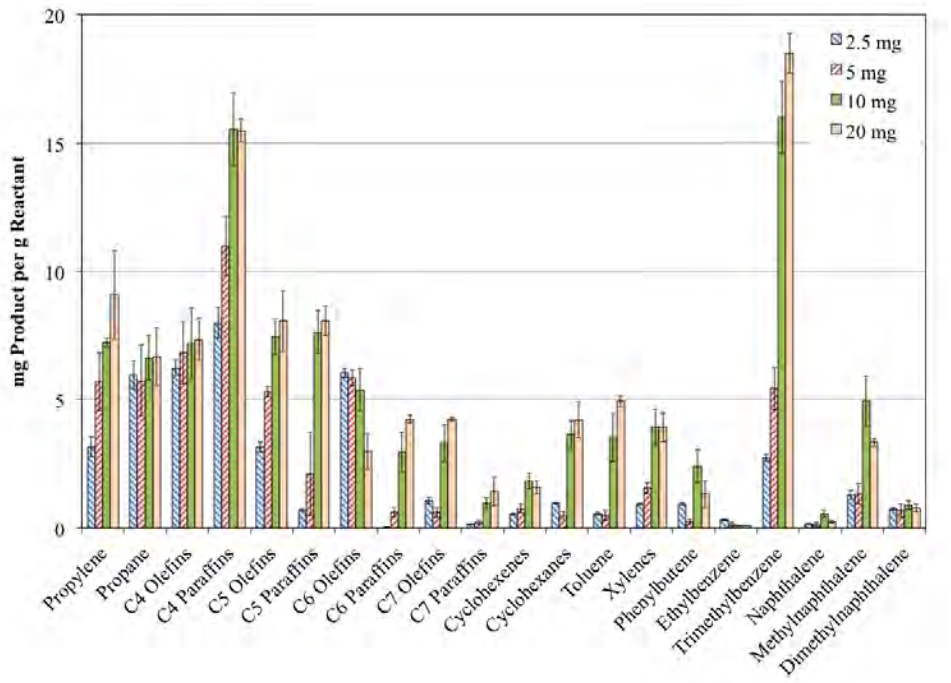


Figure I37: Effect of catalyst loading on the catalytic cracking of 1-octadecanol (Temperature: 365ºC).

Proposed Catalytic Cracking Pathway:
Zeolite catalysts are also being used for alcohol dehydration. Thus, to determine if the H^+ZSM5 catalyst used in this study favored dehydration over dehydrogenation, identification of unknown peaks seen during the thermal cracking experiments was necessary. A typical gas total ion chromatogram from gas chromatography-mass spectrometric (GC-MS) runs is shown in Figure I38. It is apparent that at 365°C, the conversion of 1-octadecanol to Unknown 1 was favored over Unknown 2. Thus, it was safe to assume that primary cracking by H^+ZSM5 primarily produced Unknown 1.

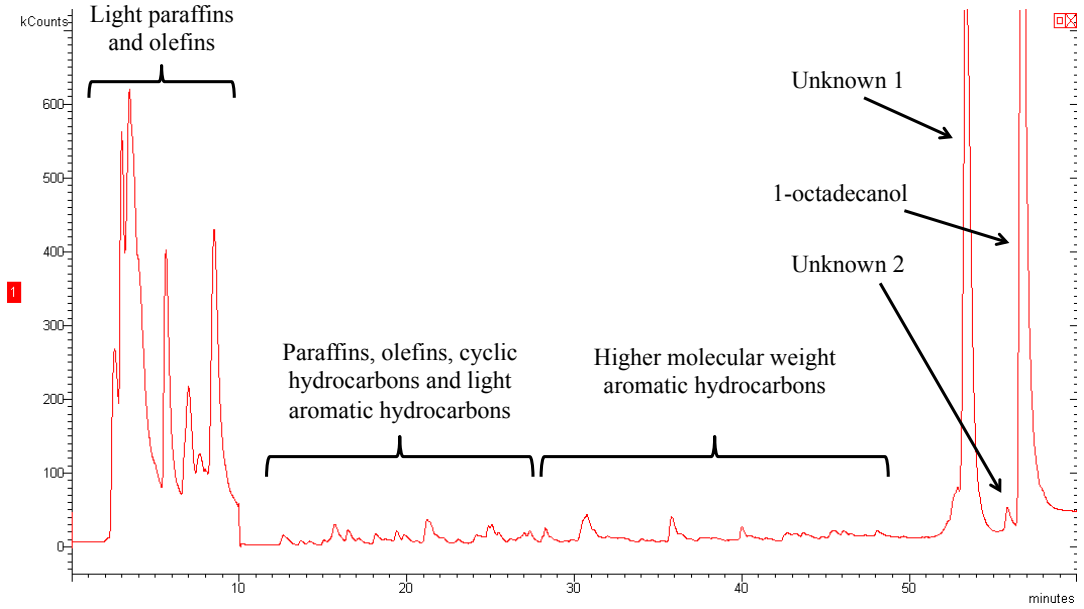


Figure I38: Typical GC/MS total ion chromatogram for cracking reaction of 1-octadecanolon H^+ZSM5 at 365ºC.*
*Scanning segmentation change at 10 min (m/z = 10 – 100 for first 10 min and then m/z = 40 – 350 for remainder of chromatographic run).

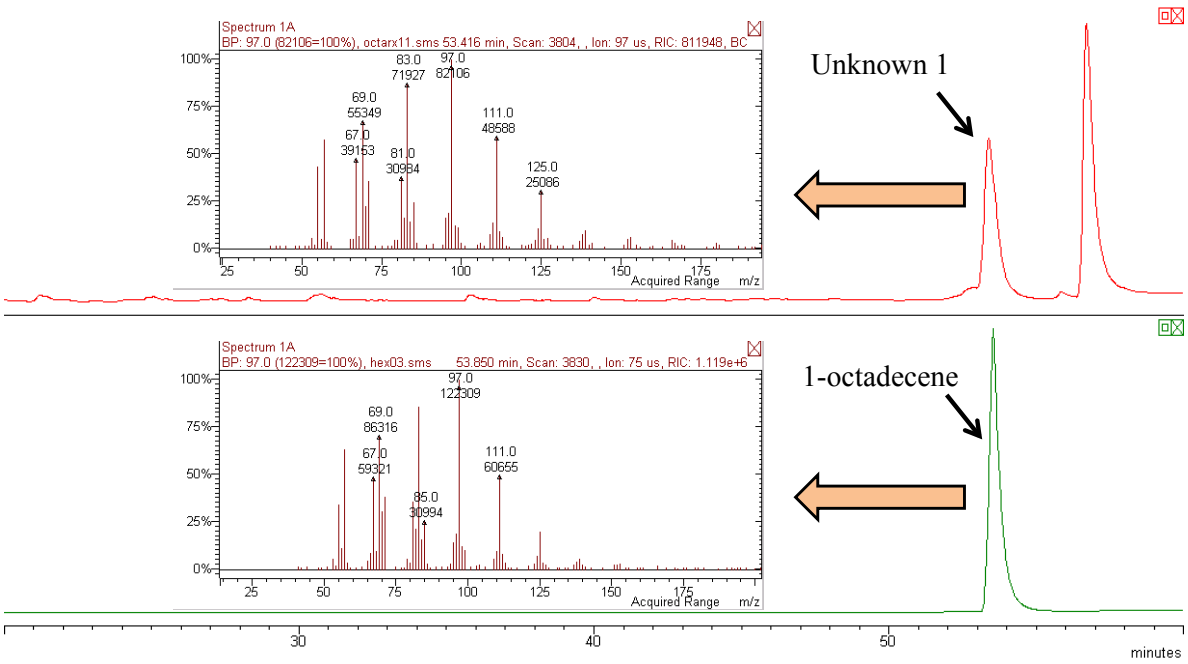


Figure I39: Comparison of unknown peak 1 and 1-octadecene.

To better understand the mechanism of primary steps in catalytic cracking of 1-octadecanol, identification of unknown 1 was necessary. As was mentioned earlier, pyrolysis of 1-octadecanol will produce mainly octadecene and octadecanal. Figures I36 and I37 show that CO and CO_2 were not detected in the cracking products. If initial cracking of 1-octadecanol produces significant amount of 1-octadecanal, CO and CO_2 should be present in the reaction products due to decarbonylation and decarboxylation reactions. Thus it was presumed that Unknown 1 was octadecene and, as shown in Figure I39, this was indeed the case.

Knowing that octadecene is the favored primary cracking product, a mechanism was developed to describe the conversion of 1-octadecanol to fuel related compounds over H^+ZSM5. The proposed mechanism is presented in Figures I40 and I41. Figure I40 covers primary cracking reactions, which starts by dehydration of 1-octadecanol catalyzed by H^+ZSM5 and heat. Figure I41 covers secondary and tertiary cracking of 1-octadecanol. For this discussion 1-octadecene was considered, although in reality it can isomerize by double bond shift. Nevertheless, the mechanism would be the same, and throughout this discussion alkene will be used in place of 1-octadecene.

Initial stages of alkene cracking were proposed to be the formation of a complex, which involves the double bond in the molecule. This complex results to the formation of carbenium ions. Primary carbenium ions are the least stable among these type of compounds, followed by secondary and then tertiary carbeniums. If a primary carbenium is produced during cracking, it rapidly decomposes or isomerizes to secondary carbenium ion. From the carbenium ions, primary cracking of alkene molecules starts [22].

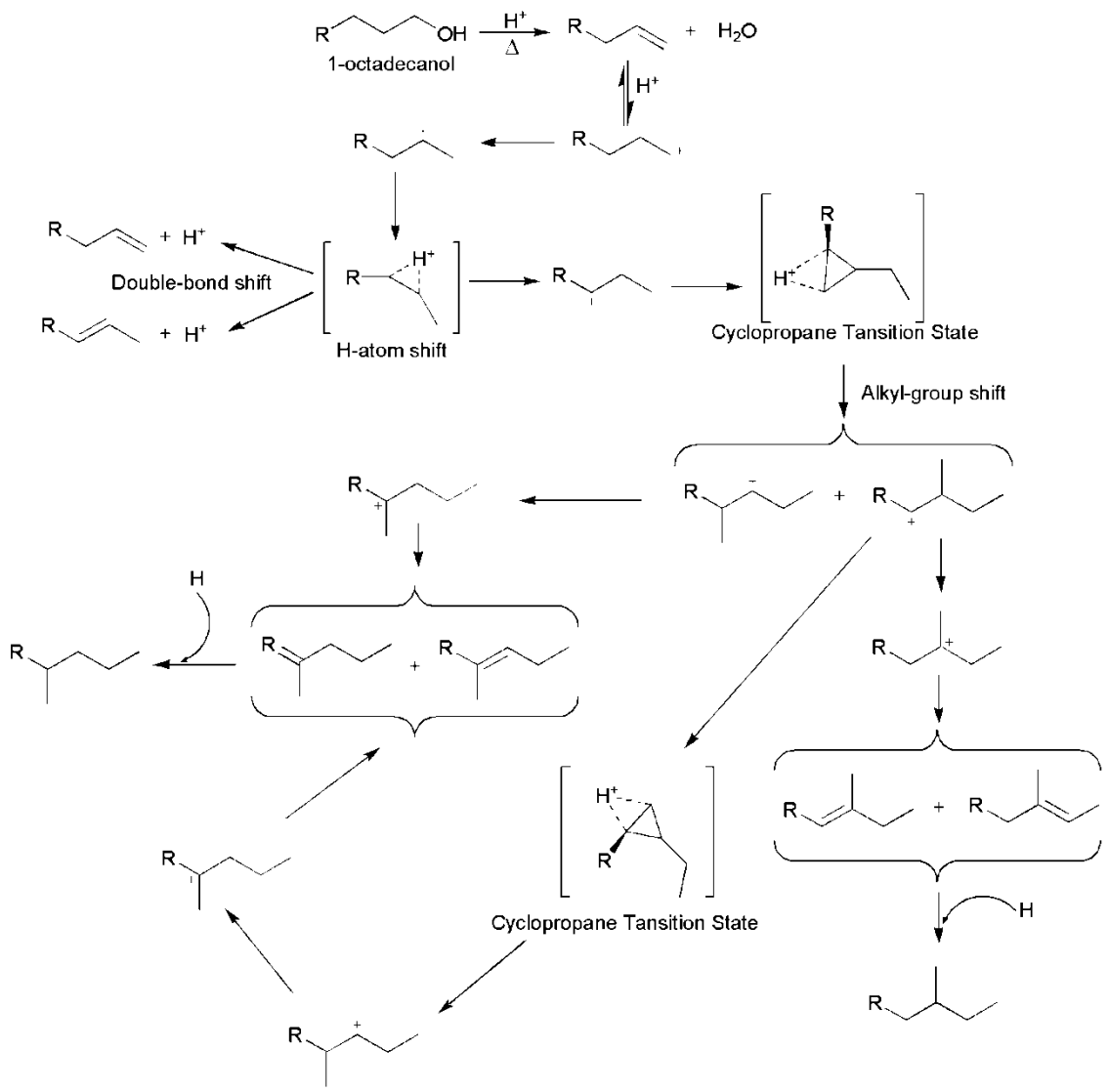


Figure I40: Primary cracking of 1-octadecanol over H^+ZSM5.

The carbenium ions can undergo H-atom shift, which could regenerate the original alkene or produce an isomer of it via double-bond shift. Branching of molecules during cracking can be made possible by an alkyl-group shift through the cyclopropane transition state. This reaction is commonly referred to as type-B skeleton rearrangement. This alkyl-group shift is followed by an H-atom shift, which generates ternary carbenium ions, which increases the profiles of products from primary cracking of 1-octadecanol. Further reaction includes methyl-group shift involving branched tertiary carbenium ions, which also involves a cyclopropane transition state. This is also called the type-A skeleton rearrangement reactions. Cracking of alkenes over acidic catalysts are usually accompanied by formation of alkanes with the same skeleton. Thus a hydrogenation reaction step occurs during catalytic cracking of these molecules. The source of hydrogen for these hydrogenation reactions is discussed below [22].

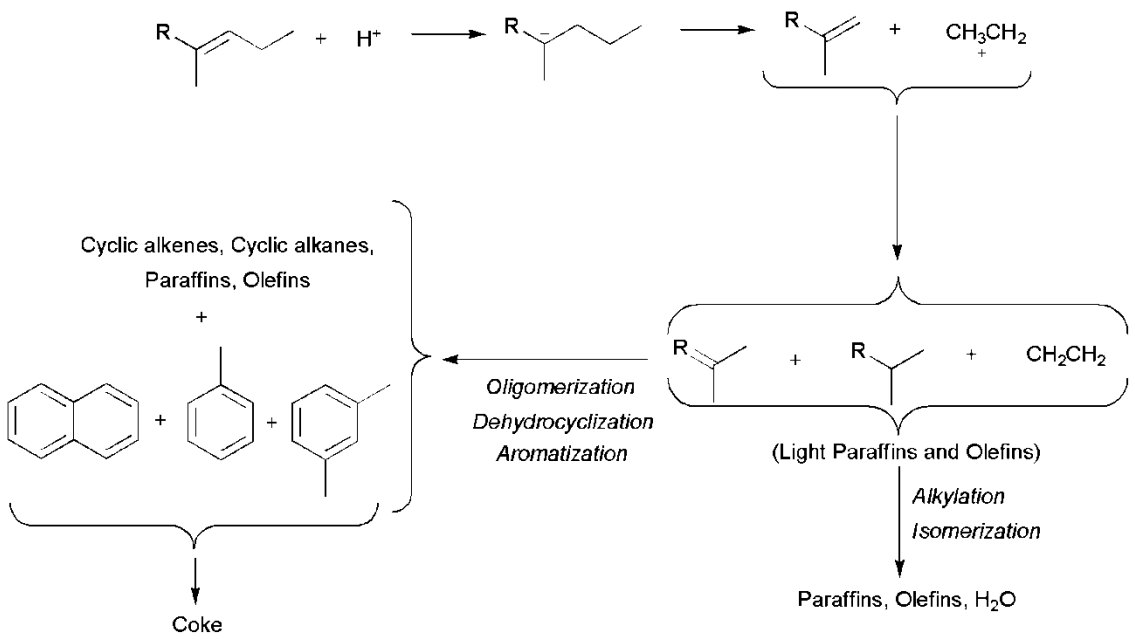


Figure I41: Secondary and tertiary cracking of 1-octadecanol over H^+ZSM5.

Primary products from 1-octadecanol cracking such as a branched alkene can react with the acidic sites on the H^+ZSM5, producing more carbenium ions. These carbenium ions can undergo C─C bond (i.e. β-C─C bond) scission, reducing the size of molecules from primary cracking steps. The products from C─C scission can also undergo cracking similar to primary cracking mechanism. These C─C scission reactions are the ones responsible for the production of light paraffins and olefins. Light paraffins and olefins can undergo alkylation and isomerization producing paraffins and olefins within the range of gasoline and diesel compounds. Light paraffins and olefins can also undergo oligomerization, cyclization, and aromatization. Oligomerization of secondary products could lead to the formation of long chain hydrocarbons, which could then undergo β-C─C bond scission, producing smaller molecules. These molecules are usually referred to as tertiary cracking products. The oligomerization, cyclization, and aromatization steps together with the coke formation reactions are believed to be the source of hydrogen for hydrogenation reactions mentioned earlier. These steps are also referred to as hydrogen redistribution reactions. Thus production of alkanes during catalytic cracking of 1-octadecanol is accompanied by the generation of hydrogen-deficient compounds such as cyclic and aromatic hydrocarbons. The production of hydrogen from oligomerization reactions usually starts with the formation of cycloalkenes. This validates the detection of cyclohexenes in the reaction products [22]. These cyclohexenes, together with cyclohexanes, could also be formed from cyclization of paraffins and olefins. Due to the decreasing amount of C6 olefins in the products as the catalyst loading was increased, they were thought to be the main intermediate for the formation of cyclic hydrocarbons. This is possible through direct cyclization or through C6 olefin cracking followed by oligomerization reactions.

Benzene, which is commonly produced during catalytic cracking of vegetable oils, was not detected in any reaction runs. This suggests the validity of the proposed reaction pathway for 1-octadecanol cracking. According to Kissin (2001), cracking of 1-hexene over ZSM5 produces light aromatics such as toluene, ethylbenzene, xylenes, and other disubstituted benzenes, while 1-octene generates mostly C8 aromatic hydrocarbons [22]. Moreover, methane and C2 hydrocarbons were not detected in the cracking products of 1-octadecanol. According to Kissin

(2001), methane, C2, and C3 are not usually observed in catalytic cracking of alkenes under mild conditions (i.e. 150°C). The observed formation of C3 hydrocarbons could be attributed to more severe cracking conditions (i.e. 365ºC) employed in this study [22]. These literature observations, and the fact that CO and CO_2 where not produced during the catalytic cracking of 1-octadecanol over H^+ZSM5, supports the validity of the proposed cracking mechanisms.

The mass balance for cracking of the model compound (1-octadecanol) considered in this study was at least 90% with the balance of the numbers presented in Figures I36 and I37 as octadecene, octadecanal, and unreacted 1-octadecanol. This is because the octadecanal was not quantitated for the catalytic runs, and as shown in Figure I33, octadecanal, which mainly comes from thermal cracking, could constitute about 10% of the cracking products. Thus for this model compound, the milestone (Complete a 70% mass balance of Biocrude components and cracking products using petroleum refining catalysts) was met.

The biocrude from activated sludge contains significant amount of polyhydroxyalkanoate, which is a polymer of short chain hydroxyl-fatty acids. This compound proved to be inert to cracking (both thermal and catalytic) at reaction temperature up to 500°C. Thus the milestone for this compound was not met. A possible alternative way to convert this compound into fuel component is by depolymerization (either acid or alkali treatment) followed by cracking of the hydroxy-fatty acid monomers. The mechanisms of cracking different fatty acids are already established in the literature and thus were not done here.

Subtask I.5 Design cost efficient biomass and biofuels supply chains

The focus of this research is identifying cost-efficient and environment-friendly supply chain designs for production of biodiesel. We consider that biodiesel is produced via the use of industrial wastes generated by pulp and paper, seafood processing, meat processing, and wastewater treatment (WWT) facilities.

The main contribution of this research is developing optimization models that aim to design cost efficient and environmentally friendly supply chains for production of biodiesel. This is accomplished by considering the impact that potential carbon regulatory policies would have on the way companies design and manage their supply chain. We consider the following carbon regulatory mechanisms: carbon cap, carbon tax, carbon cap and trade, and carbon offset. We analyze the implications that these mechanisms would have on supply chain-related costs and performance. We use our computational analysis to identify the mechanism that has a greater impact in GHG emission reductions on the supply chain. Our models highlight the trade-offs that exist between costs and emissions. The goal here is to provide insights and guide companies to make sustainable choices.

1. Planned Activities:
Milestone 1: Identify the appropriate model for conducting these analyses.
Figure I42 presents the supply chain network for production of biodiesel via wastewater sludge. The structure of this supply chain is driven by the technology requirements for this product. Initial processing of wastewater sludge happens at a biocrude plant. Sludge is shipped from wastewater treatment (WWT) plants, pulp and paper mills, poultry slaughtering and processing plants, or animal and marine processing plants to a biocrude plant for initial processing. Biocrude is then shipped to a diesel refinery for further processing. Pipelines seem to be the most appropriate mode of transportation due to the large amount of sludge that would be transported to maintain production of a considerably sized biocrude facility, as well as, the

negated environmental pollution resulting from GHG emissions and noise generated by truck transportation of wastewater sludge.

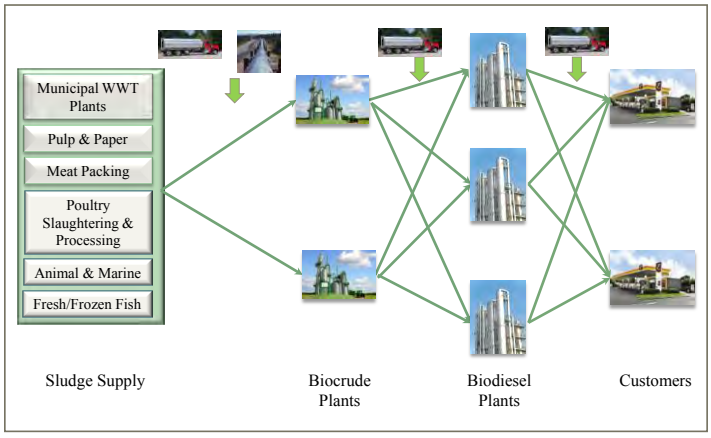


Figure I42: Biodiesel supply chain structure.

Using our mathematical model, we seek to learn what infrastructure is required to ensure a cost-efficient and environmentally-friendly production of biodiesel via wastewater sludge. The model that we present analyzes the trade-offs that exist between investment and transportation costs, as well as, analyzes the trade-offs that exist between costs and emissions in the supply chain. The optimization model that has been developed minimizes the total system costs over a planning horizon of length *T*, subject to production capacity limitations, biomass supply limitations, and transportation capacity limitations. We use dynamic, netork flow-based models. We formulate these models as Mixed Ineger Programs (MIPs) and solve these MIPs using the commercial software CPLEX. The total cost function of the MIP formulation includes investment, transportation, inventory, and penalty costs. Investment costs are the costs associated with location of biocrude plants, installation of pipelines, and purchasing of facility-owned vehicles. The transportation cost functions for pipeline and facility-owned truck consist of a fixed component (the investment costs mentioned above) and a variable component. The variable costs depend on the distance traveled and quantity shipped. Transportation cost for rented vehicles has only a variable component (given in $/(mile*tone). The model allows inventories of biomass and biofuels to be held from one period to the next, and therefore inventory holding costs occur. In this model, we also consider a penalty cost which is the penalty for not satisfying demand. One can think of this penalty cost as the market price for substitute products. This penalty plays the role of a threshold cost, which implies that there is no point of producing a product at a cost higher than the existing market price.

More details about the mathematical models we developed can be found in References 23 and 24.

Milestone 2: Estimate the cost of supply biomass, cost of distributing the fuel and sensitivity of the logistic cost to biomass yield, biomass price, biocrude price and biorefinery size.

The following tables and figures show some of the most important findings of this research. More results can be found in References 23 and 24.

Table I14: Transportation-related cost per gallon of biodiesel vs. volume of sludge transported.

Mode	Volume Shipped (m^3/day)					
	150	250	350	480	700	1000

	$ amount per gallon of biodiesel					
Single Trailer (own)	0.101	0.103	0.103	0.101	0.103	0.103
Single Trailer (rent)	0.131	0.131	0.133	0.131	0.133	0.133
Tandem Trailer (own)	0.098	0.098	0.098	0.096	0.098	0.096
Tandem Trailer (rent)	0.125	0.125	0.125	0.123	0.125	0.123
Pipeline	0.152	0.109	0.089	0.073	0.058	0.047

Table I14 presents the relationship that exists between the volume of sludge shipped and transportation-related cost per gallon of biodiesel produced. We assume that the distance traveled is 50 miles. Two important observations are made from these results. First, facility-owned tandem trailer trucks are the most cost efficient transportation mode for volumes up to 300m^3/day. Beyond this point, pipeline transportation is the most cost efficient mode of transportation. Second, truck transportation cost per gallon of biodiesel does not change with the volume transported. On the other hand, pipeline transportation cost per gallon of biodiesel decreases as the volume shipped increases. Table I15 summarizes parameters we have used to calculate these costs. This Table also compares transportation costs for sludge to other types of biomass feedstock.

Table I15: Distance fixed and variable transportation parameters.

Mode	Item Transported	DVC	Units	DFC	Units
Truck	Straw/Stover	0.14	$ / Actual t / km	5.25	$ / Actual t
	Wastewater sludge (owned) [This study]	0.04	$ / Actual t / km	3.42	$ / Actual t
	Wastewater sludge (rented) [This study]	0.05	$ / Actual t / km	4.56	$ / Actual t
Pipeline	Wastewater sludge [This study]	3.27 $C^{-0.658}$	$ / t sludge / km	1574[b]	$ / t sludge

[a] C, pipeline capacity in dry metric tons biomass per year.
[b] Calculated based on pipeline capacity of 480 ton /day.

We extended this analysis to other WWT facilities in Mississippi. Our analysis indicates that at the current level of gasoline price and labor cost, WWT facilities will not find the use of pipelines for sludge transportation economic. However, we believe that in the long run, investing in pipelines is beneficial. We came to this conclusion by looking at the impact that fuel price and labor costs have on transportation costs, as well as by considering the positive impacts that pipeline transportation have to the environment. The amount of carbon released during pipeline transportation is negligible as compared to truck transportation. Also, pipeline transportation reduces the noise associated with truck movements.

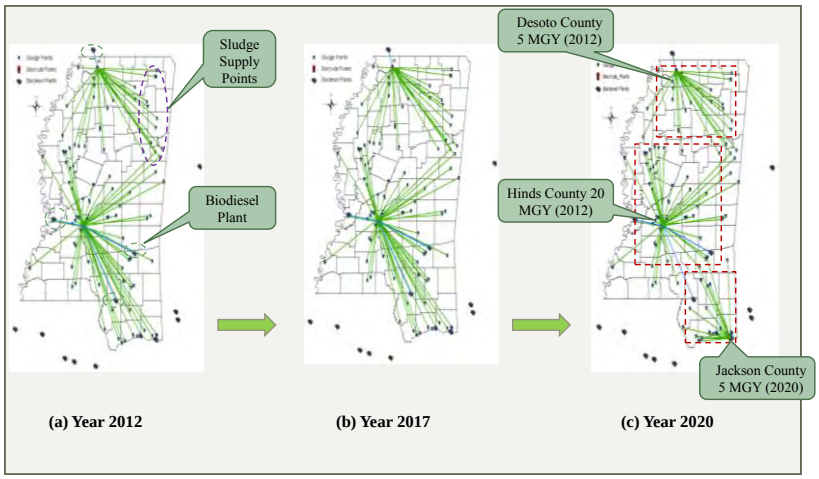


Figure I43: Biodiesel supply chain structure in Mississippi.

Figure I43 presents locations for Biocrude plants in MS to make the best use of the available sludge generated by existing WWT facilities in MS. Our analysis suggests that a 20MGY biocrude plant could be opened in Hinds County, and a 5MGY biocrude plant could be opened in Desoto County. Assuming that the population in Mississippi will grow at the same rate as the last few years, one additional 5MGY facility could be opened later on in Jackson County.

References

[1] JH Gary, GE Handwerk, Petroleum refining : technology and economics, 4th ed., Marcel Dekker, New York, 2001.
[2] R Sadeghbeigi, Fluid catalytic cracking handbook : design, operation, and troubleshooting of FCC facilities, 2nd ed., Gulf Pub. Co., Houston, Tex., 2000.
[3] SPR Katikaneni, JD Adjaye, RO Idem, NN Bakhshi, Catalytic Conversion of Canola Oil Over Potassium-Impregnated HZSM-5 Catalysts: C_2-C_4 Olefin Production and Model Reaction Studies, *Ind Eng Chem Res*, 35:10 (1996) 3332-3346.
[4] S Bhatia, CT Leng, P Tarnunaidu, Modeling and simulation of transport riser reactor for catalytic cracking of palm oil for the production of biofuels, *Energy Fuels*, 21:6 (2007) 3076-3083.
[5] FAA Twaiq, AR Mohamad, S Bhatia, Performance of composite catalysts in palm oil cracking for the production of liquid fuels and chemicals, *Fuel Process Technol*, 85:11 (2004) 1283-1300.
[6] TL Chew, S Bhatia, Effect of catalyst additives on the production of biofuels from palm oil cracking in a transport riser reactor, *Bioresour Technol*, 100:9 (2009) 2540-2545.
[7] TA Milne, RJ Evans, N Nagle, Catalytic conversion of microalgae and vegetable oils to premium gasoline, with shape-selective zeolites, *Biomass*, 21:3 (1990) 219-232.
[8] H Tian, CY Li, CH Yang, HH Shan, Alternative processing technology for converting vegetable oils and animal fats to clean fuels and light olefins, *Chin J Chem Eng*, 16:3 (2008) 394-400.
[9] YB Zhou, L Chen, XM Hu, J Lu, Modified Resin Coalescer for Oil-in-Water Emulsion Treatment: Effect of Operating Conditions on Oil Removal Performance, *Ind Eng Chem Res*, 48:3 (2008) 1660-1664.
[10] A Corma, GW Huber, L Sauvanaud, P O'Connor, Processing biomass-derived oxygenates in the oil refinery: Catalytic cracking (FCC) reaction pathways and role of catalyst, *J Catal*, 247:2 (2007) 307-327.
[11] SPR Katikaneni, JD Adjaye, NN Bakhshi, Catalytic conversion of canola oil to fuels and chemicals over various cracking catalysts, *Can J Chem Eng*, 73:4 (1995) 484-497.

[12] SPR Katikaneni, JD Adjaye, RO Idem, NN Bakhshi, Catalytic conversion of canola oil in a fluidized bed reactor, *Developments in Thermochemical Biomass Conversion*, 1:(1997) 633-647.
[13] T Benson, Elucidation of reaction pathways for catalytically cracked unsaturated lipids, *Dave C Swalm School of Chemical Engineering*. Mississippi State University, Mississippi State, pp. 153 (2008).
[14] N Taufiqurrahmi, S Bhatia, Catalytic cracking of edible and non-edible oils for the production of biofuels, *Energy & Environmental Science*, 4:4 (2011) 1087-1112.
[15] ED Revellame, R Hernandez, W French, WE Holmes, TJ Benson, PJ Pham, A Forks, R Callahan II, Lipid storage compounds in raw activated sludge microorganisms for biofuels and oleochemicals production, *RSC Advances*, 2:5 (2012) 2015-2031.
[16] B Xu, C Sievers, SB Hong, R Prins, JA van Bokhoven, Catalytic activity of Brønsted acid sites in zeolites: Intrinsic activity, rate-limiting step, and influence of the local structure of the acid sites, *J Catal*, 244:2 (2006) 163-168.
[17] TJ Benson, R Hernandez, WT French, EG Alley, WE Holmes, Elucidation of the catalytic cracking pathway for unsaturated mono-, di-, and triacylglycerides on solid acid catalysts, *Journal of Molecular Catalysis a-Chemical*, 303:1-2 (2009) 117-123.
[18] Agilent Technologies. *ChromatoProbe: Sample Introduction Device for Superior Analysis of Solids, Liquids, and Slurries*. http://www.chem.agilent.com/Library/datasheets/Public/WCI-pdf-0042.r1_chromatoprobe_ds.pdf. [Accessed: August 17, 2011].
[19] SC Moldoveanu, Pyrolysis of Alcohols and Phenols, in *Pyrolysis of Organic Molecules with Applications to Health and Environmental Issues*. Elsevier, London; New york, Ch. 9, pp. 259-313 (2010).
[20] AB Brown, EE Reid, The Catalytic Dehydration of Alcohols, *The Journal of Physical Chemistry*, 28:10 (1924) 1077-1081.
[21] JH Clark, CN Rhodes, Zeolitic Materials, in *Clean synthesis using porous inorganic solid catalysts and supported reagents*. Royal Society of Chemistry, Cambridge, UK, Ch. 2, pp. 17-36 (2000).
[22] YV Kissin, Chemical mechanisms of catalytic cracking over solid acidic catalysts: Alkanes and alkenes, *Catalysis Reviews-Science and Engineering*, 43:1-2 (2001) 85-146
[23] M. Marufuzzaman, S.D. Ekşioğlu, R. Hernandez, Optimization Models to Design and Manage Environmentally Friendly Biofuel Supply Chains, Proceedings of *ISERC Annual Meeting*, Orlando, FL, May 2012.
[24] M. Marufuzzaman, S.D. Ekşioğlu, A. Mondala, A Techno-Economic Analysis of Pipeline transportation for Wastewater Sludge, Proceedings of *ISERC Annual Meeting*, Orlando, FL, May 2012.

Publications:

Hall, J. I., M. Hetrick, W. T. French, R. A. Hernandez, J. Donaldson, A. Mondala, and W. Holmes. 2011. “Oil Production by a consortium of oleaginous microorganisms grown on primary effluent wastewater.” *Journal of Chemical Technology and Biotechnology,* 86: 54-60.

Hernandez, R. 2011. Petroleum displacement potential of next generation biofuels approaching commercialization. *Current Opinion in Chemical Engineering,* 1(1):43-46.

Mondala, A.H., Hernandez, R., French, W.T., Estí©vez, L.A., Meckes, M., Trillo, M., Hall, J. 2011. Preozonation of primary-treated municipal wastewater for reuse in biofuel feedstock generation. *Environmental Progress and Sustainable Energy,* 30(4):666-674.

Mondala, A., Hernandez, R., French, T., McFarland, L., Sparks, D., Holmes, W., Haque, M. 2012. Effect of acetic acid on lipid accumulation by glucose-fed activated sludge cultures. *Journal of Chemical Technology and Biotechnology.* 87(1):33-41.

Mondala, A.H., Hernandez, R., French, T., McFarland, L., Santo Domingo, J.W., Meckes, M., Ryu, H., Iker, B. 2012. Enhanced lipid and biodiesel production from glucose-fed activated sludge: Kinetics and microbial community analysis. *AIChE Journal.* 58(4)" 1279-1290.

Pham Patrisha J.; Hernandez Rafael; French William T.; et al. A spectrophotometric method for quantitative determination of xylose in fermentation medium Source: BIOMASS & BIOENERGY Volume: 35 Issue: 7 Pages: 2814-2821

Revellame,E., R. Hernandez, W.T. French, M. White, and B. Holmes, 2010. "Biodiesel from Activated Sludge via *In situ* Transesterification", *Journal of Chemical Technology and Biotechnology*, 85(5): 614-620.

Revellame, E., Hernandez, R., French, W., Holmes, W., Alley, E., Callahan II, R. 2011. Production of biodiesel from wet activated sludge. *Journal of Chemical Technology and Biotechnology,* 86(1):61-68.

Schneider, T., Graeff-Hí_nninger, S., French, W.T., Hernandez, R., Claupein, W., Holmes, W.E., Merkt, N.. (2012). Screening of industrial wastewaters as feedstock for the microbial production of oils for biodiesel production and high-quality pigments. Article No. 153410, *Journal of Combustion.*

Sparks, D.L., L.A. Estévez, R. Hernandez, J. McEwen, and T. French, 2010. "Solubility of Small-Chain Carboxylic Acids in Supercritical Carbon Dioxide." *Journal Chemical Engineering Data*, 55(11):4922-4927.

Zhang, G., W.T. French, R. Hernandez, E. Alley, and M. Paraschivescu. 2011. "Lipid Production from Acid Hydrolysate of Lignocellulosic Biomass by Rhodotorula glutinis." *Biomass and Bioenergy*, 35: 734-740.

Zhang, G., French, W.T., Hernandez, R., Hall, J., Sparks, D., Holmes, W.E. 2011. Microbial lipid production as biodiesel feedstock from N-acetylglucosamine by oleaginous microorganisms. *Journal of Chemical Technology and Biotechnology,* 86(5):642-650.

Zhang, G., French, W.T., Hernandez, R., Alley, E., Paraschivescu, M. 2011. Effects of furfural and acetic acid on growth and lipid production from glucose and xylose by Rhodotorula glutinis. *Biomass and Bioenergy,* 35(1):734-740.

Presentations:

Adkins, A., Riley, C., Carrubba, L, Zumbro, C. and Zhang, G. *Lipid extraction methods for oleaginous yeasts*. Presented at the 2011 MSU Biofuels Conference. Mississippi State University, October 5 – 7, 2011.

Callahan, R., Revellame, E., Holmes, W., Hernandez, R. and French, W.T. *Development of a fluidized-bed catalytic cracking (FCC) system with on-line product analyses for conversion of*

activated sludge to green fuels. Presented at the 2011 MSU Biofuels Conference. Mississippi State University, October 5 – 7, 2011.

Coker, A., Hernandez, R., French, W.T., Iretskii, A., White, M., Revellame, E., Holmes, W. **Biodiesel Production by Direct Transesterification of Activated Sludge using Supercritical Methanol**. Presented at the 2011 AOCS Annual meeting. Cincinnati, OH. May 1 – 4, 2011.

Coker, A., Hernandez, R., French, W.T., Revellame, E., Holmes, W., Zhang, G., Iretskii, A.V. and White, M. *Production of Biodiesel by Direct Transesterification of Activated Sludge Using Supercritical Methanol*. Presented at the 2011 AIChE Annual Meeting. Minneapolis Convention Center, Minneapolis, MN. October 16 – 21, 2011.

Coker, A., Hernandez, R., French, T., Iretskii, A., White, M., Revellame, E., Holmes, W. and Zhang, G. *Biodiesel production by transesterification of activated sludge using supercritical methanol*. Presented at the 2011 MSU Biofuels Conference. Mississippi State University, October 5 – 7, 2011.

Crymble, S., Sparks, D.L., Mondala, A., Hernandez, R. and French, T. *Characterization of Lipids Extracted From Enhanced Municipal Wastewater Via Supercritical Carbon Dioxide and Propane*. Presented at the 2011 AIChE Annual Meeting. Minneapolis Convention Center, Minneapolis, MN. October 16 – 21, 2011.

Donaldson, J.R., Barnard, J.M., Revellame, E., Hall, J.I., Biddle, K.S., Holmes, W.E., Hernandez, R., French, W.T. **A Genetically Modified Oleaginous Microorganism Capable of Accumulating Extracellular Lipids**. Presented at the 2011 ASM Annual meeting. New Orleans, LA. May 21 – 24, 2011.

Estill, B., Pham, P., Hernandez, R., Mondala, A., Zhang, G. and French, T. *A spectrophotometric method for quantitative determination of xylose and glucose in acid-catalyzed hydrolysate medium*. Presented at the 2011 MSU Biofuels Conference. Mississippi State University, October 5 – 7, 2011.

Hetrick, M., French, W.T., Hernandez, R., Holmes, B., Ryu, H., Iker, B., Santo Domingo, J., Donaldson, J. **The Use of Municipal Wastewater as a Media for Cultivation and Induction of Lipid Synthesis in the Oleaginous Yeast *Rhodotorula glutinis***. Presented at the 2010 AIChE Annual meeting. Salt Lake City, UT. November 7-12, 2010.

Holmes, W., Revellame, E., Hernandez, R. and French, W. *Development of a Fluidized-Bed Catalytic Cracking (FCC) System with On-Line Product Analyses for Conversion of Activated Sludge to Green Fuels*. Presented at the 2011 AIChE Annual Meeting. Minneapolis Convention Center, Minneapolis, MN. October 16 – 21, 2011.

Holmes, W., Revellame, E., Hernandez, R., French, W.T. **Renewable Fuel from Activated Sludge using Fluidized-bed Catalytic Cracking Process**. Presented at the 2011 AOCS Annual meeting. Cincinnati, OH. May 1 – 4, 2011.

Johnson, J., Mondala, A., Hernandez, R., French, T., McFarland, L. and Green, M. *Enhanced biocrude production by activated sludge via continuous and sequential batch fermentation of biomass sugars*. Presented at the 2011 MSU Biofuels Conference. Mississippi State University, October 5 – 7, 2011.

Lerma, L., Hernandez, R., French T. and Estévez, L.A. *Low voltage destabilization of water/oil (W/O) emulsions formed during solvent extraction of microbial lipids from wastewater treatment plant sludge*. Presented at the 2011 MSU Biofuels Conference. Mississippi State University, October 5 – 7, 2011.

Lerma-Caicedo, L., Hernandez, R., French, T. and Estévez, L.A. *Electrostatic Destabilization of W/O Microemulsions–Application to the Extraction of Phospholipids From Sludge In Wastewater Treatment*. Presented at the 2011 AIChE Annual Meeting. Minneapolis Convention Center, Minneapolis, MN. October 16 – 21, 2011.

Marufuzzaman, M., Eksioglu, S. and Hernandez, R. *Supply chain planning and designing for biocrude production via wastewater sludge and its distribution in Mississippi*. Presented at the 2011 MSU Biofuels Conference. Mississippi State University, October 5 – 7, 2011.

Mast, B., Graeff-Hönninger, S., Hernandez, R., French, W.T. and Claupein, W. *Microbial biodiesel production – screening of different lignocellulosic biomasses and crop residues for their suitability based on the sugar content*. Presented at the 2011 MSU Biofuels Conference. Mississippi State University, October 5 – 7, 2011.

Mondala, A. *Process Optimization and Economic Analysis of the Production of Biocrude and Other Lipidic Materials by Sewage Sludge Microorganisms In WastewaterTreatment Plant Biorefineries*. Presented at the 2011 AIChE Annual Meeting. Minneapolis Convention Center, Minneapolis, MN. October 16 – 21, 2011.

Mondala, A., Hernandez, R., Pham, P., French, W.T., McFarland, L. **Enhanced Lipid Accumulation for Biofuels Production by Sewage Anaerobic Sludge Microorganisms via Cultivation in Glucose-fed Aerobic Bioreactors**. Presented at the 2011 AOCS Annual meeting. Cincinnati, OH. May 1 – 4, 2011.

Mondala, A., Pham, P.J., Hernandez, R., French, T., McFarland, L., Green, M., Cain, J., Johnson, J. and Holmes, W. *Enhanced Biocrude Production by Activated and Anaerobic Digester Sludges Via Cultivation In Sugar-Fed Aerobic Bioreactors*. Presented at the 2011 AIChE Annual Meeting. Minneapolis Convention Center, Minneapolis, MN. October 16 – 21, 2011.

Mondala, A., Hernandez, R., French, W.T., Sparks, D., Holmes, W., Haque, M., Pham, P., Sweet, W. **Gas Chromatographic Quantification of Acetic Acid and Furfural in Lignocellulose Hydrolyzate Fermentations for Microbial Lipids Production**. Presented at the 2011 AOCS Annual meeting. Cincinnati, OH. May 1 – 4, 2011.

Pham, P., Hernandez, R., Revellame, E., French, W.T., Mondala, A.H., Callahan, R., Cain, J.D. **Characterization of Activated Sludge Oil Lipidic Components**. Presented at the 2011 AOCS Annual meeting. Cincinnati, OH. May 1 – 4, 2011.

Revellame, E., Holmes, W., Hernandez, R. and French, W. *Renewable Fuel From Activated Sludge Using Fluidized-Bed Catalytic Cracking (FCC) Process*. Presented at the 2011 AIChE Annual Meeting. Minneapolis Convention Center, Minneapolis, MN. October 16 – 21, 2011.

Revellame, E., Hernandez, R., French, W.T., Holmes, W., Pham, P. **Lipid Storage Compounds in Raw and Enhanced Activated Sludges**. Presented at the 2011 AOCS Annual meeting. Cincinnati, OH. May 1 – 4, 2011.

Revellame, E., Holmes, W., Hernandez, R., French, W.T. and Forks, A. *Elucidation of reaction pathway for the heterogeneous cracking of a saturated fatty alcohol on $H^{+}ZSM5$*. Presented at the 2011 MSU Biofuels Conference. Mississippi State University, October 5 – 7, 2011.

Revellame, M., Holmes, W., Hernandez, R., Brown, A. and Sparks, D.L. *Generation of renewable fuels and chemicals from Rhodotorula glutinis using sweet sorghum juice*. Presented at the 2011 MSU Biofuels Conference. Mississippi State University, October 5 – 7, 2011.

Revellame, E., Coker, A., Pham, P., Mondala, A., Hernandez, R., French, W.T., Holmes, W. Activated Sludge: A Novel Biofuel Feedstock. Presented at the 2011 AOCS Annual meeting. Cincinnati, OH. May 1 – 4, 2011.

Schneider, T., Graeff-Hönninger, S., Claupein, W., French. W.T. and Hernandez, R. *Material utilization of industrial wastewaters for the production of high-quality microbial oils and pigments*. Presented at the 2011 MSU Biofuels Conference. Mississippi State University, October 5 – 7, 2011.

Shields-Menard, S., Donaldson, J. and French, T. *Characterization and optimization of a Rhodococcus opacus mutant capable of producing extracellular triglycerides*. Presented at the 2011 MSU Biofuels Conference. Mississippi State University, October 5 – 7, 2011.

Sparks, D.L., Crymble, S., McEwen, J., Hernandez, R., French, W.T. **Solubility of Phosphatidylcholine in Supercritical Carbon Dioxide with Propane Co-solvent**. Presented at the 2010 AIChE Annual meeting. Salt Lake City, UT. November 7-12, 2010.

Zhang, G., French, W.T., Hernandez, R. and Holmes, W. *Microbial Oils As Biodiesel Feedstock From Hydrolyzate of Switchgrass*. Presented at the 2011 AIChE Annual Meeting. Minneapolis Convention Center, Minneapolis, MN. October 16 – 21, 2011.

Task J. Microbial Oil

Principle Investigators and team members:
William Todd French PI
Rafael Hernandez Co-PI
Mary Hetrick
Guochang Zhang
Bill Holmes
Magan Green

Executive Summary:

Mississippi State University has determined that the yeast *Rhodotorula glutinis* (*R. glutinis*) has the ability to produce significant quantities of triglycerides (i.e. oil) from the major lignocellulosic sugars (glucose and xylose) without any genetic modification. This yeast can produce between 52 and 79 gallons of a biodiesel or renewable diesel feedstock per ton of biomass. If the energy yield is compared to the production of ethanol from the same lignocellulosic feedstock, assuming 100 gallons of ethanol per ton of lignocellulosic sugars, the oil has a BTU value of 9,480,000, whereas ethanol has a BTU value of 7,800,000. While the volume yield of oil is lower per ton of biomass compared to ethanol, the energy yield of the oil is much greater than that of ethanol produced from the same feedstock. In terms of oil production, this organism has the ability to accumulate more than 40% of its dry weight in oil when cultivated on lignocellulosic sugars. The objective of this project is to scale up this process to better define the economics and performance of this process as can be seen in the process flow diagram below. These data would be used to determine the size of the equipment needed and the production cost of this oil at a commercial scale. This technology could be implemented near any large quantity of biomass such as switchgrass, giant miscanthus, or energy cane similar to the model proposed for DOE's lignocellulosic ethanol process. This technology could be used in conjunction with lignocellulosic ethanol to convert the traditionally non-fermentable sugars into triglycerides. Since ethanol production from starch is the baseline for comparing technologies utilizing microorganisms to convert sugars, it will also be used as the baseline in this study. However, these Tasks will focus on the production of triglycerides using *R. glutinis* grown on hydrolysate from biomass such as switchgrass, miscanthus, or corn stover, and other promising industrial wastes identified in Task I.

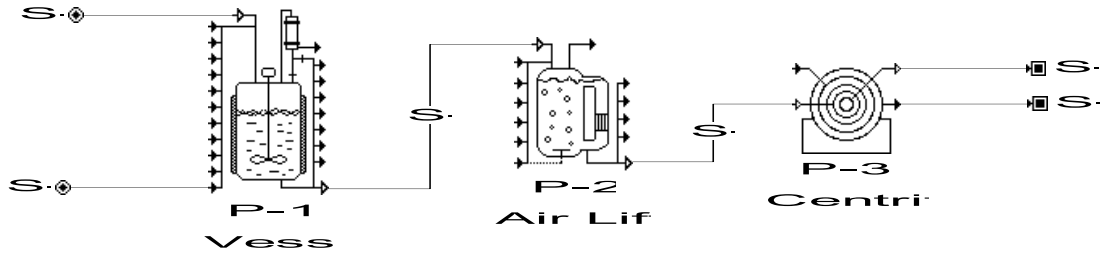


Figure J1: Process flow diagram showing biomass in (S-101) with hydrolysate out (S-103) to the bioreactor (Air Lift Fermentation) where the sugars are converted to intracellular storages of oil (S-104) followed by oil separation from the cells.

The purpose of this task is to generate the data needed to understand the economics of the process for all unit operations from feedstock through the microbial conversion process to

finished product. This will allow for the identification of areas needing research to improve the economics per gallon of oil.

The results of this investigation demonstrate the ability of the researchers to produce *Rhodoturla glutinis* at the pilot scale (1000 L) with significant quantities of oil using glucose as a substrate. *R. glutinis* was grown to a cell concentration of greater than 10 g/L and contained greater that 20% lipid content on a cell dry weight (cdw). The results of these pilot runs demonstrate the ability to produce larger quantities of this organism with significant quantities of lipids. As part of this thrust, experiments were designed to determine the optimum temperature for producing triglycerides via *R. glutinis* metabolizing glucose. The results of those investigations clearly show that 30°C was superior to the other temperatures tested and that 20°C was better than 40°C. It should be noted that incubation temperatures approaching 40°C approach the limits of life for this particular organism. There was little difference in the fatty acid profile that could significantly impact the cold flow properties of the resulting biodiesel. The research has demonstrated that with little optimization of the reactor conditions, the initial runs with *R. glutinis* could produce significant amounts of cells containing copious quantities of triglycerides. However, the cost of producing triglycerides from glucose would be cost prohibitive at current sugar prices. At yields of 0.25 g of lipids/g of sugar and glucose at $0.20/lb of sugar, the cost per gallon of oil (7.6 lbs of oil/gal) just for sugar would be ~$6 per gallon. At these prices, producing a fuel via this process is not economically feasible. In order to become more economical, the carbon source should cost no more than $0.05/lb to offer some room for the cost of cultivation, harvesting, extraction, oil purification, and fuel production. Another observation that was noted in the production of the *R. glutinis* oil is the presence of caroteniods, which could have values greater than $300/lbs. Co-products like these could greatly improve the feasibility of producing oils from expensive feedstocks. The utilization of waste feedstocks such as wastewaters from pulp and paper operations or food processing operations also could make significant improvements to the economics of producing oils via *R. glutinis*.

Subtask J.1. Confirmation of microbial growth and carbon conversion kinetics at the pilot scale

The objective of this subtask is to determine the kinetics for triglyceride production from the compounds in an acid hydrolysate of lignocellulosic biomass using MSU's oleaginous microbe *R. glutinis*. Initially, starch will be used as the basis for determining the best case scenario, followed by a comparison using hydrolysate of biomass. During these runs the growth and lipid accumulation kinetics will be determined. All of these experiments will be conducted in the pilot system developed for use in Task I. Although the Biocrude thrust will be utilizing wastewater, the system can be sterilized via steam, which will allow for studies where pure oleaginous cultures are used. The unit operations defined in Task I will be suitable to collect data to determine the information needed for full-scale deployment.

The experimental design will consist of three runs per hydrolysate source. Each run will last approximately 148 hours and will be considered complete when the sugars have been exhausted as confirmed via HPLC analysis. Time permitting, another set of experiments will be carried out using shrimp processing waste as a growth medium. Work under a contract from the MS/AL Sea Grant Consortium has demonstrated the ability of this oleaginous yeast to grow to populations of 20 g/L on hydrolysates of this material. This feedstock is abundant in Southeastern United States.

Planned Activities:

J.1.ML.1. Achieve a mass of 10 g/L of the *R. glutinis* in the pilot reactor.
J.1.ML.2 Achieve 20% dry wt. oil content *R. glutinis* in the pilot reactor.

Experimental Design:

Pilot setup and operation:
The 500-L fermenter was initialized and prepared prior to inoculation with the *R. glutinis* cultures. The sugar media was prepared by dissolving approximately 18 kg of glucose (60 g/L initial concentration in 300 L culture volume) in 260 L of warm water in the sugar mixing tank and then pumping the solution in the fermenter. The fermenter containing the sugar solution was then sterilized in place (SIP) following the recommended protocols in the equipment instruction manual. A concentrated solution of the modified synthetic wastewater (SWW) medium (components were weighed on a 300-L volume) was prepared in 10-L solution contained in a glass carboy and sterilized in an autoclave. The sterile SWW medium was then pumped into the sterile and cooled fermenter medium and mixed. The mixed medium was aerated, and the fermenter pH and DO probes were calibrated. The *R. glutinis* seed cultures in the BIOFLO 410 fermenters were then harvested and transferred into the 500-L fermenter to create a total culture volume of 300-L. The 300-L fermentation culture was then run for 7 days and samples were taken daily. After the 7-day fermentation run, the culture was automatically pumped in batches to the membrane separator to concentrate the *R. glutinis* cells. Using a 25 PSI differential pressure, we were able to process ~240 liters/hour (~4 liters/minute), and when system rate slowed down to 1 liter/minute, we stopped and collected retentate and sent it to spray dryer for further processing. After one hour of processing time, the temperature of the system had increased to 50°C. The retentate stream from the membrane separator consisting of concentrated *R. glutinis* cells was pumped in batches into the spray dryer. Using a nominal setting of inlet temperature of 285°C and outlet temp of 90°C, we were able to process at a rate of 6-8 liters/hour. This provided % moisture of 4-6% with extractable of 20-40 g/L, depending upon conditions. The dried biomass was collected and subjected to laboratory analysis for moisture content, lipid extraction, and FAME analysis. The permeate stream was discarded in the sump. The dry biomass was extracted with hexane, methanol and acetone (HMA) to remove lipids. Lipid solvent mixture was transferred to solvent recovery system to collect lipids and recovery solvent for reuse in extraction steps. Operating the solvent recovery unit at a lower temperature of 60-65°C resulted in fewer oxidized lipids At this lower temperature, less solvent is recovered (~92%) and the system requires longer operating time. A vacuum of 300mm HG was used to assist in the use of a lower temperature. No detectable levels of lipids in recovered solvent were shown, and 97% +/- 5% was recovered. Small quantities were used for testing, and an experiment is underway for extraction and recovery of 1.5Kg of extractable material to be processed and optimized.

Pilot Operation Results with Rhodotorula glutinis:
The results of the pilot run using *R. glutinis* demonstrate the ability of the system to produce cells containing significant amounts of oil. The data given in Table J1 shows the % oil extracted using a combination of non-polar and polar solvents (hexane, methanol, and acetone) performed the best. This is not surprising given the resistance of yeast cell walls to lysing. The polar solvents are known to disrupt hydrogen bonding between the membrane lipids, making it easier for the polar solvent to dissolve the polar triglycerides shown in Figure J2 However, this solvent combination also dissolves more polar cellular constituents such as proteins. With subsequent runs, the team should be able to optimize cultivation and harvesting to obtain *R. glutinis* cells containing more than 30% oil content on CDW at >20 g/L.

Table J1: Solvent recovery data using extracts from dried *Rhodotorula glutinis* biomass.

Run #	Run 4	Run 5
Solvent (L)	10	10
Mass of *R. glutinis* cells (g)	500	500
Composition	HMA	H
Results:		
Mass oil recovered (g)	100	25
Oil Recovery %	20	5

A= Acetone
M= Methanol
C= Chloroform
H= Hexane

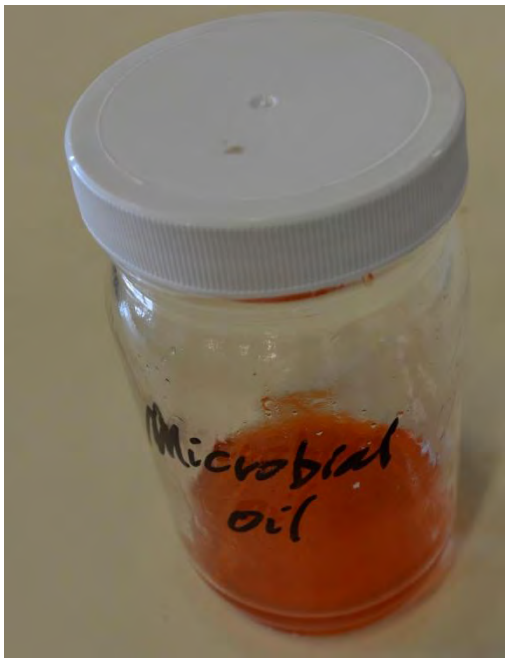


Figure J2: A photograph of a sample of the oil produced by Rhodotorula glutinis using the pilot facility's fermentors and extraction equipment.

Subtask J.2 Determination of optimal temperature for lipid accumulation using lignocellulosic sugars.

MSU's previous work with these oleaginous microorganisms has determined the optimum sugar concentration and medium pH. To date, however, no work by this group has determined the effects of temperature on the conversion kinetics. A well known biological principle is that enzyme rates can be doubled with every increase of 10ºC up to the point of denaturing the enzyme. The objective of this task is to determine the temperature at which *R. glutinis* gives the highest lipid-production rate. These experiments will be conducted in 1 L batches at incremental temperatures ranging from 30-60ºC. The cells for this experiment will be grown at 30ºC on the carbon substrate used in the lipid accumulation phase of the study. Once the cells have reached stationary phase (determined by no change in optical density), the temperature will be slowly

increased to the target temperature, and additional sugar will be added. Data will be collected to determine the yield, percent oil, sugar consumption kinetics, and lipid production kinetics.

To measure lipid accumulation, solids in collected samples will be concentrated via filtration and extracted for oil using conventional solvent extraction. The fatty-acid profiles and concentration of triacylglycerols will be determined by a GC and/or HPLC at MSU.

Planned Activities:

J.2.ML.1 To determine the optimum temperature for producing lipids using *R. glutinis* on lignocellulsoic sugars.

Experimental Design:

Preparation of Pure Culture of Rhodotorula glutinis:
The organism *R. glutinis* (204091), purchased from American Type Culture Collection (ATCC; Manassas, Virginia), was maintained on yeast peptone agar (YPD) at 4°C. YM Broth (271120), manufactured by Difco Laboratories (Becton, Dickson, and Company; Sparks, Maryland) was the media that was used to generate the pure seed culture of *R. glutinis* for all subsequent experiments listed in section 1. The medium was prepared in accordance with the listed instructions provided by the manufacturer. Following sterilization of the medium, an aliquot of *R. glutinis* was added to the medium, and the flask was incubated for 48 hours using a rotary shaker with a rotation speed of ~112 rpm.

Composition of Medium Used to Generate Increase in Lipid Production:
In order to induce lipid accumulation in this organism, it was necessary to use a medium that had a high carbon:low nitrogen ratio. All experiments listed in section 1 (with the exception of the seed culture) used a media composition in which the ratio of carbon to nitrogen was 60:1. The composition for the medium used to cultivate *R. glutinis* is as follows (g/L): Yeast Extract 1g; $Na_2HPO_4 \cdot 12\ H_20$ 1g; KH_2PO_4 1g; $MgSO_4 \cdot 7H_20$ 0.4g; $(NH_4)_2SO_4$ 1.4g; Trace Mineral Solution 10mL/L, $FeSO_4$ Solution 6 mL/L; Glucose or Xylose 60g, initial pH 6.5.

Experimental Set-Up for Batch Reactions using Flasks:
The media was prepared in 1L baffled flasks and sterilized in a Steris (Mentor, Ohio) autoclave for 15 minutes at 121°C and 15 psig. To prevent carmelization of the sugar, the carbohydrate solution (glucose or xylose) was autoclaved in a separate vessel. For the batch flask reactions, the samples were organized in triplicate. The flasks containing the pure culture of *R. glutinis* were cultivated at 20°C, 30°C or 40°C in incubators using a rotary shaker with a rotation speed of ~112 rpm. The total volume in flasks was 500 mL, with 470 mL of medium and 30 mL of pure seed culture. The total incubation time for the batch culture was 6 days.

Experimental Set-Up for Batch Reactions using Fermentation Units:
Batch cultivation experiments were conducted using a set of 3 BIOFLO 310 Bioreactors (New Brunswick Scientific; Edison, New Jersey) with an initial working volume of 3.0L. The pH of the cultures in the bioreactors was maintained at 6.5. The temperature of the culture in the bioreactors was controlled at either 20°C, 30°C, or 40°C using a platinum resistance temperature detector (RTD) and a water jacket in the fermenter vessel. Foaming was prevented by the automatic addition of 1:10 dilution of nonoil, polypropylene-based Antifoam 204 concentrate (Sigma Aldrich; St. Louis, Missouri). Aerobic batch fermentation was commenced by inoculating the sterile media with 180 mL of the pure seed culture of *R glutinis.* Air filtered through a 0.45 mm HEPA vent filter (Whatman; Kent, United Kingdom) was bubbled into the

culture at 1 vvm (volume of air per volume of media per minute). Agitation rate was set at 300 RPM in the first 24 hours of fermentation, increased to 400 RPM at 24 hours, and increased to 500 RPM at 48 hours. The total incubation time for the batch culture was 6 days.

Analyses:

Aliquots of 50 mL were taken for each of the treatments at hour 0, 12, 24, 36, 48, 72, 96, and 120. To determine cell mass, 50 mL of the sample was subjected to centrifugation at 3000 rpm for 20 minutes to form a cell pellet. Cell pellets were freeze dried overnight and the dried pellet was transferred to a weighed glass vial. The cell mass was determined based on the difference in weight of the glass vial before and after the addition of the freeze-dried cell pellet. Lipid extraction was achieved through the protocol outlined by Bligh and Dyer (Bligh and Dyer, 1959). Three sequential lipid extractions were performed for each sample in these experiments to ensure the recovery of total lipids. The extracted lipids dissolved in chloroform were dried under nitrogen. Once dried, the tubes were weighed in order to determine gravimetrically the amount of lipids present in the sample. Transesterification was achieved by dissolving dried lipids in 2.0% H_2SO_4 and incubating the samples in 60°C water bath for 2 hours. The samples were removed from the water bath and allowed to cool. Extraction of the FAMEs with toluene was carried out overnight at room temperature. The FAMEs produced by transesterification were analyzed using an Agilent gas chromatograph (model 6890; Palo Alto, California) equipped with a flame-ionization detector. Helium was used as the carrier gas. The separation was achieved with a fused-silica capillary column Stabilwax-DA with dimensions of 30m x 0.25mm and a phase thickness of 0.25mm. 1,3-Dichlorobenzene was used as an internal standard. The method consisted of injecting 1ml of sample into the gas chromatograph with a split ratio of 100:1. The temperature program began at 50°C, holding for 2 minutes. The temperature then increased by 10°C/min to 250°C. A calibration curve was prepared by injecting known concentrations of an external standard mixture comprising FAMEs. FAMEs in the samples were identified by comparing the retention times to the standard FAMEs.

Results:

Comparison of the Cell Mass Concentration of R. glutinis:
As expected, the dry cell mass data indicated that *R. glutinis* was able to grow in both the media that was supplemented with glucose as well as the media that was supplemented with xylose. Figures J3 – J6 display the change in cell mass concentration over time. Figures J3 and J4 correspond to the cultivations carried out in the flask experiments. Figures J5 and J6 correspond to the cultivations carried out in the bioreactors. Figures J3 and J5 display the change in cell mass concentration when glucose was used as the carbohydrate source and Figures J4 and J6 display the change in cell mass concentration when xylose was implemented as the sole carbohydrate source. For the cultivations that were completed in the flasks (Figures J3 and J4), it appears that 20°C was optimal for increase in cell mass concentration when glucose was the substrate, and 30°C was optimal when xylose was utilized as a substrate. In comparison, the data collected from the reactions carried out in the bioreactors (Figures J5 and J6) indicated that there is not a significant change in cell concentration at 20°C and 30°C when glucose is utilized as the carbon source. Contradictory to what was observed in the flask cultivations, the cell concentration in the bioreactors was slightly higher at 20°C than at 30°C when xylose was implemented as the carbon source. Both cultivations carried out in the flasks and in the bioreactors indicated that 40°C is not in the ideal range for the cultivation of *R. glutinis* on either substrate. As a side note, one of the reasons we carried out these experiments in the bioreactors following the completion of these experiments in the flasks was to examine whether or not the fluctuation in pH was limiting the growth of *R. glutinis.* In the flask reactions,

typically, the pH drops from 6.5 to ~2.0 between 24 and 36 hours (data not shown). When we used the bioreactors, we were able to maintain the pH at 6.5 throughout the duration of the experiment. Thus far, the data accumulated seems to indicate that the significant drop in pH observed in the batch flask experiments does not seem to hinder the growth of *R. glutinis.*

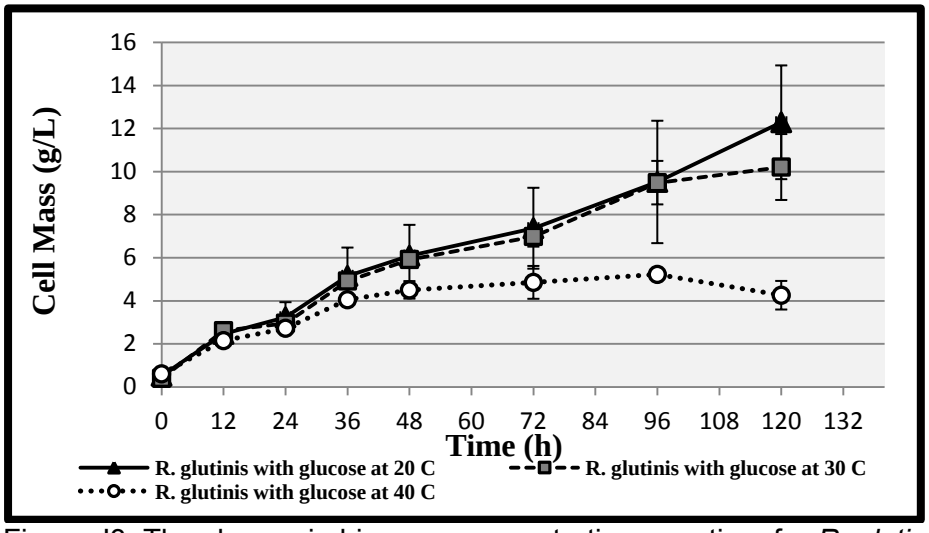


Figure J3: The change in biomass concentration over time for *R. glutinis* cultivated with glucose as the carbon source. These reactions were carried out using batch flasks.

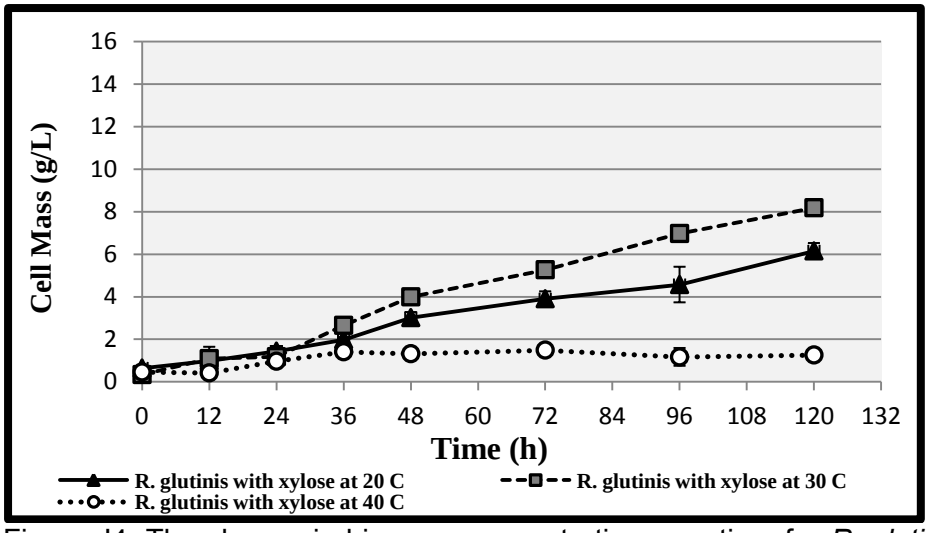


Figure J4: The change in biomass concentration over time for *R. glutinis* cultivated with xylose as the carbon source. These reactions were carried out using batch flasks.

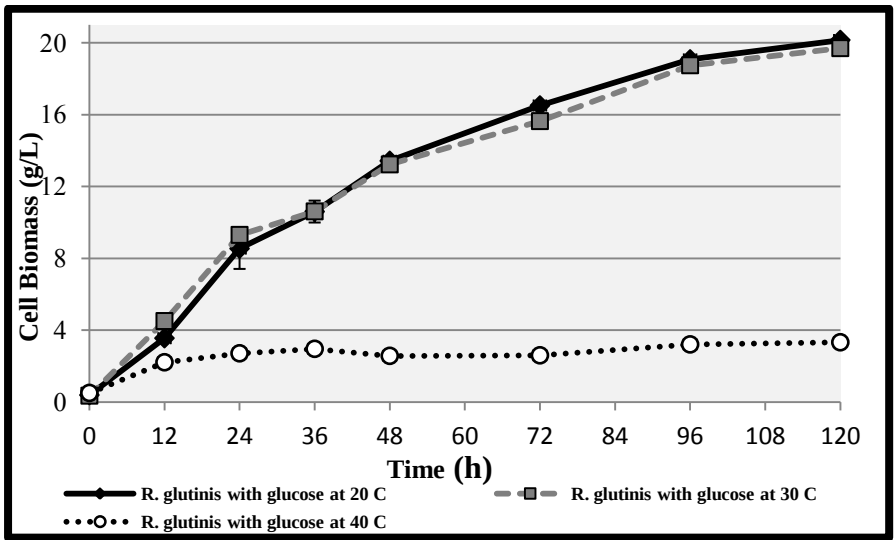


Figure J5: The change in biomass concentration over time for *R. glutinis* cultivated with glucose as the carbon source. These reactions were carried out in the bioreactors.

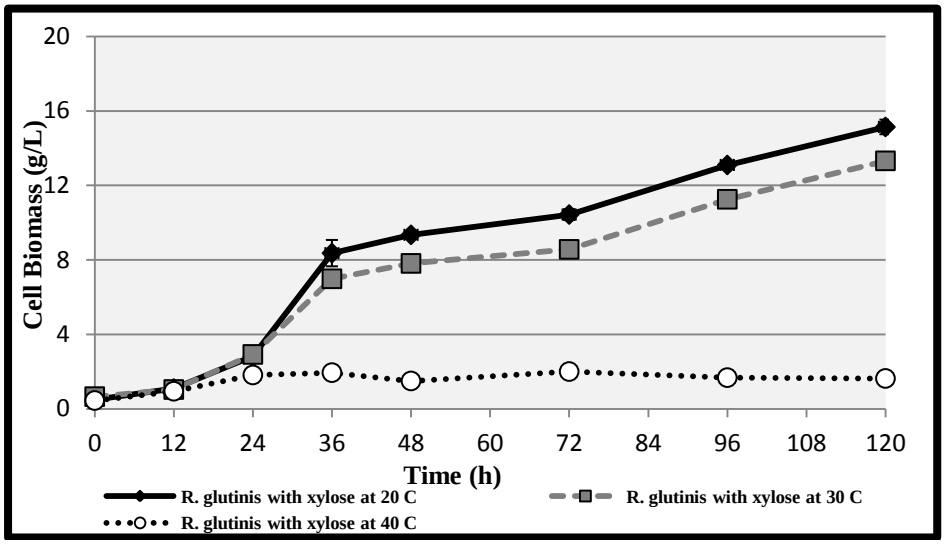


Figure J6: The change in biomass concentration over time for *R. glutinis* cultivated with xylose as the carbon source. These reactions were carried out in the bioreactors.

Comparison of Lipid Accumulation in R. glutinis at Different Temperatures:
Figures J7 – J10 display the percentage of lipids extracted from the dry cell mass pellets of *R. glutinis*. Figures J7 and J8 correspond to the experiments carried out in flask experiments. Figures J9 and J10 correspond to the experiments carried out in the bioreactors. Figures J7 and J9 display the percentage of lipids extracted from cell mass when glucose was used as the carbohydrate source. Figures J8 and J10 display the percentage of lipids extracted from cell mass when xylose was implemented as the carbohydrate source. The data collected from the flask experiments (Figures J7 and J8) indicate that when glucose is used as a carbohydrate source, the lipid accumulation occurs at a faster rate when cultivated at 20°C. It appears that by 96 hours, the accumulation of lipids is comparable at 20°C and 30°C when glucose is used as the carbohydrate source. After 96 hours, the lipids accumulated at 20°C and 30°C undergo degradation. When xylose is utilized as the substrate, results from the batch flask reactions (Figure J8) indicate that 20°C is optimal for lipid accumulation. In the bioreactor experiments

(Figures J9), 30°C appears to be optimal for lipid production when glucose is used as the substrate. Lipid accumulation at 30°C is considerably higher than at 20°C. Lipid accumulation in the bioreactors is minimal when xylose is implemented as the substrate, regardless of temperature (Figure J10). It is possible that one of the controlled variables (either pH or air flow) may be affecting the rate of lipid accumulation in *R. glutinis* when xylose is used as the substrate as these are the major differences between the flask and bioreactor experiments. There is a sharp increase in lipid accumulation at 40°C in both the flasks and the bioreactor when glucose is used as the substrate (Figure J7 and J9). This increase may be a direct result of cell death. As we observed in the previous graphs (Figure J3 and J5), there is no obvious accumulation in cell mass, so perhaps this increase in lipid yield at the end of the experiment is a direct result of cell detritus.

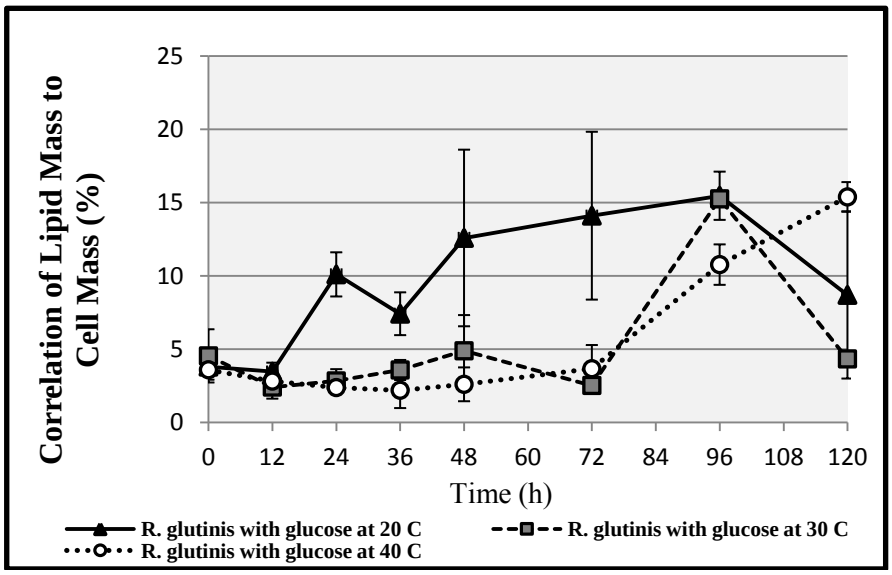


Figure J7: The percentage of lipid extracted from *R. glutinis* that were cultivated using glucose as the carbon source. Cells used in these extractions were cultivated in batch flasks.

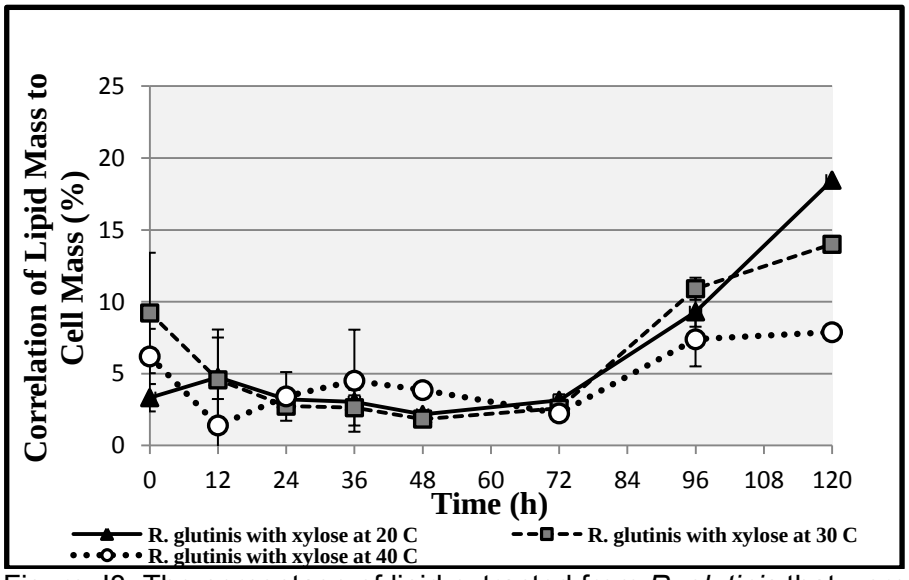


Figure J8: The percentage of lipid extracted from *R. glutinis* that were cultivated using xylose as the carbon source. Cells used in these extractions were cultivated in batch flasks.

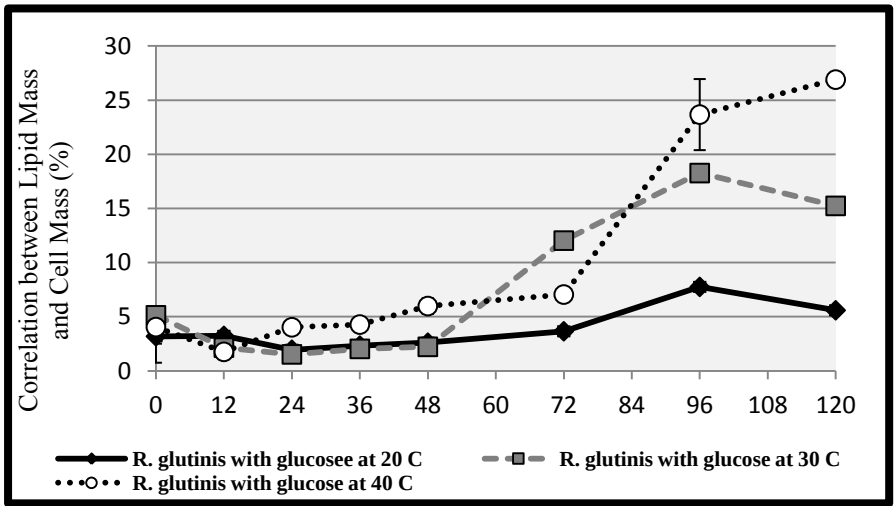


Figure J9: The percentage of lipid extracted from *R. glutinis* that were cultivated using glucose as the carbon source. Cells used in these extractions were cultivated in the bioreactors.

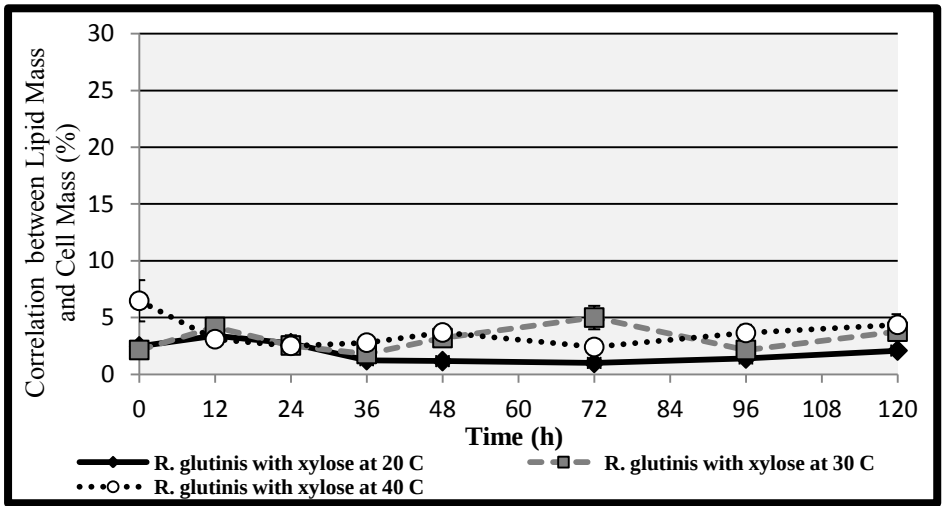


Figure J10: The percentage of lipid extracted from *R. glutinis* that were cultivated using xylose as the carbon source. Cells used in these extractions were cultivated in the bioreactors.

Analysis of FAMEs Content:
Regardless of whether the experiments were conducted in batch flasks or in the bioreactors, the FAMEs were similar among both sets of experiments. The FAMEs data indicated that lipid accumulation significantly increased between the hours of 48 and 96, regardless of the carbohydrate source.

As we have seen in previous experiments with *R. glutinis*, the three major fatty acids that are produced by this organism are palmitic acid, oleic acid, and linoleic acid. These three fatty acids comprise the majority of the total FAMEs extracted from the organism, regardless of the carbohydrate source. Total FAMEs data (Figure J11) indicated that the cells cultivated on glucose yielded a significantly higher concentration of fatty acids than the cells cultivated on xylose. Figures J12 and J13 display the percentages of saturated and unsaturated fatty acids, respectively. These graphs indicate that there is not a significant difference between the yield of

saturated and unsaturated fatty acids at the three different temperatures (20°C, 30°C, and 40°C) or between the two different substrates (glucose or xylose).

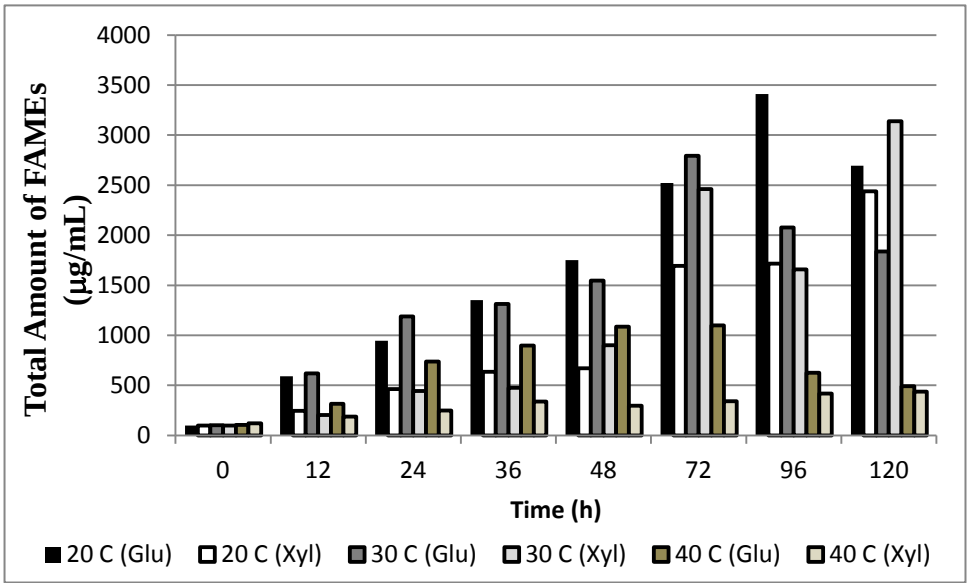


Figure J11: Total FAMEs

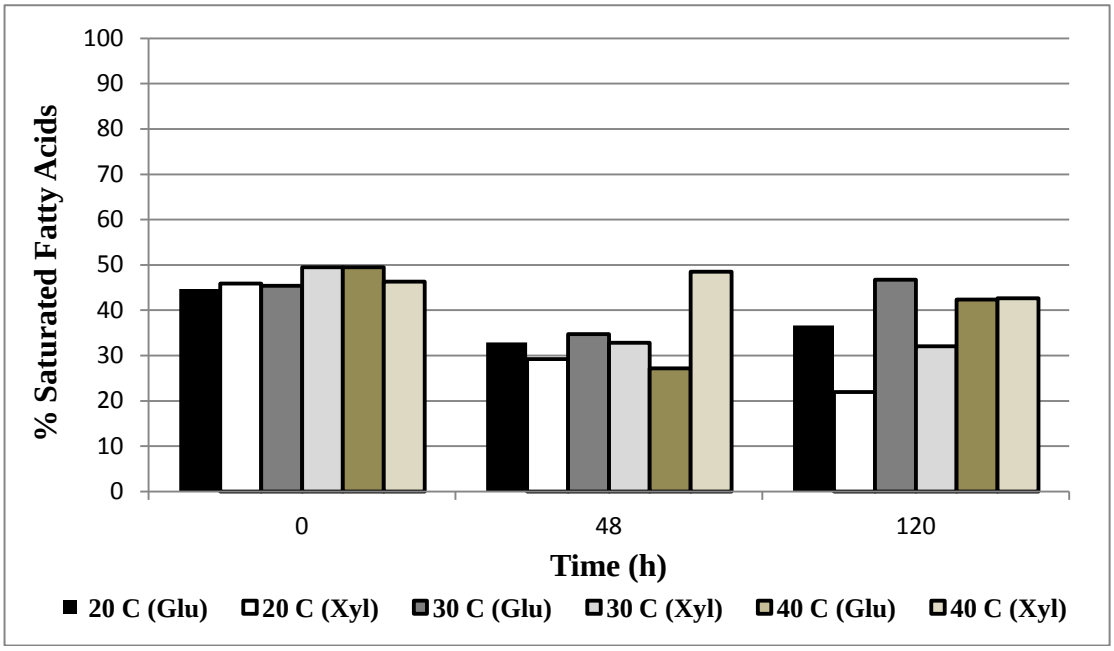


Figure J12: The percentage of saturated fatty acids detected in lipid extracted from *R. glutinis.*

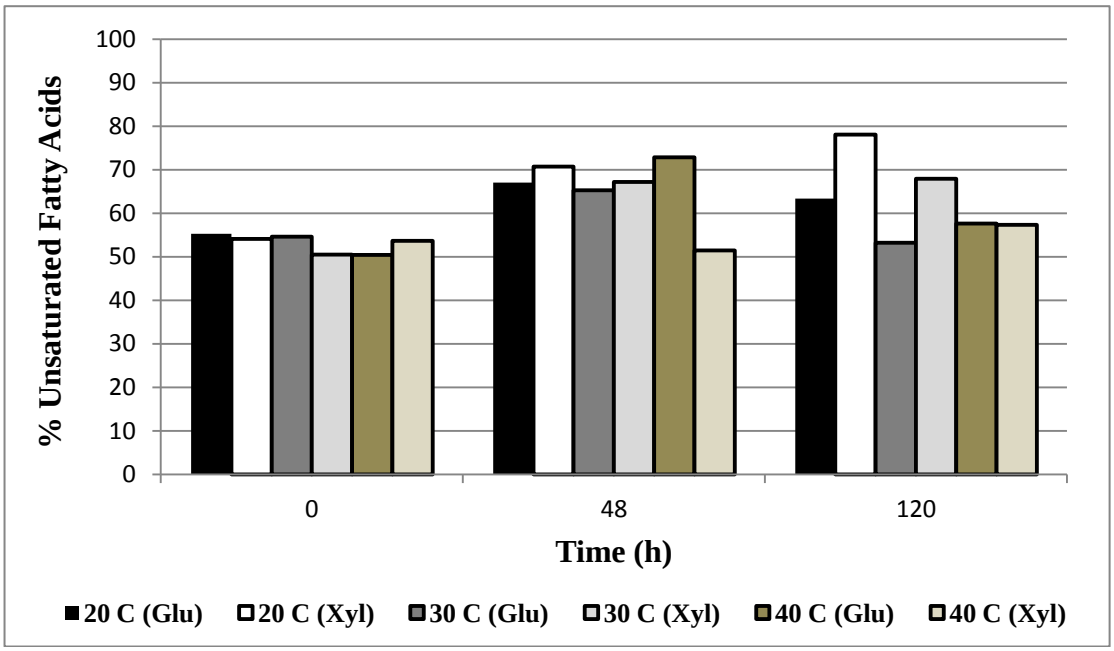


Figure J13: The percentage of unsaturated fatty acids detected in lipid extracted from *R. glutinis.*

Summary:

The data collected thus far indicates that glucose is the optimal substrate for the growth and accumulation of lipids in the organism *R. glutinis.* We have shown the xylose can be used as an acceptable carbohydrate source. The data indicates that when xylose is used as the substrate, the temperature for optimal lipid accumulation is 30°C. We can ascertain from the data collected thus far that 20°C or 30°C is ideal for growth and lipid accumulation in the organism *R. glutinis* when glucose is utilized as the carbohydrate source. Our results indicated that regardless of the sugar source, the fatty acid profile is similar at the different temperatures.

The Effects of Temperature on the Microbial Growth and Microbial Oil Production by Rhodotorula glutinis on Acid Hydrolyzate of Switchgrass

Method:

Preparation of acid hydrolysate from switchgrass:
Switchgrass was obtained from the Department of Plant and Soil Sciences at Mississippi State University. The as-received switchgrass was ground and sieved to collect material in the size range of 40 mesh to 60 mesh. A 500 g sample of switchgrass was mixed with 1418 g of the 72% (w/w) sulfuric acid solution in a 2L beaker. After the switchgrass and 72% sulfuric acid solution were thoroughly mixed, the resulting mixture was stored at 30°C for 2 hours. During the 2 hours, the mixture was agitated at least one time. The mixture was then transferred to a 10 L glass reactor with 8600 mL of deionized water. This diluted mixture was then heated up to 97°C within 2 hours and held at this temperature for 3.5 hours. The liquid hydrolyzate was filtered into a glass receiver. Barium hydroxide powder was used to adjust the pH of the hydrolysate to approximately 7. The neutralized liquid was filtered, and the filtrate was collected as the final product of switchgrass hydrolyzate.

Lipid production from acid hydrolysate by oleaginous yeast:

The oleaginous yeast *R. glutinis* (ATCC 15125) was used in all experiments. The yeast was first grown in nutrient broth media for 48 hours as inoculums. Then 50 mL of the culture was centrifuged at 2000 RPM for 15 minutes, and the cell pellet as inoculums was transferred to a 2 L shake flask with a 667 ml fresh media made of, per liter: acid hydrolyzate, 1 L, yeast extract, 0.5, 10 ml of mineral salt solution, 6.0 ml $FeSO_4$ solution (which is made of 0.4 g $FeSO_4.7H_2O$ and 100 ml water), Na_2HPO_4, 0.0545 g/l; KH_2PO_4, 0.0545 g/l; and $MgSO_4 \cdot 7H_2O$, 0.4 g/l. Before adding the media to the flask, the media was sterilized using a 0.22 µm filter membrane. The cultures were then incubated in a shake fermentor at various temperatures and 120 RMP shaking.

Analyses:

Cell dry weight determination was performed by centrifuging the cells at 3000 RPM for 15 minutes, washing with DI water, and drying in a freeze-dry system to constant weight. The lipid content of the cell was obtained by the gravimetrical method described by Bligh & Dyer.

The lipids obtained from the Bligh & Dyer extraction were transesterified with methanol. The fatty acid methyl ester (FAME) was then analyzed using an Agilent 6890 series Gas Chromatograph equipped with a Supelco SP 2380 capillary column (100 m x 0.25 mm x 0.2 micron, model number Supelco 24317) and a flame ionization detector (FID).

Glucose and xylose were analyzed by high pressure liquid chromatography equipped with an evaporative light scattering detector. The column used was a Grace-Prevail Carbohydrate ES 5u with a length of 250 mm, I.D.of 4.6 mm, particle size of 5 µm , and pH range of 2-13. The guard column was 7.5 mm long, and I.D. was 4.6 mm. Both were operated at room temperature. The mobile phase was water/acetonitrile (35:65, v/v) with a flow rate of 1ml/min. The isocratic spray chamber was controlled at 25°C, and drift tube at 55°C. The injection volume was 2 µL.

Results:

Production of sugars from lignocellulosic biomass switchgrass:
The concentrations of glucose and xylose in the product of acid hydrolysate were determined to be about 12.6 g/l and 10.4 g/l, respectively. The furfural and acetic acid were determined to be 0.221 g/L and 0.012 g/l, respectively (as shown in figure J14). The total nitrogen was 0.116 g/L. The yield of sugars (glucose +xylose) reached 42.4% based on the total dry weight of the switchgrass. The solid remnant, including lignin and all other impurity of solid soil waste, was calculated to be 31.2% of total grass weight.

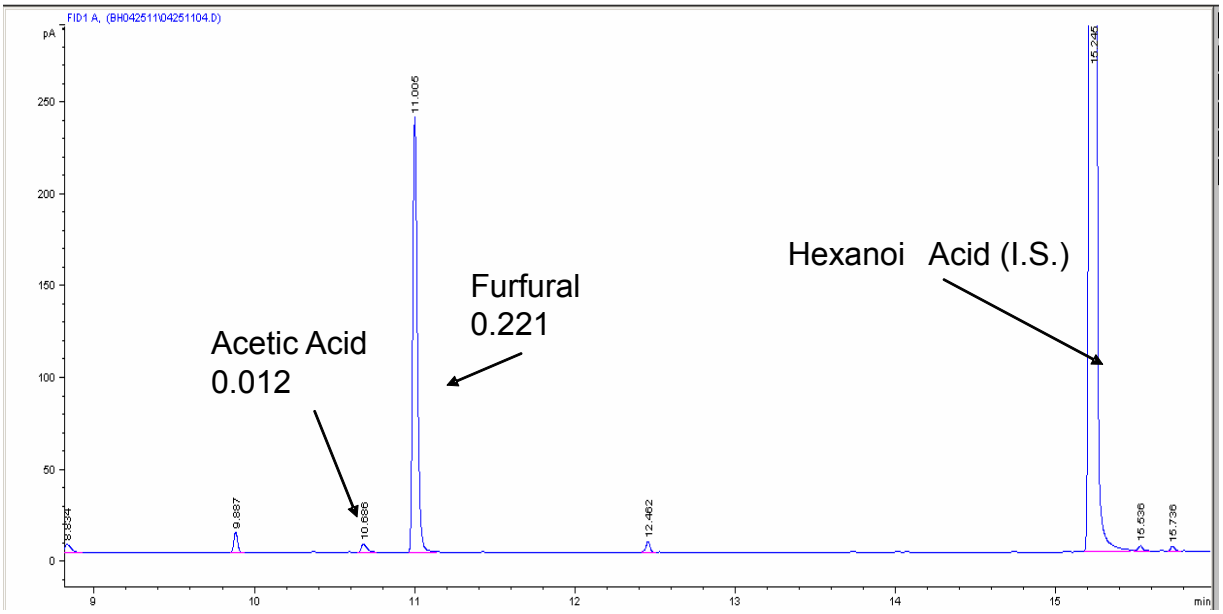


Figure J14: Analysis of furfural and acetic acid in the acid hydrolyzate by HPLC.

The growth of microorganism and microbial mass production:
The oleaginous yeast *R. glutinis* was cultivated at various temperatures of 25˚C, 30˚C, 35˚C, and 40˚C. The growth results were shown in Figure J15. Except for 40˚C, *R. glutinis* survived and grew at the other three temperatures. At 40˚C, the growth of *R. glutinis* was ceased within 24 hrs. In the first 24 hours, the growth rate of microbial mass at 35˚C was higher that at the other three temperatures. At 168 hours the cell mass concentration reached maximum of 7.34 g/L at 30˚C and 6.45 g/L at 35˚C. At 25˚C, however, it reached 6.41 g/L and kept increasing until the experiment was terminated. In view of the microbial mass production, 30˚C is the optimum temperature among the tested ones.

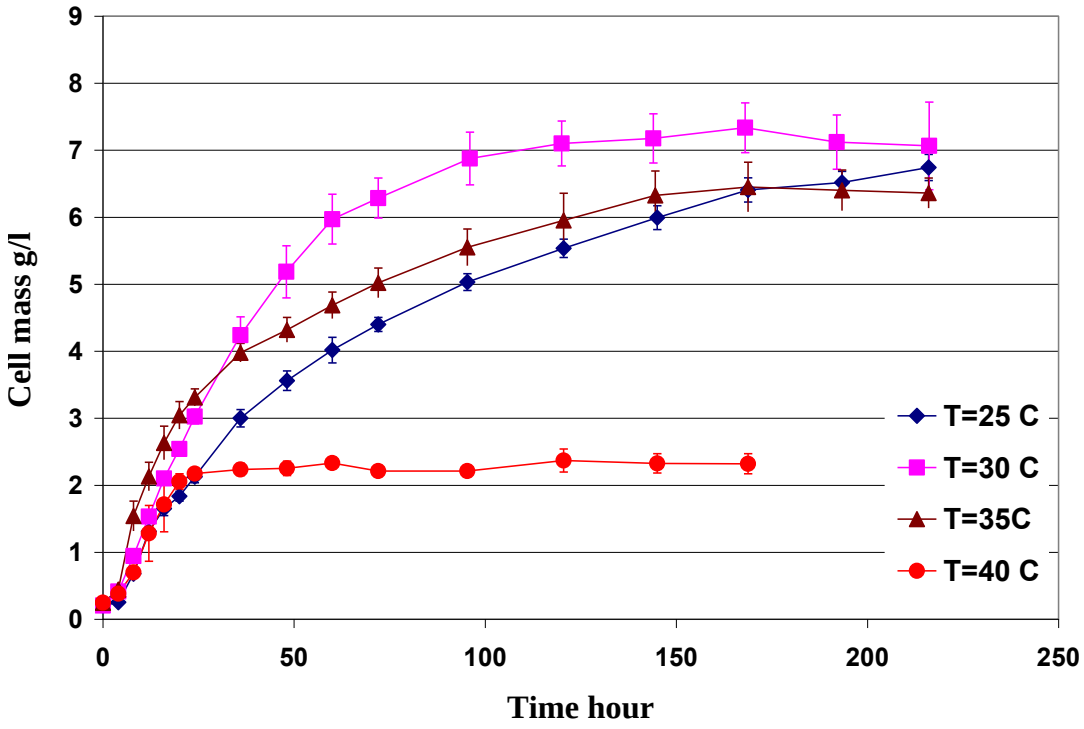


Figure J15: Growth of *Rhodotorula glutinis* at various temperatures with the acid hydrolyzate of switchgrass as sole carbon and energy source.

The lipid production:

Figure J16 presents the microbial oil production by *R. glutinis* growing on the acid hdyrolyzate of switchgrass at various temperatures. The conversion of acid hydrolyzate sugars to lipids at 25˚C and 40˚C was negligible. At 30˚C, the lipid content in the cells increased from initial 5.4% of cell dry weight to 21.2% at 96.0 hours. At 35˚C, it reached 15.8% at 120.5 hours. Considering the lipid production, the results indicated that the optimum temperature is also 30˚C.

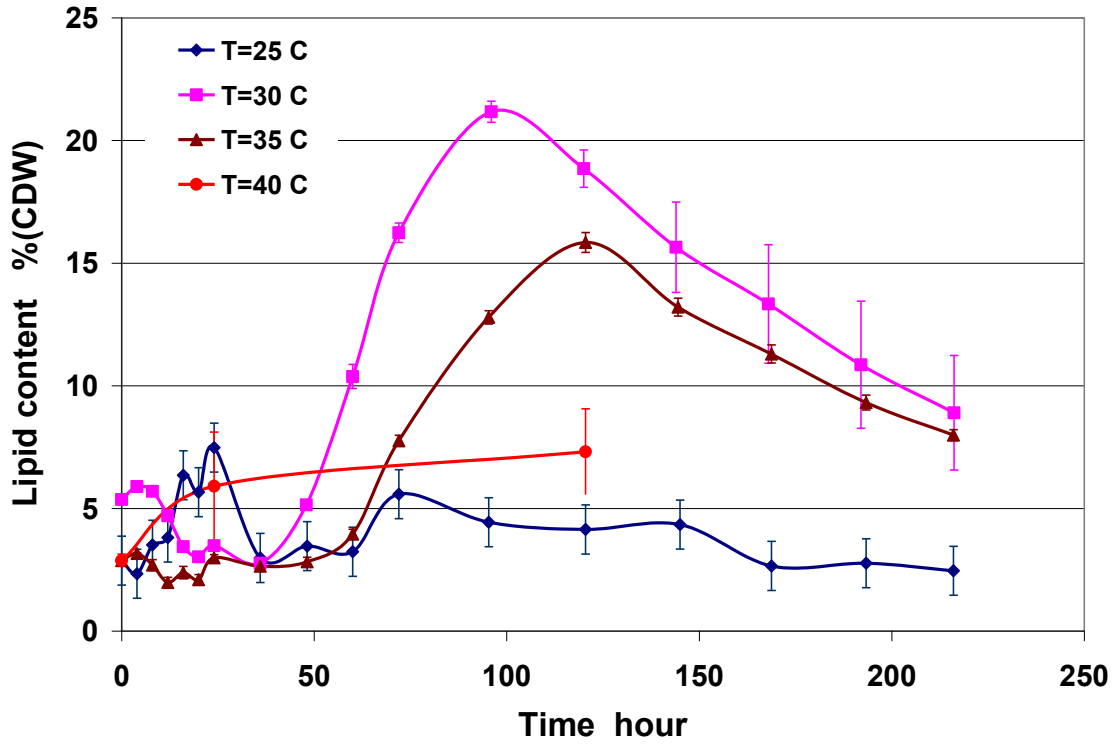


Figure J16: The microbial oil accumulation by *Rhodotorula glutinis* at various temperatures with the acid hydrolyzate of switchgrass as sole carbon and energy source.

The lipid production enhancement:
The results presented above suggested that the optimum temperature of the microbial oil production is 30˚C, and the lipid content in the cell is limited to about 21% of cell dry weight. This is most likely due to the exhaustion of the sugars in the media as the total sugars of glucose and xylose was about 23 g/L. To enhance the lipid production in this experiment, the culture was given additional fresh acid hydrolyzate media without nitrogen (yeast extract and ammonia sulphate) and phosphorous (phosphates) at the time of 120 hours. The results are shown in Figure J17.

At 120 hours, the cell mass concentration increased from initial 0.21 g/L to 8.36 g/L with lipid increasing from initial 5.4% to 8.6%. At the addition of fresh hdyrolyzate sugars, the cell mass was diluted to 4.59 g/L, and the lipid content rose to 31.0 % with cell mass of 7.26 g/L in 48 hours.

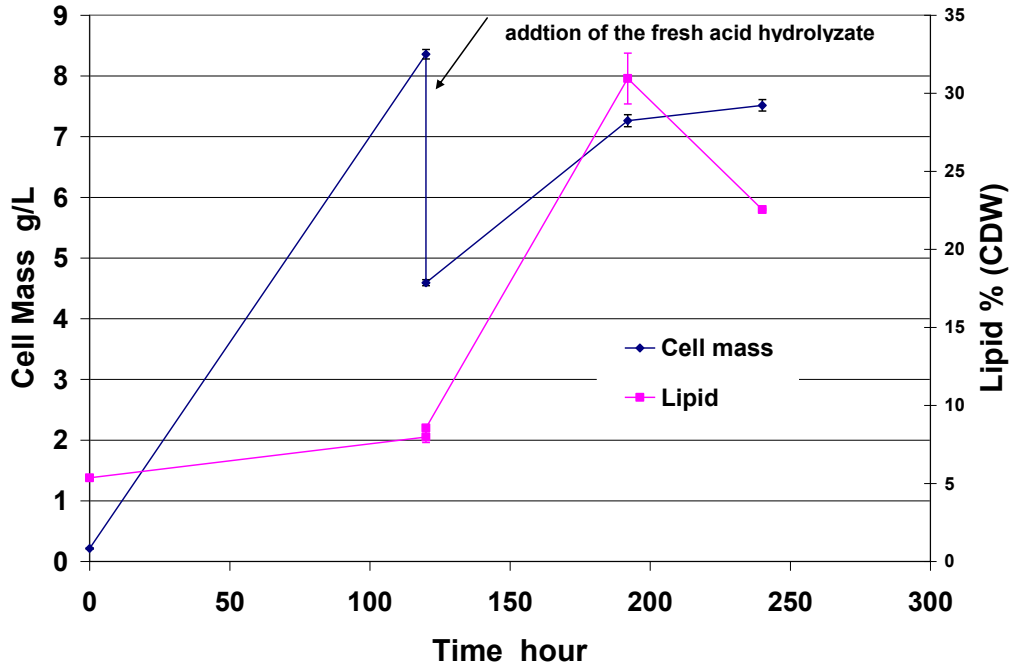


Figure J17: Enhancement of lipid production by *R. glutinis* at 30˚C.

Fatty acid profile of the generated lipids:
As indicated by the experimental results, 30˚C was the optimum temperature for the production of both microbial mass and microbial oils from the acid hydrolyzate of switchgrass. The lipids generated at 30˚C were collected and transesfterified with methanol to FAME and analyzed by GC-FID method. The gas chromatographic spectrum of the sample was shown in Figure J18. As presented in the figure, 1,3-dichlorobenzene was the internal standard, and BHT was the compound added to the samples to reduce the potential oxidization of the unsaturated fatty acids. The major peaks shown in the figures are palmitic acid (36.8%), stearic acid (13.1%), oleic acid (35.2%), and linoleic acid (7.8%).

Kinetics (the net specific growth):
The net specific growth rates of *Rhodotorula glutinis* at various temperatures were calculated and listed in Table J2. The R^2 value is larger than 0.95 for all the temperatures, which indicates that this kinetic model is suitable to describe the performance of the exponential growth of *R. glutinis* growing on acid hydrolyzate of switchgrass at 30˚C. According to the calculated rates, the optimum temperature was 35˚C for microbial mass and lipid production. This is also consistent with the results in the Figure J16. As shown in this figure, with the first 24 hours, the rate at 35˚C was the highest among the tested temperatures.

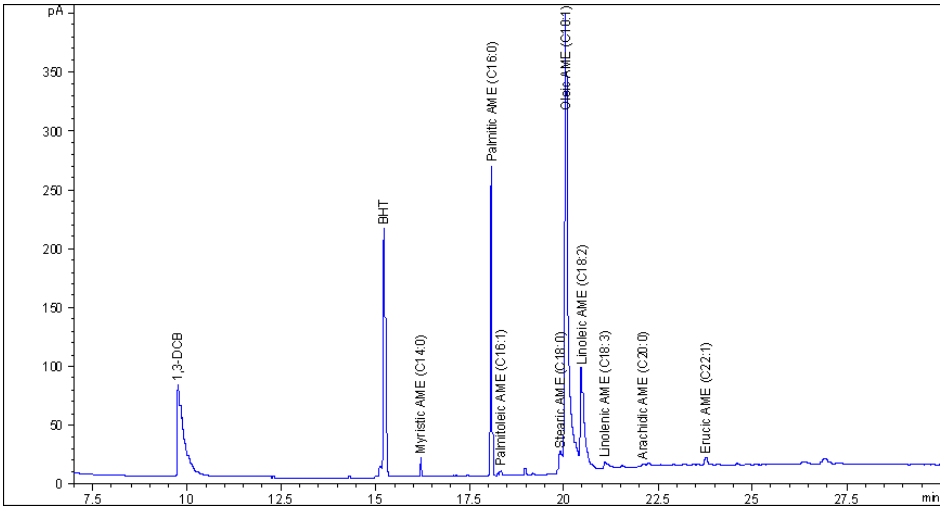


Figure J18: FAME profile from the lipid generated by *R. glutinis* at 30˚C on acid hydrolyzate.

Table J2: The net specific growth rate of *R. glutinis* at various temperatures on the acid hdyrolyzate of switchgrass.

Carbon source	Temp (˚C)	Microorganism	U_{net} (h^{-1})	T_d (h)	R^2
Acid hydrolyzate	**25**	***R. glutinis***	**0.1657**	**4.18**	**0.9545**
Acid hydrolyzate	**30**	***R. glutinis***	**0.1718**	**4.03**	**0.9905**
Acid hydrolyzate	**35**	***R. glutinis***	**0.1932**	**3.59**	**0.9546**
Acid hydrolyzate	**40**	***R. glutinis***	**0.1388**	**4.99**	**0.9946**

Summary:

The experimental data run using actual acid hydrolyzate of switchgrass as sole carbon and energy source in shake flask showed that 30˚C was the optimum temperature among 25˚C, 30˚C, 35˚C, and 40˚C, for the production of microbial oils as biodiesel feedstock. However, net specific growth rate was highest at 35˚C. The lipid content at 30˚C reached 31.0% with cell mass of 7.26 g/L. The major fatty acids of the generated lipids were identified to be palmitic acid (36.8%), stearic acid (13.1%), oleic acid (35.2%), and linoleic acid (7.8%)

Subtask J.3. Commercialization plan

In order for investors to determine the economic viability of this technology, they will need to know capital cost, fuel production cost, and other pertinent logistics. Using the data and other information from the previous subtask, a process flow diagram will be generated with the associated capital and operation cost of the entire process as well as the individual unit operations. The unit operations cost will aide in determining where the focus of future research should be placed to lower the cost per gallon of oil. A complete economic analysis of a commercial scale facility will be developed using data from the pilot facility.

Planned Activities:

J.3.ML.1 Development of a complete economic analysis of a commercial scale facility

The process of producing triglycerides via *R. glutinis* is dependent on carbon sources from which the microorganisms convert to triglycerides. The theoretical maximum amount of oil that can be produced from a pound of glucose or xylose is 0.35 pounds. This is a result of the need to remove oxygen from these sugars. In the case of *R. glutinis*, yields of 0.3 have been achieved, but routinely the yields are ~0.25 lbs of oil/lbs of sugar. With sugar prices currently selling for above $0.20/lbs, the impact on the cost of oil is substantial. Figure J19 shows the impact of carbon source costs on the cost of a gallon of triglycerides without any of the other cost to cultivate, harvest, extract, purify, or biodiesel production.

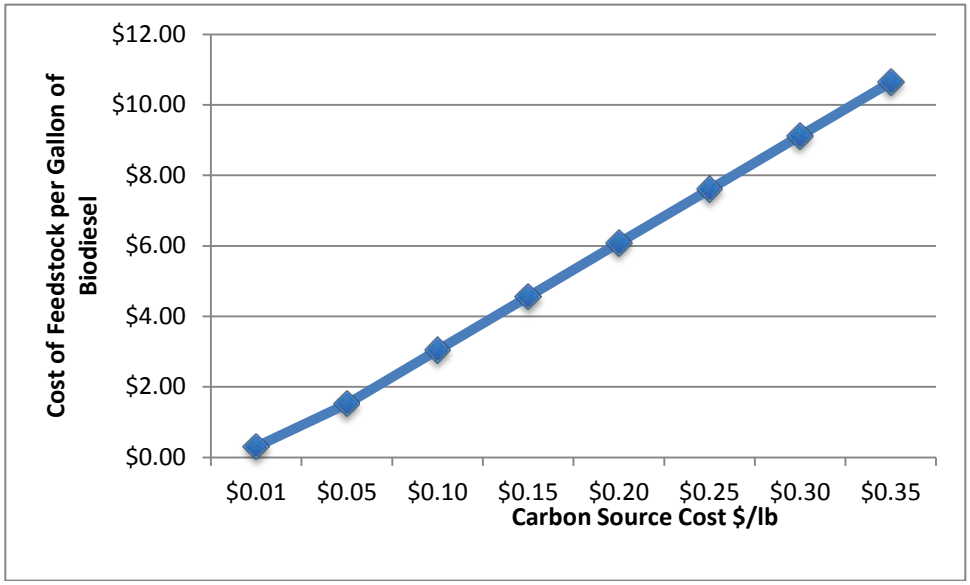


Figure J19: Effect of carbon source cost on a gallon of biodiesel.

As may be seen in the figure above, carbon source cost above $0.10/lb renders the cost of biodiesel via *R. glutinis* unfeasible. If the yield was able to reach theoretical maximum, a reduction of $0.85/gallon could be realized, but even with this savings additional improvements would still be needed. One obvious way to significantly reduce the cost is to identify feedstocks with costs of less than $0.05/lb. Free feedstocks or those that pay the producer to take feedstocks would be the most ideal to utilize. Sources of these feedstocks are industrial wastewaters such as food processors, brewery, pulp and paper, etc. These types of feedstocks have tremendous potential and will be investigated in the next phase of SERC funding.

Another area that could improve the economics of producing oils from high cost feedstocks are byproducts such as specialty chemicals. One such product that *R. glutinis* has been shown to produce by this research group as well as other groups is carotenoids. This red pigment can be observed in Figure J2. This compound and similar ones can be sold for prices in the $300/lb range. This could offset some of the high sugar cost. This investigation has demonstrated the need to find additional high value products produced by this and other organisms and identify cost effective feedstocks.

Publications:

Zhang, French*, WT., Hernandez*, R., Alley, E., and Paraschivescu, M., “Effects of furfural and acetic acid on growth and lipid production from glucose and xylose by *Rhodotorula glutinis*,” *Biomass and Bioenergy* 2011, Vol. 35, p. 734-740.

Task K. Hydrocarbons derived from synthesis gas

Principle Investigators and team members:
Principle Investigator: Fei Yu
Team members: Todd MIsna

The goal of this task is to further develop the catalyst that will convert synthesis gas to gasoline in one step and to characterize the liquid product resulting from this conversion step using synthesis gas developed from a downdraft gasifier.

The data contained in pages 1 to 35 of this report have been submitted in confidence and contain trade secrets or proprietary information, and such data shall be used or disclosed only for DOE's official evaluation of performance of the SERC Syngas Thrust Area. Therefore, this information should be disclosed to only those individuals required by DOE for this performance evaluation purpose.

Executive Summary

Subtask K.1 Larger scale catalyst testing using actual synthesis gas
A continuous process including catalyst preparation, biomass gasification, syngas cleaning, and Fischer–Tropsch synthesis (FTS) was developed and evaluated to demonstrate biomass-to-liquid (BTL) fuel technology. Oak-tree wood chips were used as the feedstock for gasification process, and they were first gasified to syngas over a commercial pilot scale downdraft gasifier. The raw wood-derived syngas contains about 47% N_2, 21% CO, 18% H_2, 12% CO_2, 2% CH_4, and trace amounts of impurities. A syngas purification system was designed to remove the impurities in the syngas after identifying the toxic or negative components for the FTS process, i.e. moisture, oxygen, sulfur, halogen elements (mainly chlorine), ammonia, tar, etc. The cleaned syngas meets the requirements for the following step of catalytic conversion to liquid fuels, i.e. total sufurs (H_2 S + COS) < 10ppb, NH_3 < 1ppm, oxygen < 1 ppm, and chlorine < 10ppb. A highly efficient carbon-encapsulated iron nanoparticle catalyst was synthesized for catalytic conversion of syngas to liquid hydrocarbons. The Fe@C core-shell nanostructures were prepared from a solution of $FeCl_2$ and wood derived sugars under hydrothermal carbonization (HTC) conditions. The obtained nanostructures were characterized by SEM, TEM, HRTEM, XRD, TPD, Raman, and FTIR. The size of these nano-spheres was about 100 to 150 nm in diameter. A multi-step mechanism of this process was proposed for the formation of carbon-encapsulated iron nanoparticles. The cleaned syngas was passed through the Fe@C nanoparticle catalyst bed; it showed excellent catalytic performance for the syngas upgrading reaction. It has high selectivity C_5^+ hydrocarbons. CO conversion rate can reach 89.5% and C_5^+ hydrocarbon selectivity can be up to 65% at 330°C. The detailed hydrocarbon analysis (DHA) showed there were 49.11% olefins, 11.82% iso-paraffins, 7.83% aromatics, 5.4% napthenes, and 5.1% paraffins in the liquid product.

Subtask K.2 Process design and economic analysis
The evaluation of biofuels processes (liquid hydrocarbons, light hydrocarbons, and oxygenates) under syngas production capacities of 65 to 10,000 Nm^3/h using economic modeling method was performed. The cost analysis was developed using VB-C# 2008 computer programming language and mathematical equations. The regression analysis and optimization sub-model was considered to help for economic evaluation. The modeling effort showed that our BTL technology was feasible. Based on the sensitivity analysis and preliminary market analysis, the results showed that the BTL technology could be profitable if ameliorating the most sensitive cost factors such as labor, project investment, and/or feedstock supply.

Subtask K.1 Larger scale catalyst testing using actual synthesis gas

In earlier work, we prepared two catalysts that demonstrated the concept of a one-step synthesis gas to gasoline conversion. These catalysts produced too much light gas and carbon dioxide to be economically feasible. However, this preliminary work has enabled us to make a second generation catalyst which showed improved yields: 15% conversion of CO, 31% selectivity to liquid hydrocarbon, and 31% selectivity to light gases (C_1-C_4). This 2nd generation catalyst will be produced in sufficient quantities to be used in larger scale testing using real synthesis gas to determine catalyst life-time and to determine sensitivity to H_2S present in the gas at small concentrations (50 ppm). A 3rd generation of catalyst is under development which shows lower yields of carbon dioxide. This catalyst will be tested for yields using real gasifier derived synthesis gas.

An existing downdraft gasifier will be used to produce synthesis gas from wood chips and other biomass. This syngas contains about 20% hydrogen, 19% carbon monoxide, 12% carbon dioxide, and 49% nitrogen and will be the feedstock for a catalytic reactor to produce liquid hydrocarbons. A unique catalyst will be used in a one step catalytic reaction for the conversion of synthesis gas to liquid hydrocarbons. Preliminary studies using this unique zeolite catalyst have shown that it is active and selective for the direct synthesis of gasoline-range branched and cyclized alkanes as well as aromatic compounds.

A pilot scale catalytic reactor will be constructed that should produce about one gallon of liquid hydrocarbon per eight hour shift. The reactor will be about 20, 1-inch diameter stainless steel tubes that contain the zeolite catalyst. The pilot scale reactor will be a continuous system and will operate under 1200 psi and 350° C.

Experiments will be conducted to evaluate the life of two types of catalysts, the effect of three temperatures and three pressures in the reactor tubes, and two throughput rates of syngas. Samples of the liquid hydrocarbons will be subjected to ASTM standard measurements for liquid hydrocarbons by the Mississippi State Chemical Laboratory. Gas chromatograph analyses will also be made to provide quality assessments during the experimental test runs. Off gases will be analyzed prior to burning them in a flare so that no hazardous gases will escape.

Planned Activities:

K.1.ML.1 Achieve 50% conversion of CO with 30% selectivity to liquid hydrocarbons using 2nd generation catalyst to determine its performance with real synthesis gas from a downdraft gasifier.

K.1.ML.2 Determine the catalyst life-time in extended, time-on-stream testing with real synthesis gas obtained from a downdraft gasifier.

K.1.ML.3 Determine the effect of trace amounts of H_2S in the actual synthesis gas upon yields.

Summarization of Activities:

A continuous process including gasification, syngas cleaning, and Fischer–Tropsch (FT) synthesis was developed and evaluated to demonstrate biomass-to-liquid (BTL) hydrocarbon fuel technology. Oak-tree wood chips were used as the raw materials and were first gasified to syngas over a commercial pilot plant downdraft gasifier. The raw wood syngas contains about

47% N_2, 21% CO, 18% H_2, 12% CO_2, 2% CH_4, and trace amounts of impurities. A purification reaction system was designed to remove the impurities in the syngas after indentifying the toxic or negative components for the FT process, i.e. moisture, CO_2, oxygen, sulfur, ammonia, tar, etc. The cleaned syngas meets the requirements for the following step of catalytic conversion to liquid fuels, i.e. total sufurs (H_2S + COS) < 10ppb, NH_3< 1ppm, oxygen< 1 ppm, and chlorine < 10ppb. A multi-functional catalyst was developed and tested for catalytic converting wood syngas to hydrocarbons in a 2-inch tubular reactor.

Preparation of syngas from wood chips:
Oak-tree wood chips were used as the raw materials for gasification process. Their moisture content was analyzed with an OHAUS MB200 balance (Certified Scale, Inc., Menomonee Falls, WI). The sample weight was measured at room temperature. The sample was heated to and held at 160 ^oC until it reached a constant value (changes < 0.01 g in 60s). The percent of weight loss was regarded as the moisture content. Wood chips with moisture content of 8.3-10.8% were used in this research for material and energy balance analysis.

The syngas composition was analyzed with an Agilent 6890N GC (Santa Clara, CA), with a TCD detector and argon as the carrier gas. The process temperatures were obtained from the host computer, which acquired the data from installed thermocouples. The volume concentrations of main syngas components were monitored online by a portable gas analyzer (7900P4C, NOVA Analytical Systems, Inc., Niagara Falls, NY).

The pilot-plant scale gasifier, BioMax 25, was purchased from Community Power Corporation (Littleton, CO). It is a downdraft gasifier with a host computer to control the gasification process. This gasification system is highly automatic. Its main components include the feeding system, the gasifier, the heat exchanger, and the filters. There are multiple thermocouples and pressure transducers installed in the system to monitor the running of the gasification system and provide input to the computer. In our experiments, the produced syngas flow rate was set at 65 Nm^3/h. The computer program would adjust the air injection rate and wood chip feeding rate according to the setting syngas flow rate.

An auger feeding system is installed with the gasifier. When the fuel level in the gasifier falls below the setting point, the motor of the feeder will be turned on and feed new fuels. The gasifier is the place where the gasification reactions occur and complete. It is designed with five levels of air injection loops and each loop has six injection points into the gasifier, which ensure the air is distributed into the gasifier evenly at the same level. The amount and rate of air injection are controlled by the computer and vary according the temperatures inside the gasifier. The heat exchanger cools down the producer gas from 500-700^oC to about 110^oC. This system uses room-temperature air to cool the producer gases. The producer gas then goes through parallel bag filters to remove fine particles. After filtration, the producer gases then go through a filter with activated carbon to remove the tars. The outlet syngas contains about 47% N_2, 21% CO, 18% H_2, 12% CO_2, 2% CH_4, some water vapor, and trace amounts of other gases. The cool syngas is then compressed to a storage tank or sent to a burner.

Cleaning and compression of wood syngas:
The syngas from the gasifier was first compressed to approximately 50 psig. After compression, a water scrubber and gas drying apparatus were assembled to scrub the wood syngas from the gasifier. Two 25-gallon 304 stainless steel (SS) wide mouth tanks were connected for the water scrubber. The first tank was outfitted with 13 SS exhaust mufflers with a filtration rating of 50 microns. These mufflers were used to create the maximum amount of syngas bubbles so that the utmost possible surface area of syngas could come in contact with the water, and

contaminates (i.e. ammonia) could be scrubbed by dissolving in the water. After the water scrubber process, the gasifier syngas was flowed through another 25-gallon tank, which contained 80 lbs of silica gel desiccant to remove moisture in the wood syngas. Finally, the gasifier syngas was compressed to approximately 2000 psig using a 2-stage pneumatic air pump obtained from Hydraulics International (Chatsworth, CA).

Deep purification of the compressed wood syngas:
A syngas purification process was designed after indentifying the possible poisoning or negative components for the FTS process, i.e. moisture, CO_2, O_2, sulfur, ammonia, and tar. The catalysts and adsorbents were selected from alumina-supported metal catalysts, 13X molsieve, active carbon, silica gel, and other high surface area materials. These catalysts/adsorbents were loaded into reactors in series. The reactor system was built with controlling parameters of temperature, pressure, and flow rate. The pilot-plant scale cleaning unit is built in the Pace Seed Laboratory of Mississippi State University. The cleaned syngas meets the basic requirements for the following step of catalytic conversion to liquid fuels and chemicals, i.e. total sufurs (H_2S + COS) < 10ppb, NH3< 1ppm, and oxygen< 1 ppm.

Preparation of Fe@C nanostructure catalyst:
Fe@carbon core-shell nano structures were synthesized hydrothermally by the reduction of Fe^{2+} in a pine wood derived sugar solution. Ten grams of $FeCl_2 \cdot 4H_2O$ were dissolved in 250 ml pine wood derived sugar solution (containing ~30 g sugars, the pH value of the reaction solution was 3.0). The mixture was stirred for 30 min and then was transferred into a one-liter Parr reactor. After the autoclave was sealed, it was heated and maintained between 160 to 180°C for eight hours. After the reaction, a black product was obtained. The product was collected and washed three times with DI water and ethanol to remove soluble ions and sugar residues. The final product was oven-dried at 110 °C overnight. The dried sample was calcined under a high purity nitrogen flow for one hour.

Catalytic reaction:
The synthesis gas conversion reaction was carried out in the 2'' continuous flow fixed-bed reactor system. The Fe based catalyst was loaded to the reactor. The system was first purged by a helium flow for 30 min, followed by prereducing with a syngas mixture at 400°C for eight hours. Syngas was then fed in until reaching the desired pressure with slow adjustment of the system to the desired temperature. The reaction was operated under the following conditions: 250- 400 °C, a gas volume hourly space velocity (GHSV) of 500 to 5,000 h^{-1} and a pressure of 500-1500 psig.

Analysis of gas and liquid products using GC and GC/MS:
The analysis of gas phase product has been carried out with an on-line Agilent 6890 gas chromatograph provided with a thermal conductivity detector (TCD) and a flame ionization detector (FID). A 30 m long and 0.53 mm i.d. Carboxen-1010 PLOT column (Supelco) was used. Argon was used as a carrier gas; its flow rate was 4.2 ml/min (30 cm/sec). Liquid products were collected using a condenser kept at 270 K. Liquid samples were analyzed using an Agilent 7683B Series Injector coupled to an Agilent 6890 Series gas chromatograph system and a 5973 Mass Selective Detector (i.e. a quadrupole type GC–MS system) as well as a FID detector. An Agilent DB-WAXetr(50 m x 0.32 mm I.D., 1.0 µm) capillary column was used. A constant column flow of 1 ml/min (24cm/sec) helium was applied. The injector was kept at 250 °C. Samples were injected (1 µl) with split ratio of 100:1. The temperature programmed separation started at 40°C for 5 min, and then ramped by 10°C/min to 250 °C for 10 min. The FID detector worked at 250°C with helium makeup gas at 30 ml/min. For the MS, the transfer line and EI source temperature were 250 and 200 °C,and Quadrupole conditions were electron energy

70 eV and emission current 150 μA. This gasoline was dried using sodium sulfate and subjected to an engine knock test (ASTM D2699; D2700), API gravity, distillation range (ASTM D86), and Reid vapor pressure (ASTM 5191).

Detailed hydrocarbon analysis (DHA) of liquid hydrocarbons:
Detailed hydrocarbon analysis (DHA) was performed over a Perkin Elmer Clarus 680 GC with a FID detector using the PIANO method. PIANO stands for Paraffins (P), Iso-paraffins (I), Aromatics (A), Naphthenes (N), and Olefins (O). About one microliter or less of liquid sample is injected into a 100-meter GC column with about 200:1 split ratio. A flame ionization detector and retention time library is used to identify compounds with a carbon number up to 14. This method is based on ASTM test method D 5134-92 but uses a 100-meter capillary column instead of a 50-meter column. The PIANO method is mainly used for gasoline-type samples, which is why it is limited to compounds with carbon numbers less than 14. Any C15 compounds or heavier are reported as unknown. The initial temperature of the GC injector was set at 200°C and held at this temperature for 43.15 min. The sample injector of the GC was heated to 450°C at 100°C/min and held at this temperature for the rest of entire run. A DHA analytical column (100m × 0.25 μm ID) was used to separate sample components. Hydrogen was used as a carrier gas; its flow rate was 100 ml/min. The initial oven temperature was initialed at 35°C for 5 min, followed by heating to 50 ^{o}C at 10°C/min and held for 21.5 min, and then the oven temperature was ramped to 150°C with a rate of 3°C/min and kept at 150°C for 4.67 min. The FID detector temperature was 250°C with a hydrogen flow of 42 ml/min and an air flow of 450 ml/min.

Characterization of Catalyst Samples:
The physical properties of the catalysts have been determined by N2 adsorption-desorption (Quantachrome, Autosorb-1C). Prior to measurements, the samples were degassed at 300°C overnight.

Temperature Programmed Reduction (TPR):
Prior to temperature programmed reduction experiments, each catalyst sample was activated under flowing O_2 (10 vol. %; balance He) at 400°C for 90 min. TPR experiments were carried with a heating rate of 10°C/min. The reactive gas compositions were H2 (4.0 vol. %/balance Ar). The TPR experiments were performed up to a temperature 1050°C at which the sample was maintained for 5 min. A TCD detector was used to monitor the change of hydrogen level in the carrier gas.

X-ray diffraction (XRD):
The samples of the catalysts were ground into powder and put into a sample cell. X-ray powder diffraction (XRD) patterns of the catalyst samples were obtained in an X-ray diffractometer operated at 40 kV and 40 mA using Cu Kα radiation with a wavelength of 1.5406 Å, from 5° to 80° at a scan rate of 0.02 s^{-1}.

Scanning electron microscopy (SEM):
The morphology of the samples was investigated with an SEM equipped with energy-diffusive X-ray spectroscopy (EDX) (JEOL JSM-6500F). This instrument is also coupled to X-EDS and WDS spectrometers and Oxford Instruments INCA Energy+ software for electron beam-induced X-ray elemental analysis. All samples were pre-coated with gold before being introduced into the vacuum chamber. The system was operated with accelerating voltage of 5 kV.

Transmission electron microscopy (TEM):

The sample particle sizes were examined with a JEOL JEM-100CX II Transmission Electron Microscope operated at accelerating voltage of 100 kV. All samples were sonicated in ethanol solution for 20 min before transferred to copper supporters.

Syngas production from wood chips:
The composition of the producer gas was stable during gasification, which was monitored by a portable gas analyzer (7900P4C, NOVA Analytical Systems, Inc.). Figure K1 showed the gas concentration variations during one run. The portable gas analyzer was not calibrated and was used only for monitoring the fluctuation of main gas concentrations. The gas concentrations measured by Agilent 6890 GC were used for material and energy balance analysis.
The flow rate of producer gas was set at 65 Nm^3/h. The feeding of wood chips was also automatically controlled by the computer according to the fuel level in the gasifier. Table K1 shows the raw syngas properties for a typical run test with oak chip feedstock. The consumption of wood chips was 26-30 kg/h, with a syngas yield of 2.3-2.5 Nm^3/ kg wood. The carbon conversion rate and hydrogen conversion rate were calculated by Equations 1 and 2, respectively. The carbon conversion rate was above 95% (from wood to CO, CO_2, and CH_4) and the hydrogen conversion rate was 67-75% (from wood to H_2 and CH_4). The produced syngas was composed of about 47% N_2, 21% CO, 18% H_2, and 12% CO_2 (See Table K1). The tar and particulate contents in the produced syngas are significantly lower than those of syngas produced by other gasifier system types.

$$\text{Carbon Conversion Rate} = \frac{\Sigma\,\text{Carbon Content}_{gas} * \text{Weight}_{gas}}{\text{Carbon Content}_{\text{wood chip}} * \text{Weight}_{\text{wood chip}}} X\ 100\% \quad (1)$$

gas = CO, CO2 or CH4

$$\text{Hydrogen Conversion Rate} = \frac{\Sigma\,\text{Hydrogen Content}_{gas} * \text{Weight}_{gas}}{\text{Hydrogen Content}_{\text{wood chip}} * \text{Weight}_{\text{wood chip}}}\ X\ 100\% \quad (2)$$

gas = H_2 or CH4

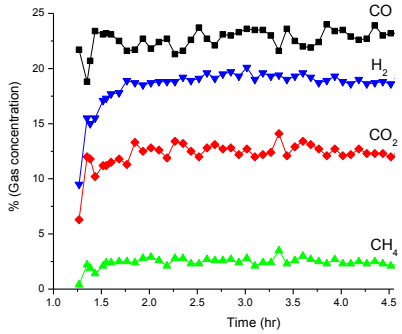


Figure K1. Typical syngas composition monitored by a portable gas analyzer.

Table K1. Raw syngas properties for a typical run test with oak chip feedstock.

Parameters	Unit	Average	Standard deviations
Wood chip consumption rate	kg/h	27.9	3.5
Syngas production rate	kg/h	71.5	3.0

Sygngas yield	kg/kg wood	2.7	2.5
	Nm^3/kg wood	2.4	2.2
Carbon conversion rate (%)	%(wt)	98.5	1.2
Hydrogen conversion rate (%)	% (wt)	75.4	1.5
CO	%(Vol)	21.0	2.1
H_2	%(Vol)	18.1	1.5
CO_2	%(Vol)	11.8	1.6
CH_4	%(Vol)	2.3	1.8
N_2	%(Vol)	47.0	0.8
O_2	%(Vol)	0.8	3.5
Tar	mg/Nm^3	50	15
Particulate	mg/Nm^3	95	26

Syngas cleaning and compression:
The syngas from the gasifier contained about 18 % hydrogen, 21 % CO, 12 % CO_2, 2% CH_4, and 47% N_2. Besides these main components, wood syngas from the gasifier typically contains 500-3,000 ppm of tars, 0.5~2% O_2, 200-1000 ppm of ammonia, and 200-400 ppm of sulfur components (H_2S and COS) (Table K2).

Table K2. Impurities identified from wood syngas before and after cleaning.

Components	**Tar**	**Oxygen**	**NH_3**	**H_2S + COS**
Before Cleaning	1000 ppm	0.8%	500ppm	250 ppm
After Cleaning	<1ppm	<0.1ppm	<1ppm	<1ppb

Impurities must be removed from syngas before CO hydrogenation since tars can cause fouling of FT catalysts; oxygen will deactivate FT and alcohol synthesis catalysts by oxidizing active metals, sulfur components (H2S + COS) can poison metal catalysts by forming metal sulfides, and ammonia can decrease catalyst performance due to it blocking active sites as a result of competitive adsorption. There are a couple of purification strategies to achieve a clean syngas. The first approach to minimize the impurities is to optimize properties of the biomass gasifier and its operating conditions. The second approach is to remove these impurities in a downstream cleaning system based on physical (such as scrubbers, filters) or catalytic strategies. This secondary treatment is also known as hot gas clean-up of biomass gasification gas. In current work, impurities are removed with the second approach, i.e. a downstream cleaning reactor system is built and attached after the gasifier. Both physical and catalytic methods are applied in the process. The cleaning procedure is generally described as follows: The syngas was compressed to approximately 50 psig. After compression, a water scrubber and gas drying apparatus were assembled to scrub the wood syngas from the gasifier. Two 25-gallon 304 stainless steel (SS) wide mouth tanks were connected for the water scrubber. The first tank was outfitted with 13 SS exhaust mufflers with a filtration rating of 50 microns. These mufflers were used to create the maximum amount of syngas bubbles so that the utmost possible surface area of syngas could come in contact with the water, and contaminates (i.e. ammonia) could be scrubbed by dissolving in the water. After the water scrubber process, the gasifier syngas was flowed through another 25-gallon tank which contained 80 lbs of silica gel desiccant to remove moisture in the wood syngas. After two tanks, a chemical/catalytic syngas purification system was attached to remove the possible poisoning or negative components for the FTS process, i.e. oxygen, sulfur, and rest of ammonia. The catalysts and adsorbents were selected from alumina-supported metal catalysts, 13 X molecular sieves, active carbon, silica gel and other high surface area materials. Finally, the gasifier syngas was compressed to approximately 2000 psig using a 2-stage pneumatic air pump. After passed through this syngas

cleaning unit, impurities level in the wood syngas were reduced as: tars < 1ppm, oxygen <0.1 ppm, ammonia < 1ppm, and total sulfur components (H_2S and COS) < 1ppb (as shown in Table K2). The cleaned syngas meets the industrial requirements for the following step of catalytic conversion to liquid fuels, i.e. total sufurs (H_2S + COS) < 10ppb, NH_3< 1ppm, and oxygen< 1 ppm.

Fe@C formation by hydrothermal treatment of pine wood derived sugar solution:
Lignocellulosic composition, including glucose, xylose, arabinose, galactose, mannose, and lignin, was determined by the NREL method. Sugars like glucose, xylose, arabinose, galactose, and mannose are formed after the pine wood hydrolysis from 1% H_2SO_4 acid pretreatments. The composition of the hydrolysis solution includes 33.3% glucose, 4.75% xylose, 1.42% arabinose, 2.90% galactose, and 15.4% mannose. There is also 41.6% lignin and 0.6% ash. All the above sugars are important sources for preparation nano-carbon materials through the HTC process. The hydrothermal carbonization of sugars was carried out in a one-liter Parr reactor. The autoclave was heated to 180°C and maintained for eight hours. A black product was obtained from the liquid phase. The product was collected and washed with DI water and ethanol to remove soluble ions and sugar residues until the filtered solution was clear. The final product was oven-dried at 110°C overnight. The results from previous work showed the highest nano-carbon yield for xylose, i.e. 80.2 g of nano-carbon spheres were obtained per 100 g of xylose, while the lowest nano-carbon yield was observed for cellulose at 28 g per 100 g cellulose. The different nano-carbon yield is possible due to different carbonization tendencies of these sugars. Xylose begins to decompose and carbonize at ~ 140°C while the decomposition temperature of glucose, arabinose, galactose, and mannose is between 160 to 180 °C.

Gas phase composition in the Parr reactor of iron ion and sugar solution after the HTC process at 180°C was analyzed by an Agilent 7890 GC. CO, CO_2, H_2, CH_4, C_2H_6, and C_3H_8 were found in the gas phase product, and the relative amount of these products are 37.0% H_2, 10.6% CO, 45.3% CO_2, 0.05% C_2H_6, 0.001% CH_4, 0.01% C_3H_8, and 3.8% N_2 in the gas phase after the liquid mixture reacted at 180°C for eight hours. Trace of ethylene (less than 0.001%) was identified by the on-line GC. Trace of benzene was previously detected using an on-line residue gas analyzer (RGA) from gas phase of glucose, xylose, sucrose, and cellulose after HTC. The detection of benzene in the gas phase meant that aromatic species were important intermediates in the HTC process.

Characterization of Fe@C nano-spheres from pine wood derived sugar solution:
Figure K2 shows the XRD patterns of the fresh Fe@C core-shell structures synthesized hydrothermally by the reduction of Fe^{2+} in a pine wood derived sugar solution, the Fe@C calcined under a nitrogen flow at 700 °C, and the calcined Fe@C after being used in the catalytic conversion process. Slight diffraction peaks were observed for the fresh sample (Figure K2a), which indicates both the core and the shell are in amorphous structure.

For the pattern of the sample calcined under a N_2 flow at 700°C (Figure K2b), one peak at 44.68° corresponded to the α-iron (110) planes respectively (PDF#97-005-3802). The peaks 37.75°, 40.7°, 42.6°, 43.75°, 44.56°, 44.94°, 45.86°, 49.12°, and 57.8° are assigned to cementite (Fe_3C) with correspondence planes of (121), (210), (201), (211), (102), (220), (031), (112), and (221), respectively (PDF#00-035-0772). The pattern of the Fe@C after being used in catalytic conversion process is similar to the calcined one (Figure K1c). There is no peak at 26.55°, which corresponds to carbon (002) plane observed for all samples. This means that the carbonaceous shell was not graphited after either the calcination at 700°C or after FTS process,

and it still exists as an amorphous state. The existence of α-iron and Fe_3C confirms both metal iron and iron carbide are the active phase of the catalyst during bio-syngas catalytic conversion.

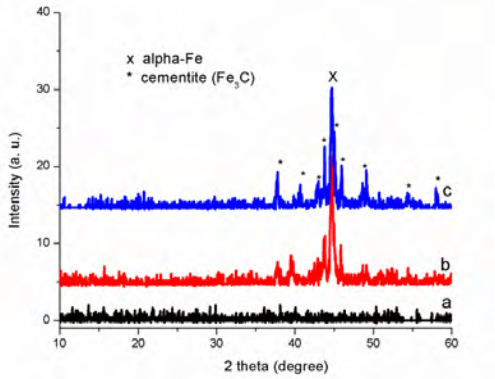


Figure K2. XRD patterns of samples. a: fresh Fe@C catalyst; b: Fe@C calcined under a nitrogen flow at 700°C; c: Fe@C after catalytic reaction.

SEM images of the Fe@C core-shell spheres are shown in Figure K3. The core-shell structure is spherical in shape. Spherical particles with a uniform particle size were observed for the product. The morphology of the single micro-sphere exhibits a porous structure surface. The diameters of the fresh core-shell structure were between 100 to 200 nm. The SEM image of the calcined carbon nano-spheres at 700°C shows the particle size is almost uniform at 50 to 100 nm. These calcined nano carbon spheres showed more uniform distribution compared to fresh ones.

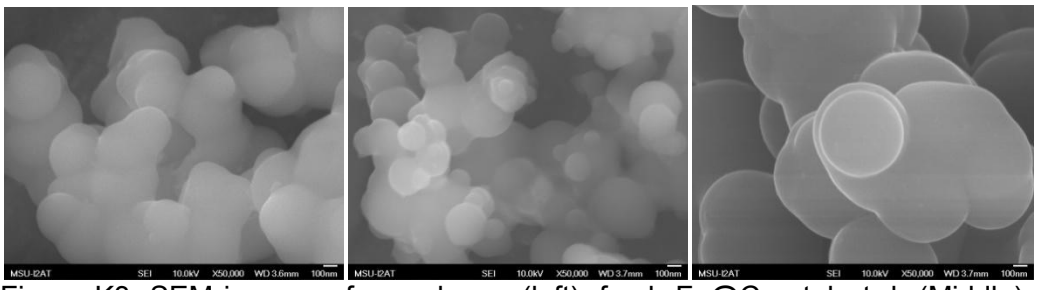


Figure K3. SEM images of samples. a (left): fresh Fe@C catalyst; b (Middle): Fe@C calcined under a nitrogen flow at 700°C; c (right): Fe@C after catalytic reaction.

The TEM images of Fe@C nano particles are shown in Figure K4. The TEM image of the fresh core-shell catalyst shows that the diameter of core-shell was about 100 to 200 nm. The diameter of the iron core structure is between 15 and 25 nm. The TEM image of the calcined carbon nano-spheres at 700°C shows the particle size is at 50 nm. The diameter of the iron core structure of the calcined one is between 10 and 20 nm. Fe@C nano particles were shrunk due to decomposition of the functional groups of the carbonaceous shell and the reduction of iron oxide during calcination process.

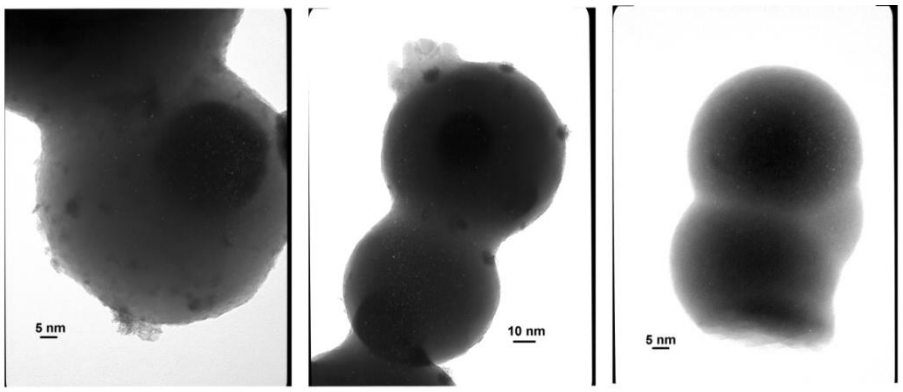
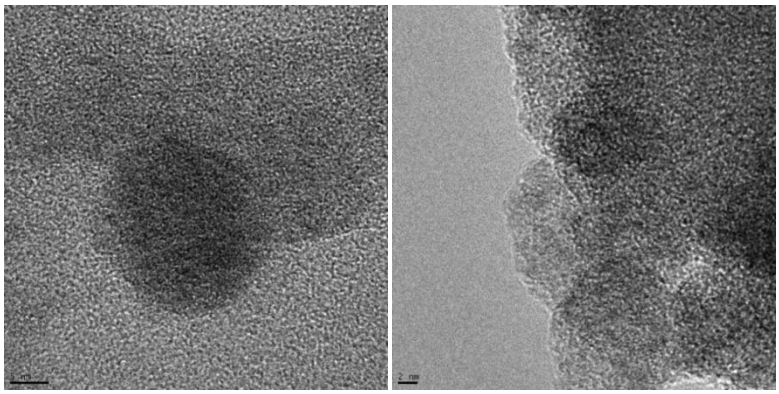


Figure K4. TEM images of samples. a (left): fresh Fe@C catalyst; b (middle): Fe@C calcined under a nitrogen flow at 700°C; c (right): Fe@C after catalytic reaction.

HRTEM images of carbon nano-spheres from pine wood derived sugars by HTC at 180°C are shown in Figure K5. HRTEM images of carbon nano-spheres show that the diameter of core nano-spheres is approximately 10 to 20 nm. The carbon shell exhibited a porous structure and an amorphous structure since no ordered planes of the natural graphite structure were observed.


Figure K5. HRTEM images (magnification 500,000X) of calcined Fe@C catalyst.

The Raman spectra can identify the presence of the graphite and disordered amorphous carbon in the samples. The Raman spectrum obtained for the fresh Fe@C core-shell nanostructures is presented in Figure K6a. Only a peak at 1610 cm^{-1} was clearly seen in the Raman spectra of the fresh Fe@C nanostructure, while a higher background of the fresh Fe@C core-shell nanostructures was also observed, which should be attributed to the high photoluminescence properties of the core nano iron particles. The Raman spectrum of the calcined sample was also obtained (Figure K6b). The sample was thermally treated at 700°C with a heating rate of 2°C/min in a N_2 atmosphere and kept for 1 hour. Two peaks around 1587 and 1366 cm^{-1} are attributed to the stretching modes of C−C bonds of the G band (in-plane vibrations of graphitic carbon) and D band (disorder-induced band due to double-resonance effect) in the carbonaceous solid, respectively. Raman spectra reveal the presence of C sp2 atoms in benzene or condensed benzene rings of amorphous (partially hydrogenated) carbon. Small aromatic clusters must therefore be present in the Fe@C samples. The difference of the spectra means thermal treatment promoting carbonization of the carbonaceous shell of the Fe@C nanostructures.

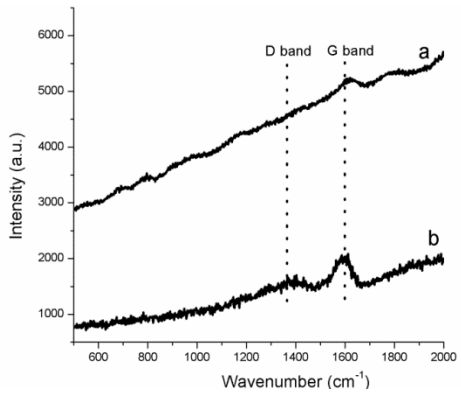


Figure K6. Raman spectra of Fe@C catalysts. a: fresh Fe@C catalyst; b: Fe@C calcined under a nitrogen flow at 700°C.

FT-IR has been one of the most frequently used analysis methods to characterize qualitatively the surface functionalities in carbon-based materials. As in organic chemistry, the assignment of the IR absorption bands and peaks to the different carbon surface functional groups is made by comparison with the absorption bands of specific organic compounds [46]. The FTIR spectrum obtained for the fresh Fe@C core-shell nanostructures is presented in Figure K7a. Several bands reveal that aromatization processes take place during hydrothermal carbonization (HTC). The characteristic vibration peaks of benzene framework positioned at 1605 and 1510 cm^{-1} indicate the existence of benzene ring structure in the carbonaceous shell, which confirms the idea of aromatization of sugar during hydrothermal treatment. The presence of aromatic rings is also evidenced by the band at 1620 cm^{-1}, attributing to C-C vibrations [49], and to the bands in the 875-750 cm^{-1} region due to aromatic C-H out-of-plane bending vibrations. The vibration band at 1710 cm^{-1} was attributed to C=O vibrations of carboxylic acids and carboxylic anhydrides and lactones, and the band at 3000-4000 cm^{-1} was assigned to the –OH stretching vibrations, implying the existence of hydroxyl groups. The carbonaceous shell also possesses aliphatic structures, as can be deduced from the band at 2980 cm^{-1}, which corresponds to stretching vibrations of aliphatic C-H.

The IR technique has been used widely to study changes in the carbon surface upon heating. In the approach, a decrease in the intensity of the characteristic IR bands reflects changes in the surface chemistry upon decomposition of the surface functional groups during thermal heating of the carbon-based materials. The IR spectrum of the calcined sample was illustrated in Figure K7b. The infrared bands associated to oxygen containing surface groups disappear or decrease in the intensity of the bands after calcined at 700°C for one hour. For instance, the decrease (compared to the fresh one) in the intensity of the bands at 1000-1450 cm^{-1} and at 3000-3700 cm^{-1} suggests that dehydration occurred during the thermal treatment of the Fe@C nanostructures and carbonization of the carbonaceous shell continued. The decrease of the intensity in the band at 1710 cm^{-1} has been associated with the decomposition of carboxylic anhydrides and lactones which contain C=O groups. When it is heated, the weakened band of 1710 cm^{-1} indicates that most of these functional groups were removed. At the peak at the 875-750 cm^{-1} region, the aromatic C-H out-of-plane bending vibrations showed similar behavior compared to the peak at 1710 cm^{-1}, which can be explained in terms of internal structural reorganizations of aromatic structures and the acceleration of carbonization of the shell during thermal treatment at higher temperature. Due to the vibration of benzene framework, the peak at 1605 cm^{-1} showed opposite behavior compared to the peak at 1710 cm^{-1}, which indicates reorganizations of aromatic structures during carbonization. The band of 2980 cm^{-1}, which corresponded to the vibrations of C–H groups of saturated alkyl hydrocarbon, was kept

unchanged after calcinations. This results because the C–H group is so strong that it won't be broken until 800°C.

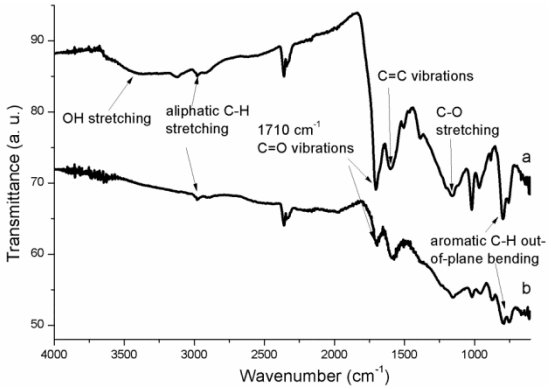


Figure K7. FT-IR spectra of Fe@C catalyst. a: fresh Fe@C catalyst; b: Fe@C calcined under a nitrogen flow at 700°C.

TPD experiments followed by an on-line GC were conducted to detect the gases produced during the calcinations of Fe@C core-shell structures. The surface functionalities chemically bound to the carbonaceous shell decompose upon heating by releasing gaseous compounds at different temperatures. The interpretation of the thermal desorption profiles provides useful information on the types of species desorbed from the shell surface and on the nature of interactions of the gaseous species and carbon. The amounts of these different surface groups can be estimated from the TPD spectra. Figure K8 shows a typical profile recording the evolution of six species in gas phase: H_2, CH_4, CO, C_2H_6, C_3H_8, and CO_2. Oxygen-containing functional groups decompose mostly as CO and CO_2. Surface complexes yielding CO_2 groups decompose at two different temperatures corresponding to two types of functional groups. Carboxylic acids (— COOH $\rightarrow$ CO_2) are responsible for the low-temperature peak (100-400°C), and the high-temperature CO_2 evolution is attributed to carboxylic anhydrides and lactones (450-700°C). The CO-yielding groups are represented by three distinct groups of peaks and the corresponding peak temperatures of CO desorption centered at 400°C for the anhydride and lactone groups. The CO peak centered at 500°C is assigned to the ether decomposition, and the CO peak above 550°C is contributed to the phenols and quinine. The methane peak at 500°C originates from decomposition of the methyl group attached to aromatic units. Hydrogen is on a carbon surface as chemisorbed water or as surface functionalities (e.g. carboxylic acids and phenolic groups), or is bonded directly to carbon atoms as a part of aromatic or aliphatic structures. The C-H bond is very stable and breaks until about 800°C without any catalyst. However, the desorption of hydrogen does happen at temperatures below 400°C when transitional metals like iron, nickel, and cobalt exist since these metals are excellent catalysts to break down C-H bonds. Heat treatment in an inert atmosphere eliminates part of the hydrogen via surface reduction. The carbonaceous shell contains a lot of oxygen-containing aromatic heterocyclic structures, which decompose with the formation of carbon monoxide, methane, and other low hydrocarbons.

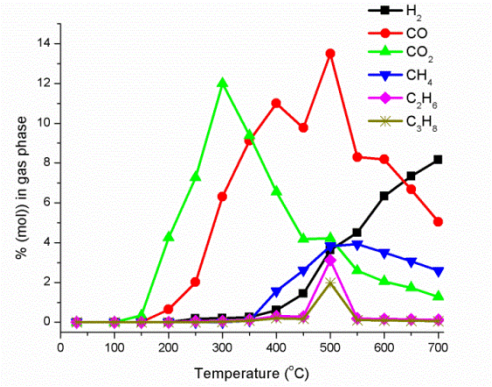


Figure K8. TPD curves for the temperature-programmed calcination of Fe@C catalyst from pine wood derived sugars, 5°C/min to 700°C purging gas: 20 ml/min nitrogen.

Thermoanalytic techniques have been widely used to study the thermal behavior of biomass. The thermal decomposition of Fe@carbon core-shell spheres was analyzed using TGA in N_2. The TG and DTG curves for Fe@carbon core-shell spheres between room temperature and 700°C in N_2 atmosphere are shown in Figure K9. The TGA mass loss of Fe@carbon core-shell spheres at 10°C/min in nitrogen was normalized over the initial mass and the DTG/mass-loss rate against temperature. A continuous weight loss with increasing temperature is observed, which denotes breaking of chemical linkages and removal of volatile products from Fe@carbon core-shell spheres. There are three possible steps of weight loss that can be observed from Figure K8. The initial weight loss corresponds to the loss of physically adsorbed water and occurs between ambient temperature and 130°C with a peak temperature of 70°C. It is followed by a plateau region for the rate of weight loss from 130 to 200°C. The strong weight loss observed at around 200 to 700°C corresponds to the decomposition of all the functional groups in the carbonaceous shell. These results indicate that oxygen functional groups start releasing in this temperature zone, leading to the initialization aromatization of the char matrix. The most weight loss of the char is in the temperature zone from 350 to 700°C. This mass loss step mainly corresponds to the decomposition of the rest of the carboxylic anhydrides and lactones, part of phenols, quinine, and ether. They release as volatile product such as CO_2, CO, CH_4, H_2O, and H_2.

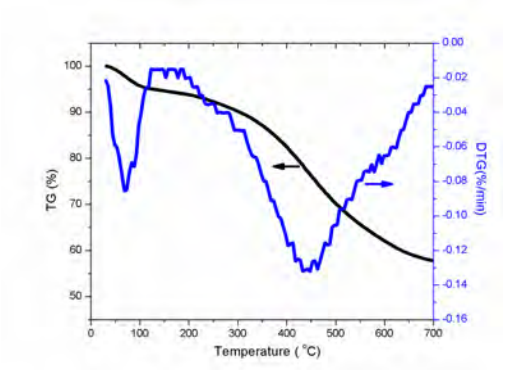


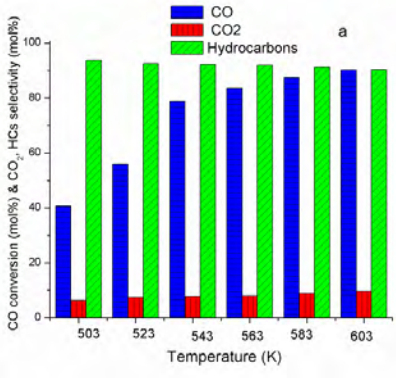
Figure K9. TG and DTG curves of Fe@C catalyst from pine wood derived sugars heated at a rate of 10°C/min in N_2 atmosphere.

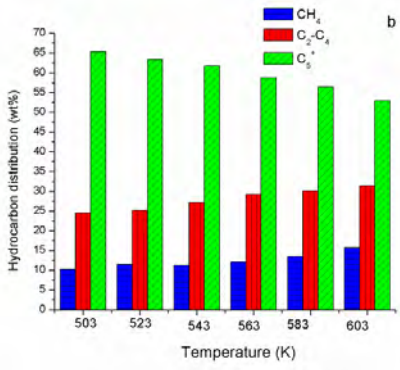
Fe@C core-shell spheres as a catalyst for Fischer−Tropsch synthesis:
Iron-based catalysts are the most important catalysts for FTS. The particle size of the iron-based catalysts has been reported to significantly influence FTS activity and selectivity. Fe@C

nanoparticles synthesized by the hydrothermal process were used as a FTS catalyst. The CO conversion and hydrocarbon distribution were measured in a fixed bed flow reactor, operating at 230 to 330°C, 2000 to 8000 h^{-1} gas hourly space velocity (GHSV), and 500 to 1000 psig pressure.

Effect of temperature:
The temperatures were performed at 230, 250, 270, 290, 310 and 330°C, with the other conditions kept constant. The operating pressure was controlled at 1000 psig while the gas hourly space velocity was maintained at 4000 h^{-1}. The feed gas was biosyngas from gasifier. Figure K10 shows the CO conversion, carbon dioxide, and hydrocarbon selectivity, gas phase hydrocarbon distribution (wt%), liquid hydrocarbon and olefin distribution with temperature. CO conversion increased from 53.7% at 230°C to 89.8% at 330°C. The hydrocarbon distribution also changed with temperature.The light hydrocarbons were favored at higher temperatures, and light hydrocarbons (C_1-C_4) increased from 34.7% at 230°C to 47.1% at 330°C. Previous work has also shown that the increase of process temperature resulted in the increase of CO conversion, a shift towards products with a lower carbon number on iron catalysts. Higher hydrocarbons are more sensitive to temperature change, undergoing cracking and de-alkylation reactions that become increasingly important with increasing temperature. FigureK10c shows the liquid fuel distribution in six groups, i.e. paraffins, iso-paraffins, aromatics, naphthenes (cycloalkanes), olefins, and oxygenates. Results indicate that as the temperature increased from 230 to 330°C, paraffins decreased from 17.80% to 3.90%. Iso-paraffins first increased from 7.3% at 230°C to 11.8% at 290°C, then decreased to 10% at 330°C. Olefins increased from 36.3% at 230°C to 49.8% at 290°C, then decreased to 46.3% at 330°C. Aromatics increased from 5.2% to 8.3%.

Olefins in the liquid fuels were analyzed; C_7, C_6, and C_5 are the main components. Figure K10d shows the liquid olefin distribution between C_4 and C_{13}. The effect of temperature on olefin distribution is complex. There is no significant trend of the olefin changes with the temperature.





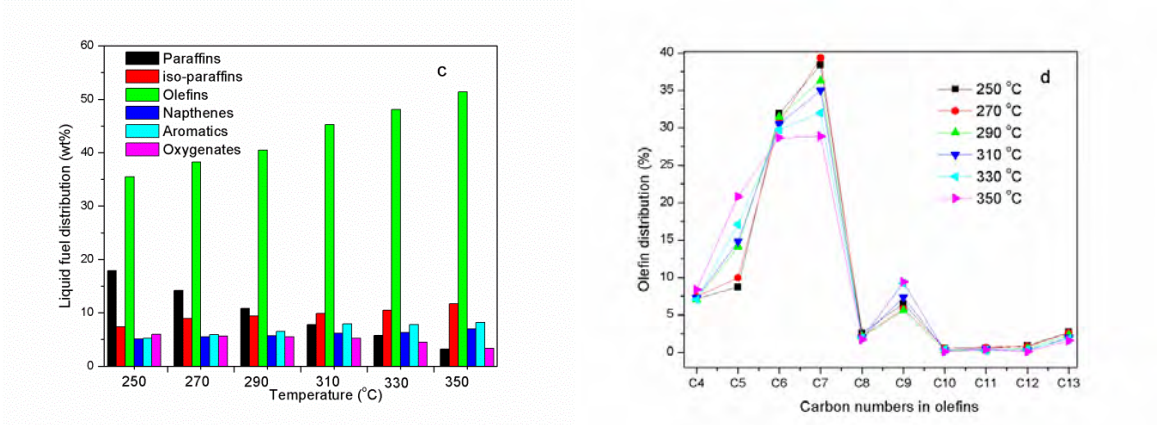
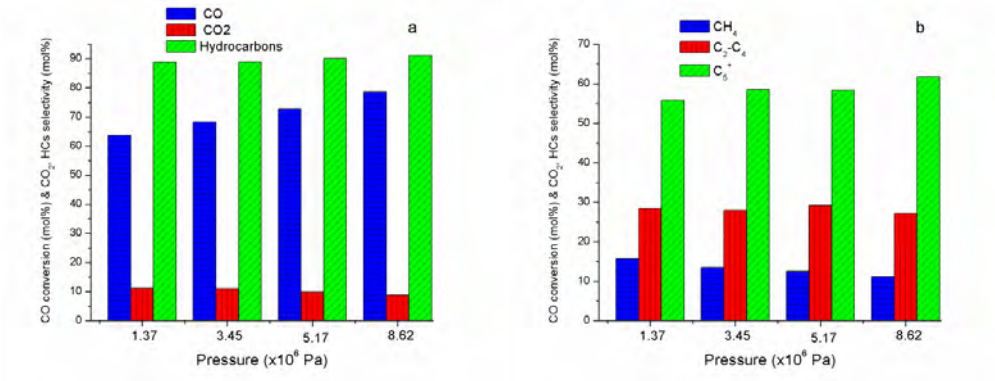


Figure K10. Effect of temperature on a: CO conversion, b: hydrocarbon selectivity, c: hydrocarbon distribution, and d: liquid hydrocarbon distribution.

Influence of pressure on the catalyst performance:
An increase in total pressure will shift the equilibrium toward the product side of the reaction and increase the CO conversion. Experiments under pressures of 500, 750, 1000, and 1250 psig were conducted. Temperature was held constant at 270°C, and the bio-syngas was employed as the feed gas. The space velocity was maintained at 4000 h^{-1}. The effect of pressure on both CO conversion and process selectivity showed that when pressure increased, CO conversion increased. Within the C_5^+ fraction, an effect of pressure on selectivity was observed. The increase in pressure slightly favored the formation of C5+.

Figure K11 shows CO conversion increased from 83.7% to 91.2% as the pressure increased from 500 psig to 1250 psig. The increase in pressure clearly favored the formation of C_5^+, while C_1~C_3 gaseous hydrocarbons remarkably decreased with the increasing of the pressure. Figure K11c shows the liquid fuel distribution by six groups. The results show that with the increasing of the reaction pressure, paraffins, iso-paraffins, aromatics, naphthenes, and olefins almost kept unchanged, except oxygenates increased from 2.9% to 6.6%. Some previous FTS studies also showed that the product selectivity shifts to heavier products and to more oxygenate compounds with increasing total pressure. Olefin distribution showed the olefin selectivity shifted to heavier products with increasing pressure (Figure K11d), C_4 and C_5 decreased with increasing of pressure, C_7^+ olefins increased with increasing pressure, and C_6 olefin kept unchanged.



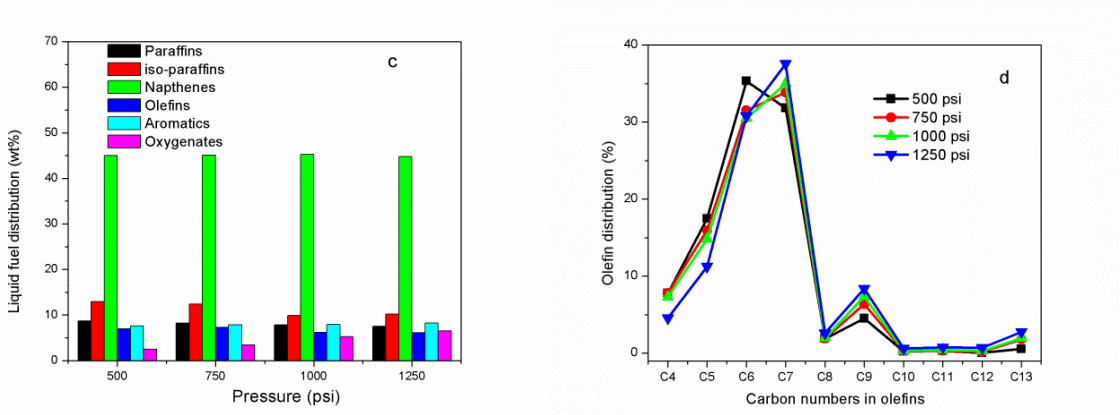


Figure K11: Effect of pressure on (a) CO conversion, (b) hydrocarbon selectivity, (c) hydrocarbon distribution, and (d) liquid hydrocarbon distribution.

Impact of space velocity on the catalyst performance:
Experiments were completed with different GHSV of 2000, 4000, and 8000 h^{-1} while the other operating conditions held constant at 270°C, 1000 psig, and clean bio-syngas. The effect of the space velocity on CO conversion and hydrocarbon distribution showed that when the space velocity increased, CO conversion decreased as expected. Figure K12 shows CO conversion decreased from 89.5% to 72.2% as the GHSV increased from 2000 to 8000 h^{-1}. At the same time, C_5^+ hydrocarbon production decreased. The effect of space time on product distribution was significant. It was observed that the yields of hydrocarbons decreased with increasing space velocity. The gasoline fraction (C_5^+) continuously decreased with increasing space velocity.

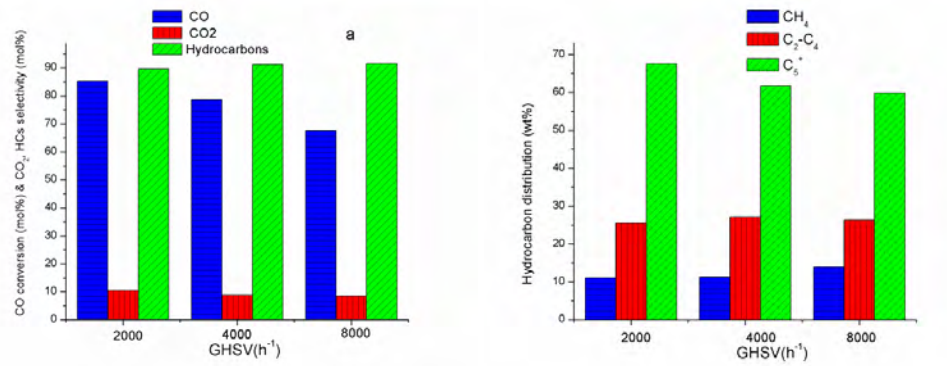


Figure K12. Effect of gas hourly space velocity (GHSV) on CO conversion, hydrocarbon selectivity, hydrocarbon distribution, and liquid hydrocarbon distribution.

Time-on-stream performance:
The time-on-stream effect on the performance of the Fe@C catalyst was studied at 310°C over a period of 160 hours. The evolution of CO conversion, light hydrocarbon, and liquid product selectivity with time-on-stream are shown in Figure K13. CO conversion was 87.8% at the beginning of the reaction, and then decreased gradually to 82.5% at 100 hours on stream. After 100 hours on stream, no further change was observed over prolonged reaction times.

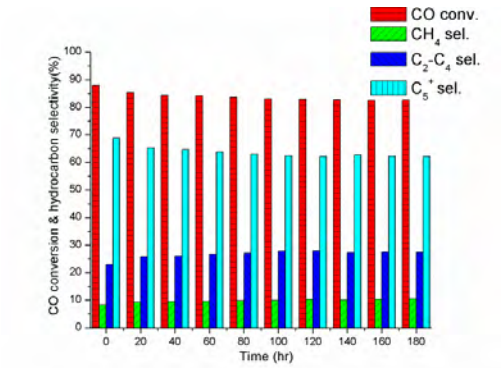


Figure K13. Time-on-stream of CO conversion, light hydrocarbon, and liquid product selectivity on the thermal treated iron-char catalyst at 310°C, 8.62 x 10^6 Pa, 3000 h^{-1} with cleaned biosyngas.

Properties and detailed liquid hydrocarbon distributions:
After reaction, liquid hydrocarbon samples were collected from the condenser during the biomass gasification run. The typical GC-MS spectrum is given in Figure K14, which shows the distribution of liquid hydrocarbons. The liquid products from bio-syngas were performed by a gas chromatography analysis. Liquid oil products were quantitatively reported in the volatile range up to molecules with 13 carbons of five families of hydrocarbon groups, i.e. paraffins, isoparaffins, aromatics, naphthenes (cycloalkanes), and olefins (PIANO). Table K3 shows typical liquid product fuels obtained using the carbon-encapsulated iron nanoparticles.

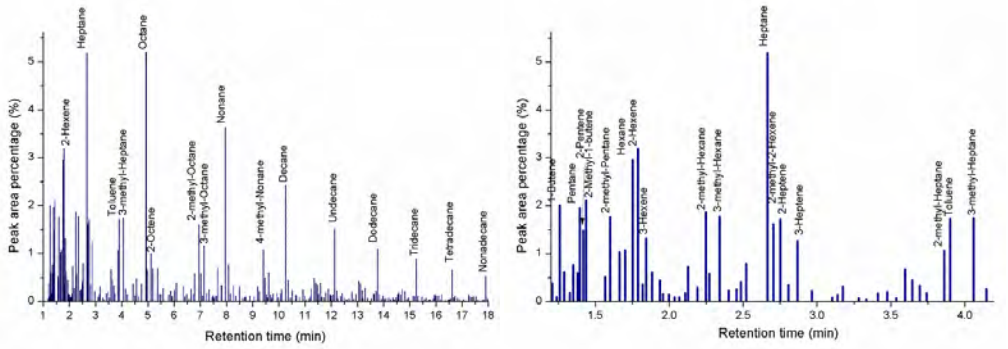


Figure K14. GC-MS of liquid hydrocarbon.

In general it was observed that the main reaction products were olefins (total about 49.11 mol%) with predominance of C_5 (11.79%), C_6 (16.51%), C_7 (17.62%), and C_9 (1.97%) components. The second most prosperous group was iso-paraffins, which totally contribute 11.82 mol% with main components of C_5 (0.7%), C_7 (1.3%), C_8 (1.42%), C_9 (4.65%), C_{10} (2.4%), and C_{11} (1.15%). Aromatics contributed 7.83 mol% overall from C_8~C_{12} components. Napthenes, and paraffins comprised 5.4 mol% and 5.1 mol% liquid product, respectively. There were also 10.74% unidentified components in the liquid product due to the limitation of the data base. If the liquid hydrocarbons were reported according to carbon numbers, C_7s contributed the most, 21.22% overall, followed by C_6s (18.93%), C_5s (16.24%), C_8s (11.04%), C_9s (10.79%), C_{10}s (9.19%), C_{11}s (4.74%), C_{12}s (3.37%), and C_{13}s (2.27%). Besides hydrocarbons, there were also 3 to 6% oxygenates found in the liquid oil phase. They were iso-propanol, ethanol, t-butanol, and methanol.

Table K3. Typical product distribution of the C_5+ liquid fraction for the Fe@C nanoparticle catalyst by group type & carbon number (in Mol Percent).

	Paraffins	**I-Paraffins**	**Olefins**	***Naphthenes***	**Aromatics**	**Unknowns**	**Total**
C5	3.63	0.7	11.79	0.12	0	0	16.24
C6	0.67	0.12	16.51	0	0	1.63	18.93
C7	0.56	1.3	17.62	0.55	0	1.19	21.22
C8	0.05	1.42	0.58	1.96	0.4	6.68	11.04
C9	0.06	4.62	1.97	1.81	0.41	1.98	10.79
C10	0.22	2.4	0	0.73	4.62	1.22	9.19
C11	0.016	1.15	0.043	0.2	1.55	1.78	4.74
C12	0.0022	0.11	0	0.013	0.85	1.39	2.37
C13	0.001	0.0013	0.6	0	0	1.87	2.47
Total	5.10	11.82	49.11	5.38	7.83	17.74	96.99

Possible mechanism of sugar carbonization and formation of Fe@C nanostructures under HTC process:

The carbonization of sugar and the formation of Fe@C nanostructures are very complex. When an aqueous sugar solution is hydrothermally treated at temperatures of 180°C, the sugar molecules hydrolyze with the catalytic promotion of iron ions which leads to small carbonaceous colloids with a low degree of polymerization. Meanwhile, iron ion is also hydrolyzed to FeOOH under the hydrothermal conditions. Then, both polymerization and condensation processes lead to the formation of soluble polymers. Polymerization and condensation reactions may be induced by intermolecular dehydration, dehydrogenation, or aldol condensation, and reduction gases CO and hydrogen will be released in this process. FeOOH will continue to be condensed and further reduced to Fe_xO_y by CO and H_2 released from the sugar carbonization process. The Fe_xO_y nanoparticles then combine with small carbonaceous colloids through Coulombic interactions with the surface functional groups (i.e. OH and C═O) and condense to form Fe_xO_y-in-C nanorods. These Fe_xO_y-in-C nanorods will be further self-assembled to Fe_xO_y@C core/shell nanospheres via further intermolecular dehydration of the surface functional groups. Figure K15 is the TEM image of the one-hour HTC sample. It displays a lot of needle-like nanorods in the early stage sample of the HTC process and confirms the formation of Fe_xO_y nanoparticles and the combination of the Fe_xO_y nanoparticles with carbonaceous colloids from sugar carbonization. The Fe_xO_y nanoparticle will further catalytically promote the condensation and aromatization of carbonaceous colloids around it. Aromatic clusters may be produced by the condensation of the aromatized molecules generated in the decomposition/dehydration of the oligosaccharides or monosaccharaides. Raman and FTIR results reveal that aromatization processes take place during hydrothermal carbonization (HTC) (Figures K6a and K7a). The characteristic vibration peaks of benzene framework indicate the existence of benzene ring structure in the carbonaceous shell, which confirms the idea of aromatization of sugar during hydrothermal treatment (Figure K7a). The presence of aromatic rings is also evidenced by the bands of the C-C vibrations and the aromatic C-H out-of-plane bending vibrations. Previous work also has proven the presence of benzene in the gas phase after the HTC reaction using a residue gas analyzer (RGA). When the concentration of aromatic clusters reaches the critical super saturation point, the formation of carbon nucleation takes place. The formed nuclei of carbon grow by diffusion of the chemical species present in the solution toward the surface of the Fe_xO_y nanoparticle. These species are linked to the surface of the microspheres via the reactive surface functional groups (hydroxyl, carbonyl, carboxylic, etc.) present in the particles.

The FTIR results show C=O vibrations of carboxylic acids, carboxylic anhydrides and lactones, and the –OH stretching vibrations, implying the existence of hydroxyl groups (Figure K7a). TPD spectra of the Fe@C nanoparticles by the HTC process in this research further demonstrated the surface functional groups (hydroxyl, carbonyl, carboxylic, etc.) in these nano-carbon spheres (Figure K8). Stable surface functional groups such as ether or quinone are also formed.

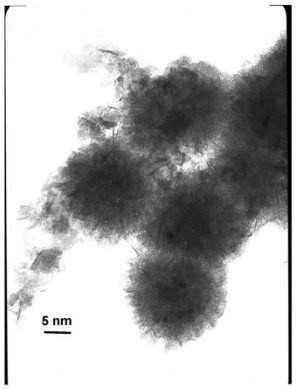


Figure K15. TEM image of the one-hour HTC sample

Based on the above discussion and the characterizations results of catalysts, a possible mechanism of the formation process of the Fe@C spheres is proposed. The mechanism is comprised of three steps. In the first step, sugar molecules are first hydrolyzed with the catalytic promotion of iron ions when the aqueous sugar solution is hydrothermally treated at 180 °C. In the second step, reactions consisting of polymerization and condensation processes lead to the formation of soluble polymers. The Fe_xO_y nanoparticles combine with small carbonaceous colloids by the surface functional groups and condense to form Fe_xO_y-in-C nanorods. Finally, these Fe_xO_y-in-C nanorods will be further self-assembled to Fe_xO_y@C core/shell nano-spheres via further intermolecular dehydration of the surface functional groups. Stable surface functional groups such as ether or quinone are also formed. Once the growth process stops, nano-carbon shells over nano Fe_xO_y particles are completed.

Performance of carbon-encapsulated iron nanoparticle catalysts:
DHA analysis of liquid hydrocarbons showed C_7 hydrocarbons contributed 21.22% of the product, 18.93% of C_6s, 16.24% of C_5s, 11.04% of C_8s, 10.79% of C_9s, 9.19% of C_{10}s, 4.74% of C_{11}s, 3.37% of C_{12}s, and 2.27% of C_{13}s. The ASF plot (Figure K16) was plotted for the C_5^+ liquid fraction data to examine the product distribution over Fe@C nanoparticles. The ASF plot showed a nearly straight-line in the C_5–C_{13} region. The slope ln(α) of the linear fitting result was -0.389. The chain growth probability *α* was calculated as 0.68. The chain growth probability *α* over Fe@C nanoparticles was 0.68. This indicates that the step-wise mechanism is predominant, and Fe@C nanoparticles showed high selectivity to liquid hydrocarbon products.

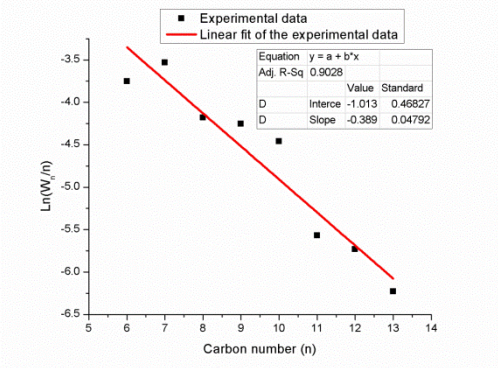


Figure K16. ASF plot of the liquid hydrocarbon distribution during FT synthesis catalyzed by Fe@C nanoparticles.

The prepared Fe@C spheres were thermally treated in nitrogen at 700°C for one hour before being used for catalytic conversion of bio-syngas to liquid fuels. Raman and FTIR results showed the further carbonization of the carbonaceous spheres occurred at higher temperatures; TEM images illustrated Fe@C nano particles were shrunk due to decomposition of the functional groups of the carbonaceous shell and the reduction of iron oxide during calcination process. The diffraction peaks of α-iron and Fe_3C confirmed both the metal iron and iron carbide are the active phase of the catalyst during bio-syngas catalytic conversion (Figure K2). The particle size of the iron species inside the carbonaceous spheres was 15 to 25 nm (Figures K4 and K5) as a result of the transformation of Fe_xO_y to iron carbides (θ-Fe_3C and α-Fe). Moreover, because of the further gasification of the carbonaceous matter during the activation process ensuring better accessibility of the embedded iron species to the reactants, Figures K11-K13 presented the FTS results over the reduced Fe@C spheres. The CO conversion was about 90%, C_5^+ hydrocarbon selectivity can be up to 65% at 330°C, and olefins contributed ~50% of the liquid fuels. The time-on-stream effect on the performance of Fe@C catalyst showed that CO conversion was kept constant at 82.5% after 180 hours running. The carbon-encapsulated iron nanocomposite core-shell catalysts showed highly stable activity for catalytic conversion of bio-syngas, which is in strong contrast with the general carbon-supported nanoparticle catalyst. Often in carbon-supported metal catalyst system, discrete metal nanocrystals are dispersed on support carbon particles that are one to several orders of magnitude larger than the supported metal nanoparticles. The most important function of a support is to provide proper texture/pore structure and high surface area to disperse and maintain the active metal catalyst. Structure-sensitive or insensitive concepts are developed to describe the observations that catalysis of metal catalyst is dependent or independent of the size of the metallic nanocrystals. These discrete metal active sites cannot keep stable and will be aggregated and then lose the catalytic activity under the severe reaction condition of FTS. Carbon-encapsulated iron nanocomposite core-shell catalysts become so stable because a much higher percentage of metal/carbon boundaries or perimeters exist in the core-shell nanocomposite system. The present data raise the general issue that a lower limit in the nanometer range may exist for metal Fe core and carbon shell in the nanocomposite catalysts. When the nanoparticle metal iron active site was fully packed by carbon shell, Fe nanopartilces were protected and would not sinter even if under the condition of bio-syngas FTS reaction. More importantly, the catalyst samples had been pretreated up to 700°C. This carbonaceous shell calcination at high temperature is very stable during bio-syngas FTS reaction. Moreover, the metal Fe core also provided the strong support for the nanobelt carbon shell to prevent the collapse of the shell. Thus, the iron/carbon catalyst synergically forms core-shell nanocomposites that could show distinctive catalytic performances. In particular, the C_{5+} fraction amounted up to 60% in the products, which is better

than the values reported to date for iron catalysts without promotion, including the Fe-*in*-CNT, Fe-*out*-CNT, and Fe/activated carbon catalysts. The high liquid product selectivity is probably contributed to the formation of nano ferrite (α-Fe), cementite (Fe_3C) in the nanocomposites after high temperature pretreatment.

Subtask K.2 Process design and economic analysis

The data from the larger scale testing of second and third generation catalysts will be used to develop a process design for a commercial process and then estimate the economics for a "brown-field" plant to make hydrocarbon liquids from an existing gasifier. An economic analysis will be performed to determine the total cost of the liquid hydrocarbons. In the analysis, the cost of feedstock to the gasifier, cost of operating the gasifier, cost of operating the compressor, and cost of operating the reactor system will be used. In addition to these variable costs, all fixed costs of the system will be calculated and used in the final analysis to obtain a cost per gallon of liquid hydrocarbons.

Planned Activities:
K.2.ML.1 Complete process design for a commercial plant to make liquid hydrocarbons from synthesis gas derived from biomass-synthesis gas.
K.2.ML.2 Complete economic analysis for the plant described in K.2.ML.1 assuming a "brown-field" installation.

Summarization of Activities:

Process design:
The purpose of this process design was to determine if the size and amount of catalyst used in a scaled up reactor (2'' in diameter) could feasibly be used due to the exothermic nature of the reaction. The effect of cooling coils on the temperature profile within a reactor system was investigated.

A simple, two-dimensional (2-D) model was used to approximate the energy transport within the system along with a three-dimensional (3-D) model. One major objective was to determine the effectiveness of using an internal fin with inter-cooling to control the extreme exothermic reactions within the reactor. Comsol was used to computationally determine the temperature profile due to the program's ability to easily change the variables that contribute to the ability to effectively control the temperature.

Two different reactor models were used which both contained fins made out of inert material with levels of catalyst. One model made use of cooling coils with water to cool the exothermic reaction and one did not. A calculated heat generation based on a literature rate equation was used in each of the models, and an obtained heat generation from literature was also used in each model to determine the accuracy of the models. A model for strictly gasoline creation was modeled along with a model for strictly CO2 creation (worst case scenario). Another model was used from a group doing similar research with a H_2 mole ratio of 40% and a CO mole ratio of 20% contained in their syngas.

Comsol Model Equations:
The equations implemented for the Comsol models made use of convection and conduction equations. These equations were adapted from Blanks to determine the heat produced from the

exothermic reactions and the amount of heat that could be dissipated using the cooling coils or inert materials throughout the reactor.

Convection and Conduction Equations

(1) Subdomain Setting Equation:

$$\nabla\cdot(-k\nabla T) = Q - \rho C_p \mathbf{u}\cdot\nabla T$$

(2) Boundary Setting Equation:

Temperature (assuming constant radial temperature):

$$T = T_0$$

Continuity:

$$\mathbf{n}\cdot(\mathbf{q_1}-\mathbf{q_2}) = 0;\ \mathbf{q_i} = -k_i\nabla T_i$$

Convective flux:

$$\mathbf{n}\cdot(-k\nabla T) = 0$$

System Parameters:

The two-dimensional system included a geometry that was proposed. There were sections dealing with the reactor itself (stainless steel), the inert fin material (steel) and the catalyst particles. For simplification purposes, this particular model only showed the top view of the temperature profile. This particular reactor has a reactor width (diameter) of 1.9358. Of the different heat generation models shown, there was one using a water cooling system and one where cooling was absent. The model used for Rahmati consisted of using the following rate equation (Equation 1) with Table K4. This table was used to calculate the heat produced from both gasoline and CO_2 creation.

$$r_i = K_{i,0} \exp(-E_{a,i}/RT)\ P_{CO}^{mi}\ P_{H_2}^{ni} \qquad \text{(Equation 1)}$$

Table K4. Kinetic Models from Rahmati.

	Kio	Ea (J/mol)	mi	ni
CH4	0.1627	83400	-1.08	1.57
C2H4	9.571E-07	65000	0.76	0.07
C2H6	0.000001207	49800	-0.56	1.32
C3H8	5.841E-10	34900	0.4	0.66
n-C4	1.151E-14	25700	0.47	1.14
i-C4	5.608E-13	25700	0.82	0.5
C5+	7.806E-12	23500	0.59	0.6
CO2	4.799E-08	58800	0.57	0.7

According to the Comsol models, the 2-D models had very little temperature differences, and cooling helped to better control the heat given off from the 40% H_2 and 20% CO model by 3 K. For the other models, implementing cooling within the reactor caused higher temperature differences shown in the 2-D models.

Modeling using 3-D showed a much larger difference in the final temperature reached at steady state. The heat generated by the 40% H_2 and 20% CO model was so extreme that a steady

state temperature was reached at 1935.34 K without cooling and 1371.208 K with cooling using Uk_air. When using Uk_t the highest temperature was 577.637. The other results were promising because they used similar mole ratio of H_2 and CO that the gasifier produces. The model used from Rahmati [1] showed that when only gasoline was generated, the highest temperature shown at steady state was 605.032 K without cooling, a high temperature of 573 K with cooling using Uk_air, and a high temperature of 573 K using Uk_t. When only CO_2 was generated, the highest temperature shown at steady state was 955.551 K without cooling, a high temperature of 736.77 K with cooling, and a high temperature of 573 K using Uk_t. The model used from Blanks showed that the highest temperature shown at steady state was 643.807 K without cooling, a high temperature of 573 K with cooling, and a high temperature of 573 K using Uk_t.

One way to improve the ability of the reactor to maintain the desired temperature is to wrap the tubing around the reactor radially in certain sections as seen in Figure K17. This will help maintain the temperature set-point throughout different levels of the reactor.

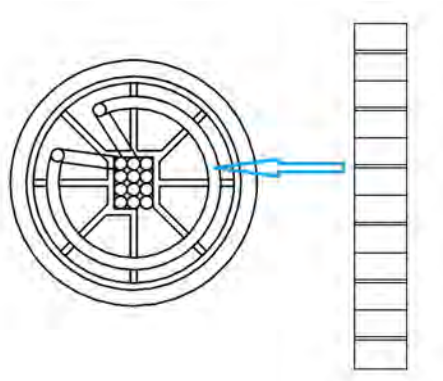


Figure K17. Schematic of wrapping tubing through catalyst beds in the reactor.

There are many ways that the model could be improved, including changing the sections of the reactor so that it imitates the catalyst/inert particles. Other models could be used that simulate turbulent flow and mass transfer of the system. Overall, this is a very simple model and will be tested in the future. The experimental set-up will consist of controlling the outer reactor temperature with a PID (proportional-integral-derivative) control loop and the internal cooling will be modified using the same type of set-up to properly control the temperature of the reactor based on these models.

Economic analysis:
The general analysis approach used in the economic evaluation of biofuels through cost analysis model including process design and analysis, cost configuration, cost evaluation model, economic evaluation with sensitivity analysis to every cost component and profitability analysis to the market is depicted in Figure K18.

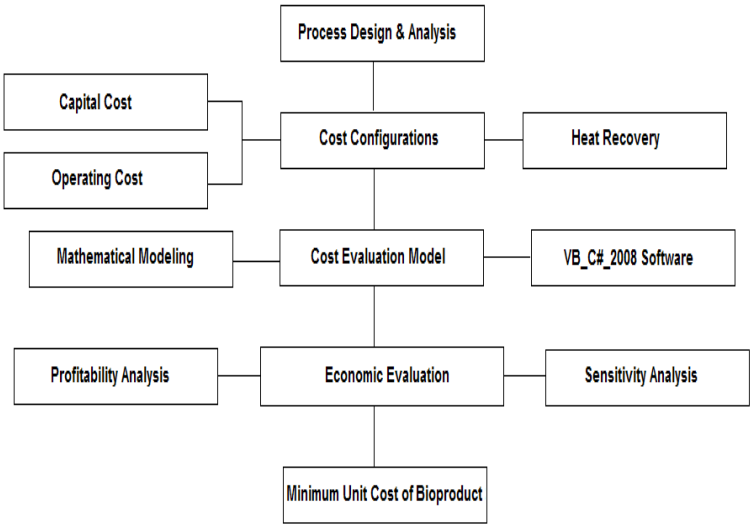


Figure K18. Analysis approach of economic evaluation

The first step was to assemble a general process flow schematic or more detailed process flow diagrams. The data from this BTL process was then used to properly size all process equipment and fully develop an estimate of the cost configuration including capital cost, operating cost, and heat recovery. These costs could have potentially been used in several types of economic analysis. In addition, since the biofuels included oil, gas, and aqueous, we needed to obtain the yield of biofuels by using the ratio of CO and H_2 in the reaction. For this design, however, a cost analysis model developed by mathematical modeling with VB_C# software was used to determine the cost composition, cost output, and minimum unit cost of biofuels to meet a requirement of biomass gasification power facility.

Cost Configurations:
In this study we chose feedstock preparation as the start point of our analysis and the bio-product output, including oil, gas, and aqueous, as the end point, using the micro-scale power facility with equivalent syngas production capacity of 65 Nm^3/h as the sample and to develop to the middle-scale power facility with equivalent syngas production capacity of 10,000 Nm^3/h.

The cost configuration of a bio-gasification facility included many factors. These factors were not only affected by external conditions such as equipment type and size of operating mode, but also influenced by internal conditions like production market price. The production cost was generally divided into capital cost, operating cost, and heat recovery, which can be further sub-divided into several cost compositions associated with the bio-gasification process (Figure K19).

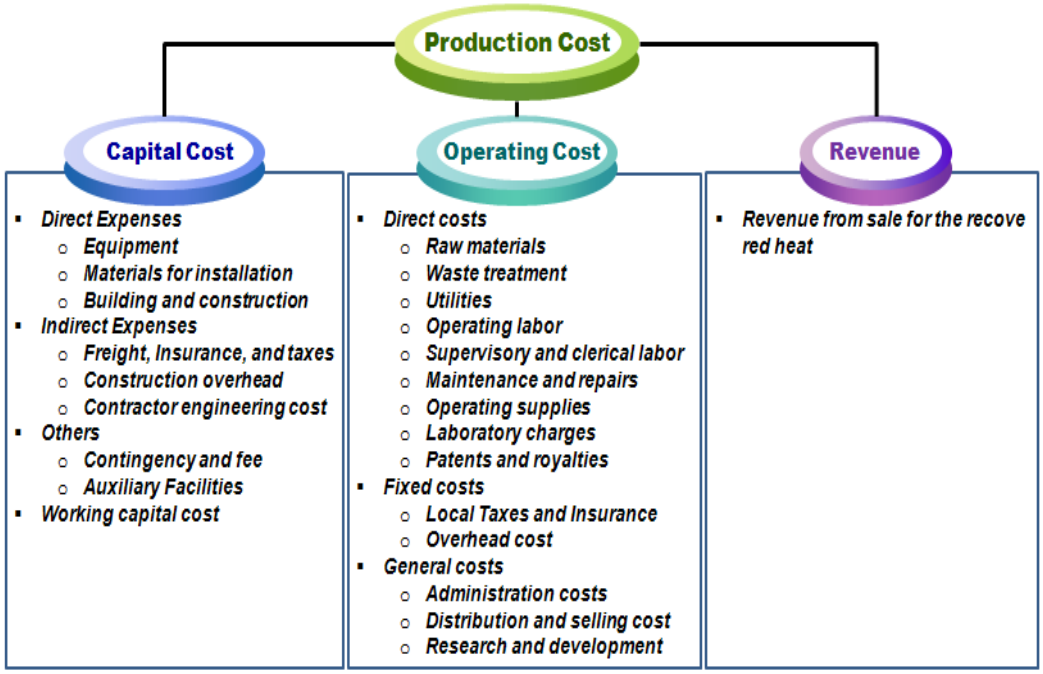


Figure K19. Cost configuration of bio-gasification power facility.

Cost Information and Assumption:
From the cost configuration, we assumed the total of annual production cost was the annual total cost with the revenue from sale for the recovered heat. The annual total cost was the sum of annual capital cost and operating cost. The revenue of the heat recovery was calculated based on the syngas yield and low heat value (LHV) of syngas. The LHV of the syngas was assumed to be 5.5 MJ Nm^{-3}. The recovery rate of the heat produced in gasification was assumed to be 20%, and the recovered heat could be sold at \$0.01 MJ^{-1}.

The total of syngas yield, depending on the type of biomass gasifier system, was the production capacity of the gasifier multiplied by its running hours. The biomass gasifier was run at full capacity at this time. In addition, one hour was needed to start up and shutdown the gasifier system for one shift or two shifts of each working day; in the case of three shifts per day, only one hour was needed for each working week. In our model we took about the operating mode in following section. The annual operating hour was the the annual working hour subtracted by 260 hours. The woodchips used in gasification had 18.7 MJ kg^{-1} of low heating value, which can be transferred to 2.4Nm^3kg^{-1} for bio-syngas to feedstock. There was no need for sizing and drying. The annual consumption of woodchips (feedstock) can be calculated from the annual total syngas yield divided by the coefficient of 2.4Nm^3kg^{-1}. In order to better understand the economic feasibility, the daily biomass consumption was obtained by annual biomass consumption divided by annual working days. The unit cost of woodchips was denoted by \$/ton; therefore we needed to do the unit transformation.

The unit cost of bio-syngas production can be obtained by the annual total production cost divided by the annual total syngas yield. Since the bio-product from bio-gasification and catalytic conversion was not unique, the unit cost of each bio-product was obtained by the weight estimate method. The weight ratio was given by the market price of the bio-product from bio-gasification and catalytic conversion including oil, gas, and aqueous. The unit weight was calculated by the total cost after heat recovery divided by the sum of the product of the market

price times the annual total yield of the corresponding bio-product. The unit cost of related bio-product was the product of the unit weight times the market price of the bio-product.

If enough costing parameters or information of the facility is available, the costing of bio-product can be carried out with a series of mathematical equations shown below that can be easily applied in computer programs of the cost evaluation model.

Annual Total Production Cost

$$C_{ta} = C_{ac} + C_{ao} - R_h \quad (1)$$

Annual Total Syngas Yield

$$Y_s = P_c \times H \quad (2)$$

Annual Operating Hours for Bio-gasification Power Facility

$$H = H_0 - 260$$

$$(H = H_0 - 52) \quad (3)$$

Annual Revenue from Sale of Heat Recovery

$$R_h = 0.2Y_s \times 5.5MJ / Nm^3 \times \$0.01MJ^{-1} \quad (4)$$

Annual Syngas Production Unit Cost

$$C_{ups} = \frac{C_{ta}}{Y_s} \quad (5)$$

Annual Bio-product Unit Cost

$$C_{upi} = \frac{C_{ta}}{\sum_i P_i Y_i} \times P_i \quad (6)$$

Annual Feedstock (Woodchips) Consumption (ton)

$$W_{festo} = \frac{Y_s}{2.4 \times 1000} \quad (7)$$

Daily Feedstock (Woodchips) Consumption (ton)

$$D_{festo} = \frac{W_{festo}}{365 - 52 \times 2} \quad (8)$$

Where:
Cta = the annual total production cost;
Cac = the annual total capital cost;
Cao = the annual total operating cost;
R_h = the annual revenue from sale of the heat recovery;
Y_s = the annual total syngas yield;
Pc (Pc_new) = the production capacity of gasification facility;
H_0 = the annual working hours for running the gasification facility;
H = the annual operating hours of the gasification facility;
C_{ups} = the annual syngas production unit cost;
C_{upi} = the annual ith bio-product unit cost;
P_i = the market price of ith bio-product;
Y_i = the annual ith bio-product yield;
W_{festo} = the annual feedstock consumption;
D_{festo} = the daily feedstock consumption

Biofuels Yield

Promoters were used to enhance activity and modify the selectivity to target products. The annual yield of each bio-product including oil, gas, and aqueous was obtained by the calculation of mass balance and energy balance based on the production selectivity and annual syngas yield. The bio-char generated from the woodchips was left in the gasifier and the composition of bio-char from annual biomass consumption was 2%.

The conversion rate of syngas was 40% from annual syngas yield after cleaning and conditioning. The ingredients of cleaned syngas included CO and H_2. The conversion rate of CO was assumed 80% from the cleaned syngas. In order to obtain the mass and volume of bio-product, the total CO moles were calculated based on the CO conversion rate and the cleaned syngas volume.

The product from syngas generation and catalytic conversion included CO_2, water (H_2O), gas (Light hydrocarbons), oil (Liquid hydrocarbons), aqueous (Oxygenates CxHyOz), and un-reacted syngas. The unreacted syngas was released after bio-gasification, and it was not considerable in our economic analysis. The selectivity of CO_2, gas, oil, and aqueous were given by 0.08, 0.2, 0.42 and 0.3. The mass and volume with recycle were calculated based on the selectivity and total CO moles with CO conversion rate. In addition, the mass of water was obtained based on the aqueous yield and the cost of waste water treatment was considered in the operating cost section. After all the calculations to bio-product yield, the total weight was obtained by the sum of each product. The total cleaned syngas (CO and H_2) weight was calculated to compare the total product weight in order to get the mass balance error. The mass balance error was 3.47%, which was in an acceptable range.The mass balance error was unchangeable with any change to the biomass consumption.

The mathematical equation for the bio-product yield including CO_2, water, gas, oil, and aqueous from syngas generation and catalytic conversion was shown below with the explanations of each denotation:

Annual Total Cleaned Syngas (CO and H_2) Yield

$$Y_{CO+H_2} = 0.4Y_s \quad (9)$$

Annual Total CO Moles

$$Y_{CO} = Y_{CO+H_2} \times 1000 / 22.4 / 2 \quad (10)$$

Annual Total CO_2 Yield

$$Y_{CO_2} = 0.8Y_{CO} \times S_{CO_2} \times 44 / 1000 / 0.8 \quad (11)$$

Annual Total Gas (Light hydrocarbons) Yield

$$Y_{LightHCs} = 0.8Y_{CO} \times S_{LightHCs} \times 14 / 1000 / 0.8 / 16 \times 22.4 / 28.26 \quad (12)$$

Annual Total Oil (Liquid hydrocarbons) Yield

$$Y_{LiquidHCs} = 0.8Y_{CO} \times S_{LiquidHCs} \times 14 / 1000 / 0.8 \times 1000 / 0.716 / 1000000 / 0.003785411 \quad (13)$$

Annual Total Aqueous (Oxygenates CxHyOz) Yield

$$Y_{CxHyOz} = 0.8Y_{CO} \times S_{CxHyOz} \times 22 / 1000 / 0.8 \times 0.334819866576961 \quad (14)$$

Annual Total Water (H_2O) Yield

$$Y_{H_2O} = Y_{CxHyOz} / 0.4 \times 0.6 / 0.8 \quad (15)$$

Where:
Y_s = the annual total syngas yield;
Y_{CO+H2} = the annual total cleaned syngas (CO and H_2) yield;
Y_{CO} = the annual CO moles;
Y_{CO2} = the annual total CO_2 yield;
$Y_{LightHCs}$ = the annual total gas (Light hydrocarbons) yield;
$Y_{LiquidHCs}$ = the annual total oil (Liquid hydrocarbons) yield;
Y_{CxHyOz} = the annual total aqueous (Oxygenates CxHyOz) yield;
Y_{H2O} = the annual total water (H_2O) yield;
S_{CO2} = the CO_2 selectivity;
$S_{LightHCs}$ = the Light hydrocarbons selectivity;
$S_{LiquidHCs}$ = the Liquid hydrocarbons selectivity;
S_{CxHyOz} = the CxHyOz selectivity

Capital Cost:
Capital costs in this model mainly included annual investment and loan interest cost. The annual investment included the annual total installed cost and the annual total indirect cost. These two kinds of cost were obtained based on the equipment purchase cost and the cost factor. The equipment purchase cost can be estimated by using capacity factored methods.

For the estimated annual total installed costs, the purchased cost of the equipment was calculated and then cost factors were used to determine it. This method of cost estimation had an expected accuracy of roughly +30% to -10%. The factors used in determining the total installed cost of each piece of equipment are shown in Table K5 below. The cost factors can be obtained by referring to existing plants or the literature. The annual total installed cost was affected by many factors, including purchased equipment installation, instrumentation and controls, piping, electrical systems, buildings, and yard improvements. Those cost factors were dependent on the equipment cost and estimated with the economic analysis model. The costs of equipment and construction should be depreciated for their economic lifetimes. Normally, economic lifetimes of equipment vary from 7 to 15 years, depending on the type and working conditions of the equipment. Economic lifetimes of buildings may be up to 20 years or more. The depreciations were significantly affected by the lifetime of the equipment and construction. Straight line depreciation method was used in this economic analysis modeling.

Table K5. General cost factors in determining total installed cost.

	% of TPEC	**Reference**
Total Purchased Equipment Cost (TPEC)	**100**	Wyman, C.E., R. L. Bain, N.D. Hinman, and D.J. Stevens, 1993;
Purchased Equipment Installation	39	
Instrumentation and Controls	26	
Piping	31	
Electrical Systems	10	
Buildings	29	
Yard Improvements	12	
Total Installed Cost	147	

The indirect costs (non-manufacturing fixed-capital investment costs) were also estimated using cost factors. The factors are shown in Table K6 and have been put as percentages in terms of total installed cost (TIC). The annual total indirect cost includes engineering, construction, legal and contractors fees, and project contingency. The annual total indirect cost can be calculated by the product of annual total installed cost multiplied by cost factor.

Table K6. General cost factors in determining total indirect cost.

Indirect Cost	% of Total Installed Cost	Reference
Engineering	13	Wyman, C.E., and D.J. Stevens, 1993;
Construction	14	
Legal and Contractors Fees	9	
Project Contingency	3	
Total Indirect Costs	39	

The cost for loan interest of the annual total investment depends on the loan rate that was the fraction of financing covered by loan and the interest rate on the loan. Hence, the loan interest was calculated by the annual total investment times the loan rate and the annual loan interest rate.

The mathematical equation for the capital cost was shown below with the explanations of each denotation:

Annual Total Capital Cost

$$C_{ac} = C_{\text{int}} + C_{ainstr} \quad (16)$$

Annual Total Investment

$$C_{\text{int}} = C_{tins} + C_{tind} \quad (17)$$

Annual Equipment Purchas Cost

$$C_{eq} = C_{ex}\left(\frac{P_{c_new}}{P_{c_ex}}\right)^{0.6} \quad (18)$$

Annual Total Installed Cost

$$C_{tins} = C_{eq} \times (1 + F_{\text{int}s}) \times R_{de} \quad (19)$$

Annual Total Indirect Cost

$$C_{tind} = C_{eq} \times (1 + F_{\text{int}s}) \times F_{ind} \times R_{de} \quad (20)$$

Annual Cost of Loan Interest

$$C_{ainstr} = C_{eq} \times (1 + F_{\text{int}s}) \times R_{loan} \times R_{\text{int}r} \quad (21)$$

Where:

C_{tin} = the annual total investment;
Cainstr = the annual loan interest cost;
Ctins = the annual total installed cost;
Ctind = the annual total indirect cost;
Ceq = the total of equipment purchase cost;
Cex = the purchase cost of existing gasifier and generator;
Pc_ex = the production capacity of an existing power facility;
Pc_new = the production capacity of gasification facility;
Rdec = the depreciation rate of construction cost;
Ftins = cost factor of total installed cost;
Ftind = cost factor of total indirect cost;
Rloan = the loan rate;
Rintr = the loan annual interest rate

Operating Cost:

There were two kinds of operating costs in the model: variable and fixed costs. The following sections discuss the operating costs including the assumptions and values for these costs. The variable costs were proportional to actual production capacity and included the costs of feedstock, electricity, waste water treatment, and catalyst. These costs were obtained by the related mathematical equation depending on the economic analysis. The fixed costs were charged annually depending on whether the facility was run at high or low production capacity. The fixed costs included labor costs, maintenance cost, general expense, insurance, and taxes. These costs were calculated by the factor method with corresponding cost rate to the labor cost and capital cost.

The feedstock cost was obtained by the product of feedstock price multiplied by the amount of annual consumption which we have obtained from the section of basic cost information. As in the model, the biomass species have been set to woodchips. Since we have already considered the quality of woodchips, transportation cost, and storage cost, and there was no extra charge for drying and sizing, the wood chips used in the model were estimated to be supplied at $35/ton.

The cost of electricitywas calculated by the product of electricity price, which is 0.0718 $/Kwh (EIA, 2009a), multiplied by the amount of annual consumption. The annual consumption of electricity can be estimated by using the capacity factor method based on the consumption and capacity of existing equipment. Waste treatment cost was the product of the rate of disposal fee multiplied by the amount of waste produced. For the bio-gasification process, the main disposal output is the bio-char and the waste water. The cost of treatment to bio-char was not considered in the analysis since the bio-char can be processed for future use of agriculture. The cost of waste water treatment was the product of the unit fee, which is 2.07 $/100ft^3, multiplied by the amount of waste water produced. The amount of waste water was obtained in the section of bio-product from syngas generation and catalytic conversion.

The cost of catalyst was calculated by the product of catalyst unit price, which was 145.15 $/lb (EIA, 2009a) in our model, multiplied by the amount of annual consumption. The annual consumption of catalyst can be estimated by using the capacity factor method based on the consumption and capacity of existing equipment. The unit consumption of equipment was reflected by the base case for equipment capacity and catalyst consumption. An exponential scaling expression was used to adjust the bare equipment catalyst consumption:

$$W_{new} = W_{base} \times (\frac{P_{new}}{P_{base}})^n \quad (22)$$

Here W_{new} was the unit catalyst consumption of new purchased equipment; W_{base} was the unit catalyst consumption of existing equipment, which was 10 lb for the capacity of 120 Nm^3/h; P_{new} was the capacity of new purchased equipment; P_{base} was the capacity of existing equipment; n was a characteristic scaling exponent, which was set equal to 0.6. We assume that the catalyst can be used for 3-5 years for one period of gasification process.

Labor costs included salary of employees and federal insurance contribution act (FICA). The salary was determined by the product of pay rate multiplied by the number of employees. FICA was proportional to the salary with the FICA rate. Pay rates varied for different employee positions. In order to help the calculation, we unified the pay rate as $16/h including the FICA, which means that the FICA rate was set equal to zero. The number of employees increased by

one as per 1,000 Nm^3/h increased of production capacity. There were two employees for the production capacity of 65 Nm^3/h.

Other fixed costs included maintenance cost, general overhead, and insurance and taxes. These costs can be obtained by the product of annual rate multiplied by the total project investment or the total salaries. The factors of maintenance cost (2% of total project investment), general overhead (95% of total project investment), and insurance and taxes (2% of total project investment) were assumed for the next calculation.

The mathematical equation for the operating cost was shown below with the explanations of each denotation:

Annual Total Operating Cost

$$C_{ao} = C_{fsto} + C_{el} + C_{labo} + C_{wast} + C_{cata} + C_{main} + C_{gen} + C_{ins} \quad (23)$$

Annual Feedstock Cost

$$C_{fsto} = P_{fsto} W_{fsto} \quad (24)$$

Annual Electricity Cost

$$C_{el} = P_{el} W_{el} \quad (25)$$

Annual Labor Cost

$$C_{labo} = mR_{labo}(1 + R_{fica})H_0 \quad (26)$$

Annual Waste Treatment Cost

$$C_{wast} = P_{wast} Y_{H_2O} \quad (27)$$

Annual Catalyst Cost

$$C_{cata} = P_{cata} W_{cata} \quad (28)$$

Annual Maintenance Cost

$$C_{main} = R_{main} C_{int} \quad (29)$$

Annual General Expense for Operating the Power Facility

$$C_{gen} = R_{gen} C_{labo} \quad (30)$$

Annual Contingency Cost for Operating the Power Facility

$$C_{ins} = R_{ins} C_{int} \quad (31)$$

Where:
Cfsto = the cost of feedstock;
Cel = the cost of electricity;
Clabo = the labor cost;
Cwast = the cost of waste treatment;
Ccata = the cost of catalyst;
Cmain = the cost of repairing of equipment;
Cgen = the general expense for operating the power facility;
Cins = the insurance and taxes;
Pfesto = the price of feedstock;
Wfesto = the annual feedstock consumption;
Rfica = the pay rate of FICA (federal insurance contribution act);
M = the number of employees;
Rlabo = the pay rates of the employees;

Pel = the unit price of electricity;
Wel = the annual electricity consumption;
Pwast = the price of waste treatment;
Y_{H2O} = Wwast = the weight of waste water produced;
Pcata = the unit price of catalyst;
Wcata = the annual catalyst consumption;
Rmain = the repairing rate of equipment;
Rgen = the ratio of general expense for operating the facility;
Rins = the ratio of insurance and taxes for the power facility

Operating Mode:
Operating costs were significantly affected by the operating mode of a gasification facility. Operating mode in this research to economic analysis of the gasification power facility includes the working hours, the ways of operating equipment, and the facility's management. The operating mode was classified into three different shifts with related working hours and operating hours in Table K7.

Table K7. Three working hours of small- or micro-scale gasification facilities operating indifferent modes.

Mode	Unit	Working Hours	Operating Hours
One Shift	h/yr	2080	1820
Two Shifts	h/yr	4160	3900
Three Shifts	h/yr	6240	6188

Working hours of operating mode were set at 52 weeks per year, 5 days per week, and 8 hours per day for one shift, 16 hours per day for two shifts, and 24 hours per day for three shifts. One hour was needed to start up and shut down a gasification facility in each working day for one and two shifts working modes;just one hour was needed in a week for the three shifts working mode.

Model Design and Programming:
The cost analysis model software possessed functions including data saving, data download, data input and output, and the cost composition graph. We can save and compare the results for each cost analysis of bio-gasification process under different scenarios. For multiple inputs to each cost component and economic assumption, we would have all the cost outputs and the par chart of the annual production cost composition of the power facility operating at different capacities. The model design mainly includes 5 parts: Interface Design, Mathematical Equation Implantation, Text Notes, Data Storage System, and Cost Composition Graph System. The model design and test was processed below by the slides of Home, Data Storage, Basic Cost Information, Production Information, Capital Cost, Operating Cost, and Cost Summary.

Cost Summary:
A summary of economic analysis for the pilot plant based on our biomass gasification, syngas cleaning, and catalytic conversion system is given below. In order to enhance the working efficiency, we set the working mode to three working shifts to maximize the operating hours. The basic cost information and the hydrocarbon yield information is presented in Tables K8 and K9. The summaries of annual production capital costs and operating costs are presented in Tables K10 and K11. The cost summary of unit price of bio-syngas and biofuels are presented in Table K12.

Table K8. Basic cost information based on our biomass gasification, syngas cleaning, and catalytic conversion system in three working shifts mode.

Basic Cost Information	**Unit**	**Value**
Biomass Gasifier Capacity	Nm^3/h	65.00
Annual Working Hours	h	6,240.00
Gasifier Actually Operating Hours	h	6,188.00
Annual Syngas Yield	Nm^3	402,220.00
Annual Biomass Consumption	Kg	167,591.67
Dayly Biomass Consumption	ton	0.64
$CO+H_2$	Nm^3	160,888.00
Total Syngas Weight	Kg	107,737.50
CO Conversion Rate	None	0.80
Total CO Moles	Mole	3591,250.00
Char	Kg	3,351.83
Mass Balance Error	%	-3.47

Table K9. Biofuels information in three working shifts mode.

Production	**Selectivity**	**Mass(Kg)**	**Mass With Recycle(Kg)**	**Volume**	**Unit**
CO_2	0.08	10,112.96	12,641.20		
Liquid Hydrocarbons	**0.42**	**16,893.24**	**21,116.55**	**7,791.07**	**Gallon**
Oxygenates	**0.30**	**18,961.80**	**23,702.25**	**7,935.98**	**Gallon**
Light Hydrocarbons	**0.20**	**8,044.40**	**10,055.50**	**498.15**	**MMBTU**
H_2O	None	28,442.70	35,553.38		
Unreacted Syngas	None	21,547.50			
Total Weight	None	104,002.60			

Table K10. Annual production capital cost information based on our biomass gasification, syngas cleaning, and catalytic conversion system in three working shifts mode.

Capital Cost	**Unit**	**Value**
Total Purchased Equipment Base Cost	$	385,000.00
Total Purchased Equipment Cost	$	266,501.71
Total Installed Cost	$	658,259.22
Total Indirect Cost	$	256,721.09
Total Project Investment	$	914,980.31
Annual Total Project Investment	$	45,749.02
Annual Loan Interest Cost	$	23,697.33
Annual Capital Cost	$	69,446.35

Table K11. Annual production operating cost information based on our biomass gasification, syngas cleaning, and catalytic conversion system in three working shifts mode.

Operating Cost	**Unit**	**Value**
Annual Feedstock Cost	$	5,865.71
Annual Electricity Cost	$	1,197.11
Annual Waste Water Treatment Cost	$	25.99
Annual Catalyst Cost	$	1,004.75
Annual Variable Operating Cost	$	8,093.56

Annual Labor Cost	$	199,680.00
Annual Maintenance Cost	$	914.98
Annual General Expense	$	189,696.00
Annual Insurance & Taxes	$	914.98
Annual Fixed Operating Cost	$	391,205.96
Annual Operating Cost	$	399,299.52

Table K12. Cost summary based on our biomass gasification, syngas cleaning, and catalytic conversion system in three working shifts mode.

Cost Summary	**Unit**	**Value**	**Market Price**	**Unit**
Annual Total Capital Cost	$	69,446.35		
Annual Total Operating Cost	$	399,299.52		
Annual Total Production Cost	$	468,745.87		
Annual Heat Recovery	$	4,424.42		
Annual Total Production Cost*	$	464,321.45		
Liquid Hydrocarbons Volume Unit Cost	**$/Gallon**	**30.89**	**3.00**	**$/Gallon**
Oxygenates Volume Unit Cost	**$/Gallon**	**25.74**	**2.50**	**$/Gallon**
Light Hydrocarbons Volume Unit Cost	**$/MMBTU**	**38.92**	**3.78**	**$/MMBTU**
Syngas Volume Unit Cost	$/Nm3	1.15		

The results showed that the total annual production cost of biofuels was $ 46,8745.87 with the annual total capital cost of $ 69,446.35 and the annual total operating cost of $ 399,299.52, thereby giving a syngas unit cost of $1.15 /Nm3 in three shift operating mode. This unit cost is equivalent to $0.01 /MJ of energy cost. The term of energy cost is defined as the cost per unit low heating value (MJ) of the syngas. Therefore the annual total production cost with heat recovery was $ 464,321.45. The biofuels unit cost of gas was $38.92 /MMBTU. The biofuels unit cost of oil was $30.89 /Gallon. The biofuels unit cost of aqueous was $25.74 /Gallon. The market price was also listed to help compare and calculate for the biofuels unit cost.

According to the above configuration analysis, the total annual production cost compositions of product were significantly changed when the gasification facilities operated at different capacities. The results of percentages of operating and capital costs to the total annual production costs of gasification operating at different capacities is shown in Figure K20. The percentages of operating costs decreased as production capacity increased to 1,800 from 60 Nm^3/h. The percentages of operating costs kept increasing as the production capacity increased to 10,000 Nm^3/h. This was because the increasing rate of capital costs for larger production capacity facility was higher than that of operating costs for the micro-scale bio-gasification power facility with capacity range from 60 through 1,800 Nm^3/h. The percentage of capital costs was up to about one third of total annual production cost when the gasification facility was operating at 1,800 Nm^3/h. When the production capacity kept increasing to 10,000 Nm^3/h the requirement of labor was up to 10 people for one working shift. The feedstock need was also increasing to satisfy the biomass consumption of larger production capacity. The increasing of the labor cost and feedstock cost was the main reason that the percentages of operating costs increased as production capacity increased to 10,000 Nm^3/h.

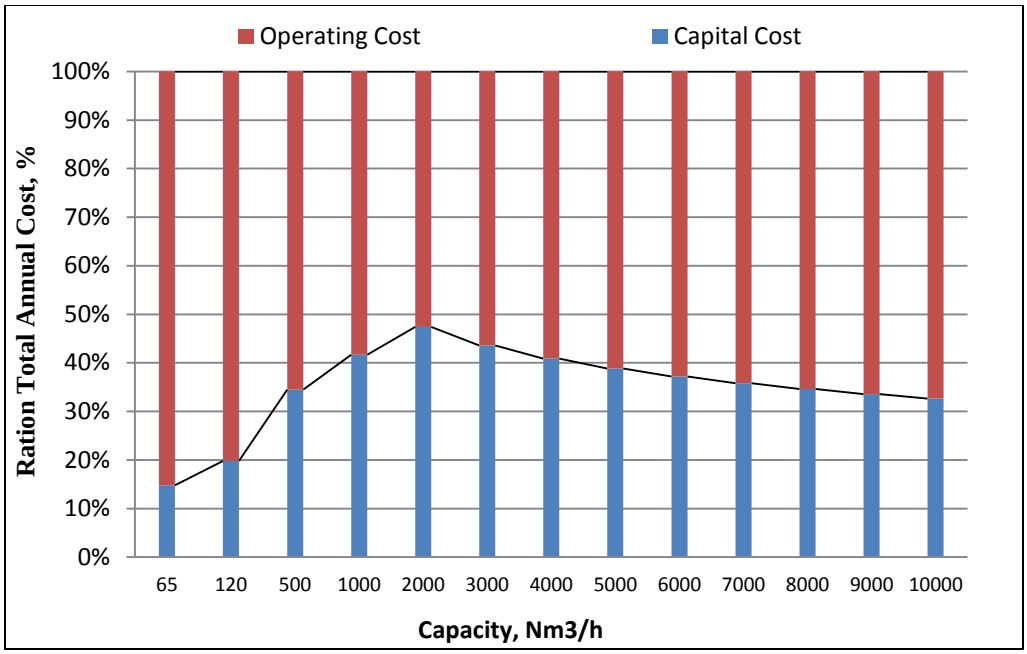


Figure K20. Percentages of capital and operating cost under different production capacities.

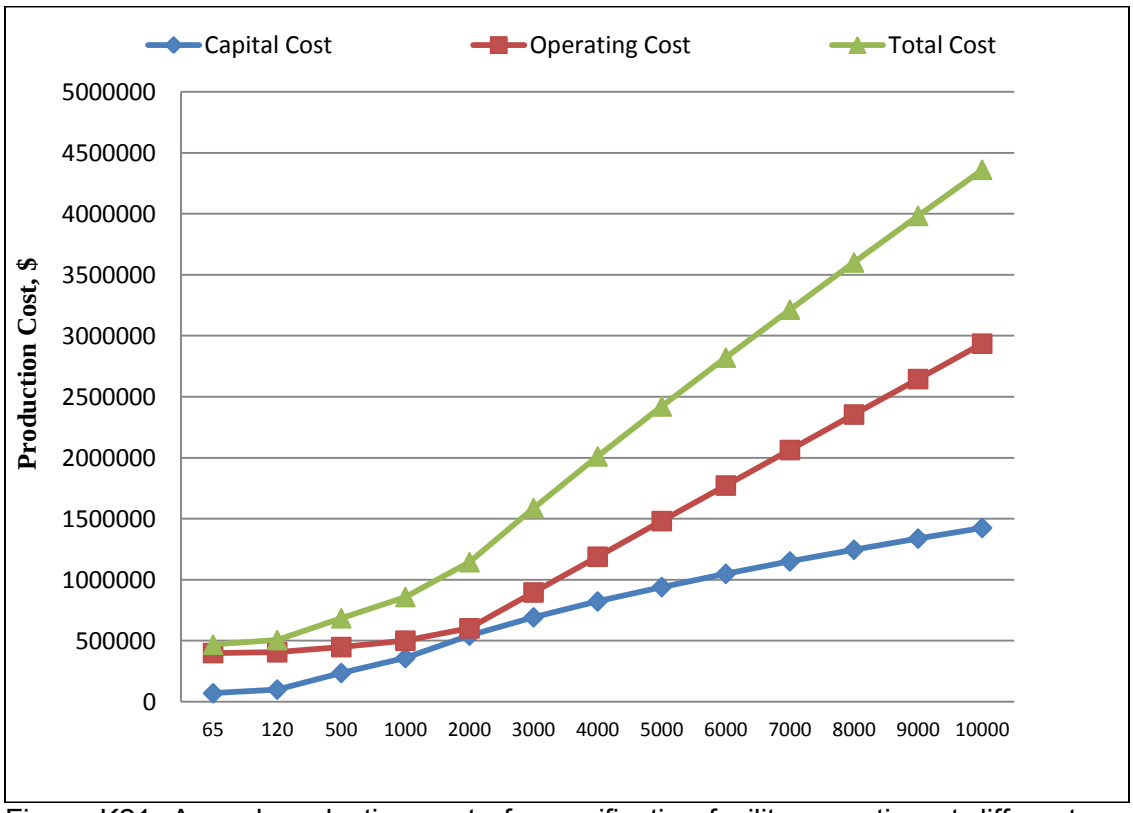


Figure K21. Annual production cost of a gasification facility operating at different capacities in three working shifts mode.

The effect of gasification facility production capacity on annual production costs is shown in Figure K21 and the effect on product unit cost is shown in Figure K22. Although total annual production cost continually increased as production capacities scaled up (Figure K21), product

unit cost still significantly decreased as the production capacity increased from 60 to 1,800 Nm^3/h (Figure K22). After the capacity of 1,800 Nm^3/h, the rate of decrease was decreasing. This resulted from the higher increasing rate of product yield compared to that of total annual production cost when production capacity was scaled up.

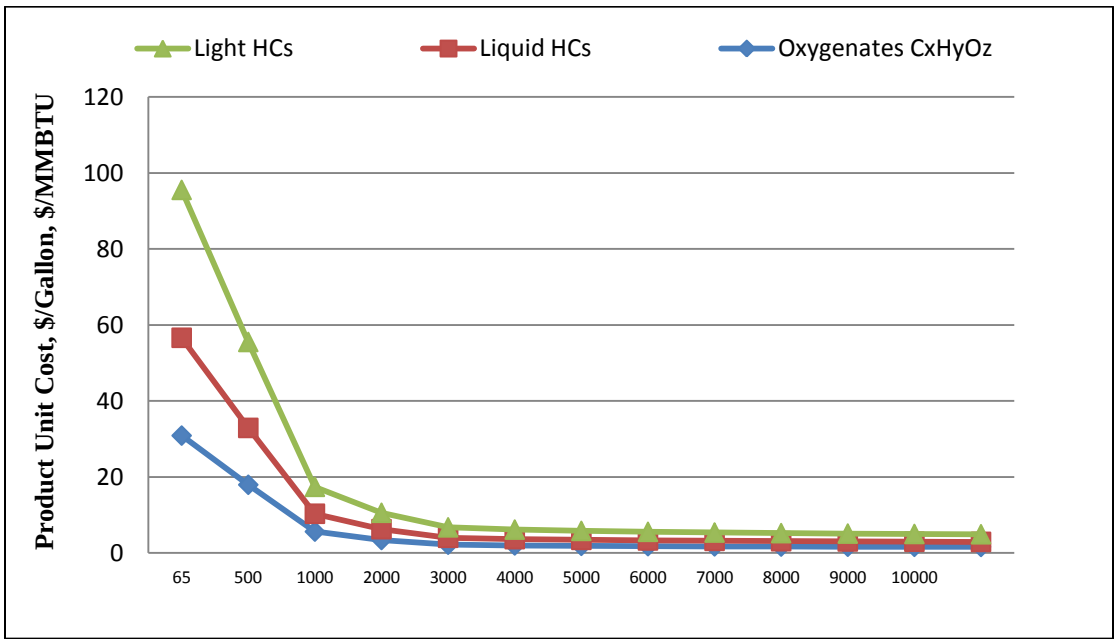


Figure K22. Product unit costs of gasification facility operating at different capacities in three working shifts mode.

As the production capacity increased from 65 to 10,000 Nm^3/h, the product unit cost of gas, oil, and aqueous decreased from $38.92 /MMBTU, $30.89 /Gallon, and $25.74/Gallon to $2.01/MMBTU, $1.59/, and $1.33/Gallon, respectively. At this point, the hydrocarbon products would be fully competitive economically compared with market price. The modeling displayed a trend of product unit cost going down as the production capacity of gasification facilities increased. These indicated that increasing gasification facility production capacity was an effective way of reducing product unit cost and improving its economic feasibility.

Publications:

Street, J., Yu, F., Wooten, J., Columbus, E., White, M., and Warnock, J., "Gasoline-range hydrocarbon production using biomass derived synthesis gas over Mo/H+ZSM-5," *Fuel,* Vol. 96, 2012, pp. 239–249.

Street, J. and F. Yu. 2011. Production of high-value products including gasoline hydrocarbons from thermochemical conversion of syngas. Biofuels 2(6):677-691.

Conference Presentations:

Yan, Q. and Yu, F., "Process development and demonstration of biomass to aviation kerosene via gasification and catalytic conversion," Paper 131503, 243rd ACS National Meeting, San Diego, CA, March 25 – March 29, 2012.

Yu, F. 2011. Higher Alcohol Synthesis from Syngas over Copper-Iron Based Catalyst. Strategic Environmental Research and Development Program (SERDP) and Environmental Security Technology Certification Program (ESTCP) annual Technical Symposium & Workshop. Washington, D.C. November 29 – December 1, 2011.

Yu, F. 2011. Liquid Hydrocarbon Production over MO/HZSM-5 Using Gasified Biomass. Strategic Environmental Research and Development Program (SERDP) and Environmental Security Technology Certification Program (ESTCP) annual Technical Symposium & Workshop. Washington, D.C. November 29 – December 1, 2011

Yu, F. Yan, Q., Columbus, E., and Wooten. J. 2011. Catalytic Conversion of Biomass Derived Synthesis Gas to Liquid Hydrocarbons. 107th Gulf Coast Conference. Galveston, TX. October 11-12, 2011.

Yan, Q., Street, J., Wooten, J., Columbus J., and Yu. F. 2011. Biomass to liquid (BTL) fuels via gasification and catalytic conversion. A Poster Presentation presented for the Mississippi State 2011 Biofuels Conference. Mississippi State, MS, October 5-7, 2011.

Lu, Y., Yan, Q., Hu, J., Street, J., Wooten, J., Columbus, E., Yu, F. 2011. Higher Alcohols Synthesis from Syngas over Copper-Iron Based Catalyst. A Poster Presentation presented for the Mississippi State 2011 Biofuels Conference. Mississippi State, MS, October 5-7, 2011.

Hu, J., Yu, F., Lu, Y., Yan, Y., Wooten, J., Columbus. E. 2011. Green Flight: Renewable Jet Fuel Production Through Integrated Biomass Gasification, Gas Cleaning and Catalytic Conversion System. A Poster Presentation presented for the Mississippi State 2011 Biofuels Conference. Mississippi State, MS, October 5-7, 2011.

Street, J., Columbus, E., Wooten, J., White, M., and Yu, F. Scale-up of Gasoline-Range Hydrocarbon Production from Biomass Synthesis Gas over Mo/HZSM-5 and other Bi-functional Catalysts. A Poster Presentation presented for the Mississippi State 2011 Biofuels Conference. Mississippi State, MS, October 5-7, 2011.

Yan, Q., Mlsna, T., Wooten, J., Columbus, E., and Yu, F. Liquid Hydrocarbons Production via Biomass Gasification and Catalytic Conversion. 4th Annual Waste-to-Fuels Conference & Trade Show. San Diego, CA, September 25-27, 2011.

Hu, J., Yu, F., Lu, Y., Yan, Q., Wooten, J., Columbus, E., and Lin, W. Catalytic Conversion of Biomass-derived Syngas to Gasoline Range Hydrocarbons. Paper: 1110878, An ASABE Meeting Presentation written for the 2011 ASABE Conference, Louisville, KY, August 7-10, 2011.

Lu, Y., Yan, Q., Hu, J., Street, J., Wooten, J., Columbus, E., and Yu, F. Mixed Alcohols Synthesis from Syngas Over Copper-Iron Based Catalyst. Paper: 1110834, An ASABE Meeting Presentation written for the 2011 ASABE Conference, Louisville, KY, August 7-10, 2011.

Street, J., Columbus, E., Warnock, J., Wooten, J., White, M., and Yu, F. Liquid Hydrocarbon Production over Mo/HZSM-5 Using Gasified Biomass. Paper: 1110541, An ASABE Meeting Presentation written for the 2011 ASABE Conference, Louisville, KY, August 7-10, 2011.

Yan, Q., J., Wooten, J., Columbus, E., and Yu, F., Synthesis of Liquid Hydrocarbons from Biomass Derived Syngas, An ASABE Meeting Presentation written for the 2011 ASABE Conference, Louisville, KY, August 7-10, 2011.

Yan, Q., Yu, F., Toghiani, H., Zhang, J., Thermal Treatment and Characterization of A Biochar Obtained from Pinewood Fast Pyrolysis, An ASABE Meeting Presentation written for the 2011 ASABE Conference, Louisville, KY, August 7-10, 2011.

Lu, Y., Yan, Q., Hu, J., Hu, J., Street, J., Wooten, J., Columbus, E., and Yu, F. Development of copper-iron based catalyst for mixed alcohol synthesis from syngas. Microscopy & Microanalysis meeting, Nashville, TN, August 7-11, 2011.

Eugene P. Columbus, E., F. Yu, and J. Wooten. 2011. Bio-feedstock engineering. 1st World Congress of Bioenergy (WCBE-2011). Dalian, China. April 25-30.

To F., F. Yu, Y. Zhang, R. Li, J. Wooten, and E. Columbus. 2011. Biomass syngas production from downdraft gasification system. 1st World Congress of Bioenergy (WCBE-2011). Dalian, China. April 25-30.

Yu, F., Q. Yan, J. Hu, Y. Lv, J. Street, J. Wooten, F. To, and E. Columbus. 2011. Production of mixed hydrocarbons via biomass gasification, biosyngas cleaning and catalytic conversion. 1st World Congress of Bioenergy (WCBE-2011). Dalian, China. April 25-30.

Process and catalysts for Converting Biomass/Municipal Solid Wasters (MSW) derived syngas to liquid hydrocarbon mixtures and oxygenates by a single stage. Fei Yu, Qiangu Yan, and William Batchelor. Provisional patent. 61/632,348.

Task L. Biomass Combustion

Principle Investigators and team members:
Sundar R. Krishnan (PI)
Kalyan K. Srinivasan (Co-PI)

Executive Summary:

Current engines are designed to operate on refined petroleum fuels. However, given emerging economic, environmental and strategic concerns, this will likely change. Clean and efficient energy-conversion technologies to fuel the transportation sector need to be developed. We envision that biomass-derived oxygenated fuels, co-designed with new low temperature combustion strategies, will meet these challenges by improving fuel efficiencies and power densities, while reducing pollutant and greenhouse gas emissions.

Fuels manufactured from non-food biomass have numerous compounds whose ignition, combustion, and emissions characteristics are significantly less understood than conventional petroleum fuels. This knowledge gap is a roadblock in the immediate utilization of biomass-derived fuels in combustion engines. Further, it is also important to understand which fuel components are conducive or detrimental for engine combustion before embarking on the development of large-scale production strategies of these fuels from biomass. To enable and optimize engine utilization of non-food biomass-derived fuels, the proposed research will characterize the ignition, combustion, and emissions characteristics of these fuels and/or appropriate surrogates through the experimental efforts discussed below.

The present research effort helped in understanding the influence of various fuels on combustion characteristics relevant to transportation and stationary engines. The fuels examined included biodiesel, methane, propane, diesel, and blends of diesel and a proprietary renewable fuel sourced from non-food biomass. Several sets of experiments were performed with different experimental setups: (1) Detailed single and dual fuel experiments on a compression ignition engine and (2) Investigation of non-intrusive diagnostic methodologies for flame measurements in a rectangular slot burner. The single fuel experiments focused on quantifying the performance, combustion, and emissions associated with diesel, biodiesel, and blended renewable fuels usage in a multi-cylinder light duty engine. The dual fuel experiments investigated the possible performance and emissions improvements with combinations of high-cetane pilot fuels (diesel or biodiesel) and low-cetane gaseous fuels (methane or propane). All of these fuels are currently available and all (except diesel) can be sourced from renewable resources. Therefore, these results are useful indicators of the performance and emissions benefits when such fuels are utilized in diesel engines. The slot burner experiments were performed to test natural flame chemiluminescence spectroscopy and laser-induced breakdown spectroscopy (LIBS) for fuel-air equivalence ratio measurements in premixed atmospheric methane-air flames. The slot burner was used for these experiments because the rapid compression machine (RCM) delivery was delayed due to unforeseen manufacturing difficulties. However, these diagnostic methodologies are expected to be used when the RCM experiments are performed in the next phase. In addition to these experiments, two combustion simulations were also developed to understand the fundamental issues that exacerbate the twin challenges of high fuel conversion efficiencies and low emissions. One was a multi-zone combustion model used to predict dual fuel low temperature combustion and led to an award-winning journal article while another was a single-zone constant internal energy-volume (UV) combustion model used to understand entropy generation in combustion processes and identify strategies for improving fuel conversion efficiencies. The knowledge gained from all of these efforts has been

disseminated in numerous refereed journal articles, national and international conference publications, and invited technical presentations given by the PIs across the country. Overall, the outcomes of the present efforts have provided the foundations for understanding and improving combustion of next-generation biofuels in combustion engines.

Goals for Subtask L.1:
L.1.ML.1 To measure ignition and combustion pressure histories of carefully chosen biomass fuel surrogates.
L.1.ML.2 To characterize ignition delays and combustion behavior of non-food biomass fuels at various engine-like operating conditions.

Actual Accomplishments for Subtask L.1:
- Three peer-reviewed journal articles, two peer-reviewed conference papers, and one non-peer-reviewed conference paper.
- Ignition characteristics in diesel-ignited methane and diesel-ignited propane dual fuel combustion were quantified and carefully analyzed.
- The manufacturing and delivery of the rapid compression machine (RCM) were delayed due to unforeseen circumstances. Therefore, two distinct optical diagnostic techniques were investigated in atmospheric, premixed methane-air flames generated in a rectangular slot burner. A McKenna burner was also procured and this device will be set up and used as the primary test bed for initial development of future diagnostics.
- Natural chemiluminescence coupled with multivariate data analysis was used to quantify fuel-air equivalence ratios in the methane-air flames. This technique is expected to be directly applicable in understanding alternative fuel combustion in the RCM experiments.
- Laser-induced breakdown spectroscopy (LIBS) was used to quantify fuel-air equivalence ratios in methane-air flames. Again, multivariate calibration models were developed and found to be very useful for equivalence ratio determination from LIBS measurements.
- The experimental results and experience gained from the burner experiments are expected to be very useful when RCM experiments are performed in the near future.

Goals for Subtask L.2:
L.2.ML.1 To investigate fuel injection and engine combustion strategies for surrogate blends of non-food biomass-derived fuels.
L.2.ML.2 To measure baseline engine performance, combustion heat release, and exhaust emissions from non-food biomass-derived fuels and/or suitable surrogate blends.

Actual Accomplishments for Subtask L.2:
- Four peer-reviewed journal articles, two peer-reviewed conference papers, and four non-peer-reviewed conference papers and posters. Two additional journal articles currently under preparation for submission.
- All experiments were performed on a Volkswagen 1.9L TDI engine. Four different types of alternative fuels were considered: biodiesel, methane, propane, and a renewable non-food biomass-derived distillate fuel provided by a US biofuels manufacturer (KiOR).
- Ignition, combustion, fuel conversion efficiencies, and engine-out exhaust emissions were measured for straight biodiesel fueling and for biodiesel-ignited methane and propane

dual fuel combustion. Additional experiments are underway for understanding the combustion of other non-food biomass-derived fuels.

- A multi-zone model of pilot-ignited natural gas engine combustion was developed. This model and results for dual fuel low temperature combustion were published in the Proceedings of the Institution of Mechanical Engineers (UK): Journal of Automobile Engineering. This article was cited for its high quality and won the 2010 SAGE Best Paper Award from the Editor and Editorial Board of the Journal.
- A single-cylinder research engine (SCRE) was also set up along with a new AC dynamometer and complete engine instrumentation. The SCRE is scheduled to be used for future experiments with advanced combustion concepts and alternative fuels.
- An air compressor-dryer system was purchased and installed in the advanced combustion engines (ACE) laboratory at MSU. This system will support "simulated turbocharging" that is critical to enable advanced combustion strategies in the research phase.
- Cyclic combustion variations in dual fuel partially premixed low temperature combustion were studied and presented at the ASME 2012 IC Engines Division Spring Technical Conference in Torino, Italy.
- As part of the overall effort to improve engine fuel conversion efficiencies, entropy generation in a constant internal energy-volume (UV) combustion process was modeled. The effects of different fuels and diluents on entropy generation were examined and guidelines for practical IC engine fuel conversion efficiency improvements were established.
- A computational fluid dynamics (CFD) model of biodiesel combustion in the Volkswagen TDI engine was developed and validated with experimental combustion data from the ACE lab at MSU. These results were presented at the 2012 Spring Technical Meeting of the Central States Section of the Combustion Institute.

Subtask L.1 Investigate ignition and combustion signatures of non-food biomass-derived fuels and/or relevant surrogates in a rapid compression machine

The goal of this task is to understand the ignition and combustion behavior of non-food biomass-derived fuels. A rapid compression machine (RCM), which emulates the compression process of an IC engine, will be used for this purpose. Combustion pressure histories and ignition delays of biomass-derived fuels and/or relevant surrogate compounds will be analyzed under *well-controlled* engine-like conditions. This understanding, which cannot be achieved with standard engines, will facilitate the evolution of strategies for better utilization of these fuels in advanced combustion engines. In addition, the results from RCM experiments will also provide valuable feedback to enhance biomass fuel manufacturing pathways and processes. Several gaseous and liquid fuels may be considered for combustion investigations with the RCM, including syngas, cyclic oxygenates, and oxygenated hydrocarbon fuels.

Summary of Activities for Subtask L.1:
RCM: The rapid compression machine (RCM) is a sophisticated single-shot device that utilizes pneumatic, hydraulic, and electronic controls to simulate one compression stroke and a partial expansion stroke of an IC engine. The RCM will provide unprecedented optical access to

perform both laser-based and combustion pressure-based combustion diagnostics. After an extensive search for commercial manufacturers of RCMs, we narrowed down two manufacturers based in Europe. Of these two, only one manufacturer could provide us with an RCM, which is comparable in geometry to a light-duty IC engine and which also provides complete optical access while allowing easy variation of effective compression ratios. Therefore, a purchase order was placed to this Germany-based manufacturer in February 2011. The original lead time for the RCM delivery at MSU was 4-5 months until the first acceptance test and 1-2 months after that for shipment, customs, clearance, and delivery.

The RCM was custom-designed according to our specifications and requirements and manufactured by the vendor in Germany. We worked closely with the RCM vendor to coordinate their design and manufacturing efforts to meet our requirements (e.g., piston crown design, overall RCM features, etc.). In addition, a “special gas option” was identified during the design phase and subsequently requested by MSU to provide an alternative pathway for adding diluents and/or secondary fuels into the RCM. Several other unexpected issues were identified with the motor (in the RCM drive unit) and other components and were resolved with multiple conference calls between the vendor and MSU during the manufacturing process. These issues delayed construction of the RCM and the performance of the first quality control acceptance tests on-site in Germany until February 2012. The MSU PIs witnessed these tests via video conferencing and accepted the results of these preliminary tests. Subsequently, the RCM was shipped to MSU from Germany in May 2012. After clearing customs in Houston, the RCM was finally delivered at MSU on June 12, 2012. Consequently, the setup and commissioning of the RCM will occur in the next phase of the project and the proposed RCM experiments will continue soon thereafter.



Figure L1: Photograph of RCM with the driver section and controls all mounted on a cart.

Fuel injection system: To enable ignition and combustion studies in the RCM with liquid non-food biomass fuels, a high-pressure fuel injection system was needed. A US-based supplier of turnkey fuel injection systems that can be adapted to function with the RCM was identified. After lengthy technical discussions on the injection system capabilities, quotes were obtained from this supplier. The new, standalone, turnkey fuel injection system was ordered in September 2011 and delivered in January 2012. This injection system will need only compressed shop air for operation and can provide fuel injection pressures as high as 2000 bar to simulate state-of-the-art diesel injection pressures. A custom-made single-hole injector and related equipment were also ordered to ensure proper interfacing between the RCM and the fuel injection system. The fuel injection system will be integrated with the RCM in the next phase of the project.

Burner experiments: To characterize combustion temperature and mixture concentrations in flames, two different diagnostic techniques have been investigated. These include natural chemiluminescence imaging and laser-induced breakdown spectroscopy (LIBS). We have completed detailed chemiluminescence-based measurements for premixed atmospheric methane-air flames in a rectangular slot burner. A partial least-squares regression (PLS-R)-based calibration model was developed to correlate chemiluminescence data with fuel-air equivalence ratios. These results showed that the PLS-R-based model could be used effectively with chemiluminescence measurements to predict equivalence ratios in premixed methane-air flames. A peer-reviewed journal paper (in *Fuel*) and a non-peer-reviewed conference paper were published out of this effort. Subsequent efforts were directed toward performing LIBS-based measurements of fuel-air equivalence ratios on the same burner. A second peer-reviewed journal paper that presents these LIBS results has been submitted to *Fuel* is currently under review. In parallel, to continue these measurements with a more standard McKenna burner, additional modifications are also being contemplated to accommodate the McKenna burner within the present experimental setup. The basic idea in all of these efforts is to initiate and develop these diagnostics first in atmospheric flames and then translate them over to the high-pressure, high-temperature environment in the RCM.

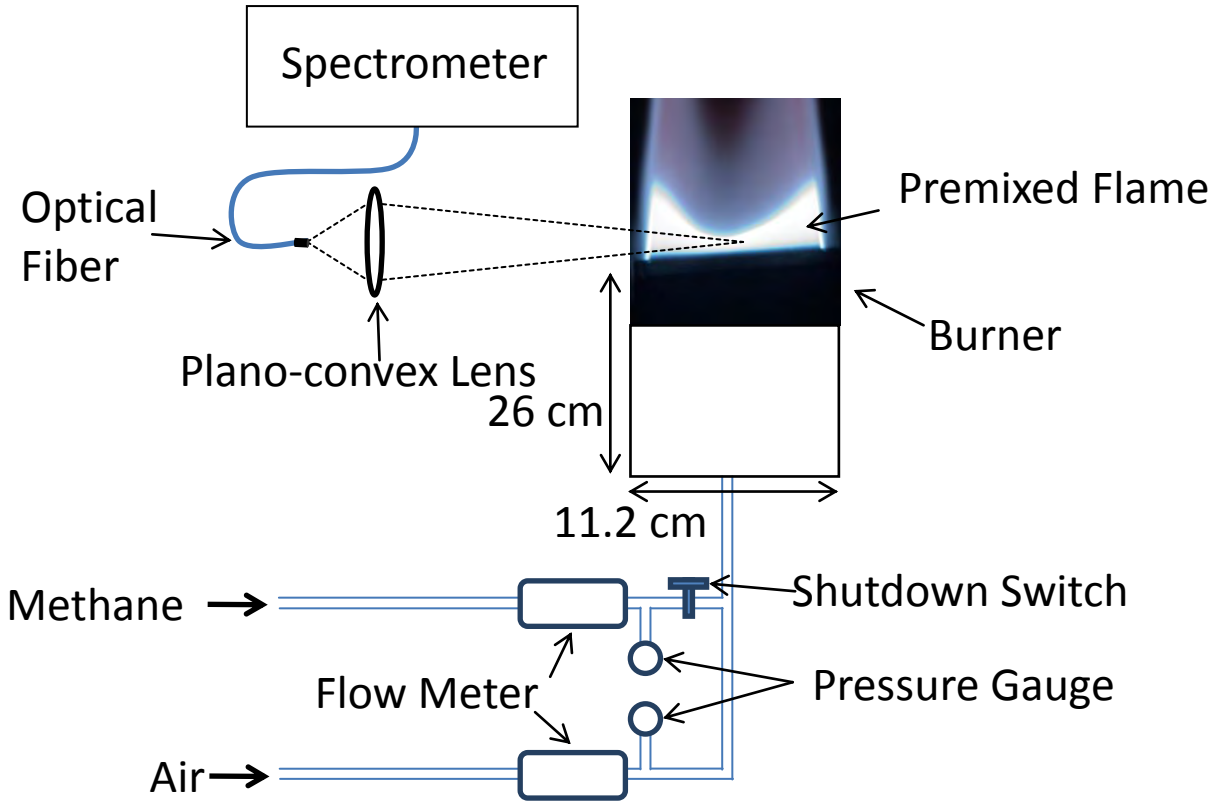


Figure L2: Schematic diagram of the experimental burner setup for spectroscopy experiments (Tripathi et al. (2012), *Fuel, 93:684-691*).

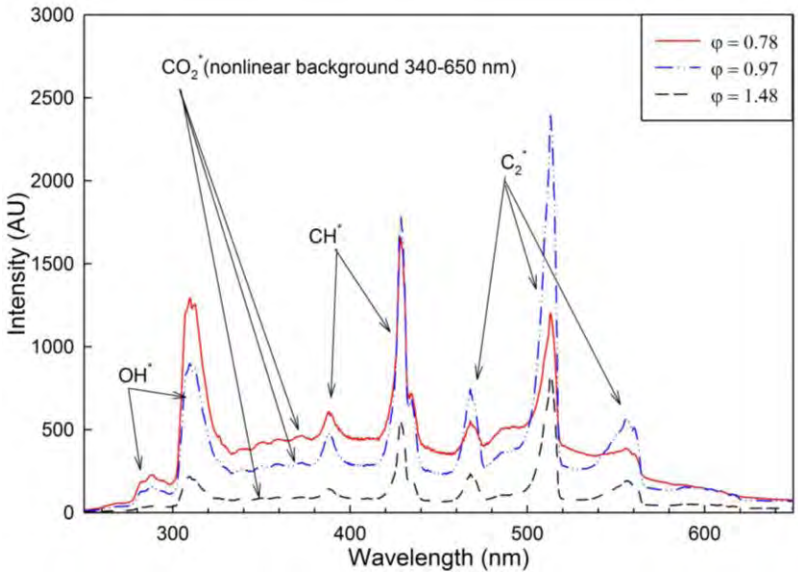


Figure L3: Chemiluminescence spectra of premixed atmospheric methane-air flames at different measured equivalence ratios (Tripathi et al. (2012), *Fuel, 93:684-691*).

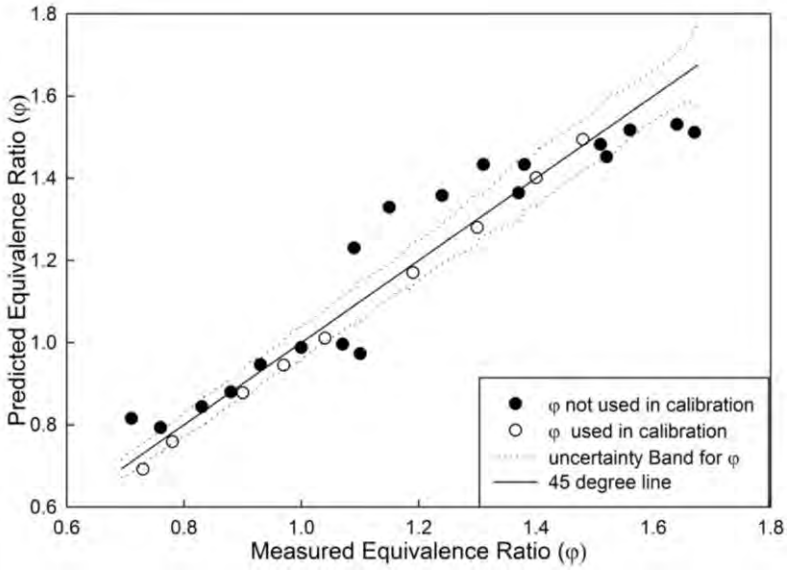


Figure L4: Comparison of equivalence ratios predicted using PLS-R-based multivariate calibration model and measured equivalence ratios for an unknown data set (Tripathi et al. (2012), *Fuel, 93:684-691*).

Ignition characteristics of dual fuel combustion: Ignition characteristics in diesel-ignited methane and diesel-ignited propane dual fuel combustion were quantified and carefully analyzed. Cyclic variations in ignition and ensemble-averaged ignition delay trends were characterized for different substitution level of the gaseous fuels and for different overall and pilot-only equivalence ratios. These results were presented in a conference paper at the ASME IC Engines Division 2011 Fall Technical Conference in Morgantown, WV. A journal manuscript based on these results is currently under review in the *Trans. ASME: Journal of Energy Resources Technology*.

Explanation of Variance:
The ignition and combustion experiments proposed in this subtask required the delivery of the RCM. Since the RCM was a custom-built device and its manufacturing faced several unforeseen difficulties as described above, its delivery was delayed due to factors outside the control of the MSU investigators. However, the RCM was finally delivered on June 12, 2012 and the proposed experiments will continue to be performed in the next phase of this project. Meanwhile, significant efforts were taken to investigate two different optical diagnostic techniques (natural chemiluminescence and LIBS) for combustion measurements in a rectangular slot burner. In addition, ignition characteristics of diesel-ignited methane and propane combustion were quantified and analyzed. These efforts provide the much needed foundation on which ignition and combustion characteristics of non-food biomass-derived fuels can be measured with the RCM in future experiments.

Subtask L.2 Demonstrate fuel injection and engine combustion strategies for non-food biomass-derived fuels

This task will focus on the demonstration of advanced fuel injection and engine combustion strategies with non-food biomass-derived fuels. Emphasis will be placed on the measurement of fuel conversion efficiencies, combustion heat release histories and mean effective pressures,

and exhaust emissions (NO_x, smoke, CO, HC, and CO_2) when operating the engine with biomass-derived fuels, and/or suitable surrogate blends. Subsequently, with input from new knowledge gained in Subtask L.1, engine performance optimization strategies will be explored with appropriate biomass-derived fuel compositions.

L.2.ML.1 To investigate fuel injection and engine combustion strategies for surrogate blends of non-food biomass-derived fuels.
L.2.ML.2 To measure baseline engine performance, combustion heat release, and exhaust emissions from non-food biomass-derived fuels and/or suitable surrogate blends.

Summary of Activities for Subtask L.2:
Detailed experiments on Volkswagen (VW) engine: A Volkswagen (VW) 1.9L 4-cylinder TDI engine was modified to operate on a variety of alternative fuels. Initially, experiments were performed with diesel to benchmark engine performance and exhaust emissions. This data facilitated later comparisons with the performance and emissions from non-food biomass fuel combustion. Four different types of alternative fuels were considered: biodiesel, methane, propane, and a renewable non-food biomass-derived liquid distillate fuel provided by a US biofuels manufacturer (KiOR) (discussed below). In the second set of experiments, straight biodiesel and biodiesel-diesel blends were tested on the engine. Subsequently, a series of "dual fueling" experiments were performed in an attempt to reduce exhaust emissions and improve engine performance. In these experiments, diesel or biodiesel were used as the "pilot" fuel (the ignition source) while methane or propane were used as the "main" fuel (providing most of the total fuel energy input). A conference paper based on the biodiesel dual fueling experiments with methane and propane was presented at the ASME IC Engines Division 2011 Fall Technical Conference. In addition, this paper has been accepted for publication in the Transactions of the ASME: Journal of Engineering for Gas Turbines and Power. Several additional refereed journal and conference papers have been published from this subtask. Sample results for combustion heat release behavior and NOx-smoke tradeoffs with biodiesel dual fueling are provided in Figs. L5 and L6.

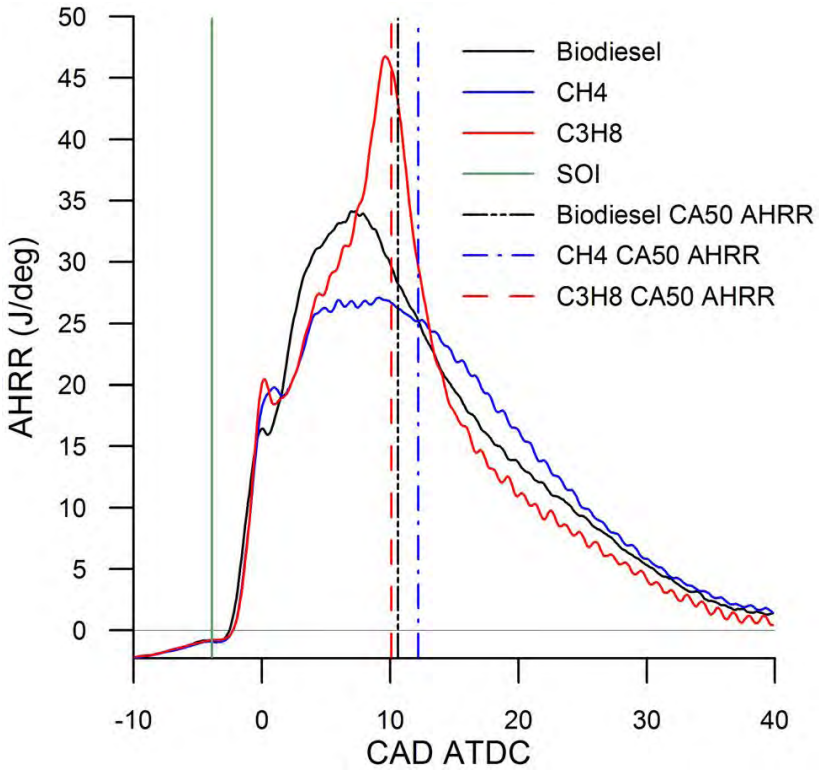


Figure L5. Apparent heat release rate (AHRR) versus CAD ATDC at 5 bar bmep. CH_4 and C_3H_8 are shown at maximum percent energy substitutions (PES) of 51% and 50%, respectively (Shoemaker et al. (2012), *Trans. ASME: J. Eng. Gas Turb. Power*).

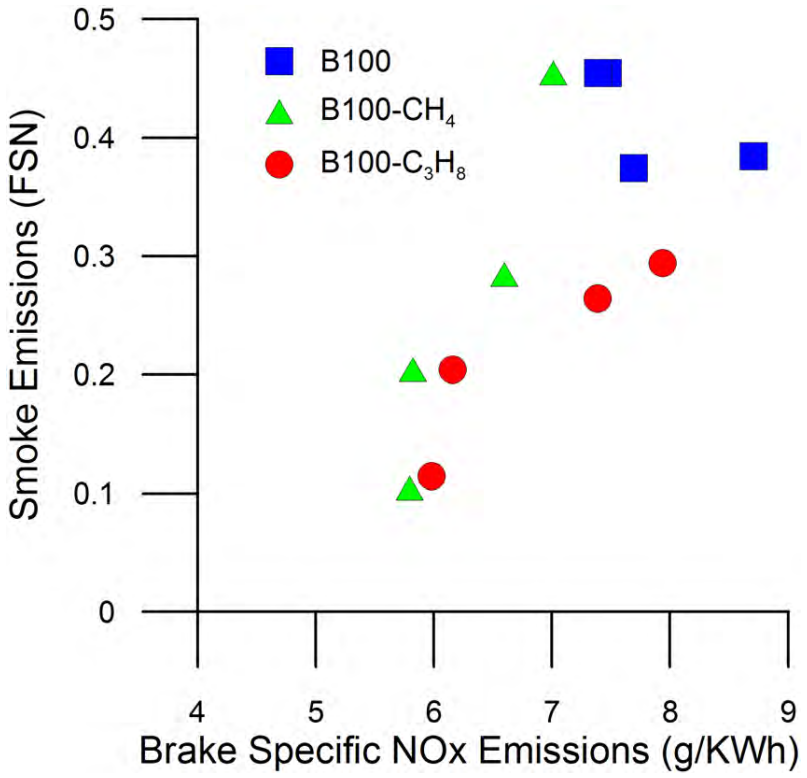


Figure L6: Smoke and NOx tradeoffs for straight biodiesel and for maximum PES of CH_4-biodiesel and C_3H_8-biodiesel dual fueling (Shoemaker et al. (2012), *Trans. ASME: J. Eng. Gas Turb. Power*).

Non-food biomass fuel experiments: Discussions were initiated with a US-based renewable second-generation biofuels manufacturer (KiOR) to obtain non-food biomass fuels (in sufficiently large quantities) for testing with the VW engine. The KiOR fuel was made available to MSU in the month of May 2011 and preliminary engine experiments were performed in the last two weeks of May. Engine performance and emissions were quantified using blends of the KiOR fuel with ultra low sulfur diesel fuel. Additionally, the effects of these fuel blends on conventional diesel engine combustion were also characterized. Since these results are proprietary, they are not included here. It is expected that these collaborative research efforts will continue in the next phase of this project.

Dual fuel low temperature combustion: Cyclic combustion variations in dual fuel low temperature combustion with diesel pilot ignition of natural gas were studied and these results were presented at the ASME 2012 IC Engines Division Spring Technical Conference in Torino, Italy.

Multi-zone model of dual fuel combustion: A multi-zone model of pilot-ignited natural gas engine combustion was developed. This model and results for dual fuel low temperature combustion were published in the Proceedings of the Institution of Mechanical Engineers (UK): Journal of Automobile Engineering. This article was cited for its high quality and won the 2010 SAGE Best Paper Award from the Editor and Editorial Board of the Journal.

Single-cylinder research engine (SCRE) setup: A single-cylinder research engine (SCRE) was set up in the new lab-space for the Advanced Combustion Engines (ACE) laboratory at MSU.

The SCRE is expected to be a complementary test platform to the VW TDI engine discussed above for understanding alternative fueled engine combustion. To facilitate operation of the SCRE, an AC (motoring) dynamometer was commissioned in one of the new test beds with the SCRE. This process involved coupling of the SCRE to the AC dynamometer, instrumenting the engine, and ensuring proper functioning of all components. The plumbing work for routing water and air into and out of the new ACE laboratory building was also completed. These plumbing efforts will facilitate the successful performance of SCRE experiments. The SCRE has been motored, some issues that need to be addressed in the drivetrain have been identified, and corrective measures were implemented to ensure proper operation of the drivetrain. The SCRE has been recently test-fired with conventional diesel fuel. Additional troubleshooting is currently underway to resolve outstanding issues with the fuel injection and data acquisition systems. Once the engine-dynamometer arrangement is functioning properly, baseline diesel experiments will be performed in the next phase of the project. Subsequently, the SCRE will be used for experiments with non-food biomass fuels.

Air compressor/dryer ordered and installed: A high-volume air compressor that is required to supply pressurized dry air to simulate turbocharging in the SCRE was purchased and installed. In addition, a heatless dessicant air dryer and an air receiver tank have also been installed. The compressor/dryer combination was commissioned in January 2012 and this currently functional system is expected to support the operation of several engines in our laboratory. The air compressor will be used to simulate turbocharging for future experiments on the SCRE.

Fundamental thermodynamic studies for engine efficiency improvements: As part of the overall effort to improve engine fuel conversion efficiencies, entropy generation in a constant internal energy-volume (UV) combustion process was modeled. The effects of different fuels and diluents on entropy generation were examined and guidelines for practical IC engine fuel conversion efficiency improvements were established. These results were recently published in a peer-reviewed research paper in the journal *Energy*. This effort involved a close collaboration between MSU engines researchers and an experimental engine combustion researcher from Argonne National Laboratory in Argonne, Illinois. We expect to continue this collaboration through the next phase of this project.

Multi-dimensional modeling of biodiesel combustion: A computational fluid dynamics (CFD) model of biodiesel combustion in the Volkswagen TDI engine was developed and validated with experimental combustion data from the ACE lab at MSU. These efforts supported the Master's thesis of an MSU graduate student who was co-advised by the MSU combustion PIs and a combustion simulation specialist from Argonne National Laboratory. The results from these efforts were presented at the 2012 Spring Technical Meeting of the Central States Section of the Combustion Institute.

Publications:

REFEREED JOURNAL PAPERS

Polk, A.C., Gibson, C.M., Shoemaker, N.T., Srinivasan, K.K., and Krishnan, S.R. (2012). Analysis of ignition behavior in a dual fuel turbocharged direct injection engine using propane and methane as primary fuels. (Under review), *Trans. ASME: Journal of Energy Resources Technology*.

Tripathi, M.M., Srinivasan, K.K., Krishnan, S.R., Yueh, F.-Y., and Singh, J.P. (2012). A comparison of multivariate LIBS and chemiluminescence-based local equivalence ratio measurements in premixed atmospheric methane-air flames. (Under review), *Fuel*.

Shoemaker, N.T., Gibson, C.M., Polk, A.C., Krishnan, S.R., and Srinivasan, K.K. (2012). Performance and emissions characteristics of bio-diesel (B100)-ignited methane and propane combustion in a four cylinder turbocharged compression ignition engine. (Accepted for publication), *Trans. ASME: Journal of Engineering for Gas Turbines and Power*.

Knizley, A.A., Srinivasan, K.K., Krishnan, S.R., and Ciatti, S.A. (2012). Fuel and diluent effects on entropy generation in a constant internal energy-volume (UV) combustion process. *Energy*, *43*(1), 315-328.

Tripathi, M.M., Krishnan, S.R., Srinivasan, K.K., Yueh, F.-Y., and Singh, J.P. (2012). Chemiluminescence-based multivariate sensing of local equivalence ratios in premixed atmospheric methane-air flames. *Fuel*, *93*, 684-691.

Gibson, C.M., Polk, A.C., Shoemaker, N.T., Srinivasan, K.K., and Krishnan, S.R. (2011). Comparison of propane and methane performance and emissions in a turbocharged direct injection dual fuel engine. *Trans. ASME: Journal of Engineering for Gas Turbines and Power, 133*(9), Article GTP-092806. (DOI: 10.1115/1.4002895).

Krishnan, S.R. and Srinivasan, K.K. (2010). Multi-zone modelling of partially premixed low-temperature combustion in pilot-ignited natural-gas engines. *Proc. IMechE, Part D: J. Automobile Engineering, 224*(D12), 1597-1622. (DOI 10.1243/09544070JAUTO1472). **NOTE:** This paper won the 2010 SAGE Best Paper Award, which was voted by the Editor and Editorial Board of the Proceedings of the Institution of Mechanical Engineers, Part D: Journal of Automobile Engineering.

Conference Papers and Posters

Peer-Reviewed Papers

K.K. Srinivasan, S.R. Krishnan, and Qi, Y., 2012, "Cyclic Combustion Variations in Dual Fuel Partially Premixed Pilot-ignited Natural Gas Engines," Paper No. ICEF2012-81145, Proceedings of the ASME 2012 Internal Combustion Engine Division Spring Technical Conference (ICES2012), May 6-9, 2012, Torino, Italy.

A. Polk, C.M. Gibson, N. Shoemaker, K.K. Srinivasan, and S.R. Krishnan, 2011, "Analysis of Ignition Behavior in a Dual Fuel Turbocharged Direct Injection Engine Using Propane and Methane as Primary Fuels," Paper No. ICEF2011-60080, Proceedings of the ASME IC Engines Division 2011 Fall Technical Conference (ICEF2011), October 2-5, Morgantown, WV.

N. Shoemaker, C.M. Gibson, A. Polk, S.R. Krishnan, and K.K. Srinivasan, 2011, "Performance and Emissions Characteristics of Bio-diesel (B100)-ignited Methane and Propane Combustion in a Four Cylinder Turbocharged Compression Ignition Engine," Paper No. ICEF2011-60081, Proceedings of the ASME IC Engines Division 2011 Fall Technical Conference (ICEF2011), October 2-5, Morgantown, WV.

C.M. Gibson, A. Polk, N. Shoemaker, K.K. Srinivasan, and S.R. Krishnan, 2010, "Comparison of Propane and Methane Performance and Emissions in a Turbocharged Direct Injection Dual Fuel Engine," Paper No. ICEF2010-35128, Proceedings of the ASME IC Engines Division 2010 Fall Technical Conference (ICEF2010), September 12-15, San Antonio, TX.

Non-Peer-Reviewed Papers and Posters

Z. Wang, K.K. Srinivasan, S.R. Krishnan, S. Som, "A computational investigation of diesel and biodiesel combustion and NOx formation in a light-duty compression ignition engine," presented at the Spring Technical Meeting of the Central States Section of the Combustion Institute, Dayton, Ohio, April 22–24, 2012.

C.M. Gibson, N.T. Shoemaker, A.C. Polk, K.K. Srinivasan, and S.R. Krishnan, "Analysis of Performance and Emissions of E85 and Diesel Dual Fueling in a Turbocharged Direct Injection Compression Ignition Engine," poster presented at MSU Bio-Fuels Conference, Starkville, MS, October 5-7, 2011.

A.C. Polk, C.M. Gibson, N.T. Shoemaker, S.R. Krishnan, and K.K. Srinivasan, "Analysis of Ignition Behavior in a Turbocharged Direct Injection Dual Fuel Engine using Propane and Methane as Primary Fuels," poster presented at MSU Bio-Fuels Conference, Starkville, MS, October 5-7, 2011.

M.M. Tripathi, S.R. Krishnan, K.K. Srinivasan, F.-Y. Yueh, J.P. Singh, "Development of a Robust Sensor for Monitoring Equivalence Ratio in Premixed Flames Using Chemiluminescence and Multivariate Data Analysis," paper presented at the 7th US National Technical Meeting of the Combustion Institute, Hosted by the Georgia Institute of Technology, Atlanta, GA, March 20-23, 2011.

A.A. Knizley, K.K. Srinivasan, S.R. Krishnan, "Fuel and Diluent Effects on Entropy Generation in a Constant Internal Energy-Volume (UV) Combustion Process," paper presented at the 7th US National Technical Meeting of the Combustion Institute, Hosted by the Georgia Institute of Technology, Atlanta, GA, March 20-23, 2011.

Invited Presentations

"Sustainable Internal Combustion Engines: Challenges and Opportunities," presented by S.R. Krishnan at the Dave C. Swalm School of Chemical Engineering, Mississippi State University, November 8, 2011.

"Dual Fuel Low Temperature Combustion - A Practical Strategy for In-Cylinder Emissions Reduction," (Invited by Session Organizer), presented by S.R. Krishnan at the 2011 Annual Meeting of the American Filtration and Separations Society, Louisville, KY, May 11, 2011.

"Next-Generation Internal Combustion Engines: Challenges, Tradeoffs, and Opportunities," presented by S.R. Krishnan at the Department of Mechanical Engineering, The University of Alabama, Tuscaloosa, AL. November 11, 2010.

"Dual Fuel Low Temperature Combustion: Opportunities and Challenges," presented by S.R. Krishnan (Opportunities) and K.K. Srinivasan (Challenges) at the Engine Research Center, University of Wisconsin-Madison, October 19, 2010. Presentation is available at the following website:

(http://mediasite.engr.wisc.edu/Mediasite/Viewer/?peid=2dc9c5e9d6f1411587f033240f55e6371d)

Task M. Biomass Feedstocks Development

Principle Investigators and team members:
Brian Baldwin, Dept. of Plant & Soil Sciences
Mike Cox, Dept. of Plant & Soil Sciences
Jeremiah Davis, Dept. of Ag. & Biological Engineering
Janet Donaldson, Dept. of Biological Sciences
Don Grebner, Dept. of Forestry
David Lang, Dept. of Plant & Soil Sciences
Rocky Lemus, Dept. of Plant & Soil Sciences
Bisoondat Macoon, Dept. of Plant & Soil Sciences, Raymond Station
Prem B. Parajuli, Dept. of Ag. & Biological Engineering
Joel O. Paz, Dept. of Ag. & Biological Engineering
Mark Shankle, Dept. of Plant & Soil Sciences, Pontotoc Station

Biomass feedstock that can be converted into liquid fuel has become the cornerstone of the US strategy to replace petroleum with renewable fuel. In addition to wood residue, this project focuses on grasses because of their substantial efficient productivity. Two perennial grass species, switchgrass and giant miscanthus, have shown promise of producing high yields in the southeastern US. In this project, we will conduct studies to determine yields and handling of several feedstocks that contribute to the DOE cellulosic platform. We have narrowed our focus to a limited number of grass species, in addition to woody residue, in order to assess sustainability of these crops.

Establishment of switchgrass and giant miscanthus is critical for their acceptance by the producer. Minimal herbicide options are available for control of weedy grass species during the establishment year of these species. Weed control during the establishment year directly impacts yields of subsequent fields. Challenging the sustainable production of cellulosic biomass is low cost availability of nitrogen (N). Grass feedstock yields are typically limited by soil N availability, yet the expense of producing N fertilizer can undermine the cost-effective production of biomass. Single, end-of-season harvest testing will be evaluated for nutrient origin and cycling. Application of char, a by-product of gasification and bio-oil production, has the potential to raise the soil organic matter and enhance soil structure, water holding capacity, and productivity. Little is known about suitable application rates and how these amendments will enhance soil sustainability and crop yields. High value crops (i.e. corn, soya, cotton, rice) are typically planted on rich land while forage and biomass crops are usually planted on more marginal/poor land. To avoid competition with food cropping systems, an effort to establish these grasses on marginal pasture and Conservation Reserve Program (CRP) lands will be made, but herbicides that will kill existing vegetation without adversely affecting the biomass crop need to be researched. Mississippi has wood residue resources estimated at four million dry tons with capturable wood residues estimated at 2.1 million dry tons each year. This quantity could support the production of 131 million gallons of cellulosic ethanol, but optimal location and production efficiencies have yet to be determined. While feedstock is widely available, the cost of feedstock may not be economical to convert it into transportation fuel. Determination of handling, densification, and bottlenecks in preparing biomass-based feedstocks for conversion is also necessary.

The primary objectives of this research include the following: 1) field establishment of candidate species and yield comparisons utilizing larger scale plots in coordinated field trials; 2) initiation of methods to determine N and carbon (C) cycling within the soil-plant continuum, and effect of fertilizer type and weathering on the feedstock; 3) augmentation of sustainability with the integration of winter N_2 fixing legumes into the system and assessing potential associative nitrogen fixation; 4) estimation of wood residue volumes generated from the forest products industry of Mississippi; and 5) evaluation of the economics of different harvesting, densification, storage, and transportation systems in the southeastern US.

While there is patentable IP disclosed in this report, the process for "Freedom" giant miscanthus, "Tusca II" and "Expresso" switchgrass are far enough ahead to make disclosure in this document moot.

Executive Summary:

M1, ML1 Testing candidate species, establishment, land conversion:
Establishment of seeded materials to give an advantage over weeds has been extremely difficult. Four seed coatings/treatments designed to enhance germination and therefore establishment failed to perform as expected. Seed safener, an antidote to broad spectrum herbicides, worked extremely well at Starkville, MS, and four other locations around the country. Weed control was so complete that the crop was fertilized in the establishment year, which isnot a normal practice. Uniform variety trials from 2011 failed due in part to very hot, dry weather. Establishment of seeded and rhizome propagated materials indicated significantly better establishment with complete control of competing species. Giant miscanthus was negatively impacted by any competition. Energycane screening for cold hardiness, a collaborative effort with USDA-ARS, continues. Energycane's high yields (10-23 US T/A) make it a potential candidate for biomass production. We have accepted newly developed genotypes for screening.

M2 ML1 Management, nutrient cycling and biochar use:
Warm season annual grasses have a niche in the new-to-biofuel user. These species can be incorporated into a farming situation without long term investment in establishment, which for perennial grasses is about three years. Sorghum and pearl millet fit this niche. Testing of these indicate Pacesetter (sorghum) and pearl millet have the highest yield (~2.5 ton/acre). Across years of testing, annual sorghum dry matter yield was greater at the lower N application rate. Both single and double harvest produced equal yields. As harvest frequency increased to three and six harvests per year, yield decreased. Experiments to determine soil-borne nitrogen fixing bacteria aid in the nutrition of these plants seem to suggest that neither switchgrass nor giant miscanthus benefit from associations with these bacteria, but energycane may. Application of the "waste product" biochar from pyrolysis processes would be a method of raising soil carbon and retaining nutrients against leaching. Pot studies with varying amounts of biochar indicate a linear decrease in soybean and corn biomass with increasing char application.

M3 Wood residue:
Survey of wood mills resulted in a 22% return rate. The survey indicated 63% of the waste wood was chips, but of that, 99% was reused and contributed $35,000/month to mill revenue. This indicates that about 1% (120,000 T/yr) of wood residue would be available for use in the biofuels industry. Transportation costs were the main constraint.

M4 Feedstock engineering:

A maize stover yield model was used to determine its potential as a feedstock. Net energy value and carbon credit balance were positive for corn in the western region of the Mississippi Delta. Transportation costs were the primary limitation to use. In an effort to enhance adoption of these grasses, potential use as poultry litter, replacing pine shavings, was attempted. Estimates of 3-6 acres/house (30 tons) were used. One inch to three inch grass was an excellent replacement for pine shavings; however, there was difficulty in grinding the straw. Harvesting this straw for use requires safe storage. Methods to evaluate various storage methods indicated baling was probably still the best storage method. Moisture probes were tested with poor accuracy. Increasing straw density increased accuracy.

Native warm season grasses (NWSG) have received much attention over the last 25 years for their ability to persist under hot, dry conditions and thrive in marginal soils (Smith et al., 2009). With increased research in genetics and breeding, many species have shown promise for use as forage and hay crops, wildlife habitat, in land reclamation, and for bio-fuel/cellulosic ethanol production. Many popular NWSG species exhibit several forms of seed dormancy, which contribute to increased cost associated with establishment. Four species (lowland switchgrass[*Panicum virgatum* (L.)], eastern gamagrass [*Tripsacum dactyloidies* (L.)], indiangrass [*Sorghastrum nutans* (L.)(Nash)], and little bluestem [*Schizachyrium scoparium* (Michx. (Nash)]) were studied for effects of seed coating and exogenous chemical application on seed germination and establishment. Annual warm-season grasses such as forage sorghum, sorghum x sudangrass hybrid, and sundangrass are highly productive and valuable feed crops (rotational crop and silage). Many of these crops could also be used as possible biofuel crops. Sugar in the stems of these warm-season grasses can be extracted and fermented, while the cellulose in the bagasse (pressed stalk) can be used for feedstock for cellulosic ethanol, making these very versatile crops. Twelve annual warm-season grasses, including forage sorghums, sudangrass, sorghum x sudangrass hybrid, and pearl millet, were planted in 1.82 x 3.35 m plots and harvested as silage and hay before sap and after sap removal. Varieties were evaluated for sap production, dry matter yield (DM), °Brix, crude protein (CP), Neutral Detergent Fiber (NDF), and Acid Detergent Fiber (ADF). Ensiling the residual biomass after pressing to remove sap did not reduce the quality of the silage, suggesting that it is possible to utilize annual warm-season grass for sap production and still ensile the biomass to provide high quality feed for ruminants.
Recruiting large numbers of producers to begin growing energy crops such as switchgrass and giant miscanthus has been difficult without incentives because there is not a strong and sustained commodity market. The U.S. commercial poultry industry (roughly 100,000 broiler house or 25,000 growers) provides a unique entry-point opportunity for biomass feedstock production in the Southeast US. Poultry growers can grow energy grasses for both poultry bedding and for energy feedstock. Data shows that we can successfully use chopped energy grasses such as switchgrass and giant miscanthus to provide poultry bedding as an alternative to pine shavings (Davis et al., 2011). The grasses can be processed in commercially available machines, but industry cooperators are making refinements. Many growers are volunteering their farms for bedding opportunities alone. This project is a benefit to farmers and growers because it provides a direct benefit for energy grass production until a dependable commodity price is stabilized.

The goal of our second set of studies was to determine the spatial distribution of the potential bio-energy crops and their environmental benefits, such as soil organic carbon (SOC) and water quality in Mississippi for renewable fuels through economic modeling and analysis. The

objective of this research was to monitor SOC due to the change of agricultural management practices in agricultural fields and use models to identify the relationships between SOC and other hydrologic and water quality parameters. Our work toward meeting those objectives will be continued in SERC IV.

The preliminary carbon analysis of the soil samples showed that the majority of carbon was determined in the 6 inch depth (compared to 12 inches and 24 inches); more carbon was available in forestland and pastureland than in the cropland. Model simulations from the two watersheds (Town Creek and Upper Pearl River) determined the negative correlation between available moisture content and carbon content in the soil, which may be sample size dependent. The economic model, including a cost calculator, was developed for the economic analysis of bio-gasification systems.

The only project in this group that was not completed on time was the Uniform Variety Trials, due in part to dry weather. Those materials were propagated during the fall and winter of last quarter and are going into the ground as of March 2012.

Subtask M.1 Testing, establishment of candidate species, and conversion of pasture/CRP land to candidate species

Conduct coordinated yield trials with uniform cultivars of primary grassy cellulosic crops at multiple locations around Mississippi. Assess labeled herbicides for tilled establishment and no-till establishment of switchgrass and giant miscanthus.

Planned Activities:

M.1.ML.1 Successful establishment of Uniform Variety Trials at six to eight locations around Mississippi, with continued testing of herbicides to enhance successful establishment under both tillage and no-tillage conditions.

Summarization of Activities:

Uniform Variety Trials:
Establishment of the Uniform Variety Trials was a failure at all locations in 2011. Failure was primarily due to hot, dry weather. Dr. Lemus, in collaboration with Josh White, has taken over that portion of the project, and since the first quarter of 2012 has moved forward with establishment of the replacement trials. Nine switchgrass cultivars and three giant miscanthus clones have been entered in the test at six locations in Mississippi from Holly Springs in the north to White Sands in the south.

Establishment of Candidate species:
Seed coatings, chemical and hormonal
The term native warm-season grass (NWSG) refers to a group of grasses – and occasionally native forbs – that are historically native to the Great Plains states and most of North America, from California to the Southeast (Hamrick et al., 2007). The NWSG group is comprised of annual and perennial plants that grow during the late spring through the warm months of the year, initiate jointing in the late summer, and typically go dormant through most of the fall and winter (Harper et al., 2004). Many of the native grasslands that existed in North America centuries ago were eventually developed as cultivated cropland or pasture for livestock, while native plants were replaced with exotic grasses for their higher forage quality, ease of establishment, and ability to withstand heavy grazing (Hamrick et al., 2007).

Native warm season grasses have seen a resurgence in popularity over the last 25 years for use as quality forage and hay crops, wildlife habitat, and land reclamation. Another interest in NWSG is in the field of renewable energy in the form of cellulosic biofuel production and co-firing. While switchgrass has become by far the most popular NWSG for consideration in the renewable energy forum, improved varieties of eastern gamagrass, little bluestem, and indiangrass have shown promise as feedstocks for renewable energy production as well as productive forage crops and quality wildlife habitat.

While NWSG have been growing on the plains of the Unites States for centuries, modern production of many species has been slow to evolve due to difficulties with germination and establishment. All NWSG do not exhibit the same types or levels of dormancy, nor do they maintain their dormancies with the same severity. Traditionally**,** after-ripening (dry storage of freshly harvested, mature seeds at room temperature for a period of several months) is used to break primary dormancy and to promote germination in many grass species (Bewley, 1997; Finch-Savage and Leubner-Metzger, 2006; Kucera et al., 2005; Leubner-Metzger, 2003). In laboratory tests, after-ripened seeds display increased vigor and germination percentage when compared to freshly harvested seed as well as an ability to germinate under a wider range of temperatures (Leubner-Metzger, 2005). This period of after-ripening is also reported to affect levels of and sensitivity to endogenous abscisic acid (ABA), increased gibberellic acid (GA) sensitivity, and increased sensitivity and response to light treatment (Leubner-Metzger, 2002). While the process of after-ripening has been shown to increase germination of many NWSG, percentages remain low and inconsistent.

Modern research has shown that several species require long periods of cold, moist stratification to break primary dormancy of seeds before they can be planted. Mechanical scarification is also a popular method to improve germination of seeds that exhibit physical or mechanical dormancy. Recent studies have shown that the use of hydrogen peroxide (H_2O_2) can substitute for the long process of stratification in many native grass species (Klein et al., 2007).

The current research project is focusing on improving germination and establishment of NWSG and evaluating their capacity to serve as dual purpose (forage and biomass) crops. This project has two major objectives: 1) to evaluate the effects of seed coatings and various exogenous chemical and hormonal treatments on seed germination, coleoptile elongation, and seedling health; and 2) to quantify these effects in relation to planting date via controlled laboratory experiments and field studies.

Materials and Methods:
This project incorporates two commercial seed coatings, a corn starch-based hydration polymer and a proprietary abiotic micro- and macronutrient blend, along with two exogenous chemical and hormonal treatments tested at 5 different rates. These treatments are being applied to four species (11 cultivars total) of NWSG. The species being studied are lowland switchgrass (*Panicum virgatum)*, eastern gamagrass (*Tripsacum dactyloidies*), indiangrass (*Sorghastrum nutans*), and little bluestem (*Schizachyrium scoparium*). These species were chosen based on their proven value as long living perennial forage species and their high biomass yield potential.

Planned activities include the incorporation of these species into laboratory experiments with the aforementioned treatments to establish dose-response curves. After completion of dose-response testing, treatments with significant contributions to increasing germination will be utilized in field studies. Field studies will include the planting of all species and significant

treatments in single ten foot rows with three replications in Starkville, MS. This planting study will be replicated in April, June, and August of 2012 and again on the same dates in 2013. Concurrently with this study, a replicate study will be carried out in the laboratory using temperature and daylight controlled growth chambers. Growth chamber studies will include all treatments from the field study, replicated three times at six temperature and light regimes. Seed coating treatments may not be evaluated in lab studies, as previous literature has cited the inability of laboratory materials to replicate acceptable soil aggregate and moisture qualities for coatings to maintain their structural integrity.

Field plantings will be evaluated at 30, 60, and 90 days after planting to track germination and establishment. These studies will be harvested in November of 2012 and 2013 and measured for biomass accumulation relative to planting date and treatment. Germination, establishment, and total biomass accumulation will also be evaluated for effects due to air temperature, soil temperature, and available soil moisture.

Results and Discussion:
Preliminary laboratory research has utilized temperature, light, and day-length controlled growth chambers to simulate optimum environmental conditions for germination. This experiment was a completely randomized factorial study replicated four times where seed germination was recorded daily for 28 days. During this study, chemical and hormonal treatments generated significant increases in germination of several NWSG cultivars in 1-3 days over controls. Hydrogen peroxide treatments have increased germination of eastern gamagrass cultivars significantly (20%) over control treatments at 28 days, while exogenously applied gibberellic acid (GA) has yielded increases in germination, root, and shoot lengths at 3-5 days after emergence in indiangrass and little bluestem. Indiangrass germination rates of 40-50% have been achieved using GA treatments, compared to 25-30% germination in control treatments. Little bluestem germination has reached >70% in GA treated lots, while untreated lots average 50-55%. Switchgrass has responded to lower concentrations of GA and hydrogen peroxide, but laboratory results have been mixed. In some cases, chemical and hormonal treatments have yielded germination rates in excess of 90% in less than 7 days. Seed viability of some NWSG cultivars was also discovered to be very low in preliminary studies.

Freedom Pilot Plant Feedstock:
Twenty acres of Freedom giant miscanthus were planted at the MSU dairy in Sessums, MS, near Starkville on May 18, 2011. These 20 acres will serve as the primary feedstock source for a cellulosic pilot plant scheduled to be built on the Starkville campus. Planting materials and equipment were supplied by Repreve Renewables.

Foundation blocks of Freedom germplasm were sprayed for broadleaf weed control (2,4-d Amine) and fertilized with nitrogen, phosphorous, and potassium (50 lbs of N using 15-5-10). Due to unseasonably warm late-winter temperatures, emergence was recorded at the first week of March. Freedom plantings at the dairy emerged a week later due to wetter soil conditions on the site. No fertilizer or herbicide was applied. The eastern portion of the planting (5 acres) did not establish well, and therefore did not emerge in the spring. However, the western field (20 acres) did establish fairly well, with roughly 50% coverage in miscanthus seedlings.

Cold Screening of Energycane:
Energycane genotypes reported on last quarter for cold screening were planted in Starkville on May 10, 2011. Originally, 41 genotypes were scheduled to be planted but were reduced to 28 genotypes due to insufficient planting materials. Additionally, seedlings of new energycane families that were transported from USDA-ARS in Houma, LA to Starkville were planted on May

2, 2011. Mortality of several energycane families was suffered during transportation, resulting in the planting of 22 new families instead of the original 27 families.

All entries for the cold-tolerance screening emerged this spring. Some half-sibs within each row were slower to emerge than others. All rows were sprayed with glyphosate (Cornerstone Plus®) prior to emergence to control all cool-season weeds. The plots were then fertilized with nitrogen, phosphorous, and potassium (50 lbs of N using 15-5-10) just following emergence. Spot treatment weed control was conducted using the aforementioned glyphosate as weed problems arose.

Establishment of Candidate Species:
Information from SERC II on seed safening indicated good control of weedy species in switchgrass establishment. The results of that testing have been expanded to the establishment of this phase's Uniform Variety Trials. Inspection of those locations planted the longest indicate excellent weed control.

Dose response testing of the safener Concep III® (fluxofenim) and the effects on germination of little bluestem, big bluestem, and indiangrass was conducted. Five rates of safener were applied as a seed soak to the candidate species to determine optimum rate to apply to field planted seed. Germination trials and statistical analysis were completed.

Successful establishment of switchgrass into existing pasture or CRP land under no-tillage conditions:
Giant miscanthus and switchgrass were planted into existing pasture and CRP land without tillage. Plants were transferred to the field by mid-July 2011 with 96% survival into pasture as of March 2012 and 68% survival into CRP land. Miscanthus plants were spaced on 2 meter centers into killed vegetation, and spreading of miscanthus will be followed over 1 to 3 years. This would be similar to planting trees by hand, and may allow for miscanthus to be established into existing vegetation without tillage. Plots are replicated four times. Diameter of the plants in March 2012 range from 15 to 45 cm. Switchgrass stands ranged from 5 to 50%.

Weed management practices and planting systems for the establishment of switchgrass:
Weed management practices and planting systems for the establishment of switchgrass were evaluated in 2010 and 2011 at the Pontotoc Ridge-Flatwoods Experiment Station in Pontotoc County, MS. Weed control studies were established on a Bude silt loam (fine-silty, mixed, thermic Glossaquic Fragiudalfs) with a history of row crop production in 2010 and an Atwood silt loam (fine-silty, mixed, thermic Typic Paleududalfs) with a history of being fallow for at least tenyears in 2011. The design was a randomized complete block (RCB) with 4 replications. Plot size was 6 x 30 ft with a 6 ft buffer strip between plots to ensure no overlapping of herbicide treatments. Due to the inherent nature of switchgrass to germinate and emerge erratically, fertilizer was not applied in order to minimize rapid weed growth that would compete and interfere with switchgrass establishment. Switchgrass was planted with a Great Plains™ no-till grain drill equipped with a small seed attachment sectioned to deliver 9 rows spaced 7.5 in apart.

In 2010, a field utilized for production of glyphosate tolerant no-till soybean the previous year received a burndown treatment of Roundup WeatherMax at 21 oz/ac (0.75 lb ae/ac) applied two weeks prior to planting. Switchgrass was planted into the no-tillage environment at a rate of 6 lb of Pure Live Seed (PLS)/ac on June 2. In 2011, a field left fallow for at least 10 years was prepared by conventional tillage methods in March followed by an undisturbed two month period to establish a firm seedbed. At two weeks prior to planting, Roundup WeatherMax at 21 oz/ac

was applied to remove any emerged weeds prior to planting. Switchgrass was planted into a stale seed bed on June 9 at a rate of 6 lb/PLS/ac. Herbicide treatments included in both 2010 and 2011 studies were the following: Ally 0.25 oz/ac; Accent 0.75 oz/ac; Pastora 0.881, 1.0, and 1.5 oz/ac; Atrazine 2 qt/ac; Accent 0.75 oz/ac + Atrazine 2 qt/ac; Pastora 1.0 oz/ac + Atrazine 2 qt/ac; Pastora 1.0 oz/ac + Atrazine 2 qt/ac; and an Untreated Check. In addition to herbicide treatments, mowing/clipping treatments were made at approximately 3, 4, and 5 weeks after herbicide treatment to evaluate their impact on weed control, switchgrass establishment, and yield. In 2010, additional herbicide treatments were included but were not repeated in 2011 due to an unacceptable level of phototoxicity to switchgrass. Data was collected throughout the growing season for weed control, switchgrass injury, and percent stand of switchgrass in both years. Switchgrass was harvested January 11, 2011, and February 9, 2012, for 2010 and 2011 establishment years, respectively. Second year stand ratings were made in the spring following the establishment year.

Planting Systems for Switchgrass on Marginal Land:
Studies of switchgrass planting systems were established in 2010 and 2011 on marginal land that would qualify to be entered into the Conservation Reserve Program (CRP). The soil type for both years was an Atwood silt loam (fine-silty, mixed, thermic Typic Paleududalfs). The design was an RCB with 3 replications in 2010 and an RCB with 4 replications in 2011. Plot size was 12 x 50 ft. Fertilizer was not applied in order to minimize a weed growth that would compete and interfere with switchgrass emergence. Switchgrass plantings were made with a Great Plains™ no-till grain drill equipped with a small seed attachment sectioned to deliver nine rows spaced 7.5 in. apart or broadcast with a mechanical seed sower. Switchgrass was planted on July 1, 2010, and June 9, 2011, at 6 lb/PLS/ac. Roundup WeatherMax at 21 oz/ac was applied two weeks prior to planting to ensure a clean seedbed at planting. Planting system treatments included the following: No-till Drilled; No-till Drilled + Cultipacking; No-till broadcast; No-till broadcast + Cultipacking; Conventional-till + Cultipacking + Drilled; Conventional-till + Cultipacking + Drilled + Cultipacking; Conventional-till + Cultipacking + Broadcast + Cultipacking; Conventional-till + Cultipacking + Broadcast; and Conventional-till + Broadcast + Cultipacking. Ratings for percent stand of switchgrass were made during the establishment year for both trials. Weed management practices employed to minimize competition include rotary mowing, broadcast, and wick-bar herbicide applications. The 2010 study was not harvested following the establishment year due to insufficient biomass production. Both studies were harvested on February 9, 2012; second year yield for the 2010 trial and first year yield for the 2011 trial. The studies were rated for percent stand and vigor in the spring of 2012. In the spring of 2012, plots were split and ammonia nitrate at 60 lb N/ac was applied to half the plot to evaluate the effects of N on second and third year switchgrass growth.

Subtask M.2 Management, nutrient cycling, and char usage

Experiments will be initiated on existing plots of feedstocks to study several very important production elements. The experiments will follow standard agronomic field experimental methods and include:

- determine N translocation, removal, and nutrient use efficiency
- study the potential of associative nitrogen fixation (ANF) with feedstock species
- determine the N value of seeding winter annual legumes to the production system
- conduct preliminary greenhouse and field experiments on application of char to soil, its affect on plant production, and potential effect on soil properties

Planned Activities:
M.2.ML.1 Provide a second year assessment of the movement of N within feedstock species, assessing feedstock species' potential of associative nitrogen fixation, determine N value of legume mediated nitrogen fixation, and obtain baseline data on appropriate char application rates.

Summarization of Activities:

Utilization of Annual Warm Season Grasses as a Biofuel Source and Feedstock By-Product:
Although millets, sorghums, and sudangrass only encompass a small percentage of hectares in Mississippi (25,000 ha), variety trials have shown that acceptable yields can be obtained. Variety trials in Mississippi have reported millet annual DM yields of 8519 kg ha^{-1} and sorghum-sudangrass yields of 6422 kg ha^{-1}(Edwards Ned C., 1991). Due to the high moisture content and digestibility of these grasses, they are most commonly utilized as silage or greenchop. Sap of most sorghum is mainly sucrose, which can be easily fermented for ethanol production without any pretreatment. Related literature considering the use of sorghums for ethanol focuses on the utilization of the entire plant (cellulose and hemicelluloses) for eventual fermentation. However, this involves a pretreatment of the whole plant and usually considers BMR varieties with lower lignin content (Corredor et. al, 2009). Other trials utilized sweet sorghum varieties common in syrup production for sap removal with the bagasse (residual biomass) being alternatively converted to energy via co-firing or further enzymatic treatment (Vermerris et. al, 2011). More data is needed that considers the use of annual grasses for sap production and simple ethanol production while utilizing the bagasse for silage, which would simplify the fermentation process while still providing on-farm feedstock for ruminants. The purpose of this project was to evaluate the performance of several varieties of annual warm season grasses with high sugar content as dual purpose crops for simultaneous ethanol and silage production.

Materials and Methods:
The experimental design was a randomized complete block replicated four times. The study included 12 annual warm season grasses, which included forage sorghums, sudangrass, sorghum x sudangrass hybrid, and pearl millet. All plots were planted at a seeding rate of 28 kg ha^{-1} in a 1.82 m x 3.35 m plot and were located in Starkville, MS with Marietta fine sandy loam. Plots were harvested when 50% of the plots were in the boot stage. Plots were fertilized with 56 kg N ha^{-1} using urea ammonium sulfate. Prior to harvest, plant population measurements were taken using two 1m^2 quadrants placed sequentially in the middle of each plot. Eight stalks were cut at a height of 7.5 cm from the ground for sap extraction; fresh weight (including leaves and stems) was recorded. Sap was extracted from whole plant using a sugar cane press and sap weight, and volume and °Brix were recorded. Estimated sap production (ESP) was calculated using the total volume of sap production from 4 plants multiplied by the number of plants in a 1m^2. Half of the bagasse was processed for silage and half was oven dried at 66°C and analyzed for nutritive value. Plots were harvested (chopped) for total yield and a subsample was collected for dry matter determination and ensiling. Data was analyzed using the General Linear Model of SAS and mean separation was done using the least significant difference (LSD) at $\alpha = 0.05$.

Results and Discussions:

When considering DM yields, Piper sudangrass and King BMR had the lowest yields. Pearl millet, Green Grazer V, and Pace Setter had the greatest DM yields (Table M1). When observing ESP, however, DM yield did not always similarly describe sap production. Sweet-N-Honey II was one of the greatest sap producers 11244 L ha^{-1}, producing 66% more sap than pearl millet. Quality of sap measured in °Brix was similar among all varieties.

Hay and silage samples that were not crushed and removed of sap had greater ADF and NDF values than silage samples that were crushed before ensiling. However, silage subjected to crushing was higher in TDN and CP. The relative better quality observed in the silage that was crushed for sap production may have been due to the removal of fermentable simple sugars from the biomass, thus inhibiting microbial processes and the production of lactic acid. Data suggest that utilizing warm season annual grasses such as sorghums may be a viable source for fermentable sugars while the remaining bagasse can still provide adequate forage for ruminants through ensiling.

Table M1: Dry Matter (DM) yield and Estimated Sap Production (ESP) of 12 different sorghum/sudangrass species and varieties.

Variety	DM Yield	Estimated Sap Production†
	kg ha^{-1}	L ha^{-1}
Piper	1389	1170
Green Grazer V	5573	7556
Forage King BMR	4399	7475
King BMR	2455	1260
Monarch V	3568	1305
Pace Setter	6113	9861
Pace Setter BMR	3045	5100
Sweeter-N-Honey II BMR	2622	6370
Sweeter-N-Honey II	5154	11243
Sweeter-N-Honey BMR	2656	10205
Pearl Millet FSG300	6398	3861
Cowvittles	4404	7940
Mean	3981	6442
LSD (0.05)	1192	2444

†ESP was calculated using sap production from 4 random plants in the plots and multiplied by the number of plants within a m^2

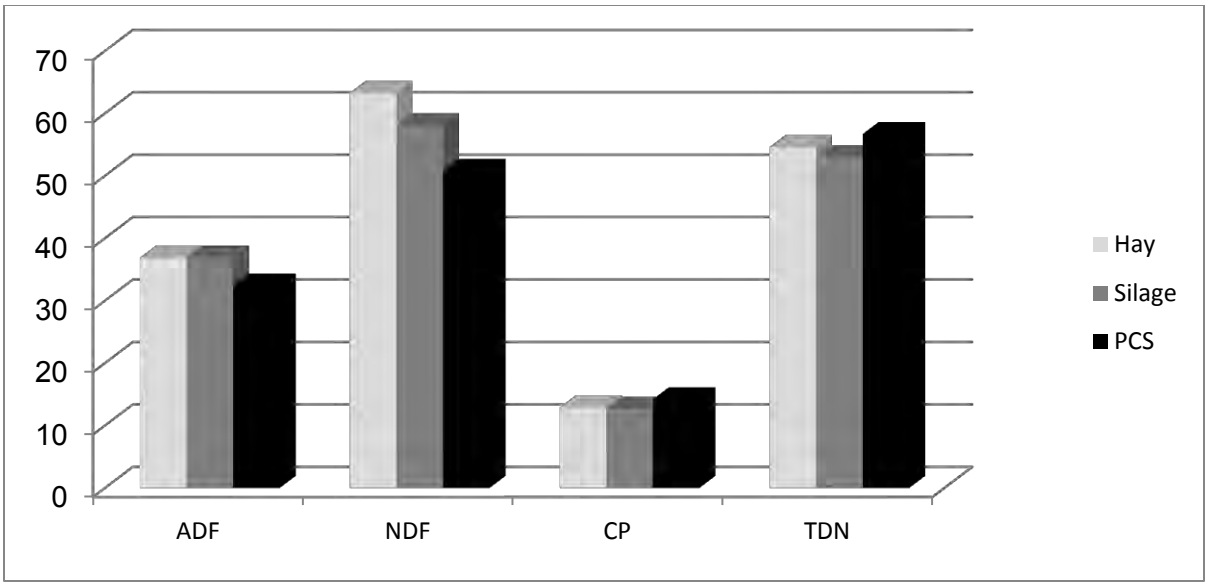


Figure M1: NDF, ADF, CP and TDN of values pooled from 12 different annual grass varieties and treated as hay, silage, and post crushed silage (PCS).

Potential of associative nitrogen fixation (ANF) with feedstock species:

The hypothesis for this subtask was that feedstock grasses will have different capabilities of supporting the growth of associative nitrogen fixing bacteria, and therefore will exhibit different amounts of nitrogen fixation. To test this hypothesis, two experiments were designed to assess the net flux of N into plants and soils growing grass-based feedstocks (giant miscanthus, switchgrass, energycane, and sugarcane). The first experiment entailed a field study including four replicates of each feedstock to each treatment. These grasses were established between Nov 2009 and March 2010 in a replicated block design (~18ft^2) at South Farm at Mississippi State University. Unfortunately, sugarcane had very low survival rates and was removed from the field study experiment. Soil was collected from the plots on May 2010 and again in December 2010, May 2011, and December 2011. Soil samples were collected from each plot at two depths (0-10cm and 10-30cm from surface), and dN^{15} values were analyzed using isotope ratio mass spectrometry. Our results show that energycane and miscanthus exhibited a significant decrease in dN15 values, indicating that these feedstock grasses may have efficient associative nitrogen fixing bacteria (Table M2).

Table M2: Field Study Data with dN15 values obtained from Switchgrass (SWG), Energycane (ECN), and Miscanthus (MSC) in relation to Sorghum control (CTR).

	2010 May		**2010 December**		**2011 May**	**2011 December**
Grass Type	**0-10cm depth ±SE**	**10-30cm depth ±SE**	**1-10cm depth ±SE**	**10-30cm depth ±SE**	**0-10cm depth ±SE**	**0-10cm depth ±SE**
SWG	6.5 ±0.2^{cd}	7.3 ±0.31	6.4 ±0.1^{cde}	7.7 ±0.2	6.5 ±0.4^{cd}	6.7 ±0.02^{bc}
ECN	6.4 ±0.2^{cde}	7.0 ±0.1	6.3 ±0.2^{de}	7.6 ±0.1	6.1 ±0.2^{ef}	5.6 ±0.03^{f}
MSC	6.3 ±0.3^{de}	7.2 ±0.1	6.5 ±0.2^{cd}	7.5 ±0.1	6.4 ±0.4^{cde}	5.9 ±0.02^{f}
CTR			6.9 ±0.1^{b}	7.8 ±0.04	6.6±0.1^{bcd}	7.3 ±0.2^{a}
Values with different superscripts within a row are significantly different (p < 0.05)						

The dN15 values have also been determined for the roots and shoots, specifically for giant miscanthus, switchgrass, and energycane. Our data indicate that energycane had a significantly higher amount of nitrogen fixation associated with the roots in comparison to giant miscanthus and switchgrass.

To verify the field studies, a second experiment was designed utilizing a greenhouse-based approach to study the associative nitrogen fixation properties of giant miscanthus, switchgrass, energycane, and sugarcane. For this study, three pots for each feedstock were utilized and injected with $^{15}N_2$. Root and shoot samples were collected from each grass and analyzed by isotope ratio mass spectrometry. Our results indicate that the shoots of energycane and sugarcane both have efficient nitrogen fixing potentials. Values were not significantly different for giant miscanthus and switchgrass.

Together, these data suggest that giant miscanthus and switchgrass do not have associative nitrogen fixing bacteria. It will be necessary to further analyze the microbial communities associated with these four feedstocks to determine what differences do exist and to determine whether the community can be altered in order to increase nitrogen fixation.

Nitrogen and Biomass Yield:
Three separate experiments were planned for Phase III studies at the Raymond location. Experiment 1 studied defoliation frequency and N fertilizer effect on biomass yield, nutrient removal, soil carbon accumulation, and plant persistence of Alamo switchgrass. This experiment was initiated during SERC II, but because of the long-term nature of this study, it was continued during Phase III. Experiment 2 quantified physiological changes in switchgrass plants throughout the seasonal cycle in response to N fertilizer at different levels. Experiment 3 was planned to evaluate effects of different fertilizer management on two switchgrass entries, the industry standard variety Alamo and an experimental line from the Noble Foundation, which was selected because it produced the greatest biomass yield among 10 entries tested during three years during SERC Phase 1 at our experiment station. Management treatments to be imposed were to be control (no fertilizer source), various winter legumes as bio-fertilizer (monocultures as well as mixtures), and animal manures compared to inorganic N fertilizer. Biomass yield; N, P, and K uptake; NDF; cell wall constituents concentration; physiological responses (mainly tiller density and plant height); and changes in soil nutrient status were to be quantified in each experiment.

For Experiment 1, treatments were two rates of N fertilizer application (80 or 160 kg N ha^{-1}) and defoliation frequencies of one, two, three, or six harvests per year. The first harvest started in June each year and plots were harvested every one, two, or three months, or there was a single end-of-season harvest. Across years, annual dry matter yield was 17.8 vs. 15.1 Mg ha^{-1} at the higher compared to the lower N application rate. A single harvest in fall (18.9 Mg ha^{-1}) or two harvests annually (20.5 Mg ha^{-1}) produced the greatest annual yield. As harvest frequency increased to three (14.5 Mg ha^{-1}) and six (11.7 Mg ha^{-1}) harvests per year, yield decreased. Neutral and acid detergent fiber, hemicellulose, cellulose, and lignin concentrations decreased while concentrations of N and macro-minerals P, K, Ca, and Mg increased with harvest frequency.

For Experiment 2, Alamo switchgrass was germinated in a greenhouse and transplanted by hand in the field to ensure uniform plant stand. Plots were planted during 2010, and the first season of treatment imposition and data collection was done in 2011. Tissue and soil samples

from 2011 as well as field data are currently being analyzed. This experiment is currently in its second year of data collection.

Experiment 3 was first planted in 2010, but there was poor stand establishment due to extremely poor germination. The existing stands were killed with plans to replant during that year, but replanting was not done because of extremely dry conditions throughout the planting season. The experiment was seeded again in 2011, but again there was poor germination and stand establishment. The study was discontinued.

Use of biochar as soil enhancement:
The purpose of this study was to determine the effects of biochar addition on soil properties and plant production. The application of significant amounts of biochar, which is essentially organic matter, has the potential to increase soil tilth and thus plant production.

A preliminary study of the effect of biochar addition on water content at -0.03 bar, soil cation exchange capacity, soil test nutrient concentrations, and pH has been conducted. Biochar rates up to 200 Mg/Ha had little, if any, effect on soil nutrient concentration and pH levels of two soils selected to encompass properties common in Mississippi. As expected, total C content of both soils increased with char rate. Total C in the Houston silty clay increased from 1.4% (0 Mg\Ha) to 6.3% (200 Mg\Ha). Increases in the Marietta fine sandy loam ranged from 0.17% (O Mg\Ha) to 5% (200 Mg\Ha). Total N concentrations, however, did not increase with char rate, suggesting that N was removed during the pyrolysis procedure.

Based on the initial study of the effect of pine char addition on soil fertility, a
greenhouse study investigating the effect of pine char addition to soil on the growth of two warm season crops has been completed. Pine char was added to the same soils used in the preliminary study at rates equivalent to 0, 50, 100, and 200 Mg/ha. Pre-germinated soybean and corn were grown for 21 days in the char amended soils. Pots with no plants were also included as a check. A nitrogen fertilizer treatment was also included. Nitrogen was applied at rates equivalent to 0, 0.5 recommended rate, and recommended rate. As there are no N recommendations for soybean, seeds were inoculated with rhizobium prior to planting. In general, both 21 day old soybean and corn dry weights decreased with increasing char additions when no extra fertilizer was added.

Corn dry weights decreased linearly from 1.6 g/pot to 0.7 g/pot with increasing char addition when grown in the Marietta soil without addition of N fertilizer. There was no significant change in corn dry weight in this soil when supplemental N was added at either 0.5 times the recommended rate or the recommended rate. Soybean dry weights also decreased with char addition in this soil. Soybean dry weights decreased from 1.5 g/pot in the control to 0.8 g/pot at the highest rate of char addition. As soybean is a legume, no N was added to this portion of the study.

As in the Marietta soil, corn dry weight decreased linearly at the 0 N rate in the Houston soil. Dry weights decreased from 5.7 g/pot (O Mg char/Ha) to 2.6 g/pot (200 Mg char/pot). However, unlike the Marietta soil, corn dry weight in the Houston soil also decreased linearly when 0.5 times the recommended rate of N was added. Dry weight in this treatment decreased from 7.6 g/pot (0 Mg char/Ha) to 2.5 g/pot (200 Mg char/Ha). Corn dry weight in this soil did not change when the recommended rate of N was applied to the soil. The addition of N fertilizer did not affect corn dry weight within char rate in either of the soils used in this study. Soybean dry weight from the Houston soil also decreased with char addition. Dry weights decreased from

3.63 g/pot (0 Mg char/Ha) to 2.75 (200 Mg char/Ha). As in the Marietta, no N treatment was included in the soybean portion of the experiment

Tissue nutrient content from the warm season crops greenhouse study was also determined. Tissues were dried and ground and have been decomposed by combustion for analysis of Ca, Mg, K, and P. Results from this analysis will be used to determine the effect of soil biochar addition on nutrient uptake by warm season crops.

A second greenhouse study investigating the effect of pine char addition to soil on the growth of three cool season crops was also conducted using the same soil as the previous studies. As in the warm season study, pine char was added to the soils at rates equivalent to 0, 50, 100, and 200 Mg/ha. Wheat, rye, and alfalfa were planted. Pots with no plants were also included as a check. A nitrogen fertilizer treatment was also included. Nitrogen was applied at rates equivalent to 0, 0.5 recommended rate, and recommended rate. Plants were harvested after 21 days, and shoot dry weight was collected. Tissue nutrient analysis from the cool season crops study continues. Tissues have been dried and ground and have been decomposed by combustion for analysis of Ca, Mg, K, and P.
Statistical analysis of all of the data continues.

Subtask M.3 Wood residue assessments

We will develop and assess a survey instrument using on-site surveys preceded by an introductory letter and copy of the survey to prepare participant mills. Using a list of primary and secondary wood manufacturing facilities in Mississippi, we propose conducting our on-site interviews to collect the necessary mill wood residue data. Descriptive statistics will be developed, and derived data will be used to re-calibrate the previous work by Perez-Verdin et al. (2009).

Planned Activities:
M.3.ML.1 Development of a survey and data regarding recoverable wood residue for bioenergy conversion.

Summarization of Activities:

Wood residue assessments:
The forest product industry is an important economic contributor in Mississippi, which generates more than 56,000 jobs and contributes over $14 billion in the state economy (Munn and Tilley, 2007). Earlier accounted wood-based biomass estimations indicated that approximately 4.0 million dry tons of additional woody biomass can be sustainably supplied from Mississippi's forest (Grebner et al., 2009) for new oppurtunities such as wood-based bioenergy. This estimate was based on data from the Mississippi Institute of Forest Inventory (MIFI) and Forest Inventory and Analysis (FIA) program of USDA Forest Service. The authors indicated that only 3% of the potential wood-based biomass feedstock, which accounted for slightly more than 100 thousand tons per year, consisted of mill residues (Grebner et al., 2009). In a separate study, however, Garrad and Leightley (2005) reported that different wood processing mills, including sawmills and chip mills, produced about 2.3 million tons of wood waste per year from 31 counties in northeastern Mississippi. While the unused wood waste in the estimates of Garrad and Leightley (2005) was around 3%, these results raised the concern that estimates based on FIA data perhaps underestimated the available mill residue for wood-based bioenergy production in Mississippi.

Undoubtedly, recalibration of available woody residue is important for the fact that feedstock plays an important role in the development of wood-based bioenergy in the state of Mississippi. Therefore, based on survey data, this study has reestimated the total amount of woody residues produced in the state. Similarly, the amount of currently unused woody biomass, which was either disposed of or given away, was also estimated. Apart from this, since none of the studies in the past have analyzed the prospect and potential of secondary wood processing facilities in supplying sustainable biomass for wood-based bioenergy industry, we further analzyed the differences and similarities among different wood processing facilities in connection to utilizing excessive woody residues.

Methodology:
A survey instrument was developed to ask the information about available woody residues in primary and secondary wood processing facilities in Mississippi. The data was collected through mail survey followed by phone calls. Contact information of primary and secondary forest product industries within Mississippi was obtained from the Mississippi Development Authority's online searchable SIC Code 24/25 and 26/27 database for 2011. Targeted respondents for this survey were the 582 key persons involved in the wood processing business such as millowners, managers, and/or their representatives. Following the survey method recommended by Dillman et al. (2000), a cover letter with the survey instrument was mailed to the selected potential respondants in the first week of August 2011. One week after the initial mailing, a postcard reminder was mailed to all selected potential respondants. One month after the first survey mail out, a new mailing with a cover letter and survey was sent to those who did not respond to the first survey. Finally, to increase the number of survey respondents, telephone interviews were also made to the randomly selected individuals who did not respond to both mailout surveys.

To segregate the information on woody residues from primary and secondary sources separately, companies were divided into two groups. The first group, which accounted for primary wood product industry, consitituted the forest products: hardwood lumber, softwood lumber, hardwood dimension parts, softwood dimension parts, hardwood plywood, softwood plywood, hardwood logs, particleboard, medium densitty fiberboard, hardboard, OSB, and wood veener. Similarly, the second group, which accounted for secondary wood product industry, constituted the forest products: furniture, flooring, cabinet/millwork, pellets, and panels. The survey contained approximately 29 questions pertaining to the issues related to unused mill residues from primary and secondary woody processing facilities.

Results:
The survey was sent to all wood processing facilities listed in SIC codes. The total response was 99 returns from 458 successful mailings with an adjusted response rate of 21.6%. Given the unreceptive nature of entrepreneurs, who were the survey respondents for this study, the adjusted response rate of survey was considered satisfactory. To check for the non-response bias, socio-demographic variables such as total number of employees, total annual sales, and ownership duration from first and second mailings were compared. Similarly, the number of employees reported in our survey was also compared with employee numbers reported in the relevant SIC codes. The non-significant difference at the 5% level of significance among the above mentioned attributes reduced the concern for non-response bias, if any existed, in this survey. Some useful information from the survey is reported in the form of descriptive statistics in following sections.

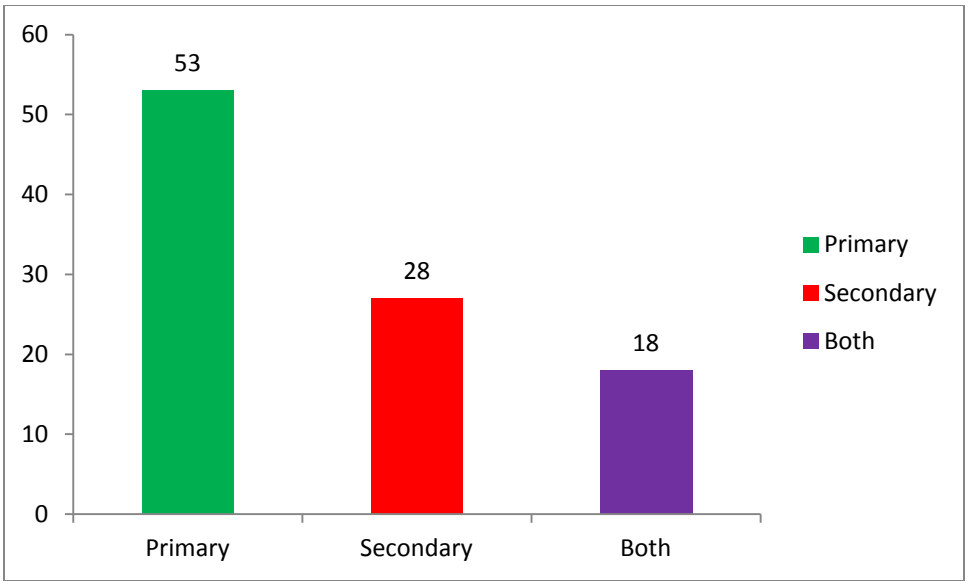


Figure M2: Primary and secondary wood processing facilities.

Among the respondents who reported the type of business activities that they were engaged in, 54% (53) were involved into the primary wood processing business. Similarly, 28% (28) were involved in secondary wood processing business. Finally, 18% (18) respondents reported that they were involved in both types of business.

Wood residue generated:
Monthly wood residue generated from all the firms that responded to the question of interest was 208,489.73 tons per month, or 2,501,913.24 tons per year. The residue was composed of variety of materials including bark, chips, sawdust, scrap lumber, shavings, and wood floor. Table M3 reports the wood residues generated by all wood processing facilities.

Table M3: Residue generated from respondent wood processing facilities (each month) in Mississippi.

Type	Amount (ton)	Percent	Type	Amount (ton)	Percent
			Scrap Lumber	2242.55	1.08
Bark	22747.91	10.91	Shavings	7541.27	3.62
Chips	131894.95	63.26	Others	1639.00	0.79
Sawdust	42374.10	20.32	Total	208489.73	100

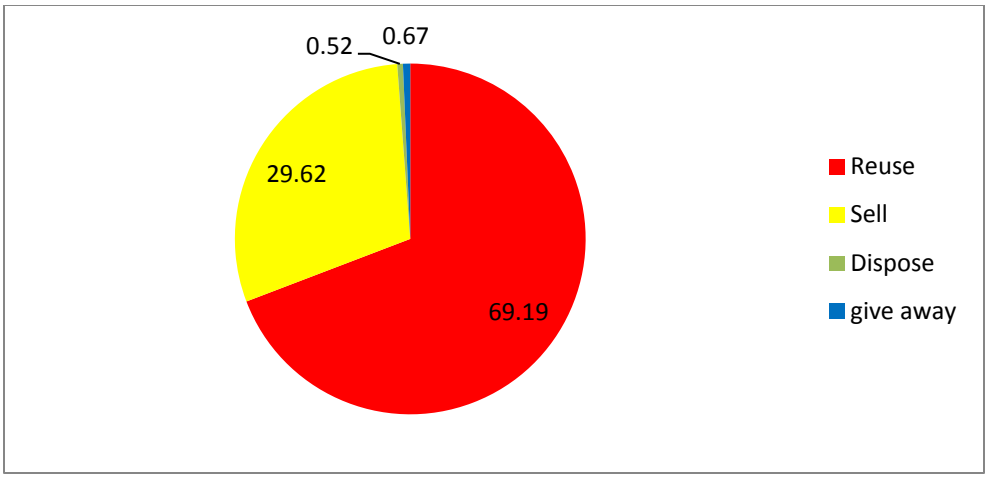


Figure M3: Method of disposal.

The results revealed that most common method of disposing excess wood residues in the facility of respondent firm was by re-using wood residue. About 69% of total wood residue produced was re-used in the site, and 30% was sold. Similarly, 1% of wood residue, which accounted for approximately 2,140.8 tons per month, was either disposed of or given away. Table M4 reports the comparison among different types of wood processing facilities, based on chi-square test of independence, in terms of using wood residues.

Table M4: Comparing differences between primary and secondary wood processing facilities on use of wood residues based on the chi-square test of independence.

	P-value[1]	Primary wood processing facility (n=53)	Secondary wood processing facilities (n=28)	Both (n=18)
Residue sale	0.04	34 (64%) [a]	11 (39%) [b]	7 (38%) [a,b]
Residue disposal	0.003	10(19%)[b]	7(25%)[b]	11(61%)[a]
Residue Given Away	0.4	11(21%)	9(32%)	6(33%)

[1] P value is reported for chi-square test of independence among all three different types of firms. The letters a, b indicate significant differences between two types of firms.

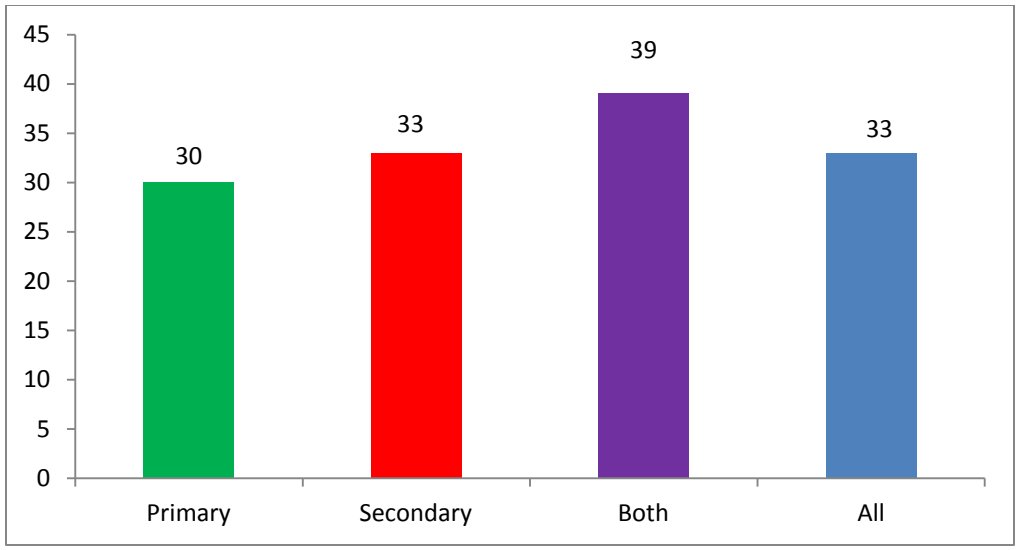


Figure M4: Years of business.

With an average of 33 years, number of years in business for wood processing industries in Mississippi ranged from 1 to 119 years. The average year of operation for primary, secondary, and both types of wood processing facilities was 30 years, 33 years, and 39 years, respectively.

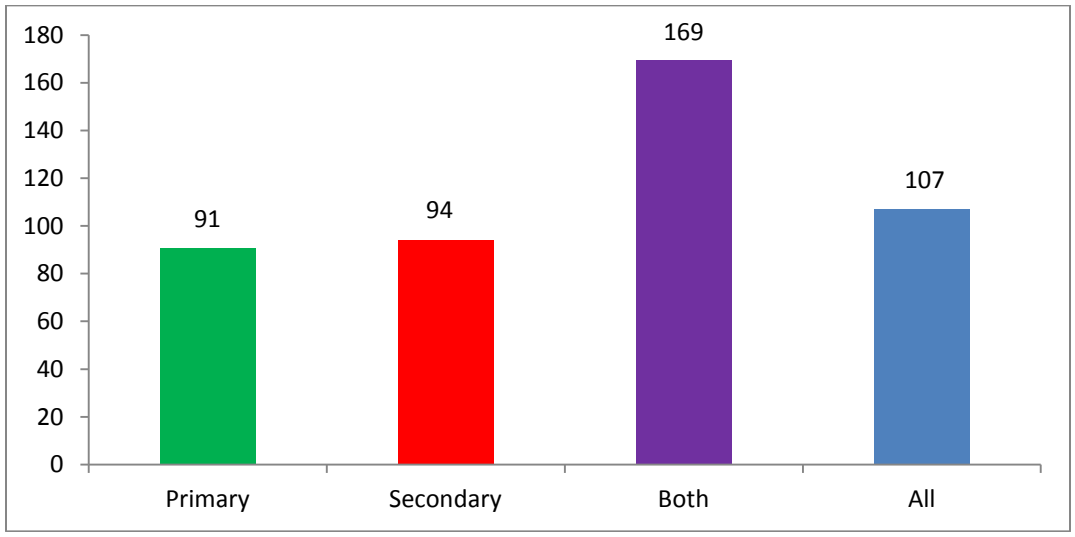


Figure M5: Number of employees.

A total of 10,041 employees, with an overall average of 107 employees, were working in the respondent wood processing firms in Mississippi. On average, 91 employees were in the primary wood processing facilities, 94 employees were in the secondary wood processing facilities, and 169 employees were in the firm which operated both facilities.

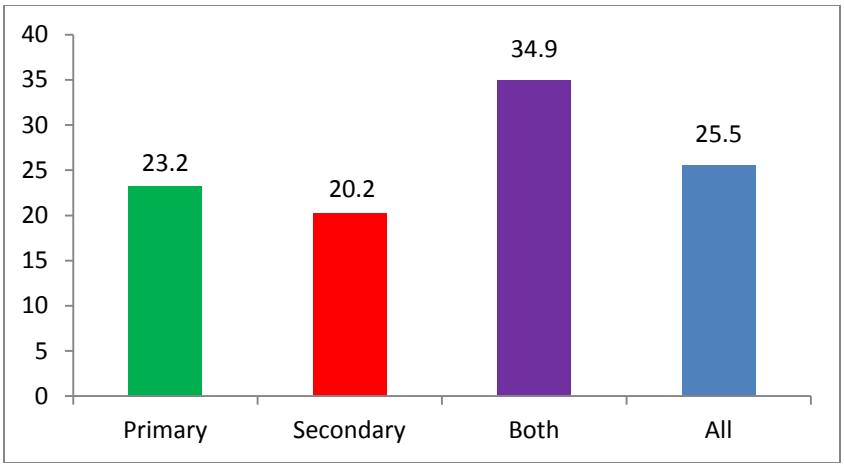


Figure M6: Annual sales.

A total of $1603 million annual sales, with an average of $25.46 million sales, were reported by the respondent wood processing facilities in the state of Mississippi. On average, primary and secondary wood processing facilities had an annual sale of $23.2 million and $20.2 million, respectively. Similarly, firms operating both facilities had average annual sales around $34.9 million.

Wood residue sales:
Results indicated that the average revenue generated by selling wood residue was approximately $35,000 per month. Categorically, the primary and secondary wood processing facilities generated the average revenue of approximately $49,000 and $11,000 per month, respectively. Likewise, the average revenue generated by the firms having both facilities was approximately $8,000 per month. Respondents reported that most of the buyers (>90%) either used the wood residue to manufacture another product or to generate energy. Table M5 provides summary information about wood residue sales in Mississippi.

Table M5: Summary statistics of wood residue sell from different wood processing facilities in Mississippi.

Wood processing facility	Average miles transported to destination	Average estimated cost to transport ($/ton)
Primary	65.71	8.83
Secondary	29.8	7.55
Both	75.07	19.09
All	59.18	10.24

Wood disposal:
Results revealed that, on average, the cost incurred in disposing the wood waste was approximately $2,000 per month. Categorically, the primary and secondary wood processing facilities, on average, had to incur a cost of approximately $2,300 and $2,700 per month respectively. Likewise, the average cost incurred during wood disposal by the firms having both primary and secondary wood processing facilities was approximately $1,500 per month. Table M6 provides summary information on cost incurred in disposing wood waste in Mississippi.

Table M6: Summary data of wood waste sell from different wood processing facilities in Mississippi

Wood processing facility	Average miles transported to destination	Average estimated cost to transport ($/ton)
Primary	20.28	15.25
Secondary	13.8	50
Both	18	23.16
All	17.68	22.56

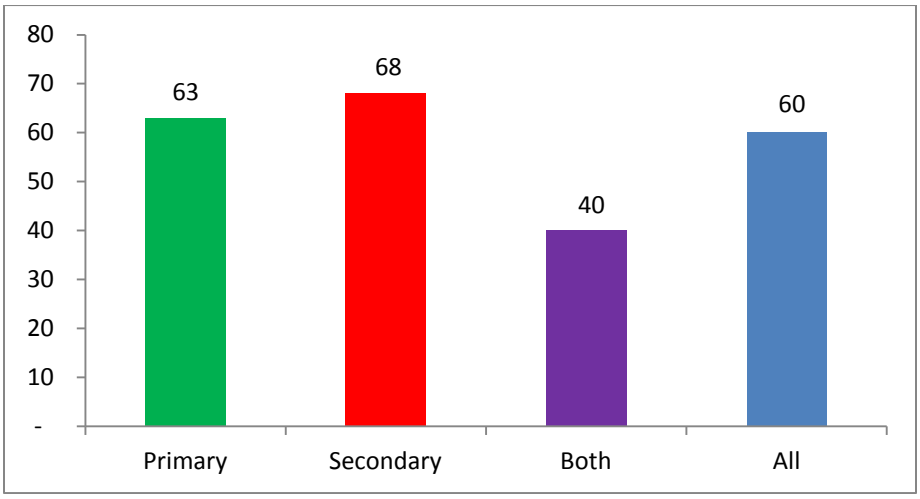


Figure M7: Market for wood residue.

Among all respondents, only 60% indicated that there is a potential market for wood residues near their facility. Explicitly, only 63% of the mill owners having primary wood processing facilities, 68% of the mill owners having secondary wood processing facilities, and 41% of the mill owners having both facilities indicated that there is potential market for wood residues near their facility. This means 40% of all respondents recognized a need for new market opportunity for wood residue near their facility.

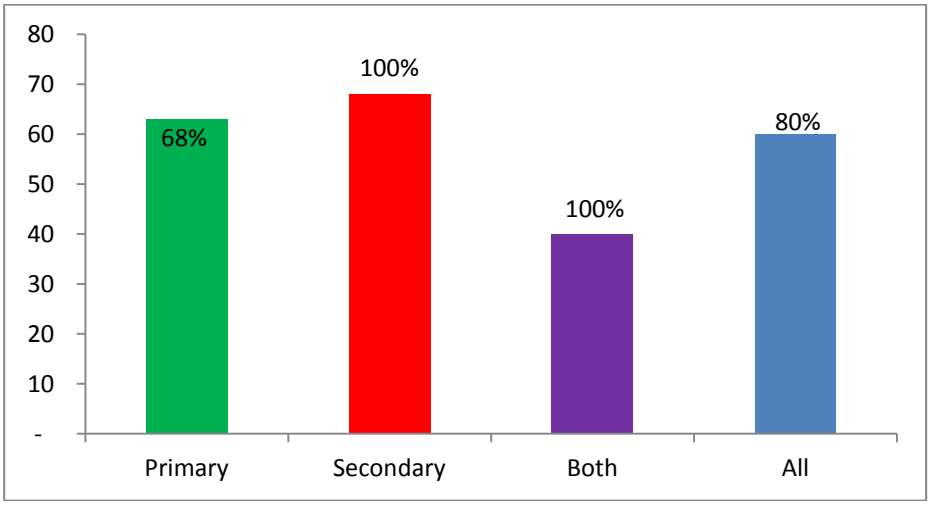


Figure M8: Distance between potential market and mill.

As reported earlier, 60% of all respondents indicated that there is a potential market for wood residue. Among those, approximately 81% reported that potential market for wood residue generated was within 60 miles of their facility. 68% of the primary wood processing facilities and

all the secondary wood processing facilities reported that the potential market was within the radius of 60 miles. Likewise, all the respondent firms having both facilities also reported a market for wood residue within 60 miles from their mill.

Estimates on available woody biomass for wood based bioenergy:
Garrard and Leightley (2005) indicated that wood waste generated by all 108 responding firms in Northern Mississippi was approximately 194,300 tons per month. The authors also reported that 3% of the total available mill residue, which equaled 5,136 tons per month, was either disposed or given away. Our results revealed that approximately 208,492.8 tons of mill residues per month were obtained from 99 responding firms in Mississippi. Similarly, since nearly 99% percent of total wood residue from the responding mills was either reused in the same facility or sold, only the remaining 1% percent, which equaled 2,140.865 tons per month, was available for supplement or additional use. Likewise, total volumes of the logging residues sold by respondent firms equaled 53,427.5 dry tons per month. Therefore, the total internally unused volumes of the mill residues, by summing up the volumes sold, given away, or disposed of, equaled 55,568.37dry tons per month, or 1,852.279 dry tons per day.

Discussion and Conclusion:
Results provided some important facts regarding availability of residues in primary and secondary wood processing facilities in the state of Mississippi. Extrapolation of our results showed that approximately 11.6 million tons of woody residues were generated by all types of wood processing industries in Mississippi. An inherent variability among wood processing industries in scale of production and efficiency dictates a cautious interpretation of extrapolated results.

Garrard and Leightley (2005) indicated that wood waste generated by all 108 respondent firms in Northern Mississippi was approximately 194,300 tons per month. Our results indicated the presence of approximately 208,489.8 tons of woody residues per month from 99 respondent firms. Given that the average number of employees of the respondent firms in our survey was considerably larger than that reported by Garrard and Leightley (2005), both results are comparable and intuitive. However, we argue that all the woody residues generated by wood processing facilities in Mississippi, unlike reported by Garrard and Leightley (2005), could not be considered as a waste. Since nearly 99% percent of total wood residue was either re-used in the same facility or sold, only the remaining 1% percent, which equaled 120,048.5 tons annually, was available for supplement or additional use. Findings of our study resonate with recent research (Indiana report 2011, GC and Potter-Witter, 2010) conducted in other parts of the country, which revealed that available mill residues for other use are limited throughout the nation.

This study provided some interesting results related to utilization of excesswood residue among the firms having primary, secondary, and both types of wood processing facilities in Mississippi. For instance, results indicated that 64% of the mill owners having primary wood processing facilities, 39% of the mill owners having secondary wood processing facilities, and 38% of the mill owners having both facilities were involved in a wood residue sale. Chi-square test of independence indicated that primary wood processing mill owners had significantly higher involvement in wood residue sale than the other two types (Table M4).

Despite the fact that approximately one third of primary wood processing mill owners do not have a potential market within the radius of 60 miles, their active involvement in wood residue sale is commendable. Given that their existing net benefits obtained from wood residue sales are likely be low due to higher transportation costs (Tables M5 and M6), it is possible that such

firms may prefer to supply wood residue to an industry such as bioenergy if it is located near their facility. On a separate note, 61% of the entrepreneurs having both wood processing facilities, which is significantly higher than other two groups (Table M4), disposed of unused woody residues at their own cost. Since the majority of the entrepreneurs operating both facilities in a single firm are currently underutilizing woody residues, these firms can also be viewed as a potential supplier of biomass for wood-based bioenergy industries in Mississippi.

The market price of woody residue, to a large extent, will determine the availability of woody residue for use in bioenergy versus existing operations (GC and Potter-Witter, 2010). Furthermore, since a considerable percentage of the survey respondents (40%) realized the need of a potential market for wood residues near their facility, these entrepreneurs could prefer to sell woody residue to a new opportunity, such as a bioenergy facility, near their mill. Therefore, a careful consideration of finding an appropriate location for potential bioenergy facility would likely reduce the short-term competition of resource use between bioenergy facilities and existing industries in the state of Mississippi.

Subtask M.4 Feedstock engineering

Planned Activities:

M.4.ML.1 Define several potential harvesting and delivery systems that could be implemented in the SE-US.
M.4.ML.2 Develop economic and performance data for at least one feedstock system that could be reasonably implemented for grass crops in the SE-US taking into account farm size, equipment availability, and farmer acceptance.

Summarization of Activities:

Spatial distribution of the potential bio-energy crops and their environmental impact on Mississippi watersheds are being studied using models. Our modeling efforts also considered developing and using economic models (Kim et al., 2012; Deng et al., 2011) to evaluate pilot-scale bio-gasification systems such as “Cost Calculator” (Figure M9).



Figure M9: A cost calculator developed for economic modeling and analysis.

A second project examined the effects of soil and management on the sustainability and ecosystem benefit of maize stover-based ethanol production systems in the Mississippi Delta.

Using CERES-Maize model, maize stover yields (MSYs) were simulated for several scenarios of cultivars, irrigations, planting dates, and soils. Net energy value (NEV) and carbon credit balance (CCB) were used as indicators of sustainability and ecosystem services benefit, respectively. Soil and management effects on MSY, NEV, and CCB were determined using analysis of variance (ANOVA). The MSYs associated with sandy loam, silt loam, and silty clay loam soils were different in all locations, as were MSYs associated with high-, mid-, and low-yielding cultivars. With an increase in irrigation amount, as well as for each delay in planting, MSY increased initially and decreased after reaching a peak. Soil and management effects on NEV and CCB were the same as on MSY because NEV and CCB were computed as linear functions of MSY. Stover yield had a positive effect on NEV and CCB, whereas the effect of travel distance was negative. However, the influence of stover yield was far more than that of travel distance because the latter affected only transportation costs, whereas the former affected the costs of all activities in the feedstock supply chain. Values of NEV and CCB were positive for all scenarios, indicating that stover-based ethanol production system in the Mississippi Delta is sustainable and also beneficial to the regulating service of the ecosystem.

A third project created the justification for poultry growers to become the early adopters of energy grasses as both poultry bedding and energy feedstocks. It has been difficult to get farmers to install and grow energy crops without incentives or credits due to the lack of a strong and sustained commodity market. The U.S. commercial poultry industry (roughly 100,000 broiler houses or 25,000 growers) provides a unique entry-point opportunity for biomass feedstock production in the Southeast US. As wood shavings are being diverted for other uses, poultry growers are finding it difficult to purchase low-cost bedding for broiler production.

A 2010 study showed that chopped switchgrass (SG) and chopped bermudagrass (BG) performed as well as pine shavings (PS) for broiler litter in small pen trials. A second field demonstration compared chopped giant miscanthus (GM), SG, BG, and PS as poultry bedding in a 40x500 ft commercial broiler house (Figure M10). The chopped grasses performed as well as PS. A full scale housing study with GM is being undertaken by Repreve Renewables (Soperton, GA) in an independent collaboration to demonstrate the feasibility of “growing your own litter” to growers.



Figure M10: left) Chopped switchgrass, and right) chopped giant miscanthus used a litter bedding in a commercial broiler house.

As part of a required nutrient management plan, many poultry growers currently own an assortment of machinery (mowers, balers, loaders, etc.) and labor to manage the land they are

required to own in the operation. The growers will be able to grow enough litter on a small portion of their land (3-6 acres per house) and sell the remaining energy grass as a feedstock. Over the last year, many growers have expressed interest in collaboration as they understand the fundamentals of production and are in need of a short-term solution. The major barrier these growers faced was chopping the grasses at sufficient rates to provide materials in a timely manner. Each 40x500 ft house required approximately 30 tons of material (assuming density of 9 lb/ft^3). A test was conducted with a portable industrial tub grinder (Figure M11). Large square bales of GM were ground with a 1x3 in grinding screen. The machine provided a fast feed rate, but many farmers are concerned about the $100,000 to $300,000 capital investment. A forage chopper was tested next with standing SG in the field. The machine did not have a screen to maintain a required uniform chop. Vermeer (Pella, IA) is providing us a machine to test this quarter. Vermeer's machine requires a double grind to reach the required < 1 in. chop. However, the company is interested in machine development for this production system.



Figure M11: A tub grinder was used to grind large square bales of giant miscanthus.

Potential storage methods included no cover, plastic sleeve, silo bag tarp, and barn. Initial costs were highest for barns due to materials and construction labor and least for tarped materials. However, bale losses were inversely proportional. We are preparing to install chopped grasses in silo bagging systems (Figure M12). The bags provide complete coverage as a barn system, but at a much cheaper cost. The bags would provide a flexible storage system for both new and used litter materials in the poultry system. Bales will be the likely choice for materials becoming energy feedstock.



Figure M12: Silo bag storage system on MSU farm.

In the field, we noticed moisture probe measurements were much different than our oven measurements. A study was conducted to characterize the effects of pressure and orientation (axial or transverse to stalks) on two commercially available electrical resistance probe-type moisture meters for switchgrass. A forage compression apparatus (Figure M13) was designed and constructed with on-farm materials and methods to provide a simple system of applying pressure achievable by any producer or researcher in the field. Results indicated that meter accuracy increased as pressure increased. Regression models were best for both probes at a pressure of 95 lb/ft^2 and a transverse probe orientation. Calibration equations were developed for both meters to improve moisture measurement accuracy.



Figure M13: Compression apparatus pressurized with weights. Meter 1 (left) and Meter 2 (right) inserted into the grass sample axially and transversely, respectively.

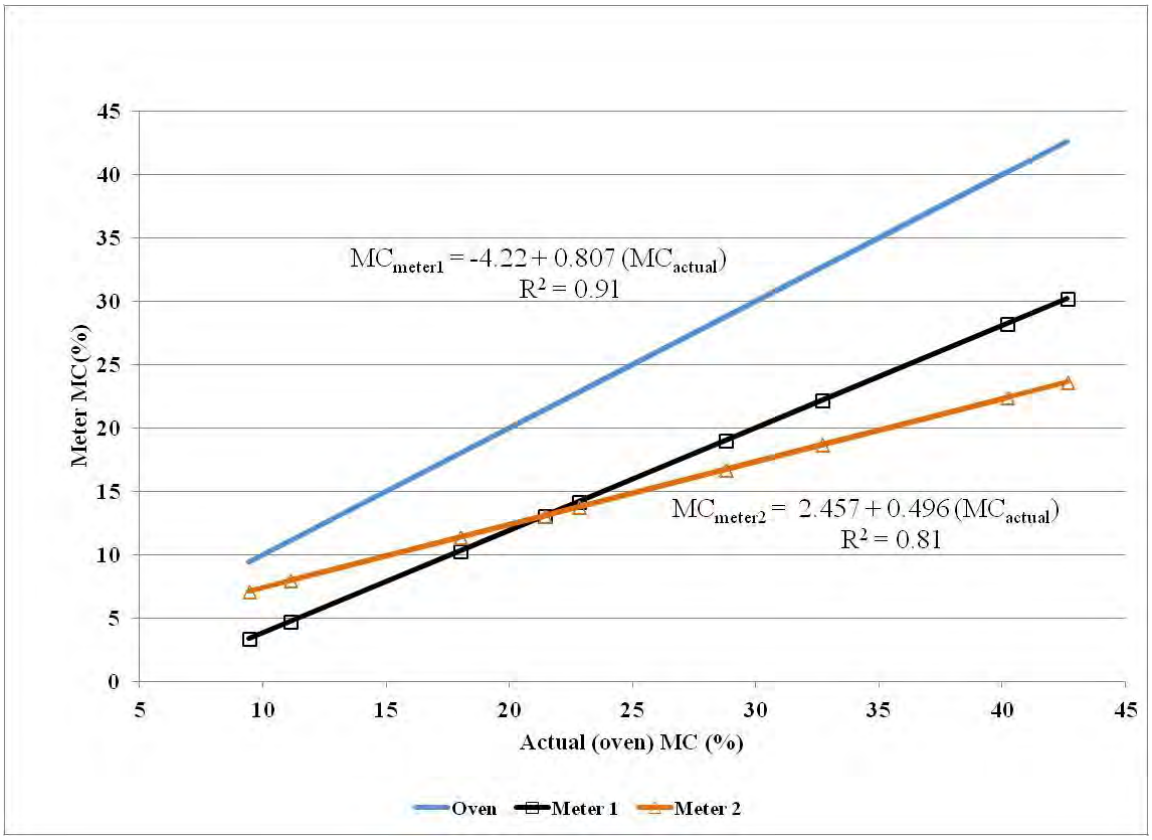


Figure M14: Linear regressions for Meter 1(Farmex HT-Pro) and Meter 2 (Delmhorst F-2000) using a pressure of 95 lbs/ft^2 and transverse probe orientation.

References:

Bewley, J.D. 1997. Seed germination and dormancy. The Plant Cell. Vol. 9: 1055-1066.

Corredor, D.Y., J.M. Salazar, K.L. Hohn, S. Bean, B. Bean, D. Wang. 2008. Evaluation and characterization of forage forghum as feedstock for fermentable sugar production. Appl biochem biotechnol 158:164-179.

Davis, J.D., J.L. Purswell, and A.S. Kiess. 2011. Evaluation of chopped switchgrass and chopped bermuda grass as sustainable litter materials over multiple broiler flocks. Proceedings of the 2011 International Poultry Scientific Forum, Jan. 24-25. Atlanta, GA. p 26. (abstract)

Dillman, D.A. 2000. Mail and internet surveys: The tailored design method. 2nd ed. New York: John Wiley & Sons, Inc. 464p.

Edwards, Ned C., Robert Elmore, Carl Hovermale, David Ingram, Roscoe Ivy, Billy Johnson, David Lang, Vance Watson. 1991. Performance of warm season forage crop varieties 1988-1990. Mississippi Agricultural and Forestry Experiment Station. Information Bulletin 192.

Finch-Savage, W.E. and G. Leubner-Metzger. 2006. Seed dormancy and the control of germination. Tansley Review. New Phytol. 171: 501-523.

Garrad, A.W. and L. Leightley. 2005. Characterizing wood waste from wood products companies in north Mississippi. Research Report, Forest and Wildlife Research Center, Mississippi State University, 14p.

GC, S. and K. Potter-Witter.2011. Status of Michigan's forest product industry in the changing market environment. Forest Products Journal. 61(1):77-82.

Hamrick, R., L.W. Berger, J. Jones and B. Strickland. 2007. Native warm season grass restoration in Mississippi. Mis. St. Ext. Ser. Pub. # 2435.

Harper, C. A., G.E. Bates, M.J. Gudlin and M.P. Hansbrough. 2004. A Landowner's Guide to Native Warm Season Grasses in The Mid-South. Univ. Tenn. Ext. Pub. #1746.

Indiana Department of Natural Resources. 2011. Woody biomass feedstock for the bioenergy and bioproducts industries. Available online at: http://www.in.gov/dnr/forestry/files/fo- WoodyBiomass_final.pdf. Last accessed. November 20th, 2011.

Klein, J.D., L.A. Wood, and R.L. Geneve. 2007. Hydrogen peroxide and color sorting improves germination and vigor of eastern gamagrass (Tripsacum dactyloides) seeds. Univ. of Kentucky. Master's Thesis. Electronic Correspondence.

Kucera, B., Cohn, M.A. and G. Leubner-Metzger. 2005. Plant hormone interactions during seed dormancy release and germination. Seed Sci. Res. 15: 281-307.

Leubner-Metzger, G. 2003. Functions and regulation of ß-1,3-glucanases during seed germination, dormancy release and after-ripening. Seed Sci. Res. 13: 17-34.

Leubner-Metzger, G. 2005. ß-1,3-Glucanase gene expression in low-hydrated seeds as a mechanism for dormancy release during tobacco after-ripening. The Plant J. 41: 133-145.

Leubner-Metzger, G. 2002. Seed after-ripening and over-expression of class I ß-1,3-glucanase confer maternal effects on tobacco testa rupture and dormancy release. Planta 215: 959-968.

Perez- Verdin, G., D. Grebner, C.Sun, I Munn, and S. Grado. 2008. Economic impact of woody biomass utilization for bioenergy in Mississippi. Forest Products Journal. 58(11):75-83.

Smith, S.R., G. Lacefield and T. Keene. 2009. Native warm season perennial grasses for forage in Kentucky. Univ. Kentucky Coop. Ext. Ser. AGR-145.

Tilley B. and I.A. Munn. 2007. 2001 economic impacts of the forest product industry in the South. Southern Journal of Applied Forestry. 31(4): 181-186.

Vermerris, Wlfred, John Erickson, David Wright, Yoana Newman, and Curtis Rainbolt. 2011. Production of Biofuel crops in Florida: Sweet Sorghum. University of Florida IFAS Extension. SS-AGR-293.

Publications:

Referred Journal Publications:

Chesser Jr. G.D., J.D. Davis, J.L. Purswell, D.E. Rowe, and R. Lemus. 2012. Moisture Determination in Switchgrass Windrows Using Electrical Resistance Probes. J. ASABE.

Chouvarine, P. A.M. Cooksey, F.M. McCarthy, D.A. Ray, B.S. Baldwin, SM. Burgess, D.G. Peterson. 2011. Phylogenetic and functions analysis of *Miscanthus*. Public Library of Science http://www.plosone.org/article/info%3Adoi%2F10.1371%2Fjournal.pone.0029850

Gruchy, S R, D L Grebner, I A Munn, O Joshi, A Hussain. 2011. An assessment of nonindustrial private forest landowner willingness to harvest woody biomass in support of bioenergy production in Mississippi: A contingent rating approach. For. Pol. Ec.

Seepaul, R., † B. Macoon, K.R. Reddy, and B. Baldwin. 2011. Switchgrass (*Panicum virgatum* L.) intraspecific variation and thermotolerance classification using in vitro seed germination assay. American J. Plant Sci. 2:134-147.

Woli, P. and J.O. Paz. 2011. Analyzing the effects of variations in soil and management practices on the sustainability of corn stover-based bioethanol production in Mississippi. ASABE Paper No. 1111062. 2011 ASAE Annual International Meeting. Louisville, KY.

Woli, P. and J.O. Paz. 2012. Evaluation of various methods of estimating global solar radiation for crop model application in the Southeastern USA. J. Appl. Meteor. and Climatol. doi:10.1175/JAMC-D11-0141.1

Zheljazkiov, V.D., B.A. Vick, B.S. Baldwin, N. Buehring, T. Astatkie, and B. Johnson. 2011. Oil productivity and composition of sunflower as a function of hybrid and planting date. J. Indus. Crops Prod. 33:537-543.

Extension Publication:

Lemus, R., B. Baldwin, and D. Lang. 2011. Agronomic Suitability of Bioenergy Crops in Mississippi. Mississippi State Univ. Coop. Ext. Serv. Pub-2713. Pp7

Referred Proceedings:

Duffy, Sarah and Parajuli Prem B. 2011. Assessing the Correlation between Predicted Soil Moisture Content and Observed Soil Organic Carbon Using SWAT and Field Studies. ASABE Publication No. 1111557, ASABE, St. Joseph, MI.

Hakkwan Kim, Parajuli P. B., Yu F., and Columbus E. P. 2011. Economic Analysis and Assessment of Syngas Production using a Modeling Approach. ASABE Publication No. 1110814, ASABE, St. Joseph, MI. Available at: http://asae.frymulti.com/azdez.asp?search=1&JID=5&AID=37322&CID=loui2011&v=&i= &T=2.

Lang, D.J., Shankle, B, Oswalt, E., Duckworth, J. Sanborn, Buell, R. and B. Robertson. 2010. Establishment and evaluation of switchgrass on reclaimed minesoil. *IN:* R.I. Barnhisel (Ed.) Proc. 2010 Nat Meeting Amer Soc Mining Reclam. Pittsburgh, PA. 27:536-550

Parajuli P. B. 2011. Bio-energy Feedstock Yields and their Water Quality Benefits in Mississippi. ASABE Publication No. 1111416, ASABE, St. Joseph, MI. Available at: http://asae.frymulti.com/azdez.asp?search=1&JID=5&AID=38511&CID=loui2011&v=&i= &T=2.

Yangyang Deng, and Parajuli P. B. 2011. Evaluation of Syngas Production Unit Cost of Bio-Gasification Facility using Regression Analysis Techniques. ASABE Publication No. 1110711, ASABE, St. Joseph, MI. Available at: http://asae.frymulti.com/azdez.asp?search=1&JID=5&AID=37284&CID=loui2011&v=&i= &T=2.

Dissertation and Theses:

Horton, D. Scott. Evaluation of sweet sorghum as a potential ethanol crop in Mississippi. M.Sc. Mississippi State Univ. Plant and Soil Sci. Aug. 2011.

Michel, Himaya Mula. Bacterial community dynamics during lignocellulose decomposition as affected by soil and residue types. Mississippi State Univ. Plant and Soil Sci. May 2011.

Sandlin, Tyler N. Row spacing and population density effect on seed yield of okra and seed oil as a source of biodiesel. M.Sc. Mississippi State Univ. Plant and Soil Sci. Aug. 2011

Conference Presentations:

Baldwin, Brian. 2011. The southeastern US: Biomass powerhouse. Soil and Water Conserv. Soc. Ann. Conf. Washington, D.C. 17 Jul.

Baldwin, B. 2011. Miscanthus 101: Focus on giant miscanthus. First Repreve Field Day. Soperton, GA 13-14 Jan.

Baldwin, Brian S. 2012. Giant miscanthus (*Miscanthus xgiganteus*) as a biofuel feedstock for the South. Alabama Bioenergy Workshop. Tuskegee University, Tuskegee AL. 11-13 Apr.

Chesser, Jr. G.D., J.D. Davis, J.L. Pursell, D.E. Rowe, and R. Lemus. 2011. Using Electrical Resistance Probes for Moisture Determination in Switchgrass Windrows. Paper No. 1111253. Annual Meetings of the Am. Soc Agric Biol Eng. Louisville, KY. 7-10 Aug.

Gilley, M.D. M. Tomaso-Peterson, B.S. Baldwin, and T.W. Allen. 2011. Frequency and identification of fungi associated with giant miscanthus in Mississippi. 2011 Mississippi Assoc.Plant Path Nema (MAPPAN) Conf. Starkville, MS. 24-25 Oct.

Hakkwan Kim, and Parajuli P. B. 2011. Assessment of the Potential Crop Yield for Bio-Energy Production Using the SWAT Model. ASA/CSSA/SSSA, Intern Ann Meeting, San Antonio, TX. 16-19 Oct.

HakKwan Kim, Parajuli P. B., Fei Yu, Joel O. Paz, and Eugene Columbus. 2011c. Economic Model for Evaluating Syngas Production Cost of Bio-gasification Facility. IBE Ann Conf, Loews Atlanta, GA 3-5 Mar.

Knoll, J.E. W. F. Anderson, B. Baldwin, E. Richard. 2010. Harvest date effects ono biomass yield and quality of new energycane (*Saccharum* hybrid) genotypes in the southeastern USA. ASA/CSSA/SSA Meetings. Long Beach, CA. 31 Oct - 4 Nov.

Lang, D., J. Duckworth, B. Shankle, N. Rebecca Buell-McGraw, B. Robinson, and R. Lemus. 2011. Establishment of switchgrass on reclaimed coal mine soil. ASA Meeting. San Antonio, TX. 18 Oct. http://a-c-.confex.com/crops/2011am/webprogram/Paper65151.html

Lemus, R., J. Morrison, and B. Rushing. Evaluation of sorghum varieties as a bioenergy crop and forage quality. *In:* Proceedings of the Southern Branch ASA. Corpus Christi, TX,. 6- 8 Feb

Seepaul, R., B. Macoon, K.R. Reddy, B. Baldwin, "A Simple *in vitro* Seed Germination Assay to Classify Switchgrass Genotypes for Thermotolerance," Southern Branch ASA Orlando, FL, 7 – 8 Feb.

Yangyang Deng, and Parajuli P. B. 2011c. Economic Evaluation of Electricity Generation from a Small-Scale Bio-Gasification Facility using an Optimization Model. IBE Annual Conference, Loews Atlanta, GA. 3-5 Mar.

Field Day Presentations:
Baldwin, B. 2011. Miscanthus 101: Focus on giant miscanthus. First Repreve Field Day. Soperton, GA 13-14 Jan.

Posters:
Baldwin, Brian, Rocky Lemus, Davis Lang. 2011. Grassy feedstocks for biomass energy Mississippi Biofuels Conf. Starkville, MS. 5-7 Oct.

Baldwin, Brian, Randy Rousseau, Scott Roberts, Mark Shankle. 2011. Woody feedstocks for biomass energy. Mississippi Biofuels Conf. Starkville, MS. 5-7 Oct.

Barnes, D.J., N.A. Reichert and B.S. Baldwin. 2011. Silencing of ricin production in castor (*Ricin communis* L.) by genetic modification. Soc. In Vitro Biol. Raleigh, NC. 4-8 June.

Barnes, D.J., N.A. Reichert, and B.S. Baldwin. 2011. Advances toward the removal of ricin toxicity from castor seed via genetic modification. Mississippi Biofuels Conf. Starkville, MS. 5-7 Oct.

Cobb, J.L., J.B. Rushing, and B.S. Baldwin. 2011. Effects of planting method, rhizome size, number of buds, and cold storage on giant miscanthus propagation. Mississippi Biofuels Conf. Starkville, MS. 5-7 Oct.

Cooksey, A.M., P. Chouvarine, D.A. Ray, B. Baldwin, S.C. Burgess, and D. G. Peterson. 2011. Transcriptome profiling of Miscanthus. MCBIOS - Mid-south Comp Biol and Informatics Soc. Seventh Ann. Mtg. Jonesboro, AR. 19-2 Feb.

Duffy, Sarah and Parajuli P. B. 2012. Assessing Water Balance Using a Hydrologic Model. 2012 Mississippi Water Res Conf., Jackson, MS. 1-3 Apr.

Gilley, M.D. M. Tomaso-Peterson, B.S. Baldwin, and T.W. Allen. 2011. Survey of phytopathogenic fungi associated with giant miscanthus in Mississippi. 2011 Misssissippi Biofuels Conf.. Starkville, MS. 5-7 Oct.

Gilley, M.D. M. Tomaso-Peterson, B.S. Baldwin, and T.W. Allen. 2011. Identification of phytopathogenic fungi associated with giant miscanthus in Mississippi. Amer Phytopath. Soc.. Honolulu, HI. 2-10 Aug.

Holmberg, M.B., J.B. Rushing, and B.S. Baldwin. 2011. Alternative nitrogen for subsequent southern switchgrass production using cool season legumes. Mississippi Biofuels Conf. Starkville, MS. 5-7 Oct.

Joshi, O. and D.L. Grebner. 2010. An assessment of potential economic impacts associated with wood-based bioenergy industries in Mississippi. 9th Annual Southern BioProducts & Renewable Energy Conf, Tunica, MS. 13-14 Apr

Joshi, O. and D.L. Grebner. 2010. An assessment of potential economic impacts associated with wood-based bioenergy industries in Mississippi. Southern Forest Econ Workshop, Pinehurst, NC. 15-17 Mar.

Perera, D., B.S. Baldwin and N.A. Reichert. 2011. Optimization of *Miscanthus x giganteus* in vitro regeneration. Soc. In Vitro Biol. Raleigh, NC. 4-8 Jun.

Perera, D. B.S. Baldwin, and N.A. Reichert. 2011. An optimized protocol for *Miscanthus Xgiganteus* in vitro propagation. Mississippi Biofuel Conf. Starkville, MS. 5-7 Oct.

Wewalwela, J, JR Donaldson, and M Williams. 2012. Evidence for associate nitrogen fixation in feedstock grasses. Ecological Society of America Mid-Atlantic Chapter Annual Meeting. Blacksburg, VA 14 - 15 Apr.

Wewalwela, J, M Williams, and JR Donaldson. 2011. Identifying diazotrophic bacterial communities contributing to associated nitrogen fixation in feedstock grasses. South Central Branch Amer Soc Micro Ann Meeting. Monroe, LA. 2-3 Dec.

Wewalwela, J, JR Donaldson, and M Williams. 2011. Identifying endophytic bacterial communities contributing to associative nitrogen fixation in feedstock grasses. Mississippi Biofuels Conf. Starkville, MS. 5-7 Oct.

Woli, P. and J.O. Paz. 2011. Evaluation of various methods of estimating solar radiation for crop model application in the Southeastern USA. ASA-CSSA-SSSA Ann Meet. San Antonio, TX. 16-19 Oct.

Yangyang Deng, Parajuli P. B., and Columbus E. 2011. Economic Analysis and Optimization of Syngas Production: Model Development and Application. Mississippi Biofuel Conf. Starkville, MS. 5-7 Oct.

External Grants:

DoE SunGrant Initiative. 2011. Herbaceous Feedstocks Partnership, Energycane Group. Baldwin, B., W. Anderson, D. Brummer, K. Gravois, T. Wilson, J. daSilva and J Parish et al. (Baldwin, team leader) $70,000 (Baldwin) plus $22,000 (Baldwin and Parish) annually for 5 years.

DoE SunGrant Initiative. 2011. Herbaceous Feedstocks Partnership, Sorghum Group. William L. Rooney, Scott A. Staggenborg, Gary N. Odvody, Ron W. Heiniger, Bisoondat Macoon, Ken J. Moore, Michael Barrett, Jeff F. Pedersen (Rooney, team leader) $22,000 (M:acoon) annually for 5 years.

North American Coal Lang, D. 2011. Evaluation and utilization of switchgrass on reclaimed mine soil. Funded for $28,056 by, 1 March, 2010 to 30 June, 2011 (extended to 31 Dec, 2011).

Repreve Renewables, Inc. 2011. Baldwin, B. and M. Tomaso-Peterson. A research plan for Mxg: Cultivar development and disease identification ands screening. $210,184 (Baldwin $114,240).

USDA Forest Service . 2011. Grebner, An economic model for evaluation the use of short rotation woody crops in the Lower Mississippi Alluvial Valley. , $80,000.

USDA-NRCS, Gulf Coast Coop Ecosystem Studies Unit. 2011. Baldwin, B.S. and J. Douglas. Mineral and proximate analysis of biomass species from weathering. ($12,000, Baldwin, lead PI).

Patent/Intellectual Property:
Baldwin, B.S. 2011. Miscanthus plant named 'MSU-MFL1' Miscanthus x giganteus . Plant patent submitted and pending - 5 Mar 2011.

Task N. Pilot Plant Construction and Support

The objective of this task is to establish and operate infrastructure to achieve pilot testing for Tasks H and I, Bio-oil and Biocrude. This objective will include a contract to build an approximately 7,000 square foot building. Pilot equipment will be installed, commissioned, and subsequently operated according to Task H and Task I objectives and milestones. The systems will be controlled through a distributed network with a Wonderware interface and data storage capability. A centrally located control room will be supplemented with local area control stations to provide maximum versatility during pilot operations. Safety and environmental standards will be implemented by control system protocol and supervised by onsite personnel.

Milestone: Completion of construction and commissioning of a building housing two pilot plants.

Executive Summary:

The objective of Task N was to design, install, and commission infrastructure to allow operation of pilot testing as detailed in Tasks H and I, Bio-oil and Biocrude. This objective consisted of the construction of a building with associated operations areas, utilities, and monitoring capabilities required for the safe and environmentally compliant operation of small-scale research facilities.

The building was installed on a 7,000 square foot concrete slab under a single roof, of which 3,000 square feet are totally enclosed with temperature and humidity control. The remaining 4,000 square feet outside area is open on 3 sides. The indoor area is further divided to contain a 1,500 square foot process area, a common control room that is shared with the outdoor process area, a conference room, an electrical room, and restroom facilities. Installed utilities include instrument/process air, 100 psig saturated steam, process water, and natural gas. These utilities are accessible from a system of elevated piping headers that are located adjacent to the indoor area, as well as around the outdoor area perimeter. Single phase and three-phase electrical power are routed from the electrical room panels to equipment and/or subpanels using overhead cable trays. Instrument and communication cable trays are also located overhead and are arranged to provide coverage of the entire process areas.

A distributed network control system with a Wonderware interface and data storage capability is located in the control room adjacent to local process area control stations. This allows for oversight of the individual project operations with regards to safety and environmental protocol while allowing local, independent process control of each system. Additionally, process area monitoring is provided by local sensors which continuously provide measurement of carbon monoxide and combustible gas levels.

Equipment for the Task H Bio-oil project has been located in the outdoor process area. The Task I Biocrude equipment has been located in the indoor process area. All currently active equipment has been connected to the appropriate utilities and commissioned for operations. Installation and/or modification of equipment and utility infrastructure will continue as dictated by project requirements.

Summarization of Activities:

Task N activities were focused on the construction of a building to provide space, utilities, and safety and environmental overview for the Task H and Task I projects, Bio-oil and Biocrude. Additionally, provisions were made for future projects or for modification/expansion of the

current projects. The building was completed and commissioned with 1,500 square feet of indoor space allocated to Biocrude and approximately 2,000 square feet of outdoor space allocated to Bio-oil. An air compressor system was installed to provide conditioned air site-wide. A natural gas-fired 100 psig saturated steam boiler was installed primarily for Biocrude requirements. Additional piping headers were installed to provide natural gas and process water for all areas.

Equipment for the Bio-oil and Biocrude projects was installed, connected to the appropriate utilities, and commissioned for process operations. A site-wide safety and environmental monitoring system utilizing a Wonderware interface and data storage capability was installed. As part of this system, carbon monoxide and combustible gas measurements are collected in the Bio-oil process area. Commissioning will continue as existing equipment is modified or expanded and as equipment is added.

Ill. I. SERC Pilot Scale Facility – Front view



Ill II. SERC Pilot Scale Facility – Back view



Ill. III. SERC Pilot Scale Facility – Biofuels



Ill. IV SERC Pilot Scale Facility – Biocrude



Task O. Project Management and Reporting

This project is divided into seven tasks (bio-oil, biocrude, microbial oil, hydrocarbons derived from syngas, biomass combustion, feedstock development and pilot plant operation). Each task is led by a task leader and a group of faculty, graduate students and staff who report to the task leader. Task groups will meet monthly to discuss the progress toward milestones, intellectual property, and the status of national laboratory, industry and other relevant partnerships. Each task will compile quarterly reports and a final report as part of their responsibility.

O.1 Quarterly reports for this project for two years

1. Planned Activities:
O.1.DL.1 Prepare and submit quarterly reports for the project.

2. Actual Accomplishments:
Quarterly report submitted.

O.2 Final reports for each task

Milestone:
O.2.DL.1 Prepare and submit final reports for each task.
O.3 Develop partnerships with national laboratories, industries and other research groups

1. Planned Activities:
Provide leadership to each task to develop partnerships with national laboratories, industries and other research groups and report these in quarterly reports.

2. Actual Accomplishments:

The SERC team met frequently with companies and agencies to promote economic development of the institute's technologies. Representatives from SERC met with a number of companies, laboratories, government agencies, and universities to discuss collaboration. The list of partnerships and collaborations is given in the spreadsheet.

SERC established collaborations with HY-TEK Bio, Mississippi Power, KiOR, Tellus Operating Group, ROI, Inc., Chemical Products Co., JBS United, AST, Inc., Piedmont BioProducts, Inc., Eclipse Renewables, Harrelson and Associates, LLC, American Science and Technology, REPREVE Renewables, LLC, Parker Towing Co, Inc, MCB, LLC, Biomass Working Groups, LLC, Morrison and Co, Biomass Energy Resources, LLC, Bass Realty Co, Replogle Hardwood Flooring Co, LLC, Oliver Mayhew, Robert Diamond, Stockbridge Associates, Resource Recovering, Inc, Terrenova, LLC, Charles Rivenburgh, Gas Technology Institute, Moon Kim, Forsythe and Long Engineering, ARCADIS US, Inc, Steve Vegte, Chris Albrick, and United Technologies Corporation.

Final Report

Project Title: Mississippi State University Sustainable Energy Research Center, Phase IV

Award Number: DE-FG36-06GO86025

Recipient: Mississippi State University

Project Location: Mississippi State University, Starkville, Mississippi

Reporting Period: January 1, 2012 – June 30, 2014

Date of Report: September 26, 2014

Written by: W. Glenn Steele

Principal Investigator: W. Glenn Steele

The data and information contained in Pages 10-79 and 160-201 of this report have been submitted in confidence and contain trade secrets and/or patentable intellectual property.

Acknowledgment: This material is based upon work supported by the Department of Energy under Award Number DE-FG36-06GO86025.

Disclaimer: This report was prepared as an account of work sponsored by an agency of the United States Government. Neither the United States Government nor any agency thereof, nor any of their employees, makes any warranty, express or implied, or assumes any legal liability or responsibility for the accuracy, completeness, or usefulness of any information, apparatus, product, or process disclosed, or represents that its use would not infringe privately owned rights. Reference herein to any specific commercial product, process, or service by trade name, trademark, manufacturer, or otherwise does not necessarily constitute or imply its endorsement, recommendation, or favoring by the United States Government or any agency thereof. The views and opinions of authors expressed herein do not necessarily state or reflect those of the United States Government or any agency thereof.

Number of Task, Subtask or Milestone	Title of Task, Subtask or Milestone	Task or Milestone Completion Criteria	Actual Accomplishments
P.	Bio-oil		
P.1	Maintain, improve, and commercialize one-ton/day pilot-scale pyrolysis reactor and bio-oil upgrading systems		
P.1.1.	Design and fabricate a char furnace for production of reactor pyrolysis heat.	The development of a prototype char furnace to replace at least 5% of the heat currently supplied by electricity. Temperature entering the pyrolysis reactor will be 600 C or higher.	The char furnace was attached to the pyrolysis reactor and the heat supplied for the pyrolysis process was measured. Seven percent to the total pyrolysis heat was supplied by the char furnace in this small prototype furnace. The furnace employs a small amount of natural gas to ignite small particles of char blown into the furnace. A temperature of 850 C is produced in the furnace and a temperature of 750 C enters the reactor heating system.
P.1.2.	Produce bio-oil for analysis and testing.	Bio-oil to be produced at 7 kg/h for the laboratory scale and pilot scale pyrolysis reactor and at one-ton per day at maximum output without significant down time.	A one-ton per day auger pyrolysis reactor was successfully designed and fabricated. All biomass handling equipment including dryer were developed to process and deliver feedstock to the reactor at more than required to process one-ton per day; particle size is 1-3 mm and biomass water content is below 30%. Bio-oil filtration removed all but nano-sized particles and total solids content was below 0.5%. Large quantities of bio-oil at a rate of 3-gal per hour have been produced over numerous 8 h days without down time. Bio-oil was produced by both the 7kg/h laboratory scale pyrolysis reactor and by the one-ton per day pilot plant reactor. Numerous species of biomass were tested for bio-oil and char quality.
P.2	Further testing and development of a laboratory scale catalytic pyrolysis reactor		
P.2.1.	Utilize various catalysts and modified catalytic pyrolysis reactor designs for bio-oil upgrading.	Utilize a novel fluidized bed reactor and test numerous catalysts to produce an upgraded bio-oil via catalytic pyrolysis.	A catalytic pyrolysis system based on a fluidized bed design was fabricated. Biomass was pyrolyzed in the fluidized bed with sand alone as control and with several catalysts mixed with the sand. The pyrolysis vapors were condensed with two condensers. The optimum pyrolysis temperature among those tested (450, 500 and 550 C) was 450 C.
P.2.2.	Optimize system with the best-performing catalyst.	Choose best performing catalyst(s) from those tested and optimize yield. Produce a liquid yield higher than 40% with an oxygen value lower than 40% and with a HHV of greater than 30 MJ/Kg.	Various catalysts were tested with the best performance produced by mesoporous acidic catalysts. The best performing catalysts were Si-Al and HZSM5. The liquid yield for the Si-Al at 42.8% was 25% higher than the 34.5% yield for HZSM5. However, the oxygen value for the Si-Al was 30% higher at 38.57% than for the 29.58% value for the HZSM5 catalyst. The high oxygen content and somewhat lower carbon content for the Si-Al liquid product resulted in a somewhat lower (31.61 MJ/Kg) value compared to that of the HZSM5 liquid product at 34.0 MJ/Kg. These results indicate that it is somewhat of a toss-up in the choice between these catalysts. It was not possible to perform an analytical test to identify hydrocarbons in the liquid products. However, the high HHV values for the liquid products of the two best catalysts indicate that considerable hydrocarbons were produced during the deoxygenation that occurred during catalytic pyrolysis.
P.3	Produce hydroxymethylfurfural (HMF) from maximized bio-oil anhydrosugars		

Number of Task, Subtask or Milestone	Title of Task, Subtask or Milestone	Task or Milestone Completion Criteria	Actual Accomplishments
P.3.1.	Utilize various heterogeneous and homogeneous catalysts to produce maximum yield of HMF.	Test numerous catalysts and reactor conditions to produce HMF at >30% yield.	Numerous catalysts and methods to produce HMF were tested and many of these were actually effective. The best catalyst for production of HMF, furfural and total furans was 1.5 M formic acid catalyst with addition of hydrolyzed aqueous solution in a ratio of 7 to 3 with DMSO. With this catalyst and methods the highest yields of HMF (39.9%), furfural (31.7%) and total furans (71.2%) were obtained. Optimal reaction time and temperature were also tested using various levels and it was found that the best temperature was 170 C for a reaction time of 45 min.
P.3.2.	Develop a method to separate clean cuts of HMF.	Test various solvents to produce clean cuts of HMF after catalysis of the aqueous bio-oil fraction to produce a treated liquid product with high HMF content.	Separation of clean HMF cuts from the un-hydrolyzed aqueous fraction was performed by using various solvent-solvent extraction steps in combination with Amberlyst 16 wet cation exchange catalyst. The un-hydrolyzed aqueous fraction was treated with 2-butanone (solvent:un-hydrolyzed aqueous fraction ratio=3:1) at 120 C for 60 min. The treatment was catalyzed with 10% Amberlyst 16 wet catalyst (weight to volume of un-hydrolyzed aqueous fraction). The treatment was performed in a Parr reactor and the heating time was 25 min. After completion of the treatment, separation of clean cuts from HMF from aqueous layer was achieved by separating funnel.
P.4	Bio-oil upgrading: continue refinement of bio-oil upgrading processes to esterified, esterified/olefinated, and hydroprocessed bio-oils; maximize and utilize sugar hydrolyzates; produce stabilized bio-oil from pine bark feedstock.		
P.4.1.	Utilize various catalysts and modify reactor designs for bio-oil upgrading and sugar production.	Produce high HHV (>30) and low acid value (<30) boiler fuels; remove 100% of bio-oil aqueous fraction inhibitors to allow production of ethanol. Develop a pyrolysis reactor design that produces higher levoglucosan levels.	A novel method of spraying a water mist into the pyrolysis vapor was developed to reduce the reactivity of the vapor during condensation. This reduced the degradation of levoglucosan and doubled its production in the aqueous fraction. This invention was patented. Multiple treatments were applied to the aqueous fraction of bio-oil and all inhibitors were fully removed. Ethanol production was maximized at 98% of theoretical level.
P.4.2.	Optimize hydroprocessing, esterification, esterification/olefination, and sugars production systems with the best-performing catalyst and/or other additives.	Produce high HHV (>30) and low acid value (<30) boiler fuels; remove 100% of bio-oil aqueous fraction inhibitors to allow production of ethanol.	A novel pretreatment method which oxidizes bio-oil allowed the increased production of carboxylic acids to provide an increased degree of esterification with a relatively low percentage of alcohol (20%). This led to production of a high HHV boiler fuel. Ozone/H2O2 pretreatment was utilized and increased the AV of raw bio-oil from 90.3 to 165.4 mg KOH/g. The boiler fuel produced had an HHV of 35.3 MJ/Kg; the energy density of boiler fuel produced by this method was increased by 120.62% from raw bio-oil at 16.0 MJ/Kg. Boiler fuel viscosity was reduced to 10.1 cSt.

Number of Task, Subtask or Milestone	Title of Task, Subtask or Milestone	Task or Milestone Completion Criteria	Actual Accomplishments
P.4.3.	Produce bio-oil from bark with various treatments and compare properties to bio-oil from clear woods.	Determine the mechanisms causing bio-oil produced from bark to have increased aging issues and lower yields.	Four bio-oils were produced that contained various percentages of bark (0%, 50%, 60% and 80%). Liquid yields decreased and char yields increased as bark content increased. pH values were about the same regardless of the bark contained in the pyrolyzed feedstock. Generally the bio-oil solids content rose for each increased percentage of bark addition. Solids content and viscosity increased with increasing bark content during accelerated aging. Chemical analysis showed that the primary and secondary alcohols reacted to produce aromatics or ketones. Each of the findings described for the study can be explained from the fact that bark contains considerably higher mineral content than clear wood. In addition, the results indicate that the bark is more highly frangible and that the increased number and size of bark fragments result in a higher amount of mineral-containing solids being entrained into the condensed bio-oil than for clear wood. It is known that minerals catalyze both gasification and char formation during pyrolysis. In addition, mineral content increases the catalysis which leads to polymerization of bio-oil during aging. For bark to be usable as a pyrolytic feedstock to produce high-quality bio-oil it is clear that means to reduce the mineral content of the bark are required or char entrainment into the bio-oil during pyrolysis needs to be greatly reduced or eliminated.
Q.	Biocrude		
Q.1	Develop a novel in-situ process for the depolymerization of lignocellulose	Evaluation of the catalytic thermal conversion of waste lignocellulosic biomass into mixtures of carbon source as substrate for oil accumulation of oleaginous microorganisms.	Hardwood bark chippings and fibrous sludge were depolymerized using supercritical methanol and doped hydrotalcites. The liquid contained numerous organic compounds. The mixture was tested for growth of oleaginous microorganisms.
Q.1.1	Produce biocrude from liquefied lignocellulose using supercritical methanol	Accumulation of >20% lipid content via oleaginous microorganisms	
Q.1.2.	Produce the carbon source at a cost consistent with U.S. DOE price targets.	A carbon source was produced and used as a media to grow oleaginous microorganisms. The carbon source cannot be compared with regular sugars because it is a liquid mixtures	The process generates a liquid mixture containing numerous organic compound, and thus, cannot be compared with the DOE target for the price of sugar.
Q.2	Expand the oil production capacity of the biocrude pilot facility.	Produce cells with >20% (wt/wt) biocrude	Data showed that under the correct conditions cells with >20% (wt/wt) biocrude could be produced.
Q.2.1.	Demonstrate biocrude production from industrial wastes.	Experiment with various industrial wastes to produce >20% lipid content	Various industrial wastes were evaluated and some (pulp and paper wastewaters) were able to produce >20% lipid content during experimentation.
Q.2.2.	Prepare a conceptual plant design for the generation of biocrude from candidate industrial wastewaters, sludge/oleaginous/algae consortiums, and/or solid residues, which will be used as carbon sources.	Prepare a PFD	A PFD was prepared.
Q.3	Develop in-situ production of biodiesel.		

Number of Task, Subtask or Milestone	Title of Task, Subtask or Milestone	Task or Milestone Completion Criteria	Actual Accomplishments
Q.3.1.	Reduce or eliminate the cost of biocrude extraction and conversion into biodiesel.	Compare various methods for lipid extraction	Various methods for lipid extraction were compared with the supercritical methanol process looking promising.
Q.4	Generate a new consortium of biocrude producing microorganisms using a combination of novel biomolecular and traditional microbiological techniques.		
Q.4.1	Develop a robust microbial consortium capable of yielding over 25 lbs of oil/100 lbs of carbon.	>25% lipid content	Since it was found in the earlier phases of the study that the lipid productivity of activated sludge microorganisms was highest (>25%) at C:N ratio 70:1, the dominance of members of the alpha *Proteobacteria* group in the resulting activated sludge culture at this condition could point to the specific microorganisms potentially responsible for high lipid accumulation among the numerous members of the activated sludge microbiota for potential isolation and use in pure culture fermentations.
Q.5	Supply chain design and management	Develop model for production and delivery of biodiesel	A mixed integer, two-stage stochastic programming model to design and manage biodiesel supply chains was developed.
Q.5.1.	Build solution procedures for the problems proposed that provide good quality solutions.		
R.	Microbial Oil		
R.1	Determine the yield and rate of the cells and oil production from selected carbon sources		
R.1.1.	Convert 75% of the carbon source by these organisms.	>75% of initial sugars input consumed	Data showed that >75% of sugars were consumed by the organism if the carbon source was favorable for growth.
R.1.2	Achieve cell densities of greater than 5 g/L with lipid contents greater than 20%.	>5 g/l cell mass with >20% lipid content	A cell mass of >5g/l and lipid content of >20% was achieved.
R.1.3.	Maximize yield of lipids/g of substrate.	> 0.15 g of lipid/g of sugar	Lipids/g of substrate were maximized to >0.15g of lipid /g of sugar.
R.2	Pure culture growth and oil accumulation on industrial waste streams.		
R.2.1.	Identify candidate oleaginous microorganisms.	Identify at least one oleaginous culture that could work in industrial wastewater	R. glutinis was identified to work in industrial wastewater.
R.2.2.	Reduce 70% in the COD of the wastewaters	>70% Reduction in COD of added COD	The maximum COD removal efficiency of 60% is achieved when R. glutinis is cultivated in amended pulp and paper wastewater. However, low COD removal could be due to the presence of non-degradable organic compounds.
R.3	Develop in-situ production of biodiesel using oil-fat microorganisms		
R.3.1.	Convert of 80% of the lipids into biodiesel.	80% of lipids transesterified	Data showed 80% of lipids could be transesterified in-situ.
R.3.2.	Reduce the cost of biocrude extraction and conversion into biodiesel by 10% compared to conventional biodiesel process.	10% Cost reduction in lipid extraction	10% cost reduction in lipid extraction was achieved.
R.4	Evaluate the value of the products contained in the residual cell mass post-oil extraction		
R.4.1.	Identify uses for the residuals remaining post oil extraction.	Identify uses of cell cake	The hydrolysate of the cell cakes demonstrated to be a highly efficient inhibitor on the natural gas hydrate formation, which was proved to be contributed to the compounds like the peptone and the resultant hydrolysates.
S.	Liquid Hydrocarbons from Bio-derived Synthesis Gas (syngas)		

Number of Task, Subtask or Milestone	Title of Task, Subtask or Milestone	Task or Milestone Completion Criteria	Actual Accomplishments
S.1	Syngas composition adjustment and syngas purification suitable for hydrocarbon synthesis		
S.1.1.	Utilize steam addition and oxygen enrichment with multiple feedstocks.	Evaluation of the possibility of steam gasification and oxygen blown gasification to the existed downdraft gasifier.	Evaluated syngas composition from woody biomass. Determined impurities which will affect the hydrocarbon production. Two refereed journal articles published.
S.1.2.	Design, build, and test a bio-syngas purification system.	Establishing the whole system for syngas cleaning. Testing oxygen removal catalyst in the syngas purification system.	Setup and tested the syngas cleaning system in both lab scale and pilot scale.
S.2	New generation catalyst with improved activity and stability		
S.2.1.	Develop a new-generation catalyst with improved activity and selectivity.	Obtaining high conversion and high selectivity catalyst for hydrocarbon production.	Several multifunctional catalysts were obtained for gasoline range, or diesel range, or jet fuel range hydrocarbons production. Four refereed journal articles published.
S.2.2.	Optimize the catalytic process conditions to account for the effects of impurities in the synthesis gas derived from biomass gasification.	Evaluation of proper conditions for the whole process from biomass to liquid hydrocarbon.	Set up the whole process for liquid hydrocarbon production including gasification, syngas cleaning and catalytic conversion.
S.2.3.	Run a 1000-hr life-time test of the new-generation catalyst to validate its activity and stability with the bio-syngas. The life-time test will be conducted under the optimized operating conditions.	Evaluation of the longevity of new generation catalysts.	Tested the longevity of new generation catalysts.
S.2.4.	Develop more understanding of catalyst deactivation and regeneration issues in syngas conversion.	Surveys the catalyst deactivation and regeneration problems if happens.	Developed a method for catalyst regeneration.
S.3	Process design and economic analysis		
S.3.1.	Complete the process design (based on ChemCAD or Aspen plus), including the syngas purification system.	Establishing the whole process design by Aspen plus.	Data obtained for Aspen plus analysis on process design and economic analysis.
T.	Biomass Combustion		
T.1	Real-time visualization of combustion of non-food biomass fuels using advanced laser diagnostic techniques		Two peer-reviewed journal articles were published and seven new research grant proposals were submitted to DOE, NSF, ACS, etc., by leveraging the RCEM experiments performed in this Subtask.
T.1.1.	Obtain spatially-resolved images of combustion of non-food biomass fuels.		Ignition characteristics in diesel-ignited methane and diesel-ignited propane dual fuel combustion were quantified and carefully analyzed. A reliable methodology was developed to estimate the compression ratios in the RCEM and several combustion shots have been completed to obtain combustion pressure and heat release rates.
T.1.2.	Characterize species evolution during non-food biomass fuel combustion		Diagnostics based on LIBS were used to quantify fuel-air equivalence ratios in premixed methane-air flames in a rectangular slot burner and a McKenna burner. A new multi-hole injector was installed in the RCEM. MSU was invited to participate in the Engine Combustion Network (ECN) after further experiments are completed on the RCEM.

Number of Task, Subtask or Milestone	Title of Task, Subtask or Milestone	Task or Milestone Completion Criteria	Actual Accomplishments
T.2	Quantification of particulate matter (PM) emissions from combustion of non-food biomass fuels		One invited peer-reviewed journal article, seven peer-reviewed journal articles, three peer-reviewed conference papers, four invited presentations (given within the US and abroad), and one non-peer-reviewed conference paper were published from this Subtask. This Subtask also facilitated one completed Ph.D. dissertation, three completed M.S. theses, one ongoing Ph.D. dissertation, and two ongoing M.S. theses.
T.2.1.	Measure filter paper-based smoke emissions for combustion of non-food biomass fuels.		Filter-paper based smoke emissions were quantified for a variety of fuels on the single-cylinder research engine: methane, propane, and a renewable non-food biomass-derived distillate fuel from KiOR. Cyclic variations in dual fuel low temperature combustion and CFD analysis of gasoline compression ignition combustion were also completed.
T.2.2.	Characterize particle size distributions in the sub-micron/nanometer range for combustion of non-food biomass fuels.		Particle size distributions were characterized over a range of operating conditions for a variety of fuels. Ignition, combustion, fuel conversion efficiencies, and engine-out exhaust emissions (including particle number and size distributions from the EEPS) were measured for straight diesel fueling and for diesel-ignited methane, gasoline, and propane dual fuel combustion. Additional state-funded experiments were also completed for understanding the combustion of KiOR's non-food biomass-derived distillate fuel and its blends with ULSD.
U.	Biomass Feedstocks Development		
U.1	Testing, establishment of candidate species, and conversion of pasture/CRP land to candidate species	Evaluation of candidate species for establishment and chemical suitability. Determination of effective planting of switchgrass and giant miscanthus in CRP or pasture conditions. And herbicides to aid in establishment.	Evaluated energycane, switchgrass, big bluestem, little bluestem, indiangrass, giant miscanthus, sweet sorghum, maize, gamagrass.. Establishment aids of seed safeners tested and worked for the most part. Field testing indicated burndown necessary in field establishment in CRP and pasture conversion. Gamagrass foliage being evaluated as an a perennial maize stover replacement
U.1.1.	Continue establishment of Uniform Variety Trials at six to eight locations around Mississippi with testing of herbicides to enhance successful establishment under both tillage and no-tillage conditions.	Sites planted or needed to be replanted.	Data obtained for rapid emergence of four species breed for such. Data on emergence and yield obtained from five Mississippi sites. New tests planted again this spring.
U.2	Management, nutrient cycling, and char usage		
U.2.1.	Provide a second year assessment of the movement of N within feedstock species, assessing feedstock species' potential of associative nitrogen fixation, determine N value of legume mediated nitrogen fixation, and obtain baseline data on appropriate char application rates.	Testing using gaseous N15 probing to determine if plants obtain nitrogen from associated bacteria. Assessment of likely species. Testing of cool season legumes to determine if they provide nitrogen to subsequent switchgrass plot. Biochar applications in field a pot studies to determine their effect on crop.	Data indicated associative nitrogen fixation was higher for energycane and switchgrass than giant miscanthus. Likely bacterial families identified. Testing of cool seasons legumes to supply nitrogen completed, but inconclusive. Biochar pot studies and field studies completed.
U.3	Wood residue assessments		
U.3.1.	Develop a survey and data regarding recoverable wood residue for bioenergy conversion.	Surveys initiated with industry and waste providers	Data from survey obtained and completed. Six refereed journal articles published
U.4	Feedstock engineering		
U.4.1.	Determine the effects of economical binders on the efficacy of densifying switchgrass through in-field cubing.	Binders will improve cubing efficacy by at least 5% as was seen in bermudagrass	Two binders and three application rates were tested pre and post-senescence in switchgrass. Though pre-senescence cubing was better than post-senescence, all binders and rates performed worse than the controls.

Number of Task, Subtask or Milestone	Title of Task, Subtask or Milestone	Task or Milestone Completion Criteria	Actual Accomplishments
U.4.2.	Determine the spatial distribution of the potential bio-energy crops and their environmental benefits in Mississippi for renewable fuels through economic modeling and analysis.	Developed models with watershed or physical data. Model calibration and validation were performed. Model results were analyzed with statistics.	Potential bio-energy crops in the watersheds were researched. Economic modeling and analysis were performed. Six peer-reviewed articles published in the journals (Trans ASABE, Ag & Forest Meteorology etc.)
U.4.3.	Assess the effects of environmental conditions and management systems on the net energy value of feedstocks.	Determine the sustainability and eco-friendliness of ethanol production associated with maize stover and switchgrass.	Two indices of sustainability and environment-friendliness – net energy value (NEV) and carbon credit balance (CCB) - were found to increase with an increase in yield level and utilization rate of biomass feedstock. This increase was due to less land requirement for biomass production, smaller draw area, shorter travel distance, and ultimately less non-renewable energy consumption for the collection and transportation of biomass feedstock. The environment-friendliness of switchgrass-based ethanol production was found to be higher than that of maize stover for all yield levels and utilization rates. This difference
V.	Pilot Plant Operations		
V.1.1	Successfully operate the pilot scale facility to produce biocrude/microbial oil and bio-oil.		Activities included maintenance and modification of both utility and pilot system infrastructure, as required, to assist in the successful production of biocrude and bio-oil. In addition, maintenance was provided for the pilot building structure and non-process related components.
W.	Project Management and Reporting		
W.1	Quarterly reports for this project for two years		
W.1.1.	Prepare and submit quarterly reports for the project.		Quarterly reports were submitted.
W.2	Final reports for each task		
W.2.1.	Prepare and submit final reports for each task		Report was submitted.
W.3	Develop partnerships with national laboratories, industries and other research groups		
W.3.1.	Provide leadership to each task to develop partnerships with national laboratories, industries and other research groups and report these in quarterly reports.		The SERC team met frequently with companies and agencies to promote economic development of the institute's technologies. Representatives from SERC met with a number of companies, laboratories, government agencies, and universities to discuss collaboration.

SERC IV Final Report

The data and information contained in Pages 10-79 and 160-201 of this report have been submitted in confidence and contain trade secrets and/or patentable intellectual property.

Begin confidential information.

Task P. Bio-oil

Principle Investigators and team members:
Philip H. Steele, Dept. of Sustainable Bioproducts
El Barbary Hassan, Dept. of Sustainable Bioproducts
Keisha Walters, Dept. of Chemical Engineering
Radha Srinivasan, Dept. of Agricultural & Biological Engineering

Executive Summary:
The goal of the SERC Bio-Oil Research Group Thrust Area is to produce and characterize high-quality bio-oils from southern forestry and agricultural feedstocks. The focus of this project proposal was operation, maintenance, and improvement of the one-ton/day pilot-scale pyrolysis and bio-oil upgrading systems developed under SERC III funding. Cooperation with two industrial cooperators to commercialize the MSU auger reactor design continued. Development of a catalytic pyrolysis system continued based on the laboratory scale reactor developed under SERC III. Production of fuels from the high-sugars content aqueous fraction system developed by MSU was also continued by adding production of hydroxymethylfurfural. Refinements to the upgrading of bio-oils by hydroprocessing, esterification, and sugars maximization was pursued, and a system to produce stable bio-oils from pine bark suitable for liquid fuels production was developed.

The research results produced by the Mississippi State University (MSU) DOE-funded Sustainable Energy Research Center will add significantly to the general and specific understanding of both bio-oil production and bio-oil conversion to fuels. Numerous papers have been published and numerous presentations have been made to transfer our findings. Patents have been filed to protect important intellectual property developed by our research. Several M.S. and Ph.D students have graduated who performed research in this project and they are entering both academia and industry to extend the knowledge that they have acquired here to other organizations and into the future. The results summarized in this final report show that all milestones sought have been fully accomplished.

The pilot scale one-ton per day pyrolysis reactor has been fully tested and is producing at the rated capacity. Mean bio-oil yield is 60% and water content is below 30%. The bio-oil produced by the pyrolysis system differs very little from the bio-oil produced in our laboratory-scale pyrolysis reactor which has been compared to bio-oil produced by other systems in several published studies. The biomass handling system functions well and biomass is delivered to the pyrolysis reactor dried and at a known mass. A prototype char furnace has been developed that replaces 7% of the heat required for pyrolysis. The centrifugal filtration unit has been fully tested and separates all but nano-sized particles from the bio-oil.

Comparison of the bio-oil from the one-ton per day and our laboratory-scale pyrolysis reactor was performed. The bio-oil quality from the laboratory-scale reactor has been compared to bio-oils produced by various researchers in several publications and no significant difference in qualities

has been shown. The comparison of bio-oil by mass balance, elemental analysis, physical properties, exit gases and by GC-MS indicated no significant difference in the bio-oil produced by the one-ton per day pyrolysis reactor compared to the MSU laboratory scale reactor. GC/MS results were compared between the SERC one-ton per day bio-oil reactor and that produced by the laboratory scale reactor processing 7 kg/h which is located in the Department of Sustainable Bioproducts (DSB) at MSU. The DSB bio-oil pyrolysis reactor has been compared to the bio-oil produced by other practitioners numerous times and in several published papers with little difference noted. Therefore a comparison between the SERC and DSB product produced during pyrolysis will confirm that the SERC reactor products are similar to that produced by most pyrolysis methods. The comparison of the SERC and DSB reactor bio-oils showed that the SERC bio-oil had much higher phenol content (15 percentage points higher) and that furfural was also higher with 2.75% produced versus zero for the DSB reactor. In addition, a comparison of bio-oil properties between the bio-oils produced by the two reactors showed that the water content, AV and HV values differed somewhat. SERC bio-oil water content was about 2 percentage points higher, the AV value was about 12 mg KOH/g lower and the HHV value was about 2 percentage points higher. The viscosity value difference is undoubtedly due to the higher water content of the SERC bio-oil. The HHV increase for the SERC bio-oil is likely due to the reduced acid value.

These differences in phenol, furfural, carbon and oxygen content were attributed to the design of the SERC pyrolysis reactor that routes char back to heat a central tube inside the main reactor tube. This process allows the char to continue to pyrolyze and emit CO and CO_2. These gases appear to initiate reaction(s) in the bio-oil during the pyrolysis reaction rather than change the species of compounds produced.

A catalytic pyrolysis system based on a fluidized bed design was fabricated. Biomass was pyrolyzed in the fluidized bed with sand alone as control and with several catalysts mixed with the sand. The pyrolysis vapors were condensed with two condensers. The optimum pyrolysis temperature among those tested (450, 500 and 550 ^oC) was 450 ^oC. Various catalysts were tested with the best performance produced by mesoporous acidic catalysts. The best performing catalysts were Si-Al and HZSM5. The liquid yield for the Si-Al at 42.8% was 25% higher than the 34.5% yield for HZSM5. However, the oxygen value for the Si-Al was 30% higher at 38.57% than for the 29.58% value for the HZSM5 catalyst. The high oxygen content and somewhat lower carbon content for the Si-Al liquid product resulted in a somewhat lower HHV (31.61 MJ/Kg) compared to that of the HZSM5 liquid product at 34.0 MJ/Kg. These results indicate that it is somewhat of a toss-up in the choice between these catalysts. It was not possible to perform an analytical test to identify hydrocarbons in the liquid products. However, the high HHV values for the liquid products of the two best catalysts indicate that some hydrocarbons were produced during the deoxygenation that occurred during catalytic pyrolysis.

The project to convert bio-oil aqueous fraction anhydrosugars to hydroxymethylfurfural (HMF) was highly successful. The bio-oil used in the study was produced on the MSU laboratory scale reactor that sprays water into the vapor stream of the pyrolysis vapors. This has been shown to nearly double the yield of anhydrosugars. Several methods, solvents and catalysts were tested to determine the best route to convert bio-oil anhydrosugars to HMF. The best method for maximum production of HMF and total furans was for 1.5 M (moles) formic acid catalyst with addition of hydrolyzed aqueous solution in a ratio of 7 to 3 with DSMO. Yield of combined HMF and furfural was 45.8% with this method with it comprising 25.5 percentage points of the total yield. Optimal reaction time and temperature were also tested using various levels and it was found that the best temperature was 170 ^oC for a reaction time of 60 min.

Continued research on bio-oil upgrading processes has added significant knowledge to the development of fuels. A study was performed to attempt to improve the understanding of pyrolysis means to produce a bark-based bio-oil with improved properties. Current pyrolysis oil from bark feedstocks polymerizes rapidly and contains high amounts of solid matter.

Four bio-oils were produced that contained various percentages of bark (0%, 50%, 60% and 80%). The yields and char wt% values for each of these bio-oils were determined. Yields of liquid bio-oil for 0%, 50%, 60% and 80% bark content had respective liquid bio-oil yields of 58.3, 51.7, 43.0 and 41.2% while the respective values for char were 23.7, 25.7, 29.1 and 30.9%. Therefore, liquid yields decreased and char yields increased as bark content increased. pH values were about the same regardless of the bark contained in the pyrolyzed feedstock. However, the solids content rose for each increased percentage of bark except for the 50% bark addition which increased above that of the 0% bark sample but was lower than for the 30 and 40% bark samples. There is no known reason for this result. Aging studies showed that the solids contained in the increasing bark content bio-oils all increased as the time of accelerated aging increased. Viscosity of the bark was also observed to increase as the accelerated aging time increased. Chemical analysis showed that the primary and secondary alcohols are reacting to produce aromatics or ketones. Each of the findings described for the study can be explained from the fact that bark contains considerably higher mineral content than clear wood. In addition, the results indicate that the bark is more highly frangible and that the increased number of bark fragments result in a higher amount of solids being entrained into the condensed bio-oil than for clear wood. It is known that minerals catalyze both gasification and char formation during pyrolysis. In addition, mineral content increases the catalysis which leads to polymerization of bio-oil during aging. For bark to be usable as a pyrolytic feedstock to produce high-quality bio-oil it is clear that means to reduce the mineral content of the bark will be necessary.

Removal of water by hydraulic compression at the harvest site would allow more economic transportation of wood mass as compared to water mass. A hydraulic press process was applied for water removal from green juvenile wood chips. The compressing process simulated a whole tree chipping operation in which loblolly pine chips were processed on the harvest site immediately after production. 50,000 psi of pressure was applied to green loblolly pine chips. The reduction of water content in the chips was disappointing with a reduction only to 42.2 from 44.5%. Numerous attempts were made to increase the efficacy of water removal by compression. It appeared that the design of our high pressure rollers was not as effective as hoped and no solution to this issue was found. The press water produced had high BOD and COD values which attributes to suspended solids and volatile compounds such as essential oils from the raw wood. Surprisingly, no water-soluble sugars were detected in the press water. This result indicated that the hydraulic pressing did not result in the extraction of non-structural carbohydrates contained in the wood chips. SEM images of the fresh and compressed chips showed morphological changes. The compressed wood chips shrunk slightly after processing. TGA and DTG analysis showed a continuous mass loss associated with increasing temperature. During TGA thermal heating the degradation was higher for raw pine wood chips compared to compressed wood chips. FTIR analysis showed that most of the oxygen-containing surface groups were removed by hydraulic compression.

Additional research to remove inhibitors from the aqueous phase containing hydrolyzed anhydrosugars was performed. Under SERC III we were partially successful but it was necessary to add 50% of glucose to the hydrolyzed bio-oil aqueous fraction to produce ethanol at the highest level. In the current study several new procedures were tested consecutively to determine the possibility of complete removal of inhibitors if cost were not an issue. This is research that has not been previously performed. Solvent separation, membrane filtration and freeze drying were

applied to the aqueous fraction of bio-oil following hydrolysis. Following all treatments to remove inhibitors the organism S. pastorianus fermented and consumed all glucose and mannose in the hydrolyzed aqueous fraction in 36 h. Ethanol yield reached its maximum at 12.12 g/L (0.50 g/g). This value is 98% of the maximum theoretical value of ethanol.

Synthesis gas was utilized as the hydrotreating step followed by hydrocracking utilizing hydrogen as is the practice. Synthesis gas contains considerable CO which assists in the water gas shift reaction to produce hydrogen when a suitable water gas shift catalyst is used. This study performed both hydrotreating and the water gas shift simultaneously. It was found that both the synthesis gas hydrotreated product and the final hydrocracked hydrocarbon mixture were nearly identical to utilization of only pure hydrogen to perform hydroprocessing of bio-oil. For this reaction to be successful the researchers found it necessary to oxidize the bio-oil to produce a highly acid intermediate containing increased amount of carboxylic acids from aldehydes. The final hydrocracked hydrocarbon mixture had an HHV of 45.3; oxygen content and acid value were zero. Water content was negligible at 0.08%. Viscosity was dramatically reduced from 28.3 to 2.4 cSt. A simulated distillation analysis estimated that the hydrocarbon mixture was comprised of 45% gasoline weight compounds, 20% jet fuel compounds, 30% diesel weight compounds and 5% weight of heavy uncracked oil that could be recracked, if desired. A detailed hydrocarbon analysis (DHA) showed that the hydrocarbon mixture contained n-paraffins of 6.8%, iso-paraffins of 17.5%, olefins of 26.9%, napthenes of 13.8% and aromatics of 7.2%. Total C14 and above weight carbons comprised 15.0% of the mixture and 10.0% were unidentified compounds. Octane number was also shown to be 61.8 by the DHA. Hydrogen utilization during the hydrotreating step was reduced by nearly 18%. It is clear that this technology has promise for reducing hydrogen utilization during hydroprocessing of bio-oil to hydrocarbon fuels. A patent has been filed to protect this intellectual property.

Most practitioners treat HDO bio-oil with a two-stage treatment consisting of a 1st-stage mild low-temperature (<300 ^{o}C) hydrotreatment followed by a higher temperature hydrocracking 2nd-stage. This study tested the potential for applying direct HDO of one stage in a continuous flow reactor to oxidized bio-oil which has been shown in the previously described synthesis gas study to be easier to hydrotreat with syngas than is raw bio-oil. The oxidized bio-oil was treated by 3 wt% oxone and 10 wt% H_2O_2. Butyric anhydride was added as a final step based on the known fact that butyric anhydride reacts with water to produce alcohol thereby reducing bio-oil water content with the hope of producing a better quality hydrocarbon mixture. Several catalysts were tested but sulfided CoMo/γ-Al_2O_3 produced the best quality HDO product. The acid value of the HDOed oxidized bio-oil was 2.1, HHV was 43.1 MJ/kg and water content was only 0.2%. Yield was lower at 0.34 g/g feed but qualities were much superior. A DHA performed on the hydrocarbon mixture showed that olefin, iso-paraffins and C14+ compound dominated followed by naphthenes and aromatics. The octane of the hydrocarbon mixture was higher than 50.

Catalyst life experiments were performed on the hydrocarbon mixture produced by sulfided CoMo/γ-Al_2O_3. These were somewhat disappointing and indicated that the longest life possible for oxidized bio-oil containing butyric anhydride as 19.1 h. As for all current HDO catalysts premature deactivation was a problem when treating oxidized bio-oil.

Subtask P.1 Maintain, improve, and commercialize one-ton/day pilot-scale pyrolysis reactor and bio-oil upgrading systems

The pilot-scale, one-ton/day pyrolysis reactor will produce large volumes of bio-oil for upgrading by hydroprocessing and esterification/olefination. The pyrolysis reactor, hydrotreater, and esterification/olefination reactor were installed with previous SERC funding. Various feedstock types will be pyrolyzed to provide the bio-oils for upgrading under this subtask. During their

operation, these systems will require continuing maintenance and potential part replacement. In addition, the current pyrolysis reactor pyrolysis heat provided by electrical resistance will be partially replaced by a char furnace to provide pyrolysis heat. Biomass handling and preparation systems for storage, drying, and conveyance were not funded in SERC III; however, these capabilities will be added under the current task. Cooperation with industrial partners to commercialize the MSU pyrolysis reactor design will continue, and chemical and physical analyses of biomass, bio-oils, and upgraded bio-oils will be performed.

Experiments were performed on a laboratory-scale catalytic pyrolysis reactor designed and fabricated in the Department of Sustainable Bioproducts at MSU. A fluidized bed system to pyrolyze the biomass prior to vapor flow through a catalyst bed was developed. After vapor catalysis the vapors were condensed. Numerous catalysts were tested. The best liquids of 38% were obtained at 450 ^{o}C as opposed to lower yields obtained at 500 and 550 ^{o}C. Among the catalysts tested mesoporous catalysts such as MCM-41 and SBA-15 provided the highest amounts of GC-MS identifiable chemical species. Acidic catalysts performed better than mixed oxide catalysts and the basic catalysts. The conclusion from these results was that the most effective catalyst for catalytic vapor pyrolysis should have mesoporosity and be acidic in nature. The catalytic treating experiments showed significant (nearly 50%) reductions in acid value and an increase in water content compared to the blank control. Increased water content indicates that dehydration reaction was predominant in catalytic vapor pyrolysis. An attempt to utilize formic acid as a hydrogen donor to reduce oxygen in the catalyzed product was unsuccessful. Recycling of noncondensable gases through the pyrolysis reactor during pyrolysis was also tested as some practitioners have shown this to significantly reduce oxygen. This experiment also failed to reduce oxygen content; this may have been due to the utilization of nitrogen as a blanket gas that interfered with oxygen reducing reactions.

Production of hydroxymethylfurfural (HMF) from bio-oil anhydrosugars was highly successful. Bio-oils were fractionated into organic and aqueous fractions by 1:1 water addition to raw bio-oil. The bio-oil was produced on the MSU auger reactor which uses a patented method to nearly double the anhydrosugars produced during pyrolysis. Several methods and applications of solvents and catalysts were performed. The most successful of the systems for conversion of anhydrosugars to HMF was for formic acid catalyst at 1.5 m at 170 ^{o}C for a 60 min reaction time with addition DMSO at a ratio of 7:3 (hydrolyzed aqueous solution:DMSO) which led to highest yields of HMF (39.9%), furfural (31.7%) and total furans (71.2%).

Planned Activities:
P.1.ML.1 Design and fabricate a char furnace for production of reactor pyrolysis heat.
P.1.ML.2 Produce bio-oil for analysis and testing.

Summarization of Activities:
The samples for this study were pine clear wood produced from MSU's Forest Products laboratory-scale auger pyrolysis reactor. To perform the lab-scale centrifugal filtration study, the parameters were mimicked as closely as possible to the prior testing performed by Westfalia on the pyrolysis oil produced by MSU (Figure P1).

Glass centrifuge cups
Spin Conditions:

- T = 80 °C
- 6000 rpm
- Mean centrifugal acceleration 4,500 x g (m/s^2)
- 0.5, 1, and 2 min spin times
- 2 sets, 1st group 100 vol% pyrolysis oil, 2nd group 0.1 vol% citric acid & 2 vol% water added prior to spin testing

3 phases occurred:

- Top – water-rich, light brown/translucent, 20 vol%, ρ = 1.177 g/cm3 at 20 °C
- Middle – oil-rich, dark brown/opaque, 79.5 vol % (78.5 vol % for 2nd group), ρ = 1.185 g/cm3 at 20 °C
- Bottom – solids, black, 0.5 vol% (1.5 vol% for 2nd group)

Figure P1. *Spin parameters and summarized results from Westfalia testing*.

Water addition, acid addition, and elevated feed temperature being the three main parameters examined to cause three-phase (light liquid-heavy liquid-solid) separation. Next, increased spin times were examined; however, increasing the spin time also did not induce three-phase separation. It was concluded that storage and shipment of the samples to Westfalia—during which time temperature was not controlled—may have caused 'aging' and resulted in a propensity of the samples to triple-phase separate when centrifuged by Westfalia in Germany.

Samples were next stored for approximately 2 months (5/31/12 – 7/26/12) before being centrifuged following the same procedures used for the acid addition and elevated temperature testing, except the time was again lengthened to 30 min. The 30 min time was split into two 15 min runs, with the 80 °C samples reheated and all tubes rotated 90° inside the centrifuge to better mimic swing bucket centrifuge forces. Top and bottom aliquots from all test conditions were collected and characterized for change in density, water content (wt%), molecular weight distribution and chemical composition.

There was a slight increase in density in the bottom aliquots, but no statistical difference between the top layers and the control (non-separated) sample. This indicates that the solid and tar-like materials were separated into a low-volume, bottom phase, without significantly altering the density of the top phase. Water content was lower in the bottom aliquots, as expected. No strong effects on separation were observed due to water addition, acid addition or both water and acid addition.

To identify chemical composition changes, FTIR spectroscopy was used. Spectra for acid addition and elevated temperature samples did not cause major composition changes in comparison to the water-addition spectra. One interesting factor about the control samples was that the room temperature control resembled the top layer of the centrifuged samples, while the 80 °C control sample resembled the bottom of the centrifuge samples; this is a result that was also obtained by Naske and Walters in a prior SERC project. At longer centrifugation times, there were some notable spectral changes. The top layer showed a stronger –OH stretch peak, possibly from carboxylic acid. The C-H stretching peaks were stronger for the bottom layers, indicating a higher alkane composition. The bottom layers also showed stronger aromatic phenyl bonding, C-C scissoring vibrations, and ketone methyl bending, all indicative of aromatics and heavier molecular weight compounds. Bottom and solid samples indicated conjugation and phenyl naphthalene bonding which is not present in most control and top samples. Possible loss of C=C

alkene stretching and gain of C=C aromatic stretching were also noticed. A stronger conjugation of carbon, seen with polymerization reactions or polymerized samples was observed. Stronger ester bending was also observed in the bottom samples.

To determine molecular weight distribution, gel permeation chromatography (GPC) was utilized. There were generally 3 peaks (fractions) identified in each sample demonstrating a fairly large variation in molecular weight. For each peak, the polydispersity index (PDI) was measured. Overall, the addition of water and/or acid did not seem to have any effect on molecular weight distributions or PDI.

To determine the particle sizes found in pyrolysis oil control samples and what is removed with centrifugation, optical microscopy was performed. The samples centrifuged for 6 and 2 min with water addition were analyzed. The data showed that centrifugation did remove particulate matter, although it was mostly larger particles (>5 μm^2) and that more particles were removed at the longer centrifugation times. From this small study, preliminary results indicate water addition prior to centrifugation might improve particulate removal.

The centrifugal filtration system installed was a GEA Westfalia Separator SSD2-02-107 Centrifuge with self-cleaning bowl. It has a maximum solid capacity of 0.5 L at maximum density of 1.4 kg/dm^3 and a total capacity of 1 L. It has a maximum bowl speed of 10,000 rpm with output of 1,170 L/h and maximum operating temperature of 100 °C and pressure of 2.5 bars. A 200 gal stainless steel jacketed tank with stirrer was available for storing oil prior to centrifugation and for collecting the light phase from the centrifuge. Two 50 gal tanks were available for collecting the heavy liquid phase and solids. The feed, light phase outlet and heavy phase outlet lines were equipped with flow meters. A hot water recirculation system was available to increase the temperature of the feed and product (light-phase), if required. The centrifuge is designed to be fully operational with control and monitoring by computer process, allowing for unmanned operation. For the three-phase separation, a regulating ring was inserted to force liquids of different densities to separate. The capacity of the separator does not change and ejection and flow rate are dependent upon particle/solid concentration, water concentration, viscosity, temperature, density, pressure, and desired purity of product [GEA Westfalia 2012]. For this reason, the characteristics of the feedstock need to be known before running the centrifuge system. The ejection time is very important for efficient operation of the centrifuge system. The bowl separates slightly when ejecting, forcing the solid content out the ejection line. If the time is too long, the solids hold will overflow and remix with the sample mass and if the time is too short, sample loss is increased with loss of pressure and sample from the opening of the centrifuge. During ejection, the opening of the bowl is facilitated by the operating water. So the operating water discharge time should also be monitored to facilitate complete ejection of solids. It should be noted that filling water sequence is there in the three-phase separation mode which will fill the bowl with water before the start of each run to create a zone for liquid-liquid separation. Due to this, during ejection one can see lots of water coming out along with solids.

Post-condensation filtration was performed using the pilot plant centrifuge for both the two-phase and three-phase separation. All the liquid and solid samples were collected.

Two-phase separation was performed for three different separation times (2, 5, 10 min) to determine the effects of separation time on the centrifuge separation efficiency. The liquid samples were characterized, including pH, density, water content (wt%), and solids content (as ethanol insoluble materials (EIM), wt%). To determine the change in chemical composition, FTIR spectroscopy was utilized. Particle size distribution was also determined. An important observation was that solids content in the liquid phase of the pyrolysis oil decreased as the

separation time (ST) was reduced. This might be due to less entrainment of the removed solids into the liquid phase when the deposited solids are ejected frequently. This supports the need to determine separation time before running the centrifuge, as either sample loss or solids entrainment into the separated liquid phase could result at non-ideal separation times. Overall, centrifugation reduced the oil solids content from 0.58% to as low as 0.05%. In addition, the measured water content of the liquid phase decreased as the amount of solids removed increased; this indicates that there was water associated with the removed solids in the centrifugal filtration process. Density of the liquid phase decreased when more solids were removed, as expected.

No significant chemical composition changes between the control sample and centrifuged oil samples could be identified visually from the spectra obtained using FTIR spectroscopy. Therefore, a peak height ratio (PHR) method was used to quantify the presence of the major functional groups. PHR was calculated by dividing the height of a peak of interest by the peak height corresponding to the C-H stretch, which is not expected to deviate from sample to sample. FTIR spectra and PHR data were given in the Q7 report. PHR for O-H stretch decreased for the centrifuged oils compared to the control sample. This result might be due to the removal of some water along with the solids. In addition, a peak was observed for the solid samples at 1452 cm^{-1} which was not seen in liquid phase samples, and indicates the presence of aromatics and heavier molecular weight compounds. No significant peak was observed around 1600 cm^{-1} which indicates an absence of alkene stretching. An increase in C-O and C=O stretching related to primary and secondary alcohols was observed which could indicate acetalization and hemiacetal formation. A decrease in C=O stretching was observed which narrowed the list of probable chemical mechanisms to those involving aldehydes and carboxylic acids. The proposed decrease in carboxylic acid content correlates well with the slight increase in pH that was observed. To determine the particle size distribution, dynamic light scattering (DLS) and optical microscopy with image analysis software were utilized. These results indicate that centrifugal filtration of the post-condensate pyrolysis oil remove larger-sized particles.

Three-phase separation trials run with the pilot plant reactor and centrifugal filtration system were unsuccessful. With the presence of the technician from Westfalia separators, a trial was performed using a lab-scale centrifuge, with the aim of examining three-phase separation. Parameters that were varied during the trial were rpm, time and temperature. Samples were also run after the addition of 20% (v/v) water to see if high water content would aid in destabilizing the emulsion. All the test conditions were mentioned in the Q6 report. The lab trial was unsuccessful and it was conlcuded that three-phase separation using the centrifuge is not possible for our unaged pine, clearwood bio-oil. As the organic fraction and water in pyrolysis oil forms an emulsion, this is an avenue to be pursued in the destabilization of the emulsion if organics-water separation is desired.

A study was conducted to examine the effects of $CaCl_2$ in destabilizing the emulsion and thereby improving centrifugal separation of oil- and water-rich liquid phases. The calcium cation causes the oil droplet to coalesce by neutralizing the initial negative surface charge of the oil droplet. The coalescence of the oil droplet can be ascertained by the increase in oil droplet size. Droplet size distribution measurements were performed to understand the destabilization. A Hermle Labnet Z206 lab-scale centrifuge (6000 rpm max) with fixed angle rotor was used for this study. An Olympus Bx51 optical microscope and dynamic light scattering were used to perform droplet size distribution analyses. Initially the solids content from the oil was removed to facilitate the accurate measurement of droplet size. Anhydrous $CaCl_2$ was added at 0.1, 0.5 and 1.0 M concentrations to samples with solids previously removed (6000 rpm, 3 x 35 min). The sample was stirred in a vortex mixer to facilitate the dissolution of $CaCl_2$ and the sample was allowed to stabilize for about

30 min. The $CaCl_2$ samples were centrifuged at 6000 rpm for 15 min and then smeared onto microscope slides. Oil and water separation after $CaCl_2$ addition and centrifugation is shown in Figure P2. Separation was observed with 0.5M and 1.0M $CaCl_2$; only a small amount of separation was observed with 0.1M and 0.3M $CaCl_2$. Mass balances of oil and water after separation are presented in Table P1.

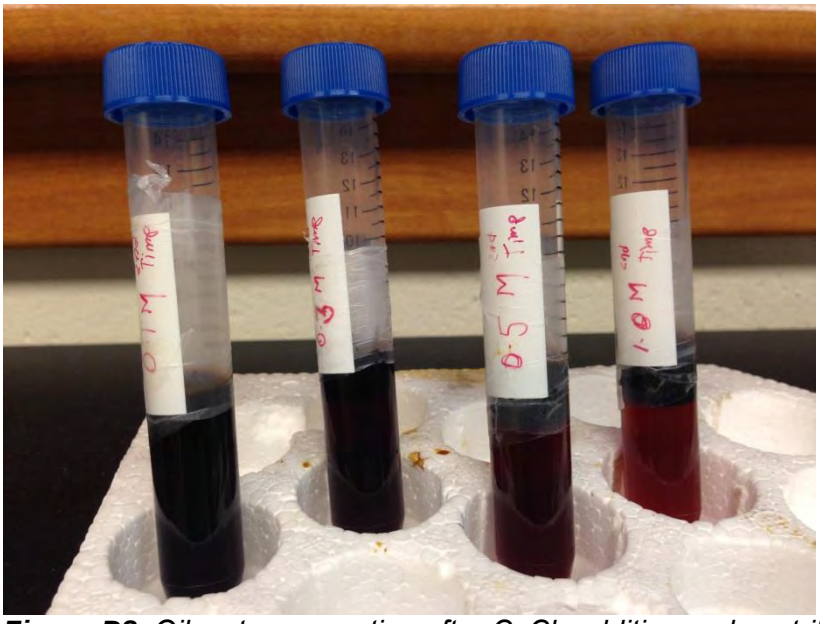
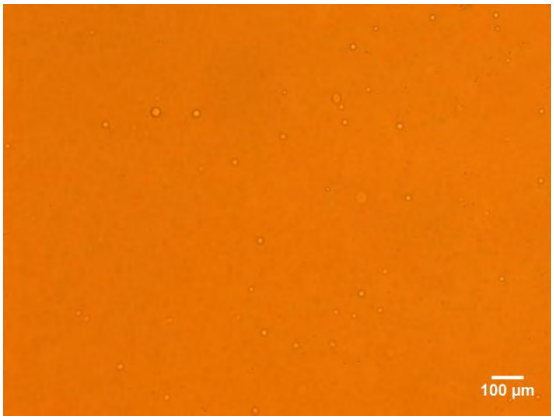


***Figure P2**. Oil-water separation after $CaCl_2$ addition and centrifugation*.

***Table P1**. Mass balance of oil- and water-rich phases after separation.*

$CaCl_2$ concentration (M)	Sample wt. (g)	Oil -- top phase (g)	Water-- bottom phase (g)	Loss	Oil (wt%)	Water (wt%)
0.1	7.62	1.4466	5.9167	0.2567	18.98	77.65
0.3	7.82	1.7436	5.6996	0.3768	22.30	72.89
0.5	8.23	2.0258	5.8649	0.3393	24.61	71.26
1.0	8.28	2.138	5.7738	0.3682	25.82	69.73

Oil-water separtion was observed in the samples at 0.3M and higher concentrations of $CaCl_2$. Increased oil droplet size was also observed and can be clearly seen when 1.0M $CaCl_2$ was added (Figure P3).



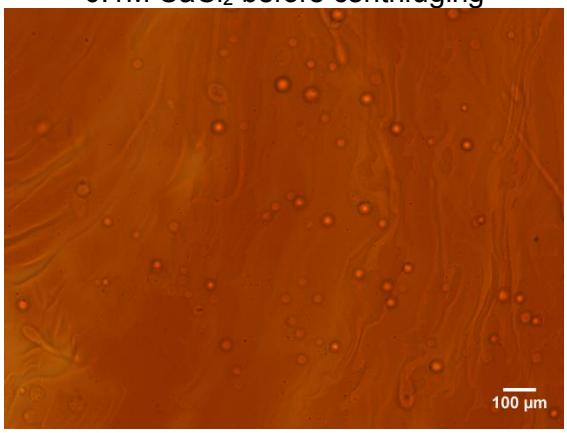
Control



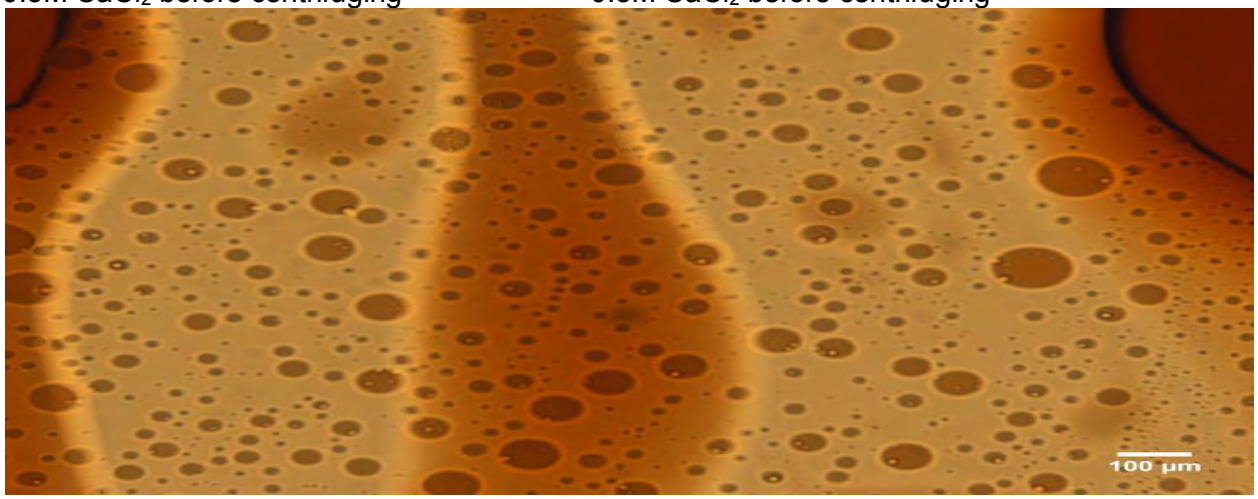
0.1M $CaCl_2$ before centrifuging



0.3M $CaCl_2$ before centrifuging



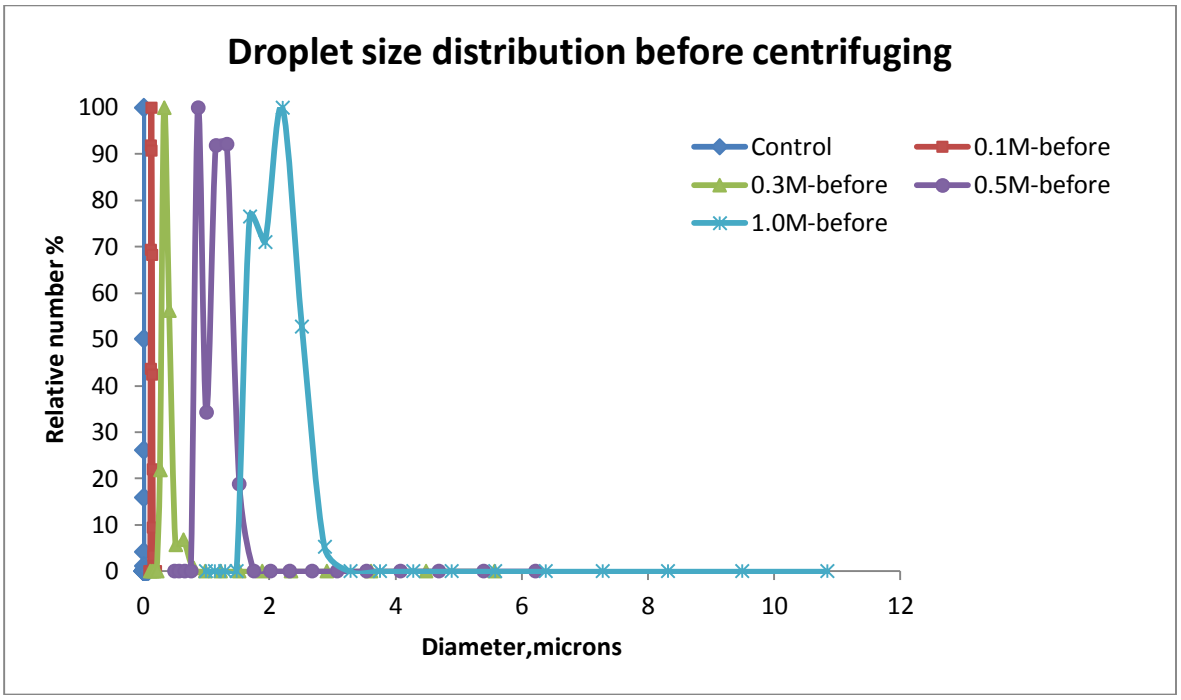
0.5M $CaCl_2$ before centrifuging



1.0M $CaCl_2$ before centrifuging

Figure P3*. Representative optical micrographs as a function of $CaCl_2$ concentration*.

In order to obtain droplet size distribution, dynamic light scattering was utilized. Samples were diluted in water due to the technique's requirement of low concentration. After centrifuging the samples, the separated bottom phase was analyzed. A decrease in droplet size was observed which confirms the separation of oil in the emulsion (Figure P4).



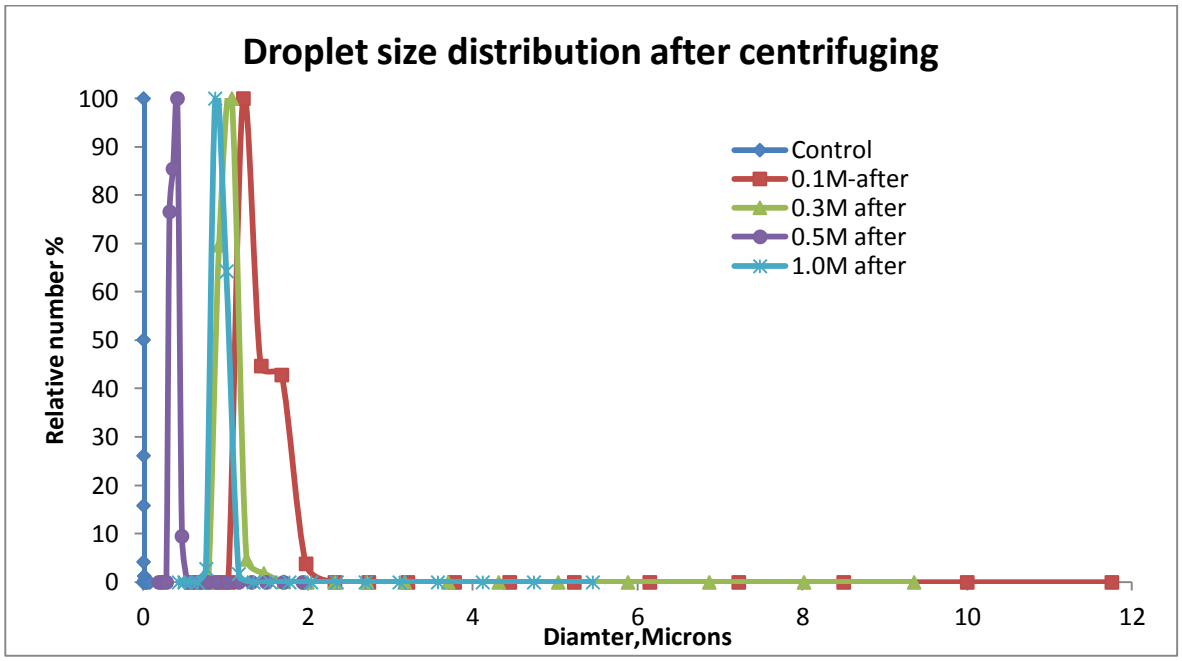


***Figure P4**. Effect of feed temperature on the separation efficiency of the centrifuge.*

The key variable in the separation process is the terminal velocity. At higher terminal velocities, the radial velocity will be higher and the separation will be improved. The terminal velocity increases with the decrease in the viscosity of the medium. When the temperature of the medium is increased, the viscosity can be reduced. A study was conducted to understand the effects of feed temperature on the separation efficiency of the centrifuge. The bio-oil used for this study was produced from the SERC pilot plant one-ton per day auger reactor using pine clear wood as feedstock. The feed to the centrifuge was heated to 25, 30, 35 and 40 °C using a hot water circulation system. The separation time was constant at 10 min. A two-phase separation study

was performed. The feed volume and the volume of the liquid phase outlet were measured and the volume of solid collected is given as the difference between the feed and liquid phase as shown in Table P2. More solids were separated when the temperature was increased (Table P3). The solids separated in the centrifuge had some oil and/or water associated with it, so solids content (as MIM) was also measured for the solid samples to determine the actual mass of solids separated (Table P4).

***Table P2**. Volumes of feed, separated liquid and solid phases.*

Feed Temperature,°C	Feed,gal	Liquid,gal	solid,gal	Vol.% liquid	Vol.% solid
25	3.07	2.7	0.37	87.95	12.05
30	4	3.65	0.35	91.25	8.75
35	3.6	3.1	0.5	86.11	13.89
40	3.06	2.1	0.96	68.63	31.37

***Table P3**. Solid contents of the liquid phase*.

Temperature,°C	MIM (wt%)
25	0.88
30	0.26
35	0.13
40	0.19

***Table P4**. Solid contents of the 'solids' phase*.

Temperature,°C	MIM (wt%)
25	2.82
30	11.72
35	7.41
40	6.09

When the oil temperature was raised, the solids content of the resultant separated liquid phase was considerably reduced. Also, the true solids removed were higher when the operation temperature was increased. So raising the feed temperature helped in enhancing solids separation. However, since pyrolysis oil 'ages' at high temperatures, the centrifugal filtration needs to ideally be performed just after condensation or the oil temperature raised to 40°C only just prior to centrifugation if it has been stored at ambient or reduced temperatures for some period of time after production.

Particle size distribution analysis was performed for the samples separated at different temperatures. The liquid samples collected were smeared onto microscopic slides and images collected using an Olympus Bx51 optical microscope with 10x magnification. Particle sizes were measured using ImageJ (1.45s) software (Figure P5). More particles were removed when the feed temperature was increased. Most of the particles greater than 10 μm in diameter were removed when the feed temperature was raised to 40 °C.

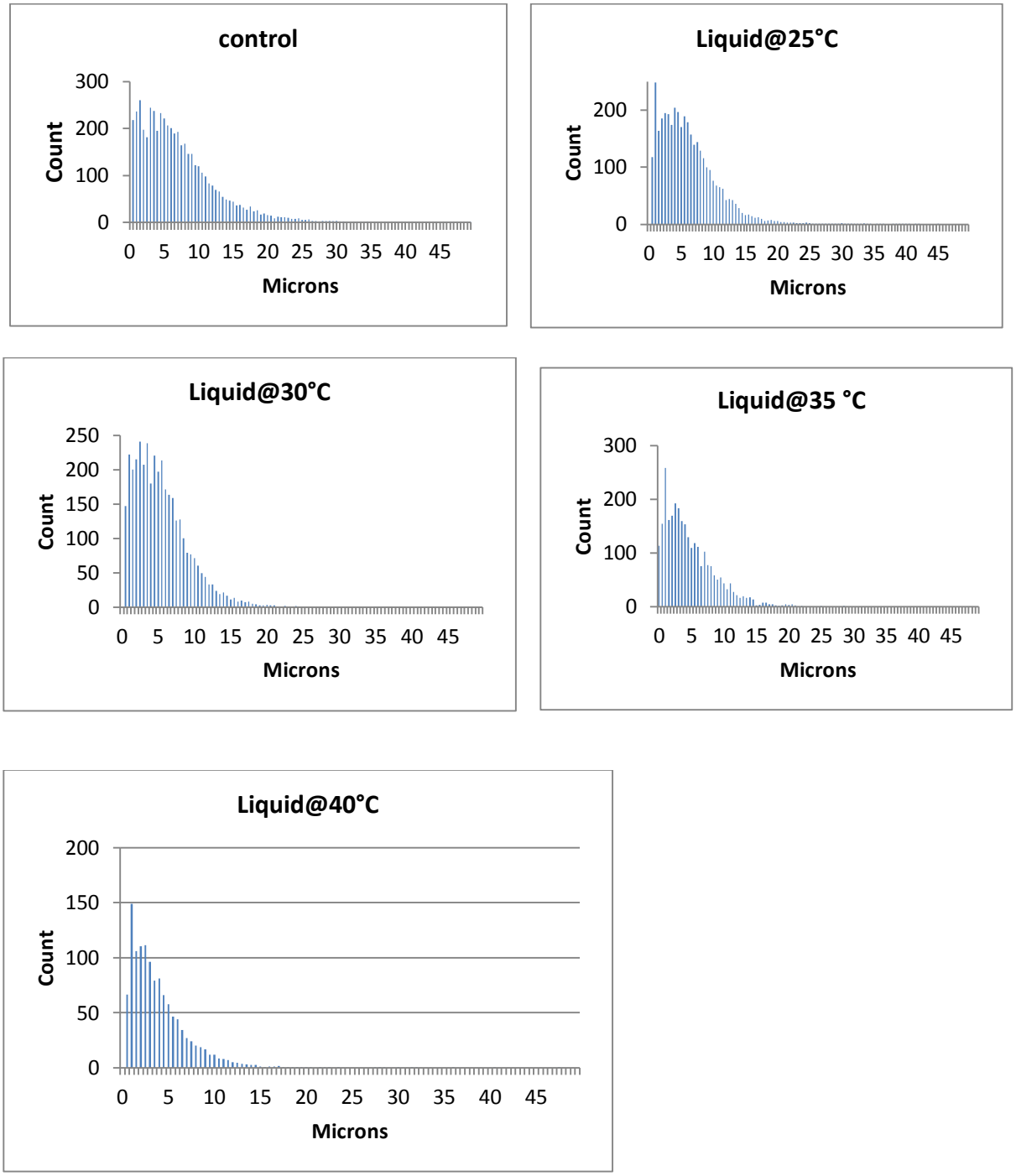


***Figure P5**. Particle sizes observed in pyrolysis oil samples centrifuged at different feed temperatures.*

A one-ton per day auger pyrolysis reactor was designed and fabricated in the Energy Institute Pilot Plant and is shown in Figure P6. The main reactor tube is 12" in diameter. Heating of the tube is accomplished by direct heating of the biomass with hot steel shot, externally by heating the outside of the reactor tube with electric ring heaters, and internally by routing the char and shot following pyrolysis through the center of the auger pipe. The hot shot enters the reactor tube

just after entry of the biomass thourgh a rotary airlock valve. Auger rotation mixes the hot shot with the biomass to provide part of the total pyrolysis heat. Heat is applied on the external surface of the main reactor tube with 14 electric ring heaters spaced along 12 ‘ of the total 16’ of the mian reactor tube length. Internal heat is provided by hot steel shot/char transferred through a 6” internal auger. The hot shot/char are provided by transferring the pyrolyzed biomass and hot shot to an entry port on the 6” internal tube that is near the entry point of the biomass and hot shot. An internal auger moves the hot shot/char through the internal 6” heating tube. At the exit of the 6” internal auger tube the hot shot/char enter a port on a shot sifter that separates the hot shot from the char. The hot shot is transported via 4” diamter return augers to the hot shot entry port previously mentioned to be just after the entry of the biomass from the rotary airlock valve. The char cooled via a heat exchanger and is stored in a 55 gallon air-tight vessel for later disposal.



Figure P6. *One-ton per day auger pyrolysis reactor*.

The auger reactor is fully computer automated with heat monitored by 83 thermocouples. Ten motors are also computer controlled in respect to speed of rotation. Heater temperatures are also controlled between 50 and 600 ^{o}C.

The pyrolysis vapors are drawn off through three transfer pipes for delivery to enter a series of three shell and tube condensers. The three condensers are shown in Figure P7. Bio-oil is periodically drawn from each condenser through lower valves as shown in Figure P7. At the maximum SERC pyrolysis reactor production of one-ton per day the liquid bio-oil production is 5

gal per h or 2.9 barrels of production over a 24 h period. The mean bio-oil yield of the SERC reactor is 60%.



Figure P7*. The three shell and tube condensers that condense the pyrolysis vapor on the one-ton per day auger pyrolysis reactor.*

Figure P8 shows the entry into the biomass handling and drying system. Chipped biomass is transferred into the biomass hopper and is then fed via an auger tube to the biomass dryer. The biomass dryer (Figure P9) is able to dry the biomass to 1.5% at a rate of 400 lbs/h. The biomass is then transported by an auger to a weigh belt conveyor that weighs the biomass. As shown in Figure P10, the biomass is then transported to a final hopper to allow for turning at a 90° angle. An auger hopper transports the biomass to a small hopper at the top of the auger from which the biomass is fed into the rotary airlock valve.



***Figure P8**. Biomass feed hopper with auger to biomass dryer*.



***Figure P9**. Side view of biomass dryer showing explosion proof baghouse.*



Figure P10. *Weigh belt conveyor and hopper/feeder with inclined auger*.

Nitrogen, as a blanket gas, is fed into the auger reactor at 35 liters/min (LPM) just below the rotary airlock valve. The nitrogen is produced on site by a nitrogen generator.

The bio-oil from test runs of the SERC pyrolysis reactor were performed and a bio-oil and gas sample were collected. Data from a gas flow meter monitoring gas volume produced allowed computation of a complete mass balance as shown in Table P5. Table P5 shows the one-ton per day mass balance compared to the smaller laboratory scale reactor located at the Department of Sustainable Bioproducts (DSB). This reactor has been tested for years and its bio-oil production and qualities compared to published data many times. The mass balance comparison shows that bio-oil, char, and gas yields are very similar indicating that scale-up did not influence the process.

Table P5. *Mass balance from test run of one ton/day auger pyrolysis reactor*.

Reactor	Bio-oil Yield(%)	Char Yield(%)	Gas Yield(%)	Total Yield(%)
SERC	58.2	22.13	14.84	96.37
DSB	62	24.2	13.1	99.3

The SERC and DSB bio-oil elemental analyses are compared in Table P6. Again, the only property that differs substantially is that the nitrogen value for the SERC bio-oil is about 3 times higher than for the DSB bio-oil. It is likely that this is due to the use of relatively more nitrogen as a blanket gas in the SERC reactor. This can be adjusted if it is a problem in the final bio-oil.

Table P6. *Bio-oil elemental analysis from test run of one ton/day auger pyrolysis reactor.*

Reactor	Carbon (%)	Hydrogen (%)	Nitrogen (%)	O (%)
SERC	39.59	7.97	0.34	52.10
DSB	41.10	7.56	0.10	51.24

The SERC and DSB bio-oil physical properties are compared in Table P7. The pH and density values do not differ greatly. However, the water content, AV and HV values differ somewhat. SERC bio-oil water content was about 2 percentage points higher, the AV value was about 12 mg KOH/g lower and the HHV value was about 2 percentage points higher. The viscosity value difference is undoubtedly due to the higher water content of the SERC bio-oil. The HHV increase for the SERC bio-oil is likely due to the reduced acid value.

***Table P7**. Bio-oil physical properties from test run of one ton/day auger pyrolysis reactor.*

Reactor	Water(%)	Acid Value	Density(g/cm3)	Viscosity(mm2/s)	HHV(MJ/Kg)
SERC	27.57	79.01	1.14	9.87	17.45
DSB	25.85	91.4	1.18	8.53	15.64

GC/MS analyses were performed on each of the two reactor bio-oil types: SERC one-ton per day reactor and the DSB laboratory scale reactor. The results of these analyses are compared in Table P8. One major difference is that the total phenolic compounds contained in the SERC bio-oil (47.21%) were much higher than that in the DSB bio-oil (34.19%). Especially, the content of 2, methoxy-4-methyl-phenol in the in the SERC oil was 11.67%, much higher than 7.59% in the DSB oil. This explains the higher HHV of the SERC oil. A second major difference is the furfural content increased from zero in the DSB bio-oil to 2.75% in the SERC bio-oil.

Both the decreased phenols and the increased furfural values for SERC bio-oil apparently stem from the design of the SERC pyrolysis reactor that routes char back to heat a central tube inside the main reactor tube. This process allows the char to continue to pyrolyze and emit CO and CO_2. These gases appear to initiate reaction(s) in the bio-oil during the pyrolysis reaction than change the species of compounds produced.

***Table P8**. GC/MS analysis comparing the major compounds detected in both the SERC one-ton per day reactor bio-oil to the DSB laboratory scale reactor bio-oil.*

Compound Name	SERC OIL (% area)	DSB OIL (% area)
acetic acid	6.87	5.22
furfural	2.75	0.00
1-(acetyloxy)-2-propanone	0.00	0.42
tetrahydro-2,5-dimethoxy-furan	0.00	1.55
2-hydroxy-2-cyclopenten-1-one	2.24	1.59
phenol	0.76	0.45
2-hydroxy-3-methyl-2-cyclopenten-1-one	2.36	1.50
2-methyl-phenol	1.04	0.00
4-methyl-phenol	1.10	0.00
2-methoxy-phenol	4.20	3.93
2,4-dimethyl-phenol	1.20	0.00
2,methoxy-4-methyl-phenol	11.67	7.59
3-methyl-1,2-benzenediol	1.87	1.12
4-ethyl-2-methoxy-phenol	2.97	2.42

4-methyl-1,2-benzenediol	3.04	1.70
2-methoxy-4-vinylphenol	3.65	2.58
Eugenol	2.08	1.28
2-methoxy-4-propyl-phenol	1.13	0.79
vanillin	1.20	0.83
2-methoxy-4-(1-propenyl)-phenol	8.94	10.00
Levoglucosan	14.12	13.50
4-hydroxy-3-methyl-benzeneacetic acid	1.96	3.56
n-hexadecanoic acid	0.72	0.46
bis(2-ethylhexyl)-hexanedioic acid	2.76	2.73

Figure P11 shows the test char furnace attached to the pyrolysis reactor. The combusted char produces a temperature of 860 ^{o}C inside the furnace. With some cooling occurring in the heat delivery pipe the heat entering the pyrolysis reactor is 750 ^{o}C. The electrical load replaced by this small char furnace is 7%. A larger char furnace could supply a much larger percentage of electrically produced heat.



Figure P11*. The test char furnace attached to the pyrolysis reactor providing heat from combustion of char to replace that produced by 3 ring heaters.*

Figure P12 shows a back view of the char furnace showing the char feeding system. The system is composed of the square black hopper that supplies the char. An auger inside the hopper feeds to a T and the char drops by gravity. At the bottom of gravity pipe a second T is pressurized pneumatically to force the powdered char into the char furnace at high velocity. A gas ignition system provides the initiating heat to begin the combustion of the char which is self-combusting.

Table P9 compares the HHV and elemental analysis (CHNO with O by subtraction) between SERC and DSB chars. The only substantial differences in the values of Table P9 are that the carbon is higher by about 8 percentage points for the DSB char and the oxygen is about 8 percentage points lower for the DSB char. Again, the lower carbon and higher oxygen in the SERC char likely stems from the design of the SERC pyrolysis reactor that routes char back to heat a central tube inside the main reactor tube. This process allows the char to continue to pyrolyze and emit CO and CO_2. These gases appear to initiate reaction(s) in the bio-oil during the pyrolysis reaction that change the nature of the final char produced by the two systems.

***Table P9**. Comparison of the char elemental analysis between the SERC and DSB reactors showing that there is negligible difference in the char CHNO values (oxygen by subtraction).*

Reactor	HHV(MJ/Kg)	Carbon (%)	Hydrogen (%)	Nitrogen (%)	O (%)
SERC	29.14	70.76	3.18	0.47	25.59
DSB	31.15	77.79	4.08	0.84	17.28



***Figure P12**. A view of the char furnace from the back side showing the feeding system for the char into the furnace.*

The completed one-ton per day reactor operates very successfully to produce 5 gal per hour of bio-oil. Several commercial entities are interested in having scaled up versions (10-15 tons per day) of our pilot reactor built for their operations. Negotiations continue.

Subtask P.2 Further testing and development of a laboratory scale catalytic pyrolysis reactor

Partial upgrading of bio-oil by deoxygenation during the pyrolysis step has the potential to produce a product that is directly usable as heating fuel and stabilized for transport. In addition, the partially deoxygenated product will be more easily upgraded by full deoxygenation at a later stage. A proprietary MSU technology to increase the reaction speed of low-cost catalysts in the pyrolysis reactor for partial deoxygenation was developed under previous SERC III funding. This technology will be further refined and tested with SERC IV funding.

Planned Activities:

P.2.ML.1 Utilize various catalysts and modified reactor designs for bio-oil upgrading.
P.2.ML.2 Optimize system with the best-performing catalyst.

Summarization of Activities:

Catalytic pyrolysis is performed at fast pyrolysis conditions using catalysts in-situ, either by mixing catalysts with the biomass feedstock or by passing the pyrolysis vapors over a bed of fluidized catalyst particles. Catalytic pyrolysis favors deoxygenation of pyrolysis vapors generated during the fast pyrolysis process by catalytic cracking. Catalytic pyrolysis is often performed at atmospheric pressure mostly using acid cracking catalysts; zeolites are widely employed. The final liquid product from catalytic pyrolysis is a mildly deoxygenated bio-oil which is produced in yields lower than those obtained directly from fast pyrolysis. Fast pyrolysis produces bio-oils in yields up to 65% while catalytic pyrolysis usually limits bio-oil yields lower than 50%, based on dry biomass weight. Application of acid cracking catalysts in catalytic pyrolysis cracks pyrolysis vapors and generates higher yields of non-condensable gases (e.g., CO, CO_2, C_2H_4, etc.), compared to conventional fast pyrolysis, while also producing more water. Partially deoxygenated bio-oil produced from catalytic pyrolysis is more favorable for further upgrading using hydrotreating techniques (e.g., HDO) than directly being used as a liquid transportation fuel. Presence of lower oxygen content than that in the bio-oil produced from fast pyrolysis favors longevity of the hydrotreating catalysts while also minimizing the amount of hydrogen required for hydrodeoxygenation process. Greater amounts of aromatic hydrocarbons than aliphatic hydrocarbons are produced during catalytic pyrolysis. Catalytic pyrolysis is advantageous over other crude oil upgrading techniques in that it does not require hydrogen and high reaction pressures while being an integrated fast pyrolysis process. However, catalytic pyrolysis does not favor the production of a highly deoxygenated bio-oil, thereby requiring one or more additional refining steps. Catalyst coking is also a significant factor limiting the potential of catalytic pyrolysis process.

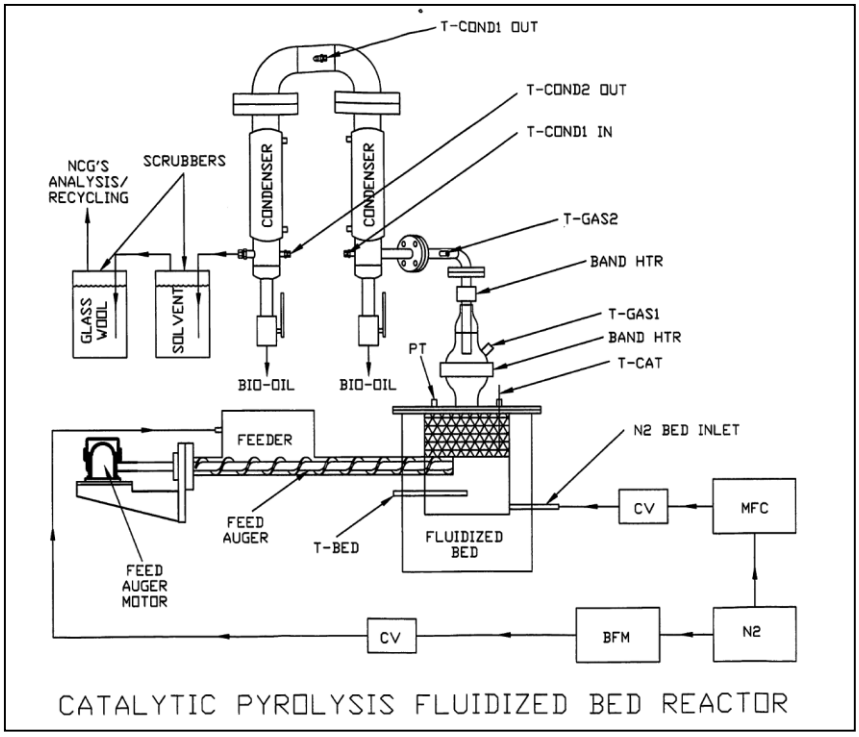


***Figure P13**. Schematic of the fluidized bed reactor used for catalytic pyrolysis.*

Catalytic pyrolysis research in SERC-IV was focused on developing a laboratory scale fluidized bed reactor (FBR) to employ and test a wide variety of catalyst compositions. We have been partially successful in developing a laboratory-scale fluidized bed reactor and in identifying a suitable catalyst composition for catalyst pyrolysis. The following information on results and the discussion on the obtained results provide insight into the research performed in the area of catalytic pyrolysis as a part of SERC-IV.

Figure P13 shows the schematic of the fluidized bed reactor developed for the catalytic pyrolysis. Biomass of the particle size 2-3 mm is fed into the FBR using an auger. The biomass feed rates can be varied from 5 to 50 g/min. N_2 is used as the fluidizing gas as well as the carrier gas. N_2 flow rate into the FBR is controlled using a mass flow controller (MFC), while the N_2 flow rate into the feeder (to maintain inert atmosphere as well as to restrict the back flow of N_2 from the FBR into the feeder) is controlled using a ball flow meter (BFM). Temperature inside the FBR is monitored using thermocouple (T-BED) placed at the center of the FBR. The pyrolysis vapors generated in the FBR are carried into condensers 1 and 2 (using N_2), which are pre-cooled to -5 °C using antifreeze (ethyleneglycol and water mixture). The inlet and outlet temperatures of the condensers are monitored using K-type thermocouples (T-Cond IN, T-Cond1 OUT, T-Cond2 OUT). The gases (uncondensed pyrolysis vapors and non-condensable gases) exiting condenser 2 are cleaned by passing them through scrubbers (containing solvent and glass wool) and are later sampled for gas analysis.

Pyrolysis test runs were conducted to check the functionality of the FBR as well as to optimize the biomass pyrolysis conditions prior to testing catalysts. Pyrolysis temperature, biomass feed rate, and nitrogen flow rate are the main variables that aid in optimizing the pyrolysis conditions. However, only one variable, i.e. pyrolysis temperature, was tested during the past quarter and the test runs regarding the biomass feed rate are underway. Three different pyrolysis temperatures (450, 500 and 550 °C) were tested, keeping the N_2 flow rate and the biomass feed rate constant

at 5 L/min and 10 g/min, respectively. Run time of the pyrolysis experiments was one hour and no catalysts were used. Figure P14 summarizes the product yields of the experiments showing the effect of temperature on biomass pyrolysis.

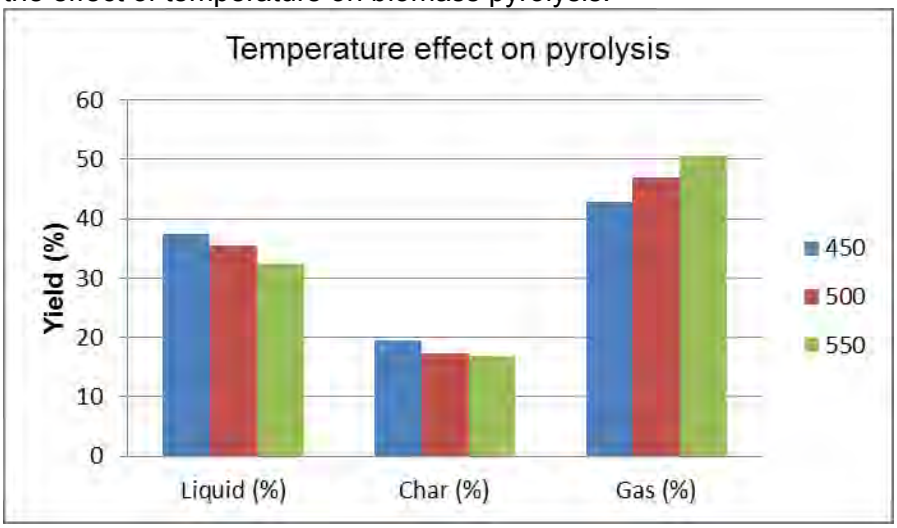


***Figure P14**. Effect of pyrolysis temperature on the product distribution.*

Analysis of the liquid products

GC-MS analysis of the liquid product obtained from the pyrolysis experiments was performed, yielding both quantitative as well as qualitative information. The quantitative data from GC-MS gives the concentration of the bio-oil components in the sample taken for data analysis. From the quantitative data, the mass (g) of the compound of interest present in 1 g of liquid product obtained from an experiment was calculated using:

$$= \frac{C\left(\frac{\mu g}{mL}\right) X10\ (mL) X10^{-6}\left(\frac{g}{\mu g}\right)}{S\left(\frac{g}{10\ ml}\right)}$$

Where *C* is the concentration of the compound of interest obtained from the quantitative analysis of the liquid sample using GC-MS$\left(\frac{\mu g}{mL}\right)$ and *S* is the amount of liquid product sample dissolved in 10 mL of solvent for GC-MS analysis (g). These computations were performed for the liquid product from each catalytic run as well as from the blank run. The resulting mass of each compound was then distributed according to the functional group(s) present in the compound, and the total mass of compounds in a particular functional group contained in 1 g of liquid product was determined.

Using high temperatures (550 °C) resulted in severe cracking of pyrolysis vapor and, therefore, generated very high gaseous yields (~50%) at the expense of liquid products. The gas yields may further increase in the presence of catalysts if the pyrolysis temperature is set greater than 500 °C. Therefore, it was decided to test the pyrolysis temperatures no greater than 500 °C for further optimization experiments as well as catalytic pyrolysis experiments. However, use of higher temperatures (500-550 °C) favored the conversion of higher oxygenates such as eugenols, guaiacols and catechols to lower oxygenates like phenols. This is due to the increase in cracking of higher oxygenates at high temperatures. Pyrolysis temperature studies show that the cracking of guaiacols, vanillins and acetovanillones comprise the predominant reactions that result in the formation of catechols which can further be cracked to phenols at higher temperatures.

A suitable catalyst composition was identified prior to its use in the FBR for the optimization of process variables. For this purpose the readily available commercial catalyst supports – acidic, basic and mixed oxides – which have been reported in the literature for cracking and reduction reactions were tested for catalytic pyrolysis of pinewood. Catalytic pyrolysis was performed in nitrogen atmosphere at 450-500 °C. Table P10 shows the composition of the product pyrolysis vapors; it is evident that the predominant functionalities in the product vapors include acids, aldehydes & ketones (carbonyls), furans, and phenols. The selectivity of the compounds in the product vapors varied with catalyst composition and did not follow a specific pattern. Among all the tested catalysts, mesoporous catalysts such as MCM-41 and SBA-15 resulted in the highest amount of GC-MS identifiable chemical species (Figure P15). Acidic catalysts, including γ-Al2O3, ZrO2, performed better than mixed oxide catalysts (SiO2-Al2O3, ZrO2-TiO2), as well as the basic catalysts (CeO2, TiO2, hydrotalcite) (Figure P13). The cracking nature of the acid catalysts was responsible for the breakdown of heavy molecular weight compounds to lighter fractions that are easily identifiable and quantifiable by GC-MS. Hydrotalcite yielded the least amount of GC-MS identified chemical compounds at 35.3%. This indicates that the catalyst, to be effective for the cracking of heavy molecular weight pyrolysis vapors, should possess mesoporosity and be acidic in nature.

Table P10. *Distribution of various functional groups in the product pyrolysis vapors as a function of catalyst composition.*

	Product distribution as a function of catalyst composition								
	CeO_2	**ZrO_2-TiO_2**	**γ- Al_2O_3**	**Hydrotalcite**	**MCM-41**	**SBA-15**	**SiO_2-Al_2O_3**	**TiO_2**	**ZrO_2**
Acid	14.2	12.1	4.7	7.0	14.8	12.6	0.7	11.1	2.0
Ketone	12.1	14.0	15.2	13.5	4.3	8.9	10.6	10.0	21.8
Furans	4.4	6.0	9.8	4.7	17.5	6.4	18.2	10.9	5.4
Olefins	2.0	1.1	15.6	1.3	8.4	0.6	7.0	1.8	16.8
Aldehydes	1.9	4.4	0.9	3.3	6.1	13.7	2.2	3.5	
Oxgenates	3.0			0.8	2.8	7.4	12.3	7.6	5.3
Alcohols	2.2	1.6		0.5		1.6		2.3	
Alkane			0.6						
Ester					1.4		1.2	0.8	1.4
Phenol	26.4	18.7	4.4	14.9	7.0	14.2	9.9	23.2	9.4
Benzene			5.1		4.7				
Others	3.3	7.6	4.4	4.3	0.8	5.1	0.5		1.1
Total	43.1	46.8	56.2	35.3	60.6	56.4	52.7	48.0	53.8

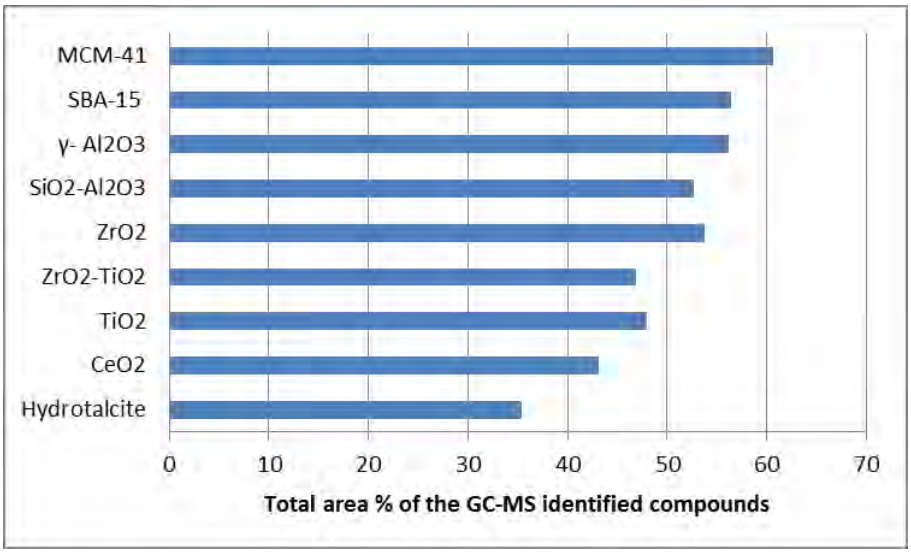


***Figure P15**. Total area% of the GC-MS identified compounds in the product vapors, as a function of catalyst composition.*

Further testing involved amorphous and crystalline Si-Al catalysts including Si/Al, γ-alumina and HZSM-5 (Si/Al=30). Experiments conducted are summarized in Table P11.

***Table P11**. Summary of catalytic pyrolysis experiments*.

		Yield (%)		Catalyst coke* (c)	Gas Yield (%) {100-(a+b+c)}
Catalyst	WHSV (h^{-1})	Liquid (a)	Char (b)		
Sand	-	41.7	14.5	-	43.8
Si/Al	12	42.8	14.7	1.25	41.25
γ-alumina	12	37.2	14.1	1.1	47.6
HZSM-5	12	34.23	15.6	1.6	48.57

* Difference in the weight of catalyst before and after the respective experiment; - not determined

***Table P12**. Acid values and water percent of liquid products from catalytic pyrolysis experiments.*

Catalyst	Acid value (mg KOH/ ml Oil)	H_2O, %
Sand	77.878	48.0%
Si/Al	74.140	42.8%
γ-Al_2O_3	61.184	60.4%
HZSM-5	46.407	66.4%

Compared to the blank experiment where no catalyst was employed, all the catalytic pyrolysis experiments showed a decrease in the acid value. Also, a significant increase in the water % of the product oil was observed using acid catalysts γ-Al_2O_3 and HZSM-5 (Figure P16). The water % values of the catalytic experiment samples indicated that dehydration reactions were predominant in the catalytic vapor pyrolysis. Moreover, dehydration reactions were one of the

favorable reaction routes on the surfaces of the acid catalysts which resulted in the formation of more water in the product bio-oil. Among all the catalysts tested, HZSM-5 showed relatively more activity for dehydration reactions and resulted in the formation of more water. From the acid values of the product oils, it was easy to see that some of the carboxylic groups were eliminated by decarboxylation and decarbonylation reactions resulting in the formation of CO and CO_2 in the gas phase (Table P12). However, from the acid value and water content analysis of the product oil, it can be concluded that deoxygenation of bio-oil was attained via catalytic pyrolysis.

Table P13 shows the liquid yields elemental analysis and HHV for the Si-Al and HZSM5 catalysts that performed the best for catalytic pyrolysis. The liquid yield for the Si-Al at 42.8% is 25% higher than the 34.5% yield for HZSM5. However, the oxygen value for the Si-Al is 30% higher at 38.57% than for the 29.58% value for the HZSM5 catalyst. The high oxygen content and somewhat lower carbon content for the Si-Al liquid product resulted in a somewhat lower (31.61 MJ/Kg) value compared to that of the HZSM5 liquid product at 34.0 MJ/Kg. These results indicate that it is somewhat of a tossup in the choice between these catalysts.

It was not possible to quantify the hydrocarbons via detailed hydrocarbon analysis due to the high water content of the liquid.The relatively high HHV values indicate that some hydrocarbons were produced via deoxygenation during the catalytic pyrolysis.

***Table P13**. Liquid yields, elemental analysis and HHV for the two best catalysts tested for catalytic pyrolysis*.

Catalyst	Liquid yield %	C %	H %	N %	O %	HHV (MJ/Kg)
Si-Al	42.8	53.94	7.46	0.03	38.57	31.61
HZSM5	34.2	62.08	7.86	0.48	29.58	34.00

Liquid product analysis

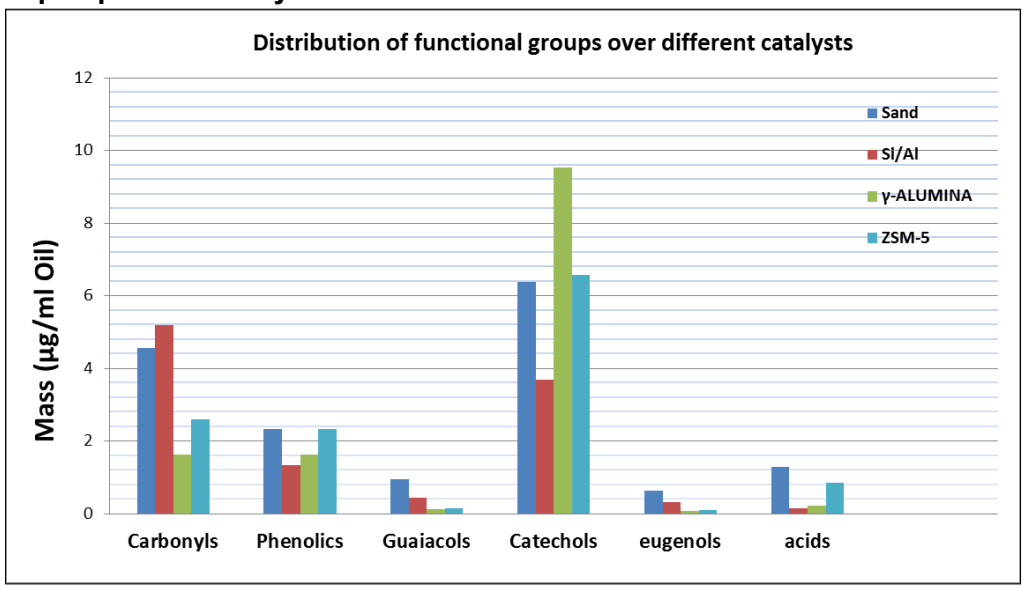


***Figure P16**. Product distrubition in the bio-oils obtained in catalytic pyrolysis experiments.*

A different approach was also tested by pretreating pyrolysis feedstock with a hydrogen donor to check the in-situ deoxygenation. Pine wood was pretreated with 5 and 10 wt% HCOOH by spray method prior to fast pyrolysis. Formic acid was previously used as an in-situ hydrogen donor for catalytic upgrading of heavy oils. Table P13 shows the liquid, char, and gas yields of pine wood treated with 5 and 10% HCOOH.

Table P13. *Product distribution of bio-oils obtained from fast pyrolysis of pine wood pretreated with 5% and 10% HCOOH.*

			Yield (%)		
Dry Feed (g)	HCOOH (g)	Total (g)	Bio-oil	Char	Gas (100-a+b)
2400	150	2543	1425 (56%)	566 (22.3%)	21.7 %
2250	250	2492	1347 (54%)	507 (20.3%)	25.7%

Table P13 shows that the increase in HCOOH percentage in the pretreatment process slightly decreased the liquid yields. This observation could be attributed to the acidic character of HCOOH which might have resulted in acidic cracking of the pyrolysis vapors. Higher HCOOH concentration in the pretreated biomass decreased the lignin derived compounds such as phenols and alkylated phenols while slightly increasing the cellulose derived compounds such as levoglucosan. Table P14 shows the elemental analysis, water content and the acid value of the bio-oils produced by the 5 and 10% addition of HCOOH.

Table P14*. Elemental analysis, water content, and acid values of the pyrolysis oils post fast pyrolysis. Oxygen was determined by subtraction.*

Experiment	% C	% H	% N	% O	H_2O (%)	Acid Value (mg KOH/g Oil)
5% HCOOH	42.64	8.04	0.25	49.07	20.71	120.4
10% HCOOH	35.59	8.20	0.17	56.04	29.84	151.2

Our experiments indicated that HCOOH did not serve as an in-situ hydrogen donor; instead, it provided an acidic environment for the cracking of pyrolysis vapors. However, such an increase in acid value hints at increasing the acidic nature of the pyrolysis oil compounds which can provide higher stability (compared to the stability of the carbonyl compounds) when processed at hydrodeoxygenation conditions. Later, the bio-oils obtained by the fast pyrolysis of pinewood pretreated with formic acid were hydrotreated in a Parr batch reactor using a hydrotreating catalyst, Ni/SiO_2-Al_2O_3. Hydrotreating was performed under 1000 Psig H_2 pressure for a run time of 3 hours at the reaction temperature 400 ^oC. Table P15 shows the elemental analysis, water content and the acid value of the hydrotreated bio-oils.

Table P15. *Elemental analysis, water content, heating and acid values of the hydrotreated bio-oils*.

Feedstock	% C	% H	% N	% O	HHV (MJ/Kg)	Acid Value (mg KOH/g Oil)
Bio-oil from 10% HCOOH pretreatment	70.55	9.60	0.37	19.47	33.1254	70.41
Bio-oil from 5% HCOOH pretreatment	72.35	10.19	0.00	17.46	35.2764	68.885

Table P15 shows that hydrotreatment resulted in a substantial decrease in the oxygen percentage compared to the bio-oils obtained from fast pyrolysis. Acid values are almost halved by hydrotreatment, while heating values almost doubled (from 17-18 MJ/Kg for raw bio-oil to 33-35 MJ/Kg for hydrotreated bio-oil). However, further catalyst testing is required to improve the heating value of the liquid products while also decreasing the acid values.

Another approach for deoxygenation of pyrolysis vapors included recycling the non-condensable pyrolysis exit gases into the fast pyrolysis process to examine the reducing activity of the CO + H_2 present in the pyrolysis non-condensable exit gases. In our experiments, approximately 70% of the total non-condensable exit gases from fast pyrolysis were recycled into the pyrolysis reactor. Nitrogen was used to provide inert medium for fast pyrolysis. Table P16 shows the elemental analysis of the bio-oils obtained using product gases as reaction medium.

Table P16. *Elemental analysis and water content results of bio-oils obtained by product gas recycling method.*

Sample	% C	% H	% N	% Remaining	H_2O (%)
Sample 1	41.30	7.85	0.15	50.69	25.1315
Sample 2	40.46	7.90	0.23	51.41	27.3451

Table P16 shows no observable changes in the elemental composition of the bio-oils obtained using product gas recycling method. This may be due to the use of nitrogen as carrier gas, due to which the product gas composition might have been diluted and couldn't provide the required reducing environment for deoxygenation of pyrolysis vapors. The presence of excessive nitrogen in the pyrolysis environment is evident by the gas analysis of the product gases shown in Table P17. Moreover, no hydrogen was observed in the product gas which indicates that the lighter hydrogen might have been driven away when the product gas was slip-streamed to provide 70% of the total gases for pyrolysis.

Table P17. *GC analysis of the gas samples obtained from product gas recycling experiments.*

Sample	H_2%	O_2%	N_2%	CH_4%	CO%	CO_2%	C_2H_6%	Sum
Gas - 1	0.00	4.44	43.23	2.49	19.02	21.86	0.27	91.31
Gas - 2	0.00	1.67	31.58	3.69	27.10	29.21	0.31	93.57
Gas - 3	0.00	4.61	33.56	3.73	25.24	25.79	0.29	93.22

Each approach, catalytic pyrolysis using cracking catalysts, recycling pyrolysis exit gases, and pretreating biomass feedstock with a hydrogen donor solvent, has proven to have its advantages and disadvantages. Catalytic pyrolysis using acid cracking catalysts produce bio-oils with lower oxygen content than produced using a conventional fast pyrolysis method. However, low bio-oil yields and catalyst deactivation inhibited better results. Pyrolysis of an acid-pretreated biomass feedstock, though it did not substantially deoxygenate the pyrolysis vapors, produced a bio-oil with higher stability. More research into other hydrogen donor solvents is essential prior to concluding this approach. Product gas recycling method did not provide any notable difference in the quality of bio-oil produced from fast pyrolysis. However, use of nitrogen as carrier gas is assumed to decrease the concentration of reductive gases limiting their efficacy in reducing bio-oil functionalities. Further examination on product gas recycling, use of different hydrogen donor solvents and mechanistic study of catalytic pyrolysis is required to identify an effective deoxygenation approach. Integration of two or more processes, such as recycling pyrolysis exit gases into the catalytic fast pyrolysis of a pretreated (with a hydrogen donor solvent) biomass feedstock using an effective cracking catalyst, might prove to be a step forward in the area of catalytic pyrolysis to produce a stable, deoxygenated bio-oil liquid product.

Subtask P.3 Produce hydroxymethylfurfural (HMF) from maximized bio-oil anhydrosugars
MSU research has developed a proprietary method to increase anhydrosugars approximately 50% above yields attained by previously applied technologies. This method will be refined to determine optimal parameters of the process. The method will depend on the water fractionation of raw bio-oil into pyroligneous and aqueous components. Anhydrosugars will be contained in the aqueous fraction. This fraction will be hydrolyzed to monomeric sugars, and HMF will be produced by both homogeneous and heterogeneous catalytic methods.

Planned Activities:
P.3.ML.1 Utilize various heterogeneous and homogeneous catalysts to produce maximum yield of HMF.
P.3.ML.2 Develop a method to separate clean cuts of HMF.

Summarization of Activities:
Our planned activities to produce high yield from furan derivatives (HMF and furfural) and separation of clean cuts from HMF were completely achieved. Various conversion methods were optimized in this study producing four peer-reviewed publications and several presentations from this work. Summary for the approaches used and the obtained results are given below:

We first tested the effect of different reaction parameters (solvent, catalyst, time and temperature) on the yield of HMF produced from cellulose hydrolysis. In this series of experiments we tested the effect of different parameters (solvent, catalyst, time and temperature) on the yield of HMF produced from hydrolysis of different cellulosic materials. We tested the following parameters:

1. Effect of acid-catalyzed hydrolysis of waste paper in different solvents.
2. Effect of using co-catalysts (acid/metal chloride) on the yield of HMF produced from hydrolysis of cellulose in a biphasic (*n*-butanol/water) system.
3. Effect of using zeolite/$CrCl_2$ co-catalyst on the yield of HMF produced from hydrolysis of microcrystalline cellulose in one-phase system.
4. Effect of using zeolite/$CrCl_2$ co-catalyst on the yield of HMF produced from hydrolysis of microcrystalline cellulose in the MIBK/water biphasic system.
5. Optimization of the MIBK/water biphasic system for HMF production from monosugars by using zeolite-metal chloride co-catalyst.
6. Effect of using ionic liquids with different metal chloride catalysts on the yield of HMF produced from hydrolysis of microcrystalline cellulose. We studied the effect of catalyst type and effect of using single and combined metal chloride catalyst.

Our preliminary study on cellulose gave us valuable insights as to the conditions we need to apply to convert aqueous fraction bio-oil sugars to HMF. Two peer-reviewed publications were obtained from this work.

Bio-oil with high sugar content was prepared from pine wood as follows: pine wood was pretreated with an aqueous solution of phosphoric acid (1%, w/w) and the pretreatment solution ratio to pine wood was 1:5. The pretreatment solution was mixed with pine wood in a mixer for 30 min at room temperature to allow complete mixing of the wood and pretreatment solution. After pretreatment, the biomass was filtered from the pretreatment solution and dried at 100 °C in a drying oven until the moisture content reached 5-7%. After drying, the treated pine wood feedstock was pyrolyzed at a temperature of 450 °C according to the MSU patented system that produces higher levoglucosan anhydrosugars in the bio-oil. The bio-oil was fractionated into oil and aqueous fractions using a separatory funnel by adding an equivalent amount of water to the bio-oil. The

separating funnel components (bio-oil and water) were mixed thoroughly and left overnight until two distinct layers from aqueous and pyroligneous fractions were formed. The bottom oil fraction was withdrawn from the separating funnel and the remaining aqueous fraction was transferred into another container for hydrolysis. The sugar contents for the hydrolyzed aqueous fraction (HAF) and un-hydrolyzed aqueous fraction (Un-HAF) are summarized in Table P18.

***Table P18**. Sugars analysis of un-hydrolyzed aqueous fraction (Un-HAF), and hydrolyzed aqueous fraction (HAQ).*

Sample	Glucose, mg/ml	Xylose, mg/ml	Levoglucosan, mg/ml	Hexoses, mg/ml	Total sugars mg/ml	HMF, mg/mL
Un-HAF	18.80	44.70	143.80	12.20	219.50	10.26
HAF	123.70	13.40	21.30	60.70	219.10	2.14

Table P18 shows the sugar concentrations for un-HAF and HAF aqueous fraction. Levoglucosan was the main sugar component in the un-HAF aqueous fraction. After the hydrolysis step, glucose and the other monosugars (hexoses and xylose) were the major components. Sugar analysis showed also that the un-HAF aqueous fraction bio-oil contained high yields of 5-hydroxymethyl furfural (HMF). Hydrolysis of anhydrosugars to monosugars in acidic medium apparently led to the decomposition of HMF. Therefore, we proposed a new treatment step for separation of clear cuts from the HMF contained in the un-HAF before the hydrolysis and conversion steps.

For this purpose, different solvent-solvent extraction steps in combination with cation exchange resins were used. The efficiency of using cation exchange as catalyst for the conversion of hydrolyzed monosugars to HMF was also tested. Separation of un-HAF was performed by solvent treatment in the presence of Amberlyst 16 wet cation exchange catalyst. The un-HAF was treated with 2-butanone (solvent: un-HAF ratio=3:1) at 120 °C for 60 min. The treatment was catalyzed with 10% Amberlyst 16 wet catalyst (weight to volume of un-HAF). The treatment was performed in a Parr reactor for a heating time of 25 min. After completion of the treatment, separation of the organic layer from the aqueous layer was achieved by using a separating funnel. The produced un-hydrolyzed aqueous layer was hydrolyzed with 4% sulfuric acid at 120 °C for 60 min to give HAF containing monosugars.

***Table P19**. HMF concentration (mg/ml) before and after Amberlyst 16 treatment.*

Sample	HMF, mg/mL
Unhydrolyzed aqueous fraction before Amberlyst 16 treatment (75 ml).	10.26
Aqueous fraction after Amberlyst 16 treatment.(75 ml)	2.04
Organic fraction after Amberlyst 16 treatment.(225 ml)	2.73
Hydrolyzed (4% sulphuric) Aqueous fraction after Amberlyst 16 treatment.	0.04

Table P19 shows the concentration of HMF before and after the pretreatment with Amberlyst 16 wet catalyst. The initial HMF concentration in the un-hydrolyzed aqueous solution was 10.26 mg/ml. After the pretreatment, the concentration of HMF was reduced to 2.04 mg/ml and 2.73 mg/ml in both aqueous and organic layers, respectively. This means that almost 80.12% of the HMF already existing in un-hydrolyzed aqueous solution was extracted by the organic phase (2-butanone) through the treatment step. After hydrolysis the concentration of HMF was reduced to

a very low level of 0.04 mg/ml. The above results led us to perform the further conversion processes on the hydrolyzed aqueous solution with 0.04 mg/ml HMF.

A series of experiments was performed to determine the best catalyst and organic solvent combination for conversion of monosugars to HMF. In these experiments the conversion of sugars to HMF experiments were performed in a 70 ml stainless steel reactor. The reactor was charged with 5 mL of HAF bio-oil, 15 mL solvent and the catalyst. The biphasic acid catalyzed dehydration reactions were performed by heating the reactor in a thermostatic oil bath at 170°C for 60 min. After the reaction was complete both the organic and the aqueous phase were separated with a separatory funnel and the volumes of both phases were determined. Furan derivatives were determined in both layers by using 1100 Agilent High Performance Liquid Chromatography (HPLC) equipped with a ZORBAX eclipse C_{18} column and UV detector. The column temperature was constant at 30 °C, and the mobile phase was methanol in water (1: 5 v/v acidified by 5% acetic acid) at a flow rate of 1 ml/min with UV detection at 282 nm, and 10 µL of each sample was injected manually and the yield of HMF and furfural were determined.

Two techniques (one stage and two stage) were performed in order to convert the monosugars in HAF into HMF and furfural chemicals by using (Amberlyst 70 wet) cation exchange catalyst.
In the one-stage conversion technique monosugars conversion was performed in a biphasic reaction system consisting of 2-butanone and the HAF in ratio 3:1, respectively. Concentrations of Amberlyst of 5, 10, 20 and 30% were applied and the conversion was tested a several reaction temperatures and times. Table P20 shows the yields of HMF and furfural produced from the conversion of monosugars under different reaction conditions.

Table P20*. Effect of catalyst concentration on the yields of HMF, furfural and total furans produced from the conversion of HAF with high yield sugars at different reaction temperatures and times.*

(Amberlyst 70), %	Temp. (°C)	Time (min)	Yield $_{HMF}$, %	Yield $_{FF}$, %	Total Furan Yield, %
5	130	120	6.28	5.04	11.33
10	130	120	6.22	7.01	13.23
20	130	120	4.07	4.30	8.38
30	130	120	6.12	6.14	12.27
5	150	60	10.06	2.43	12.49
10	150	60	7.94	1.29	9.23
20	150	60	5.46	5.36	10.86
30	150	60	6.87	3.69	10.56
5	170	60	17.09	7.31	24.41
10	170	60	15.49	6.37	21.82
20	170	60	18.14	6.89	25.03
30	170	60	12.61	4.94	17.56
5	190	30	17.25	5.53	22.78
10	190	30	17.18	7.68	24.87
20	190	30	12.52	6.10	18.63
30	190	30	13.29	6.44	19.73

As shown in Table P20 regardless of reaction temperature, increasing the catalyst concentration did not change the yield of HMF or total furans markedly. The highest yields of total furan compounds obtained at (130 °C for 120 min) and (150 °C for 60 min) were 13.23 and 12.49%, respectively. The total furans yields were improved to 25.03 and 24.87% at higher reaction temperatures (170 °C for 60 min) and (190 °C for 30 min), respectively. Applying the highest

concentration of catalyst (30%) at higher reaction temperatures of 170 °C or 190 °C decreased the total furans yields to 17.56 and 19.73%, respectively. Accordingly, the high catalyst concentration (30%) resulted in lower total furan yields. The catalyst concentrations of 20 and 10% were the optimum catalyst concentrations at 170 and 190 °C as they gave high HMF yields.

Another series of experiments were performed to optimize the reaction time at the best temperature and catalyst conditions. Table P21 summarizes the effect of reaction time on HMF and total furans yields at 170 and 190 °C. It is clear from the table that the optimum reaction time of 170 °C was 30 min. At 190 °C, the highest HMF and total furan yields were obtained after 20 min.

Table P21*. Effect of reaction times on the yields of HMF, FF, and total furans produced at reaction temperatures of 170 °C and 190 °C and optimum catalyst concentration*.

(Amberlyst 70), %	Temp. (°C)	Time (min)	Yield $_{HMF}$, %	Yield $_{FF}$, %	Total Furan Yield, %
20	170	15	8.53	3.88	12.42
20	170	30	19.74	8.77	28.51
20	170	45	16.20	6.15	22.36
20	170	60	18.14	6.89	25.03
20	170	90	12.37	5.09	17.46
10	190	5	5.21	4.36	9.57
10	190	10	11.79	6.28	18.07
10	190	15	15.69	7.44	23.14
10	190	20	16.94	8.07	25.01
10	190	30	17.18	7.68	24.87
10	190	45	15.33	4.47	19.80
10	190	60	12.26	5.34	17.60

A two-stage conversion process technique was also tested for the conversion of monosugars to furans. In the first stage, the biphasic system (butanone: HAF with ratio = 3:1) was catalyzed either by 0.2 M phosphoric acid or 1.5 M formic acid (the concentration of acid was calculated based on the volume of HAF in the reaction). The reaction conditions for the first stage chosen based on our previous results in which 0.2 M phosphoric acid and 1.5 M formic acid were found to be the optimum catalyst concentrations at 170 °C for 60 min. The produced liquid in the first stage was subjected to the second stage in which the reaction was catalyzed with 20% (based on the initial total sugar content involved in the first stage) of Amberlyst 70 wet at 170 °C for 30 min. As shown in Table P22, low furan derivative yields (HMF, total furans) were produced when liquid acids were used as catalysts in the first stage with and without the addition of DMSO. The produced liquors from the first stage were subjected to the second stage conversion process which was catalyzed by Amberlyst 70 wet at 170 °C for 30 min. After the second stage the produced amount of HMF was remarkably increased. The highest HMF yields were produced from the second stage catalyzed by formic acid or phosphoric acid with the addition of DMSO, respectively.

Table P22*. Two-stage conversion process of monosugars in high concentrated aqueous solution into HMF and FF.*

After the first stage				After the second stage		
Catalyst	HAF:DMSO	HMF, %	FF, %	HMF, %	FF, %	Total Furans, %
HCOOH	-	7.00	7.11	28.44	-	28.44

HCOOH	8 : 2	8.69	3.35	35.38	1.00	36.38
H_3PO_4	-	9.35	1.06	29.57	1.35	30.92
H_3PO_4	8 : 2	8.94	5.90	33.58	1.25	34.83

The two-stage conversion process was also performed on the HAF produced from low water content bio-oil. In the first stage the conversion reactions were catalyzed by solid acids (aluminum silicate or zeolite) in the presence of 2-butanone (butanone: HAF ratio = 3:1) at reaction conditions shown in Table P23. The produced organic layer from the first stage was subjected to the second stage of cation exchange treatment using Amberlyst IR-120 Na at 120 °C for 60 min. As shown in Table P23, this two-stage conversion process resulted in high selective conversion into HMF with yields of 46.17 and 43.26%.

Table P23. *Effect of different pretreatment conditions of the HMF produced from the conversion of monosugars*.

HMF Yield, % after the first stage					HMF Yield, % after the second stage		
Catalyst	Temp. °C	Time, min	HMF, %	FF, %	HMF,%	FF,%	Total Furans,%
aluminum silicate	170	60	17.85	5.20	41.89	-	41.89
Zeolite (ZSM-5)	170	60	18.09	4.10	43.26	-	43.26
Zeolite (CBV400)	170	60	23.50	1.75	37.15	-	37.15
Aluminum silicate	190	60	12.49	1.00	46.17	-	46.17
Zeolite (ZSM-5)	190	60	12.62	1.00	42.36	-	42.36

The effect of phosphoric acid catalyst on the catalyzed biphasic process was tested with various solvents. The concentration of phosphoric acid used in all runs (0.2M) was calculated based on the volume of the aqueous fraction used in the run. The results of this study are summarized in Table P24.

Table P24. *Yields of hydroxymethylfurfural (HMF) and furfural (FF) produced from phosphoric acid- catalyzed dehydration reaction at 170 °C for 60 min*.

Solvent	HMF yield, %	FF yield, %	Total furans yield, %
n-propanol	3.86	0.00	3.86
n-butanol	8.92	0.71	9.63
n-pentanol	3.67	0.00	3.67
n-hexanol	8.94	2.21	11.15
Isopropanol	12.74	8.00	20.74
isobutanol	8.32	5.07	13.39
2-butanone	15.28	16.51	31.79
2-pentanone	15.19	6.51	21.7
MIBK	20.48	6.25	26.73
DMSO	18.41	9.11	27.52
THF	19.64	6.03	25.67

Two more series of experiments were performed to study the effect of replacing mineral phosphoric acid with organic acids. Two different organic acids (formic and triflouroacetic acid) were used and the results of this study are summarized in Tables P25 and P26.

Table P25. *Yields of hydroxymethylfurfural (HMF) and furfural (FF) produced from formic acid-catalyzed dehydration reaction at 170 °C for 60 min.*

Solvent	HMF yield, %	FF yield, %	Total furans yield, %
n-propanol	16.50	8.21	24.71
n-butanol	17.97	7.62	25.59
n-pentanol	18.94	9.43	28.37
n-hexanol	17.36	5.05	22.41
Isopropanol	12.81	6.96	19.77
isobutanol	12.43	7.14	19.57
2-butanone	18.10	23.43	41.53
2-pentanone	19.29	12.42	31.71
MIBK	23.12	15.33	38.45
DMSO	14.62	9.04	23.66
THF	14.75	7.09	21.84

Table P26*. Yields of hydroxymethylfurfural (HMF) and furfural (FF) produced from triflouroacetic acid-catalyzed dehydration reaction at 170 °C for 60 min.*

Solvent	HMF yield, %	FF yield, %	Total furans yield, %
n-propanol	21.89	11.36	33.25
n-butanol	11. 49	10.61	22.10
n-pentanol	11.07	5.14	16.21
n-hexanol	8.57	3.51	12.08
Isopropanol	11.60	7.6	19.2
isobutanol	10.94	7.47	18.41
2-butanone	8.87	12.06	20.93
2-pentanone	5.91	4.08	9.99
MIBK	7.42	3.8	11.22
DMSO	14.02	5.07	19.09
THF	8.61	5.84	14.45

In general, the total yield of furan derivatives in the case of formic acid catalyst was higher than for phosphoric acid. We concluded from this study that the application of MIBK and 2-butanone as solvent with formic acid catalyst is the most promising biphasic system for production of HMF and other furan derivatives from aqueous fraction bio-oil sugars. Therefore, a series of experiments was performed to optimize this system. The effects of formic acid concentration, reaction temperatures, times, and the modification of the aqueous phase by addition of DMSO were studied.

Conversion experiments were performed in a 70 mL stainless steel reactor. A biphasic solution consisting of 5 mL of hydrolyzed aqueous solution (HAS) and 15 mL of methylisobutylketone (MIBK) with different formic acid catalyst concentrations (0.1- 4 molar) was placed in the reactor and mixed together. The concentration of formic acid used in each run was calculated based on the volume of aqueous phase in the biphasic solution, 5 ml. The reactor was then immersed in a preheated oil bath connected with a temperature controller and heater. This point was considered to be the starting reaction time. The conversion experiments were performed at three different temperatures (150, 170 and 190 °C) and different reaction times (30-90 min). Experiments with optimum conditions were performed again by adding dimethyl sulfoxide (DMSO) to the HAS/MIBK biphasic system. The total volume of HAS and DMSO was kept constant (5 mL) for each composition and the ratios of HAS to DMSO were 8:2, 7:3, 6:4, and 5:5. The MIBK volume was

also kept constant at 15 mL after DMSO addition. After each run, the biphasic solution was filtered by Whatman 42 filter paper to separate any solid particles from the solution. The filtered biphasic solution was poured into a measuring cylinder to determine the volume of the organic layer (upper layer) and the aqueous layer (lower layer). The two layers were separated by using a separating funnel and filtrated again with 0.2 µm syringe nylon membrane (Millex-GN). HMF and other furans were detected in both the organic and aqueous layers by using HPLC.

HPLC analysis for the converted HAS sugars showed two pronounced peaks for HMF and furfural. Figure P17 illustrates the effect of formic acid concentration on the yields of HMF and furfural produced from the conversion of sugars in the HAS-MIBK biphasic system at three different reaction temperatures of 150, 170, and 190 °C for 60 min. The choice of optimum conditions for the effect of temperature and formic acid concentration was mainly based on the total yield of furan derivatives produced from the conversion process. As shown in Figure P17a–c, the yields of HMF and furfural were gradually increased until they reached a maxima, then decreased with increasing formic acid concentration from 0.1- 4 molar. The concentration of formic acid that gave a maxima was highly dependent on the reaction temperature. As shown in Figure P17a, the reaction temperature of 150 ºC was far below the required temperature to efficiently convert HAS sugars because the highest total yield of HMF and furfural was 23.4% (14.4% HMF and 9% furfural) at 3M formic acid concentration. Increasing the reaction temperature to 170 °C led to remarkable increase in the yields of both HMF and furfural compounds at 1.5M catalyst concentration (Figure P17b). The highest total yield of both HMF and furfural reached 45.8% and the process was slightly more selective toward the production of HMF (25.5% HMF yield and 20.3% furfural yield). The total yield of furan compounds obtained at 170 ºC and 1.5M formic acid was almost twice of that obtained at 150 ºC and 3M formic. As shown in Figure P17c increasing the reaction temperature to 190 °C led to a greater increase in the total furans and the yield reached 52.7% (39.2% HMF and 13.5% furfural) at 0.5M catalyst concentration. The selectivity of the process toward HMF production was three times higher than the selectivity toward furfural production. Accordingly, we can conclude from the results shown in Figure P17a-c that the reaction temperature had more significant effect than formic acid concentration on the conversion of sugars in the (HAS-MIBK) biphasic system. The highest total furans yield was shifted toward lower formic aid concentration with increasing reaction temperature. This conclusion was supported by the inefficient conversion yield obtained below 170 ºC even at high formic acid concentration.

***Figure P17**. Effect of formic acid concentration on the yields of HMF and furfural at different reaction temperatures (Time = 60 min).*

Effect of reaction time

Optimization of reaction time was performed at the optimum conditions determined for temperature and formic acid concentration. Figure P18a shows the effect of reaction time on the yields of HMF, furfural and their combined yield at 170 ºC and 1.5M acid concentration. The highest yield of 52.2% (29.6 for HMF and 22.6% for furfural) for the combined furan derivatives was obtained at 45 min reaction time. Further increase in the reaction time resulted in gradual decrease in the yield of both HMF and furfural. Therefore, the optimum conversion time for the process at 170 °C and 1.5M acid was 45 min. Figure P18b shows the effect of reaction time on the yields of furan derivatives at the second optimum conditions (190 °C and 0.5M acid). The highest yield of 52.5% (39.2 for HMF and 13.5% for furfural) for the furan derivatives was obtained at 60 min reaction time. Further increase in the reaction time resulted in gradual decrease in the total yield of 34.2% at 90 min. The decrease in the furan derivatives yield with increasing the reaction time might be related to the conversion of furan derivatives to levulinic and formic acids at the extended time. Therefore, the two optimum conversion conditions selected for further study were 170 ºC with 1.5 M formic for 45 min and 190 ºC with 0.5 M formic for 60 min.

***Figure P18**. Effect of reaction time on the yields of HMF and furfural at the optimum formic acid concentration.*

As shown in Figure P19, the conversion reaction conditions, with addition of DMSO, were performed at the two optimum conditions previously determined. Figure P19a shows the effect of DMSO addition on the yield of conversion products at 170 °C. It was found that the addition of DMSO with a ratio of 7:3 led to highest yields of HMF (39.9%), furfural (31.7%) and total furans (71.2%). In comparison with the results of conversion without DMSO, the addition of DMSO with a 7:3 ratio with HAS enhanced the yields of HMF, furfural and total furans by about 26%, 64% and 36%, respectively. Figure P19b shows the effect of DMSO addition on the yield of conversion products at 190 °C. It was found that increasing the ratio of DMSO to the ratio of 6:4 resulted in a pronounced increase in the yield of furfural from 13.5% to 33.5%. Consequently, the total furan yield was increased from 52.5% to 72.0%. It is obvious that the HAS/DMSO composition (6:4) increased the selectivity of furfural production by more than 100% and total furans by 27.0% compared with the analog experiments without DMSO. Our results are consistent with previous researchers that showed an effect of DMSO in shifting the reaction toward more furan compounds.

***Figure P19**. Effect of addition of DMSO to the hydrolyzed aqueous solution (HAS) at the optimum conditions.*

In the next series of experiments we chose a solid acid catalyst system to overcome the environmental and cost disadvantages of the liquid acid catalyst. Also, solid acid catalyst is easily separated from the reaction medium and can be reused. The use of a combination of zeolite and transition metal chlorides was designed to utilize the advantages of both zeolite and transition metal chloride catalysts. Zeolite is characterized by functionalized acidic centers which can promote the reaction acidity with metal chloride. Also, the presence of transition metal chlorides can increase the isomerization stage of glucose (a major component in the aqueous fraction) to produce fructose which can easily be converted to HMF. The effects of zeolite and metal chloride concentration, reaction temperatures and time were tested.

As shown in Figure P20, the effect of catalyst systems was tested at reaction temperatures (180 °C) for time intervals ranging from 15 to 90 min. The results showed that the highest yields for HMF and total furan yields resulted from the conversion process of catalyzed zeolite/$CrCl_3$ at 180 °C for 60 min. The catalyst system zeolite/$CuCl_2$ gave the lowest efficiency of all tested time intervals. The catalyst system zeolite/$FeCl_3$ had comparable efficiency with zeolite/$CrCl_3$ at 180 °C for 45 and 60 min. At 180 °C and 60 min, zeolite/$FeCl_3$ produced the highest HMF and total furans.

***Figure P20**. Effect of metal chloride catalysts on the yields of HMF, FF and the total furans at different reaction time intervals (Temperature = 180 ℃).*

Figure P21 shows the effect of catalyst systems at reaction temperatures (200 °C) for different time intervals ranging from 15 to 90 min. The optimum results for HMF and furans yields were achieved at a shorter (30 min) reaction time. The optimum HMF yields (34.07, 37.03, and 31.9%) were achieved by using FeCl3, CrCl3, and CuCl2 with zeolite, respectively. Also, the optimum total furans yields (59.7, 67.49 and 56.84%) were produced at the same reaction time. Based on the above data, the zeolite/CrCl3 system was considered to be the most successful catalyst among the zeolite/single metal chloride catalyst systems tested. The high catalytic power for zeolite/CrCl3 may be attributed to the high efficiency of CrCl3 for performing the isomerization stage in which glucose can be converted to fructose conformation.

***Figure P21**. Effect of metal chloride catalysts on the yields of HMF, FF and the total furans at different reaction time intervals (Temperature = 200 ℃).*

In another series of experiments a pair of metal chlorides combined with zeolite was applied at optimum reaction conditions of temperature and time (180 °C/60 min and 200 °C /30 min). As shown in Figure P22, at reaction conditions (180 °C and 60 min), using a pair of metal chlorides with zeolite improved only the catalytic efficiency of zeolite/$CuCl_2$, while both zeolite/$FeCl_3$ and zeolite/ $CrCl_3$ were still better than all pairs of metal chlorides used with zeolite. At reaction conditions (200 °C and 30 min), two promising zeolite/pair metal chloride systems were established, zeolite/$FeCl_3$-$CrCl_3$ and zeolite/$CuCl_2$- $CrCl_3$. These catalytic systems had higher catalytic efficiency than all zeolite/single metal chloride systems tested. The use of zeolite/ $FeCl_3$-$CrCl_3$ system led to an increase in yields of HMF and total furans.

***Figure P22**. Effect of using a pair of metal chloride catalysts on the yields of HMF, FF and the total furans at the optimum reaction conditions (Temperature = 180 °C and time =60 min; Temperature = 200 °C and time =30 min).*

Subtask P.4 Bio-oil upgrading: continue refinement of bio-oil upgrading processes to esterified, esterified/olefinated, and hydroprocessed bio-oils; maximize and utilize sugar hydrolyzates; produce stabilized bio-oil from pine bark feedstock

MSU is a leader in hydroprocessing bio-oil to hydrocarbons, producing esterified and esterified/olefinated bio-oil suitable for boiler fuel, and producing glucose from the bio-oil aqueous fraction. While considerable progress has been made in upgrading these systems, they require refinement prior to commercialization. This refinement will take place under SERC IV funding. Cooperation with a catalyst company to refine MSU hydroprocessing technology is expected. There will be cost share from this company based on the cooperative research in this event. Cooperation with a company to license and produce esterified and/or esterified/olefinated bio-oil as a boiler fuel is expected. There will be cost share from this company based on the cooperative research in this event. Bark is a low-cost resource that has been avoided for production of bio-oil because its highly reactive nature results in high instability. MSU has performed extensive research into the cause for the high reactivity of bio-oil produced from bark. Based on this information, treatments to counter this reactivity will be developed. Production of bio-oil with less reactive properties from the bark resource will allow a low-cost biomass to be pyrolyzed to bio-oil followed by conversion to fuels.

Planned Activities:

P.4.ML.1 Utilize various catalysts and modify reactor designs for bio-oil upgrading and sugar production.

P.4.ML.2 Optimize hydroprocessing, esterification, esterification/olefination, and sugars production systems with the best-performing catalyst and/or other additives.

P.4.ML.3 Produce bio-oil from bark with various treatments and compare properties to bio-oil from clear woods.

Summarization of Activities:
The bark addition study involving percentages of bark added to clear wood of pine was performed to determine the effect bark feedstock has on the physicochemical characteristics and stability of pyrolysis oil. Pyrolysis oil used for this study was produced using a lab scale auger reactor at MSU's Forest Products laboratory. The oil was produced using 0, 20, 40 and 50 wt% of pine bark, with the remainder of the feedstock being pine clear wood. Multiple condensers were utilized to condense the hot gases to oil. The samples were collected as total (from all the condensers), Fractionate I (excludes product from one condenser with high water content) and Fractionate II (product from condenser with high water content). Decreased overall oil yield and increased char was observed when bark was added to the feedstock. The yield and the char content for each production run are shown in Table P27.

Table P27*. Yield and char content in pyrolysis oil produced from different ratios of bark in the feedstock.*

	Feedstock			
	100% CW	80%CW/20%Bark	60%CW/40%Bark	50%CW/50%Bark
Oil (Wt%)	58.3	51.7	43	41.2
Char (Wt%)	23.7	25.7	29.1	30.9

Oil produced from 100% clear wood (CW) was mostly homogenous with solid particles dispersed throughout. Larger size particles were observed in all the samples produced with bark. Phase separation was observed in some of the bark samples. The non-fractionated sample (total) produced from 50%CW/50%Bark had a layer of solids content settled at the bottom. Particles precipitated quickly in the high water content sample and may be materials derived from the lignin content. The Fractionate II samples from 50%CW/50%Bark had a less dense sticky, slimy layer at the top that may be agglomerated particles that are rich in waxy materials such as fatty acids.

Physical properties such as pH, density, viscosity, solids content (as MIM wt%) and water content were measured. To determine the change in chemical composition, FTIR spectroscopy was utilized. Though pH was increased when bark was added to the feedstock, no difference was observed with the change in ratio of the bark added as shown in Table P28. It was observed that the density increased when bark was added to the feedstock. In all the sample sets, the density for Fractionate I was higher as it excludes product from the condenser with high water content. The solid content also increased with the addition of bark in the feedstock and it increased with the increase in the bark ratio. A slight decrease was observed in the sample from 50% bark feedstock as the solids were precipitating out quickly even after vigorous shaking which could be due to high lignin content in the feedstock. Solid content data is shown in Table P29. This might have caused error when an aliquot of sample was taken for analysis. Around 30% increase in water content was observed for the oil produced 50%CW/50%Bark when compared with 100% CW oil. Oil showed a higher pH due to acid content of precipitated phase and apparent increase in water content. The Fractionate I sample showed decrease in water content as it excludes the product from one of the condensers with high water content. The Fractionate II sample showed high water content as expected. The plot can be seen in the Q8 report.

Table P28. *Bark-feedstock pyrolysis oil pH data.*

Feedstock	pH
0%bark	2.40±0.07
20%bark	2.50±0.06
40%bark	2.50±0.06
50%bark	2.52±0.03

***Table P29**. Bark-feedstock pyrolysis oil solids content (as MIM wt%).*

Feedstock	MIM wt.%
0% bark	0.18
20% bark	1.05
40% bark	1.44
50% bark	0.71

Particle size distribution analysis showed increase in particle size with the addition of bark. Detailed discussion and plot is shown in the Q8 report. ATR-FTIR spectroscopy was performed to identify any change in chemical composition. The spectra obtained for the total samples from all the feedstock using ATR-FTIR were compared and no significant change was found. To determine the quantitative change peak height ratio (PHR) was measured. Normalization for the PHRs are based on the peak height for the peak apex falling in the 1265-1277 cm^{-1} wavelength (C-C, C-O, C=O -st) a common and very consistent peak from sample-to-sample. When bark was added in the feedstock PHR for the O-H stretch (3390-3412 cm^{-1}) increased which indicates the increase in phenolic concentration. It correlates with the presence of lignin-derived compounds. Aromatics increased which is shown by the increase in PHR for the C-H_3 (rocking)/C-C (skeleton) (1052 cm^{-1}). Increased ether and ester content was also observed which corresponds to C-H (deformation vibration/scissoring), C-H(asymmetric deformation), C-H_2 (symmetric deformation) at 1463 cm^{-1}.

An aging study was performed to understand the effects of bark on the stability pyrolysis oil. All the samples were aged at 80°C for 6, 24 and 48 h. For the aging studies 27mL of oil was placed in 30 mL of jars and heated in the convection oven at 80 °C. The caps were retightened often to avoid loss of mass. Initial and final weights were recorded to determine any loss in mass if any. The weight loss for all the samples was within 0.1wt%.The solid content increased when the samples were aged for long hours as shown in Table P30. It was difficult to take representative samples since all the bark added samples were non-homogenous and the particle sizes detected were large due being separated from the liquid even after vigorous shaking which caused the difference in solid content for the samples taken for aging with the control.

***Table P30.** Bark-feedstock pyrolysis oil solids content (MIM wt%) for aged samples.*

	MIM Wt.%		
Feedstock	6h	24h	48h
0% bark	0.39	0.50	0.92

20% bark	0.35	0.44	0.54
40% bark	0.54	0.58	0.77
50% bark	0.56	0.44	0.91

Rheology data were collected using a TA Instruments AR 1500x rheometer with a 60 mm aluminum parallel plate accessory, Rheology Advantage Instrument Control AR software (version V5.7.0), and Rheology Advantage Data Analysis software (version V5.7.0). Step-flow shear data were collected at 40 °C over the 0.1 to 100 s^{-1} shear rate range with 10 points per decade. The measurements were taken for the control and the samples aged for 6 h and 48 h. The data reported are the average values for the region where the data was almost constant (shear rate of 10-100 s^{-1}) for the samples produced from 100% CW and 50%CW/50%Bark feedstock. The data is shown in Table P31.

***Table P31**. Bark-feedstock pyrolysis oil viscosity measurements (measured at 40 °C).*

Feedstock	Viscosity,cP		
	Control	6 h	48 h
0% bark	12.30	11.85	14.08
50% bark	2.96	2.81	4.70

From the data it was observed that no difference was seen when the samples were aged for 6 h. Increase in viscosity was observed for the samples aged for 48 h. Again, due to the larger size of the particles in the sample produced from the bark-added feedstock, it was difficult to take the representative samples for analysis. The torque for the rheometer exceeded the limit when the particles were used for the measurement. Performing the aging studies after filtration might help to obtain more valid results.

To determine the change in chemical composition with aging, the spectra for the 48 h aged sample was compared with the spectra for the control. For the sample produced from 100% CW, peaks were observed at 48 h at 1153, 1124, 1034 cm^{-1} which was not observed for unaged samples. This indicated the occurrence of etherification and esterification reactions. For most of the samples aged for 48 h, increase in PHR was observed for C=O (stretching) (1700cm^{-1}) and C-H,C=C-C (ring stretching) / N=O (stretching) (1515 cm^{-1}) which indicates the increase in aromatics and ketones. Decrease in C-O stretching was observed which indicates that the primary and secondary alcohols are reacting to produce aromatics or ketones.

The ratio of energy available in biomass is low in relation to its bulk density. This is particularly true if the original water content of the tree stem has not been reduced. In addition, the economics of transportation of biomass requires that the bulk density be about 286 kg/m^3 to allow full truck weight capacity. The bulk density of green loblolly pine chips has been estimated to be 245 kg/m^3.Compression to remove water is a viable method to reduce water content in tree stems at the harvest site such that transportation of greater quantities of dryer biomass can be achieved. Compression to remove water has the benefit of reducing the drying usually required prior to production of bioenergy or chemicals from biomass. In this project, water content of young loblolly pine is expected to be reduced from 55% to less than 35% of green weight by hydraulic pressure in conjunction with a whole tree chipping operation. The pressed chips will be both dried and compressed such that full truck weight capacity will be easily achieved.

Removal of water by hydraulic compression at the harvest site would allow more economic transportation of wood mass as compared to water mass. A hydraulic press process was applied for water removal from green juvenile wood chips (Figure P23). The compressing process

simulated a whole tree chipping operation in which loblolly pine chips were processed on the harvest site immediately after production. Each simulation was comprised of 500 lbs of green chips. The green chips from juvenile wood were obtained immediately after production at a local sawmill and placed into plastic bags to prevent moisture loss during transportation. The chips were pressed by a hydraulic press at up to 120,000 psi. Raw chips and crushed chips along with process water were collected for physicochemical property analysis (Figure P24).

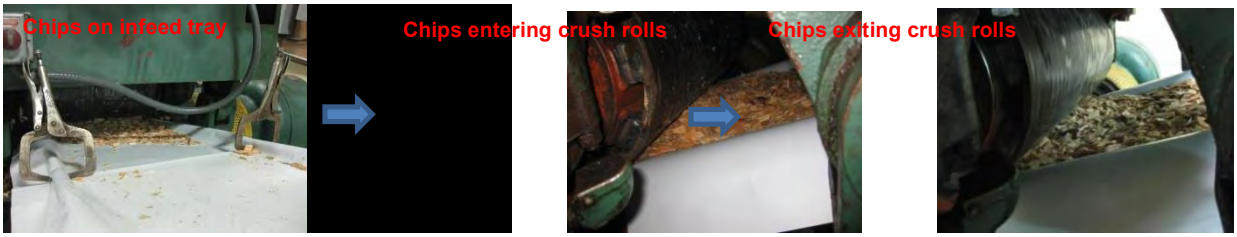


Figure P23. *High pressure hydraulic press process on green juvenile pine wood chips.*



Figure P24*. Pine wood chips and process water samples collected from hydraulic press process conducted at 50,000 psi.*

In order to test the effect of hydraulic pressure on densification of raw green loblolly pine chips, hydraulic pressure at 50,000 psi was applied to press freshly cut loblolly pine chips which originally contained about 45% water. Both raw and pressed pine chips were characterized and compared in order to show the effectiveness of hydraulic pressure. The process water collected from the hydraulic press process was also analyzed for physiochemical properties. All tests were conducted in triplicates and the average values were reported.

Green loblolly pine chips before and after hydraulic press conducted at 50,000 psi were characterized and compared. As summarized in Table P32, the water content of pine chips was reduced from 44.46% to 42.15% after hydraulic pressing. This small change in water content indicated that the hydraulic press process was not effective for compressing raw wood chips to meet the expected weight capacity for transportation. Furthermore, other properties of raw and pressed wood chips, such as ash content, higher heating values, and elemental contents, were similar to each other (Table P32). The results obtained showed that no significant change in physicochemical properties occurred during the hydraulic pressing process. To further test the hypothesis with regards to efficient reduction of water removal by compressing, a higher pressure may be applied or raw chips with more moisture may be used in a future study.

Table P32*. Comparison of raw and pressed pine chips.*[a]

Parameters	Raw	Pressed
Solid (wt%)	55.44±0.19	57.85±0.60
Water (wt%)	44.46±0.19	42.15±0.60
Ash (wt%)	0.25±0.03	0.20±0.02
Higher heating value (HHV) (MJ/KG)	16.59±0.26	16.73±0.10
Elemental analysis		

Carbon (%)	45.73±0.25	45.86±0.16
Hydrogen (%)	6.35±0.16	6.26±0.02
Nitrogen (%)	0.20±0.05	0.22±0.06

[a] means of three replicates reported.

As presented in Table P33, the press water had high BOD and COD values which could be attributed to suspended solids and volatile compounds, such as essential oils from raw wood. However, no water soluble sugars were detected via HPLC analysis. These results indicated that hydraulic press did not result in extraction of non-structural carbohydrates in wood chips.

***Table P33**. Physicochemical property of the press water.[a]*

Parameters	value
BOD (mg/L)	4,680
COD (mg/L)	12,470
Suspended solids (wt%)	1.60
Ash (wt%)	4.61
Water soluble sugars (mg/L)	ND

[a]means of three replicates reported

The process water was analyzed for its compositions using GC-MS. The result showed that trace amounts of organic compounds, such as short chain fatty acids, dissolved in the process water.

Figure P25 shows SEM images of raw and squeezed pine wood chips. As can be seen from the images, the hydraulic compression slightly changed the morphology of the wood chips. The squeezed wood chips shrunk slightly after compression. SEM images of cross-sections of these wood chips will be studied in the next quarter.

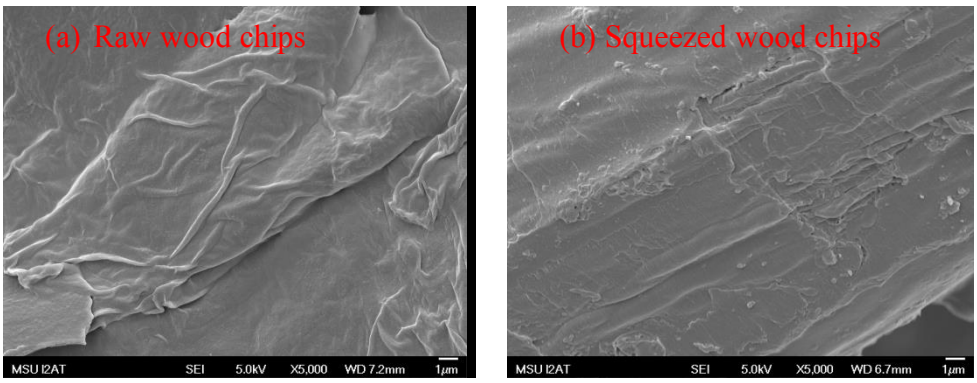


***Figure P25**. SEM images of raw and squeezed pine wood chips.*

TGA profiles of raw and squeezed pine wood chips are depicted in Figure P26. TGA and DTG data displayed a continuous mass loss associated with increasing temperature. The significant mass loss of both wood chips, mainly due to decomposition of lignin and carbohydrate, occurred at 380-400 °C. Raw pine wood chips degraded at a lower temperature (380 °C) than squeezed pine wood chips (393 °C). Moreover, for raw wood chips, more mass was lost during the thermochemical degradation. The results indicate that hydraulic compression resulted in an increased thermal stability of wood chips.

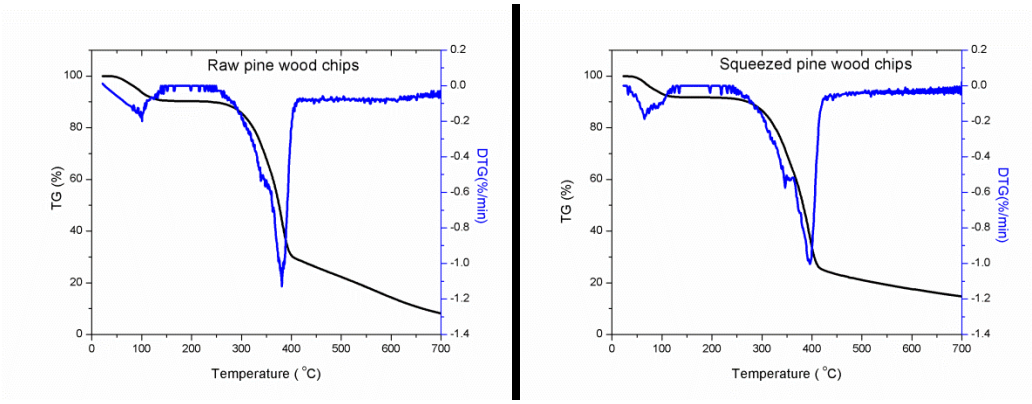


Figure P26. *TGA profiles of raw and squeezed pine wood chips.*

Figure P27 shows SEM images of raw and pressed pine wood chips (cross-section). These images indicate that after the hydraulic compression wood chips were loosened and wood fibers appeared to be much softer.

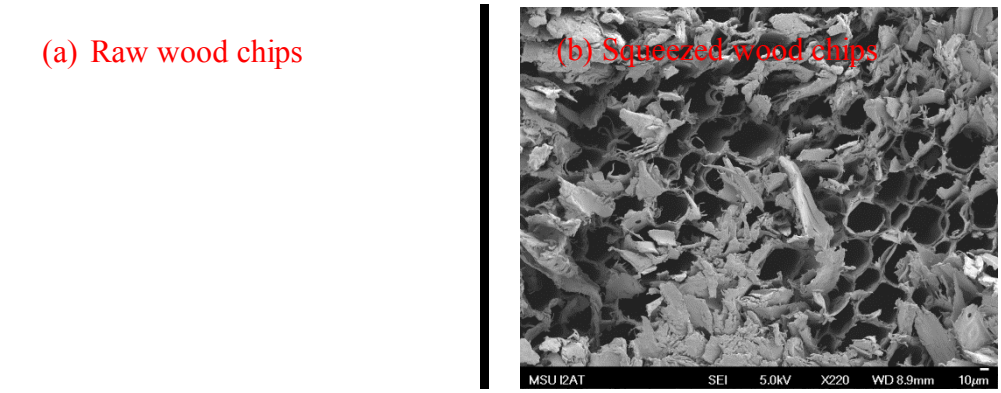


Figure P27. *SEM images of raw and squeezed pine wood chips (cross-section).*

FT-IR was performed to investigate the changes in surface functional groups of wood chips. The broad band at 3320 cm^{-1} was associated to O-H stretching vibration mode of hydroxyl functional groups. The band at 2998 cm^{-1} was associated with symmetric C-H stretching of alkyl groups. The bands between 950 and 1710 cm^{-1} showed the presence of oxygen containing functional groups. As compared to raw wood chips (Figure P28), some FTIR bands disappeared or decreased in intensity for pressed wood chips (Figure P28). Such changes revealed the removal of surface functional groups during hydraulic pressing. Decrease or disappearance of the bands between 950 and 1710 cm^{-1} indicated that most of the oxygen-containing surface groups were removed by hydraulic compression.

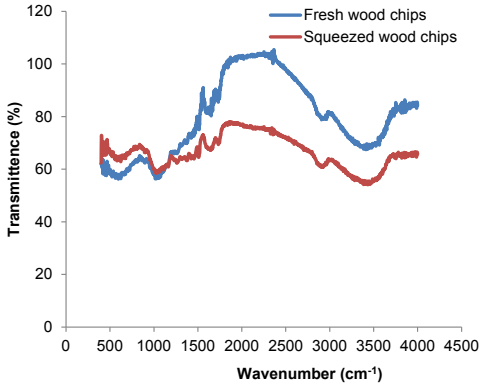


Figure P28. *FT-IR spectra of raw and squeezed pine wood chips.*

Research performed under SERC III developed a method to nearly double the anhydrosugars production during pyrolysis. Inhibitor removal to allow production of ethanol was partially successful. However,further research was necessary to determine the potential for fully removing all inhibitors from the hydrolyzate produced from bio-oil anhydrosugars.

Levoglucosan is the major anhydrosugars component of bio-oil produced by fast pyrolysis. Previous research has shown that levoglucosan yield can be greatly increased if a mild acid pretreatment is applied to demineralize the feedstock prior to pyrolysis. The interest in levoglucosan production is that it provides a route to production of monomeric sugars, primarily glucose, which can be utilized to produce biochemically derived fuels (ethanol, butanol, etc.). SERC III developed a novel method based on pyrolysis of clear pine wood particles with acid pretreatment and modification of the pyrolysis process. This new method resulted in a 30.7% increase in levoglucosan yield in the bio-oil when water spray was applied with a novel condenser temperature manipulation method (shown in Table P34). This increase may change the process economics of production of anhydrosugars via pyrolysis.

Table P34*. Water, levoglucosan, acetic acid and furfural concentrations in weight percentage for all four treatments.*

	Concentrations in weight percentage (wt%)			
Treatment applied	Water content in whole bio-oil sample	Levoglucosan in bio-oil organic portion	Acetic acid in bio-oil organic portion	Furfural in bio-oil organic portion
biomass untreated; no spray	28.53 ± 0.32	6.58 ± 0.10	7.83 ± 0.07	0.14 ± 0.02
biomass pretreated; no spray	22.21 ± 1.69	12.57 ± 0.67	5.42 ± 0.23	0.27 ± 0.04
biomass untreated; spray	34.55 ± 0.69	6.66 ± 0.16	7.63 ± 0.35	0.18 ± 0.02
biomass pretreated; spray	34.32 ± 0.54	16.43 ± 0.71	5.01 ± 0.39	0.37 ± 0.02

The device and method developed in this study provided a means to greatly increase anhydrosugars yield produced from pyrolysis of biomass feedstock. This increase was achieved by injection of a liquid spray into the vapor stream of any pyrolysis reactor type just prior to the

reactor condensers. The high amount of water contained in this condenser caused self-fractionation which allowed separation of the aqueous and pyroligneous fractions of bio-oil. The aqueous fraction contained a high percentage of anhydrosugars that may be utilized to produce fuels or chemicals. The pyroligneous fraction, with the removal of compounds that foul catalysts, is more easily utilized for catalysis to hydrocarbon fuels.

In SERC IV, continuous research was performed on fermentation of anhydrosugars into ethanol. Utilization of 1, 6-anhydro-β-d-glucopyranose (levoglucosan) present (11% w/v) in the water fraction of bio-oil for ethanol production will facilitate improvement in comprehensive utilization of total carbon in biomass. One of the major challenges for conversion of anhydrous sugars from the bio-oil water fraction to bio-ethanol is the presence of inhibitory compounds that slow or impede the microbial fermentation process. Removal of inhibitory compounds was first approached by n-butanol extraction. Optimal ratio of n-butanol and bio-oil water fraction was 1.8:1. Removal of dissolved n-butanol was completed by evaporation. Concentration of sugars in the bio-oil water fraction was performed by membrane filtration and freeze drying. Fermentability of the pyrolytic sugars was tested by fermentation of hydrolyzed sugars with *Saccharomyces pastorianus* lager yeast.

Inhibitors were successfully removed from the bio-oil water fraction by sequential treatments (Figure P29). Levoglucosan produced by fast pyrolysis of biomass was fermented to bioethanol. n-butanol extraction was effective in removing organic inhibitors. Membrane filtration and freeze drying improved the fermentability.

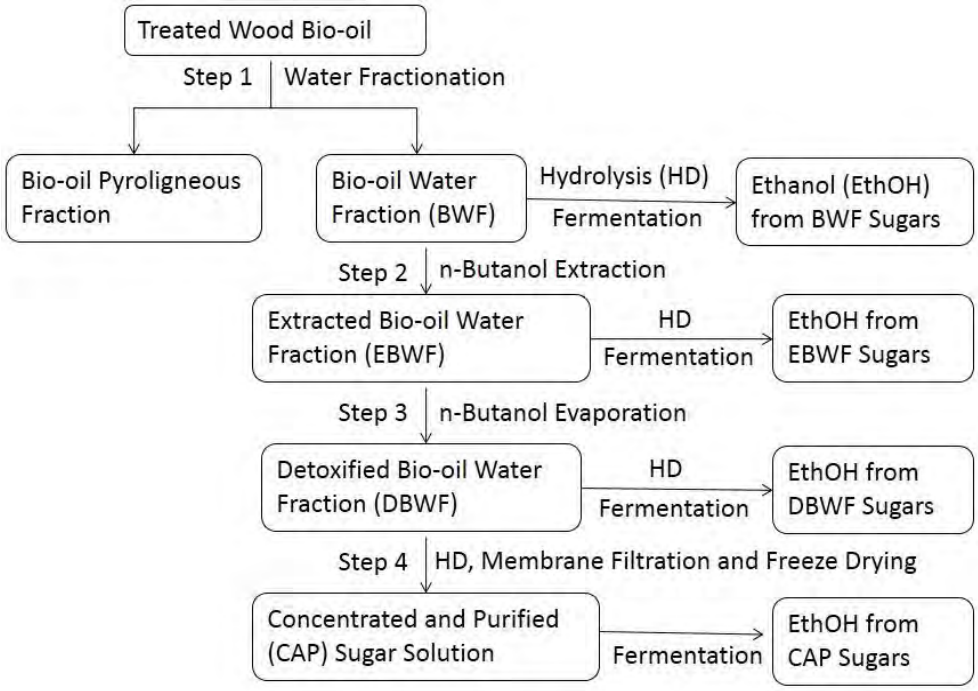


***Figure P29**. Schematic diagram of the methods applied to remove inhibitors.*

Figure P30 shows the relationship between sugar consumption of concentrated and purified (CAP) sugars solution and ethanol production over fermentation time. Glucose, mannose and galactose consumption is depicted on the secondary axis. Figure P30 shows that all glucose and mannose were consumed after 36 h of fermentation and at the same time ethanol production

(primary axis) reached its maximum (12.12 g/L) (0.50 g/g). Since *S. pastorianus* only consumes 6-carbon (glucose, mannose and galactose) sugars, it was expected that galactose would be consumed by this yeast as well. In the current study, the galactose present in the CAP sugar solution was not consumed by *S. pastorianus* and the amount of galactose content during the fermentation remained unchanged. Thus, for the calculation of the theoretical yield of ethanol only glucose and mannose in the CAP sugar solution were considered to be converted into ethanol. The CAP sugar solution, with inhibitors removed, gave an ethanol yield of 98% (0.5g EthOH/g glucose) of the theoretical yield.

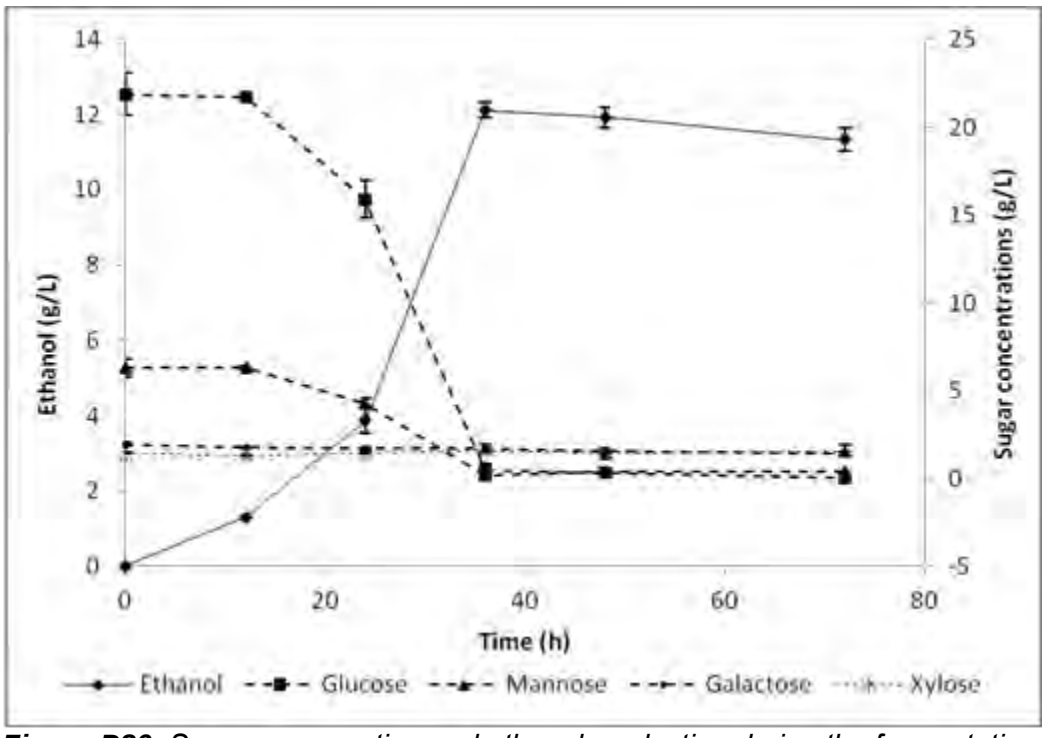


***Figure P30**. Sugar consumption and ethanol production during the fermentation of CAP.*

This study demonstrates the technical potential for removal of inhibitors to obtain high ethanol yield with bio-oil sugars. However, further research is required to reduce the inhibitor removal costs to render the process economically feasible.

One hindrance to commercialization of both hydroprocessing and catalytic pyrolysis is the high cost of hydrogen required to produce transportation fuels. This study utilized syngas to replace the hydrogen required for the hydrotreating stage of hydroprocessing.

Synthesis gas produced purposely by biomass gasification contains significant percentages of both hydrogen and CO in addition to other gases with nitrogen and CO_2 being the major additional gases. Despite the presence of other gases a water gas shift (WGS) reaction will occur when the syngas is pressurized, the proper heat is applied and in the presence of an effective WGS catalyst and water. Bio-oil water content typically ranges from 25 to 30 wt%. Therefore, the theoretical conditions (CO and H_2O) are present for utilization of the WGS reaction to produce increased hydrogen content in biomass syngas during bio-oil catalysis.

$$CO + H_2O \xleftrightarrow{\text{Catalyst}} H_2 + CO_2 \qquad \text{Scheme 2}$$

The objective of this research was to conserve hydrogen by utilization of syngas which contains a low percentage of hydrogen. We hypothesized that the WGS reaction would take place by reaction of the CO contained in the syngas with the water contained in the oxidized bio-oil during partial deoxygenation. This was hypothesized to produce sufficient additional hydrogen to allow the partial deoxygenation reaction to occur during the 1st stage of partial deoxygenation. The 2nd stage of full deoxygenation of the partially deoxygenated product was performed in the presence of pressurized pure hydrogen. We will term this combination of 1st-stage syngas partial deoxygenation followed by 2nd-stage full hydrogen deoxygenation as catalytic deoxygenation (CDO).

Bio-oil required for this research was produced from loblolly pine wood chips with a particle size of 1-3 mm and moisture content of 8-10% on a dry weight basis. Bio-oil was produced by fast pyrolysis performed at a temperature of 450 °C with nitrogen carrier gas at a rate of 7-kg/h with an auger-feed pyrolysis reactor located in the Department of Sustainable Bioproducts, Mississippi State University (MSU). The MSU auger fast pyrolyzer produced 60-65 wt% of liquid product, 10-15% of non-condensable gases and 20-25% of char on a dry biomass weight basis.

Biosyngas utilized in this study was produced in a downdraft gasifier at Mississippi State University and compressed to 1500 psi in laboratory tanks for our experiments. Production of synthesis gas was performed with a Bio Max 25 gasifier. This syngas was comprised of approximately 18-20% hydrogen, 19-22% carbon monoxide, 11% carbon dioxide, 2% methane and 47-49% nitrogen. Hydrogen gas used in this research was obtained from nexAir.

Potassium carbonate, hydrogen peroxide (H_2O_2) 50 wt% solution in water, chloroform-d ($CDCl_3$) 99.96 atom % D contains 0.03 % (v/v) TMS, oxone (potassium monopersulfate triple salt) and copper(II)oxide were obtained from Sigma-Aldrich. Nickel on silica-alumina (66±5% Ni) catalyst powder was obtained from Alfa Aesar. All chemicals were used with no further purification.

Oxidation pretreatment was performed in a stainless steel, high-pressure batch autoclave reactor equipped with an overhead magnetic stirrer, a pressure indicator with a maximum capacity of 5000 psig and a thermocouple for temperature monitoring in the range of 0-500 °C. The autoclave was equipped with an electrical heating and cooling system to control the reactor temperature. Oxidation pretreatment was applied to raw bio-oil by addition of a mixture of oxone/H_2O_2 (oxidizing agent) followed by stirring for 90 min at room temperature and without applied pressure. This oxone/H_2O_2 solution was prepared by dissolving 5 wt% of oxone in 10 wt% of commercial 50 wt% H_2O_2 solution in water. This oxidation pretreatment significantly increased the bio-oil acid value by converting aldehydes into carboxylic acids. This pretreated bio-oil (oxidized product) was utilized as a precursor material to produce hydrocarbons by CDO.

CDO comprised of partial deoxygenation followed by full deoxygenation was performed in the same Parr batch autoclave described above. The 1st-stage partial deoxygenation of the oxidized product was performed in the presence of a mixture of nickel on silica-alumina (5 wt%), potassium carbonate (3 wt%) and copper(II)oxide (2 wt%) catalyst at a temperature of 360 °C and under pressurized syngas at 5.5 MPa for about 90 min. In the 2nd-stage, the partially deoxygenated top oil fraction was separated and fully deoxygenated by a mixture of nickel on silica-alumina (5 wt%) and copper(II)oxide (2 wt%) catalyst at a temperature of 425 °C and under pressurized hydrogen at 9.6 MPa for about 150 min. As a control, partial deoxygenation of direct raw bio-oil with syngas was also performed at the same 1st-stage partial deoxygenation reaction conditions. However, no product was able to be produced due to heavy coke formation during the reaction. It appears that partial deoxygenation of raw bio-oil with pressurized syngas is not possible unless applied to oxidized bio-oil.

In each experiment, once the reaction was complete, the liquid products were cooled in the reactor. The mixture was collected in centrifuge test tubes and centrifuged for 2-4 h to separate the resulting aqueous and organic phases. Both phases were separated and weighed for mass balance computation. The byproducts produced in this process included water and off-gas. Yields were calculated by Eq. 1.

Yield (wt%) of organic fraction = (P (g) × 100)/ bio-oil weight (g) Eq. 1
Where: P = products obtained

The raw bio-oil, oxidized product, partially deoxygenated product (boiler fuel) and fully deoxygenated product (hydrocarbon mixture) produced were characterized following ASTM methods. Higher heating values (HHV) were determined by Ika-5000 bomb calorimeter by applying the ASTM D240 method. Acid values were determined by dissolving 1 g of bio-oil in 50 ml of 35:65 ratio of isopropanol to water mixture and titrating to a pH of 8.5 with 0.1N KOH solution following the method of ASTM D664. pH values were determined by ASTM E70. Densities were determined by Anton Parr DMA 35n portable density meter by ASTM D4052. Viscosities were determined by Ubbelohde capillary viscometer at 40 ^{o}C water bath temperature according to the ASTM D445. Elemental carbon, hydrogen, and nitrogen were determined by EAI CE-440 elemental analyzer with oxygen content determined by difference according to ASTM D5291. Water content was determined by Karl-Fisher titration by ASTM E203. Fourier Transform Infrared Spectroscopy (FTIR) spectra were obtained by a Varian 3500 FTIR analyzer with standard potassium bromide disk technique and spectra were analyzed by Varian-Resolutions software. A Varian CP-4900 Micro GC analyzed the gas composition of the remaining gas stream after each batch experiment. A mass balance for the fuels from the best performing catalyst was calculated. Simulated distillation data analysis was performed by ASTM D2887 with gas chromatography. A detailed hydrocarbon analysis (DHA) was performed by ASTM D6730-01.

Table P35 compares some raw bio-oil and oxidized product physical and chemical properties. As shown in Table P 35 raw bio-oil acid value increased from 90.28 to 161.0 mg KOH/g following oxidation; viscosity decreased by 45.16% and water content increased by about 11%. The HHV of the oxidized product decreased from raw bio-oil's 16.01 to 15.40 MJ/kg probably due to water content increase in oxidized product. Density decreased from 1.22 to 1.14 g/ml and pH was reduced to 2.87 from 3.16. Oxygen content of the bio-oil following oxidation increased somewhat from 53.58 to 58.96. This likely resulted from both increased acid and water content.

Table P35*. Comparison of raw bio-oil and oxidized product physical and chemical properties.*

Properties	Raw bio-oil	Oxidized product
Density, g/mL	1.22	1.14
HHV, MJ/kg	16.01	15.40
Oxygen, wt%	53.58	58.96
Total acid value, mg KOH/g	90.28	161.0
pH	3.16	2.87
Water content, vol%	30.45	33.75
Kinematic viscosity, 40°C, cSt	12.09	6.63

The oxidized product was then partially deoxygenated in the presence of pressurized syngas at 5.5 MPa at a reaction temperature of 360 °C as described in section 2.2.2. After cooling, the partially deoxygenated product had an aqueous phase at the bottom of the vessel and an oil phase at the top. The aqueous fraction was separated from the oil fraction. A portion of the organic fraction was maintained for testing as a boiler fuel product. The remainder of the organic fraction was subjected to full deoxygenation under hydrogen pressure at 9.6 MPa at a temperature 425 °C for 150 min as described in section 2.2.2. The resulting liquid contained both hydrocarbons as a top layer and a small percentage of an aqueous phase at the bottom.

The properties of the oxidized product, the resultant boiler fuel following partial deoxygenation and the hydrocarbon mixture produced by full deoxygenation are given in Table P36. The HHV of the boiler fuel at 35.40 MJ/kg was more than double the 15.40 MJ/kg value of the oxidized product. Boiler fuel oxygen content was dramatically reduced from 58.96 to 14.0. Acid value was reduced from 161.0 to 51.6 and pH was increased from 2.87 to 4.24. Water content of the boiler fuels was only 2.7 vol% compared to that of the oxidized product at 33.75 vol%. Density was reduced to 1.04 for boiler fuel compared to 1.14 for the oxidized product. Viscosity increased greatly from 6.63 to 28.25 cSt.

As a control, partial deoxygenation of raw bio-oil was also performed several times at the same 1st-stage partial deoxygenation reaction conditions but the reaction was hindered due to coke formation. The partial deoxygenation of raw bio-oil was not able to be performed with pressurized syngas. It appears that the bio-oil oxidation step is required to produce a product that can be partially deoxygenated with syngas.

The properties of the hydrocarbon mixture were greatly improved above those of the boiler fuel. HHV of hydrocarbon mixture was increased to 45.30 from the boiler fuel HHV of 35.40 MJ/kg, an increase by 27.97%. Oxygen content was reduced from 14 wt% to zero and acid value was also decreased to zero from 51.6 mg KOH/g; pH was on the basic side at 9.5. Water content was decreased from 2.7 vol% to 0.08 vol%, a decrease by 97.0%. Density was considerably lowered from 1.04 to 0.88 g/ml; viscosity was reduced significantly from 28.25 cSt to 2.38 cSt, a decrease of 91.57%.

Table P36*. Comparison of oxidized product, boiler fuel and hydrocarbon mixture physical and chemical properties.*

Properties	Oxidized product	Boiler fuel	Hydrocarbon mixture
HHV, MJ/kg	15.40	35.40	45.30
Oxygen, wt%	58.96	14.0	0
Total acid value, mg KOH/g	161.0	51.6	0
pH	2.87	4.24	9.5
Water content, vol%	33.75	2.7	0.08
Density, g/ml	1.14	1.04	0.88
Kinematic viscosity, 40°C, cSt	6.63	28.25	2.38

Figure P31 shows the elemental composition weight percentages of the oxidized product, boiler fuel and hydrocarbon mixture. The carbon content of the boiler fuel of 76.4 wt% increased from that of the oxidized product at 33.10 wt%. Carbon content of the hydrocarbon mixture was 87.06. The oxygen content of the oxidized product decreased from 58.96 wt% to 14.0 wt% for boiler fuel to zero for the hydrocarbon mixture. Nitrogen content was not altered by CDO.

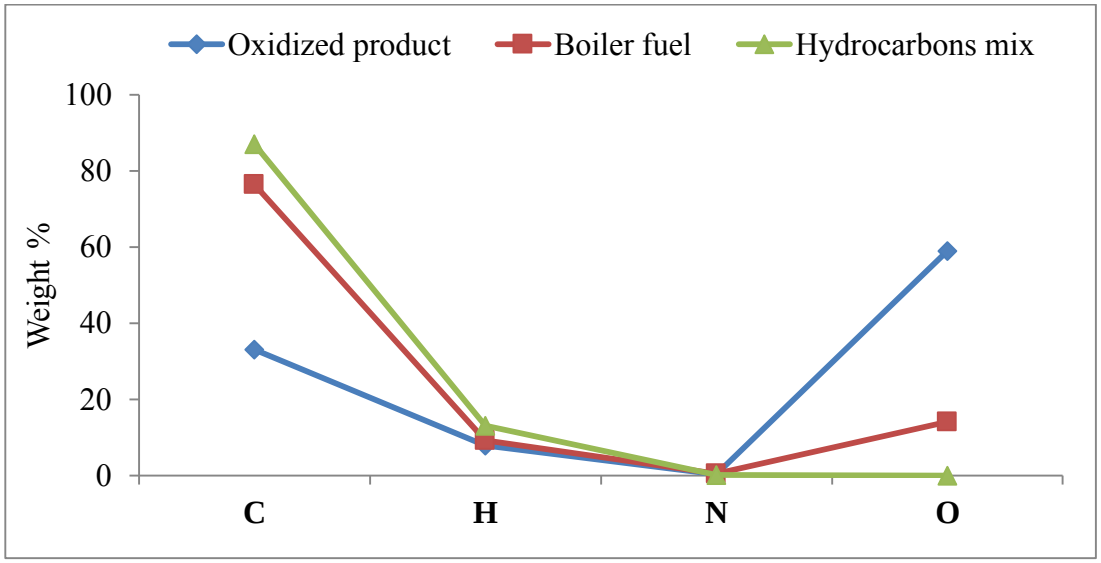


***Figure P31**. Oxidized product, boiler fuel and hydrocarbon mixture elemental analysis comparison.*

A DHA was performed by ASTM D6730-01. This test is often referred to the as PIANO method (paraffins, iso-paraffins, aromatics, naphthenes and olefins) to classify the hydrocarbons present in the hydrocarbon mixture. The results of the DHA are given in Figure P32. These results show that the hydrocarbon mixture contained n-paraffins of 6.84 mass%, iso-paraffins of 17.51 mass%, olefins of 26.90 mass%, naphthenes of 13.78 mass%, aromatics of 7.21 mass%, total C14+ of 15.02 mass% and unknown compounds of 10.04 mass%. This DHA analysis also calculated the liquid hydrocarbon mixture octane number of 61.8.

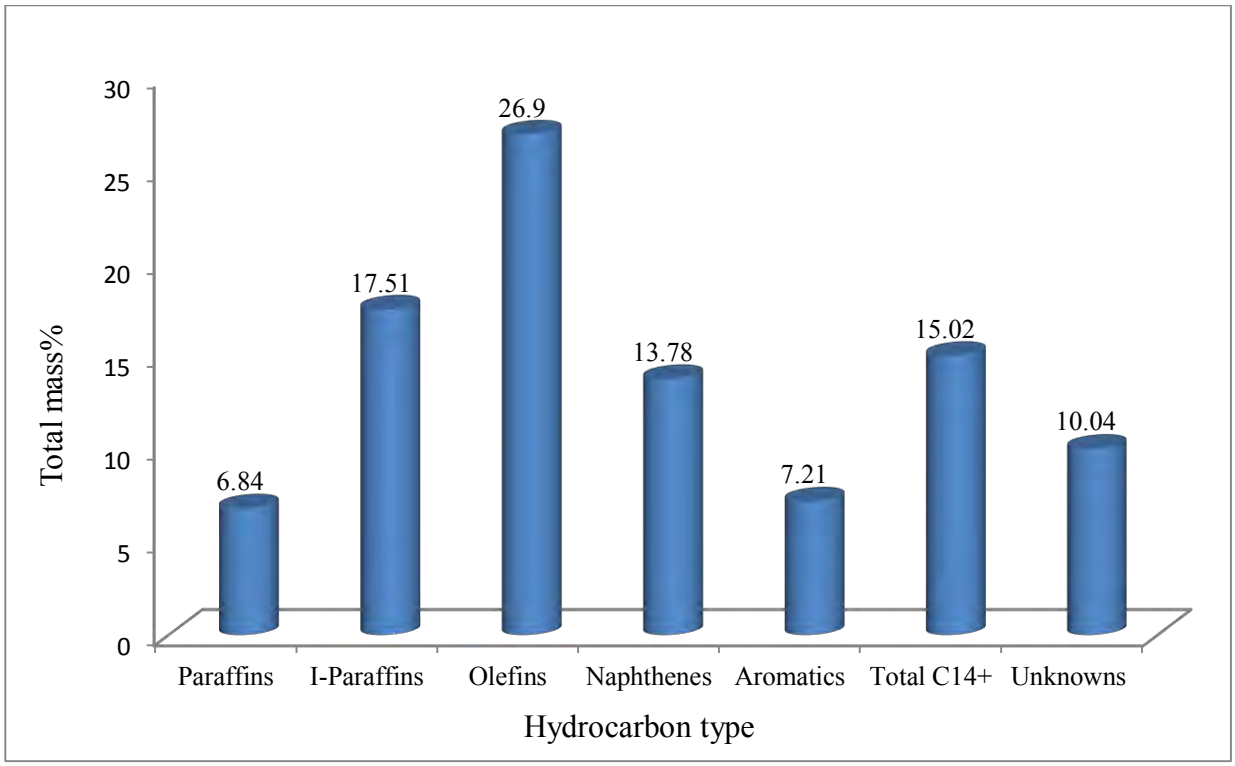


Figure P32. *Hydrocarbon types and their mass percentages present in liquid hydrocarbon mixture results analyzed by DHA ASTM D6730-01.*

Simulated distillation of the hydrocarbon mixture was performed by ASTM D2887 for boiling range distribution of petroleum fractions by gas chromatography. Simulated distillation of the hydrocarbon mixture results are shown in Figure P33 as the petroleum fuel equivalent based on vaporization temperature. These boiling temperatures are given below the named petroleum equivalents. These petroleum equivalents were of the molecular weights of gasoline (45%), jet fuel (20%) and diesel (30%). Not shown in Figure P33 is the 5% of heavy fuel produced at temperatures above 350 ^{o}C.

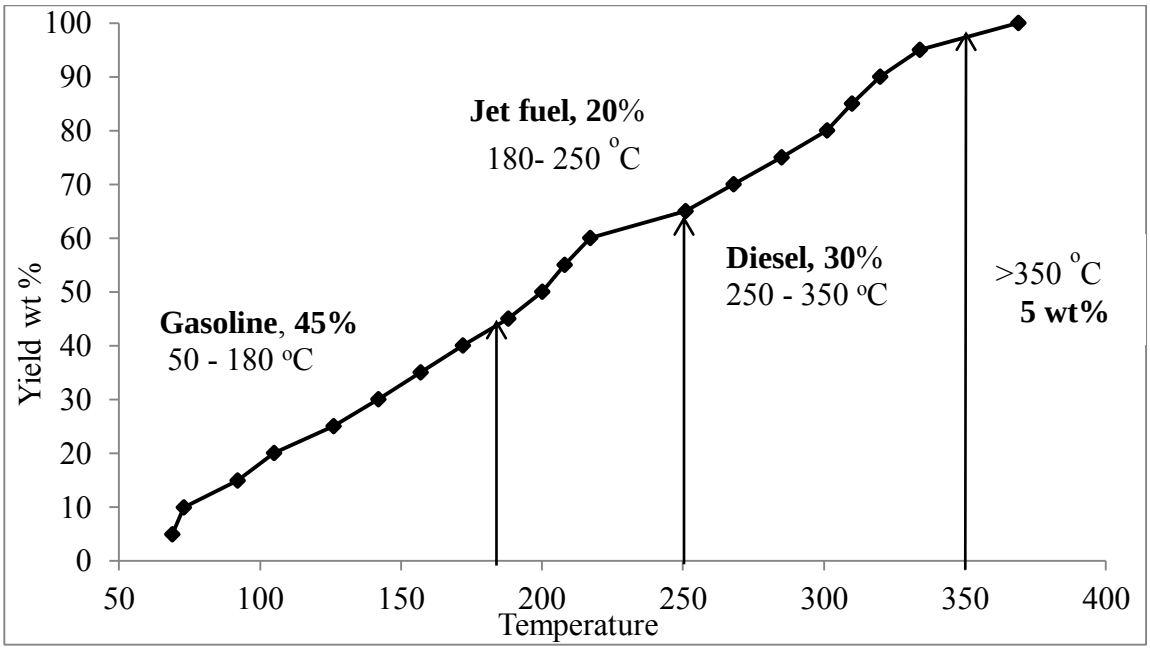


***Figure P33**. Gasoline, jet fuel and diesel fuels weight percentages present in hydrocarbon mixture results from simulated distillation analysis by the ASTM D2887.*

Figure P34 shows the comparison of oxidized product, boiler fuel and hydrocarbon mixture FTIR spectra. These spectra identified the functional groups present in the product types. Characteristic vibrational modes were observed at 3200-3600 cm^{-1} (OH stretch), 2800-3100 cm^{-1} (CH aliphatic stretch), 1600-1750 cm^{-1} (C=O stretch), 1350-1470 cm^{-1} (CH bending) and 1000-1250 cm^{-1} (C-O stretch). The OH (carboxylic acids) stretching was decreased and CH (alkanes) aliphatic stretch and CH bending stretch absorption bands were significantly increased from oxidized product to boiler fuel and for the hydrocarbon mixture. The decrease in both OH and C=O stretch absorption bands and increase in CH aliphatic stretch absorption band indicate that the carboxylic acids and other oxygenated chemical compounds were converted into hydrocarbons. The findings of the FTIR spectra are in good agreement with the physical and chemical properties described in Table P36 and DHA results in Figure P32.

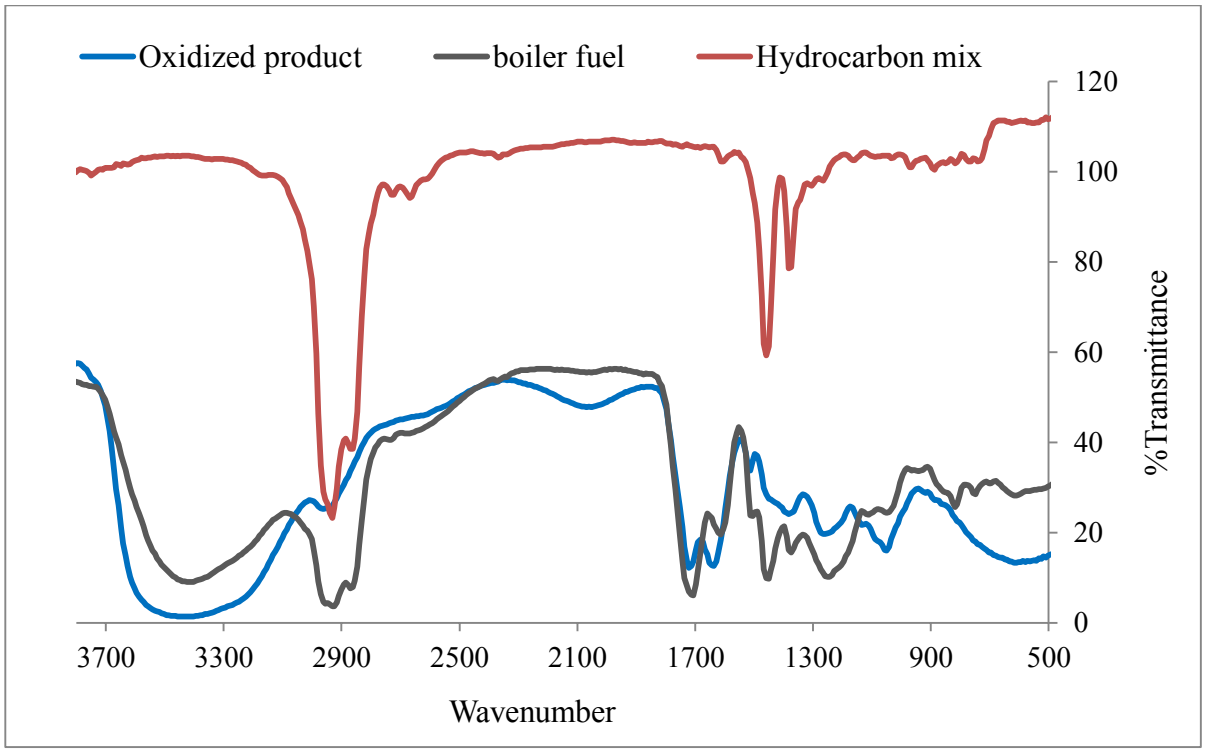


***Figure P34**. FTIR spectra comparing oxidized product, boiler fuel and hydrocarbon mixture.*

Table P37 shows the micro GC analysis of the input pressurized syngas applied for partial deoxygenation and exit gas compositions resulting from the partial deoxygenation reactions of both input syngas and hydrogen. As shown in Table P37, input syngas was comprised of 18.0% of H_2, 22.0% of CO and 11% of CO_2; exit gas from the syngas partial deoxygenation reaction was comprised of 1.1% of H_2, 5% of CO and 38.8% of CO_2. The exit gas produced from the syngas partial deoxygenation reaction indicates consumption of 17 percentage points of CO; in addition, the reaction resulted in the production of an additional 28.8 percentage points of CO_2. This high consumption of CO and the high production of CO_2 during the syngas partial deoxygenation step indicate that the Scheme 2 WGS reaction occurred between the CO present in the syngas and H_2O present in the bio-oil to produce hydrogen and CO_2 as a byproduct.

***Table P37**. Partial deoxygenation reaction In-gas and Exit-gas components analysis by micro GC analyzer.*

Sample Name	H_2%	CO%	CO_2%
Syngas [In gas]	18.0	22.0	11.0
Syngas partial deoxygenation [Exit gas]	1.1	5.0	38.8
Hydrogen [In gas]	100	0.0	0.0
Hydrogen partial deoxygenation [Exit gas]	51.0	0.6	15.9

Pure hydrogen was also applied to perform the partial deoxygenation of the oxidized product as a comparative control of exit gas composition. As shown in Table P37 the exit gas from the hydrogen partial deoxygenation reaction was comprised of 51.0% of H_2, 0.6% of CO and 15.9% of CO_2. This result indicated that 49% of the input 100% hydrogen was required (leaving 51% in

the exit gas) to perform the partial deoxygenation under the conditions applied. The release of the small respective percentages of 0.6% CO and 15.9% CO_2 would be expected during the pure hydrogen partial deoxygenation reaction.

A remaining question is whether the H_2 contained in the input syngas combined with the H_2 produced by the WGS reaction performed satisfactory deoxygenation of the oxidized bio-oil. Table P38 repeats the description of the syngas partial deoxygenated product given in Table P36 above to allow a comparison to the study results of pure hydrogen partial deoxygenated product performed on oxidized bio-oil. A comparison of these Table P38 results shows that there was very little difference between the partially deoxygenated product produced by pure hydrogen and syngas partial deoxygenation product. HHV, acid value, pH, water content, density and viscosity have nearly equivalent values with the greatest difference in the oxygen content values. The oxygen value difference showed a lower oxygen content value (14.00 wt%) for the syngas partial deoxygenation product compared to the pure hydrogen partial deoxygenated product (15.10 wt%), a 7.2% decrease. Therefore, it can be concluded that the syngas partially deoxygenated and hydrogen partially deoxygenated products are nearly identical. This indicates that the H_2 contained in the raw syngas combined with that added by the WGS reaction provided sufficient H_2 to drive the partial deoxygenation reaction to the same degree as for pure hydrogen when performed on identical samples of oxidized bio-oil.

Table P38. *Comparison of some physical and chemical properties of boiler fuels produced from both syngas and hydrogen partial deoxygenation reactions*.

Properties	Boiler fuel [Syngas]	Boiler fuel [Hydrogen]
HHV, MJ/kg	35.40	34.50
Oxygen, wt%	14.00	15.10
Total acid value, mg KOH/g	51.60	48.60
pH	4.24	4.20
Water content, vol%	2.70	2.70
Density, g/ml	1.04	1.00
Kinematic viscosity, 40°C, cSt	28.25	28.00

The pretreatment of raw bio-oil followed by a partial deoxygenation in the presence of pressurized syngas and full deoxygenation with pure hydrogen successfully produced liquid hydrocarbons of transportation fuel quality. Upgrading with syngas appears to provide sufficient hydrogen required for CDO of oxidized bio-oil reactions. Simultaneously, the CDO large reduction in water content in the partially deoxygenated product that is produced by the WGS should render the final hydrogen deoxygenation step more efficient in hydrogen utilization. The liquid hydrocarbons produced from CDO had an HHV of 45.30 MJ/kg. The oxygen content of raw bio-oil was decreased from 53.58 wt% to 0.0 wt% of the syngas CDO hydrocarbon mixture. Acid value and water content were nearly zero. pH was on the basic side at 9.5. Density and viscosity were considerably lowered at 0.88 g/ml and 2.38 cSt, respectively. The energy density of hydrocarbons produced by this method was increased by approximately 182% from raw bio-oil. Our results indicated that the syngas partially deoxygenated and hydrogen partially deoxygenated products were nearly identical. DHA, ^{1}H-NMR, FTIR and simulated distillation analysis resulted that the

liquid hydrocarbon mixture produced by this study (CDO) were comprised of petroleum equivalent molecular weights of gasoline (45%), jet fuel (20%) and diesel (30%).

Raw bio-oil cannot be combusted as transportation fuel directly because of its high acidity, high water content, lower heating value and variable viscosity over time. These negative bio-oil properties are due to the presence of high proportion of oxygenated compounds. Moreover, the reactive oxygenates are also thermally unstable and decompose to carbon residue on the catalyst when heated to reaction temperature. Therefore, bio-oil should be chemically converted to a more stable liquid product before subjecting it to hydrodeoxygenation conditions, and to minimize the formation of thermal coke in the fixed-bed reactor. This modified bio-oil is upgraded to hydrocarbons in a continuous packed bed reactor.

Various techniques have been adopted by researchers for upgrading bio-oil. It has been observed in studies that hydroprocessing in a continuous packed bed reactor is an easy and simple approach with better results than for batch processing. It has become customary to practice the hydroprocessing of bio-oil by utilizing a 2-stage approach in which the 1st-stage comprises a hydrotreating stage utilizing a mild temperature (<300 ^{o}C) for the reaction. This 1st-stage eliminates the polymerization of bio-oil that occurs when raw bio-oil is subjected to high temperatures. Hydrocracking the hydrotreated product is then practiced in a 2nd-stage reaction at higher temperature (>350 ^{o}C). The 2-stage hydroprocessing method usually required 2 reactors which increases the capital cost of the hydroprocessing technology; more reaction time is also required increasing variable costs. It was the objective of this study to test a pretreatment that allows application of single-stage hydroprocessing, without bio-oil polymerization, to produce 100% mixed hydrocarbons.

Hydrodeoxygenation is one of the upgrading methods reported to produce a highly de-oxygenated (as low as zero wt% oxygen in the upgraded product), high energy liquid fuel. Previous hydrodeoxygenation studies over nearly three decades have provided considerable information about methods to upgrade bio-oil by this technology. However, rapid catalyst deactivation (by coking), reactor plugging, and low product yields continue to be problematic and further research is required to refine current hydrodeoxygenation methods and catalysts. Our studies employed an oxidatively pre-treated bio-oil (PTBO) processed by the HDO method to upgrade bio-oil to mixed liquid hydrocarbons. The results showed that PTBO is a better feedstock, compared to raw bio-oil, in terms of producing higher yields of liquid hydrocarbons and in prolonging catalyst life.

PTBO was used as a feedstock for the hydrotreatment process. Raw bio-oil was produced from an augur pyrolysis reactor operated at a temperature between 400-550 ^{o}C. The pretreatment (oxidation) of raw bio-oil was performed at ambient temperature and pressure in a Parr autoclave (450 ml) equipped with an electronic stirrer. Bio-oil oxidation was performed by the addition of 3 wt% oxone and 10 wt% H_2O_2 and the mixture was stirred for 90 min at room temperature. Following this step, 25 wt% butyric anhydride was added and the reaction mixture was stirred for 90 min at 90 ^{o}C to obtain the final experimental PTBO.

CoMo/γ-Al_2O_3 and Ru/γ-Al_2O_3 were purchased commercially from Alfa Aesar and Acros Organics, respectively. Catalyst supports such as Si-Al, γ-alumina and the required inorganic metal salts for preparation of Ni/Si-Al and FeW/Si-Al catalysts were also commercially purchased. The Ni/Si-Al and FeW/Si-Al catalysts were prepared using the wet-impregnation method, where by the metal salts were impregnated on catalyst supports and then dried at 120 ^{o}C for 12 hours before calcining them at 550 ^{o}C for 4 hours. The calcined metal dispersed catalysts were then reduced at 700 ^{o}C using hydrogen flow (100 mLpm) for 4 hours.

Continuous packed bed reactor

The continuous packed bed reactor (Figure P35) consisted of a 1" I.D tubular reactor enclosed in a three-zone furnace (three 6" zones independently controlled by 3 temperature controllers) followed by a condensation system. The temperatures inside the reactor were monitored with a point profile thermocouple with ten sensing points (Omega Instruments). The catalyst bed temperature was maintained at a desired set point through the course of the experiment. The bio-oil was fed using a high-pressure dual-pump system (Teledyne Isco 500D) and the hydrogen flow was controlled by a mass flow controller (MFC; Brooks Instruments). The reactor pressure was controlled using a back-pressure regulator.

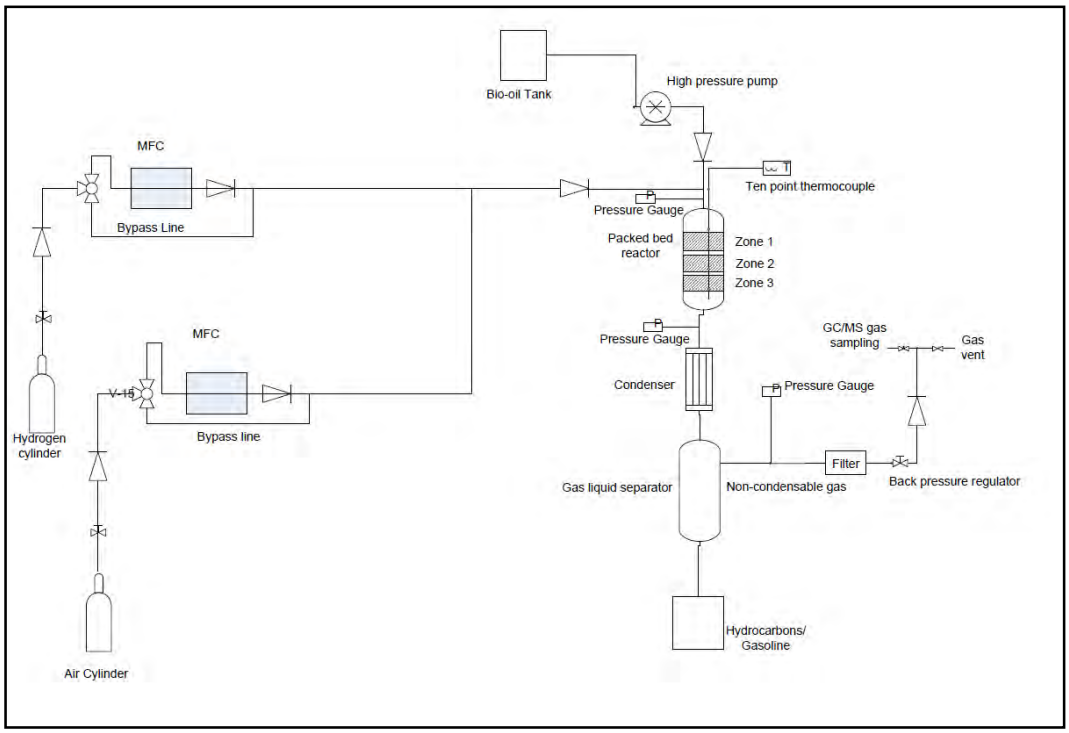


***Figure P35**. Schematic of the continuous packed bed reactor.*

The reactor was loaded with catalyst and set to the reaction temperature of 250 °C which was attained as rapidly as possible (15 minutes approximate waiting time). Following attaining 250 °C the reactor temperature was immediately set to 350 °C. Over the course of the reaction the temperature fluctuated between 300 to 375 °C due to adiabatic conditions due to the catalytic reaction. The reactor was then pressurized to the desired hydrogen reaction pressure using a by-pass valve. Once the system reached the desired pressure of 1500 psi, hydrogen was supplied to the reactor through a mass flow controller set at a desired flow rate to maintain a LHSV of 0.2 to 0.3 h^{-1}. The exit gas flow rate was monitored using an Agilent flow meter. Products exiting from the packed bed reactor were cooled in the condenser and the liquid products were collected in a sampling bottle at regular intervals while gas sampling was performed using Tedlar sampling bags.

The liquid products produced from the HDO treatments were analyzed for acid value (AV), water content (H_2O%), higher heating value (HHV), elemental analysis and GC-MS analysis. AV was obtained by dissolving one gram of bio-oil in an isopropanol/water mixture and titrating to a pH of 8.5 with 0.1 N KOH by ASTM D 664. Percent water was determined by ASTM Method E 203 by a Cole-Parmer Model C-25800-10 titration apparatus. The HHV was determined with Parr 6400

automatic isoperibol calorimeter by ASTM D 240. Elemental analyses of raw bio-oil were performed with an EA920 elemental analyzer by ASTM D 5291.

Our study focused on testing the effect of various catalyst compositions on the quality of the liquid product by one-stage HDO of PTBO. The catalysts employed for this study included FeW/Si-Al, sulphided CoMo/γ-Al_2O_3, iron oxide-chromium oxide (Fe-Cr) catalyst, and 1:2 ratio of Ru/γ-Al_2O_3:Ni/Si-Al. The collected liquid products were centrifuged for 1 hour to separate the aqueous and hydrocarbon fractions. The hydrocarbon fractions of the liquid products were subjected to characterizations such as elemental analysis, HHV, AV, and H_2O% analysis to determine quality, based on which the catalyst performance was interpreted. The reduction in AV, increase in HHV accompanied by decreased elemental oxygen in the hydrocarbon fraction of the product indicates reduction of bio-oil oxygen.

***Table P39**. Hydrotreating catalysts, experimental conditions applied and properties (AV, HHV, H_2O%) of the hydrocarbon fraction of the liquid products.*

Catalyst	Temperature (°C)	P (Psig)	LHSV (h^{-1})	AV	HHV	H_2O %	Yield g/g of feed
Control- Pretreated bio-oil (PTBO)					19.0	21.0	
FeW/Si-Al	300-375	1500	0.2-0.3	51.9	33.0	7.6	0.34
Sulphided CoMo/ γ-Al_2O_3				2.1	43.1	0.2	0.34
Fe-Cr mixed oxide				24.8	35.4	4.9	0.44
1:2 ratio of Ru/γ-Al2O3 & Ni/Si-Al				16.5	41.6	0.3	0.47

***Table P40**. The elemental analysis of the hydrocarbon fraction produced by catalyst type.*

Catalyst	%C	$\%H_2$	$\%N_2$	$\%O_2$ (100 -%C+$\%H_2$ +$\%N_2$)
PTBO	43.1	8.9	0.2	47.8
FeW/Si-Al	81.7	10.0	0.4	7.9
Sulphided CoMo/ γ- Al2O3	86.3	13.4	0.4	0.1
Fe-Cr mixed oxide	69.1	11.2	0.2	19.5
1:2 ratio of Ru/ γ-Al_2O_3 and B: Ni/ Si-Al	85.5	13.8	0.1	0.6

Results were compared between the control sample (PTBO) and the hydrocarbon liquid fractions from catalytic hydroprocessing experiments using catalysts FeW/Si-Al, sulfided CoMo/γ-Al_2O_3, Fe-Cr mixed oxide catalyst, and 1:2 ratio of Ru/γ-Al_2O_3, Ni/Si-Al. Applying these catalysts to the PTBO hydroprocessing produced respective AV's of 51.9, 2.1, 24.8 and 16.5 mg KOH/g. Relative yields were 0.34, 0.34, 0.44 and 0.47 g/g feed. As is evident from Table P39, all the catalysts significantly decreased the AV, with sulphided CoMo/ γ-Al_2O_3 being the most effective catalyst. HHVs produced by these catalysts were 33.0, 43.1, 35.4 and 41.6 MJ/kg, respectively. Elemental oxygen (Table P40) in the liquid products obtained using the above mentioned catalysts were 7.9%, 0.06%, 19.5%, and 0.6 %, respectively. The best results were obtained using the sulphided CoMo/ γ- Al_2O_3 catalyst with an AV of 2.14, HHV of 43.1, H_2O of 0.2% and oxygen of 0.06%. Yield was lower at 0.34 g/g feed than for Fe-Cr mixed oxide and 1:2 ratio of Ru/ γ-Al_2O_3 and B: Ni/ Si-Al but qualities of the hydrocarbons were much superior.

Figure P36 shows the effect of hydrotreating catalysts in increasing the HHV of the hydrocarbon fractions. All hydrocarbon fractions demonstrated increased HHVs compared to the PTBO. While sulphided CoMo/ γ-Al_2O_3 was the most effective catalyst in improving the HHV of the hydrocarbon fraction (~43 MJ/Kg), 1:2 ratio of Ru/γ-Al_2O_3, Ni/Si-Al was also effective in increasing the HHV (~42). From Figure P36, it can be determined that the increase in HHV of the hydrocarbon fractions was largely a function of the decrease in the water content and AVs.

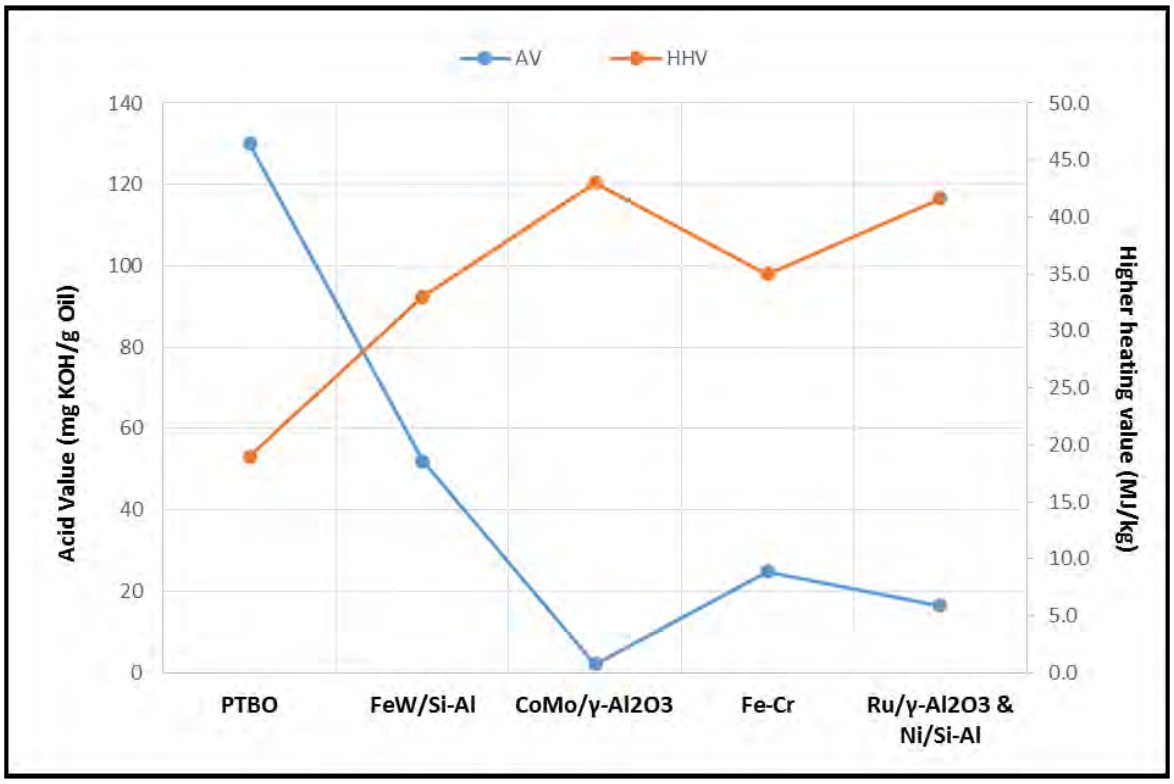


Figure P36. *Effect of catalysts on AV and HHV of the liquid products.*

Table P41 gives the detailed hydrocarbon analysis (DHA) of three replicates of mixed liquid hydrocarbons obtained with sulphided CoMo/γ-Al_2O_3 as a hydroprocessing catalyst. The olefins, iso-paraffins, and C14+ compounds dominated the mixed liquid hydrocarbons followed by naphthenes and aromatics. The octane value of each replicate exceeded 50.

Table P41. *DHA mass percentage of sulphided CoMo/γ-Al_2O_3 upgraded oil fractions.*

	Sulphided CoMo/γ-Al_2O_3		
Group Type	Replication 1	Replication 2	Replication 3
Paraffins	2.6	3.2	3.13
I-Paraffins	19.1	16.3	19.17
Olefins	16	18.02	18.5
Naphthenes	17.7	16.6	8.25
Aromatics	8.4	7.4	8.1

Total C14+	10.9	11.6	16.5
Unknowns	25.3	26.8	24.64
Octane #	54	52	51

Table P42 shows the analysis of gas samples collected during the hydroprocessing experiments. Gas samples were collected 10-15 minutes prior to collecting the liquid samples. Gas analysis was used to interpret the H_2 percentage in the exit gas as well as the formation of low molecular weight hydrocarbon gases such as CH_4, C_2H_6, etc. As seen in Table P41, exit gases from the sulphided CoMo/γ-Al_2O_3 experiment contained the lowest hydrogen percentage, indicating that more hydrogen was consumed for hydroprocessing PTBO. This observation is in agreement with the elemental analysis results that showed the presence of 13.4% hydrogen in the suphided CoMo/γ-Al_2O_3 upgraded hydrocarbon fraction compared to 10.6% and 11.2 % hydrogen present in the FeW/ Si-Al and Fe-Cr mixed oxide upgraded hydrocarbon fractions. The exit gases from the experiment using Ru/γ-Al_2O_3 + Ni/Si-Al catalyst combination had 74% hydrogen which had the next best performance to the sulphided CoMo/ γ-Al_2O_3 gas samples.

***Table P42**. Gas analysis results from hydroprocessing experiments by catalyst type.*

Catalyst	H_2%	O_2%	N_2%	CH_4%	CO%	CO_2%	C_2H_6%
FeW/Si-Al	79.21	0.41	1.36	0.06	0.44	1.01	0.02
Sulphided CoMo/γ-Al_2O_3	69.79	0.25	0.72	5.73	0.16	1.66	0.93
Fe-Cr	81.74	0.48	1.5	0.25	0	1.84	0.06
Ru/ γ-Al_2O_3 + Ni/Si-Al	74.38	0.15	0.38	7.23	0	0.36	0.29

Figure P37 gives the FTIR spectral overlay of PTBO and sulphided CoMo/γ-Al_2O_3 upgraded liquid fuel showing a very broad band in the region of 2500-3300 cm^{-1}in the PTBO spectra for the carboxylic acid O–H stretch. Also, for the PTBO, an intense band ranging from 1760-1690 cm^{-1} representing carbonyl stretch C=O of a carboxylic acid was observed. Whereas, for the upgraded liquid fuel, the absence of peaks representing carboxylic acid groups as well as the evidence of aromatic C-H stretch as a strong peak at 3000-3100 cm^{-1} and a C–C stretch (in-ring) ranging from 1500-1400 cm^{-1} indicated a significant decrease in elemental oxygen and acid (no carboxylic acid O–H stretch).

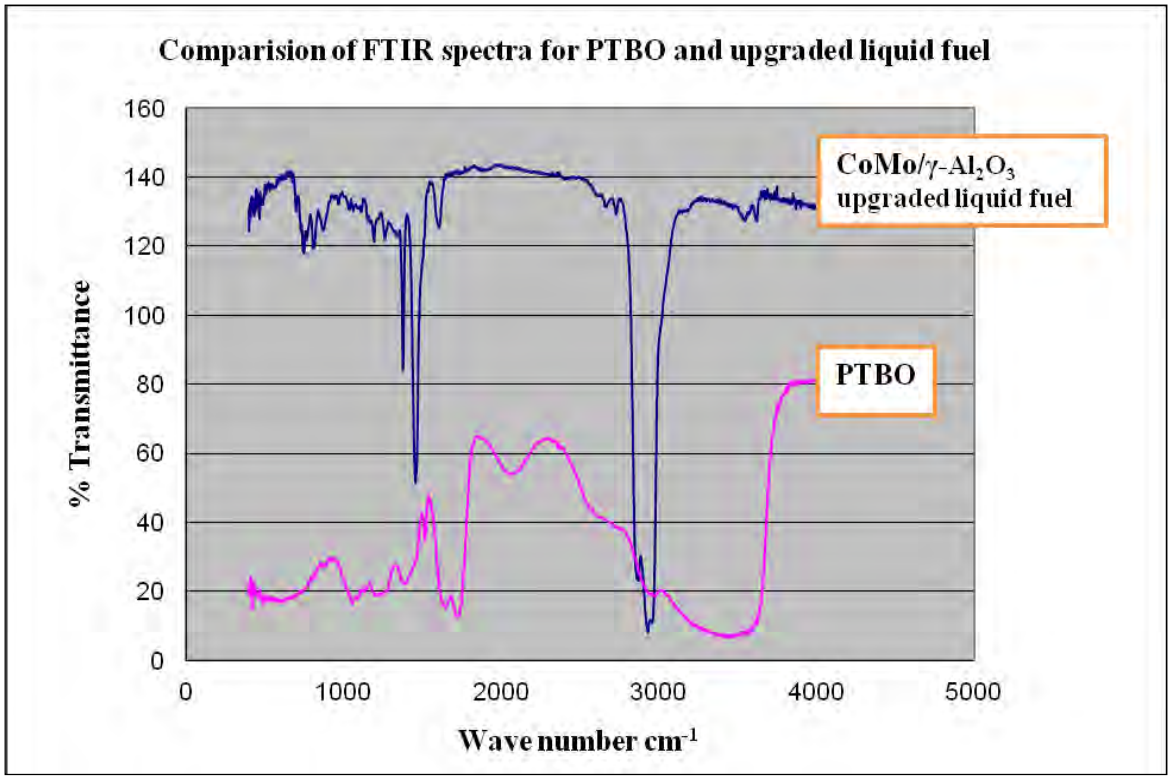


Figure P37. *Comparision between the FTIR spectras of the PTBO and the sulphided CoMo/γ-Al_2O_3 upgraded liquid fuel.*

Simulated distillation was perfomed on the sulphided CoMo/γ-Al_2O_3 upgraded liquid fuel and the plot is shown in Figure P38. The Initial Boiling Point (IBP) of the fuel, which is the temperature detected as the first drop of condensate falls into the distillate receiver, was observed to be 69 ºC; at this temperature 15% of the fuel was distilled. The Final Boiling Point (FBP) was the maximum temperature recorded during the test, shown to be 304 ºC; at this temperature 99.5% of the sample was distilled. This indicates that almost no residue was left in the distillation flask (had there been any residue left, the dry point, instead of FBP, would be recorded). From the simulated distillation results, it can be reported that the obtained liquid fuel had a boiling temperature range of 69 to 304 ºC. Using distillation temperatures for petroleum gasoline, jet fuel and diesel the molecular weight hydrocarbons were petroleum equivalents of 50% gasoline (38 - 170 ºC), 30% jet fuel (170-250 ºC) and 20% diesel (250-350 ºC) range hydrocarbons.

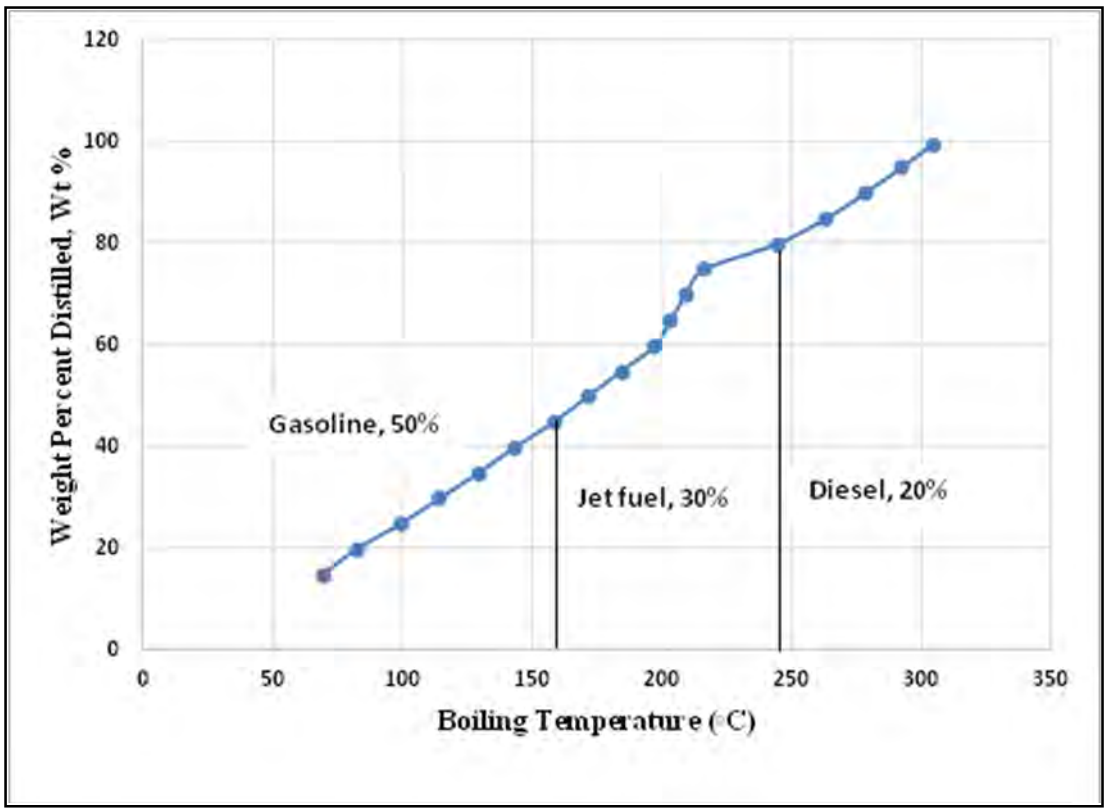


***Figure P38**. wt% distilled vs boiling temperature T_b (°C) of the sulphided CoMo/γ-Al_2O_3 upgraded liquid fuel determined by simulated distillation GC.*

To study the lifetime of the catalyst (deactivation), the hydroprocessing experiments were performed in a temperature range of 375-400 °C, pressure 1500 psig, hydrogen flow rate of 1000 ml/min and liquid hourly space velocity of 0.3 h^{-1} in the presence of sulfided CoMo/γ-Al2O3 catalyst. Three different types of feedstocks such as raw bio-oil (RBO (0)), pretreated oil without butyric anhydride treatment (PTBO (1)) and pretreated oil with butyric anhydride treatment (PTBO (2)) were utilized in this study. The results were compared with control samples of RBO (0), PTBO (1) and PTBO (2). The comparison of experimental run times and properties of hydrocarbon mix obtained with RBO, PTBO (1) and PTBO (2) was also made. A detailed description of the reactor, the CoMo/γ-Al_2O_3 sulfiding process, and a description of hydroprocessing and chemical analysis methods were provided in the last quarterly report and will not be repeated here. The properties acid value (AV), higher heating value (HHV), elemental carbon, hydrogen, nitrogen and oxygen (CHNO) and water content (WC) are described in Table P43 and Figure P39. Different run times in Table P43 indicate that the hydroprocessing experiments were performed with varied time periods depending on two factors – pressure drop indication in the reactor and color change indication in the product collected at different time intervals.

***Table P43**. Results (AV, HHV, CHNO, %WC, TL, hydrocarbon fraction and AF) of sulfided CoMo/γ-Al2O3 catalysis at temperature (T) range of 375-400 °C, pressure (P)1500 psig, hydrogen*

flow rate of (HFR)1000 ml/min and liquid hourly space velocity (LHSV) of 0.3 h^{-1} for feedstocks, RBO (0), PTBO (1) and PTBO (2) by hydroprocessing treatments.

T.No	Feedstock	Run-Time (h)	AV (mg of KOH/g)	HHV (MJ/kg)	C %	H %	N %	O %	WC %
0	RBO control	NA	96.8	16.5	37.2	7.7	0.3	54.5	29.8
0	RBO (0)	11	2.9	42	84.9	35.3	0.2	3.1	1.2
1	PTBO 1 control	NA	147.2	16	29.1	8	0.3	62.8	36.9
1	PTBO (1)	12.1 h	0.5	44	84.5	12	0.3	2.8	0.8
2	PTBO 2 control	NA	266.4	17.5	39.8	8	0.3	51.6	23.3
2	PTBO (2)	19.19 h	1.3	43	86.3	12	0.2	1.7	0.05

Table P43 and Figure P39 describe the properties of hydrocarbon fraction obtained by the hydroprocessing of raw bio-oil (RBO (0)), (PTBO (1)) and (PTBO (2)) treatments. The properties of the upgraded products from the above mentioned three treatments were compared with the control samples of RBO control, PTBO control 1 and PTBO control 2.

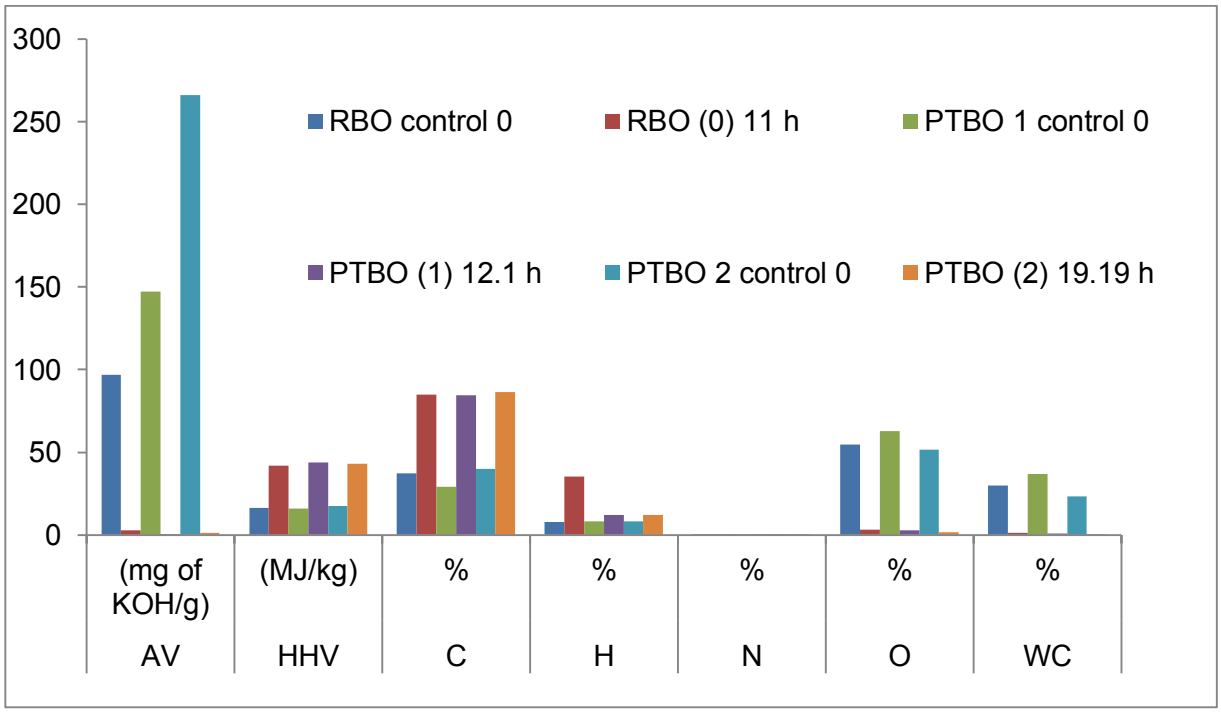


Figure P39. *Results (AV, HHV, CHNO, %WC, TL, hydrocarbon fraction and AF) of sulfided CoMo/γ-Al2O3 catalysis at temperature (T) range of 375-400, pressure (P)1500 psig, hydrogen flow rate of (HFR)1000 ml/min and liquid hourly space velocity (LHSV) of 0.3 h-1 for feedstocks, RBO (0), PTBO (1) and PTBO (2) by hydroprocessing treatments.*

The AV of the treated bio-oil RBO (0) was 2.9 mg KOH/g and the AV was considerably low in comparison to the control RBO AV of 96.8 mg KOH/g. Whereas, the AV of PTBO (1) treatment and PTBO (2) treatment was 0.5 and 1.3 mg KOH/g, respectively, which was less than the AV of the treated RBO (0) treatment (2.9 mg KOH/g) and PTBO 1 control (147.2 mg KOH/g) and PTBO 2 control (266.4 mg KOH/g). Among the above tested treatments the lowest AV of 0.5 mg KOH/g was obtained with PTBO (1) treatment for a run time of 12 h 10 min; the next lowest AV of 1.3 mg

KOH/g was obtained with PTBO (2) treatment for a run time of 19 h 19 min. The HHV of the treated RBO (0) was 42 MJ/Kg, which was more than double the value of the RBO control HHV. The HHV of PTBO (1) and PTBO (2) treatments had an HHV of 44 and 43 MJ/Kg respectively, whereas the PTBO control (1) and PTBO control (2) had an HHV of 16 and 17.5 MJ/Kg, respectively. From the tested treatments the highest HHV was obtained with PTBO (1) treatment followed by PTBO (2) treatment and then RBO (0) treatment for a run time of12 h 10 min, 19 h 19 min and 11 h, respectively.

The CHNO properties of RBO (0) treatment were 84.9, 35.3, 0.2 and 3.1% and the CHNO properties were compared to the control RBO which had the CHNO values of 37.2, 7.7, 0.3 and 54.5%, respectively. The PTBO (1) treatment had a CHNO values of 84.5, 12, 0.3, and 2.8%, respectively compared to the control PTBO (1) which had the CHNO values of 29.1,8, 0.3 and 62.8%, respectively. The control PTBO (2) had the CHNO values of 39.8, 8, 0.3 and 51.6%, whereas, the treated PTBO (2) had the CHNO values of 86.3, 12, 0.2 and 1.7%, respectively. The lowest elemental O value of 1.7% was observed with the PTBO (2) treatment followed by PTBO (1) treatment with O value of 2.8 and then RBO (0) with an O value of 3.1%.

The WC value of the treated RBO (0) is 1.2% compared to the control RBO which had the WC value of 29.8%. Whereas, the WC values of PTBO (1) and (2) treatments were 0.8 and 0.05% and the control PTBO (1) and (2) had the WC value of 36.9 and 23.3, respectively. The hydrocarbon fraction from PTBO (2) treatment had the lowest WC value of 0.05% among the tested treatments; this may be due to the presence of low water content in the feedstock PTBO (2) control.

Among the tested treatments better properties were obtained with PTBO (1) and PTBO (2) in comparison to RBO (0). Based on the run time, highest run time was demonstrated with PTBO (2) with reasonable better properties in terms of O value (Oxygen content) and WC. However, in terms of AV, HHV values are slightly lower than the AV and HHV values of PTBO (1). Still, PTBO (2) was considered a better feedstock than PTBO (1) and RBO (0) with respect to run time and the hydrocarbon fraction yields.

Patents*:*
Steele, P.H., et al. Composition and Method for Improved Fuel Production. 5/1/13.

Publications:
Pittman, C., D. Mohan, A. Eseyin, Q. Li, L.L. Ingram, Jr., E.M. Hassan, B.K. Mitchell, H. Guo, P.H. Steele. 2012. Characterization of bio-oils produced from fast pyrolysis of corn stalks in an auger reactor. Energy and Fuels. 26:3816-3825.

Srinivasan, R., P.H. Steele, Q. Li, F. Yu, B.K. Mitchell. 2012. Effect of acid, steam explosion and size reduction pretreatments on bio-oil production from sweetgum, switchgrass and corn stover. Applied Biochemistry and Biotechnology. 167(2):285-297.

Steele, P.H., D.R. Parish, J.E. Cooper. 2012. Demonstration results from greenhouse heating with liquefied wood. SNA Research Conference Proceedings. 56:421-428.
Abouyousef, H., E.M. Hassan, P.H. Steele. 2013. Rapid conversion of cellulose to 5-hydroxymethylfurfural using single and combined metal chloride catalysts in ionic liquid. Journal of Fuel Chemistry and Technology. 41(2):214-222.

Bhattacharya, P., K. Penmetsa, P.H. Steele, B.K. Mitchell. 2013. Production of bio-energy feedstocks from forest understory vegetation. Journal of Forest Products and Industries. 2(1):47-

57.

Hassan, E.M., H. Abouyousef, P.H. Steele. 2013. Increasing the efficiency of fast pyrolysis process through sugar yield maximization and separation from aqueous fraction bio-oil. Fuel Processing Technology. 110:65-72.

Li, Q., P.H. Steele, B.K. Mitchell, L.L. Ingram, Jr., F. Yu. 2013. The addition of water to extract maximum levoglucosan from the bio-oil produced via fast pyrolysis of pretreated loblolly pinewood. BioResources. 8(2):1868-1880.

Li, Q., P.H. Steele, F. Yu, B.K. Mitchell, E.M. Hassan. 2013. Pyrolytic spray increases levoglucosan production during fast pyrolysis. Journal of Analytical and Applied Pyrolysis. 100:33-40.

Steele, P.H., D.R. Parish, J.E. Cooper. 2013. Demonstration results from greenhouse heating with bio-oil. Technical Note: Forest Products Journal. 62(6):474-479.

Steele, P.H., M. Puettmann, K. Penmetsa, J.E. Cooper. 2013. Life cycle assessment of pyrolysis bio-oil production. Forest Products Journal. 62(4):326-334.
Abou-Yousef, Hussein, El Barbary Hassan. (In press). A novel approach to enhance the activity of H-form zeolite catalyst for production of hydroxymethylfurfural from cellulose. J. Ind. Eng. Chem. (2013), http://dx.doi.org/10.1016/j.jiec.2013.09.016.

Sukhbaatar, B., E.M. Hassan, M.G. Kim, P.H. Steele, L.L. Ingram, Jr. 2013. Optimization of hot-compressed water pretreatment of bagasse and characterization of extracted hemicelluloses. Carbohydrate Polymers. 101:196-202.

Abou-Yousef, H. and E.B. Hassan. 2013. A novel approach to enhance the activity of H-form zeolite catalyst for production of hydroxymethylfurfural from cellulose. J. Ind. Eng. Chem. http://dx.doi.org/10.1016/j.jiec.2013.09.016.

Abou-Yousef, H. and E.B. Hassan. 2014. Efficient utilization of aqueous phase bio-oil to furan derivatives through extraction and sugar conversion in acid-catalyzed biphasic system. Fuel (submitted 4/2014).

Sukhbaatar, B., Q. Li, C. Wan, F. Yu, E.M. Hassan, P.H. Steele. 2014. Inhibitors removal from bio-oil aqueous fraction for increased ethanol production. Biores. Tech. 161:379-384.

Scientific/Professional Papers/Presentations:

Steele, P.H. 2013. Production of multiple fuel types from bio-oil. SEC Symposium. Atlanta, GA. 2/10/2013 - 2/12/2013.

Steele, P.H. 2013. MSU SERC bio-oil research and commercialization. Coastal Plain Branch Experiment Station. Newton, MS. 3/19/2013 - 3/19/2013.

Hassan, E. and Abouyousef, H. Conversion of bio-oil anhydrosugars to furan derivatives using formic acid catalyzed biphasic system. 67th International Convention, Forest Products Society. Austin, TX. June 9-12, 2013.

Tanneru, S.K., P.H. Steele. 2013. Production of hydrocarbons via low hydrogen hydroprocessing of pyrolysis oil. 67th International Convention, Forest Products Society. Austin, TX. June 9-12, 2013.

Parapati, Divya R., Venkata K. Penmetsa, Vamshi K. Guda, Philip H. Steele. 2013. Upgrading of pyrolysis oil by hydroprocessing in a packed bed flow reactor. 246th American Chemical Society National Meeting. Sept. 8-12. Indianapolis, IN.

Parapati, D.R., V.K. Guda, V.K. Penmetsa, P.H. Steele. 2013. Poster. Upgrading of pretreated bio-oil by direct hydrocracking in a continuous packed bed flow reactor. 12th Annual Southern BioProducts and Renewable Energy Conference. Sept. 17-18. Tunica, MS.

Penmetsa, K., P.H. Steele, D. Parapati, V. Guda. 2013. Poster. Single-stage hydroprocessing of pyrolysis oil in a continuous packed bed reactor. TCBiomass2013, International Conference on Thermochemical Conversion Science. Sept. 3-6. Chicago, IL.

Steele, P.H., K. Penmetsa. 2013. Progress in production and upgrading bio-oil at Mississippi State University. International Symposium of Forestry and Ecology, Shandong Provincial Education Dept., Shandong Agricultural University. Aug. 28-31. Taian, China.

Steele, P.H., S.K. Tanneru. 2013. Conversion of bio-oil to hydrocarbons via a low hydrogen route. TCBiomass2013, International Conference on Thermochemical Conversion Science. Sept. 3-6. Chicago, IL.

Steele, P.H. 2013. Progress in production and upgrading of bio-oil at Mississippi State University. Fall 2013 Auburn University School of Forestry and Wildlife Sciences Seminar Series. 10/23/2013 - 10/23/2013. Auburn, AL. Invited.

Steele, P.H., S.K. Tanneru, D. Parapati, Y. Luo, Q. Li, B.K. Mitchell, K. Penmetsa, V. Guda. 2013. Production of hydrocarbons from bio-oil by biomass syngas catalysis. The Role of Natural Renewable Resources in Energy Sustainability and Global Warming Mitigation: A Symposium. Mississippi State University, The Maroon Edition, FWRC. 11/21/2013 - 11/21/2013. Mississippi State, MS. Invited.

Tanneru, S.K., P.H. Steele. 2013. Production of transportation fuels range hydrocarbons from pyrolysis oil via a low hydrogen catalytic deoxygenation. AICHE Annual Conference. 11/3/2013 -11/8/2013. San Francisco, CA. Plenary.

Varadarajan, A., K.B. Walters. 2013. Effects of centrifugal filtration on the physicochemical properties of pyrolysis oil. Podium presentation at AIChE Annual Meeting. 11/3/2013 – 11/8/2013. San Francisco, CA. Plenary.

Luo, Y., P.H. Steele, S.K. Tanneru. 2014. Bio-oil upgraded by sulfided CoMo/γ-Al2O3 catalysts. Graduate Student Research Symposium. 3/22/2014. Mississippi State, MS.

Luo, Y., P.H. Steele, S.K. Tanneru. 2014. Sulfided CoMo/γ-Al_2O_3 catalysts for hydrodeoxydation of bio-oil. Southeastern Natural Resources Graduate Student Symposium. 3/5-7/2014. Mississippi State, MS.

Parapati, D., P.H. Steele. 2014. Comparison of reduced and sulfided CoMo/γ-Al2O3 catalyst on hydroprocessing of pretreated bio-oil in a continuous packed-bed flow reactor. Graduate Student

Research Symposium. 3/22/2014. Mississippi State, MS.

Parapati, D., P.H. Steele. 2014. Upgrading bio-oil at supercritical conditions. Southeastern Natural Resources Graduate Student Symposium. 3/5-7/2014. Mississippi State, MS.

Parapati, D., V. Guda, K. Penmetsa, S.K. Tanneru, P.H. Steele. 2014. Upgrading of pretreated bio-oil by direct hydrocracking in a continuous packed bed reactor. 247th ACS National Meeting & Exposition. 3/16-20/2014. Dallas, TX.

Tanneru, S.K., D. Parapati, P.H. Steele. 2014. Boiler fuel production from fast pyrolysis oil by an oxidation pretreatment to bio-oil followed by esterification. 247th ACS National Meeting & Exposition. 3/16-20/2014. Dallas, TX.

Tanneru, S.K., P.H. Steele. 2014. Catalytic deoxygenation of bio-oil with low hydrogen to produce transportation fuels. Southeastern Natural Resources Graduate Student Symposium. 3/5-7/2014. Mississippi State, MS.

Tanneru, S.K., P.H. Steele. 2014. Production of transportation fuels range liquid hydrocarbons from pretreated bio-oil via catalytic deoxygenation with syngas. Graduate Students Research Symposium. 3/22/2014. Mississippi State, MS.

Varadarajan, A., A.F. Chaparro, K.B. Walters. 2014. Can we use timber residue to produce pyrolysis oil? Effects on the physicochemical properties of pyrolysis oil from the inclusion of bark in the feed stock. Podium presentation at Graduate Student Research Symposium. 3/22/2014. Mississippi State, MS.

Poster Presentations:

Luo, Y., P.H. Steele. 2014. Poster. Bio-oil upgrading to hydrocarbons by the water gas shift reaction with syngas. 247th ACS National Meeting & Exposition. 3/16-20/2014. Mississippi State, MS.

Varadarajan, A., A.F. Chaparro, K.B. Walters. 2014. Can we use timber residue to produce pyrolysis oil? Effects on the physicochemical properties of pyrolysis oil from the inclusion of bark in the feed stock. Poster presentation at Graduate Research poster competition. 3/24-25/2014. Mississippi State, MS.

End confidential information.

Task Q. Biocrude

Principle Investigators and team members:
Rafael Hernandez, University of Louisiana at Lafayette, Department of Chemical Engineering
Sandra Eksioglu, Dept. of Industrial and Systems Engineering
Todd French, Dave C. Swalm School of Chemical Engineering

Executive Summary:
The Biocrude thrust area focuses on the generation of oils by microorganisms conventionally used for treating municipal and industrial wastewaters. Over the last three years, systems have been scientifically developed and engineered to produce microbial oils ready for conversion into biodiesel and/or renewable diesel. Microorganisms collected from wastewater treatment facilities and grown on wastewater have been demonstrated to accumulate significant quantities of acyl glycerides (biocrude) under stress (high carbon:nitrogen ratios). These systems have been developed at a relatively small scale. Many of the proposed research and development activities for SERC IV were conducted in partnership with industry, universities, and government, taking advantage of the unique pilot facilities developed during SERC III.

The biocrude technology was integrated with heterotrophic algae to maximize oil production. Hybrid biocrude-algae-oleaginous consortiums were evaluated to generate oils that can used to produce diesel fuel to potentially operate a demonstration vehicle at MSU. Biocrude thrust area researchers continued research and development activities in the areas of oil separation and catalysis. These activities were conducted in partnership with the selected industries. This strategic research and development partnership generated intellectual property of mutual benefit to MSU and the renewable energy industry. New catalysts were specifically developed for biocrude conversion into fuels of interest to industrial partners. Separation technologies were developed to minimize energy inputs for biocrude and algae related processes.

Subtask Q.1 Develop a novel in-situ process for the depolymerization of lignocellulose

Numerous lignocellulose samples from Mississippi biomass will be depolymerized, and the liquid will be characterized using analytical techniques developed during SERC II and III. Some of the samples/processes may require development of specific analytical methods. Once products are identified, efforts will focus on developing chemical reaction pathways. The solid residue of samples (lignin) will also be depolymerized with supercritical methanol using heterogeneous catalysts. Once the liquid fraction is characterized, efforts will focus on developing chemical and/or biological processes to generate value added chemicals. The liquids generated will be used as a carbon source for producing biocrude.

Planned Activities:
Q.1.ML.1 Produce biocrude from liquefied lignocellulose using supercritical methanol
Q.1.ML.2 Produce the carbon source at a cost consistent with U.S. DOE price targets.

Summary of Activities:
Lignocellulosic Materials Deconstruction and Upgrading Using Supercritical Methanol in the Presence of Base Catalysts

Background of the Study:

The main objective of this study was the evaluation of the catalytic thermal conversion of waste lignocellulosic biomass into mixtures of oxygenated hydrocarbons to be used as substrate for oil accumulation by oleaginous microorganisms.

Study Design:
This study specifically uses samples of hardwood bark chippings and fibrous sludge from pulp and paper wastewater treatment operations as feedstocks (Figure Q1). Two hydrotalcite catalysts were used: Fe(III)-doped Al-Mg hydrotalcite and Cu(III)-doped Al-Mg hydrotalcite. These catalysts were prepared in the laboratory using established procedures. The design of the experiment considers the amount of catalyst, type of catalyst and type of feedstock as the important factors. Each factor-level combination was run in duplicate (Table Q1). The other pertinent factors were set to levels equal to previous studies: $T_{reaction}$ = 250°C, $P_{reaction}$ = 1,200 psi, $t_{reaction}$ = 1 hour, $N_{stirring}$ = 240 rpm, $V_{reaction}$ = 500-mL, V_{MeOH} = 100-mL, $m_{feedstock}$ = 5-g (Coker, et al., 2012).



(a) Hardwood bark chippings



(b) Fibrous sludge from wastewater

***Figure Q1**. Feedstocks: (a) hardwood bark chippings and (b) fibrous sludge*

***Table Q1**. Design of the experiment.*

Ordered Run	Catalyst Amount (g)	Catalyst Type	Feedstock Type
1	0.5	Cu-doped	Sludge
2	0.5	Cu-doped	Sludge
3	0.5	Fe-doped	Bark
4	0.5	Fe-doped	Bark
5	0 (control run)	Cu-doped	Bark
6	0 (control run)	Cu-doped	Bark
7	0 (control run)	Fe-doped	Sludge
8	0 (control run)	Fe-doped	Sludge
9	0.5	Fe-doped	Sludge
10	0.5	Fe-doped	Sludge
11	0.5	Cu-doped	Bark
12	0.5	Cu-doped	Bark

Methodology:

Preparation of the Lignocellulosic Feedstocks

The wet raw feedstocks were dried for 1 day in the oven at 105°C. After oven drying these were ground using laboratory blender and grinder (Figure Q2).



(a) Hardwood bark chippings *(b) Fibrous sludge from wastewater*

***Figure Q2**. Ground feedstocks: (a) hardwood bark chippings and (b) fibrous sludge*

Preparation of the Hydrotalcite Catalysts (HTCs)

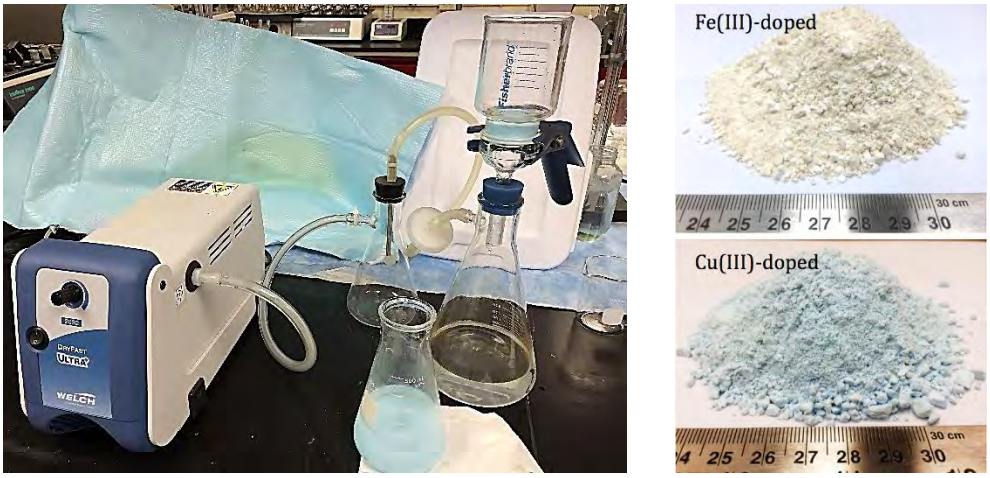
The preparation procedure for the two catalysts was based on earlier studies (Di Cosimo, J. I., et al., 1998; Macala, G., et al., 2008). The reactive production of the catalysts was conducted in a 1-L glass reactor shown below (Figure Q.3a). A 375-mL of 0.14M $Na2CO_3$ was fed and heated to 60°C under vigorous stirring (180 rpm). The temperature and stirring were maintained while adding 250-mL of 1.2M $MgCl_2.6H_2O$ solution and 250-mL of the solution containing 0.32M $AlCl_3$ and 0.08M dopant ($CuCl_3.6H_2O$ for Cu(III) dopant and $FeCl_3.6H_2O$ for Fe(III) dopant). This was accomplished by adding 10-mL aliquots of each solution at a time. The reaction pH 10 was maintained by adding 1M NaOH. Then the suspension obtained was heated at 80°C for 3 days.



(a) Catalysts preparation *(b) The Fe-doped and Cu-doped HTCs suspensions*

***Figure Q3.** Preparation of the Fe(III)-doped and Cu(III)-doped Al-Mg hydrotalcite catalysts: (a) 1-L reactor preparation and (b) catalyst and supernatant mixture.*

The resulting mixture (Figure Q3b) was filtered using a suction filter (Figure Q4a). The filtered cake was washed on the filtration setup using ample amount of deionized H_2O and was dried in the oven at 105°C for 24h. The lump dried catalysts were then ground using mortar and pestle (Figure Q4b). The catalysts were stored in sealed bottles until use.

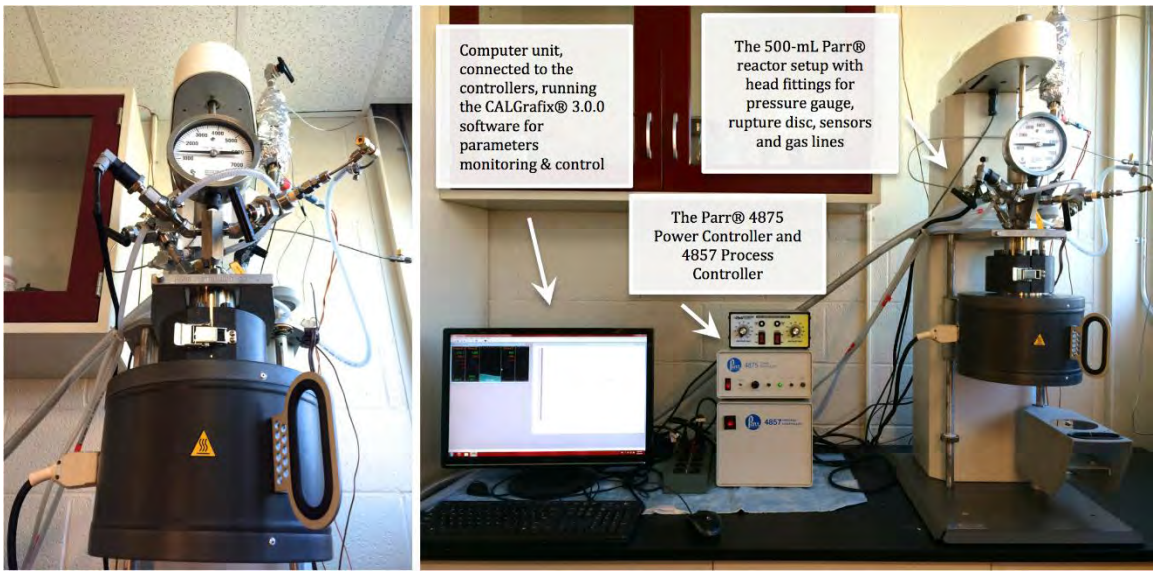


(a) Catalyst suspension filtration *(b) Ground dry catalysts*

***Figure Q4**. Separation and drying of the Fe(III)-doped and Cu(III)-doped Al-Mg hydrotalcite catalysts: (a) catalyst suspension filtration and (b) ground dry catalysts.*

Experimental Runs

The treatment runs (Table Q1) were conducted in a Parr® Reactor Setup with temperature, pressure, and stirring controls (Figure Q5). For each run, the catalyst was calcined in air at 460°C for 1 hour using a furnace and then cooled in a desiccator containing NaOH to protect it from carbon dioxide and moisture adsorption. A 5 grams of the solid feedstock, 100-mL of methanol, and 0.5-g of the freshly calcined catalyst were fed into the 500 mL Parr® batch reactor vessel as the reactor setup was assembled. The vessel was purged with nitrogen and the pressure was set back to around 20 psig. The openings were then closed and the reaction temperature was set at 250°C, and stirring at 500 rpm. The reaction vessel took around 30 minutes to reach the reaction condition 250ºC and 1200 psig. The reaction time was 1 hour. Cooling the reaction vessel with an ice bath quenched the reaction. When the reactor reached room temperature and pressure (around 25º and 20psig), the reaction products were withdrawn by opening the reactor vessel. The reactor contents were transferred to a 250 mL beaker and the inside of reactor vessel was rinsed with methanol. The liquid and solid portions of the reaction products were separated by suction filtration. The solids were kept and weight for mass balancing, and the filtrates were kept in refrigerated tubes for chemical analysis.



(a) The 500-mL Parr® reactor setup (b) Automatic control system for the reactor

***Figure Q5**. The Parr® reactor used in the experimental runs: (a) 500-mL Parr® reactor, and (b) Automatic control system for the reactor*.

Chemical Analysis

The target products of the experiment are the liquid phase mixtures. Gas chromatography mass spectroscopy (GCMS) was used for chemical analysis and the settings of the equipment are summarized in Table Q1-2 below. Since there is no other similar process published in the literature, the quantification of product compounds was difficult, while the identification of possible product compounds is a more probable chemical analysis. To have an idea of the amount of organic compounds, phenol was chosen as a reference chemical for approximate quantification. The identification of possible compounds was based on the NIST (National Institute of Standards and Technology) MS database.

Table Q2*. Settings of the GCMS used for chemical analysis of the liquid products.*

COLUMN	
Type:	Capillary
Model Number:	Restek 13623 RXI5SIL-MS
Max Temperature:	350 ºC
Nominal length:	30.0 m
Nominal diameter:	250.00 um
Nominal film thickness:	0.25 um
Mode:	Constant flow
Initial flow:	1.2 mL/min
Nominal init. pressure	8.47 psi
Average velocity:	39 cm/sec
Inlet:	Back inlet
Outlet:	MSD
Outlet pressure:	vacuum
BACK INLET	
Mode:	Splitless
Initial temp:	300 ºC
Pressure:	8.46 psi
Purge flow:	50.0 mL/min
Purge time:	0.75 min
Total flow:	54.8 mL/min
Gas Type:	Helium
OVEN	
Initial temp:	30 ºC
Initial time:	3.00 min
Ramps:	
	1) Rate=25, Final temp=100, Final time=0
	2) Rate=10, Final temp=300, Final time 4.20
	3) Rate=0 (off)
Post temp:	0 ºC
Run time:	30 min
INJECTOR	
Injection volume:	2.00 uL
Syringe size:	10.0 uL
SCAN PARAMETERS	
Low mass:	40.0
High mass:	500.0

Results:

Qualitative Descriptions

The liquid portions and solid portions of the treatment products are shown in Figure Q6 and Q7. The liquid products are solutions of deep brown color. The solid residues also turned darker without significant physical differences among the bark residues and among the sludge residues in the control and treatment runs.



Figure Q6. *Filtrates from the duplicated treatment runs*.

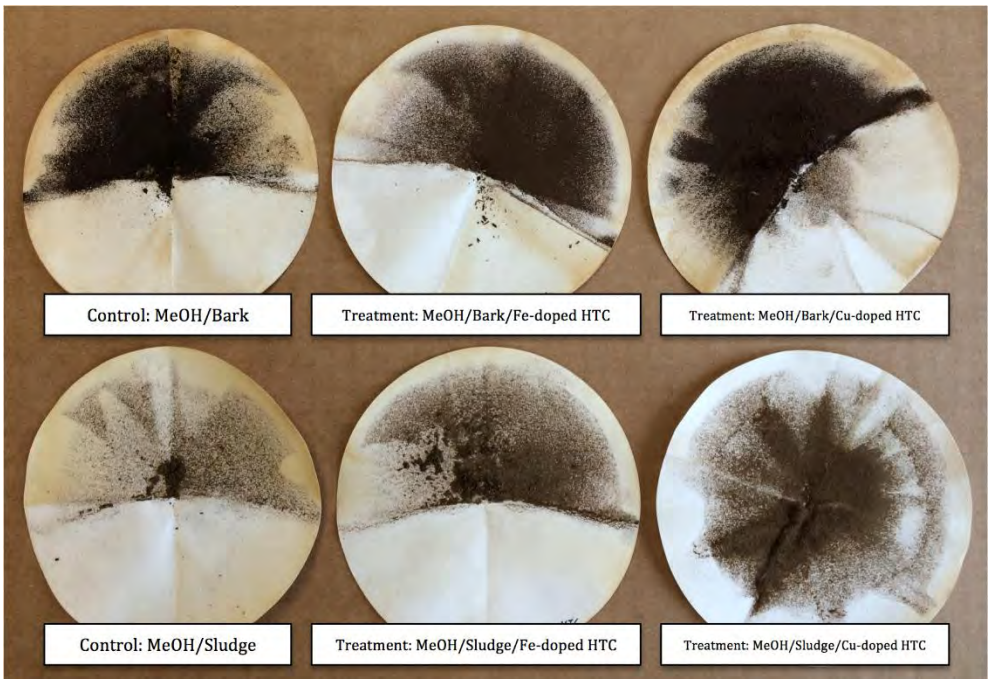


Figure Q7*. Sample solid residues from the treatment runs*.

Some of the liquid portions were stored in sealed and labeled PET bottles for shipment to partner research team at Mississippi State University (Figure Q8). These were shipped a few days after

the completion of the runs. These were kept refrigerated in the shipping package and arrived in good condition at the destination.



***Figure Q8**. Filtrate samples sent to Mississippi State University for fermentation testing.*

Quantitative Results

After evaluating the chromatographs, the possible compounds that correspond to the various peaks were identified using the mass spectroscopy database of NIST. This database allows inspection of the detailed spectra of the possible compounds in addition to the suggested matching compounds automatically generated in the software of the GCMS. The identified possible compounds with peak areas of at least 1% of the total area of the chromatographs for the six treatments were taken and are summarized in Table Q3, Q4, Q5, Q6, Q7, and Q8. The percentages are proportional to the concentration of the compounds.

Overall, the majority of the organics produced are of the following types: methyl ester, alcohols, phenols, ketones, alkanes, and anhydrides. There are few occurrences of ethyl ester and organic acids. A common and high percentage compound in all treatments is propanoic acid, 2-hydroxy-, methyl ester followed by propanoic acid, 2-methyl-, anhydride, and phenol derivatives.

Comparing the feedstocks, the wood bark decomposed to more types of compounds while the sludge decomposed to fewer products. This is most likely due to the fact that the fibrous sludge is mostly cellulose, while the wood bark is a lignocellulose containing cellulose, hemicellulose, and lignin. The percentages of compounds from the wood bark are lower as compared to the percentages of products from the sludge. The sludge depolymerized to a larger extend compared to the bark.

The types of compounds generated with the addition of the two types of HTCs are similar for each feedstock. However, the results presented in Figure Q9 suggest the addition of HTC increases product yield for the sludge. Fe (III)-HTC was more effective depolymerizing sludge compared to the control and Cu (III)-HTC. Depolymerization of wood bark was less dependent on catalyst addition. There was no difference in the gravimetric yield (~20%) of wood bark depolymerization using HTCs doped with Fe (III) or Cu (III). Differences in product yield between the two catalysts (see Figure Q9) may have been caused by the product distribution. Fe (III)-HTC may generate more volatile products from bark, which are loss during solvent evaporation prior to sample analysis, giving the appearance of lower performance compared to Cu (III)-HTC.

***Table Q3**. Tentative identification results for **BARK** deconstructed in supercritical methanol **without catalyst**.*

Retention Time (min)	Possible Compound	CAS No.	Percent of Total Area (%)
4.762	Acetic acid, hydroxy-, methyl ester	96-35-5	4.338
4.863	Propanoic acid, 2-hydroxy-, methyl ester*	2155-30-8	1.181
4.963	Propanoic acid, 2-hydroxy-, methyl ester*	2155-30-8	8.269
5.482	1,2-Butanediol	26171-83-5	3.935
6.928	trans-2-Methyl-4-hexen-3-ol	96346-76-8	3.570
7.129	Butanedioic acid, dimethyl ester	106-65-0	1.537
7.172	2-Cyclopenten-1-one, 2-hydroxy-3-methyl-**	80-71-7	1.480
7.410	2-Cyclopenten-1-one, 2-hydroxy-3-methyl-**	80-71-7	1.524
7.601	Cyclopropanecorboxylic acid, 2-methoxy-, methyl ester, trans-	122775-09-1	1.639
7.728	Phenol, 2-methoxy-	90-05-1	5.661
7.775	Pentane, 2,2,4,4-tetramethyl-3-methoxy-***	Not available	1.197
7.871	Pentane, 2,2,4,4-tetramethyl-3-methoxy-***	Not available	2.559
7.908	Pentane, 2,2,4,4-tetramethyl-3-methoxy-***	Not available	3.549
8.024	2-Cyclopenten-1-one, 3-ethyl-2-hydroxy-	21835-01-8	1.525
8.787	Phenol, 2-methoxy-4-methyl-	93-51-6	1.211
9.300	Butanedioic acid, 2-hydroxy-3-methyl-, dimethyl ester	50460-80-5	1.128
9.745	Phenol, 4-ethyl-2-methoxy-	2785-89-9	2.774
10.370	Phenol, 2,6-dimethoxy-****	91-10-1	1.176
10.645	Phenol, 2,6-dimethoxy-****	91-10-1	5.443
10.767	Phenol, 2-methoxy-4-propyl-	2785-87-7	2.026
11.731	Phenol, 4-methoxy-3-(methoxymethyl)-	59907-65-2	1.194
11.794	Phenol, 2-methoxy-4-(1-propenyl)-	97-54-1	1.701
13.563	2,4-Hexadienedioic acid, 3,4-diethyl-, dimethyl ester, (Z,Z)-	31447-54-8	2.612
14.384	Phenylacetylformic acid, 4-hydroxy-3-methoxy-	1081-71-6	1.201
14.627	Phenol, 2,6-dimethoxy-4-(2-propenyl)-	6627-88-9	1.590
16.751	Hexadecanoic acid, methyl ester	112-39-0	1.400
18.403	10-Octadecenoic acid, methyl ester	13481-95-3	1.366
20.627	1-Phenanthrenecarboxylic acid, 1,2,3,4,4a,9,10,10a-octahydro-1,4a-dimethyl-7-(1-methylethyl)-, methyl ester	1235-74-1	4.332
21.183	Linoleic acid ethyl ester	544-35-4	2.119

*, **, ***, **** - Possible isomers which maybe verified using nuclear magnetic resonance (NMR) or higher resolution GCMS.

***Table Q4**. Tentative identification results for **BARK** deconstructed in supercritical methanol **with Fe(III)-doped hydrotalcite catalyst**.*

Retention Time (min)	Possible Compound	CAS No.	Percent of Total Area (%)
4.482	Acetic acid, hydroxy-, methyl ester*	96-35-5	2.509
4.503	Acetic acid, hydroxy-, methyl ester*	96-35-5	1.957
4.699	Propanoic acid, 2-hydroxy-, methyl ester**	2155-30-8	2.355
4.789	Propanoic acid, 2-hydroxy-, methyl ester**	2155-30-8	17.852
4.815	Acetic acid, methoxy-, methyl ester	6290-49-9	2.357
5.440	1,2-Butanediol***	26171-83-5	2.492
5.493	1,2-Butanediol***	26171-83-5	4.792
6.727	Pentanoic acid, 4-oxo-, methyl ester	624-45-3	1.279
6.907	Propanoic acid, 2-methyl-, anhydride	97-72-3	5.864
7.108	Butanedioic acid, dimethyl ester	106-65-0	1.604
7.405	2-Cyclopenten-1-one, 5-hydroxy-2,3-dimethyl-	58649-31-3	2.733
7.595	Cyclopropanecorboxylic acid, 2-methoxy-, methyl ester, trans-	122775-09-1	1.599
7.728	Phenol, 2-methoxy-	90-05-1	4.667
7.860	Pentane, 2,2,4,4-tetramethyl-3-methoxy-****	Not available	1.645
7.892	Pentane, 2,2,4,4-tetramethyl-3-methoxy-****	Not available	1.839
8.305	Ocatanoic acid, 6-hydroxy-8-methoxy-, .epsilon.-lactone	102541-04-8	1.398
8.787	Phenol, 2-methoxy-4-methyl-	93-51-6	1.313
9.745	Phenol, 4-ethyl-2-methoxy-	2785-89-9	2.951
10.630	Phenol, 2,6-dimethoxy-	91-10-1	2.460
10.762	Phenol, 2-methoxy-4-propyl-	2785-87-7	1.456
12.610	5-tert-Butylpyrogallol	20481-17-8	2.256
16.751	Hexadecanoic acid, methyl ester	112-39-0	1.104
20.616	1-Phenanthrenecarboxylic acid, 1,2,3,4,4a,9,10,10a-octahydro-1,4a-dimethyl-7-(1-methylethyl)-, methyl ester	1235-74-1	3.364
23.375	Tetracosanoic acid, methyl ester	2442-49-1	1.322

*, **, ***, **** - Possible isomers which maybe verified using nuclear magnetic resonance (NMR) or higher resolution GCMS.

***Table Q5**. Tentative identification results for **BARK** deconstructed in supercritical methanol **with Cu(III)-doped hydrotalcite catalyst**.*

Retention Time (min)	Possible Compound	CAS No.	Percent of Total Area (%)
4.657	Acetic acid, hydroxy-, methyl ester	96-35-5	3.008
4.821	Propanoic acid, 2-hydroxy-, methyl ester*	2155-30-8	2.749
4.858	Propanoic acid, 2-hydroxy-, methyl ester*	2155-30-8	9.220
4.905	Propanoic acid, 2-hydroxy-, methyl ester*	2155-30-8	12.785
5.064	Propanoic acid, 2-methoxy-, methyl ester**	17639-76-8	1.184
5.498	Butanoic acid, 2-hydroxy-, methyl ester***	29674-47-3	4.672
5.541	Butanoic acid, 2-hydroxy-, methyl ester***	29674-47-3	2.073
5.726	Pentane, 3-methoxy-	36839-67-5	1.020
6.748	Pentanoic acid, 4-oxo-, methyl ester	624-45-3	1.276
6.923	Propanoic acid, 2-methyl-, anhydride	97-72-3	4.583
7.124	Butanedioic acid, dimethyl ester	106-65-0	1.703
7.177	2-Cyclopenten-1-one, 2-hydroxy-3-methyl-	80-71-7	1.082
7.415	2-Cyclopenten-1-one, 5-hydroxy-2,3-dimethyl-	58649-31-3	1.938
7.437	2-Cyclopenten-1-one, 3-ethyl-2-hydroxy-	21835-01-8	1.081
7.606	2,4-Dimethylhexanedioic acid	40933-45-7	1.419
7.733	Phenol, 2-methoxy-	90-05-1	3.791
7.865	Pentane, 2,2,4,4-tetramethyl-3-methoxy-****	Not available	1.603
7.903	Pentane, 2,2,4,4-tetramethyl-3-methoxy-****	Not available	1.693
8.316	Ocatanoic acid, 6-hydroxy-8-methoxy-, .epsilon.-lactone	102541-04-8	1.320
8.792	Phenol, 2-methoxy-4-methyl-	93-51-6	1.254
9.295	2-Ethylnon-1-en-3-ol	Not available	1.067
9.745	Phenol, 4-ethyl-2-methoxy-	2785-89-9	2.751
10.630	Phenol, 2,6-dimethoxy-	91-10-1	1.911
10.762	Phenol, 2-methoxy-4-propyl-	2785-87-7	1.197
12.610	Benzene, 1,2,3-trimethoxy-5-methyl-	6443-69-2	1.867
13.553	2,4-Hexadienedioic acid, 3,4-diethyl-, dimethyl ester, (E,Z)	31545-75-2	1.246
16.751	Pentadecanoic acid, 14-methyl-, methyl ester	5129-60-2	1.085
18.398	10-Octadecenoic acid, methyl ester	13481-95-3	1.027
19.759	Eicosanebioic acid, dimethyl ester	42235-38-1	1.008
20.622	1-Phenanthrenecarboxylic acid, 1,2,3,4,4a,9,10,10a-octahydro-1,4a-dimethyl-7-(1-methylethyl)-, methyl ester	1235-74-1	2.973
21.178	Linoleic acid ethyl ester	544-35-4	1.545
23.375	Tetracosanoic acid, methyl ester	2442-49-1	1.075

*, **, ***, **** - Possible isomers which maybe verified using nuclear magnetic resonance (NMR) or higher resolution GCMS.

***Table Q6**. Tentative identification results for **SLUDGE** deconstructed in supercritical methanol **without catalyst**.*

Retention Time (min)	Possible Compound	CAS No.	Percent of Total Area (%)
4.397	2-Propanone, 1-hydroxy-	116-09-6	2.314
4.492	Acetic acid, hydroxy-, methyl ester*	96-35-5	1.738
4.572	Acetic acid, hydroxy-, methyl ester*	96-35-5	4.443
4.593	Acetic acid, hydroxy-, methyl ester*	96-35-5	2.810
4.757	Propanoic acid, 2-hydroxy-, methyl ester	2155-30-8	22.474
5.467	1,2-Butanediol	26171-83-5	6.958
5.689	2-Furanmethanol	98-00-0	2.128
6.218	Pentanoic acid, 2-hydroxy-, methyl ester	7445-76-3	1.496
6.732	Pentanoic acid, 4-oxo-, methyl ester	624-45-3	1.546
6.917	Propanoic acid, 2-methyl-, anhydride	97-72-3	14.712
7.103	Butanedioic acid, dimetyl ester	106-65-0	1.445
7.172	2-Cyclopenten-1-one, 2-hydroxy-3-methyl-	80-71-7	3.933
7.399	2-Cyclopenten-1-one, 3-ethyl-2-hydroxy-	21835-01-8	1.995
7.585	Cyclopropanecarboxylic acid, 2-methoxy-, methyl ester, trans-	122775-09-1	1.661
7.706	Phenol, 2-methoxy-	90-05-1	1.548
7.855	Pentane, 2,2,4,4-tetramethyl-3-methoxy-**	Not available	1.737
7.897	Pentane, 2,2,4,4-tetramethyl-3-methoxy-**	Not available	4.077
8.029	2-Cyclopenten-1-one, 3-ethyl-2-hydroxy-	21835-01-8	1.426
8.114	Pentanedioic acid, dimethyl ester	1119-40-0	1.212
8.310	2-Hydroxyhexadecyl butanoate	77899-01-5	1.632
8.930	Acetic acid, 3,4-dihydorxy-3-methyl-butyl ester	Not available	1.566
9.279	Hexanedioic acid, dimethyl ester	627-93-0	2.337

*, ** - Possible isomers which maybe verified using nuclear magnetic resonance (NMR) or higher resolution GCMS.

Table Q7. *Tentative identification results for* ***SLUDGE*** *deconstructed in supercritical methanol* ***with Fe(III)-doped hydrotalcite catalyst****.*

Retention Time (min)	Possible Compound	CAS No.	Percent of Total Area (%)
4.317	2-Butanol	14898-79-4	1.048
4.503	2-Propanone, 1-hydroxy-	116-09-6	1.260
4.752	Propanoic acid, 2-hydroxy-, methyl ester*	2155-30-8	2.339
4.826	Propanoic acid, 2-hydroxy-, methyl ester*	2155-30-8	6.141
4.884	Propanoic acid, 2-hydroxy-, methyl ester*	2155-30-8	1.520
5.006	Propanoic acid, 2-hydroxy-, methyl ester*	2155-30-8	19.605
5.482	Butanoic acid, 2-hydroxy-, methyl ester**	29674-47-3	2.042
5.509	Butanoic acid, 2-hydroxy-, methyl ester**	29674-47-3	2.460
5.546	Butanoic acid, 2-hydroxy-, methyl ester**	29674-47-3	1.060
5.599	Butanoic acid, 2-hydroxy-, methyl ester**	29674-47-3	2.789
5.795	2-Furanmethanol	98-00-0	1.331
6.234	Pentanoic acid, 2-hydroxy-, methyl ester***	7445-76-3	1.393
6.287	Pentanoic acid, 2-hydroxy-, methyl ester***	7445-76-3	1.072
6.790	Pentanoic acid, 4-oxo-, methyl ester	624-45-3	1.272
6.965	Propanoic acid, 2-methyl-, anhydride	97-72-3	14.128
7.235	2-Cyclopenten-1-one, 2-hydroxy-3-methyl-	80-71-7	2.254
7.463	2-Cyclopenten-1-one, 3-ethyl-2-hydroxy-	21835-01-8	1.302
7.606	Cyclopropanecarboxylic acid, 2 methoxy-, methyl ester, trans-	122775-09-1	1.555
7.749	Phenol, 2-methoxy-	90-05-1	1.231
7.918	Pentane, 2,2,4,4-tetramethyl-3-methoxy-	Not available	4.961
8.347	Octanoic acid, 6-hydroxy-8-methoxy-, .epsilon.-lactone	102541-04-8	1.974
9.290	Hexanedioic acid, dimethyl ester	627-93-0	1.358

*, **,*** - Possible isomers which maybe verified using nuclear magnetic resonance (NMR) or higher resolution GCMS.

***Table Q8**. Tentative identification results for **SLUDGE** deconstructed in supercritical methanol **with Cu(III)-doped hydrotalcite catalyst**.*

Retention Time (min)	Possible Compound	CAS No.	Percent of Total Area (%)
4.264	2-Propanone, 1-hydroxy-	116-09-6	1.287
4.492	Propanoic acid, 2-hydroxy-, methyl ester*	2155-30-8	6.912
4.783	Propanoic acid, 2-hydroxy-, methyl ester*	2155-30-8	32.490
5.440	1,2-Butanediol**	26171-83-5	3.278
5.493	1,2-Butanediol**	26171-83-5	9.534
6.229	Pentanoic acid, 2-hydroxy-, methyl ester	7445-76-3	2.501
6.727	Pentanoic acid, 4-oxo-, methyl ester	624-45-3	1.232
6.912	Propanoic acid, 2-methyl-, anhydride	97-72-3	11.230
7.103	Butanedioic acid, dimethyl ester	106-65-0	1.366
7.161	2-Cyclopenten-1-one, 2-hydroxy-3-methyl-	80-71-7	2.704
7.399	2-Cyclopenten-1-one, 3-ethyl-2-hydroxy-	21835-01-8	2.046
7.585	Cyclopropanecorboxylic acid, 2-methoxy-, methyl ester, trans-	122775-09-1	2.276
7.706	Phenol, 2-methoxy-	90-05-1	1.663
7.855	Pentane, 2,2,4,4-tetramethyl-3-methoxy-***	Not available	2.734
7.897	Pentane, 2,2,4,4-tetramethyl-3-methoxy-***	Not available	4.189
8.305	Octanoic acid, 6-hydroxy-8-methoxy-, .epsilon.-lactone	102541-04-8	1.752
8.919	4-sec-Butoxy-2-butanone	57545-63-8	2.142
9.274	Hexanedioic acid, dimethyl ester	627-93-0	2.170

*, **,*** - Possible isomers which maybe verified using nuclear magnetic resonance (NMR) or higher resolution GCMS.

An estimate of the yields of organics in the liquid products is shown in Figure Q9. These are yields reported as phenol equivalents of all the organics. The phenol equivalent of total organics for each of the treatments was calculated based on the area under the curves of the chromatographs. The yield calculation is based on the 5-gram feedstock fed into the reactor for each run. It is evident that the values are high but it should be noted that these are approximate yields.

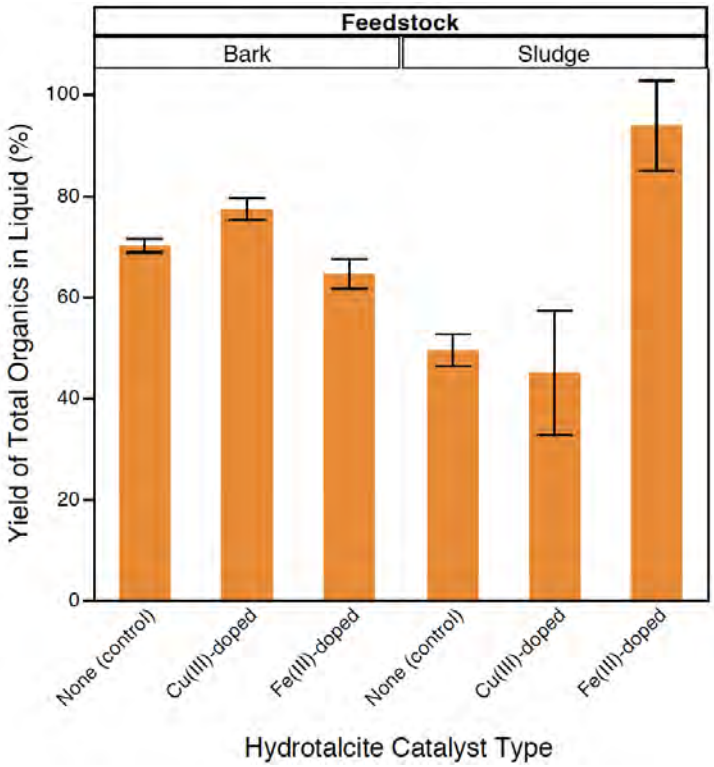


***Figure Q9**. Organics yield in the liquid product. The reference compound is phenol and the yield is based on the 5-gram feedstock fed into the reactor. Error bars are 1 S.D. from the mean.*

References:

Coker, A.T., Hernandez, R., Revellame, E.D., French, W.T., Iretskii, A.V., Holmes, W., & White, M.G. (2012). *Comparison of 1- and 2- Step Biodiesel Production From Activated Sludge Using Supercritical Methanol and Economic Analysis*. Paper presented at the 2012 AIChE Conference.

Di Cosimo, J. I., Díez, V. K., Xu, M., Iglesia, E., & Apesteguía, C. R. (1998). Structure and Surface and Catalytic Properties of Mg-Al Basic Oxides. *Journal of Catalysis, 178*(2), 499-510.

Macala, GeraldS, Robertson, AndrewW, Johnson, CharlesL, Day, ZacharyB, Lewis, RobertS, White, MarkG, . . . Ford, PeterC. (2008). Transesterification Catalysts from Iron Doped Hydrotalcite-like Precursors: Solid Bases for Biodiesel Production. *Catalysis Letters, 122*(3-4), 205-209.

Subtask Q.2 Expand the oil production capacity of the biocrude pilot facility

Oil accumulation will be evaluated using wastewaters or solid residues from refineries, animal-raising facilities, and the pulp and paper industry. Wastewaters and/or solid residues producing oil accumulation higher than 10% by weight of cell dry mass will be evaluated in the pilot facility. The extracts will also be characterized for other chemicals of importance to industry.

Planned Activites:

Q.2.ML.1 Demonstrate biocrude production from industrial wastes.
Q.2.ML.2 Prepare a conceptual plant design for the generation of biocrude from candidate industrial wastewaters, sludge/oleaginous/algae consortiums, and/or solid residues, which will be used as carbon sources.

Summary of Activites:

Failure to improve lipid production during earlier fermentations (Figure Q10, Figure Q11, Figure Q12, Figure Q13) led to an investigation of potential differences between the laboratory parameters and the scaled-up pilot plant parameters. Equipment parameters, as well as air and water sources at the facility were examined. Agitation rate in the fermentation units were found to be too low. This error was corrected.

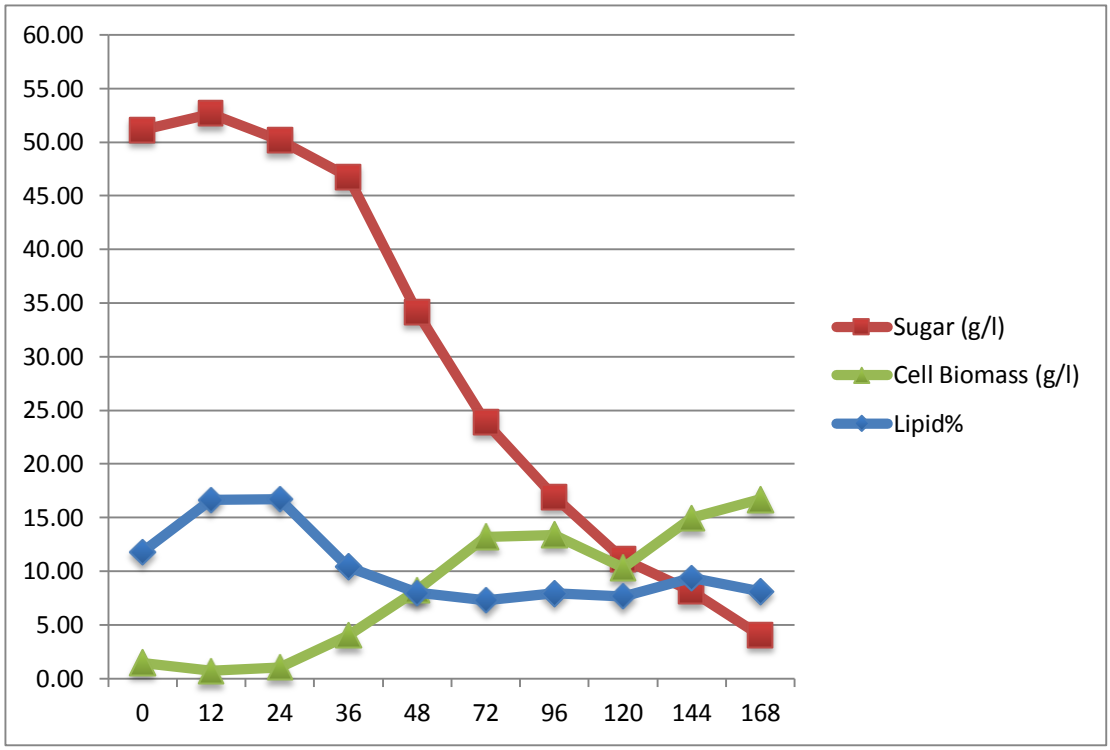


Figure Q10. *Pilot 11A Results*

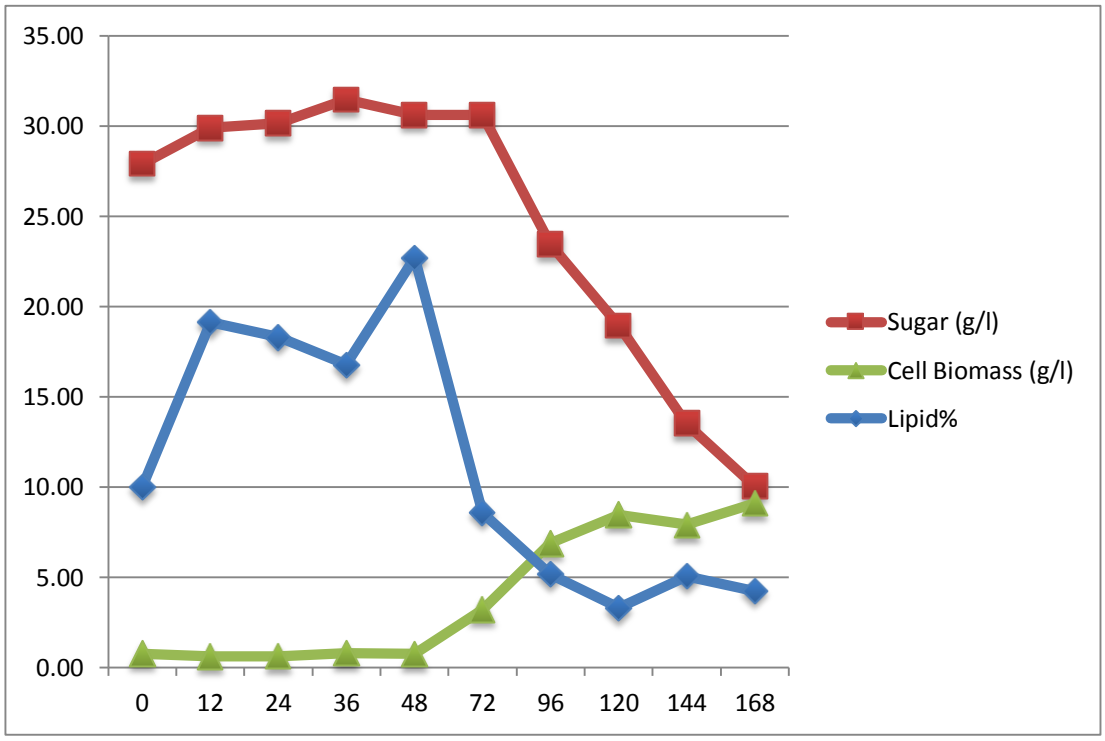


Figure Q11. *Pilot 11B Results*

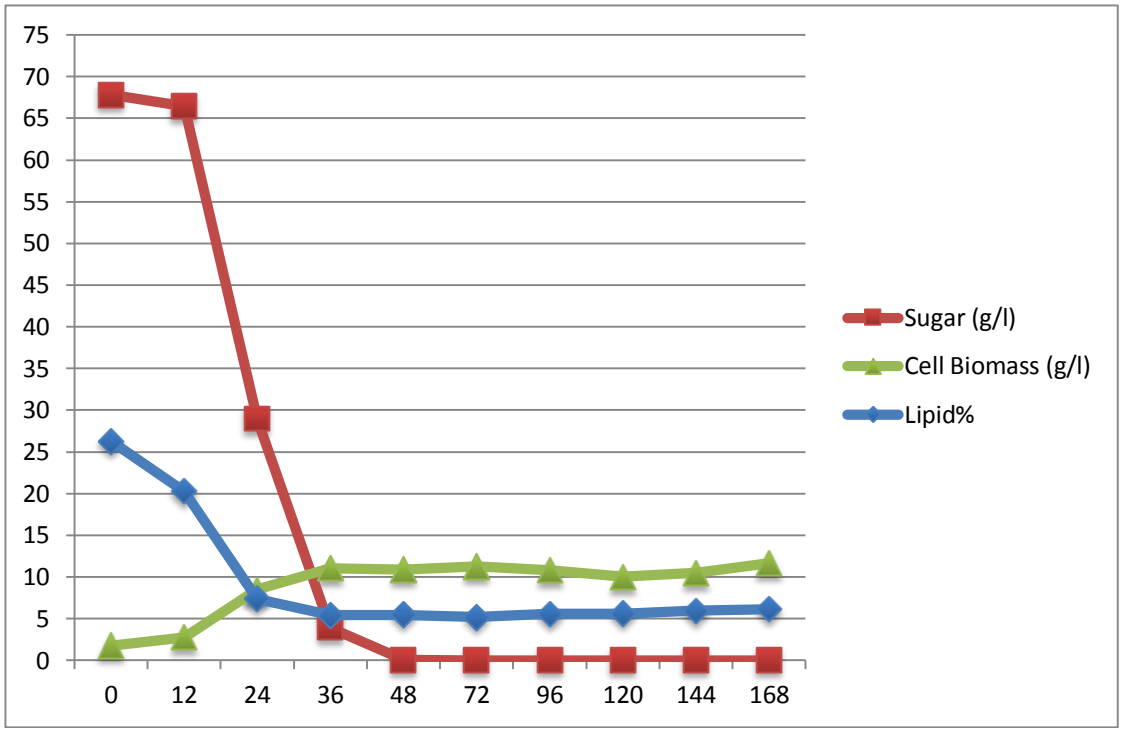


***Figure Q12**. Pilot 12A Results*

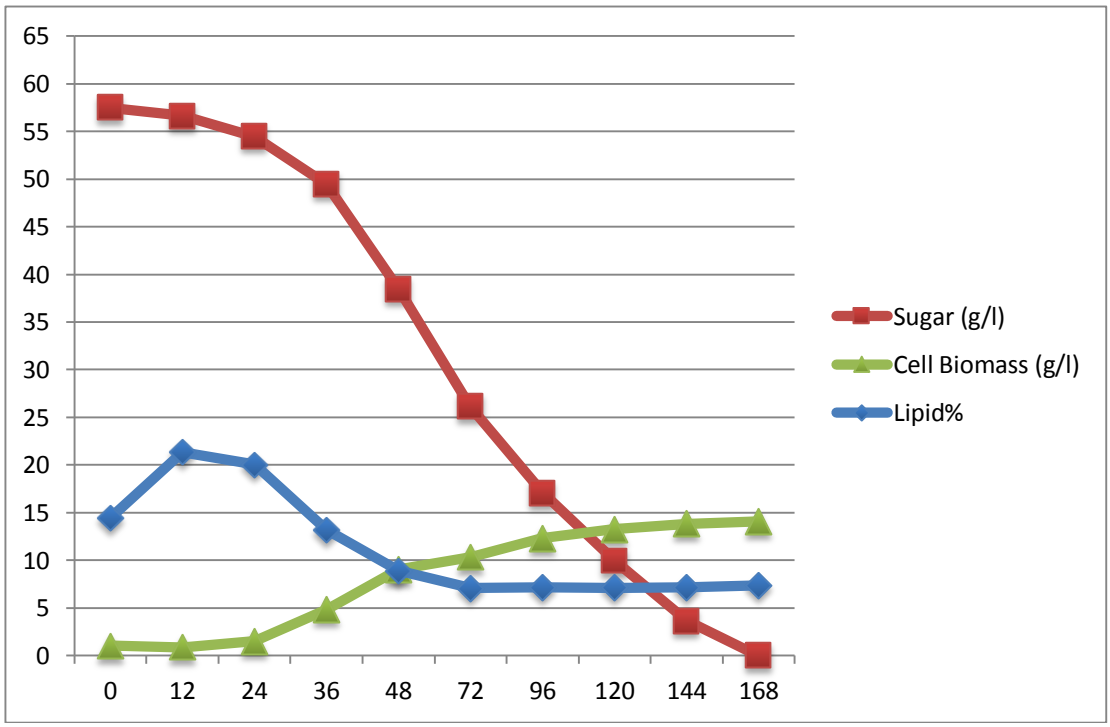


***Figure Q13**. Pilot 12B Results*

Two parallel fermentations were run using a 60:1 C:N ratio, with glucose as the carbon source. Fermentation 13A (Figure Q14) was run with a pure culture of Rotatarula Glutinis and Fermentation 13B (Figure Q15) was run with municipal wastewater sludge as a microbial source.

With the new operational parameters, fermentations resulted in faster substrate consumption and higher lipid concentrations.

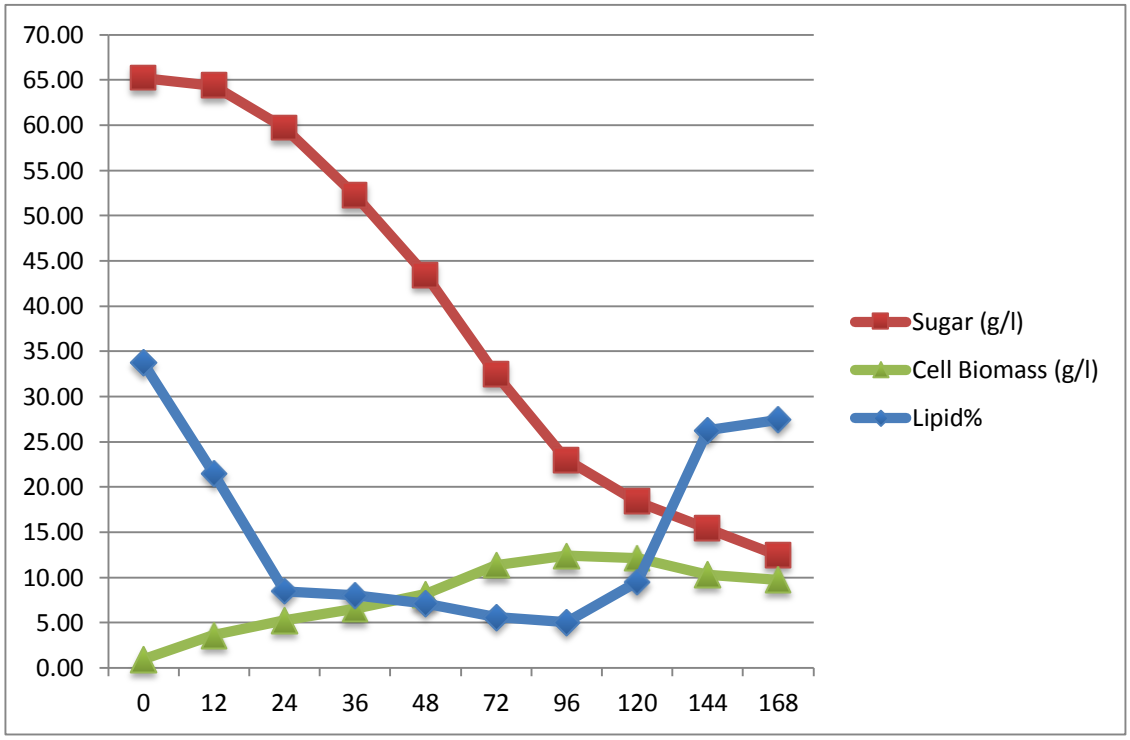


Figure Q14. *Pilot 13A Results*

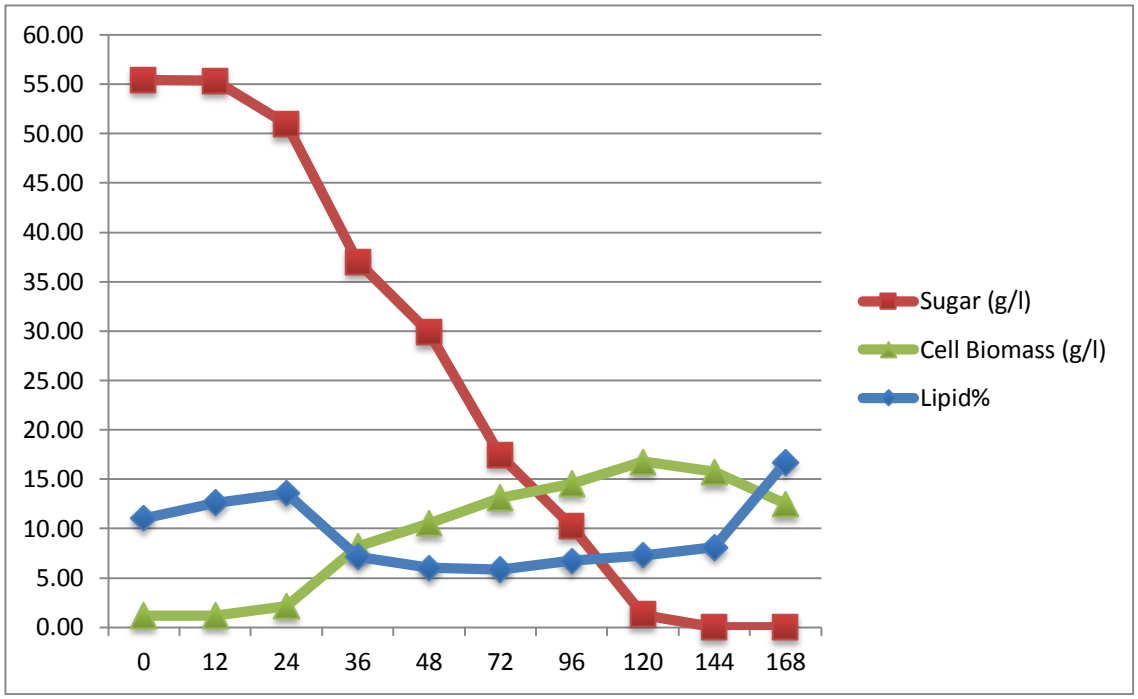


Figure Q15. *Pilot 13B Results*

Biocrude production using Georgia Pacific wastewater and seeds from their facility compared to the seed obtained from Tuscaloosa Wastewater Treatment facility. Pilot 14A contained Georgia Pacific wastewater, 60g/l glucose, nutrients, and Georgia Pacific sludge as the microbial source. Results are shown in Figure Q16. Pilot 14B contained synthetic wastewater, 60g/l glucose, and sludge from Tuscaloosa Wastewater Treatment facility as the microbial source. Results are shown in Figure Q17.

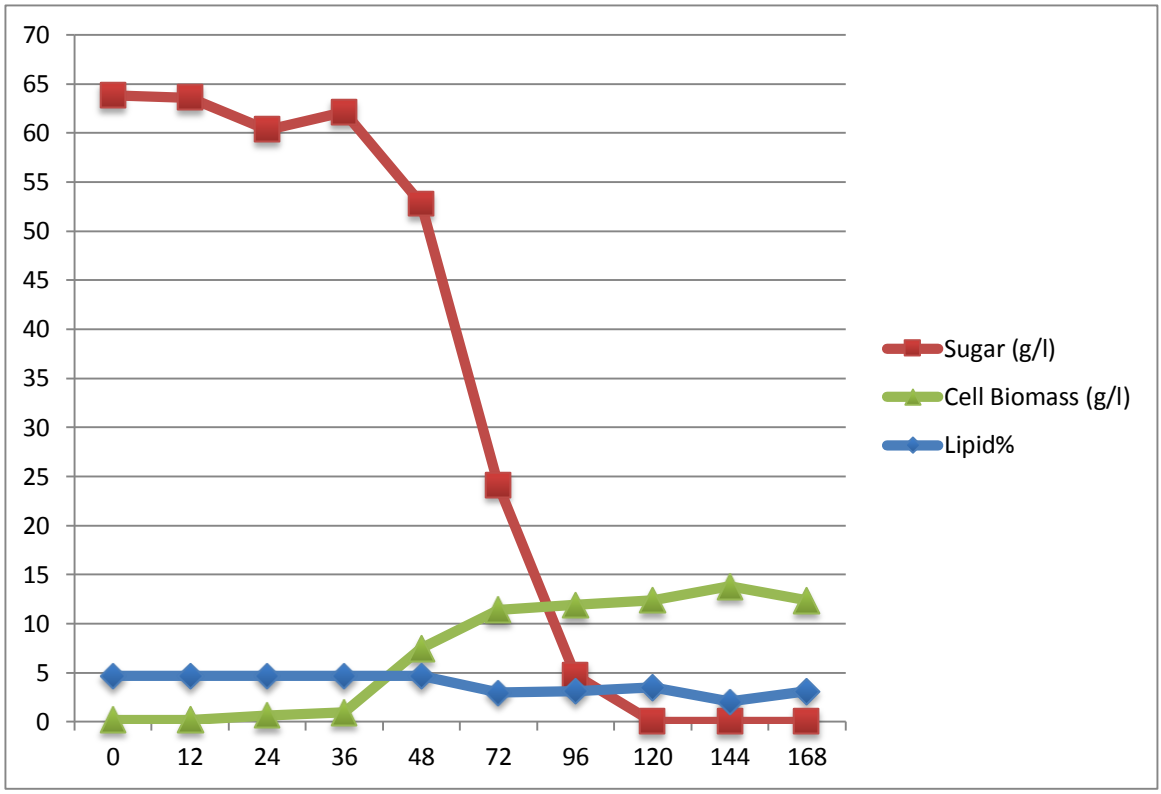


***Figure Q16**. Pilot 14A Results*

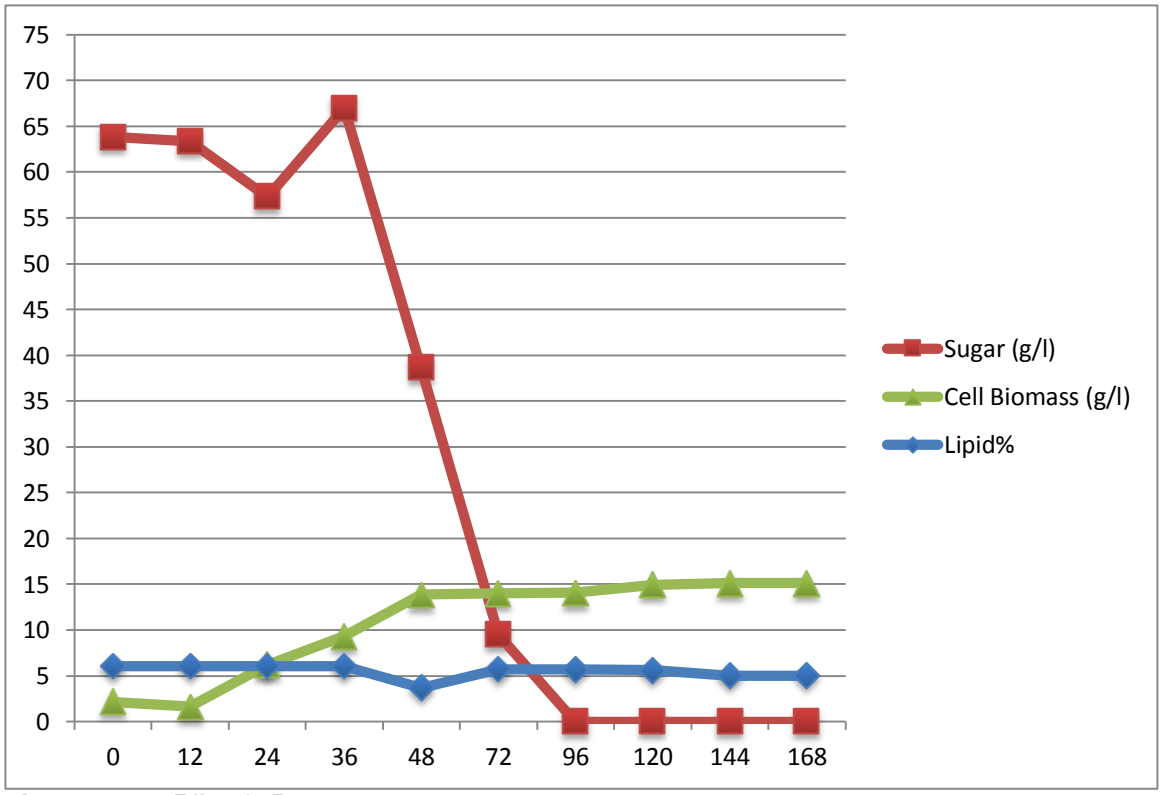


***Figure Q17**. Pilot 14B*

Pilot fermentation 15 contained a 70:1 carbon to nitrogen ratio using 20% glycerol and balanced with glucose in sugar broth. It was inoculated with a pure culture of *Rhodotorula Glutinis*. Results are shown in Figure Q18. In an effort to provide baseline data nutrients were not added during the initial phase of the experiment. Fermentation 16A contained 60g/l glucose and municipal wastewater sludge from Tuscaloosa, AL. Results are shown in Figure Q19. Fermentation 16B contained 60g/l of glucose and municipal wastewater sludge from Jackson, MS. Nutrients were added at 133 hrs because the carbon source was not being utilized. Results are shown in Figure Q20.

During the centrifugation stage 8.86kg of solids with 50% moisture content was recovered for pilot 15A. For pilot 16A 1.425kg solids with 58% moisture content was recovered. For pilot 16B 9.0kg of solids were recovered with 50% moisture content was recovered.

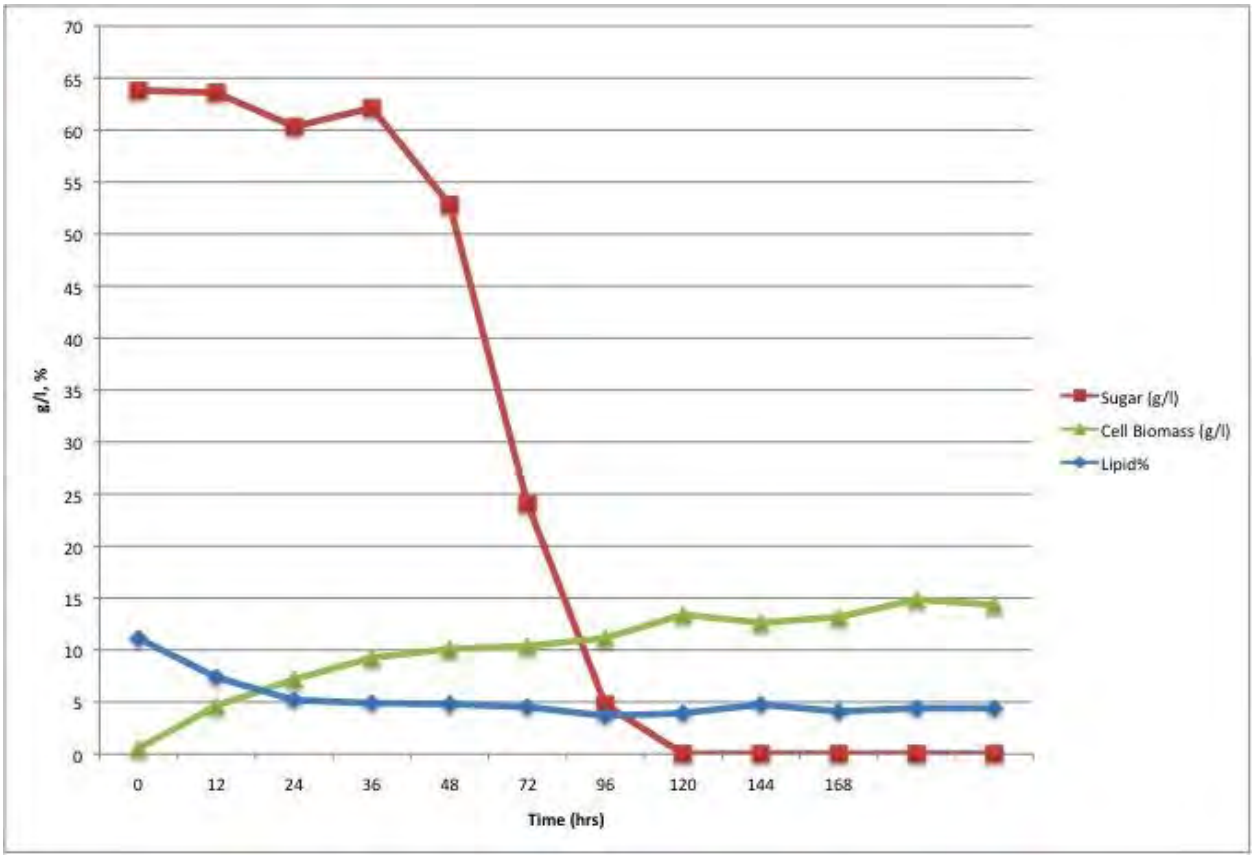


Figure Q18. *Pilot 15 Results.*

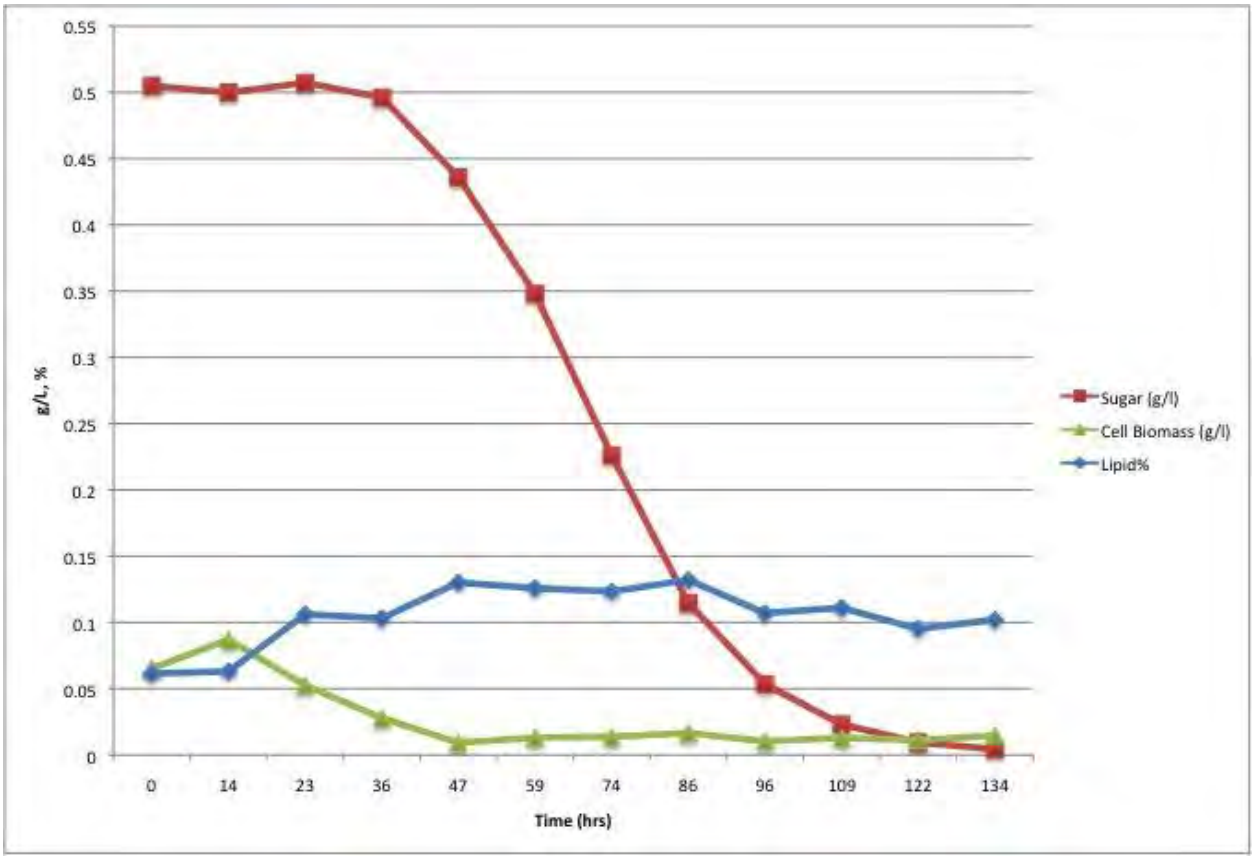


Figure Q19. *Pilot 16A Results.*

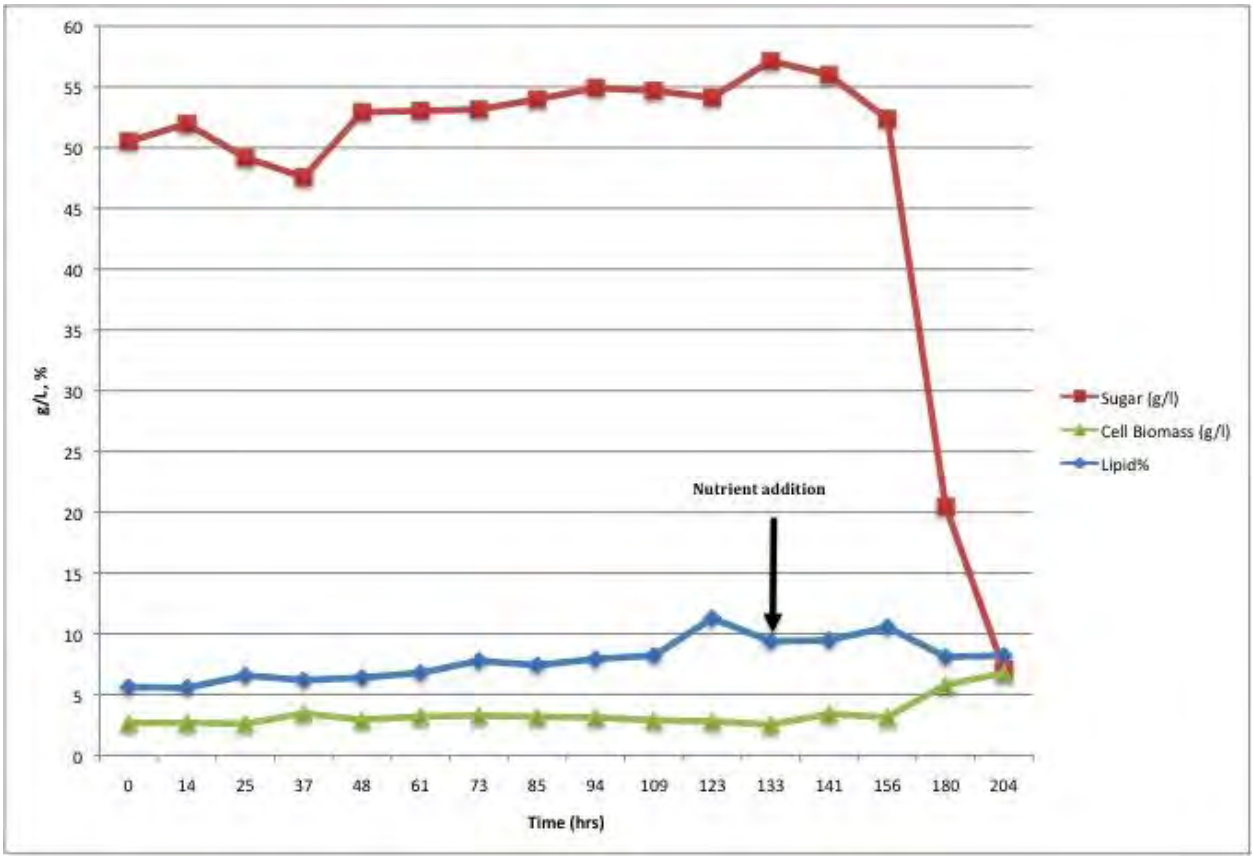


Figure Q20. *Pilot 16B Results.*

Downstream processing bio-crude yields did not match daily samples. It was determined that the membrane separation unit could be replaced by a centrifugation unit to optimize the isolation of lipid-filled oleaginous cells without losing lipids to the permeate stream. Utilizing the centrifugation unit allowed for much time to be conserved because of the efficiency of the centrifuge rather than the membrane separator. Preliminary operation has resulted in a centrifuge cake below 36 wt% moisture content. Solvent extraction unit operation was also reviewed. It was determined that this operation required an improvement in the physical separation of the solid/extracted liquid as well as an improvement in the solvent recovery procedure. A new solvent extraction unit was designed along with a more efficient way of recovering the solvent.

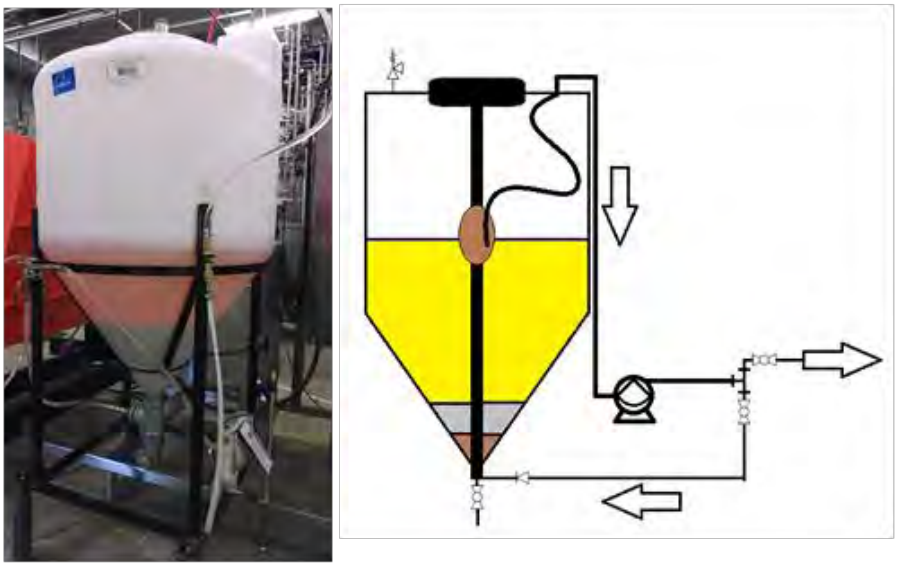


Figure Q21. *Solvent recovery system.*

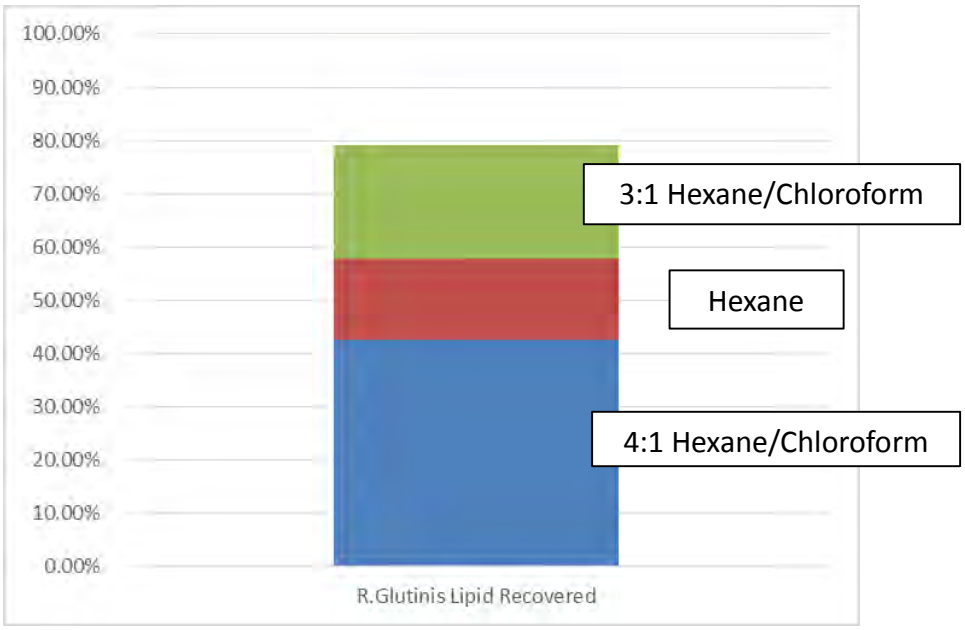


Figure Q22. *Total Lipid Recovery from R. Glutinis Centrifugate Using Multiple Extraction Solvent Mixtures*

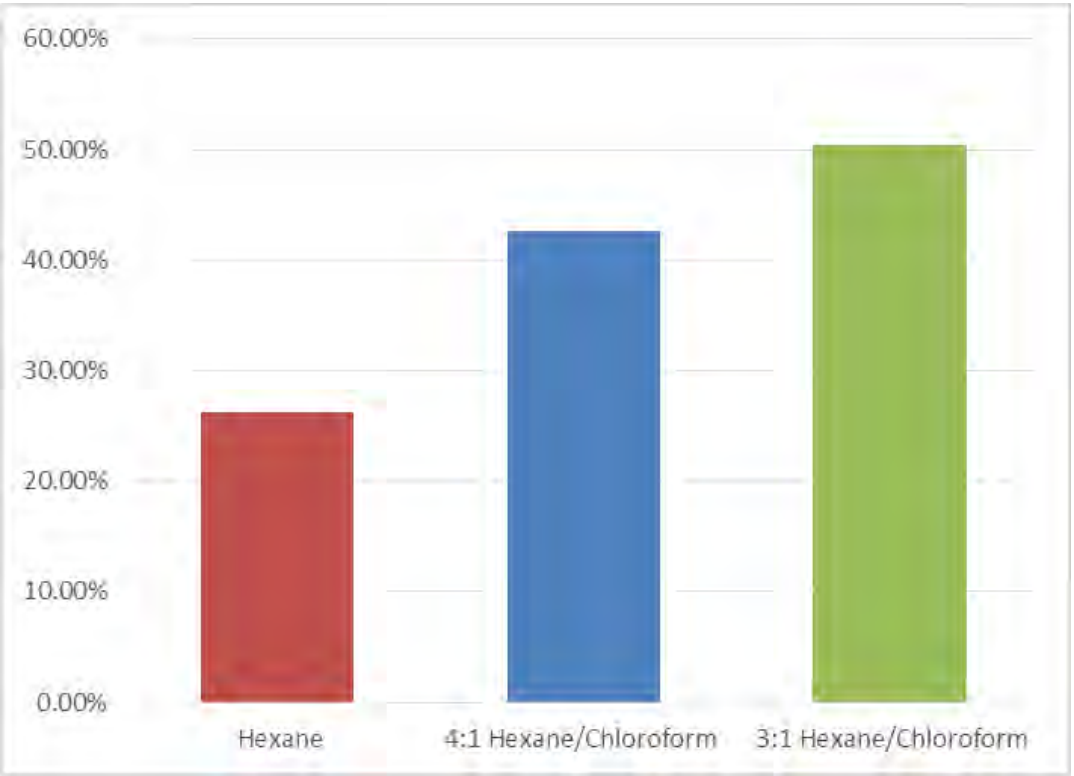


Figure Q23. *Single Extraction Efficiency as a percentage of remaining R. Glutinis Lipid Centrifugate*

Lipid production by *R. glutinis* in waste paper hydrolysate.

Conversion of lignocellulosic sugars existing in waste paper hydrolysate to triacylglycerols using oleaginous yeast is a viable approach to reduce the cost for production of biofuel. According to Environmental Protection Agency report (2011), in America 70 million tons of paper products were produced. Out of 70 million tons 46 million tons of paper products have recovered. However, 42% of recovered paper products were exported to overseas markets and 58% of recovered paper products were recycled in US. Utilization of recovered paper products as carbon source for oleaginous yeast can be an excellent economic way for biofuel production.

Method:

Optimization of paper hydrolysis condition:
The objective of the experiment was to determine the optimum hydrolysis condition that will produce the highest amount of monomeric sugars (glucose (Glc) and xylose (Xyl)), which can be used as carbon source for oleaginous yeast for lipid production. Office waste paper with black-ink print was chosen for the preparation of hydrolysate as a representative of waste paper. Optimization experiments were conducted by considering (1) acid concentration, (2) ratio of pure sulfuric acid to cellulose in biomass, (3) duration of oligo-sugar hydrolysis.

Office paper composed of 71+/-6.1% Glc, 13+/-0.7% Xyl, 12.71+/-1.2% lignin in extractive (12%) in moisture free (4.7%) basis. Plain office paper was shredded and cut into small pieces, ~5x10 mm. First, to determine sulfuric acid (SA) concentration that will be used for further hydrolysis, 4 ml of 50, 55, 60, and 65% SA was added to 1.2 g of paper each and hydrolyzed for one hour in

30°C water bath. Then, 13-15 ml of DI water was added to obtain ~45 g/L Glc in hydrolysate and autoclaved at 121^{0}C for 15 min. After cooling to room temperature hydrolysate was neutralized with calcium carbonate and the sugar contents were analyzed with Agilent 1100 HPLC system.

Optimal ratio of paper and SA was determined by following experiment. Ten grams of paper was treated with 2.7, 5.4, 8.1, 10.8, 13.5 and 16.2 ml of 65% SA assuming that 10 g of paper would contain 7.1 g of Glc (71% Glc w/w) in the form of cellulose. The ratio of pure SA to cellulose were 1:0.33, 1:0.67, 1:1, 1:1.33, 1:1.67, and 1:2, respectively. Theoretically, to cleave one Glc unit from cellulose needs one H^+ of SA (1 mol Glc: 0.5 mol SA). Thus, to convert 7.1 g cellulose to glucose needs 4.2 g of SA, which exists in 2.7 ml 65% SA (d=1.5533 g/cm^3 at 20 °C). Based on this calculation the amount of SA increased 2, 3, 4, 5, and 6 times to find out the optimal amount of SA.

Duration of autoclaving after diluting with DI water was also considered. Autoclaving time at elevated temperature (121°C) was 0, 5, 10, 15, 20 and 25 min.

*Lipid production from acid hydrolysate by **R. glutinis:***
Inocula
The yeast *Rhodotorula glutinis* (ATCC 15125) was obtained from American Type Culture Collection, Manassas, VA. *R. glutinis* cells were inoculated into sugar broth medium containing (per liter) 1 g yeast extract, 60 g glucose , 1.6 g $(NH_4)_2SO_4$, 1 g KH_2PO_4, 1 g NaH_2PO_4 x $12H_2O$, 0.4 g $MgSO_4$ x $7H_2O$, 10 mL trace mineral, and 6 mL $FeSO_4$ solution (4 g/ L FeSO4 x $7H_2O$) at 30 °C on a rotary incubator at 130 rpm. The trace mineral solution consisted of (per liter) 3.6 g $CaCl_2$ x $2H_2O$, 0.75 g $ZnSO_4$ x $7H_2O$, 0.13 g $CuSO_4$ x $5H_2O$, 0.5 g $MnSO_4$ x H2O, 0.13g $CoCl_2$ x $6H_2O$, and 0.17g Na_2MoO_4 x $2H_2O$.

Fermentation media and fermentation
After 5 days of cultivation, 20% (v/v) of *R. glutinis* culture was inoculated into the waste paper hydrolysate medium, containing glucose and xylose as carbon source, and nutrients. The nutrients for hydrolysate medium consisted of (per liter) 0.07 g yeast extract, 0.01 g casamino acids, 1.5 g NaH_2PO_4, 1 g K_2HPO_4, 0.15 g gelatin, 0.07 g starch, 5 ml of trace mineral solution and $(NH_4)_2SO_4$ as nitrogen source. The amount of $(NH_4)_2SO_4$ added was calculated based on the amount of carbohydrates (glucose and xylose) existed in hydrolysate to obtain a high carbon-to-nitrogen ratio of 70:1.

This amended hydrolysate medium was used as a fermentation medium for lipid accumulation during the 9 days of cultivation time in a 5-L aerobic batch fermenter New Brunswick Scentific Bioflo 310 bioreactors (Eppendorf, Hauppauge, New York, USA). The starting volume of the media was 3 L.

Analyses:
Glucose and xylose were analyzed by Agilent 1100 HPLC system equipped with HPX-87P column and evaporative light scattering detector (ELSD). The mobile phase was water (HPLC grade) with flow rate of 0.6 ml/min. The isocratic spray chamber of ELSD was controlled at 40°C and the drift tube at 79°C.

Sugar degradation compounds such as acetic acid, furfural, 5-hydroxymethyl furfural (5-HMF) produced during hydrolysis process were analyzed on Agilent 1100 HPLC system equipped with ROA+ acid column and Diode Array detector at wavelength range XXX mn.

Cell dry weight determination was performed by centrifuging the cells at 3000 RPM for 15 minutes, washing with DI water, and drying in a freeze-dry system to constant weight. The lipid content of the cell was obtained by the gravimetrical method described by Bligh & Dyer.

The lipids obtained from the Bligh & Dyer extraction were transesterified with methanol. The fatty acid methyl ester (FAME) was then analyzed using an Agilent 6890 series Gas Chromatograph equipped with a Zebron FFAA capillary column (30 m x 0.25 mm x 0.2 micron) and a flame ionization detector (FID).

Results:

Optimization of paper hydrolysis condition:
The yield of glucose obtained after treating with different strength SA is shown in Figure Q24. Apparently, as concentration of SA goes high the de-crystallization goes close to complete. The results indicated a maximum glucose 90+/-1.0% (% of total Glc) yield when hydrolyzed with 65% SA. Higher concentration than 65% was not considered because high concentration will lead to elevated amount of degradation compounds content.

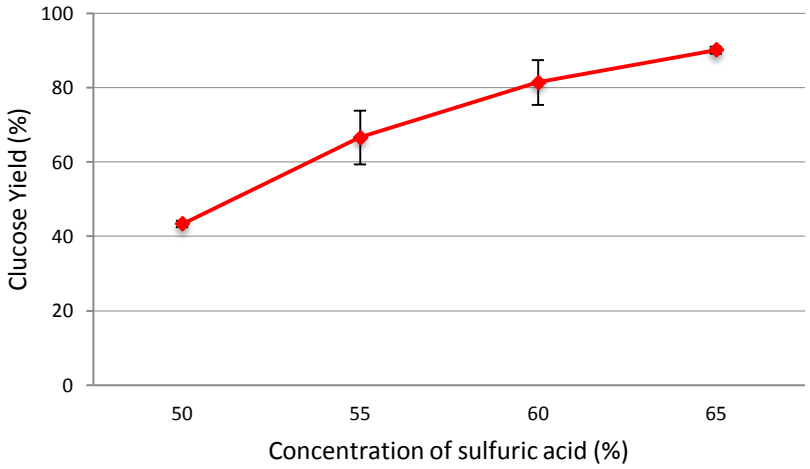


***Figure Q24**. Paper hydrolysis by different strength sulfuric acid.*

Results of the experiments in terms of yield of Glc (% of total Glc) in relation to the ratio of pure SA to cellulose and the duration of hydrolysis process in the autoclave are shown in the Figure Q25. Maximum amount of Glc was obtained during the 15 min hydrolysis when the ratios of pure SA to carbohydrate were 1:1, 1:1.33, 1:1.67, and 1:2. The yield of Glc was the highest among the other conditions and the yield of Glc was close to each other 86.4, 91.5, 91.9 and 93.2% (% of total Glc). In order to use less amount of SA and for other economical reason (utilization of less neutralization reagent), the ratio for the hydrolysis of the paper was chosen 1:1.33. The optimum condition for further hydrolysis is (1) 65% strength SA, (2) ratio of pure sulfuric acid to cellulose in biomass is 1:1.33, (3) duration of oligo-sugar hydrolysis in autoclave is 15 min.

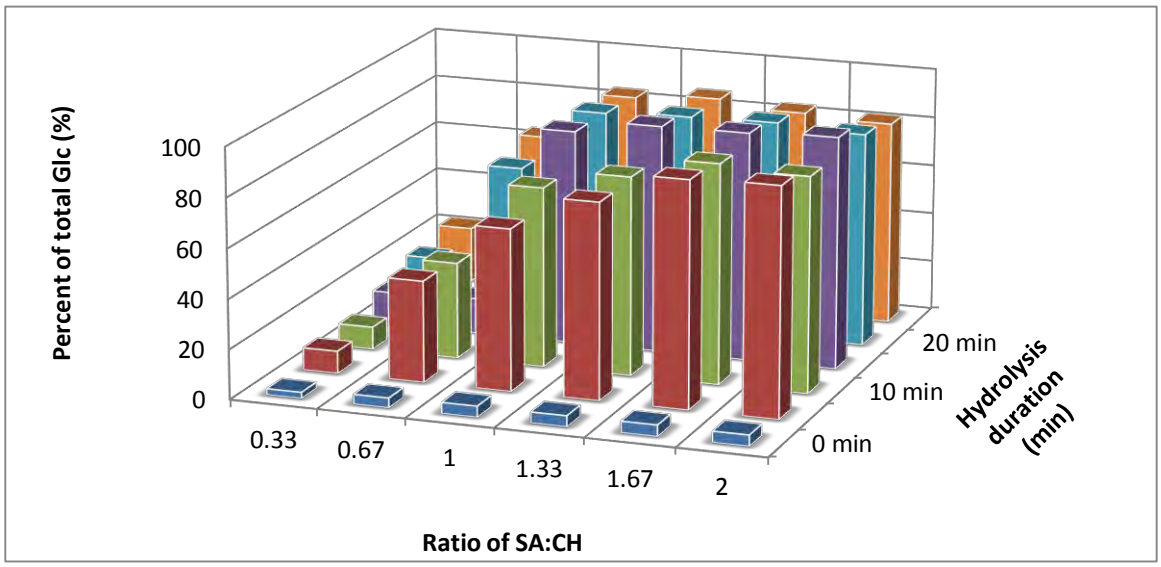


***Figure Q25**. Effect of acid concentration and hydrolysis time to the yields of glucose.*

Furfural, acetic acid analysis:

Furfural, 5-HMF and acetic acid are common degradation products of cellulosic sugar hydrolysis. Presence of these compounds tends to suppress the cell growth of microorganisms. Thus, elevated concentration of inhibitory compounds in hydrolysate is not preferred. The content of those compounds in paper hydrolysate at various hydrolysis conditions were quantified and presented in Figure Q26 and Q27. At the optimum condition the amount of furfural and 5-HMF was 0.211 g/L and 0.095 g/L, respectively. As expected the amount of 5-HMF and furfural were increasing as the hydrolysis condition become severe. However, acetic acid in hydrolysates was not detected. It can be explained that during the paper pulping process hemicelluloses with acetate side chain were removed.

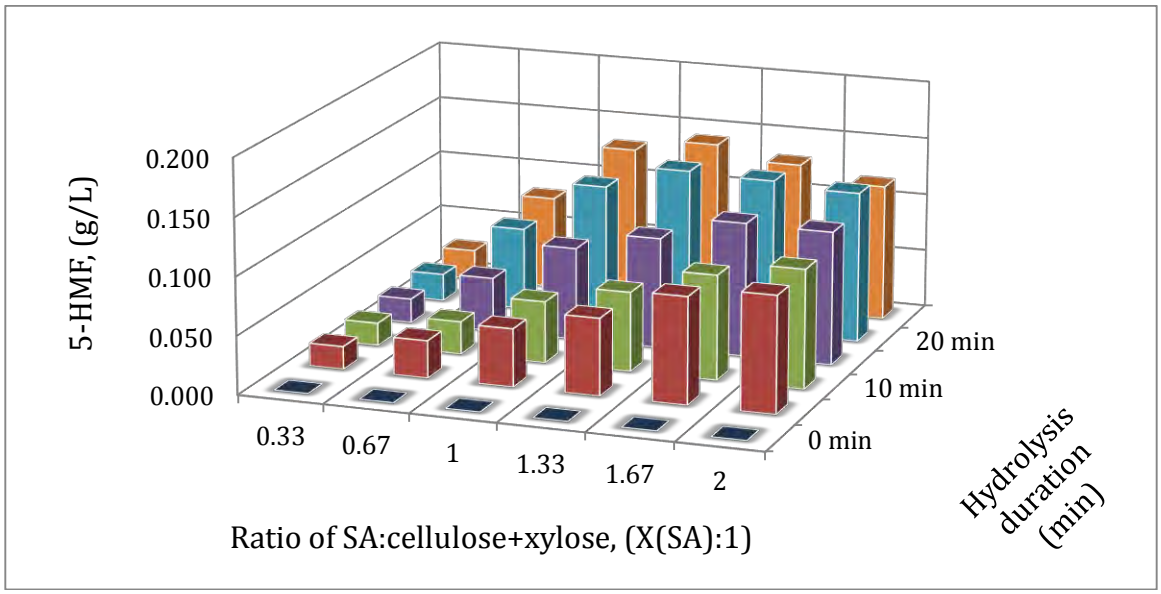


***Figure Q26**. 5-HMF produced at different hydrolysis conditions.*

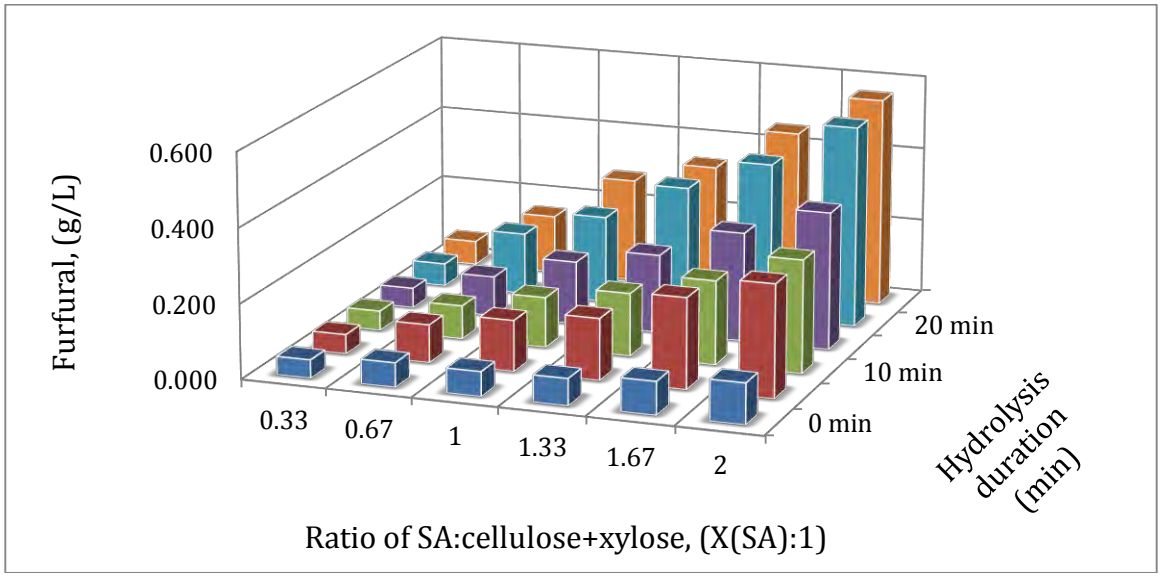


***Figure Q27**. Furfural produced at different hydrolysis conditions.*

Lipid production by R. glutinis in paper hydrolysate.

Seven liter paper hydrolysate was produced at optimum condition with moderate modification. The hydrolysis time in autoclave was increased from 15 to 45 min. It was necessary because the initial optimization was conducted in screw top test tubes with total volume of 15-20 ml of hydrolysate. In order to complete hydrolysis process in large volume (2 L volume pressure tubes) the duration of autoclaving was extended. Total 7 L hydrolysate containing 55 g/L Glc and 11 g/L Xyl was prepared. In order to support microorganisms growth the hydrolysate was neutralized with 19 M sodium hydroxide until pH 7. It was crucial to remove sodium sulfate salt because it was toxic for the yeast due to the existence of large quantity salt. Thus, the hydrolysate was placed in the fridge over night to crystallize sodium sulfate salt in the form of $Na_2SO_4x10H_2O$. Since the sodium salt uses ten molecules of water the volume of hydrolysate was noticeably reduced and the concentrations of Glc and Xyl were elapsed to ~30 g/L and 6.2 g/L, respectively. It is suggested to perform neutralization alternatively with calcium or barium hydroxide to reduce the loss of volume and perhaps sugars.

Starting hydrolysate along with controls were inoculated with 20% v/v yeast. The first control started with 64 g/L Glc only in order to control the performance of the yeast. The second control was synthetic hydrolysate and it contained 24 g/L Glc and 5.7 g/L Xyl. Nitrogen source was added to obtain 70:1 ratio of N:C. Results for sugar consumption and lipid accumulation of *R. glutinis* are presented in the following figures.

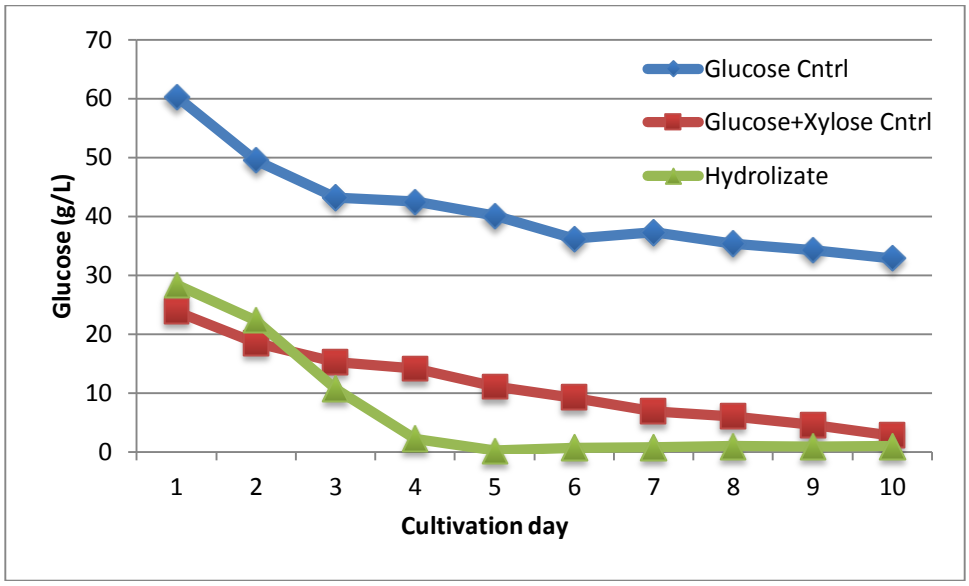


***Figure Q28**. Glucose consumption by R. glutinis during the cultivation period.*

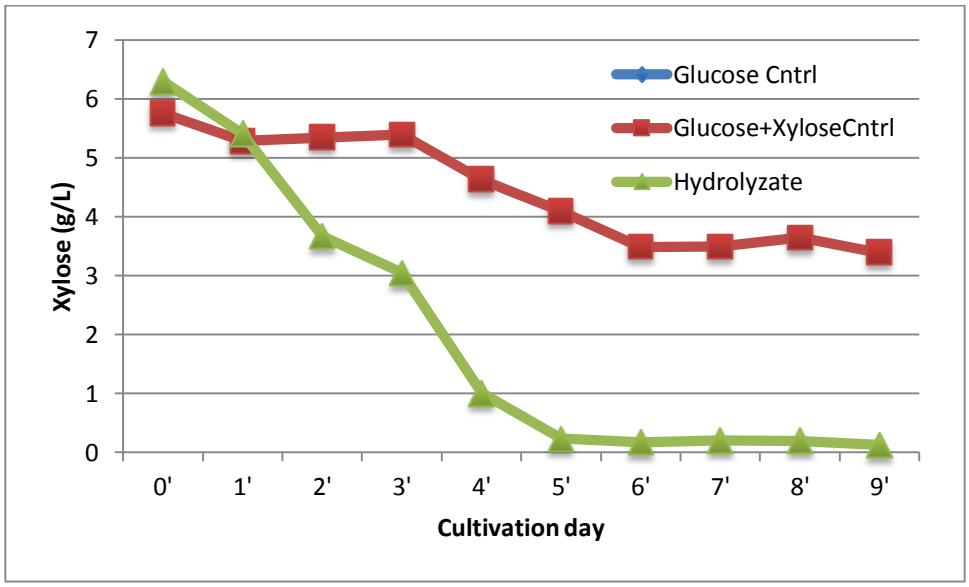


***Figure Q29**. Xylose consumption by R. glutinis during the cultivation period.*

Figures Q28 and Q29 shows the sugar consumption profile of controls and hydrolysate during the cultivation period. Glucose and xylose existing in the hydrolysate were consumed completely in 5 days. However, in controls moderate amount of sugars remained. This could be because of the excess amount of glucose existing in first control and pH shift from 6.5 to ~2.5 between day 2 and 3 and remained at that range throughout the duration of the experiment. However, the pH of hydrolysate dropped down to ~2.7 during the day 2 and went back to pH 6.1 during the third day and gradually increased during the experiment and at day 9 reached pH 6.8. This could be the explanation to the complete consumption of sugars in hydrolysate.

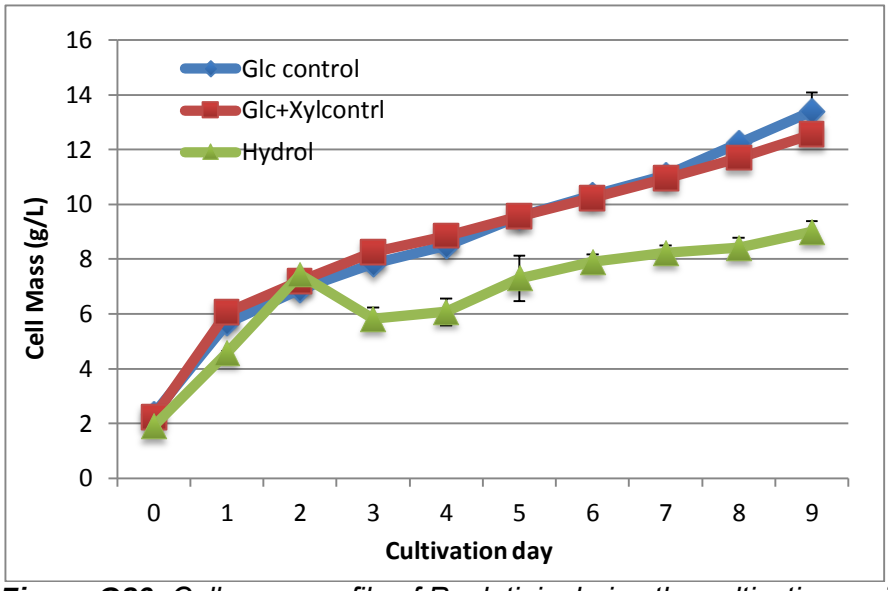


***Figure Q30**. Cell mass profile of R. glutinis during the cultivation period.*

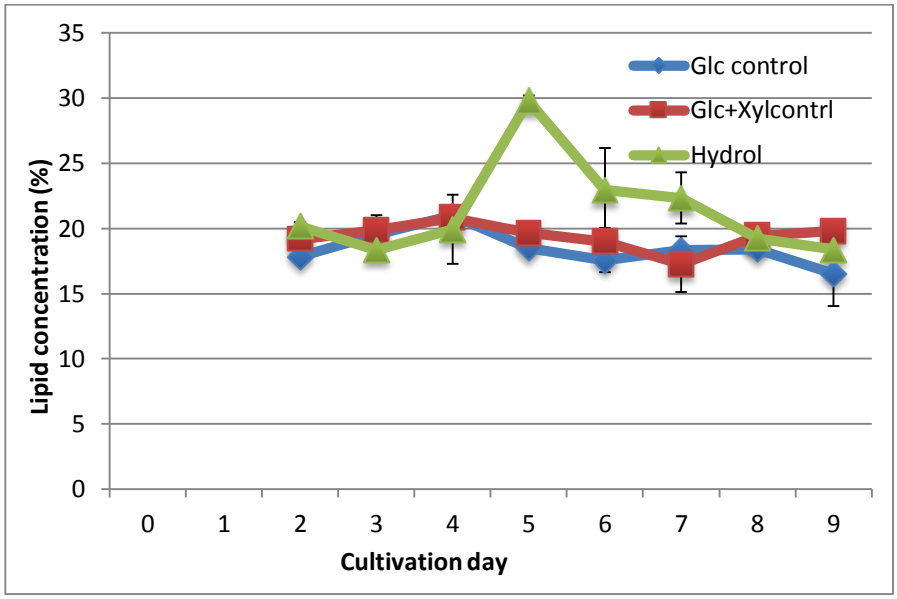


***Figure Q31**. Lipid accumulation profile by R. glutinis.*

In both controls the amount of cells was increasing during the cultivation period and the concentration of the cells produced was similar (Figure Q30). In case of hydrolysate the concentration of the cells were comparable during the first two days and remained slightly low throughout the duration of the experiment. Lipid concentration accumulated in the cells grown in hydrolysate reached to 30% of CDW at day 5. This could be the direct result of the pH that remained ~pH 6.5.

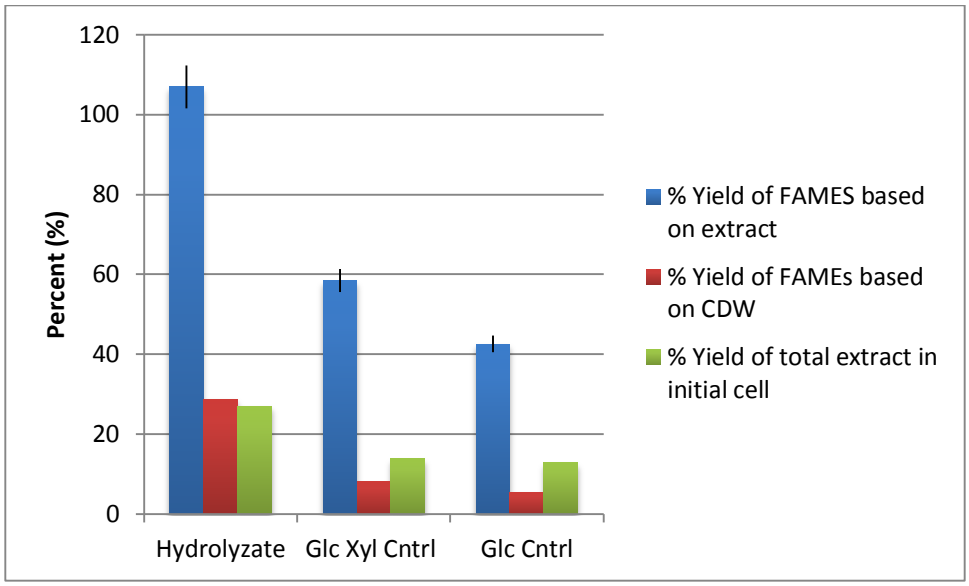


***Figure Q32**. Percentage of FAMEs extracted from R. glutinis*.

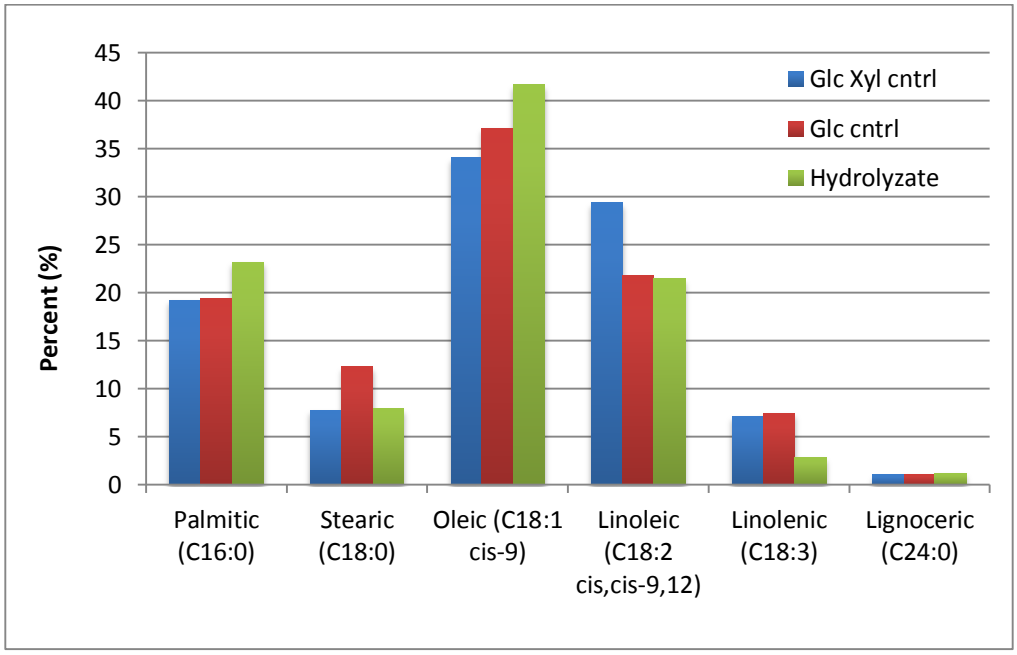


***Figure Q33**. FAMEs composition profile.*

The FAMEs data indicate that lipid content in hydrolysate at day 5 almost fully converted to FAMEs (Figure Q32). This could be due to the ink content or could be due to the neutral pH. The FAMEs profile shows that *R. glutinis* accumulated mainly Oleic, Linoleic and Palmitic acids in all three cases (Figure Q33).

Summary

In conclusion, production of lipid via oleaginous yeast in paper hydrolysate is a possible approach for biodiesel production. Data shows that the sugars in hydrolysate can be used as the substrate when there are limited amounts of inhibitory compounds in the hydrolysate.

Subtask Q.3 Develop *in-situ* production of biodiesel
Conventional in-situ reactions (60 °C, atmospheric pressure, and catalyst) of modified (e.g., oil accumulation stage) and unmodified activated sludge were compared with in-situ supercritical methanol treatment (relatively high temperatures and pressures, and no catalyst). The wet microbial mixture was loaded into a reactor with the reactants, eliminating the drying, and combining extraction and reaction in one step. The supercritical methanol process eliminates the need for a catalyst, and could potentially increase the biodiesel yield.

Planned Activities:
Q.3.ML.1 Reduce or eliminate the cost of biocrude extraction and conversion into biodiesel.

Summary of Activities:
The aim of this study was to evaluate the optimal reaction conditions for the direct transesterification of sludge while increasing biodiesel yield; and then comparing yields and efficiency to the 2-step method of hydrolysis and esterification to evaluate the possibility of reducing methanol consumed, while increasing biodiesel yield. *Rhodotorula glutinis* is used as a surrogate for sludge to optimize reaction conditions. This study allowed the determination of the mechanism occurring in the reaction and the effect of water in the system. The overall aim was to evaluate an alternative, cost-efficient method for producing biodiesel from sludge directly and avoiding the costs involved with drying the sludge, adding and separating catalysts.

A new batch of *Rhodotorula glutinis* was grown and samples were analyzed for lipid content using the Bligh-Dyer method. Gravimetric analysis showed a Bligh-Dyer lipidic extract of 41 $\pm$ 1.7 % cell dry weight (CDW). The percent fraction of total mono-, di-, and tri- glycerides in this unreacted extract was 44 $\pm$ 1%. Of which 2 $\pm$ 1% were monoglycerides, 5 $\pm$ 2% were diglycerides, and the bulk, 38 $\pm$ 1% were triglycerides.
<u>In situ transesterification yield at 60 °C</u>

To estimate biodiesel yield and fatty acid profile, Bligh-Dyer extraction was conducted on 0.2mg of dry RG cells and the in-house method of tranesterification of the Bligh-Dyer lipid extracts was used to produce FAMEs, which were analyzed and quantitated by gas chromatography.

For the transesterification, 2ml of a 2% (v/v) sulfuric acid in methanol was added to the lipid extract samples, vortex-mixed, and heated at 60 °C in a water bath for 2 hours. The samples were cooled to room temperature and quenched with 5 mL of an aqueous solution containing 3% (w/v) NaCHO3 and 5% (w/v) NaCl. FAMEs were extracted from the reaction mixture with two washings of 2 mL toluene containing 200 ug/ml of 1,3-dichlorobenzene as the internal standard and 100 ug/ml of BHT as an antioxidant. The toluene extracts were dried using anhydrous sodium sulfate and diluted as needed.

The yield of FAMEs from this reaction was 14.8 $\pm$ 1.2% based on the extract mass and 19% $\pm$ 1.7 % based on the initial 0.2g of dry RG cells.
<u>Timed results at 250 °C, 90% water content from 10 – 60 minutes</u>

Previous experiments varying reaction time from 30min to 1.5hr for 0.2g of RG with 90% water content at 300 °C showed that FAME yields (based on initial 0.2g of cells) were not significantly different, as seen in Figure Q34 below.

FAME Yield on *Rhodotorula glutinis* as a function of Time
At 30 ml:1 g, 300 °C

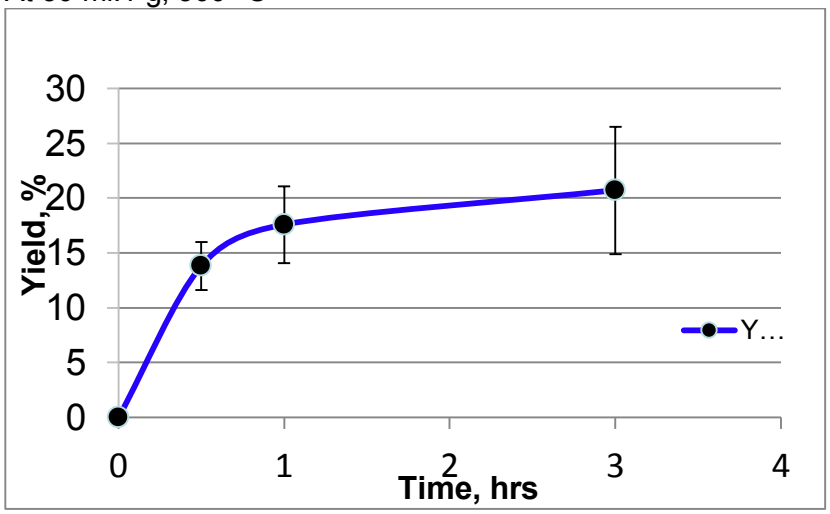


Figure Q34 *- Data on effect of reaction time*

Therefore, we conducted some more experiments to study conversion of glycerides and generation of FAMEs in a lower range of 1 hour total reaction time at 10-minute intervals. Since the internal temperature probe could take 12 – 20 minutes to settle at the temperature setpoint for a given reaction, the reaction time for these tests was started immediately after dropping the reactors into the sand bath to not miss the conversions that take place in the first couple minutes of heating. This helped us investigate if there were any significant changes in FAME yield at a lower reaction period (region between 0 and 1 hour as seen in Figure Q.34 above) and to investigate the concentration changes in glycerides and FAMEs as reaction time progressed. We chose a reaction time of 250 °C for this test because previous data collected comparing 275, 300 and 325 °C showed that the FAME yields at the same condition were not significantly different and we wanted to test if the results achieved at 250 °C were comparable to yields between 270 and 325 °C, which would help reduce costs. Figure Q.35 below shows the progression of the glyceride and FAME components in the reaction with time:

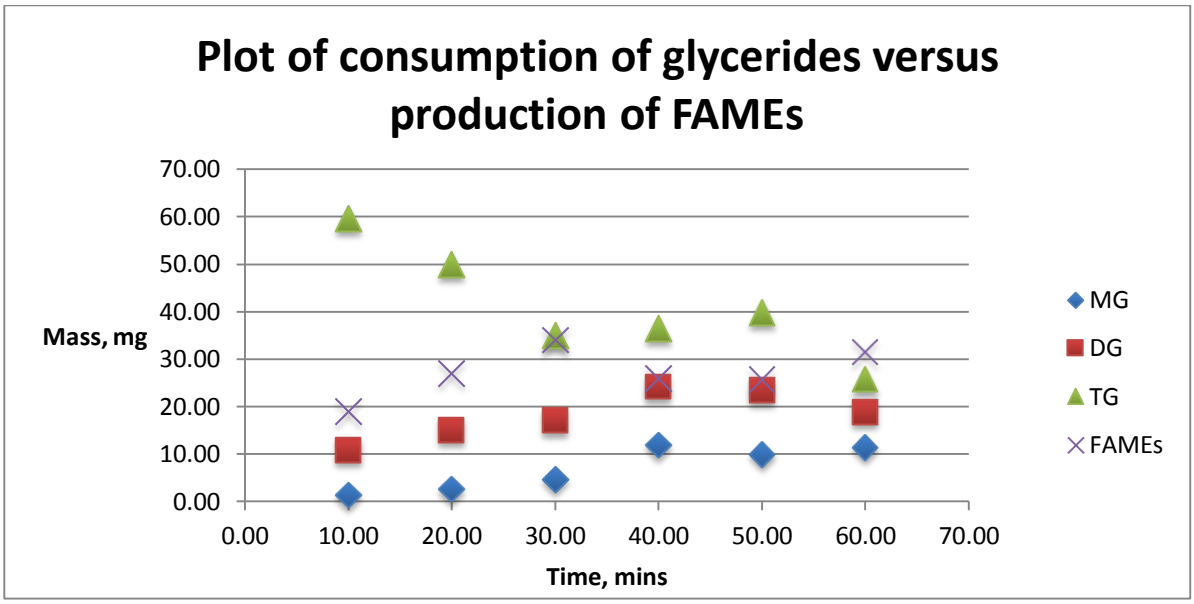


Figure Q35 - *Reaction progression between 0 and 60mins*

In the first 30 minutes, the trends on the 4 components are as expected with triglyceride amounts decreasing as it is being converted to diglycerides and monoglycerides, and FAMEs increasing as it is being produced from the glycerides as seen in the mechanism below.

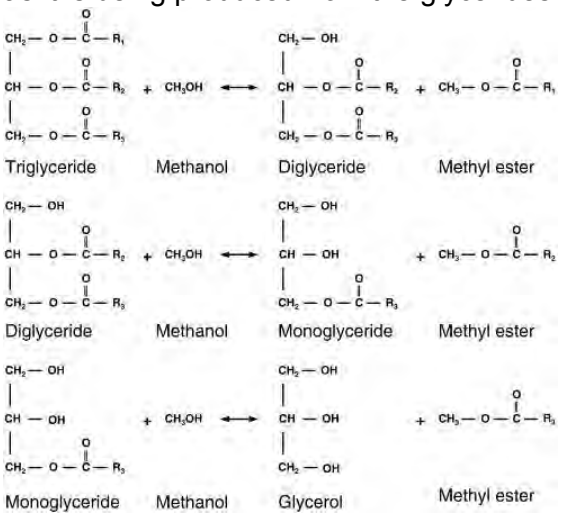


Figure Q36 - *Triglyceride conversion mechanism*

After the 30 minute sample, the glyceride amounts seem to stabilize at the 40 and 50 minute times although the triglyceride amount still decreases a little at the 60 minute sample and the FAME increases at the 60 minute time. These results between the 40 – 60 minute time periods might be due to equilibrium occurences or could also include some experimental error as there were some accuracy issues with the replicates unlike the 10 – 30 minute samples which have 2 replicates. Also, the 40 – 60 minute reactions were run on a different day. (Typically, the method used is to place 3 reactors with the internal probe reactor in the sandbath once it's at the set point, and then remove each reactor at the respective time interval).

Based on the glyceride consumption and FAME production, we can conclude that the reaction time does not need to be higher than 30 minutes as we didn't get a higher yield in FAMEs past that. This time determined can be used as a basis for running other reactions.

Most of the reaction conversions take place in the first 30 minutes after which they seem to equilibrate. For studying kinetics and proposing a mechanism, it would be ideal to have more sample points in the first 30 minutes. Although that brings a concern about studying the mechanism at a set temperature since it takes 12 – 20 minutes for the internal temperature probe to reach the set point. For this we could try increasing the temperature of the sand bath way 30 °C higher than the setpoint before dropping in the reactors and then switching the controller temperature back to the desired setpoint to reduce the heat up time. Currently we've tried his method but usually use only about 15 °C higher. If that works favorably, then we might be able to take more samples within the 30 minute period and still capture the early reaction conversions e.g. at 5-minute intervals.

All glyceride samples were derivatized using a modified ASTM D6584 method before analysis. 125ul of 8mg/ml tricaprin in pyridine and 100ul mstfa were added to the mass being analyzed, allowed to sit at least 20 mins, and diluted with 3775 ul of plain chloroform before being shot on the high-temperature GC.

Conclusions:

The 2 hour *in situ* transesterification at 60 °C of the bligh-dyer extract from the same 0.2g mass of cells used yielded only approximately 4.8% while the FAME yield obtained from 10 minutes of 250 °C reaction with supercritical methanol was 10% (based on initial 0.2g of dry RG cells). The 10-minute time being the lowest tested so far and not yet optimized for maximum yield, the supercritical methanol process still looks promising.

Another key component that could produce FAMEs in the mixture is fatty acids since hydrolysis of triglycerides could also occur in the bligh-dyer procedure to produce fatty acids. Identifying the fatty acids in the sample will help close the mass balance and that work is in progress. This would also help in optimizing and increasing FAME yield when we study the 2-step mechanism in detail, evaluating if the combination of hydrolysis followed by esterification could bring higher yields in a relatively short time and still be economical.

Subtask Q.4 Generate a new consortium of biocrude producting microorganisms using a combination of novel biomolecuar and traditional microbiological techniques.
Samples from experiments in Task Q.2 were sent to the EPA for DNA extraction and PCR assays. PCR products were be used for cloning, and the transformed cell plated for later sequencing. Primers were developed to measure growth and survival of oil-accumulating microorganisms under specific experimental conditions. A consortium of these identified microorganisms were developed and tested using industrial and/or municipal wastewaters and different carbon sources.

Planned Activities:
Q.4.ML.1 Develop a robust microbial consortium capable of yielding over 25 lbs of oil/100 lbs of carbon.

Summary of Activities:
The variation in the composition of the activated sludge microbial population with fermentation time and C:N ratio is illustrated in Figs. Q37-Q39. Although **t**he composition of activated sludge microbiota has been studied previously [Snaidr, et al., 1997], to our knowledge this is the first time sludge microbial communities have been studied under conditions conducive to enhanced lipid

accumulation. 16S rRNA gene clone libraries were developed from the samples obtained at different C:N ratios since C:N ratio was found to exert a significant effect on lipid accumulation in activated sludge. As shown in Fig. Q37, members of the *Proteobacteria* (gram-negative bacteria) phylum dominated the raw sludge samples (Day 0) prior to the treatments (58.4 %) followed by *Bacteriodetes* (26.6 %). Similar results have been found in previous studies conducted by other researchers on different activated sludge systems [Wagner and Loy, 2002; Eschenhagen, et al., 2003]. Among the *Proteobacteria,* gamma- and beta-like sequences dominated, accounting for 40.5 and 29.3 % of the *Proteobacteria* sequences, respectively. Alpha and delta-like Proteobacteria sequences were approximately 14.6 and 13.1 % of the total *Proteobacteria* sequences, respectively. On the other hand, most of the *Bacteriodetes* sequences identified (85 %) were found to be closely related to *Sphingobacteria*. *Verrucomicrobia*-like sequences were close to 7 % of the Day 0 library, while other groups represented less than 1 % each (i.e., gram-positive bacteria or *Firmicutes*, TM7, *Gemmatimonadetes*, OP10, SR1, *Chloroflexi*).

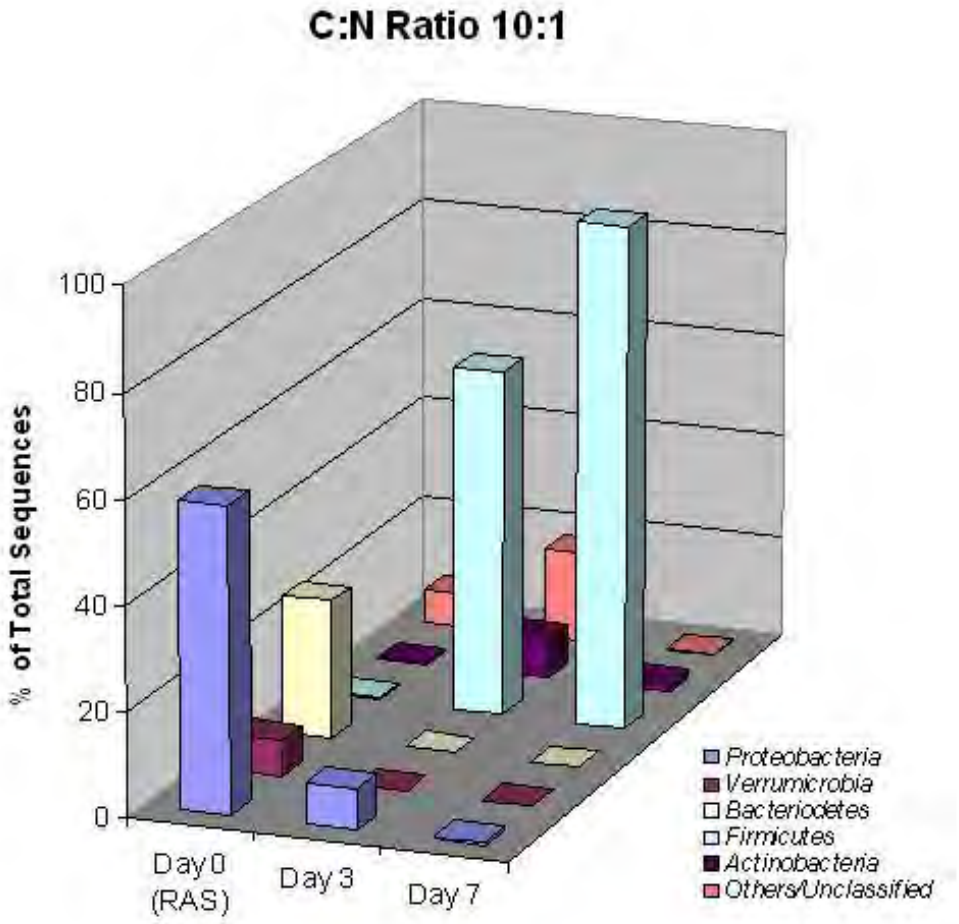


Figure Q37*: Variation in activated sludge microbial composition with cultivation time at C:N ratio 10:1. Total sequences: Day 0 (274), Day 3 (166), and Day 7 (180).*

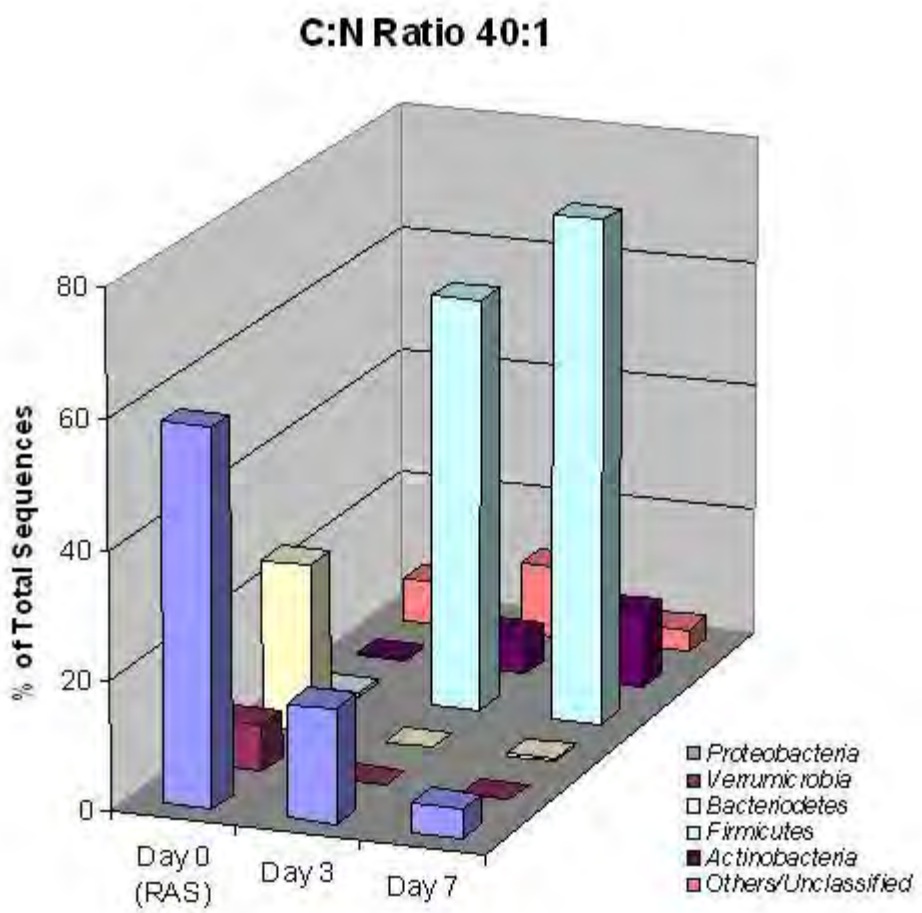


Figure Q38: *Variation in activated sludge microbial composition with cultivation time at C:N ratio 40:1. Total sequences: Day 0 (274), Day 3 (185), and Day 7 (183).*

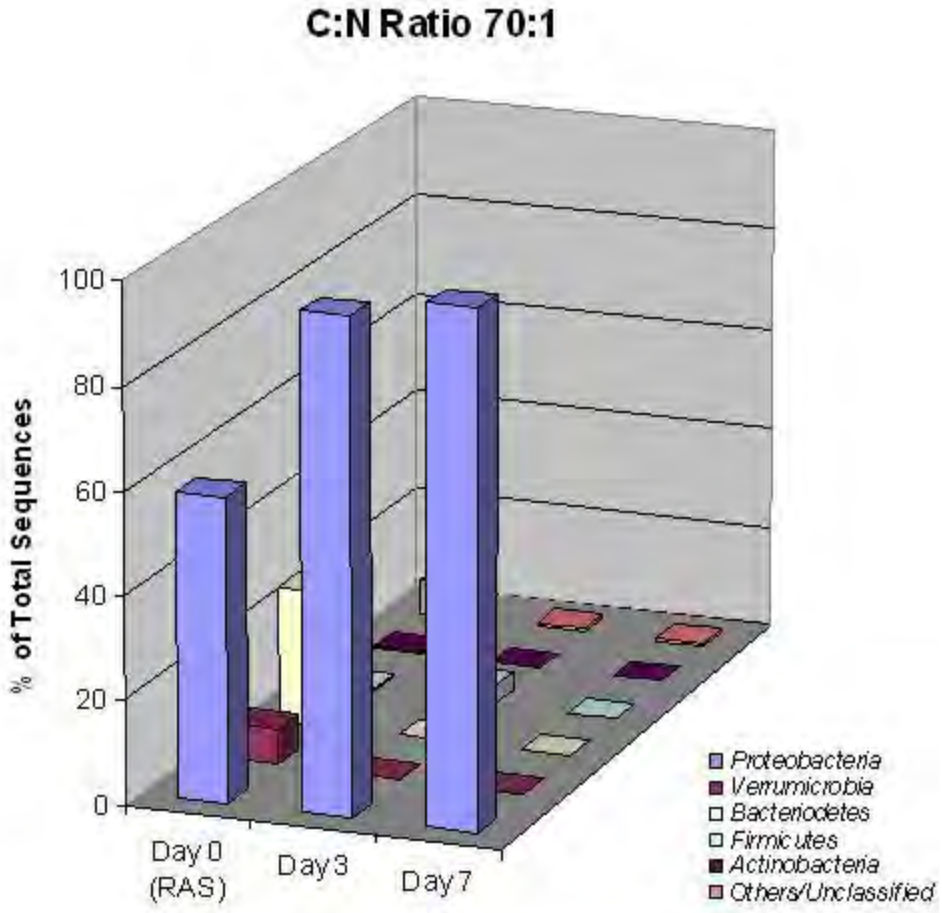


Figure Q39: *Variation in activated sludge microbial composition with cultivation time at C:N ratio 70:1. Total sequences: Day 0 (274), Day 3 (175), and Day 7 (189).*

Significant changes in microbial composition were observed for each of the treatments after 3 d, which corresponded to the onset of the stationary phase and lipid accumulation in the case of C:N ratio 70:1 (Fig. Q39). At C:N ratio 10:1 (Fig. Q37) and C:N ratio 40:1 (Fig. Q38), *Firmicutes* increased from 0.6 to 67 and 65 % of all sequences, respectively. Most *Firmicutes* sequences (78-86 %) were closely related to members of the *Clostridia* class and the rest belong to the *Erysipelotrichi* class. *Proteobacteria* decreased considerably in numbers, representing less than 18% (i.e., 7.8 % for C: N 10:1 and 17.8 % for C:N 40:1) of the sequences, most of which were gamma-like sequences. In contrast, *Actinobacteria* increased to 7.8 and 5.9 % in the C:N ratio 10:1 and C:N ratio 40:1 Day 3 libraries, respectively and no *Bacteroidetes* sequences were found in any of the treatments. After 7 d, *Firmicutes* proportion increased further to 97.2 and 79.2 % of the total sequences at C:N ratio 10:1 and C:N ratio 40:1, respectively. In this group, *Clostridia* was the dominant class, accounting for around 85 % of the *Firmicutes* sequences. Within the *Clostridia* class, *Sporacetigenium*- and *Turicibacter*-like sequences were the majority. Similar to other *Clostridia*, *Sporacetigenium*- and *Turicibacter*-type species are considered obligate anaerobic bacteria. The fact that these microorganisms dominated in aerated bioreactors suggest that some of their close relatives might be tolerant to aerobic conditions or that there are microniches within these systems that can promote anaerobic growth. The changes in composition favoring *Clostridia* as abundant bacteria in the C:N ratio 10:1 and C:N ratio 40:1

samples can be explained by the utilization of potentially available carbohydrates such as glycerol, a process that could result in the production of value added products such as butanol [Taconi, et al., 2009].

As shown in Fig. Q39, the C:N ratio 70:1 microbial community was vastly dominated by Proteobacteria (96 %) after 3 d, most of which were gamma *Proteobacteria* (90.4 % of *Proteobacteria* sequences). Some of the most abundant gamma *Proteobacteria* at this stage of the fermentation were members of orders *Enterobacteriales, Pseudomonadales,* and *Aeromonadales*, which were below detection limits in the initial sludge community. In a previous study, some members of these orders (genera *Pseudomonas* and *Aeromonas*) have been isolated from municipal sewage sludge as producers of polyhydroxyalkanoates (PHA) under similar conditions with the present study [Reddy, et al., 2008]. Further, extracellular polysaccharide (EPS) formation has been detected in bacteria of the orders *Rhodospirillales, Sphingomonadales, Xanthomonadales, Enterobacteriales* and *Pseudomonadales* [Vu, et al., 2009]. These microbial storage products could possible take into account the unsaponifiable fraction of the lipids not converted to biodiesel, which constitutes a significant fraction (40 to 50 %) of the total lipid extracts.

Nearly all of the C:N ratio 70:1 sequences (99%) were alpha *Proteobacteria* after 7 d, indicating a significant shift in microbial composition, specifically from gamma to alpha *Proteobacteria*, at which time span maximal lipid contents in the activated sludge biomass were obtained. Most of the alpha-like sequences (99.5 % of total *Proteobacteria* sequences) were closely related to *Acidomonas methanolica*, a member of the *Rhodospirillales* order under the *Acetobacteraceae* family, which are known acetic acid producers [Wilkinson, 1988], which interestingly was not detected in the initial sludge community. No mention has yet to be found in literature regarding lipid accumulation by any member/s of this bacterial groups; however, the dominance of oleic acid (C18:1) followed by palmitic acid (C16:0) in the fatty acid profile of lipid extracts obtained from activated sludge grown in the same conditions could be accounted for by the dominance of this particular group in the late stages of the C:N ratio 70:1 culture. Bacteria belonging to the *Acetobacteraceae* family have characteristic fatty acid profiles having 70 – 80 % oleic acid and 10 – 20 % palmitic acid [Wilkinson, 1988] while the final activated sludge biomass contained lipids with 50 – 60 % oleic acid and around 20 % palmitic acid. It should be noted however that the lower oleate levels in activated sludge compared with the specific *Acetobacteraceae* family is probably due to the fact that activated sludge is a mixed culture. Despite the apparent dominance of one family in the total bacteria, it should also be considered that other microbial groups such as yeasts and fungi have not been investigated for their population dynamics in activated sludge; hence it is possible that these eukaryotes are present in the sludge community as well contributing to the enhanced lipid production.

Conclusions:

The composition of the microbial community in municipal sewage sludge was analyzed at different initial C:N ratios of the fermentation media for enhanced lipid accumulation. Results showed that the microbial composition of activated sludge changed considerably from being in its raw form in the municipal wastewater treatment plant and after aerobic cultivation in synthetic wastewater supplemented with sugars (glucose) at different initial C:N ratios. After 3 and 7 d of fermentation, the microbial composition of cultured activated sludge was very similar at low (10:1) and medium (40:1) C:N ratios and both were significantly from that at obtained at high C:N ratio (70:1). The results also suggested that prolonged exposure to any of these conditions led to a significant reduction in the diversity of the activated sludge microbiota, in terms of the bacterial population. Since it was found in the earlier phases of the study that the lipid productivity of activated sludge microorganisms was highest at C:N ratio 70:1, the dominance of members of the alpha

Proteobacteria group in the resulting activated sludge culture at this condition could point to the specific microorganisms potentially responsible for high lipid accumulation among the numerous members of the activated sludge microbiota for potential isolation and use in pure culture fermentations.

Subtask Q.5 Supply chain design and management

Designing the biocrude supply chain means identifying for each municipal and industrial wastewater treatment facility the refinery where biocrude would be shipped for further processing, the location of the plant that will provide lignocellulosic sugars, and companies that will provide waste. Managing the biocrude supply chain means identifying a production schedule for biocrude and identifying a transportation schedule that minimizes biocrude-supply-chain-related costs. Mathematical (mixed integer programming) models will be used to design these supply chains and estimate the cost of biocrude.

Planned Activities:

Q.5.ML.1 Build solution procedures for the problems proposed that provide good quality solutions.

Summary of Activities:

The work is focused on developing mathematical models in support of supply chain decisions for production and delivery of biodiesel via wastewater treatment. We develop a mixed integer, two-stage stochastic programming model to design and manage biodiesel supply chains. This model is an extension of the classical two-stage stochastic location-transportation model. The proposed model optimizes not only costs but also emissions in the supply chain. The model captures the impact of biomass supply and technology uncertainty on supply chain-related decisions; the tradeoffs that exist between location and transportation decisions; and the tradeoffs between costs and emissions in the supply chain. The objective function and model constraints reflect the impact of different carbon regulatory policies, such as carbon cap, carbon tax, carbon cap-and-trade, and carbon offset mechanisms on supply chain decisions. We solve this problem using algorithms that combine Lagrangian relaxation and L-shaped solution methods, and we develop a case study using data from the state of Mississippi. The results from the computational analysis point to important observations about the impacts of carbon regulatory mechanisms as well as the uncertainties on the performance of biocrude supply chains

See appendix for computer models.

Publications:

B. Sukhbaatar, W.T. French, M. Green, L. McFarland. Production of biodiesel via *Rhodotorula glutinis* using waste paper hydrolysate. Bioresource Technology. (In preparation).

Marufuzzaman, M, S.D. Ekşioğlu, Y. Huang, "Two-Stage Stochastic Programming Model for Biocrude Supply Chain," *Computers and OR*, Vol. 49, 2014, 1-17. http://dx.doi.org/10.1016/j.cor.2014.03.010

Presentations:

B. Sukhbaatar, M. Green, L. McFarland, W.T. French. Lipid accumulation of *Rhodotorula glutinis* grown in waste paper hydrolysate. 105th AOCS Annual Meeting & Expo, American Oil Chemist Society, San Antonio, TX. May 3-7, 2014.

Task R. Microbial Oil

Principal Investigators and team members
Todd French, Dave C. Swalm School of Chemical Engineering
Rafael Hernandez, University of Louisiana at Lafayette, Department of Chemical Engineering

Executive Summary
The Microbial Oil thrust area focuses on the generation of oils by single or consortiums of oleaginous microorganisms using a variety of carbon sources, either singularly or in combination. The composition of these oils is primarily triglycerides and as such can be readily converted into biodiesel or renewable diesel. The Microbial Oil thrust utilizies the biocrude pilot system to conduct experiments to confirm growth and oil production kinetics, yield, and nutritional requirements at a larger scale. Many of the proposed research and development activities for SERC IV were conducted in partnership with industry and government. As part of these efforts, the microbial oil technology was integrated with heterotrophic algae to maximize oil production. Pure oleaginous microorganisms, consortiums of oleaginous microorganisms, pure oleaginous heterotrophic algal strains, and hybrid algae-oleaginous consortiums were evaluated to generate oils from a variety of different carbon inputs, including timber waste, cultivated crops, paper waste, glycerol, chitin-containing waste, and selected industrial waste streams. The resulting oils were used to produce diesel fuel to potentially operate a demonstration vehicle at MSU. An important milestone was to comply with oil specifications for oil refining and ASTM fuel standards. In addition to the biofuels from the lipids, Microbial Oil thrust-area researchers continue research and development activities in the areas of value-added products from the residuals. Extraction and production of new products, such as pigments, animal feeds, and specialty chemicals, from the oils and residuals were explored. In cooperation with the Biocrude thrust, separation technologies were developed to minimize energy inputs for oleaginous microorganisms and algae-related processes.

Subtask R.1 Determine the yield and rate of the cells and oil production from selected carbon sources

Sugars are a major cost in the production of biofuels. Microbial processes that are flexible in terms of their ability to convert multiple carbon inputs into fuel or fuel feedstocks would have an obvious advantage over systems that have specific sugar requirements. The objective of this task is to determine the effect that combinations of carbon sources would have on the growth of the oleaginous microorganisms and their oil yields. The carbon sources to be investigated are lignocellulosic hydrolyzates from cultivated crops, such as switch grass and trees, waste paper hydrolyzates, chitin-containing wastes, such as shrimp, crab, and crawfish shells (also a source of nitrogen), waste-paper hydrolyzates, glycerol, and wasted flour from breading processes. The Microbial Oils thrust has demonstrated that pure oleaginous yeast has the ability to convert all of the previously mentioned carbon sources into cellular mass and lipids. This study will investigate the next step, combining the carbon sources.

Planned Activities:
R.1.ML.1 Convert 75% of the carbon source by these organisms.
R.1.ML.2 Achieve cell densities of greater than 5 g/L with lipid contents greater than 20%.
R.1.ML.3 Maximize yield of lipids/g of substrate.

Summary of Activities:
Characterization of Lipid Accumulation by Rhodococcus rhodochrous When Grown in Model Lignocellulosic Sugars and Inhibitors

Rhodococcus rhodochrous is a gram-positive bacterium with a wide array of degradative capabilities. Our interest in R. rhodochrous is in its potential ability to utilize lignin-derived compounds as carbon sources for lipid accumulation. While we have previously shown the survival of R. rhodochrous in phenol, the most basic component of lignan, we are currently working on optimizing culture conditions for maximum cell mass and lipid yield by using glucose as the sole carbon source. Despite the widespread use of R. rhodochrous in degradation research, the understanding of its ability for lipid accumulation is limited.

Previous experiments have shown promise of lipid accumulation by *R. rhodochrous* along with the ability to utilize both glucose and phenol as carbon sources. However, growth in these conditions was slow and yielded minimal cell mass. The overall goal of this research was to identify lignocellulosic substrates that would encourage lipid accumulation by *R. rhodochrous*. The first objective was to characterize *R. rhodochrous* as oleaginous and so optimization of growth conditions was necessary to produce a large biomass of *R. rhodochrous* to evaluate its lipid accumulation capabilities. The second objective was to use model lignocellulosic sugars (glucose and xylose) and inhibitors (acetic acid, furfural, and phenol) to evaluate growth and lipid accumulation of *R. rhodochrous*. A series of shake-flask experiments were used to optimize media conditions and evaluate carbon sources that encourage lipid accumulation. A BioFlo 410 fermenter was used to show lipid accumulation on a larger scale. Lipids were analyzed using thin-layer chromatography and FAMEs analysis. A collaboration with ORNL allowed for genomic sequencing of our strain to provide further insight into the lipid accumulation capabilities of *R. rhodochrous*.

Experimental Set-up

Organism Culture

A freezer stock of *R. rhodochrous* was streaked on nutrient agar plates, which were then incubated for 4 days at 30C. Plates with pure culture growth were scraped using sterile loops and cells were collected in an aliquot of the Sorkhoh medium. Cells were vortexed to create a homogenous solution and then equal amounts of cell suspension were distributed to each flask or directly into the fermenter.

Media optimization

A shake-flask experiment was designed to culture *R. rhodochrous* in two different minimal salts medium (30g/L and 10g/L glucose), sugar broth (60g/L glucose), and Sorkhoh medium (10g/L glucose). Glucose concentration was analyzed using a YSI 2900. Absorbance was taken to monitor growth. Cells from all treatments were harvested daily and lipids were extracted from total cell dry weight.

Based on the previous experiment, a shake-flask experiment was then designed to culture *R. rhodochrous* in 10g/L, 20g/L, or 40g/L glucose-supplemented Sorkhoh media.

Shake-Flask experiments

The medium was supplemented with 20g/L glucose for inhibitor experiments and glucose controls and 10g/L xylose with or without 10g/L of glucose for xylose experiments. Acetic acid (3g/L) and furfural (0.3ml/L) were sterile filtered and added to the glucose medium as model inhibitor compounds and the pH was adjusted to 7.0 using sterile sodium hydroxide. Phenol experiments used 1g/L phenol supplemented Sorkhoh medium and a mix of 1g/L phenol and 20g/L glucose. All experiments were conducted in triplicate and incubated in baffled flasks at 30°C in a shaking incubator at 125 rpm (New Brunswick Scientific Model I26, Edison, New Jersey). The mean and standard deviation were calculated for all analyses.

Fermenter Set-up
A glucose solution was sterilized in the Bioflo410 and a separate nutrient solution (Sorkhoh medium) was added after the glucose had cooled. The fermenter was inoculated as described in 2.1. Agitation was set at 200 rpm and the initial pH was 6.8. Samples of 100mL were collected every 12 hours for 48 hours and then every 24 hours until 168 hours.

Analysis
Daily samples of 50 mL of culture were transferred to a 50 mL conical tube and centrifuged (Eppendorf Centrifuge 5810R, Eppendorf, Hamburg, Germany) at 4500 rpm for 10 minutes. The supernatant was removed and used for pH (Accumet pH meter) and sugar measurements and the pellet was frozen at -20°C. Glucose and xylose concentrations were measured using an YSI 2900 Biochemistry Analyzer (YSI Incorporated Life Sciences, Yellow Springs, Ohio). Residual nitrate in the supernatant was determined using the manufacturer methods of an ICS 3000 ion chromatography system (Dionex Corp., Sunnyvale, CA) equipped with an IonPac AS16 anion exchange analytical column (250 x 4mm), AG16 guard column (50 x 4mm), and a conductivity detector.

Lipids were extracted from a freeze-dried pellet using modified Bligh and Dyer (1959) method as described by Revallame et al. (2012). The extract was filtered through glass wool into a tared amber vial. The solvent was removed using a TurboVap LV (Caliper Life Sciences, Hopkinton, MA, USA) at 50°C and a constant flow of nitrogen gas at a rate of 15psi for 50 minutes. The recovered extract was weighed to determine gravimetric lipid yield. The solvent extractables were then transesterified into fatty acid methyl esters (FAMEs) and analyzed using an Agilent 6890N gas chromatogram with a flame-ionization detector (GC-FID; Agilent Technologies Inc., Wilmington, Delaware) with a fused silica column Stavilwax-DA (30 m x 0.25 mm, film thickness 0.25 um). Oven temperature was 50-250°C with a rate of 10°C per minute. Helium was used as the carrier gas with a flow rate of 1.5 mL per minute. The detector temperature was 260°C. The retention times of internal standards were used to identify FAMEs.

Thin layer chromatography analysis was used to investigate lipid classes present in *R. rhodochrous* extractables (Fig R1-1). The dried lipid extracts were reconstituted in 1mL of chloroform and applied to a 20 x 20 cm glass-backed Analtech Uniplate™ pre-coated with 250 um silica gel-G (Sigma-Aldrich, St. Louis, MO, USA). Drummond microcaps® disposable pipettes (Fisher Scientific, Pittsburg, PA, USA) were used to apply samples (20uL) and standards (30uL). Standards of phospholipid mixture, mono-,di-, and triglycerides, and palmityl palmitate (Sigma-Aldrich, St. Louis, MO, USA) were used to represent lipid classes of interest. Plates were developed in either 94/6 (v/v) n-hexane/diethyl ether or 85/15/2 (v/v/v n-hexane/diethyl ether/acetic acid and then sprayed with a 10% (w/v) cupric sulfate in 8% (v/v) phosphoric acid to visualize bands. The plates were allowed to dry and then charred in a 150°C oven.

Genomic Sequencing
To develop a better understanding of the lipid accumulation capabilities of *R. rhodochrous*, a draft genome sequence was generated for strain ATCC 21198. The isolate of *R. rhodochrous* ATCC 21198 was purchased from American Type Culture Collection (ATCC). Genomic DNA was isolated from frozen cell pellets using the MoBio PowerSoil DNA isolation kit modified with the addition of lysozyme. 16S sequencing was used to confirm a pure culture. Sequencing was performed by the Oak Ridge National Lab.

Actual Accomplishments:
Objective 1: Characterization of *R. rhodochrous* as Oleaginous

R. rhodochrous grew better in Sorkhoh media than in the other minimal salts media and sugar broth (Fig R1). Based on this data, Sorkhoh media was used for all further experiments.

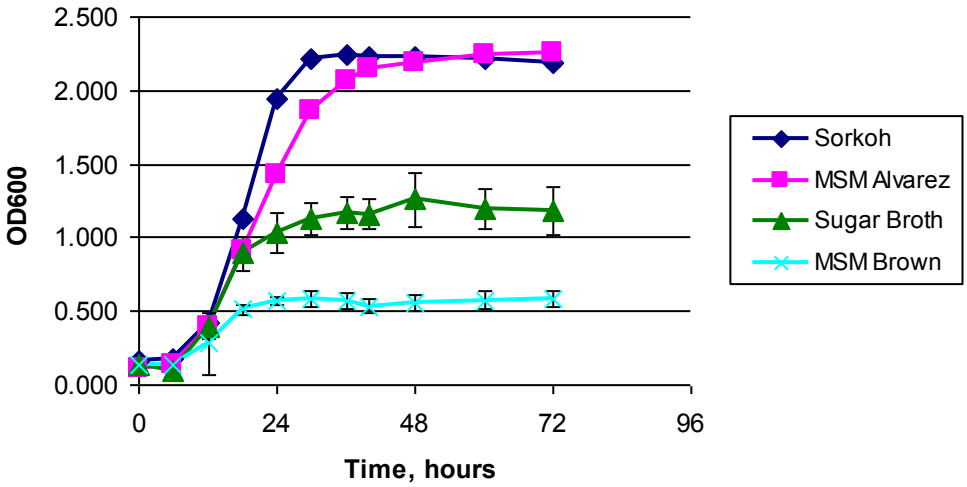


***Figure R1**. Absorbance at 600nm of R. rhodochrous grown in various media.*

Sorkhoh media was also used to evaluate glucose concentrations for optimal growth and lipid accumulation. While *R. rhodochrous* showed similar growth rates in the different concentrations of glucose supplemented Sorkhoh media (Fig R2), 54% lipid accumulation per cell dry weight was observed in the 20g/L glucose condition (Fig R3). These results suggest that given the correct media, *R. rhodochrous* can achieve cell densities over 4g/L and lipid accumulation of over 50% when grown in glucose.

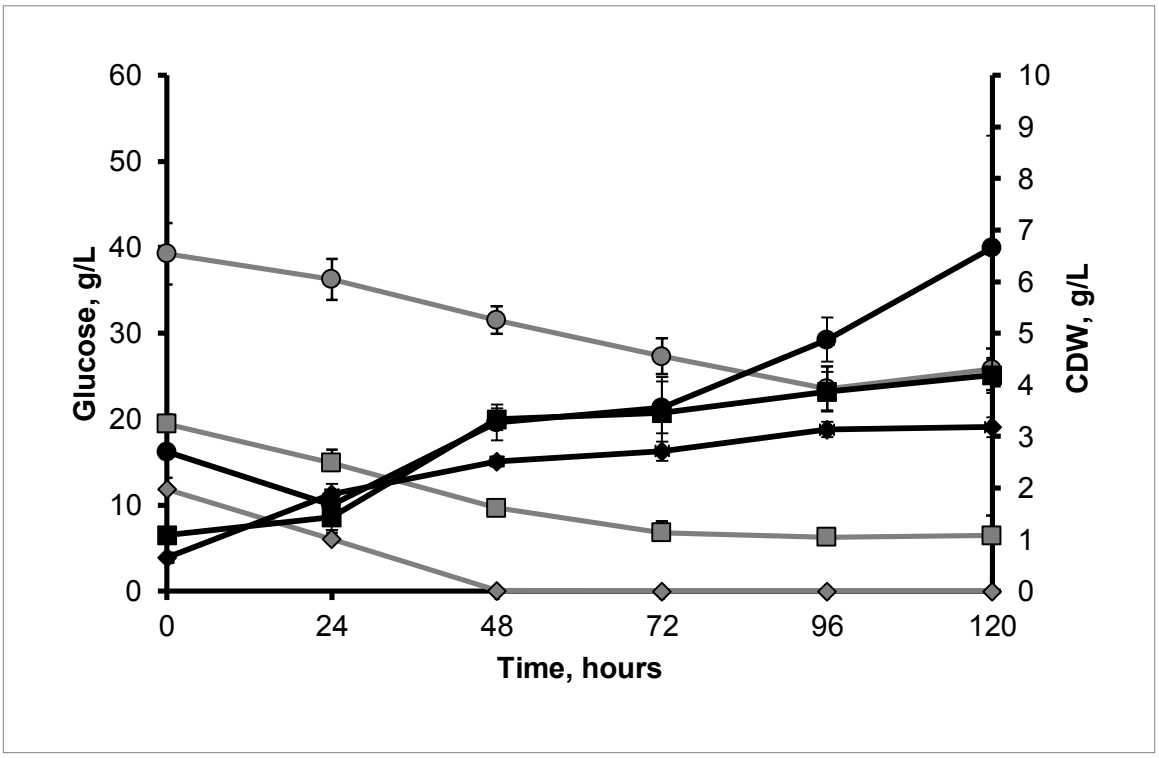


***Figure R2**. Glucose concentration (grey; g/L ±SD) and R. rhodochrous cell dry weight (black; g/L ±SD) of shake flask cultures supplemented with 10 (□), 20 (□), or 40g/L (□) of glucose.*

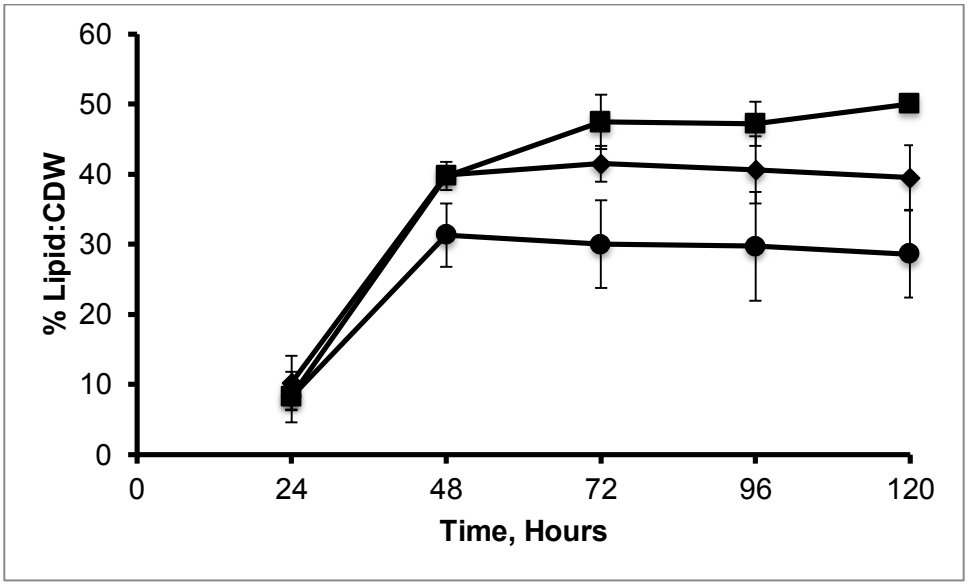


***Figure R3**. Percent lipid (±SD) of cell dry weight accumulated by R. rhodochrous shake flask cultures supplemented with 10 (□), 20 (□), or 40g/L (□) of glucose.*

R. rhodochrous was grown in a BioFlo 410 Fermenter with 7L total media volume. Despite the slow start of growth of *R. rhodochrous* in the fermenter, a 7g/L cell dry weight was still achieved (Fig R4) and gravimetric lipid results show accumulation over 40% (Fig R5). Glucose was consumed to less than 5g/L remaining sugar (Fig R4). These results are comparable to the shake flask results from previous experiments suggesting that *R. rhodochrous* can achieve replicable results at a larger scale.

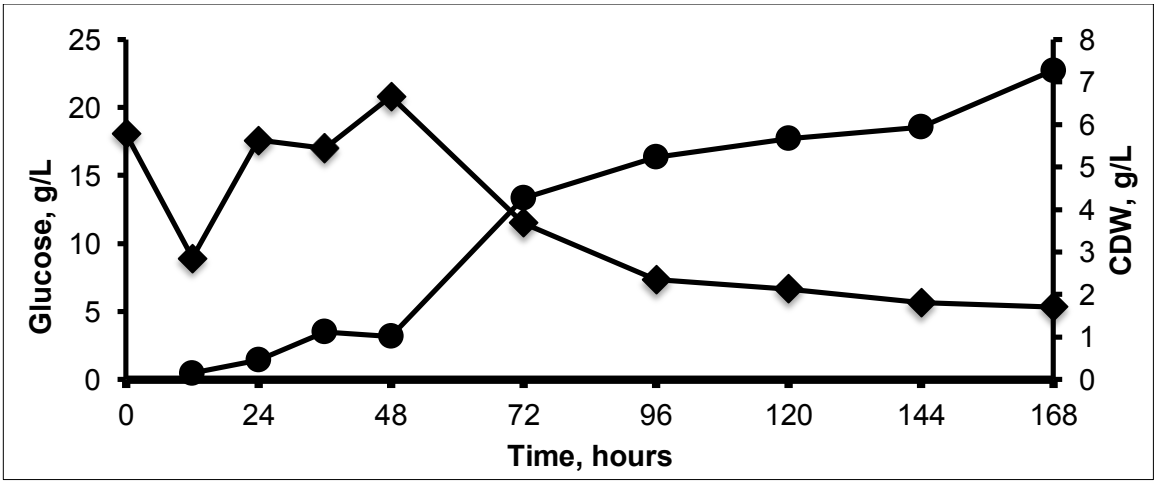


***Figure R4**. Glucose concentration (□) and R. rhodochrous cell dry weight (□; g/L ±SD) of fermenter experiment using 20g/L of glucose-supplemented medium.*

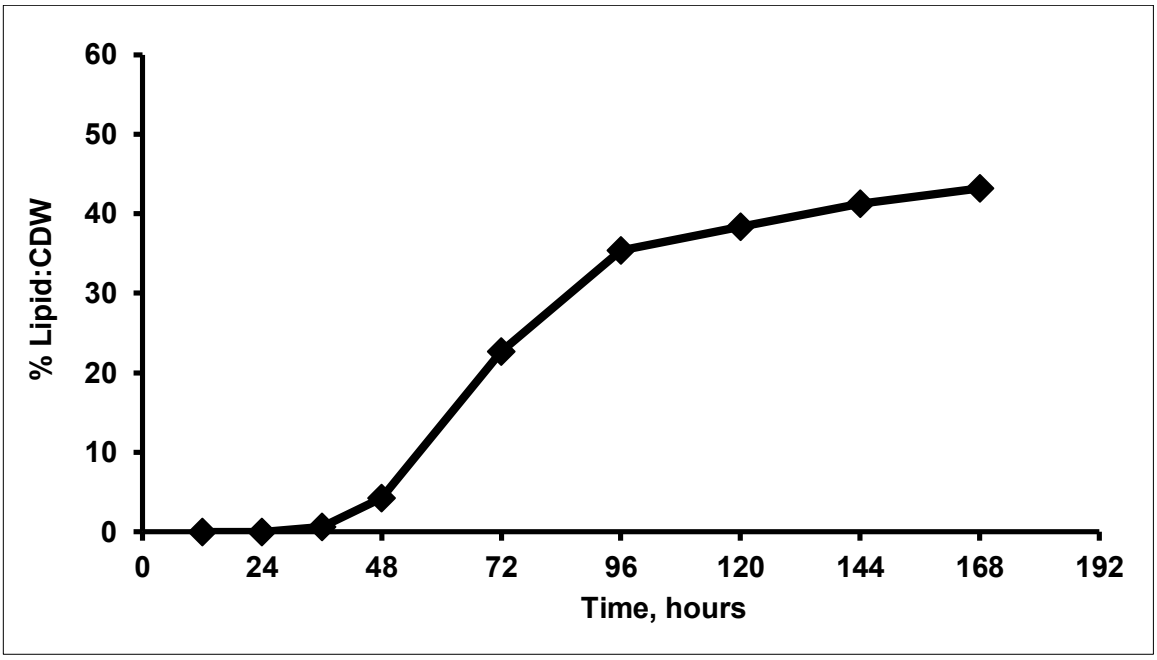
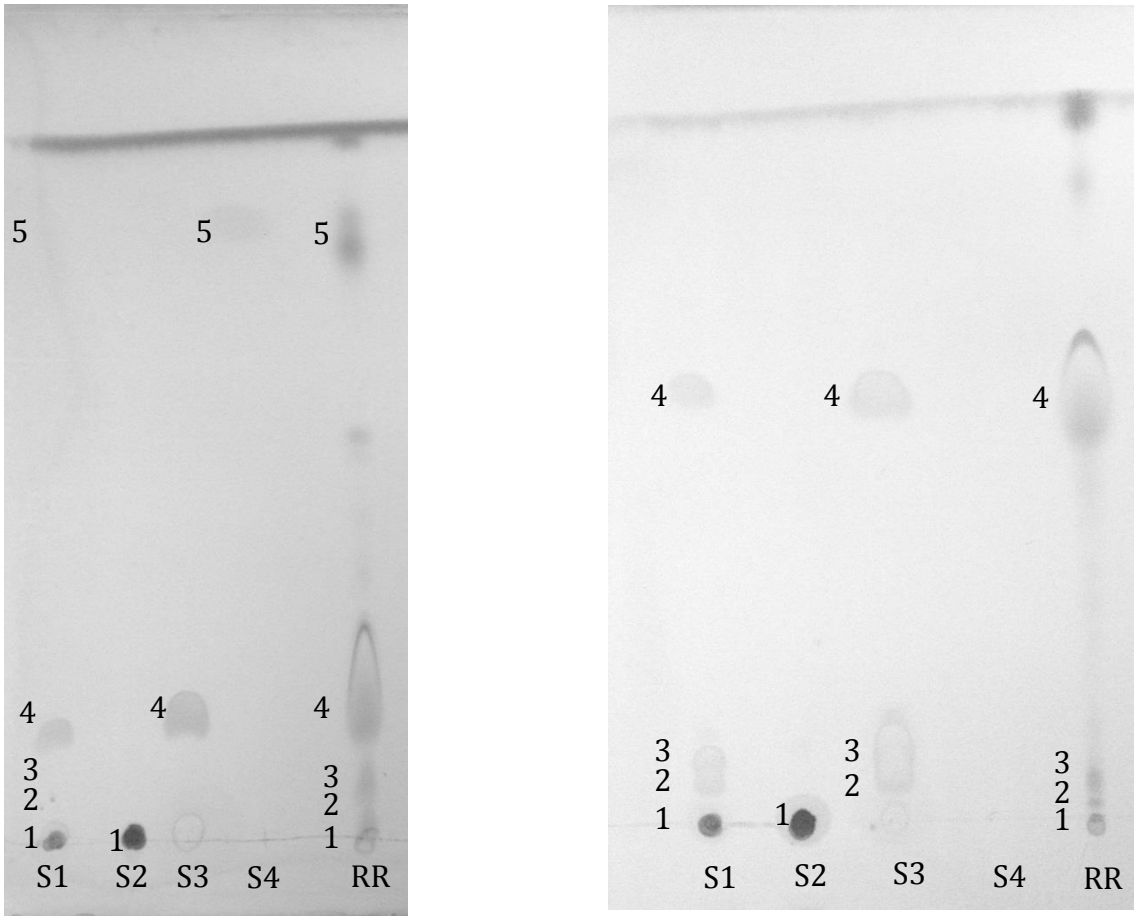


Figure R5. *Percent lipid (±SD) of cell dry weight accumulated by R. rhodochrous grown in a fermenter using 20g/L of glucose-supplemented medium.*

To further characterize *R. rhodochrous* as oleaginous, a thin layer chromatography plate was used to assess the lipid profile. The lipid extract from *R. rhodochrous* cultivated in the BioFlo410 fermenter (Fig R6-lane RR) showed bands corresponding to triglycerides (Fig R6-lanes S1 and S3), wax esters (Fig R6-lanes S1 and S4), and phospholipids (Fig R6-lanes S1 and S2).

The genomic sequencing results further support these data by identifying putative lipid associated genes. *Rhodococcus* species have been shown to produce large amounts of lipid in the form of TAGs, which is most likely due to high activity of the enzyme, acyl-CoA:Diacylglycerol acyltransferase (DGAT). Blast analysis of *R. rhodochrous* gene or2612 revealed a 90% sequence similarity to the *Rhodococcus* sp. DGAT gene. Other putative fatty acid and TAG synthesis genes were also discovered in the *R. rhodochrous* genome such as acetyl-CoA carboxylase, acyl carrier proteins, 1-Acyl-G3P acyltransferase, glycerol kinase, and glycerol-3-phosphate dehydrogenase.



(A) (B)

Figure R6*. Thin layer chromatography of lipid extract from R. rhodochrous fermenter culture (RR).*

(A) Lipid extract developed in hexane/diethyl ether (96/4). (B) Lipid extract developed in hexane/diethyl ether/acetic acid (85/15/2). S1 is a standard mixture of S2, S3, and S4. S2 is a (1) phospholipid standard mixture (S2). S3 is a mixture of (2) monoolein, (3) 1, 2-diolein, and (4) triolein. S4 is (5) palmityl palmitate.

Objective 2: To evaluate growth and lipid accumulation of *R. rhodochrous* when grown on Model Lignocellulosic sugars and in the presence of inhibitors

R. rhodochrous grew to 4g/L of cell dry weight in shake flasks with both glucose and xylose supplemented medium (Fig R7). Glucose was consumed within 48 hours, but xylose was not reduced in either treatment (Fig R7 and R8). Despite the growth observed in the glucose and xylose mixed medium, *R. rhodochrous* did not accumulate over 20% of cell dry weight as lipid (Fig R7), suggesting that xylose is not a favorable carbon source for promoting lipid accumulation in *R. rhodochrous*.

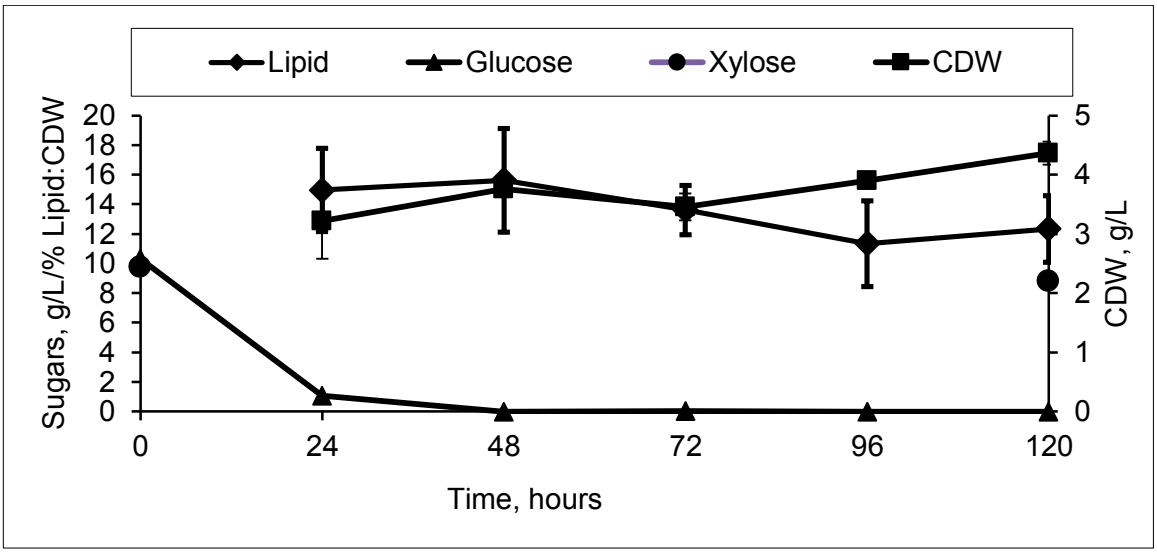


Figure R7. *Cell dry weight, lipid yield, and sugar concentration of R. rhodochrous grown in a shake-flask with xylose and glucose supplemented Sorkhoh medium.*

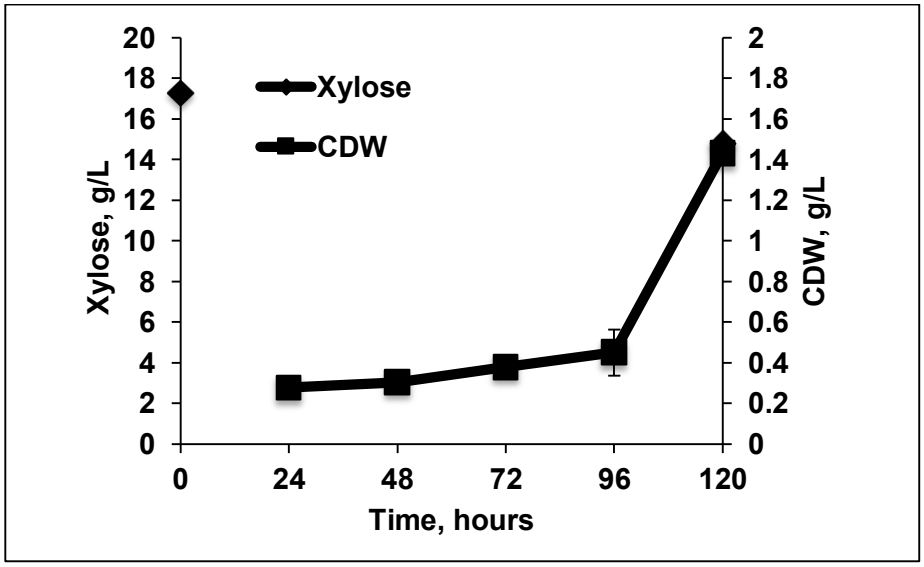


Figure R8. *Cell dry weight, and xylose concentration of R. rhodochrous grown in a shake-flask with xylose-supplemented Sorkhoh medium.*

Growth of *R. rhodochrous* as observed by cell dry weight was similar across all inhibitor treatments (Fig R9). *R. rhodochrous* achieved over 50% lipid accumulation in the glucose control and acetic acid (sodium acetate) treatments and 40% lipid accumulation in inhibitor treatments containing furfural (Fig R10), suggesting that furfural and acetic acid do not inhibit lipid accumulation. Gravimetric lipid analysis showed the largest lipid accumulation at 72H (Fig R10) and yielded 12-14% FAMEs (Fig R11). Palmitic and oleic methyl esters were most prevalent of the FAMEs in all treatments (Fig R12).

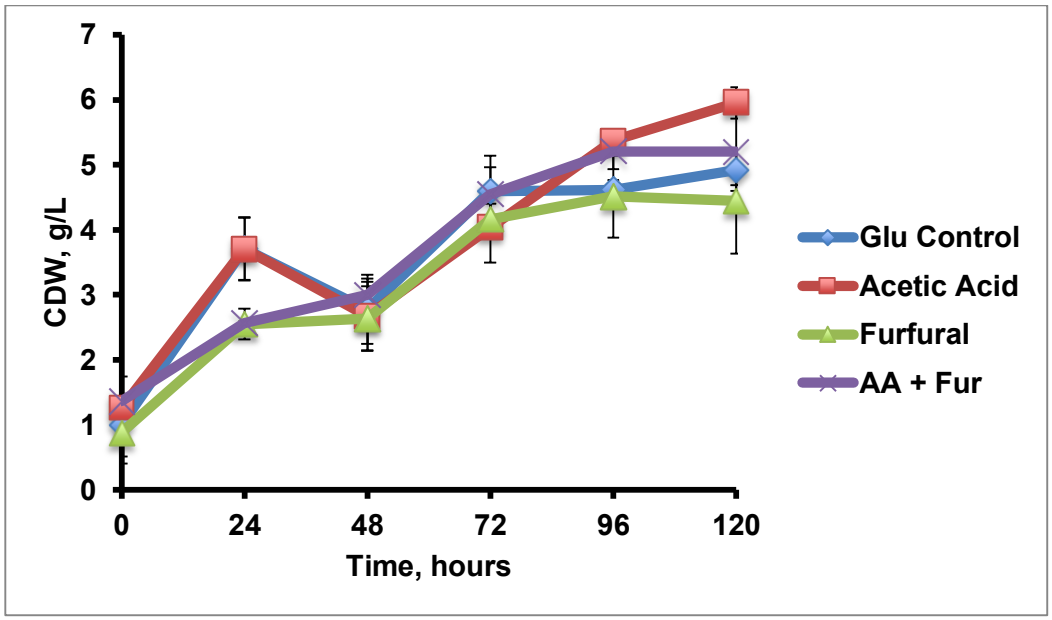


***Figure R9**. R. rhodochrous cell dry weight (g/L ±SD) of shake flask cultures with glucose and supplemented with acetic acid, furfural, or a mix of acetic acid and furfural.*

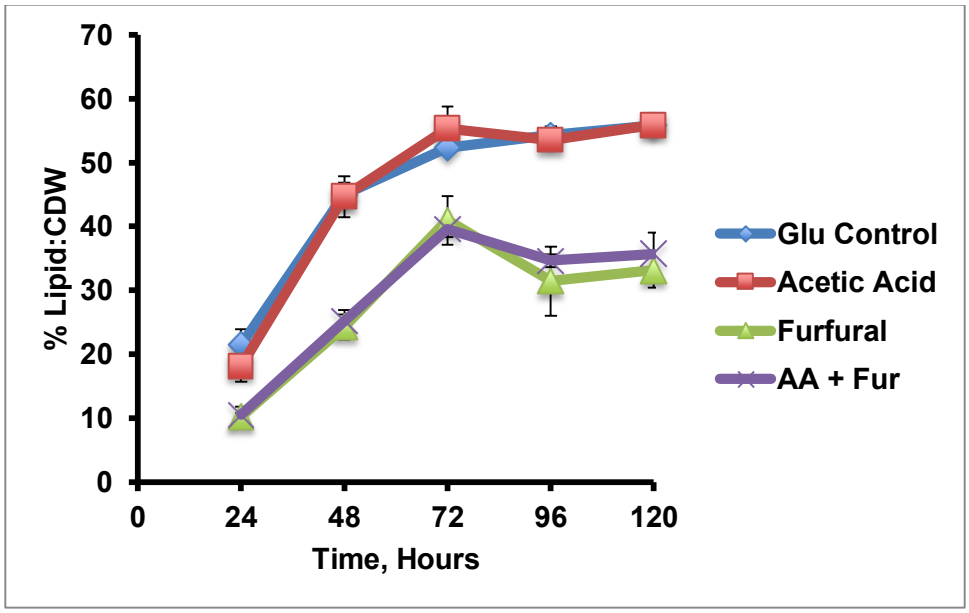


***Figure R10.** Percent lipid (±SD) of cell dry weight accumulated by R. rhodochrous shake flask cultures with glucose and supplemented with acetic acid, furfural, or a mix of acetic acid and furfural.*

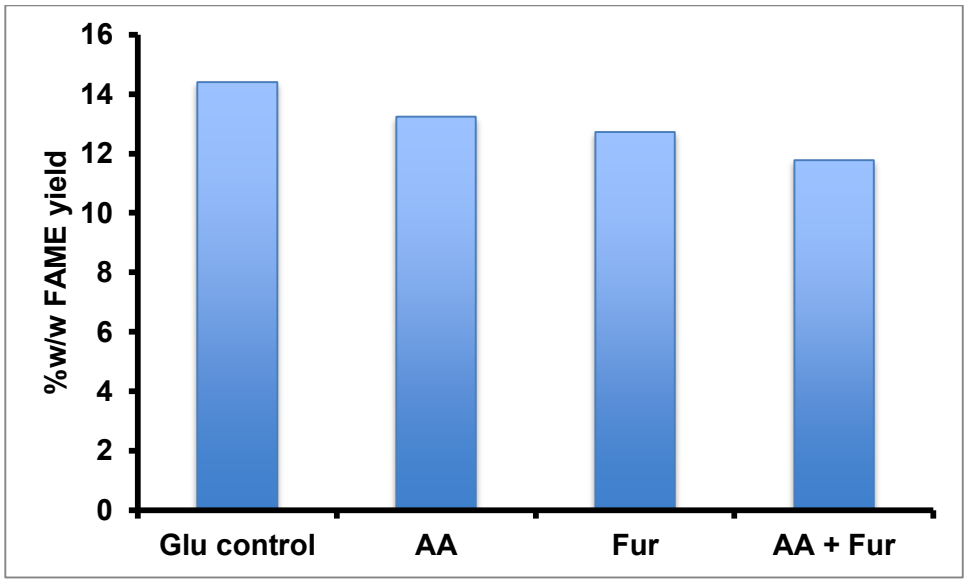


***Figure R11**. Percent yield of FAMEs (±SD) based on CDW of R. rhodochrous cultures at 72H grown in glucose and supplemented with acetic acid, furfural, or a mix of acetic acid and furfural. All treatments are significantly different ($p<0.01$).*

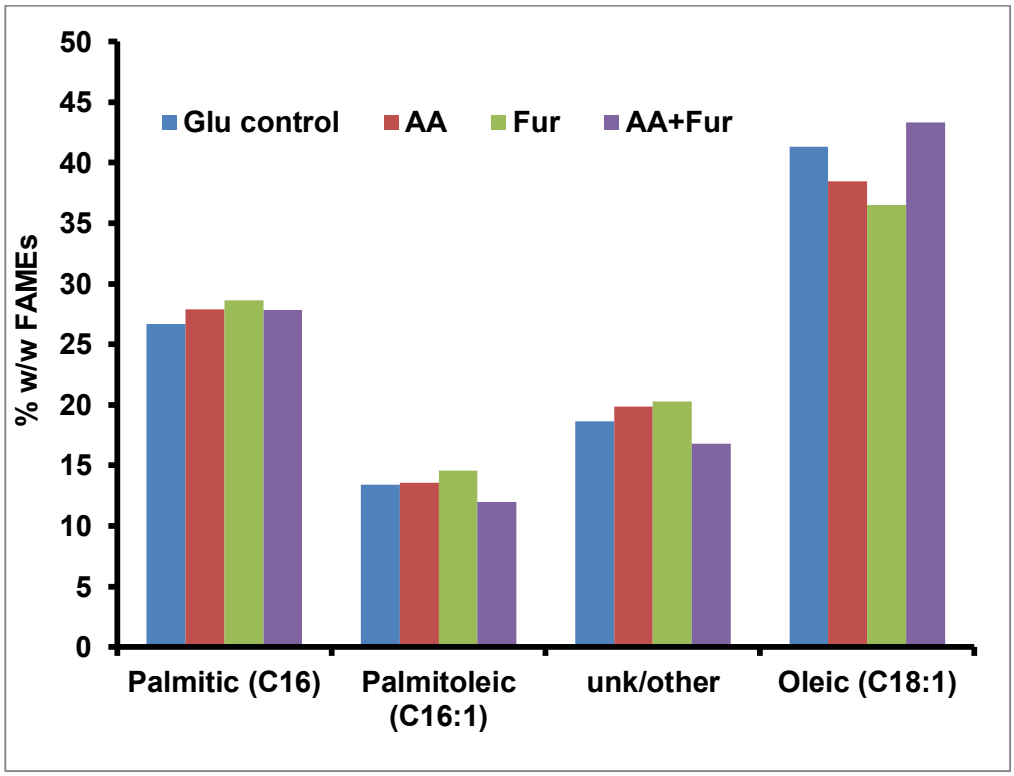


***Figure R12**. FAME profile of R. rhodochrous cultures at 72H grown in glucose and supplemented with acetic acid, furfural, or a mix of acetic acid and furfural.*

Preliminary results from experiments using phenol-supplemented medium suggest that phenol alone inhibits cell growth and lipid accumulation. However, when glucose media was

supplemented with phenol, cell growth was delayed, but still achieved over 4g/L of biomass (Fig R13). Furthermore, although lipid accumulation by *R. rhodochrous* grown in phenol and glucose was less than that achieved in the glucose control, it was still over 20% of the cell dry weight indicating oleaginous status (Fig R14).

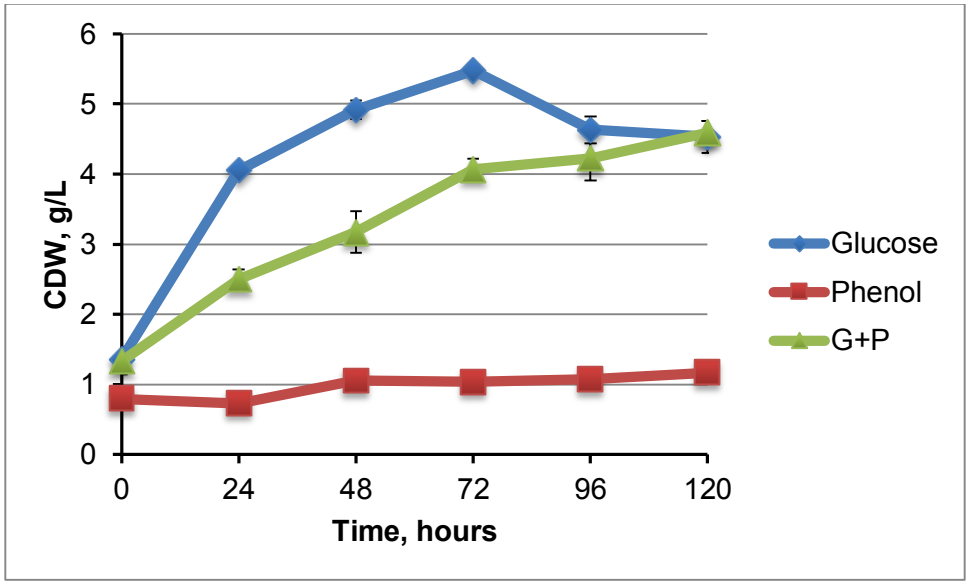


Figure R13. *R. rhodochrous cell dry weight (g/L ±SD) of shake flask cultures with phenol supplemented media.*

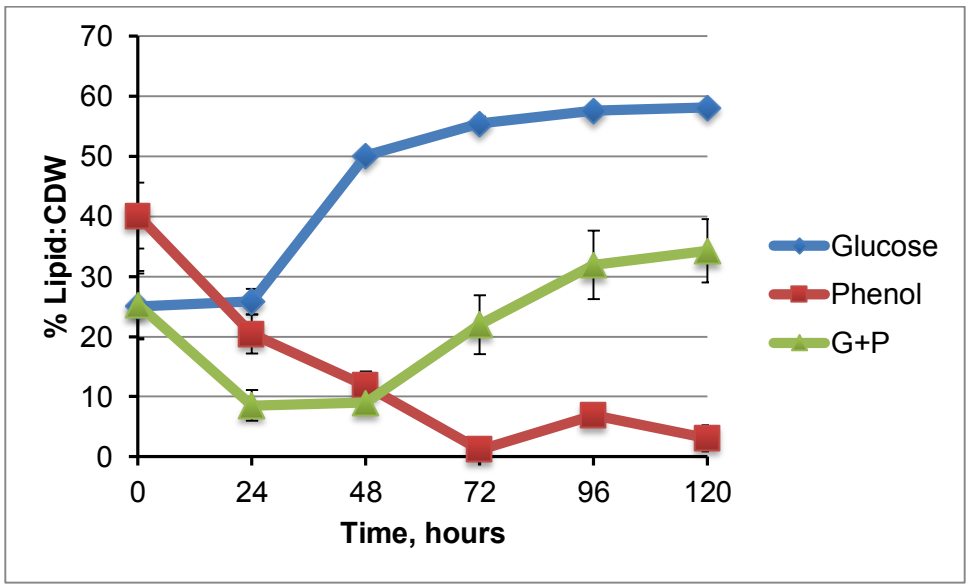


Figure R14. *Percent lipid (±SD) of cell dry weight accumulated by R. rhodochrous shake flask cultures supplemented with phenol.*

Summary:
This research investigated the growth and lipid accumulation of *R. rhodochrous* when grown in lignocellulosic sugars and inhibitors. After media optimization and confirmation of *R. rhodochrous'* lipid producing capability, we were able to analyze other carbon sources that would encourage lipid accumulation. *R. rhodochrous* grew in glucose, glucose and xylose, glucose and inhibitors, and glucose and phenol. Lipid accumulation was inhibited by xylose and reduced by furfural and phenol. These results suggest that lignocellulosic hydrolysate could be used by *R. rhodochrous* to produce lipids. Further work must be done to understand the mechanisms of inhibition to provide a more efficient process.

Subtask R.2 Pure culture growth and oil accumulation on industrial waste streams

Many industrial waste streams, such as processing water from vegetable preparations and pulp and paper production, are rich in carbon and free of competing microorganisms. These conditions are favorable for the production of microbial oils using oleaginous microorganisms, heterotrophic algae, or a combination of the two. These types of waste streams could provide a low-cost carbon substrate for the production of copious quantities of microbial oil.

The kinetics of substrate consumption during the lipid-accumulation stage, identified by constant OD readings (no cell growth), will be measured, and all rate parameters necessary for pilot-reactor operation will be determined. To measure lipid accumulation, solids in collected samples will be concentrated via filtration and extracted for oil using conventional solvent extraction. The fatty-acid profile will be determined by converting the oil into fatty acid methyl esters (FAMEs) produced by transesterification and analyzed on a GC/FID. Another GC/FID method will be used to determine concentration of acylglycerols. Once oil accumulation data is determined at the bench scale, the best operating conditions will be selected and applied during pilot studies. The process is expected to generate sufficient oil to operate an MSU demonstration vehicle and/or diesel engine.

Planned Activities:
R.2.ML.1 Identify candidate oleaginous microorganisms.
R.2.ML.2 Reduce 70% in the COD of the wastewaters.

Summary of Activities:
High Strength Industrial Wastewaters as Substrates for Biocrude Production
High BOD and COD wastewaters from various industries could prove to be excellent sources of water, nutrients, and carbon for production of renewable biocrude via fermentation by oleaginous microorganisms. In this study, the potential of utilizing pulp and paper mill wastewater effluents as cultivation media has been evaluated for the sustainable production of microbial lipids as biodiesel feedstock by oleaginous microorganisms. Pulp and paper industry ranks as a top producer of huge amounts of wastewater effluents amounting to approximately 20000 – 60000 gallons per ton of product. The biochemical behavior (production of biomass, lipid accumulation, substrate utilization, and fatty acid composition) of oleaginous yeast, Rhodotorula glutinis was studied when grown on pulp and paper wastewater supplemented with glucose, xylose, and glycerol as carbon sources singularly or in mixtures under nitrogen-limited conditions. The initial characteristic of the wastewater and its place of origin are provided in Table R1. Based on the initial characteristic of the wastewater, almost no detectable sugars as carbon sources were observed. Also, low nutrients levels and moderately low COD values were reported. Therefore, the wastewater was supplemented with 60 g/L carbon sources and nutrients (1 g/L K2HPO4, 1.5 g/L Na2H2PO4, and NH4Cl) prior to the experiment. The concentration of ammonium chloride as nitrogen source is calculated to obtain the C:N ratio of 70:1. For culture preparation, the pure

culture of Rhodotorula.glutinis (ATCC 15125) was grown in sugar broth media (1 g/L Yeast Extract, 1 g/L Na2HPo4.12 H2o, 1 g/L KH2Po4, 0.4 g/L MgSo4.7H2o, 1.6 g/L (NH4)2So4, 10.0 ml Trace Mineral Solution, 6.0 ml Iron Solution, 60 g/L glucose) for 4 days prior to the experiment. Then, the media was inoculated with 20% (v/v) R. glutinis culture.

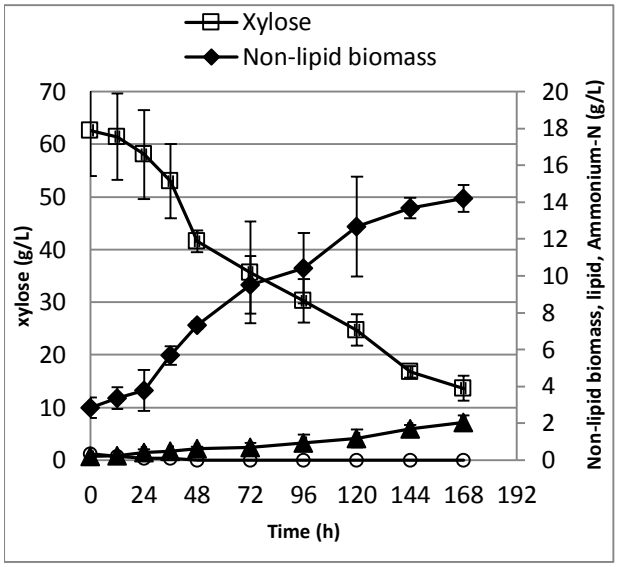
***Table R1**. Pulp and paper wastewater initial characteristics (before treatment)*

Characteristics	Pulp Wash
Place of Origin	Post pulping and bleaching process
pH	2.25
COD (mg/L)	1478
Ammonium (mg/L)	3.95
Sulfate (mg/L)	1400

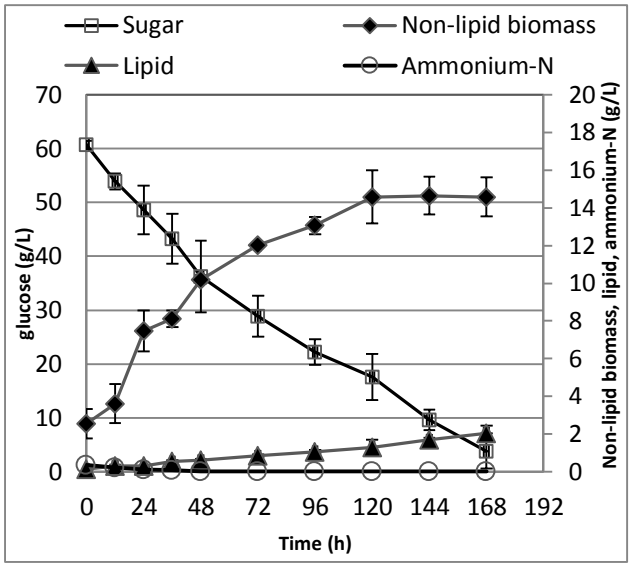
In fermentation experiment, the wastewater (2.4 L) was amended with 60g/L carbon sources and nutrients as previously described and seeded with 20% initial inoculum of R.glutinis (600 ml) in 3L Bioflo 310 fermenter (New Brunswick Scientific, Edison, NJ). The pH of the amended wastewater was adjusted to 6.5 using 1 M NaOH solution, and the temperature was controlled at 25°C. The aeration rate was adjusted at 3 volume of air per volume of medium and per minute (VVM), and the agitation rate was set at 300 rpm and was adjusted to maintain a dissolved oxygen (DO) level no lower than 60 % saturation during the experiment. An antifoam agent (Sigma-Aldrich, St. Louis, MO) was periodically added to prevent foaming in the vessel. Samples were obtained from aerobic batch fermenter regularly every 12 h during the first 48 h of the experiment and then every 24 h during the 10 days of incubation time. Duplicate samples were collected and analyzed for biomass concentration (centrifugation and freeze-drying), lipid content (Bligh and Dyer extraction method and solvent evaporation by Turbovap), residual sugar (YSI 2900), residual ammonium (IC), and residual COD (Standard digestion method). DO and pH were monitored using the built-in probes in the fermenters. The lipid extracts (biocrude) are currently being processed for GCFID analysis of biodiesel yield (saponifiable fraction) and fatty acid profile.

The results shown in Figures R15a to R15f indicate that R. glutinis culture were able to grow and increase their lipid content and produce biocrude using the pulp and paper wastewaters as media supplemented with different sugars and nutrients. In all the treatments, growth and lipid accumulation of the R.glutinis reached the maximum non-lipid biomass and lipid concentration of around 12-17 g/L and 1.3-2.9 g/L, respectively which are corresponded to the intracellular lipid contents of 8-15% CDW. An average maximum lipid content of 15% CDW of oleaginous yeast was obtained when glycerol used as a substrate. After glycerol, xylose grown R.glutinis media reached the maximum lipid content of 12.6 % CDW which was comparable to glycerol and higher than the one obtained when glucose used as a sole carbon source.

(a)


Xylose
Non-lipid biomass
xylose (g/L)
Non-lipid biomass, lipid, Ammonium-N (g/L)
Time (h)
0
24
48
72
96
120
144
168
192

(b)


Sugar
Non-lipid biomass
Lipid
Ammonium-N
glucose (g/L)
Non-lipid biomass, lipid, ammonium-N (g/L)
Time (h)
0
24
48
72
96
120
144
168
192

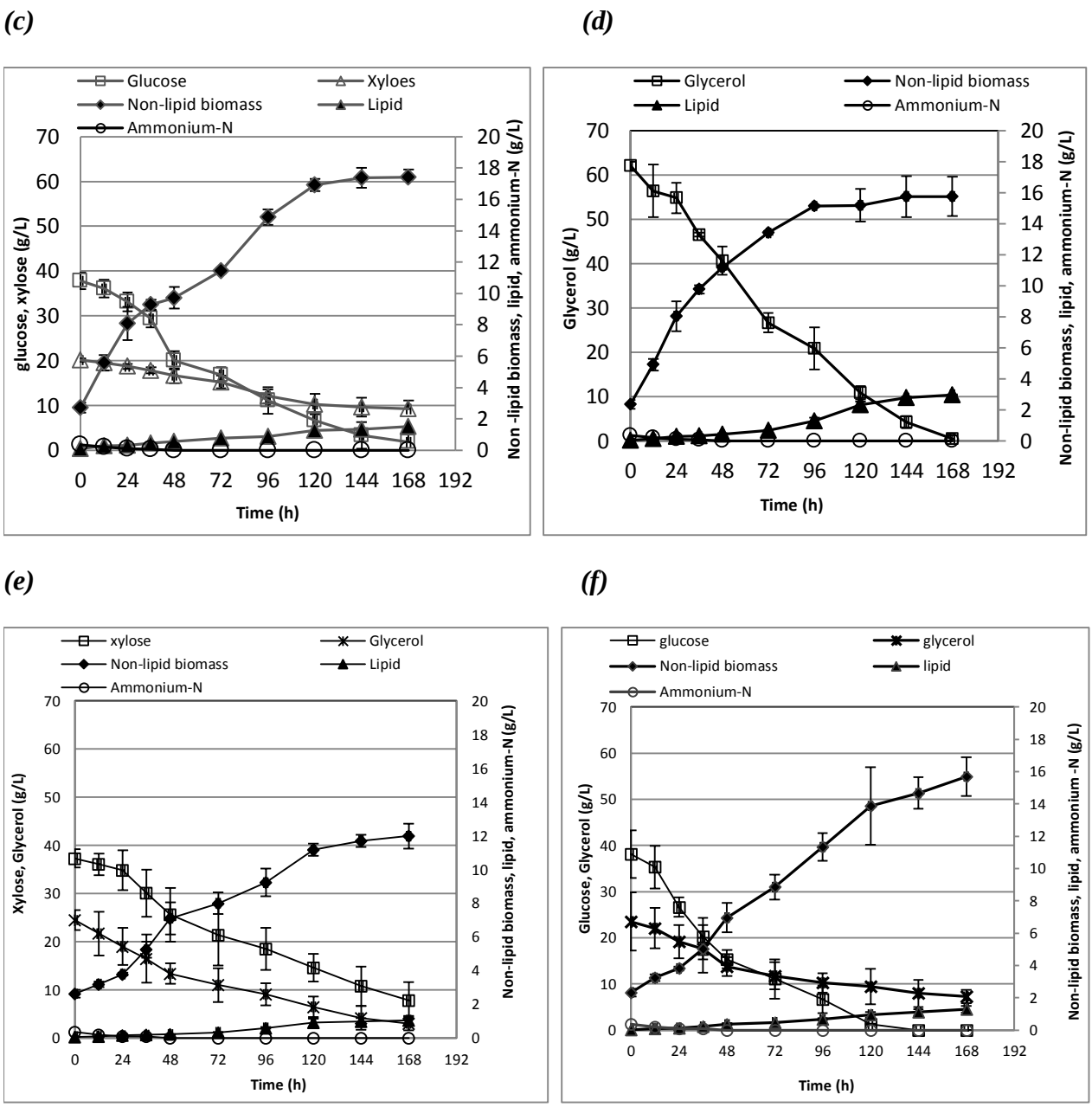


***Figure R15a-R15f**: Growth and lipid accumulation of the R.glutini.*

The results of the characterization of total extracted lipid from produced biomass and biodiesel (FAMEs) yield by transesterification of the harvested lipids are shown in figure R16. The transesterification yield of approximately 40-60(w/w) based on extracted lipid is achieved regardless of the type of substrate used.

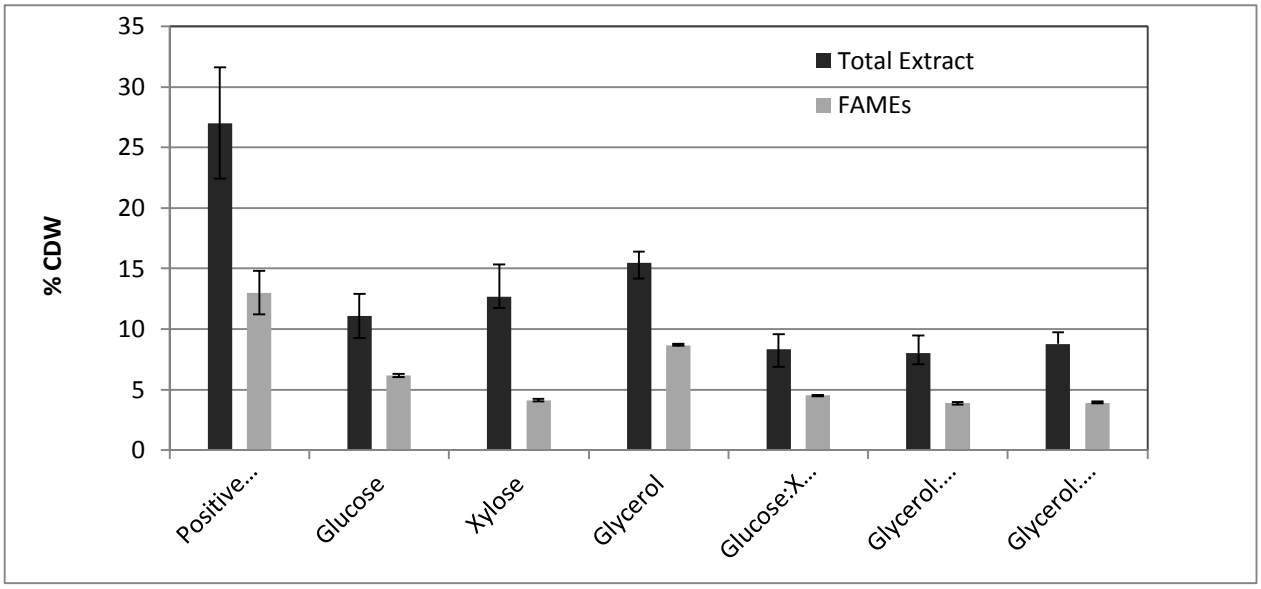


Figure R16. *Percentage of total lipid extract and FAMEs yield based on cell dry weight (CDW)*

The fatty acid profile of R.glutinis was determined using FAMEs analysis in order to evaluate the potential of using this oleaginous yeast as biodiesel feedstock. Figure R17 shows the composition of the produced FAMEs from transesterified lipids. According to Figure R17, palmitic acid (C16:0), and Oleic acid (C18:1) are the two main intracellular fatty acid methyl esters in the produced biodiesel from R. glutinis which accounted for approximately 22-25% and 26-35 % of the total FAMEs for all the substrates, respectively. The palmitic acid ME (C16:0) levels which is considered as the majority of saturated fatty acids did not change considerably by the type of carbon sources and remained in the order of 22-25%.

The Composition of the FAMEs was comparable to the fatty acid profile of the soybean oil used to produce biodiesel. Comparing the fatty acid composition of R.glutinis in this study with the soybean oil indicates that the FAMEs derived from transesterification of lipids from R.glutinis were more saturated. The quality of the produced biodiesel in this study improved compared to the biodiesel produced by soybean in terms of oxidative stability, cetane number, and nitrogen oxide level which is attributed to the higher levels of saturated fatty acids and lower levels of polyunsaturated fatty acids.

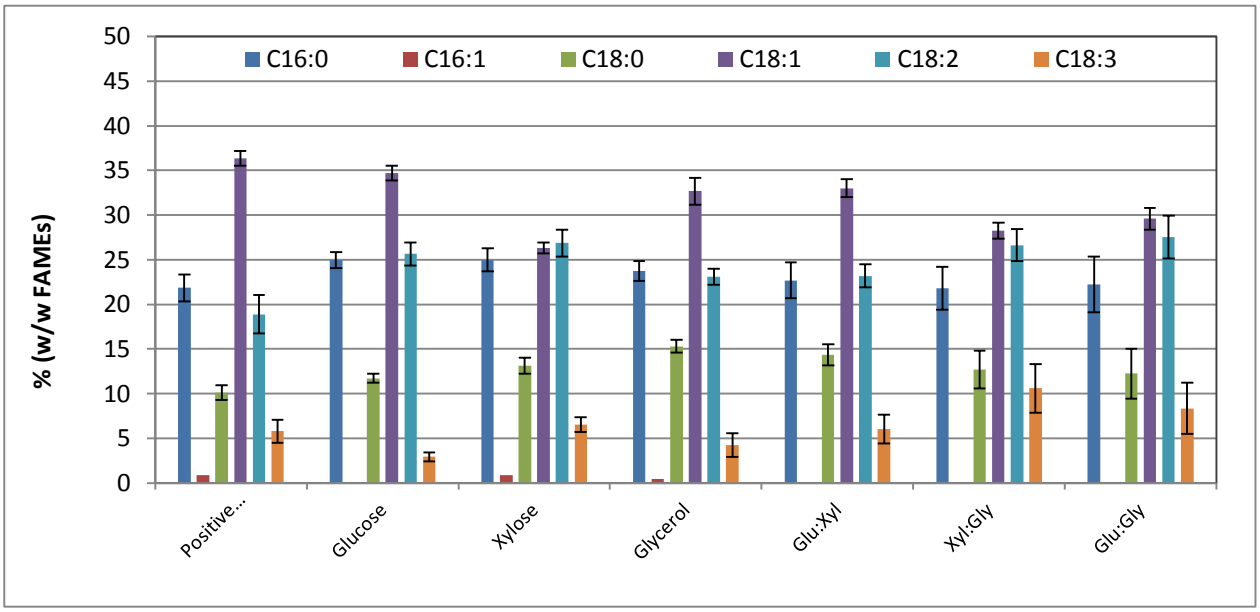


***Figure R17**. Fatty acid composition of transesterified lipids produced by R. glutinis grown in pulp and paper wastewater*

To predict the quality of the biodiesel which can be produced from R. glutinis lipids, some fuel properties such as cetane number, iodine value, saponification value, and higher heating value were estimated using its fatty acid composition and available published models.

$$Cetane\ number(CN) = 61.1 + (0.088 \times M) + (0.133 \times P) + (0.152 \times S) - (0.101 \times PA) - (0.039 \times O) - (0.243 \times L) - (0.395 \times LL) \quad (1)$$

$$Iodine\ value\ (IV) = 35.9 - (0.212 \times P) + (0.660 \times S) + (0.448 \times O) + (1.23 \times L) + (1.73 \times LL) \quad (2)$$

$$Saponification\ value\ (SV) = 268 - (0.418 \times P) - (1.3 \times S) - (0.695 \times O) - (0.77 \times L) - (0.847 \times LL) \quad (3)$$

Where, $M = Myristic$ $P = Palmitic$ $S = Stearic,$ $PA = Palmitoleic$ $O = Oleic,$ $L = Linoleic,$ $and\ LL = Linolenic$

$$Higher\ heating\ value\ (HHV) = 49.43 - (0.015 \times IV) - (0.041 \times SV) \quad (4)$$

Table R2 shows the comparison of these four biodiesel properties of the R. glutinis lipid raw material with the most common plant oils used lipid feedstock indicates that these chemical values were in the range of these vegetable oils (soybean, rapeseed, palm, and sunflower).

***Table R2**. Comparison of the saturated, monosaturated, and polyunsaturated fatty acids and their corresponded Cetane number, iodine value, saponification value, and the higher heating value of the common vegetable oils biodiesel feedstock with R. glutinis lipids biodiesel feedstock*

Biodiesel	Soybean	Rapeseed	Palm	Sunflower	This study (R. glutinis)
Saturated	14.2	7.1	51	11	36.57
Monounsaturated	23.2	58.6	39	20	30.7
Polyunsaturated	57.8	29.6	10	69	31.72
Cetane number (CN)	45-60	44-65	58-70	49-61.2	56.4
Iodine value (IV) (g iodine/ 100 g oil)	120.52	108	59	136	95
Saponification value (mg KOH/ g oil)	194.61	197	205	193	194.8
Higher heating value (MJ/Kg)	39.63	39.73	41	39.45	40

For environmental concerns, the water quality must be enhanced before releasing to receiving waters. Therefore, in this study the quality of the water is determined by measuring the chemical oxygen demand (COD) in addition to the growth and lipid accumulation of R. glutinis. Figure R18 presents the COD reduction from pulp and paper wastewater tested with different renewable carbon sources which inoculated with R. glutinis culture. The maximum COD value is obtained for the case of glycerol used as a substrate. The maximum COD removal efficiency of 60% is achieved when R. glutinis is cultivated in amended pulp and paper wastewater. However, low COD removal could be due to the presence of non-degradable organic compounds. Consequently, the aim of the treatment of pulp and paper mill using lipid producing R. glutinis becomes more challenging due to the presence of possible contaminants in the wastewater. The presence of lignin and its derivatives in pulp and paper wastewater can form recalcitrant complex which may be responsible for the non-biodegradable COD.

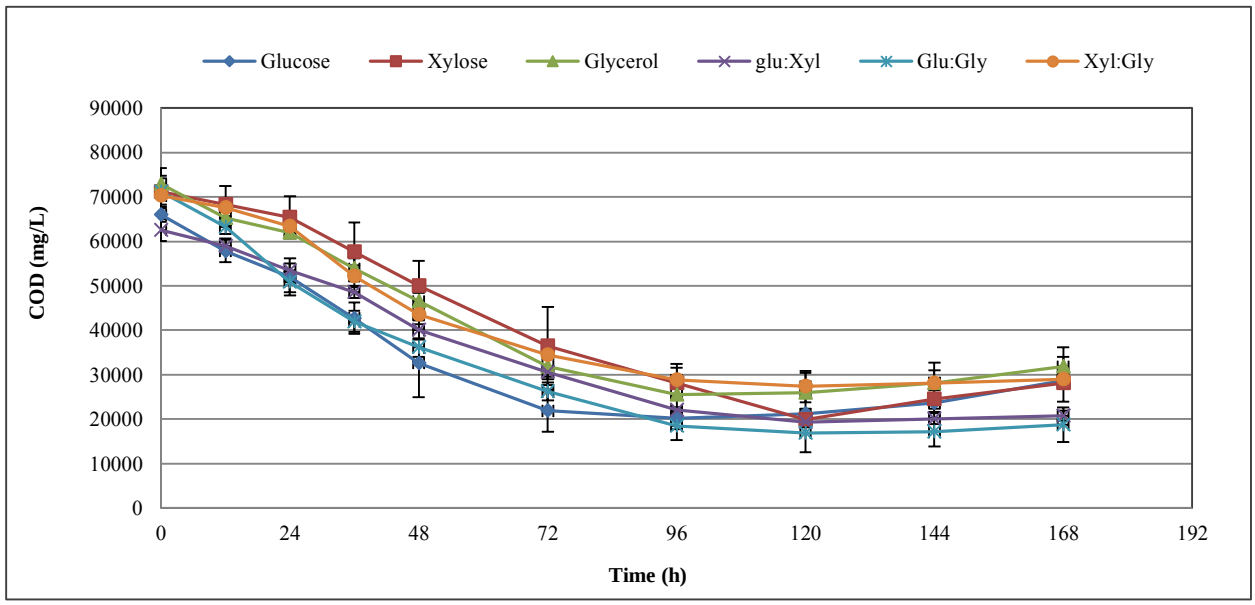


***Figure R18**. COD reduction of the pulp and paper wastewater using R. glutinis growing on different carbon sources*

This study has shown that oleaginous yeast Rhodotorula glutinis is able to grow and accumulate lipids in amended pulp and paper wastewater. In order to enhance the growth and lipid production by R. glutinis in pulp and paper wastewater media, fermentation optimization has been investigated using response surface techniques. A Box–Behnken design with total of four variables (k=4) including initial glucose concentration (x1), initial nitrogen concentration (x2), the initial inoculum concentration (x3) and fermentation time (x4) was selected as design variables. The synergy between four independent variables was determined with respect to their effects on the biomass (Y1) and lipid production (Y2) as responses. Four independent variables were studied at three different levels, low (-1), medium (0), and high (+) to determine the response pattern, which is shown in Table R3.

***Table R3.**Minimum and maximum levels of 4 factors in terms of coded and uncoded* symbols

Factor	**Symbols**		**Code level**		
	coded	uncoded	**-1**	**0**	**1**
Initial carbon (g/L)	x_1	X_1	40	60	80
Initial Nitrogen (g/L)	x_2	X_2	0.6	1	1.4
Inoculum concentration % (v/v)	x_3	X_3	10	15	20
Fermentation time (day)	x_4	X_4	5	7	9

According to this design, the experimental plan contains 27 trials which were conducted with three replications at the central point to estimate the purely experimental uncertainty variance. The experiments were conducted in 1L Erlenmeyer flasks. The glucose and ammonium sulfate are loaded to obtain the initial concentration of 40-80, and 0.6-1.4 g/L respectively. The studied carbon to nitrogen ratio is 50-250. The pH is adjusted to 6.5 prior to the experiments, and then

the flasks are located in the rotary incubator with shaking speed of 120 rpm. The seed culture levels of 10-20% (v/v) is used as inoculum culture to 200 mL medium and incubated at 30 °C for 5-9 days. To determine the correlation between four independent variables the second order polynomial equation was fitted to data resulting from the 27 trials. The low, middle, and high levels of each variable and the experimental design and respective experimental results and its corresponded predicted values are given in Table R4.

The general equation for the second –degree polynomial equation which is based on the multiple linear regressions is shown as equation 5. This equation takes account of main, quadratic and interaction effects for the independent variables.

$$Y = \beta_0 + \sum \beta i\, xi + \sum \beta ij\, xi\, xj + \sum \beta ii\, xi^2 \qquad (5)$$

Where Y is the predicted response, xi and xj stand for the input variables which affect the response variable (Y), βo is the intercept, βi is the linear coefficient, βij is the linear-by-linear interaction effect between xi and xj and βii is the squared interaction effect.

Table R4*.Box-Benhken experimental design matrixes and the response values*

Trial	Code level				Biomass (g/L)		Lipid productivity (g/L)	
	X_1	X_2	X_3	X_4	Experimental	Predicted	Experimental	Predicted
1	0	-1	1	0	14.71333	14.12778	2.207	2.072868
2	-1	1	0	0	12.14667	11.7102	0.585382	0.593131
3	1	0	0	1	15.45	15.35248	1.650149	1.501782
4	1	0	-1	0	13.15667	13.1733	1.667934	1.716587
5	1	-1	0	0	11.82667	12.07797	1.397219	1.459842
6	0	1	0	1	14.41667	15.0584	1.315401	1.444227
7	0	1	0	-1	13.31667	13.82399	1.085454	1.082229
8	-1	-1	0	0	9.926667	9.868529	0.693146	0.762738
9	0	0	1	-1	14.21	14.45866	1.45507	1.555337
10	0	0	1	1	13.99333	13.80817	1.080701	1.151074
11	-1	0	-1	0	9.45	9.86719	0.904582	0.885824
12	0	-1	0	-1	12.52667	12.65565	1.811882	1.746815
13	1	1	0	0	14.12	13.99297	1.263043	1.263825
14	-1	0	0	-1	13.07	12.58196	0.923424	0.937658
15	0	1	1	0	12.27333	11.68778	0.967475	0.833343
16	-1	0	1	0	11.19667	11.95075	0.734831	0.749938
17	0	0	-1	-1	12.20667	12.47007	1.078281	1.145266
18	0	-1	0	1	12.78333	13.13686	1.204455	1.286973
19	1	0	1	0	13.56667	13.16974	1.068293	1.022084
20	1	0	0	-1	11.63667	11.44804	0.306334	0.218411
21	-1	0	0	1	14.39333	13.95951	1.748206	1.718312
22	0	1	-1	0	11.70333	12.32333	1.526268	1.526801
23	0	-1	-1	0	12.06	12.32333	1.440766	1.526801
24	0	0	-1	1	13.20667	12.32333	1.613368	1.526801
25-27	0	0	0	0	12.32333333	12.88521	1.502642	1.512503

The second order regression equations for biomass (Y_1), and lipids content (Y_2) as a function of initial glucose concentration (x_1), initial nitrogen concentration (x_2), initial inoculums size of the

culture (x_3), and fermentation time (x_4) which is the empirical relation between biomass and lipid production values and the test variables (as coded values) are given as follows:

$$(Biomass)Y_1 = 0.9293 + 0.1045\,x_1 + 15.5913\,x_2 + 1.7958\,x_3 - 4.8828\,x_4 - 0.0010\,x_1^2 - 0.1467\,x_2^2 + 0.0038\,x_3^2 + 0.3005\,x_4^2 + 0.0023\,x_1x_2 - 0.0053\,x_1x_3 + 0.0207\,x_1x_4 - 1.0796\,x_2x_3 + 0.4437\,x_2x_4 - 0.0587\,x_3x_4$$

$$(lipid)Y_2 = -4.74343 + 0.11772x_1 + 2.12758x_2 + 0.25496x_3 - 0.09117x_4 - 0.00118x_1^2 - 0.22583x_2^2 + 0.00415x_3^2 - 0.03401x_4^2 - 0.00083x_1x_2 - 0.00073x_1x_3 + 0.00749x_1x_4 - 0.26418x_2x_3 + 0.30111x_2x_4 - 0.01422x_3x_4$$

The model accuracy was checked by comparing the predicted and experimental values for biomass and lipid production. Fig. R19 shows the linear relationship between the predicted and experimental results for (a) biomass, and (b) lipid production. The R^2 values of 0.89, and 0.94 for biomass and lipid productivity indicates that the model is fitted with the experimental values and the suggested model is accurate to estimate the biomass and lipid productivity.

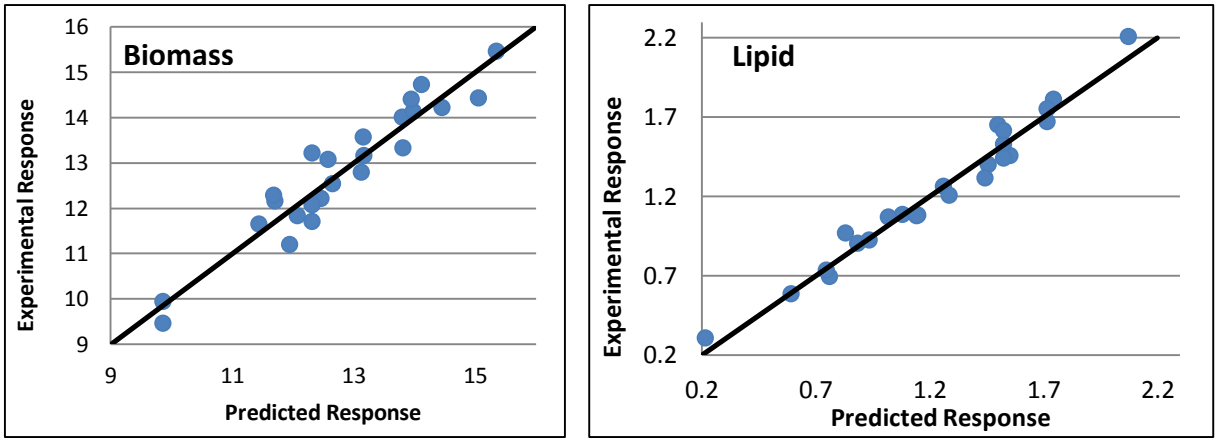


***Figure R19**. Comparison of predicted and experimental biomass and lipid productivity*

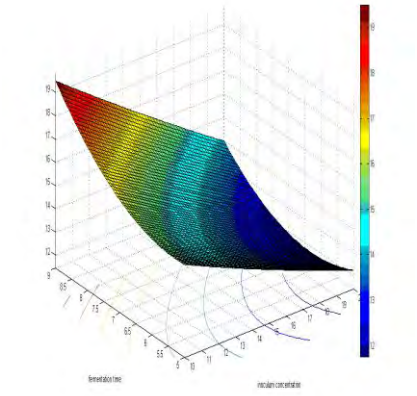
Response Surface and contour Plots for biomass

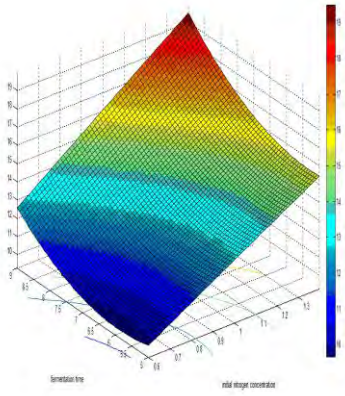
Response surface plots were developed to indicate an optimum condition using the fitted quadratic polynomial equations obtained by holding 2 of the independent variables at a constant value and changing the levels of the other two variables. The relationships between the biomass and these 4 factors are shown in Figs R20a-f. Each plot shows the effects of two variables within their studied ranges, with the other variable fixed to the zero level. The interaction between (a) initial glucose concentration and initial nitrogen concentration, (b)) initial glucose concentration and inoculum concentration, (c) initial nitrogen concentration and inoculum concentration, (d) initial glucose concentration and fermentation time, (e) initial nitrogen concentration and fermentation time (f) inoculum concentration and fermentation time.

Figure 6-a: initial glucose concentration and initial nitrogen concentration interaction

Figure 6-b: initial glucose concentration and inoculum concentration interaction

Figure 6-c: initial nitrogen concentration and inoculum concentration interaction





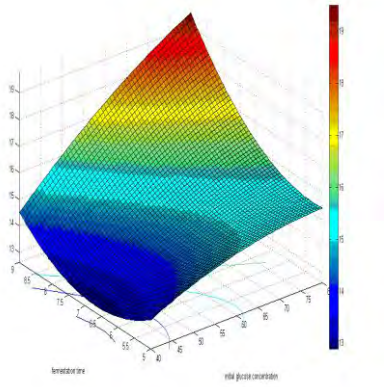


Figure 6-d: initial glucose concentration and initial nitrogen concentration interaction

Figure 6-e: initial nitrogen concentration and fermentation time interaction

Figure 6-f: inoculum concentration and fermentation time interaction

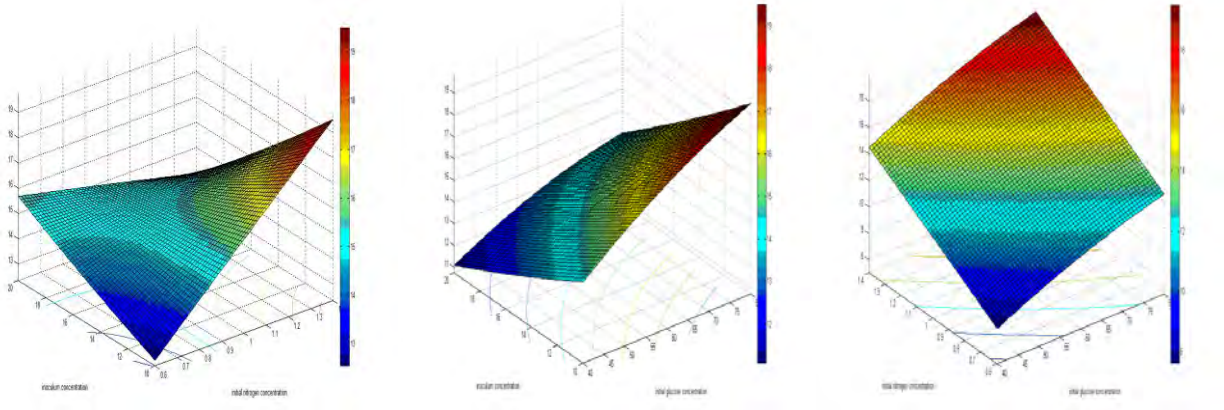


Figure R20a-f

The response surface better visualizes the tendency of each factor to influence the biomass and lipid production. The shape of the contour plot shows the natures of the interactions between factors. An elliptical contour plot indicates a prominent interaction, whereas a negligible effect appears as a circular contour plot. After the significance of the parameters has been evaluated by the shape of the contour plots, the model can be improved by eliminating the terms that are not very significant. The modified model for describing the relationship between biomass and 4 studied factors is shown in Equation below:

$$(Biomass)Y_1 = 0.9293 + 0.1045\,x_1 + 15.5913\,x_2 + 1.7958\,x_3 - 4.8828\,x_4 - 0.1467\,x_2^2 + 0.3005\,x_4^2 + 0.0207\,x_1x_4 - 1.0796\,x_2x_3 + 0.4437\,x_2x_4 - 0.0587\,x_3x_4$$

Response Surface and contour Plots for lipid productivity

Figure 7-a: initial glucose concentration and initial nitrogen concentration interaction

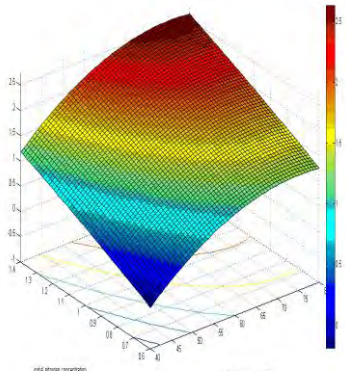


Figure 7-b: initial glucose concentration and inoculum concentration interaction

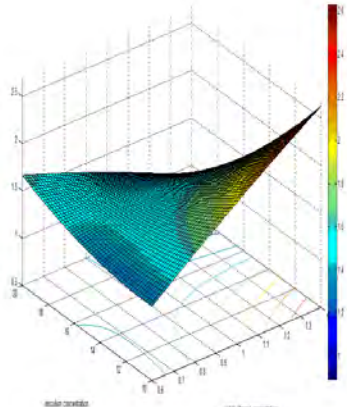


Figure 7-c: initial nitrogen concentration and inoculum concentration interaction

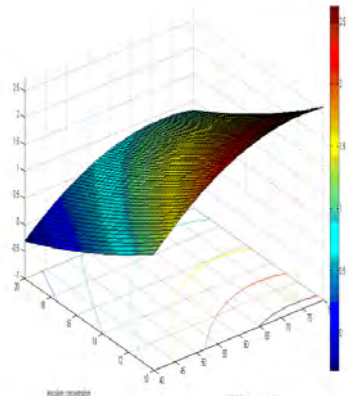


Figure 7-d: initial glucose concentration and initial nitrogen concentration interaction

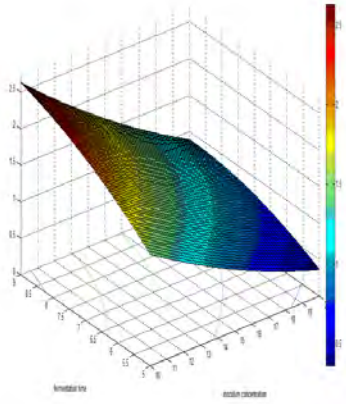


Figure 7-e: initial nitrogen concentration and fermentation time interaction

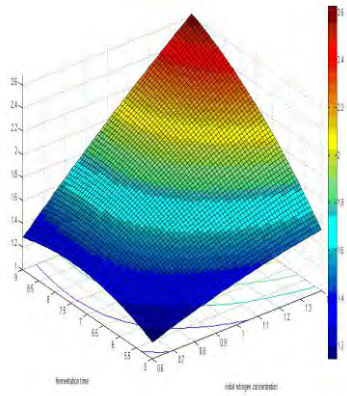


Figure 7-f: inoculum concentration and fermentation time interaction

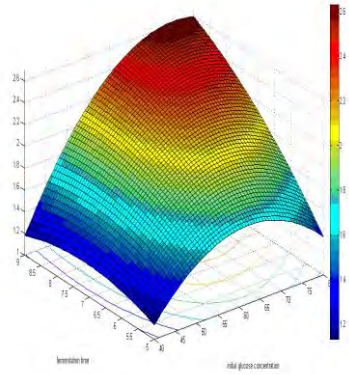


Figure R21a-f

Similarly the modified model for describing the relationship between lipid productivity and 4 studied factors is shown in Equation below:

$$(lipid)Y_2 = -4.74343 + 0.11772x_1 + 2.12758x_2 + 0.25496x_3 - 0.09117x_4 - 0.22583x_2^2 - 0.03401x_4^2 - 0.26418x_2x_3 + 0.30111x_2x_4 - 0.01422x_3x_4$$

The optimization function in Matlab was used to obtain the optimal conditions for biomass and lipid production. The optimal conditions for the biomass and lipid production were at initial glucose concentrations of 73 g/l, and 80 g/L, an initial nitrogen concentration of 1.4, and1.4 g/L, inoculum concentration of 10, and 10%, and the fermentation time of 9 days respectively.

Subtask R.3 Develop in-situ production of biodiesel using oil-fat microorganisms

In this task, the Biocrude thrust's efforts will be repeated using the oleaginous microorganisms and/or heterotrophic algae. Previous SERC II results have shown that in-situ esterification\transesterification yields the highest lipids/FAMEs extraction/conversion efficiency for microbial mixture. This one-step process works efficiently even at moisture contents as high as 50%. One of the disadvantages of the process is the high concentration of acid or base necessary to overcome mass transfer limitations. Another in-situ technique that will be evaluated during SERC IV is supercritical methanol in the absence of catalyst. Preliminary data have shown that 20 g of activated sludge (15% solid) reacted with 70 mL MeOH in the absence of base or acid at 300°C overnight in a Batch Parr reactor produces a crude biodiesel mixture (FAMEs). The product was filtered and analyzed via gas chromatography. More detailed experiments will be conducted to optimize the yield of biocrude, reduce reaction times, and determine the effect of water in the mixture. Microbial mixtures from Task R.2 will be selected to investigate the efficiency of this novel in-situ technique.

Planned Activities:
R.3. ML.1 Convert of 80% of the lipids into biodiesel.
R.3. ML.2 Reduce the cost of biocrude extraction and conversion into biodiesel by 10% compared to conventional biodiesel process.

Summary of Activities:
In the experiments, oil-fat microorganism Rodotorula glutinis was grown on the pure glucose or xylose or acid hydrolyzate of switchgrass as sole carbon and energy source, the biodiesel was then produced directly from the cells of Rodotorula glutinis.

Method:

Preparation of the oil-fat microorganism Rodotorula glutinis

The oleaginous yeast *Rhodotorula glutinis* (ATCC 15125) was used in all experiments. The yeast was first grown in nutrient broth media for 48 hours. Then 50 ml of the culture was centrifuged at 2000 RPM for 15 minutes and the cell pellet as was transferred to a 2 L shake flask with 667 ml fresh media made of, per liter: yeast extract, 0.5 g, mineral salt solution, 10 mL, $FeSO_4$ solution (which is made of 0.4 g $FeSO_4.7H_2O$ and 100 ml water), 6.0 mL, Na_2HPO_4, 1.0g KH_2PO_4, 1.0g $MgSO_4 \cdot 7H_2O$, 0.4 g $(NH_4)_2SO_4$, 0.5 g sugar (glucose or xylose), 60 g/L. The cultures were then incubated in shake flasks at 30 ˚C and 120 RMP. After growing for 7 days on glucose or 9 days on xylose, the cells were collected and freeze-dried. The cells are then used for biodiesel production. .

While using acid hydrolyzate of switchgrass as sole carbon and energy source, 1 L of the actual acid hydrolyzate of switchgrass was used instead of sugar and 1 L of water in the preparation of the media. The fermentation was conducted in BIOFLO 310 fermenters with a total volume of 3 liters and samples were taken during the cultivation.

Biodiesel production

Biodiesel production from the lipid extraction and acid transesterification of extracted lipids (E & T)

To determine the oil content of the cells and separation of oils from the cells, Bligh Dyer extraction method was performed on the cells and the oils were collected and transesterified with methanol with 2%(v/v) H_2SO_4 as catalyst at 65 ˚C for 2 hours.

Biodiesel production directly from in- situ transesterificaton the cells of Rodotorula glutinis (DT)

Dried cells grown on glucose or xylose or acid hydrolysate of switchgrass were added to grass tube with methanol having 2%(v/v) sulfuric acid as catalyst. The grass tubes were put into thermal reservoir at 65 ˚C for reaction to produce FAME. After the termination of reaction, the samples were cooled down to room temperature, and followed by neutralization with solution of 2% $NaHCO_3$ and 5%NaCl. For the extraction of FAME, toluene was added to the samples and they were thoroughly mixed followed by centrifugation at 1800 RPM for 20 minutes. The Toluene on the top with FAME was collected for GC analysis to determine the lipid content and fatty acid profiles. For the gravimetric measurement, the Toluene was evaporated in a turbovap at 45 ˚C under the blowing of N_2, the remaining FAME was weighed.

Analysis of the biodiesel (fatty acid methyl ester, FAME).

The fatty acid methyl ester (FAME) were analyzed using an Agilent 6890 series Gas Chromatograph equipped with a Supelco SP 2380 capillary column(100 m x 0.25 mm x 0.2 micron, model number Supelco 24317) and a flame ionization detector (FID).

Results:

Biodiesel production

With Bligh-Dyer extraction, lipids produced by *Rodotorula glutinis* grown on glucose or xylose composed 40% and 30% of dry cell mass, respectively. However, as determined by the in-situ method, FAME produced on *Rodotorula glutinis* grown on glucose and xylose was 60% and 55% of dry cell mass, respectively.

Table R5 biodiesel production form Rhodotorula glutinis grown on acid hydrolyzate of switchgrass (*DCW: dry cell weight, LW: Lipid weight)*

Time	Cell mass	Extraction-transesterification			DT
hour	g/l	Lipid % (DCW)	FAME%(DCW)	FAME% (LW)	FAME%(DCW)
0	0.40	2.47	1.82	73.91	3.57
12	4.71	3.44	2.36	68.75	7.78
48	8.78	4.20	2.27	54.11	31.95
60	9.73	6.70	3.81	56.92	37.07
72	10.16	6.41	4.50	70.10	39.97
96	11.11	9.09	5.20	57.24	43.74
120	12.41	12.94	3.80	29.35	43.61
144	13.61	14.03	4.08	29.10	44.52
169	14.57	12.73	4.47	35.14	45.02
216	16.66	8.88	1.92	21.61	43.91

For the cells grown on acid hydrolyzate of switchgrass, the biodiesel yields are listed in table R5. Obviously, the lipid content and FAME yield from the extracted lipids were both lower than the value from the direct acid transesterification process. Especially, for samples taken after 48 hrs,

the lipid content and biodiesel yield were significantly under estimated by the E & T process. For example, at 48 hours, the lipid% by Bligh& Dyer was 4.20% (DCW), and FAME yield was 31.95%(DCW) by DT process. And at 96 hours, the lipid% by Bligh& Dyer was 9.09% (DCW), and FAME yield was 43.74%(DCW) by DT process.

As 100 lbs of lipid produces about 100 lbs of biodiesel, the results showed that in-situ transesterification is more effective on the bidiesel production while using oil-fat microorganism *Rodotorula glutini* as feedstock. These results also showed that Bligh&Dyer extraction gives significantly lower estimates of the lipid content in the oleaginous microorganism *Rhotorula glutinis*. The carbon source of glucose or xylose has no significant effects on the lipid accumulation in *Rhotorula glutinis*

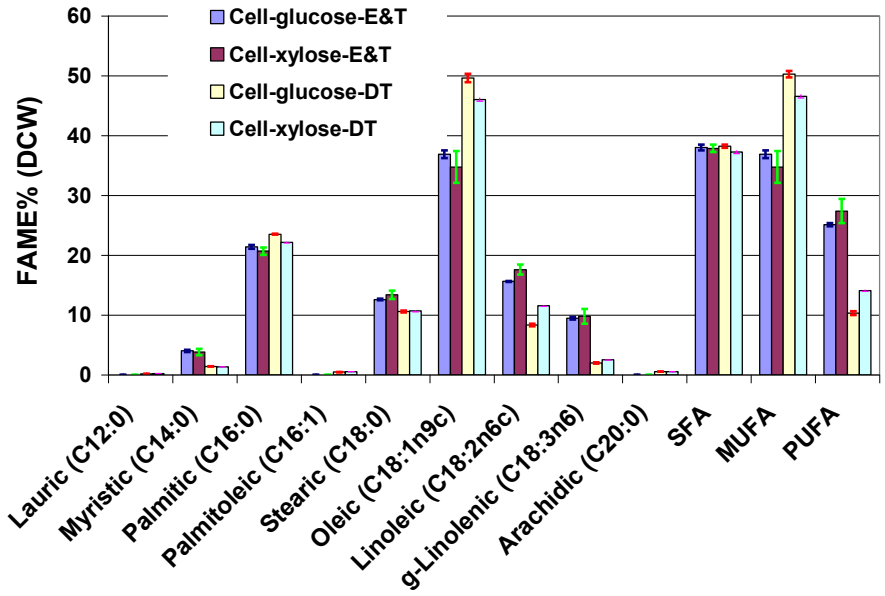


Figure R21 *Fatty acid profiles of the lipids from B&D extraction and FAMEs from in-situ transesterification for the cells grown on pure glucose or xylose.*

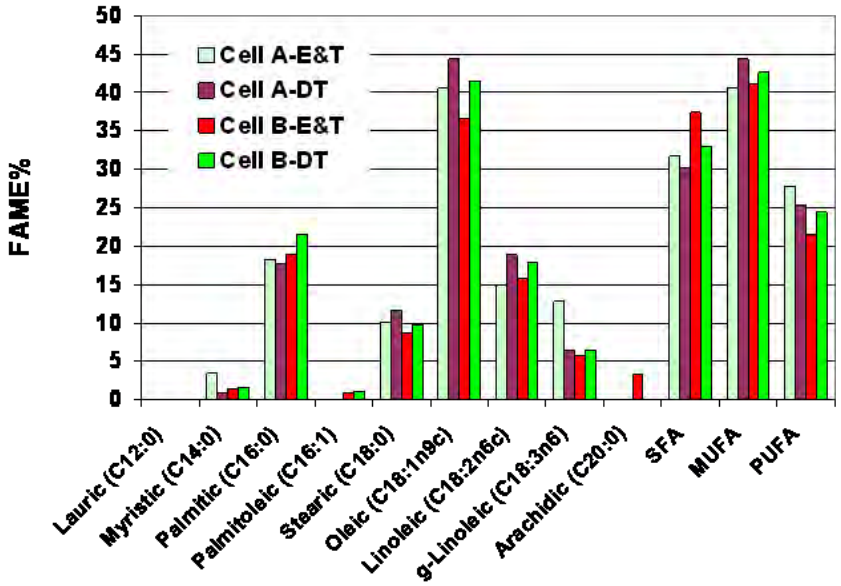


Figure R22 *Fatty acid profiles of the FAMEs produced from Rhodotorula glutinis grown on acid hydrolyzate of switchgrass (Cell A: lipid% by Bligh Dyer was 3.4% (DCW) and FAME yield was 2.36% (DCW), By DT, FAME yield was 7.78% (DCW); Cell B: lipid% by Bligh Dyer was 14.03% (DCW) and FAME yield was 4.08% (DCW), By DT, FAME yield was 44.52% (DCW*

The fatty acid profiles of the lipids from E&T or DT process were characterized by using gas chromatography, and the results were shown in figure R21 and figure R22. As presented in the figure, there is a slight difference for the fatty acid profiles. Results showed that direct transesterication method had a higher yield of oleic acid methyl esther and as well as a lower yield of linoleic acid methyl ester from *Rhotorula glutinis.*

Subtask R.4 Evaluate the value of the products contained in the residual cell mass post-oil extraction

Using pure cultures or a consortium of pure cultures of oil-producing microorganisms is expensive and decreases the cost-value needed for the residuals remaining post-oil extraction. Contained in the residuals is an abundance of nitrogen and phosphorus that could be used to cultivate additional oleaginous microorganisms or as a plant supplement. Also contained in the residuals are the antioxidants produced by some of the oleaginous yeast and algae. If these oil-bearing cells are produced from non-pathogenic-containing media, then the residuals may also have an animal-feed value.

Planned Activities:
R.4.ML.1 Identify uses for the residuals remaining post oil extraction.

Summarization of Activities:
Cell Cakes from pilot plant were used to test the effects on the gas hydrate formation. Two pretreated cell cakes were investigated; the one is that the cell cakes were simply washed with water for five times; the other is that the cell cakes were pretreated with Bligh & Dyer lipid extraction and washed with water to remove all potential water soluble surfactants. Also the hydrolysis was conducted on the cell cakes and influence of the resultant hydrolysates was evaluated on the inhibition of gas hydrate formation.

Effects of the residual cell mass post-oil extraction on gas hydrate formation
In these experiments, the cell cakes were collected from the plot plant. And the cells were extracted only with hexane at the pilot plant. Before natural gas hydrate formation test, the cell cakes were washed with water for five times and then freeze-dried (CW2). Microbes have been reported to be able to produce biosurfactants which promote the hydrate formation by reducing hydration induction time and increasing the formation rate. To remove all potential water soluble surfactants in the residual, the cell cakes were treated by Bligh & Dyer lipid extraction and then washed with water until the surface tension of the washing supernatant reached over 65.0 mN/m; the cell residual was then freeze-dried for the next hydrate test (CW1). The results of hydration induction time, average formation rate of natural gas hydrate and the total pressure drop during the hydrate formation were shown in figure R23, figure R24 and figure R25, respectively.

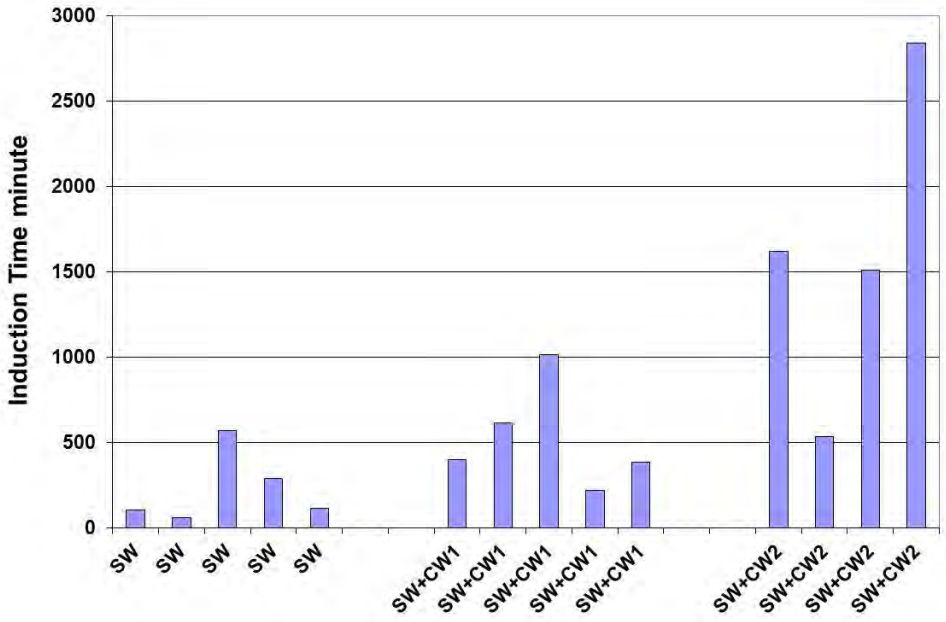


Figure R23*. Hydration induction time of the natural gas hydrate formation with a mixture of seawater and the cell wall materials;* ***SW:*** *Seawater;* ***CW1****: The cell cakes that were very well washed with water and freeze-dried.* ***CW2****: The residual cell cakes that were washed with water 5 times and freeze-dried.*

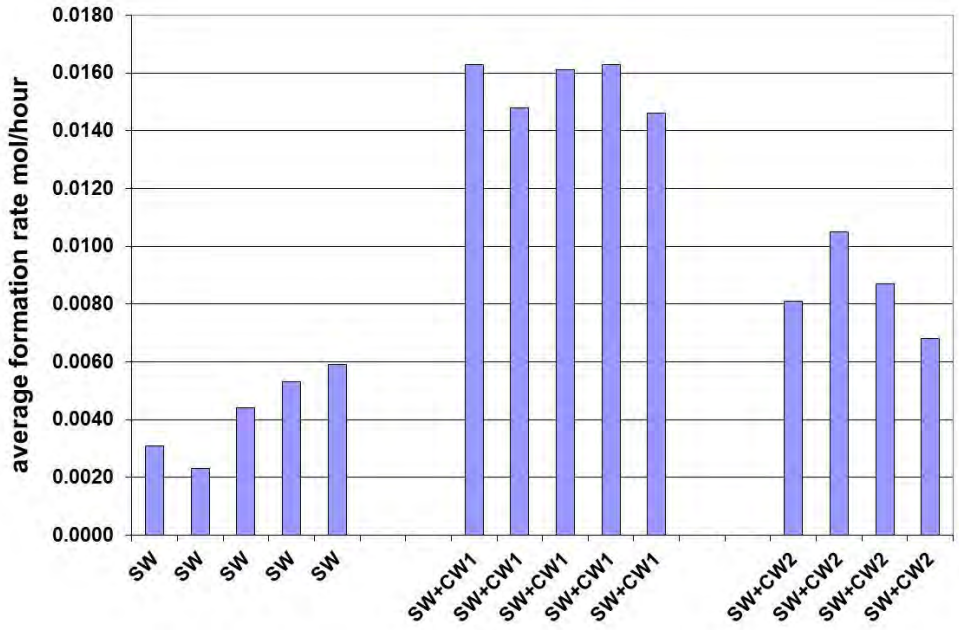


Figure R24. *Average hydrate formation rate of natural gas hydrate formation with a mixture of seawater and the cell wall materials.* ***SW:*** *Seawater;* ***CW1****: The residual cell cakes that were very well washed with water and freeze-dried.* ***CW2****: The residual cell cakes that were washed with water 5 times and freeze-dried.*

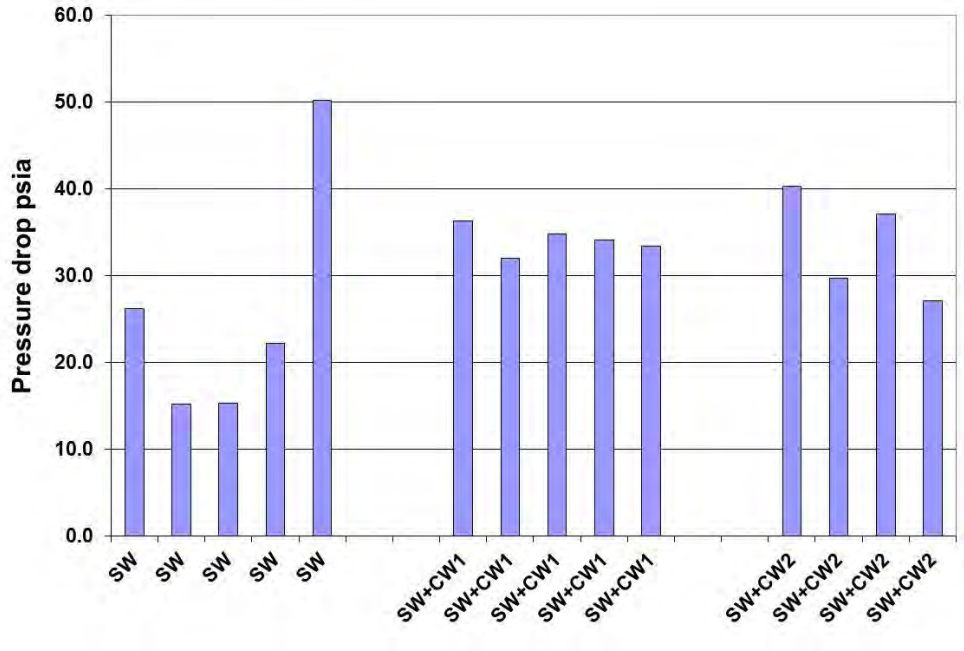


Figure R25 *Total pressure drop of natural gas hydrate formation with a mixture of seawater and the cell wall materials.* ***SW:*** *Seawater;* ***CW1****: The residual cell cakes that were very well washed with water and freeze-dried.* ***CW2****: The residual cell cakes that were washed with water 5 times and freeze-dried.*

In figure R23, most of the hydration induction times for seawater were less than 500 minutes, and the average of the five tests was 226 minutes. Upon the addition of the CW1 the cell cakes were treated with Bilgh & Dyer lipid extraction and were washed with water. The hydration induction times became a little longer; the average of five was 526. When the CW2 was added the cell cakes were simply washed with water for five times and the induction time became much longer. The average of five increased from 226 to 1626 minutes. Apparently, with the water soluble compounds remaining in the cell cakes, the induction time was much longer. The data indicates that the cell caked did interfere with the hydrate nucleation process during the hydrate formation; and the water soluble compounds could apparently inhibit hydrate formation by increasing the induction time.

As presented in figure R24, the average formation rate of natural gas hydrates rose at the addition of the cell cakes for both CW1 and CW2. Compounds in the cell cakes as shown above, could inhibit hydrate formation by increasing the induction time, but also increased the hydrate formation rate upon hydrate foramtion. This could be explained by the compounds of lipids, such as lecithin, which could promote mass transfer of the natural gas in the solution during the hydrate formation. The effects of the lecithin on hydrate formation will be discussed in the next section. The results of the total pressure drop which could tell the amount of natural gas hydrates were formed in the system, were shown in figure R25. It indicated that there was no obvious difference.

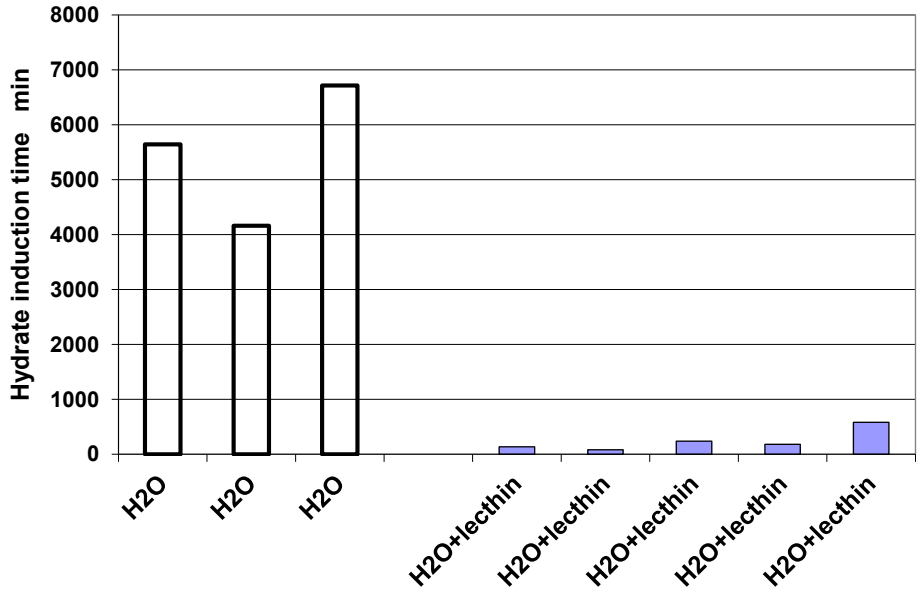


***Figure R26**. Hydration induction time of the natural gas hydrate formation with a mixture of HPLC grade water and lecithin. Blank bar means that no hydrate formed during the tested period of time and the experiment was terminated manually.*

The effects of lecithin on hydrate formation were investigated. The results of hydrate induction time, average formation rate and the total pressure drop during the hydrate formation were show in figure R26, figure R27 and figure R28, respectively. For the pure HPLC grade water, no hydrate formation occurred during the tested period for all three experiments. However, upon the addition of lecithin, the hydrates formed very quickly. The average of hydrate formation rate and total pressure drop were almost the same as the system of seawater with CW2. This data suggested that the compounds of lipids like lecithin could promote hydrate formation by decreasing induction time and increasing the formation rate.

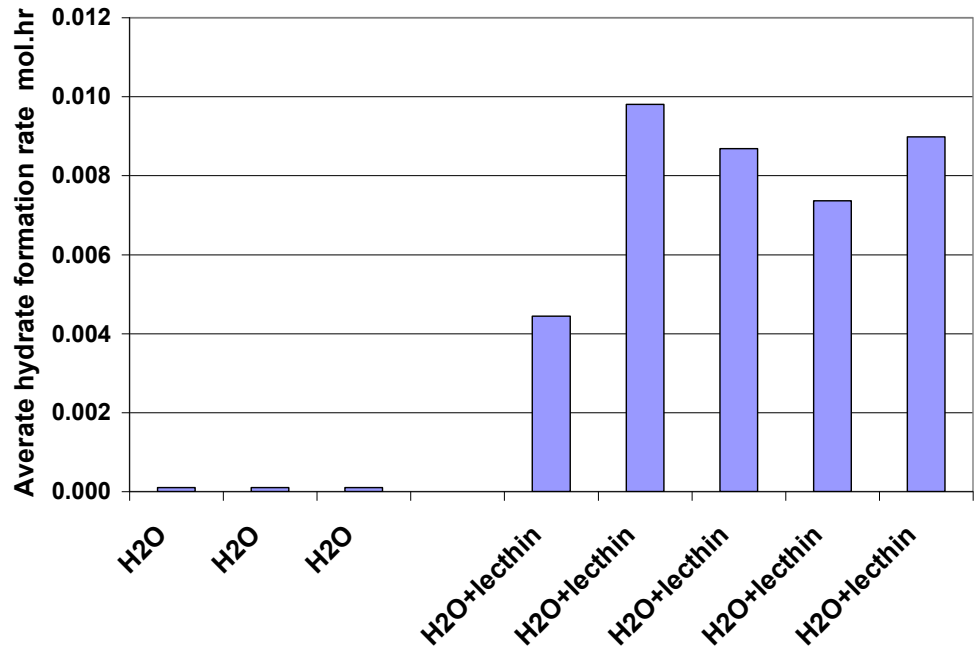


***Figure R27**. Average hydrate formation rate of the natural gas hydrate formation with a mixture of HPLC grade water and lecithin.*

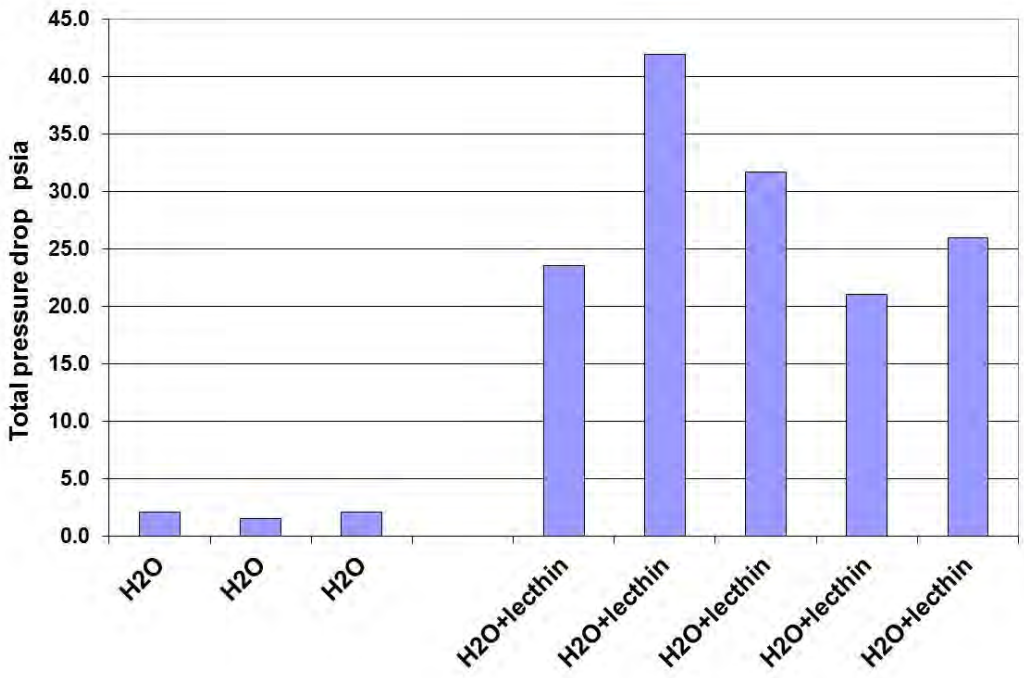


***Figure R28**. Total pressure drop for hydrate formation of the natural gas hydrate formation with a mixture of HPLC grade water and lecithin.*

Generally, the cell cakes showed inhibitive effects on natural gas hydrate formation by increasing the hydration induction times, and the water soluble compounds in the cell cakes demonstrated much longer hydration induction time. Compounds of lipids like lecithin could promote hydrate formation by reducing the induction time and increasing the hydrate formation rate.

Effects of hydrolysate of cell cakes on the gas hydrate formation.

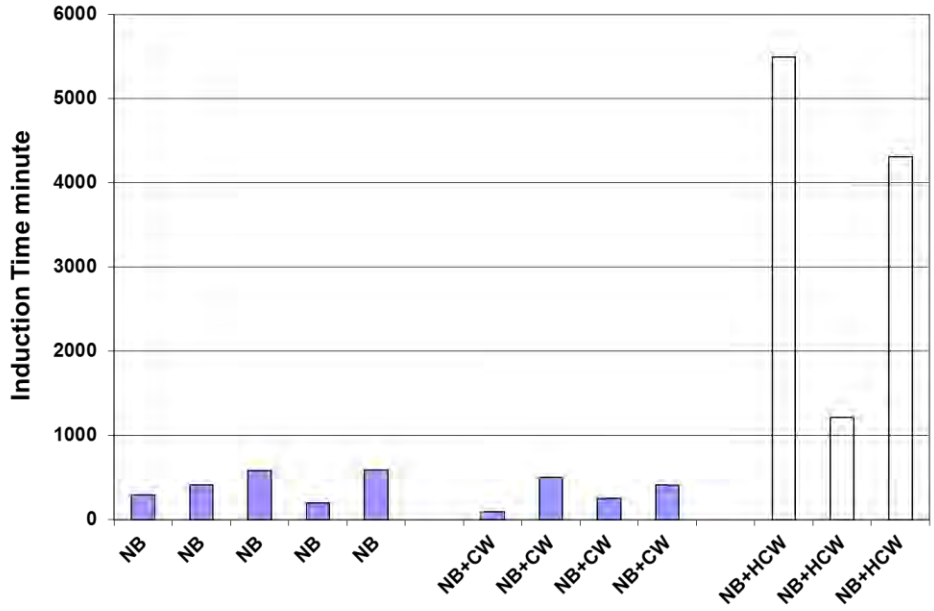


Figure R29. *Hydration induction time of the tested natural gas hydrate formation with a mixture of nutrient broth (**NB**), cell cakes (**CW**) and hydrolysate of cell cakes (**HCW**). The blank bar refers to the test that no hydrate formed during the tested time and was terminated manually*.

To further investigate the effects of the cell wall materials on the hydrate formation. The acid hydrolysis was conducted on the cell cakes using 5% HCl (wt) at 80°C. To demonstrate the inhibitive effects, nutrient broth media was used as control in the experiment. The results of hydration induction time, average formation rate and the total pressure drop during the hydrate formation were show in figure R29, figure R30 and figure R31, respectively.

In figure R29, there was no significant difference for the induction time when the cell cakes were added to the nutrient broth media. However, upon the addition of hydrolysate of the cell cakes, the induction time was greatly increased and no massive hydrate formation occurred during the tested period of time for the three tests. This date indicated that the hydrolysate of the cell cake demonstrated significant inhibitive effects on natural gas hydrate formation.

As presented in figure R30 and figure R31, the average formation rate and total pressure drop were also decreased when the cell cakes were added to the media. This showed that the cell cake could interfere with the hydrate formation. The results were consistent with the ones in figure R23, R24, R25 shown above.

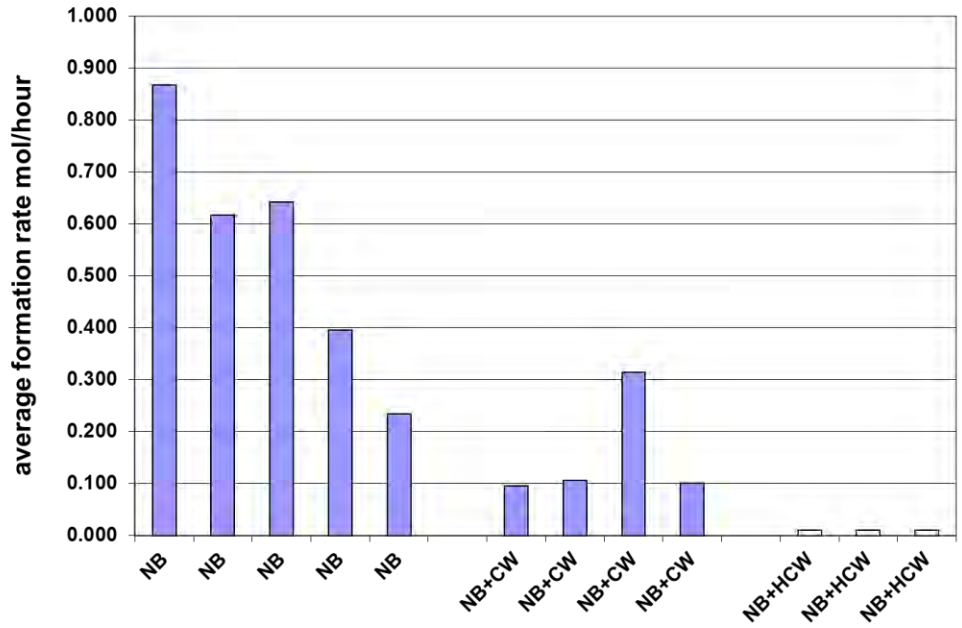


Figure R30. *Average hydrate formation rate of the tested natural gas hydrate formation with a mixture of nutrient broth (**NB**), cell cakes (**CW**) and hydrolysate of cell cakes (**HCW**). The blank bar refers to the test that no hydrate formed during the tested time and was terminated manually.*

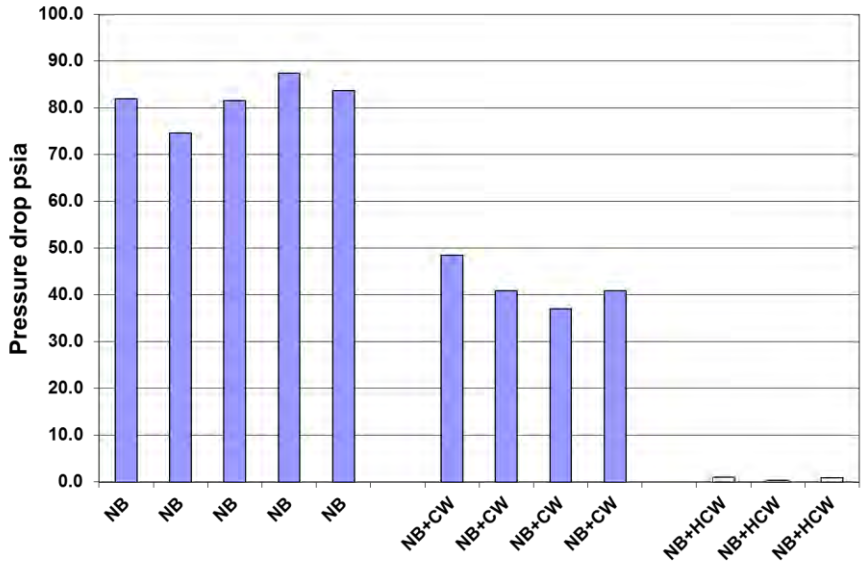


Figure R31 *Total pressure drop of the tested natural gas hydrate formation with with a mixture of nutrient broth (**NB**), cell cakes (**CW**) and hydrolysate of cell cakes (**HCW**). The blank bar refers to the test that no hydrate formed during the tested time and was terminated manually.*

The cell wall materials of the *Rhodotorula glutinis* were reported to be mannoprotein, β-glucan and chitin. The hydrolysis of glucan produces sugars and chitin produces N-acetylglucosamine. The analysis on the hydrolysate by HPLC was performed and spectra were shown in figure R32. In the hydrolysates, the N-acetylglucosamine , mannose, glucose, and galactose were identified. To test the effects of protein in the hydrolysate, the peptone was selected as representative protein in the research. The results of hydrate induction time, average formation rate and the total

pressure drop during the hydrate formation were show in figure R33, figure R34 and figure R35, respectively. The effects of Chitin, the N-acetylglucosamine and mannose were also studied and results were represented in figure R36, R37, R38.

Results given in figure R33, R34, R35, show the addition of both peptone or the hydorlysate of peptone remarkably prolonged the hydration induction time and no massive hydrate formed during the tested time of over 2746 minutes. It proved that both the peptone and the hydrolysate of peptone shown great inhibitive influence on natural gas hydrate formation.

To study the compounds that could be generated from the hydrolysis of chitin and glucan, chitin **(CT)**, N-acetylglucosamin **(NGC)** and mannose **(MN)** were evaluated on the natural gas hydrate formation. Results were displayed in figure R36, R37, R38. These data indicated that chitin **(CT)**, N-acetylglucosamin **(NGC)**, Mannose **(MN)** in the media of nutrient broth showed negligible effects on the induction time, average formation rate and total pressure drop in the formation of natural gas hydrate. This suggested that the inhibitive effects of the hydrolysate of cell cakes on hydrate formation was contributed to the proteins and the hydrolysate of the proteins.

In a summary, the hydrolysate of the cell cakes demonstrated to be a highly efficient inhibitor on the natural gas hydrate formation, which was proved to be contributed to the compounds like the peptone and the resultant hydrolysates.

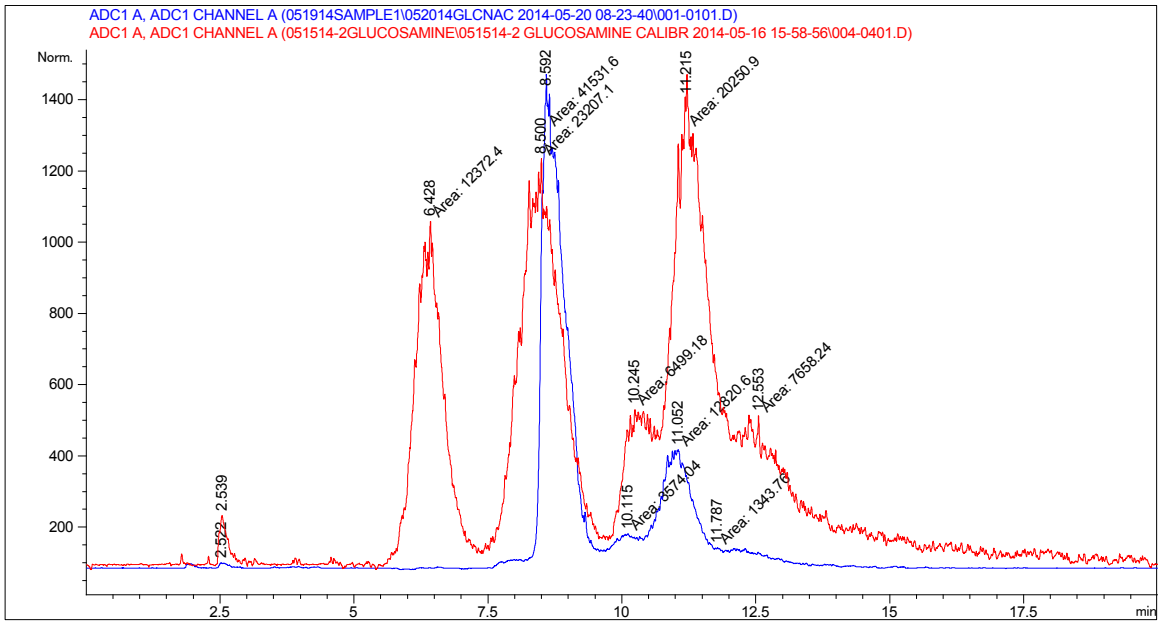


Figure R32. *the spectra by HPLC for the hydrolysate sample (blue line) compared with standard (red line). Peaks of 6.428, 8.592, 10.245, 11.215 and 12.53, were fucose, N-acetylglucosamin, mannose, glucose and galactose, respectively.*

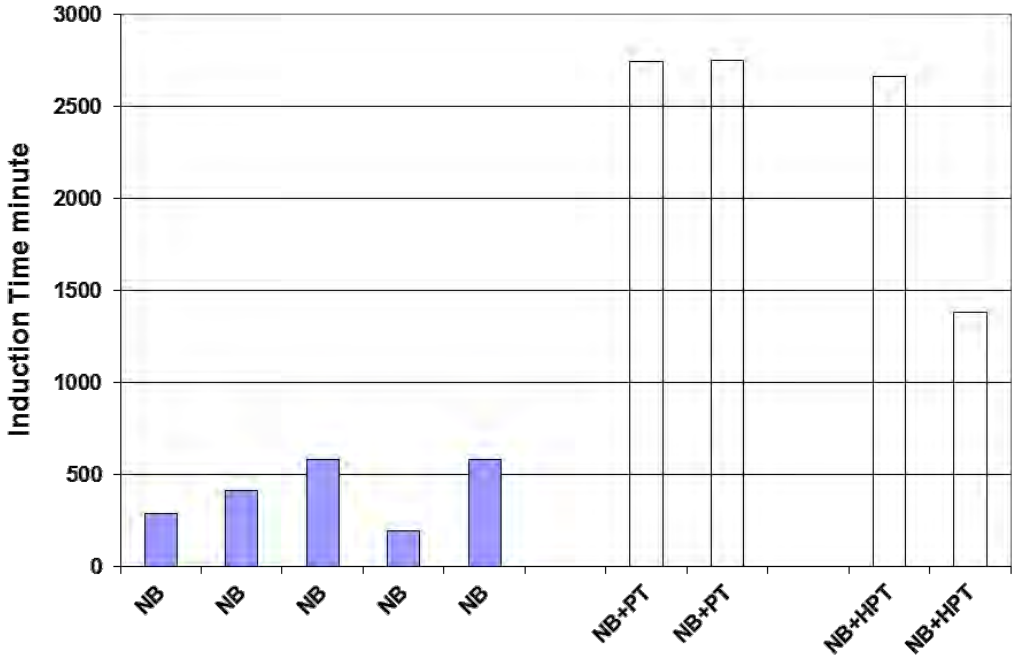


Figure R33. *Hydration induction time of the tested natural gas hydrate formation with a mixture of nutrient broth (**NB**), Peptone (**PT**), and hydrolysate of Peptone (**HPT**). The blank bar refers to the test that no hydrate formed during the tested time and was terminated manually.*

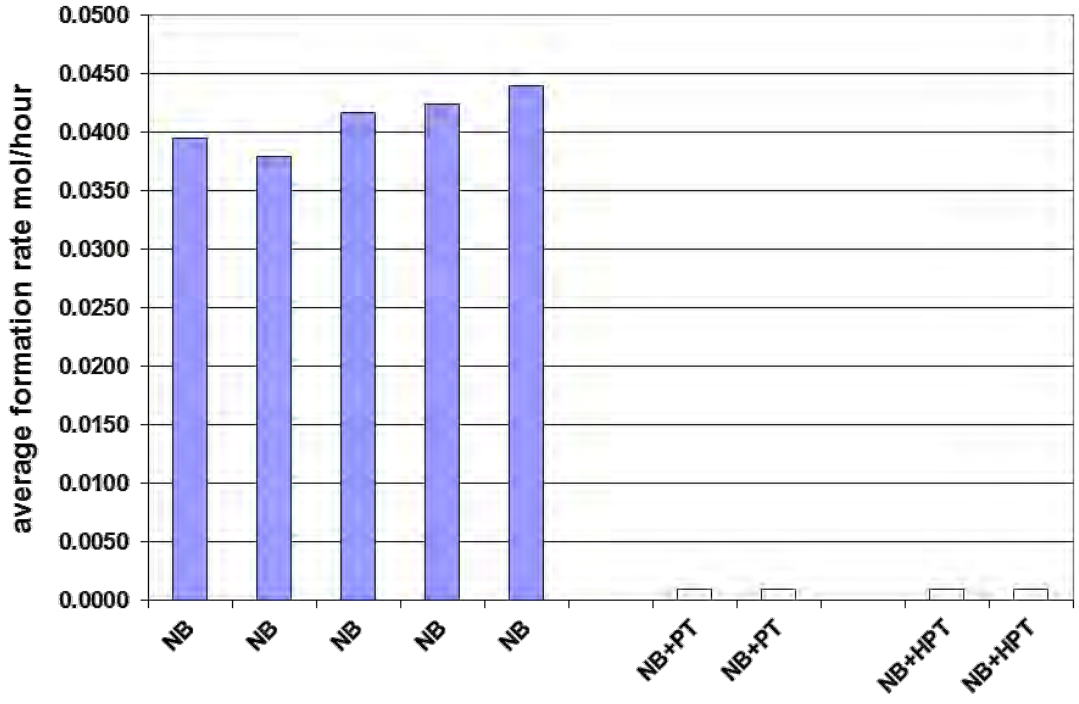


Figure R34. *Average hydrate formation rate of the tested natural gas hydrate formation with a mixture of nutrient broth (**NB**), Peptone (**PT**), and hydrolysate of Peptone (**HPT**). The blank bar refers to the test that no hydrate formed during the tested time and was terminated manually.*

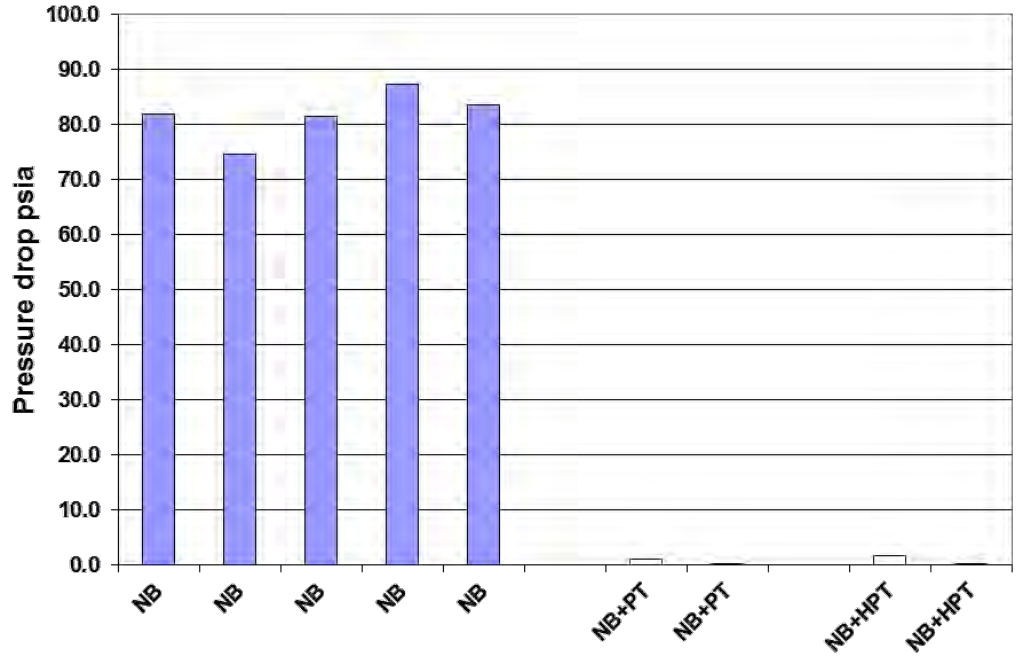


Figure R35 *Total pressure drop of the tested natural gas hydrate formation with with a mixture of nutrient broth (**NB**), Peptone (**PT**), and hydrolysate of Peptone (**HPT**). The blank bar refers to the test that no hydrate formed during the tested time and was terminated manually.*

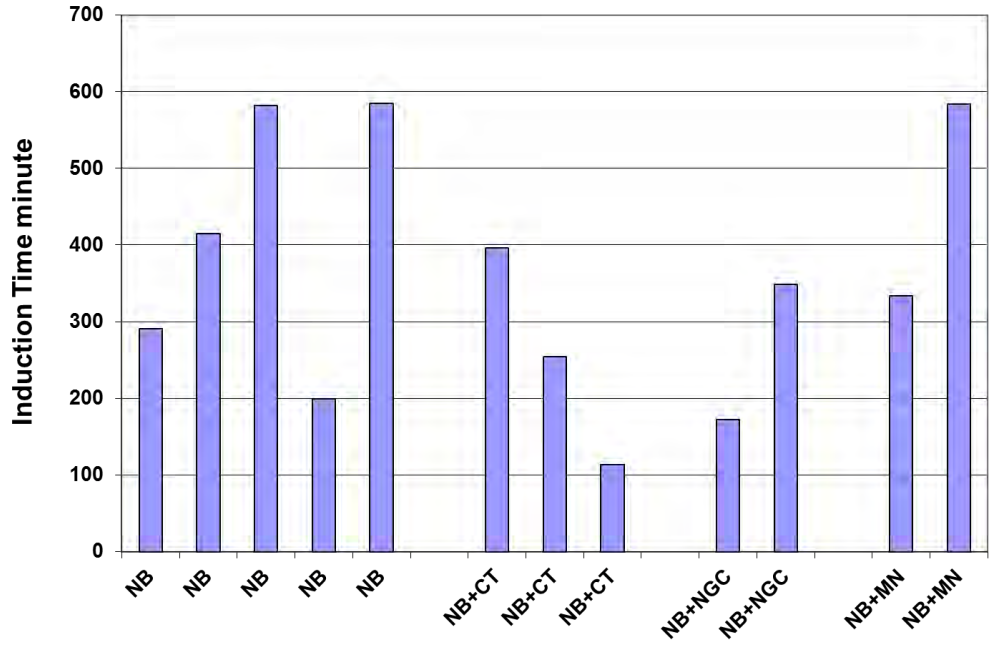


Figure R36*. Hydration induction time of the tested natural gas hydrate formation with a mixture of nutrient broth (**NB**), Chitin **(CT)**, N-acetylglucosamin **(NGC)**, Mannose **(MN)**.*

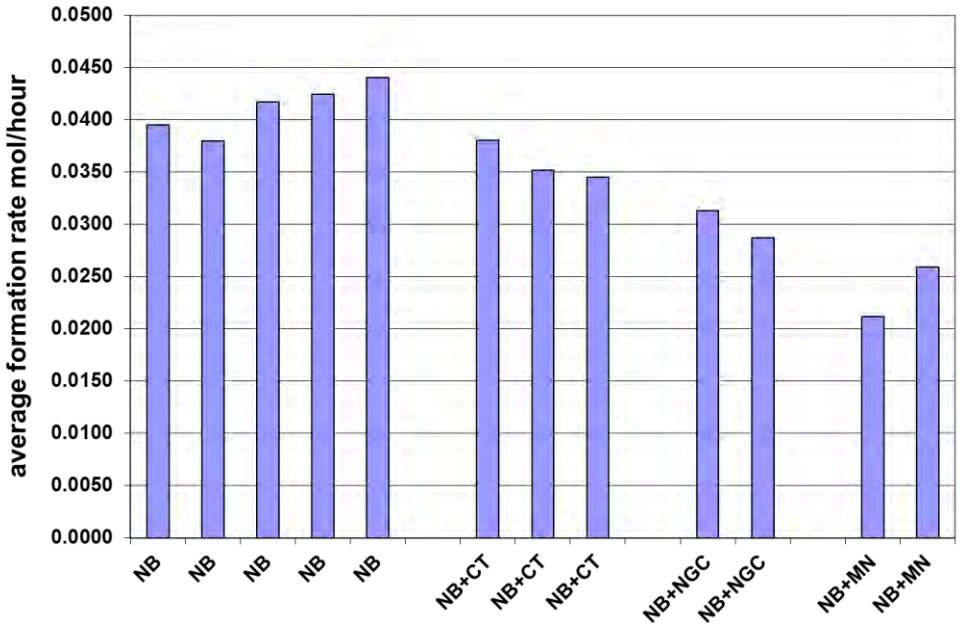


Figure R37. *Average hydrate formation rate of the tested natural gas hydrate formation with a mixture of nutrient broth (**NB**), Chitin **(CT)**, N-acetylglucosamin **(NGC)**, Mannose **(MN)**.*

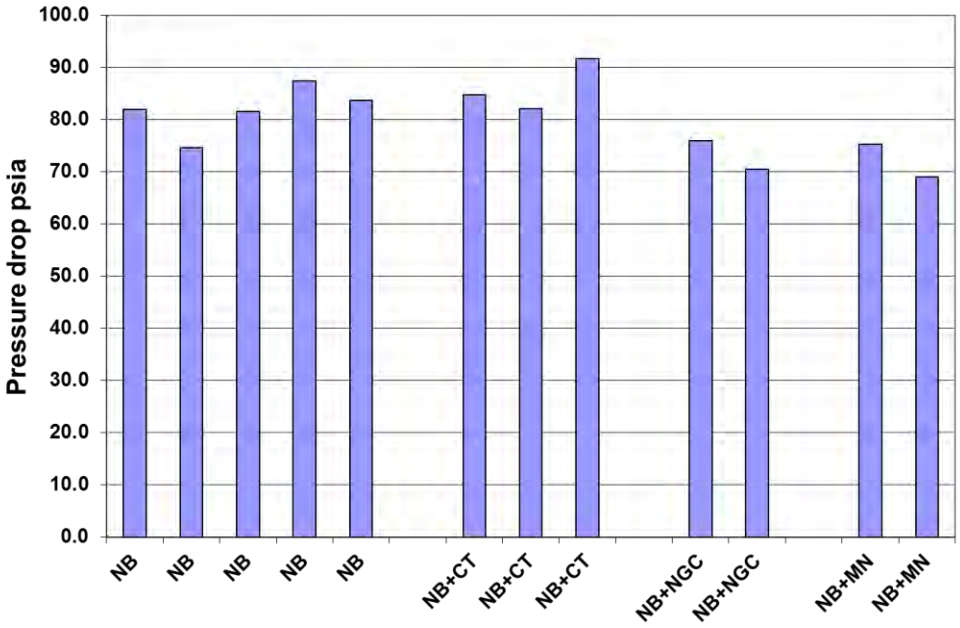


Figure R38 *Total pressure drop of the tested natural gas hydrate formation with with a mixture of nutrient broth (**NB**), Chitin **(CT)**, N-acetylglucosamin **(NGC)**, Mannose **(MN)**.*

Publications:

Shields-Menard, SA., SD Brown, DM Klingeman, K Indest, D Hancock, JJ Wewalwela, WT French, and JR Donaldson. 2014. Draft Genome Sequence of *Rhodococcus rhodochrous* strain ATCC 21198. Genome Announcements. 13;2(1).

Presentations:

Shields-Menard, S.A., B. Sukhbaatar, J.R. Donaldson, and W.T. French. Lipid Accumulation by *Rhodococcus rhodochrous* Grown on Model Lignocellulosic Sugars. Poster presentation at the Society for Industrial Microbiology and Biotechnology 2014 Symposium on Biotechnology for Fuels and Chemicals. Clearwater Beach, FL. April 28-May 1, 2014.

Shields-Menard, S.A., B. Sukhbaatar, J.R. Donaldson, and W.T. French. Lipid Accumulation by *Rhodococcus rhodochrous* Grown on Model Lignocellulosic Sugars. Oral presentation at the 2014 Graduate Student Research Symposium. Mississippi State University, MS. March 22, 2014.

Begin Confidential Information.

Task S. Liquid Hydrocarbons from Bio-derived Synthesis Gas (syngas)
The objective of the Liquid Hydrocarbons from Bio-derived Synthesis Gas thrust at MSU is to develop technologies for biomass gasification to syngas and for the catalytic conversion of clean syngas to alcohols, gasoline and diesel fuels. This is accomplished through the design and optimization of the syngas-to-hydrocarbons pilot plant, including biomass gasifier, syngas purification reactors, syngas upgrading reactors as well as new catalyst material development.

Principle Investigators and team members:
Fei Yu
Todd Mlsna

List of authorized distribution limitation notices
The data contained in pages 153 to 195 of this report have been submitted in confidence and contain trade secrets or proprietary information, and such data shall be used or disclosed only for DOE's official evaluation of performance of the SERC Syngas Thrust Area. Therefore, this information should be disclosed to only those individuals required by DOE for this performance evaluation purpose.

Executive summary
S.1 Syngas composition adjustment and syngas purification suitable for hydrocarbon synthesis
Sulfur content is relatively low in the wood chip feedstock, and sulfur removal is out of the scope of syngas purification in this subtask. Selective oxygen (O_2) removal from wood-derived syngas was investigated over three types of ceria-modified alumina supported metal catalysts (i.e., Pt, Pd, and Cu). Complete O_2 removal was observed with the Pt and Pd catalysts at a lower temperature than with the Cu catalyst. Gas hourly space velocity (GHSV) was another critical parameter affecting O_2 removal, substantially reducing O_2 conversion by all three catalysts at 4000 h^{-1} or above. The Cu catalyst appeared to be most sensitive to GHSV. Among three catalysts, the Pd catalyst had the best performance on O_2 removal. In addition to reaction conditions, CO_2 and water vapor in the syngas also influenced O_2 removal, both of which had adverse effects on O_2 conversion. Stability tests indicated that both Pt and Pd catalysts were quite stable over a 300 h testing period while the Cu catalyst was deactivated after 50 h and regenerated by elevating reaction temperature.

S.2 New generation catalyst with improved activity and stability
An integrated continuous process involving gasification, syngas cleaning, and Fischer–Tropsch (FT) synthesis was developed to efficiently produce liquid hydrocarbons. Oak-tree wood chips were first gasified to syngas over a commercial pilot plant downdraft gasifier. The raw wood syngas contains about 47% N_2, 21% CO, 18% H_2, 12% CO_2, 2% CH_4 and trace amounts of impurities. A purification reaction system was designed to remove the impurities in the syngas such as moisture, oxygen, sulfur, ammonia, and tar. The purified syngas meets the requirements for catalytic conversion to liquid fuels. Several multi-functional catalysts were developed and tested for the catalytic conversion of wood syngas to liquid hydrocarbons. As an example, in this report it was demonstrated that liquid fuels similar to commercial aviation turbine fuels (Jet A) was successfully synthesized from bio-syngas. Other findings of catalyst development and catalytic conversion for diesel range hydrocarbons and aromatic range hydrocarbons could be addressed in the published articles.

S.3 Process design and economic analysis

The Aspen Plus model has been run with both wood and coal feedstock plants with biomass feeds of 50, 500 and 5000 tons per day. It was discovered that to be viable, a plant with approximately 5000 tons per day would need to be used unless some of the equipment can be purchased at far less price points than were used in the model. An oxygen fed gasifier must also be used (not air fed) or the compressor will use so much power to compress the inert nitrogen in the gas so that the plant becomes economically unfeasible. Other discoveries from the study include that a catalyst is needed which will not form products that need further cracking. The plant can also become economically unfeasible if energy is not recycled from the gasifier or FT reactors. This model is highly dependent on the energy being recycled and only 80% of the energy was recycled (as a rule of thumb for energy recovery for large scale plants). Several items can be addressed to increase the profitability of the plants including selling the carbon dioxide created, recovering more than 80% of the energy from the gasifier and increasing catalyst conversion to more than 83% which was used in the model.

S.1 Syngas composition adjustment and syngas purification suitable for hydrocarbon synthesis

The existing downdraft gasifier is producing syngas from wood chips and other biomass. Currently, the syngas from the gasifier contains about 20% H_2, 19% CO, 12% CO_2, and 49% N_2. The nitrogen content is too high for hydrocarbon synthesis; therefore, the composition of the syngas must be adjusted to that which is suitable for liquid hydrocarbon formation. One option to decrease nitrogen in the syngas is to feed steam into the gasifier; using oxygen-enriched air is another option. These options will be explored as a means of improving the syngas.

In addition to the gases listed above, the bio-syngas also contains some tars, ammonia, H_2S, and particulates as impurities. Syngas must be cleaned prior to CO hydrogenation to liquid fuels because H_2S can poison metal catalysts, tars can cause fouling of hydrogenation catalysts, and ammonia can block catalyst sites as a result of competitive adsorption. The target level of cleanup depends on the contaminant tolerance of the downstream conversion catalyst. One of the cleaning approaches is to remove these impurities in a downstream cleaning system based on physical or chemical strategies.

Planned Activities:
S.1.ML.1 Utilize steam addition and oxygen enrichment with multiple feedstocks.
S.1.ML.2 Design, build, and test a bio-syngas purification system.

Summarization of Activities:
Steam gasification and oxygen blown gasification processes were tested by the current downdraft gasifier, and no success were achieved during the performance due to the construction limitation of the existed gasifier.

The syngas from the gasifier was first compressed to approximately 50 psig. After compression, a water scrubber and gas drying apparatus were assembled to scrub the wood syngas from the gasifier. Two 25-gallon 304 stainless steel (SS) wide mouth tanks were connected for the water scrubber. The first tank was outfitted with 13 SS exhaust mufflers with a filtration rating of 50 microns. These mufflers were used to create the maximum amount of syngas bubbles so that the utmost possible surface area of syngas could come in contact with the water and contaminates (i.e. ammonia) could be scrubbed by dissolving in the water. After the water scrubber process, the gasifier syngas was flowed through another 25-gallon tank which contained 80 lbs of silica gel desiccant to remove moisture in the wood syngas. Finally, the gasifier syngas was compressed

to approximately 2000 psig using a 2-stage pneumatic air pump obtained from Hydraulics International (Chatsworth, CA).

A benchtop scale syngas purification process was designed after identifying the possible poisoning or negative components for the FTS process, i.e., moisture, CO_2, oxygen, sulfur, ammonia and tar (Figure S1). The pilot scale syngas compression system was ordered and received as shown in Figure S2. The catalysts and adsorbents were selected from alumina-supported metal catalysts, 13X molecule sieve, active carbon, silica gel and other high surface area materials. These catalysts/adsorbents were loaded into reactors in series. The reactor system was built with controlling parameters of temperature, pressure, and flow rate. The pilot-plant scale cleaning unit is built in the Pace Seed Laboratory of Mississippi State University. The cleaned syngas should meet the basic requirements for the following step of catalytic conversion to liquid fuels and chemicals, i.e., total sufurs (H_2S + COS) < 10 ppb, NH_3< 1 ppm, oxygen< 1 ppm.

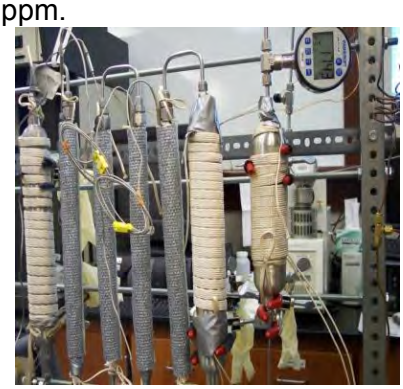


Figure S1*. Syngas cleaning lab-scale unit.*



Figure S2 *Pilot scale syngas compression system.*

Catalytic tests for oxygen removal from wood syngas

Three oxidative catalysts (i.e., 1wt % $Pt/CeO_2/Al_2O_3$, 1wt %$Pd/CeO_2/Al_2O_3$, 8wt %$Cu/CeO_2/Al_2O_3$) were examined for selective O_2 removal from wood syngas. The wood syngas used in this study contained about 46% N_2, 21% CO, 18% H_2, 12% CO_2, 2% CH_4, and 0.82% O_2. The wood syngas was free of other potential toxic component, such as moisture, ammonia, sulfur compounds (H_2S, and COS) and tar, by passing through a pre-cleaning system. The reaction pressure and gas hourly space velocity (GHSV) were 206.8 kPa and 4000 h^{-1} GHSV, respectively, unless stated otherwise.

Figure S3 compares the temperature dependence of O_2, CO and H_2 conversion during O_2 removal from wood syngas over different catalysts. O_2 was completely removed over the Pt catalyst at the reaction temperature of 75 °C or above (Figure S3a). CO conversion first increased with temperature and reached a maximum value of 5.4% at 100°C, then decreased (Figure S3b), while H_2 conversion increased with the temperature (Figure S3c). The results suggested that O_2 was mainly consumed by CO oxidation reaction below 100 °C over the Pt catalyst. However, the amount of O_2 consumed by CO decreased when the temperature was above 100°C (Figure S3b). This may be due to the fact that increasing temperature limited the CO oxidation reaction as this reaction was an exothermic process. In contrast, the amount of oxygen used by H_2 increased with the increasing temperature. H_2 oxidation reaction proceeded in competition with CO oxidation since all reactive gases were adsorbed over active metal Pt surface during the catalytic oxidation process. As the reaction temperature increased, H_2 oxidation became faster than CO oxidation reaction, leading to a higher selectivity towards H_2 oxidation. The Cu catalyst was not very active at the temperature below 100 °C for selective oxygen removal. Oxygen conversion of 100% was

achieved above 150 °C (Figure S3a). Similar to the Pt catalyst, O_2 mainly reacted with CO at low temperature (below 150 °C for the copper catalyst). The oxygen conversion decreased with increasing reaction temperature because of predominant H_2 oxidation at high temperatures. The Pd catalyst demonstrated the best oxygen removal performance at low temperature (Figure S3a). The oxygen conversion was very high at low temperatures, i.e., 98% at 50 °C. A complete oxygen conversion was observed at temperatures higher than 75 °C. It should be noted that the Pd catalyst showed very higher selectivity for the O_2 reduction reaction with H_2 than the Pt and Cu catalysts. However, this catalyst showed much lower selectivity towards CO oxidation, especially at low temperatures (Figure S3b).

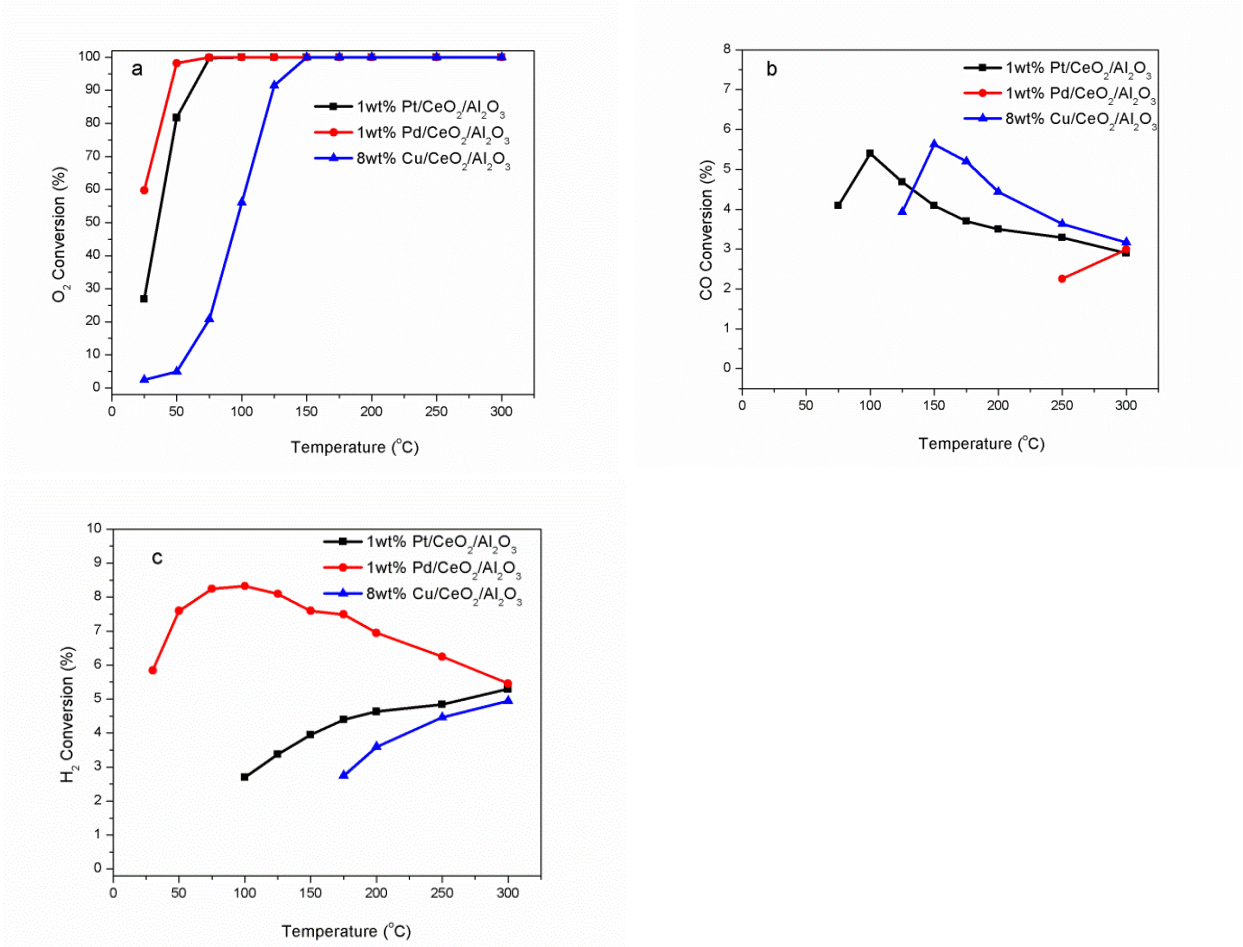


Figure S3 *Effect of temperature on the performance of the catalysts: (a) O_2 conversion, (b) CO conversion, and (c) H_2 conversion.*

Effect of GHSV on oxygen removal

The effects of hourly space velocities (GHSV) on oxygen removal from wood syngas were evaluated at varying temperatures. For the Pt catalyst (Figure S4a), complete oxygen conversion was obtained at GHSV below 4000 h^{-1} when the reactor was run at 100 °C. Further increasing of GHSV led to an increased O_2 level in the exit gas (Figure S4a), regardless of reaction temperatures. For the Pd catalyst O_2 conversion reached 100% at GHSV below 6,000 h^{-1} when the reaction temperatures were 125 and 150 °C (Figure S4b). The residual oxygen in the exit gas increased with the increasing of GHSV above 8000 h^{-1}. For the Cu catalyst, when it was tested at 150 °C, the lowest exit oxygen was 1.5 ppm at GHSV of 2000 h^{-1}, while the highest oxygen level of 0.12% was detected at GHSV of 12000 h^{-1} (Figure S4c). O_2 conversion reached 100% at

GHSV below 4,000 h^{-1} at 175 and 200 °C. Significant decrease in oxygen conversion at the higher GHSV can be due to the short residence time of the reactants. The contact time decreased from 1.8 s to 0.3 s when GHSV increased from 2000 to 12,000 h^{-1}.

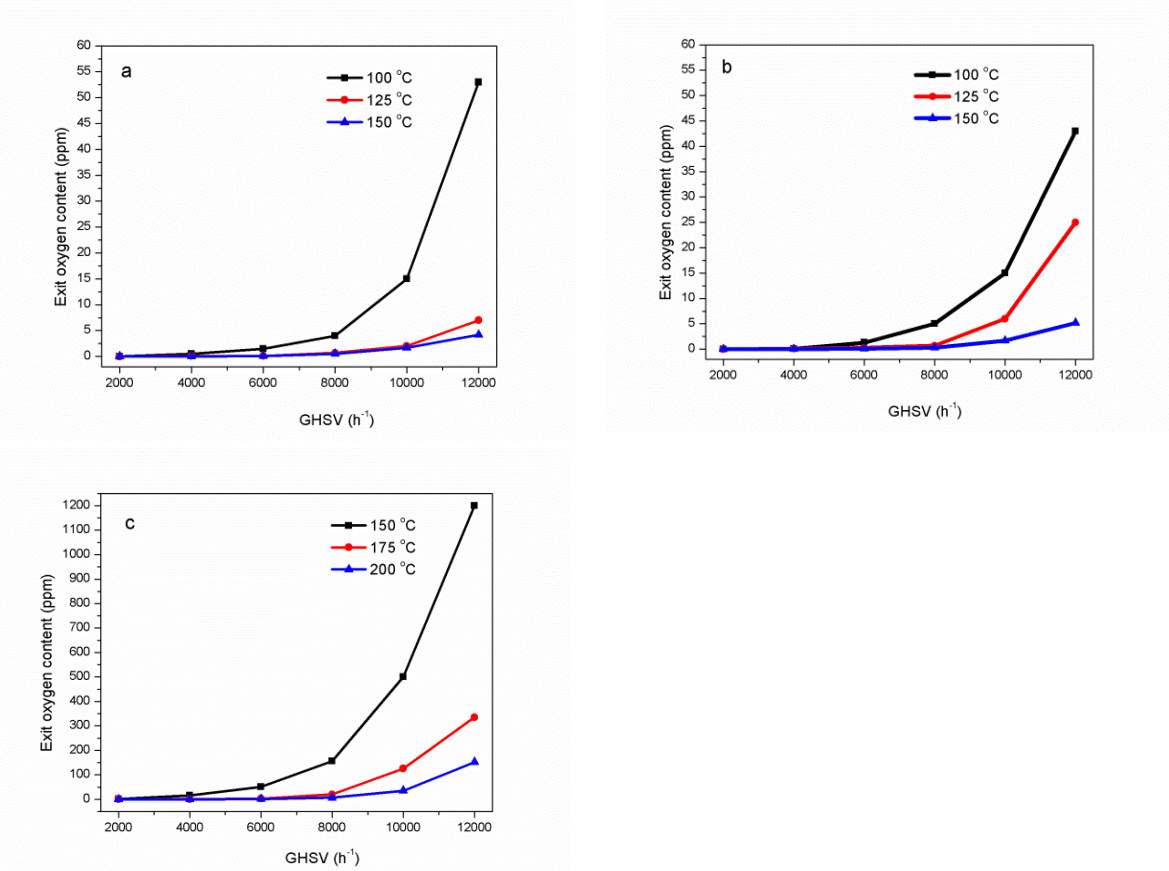


Figure S4 *Effect of GHSV on oxygen removal by (a) Pt, (b) Pd, and (c) Cu catalysts*.

Effect of CO_2 pre-capture on oxygen removal

CO_2 may have a negative effect on oxygen removal since there was up to 12% CO_2 in the pre-cleaned wood syngas. To investigate the effect of CO_2 on the oxygen removal performance, wood syngas passed through a CO_2 capture system packed with absorbents of active carbon, zeolites, and CaO. After CO_2 capture, the syngas contained 23.8 % CO, 20.5% H_2, 2.2% CH_4 and 1.0% O_2, and 52% N_2. The results showed that the presence of CO_2 resulted in slight decrease in oxygen conversion at the low temperature (<50 °C) by both Pt and Pd catalysts. For the Cu catalyst, O_2 conversion increased by 9% after CO_2 pre-capture. Moreover, the absence of CO_2 resulted in a shift of the maximum CO conversion temperature to a lower temperature. The reasons for the difference in catalytic behavior with the presence of CO_2 are unclear so far. However, the negative effect of CO_2 on catalyst activity can be due to formation of carbonate or carboxylate species during oxidative reaction which in turn block the active sites of the catalysts and prevent adsorption and reaction of the reactants on the catalyst surfaces. On the other hand, the reverse water gas shift reaction (RWGS, $CO_2 + H_2 \leftrightarrow CO + H_2O$) between CO_2 and H_2 could lead to the CO formation and CO conversion thus decreased in the presence of CO_2 in the feed gas. As mentioned above, CO_2 had an unfavorable effect on the catalytic activity. In other words, CO_2-free wood syngas allowed the catalyst to have a good performance.

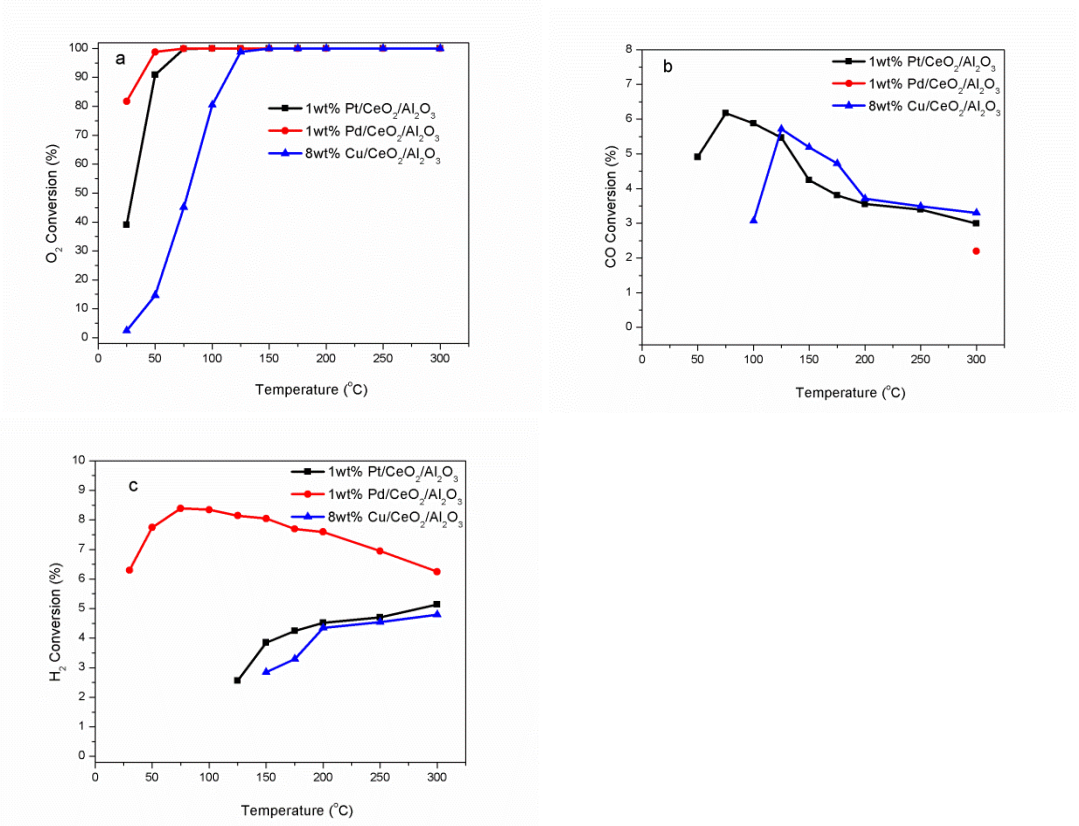


Figure S5 *Effect of pre-captured CO_2 on performance of the catalysts: (a) O_2 conversion, (b) CO conversion and (c) H_2 conversion.*

Effect of moisture on oxygen removal

The catalytic activity of a catalyst can be significantly depressed with the presence of water in the feed stream. The wood syngas that exits the gasifier usually contains 5-10% water. Therefore, it is important to investigate the effect of moisture on catalytic removal of oxygen. In the current work, pre-cleaned wood syngas was adjusted with 5% moisture and then used for oxidative reaction. The results showed that for the Pd catalyst moisture negatively affected both O_2 and H_2 conversion while positively affecting CO conversion at the low temperatures (<100°C) (Figure S6a and S6c). Similar performance was also observed with the Pd catalyst (Figure S6a and S6c). In contrast, a significant decrease in O_2 conversion was observed with the Cu catalyst at the temperature below 150 °C (Figure S6a and S6c). The CO conversion also increased a little bit but with conversion peak temperature shifting to 175 °C. H_2 conversion declined slightly. However, the oxidative activities of all three catalysts were not significantly influenced by the moisture at higher temperatures (Figure S6a-c).

The negative effect of the moisture in the feed gas on the catalytic performance may be due to water molecular competing with adsorption of O_2, CO and H_2 on the metal surface and water molecular blocking parts of the active sites. The increasing of CO conversion and decreasing of H_2 conversion over the entire temperature range might be due to the water-gas shift reaction (WGSR, $CO + H_2O \leftrightarrow CO_2 + H_2$), through which part of CO was converted while H_2 and CO_2 were formed in the presence of water. Loss of catalyst activity caused by water vapor could diminish at higher temperatures.

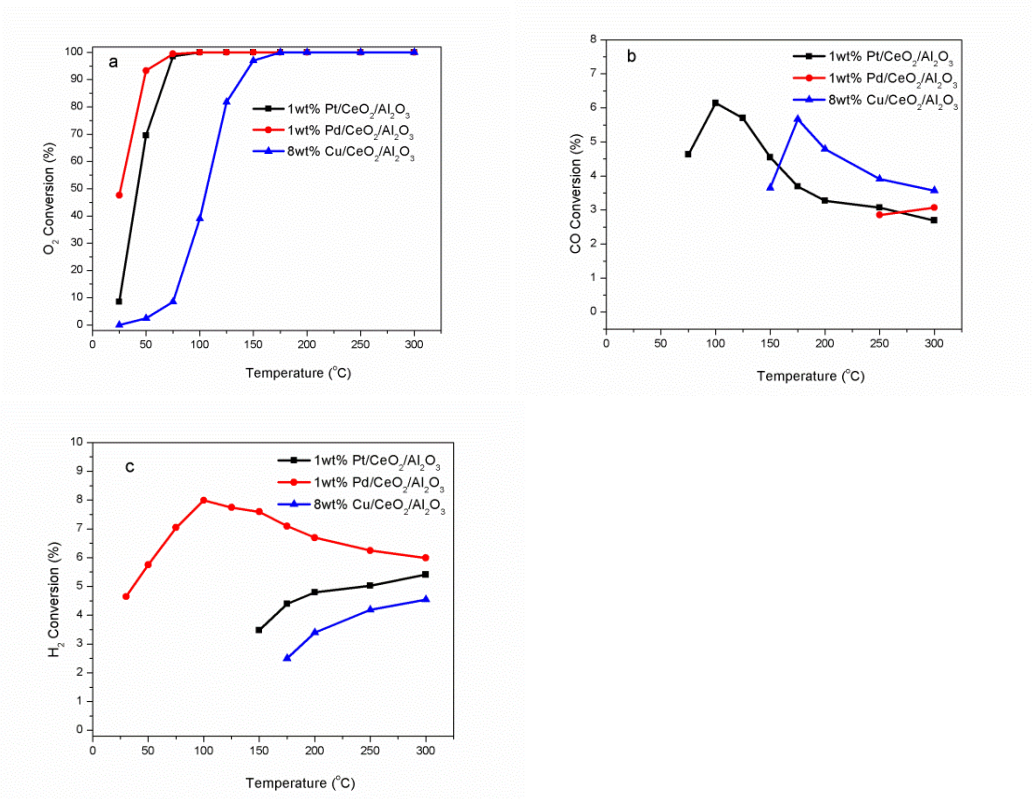


Figure S6 Effect of moisture on the performance of the catalysts: (a) O_2 conversion, (b) CO conversion, and (c) H_2 conversion.

Stability test

The long-term activity and stability of the catalysts were examined for up to 300 hours. The reaction temperature was100 °C for both Pt and Pd while 150 °C for the Cu catalyst. GHSV of 4000 h^{-1} was for all three catalysts. As shown in Figure S7, both Pt and Pd catalysts exhibited high stability with the exit oxygen concentration kept below 0.5 ppm over 300 hours testing period. For the Cu catalyst, the exit oxygen level was below 1.0 ppm at first 40 hours and then kept increasing, reaching 5.0 ppm after 90 hours. It drastically increased to 205 ppm after 220 hours, indicating catalyst deactivation. Attempt was made to recover the activity of the Cu catalyst by increasing reaction temperature to 200°C. It was found that the catalyst activity was gradually recovered after 20 hours and the exit oxygen level was kept below 0.5 ppm throughout the rest of the reaction period (Figure S7). Deactivation of the catalyst at 150°C may be due to accumulation of carbonates on active sites of copper. When the reaction temperature increased to 200 °C, carbonates accumulated could be decomposed and the Cu oxide species could be reduced.

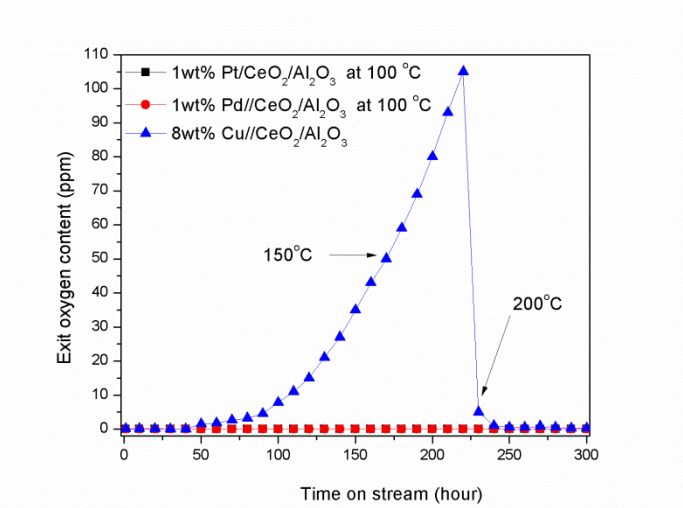


Figure S7 *Stability test of the catalysts for oxygen removal.*

Among syngas impurities, O_2 has been found to be one of the most toxic compounds to FTS catalysts, especially iron and cobalt-based catalysts. O_2 can temporarily or permanently deactivate an FT catalyst even at a trace level. Frequent regeneration of FT catalysts not only increases the difficulty of operation but also significantly increases the associated costs. As raw bio-syngas generally contains a significant amount of O_2 (~1%), efficient O_2 removal is particularly important for its downstream FTS process. In this task, we aimed to develop ceria modified alumina supported metal-based catalysts for selective O_2 removal from the bio-syngas by.

Catalyst characterization

As compared to γ-Al_2O_3, ceria modified support and all catalyst samples had decreased BET surface area and pore sizes (Table S1). Both Pt and Pd catalysts had similar properties while the Cu catalyst had the smallest surface area and pore size. The catalyst preparation process, especially with steps involving drying and calcination, mainly contributed to changes in physical properties of the catalysts.

TPR was carried out to elucidate the state of metal oxides and metallic platinum, palladium, and copper. The reduction peak at 89 ºC was observed with the Pt catalyst (Figure S8a), which related to reduction of PtO_2. In contrast, the Pd catalyst was more easily reduced than the Pt catalyst, exhibiting one positive peak at 65 ºC and one negative peak at 118 ºC (Figure S8b). The positive peak was attributed to the reduction of PdO, and the negative peak most likely attributed to the decomposition of palladium hydride. The TPR profile of the Cu catalyst shows a distinct profile from which a single large peak was observed at 207 ºC (Figure S8c), elucidating the reduction of CuO at that temperature.

Table S1 *Physical property of the catalysts*

Catalyst	BET Surface Area (m^2/g)	Pore Volume (cm^3/g)	Average Pore diameter (nm)
$\gamma-Al_2O_3$	252	0.95	10.5
CeO_2/Al_2O_3	193	0.73	8.2
$Pt/CeO_2/Al_2O_3$	185	0.5	7.5
$Pd/CeO_2/Al_2O_3$	187	0.49	7.2
$Cu/CeO_2/Al_2O_3$	129	0.31	4.7

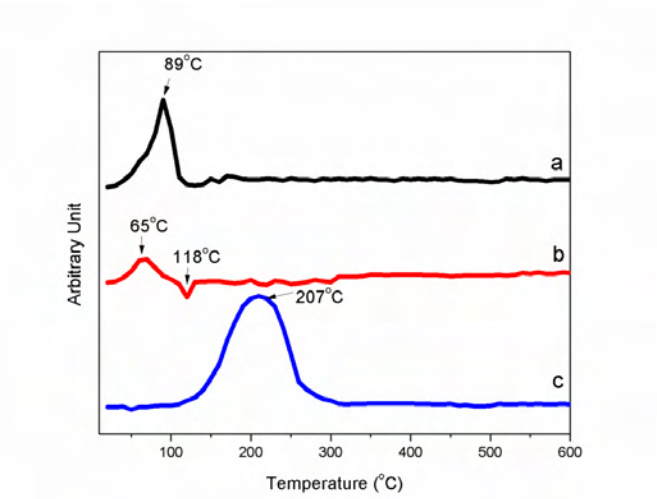


Figure S8 *TPR profiles of the (a) Pt, (b) Pd, and Cu (c) catalysts*

O_2 content of producer gas during the gasification process

The gas composition of producer gas was monitored by an on-line GC at 20 minute intervals during the gasification process. The gasifier was first purged with air for 20 min and then ignited for wood gasification. As shown in Figure S9, O_2 decreased quickly from 21% to 3.8% after the gasifier was ignited for 20 min, and then to 1.7% for another 20 min. After this point, the O_2 levels dropped to about 0.4~0.5% for the remaining period of gasification. Incomplete conversion of O_2 during gasification was most likely due to a high flow rate ($65 m^3/h$) of the gas through the fixed downdraft gasifier bed. In this scenario, air was forced to pass through "short cut channels" of the gasifier bed before it can be exposed to the wood chips or char. Other gaseous products formed during gasification included CO_2, CO, H_2 and CH_4, which increased with prolonged gasification time and reached steady levels after the gasifier was fully started up at around 90 min. The producer gas collected during the steady gasification run was composed of 21% CO, 18% H_2, 12% CO_2, 2.5% CH_4 and 0.5% O_2. N_2 was the balance gas in the producer gas.

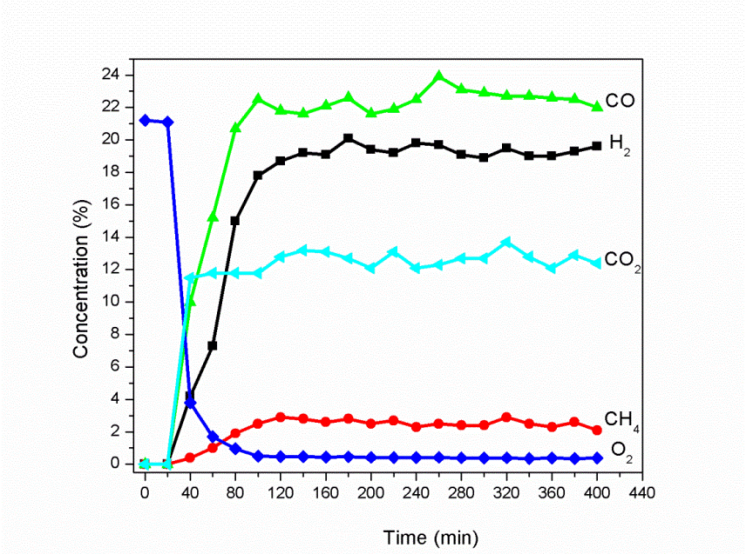


Figure S9 *Syngas composition monitored throughout the gasification process*

Influence of O_2 in syngas conversion

The producer gas was pre-cleaned and tested for the effects of O_2 on the FTS process. As shown in Figure S10, O_2 content as low as 0.5% was highly toxic to the FT catalyst which deactivated the catalyst within several hours. As a result, conversion efficiency of raw syngas drastically decreased. In contrast, a stable conversion was obtained with O_2-free syngas (cleaned). Since frequent regeneration of the FTS catalyst generally leads to increased operation costs and reduced catalyst lifetime, it is necessary to remove O_2 from bio-syngas before it can be used as a feedstock gas for FTS.

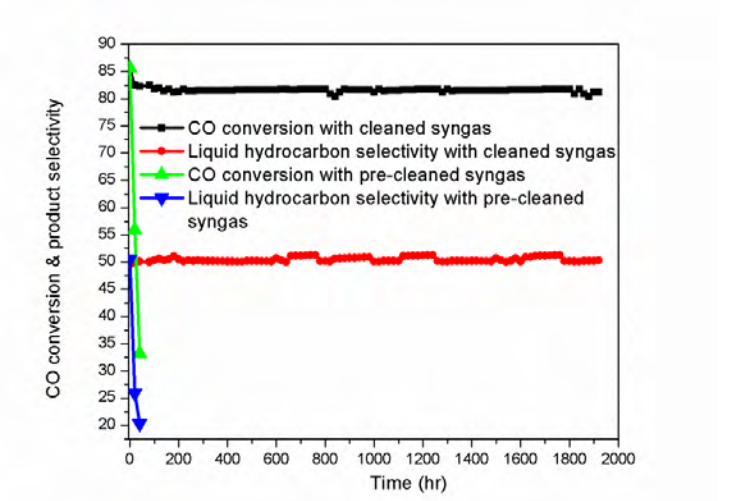


Figure S10 *Influence of O_2 on syngas conversion.*

S.2 New generation catalyst with improved activity and stability

Developing high activity and high stability catalysts is the key for a better overall performance of this process. A new-generation catalyst will be designed and fabricated with improved activity and selectivity. More importantly, the new generation catalyst will have a high stability when using bio-syngas. The syngas-conversion catalysts can be deactivated by metal sintering, carbon

deposition, poisoning, and attrition. Improving life and impurity tolerance of the catalysts is essential. A fundamental understanding of the catalytic process will be pursued to help improve the catalyst durability.

Planned Activities:
S.2.ML.1 Develop a new-generation catalyst with improved activity and selectivity.
S.2.ML.2 Optimize the catalytic process conditions to account for the effects of impurities in the synthesis gas derived from biomass gasification.
S.2.ML.3 Run a 1000-hr life-time test of the new-generation catalyst to validate its activity and stability with the bio-syngas. The life-time test will be conducted under the optimized operating conditions.
S.2.ML.4 Develop more understanding of catalyst deactivation and regeneration issues in syngas conversion.

Summarization of Activities:

Design of multifunctional catalysts for jet fuel synthesis from wood derived syngas
Paraffins, iso-paraffins, aromatics, and naphthenes are the main hydrocarbon components in jet fuel, while straight chain paraffins and/or olefins are the main products over iron and cobalt-based FT catalysts (Leckel, et al., 2009a and Leckel, et al., 2009b). Multiple processing steps are usually followed after FTS to reach these specifications of Jet fuel (Huber, et al, 2006). However, too many processing steps will increase the cost of the product and decrease the overall efficiency of the process. Therefore, to explore fewer steps for synthesizing ATF via FTS that meets all these specifications, new catalysts are needed to produce the desired range of ATFs or jet fuels from syngas. One of the alternatives to improve the selectivity and quality limitations of the FT process is to use hybrid or composite catalysts which comprise a FT base catalyst and a co-catalyst containing the appropriate functionality to increase the yield and selectivity of the desired products. The combination of an iron-based FT catalyst displaying high selectivity to olefins and oxygenates with ZSM-5 or HY zeolites (Botes, 2005; and Yan, et al., 2008) results in an enhanced gasoline selectivity and an increased concentration of high-octane branched and aromatic hydrocarbons by promoting oligomerization, cracking, isomerization, and aromatization reactions on the zeolite acid sites. Another approach is to convert syngas to alcohols over an alcohol synthesis catalyst, and alcohols subsequently convert to hydrocarbons over solid acid catalysts like ZSM-5 (Yan, et al., 2008).

Multifunctional catalysts are needed to chemically convert syngas to jet fuel range hydrocarbons like paraffins, iso-paraffins, aromatics, and naphthenes; therefore, the catalyst should include CO hydrogenation, FTS, alcohol dehydration, and hydrotreating/hydrocracking activity. As mentioned previously, bio-syngas (producer gas) will be used as sole feedstock in the process. In the designed process, alcohols are formed from syngas by CO hydrogenation. Hydrocarbons are produced from syngas through alcohol dehydration and/or the FTS process over heterogeneous catalysts. The designed catalyst has functions of CO hydrogenation for alcohol formation, FTS for paraffin production, and alcohol dehydration for producing iso-paraffins, aromatics, naphthenes from alcohols. The isomerization function is also needed since branched paraffins are the favored component for jet fuels, while FTS and alcohol synthesis processes are principally used for producing linear hydrocarbon molecules (Gujar, et al., 2009). Branched paraffins, aromatics, naphthenes and/or iso-alcohols are produced from their linear counterparts by the isomerization process.

Alcohols are synthesized from syngas through the CO hydrogenation process. Various catalyst systems, such as modified Cu/ZnO, modified MoS_2, and modified Fe or Co FT catalysts, have

been found to produce higher alcohols from syngas (Freerks and Muzzell, 2004). Cobalt-promoted Mo based catalysts have been extensively used in the hydrotreating process (Davis, 2005), and it was also reported Co-Mo based bimetallic catalysts were active to produce mixed higher alcohols from syngas (Ancheyta-Juárez, et al., 1999). C1-C7 mixture alcohols were produced from syngas over Co-Mo based catalysts (Bian, et al., 1999).

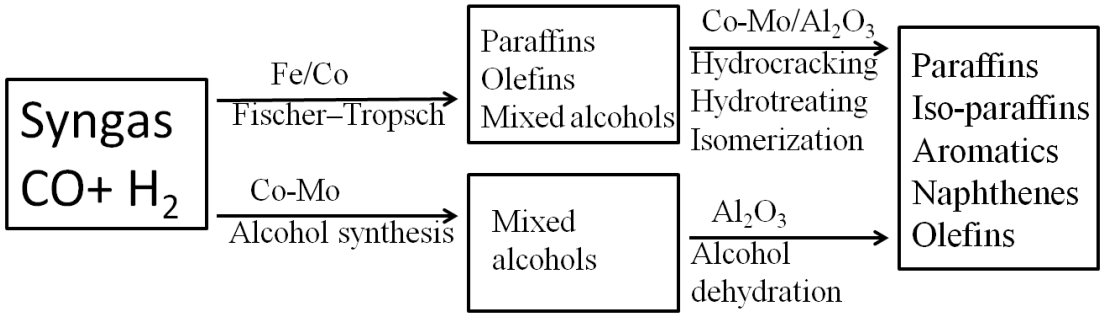
Only Fe, Co, Ni and Ru metals have sufficiently high activities for the FTS process (Li, et al., 1998). Among these four metals, only cobalt and iron-based catalysts can be considered as practical FT catalysts (Li, et al., 1998). Co catalysts are generally 5-10 times more active than iron catalysts for comparable conditions. Moreover, carbon selectivities to C5+ of Co catalysts are also generally higher relative to Fe catalysts, since Co produces very little or no CO_2. Co is already used as the alcohol synthesis active component, so iron is also selected for the designed catalyst due to its low cost, low H_2/CO usage ratio (near 0.7), and tendency to yield high amounts of olefins in hydrocarbon distribution. Iron can also be operated at high temperatures (>300 °C).

One of the alternative ways to synthesize hydrocarbons is by the condensation of alcohols. This is a process in which alcohols lose water and form olefins and/or cyclic hydrocarbons and/or aromatics. Alcohol dehydration reactions generally occur by heating the alcohol with strongly acidic zeolites and oxides like SiO_2, Al_2O_3, TiO_2, ZrO_2, and ZnO. These have been extensively used as heterogeneous catalysts for alcohol dehydration to hydrocarbons (Davis, 2007). Our previous work on conversion of alcohols to hydrocarbons demonstrated that the methanol reaction over H^+/ZSM-5 produced aromatics including *p*-xylene, 1,2,3-trimethylbenzene, and 1,2,4,5-tetramethylbenzene and oxygenates including dimethyl ether, 3-methyl-2-butanone, and acetone among others (Gujar, et al., 2009). The reaction of ethanol under similar conditions produced ethyl-substituted aromatic compounds including 1, 3-diethylbenzene and 1,2-diethylbenzene and alkanes like 3-methylheptane and 4-methyloctane among others. When ethanol was used, the production of oxygenates was less than that obtained for methanol. When 1-propanol reacted over H^+-ZSM-5, products exclusively composed of alkenes and branched alkanes like 2-methyl-1-propene, 4-methylhexane, and 4-methylheptene were formed. Employing 2-propanol as a reactant resulted in a product distribution containing aromatics including p-xylene and 1-ethyl-2-methylbenzene and olefins including 3-methyl-2-hexene and 3-methyl-2-pentene. Of all the butanols reacted over H^+-ZSM-5, only 2-methyl-2-propanol (*tert*-butanol) gave the most significant aromatic yield. The remaining butanol isomers mainly gave branched alkanes and alkenes (Li, et al., 2001).
Solid acid catalysts have been widely used and are industrially important because of the hydrocarbon isomerization process (Nel and de Klerk, 2007). Zeolites are also used as a catalyst for the isomerization process (Kriz, et al., 1998). γ-Alumina also showed good activity on the reconstruction of straight chain hydrocarbons to branched, cyclic, and aromatic compounds (Sotelo-Boyas, et al., 2011).

Hydrotreating and/or the hydrocracking process usually follows the FTS process to upgrade these long chain paraffins to the desired range of ATFs or jet fuels. The designed catalyst contains these hydrotreating/hydrocracking functions. The Co-Mo/γ-Alumina catalyst has been widely used as a hydrotreating/hydrocracking catalyst in the petroleum industry (Baumgarten, et al., 1983). Supported Co-Mo catalysts have been used in the petroleum refining industry for the past half century due to their reliable activity and thermal resistance (Lamprecht, 2007). Co-Mo bimetallic nanocatalysts were found to enhance the CO conversion in FTS. Incorporation of Mo into Co nanocatalyst led to better reducibility and higher H_2-consumption which would have resulted in more metal active sites available for FTS. Thus, it enhanced catalytic activity compared to those of the monometallic nanocatalysts (Reddy, et al., 1998).

Promoters are also an important part of a catalyst. K_2O has shown a superior ability to improve the selectivity and stability of catalysts. It is an important promoter for both the FTS and CO hydrogenation catalysts, and therefore, K_2O was chosen as the promoter of the multifunctional catalyst used in this study.

Overall, the K-Fe-Co–Mo-γ-Alumina catalysts designed for this study were expected to be capable of converting syngas to jet fuel-range hydrocarbons in a single reaction step since they contain several catalytic functions. Scheme S1 illustrates the reactions and the selected active phases involved over the K-Fe-Co–Mo/γ-Al_2O_3 catalyst. The bimetallic Co-Mo provides the active sites to convert CO into a mixture of alcohols from syngas. Iron and cobalt contain the hydrocarbon synthesis active sites for forming paraffins from syngas. γ-Al_2O_3 has the capability to dehydrate alcohols to paraffins, iso-paraffins, aromatics, naphthenes, and olefins. γ-Al_2O_3 also acts as the isomerization active components to restructure straight chain paraffins to branched paraffins and naphthenes. Co–Mo/Al_2O_3 is well known as a hydrotreating/hydrocracking catalyst to upgrade long chain paraffins to iso-paraffins, aromatics, and naphthenes. Alkaline metal K is the promoter to improve catalyst selectivity and stability.



Scheme S1 *Illustration of the reactions of syngas to synthetic aviation turbine fuels over the K–Co–Mo-γ-Alumina catalyst*.

Syngas production from wood chips

Many studies have been carried out to produce high quality syngas from natural gas or coal (Labrecque and Lavoie, 2011). In current work, syngas was generated from wood chips through gasification process. The composition of the producer gas was stable during gasification, which was monitored by a portable gas analyzer (7900P4C, NOVA Analytical Systems, Inc.). Fig. S11 showed the gas concentration variations during one run. The portable gas analyzer was not calibrated and was used only for monitoring the fluctuation of main gas concentrations. The gas concentrations measured by Agilent 6890 GC were used for material and energy balance analysis.

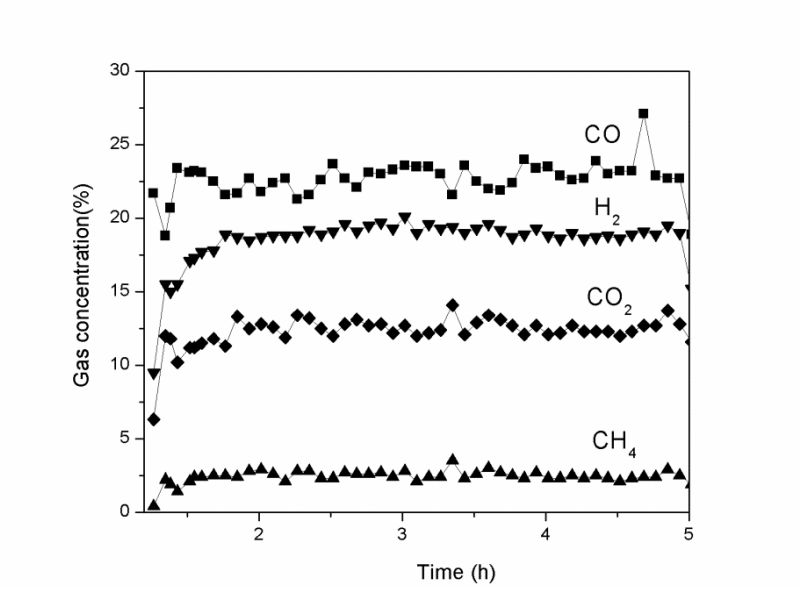


***Figure S11**. Typical syngas composition monitored by a portable gas analyzer*.

The syngas from the gasifier contained about 18 % H_2, 21 % CO, 12 % CO_2, 2% CH_4 and 46% N_2. Besides of these main components, producer gas typically contains 500-3,000 ppm of tars, 0.5~2% oxygen, 200-1000 ppm of ammonia, and 200-400 ppm of sulfur components (H_2S and COS). After passing through the syngas cleaning unit, impurities in the producer gas were removed; the cleaned producer gas met the industrial requirements for catalytically converting the syngas (CO + H_2) to liquid fuels. The sulfur content (H_2 S + COS) was less than 10ppb, the ammonia content (NH_3) was less than 1ppm, and the oxygen content (O_2) was less than 1 ppm (Yan and Yu, 2012).

Catalytic conversion wood syngas to liquid hydrocarbons

The influence of different operation parameters (catalyst bed temperature, reactor pressure, and GHSV) on the behavior of the FTS process was studied. Producer gas passed through the single tube reactors and was converted to liquid hydrocarbons. The effluent flow was cooled and condensed, and then water was separated from oil phase. The CO conversion and hydrocarbon distribution were measured in a fixed bed flow reactor operating at a temperature of 250 to 350 °C, a gas hourly space velocity (GHSV) of 500 to 3000 h^{-1}, and a pressure of 3.14 to 8.62 MPa.

Effect of temperature

The temperatures studied were 250, 270, 290, 310, 330 and 350 °C, with the remaining conditions maintained constant. Three grams of catalyst were loaded into the reactor, and producer gas was fed into the reactor. The operating pressure was maintained at 6.89 MPa while the gas hourly space velocity was maintained at 3000 h^{-1}. The control of the reaction temperature is an extremely critical step since the FTS is a highly exothermic process, and high temperature may lead to the sintering of the catalyst, a decrease in the CO conversion rate, and a product selectivity shift to light hydrocarbons with increasing temperature.

Fig. S12 shows the CO conversion, the carbon dioxide and hydrocarbon selectivity, the gas phase hydrocarbon distribution (wt %) and the liquid hydrocarbon distribution with temperature. CO conversion increased from 53.2% at 250 °C to 85.6% at 350 °C, and the hydrocarbon distribution also changed with temperature; the C5+ hydrocarbons decreased with increasing of temperatures

from 66.5% at 250°C to 57.4% at 350°C. Fig. S12c shows the liquid fuel distribution in six groups, i.e., paraffins, iso-paraffins, aromatics, naphthenes, olefins, and oxygenates. Results indicate that paraffins decreased from 35.20% to 14.90% as the temperature elevated from 250 to 350 °C; iso-paraffins increased from 20.3% at 250 °C to 25.8% at 350 °C; olefins decreased from 21.3% at 250 °C to 14.2% at 350 °C; aromatics increased from 18.1% at 250 °C to 30.8% at 350 °C; naphthenes increased from 6.3% to 12.8%; while oxygenates decreased from 1.21 to 0.03%. Fig. S.2.2d illustrates the liquid fuel yield versus reaction temperature, the yield rate of the liquid hydrocarbons increased from 0.146 g/(g cat·h) at 250 °C to 0.203 g/(g cat·h) at 350 °C.

The results show that there is a balance between two trends: the CO hydrogenation reactions yielding alcohols, mainly due to the bimetallic Co-Mo, with an optimum temperature of 250−300 °C, and the acid function-based reactions, i.e, the conversion of oxygenates to hydrocarbons or aromatization, mainly due to the γ-Al_2O_3, with an optimum temperature of 300−350 °C. A compromise between these two trends leads to an optimum reaction temperature to give the maximum aromatics, iso-paraffins, and naphthenes yield. On the other hand, although the $C5^+$ fraction decreases in absolute terms, the aromatics, iso-paraffins, and naphthenes fractions increase relative to the total $C5^+$ fraction when the temperature increases above 300 °C, so that the liquid fraction becomes richer in aromatics, iso-paraffins, and naphthenes. It has been proven that increasing the operating temperature results in a shift in selectivity toward lower carbon number products and more hydrogenated products for all FT catalysts (Yan, et al., 2008; Gujar, et al., 2009). The degree of branching increases, and the amount of secondary products formed (such as ketones and aromatics) also increases as the temperature is raised. These shifts are in line with thermodynamic expectations and the relative stability of the products. As Co is a more active hydrogenating catalyst, the products are generally are more hydrogenated, and the CH_4 selectivity rises more rapidly with increasing temperature.

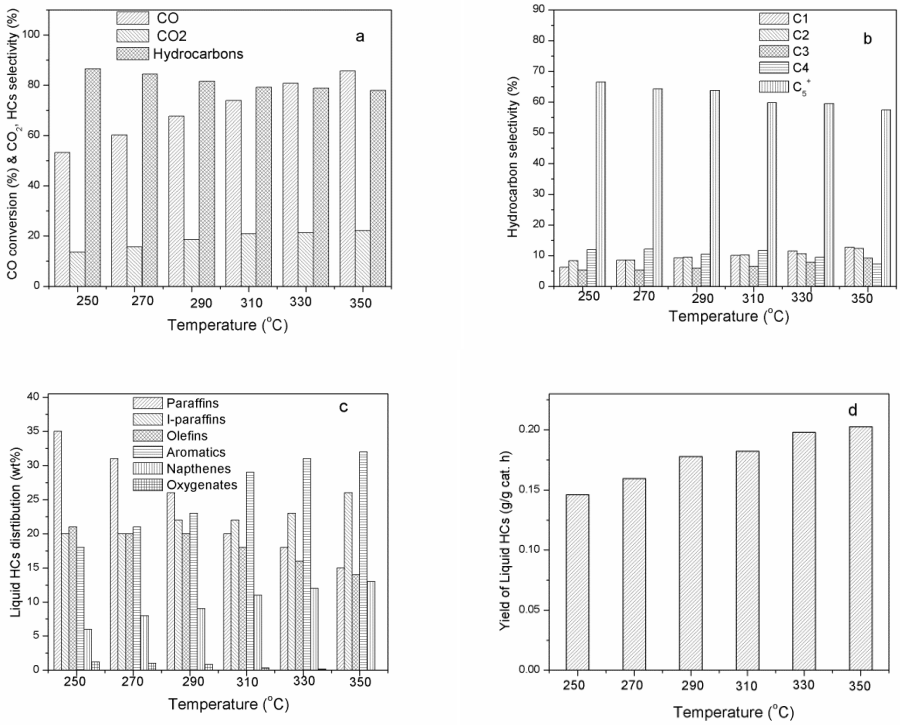


***Figure S12**. Effect of temperature on (a) CO conversion, CO_2 and hydrocarbon selectivity, (b) hydrocarbon distribution, (c) liquid hydrocarbon distribution, and (d) yield of liquid hydrocarbons*

at 6.89 MPa, with wood syngas, GHSV of 3000 h^{-1}; 3 g of catalyst was used in the reaction. Time on stream was 48-100 h.

Influence of pressure on the catalyst performance

An increase in total pressure will shift the equilibrium towards the product side of the reaction, and increase the CO conversion. Experiments under pressures of 3.45, 5.17, 6.89, and 8.62 MPa were conducted. Temperature was held constant at 310 °C, and the producer gas was employed as the feed gas. The space velocity was maintained at 3000 h^{-1}. The effect of pressure on both CO conversion and process selectivity showed that CO conversion increased with the increase of reaction pressure. Within the C5+ fraction, an effect of pressure on selectivity was observed. The increase in pressure clearly favored the formation of C_5^+, while C_1~C_3 gaseous hydrocarbons clearly decreased with an increase of the pressure. Fig. S13c shows the liquid fuel distribution in six groups. The results show that with the increasing of the reaction pressure, paraffins decreased from 25.7% to 19.5%; iso-paraffins increased from 18.3% to 23.0%; olefins decreased from 22.3% to 16.5%, aromatics increased from 21.6% to 31.5%; naphthenes were approximately unchanged and oxygenates increased from 0.21% to 1.56%. Fig.S13d shows the effect of pressure on the liquid fuel yield, the yield rate of the liquid hydrocarbons increased from 0.153 g/(g cat·h) at 3.45 MPa to 0.230 g/(g cat·h) at 8.62 MPa.

The effect of pressure on both CO conversion and process selectivity showed that when pressure increased, CO conversion increased. Within the C5+ fraction, an effect of pressure on selectivity was observed. The increase in pressure slightly favored the formation of carbon molecules of the C5+ range. The synthesis rates of both alcohols and hydrocarbons are dependent on the syngas pressure over the K-Fe-Co–Mo-γ-Alumina catalyst. Therefore, increasing syngas partial pressure results in an increased productivity of all products with the exception of CO_2, which is not very sensitive to the change in syngas pressure. In the present study, a stoichiometric H_2/CO ratio of 1 seems to be an appropriate syngas composition for the synthesis of hydrocarbons.

The increase in pressure clearly favored the formation of C_5^+, while C_1~C_3 gaseous hydrocarbons clearly decreased when the pressure was increased. Fig. S13c shows that when the reaction pressure was increased, the mole percentage of paraffins decreased from 25.7% to 19.5%, iso-paraffins increased from 18.3% to 23.0%, olefins decreased from 22.3% to 16.5%, aromatics increased from 21.6% to 31.5%, naphthenes remained relative, and oxygenates increased from 0.21% to 1.56%. Some previous FTS studies also showed that the product selectivity shifts to heavier products and more oxygenates (mainly alcohols) when the total pressure is increased (Li, et al., 1998). More alcohols were generated under higher pressure, and more aromatics were formed since they are mainly formed from alcohol condensation over acid catalysts. Increasing pressure strongly affects performance of FT synthesis, and it was discovered that the type of reaction would change from FTS synthesis to hydroformylation when using cobalt catalysts as pressure increased (Iglesia, 1997).

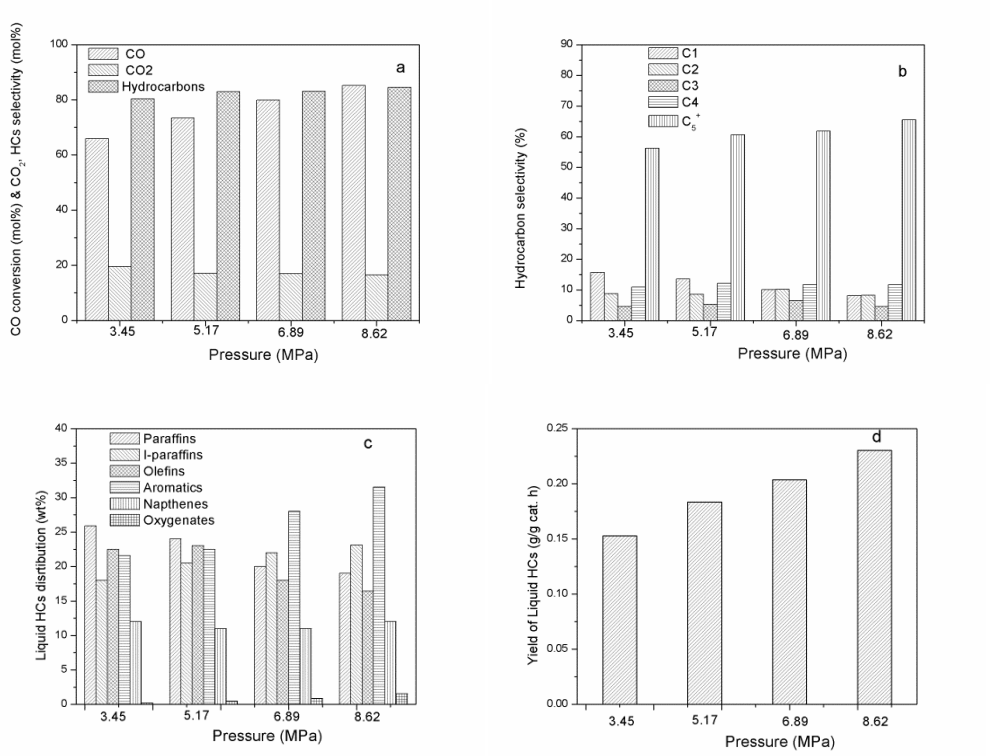


Figure S13 *Effect of pressure on (a) CO conversion, CO_2 and hydrocarbon selectivity, (b) hydrocarbon distribution, (c) liquid hydrocarbon distribution, and (d) yield of liquid hydrocarbons at 310 ºC with wood syngas, GHSV of 3000 h^{-1}; 3 g of catalyst was used in the reaction. Time on stream was 48-100 h.*

Impact of space velocity on the catalyst performance

Experiments were completed with different GHSVs of 500, 1000, 2000, 2500 and 3000 h^{-1}. The remaining operating conditions of the producer gas were held constant at 310°C and 6.89 MPa. The effect of the space velocity on CO conversion and hydrocarbon distribution showed that when the space velocity increased, CO conversion decreased as expected (Fig. S14). At the same time, C5+ hydrocarbon production decreased. The effect of space time on product distribution was significant. It was observed that the yields of hydrocarbons decreased with increasing space velocity. The gasoline fraction (C5+) continuously decreased with increasing space velocity. Fig. S14c shows that with the increasing of the GHSV from 500 to 3000 h^{-1}, paraffins increased from 17.1% to 30.0%.Olefins decreased with the increasing of GHSV. Iso-paraffins, aromatics, and naphthenes were approximately unchanged, and oxygenates increased from 0.25% to 2.06%. Fig.3d shows the effect of GHSV on the liquid fuel yield, the yield rate of the liquid hydrocarbons increased from 0..08 g/(g cat·h) at 1000 h^{-1} to 0.276 g/(g cat·h) at 5000 h^{-1}.The increasing paraffin selectivity with increasing space velocity in this work may results from a decreased isomerization reaction and hydrotreating/hydrocracking rates for restructure straight chain paraffins to branched paraffins, aromatics, and naphthenes in the short contact time, while olefin selectivity decrease with decreased with increasing of GHSV may be due to less of alcohols condensed to olefins under high space velocity.

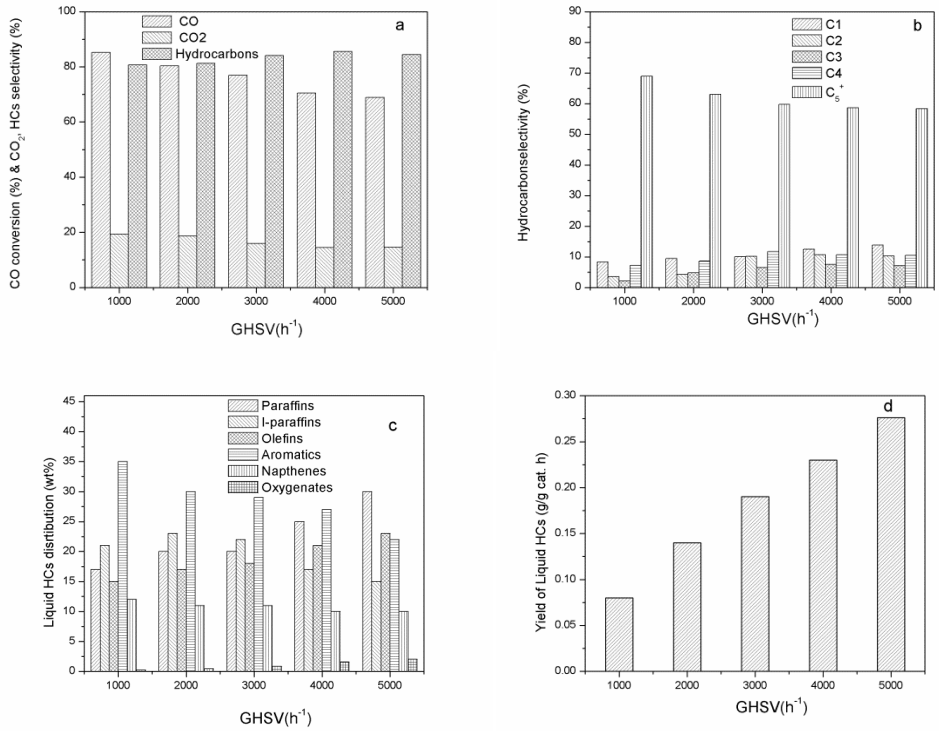


Figure S14 *Effect of GHSV on (a) CO conversion, CO_2 and hydrocarbon selectivity, (b) hydrocarbon distribution, (c) liquid hydrocarbon distribution and (d) yield of liquid hydrocarbons at 310 °C, 6.89 MPa with wood syngas; 3 g of catalyst was used in the reaction. Time on stream was 48-100 h.*

Time-on-stream performance

The time-on-stream effect on the performance of the K-Fe-Co–Mo-γ-Alumina catalyst was studied at 310 °C over a period of 160 h. The evolution of CO conversion, light hydrocarbon and liquid product selectivity with time on stream are shown in Figure S15. CO conversion was 78.3% at the beginning of the reaction and then decreased gradually to 72.5% after 160 h on stream. After 80 h on stream, no further change was observed over prolonged reaction times.

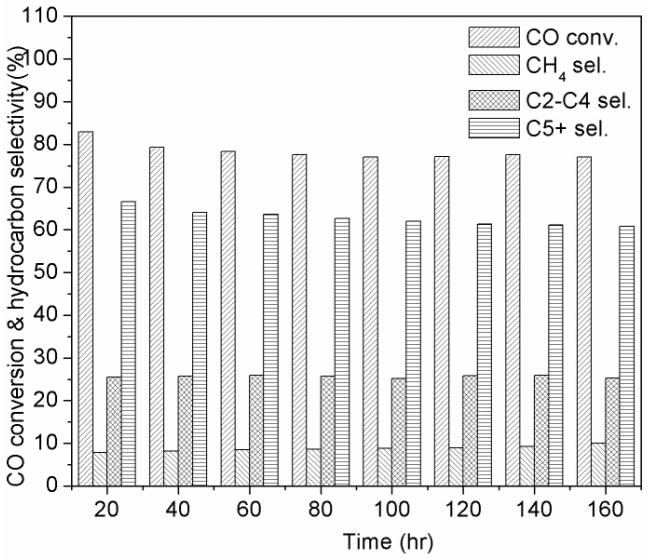


***Figure S15**. Time on stream of CO conversion, hydrocarbon selectivity and distribution on the catalyst at 310°C, 6.89 MPa, 3000 h^{-1} with wood syngas.*

Analysis of liquid fuel from wood syngas

After the reaction, liquid hydrocarbon samples were collected from the condenser. The typical GC-MS spectrum shows the product distribution can be separated into three zones, i.e., renitent time of 1.5 to 5.5 minutes, which includes C4-C8 products (olefins, iso-paraffins, paraffins, aromatics, naphthenes, and oxygenates). In the zone of 6.8~23.1 minutes, C8 (aromatics) and ~C19 hydrocarbons are located in this period of time, and the main products are aromatics, iso-paraffins, and naphthenes. The third zone is retention time between 24.3 and 37.4 minutes, and this zone includes products of C20 ~C26. These products are mainly long chain paraffins and iso-paraffins.

The liquid product characterization from the producer gas was performed by gas chromatography using the PIANO analysis. Liquid oil products were quantitatively reported in the volatile range up to molecules with 13 carbons with the five families of hydrocarbon groups (paraffins, iso-paraffins, aromatics, naphthenes, and olefins).

Table S2 shows typical liquid product fuels obtained with the catalyst. In general, it was observed that the main reaction products were olefins (totally about 25.33%) with a predominance of C7 (10.37%), C9 (5.07%), C6 (4.68%), and C13 (2.1%) components. The second largest group included aromatics, which contributed 19.84% (mol) from C7~C12 components with main components of C10 (13.78%), C12 (1.99%), C11 (1.91%), and C9 (1.55%). The largest amount of aromatic molecules include sec-butylbenzene (5.8211%), 1,2-dimethyl-3-ethylbenzene (4.7077%), 1,3-dimethyl-4-ethylbenzene (1.0227%) , 1,2-ethyl-i-propylbenzene (0.5801%), 1,3-methyl-i-propylbenzene (0.5822%), 1,3-methylethylbenzene (0.5224%), and 1,3-dimethylbenzene (0.5935%). Iso-paraffins contribute 15.02% overall, from C6~C13 components. Naphthenes and paraffins comprised 8.05% and 12.94% of the liquid product, respectively. There are also 19.74% unidentified components in the liquid product due to the limitation of the data base. If reporting the liquid hydrocarbons by carbon numbers, C9s and C10s contribute 23.0% and 23.01%, respectively. The other carbon numbers are made up of the following: C7s (15.92%), C8s (15.28%), C12s (5.96%), C6s (5.81%), C11s (5.49%), C13s (5.13%), and C5s (0.74%). C8~C13 hydrocarbons contribute 77.87% of the liquid product. Besides hydrocarbons, there are also 3.1% oxygenates found in the liquid oil phase. These oxygenates are iso-propanol, ethanol, and tert-butanol.

***Table S2.** Typical product distribution of the C_5+ liquid fraction for the K-Fe-Co-Mo/γ-Al_2O_3 catalyst by group type and carbon number (in mol percent).*

	Paraffins	Iso-Paraffins	Olefins	Naphthenes	Aromatics	Unknowns	Total
C5	0.07	0	0.67	0	0	0	0.74
C6	1.1	0.025	4.68	0	0	0	5.81
C7	2.28	0.33	10.37	1.41	0.5	1.03	15.92
C8	2	0.79	1.26	1.5	0.61	9.12	15.28
C9	2.5	7.38	5.07	4.16	1.55	2.34	23
C10	2.92	4.23	0.5	0.77	13.78	0.81	23.01

C11	1.07	1.84	0.15	0.2	1.91	0.32	5.49
C12	0.503	0.41	0.032	0.012	1.99	3.01	5.96
C13	0.5	0.02	2.1	0	0	2.51	5.13
Total	12.94	15.02	25.33	8.05	19.84	19.74	81.18

Since hydrocarbons in ATFs are mainly C8~C17, the syncrude from producer gas was distilled to remove both lighter hydrocarbons and wax components. The production sample was collected by distillation with a boiling point between 110 and 310 °C. The GC-MS spectrum shows that the distilled products were located in the retention time of 5.9~21.1 minutes. The C8 (aromatics) ~C17 hydrocarbons are found from this zone, and the main products were aromatics, iso-paraffins, paraffins and naphthenes.

Table S3 shows typical liquid products of the syncrude after distillation. In general, it was observed that the main products were aromatics (22.16%), iso-paraffins (19.63%), naphthenes (14.51%) and paraffins (14.11%). Most of the olefins have been removed (from 25.33% % in the syncrude to 7.23%). This agrees with the GC-MS spectrum. By carbon numbers, C10s contribute 32.83%; followed by C9s (19%), C11s (13.14%), C12s (12.16%), C8s (9.15%), C13s (8.86%), and C8s (4.45%). C8~C13 hydrocarbons contribute 95.14% of the liquid product.

Table S3*. Typical product distribution of the C_5+ liquid fraction of the distillation by group type & carbon number (in mole percent).*

	Paraffins	**Iso-Paraffins**	**Olefins**	**Naphthenes**	**Aromatics**	**Unknowns**	**Total**
C5	0.03	0	0.02	0	0	0	0.05
C6	0.05	0.01	0.3	0	0	0	0.36
C7	1.3	0.1	0.88	0.92	0.95	0.3	4.45
C8	2.1	0.93	0.68	1.84	1.14	2.46	9.15
C9	1.52	2.8	2	5.46	2.04	5.18	19
C10	3.15	9.58	0.19	5.89	12.74	1.28	32.83
C11	2.59	4.06	0.36	0.4	2.96	2.77	13.14
C12	2.27	2.06	0.06	0	2.33	5.44	12.16
C13	1.1	0.09	2.74	0	0	4.93	8.86
Total	14.11	19.63	7.23	14.51	22.16	22.36	77.64

A commercial Jet A sample was also analyzed for comparative purposes. The DHA results of Jet A is listed in Table S5. The GC-MS spectrum shows that the distilled products are located within the retention time of 5.9~23.2 minutes, and C8 (aromatics) ~C18 hydrocarbons are found within this zone. The main products are aromatics, iso-paraffins, paraffins and naphthenes.

Table S4 shows typical component distribution of a commercial Jet A fuel. The main components in Jet A are aromatics, iso-paraffins, paraffins and naphthenes. Aromatics contribute 27.52%, iso-paraffins contribute 21.94%, naphthenes contribute 11.19% and paraffins contribute 11.95%. There are also 3.62% of olefins in the commercial sample. By carbon numbers, C10s contribute 33.73% overall; followed by C9s (19.48%), C11s (14.72%), C12s (10.91%), C13s (11.5%), and C8s (7.41%). C8~C13 hydrocarbons contribute 97.75% of the liquid product.

Table S4 *DHA results of a commercial ATF (Jet A) sample*

	Paraffins	Iso-Paraffins	Olefins	Naphthenes	Aromatics	Unknowns	Total
C5	0.01	0	0.01	0	0	0	0.02
C6	0.01	0	0.17	0	0	0	0.18
C7	1.01	0.1	0.48	0.64	0	0.01	2.24
C8	0.7	0.93	0.58	1.8	1.18	2.22	7.41
C9	2.3	7.11	0.78	5.9	2.05	1.34	19.48
C10	3	7.1	0.23	2.08	19.22	2.1	33.73
C11	2.58	3.65	0.39	0.77	3.02	4.31	14.72
C12	1.23	1.95	0.02	0	2.05	5.66	10.91
C13	2.11	1.1	0.96	0	0	7.33	11.5
Total	11.95	21.94	3.62	11.19	27.52	22.97	74.554

The properties of syncrude fuel from producer gas, distilled fuels, and a commercial Jet A sample are listed in Table S5. Average molecular weights (g/mol) of these samples are 125.5 for the syncrude fuel from producer gas, 137.98 for the distilled syncrude, and 140.65 for the Jet A. The relative density of the Jet A sample is the highest in these three samples. The properties of the distilled sample are more similar to those of the Jet A sample. These results further demonstrate the successful synthesis of aviation turbine fuels from producer gas.

Table S5 *Comparison of syncrude fuel from syngas, distilled fuels, and Jet Fuel JPA*

Properties	Syncrude	Distilled fuel	Jet Fuel JPA
Average Molecular Weight (g/mol)	125.50	137.98	140.65
Relative Density (g/ml)	0.80	0.81	0.82
Reid Vapor Pressure @ 100°F (37.8 °C) (psi)	0.55	0.16	0.04
Percent Carbon	86.58	86.61	86.95
Percent Hydrogen	13.29	13.36	13.05
Bromine Number (Calc)	26.16	6.12	3.18
Total Oxygen Content (mass %)	0.1243	0.0252	0.0044
Freeze point (°C)	-28.5	-37	-40

S.3 Process design and economic analysis

A design for a commercial process will be performed using the data from the pilot-scale testing with the new-generation catalyst and bio-syngas. The overall cost analysis of the commercial process for the syngas conversion will be performed. The cost analysis will include the feedstock process, gasifier, syngas compressing process and cleanup system, syngas conversion reactor, product-separation equipment, and overall operating cost.

Planned Activities:

S.3.ML.1 Complete the process design (based on ChemCAD or Aspen plus), including the syngas purification system.

Summarization of Activities:
Economic modeling was performed using the CapCost method outlined in Turton, et. al. with the assistance of calculations performed in Aspen Plus to obtain the material stream information, energy usage and equipment sizing.

Properties of the Feedstocks used in the Model
Feedstock Properties and differences in the Reverse WGS reaction Conversion
The proxanal (proximate analysis weight percentage), ultanal (ultimate analysis weight percentage) and sulfanal (sulfur analysis by weight percentage) values that were used in the models are shown in the tables below and were adapted from data published by Jenkins et al. The sufanal values were calculated using the same types of sulfur ratios from a report written by Hamersma et al. which summed to the total sulfur content. A moisture content of 19% was used in all the models due to Aspen Plus sensitivity analyses which showed a higher hydrocarbon output when this was used in the Gibbs free energy reactor block. The higher heating value or heat of combustion for the woody biomass was taken from a study done by Jenkins et al. Hybrid poplar was used in the Aspen Plus models because it is very fast growing and has a heat of combustion comparable to lignite coal.

Table S6. *Proxanal Values used in Aspen Plus for Wood Feed***.**

Proxanal Material	Percentage (%)
Moisture	19
Fixed Carbon	12.49
Volatile Matter	84.81
Ash	2.7

Table S7. *Ultanal Values used in Aspen Plus for Wood Feed.*

Ultanal Material	Percentage (%)
Ash	2.7
Carbon	50.18
Hydrogen	6.06
Nitrogen	0.6
Chlorine	0.01
Sulfur	0.02
Oxygen	40.43

Table S8*. Sulfanal Values used in Aspen Plus for Wood Feed.*

Sulfanal Material	Value
Pyritic	0.1669 (83.45% of total sulfur)
Sulfate	0.00186 (0.93% of total sulfur)
Organic	0.03124 (15.62% of total sulfur)

Values for the energy content, proxanal, ultanal, and sufanal values for coal are shown on the table below and are values from a report written by Yongue et al. dealing with lignite coal from

Mississippi. The sufanal values were calculated using the same types of sulfur ratios as medium volatile bituminous coal from a report written by Hamersma et al. which summed to the total sulfur content. The volatile matter was pulled from Lignite A type coal properties of page 2 of a book written by Kabe et al., and the fixed carbon was calculated by subtracting the ash and volatile matter percentage from 100 percent. The size of the coal which is pulverized for gasification is somewhat ambiguous in the real world so the values from Table S129 were assumed to be true for the model.

Table S9. *Proxanal Values used in Aspen Plus for Coal Feed.*

Proxanal Material	Percentage (%)
Moisture	19
Fixed Carbon	38.3
Volatile Matter	46.7
Ash	15

Table S10. *Ultanal Values used in Aspen Plus for Coal Feed.*

Ultanal Material	Percentage (%)
Ash	15
Carbon	45
Hydrogen	3
Nitrogen	21.5
Chlorine	0
Sulfur	0.5
Oxygen	15

Table S11.*Sulfanal Values used in Aspen Plus for Coal Feed.*

Sulfanal Material	Percentage (%)
Pyritic	0.41725
Sulfate	0.00465
Organic	0.0781

Table S12. *The size of the coal and wood were both assumed to be the size shown on the following table to model the amount of power that would be needed to crush the material.*

Interval	Lower limit (in)	Upper limit (in)	Weight fraction	Cumulative weight fraction
1	0.05	0.083058	0.1	0.1
2	0.083058	0.137973	0.1	0.2
3	0.137973	0.229195	0.1	0.3
4	0.229195	0.380731	0.1	0.4
5	0.380731	0.632456	0.1	0.5
6	0.632456	1.05061	0.1	0.6
7	1.05061	1.74524	0.1	0.7

8	1.74524	2.89912	0.1	0.8
9	2.89912	4.81591	0.1	0.9
10	4.81591	8	0.1	1

Table S13.*This table shows the differences in the WGS CO conversion to produce H_2 and CO_2 to increase the H_2/CO ratio for a 50 ton per day process plant with an air fed gasifier using a coal biomass feedstock and known reactor yields from experimental results.(A WGS CO conversion of 40% was chosen to be used with the CapCost economic modeling (other CO conversion percentages not shown produced errors).*

WGS CO Conv (%)	H2 (Mole %)	CO (Mole %)	CO2 (Mole %)	CH4 (Mole %)	N2 (Mole %)	CH4 (kg/h)	C2H6 (kg/h)	C3-C4 (kg/h)	C5-C12 (kg/h)	C13-C20 (kg/h)	Sum of C1-C20 (kg/h)
*0	17.85	22.99	10.08	1.41	47.59	65.29	7.16	8.87	76.05	123.15	280.51
*10	19.69	20.22	12.10	1.38	46.52	65.63	5.39	9.68	64.41	128.15	273.25
*20	21.46	17.58	14.04	1.35	45.50	65.97	6.59	10.63	62.83	130.53	276.55
*30	23.15	15.05	15.88	1.32	44.52	66.31	7.71	11.59	61.85	132.20	279.66
**40	24.76	12.63	17.65	1.29	43.58	68.77	17.04	29.80	163.93	195.66	475.20
**50	26.32	10.31	19.35	1.27	42.68	67.75	8.59	13.47	155.70	167.43	412.95
**60	27.80	8.08	20.98	1.24	41.82	66.73	0.00	10.78	103.05	134.03	314.59
**70	29.23	5.94	22.55	1.22	40.99	65.71	0.00	8.08	70.55	100.52	244.87

*H_2 is the limiting reactant in the FT reactions, **CO is the limiting reactant in the FT reactions

Table S14. *This table shows the differences in the WGS CO conversion to produce H_2 and CO_2 to increase the H_2/CO ratio for a 500 ton per day process plant with an air fed gasifier using a coal biomass feedstock and known reactor yields from experimental results. A WGS CO conversion of 40% was chosen to be used with the CapCost economic modeling (other CO conversion percentages not shown produced errors).*

WGS CO Conv (%)	H2 (Mole %)	CO (Mole %)	CO2 (Mole %)	CH4 (Mole %)	N2 (Mole %)	CH4 (kg/h)	C2H6 (kg/h)	C3-C4 (kg/h)	C5-C12 (kg/h)	C13-C20 (kg/h)	Sum of C1-C20 (kg/h)
*0	17.85	22.99	10.08	1.41	47.59	652.89	71.56	88.67	760.51	1231.48	2805.10
*10	19.69	20.22	12.10	1.38	46.52	656.29	53.88	96.77	644.06	1281.53	2732.53
*20	21.46	17.58	14.04	1.35	45.50	659.69	65.91	106.29	628.31	1305.26	2765.45
*30	23.15	15.05	15.88	1.32	44.52	663.09	77.15	115.86	618.48	1322.04	2796.62
**40	24.76	12.63	17.65	1.29	43.58	687.70	170.37	297.98	1639.31	1956.61	4751.96
**50	26.32	10.31	19.35	1.27	42.68	677.50	85.87	134.74	1557.05	1674.34	4129.50
**60	27.80	8.08	20.98	1.24	41.82	667.30	0.00	107.79	1030.48	1340.31	3145.88
**70	29.23	5.94	22.55	1.22	40.99	657.10	0.00	80.84	705.55	1005.23	2448.72
**80	30.61	3.88	24.05	1.19	40.20	646.89	0.00	53.90	345.88	670.15	1716.82

*H_2 is the limiting reactant in the FT reactions, **CO is the limiting reactant in the FT reactions

Table S15. *This table shows the differences in the WGS CO conversion to produce H_2 and CO_2 to increase the H_2/CO ratio for a 5000 ton per day process plant with an air fed gasifier using a coal biomass feedstock and known reactor yields from experimental results. A WGS CO conversion of 40% was chosen to be used with the CapCost economic modeling (other CO conversion percentages not shown produced errors).*

WGS CO Conv (%)	H2 (Mole %)	CO (Mole %)	CO2 (Mole %)	CH4 (Mole %)	N2 (Mole %)	CH4 (kg/h)	C2H6 (kg/h)	C3-C4 (kg/h)	C5-C12 (kg/h)	C13-C20 (kg/h)	Sum of C1-C20 (kg/h)
*0	17.85	22.99	10.08	1.41	47.59	6528.90	715.57	886.65	7605.06	12314.84	28051.02
*10	19.69	20.22	12.10	1.38	46.52	6562.91	538.79	967.69	6440.59	12815.28	27325.26
*20	21.46	17.58	14.04	1.35	45.50	6596.92	659.13	1062.87	6283.07	13052.56	27654.54
*30	23.15	15.05	15.88	1.32	44.52	6630.92	771.48	1158.63	6184.76	13220.41	27966.20
**40	24.76	12.63	17.65	1.29	43.58	6877.04	1703.67	2979.78	16393.10	19566.06	47519.65
**50	26.32	10.31	19.35	1.27	42.68	6775.02	858.72	1347.38	15570.49	16743.40	41295.01
**60	27.80	8.08	20.98	1.24	41.82	6672.99	0.00	1077.90	10304.81	13403.06	31458.77
**70	29.23	5.94	22.55	1.22	40.99	6570.96	0.00	808.43	7055.45	10052.24	24487.08

*H_2 is the limiting reactant in the FT reactions, **CO is the limiting reactant in the FT reactions

The mole fraction of the gas could be changed by adding a water gas shift reactor with steam to increase the H_2/CO ratio and the results of changing the conversion of CO under the WGS reaction to hydrogen and carbon dioxide can be seen in Table S13 - Table S15. The ratio produced by the gasifier in the Gibbs free energy model was similar to the gasifier that we have on site at MSU so based on the results, the Gibbs free energy reactor model is assumed to also suffice as a good model to predict the end products of an oxygen fed gasifier using wood and coal feedstocks, as well as a coal air-fed gasifier. Table S13 - Table S15 depict the gas composition (mole %) before the gasified biomass is fed into the compressor as well as the mass flow rate after the products are fed through a distillation tower. Since the C13-C20 chain hydrocarbons have a higher cost per kg, to determine the appropriate WGS conversion of CO which would output the product with this as the majority yield was chosen as the model to perform the economic analysis in CapCost. After running the sensitivity analysis for both coal and wood to convert CO to H_2 and CO2 through the WGS reaction, the best yield with a wood feedstock was 20% CO conversion, while the best yield for the coal feedstock was 40% CO conversion to give the best stoichiometric values for a 2:1 ratio of H_2 to CO.

Aspen Plus Process Flow Diagram

The Aspen Plus diagram is split up in Figure S16-Figure S21. This diagram was used for both the wood and coal economic models. Figure S16 shows the feedstock handling process (temperature is in Kelvin and pressure is in atmospheres). The biomass is chipped and dried in a heater with airflow to remove moisture. The chipper was modeled as an Aspen Plus crusher block with a multiple roll crusher type. The maximum particle diameter chosen was 5 inches and Rattanakawin et al. mentions that all coal samples can be "classified as lignite with the Hargrove grindability indices ranging from about 40 to 50" so a Hargrove grindability index of 45 was chosen for the coal models. The biomass dryer was modeled with the RStoic block (using a 20% conversion of coal to water) in Aspen Plus with the following reaction as outlined in the Aspen Plus solids handling worksheet tutorial using equation S1. The fractional conversion was modified using a calculator block to achieve the desired moisture content at the output.

$$Coal \longrightarrow 0.0555084 \quad H_2O \tag{S1}$$

$$CONV = \frac{H_2O_{IN} - H_2O_{OUT}}{100 - H_2O_{OUT}} \tag{S2}$$

The H_2O removal after the biomass heater was modeled with a Flash2 block in Aspen Plus to model the removal of the extra water in the system that is not desired in the gasifier reactions down the line.

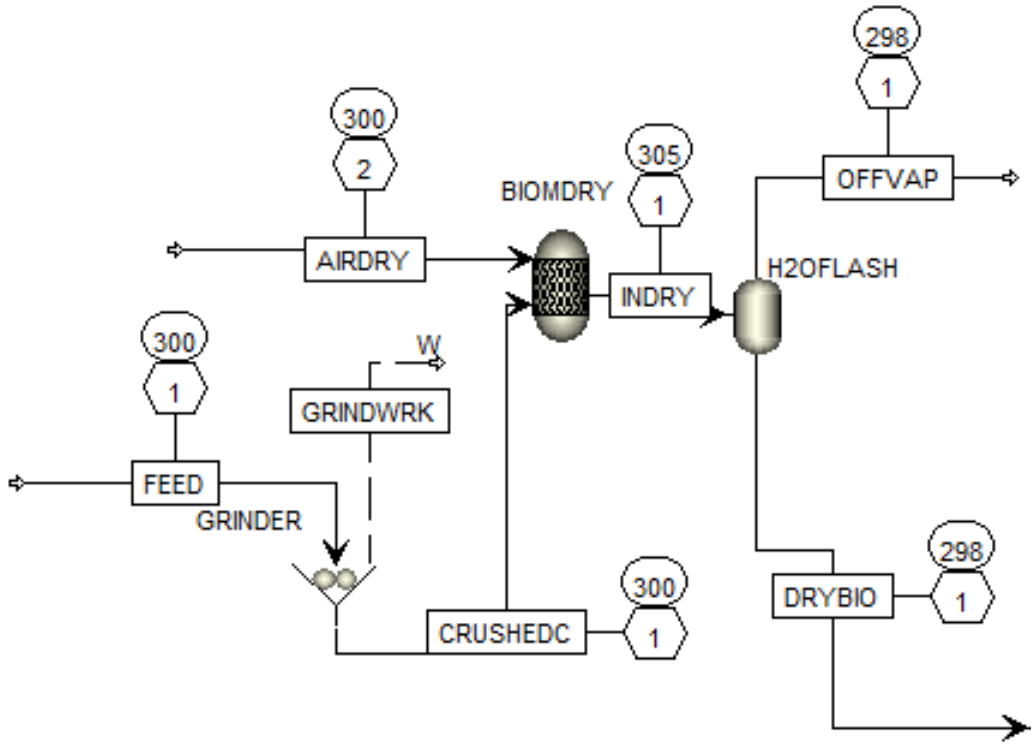


Figure S16. *Feedstock handling process (temperature is in Kelvin and pressure is in atmospheres). The biomass is chipped and dried in a heater with airflow to remove moisture.*

Figure S16 describes the gasification process of the model with elements of the biomass being simulated as being broken down with the CRUSHER block. The Hardgrove Grindability Index was used to model how much energy would be required to break down the biomass. For coal a study from Rattanakawin et al. was used and an HGI of 45 was used in the coal feedstock models. Woodchip data from a Ph.D. Thesis by Shang showed that an HGI of 19 would be appropriate when dealing with woody biomass feedstocks. The elements of the biomass are divided in the RYIELD reactor block. The components that were broken down were modeled using equation S.3.3 in a calculator block in Aspen Plus to calculate the mass yield (all except moisture).

$$EMass = (1 - Moisture) * Ultimate * TotalMass_{Feed} \quad \text{(S3)}$$

Where EMass is the mass percentage of the particular component in question (H_2, O_2, N_2, S, C or Ash), Moisture is the moisture content of the gas, Ultimate is the percentage of the ultimate analysis the component originally was, and $TotalMass_{Feed}$ is the total mass flow rate of the biomass in the inlet stream. A sensitivity analysis was carried out with each model to determine the amount of oxygen or air that would be best suited to produce the greatest amount of hydrocarbons. In Figure S17 the first stage of the gasifier was modeled as an RGibbs reactor block which considered all components as products. The RGibbs reactor models the reactions as the components having infinite time in the reactor and perfect mixing. Although this is not the case, the results when using air gave similar results to real world situations. The (reverse) water gas shift (WGS) reactor was modeled with an RStoic reactor with equation S4 a particular conversion of CO depending on whether the wood or coal feedstock was used. The amount of the conversion was determined using a sensitivity analysis to produce the greatest amount of liquid hydrocarbons.

$$CO + H_2O \rightarrow H_2 + CO_2 \quad \text{(S4)}$$

Air or pure oxygen (depending on the desired model) and the elements of the wood in a Gibbs free energy reaction model. The second stage of the gasification is modeled with a stoichiometric reactor which uses a water gas shift reaction to increase the hydrogen to carbon monoxide ratio. A heat exchanger is used to cool the outlet stream from the water gas shift (RStoic block) reactor to 500 °C.

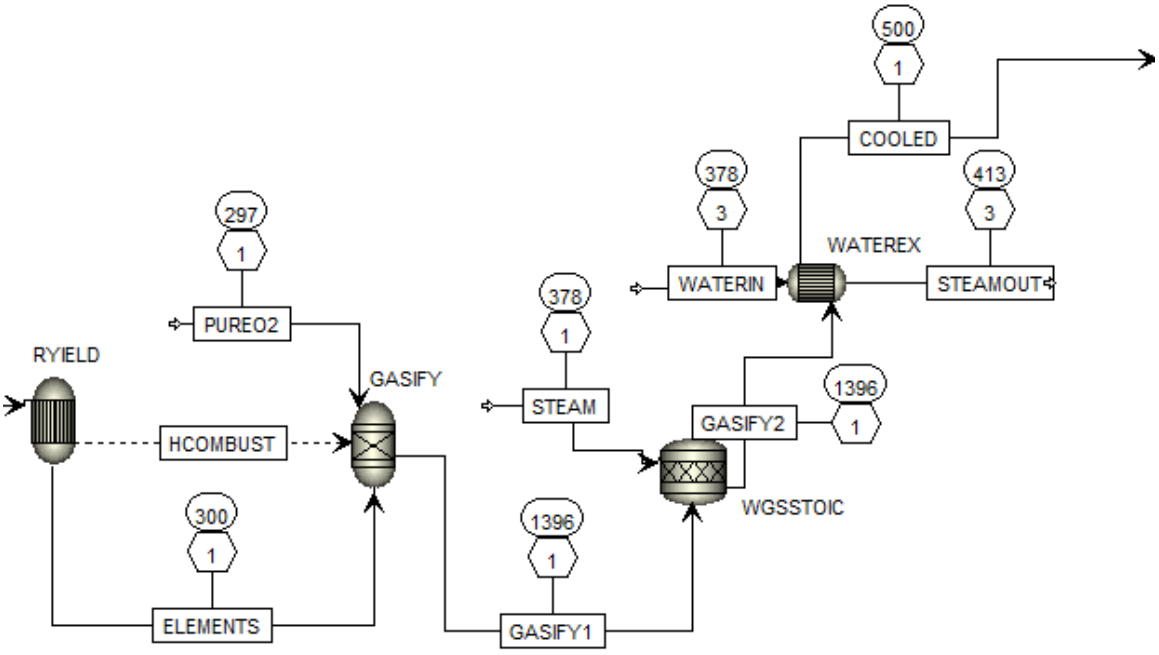


Figure S17. *The Aspen Plus diagram showing elements of the wood first simulated as being broken down in the RYIELD reactor. The heat of combustion from this block is forwarded onto the first stage of the gasification model called 'GASIFY' . The second stage of the gasification is modeled with a stoichiometric reactor which uses a water gas shift reaction to increase the hydrogen to carbon monoxide ratio. A heat exchanger is used to cool the outlet stream from the water gas shift (RStoic block) reactor to 500 °C.*

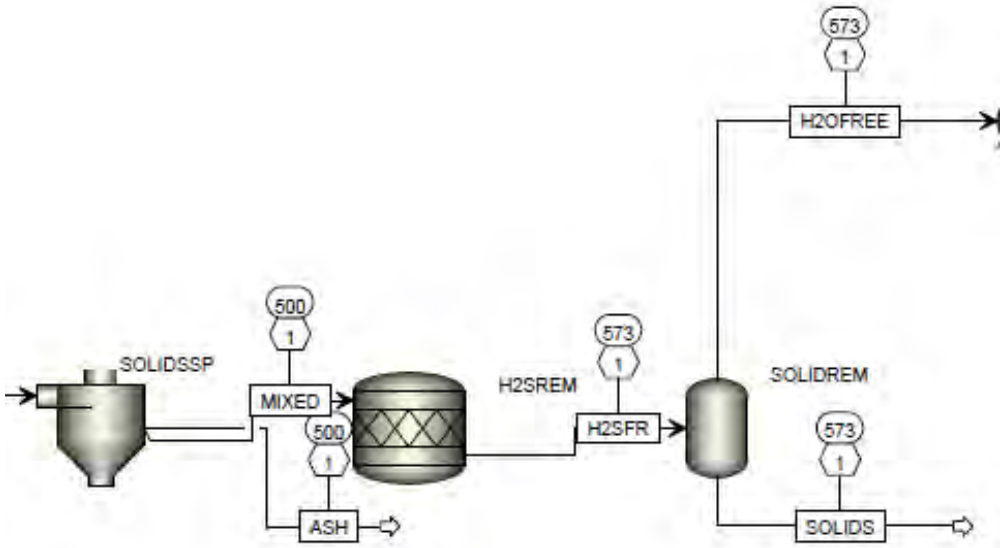


Figure S18. *Aspen Plus diagram showing the ash separation that is done immediately after the gasifier using the SSplit block. After this step, the H2S removal reactor is modeled as a RStoic block reactor.*

Figure S18 *describes the first part of the gas clean-up process by removing the ash from the stream. This is followed by the removal of any H_2S that is in the system using the RStoic block. The reactions used in this block are given by equations 57 and 58 (which is the Claus reaction).*

$2\ H_2S + 3\ O_2 \rightarrow 2\ SO_2 + 2\ H_2O$ (S5)

$2\ H_2S + SO_2 \rightarrow 3\ S + 2\ H_2O$ (S6)

Although equation S6 does take place at temperatures higher than what is shown in Figure S18, the energy requirement was taken into account in the CapCost models in the economics section. This is an exothermic reaction that gives multiple side products but they were ignored for this model. The sulfur created from this block was removed with the Flash block so that the gas stream could flow free of particulates.

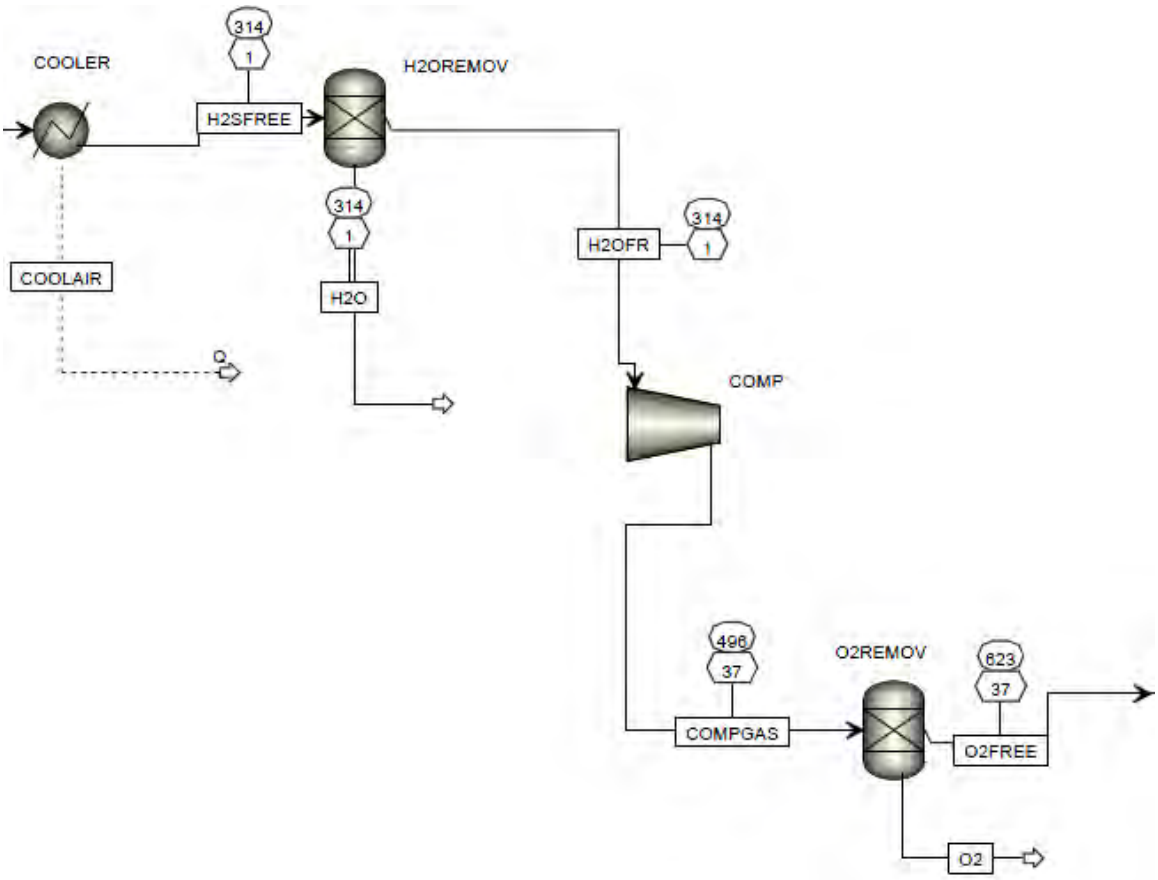


Figure S19. *The gasified biomass passes through an air cooler modeled with the Heater Block. In the 'Sep' block the water is removed from the gas before flowing into the compressor. After the compressor, another 'Sep' block was used to model the removal of* O_2.

Figure S19 shows the modeling of cooling, water removal, compression and oxygen removal of the gasified biomass. The air cooling energy requirement was calculated by Aspen Plus and the area of the heat exchanger to use in the economics modeling was done using equation S7.

$$A = \frac{Q}{U \cdot \Delta T} \qquad \text{(S7)}$$

Where A is the area of the heat exchanger, Q is the energy required to cool the gas to a specific temperature, U is the overall heat transfer coefficient of air (5.7 $Wm^{-2}K^{-1}$) and ΔT is the temperature difference of the gasified biomass before entering the heat exchanger and after exiting the heat exchanger. The compressor was modeled so that a partial pressure of 130.66 psig for CO was used in all the models.

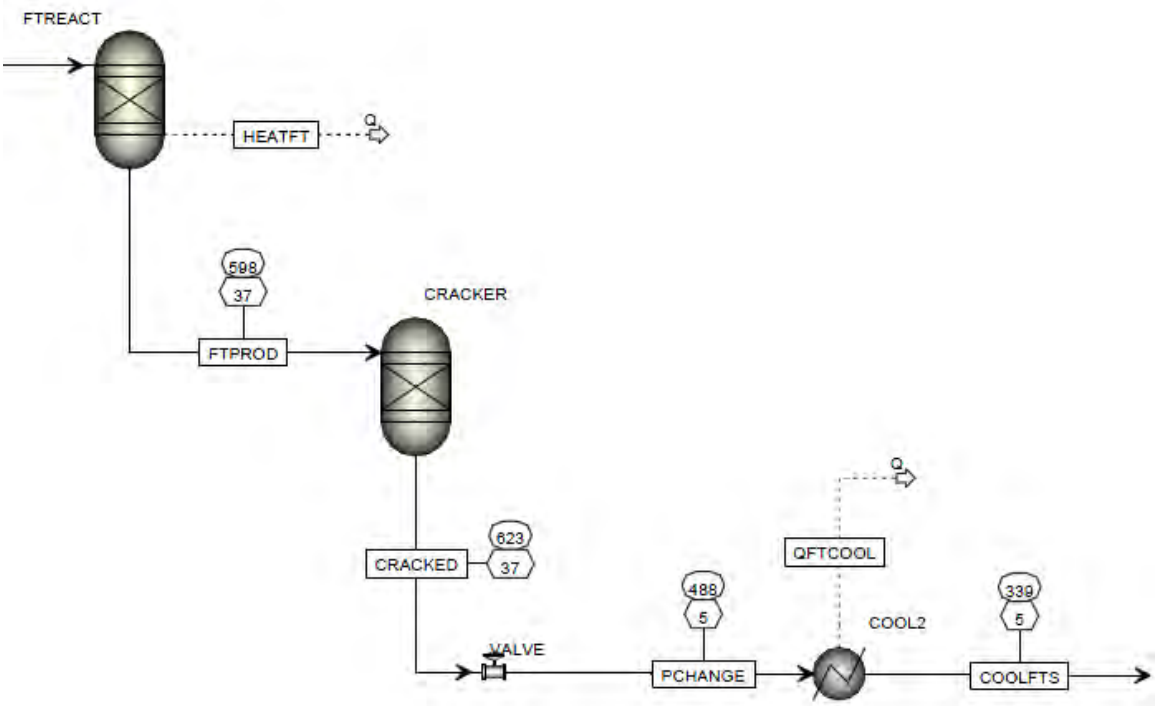


Figure S20. *The FT reactor and cracker were both modeled with the RStoic block. A back pressure valve was also modeled to show the temperature change and an air cooler was modeled as the Heater block to further cool the gas before distillation.*

The FT reactor was modeled with the following chemical equations shown in Table S16. For the purposes of this model the simple alkane formation equation shown in equation S8 was used to determine the types of hydrocarbons that would be created.

$(2n + 1)\ H_2 + n\ CO \rightarrow C_nH_{(2n+2)} + n\ H_2O$ (S8)

Each of the specific conversion percentages of CO are also shown as well and were derived using the Anderson–Schulz–Flory distribution shown in equation S9.

$W_n = n(1-a)^2 * (a^{n-1})$ (S9)

Where W_n is the is the weight percent fraction of hydrocarbons, and a is the probability for chain growth (0.9 was used).

Table S16. *The alkane equation and Anderson-Schulz-Flory weight percent fraction of hydrocarbons when using an alpha of 0.9.*

Wn at alpha = 0.9	Equation	Equation Number
1	$CO + 3\ H_2 \rightarrow CH_4 + H_2O$	S.3.10
1.8	$2\ CO + 5\ H_2 \rightarrow C_2H_6 + 2\ H2O$	S.3.11
2.43	$3\ CO + 7\ H_2 \rightarrow C_3H_8 + 3\ H_2O$	S.3.12
2.916	$4\ CO + 9\ H_2 \rightarrow C_4H_{10} + 4\ H_2O$	S.3.13
3.2805	$5\ CO + 11\ H_2 \rightarrow C_5H_{12} + 5\ H_2O$	S.3.14
3.54294	$6\ CO + 13\ H_2 \rightarrow C_6H_{14} + 6\ H_2O$	S.3.15

3.720087	$7\ CO + 15\ H_2 \rightarrow C_7H_{16} + 7\ H_2O$	S.3.16
3.826375	$8\ CO + 17\ H_2 \rightarrow C_8H_{118} + 8\ H_2O$	S.3.17
3.874205	$9\ CO + 19\ H_2 \rightarrow C_9H_{20} + 9\ H_2O$	S.3.18
3.874205	$10\ CO + 21\ H_2 \rightarrow C_{10}H_{22} + 10\ H_2O$	S.3.19
3.835463	$11\ CO + 23\ H_2 \rightarrow C_{11}H_{24} + 11\ H_2O$	S.3.20
3.765727	$12\ CO + 25\ H_2 \rightarrow C_{12}H_{26} + 12\ H_2O$	S.3.21
3.671584	$13\ CO + 27\ H_2 \rightarrow C_{13}H_{28} + 13\ H_2O$	S.3.22
3.558612	$14\ CO + 29\ H_2 \rightarrow C_{14}H_{30} + 14\ H_2O$	S.3.23
3.431519	$15\ CO + 31\ H_2 \rightarrow C_{15}H_{32} + 15\ H_2O$	S.3.24
3.294258	$16\ CO + 33\ H_2 \rightarrow C_{16}H_{34} + 16\ H_2O$	S.3.25
3.150134	$17\ CO + 35\ H_2 \rightarrow C_{17}H_{36} + 17\ H_2O$	S.3.26
3.001893	$18\ CO + 37\ H_2 \rightarrow C_{18}H_{38} + 18\ H_2O$	S.3.27
2.851798	$19\ CO + 39\ H_2 \rightarrow C_{19}H_{40} + 19\ H_2O$	S.3.28
2.701703	$20\ CO + 41\ H_2 \rightarrow C_{20}H_{42} + 20\ H_2O$	S.3.29
2.55311	$21\ CO + 43\ H_2 \rightarrow C_{21}H_{44} + 21\ H_2O$	S.3.30
2.407218	$22\ CO + 45\ H_2 \rightarrow C_{22}H_{46} + 22\ H_2O$	S.3.31
2.264973	$23\ CO + 47\ H_2 \rightarrow C_{23}H_{48} + 23\ H_2O$	S.3.32
2.127105	$24\ CO + 49\ H_2 \rightarrow C_{24}H_{50} + 24\ H_2O$	S.3.33
1.994161	$25\ CO + 51\ H_2 \rightarrow C_{25}H_{52} + 25\ H_2O$	S.3.34
1.866535	$26\ CO + 53\ H_2 \rightarrow C_{26}H_{54} + 26\ H_2O$	S.3.35
1.744492	$27\ CO + 55\ H_2 \rightarrow C_{27}H_{56} + 27\ H_2O$	S.3.36
1.628193	$28\ CO + 57\ H_2 \rightarrow C_{28}H_{58} + 28\ H_2O$	S.3.37
1.517708	$29\ CO + 59\ H_2 \rightarrow C_{29}H_{60} + 29\ H_2O$	S.3.38
1.413039	$30\ CO + 61\ H_2 \rightarrow C_{30}H_{62} + 30\ H_2O$	S.3.39
SUM: 83.0435		

The cracker used in the model was used to break down waxes and although more side reactions would and do happen, equations S.3.40 - S.3.49 show the reactions used in the cracker model to convert the higher wax hydrocarbons into liquid. The assumption was made that the conversion for the main reactant percentage was 90%.

$H_2 + C_{21} \rightarrow C_{10} + C_{11}$ (S.3.40)
$H_2 + C_{22} \rightarrow C_5 + C_{17}$ (S.3.41)
$H_2 + C_{23} \rightarrow C_5 + C_{18}$ (S.3.42)
$H_2 + C_{24} \rightarrow 2\ C_{12}$ (S.3.43)
$H_2 + C_{25} \rightarrow C_{12} + C_{13}$ (S.3.44)
$H_2 + C_{26} \rightarrow 2\ C_{13}$ (S.3.45)
$H_2 + C_{27} \rightarrow C_{13} + C_{14}$ (S.3.46)
$H_2 + C_{28} \rightarrow 2\ C_{14}$ (S.3.47)
$H_2 + C_{29} \rightarrow C_{14} + C_{15}$ (S.3.48)
$H_2 + C_{30} \rightarrow 2\ C_{15}$ (S.3.49)

The area for air cooler that cooled the gas before it entered the distillation tower was calculated the same way as the air cooler mentioned previously with equation S7.

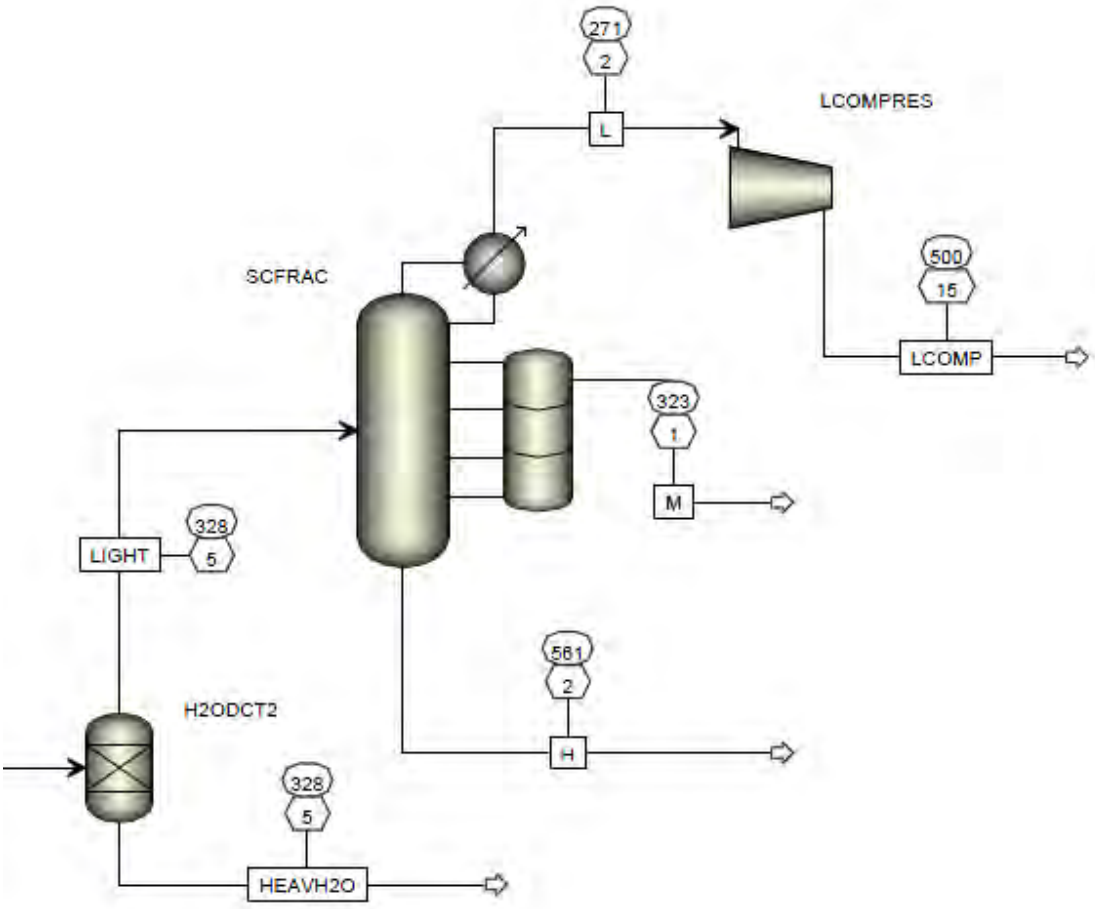


Figure S21. *Aspen Plus diagram showing water being separated using the 'Sep' block and the product was input into the shortcut distillation column block. The lighter hydrocarbons were compressed with the 'Compr' block to a pressure of 200 psig*.

Figure S21 shows the product being put through a water decanter and then distilled into 3 main product groups. In real world scenarios the distillation products are separated into many more denominations of specific products, but to keep the model simple so that economics could be performed easier, only three were chosen. Those three groups are shown in Table S17.

Table S17. *Groups of hydrocarbons that were distilled from the Shortcut distillation column.*

Stream Name	Components
L	CO, H_2, CO_2, H_2O, H_2S, N_2, CH_4, C_2H_6, C_3H_8, C_4H_{10}
M	C_5H_{12}, C_6H_{14}, C_7H_{16}, C_8H_{18}, C_9H_{20}, $C_{10}H_{22}$, $C_{10}H_{22}$, $C_{12}H_{26}$
H	$C_{13}H_{28}$, $C_{14}H_{30}$, $C_{15}H_{32}$, $C_{16}H_{34}$, $C_{17}H_{36}$, $C_{18}H_{38}$, $C_{19}H_{40}$, $C_{20}H_{42}$

The shortcut distillation column also made use of the calculator block to be sure that the proper mole percent of products were distributed properly and the mass balance was properly maintained. The calculator block summed the mole percentage of each of the light-, mid- and heavy-range products coming into the distillation column and inputted this number into the appropriate feed fraction.

Equipment and Energy calculations completed for the Economic Analysis

When modeling the distillation tower in CapCost, the following assumptions were made. Each reactor for the 500 and 5000 ton/day plant was assumed to be made out of 419 2 inch nominal schedule 40 pipes that were 30 ft long with a total enclosed diameter of 8 feet with a gas hourly space velocity (GHSV) of 3000 h^{-1}. This flow rate was divided into the total flow rate depending on the model to give how many reactors would be needed for the CapCost economic model. The heat required to heat the reactors was calculated using equation S.3.50, S.3.51 and S.3.52.

$$Q_r = \frac{W * C_p * \Delta T}{3412 \left(\frac{kWh}{BTU}\right) * time(hr)} \qquad \text{(S.3.50)}$$

Where Q_r is the required power to raise the temperature, W is the weight of the material, C_p is the specific heat of the material (0.12 BTU/lb) , and ΔT is the change in temperature (809 ^oF).

$$Q_l = \frac{k * S_{Area} * \Delta T}{3412 \left(\frac{kWh}{BTU}\right) * time(hr)} \qquad \text{(S.3.51)}$$

Where k is the thermal conductivity of the insulation (assumed to be 0.67 (BTU*in)/(ft^2* ^oF * hr), S_{Area} is the surface area to be heated and and ΔT is the change in temperature.

As the engineering guide source for heating material shows, a safety factor was used when using both equation S.3.50 and S.3.51 together so that equation S.3.52 was formed to give the overall power needed to heat the reactor to the desired reaction temperature.

$$Q_{Total} = 2 * (Q_r + \frac{2}{3} Q_r) \qquad \text{(S.3.52)}$$

The total amount of power that needed to be provided was calculated by adding the power needed for the FT reactor, the oxygen removal reactor, the hydrogen sulfide removal reactor, the power required for the drive shafts of the compressors, the feedstock grinder and steam that needed to be generated. Most of these values were found from the Aspen Plus model but the FT reactor would also produce a certain amount of power due to the exothermic reactions. An assumption was made that the FT reaction would produce approximately 0.5 MW/m^3 based on literature results. The energy calculated (based on the volume of the reactor) was subtracted from the total power requirement (along with 80% of the gasifier energy in the Aspen Plus model). Without this use of power from the gasifier and the FT reactor, the CapCost models all became economically unfeasible. The distillation tower trays usually have an efficiency of 50%-70% so the theoretical trays that were calculated by Aspen Plus were multiplied by 2 to give the total number of trays used in the CapCost model. Fair's method was used to calculate the column diameter by using equations S.3.53, S.3.54, and S.3.55.

$$u_{flood} = C_{abf} \left(\frac{\sigma}{20}\right)^{0.2} \sqrt{\frac{p_L - p_V}{p_V}} \qquad \text{(S.3.53)}$$

Where u_{flood} is the flooding vapor velocity, C_{abf} is the capacity factor (found chart found in the book Separation Process Engineering), $p_L$is the liquid density, p_v is the vapor density and σ is the surface tension. The flooding vapor velocity was used to find the diameter using equation S.3.54.

$$D = \sqrt{\frac{4 * V_{mass}}{\pi * \eta * p_V * u_{flood} * 0.75}} \qquad \text{(S.3.54)}$$

Where V_{mass} is the mass flow rate of the vapor and η is 1 minus the ratio of the tray hole area to the active tray area (0.9). The distillation reflux drum dimensions were calculated based on chapter 18 of Couper's book using equation S.3.55.

$$V_d = 2 * F_4 * (F_1 + F_2) * (L_{rf} + F_3 * Q) \quad \text{(S.3.55)}$$

Where V_d is the volume of the reflux drum, F_1,F_2, F_3, and F_4 are specific factors shown in chapter 18 of Couper and were assumed to have values of 1, 1.5, 3, and 1.5 respectively. L_{rf} is the reflux flow rate and Q is the overhead net product flow rate. The reflux pump calculation for the distillation tower was calculated using equation S.3.56.

$$P = \frac{q*\rho*g*h}{3.6*10^6} \quad \text{(S.3.56)}$$

Where P is power (kW), q is flow rate (m^3h^{-1}), ρ is the fluid density (kgm^{-3}), g is the acceleration due to gravity (9.81 ms^{-2}), and h is the differential head (m). The distillation reboiler and condenser power requirement were calculated in the Aspen Plus model and to obtain the appropriate surface area, equation S.3.7 was used (same equation used with the air coolers mentioned previously). The only difference was that the overall heat transfer coefficients. The heat transfer coefficient of stainless steel to steam (used for the reboiler) was 680 $Wm^{-2}K^{-1}$ and the heat transfer coefficient used for the condenser was 11.3 $Wm^{-2}K^{-1}$ for water to stainless steel. Storage tanks were calculated by assuming that they needed to store a week's worth of product before shipment could take place. Besides the compressor, the most expensive equipment for the plant was the gasifier. The MSU bioenergy lab spent approximately $250,000 on a 0.66 ton per day gasifier, and another source from Karnataka, India (Goodrich Sugar & Chemical Complex Limited) has a 220 ton per day gasifier at an American installation cost of $12,000,000. The gasifier cost estimate was done my using a method mentioned by Sweeting using equation S.3.57 to find the slope of the line needed to obtain the cost of scaled up equipment. This value was used to obtain the results of the costs of the scaled up equipment.

$$m = \frac{\log(12000000) - \log(250000)}{\log(220) - \log(0.66)} \quad \text{(S.3.57)}$$

The value of m was calculated to be 0.666. This value was used to find the 'B' value of equation S.3.58.

$$\log(250000) = \log(B) + m*\log(0.66) \quad \text{(S.3.58)}$$

The log of 0.66 is the tons/day (not to be confused with the 0.666 value of m). This 'B' value was solved for (329758.1675) and used to find the new cost of a scaled up gasifier based on the tonnage per day of biomass using equation S.3. 59 (5000 tons/day is used in this equation).

$$\log(Cost_{5000}) = \log(329758.1675) + (0.666)*\log(5000) \quad \text{(S.3.59)}$$

The bare module cost for the gasifier was solved for by using methods outlined on page 200 of Turton with equation S.3.60 and S.3.61.

$$C_{BM} = C_{p0} * (B_1 + B_2 * F_M * F_p) \quad \text{(S.3.60)}$$

Where C_{p0} is the cost calculated using equation S.3.59 above, B_1 = 2.25, B_2 = 1.82, F_M = 3.1 (as outlined in pages 200 and 945 of Turton and F_p was solved for using equation S.3.61.

$$F_p = \frac{(P_{gasifier} + 1bar) * D_{gasifier}}{\frac{2(S_{gasifier}) * E_{gasifier} - 1.2 * (P_{gasifier} + 1bar)}{t_{min}}} \quad \text{(S.3.61)}$$

Where $P_{gasifier}$ is the working pressure of the gasifier (1atm), $D_{gasifier}$ is the diameter of the gasifier (1m), $S_{gasifier}$ is the maximum allowable stress of the stainless steel used in the gasifier (1305 psig), $E_{gasifier}$ is the weld efficiency (1) and t_{min} is the minimum thickness of the gasifier (1 inch).

The cost was solved for this way for the 50, 500 and 5000 ton per day biomass plants. The oxygen concentrator was solved for using the well-known sixth-tenths rule and was also mentioned by Sweeting. (The calculation for a 5000 ton per day plant is shown with equation S.3.62.)

$O_2cost_{5000} = Base_{COST} * (5000/0.66)^{0.6}$ (S.3.62)

The initial valued of the oxygen concentrator was obtained from PCI with a base cost of $65,500 ($Base_{COST}$ variable) for the 0.66 ton/day plant that we have on site at MSU. The bare modulus cost was assumed to have the same kind of cost associated with a compressor so the value of the direct cost was multiplied by 5.7 to obtain the bare modulus cost of the oxygen concentrator.

CapCost base case scenario

The base case for this study assumes that the biomass moisture is at 19% and is modeled after an oxygen fed gasifier using single investment discounted rate with a 5 year MACRS depreciation.. Each of the following cases Net Present Value (NPV) and rate of return on investment (ROROI) are shown in
Table *S19*,
Table *S20*, Table S22 and
Table *S23*. The cost of Mississippi lignite coal s assumed at $25/ton. A report from the EPA has stated that the average cost for hybrid poplar is approximately $49.5/ton but the forest residue is only approximately $20/ton. To best compare with the coal, the model in CapCost used the same price of $25/ton. The $49.50 price point was used per ton but was not economically viable at this level. Most investors would like a minimum of 20% rate of return on their investment and this could not be achieved until a price point of approximately $6 per gallon of gasoline.
Table *S28* gives the price points used to find the values in
Table *S19* and
Table *S20* and
Table *S21* gives the price points used to find the values in Table S2222 and
Table *S23*.

Table S28. *Variables used to calculate values for*

Table ***S19*** *and S41.*

Material Name	Classification	Price ($/kg)	Flow rate (kg/h)	Annual Cost
Biomass	Raw Material	Varies	189000.00	Varies
C_5-C_{12} Gasoline Range	Product	$ (1.65)	11981.96	$ (164,627,601)
Methane	Product	$ (0.24)	6027.98	$ (12,089,737)
Ethane	Product	$ (0.29)	619.84	$ (1,480,446)
LPG C_3/C_4	Product	$ (0.39)	888.03	$ (2,874,792)
C_{13}-C_{20} Diesel Range	Product	$ (1.82)	11908.78	$ (179,974,439)
Hydrogen	Product	$ (4.00)	1323.75	$ (44,064,990)
Pure O_2	Raw Material	$ 0.04	126783.00	$ 42,203,525

Waste Water	Non-Hazardous Waste	0.036	76497.8	$ 22,918,129

Table S19. *Net Present value (in millions of dollars) and rate of return on investment (%) of running the plant for 20 years using a wood feedstock. This study uses the base case scenario of an O_2 fed gasifier, no extra costs to dry the biomass and no need for a wax cracking reactor.*

	50 tons/day (tons/day)		500 tons/day (tons/day)		5000 tons/day (tons/day)	
Wood Price Point ($/ton)	NPV (million $)	ROROI (%)	NPV (million $)	ROROI (%)	NPV (million $)	ROROI (%)
15	(26.08)	N/A	(221.70)	N/A	319.04	18.82
25	**(26.93)**	**N/A**	**(230.11)**	**N/A**	**234.90**	**15.97**
35	(27.77)	N/A	(238.53)	N/A	150.76	13.12
45	(28.61)	N/A	(246.94)	N/A	66.62	10.27
55	(29.45)	N/A	(255.35)	N/A	(17.52)	N/A

***Base case scenario is in Bold**

Table S20 *Net Present value (in millions of dollars) and rate of return on investment (%) of running the plant for 20 years using a coal feedstock. This study uses the base case scenario of an O_2 fed gasifier, no extra costs to dry the biomass and no need for a wax cracking reactor.*

	50 tons/day (tons/day)		500 tons/day (tons/day)		5000 tons/day (tons/day)	
Coal Price Point ($/ton)	NPV (million $)	ROROI (%)	NPV (million $)	ROROI (%)	NPV (million $)	ROROI (%)
15	(33.43)	N/A	(75.71)	N/A	349.59	18.86
25	**(34.27)**	**N/A**	**(84.12)**	**N/A**	**265.45**	**16.25**
35	(35.11)	N/A	(92.54)	N/A	181.31	13.63
45	(35.95)	N/A	(100.95)	N/A	97.17	11.02
55	(36.79)	N/A	(109.37)	N/A	13.03	8.41

***Base case scenario is in Bold**

Table S21. *Variables used to calculate values for Table S22 and*

Table ***S23.***

Material Name	Classification	Price ($/kg)	Flow rate (kg/h)	Annual Cost
Biomass	Raw Material	$ 0.028	189000.00	$ 44,040,024
C_5-C_{12} Gasoline Range	Product	Varies	11981.96	Varies
Methane	Product	$ (0.24)	6027.98	$ (12,089,737)
Ethane	Product	$ (0.29)	619.84	$ (1,480,446)
LPG C_3/C_4	Product	$ (0.39)	888.03	$ (2,874,792)

C_{13}-C_{20} Diesel Range	Product	Varies	11908.78	Varies
Hydrogen	Product	$ (4.00)	1323.75	$ (44,064,990)
Pure O_2	Raw Material	$ 0.04	126783.00	$ 42,203,525
Waste Water	Non-Hazardous Waste	0.036	76497.8	$ 22,918,129

Table S22. *Net Present value (in millions of dollars) and rate of return on investment (%) of running the plant for 20 years using a wood feedstock. This study uses the base case scenario of an O_2 fed gasifier, no extra costs to dry the biomass and no need for a wax cracking reactor.*

	50 tons/day (tons/day)		500 tons/day (tons/day)		5000 tons/day (tons/day)	
Price of Gasoline | Diesel ($/gallon)	NPV (million $)	ROROI (%)	NPV (million $)	ROROI (%)	NPV (million $)	ROROI (%)
3.00 | 3.50	(31.57)	N/A	(276.35)	N/A	(277.09)	N/A
4.00 | 4.50	(29.25)	N/A	(253.23)	N/A	(21.10)	N/A
5.00 | 5.50	**(26.93)**	**N/A**	**(230.11)**	**N/A**	**234.90**	**15.97**
6.00 | 6.50	(24.60)	N/A	(206.99)	N/A	490.90	24.76
7.00 | 7.50	(22.27)	N/A	(183.80)	N/A	747.67	33.57
8.00 | 8.50	(19.95)	N/A	(160.68)	N/A	1003.67	42.36
9.00 | 9.50	(17.62)	N/A	(137.57)	N/A	1259.66	51.14

***Base case scenario is in Bold**

Table S23. *Net Present value (in millions of dollars) and rate of return on investment (%) of running the plant for 20 years using a coal feedstock. This study uses the base case scenario of an O_2 fed gasifier, no extra costs to dry the biomass and no need for a wax cracking reactor.*

	50 tons/day (tons/day)		500 tons/day (tons/day)		5000 tons/day (tons/day)	
Price of Gasoline | Diesel ($/gallon)	NPV (million $)	ROROI (%)	NPV (million $)	ROROI (%)	NPV (million $)	ROROI (%)
3.00 | 3.50	(40.50)	N/A	(146.40)	N/A	(357.34)	N/A
4.00 | 4.50	(37.39)	N/A	(115.26)	N/A	(144.57)	N/A
5.00 | 5.50	**(34.27)**	**N/A**	**(84.12)**	**N/A**	**265.45**	**16.25**
6.00 | 6.50	(31.16)	N/A	(52.98)	N/A	576.84	26.05
7.00 | 7.50	(28.04)	N/A	(21.75)	N/A	889.18	35.89
8.00 | 8.50	(24.92)	N/A	9.39	10.04	1200.58	45.69
9.00 | 9.50	(21.81)	N/A	40.53	16.13	1511.98	55.50

***Base case scenario is in Bold**

CapCost Results when bringing moisture from 42% to 19%

Yongue et al. described their onsite delivery of coal as having a moisture content of 42% and then they dried it to 19% before gasification. Some of this moisture needs to be removed so

that the gasifier can run at the desired temperature to produce the desired H_2 and CO for hydrocarbon production. Aspen plus models were used to mimic this data to immediately dry the coal from 42 percent moisture to 19 percent moisture before gasification. The biomass required when using the reactor block to remove moisture from 42% to 19% was calculated using Aspen Plus with equations 53 and 54. To feed 5000 ton/day into a gasifier, the feed for both the coal and wood would need to be approximately 7000 ton/day of biomass. The largest plant was chosen first to see going through the drying process would be economical and if not, because of economy of scale the process would not be economical for smaller plants.
Table *S24* shows that the Net Present Value (NPV) is negative for the largest plant evaluated in this study so the amount of energy required to dry smaller plants would not be economical as well. The area of the dryer was calculated using equation S.3.63 and this value was input into CapCost with the energy required to remove the water from the coal so that the moisture content was only 19%.

$$Area_{dryer} = \frac{m_{air}}{G_{air}} \qquad \text{(S.3.63)}$$

Where $Area_{dryer}$ is the area of the rotary dryer input into CapCost, m_{air} is the mass flow rate of air (kg/hr) and G_{air} is the assumed maximum superficial air mass velocity (800 lb/(hr*ft^2). The extra energy required to heat the biomass and the extra amount of biomass was also added. The extra cost due to drive power of having to crush up more material was also negligible so it was left out of this analysis (the cost to dry the material is shown to be uneconomical regardless of these types of smaller costs).
Table *S24* illuminates the fact that drying this amount of coal with a rotary dryer is not cost effective and it is better economically to let the coal dry in the elements so that no extra energy costs are incurred.

Table S24. *Net Present value of running the plant for 20 years using a rotary drier to dry coal and using the base case scenario of an O_2 fed gasifier.*

	5000 tons/day ($ million)
Coal Feedstock	(481.67)
Wood Feedstock	(215.04)

The energy content required was also calculated for the compressor using the base case for coal with a pure oxygen feed of a partial pressure of 231.18 psig for H_2 and a partial pressure of 130.66 psig for CO with an overall pressure of 525 psig. To obtain the same partial pressure of CO when using wood, the overall pressure of 595 psig was used so that the partial pressure of CO was 130.6 psig and the partial pressure of H_2 was 267.7 psig.

CapCost Results if a Catalytic Cracker must be used
The original base case takes into account the ability of the catalyst to keep the hydrocarbons in a liquid phase without any extra cracking (although this is modeled as two separate blocks). If a catalyst was used that could not keep the hydrocarbons in only a liquid or gaseous phase, then a catalytic cracker would have to be used. When modeling this in CapCost, the largest plant was first used to determine if it would be economical to add in plants with a smaller capacity and if so, other smaller capacity plants would be studied with this. In each of the wood and coal feedstock plants, the catalytic crackers were assumed to need the same volume of space as the original FT reactors but would require more energy since cracking reactions are endothermic and the energy usually released during the FT reactors would not be there for the cracking

reactors to supplement the heat required for the cracking reactions. Industrial catalytic crackers usually operate at a temperature of approximately 475 ^{o}C and approximately 20 psig so these operating conditions were used in the CapCost model. The endothermic reactions were not calculated to find any extra heat that would needed because after only calculating the amount of heat needed to heat the reactor tube and keep the reactor heated at 475°C, the extra cracker was found to not be economical.
Table *S25* shows that the plant would not be economically viable so to run a plant using the gasified biomass, a catalyst like the one used in previous chapters would be needed that transforms the gas into mainly liquid hydrocarbons without forming wax.

Table S25. *Net Present value of running the plant for 20 years using catalytic crackers (with the same volume as the original FT catalyst)*

	5000 tons/day ($ million)
Coal Feedstock	(108.80)
Wood Feedstock	(131.90)

CapCost Results if a Air was used as the feed gas in the Gasifier
The original base case assumes that pure oxygen would be used for the feed gas into the gasifier, so a study was done that used air as the feed gas. When modeling this in CapCost, the largest plant was first used to determine if it would be economical to add in plants with a smaller capacity and if so, other smaller capacity plants would be studied with this variation. To properly evaluate this situation, the same partial pressures of CO and H_2 were used to be sure that the same catalyst reactions would take place to produce similar results as the base case in a real world scenario. The amount of CO conversion in the WGS reaction was determined using a sensitivity analysis and the most efficient conversion was found to be 10% (when using the wood feedstock) and 40% (when using the coal feedstock) to create the largest amount of hydrocarbon products. The overall pressure of the air fed gasifier plants would need to be higher due to the nitrogen content that would be introduced with the air, so a partial pressure of 130.66 psig was used (to compare to previous scenarios) for CO and a partial pressure of 253.02 psig was used for H_2 (with the wood feedstock plant) with an overall pressure of 1023.42 psig for the wood feedstock scenario. The coal feedstock plant scenario had a partial pressure of 130.66 psig for CO, a partial pressure of 240.65 psig for $H_2$and an overall pressure of 985.82 psig when using the coal feedstock. Even though an oxygen concentrator and the cost for making the extra oxygen are negated,

Table ***S26*** shows that the amount of energy required for the compressor makes using an air fed gasifier unfeasible unless the nitrogen could possibly be removed before compression.

Table S26. *Net Present Value (NPV) of using an Air fed (78% N_2 and 22% O_2) gasifier*.

	$ millions
Coal (air fed gasifier)	(95.37)
Wood (air fed gasifier)	(249.82)

Publications:
Yan, Q., Y. Lu, C. Wan, J. Han, J. Rodriguez, J. Yin, and F. Yu. *2014.* Synthesis of Aromatics-rich Gasoline Range Hydrocarbons from Biomass-derived Syngas over Pd-promoted Fe/HZSM-5 Catalyst. *Energy and Fuels*. 28 (3):2027–2034.

Lu, Y., B. Cao, F. Yu, J. Liu, Z. Bao, and J. Gao. *2014*. High Selectivity Higher Alcohols Synthesis from Syngas over Three-dimensionally Ordered Macroporous Cu-Fe catalysts. *ChemCatChem*. 6:473-478.

Wan, C., F. Yu, Y. Zhang, Q. Li, and J. Wooten. *2013*. Material Balance and Energy Balance Analysis for Syngas Generation by a Pilot-plant Scale Downdraft Gasifier. *Journal of Biobased Materials and Bioenergy*. 7: 690-695.

Yan, Q., C. Wan, J. Street, D. Yan, J. Han, and F. Yu. *2013.* Catalytic Removal of Oxygen from Biomass-derived Syngas. *Bioresource Technology.* 147:117–123.

Zhang, Y., C., Wan, Q. Li, P.H. Steele, and F. Yu. *2013.* Studies of Biochars Generated from Pilot-scale Downdraft Gasification. *Transactions of the ASABE. 56(3): 995-1001.*

Yan, Q., C. Wan, J. Liu, J. Gao, F. Yu, J. Zhang, and Z. Cai. *2013.* Iron Nanoparticles in situ Encapsulated in Biochar-based Carbon as an Effective Catalyst for Conversion of Biomass-derived Syngas to Liquid Hydrocarbons *Green Chemistry.* 15:1631-1640.

Yan, Q., F. Yu, Z. Cai, and J. Zhang. 2012. Catalytic upgrading nitrogen-riched wood syngas to liquid hydrocarbon mixture over a Fe–Pd/ZSM-5 catalyst. Biomass and Bioenergy. 47: 469-473.

Yan, Q., F. Yu, J. Liu, J. Street, J. Gao, Z. Cai, and J. Zhang. 2012. Catalytic Conversion Wood Syngas to Synthetic Aviation Turbine Fuels over A Multifunctional Catalyst. Bioresource Technology.127:281-290.

Wang, H., D. Livingston, R. Srinivasan, Q. Li, P. Steele, and F. Yu. 2012. Detoxification and fermentation of pyrolytic sugar for ethanol production. Applied Biochemistry and Biotechnology. 168:1568–1583.

Hu, J., F. Yu, and Y. Lu. *2012.* Application of Fischer-Tropsch Synthesis in Biomass to Liquid Conversion. *Catalysts.* 2:303-326.

Street, J., F. Yu, J. Warnock, J. Wooten, and M. G. White. *2012.* Design and testing of a labview controlled catalytic packed-bed reactor system for production of hydrocarbon fuels. *Transactions of the ASABE.* 55(3): 1047-1055.

Lu, Y., F. Yu, J. Hu, and J. Liu. *2012.* Catalytic conversion of syngas to mixed alcohols over Zn-Mn promoted Cu-Fe based catalyst. *Applied Catalysis A, General.* 429–430:48-58.

Kunwar B, Wijaylapala H, Thieme J, Patel SV, Mlsna TE. 2013. A Simple Portable Gas Chromatograph for the Monitoring of Biomass Gasification. *Journal of Sensors and Instruments.* 1:1-16.

Rangana Wijayapala, Charles Pittman, Fei Yu and Todd Mlsna. 2014. Synthesis of alkylated aromatic hydrocarbons from CO/H_2 mixtures over Molybdenum/ZSM/Water Gas Shift Catalysts. *Applied Catalysis A: General.* (*Accepted* Ms. No.: APCATA-D-13-01624).

Conference Presentation:

Street, J., Yu, F., Columbus, E., amd Wooten, J. 2014. The Design and Economics of Gas-to-Liquid Plant using Wood Feedstocks. A Poster Presentation presented for the Southeastern Natural Resources Graduate Symposium. Mississippi State, MS, March 5-7, 2014.

Yu, F. 2013. Wide-cut diesel production from an integrated gasification, syngas cleaning, and catalytic conversion process. 2013 Mid-South Area Engineering and Sciences Conference. October 28-29. Oral presentation.

Zhang, L., P. Zhou, F. Yu, and K. Walters. 2013. Production of Hydrogen Via Steam-Reforming Reactions of Bio-Oil Over Nickel Based Catalysts. 2013 AIChE Annual Meeting. November 3-8. Poster presentation.

Lu, Y., F. Yu, J. Hu, and P. Zhou. 2013. CO hydrogenation to higher alcohols over three-dimensionally ordered macroporous Cu-Fe catalysts. 246th American Chemical Society National Meeting. Indianapolis, IN. September 8-12. Oral presentation.

Lu, Y., F. Yu, J. Hu, and P. Zhou. 2013. Catalytic conversion of syngas to higher alcohols via Zn-Mn promoted Cu-Fe based catalysts. 246th American Chemical Society National Meeting. Indianapolis, IN. September 8-12. Poster presentation.

Street, J., Yu, F., Columbus, E., and Wooten, J. 2013. Process Design and Economic Analysis of a Gas-to-Liquid Plant with Aspen Plus using a Woody Biomass Feedstock. Mississippi Biomass and Renewable Energy Council Conference. Tunica, MS. September 17-18. Poster presentation.

Lu, Y., F. Yu, J. Hu, and P. Zhou. 2013. Higher alcohols synthesis from syngas over three-dimensionally ordered macroporous Cu-Fe bimetallic catalyst. 23rd North American Catalysis Society Meeting. Louisville, KY. June 2-7. Poster.

Yan, Q., and F. Yu. 2013. Catalytic Conversion Wood Syngas to 'Wide Cut' Diesel over A Multifunctional Catalyst. 23rd North American Catalysis Society Meeting. Louisville, KY. June 2-7. Poster.

Lu, Y., Yu, F., Hu, J., Zhou, P. Syngas to Higher Alcohols via Three-dimentionally Ordered Macroporous Cu-Fe Bimetallic Catalyst. A Poster Presentation presented for the 2013 SEC Symposium. Atlanta, GA, February 10-12, 2013.

Street, J., Yu, F., Columbus, E., Wooten, J., and Yan, Q. Scale up of Gasoline-Range Hydrocarbon Production from Gasified Woody Biomass using a Bi-Functional Catalyst. A Poster Presentation presented for the 2013 SEC Symposium. Atlanta, GA, February 10-12, 2013.

Hu, J., Yu, F., Lu, Y., Street, J., Wooten, J., Columbus, E. 2012. Transportation Fuels Production from Biomass through Biomass Gasification, Gas Cleaning and Fischer-Tropsch Synthesis: A Technical and Economic Analysis, Paper: 121337425, An ASABE Meeting Presentation written for the 2012 ASABE Conference, Dallas, TX, July 29-August 1, 2012.

Lu,Y., Hu,J., Zhou, P., Street, J., Wooten, J, Columbus, E., Yu, F. 2012. Catalytic conversion of syngas to mixed alcohols via three-dimentionally ordered macroporous Cu-Fe based catalyst. Paper:121337229, An ASABE Meeting Presentation written for the 2012 ASABE Conference, Dallas, TX, July 29-August 1, 2012.

Street, J., Yu, F., Columbus, E., Wooten, J. 2012. Scale-Up of Liquid Hydrocarbon Production using Gasified Biomass. Paper: 121337524, An ASABE Meeting Presentation written for the 2012 ASABE Conference, Dallas, TX, July 29-August 1, 2012.

Lu, Y., Yu, F., Hu, J., Zhou, P. Mixed alcohols Synthesis from Syngas via Zn-Mn promoted Cu-Fe based catalyst. 2012. A Poster Presentation presented for the 2012 Southeast Biofuels Conference. Jackson, MS, August 8-9, 2012.

Street, J., Wooten, J., Columbus, E., and Yu, F. 2012. Scale-up of Gasoline-Range Hydrocarbon Production from Gasified Woody Biomass using Bi-functional Catalysts. A Poster Presentation presented for the 2012 Southeast Biofuels Conference. Mississippi State, MS, August 8-9, 2012.

Lu, Y., Yu, F., Hu, J., Zhou, P. 2012. Syngas to mixed alcohols via 3D ordered macroporous Cu-Fe based catalyst. Paper number: 172, An oral presentation presented for 244th American Chemical Society National Meeting & Exposition. Philadelphia, PA, August 19-23, 2012.

Yan, Q., Yu, F., Liu, J. 2012. Carbon encapsulated iron nanoparticles for catalytic conversion biosyngas to liquid hydrocarbons. 244th ACS National Meeting, Philadelphia, PA, August 19-25, 2012.

Hu, J., Yu, F., Lu, Y., Yan, Q., Wooten, J., Columbus, E. Green Flight: Renewable Jet Fuel Production Through Integrated Biomass Gasification, Gas Cleaning and Catalytic Conversion System. A Poster Presentation presented for the Lignocellulosic Biofuels Workshop. Auburn, AL, June 13-15, 2012.

Lu, Y., Yu, F., Hu, J., Zhou, P. Syngas to mixed alcohols via Zn-Mn promoted Cu-Fe based catalyst. A Poster Presentation presented for the Lignocellulosic Biofuels Workshop. Auburn, AL, June 13-15, 2012.

Street, J., Yu, F., Columbus, E., Wooten, J. Gasoline-range Hydrocarbon Production from Gasified Woody Biomass Using an Iron Bi-functional Catalyst. A Poster Presentation presented for the Lignocellulosic Biofuels Workshop. Auburn, AL, June 13-15, 2012.

Yan Q., and Yu, F. 2012. Process Development and Demonstration of Biomass to Liquid (BTL) Fuels via Gasification and Catalytic Conversion. AIChE's 2012 Spring Meeting. Houston, TX. April 1-5, 2012.

Akila G Karunanayake, Rangana T Wijayapala, Huidong Qiu, Todd E Mlsna. 2014. **Dual Cu based water gas and ZSM-5 supported iron catalysts for Fischer-Tropsch production.** *ACS 247th National Meeting*, Dallas, TX. *March 2014*.

Rangana Wijayapala, Fei Yu, Charles U. Pittman, Jr., Todd E. Mlsna. 2014. **K-promoted Mo/Co- and Mo/Ni-catalyzed Fischer-Tropsch synthesis of aromatic hydrocarbons with and without a Cu water gas shift catalyst.** *ACS 247th National Meeting*, Dallas, TX. *March 2014*.

Rangana Wijaylapala. 2013. Hydrodeoxygenation (HDO) of Guaiacol and Furfural using WGS and Mo/Co/K catalyst system, *ACS 245th National Meeting*, New Orleans, LA. April *2013*.

Bidhya Kunwar. 2013. Upgrading bio-oil with a combination of synthesis gas and alcohol, *ACS 245th National Meeting*, New Orleans, LA. April *2013*.

Bidhya Kunwar. 2012. Portable Gas Chromatograph for the Monitoring of Biomass Gasification, *39th Annual Meeting of FACSS*, Kansas City, MO. September *2012*.

Patent Applications:

Catalysts for converting syngas into liquid hydrocarbons and methods therof. Fei Yu, Qiangu Yan, and William Batchelor. Final patent application. US 14/162,606. January 23, 2014.

Upgrading Bio-Oil with Synthesis Gas. Todd Mlsna, Phillip Steele, Fei Yu. US provisional patent application. September *2013*.

End Confidential Information.

Task T. Biomass Combustion

Principal Investigators and team members:
Sundar R. Krishnan (PI), Kalyan K. Srinivasan (Co-PI)

Executive summary:
The focus of the Biomass Combustion research thrust was to understand the influence of various fuels on combustion processes relevant to transportation and stationary engines. The fuels examined included methane, propane, ethanol (E-85), diesel, and blends of diesel and a proprietary renewable fuel sourced from non-food biomass. Several sets of experiments were performed with different experimental setups: (1) Detailed dual fuel low temperature combustion (LTC) experiments on a single cylinder research engine (SCRE) and on multi-cylinder light-duty and heavy-duty diesel engines and (2) Combustion pressure diagnostics in a rapid compression expansion machine (RCEM) and non-intrusive laser-induced breakdown spectroscopy (LIBS) for flame measurements in a rectangular slot burner. The dual fuel LTC experiments focused on quantifying the performance, combustion, and emissions associated with diesel ignition of methane, gasoline, propane, and E-85 in the SCRE. The dual fuel experiments investigated the possible performance and emissions improvements with combinations of different low-cetane gaseous fuels (methane, propane, E-85, gasoline). All of these fuels are currently available and all (except diesel and gasoline) can be sourced from renewable resources. Therefore, these results are useful indicators of the performance and emissions benefits when such fuels are utilized in diesel engines. A proprietary second-generation non-food biomass fuel was blended with ultra low sulfur diesel and the effects on combustion, performance, efficiency, and emissions were investigated on both the multi-cylinder light-duty and heavy-duty engines. The slot burner experiments were performed to employ LIBS for fuel-air equivalence ratio measurements in premixed atmospheric methane-air flames. In addition, pure air compression and diesel combustion studies were performed with combustion pressure diagnostics on the RCEM. A high-speed laser-based optical diagnostics system was purchased to facilitate planar laser-induced fluorescence (PLIF) and chemiluminescence imaging on the RCEM. However, due to unforeseen hardware and software issues with RCEM operation, it was not possible to commission the PLIF/chemiluminescence system before the end of this project; this is expected to occur in the near future. The knowledge gained from all of these efforts has been disseminated in numerous refereed journal articles, national and international conference publications, and invited technical presentations given by the MSU PIs at US and international institutions. In addition, the MSU PIs leveraged the RCEM and PLIF/chemiluminescence facilities to collaborate with ten partner institutions, including universities and national laboratories, to submit 7 new research grant proposals. Overall, the outcomes of the present efforts have provided the foundations for understanding and improving combustion of next-generation biofuels in combustion engines.

T.1 Real-time visualization of combustion of non-food biomass fuels using advanced laser diagnostic techniques

- Two peer-reviewed journal articles were published from this Subtask.

- Ignition characteristics in diesel-ignited methane and diesel-ignited propane dual fuel combustion were quantified and carefully analyzed. One journal paper was published in the *Proceedings of the Institution of Mechanical Engineering, Part D: Journal of Automobile Engineering* from these efforts.

- We have developed a reliable methodology to estimate the compression ratios in the rapid compression expansion machine (RCEM). In addition, we have performed several combustion shots to obtain cylinder pressure and heat release rates.

- A new multi-hole injector was installed on the RCEM to simulate engine-like combustion. MSU was invited to participate in the Engine Combustion Network (ECN) – an online repository of knowledge where researchers share the knowledge from their experiments on diesel sprays. MSU researchers plan to work with the ECN once additional results are obtained from the RCEM. In addition, researchers at a renowned university in Spain have shared their research results obtained on a similar RCEM with MSU to enable a mutually beneficial collaboration between both universities.

- The manufacturing and delivery of the PLIF/OH* chemiluminescence system was delayed due to unforeseen circumstances. In addition, the RCEM developed unexpected hardware and software problems that prevented the performance of optical diagnostic experiments. Therefore, optical diagnostic experiments based on laser-induced breakdown spectroscopy (LIBS) were performed on atmospheric, premixed methane-air flames generated in a rectangular slot burner and a McKenna burner.

- Diagnostics based on LIBS were used to quantify fuel-air equivalence ratios in methane-air flames. Multivariate calibration models were developed and found to be very useful for equivalence ratio determination from LIBS measurements. Another journal paper was published in the journal *Fuel* based on these efforts.

- The experimental results and experience gained from the burner experiments are expected to be very useful when RCEM experiments are performed in the near future.

- The experience gained in performing RCEM experiments through this Subtask was also leveraged to write ***7 new research grant proposals*** (in 2013-2014) to DOE, NSF, ACS, etc., in collaboration with several external partner institutions including Lawrence Berkeley National Laboratory, Argonne National Laboratory, University of California-Berkeley, Michigan Technological University, Carnegie Mellon University, Georgia Institute of Technology, Michigan State University, University of Alabama, Colorado School of Mines, and University of Alabama-Huntsville.

T.2 Quantification of particulate matter (PM) emissions from combustion of non-food biomass fuels

- Seven peer-reviewed journal articles, three peer-reviewed conference papers, and one non-peer-reviewed conference paper were published from this Subtask. An ***invited*** journal article is currently under review for publication in the *ASCE Journal of Energy Engineering.* Two additional journal articles currently under preparation for submission to the journals *Fuel* and *Energy*.

- This Subtask facilitated one completed Ph.D. dissertation, three completed M.S. theses, and one more ongoing Ph.D. dissertation and two more ongoing M.S. theses.

- For this subtask, experiments were primarily performed on two different engine platforms: a single cylinder research engine (SCRE) and a Volkswagen 1.9L multi-cylinder diesel engine. Three different types of alternative fuels were considered: methane, propane, and a renewable non-food biomass-derived distillate fuel provided by a US biofuels manufacturer (KiOR).

- An air compressor-dryer system, which was purchased in the previous phase of the project was commissioned and used successfully to "simulate turbocharging" on the SCRE for investigating and achieving controlled low temperature combustion (LTC) strategies.

- Ignition, combustion, fuel conversion efficiencies, and engine-out exhaust emissions were measured for straight diesel fueling and for diesel-ignited methane, gasoline, and propane dual fuel combustion. Additional state-funded experiments were also completed for understanding the combustion of KiOR's non-food biomass-derived distillate fuel and its blends with ultra low sulfur diesel (ULSD) on both light-duty (VW 1.9L) and heavy-duty multi-cylinder diesel engines.

- Four different invited presentations were given by the co-PIs on various combustion strategies with conventional and alternative fuels both within the US and in several international universities.

- The engine exhaust particle sizer spectrometer (EEPS), which was purchased to fulfill the objectives of this Subtask, has become an excellent state-of-the-art instrument for use with other ongoing projects the Advanced Combustion Engines (ACE) lab at MSU. For example, particle emissions results (measured with the EEPS) from various dual fuel LTC strategies were presented at the 2014 Spring Technical Meeting of the Central States Section of the Combustion Institute in Tulsa, OK. The EEPS was also leveraged to investigate particle emissions from diesel-ignited propane LTC in a multi-cylinder heavy-duty diesel engine, and the results were published at the ASME 2013 Internal Combustion Engine Division Fall Technical Conference (ICEF2013) in Dearborn, MI as well as the *Trans. ASME: Journal of Engineering for Gas turbines and Power.*

- Cyclic combustion variations in diesel-ignited natural gas dual fuel LTC were studied and presented at the ASME 2012 IC Engines Division Spring Technical Conference in Torino, Italy, and later published in the *Trans. ASME: Journal of Energy Resources Technology*.

- A new exhaust gas recirculation (EGR) system has been designed for the SCRE and is being built to facilitate future LTC experiments.

- A computational fluid dynamics (CFD) model of gasoline compression ignition combustion in a light-duty diesel engine was developed in a separate collaborative effort with researchers at Carnegie Mellon University and validated with experimental results from colleagues at Argonne National Laboratory. A joint paper was authored on this topic and presented at the Proceedings of the ASME 2013 Internal Combustion Engine Division Fall Technical Conference (ICEF2013) in Dearborn, MI as well as the *Transactions of the ASME: Journal of Engineering for Gas turbines and Power.*

Refereed Journal Papers

Raihan, M.S., Guerry, E.S., Dwivedi, U., Srinivasan, K.K., and Krishnan, S.R. (2014). Experimental analysis of diesel-ignited methane dual fuel low temperature combustion in a single cylinder diesel engine. Under review, *Trans. ASCE: Journal of Energy Engineering*.

Kavuri, C., Singh, S., Krishnan, S.R., Srinivasan, K.K., and Ciatti, S.A. (2014). Computational analysis of combustion of high and low cetane fuels in a compression ignition engine. Accepted for publication, *Trans. ASME: Journal of Engineering for Gas Turbines and Power*.

Polk, A.C., Carpenter, C.D., Srinivasan, K.K., and Krishnan, S.R. (2014). An investigation of diesel-ignited propane dual fuel combustion in a heavy-duty diesel engine. *Fuel*, *132*, 135-148. (http://dx.doi.org/10.1016/j.fuel.2014.04.069).

Dwivedi, U., Carpenter, C.D., Guerry, E.S., Polk, A.C., Krishnan, S.R., and Srinivasan, K.K. (2014). Performance and emissions characteristics of diesel-ignited gasoline dual fuel combustion in a single cylinder research engine. *Trans. ASME: Journal of Engineering for Gas Turbines and Power*, *136*(10), 101504 (May 02, 2014), Paper No: GTP-14-1088; doi: 10.1115/1.4027273.

Polk, A.C., Carpenter, C.D., Guerry, E.S., Dwivedi, U., Srinivasan, K.K., Krishnan, S.R., and Rowland, Z.L. (2014). Diesel-ignited propane dual fuel low temperature combustion in a heavy-duty diesel engine. *Trans. ASME: Journal of Engineering for Gas Turbines and Power*, *136*(9), 091509 (Apr 18, 2014), Paper No: GTP-14-1085; doi: 10.1115/1.4027189.

Srinivasan, K.K., Krishnan, S.R., and Qi, Y. (2013). Cyclic combustion variations in dual fuel partially premixed pilot-ignited natural gas engines. *Trans. ASME: Journal of Energy Resources Technology*, *136*(1), 012003 (10 pages), (doi:10.1115/1.4024855).

Polk, A.C., Gibson, C.M., Shoemaker, N.T., Srinivasan, K.K., and Krishnan, S.R. (2013). Detailed characterization of diesel-ignited propane and methane dual fuel combustion in a turbocharged DI diesel engine. *Proc. IMechE, Part D: J. Automobile Engineering*, *227*(9), 1255-1272, (doi:10.1177/0954407013487292).

Polk, A.C., Gibson, C.M., Shoemaker, N.T., Srinivasan, K.K., and Krishnan, S.R. (2013). Analysis of ignition behavior in a dual fuel turbocharged direct injection engine using propane and methane as primary fuels. *Trans. ASME: Journal of Energy Resources Technology*, *135*(3), 032202, (10 pages), (doi:10.1115/1.4023482).

Tripathi, M.M., Srinivasan, K.K., Krishnan, S.R., Yueh, F.-Y., and Singh, J.P. (2013). A comparison of multivariate LIBS and chemiluminescence-based local equivalence ratio measurements in premixed atmospheric methane-air flames. *Fuel*, *106*, 318-326. (http://dx.doi.org/10.1016/j.fuel.2012.10.079)

Shoemaker, N.T., Gibson, C.M., Polk, A.C., Krishnan, S.R., and Srinivasan, K.K. (2012). Performance and emissions characteristics of bio-diesel (B100)-ignited methane and propane combustion in a four cylinder turbocharged compression ignition engine. *Trans. ASME: Journal of Engineering for Gas Turbines and Power*, *134*(8), 082803 (10 pages) (http://dx.doi.org/10.1115/1.4005993).

Conference Papers and Posters

Peer-Reviewed Papers

U. Dwivedi, C.D. Carpenter, E.S. Guerry, A.C. Polk, S.R. Krishnan, and K.K. Srinivasan, 2013, "Performance and Emissions Characteristics of Diesel-Ignited Gasoline Dual Fuel Combustion in a Single Cylinder Research Engine," Paper No. ICEF2013-19108, Proceedings of the ASME 2013

Internal Combustion Engine Division Fall Technical Conference (ICEF2013), October 13-16, 2013, Dearborn, MI.

C. Kavuri, S. Singh, S.R. Krishnan, K.K. Srinivasan, and S.A. Ciatti, 2013, "Computational Analysis of Combustion of High and Low Cetane Fuels in a Compression Ignition Engine," Paper No. ICEF2013-19178, Proceedings of the ASME 2013 Internal Combustion Engine Division Fall Technical Conference (ICEF2013), October 13-16, 2013, Dearborn, MI.

K.K. Srinivasan, S.R. Krishnan, and Qi, Y., 2012, "Cyclic Combustion Variations in Dual Fuel Partially Premixed Pilot-ignited Natural Gas Engines," Paper No. ICEF2012-81145, Proceedings of the ASME 2012 Internal Combustion Engine Division Spring Technical Conference (ICES2012), May 6-9, 2012, Torino, Italy.

Non-Peer-Reviewed Papers and Posters

Krishnan, S.R., Srinivasan, K.K., Raihan, M.S., and Guerry, E.S. (2014). Characterization of particle emissions from dual fuel partially premixed low temperature combustion, presented at the 2014 Spring Technical Meeting of the Central States Section of the Combustion Institute, March 16-18, 2014, Tulsa, OK.

Invited Presentations

Srinivasan, K.K. "Dual Fuel Low Temperature Combustion Technologies for Future Transportation Applications: Opportunities and Challenges," presented at the Centre for Energy Studies, Indian Institute of Technology – Delhi, New Delhi, India, May 19, 2014.

Krishnan, S.R. "Sustainable Internal Combustion Engines for the Future," presented at Government College of Engineering, Tirunelveli, Tamil Nadu, India, July 23, 2013.

Krishnan, S.R. "Advanced Combustion Strategies for Future Internal Combustion Engines," *and* "Dual Fuel Low Temperature Combustion Strategies for Next-Generation IC Engines," presented at National Engineering College, Kovilpatti, Tamil Nadu, India, July 11, 2013.

Krishnan, S.R. "Tailoring Renewable Biofuels for Future Engine Combustion Strategies," presented at the Southeast Biofuels and Renewable Energy Conference, Jackson, MS, August 8, 2012

Graduate Student Theses and Dissertations

Ph.D. dissertation: Andrew Clayton Polk (2013). Detailed characterization of conventional and low temperatures dual fuel combustion in compression ignition engines. Ph.D. dissertation, Department of Mechanical Engineering, Mississippi State University, Starkville, MS.

MS thesis: Robert Dennis McElmurry (2014). Development of a flexible open architecture controller for a six-cylinder heavy-duty diesel engine. MS thesis, Department of Mechanical Engineering, Mississippi State University, Starkville, MS.

MS thesis: Edward Scott Guerry (2014). Injection timing effects of diesel-ignited methane dual fuel combustion in a single cylinder research engine. MS thesis, Department of Mechanical Engineering, Mississippi State University, Starkville, MS.

MS thesis: Umang Dwivedi (2013). An experimental investigation of diesel-ignited gasoline and diesel-ignited methane dual fuel concepts in a single cylinder research engine. MS thesis, Department of Mechanical Engineering, Mississippi State University, Starkville, MS.

Subtask T.1 Real-time visualization of combustion of non-food biomass fuels using advanced laser diagnostic techniques

The goal of this task is to utilize advanced laser diagnostic techniques, such as planar laser induced fluorescence (PLIF), to enable real-time visualization of combustion of novel non-food biomass fuels. Real-time combustion images will be obtained to characterize species evolution during combustion. This approach will provide important data to design smart fuel injection strategies to optimize fuel conversion efficiency and to minimize pollutant formation while using biomass-derived fuels.

Planned Activities:

T.1.ML.1 Obtain spatially-resolved images of combustion of non-food biomass fuels.
T.1.ML.2 Characterize species evolution during non-food biomass fuel combustion.

Summary of Activities for Subtask T.1:

1. *RCEM commissioning for performing combustion visualization experiments*: For Subtask T.1, the high-speed combustion visualization experiments were planned to be performed on the MSU rapid compression-expansion machine (RCEM). The MSU RCEM, shown in Fig. T.1, is a sophisticated, computer-controlled single-shot device that utilizes pneumatic, hydraulic, and electronic controls to simulate one compression stroke and a partial expansion stroke of an IC engine. The RCEM provides excellent optical access to perform both laser-based and combustion pressure-based combustion diagnostics. Before the laser-based combustion diagnostics hardware could be installed, the RCEM had to be commissioned. The initial commissioning of the RCEM was completed between January and August 2013.

   The experimental efforts during the initial commissioning involved the following important steps:

   - *RCEM Driving Gas Pressure Calibrations:* Since the RCEM is an experimental research machine, its operating parameters are not pre-defined but customizable for the end-user's requirements. For this purpose, specific experiments were performed to build a matrix of "driving gas pressures" required to achieve different compression ratios, loading pressures (initial combustion chamber or charge pressures), and simulated engine speeds.

   - *Injection System Commissioning and Calibration*: As mentioned in previous quarterly reports, a custom-built, high-pressure diesel injection system is currently available with the RCEM to enable the performance of the experiments in this Subtask. This fuel injection system was commissioned for operation. Compressed air supply for the air-hydraulic pump was provided, and after successful setup and troubleshooting of the injector control hardware/software, a specially modified single-hole solenoid diesel injector was carefully calibrated. In this calibration process, for a given injection pressure and injector open duration, the amount of fuel injected per injection pulse was measured by capturing a known number of injections (e.g., for 1000 injection

pulses) in a graduated beaker. By repeating this process over a range of injection pressures and injector open durations, “injector calibration maps” were developed. A sample fuel calibration map for the single-hole diesel injector is shown in Fig. T.2. The calibration maps for the fuel injector will be helpful in determining the mass of fuel injected into the RCEM during one combustion event. The calibrated fuel injector was installed in the RCEM and preliminary diesel combustion experiments were performed. A standard multi-hole solenoid diesel injector was also purchased and is currently available for use with the RCEM.

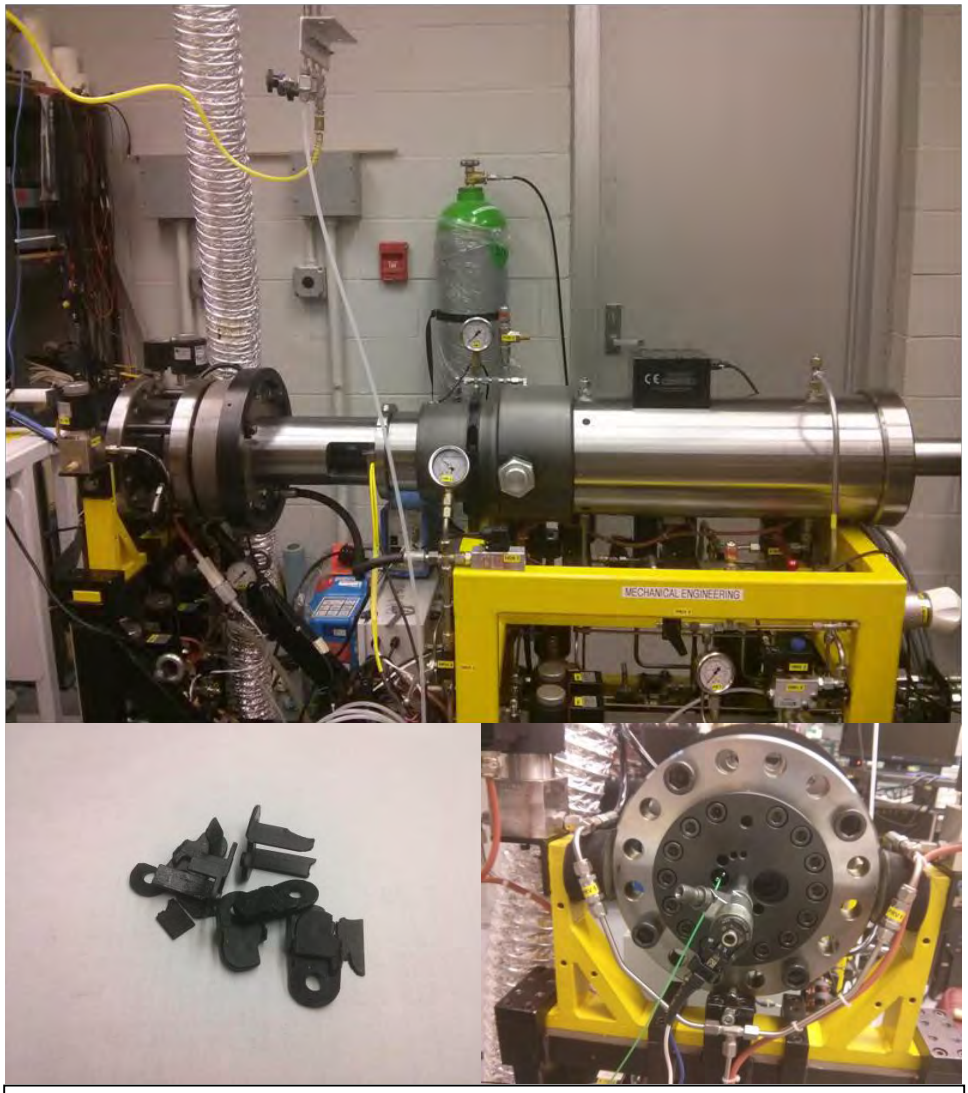


***Figure T.1**: (Clockwise from top) – Photograph of MSU RCEM with the driver section and controls; cylinder head insert showing fuel injector and combustion pressure sensor wiring; and broken links of chain used to anchor displacement sensor wiring, which prevented combustion image acquisition.*

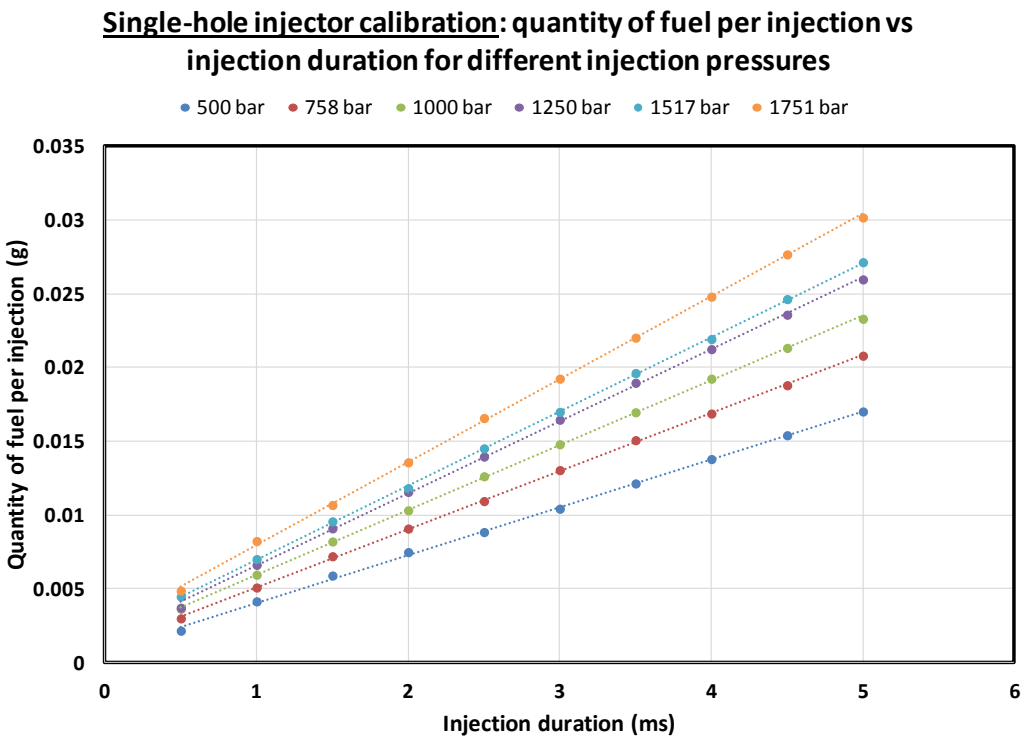


***Figure T.2**: A calibration map developed for the single-hole diesel injector used with the RCEM.*

- *"Pure Air Compression" Experiments*: Several compression shots of pure air (with no fuel) were performed at various stroke lengths, driving gas pressures, and initial charge pressures. These pure air compression shots were useful to determine the range of driving gas pressures needed to achieve different stroke lengths (e.g., from 190 to 240 mm). Since the RCEM is a "free piston" device, i.e., since there is no connecting rod to ensure rigid motion of the piston, the actual stroke length executed by the piston is dependent not only on the driving gas pressure, which "drives" the piston, but also on the pressure inside the combustion chamber, which opposes piston motion toward the end of the rapid compression process. Since combustion chamber pressure (in the absence of combustion) is directly dependent on the initial charge pressure, it was important to adjust the driving gas pressures appropriately to achieve a desired stroke length as initial charge pressure was varied. Another parameter that was investigated was the so-called "throttle distance," which allowed the simulation of different time-resolved piston displacement profiles to simulate different engine speeds. In addition to determining the driving gas pressures, several pure air compression shots were also repeated multiple times to characterize the shot-to-shot repeatability of the device without the random uncertainties associated with combustion. During these preliminary experiments, the shot-to-shot variability for pure air compression was very small as evident from Fig. T.3.

- *Effective Compression Ratio Estimations*: During these pure air compression experiments, it was noticed that since the RCEM had a "free piston" the effective compression ratio achieved was both a function of the driving gas pressure as well as the initial charge pressure. Since the final piston position (i.e., the top dead center or

TDC) is not fixed *a priori* as in a normal IC engine, it was necessary to determine the actual (effective) compression ratio after each shot. Several thermodynamics-based approaches for both ideal (e.g., isentropic) and actual compression processes were considered for estimating the effective compression ratios. A Matlab code was written to automate the effective compression ratio calculations and the code was validated over a range of stroke lengths.

- *Diesel Combustion Experiments*: Following the pure air compression experiments, diesel combustion experiments were performed with the single-hole diesel injector at different diesel injection durations (i.e., for different diesel quantities) and stroke lengths. A sample of the time-resolved measured pressure and piston displacement histories for diesel combustion is provided in Fig. T.4 for an injection pressure (Pinj) of 1000 bar, an injection duration of 2 ms, and a start of injection (SOI) of 190 mm (with respect to piston position). Clearly, these experiments demonstrated that the RCEM is conducive for achieving compression ignition of diesel over a range of conditions.

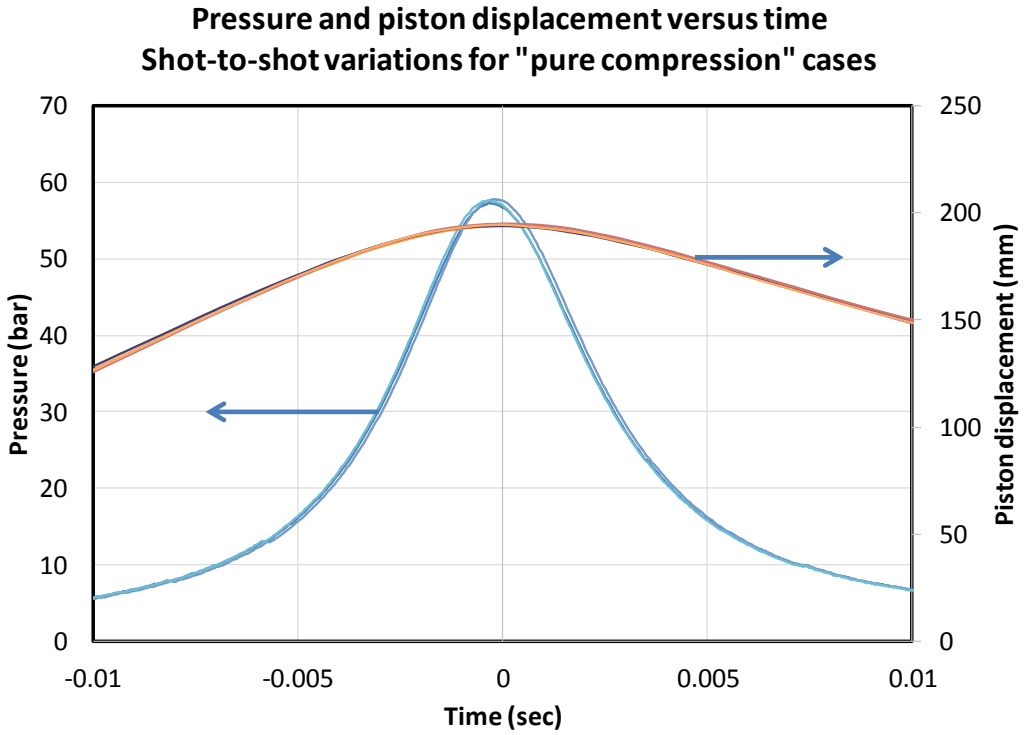


***Figure T.3**: Time-resolved pressure and piston displacement histories for pure compression in the RCEM showing shot-to-shot variations (195 mm max. stroke length).*

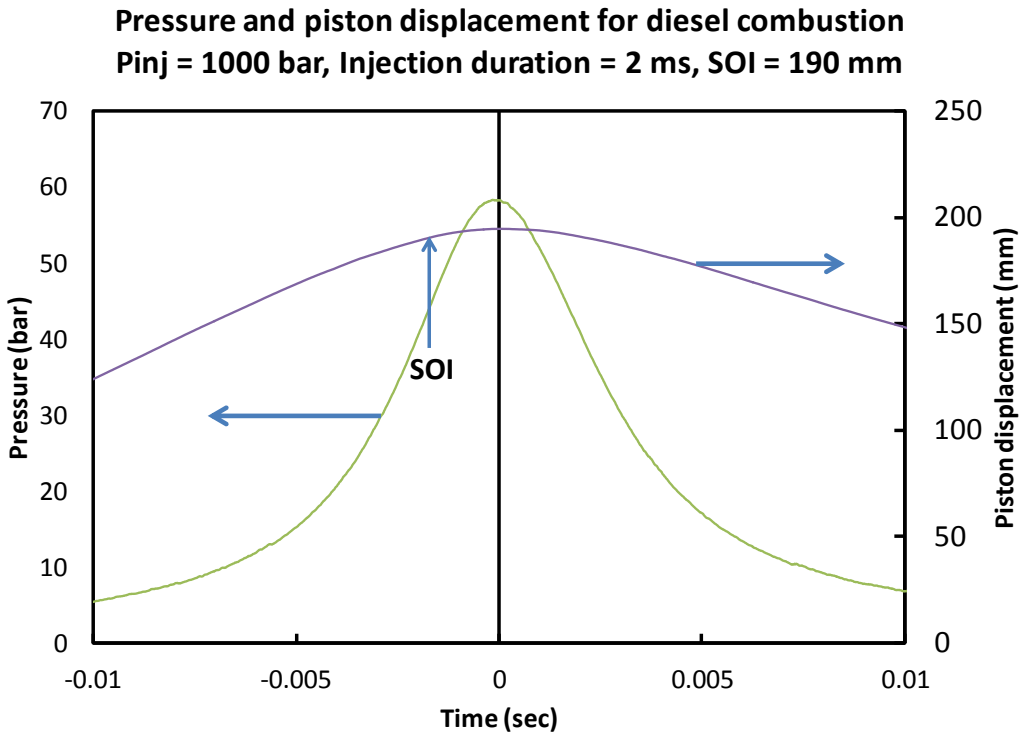


***Figure T.4**: Time-resolved pressure and piston displacement histories for diesel combustion in the RCEM for an injection pressure (Pinj) of 1000 bar, an injection duration of 2 ms, and a start of injection (SOI) of 190 mm (with respect to piston position).*

Hardware and Software issues with the RCEM: After completing the preliminary pure compression and diesel combustion experiments, we attempted to get the RCEM ready for accommodating laser-based diagnostics. However, several hardware and software issues were identified with the RCEM during this process (both persistent old issues as well as new ones). These included:

- Displacement sensor malfunction and reset issues
- "RCM CAMAS" software issues such as periodic hanging, inability to retrieve the entire data, and lack of flexibility in software for altering experimental procedure
- Broken links of chain used to anchor displacement sensor wiring and cabling (please see photograph to the bottom-left in Fig. T.1)
- Excessive vibration of the 45° mirror during piston movement
- Shot-to-shot inconsistencies during combustion shots
- Inconsistencies in piston retraction to initial position upon shot completion.

While the RCEM had initially been sufficiently stable to obtain sample combustion pressure and piston displacement histories, shot-to-shot inconsistencies during combustion shots and the other hardware and software issues described above became increasingly problematic. Despite repeated attempts to get the RCEM working satisfactorily, the broken chain links and various other unforeseen issues (e.g., displacement sensor inconsistencies, excessive mirror vibrations, etc.) and software issues prevented the expected commissioning of the laser diagnostics equipment. Since the RCEM is a custom-built device, we had to work closely with the RCEM manufacturer in Germany to try to resolve these issues, which were outside our

control (e.g., only the RCEM manufacturer had the wherewithal to resolve complicated hardware and software issues). Unfortunately, we were unable to resolve all outstanding issues in time to use the RCEM to perform the real-time visualization experiments. As soon as the RCEM issues are resolved, we plan to commission the OH-PLIF/chemiluminescence system in the next few months. Meanwhile, significant efforts were taken to investigate laser-induced breakdown spectroscopy (LIBS) for equivalence ratio measurements of premixed methane-air flames in a rectangular slot burner as described below.

2. *Laser-Based and Optical Diagnostics*: To enable real-time visualization of ignition and combustion processes in the RCEM, a high-speed laser-based and optical diagnostics system manufactured by TSI, Inc., was purchased. This system comprises laser hardware for performing planar laser-induced fluorescence (PLIF) of the hydroxyl (OH) radical, a camera/intensifier system for performing either 10 Hz OH-PLIF imaging or high-speed chemiluminescence and natural luminosity (NL) imaging as needed, all necessary optical lenses and filters, and a comprehensive software package to coordinate, acquire, and post-process all of these measurements. Delivery of the new diagnostics system was taken in October 2013.

   With the high-speed chemiluminescence system, ignition and combustion evolution in *a single RCEM cycle* can be analyzed both from line-of-sight OH* chemiluminescence and NL images, which are time-resolved. The camera available for these studies is a high-speed Phantom v611 CMOS camera (20.9 kHz @ 512 x 512 pixel resolution, ~48 μs time resolution or ~0.5 CAD resolution at 1500 rpm). Camera gain settings and exposure times can be optimized to obtain the best possible image quality. The high-speed NL and chemiluminescence images can be obtained by viewing through the bottom of the quartz piston crown with the 45° mirror available in the RCEM as shown in Fig. T.5. The two main advantages of the OH* chemiluminescence measurements compared to single-shot OH-PLIF is: (i) OH* can yield cycle-resolved information, and (ii) only the OH from the high-temperature flame (not the OH in the post-flame burned gases) will contribute to the OH* signal. The Phantom v611 camera can be coupled to the high-speed UV image intensifier (Invisible Vision UVi Model 1850-10; 200-700 nm sensitivity) and a short wave pass (SWP) filter with a cut-off near 348 nm for isolating OH* signals.

   For OH-PLIF experiments, a Nd:YAG-pumped Continuum tunable dye laser (10 Hz, 25 mJ) is available to pump the overlapping $Q_1(9)$ and $Q_2(8)$ lines of the (1,0) band of the $A \rightarrow X$ transition of OH near 284 nm. Cylindrical and spherical lenses are available to convert the laser beam into a laser sheet before it enters the RCEM in one of the two orientations shown in Fig. T.5 (i.e., either parallel to the piston crown or along the diesel jet axis). The intensified Phantom v611 camera with a Nikon UV-VIS (220-900 nm), 105 mm, f/4.5 lens can be used to collect OH fluorescence from multiple rotational transitions in both the (0,0) and (1,1) vibrational bands in the 308-320 nm range. A set of three filters are available: (i) a 313 nm bandpass (BP) filter (10 nm FWHM) to isolate OH fluorescence, (ii) a 348 nm SWP filter to reject red-shifted fluorescence, and (iii) a WG305 long wave pass (LWP) filter to remove elastically scattered laser light. The OH-PLIF will provide 2D images viewed through the bottom of the quartz piston crown. The TSI Insight4G software with the MODULE4G-PLIF module is available for in-situ PLIF image calibration, background removal, corrections for variations in laser light sheet intensity, shot-to-shot variations in laser pulse energy, customized image processing, and integrated data presentation. Built-in flame front detection algorithms in Insight4G can also be used when necessary. As mentioned above, as soon as the persisting hardware and software issues are resolved in the near future, the high-speed

chemiluminescence, NL, and OH-PLIF systems will be commissioned for future experiments on the RCEM.

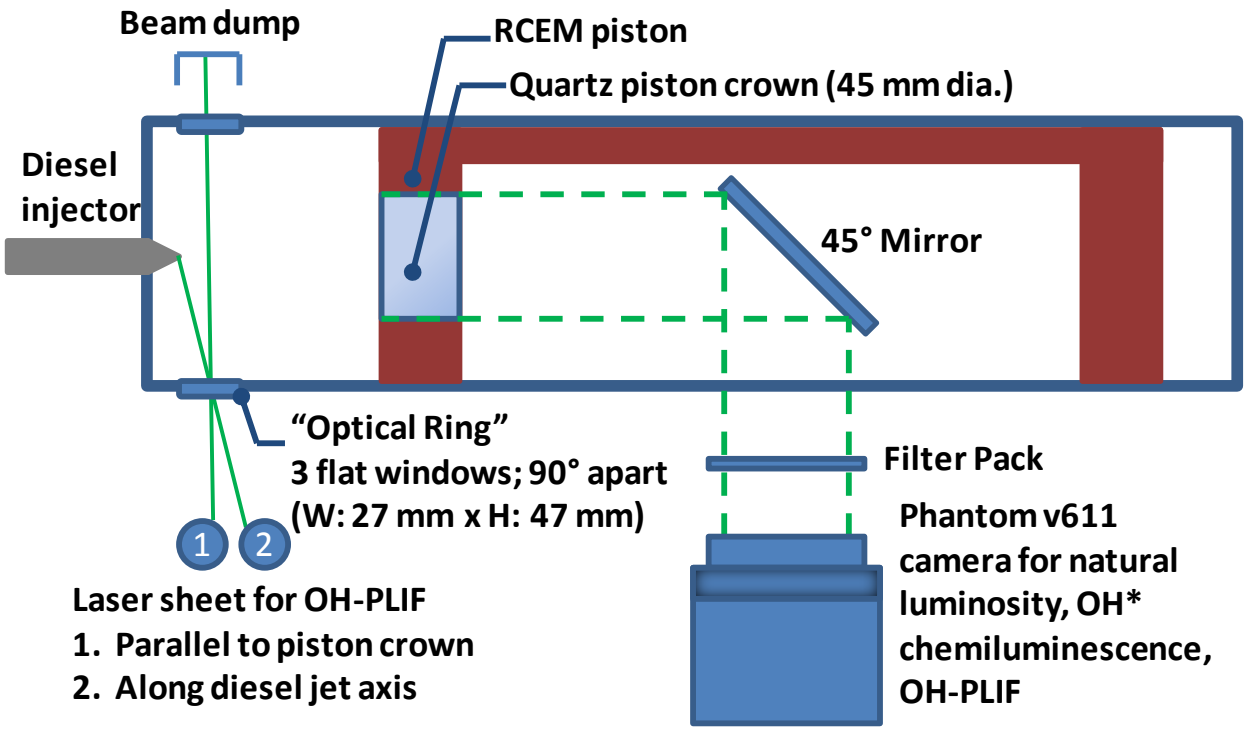


***Figure T.5**: Schematic of the MSU RCEM with the available optical diagnostics (optical visibility ring for laser beam introduction and 45° mirror for obtaining the bottom view of the combustion chamber through a quartz-crowned piston).*

3. *Laser-induced breakdown spectroscopy (LIBS) experiments on a premixed burner*: To characterize combustion temperature and mixture concentrations in flames, detailed laser-induced breakdown spectroscopy (LIBS) measurements were completed for premixed atmospheric methane-air flames in a rectangular slot burner. A partial least-squares regression (PLS-R)-based calibration model was developed to correlate LIBS data with fuel-air equivalence ratios. These results showed that the PLS-R-based model could be used effectively with LIBS measurements to predict equivalence ratios in premixed methane-air flames. A peer-reviewed journal paper (in *Fuel*) was published out of this effort. In parallel, to calibrate the LIBS measurements, preliminary measurements were performed with laser Rayleigh scattering on a more standard McKenna burner. The basic idea in all of these efforts is to initiate and develop these diagnostics first in atmospheric flames and then translate them over to the high-pressure, high-temperature environment in the RCEM.

   A schematic of the experimental setup used for LIBS measurements on methane-air flames generated in the rectangular slot burner (length: 11.2 cm, width: 0.55 cm, and height: 26 cm) is shown in Fig. T.6. A frequency-doubled Nd:YAG pulse laser (BigSky/Quantel CFR 400 10 Hz, 532 nm, 180 mJ, 9 mm beam diameter) was used to create laser-induced-breakdown in the premixed flame. The laser beam of 87 mJ pulse energy was focused approximately 2 mm above the burner by employing a plano-convex lens of 200 mm focal length. The LIBS signal was collected by employing the ungated detection technique. A polarizer (Karl Lambrecht

Corporation, MGLS-SW-15) was employed to suppress the elastically scattered laser light. In the performance comparison experiments, the polarizer was replaced with a notch filter (Kaiser Optical Systems, Inc., HSPF-532-1.5) to evaluate its performance. A fused silica, plano-convex, spherical lens with 100 mm focal length and 12.7 mm diameter collected and coupled the optical signal to the single end of a bifurcated optical fiber (Ocean Optics, QBIF400-UV–VIS). One of the bifurcated ends of the optical fiber was connected to an Ocean Optics USB 2000 spectrometer (600 grooves/mm grating) with a spectral resolution of 3.8 nm (full-width half-maximum) to record the LIBS spectra. The other end was used for optical alignment in the flame by sending a separate laser beam through it before the experimental measurements were performed.

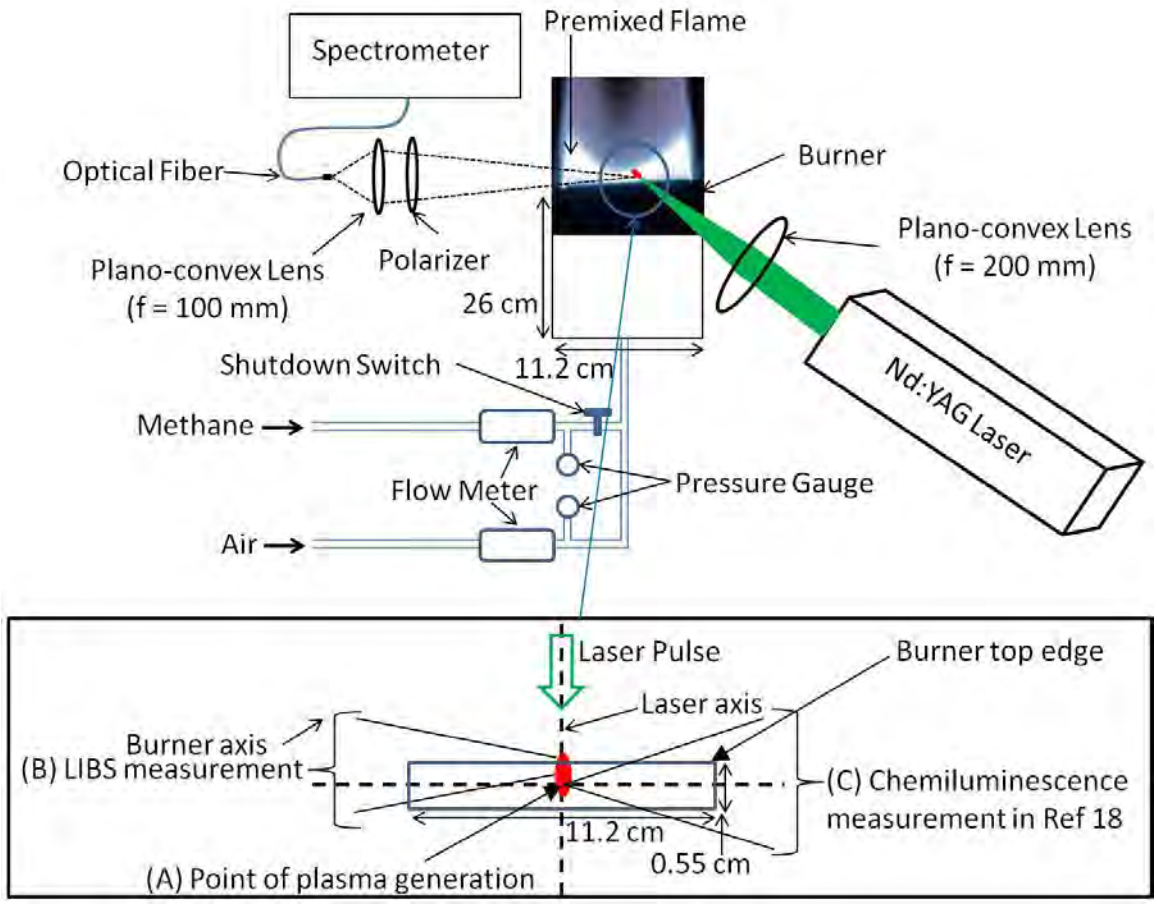


Figure T.6. *Schematic diagram of the experimental burner setup for LIBS experiments (Tripathi et al. (2013), Fuel, 106, 318-326.*

In Fig. T.7, the performances of the two most commonly used methods for suppressing the scattered laser light are compared (for ungated LIBS in combustion diagnostics) – a notch filter and a polarizer. The notch filter used in this work was a holographic SuperNotch-Plus™ filter (Kaiser Optical System, Inc.) with optical density attenuation > 6.0 and bandwidth < 10 nm at 532 nm wavelength and the polarizer was a Glan laser prism polarizer (Karl Lambrecht Corporation) with single escape window and 15 mm clear aperture. Figure T.7 shows the LIBS spectra collected from a premixed methane-air flame with both arrangements. The LIBS spectrum without both arrangements was not recorded as the elastically scattered laser light would have saturated the detector. It can be observed from Fig. T.7 that the polarizer

performed better in suppressing the laser light. Also, the LIBS spectra with the polarizer had more spectral features (specifically at shorter wavelengths) in comparison with the LIBS spectra with the notch filter. In the laser-induced plasma, the LIBS spectra were collected from a location that was ~2 mm away axially from the point of plasma generation (see inset Figure T.6). The sampling location was varied while closely watching the real-time LIBS signal and finally optimized to this value. This arrangement also helped in reducing the presence of scattered laser light.

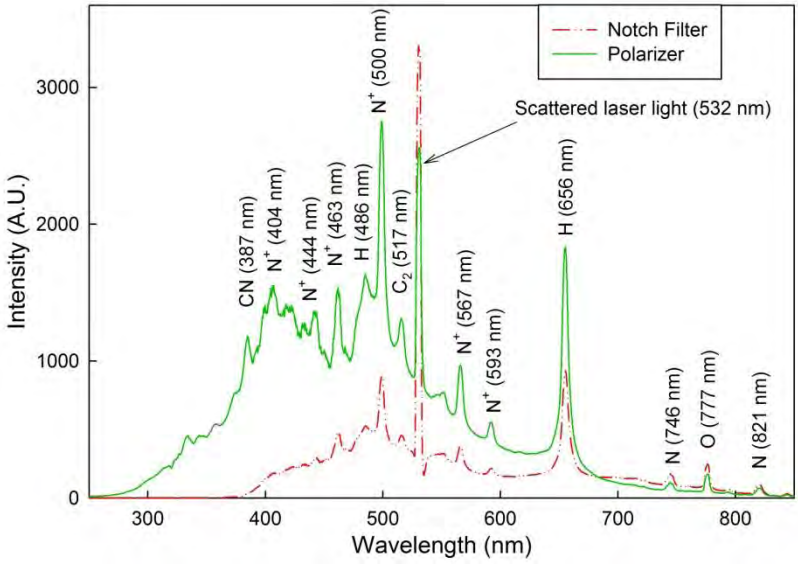


Fig. T.7. *Comparison of LIBS spectra collected from a premixed methane–air flame with a notch filter and a polarizer (Tripathi et al. (2013), Fuel, 106, 318-326.*

Measured LIBS spectra were used to develop intensity ratio calibrations for fuel-air equivalence ratios based on the $H_{656\ nm}/N^{+}_{500\ nm}$ and $H_{656\ nm}/O_{777\ nm}$ intensity ratio. Subsequently, these calibrations were tested with an unknown, independent spectral data set that was collected separately. Equivalence ratios predicted from the $H_{656\ nm}/N^{+}_{500\ nm}$, $H_{656\ nm}/O_{777\ nm}$ intensity ratio calibrations and the partial least squares regression (PLS-R)-based multivariate calibration are presented versus measured equivalence ratios in Fig. T.8. For a similar range of equivalence ratios, the prediction results from the chemiluminescence-based multivariate calibration model developed in our previously published paper (Tripathi et al. (2012), *Fuel*, *93*, 684-691) are also shown in Fig. T.8. The chemiluminescence experiments were performed on the same setup under similar experimental conditions. A detailed description of the experimental parameters for the chemiluminescence experiments can be found in Tripathi et al. (2012). It is important to mention here that although the chemiluminescence and the LIBS measurements were performed at slightly different locations (see inset Fig. T.6), the LIBS spectral data were collected from the secondary plasma that originated from the same spot where the chemiluminescence measurements were performed. Hence, the LIBS spectral data will provide spectral information pertaining to the equivalence ratio value at the same location as the chemiluminescence measurements.

Comparing the LIBS prediction results, it can be observed that the predictions from the $H_{656\ nm}/O_{777\ nm}$ intensity ratio calibration and the PLS-R based multivariate calibration are closer to the 45 degree line (indicating perfect predictions) in comparison to the $H_{656\ nm}/N^{+}_{500\ nm}$ intensity ratio calibration. However, between the $H_{656\ nm}/O_{777\ nm}$ intensity ratio calibration and

the PLS-R based multivariate calibration, one of the key advantages with the multivariate calibration is that it does not involve any intensity corrections for the overriding continuum plasma emission. Also, the oxygen line at 777 nm has a relatively low intensity (see Fig. T.7). So in a noisy environment (with low signal-to-noise ratio), predictions from the $H_{656\ nm}/O_{777\ nm}$ intensity ratio calibration may relatively more error-prone. On the other hand, the multivariate calibration incorporates more spectral information, which will improve the robustness of the calibration model even in noisy environments.

Comparing the chemiluminescence-based prediction results with the LIBS-based prediction results, it is clearly evident that the LIBS-based calibrations provide better predictions. The main reason behind this difference is that LIBS is a "point" measurement while chemiluminescence is a "line-of-sight" measurement. In LIBS, the laser pulse is tightly focused with a spot diameter of the order of a micron. Hence, the generated plasma carries spectroscopic information from a "point-like volume". On the other hand, with chemiluminescence, the spectral information from the entire line-of-sight is collected by the collection lens. Therefore, it may be argued that while performing LIBS experiments, the laser can be precisely focused in a very small control volume in the premixed zone resulting in more "local" measurements of equivalence ratios and better predictions from the developed calibration.

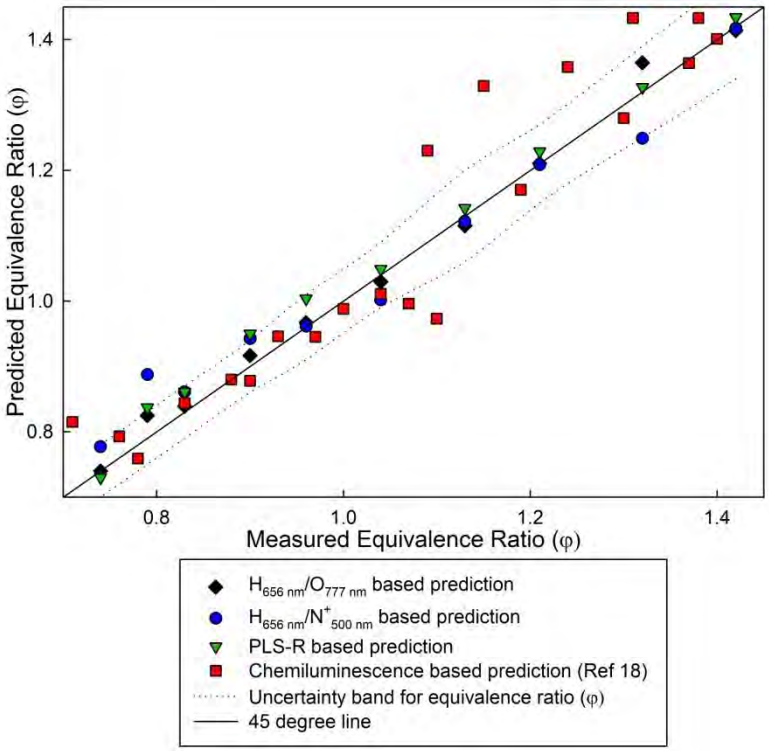


***Fig. T.8**. Prediction results from $H_{656\ nm}/N^{+}_{500\ nm}$ intensity ratio calibration, $H_{656\ nm}/O_{777\ nm}$ intensity ratio calibration, PLS-R based multivariate calibration, and chemiluminescence-based multivariate calibration (Tripathi et al. (2013), Fuel, 106, 318-326.*

4. *Ignition characteristics of dual fuel combustion for future RCEM comparisons*: To obtain baseline data for future comparisons with the RCEM experiments, ignition characteristics in diesel-ignited methane and diesel-ignited propane dual fuel combustion on the VW 1.9L

engine were quantified and carefully analyzed. Cyclic variations in ignition and ensemble-averaged ignition delay trends were characterized for different substitution levels of the gaseous fuels and for different overall and pilot-only equivalence ratios. These results were published in Polk, A.C., Gibson, C.M., Shoemaker, N.T., Srinivasan, K.K., and Krishnan, S.R. (2013). Analysis of ignition behavior in a dual fuel turbocharged direct injection engine using propane and methane as primary fuels. *Trans. ASME: Journal of Energy Resources Technology*, *135*(3), 032202, (10 pages), (doi:10.1115/1.4023482).

Explanation of Variance

As discussed above, the laser-based diagnostics equipment for performing OH-PLIF and high-speed chemiluminescence measurements were delivered in October 2013. However, the real-time ignition and combustion visualization experiments proposed in this subtask required proper functioning of the RCEM, especially stability of the 45° mirror arrangement as well as consistency between shots at identical conditions. While the RCEM had initially been sufficiently stable to obtain sample combustion pressure and piston displacement histories, shot-to-shot inconsistencies during combustion shots became increasingly problematic. Despite repeated attempts to get the RCEM working satisfactorily, the broken chain links and various other unforeseen hardware (e.g., displacement sensor inconsistencies, excessive mirror vibrations, etc.) and software issues prevented the expected commissioning of the laser diagnostics equipment. Since the RCEM was a custom-built device, we had to work closely with the RCEM manufacturer in Germany to try to resolve these issues, which were outside our control (e.g., only the RCEM manufacturer had the expertise to resolve deep hardware and software issues). Unfortunately, we were unable to resolve all outstanding issues in time to use the RCEM to perform the real-time visualization experiments. As soon as the RCEM issues are resolved, we plan to commission the OH-PLIF/chemiluminescence system in the next few months. Meanwhile, significant efforts were taken to investigate laser-induced breakdown spectroscopy (LIBS) for equivalence ratio measurements of premixed methane-air flames in a rectangular slot burner. In addition, ignition characteristics of diesel-ignited methane and propane combustion were quantified and analyzed on a multi-cylinder engine. *Finally, the RCEM and the OH-PLIF/chemiluminescence system have been leveraged to submit 7 new research grant proposals from various funding agencies including NSF, DOE, American Chemical Society, etc.* These efforts provide an effective foundation to continue our efforts in the near future to understand ignition and combustion characteristics of conventional and non-food biomass-derived fuels on the RCEM.

Subtask T.2 Quantification of particulate matter (PM) emissions from combustion of non-food biomass fuels

This task will focus on the measurement of particulate matter (PM) emissions from advanced combustion strategies with non-food biomass-derived fuels. Emphasis will be placed on detailed characterization of PM emissions using filter-paper based average smoke measurements along with particle size distributions. Although it is likely that the net PM emissions will be low for non-food biomass fuel combustion and therefore will not warrant mass-based estimation, the size and number density of PM emissions is expected to be in the sub-micron to nanometer range, and they will need to be characterized to identify possible health risks from PM emissions.

Planned Activities:

T.2.ML.1 Measure filter paper-based smoke emissions for combustion of non-food biomass fuels.

T.2.ML.2 Characterize particle size distributions in the sub-micron/nanometer range for combustion of non-food biomass fuels.

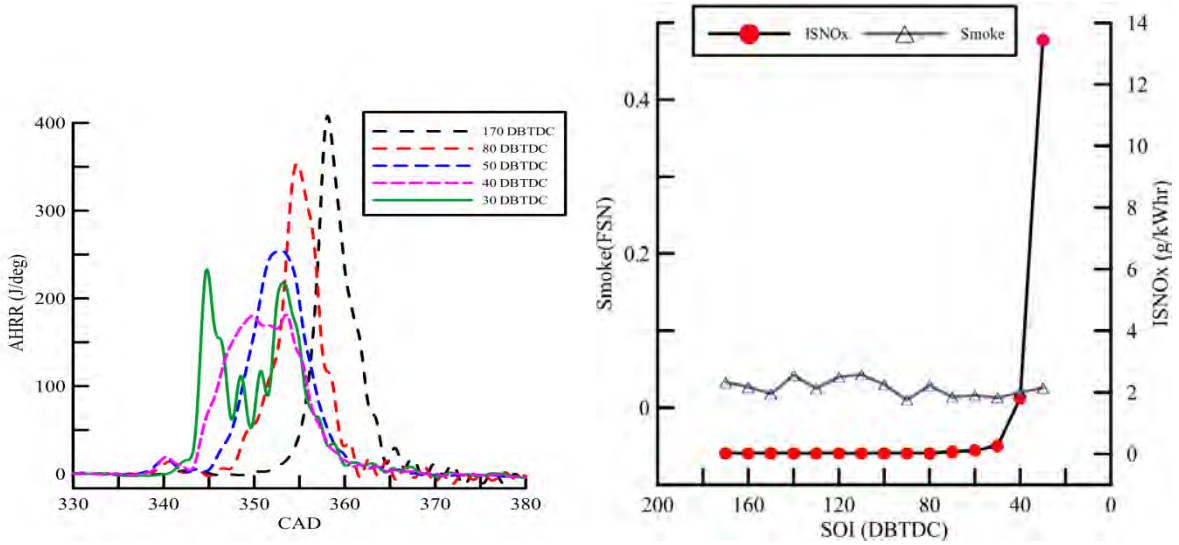
Summary of Activities for Subtask T.2:

1. *Single-cylinder research engine (SCRE) experiments*: A single-cylinder research engine (SCRE) was installed, instrumented, and commissioned in the new lab-space for the Advanced Combustion Engines (ACE) laboratory at MSU. To facilitate operation of the SCRE, an AC (motoring) dynamometer was also commissioned. A high-volume air compressor, a heatless dessicant air dryer, and an air receiver tank that were purchased and installed in the previous project phase were used to supply pressurized dry air to simulate turbocharging in the SCRE. The SCRE was operated at a constant speed of 1500 rev/min and with various conventional and alternative fuels including diesel, gasoline, methane, propane, E-85 ethanol, and a proprietary non-food biofuel manufactured by KiOR, Inc. One of the primary combustion modes investigated on the SCRE was dual fuel LTC, in which a high-cetane fuel (e.g., diesel) is directly injected into the cylinder to ignite premixed mixtures of a low-cetane fuel (e.g., methane, propane, gasoline, E-85 ethanol) and air.

   Figure T.9 (a) shows the apparent heat release rate (AHRR) profiles at different injection timings for diesel-ignited gasoline LTC. For these experiments, engine load was fixed at 5.2 bar IMEP, and gasoline percent energy substitution (PES) was maintained at 80% while diesel pilot injection timing was varied from 30 DBTDC to 170 DBTDC. Diesel injection pressure was held constant at 500 bar, intake manifold pressure was set at 1.5 bar, and no EGR was used. As SOI is advanced from 30 to 170 DBTDC, the AHRR shape changes significantly. At 30 DBTDC, fuel injection begins at 330 CAD and ends at about 340 CAD. Also there are two distinct peaks and no significant low temperature heat release (LTHR) peak. Combustion is observed to start around 341 CAD, which indicates that the separation between the end of injection (EOI) and start of combustion (SOC) is very small, about 1 CAD. As a result, the diesel spray is stratified and retains its heterogeneity. This also indicates that the diesel is injected at high enough cylinder temperatures; as a result, there are no significant low temperature reactions that would warrant LTHR. Moreover, the occurrence of two AHRR peaks suggests that the first peak is likely due to the combustion of diesel and entrained gasoline and the second peak is likely due to mixing controlled burn of the lean (phi ~ 0.23) gasoline-air mixture. As SOI is advanced to 50 DBTDC, the separation between EOI and SOC is increased to 28 CAD. The overall shape of the AHRR indicates predominantly a premixed burn. It is hypothesized that the early injection allows the injected diesel to attain a “premixed enough” state, which results in faster local burn rates while maintaining “slow enough” overall burn in the surrounding lean gasoline-air mixture as indicated by the smooth sinusoidal AHRR profile. As SOI is advanced further to 80 and 170 DBTDC, the AHRR peak magnitude increases, and is phased almost at TDC. At 170 DBTC, the separation between injection and combustion is about 155 CAD. With increasing SOI advance, the state of the injected diesel fuel transitions from “premixed enough” to “well-mixed”, leading to diesel-assisted gasoline HCCI-type combustion, which is characterized by high maximum pressure rise rates and short combustion durations. The “overmixing” also results in a loss of the “heterogeneity” required to maintain combustion control. In other words, the window of SOIs between 50 - 80 DBTDC maintain the “premixed enough” state for the low cetane diesel fuel, which is required for overall combustion control.

Trends for ISNOx and smoke emissions are shown in Fig. T.9 (b). On advancing the SOI from 30 DBTDC to 40 DBTDC, the ISNOx emissions decrease sharply from 14 g/kWhr to 2 g/kWhr and further SOI advance reduces the NOx emissions down to near-zero levels, while the smoke emissions remain unchanged throughout the SOI sweep at less than 0.1 FSN. The dramatic NOx

reduction is related to the increased residence times available for the diesel pilot to mix with the surrounding gasoline-air mixtures. This increased mixing with more advanced injection results in increasingly homogeneous in-cylinder mixtures, which in-turn results in low local temperatures, well below the thermal NOx formation threshold temperatures of ~1900 K. Consequently, the NOx emissions are reduced to near-zero levels. The simultaneous reduction of NOx and smoke emissions is an indirect proof of the occurrence of low temperature combustion (LTC) under these conditions.



(a) (b)

Figure T.9. *(a) Apparent heat release rate (AHRR) profiles and (b) Indicated-specific NOx (ISNOx) and smoke emissions for diesel-ignited gasoline LTC at various injection timings at 5.2 bar IMEP, 80 PES, N= 1500 RPM, Pin = 1.5 bar (Dwivedi et al. (2014), Trans. ASME: J. Engg. Gas Turb. Power, 136(10), 101504 (May 02, 2014), Paper No: GTP-14-1088).*

2. <u>*Particle emissions from various dual fuel LTC concepts on SCRE*</u>: After initial diesel-gasoline LTC experiments were completed, the research efforts focused on characterizing particle emissions from various dual fuel LTC strategies on the SCRE, including diesel-methane, diesel-gasoline, diesel-propane, and diesel-E85 ethanol LTC. The following paragraphs discuss sample particle emissions results from these studies.

   Kittelson (*Journal of Aerosol Science*, **29**(5-6): pp. 575-588, 1998) defined several classes of atmospheric particles arising from engine exhaust: PM10 (D_p < 10 µm), fine particles that are sometimes referred to as PM2.5 (D_p < 2.5 µm), ultrafine particles (D_p < 100 nm), and nanoparticles (D_p < 50 nm). Kittelson also characterized the so-called accumulation mode as particles in the 100-300 nm range and the nucleation mode as particles in the 5-50 nm range. Particles larger than 1µm and up to 10 µm constitute the coarse mode. The nucleation mode usually consists of volatile organic and sulfur compounds that form during exhaust dilution and cooling and also includes solid carbon and metallic particles. On the other hand, accumulation mode particles consist of carbonaceous agglomerates and associated adsorbed compounds while coarse mode particles consist of accumulation mode particles that were originally deposited on cylinder and exhaust piping surfaces and later re-entrained into the exhaust stream. Most of the particle mass exists in the accumulation mode (> 60%) but the nucleation (1-20%) and coarse (5-20%) modes also contribute to the overall PM mass. By

contrast, 90% of the particle numbers are found in the nucleation mode, i.e., nearly all of the particles emitted by diesel engines are nanoparticles.

Figure T.10 (a) shows the normalized particle number concentration $dN/dlogD_p$ versus particle diameter (D_p) for a PES sweep of diesel-methane LTC from 0 PES (pure diesel) to 90 PES of methane at 3.3 bar BMEP while maintaining P_{inj} = 500 bar, P_{in} = 1.5 bar, and SOI = 10° BTDC. It is evident that the shape of the particle concentration curve changes from clearly bimodal (both nucleation and accumulation modes) to somewhat less bimodal as PES is increased. For 0 PES, both the nucleation mode and the accumulation mode particles are substantially higher compared to higher PES conditions. *As PES is increased, the particle concentrations in both the nucleation and accumulation modes decrease. By comparison, the measured smoke trends (not shown here) indicate that the smoke emissions also decreased from about 0.49 FSN at 0 PES to about 0.09 FSN at 90 PES.* These trends may be attributed to the transition from classic mixing controlled heterogeneous diesel combustion at 0 PES to substantially more premixed combustion in the diesel-methane-air mixture at 90 PES, which suppresses both the smoke and the particle emissions at 90 PES.

Figure T.10 (b) shows $dN/dlogD_p$ trends for SOI variations from 10° BTDC to 100° BTDC for fixed P_{in} and P_{inj} at 80 PES and 3.3 bar BMEP. Since the methane PES was relatively high (80%) at all SOIs, the smoke emissions remain very low (< 0.1 FSN) for all SOIs. Also, since all other engine operating parameters except SOI are held constant, only the diesel spray penetration and mixing with the surrounding methane-air mixture are affected, and in turn, affect the local heterogeneity of the diesel-methane-air mixture. As SOI is advanced from 10° BTDC to 100° BTDC, the diesel sprays are injected into methane-air mixtures that are progressively cooler and less dense and so the ignition delays are increasingly long. Consequently, the sprays likely penetrate farther into the combustion chamber and mix more completely with the methane-air mixture. Therefore, the particle concentrations decreased with advancing SOI up to about 50° BTDC. On the other hand, as SOI is advanced to 70° BTDC and beyond, the particle concentrations are increased slightly. This may be caused by the possible impingement of the diesel sprays on the cylinder walls for very early SOIs, causing locally fuel-rich regions and higher particle concentrations (with slightly larger D_p), despite the overall smoke emissions remaining very low.

The effects of P_{in} on particle emissions for diesel-methane LTC at 3.3 bar BMEP, SOI = 50° BTDC, P_{inj} = 500 bar, and 80 PES are shown in Fig. T.10 (c). As P_{in} is increased from 1.1 bar to 1.7 bar, the overall fuel-air equivalence ratio decreases; however, the measured smoke emissions are very low (< 0.1 FSN) due to the high PES and relatively early SOI, and remain invariant with P_{in}. On the other hand, nanoparticle emissions decreased by a factor of four with increasing P_{in}. This is likely due to a combination of different factors including leaner local equivalence ratios, higher in-cylinder densities, and greater spray entrainment and mixing. All of these factors may have led to the suppression of nanoparticle emissions without an attendant increase in the accumulation mode particles. It is also possible that volatile and semi-volatile particles may have escaped the engine exhaust without condensation due to relatively higher bulk in-cylinder temperatures at higher P_{in}.

Figure T.10 (d) shows the influence of diesel injection pressure (P_{inj}) on particle emissions for diesel-methane LTC at 3.3 bar BMEP, SOI = 50° BTDC, P_{in} = 1.5 bar, and 80 PES. Again, due to the high PES, the smoke emissions are very low (< 0.1 FSN) for all P_{inj}. In general, nanoparticle concentrations decrease with increasing P_{inj} until 600 bar. This trend can be explained based on the consideration that, at the early SOI of 50° BTDC, lower P_{inj} leads to more stratified sprays, and therefore, increases the possibility of forming more nanoparticles.

On the other hand, for very high P_{inj} such as 1300 bar, the particle concentrations as well as the effective particle size increase slightly, again likely due to spray impingement on the cylinder walls.

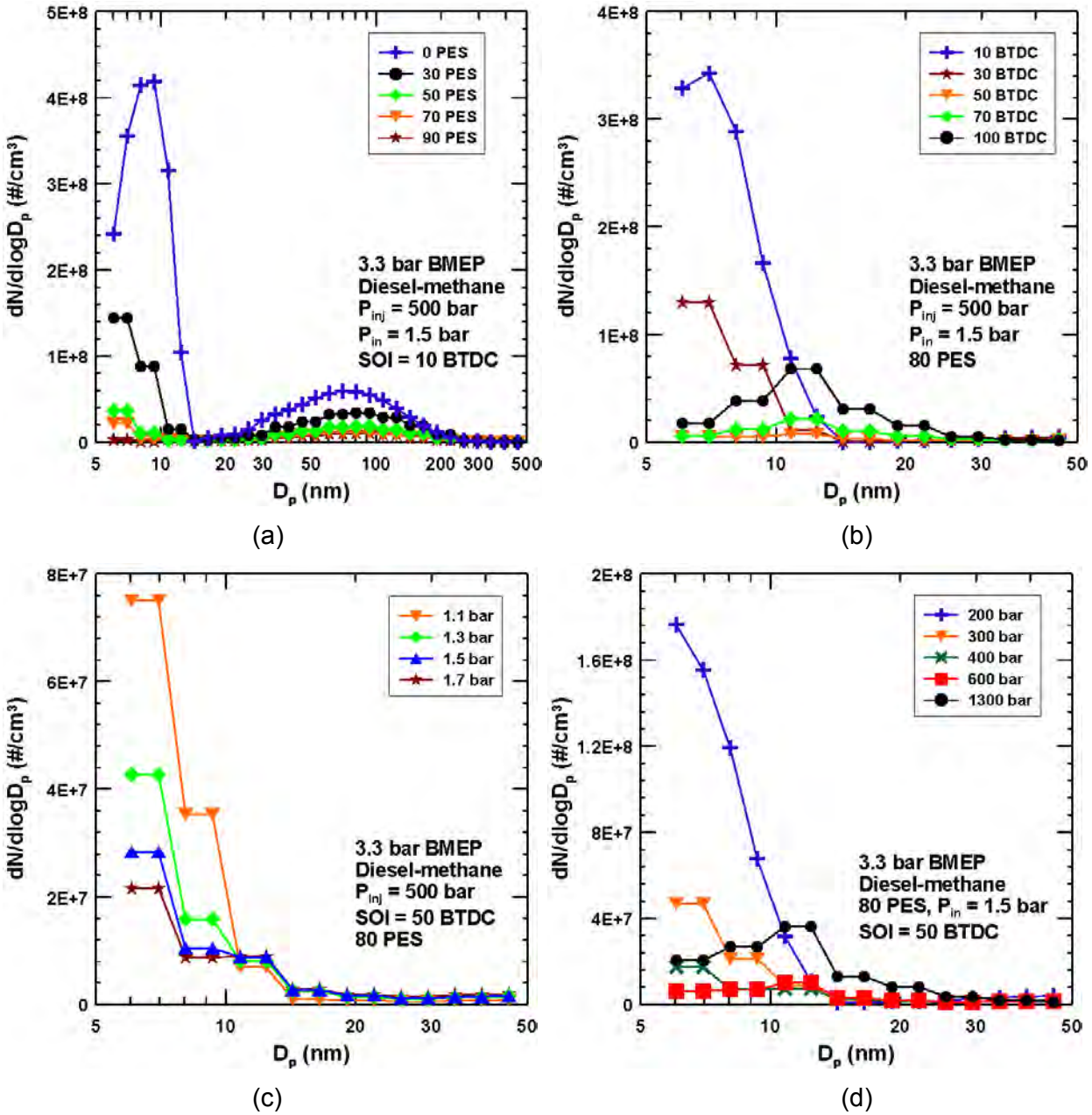


Figure T.10. *Measured normalized particle concentrations and size distributions for sweeps of (a) PES, (b) SOI, (c) P_{in}, and (d) P_{inj} for diesel-methane LTC at 3.3 bar BMEP (Krishnan et al. (2014), Characterization of particle emissions from dual fuel partially premixed low temperature combustion, presented at the 2014 Spring Technical Meeting of the Central States Section of the Combustion Institute, March 16-18, 2014, Tulsa, OK).*

Figures T.11 (a) shows dN/dlogD_p trends for a PES sweep of diesel-gasoline LTC at 3.3 bar BMEP. These results are somewhat comparable to the diesel-methane LTC results presented

above. However, there are some differences in the experimental conditions. For example, the PES sweep was performed at an SOI of 50° BTDC (compared to 10° BTDC for the diesel-methane LTC tests) to characterize the influence of PES at early SOIs. It is important to note that the PES sweep for diesel-gasoline LTC is restricted to the 50-90% range because lower PES values led to high pressure rise rates and engine knock. Nevertheless, the $dN/dlogD_p$ trends for the diesel-gasoline LTC PES sweep are similar to those for diesel-methane LTC in that the particle concentrations decrease with increasing PES. The only exception is observed in the lack of an accumulation mode, likely due to the high PES values examined for diesel-gasoline LTC. Figure T.11 (b) shows sample particle concentration results for a PES sweep from 0 to 85% for diesel-ignited E85 ethanol LTC at 5 bar BMEP, SOI = 5° BTDC, P_{inj} = 500 bar, and P_{in} = 1.5 bar. For diesel-E85 LTC, the particle concentration trends follow expectations in that they decrease with increasing PES and transition from the bi-modal (nucleation plus accumulation mode) shape at 0 PES to the virtually unimodal (only nucleation mode) shape at 85 PES.

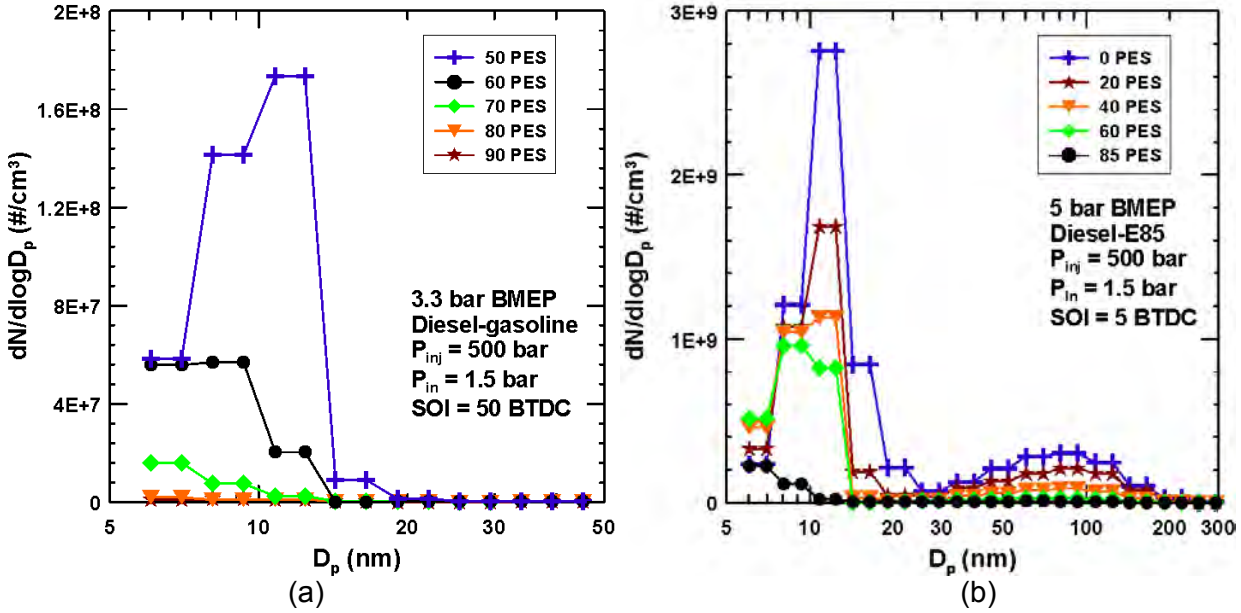


Figure T.11. *Measured normalized particle concentrations and size distributions for PES sweeps of (a) diesel-ignited gasoline LTC at 3.3 bar BMEP and 50 BTDC SOI, and (b) diesel-ignited E85 LTC at 5 bar BMEP and 5 BTDC SOI (Krishnan et al. (2014), Characterization of particle emissions from dual fuel partially premixed low temperature combustion, presented at the 2014 Spring Technical Meeting of the Central States Section of the Combustion Institute, March 16-18, 2014, Tulsa, OK).*

3. *Particle emissions from diesel-ignited propane LTC on multi-cylinder heavy-duty engine*: While the focus of Subtask T.2 was to quantify particle emissions from various LTC strategies and to investigate the combustion of non-food biomass fuels, the EEPS was also leveraged for diesel-ignited propane LTC experiments in a multi-cylinder heavy-duty diesel engine, which were performed as part of another concurrent research project funded by the Propane Education and Research Council (PERC). The results from these experiments were presented and published at the ASME 2013 Internal Combustion Engine Division Fall Technical Conference (ICEF2013) in Dearborn, MI as well as the *Transactions of the ASME:*

Journal of Engineering for Gas turbines and Power. A sample of particle emissions trends for diesel-ignited propane LTC, excerpted from Polk et al. (2014), is shown in Fig. T.12.

Smoke emissions were consistently lower than 0.1 FSN for diesel-ignited propane LTC and exhibited very little change with SOI. However, the normalized particle number concentration ($dN/dlogD_p$) plotted versus particle size changed with SOI, as shown in Fig. T.12. The most noticeable difference in size distribution was between the diesel baseline condition and the dual fuel conditions. The diesel baseline condition produced more particles in both the nucleation and accumulation mode regimes, also indicated by the relatively higher FSN of 0.26. As SOI was advanced with dual fueling, the peak particle number concentration decreased. Longer ignition delays provided more time for better fuel-air mixing and fewer fuel-rich areas, preventing initial soot formation. This change was likely not indicated by FSN trends because larger particles have a more significant effect on FSN, having a greater chance to be trapped in the filter paper, and the number of larger particles at each SOI (greater than 100 nm) varied far less than the number of smaller particles. Particles in the nucleation mode remained relatively unchanged in the dual fuel combustion mode, regardless of SOI but were significantly fewer in number than the nucleation mode particles resulting from baseline diesel combustion.

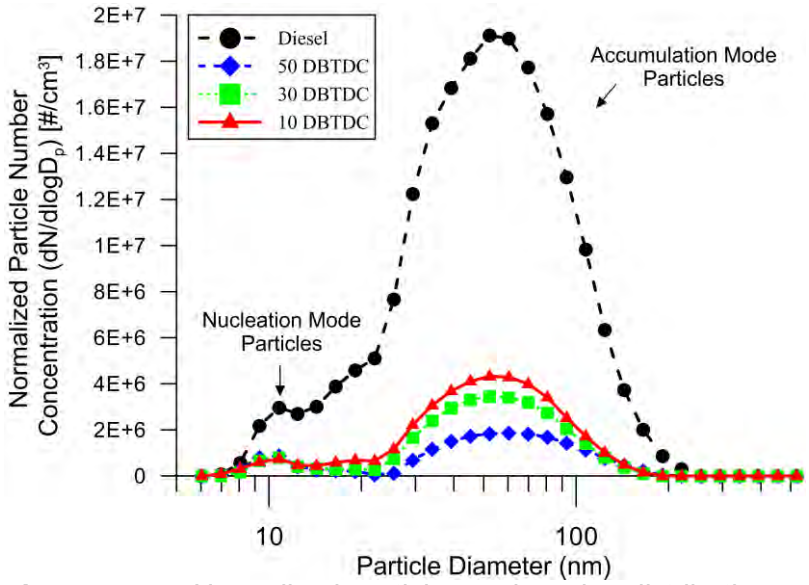


Figure T.12. *Normalized particle number size distributions at different SOIs for 84 PES of propane for diesel-propane LTC and diesel baseline on multi-cylinder heavy-duty diesel engine; BMEP = 5 bar, N = 1500 RPM, EGR = 10.6%, P_{in} = 1.88 bar, T_{in} = 20.1°C (Polk et al. (2014), Trans. ASME: J. Engg. Gas Turb. Power, 136(9), 091509 (Apr 18, 2014), Paper No: GTP-14-1085).*

4. ***Invited*** *journal article on dual fuel LTC*: The MSU PIs in the biomass combustion thrust were invited to write a journal article for a special issue of the American Society of Civil Engineers: Journal of Energy Engineering. We have contributed an article on diesel-ignited methane dual fuel LTC for the special issue titled "Combustion for Clean and Efficient Power Generation," which is currently under review.

5. *Leveraged additional state funding for non-food biomass fuel experiments*: Subsequent to experiments performed on a Volkswagen 1.9L TDI engine in the previous phase of the project, discussions were continued with a US-based renewable second-generation biofuels manufacturer (KiOR) to obtain non-food biomass fuels (in sufficiently large quantities) for testing with the multi-cylinder heavy-duty diesel engine. A separate project was leveraged from the Mississippi Development Authority in partnership with KiOR. The KiOR fuel was made available to MSU in October 2013 and preliminary engine experiments based on the ESC 13 mode test cycle were performed in the last two months of 2013. Engine performance and emissions were quantified using blends of the KiOR fuel with ultra low sulfur diesel fuel. Additionally, the effects of these fuel blends on exhaust particle emissions were also characterized using the EEPS. Since these results are proprietary, they are not included here. Additional experiments are also planned for this leveraged project in late summer 2014.

6. *Cyclic variations in dual fuel LTC*: Cyclic combustion variations in dual fuel low temperature combustion with diesel pilot ignition of natural gas were studied and these results were presented at the ASME 2012 IC Engines Division Spring Technical Conference in Torino, Italy. Subsequently, these results were also published in the *Transactions of the ASME: Journal of Energy Resources Technology* in 2013. A sample of the cyclic combustion variation results is provided in Fig. T.13, which shows maximum cylinder pressure (Pmax) versus the relative combustion phasing (Ca50-SOI) for different SOIs from 20°-60° BTDC. In addition, fuel conversion efficiency (FCE) and unburned hydrocarbon (HC) emissions are also plotted against the relative combustion phasing. This plot shows the relevance of the relative combustion phasing for dual fuel LTC. Larger magnitudes of the relative combustion phasing indicate that the injection and combustion event are significantly separated. From Fig. T.13, it is evident that the relative combustion phasing affects Pmax significantly, both across SOIs and within a given SOI. For instance, it can be seen that the magnitude of Pmax for all cycles at a given SOI tends to increase with advancing SOI up to 40° BTDC and then decrease with further advancement to 60° BTDC. It is also seen that the FCE and HC trends mirror one another; as FCE increases, HC decreases. Interestingly, they are correlated with the Pmax behavior at different relative combustion phasings. For example, the FCE increases and the HC emissions decrease as the SOI is advanced to 40° BTDC, where the Pmax values also peak. Further advancement of the SOI decreases Pmax and FCE and leads to a more modest increase in HC emissions. The HC emissions are highest for 20° BTDC, which shows high cyclic variability in the relative combustion phasing and the lowest Pmax values. It is clear that the lower Pmax and the slower combustion rates for 20° BTDC result in lower local temperatures and incomplete HC oxidation. By contrast, for 40° BTDC, the combustion rates are faster, resulting in higher FCE, higher local temperatures, lower HC, and higher Pmax. An additional fact that is evident at all SOIs is that the lower the relative combustion phasing (i.e., the closer the combustion event is to the injection event) for a given engine cycle, the higher the corresponding Pmax value. The slope of this correlation between Pmax and relative combustion phasing appears to have a direct impact on the observed FCE trends. For 60° BTDC, despite the higher average relative combustion phasing, the Pmax values are higher than for 20° BTDC, leading to higher FCE for the more advanced SOI.

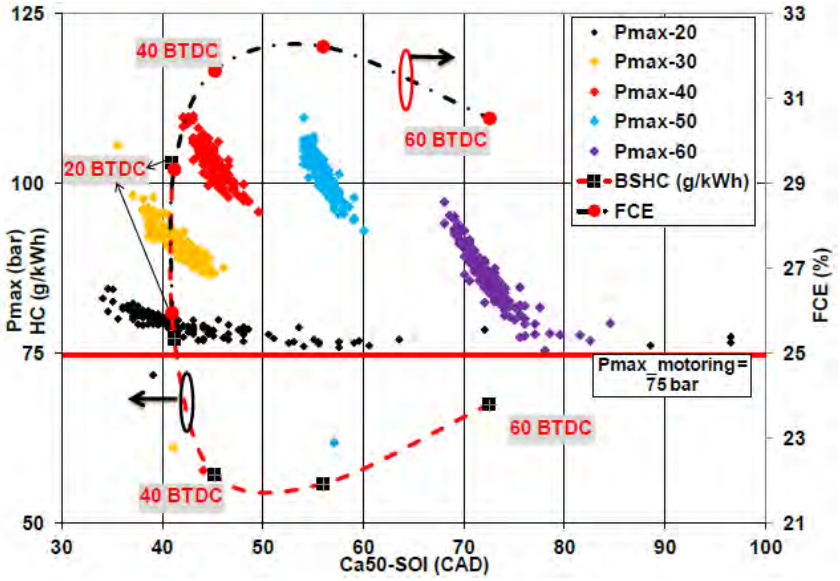


Figure T.13. *Cyclic variations in Pmax and steady-state HC and FCE vs. relative combustion phasing at different SOIs for diesel-natural gas LTC on a single-cylinder heavy-duty diesel engine; BMEP = 6 bar, N = 1700 RPM, P_{in} = 1.81 bar, T_{in} = 75°C (Srinivasan et al. (2013), Trans. ASME: J. Energy Resources Tech., 136(1), 012003 (10 pages)).*

7. *EGR setup for the SCRE*: While the dual fuel LTC experiments performed on the multi-cylinder heavy-duty engine took advantage of the built-in cooled EGR system, the SCRE experiments were somewhat limited by the absence of an EGR system. To facilitate higher efficiencies and better control of dual fuel LTC and to further reduce engine-out NOx, HC, and CO emissions, an EGR system (shown in Fig. T.14) has been designed to provide temperature-controlled EGR to the SCRE. This EGR system will have the ability to provide a wide range of EGR ratios for the SCRE at precisely controlled temperatures. Since HC and CO emissions are persisting issues with virtually all LTC strategies, the ability of the proposed EGR system to provide uncooled, partially cooled, or fully cooled EGR at various levels will provide an excellent lever to reduce HC and CO emissions in future LTC experiments. Critical components (e.g., electronically controlled valves, EGR cooler, etc.) are under order and we expect that the EGR system will be fully functional by the end of summer 2014.

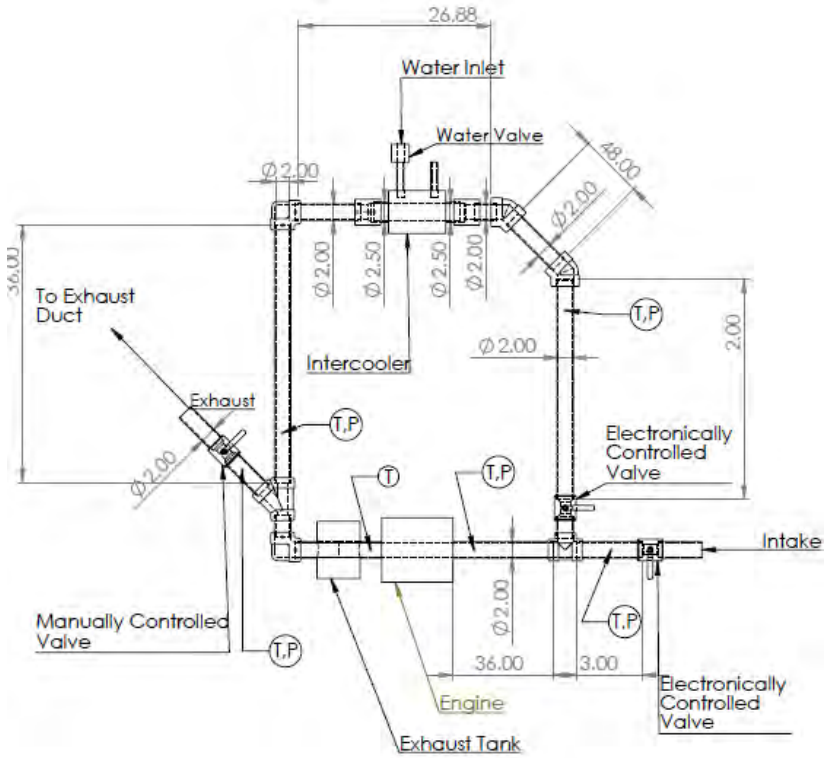


Figure T.14. *Design of temperature-controlled EGR system for SCRE.*

8. *Conventional dual fuel experiments on Volkswagen (VW) light-duty diesel engine:* The Volkswagen (VW) 1.9L 4-cylinder TDI engine was modified to operate on a variety of alternative fuels. In the previous project phase and the current phase, four alternative fuels were considered in all: biodiesel, methane, propane, and a renewable non-food biomass-derived liquid distillate fuel provided by KiOR (as discussed above). Conventional dual fuel combustion experiments were performed in an attempt to reduce exhaust emissions and improve engine performance. In these experiments, diesel or biodiesel was used as the "pilot" fuel (the ignition source) while methane or propane were used as the "main" fuel (providing most of the total fuel energy input). A journal paper based on these dual fuel experiments was published in the *Proceedings of the IMechE: Journal of Automobile Engineering*. Several additional refereed journal and conference papers have also been published from these efforts. Sample results for combustion heat release behavior and brake-specific NOx, CO, HC, and smoke emissions with varying PES for conventional diesel-methane and diesel-propane dual fuel combustion are provided in Figs. T15 through T17.

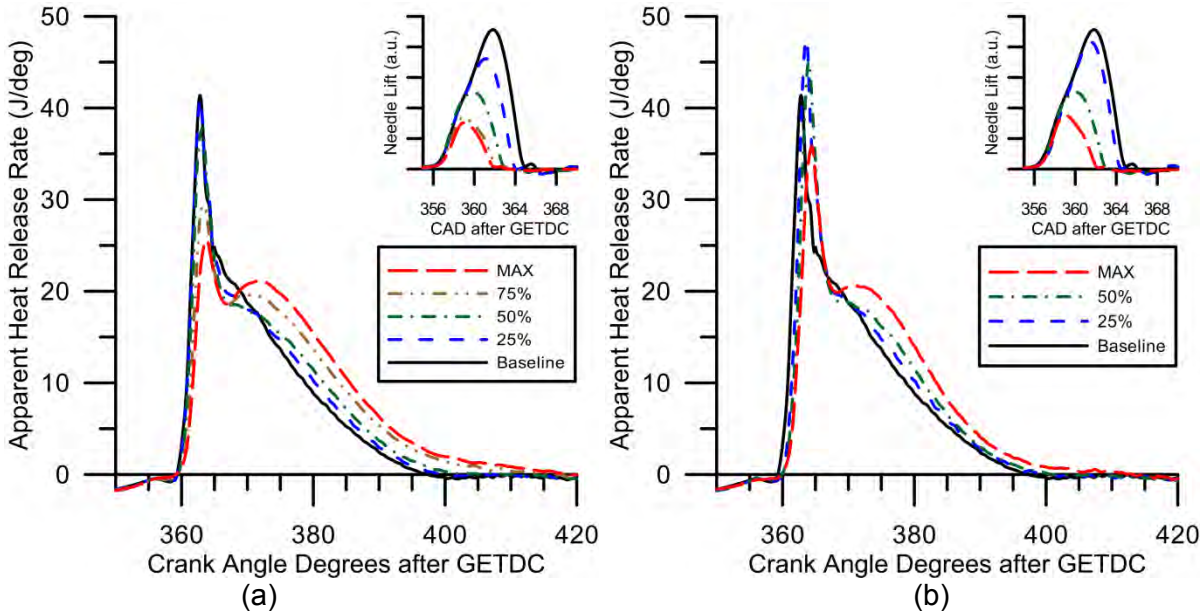


Figure T.15. *Apparent heat release rate and needle lift profiles for (a) diesel-ignited methane combustion and (b) diesel-ignited propane combustion at a fixed BMEP of 2.5 bar; the PES ranges from 0% to 83% (Polk et al. (2013), Proc. IMechE, Part D: J. Automobile Engineering, 227(9), 1255-1272).*

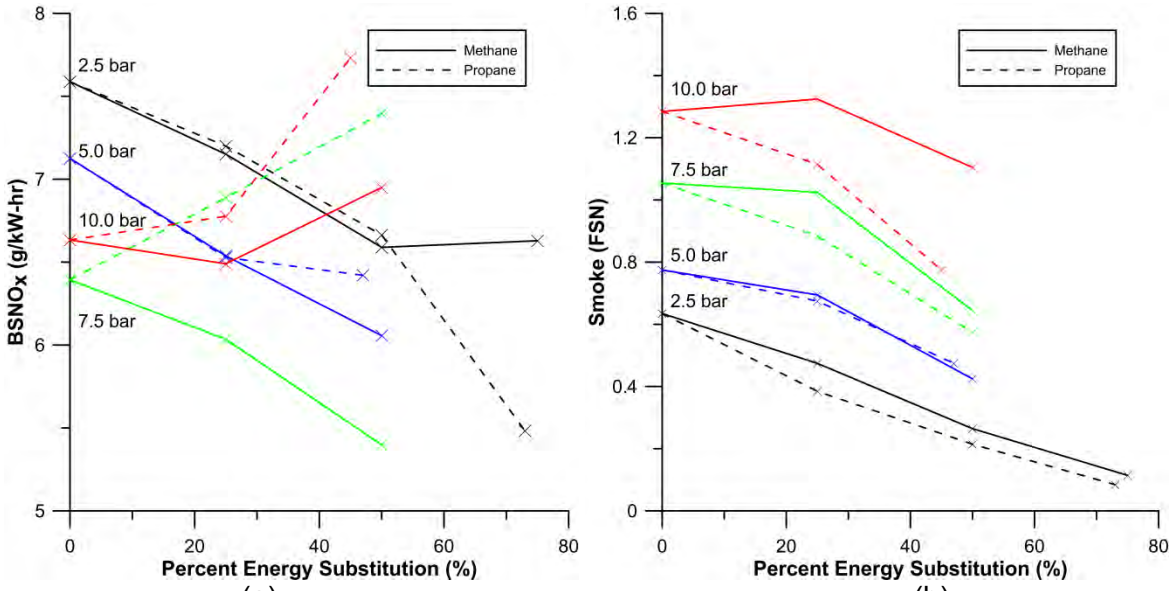


Figure T.16. *(a) $BSNO_x$ emissions and (b) smoke emissions for diesel-ignited methane combustion (solid curves) and diesel-ignited propane combustion (dashed curves) versus PES at various fixed BMEPs (Polk et al. (2013), Proc. IMechE, Part D: J. Automobile Engineering, 227(9), 1255-1272).*

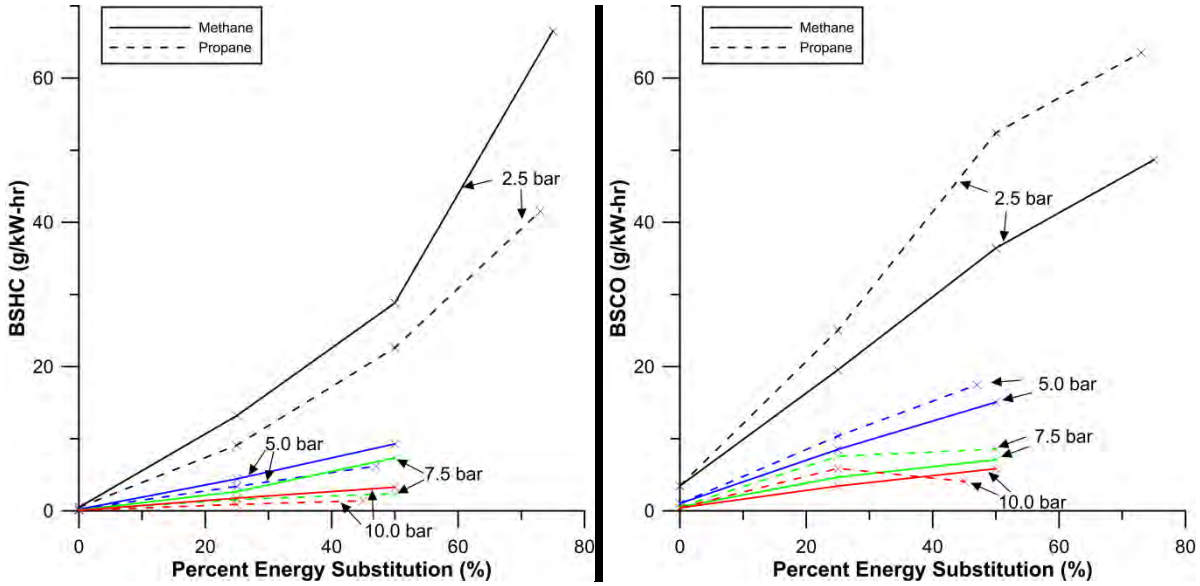


Figure T.17. *(a) Brake-specific HC emissions and (b) brake-specific CO emissions for diesel-ignited methane combustion (solid curves) and diesel-ignited propane combustion (dashed curves) versus PES at various fixed BMEPs (Polk et al. (2013), Proc. IMechE, Part D: J. Automobile Engineering, 227(9), 1255-1272).*

9. *Multi-dimensional modeling of gasoline compression ignition (GCI) combustion*: Leveraging an existing close collaboration between MSU engines researchers, an experimental engine combustion researcher from Argonne National Laboratory, and a computational engine simulation expert from Carnegie Mellon University (CMU), a computational fluid dynamics (CFD) model of gasoline compression ignition combustion in a light-duty diesel engine was developed at CMU and validated with experimental combustion data from ANL with consulting assistance provided by MSU researchers. A joint paper was authored on this topic and presented at the Proceedings of the ASME 2013 Internal Combustion Engine Division Fall Technical Conference (ICEF2013) in Dearborn, MI as well as the *Transactions of the ASME: Journal of Engineering for Gas turbines and Power.*

Task U. Biomass Feedstocks Development

Biomass feedstock that can be converted into liquid fuel has become the cornerstone of the US strategy to replace petroleum with renewable fuel. In addition to wood residue, this project focuses on grasses because of their substantial efficient productivity. Two perennial grass species have shown promise (switchgrass and giant miscanthus) of producing high yields in the southeastern US. In addition they naturally senesce at the end of the growing season making harvest using conventional haying equipment possible. Toward the closure of this research funding an additional grass (gamagrass) was investigated, due in part to its high yield potential, but also because of its fiber characteristics that are similarity to maize. Gamagrass is perennial, making it economically friendlier than corn stover in the South. I is also adapted to marginal lands.

In this project, we will conduct studies to determine yields and handling of several feedstocks that contribute to the DOE cellulosic platform. We have narrowed our focus to a limited number of grass species (in addition to woody residue) in order to assess sustainablity of these crops.

Establishment of switchgrass and giant miscanthus is critical for its acceptance by the producer. There are minimal herbicide options for control of weedy grass species during the establishment year of these species. Weed control during the establishment year directly impacts yields of subsequent fields. Challenging the sustainable production of cellulosic biomass is low cost availability of nitrogen. Grass feedstock yields are typically limited by soil N availability, yet the expense of producing N fertilizer can undermine the cost-effective production of biomass. Single, end-of-season harvest testing will be evaluated for nutrient origin and cycling. Application of biochar, a by-product of gasification and bio-oil production, has the potential to raise the soil organic matter, enhance soil structure, water holding capacity and productivity. Yet little is known about suitable application rates and how these amendments will enhance soil sustainability and crop yields. High value crops will always command the best land. To avoid competition with food cropping systems, a focus on establishment of these grasses on marginal pasture and Conservation Reserve Program (CRP) lands will be made, but herbicides to kill existing vegetation without adversely affecting the biomass crop need to be researched.

Mississippi has wood residue resources, estimated at four million dry tons, with capturable wood residues estimated at 2.1 million dry tons each year. This quantity could support the production of 131 million gallons cellulosic ethanol, but location and production are unknown. While feedstock is widely available, the cost of feedstock may not be economical to be converted into transportation fuel. Determination of handling, densification, and bottlenecks in providing biomass-based feedstocks for conversion are also necessary.

The primary objectives of this research include: 1) field establishment of candidate species and yield comparisons utilizing larger scale plots in coordinated field trials; 2) initiation of methods to determine N and C cycling within the soil-plant continuum and effect of fertilizer type and weathering on the feedstock; 3) augmentation of sustainability with the integration of winter N_2 fixing legumes into the system and assessing potential associative nitrogen fixation; 4) estimation of wood residue volumes generated from the forest products industry of Mississippi; 5) evaluation of the economics of different harvesting, densification, storage, and transportation systems in the southeastern US.

Principle Investigators and team members:

Principle Investigators: Brian Baldwin, Mike Cox, Jeremiah Davis, Janet Donaldson, Don Grebner, David Lang, Rocky Lemus, Bisoondat Macoon, Joel Paz, Prem Parajuli, Fei Yui.

Team Members: Melinda Josey, John Wes Lowe, Jesse Morrison, J. Brett Rushing, Joshua White, Prem Woli

Graduate Students: Tyler Behel, Matt Hock, Mitchell Holmberg, Omkar Joshi, Puskar Khanal, Emile Trey Koury, Jacob Mayer, Derek McCain, Marc Measells, Jonathan Richwine, Charles Robinson, Patton Slusher, J. Spencer Smith, Jayani Wewalwela,

Authorized distribution/limitations:
There are no limitations placed on the distribution of the information contained in this section of the closing report.

Executive summary:
Perennial grasses and wood are the cornerstone of cultured feedstock production for liquid fuel. Forest inventory was obtained in an earlier granting cycle. This cycle focused on obtaining was wood from urban areas and industry. Establishment of high yielding perennial grasses is critical for acceptance by the producer. Options to aid in establishment include: breeding for precocious germination and use of seed safeners that would preclude weeds from establishing, but allow desired species to germinate. Breeding in four perennial grass species has been successful as far as we have gone. Seed safening which proved to be an excellent option in switchgrass was effective for big bluestem, less effective for little bluestem and not effective for indiangrass. Studies on ethanol conversion efficiency indicate corn stover is better than switchgrass or giant miscanthus, largely due to its lower lignin content. However, tillage for the production of corn is a significant drawback. Gamagrass is being evaluated as a high-yielding perennial relative of corn with similar feedstock characteristics. The sugar (to ethanol) platform for energy is dominated by sugarcane. Starkville is well north of sugarcane production areas, as such we evaluated putative cold-hardy energycane (for biomass), and sweet sorghum (for sugar). Of the nearly 400 energycane genotypes from USDA-ARS tested, 32 survived the winter of 2013/2014. Sweet sorghum can be improved and managed for high sugar yields and production volumes. Seeding rates/plant density impacts sugar and fiber production in sweet sorghum.

Nitrogen is the largest carbon input and most costly. Grass yields are typically limited by soil N availability, yet its expense can undermine the cost-effective production of biomass. A single, end-of-season harvest was determined to be best for nitrogen-use-efficiency, but resulted in higher fiber compared to multiple intra-seasonal harvests. Microbial screening indicated switchgrass, energycane obtain significant amounts of nitrogen from an association of bacteria in the soil, but giant miscanthus was less efficient. A by-product of syngas, biochar application to soil profiles raised soil organic matter, negatively impacted mineral uptake of the seven crops tested. Positive effects may be expected from long term field studies.

High value crops will always command the best land. To avoid competition with food cropping systems, a focus on establishment of these grasses on marginal pasture and Conservation Reserve Program (CRP) lands was evaluated. Establishment trials were made with switchgrass and giant miscanthus. Greatest establishment values were possible with burn-down herbicides and early plantings in both pasture situations and CRP lands. Subsequent growth was better in pasture situations compared to CRP.

A survey on capturable wood inventory indicated there is about 280,000 tons of recoverable urban wood-waste in Mississippi. The ability to capture urban would waste as a feedstock indicate a favorable possibility, most derived by diverting material from rubbish. However, waste collection

facilities are uncertain about their willingness to supply biomass for emerging market such as bioenergy.

This quantity could support the production of 131 million gallons cellulosic ethanol, but location and production are unknown. Determination of handling, densification, and bottlenecks in providing biomass-based feedstocks for conversion is necessary.

Production of syngas from pine and oak chips provides indicated an efficiency of 13% when targeting jet-fuel range hydrocarbons. Cost of production was estimated at $3.5-5/ gallon. Critical barriers regarding the success of the pathway are 1) feedstock selection and preprocessing; 2) highly functional cleaning systems for maintaining high quality syngas; 3) development of cost-effective synthesis catalysts; 4) extensive investigation of fundamental kinetics of the complex FTS system; 5) process integration for CO2 utilization.

Biomass yield level and utilization rate affect the sustainability and eco-friendliness associated with maize stover and switchgrass as a feedstock. Conversion efficiency indicates that stover is better than switchgrass in conversion to ethanol, though switchgrass production is more ecofriendly.

Identify Products Developed/Technology transferred:

Patents:
Baldwin, B.S. 2013. Miscanthus plant named 'MSU-MFL1' *Miscanthus x giganteus*. ['Freedom'] Plant patent granted - 8 April 2013 (funds **not** from DoE)

Other Intellectual Property Developed
Baldwin, Brian S. and J. Brett Rushing. 2011. Generation of Imazapic Resistance Switchgrass Population (Expt. Desgn. LL PANVI AL IR) ['Tusca II']. Preliminary patent submitted, conversion to Plant Variety Protection underway.

Baldwin, Brian S. 2013. Selection of lowland switchgrass to enhance precocious germination (Reduced seed dormancy in lowland switchgrass) ['Expresso'].

Intellectual Property Licensed
Baldwin, Brian S. 2010. The giant miscanthus cultivar known as "MSU-MFL1 'Freedom' giant miscanthus, licensed to Sunbelt BioFuels, Soperton, GA (bought out by Repreve Renewables, Inc. Greensboro, NC).

Baldwin, Brian S. 2013. Selection of lowland switchgrass to enhance precocious germination (Reduced seed dormancy in lowland switchgrass) ['Expresso']. Licensed to: Prairie Creek LLC. Newburn, AL.

Publications/Presentations:

Peer-Reviewed Articles
Duffy, Sarah E. and Prem B. Parajuli. 2014. Simulating Soil Moisture Content Variability and Bio-energy Crop Yields Using a Hydrological Model. American Journal of Environmental Engineering, 4(3): 46-55. DOI: 10.5923/j.ajee.20140403.02.
Available at: http://article.sapub.org/10.5923.j.ajee.20140403.02.htm.

Grado, S.C., Measells, M., and D.L. Grebner. 2013. Revisiting the status, needs, and knowledge levels of Mississippi's governmental entities relative to urban forestry. *Journal of Arboriculture & Urban Forestry*, 39(4): 149-156.

Henderson, J., Roberts, S.D., Grebner, D.L, and I.A Munn. 2013. A graphical comparison of Loblolly Pine Growth and Yield Models. *Southern Journal of Applied Forestry,* 37(3): 169-176.

Joshi, O., Grebner, D.L., Hussain, A., and S.C. Grado. 2013. Landowner Knowledge and Willingness to Supply Woody Biomass for Wood-Based Bioenergy: Sample Selection Approach. *Journal of Forest Economics,* 19(2013): 97-109.

Joshi, O., Grebner, D.L., Henderson, J.E., Grado, S.C., and I.A. Munn. 2013. Input-output modeling of wood-based bioenergy industries in Mississippi. *Forest Products Journal,* 62(7/8): 528-537.

Factors influencing utilization of woody biomass from wood processing facilities in Mississippi. *Forest Products Journal*, 64(1/2): 64-71.

Joshi, O., Grebner, D.L., Munn, I.A., Hussain, A. and S.R. Gruchy. 2013. Understanding landowner preferences for woody biomass harvesting: A choice experiment-based approach. *Forest Science*, 59(5): 549-558.

Knoll, Joseph E., William F. Anderson, Edward P. Richard Jr., Joy Doran-Peterson, Brian Baldwin, Anna L. Hale, Ryan P. Viator. 2013. Harvest date effects on biomass quality and ethanol yield of new energycane (*Saccharum* hyb.) genotypes in the Southeast USA. Biomass and Bioenergy 56:147-156.

Krapfl, Kurt, J., Jeff A. Hatten, Scott D. Roberts, Brian S. Baldwin, Randall J. Rousseau, and Mark W. Shankle. 2014. Soil properties, nitrogen status and productivity of switchgrass following biochar application to a silty clay loam. J. Soil Science Soc. Am. doi:10.2136/sssaj2013.07.0304

Nepal, P., Grala, R.K., Grebner, D.L., and R. Abt. 2013. Impact of harvest-level changes on carbon accumulation and timber stumpage prices in Mississippi. *Southern Journal of Applied Forestry*, 37(3): 169-168.

Parajuli Prem B., and Duffy S. 2013. Quantifying Hydrologic and Water Quality Responses to Bioenergy Crops in Town Creek Watershed in Mississippi. Journal of Sustainable Bioenergy Systems, 3:202-208. DOI: 10.4236/jsbs.2013.33028.
Available at: http://www.scirp.org/journal/PaperInformation.aspx?PaperID=36925.

Parajuli Prem B., and Duffy S. 2013. Evaluation of Soil Organic Carbon and Soil Moisture Content from Agricultural Fields in Mississippi. Open Journal of Soil Science (OJSS), 3(2): 81-90. DOI: 10.4236/ojss.2013.32009.
Available at: http://www.scirp.org/journal/PaperInformation.aspx?PaperID=32580.

Radhakrishnan, S., Paz, J.O., Yu, F., Eksioglu, S., and D.L. Grebner. 2013. Assessment of Potential Capacity Increases at Combined Heat and Power Facilities Based on Available Corn Stover and Forest Logging Residue. *Energies*, 6(9): 4418-4428.

Rushing, J. B., B. S. Baldwin, A.G. Taylor, V.N. Owens, J.H. Fike, and K.J. Moore. 2013. Seed safening from herbicide injury in switchgrass establishment. Crop Sciences 53:(4):1650-1657 / doi: 10.2135/cropsci2013.01.0050.

Wewalwela, Jayani, J., Janet R. Donaldson, Jac J. Varco, Brian S. Baldwin, J. Brett Rushing, Mark A. Williams. 2014. Isotopic $\delta^{15}N$ evidence consistent with high rates of associative nitrogen-fixation in the root zone of three perennial feedstocks growing on marginal lands. Soil Biology and Biochemistry (under review)

White, J.A. and R. Lemus. 2014. Utilization of Annual Warm-Season Grasses as a Biofuel Source and Feedstock By-Product. Agronomy Journal (In review, AJ-14-0105).

Woli P, Paz JO. (2011). Analyzing the effect of variations in soil and management practices on the sustainability of corn stover-based bioethanol production in Mississippi. *ASABE* Paper # 1111062.

Woli P, Paz JO. (2012). Evaluation of various methods for estimating global solar radiation in the southeastern USA. *J. Appl. Meteorol. Climatol*., 51:972-985.

Woli P, Paz JO, Lang DJ, Baldwin BS, Kiniry JR. (2012). Soil and variety effects on the energy and carbon balances of switchgrass-derived ethanol. *J. Sustainable Bioenergy Syst*., 2:65-74.

Yan, Q., Yu, F., Liu, J., Street, J., Gao, J., Cai, Z., and Zhang. J. **2012**. Catalytic Conversion Wood Syngas to Synthetic Aviation Turbine Fuels over A Multifunctional Catalyst. *Bioresource Technology*, 127:281-290.

Yan, Q., Wan, C., Street, J., Yan, D., Han, J., and Yu. F. **2013**. Catalytic Removal of Oxygen from Biomass-derived Syngas. *Bioresource Technology.* 147:117–123.

Yan, Q., Lu, Y., Wan, C., Han, J., Rodriguez, J., Yin, J., Yu, F. Synthesis of Aromatic-rich Gasoline-Range Hydrocarbons from Biomass-Derived Syngas over a Pd-Promoted Fe/HZSM-5 Catalyst. **2014**. *Energy Fuels* 28, 2027–2034.

Non-Peer Reviewed Articles

Grebner, D.L., Grala, R.K., and O. Joshi. 2013. Current status of woody biomass research in the United States Mid-South. In: Book of Abstracts, Forest Biomass Conference in Mierzęcin, Poland. Sponsored by the Faculty of Forestry, Poznań University of Life Sciences, Poznań, Poland, October 6th-9th, 2013.

Lemus, R., B. Baldwin, and D. Lang. 2011. Agronomic Suitability of Bioenergy Crops in Mississippi. Mississippi State Univ. Coop. Ext. Serv. Publication 2713. (January 2012)
http://msucares.com/pubs/publications/p2713.pdf

White, J., R. Lemus, B. Rushing, B. Johnson, J.R. Saunders, D. Rivera, and P. Slusher. 2014. Mississippi Biomass Feedstock Variety Trials, 2013. IS 1363.

Presentations:

Baldwin, B.S. 2012. Factors Impacting Feedstock and Bio-based Fiber Composition. Keynote Presentation. 2012 BioEnvironmental Polymer Society Conference, Sept 18-21, 2012, Denton, TX. Oct 8

Baldwin, B.S., W. Anderson, C. Brummer, J.R. Parish, K. Gravois, L.T. Wilson, J. Blumenthal, A. Hale. 2013. Southeast regional evaluation on energycane (*Saccharum* spp) genotypes as a potential bioenergy crop. SEC Conf. Atlanta GA. 10-12 Feb. http://www.youtube.com/watch?v=nIkf8NZSzwc

Baldwin, B.S., J.B. Rushing, J.I. Morrison, K.B. Holmberg, K.D. Jones, J.L. Douglas, J.M. Grabowski. 2013. Reducing seed dormancy: The first temp in domesticating native forage grasses.In: Proceedings of the 67th Southern Pasture & Forage Crop Improvement Conference. Tyler, TX. April 22-24, 2013. P 16. http://agrilife.org/spfcic/files/2012/05/20013-Proceedings-67th-SPFCIC1.pdf

Duckworth, J. and D.J. Lang. 2012. Establishment of Miscanthus into Pasture or Conservation Reserve Land. Poster Presented at the American Society of Agronomy National Meeting, Cincinnati, OH 21-24 October, 2012 http://scisoc.confex.com/scisoc/2012am/webprogram/Paper75479.html

Gilley, M.D., Tomaso-Peterson, M., Allen, T.W., and Baldwin, B.S. 2013. Foliar disease incidence associated with giant miscanthus (*Miscanthus x giganteus*) and switchgrass (*Panicum virgatum*) cultivars in Mississippi. American Phytopathological Society Annual Meeting. Aug. 10-14.

Grebner, D.L., Grala, R.K., Henderson, J.E., and O. Joshi. 2014. An approach and framework for assessing the use of woody biomass as a bioenergy feedstock in the United States West Gulf Coast Region. Presented at: Adaptation in forest management under changing framework conditions, International Symposium of International Union of Forestry Research Organizations (IUFRO), Joint Units 4.05.00 and 3.08.00. Sopron, Hungary. May 19-23, 2014. (Invited)

Grebner, D.L., Grala, R.K., and O. Joshi. 2014. Current status of woody biomass research in the United States Mid-South. Presented at Northern Arizona University Graduate Forestry Seminar Series, Flagstaff, Arizona, January 29, 2014. (Invited)

Grala, R.K. and D.L. Grebner. 2013. Monetary value of ecosystem services provided by Mississippi's forest landowners. Presented at the Society of American Foresters National Convention, North Charleston, South Carolina, October, 2013.

Grala, R.K. and D.L. Grebner. 2013. Technical and economic availability of logging residues for bioenergy production. Presented at the Society of American Foresters National Convention, North Charleston, South Carolina, October, 2013.

Grala, R.K., Grebner, D.L., Munn, I.A., and A. Hussain. 2013. Capacity of southern mills to utilize woody residues for bioenergy production. Presented at the Southern Forest Economics Workers Annual Meeting in Auburn, Alabama, March 10-12, 2013.

Grala, R.K., Mutandwa, E., Munn, I.A., Grebner, D.L., Grado, S.C., Hussain, A., and D.R. Petrolia. 2013. Willingness to Mississippi's forest landowners to manage their forests for ecosystems services. Presented at the Southern Forest Economics Workers Annual Meeting in Auburn, Alabama, March 10-12, 2013.

Grebner, D.L., Grala, R.K., and O. Joshi. 2013. Current status of woody biomass research in the United States Mid-South. Presented at the Forest Biomass Conference in Mierzęcin, Poland. Sponsored by the Faculty of Forestry, Poznań University of Life Sciences, Poznań, Poland, October 6th-9th, 2013. (Invited)

Joshi, O., Grebner, D.L., Henderson, J.E., Grado, S.C., and I.A. Munn. 2013. Input-output modeling of wood-based bioenergy industries in Mississippi. Presented at the Southern Forest Economics Workers Annual Meeting in Auburn, Alabama, March 10-12, 2013.

Knoll, Joseph E., William F. Anderson, Edward P. Richard Jr., Joy Doran-Peterson, Brian Baldwin, Anna L. Hale, Ryan P. Viator. 2013. Harvest date effects on biomass quality and ethanol yield of new energycane (*Saccharum* hyb.) genotypes in the Southeast USA. Biomass and Bioenergy 56:147-156.

Lang, D., J. Duckworth, B. Shankle, N. Rebecca Buell-McGraw, B. Robinson, and R. Lemus. 2011. Establishment of Switchgrass on Reclaimed Coal Mine Soil. Paper Presented at National Agronomy Society of America Meeting, Oct. 18, 2011. San Antonio, Texas. http://a-c-s.confex.com/crops/2011am/webprogram/Paper65151.html

Lang, David, Barry Stewart, Richard Barnhisel and Kim Vories. 2012. Sustainable Reclamation – the 29th Annual Meeting of the American Society of Mining and Reclamation. Reclamation Matters. Spring 2012, pp. 6-18. http://www.asmr.us/Publications/ReclamationMatters/2012/ASMR_Sprring%202012.pdf

Lowe, J.W., J.D. Davis, J.L. Pursewell, and B.S. Baldwin. 2012. Effect of lignin-based binder on densification of bermudagrass through in-field cubing. Lignocellulosic Biofuels using Thermochemical Conversion Workshop. Auburn, AL. 14-15 Jun.

Morrison, J.I., R. Lemus, B. Baldwin, P. Meints and G. Munshaw. 2013. Efficacy of Seed Coatings, Chemical and Hormonal Treatments to Hasten Germination of Native Warm-Season Grasses in Mississippi. In: Proceedings of the 67th Southern Pasture & Forage Crop Improvement Conference. Tyler, TX. April 22-24, 2013. p. 27. http://agrilife.org/spfcic/files/2012/05/20013-Proceedings-67th-SPFCIC1.pdf

Morrison, Jesse I. and Brian S. Baldwin. 2012. Responsibilities with the evolution of land use: Is the bioeconomy bad for biodiversity. ORAL *3rd of 58 entries. Proc. Growing the Bioeconomy Conf: Social, Environmental and Economic Implications. Banff, AB. P 64. Oct 2-5.

Owens, V., B.S. Baldwin, D.K. Lee, and T.B. Voigt. 2013. Perennial herbaceous energy crops and CRP land for biomass production in the USA: A five year regional feedstock partnership report. 10th World Congress on Industrial Biotechnology. 16-19 June.

Smith, J. Spencer, J. Brett Rushing, Brian S. Baldwin. 2012. Herbicide safening to aid in the establishment of three native warm season grass species. Eighth Eastern Native Grass Symp. Charlottesville, VA Oct 1-4.

Steen, J.D., Grado, S.C., Munn, I.A., Measells, M.K., Hussain, A., Henderson, J.E., Grala, R.K., Grebner, D.L., and R.J. Rousseau. 2013. Factors influencing nonindustrial private forest landowner willingness to grow short-rotation woody crops for bioenergy in Mississippi. Presented at the Southern Forest Economics Workers Annual Meeting in Auburn, Alabama, March 10-12, 2013.

Task U. Biomass Feedstocks Development
PI: Brian Baldwin

General Narrative:
Biomass feedstock that can be converted into liquid fuel has become the cornerstone of the US strategy to replace petroleum with renewable fuel. In addition to wood residue, this project focuses on grasses because of their efficient productivity. Two perennial grass species have shown promise (switchgrass and giant miscanthus) of producing high yields in the southeastern US. In this project, we will conduct studies to determine yields and handling of several feedstocks that contribute to the DOE cellulosic platform. Due to the nature of agronomic practices (in the field), repeated and follow up monitoring of existing tests is required. Our focus is on a limited number of grass species (in addition to woody residue) in order to assess sustainability of these fuel sources.

Establishment of switchgrass and giant miscanthus is critical for its acceptance by the producer. There are minimal herbicide options for control of weedy grass species during the establishment year of these species. Weed control during the establishment year directly impacts yields of subsequent fields. Challenging the sustainable production of cellulosic biomass is low cost availability of N. Grass feedstock yields are typically limited by soil N availability, yet the expense of producing N fertilizer can undermine the cost-effective production of biomass. Single, end-of-season harvest testing will be evaluated for nutrient origin and cycling. Application of char, a by-product of gasification and bio-oil production, has the potential to raise the soil organic matter, enhance soil structure, water holding capacity and productivity. Yet little is known about suitable application rates and how these amendments will enhance soil sustainability and crop yields. High value crops will always command the best land. To avoid competition with food cropping systems, a focus on establishment of these grasses on marginal pasture and Conservation Reserve Program (CRP) lands will be made, but herbicides to kill existing vegetation without adversely affecting the biomass crop need to be researched. Mississippi has wood residue resources, estimated at four million dry tons, with capturable wood residues estimated at 2.1 million dry tons each year. This quantity could support the production of 131 million gallons cellulosic ethanol, but location and production are unknown. Determination of handling, densification, and bottlenecks in providing biomass-based feedstocks for conversion is necessary.

The primary objectives of this research include: 1) field establishment of candidate species and yield comparisons utilizing larger scale plots in coordinated field trials; 2) initiation of methods to determine N and C cycling within the soil-plant continuum and effect of fertilizer type and weathering on the feedstock; 3) augmentation of sustainability with the integration of winter N2 fixing legumes into the system and assessing potential associative nitrogen fixation; 4) estimation of wood residue volumes generated from the forest products industry of Mississippi; 5) evaluation of the economics of different harvesting, densification, storage, and transportation systems in the southeastern US; 5) assess the sustainability of different feedstocks for bioethanol production.

U.1 Testing, establishment of candidate species, and conversion of pasture/CRP land to candidate species

Conduct coordinated yield trials with uniform cultivars of primary grassy cellulosic crops at multiple locations around Mississippi. Assess labeled herbicides for tilled establishment and no-till establishment of switchgrass and giant miscanthus.

Planned Activities:

U.1.ML.1 Continue establishment of Uniform Variety Trials at six to eight locations around Mississippi with testing of herbicides to enhance successful establishment under both tillage and no-tillage conditions.

Baldwin/Morrison/Rushing/Smith

Safening seed, an aid to grass establishment:

Difficulties with stand establishment are a major factor limiting further agronomic use of native warm season grasses. One significant cause of stand failure is competition with rapidly growing annual weed species during the early development of the perennial native grass. Seed safening was an extremely successful experiment in switchgrass, a known bioenergy crop. Seed safening studies on three additional native grasses (indiangrass and big and little bluestem) that are candidates for biomass were undertaken. Broad spectrum preemergent herbicides can provide the needed weed control, but only if tolerance exists in the desired grass. Herbicide safeners, synthetic compounds that protect crops from herbicide injury, applied as seed treatments offer a potential strategy to achieving the needed herbicide tolerance where it does not naturally occur. This study tested the efficacy of five herbicide safeners (benoxacor, fenclorim, fluxofenin, naphthalic anhydride, and oxabetrinil) in protecting three native perennial warm season grass species (big bluestem, *Andropogon gerardii* Vitman; little bluestem, *Schizachyrium scoparium* (Michx.) Nash; indiangrass, *Sorghastrum nutans* (L.) Nash) from herbicidal injury caused by preemergent application of S-metolachlor and quantifies this establishment method's impact on early stand performance. Stands established well in 2012, but performed poorly across all treatments, including the positive control, in both trial locations in 2013. However, results were consistent across years and locations despite the overall poor performance in 2013. Given that treatment effects on stand performance were swamped by the environmental effect due to year in 2013, comparisons of stand performance between treatments were inconclusive for 2013. As such, this discussion of the impact on stand performance is based largely on the end of season data from the Starkville 2012 trial.

Indiangrass

Unsafened indiangrass plots demonstrated severe sensitivity to S-metolachlor, based on the significant differences in seedling emergence between the no herbicide positive control and the no safener with herbicide negative control. No safener treatment tested provided any degree of protection to indiangrass.

Big Bluestem

Unsafened big bluestem demonstrated a degree of tolerance to S-metolachlor, although stand density was significantly reduced as compared to the positive control plots that did not receive herbicide application. Complete protection was provided to big bluestem by fluxofenin, and partial protection was provided by all other safeners, in Starkville 2012. Fluxofenin was the only safener, though, to provide big bluestem complete protection in 2012 and protection in both 2013 trials.

The most important measure of stand performance is obviously yield. Although big bluestem was successfully safened from S-metolachlor, and S-metolachlor significantly reduced weed competition, yields were not increased in either the establishment year or the year after planting in the herbicide treated plots as compared to the untreated control plots. Therefore, no practical benefit on big bluestem early stand performance was observed from the extra work and expense involved in seed treatments and preemergent herbicide application.

Little Bluestem

Unsafened little bluestem demonstrated severe sensitivity to S-metolachlor, as indicated by significantly reduced seedling emergence between the unsafened negative (with herbicide) and

positive (no herbicide) control plots. No safener provided little bluestem complete protection, but partial protection of little bluestem was provided by fluxofenin and naphthalic anhydride in Starkville 2012.

Discussion of stand performance focused on Starkville 2012. Greater end of season crown counts and coverage ratings were observed in the positive control plots than all other plots. However, fluxofenin and naphthalic anhydride, the two safeners providing partial protection, did increase both measures compared to the negative control. Importantly, fluxofenin and naphtahlic also resulted in statistically similar yields as the positive control in the establishment year. The weed competition suffered by seedlings in the positive control plots and the reduced stand density resulting from only partial protection, therefore evened one another out with regard to establishment year yields.

The same general trend was observed in the year after planting. Coverage was significantly increased in the positive control plots and the fluxofenin treated plots compared to all others. However, the failure to increase yields again points to the conclusion that the increased costs in seed treatment and preemergent herbicide application are not practically justified in establishing little bluestem.

Baldwin/Morrison/Rushing/White

Baldwin, Morrison, and Rushing as a group assisted in data collection with White on the Uniform Varieties Trials for native perennial grasses and biomass crops. These trials were first established in 2012. The objective was to test emergence of a number of our breeding lines. Commercially available switchgrass and giant miscanthus lines were included. In an effort to include testing and speed release, available seed of the most advanced generations of each of the species have been included in the 2013 MAFES Forage Variety Testing at: Holly Springs, Starkville, Brooksville, Newton and Poplarville. Twenty-eight day emergence data is below. Our material (Expresso and the "C7" series) was compared with released varieties of the same species. All seedlots were produced at Starkville in an effort to eliminate yearly and locational effects on seed dormancy. Because of limited seed production, 'Kaw' big bluestem was only planted at two of the five test sites. Depending on test location, our material performed from twice to 7x better that their respective checks over the 28-day establishment period.

Table U1*. Field emergence of germplasm selected for rapid germination as an aid to field establishment at five Mississippi locations.*

Holly Springs (Number of field emergent seedling per linear foot of row after 28 days)							
Lowland switchgrass		Upland switchgrass		Big bluestem		Indiangrass	
Alamo	8.3	Cave-in-Rock	5.3	Kaw	4.5	Cheyenne	5.7
Expresso (MSU)	11.9	C7UPSG	14.8	C7BBS	13.1	C7IG	14.5
Starkville (Number of field emergent seedling per linear foot of row after 28 days)							
Lowland switchgrass		Upland switchgrass		Big bluestem		Indiangrass	
Alamo	9.7	Cave-in-Rock	5.1	Kaw	2.7	Cheyenne	8.3
Expresso (MSU)	20.8	C7UPSG	25.6	C7BBS	15.8	C7IG	21.3
Brooksville (Number of field emergent seedling per linear foot of row after 28 days)							

Lowland switchgrass		Upland switchgrass		Big bluestem		Indiangrass	
Alamo	3.8	Cave-in-Rock	5.9	Kaw	-	Cheyenne	6.3
Expresso (MSU)	11.4	C7UPSG	14.6	C7BBS	-	C7IG	17.1
Newton (Number of field emergent seedling per linear foot of row after 28 days)							
Lowland switchgrass		Upland switchgrass		Big bluestem		Indiangrass	
Alamo	1.7	Cave-in-Rock	1.8	Kaw	-	Cheyenne	1.8
Expresso (MSU)	5.1	C7UPSG	6.3	C7BBS	-	C7IG	15.0
Poplarville (Number of field emergent seedling per linear foot of row after 28 days)							
Lowland switchgrass		Upland switchgrass		Big bluestem		Indiangrass	
Alamo	9.8	Cave-in-Rock	7.6	Kaw	-	Cheyenne	6.8
Expresso (MSU)	18.5	C7UPSG	20.0	C7BBS	-	C7IG	19.1

In comparison of the data above (actual field establishment) with the laboratory germinations, below, it is apparent the growth chamber germinations tend to show an excessively optimistic view, however, they do indicate the level of achievement we have obtained (in most cases).

***Table U2**. Mean laboratory germination percentage of all generations of advancement*

Lowland switchgrass	Cycle	%	Upland switchgrass	%	Indiangrass	%	Big bluestem	%
	0	0.9		1.4		0.6		0.7
	1	19.1		4.0		2.7		1.4
	2	30.3		5.5		10.2		3.6
	3	31.3		6.1		12.6		9.3
	4	41.3		12.8		11.3		11.3
	5	50.7		1.1		13.5		15.1
	6	63.9		23.0		24.5		16.5
	7	78.4		56.5		28.9		21.5

Baldwin/Lemus/Morrison/ Rushing/White

Biomass Crop Variety Testing

Biomass feedstock species established in 2012, were harvested in two locations (Newton and Starkville) for yield. Biomass samples are being process for quality analysis. Yields are shown in Table U3.

Table U3. *Dry matter yields for switchgrass and giant miscanthus varieties in Starkville and Newton in 2013*

Species	**Variety**	**Location**		
		Newton	**Starkville**	**Avg.**
		lb/ac		
Switchgrass	Alamo	8,337	10,220	9,605
	Blackwell	5,235	6,733	6,973
	BoMaster	7,644	8,136	7,922
	Cave 'n' Rock	9,466	6,640	7,112
	Colony	7,745	8,260	7,682
	Kanlow	5,738	7,411	6,756
	Miami	11,304	4,606	6,255
	Performer	7,971	8,252	8,316
	Stuart	11,208	8,796	9,957
Giant Miscanthus	Freedom	16,811	17,823	17,317
	Illinois	13,143	12,420	12,782
	Nagara	14,143	14,234	14,188
Mean		9,895	9,461	9,572
$LSD_{0.05}$		5,034	3,858	3,056
CV%		31	28	22
Newton: Planted 4-25-2012 Harvested: 11-8-2013 Starkville: Planted 4-27-2012 Harvested: 10-22-2013 Newton soil type: Prentiss fine sandy loam Starkville soil type: Marietta fine sandy loam				

Giant miscanthus produced greater biomass than switchgrass at both locations. 'Freedom' giant miscanthus produced more than 'Illinois' in Starkville, but yields were similar among the three varieties in Newton. Switchgrass was more variable between locations. 'Miami' produced less than half the yield in Starkville compared with Newton. 'Alamo' was the only switchgrass variety in Starkville that preformed over the mean of the trial. In Newton, Miami and 'Stuart' were the only varieties that produced yields above the mean. However, when averaged between locations, 'Stuart' and 'Alamo' produced superior yields. Much of the variability in switchgrass yield is likely due to the rate of establishment.

Lang:

Establishment of giant miscanthus into existing pasture

Giant miscanthus *Miscanthus giganteus* cultivar Illinois was developed as a bioenergy crop. Giant miscanthus was planted into existing pasture and CRP land without tillage. Miscanthus plants were spaced on 2 meter centers into herbicide-killed vegetation, similar to planting trees by hand and may allow for miscanthus to be established into existing vegetation without tillage. Spread of miscanthus was followed over 2 to 3 years. Plots were replicated three times. Plants transferred to the field by mid-July, 2011 had 96% survival into pasture as of March 2012 and 68% survival into CRP land. Diameter of the plants increased 15 to 45 cm and to 56 cm into pasture by June, 2012. By May 2013 the diameter of giant miscanthus growing in a pasture was 77 cm and in CRP land they were 50 cm and diameter by November, 2013 was 90 cm in the pasture and 70 cm in the CRP land. Switchgrass stands were 70 to 90% as of September 2013 in CRP land and 60 to

80 established into pasture. This establishment will enable production of a bioenergy crop on marginal lands without tillage. Crabgrass (*Digitaria sanguinalis*) volunteered late in the season, between miscanthus plants and provided an opportunity to provide grazable excellent forage during miscanthus establishment and while the bioenergy conversion process of lignocellulostic crops such as giant miscanthus and switchgrass becomes economically viable. Crabgrass provided 2-3 Mg ha^{-1} and could be grazed particularly since miscanthus is unpalatable to livestock. This would provide an income stream to landowners in addition to government payments CRP and for developing crop plantings in the Bioenergy Program for Advanced Biofuels (BPAB) program. Switchgrass stands established at 76% in CRP land and 56% into pasture. This establishment will enable production of a bioenergy crop on marginal lands without tillage. Biomass yield of Illinois giant miscanthus in January was 3.6 Mg ha^{-1} in 2013 and 5.5 Mg ha^{-1}in 2014. Biomass yield of first year switchgrass was 1.6 Mg ha^{-1} in the pasture and 4.5 Mg ha^{-1} at the CRP site in January 2014. Samples of giant miscanthus, switchgrass and crabgrass were analyzed by NIRS by two equations: Bioenergy and Grass Hay. Samples were also sent to the Essig Nutrition Laboratory for ANKOM fiber and IVDMD analysis and to the Soils Laboratory for mineral analyses by Inductively Coupled Plasma (ICP). Winter weathered biomass samples harvested in January and February to reduce ASH levels are not estimated very well by NIRS. Potassium (K) is particularly underestimated by NIRS compared with ICP chemistry.

Giant miscanthus and switchgrass established into existing pasture and CRP land were harvested in January 2013 and 10 February 2014. Samples collected in 2013 and 2014 will be analyzed for energy content and various carbohydrate and lignin components to assess these as bioenergy sources. This was conducted by both wet chemistry and NIRS to contribute to the NIRS Energy Prediction Calibration equations being developed for giant miscanthus and switchgrass. Cultivars, Freedom and Illinois giant miscanthus was planted in October, 2013 into a pasture at 1 and 2 m spacing to repeat the study of following diameter expansion and assess volunteer crabgrass as grazable forage without damaging the establishment of giant miscanthus. Diameter of the giant miscanthus plants will continue to be measured.

Baldwin/Rushing/Morrison

Genetic screening of energycane

Starkville, MS at 33º latitude is roughly 250 miles north of the northern most sugarcane production areas. In 2011, 367 genotypes of energycane (a cold-hardy low sugar/high fiber relative of sugarcane) were obtained from USDA-ARS Sugar Research Center (Houma LA) and established at Starkville for cold hardiness screening. During the first two years of screening, winters were only cold enough to kill checks (true sugarcane types). Growth parameters (height and yield) have been taken during the past two years to determine genetic families with the greatest growth potential this far north. There was little indication of differences in winter hardiness. Temperatures during 2013/2014 made this past year a particularly important screening year for this germplasm. Differences in survival of this material though this past winter were evident. All but 32 of the nearly 400 individuals being screened at Starkville were killed. Slips of surviving genotypes have been lifted from the field and are being held in a greenhouse for return to the energycane breeder (Dr. Anna Hale) at USDA-ARS, Houma, LA.

Baldwin/Morrison

Testing of somaclonal variants in giant miscanthus

A project funded by Repreve Renewables, Inc. to induce genetic variation through mutagenics in the seed-sterile giant miscanthus cultivars has finished. That material was taken to the field for increase. Individual plant crowns were divided and rhizome numbers counted (an indication of growth potential). These rhizomes were used to establish two - replicated field trials to determine if any of the mutations caused marketable changes in giant miscanthus physiology that equals

greater yield. Heat tolerance, herbicide tolerance were selected for in callus culture. Also a group of general (unguided induced mutations) were produced. This work was funded by Repreve Renewables. In spring of 2014, replicated field trials in Georgia (Moultrie) and Fayetteville, NC were established. A replacement/backup nursery has been re-established at the South Farm of Mississippi State University. This grant covered the cost of field establishment and distribution of the material to Georgia and North Carolina.

Baldwin/Hock

In conjunction with Paz (Feedstocks Engineering section U.4.ML.2; maize as a feedstock) graduate student Matt Hock looked at multiple commercial hybrids and their response to a simulated frost (negative above ground biomass accumulation) at pre-determined vegetative growth stages. Commercial hybrids were planted in a randomized strip trial design with four replications. Hybrids underwent two types of biomass removal. One consisting of cutting plants off at ground level and the other burning plants with a propane torch. Plant height of all treatments (untreated control and the regrowth of the treated plots) was recorded throughout the season with total biomass recorded at the end of the season along with yield. Literature indicates the growing point of maize remains beneath the ground until approximately V5 or V6; therefore, in theory, fairly large plants should "survive" our treatments, but the question remains on how much this type of cold event influences yield. Planting early is a risk/reward scenario because hard, late freeze can occur, and that extreme cold weather severely injures small corn plants. With the occurrence of frost damage, insurance companies, seed companies, consultants, and especially producers need data to make informed decisions about replanting. Producers who consider planting early and exposing themselves to risk on the front end of the season will have replanting decision support tools available to them should they experience a damaging frost. These are the questions we hope to address with this research project. This study will be continued by other grant sources. Conclusions will be obtained at the end of the summer 2014.

Baldwin/Morrison/Richwine

Gamagrass as a feedstock for ethanol production

Gamagrass is a high yielding, low lignin native perennial grass well adapted to the South. It has the potential to provide maize-like feedstock while being planted in a no-till situation. Yields of gamagrass in the South range from 7,000 ton 21,700 lbs of dry matter per season. The main drawback is difficulties in seed production and retention. A breeding program is underway to ameliorate these short comings and will be funded by subsequent granting opportunities. Additionally, a collection of genotypes from five southeastern states has been made. Tissue samples from 370 diploid and tetraploid genotypes have been submitted for wet chemical analysis to determine which would be suitable for exploitation in the biomass arena. Wet chemistry will be used to develop a Near Infrared Spectroscopic equation to allow easier (and cheaper) evaluation of plant material from this species. Results won't be realized until after the closure of SERC IV.

Baldwin/Holmberg

Alternative nitrogen sources for switchgrass from cool season legumes

Switchgrass is the model bioenergy grass. Nitrogen inputs to maximize yield are the single costliest input. Warm, winter temperatures in the southern USA allow for fall establishment and winter growth of cool-season legumes that may provide sufficient nitrogen to a subsequent spring perenniating crop of switchgrass. Data from this two year, two location study of five cool season legumes indicated that hairy vetch seeded to fall dormant switchgrass plots provided the greatest nitrogen percentage to the subsequent switchgrass. In 2011, switchgrass fertilized with 56 kg ha-1 N had a yield that was greater than the control (no supplemental nitrogen) and in 2012 it was greater than the 28 kg ha-1 N treatment. Variation around the means prevented clear separation among other treatments, but a clear trend was that the legume crops that established provided

sufficient nitrogen to maintain a switchgrass crop in a one-cut end of season system. The data also showed the cool season legume, hairy vetch, had the greatest volunteer frequency and cover percentage throughout the year. Established switchgrass was able to maintain growth and was not smothered by the vigorous hairy vetch growth. Data from the second location (Dairy Farm) showed no differences in yields due primarily to a lack of field management the previous years (low soil pH). Only ball clover increased its coverage over time.

Baldwin/Morrison/Richwine

Insects and fungi compromise switchgrass yield

We initiated a new trial, whose data won't be realized until after the closure of SERC IV. Breeding programs have been funded under the SunGrant at University of Georgia, Athens to develop switchgrass lines resistant to fungus. In addition, there have been a number of insects discovered feeding on switchgrass at South Dakota State University. When asked about the losses due to these pests, none of the breeders can answer how much that lose is. We (Baldwin, Morrison and Richwine) initiated a test with four treatments – systemic insecticide, systemic fungicide, combination of the two, and control. These treatments were applied to two existing switchgrass fields to total eight replications in early October 2013. Additional fungicide/insecticide applications are being made during spring 2014 green-up and seasonal growth. The objective is to see if there is a switchgrass yield change due to control of these pests. The data from this project will be used to leverage additional grant submissions.

Baldwin/Morrison/Smith

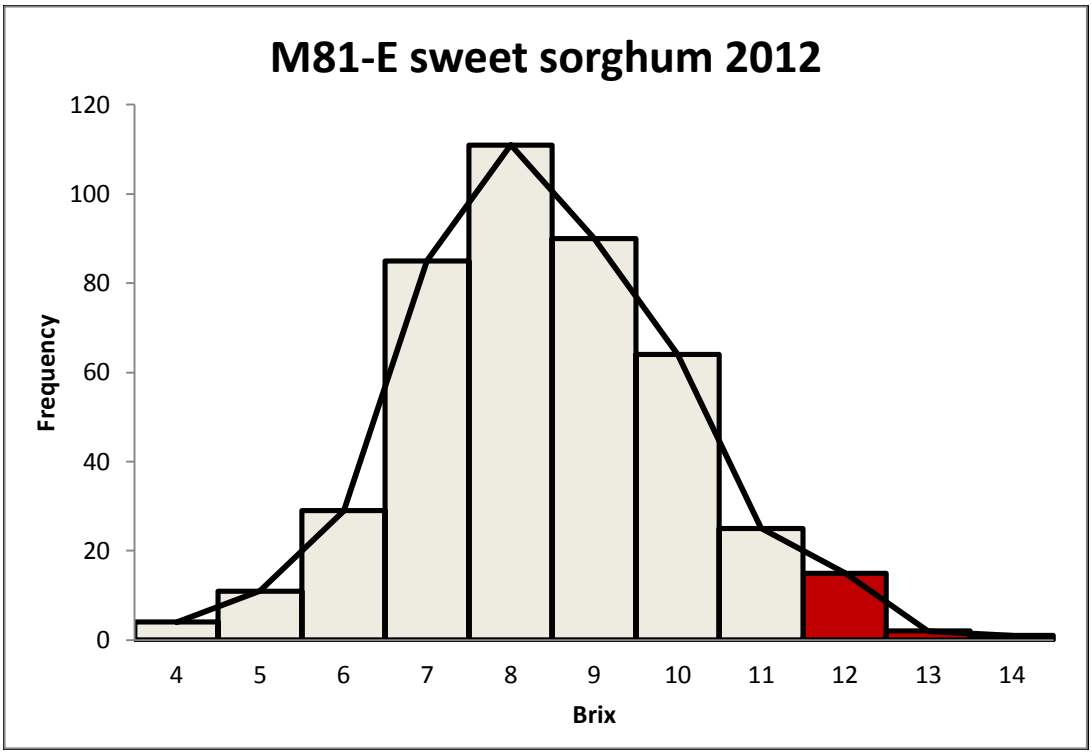
Selection for enhanced sugar production in sweet sorghum

Work to determine if we can clean up and reselect (or otherwise increase sugar accumulation) in sweet sorghum lines has indicated significant progress in selecting for higher sugar concentration in the Mississippi State/Miss. Expt. Station line M81-E. While Brix levels were extremely low due to rainfall events in 2013, there was a significant gain in sugar concentration (Brix = 3.3) compared to the unselected control (Brix = 3.1).

Sorghum population M81-E was planted on the south farm in spring of 2012. The field was divided in half. In one half of the field Brix were taken on 437 plants. The base population had a range from 4 to 14, a mean of 8.405, and a standard deviation of 1.652. Every plant with a value of 12 or higher was selected and all others removed. Of the 437 plants sampled, 18 plants were selected (4.12% of the population). The selected population had a mean of 12.2 and a standard deviation of 0.55. The selection differential was therefore 3.82, and the selection intensity was 2.31. Seed from the 18 selected plants was harvested and bulked. This seed constituted the 'select population.'

In the second half of the field no measurements or selections were made. Given that the entire field was planted at once and from the same seed lot, no difference in mean or standard deviation was expected. Seed from the second half of the field was harvested and bulked and constituted the 'general population.'

Figure U1*. Distribution of sugar concentration (Brix) in the general population of M81-E, and the selected parents pollinated for superior progeny (in red).*

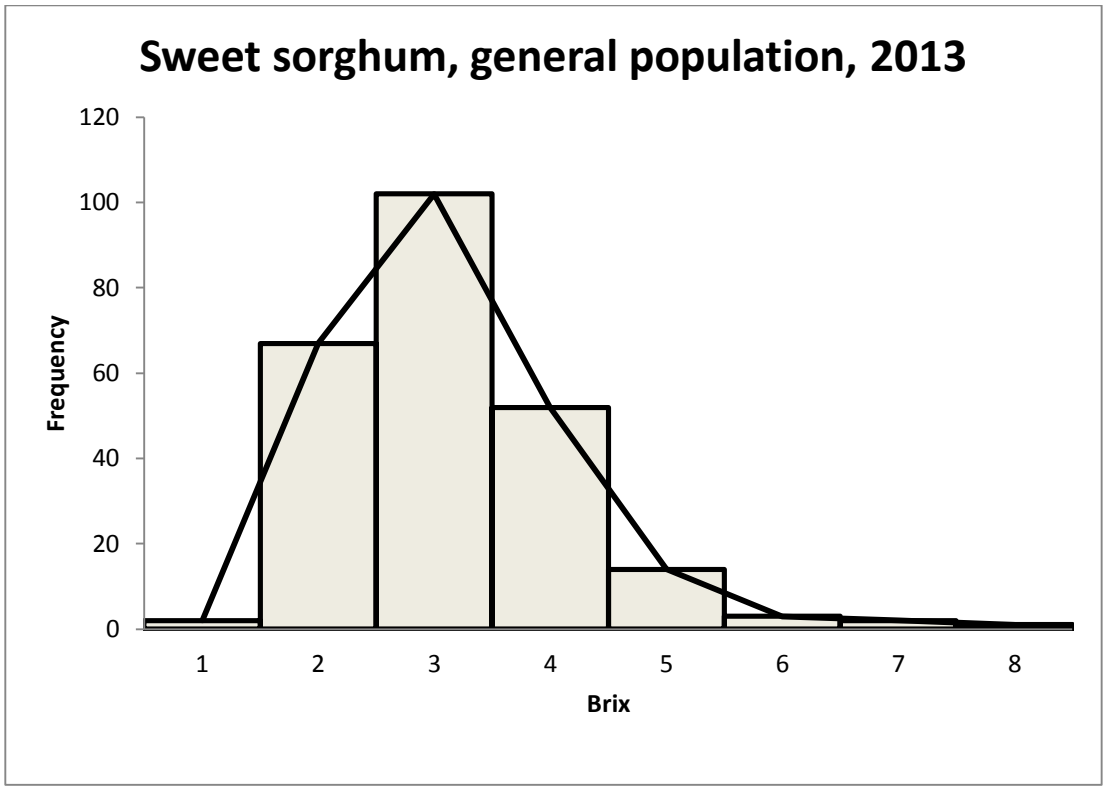


The select and general populations were both planted in the spring of 2013 in two separate fields separated by 1000 meters in order to prevent pollen flow between populations. Brix were taken on both populations. The general population had a range from 1 to 8, a mean of 3.13, and a standard deviation of 1.04. The select population had a range from 1 to 6, a mean of 3.30, and a standard deviation of 0.92. The smaller range and standard deviation of the select population was presumably due to variation eliminated during the selection process but still present in the general population.

The general population was planted to serve as an unselected control population in order to control for environmental variation of population means between years. The large difference between the mean of the base population in 2012 (8.41) and the mean of the general population in 2013 (3.13) demonstrated the need for a control population. Subsequent comparisons between populations are therefore made between the select and general populations planted in the same year and not between the select population and base population from which it was derived.

The mean of the select and general populations were statistically significantly different from one another at the alpha=0.05 level of significance. The means were separated by way of an LSD test. The select population's mean was 0.174 greater than the mean of the general population, a difference which exceeded the least significant difference of 0.168. The LSD number was relatively small in this test due to the large sample size and the subsequent large error degrees of freedom (520). The effect due to selection was also shown to be statistically significant by way of an ANOVA test at the alpha=0.05 level of significance, but with a P-value of 0.0434 which cleared the 0.05 threshold. The results of our selection were, therefore, while statistically significant, practically modest.

Figure U2*. Distribution of sugar concentration (Brix) in the general population of M81-E showing the impact of recent rain*.



Lemus/ Slusher/White

Utilization of annual warm-season grasses as biofuel sources and feedstock by-product

Annual warm-season grasses such as forage sorghum, sorghum x sudangrass hybrid and sundangrass are highly productive and valuable feed crops (rotational crop and silage). Many of these crops could also be used as possible biofuel crops. Sugar in the stems of these warm-season grasses can be extracted and fermented, while the cellulose in the bagasse (pressed stalk) can be used for feedstock or cellulosic ethanol, making these very versatile crops. Twelve annual warm-season grasses including forage sorghums, sudangrass, sorghum x sudangrass hybrid, and pearl millet were planted in 1.82 x 3.35 m plots and harvested as silage and hay before sap and after sap removal. Dry matter (DM) yield from single harvest in 2011 and 2012 were collected and analyzed (Table 4). Further analysis from the varieties includes evaluation for sap production, Brix, crude protein (CP), Neutral Detergent Fiber (NDF), and Acid Detergent Fiber (ADF). Forage quality in silage was negatively affected when first removed of sap before ensiling, producing quality similar to that of hay samples. Sugar yields (SY) were not comparable to sweet sorghum yields, but when considering SY along with bagasse yield a few varieties may offer a proper compromise as a dual purpose crop.

Table U4. *Estimated fermentable sugar yield from 12 varieties of summer annuals from harvest in 2011, 2012 and the average of those years*

		Years		
Varieties	Species	2011	2012	AVG
		kg ha^{-1} †		
Cowvittles	Sorghum	381	467	425
Forage King BMR	Sorghum/Sudan	435	253	344
GreengrazerV	Sorghum/Sudan	491	279	385

King BMR	Sudangrass	73	26	49
Monarch V	Sudangrass	93	28	61
Pace Setter	Sorghum/Sudan	417	182	299
Pace Setter BMR	Sorghum/Sudan	308	148	228
Pearl Millet FSG300	Millet	243	55	149
Piper	Sudangrass	73	8	40
Sweeter-N-Honey BMR	Sorghum/Sudan	492	133	313
Sweeter-N-Honey II	Sorghum/Sudan	589	405	497
Sweeter-N-Honey II BMR	Sorghum/Sudan	361	191	276
Mean		330	182	256
CV %		38	40	31
$LSD_{0.05}$		191	106	115

†Sugar Yield = Juice yield * Brix * 0.75

Subtask U.2 Management, nutrient cycling, and char usage

Experiments will be initiated on existing plots of feedstocks to study several very important production questions that will address questions that this research team is asked frequently by stakeholders. The experiments will follow standard agronomic field experimental methods and include:

- *determine N translocation, removal and nutrient use efficiency*
- *study the potential of associative nitrogen fixation (ANF) with feedstock species*
- *determine the N value of seeding winter annual legumes to the production system*
- *conduct preliminary greenhouse and field experiments on application of char to soil, its effect on plant production, and potential effect on soil properties*

Planned Activities:

U.2.ML.1 Provide a second year assessment of the movement of N within feedstock species, assessing feedstock species' potential of associative nitrogen fixation, determine N value of legume mediated nitrogen fixation, and obtain baseline data on appropriate char application rates.

Actual Accomplishments:

Donaldson:

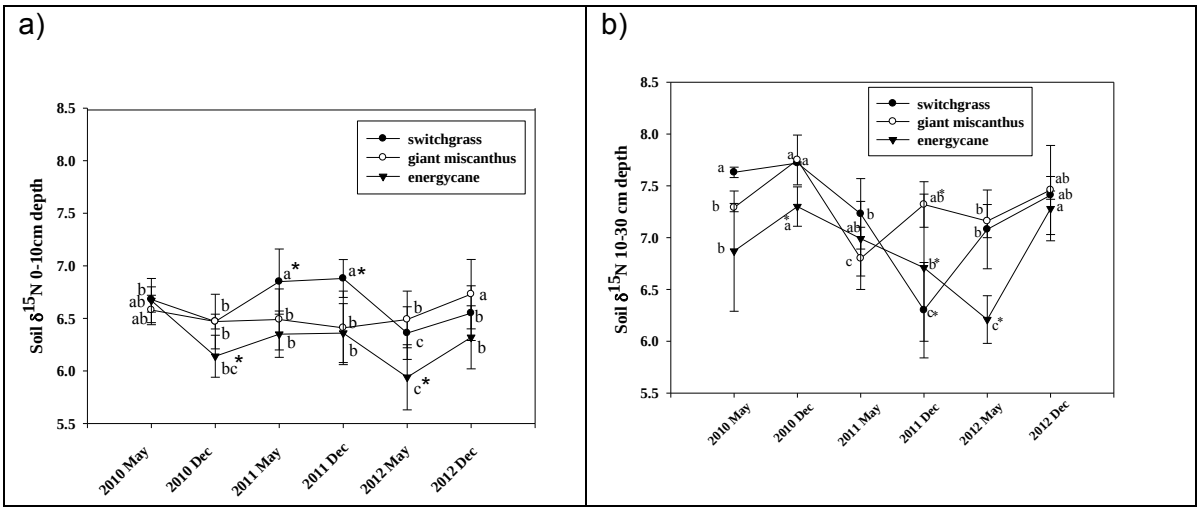
Associative nitrogen fixation

Associative nitrogen fixation is a lose association of free living nitrogen fixing bacteria in and around the root zone of a plant, allowing the plant to obtain nitrogen from the bacteria while giving up some carbohydrates to feed the bacteria. The hypothesis for this research study was that associative nitrogen fixing bacteria varied in the population composition and in their ability to support the growth of bioenergy grasses on marginal lands. The specific aims for this project were as follows:

1. Isotopic $\delta^{15}N$ evidence consistent with high rates of associative nitrogen-fixation in the root-zone of three perennial bioenergy grasses growing on marginal lands
2. Identification and characterization of putative endophytic and rhizosphere nitrogen fixing bacteria associated with three feedstock grasses
3. Quantification of biological nitrogen fixation associated with three bioenergy grasses using $^{15}N_2$ enriched soil
4. Evaluate the growth of three feedstock grasses by co-inoculation of bacteria isolated form field

We were able to assess the associative nitrogen fixation through isotopic technique as well as using molecular techniques. In previous years of the SERC funding period, we were able to collect data from a three year field study where the bioenergy grasses switchgrass, giant miscanthus, and energycane were grown. Samples from the soil, roots, shoots, and biomass were collected and analyzed for alterations in the presence of N15. Our results indicate that the three grasses were able to fix nitrogen with the addition of nitrogen fertilizers (Fig. U3). These grasses were further found to associate with nitrogen fixing bacteria (Fig. U4). This manuscript has been submitted to Soil Biology and Biochemistry we are currently editing the manuscript for resubmission to this journal.

Figure U3. *Mean soil $\delta^{15}N$ in switchgrass, giant miscanthus and energycane grown over three years in field plots of a) 0-10 cm depth, and b) 10-30 cm depth at different time points. Letters (^{a,b,c}) denote significant difference between the time points within same grass species and error bars represent standard error (n=4; P < 0.05). Asterisk (*) following the values indicate significant difference within soils of each time point of different grasses.*



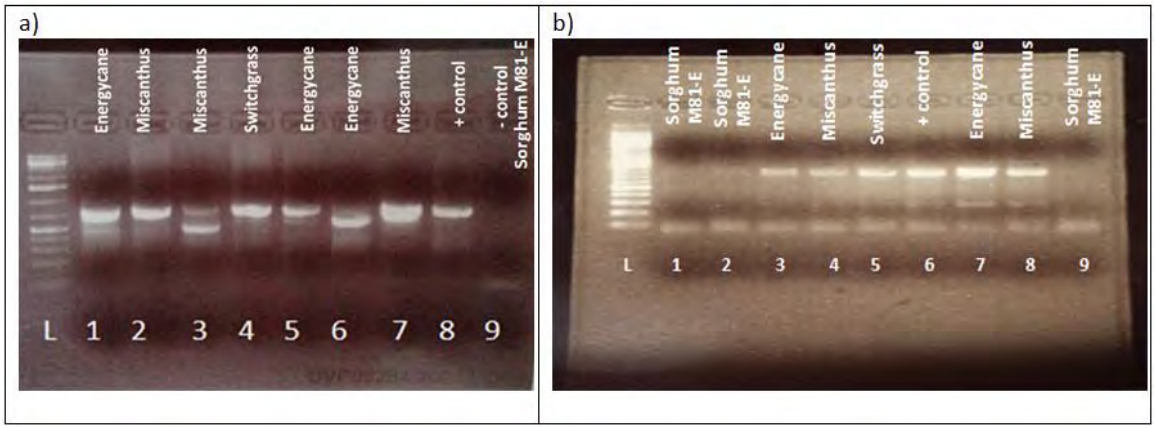


Figure U4*. The nifH genes were identified in samples associated with energycane, giant miscanthus, and switchgrass, suggesting associative nitrogen fixing bacteria were present. A) Lane L, 100 bp ladder; lane 1 rhizosphere; lane 5 root, and lane 6 root of energycane of 2012 May. Lane 2- rhizosphere, lane 3-root, lane 7-root of giant miscanthus of 2012 May. Lane 4- root of switchgrass of 2012 May. Lane 8 positive control Gluconoceobacter diazotrophicus (ATCC 49037); Lane 9-root of Sorghum of 2012 May (negative control). B) Lane L, 100bp ladder; lane 1-rhizosphere, lane 2-root; lane 9-root of Sorghum of 2012 December. Lane 2- rhizosphere, lane 7-root of energycane of 2012 December. Lane 4-rhizosphere, lane 8-root of giant miscanthus of 2012 December. Lane 5-root of switchgrass; Lane 6 G. diazotrophicus. Bands were ~600-750 bp.*

We were also able to identify and characterize putative endophytic and rhizosphere nitrogen fixing bacteria associated with Energycane, Miscanthus, and Switchgrass. From the sequencing of the *nifH* gene products from root and soil samples, we identified that variations existed between all three grasses in their bacterial populations (Table U5).

Table U5. Associative nitrogen fixing bacteria associated with rhizospheres (May 2012 samples)

	Switchgrass	Giant miscanthus	Energycane
Bacillus sp. IHB B 2269	+	+	+
Ramlibacter sp	+		
Burkholderia sp.		+	
Azospirillum lipoferum			+
Azospirillum sp. B510			+
Beijerinckia indica			+

Differential gradient gel electrophoresis was used to characterize the populations with these samples (Fig. U5). The bands were then excised and sequenced to identify the common and specific aspects for each of these communities (Fig. U6).

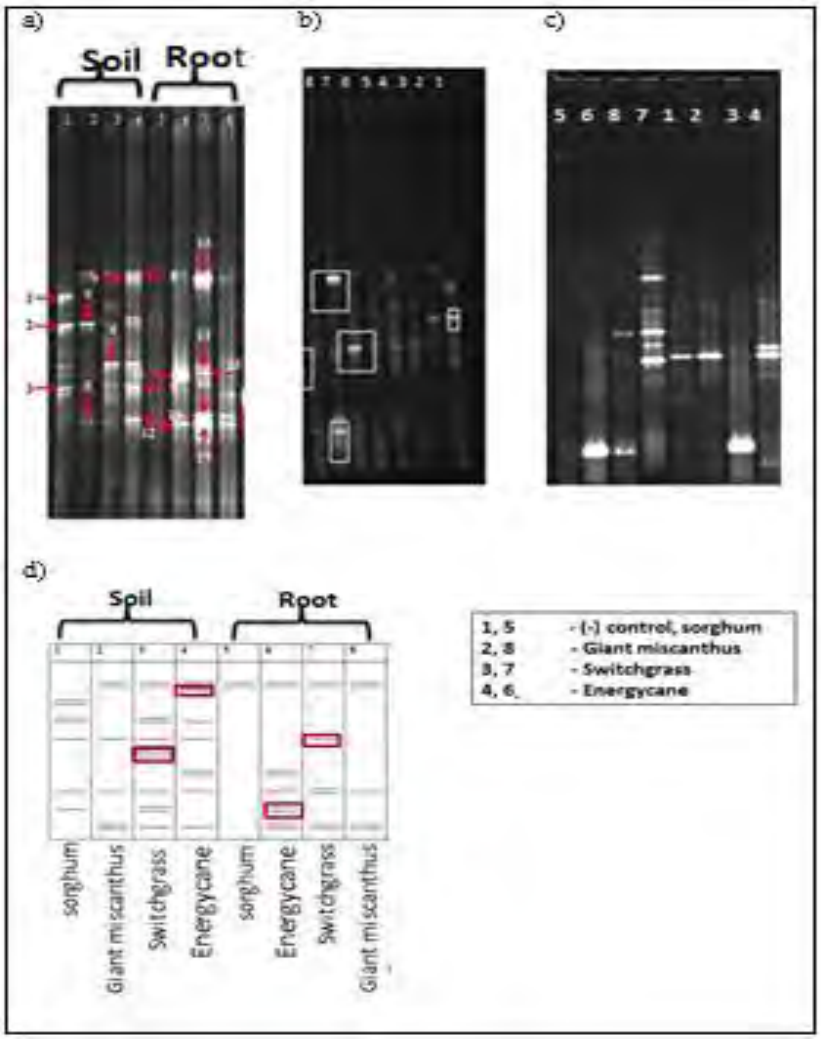


Figure U5*. Denaturing Gradient Gel Electrophoresis profiles of PCR amplified V3 region of 16S rRNA gene in bacterial DNA from three bioenergy grasses; 1-4 rhizosphere soil and 5-8 roots. Each bioenergy grass has unique banding patterns, although many energy grasses have common bands. a.) DGGE gel image of four plant type in soil and root b.) Replicate of gel a. c.) DGGE gel image of four plant type in soil and root in different plot at same area d.) Diagram of DGGE gel*

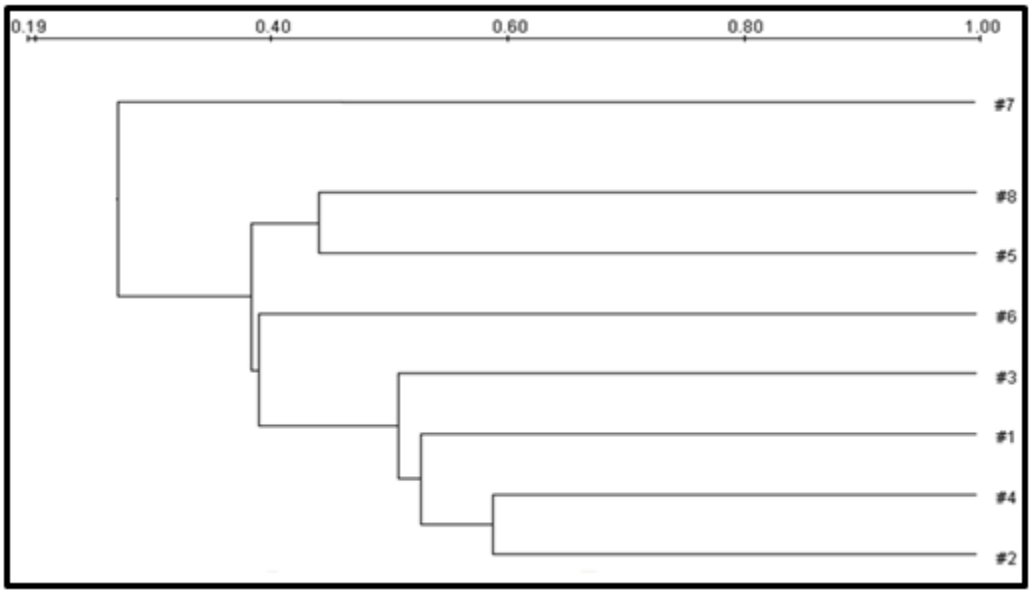


***Figure U6**. Phylogenetic analysis switchgrass, giant miscanthus and energycane along with negative control Sorghum bicolor M81-E, rhizosphere soil and root of bacterial 16S rRNA gene. Numbers indicate as follows: 1-4 were rhizosphere soil and 5-8 were roots of three bioenergy grasses. 1 and 5 were Sorghum bicolor M81-E, 2 and 8 were giant miscanthus, 3and 7 were switchgrass, 4 and 6 were energycane. The amount of similarity was reflected by the relatively closeness or grouping and was indicated by the percentage similarity coefficient bar located above each dendrogram.*

The biological nitrogen fixation was also analyzed through inoculations of ^{15}N-isotopic dilution experiments for all three energy grasses within a controlled (greenhouse) experiment. Table U6 indicates that energycane and switchgrass were able to fix nitrogen more efficiently than giant miscanthus.

***Table U6**. Percentage Ndfa of three bioenergy grasses grown in green house with $^{15}N_2$ injected and un-injected into greenhouse pots.*

Bioenergy grass species	%N fixation in un-injected plants	%N fixation in injected plants
Energycane	62 a*	28 b*
Switchgrass	44 a*	28 b*
Giant miscanthus	14 a	13 a

Our final target for this study was to inoculate the nitrogen-fixing bacteria isolated from field into greenhouse pots. We have grown the single isolated colonies in nitrogen free medium and inoculated into greenhouse grown plants. However, we have been unsuccessful in obtaining

significant results from this experiment. This may be due to an impure inoculation, isolation of a strain that is not conducive to growth outside of its "normal" microbial community, lack of phosphorous or potassium fertilizer or lack of nitrogen in soil for initial establishment. We are continuing to trouble shoot this experiment.

Cox:

Impact and use of biochar

To investigate the effects of soil application of biochar on plant growth, two greenhouse experiments were conducted. The first greenhouse experiment evaluated soil biochar application to warm season crops. Corn (*Zea mays* L.) and soybean (*Glycine max* L.) were grown on the soils where biochar application is likely to take place. On the same soils wheat (*Triticum aestivum* L.), cereal rye (*Secale cereal* L.) and alfalfa (*Medicago sativa* L.) were grown representing common cool-season forages. In both experiments a pine biochar, burned at 450˚C, and was applied at 4 rates (0, 45, 90 and 180 Mg ha^{-1}) to a Marietta fine sandy loam (fine-loamy, siliceous, active, thermic Fluvaaquentic Eutrudept) and a Houston silty clay (very fine, smectitic, thermic Oxyaquic Haplaudert). To investigate a possible nitrogen effect three nitrogen rates (0, 0.5 and 1.0X the recommended rate for each crop) were added to non-legume species. The two legume crops were inoculated upon planting. Twenty-one days after planting, plants were harvested and shoots were analyzed for nutrient uptake, forage quality and shoot dry weight. The results showed significant decreases in uptake of N, P, K, Mg, Ca and Na for both soils in corn, soybean and alfalfa at the higher rates of char. In the Marietta soil, wheat and rye showed no significant effects in nutrient uptake due to char rates, while wheat grown in the Houston soil showed significantly decreased nutrient uptake with increasing char rates. Proximate analysis showed significant increases in crude protein (CP), acid detergent fiber (ADF), neutral detergent fiber (NDF) and lignin when N fertilizer was added for corn, wheat and soybean on the Marietta soil. However, increasing char rates significantly increased ADF and NDF in wheat grown on the Houston soil. The higher char rates significantly increased shoot dry weight in wheat and soybean grown on the Marietta soil, while the same occurred in rye and soybean grown on the Houston soil

A field trial was initiated investigating the effects of biochar and poultry litter application on soil physical properties affecting skinning in sweetpotato production was started in 2012. We were asked to join this study to investigate the influence of the biochar, poultry litter, and biochar/poultry litter interaction on soil physical and chemical properties related to soil tilth. In this study, poultry litter treatments of 0 and 1.5 Mt/ha were applied as the whole plot treatment while 0, 2.2, 4.4, 6.6, and 8.8 Mt/ha of biochar (pine chip source) were applied as the split plot treatment. Both treatments were incorporated into the soil using common tillage techniques. Plot were arranged in a randomized complete block design with four replications. Sweetpotatoes (*Ipomoea batatas*) were grown and harvested using conventional techniques. After harvest, soil samples were collected 0-15cm and analyzed for total C and N, soil test extractable Ca, Mg, K, P, and Na, pH and water stable aggregation (WSA). Biochar analysis was also conducted and the material found to be primarily lignin (a very slowly reactive organic compound). Data was analyzed using an ANOVA in Proc Glimmix of SAS.

No explainable differences in any of the treatments were found for WSA, extractable Ca, K, Mg, Na or P, CEC, or pH indicating the addition of biochar or biochar and poultry litter would detrimentally change or enhance common indicators of soil fertility. Water stable aggregation ranged from 0.34 in the 0 Mt/ha biochar rate to 0.43 in the 8.8 Mt/ha rate with all rates numerically higher than the control. Values for WSA ranged from 0.33 (O Mt litter/ha) to 0.42 (1.5 Mt litter/ha). However these neither the differences due to biochar nor poultry litter were statistically significant at alpha = 0.05. Subsequent soil samplings found essentially identical results. While the influx of organic matter due to both the poultry litter and the biochar would be expected to encourage the

formation of stable soil aggregates, this result was not found in this study. The structure of the biochar provides a possible explanation for this lack of change in the WAS. The influence of organic matter to soil aggregate formation is due primarily to its degradation and the formation of new organic compounds that bind the individual soil particles (sand, silt, and clay) together. The biochar used in this study was primarily lignin which is highly resistant to breakdown in the soil. Hence, the increase in WAS due to the addition of this type of biochar may take much longer to become apparent than if fresh (unpyrolyzed) residue was added to the soil. The presence of numerically higher WSA in the amended soil may be indicative of a statistical increase in the future. Biochar application to soil may also have positive effects on soil fertility. However, this study showed no statistical increases in extractable nutrients. Unlike WSA, the addition of biochar did not result in any numerical differences either. Biochar did not affect CEC or soil pH. Biochar addition did appear to reduce total N at the 8.8 Mt/ha rate only. This is possibly due to N depression which commonly occurs when organic material with a high C:N ratio is added to the soil.

***Table U6**. Extractable soil nutrient levels after addition of five rates of biochar and two rates of poultry litter in a field test on sweetpotato. The poultry litter application did not have a significant effect, thus data was pooled.*

Rate	Ca	Mg	K	P	pH	CEC	N	C
Mt ha^{-1}	mg kg^{-1}				-	$cmol_c$ kg^{-1}	%	
0	742.2a	28.7a	91.5a	76.4a	6.4a	4.3a	0.074a	0.342a
2.2	723.8a	28.9a	90.9a	73.2a	6.4a	4.2a	0.066ab	0.358a
4.4	628.8b	28.7a	76.7a	71.9a	6.0b	3.7b	0.063ab	0.324a
6.6	771.6a	27.1a	79.7a	66.9a	6.6a	4.4a	0.063ab	0.264a
8.8	710ab	29.0a	81.6a	69.8a	6.3ab	4.1ab	0.058b	0.345a

These results are not unexpected as biochar is comprised of highly recalcitrant lignin and we expect changes to occur over longer periods of time. Soil analysis after sweetpotato harvest in the fall and before planting in the spring of 2014 have been completed and no differences in soil properties were found. As mentioned before, we expect any differences in soil chemistry to occur slowly over a much longer time period.

Baldwin/Lemus

Carbon Sequestration

Core samples collected across different warm-season grasses were processed for bulk density, nitrogen and carbon content. Core samples ready for are being process for N and C content. Equipment was recently purchased to conduct the C:N ratios. Bulk density was influence by soil type as also by the length the native grasses have been established. Older stands (Cycle 7) had higher root mass and lower bulk density. Miscanthus had lower bulk density when compared to energycane and/or switchgrass across the same locations.

Lemus/Slusher/White

Physiological responses of sweet sorghum cultivars to seeding rates

The study was conducted at the Henry H. Leveck Research Farm at Mississippi State University. The soil is a Marietta soil (Fine-loamy, siliceous, active, thermic Fluvaquentic Eutrudepts). The experimental design was a strip-plot and replicated three times. The main plots were varieties,

while subplots were seeding rate. The study included eight sweet sorghum varieties (Dale, Della, KN Morris Cane Seed, M81-E, Simon, Sugardrip, Theis and Top 76-6) (Table 1). Varieties were planted in a 6'x 20' plot at two seeding rates (5 and 10 lb/ac). All plots were fertilized with 50 lb N/ac (33-0-0) when plants reached 3-5". Brix was measure at harvest. Biomass subsamples were collected for dry matter determination. Samples were dried a forced-air oven at 110 °F for 3-5 days and ground to pass a 2-mm screen and analyzed for forage quality [crude protein (CP), acid detergent fiber (ADF), nutrient detergent fiber (NDF), ash, and water soluble content (WSC) using the hay equation from the NIRS Feed Consortium. The original 1996 NIRS machine started to fail with wavelength deterioration. The replacement has just arrived. We await the Foss representative to assemble components and load equations/software. Data will be analyzed using NIRS and characteristics will be assessed via PROC GLIMMIX of SAS and means separated using Least Significant Differences (LSD) at α=0.05.

Macoon:

Nitrogen and biomass yield

At the Raymond, MS location, completion of fieldwork, laboratory analyses, data analyses, and preparation of manuscripts for three experiments were the main accomplishments during the year. Experiment 1 evaluated harvest frequency and N fertilizer effects on biomass yield, nutrient removal, soil carbon accumulation, and plant persistence of Alamo switchgrass initiated during SERC II and continued during Phase III. Treatments were two rates of N fertilizer application (80 or 160 kg N ha^{-1}) and defoliation frequencies of 1, 2, 3, or 6 harvests per year (first harvest started in June each year and plots were harvested every 1, 2, or 3 months or a single end-of-season harvest). Experiment 2 was conducted during Phases III – IV evaluating yield and chemical composition responses of four cultivars of switchgrass to four levels of N fertilizer application. Experiment 3 initiated during late Phase III and continued into Phase IV quantified physiological changes in switchgrass plants throughout the seasonal cycle in response to N fertilizer at different levels. Treatments were all factorial combinations of four N application rates (0, 40, 80 and 120 kg ha^{-1}) and six monthly harvest times (May to October) in a RCBD with treatments allocated in a split-plot arrangement.

Results for Experiment 1 indicate that less frequent annual harvests resulted in greater yields with lesser nutrient concentration, resulting from the greater potential for nutrient translocation, and therefore may require less agronomic inputs. A single post-frost kill harvest resulted in reduced tissue N, P, and K concentrations. Nitrogen removal responded to both harvest frequency and N application rate while P, K, Ca, and Mg removal differences were due more to harvest frequency than N application rate. Increased harvest frequency changed the plant physiology and phenology and increased the nutrient removal capacities from multiple harvest systems. In addition, less annual harvests resulted in increased cell wall constituents concentration, thus improving feedstock quality factors. Generally, the feedstock quality increased with switchgrass maturity.

In Experiment 2, biomass production and nutrient removal was affected by both cultivar and N rate. Nutrient removal was driven primarily by biomass yield that was, in turn, dependent on cultivar-inherent biomass production capacities and their response to N rather than tissue nutrient concentration. Nitrogen use efficiency and apparent nitrogen recovery decreased with increased N application. Application rates above 80 kg N ha^{-1} reduced N use efficiency and apparent nitrogen recovery and are likely to result in increased N leaching and volatilization. Biomass production, nutrient removal, N use efficiency and apparent nitrogen recovery for Cave-in-Rock were less than Alamo and the two experimental lines derived from Alamo. Coupled with soil chemical characteristics, nutrient removal rates can be used to develop cultivar-specific fertility recommendations. Although compositional differences exist among entries, nitrogen application

had no effect on cell wall properties and several sugars. The differences in yield had greater importance than the differences in biomass quality. Ethanol yield was more dependent on the biomass yield rather than the small differences in compositional traits among the entries. A manuscript reporting the results of this study is currently being revised based on internal review.

In Experiment 3, in the total aboveground biomass, stem, and leaves, concentrations of the chemical constituents of fiber, namely, acid detergent fiber, neutral detergent fiber, lignin, cellulose and hemicellulose increased from the May to October harvest time in both years. Fiber concentration of aftermath, on the other hand, decreased from May to August harvest time with stems components accumulating greater fiber concentrations than leaf. Crude protein and in vitro dry matter digestibility decreased with plant maturity and were greatest in the leaf component. Similar to fiber concentration, the concentrations of major sugars increased with maturity and were greatest in the most mature stand in the aftermath. Total ethanol yield was greatest in the least mature stands, however, total ethanol production increased with maturity and is largely a result of biomass yield. Nitrogen fertilizer application rate did not influence the forage nutritive value or feedstock composition in either the primary or aftermath harvests. These results indicate that a two-harvest system (early season and end-of-season) has potential for both forage and feedstock use, however, dual use will depend on the economics of forage vs. feedstock use. A manuscript from this work is currently undergoing internal review.

Subtask U.3 Wood residue assessments

A survey instrument will be developed and assessed using on-site surveys preceded by an introductory letter and copy of the survey to prepare participant mills. Using a list of primary and secondary wood manufacturing facilities in Mississippi, interviews will be conducted to collect the necessary mill wood residue data. Descriptive statistics will be developed and derived data will be used to re-calibrate the previous work by Perez-Verdin et al. (2009).

Planned Activities:
Milestone:
U.3.ML.1 Develop a survey and data regarding recoverable wood residue for bioenergy conversion.

Actual Accomplishments:

Grebner:
Urban and rural wood recovery and usage
Urban wood waste is characterized as available volume of wood waste in commercial, industrial and municipal waste landfill sites or processing facilities including: wooden pallets and shipping containers, wood volumes in the form of construction and demolition debris, railroad ties, given away or disposed volumes of logging residues and wood products from primary and secondary mill processing facilities (Fehrs et al. 1999). Forest industry generates large amount of industrial bi-products, which approximately account one-tenth of all waste generated in North America (Falk and McKeever 2012, USEPA 2009, NRCan 2006). Nearly half of the 280 million metric tonnes of wood resource harvested in the United States have been used as industrial material, a significant proportion of which finally gets discarded as manufacturing waste or disposal products (Falk 1997). Falk and McKeever (2012) revealed that 70.6 million tons of urban wood wastes were generated in year 2010 in United States. Out of this, 48 percent was contributed by municipal solid waste (MSW) and 52 percent was contributed by construction and demolition debris. This signifies that a substantial proportion of our industrial raw material and many products contain wood fiber that is recoverable.

MSW includes both biological and non-biological waste items such as: product packaging, glass, plastics, food, bottles, and wood materials (EPA 2010, McKeever 2004), of which biological materials constitute a substantial share (EPA 2010). Recent estimates suggest that there were about 250 million tons of MSW generated in United States in 2010 (Falk and Mckeever 2012). About 14 percent of the MSW contained wood component, which include discarded waste from secondary wood products such as: furniture, pallets and wooden panels among others (Falk and McKeever 2012). About11.2 million dry tons of MSW wood waste was available for recovery in United States (Falk and Mckeever 2012).

Construction and demolition wastes are another major source of wood waste in the United States. While both construction and demolition wastes are given away together, they originate from different sources (Falk and McKeever 2012, Perlack et al. 2005). For instance, construction waste are obtained from the construction, repair and remodeling of residential and nonresidential structures. Therefore, construction waste is relatively clean and has higher recovery rate (Perlack et al. 2005). Given that demolition waste is contaminated with paints, fasteners, adhesives, and other dirt, its separation can be time-consuming and costly in the landfill sites (McKeever 2004). These factors make recovery from demolition relatively difficult than from construction wastes (McKeever 2004, Folk 1997). In addition, factors such as type and location of facility, and the age of the demolished product also have some role in wood-waste recovery (McKeever 2004).

Urban wood waste has the potential to become an important reusable resource though it has long been regarded as a cumbersome disposal problem (Minnesota DNR 1993). For example, urban wood waste is an inexpensive but underutilized feedstock in wood-based bioenergy. In billion ton vision document, U.S. Department of Energy (2011) estimated potentially available urban wood-waste for bioenergy use in United States. About 32 million dry tons of feedstock is potentially available for bioenergy from urban wood waste, 75 percent of which was available at $20 per ton (U.S. Department of Energy, 2011). Of importance, given the population growth, more recoverable wood waste volumes were expected in the future and the rate was estimated to be one half of the population growth (Department of Energy, 2011). MacFarlane (2009) also reported that currently underutilized dead urban trees are available for bioenergy use in Michigan.

Nzokou (2009) estimated recoverable volumes of urban wood waste in southern Michigan and found that 84 percent of total wood yard volumes came from large yards. While recoverable wood waste contributions were mostly from large facilities, small facilities having four to five employees on average were deemed flexible in producing diverse product line in the state of Michigan (Nzokou 2009). In a related note, Falk (1997) cited various factors such as: type and available volumes of wood waste, cost of sorting and cleaning, and the cost of alternative raw materials available in market being the primary factors affecting recoverability in waste processing facilities.

Recovery rate varies widely for different urban wood waste sources. For instance, almost all of waste coming from primary timber processing industry is recovered due to relative cleanliness in such woody residues. As explained earlier, recoverable volumes of demolition debris, which largely depend upon factors such as: type, location, and age of the demolished structure, are small and even difficult to estimate (McKeever 2004). McKeever and Falk (2012) reported that about 48 percent of the total construction and demolition wood waste were available for recovery. Similarly, total available volumes for recovery in case of municipal wood waste were approximately 33 percent (McKeever and Falk 2012). Research also suggests that there are regional variations in the rate of wood waste recovery as well. For example, Camas Creek Enterprises (2009) found that 45 percent of the wood wastes in waste disposal sites were processed in Kansas. In contrast, average conversion rate was 30 percent in the state of

Michigan. Inefficient sorting mechanism was cited as a primary reason for very small wood waste recovery rate (Nzokou 2009). Staley and Barlaz (2009) also found significant variations in the amount of collected waste volumes and recovery rate within various regions in the United States. While all disposed MSW in the Delaware and Kanas were landfilled, the rate of disposal was only 60% in Minnesota (Staley and Barlaz 2009). Given such variations in recovery rates, one size fits all formula might not work to estimate recoverable urban wood waste. Therefore, research in smaller geographical extent is important.

The State of Mississippi has abundant forest resources and proper waste management could provide an opportunity to generate energy from these sources. Perez-Verdin et al. (2009) estimated annual availability of approximately 4.0 million dry tons of woody biomass in Mississippi and Seven percent of it was obtained from urban wood waste sources. While this study provided general information on recoverable urban waste, these estimates utilized secondary data sources, conducted in other states, for generating recoverable waste and used published recovery percentages for different product classes. As Kittler and Beauvais (2010) cautioned, recoverability of urban wood waste varies by product types and region. Therefore, accurate estimates are difficult obtain without having a region specific study. Moreover, conversion of urban wood waste volumes to a viable product such as bioenergy is a considerable financial investment and hence requires careful consideration for reliable availability of woody materials (Nzokou 2009, Perez-Verdin et al. 2009). Similarly, as Nzokou (2009) acknowledged, factors affecting availability and utilization of wood waste in disposal yard are critically important for sustainable production and maximization of the economic benefits. Therefore, the focus of this study is to estimate the quantity of urban wood waste in Mississippi solid waste management facilities for different product classes and to understand the factors affecting recoverable volumes of wood-waste in study area.

Data Sources

The data for this study were primarily obtained from a mail survey of waste processing facilities in Mississippi. State of Mississippi solid waste management listing by Solid Waste Management Program was used for survey data collection. Total population for this census survey was 229 waste collection facilities in Mississippi. The survey instrument consisted of three sections. The first section collected information on type of solid waste management facilities, annual estimated quantity of solid waste, volume and percentage of wood based waste, recoverable volumes of wood waste were obtained. The second section included questions on wood-waste types, condition of collected wood-waste, cost in and benefits from wood recovery, potential markets, and interest in generating wood-based bioenergy among others. The third and final section included socio-demographic information such as: location, year of operation, number of employee, organization structure and technological capabilities associated with a waste processing facility. The draft survey was pilot tested among few wood processing facilities and the feedbacks were incorporated before its final distribution in March 2013. Data collection followed the Tailored Design Method, which included a reminder postcard and three mailings (Dillman 2000). Apart from the survey data, number of primary and secondary wood processing mills reported by Mississippi Development Authority and the county population of waste processing facilities were supplemented in econometric analysis.

Estimates on available and recoverable volumes

Descriptive statistical analysis was used to obtain available and recoverable volumes of urban wood waste in Mississippi. Total volumes of waste from different collection facilities, distribution of waste based on facility types, recoverable wood waste percentage and volumes were estimated. Similarly, relative cleanliness of collected urban wood-waste in different facilities in Mississippi was also estimated. Other information included available market opportunities for recovered wood-waste, new markets such as bioenergy, and the organization structure of facility. Mathematical extrapolation was done to obtain statewide estimations on recoverable urban wood waste. Conservative extrapolation approach, which estimated volume weighted average of the recovery rates in all facility types, was implemented to avoid over-estimation of the recoverable volumes.

Econometric Modelling

A decision to recover wood-waste by a waste processing facility depends upon comparative analysis of current or potential benefits of recovered wood-waste to the expected costs. Recoverable rates or volumes are determined by numerous factors including relative cleanliness of waste, current or potential market for recoverable material, technology, available volumes of waste, size of facility, and the years of operation. Therefore, an ordinary least square regression was used for empirical analysis. In our model, the observed rate of recovery was a continuous variable. The relationship between the dependent (Y_i) and independent variables (x_i) can be expressed by a multiple linear regression model (Greene, 2008):

$$Y_i = \beta_i x_i + \varepsilon_i \qquad \text{Eq.1}$$

Where β_i represents the vector of parameter coefficients, and ε_i is the random component. The empirical relationship between the waste recovery rate and these factors can be written as:

$$\text{RECOVERY RATE} = \beta_0 + \beta_1 \text{CLEAN} + \beta_2 \text{WOOD} + \beta_3 \text{ORG} + \beta_4 \text{RUB} + \beta_5 \text{POP} + \beta_6 \text{SEASON} + \beta_7 \text{MARKET} + \beta_8 \text{YEAR} + B_9 \text{MILL} + \varepsilon_i \qquad \text{Eq.2}$$

The dependent variable in econometric model was wood-waste recovery rate provided by surveyed waste processing facilities in Mississippi. The definition and descriptive statistics of all explanatory variables are reported in Table U1. First set of independent variables included the factors characterizing the waste collection facility. The variable CLEAN represented percentage of clean volume of wood-waste in wood-waste collection facility. Since facilities having higher volumes of clean wood-waste are more likely to recover than others, it was expected to have a positive sign. Similarly, a total volume of available wood-waste (WOOD) in processing facility was expected to have a positive sign. It is because higher volumes would justify for a need of wood-waste recovery. Among facility types, rubbish landfills (RUB) '1' indicated if facility was rubbish landfill and '0' others. Since rubbish landfills do not allow other mainstream waste coming in the form of discarded food or chemical (Cook cogin engineers, 2011), the variable was expected to have a positive coefficient. Organization structure (ORG), which was assigned as '1' if the facility had a private ownership and '0' otherwise, was also considered as explanatory variable in the model. Since private ownerships are highly flexible in terms of industrial modifications and aim to obtain multiple benefits out of their business, the variable was expected to have a positive coefficient. Duration of facility ownership (YEAR) was another attribute considered in the model. Since duration of ownership provides necessary experience among entrepreneurs to seek for multiple benefits, this variable was expected to have a positive coefficient. Number of employee (EMPLOYEE) was also considered in this analysis. Since number of employee represent the size of a facility (Joshi et al. 2013), this attribute was expected to have a positive sign. Finally, we were interested to see impact of seasonal variations on rate of wood recovery. It was assigned as '1' if

the facility operates with seasonal variations (SEASON) in volumes of received wood-waste and '0' otherwise. Mississippi delta is a vulnerable zone and periodic natural disasters are not uncommon in the region (Costanza et al. 2006). Seasonal fluctuations are likely to occur due to collection of disaster debris aftermath of hurricane or any other form of inclement weather. While seasonal fluctuations might result with unsteady flow of wood-waste intake, disaster debris are relatively clean and don't require excessive mechanical or chemical treatment for recovery. Therefore, we could not predict the sign of this attribute.
Second category of the variables represented neighborhood characteristics and the market opportunities. To account for neighborhood attributes, total population (POP) of the county having waste collection facility in logarithmic scale was considered in the model. Since the counties having higher population are likely to collect more waste, we expected to have positive sign of this attribute.

Finally, number of primary and secondary wood processing mills (MILL) in the county having waste collection facility was considered as explanatory variable. Since higher number of mill will provide sufficient wood-waste in waste collection facilities, the attribute was expected to have a positive coefficient.

Results:

Descriptive statistics:

Out of total 229 surveys, there were 64 returns from 208 deliverable mailings leading to an adjusted response rate of 30.77 percent. Study results suggested that about 68 percent of the survey respondents represented rubbish sites, 18 percent were from transfer stations, and 11 percent were from landfill sites. However, this trend was reversed with the total collected volumes of waste. Almost 62 percent of the total collected waste came from solid waste landfill sites, whereas rubbish sites constituted about 26 percent. Survey results suggested that wood-waste constituted 32 percent share of the total collected volumes. Out of all collected wood-waste, approximately 29 percent was considered as recoverable wood-waste volumes in Mississippi.

Rate of recovery and the cleanliness of the collected wood-waste varied across major waste collection facilities in Mississippi. For example, approximately half (47 percent) of collected wood-waste in rubbish site was available for recovery. In contrast, very small portion (10 percent) of the total collected waste could be recovered in municipal solid waste landfill sites. Survey results suggested that wood-waste collected in rubbish sites were relatively clean (40 percent) compared to municipal solid waste landfill sites (0 percent). Of note, minimal or no chemical or mechanical treatments are needed for a "clean" waste recovery. Survey results suggest that 42 percent of the total collected wood-waste contained municipal solid waste such as: pallets/shipping container, 29 percent was construction and demolition wood-waste and 16 percent was woody yard trimming. Remaining 12 percent was an industrial or any other form of wood-waste.

More than half (53 percent) of the respondents reported seasonal variations in the amount of wood-waste obtained at their facility. Those received highest volumes of wood-waste during spring or summer season. Majority of the wood-waste collection centers (67 percent) were publicly owned. On average, facilities were slightly over 20 years old. When asked about market for recovered wood-waste, more than half (60 percent) were unsure and very few (10 percent) had an affirmative response. Similarly, more than half (55 percent) were not aware of concept of wood-based bioenergy. Perhaps due to lack of awareness, 58 percent were not sure whether they will supply recovered wood-waste for a bioenergy use. Finally, conservative extrapolation of the survey suggested that about 390,076 tons of urban wood-waste were recoverable from 208

waste collection facilities in state of Mississippi. Majority of recoverable wood-waste volume (75 percent) came from rubbish sites.

Econometric analysis:

The generalized least square regression model was an overall fit with a significant F statistic value at 1 percent level of significance. Diagnostics test revealed that model did not suffer from autocorrelation, and multicolinearity. Similarly, White's robust standard errors in the generalized least square regression alleviated a potential issue of heteroscedasticity in the model (Greene, 2008). A full and reduced form[1] of generalized least square regression model is reported in Table 2. Five out of six variables in the econometric model were statistically significant at 10 percent or lower. The attributes: SEASON, CLEAN, and RUB had positive coefficient and were significant at 10 percent level. The attribute representing organization structure of the waste collection facility (ORG) significantly influenced the availability of recoverable volumes of wood residues in waste collection facility at 5 percent level. While population of the county having waste collection facility (POP) was significant at full model, it did not significantly influence the availability of recoverable volumes in restricted model. Since dependent variable was in logarithmic scale, dummy variables such as SEASON, CLEAN, RUB, and ORG required additional calculations for a meaningful interpretation (Halvorsen and Palmquist, 1980). For example, results from reduced econometric model suggested that wood-waste recovery in year round facility recoverable wood-waste in year round facility were 41 percent higher than in a seasonal facility. Similarly, facilities with private ownerships were likely to have 41 percent more waste recovery than public ownerships. Finally, WOOD was positive and significant at 1 percent level suggesting that 1 percent increase in volume of wood waste increases recovery rate by 24 percent.

Discussion and Conclusion

Study results provided insightful information on total collected and recoverable volumes of wood-waste in Mississippi. Estimates on recoverable volumes of urban wood waste volumes have significant practical implications as none of the previous studies to the best of our knowledge have used primary data sources for such estimations. Perez-Verdin et al. (2009) estimated about 280,000 tons of recoverable urban wood-waste in Mississippi. Sixty-eight percent of those recoverable volumes were estimated to be obtained from rubbish sites (Perez-Verdin et al. 2009). Compared to our estimates, these results seem slightly conservative. As explained earlier, we estimated 39 percent more recoverable wood-waste volumes. Since statewide results are based on mathematical extrapolation, results need a cautious interpretation. To this end, our results are comparable or conservative to the estimates done in other states (Camas Creek enterprises 2009, Kittler and Beauvais 2010). For example, more than 67,000 green tons of woody biomass was available for bioenergy use in the state of Kansas (Camas Creek enterprises 2009). Similarly, estimates done in Maryland suggest availability of more than 600,000 dry tons of urban wood waste in the state. Given that Mississippi has significantly large forestland compared to both states, our estimates seem realistic. Nevertheless, a careful interpretation is suggested as estimates are based on mathematical extrapolation.

State of Mississippi 2012 status report on solid waste management facility indicated that about 83 percent of the total received solid waste was coming from landfill sites in Mississippi (MDEQ 2012). However, as our results suggest, recovery percentage in landfill sites are very small. There were 79 active rubbish sites in Mississippi receiving approximately 17 percent of total received solid waste. Rubbish sites are considered as a better source for recoverable wood-waste as they generally receive the less contaminated woody materials such as: natural vegetation, salvaged

[1] Reduced form regression model is used given smaller sample size in this study.

furniture, saw dust, wood savings, and wood chips among others (MDEQ 2012).

Consistent with our expectations, probability of obtaining recoverable volumes of urban wood-waste is higher in rubbish sites and private waste collection centers. Since wood-waste collected in rubbish sites are less contaminated and require minimal chemical or mechanical treatments for recovery, these facilities might have more incentives to recover woody materials as compared to others. While there are very few waste collection facilities with a private ownership in the state, study results suggest private entrepreneurs in this business are seeking every opportunity to maximize profits compared to their public counterparts.

Study results suggested that recovery was higher with facilities having seasonal variations in the flow of wood-waste intake. Descriptive statistics suggests that majority waste collection facilities in Mississippi had seasonal fluctuations in amount of wood-waste collection. Natural disasters such as straight line winds, tornedoes and winter ice storms are common in Mississippi and are likely to bring such variations. Since trees and limbs are the major disaster debris, rubbish sites become preferred disposal options (Cook Cogin Engineers 2011). Since disaster debris is relatively clean and requires minimal cost during recovery, positive relationship between seasonal variations and a recovery rate makes intuitive sense. However, consistent with the argument forwarded by Perlack et al. (2005), seasonal variations in intake wood-waste volumes can affect the viability of these feedstocks in bioenergy use.

While the probability of recovery was higher in a facility having more wood-waste, unlike what we expected, better proximity with primary wood processing facility did not contribute to the rate of recovery. These results indicate that woody residues from primary wood processing facilities are largely utilized internally and very small portions are disposed or given away in a waste collection facility. As descriptive and econometric results suggest, availability of nearby market did not motivate facilities for wood-waste recovery. It was because majority of these facilities were unsure about potential market such as bioenergy for recoverable wood-waste. This could be the reason behind suppressed wood-waste recovery percentage in Mississippi and other neighboring southern states.

Study results have several policy implications. Firstly, while urban wood wastes are reliable contributors, available biomass feedstock as such are not sufficient to operate a bioenergy industry independently. However, there are more than 200 waste collection facilities located in every smaller city in Mississippi and therefore are easily available for use in a minimal hauling cost. Per units feedstock costs will be smaller if bioenergy industries could use a mix of logging residues, mill residues as well as urban wood-waste. To this end, urban wood-waste can become important supplement to logging residues or small-diameter trees in Mississippi.

Secondly, majority of the urban waste collection facilities are unsure of any market for recoverable urban wood waste in Mississippi. Bioenergy has received wide attention in Mississippi and a number of industries are already in operation in the state (Timber-Mart South 2013). However, waste collection facilities are uncertain about their willingness to supply biomass for emerging market such as bioenergy. Any investment in wood-waste recovery is difficult to justify with an unsure mindset. Therefore, higher recovery rates are associated with rubbish sites, which typically accept minimally contaminated wood-waste and do not require higher expenditures during wood-waste recovery. An extension strategy is needed for better communication between both industry types.

Finally, urban wood waste can become primary source of biomass feedstock if waste collection centers could integrate with smaller sized bioenergy industry. More than 80 percent of the total

wastes are collected in landfill sites (MDEQ 2012), large volumes of wood-waste in these facilities are not recovered yet. Unlike rubbish sites, landfill sites contain contaminated wood-waste and might require additional costs during recovery. However, there is about $21 per ton waste disposal tipping fee in Mississippi (Product Stewardship institute 2012). Since the wood-waste recovery and its potential use for bioenergy will reduce the volume of disposable waste and per unit costs, biomass feedstock from landfill sites might still be justifiable as small diameter trees and the logging residues are the most expensive form of woody biomass in Mississippi (Perez-Verdin et al. 2009). Nonetheless, future research to explore costs associated with landfill wood-waste recovery and its potential use in bioenergy is suggested.

References

Cook Cogin Engineers 2011.Three rivers solid waste management authority, solid waste management plan. Available online: http://www.trpdd.com/gov/swp_rev.pdf [[Last accessed January 20th, 2014].

Costanza R., W.L. Mitsch., and J. W. Day Jr. 2006. A new vision for New Orleans the Mississippi delta: applying ecological economics and ecological engineering. Frontiers in Ecology and Environment. 4(9):465-472.

Dillman, D.A. 2000. *Mail and internet surveys: The tailored design method*. 2nd ed. New York: John Wiley & Sons, Inc. 464 p.

EPA. 2010. 2010 facts and figure fact sheet. Environmental Protection Agency, Washington DC. Available online at http://www.epa.gov/osw/nonhaz/municipal/msw99.htm[Last accessed January 20th, 2014].

Falk B. Opportunities for the wood waste resource. Forest Product Journal. 47(6): 17-22.

Falk, B., and D. McKeever. 2012. Generation and recovery of solid wood waste in the United States. Biocycle. P. 30-32. Available online at http://www.fpl.fs.fed.us/documnts/pdf2012/fpl_2012_falk001.pdf. [Last accessed January 17th, 2014].

Ferhs, J.E. 1999. Secondary mill residues and urban wood waste quantities in the United States. Northeast Regional Biomass Program. Available online at http://www.nrbp.org/pdfs/pub21.pdf [Last accessed January 17th, 2014].

Greene, W.H., 2008. Econometric analysis, 6th edition Prentice-Hall International, Inc.,New Jersey, NJ. 1178 pp.

Halvorsen, R., and R. Palmquist. 1980. The Interpretation of Dummy Variables in Semilogarithmic Equations. *The American Economic Review.* 70(3): 474-475.

Joshi, Omkar, D.L. Grebner, I. A. Munn, S. C. Grado, R. K. Grala, and A. Hussain. 2013. Factors influencing utilization of woody biomass from wood processing facilities in Mississippi. *Forest Products Journal* (accepted).

Kittler, B.A. and C.M. Beauvais. 2010. *The potential for sustainable wood-based bioenergy in Maryland.* Developing safeguard for woody biomass harvests and evaluating wood-based bioenergy markets. Pinchot Institute for Conservation. 196 p.

MacFarlane, D.W.2009. Potential availability of urban wood biomass in Michigan: Implication for energy production, carbon sequestration, and sustainable forest management in the U.S.A. *Biomass and Bioenergy*. 33: 628-634.

Minnesota Department of Natural Resources. 1994. Minnesota wood waste studies. Available online at http://files.dnr.state.mn.us/forestry/um/woodwaste.pdf [Last Accessed April 11th, 2014].

Nzokou, P.2009.Wood waste processing and utilization in Southeastern Michigan. Technical report. Department of Forestry, Michigan State University. 50 p.

NRCan. 2006. An analysis of resource recovery opportunities in Canada and the projection of greenhouse gas implications. Prepared by: Sinclair, R. for Natural Resources Canada. March]. 343 p. http://www.nrcan.gc.ca/sites/www.nrcan.gc.ca.minerals-metals/files/pdf/ mms-smm/busi-indu/rad-rad/pdf/rrd2eng.pdf.

McKeever, D.B. 2004. Inventories of woody residues and solid wood waste in the United States, 2002. In: Proceedings of the ninth international conference, inorganic-bonded composite materials. October 10-13. 2004.

MDEQ. 2012. State of Mississippi status report on Solid waste management Facilities and activities Calendar year 2012. Solid waste policy, planning & grants branch Office of pollution control Mississippi department of environmental quality. 40 p.

Perez-Verdin, G., D. Grebner, C.Sun, I Munn, and S. Grado. 2008. Economic impact of woody biomass utilization for bioenergy in Mississippi. *Forest Products Journal*. 58(11):75-83.

Perlack, R.D., L.L. Wright, A. Turhollow, R.L. Graham, B. Stokes and D.C. Erbach. 2005. *Biomass as feedstock for a bioenergy and bioproducts industry: The technical feasibility of a billion-ton annual supply*. U.S. Department of Energy and USDA Forest Service, Washington, DC. 73 p.

Product Stewardship Institute. 2012. Mississipians landfill $210 millions recyclables annually. Available online: http://www.msrecycles.org/spotlight/255-prodsteward082012.html. Last accessed, March 23,2014.

USEPA. 2009. Estimating 2003 building-related construction and demolition materials amounts. Washington, DC: U.S. Environmental Protection Agency. [March]. 60 p. http://www.epa.gov/osw/conserve/rrr/imr/cdm/pubs/cdmeas.pdf.

U.S. Department of Energy. 2011. U.S. Billion-Ton Update: Biomass Supply for a Bioenergy and Bioproducts Industry. R.D. Perlack and B.J. Stokes (Leads), ORNL/TM-2011/224. Oak Ridge National Laboratory, Oak Ridge, TN. 227 p.

Timber Mart-South. 2013. Timber Mart-South Market News Quarterly. The Journal of Southern Timber Market News. 18(4): 1-40.

Subtask U.4 Feedstock engineering (Paz, Davis, Parajuli)

One of the limiting factors in the production of cheaper biofuels is the cost of transporting biomass to conversion facilities. Densification of biomass in the field reduces the number of processing steps before conversion and allows more material to be transported each trip. This subtask will

focus on two areas: a) collecting economic and engineering data on feedstock harvesting, handling, densification, and particle size reduction and storage, and b) assessing the sustainability of feedstocks. We will collect data to refine estimates of these processes for several common biomass systems in the Southeastern US. Using economic models, data will be used to refine estimates of costs associated with providing biomass to a plant gate. The sustainability of bioenergy produced from a particular source may be measured using net energy value (NEV), an established measure for the energy gain and sustainability of bioethanol. We will examine the sustainability of different feedstocks such as agricultural and forestry residues and bioenergy crops, in terms of the net energy value and CO_2 emissions.

Planned Activities:
U.4.ML.1 Determine the effects of economical binders on the efficacy of densifying switchgrass through in-field cubing. (Davis)

U.4.ML.2 Determine the spatial distribution of the potential bio-energy crops and their environmental benefits in Mississippi for renewable fuels through economic modeling and analysis. (Paz)

U.4.ML.3 Assess the effects of environmental conditions and management systems on the net energy value of feedstocks. (Yui)

U.4.ML.1 Determine the effects of economical binders on the efficacy of densifying switchgrass through in-field cubing. (Davis)

The objective of this work was to compare the efficacy of two economical binders applied at varying rates during switchgrass cubing at two times in the year (before and after senescence). Two field trials were conducted in a switchgrass pasture at the Joe Bearden Dairy Research Center, Mississippi State University, Sessums, MS. The first trial was conducted in November after the grass has entered the senescence stage (typical in a one-time per year cutting). The second trial was conducted in June before senescence to simulated the first of a two-time per year cutting system. Switchgrass was cut and conditioned with a mower conditioner (635 MoCo, Deere and Co. Ottumwa, IA). The hay material was allowed to dry for 48 h before attempting to rake and windrow using a hay rake (WR1008, Deere and Co, Ottumwa, IA). Eight windrows were formed across the field. At the beginning of each windrow, a 7.6 m (25 ft) section of grass provided material to ensure treatment discharge from the previous windrow. After the 7.6 m section, four 30.5 m (100 ft) sections were established to collect treatment samples randomized within two rows (fig U7).

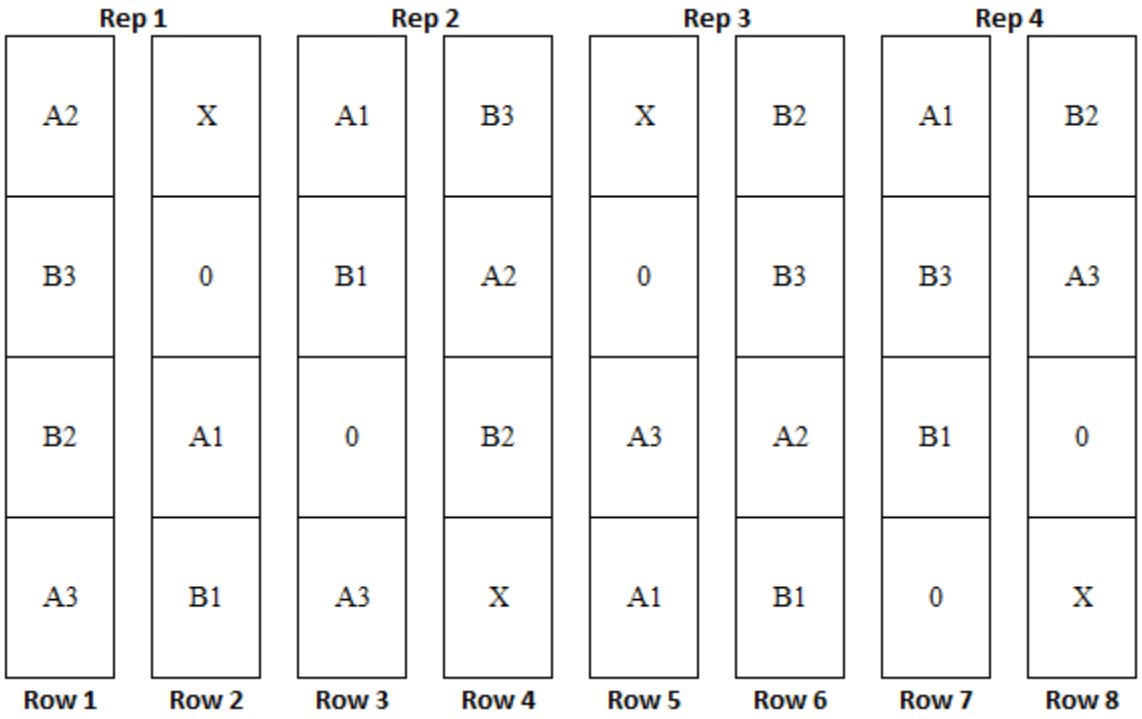


Figure U7: *Binder treatment design across eight windrows of switchgrass. (0 = no binder control; A1 = 25 kg/tonne, A2 = 32 kg/tonne , A3 = 40 kg/tonne lignin sulfonate binder; B1 = 2.5 kg/tonne, B2 = 3.7 kg/tonne, B3 = 5 kg/tonne starch binder; X = not collected).*

Two readily available binders were used; a liquid lignin sulfonate binder (Super-Bind® Liquid, Uniscope, Inc., Johnstown, CO) and a starch binder (Pro-Bind, Uniscope Inc., Johnstown, CO). A control and three binder application rates were used for a total of seven treatements [0 = no binder control; A1 = 25 kg/tonne, A2 = 32 kg/tonne , A3 = 40 kg/tonne lignin sulfonate binder; B1 = 2.5 kg/tonne, B2 = 3.7 kg/tonne, B3 = 5 kg/tonne starch binder]. Binder was applied to treatments with a backpack sprayer (Model T, Bellspray, Inc, Opelousas, LA) (fig. U8). The backpack sprayer was calibrated for each treatment flow rate.



Figure U8: *Application of binder to switchgrass windrow using a pressurized backpack sprayer.*

A standard warm-up procedure was used to prepare the hay cuber (425, John Deere, Ottumwa, IA) for operation. The machine was started and run at full throttle with the cubing mechanism engaged for a period of five minutes to allow the dies to warm up. Once machine reached full operational level, the machine was moved to the first row of the trial. Cubes and fines for each section of windrow were collected in a plastic container (fig. U9) and transferred to large heavy-duty plastic bags.



Figure U9: *In-field hay cuber cubing switchgrass windrows. Students are collecting samples for each treatment through a plastic drop chute at the rear of the machine. Picture insert shows cubes exiting the dies at the top of the machine.*

Collected materials were sifted to determine efficiency of cube production (eq. 1) for each treatment. Each sample was weighed on a balance (SX-1002, Circuits and Systems, Inc., East Rockaway, NY) and placed on an inclined sifting table to remove fines (fig. U10). The table was constructed with expanded metal grating with two vibrators (SPWT-80, Vibco, Wyoming, RI)

attached at one-third and two-third of table length. An 11.3 kg weight suspended from the center of the table produced an oscillation with the vibrators. This assisted in the conveyance of the material cubes across the table and fines dropped through the grates. Both materials were weighed and compared to initial weight for recovery determination.

$$\%_{Cubes} = \frac{Weight_{Cubes}}{Weight_{Total}} * 100 \qquad \text{(eq. 1)}$$



Figure U10: *Students sifting the fines from the cubes on a inclined vibratory table.*

One grab sample was taken across each treatment test section before cubing. A second grab sample was taken from the cubing machine discharge during collection. Initial moisture content ($MC_{initial}$) and post-cubing moisture content (MC_{cube}) were determined according to ASAE S358.2 Moisture Measurement – Forages standard (ASAE, 1993). Grab samples were placed in pre-weighed aluminum sample dishes and contents weighed using a balance (Excellence XA, Mettler Toledo, and Columbus, OH). Each sample was placed in a preheated oven (LB305565G, Lindberg Blue/M, Waltham, MA) at 103 °C for 24 h. Moisture content (wet-basis) was calculated using equation 2.

$$MC_{Wet\ Basis} = \frac{Weight_{Wet} - Weight_{Dry}}{Weight_{Wet}} * 100 \qquad \text{(eq. 2)}$$

Data were analyzed in an analysis of variance using the PROC MIXED model (Version 9.2, SAS, Cary, NC). Least square means were calculated for each treatment and separated with Fisher's LSD (α = 0.05).

Senescence Cutting Results

Switchgrass treatments were cubed in the month of November to simulate a single harvest per year; late spring and after senescence. The switchgrass had an average moisture content of 34.7%. In Figure U11, the control (no binder) was significantly higher and provided the best cube production of 14.4% compared to the six binder treatments. All six binder treatments created fewer cubes than the control. Switchgrass cube production was much lower than the previously reported in-field cubing of bermudagrass (78.9% with a binder). The best cubes were formed

immediately after startup when the die rings were cold and material in the die helped maintain backpressure on the cube material. Once back pressure was lost, the cubes wouldn't maintain their shape.

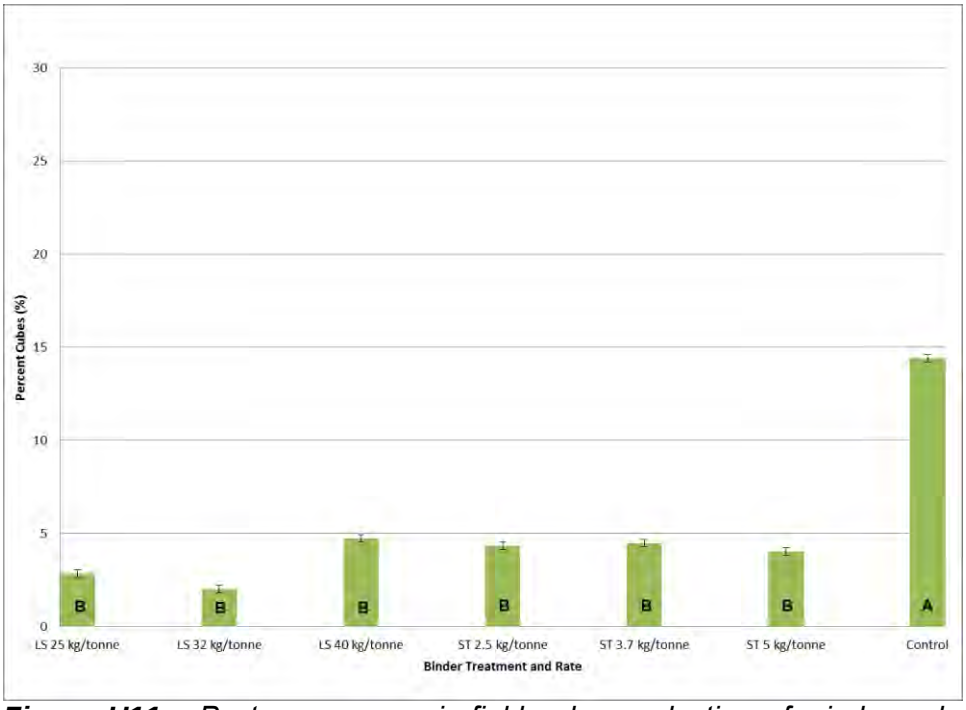


Figure U11: *Post-senescence in-field cube production of windrowed switchgrass by binder treatment and application rate.*

Pre-senescence Cutting Results

Switchgrass treatments were cubed in the month of June to simulate two harvests per year. The switchgrass had an average moisture content of 12.4%. At best, cube production was 27.7%. In Figure U12, none of the starch binder treatments improved cubing when compared to the control. The lignin sulfonate binders produced fewer cubes as compared with the control. The highest rate of lignin sulfonate (40 kg/tonne) was significantly lower than the control or starch binder treatments. Using lignosulfonate and starch binders at the specified rated did not improve cube production of switchgrass. However, cube production pre-senescence was almost doubled that of cubing after senescence.

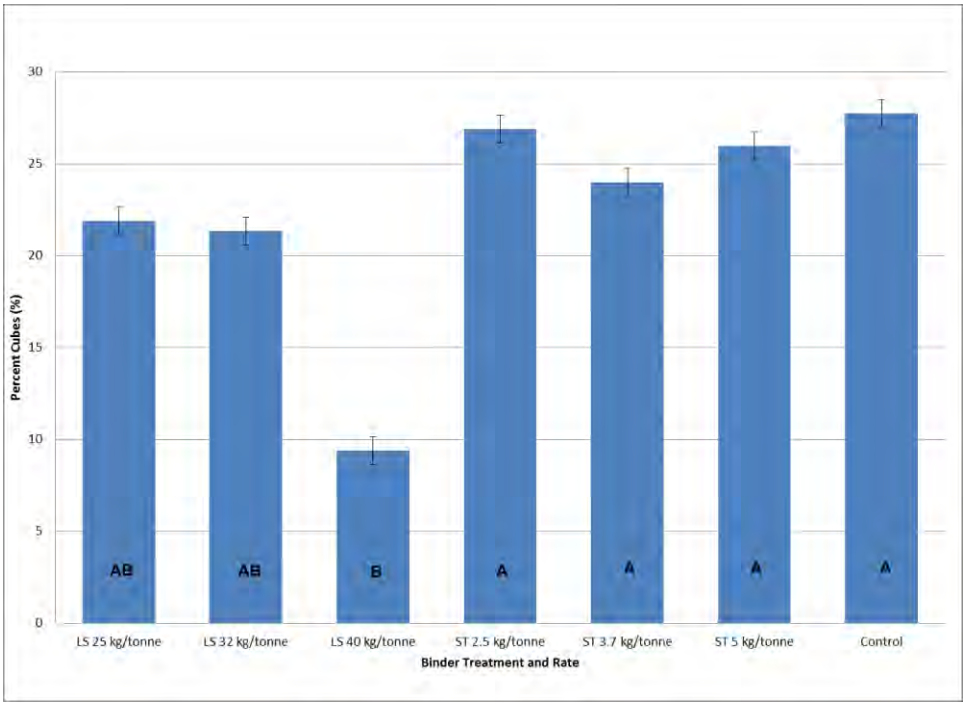


Figure U12: *Pre-senescence in-field cube production of windrowed switchgrass by binder treatment and application rate (LS = lignin sulfonate, ST = starch)*

This research concluded that in-field cubing of switchgrass is not an efficient means of densification without significant modifications to the in-field hay cuber. Though efficiency of cubing was improved during pre-senescence, the team was unable to achieve throughput capacities equivalent to commercial hay balers. Real-time moisture sensing and the ability to control die temperature separately from cubing operation are needed. The team worked to improve the consistency of this operation but a major design change (rotating the drum to operate on its side) would be needed to keep all dies loaded with the same quantity of material. Because the team only achieved a cubing efficiency of 27% for switchgrass, the machine needs a return belt for fines so the material gets recubed and not left on the ground. Though the cuber produced bermuda grass cubes at 79% with a binder, the team hasn't been able to consistently cube switchgrass with any uniformity. In-field cubing of switchgrass has not been achievable to contend with baling in the field and densifying in a facility.

Publications:

Lowe, J.W., G.D. Chesser, J.D. Davis and J.K. Ward. 2013. Effect of two binders at three rates on densification of switchgrass through in-field cubing. Presentation for the 2013 ASABE International Meeting. Jul 21-24. Kansas City, MO.

U.4.ML.2 Determine the spatial distribution of the potential bio-energy crops and their environmental benefits in Mississippi for renewable fuels through economic modeling and analysis. (Paz)

Renewability of biofuel

The sustainability of biofuel production in terms of non-renewable energy displacement can be quantified using net energy value (NEV) – the renewable energy produced minus non-renewable energy used to produce the renewable energy. A positive NEV indicates that the biofuel production system is sustainable in terms of energy security, and a larger value signifies that the system is more sustainable. The eco-friendliness of biofuel production in terms of reduction in carbon emissions can be quantified using carbon credit balance (CCB) – the amount of CO2 (Mg) fixed by a crop plant from the atmosphere and stored in the harvested biomass minus the amount of CO2 (Mg) emitted to the atmosphere while producing and supplying a given quantity of the biomass to a refinery, processing the ethanol at the refinery, and transporting, distributing, and combusting the ethanol after its production (Woli et al., 2012). One carbon credit may be regarded as a reward for extracting 1 Mg of CO2 gas from the atmosphere. A positive CCB indicates that the ethanol production system is environmentally friendly in terms of carbon emissions reduction, and a larger value is indicative of a more environmentally friendly system.

We examined the effects of biomass yield and utilization rate on the sustainability (in terms of non-renewable energy displacement) and eco-friendliness (in terms of carbon emissions reduction) of ethanol production associated with two different feedstocks – maize stover and switchgrass – using NEV and CCB as the indicators of sustainability and eco-friendliness, respectively, for the state of Mississippi. This study also compared the two feedstocks in terms of the land required for producing a given quantity of ethanol.

Sites and Data

The sustainability and eco-friendliness of ethanol derived from maize stover and switchgrass were examined for ten biomass yield levels and four utilization (harvest removal) rates for ten locations in Mississippi: Poplarville (30.8°N, 89.5°W), Natchez (31.6°N, 91.4°W), Mendenhall (32.0°N, 89.9°W), Meridian (32.4°N, 88.7°W), Vicksburg (32.4°N, 90.9°W), Columbus (33.5°N, 88.4°W), Indianola (33.5°N, 90.7°W), Grenada (33.8°N, 89.8°W), Booneville (34.7°N, 88.6°W), Tunica (34.7°N, 90.4°W). These locations were selected taking into account potential acreage of these crops and geographical coverage. For each location, maize grain yield data for the climatic normal period of 1971-2000 (30 years) were obtained from the USDA National Agricultural Statistics Service (http://quickstats.nass.usda.gov/). A 3-decade climatic period is long enough to filter out many short-term annual fluctuations and anomalies, but short enough to reflect long-term climatic trends (WSCO, 2003). The grain yields then were converted to stover yields using the stover to grain ratio of 1:1 (Kim and Dale, 2004; Sheehan et al., 2004).

Because the biomass yield data of switchgrass were not available for these locations and years, they were simulated using Agricultural Land Management Alternatives with Numerical Assessment Criteria (ALMANAC) (Kiniry et al., 1992), a widely-tested and used crop model that can reliably simulate switchgrass biomass yields for a wide range of environments. This is a process-based model and simulates plant growth for several species using leaf area index, light interception, radiation use efficiency, and soil water and plant nutrient balances (Kiniry et al., 2005). Maximum and minimum air temperatures, precipitation, and solar irradiation are its inputs. It needs several parameters related to crop, soil, and tillage.

For each location, daily weather data for the 30 years were obtained from the Delta Agricultural Weather Center (www.deltaweather.msstate.edu) and the National Climate Data Center (www.ncdc.noaa.gov/oa/climate/stationlocator.html). These data contained air temperatures and precipitation, but not solar irradiation. Thus, the daily values of solar irradiation were generated using the WP method described by Woli and Paz (2012). Using the weather data, switchgrass biomass yields were simulated for the above locations and years. Because the model had already been calibrated and evaluated for switchgrass yield simulation for Mississippi conditions by Woli et al. (2012), the model was directly used to simulate the biomass yields of this energy crop.

Factors and Treatments

From the 30 biomass yield values of each feedstock, 10 yield levels (minimum, maximum, and 8 intermediate values with equal interval) were computed for each location (Table U7). The ten yield levels were used as the representative yields produced under a wide range of environment, technology, and management. For each feedstock, four utilization rates were considered. Because from an environmental sustainability point of view the harvest removal percent for maize stover should not exceed 40 (Kim and Dale, 2004; Petrolia, 2009; Sheehan et al., 2004), the four utilization rates considered for this feedstock were 10%, 20%, 30%, and 40% of the biomass yield (presented in Table U7). For switchgrass, the utilization rates considered were 60%, 70%, 80%, and 90% of the biomass yield. Because switchgrass is a dedicated energy crop and has no or little environmental issues associated with its harvest removal rates (McLaughlin et al., 1999; McLaughlin and Kszos, 2005), larger utilization rates were considered.

NEV and CCB Computation

Each of the ten yields of each feedstock for each utilization rate and location was then used as an input to the Integrated Biomass Supply Analysis and Logistics (IBSAL) model (Sokhansanj et al., 2006) to compute the amounts of non-renewable energy consumed and CO_2 emitted during various operations in the feedstock supply chain (biomass production field to refinery facility). As the IBSAL simulations were carried out for four utilization rates for each location and yield level, the total number of yield scenarios analyzed for each feedstock was 400. The IBSAL is a dynamic logistics model to simulate delivered cost, energy use, and carbon emissions associated with various operations in a feedstock supply chain. Its key inputs are biomass yield, crop harvest progress, air temperature, precipitation, relative humidity, snow fall, and wind speed. It also needs several parameters related to equipment and machinery costs. The model includes several energy crops and crop residues.

The energy use and CO_2 emissions values estimated by the IBSAL model were then used to compute NEV and CCB. The NEV of ethanol production associated with a yield scenario was computed as renewable energy obtained from ethanol minus the non-renewable energy used to obtain the renewable energy as

$$\mathrm{NEV} = \mathrm{E_e} - (\mathrm{E_f} + \mathrm{E_l} + \mathrm{E_p} + \mathrm{E_t}) \quad (1)$$

where NEV is net energy value (MJ L^{-1}); E_e is the energy obtained from ethanol; and E_f, E_l, E_p, and E_t are the energy used for biomass production, biomass logistics (harvesting, collection, storage, and transportation), ethanol processing, and ethanol transport and distribution, respectively. Except for E_l, which was computed by IBSAL, values for the other variables were obtained from literature.

Table U7. *Biomass yields (Mg ha^{-1}) of two feedstocks for various yield levels and locations in Mississippi, USA*

Feedstock	Location	Yield level									
		1	2	3	4	5	6	7	8	9	10
Maize stover	Tunica	1.6	2.3	3.1	3.8	4.6	5.3	6.1	6.8	7.6	8.3
	Booneville	2.1	2.5	3.0	3.4	3.9	4.3	4.8	5.2	5.6	6.1
	Grenada	1.6	2.3	2.9	3.6	4.3	5.0	5.7	6.4	7.1	7.8
	Indianola	1.8	2.6	3.5	4.3	5.1	6.0	6.8	7.6	8.5	9.3
	Columbus	1.3	2.0	2.7	3.4	4.2	4.9	5.6	6.3	7.0	7.8
	Vicksburg	2.0	2.9	3.7	4.6	5.4	6.3	7.2	8.0	8.9	9.7
	Meridian	1.3	1.5	1.6	1.8	2.0	2.2	2.4	2.6	2.8	3.0
	Mendenhall	1.3	1.8	2.3	2.8	3.3	3.7	4.2	4.7	5.2	5.7
	Natchez	1.5	2.1	2.7	3.3	3.9	4.5	5.1	5.7	6.4	7.0
	Poplarville	1.7	2.1	2.6	3.0	3.5	3.9	4.3	4.8	5.2	5.6
Switch-grass	Tunica	12.7	13.7	14.7	15.7	16.7	17.7	18.7	19.7	20.7	21.7
	Booneville	4.8	5.7	6.7	7.6	8.5	9.4	10.3	11.3	12.2	13.1
	Grenada	13.4	14.3	15.2	16.1	17.0	18.0	18.9	19.8	20.7	21.6
	Indianola	9.4	10.2	11.0	11.8	12.6	13.4	14.2	15.1	15.9	16.7
	Columbus	7.7	8.4	9.1	9.8	10.5	11.2	11.9	12.6	13.3	14.0
	Vicksburg	7.2	8.4	9.5	10.7	11.8	13.0	14.1	15.3	16.5	17.6
	Meridian	9.9	10.6	11.3	12.0	12.7	13.4	14.1	14.8	15.5	16.2
	Mendenhall	10.2	10.7	11.3	11.8	12.3	12.8	13.4	13.9	14.4	15.0
	Natchez	12.1	12.6	13.0	13.5	14.0	14.5	14.9	15.4	15.9	16.4
	Poplarville	7.1	7.9	8.6	9.4	10.1	10.9	11.7	12.4	13.2	13.9

The CCB of ethanol production associated with a yield scenario was computed as the amount of CO_2 (Mg) fixed from the atmosphere by the harvested biomass minus the amount (Mg) released back into the atmosphere as

$$\mathrm{CCB} = \frac{\alpha\beta}{\gamma} - (\mathrm{C_f} + \mathrm{C_l} + \mathrm{C_p} + \mathrm{C_t} + \mathrm{C_c}) \qquad (2)$$

where CCB is carbon credit balance (credits m^{-3}); α is the carbon content of biomass (kg kg^{-1}); β is the CO_2 to C ratio (kg kg^{-1}); γ is the biomass to ethanol conversion ratio (L kg^{-1}); and C_f, C_l, C_p, C_t, and C_c are the amounts of CO_2 emitted (kg CO_2 L^{-1}) through energy consumption for biomass production, biomass logistics, ethanol processing, ethanol transport and distribution, and ethanol combustion, respectively. Except for C_l, values for the other variables were obtained from literature.

Sustainability

Based on the results, the long-term energy sustainability (in terms of non-renewable energy displacement) of ethanol production associated with maize stover and switchgrass each varied by both biomass yield level and utilization rate (Figure U13). The results regarding the impact of yield on sustainability were in agreement with those of several previous studies (Persson et al., 2009, b; Woli and Paz, 2011; Woli et al., 2012). Those results, however, were not directly based on a number of yield levels considered in this study. For each feedstock and utilization rate, the values of NEV (i.e., energy sustainability) increased at a decreasing rate with an increase in yield level. This increase was due to decrease in energy consumption during various logistics operations such as harvesting, collection and transportation. The energy used for these operations decreased with an increase in yield because the land required for producing a given quantity of ethanol decreased for each increase in yield (Figure 8). With a decrease in land required for growing the feedstock (draw area), the quantity of fuel needed for collection and transportation operations decreased due to decrease in travel distance.

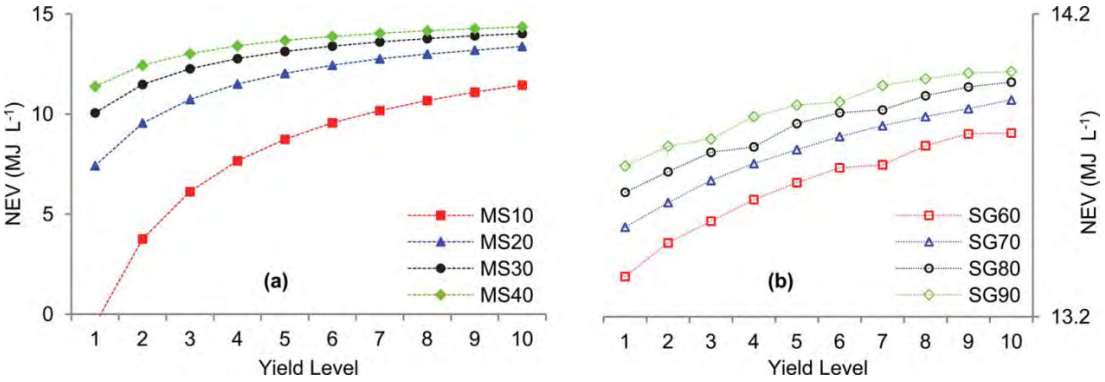


Figure U13. *The net energy value (NEV; MJ L^{-1}) of ethanol produced from: (a) maize stover and (b) switchgrass for various yield levels and utilization rates for Mississippi, USA.*

Note: 1 = lowest yield, …, 10 = highest yield; MS10 = maize stover at 10% utilization rate, …, SG90 = switchgrass at 90% utilization rate

The values of NEV also increased with an increase in utilization rate for all yield levels of each feedstock (Figure U13). This increase in NEV was likely because the increase in utilization rate increased the quantity of biomass to be used for ethanol production. An increase in utilization rate, thus, was equivalent to an increase in yield level. As explained in the preceding paragraph, the yield increase led to a decrease in land requirement, draw area, travel distance, and ultimately transport fuel. The above results, therefore, demonstrated that the sustainability of ethanol production associated with maize stover and switchgrass each increases with an increase in biomass yield as well as utilization rate.

Eco-friendliness

As energy sustainability, the eco-friendliness (in terms of carbon emissions reduction) of ethanol production associated with maize stover and switchgrass each varied by both biomass yield level and utilization rate. These results were consistent with those of previous studies (Woli and Paz, 2011; Woli et al., 2012), where eco-friendliness was found to have been impacted by biomass yield. According to the current study results, the eco-friendliness of ethanol derived from both maize stover and switchgrass increased with an increase in biomass yield as well as utilization rate (Figure U14). Like NEV, the values of CCB increased at a decreasing rate with an increase in yield level for each feedstock and utilization rate. Similarly, the CCB values increased with an increase in utilization rate for all yield levels of each feedstock. The similarity between NEV and CCB was because the latter was linearly associated with the former. For various operations in the biomass logistics, the IBSAL model computed the amount of CO_2 emitted as a linear function of the energy consumed as:
CO_2 emitted (kg) = 0.0686 × energy consumed (MJ).

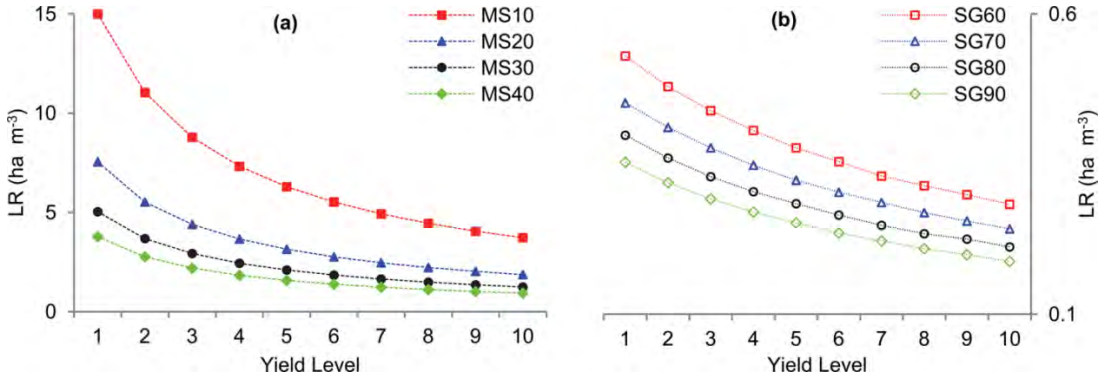


Figure U14. *Land required to producing 1 m^{-3} of ethanol (LR; ha m^{-3}) from: (a) maize stover and (b) switchgrass for various yield levels and utilization rates for Mississippi, USA.*

Note: 1 = lowest yield, …, 10 = highest yield; MS10 = maize stover at 10% utilization rate, …, SG90 = switchgrass at 90% utilization rate

Maize Stover vs. Switchgrass

The quantity of land required to produce a given amount of ethanol (ha m-3) from maize stover was larger (>0.9 ha m-3) than that from switchgrass (<0.6 ha m-3) for all yield levels and utilization rates (Figure U14). Thus, the results suggested that producing a certain quantity of ethanol from maize stover requires more land (2-80 times, depending on yield level and utilization rate) than from switchgrass. The requirement of more land for maize stover was due to its lower yields (0.7-156 times, depending on yield level and utilization rate) than that of switchgrass.

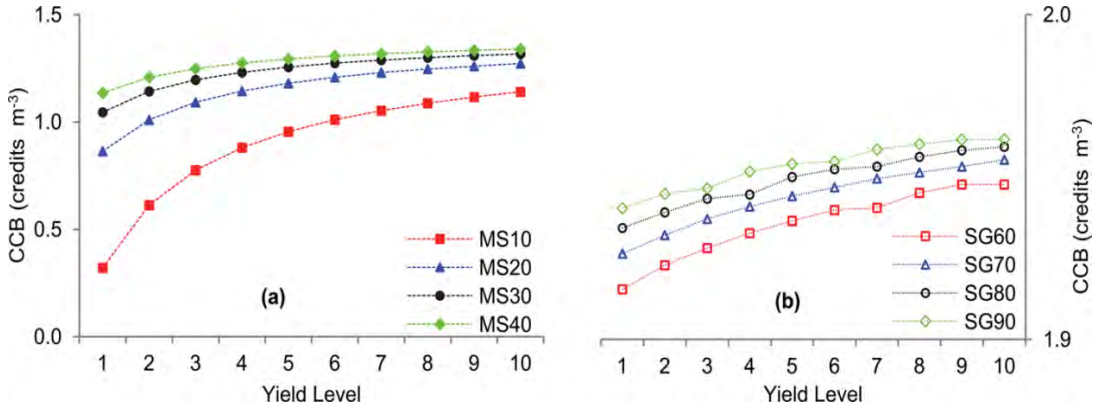


Figure U15. *The carbon credit balance (CCB; credits m^{-3}) of ethanol produced from: (a) maize stover, and (b) switchgrass for various yield levels and utilization rates for Mississippi, USA.*

Note: 1 = lowest yield, …, 10 = highest yield; MS10 = maize stover at 10% utilization rate, …, SG90 = switchgrass at 90% utilization rate

The values of CCB for switchgrass for all scenarios were larger than 1.9 credits m-3, whereas those for maize stover were smaller than 1.5 credits m-3 (Figure U15). The results indicated that ethanol produced from switchgrass were more eco-friendly (1-6 times, depending on yield level and utilization rate) than that produced from maize stover for all yield levels and utilization rates. The larger CCB values for switchgrass were mainly due to its higher carbon content (α) and lower biomass to ethanol conversion ratio (γ), which gave rise to a larger value of the carbon credits earned per unit of ethanol produced (αβ/γ in Equation 2). The larger values were also due to less carbon emissions per unit of ethanol produced during logistics operations (harvesting, collection, and transportation), which in turn were due to higher yields, and thus shorter distances to travel.

The effects of yield level and utilization rate on the sustainability of ethanol production, however, were different depending on the yield level and the utilization rate (Figure U18). The results indicated that at higher productivity conditions and higher utilization rates, maize stover-based ethanol production is more sustainable than the one based on switchgrass. For instance, for yield levels of 7-10, the maize stover at 40% utilization (MS40) scenario was more sustainable than all switchgrass scenarios. For the yield level of 6, the MS40 scenario was more sustainable than the switchgrass at 60% utilization (SG60) and SG70 scenarios. For the yield level of 5, MS40 was more sustainable than SG60. The MS30 scenario was more sustainable than the SG60 and SG70 scenarios for the yield level of 9 and all switchgrass scenarios for the yield level of 10. For low productivity levels, on the other hand, using switchgrass was found to be more sustainable than using maize stover, regardless of utilization rates. For instance, for the yield levels of 1-4, all switchgrass scenarios had larger values of NEV than those of maize stover of all scenarios. Similarly, selecting switchgrass was more sustainable than selecting maize stover with lower utilization rates, regardless of yield levels. For instance, all switchgrass scenarios were more sustainable than the MS10 and MS20 scenarios for all yield levels.

The results also demonstrated which ethanol production system would be made more sustainable when two different feedstocks had different productivity levels and were utilized at different rates. Specifically, the results showed that the sustainability of ethanol production could be maximized

by selecting one of the two feedstocks depending on the productivity (yield) level and harvest removal rate available for each feedstock. For instance, for a farmer whose land productivity for maize stover and switchgrass was of level 7 and 3, respectively, and who had the option of utilizing 30% of maize stover and 70% of switchgrass biomass, growing maize stover would be more sustainable than growing switchgrass (Figure U16).

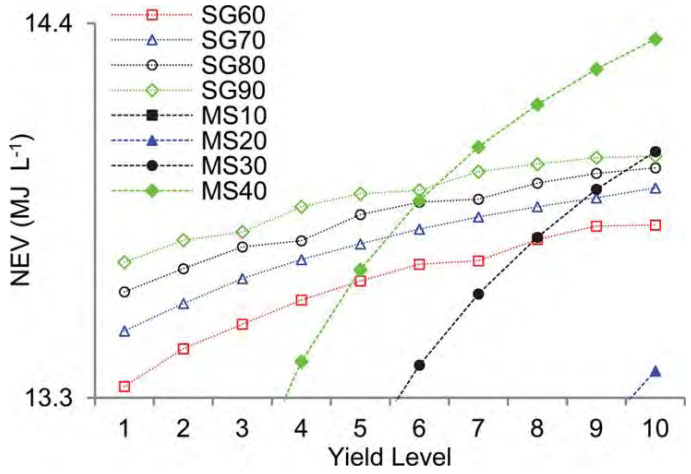


Figure U16. *The net energy value (NEV; MJ L^{-1}) of ethanol produced from maize stover and switchgrass for various yield levels and utilization rates for Mississippi, USA.*

Note: yield level 1 = lowest yield, …, 10 = highest yield; MS10 = maize stover at 10% utilization rate, …, SG90 = switchgrass at 90% utilization rate. MS10 has not been shown in the figure because its values were far smaller than those of switchgrass. Its inclusion would not clearly show the differences across switchgrass utilization rates.

Conclusions

The results demonstrated that biomass yield level and harvest removal (utilization) rate affect the sustainability and eco-friendliness of ethanol production associated with two major biomass feedstocks, namely maize stover and switchgrass. Both indices of sustainability and environment-friendliness – NEV and CCB, respectively – were found to increase with an increase in yield level and utilization rate. This increase was due to less land requirement for biomass production, smaller draw area, shorter travel distance, and ultimately less non-renewable energy consumption for the collection and transportation of biomass feedstock.

The environment-friendliness of switchgrass-based ethanol production was found to be higher than that of maize stover for all yield levels and utilization rates. This difference was due to higher carbon content, lower biomass to ethanol conversion ratio, and higher biomass yield of switchgrass. In terms of the sustainability of ethanol production, maize stover was better than switchgrass at higher yield levels (>6) with the highest utilization rate studied (40%). For other scenarios, however, switchgrass was better than maize stover. The study results might be helpful to energy crop farmers in maximizing the sustainability of ethanol production through the selection of one of the two feedstocks depending on the productivity level and harvest removal rate available for each feedstock.

The exact quantity of a crop residue that can be harvested for biofuel production has always been a subject of debate. So far, factors that determine how much residue needs to remain in the field include mainly soil sustainability-related environmental issues such as erosion, organic matter content, and fertility (nutrients). Previous studies have shown that an increase in the utilization rate of biomass for ethanol production decreases environmental sustainability (Kim and Dale, 2004; Petrolia, 2009; Sheehan et al., 2004). This study, however, showed that the energy sustainability as well as the eco-friendliness of ethanol production increases with an increase in utilization rate. These contrasting results, therefore, have again raised the question of the optimum utilization rate that is both environmentally and energetically sustainable. Thus, to find the complete picture of the effect of utilization rate on the environment and sustainability, a comprehensive analysis accounting for both types of sustainability (energetic and environmental) needs to be performed by including two additional variables – net energy value and carbon credit balance – in the list of the factors that are being considered as criteria for determining the amount of residue needed to be left in the field. This comprehensive analysis can be a subject matter for future studies.

References

Kim S, Dale BE. (2004). Global potential bioethanol production from wasted crops and crop residues. *Biomass Bioenergy*, 26:361-375.

Kiniry JR, Williams JR, Gassman PW, Debaeke P. (1992). A general, process-oriented model for two competing plant species. *Trans. ASAE*, 35:801-810.

Kiniry JR, Tischler CR, van Esbroeck GA. (1999). Radiation use efficiency and leaf CO_2 exchange for diverse C4 grasses. *Biomass Bioenergy*, 17:95-112.

Kiniry JR, Cassida KA, Hussey MA, Muir J P, Ocumpaugh WR, Read JC, Reed RL, Sanderson MA, Venuto BC, Williams JR. (2005). Switchgrass simulation by the ALMANAC model at diverse sites in the southern US. *Biomass Bioenergy*, 29:419-425.

McLaughlin SB, Bouton J, Bransby D, Conger BV, Ocumpaugh WR, Parrish DJ, Taliaferro C, Vogel KP, Wullschleger SD. (1999). Developing switchgrass as a bioenergy crop. In *Perspectives on New Crops and New Uses*; Janick J, Ed.; ASHS Press: Alexandria, VA, USA, pp. 282-299.

McLaughlin SB, Kszos LA. (2005). Development of switchgrass (*Panicum virgatum*) as a bioenergy feedstock in the United States. *Biomass Bioenergy*, 28:515-535.

Persson T, Garcia y Garcia A, Paz JO, Jones JW, Hoogenboom G. (2009). Maize ethanol feedstock production and net energy value as affected by climate variability and crop management practices. *Agric. Syst*., 100:11-21.

Persson T, Ortiz BV, Bransby DI, Wu W, Hoogenboom G. (2011). Determining the impact of climate and soil variability on switchgrass (*Panicum virgatum* L.) production in the southeastern USA: A simulation study. *Biofuels Bioprod. Biorefin*., 5:505-518.

Petrolia DR. (2009). Economics of crop residues: corn stover. In *The Role of Extension in Energy*; English BC, Menard J, Jensen K, Eds.; Farm Foundation: Oak Brook, IL, USA, pp. 58-59.

Sheehan J, Aden A, Paustian K, Killian K, Brenner J, Walsh M, Nelson R. (2004). Energy and environmental aspects of using corn stover for fuel ethanol. *J. Ind. Ecol*., 7:117-146.

Sokhansanj S, Kumar A, Turhollow AF. (2006). Development and implementation of Integrated Biomass Supply Analysis and Logistics model (IBSAL). *Biomass Bioenergy*, 30:838-847.

USDE. (2007). *Fact Sheet: Energy Independence and Security Act 2007*; United States Department of Energy (USDE): Washington DC, USA.

Woli P, Paz JO. (2011). Analyzing the effect of variations in soil and management practices on the sustainability of corn stover-based bioethanol production in Mississippi. *ASABE* Paper # 1111062.

Woli P, Paz JO. (2012). Evaluation of various methods for estimating global solar radiation in the southeastern USA. *J. Appl. Meteorol. Climatol*., 51:972-985.

Woli P, Paz JO, Lang DJ, Baldwin BS, Kiniry JR. (2012). Soil and variety effects on the energy and carbon balances of switchgrass-derived ethanol. *J. Sustainable Bioenergy Syst*., 2:65-74.

WSCO. (2003). Climatic Normals; Wisconsin State Climatology Office (WSCO): Madison, WI, USA. www.aos.wisc.edu/~sco/normals.html (accessed: 30 January 2013).

Parajuli:

Validation of forest biomass usage

Graduate student Trey Robinson continued his study in the Big Black River Watershed (BBRW) using the Soil and Water Assessment Tool (SWAT). The SWAT model calibration and validation process has been completed for forest biomass using different plant growth parameters (e.g. leaf area index, harvest index, biomass energy index, and plant height) and field observed data. Land use data was acquired from the USDA Crop Data Layer. Soil data was acquired from the NRCS, SSURGO soils database. The observed harvested biomass data for loblolly pine tree forests in Mississippi was obtained from the Mississippi State University Extension Service website (msucares.com). This data was used to calibrate and validate the SWAT model.

The first step to setting up the model was to calibrate for stream flow. Once stream flow was calibrated for the BBRW, annual pine tree biomass yields calibration was attempted. The preliminary results of the annual biomass yield calibration and validation process showed good correlation (R^2 = 0.38 and NSE = 0.33) in this study (Fig. U17).

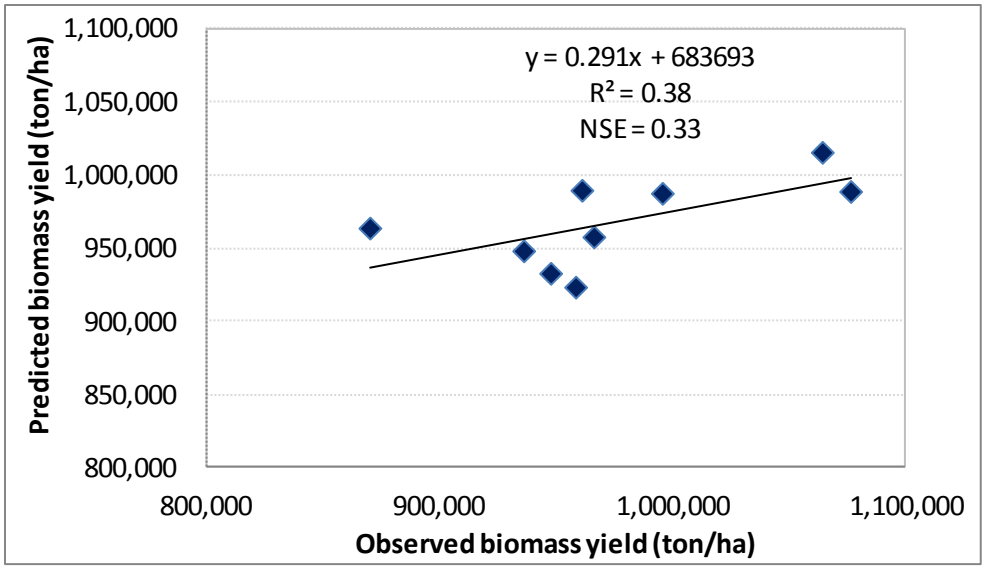


***Figure U17**: Model predicted vs. observed pine tree annual biomass yields (ton/ha)*

U.4.ML.3 Assess the effects of environmental conditions and management systems on the net energy value of feedstocks. (Yui)

Syngas upgrading to hydrocarbon fuels

Clean jet fuels production from biomass via gasification and conversion using a multifunctional catalyst

Currently commercial production of liquid hydrocarbon fuels is predominantly based on petroleum oil in the United State. Stringent environmental regulations have pushed conventional refineries to use more costly hydrogenation technologies to remove impurity in the raw oil and to improve the fuel quality. In the view of both energy efficiency and environmental impact, converting syngas into clean liquid fuels via advanced Fisher-Tropsch synthesis (FTS) routes has attracted industrial application interests for displacement of petroleum oil-based energy frame. Syngas can be derived from various non-petroleum resources, such as biomass. Biomass gasification releases a significantly lower amount of CO_2 than coal-based power generation in which no CO_2 capture is usually involved. Biomass is a renewable and low-carbon footprint source for syngas production. Biomass-derived syngas is further transformed into another form of energy resource, liquid hydrocarbons, which are readily blended with commercial fuels. Super clean fuels via FTS are achievable from biomass-derived syngas and believed to contribute to the environmental improvements in comparison with the best fuels available from conventional oil refineries.

The basis of this RFI is to design, build and operate a demonstration scale plant to produce mil-spec grade jet fuel using MSU's multifunctional catalyst technology. The proposed technology for converting biomass into jet fuel is based on gasification followed by syngas cleaning and FTS using multifunctional catalysts. Biomass, such as agricultural wastes and forestry wastes, will be used for gasification.

Central to this demonstration plant is the multifunction catalyst that has been developed and piloted by MSU. We believe this has the potential to make a significant advancement in the design of a BTL plant meeting the specific goals:

- Produce products that almost meet military specifications for jet fuel (JP-8 MIL-DTL-83133) (Wright-Patterson, 2013);
- Make significant progress toward compliance with the EISA 2007 §526 lifecycle GHG emission requirements; this can be achieved by using biomass feedstock.
- Make significant progress toward being cost competitive with conventional petroleum-based jet fuel.

Syngas Upgrading to Hydrocarbon Fuels' pathways regarding:

a. Key process characteristics (including feedstock type(s), intermediate product(s), deconstruction and intermediate upgrading technologies, primary product(s), and co-products);
Syngas upgrading to hydrocarbon fuels using oak or pine woodchips as feedstock yielded intermediate products of syngas, alcohol, and other fuels with upgrading (i.e. jet fuel). Co-products included other gases, liquid hydrocarbon, and biochar

b. Product yields;
Currently, the overall carbon monoxide conversion rate is about 80%, and the total liquid hydrocarbon selectivity is about 40%, and the jet-fuel range hydrocarbon selectivity accounts for 40% in the total liquid hydrocarbon fuels. Therefore, the carbon selectivity to jet-fuel range hydrocarbon is about 13%.

c. Current state of technology (including technology readiness level);

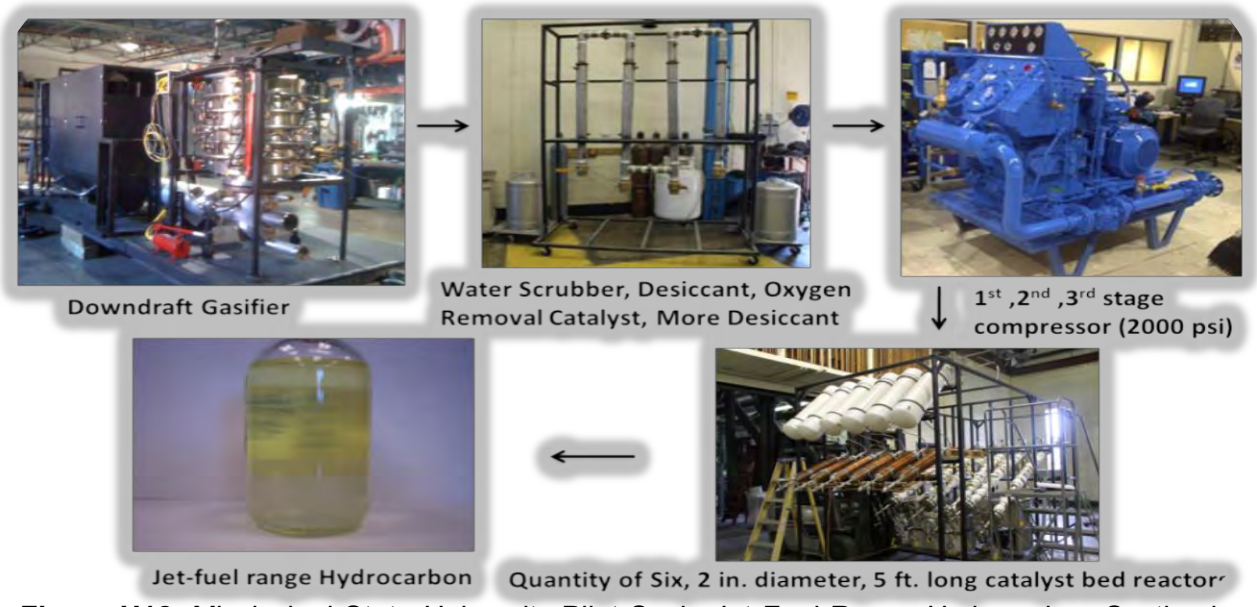


Figure U18. Mississippi State University Pilot Scale Jet-Fuel Range Hydrocarbon Synthesis via Biomass Gasification, Biomass-derived Syngas Cleaning, and Fischer–Tropsch Synthesis

The current state of technology readiness level is level 4 (fig. U18). Woody syngas was produced from oak chips (a moisture content 8.3% -10.8%) in a pilot-scale downdraft gasifier and passed through a cleaning system for impurity removal. The pilot-scale downdraft gasifier BioMax 25 was purchased from Community Power Corporation. The Capability of the production of biomass-derived syngas is about 65 m^3/h. The effluent raw biomass-derived syngas contained about 47% N_2, 21% CO, 18% H_2, 12% CO_2, 2% CH_4, some water vapor, and a trace amount of other gases.

The raw biomass-derived syngas from the gasifier was first passed through a pre-cleaning system under 0.34 MPa to remove the poisoning or negative components, e.g., sulfur, ammonia, tar, and moisture. Then, the cleaned gas was compressed to approximately 13.8 MPa using a two-stage pneumatic air pump obtained from Hydraulics International (Chatsworth, CA). A deep purification process was designed and installed before the Fischer – Tropsch reactor to eliminate oxygen, sulfur, ammonia, and tars under 6.89 MPa. The catalysts and adsorbents were selected from alumina-supported metal catalysts, molecular sieve 13 X, active carbon, silica gel and other high surface-area materials. The reactor system for cleaning was built with controlling parameters of temperature, pressure, and flow rate. The cleaned syngas meets the basic requirements for the following steps of catalytic conversion to liquid fuels; i.e., total sulfurs (H_2S + COS) < 10 ppb, NH_3 < 1 ppm, oxygen < 1 ppm, and tars < dew point. The cleaned biomass-derived syngas, which contained 47% N_2, 21% CO, 18% H_2, 12% CO_2, and 2% CH_4 was for the catalytic tests.

d. Current process economics (including finished product cost);
Our preliminary results showed that jet fuels were successfully synthesized from biomass-derived syngas over a 'cocktail'-type multifunctional catalyst (Yan et al. 2012). A cost analysis conducted based on the preliminary data shows that the operation cost mainly consisting of labor cost and general cost of the system accounts for around 50% of the total cost. Feedstocks and gasification capacity are also other major costs affecting the unit price of jet fuels. A reduction in the feedstock cost by 40% lowers the jet fuels cost by 10-20%. Biomass-derived jet fuel is projected around $3.5-5/ gallon when the gasification capacity is higher than 3000 Nm^3/h. Overall, our preliminary cost estimation indicates that biomass-derived jet fuels produced at a large scale appear to be cost competitive with commercial petroleum-based jet fuels.

e. Near/Mid/Long-term techno-economic potential (including target costs for primary product(s) and finished fuel);
Techno-economic analyses are performed on the syngas to mixed alcohols to hydrocarbons process. The target costs for primary products and finished fuel are.

f. Time horizon for commercial relevance (including when first commercial plant is expected to be built);
The first commercial plant is expected to be built in 2025.

g. Feedstock availability/flexibility;
The state of Mississippi is rich in oak and pine production (20 M acres of pine alone; MSU ES).

h. Potential volumetric impact in 2030;
The potential volumetric impact in 2030 will be about 2% among petroleum derived jet fuel.

i. Environmental performance (including life-cycle greenhouse gas emissions, water use, and water and air quality impacts);
Life-cycle analyses including greenhouse gas emissions, water use, and water and air quality impacts will be performed on the syngas to mixed alcohols to hydrocarbons process for jet fuel range hydrocarbon synthesis.

j. Co-product economics.
The co-product economics of gas hydrocarbon, other liquid hydrocarbon, and biochar will be carried out.

Critical barriers regarding the success of 'Syngas Upgrading to Hydrocarbon Fuels' pathway.

We believe that the demonstration of a multifunction catalyst FTS process can significantly improve the likelihood of the commercial production of biomass-derived jet fuel with environmental sustainability and economic viability. Construction and operation of the demonstration plant would enable development and advancement of many issues relating to economic and environmental benefits of BTL. The critical barriers regarding the success of the pathway are as follows: 1) feedstock selection and preprocessing; 2) highly functional cleaning systems for maintaining high quality syngas; 3) development of cost-effective synthesis catalysts; 4) extensive investigation of fundamental kinetics of the complex FTS system; 5) process integration for CO_2 utilization. The suggested technical approaches for addressing the above issues are described below:

1) Feedstock selection and preprocessing

Biomass with a low alkali content, such as wood, is preferred for gasification since potassium in biomass reacts with other silica in the ash, resulting in lower melting temperature that may form slag. These deposits can make syngas equipment cleanup difficult and would negatively impact a catalyst reactor tube.

2) Highly functional cleaning systems for maintaining high quality syngas

Raw syngas derived from biomass contains H_2 and CO as well as some impurities (e.g., CO_2, H_2O, tars, O_2, ammonia, H_2S, and particulates). Most of the impurities, especially sulfur compounds generated from biomass gasification, are highly toxic to the FTS catalysts and thus reduces syngas conversion efficiency (Yan et al. 2013). Therefore, syngas must be cleaned and purified for impurity removal before it is fed to the synthetic reactors. The target level of cleanup depends on the contaminant tolerance of FTS catalysts. Better understanding of detrimental effects of impurities on FTS catalysts will help select proper adsorbent media and methods for impurity removal. Adsorbent media, such as alumina-supported metal catalysts (e.g., Cu, Mn), 13 X molecular sieves, active carbon/biochar, and other high surface area materials have relatively low costs and can be explored for syngas cleaning. A cleaning system incorporating multiple cost-effective adsorbent media are essential for selective and efficient removal of syngas impurity.

3) Development of efficient and low cost heterogeneous synthesis catalysts

Fischer–Tropsch synthesis (FTS) is a major part of gas-to-liquids (GTL) technology. Controlling and maximizing selectivity is one of the main challenges with the FTS. Moreover, traditional FTS involves multiple processes to achieve the desired products. The use of a hybrid multifunctional FTS catalyst allows for simultaneous synthesis of methanol from syngas over the metallic function and transformation of methanol into target hydrocarbons over the acidic function. Selective synthesis of jet fuel-rich hydrocarbons from syngas can be accomplished in one-stage reaction by developing novel multifunctional catalysts. High selectivity towards target products ensures clean production of jet fuels since a low amount of impurities is produced. Moreover, one-stage reaction process is more efficient and more economic than two or multiple-stage synthesis.

4) Extensive investigation of fundamental kinetics of the complex FTS system

Probing into active sites of the catalysts and *in situ* measurement of the reaction intermediates provides a comprehensive understanding of FTS reaction mechanism behind the selective synthesis of jet fuels from syngas. Physics/imaging/chemistry tools can be used to study the molecular and atomic nature of FTS catalysts during their interaction with CO and H_2 as well as reaction intermediates. Detailed kinetics results along with an understanding of the thermodynamics provide a solid basis for reaction engineering. Studies of the catalysts, kinetics and reactors, and other fundamental aspects of FTS form all important concepts of the further scaling-up efforts. These investigations are also helpful in reducing operational risks in large-scale plants.

5) Process integration for CO_2 capture and utilization

Through the biomass to liquid technology, most of carbon is transformed into liquid hydrocarbons. A small amount of carbon releases as a form of CO_2 from gasification and catalytic conversion process. Thus, this technology itself appears to have a significantly lower CO_2 emission than petroleum-based jet fuel production. In order to further reduce CO_2 emission, generated CO_2 can be captured and then used as a reactant agent to gasify chars that are produced as a by-product during biomass gasification. This integrated process provides an enclosed loop for maximizing carbon utilization and significantly reducing CO_2 emission. Process integration for CO_2 capture and utilization makes the proposed technology more environmental sustainable and energy efficiency.

References:

Wright-Patterson jet fuel analysis report number: POSF 10293. **2013**.

Yan, Q., Yu, F., Liu, J., Street, J., Gao, J., Cai, Z., and Zhang. J. **2012**. Catalytic Conversion Wood Syngas to Synthetic Aviation Turbine Fuels over A Multifunctional Catalyst. *Bioresource Technology*, 127:281-290.

Yan, Q., Wan, C., Street, J., Yan, D., Han, J., and Yu. F. **2013**. Catalytic Removal of Oxygen from Biomass-derived Syngas. *Bioresource Technology.* 147:117–123.

Yan, Q., Lu, Y., Wan, C., Han, J., Rodriguez, J., Yin, J., Yu, F. Synthesis of Aromatic-rich Gasoline-Range Hydrocarbons from Biomass-Derived Syngas over a Pd-Promoted Fe/HZSM-5 Catalyst. **2014**. *Energy Fuels* 28, 2027–2034.

Task V. Pilot Plant Operations

Principle Investigators and team members:

Larry Pearson, Institute of Clean Energy Technology
Tony Wofford, Institute of Clean Energy Technology

The objective of this task is to provide infrastructure and operational support to achieve pilot testing goals for Tasks P, Q, and R. This objective will include modifications to existing pilot equipment, as well as, installation of additional equipment according to testing plans or results. Safety and environmental monitoring will be conducted by onsite personnel.

Executive Summary:

The objective of Task V was to provide support for pilot operations as detailed in Tasks P, Q, and R. This objective consisted of the installation, modification, and maintenance of utility and pilot system infrastructure required for the safe and environmentally compliant operation of the Biocrude/Microbial Oil and Bio-Oil Pilot Test Facilities. In addition, maintenance was to be provided for the pilot building structure and non process related components.

Activities supporting the Task P Bio-oil pilot system included modifications to detect and prevent hazardous conditions involving gases produced during pilot system operation. These modifications included installation of area monitors for carbon monoxide and combustible hydrocarbons above and around process equipment. In addition, an oxygen sensor was installed in the flare header to allow rerouting of gases in the event of the production of a combustible mixture during pilot plant operation.

Support was also provided to allow increased pilot plant capacity. These included installation of a larger peristaltic process gas pump and replacement of the chilled water system for condensation of the product bio-oil. In addition, equipment was installed to allow testing of a fluid bed dryer and related sawdust feed conveyors.

Activities supporting the Task Q and Task R Biocrude pilot plant operations included modifications to the waste water collection system and feed tanks. A centrifuge was tested as a replacement for the original membrane filter system for solids removal. In addition, an extraction vessel was installed and tested for oil removal from collected solids.

For all tasks, Task P, Q, and R, routine maintenance on utility infrastructure and pilot plant equipment was required. In addition, maintenance was required on building infrastructure which included modifications to the air conditioning system.

Planned Activites:
V.1.ML.1 Successfully operate the pilot scale facility to produce biocrude/microbial oil and bio-oil.

Summarization of Activities:
Task V activities were focused on support for pilot operations as detailed in Tasks P, Q, and R. These activities included maintenance and modification of both utility and pilot system infrastructure, as required, to assist in the successful production of biocrude and bio-oil. In addition, maintenance was to be provided for the pilot building structure and non-process related components.

The Task P Bio-oil pilot system is located in the outdoor process area. Support for the initial operation and production of bio-oil required the installation and commissioning of electrical, air, and process water utilities. Continued testing and operations of the bio-oil pilot system required additional support. Area monitors were installed to detect the presence of carbon monoxide and combustible hydrocarbons above and around process equipment that could potentially create an explosion or personnel exposure hazard. An oxygen sensor and process piping was installed in the flare line to prevent an explosion from the production of a combustible mixture in the bio-oil reactor system. This arrangement allowed for the feeding of methane into the flare header to lower the oxygen level or for bypassing the flare if required. Instrumentation was also installed to monitor and database the pyrolysis reactor electrical heating load in real time. The distributed network control system was deleted due to integration issues with the Adams Control Modules, which were used to control the majority of the bio-oil pilot system. Process variables were instead sent directly to the Adams control system.

To allow a higher biomass throughput, the peristaltic gas pump on the system was resized. To accommodate the higher gas flow, a larger flare line seal vessel was installed immediately upstream of the flare. In addition, the bio-oil condensers required more cooling capacity than was available with the original chilled water system. This system was replaced with a larger chiller system, which included a reservoir, transfer piping, and electrical switchgear. As part of Task P, a wood handling system was installed adjacent to the bio-oil pilot system outside of the covered area. This system consisted of a tote bag unloading hoist, a natural gas fluid bed dryer, a weigh feed device, and associated transfer screw conveyors. Electrical, air, and natural gas utility connections were installed and tested. To alleviate weather related concerns, the entire wood handling system was covered with a tin structure.

Activities for the Bio-crude/Microbial oil projects, Task Q and R, were conducted within the indoor pilot area. Utility infrastructure supporting these tasks included 100 psig steam, process water, process air, chilled water, and electrical power. Continued testing and modifications to the pilot systems required additional support. A waste water collection system was installed to handle flushes, as well as, membrane filter and steam trap discharges. The exhaust from the spray drying system was routed outside to alleviate noise and humidity issues within the indoor process area. Additional steam piping was run to provide heating to feed vessels. Tank mixers were modified to increase low volume mixing efficiency.

As part of Task Q and R activities, a centrifuge was installed and operated as a replacement for membrane filter solids separation. A stand was also constructed to allow solvent extraction experimentation on the collected oil-containing solids.

For all tasks, Task P, Q, and R, routine maintenance on utility infrastructure and pilot plant equipment was required. In addition, maintenance was required on building infrastructure which included modifications to the air conditioning system.

Task W. Project Management and Reporting

This project is divided into seven tasks (bio-oil, biocrude, microbial oil, hydrocarbons derived from syngas, biomass combustion, feedstock development and pilot plant operation). Each task is led by a task leader and a group of faculty, graduate students and staff who report to the task leader. Task groups will meet monthly to discuss the progress toward milestones, intellectual property, and the status of national laboratory, industry and other relevant partnerships. Each task will compile quarterly reports and a final report as part of their responsibility.

W.1 Quarterly reports for this project for two years

Milestone:
W.1.DL.1 Prepare and submit quarterly reports for the project.

Summarization of Activities:
Quarterly reports were submitted.

W.2 Final reports for each task

Milestone:
W.2.DL.1 Prepare and submit final reports for each task

Summarization of Activities:
Final report was submitted.

W.3 Develop partnerships with national laboratories, industries and other research groups

Milestone:
W.3.DL.1 Provide leadership to each task to develop partnerships with national laboratories, industries and other research groups and report these in quarterly reports.

Summarization of Activities:

The SERC team met frequently with companies and agencies to promote economic development of the institute's technologies. Representatives from SERC met with a number of companies, laboratories, government agencies, and universities to discuss collaboration.

SERC Report

F. Information Regarding Projects involving Computer Modeling:

a. Model description, key assumptions, version, source and intended use:

Problem Description:
The main objective of this research is to build models that aid the design and management of biodiesel supply chains while taking uncertainties into account. We propose an extension of the two-stage location-transportation stochastic programming model in order to capture the tradeoffs that exist between location and transportation costs; the tradeoffs that exist between cost and emission in this supply chain; and the uncertain nature of sludge supply and technology development. The model we propose identifies locations for biocrude plants, selects one or a combination of transportation modes for delivering sludge, and finally identifies transportation quantities between different stages of the supply chain. Figure 1 presents the structure of the biodiesel supply chain consisting of three sludge suppliers, two potential locations for biocrude plants, two diesel production plants, and three customers.

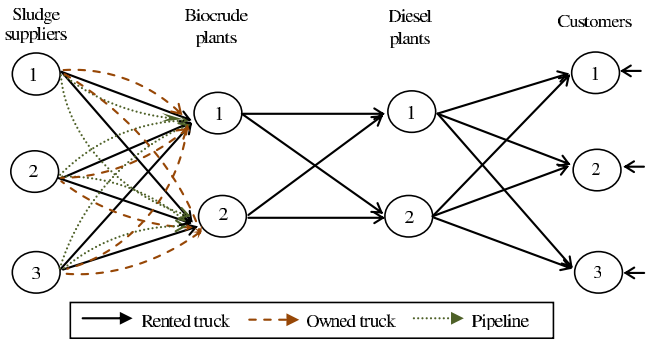


Figure 1: Network representation of Biodiesel Supply Chain (BSCN).

The Biodiesel Supply Chain Network (BSCN) for production of biodiesel consists of a set of nodes $\mathcal{N}$ and a set of arcs $\mathcal{A}$. The set of nodes consists of subset $\mathcal{K}$ representing sludge supply nodes, subset $\mathcal{J}$ representing potential biocrude plant locations, subset $\mathcal{I}$ representing diesel plants, and subset $\mathcal{G}$ representing customer locations. In this network, nodes in $\mathcal{K}$ have a sludge supply which could be used to produce biocrude and eventually biodiesel. Existing diesel plants process biocrude into biodiesel. The demand in each node of $\mathcal{G}$ represents a customer's demand for biodiesel. Nodes in $\mathcal{J}$ and $\mathcal{I}$ are transshipment nodes.

Three different products flow along the arcs of this network: sludge flows from supply to biocrude plant nodes; biocrude flows from biocrude plants to diesel plant nodes; and biodiesel flows from diesel plants to customer nodes. There are three arcs between each supply and biocrude plant nodes. We use these arcs to represent the fact that three different modes of transportation could be used to ship sludge: pipeline, facility owned truck, and rented truck. A single transportation arc exists between each biocrude plant and diesel plant node and between diesel plant and customer node, which represent the use of rented trucks for shipment of biodiesel and diesel. We consider additional transportation modes are used for shipping sludge when the transportation volume is high.

The transportation cost function for facility owned trucks and pipelines consists of a fixed and a variable component. The fixed cost component for facility owned trucks consists of the annual sales tax, insurance cost, management cost, and overhead cost. These costs are not a function of the distance traveled or quantity shipped, and this is why we consider them to be fixed. The variable costs include the fuel, labor, tire, maintenance and repair costs. The fixed costs for pipeline transportation represent the cost of establishing a pipeline of a particular capacity, and the variable cost represents the cost of operating the pipeline. Transportation costs for rented trucks have only a variable component (given in \$/(mile*ton)) which represents a fixed \$ amount typically charged by third-party service providers per mile and per ton shipped [8, 18].

Let ν_m^p be the fixed transportation cost (\$ per full-truck load) for product p ($p \in \mathcal{P}$) when using transportation mode m (m = Facility owned truck, Rented truck). Let, β_m^p be the variable transportation cost (\$/mile per full-truck load) for product p when using transportation mode m, and ξ_m^p transportation capacity of mode m to ship product p. Let α_f be the variable unit cost for operating a pipeline of capacity f, d_{ij} distance from node i to node j.

Equation (1) presents the unit cost (\$/ton) for transporting sludge from a supply node $k \in \mathcal{K}$ to a biocrude plant $j \in \mathcal{J}$.

$$c_{kjm}^1 = \begin{cases} \frac{\beta_1^1 * d_{kj}}{\xi_1^1} & \text{for } m = \text{Rented truck}, \\ \frac{\nu_2^1 + \beta_2^1 * d_{kj}}{\xi_2^1} & \text{for } m = \text{Facility-owned truck}, \\ \alpha_f * d_{kj} & \text{for } m = \text{Pipeline}; f = 1, \ldots, \mathcal{F}. \end{cases} \tag{1}$$

Equations (2) and (3) present unit transportation costs (\$/gallon) for a rented truck when used for biocrude and biodiesel shipments.

$$c_{ji}^2 = \frac{\nu_2^2 + \beta_2^2 * d_{ji}}{\xi_2^2} \qquad \text{for } j \in \mathcal{J}, i \in \mathcal{I}. \tag{2}$$

$$c_{ig}^3 = \frac{\nu_2^3 + \beta_2^3 * d_{ig}}{\xi_2^3} \qquad \text{for } i \in \mathcal{I}, g \in \mathcal{G}. \tag{3}$$

With each arc of the network we associate not only transportation costs but also transportation-related emissions. Let e_{kjm}^1 denote emissions (kg of CO_2) due to shipping 1 ton of sludge from location $k \in \mathcal{K}$ to $j \in \mathcal{J}$ using transportation mode m. Let, e_{ji}^2 denote emissions due to shipping 1 gallon of biocrude from $j \in \mathcal{J}$ to $i \in \mathcal{I}$ using trucks, and let e_{ig}^3 denote emissions due to shipping 1 gallon of biodiesel from $i \in \mathcal{I}$ to $g \in \mathcal{G}$ using trucks. Equations (4) to (7) are used to calculate emissions along the transportation arcs. These equations were developed in a recent work by [16]. Appendix A presents the formulas we use to calculate emissions for each mode of transportation.

$$\begin{aligned} e_{kjm}^1 &= \zeta_m^1 + \tau_m^1 * d_{kj} \\ &\quad \text{for } \ m = \text{Facility owned, Rented truck} && (4) \\ e_{kjm}^1 &= (0.746 * P_p * \pi_h * E^e * n_{kj}) / \Upsilon_p * C_p \\ &\quad \text{for } \ m = \text{Pipeline} && (5) \\ e_{ji}^2 &= \zeta_2^2 + \tau_2^2 * d_{ji} && (6) \\ e_{ig}^3 &= \zeta_2^3 + \tau_2^3 * d_{ig} && (7) \end{aligned}$$

In these equations, ζ_m^p and τ_m^p denote the fixed (kg/ton) and variable (kg/(ton*mile)) emissions. Fixed emissions are a function of the power requirements and the efficiency of the pump used during loading and unloading of a truck or a pipeline. For truck transportation, variable emissions depend on the distance traveled and the type of truck used. The definition of variable emissions for pipeline transportation is somewhat different because emissions are a function of capacity and length of the pipeline. For pipeline transportation, variable emissions depend on the power of the pump used P_p (hp), pump efficiency Υ_p, number of operating hours per year π_h (hr/year), number of booster pumps required from origin k to destination j, n_{kj}, pipeline capacity C_p (tons/year), and the amount of CO_2 emitted per kWh of electricity generated E^e (kg/kWh).

Formulation of the Two-Stage Stochastic Programming Model without Carbon Emissions Considerations: The two-stage stochastic programming model we present below allows us to capture the impact of the stochastic nature of sludge supply on location and transportation decisions in the supply chain; it also allows us to capture the timing of decisions in the supply chain. Facility location decisions, pipeline establishment decisions, and decisions about the number of trucks to purchase are long-term decisions made prior to observing the realization of biomass supply. These are the first-stage decisions in our model, which define the structure of the supply chain. Once these decisions are made, then, based on the availability of biomass supply -the realization of supply - the operational decisions related to biocrude and biodiesel production and transportation are made. For simplicity, the formulation below only captures sludge supply uncertainties.

The first-stage decision variables for our model are X_{lj} which is a binary variable that takes the value 1 if a biocrude plant of capacity $l \in \mathcal{L}$ is located at site $j \in \mathcal{J}$, and 0 otherwise; Z_{fkj} which is a binary variable that takes the value 1 if a pipeline of capacity $f \in \mathcal{F}$ is installed between supplier $k \in \mathcal{K}$ and biocrude plant $j \in \mathcal{J}$, and 0 otherwise; V_j which is the total number of trucks purchased for shipping sludge to biocrude plant $j \in \mathcal{J}$. Due to the physical characteristics of sludge and biocrude, the same trucks cannot be used to ship both products.

The investment cost for a biocrude plant of capacity $l \in \mathcal{L}$ is denoted by ψ_l. The investment costs for establishing a pipeline of capacity $f \in \mathcal{F}$ are denoted by ϑ_f. The purchase cost of a truck is denoted by v_1^1. Let $s_k(\omega)$ denote the amount of sludge available at site $k \in \mathcal{K}$ under scenario $\omega \in \Omega$. The model considers a fixed number of scenarios ($|\Omega|$), each of which represents a particular realization of biomass supply in each supply node. There is a positive probability ($prob(\omega)$) associated with each scenario.

Here are the second stage decision variables. The amount of sludge available for production of biodiesel at node $k \in \mathcal{K}$ under each scenario ω affects the amount of sludge transported to biocrude plant $j \in \mathcal{J}$. This amount in our model is represented by the decision variable $Y_{kjm}^1(\omega)$. Sludge availability under a particular scenario ω also impacts the values of the following decision variables: $W_{lj}(\omega)$ which is the amount of biocrude produced at plant $j \in \mathcal{J}$ of capacity $l \in \mathcal{L}$; $Y_{ji}^2(\omega)$ which is the amount of biocrude shipped from plant $j \in \mathcal{J}$ to diesel refinery $i \in \mathcal{I}$; $Y_{ig}^3(\omega)$ which is the amount of biodiesel shipped from diesel refinery $i \in \mathcal{I}$ to customer $g \in \mathcal{G}$; and $U_g(\omega)$ which is the amount of biodiesel shortage at customer g. The decision variables introduced in this paragraph are scenario-specific and are known as the second-stage or recourse variables. We assume that there are substitute products (such as, soybean-, canola-, sunflower-, palm- or coconut oil-based biodiesels) which can be used to satisfy customers' demand for biodiesel. The best market price for a substitute product is denoted by ρ. This price, which is exogenously determined, equivalently represents the penalty paid for not satisfying customers' demand. The value of this penalty serves as a threshold level for the unit cost of delivering biodiesel to the market since there is no point in producing a product at a cost higher than the existing market price.

Other parameters that we use in the model formulation are ϕ which is the conversion rate (tons/gallon) of sludge to biocrude; γ which is the conversion rate (gallon/gallon) of biocrude to biodiesel; p_l^1 which is the unit production cost at a biocrude plant of capacity $l \in \mathcal{L}$; p_i^2 which is the unit production cost of biodiesel at diesel refinery $i \in \mathcal{I}$; b_g which is the demand for biodiesel at customer $g \in \mathcal{G}$; and q_i which is production capacity of biodiesel plant $i \in \mathcal{I}$.

The objective function of the biocrude supply chain network (BSCN) design model we propose minimizes the expected annual costs of the supply chain. This objective totals the first-stage costs and the expected second-stage costs. The first-stage costs comprise the annual equivalent investment costs to locate biocrude plants, to install pipelines, and to purchase trucks at biocrude plants. The second stage costs comprise the expected production, transportation, and penalty costs. The following is our model formulation.

$$\text{(BSCN): Minimize z}= \sum_{j\in\mathcal{J}}\sum_{l\in\mathcal{L}} \psi_l X_{lj} + \sum_{f\in\mathcal{F}}\sum_{k\in\mathcal{K}}\sum_{j\in\mathcal{J}} \vartheta_f Z_{fkj} + \sum_{j\in\mathcal{J}} v_1^1 V_j + E_\omega\{\sum_{k\in\mathcal{K}}\sum_{j\in\mathcal{J}}\sum_{m\in\mathcal{M}} c_{kjm}^1 Y_{kjm}^1(\omega)$$

$$+ \sum_{j\in\mathcal{J}}\sum_{i\in\mathcal{I}} c_{ji}^2 Y_{ji}^2(\omega) + \sum_{i\in\mathcal{I}}\sum_{g\in\mathcal{G}} (c_{ig}^3 + p_i^2) Y_{ig}^3(\omega) + \sum_{l\in\mathcal{L}}\sum_{j\in\mathcal{J}} p_l^1 W_{lj}(\omega) + \sum_{g\in\mathcal{G}} \rho U_g(\omega)\}$$

Subject to

$$\sum_{l\in\mathcal{L}} X_{lj} \leq 1 \qquad \forall j \in \mathcal{J} \tag{8}$$

$$\sum_{j\in\mathcal{J}}\sum_{m\in\mathcal{M}} Y^1_{kjm}(\omega) \leq s_k(\omega) \quad \forall k \in \mathcal{K}, \omega \in \Omega \tag{9}$$

$$Y^1_{kjm}(\omega) - \xi^1_1 t_{kj} V_j \leq 0 \quad \forall k \in \mathcal{K}, j \in \mathcal{J}, \omega \in \Omega, m = \text{Fcl. own. truck} \tag{10}$$

$$Y^1_{kjm}(\omega) - \sum_{f\in\mathcal{F}} f * Z_{fkj} \leq 0 \quad \forall k \in \mathcal{K}, j \in \mathcal{J}, \omega \in \Omega, m = \text{Pipeline} \tag{11}$$

$$W_{lj}(\omega) \leq l * X_{lj} \quad \forall l \in \mathcal{L}, j \in \mathcal{J}, \omega \in \Omega \tag{12}$$

$$\sum_{k\in\mathcal{K}}\sum_{m\in\mathcal{M}} \phi Y^1_{kjm}(\omega) = \sum_{l\in\mathcal{L}} W_{lj}(\omega) \quad \forall j \in \mathcal{J}, \omega \in \Omega \tag{13}$$

$$\sum_{i\in\mathcal{I}} Y^2_{ji}(\omega) = \sum_{l\in\mathcal{L}} W_{lj}(\omega) \quad \forall j \in \mathcal{J}, \omega \in \Omega \tag{14}$$

$$\sum_{j\in\mathcal{J}} \gamma Y^2_{ji}(\omega) = \sum_{g\in\mathcal{G}} Y^3_{ig}(\omega) \quad \forall i \in \mathcal{I}, \omega \in \Omega \tag{15}$$

$$\sum_{g\in\mathcal{G}} Y^3_{ig}(\omega) \leq q_i \qquad \forall i \in \mathcal{I}, \omega \in \Omega \tag{16}$$

$$\sum_{i\in\mathcal{I}} Y^3_{ig}(\omega) + U_g(\omega) = b_g \qquad \forall g \in \mathcal{G}, \omega \in \Omega \tag{17}$$

$$X_{lj} \in \{0,1\} \quad \forall l \in \mathcal{L}, j \in \mathcal{J} \tag{18}$$

$$Z_{fkj} \in \{0,1\} \quad \forall f \in \mathcal{F}, k \in \mathcal{K}, j \in \mathcal{J} \tag{19}$$

$$V_j \in Z^+ \qquad \forall j \in \mathcal{J} \tag{20}$$

$$Y^1_{kjm}(\omega) \geq 0 \quad \forall k \in \mathcal{K}, j \in \mathcal{J}, m \in \mathcal{M}, \omega \in \Omega \tag{21}$$

$$Y^2_{ji}(\omega) \geq 0 \quad \forall j \in \mathcal{J}, i \in \mathcal{I}, \omega \in \Omega \tag{22}$$

$$Y^3_{ig}(\omega) \geq 0 \quad \forall i \in \mathcal{I}, g \in \mathcal{G}, \omega \in \Omega \tag{23}$$

$$W_{lj}(\omega) \geq 0 \quad \forall l \in \mathcal{L}, j \in \mathcal{J}, \omega \in \Omega \tag{24}$$

$$U_g(\omega) \geq 0 \quad \forall g \in \mathcal{G}, \omega \in \Omega \tag{25}$$

Constraints (8) ensure that at most one biocrude plant of capacity $l \in \mathcal{L}$ is operating at a particular location $j \in \mathcal{J}$. Constraints (9) ensure that the amount of sludge shipped from supplier $k \in \mathcal{K}$ is less than or equal to the amount of sludge available under scenario ω. Constraints (10) limit the amount of sludge transported by facility owned trucks at plant $j \in \mathcal{J}$. This amount depends on the number of trucks purchased, truck capacity, and the number of trips between supplier k and plant j (denoted by parameter t_{jk}). Constraints (11) show that the maximum amount of sludge transported by pipeline is limited by pipeline capacity. Note that in our model we assumed that the number of available rented trucks is not limited; therefore, we did not impose any capacity constraints for the rented trucks. Constraints (12) connect the binary biocrude facility location variables with the continuous biocrude production variables. These constraints also show that the total amount of biocrude produced is limited by production capacity of the plant. Constraints (13) calculate the total amount of biocrude produced from sludge at plant $j \in \mathcal{J}$ under scenario ω. Constraints (14) are the flow balance constraints at biocrude plant $j \in \mathcal{J}$. Constraints (15) are the flow balance constraints at diesel refinery $i \in \mathcal{I}$. Constraints (16) show that the total amount of biodiesel shipped from a diesel refinery is limited by its production capacity. Constraints(17) are the flow conservation constraints at customer $g \in \mathcal{G}$. These constraints indicate that customers' demand for biodiesel will be fulfilled either by using biocrude or other substitute products. Constraints (18) and (19) are binary constraints, and constraints (20) are the integrity constraints. Finally, (21) to (25) are the nonnegativity constraints.

Model Extension with Carbon Emission Considerations: This section presents four extensions of the (BSCN) model formulation to capture the impact that different carbon regulatory policies have on the supply chain design and management decisions. These policies include carbon cap, carbon tax, carbon cap-and-trade, and carbon offset. These extensions were inspired by recent work from Benjaafar et al. [3] who explores the impact of those carbon-regulatory policies on supply chain operations. The authors also provide similar extensions for the classical economic lot-sizing problem.

In this research we focus only on CO_2 emissions due to production and transportation in the supply chain since they contribute more than 95% of the total GHG emissions. The goal is to show later on in the computational results that certain modifications to production and transportation-related decisions (such as transportation mode selection, production schedule, and shipment schedule) can significantly reduce system-wide emissions at minimum cost.

Model Formulation of Carbon Cap Policy: Under a carbon cap policy, a company has a limited amount of carbon allowances to use, which is referred to as the *carbon cap* and denoted by c^{cap}. The World Resources Institute (WRI) has developed tools which support consistent and transparent public reporting of corporate value chain emissions [1]. Based on these standards, companies should account for emissions within their facility as well as emissions due to related upstream and downstream activities. That means, a biocrude plant should also be counting emissions due to in-bound and out-bound supply chain activities. In order to present this limitation posed on the supply chain operations due to the carbon cap policy, we add the following constraints to (BSCN) model formulation. We refer to this new formulation as (BSCN-Cap) model.

$$\sum_{k\in\mathcal{K}}\sum_{j\in\mathcal{J}}\sum_{m\in\mathcal{M}} e^1_{kjm}Y^1_{kjm}(\omega)+\sum_{l\in\mathcal{L}}\sum_{j\in\mathcal{J}} e^4_{lj}W_{lj}(\omega)+\sum_{j\in\mathcal{J}}\sum_{i\in\mathcal{I}} e^2_{ji}Y^2_{ji}(\omega)+\sum_{i\in\mathcal{I}}\sum_{g\in\mathcal{G}}(e^3_{ig}+e^5_{ig})Y^3_{ig}(\omega)\le c^{cap} \quad \forall\omega\in\Omega \tag{26}$$

Here, e^4_{lj} denotes emissions per gallon of biocrude produced at a facility of capacity $l\in\mathcal{L}$, and e^5_{ig} denotes emissions due to biodiesel production at a diesel refinery.

Model Formulation of Carbon Tax Policy: A carbon tax policy imposes a financial penalty per unit of CO_2 emitted. Such a mechanism sets no limit on CO_2 emissions in the supply chain. This formulation assumes a linear relationship between emissions and carbon taxes. Let c^{tx} be the amount of tax paid per unit of CO_2 emitted. The objective function of the (BSCN) model is updated as follows to account for these taxes. We refer to this new formulation as (BSCN-Tax) model.

$$\text{Minimize z}=\sum_{j\in\mathcal{J}}\sum_{l\in\mathcal{L}}\psi_l X_{lj}+\sum_{f\in\mathcal{F}}\sum_{k\in\mathcal{K}}\sum_{j\in\mathcal{J}}\vartheta_f Z_{fkj}+\sum_{j\in\mathcal{J}} v^1_1V_j+E_\omega\{\sum_{k\in\mathcal{K}}\sum_{j\in\mathcal{J}}\sum_{m\in\mathcal{M}}(c^1_{kjm}+c^{tx}e^1_{kjm})Y^1_{kjm}(\omega)$$
$$+\sum_{j\in\mathcal{J}}\sum_{i\in\mathcal{I}}(c^2_{ji}+c^{tx}e^2_{ji})Y^2_{ji}(\omega)+\sum_{i\in\mathcal{I}}\sum_{g\in\mathcal{G}}(c^3_{ig}+p^2_i+c^{tx}(e^3_{ig}+e^5_{ig}))Y^3_{ig}(\omega)+\sum_{l\in\mathcal{L}}\sum_{j\in\mathcal{J}}(p^1_l+c^{tx}e^4_{lj})W_{lj}(\omega)+\sum_{g\in\mathcal{G}}\rho U_g(\omega)\}$$

Model Formulation of Carbon Cap-and-Trade Policy: A carbon cap-and-trade policy imposes a carbon cap on supply chain operations. However, a carbon market exists where companies can trade their carbon allowances. A company can sell unused carbon allowances, or it can purchase additional carbon allowances to maintain supply chain operations. We make the following reasonable assumptions to reformulate the (BSCN) model under a carbon cap-and-trade policy: (a) carbon selling and purchasing prices are equal; (b) there is no limit on the amount of carbon allowances sold/purchased, and carbon trading decisions of this supply chain do not impact the market price; (c) the total cost/benfit function due to purchasing/selling carbon allowances is linear.

Let, c^p denote the market price per unit (kg) of carbon traded, and $c^{t+}(\omega)$ and $c^{t-}(\omega)$ denote the amount of carbon allowance purchased and sold under scenario ω. We propose the following formulation for this problem which we refer to as the (BSCN-CAT) model.

$$\text{Minimize z}=\sum_{j\in\mathcal{J}}\sum_{l\in\mathcal{L}}\psi_l X_{lj}+\sum_{f\in\mathcal{F}}\sum_{k\in\mathcal{K}}\sum_{j\in\mathcal{J}}\vartheta_f Z_{fkj}+\sum_{j\in\mathcal{J}} v^1_1V_j+E_\omega\{\sum_{k\in\mathcal{K}}\sum_{j\in\mathcal{J}}\sum_{m\in\mathcal{M}} c^1_{kjm}Y^1_{kjm}(\omega)+\sum_{j\in\mathcal{J}}\sum_{i\in\mathcal{I}} c^2_{ji}Y^2_{ji}(\omega)+$$
$$\sum_{i\in\mathcal{I}}\sum_{g\in\mathcal{G}}(c^3_{ig}+p^2_i)Y^3_{ig}(\omega)+\sum_{l\in\mathcal{L}}\sum_{j\in\mathcal{J}} p^1_lW_{lj}(\omega)+\sum_{g\in\mathcal{G}}\rho U_g(\omega)+c^p(c^{t+}(\omega)-c^{t-}(\omega))\}$$

subject to: (8)-(25)

$$\sum_{k\in\mathcal{K}}\sum_{j\in\mathcal{J}}\sum_{m\in\mathcal{M}} e^1_{kjm}Y^1_{kjm}(\omega)+\sum_{l\in\mathcal{L}}\sum_{j\in\mathcal{J}} e^4_{lj}W_{lj}(\omega)+\sum_{j\in\mathcal{J}}\sum_{i\in\mathcal{I}} e^2_{ji}Y^2_{ji}(\omega)+$$
$$\sum_{i\in\mathcal{I}}\sum_{g\in\mathcal{G}}(e^3_{ig}+e^5_{ig})Y^3_{ig}(\omega)+c^{t-}(\omega)\le c^{cap}+c^{t+}(\omega)\quad\forall\omega\in\Omega \tag{27}$$
$$c^{t+}(\omega)\ge 0\quad\forall\omega\in\Omega \tag{28}$$
$$c^{t-}(\omega)\ge 0\quad\forall\omega\in\Omega \tag{29}$$

Model Formulation of Carbon Offset Policy: A carbon offset policy works like a carbon cap-and-trade policy. This policy imposes a carbon cap. A carbon market exists where additional carbon allowances can be purchased, if necessary, to maintain operations. However, unused carbon allowances cannot be sold. This implies that the supply chain of a product does not benefit from emitting less carbon than the corresponding cap.

Let, c^o be the unit price of carbon offset and $c^{t+}(\omega)$ denote the amount of carbon allowance purchased under scenario ω. We propose the following formulation for this problem which we refer to as (BSCN-CO) model.

$$\text{Minimize z}= \sum_{j\in\mathcal{J}}\sum_{l\in\mathcal{L}}\psi_l X_{lj}+\sum_{f\in\mathcal{F}}\sum_{k\in\mathcal{K}}\sum_{j\in\mathcal{J}}\vartheta_f Z_{fkj}+\sum_{j\in\mathcal{J}}v_1^1 V_j+E_\omega\{\sum_{k\in\mathcal{K}}\sum_{j\in\mathcal{J}}\sum_{m\in\mathcal{M}}c_{kjm}^1 Y_{kjm}^1(\omega)+\sum_{j\in\mathcal{J}}\sum_{i\in\mathcal{I}}c_{ji}^2 Y_{ji}^2(\omega)$$

$$+\sum_{i\in\mathcal{I}}\sum_{g\in\mathcal{G}}(c_{ig}^3+p_i^2)Y_{ig}^3(\omega)+\sum_{l\in\mathcal{L}}\sum_{j\in\mathcal{J}}p_l^1 W_{lj}(\omega)+\sum_{g\in\mathcal{G}}\rho U_g(\omega)+c^o c^{t+}(\omega)\}$$

subject to: (8)-(25)

$$\sum_{k\in\mathcal{K}}\sum_{j\in\mathcal{J}}\sum_{m\in\mathcal{M}}e_{kjm}^1 Y_{kjm}^1(\omega)+\sum_{l\in\mathcal{L}}\sum_{j\in\mathcal{J}}e_{lj}^4 W_{lj}(\omega)+\sum_{j\in\mathcal{J}}\sum_{i\in\mathcal{I}}e_{ji}^2 Y_{ji}^2(\omega)+$$

$$\sum_{i\in\mathcal{I}}\sum_{g\in\mathcal{G}}(e_{ig}^3+e_{ig}^5)Y_{ig}^3(\omega)\le c^{cap}+c^{t+}(\omega)\quad\forall\omega\in\Omega \tag{30}$$

$$c^{t+}(\omega)\ge 0\quad\forall\omega\in\Omega \tag{31}$$

b. Performance criteria for the model related to the intended use:

The main contribution of this research is to develop a mathematical model that aids to the design and management of the supply chain of biodiesel when produced through wastewater treatment. The model captures the stochastic nature of biomass supply and technology development. The model is an extension of the classical two-stage stochastic location-transportation model [5]. The model integrates location, transportation and production-related decisions in the supply chain. The model captures the tradeoffs that exists between costs and emissions in the supply chain. More specifically, the model proposed minimize transportation and production costs, and at the same time, minimize the carbon emissions due to supply chain related activities.

We use the following performance criteria to evaluate the impact of our model:

- We use this model to understand the impacts that potential carbon regulatory policies such as carbon cap, carbon tax, carbon cap-and-trade, and carbon offset mechanism, will have on supply chain designs and operation decisions. We note that currently, there is no federal regulation in the U.S. that restricts carbon emissions resulting from transportation, except for electrically powered transport [14]. However, some regulations have already been enacted at the State level [31]. These regulations force companies to seek additional opportunities to reduce emissions. Our numerical analysis provides interesting observations with respect to the trade-offs that exist between costs and emissions under different regulatory mechanism.
- An important contribution of this research is developing an L-shaped based algorithm to solve the two-stage stochastic programming model. The development of this algorithm was inspired and reflects characteristics of the problem on-hand. Numerical experiments show that the algorithm provides high quality solutions in a reasonable amount of time. We implement the algorithm on a case study developed using real-life data from the state of Mississippi. The numerical analysis provides several managerial insights to aid companies in making supply chain-related decisions.

c. Test results do demonstrate the model performance criteria were met:

Results from Problem Formulation Without Carbon Emissions Considerations:
Based on our experiments, the total expected cost of delivering biodiesel is \$2.72 per gallon. Recall that, we consider sludge is obtained at no cost. 77.94% of the delivery cost represents biocrude plant investment and operating costs, 16.54% represents biodiesel production costs, and 5.52% represents transportation costs. Investment and operating costs contribute the most to the final product's cost for several reasons. This is mainly because investment costs for building a biocrude plant are typically high. This is the case with facilities that produce other types of second-generation biofuels. Second, plant capacities considered in this analysis are relatively small due to biomass availability in the state and high transportation costs for shipping sludge over long distances. Therefore, companies

cannot take advantage of economies of scale associated with high production capacities. Finally, the conversion rates used in our experiments are relatively low.

Our model considers that alternative products, such as petroleum-based diesel, or refined soy-based biodiesel can be used to meet demand in case biodiesel production is low. observed that the market price for petroleum-based diesel has fluctuated between \$4.50/gallon and \$5.00/gallon, and the market price for refined soy-based biodiesel has fluctuated between \$4.00 and \$4.50/gallon [20]. The \$2.72 is not a market price; it only represents costs, but not profits made by different players in the supply chain. We perform a sensitivity analysis to evaluate the impact that the cost/price of competitive products has on sludge-based biodiesel production. This is accomplished by changing the value of the penalty cost, π_g, from \$2.20/gallon to \$3.00/gallon. The graph in Figure 2 presents the results of this analysis. Based on these results, substitute products would satisfy all market demand when the market price is between \$2.20/gallon to \$2.50/gallon. as the cost/price for substitute products increases, the use of sludge-based biodiesel increases. However, about 31% of the demand for biodiesel is not met even in the case when substitute products are more expensive. This is due to the limited availability of sludge in Mississippi, which consequently limits biodiesel production.total system cost line represents the cost of satisfying market demand. For small values of penalty costs, the graph represents the penalty (the loss of profit) for not satisfying market demand. For high values of the penalty costs, the graph represents the total of biodiesel production and transportation costs, as well as the penalty cost of not satisfying 31% of the market demand.

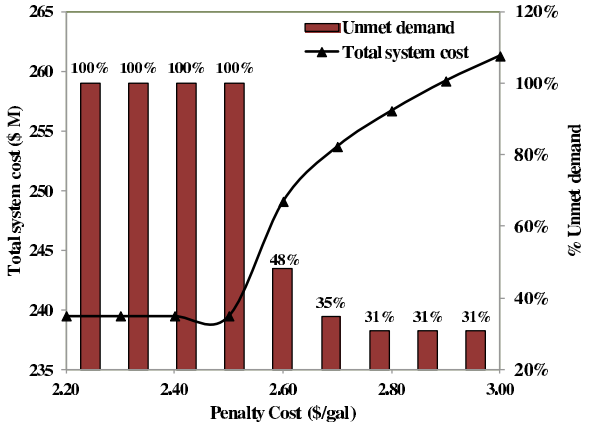
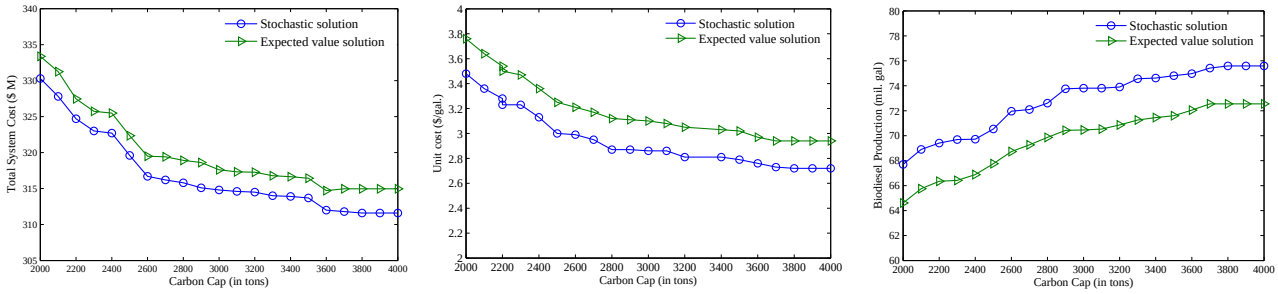


Figure 2: Penalty costs versus total system costs and performance

Results from Problem Formulations with Carbon Emission Considerations:

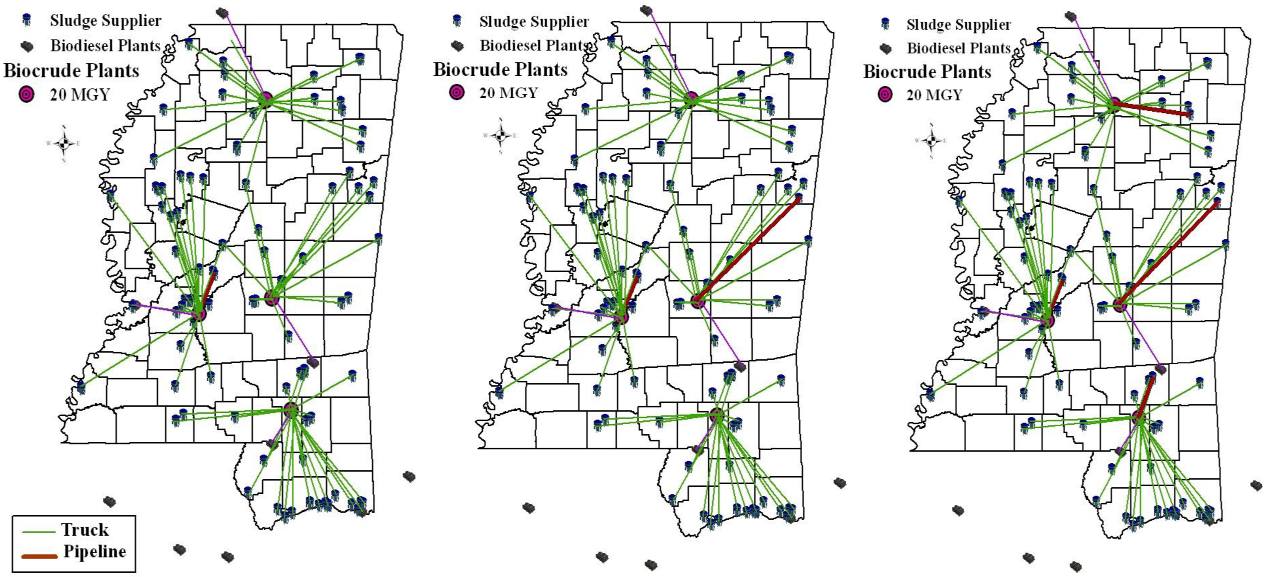
Computational analysis of (BSCN-Cap) : Figure 3 shows the impact of varying emissions caps on total system costs and biodiesel production. Each graph has two lines, one that presents the results from the stochastic solution for model (BSCN-Cap) and the other that presents the results of the corresponding expected value solution. In order to generate these results, we consider only supply uncertainties. Figure 3(a) presents the relationship between the carbon cap and total system costs; 3(b) presents the relationship between the carbon cap and the unit cost; and 3(c) presents the relationship between the carbon cap and biodiesel production. Comparing the stochastic and expected value lines shows that the stochastic solution outperforms the expected value solutions. The stochastic models identify solutions which result in, on average, savings of \$2.99 million per year and an average increase of production by 3.08 MGY.

The results indicate that biodiesel production decreases and total system costs increase as the carbon cap gets tighter. However, note the stepwise shape of the graphs as the carbon cap decreases. This shape indicates that the decrease in production and increase in costs is not smooth with the decrease of the carbon cap. A carbon cap is a hard constraint for the system and directly impacts its emissions (see Figure 8(a)). As the cap gets tighter, the system design and management is adjusted to meet emissions requirements at a slight increase in costs. For example, reducing the carbon cap from 3,200 tons/year to 2,900 tons/year does not impact biocrude production (see the stochastic solution in Figure 3(c)), but it does impact costs. Total systems cost increases from \$314 million to \$317 million. The 9.7% reduction in emissions, due to the change on the carbon cap, results in a 0.96% increase in the total system costs. This indicates the potential to reduce carbon emissions in the supply chain through changes in supply chain operations at minimum cost.



(a) Carbon cap vs. total system cost (b) Carbon cap vs. unit cost (c) Carbon cap vs. biodiesel production

Figure 3: Carbon cap versus total system costs and biodiesel production under feedstock supply uncertainty



(a) 2800 tons/year (b) 2400 tons/year (c) 2000 tons/year

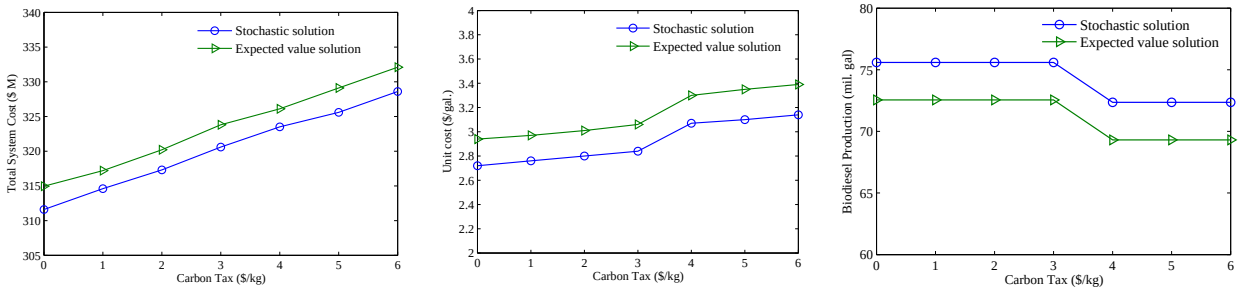
Figure 4: Supply chain designs for different carbon caps

Figure 4 presents supply chain designs for different carbon caps. The darker lines in the graphs represent pipelines established between biocrude plants and their suppliers. For example, at a cap of 2,800 tons/year, a pipeline of capacity 31,500 TPD is established between Peco Foods Poultry Processing Plant in Madison County and the biocrude plant located in Hinds County. Note that, as the cap gets tighter, more pipelines are established. In Mississippi, truck transportation of sludge is less expensive than pipeline transportation. This is mainly due to the low volume of sludge available and short transportation distances. However, pipeline transportation is more environmentally friendly than truck transportation. This is the reason why more pipelines are established when carbon caps get tighter.

Note that, we assume the fuel efficiency of trucks remains unchanged despite the decrease in the carbon cap or increase in the carbon tax and carbon market price. A related study [17] depicts the positive impact on improvements in truck's fuel efficiency that is reducing supply chain-related emissions.

Computational analysis of (BSCN-Tax): Figure 5 presents the impact of the carbon tax on biodiesel production and total unit costs. Figure 5(a) indicates that increasing the carbon tax directly (linearly) increases total unit costs. However, biodiesel production (Figure 5(c)) is not impacted when the tax rate is less than \$3/kg (or equivalently \$3,000/ton) of CO_2 because the unit delivery cost of biodiesel is less than \$3/gallon. The increase in tax beyond \$3/kg of CO_2 increases the unit cost of biodiesel beyond \$3/gallon, and therefore, other substitute products are used instead. The graphs in Figure 5 also indicate that the stochastic model outperforms the expected value solution. The average cost savings from the stochastic solutions are \$3.16 million/year and the average production increase is 3.05 MGY.

A recent survey conducted by the Intergovernmental Panel on Climate Change (IPCC) found that an optimal carbon tax rate would be between \$3 and \$95 per metric ton. 100 related studies were used to estimate a range

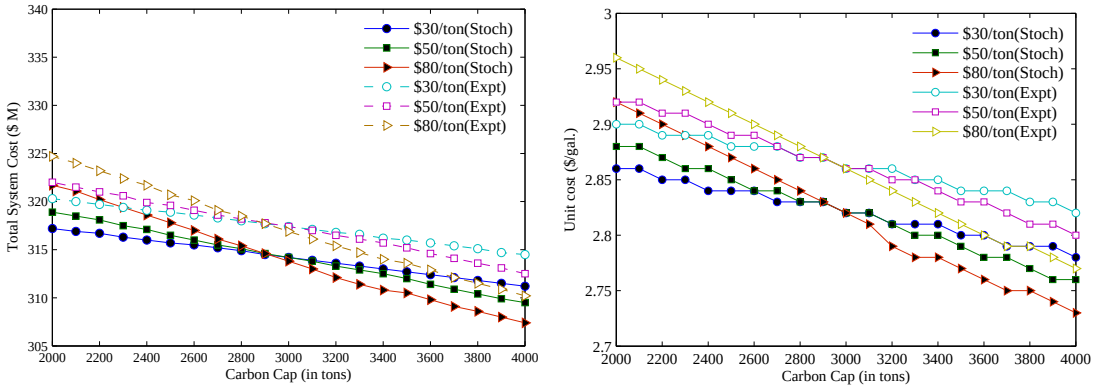


(a) Carbon tax vs. total system cost (b) Carbon tax vs. unit cost (c) Carbon tax vs. biodiesel production

Figure 5: Carbon tax versus costs and biodiesel production under feedstock supply uncertainty

for the optimal tax rate [19]. The values of tax rates we use in our analysis are very high. We used such values in order to identify the level of tax rate which impacts decisions about supply chain design and management.

Computational analysis of (BSCN-CAT):



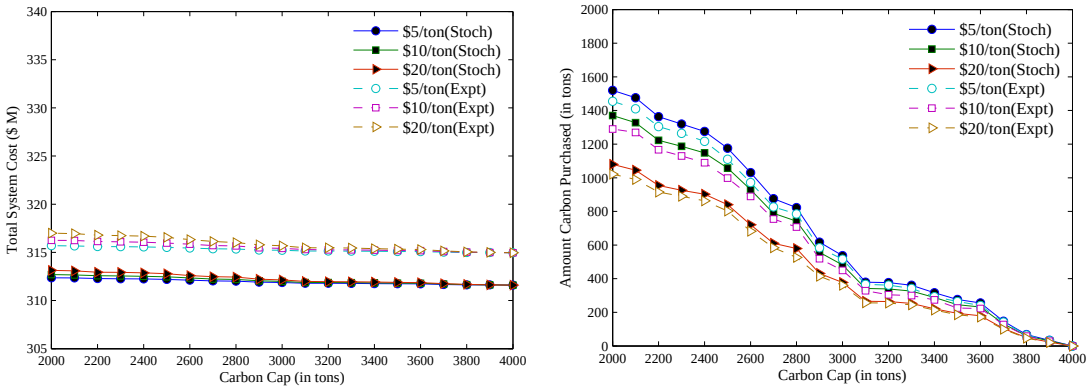
(a) Carbon cap versus total system cost (b) Carbon cap versus unit cost

Figure 6: Carbon price versus costs under a carbon cap-and-trade policy

Figure 6 represents the relationship between carbon cap, total system costs, unit cost at different carbon market prices. The figure indicates that an increase in the carbon market price would result in lower supply chain costs when the cap is loose and higher costs when the cap is tight. This is because at low cap and at high carbon price, there is an incentive for companies to sell carbon credits which are considered an additional source of income. However, as the cap becomes tighter, it costs more to buy additional credits and results in higher supply chain costs. In all the experiments we performed, biodiesel production was maintained because the unit cost of biodiesel is less than the $3/gallon, which is assumed to be the market price for substitute products. Figure 6 plots the stochastic and expected value solutions. The average cost savings under the stochastic solution are $3.12 million/year.

Computational analysis of (BSCN-CO): Figure 7 shows the effect of a carbon offset mechanism on total system cost and on the amount of carbon credits purchased. We consider three different carbon offset prices c^o ($/ton) $\in \{5, 10, 20\}$. The motivation for selecting these values was the observation that in the last few years the carbon offset price has varied from $2.75/ton-$12/ton (Chicago Climate Exchange). Decreasing the carbon cap implies that the amount of carbon credits available to maintain supply chain activities is decreasing. Thus, in order to maintain its operations, this supply chain is faced with these decisions: (a) reduce production; (b) purchase additional carbon credits in the market; or (c) modify supply chain operations. Figure 7 indicates that the amount of carbon credits purchased increases as the carbon cap gets smaller. The higher the market price, the smaller the amount of credits purchased. There is a difference in the total system costs and the amount of carbon traded as we move from the stochastic to the expected value solution. The average savings from the stochastic solution are $3.46 million/year.

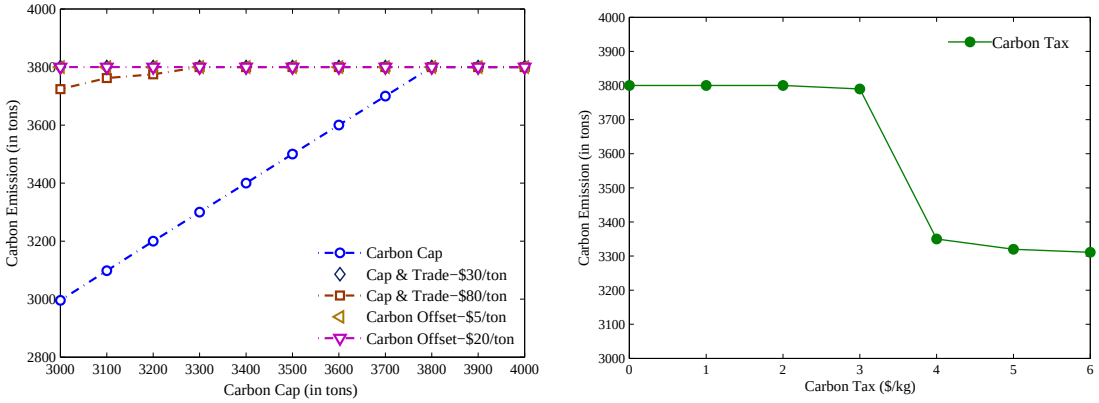
Figure 8 shows the impact of different regulatory mechanisms on carbon emissions in the supply chain. The results are grouped in two figures. Figure 8(a) shows the impact of a carbon cap on emissions. A carbon cap is enforced by the carbon cap, carbon cap-and-trade and carbon offset mechanisms. Figure 8(b) shows the impact



(a) Total system cost vs. carbon cap

(b) Amount carbon purchased vs. carbon cap

Figure 7: Carbon price versus total system costs and amount of carbon purchased under carbon offset policy



(a) Carbon emission vs. carbon cap

(b) Carbon emission vs. carbon tax

Figure 8: The effect of carbon caps and tax prices on carbon emissions under different carbon regulatory policies

of the carbon tax on emissions. The results of Figure 8(a) indicate that the carbon cap is a hard constraint in a carbon cap mechanism. The amount of CO_2 emitted equals the cap. Emissions under the carbon cap-and-trade and carbon offset mechanisms are affected less by the cap. The existence of a market gives this supply chain the opportunity to purchase carbon credits necessary to maintain the operations. A company would purchase carbon credits as long as the additional costs incurred are less than the benefits from maintaining supply chain operations. Figure 8(b) indicates that CO_2 emissions are not affected by the carbon tax when the tax is less than \$3/kg. The tax adds to the cost of the final product. However, for taxes less than \$3/kg, the total unit cost is less than the market price of substitute products. Higher taxes impact production costs and, consequently, impact production quantity and CO_2 emissions.

The focus of regulatory mechanisms such as the ones discusses here is to curb the total carbon emissions in the supply chain of a particular region, or a county, or the whole world. The parameters used in the calculations will differ, but, the mathematical models we propose and the methods we use to calculate emissions can easily adopted to other regions.

Analyzing the Performance of Solution Algorithms: This section describes our computational experiences related to the algorithms proposed in Section when solving the biodiesel supply chain problem. The dimensions of the deterministic equivalent problem are presented in Table 1.

Table 1: Problem size of the deterministic equivalent of the model

$\mid \mathcal{K} \mid$	$\mid \mathcal{J} \mid$	$\mid \mathcal{I} \mid$	$\mid \mathcal{G} \mid$	$\mid \mathcal{M} \mid$	$\mid \mathcal{L} \mid$	$\mid \mathcal{F} \mid$	No. of binary variables	No. of integer variables	No. of continuous variables	No. of constraints
94	26	10	52	3	3	3	104	7,332	8,243	7,732

Table 2 summarizes the results of the algorithms proposed. We use the following terminating criteria for these algorithms: (a) $\varepsilon = 0.01$ (b) $time_{max} = 36,000$ seconds and, (c) $iter_{max} = 1,000$. The first column of Table 2 presents the number of scenarios studied, followed by the solution method used, the corresponding objective function value found, error gap, number of iterations, and running time. The error gap is calculated as follows: Error (in %) $= 100 * (UB - LB)/UB$.

Our computational experience in solving the problem using (BSCN-ML) and (BSCN-LR-ML) algorithms has been very good. The algorithm finds high quality feasible solutions for the master problem in all problem instances. This impacts the quality of solution of the subproblem, and consequently the quality of the overall solution. Algorithms (BSCN-ML) and (BSCN-LR-ML) outperform (BSCN-L) and (BSCN-LR-L) since the multiple optimality cuts added in each iteration do a better job in approximating $\Theta(X, Z, V)$. Both (BSCN-ML) and (BSCN-LR-ML) algorithms provide solutions within 1% error gap in a reasonable amount of time. The other algorithms stop because of the time limit or iteration limit.

We observed that during the initial iterations of the algorithm, the master problem did not receive enough information from the subproblem and therefore, the quality of solutions was poor. We were able to find feasible solutions to the master problem as the number of the optimality cuts increased. Thus, in order to reduce the running time of the Lagrangean-relaxation during the initial iterations of the L-shaped algorithm, we set the error gap for the Lagrangian relaxation algorithm (ε_{LR}) to 0.05. This error gap is dynamically adjusted to 0.01 as the algorithm progresses and the gap between upper and lower bound of the L-shaped algorithm improves. Often, during the initial iterations of the L-shaped algorithm, the Lagrangian-relaxation algorithm did not converge to the pre-specified error gap. This is why we terminate the Lagrangian-relaxation algorithm when one of the following criteria is met: (i) the improvement on the lower bound after r consecutive iterations is below a threshold value; or (ii) the maximum number of iterations is reached. We proceed solving the subproblem by using the best known feasible solution of the master problem obtained so far.

When solving problems of large size, the chances are that the optimality gap of Lagrangian-relaxation algorithm may still be greater than zero. In this case the readers are encouraged to apply well-known techniques, such as, branch and bound [9], variable fixing [29] and reduction tests [9] to reduce this optimality gap.

Note that, CPLEX also emerges as a good tool to solve the problem within 1% error gap for all the instances studied. However, the running time of CPLEX is, on average, 3.3 and 25.7 times higher as compared to (BSCN-ML) and (BSCN-LR-ML).

Table 2: Comparison of solution quality

$\|\Omega\|$	Solution Method	Obj. Val. ($ M)	Error (%)	No. of iter.	CPU time (sec)
5	CPLEX	311.5	0.91	N/A	3,487.1
	BSCN-L	312.4	3.09	1,000	3,541.8
	BSCN-ML	312.3	0.90	97	974.7
	BSCN-LR-L	313.3	3.46	1,000	2,812.3
	BSCN-LR-ML	312.4	0.97	43	192.4
6	CPLEX	309.9	0.97	N/A	4,712.4
	BSCN-L	311.9	3.42	1,000	8,816.8
	BSCN-ML	311.4	0.94	194	1,214.9
	BSCN-LR-L	312.8	3.48	1,000	4,221.7
	BSCN-LR-ML	311.5	0.90	47	201.9
7	CPLEX	312.9	0.94	N/A	5,489.7
	BSCN-L	316.8	3.95	1,000	9,845.7
	BSCN-ML	314.5	0.92	210	1,411.1
	BSCN-LR-L	317.6	4.18	1,000	4,301.4
	BSCN-LR-ML	315.0	0.95	56	248.6
8	CPLEX	310.4	0.93	N/A	6,626.5
	BSCN-L	313.9	3.66	1,000	11,341.2
	BSCN-ML	313.4	0.86	256	2,089.1
	BSCN-LR-L	316.8	4.13	1,000	6,097.6
	BSCN-LR-ML	313.8	0.96	68	281.8
9	CPLEX	311.4	0.87	N/A	8,478.9
	BSCN-L	315.6	2.76	1,000	14,749.1
	BSCN-ML	313.2	0.89	281	3,161.2
	BSCN-LR-L	316.9	5.05	1,000	6,229.4
	BSCN-LR-ML	313.4	0.96	82	303.9
10	CPLEX	310.6	0.98	N/A	13,247.4
	BSCN-L	315.2	4.27	1,000	21,779.1
	BSCN-ML	312.4	0.92	344	3,881.5
	BSCN-LR-L	315.9	4.44	1,000	7,582.8
	BSCN-LR-ML	313.0	0.93	126	409.3

Performance evaluation of stochastic solutions: This section evaluates the performance of the stochastic programming models developed to capture supply and technology development uncertainties. For this purpose, we calculate the expected value of perfect information ($EVPI$) and the value of stochastic solution (VSS). $EVPI$ measures the value of knowing the future with certainty [5]. Thus, $EVPI$ represents the difference between the wait and see solution (WSS) and the objective function value from solving (BSCN). VSS measures the value of stochastic solution and it is calculated as the difference between the objective function value of (BSCN) and the expected value solution (EEV). A summary of these results is reported in Tables 3 and 4.

$EVPI$ is calculated using the results listed in Table 3. The WSS for each scenario are calculated by solving (BSCN) assuming in the future we face this single scenario only. Then, we use these results to calculate $WSS = (\$316.77M + \$287.10M + \$319.67M + \$284.02M + \$298.66M) * 0.15 + (\$269.15M + \$338.22M + \$276.45M + \$304.57M + \$287.69M) * 0.05 = \$299.73M$. Therefore, $EVPI = \$310.9M - \$299.73M = \$11.17M$. This means, if it were possible to know perfectly the future of annual sludge supply, then the total system costs would only be \$299.73M. However, since no one can predict the future, by solving the stochastic programming model, we identify a supply chain with total costs of \$310.9M. The value of $EVPI$ - $\$11.17M$ - indicates how much is worth knowing the future with certainty.

In order to calculate VSS we first need to calculate EEV. Calculating EEV requires two simple steps. We first solve the deterministic version of (BSCN) by using expected values of biomass supply instead. Next, we use this solution to set the values of the first-stage variables in formulation (BSCN) and then resolve. The corresponding objective function value is EEV. Then, $VSS = EEV$ - \$310.90M = \$314.15M - \$310.90M = \$3.25M. Therefore, \$3.25M represents the savings realized by solving the stochastic model formulation (BSCN) rather than solving the corresponding deterministic formulation of our problem.

Table 3: Comparison of stochastic and deterministic solutions under feedstock supply uncertainty

Strategies	Value ($M)	Biodiesel Production (MGY)
Stochastic programming	310.9	75.83
Wait and see solutions		
Scenario-1	316.77	69.98
Scenario-2	287.10	80.34
Scenario-3	319.67	67.74
Scenario-4	284.02	81.62
Scenario-5	298.66	77.56
Scenario-6	269.15	90.71
Scenario-7	338.22	60.48
Scenario-8	276.45	83.96
Scenario-9	304.57	74.40
Scenario-10	287.69	80.25
Expected value solution	314.15	72.71

Similarly, we use the data in Table 4 to calculate $EVPI$ and VSS for the case when we solve (BSCN) under technology development uncertainty. In this case, $WSS = \$303.32M$, and the corresponding $EVPI = \$3.70M$. This means, the value of knowing perfectly the future of technological innovations is \$3.70M. The value of $EEV = \$309.25M$, and $VSS = \$2.23M$. Thus, \$2.23M are the total savings which can result from modeling and solving this supply chain problem as a two-stage stochastic program, rather than solving the corresponding deterministic model.

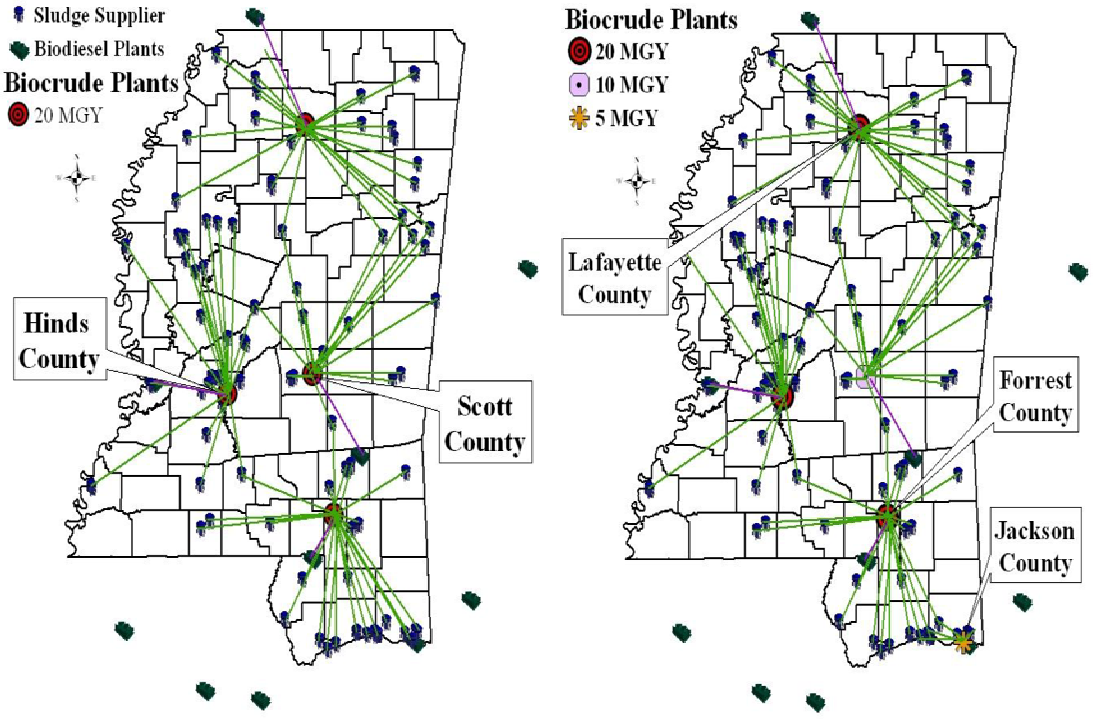
Tables 3 and 4 also present the amount of biodiesel produced under each scenario. The results of Table 4 indicate that, as the conversion rate increases, the amount of biodiesel produced increases.

Figure 9(a) depicts the network design resulting from solving formulation (BSCN). Figure 9(b) depicts the network design of the expected value solution of (BSCN). Both figures consider only sludge supply uncertainties. The structure of the supply chain in these graphs is different. For example, the stochastic model locates biocrude plants with a capacity of 20 MGY in the following counties Hinds, Scott, Lafayette, Forrest. The expected value solution locates biocrude plants in the following counties Hinds, Lafayette, Forrest, Scott and Jackson. The corresponding capacities are 20 MGY, 20 MGY, 20 MGY, 10 MGY and 5 MGY, respectively. As a result, the total system cost from the stochastic solution is \$310.9 M, and the expected value solution is \$314.15 M. The total biodiesel production from the stochastic solution is 75.83 MGY and from the expected value solution it is 72.71 MGY.

In summary, the performance of supply chain is impacted by uncertainties in sludge supply and technology

Table 4: Comparison of stochastic and deterministic solutions under technology development uncertainty

Strategies	Value ($M)	Biodiesel Production (MGY)
Stochastic programming	307.02	74.62
Wait and see solutions		
Scenario 1	344.45	57.62
Scenario 2	317.51	69.14
Scenario 3	303.16	74.70
Scenario 4	288.10	79.68
Scenario 5	266.42	91.30
Expected value solution	309.25	73.34



(a) Stochastic Model Solution

(b) Expected Value Solution

Figure 9: Network representation of the supply chain under stochastic and expected value solution

development. Therefore, it is worthwhile to adopt stochastic programming modeling to design and manage biodiesel supply chains. Experimental results indicate that total cost savings result when a stochastic approach is used to solve the problem as opposed to an expected value approach.

d. Theory behind the model, expressed in non-mathematical terms:

The two-stage stochastic programming model we present allows us to capture the impact of the stochastic nature of sludge supply on location and transportation decisions in the supply chain; it also allows us to capture the timing of decisions in the supply chain. Facility location decisions, pipeline establishment decisions, and decisions about the number of trucks to purchase are long-term decisions made prior to observing the realization of biomass supply. These are the first-stage decisions in our model, which define the structure of the supply chain. Once these decisions are made, then, based on the availability of biomass supply -the realization of supply - the operational decisions related to biocrude and biodiesel production and transportation are made.

The objective function of the biocrude supply chain network (BSCN) design model we propose minimizes the expected annual costs of the supply chain. This objective totals the first-stage costs and the expected second-stage costs. The first-stage costs comprise the annual equivalent investment costs to locate biocrude plants, to install

pipelines, and to purchase trucks at biocrude plants. The second stage costs comprise the expected production, transportation, and penalty costs.

e. Mathematics to be used, including formulas and calculation methods:

Algorithmic Approaches:
The computational challenges faced when solving the models presented above motivated the development of a number of solution approaches discussed in this section. These computational challenges were inevitable since they represent a special case of the deterministic uncapacitated facility location problem, which has been shown to be NP-hard [10].

In this two-stage stochastic programming model, the first-stage decision variables are integer, but the second-stage decision variables are continuous. Laporte and Louveaux [15] present an algorithm to solve problems which include integer variables in the first-stage. The solutions algorithms we develop rely on and are extensions of the L-shaped method developed by Laporte and Louveaux.

L-Shaped Algorithm: Let $\Theta(X, Z, V)$ denote the expected value of the second-stage sub-problem of (BSCN) for the given values in the first-stage variables. The following is the deterministic equivalent formulation of (BSCN), referred to as (D-BSCN).

$$\text{(D-BSCN)}\quad \text{Minimize z}=\sum_{j\in\mathcal{J}}\sum_{l\in\mathcal{L}}\psi_l X_{lj}+\sum_{f\in\mathcal{F}}\sum_{k\in\mathcal{K}}\sum_{j\in\mathcal{J}}\vartheta_f Z_{fkj}+\sum_{j\in\mathcal{J}}v_1^1 V_j+\Theta(X,Z,V)$$

subject to:

$$\sum_{l\in\mathcal{L}} X_{lj} \leq 1 \qquad \forall j\in\mathcal{J} \tag{32}$$

$$X_{lj} \in \{0,1\} \qquad \forall l\in\mathcal{L}, j\in\mathcal{J} \tag{33}$$

$$Z_{fkj} \in \{0,1\} \qquad \forall f\in\mathcal{F}, k\in\mathcal{K}, j\in\mathcal{J} \tag{34}$$

$$V_j \in Z^+ \qquad \forall j\in\mathcal{J} \tag{35}$$

The L-shaped algorithm is an iterative method. In each iteration, the problem solved is a relaxation of (D-BSCN), which instead of minimizing $\Theta(X, Z, V)$, minimizes an outer approximation of $\Theta(X, Z, V)$. Birge and Louveaux [5] show that $\Theta(X, Z, V)$ is a piecewise linear convex function when the number of scenarios considered $|\Omega|$ is finite. Thus, the linear functions generated by the algorithm lie on or below $\Theta(X, Z, V)$. Iteratively, the algorithm improves this approximation till an optimal solution is found. Laport and Louveaux [15] show that the L-shaped method converges to an optimal solution in a finite number of steps when the optimality and feasibility cuts added are valid; and when for a given set of first stage variables, the value of $\Theta(X, Z, V)$ can be computed.

The performance of the L-shaped algorithm relies on its ability to approximate $\Theta(X, Z, V)$. The following formulation (M-BSCN) is an approximation of model (D-BSCN). This formulation is solved iteratively, and Φ^n is the objective function value obtained at iteration n.

$$\text{(M-BSCN)}\ \Phi^n := \text{Minimize}\ \sum_{j\in\mathcal{J}}\sum_{l\in\mathcal{L}}\psi_l X_{lj}+\sum_{f\in\mathcal{F}}\sum_{k\in\mathcal{K}}\sum_{j\in\mathcal{J}}\vartheta_f Z_{fkj}+\sum_{j\in\mathcal{J}}v_1^1 V_j+\theta$$

subject to: (32)-(35)

$$V_j \leq \sum_{l\in\mathcal{L}} N_l^T X_{lj} \qquad \forall j\in\mathcal{J} \tag{36}$$

$$\sum_{k\in\mathcal{K}}\sum_{f\in\mathcal{F}} Z_{fkj} \leq \sum_{l\in\mathcal{L}} X_{lj} \qquad \forall j\in\mathcal{J} \tag{37}$$

$$\theta \geq \theta^n + \sum_{j\in\mathcal{J}}\{\sum_{l\in\mathcal{L}}\lambda_{lj}^n(X_{lj}-X_{lj}^n)+\sum_{f\in\mathcal{F}}\sum_{k\in\mathcal{K}}\delta_{fkj}^n(Z_{fkj}-Z_{fkj}^n) + \Upsilon_j^n(V_j^n-V_j)\} \qquad \forall n=1,\ldots,N \tag{38}$$

Constraints (36) and (37) are valid inequalities for problem (BSCN). Constraints (36) set an upper bound on the number of trucks (denoted N_l^T) that can be purchased by a facility of capacity $l \in \mathcal{L}$. These two sets of constraints allow investments on purchasing trucks and building pipelines to those locations where facilities are

located. Computational performance indicates that adding these constraints improves the running time of the algorithm.

Let N represents the number of iterations the algorithm has performed so far. In each iteration, (M-BSCN) is solved and the values for (X, Z, V) are obtained. These values become an input for the scenario-based problems (S-BSCN(ω)). The solutions obtained from solving these problems are used to calculate the value for $\Theta(X, Z, V)$. Each scenario-based problem is a linear, capacitated minimum cost network flow problem. The following is the formulation for the scenario-based problem ω during the $n-th$ iteration of the L-shaped algorithm.

(S-BSCN(ω)) $\theta^n(X_{lj}, Z_{fkj}, V_j, \omega) :=$ Minimize

$$\{\sum_{k\in\mathcal{K}}\sum_{j\in\mathcal{J}}\sum_{m\in\mathcal{M}} c^1_{kjm}Y^1_{kjm}(\omega) + \sum_{j\in\mathcal{J}}\sum_{i\in\mathcal{I}} c^2_{ji}Y^2_{ji}(\omega) + \sum_{i\in\mathcal{I}}\sum_{g\in\mathcal{G}}(c^3_{ig}+p^2_i)Y^3_{ig}(\omega) + \sum_{l\in\mathcal{L}}\sum_{j\in\mathcal{J}} p^1_l W_{lj}(\omega) + \sum_{g\in\mathcal{G}}\rho U_g(\omega)\}$$

subject to: (9)-(17) and (21)-(25)

$$X_{lj} = X^n_{lj} \quad : \Lambda^n_{lj}(\omega) \qquad \forall l \in \mathcal{L}, j \in \mathcal{J} \tag{39}$$

$$Z_{fkj} = Z^n_{fkj} \quad : \Delta^n_{fkj}(\omega) \qquad \forall f \in \mathcal{F}, k \in \mathcal{K}, j \in \mathcal{J} \tag{40}$$

$$V_j = V^n_j \quad : \Upsilon^n_j(\omega) \qquad \forall j \in \mathcal{J} \tag{41}$$

The linear equations (38) are constructed for specific sets of values for (X, Z, V). The generation of the $n-th$ linear equation is based on the value of partial derivatives of $\Theta(X, Z, V)$ for changes in X, Z, and V. These values are in fact the dual variables from constraints (39), (40) and (41). Let $\Lambda^n_{lj}(\omega)$, $\Delta^n_{fkj}(\omega)$ and $\Upsilon^n_j(\omega)$ denote the dual variables for the ω scenario-based problem during the $n-th$ iteration of the L-shape algorithm, then the slope coefficients used in the linear equation (38) are computed as:

$$\Lambda^n_{lj} = \sum_{\omega\in\Omega} prob(\omega)\Lambda^n_{lj}(\omega) \tag{42}$$

$$\Delta^n_{fkj} = \sum_{\omega\in\Omega} prob(\omega)\Delta^n_{fkj}(\omega) \tag{43}$$

$$\Upsilon^n_j = \sum_{\omega\in\Omega} prob(\omega)\Upsilon^n_j(\omega) \tag{44}$$

The intercept term is:

$$\theta^n = \sum_{\omega\in\Omega} prob(\omega)\theta^n(\omega). \tag{45}$$

For any given set of values in first-stage decision variables, problems (S-BSCN(ω)) are always feasible. The feasibility of these problems is always maintained because of constraints (17). These constraints enforce customer demand to be satisfied either through production, or through substitute products available in the market. Thus, even in the case when the value of all the first-stage variables is zero, customer demand is still satisfied.

The objective function value of problem (M-BSCN) is a lower bound for (D-BSCN) [5]. This is because (M-BSCN) minimizes instead an outer approximation of the convex function $\Theta(X, Z, V)$. For a given set of first stage variables, the scenario based problems are used to calculate the actual value of $\Theta(X, Z, V)$. At each iteration, a solution of the master problem and its subproblem provides an upper bound for the original problem (BSCN). The L-shaped algorithm terminates when the relative error gap between the generated lower and upper bounds is less than ϵ.

Table 5, in Appendix B, describes the L-shaped algorithm. We use CPLEX to solve (M-BSCN) and (S-BSCN(ω)) for all $\omega \in \Omega$. The computational efficiency of this algorithm depends mainly on the computational efforts required to solve (M-BSCN). The algorithms discussed next aim to reduce the running time of this algorithm.

Multi-cut L-Shaped Algorithm: The L-shaped algorithm adds a single optimality cut in each iteration of the master problem (M-BSCN). This cut aims to approximate the solution space of the scenario-based subproblems (S-BSCN(ω)). Instead, in every iteration of the multi-cut L-shaped algorithm, $|\Omega|$ linear equations are added to the first stage problem. These additional constraints are generated by disaggregating the single cut (38) used in the L-shaped algorithm. The following (MC-BSCN) is the first stage problem solved when using this algorithm.

(MC-BSCN) $\Phi^n :=$ Minimize $\sum_{j\in\mathcal{J}}\sum_{l\in\mathcal{L}} \psi_l X_{lj} + \sum_{f\in\mathcal{F}}\sum_{k\in\mathcal{K}}\sum_{j\in\mathcal{J}} \vartheta_f Z_{fkj} + \sum_{j\in\mathcal{J}} v^1_1 V_j + \sum_{\omega\in\Omega} prob(\omega)\theta_\omega$

Subject to: (32)-(35)

$$\theta_\omega \geq \theta_\omega^n + \sum_{l\in\mathcal{L}}\sum_{j\in\mathcal{J}} \Lambda_{lj\omega}^n (X_{lj} - X_{lj}^n) + \sum_{f\in\mathcal{F}}\sum_{k\in\mathcal{K}}\sum_{j\in\mathcal{J}} \Delta_{fkj\omega}^n (Z_{fkj} - Z_{fkj}^n) + \sum_{j\in\mathcal{J}} \Upsilon_{j\omega}^n (V_j^n - V_j) \quad \forall n = 1,\ldots,N, \omega \in \Omega \tag{46}$$

To solve this problem we slightly adjust the algorithm presented in Table 5, in Appendix B. These modifications are: STEP 3 is not executed, and STEP 4 solves (MC-BSCN) instead.

The multi-cut L-shaped algorithm was introduced by Birge and Louveaux [4] to enhance the convergence of the L-shaped algorithm. The algorithm is expected to take fewer number of iterations to reach optimality. However, each iteration is likely to take longer due to the larger set of constraints in (MC-BSCN). This is particularly true when the restricted master problem is a mixed integer program.

Lagrangian Relaxation with L-Shaped Algorithm: We developed a problem-specific, Lagrangian relaxation-based algorithm to solve (M-BSCN) problem within the L-shaped algorithm. We relax constraints (32) and obtain the following Lagrangian relaxation problem.

(LR-BSCN) $L(\Xi) = \min \sum_{j\in\mathcal{J}}\sum_{l\in\mathcal{L}} \psi_l X_{lj} + \sum_{f\in\mathcal{F}}\sum_{k\in\mathcal{K}}\sum_{j\in\mathcal{J}} \vartheta_f Z_{fkj} + \sum_{j\in\mathcal{J}} v_1^1 V_j + \theta + \sum_{j\in\mathcal{J}} \Xi_j (\sum_{l\in\mathcal{L}} X_{lj} - 1)$

subject to: (33)-(38).

Ξ_j are the Lagrangian multipliers where $\Xi_j \geq 0; \forall j \in \mathcal{J}$. We use a subgradient method [21] to solve the Lagrangian dual problem. Table 6 in Appendix B provides the details of the Lagrangian relaxation algorithm. Within the L-shaped algorithm presented in Table 5, this algorithm is used instead of STEP 1.

The algorithm starts by initializing the decision variables, iteration number (r), and a threshold value of the error gap (ε_{LR}). The purpose of initializing the decision variables is to start the algorithm with an upper bound value which is better than some arbitrarily high value. We use a simple procedure that opens the minimum number of facilities to ensure that the expected customer demand is satisfied. Next, the algorithm calculates a minimum number of trucks to purchase to ensure the delivery of biomass supply to each facility. Formulation (LR-BSCN) is then solved using CPLEX. The solution to this relaxation is a lower bound for (M-BSCN). Thus, it is also a lower bound for model (BSCN). When the relative gap between the lower and the upper bounds generated is smaller than the threshold value ε_{LR}, the algorithm stops. Otherwise, the values of Lagrangian multipliers are updated, and problem (LR-BSCN) is resolved.We refer the readers to a recent study by Rawls and Turnquist [23] for details about the convergence and computation performance of this heuristic approach.

Lagrangian Relaxation with Multi-cut L-Shaped Algorithm: The Lagrangian relaxation algorithm is also used with the Multi-cut L-shaped algorithm to solve the first-stage problem. The following is the corresponding Lagrangian relaxation problem obtained by relaxing constraints (32).

(LR-M-BSCN)

$$L(\Xi) = \min \sum_{j\in\mathcal{J}}\sum_{l\in\mathcal{L}} \psi_l X_{lj} + \sum_{f\in\mathcal{F}}\sum_{k\in\mathcal{K}}\sum_{j\in\mathcal{J}} \vartheta_f Z_{fkj} + \sum_{j\in\mathcal{J}} v_1^1 V_j + \sum_{\omega\in\Omega} prob(\omega)\theta_\omega + \sum_{j\in\mathcal{J}} \Xi_j (\sum_{l\in\mathcal{L}} X_{lj} - 1)$$

subject to: (33)-(37), and (46)

$$\Xi_j \geq 0 \qquad \forall j \in \mathcal{J}.$$

Similar to the Lagrangian-relaxation algorithm in Table 6, the algorithm developed to solve $L(\Xi)$ relies on using the subgradient algorithm to determine the value of the Lagrange multipliers. We follow the same steps as explained in Algorithms 1 and 2. Algorithm 2 finds lower bounds to (BSCN) by solving the (LR-M-BSCN) formulation using the Lagrangian relaxation algorithm.

f. Whether or not the theory and mathematical algorithms were peer reviewed, and, if so, include a summary of theoretical strengths and weaknesses:

Efficient solution approaches have been developed for solving two-stage stochastic mixed integer programming problems. Some of the approaches use variations of branch-and-bound algorithm to solve the problem, or, when

Table 5: **Algorithm 1:** L-shaped algorithm for BSCN problem (BSCN-L)

STEP 0:
Initialize, ε. Set, $n \leftarrow 1$, $LB \leftarrow -\infty, UB \leftarrow +\infty$
STEP 1:
Solve (M-BSCN) to obtain Φ^n, X_{lj}^n, Z_{fkj}^n, V_j^n
If $(\Phi^n > LB)$ **Then**
$LB \leftarrow \Phi^n$
End If
STEP 2:
For all $\omega \in \Omega$ **Do**
Solve (S-BSCN(ω)) to obtain $\theta_\omega^n, \Lambda_{lj}^n(\omega), \Delta_{fkj}^n(\omega), \Upsilon_j^n(\omega)$
End for
Calculate θ^n using (45)
$\varrho^n \leftarrow \theta^n + \sum_{j\in\mathcal{J}}\sum_{l\in\mathcal{L}} \psi_l X_{lj} + \sum_{f\in\mathcal{F}}\sum_{k\in\mathcal{K}}\sum_{j\in\mathcal{J}}$
$\vartheta_f Z_{fkj} + \sum_{j\in\mathcal{J}} v_1^1 V_j$
If $(\varrho^n < UB)$ **Then**
$UB \leftarrow \varrho^n$
End If
STEP 3:
Calculate $\Lambda_{lj}^n, \Delta_{fkj}^n, \Upsilon_j^n$ using (42), (43), (44)
STEP 4:
If $((UB - LB)/UB < \varepsilon)$ **Then STOP**
Else
Add to (M-BSCN):
$\theta \geq \theta^n + \sum_{l\in\mathcal{L}}\sum_{j\in\mathcal{J}} \Lambda_{lj}^n(X_{lj} - X_{lj}^n) + \sum_{f\in\mathcal{F}}\sum_{k\in\mathcal{K}}$
$\sum_{j\in\mathcal{J}} \Delta_{fkj}^n(Z_{fkj} - Z_{fkj}^n) + \sum_{j\in\mathcal{J}} \Upsilon_j^n(V_j^n - V_j)$
$n \leftarrow n + 1$; **GoTo STEP 1**
End If

appropriate, use extensions of Benders decomposition algorithm. Escudero et al. [11] provide an efficient branch-and-fix coordination method for solving large-scale, two-stage stochastic problems with mixed 0-1 first stage variables. Ahmed et al. [2] developed a branch-and-bound algorithm for solving two-stage stochastic integer programs with mixed-integer first-stage variables, and pure-integer second-stage variables. Sherali and Fraticelli [28], Sen and Higle [25] and Ntaimo and Sen [22] propose branch-and-cut algorithms for solving two-stage stochastic programs having first stage pure 0-1 variables and 0-1 mixed-integer recourse variables.

Caroe and Tind [7] propose a generalized Benders decomposition algorithm to solve two-stage stochastic programming problems that contain 0-1 mixed-integer recourse variables, which are either pure continuous or pure first stage 0-1 variables. Sen and Sherali [26] and Sherali and Zhu [27] propose a modified Benders decomposition algorithm where the integer sub-problems are solved using a branch-and-cut decomposition algorithm. Caroe and Schultz [6] and Hemmecke and Schultz [13] present a branch-and-bound algorithm for solving stochastic programming problems with mixed-integer variables in both stages. Instead of finding an optimal solution, the authors focused on obtaining high quality feasible solutions using a Lagrangian relaxation approach. Takriti and Birge [30] extended these works by developing a Lagrangian relaxation solution method. This method incorporates a Progressive Hedging algorithm [24] which updates the Lagrange multipliers.

Most recently, Rawls and Turnquist [23] propose a Lagrangian based L-shaped algorithm that can solve large scale problem instances in a reasonable amount of time. The general idea behind this extension is to develop an algorithm for finding feasible solutions for the integer variables of the master problem. This is important when the master problem is considered difficult to solve. The Lagrangian based L-shaped algorithm proposed in this paper is an extension of the algorithm proposed in [23]. We have improved the performance of the algorithm by adding valid cuts into the master problem. The computational experience with the biocrude supply chain network model indicates that the algorithm provides high quality solutions.

g. Hardware requirements:

All the algorithms are coded in GAMS 24.2.1 [12] on a desktop with Intel Pentium Centrino Dual computer with 2.80 GHz processor and 1.0 GB RAM. The optimization solver used is ILOG CPLEX 12.6.

Table 6: **Algorithm 2:** Lagrangian relaxation algorithm

STEP 1

Initialize, ε_{LR}, $\overline{X}_{lj}$, $\overline{Z}_{fkj}$, $\overline{V}_j$.

Set, $r \leftarrow 1$, stop $\leftarrow$ **False**, $\Xi_j^r \geq 0$, $no_{impr} \leftarrow 0$, $\eta^r \leftarrow 2$, $s_s \leftarrow 0$

While (stop = **False**) **Do**

Solve (LR-BSCN) to obtain $L(\Xi)^r$, X_{lj}^r, Z_{fkj}^r, V_j^r

If $(L(\Xi)^r > LB)$ **Then**

$LB \leftarrow L(\Xi)^r$

$no_{impr} \leftarrow 0$

Else

$no_{impr} \leftarrow no_{impr} + 1$

If$(no_{impr} > 5)$ **Then**

$\eta^{r+1} \leftarrow \eta^r/2$

$no_{impr} \leftarrow 0$

End If

End If

$\overline{UB} = min\{UB, \sum_{j\in\mathcal{J}}\sum_{l\in\mathcal{L}}\Psi_l\overline{X}_{lj} + \sum_{f\in\mathcal{F}}\sum_{k\in\mathcal{K}} \sum_{j\in\mathcal{J}}\vartheta_f\overline{Z}_{fkj} + \sum_{j\in\mathcal{J}}\nu_1^1\overline{V}_j\}$

If $((\overline{UB} - LB)/\overline{UB} \leq \varepsilon_{LR})$ **Then**

stop $\leftarrow$ **True**

Else

$s_s \leftarrow \eta^r \frac{\overline{UB}-LB}{\sum_{j\in\mathcal{J}}(\sum_{l\in\mathcal{L}} X_{lj}-1)^2}$

$\Xi_j^{r+1} = \max\{0, \Xi_j^r + s_s(\sum_{l\in\mathcal{L}} X_{lj} - 1)\}$

End If

$r \leftarrow r + 1$

End While

h. Documentation (e.g., users guide, model code):

The following GAMS code are attached under the *"GAMS Code-COR Paper"* folder:

- **Deterministic Solution.gms**: Contains the code for the deterministic equivalent of the original model formulation
- **Stochastic Formulation.gms**: Contains the code for the stochastic programming model formulation
- **L-shaped method.gms**: Contains the code for the L-shaped algorithm
- **Multicut L-shaped Algorithm.gms**: Contains the code for the Multi-cut L-shaped algorithm
- **Lagrangian Relaxation with L-shaped (subgradient).gms**: Contains the code for the Lagrangian relaxation with L-shaped algorithm
- **Lagrangian Relaxation with Multicut (subgradient).gms**: Contains the code for the Lagrangian relaxation with Multi-cut L-shaped algorithm

The associated data files needed to run the code are also included in the *"GAMS Code-COR Paper"* folder.

References

1. Corporate Value Chain (Scope 3) Accounting and Reporting Standard. Technical report, World Recourse Institutes.
2. S. Ahmed, M. Tawarmalani, and N.V. Sahinidis. A finite branch-and-bound algorithm for two-stage stochastic integer programs. *Mathematical Programming*, 100:355–377, 2004.
3. S. Benjaafar, Y. Li, and M. Daskin. Carbon footprint and the management of supply chains: Insights from simple models. *IEEE Transactions on Automation Science and Engineering*, 2012. *doi* : 10.1109/$TASE$.2012.2203304.
4. J. R. Birge and F. V. Louveaux. A multicut algorithm for two-stage stochastic linear programs. *European Journal of Operational Research*, 34(3):384–392, 1988.
5. J. R. Birge and F. V. Louveaux. *Introduction to stochastic programming.* Springer, New York, 1997.
6. C. C. Caroe and R. Schultz. Dual decomposition in stochastic integer programming. *Operations Research Letters*, 24:37–45, 1999.

7. C. C. Caroe and J. Tind. L-shaped decomposition of two-stage stochastic programs with integer recourse. *Mathematical Programming*, 83:451–464, 1998.

8. C. W. Chen and Y. Fan. Bioethanol supply chain system planning under supply and demand uncertainities. *Transportation Research Part E*, 48:150–164, 2012.

9. I. Contreras, J. Cordeau, and G. Laporte. The dynamic uncapacitated hub location problem. *Transportation Science*, 45(1):18–32, 2011.

10. G. Cornuejols, G. L. Nemhauser, and L. A. Wolsey. *Discrete Location Theory*, chapter The uncapacitated facility location problem, pages 119–171. John Wiley and Sons, New York, 1990.

11. L. F. Escudero, A. Garin, M. Merino, and G. Perez. A general algorithm for solving two-stage stochastic mixed-integer programs. *Computers & Operations Research*, 36:2590–2600, 2009.

12. General Algebraic Modeling System (GAMS). Available from: `http://www.gams.com/`, 2012.

13. R. Hemmecke and R. Schultz. *Decomposition methods for two-stage stochastic integer programs.*, chapter Online Optimization of Large Scale Systems, pages 601–622. Springer, 2001.

14. K. M. R. Hoen, T. Tan, J. C. Fransoo, and G. J. van Houtum. Effect of carbon emission regulations on transport mode selection in supply chains. Available from: `http://cms.ieis.tue.nl/Beta/Files/WorkingPapers/Beta_wp308.pdf`, 2010.

15. G. Laporte and F. V. Louveaux. The integer L-shaped method for stochastic integer programs with complete recourse. *Operations Research Letters*, 13(3):133–142, 1993.

16. M. Marufuzzaman, S. D. Eksioglu, and R. Hernandez. Environmentally friendly supply chain planning and design for biodiesel production via wastewater sludge. Technical report. Department of Industrial and Systems Engineering, Mississippi State University, 2011.

17. M. Marufuzzaman, S. D. Eksioglu, and R. Hernandez. Optimization models to design and manage environmentally friendly biofuel supply chains. Proceedings of the Industrial & Systems Engineering Research Conference (ISERC), May 19-23, Orlando, Fl, USA, 2012.

18. M. Marufuzzaman, S. D. Eksioglu, and A. Mondala. A techno economic analysis of pipelining wastewater sludge transportation. Proceedings of the Industrial & Systems Engineering Research Conference (ISERC), May 19-23, Orlando, Fl, USA, 2012.

19. G. E. Metcalf and D. Weisbach. The design of a carbon tax. Available from: `http://www.law.harvard.edu/students/orgs/elr/vol33_2/Metcalf%20Weisbach.pdf`, 2009.

20. A. Mondala, K. Liang, H. Toghiani, R. Hernandez, and T. French. Biodiesel production by in situ transesterification of municipal primary and secondary sludges. *Bioresource Technology*, 100:1203–1210, 2009.

21. G. L. Nemhauser and L. A. Wolsey. *Integer and combinatorial optimization*. John Wiley & Sons, Inc., 1988.

22. L. Ntaimo and S. Sen. The million variable 'march' for stochastic combinatorial optimization. *Journal of Global Optimization*, 32:385–400, 2005.

23. C. G. Rawls and M. A. Turnquist. Pre-positioning of emergency suppliers for disaster response. *Transportation Research Part B*, 44:521–534, 2010.

24. R.T. Rockafellar and R.J-B Wets. Scenario and policy aggregation in optimisation under uncertainty. *Mathematics of Operations Research*, 16:119–147, 1991.

25. S. Sen and J.L. Higle. c3 theorem and the d2 algorithm for large scale stochastic mixed-integer programming: set convexification. *Mathematical Programming*, 104:1–20, 2005.

26. S. Sen and H. Sherali. Decomposition with branch-and-cut approaches for two-stage stochastic mixed-integer programming. *Mathematical Programming Ser. A.*, 105:203–223, 2006.

27. H. Sherali and X. Zhu. On solving discrete two-stage stochastic programs having mixed-integer first- and second-stage variables. *Mathematical Programming Ser. B.*, 108:597–611, 2006.

28. H.D. Sherali and B.M.P. Fraticelli. A modification of Benders' decomposition algorithm for discrete subproblems: An approach for stochastic programs with integer recourse. *Journal of Global Optimization*, 22:319–342, 2002.

29. L. V. Snyder and M.S. Daskin. Reliability models for facility location: The expected failure cost case. *Transportation Science*, 39(3):400–416, 2005.

30. S. Takriti and J. Birge. Lagrangean solution techniques and bounds for loosely coupled mixed-integer stochastic programs. *Operations Research*, 48:91–98, 2000.

31. R. B. Williams, B. M. Jenkins, and M. C. Gildart. California biofuel goals and production potential. 15th European Biomass Conference & Exhibition, May 7-11, Berlin, Germany, 2007.